

Scientific Programme - Abstracts

A Postgraduate Educational Programme 3

Session numbers are prefixed by HL, EM, E³, NH, SA, SF, CC, RC, WS, PR, ER, EF
Presentation numbers are prefixed by the letter A

B Scientific Sessions 129

Daily overviews display all sessions' basic details and indicate the page on which the related abstracts can be found.

Sessions and abstracts are listed by days.
Presentations for which the author(s) have submitted additional material and images to EPOST™ are marked with the icon.

Session numbers are prefixed by SS
Presentation numbers are prefixed by the letter B

C Scientific and Educational Exhibits 345

Daily overviews display all sessions' basic details and indicate the page on which the related abstracts can be found.

Sessions and abstracts are listed by days.

Presentations for which the author(s) have submitted additional material and images to EPOST™ are marked with the icon.

Presentation numbers are prefixed by the letter C

D IMAGINE - The Intelligent Department 569

Abstracts are grouped by topics.
Presentations selected for an electronic poster session (EPS) are marked with the icon.
Presentations by ECR Research Grant winners can be viewed in EPOST™.

Presentation numbers are prefixed by the letter D

E Satellite Symposia 577

Presentation numbers are prefixed by the letter E

F Authors' Index 589

This part lists all first authors (including co-authors) and presentation titles, followed by the session number/topic header/identifier in brackets, and the presentation number in italic letters.

G List of Authors & Co-authors 649
List of Moderators 686

This part lists all authors and co-authors followed by the presentation number in italic letters.

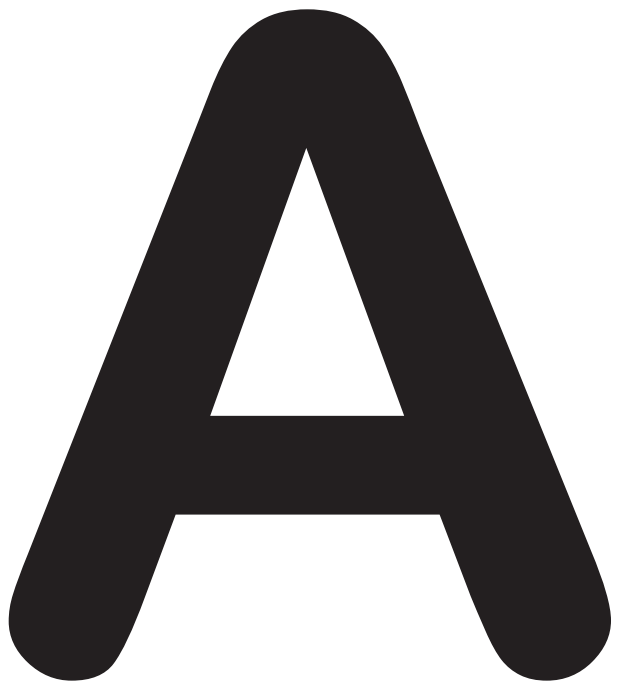
This part lists all moderators followed by the session number in italic letters.

© 2005, European Congress of Radiology, ECR 2005

All articles published herein are protected by copyright, which covers the exclusive rights to reproduce and distribute the articles, as well all translation rights. No material published herein may be reproduced or stored electronically without first obtaining written permission from the publisher. The use of general descriptive names, trade names, trademarks, etc., in this publication, even if not specifically identified, does not imply that these names are not protected by the relevant laws and regulations. While the advice and information in this publication is believed to be true and accurate at the date of publishing, neither the authors, the editors, nor the publisher can accept any legal responsibility for any errors or omissions that may be made. The publisher makes no warranty, express or implied, with respect to the material contained herein.

ECR accepts no responsibility for errors or misprints.

The abstractbook is printed on environment-friendly paper.



Postgraduate Educational Programme

Honorary Lectures (HL)
"ECR meets" (EM)
European Excellence in Education (E³)
New Horizons Sessions (NH)
State-of-the-Art Symposia (SA)
Special Focus Sessions (SF)
Categorical Courses (CC)
Refresher Courses (RC)
Workshops (WS)
Primer (PR)
Joint ECR/EAR Sessions (ER)
EFOMP Workshop (EF)

Friday.....	5
Saturday	31
Sunday	61
Monday	89
Tuesday	115

Postgraduate Educational Programme

Friday, March 4

Postgraduate Educational Programme

		room A 2nd level	room B 2nd level	room C 2nd level	room E1 entr. level	room E2 entr. level	room F1 entr. level	room F2 entr. level	room G lower level	room H lower level		
07:00											07:00	
07:30											07:30	
08:00											08:00	
08:30											08:30	
09:00		CC 117 Essentials of Neuroradiology Ischemic stroke (p. 8)	RC 110 Musculoskeletal Sports injuries (p. 8)	SF 1 Special Focus Session Computer assisted diagnosis (p. 9)	RC 102 Breast Breast MR imaging (p. 10)	RC 101 Abdominal and Gastrointestinal MR of the colon and rectum (p. 11)	RC 104 Chest Smoking-related diseases (p. 11)	RC 111 Neuro Imaging of normal anatomy and function (p. 12)	RC 108 Head and Neck Salivary glands (p. 13)	ER 126 Joint ECR/EAR sessions: Challenges for European Radiology Harmonization of training programmes: Myth or reality? (p. 13)		09:00
09:30											09:30	
10:00											10:00	
10:30											10:30	
11:00		SA 2 State-of-the-Art Symposium Whole-body imaging (p. 17)	SS 210 Musculoskeletal Imaging in orthopedic and traumatologic disorders (p. 134)	SS 201a GI Tract Upper GI tract cancer: Diagnosis and staging (p. 136)	SY 1 Satellite Symposium Real-time virtual sonography (RVS) (p. 578)	SS 202 Breast New developments in breast imaging (p. 138)	SS 204 Chest Pulmonary nodule: Detection and significance (p. 140)	SS 201b Abdominal Viscera (Solid Organs) Focal liver lesions: MR imaging contrast agents (p. 142)	SS 208 Head and Neck Salivary glands, mandible and thyroid imaging (p. 144)	SS 209a Interventional Radiology Intervention in the thoracic aorta (p. 146)		11:00
11:30											11:30	
12:00											12:00	
12:30		Opening Ceremony/ Inauguration Lecture/ Presentation of Honorary Members (p. 19)									12:30	
13:00											13:00	
13:30											13:30	
14:00											14:00	
14:30		SS 306 Contrast Media US contrast media (p. 159)	SS 310 Musculoskeletal Invasive and interventional procedures (p. 161)	SS 301a GI Tract Colorectal cancer and staging (p. 163)	SY 2 Satellite Symposium Advances in MR contrast media imaging (p. 578)	SS 302 Breast Digital mammography (p. 165)	SS 304 Chest Computer aided detection (CAD) and volumetry of pulmonary nodules (p. 167)	SS 301b Abdominal Viscera (Solid Organs) Benign biliary disease and liver transplantation (p. 169)	SS 308 Head and Neck Oncologic imaging (p. 172)	SS 309a Interventional Radiology Non-vascular interventional procedures (p. 174)		14:30
15:00											15:00	
15:30											15:30	
16:00											16:00	
16:30											16:30	
17:00											17:00	
17:30											17:30	
18:00		ECR Opening Concert									18:00	
18:30											18:30	
19:00											19:00	

Postgraduate Educational Programme

	room I lower level	room K lower level	room L/M 1st level	room N/O 1st level	room P lower level	room W basement	room R 1st level	room Y 1st level	room Z entr. level	La Scala 2nd level	
07:00											07:00
07:30											07:30
08:00											08:00
08:30											08:30
09:00	WS 118 Workshops on Interventional Radiology Abdominal intervention (p. 14)	RC 107 Genitourinary Imaging of the female pelvis (p. 15)	CC 116 Infection in the Adult Today Spinocranial infection (p. 16)	RC 106 Contrast Media Contrast media for MR imaging and US liver imaging (p. 16)						E ³ 120 Foundation Course: Chest Radiology Anatomy and basic signs in imaging (p. 17)	09:00
09:30											09:30
10:00											10:00
10:30											10:30
11:00	SS 209b Interventional Radiology Experimental interventions in models and animals (1) (p. 148)	SS 203 Cardiac MR imaging in cardiomyopathy (p. 150)	SS 211 Neuro Inflammatory, infectious and degenerative CNS disease (p. 153)	SS 205 Computer Applications Advanced image processing (p. 155)	SS 215 Vascular Plaque imaging/ Thrombo- embolic disease (p. 157)	WS 222 Vertebroplasty "Hands on" Workshop				E ³ 220a Radiology on the web (p. 18)	11:00
11:30											11:30
12:00											12:00
12:30											12:30
13:00											13:00
13:30											13:30
14:00											14:00
14:30	SS 309b Interventional Radiology Experimental interventions in models and animals (2) (p. 176)	SS 303 Cardiac MR imaging in myocardial infarction (p. 178)	SS 311 Neuro The young and the old brain (p. 180)	SS 305 Computer Applications New developments in PACS (p. 182)	SS 315 Vascular Peripheral circulation (p. 184)	WS 325 Tips and Tricks in Radiofrequency Ablation "Hands on" Workshop				E ³ 320 Interactive Image Teaching Acute abdomen (p. 19)	14:30
15:00											15:00
15:30											15:30
16:00											16:00
16:30	WS 418 Workshops on Interventional Radiology Arterial and venous liver intervention (p. 26)	RC 407 Genitourinary Imaging problem lesions (tumors) (p. 27)	CC 416 Infection in the Adult Today Chest (p. 27)	PR 419 Primer: Molecular Imaging New imaging methods and technologies (p. 28)	RC 405 Computer Applications Tele-imaging in Europe today (p. 29)					E ³ 420 Foundation Course: Chest Radiology Interstitial and alveolar disorders (p. 30)	16:30
17:00											17:00
17:30											17:30
18:00											18:00
18:30											18:30
19:00											19:00

Friday

Postgraduate Educational Programme

08:30 - 10:00

Room A

Essentials of Neuroradiology

CC 117

Ischemic stroke

Moderator:

C. Cognard; Toulouse/FR

A-001

A. Imaging in acute stroke

M.M. Thurnher; Vienna/AT

Although the diagnosis of acute stroke is essentially clinical, neuroimaging plays an important role in the diagnosis of acute ischemia, while it continues to improve our understanding of the underlying pathophysiology. Because of its 24-hour availability, computed tomography (CT) maintains its role as a primary modality in the evaluation of patients with acute stroke. It is still generally considered the "gold standard" for the exclusion of acute cerebral haemorrhage. Typical signs of acute ischemia on CT will be discussed. Recent investigations using perfusion CT have shown major advances in the assessment of acute stroke patients. Compared with CT imaging, abnormal findings are present earlier on magnetic resonance imaging (MR) following acute cerebral ischemia. Diffusion-weighted MR imaging (DWI) is superior to conventional MR imaging, initial CT, and follow-up CT in examination of patients with acute stroke within 24 hours of presentation. Cerebral perfusion can be measured with MR using two different technical approaches: one measures contrast agent bolus through the brain, while the other uses radiofrequency pulses to image inversion of the magnetization inside or outside the imaged slice (spin tagging). Imaging algorithm for examining patients in acute stroke, as well as the "optimal method" for stroke detection, and the "optimal time" to image stroke patient will be described. Thrombolytic therapy has been reported to be most beneficial in patients with cytotoxic edema involving 33% or less of the MCA territory. It is crucial to distinguish patients who will benefit and those who will not have any benefit from thrombolytic therapy.

Learning Objectives:

1. To review the physiology of cerebral blood flow and explain the mechanism of cytotoxic edema.
2. To review the CT imaging findings in acute cerebral infarction.
3. To review the imaging findings in acute cerebral infarction on conventional MR sequences, diffusion-weighted MR imaging (DWI) and MR perfusion.
4. To suggest the algorithm for optimal imaging protocol in acute stroke, discuss optimal time to image the stroke patient, and optimal method for infarct detection.
5. To learn how to select patients which may benefit from treatment with thrombolytics.

A-002

B. Cerebrovascular distribution territories

A. Rovira-Cañellas¹, E. Grivé¹, A. Rovira-Gols², J. Alvarez-Sabin¹;

¹Barcelona/ES, ²Sabadell/ES

Ischemic stroke prognosis, risk of recurrence, clinical assessment and treatment decisions are influenced by stroke subtype (anatomical distribution and causative mechanism of infarction). Stroke subtype diagnosis is better achieved in the early phase of acute ischemia with the use of multimodal MR imaging (diffusion-weighted imaging, and MR angiography).

The pattern of brain lesions as shown by brain MR imaging can be classified according to a modified Oxfordshire method, based on the anatomical distribution of the infarcts into six groups: 1) total anterior circulation infarcts, 2) partial anterior circulation infarcts, 3) posterior circulation infarcts, 4) watershed infarcts, 5) centrum ovale infarcts, and 6) lacunar infarcts.

The subtype of stroke according to its causative mechanism is based on the TOAST method, which classifies stroke into five major etiological groups: 1) large-vessel atherosclerotic disease, 2) small-vessel atherosclerotic disease, 3) cardioembolic source, 4) other determined etiologies, and 5) undetermined or multiple possible etiologies.

The different MR imaging patterns of acute ischemic brain lesions (topography, size and multiplicity) visualized using diffusion-weighted imaging, the pattern of vessel involvement demonstrated with MR angiography, and the presence of previous ischemic lesions detected with conventional MR imaging are essential factors that can suggest the most likely causative mechanism of infarction. This information may have an impact on decisions regarding therapy and the performance of additional diagnostic tests.

Learning Objectives:

1. To be familiarized with the different topographic patterns of ischemic stroke
2. To understand the various causative mechanisms of ischemic stroke.
3. To illustrate the capability of diagnostic imaging for establishing early stroke subtype, which has implications regarding therapeutic decisions and indication for additional diagnostic tests.

A-003

C. Carotid and vertebral artery disease

A. Goulão; Almada/PT

Ischemic strokes may have distinct aetiologies including several different intrinsic arterial pathological disorders. The diagnosis and understanding of these arterial diseases is critical for the correct management of stroke as different treatment approaches are undertaken according to the aetiology. Atherosclerosis is, by far, the most common arterial disease among adults and other pathological processes include arterial dissection, small-vessel disease, inflammatory and noninflammatory vasculopathy and vasomotor disorders. In children there are several vasculopathies responsible for vaso-occlusive disease like sickle-cell anemia, acute regressive angiopathy and Moya-Moya disease, neurofibromatosis, dissections, vasculitis associated with intracranial and systemic infections.

An overview of the major carotid and vertebral pathological diseases responsible for ischemic stroke in adults and children, highlighting the accuracy of the different imaging modalities for its diagnosis and the imaging appearance of these diseases, is given.

Learning Objectives:

1. To recognize the most common causes of carotid and vertebral pathology responsible for stroke for children and adults.
2. To learn the technical principles underling the vascular imaging modalities and realize its accuracy and limitations.
3. To comprehend the value of the different imaging modalities to evaluate the arterial system and establish an imaging protocol for the stroke study in adults and children.
4. To glimpse into the recent applications of MR vascular imaging to study the structure of arterial wall.

08:30 - 10:00

Room B

Musculoskeletal

RC 110

Sports injuries

Moderator:

V.M. Metz; Vienna/AT

A-004

A. Ligamentous injuries of the knee revisited

O. Papakonstantinou; Iraklion/GR

MR imaging of the knee is the most frequently requested MR imaging study of the musculoskeletal system. Due to its multiplanar capabilities and excellent soft tissue resolution MR imaging has provided a new insight into the specific patterns of knee injuries produced by different mechanisms of injury. Normal and abnormal appearances of the ligamentous structures of the knee will be discussed, as well as ancillary findings to the ligamentous injuries, such as meniscal tears and bone marrow contusions. Patterns of knee injuries will be identified with regard to different mechanisms of injury. In recent radiologic literature, it has been emphasized that the distribution of bone marrow contusions may be indicative of the forces that produced the injury. Awareness of the mechanism of injury results in higher detection rates of the abnormalities of the individual anatomic structures that have been involved in a knee injury.

Learning Objectives:

1. To review the normal MR imaging anatomy of the knee ligaments and to describe optimized MR imaging sequences and imaging planes.
2. To describe the MR imaging findings that are diagnostic of or associated to a specific ligamentous injury.
3. To correlate the mechanisms of injury that produce the individual ligamentous injuries, the patterns of knee instability and the patterns of MR imaging findings.

Postgraduate Educational Programme

A-005

B. Sports-related degenerative disease of joints

C. Masciocchi; L'Aquila/IT

Amateur and professional sports activities are of increasing importance in our daily life. This means a correspondingly higher frequency of sports-related injuries, leading to muscular, tendinous, ligamentous and bony pathology. Usually in these conditions, an early and correct diagnosis is required to avoid subsequent joint instability and/or functional impairment. Many of the diagnostic techniques now available play an important role in sports-related diseases; however to choose the right diagnostic protocol it is always necessary to know how traumatic forces acted. The most frequently involved joints are those provided by the largest range of motion: shoulder, knee and ankle. As this field of diseases comprehend both acute and chronic trauma we will consider only the degenerative conditions caused by long-lasting microtraumas and overloads which may lead to stress fractures, synovial hyperplastic reactions, chondral and subchondral suffering, tendinous degeneration, impingement syndromes and entrapment neuropathies (typically involves structures narrowed into bony or ligamentous channels). Plain films are usually the first examinations to perform as they allow the best detection of bony alterations as a consequence of altered loads; being able to clearly depict osteophytes, bone sclerosis and osteochondral fragments. However in many cases plain films may be completely negative as in stress fractures, impingement syndromes and ligament derangements. In these cases Ultrasound, Magnetic Resonance and Computed Tomography allow a complete evaluation of all the remaining soft joint components.

Learning Objectives:

1. To identify critical areas of the joints submitted to dynamic stress related to the athletic movements.
2. To define the different sports-related lesions by means of diagnostic imaging techniques.
3. To emphasize the relevance of the information obtained by means of diagnostic imaging techniques for the subsequent therapeutical approach.

A-006

C. Trauma of the appendicular skeleton

N. Boutry; Lille/FR

Appendicular skeleton injuries are common, often resulting from multiple forces. After a review of the main diagnostic pitfalls, different types of traumatic lesions that affect the appendicular skeleton and their common associations are described. The ability of ultrasonography to evaluate appendicular skeleton injuries is also presented.

Learning Objectives:

1. To provide an overview of the different types of traumatic lesions that affect the appendicular skeleton and their common associations.
2. To review the role of imaging techniques in clinical management and surgical planning of these injuries.

08:30 - 10:00

Room C

Special Focus Session

SF 1

Computer assisted diagnosis

Moderator:

K.-J. Klose; Marburg/DE

A-007

Computer assisted diagnosis (Introduction)

K.-J. Klose; Marburg/DE

The session will reflect basic scientific aspects and the computational background of different clinical application of Computer Assisted Diagnosis (CAD). The first presentation will concentrate on CAD in mammography, which has a long history in the science of CAD. It will highlight, which problems CAD has solved already and how it can be used today. It will also discuss still existing caveats and restriction of this exciting technology.

The second presentation will expand the application of CAD into the field of therapy planning. Radiologists are aware of the goal, that the result of a radiological examination should help the referring physicians, to treat their patients better.

Especially in the demanding field of surgery, not all surgical questions can be reflected in every single radiology report by reading the pictures in traditional

manner, even in a softcopy reading environment. In order to squeeze volume-data-sets for all their inherent information, dedicated post-processing programs (software assistants) are needed. These have to be based on diagnostic radiological aspects as well as on surgical therapy planning considerations, if they should help to reduce information to its maximal benefit in an individual patients situation.

Support of the therapeutic decision making process can also be applied to field of interventional radiology and is addressed by the principles of RF ablation planning tools.

In the last presentation, we will see that the radiologist must learn, that reading competence relies mainly on lesion detection, which can be improved by the support of dedicated CAD software tools.

Learning Objectives:

1. To learn, how CAD can help the individual radiologist to improve the quality of his diagnostic capabilities.
2. To learn, how structured reporting supports the radiological decision process.
3. To understand, that radiological findings mostly represent intermediate outcome parameters, which guide therapeutic reasoning and how this can be linked by software assistants.
4. To discuss, how CAD will alter the way, how radiologists will work and perform in a CAD-supported future.

A-008

CAD of the breast

N. Karssemeijer; Nijmegen/NL

In breast cancer screening, Computer Aided Detection has evolved into a technology that is widely used in practice to help radiologist to perceive subtle signs of cancer. Current CAD systems can achieve very high sensitivity in the detection of clustered microcalcifications. Some radiologists consider it acceptable to rely on CAD for this feature and restrict search for microcalcifications to areas prompted by CAD. In particular, with soft-copy reading of digital mammograms this can increase productivity dramatically, as time consuming user interaction to fully magnify on the displays each part of all mammograms in an exam can be avoided in that way. For detection of masses and other signs of malignancy current CAD systems are less sensitive, but gradual progress is being made to improve algorithms. In practice the use of CAD appears to be more difficult for detection of masses. Radiologists find it more difficult to dismiss false positives of CAD and appear to need much more training to learn how to use CAD for masses effectively. Detection of masses is to a large extent a problem of interpretation. Fewer errors are made in the initial detection process. Therefore, CAD systems are being developed that are aimed at helping radiologists to characterize suspect abnormalities and to help them making a more reliable estimate of the likelihood that cancer is present. In the future, CAD systems will not be restricted to mammography. New programs are being developed to deal with ultrasound and breast MR imaging.

Learning Objectives:

1. To understand the strengths and weaknesses of current CAD systems.
2. To learn about new developments of CAD technology in breast imaging.

A-009

CAD and intervention planning of the liver

H.-O. Peitgen; Bremen/DE

We will report on new software assistants for the radiological work towards surgery and intervention planning for the liver.

For oncological liver surgery, the issue at hand is to detect and quantify the lesions and evaluate the risks of compromised liver function after resection. To that end the assistant permits the user to choose variable safety margins, determines which vessels are compromised, and then computes the territories supplied or drained by these. As a result the assistant determines the parenchyma at risk from the point of view of compromised branches of the portal vein, hepatic vein, hepatic artery and bile ducts. Finally, based on volumetry and visualization the assistant supports the choice of optimal resection proposals.

For living-donor-liver transplantation the issue at hand is to quantify the risks when a graft or remnant lobe has critical volume; determine, quantify and visualize the risks when grafts or remnant lobes are left with compromised territories (parts that are not properly drained or supplied by the hepatic vascular systems); to determine the appropriate cutting lines interactively and evaluate the risks for the resulting remnants and grafts.

For intervention planning we will demonstrate a new software assistant which simulates an entire RF ablation procedure based on individual patient data. As a

Postgraduate Educational Programme

result of the bio-physical simulation the interventional radiologist can determine whether a lesion can be ablated at all, or is assisted in the optimal placement of the applicator.

Learning Objectives:

1. To comprehend compromised liver function based on CT imaging in liver tumor surgery and living-donor-liver surgery.
2. To understand the radiological role of new preoperative planning tasks for oncological liver surgery, living-donor-liver transplantation, interventional ablation procedures.
3. To become familiar with new risk assessment strategies in the radiological work up for liver surgery and intervention planning.

A-010

CAD of the chest

P. Herzog, C.R. Becker, M.F. Reiser; Munich/DE

Purpose: To assess the performance of a computer aided diagnosis tool for the detection of pulmonary nodules in comparison with three radiologist readers.

Methods and Materials: 75 datasets of MDCT studies of the chest were randomly selected, axial images of 2 mm slice width were obtained and read independently by three readers. Readers were asked to report every pulmonary nodule on a special evaluation form. Furthermore all studies were submitted to a CAD tool (ICAD L, Siemens, Princeton, USA). To evaluate the performance of the CAD tool and the performance of readers, a consensus panel of two experienced chest radiologists validated the nodules found by the readers and the CAD tool.

Results: 772 pulmonary nodules with diameters from 2.5-18 mm were confirmed by the consensus panel. Only 238 nodules were found by the readers (39%), while 402 were missed (61%). The CAD tool detected 730 candidate nodules; 515 were confirmed by the consensus panel (70%) while 223 were dismissed as false positives (30%). Each reader working alone had an average sensitivity of 39%, whereas an individual reader plus ICAD would have had an average sensitivity of 88%, an increase of 49%.

Conclusion: CAD tools have the potential to significantly increase the number of detected pulmonary nodules. Also due to the relatively high rate of false positive findings the most beneficial way of inserting computer aided diagnosis into a the clinical context appears to be in a supportive role, as an aid for experienced human readers.

Learning Objectives:

1. To learn how to use CAD-tools to detect and to evaluate pulmonary nodules.
2. To learn how to avoid pitfalls.
3. To learn how to manage screenees or patients.
4. Indications.

08:30 - 10:00

Room E1

Breast

RC 102

Breast MR imaging

Moderator:

S.H. Heywang-Köbrunner; Munich/DE

A-011

A. When and how

J. Danes; Prague/CZ

MR mammography (MRM) occupies a strong position among other diagnostic imaging methods. The task of a radiologist specialized in "breast imaging" is to rule out malignancy, staging of tumour extent or to set the diagnosis in the easiest and cheapest way, shortest possible time and with minimal patient discomfort. Combination of high quality mammography and sonography is essential. According to our experience as many as 30% of all indications to MRM are incorrect: these are mostly ambiguous focal changes (core biopsy is a method of choice) or findings of dubious microcalcifications. MRM is relatively often indicated on basis of an interpretation of low quality mammograms or substitutes an image with spot compression or magnification. In studies of comparing routine methods, mammography and sonography also underestimated and minimal signs of carcinoma are missed.

Main indications of MRM are: Exclusion of rupture of silicon implant, assessment of scarring after breast conserving therapy, exclusion of multifocality and preoperative assessment of the extent of carcinoma in mammographically dense breast. It is suitable for screening of women with quite high risk of carcinoma (BRCA1, 2

positive) and monitoring of an impact of chemotherapy. On the other hand it is inappropriate for young symptomatic women with dense breasts, in cases of clustered microcalcifications or for differentiation of inflammation from inflammatory (erysipeloid) carcinoma.

Author also describes recommended techniques of imaging and evaluation with emphasis on standardization of procedure. He shows typical examples and cases, where MR mammography was incorrectly indicated or failed.

Learning Objectives:

1. To discuss usual indications and contraindications.
2. To present basic principles and technical aspects.
3. To present analysis and interpretation criteria as well as their results.
4. To present typical cases and common pitfalls.

A-012

B. MR guided interventional procedures

T.H. Helbich; Vienna/AT

Contrast-enhanced MR imaging of the breast has proved to be a valuable tool in the detection and work-up of breast lesions. Most of these lesions are small and not visible by other imaging modalities such as mammography or US. Thus, MR-guided preoperative localization techniques or MR-guided percutaneous biopsy can provide a histologic work-up of such lesions. MR-guided preoperative localization seems to be a well-established procedure. However, MR-guided biopsy is still problematic. Although prototypic biopsy systems have been developed, considerable progress is still required. Thus, needle biopsy currently is not recommended for lesions smaller than 10 mm.

Beside the potential of MR imaging of the breast for monitoring of interventional procedures, MR imaging provides also the impetus for the development of dedicated systems for MR-guided therapy. A variety of minimally invasive procedures have already been used to characterize and treat breast lesions. These therapies include thermal treatments, percutaneous excision or breast lumpectomy, and interstitial radiotherapy.

This course reviews current techniques for MR-guided preoperative localization and percutaneous biopsy in breast lesions. The diagnostic accuracy achievable with these techniques will be discussed. Potential for new research opportunities and directions will be provided.

Learning Objectives:

1. To review current techniques for MR-guided preoperative localization and percutaneous biopsy.
2. To discuss problems related to MR guided interventional procedures (needle artifacts, tissue shift).
3. To present the diagnostic accuracy achievable with these techniques.
4. To provide potentials for new research opportunities and directions.

A-013

C. Future trends: Technique, indications, contrast media

A. Tardivon; Paris/FR

New indications of breast MR imaging are emerging, such as screening in high risk patients with several reports demonstrating its effectiveness for detecting breast cancer. Dynamic contrast-enhanced MR imaging has a high sensitivity but a limited specificity, due to the non selective extravasation of gadolinium chelates from blood into the interstitium of both normal and pathological tissues. New techniques can be added to improve these results. The high capillary perfusion of cancers can be assessed with T2*-weighted first-pass MR imaging (detection of a signal intensity loss after contrast agent injection). Hydrogen MR spectroscopy allows the detection of an abnormal choline resonance peak in cancers. First results of combined MR studies are encouraging with a reported specificity of 100%. MR elastography is an imaging-based method for quantitatively imaging the elastic properties of breast tissue. Preliminary results show a significant difference between normal and malignant tissues. New different contrast agents are under evaluation. Macromolecular contrast media (molecular weight > 10 kDa, large size) should diffuse only across the pathological endothelium of malignant tumours. These agents seem promising and allow quantitative assessment of tumor blood flow and microvascular permeability. Current clinical applications have to define the optimal MR protocols. Ultrasmall superparamagnetic iron oxide agents increase the detection of malignant axillary lymph nodes (no captation after intravenous injection, T2*-weighted sequence) and can be used in association with gadolinium chelates for the staging of breast cancers. Intramammary injection of this contrast medium seems possible for the detection of the sentinel lymph node.

Postgraduate Educational Programme

Friday

Learning Objectives:

1. To present new sequences and new techniques (MR-spectroscopy, MR-elastography, thermo IRM).
2. To focus on new indications (high risk patients, genetic risk).
3. To present new aspects in contrast media research.
4. To present the potentials of MR imaging in axillary lymph node staging.

08:30 - 10:00

Room E2

Abdominal and Gastrointestinal

RC 101

MR of the colon and rectum

Moderator:

B. Marincek; Zürich/CH

A-014

A. Contrast agents and sequences in MR colonography

N. Papanikolaou; Iraklion/GR

MR colonography (MRC) is proposed as an alternative non-invasive technique to CT colonography (CTC) to study the large bowel. The main advantages of MRC include multiplanar imaging capabilities providing cross-sectional and virtual endoscopic views of the colon, superb soft tissue contrast and absence of radiation exposure. Two MRC protocols have been proposed. According to the first, termed as "bright lumen MRC", a gadolinium spiked water solution is administered endorectally to the patient who has previously undergone colonic cleansing to distend the colon, resulting in a homogeneous high signal intensity on heavily T1 weighted 3d gradient echo images. Polyps are demonstrated as filling defects while air bubbles can be differentiated by performing the examination in both supine and prone position. According to the second approach termed as "dark lumen MRC", dense barium or tap water is used to distend the colon in conjunction with post gadolinium 3d gradient echo with fat saturation sequences. The colonic wall and the corresponding polyps exhibit high signal intensity due to gadolinium uptake while the colonic lumen presents with low signal intensity. Recent technical developments are focused on avoiding colon cleansing. According to this method the patient drinks, at each meal, a gadolinium or barium containing contrast agent, 36 hours prior to the examination. The contrast agent is mixed up with stools and consequent changes in their signal intensity resulted in masking of the fecal material during MRC. Spatial resolution of MRC needs to be increased in the future to provide equivalent image quality to CTC.

Learning Objectives:

1. To discuss the relevant merits of individual contrast agents.
2. To review the sequences used in MR colonography.
3. To consider further technical developments.

A-015

B. Clinical applications and results of MR colonography

T.C. Lauenstein; Essen/DE

Magnetic resonance colonography (MRC) has been shown to be an appropriate diagnostic tool for the detection of colorectal pathologies. Similar to contrast-enhanced three-dimensional (3D) MR angiography, MRC is based on the principles of ultra-fast, T1-weighted 3D gradient-echo acquisitions collected within the confines of a single breath-hold. Therefore, the use of an MR system equipped with high-performance gradients is crucial. Two additional requirements need to be fulfilled: bowel distension and a sufficient contrast between the bowel wall and bowel lumen. While bowel distension can be gained by the rectal administration of either liquid or gaseous media, the contrast mechanism strongly depends on the acquired MR-sequences. Initial approaches of MRC were based on the rectal application of water spiked with paramagnetic contrast (bright-lumen MRC). Recently, dark-lumen MRC has been introduced. This technique is based on the acquisition of a T1-weighted sequence after the administration of a water enema and the intravenous administration of paramagnetic contrast. Dark-lumen MRC has turned out to be more accurate and less time consuming than bright-lumen techniques.

Learning Objectives:

1. To review the procedure and performance of MR colonography.
2. To compare patient acceptance and accuracy with other imaging modalities.
3. To consider problems and pitfalls in MR colonography.

A-016

C. MR staging of rectal tumors, problems and pitfalls

R.G.H. Beets-Tan; Maastricht/NL

One of the concerns after rectal cancer surgery is the local recurrence rate. It is now proven through randomized trials that the best local control rate for rectal cancer patients taken together as a whole group is obtained by a short preoperative course of radiotherapy followed by a total mesorectal excision¹⁻³. There are however subgroups of rectal cancer patients with different risks for recurrence. On one side of the spectrum there is the stage I disease who are at very low risk for local recurrence. At the other end of the spectrum is the group of patients with a locally advanced tumor who are at very high risk and who would benefit from a more extensive neoadjuvant treatment schedule. Paramount for the selection and differentiation of treatment is a reliable preoperative test that can distinguish between these groups.

There is recent evidence suggesting that MR imaging can accurately predict the tumor free circumferential resection margin at TME⁴⁻⁷. Our study, published in The Lancet 2001, showed that phased array MR imaging is highly accurate and reliable for the prediction of the circumferential resection margin. The prediction of the T stage however was less accurate and more affected by the experience of the observer.

In this lecture, a review will be given of the different imaging methods for rectal cancer including the appropriate MR technique and problems and pitfalls in interpreting the MR images.

Learning Objectives:

1. Preparation of the patient and contrast agents.
2. To compare staging of rectal cancer by different imaging modalities.
3. To discuss problems and pitfalls in relation to MR staging.

08:30 - 10:00

Room F1

Chest

RC 104

Smoking-related diseases

Moderator:

M. Bellomi; Milan/IT

A-017

A. Emphysema: State-of-the-art

A.A. Bankier; Vienna/AT

Pulmonary emphysema is a common, dangerous, and expensive disease. Because the definition of emphysema is based on pathological morphology, imaging techniques play a major role in the in-vivo assessment of pulmonary emphysema. Beyond a descriptive approach, these imaging techniques can be used to objectively quantify emphysema. This is at the base of the rational allocation of treatment, training or surgery.

This presentation will detail the typical and atypical radiological presentations of emphysema. It will also emphasize the limitations of the subjective assessment of emphysema. To overcome these limitations, methods for the objective quantification of emphysema will be presented. Clinical and pre-clinical applications of objective quantification of emphysema will be presented. Finally, the potential impact of new technologies on the clinical work-up of pulmonary emphysema will be discussed.

Learning Objectives:

1. To increase the awareness of the epidemiological and socioeconomic importance of pulmonary emphysema.
2. To demonstrate typical and atypical radiological features of pulmonary emphysema.
3. To familiarize with the basic technical tools and parameter used and required to accurately quantify emphysema on CT.
4. To inform about the emerging role of functional imaging and the use of advanced techniques in the quantification of pulmonary emphysema on CT.
5. To suggest how emerging new tools for analyzing emphysema could affect the diagnosis and the treatment of this disease.

A-018

B. Smoking-related interstitial diseases

K. Marten; Munich/DE

The spectrum of smoking-related interstitial lung diseases (ILD) encompasses respiratory bronchiolitis, respiratory bronchiolitis-associated interstitial lung dis-

Postgraduate Educational Programme

ease, desquamative interstitial pneumonia, and Langerhans' cell histiocytosis as the most important disorders. Although traditionally being considered as discrete entities, these smoking-related ILD frequently coexist, accounting for the sometimes complex patterns encountered on high-resolution computed tomography. This refresher course discusses the radiologic and pathologic appearances of smoking-related ILD, with emphasis placed on their frequent coexistence.

Learning Objectives:

1. To recognise the variety of interstitial lung diseases that are encountered in cigarette smokers.
2. To understand the HRCT appearances of the "pure" smoking-related interstitial lung diseases.
3. To appreciate the inter-relationship between the various smoking related lung pathologies, particularly the development of interstitial fibrosis.

A-019

C. Sites of airflow obstruction in cigarette smokers

A. Oikonomou; *Alexandroupolis/GR*

Cigarette smoking accounts for most cases of Chronic Obstructive Pulmonary Disease (COPD) - a leading cause of disability and death. Anatomical sites affected in COPD are large and small airways (chronic bronchitis and bronchiolitis) and distal airspaces (centrilobular emphysema). The two major causes of airflow obstruction are: increased airflow resistance related to luminal narrowing (chronic bronchitis) and reduced outflow pressure caused by loss of elastic recoil (emphysema).

In saber sheath trachea - strongly related to COPD - the coronal diameter of intrathoracic trachea is two-thirds of the sagittal one at the same level.

Chronic bronchitis is a clinical diagnosis and radiography has little to offer. Its principal role is to exclude other diseases that may mimic chronic bronchitis. Limited information is also available about HRCT in chronic bronchitis, perhaps reflecting the nebulous nature of this clinical entity; the most common findings being bronchial wall thickening, air-trapping and bronchiolectasis.

HRCT is more sensitive than radiography and PFTs in determining the type, and severity of emphysema and is the best noninvasive technique for detecting early emphysema. Localization of smoking induced emphysema within the secondary pulmonary lobule with radiologic-pathologic correlation and distinction from other types of emphysema (panlobular, paraseptal) as well as the functional - CT correlation will be explored.

The entity of respiratory bronchiolitis - invariably associated with cigarette smoking- will be discussed as a possible mechanism of (early) mixed obstruction and restriction.

Finally the emerging role of hyperpolarized 3He MR imaging ventilation imaging in the evaluation of COPD will be briefly reviewed.

Learning Objectives:

1. To review the anatomy of the structures that can contribute to airflow obstruction as well as the pathophysiology of smoking-related COPD.
2. To discuss the radiologic and CT findings of specific diseases of the large and small airways (chronic bronchitis-bronchiolitis), and distal airspaces (centrilobular emphysema) that cause airflow obstruction in smokers and explore the functional - CT correlation.
3. To describe the entity of respiratory bronchiolitis and discuss its functional significance.
4. To summarise new imaging techniques, such as hyperpolarized 3He MR imaging ventilation imaging offering new insights in the evaluation of COPD.

08:30 - 10:00

Room F2

Neuro

RC 111

Imaging of normal anatomy and function

Moderator:

P.H. Nakstad; *Oslo/NO*

A-020

A. Brain morphology and function

F. Di Salle; *Naples/IT*

Among the astonishing progresses brain imaging has undergone in the last decades, of particular importance is the unveiling of structural details and functional processes of the human brain with unprecedented sensitivity and precision, which has provided revolutionary contributions to neuroscience research. An important

role in these developments has been played by the diffusion of high field MR imaging units for humans. While a few research centres are equipped with very high field MR imaging units, up to 8 T, magnets with field intensity ranging between 3 and 5 T have become relatively common. Consequently, studies of brain structures with high spatial resolution have become possible, as well as the use of high definition 3D sequences, which further enhance the detail of structural analysis of the brain. At the same time, also favoured by the availability of high field units, functional magnetic resonance (fMRI) has become the most widely used approach for studying brain function in humans. The diffusion of fMRI has been favoured by its sensitivity in analysing brain functional phenomena and by the lack of biological invasiveness, resulting in a remarkable flexibility of use. These properties brought the functional examination of the brain within the reach of many researchers and appreciably stimulated the research on brain functional processes. The convergence in one single machine of the potential for highly detailed anatomy and for remarkably precise studies of brain function, created the fertile ground that has promoted the incredible development of our knowledge on brain functional anatomy we have witnessed in these last years.

Learning Objectives:

1. To identify the potential of the new MRI techniques in the study of brain cortical and subcortical anatomy and in the evaluation of white matter connections.
2. To integrate the growing knowledge on brain anatomy with the evaluation of brain functions with fMRI.

A-021

B. Brain stem and cranial nerves

J. Casselman; *Bruges/BE*

The nuclei of cranial nerves III-XII are located in the brain stem and cervical medulla. The nuclei cannot be identified on MR but their location can be deduced if one can visualise the surrounding myelinated structures. This is best achieved using high resolution thin proton density and T2W TSE images with a long TR. In the same way, their fascicular course inside the brain stem can be found.

The cisternal segments, surrounded by CSF, are best seen on axial high resolution GE or TSE T2W images with a thickness of 0.35-1.0 mm. The parasellar course of nerves III-VI, the complete course of the olfactory nerve and optic nerve and tract and the extracranial course of all nerves are best seen on coronal high-resolution gadolinium-enhanced T1W SE images. Axial gadolinium-enhanced MRA TOF images are used to visualise cranial nerves IX-XII inside the jugular foramen.

The function of nerves V-VII-VIII-IX and X are more complex and must be known so that the neuroradiologist is aware which nerve (segment) he must visualise to find the cause of a certain clinical sign. This is sometimes impossible as the correlation between "clinical sign" and "involved nerve branch" can be poor (e.g. trigeminal nerve). Moreover, connections exist between cranial nerves (e.g. V-VII-IX) and their brain stem nuclei (e.g. IX-X-XI). Therefore certain nerves are best imaged as a group. Small peripheral branches of the cranial nerves and the connections between the cranial nerves must be known as lesions and tumors can involve/follow these branches and connections.

Learning Objectives:

1. To learn how to localize nuclei and fascicular segments of the cranial nerves in the brain stem.
2. To find out which technique must be used to visualise the different cranial nerves and nerve segments.
3. To know the major connections between different cranial nerves and brain stem nuclei.
4. To understand which clinical sign correlates with which nerve (segment) involvement.

A-022

C. Spine, spinal cord and circulation of cerebrospinal fluid

M. Schumacher; *Freiburg/DE*

The normal anatomy of the spine and its contents will be presented in terms of function with respect to the biomechanics of the skeletal structures as well as the movements of the spinal cord and the cerebral spinal fluid. It is shown how the spinal cord is adapted to these movements by tension, stretching and displacement. The biomechanical factors that are responsible for the development of chronic vertebrogenic myelopathy as well as the meaning of the axial spinal load will be explained. The anatomical background for loading tests is elucidated. The involvement of different anatomical structures such as viscous, elastic and bony elements is analyzed with regard to the explanation of the functional spinal unit and spinal instability and regions of motion.

Postgraduate Educational Programme

Learning Objectives:

1. To learn how anatomy and function in diseases of the spine is related to each other.
2. To learn, that static investigation of the spine and spinal cord is not enough and how it has to be combined with functional tests.
3. To know, how biomechanical stress produces pain and immobilisation.

08:30 - 10:00

Room G

Head and Neck

RC 108

Salivary glands

Moderator:

J.E. Kabala; Bristol/UK

A-023

A. Choice of imaging technique in patients presenting with salivary gland problems

A. Borges; Lisbon/PT

A variety of imaging modalities are used to visualize the salivary glands including plain films, conventional sialography, ultrasound, CT, CT sialography, MR imaging, MR sialography and nuclear medicine studies. For a rational, cost-effective use of diagnostic imaging it is necessary to tailor the imaging approach to patient's clinical problem/presentation. Two main clinical syndromes determine the appropriate imaging approach: inflammatory/obstructive and mass lesion syndromes. Whereas patients presenting with an inflammatory/obstructive syndrome are best evaluated with ultrasound or CT and some form of sialography, patients presenting with a mass lesion syndrome are preferably evaluated with MR or CT. Sialolithiasis and infectious/non-infectious sialoadenitis are the most common entities presenting with obstructive/inflammatory syndrome whereas benign and malignant neoplasms present as a mass lesion.

Imaging differentiates sialolithiasis from other causes of sialoadenitis. It also identifies the location and number of calculi, detects post-obstructive changes and may establish the etiology of acute and chronic sialoadenitis. Patients with mass lesion syndrome present with a palpable mass. Imaging is tailored to determine its precise anatomic location, the relationship with the facial nerve and to characterize the mass (cystic/solid, single/multiple, benign appearing/aggressive); features which will help to narrow the differential diagnoses. Imaging is also used to guide fine needle aspiration.

Learning Objectives:

1. To become familiar with the most common clinical presentations of salivary gland pathology.
2. To be able to do a cost-effective imaging approach of the most common salivary clinical syndromes.
3. To understand the advantages and limitations of the available imaging modalities.
4. To be able to build a clinically useful differential list based on imaging features.

A-024

B. The value of MR sialography today

M. Becker; Geneva/CH

Similar to MR cholangio-pancreatography, MR sialography is based on the principle that stationary fluids are hyperintense on heavily T2-weighted images. This lecture will first review the different pulse sequences that can be used to perform MR sialography, such as 2D and 3D FSE, RARE, HASTE, GRASE, 3D CISS and 3D EXPRESS. It will discuss their relative advantages and disadvantages, as well as their performance in the diagnosis and management of non-neoplastic diseases affecting the major salivary glands. Emphasis will be placed on the assessment of sialolithiasis, chronic recurrent sialadenitis and sialodochitis, autoimmune diseases, sialosis and cysts. Data from the literature comparing the performance of MR sialography with conventional X-ray sialography will be discussed. Sensitivity, specificity, positive and negative predictive values of the most useful MR sialography sequences will be discussed, as well as how to integrate the information available from these imaging studies with the clinical findings and non-radiologic diagnostic tests. Emphasis will be placed on the correlation between clinico-pathologic presentation and MR sialography findings. In addition, the implications of a precise pre-therapeutic work-up, as well as the key questions that the radiologist has to answer in a specific clinical context will be discussed with respect to treatment.

Learning Objectives:

1. To understand the role, advantages and disadvantages of MR sialography for imaging of non-neoplastic diseases of the salivary glands.
2. To recognize the diagnostic features of sialolithiasis, ductal stenoses, autoimmune diseases and cysts on MR sialography images.
3. To understand the role of MR sialography for the pretherapeutic work-up of these different pathologic entities.

A-025

C. Differential diagnosis in major and minor salivary gland tumors

N.J.M. Freling; Amsterdam/NL

Differential diagnosis of salivary gland masses depends largely on the location of the lesion: preauricular area, parapharyngeal space (PPS), oral cavity (OC), sublingual /submandibular space (SMS). Depending on the tissue constituents within these specific areas, one may assume a different origin of the lesion: major or minor salivary gland, lymph nodes, bone (mandible, skull base), odontogenic, masticator muscles, PPS, subcutaneous origin, vascular. Imaging will help differentiate a solid from a cystic or vascular lesion, and solitary from multiple lesions. To differentiate benign from malignant salivary gland lesions is not always possible. Salivary gland tumours are rare and make up about 3% of all tumours in the general population. About 1% of all head and neck tumours are of salivary origin. Parotid tumours are benign in up to 75%, submandibular and minor salivary gland tumours are malignant in about 50%, sublingual gland tumours are malignant in more than 90%. The age of the patient at presentation will greatly influence differential diagnosis: although solid salivary gland tumours may also occur in children, most of the mass lesions presenting at a very young age are due to vascular or lymphatic malformations. In the adult or elderly, solid salivary tumours outweigh vascular lesions.

Learning Objectives:

1. To locate salivary gland lesions.
2. To know relevant statistical facts about salivary gland tumours.
3. To make a differential diagnosis in view of patient data, clinical data and imaging results.
4. To advise next steps in making a final diagnosis (more imaging, FNAC, biopsy, medical treatment).
5. To consider rare minor salivary gland disease at specific anatomic locations.

08:30 - 10:00

Room H

Joint ECR/EAR sessions: Challenges for European Radiology

ER 126

Harmonization of training programmes: Myth or reality?

Moderator:

P.A. Grenier; Paris/FR

A-026

Current status from a survey

A.H. Karantanas; Iraklion/GR

Harmonization of training programmes in Europe is mandatory if communication and scientific interactions-including professional contracts- among European radiologists is to be attained. To assess the possible success of this endeavour, information on the various systems of training in different countries is required. A survey has been performed in European countries with regard to their radiology training programmes. The survey included questions on the qualifications needed upon entry into training schemes; description of the training schemes; examinations and professional evaluation; current status of sub-specialties with emphasis on the opportunities; statistics on the number of both general or sub-specialized radiologists working in each country.

The survey disclosed similarities and differences on every single topic of the questionnaire. Similarities occur mostly in the duration of training, the obligatory character of formal teaching and the professional evaluation. Differences have been mainly detected in qualification requirements upon entry into training schemes, rotation in sections and departments, check list availability for the trainees, independent action of trainees, opportunities for sub-specialty training and the number of working radiologists per million.

Learning Objectives:

1. To provide information on the current status of radiology training programmes in Europe.

Postgraduate Educational Programme

2. To assess if the differences and similarities in the radiology training programmes among different European countries can be harmonized in terms of efficiency and scientific inter-communication.

A-027

Examples from the West and the East

L. Bonomo¹, A. Urbanik²; ¹Rome/IT, ²Krakow/PL

To attempt a progressive reduction in the gap currently existing between training programmes throughout European countries it is necessary to provide guidelines and curricula for harmonization of training programmes.

At the moment there are big differences of training programmes not only between Western and Eastern in Europe, but even amongst Western European countries. Examples of training programmes will be illustrated underlying some differences. Ways to reduce the main differences will be proposed.

Learning Objectives:

1. To know some examples of training programmes in Western countries.
2. To understand some big differences of training programmes.
3. To learn how it is possible to reduce the existing gaps in training programmes.

A-028

Specific issues for training in a subspecialty

J.-I. Bilbao Jaureguizar; Pamplona/ES

There is a constant expansion of the speciality of Radiology into new areas. The permanent innovation and the continuous search for new applications result in an important expansion of both diagnostic and therapeutic interventional radiology. The concept of a common trunk in the speciality is supporting that, within the homogeneity, it is favoured the training in different radiological subspecialties. Furthermore, and not less important, the multi-disciplinary involvement of radiology in the management of the patient, needs specialists trained in determined abilities and attitudes, who are capable of responding and moulding to such objectives. Therefore, sub-specialisation in radiology is the consequence of the enormous growth in knowledge, and at the same time, is the response to the needs that the new clinical scenarios require.

The radiological subspecialties are based in "organs" (e.g. gastrointestinal), "ages" (e.g. pediatric), and types of pathology (e.g. oncology) or in therapeutic intervention. A radiologist expert in one of these areas, with clinical knowledge and working within a multi-disciplinary team will be of great value to the clinical process. Nevertheless, it is likely that the most demanded sub-specialty, with a greater impact in the composition of a hospital will be the "general radiologist", expert in several areas and with knowledge of basic interventional techniques (biopsy and drainage).

Learning Objectives:

1. To understand the need for the different subspecialties to be able to provide solutions to the particular problems of each patient.
2. To recognise the need for a multidisciplinary approach in patient care and increase our responsibility in the management of patients.
3. To realise the need to focus in a subspecialty area of interest within a broad general radiology training.
4. To envisage and be ready to adapt to the changes that the future may bring.

A-029

Objectives for the future

P.A. Grenier; Paris/FR

To target a future harmonization of training programmes in Europe, EAR will offer information and services to define common education standards, to facilitate exchanges between universities and countries, and to create a European network of excellence in education. The plan of action includes: 1) guidelines and curricula for training in radiology regularly updated and available on the EAR website, 2) recommendations and common procedures for assessing training centres through Europe, 3) development of a self-assessment system and a European diploma, both computer-based and designed through the internet, 4) identification of centers of reference offering training programme in a particular field of interest during the training time (for non certified trainees), or as a CME training (for board-certified radiologists), 5) identification of centers of excellence in the different fields of imaging for teaching the teachers, 6) selection of high quality educational material and courses for recognition and awarding.

Learning Objectives:

1. To present the plan of actions of EAR in the development of a European house for education in radiology.

2. To suggest the promotion of centers of reference in Europe for training in radiology.
3. To suggest the promotion of centers of excellence in Europe to teach the teachers.

08:30 - 10:00

Room I

Workshops on Interventional Radiology

WS 118

Abdominal intervention

Moderator:

R. Morgan; London/UK

A-030

A. Thermal ablation of liver tumors

P. Cabassa; Brescia/IT

In the last 10 years different percutaneous therapies have been used in the curative management of primary and secondary liver tumors in patients not candidate for surgery. The field of image-guided tumor ablation includes chemical ablation (ethanol or acetic acid) and thermal therapies, such as radiofrequency, laser, microwave, ultrasound, and cryoablation. Radiofrequency (RF) is a relatively new image-guided procedure; results are encouraging that this minimally invasive technique could assume a primary role of in the treatment management of patients with both primary and secondary liver neoplasms. In RF ablation, a current induces ionic agitation which results in frictional heat production within the tissue. This heat induces cellular death via coagulation necrosis. Different RF devices are commercially available for RF. These include single tip electrodes or expandible hooks electrode. Electrodes can be placed under US (most frequently), CT or MR guidance.

Treatments are performed under conscious sedation or general anesthesia.

Patient selection is mandatory: Multifocal disease ($n > 5$), lesions adjacent to bowel loops, or patients with severe coagulopathy should be considered not suitable for treatment. Lesion size is the most important factor in determining local therapeutic efficacy. Lesions larger than 4 cm have a high probability of tumor persistence after ablation. The introduction of combined procedures such as RF+embolisation (to reduce blood flow) or RF+saline injection (to increase ionic conductivity) can achieve better results especially in large lesions. The procedure is safe and well tolerated. Major complications are rare and include peritoneal hemorrhage, neoplastic seeding, intrahepatic abscesses, and intestinal perforation.

Learning Objectives:

1. To understand the principles, equipment and techniques of radiofrequency ablation.
2. To know how to do an appropriate case selection.
3. To know the imaging features of the lesions after radiofrequency ablation and their follow-up with regards to local recurrence.
4. To know the place of combined procedures and their potential role in difficult case management.

A-031

B. Management of gastrointestinal bleeding

A. Denys, F. Doenz, S. Qanadli, B. Bessoud, P. Schnyder; Lausanne/CH

Embolization of digestive haemorrhage necessitate a perfect knowledge of arterial and venous anatomy of the abdominal vessels. Indications of embolization of low and upper digestive system will be discussed in the perspective of other therapeutic methods like endoscopy and surgery. Basic technique of embolization (temporary vs. definitive) will be detailed depending of the vascular territory. Follow-up of patients as well as complications will be presented.

Learning Objectives:

1. To be familiar with the arterial anatomy of celiac trunk, superior and inferior mesenteric artery.
2. To understand what are the indications of an endovascular treatment of upper and lower GI bleeding.
3. To detail the technique of embolization in these different territories.
4. To know about other endoscopic or surgical treatment options.
5. To understand how complications and treatment failure occurs in these different vascular territories.

Postgraduate Educational Programme

A-032

C. Percutaneous gastrostomy/Gastrojejunostomy

J. Seitz; Regensburg/DE

The most common indications for gastrostomy or gastrojejunostomy are malignant tumors of the throat or esophagus as well as different neurological diseases. Several conditions make the endoscopic approach of gastrostomy impossible or lead to an unsuccessful endoscopic procedure. This is the indication for radiological guided gastrostomy or gastrojejunostomy. There are two common radiological methods: (1) the fluoroscopically guided procedure and alternatively the CT-guided gastrostomy. Contra-indications for both procedures are severe uncorrectable coagulopathy and major perigastric ascites. Additional contra-indications for the fluoroscopically guided technique are hypertrophy of the left lobe of the liver, interposition of the colon and major surgical procedures of the upper abdomen. The preparation of the patient with a nasogastral catheter is the same for both procedures. The fluoroscopically guided method requires an additional enema of the colon with contrast media or an oral application of barium the day before. Before imaging an intravenous application of a parasympatholytic agent or Glucagon is required. Additionally room air must be insufflated over the nasogastral tube to distend the stomach. After local anesthesia the stomach is punctured and an anchor is placed inside. This access has to be dilated in seldingers technique up to 17 F. Next the 14 F gastrostomy catheter is inserted via a peel-away sheath. The balloon of the catheter has to be blocked with 5 ml of a mixture consisting of 0.9% NaCl and contrast media.

Learning Objectives:

1. To know the indications and contra-indications of gastrostomy/gastrojejunostomy.
2. To be familiar with the preparation of the patient and the information about the procedure itself.
3. To understand the complications, pitfalls and their management.

08:30 - 10:00

Room K

Genitourinary

RC 107

Imaging of the female pelvis

Moderator:

E. Kuligowska; Boston, MA/US

A-033

A. Infertility

A.J.M. Maubon¹, B. Caire-Gana¹, M. DeGraef², P. Piver¹, Y. Aubard¹, J. Rouanet²; ¹Limoges/FR, ²Montpellier/FR

Epidemiological studies show that 12-20% of couples have an infertility problem. On the female side they can be classified according to the localization of the fertility impairment - uterine factors (Müllerian malformations, DES syndrome, synechia, adenomyosis, ...), tubal factors (tubal obstruction, tubal infection, salpingitis isthmica nodosa, ...), peritoneal factors (endometriosis, inflammatory adhesions, ...), ovarian or central factors (dysovulations, pituitary adenomas, ...). Ancient and more recent imaging modalities (Hysterosalpingogram, tubal catheterization techniques, ultrasound, doppler ultrasound, sonohysterogram, MRI) play an essential role in the diagnostic and therapeutic assessment of these various infertility factors. This lecture will focus on recent developments in this rapidly evolving field, with a special emphasis on pelvic magnetic resonance. Pelvic MR is specially invaluable in the non invasive diagnosis and follow-up of infertile patients. Furthermore we shall detail how, from a medical and a financial point of view, MR imaging will modify the management of patients included in an infertility program.

Learning Objectives:

1. To review the imaging work up for female infertility (ultrasound, magnetic resonance, hysterosalpingogram).
2. To review the imaging features of the main causes of female infertility (tubal obstruction, uterine malformation, adenomyosis, endometriosis, pelvic adhesions) in relationship with their potential treatment.
3. To detail the remaining indications of hysterosalpingogram and selective tubal catheterization.

A-034

B. Endometriosis

K. Kinkel; Chêne-Bougeries/CH

Endometriosis corresponds to ectopic growth of endometrial glandular tissue associated with stromal tissue. Clinical symptoms are chronic pelvic pain, mainly menstrual, and infertility. Endometriosis of the pelvis includes superficial or peritoneal endometriosis, endometriomas or endometriosis of the ovary and deep peritoneal endometriosis which can be located posteriorly (retrocervical, uterosacral ligaments, rectosigmoid, ureter), anteriorly (bladder) or in the vagina. Ultrasound is the initial imaging of choice. Characteristic sonographic features of endometriomas are diffuse, low-level internal echoes, multilocularity and hyperechoic foci in the wall. Differential diagnoses include corpus luteum, teratoma, cystadenoma, ovarian fibroid, tubo-ovarian abscess and carcinoma. Repeat ultrasound is highly recommended for unilocular cysts with low-level internal echoes to differentiate functional corpus luteum from neoplastic ovarian cysts such as endometriomas. Ultrasound is limited in the diagnosis of vaginal and posterior endometriosis. MR imaging has shown a high positive predictive value for all locations of pelvic endometriosis and often demonstrates abnormal nodular structures of T2 low or intermediate signal intensity with occasional T1 hyperintense spots. Knowledge of the most frequent anatomical location of endometriosis and a technical imaging protocol adapted to clinical symptoms are important factors to identify lesions of deep endometriosis, often missed at laparoscopy due to subperitoneal location or presence of severe adhesions. This lecture will focus on imaging signs at ultrasound and MR imaging according to lesion localization, and include clinical case presentation.

Learning Objectives:

1. To identify features of ovarian, peritoneal, vaginal, bladder, rectal and bowel endometriosis at ultrasound and MR imaging.
2. To discuss differential diagnosis in patients with pelvic pain.
3. To compare the value of preoperative imaging modalities according to symptoms and lesion location.

A-035

C. Adnexal lesions characterization and staging

C.S. Balleyguier¹, K. Kinkel², N. Perrot³, P. Morice¹, R. Sigal¹; ¹Villejuif/FR, ²Geneva/CH, ³Paris/FR

Imaging is essential for characterization and staging of adnexal masses. The role of modern imaging is to point out the originating organ, to specify if the process is congenital, functional, hemorrhagic, neoplastic, obstructive or inflammatory and finally to adequately stage the neoplastic diseases before surgery or medical treatment. Adnexal lesions may include lesions of ovaries, fallopian tubes, broad ligament, uterosacral ligaments and their blood and nervous supply. Masses may also arise from the uterus. Non gynaecologic sources of abdominopelvic masses must also be considered.

Knowledge of female anatomy, embryology and physiology is necessary to understand adnexal diseases. Awareness of previous surgery and medical treatment are also helpful for the analysis of organs. Ultrasonography and Doppler US remain the first step to detect and characterize adnexal lesions. Nevertheless, MR imaging is often more accurate, provided an excellent technique depending on the suspected disease and based on multiplanar capability, spontaneous organ contrast and optional enhancement by contrast media. MR imaging carries a better soft tissue contrast than CT and precisely delineates pelvic organs and the pelvic wall landmarks like nodal chains and bones. MR imaging is also the best imaging method for deep pelvic endometriosis and atypical endometriomas. CT can provide useful information about the extent of disease in case of malignancy, and in some ovarian lesions, like teratomas or calcified ovarian tumours.

US and MR imaging appear to be complementary tools for the examination of adnexal diseases. Multidisciplinary approach is mandatory in order to understand the possibilities and limits, advantages and pitfalls of pelvic imaging.

Learning Objectives:

1. To list the most common ovarian tumors, benign or malignant, including main features of prognosis and natural history.
2. To understand why non neoplastic diseases like infection or endometriosis may present as adnexal masses.
3. To understand the role of Doppler ultrasonography for the detection and characterization of masses.
4. To know the standard technique for MR imaging, and to understand how to optimize spatial resolution and tissue characterization.
5. To describe the role of CT, which is mandatory for staging and follow-up of tumors, and may help for tumor characterization.
6. To understand the role of the radiologist in the multidisciplinary approach for decision making.

Postgraduate Educational Programme

08:30 - 10:00 Room L/M

Infection in the Adult Today

CC 116

Spinocranial infection

Moderator:

R.D. Brüning; Munich/DE

A-036

A. Cranial viral infection

C.F. Andreula; Bari/IT

The central nervous system viral infections are very rare.

Acute encephalitides: Among them arbovirus encephalitis and Japanese B encephalitis, have diffuse lesions with the preferential sites being thalamus and basal ganglia. Enteroviruses encephalitides are very rare. Neuroradiological examination of all these forms could be negative, or in the worst diseases show edema and encephalomalacia. Herpes simplex type 1 encephalitis causes a typical necrotic hemorrhagic meningo-encephalitis. CT is often negative in the first week of infection. MR imaging discloses early initial meningeal involvement, submeningeal edema and hemorrhagic lesions.

Immunomediated encephalitis: The course of ADEM is usually monophasic with synchronous-enhancing lesions. These lesions do not differ greatly from multiple sclerosis plaques. MS lesions are mostly symmetrical, frequently involving the corpus callosum (rarely in ADEM), rarely basal ganglia and thalamus (frequently in ADEM), active plaques enhance and some inactive ones do not.

Subacute encephalitis: HIV encephalitis is caused by the virus itself with slow nervous tissue "intoxication" (atrophy and/or leucoencephalopathy) with MR imaging hyperintensity on long TRWI, with regular outer borders. PML is caused by papova with lesions often being multifocal and rarely symmetrical. MR imaging reveals zones of high signal on T2WI and almost always low signal on T1WI with finger-like outer borders.

Chronic encephalitides: These are caused by unconventional agents (spongiform encephalopathy). Lesions involve the cortex, thalamus and basal ganglia in Jakob-Creutzfeld disease whereas they are frequent in the cerebellum and brainstem in Kuru.

Learning Objectives:

1. To learn the epidemiology, neuropathology and clinical presentation of cranial viral disease in adulthood.
2. To recognise neuroradiological findings in disease, correlating these with neuropathology.
3. To know how to recommend imaging protocols appropriate to a correct examination.
4. To become familiar with differential diagnosis, pathognomonic features, and diagnostic strategies.

A-037

B. Cranial bacterial infection

P.L. Anslow; Oxford/UK

Despite many medical advances many intracranial pathologies, degenerative or neoplastic remain difficult or impossible to treat. Intracranial bacterial infection remains common, is treatable and delayed or unconsidered diagnosis is simply a tragedy.

The lecture demonstrates the various manifestations of intracranial sepsis. There are some clinical presentations which raise suspicions of the disease, other presentations which are frankly confusing. There are some radiological manifestations which are very obvious and some very subtle.

Attention should always be given to the parasite versus host question. How did the infection arrive in the cranium? How did it "beat" the efforts of the immune system to eradicate it? Are there critical numbers of bacteria which are required for an infection to become established? Blood borne infection and direct spread of infection from paranasal sinuses will be considered.

Finally how is intracranial infection treated? Despite effective antimicrobials, surgical intervention is usually required. How should this be done? Needle aspiration or excision? How often should the patient be scanned after definitive treatment?

Learning Objectives:

1. To recognise the classical radiographic features of intracranial sepsis.
2. To understand that whether infection occurs or not is a balance between the number of organisms, their virulence and the host's response.
3. To appreciate the importance of detecting intracranial infection.

A-038

C. Spinal and spinal cord infection

D. Balériaux; Brussels/BE

Spinal and spinal cord infections are severe pathological conditions that should be diagnosed in an early stage to avoid serious orthopedic and neurological complications. MR imaging has nowadays a key role to play and should be available as soon as infection is clinically suspected.

Learning Objectives:

1. To learn to identify the different types of infectious involvement of the spine and how to make an early and accurate diagnosis.
2. To be aware of the respective indications, contributions and limitations of plain films, CT, PET and MR imaging for the diagnosis of different spinal infectious diseases.
3. To be aware of the recurrence of tuberculous diseases of the spine.
4. To know how to identify severe and possibly life threatening complications of spinal infection.
5. To become more familiar with infectious diseases of the spinal cord since they are recently better disclosed by MR imaging.

08:30 - 10:00

Room N/O

Contrast Media

RC 106

Contrast media for MR imaging and US liver imaging

Moderator:

M.-F. Bellin; Villejuif/FR

A-039

A. Non-specific and liver-specific paramagnetic contrast media

G. Morana; Treviso/IT

Paramagnetic contrast media (CM) are able to modify the signal intensity of either the lesion or normal liver parenchyma and thus contribute towards the characterization of the lesion. Non-specific gadolinium chelates such as Gd-DTPA are most effective during the dynamic phase of contrast enhancement, which is an important tool in the identification and characterization of FLL. Unfortunately, dynamic phase imaging alone can, at times, prove unsatisfactory for the accurate diagnosis of hepatic lesions. The current availability of liver specific contrast media (LSCM) give the possibility to obtain an accurate diagnosis on studying focal liver lesions (FLL). It is possible to subdivide FLL into three main groups, according to the kinetic of contrast enhancement: Hypervascular FLL, hypovascular FLL and FLL with delayed enhancement. LSCM with a first phase of extra-cellular distribution give both dynamic (morphological) and late phase (functional) useful informations for lesion characterization. With LSCM it is possible to differentiate with high accuracy benign from malignant lesions and hepatocellular lesions from non hepatocellular ones. LSCM with exclusive distribution to the hepatocellular compartment has a very high sensitivity and specificity in differentiating malignant vs benign lesions and hepatocellular vs non-hepatocellular lesions. The lack of dynamic contrast enhancement by mangafodipir trisodium represents a major shortcoming of this agent. It is necessary to have an in depth knowledge either of the biological and histological characteristics of FLL either of the enhancement mechanism of LSCM to gain significant accuracy in the differential diagnosis of FLL.

Learning Objectives:

1. To illustrate the different possibilities of imaging the liver with paramagnetic contrast media.
2. To increase the confidence of the radiologist with lesion characterization.
3. To describe the different enhancement of the same focal liver lesion with multiple liver-specific contrast media.

A-040

B. Superparamagnetic contrast media for liver imaging

P.J.A. Robinson; Leeds/UK

SPIO contrast agents are stabilised aqueous suspensions of crystalline particles of mixed oxides of iron with magnetic properties. The particles are of colloidal size and are cleared rapidly by the reticulo-endothelial cells of the liver, spleen and bone marrow. Although there is a short-lived T1 enhancing effect whilst the particles are in the blood compartment, the main contrast effect is due to marked shortening of T2* producing a marked loss of signal from normal liver tissue. Of

Postgraduate Educational Programme

the two commercially available SPIO preparations, ferumoxide is given by slow IV infusion, whilst ferucarbutran may be given as a bolus injection. The bolus approach allows dynamic T1 acquisitions which show transient enhancement. A delayed (10 minutes) acquisition shows the T2* contrast effect. SPIO contrast depends upon susceptibility effects so GRE rather than FSE sequences are required.

SPIO is taken up only in normal liver tissue, so increased contrast between tumour and liver allows improved detection of tumours and optimum demonstration of their extent. A recent comparison with multi-slice CT has shown SPIO-enhanced MR imaging to be superior in detecting small metastases. Benign hepatocellular lesions, FNH and adenoma, take up SPIO, whilst metastases don't. In the cirrhotic liver, uptake of SPIO indicates benignity in a nodule, whilst nodules which take up no SPIO may be regarded as malignant.

A double-contrast approach combining post-SPIO T2* sequences with Gd-enhanced T1 images is particularly useful in differentiating benign hepatocellular lesions from metastases, and is the most effective technique for detecting HCC in the cirrhotic liver.

Learning Objectives:

1. To understand the mechanisms for liver contrast enhancement with spio.
2. To be able to prescribe a suitable sequence for using spio in a liver examination.
3. To select appropriate patients for examination with spio and interpret the results correctly.

A-041

C. Bubbles for US liver imaging

T. Albrecht; Berlin/DE

Several microbubble contrast agents for ultrasound (US) have been developed in recent years. In principle, all microbubble contrast agents are blood pool agents, some also have liver-specific properties. In the liver, US contrast agents are used for dynamic assessment of enhancement during the arterial, portal venous and delayed phase. The delayed phase is a specific property of US contrast agents. During this phase the bubbles pool in normal liver and spare malignant focal lesions, such as metastases. The delayed phase is of particular value for detection and characterisation of liver tumours.

The use of contrast agents dramatically improves detection and characterisation of focal liver lesions and has changed the role of US in clinical liver imaging. Contrast enhanced US is about as sensitive as CT in detecting metastases and comparable to MR imaging in characterising focal lesions.

US contrast agents can also be used as tracers for functional studies of liver perfusion. Hepatic transit time is shortened in certain diseases, such as cirrhosis or metastases, and transit time analysis of a microbubble bolus is a promising research tool for early detection of these diseases.

Learning Objectives:

1. To understand the pharmacological and technical basis of contrast-enhanced liver US.
2. To know the dynamic patterns of contrast enhancement of common focal liver lesions.
3. To understand the role of contrast agents in liver US.

08:30 - 10:00

La Scala

Foundation Course - Chest Radiology

E3 120

Anatomy and basic signs in imaging

Moderator:

P. Vock; Berne/CH

A-042

A. Normal anatomy

J. Cáceres; Barcelona/ES

All conventional radiology is based in the interplay of four basic densities: air, fat, soft tissues and calcium. The chest radiograph is, and will continue to be, an excellent method for detecting pulmonary abnormalities, since any pathological process is manifested as an increase in density on the dark background of the healthy lung.

A conventional PA radiograph is the first step when investigating chest disease. Unless it is physically impossible, a lateral chest radiograph should be taken.

In both lungs, there are opacities that correspond to normal structures. They are

the hila, the pulmonary vessels and the fissures. It is basic to know the normal anatomy of these structures because they act as markers of pulmonary disease. A basic question when an abnormality is found is whether it is pathological or simply a normal variant. Fat is ubiquitous in the thorax and may be confused with numerous pathological processes.

Learning Objectives:

1. To demonstrate the importance of knowing normal anatomy to understand pathological changes.
2. To emphasize the value of the silhouette sign in the understanding of normal radiological anatomy.
3. To show normal variants that may be confused with pathology.

A-043

B. Basic findings and signs in imaging

T. Franquet; Barcelona/ES

The diagnostic limitations of conventional chest radiology are well known. A thorough knowledge of roentgen signs in thoracic radiology is required for the detection and diagnosis of chest pathology. Although the discovery of a chest abnormality on conventional radiography may be of great clinical importance, it does not necessarily lead to a definitive diagnosis. Despite recent major advances in thoracic imaging, conventional plain-film still remains the first radiographic study. Recognition of special radiographic signs is useful in chest radiologic interpretation. In this lecture some of these signs are described and their value discussed. Some of the most relevant described signs include the silhouette sign, the air bronchogram, the bulging septum, the extrapleural sign, the S-line of Golden, and the patent bronchus sign. With new cross-sectional technology, signs based on the CT findings have also been described. CT signs include among others the angiogram sign, the halo sign, the mucous bronchogram, and the split pleura sign. This presentation will revisit the commonest conventional and CT signs in thoracic imaging. Emphasis will be placed on the correlation between conventional radiographic presentation and CT findings. Knowledge of these signs will permit the radiologist an accurate interpretation of images as well as a confident diagnostic approach.

Learning Objectives:

1. To describe the characteristics imaging manifestations and significance of the most common radiologic signs.
2. To recognize these signs on chest radiography and/or chest CT.

10:30 - 12:00

Room A

State-of-the-Art Symposium

SA 2

Whole-body imaging

Moderator:

M.F. Reiser; Munich/DE

A-044

Whole-body imaging (Introduction)

M.F. Reiser; Munich/DE

The healthcare systems all over the world face major financial problems. Limited resources have to be spent as effectively as possible. Moreover, the population in industrialized countries became more and more aware of the value of early diagnosis and preventive interventions. These global trends resulted in new challenges to radiology: non-invasive, accurate diagnosis, if possible in a one-step approach, instead of a cascade of multiple different diagnostic procedures.

Recently, various modalities have been introduced, which appear to be capable to fulfil these expectations by imaging the whole body. Many diseases, such as atherosclerosis, advanced stages of malignant tumours, lymphoma and rheumatic disorders manifest in various locations rather than in one single organ or body part. Therefore, disease oriented imaging is required and "whole body imaging" may be the best approach.

In this state-of-the-art symposium, the methods for whole body imaging - multi-slice-CT, whole-body MR imaging and PET/CT - will be presented. The contribution of these methods in the early detection and comprehensive diagnosis of cardiovascular and oncologic diseases will be discussed. Even if extensive scientific research is required to explore the capabilities and limitations of different types of whole body imaging, it can be anticipated that they will play an increasing role in the field of our profession.

Postgraduate Educational Programme

Learning Objectives:

1. To describe the technical background of MDCT, whole body MR imaging and PET/CT for comprehensive diagnostics.
2. To inform about the methods and results of whole body imaging in the detection and staging of malignancies.
3. To discuss the technique and diagnostic accuracy of MR imaging in the assessment of cardiovascular diseases.

A-045

Modalities

H.-P. Schlemmer; *Tübingen/DE*

Recent progress in Radiology allows to acquire three-dimensional high-resolved data sets of the whole body within one single examination thus enabling fast one-stop assessment of systemic aspects of diseases. The presentation describes cutting-edge advances in cross-sectional imaging technology radiologists are faces with as whole-body imaging is entering everyday clinical practice. Physical and technical principles of whole-body imaging using helical computed tomography (CT), magnetic resonance imaging (MRI) and the combination of positron emission tomography (PET) with CT in one hybrid scanner (PET-CT) are demonstrated. Relative virtues and limitations of the imaging modalities are discussed against the background that these technologies may shortly become an important and even initial diagnostic approach for evaluating a wide range of diseases, e.g. in oncology or cardiovascular diseases. It is illustrated how advances in information processing and communication technology are necessary and will facilitate imaging data management for improved and accelerated image interpretation. Using high-power workstations diagnostic findings can be reported interactively making whole-body imaging a great help to other clinicians. The technologies will furthermore contribute to a more rapid throughput of patients in the Radiology department. Consequently, whole-body imaging will be an important diagnostic tool in the face of not only medically but also economically optimized patient management.

Learning Objectives:

1. To understand physical and technical principles of whole-body imaging using cross-sectional modalities CT, MRI and PET-CT.
2. To learn relative opportunities and drawbacks of the modalities.
3. To become familiar with the potentials of image post-processing for improved and accelerated image interpretation.
4. To comprehend indications in the face of medically and economically optimized patient management.

A-046

Metastases

A. Baur-Melnyk; *Munich/DE*

Until now MSCT is the method of choice for screening the cerebrum, the thorax and abdomen in patients with suspected metastases. However, new technologies in MR imaging and the development of PET/CT now also allow for a whole body screening. With the introduction of special coil devices and parallel imaging in MR imaging, a whole body imaging approach for the detection of metastases is possible within a reasonable time. Since not all tumors show a pathologic FDG uptake, indications are limited to a number of malignancies, such as bronchogenic carcinoma, head and neck cancer, esophageal cancer, colorectal cancer, lymphoma and malignant melanoma. In CT and MR imaging the detection of lymph node metastases, tumor recurrences in the peritoneal cavity and postoperative tissue changes sometimes is limited. Due to the functional approach with FDG these problems can be overcome by PET/CT. In addition, response of therapy can be monitored. With the combination of PET with CT the resolution is increased, and the definition of the exact anatomic site of "hot-spot" lesions is made possible. PET/CT has shown to be superior over PET and CT alone for the detection of metastatic lesions. Since the brain and the kidney show a strong homogeneous uptake of FDG there is a constrain for the detection of metastases in the brain and kidney. Small lesions < 1 cm in size may not show enough enhancement. MR imaging shows an advantage over PET/CT for the detection of skeletal and liver metastases. MR imaging has limited sensitivity for lymph node and lung metastases.

Learning Objectives:

1. To become familiar with the appearance of metastases in the different techniques of whole body imaging (PET/CT, MR imaging/MSCT).
2. To comprehend the advantages and disadvantages of each technique concerning metastases.
3. To understand the role of whole body imaging in patients with malignant tumors.

A-047

Vascular imaging

S.G. Ruehm; *Essen/DE*

Peripheral vascular disease (PVD) is frequently associated with coronary, renal, and carotid arterial disease. Localizing and determining the severity of arterial lesions is crucial for therapeutic decision making. Recently, whole-body 3D MR-angiography has become available. The technique which is used at our department (1.5 T MR-Scanner (SIEMENS, Sonata, Erlangen, Germany)) employs a rolling table platform (AngioSURF). Five coronal contiguous 40 cm data sets are collected each with a 3D FLASH sequence over 12 s. Taking into account 3 s for table repositioning, the total scan time is 72 s. Paramagnetic contrast agent is administered using a power-injected using a biphasic injection protocol at a dose of 0.2 mmol/kg BW.

Whole body 3D MRA-approach is characterized by non-invasiveness, three-dimensionality, extended coverage and high contrast conspicuity. It allows for a quick, risk-free, and comprehensive evaluation of the arterial system from carotid to tibial arteries in patients with atherosclerosis.

Learning Objectives:

1. To discuss the role of whole-body MR angiography in the management of patients with PVD.
2. To become familiar with typical findings in whole-body MRA.
3. To discuss the role of whole-body MR angiography as a screening tool.
4. To discuss clinical indications for whole-body MRA.

10:30 - 11:15

La Scala

E³ - European Excellence in Education

E³ 220a

Radiology on the web

Moderator:

D. Caramella; *Pisa/IT*

A-048

Radiology on the web

D. Caramella; *Pisa/IT*

The Internet provides access to a huge volume of medical information that is directed toward both health care professionals and the public, and that might not be readily available through traditional sources.

Radiologists are aware that a wealth of diagnostic imaging information is accessible on the World Wide Web: this material has the potential to empower the public by improving their understanding of the diagnostic procedures as well as to enhance continuing medical education for professional users.

However, there is growing concern that a substantial proportion of such information that is free from rigorous editorial control might be inaccurate, erroneous, misleading, and thereby causing potential danger.

One of the initiatives that implemented a formal anonymous peer-review process to assure the scientific and educational quality of radiological material published on the Internet is EURORAD, the on-line educational database of the European Association of Radiology (ISSN 1563-4086) that can be accessed free of charge at the address: www.eurorad.org.

EURORAD promotes interactive learning supported by the consultation of multi-modality digital images illustrating common as well as unusual pathological situations.

Presently, EURORAD contains a large variety of teaching files (published in English, French, and Spanish) encompassing all radiological subspecialties and aims to stimulate the professional use of the World Wide Web, by providing sound and up-to-date information that can assist radiological practice and education.

EURORAD exploits the powerful features of the Internet by combining co-operative work, peer review, and universal access.

Learning Objectives:

1. To appreciate the value of Internet for distributing health-related information.
2. To realize the potential risks arising from the wide availability of medical information free from proper editorial control.
3. To understand the specific features of the educational database eurorad.org.

Postgraduate Educational Programme

11:15 - 12:00

La Scala

E³ - European Excellence in Education

E³ 220b

E-mail for the radiologist

Moderator:

E.R. Ranschaert; s'-Hertogenbosch/NL

A-049

E-mail for the radiologist

E.R. Ranschaert; s'-Hertogenbosch/NL

E-mail has become one of the most popular communication tools, and it is also increasingly being utilised in radiological practice. It is an internet service that is not only used for sending messages between two individuals, but also for participating in (radiological) discussion groups.

For sending and receiving these types of messages, the users must use either a dedicated e-mail client or one of the other mailing facilities offered on the world wide web. The principles and mechanisms of different e-mail services are explained. Several additional functionalities are highlighted, such as the possibility to attach documents and images. Potential problems and concerns, such as virus attacks, spamming and privacy matters are highlighted. It is demonstrated how e-mail can be of value in a professional radiological environment and how it can facilitate communication between radiologists and other medical professionals.

Learning Objectives:

1. To learn the principles of the different e-mail services offered on the Internet.
2. To become familiar with the advantages and disadvantages of using e-mail.
3. To learn how the most frequent problems can be solved.
4. To understand how e-mail can add value to daily radiological practice.

12:15 - 13:30

Room A

Plenary Session

Opening Ceremony

Inauguration Lecture/Presentation of Honorary Members

Presiding:

A. Chiesa; Brescia/IT

Musical Performance

Vienna Boys' Choir

Presidential Address

A. Chiesa; Brescia/IT

President ECR 2005

IL

Inauguration Lecture

A-050



Quantitative imaging: The next paradigm

J.T. Ferrucci; Boston, MA/US

Data acquired from radiological imaging modalities may be described as having three qualities; i.e., anatomical (structural), physiological (functional) and metabolic (molecular). In addition to classic visual inspection, image data is being independently processed to create new windows to diagnostic information. Automated computations can display unique numerical relationships extracted from large data sets, especially from modern CT and MR scanners. Using computer science techniques such as statistical learning theory and pattern recognition, quantitative imaging is evolving as the next paradigm for Radiology.

Principle tools for quantitative imaging include segmentation (digital extraction of voxels), computer aided detection (CAD) used for cancer screening and volumetry for organ, or tumor volumes. Computations are automated, and results can be sorted and edited for reporting. Software resides on clinical diagnostic workstations, and increasingly will be PACS/RIS integrated.

Segmentation, a user defined data separation process, is the first step for both CAD and volumetry, but has its own applications especially in displaying regional anatomy (vessels). CAD is used as a decision-support tool in mammography, lung cancer screening, CT colonography, and liver tumor detection. Automated

volumetric measurements are faster and more accurate than traditional linear or planimetric estimates of volume. Volumetry has many clinical uses, including monitoring growth of liver neoplasms, lung nodules, or colon polyps, and predicting functional organ reserve.

Learning Objectives:

1. To describe quantitative imaging techniques and applications.
2. To review segmentation, computer aided diagnosis and volumetry.

14:00 - 15:30

La Scala

E³ - European Excellence in Education

E³ 320

Interactive image teaching

Moderator:

G.P. Krestin; Rotterdam/NL

A-051

Acute abdomen

G.P. Krestin¹, B. Marincek²; ¹Rotterdam/NL, ²Zürich/CH

Acute abdomen is one of the most common and diverse syndromes in medicine. In its broad sense it refers to various disorders associated with more or less severe abdominal pain of rapid onset. Imaging diagnosis plays a crucial role in differentiating the underlying cause of the symptoms. Narrowing of the differential is based upon localisation of the main symptoms. The instructors will discuss in an interactive fashion the common and more unusual cases with main symptoms localised to the right lower abdominal quadrant, the right upper quadrant, the left lower quadrant, central abdominal pain, diffuse complaints and flank pain. The audience should be able to learn how to approach these cases and use different imaging modalities for establishing the diagnosis. The main focus will be on multidetector CT.

Learning Objectives:

1. To understand the role of different imaging modalities in acute abdomen.
2. To learn possible differential diagnosis based on localisation of main symptoms in acute abdomen.
3. To recognise some selected common and more unusual findings in acute abdominal disorders.

16:00 - 17:30

Room B

Essentials of Neuroradiology

CC 417

Hemorrhagic stroke

Moderator:

J. Neuwirth; Prague/CZ

A-052

A. Intracranial hemorrhage

T.A.G.M. Huisman; Zürich/CH

Intracranial hemorrhage is one of the most common causes of acute focal neurological deficit in children and adults. Neuroimaging including ultrasonography (US), computer tomography (CT) and magnetic resonance imaging (MRI) is essential in the diagnosis of intracranial hemorrhage. Imaging findings should guide treatment. The highly variable appearance of an intracranial hemorrhage can be challenging. A thorough knowledge of hematoma evolution and US, CT and MR-hematoma characteristics is mandatory for an adequate interpretation of findings. The purpose of this presentation is (a) to summarize the imaging characteristics of intracranial hemorrhage on various imaging techniques and (b) to review the various types of intracranial hemorrhage, and their causes.

Learning Objectives:

1. To give insight in the imaging characteristics of intracranial hemorrhage on various imaging techniques.
2. To review the various types of intracranial hemorrhage, and their causes.

Postgraduate Educational Programme

A-053

B. Intracranial aneurysms

R. Gasparotti; Brescia/IT

Intracranial aneurysms become symptomatic as a result of rupture with consequent subarachnoid hemorrhage (SAH). Unruptured aneurysms may be discovered when they cause neurological symptoms depending on the location and size. With the advent of spiral and multi-slice CT, CT Angiography (CTA) has been proposed as an adjunct to plain CT in investigating SAH and it is under debate whether it can replace intraarterial digital subtraction angiography (IAD-SA) in treatment planning.

Although MR Angiography (MRA) has given good results in detecting aneurysms in acute SAH, it is preferred as a screening modality for patients at risk and for the follow-up of aneurysms treated with endovascular coiling. MRA has the advantage of displaying cerebral vessels without contrast medium, although it provides limited coverage of the intracranial vasculature.

There are several methods to analyze CTA and MRA volumes: once the aneurysm is identified on source images, 3D reconstructions (MIP, SSD or VRT) are used for depiction of the size and orientation of the aneurysm neck and sac and characterization of arterial branching patterns. An accurate anatomical evaluation is useful for assessment of the suitability of an endovascular approach for aneurysm treatment, which has become a valid alternative to surgical clipping. IADSA is still the most sensitive tool in detecting intracranial aneurysms and should be performed within 24 hours from bleeding to ensure a correct therapeutic management of patients. The selective intraarterial injection of iodinated contrast medium ensures optimal enhancement of the intracranial arteries with superior resolution than CTA or MRA.

Learning Objectives:

1. To become familiar with the etiology and classification of intracranial aneurysms.
2. To understand imaging strategies for detecting subarachnoid hemorrhage and aneurysms.
3. To learn how to perform non-invasive screening for cerebral aneurysms.
4. To comprehend the principles, the indications and the effectiveness of the endovascular treatment of intracranial aneurysms.

A-054

C. Cerebrovascular malformations

J.V. Byrne; Oxford/UK

Arteriovenous Malformation of the Brain: The term refers to abnormal cerebral blood vessels comprising feeding arteries, draining veins and an intervening collection of abnormal vessels called the nidus. Diagnosis of large BAVM on CT and MR imaging is relatively easy. Small lesions are more difficult and recent haemorrhage may mask a small lesion. DSA remains the gold standard for excluding BAVM.

Cavernous Malformations: These occur anywhere in the brain but are usually found in subcortical white matter. They consist of closely packed thin-walled vessels without normal interposed brain. On CT they are well-demarcated hyperdense lesions but CT does not show 10% of lesions found at surgery and only 1/3rd of lesions demonstrated by MR. On MR the features are characteristic but not pathognomonic. They are not seen on DSA.

Capillary Telangiectasis: These lesions are ill-defined areas of dilated thin walled capillaries without mural smooth muscle or elastic fibres. Normal brain is found between these vessels. CT and DSA are usually unhelpful but on MR these lesions show hypointense or isointense signal.

Dural AV Fistulas: These lesions comprise arteriovenous fistula(s) situated in the meninges and supplied partly or wholly by dural arteries. CT is rarely diagnostic. Dilated vessels may be seen in the parenchyma (cortex or subcortical) on enhanced scans. Following haemorrhage the findings are those of lobar haematoma with or without subarachnoid haemorrhage. MR may show dilated vessels on the cortex (veins), meninges or extracranial tissues. CE-MRA will help. Catheter angiography is the "gold-standard".

Learning Objectives:

1. To consider 4 types of commonly encountered cerebral vascular malformations.
2. To protocol investigation of the patient presenting with spontaneous cerebral haemorrhage.
3. To logical plan imaging investigations.
4. To learn imaging features of 1. above.

16:00 - 17:30

Room C

Special Focus Session

SF 4a

Rectal carcinoma

Moderator:

S. Rafaelsen; Vejle/DK

A-055

Rectal carcinoma (Introduction)

S. Rafaelsen; Vejle/DK

Rectal cancer is a major health problem in Europe. Prognosis and treatment of the disease depend on stage at the time of diagnosis. Local recurrence, as well as liver metastases, are significant causes of morbidity and mortality. The high mortality is presumably also caused by other factors: The examinations performed, the offered treatment including operative techniques, the possible combination of operation with radiotherapy and chemotherapy and post-treatment follow-up.

The treatment of rectal carcinoma has changed over the last years, as far as surgical techniques (with introduction of total mesorectal excision) and radiotherapy are concerned. With the implementation of the new treatment options local recurrence rates have been considerably reduced. Accurate radiological evaluation of the extension of the tumour into the peri-rectal fat, distance to the mesorectal fascia, involvement of adjacent organs and lymph nodes are essential for best possible treatment planning.

Multidisciplinary teams and quality assurance are important for achievement of optimal treatment planning.

Learning Objectives:

1. To hear about the different methods in the diagnosis.
2. To understand the importance of accurate staging.
3. To discuss the possible effect of post-treatment follow-up.

A-056

Diagnosis

F.-T. Fork; Malmö/SE

Symptoms of rectal carcinoma depend on type, extent and complications, including bleeding, tenesmus, sensation of incomplete evacuation and mucous discharge. Abdominal discomfort is absent until perirectal tissue is involved.

Change in bowel habit may develop over a long period of time.
Occult blood in stool: Testing for occult blood is low in sensitivity but high in specificity and inexpensive. It demands dietary restriction. Positive tests require further examinations.

Digital exploration: Tumours in the anal part of the rectum may be explored if not soft and villous.

Flexible sigmoidoscopy: About 60 percent of colorectal cancers are within the reach of flexi sig. Rectoscopy with stiff instruments should therefore be discarded.

Total colonoscopy: If any of the above tests are positive a total colorectal exploration should be contemplated to rule out and remove suitable synchronous lesions.

Barium enema examination is sensitive for mass lesions but not for a histologically early, superficial malignancy and a protruding one less than 5-10 mm. Therefore, barium enemas ought to be replaced by colonoscopy in patients at risk for CRC.

Colonography based on CT and MR imaging techniques are still under clinical testing. Results report figures of sensitivity in detecting neoplastic lesions bigger than 5 mm in par with colonoscopy. Results based on routine studies of patients with an average risk for colorectal cancer disease show less favourable figures.

Learning Objectives:

1. To understand the role of imaging in the management of patients with colorectal cancer.
2. To understand the virtues and shortcomings of diagnostic techniques available today.
3. To select first imaging modality based on clinical patient data.

Postgraduate Educational Programme

A-057

Staging

C.I. Bartram; Harrow/UK

The Dukes classification gives an indication of prognosis, and the TNM system tumour penetration and nodal involvement. However, it does not account for the variation in T3 survival, nor relates lateral tumour extent to the mesorectal fascia, the preferred plane of surgical dissection. Fascial involvement implies total mesorectal excision (TME) will not be feasible and pre-operative chemo-radiotherapy indicated to downstage the tumour to allow TME and prevent local recurrence. Early T1 cancers may be considered for local excision provided there is no nodal involvement.

CT is valuable for large, clinically fixed lesions to determine local infiltration. Rectal endosonography (RES) remains the optimum modality for T staging, though liable to overstage T2 lesions, if an inflammatory response is not recognised. Perirectal stranding on MR imaging may be just due to desmoplastic response, though tumour infiltration is difficult to exclude. The main strength of MR is to define the mesorectal fascia and to relate the lateral tumour margin to this using high spatial resolution T2w sequences at right angles to the long axis of the tumour. The criteria for nodal involvement has been mainly size, although there is considerable overlap between reactive and involved nodes both on RES and MR imaging. Border contour and signal intensity characteristics are more discriminatory.

Learning Objectives:

1. The pathological rationale for the surgical management of rectal cancer.
2. The role of endosonography.
3. MR imaging of rectal cancer in relation to the mesorectal fascia and nodal involvement.
4. Limitations and problems imaging rectal cancer.

A-058

Post-treatment follow-up

T.J. Vogl; Frankfurt a. Main/DE

Purpose: To evaluate the role of imaging techniques and interventional procedures in the post treatment follow-up of rectal cancer.

Methods and Materials: Techniques of MR imaging protocols for the evaluation of the rectum and small pelvis are based on T1- and T2-weighted protocols and contrast-enhanced images using dynamic and diffusion imaging. MSCT protocols are based on the evaluation of raw data and 3D reconstruction protocols.

Results: Depending on the results of the primary staging, follow-up protocols will be presented using MR imaging techniques or MSCT protocols. For the evaluation of the small pelvis, PET will be discussed as well as techniques for the evaluation of distant metastases in the lung, liver, lymph nodes and bones. For the verification of a local recurrence CT- or MR imaging-based interventional biopsy techniques will be presented.

Conclusion: Cross-sectional imaging techniques allow a precise follow-up evaluation after treatment of rectal cancer. Under certain circumstances the additional use of PET and biopsy techniques is necessary.

Learning Objectives:

1. To understand the clinical question.
2. To define the examination strategy.
3. To analyze images of the rectum.

16:00 - 17:30

Room E1

Special Focus Session

SF 4b

Imaging of the lymphatic system

Moderator:

S.C. Efremidis; Ioannina/GR

A-059

Imaging of the lymphatic system (Introduction)

S.C. Efremidis; Ioannina/GR

During the past two decades technological improvements in computed tomography (CT), advances in high resolution power Doppler ultrasonography (US), the development of tissue specific contrast media in magnetic resonance (MR) imaging and refinements in lymphangioscintigraphy have severely curtailed the use of conventional oil-contrast lymphangiography, which has long been considered the

standard of reference for lymphatic imaging. However, the techniques mentioned above have neither the ability to visualize the lymphatic vessels nor have they the accuracy of conventional lymphangiography to demonstrate the internal architecture and show metastases in normal sized nodes. On the other hand, lymphangiography in contrast to CT, MR and US is a traumatic procedure, tedious to perform and time consuming, unable to routinely visualize in its entirety, the regional lymphatic system of common pelvic malignancies. All of these reasons have contributed to its dramatic decline in popularity. Therefore, despite past and current innovations, evaluation of the lymph nodes and lymphatics remains the "Achilles heel" of imaging.

Imaging of the lymphatic system is a forgotten frontier. Yet, prognosis and treatment of neoplastic diseases are not infrequently based on this art. Moreover, this system has a major role to play in the propagation and limitation of disease processes providing both a barrier to their extent and, a conduit to their spread. Finally, visualization of the lymphatics is very important in some congenital, hereditary, circulatory, traumatic and inflammatory disorders affecting this system.

Recently there has been some research devoted to visualizing univascularly the lymphatic system and identifying micrometastases in lymph nodes.

Learning Objectives:

1. To learn the anatomic- imaging correlation of the normal lymphatic drainage systems.
2. To understand the interaction of lymph vessels and nodes in the limitation and spread of diseases.
3. To discuss the role of imaging in various lymph vessel diseases (congenital, inflammatory, neoplastic).

A-060

The lymphatics: Clinical considerations

M. Bellomi; Milan/IT

Lymphatic ducts drain interstitial fluid and macromolecules, playing a major role in many diseases involving the intercellular space. Malfunction of lymphatic drainage leads to liquid stagnation within the tissues and eventually lymphoedema. This condition is common in Filariasis but may be caused by surgery or radiotherapy.

Lymphatics play a major role in tumor spread, involving both surgical approach and staging modalities. Sectorial surgery is based on the knowledge of the lymphatic drainage pathways, resecting the tumor and extending the resection to lymphatic "bed", where the diffusion of neoplastic cells is probable: This happens today in breast and colonic tumors resections, and is under research for possibly reducing demolitive surgery in tongue tumors. Imaging of lymphatic pathways draining the tumor can be obtained by lymphoscintigraphy or by injection of dyes during operation: This not only helps to decide on the surgical margins, but also the identification of sentinel node(s).

Nodal staging is a key-point in therapeutic management of many tumors and knowing the path of lymphatics is important to target the sophisticated techniques to define nodal status. The clinical impact of N staging is very important in some tumors at early stages (prostate, ovary); in other tumors (i.e. lung, rectum, pancreas) imaging is less important, since their surgical approach already foresees loco-regional nodal dissection. The detection of distant nodal metastases is always mandatory, because they are outside the conventional surgical bed, and when imaging is aimed to staging, the entire lymphatic drainage net from different tumors has to be kept in mind.

Learning Objectives:

1. To learn the function of the lymphatic drainage.
2. To understand the clinical importance of the lymphatic drainage in surgical planning of some tumors.
3. To learn how to correctly stage Nodal status of neoplastic patients.

A-061

Normal lymphatic drainage

S.C. Efremidis; Ioannina/GR

Evaluation of the lymphatic system* requires knowledge of lymph flow pathways dictated by its anatomy. The anatomy of the lymphatic system can be separated into pathways of the upper and lower extremities, neck, mediastinum, upper abdomen, lower abdomen and pelvis. This lecture will focus on the anatomy of this system in the abdomen and pelvis with emphasis on lymph drainage because of its complexity and frequently confusing pathological configuration.

The lymphatic route is composed of afferent and efferent lymphatic vessels and lymph nodes. Lymphatic vessels in the abdomen and pelvis course within the subperitoneal space (including that of peritoneal reflections i.e. ligaments, mesenteries and omenta), providing an important natural pathway for extension of the pathological processes.

Postgraduate Educational Programme

Lymph nodes in the abdomen are also extraperitoneal lying within the retroperitoneal space or its subperitoneal continuation, where they form discrete groups. Terminal groups are the retroperitoneal nodes divided into pre-aortic, para-aortic and retro-aortic groups. These groups have their own large area of visceral drainage via lymphatic trunks of intermediary nodes representing steps of the natural lymph flow from the regional nodes of the abdominal and pelvic organs to the cisterna chyli. A key to understanding the lymph drainage in the abdomen is the lymphatic anatomy of the lesser omentum which provides a conduit for disease extension from peritoneal organs such as the stomach, liver, gallbladder, bile ducts and duodenum to retroperitoneal tissues via the hepatoduodenal ligament. *Term "lymphatic system" in this lecture is used to denote lymphatic vessels and lymph nodes only.

Learning Objectives:

1. To familiarize with localization, identification and terminology of lymphatic vessels and lymph nodes.
2. To comprehend the complex anatomy of lymph drainage in the abdomen and pelvis.
3. To understand the pathophysiology of disease extension using the lymphatic route.
4. To present certain relatively discrete configurations of nodal involvement in the abdomen.

A-062

Imaging of lymph vessel disease

S.G. Ruehm; Essen/DE

Knowledge of the status of lymphatic vessels and nodes is important for various diseases. Reflecting the small size and indistinct tissue properties of the lymphatic system, display of the lymphatic system requires contrast agents that can be delivered by using different routes.

Direct lymphography, usually performed with fluoroscopic guidance with iodinated contrast agents, permits enhancement of only those lymph nodes contained within the draining route of the cannulated vessel. Although it provides the highest accumulation of contrast agent in lymph nodes, the technique has been abandoned owing to its invasiveness, technical difficulties, and potential for side effects (pulmonary embolism, local wound infection). Indirect lymphangiography, using interstitial injection of iodinated contrast agent to delineate draining lymph vessels has been proposed. However, the technique could not find its way into clinical routine. Selected display of lymph nodes is also possible after intravenous administration of contrast agent. Authors of several studies have described the use of ultrasmall iron oxide particles (USPIO) for systemic lymph node display in conjunction with magnetic resonance (MR) imaging. Results have been mixed, as nodal accumulation of contrast agent appears unreliable, and images depict many artefacts. Alternatively, the contrast agent can be administered into the subcutaneous interstitium. Several MR imaging agents have been evaluated for this purpose, including USPIOS and Gd-based compounds. New developments in contrast agents in combination with recent sequence designs might allow the implementation of MR based imaging techniques with the advantage of combining functional information about local lymphatic drainage with high resolution data acquisition.

Learning Objectives:

1. To discuss the role of MR lymphography for the diagnosis of lymphatic disease.
2. To become familiar with possible approaches for MR lymphography and its underlying principles.

16:00 - 17:30

Room E2

Abdominal and Gastrointestinal

RC 401

Abdominal trauma

Moderator:

J.S. Laméris; Amsterdam/NL

A-063

A. The radiologist's role in the trauma team (organisation and triage)

P. Huppert; Darmstadt/DE

There is no radiological field where the radiologist is more integrated into an interdisciplinary team than in trauma management. Consequently he should be aware of general principles in trauma management and the role of diagnostic and interventional radiology for patients triage.

Radiologists have to make sure that state of the art radiography, (Multislice-) Spiral-CT and diagnostic and therapeutic angiography are available at any time and within an appropriate distance to the emergency room. Imaging procedures have to be standardized according to protocols available at any time. Accepted rules of interdisciplinary trauma management should be discussed in advance, including standards for imaging and intervention.

Radiologists have to be familiar with typical findings in trauma patients and with specific problems of critical periods: detection and management of ongoing bleeding during the first hours and complications around the 3rd week.

Radiologists have to make sure that modalities, technicians and instruments are on stand-by if patients arrive at the hospital, that studies proceed without time delay according to protocols, that positive and suspected findings are communicated immediately and that a reliable written report and complete image folders are available to all members of the trauma team at any time.

Learning Objectives:

1. To discuss the overall organisation of radiology in the trauma team.
2. To review the essential needs of personnel and equipment.
3. To describe patient triage, logistics and outcome.

A-064

B. How to image the trauma patient

O. Chan; London/UK

The advent of small portable US machines, PACS and in particular MDCT scanners, has opened new pathways for the management of severely polytraumatised patients and hence the role of the emergency radiologist (ER) has changed dramatically over the past 10 years. Clinical evaluation in the obtunded patient has been shown to be unreliable and misleading and the role of US and CT in evaluating this group of patients is now clearly established. Subsecond imaging with > 32 MDCTs, potentially allows up to 9600 images to be acquired in 1 minute. The delay in transporting patients into CT from the emergency resuscitation room is no longer acceptable in these scenarios. Patients should be transferred from the ambulance or helicopter, directly to the CT scanner, where basic resuscitation can be carried out with simultaneous imaging of the whole body.

This will allow patients to be accurately and rapidly assessed both clinically and radiologically, regardless of the patient's haemodynamic status. "Conventional wisdom"/management can now be challenged using this form of algorithm and hopefully, the doughnut of death can be renamed "The doughnut of life"!

Learning Objectives:

1. To discuss the relative merits of individual radiological techniques.
2. To learn who, when and where to image polytraumatised patients.
3. To understand the changing face of trauma imaging - role of MDCTs and the ER.

A-065

C. The role of intervention

P. Goffette; Brussels/BE

Investigation of polytraumatized patients with multidetector CT, which enables precise evaluation of solid organ trauma, leads to a more conservative management of all abdominal trauma irrespective of their grading.

Advances in CT technology have improved the identification of both contrast extravasation and non-bleeding vascular injuries and can predict the need for embolization in low-grade trauma. Contrast blush (CB) on CT after splenic fracture is not an absolute indication for immediate angio-intervention. Conversely, CB after liver trauma is associated with a significantly greater risk of mortality and needs systematic angio-embolization.

The liberal use of angiography and the technical refinements in embolization have broadened the indications and improved the results of the non-operative management in high-grade injuries.

Immediate angiography should be performed in the following settings:

1. As primary damage control modality in lieu of devastating surgery in unstable patients suspected to develop massive retroperitoneal or pelvic hemorrhage.
2. After damage control laparotomy for complex hepatic or mesenteric injuries in order to detect and treat deeply located vascular lesion not detected at surgery.
3. For all high-grade (IV-V) hepato-splenic or renal injuries, irrespective of the hemodynamic status.
4. To stop visceral bleeding in stable patients and obviate otherwise unnecessary surgery.
5. To differentiate CT findings of "ongoing hemorrhage" from small intra-parenchymal or intra-muscular CB or venous bleeding which don't require intervention.

Postgraduate Educational Programme

Endovascular hemostasis is achieved in 88 to 100% of the cases. Failures are nearly always due to delayed intervention or underestimation of the severity of injury on CT. Post-embolization complications are rare.

Learning Objectives:

1. To discuss the indications and contraindications of vascular intervention.
2. To identify the CT findings which should lead to angiographic intervention.
3. To learn the principles and technical rules of hemostatic embolization in polytraumatised patients.

16:00 - 17:30

Room F1

Cardiac

RC 403

Cardiomyopathies

Moderator:

R. Couliden; Cambridge/UK

A-066

A. Hypertrophic cardiomyopathy

J. Bogaert; Leuven/BE

The characteristic finding of hypertrophic cardiomyopathy (HCM) is an inappropriate myocardial hypertrophy in the absence of an obvious cause for the hypertrophy, such as systemic hypertension or aortic stenosis. Familial clustering is often observed, and the disease is genetically transmitted in about half of the cases. The natural history and clinical presentation of HCM are variable. Symptoms are caused by intraventricular, usually left ventricular outflow tract (LVOT) obstruction; myocardial ischemia and reduced coronary vasodilator flow reserve; diastolic dysfunction; and arrhythmias. Although patients might be completely asymptomatic, HCM is the most common identified cause of sudden cardiac death in young people, due to arrhythmia. Histologically, HCM is characterized by a disorganization and malalignment of the myofibrils, i.e., myofibrillar disarray, which is not unique to HCM but is clearly more extensive in this disorder than in secondary myocardial hypertrophy from pressure overload or congenital heart disorders. In this presentation, the contribution of new cardiac imaging modalities, such as magnetic resonance imaging, in the diagnosis, differential diagnosis and follow-up of patients with HCM will be highlighted.

Learning Objectives:

1. To give an overview of the clinical problem.
2. To learn the techniques.
3. To discuss usefulness and limitations of imaging.

A-067

B. Restrictive cardiomyopathy

O. Vignaux; Paris/FR

Restrictive cardiomyopathy, the least common form of cardiomyopathy, is defined as heart-muscle disease that results in impaired ventricular filling due to increased myocardial stiffness, with normal or decreased diastolic volume of either or both ventricles. Systolic function usually remains normal, at least early in the disease, and wall thickness may be normal or increased, depending on the underlying cause. Outside the tropics, cardiac amyloidosis is the most frequent cause. A number of other infiltrative conditions can result in restrictive cardiomyopathy such as tropical endomyocardial fibrosis and eosinophilic cardiomyopathy (Loffler's endocarditis), glycogen storage diseases, hemochromatosis and cardiac sarcoidosis. Other restrictive conditions include carcinoid heart disease, radiation-induced and anthracycline-induced endomyocardial fibrosis and idiopathic myocardial fibrosis. Clinical signs and symptoms may be similar to those in constrictive pericarditis and Cardiac Magnetic Resonance imaging (CMR) plays an important role in the differential diagnosis (pericardial thickness < 4 mm in restrictive cardiomyopathy). CMR examination with steady-state free precession and velocity-encoded sequences may show biventricular enlargement with normal left ventricular size, increased left ventricular thickness and mass, severe diastolic dysfunction (abnormal E/A velocity ratio), and normal systolic function. Infiltrative cardiomyopathies may exhibit specific CMR findings on T1- and T2-weighted black blood fast spin echo and Gadolinium-DTPA-enhanced sequences (patchy area of increased signal intensity and enhancement reflecting interstitial inflammation or granuloma in sarcoidosis, T2-weighted signal loss due to extensive iron deposit in hemochromatosis). Fibrosis or collagenous scar with expanded interstitial space appears as mid-wall hyperenhancement on delayed Gadolinium CMR.

Learning Objectives:

1. To give an overview of the clinical problem.
2. To learn the techniques.
3. To discuss usefulness and limitations of imaging.

A-068

C. Arrhythmogenic right ventricular cardiomyopathy

E. Di Cesare; L'Aquila/IT

Right ventricular dysplasia is a new entity of unknown origin in the classification of cardiomyopathies. Also known as arrhythmogenic right ventricular cardiomyopathy (ARVC) or arrhythmogenic right ventricular dysplasia, it is a disease of the heart muscle characterised by fibro-adipose atrophy mainly involving the right ventricle and responsible for cardiac electric instability. ARVC is also considered responsible for severe ventricular arrhythmias and sudden death also in young people. Symptomatology includes palpitations, syncope, congestive heart failure. Symptoms usually appear during exercise and progress over time.

MR imaging provides evidence of ventricular dilatation at the outflow tract, thinning and thickening of the wall, kinetic alterations, diastolic bulging areas (especially located at the level of the right ventricle outflow tract) and fatty substitution of the myocardium mainly at the level of the right ventricle. Many radiologists erroneously consider the previously described fatty substitution as the main sign of ARVC, even though an evaluation of fat substitution alone may be a source of error: firstly because isolated areas of fatty replacement are not synonymous with ARVC since small focal fatty areas of fat are also present in the normal patients, and secondly because the MR imaging detection of fat may be overestimated due to partial volume artefacts with normal subepicardial fat.

Moreover, considering the evolutive nature of the disease, the non invasiveness of MR imaging allows the follow-up of these patients and may be considered an excellent screening modality for the diagnosis of ARVC in family members.

Learning Objectives:

1. To give an overview of the clinical problem.
2. To learn the techniques.
3. To discuss usefulness and limitations of imaging.

16:00 - 17:30

Room F2

Neuro

RC 411

Functional MR imaging

Moderator:

M. Papathanassiou; Athens/GR

A-069

A. Technique, protocols and stimulation equipment

S. Sunaert; Leuven/BE

Functional MR imaging is a non-invasive technique capable of depicting brain activity. It is extensively used in the neurophysiological study of the human brain, and more recently clinical applications have appeared in the presurgical workup of patients with brain tumours as well as in the study of the diagnosis and treatment of different neurological and psychiatric diseases.

This refresher course will review both the MR physics and physiological principles underlying the functional MR imaging technique. The Blood Oxygen Level Dependent (BOLD) contrast, as well as other techniques will be discussed. Pitfalls regarding false positive and false negative fMRI imaging activation will be addressed.

It will review the most widely used (clinical) protocols to visualise brain activity during sensory (visual, taste, sensation, auditory, ...), motor and cognitive actions. The difference, advantages and challenges of block and event-related paradigms will be discussed. Details of acquisition and post-processing relevant to the study of specific brain activations will be elaborated on, e.g. on the use of adapted fMRI imaging sequences for the study of the auditory system, where auditory stimuli have to be delivered without interference of the MR imaging scanner noise. Finally, stimulation equipment to deliver visual, auditory, and other stimuli, as well as monitoring equipment to record responses, eye movements, etc. will be covered.

In summary, this part of the RC will introduce the audience to the basic principles, techniques, paradigms and stimulation equipment that is at present used in state-of-the art fMRI imaging studies.

Postgraduate Educational Programme

Learning Objectives:

1. To understand the basic physiological and physical principles underlying blood oxygenation level dependent functional MR imaging.
2. To understand the problems and merits of the most common imaging techniques in functional MR imaging.
3. To learn about the setup of both block and event-related fMR imaging paradigms in a clinical setting.
4. To understand imaging problems in fMR imaging and how to cope with these during fMR imaging data analysis.
5. To learn about the validity, pitfalls, accuracy and limitation of fMR imaging in a clinical setting.

A-070

B. Clinical applications of fMR imaging for intracranial tumors and epilepsy

C. Stippich; Heidelberg/DE

Preoperative fMR imaging of motor, somatosensory and language function is used worldwide by an increasing number of medical centers for safer surgery on brain tumors and epileptogenic foci. The method has not yet reached the status of a standardized diagnostic procedure. Therefore this talk provides the information that is relevant for the successful and responsible application of fMR imaging prior to brain surgery: The functional neuroanatomy of the motor and somatosensory systems and of language is summarized. Optimised clinical fMR imaging protocols and reference data are presented. Physiological and important pathological diagnostic findings are presented as well as the intraoperative validation of the functional localizations in neuronavigators using electrocorticography. Multimodality integration with MEG is presented. Important limitations and pitfalls of preoperative fMR imaging are discussed

Learning Objectives:

1. To learn about the functional neuroanatomy of motor, somatosensory and language associated brain activation.
2. To identify the indications for preoperative fMR imaging in patients with brain tumors.
3. To identify optimized preoperative fMR imaging protocols for patients with preexisting deficit.
4. To learn about normal and atypical findings in preoperative fMR imaging (illustrative cases).
5. To understand the use of fMR imaging in neuronavigation (illustrative cases).
6. To learn about the validity, intrinsic problems, pitfalls and limitations of preoperative fMR imaging.
7. To understand the possibilities of preoperative multimodality functional brain imaging using fMR imaging and magnetoencephalography (MEG) (illustrative cases).

A-071

C. fMR imaging for evaluation of brain plasticity in multiple sclerosis, stroke and trauma

A. Bizzì, V. Blasi; Milan/IT

Plasticity means different things to different scientists, but most would agree with the following definition: a change in structure over time resulting in a change of function.

Plastic changes occur at the level of the synapse, and are consequently reflected at the level of neuronal networks. It has been established that human brains show considerable plastic changes during development and that plasticity is also present in injured adult brains. In patients with lesions of the nervous system plasticity is the active or passive process of reorganizing connections and re-coordinating a network of areas while function is recovering.

Brain functions may be localised in functionally segregated brain regions but are mainly represented in extended, connected, overlapping and highly parallel processing networks. In normal subjects, it is characterised by a decrease of focal brain activity going along with an increased connectivity between the collaborating nets. Recovery of function seems to imply the "reconnection" or the recoordination of a network of areas.

Non-invasive functional neuroimaging methods such as fMR imaging offer the experimental opportunity for measuring changes in connectivity and functional segregation that accompany and underpin behavioural change or functional improvement after brain injury. This presentation will review the potential and limitations of fMR imaging to illustrate plastic changes occurring in patients after a stroke, a head injury or along the course of a relapsing remitting disease such as multiple sclerosis.

Learning Objectives:

1. To learn about acute changes in functional segregation and connectivity occurring after a focal brain lesion.
2. To learn about adaptive changes in functional segregation and connectivity occurring during recovery and their relationship with functional improvement.
3. To learn about changes in motor and language network re-organization induced by rehabilitation.

16:00 - 17:30

Room G

Head and Neck

RC 408

Radiological approach to stage head and neck squamous cell carcinoma

Moderator:

J.A. Castelijns; Amsterdam/NL

A-072

A. What the clinician needs to know and why

E.J. Adam; London/UK

Head and neck cancer is uncommon, accounting for only 3% of newly diagnosed cancers per annum. Benign disease far outweighs malignant disease in general ear, nose and throat surgical practice and the radiologist has an important role in alerting the clinician to the possibility of underlying malignancy.

Some "benign" presentations, for example middle ear effusions, sinus opacity and cystic neck masses, may indicate underlying malignancy and the radiologist needs to be aware of these potential pitfalls.

Once diagnosed, direct inspection provides excellent assessment of the extent of mucosal involvement by squamous cell carcinoma, but imaging is essential for evaluating the deep extent of disease and involvement of adjacent critical structures. Because these are uncommon cancers, the evidence base for treatment is small with few randomised controlled trials, and there is considerable variation in treatment strategies. The radiologist must be aware of local treatment protocols so that imaging is tailored to evaluate the critical radiological features which may affect the treatment offered to the patient.

The status of the cervical lymph nodes is the single most important prognostic factor. Clinical assessment is generally regarded as inaccurate (sensitivity and specificity 60-70%) and radiological staging is used to increase accuracy. It has a particular role in upstaging disease in the clinically negative neck and in the detection of contralateral disease, both of which will affect therapy. It is also important that radiologists and clinicians working together in this field use the same system for describing the sites of abnormal nodes for surgical planning.

Learning Objectives:

1. To appreciate the clinical context of head and neck image interpretation.
2. To be aware of radiological features which will influence treatment.
3. To understand the value of clear communication between radiologists and clinical teams.

A-073

B. Nasopharynx

M.G. Mack, T.J. Vogl; Frankfurt a. Main/DE

The nasopharynx forms an important boundary zone between the anterior and middle skull base and the parapharyngeal space. Diagnostic imaging is used in this region for morphologic evaluation, localization and staging of primary lesions of the nasopharynx.

The nasopharynx forms the upper portion of the pharynx and is continuous anteriorly with the nasal cavity. Its' roof is formed by the sphenoid bone, while its' floor and junction with the oropharynx are at the level of the soft palate. The pharyngeal recess (Rosenmüller fossa) is a pouch-like recess in the lateral wall of the nasopharynx directed toward the parapharyngeal space and lying directly adjacent to the Eustachian tube orifice. This region is a common site of origination for nasopharyngeal malignancies. Five percent of all malignant tumors of the head and neck originate in the nasopharynx and more than 90% of these are carcinomas. MR imaging is extremely helpful to demonstrate the extent of a mass in three dimensions and, most importantly, MR imaging can define the relationship of the mass to cranial nerves V, IX and X. However Multidetector CT (MDCT) is also helpful in the evaluation of the nasopharynx, especially if multi-planar reconstructions are used.

This presentation will focus on normal anatomy, benign and malignant tumors,

Postgraduate Educational Programme

congenital variations and malformations as well as the differential diagnosis.

Learning Objectives:

1. To learn the normal anatomy.
2. To learn the examination technique.
3. To know about different tumors, variants, differential diagnosis and imaging criteria.
4. To learn about tumor staging.

A-074

C. Oral and oropharyngeal cancer

R.C. Sigal; Villejuif/FR

In the oral cavity and oropharynx, cancer most often arises from the oral mucosa. Therefore the radiologist only plays a minor role in the detection of the disease but helps to define the exact extent of the lesion. Imaging plays an important role in therapeutic planning. The choice for the various types of surgery (partial or complete glossectomy, mandibulectomy) is dictated by invasion of the muscles of the tongue and the neurovascular bundle of the tongue, as well as the various subregions of the oropharynx (faucial area, soft palate, posterior oropharyngeal wall). Evaluation of the mandible is of paramount importance. Computed Tomography and Magnetic Resonance Imaging are the imaging modalities of choice. Imaging is also important in the follow-up and in the early tumor recurrence detection.

Learning Objectives:

1. To present the CT and MR techniques in the exploration of the tongue and oropharynx area.
2. To show the main patterns of tumor spread.
3. To explain the value of imaging at the posttherapeutic stage.

A-075

D. Laryngeal cancer

R. Hermans; Leuven/BE

About one quarter of head and neck tumours arise in the larynx. The majority are squamous cell carcinoma. As most laryngeal malignancies are mucosal lesions, inspection is important in staging the lesion. Imaging is needed to detect deep tumour spread into the paraglottic space, cartilage involvement and extralaryngeal tumour spread.

Criteria for tumour involvement are abnormal contrast enhancement, soft tissue thickening, presence of a bulky mass, infiltration of fatty tissue, or a combination of these features. CT can detect gross cartilage invasion, but often fails to detect early invasion. MR imaging is a more sensitive technique to detect cartilage invasion, but may yield false positive results. Overall, CT and MR imaging show comparable results in defining laryngeal tumour extent. In selected cases, these modalities may be considered to be complementary.

Surgery and radiotherapy are the only curative treatments for laryngeal cancer; chemotherapy can be used as an adjunct to one or both of these treatment modalities. Most early-staged laryngeal cancer can be cured by either surgery or radiotherapy, with similar cure rates for similar lesions. Patients with moderately advanced lesions may benefit from combined therapy. Advanced lesions often can only be treated palliatively.

The treatment plan for a particular patient is the result of a multifactorial decision process including tumour characteristics, tumour staging and volume, patient condition, and patient and institutional preferences. Objective tumour data, obtained from imaging studies, can be helpful to ensure a firm basis for informing the patient about his prognosis and for treatment decision making.

Learning Objectives:

1. To know the CT and MR appearances of laryngeal carcinomas.
2. To know the appearance of tumoral extensions into deep laryngeal structures.
3. To know the involvement of imaging modalities in the establishment of tumoural staging.
4. To understand the role of the TNM classification in the determination of the appropriate therapeutic modality.

16:00 - 17:30

Room H

Special Focus Session

SF 4c

History of contrast media

Moderator:

G. Livadas; Athens/GR

A-076

History of contrast media (Introduction)

G. Livadas; Athens/GR

This year's history session has been arranged so that it focuses on a single subject, the development of contrast media. The theoretical concept for a medium that would assist the visualisation and investigation of hollow organs is almost as old as the X-ray, since the first experimental papers on the subject appeared as early as 1896. In this session we will explore the evolution of contrast media from the primitive form of toxic and harmful compounds used in cadavers or guinea pigs, to the most sophisticated organ-specific, pathology-specific or modality-specific agents used in today's radiological practice. The speakers will present the pioneers and how they strove to excel and conquer the unknown, in an effort to understand the ideals and virtues of the talented individuals in relation to their social environment.

Learning Objectives:

1. To comprehend that any single product that commercially reaches the market is a result of a multitude of contributors' brainwork, research, trials, attempts and errors.
2. To discuss the intricate ramifications of ideas, starting as an individual conception and either ending as a failure or leading to a remarkable invention.
3. To promote the necessity of the recording and the study of all aspects of the history of radiology.
4. To stimulate younger radiologists to look into their history as a source of inspiration.
5. To stress the responsibility we all have not only to the patients but equally importantly, towards the future generations of radiologists to come.

A-077

The early years of contrast media

A.M.K. Thomas; Orpington/UK

The latter part of the 19th Century was a time of rapid development. In surgery, antisepsis was introduced by Joseph Lister and in 1865 the first operation was performed using his technique. The first anaesthetic was given in 1846 by William Morton. Unfortunately the visualization of the body prior to surgery was limited, although the first cystoscope had been introduced by Max Nitze in 1879. It was only when Wilhelm Röntgen discovered X-rays in 1895 that medical radiology was born with abdominal imaging becoming a reality. However, imaging of the abdomen was poor owing to the lack of contrast between the abdominal viscera. The use of contrast media enabled abdominal structures to be visualized, and normality and pathology defined.

In the renal tract, radiographs could be made after the passage of opaque ureteric catheters and the location of the ureters determined. This was first performed in 1901 by Schmidt and Kollscher. Opaque liquids could be injected as suggested by Klose in 1904. A suspension of bismuth sub-nitrate was initially used, however this was toxic in the renal tract. The technique of retrograde pyelography was refined in 1906 by Voelcker and von Lichtenberg and they produced the first complete outline of the ureters and renal pelvis. The problem of toxicity of the early agents was solved in 1918 when Douglas Cameron recommended the use of sodium and potassium iodide.

The retrograde contrast agents were the mainstay of renal imaging for 30 years and much knowledge of renal pathology was acquired.

Learning Objectives:

1. To understand the 19th century medical background to diagnostic radiology.
2. To learn about the development of clinico-radiological correlation in the diagnosis of normality and disease.
3. To learn about the early use of contrast material in abdominal imaging.

Friday

Postgraduate Educational Programme

A-078 ♀

The classical ionic contrast media

C. de Haén; Milan/IT

Technological innovation comprises the affirmation on the market of a product that responds to a unmet societal need. Solutions of water-soluble iodinated organic compounds for intravascular injection as X-ray contrast media (CM), which in 1930 made excretion urography and angiography practical and commercially viable, responded to this criterion. The innovation process involved both institutions and individuals, who with their background contributed to constructive interference of different knowledge cultures.

By the mid 1920's CM for excretion urography and angiography assumed the character of a vision of technology, namely the locus on the perceptive horizon where the line of temporal extrapolation of feasibility meets with that of desirability. Under its spell a web of interactions between numerous academic investigators (Hryntschat, Binz, Räth, Lichtwitz, Swick, von Lichtenberg) and three industries (DEGUSSA, Bayer, Schering-Kahlbaum) with their researchers (Ossenbeck, Tietze, Hecht, Schoeller, von Schickh) formed. Since 1897 through a series of commercial injectable CM, iodine had acquired the status of a preferred constituent. Only a few months apart in 1930 two iodinated uro-angiographic CM reached the market, uroselectan (Schering-Kahlbaum) and methiodal (Bayer/IG Farben). These CM bore a salified acid function. The ratio of iodine atoms per particle formed in solution was $I/P = 0.5$. Although osmolality at the time was not considered, soon CM with ratios of 1 and 1.5, i.e. reduced osmolality, became available. Along with reduced osmolality came reduced toxicity. In particular, numerous products with $I/P = 1.5$, epitomized by diatrizoate, conquered the markets in the 1950s and are still widely used in certain parts of the world.

Learning Objectives:

1. To become conscious of the social dimension of technological innovation, contrast media in the three decades following 1925 illustrating this.
2. To recognize the interplay of multiple knowledge cultures in innovation, for contrast media in particular those of chemistry, physiology, pharmacology, pharmaceuticals, radiology, internal medicine, patenting, industrial production, project management, entrepreneurship, communication, marketing and sales.
3. To appreciate the historical heritage recognizable in modern contrast media.

A-079

The development of the non-ionic contrast agents

T. Almén; Malmö/SE

I try to remember how the concept "non-ionic contrast media with high water solubility" arose. Ingredients were:

1. A desire to reduce pain caused by the iodine contrast media of the 1950s when injected for arteriography.
2. An interest in chemistry stimulated by arteriographies in animals.

Basics: The water soluble media for arteriography were salts. Three iodine atoms (with high X-ray absorption) covalently bound to a benzene ring constituted the anion. Sodium or methylglucamine (with low X-ray absorption) constituted the cation. The media had an osmolality 5-8 times greater than plasma.

Impulses: Some episodes during clinical arteriography gave me the belief that the pain might be decreased if contrast media isotonic to plasma could be created.

Logic: The question arose: "How do you design contrast media based on three-iodinated benzene rings, which gives a higher water solubility, lower osmolality and lower viscosity for the same amount of iodine?" My naïve thinking suggested: 1) Eliminate the positive ions and make the iodo-benzenes watersoluble by covalently bonded, hydrophilic hydroxyl groups. This means a 50% reduction in osmolality. 2) For further reduction dimers, trimers, oligomers of such three-iodinated benzene rings could be tried. 3) Make the molecules small and spherical for low viscosity.

The real world: These ideas were discussed in 1968 with Dr Hugo Holtermann, head of research at Nyegaard & Co, a small Norwegian pharmaceutical company. This resulted in a non-ionic medium, metrizamide, primarily intended for the subarachnoid space. Development has continued and today various non-ionic monomers and dimers are produced by different companies for various indications.

Learning Objectives:

1. To become conscious of the social dimensions in technological innovation.
2. To recognize the interplay of multiple knowledge cultures in innovations. For contrast media this concerns chemistry, physiology, pharmacology, pharmaceuticals, diagnostic radiology, internal medicine, patenting, industrial production, project management, entrepreneurship, communication, marketing and sales.
3. To appreciate the historical heritage recognizable in modern contrast media.

A-080

MR imaging contrast agents

H.-J. Weinmann; Berlin/DE

In the early eighties NMR tomography (today MRI, Magnetic Resonance Imaging) became a new, exciting imaging technology. Lauterbur, Brady and others demonstrated that paramagnetic salts could effectively change relaxation times and create contrast in MRI.

In 1981, Gries, Rosenberg and Weinmann synthesized and characterized paramagnetic chelates as contrast agents for MRI. The Schering patents covered the fundamentals of this class of MRI contrast agents.

Independent of the activities in Berlin, paramagnetic contrast agents (e.g. Cr EDTA, ferrioxamine B, stable free radicals) were tested at the UC in San Francisco, the Vanderbilt University in Nashville, and Mallinckrodt Inc. in St. Louis. The first clinical trials started in 1983 (FU Berlin). The first successful contrast enhancements in patients were at the Hammersmith Hospital in London in 1983. In 1988, various health authorities granted marketing authorization for Gd DTPA (Magnevist®). Other gadolinium-based agents were introduced into the market several years later.

Independent of the described contrast agent technology, superparamagnetic particles were investigated. Advanced Magnetics (Cambridge, MA, USA) received FDA approval for ferumoxides, introduced in 1995 (Endorem, Guerbet, France, or Ferridex, Berlex Laboratories Inc., USA). The second generation of superparamagnetic iron oxides became available in Europe (Resovist®, Schering AG, Germany) in 2001.

Gadolinium-based contrast agents with a specific distribution in the organism are in clinical development and may reach the market within the near future. MRI technology is still in a development phase and it is very likely that improvements in technology and contrast agent development will result in more tissue- and disease-specific agents.

Learning Objectives:

- To understand the historical development of MR contrast agents.

16:00 - 17:30

Room I

Workshops on Interventional Radiology

WS 418

Arterial and venous liver intervention

Moderator:

J.B. Karani; London/UK

A-081

A. Portal venous embolization

A.J. Roche; Villejuif/FR

Curative resection of malignant liver tumors closely depends on the volume of the remnant liver (RL) after hepatectomy. The aim of portal vein embolization (PVE) is to selectively induce hypertrophy of the RL during the preoperative period. This is achieved by embolization of portal branches of the future resected liver parenchyma. Basis for understanding the mechanisms involved in inducing hypertrophy after PVE will be given. Technical choices (approach, embolic agents) will be detailed and discussed. Indications for patients with hepatocellular carcinoma or metastases will be presented as well as short and long term results. An adverse effect of PVE might be stimulation of tumor growth in the RL. This critical point will be specifically discussed. State of the art of known prognostic factors for predicting hypertrophy after PVE and liver failure after surgery will be presented for patients with normal or compromised liver (chronic hepatitis, cirrhosis, long term previous chemotherapy, cholestasis).

Learning Objectives:

1. To understand the mechanisms of induced hypertrophy after portal vein embolization.
2. To choose the appropriate technique: Surgical or endovascular proximal ligation versus distal embolization, type of embolus to use.
3. To know the indications and results in liver metastases and hepatocellular carcinoma.
4. To know the effect of embolization upon tumor growth in the non-embolized liver.
5. To know the efficiency in compromised liver (previous IV or IA chemotherapy, cirrhosis).

Postgraduate Educational Programme

A-082

B. Chemoembolization

I. Battyány; Pécs/HU

The effectiveness of intraarterial selective cytostatic treatment and chemoembolization was analysed separately and in combination with surgery and/or RF ablation in patients suffered from liver malignancies. The duration of the selective intraarterial cytostatic treatment took 5 days and ended with chemoembolization. Mytomycin (1 x 10 mg), Farmorubicin (5 x 10 mg), Carboplatin (5 x 40 mg) for intraarterial cytostatic treatment and for chemoembolization Farmorubicin (10 mg), Lipiodol Ultrafluid (3-6 ml) and Iodamide 380 (1 ml) suspension were applied. The treatment was repeated six times in period of 4-6 weeks. Results of the treatment were controlled by US and CT. The chemoembolisation applied in combination with 5 days selective cytostatic treatment showed better results than chemoembolisation applied alone or together with less than 5 days selective cytostatic treatment. The surgery or RF ablation combined with intraarterial cytostatic treatment and chemoembolization are highly increased the survival time in HCC patients and significantly in metastatic patients. In vitro effectiveness of RF treatment alone and in combination with intraarterial liver chemoembolization was also analysed with help of perfused in vitro (pig) liver model.

Learning Objectives:

1. To know how to increase the effect of radiofrequency with chemo-embolization.
2. To know what is the correct order in the combination of different oncoradiotherapy methods to improve the therapeutic result.
3. To know the benefits of multimodality treatment.

A-083

C. Budd Chiari syndrome

J.-I. Bilbao Jaureguizar, A. Martínez-Cuesta; Pamplona/ES

Budd-Chiari syndrome (BCS) is caused by obstruction of the hepatic venous flow and characterized by the presence of ascites, hepatomegaly and abdominal pain. Clinically indistinguishable from hepatic venous occlusive disease, BCS is secondary to an obstruction of the major hepatic veins or even the inferior vena cava that can be secondary to multiple clinical situations. Different surgical procedures have been described to improve the decompression of the portal system when medical treatments become ineffective. As an alternative, several percutaneous techniques have been reported for treating BCS. The reported long term results with such techniques are at least as good as with surgery.

Learning Objectives:

1. To know the different etiologies of Budd-Chiari syndrome (BCS).
2. To understand the embryologic origin of the inferior vena cava.
3. To be familiar with the different radiologic modalities for establishing the diagnosis of BCS.
4. To know the different percutaneous approaches that may be performed for the treatment of BCS.
5. To know when to place a stent or perform a percutaneous transluminal balloon angioplasty in BCS.

16:00 - 17:30

Room K

Genitourinary

RC 407

Imaging problem lesions (tumors)

Moderator:

A. Magnusson; Uppsala/SE

A-084

A. Adrenal imaging

G.P. Krestin; Rotterdam/NL

Clinical symptoms of adrenal diseases are due to hormonal hyper- and hypofunction and to the large size of an adrenal mass. Incidentally found asymptomatic adrenal masses are very common findings on cross sectional examinations. Therefore differentiation of "incidentalomas" is important and may be challenging. Besides non-hyperfunctioning adenomas and metastasis - the two most common adrenal incidentally found masses - other diseases like cysts and pseudocysts, fatty lesions, mesenchymal tumors, solid cortical tumors, medullary neurogenetic tumors, infections and granulomas have to be considered. Imaging features of these different entities will be presented and the differential diagnostic approach based on clinical and morphologic appearance will be discussed.

Learning Objectives:

1. To understand the clinical context that allows a pragmatic approach to imaging of adrenal lesions.
2. To become familiar with the imaging techniques and their specific features in different common adrenal tumours.
3. To learn about the differential diagnostic approach to some rare conditions affecting the adrenal glands.

A-085

B. Renal imaging

R. Pozzi-Mucelli; Verona/IT

Although diagnostic imaging modalities are extremely accurate in the diagnosis of renal masses, diagnostic difficulties are sometimes encountered with US, CT and MR imaging. The main diagnostic problem is the differential diagnosis between benign and malignant tumors, mainly in cases of complex cystic masses and in some solid masses.

A greater number of problematic masses are found with US. Diagnostic difficulties with US are due to technical limitations and/or the complexity of the lesion itself. Technical limitation are due to limited spatial and contrast resolution. Other limitations are due to artefacts and obese patients. For complex cystic masses, the difficulties in the definition of the benign or malignant nature of the lesion is due to the presence of some findings such as calcifications, septae, vegetations, blood and purulent debris. For solid masses, problems concern the identification of small tumors, the differentiation among the anatomical variants, the differentiation between benign (i.e. atypical angiomyolipoma, oncocytoma) and malignant (renal cell carcinoma) tumors. The contribution of colour-power Doppler and contrast media in the solution of some of the diagnostic difficulties will be illustrated. Problematic renal masses can be seen, although in a less number of cases, with CT and MR imaging. Indeterminate masses in CT are due to very small size, internal septae, blood, debris. Also with CT the differential diagnosis between some benign tumors (atypical angiomyolipoma and oncocytoma) and malignant tumors is difficult. MR imaging has similar difficulties but it provides a higher contrast resolution enabling better characterization of fluid content in cases of hemorrhagic cysts.

Learning Objectives:

1. To show the problematic renal masses with US, CT and MR imaging.
2. To demonstrate the possible solutions in order to differentiate benign from malignant lesions.
3. To show the importance of integration of diagnostic imaging modalities.
4. To report the advances of US, CT and MR imaging and the role of contrast agents.

16:00 - 17:30

Room L/M

Infection in the Adult Today

CC 416

Chest

Moderator:

M.-F. Carette; Paris/FR

A-086

A. Community-acquired and nosocomial infections

C.J. Herold; Vienna/AT

Pulmonary infections are among the most frequent causes of morbidity and mortality throughout the world. In the non-immunocompromised population, pneumonia is one of the top two infectious diseases and represents the most prevalent community-acquired infection (CAP). Nosocomial pneumonia (NP) is the leading cause of death from infection acquired in the hospital.

In CAP, most individuals are infected through person-to-person transmission of microorganisms bound to or suspended in water-mucus droplets. NP is the result of aspiration of gastric contents or contaminated oropharyngeal secretions.

Infections in CAP are commonly caused by gram-positive bacteria, atypical bacteria, and viruses. The most important pathogens in NP include aerobic gram-negative organisms and *Staphylococcus aureus*. Viruses, protozoa, and fungi play an increasing role in patients with impaired defense mechanisms.

In CAP and NP, the typical radiologic findings include lobar pneumonia, bronchopneumonia (lobular pneumonia), and rarely, diffuse bilateral interstitial disease. Nodules may be seen in mycobacterial infections. Complications include necrosis, cavitation, bronchopleural fistula, and pleural effusions.

Postgraduate Educational Programme

In both entities, the role of radiology includes detection and exclusion of pulmonary infiltrates (which may be difficult in NP), narrowing of the differential diagnosis, guidance of additional (invasive) procedures, and patient follow-up.

Learning Objectives:

1. To help understand the epidemiology and the causative factors of CAP and NP.
2. To elucidate the spectrum of causative microorganisms in both forms of pneumonia.
3. To present the radiologic features and patterns of different infections.
4. To discuss the role of imaging methods in the investigation of patients with suspected pneumonia.

A-087

B. Infection in AIDS and the immunocompromised patient

T. Franquet; Barcelona/ES

Pulmonary infection is a major cause of morbidity and mortality in patients with impaired immune function. In the last several decades, the AIDS epidemic, advances in the treatment of cancer, organ transplantation, and immunosuppressive therapy has resulted in large numbers of patients who develop abnormalities in their immune system. Mildly impaired host immunity, as it occurs in chronic debilitating illness, diabetes mellitus, malnutrition, alcoholism, advanced age, prolonged corticosteroid administration and chronic obstructive lung disease, has also been regarded as a predisposing factor for pulmonary infections. Although plain chest radiography, in most cases, provides adequate information and CT is usually not required for diagnosis, in some cases CT might be used as a problem-solving tool.

Learning Objectives:

1. To summarize the high-resolution CT findings of some of the most common infectious processes seen in AIDS and in immunocompromised non HIV patients.
2. To describe some complications associated with pulmonary infections.
3. To learn key points in distinguishing infectious diseases from other non-infectious pulmonary disorders.

A-088

C. The spectrum of tuberculosis and non-mycobacterial tuberculous infection

S.M. Ellis; London/UK

The spectrum of radiographic findings in pulmonary infections due to *M.tuberculosis* (TB) and non-tuberculous mycobacteria (NTM) are being increasingly discussed, primarily as a result of the increasing prevalence of these infections. NTM organisms are often overlooked as potential infecting organisms, diagnosis is often delayed and radiologists tend not to include NTM in their differential diagnosis. The literature on the imaging appearances of NTM pulmonary infections is now sufficiently large as to identify some features that would help to distinguish an NTM infection from conventional pulmonary tuberculosis (TB), allowing the radiologist at least to raise the possibility of NTM infection. This review is intended to describe the radiological features, in the immunocompetent host, that accompany TB and NTM pulmonary infections and highlight the imaging features that would favour an NTM as the causative organism.

Learning Objectives:

1. To increase awareness of radiographic appearances of mycobacterial infections in the chest.
2. To highlight features that may help distinguish different mycobacterial organisms.
3. To understand the implications the organism type has on management.

16:00 - 17:30

Room N/O

Primer: Molecular Imaging

PR 419

New imaging methods and technologies

Moderator:

H. Alfke; Marburg/DE

A-089

What molecular imaging actually is

C. Bremer; Münster/DE

Molecular imaging is one of the emerging research arenas for imaging related sciences. This talk intends to provide a brief definition of the term "Molecular Imaging". Selected imaging examples will be given in order to present the whole scope of this research field. Moreover an overview of the "Primer on Molecular Imaging" is provided including a presentation of the speakers and aspects covered in this new lecture series.

Learning Objectives:

1. To briefly explain the main goals of molecular imaging.
2. To introduce the speakers of the "Primer on molecular imaging".

A-090

A. Parametric and molecular MR techniques

C. Moonen; Bordeaux/FR

Molecular Imaging (MI) includes all imaging modalities and builds on the full deciphering of the human genome by looking at spatio-temporal maps of gene expression levels and its consequences. Selected examples of MI approaches using MR imaging are:

1. Visualization of tumor activity by targeting angiogenesis by directly mapping altered gene expression levels or indirectly using biomarkers such as perfusion. Processes related to apoptosis and degradation of the extracellular matrix can be mapped based on specific contrast agents targeting annexin V and Matrix Metalloproteases, respectively. Once specific markers are found, radiopharmaceuticals, and/or drugs can be attached to locally deliver therapy.
2. Local delivery of a gene therapy vector using real-time image guidance, and mapping expression of a marker gene. Spatial and temporal control of transgene expression can be achieved based on a combination of MR imaging-guided local hyperthermia and a heat-sensitive promoter.
3. Homing of stem cells as gene therapy vectors and for tissue repair. Stem cells have been isolated, labeled with MR contrast agents, then re-injected and tracked towards their target using serial MR imaging.

Recent advances have demonstrated the large potential of multi-modality MI. MR imaging requires amplification strategies to reach the high specific sensitivity of optical and Nuclear Medicine techniques. Its role in translational MI research and development of biomarkers will be significant. Further progress is needed in:

1. development of clinically relevant biomarkers,
2. specific contrast agent design,
3. development of combined diagnostic/therapeutic agents,
4. development of image-guided technologies for local drug delivery and local gene therapy.

Learning Objectives:

1. To review the emerging field of molecular imaging using MR imaging.
2. To illustrate the strategies to develop targeted MR contrast agents to evaluate endogenous and exogenous gene expression.
3. To understand the concept of MR biomarkers in the field of (anti)angiogenesis, macrophage activity, metabolism.
4. To illustrate the concept of MR image guided local molecular therapy.

A-091

B. Optical imaging

V. Ntziachristos; Charlestown, MA/US

The ability to non-invasively image molecular processes in-vivo is an emerging reality using different reporter and detection approaches. Molecular imaging has been heralded to lead to earlier detection than current anatomical imaging approaches, which typically detect late stage abnormalities. By construction the approach is highly specific as reporting probes can be engineered to be reporting on certain molecules with good discrimination capacity. Another important prospect of molecular imaging is the ability to examine and quantify treatment responses in-vivo by monitoring specific primary molecules or downstream tar-

Postgraduate Educational Programme

gets. Therapeutic efficacy could then be probed dynamically on time-scales of hours to days. This is in contrast to the mainstay of today's healthcare with traditionally late end points of drug efficacy, a practice that often impairs prompt revision and exclusion of ineffective treatment strategies with potentially lethal results. Still we are significantly limited in the ways we can accurately detect such reporter technologies in tissues associated with high photon scattering and non-linear light propagation. This talk presents the current state of the art as well as revolutionary new technologies that enable accurate and sensitive optical molecular imaging. These technologies enable practical strategies for recording of proteomics and genomics in-vivo and are designed with the clinical application in mind. Therefore they attain high potential for clinical translation and impact.

Learning Objectives:

1. To understand the basic principles of optical imaging and tomography.
2. To outline optical imaging strategies and applications.
3. To gain insights on potential clinical applications.

A-092

C. Nuclear imaging including PET

M. Schäfers; Münster/DE

The spectrum of clinically available imaging methods has a wide range of modalities capable of investigating morphology, function and molecular processes. Within this spectrum scintigraphic (nuclear) imaging modalities are widely used to characterize organ function and molecular pathways in the whole body *in vivo*. These techniques are based on the concept of labelling authentic or analog molecules with radioactive isotopes, which either are detected by direct gamma-emission (single photon emission tomography SPECT: Tc-99m, I-123 etc.) or indirect by coincidence of two high energy gamma quants (512 keV) originating from an annihilation of a positron in the tissues (positron emission tomography PET: F-18, C-11, O-15 etc.). These radiopharmaceuticals are then injected intravenously, their distribution in space and time are assessed three-dimensionally by either SPECT or PET.

Especially when used in molecular imaging, *in vivo* scintigraphic imaging approaches are uniquely able to assess molecular processes with a very high sensitivity without influencing the physiology/pathophysiology.

The state-of-the-art role of scintigraphic imaging in research and clinical applications will be reviewed.

Learning Objectives:

1. To learn about the high molecular sensitivity of scintigraphic approaches as compared to MR, CT and ultrasound.
2. To know the spectrum of currently available radiopharmaceuticals and molecular scintigraphic techniques.
3. To understand the principles and challenges of quantification (compartment models etc.) of molecular metabolism *in vivo*.
4. To hear about potential clinical scintigraphic applications.

16:00 - 17:30

Room P

Computer Applications

RC 405

Tele-imaging in Europe today

Moderator:

K.-J. Klose; Marburg/DE

A-093

A. Introductory lecture on teleradiology

L. Donoso; Sabadell/ES

Teleradiology is the electronic transmission of radiographic images from one geographical location to another for the purposes of interpretation and consultation. In many respects teleradiology is the best telemedicine service. It is already part of daily practice. The current clinical uses of teleradiology will be discussed from primary interpretations to on-call coverage in inter and intra-institutional scenarios.

There are many technical challenges in teleradiology, including image acquisition, transmission and interpretation. It is important to recognize that image distribution in teleradiology scenarios is only an enabling component of a much larger goal that requires both new technology (integrated information system) and new practical culture. The term "teleradiology" itself will be obsolete, remote interpretations and consultations will be such an integral part of radiology practice that referring to them will neither require nor occasion a special term.

Teleradiology clearly has a number of advantages but it also has the potential to create considerable difficulties for radiologists unless their role and the legal responsibilities involved are defined and debated.

Radiologists must now fundamentally become partners in the leadership of the process: rethink the approach to image management and distribution, promote integration of information, bearing in mind that radiology is a clinical specialty rather than just a reporting service.

Learning Objectives:

1. To discuss the impact of IT in health scenario from the radiology focus.
2. To share our experience in new working scenarios using teleradiology.
3. To recognise key factors in the process.
4. To introduce the concept of replacing teleradiology with inter-institutional networking.

A-094

B. The mobile teleradiology

J. Reponen; Oulu/FI

The development of wireless networks and terminal devices has made mobile communication to image archive systems possible. The access is nowadays possible outside the fixed hospital network and even outside physical hospital boundaries.

The mobile teleradiology units are based on different technical platforms ranging from laptop computers to mobile phones. Most promising terminal types for medical purposes are Smartphones with computer functions, Personal Digital Assistants (PDA) with phone capabilities or tablet PC devices with networking capabilities. Various wireless networks are available ranging from WLAN to GSM and GPRS.

The main limitations of current technology are relatively slow network speed, restricted computational power and a small display for image viewing purposes. For selected tasks their service is acceptable even today.

The clinical needs are basically twofold: within a hospital there is a need to serve the users of electronic patient record with radiological images. A tablet PC might be one mobile tool replacing a paper journal on wards. On the other hand, mobile teleradiology terminals have so far been used for viewing images needing a secondary consultation. A Neuroradiologist on duty can make his remarks on an emergency CT scan with a help of an image phone. A Neurosurgeon can make decisions based on image data even before entering the hospital. The benefit of mobile devices will be greatest, if they can be connected to a comprehensive electronic patient record. Especially well they perform together with a web type multimedia medical record where only a thin client software is needed.

Learning Objectives:

1. To understand the different technical platforms for mobile teleradiology and their restrictions.
2. To understand the clinical needs of multimedia terminals for radiologists and other specialities.
3. To evaluate the present and future role of mobile image viewing service.

A-095

C. Results in practice: The Norwegian experience

J. Størmer; Tromsø/NO

Norway had early pilot projects in Teleradiology (first one reported in 1984) converted to permanent services with a considerable volume per site (7,000 – 8,000 exams a year) since 1992.

PACS also has been rapidly and largely accepted in almost 100% of the 50 hospitals since the very first was installed in the Lofoten Islands in 1996.

Since 2002 the Norwegian health care system has changed fundamentally in its organisation with a shift from local/regional ownership shared between the 20 counties to a more centralized and government based ownership. Actually the country with close to 4,6 million inhabitants is divided in five independent regions, each organised as private enterprises with government as majority owner and thereby protected from bankrupts. Each region has adopted different strategies in order to create interoperability between the PACS and other clinical information systems (HIS) in their medical institutions. National authorities have since year 2,000 planned for a nationwide Health Intranet. Different local and regional initiatives (mainly proprietary Teleradiology solutions since early nineties) has resulted in a convergence ending up in an applicable and standardized National Health Net in operation since October 2004. This has facilitated and accelerated the different initiatives to interconnect PACS's. Still difficulties in interoperability between PACS and RIS from different vendors are an obstacle in the process of integration. Legal aspects are another challenge for the developers or pioneers in connecting medical information systems to the benefit for the constantly more mobile and demanding modern patient.

Postgraduate Educational Programme

Learning Objectives:

1. To discuss the basis of a nationwide teleradiology system.
2. To understand the key of the success for a teleradiology system.

16:00 - 17:30

La Scala

Foundation Course - Chest Radiology

E3 420

Interstitial and alveolar disorders

Moderator:

C. Schaefer-Prokop; Amsterdam/NL

A-096

A. Diffuse infiltrative lung disease

D.M. Hansell; London/UK

High resolution computed tomography (HRCT) is a powerful and accepted technique which is now routinely used for the investigation of patients with suspected or known diffuse infiltrative lung disease. However, when interpreting the results of the various studies that have evaluated the diagnostic accuracy of HRCT, and encouraged its widespread clinical application, several factors need to be borne in mind: a) there is inevitably a selection bias with a relatively high proportion of conditions which have distinctive HRCT appearances. In this respect, the study populations do not reflect the case mix encountered in "normal" clinical practice, b) such studies are retrospective and are usually undertaken by highly experienced observers, and c) new or "difficult" conditions (e.g. non-specific interstitial pneumonitis) and normal individuals are under-represented.

HRCT provides a similar view of the lung as a low power scan of an autopsy or lung biopsy specimen and it is not an overstatement to suggest that HRCT images reflect histological appearances. Once the mechanism behind the generation of the basic HRCT signs is understood, interpretation is greatly facilitated. For example, the situations in which ground glass opacification on HRCT (essentially caused by nothing more or less than the displacement of air) will be encountered can readily be predicted. It must be emphasized that the *indirect* HRCT signs of fundamental pathologic processes are not wholly reliable. An appreciation of the limits of HRCT and a basic understanding of the pathophysiology of diffuse lung diseases increases the quality of HRCT interpretation.

Learning Objectives:

1. To clarify the borderland between normal state and early diffuse lung disease.
2. To understand the generation of basic HRCT features of diffuse lung disease.
3. To appreciate the limits of sensitivity and specificity of HRCT.
4. To avoid some of the obvious pitfalls in HRCT interpretation.

A-097

B. Alveolar lung disease and atelectasis

P.A. Grenier; Paris/FR

Alveolar lung diseases can manifest on chest radiographs or CT as a nodular pattern, ground glass opacification or consolidation. These features express the displacement of air from the alveoli by accumulation of fluid, cells, tissue or amorphous material.

A nodular pattern is made up of rounded opacities that measure 5-10 mm in diameter. Most often the nodular opacities have a patchy distribution and are often associated with airspace consolidation. Nodular pattern is most frequently encountered in the context of bacterial infection. Ground glass opacification is present when there is increased lung density; on CT scans, it appears as a patchy or diffuse hazy increase in lung attenuation with preservation of bronchial and vascular markings. Reticulation may be present in the same areas as ground glass opacification, giving the crazy paving pattern. Airspace consolidation is seen as homogeneous increased opacity with obscuration of underlying pulmonary vessels. This opacity extends to pleural surfaces and presents with fuzzy borders and may contain air bronchograms. Consolidation can be diffuse, patchy or lobar in distribution; it can also appear as rounded, linear or curvilinear opacities. The distribution of changes and the evolution pattern, on both radiographs and CT scans, may be helpful differential features.

Atelectasis or lung collapse is defined by a loss of lung volume. Mechanisms are obstructive, passive, cicatricial or adhesive. The imaging features of atelectasis include decrease in volume of the lobe or segment involved (movement of fissures), hilar and large airway rearrangement, mediastinal shift, compensatory hyperinflation, chest wall and diaphragm positional changes.

Learning Objectives:

1. To enhance the understanding of mechanisms and causes of alveolar lung diseases and lung atelectasis.
2. To illustrate the typical and atypical patterns at chest radiograph and CT of alveolar lung diseases.
3. To familiarize with anatomical displacement of structures in case of lobar atelectasis.
4. To illustrate the typical and atypical patterns at chest radiograph and CT scan of lobar atelectasis.

Saturday, March 5

Postgraduate Educational Programme

		room A 2nd level	room B 2nd level	room C 2nd level	room E1 entr. level	room E2 entr. level	room F1 entr. level	room F2 entr. level	room G lower level	room H lower level	
07:00											07:00
07:30											07:30
08:00											08:00
08:30											08:30
09:00		CC 517 Essentials of Neuroradiology Cerebral tumors and infections (p. 34)	RC 510 Musculoskeletal Osteoporosis and osteopenia (p. 34)	SF 5 Special Focus Session High-field body MR imaging: The new standard? (p. 35)	RC 502 Breast Open questions (p. 36)	RC 501 Abdominal and Gastrointestinal Liver imaging: Characterisation and pitfalls (p. 36)	RC 504 Chest CT angiography of the chest (p. 37)	EF 1 EFOMP Workshop State-of-the-art in information technology (p. 38)	RC 508 Head and Neck Imaging in cochlear implant candidates (p. 39)	RC 509 Interventional Radiology Endovascular treatment in female pelvis (p. 39)	
09:30											09:30
10:00											10:00
10:30		EM 1 “ECR meets” Italy Imaging of focal lesions (p. 45)	NH 6 New Horizons Session Nanotechnology (p. 46)	SS 610 Musculoskeletal Bone structure imaging and quantification (p. 190)	SY 3 Satellite Symposium Implementation of clinical system solutions in an e-health environment (p. 580)	SS 602 Breast MR mammography (1) (p. 192)	SY 4 Satellite Symposium Work safety in the daily routine for technical staff in radiology (p. 580)	EF 2 EFOMP Workshop How to get the best from information technology for patient care (p. 47)	SS 608 Head and Neck Acoustic pathway and base of the skull imaging (p. 194)	SS 609a Interventional Radiology Skeletal interventions (p. 196)	
11:00											11:00
11:30											11:30
12:00											12:00
12:30											12:30
13:00											13:00
13:30											13:30
14:00											14:00
14:30		SS 703a Cardiac MDCT of the coronary arteries (p. 208)	SS 710 Musculoskeletal MR imaging of the cartilage (p. 210)	SS 701a GI Tract Acute abdomen (p. 212)	SY 7 Satellite Symposium Ultravist: Two decades of partnership in CT: Answers to current topics (p. 582)	SS 702 Breast MR mammography (2) (p. 215)	SS 704 Chest Malignant tumors: Screening, staging and outcome (p. 217)		SS 707 Genitourinary Renal and adrenal tumors (p. 219)	SS 709 Interventional Radiology MR, CT and US guided procedures (p. 221)	
15:00											14:30
15:30											15:00
16:00											15:30
16:30		CC 817 Essentials of Neuroradiology Epilepsy, white matter diseases and ageing (p. 49)	RC 810 Musculoskeletal Bone marrow disorders as a manifestation of disease (p. 50)	SF 8a Special Focus Session Imaging ICU patients (p. 50)	RC 803 Cardiac Coronary vessels (p. 51)	RC 801 Abdominal and Gastrointestinal Crohn's disease of the intestinal tract: Advances in imaging (p. 52)	RC 804 Chest Imaging of lung cancer (p. 53)	RC 811 Neuro Orbit and visual system (p. 53)	SF 8b Special Focus Session Diagnostic and interventional radiology of transplants (p. 54)	RC 813 Physics in Radiology Special issues of radiation exposure in diagnostic radiology (p. 55)	
17:00	registration										16:00
17:30	EPOS™ - scientific exhibition										16:30
18:00											17:00
18:30											17:30
19:00											18:00
											18:30
											19:00

Postgraduate Educational Programme

	room I lower level	room K lower level	room L/M 1st level	room N/O 1st level	room P lower level	room W basement	room R 1st level	room Y 1st level	room Z entr. level	La Scala 2nd level	
07:00											07:00
07:30											07:30
08:00											08:00
08:30											08:30
09:00	RC 515 Vascular Venous imaging and intervention (p. 40)	RC 507 Genitourinary Imaging of the uterus (p. 41)	CC 516 Infection in the Adult Today Gastrointestinal infection: A changing scene (p. 42)	RC 514 Radiographers MR imaging/ Neuroimaging (p. 43)	ER 526 Joint ECR/EAR sessions: Challenges for European Radiology Assessment and accreditation in radiology in Europe (p. 43)				WS 23A1 Screening Mammography Interpretation Test "Hands-on" Workshop	E ³ 520 Foundation Course: Chest Radiology Airways and infection (p. 44)	09:00
09:30											09:30
10:00									WS 23A2 Screening Mammography Interpretation Test "Hands-on" Workshop		10:00
10:30									WS 624 Basic Life Support for Radiologists "Hands-on" Workshop	E ³ 620a Logistic implications of MSCT (p. 48)	10:30
11:00	SS 609b Interventional Radiology Abdominal aortic aneurysms (p. 198)	SS 603 Cardiac Coronary plaque imaging (p. 200)	SS 611 Neuro Stroke imaging (p. 202)	SS 605 Computer Applications Computer aided deduction and diagnosis (p. 204)	SS 615 Vascular Post therapeutic follow up and monitoring of disease (p. 206)	WS 622 Vertebraloplasty "Hands-on" Workshop			WS 23A3 Screening Mammography Interpretation Test "Hands-on" Workshop	E ³ 620b How to write a successful grant proposal (p. 48)	11:00
11:30											11:30
12:00											12:00
12:30											12:30
13:00											13:00
13:30											13:30
14:00									WS 23B1 Screening Mammography Interpretation Test "Hands-on" Workshop	E ³ 720 Foundation Course: Chest Radiology Vascular, emergency and ICU imaging (p. 48)	14:00
14:30	SS 701b Abdominal Visera (Solid Organs) Pancreatic and bile duct cancer (p. 223)	SS 703b Cardiac Cardiac function (p. 225)	SS 711 Neuro Epilepsy and brain tumors: Advanced diagnostic imaging (p. 227)	SS 713 Physics in Radiology CT: Radiation dose (p. 229)	SS 715 Vascular Carotid imaging (p. 231)				WS 23B2 Screening Mammography Interpretation Test "Hands-on" Workshop	WS 724 Basic Life Support for Radiologists "Hands-on" Workshop	14:30
15:00											15:00
15:30											15:30
16:00									WS 23B3 Screening Mammography Interpretation Test "Hands-on" Workshop		16:00
16:30	WS 818 Workshops on Interventional Radiology Pediatric intervention (p. 56)	RC 807 Genitourinary Imaging of stones (p. 57)	CC 816 Infection in the Adult Today Musculoskeletal infection (p. 57)	PR 819 Primer: Molecular Imaging MR approaches to molecular imaging (p. 58)	JRF Highlighted Lectures					E ³ 820 Interactive Image Teaching Mediastinal masses (p. 59)	16:30
17:00											17:00
17:30											17:30
18:00											18:00
18:30											18:30
19:00											19:00

Saturday

Postgraduate Educational Programme

08:30 - 10:00

Room A

Essentials of Neuroradiology

CC 517

Cerebral tumors and infections

Moderator:

N. Besenski; Charleston, SC/US

A-098

A. Extra-axial brain tumors

A. Drevelegas; Thessaloniki/GR

Extra-axial are tumors with an extracerebral location. They are usually benign. Meningiomas are the most common extra-axial neoplasms in the supratentorial compartment. Other extra-axial neoplasms are: schwannomas, metastatic lesions, arachnoid cysts, epidermoids, dermoids, chordomas and eosinophilic granulomas. Schwannomas are by far the most common neoplasms of the posterior fossa.

The clinical image depends on the size and the location of the tumor. The location of the brain tumors affects treatment planning and predicts their prognosis.

In the evaluation of extra-axial brain tumors CT and MR imaging represent the two most important and commonly used imaging modalities. CT is superior for detecting areas of calcification and for evaluating bony changes related to the tumor. Multidetector CT (MDCT) is also very helpful in the presurgical evaluation of the tumors. The multiplanar capability and the superior contrast resolution of MR imaging makes it the best technique in the evaluation of extra-axial brain tumors. MR imaging permits more reliable distinction between intra- and extra-axial tumors and provides better delineation of the relationship of extra-axial tumors to the surrounding brain and vital structures involved by the tumor. Additionally MR imaging is also more useful in delineating tumors of the posterior cranial fossa where the beam hardening artifacts obscures their delineation on CT. Imaging studies play an important role in the diagnosis of extra-axial tumors and provide crucial information to the neurosurgeon in preoperative planning.

Learning Objectives:

1. To define and classify extra-axial brain tumors.
2. To demonstrate the imaging characteristics of extra-axial brain neoplasm.
3. To describe the appropriate imaging protocols.
4. To identify some clues for differential diagnosis.
5. To learn how to image the post-operative patient.

A-099

B. Intra-axial brain tumors

G. Wilms; Leuven/BE

Neuroradiology plays a key-role in the diagnosis and preoperative setup of patients with brain tumours. State-of-the-art imaging requires a standardised imaging protocol, careful and systematic study of the images and finally an attempt at characterisation of the lesion.

The radiological diagnosis and differential diagnosis of intra-axial tumours no longer relies on CT-scan and routine MR-sequences alone. Standard multiplanar imaging has to be combined with fMR imaging to allow exact anatomic location of the lesion and precise determination of the extent of the tumour. Perfusion and diffusion MR become more and more important in the differential diagnosis of cerebral mass lesions and in grading and typing of gliomas. More sophisticated techniques such as diffusion tensor imaging and spectroscopy will further enhance the value of radiological studies.

Learning Objectives:

1. To learn the standard imaging protocols for the radiological study of intra-axial brain tumors.
2. To underline the importance of new imaging techniques in the diagnosis and differential diagnosis of intra-axial brain tumors.
3. To give some clues for the differential diagnosis of intra-axial brain tumors.

A-100

C. Cerebral infections

S. Karampekios; Iraklion/GR

In spite of the development of many effective antimicrobial therapies and the general improvement in hygiene and health care systems all over the world, the incidence of central nervous system (CNS) infection has increased significantly in the past 15 years. This can be attributed primarily to the acquired immunodeficiency syndrome (AIDS) epidemic and its devastating effect on the immune sys-

tem and secondarily to various immunosuppressive agents that are being used in aggressive cancer treatment and in organ transplantations.

The brain is relatively protected from infection by the calvarium, meninges, and blood-brain barrier. However, a large number of pathogens, including bacteria, viruses, fungi, and parasites, can reach the brain hematogenously or less likely by direct extension from an adjacent infected focus. When an intracranial infection does occur, the precise localization is of great importance, because it narrows the differential diagnosis, sometimes determining the type of the pathogen, allowing institution of more appropriate treatment, and eventually leading to a more favourable outcome. Magnetic resonance imaging (MRI) is the most sensitive imaging modality in detecting focal or diffuse parenchymal infectious lesions, and today it has clearly replaced computed tomography (CT). By using advanced MRI techniques, such as Proton MR Spectroscopy (¹H-MRS), Diffusion-Weighted (DW) imaging, Perfusion-Weighted (PW) imaging and Magnetization Transfer (MT) sequences, further improvement in the detection and characterization of infectious brain lesions is possible.

Learning Objectives:

1. To become familiar with the different types of cerebral infections, using some broad categories to localize them, by the anatomic compartment involved.
2. To present the various manifestations of AIDS-related infections.
3. To understand the role of advanced MR techniques, such as DWI, PWI, MRS, MT, for the detection and characterization of intracranial CNS infections.

08:30 - 10:00

Room B

Musculoskeletal

RC 510

Osteoporosis and osteopenia

Moderator:

B. Vande Berg; Brussels/BE

A-101

A. Acquired osteoporosis

J.E. Adams; Manchester/UK

During childhood the bones grow in size, alter in shape and increase in mineral content, particularly at puberty. Peak bone mass (PBM) is reached around 20 and bone mineral density (BMD) remains stable for the next two to three decades. PBM is determined by genetic factors (80%), but lifestyle factors (physical activity, nutrition and hormonal status) are also relevant.

Bone "turnover" continues, with old bone being resorbed (osteoclasts) and replaced by new bone (osteoblasts), to maintain integrity and strength. Normal bone mineralization depends on the supply of vitamin D (1,25(OH)₂D), calcium, phosphorus and alkaline phosphatase; deficiencies cause rickets/osteomalacia. Bone formation and resorption are balanced (Basal Metabolic Unit - BMU), but in some diseases become "uncoupled". Formation may be defective (osteogenesis imperfecta, corticosteroid therapy) or resorption excessive (oestrogen deficiency, hyperparathyroidism). Bone deficiency/loss (osteoporosis), reduced BMD and insufficiency fractures result. Characteristic radiological features may have prognostic significance (a prevalent vertebral fracture predicts future fracture risk of vertebra x5 and hip x2). Bone densitometry (DXA) is important to identify those at risk before fractures occur. Effective preventative and therapeutic measures (bisphosphonates, SERMS, vitamin D and calcium supplementation) are available to increase BMD and reduce fractures.

Learning Objectives:

1. To describe the normal growth and development of the skeleton and the factors that influence the attainment of peak bone mass.
2. To explain normal bone turnover and the basal metabolic unit (BMU), and how "uncoupling" through diseases may lead to bone loss and osteoporosis.
3. To outline preventive and therapeutic measures available for secondary osteoporosis.

A-102

B. How to measure and monitor it

S. Grampp; Vienna/AT

The basis for diagnosing osteoporosis is the conventional radiograph, dual X-ray absorptiometry (DXA) (femur, lumbar spine), and quantitative computed tomography (QCT) (lumbar spine).

Conventional radiographs yield a relatively low sensitivity and cannot be used as a screening method.

Postgraduate Educational Programme

For economical reasons and because of the low radiation dose, DXA is of the most clinical relevance. After an initial radiograph of the lumbar spine either a DXA of this region (patients up to 65 and without significant degenerative changes) or at the hip (patients above 65 or with significant degenerative changes) should be performed.

In special cases or if such a device is readily available a QCT of the lumbar spine might be a first-evaluation technique.

General data for the application of densitometry with quantitative ultrasound (QUS) does not currently allow a general recommendation for its' use in diagnosis. The method is currently regarded as an additional technique and can be used for pre-screening to identify healthy women and men.

Learning Objectives:

1. To know the clinically relevant methods to measure and monitor the skeletal status such as DXA, QCT and conventional radiographs.
2. To get the ability in using strategies to apply the radiological methods in the primary diagnosis as well as in follow-up studies and in different patient groups.
3. To know about the major weaknesses and strength of each method.
4. To realize about the major pitfalls related to each method.

A-103 ♀

C. Juvenile osteopenia

T.M. Link; San Francisco, CA/US

Children are not simply small adults and bone mineral density (BMD) measurements in childhood and adolescence are an extremely complex issue. Since bone size, shape and volumetric density vary substantially with age, T-scores are of no use in this population. In addition timing of growth and puberty may also be variable. It is extremely important, however, to diagnose osteoporosis and osteopenia in these patients at an early stage since these deficits will translate into permanent deficits in bone mass in the adult.

The ideal densitometric technique should (1) provide a low radiation exposure, (2) assess true volumetric BMD, (3) provide information on fracture risk and (4) be based on normative data collected from a representative healthy population with various age ranges. Such a technique, however, does not exist at present. Currently, dual energy X-ray absorptiometry (DXA) is most frequently used, since it is fast, has a low radiation exposure and the best-established pediatric reference data. However, areal BMD is extremely dependent on bone size, which may be a big handicap in children with accelerated or delayed development. Quantitative CT (QCT) provides true volumetric density but has a higher radiation dose and there is little reference data.

Indications for bone densitometry in children and adolescents include chronic disorders such as anorexia nervosa and endocrine disorders as well as systemic diseases such as cystic fibrosis, rheumatoid arthritis, osteogenesis imperfecta and neoplastic diseases. Additionally, normal children with fractures due to low impact trauma and patients with the rare idiopathic juvenile osteopenia warrant study.

Learning Objectives:

1. To understand the limitations of diagnostic techniques in a pediatric and adolescent population.
2. To learn the strengths and weaknesses of bone densitometry techniques used for diagnosing juvenile osteoporosis and osteopenia.
3. To be aware of potential indications for BMD measurements in children and adolescents.

08:30 - 10:00

Room C

Special Focus Session

SF 5

High-field body MR imaging: The new standard?

Moderator:

G.P. Krestin; Rotterdam/NL

A-104

High-field body MR imaging: The new standard? (Introduction)

G.P. Krestin; Rotterdam/NL

High-field MR imaging is one of the most exciting, challenging but also controversial areas of development in Magnetic Resonance Imaging during the last years. While there is no doubt that for applications in the central nervous system high-field strengths have clear benefits, the use of whole body 3 T systems for imaging the heart, the abdomen or the musculoskeletal system are much more

controversial. Three experts in the area will discuss body applications of high-field MR imaging.

Learning Objectives:

1. To learn about the technical challenges of high-field body MR imaging in the three different areas of application.
2. To understand the current indications for high-field MR imaging in the cardiovascular and musculoskeletal systems and in the abdomen.
3. To learn about the future trends and developments of high-field body MR imaging.

A-105

Cardiovascular

S. Dymarkowski; Leuven/BE

The intrinsic advantage of an increased signal-to-noise ratio(SNR) at 3 T has stimulated many researchers to use this ultra-high field equipment for studies outside the brain. However, the higher field strength presents specific obstacles to 3 T MR imaging determined by the laws of physics, therefore making the transition from CMR at 1.5 T to 3 T not straightforward. The increased RF-energy deposition (SAR), the larger chemical shift and the stronger susceptibility effects have to be considered as challenges, especially in cardiovascular studies. Development of specific higher order shimming procedures, optimized surface coils and proper sequence adaptation has so far allowed highly detailed anatomical imaging, but has also opened the door for functional exams, including high quality MR tagging studies, contrast-enhanced imaging of myocardial perfusion and infarction, and offers the possibility of coronary artery imaging with formerly unseen spatial resolution.

Cardiac MR imaging exams performed at 3 Tesla are gradually finding clinical acceptance. Looking at the present results and taking in consideration the present advantages and disadvantages of using 3 T for cardiovascular work, it is still unclear to most researchers and clinicians if this is the right path to pursue. Future scientific investments will still need to tackle many currently unresolved issues and to carefully deliberate at which field strength cardiac MR imaging is best performed.

Learning Objectives:

1. To understand the signal-to-noise, imaging speed and SAR trade-offs associated with transferring cardiac MR imaging from 1.5 T to 3 T.
2. To understand how imaging at 3 T requires significant changes in pulse sequence parameters.
3. To understand how inherent benefits at 3 T can be used as an advantage in cardiac MR imaging.

A-106

Abdomen

S.M. Hussain; Rotterdam/NL

The development of a body coil and radio frequency coils for a 3 Tesla MR imaging system, and their recent approval in Europe and North America, facilitated its application as a whole body MR system. With about double the signal-to-noise ratio of a 1.5 T system, the 3.0 T MR systems dramatically improve the image quality and image acquisition speed. Higher signal-to-noise allows more imaging flexibility. Theoretically, 3.0 T can deliver half the voxel size or, in certain cases, enable one-quarter of the acquisition time of a comparable study done at 1.5 T. Additional resolution and speed could be used in a number of ways: 1) increased resolution: to visualize small structures in greater detail; 2) shorter acquisition times to reduce motion artifacts when imaging patients unable to perform extended breath holds; 3) improve both acquisition speed and resolution. Anatomy that is difficult to image at lower field strengths, such as the prostate, rectum, uterus, and ovaries, could be imaged without an internal coil, significantly reducing patient discomfort and preparation time. Faster breath-hold body imaging - with or without parallel imaging capability such as SENSE - is offered as a standard feature by several vendors. In this lecture, we will present our experience concerning the body applications of 3 T based on volunteer studies and patients, and will explain some of the difficulties that occur during sequence optimization.

Learning Objectives:

1. To review the differences between 3 T and 1.5 T for body imaging.
2. To point out the current advantages and possible future directions of 3 T for body imaging.

Postgraduate Educational Programme

A-107

Musculoskeletal

D. Weishaupt; Zürich/CH

Magnetic resonance (MR) has revolutionized musculoskeletal imaging because of high spatial resolution, multiplanar imaging capabilities and exquisite soft-tissue contrast. So far, clinical MR imaging of the musculoskeletal system is performed at magnetic field strengths ranging from 0.2 to 1.5 T with dedicated surface coils. Recently, whole body MR systems working at 3.0 T have become available for clinical use. 3.0 T MR systems provide various benefits for body MR imaging including increased signal-to-noise ratios (SNR), enhanced T2^{*} contrast, increased chemical shift resolution, and probably better diagnostic performance compared to magnets working at lower field strengths. The higher intrinsic SNR of 3.0 T systems can also be used to improve imaging speed. However, when imaging at 3.0 T there are several changes to consider including changes in relaxation time, increased artifacts and increased radio-frequency (RF) power deposition.

Learning Objectives:

1. To discuss advantages and limitations of musculoskeletal imaging at 3.0 T.
2. To understand the changes in RF- and relaxation characteristics with 3.0 T.
3. To review the differences of imaging at 3.0 T compared to imaging at lower field strength.
4. To identify potential applications of 3.0 T imaging for musculoskeletal diseases.

08:30 - 10:00

Room E1

Breast

RC 502

Open questions

Moderator:

G. Forrai; Budapest/HU

A-108

A. Technology assessment

E. Azavedo; Stockholm/SE

Technology Assessment is an important step in managing modern health care. This assessment can be divided into several parts and the most common way usually is seen from a technical point of view assessing physical details of a radiological image. The next part is assessment of the overall quality of an image to see the diagnostic details that one wishes to see. The modern approach to Technology Assessment is to assess the role and place of modern technology in a health system.

The lecture will show examples and discuss how new technology is and will be assessed by the health providers because it is a matter of economy that has to be related to the additional information that new technology may give us. We could also have new technology giving us the same old information but at a more economically attractive level and these kind of economic aspects will probably dominate the choice of future technology investments.

If a new technology needs more time and/or more total costs are involved in this new technology than the costs of existing modalities than it may be hard to convince our health providers to approve the usage of such a modality in routine clinical practice. On the other hand medico-legal implications will also force us to turn our eyes to modalities with the highest sensitivity and specificity and this type of equations are not easily solved. The lecture will cover these above mentioned aspects by showing examples of published data.

Learning Objectives:

1. To present the basics of technology assessment.
2. To discuss two cases: Introducing full-field digital mammography and large vacuum biopsy.
3. To discuss the use of technology assessment within Europe.

A-109

B. Reporting standards

H. Zonderland; Leiden/NL

In mammography, reporting a classification, based on risk assessment is the cornerstone of good patient care, as it improves the clarity of the findings and leads to optimal interdisciplinary communication. The Breast Imaging Reporting and Data System™ (BI-RADS) has been developed and revised three times since 1992 by the American College of Radiology. The newest edition also includes Ultrasound and MR imaging. It is not restricted to final assessment categories

alone, but also attempts to unify morphologic descriptive features, follow-up and outcome monitoring. It has become obligatory in accredited institutions in the US and utilization of BI-RADS in Europe is increasing. This presentation will outline considerations needed in order to consider implementing the use of BI-RADS in the European community. There are distinct advantages: Optimal inter-professional and inter-institutional communication, standardization of reporting and ease of outcome monitoring. On the other side, sometimes fine-tuning, tailored to local conditions, is missing. Also interobserver variability can hamper good comparison. One can discuss some morphologic definitions as well as definitions with respect to outcome monitoring. They are undoubtedly well-suited for the American system of health care, but sometimes need some adaptations in situations or studies performed on other grounds. The system is the product of an excellent collaborative effort between members of various committees of the American College of Radiology, but should also be discussed on European level, before full acceptance can be achieved.

Learning Objectives:

1. To discuss the need of correlation between mammography, ultrasound and pathology reports.
2. To discuss the benefits and limitations of BI-RADS.
3. To propose a method for breast imaging audit.

A-110

C. Screening planning

A. Evans; Nottingham/UK

Mammographic screening is only effective if the intervention is of high quality. To achieve this level of performance obligatory training of professional groups and a rigorous quality assurance process are essential. Screening centres have to be large enough to allow statistical evaluation of performance and for the staff to gain sufficient experience. Screening and symptomatic breast work is often best done by the same team.

Small invasive cancer detection rate is a good surrogate for overall screen performance but quality assurance visits to screening centres to assess multi disciplinary team work are also invaluable. Mammographic screen reading should be done by a limited number of high volume readers all of whom participate in screening assessment, as a number of studies have correlated performance with volume and access to feedback. Volume and performance are also seen to correlate in performance of breast pathologists and surgeons.

The best film reading practice is double reading with arbitration and given the shortage of radiologists across Europe this is often done by radiographic technicians. There is good evidence that radiographers have identical sensitivity and specificity as radiologists of similar experience. The introduction of full field digital mammography will make the use of CAD a practical possibility. As yet there is no evidence that single reading with CAD is equal to double reading with arbitration.

Learning Objectives:

1. To present the basics of screening planning.
2. To correlate with the problems of screening in Europe (enhance radiologists shortage).
3. To discuss the helping of radiographers and CAD.

08:30 - 10:00

Room E2

Abdominal and Gastrointestinal

RC 501

Liver imaging: Characterisation and pitfalls

Moderator:

A. Palkó; Szeged/HU

A-111

A. Calcifications

C. Stoupis; Berne/CH

Although calcified liver lesions are not often seen in imaging studies in daily practice, many represent inflammatory lesions or benign and malignant liver neoplasms. Even though a specific diagnosis of a calcified mass is not always possible, there are some additional imaging features (presence of mass effect, nature of the calcified mass -cystic, solid- and the presence of scar) that may indicate the correct diagnosis. In calcified granulomatous disease (e.g., tuberculosis), the calcification (solitary, multiple) typically involves the entire lesion (no mass effect) and produces artifacts on CT. Echinococcus cysts have curvilinear or ring

Postgraduate Educational Programme

calcifications. E. alveolaris appears with calcification in a mass, mimicking malignancy. Chronic abscess may have discrete calcifications, mimicking treated metastases. In the case of hemangiomas, calcifications are solitary, large, coarse and centrally located in areas of fibrosis (CT 20%, plain film 10% of cases). In the case of hepatocellular adenoma, calcifications may be multiple, heterogeneous and usually located eccentrically within a heterogeneous mass. Primary malignant neoplasm, such as fibrolamellar carcinoma (CT 15%-25% of cases), demonstrate solitary, stellate, calcifications located in a scar (very rare, focal nodular hyperplasia, may calcify, in 1-2% of cases!). Calcifications in intrahepatic cholangiocarcinoma (18% of cases) are typically accompanied by a desmoplastic reaction and are ill defined. Calcifications in cystadenocarcinoma are associated with multiloculated, inhomogeneous cystic masses with solid components. Calcified hepatic metastases are most frequently associated with mucin-producing neoplasms such as colon carcinoma, are multiple, ill defined, amorphous and associated with a mass.

Learning Objectives:

1. To learn the pathological characteristics of calcified liver lesions.
2. To define the technical imaging aspects for the study of the liver in case of calcifications.
3. To learn the imaging characteristics of calcified liver entities.

A-112

B. Fat

C. Valls; Barcelona/ES

Diagnosis and characterization of fat in the liver is a diagnostic challenge because with most diagnostic techniques the presence of fat in the liver will significantly impair the quality of the examination. MR imaging offers significant advantages in that setting. There are two basic MR techniques that can be used to detect and characterize fatty lesions in the liver: Chemical shift imaging and fat saturation techniques. Chemical shift imaging techniques take advantage of the difference in resonance frequency between triglycerides and water protons. In in-phase images the signal from water and lipid protons is additive leading to a high signal intensity of fatty lesions. In opposed-phase images tissues containing fat and water show a significant loss of signal because the signal from water cancels the signal from fat.

Liver steatosis is defined as an abnormal accumulation of triglycerides within hepatocytes. US and CT examinations are severely impaired in cases of steatosis and the ability to detect focal lesions is decreased. Both focal fatty change and focal sparing of the liver parenchyma may have a troublesome appearance that may lead to a misdiagnosis of hepatic mass. MR imaging can readily differentiate these lesions from other tumoral lesions because focal fatty change is hyperintense on in-phase sequences and hypointense on opposed phase sequences. The differential diagnosis of incidental fat-containing liver lesions includes focal fatty change, hepatic lipoma, angiomyolipoma, liver cell adenoma and hepatocellular carcinoma. In the setting of chronic liver disease, a fat containing focal liver lesion is highly suggestive of HCC.

Learning Objectives:

1. To provide an update on technical factors and MR imaging contrast agents useful for detection and characterization of fat containing liver lesions.
2. To learn the imaging findings in fat containing liver lesions and fatty infiltration.
3. To review atypical presentations of focal liver lesions and to optimize imaging strategies in the setting of diffuse steatosis.

A-113

C. Vascular abnormalities

Y. Menu, A.-S. Rangheard; Le Kremlin-Bicêtre/FR

Flow related liver abnormalities are extremely common. Some are relevant for the diagnosis or the prognosis while others carry no clinical importance. Complexity of liver flow physiology and anatomy is the main explanation for the multiple features of liver perfusion on CT and MR imaging. Arterial obstruction or dilatation, portal or hepatic obstruction and fistulas may interfere with liver perfusion alone or in association. Liver blood volume is somewhat limited by the liver capsule, leading to a balance between different compartments. Other conditions like diffuse diseases (fatty liver disease, fibrosis or cirrhosis) or liver tumors are commonly associated with flow abnormalities. Special attention will be given to portal hypertension including portal thrombosis, arterio-portal balance, fistulas, the relationship between liver tumors and flow abnormalities, hepatic vein obstruction, peliosis and associated conditions. In this presentation, a simple method based on the recognition of anatomical landmarks and temporal analysis of liver images (plain images, arterial phase, portal phase and sometimes delayed

images) will be detailed. At the end of this talk, it should be possible to identify the abnormal flows that are clinically relevant, to recognize the most common pitfalls, to determine if an underlying disease is present and to evaluate the practical importance of flow abnormality to establish the overall prognosis.

Learning Objectives:

1. To understand normal liver flow physiology.
2. To be able to determine which vessel or flow is abnormal.
3. To understand the significance of flow abnormalities in main liver diseases.

08:30 - 10:00

Room F1

Chest

RC 504

CT angiography of the chest

Moderator:

L. Heuser; Bochum/DE

A-114

A. Technique for imaging the great vessels

M. Rémy-Jardin, J. Rémy; Lille/FR

Volumetric techniques are greatly improved by multislice spiral CT scanners that can scan large volumes with narrow slice collimation. These new scanners confirm that they now allow the radiologists to increase the diagnostic accuracy and clinical indications of volumetric scanning not only by means of high-resolution transverse CT sections but also by means of high-quality 2D and 3D images. Multiplanar reformatting creates sagittal, coronal or curved imaging planes providing unique displays for the transverse images. Volume rendering techniques address some of the limitations of shaded-surface display techniques. MIP rendering can be applied to either the entire imaged volume or can be targeted to a thin slab of tissue. All reformatting and volume-rendering techniques provide optimal results when applied to motion-free, three-dimensional data sets composed of isometric voxels. The purpose of this lecture is to focus on practical aspects of CT angiographic techniques aimed at evaluating thoracic vessels (aorta excepted).

Learning Objectives:

1. To review the acquisition and reconstruction protocols for optimal imaging of thoracic vessels.
2. To become familiar with the most commonly used reconstructions.
3. To understand the pitfalls and limitations of postprocessing techniques used as diagnostic tools.

A-115

B. Normal and variant anatomy

M.L. Storto; Chieti/IT

The normal radiographic and cross-sectional anatomy of thoracic aorta, great vessels, and mediastinal veins will be reviewed along with a description of the most common variants.

A detailed knowledge of the wide range of congenital abnormalities that may involve the aortic arch is fundamental for a correct interpretation of mediastinum, in order to avoid misdiagnoses.

The most common anomaly of the aorta is an aberrant right subclavian artery originating from a normal left-sided arch, occurring in approximately 0.5% of the population. The proximal portion of the aberrant artery is frequently dilated, a finding known as diverticulum of Kommerel.

A right aortic arch is present in about 0.1-0.2% of subjects and in approximately 70% of cases is associated with an aberrant left subclavian artery. The presence of a left ligamentum arteriosum completes the vascular ring in most of such patients. A right aortic arch with mirror-image branching can also occur; in these cases, the left innominate artery arises as the first branch of the aorta.

In patients with double aortic arch, the right common carotid and subclavian arteries arise from the right arch, whereas the left common carotid and subclavian arteries arise from the left arch. The two arches join posteriorly to form one descending aorta.

A persistent left SVC draining to a coronary sinus is the most common thoracic venous anomaly that occurs in 0.3% of healthy subjects and 4.3% of patients with congenital heart disease. Rarely, the left SVC drains into the left atrium, thus creating a right-to-left shunt.

Postgraduate Educational Programme

Learning Objectives:

1. To describe the normal anatomy of the aorta, great vessels, and mediastinal veins.
2. To become familiar with the most common arterial and venous variants in the mediastinum.
3. To discuss possible pitfalls of interpretation.

A-116

C. Current role of CT in the evaluation of aortic diseases

M. Prokop; Utrecht/NL

For evaluation of the thoracic aorta, CT angiography became a substitute for angiography already in the mid 1990s. Multislice scanning has made it possible to improve spatial resolution for thoracic CTA and, if necessary, include the abdomen into the evaluation. Technological advances include suppression of pulsation effects by fast retrospective ECG gating or prospective triggering. Such techniques can be considered in patients with suspected type A aortic dissections or atypical chest pain. With the newest generation of 32- to 64-slice scanners, evaluation of the heart and thoracic aorta can be combined. Dose issues then become an important limiting factor. The course will discuss how radiation dose can be kept to a minimum while maintaining diagnostic image quality. Optimized techniques of contrast material administration with the new scanners can ensure evaluation of aorta, coronaries and pulmonary arteries within one scan. The course will also review the most critical clinical questions for aortic dissection, aortic aneurysm, aortic rupture as well as aortitis. Because of its speed, ease and diagnostic yield, multislice CTA is now the gold standard for the evaluation of the thoracoabdominal aorta. MRA, however, should be preferred in young individuals (radiation exposure) and in patients with impaired renal function.

Learning Objectives:

1. To learn how to choose scanning and contrast injection parameters for CTA of aortic diseases.
2. To recognize typical artifacts and learn how to avoid them.
3. To understand the most critical questions to be answered in patients with aortic dissections, aneurysms, rupture and aortitis.
4. To comprehend the relative roles of CTA and MRA for the thoracic aorta.

08:30 - 10:10

Room F2

EFOMP Workshop

New technology in diagnostic radiology: The inescapable growth of information technology

EF 1

State-of-the-art in information technology

Moderators:

D. Caramella; Pisa/IT

S. Christofides; Nicosia/CY

A-117

Welcome address

A. Del Guerra; Pisa/IT, A. Chiesa, Brescia/IT

Information Technology (IT) has become a fundamental issue in Radiology. It opens new frontiers in diagnosis, but also creates the need for additional expertise and for new evaluation and quality control criteria. More and more advanced devices are now available with built-in capability for CAD, GRID, image analysis and quantitative image processing. Additionally PACS and Teleradiology are receiving a lot of attention in the clinical arena. This workshop is the 7th of the series EFOMP Workshop in "New Technology in Diagnostic Radiology". It has been organized by EFOMP in collaboration with ECR and COCIR to address the technological aspects, the medical requirements and the industry perspective of IT in Diagnostic Radiology.

A-118

Advances in CAD for cancer detection

N. Karssemeijer; Nijmegen/NL

Computer aided detection (CAD) of cancer is gaining acceptance as a new way of improving reader performance in radiology. In particular in screening applications the use of CAD seems to be advantageous. By using a computer that marks suspicious areas in images the risk of overlooking important lesions is greatly reduced. For effective use of CAD systems a high sensitivity is required. In general, CAD systems have a threshold for display of markers that can be adjusted

to increase sensitivity. However, display of more markers goes at the cost of specificity. Finding the right operating point is an important issue. If a CAD system has poor performance the number of false positive markers may be too high at acceptable levels of sensitivity.

The use of CAD is particularly effective in combination with dedicated workstations. On electronic display systems CAD results can be presented as overlays that can be switched on or off, allowing the radiologist to identify exactly what the computer has detected. For instance, in mammography microcalcification clusters can be displayed by highlighting individual calcifications. This allows the user to conveniently judge their spatial distribution. In lung cancer detection with CT dedicated 3D workstations allow the user to automatically move to slices in which CAD has found nodule candidates. Navigation is also possible using a 3D volume renderer in which nodules are marked. Image registration can be applied to match nodules in a temporal image pair, which greatly enhances the efficiency of the reading process.

Learning Objectives:

1. To learn about the state of art of computer aided detection of breast and lung cancer.
2. To understand the advantage of using CAD in combination with dedicated workstations for visualization.
3. To gain insight in future development of CAD.

A-119

Use of the GRID in medical imaging data management

S.R. Amendolia; Geneva/CH

A GRID can provide a seamless and secure access to distributed information and to high-level applications, a transparent use of local and remote computing resources, and constitutes a way of implementing a framework for collaborative work. GRID thus becomes a necessary tool in modern e-Health implementations: individualised healthcare requires access to all patient information regardless of place. Epidemiology demands large datasets to be addressable transparently, quality control implies quick comparison of image quality across borders, screening and early prevention rely on the possibility of exploiting in a efficient way the experts and the emerging IT tools, like CADetection systems. All this has to be carried out respecting the particularly demanding privacy and security criteria that govern the clinical data usage. Medical data are more and more based on images; multimedia, large, increasing in size and are relevant in the long term. As an example, a mammography exam can require as much as 120 Mbytes of information in terms of images, plus the associated metadata. A countrywide screening programme in a European country ends-up with terabytes of data each year on distributed storage media. Managing such an amount of information in a coherent way is outside the reach of the customary IT tools (web). This is where the GRID can make the difference, also because its intrinsic structuring in Virtual Organisations naturally matches the structure of healthcare users. Examples will be given, in particular a running GRID system for mammography data handling will be shown and discussed.

Learning Objectives:

1. To understand the basics of a GRID IT system.
2. To match the potential of GRID to the requirements of healthcare provision.
3. To verify from a practical implementation the ease of use and the scope of a GRID applied to the management of medical imaging data.

A-120 ♀

Designing image analysis algorithms for molecular imaging

B.M. ter Haar Romeny; Eindhoven/NL

Molecular imaging (MI) promises to be the next revolution in medical and biomedical imaging. As a direct extension to nuclear medicine imaging, a wide variety of molecular processes can now be monitored for the understanding of diseases and life's fundamental processes. Investments worldwide are huge, both by industry and by governmental and university research institutes.

At this moment, MI is still in the research phase. The images originate from PET, MR imaging, ultrasound and optical methods such as fluorescence microscopy. A new feature is the multi-spectral nature of the resulting image data, e.g. multiple values in a single pixel/voxel, e.g. from MR imaging scanning sequences, from different molecular target marker responses, and from combining different physical measurement parameters, e.g. fluoroscopic decay times and interaction parameters. Even full matrices and tensors become common as pixel values. Image analysis aims to answer quantitative questions by computer vision technology about the images, and visualize this complex data.

We discuss the following applications in detail:

- statistical analysis of high resolution multi-modal MR imaging data for the in-vivo classification of atherosclerotic plaque in the human internal carotid artery;

Postgraduate Educational Programme

Saturday

- visualization of tensorial data, such as for diffusion tensor imaging of human brain fibre bundles and heart muscle fibre orientation;
- analysis of functional shape parameters in remodelling vessel wall cells of the mouse from high resolution 2-photon microscopy images;
- segmentation of lysosomes in noisy 3D images of macrophages;
- the use of *Mathematica 5* as a versatile high level design language for complex image analysis algorithms by geometric reasoning.

Learning Objectives:

1. To understand the role and comprehend the design challenges of new algorithms for molecular imaging analysis.
2. To learn from examples to develop new and complex image analysis algorithms for molecular imaging.
3. To become familiar with a modern computer system for doing mathematics on images.
4. To learn the principles underlying the techniques used in the analysis of molecular images and sequences.

08:30 - 10:00

Room G

Head and Neck

RC 508

Imaging in cochlear implant candidates

Moderator:

P.A. Dimopoulos; Patras/GR

A-121

A. What the clinician needs to know and why

F.E. Offeciers; Antwerp/BE

I will give an overview of:

1. How and why cochlear implants function well as a replacement of the cochlear sensory function,
2. the surgical procedure,
3. the components of a cochlear implant.

The essential questions a Cochlear Implant surgeon wants answers on are:

1. Is the cochlea implantable, i.e. accessible for a standard CI electrode?
2. Is the cochlear nerve morphologically normal?
3. Are there any central auditory lesions or malformations which could hamper the normal functional outcome of a CI?
4. Is there any kind of concomitant pathology throughout the auditory system which would jeopardize safe implantation or preclude a favorable and stable long-term outcome?

Imaging also helps answering other questions. We distinguish 5 specific levels of interest, or if you will, 5 sets of goals, which are:

1. To help identifying the etiology of deafness
2. To help in selecting and counselling the CI candidates
3. To pre-operatively visualize useful surgical landmarks
4. To post-operatively evaluate the position of the CI-electrode
5. To provide important data in CI-related research

All these categories of questions will be discussed using practical examples from our clinical experience, emphasizing the impact of each set of imaging data on clinical decision making and on the functional outcome.

We will try to make this session as interactive as possible, welcoming questions from the floor throughout the session.

Learning Objectives:

1. To understand the rationale behind performing cochlear implants.
2. To be familiar with the surgical procedure and type of implants available.
3. To know which information is essential for the surgeon prior to performing a cochlear implant.
4. To know which information is essential for the surgeon in case of cochlear implant dysfunction.

A-122

B. Pre-implant imaging

J.-W. Casselman; Bruges/BE

Both CT and MR are needed in prospective cochlear implant candidates if one wants to provide the surgeon with all necessary information.

Inner ear malformations in congenitally deaf children can be seen on CT and MR. However MR better detects the intralabyrinthine malformations. In the internal auditory canal (IAC), only MR is able to detect aplasia or hypoplasia of the VIIIth nerve and its cochlear branch. Inner ear and IAC malformations are best seen on thin TSE or GE T2W images. Congenital malformations in the brainstem or audi-

tory cortex (e.g. pachygryria) can also jeopardize the success of cochlear implantation.

Meningitis is the most frequent cause of acquired deafness in children. Calcified obliterations of the cochlea can be detected on CT, whereas MR can detect fibrous intracochlear obliteration. However, MR cannot distinguish calcified from fibrous obliteration. Therefore both MR and CT are needed to tell the surgeon if cochlear implantation is possible. Acute labyrinthitis can be seen as intralabyrinthine enhancement on Gadolinium-enhanced T1W images. CT is still needed to evaluate the mastoid pneumatisation and to exclude anatomical variations/congenital malformations on the route towards the basal turn of the cochlea, even if the inner ear and nerves in the IAC are normal on MR.

In adults otosclerosis, neurofibromatosis and labyrinthitis (acquired deafness) are the most frequent causes leading to cochlear implantation. Infarction, MS, tumor or post-traumatic lesions along the auditory pathway or in the auditory cortex can also be the cause of bilateral deafness and are best seen on MR.

Learning Objectives:

1. To know which are the imaging modalities and the pertinent protocols needed to image the temporal bone and brain prior to performing a cochlear implant.
2. To know the anatomy of the auditory pathway and recognize normal and abnormal findings.
3. To know how to recognize contraindications for performing cochlear implants.
4. To be able to report the essential findings to the ENT surgeon.

A-123

C. Post-implant imaging

C. Czerny¹, W.D. Baumgartner¹, W. Gstöttner²; ¹Vienna/AT, ²Frankfurt

a. Main/DE

Introduction: This paper explains the techniques of digital radiography(DR) in one projection and Computed Tomography, presenting their indications and showing the imaging findings of normally and abnormally inserted implant electrodes in the postoperative assessment of multichannel cochlear implant (CI) patients.

Methods: To explain the radiological techniques of DR in a modified Chausse III projection and in CT imaging. To show how the position and insertion depth of the CI electrodes can be determined.

Results: The radiographic findings were found to be similar to the CT findings regarding the detection of electrode position. Excellent correlation exists between the radiological and surgical results with regard to insertion depth ($r = 0.92$). Abnormally inserted electrodes show bent electrodes, incomplete insertion, and misplaced electrodes. The radiation dose of one CT examination is about 200 times higher than that of one radiographic examination, and the examination time of one CT is 20 times longer than that of one X-ray. The costs for one CT examination are about 5.5 times higher than those of one X-ray.

Conclusions: Digital radiographs obtained in a modified Chausse III projection enable accurate assessment of the CI electrode position and insertion depth correlated to surgical results and compared to CT. The radiation dose and the costs of the examination are considerably lower than those of CT, and these facts might favour the use of digital radiographs in the modified Chausse III projection. CT might be indicated in those cases in which the radiographs can not explain any problems concerning the implant electrode.

Learning Objectives:

1. To know the modalities of exact depiction of cochlear implants and the accuracy of the different imaging modalities.
2. To know which is the most effective imaging technique for the assessment of inserted cochlear implants and to be able to recognize the features of correctly and incorrectly inserted cochlear implants by using different imaging modalities.
3. To delineate potential complications of cochlear implant insertion failure.

08:30 - 10:00

Room H

Interventional Radiology

RC 509

Endovascular treatment in female pelvis

Moderator:

E. Brountzos; Athens/GR

A-124

A. Leiomyomata

I. Pinto Pabón; Madrid/ES

Indications: The main indication for UAE is the treatment of symptomatic fibroids,

Postgraduate Educational Programme

intra-mural less than 10 cm in diameter, in a patient with no wish of future pregnancy.

Anatomy: In 77% of the cases the internal iliac artery has an anterior and a posterior trunk. The anterior trunk usually has three parietal branches (obturator, inferior gluteal, and internal pudendal) and three visceral branches (vesical, uterine, and middle rectal). We can recognize the uterine arteries, because they are highly twisted; and the characteristic course is a parietal segment, an arch part and a marginal or ascending segment.

Technique: Adequate sedation and analgesia is achieved with midazolam and fentanyl. Concerning the approach the unilateral right common femoral artery is preferred for access. Beginning with a Sidewinder catheter 4 F to catheterize the left internal iliac artery and after that, selective uterine artery catheterization is performed, with catheter tips placed within the transverse portion of the uterine artery. Embolization is performed with particles bigger than 400 μ (PVA particles or microspheres).

Complications:

* During the procedure:

- Arterial spasm (13-17%)
- Dissection or vessel perforation (5%).
- Non-target embolization.

* After the procedure: Post-embolization syndrome (15-25%), Vaginal discharge (20-50%), Sloughing Fibroids (3%-6%), Infection, piometra or uterine perforation that makes hysterectomy necessary in just 1% of cases and death (3/10,000). Amenorrhea has been reported to occur in 0%-14% of patients undergoing uterine fibroid embolization.

Follow-up: MR imaging at 3 months and after one year.

Learning Objectives:

1. To understand indications for UAE in uterine leiomyomata.
2. To discuss different uterine arteries anatomy.
3. To discuss different techniques of UAE.
4. To know possible complications.
5. To understand follow-up of UAE leiomyomata.

A-125

B. Ovarian varicocele

A. Nicholson; Leeds/UK

Chronic pelvic pain is defined as "pain that is present for at least 6 months". One third of patients have endometriosis, one third have other structural abnormalities, and one third have no obvious findings. There is often significant psychological overlay. Therefore, chronic pelvic pain can be difficult to manage and is often refractory to surgery.

Indications for ovarian venography and embolization include:

1. Unexplained chronic pelvic pain. Laparoscopy and pelvic ultrasound to exclude other pathologies is mandatory. Lack of abnormal vasculature at either of these studies does not preclude the possibility of ovarian vein reflux.
2. Lower extremity varicose veins immediately recurrent after adequate surgical treatment.
3. Severe labial/perineal varicosities. These are difficult to treat. Conservative therapy should be contemplated. If intervention is undertaken and the patient has ovarian vein reflux, these veins will recur immediately after sclerosis unless the ovarian vein "pressure column" is interrupted.

Varicosities in the pelvis secondary to retrograde flow in the ovarian vein causing pelvic pain worsening after long periods of standing or at the end of the day, labial varicosities, and dyspareunia is termed *pelvic congestion syndrome*. If the patient has reflux sufficient to cause pelvic pain, it is obvious on left renal vein or proximal right ovarian vein injection. If ovarian vein reflux is confirmed in a patient with the appropriate clinical symptoms, embolisation will cure or symptomatically improve 73%-78% of patients. This compares with 66% after surgery. Ultrasound CT and MR imaging also can aid diagnosis.

Learning Objectives:

1. To discuss the indications and technical aspects for ovarian venography.
2. To discuss the use of embolization to treat this and varicosities of the lower extremity and perineum.
3. To discuss the difference between ovarian vein syndrome and pelvic congestion syndrome.

A-126

C. Post-partum haemorrhage

J.-P. Pelage; Boulogne/FR

Post partum haemorrhage remains a major cause of maternal mortality throughout the world. Uterine atony, genital tract lacerations and abnormal placentation

account for the majority of cases. Uterine atony is usually controlled with early introduction of oxytocin or prostaglandin analogues. Surgical repair is effective to treat cervical tears and curettage may be sufficient to remove retained placental tissue. For patients whose clinical condition continues to deteriorate, arterial ligation or hysterectomy is often the favored treatment. However, surgical procedures are associated with significant failure and morbidity rates particularly in patients with coagulation disorders. The successful use of embolisation was first reported in 1979 in a patient who underwent hypogastric artery ligation and hysterectomy. Since then, many reports have emphasized the advantages of embolisation over surgery. In the majority of cases, selective embolisation of both uterine arteries is performed. In case of failure to control bleeding, additional blood supply may originate from the cervicovaginal, ovarian or round ligament arteries. In case of arterial vasoconstriction, embolisation of the anterior division of the hypogastric arteries is safe and effective. Gelatin sponge pledges, which provide a temporary occlusion are particularly suitable for hemostatic embolisation. Embolisation is effective in 70-90% of cases following cesarean section and uterine atony respectively. Pluridisciplinary management for patients with postpartum haemorrhage should be realized in highly specialized centers open 24 hours a day. If applied early in the course of events, embolisation is a valuable and safe alternative to surgery in the management of intractable postpartum hemorrhage.

Learning Objectives:

1. To understand the indications for uterine artery embolization for PPH.
2. To discuss different embolization strategies.
3. To identify and prevent failures associated with embolization.
4. To understand the need for a pluridisciplinary approach of patients with severe PPH.

08:30 - 10:00

Room I

Vascular

RC 515

Venous imaging and intervention

Moderator:

M.W. de Haan; Maastricht/NL

A-127

A. CT of thromboembolic disease

E.J.R. van Beek; Sheffield/UK

Venous thromboembolism (VTE) is now recognised as a single clinical entity, encompassing thrombosis in leg and arm veins (DVT) and their common complication of pulmonary embolism (PE). It is one of the most frequently encountered clinical problems with 3 per 1,000 population suspected of having the disease. The main diagnostic dilemma is to exclude those patients who should not run the risks of anticoagulant therapy from those where the disease can be demonstrated and treatment can take place to avoid recurrent events and late sequelae, such as chronic thromboembolic pulmonary hypertension.

After the initial start of CT for the diagnosis of PE in 1992, technology rapidly overtook the pace of clinical trials. As a result, only a few management studies have been performed using single helical CT (sCT). Subsequently, the rise of multidetector row CT (MDCT) has significantly improved the visualisation of subsegmental PE, while the increased speed of these systems allow direct imaging of the entire deep venous system. The technical aspects of sCT and MDCT will be discussed.

The findings that are characteristic of PE and DVT will be discussed, together with the findings of chronic PE. Pitfalls of diagnosis and alternative findings will also be shown. Diagnostic algorithms for the diagnosis of PE will be discussed in the context of other diagnostic tests.

Learning Objectives:

1. To be able to interpret the common findings and pitfalls of VTE.
2. To be able to make distinction between acute and chronic PE.
3. To be able to understand the literature in respect of CT for VTE.
4. To be able to integrate CT in the diagnostic management of VTE.

A-128

B. MR venography

J.F.M. Meaney; Dublin/IE

Magnetic resonance venography is a valuable cost-efficient and accurate technique for non-invasive evaluation of the venous system. Although traditional non-contrast methods are effective for evaluation of the venous system, they are

Postgraduate Educational Programme

time-consuming and prone to artefacts, predominantly because of slow flow-rates encountered in the veins. Because of rapid scan times, freedom from artefacts and high accuracy, contrast-enhanced techniques have become the reference-standard for demonstration of venous anatomy, venous anomalies and venous pathology. Depending on the anatomic location, different approaches may be appropriate. For example, injection of dilute contrast into an extremity vein allows high quality imaging of extremity veins "upstream" to the injection, however, the visceral veins (portal, mesenteric, renal) cannot be evaluated by this "direct" method and must be evaluated by other "indirect" methods (non-contrast techniques or during the "venous" phase of a contrast-enhanced MRA). Because blood T1 shortening is not as marked during the "venous" phase, elimination of fat by subtraction of a pre-contrast mask offers an advantage in most instances. Additionally, subtraction of the arterial phase from the venous phase (VESPA - Venous Subtracted Peak Arterial Phase) has the added value of subtracting not only the bright fat but also the overlapping arterial signal which results in depiction of the veins in isolation.

Evaluation of the venous component of vascular malformations can be performed using a variety of techniques.

More recently balanced sequenced (e.g. True FISP) have shown promise for venous imaging.

This presentation will describe tailored evaluation of the veins throughout the body in a time-efficient manner.

Learning Objectives:

1. To understand the clinical indications for MR venography.
2. To describe the advantages and limitations for both non-contrast techniques and contrast-enhanced techniques.
3. To explain the rationale for and technique of "indirect" and "direct" contrast-enhanced MR venography.
4. To illustrate the spectrum of findings in venous thrombosis.
5. To describe the strengths, limitations and pitfalls of MR venography in diagnosis of visceral, central and peripheral venous occlusion.

A-129

C. DVT and interventional therapy: Fact or fiction

M.J. Sharafuddin; Iowa, IA/US

Deep vein thrombosis (DVT) of the lower extremities is a common medical problem with a high risk of mortality and morbidity, and substantial immediate and long-term costs to society. Acute complications DVT include pulmonary embolism (PE), and venous ischemia. Delayed complications include a spectrum of debilitating symptoms referred to as the post-thrombotic syndrome. Anticoagulation therapy remains the mainstay of therapy in acute DVT. However, there is little data to suggest any major beneficial effect on the post-thrombotic syndrome, which is thought to be mediated by valve damage and/or occlusive chronic thrombus and venous scarring. Several experimental as well as clinical studies have indicated a potential role for early thrombolysis in preservation of venous valve function and prevention of venous occlusive pathology. Endovascular catheter-directed thrombolysis techniques using pharmacologic thrombolytic agents alone or in combination with mechanical thrombectomy devices have been proven highly effective in clearing acute DVT. In patients with underlying occlusive abnormalities, definitive management via endovascular stenting can also be undertaken. Another group of patients that benefit from endovascular therapy are those with chronic symptoms attributable to venous occlusive pathology, where endovascular stenting can play a role in alleviating symptoms attributable to venous hypertension. Management of post-thrombotic venous valve dysfunction remains one of the most formidable problems in patients suffering from chronic venous insufficiency. Although the role of endovascular techniques in the management of valvular insufficiency has been limited, a number of emerging paradigms are being explored. Endovascular obliteration is currently an effective option in solitary superficial venous insufficiency.

Learning Objectives:

1. To summarize the current indications for endovascular therapy in acute DVT.
2. To describe the current approaches and techniques for the treatment of acute DVT and chronic post-thrombotic venous disease.
3. To summarize the current outcomes of endovascular therapy in venous disease.
4. To describe the current status of endovenous ablative therapies of superficial varicose veins.

08:30 - 10:00

Room K

Genitourinary

RC 507

Imaging of the uterus

Moderator:

D. Babnik Peskar; Ljubljana/SI

A-130

A. Ultrasound imaging techniques

G. Serafini; Pietra Ligure/IT

A variety of examination techniques can be used for the US study of the uterus. Transabdominal sonography can still be considered the first approach to the uterus, but transvaginal sonography is the best examination technique for evaluating the endometrium and small intrauterine lesions.

A special technique called hysterosonography has been developed to obtain better analysis of the endometrial surface and uterine cavity.

Enlarged uterus: US is commonly requested to characterize structural changes of the uterus and to measure it. Fibroids are the most common tumor of the uterus and most common cause of uterine enlargement.

On US studies, uterine fibroids usually appear as solid, discrete, well-defined masses. They may be hyper, iso or hypoechoogenic related to the myometrium. Uterine leiomyosarcomas are rare and usually occur in the elderly. At US they appear as bulky uterine masses that are indistinguishable from large non-malignant fibromas. However, the clinician can be alerted to diagnosis by their rapid progression over time.

Abnormal bleeding: In clinical practice, transvaginal US is commonly employed for three main purposes:

- determining which patient should undergo endometrial biopsy. US-pathological correlation studies have demonstrated that, considering a bi-endometrial thickness cutoff value of 4 mm, in patients with endometrial measurement below this point, postmenopausal bleeding can be related to atrophy with a high degree of confidence.
- accurate analysis of the endometrium to detect polyps or submucosal fibroids.
- local staging of myometrial invasion from endometrial cancer.

Learning Objectives:

1. To understand the role of transvaginal vs. transabdominal ultrasonography in the evaluation of the uterus.
2. To be able to recognize the US findings of uterine diseases.
3. To learn the scanning technique and clinical indications of US hysteroscopy.
4. To learn the role of color Doppler in patients with uterine disorders.

A-131

B. Abnormal gynecological bleeding: What the gynecologist wants to know

R. Forstner; Salzburg/AT

Abnormal gynecologic bleeding refers to bleeding other than the expected menstrual pattern.

It is usually attributed to a uterine source, but may also arise from other pelvic sites.

In the diagnostic work-up of abnormal gynecological bleeding transvaginal sonography is the primary imaging modality in pre- and postmenopausal women. The purpose of pelvic sonography is to identify uterine or extrauterine abnormalities, and to analyze endometrial and myometrial morphology. In case of abnormal bleeding and indeterminate sonography MR imaging serves as an adjunct in localizing the source of hemorrhage, in establishing the definite diagnosis, and in determining the feasibility of conservative uterine surgery.

In patients with bleeding in childbearing age and sonographically diagnosed uterine fibroids MR imaging helps to guide to the appropriate myomectomy technique. In pre-and perimenopausal women with a sonographically enlarged uterus MR imaging allows differentiation between leiomyomas and adenomyosis.

In bleeding caused by uterine malignancies pretherapeutic MR imaging findings will directly influence the choice of therapy and guide in therapy planning.

In patients with vaginal bleeding and a large pelvic mass MR imaging helps to define the origin of the tumor and may also be able to differentiate between a neoplastic and inflammatory etiology.

Learning Objectives:

1. To become familiar with the etiologies of abnormal gynecological bleeding in pre and post menopausal patients.
2. To learn diagnostic imaging features for benign and malignant endometrial and myometrial pathologies.

Saturday

Postgraduate Educational Programme

3. To understand the value of MR imaging as adjunct to US in uterine disorders presenting with abnormal bleeding.
4. To learn what the gynecologist wants to know for treatment planning.

A-132

C. Staging and follow-up of cervical cancer

P. Petrow; Geneva/CH

MR imaging provides excellent spontaneous soft tissue contrast of all female pelvic organs, permits a multiplanar exploration of the entire pelvis including lymph nodes and the pelvic floor. Therefore MR imaging is the imaging modality of choice for the initial work-up of invasive cervical cancer. This course reviews the technical aspects of MR imaging exploration of invasive cervical cancer such as choice of sequences, slice orientation, intracavitary and intravenous contrast media injection for MR examination for initial staging, follow-up examinations during radiation therapy (external RT and brachytherapy) and suspected recurrence. The imaging features encountered during initial staging such as parametrial, bladder, ureteral and rectal invasion are reviewed with particular emphasis on findings to guide fertility conserving surgery, external radiation therapy or brachytherapy. These findings can be correlated to the FIGO classification for invasive cervical cancer. Lymph node involvement of cervical cancer and its repercussions on MR imaging are highlighted.

During follow-up, especially if cervical cancer is treated by chemoradiation, post radiation changes of the pelvic organs and spaces can render difficult the interpretation of MR images and the use of dynamic-acquisition contrast-enhanced T1-weighted SE MR images is useful to distinguish post-radiation fibrosis from recurrence.

In conclusion, MR imaging is the imaging modality for evaluation initial tumor volume and extension, response to treatment and to rule out recurrence.

Learning Objectives:

1. To become familiar with basic principles and imaging protocols to explore cervical cancer, with special emphasis on MR imaging.
2. To enhance the utility of MR imaging in the follow-up when treated with radiation therapy.
3. To show the features of recurrence.

08:30 - 10:00

Room L/M

Infection in the Adult Today

CC 516

Gastrointestinal infection: A changing scene

Moderator:

M.A. Lucic; Novi Sad/CS

A-133

A. Gastrointestinal infection in the immunocompromised patient

J.W.A.J. Reenders; Curaçao/AN

In less than three decades AIDS has become one of the most devastating illnesses in human history. The AIDS epidemic differs from most others in many ways, has challenged conventional medical thinking and has broadened the boundaries of the knowledge of human biology and medicine. The patterns of disease and pathological changes seen in AIDS patients can be perplexing and challenging, particularly in the medical imaging department. Although astonishing progress has been achieved during recent years in the treatment of patients afflicted with AIDS, with the introduction of highly active antiretroviral therapy (HAART), the epidemic still continues to spread. AIDS patients are no longer confined to a few specialized AIDS hospitals and are now seen in general hospitals and clinics everywhere. The value of imaging of AIDS is well established. This CC provides a comprehensive overview of our current knowledge about radiologic imaging features of the wide range of gastrointestinal, hepatic, splenic, biliary and retroperitoneal manifestations in the immuno-compromised patient and how the role of modern medical imaging techniques and diagnosis and treatment can be applied. The imaging aspects (conventional double contrast gastrointestinal studies, ultrasound, CT and MR) of the diseases of the luminal gastrointestinal tract, liver, spleen, biliary tract and retroperitoneum will be systematically discussed. Candidiasis, herpes, cytomegalovirus, cryptosporidiosis, histoplasmosis, isosporiasis, salmonellosis, unusual mycobacterial and viral infections account for the majority of non-neoplastic disorders. This CC is not only comprehensive, but also practical and easy to apply to daily clinical problem solving.

Learning Objectives:

1. To learn the wide range of radiological manifestations in AIDS of the GI tract.
2. To understand how modern medical imaging can assist in diagnosis and treatment.
3. To understand the needs of investigating AIDS patients in clinical practice.

A-134

B. Gastrointestinal and abdominal tuberculosis

F.M.H.M. Vanhoenacker, A.I. DeBacker, P.M. Parizel; Antwerp/BE

In this educational lecture the range of manifestations of tuberculosis (TB) of the abdomen will be discussed, including involvement of the gastrointestinal tract, the peritoneum, mesentery, omentum, abdominal lymph nodes, solid abdominal organs, the genital system and the abdominal aorta.

Abdominal TB is a diagnostic challenge, particularly when pulmonary TB is absent. It may mimic many other abdominal diseases, both clinically and radiologically. An early correct diagnosis, however, is important in order to ensure proper treatment and a favourable outcome.

Modern imaging is a cornerstone in the early diagnosis of abdominal TB and may prevent unnecessary morbidity and mortality. Generally, Computed Tomography (CT) appears to be the imaging modality of choice in the detection and assessment of abdominal tuberculosis, other than gastrointestinal TB. Barium studies remain superior for demonstrating mucosal intestinal lesions. Ultrasound (US) may be used for follow-up to monitor therapy response. The role of MR imaging has to be further defined.

Ileocaecal involvement, free or loculated high density ascites with thin-mobile septa, omental thickening, a thickened and enhancing peritoneum, a misty mesentery, low density adenopathies and focal hepatosplenic lesions are suggestive imaging findings demonstrated by either gastrointestinal series, US, CT and MR imaging.

The diagnosis of abdominal TB should be considered if suggestive imaging findings are found in patients with a high index of suspicion.

Learning Objectives:

1. To recognise the range of imaging characteristics of abdominal TB.
2. To define the strength of each imaging modality in detecting (specific) changes encountered in abdominal tuberculosis.

A-135

C. Gastrointestinal parasite infestation

M.E.A. El Bagi; Riyadh/SA

25% of the world population could be suffering from parasitic infestation. The highest prevalence is in underdeveloped agricultural and rural areas in the tropical and subtropical regions. In some areas the incidence may reach 90% of the population. In contrast, some major economic projects intended to promote local development have, paradoxically caused parasitic proliferation e.g. Bilharziasis in Egypt and Sudan and Chagas disease in Brazil. The commonest cosmopolitan gastrointestinal parasite is Entamoeba histolytica. Some intestinal parasites are endemic in temperate climates e.g. Enterobius vermicularis. The AIDS epidemic has increased the prevalence and severity of parasitic disease particularly Strongyloides stercoralis. Tropical parasites are seen in Western people who travel to tropical countries. Radiology has acquired a major role in diagnosis and management of gastrointestinal parasite infestations and their complications.

Learning Objectives:

1. To summarize the worldwide prevalence of the commonest gastrointestinal parasites.
2. To describe the various radiologic presentations of gastrointestinal parasites.
3. To highlight the role of radiology in the management of gastrointestinal parasites.

Postgraduate Educational Programme

Saturday

08:30 - 10:00	Room N/O	08:30 - 10:00	Room P
Radiographers RC 514 MR imaging/Neuroimaging <i>Moderators:</i> P.C. Maly Sundgren; Ann Arbor, MI/US F. Olsen; Trondheim/NO		Joint ECR/EAR sessions: Challenges for European Radiology ER 526 Assessment and accreditation in radiology in Europe <i>Moderator:</i> I.W. McCall; Oswestry/UK	
A-136 A. 3 Tesla whole body system MR imaging: Experiences from Lund University Hospital B. Hansson; Lund/SE		A-138 Assessment and accreditation of training centres in Europe I.W. McCall; Oswestry/UK	
In September 2003, we installed a 3 T Philips whole body scanner at the Lund University Hospital. Like our three Philips 1.5 T and our 3 T Siemens head scanners, it is mostly used to examine clinical patients. It is both interesting and challenging to be part of the development of a new technique such as the 3 T whole body system. During the first year, we received the various coils and could start to examine different body parts. We learned about the merits and disadvantages of the system, and developed techniques to work around problems. For brain examinations we already knew that 3 T was excellent e.g. in MRS (MR Spectroscopy), MRA (MR Angio) and high resolution. For other examinations, there were not many protocols optimised for 3 T and we had to explore the parameter space to find the suitable settings for a 3 T system. For example, one difficulty we encountered was to obtain a sufficient contrast between white and grey matter in a T1 weighted image. Also, to use the gradient echo instead of the spin echo produces susceptibility artefacts. One large issue with the 3 T scanner is artefact reduction. All artefacts will increase compared to using a lower field-strength. Fortunately, Philips has provided several new techniques that reduce artefacts, e.g. SENSE (SENSitivity Encoding) can help us get rid of motion artefacts by running the scan more rapidly. <i>Learning Objectives:</i> 1. To learn about the Lund university hospital experiences with 3 T whole body scanner. 2. To identify the advantages of a 3 T system. 3. To identify the difficulties with a 3 T system.		The structure of radiology training varies between and within countries in Europe. Some have a unified national training scheme, while others are managed independently by individual universities or hospitals. Practice in radiology within the EU, requires a certificate of specialist training, awarded nationally or by individual institutions. Radiologists can practice in another country or may provide services across state boundaries and patients and employers must have confidence that their training is good. To enhance and standardise training across Europe, the EAR and the radiology section of the UEMS has instigated a training assessment program. Assessment of training centres in each EAR member country are undertaken by two experienced trainers from other European countries. The host centre completes a questionnaire, which provides details of the trainers and trainees, the facilities, equipment, workload and case-mix. Information is also provided on training programs, lectures, tutorials and sub-specialty training. A separate confidential questionnaire is completed by each trainee on the strengths and weaknesses of their training. The assessors visit the centre and review the facilities, talk to both trainers and trainees and the management. Finally the assessors report to the centre identifying their strengths and weaknesses and suggesting improvements if appropriate. The reports are collated by EAR and UEMS to identify key training issues. These include instituting the EAR curriculum, providing formal tutorials and lectures and structured trainee appraisal. Provision of sub-speciality training is not available in many centres. Involvement of trainees in clinico-radiological conferences and audit is encouraged. These will be discussed. <i>Learning Objectives:</i> 1. To recognize of the need for training centre assessment throughout Europe. 2. To understand the structure and mechanisms of the EAR assessment program. 3. To appreciate the variability of training structures and opportunities in training centres in different European countries. 4. To evaluate some of the key areas where training programs may improve their structure and performance.	
A-137 B. Neuroimaging and analysis techniques for research into brain structure and function V. Sluming; Liverpool/UK		A-139 Appraisal and assessment of trainees during training C.D. Becker; Geneva/CH	
A wide range of imaging and image analysis techniques now exist for demonstrating the structure and neural activity of the living human brain. This presentation will chart the development of these techniques and describe their respective advantages and limitations. There have been major advances in recent years in analysing the structure of the human brain in-vivo using computerised statistical voxel based analysis techniques which have made the visualisation of, for example, wide spread degenerative changes of cortical tissues easier and more objective. Functional neuro-imaging is making a significant contribution to our understanding of neural substrates with studies of higher cognitive function, perception, action and emotion. Furthermore, results obtained from healthy human volunteers are leading to new ideas about depression, schizophrenia, pain syndromes, multiple sclerosis and other psychiatric and neurological disorders. The spatial mapping techniques which have been demonstrated to provide powerful insights into the structure and function of the brain include: structural and functional magnetic resonance imaging, positron emission tomography, source localisation with electroencephalography and magnetoencephalography and functional transcranial Doppler ultrasound. The physical principles underlying these techniques will be briefly outlined and important assumptions and limitations identified. A range of applications for each technique will be indicated. <i>Learning Objectives:</i> 1. To discuss the choice of appropriate imaging modality to answer a particular research question relating to structure and/or function of the human brain. 2. To appreciate the different image analysis techniques for analysing structural and functional brain data.		A primary goal of appraisal of Radiology trainees during training is to assess the adequacy of postgraduate training. The legal responsibility for the training standards vary from one country to another but the director of the training programme certainly holds a key role in this process. Appraisal must be done at each stage of training and must be based on defined methods, including regular, constructive feedback at least annually, and standardised Radiology board examinations. Assessment and feedback should be based on a written evaluation protocol containing more general as well as specific radiologic criteria. A logbook for certain invasive procedures may be helpful in order to document personal practical experience. Radiology board examinations may be written (eg, multiple-choice) or oral; their content must be based on the objectives of the postgraduate training programme in Radiology. <i>Learning Objectives:</i> To understand the process of evaluation of radiology trainees during postgraduate training.	

Postgraduate Educational Programme

A-140

Delivering a national continuing medical education programme

J. Freyschmidt; Bremen/DE

The German Academy for Continuing Education in Diagnostic Radiology was founded in 1998, 6 years before vocational training became legally mandatory for the medical profession in Germany. The Academy was founded and is supported by the German Radiological Society and the Association of German Radiologists. In Germany the fulfillment of the legal requirements which are mandatory in medical training since 2004 are being controlled by the medical associations of the individual federal states which in turn are members of the German Medical Association. The legal requirements ask for the verification of 150 CME credits every 3 years or 250 CME credits every 5 years. On recommendation of the German Medical Association, the medical associations of the federal states acknowledge 3- or 5-year-certificates of the German Academy for Continuing Education in Diagnostic Radiology, provided that the Academy can prove the fulfillment of the requirements for continuous medical education set up by the federal medical associations. Starting in 2005, the exchange of data between the Academy and the federal medical associations will run on a common server, facilitating the acknowledgement of these credits.

The German Academy for Continuing Education in Diagnostic Radiology distinguishes two categories of continuing education. Courses can only be acknowledged as category I, if they are certified by a written evaluation. The evaluation is being analysed electronically at the Academy, the participants can be identified by means of a barcode. The lecturers will receive a printout of their respective evaluations. From its beginning the Academy carried out about 15,000 evaluations. Since we started our category I courses, the level of the courses as well as that of the lecturers has risen tremendously. All category-I-courses have to be registered at the Academy, where they are also tested and rated regarding the maximum of possible credits. One training unit (1 CME-credit) corresponds to a lecture or course of 45 minutes.

Among the category-II-activities are the attendance of scientific lectures at national and international meetings, visits at medical institutions, scientific publications and lectures, basically all training activities that are not being evaluated. Private studies of scientific books and journals can be acknowledged with a maximum of 30 credits in 3 or 50 credits in 5 years. Detailed interactive studies with print media, online media or audio-visual media with a certified qualification and evaluation of the learning results are acknowledged with 1 credit per training unit. The participants of the Academy are supposed to acquire 25 CME-credits in category I and 25 CME-credits in category II per year. After 3 and/or 5 years they obtain a certificate from the Academy, which can be submitted to the German Medical Association.

From its very start, the German Radiological Academy has been extremely successful and functions as a role model for the academies of other disciplines, which were mostly initiated at a later date. In the meantime we count more than 2750 participants or, in other words, about 70% of all practicing radiologists in Germany. The Academy is directed by a board, whose chairman is the author of this abstract. It is financed mainly by fees from participants and organisers of scientific workshops and training courses, by subsidies from the German Radiological Society and the Association of German Radiologists and - after strong initial support - now only by a minor part by sponsoring from the industry.

Learning Objectives:

1. To demonstrate how a national academy for continuing education in radiology can be established on a voluntary basis, finding approval from the national medical authorities, especially as continuing education became legally compulsory for the medical profession.
2. To demonstrate that an academy run by a medical society (in this case in radiology) can stimulate its members to continuing education on a high level.
3. To demonstrate that at least 50% of the activities in continuing education should be evaluated regarding their quality in order to raise their level evidently.

A-141

Revalidation and re-certification of radiologists in Europe

A.P. Brady; Cork/IE

The concept of recertification of medical specialists was first raised in the US in 1940, and the introduction of time-limited specialist certification began there in 1969. The impetus for recertification of medical specialists comes from the desire to ensure and maintain competence of medical service delivery, driven by public demand. This demand has accelerated in recent years, at least in part, as a response to publicity relating to medical malpractice and misadventure, and an increase in litigation following adverse medical outcomes in many populations. It

is no longer publicly acceptable that lifelong competence be assumed following completion of training and passing an examination in the early years of one's medical career, and the medical profession must develop robust mechanisms by which competence of physicians can be maintained and verified throughout their careers, just as is the case with many other professions. The mechanisms developed must be unbiased and fair, appropriate to the work being done by the doctor, and acceptable to the public. This lecture will review the background behind the demand for revalidation, the arguments for and against revalidation and the methods being employed for revalidation within and outside Europe, in the context of diagnostic radiology.

Learning Objectives:

1. To understand why the demand for revalidation and recertification has arisen.
2. To understand the importance of developing unbiased and robust methods of revalidation.
3. To understand various methods of revalidation being considered or introduced.

08:30 - 10:00

La Scala

Foundation Course - Chest Radiology

E3 520

Airways and infection

Moderator:

S.J. Copley; London/UK

A-142

A. Airway disorders and hypoluent lungs

J.A. Verschakelen; Leuven/BE

Disorder of the airways can be divided into disorders of the (large) proximal and disorders of the (small) distal airways. Chest radiograph and especially spiral computed tomography can provide very accurate information on diseases that affect the proximal airways and are often helpful for diagnosis and workup before treatment of these diseases. Small airways involvement is best seen with high resolution CT. This technique is particularly valuable in showing small airways involvement not only when it is part of widespread diseases but also when bronchiolitis is the primary finding. Focal or widespread reduction in lung attenuation is one of the important CT features of some small airways diseases and should be differentiated from other causes of hypoluent lungs.

Learning Objectives:

1. To illustrate the radiographic and CT features of airway diseases.
2. To familiarize the participants with the different causes of hypoluent lungs.

A-143

B. Pneumonia and disorders in the immunoincompetent host

C.J. Herold; Vienna/AT

Individuals with an impaired immune system are prone to a variety of infections, neoplasms, and cardio-vascular disorders. Among those, pneumonia is the most common infectious disorder, and can occur in up to 80% of patients with acute leukaemia, and in up to 50% of organ transplant recipients, respectively. Neoplasms may develop due to the primary disease, but also as a consequence of chemotherapy or radiation. Cardiovascular disorders appear most commonly as a short term or long term complication of treatment.

In this course, the underlying factors for the development of different disorders in the immunocompromized host will be revisited. Furthermore, the spectrum of causative organisms and radiologic features of various opportunistic pulmonary infections will be discussed. Specific attention will be paid towards narrowing the differential diagnosis by integrating clinical laboratory and radiologic information. Finally, the role of imaging methods in the evaluation of patients with different disorders will be reevaluated.

Learning Objectives:

1. To familiarize the audience with epidemiology, pathophysiology and etiology of infections in the immunocompromized host.
2. To elucidate the spectrum of noninfectious disorders in this specific patient population.
3. To review the morphologic findings and radiologic patterns of infectious and noninfectious diseases.
4. To illustrate the role of the radiologists in dealing with these disorders.

Postgraduate Educational Programme

10:30 - 12:00

Room A

"ECR meets" Italy

EM 1

Imaging of focal lesions

Presiding:

A. Chiesa; Brescia/IT
F. Dalla Palma; Trento/IT

A-144

Imaging of focal lesions (Introduction)

L. Bonomo; Rome/IT

Focal lesions are a common finding in daily radiological practice. In the evaluation of focal lesions, the role of imaging is different according to the diagnostic task (detection, characterization, staging and follow-up) and to the examined body organ. In "ECR meets" Italy five Italian radiologists present their experience regarding the role of different imaging modalities (conventional radiology, US, CT, MR and MN) in the evaluation of focal cerebral, pulmonary, hepatic, renal and muscular lesions.

Learning Objectives:

To introduce the role of different imaging modalities in focal lesion assessment.

A-145

Brain

G. Polonara; Ancona/IT

Neuroimaging plays a pivotal role in the diagnosis of CNS disorders. The most frequent focal pathologies of the CNS are vascular accidents, tumours and infections. The imaging techniques used for evaluating brain focal lesions include CT and MR. The multiplanar capability of MR gives better definition of the lesion extent and location. The use of a non-conventional MR technique allows for an accurate characterization of lesions compared to standard approaches. Diffusion-weighted imaging (DWI) is widely used to investigate hyper-acute cerebral ischemia, detecting early ischemic abnormalities related to reduction of ADC. DWI can also help in differentiating a brain abscess from a cystic brain tumour. Perfusion weighted imaging (PWI) provides information on the hemodynamic status of brain tissue and detects regions with impaired cerebral perfusion. PWI has been shown to be clinically useful, particularly in the initial investigation of stroke, in tumour imaging and in assessing brain tumour responses to therapies. In acute ischemic stroke patients, the difference between DWI and PWI abnormalities, termed as diffusion/perfusion mismatch, represents potentially salvageable brain tissue with timely and appropriate therapy. MR imaging is a sensitive tool for identifying space-occupying CNS lesions, but it is relatively non-specific in distinguishing between benign and malignant lesions. Proton MR-Spectroscopy can non-invasively provide a chemical profile of the lesions that help in this determination. It can also give useful information on brain tumour type and grade, even obviating stereo-tactic biopsies in some cases, and is of help in monitoring the response to therapeutic surgical/medical intervention.

Learning Objectives:

1. To become more familiar with the typical MR features of the most frequent brain focal lesions.
2. To examine the potential of new MR imaging techniques in the characterization of cerebral focal lesions.
3. To identify an acute stroke lesion with DWI and PWI.
4. To know how to distinguish between focal and infiltrating lesions.
5. To know how to differentiate a brain abscess from a cystic brain tumour.
6. To examine the potential of proton MR spectroscopy for giving useful information on brain tumour type and grade.

A-146

Chest

M.L. Storto; Chieti/IT

Pulmonary nodules are frequently detected on chest radiographs and CT scans and often represent a diagnostic challenge. As a matter of fact, all pulmonary nodules should be considered malignant until proven otherwise. However, most of them are benign, especially if their diameter is ≤ 10 mm and do not require invasive assessment.

Numerous radiographic and CT criteria have been traditionally used to differentiate benign from malignant nodules including size, morphology, contrast enhance-

ment, and lesion growth over time. Although small nodules have a higher probability of being benign, size alone is not a reliable indicator of benignity. Morphologic features are only useful in a limited number of nodules showing a benign pattern of calcification. Contrast enhancement on dynamic CT scans seems to be a valuable method to rule out malignancy in nodules enhancing less than 15 HU (negative predictive value of 96%) and can be proposed in the diagnostic workup of nodules ranging between 8 and 20 mm in diameter, which are more difficult to reach with percutaneous biopsy. Growth rate assessment, which is commonly measured in terms of doubling time, is gaining particular importance in the context of lung cancer screening trials which lead to a large number of incidentally detected small nodules. In this regard, 3D estimations of doubling time are more accurate than 2D measurements, since asymmetric nodular growth can occur in malignant lesions.

Learning Objectives:

1. To review radiographic and CT criteria most useful in characterizing pulmonary nodules as benign or malignant.
2. To discuss the role of imaging in non-invasive assessment of pulmonary nodules.
3. To provide a management algorithm for small pulmonary nodules.

A-147

Liver

L. Graziosi; Brescia/IT

The last 10 years of experience demonstrate that the technological progress of non-invasive modalities has reduced the need for liver biopsy or other invasive diagnostic techniques in the diagnosis of focal liver lesions. At present, Doppler US with echo-enhancement, fast multi-detector CT and contrast enhanced MR represent complementary tools in terms of image quality, diagnostic accuracy and functional data in the identification and characterization of focal liver lesions. Contrast enhanced US with second generation contrast material completes the ultrasound diagnostic capability through dynamic vascular evaluation of focal liver lesions, offering additional morphologic elements useful for the final diagnosis.

Imaging multirow detector technology can provide enhanced focal lesion detection and characterization, as well as high-quality vascular studies increasingly requested in the context of liver transplantation. The most flexible applications in liver imaging result from the clear separation of the three distinct phases of contrast enhancement: the arterial, the portal venous in flow and the venous phase of parenchymal enhancement, which are very useful for differential diagnosis of focal liver lesions considering their different vascularization.

Recent technological developments have considerably broadened the role of MR imaging in the evaluation of liver pathology. Today, MR imaging is not looked upon merely as a problem-solving technique, but is widely considered the principal imaging modality for both the detection and accurate diagnosis of focal liver lesions. Advances in hardware and sequence design, and the advent of novel contrast agents with liver specific properties, have contributed towards making MR of the liver a routine clinical application.

Learning Objectives:

1. To describe US, CT, and MR imaging techniques to optimize detection and characterization of focal liver lesions.
2. To identify characteristic US, CT, and MR features of various primary and secondary hepatic neoplasms.

A-148

Kidney

M. Bertolotto; Trieste/IT

New and improved imaging modalities have increased the proportion of focal renal lesions discovered during US, CT and MR imaging. The main diagnostic problem is to differentiate benign from malignant lesions.

Among solid renal lesions, imaging modalities enable one to distinguish typical pseudotumors (normal variants), typical RCCs and show some distinctive features for angiomyolipomas in most cases. No definite imaging features have been described that allow adenoma to be differentiated from adenocarcinoma. Similar difficulties occur with oncocytomas, which may exhibit some specific features only in few instances. The clinical history and CT findings may help suggest the histopathologic nature of an indeterminate renal mass in chronic or acute inflammatory lesions, renal lymphoma, metastasis and multiple hereditary renal neoplasms.

Characterization of cystic masses relies on Bosniak's classification which consists of four categories: Benign (I) and minimally complicated cysts (II), Indeterminate cystic masses (III) including cystic tumors and complex cysts and Cystic RCCs (IV).

Saturday

Postgraduate Educational Programme

With the exception of typical renal cysts, most renal masses remain indeterminate at grey-scale US. Color Doppler US can allow identification of pseudotumors when the vascular architecture of the normal renal parenchyma is identified. MR imaging can be used in characterising very small cysts and some complex cystic or pseudo-cystic indeterminate masses. It provides higher contrast resolution compared to CT enabling better characterization of the fluid content of atypical hemorrhagic cysts. MR imaging and contrast enhanced US can be useful in demonstrating minimal contrast enhancement in solid tumors with poor vascularity or within the wall of cystic RCCs.

Learning Objectives:

1. To be aware of the capabilities of CT and the role of US and MR imaging in diagnosis of focal renal lesions.
2. To know the CT appearance of solid and cystic focal renal lesions.
3. To be aware of the difficulties in the differential diagnosis of benign and malignant focal renal lesions.

A-149

Muscles and tendons

C. Martinoli, R. Podestà, G. Succio, C. Gauglio, F. Zuccarino; Genova/IT

Diagnostic imaging plays an important role in directing the work-up of space-occupying lesions affecting muscles and tendons. The objective of this lecture is to provide an overview of the ultrasound and MR imaging appearances of a spectrum of tumors and tumor-like conditions affecting muscles (including intramuscular lipoma, haemangioma, ganglion, mixoma, desmoid tumor, sarcoma and metastasis) and tendons (including giant cell tumor of the tendon sheath and intratendinous ganglia). Epidemiology and clinical features of these tumors will briefly be discussed. Although a certain overlap is observed, ultrasound and MR imaging are able to demonstrate several characteristic features of these masses that may lead, in some instances, to a conclusive diagnosis. When imaging findings are non-specific, these techniques may help to differentiate benign from malignant forms and to establish the indication for a biopsy. Potential pitfalls in imaging interpretation of pathology and the advantage of one imaging technique over the other will be discussed.

Learning Objectives:

1. To learn the ultrasound and MR imaging appearance of a wide variety of benign and malignant tumors of muscles and tendons.
2. To understand potential advantages and limitations of ultrasound and MR imaging in characterization of tumors of muscles and tendons.
3. To identify other pathologic entities mimicking these tumors.
4. To discuss the imaging features so that when a tumor arising from a muscle or a tendon is encountered the diagnosis may be considered.

10:30 - 12:00

Room B

New Horizons Session

NH 6

Nanotechnology

Moderator:

M.J. Lee; Dublin/IE

A-150

Nanotechnology (Introduction)

M.J. Lee; Dublin/IE

Nanotechnology refers to the process of building devices from the bottom up i.e. when a large product is constructed atom by atom into larger more complex structures. All this takes place on the nanoscale, which refers to one-billionth. One of the main requirements for doing this is the scanning tunneling microscope, which has allowed nanotechnology to develop. Properties of materials constructed from nanoscale objects are often different from properties of the same material created from larger molecules. Strength, melting point, electrical conductivity and magnetic properties may all change at the nanoscale level. Nanoscience therefore, can create novel products with unique characteristics. Examples of objects made from nanoparticles include: materials used in the computer industry to decrease the size required for storing memory, electronic circuitry, CD players and LED-based traffic signals.

In the area of Medicine and Health: proteins, nuclear gases, lipids etc. have properties at the nanoscale level. Medical research is currently underway to develop tools capable of probing this biologic nanometer world. Non-invasive sensing systems are being developed in an attempt to try and detect emerging diseases.

Treatment in terms of nanoscale drug delivery devices are being developed as well as implantable drug synthetic systems and others.

This New Horizons Series will provide a basic understanding of nanotechnology concepts and will also detail the implications of nanotechnology for medicine and health and for imaging sciences.

Learning Objectives:

1. To provide a basic understanding of the fundamentals of nanotechnology.
2. To describe in general, current and future interactions with medicine.
3. To describe possible interfaces between nanotechnology and diagnostic imaging.
4. To stimulate future areas of research.

A-151

Basic tools and concepts

D. Fitzmaurice; Dublin/IE

Nanotechnology has emerged as a key enabling technology, which will impact on all areas of science and engineering, including those that underpin the field of radiology.

This presentation will provide a societal and economic context for nanotechnology. It will present and illustrate a practical definition of nanotechnology. It will consider current and possible future applications of nanotechnology in diverse fields.

In doing so, the basic concepts and tools that have underpinned the emergence of nanotechnology will be reviewed.

Learning Objectives:

1. To be able to define nanotechnology and illustrate this definition by reference to both the underpinning concepts and tools and by reference to recent developments in areas of science and engineering that are relevant to the field of radiology.
2. To be able to discuss the current and possible future social and economic impacts of the emergence of nanotechnology as a key enabling technology.

A-152

Implications for medicine and health

D. Kelleher; Dublin/IE

Nanoparticle technology offers many new and exciting advantages in biomedicine with particular applications both in laboratory and radiological diagnostics and potentially in therapeutics. Nanoparticles can be generated from a variety of materials and constructed to dimensions that have the potential to mimic the size of viruses, proteins or genes. Nanoparticles have significant advantages as fluorescent probes, including wide absorption profiles, allowing excitation of varying particles at different times simultaneously, large linear absorption cross-section, narrow emission spectra which are tunable by size and excellent photo stability. One of the major advantages of nanoparticle technology is the capacity to synthesise in organic solvents and functionalise for biological use including biologically labelling with proteins, antibodies, genes, antisense or RNAi. Latterly, nanoparticles have been designed to target cellular and subcellular compartments.

Overall, therefore, such technology offers significant advantages in biomedicine. In terms of drug delivery, the wide tissue distribution of nanoparticles permits selective localisation of pharmaceutical agents carried on pre-tagged nanoparticles. In addition, magnetic carriers have also been used in imaging, and for similar reasons, may permit detection of specific tumours based on their physical and/or antigenic properties. Lastly, the capacity to generate self-assembling nanowires in physiological solution from nanoparticles has enormous potential in a range of both neurological and inflammatory conditions. Finally, nanoparticles are currently at a relatively early stage of development and it is anticipated that major breakthroughs in the coming years will have a significant impact on human health care.

Learning Objectives:

1. Basic principles of nanoparticle composition and synthesis.
2. Potential for functionalisation of nanoparticles with drugs, proteins, DNA, RNAi.
3. Applications of functionalised nanoparticles in diagnostics, imaging and therapeutics.

A-153

Nanotechnology and diagnostic imaging

M. Harisinghani; Boston, MA/US

Magnetic nanoparticles containing superparamagnetic iron oxides are providing researchers with exciting new opportunities to study molecular and cellular proc-

Postgraduate Educational Programme

esses in various diseases. On the basic science front, derivatives of these nanoparticles have been modified into "smart" sensing probes allowing us for the first time to detect DNA mismatches or proteins/protein interactions. In some more applied research, derivatized nanoparticles have also been used to target the growth of new blood vessels (angiogenesis), cell death (apoptosis) or specific cell types (stem cells, immune cells). Specifically, a new physiologically inert nanoparticle (highly derivatized crosslinked iron oxide nanoparticle derivatized with tat peptide sequences; CLIO-HD) has been shown to allow in-vivo MR imaging tracking of systemically injected cells at near single-cell resolution. On the clinical front a commercial preparation of magnetic nanoparticle is being successfully used for the MR detection of minimal nodal metastasis disease and study early perfusion changes in the pancreas of patients with type I diabetes. The proposed talk will provide a systematic overview of magnetic nanoparticle applications from bench to bedside as well as emerging techniques. Clinical applications such as detection of minimal metastatic disease in lymph nodes, imaging of angiogenesis, imaging inflammation will be covered.

Learning Objectives:

1. To provide a broad overview of the current and emerging applications of nanoparticles.
2. To become familiar with the potential clinical applications of nanoparticles.
3. To understand the optimal techniques for imaging with nanoparticles.

10:30 - 12:00

Room F2

EFOMP Workshop

New technology in diagnostic radiology: The inescapable growth of information technology

EF 2

How to get the best from information technology for patient care

Moderators:

J. Damilakis; Iraklion/GR

B.M. ter Haar Romeny; Eindhoven/NL

A-154

PACS and teleradiology in Europe

D. Caramella; Pisa/IT

The 22nd International Conference of EuroPACS, that was held in Trieste in September 2004, offered a comprehensive update on the development of PACS and teleradiology in Europe (www.europacs.org).

The conference showed that a wealth of experience has been gathered both from the clinical and the research points of view in many European countries, including those of central and eastern Europe. Topics of relevant interest included the development of regional PAC systems with innovating networking strategies and the progressive convergence between PACS and teleradiology. The purchase of PACS services is no longer limited to traditional approaches, as ASP is emerging as a possible alternative attractive to both vendors and hospital managers. Another important aspect is the increasing role of standards in supporting filmless hospitals: in the past, interface standards such as HL7 and DICOM already facilitated systems integration, now integrating the health enterprise (IHE) promises to allow functionally driven system integration. Finally, there is an increasing interest towards the E-learning applications that use PACS systems as tools for fostering education in radiology.

Learning Objectives:

1. To analyze the organizational and networking strategies needed for the development of regional PACS.
2. To evaluate if ASP is a viable alternative in the purchase of PACS services.
3. To verify the importance of the IHE standard initiative.
4. To assess the value of PACS as a learning tool for radiologists.

A-155

Quantitative image processing

A. Jackson; Manchester/UK

The lecture should provide an understanding of the basic concepts of quantitative image analysis. In particular the lecture is intended to provide the radiologist with some insight of the potential errors that can occur in quantitative image analysis techniques.

Background: The increasing availability of stable digital imaging platforms has led to an explosion in the use of quantitative image analysis techniques many of

which are now available on commercial platforms. Typical examples include software to perform tissue segmentation, measurements of tissue perfusion or to detect differences between scans over time. All of these techniques are designed to produce quantitative data so that an understanding of the potential errors which may occur is essential.

Procedure Details: This talk will introduce the basic generic concepts of image processing using tissue segmentation and dynamic contrast enhanced MR techniques as examples. We will focus on commonly commercially available techniques and examine in detail the potential advantages and disadvantages of them by illustrating the analysis process. We will also discuss the concept of the generation of models underlying analysis techniques and the implications of their use.

Conclusions: Clinical use of quantitative image analysis techniques is increasingly common. This lecture will highlight generic issues associated with this type of analysis which must be appreciated by clinicians intending to use these methodologies.

Learning Objectives:

1. To understand the basic approaches that can be taken to segment individual tissues from MR image.
2. To understand the advantages and disadvantages of different approaches.
3. To understand the concept of dictated model based analysis of imaging data and its advantages and disadvantages.
4. To understand the basic analysis concepts applied to dynamic contrast enhanced data from MR imaging and CT.
5. To understand the range of models that can be applied to dynamic contrast enhanced data and the implications of the choice of analysis technique.

A-156

Industry, integrating solutions towards a better practice

E. Cordonnier; Rennes/FR

Due to the digitization of equipment, the medical imaging industry increasingly integrates its products, and, more, integration is becoming a crucial part of the quality of solutions.

Initially, integration was considered by vendors as:

- losing product specificity by leveraging common minimal features,
- decreasing competitive advantages by opening solutions to products from competitors,
- increasing complexity by introducing external constraints.

However, users have clearly notified vendors that without integration, products have no future. Medical imaging equipment support some of the most complex clinical processes, and data produced by devices (images, signal^{1/4}) are to be associated to and manipulated with other information originating from various sources (electronic patient record^{1/4}).

Through an increasing global and active cooperation between users and vendors, the medical imaging community has designed standards and an integration framework which enable to connect and associate multiple products without losing any advantages of any products. It has been possible to respect cultural and local clinical practices through option and configuration parameters.

The DICOM and HL7 standards, as well as general-purpose standards (Internet^{1/4}), enabled to define proper interfaces (objects, services) between systems. IHE, a worldwide initiative, defines how to implement integrated solutions complying with these standards for common clinical scenarios. This approach was first applied to radiology and then to the laboratory sector, and it is now gradually spreading to all medical sectors including cardiology and other medical imaging sectors as well as IT infrastructure, within and also across healthcare facilities. This contributes to the Cross-Enterprise Electronic Patient Record.

Learning Objectives:

1. To comprehend what is the evolution of the medical imaging industry towards integration of standards.
2. To understand what is the impact of the IHE approach for the users and clinical practice.
3. To anticipate what are the biggest challenges for the next five years around the cross-enterprise Electronic Patient Record.
4. To learn what are behind the different Acronyms: DICOM, HL7, IHE and COCIR.

Postgraduate Educational Programme

10:30 - 11:15

La Scala

E³ - European Excellence in Education

E³ 620a

Logistic implications of MSCT

Moderator:

A.K. Dixon; Cambridge/UK

A-157

Logistic implications of MSCT

A.K. Dixon, B. Housden; Cambridge/UK

The advent of Multislice CT has profoundly changed the way we practice radiology, let alone CT. The pressure to maximise throughput on modern CT systems is intense. Various novel methods of streamlining the workflow will be presented. Meanwhile the clinical indications for MSCT expand, often with little or no extra revenue for the CT unit itself. This puts yet more pressure on the hard-pressed radiographers who feel that they are running faster and faster on the treadmill and only just keeping up! Such pressures may lead to a compromise on quality. It is very hard to provide an excellent high quality, large volume service at low cost. Some of the inevitable compromises will be discussed. So too will issues related to reporting and filming/PACS storage. The single most important factor in the smooth running of a CT Unit is mutual respect between radiographers and radiologists. Only by close co-operation between the two essential groups within a modern Radiology Department will MSCT be used to its full potential.

Learning Objectives:

1. To comprehend the ever increasing indications for MSCT.
2. To understand the role and importance of vetting requests.
3. To become familiar with methods of streamlining workflow.
4. To learn the principles of archiving dilemmas and reporting practices.

11:15 - 12:00

La Scala

E³ - European Excellence in Education

E³ 620b

How to write a successful grant proposal

Moderator:

L. Everse; Rotterdam/NL

A-158

How to write a successful grant proposal

L. Everse; Rotterdam/NL

Grant support is increasingly important to the radiological researcher. Yet even the most brilliant idea is not always funded. In order to score well, you have to show that your proposal fulfils the granting agency's objectives and that it is likely that your project will have an important impact on the population of interest. Some simple techniques can aid us in gaining that coveted letter of approval.

This lecture will cover the basic points inherent in determining ranking of grant proposals and make suggestions as to how grant proposals can be fine-tuned to increase their ranking. By identifying the objectives of granting organizations, you can select the most suitable granting agency and adapt your proposal to fit their priorities. By understanding the grant application process, you can identify the information that the reviewer needs to judge your proposal. Putting yourself in the reviewer's shoes teaches you to use lucid text that provides the reviewer with the required information and to use appropriate buzz-words that link your proposal to the organization's objectives and priorities. In order to show potential impact of your research, you should clearly state what the target population is and how exactly this project will change their lives. The feasibility of the project should be clear. Feasibility includes investigator expertise, predicted inclusion rates, the estimated sample size needed, and the appropriateness of the experimental design. Finally, how the project will transition from research to clinical practice should be specified (implementation plans).

Learning Objectives:

1. To identify the priorities of granting agencies from their literature.
2. To understand what the reviewer needs to know to judge your grant properly.
3. To understand the structure of grant application forms - what information goes where?
4. To optimally describe the impact that your proposal will have on the population of interest, including feasibility parameters.

12:15 - 12:30

Room B

Plenary Session

ECR Research and Education Fund Awards

Presiding:

A. Chiesa; Brescia/IT

H.M.L. Carty; Liverpool/UK

Presentation of the ECR Research and Education Fund Winners

A.H. Mahnken; Aachen/DE

A. Fausto; Milan/IT

O.R. Lucidarme; Paris/FR

C.P. Heussel; Mainz/DE

J.E. Wildberger; Aachen/DE

12:30 - 13:00

Room B

Plenary Session

HL 1

Wilhelm Conrad Röntgen - Honorary Lecture

Presiding:

A. Chiesa; Brescia/IT

A-159

Would W.C. Röntgen get along with hospital managers?

J.F. Debatin; Hamburg/DE

The work of W.C. Röntgen stands for hard work, creativity, and unrelenting curiosity spiced up by a bit of luck - ingredients which are best summarized by the term "serendipity".

Since the death of W.C. Röntgen both Radiology research and clinical Radiology have become more and more organized, requiring ever more management input. The results are evident at ECR 2005. Every angle of every new research development is being explored resulting in a vast increase in research quantity, accuracy and reliability. A visit of the industrial exhibit underscores the impact of management requirements onto clinical radiology. Thus the dominance of high tech machinery is being increasingly eroded by the omnipresence of IT management tools.

The need for structured management thus appears to be part of the Röntgen heritage. There is more, however: a modern W.C. Röntgen would insist on leaving sufficient space for creativity to assure "serendipity" not merely in research but also in clinical Radiology. Hospital managers, particularly those involved in a research environment seem well advised to consider both aspects of the Röntgen heritage. A balance needs to be struck between structured management on one hand and managed freedom on the other.

Learning Objectives:

1. To explore the skills sets required by the imaging researcher and practitioner in the 21 century.
2. To define the future role of diagnostic imagers in an evermore intriguing and complex health care system.

14:00 - 15:30

La Scala

Foundation Course - Chest Radiology

E³ 720

Vascular, emergency and ICU imaging

Moderator:

D. Fleischmann; Stanford, CA/US

A-160

A. Vascular disease and lung edema

M. Prokop; Utrecht/NL

Pulmonary embolism (PE), if left untreated, is a highly lethal disease and therefore requires a rapid diagnostic workup. There are a vast number of potential diagnostic strategies, which all prominently feature imaging techniques such as scintigraphy, CT angiography (CTA) and ultrasound. Multislice CTA has de-facto substituted for angiography as the gold standard for diagnosis of but it need not always be the first technique to be performed for this indication. The course will discuss under which conditions D-dimer assays can be used to rule out PE, and

Postgraduate Educational Programme

under which circumstances scintigraphic techniques still play a role. It will describe the dilemmas of pulmonary angiography and cover the future potential of MRA. Technical and interpretational pitfalls of CTA will be demonstrated. Radiation dose issues will also include the question which technique to use in pregnant women.

Aortic dissection and traumatic aneurysms are the most important acute diseases of the thoracic aorta and are primarily diagnosed by (multislice) CT. Chronic dissections, congenital abnormalities, aneurysms, and aortitis are diseases where MRA also plays a major role. Typical diagnostic questions and imaging pitfalls will be reviewed. In the last part, this course will provide the pathophysiologic concepts behind the development of the various types of pulmonary edema and focus on patterns that help distinguish them on plain chest radiographs. It will describe particular criteria that have to be known when interpreting bedside chest radiographs and will correlate findings with CT morphology.

Learning Objectives:

1. To learn how to diagnose pulmonary embolism and avoid diagnostic pitfalls.
2. To learn to use CTA and MRA for diagnosis of aortic disease.
3. To understand the criteria for distinguishing different types of pulmonary edema.

A-161

B. Trauma, emergency and ICU imaging

P. Schnyder; Lausanne/CH

The first part of the topic will familiarize young radiologists with the modern concept of radiological investigations of polytrauma patients, with particular focus on the impact of multidetector CT installed within or adjacent to the emergency room. The most striking life-threatening thoracic conditions will be considered, including chest wall lesions, occult and tension pneumothoraces, hemotorax, tracheobronchial ruptures, hemomediastinum and aortic lesions, diaphragm ruptures and frequently associated abdominal lesions which urge total body survey of polytrauma patients.

The second part of the presentation will deal with the importance of daily film reading sessions in the ICU held by a senior and junior radiologists together with ICU physicians. The most frequent conditions encountered daily in the ICU will be considered, including: early identification and characterization of lung infiltrates and consolidations, usual and unusual presentation of lung edema, intrathoracic fluid collections, intravascular fluid overload, postoperative complications, bone abnormalities previously missed, knowledge and identification of correct positioning of all lines or misplacement, with corresponding consequences, including mainly tracheal tubes, central venous catheters, Swann-Ganz catheters, nasogastric tubes, pleural drains, intraaortic balloon pumps and some other more specific devices.

This topic also emphasizes the importance of the close relationship between radiologists and intensive care physicians urged by ICU patients and on the role of CT applied on selected ICU patients and selected pathologic conditions for a better comprehension of physiopathological situations, for confirmation of a pending diagnosis and not infrequently for modification of the treatment.

Learning Objectives:

1. To familiarize the audience with the spectrum of findings in chest trauma.
2. To provide an overview regarding lung abnormalities in the ICU patient.
3. To present usual and unusual appearances of tubes and lines in the chest.

16:00 - 17:30

Room A

Essentials of Neuroradiology

CC 817

Epilepsy, white matter diseases and ageing

Moderator:

D. Ducreux; Le Kremlin-Bicêtre/FR

A-162

A. Epilepsy

H. Urbach; Bonn/DE

Imaging of epilepsy patients is challenging since epileptogenic lesions (defined as a structural lesions causally related to the epilepsy syndrome) may be small and often do not change during life. Prior clinical information about the epilepsy syndrome and the semiology of the seizures is needed in order to plan the examination properly. The effort to detect an epileptogenic lesion is directed to partial (focal) epilepsy syndromes whereas - by definition - no lesion is identified in

idiopathic epilepsies. Most patients with partial epilepsies suffer from mesial temporal lobe epilepsies. In these patients, 2 to 3 mm thick T2-weighted rather than FLAIR fast spin echo slices along or perpendicular to the temporal lobe length axis have the highest diagnostic efficacy. In contrast, in patients with extratemporal lobe epilepsies perpendicular FLAIR slices through the anatomic region, from which due to clinical and EEG criteria the seizures are likely to originate, are preferred. The imaging features of common epileptogenic lesions (hippocampal sclerosis, long-term epilepsy-associated tumours, focal cortical dysplasias, vascular malformations, encephalitis including limbic and Rasmussen's encephalitis, gyral scarring including ulegryia) are detailed.

Learning Objectives:

1. To become familiar with clinical informations about the epilepsy syndrome and the semiology of the seizures.
2. To use these informations as clues whether an epileptogenic lesions is likely to be present and in which part of the brain one has to look for.
3. To learn the imaging findings of common epileptogenic lesions found in patients undergoing persurgical evaluation for possible epilepsy surgery.

A-163

B. White matter diseases

E.-W. Radü; Basle/CH

This lecture will give an overview of the structure and pathology of white matter which mainly consists of myelin and supporting tissues. The presentation and specific artefacts of different examination sequences -like the spin echo sequence, the turbo spin echo sequence and the FLAIR sequence as well as other gradient echo sequences- will be discussed. Examination protocols for different types of pathologies (vascular, degenerative, inflammatory) will be introduced to make the differential diagnosis easier.

The pattern of lesions, their localization, contrast media enhancement and space occupying effects will be discussed; the lecture will present characteristic forms of congenital and acquired diseases of white matter and will suggest ways to assign them etiologically.

Furthermore the changes in white matter due to multiple sclerosis will be shown in detail. The value of T2 hyperintense areas, black holes and contrast media enhancements will be presented in connection to their distinct pathological findings. MR spectroscopy as a method of examination as well as Magnetization Transfer Imaging will be discussed. The lecture will present standardized protocols for examinations of the brain and the spinal cord in suspected multiple sclerosis and for follow-up examinations in definite multiple sclerosis. Finally, difficulties in follow-up examinations and hints on how to perform a satisfying repositioning will be shown.

Learning Objectives:

1. To demonstrate the relevant knowledge of the correlation between MR findings and histo-pathological alterations.
2. To induce a detailed report especially of alterations of the white matter.
3. To suggest a standardized examination in multiple sclerosis.

A-164

C. Normal ageing and neurodegenerative diseases

M.A. van Buchem; Leiden/NL

The most common neurodegenerative disorder is ageing. Ageing is associated with degenerative changes in the brain. With increasing life expectancy of the population, the number of elderly persons increases in industrialized societies. Therefore, radiologists in such societies will increasingly be confronted with age-related changes in the brain. Knowledge of these changes is thus essential for every radiologist. Before describing the abnormalities that occur with aging, it is important to be aware of a few facts. First, age-related abnormalities do not occur in all elderly persons. Second, age-related changes that are apparent on radiological examinations do not always have functional consequences. Third, normal ageing and neurodegenerative disorders may be difficult to distinguish. One reason is the similarity of the abnormalities that are associated with these conditions. Another phenomenon that complicates distinguishing normal ageing from other neurodegenerative disorders is the fact that due to the high prevalence of the latter, these conditions often coexist in the elderly with changes that are due to normal aging. In such circumstances it may be impossible to separate the abnormalities in terms of their origin. An important task for radiologists, when confronted with a brain study in an elderly patient, is to screen for the presence of neurodegenerative disorders. In this process, changes should not be attributed too easily to normal aging. In order to be able to separate usual ageing and other neurodegenerative disorders, a radiologist should be familiar with the changes that occur in normal ageing. In this presentation such changes will be described.

Postgraduate Educational Programme

Learning Objectives:

1. To comprehend the principles of successful, usual and pathological aging.
2. To become familiar with age-related changes in the brain that occur during usual aging.

16:00 - 17:30

Room B

Musculoskeletal

RC 810

Bone marrow disorders as a manifestation of disease

Moderator:

H. Imhof; Vienna/AT

A-165

A. How to image bone marrow

A. Stähler; Munich/DE

Introduction: MR imaging can directly visualize bone marrow. Bone marrow pathologies have low SI on unenhanced T1-weighted images and increased SI on (fat-suppressed) PD, T2w and STIR images. Differentiation of acute osteoporotic and tumor-related vertebral fracture can be difficult.

Gadolinium: The principles of percentage enhancement for bone marrow imaging and the cut-off values (> 35% in patients older 35 years) are explained. Percentage enhancement is a good and reliable tool to estimate marrow cellularity. Diffusion-weighted Imaging: On diffusion-weighted imaging benign fractures exhibit isointense or low SI compared to surrounding bone marrow, whereas metastatic vertebral compression fractures show high SI.

Whole Body Imaging: Whole body MR imaging detects more lesions than bone scintigraphy. Although bone scans tend to detect more lesions in the ribs and the skull, MR imaging detects more lesions in the clinically relevant body parts including the spine and the pelvis.

Differentiation of acute osteoporotic and tumor-related vertebral fractures:

Imaging findings characteristic for tumor-related vertebral fractures are a convex posterior cortex, diffuse low SI on T1w images, lesion extension into the pedicle, high or inhomogenous signal-intensity following Gadolinium, and a high SI of the bone marrow on T2w or STIR images. Findings indicative of osteoporotic fractures are retropulsion of a bone fragment, preservation of some fat signal on T1-weighted images, return to normal SI after Gadolinium, a horizontal bandlike signal pattern, and isointense bone marrow signal on T2w or STIR images. There is a correlation between "vacuum phenomenon" on CT and the "fluid sign" on MR imaging.

Learning Objectives:

1. To differentiate acute osteoporotic from tumor-related vertebral fractures.
2. To understand diffusion weighted imaging of bone marrow.
3. To use percentage gadolinium enhancement for bone marrow imaging.

A-166

B. Tumors

F. Lecouvet; Brussels/BE

MR imaging has a variety of roles in the setting of bone marrow tumors, depending on the patient's clinical details: unexpected observation of a tumoral lesion in patients with unknown neoplasia, confirmation of lesions detected by nuclear medicine techniques, disease staging and evaluation of response to treatment in patients with known cancer, work-up of symptoms for cancer.

Systematic screening of the bone marrow requires investigation of the pelvis and proximal femurs in addition to the spine study.

For lesion detection, T1-weighted images are often sufficient and lesions have low signal intensity. Fat-saturated T2 or intermediate-weighted images, or STIR images are also efficient in lesion detection that generally have intermediate to high signal intensity. These sequences and contrast-enhanced T1-weighted images become mandatory to differentiate diffuse neoplastic marrow infiltration from abnormally cellular albeit normal marrow.

In terms of lesion characterization, MR imaging plays little role because MR patterns of neoplastic marrow involvement are non-specific: focal lesions and diffuse infiltration are observed in metastases, lymphoma and multiple myeloma. However, some subtle features sometimes help in the differential diagnosis: concurrent observation of diffuse bone marrow signal alterations, focal lesions and compression fractures are indicative of myeloma; a combination of bone lesions with paraspinal or pelvic tumoral lymph nodes and extra-osseous tumor spread without alteration of the bone cortices suggests lymphoma.

The radiologist must be aware of some benign conditions which may mimic tumoral lesions: benign, diffuse or focal bone marrow hyperplasia, intravertebral disk herniations, acute vertebral compression fractures and infectious lesions.

Learning Objectives:

1. To illustrate general MR imaging characteristics of tumoral bone marrow involvement.
2. To describe imaging features suggestive of most frequent bone marrow tumors: Metastases, myeloma and lymphoma.
3. To underline the lack of specificity of MR imaging and illustrate several non-tumoral lesions which may mimick bone marrow tumors.

A-167

C. Non-neoplastic marrow disorders

A.H. Karantanas; Iraklion/GR

Magnetic resonance imaging is an imaging technique that allows direct visualization of bone marrow. Although MR imaging exhibits high sensitivity, we need an adequate understanding and careful choice of acquisition sequences to improve specificity. Technical improvements such as providing a moving table and developing new coils and sequences allows the study of the whole marrow in a reasonable time.

Non-neoplastic disease processes involving the marrow can induce a variety of imaging findings. These conditions are frequently undetectable by conventional radiographic techniques until they have reached an advanced clinical stage. The excellent spatial and contrast resolution provided by MR imaging facilitates early detection and evaluation of various disorders thus allowing prompt treatment. In addition, the association between marrow changes and pain such as in osteonecrosis and osteoarthritis is clinically relevant. Radiological interpretation of the marrow space requires an understanding of normal maturation, and recognition that red and yellow marrow co-exist with variable amounts depending upon age and location. With MR imaging this variability yields normal patterns ranging from very uniform and homogeneous to patchy and heterogeneous signal intensity. Signal changes also depend on the pulse sequence applied. The marrow reflects patient health and may herald developing anemia with marrow reconversion from inactive to active. Disorders to be considered include: a) marrow ischemia and infarction, b) transient osteoporosis of the hip and transient epiphyseal lesions of the knee, c) marrow oedema-like lesions secondary to trauma, stress response, osteoarthritis, tendon pathology, Sudeck's algodystrophy and previous arthroscopy, d) infection and e) marrow infiltration (Gaucher's disease - myelofibrosis).

Learning Objectives:

1. To understand the normal bone marrow reconversion observed in athletes, heavy smokers and obese patients.
2. To provide an overview of marrow changes in hemoglobinopathies, storage diseases, infection and Paget's.
3. To be familiar with the bone marrow changes in avascular necrosis and transient osteoporosis.
4. To understand the marrow changes in trauma.

16:00 - 17:30

Room C

Special Focus Session

SF 8a

Imaging ICU patients

Moderator:

L. Gattinoni; Milan/IT

A-168

Imaging ICU patients (Introduction)

L. Gattinoni; Milan/IT

The use of CT scans in ICU patients has been delayed for several years, largely because of the difficult transport of ICU patients, the cost of the technique and the absence of clear indications. The best example is ICU patients with ARDS; only in 1984 did the first report appear on the use of CT in this pathology. The CT scan images and the quantitative CT scan analysis allow us to confidently refute the common belief that ARDS is a homogeneous alteration of the lung parenchyma. Most of the more recent advances in the treatment of the patients with ALI/ARDS originated from the information obtained by CT scanning. Despite the difficulties and costs, the CT scan resulted in a change of treatment in about 30% of the patients with ALI/ARDS, making it cost-effective. Trauma, pulmonary embolism, discrepancy between clinical findings and radiological observations are all

Postgraduate Educational Programme

clear indications for CT scanning. The use of CT scan is nowadays an integral part of the assessment of most patients admitted to the ICU.

Learning Objective:

To understand the general indications for CT scanning in ICU patients.

A-169

Structure-function correlations in acute lung injury

L. Gattinoni; Milan/IT

The use of quantitative CT scanning allowed great advances in our understanding of pathophysiology of acute lung injury and ARDS. A standard voxel, characterized by a given CT number, (0.5 x 0.5 x 1.5 mm) matches the dimensions of a normal acinus at functional residual capacity, about 2,000 alveoli. If the lung collapses the same voxel may include up to 11.5 acini. In case of intra-alveolar edema the same voxel should include about 1 fluid-filled acinus. Knowing the CT number frequency and distribution, it is possible to compute the gasless, the fully aerated, the normally aerated and the hyperinflated tissue. Moreover, it is possible to compute the excess lung weight, i.e. the edema, using as reference the expected normal lung weight for any given patient. The quantitative analysis allows us to determine in ALI/ARDS if the aerated lung is small rather than stiff, and the dimensions of the baby lung are estimated by lung compliance. Regional analysis obtained at different pressure conditions led to the discovery that the lung recruitment is a continuous phenomenon along the entire volume/pressure curve. The actual modeling refers to the ARDS lung as a sponge. The increased lung mass causes the compression of the most dependent regions. The density redistribution in the prone position as well as the mechanism of positive end expiratory pressure are best explained by this model. Finally the CT scan allows an estimate of the potential for recruitment, this information may be a key clinical advance for setting PEEP and tailoring an appropriate mechanical ventilation.

Learning Objective:

To understand the use of CT scan taken in different conditions for the clinical treatment of ALI/ARDS patients.

A-170

Clinical correlation in the imaging of ARDS

L.R. Goodman; Milwaukee, WI/US

Adult respiratory distress syndrome (ARDS) is a dynamic disease due to multiple different systemic and/or local insults to the lung. Although there are some distinct differences in the imaging appearance of ARDS due to systemic insults and ARDS due to direct lung insults, in general, imaging is not specific and is used to support the diagnosis of ARDS rather than to make the diagnosis. However, in the proper clinical context, the imaging is strongly suggestive of ARDS or suggesting alternative causes for the respiratory difficulties. Imaging also aids in the understanding of the underlying clinical and pathophysiological progression. The current generation of multidetector CT scanners is also being used to study respiratory dynamics and the effect of various ventilatory measures on lung volumes and gas distribution.

Imaging's most important role is in following the progression of the disease and in the prevention and diagnosis of complications. Complications are numerous and include aspiration, nosocomial infection, atelectasis, and pulmonary embolus. Iatrogenic complications include barotrauma, fluid overload, and malposition of tubes and catheters.

Learning Objectives:

1. To understand the expected imaging progression of ARDS.
2. To understand how imaging reflects pathophysiology of ARDS.
3. To be able to detect early complications of ARDS and their treatment.

A-171

Imaging sequelae of acute lung injury

S.R. Desai; London/UK

The acute respiratory distress syndrome (ARDS) is a non-specific response to direct or indirect lung injury. Patients with ARDS are characterised by progressive dyspnoea, refractory hypoxia, decreased compliance and alveolar infiltrates on chest radiography. On histopathological examination there are progressive changes which are mirrored by the appearances on radiological studies: acutely, there are eosinophilic hyaline membranes within respiratory bronchioles and alveolar ducts. Initially, there is only a limited interstitial infiltrate. With time the interstitial infiltrate becomes more striking and there is inflammatory and haemorrhagic fluid exudation into the airspaces. In the final stages there is healing by fibrosis which, in some patients, may be marked. Imaging has an important role in the management of critically ill patients; daily chest radiography is useful for

monitoring progress and detecting complications. Computed tomography (CT) is also valuable in the acute stages: in addition to "problem-solving", CT provides insights into the pathophysiology of ARDS. The typical CT changes, in the acute stages, comprise symmetrical regions of dependent dense parenchymal opacification, non-dependent areas of ground-glass opacification and normally aerated lung parenchyma in varying proportions. In some patients it is possible to differentiate ARDS due to pulmonary and extrapulmonary injury based on CT features. Furthermore, in survivors of ARDS, there is a characteristic distribution of changes which is thought to be a consequence of barotrauma in the acute stage. The lecture will present the morphological features of ARDS both in the acute stage and at follow-up.

Learning Objectives:

1. To learn the imaging (CT) features in patients with lung injury.
2. To appreciate the relationships between histopathological changes and CT features in patients with ARDS.

16:00 - 17:30

Room E1

Cardiac

RC 803

Coronary vessels

Moderator:

M. Oudkerk; Groningen/NL

A-172

A. Clinical issues and anatomy of the coronary vessels

R. Riemann; Graz/AT

Coronary vessels serve as conduit for blood flow (F) from the aorta to the myocardium and further to the right atrium.

The task of the F is to keep permanent balance between myocardial oxygen supply and demand to prevent myocardial damage. Therefore early recognition of the presence and causes of insufficient coronary F are mandatory. This means it is necessary to control and to consider all factors which may influence the F and the demand of oxygen.

Under normal anatomical conditions the individual distribution and course of the coronary vessels and their ramification play a major role. In the presence of pathohistological changes of coronary vessel walls the F is mainly influenced by the decrease of elasticity and increase of vessel wall resistance.

The loss of normal elasticity diminishes the possibility of fast F adaptation with respect to myocardial oxygen demands.

In a simplified model, coronary F may be described by Ohm's formula $F = P/R$, whereby pressure (P) and resistance (R) are controlled by the neuro-humoral system.

The present non-invasive coronary imaging methods enable the visualisation not only of the macro-anatomy of the coronary vessels and their ramification, but also directly atherosclerotic wall changes.

As their spatial, contrast and time resolution are continuously improving, they are already superior to lumeno-graphic methods as coronary angiography. The visualisation of coronary anatomy and its wall pathology will - by simultaneously performed quantitative measurements of myocardial F and by the control of neuro-humoral system - enable to generate a new approach to individual risk stratification.

Learning Objectives:

1. To give an overview of the clinical problem.
2. To describe the radiological anatomy of the coronary arteries.
3. To discuss methods of risk stratification.

A-173

B. MRA of the coronary arteries

A. de Roos; Leiden/NL

Magnetic resonance angiography (MRA) of the coronary arteries is still suboptimal for routine clinical application. Initial results have shown the potential of breath-hold and navigator approaches for visualizing coronary artery stenoses. A multicenter trial using navigator technology has shown that the exclusion of major coronary artery disease is feasible. Recently, new technical approaches have been introduced to improve coronary artery visualization. For example, whole heart MRA acquires multiple thin slices with navigator control and is displayed in various ways for improved coronary artery visualization, including with the use of volume rendering techniques. Also the recent introduction of higher field systems

Postgraduate Educational Programme

(3 T) may help to improve coronary artery visualization. In addition, a number of contrast media are tested for improved vessel delineation. Bypass imaging is also feasible with the same technology. Not only patency, but also stenosis detection in venous bypasses is feasible with MRA. Furthermore, the versatility of MR imaging also allows flow quantification in the native coronary circulation as well as in bypass grafts. Another important goal is to detect atherosclerotic plaques and to characterize plaque composition. The versatility of MRA allows anatomic depiction of the coronary vessels as well as functional assessment of the stenosis in both the coronary arteries and bypass grafts.

Learning Objectives:

1. To discuss principles and techniques of MRA.
2. To give an overview of recent clinical outcome.
3. To discuss clinical indications of MRA.

A-174

C. MDCT of the coronary arteries

C.R. Becker; Munich/DE

The combination of multi-detector rows and fast gantry rotation together with the simultaneous acquisition of the ECG signal allows for imaging the coronary arteries with a high spatial and temporal resolution by a technique called retrospective ECG gating. With every new MDCT generation, spatial and temporal resolution is getting closer to cardiac catheter. It is therefore foreseeable that a significant number of diagnostic cardiac catheter investigations will be replaced by coronary CT angiography (cCTA) in the near to midterm future.

Assessment of the atherosclerotic plaque burden by coronary calcium screening with CT is a simple and effective way to non-invasively identify asymptomatic subjects with an increased risk for a cardiac event. cCTA may have the potential to visualize vulnerable plaques that are prone to rupture and cause acute coronary symptoms.

In patients with acute myocardial infarction cCTA may be able to display the location as well as the culprit lesion in the coronary artery.

cCTA may also provide valid information in patients with vasculitis and aneurysms, fistulas or dissections. The current strength of cCTA is the high negative predictive value as compared to cardiac catheter. In patients with unspecific complaints or ambiguous stress tests, cCTA may serve as a reliable non-invasive alternative to rule out coronary artery disease. The key application of cCTA will be to perform a non-invasive triage of patients with stable angina for conservative therapy, interventional treatment and bypass surgery and limit the use of invasive coronary angiography to patients in whom coronary interventions appears necessary.

Learning Objectives:

1. To discuss principles and techniques of MDCT.
2. To give an overview of recent clinical outcome.
3. To discuss clinical indications of MDCT.

16:00 - 17:30

Room E2

Abdominal and Gastrointestinal

RC 801

Crohn's disease of the intestinal tract:

Advances in imaging

Moderator:

A. Cieszanowski; Warsaw/PL

A-175

A. US and Doppler

C. Bru; Barcelona/ES

Ultrasonography with doppler is frequently the initial imaging study performed in patients with abdominal pain and diarrhoea. Inflammatory processes affecting the intestinal wall generally result in decreased peristalsis and bowel wall thickening, both of which tend to decrease the luminal gas content that allows a better visualization of intestinal structures.

The use of graded compression or cleansing and water enema improves the capacity of the technique to evaluate all the intestinal segments. The transperineal approach can be useful for the study of perianal pathology associated with Crohn's disease.

Technical improvements in US equipment allows us to evaluate the characteristic five layer pattern of the intestinal wall, the presence or absence of haustra, the vascularity of intestinal segments as well as the flow through the superior mesenteric artery.

The following topics will be discussed during the lecture:

- Methodology of intestinal ultrasound study
- Patterns in Crohn's disease and differential diagnosis.
- Risks and benefits of the technique
- Impact on management.

Learning Objectives:

1. To describe the US examination technique and findings in chronic inflammatory diseases of the intestinal tract.
2. To discuss the value and the limits of US for the diagnosis of Crohn's disease.
3. To discuss the impact of US on patient's management.

A-176

B. CT and CT enteroclysis

E.K. Makó; Budapest/HU

The incidence and prevalence rates of inflammatory bowel diseases show an increasing tendency worldwide.

There are efforts to find a more appropriate examination technique which is able to depict characteristic and large enough pathology of the IBD is permanent.

The diagnostic flowchart in patients with known chronic inflammatory bowel disease has changed due to wide availability of spiral or multidetector CT equipment, proceeding from multi-step diagnosis toward a "one stop shop" modality such as CT or MR enteroclysis.

When compared to US the capability of CT (enteroclysis) is less patient and operator dependent. Using thin slices and narrow collimation provides excellent spatial resolution and depicts tiny pathology of the bowel mucosa over characteristic intramural or extraintestinal changes.

Although specificity and sensitivity of CT (enteroclysis) in patients with superficial Crohn's disease still remains lower than barium enteroclysis (~90% and 98% respectively), in transmural and extraintestinal IBD it provides all the relevant pathological information needed for the correct diagnosis.

CT has the advantage of allowing simultaneous depiction of possible extra-intestinal abdominal complications of IBD and playing an important role in patient's management.

Learning Objectives:

1. To describe the CT examination technique and findings in chronic inflammatory diseases of the intestinal tract.
2. To discuss the value and the limits of CT for the diagnosis of Crohn's disease.
3. To discuss the impact of CT on patient's management.

A-177

C. MR imaging

D.J. Lomas; Cambridge/UK

Techniques: Several fast imaging sequences suitable for imaging the small bowel are now available on modern MR systems, including T1W, T2W and balanced T2/T1W. Each has particular merits for studying the small bowel. Both oral and nasojejunal tube examinations may be performed with MR imaging, paralleling the same examinations using X-ray. Most tube studies have employed methyl cellulose or dilute barium as the contrast media infused by manual or automated pump systems. As for X-ray studies, debate continues regarding the merits of the two approaches and regarding the most appropriate orally administered agent to achieve adequate luminal distension. Currently many studies are performed as static examinations with initial filling of the small bowel followed by an anti-peristaltic agent and then multiple breath-hold image sets acquired with a distended small bowel lumen.

Applications: Numerous studies have shown that MR examinations in inflammatory bowel disease can demonstrate many of the morphological features of traditional X-ray studies. MR imaging also has the benefits of avoiding ionizing radiation in a typically young population and of demonstrating the extra-luminal tissues, allowing excellent delineation of fistulae and extra-luminal changes such as fatty proliferation. Current MR systems are not well designed for these types of studies and tube insertion is usually done under X-ray guidance at present. These and other factors such as availability have limited the more widespread introduction of MR imaging in routine clinical practice. Further development of "interventional" MR imaging systems may simplify the practical aspects of these procedures and encourage more widespread use in the future.

Learning Objectives:

1. To describe the MR examination technique and findings in chronic inflammatory diseases of the intestinal tract.
2. To discuss the value and the limits of MR imaging for the diagnosis of Crohn's disease.
3. To discuss the impact of MR imaging on patient's management.

Postgraduate Educational Programme

Saturday

16:00 - 17:30

Room F1

Chest

RC 804

Imaging of lung cancer

Moderator:

H.-U. Kauczor; Heidelberg/DE

A-178

A. Screening for lung cancer: Update on results of current trials

F. Laurent; Pessac/FR

Although screening studies using chest radiograph and sputum cytology examination are still the subject of debate and the use of molecular techniques an exciting area of research, CT is the current method for ongoing screening programs. This course will focus on low dose multislice CT screening studies and updates on current trials will be reported. CT studies have shown that earlier-stage lung cancer can be detected but whether this will translate into a mortality reduction remains the subject of an intense debate because of methodological biases. Randomized trials including death as an outcome are advocated to evaluate this issue. Implications of CT screening are also great especially the number of patients who require further evaluation after CT. Current practice includes the use of non-invasive procedures to evaluate indeterminate nodules in order to minimize the cost and risk of invasive methods. Recent improvements in dedicated tools for enhancing detection (CAD) and characterization (CT volumetry) may play a significant role in decreasing the concern of the indeterminate pulmonary nodule.

Learning Objectives:

1. To understand the potential role and limitation of multislice CT in lung cancer screening.
2. To update the knowledge on results of recent and current trials.
3. To become familiar with the algorithms used for managing patients with indeterminate nodules.
4. To understand the impact of CAD and volumetric measurements in screening studies.

A-179

B. Staging and follow-up with CT and MR imaging

M. Zompatori¹, G. Battista², R. Canini²; ¹Parma/IT, ²Bologna/IT

Once the diagnosis of lung cancer has been established, attention turns to clinical staging. There is a strong relationship between the anatomical extent of tumor at diagnosis and post-treatment survival. A correct staging allows the selection of patients for surgical intervention, also reducing the rate of exploratory thoracotomies. However, misclassification is still reported in about one third of cases, particularly for lower lobe tumors. Optimal lung cancer staging and follow-up is still evolving. Today, it requires a multidisciplinary approach with a combination of MDCT and FDG-PET. Other techniques, such as MR or US, can be used as problem solving tools in particular cases. In our view, the introduction of metabolic staging (FDG-PET) is probably only the first step towards an imaging directed more at tumor biology investigation. During the presentation, T, N and M status will be discussed, along with particular problems such as: Satellite nodule evaluation, pleural disease, pancoast tumor. CT technical improvements will be evaluated, in comparison with the other anatomical methods and with brief reference to the strengths and weaknesses of functional imaging. Finally, an evidence-based, algorithmic approach will be presented, which can be used as a simplified reference for the staging of a new case of lung cancer.

Learning Objectives:

1. To understand the staging system of non-small cell lung cancer and small cell lung cancer.
2. To evaluate the role of the different imaging modalities for T-, N- and M-staging of lung cancer.
3. To characterize the different therapeutic strategies at different tumor stages and its relevance for imaging procedures.

A-180

C. Staging and follow-up with PET/PET-CT

G.K. von Schulthess; Zürich/CH

FDG (Fluorodeoxyglucose)-PET has gained major importance in diagnosis and staging of lung cancers for characterization of pulmonary nodules and for N- and M-staging of NSCLC.

PET is the best imaging modality to identify malignant pulmonary nodules (accuracy > 90%). False positives are due to infection; hence the prevalence of TBC is important. There are also some false negatives, mainly in bronchioalveolar carcinomas, which may show no FDG uptake.

N and M staging with PET has shown to be highly sensitive (85-90%) and specific (90-95%) and substantially higher than CT. PET staging is now the preferred staging modality for this disease. It can identify pathological lymph nodes at sizes 1 cm and smaller, where CT criteria for pathology are useless. It identifies bone metastases which are not seen on CT, and since the lesion to background contrast in PET is exquisite, tumor manifestations are less frequently overlooked on PET compared to CT scans. PET-CT is now rapidly replacing "PET alone" scanning and provides a "one-stop-shop" exam for patients with NSCLC. Data show that PET-CT, unlike PET alone, contributes to T staging as it can demonstrate thoracic wall infiltration and distinguish tumor involvement from atelectasis. PET-CT has higher sensitivity and specificity than either PET or CT alone, and even a painstaking side-by-side viewing of PET and CT data - while useful - is less accurate than fused images. Examples where the CT part of the examination adds information not seen on PET are small disseminated metastases, pleural effusions and calcifications.

Learning Objectives:

1. To discuss therapeutic strategies at different manifestations of lung cancer recurrence.
2. To analyse the role of different imaging modalities for detection of local recurrence, lymphatic or distant metastases.
3. To understand the advantages of PET-CT compared to separate PET and CT.

16:00 - 17:30

Room F2

Neuro

RC 811

Orbit and visual system

Moderator:

K. Karlinger; Budapest/HU

A-181

A. Imaging of orbital pathology

P. Sosnowski; Poznan/PL

The role of computerized methods in orbital imaging is established. CT remains the method of choice in most emergencies, especially with bony and ocular trauma, including detection of intraorbital metallic foreign bodies. In intraorbital pathologies, CT and MR are used interchangeably. MR is a more demanding and still less accessible method but has undisputable advantages, especially regarding eye, optic nerve and extraocular muscles. Its superiority in superficial orbital structures and ocular imaging are subsequent to better tissue characterization and application of local coils. MR is complementary to ultrasound in problematic cases of congenital eye abnormalities, for tissue characterization and for evaluation of secondary extraocular involvement, especially in retinoblastoma and melanoma.

Regarding the optic nerve, application of different MR sequences, fat-saturation techniques and contrast media enables detection of even subtle pathology, like MS plaques, and precise visualization of the extent of disease along the whole course of the nerve.

In the era of MSCT with precise multiplanar reconstructions, the main advantage of MR in extraocular muscle imaging is the ability to define the activity of the pathological process. It is especially helpful in thyroid ophthalmopathy, remaining one of the leading indications for computerized imaging of the orbit. The algorithm of MR study encompasses morphological sequences, with the especially important SE T1 and STIR, and short-lasting GRE scans used for quantitative analysis of eye motility disorders, especially diplopia.

Learning Objectives:

1. To understand advantages, disadvantages and the main indications for CT and MR of the orbit.
2. To define the role of MR imaging in tumoral and nontumoral eye and optic nerve pathology.
3. To identify the algorithm for MR evaluation of the extraocular muscles pathology, putting a stress on thyroid orbitopathy.
4. To comprehend the role of computerized imaging in the evaluation of the intraorbital reasons of diplopia and blindness.

Postgraduate Educational Programme

A-182

B. Imaging of optic chiasm and visual tract diseases

W. Müller-Forell; Mainz/DE

Most patients suffering from intracranial pathologies affecting the visual pathway complain of nonspecific visual deficits. Subtle neuro-ophthalmological examination discloses different visual field deficits, depending on the specific location of the involved area. Therefore this refresher course starts with a short review of the anatomical landmarks of the visual pathway, visible on MR imaging (the method of choice in the case of visual pathway lesions) and corresponding neurological symptoms.

The following presentation of different pathologies includes clinical and imaging characteristics of the three main groups of potential pathological lesions: Extrinsic lesions: these prefer the sellar region and include skull base meningioma, pituitary adenoma and craniopharyngioma. Vascular compression syndromes, caused by intracranial aneurysms are also included. The latter present with different neurological symptoms, related to their location in the circle of Willis. Intrinsic brain tumors mainly affect the visual tract and optic radiation. Imaging characteristics and differential diagnostic criteria of e.g. different types of glioma, ependymoma or metastasis are discussed.

In the last group vascular and/or inflammatory processes, affecting the visual pathway are presented.

Learning Objectives:

1. To learn about anatomic landmarks of the intracranial pathway.
2. To understand their corresponding function and neurologic symptoms in case of pathologic involvement.
3. To learn about differential diagnostic criteria of MR images concerning possible different intracranial pathologies.

16:00 - 17:30

Room G

Special Focus Session

SF 8b

Diagnostic and interventional radiology of transplants

Moderator:

M. Galanski; Hannover/DE

A-183

Diagnostic and interventional radiology of transplants (Introduction)

M. Galanski; Hannover/DE

The field of organ transplantation has grown continuously during the past decades. Kidney and liver transplantation are well established. Lung transplantation has become an accepted treatment for patients with end-stage pulmonary or vascular lung disease. Combined kidney and pancreas transplantation is the most effective treatment for renal insufficiency due to diabetes. Advances in organ preservation, development of sophisticated surgical techniques, progress in perioperative management and postoperative intensive care, and dramatic improvement in immunosuppression have resulted in higher rates of patient and graft survival. Nevertheless, the field of transplantation still presents many challenges. Whereas excellent short-time survival is readily achieved, graft loss due to chronic rejection remains a major problem. Another major barrier is the lifelong need for immunosuppression with the risk for associated complications such as infection and malignant disease. A further critical point is the shortage of donor organs. The need for transplants for qualified recipients by far exceeds the number of donor organs. Strong efforts are made to close this gap, e.g. better patient and donor selection criteria, including older donors and non-heart-beating donors in the organ pool, living donor transplantation and so on. A deeper understanding of the immunological processes responsible for transplant rejection, induction of immunologic tolerance to achieve specific graft tolerance, xenografting, cell transplantation, and gene therapy strategies are on the horizon and may one day solve the main problems.

Learning Objectives:

1. To review the current developments that have significantly improved graft and patient survival among solid-organ transplantation and addresses the main challenges in the future.
2. To learn the clinical and surgical considerations in the evaluation process for organ transplantation.
3. To understand the pathophysiology of immediate and late complications, their manifestation in imaging and their management.

A-184

Liver

J.B. Karani; London/UK

Liver transplantation is the accepted treatment of patients with irreversible liver cell failure, some metabolic disorders and a selected group of patients with hepatocellular carcinomas. Over the last decade, the major transplant centres have reported improving survival rates even though during this period more complex surgical techniques, including split liver, auxiliary and live related transplantation have been introduced and more 'marginal' higher risk patients have been treated. This successful outcome has been dependent on appropriate recipient selection, robust surgical technique and early recognition and treatment of complications. Radiologists are core members of the multidisciplinary team achieving this success.

Despite these developments there remains an organ shortage for potential recipients. Therefore appropriate selection of recipients, particularly those with hepatomas and acute liver failure, is mandatory. Inappropriate selection from inaccurate radiological diagnosis or staging will not only result in poor recipient survival, but will also deny an organ to another recipient with a better survival profile.

Improved surgical technique has decreased the more common vascular and biliary complications but the newer techniques present differing diagnostic and interventional challenges. Major developments in MR and MDCT allow these complications to be diagnosed non-invasively, reserving invasive techniques for intervention. Vascular techniques of angioplasty and stent placement may reverse the sequelae of graft ischaemia or portal hypertension and prolong graft survival in both adult and paediatric recipients. MRC allows early recognition of biliary strictures amenable to dilatation and stent placement.

This presentation will review the application and outcome of these techniques.

Learning Objectives:

1. To understand the indications and outcome of liver transplantation in an adult and pediatric program.
2. To understand the new surgical techniques and the importance of radiology in recipient and donor selection.
3. To understand the importance of a multimodality approach to the recognition of the complications of liver transplantation.
4. To understand the role of interventional radiology in providing a bridge to transplantation and treating vascular and biliary complications.

A-185

Kidney and pancreas (part 1)

J. Klempnauer, F. Lehner; Hannover/DE

Kidney transplantation is preferred over dialysis for management of end-stage renal disease complicating type 1 or 2 diabetes mellitus (DM). Simultaneous pancreas-kidney (SPK) or pancreas after kidney transplantation (PAK) is an important alternative to kidney transplantation alone for type 1 diabetes patients. Despite the significant risks, SPK/PAK is an effective treatment to reverse or minimize metabolic abnormalities and complications of type 1 DM. Candidates for SPK and PTA transplantation need to meet various selection criteria to exclude cardiac and other risk factors. SPK and PTA endocrine function is usually excellent, but common post-transplant medical complications, as well as complications unique to SPK and PTA transplantation may occur. The main post-transplant complications are pancreatitis, venous thrombosis of the graft, rejection and bleeding. Clinical diagnosis of these complications is often difficult. Therefore, diagnostic and interventional radiology play an important role in the interdisciplinary treatment concept. As a result of improved surgical techniques, immunosuppression and patient selection, one-year survival rates of 95, 83, and 88% for patient, pancreas and kidney survival are reported for patients with simultaneous pancreas-kidney transplantation. However, morbidity and mortality after SPK are still higher than for kidney transplantation alone in the first year. Main future goals are reducing postoperative morbidity, identifying relevant indications for single pancreas transplantation, adopting the best surgical technique for individual patient's needs (bladder versus enteric drainage with/without portal venous delivery of insulin), and developing immunosuppressive strategies with low nephrotoxic and diabetogenic potential.

Learning Objective:

Detection and identification of the cause of post-transplant pancreas graft dysfunction.

Postgraduate Educational Programme

A-186

Kidney and pancreas (part 2)

A. Chavan; Oldenburg/DE

Arterial DSA, which was generally used to clarify renal vascular anatomy in living kidney donors about a decade ago, has now largely been replaced by the non-invasive Duplex-Doppler Ultrasonography (US), supplemented either by contrast enhanced MRA or CTA. Due to the lack of ionizing radiation and non-nephrotoxic contrast agents, MRA is the modality of choice for this purpose in these otherwise healthy patients. As opposed to this, CTA is better suited for depicting calcification and narrowing of recipient pelvic vessels. Even in recipients, DSA is generally carried out only if an angioplasty (PTA) is necessary prior to surgery. Following renal transplantation (RT), complications of relevance to the radiologist include post-operative perirenal fluid collections compromising organ function, transplant vessel stenosis (RAS) as well as post-biopsy arterio-venous fistulas (AVF). The perirenal fluid collections are generally drained percutaneously using CT or US guidance. Besides US, MRA now has sensitivities and specificities exceeding 90% for non-invasively detecting RAS. Treatment of these stenoses as well as of intrarenal AVFs is the domain of the interventional radiologist; the technical success rate exceeds 85%.

Following pancreas transplantation (PT), organ perfusion can be determined using dynamic MRA and quantified by plotting the extent of organ enhancement against time. With increasing experience, MRA is also becoming a valuable tool in detecting vascular complications in the graft. AVFs in the transplanted organ are rare. Whereas most such fistulas are not significant, persistent fistulas affecting organ function can be treated interventional using metal coils and detachable balloons.

Learning Objectives:

1. To illustrate the advantages and disadvantages of various imaging modalities in the pre- and post-operative work-up of patients undergoing renal and pancreatic transplantation.
2. To provide tips for optimizing the technique of examination.
3. To present the entire spectrum of pre- and post-operative interventional procedures which help improve the long-term results in such patients.

A-187

Lung (heart and lung) (part 1)

A.A. Bankier; Vienna/AT

Since the very introduction of lung transplantation, lung transplant recipients have been the subject of imaging studies. Both conventional chest radiography and CT are widely applied in lung transplant recipients, with each technique having specific advantages and indications. Moreover, recent technical development in CT and the introduction of MR imaging open a window of opportunity for both morphological and functional imaging of lung transplant recipients. Finally, interventional techniques might contribute to the treatment of complications after lung transplantation. This presentation will review the role of imaging techniques in the diagnostic work-up and treatment of patients after lung transplantation and will indicate potential applications of imaging techniques currently under development.

Learning Objectives:

1. To summarize the imaging techniques used in the work-up of patients after lung transplantation.
2. To describe diagnostic and interventional methods in the management of posttransplant complications.
3. To discuss the role of imaging in the short- and long-term follow-up after lung transplantation.

A-188

Lung (heart and lung) (part 2)

M. Estenne; Brussels/BE

Since the first successful lung transplantation two decades ago, the procedure of lung transplantation has gained acceptance as a therapeutic option for a wide spectrum of lung disorders. For patients with a life expectancy limited by severe functional impairment, lung transplantation offers the potential of an improved quality of life and a longer survival. Nonetheless, complications of lung transplantation can occur and often result in constraints on long-term preservation of the graft and on patient survival. This presentation will review the current status of lung transplantation, with particular attention to the clinical indications for transplantation, the selection of patients, and the short- and long-term complications after lung transplantation.

Learning Objectives:

1. To review the clinical indications and the patient selection criteria for lung transplantation.
2. To describe the process of pretransplant evaluation and the techniques of lung transplantation.
3. To summarize common short- and long-term complications after lung transplantation.

16:00 - 17:30

Room H

Physics in Radiology

RC 813

Special issues of radiation exposure in diagnostic radiology

Moderator:

J. Walecki; Warsaw/PL

A-189

A. Minimizing radiation doses to pediatric patients

M. Raissaki; Iraklion/GR

There is considerably greater radiosensitivity of the organs and bone marrow in children, because of rapidly dividing cells. Any radiation dose, small or large, is expected to produce a response and a cumulative effect. Therefore, every effort should be made in the radiation protection area to keep the dose as low as reasonably achievable, trying to retrieve the best possible information when performing indicated, justified diagnostic tests.

Minimizing radiation doses should be a concept applied in a chain of actions, starting from the choice of equipment of the radiology department. Pediatric-oriented protocols, especially with regard to CT-protocols, regular quality assurance tests and continuous training of staff involved are important parts of this chain. Radiation protection rules should be meticulously applied in neonates and children. Justification of requested examinations, vetting of referrals for complex examinations, standardization of techniques and procedures as well as optimization of protection measures are crucial components for ensuring minimization of radiation exposure when imaging children. Special considerations include shielding of gonads, thyroid and lens, appropriate collimation, PA projections in females and grid removal. In addition, short exposure times, immobilization or sedation, entertainment or distracting devices should be applied in order to eliminate patient motion. All departments can benefit from self-audits and re-evaluation of their procedures.

Learning Objectives:

1. To emphasize dedicated clinical and radiological management when minimizing radiation doses to pediatric patients.
2. To stress the importance of multilevel training of all parties involved in the reduction of radiation exposure to pediatric patients.

A-190

B. Topics in radiation protection to be learned by radiologists

K. Perisinakis; Iraklion/GR

The recent advances in computed tomography and complex interventional radiology have lead in an exploding increase in the number of procedures which deliver high radiation doses to patients and staff. The challenge for radiologists is to maximize benefit, whilst minimizing radiation risk to patients and staff. Recommendations of international radiation protection bodies has been increasingly incorporated in national legislation and requires a rigorous approach to protecting patients and staff. In 2005, the International Commission on Radiological Protection plans to adopt a new set of recommendations that should be seen as a consolidation of earlier recommendations. However, radiation protection in medicine is not likely to be improved significantly simply with the addition of more standards. A combined approach by radiation safety professionals and radiologists is required to enhance training in radiation protection in a spirit of mutual benefit. Appropriate training should include awareness of the potential for radiation injury, equipment operational parameters, doses measurement and recording methods and dose reduction techniques.

In this presentation, the philosophy of current radiation protection policy will be illustrated and diagnostic radiology patient and occupational risks will be assessed. Current status and future advances of radiation protection training modules for radiologists will be discussed.

Postgraduate Educational Programme

Learning Objectives:

1. To review current knowledge on radiation induced effects and radiation protection philosophy.
2. To assess the level of radiation protection knowledge required by the radiologist.
3. To evaluate the future training programs for radiologists in radiation protection.

A-191

C. Pregnant employees working in diagnostic radiology

J. Damilakis; Iraklion/GR

The protection of the unborn children of pregnant employees working in diagnostic radiology is very important because the conceptus is particularly sensitive to the effects of X-rays. Efforts should be made to keep occupational radiation exposure of a pregnant worker as low as reasonably achievable. Special rules about radiation dose limits for the conceptus apply after a pregnant employee declares her pregnancy. A publication of the European Commission (EC, Radiation Protection 100, 1998) recommends that the protection of the child to be born shall be comparable with that provided for members of the public. The conditions for the pregnant woman in the context of her employment shall be such that the radiation dose to the conceptus will be unlikely to exceed 1 mSv during the remainder of the pregnancy. Once a pregnant worker declares her pregnancy, a program should be established to calculate and monitor conceptus dose and counsel the pregnant woman. This presentation will provide a methodology for accurate conceptus radiation dose anticipation and determination of the maximum workload allowed for the remaining gestation period for the declared pregnant employee who participates in complex fluoroscopic procedures. It is important that the pregnant worker receives radiation safety counselling and understands the risk to the conceptus from exposure to ionising radiation.

Learning Objectives:

1. To learn dose limits, regulations and recommendations concerning occupational exposure of pregnant women employed in diagnostic radiology.
2. To provide a methodology for establishing a program to calculate and monitor conceptus radiation dose as a result of the occupational exposure of the pregnant worker.
3. To learn the effects that radiation may have on the conceptus.
4. To understand the radiation protection measures that will ensure that the conceptus dose from the mother's occupation is kept as low as practicable.

16:00 - 17:30

Room I

Workshops on Interventional Radiology

WS 818

Pediatric intervention

Moderator:

D.J. Allison; London/UK

A-192

A. Oesophageal interventions in children

D. Roebuck; London/UK

Almost all oesophageal strictures in children are benign. Common causes include congenital and surgical strictures, ingestion of corrosive substances, gastro-oesophageal reflux, achalasia, immunodeficiency and dystrophic epidermolysis bullosa. The natural history, response to treatment and probability of complications all depend strongly on the underlying cause of the stricture. A number of interventional radiology techniques are used in children with oesophageal strictures. This workshop will cover endoluminal ultrasound, balloon dilatation, mitomycin application and temporary stenting. Most strictures can be treated with antegrade balloon dilatation using a simple technique. We perform this procedure under general anaesthetic, although other centres use sedation. Repeat dilatations are often necessary. In some patients this is done electively to allow progressive enlargement of the lumen. In other patients, especially those with corrosive injury or epidermolysis bullosa, repeated procedures are necessary because the stricture tends to recur. Occasionally it is impossible to cross the stricture from above. When this occurs in children who have a gastrostomy, retrograde dilatation is almost always successful. Treatment is considered successful when the interval between dilatations becomes progressively longer. Sometimes this cannot be achieved because of relentless stricture recurrence. In these patients, most of whom have corrosive strictures, mitomycin application and/or tem-

porary stenting can be performed. Clinically significant complications of oesophageal intervention are uncommon, and can usually be treated conservatively. Multidisciplinary teamwork is vital to effective treatment of oesophageal strictures in children, and the opinions and technical input of surgeons, gastroenterologists and radiologists are important. Surgical resection of oesophageal strictures is now rarely necessary.

Learning Objectives:

1. To understand the common disease processes that cause oesophageal strictures in children.
2. To be familiar with the indications for oesophageal dilatation in children.
3. To be able to discuss the anaesthetic management and perioperative care of children undergoing dilatation.
4. To understand the indications for other intervention in children with oesophageal strictures.
5. To be familiar with the results of intervention in children with oesophageal strictures.
6. To be able to treat complications of oesophageal intervention in children.

A-193

B. Treatment of vascular malformations outside the central nervous system

F. Brunelle; Paris/FR

Vascular malformations in children can be classified depending on their biological behaviour, their vascular component and their hemodynamics. Infantile haemangiomas are true vascular tumours made of endothelial cells. Two sub types are described, the classic infantile haemangioma that appears after birth and regresses slowly during the first two years of life and the RICH (rapidly involuting congenital haemangioma), that is diagnosed during pregnancy and rapidly involutes after birth. Except in rare cases with cardiac insufficiency and platelets consumption those angiomas do not need any treatment. Vascular malformations on the other hand are made of lymphatics, veins or arteries. They are called lymphangiomas, venous malformations and arterial dysplasias. True arteriovenous fistulas are rare. Arteriovenous malformations are vascular dysplasias that may involve a segment of a limb or portion of the face. Treatment depends on the macroscopic appearance, hemodynamics and localisation. Sclerotherapy of venous malformations and lymphangiomas is made thanks to injection of alcohol in the lesion. Hemodynamically active lesions can be embolised.

Learning Objectives:

1. To learn the classification of vascular malformations (VM) in children.
2. To understand the therapeutic algorithm.
3. To know the different therapeutic options and their benefit/risk ratio.
4. To learn the natural history of VM.
5. To know how to create a multidisciplinary staff.

A-194

C. Angioplasty and arterial stenting in children

C. McLaren; London/UK

There are several differences between adult and pediatric practice in angioplasty and arterial stenting. Firstly, the underlying disease processes in children are different than those in adults. Fibromuscular dysplasia is far more common than atherosclerosis, which is extremely rare in childhood. Secondly, modifications to angiographic equipment and technique are required because of the smaller size of the patients. For example, children with "mid-aortic syndrome" have a narrow aorta, and renal angioplasty and stenting are technically more difficult than in adults. In very small children the size of the femoral artery may be limiting. Thirdly, management decisions need to take into account future growth of the patient and, in most cases, a very long life expectancy. Angioplasty and stenting may be performed as definitive treatment, or with the intention of delaying surgery until the patient's growth is almost complete. Multidisciplinary teamwork is essential as this allows all treatment options to be considered. In our practice the main indication for angioplasty and stenting is renovascular hypertension. Careful patient selection is required. Children who have poorly controlled blood pressure are considered for diagnostic angiography, which provides the best information about the extent of the disease. In patients with bilateral disease, or with involvement of multiple segmental arteries, renal vein renin sampling can identify which lesion is the principal cause of the hypertension. Angioplasty is usually successful, either by reducing blood pressure on the same antihypertensive medications or by reducing the number of agents required. Stenting may be performed if angioplasty is unsuccessful.

Learning Objectives:

1. To understand the common disease processes that cause arterial abnormalities in children.

Postgraduate Educational Programme

2. To be familiar with the modern imaging modalities available for evaluation of pediatric arterial disease.
3. To be able to discuss the potential indications for angioplasty and stenting in children.
4. To be familiar with the perioperative care required in children undergoing these procedures.
5. To understand the differences between angioplasty and stenting techniques in children and adults.
6. To be able to treat complications of angioplasty and stenting in children.

16:00 - 17:30

Room K

Genitourinary

RC 807

Imaging of stones

Moderator:

G. Jager; 's Hertogenbosch/NL

A-195

A. Plain film, IVU and ultrasound

G. Heinz-Peer; Vienna/AT

Urolithiasis is a common problem in patients presenting to emergency departments. Radiologic imaging has always had a primary role in the work-up of these patients. Traditionally, evaluation consisted of conventional radiography (KUB) followed by intravenous urography (IVU). With the advent of ultrasonography (US) those patients who could not safely undergo IVU could be evaluated for primary or secondary (i.e. hydronephrosis) signs of obstruction. In the past several years, the introduction of unenhanced spiral CT has dramatically changed the role of the various imaging techniques in evaluation of urolithiasis. In the recent literature some authors believe that it is time for IVU to retire after 70 years of good performance. However, daily practice shows that urologists still like those "old" techniques. In addition, many patients have to undergo follow-up examinations for stone treatment. Complete replacement of IVU by CT for stone evaluation would excessively increase radiation dosages applied to patients with a high probability of disease recurrence.

This lecture will review the pros and cons of KUB, IVU, and ultrasound. In addition, aspects of radiation dosage, requirements for further imaging, impact on urological interventions and follow-up examinations, as well as aspects on diagnostic utility and the measured clinical outcome will be addressed.

Learning Objectives:

1. To understand advantages and disadvantages of the various imaging modalities.
2. To recognize the role of functional aspects in obstructive disease.
3. To know how to answer to clinical questions from the urologist.

A-196

B. CT(U) and MRU

C.C.A. Nolte-Ernsting; Hamburg/DE

Unenhanced multislice (MS) CT is considered the gold standard in the diagnosis of urolithiasis, reaching a sensitivity and specificity of nearly 100%. MSCT is able to determine location and exact size of a calculus. The rim-sign and tail-sign help distinguish calculi from phleboliths. Perinephric stranding is well seen on unenhanced images and even the grade of dilation may be assessed without using contrast material. Consequently, unenhanced MSCT provides the primary diagnostic information needed for the treatment of an acute stone colic. Contrast-enhanced MSCT urography using a low-dose scanning protocol may be employed supplementarily to obtain detailed demonstration of the urinary tract anatomy. Stones can be identified within the opacified urine. Exact knowledge of the urinary tract anatomy obtained with MSCT urography may help determine the potential of stone passage after lithotripsy or during endourologic removal. In MR urography (MRU), direct identification of small calcifications is difficult, regardless of whether unenhanced T2-weighted MRU or gadolinium-enhanced T1-weighted excretory MRU is performed. Hence, stones can only be found on MR urograms by identifying filling defects. Initial studies demonstrate that MRU may be as effective as CT in the diagnosis of ureterolithiasis, whereas data concerning the value of MRU in nephrolithiasis are still missing. Apart from its limited value in acute urolithiasis, MRU may be a promising alternative to CT in chronic stone disease in order to provide exact knowledge of the urinary tract anatomy without repeated radiation exposure.

Learning Objectives:

1. To understand CT- and MR-based imaging strategies in urolithiasis.
2. To be able to understand the role of saline, furosemide and contrast material in CT(U) and MRU.
3. To learn the imaging patterns of urolithiasis in CT(U) and MRU.

A-197

C. Radiation issues and economic aspects

F. Stacul; Trieste/IT

Unenhanced helical CT (UHCT) is now considered the gold standard for imaging patients with renal colic. However some disagreements exist on the radiation dose to patients undergoing the procedure and on the cost of the examination. Different CT techniques are used: not surprisingly the X-ray dose calculations in the literature vary to a large extent. The delivered dose can be up to 5 times higher than that delivered by excretory urography. With single-detector helical scanners the dose can be significantly decreased by increasing the pitch; some authors report that the accuracy rate for stone detection is not affected. Multidetector scanners provide an increased radiation dose if CT parameters are unchanged. The dose could be lowered by decreasing the mAs, with individual optimization related to body size or using a geometric X-ray modulation. However there is concern regarding alternate and additional diagnoses that could be missed if the dose is lowered too much.

The cost of a CT procedure in patients with renal colic can be compared with other radiological procedures following a careful analysis of the differential costs of each investigation (equipment, variable costs, personnel) and their common costs. In our environment UHCT has a cost which is 8% lower as compared to IVU.

However multiple variable factors, both for the dose and cost analysis, suggest the data cannot be simply applied to other environments and similar evaluations look worthwhile in other departments.

Learning Objectives:

1. To provide awareness of the X-ray dose delivered by single-detector and multidetector scanners.
2. To become familiar with the methodology of cost analysis.
3. To stimulate assessment of delivered X-ray dose and of financial costs in imaging patients with renal colic.

16:00 - 17:30

Room L/M

Infection in the Adult Today

CC 816

Musculoskeletal infection

Moderator:

K. Verstraete; Gent/BE

A-198

A. Vertebral infection

V. Jevtic; Ljubljana/SI

Vertebral infection represents 2-4% of all cases of osteomyelitis. An increase in the incidence of pyogenic as well as granulomatous spondylitis has been noticed. Early radiological diagnosis is of great importance for prompt treatment and prevention of clinically significant consequences which include neural compromise and late spinal deformities. The most frequent causative pyogenic microorganisms are gram-positive bacteria especially *Staphylococcus aureus*. An important form of non-pyogenic granulomatous infection is tuberculous spondylitis which represents the most common form of extra-pulmonary tuberculosis. The routes of spinal infection include hematogenous spread, post-operative infections, direct implantation during spinal punctures and spread from a contiguous focus. The role of imaging is early diagnosis, evaluation of extent of infection with special regard to potential neural compromise, differential diagnosis, guidance of diagnostic biopsy, planning of eventual operative procedures and assessment of therapeutic response. Imaging modalities include skeletal scintigraphy, plain radiography, computed tomography (CT) and magnetic resonance imaging (MRI). In practice usually a combination of a sensitive and a specific method is utilised. The only imaging modality which combines high sensitivity with satisfactory specificity is MRI. This is the reason that MRI has become the first imaging modality in clinically suspicious spinal infection. MRI is the method of choice for demonstration of direct extension of infection, especially of secondary epidural abscess or phlegmon and consequent neural compression. Using MRI, monitoring of therapeutic efficacy is possible.

Postgraduate Educational Programme

Learning Objectives:

1. To become familiar with the pathoanatomic background of vertebral infection.
2. To understand radiographic, CT and MR signs of spinal infection.
3. To comprehend the importance of Gd-DTPA MRI for early diagnosis, differential diagnosis, planning of therapy and evaluation of therapeutic efficiency in pyogenic and granulomatous spondylitis.

A-199

B. Infection in the appendicular skeleton

K. Bohndorf; Augsburg/DE

In relation to the clinical course, infection in bone can be divided into acute, subacute and chronic osteomyelitis. The diagnosis of acute osteomyelitis is challenging but can be best made by correlating radiography, bone scintigraphy and MR imaging with clinical information. Radiography should routinely be supplemented by sonography in newborns and infants, if applicable. Brodie's abscess, which is clinically a sub-acute form of osteomyelitis, is best diagnosed by the combination of radiography and MR imaging. Chronic osteomyelitis is divided into primary hematogenous forms and exogenous, mostly post-traumatic osteomyelitis. In the majority of patients, post-traumatic osteomyelitis is a clinical diagnosis; however, in a number of patients only the correlation of clinical findings, blood tests and imaging reveals the correct diagnosis. Often, MR imaging and scintigraphic methods, such as scanning with labelled leucocytes, together establish the diagnosis. Chronic recurrent multifocal osteomyelitis may mimic bacterial osteomyelitis but is a distinct disease probably associated with the SAPHO syndrome.

Learning Objectives:

1. To become familiar with the different imaging modalities which are available for diagnosing different forms of osteomyelitis.
2. To discuss the role of MR imaging compared to scintigraphic methods, including PET, to diagnose different forms of osteomyelitis.
3. To discuss the entity CRMO in comparison to bacterial osteomyelitis.
4. To define the criteria how CRMO can be diagnosed by the radiologist.

A-200 ♀

C. Soft tissue infections

D.J. Wilson; Oxford/UK

Soft tissue infection may be acute or chronic. It may involve the subcutaneous tissues (cellulitis) and/or deeper structures including muscle tendon and ligaments. Infections of bones or joints may spread to involve the soft tissues and less commonly soft tissue infection may extend to involve bones and joints.

Radiological appearances

Early, intermediate and late signs will be covered.

Specific infections

The following infection types will be discussed:

- Fungi
- HIV
- Leprosy
- Tuberculosis
- Management

The following topics will be discussed:

- Role in diagnosis, relationship to biopsy
- Role in planning treatment
- Radiological interventional techniques
- Role in monitoring treatment

Septic Arthritis

Acute pain, effusion and limitation of movement are the commonest symptoms of septic arthritis. The possibility of infection must be borne in mind to prevent severe joint destruction occurring without a concurrent strategy to manage the infection.

Radiological signs

Early, intermediate and late signs will be covered with discussion of infection in prosthetic joints.

Learning Objectives:

1. To understand the pathological basis for soft tissue and joint infections.
2. To appreciate how the radiological signs match the pathological stages of infection.
3. To recognise the role of imaging in the management of soft tissue and joint infection.

16:00 - 17:30

Room N/O

Primer: Molecular Imaging

PR 819

MR approaches to molecular imaging

Moderator:

P. Wunderbaldinger; Vienna/AT

A-201

A. Imaging of angiogenesis

A.R. Padhani; Northwood/UK

Several MR imaging techniques can assess the state of microscopic blood flow of tissues. These can be divided into extrinsic (contrast media enhanced) and intrinsic (non-enhanced) methods. The former can be further divided by the type of contrast medium utilized: (i) low molecular weight agents (< 1 kDa) that rapidly diffuse in the extracellular fluid space (ECF agents), (ii) intermediate (MW, 5-30 kDa) and large-molecular agents (MW, > 30 kDa) designed for prolonged intravascular retention (macromolecular contrast media, MMC, or blood pool agents) and (iii) agents intended to accumulate at sites of concentrated angiogenesis mediating molecules. This review concentrates primarily on non-invasive characterisation of human tumour neovasculature with DCE-MR imaging using low-molecular weight contrast agents and explains how perfusion and permeability related data can be extracted depending on the technique utilized. The quantification and potential human applications of MMC MR imaging will also be illustrated. Tumour angiogenesis can also be analysed using intrinsic susceptibility weighted or blood oxygenation level dependent (BOLD) contrast MR imaging. BOLD imaging can be used to monitor the effects of vascular targeting agents in humans and this application of BOLD MR imaging will be discussed. Other MR imaging techniques which provide information on tissue blood flow such as flow-related enhancement and diffusion weighted imaging will not be considered in this review.

Learning Objectives:

1. To demonstrate the differing phenomena of T1- and T2*-weighted DCE-MR imaging with low molecular weight contrast media.
 - 1.a. To explain the physiological processes that determine tissue enhancement.
 - 1.b. To show that DCE-MR imaging is dominated by tissue blood flow in tumours.
 - 1.c. Quantification of DCE-MR imaging and pathological correlates.
2. To illustrate the potential of MR imaging with macromolecular contrast agents.
 - 2.a. To show that microvessel permeability and fractional blood volume is dependent on molecular size.
3. To show that intrinsic susceptibility weighted (BOLD) contrast is sensitive to tissue oxygenation and blood flow.

A-202

B. Imaging of cell migration

M. Höhn; Köln/DE

In order to observe cell mobility in vivo using a noninvasive imaging modality, the cells must be labeled to produce sufficient contrast against the host tissue background. Depending on the chosen imaging technology, different demands on the contrast agent as well as on the labeling strategy must be considered. Selecting magnetic resonance imaging (MRI) as the imaging tool, iron oxide nanoparticles are mostly used to achieve a strong contrast on T2*-weighted images. Incorporation of the label into the cells depends on the route of labeling: i) *in vitro* labeling followed by cell implantation, or ii) *in vivo* labeling by specific injection of the contrast agent in combination with selective uptake by the desired cell population. Care must be taken to ensure that the labeling procedure is efficient enough for satisfactory contrast generation, that it is tolerated by the cells, and that, on the other hand, contrast is not lost upon dilution of the label in the wake of continuing proliferation. Finally, the technical limits of sensitivity and detectability must be considered for the lay-out of a project investigating cell migration in vivo. The learning objective is to understand the potential and limits of the above listed facets of *in vivo* cell labeling and detection using MRI. Consideration regarding application to different examples of (patho-)physiological studies are also discussed.

Learning Objectives:

1. To understand the issues of cell labeling.
2. To understand the issues of cell label efficiency for *in vivo* MRI and toxicity.
3. To understand the methodological aspects of *in vivo* cell detection with MRI.

Postgraduate Educational Programme

Saturday

4. To understand the spatial and temporal resolution requirements to observe cells *in vivo*.
5. To discuss various experimental applications under physiological and pathophysiological conditions.

A-203

C. Targeted MR contrast agents

S.A. Wickline, G.M. Lanza; St. Louis, MO/US

The next generation of pharmaceutical agents will be targeted against specific molecular pathways and/or locales within the body. Our laboratory is engaged in a multidisciplinary effort to develop systemically deliverable ligand-targeted nanoparticles for noninvasive *in vivo* image-based detection of picomolar quantities of pathological epitopes that are the sources of cancer and cardiovascular disease. We have devised strategies for the delivery of drugs or genes to those sites with the use of targeted nanoparticle carriers that can incorporate various classes of ligands (e.g., antibodies, small molecules) and selected drugs active against cancer and atherosclerosis and thrombosis. These particles also can be imaged *in vivo* with MR imaging, nuclear, CT, or ultrasound methods based on incorporation of payloads of gadolinium chelates, radionuclides, iodinated compounds, or perfluorocarbon content respectively. Drugs such as doxorubicin, paclitaxel, fumagillin can be incorporated and delivered selectively to individual cells of choice through a novel process of "contact facilitated drug delivery", which is proving to dramatically enhance tumor lysis and plaque regression.

Learning Objectives:

1. To understand the potential clinical applications of molecular imaging for early diagnosis of cardiovascular disease and cancer.
2. To understand the comparative advantages and limitations of molecular MR-imaging as a component of various imaging technologies such as nuclear, optical, ultrasound, etc.
3. To understand the role of nanotechnology in molecular MR-imaging and targeted drug delivery.

16:00 - 17:30

La Scala

E³ - European Excellence in Education

E³ 820

Interactive image teaching

Moderator:

J. Cáceres; Barcelona/ES

A-204

Mediastinal masses

J. Cáceres¹, J. Vilar²; ¹Barcelona/ES, ²Valencia/ES

The study of the mediastinum is performed with cross-sectional imaging (CT or MRI), due to the lack of contrast among the different mediastinal structures in conventional radiography. Nevertheless, the PA and lateral chest radiograph may be very useful as the initial examination to detect mediastinal masses and to suggest the next procedure to perform.

The study of the mediastinum starts with a thorough knowledge of the radiographic anatomy and most common variants. Differentiation of pulmonary from mediastinal masses is easily made by knowing basic semiology (pregnancy sign). To facilitate the differential diagnosis among different pathologies it is convenient to divide the mediastinum into different areas (thoracic outlet, anterior middle and posterior, including supra and infravascular compartments). The radiographic appearance and location of masses on cross-sectional imaging will contribute to narrowing the differential diagnosis.

Learning Objectives:

1. To review the anatomy and normal variants of the mediastinum.
2. To describe the signs that allow recognition of mediastinal masses and their differential diagnosis.
3. To emphasize that fat and vascular structures are not uncommon causes of mediastinal masses.

Postgraduate Educational Programme



Sunday, March 6

Postgraduate Educational Programme

		room A 2nd level	room B 2nd level	room C 2nd level	room E1 entr. level	room E2 entr. level	room F1 entr. level	room F2 entr. level	room G lower level	room H lower level		
07:00											07:00	
07:30											07:30	
08:00											08:00	
08:30		CC 917 Essentials of Neuroradiology Three common neurological problems: Loss of vision, hearing loss, trigeminal and facial nerve palsy (p. 64)	RC 910 Musculoskeletal Wrist (p. 64)	SF 9a Special Focus Session Radiology of the elderly (p. 65)	RC 902 Breast Diagnostic highlights (p. 66)	RC 901 Abdominal and Gastrointestinal Impact of multislice CT on imaging of the upper abdomen (p. 67)	ER 926 Joint ECR/EAR sessions: Challenges for European Radiology European research network in biomedical imaging (p. 67)	RC 911 Neuro Radiological vascular interventions (p. 68)	SF 9b Special Focus Session PACS pitfalls (p. 69)	RC 909 Interventional Radiology Endovascular treatment of lower limb vascular occlusion (p. 70)		08:30
09:00											09:00	
09:30											09:30	
10:00											10:00	
10:30		EM 2 “ECR meets” Hungary The present and future of Hungarian radiology: Contribution of a new generation (p. 73)	NH 10 New Horizons Session Drug-eluting stents (p. 75)	SS 1010 Musculoskeletal Tumor imaging (p. 238)	SY 9 Satellite Symposium MDCT imaging: New challenges for scan and contrast optimisation (p. 584)	SS 1004 Chest CT and MR imaging of the pulmonary vessels and right heart (p. 239)	SY 10 Satellite Symposium Contrast-induced nephropathy (p. 586)	SS 1001 Abdominal Viscera Pancreas: MR imaging evaluation of pancreatic duct and pancreatic cystic lesions (p. 242)	SS 1007 Genitourinary MR imaging of the prostate (p. 244)	SS 1009a Interventional Radiology Hepatic interventions (p. 246)		10:30
11:00											11:00	
11:30											11:30	
12:00											12:00	
12:30											12:30	
13:00											13:00	
13:30											13:30	
14:00											14:00	
14:30											14:30	
15:00											15:00	
15:30											15:30	
16:00											16:00	
16:30		CC 1217 Essentials of Neuroradiology Base of the skull, hypophysis, supra- and parasellar region (p. 77)	SA 12 State-of-the-Art Symposium Multi-dimensional imaging for guiding therapy (p. 78)	SF 12 Special Focus Session Assessment of myocardial perfusion and viability (p. 79)	RC 1203 Cardiac Pericardial diseases (p. 79)	SY 12 Satellite Symposium Advances in head and neck imaging using CT and MR (p. 586)	RC 1204 Chest Multislice CT of the thorax (p. 80)	RC 1211 Neuro Diffusion and perfusion MR imaging of the brain (p. 81)	RC 1213 Physics in Radiology Safety considerations in MR (p. 81)	WS 1209 Interventional Radiology Aortic stent grafts (p. 82)		16:30
17:00	registration										17:00	
17:30	EPOS™ - scientific exhibition										17:30	
18:00											18:00	
18:30											18:30	
19:00											19:00	

Postgraduate Educational Programme

	room I lower level	room K lower level	room L/M 1st level	room N/O 1st level	room P lower level	room W basement	room X 1st level	room Y 1st level	room Z entr. level	La Scala 2nd level	
07:00											07:00
07:30											07:30
08:00											08:00
08:30											08:30
09:00	WS 918 Workshops on Interventional Radiology Urological intervention (p. 70)	RC 912 Pediatric Neuro-imaging (p. 71)	CC 916 Infection in the Adult Today Modern imaging of infective disease in the face and pelvis (p. 72)	RC 913 Physics in Radiology Medical image registration: Methods, applications and validation (p. 72)	WS 921 Musculo- skeletal US "Hands-on" Workshop					WS 924 Basic Life Support for Radiologists "Hands-on" Workshop	E ³ 920 Foundation Course: Chest Radiology Nodules and neoplasms (p. 73)
09:30											09:30
10:00											10:00
10:30											10:30
11:00	SS 1009b Interventional Radiology Carotid stenting (p. 248)	SS 1003 Cardiac MDCT in ischemic cardiomyopathy and myocardial infarction (p. 250)	SS 1011 Neuro Brain tumor evaluation with diffusion and perfusion MR imaging (p. 252)	SS 1013 Physics in Radiology Digital radiography/ Digital mammography (p. 254)	SS 1015 Vascular Imaging of stenosis, aneurysm and dissection in the abdominal vessels (p. 256)	WS 1022 Vertebralplasty "Hands-on" Workshop	WS 1021 Musculo- skeletal US "Hands-on" Workshop	WS 23C2 Screening Mammography Interpretation Test "Hands-on" Workshop		WS 1024 Basic Life Support for Radiologists "Hands-on" Workshop	E ³ 1020 Errors in radiology (p. 76)
11:30											11:30
12:00											12:00
12:30											12:30
13:00											13:00
13:30											13:30
14:00											14:00
14:30											14:30
15:00											15:00
15:30											15:30
16:00											16:00
16:30	RC 1215 Vascular Vascular imaging (p. 83)	RC 1212 Pediatric Chest imaging (p. 84)	RC 1214 Radiographers Pediatrics/ Radiography (p. 84)	PR 1219 Primer: Molecular Imaging Imaging of gene expression: Optical and nuclear techniques (p. 85)	RC 1205 Computer Applications Building an electronic patient record system (p. 86)					E ³ 1220 Foundation Course: Chest Radiology Wrapping it up ... (p. 87)	16:30
17:00											17:00
17:30											17:30
18:00											18:00
18:30											18:30
19:00											19:00

Postgraduate Educational Programme

08:30 - 10:00

Room A

Essentials of Neuroradiology

CC 917

Three common neurological problems: Loss of vision, hearing loss, trigeminal and facial nerve palsy

Moderator:
G. Hur; Koyang-city/KR

A-205

A. Loss of vision: Imaging the visual pathways

H. Jäger; London/UK

Lesions affecting specific parts of the visual pathways have characteristic clinical manifestations. Radiological investigations should be tailored according to the type of visual defect, using different techniques for the examination of the orbits, sellar region, white matter tracts and occipital cortex. The type of pathology encountered depends on the location and the patient's age. Amongst tumours of the globe retinoblastomas are common in children and melanoma metastases are common in adults. The most frequent tumours of the optic nerve sheath/ complex are gliomas in children and meningiomas in adults. Other conditions involving the optic nerve/sheath complex include demyelination, orbital pseudotumour, sarcoidosis. Chiasmal lesions produce characteristically bitemporal hemianopia. Extrinsic compression of the optic chiasm may be due to pituitary tumours or giant aneurysms in adults, and craniopharyngiomas in children. Intrinsic chiasmal lesions include gliomas and granulomatous lesions. Lesions involving the optic radiation are most frequently infarcts, demyelination or tumours but other entities such as progressive multifocal leukoencephalopathy (PML) and posterior/reversible leuko encephalopathy syndrome (PRES) must also be considered. Lesions in the primary visual (striate) cortex produce homonymous hemianopia and infarcts and tumours are the commonest pathology in this region. Selective involvement of extra striate visual cortex can lead to inability to perceive movement or to recognize colours.

On the whole MR imaging is superior to CT for the assessment of visual pathways. CT is however the first line modality in orbital trauma and may be helpful to identify tumour calcification in optic nerve sheath meningiomas and craniopharyngiomas.

Learning Objectives:

1. To learn the anatomy of the visual pathways.
2. To acquire knowledge of the type of visual defects associated with lesions at specific sites of the visual pathways.
3. To become familiar with CT and MR techniques for examination of the orbits, sellar region, optic tracts and radiation and visual cortex.
4. To be able to provide a differential diagnosis for lesions of the visual pathways based on location, patient's age and imaging appearances.

A-206

B. Sensorineural hearing loss

F. Veillon; Strasbourg/FR

The aim of this lecture is to understand how to perform imaging and its results when exploring a sensorineural hearing loss.

CT is necessary for evaluating the oval and round windows and the inner ear (shape, size and bony structures). MR imaging is important for analyzing the fluid and membranous content of the labyrinth; the shape, size and structure of the VIII, VII, mixed nerves in the internal auditory meatus (IAM); the cerebello-pontine angle (CPA), the appearance of the brainstem and the cochlear pathways in the brain. Trauma may lead to injury of the oval and round windows with or without fractures (which are well documented with CT). Post operative complications in otosclerosis such as too long a prosthesis or intravestibular granuloma are studied with both CT and MR. CT and MR also used for the detection of bacterial, viral and autoimmune labyrinthitis and hemorrhage. Intralabyrinthine neurinomas are detected as solid masses with gadolinium enhancement. Malformations of the inner ear may be separated into minor and major lesions. Vestibular schwannomas must be considered but also meningioma, hamartoma, epidermoid cyst, lipoma, vascular malformation, metastases, lymphomas, meningitis, siderosis, in the IAM and/or CPA. Central brain lesions are presented in MR imaging; ischemia, hemorrhage, multiple sclerosis and tumors.

Learning Objectives:

1. To understand the method and results allowing to evaluate a sensorineural hearing loss with CT and MR imaging.

2. To know the indications of imaging (CT and/or MRI) in the evaluation of sensorineural hearing loss.

3. To learn the different signs in imaging allowing to know the etiology of sensorineural hearing loss and the consequences about the treatment.

A-207

C. Facial nerve paralysis and trigeminal neuralgia

A. Borges; Lisbon/PT

The trigeminal nerve is the largest of the cranial nerves. It provides sensory input from the face and motor innervation to the muscles of mastication. The facial nerve is the cranial nerve with the longest extracranial course and its main functions include motor innervation to the muscles of facial expression, sensory control of lacrimation and salivation, control of the stapedial reflex and to carry taste sensation from the anterior two thirds of the tongue. In order to be able to adequately image and follow the course of these cranial nerves and its main branches a detailed knowledge of neuroanatomy is required. As we are dealing with very small anatomic structures high resolution dedicated imaging studies are required to pick up normal and pathological nerves. Whereas CT is best suited to demonstrate bony neurovascular foramina and canals, MR imaging is preferred to directly visualize the nerve. It is also the single technique able to detect pathological processes afflicting the nerve without causing considerable expansion such as is usually the case in certain inflammatory/infectious conditions, perineural spread of malignancies and in very small intrinsic tumours. Because a long course from the brainstem nuclei to the peripheral branches is seen, it is useful to subdivide the nerve in several segments and then tailor the imaging modality and the imaging study to that specific segment. This is particularly true in cases where clinical topographic diagnosis can be used to locate a lesion in the course of these nerves.

Learning Objectives:

1. To become familiar with the anatomy and main functions of the trigeminal and facial nerves.
2. To become aware of the current imaging potential to visualize normal and pathologic trigeminal and facial nerves.
3. To be able to tailor the imaging approach in patients presenting with trigeminal and facial nerve dysfunction.
4. To understand the advantages and limitations of a topographic approach to trigeminal and facial nerve lesions.

08:30 - 10:00

Room B

Musculoskeletal

RC 910

Wrist

Moderator:
M. Padrón; Madrid/ES

A-208

A. Plain films revisited with MSCT and MR imaging

A. Blum; Nancy/FR

CT-arthrography and Magnetic Resonance Imaging are the most efficient techniques to evaluate the wrist; however, standard radiography remains a valuable method to explore this region. In most situations, it is sufficient to allow a precise diagnosis and determine therapeutic protocols. However, this method can present a real diagnostic value only when it is guided by a relevant medical history and clinical details. The purpose of this presentation is to propose a practical approach for radiographic evaluation of the wrist, suited to the main clinical scenarios. CT and MR imaging correlations will help to understand radiographic findings.

Learning Objectives:

1. To learn how to suit radiographs to the different clinical situations.
2. To know how to perform the most pertinent stress views.
3. To learn how to base the diagnostic strategy on clinical and plain films findings.

A-209

B. MR imaging and US of chronic pain

M. Zanetti; Zürich/CH

Optimal Magnetic Resonance (MR) imaging of the wrist requires a high field strength magnet and a dedicated wrist coil to achieve high-resolution images. Using current MR sequences, detailed images of articular cartilage and the sup-

Postgraduate Educational Programme

porting ligaments and tendons can be obtained. Evaluation of the triangular fibrocartilage as well as the intrinsic ligaments of the wrist is substantially improved by direct MR-arthrography. Fast inversion recovery sequences or T2 weighted sequences with fat suppression allow for detection of osteonecrosis and fractures, which are often radiographically occult. MR imaging also provides valuable information in the evaluation of tendons and synovium in rheumatoid arthritis. Normal variants (e.g. lunate II, carpal boss), pitfalls (e.g. pseudo-DISI), and findings with a high prevalence in the asymptomatic population (e.g. TFC lesion, intercarpal ligament lesion) have to be considered in the evaluation of chronic wrist pain.

With the advent of new technical improvements (high frequency probes up to 15 MHz), ultrasound is gaining acceptance as a useful modality to diagnose a variety of diseases involving the wrist. Ultrasound offers benefits in the evaluation of tendon inflammation and rupture, evaluation of palpable masses or suspected occult masses, and evaluation of suspected foreign bodies.

Learning Objectives:

1. To know the appropriate imaging technique of standard MR imaging, MR arthrography and ultrasound for triangular fibrocartilage lesions, ligament and tendon lesions, occult osseous lesions and soft tissue masses.
2. To know the diagnostic potential of standard MR imaging, MR arthrography and ultrasound for such lesions.
3. To know the differential indications for MR imaging and ultrasound in patients with chronic wrist pain.

A-210

C. Dynamic studies: MR and US clinical applications

M. Mastantuono; Rome/IT

Dynamic imaging is a mandatory step after static and morphologic assessment for the evaluation of wrist and hand. Ahead of other imaging modalities, US offers the capability of real-time depiction: continuity, position (transient dislocation) and normal sliding of the structures (stenosing tenosynovitis) are evaluated in time to assess the normal functions of tendons and muscle fibres. Kinematic MR imaging improves the diagnostic capabilities of MR imaging by allowing for the detection of dynamic instability patterns, transitory subluxation, and bony or soft tissue impingement syndromes. Dynamic MR imaging studies may passively and actively test the joint. Active movement generally provides a more physiological examination of the joint, but some techniques, like incremental passive Kinematic MR imaging, allows one to describe carpal motion and dynamic instability by using sagittal images that are acquired during progressive movement from radial to ulnar deviation. This representation is easy and directly related to the columnar concept on which the most widely accepted models for carpal instability are based. Kinematic studies performed with US and MR imaging allow one to assess pathologic conditions that are not apparent with conventional studies. They also permit an easier analysis of the radio-carpal and intra-carpal biomechanics.

Learning Objectives:

1. To choose the most suitable kinematic MR imaging protocols.
2. To review basic principles in interpreting dynamic studies (stable and unstable equilibrium in the wrist).
3. To identify the diagnostic possibility of dynamic studies in clinical applications.
4. To identify the diagnostic possibility of dynamic ultrasound studies (comparison between MR imaging and ultrasound finding).

08:30 - 10:00

Room C

Special Focus Session

SF 9a

Radiology of the elderly

Moderator:

J. Cáceres; Barcelona/ES

A-211

Radiology of the elderly (Introduction)

J. Cáceres; Barcelona/ES

In developed countries, the expected life span is 74-76 years for men and 79-82 years for women. This aging population poses new challenges for receiving medical care. The elderly behave differently to their younger counterparts. They react differently to external insults, are more prone to fractures and infection and are prey to neurological disease, such as dementia and depression. From a radiolog-

ical standpoint, handling elderly patients creates problems of logistics and interpretation that have to be addressed by the radiology department.

Learning Objectives:

1. To assess imaging changes associated with dementia in the elderly patient.
2. To evaluate the causes and differential diagnosis of dyspnea in the elderly.
3. To present an evaluation of abdominal pain in patients of advanced age.

A-212

Aging and dementia

F. Barkhof; Amsterdam/NL

When should imaging be performed?

Every patient suspected of dementia should undergo imaging at least once during the work-up. While CT may exclude surgically treatable cases (e.g. tumour, subdural haematoma), MR imaging is superior in identifying disease specific changes, such as medial temporal lobe atrophy (MTA).

A practical MR imaging protocol

To assess the pattern of atrophy, including MTA, coronal images are indispensable. Visual rating scales are available that have good predictive value. The presence of vascular pathology (infarcts, lacunes, white matter lesions, and micro-bleeds) can be assessed using T2/FLAIR and T2*-GE.

When should non-conventional techniques be considered?

Gadolinium-enhancement and DWI can be used to assess the possibility of vasculitis. Perfusion-weighted MR may reveal altered metabolism before the development of atrophy, and obviate the need for SPECT/PET studies in suspected Alzheimer's disease or fronto-temporal dementia (FTD).

Take-home messages:

- a normal hippocampus rules out Alzheimer's disease
- MTA can be indicative of AD, but does not rule out other dementias
- isolated atrophy of the temporal pole is diagnostic of FTD
- vascular pathology also occurs in AD
- small strategic infarcts (e.g. thalamic) may cause vascular dementia
- in dementia with Lewy bodies there are often hardly any abnormalities

Learning Objectives:

1. To understand normal ageing phenomena in the brain.
2. To design a robust MR imaging protocol for the evaluation of dementia patients.
3. To understand the importance of hippocampal atrophy for Alzheimer's disease.
4. To establish a diagnosis of vascular dementia

A-213

Dyspnea

J. Andreu; Barcelona/ES

Dyspnea is one of the main reasons for emergency room admission in the elderly population. The major causes of dyspnea are respiratory and cardiologic processes, but other diseases, such as abdominal and metabolic conditions have to be included in the differential diagnosis. This talk will center on the value of imaging techniques for the diagnosis and follow-up of patients with chest processes whose main presenting feature is dyspnea.

The first section will deal with common age-related limitations of the patients which can affect the quality of the technique, and the typical radiological changes seen in aging.

Following this, the most frequently encountered entities causing dyspnea in the elderly will be reviewed. Special focus will be placed on pneumonia, COPD, thromboembolism, and heart disease. The diagnostic value of the radiological features seen in each of these groups will be discussed and a practical diagnostic algorithm provided.

Chest radiology is underutilized in the elderly, but is essential for prompt diagnosis of the cause of dyspnea. The chest radiograph is still the mainstay technique for this purpose, although CT provides highly useful information in specific conditions.

Learning Objectives:

1. To present age-related features commonly seen on chest imaging in the elderly.
2. To establish a practical radiological approach to dyspnea.
3. To review the most common causes and radiological presentation of dyspnea in geriatric patients.

Postgraduate Educational Programme

A-214

Abdominal pain

W. Curati-Alasonatti; Stanmore/UK

Abdominal pain in the elderly is a symptom developing on a clinical background of aging. Aging reduces our immunity and our faculty to respond to aggression by inflammatory processes.

1. The incidence of the majority of cancers increases with age.
2. The number of cases of Multiple Malignant Tumours (MMT) increases up to the age of 90.
3. Severe inflammatory conditions may not present with significant symptoms in the elderly.

We shall present and discuss briefly at the Conference the cases of six elderly patients having presented with abdominal pain with various clinical conditions in order to illustrate the reasoning from the clinical/diagnostic problem to the result obtained.

The application of MDCT in the elderly allows for rapid and non-invasive assessment of patency (or not) of mesenteric arteries and veins, thus replacing conventional angiography. Angiography with the intention to perform an interventional procedure remains as a specific modality.

As we will illustrate in the case presentation, we are liberal with the use of MDCT in the elderly for the following reasons:

- MDCT provides a fast diagnosis or the facility to perform immediate biopsies.
- MDCT gives a complete overview of the abdomen.
- MDCT reveals all coincidental pathologies.
- MDCT is well tolerated (contrast agents limitations apply).
- MDCT is a modality of choice for teleradiology/specialist advice.
- MDCT radiation dose is relatively less significant in the elderly and,
- MDCT 2D or 3D images provide fascinating insights of the human anatomy.

Learning Objectives:

1. To comprehend the basic differences between abdominal pathologies in the adult and in the elderly.
2. To understand the principles underlying the various algorithms used in the elderly.
3. To become familiar with the arguments supporting the modality of choice.

08:30 - 10:00

Room E1

Breast

RC 902

Diagnostic highlights

Moderator:

G. Svane; Stockholm/SE

A-215

A. Increased lifetime risk

I. Saarenmaa, T. Salminen; Tampere/FI

Basic life time risk of breast cancer in women in developed countries is 4% to 6%. Most breast cancers (between 65% and 80%) occur as sporadic malignancy among women without any elevated risk. The risk increases with age. Prolonged exposure to endogenous hormones increases the risk: Early menarche and late menopause, nulliparity, late first full-term pregnancy and lack of breast feeding. The breast cancer risk is elevated in women who have a first degree relative (mother, sister or daughter) with breast cancer. Inherited mutations of BRCA1 and BRCA2 genes account for a very high relative risk of breast cancer. However, only 5% of all cancers are considered to have genetic background. 10% to 20% of breast cancers are DCIS, which carries a 30% chance of developing into invasive disease. LCIS is considered not to be a precursor lesion, but it is associated with an increased risk. Some biopsy proven benign proliferative changes, in particular ADH or ALH, increase breast cancer risk. Ionizing radiation, for instance treatment for Hodgkin's disease, increases risk. Increased weight in menopause, western diet, alcohol, dense breast parenchyma, HRT and oral contraceptives are considered to have weak association to increased risk. Risk factors increase total average risk to 11%.

The risk of secondary cancer in the same (10%-35%) or in contralateral breast (1% to 15%) depends on the size, histological type and grade of the tumour, completeness of tumour removal and postoperative therapy.

Learning Objectives:

1. To introduce the increased lifetime risk factors.

2. To discuss some specific situations: Contralateral breast cancer, local recurrence, age.
3. To propose increased risk groups and best imaging modality for selected screening projects.

A-216

B. HRT and other hormone risk markers

M.G. Wallis; Coventry/UK

The major risk factor for developing breast cancer is "oestrogen". This is affected by reproductive history and exogenous hormones (oral contraceptive pill and HRT). Additionally obesity and alcohol affect oestrogen metabolism and cellular sensitivity. HRT usage in the western population has become endemic (20 to 50% of women 47-70 years of age). Oestrogen/progestogen combinations (to protect the endometrium) have superseded earlier oestrogen only preparations. More recently synthetic oestrogen (Tibolone) has been introduced.

It has been known for a long time that current HRT usage is associated with increased risk of breast cancer. But the media were sent in to overdrive by WHI study (USA) and the Million Women Study (UK). The later implicates all preparations but combined oestrogen progestogen cause 4 times as many extra cancers as oestrogen on its own. In the UK current users are 66% more likely to develop breast cancer and 22% more likely to die from breast cancer than never users. The effect on incidence increases with increasing duration of use and wears off with in a few years of stopping therapy. Additionally HRT decreases both the specificity of screening mammography (i.e. increases recall rates) and reduces its sensitivity (i.e. increases interval cancer rates). How much of this is directly related to mammographic background density remains controversial.

Increasing affluence is associated with many benefits but at what risk? All these risks are amenable to change but the choices, evidence and explanations are not necessarily straightforward.

Learning Objectives:

1. To learn about the state-of-the-art of HRT.
2. To understand the effects of HRT on the breast and imaging accuracy.
3. To understand the potentials of life style (including cultural) change on breast cancer risk.

A-217

C. Physician-patient relationship

R. Chersevani; Gorizia/IT

Radiologist-breast patient relationship may differ from that of other physician-patient situations as it is not continuous, but sometimes rather brief, or with no real meeting among the two actors. There usually is no choice on behalf of the patient; imaging production is considered a technical and rather automatic procedure - depending mostly on "machines"; the perception or misperception is that diagnosis will always be achieved as the sensitivity of imaging techniques is always 100%.

We are surely responsible for some of these issues as we have pushed women to early diagnosis indicating our best results and not the drawbacks.

Patients want to trust their doctors, but in order to achieve this they need information. Women coming for breast diagnosis differ not only as far as being symptomatic or not, but also for age, health literacy, level of anxiety and fear, and previous experiences with illness.

There must be time for dialogue: To communicate results, to explain our diagnostic workup, obtain informed consent, explain causes of false diagnosis and show care and empathy in case of "bad news".

This will not avoid the invitations women receive from the media and the web for a review of their results, nor will it change the very easy to apply hindsight analysis - no matter the bias - or pure mathematical concepts on cancer doubling time. A correct approach requires dignity, respect, understanding and caring, for the patient and her needs, and it may not necessarily be a one-way relationship.

Learning Objectives:

1. To discuss causes and rate of litigation and troubles affecting physician-patient relationship.
2. To discuss practicing breast imaging within the margins of human error.
3. To propose effective methods to increase relationships.

Postgraduate Educational Programme

08:30 - 10:00

Room E2

Abdominal and Gastrointestinal

RC 901

Impact of multislice CT on imaging of the upper abdomen

Moderator:

C. Bremer; Münster/DE

A-218

A. Technical advances

M. Prokop; Utrecht/NL

Multislice CT has been one of the most rapidly developing techniques in the history of radiology. Since the late 1980s, performance of scanners has doubled every two years. The newest developments include 32- to 64-slice scanners that can reduce acquisition time to well below 10 s for all body applications except the heart. In the abdomen, the better spatial resolution of multislice CT has improved the evaluation of vascular structures, biliary and pancreatic ducts, the stomach and bowel, and the genitourinary system. The faster acquisition times of multislice CT have made it possible to improve arterial phase imaging of the liver and pancreas. This course will provide the technological background to understand the differences between present 4- to 64-slice systems, will evaluate the effect of various acquisition parameters on image quality and radiation dose, and will discuss how to optimize intravenous contrast administration for the abdomen. New clinical opportunities and pitfalls for interpretation will be discussed.

Learning Objectives:

1. To become familiar with the systems of multislice computed tomography.
2. To comprehend the effects of different acquisition parameters on image quality.
3. To understand the impact of multislice computed tomography on performance parameters and clinical applications.

A-219

B. Bile ducts and pancreatic ducts

C.D. Becker; Geneva/CH

In daily clinical practice computed tomography (CT) retains an important role in diagnostic imaging of biliary and pancreatic disorders. Clinical findings are often unspecific and access to MR cholangio-pancreatography is limited in many institutions, especially in the emergency setting. With the advent of multislice CT with its improved resolution and reconstruction capabilities, it appears interesting to reappraise the respective role of CT and MR imaging and to define the situations in which MR imaging is clearly superior and those in which CT may be sufficient. MR cholangio-pancreatography (MRCP) is the most reliable noninvasive technique for choledocholithiasis, and the current literature provides no evidence that multidetector CT could replace it for this indication. MRCP also appears superior in the context of benign stenoses, cystic disorders and hilar cholangiocarcinoma. On the other hand, contrast - enhanced MSCT with 2D and 3D reconstructions can often provide sufficient information with regard to resectability and palliative treatment in malignant extrahepatic bile duct obstruction, including pancreatic cancer. In the context of acute and chronic pancreatitis MSCT has some advantages over MRCP because of its excellent sensitivity for detecting and localizing parenchymal and ductal calcifications.

Learning Objectives:

1. To learn about MDCT imaging protocols optimized for imaging of the pancreas and biliary ducts.
2. To learn about the usefulness of curved planar reconstructions for visualization of biliary and pancreatic abnormalities, especially for demonstration purposes.

A-220

C. Liver

C. Catalano; Rome/IT

Multidetector-row technology has completely changed the approach with computed tomography to imaging of the upper abdomen and particularly of the liver. Several technical innovations are reflected in clear advantages in the current clinical practice of liver imaging. The use of thin collimation allows us to routinely achieve high resolution studies with the possibility to visualize the liver in multiple planes, similar to that performed with magnetic resonance, using at the same time the 3D data set to perform vascular and biliary reconstructions. Further-

more, the fast acquisition allows us to scan the liver in pure vascular phases making it possible to detect significantly more lesions or diseases and increasing significantly the sensitivity. Importance of each vascular phase after contrast agent administration will be reviewed and discussed. At the same time, improvements in post-processing allows us to exactly determine anatomy, each liver segment volume, weight, arterial, portal and systemic venous vascularization and so providing important information for advanced resection, percutaneous treatment and transplantation.

Different acquisition protocols can be used and will be reviewed keeping in mind X-ray exposure to the patient. Protocols for contrast agent administration will also be examined with attention to volume, flow rate and iodine concentration.

Learning Objectives:

1. To understand the basic principles of MDCT for liver imaging.
2. To recognize the different phases of liver enhancement.
3. To become familiar with contrast injection protocols for MDCT.
4. To learn possible new clinical applications of MDCT.

08:30 - 10:00

Room F1

Joint ECR/EAR sessions: Challenges for European Radiology

ER 926

European research network in biomedical imaging

Moderator:

G.P. Krestin; Rotterdam/NL

A-221

Fundamental biomedical imaging research in Europe

D. Le Bihan; Orsay/FR

Biomedical imaging research is becoming a major issue for European health care, especially in light of soaring care costs and population aging. Furthermore, there is a need for a European basic research and technology space to fuel the European biomedical industry. This lecture will examine the different kinds of interfaces possible between basic research and radiology, based on existing examples within Europe. Obstacles and difficulties for radiologists to engage in basic research activities will be analyzed and discussed. Finally, proposals will be made to enhance biomedical imaging research in Europe, both in terms of human resources and infrastructures.

Learning Objectives:

1. To discuss possibilities and problems for radiologists to engage in biomedical imaging research in Europe.
2. To present solutions to improve the contribution of radiologists to European biomedical research.

A-222

Role of industry in sustaining European biomedical imaging research

E.R. Reinhardt; Erlangen/DE

Many innovative modalities and systems for radiology, for example CT and MR imaging, have emerged in the past few decades. These technologies have fundamentally changed medical diagnostics and have helped increase the quality of healthcare and reduce its cost. Research in European industry has played an important role in identifying and developing such technologies.

The potential for innovation in diagnostic and therapeutic technologies to continue to improve healthcare efficiency is tremendous. The field of molecular medicine is especially promising. In-vitro molecular diagnosis will be decisive for determining pre-disposition to diseases and early detection. Molecular medicine will result in more individualized therapies, making them much more effective. Information technology is crucial to leverage the benefits of molecular medicine: the integration of medical data, including information from genomics and proteomics studies, in data-warehouses with application of data-mining technologies will be essential in enabling knowledge-driven healthcare. This will also enable efficient clinical studies and therefore, translation of biomedical research results into clinical practice.

In order to realize the potential to improve healthcare efficiency, close cooperation among healthcare participants is necessary. A global network of innovation is key: it helps in defining priorities, stimulating ideas and spin-offs, shaping healthcare systems, building common knowledge databases, and attracting the most innovative and creative minds. It is important therefore, for industry to drive such innovation networks. It is also important for industry to closely partner with clinicians and scientists in the earliest phases of its R&D activities; innovation must be driven by market needs.

Postgraduate Educational Programme

Learning Objectives:

1. To highlight the input of industry to biomedical imaging research in Europe.
2. To show the key role molecular medicine will play in improving healthcare efficiency and the importance of information technology in leveraging its benefits.
3. To show the importance of close cooperation among healthcare participants - e.g. providers, academic and research centers, and industry - through a global network of innovation.

A-223

Structuring the European research area: Possibilities for biomedical research in Europe

H. Pero; Brussels/BE

The EU (and the world) is confronted with new challenges resulting from globalisation and the new "knowledge-based economy". The IT revolution has produced a fundamental change in society and knowledge is increasingly being codified and transmitted through computer and communication networks. At the same time, innovation concepts are being challenged in an unprecedented way. It is not simply a question of a tremendous increase of scientific principles to technology and the production of goods and services in general. Knowledge and skills become central issues within the economic framework. In short, there is an urgent need to capture the benefits of the new "knowledge based economies", economies which are more strongly dependent on the production, distribution and use of knowledge than ever before.

The European Research Area and its Research Infrastructures are clearly at the basis of knowledge creation, knowledge transmission, knowledge exchanges and knowledge preservation. They are also very much linked to the industrial and health related world. They offer tools and services for the development of leading-edge research, both of basic and applied character, in particular in the field of biomedical imaging. They are therefore core elements in the implementation of the Lisbon agenda. Since research infrastructures are mainly nationally-based, their development requires however more coordination efforts across Member states. In this context, the Open Method of Coordination is increasingly being used for the development of coordinated European Roadmaps.

Learning Objectives:

1. To learn about the Community research actions.
2. To reflect on European research challenges.
3. To be stimulated to participate in future European initiatives.

A-224

Towards an European institute of biomedical imaging research

G.P. Krestin; Rotterdam/NL

Since 2002 the Executive Bureau of EAR has decided to put biomedical imaging high on its agenda. Following the report of an ad hoc Committee on Research delivered during ECR 2004 a Standing Committee for Research has been created. The mission of this Committee on Research of EAR is to create an environment and infra-structure that promotes biomedical imaging research in Europe. Specific aims include:

- building of a biomedical imaging research network throughout Europe,
- encouraging excellence in basic and clinical imaging research,
- creating opportunities for research education.

It is widely recognised that the ultimate goal could be the creation of a European research centre located in one of the EU countries. In order to fulfil this endeavour a European Institute for Biomedical Imaging Research (EIBIR) should be created and formed by a network of excellence of a large number of European institutions. The network should include both fundamental research laboratories and high quality clinical research departments. A survey among many potentially participating organisations throughout Europe allows the selection and inclusion of those institutions becoming active members of the Institute. EIBIR will offer a large number of services to its member institutions and will seek endorsement from many European scientific organisations. The structure of EIBIR will allow it to fulfil the criteria for funding by the European Union and sponsorship by industrial partners. The presentation will give an overview of the first steps leading towards the creation of the European Institute of Biomedical Imaging Research.

Learning Objectives:

1. To recognise the efforts delivered by the European Association of Radiology for creating an environment in which biomedical research can flourish.
2. To learn about the ideas and activities developed by the EAR Committee on Research.
3. To recognise the necessity for creation of a European Institute for Biomedical Imaging Research.

08:30 - 10:00

Room F2

Neuro

RC 911

Radiological vascular interventions

Moderator:

M. Leonardi; Bologna/IT

A-225

A. Aneurysms and vascular malformations

I. Szikora; Budapest/HU

Intracranial aneurysms are treated by both surgical and endovascular methods. Most endovascular techniques include packing of the aneurysm sac with platinum microcoils. While surgical clipping is more effective in preventing recanalization, the endovascular approach is significantly less invasive. For ruptured lesions, endovascular treatment is recommended whenever technically feasible, as recent studies (ISAT) demonstrated better clinical outcomes following endovascular than surgical aneurysm repair. Some morphological features, such as large size or poor neck to size ratio are associated with high incidence of recurrence. To avoid recanalization, special endovascular techniques are employed including tighter aneurysm packing by liquid embolus, using biologically active micro-coils that induce healing reaction inside the aneurysm, and flow modification within the parent vessel by applying vascular stents.

Intracranial vascular malformations are classified as capillary, venous and arteriovenous (AVM) lesions. The proper diagnosis is made by noninvasive MR imaging techniques. For AVMs, catheter angiography is necessary to choose the most appropriate therapeutic modality. These include surgical removal, transarterial embolization, radiosurgery and combinations of the above. The optimal technique is chosen based on the size, location and flow pattern of the malformation. Embolization is performed using adhesive and nonadhesive liquid embolus and employed either as a sole treatment, a preoperative measure to reduce intraoperative blood loss or to reduce the size of the AVM in preparation to radiosurgery. In general, 20-40% of all AVMs can be cured by embolization alone and 60-70% by combined techniques.

Learning Objectives:

1. To learn about treatment options for ruptured and unruptured intracranial aneurysms.
2. To understand techniques, indications and results of endovascular treatment for ruptured and unruptured aneurysms.
3. To learn about the classification of CNS vascular malformations.
4. To learn about clinical manifestation and imaging protocol of CNS vascular malformations.
5. To understand therapeutic decision and endovascular treatment of CNS vascular malformations.

A-226

B. Acute stroke and transarterial treatment

G. Wikholm; Gothenburg/SE

Stroke is today no longer without active treatment. Intravenous thrombolysis is an accepted treatment both in Europe and in the US. In more severe stroke and in a wider time window after the stroke transarterial embolectomy is a useful alternative to intravenous thrombolysis. A technique utilizing a standard intravascular retrieval snare will be presented in detail together with treatment results. The improvement in clinical status for patients treated has been encouraging. Our main problem today is to get the patients to the hospital quickly enough.

Learning Objectives:

1. To learn about active treatment in acute stroke.
2. To identify exempt from intravenous thrombolysis.
3. To understand technical aspects.
4. To learn about treatment results.

A-227

C. Carotid stenting

C. Cognard, H. Rousseau, P. Tall, A.C. Januel, F. Chollet, J.F. Albucher, A. Viguier, V. Larrue; Toulouse/FR

Carotid angioplasty and stenting is an alternative to carotid endarterectomy which is performed more and more worldwide in symptomatic and asymptomatic carotid stenosis. Several multicentric randomized international series are ongoing to compare both techniques and try to determine the safety and efficacy of each of

Postgraduate Educational Programme

them. In France, every patients presenting with a symptomatic carotid stenosis should be included in the EV3S study. Cases considered non surgical are the only candidate for stenting outside the trial. Treatment of asymptomatic carotid stenosis is very controversial and should be indicated in very selected cases only. The procedure is performed in most centers under local anaesthesia. The use of a brain protecting device is mandatory in the EVA3S study. Prestenting angioplasty is very rarely required.

The goal of this presentation is to discuss:

- Pretherapeutic diagnostic imaging including Doppler US, Angio CT or MR and digital substracted angiography
- Patients selections
- Therapeutic material and method
- Results of the main series published in the literature.
- Post-stenting patients medical care
- Long term follow-up

In conclusion, Carotid stenting is today a very frequent procedure which benefits from extremely rapid technological improvements and becomes more and more easy and safe to perform. Nevertheless, its advantages and drawbacks must be compared to surgery in term of evidence based medicine.

Learning Objectives:

1. To review previous and ongoing trials involving carotid angioplasty and stenting.
2. To discuss current clinical indications for carotid stenting.
3. To outline the current technique of carotid angioplasty and stenting and use of cerebral protection.

08:30 - 10:00

Room G

Special Focus Session

SF 9b

PACS pitfalls

Moderator:

N.H. Strickland; London/UK

A-228

PACS pitfalls (Introduction)

N.H. Strickland; London/UK

Our three speakers, all PACS experts from different parts of Europe, will give us the benefit of their experience using PACS in the clinical environment. PACS technology itself is now mature, and is available as an "off-the-shelf" product but many pitfalls still exist to trap those implementing PACS. Our experts draw particular attention to the pitfalls associated with: integration of PACS with other electronic systems, on-going maintenance of a PACS and its network infrastructure, reorganising clinical workflow optimally to exploit PACS, and the human factor involved in implementing a hospital-wide (or larger) PACS project.

Learning Objective:

How to avoid PACS pitfalls.

A-229

A typical PACS implementation: More than just the image! Organisational and infrastructural considerations

L. Sutton; Halifax/UK

A successful PACS Implementation requires a significant period of planning and organisational preparation if the organisation is to adapt to the changes the Implementation will introduce.

The key themes in managing this process are managing the organisational change, managing new ways of working and ensuring a robust infrastructure and well-managed network. This presentation addresses the change management issues under the following headings:

1. Realising the benefits of PACS.
2. Preparing the organisation.
3. Preparing the business case.
4. Implementation planning.
5. Post implementation support.

Educating members of the organisation of the benefits of PACS is essential if the full organisational benefits are to be realised. The types of benefits are discussed and consist of Clinical, Patient, Staff, Business and Strategic elements. In preparing the organisation there will be a greater degree of success if all members of the organisation are active participants in the planned changes rather than passive respondents.

Engaging active involvement is achieved through effective communication, training and education programmes and by addressing fears and unreasonable expectations. The involvement of the clinical community is essential for success. The formation of a Clinical Advocate Group is recommended.

Continuing success is dependent upon continuing training and education to ensure that the benefits described are actually realised. The central role of the PACS administrator is emphasised with stress being placed on effective communication skills with all members of the organisation.

The major measure of success following the implementation is that no-one would wish to go back to a film-based environment.

Learning Objectives:

1. To understand the main issues in planning and implementing a PACS into a health care organisation.
2. To recognise the importance of demonstrating the benefits of PACS to the organisation.
3. To understand the need to involve all members of the organisation as actively as possible to enable PACS to deliver all the clinical and non-clinical benefits.
4. To acknowledge that the PACS implementation process is not just simply an IMT exercise but an exercise in organisational change management.

A-230

Pitfalls when integrating HIS with PACS

W. Leodolter; Graz/AU

In the Austrian province of Styria the hospital group "KAGes" covers app. 85% of hospital beds. The group manages 22 hospitals with 6,700 beds and offers a wide range of ambulatory services. KAGes serves as example for describing pitfalls and opportunities in PACS-HIS-Integration.

Facing the dilemma of too many hospitals offering medical services close to where people are living, there is one way to manage such a group: Build a virtual hospital organisation. Uniform and interlinked hospital Information systems (HIS) with a single master patient index as entry point to an electronic patient record (EPR) and a "common language" are a prerequisite to offer patient related information exchange and telemedical services from centralized competence centers to local hospitals. PACS helps to enable the EPR, a HIS and especially teleradiology as driver for a virtual hospital organisation. Teleradiology is the most advanced field in telemedicine at KAGes.

PACS as learning opportunity for improved clinical workflow helps to prevent problems when implementing complex workflows in a HIS project afterwards. The evidence of integration issues with a Radiology information system (RIS) prevents the building of only poorly integrated "islands of information". Give your staff a taste of the benefits of an integrated HIS and EPR. Integrate the ordering-workflow from referring departments and the viewing of pictures in the ward. Experience the organisational changes involved with the intense use of EDP in your health care organisation. Teleradiology is an extension beyond the borders of the hospital organisation towards "healthcare unbound" and "e-health".

Learning Objectives:

1. To understand the role of PACS as a small part of the electronic patient record (EPR) and a hospital information system (HIS).
2. To learn why PACS is one of the driving forces and features implemented early on the way to an EPR and HIS.
3. To learn that the real and widely underestimated benefit of PACS is in clinical workflow
4. Why to address organisational changes in time when you implement the integration between PACS and HIS.

A-231

PACS implementation pitfalls: How to avoid a staff revolt!

T. Andersson; Örebro/SE

Traditional radiology is a proven and established technique, fine-tuned over more than a century. Filmless radiology, therefore, has until recently not really been considered an alternative, but more a business for pioneers, visionaries and crazy people in general. Today, however, technology makes it possible to go digital more easy and the PACS department is no longer a dream, but a reality that most hospitals have to prepare for.

Introducing a PACS is a major change of paradigm with far-reaching consequences for staff, routines and also the surrounding clinics and departments.

Dramatic changes are, in general, not popular among hospital staff, or human beings in general, and since PACS implementation is a typical and quite dramatic example of a major change one must be aware of the human side of a digitalisation process. To be able to really harvest the potential benefits from such a large change, traditional behaviours must be questioned, routines abandoned and new ways of working introduced. This is not done without pain and it is therefore im-

Postgraduate Educational Programme

portant to be prepared, not only for technical problems, but also for the human reactions and challenges.

The Pax Vobiscum project includes a total digitalisation of five independent radiology departments within Örebro County, Sweden. The human strategies, successful and unsuccessful, and lessons we learned in this project will form the basis for this presentation, which hopefully will give the audience a good view of the challenges in PACS implementation.

Learning Objectives:

1. To understand today's challenge in PACS. This is no longer the technology but rather the human side and how you organise your staff and your routines.
2. To be aware of that a successful PACS implementation must be driven from in-house, by the future users.
3. To be aware of that digitalisation is a matter for the whole hospital alone since the largest advantages can be expected outside radiology.
4. To be aware of size - small department - small problems, large department - large problems.
5. To be aware of the importance of a good system for image distribution.

08:30 - 10:00

Room H

Interventional Radiology

RC 909

Endovascular treatment of lower limb vascular occlusion

Moderator:

A. Besim; Ankara/TR

A-232

A. Thrombolysis

J.A. Reekers; Amsterdam/NL

Acute peripheral arterial thrombotic occlusion is still a limb-threatening situation, which needs acute intervention. Both surgical (thrombectomy) endovascular (thrombolysis or mechanical thrombectomy) have been widely used. There have been numerous trials to compare both treatment strategies (surgery versus thrombolysis) for endpoints like limb salvage, amputation and safety. Outcome for both groups was more or less equal, however morbidity and mortality seemed to be better in the thrombolysis group. The general opinion is that, whenever possible thrombolysis should be the first treatment option for acute arterial thrombosis. There has been a wide dispute in the literature about the way to administer the thrombolytic drug (pulsed or low-flow) and about which drug to use (rtPA or Urokinase) and the dosages. In a recent overview looking at Urokinase versus rtPA for peripheral occlusions forty-eight studies (22 urokinase, 22 rtPA, and 4 that included both treatments) were identified, encompassing 2226 urokinase-treated patients and 1927 rtPA-treated patients. The incidence of major hemorrhage varied widely, but the overall rate was lower among urokinase-treated patients (6.2%) than for patients treated with rtPA (8.4%. p = 0.007). The overall incidence of intracerebral hemorrhage was also significantly lower for urokinase (0.4% versus 1.1% for rtPA, p = 0.020). The major amputation rate was similar for both treatments (urokinase 7.9%, rtPA 7.2%), but the mortality rate was significantly lower for urokinase (3.0% versus 5.6% for rtPA, p < 0.001). The need for transfusions was less frequent with urokinase (11.1% versus 16.1%, p = 0.002).

Learning Objectives:

1. To discuss indications and practical cases concerning thrombolysis.
2. To evaluate technique and dose regimens.
3. To discuss other techniques for thrombus management like mechanical thrombectomy and thrombosuctie.

A-233

B. Uncovered stents vs covered stents

M. Sapoval; Paris/FR

Endovascular treatment of lower limb arterial occlusion can be often treated by Interventional Radiology procedures. Patients referred for non invasive imaging of leg arteries or arteriography should be carefully assessed clinically before to propose endovascular treatment. Balloon angioplasty can treat a wide range of lesions but stents can be implanted for the following setting: recanalisation of total chronic occlusion, occlusive dissection, embolic lesions. Uncovered stents should preferably be Nitinol stents and self expandable stent because of the risk of collapse in case of external compression. Covered stents are recommended for long total chronic occlusions and are now challenging the results of venous or

synthetic bypass grafts. Other techniques such as laser or atherectomy are not longer used.

Learning Objectives:

1. To understand the main clinical features of patients referred for revascularisation of lower limb vascular occlusion.
2. To choose for which patient interventional technique should be proposed.
3. To choose between covered stents, uncovered stents and simple angioplasty to ensure higher technical/clinical success.

A-234

C. Infrapopliteal lesions

A. Bolia; Leicester/UK

Subintimal Angioplasty of infrapopliteal occlusions has made a substantial impact on the treatment of critical limb ischaemia. The technique involves using a 5 French system and hydrophilic 0.035 guidewire. The wire is manipulated into a loop, which is then advanced through the length of the tibial occlusion. Then, after successfully crossing the lesion, a 3 mm balloon is used to dilate the artery. A number of publications are now available demonstrating the value of infrapopliteal subintimal angioplasty on the treatment of critical limb ischaemia. Primary success rates of over 80% and patencies of about 50% at 1 year can be expected. However, despite the relatively low patency rate, limb salvage of around 90% at 1 year has been demonstrated. Subintimal Angioplasty is safe, simple and a minimally invasive method of treating patients with chronic critical limb ischaemia. It is effective, inexpensive and a low risk alternative to distal reconstructive surgery.

Learning Objectives:

1. To discuss the management of critical limb ischaemia and include the indications, materials, technique and results of angioplasty.
2. To discuss the impact that the technique of subintimal angioplasty makes on CLI.
3. To briefly discuss the results of femoropopliteal subintimal angioplasty.
4. To grasp the basic technique of subintimal angioplasty.

08:30 - 10:00

Room I

Workshops on Interventional Radiology

WS 918

Urological intervention

Moderator:

U. Patel; London/UK

A-235

A. Nephrostomy and ureteric stenting

F. Cornud; Paris/FR

Percutaneous nephrostomy (PCN) is a simple interventional procedure when it is performed on a dilated collecting system to relieve a chronic hydronephrosis. When the collecting system is not dilated, failure may occur if the Interventional Radiologist is not aware of some technical points which will be shown and which permit to achieve a PCN in virtually 100% of cases on a non-dilated collecting system. In patients with complex pelviccalyeal stones, including staghorn calculi, stones within a diverticulum, access to the collecting system is governed by a series of technical rules which will be exposed to show how to render stone-free a patient harboring the most complex renal calculi. Percutaneous stone extraction of the upper third of the ureter is also governed, in difficult cases, by technical endourological recipes which will be explained to show how to clear the ureter of stones embedded within the ureteral mucosa. Concerning ureteral stenting, most of the problems encountered are due to tight stenoses which may seem to be impassable, owing to a total ureteral obstruction. In these cases, performing an uretero-neocystostomy or using the rendez-vous technique, with a combined antegrade and retrograde approach, permits passage in 100% of cases of these totally obstructed ureters. Technical aspects of this technique will be shown. The rendez-vous technique can also very successfully be used to stent ureters in case of ureteral fistula into the retroperitoneum. Other endoureteral manipulations will be shown such as ureteral embolisation in case of intractable vesico-vaginal fistulae secondary to pelvic malignancies in female patients.

Learning Objectives:

1. To show how to solve problems in case of difficulties encountered during complex percutaneous nephrostomies.

Postgraduate Educational Programme

2. To describe the rendez-vous technique to stent ureters in case of complete obstruction or ureteral fistula.
3. To give guidelines to extract complex stones.

A-236

B. Thermal ablation of renal tumors

P.R. Mueller; Boston, MA/US

This lecture will be an updated summary of where radiofrequency ablation stands in 2004. A review of the procedure with an overview of technique, results, complications and follow-up will be given. While there have been several articles in the literature on RF ablation, there has been very little description of the process and technical difficulties of performing ablation on difficult lesions in the liver and kidney. What are the most difficult lesions to treat in the liver? What are expected results with treating primary tumors of the liver vs. metastasis disease? How difficult is follow-up? What are the problems with imaging interpretation? Similarly, in the kidney: What lesion is best suited to be treated in the kidney? What are major problems with RF of the kidney? Can you treat a metastasis? These points will be emphasized and summarized in the lecture.

Learning Objectives:

1. To become familiar with the world literature on RF ablation of kidney tumors.
2. To understand the safe techniques used to ablate kidney tumors.
3. To understand patient care issues in patients who have been or are being treated with RF ablation.

A-237

C. Renal arterial intervention

P.M.T. Pattynama; Rotterdam/NL

Renal artery stent placement has evolved as the method of choice for revascularization of atherosclerotic renal artery stenosis (RAS). The initial technical success rate is 95-100%, with only low complication rate when using the newer low-profile stent systems delivered through guiding sheaths. Complications, however, do occur and may be life-threatening: Embolisation of atherosclerotic debris in severely atherosclerotic vessels may, in the rare patient, lead to kidney loss and bowel necrosis. Stent patency approximates 90% at 6 months and 80-85% at 18 months, with little data available on more long-term follow-up. Studies are underway to establish whether patency will improve when using drug-eluting stents. Current discussion centers on the appropriate patient selection for stent placement. Proper indications include hypertension and/or renal functional impairment. There is a shift towards the latter indication, treatment to preserve renal function, given the increased efficacy of anti-hypertensive medical treatment. It has been clearly shown that RAS in the absence of hypertension or renal insufficiency should not be treated with stent placement. The importance of appropriate patient selection is shown in nearly all patient series: Stent placement will hugely benefit some patients, but will show no benefit at all in others. Controversy exists about accurate predictors of clinical success: Beneficial factors may include a relatively preserved renal function and preserved intrarenal vascular microvasculature, as evidenced by a normal resistive index of better than 80% measured with doppler ultrasound. Initial reports suggest a beneficial effect of using embolic trapping devices during stent placement, such as filter-tipped guide wires.

Learning Objectives:

1. To know the different etiologies of renal artery stenosis.
2. To discuss the indications and contraindications for renal artery revascularization.
3. To understand the evolving discussion about appropriate patient selection.
4. To discuss available techniques for, and potential complications of renal artery stent placement.

08:30 - 10:00

Room K

Pediatric

RC 912

Neuro-imaging

Moderator:

T.A.G.M. Huisman; Zürich/CH

A-238

A. Large infant heads: What do we do - and when?

F. Brunelle; Paris/FR

Macrocrania in children is a common presenting clinical feature. It affects 5% of the population. Macrocrania is an associated finding in some syndromes in which mental retardation is a cardinal clinical sign. In these cases, the medical problem is of a completely different nature. However, macrocrania in some instances appears isolated. Macrocrania by definition is the consequence of an increased growth of the cranium over the brain. It cannot appear after the closure of the sutures. The role of ultrasound is to check the ventricular size and to exclude massive hydrocephalus. CT scan is usually done following the ultrasound or directly as a first procedure. It will assess the ventricular size, rule out the presence of a brain tumor and look for a chronic subdural effusion. In many cases MR imaging will be performed to make a precise diagnosis, to appreciate the extent of a tumor or to do MR angiography. Main causes of macrocrania are as follows: hydrocephalus; external hydrocephalus; brain tumors; vascular malformations; vein of galen aneurysms; metabolic diseases; idiopathic. A familial incidence is often found. Mild mental retardation is not unusual.

Learning Objectives:

1. To decide which patient should be worked-up and when.
2. To choose the technique, CT versus MR imaging.
3. To differentiate benign from conditions requiring treatment.
4. To understand the mechanisms of hydrocephalus.

A-239

B. Imaging of sensorineural hearing loss: A practical approach in children

M. Elmaleh; Paris/FR

The most frequent etiologies of sensorineural hearing loss (SNHL) are far different in children than in adults. Congenital abnormalities, infections, and trauma are, in descending order, the main causes of SNHL in children. Posterior fossa tumors are often associated with other cranial nerve involvement; IAC schwannomas are rare and, when part of neurofibromatosis type 2, manifest in the second decade of life.

Clinical and audiological data of the child (supposed time of onset, degree of the hearing loss, personal and familial history...) are essential to choose the most efficient imaging technique.

CT detects osseous labyrinth and IAC malformations, and with careful analysis of the cochlear nerve bony canal, can raise suspicion of cochlear nerve hypoplasia. Labrynthine ossification from post-meningitis deafness and temporal bone fractures are also well evaluated by CT. Recent improvements in CT technology, such as helical CT, have reduced dramatically the need for sedation. Depending on the series in the literature, CT is positive in about 20-40% in children with SNHL.

However MR imaging is the only method that looks at the cochlear nerve, the brainstem and the brain parenchyma and it can detect isolated abnormalities of the membranous labyrinth. 3D-fast spin echo technique provides sub-millimeter high-resolution T2-weighted images of the labyrinth and IAC contents. Evaluation of cochlear implant candidates include both CT and MR imaging.

Concerning congenital deafness, we would like to emphasize the increasing role of imaging in the diagnosis of deafness etiology: an increasing number of known syndromes or known genetic defects can be confidently identified by imaging.

Learning Objectives:

1. To choose the most appropriate imaging technique, CT and/or MR imaging, based on the clinical examination, history and audiologic data.
2. To propose imaging protocols, emphasising the last technical improvements in CT and MR imaging.
3. To illustrate the most frequent aetiologies of sensorineural hearing loss (SNHL) in children: Congenital abnormalities, infectious diseases and trauma.
4. To review the role of imaging in the work-up of cochlear implant candidates and after cochlear implant surgery.

Postgraduate Educational Programme

A-240

C. Pediatric MR spectroscopy: Current applications and future prospects

M.J. Beer, H. Koestler; Würzburg/DE

MR-spectroscopy (MRS) has gained an established use in paediatric neuroradiology, allowing the non-invasive assessment of multiple metabolic processes. Additionally, other potential applications currently emerge outside the central nervous system e.g. heart, musculoskeletal system or liver.

The increasing use of MRS techniques is not only a result of the fascinating non-invasive approach to fundamental biochemical processes, but also a result of recent technical advances. Reproducible quantification methods, dedicated data acquisition and postprocessing methods have been introduced. Dedicated 3 T scanners pave the way for new clinical applications of MRS, with enormously increased spatial and/or temporal resolution.

1H-MRS, which is the mostly used technique in the field of neuroimaging, allows the analysis of chemical moieties as N-acetyl aspartate (NAA), creatine (Cr/PCr) and choline (Cho). An important aspect for the use in paediatrics is the normal regional variation and age dependence of the respective moieties. The main applications are characterization of brain tumours and analysis of inborn errors of metabolism.

Using 31P-MRS, the main molecules of energy metabolism, phosphocreatine (PCr) and adenosinetriphosphate (ATP), can be studied. In heart failure, both metabolites are increasingly reduced. Detection of subclinical cardiac commitment in a variety of diseases like multiple sclerosis or different forms of neurodegenerative diseases is possible. Another use is the differentiation of liver and musculoskeletal diseases and finally as a prognostic tool in oncology.

Thus, MRS may become a clinical routine tool, which offers valuable additional information for detection and assessment of various diseases.

Learning Objectives:

1. To understand fundamental biochemical processes.
2. To propose dedicated data acquisition and postprocessing protocols.
3. To illustrate possible clinical applications inside and outside the brain.
4. To review recent technical advances including (3 T/Gating/AW-CS1/DW-CS1).

08:30 - 10:00

Room L/M

Infection in the Adult Today

CC 916

Modern imaging of infective disease in the face and pelvis

Moderator:

M. Gödeny; Budapest/HU

A-241

A. Cervicofacial infection in the immunocompromised patient

K. Marsot-Dupuch; Le Kremlin-Bicêtre/FR

Head and neck lesions are encountered in more than 40-50% in patients with immunosuppression (HIV-infection, diabetes mellitus, transplant recipients, immunosuppressive drugs or post-radiotherapy). The organs affected are mainly involved by granulation tissue, perivascular and perineural inflammation, and neoplasms.

Salivary gland involvement leads to a non-specific bilateral painless enlargement of the parotid gland and xerostomia. The high rate of salivary gland involvement is related to the presence of the HIV within the saliva. Lymphoepithelial cysts, sialosis, and lymphoma may be present simultaneously in the same patient. Sinonasal diseases (66% of IS patients) are associated with a trend of decreased survival rate. Fungal sinus disease (1-10% of transplant recipients) should be suspected whether organ rejection is considered. Invasive aspergillosis (lethal in 50-80%) is defined by submucosal hyphae and tumor necrosis without host inflammatory response. MR is the best imaging modality to perform to exclude skull base involvement, extrasinonasal extension and meningeal spread. The lesion has a characteristic hypointensity on T2-WI.

The temporal bone is the most frequent target organ in the IS pediatric population. Prompt treatment may avoid complications such as lateral sinus thrombosis and skull base spread.

Kaposi's sarcoma is an indicator of the progression of HIV infection. Often multifocal at presentation, it may affect the skin and visceral organs. Cytokines and growth factors may play a role in the pathogenesis of angiogenic sarcoma.

In conclusion, immunosuppressed patients are likely to develop virulent infection with vascular complications and tumor at an earlier age than usual.

Learning Objectives:

1. To underline pathologies leading to immunosuppression status.
2. To illustrate some characteristic pathologies occurring in immunocompromised patients.
3. To describe perineural and vascular spread and complications.
4. To discuss post transplant lymphoproliferative disorders.

A-242

B. Urinary infection

W. Torreggiani, R. Browne; Dublin/IE

Urinary tract infection (UTI) in the adult is primarily based on a combination of typical symptoms of fever, as well as urinalysis. Patients with uncomplicated pyelonephritis who respond to treatment do not necessarily require radiological evaluation. In general imaging should be reserved to those patients in whom conventional treatment has failed or those who have recurrent or unusually severe symptoms. Occasionally patients may be referred for imaging at an early stage if the symptomatology or urine analysis is uncertain and if other diseases such as ureteric colic or renal infarction are suspected. In addition, in certain patients such as those with conditions predisposing to infection such as diabetes mellitus or immunocompromised states early imaging may be beneficial. Intravenous urography (IVU) and ultrasound (US) have traditionally played leading roles in the evaluation of UTI. MR imaging is an emerging modality but it is computerised Tomography (CT) that plays the pivotal role in the diagnosis of renal tract infection and its complications.

Learning Objectives:

1. To describe the role of the various imaging modalities in the investigation of UTI in adults.
2. To depict the wide range of findings that may be present in a variety of urinary infections.
3. To indicate the important role that the interventional radiologist plays in the management of these patients.

A-243

C. The spectrum of pelvic infection

A.A. Ghiatis; Athens/GR

Pelvic infection affects approximately one million women yearly with rather serious consequences such as infertility, ectopic pregnancy and pelvic pain.

Early diagnosis of pelvic infection leads to early and successful treatment with minimal if any complications. Imaging provides significant assistance to the management of pelvic infection and appropriate selection and use of different imaging modalities and techniques is essential to the diagnostic management of this pathological entity. The purpose of this presentation is to discuss the approach as well as the use of different imaging modalities such as US, MR imaging, CT and Hysterosalpingography in the management of pelvic infection.

Learning Objectives:

1. To understand the optimal use of imaging modalities.
2. To become familiar with optimal imaging protocols.
3. To comprehend an appropriate approach to imaging patients with pelvic infection.

08:30 - 10:00

Room N/O

Physics in Radiology

RC 913

Medical image registration: Methods, applications and validation

Moderator:

M. Kachelrieß; Erlangen/DE

A-244

A. A tutorial on algorithms and methods

D. Rueckert; London/UK

This lecture will provide attendees with a basic working knowledge of methods used to register images, and a description of some examples of the wide variety of applications for which these techniques are used. Applications of image registration include combining images of the same subject from different modalities, aligning temporal sequences of images to compensate for motion of the subject between scans, providing guidance during surgical procedures, correcting for

Postgraduate Educational Programme

soft tissue deformation and aligning images from multiple subjects in cohort studies. We will review the current state-of-the-art in image registration. We will focus primarily on algorithms that use voxel-based similarity measures to automatically register images that are related by a rigid-body transformation. We will also discuss current research trends in the development of non-rigid registration algorithms that can compensate for tissue deformation or align images from different subjects.

Learning Objectives:

1. To become familiar with the basic image registration techniques.
2. To understand the concept of rigid and non-rigid registration.
3. To understand the role of image features, image similarity measures and image interpolation in registration.

A-245

B. Applications

D. Hawkes; London/UK

Image registration has emerged as a powerful tool over a wide range of medical applications. This talk will explore how the development of this technology impacted on these applications. In multi-modal imaging, complimentary information is combined to provide synergy between two (or more) imaging modalities. Examples include the combination of structural information from MR with the functional information available at lower spatial resolution from PET or SPECT. Very accurate alignment of intra-modality data allows subtle temporal changes in structure or function to be analysed. Over short time intervals image registration improves image alignment in functional MR studies and over long time intervals allows highly accurate detection of cerebral atrophy. Image registration to the physical space of the patient in the operating room is the key enabling technology in image-guided surgery.

Non-rigid registration applications range from the measurement of change, to the generation of atlases and the propagation of segmentation in the automated interpretation of images. Applications include accurate measurement of tissue growth and destruction in the monitoring of therapy and the progression of disease by analysis of deformation fields. Atlases can be built from large numbers of example images that have been aligned and the statistics of the resulting deformation models can be used to build statistical shape models. These models can then be used to propagate organ outlines to improve measurements of size and shape.

Learning Objectives:

1. To learn how to carry out very precise measurements of change, growth, atrophy.
2. To understand how to apply image registration in motion analysis.
3. To understand how to apply image registration in shape modelling, atlas generation and segmentation propagation.
4. To understand how to use image registration in image guided interventions.
5. To understand how to use image registration in multi-modality imaging.

A-246

C. Strategies for validation

A. Todd-Pokropek; London/UK

Image registration techniques require validation, which implies the availability of a gold standard. For rigid registration this then permits the definition of a target registration error and a number of successful evaluations of rigid registration techniques have been completed. Non-rigid registration includes a model of interpolation and cannot be evaluated in such a simple manner. We are interested in the accuracy of registration at all points in image space, but "weighed" by the clinical objective to be achieved. Non-rigid registration must also include a model of the process of deformation (for example a model of tissue characteristics) and can be divided into spatial deformation and material transport. It is then possible to define the registration in terms of the deformation vector field and transport field, where some methods exist for their assessment. In general, a suitable strategy for validation of such methods starts by using real clinical data and deforming it, for example using a finite element (tissue based) method. The accuracy of restoring the data back to its undeformed state provides a baseline for evaluation, although the use of circular methods (where the forward and reverse operations match) must be avoided. Finally clinical trials are required to confirm this validation on real clinical data for real applications.

Learning Objectives:

1. To enable the understanding of the processes of rigid and non-rigid registration, of constraints such as diffeomorphism and consistency, and the choice of various particularities of different methods as appropriate for different clinical applications.

2. To understand the process of validation of rigid registration and strategies for use for non-rigid registration.
3. To become familiar with the use of and the limitations of such techniques.

08:30 - 10:00

La Scala

Foundation Course - Chest Radiology

E3 920

Nodules and neoplasms

Moderator:

T. McLoud; Boston, MA/US

A-247

A. Solitary and multiple pulmonary nodules

A.A. Bankier; Vienna/AT

Pulmonary nodules are among the most common radiological findings. A wide array of diseases can manifest as solitary or multiple pulmonary nodules. At the edge of the differential diagnosis is the differentiation between benign and malignant nodules. This presentation attempts to propose a systematic approach to these lesions.

Learning Objectives:

1. To define the concept of pulmonary nodule.
2. To illustrate the spectrum of its radiological presentations.
3. To review the array of its differential diagnoses.
4. To present subjective and objective analytical approaches.

A-248

B. Staging of non-small cell and small cell lung cancer

P. Armstrong; London/UK

The treatment of lung cancer is highly dependent on its stage and cell type. Small-cell lung cancer is almost never treated surgically, whereas surgical resection is the optimum potentially curative treatment for non small-cell lung cancers in patients who are fit for surgery and whose tumours can be fully resected by surgery. The presentation will focus predominantly on the imaging information required by thoracic surgeons considering surgical resection of lung cancers. The practical approach, given the difficulty of accurately determining T, N and M stage and the diagnosis of metastases, will be emphasised.

Learning Objectives:

1. To inform about current staging classifications for non small-cell and small-cell lung cancer.
2. To review the spectrum of imaging features of different tumours in the TNM classification.
3. To enhance the understanding of the role of imaging in the differentiation between operable and non-operable tumours.

10:30 - 12:00

Room A

"ECR meets" Hungary

EM 2

The present and future of Hungarian radiology: Contribution of a new generation

Presiding:

A. Chiesa; Brescia/IT

B. Lombay; Miskolc/HU

A-249

The present and future of Hungarian radiology: Contribution of a new generation (Introduction)

A. Palkó¹, B. Lombay²; ¹Szeged/HU, ²Miskolc/HU

Being invited by the president of ECR 2005 as one of the countries "meeting ECR" is among the most important successes in the more than one hundred year history of Hungarian radiology, thus we may be very proud to have the honor to introduce the session "ECR meets" Hungary.

The list of speakers and topics discussed by them was selected to express the concept that rich traditions of Hungarian radiology today may be best represented by those young scientists who belong to a new generation, having the oppor-

Postgraduate Educational Programme

tunity to spend the most productive period of their professional life as citizens of a new member country of the European Union.

The lectures discussing results of experiments on diffusion MR imaging and automated colon CT diagnostics, applied clinical research on epilepsy diagnostics and interventions in the liver and the carotid vessels give good samples of the wide range of ongoing scientific activity in university and hospital departments and research labs in different regions of Hungary.

We hope that the ninety minutes of the session will give a good impression and provide a lot of valuable new information regarding Hungary and Hungarian radiology at the time of our arriving back home to Europe.

Learning Objectives:

1. To introduce significance of being one of the countries invited to the "ECR meets" program.
2. To introduce principles of speaker and topic selection to the "ECR meets" Hungary session.

A-250

What do we see on diffusion MR images? A lesson learned from model experiments

P. Bogner; Kaposvár/HU

Purpose: Diffusion imaging is highly sensitive to detect the changes in water movement that are characteristically reduced in ischemic stroke as a consequence of cytotoxic edema. In addition to changes in water diffusion, the osmotic properties of ischemic brain tissue are progressively altered. In cellular model experiments the impact of cellular volume changes on water diffusion as well as the relationship of diffusive and osmotic characteristics of cellular water were investigated.

Methods and Materials: Mammalian erythrocytes with different protein hydration levels were used. Along with cellular volume changes the osmotic resistance and the amount of osmotically unresponsive water were determined. Water diffusion was measured with the Stejskal-Tanner sequence (b-factor: 0-17.684 s/mm²) on a Varian ^{Inova}Unity MR microimaging system.

Results: It was shown that a two-fold change in cellular volume (protein hydration) results in only about a 20% change in water diffusion in human erythrocytes. However, cellular volume change causes a significant alteration in the osmotic behavior of the cells that, in this experimental model, is a consequence of the change in protein hydration and most likely protein aggregation.

Conclusion: Water movement is restricted in living tissues due to three major reasons, namely 1. the presence of biological membranes, 2. molecular obstruction and 3. water binding mainly to macromolecules (protein hydration). It seems likely that the osmotic behavior is closely related to protein hydration but water diffusion depends also on other mechanisms as mentioned above. The possible mechanism of reduced water diffusion and altered osmotic behaviour in brain ischemia will be discussed.

Learning Objectives:

1. To define parameters that characterize the osmotic behavior of a cell-membrane characteristics, osmotically inactive water and protein hydration water.
2. To introduce the relationship of osmotic and diffusive characteristics of cellular water.
3. To implement experimental results in diagnostics of DWI and suggest possible therapeutic consequences.

A-251 ♀

Epilepsy patient: The complex neuroradiological approach

P. Barsi; Budapest/HU

Purpose: We created a neuroradiological protocol to answer the clinicians' questions, varying with the patient's age, epilepsy type, and treatment phase (pre/postoperative).

Material and Methods: We examined more than 1,000 epilepsy patients by MR imaging (from 0.5 to 1.5 Tesla). We used the protocol containing thin T2 and PD/FLAIR slices perpendicular to the hippocampus, and 3D acquisition with multiplanar and surface reconstructions. We used T1 IR instead of 3D under 2 years of age. We performed 3D MR imaging for the localization of intracranial EEG electrodes detecting epileptic discharges during monitoring. We used the same protocol for postoperative cases. The only role of CT was to detect calcification. We discussed our findings in detail with the clinicians.

Results: 1. The commonest causative pathologies were hippocampal sclerosis and cortical dysgenesis. 2. Focusing on the hippocampus resulted in the identification of dual pathologies and hippocampal malrotation. 3. We found evolving hippocampal sclerosis in 7 cases of SMEI. 4. We found a subtype of extensive closed lip schizencephaly with mild clinical picture. 5. We found characteristic

features in different lissencephaly subtypes. 6. MR imaging of invasive EEG electrodes proved to be useful in the focus localization of dubious focal epilepsies. 7. Postoperative analysis of unsuccessful cases is a work in progress based on a volumetric approach.

Conclusions: 1. The proper epilepsy MR imaging protocol is essential in each diagnostic phases of epilepsy. 2. The protocol should be used even in cases of other pathologies or generalized epilepsy cases. 3. Interpretation of imaging results needs close cooperation with the clinicians.

Learning Objectives:

1. To comprehend the role of MR imaging in the pre-, peri-, and postoperative phases of epilepsy patients' management.
2. To become familiar with the proper MR imaging protocol for epilepsy patients.
3. To learn the causative pathologies possibly detected by the examination.

A-252 ♀

Radiological diagnosis and treatment of carotid artery stenosis

R. Szentgyörgyi; Szeged/HU

Stroke is the No. 1 cause for disability, and No. 3 among all causes of death, behind diseases of the heart and cancer. Thromboemboli originating from stenosed carotid bifurcations are the cause of stroke in 12-60%. Non-invasive imaging techniques became widely available for the diagnosis of internal carotid artery (ICA) stenosis. Carotid artery stenting (CAS) is slowly being favoured over surgical endarterectomy (CEA) for the prevention of stroke. Observations based on the series of 250 CAS procedures performed at our institute are presented.

Duplex Doppler examination is the standard tool for screening of carotid artery stenosis. For preprocedural evaluation before CAS, however, it has to be augmented with CT angiography or MR angiography for more precise stenosis measurement and additional pathological findings in the region of supraaortic vessels. Indications for CAS are similar to those of CEA, but it is also feasible for patients considered high risk for surgery. Complication rates much lower than achievable with CEA are possible with CAS in cases with careful preprocedural planning and endovascular equipment selection. Risks of anesthesia and complications related to relatively long clamp-time is avoided with stenting. Periprocedural patient care is vital for the success of CAS. Restenosis can be successfully managed with a cutting balloon.

Improvement in equipment and expertise for CAS is expected, and will surely replace CEA in the next few years.

Learning Objectives:

1. To learn the aspects for preprocedural evaluation for carotid artery stenting.
2. To learn the indications for CAS.
3. To learn the significance of "passive protection" for CAS.

A-253

Interventional radiology in portal hypertension

I. Lázár; Miskolc/HU

Background: Viral and alcoholic induced cirrhosis are the principle causes of PH in Europe. The rest of cirrhoses are the sequelae of various metabolic or idiopathic disorders of the liver. Ultrasonography (US) is the most widespread diagnostic procedure in PH combined with invasive mesenteric angiography. In the early stages of cirrhosis PH symptoms threaten the patient more than parenchymal impairment of the liver. Transjugular intrahepatic portosystemic shunt (TIPS) is indicated at that stage or later as a bridge to liver transplantation.

Procedure Details: When clinical and endoscopic signs of PH are present an assessment of portal hemodynamics is performed by US. It is essential to reveal pre- versus post hepatic PH. Portosystemic collaterals and frequent incidental hepatocellular carcinoma are evaluated by computed tomography and recently MR. Our single center experience is 80 TIPS and 27 revisions, including 12 stent-graft procedures, a pediatric case and TIPS in a patient with portal cavernoma.

Conclusion: Interventional radiology is the method of choice in the treatment of patients with PH. Up-to-date imaging methods and continuously growing experience make the TIPS procedure safe and reproducible. The use of e-PTFE covered stent-graft, compared to bare stents, reduces the re-intervention rate by prolonging TIPS patency. Procedural technical problems seem to be mostly overcome but important difficulties like restenosis and hepatic encephalopathy has still not been solved with complete satisfaction.

Learning Objectives:

1. To remind the most frequent etiology and imaging methods of portal hypertension (PH).
2. To become familiar the indications and techniques for the interventional radiological management of PH.

Postgraduate Educational Programme

3. To illustrate the results and the complications of transjugular intrahepatic portosystemic shunt.
4. To outline the pros and cons of PTFE covered stent in TIPS procedure.

A-254 ♀

Results of the virtual colonoscopy CAD project

Z. Tarján; Budapest/HU

The aim was to develop a PC based virtual colonoscopy application which needs minimal user interaction, and with automated functions may be used as a screening tool. ColVis was developed by two universities and runs on PCs or laptop computers. Interactive real time ray casting is used, which allows high speed, high resolution volume rendering. Semiautomatic region growing segments the colon and cast or transparent view is used. For fast evaluation of suspected lesion composition an oblique image perpendicular to the virtual camera plain may be adjusted to the lesion. Automatic centerline extraction generates automated videos of the whole colon. For noisy low/ultra-low dose CT data a filter volume enhancement with edge preservation is used.

For better patient compliance the patient may eat normally in the days before the examination. Digital subtraction bowel cleansing uses the combination of selective regional thresholding and seed growing. This enables smooth, reliable endoscopic views after electronic cleansing in patients without cleansing bowel preparation. The automated lesion detection CAD, which enables us to detect polypoid lesions, is based on robust shape and density analysis algorithms. It detects all simulated polyps in plastic and pig colon fomants without false positives, and also shows promising results in patient data. The lesion size threshold may be adjusted and algorithms help to discriminate residual stool balls from polyps.

The presentation demonstrates the features of ColVis in phantom models and in patients with colonoscopic correlation. Examples of primary 2D or 3D based colon evaluation and features shortening evaluation time are demonstrated.

Learning Objectives:

1. To evaluate how PC based software may aid the reading of CT colonography data.
2. To learn the 2D and 3D based evaluation methods in colonography.
3. To understand features which are needed for greater patient compliance.
4. To get familiar with features shortening the evaluation time.

10:30 - 12:00

Room B

New Horizons Session

NH 10

Drug-eluting stents

Moderator:

J.A. Reekers; Amsterdam/NL

A-255

Drug-eluting stents (Introduction)

J.A. Reekers; Amsterdam/NL

Both interventional cardiologists and interventional radiologists have been facing the huge problem of intimal hyperplasia for decades. This has truly been the "Achilles heel" of percutaneous treatment of stenotic arterial disease. Introduction of stents in the late eighties of the last century has shown not to be a solution to this problem. However, stents did improve PTA outcome, due to a better starting point by elimination the recoil problem. Drug eluting stents (DES) are the next, promising step to improve the outcome after PTA by blocking intimal hyperplasia.

The fast majority of the experience and data concerning DES comes from interventional cardiology. Although DES are a very promising development for peripheral PTA, there is one important difference with all the cardiology studies. The endpoint in most cardiology studies is an angiographic parameter and deals with reduction in intimal hyperplasia compared to a placebo. For peripheral vessels however, a statistically significant effect on an angiographic primary endpoint has to translate into a significant clinical effect, as in most cases the original disease (intermittent claudication) is not life-threatening but only lifestyle limiting. DES are an exciting new tool in the battle against intimal hyperplasia, which might change the future perspective of peripheral PTA. It is therefore interesting for every radiologist involved in peripheral interventions to know about DES, and to learn about the latest development. This special session on DES is a unique opportunity to get a complete update on this topic.

Learning Objectives:

1. To understand the current role of drug eluting stents for the treatment of peripheral vascular disease.
2. To learn about ongoing research in the field of DES.
3. To become familiar with all the specific drugs currently tested against intimal hyperplasia.

A-256

General introduction drug-eluting stents

J. Rose; Newcastle Upon Tyne/UK

The restoration of peripheral vascular patency with angioplasty and stents has long been beset with the problem of restenosis. The basic mechanisms of restenosis include early elastic recoil, vessel wall remodelling and myointimal hyperplasia. The vascular stent reduces elastic recoil but tends to increase the degree of neointimal hyperplasia and late lumen loss. Several alternative technologies including anti-platelet agents, inert stent coatings, brachytherapy, sonotherapy and gene therapy have been proposed to prevent restenosis. None of these alternatives have yet been proven and drug eluting stents have attracted steadily increasing interest over the last 5 years.

The basic principle underlying the drug eluting stent is the inhibition of cellular proliferation by local delivery of an active agent with minimal systemic effect. In general a basic stent platform is coated with a matrix polymer, which may be biodegradable, and a suitable pharmacological agent is loaded within the matrix. Stents coated with a variety of anti-inflammatory or anti-mitotic agents have produced encouraging reductions of angiographic re-stenosis in the coronary circulation and appear clinically effective in the short to medium term.

The latest trends however, seem to indicate that the problem of re-stenosis is delayed rather than abolished by the use of such devices. It may be that the ideal pharmacological agent is yet to be tested and indeed the use of new stent materials, including fully bio-degradable compounds, is proceeding apace.

Learning Objectives:

1. To understand the basic mechanisms of re-stenosis.
2. To become familiar with the principles of drug eluting stents.
3. To learn the various classes of pharmacological agent carried by drug eluting stents.
4. To understand the technological differences between the current stent platforms.
5. To gain a broad picture of the current data from coronary stent trials.

A-257 ♀

Drug-eluting stents in renal arteries

M. Zähringer; Cologne/DE

The various modalities used in the treatment of renal artery stenosis (RAS) have evolved over the years. In the late 1970's, Percutaneous Transluminal Renal Angioplasty (PTRA) was introduced as an alternative to surgical revascularization. Since then, PTRA has been accepted as the initial treatment for RAS due to its minimally invasive nature. However, restenosis after PTRA still remained a problem. The introduction of stenting in renal artery treatment did improve the results. Restenosis rate after PTRA up to 9 months has been reported in various series up to 38%. A meta-analysis of the literature showed a restenosis rate at 6 months close to 17% when .035" compatible stents are used, but also showed a lack of validated angiographic follow-up data. Restenosis rate using new low profile stents have not been reported in the literature yet.

The GREAT study, presented in the lecture, is a multicenter study on the use of bare and, at the first time, drug eluting low profile balloon expandable stents in renal artery stenosis.

The study demonstrates that low profile balloon expandable stent systems allow to obtain excellent results with a low restenosis rate of 14.3% in the bare stent group. By renal artery stenting with drug eluting Palmaz Genesis stents it is possible to cut down the restenosis rate to 6.7% with a decrease in the numbers of revascularizations with 50%.

Learning Objectives:

1. To comprehend the indications for the interventional radiological management of patients with renal artery stenosis.
2. To understand the role of interventional radiology in the management of renal artery stenosis.
3. To become familiar with the relative advantages of drug eluting stents in treating renal artery stenosis.
4. To learn the principles underlying the techniques used by interventional radiologists in the management of renal artery stenosis.

Postgraduate Educational Programme

A-258

Drug-eluting stents in SFA

J. Lammer, C. Kopp, M. Cejna, T. Rand, E. Minar; Vienna/AT

Purpose: Drug-eluting stents locally release drugs at high concentration to reduce intimal hyperplasia.

Method and Material: Metallic stents are covered by a polymer matrix or nanoporous ceramics to cause controlled release of the drug. The target of intervention can be blockage of receptor activation in smooth muscle cells. This prevents signal transduction by cytokines or growth factors. Immunosuppressive macrolites such as Rapamycin (Sirolimus) or FK506 (Tacrolimus) are drugs to suppress T-cell proliferation and release of proinflammatory cytokines. This also causes cell cycle arrest of smooth muscles in the late G1 phase. Another target of intervention is to block cell division in the M phase with cytotoxic drugs such as Paclitaxel (Taxol).

Results: Various animal experiments have shown that Rapamycin, FK 506 and Paclitaxel are able to prevent intimal hyperplasia. In coronary arteries large clinical trials such as the Sirius trial compared a Sirolimus-eluting stent with a bare stent in 1101 patients. At 2 years follow-up restenosis requiring target lesion recanalization (TLR) was significantly reduced (6.3% vs. 21.0%, p < 0.001). In the Taxus IV trial (n = 1314) the TLR rate at 12 month was 4.4% vs. 15.1%, p < 0.0001. In peripheral arteries only one clinical study was finished so far. In the Sirocco trial comparing Sirolimus-eluting versus bare stents in the SFA in 72 patients the 6-month binary angiographic restenosis rate was 0% vs. 11.6%.

Conclusion: Drug-eluting stents have proven to reduce the restenosis rate significantly in coronary arteries. Convincing data of studies in the peripheral arteries are pending.

Learning Objectives:

1. To understand the biological action of the various drugs.
2. To learn the clinical results of coronary artery trials.
3. To learn the clinical results of peripheral artery trials.

10:30 - 12:00

La Scala

E³ - European Excellence in Education

E3 1020

Errors in radiology

Moderator:

R. FitzGerald; Wolverhampton/UK

A-260

Uncertainty, discrepancy, and errors in radiology

R. FitzGerald; Wolverhampton/UK

Reporting discrepancies are common in Radiology, but fortunately only a minority affect patient management. Whilst one can categorise their aetiology as being due to problems of technique, perception, knowledge and judgement, in reality the origins are often multifactorial and systemic. We need to learn lessons from the airline industry in improving safety. Teamworking is fundamental to optimising performance. However, individual accountability still remains even in a systems-based culture, and we should have strategies for radiologists with difficulties. Learning from error and discrepancy is very important. We need to have a no blame reporting culture. Patients have the right to know of errors that have adversely affected their care. The communication of this information must be undertaken in a sensitive manner. A simplistic approach to accuracy in Radiology needs to be replaced with a more complete model of radiological performance. Innovations in radiological interpretive discrepancy collection should stimulate better knowledge sharing and targeted instruction.

Learning Objectives:

1. To learn how some "incorrect" radiological reports may be due to uncertainty or discrepancy rather than error.
2. To become familiar with the scale and causes of error in radiology.
3. To understand how a report can be diagnostically accurate but lack therapeutic impact.
4. To appreciate the relative infrequency of clinical effect on patients from radiological error.
5. To realize that complacency is not appropriate and how we should learn from error in a supportive environment including properly conducted discrepancy meetings.
6. To acknowledge that better knowledge sharing, targeted instruction and teamworking in radiology can improve patient safety and our own working lives.

A-261

Pitfalls in emergency radiology

O. Chan; London/UK

Large numbers of studies have been published in relation to errors in radiology. The "error rate" varies depending on numerous factors and on which imaging modality is studied. However, several factors have been identified, which consistently contribute to major errors. It is neither within the scope or intention of this talk to trawl through the literature, repeating what has already been published. The talk is based on personal experience in a busy emergency radiology department, with a strong emphasis on major trauma (HEMS). It will concentrate on how to reduce errors and improve communication in the emergency room, with quick, simple, cheap and practical advice.

The aim of this talk is to make you think and hopefully adjust/change your current practice, with an emphasis on the following:

- 1) Zero tolerance for poor quality radiography.
- 2) Interpret the radiographs with NO clinical history initially - don't be afraid to make mistakes!
- 3) Use a systematic approach - but relevant to your practice (ABCs approach).
- 4) Obtain a reliable history before giving a report.
- 5) Go and see patients!! Teleradiology is NOT the answer in trauma.
- 6) There is no point in providing a report which fails to get through the physician's skull vault.
- 7) Give your opinion, not a report!

Trauma radiology is FUN and unlike most of radiology, it SAVES LIVES!!

Learning Objectives:

1. To discuss ways of reducing errors in trauma radiology.
2. To emphasize the difference between a report and an opinion.
3. To ensure that your report is communicated to the physician.
4. To attract radiologists into emergency radiology.

A-262

Pitfalls in musculoskeletal MR imaging

W.C.G. Peh; Singapore/SG

Numerous pitfalls may be encountered in musculoskeletal magnetic resonance (MR) imaging. Those caused by imaging technical factors are potentially preventable, and include optimizing coil selection, slice selection, scan planes, pulse sequences, fat suppression, intravenous and intraarticular use of contrast agents, use of surface markers, and protocol-error artifacts. Common inherent MR artifacts include motion, truncation, chemical shift, susceptibility, fat suppression and the magic angle phenomenon. Normal anatomical structures and variants may also be a source of diagnostic pitfalls. Emphasis is placed on recognizing common potential pitfalls, identifying their causes with the aim of providing a remedy for correctable problems, improving diagnostic accuracy, and avoiding unnecessary treatment or surgery.

Learning Objectives:

1. To be aware of the various types of common potential pitfalls in musculoskeletal MR imaging.
2. To identify and if possible, correct or avoid these pitfalls in order to reduce errors in diagnosis.

12:15 - 12:45

Room B

Plenary Session

Gold Medal Awards

Presiding:

A. Chiesa; Brescia/IT

Presentation of the ECR Gold Medal Awards to:

W.W.M. Dihlmann; Hamburg/DE

H. Ringertz; Stanford, CA/US

J. Vignaud; Vouzon/FR

Postgraduate Educational Programme

12:45 - 13:15

Room B

Plenary Session

HL 2

Marie Curie - Honorary Lecture

Presiding:

A. Chiesa; Brescia/IT

A-263

The brain perivascular spaces in health and disease: 2005 update on anatomy, pathophysiology, advanced neuroimaging

A.G. Osborn; Salt Lake City, UT/US

The perivascular (Virchow-Robin) spaces (PVSs) are pial-lined structures that accompany the brain penetrating arteries. This lecture will demonstrate their anatomy and function, illustrating the relationship of the vessels and pia using both electron and transmission microscopy. Computer graphics model the normal PVSs in both the cortex and basal ganglia. The wide spectrum of their normal imaging appearance is demonstrated using 3 T MR scans. A spectrum of giant and "tumefactive" PVSs, extreme but normal variations that should not be mistaken for disease, will be shown. The contents of PVSs, interstitial fluid (ISF, not CSF), is documented and the potential role the PVSs play in regulating brain ISF and modulating immunological response in health and disease is illustrated. A variety of pathologic processes that involve the PVSs, ranging from congenital, infectious, vascular, and neoplasms is demonstrated.

Learning Objectives:

1. To understand the normal anatomy and physiology of the brain perivascular spaces.
2. To recognize the broad spectrum of normal PVSs seen on 3 T MR scans.
3. To become familiar with pathologic processes that involve the PVSs.
4. To learn to avoid mistaking giant, "tumefactive" PVSs for more ominous diagnoses such as neoplasm.

14:00 - 15:30

Room A

Plenary Session

IIS

Image Interpretation Session

Moderator:

P. Schnyder, Lausanne/CH

Panelists:

F. E. Avni; Brussels/BE
C. Cognard; Toulouse/FR
B. Jamar; Ljubljana/SI
A.G. Jurik; Arhus/DK
K. Malagari; Athens/GR

16:00 - 17:30

Room A

Essentials of Neuroradiology

CC 1217

Base of the skull, hypophysis, supra- and parasellar region

Moderator:

B. Góra; Nijmegen/NL

A-264

A. The skull base

J.-W. Casselman; Bruges/BE

Evaluation of the skull base requires a thorough knowledge of the skull base anatomy; the anatomy of the foramina and fissures must especially be known. The bone anatomy is best evaluated using CT. The vessels and nerves passing through the foramina and fissures and the intracranial and extracranial soft tissue structures are however best seen on MR. One can only follow or predict tumor extension along nerves and vessels and through foramina and fissures if this anatomy is known.

Many lesions occur in the anterior, central and posterior skull base and today MR is the preferred technique not only to detect but also to characterise these lesions. However, MR is only superior when the right sequences and imaging planes are used. The use of CT is more and more restricted to evaluate the presence of calcifications and involvement of thin bony walls, foramina and fissures. Many lesions can be characterised by their specific signal intensity on different MR sequences (e.g. menigioma, chondrosarcoma etc.) and by their location (e.g. esthesioneuroblastoma, glomus jugulare etc.). Nevertheless some lesions can only be characterised after biopsy. The purpose of imaging in skull base tumors remains in the first place the evaluation of the exact tumor extent and this is again best achieved with MR. Involvement of bone and sinuses, tumor spread along neurovascular structures and extension in the extra- and intracranial soft tissue structures all have their influence on the staging and therapy choice. All these extensions and involvements are again best seen on MR.

Learning Objectives:

1. To become familiar with the MR and CT technique used to study the skull base.
2. To know the normal anatomy of the bone and soft tissue structures of the skull base.
3. To understand which lesions affect the anterior, central and posterolateral skull base.
4. To learn the which routes are followed when tumor extension occurs.
5. To be able to characterize some of the lesions which are affecting the skull base.

A-265

B. Pituitary lesions

J.-F. Bonneville, F. Cattin; Besançon/FR

MR is today the only method needed for the morphological investigation of endocrine-active pituitary adenomas. In acromegaly and Cushing's syndrome, therapy is directly affected by MR data.

We present the MR aspects of pituitary adenomas according to size, sex, age, endocrine activity, and a few particular conditions such as hemorrhagic pituitary adenomas, pituitary adenomas during pregnancy, cavernous sinus invasion and postsurgical aspects.

When an intrasellar mass extending out of the sella is detected, the goal of the MR examination is to precisely locate the origin of the tumor, its extension in relation to the various anatomical surrounding structures, its structure, and its enhancement in order to help in the differential diagnosis.

Demonstration of very small pituitary adenomas remain a challenge. When SE T1 and Turbo T2-weighted sequences are non diagnostic, enhanced imaging becomes mandatory and half-dose gadolinium injection, delayed sequence, dynamic imaging can be of some help.

Learning Objectives:

1. To familiarize with the different MR techniques useful in the study of pituitary tumors.
2. To choose the MR imaging protocols according to the clinical and biological data.
3. To recognize the usual and unusual presentations of pituitary adenomas.

A-266

C. Supra- and parasellar lesions

J. Ruscalleda; Barcelona/ES

The sellar and parasellar region is an anatomically complex area that represents a crucial crossroad of important adjacent structures, e.g. orbits, cavernous sinus and its contents, circle of Willis, hypothalamus through the pituitary stalk and dural reflections forming the diaphragma sellae and the walls of the cavernous sinuses.

Although the cavernous sinus represents the most relevant parasellar structure, from the practical and clinical point of view all the structures that surround the sella turcica can be included in the parasellar region.

CT and mainly MR are the imaging modalities to study and characterize the normal anatomy and the majority of processes presenting in this region.

We present a practical short review of the most relevant CT and MR imaging characteristics such as location, nature of contrast enhancement, presence of cystic components, together with clinical findings which permit differentiation of the most frequent and less common lesions found in the parasellar region.

Learning Objectives:

1. To review the complex anatomic relationships between structures in the sellar and parasellar regions.

Postgraduate Educational Programme

2. To understand the main patterns and radiological characterisation, mainly by MR, of the many lesions that alter the structure and function of sellar and parasellar anatomy.
3. To be familiar with the description of the MR features that permit differentiation among less common lesions.
4. To learn the different protocols in the approach parasellar pathology.

16:00 - 17:30

Room B

State-of-the-Art Symposium

SA 12

Multi-dimensional imaging for guiding therapy

Moderator:
C. Bartolozzi; Pisa/IT

A-267

Multi-dimensional imaging for guiding therapy (Introduction)

C. Bartolozzi; Pisa/IT

Interventional techniques are nowadays the therapy of choice in many clinical settings and are therefore progressively substituting conventional surgical interventions.

A prerequisite for this approach is the precise anatomical display of the lesion to treat as well as the surrounding anatomical structures. This can ideally be achieved by using multi-modality volume acquisitions and advanced processing techniques (3D, image fusion, virtual reality, etc.) which allow a paramount representation of the area of interest and help to correctly plan the procedure.

Another key issue is the possibility to have a real-time feedback on the progress of the on-going interventional procedure, thus optimising the efficacy of the treatment and at the same time reducing the risks for the patient. A high degree of interactivity is therefore mandatory in these applications.

Finally, the role of computer-assisted guidance in these procedures is clearly emerging and has the potential to lead to the introduction of automated systems (robots) for performing specific interventional tasks.

Learning Objectives:

1. To discuss the role of image processing and 3D imaging in planning therapy.
2. To review the available techniques for real-time monitoring of interventional procedures.
3. To highlight present capabilities and future development of image-guided therapy and robotic applications.

A-268

3D imaging in therapy planning

A. Laghi; Rome/IT

The acquisition of volumetric data sets and the parallel development of new rendering software (in particular perspective volume rendering) allows the generation of high quality 3D reconstructions making 3D imaging part of the routine diagnostic process.

3D imaging plays a very important role in therapy planning, assisting the decisional process in conventional surgery, laparoscopic surgery and within non-surgical, interventional therapies. For upper abdominal surgery and in particular within the liver, precise definition of vascular anatomy, both arterial and venous, is determinant. The identification of a vascular anomaly, correct in over 95% of the cases, may even alter or prevent a certain type of surgery. New high-resolution data sets from 16-slice or more multi-detector spiral CT equipments allow the identification of second-order intra-hepatic branches in over 85-90% of the cases. This evaluation is particularly important in living liver donors, where some intrahepatic vascular anomalies may prevent subjects from intervention.

3D imaging offers also a better evaluation of parenchymatous lesions, in particular those small and in a sub-capsular location, thanks to the use of planes different from the axial.

Organ and lesion volumetry are two other applications of 3D imaging. Today software for automatic liver segmentation as well as calculation of segmented liver volumes are available, helping clinicians in the decision-making process regarding hepatectomy or transplantation.

In conclusion, 3D imaging does not affect the diagnosis, but it makes the diagnosis easier and faster. It offers complementary information to a simple 2D data evaluation and it facilitates the communication between radiologists and clinicians.

Learning Objectives:

1. To understand basic principles of 3D post-processing techniques.

2. To comprehend the indications for the use of different 3D post-processing techniques.
3. To understand the role of 3D imaging in different surgical planning.

A-269

Real-time monitoring of interventional procedures

A.R. Gilliams; London/UK

Successful ablation requires complete coverage of the whole tumour in three dimensions and a 1 cm margin of normal appearing tissue which often contains microscopic tumour cells. Yet, none of the available ablation techniques produce predictable zones of ablation. Tissue-mediated perfusion and adjacent vessels impact on ablation size and shape. Therefore it is important to monitor the ablation. Ideally the interventional radiologist would be provided with co-registered 3D images of the tumour with the superimposed ablation zone so that an immediate assessment can be made. Of the available techniques, CT is useful in lung ablation. A penumbra of ground-glass shadowing that encapsulates the treated lesion usually indicates successful ablation. For liver and renal ablation there are several options although the most readily available, unenhanced US, is of limited value. Contrast enhanced US has proven efficacious in the assessment of hyper-vascular tumours but is less useful in hypovascular tumours. For metastases contrast enhanced CT or MR are a better option. Ablation is indicated by absent enhancement. Intra-procedural scans can provide immediate feedback. MR has the added attraction of providing temperature mapping either by looking at changes in T1 or shifts in proton resonance frequency. This has been useful in the breast and extremities but is less useful in liver ablation where subtraction imaging is hampered by respiratory movement and tissue deformation. A more recent development uses Gadolinium-filled thermosensitive liposomes which produce T1 shortening when a specific, pre-determined temperature threshold has been reached.

Learning Objectives:

1. To understand the different options for monitoring tumour ablation, the possibilities and the drawbacks.
2. To understand how to choose the optimal technique for a particular patient.
3. To understand the importance of feedback in ensuring complete ablation.

A-270

Image-guided therapy and robotic applications

E. Sorantin¹, J. Kettenbach², R. Bale³, G. Kronreif², G. Werkgartner¹, R. Beichel¹, A. Bornik¹, B. Reitinger¹, M. Sonka⁴; ¹Graz/AT, ²Vienna/AT, ³Innsbruck/AT, ⁴Iowa, IA/US

Present capabilities of imaging modalities produce volumes of data in the range of the human genome during a single investigation. This is especially true for Multislice Computed Tomography (MSCT) and Magnetic Resonance Imaging (MRI). Together with the luckily available and affordable computer power, the development and implementation of new and challenging applications in image-guided therapy are possible.

The term 'image-guided therapy' describes applications ranging from disease quantification (e.g. tumor volumes), image fusion (e.g. functional and morphologic data - PET/CT) to intraoperative navigation. The latter, refers to a setup, where the physician can monitor the progress of a procedure by using any imaging modality (e.g. ultrasound guided biopsy). Imaging data and reality can be fused by setting up an "Augmented Reality" system, where image based 3D virtual objects can be displayed together with "Reality" around the user in real-time. Such a setup is similar to navigation systems which help aircraft pilots land an airplane safely despite unrecognizable real-life conditions (e.g. due to fog). Integration of robotics offers the possibility to exploit their precision for certain tasks such as drilling screw holes in trauma surgery or taking biopsies.

Learning Objectives:

1. To present the basics and ingredients of real time navigation and tracking.
2. To give an introduction how to set up an "Augmented Reality System".
3. To demonstrate key applications and discuss their clinical impact.

Postgraduate Educational Programme

16:00 - 17:30

Room C

Special Focus Session

SF 12

Assessment of myocardial perfusion and viability

Moderator:

A. de Roos; Leiden/NL

A-271

Assessment of myocardial perfusion and viability (Introduction)

A. de Roos; Leiden/NL

In this session, the issue of assessing myocardial viability with the use of well-accepted technology, as well as with new imaging modalities like CT and MR imaging, will be discussed. Assessment of myocardial viability is a critical clinical question for patient management. Nuclear medicine imaging is traditionally the accepted and time-honored tool for viability assessment. The role of stress echocardiography, the upcoming role of CT and the somewhat more established role of MR imaging will be discussed from different perspectives. As part of these discussions the state-of-the-art of the various technologies will be discussed. Both the current technology as well as the established or potential role of these imaging techniques for viability imaging will be put in perspective.

Learning Objectives:

1. To understand the current technical approaches.
2. To learn the current clinical applications.
3. To learn current advantages and limitations.

A-272

Ultrasound and nuclear medicine

J.J. Bax¹, D. Poldermans²; ¹Leiden/NL, ²Rotterdam/NL

Background: Assessment of viability has become an important component of the diagnostic and prognostic work-up of patients with chronic ischemic left ventricular (LV) dysfunction. This is important for risk-benefit analysis, since not all patients improve in function after revascularization. In a recent analysis with 258 consecutive patients (LVEF 29±7%), improvement in LVEF after revascularization was observed in 39% of patients.

Procedure Details: Large experience has been obtained with nuclear imaging (PET and SPECT) and stress (mainly dobutamine) echocardiography. Based on the presence of viability, it is possible to predict improvement of regional and global LV function, heart failure symptoms and exercise capacity. In addition, viability assessment carries important prognostic information. In 18 direct comparisons (563 patients) between dobutamine stress echocardiography and nuclear imaging, the sensitivity of nuclear imaging was higher than that of stress echocardiography (90% vs 74%, P < 0.05), indicating that the nuclear imaging techniques are more sensitive in detecting viable tissue.

Conclusion: Both nuclear imaging techniques and dobutamine stress echocardiography are useful techniques for assessment of viability; nuclear techniques are more sensitive to detect viability.

Learning Objective:

To explain the basics and the relative merits of nuclear imaging and dobutamine stress echocardiography for the assessment of viability.

A-273

Role of multidetector CT

J. Barkhausen; Essen/DE

Recently ECG gated multidetector spiral CT (MDCT) has emerged as a new modality for cardiac imaging. The focus of MDCT has been primarily on applications for calcium scoring and CT angiography of the coronary arteries. However, MDCT can additionally be used to assess myocardial viability and myocardial perfusion.

In the first part of the lecture different scan protocols (single- and dual-phase approaches) will be introduced. Advantages and limitations including the necessity for iodinated contrast material and radiation exposure will be discussed. Thereafter, different myocardial enhancement patterns (early defects, residual defects and late enhancement) and the clinical meaning of these findings will be explained. However, only a limited number of studies have been published so far and therefore the assessment of myocardial perfusion and myocardial viability must still be considered a challenging and controversial field of cardiac CT. Future clinical applications might include the measurement of the infarct size in

patients with acute myocardial infarction and the assessment of the success of attempted reperfusion therapy after percutaneous coronary interventions.

Learning Objectives:

1. To learn about scan protocols for the assessment of myocardial viability and perfusion.
2. To understand different myocardial enhancement patterns.
3. To discuss potential clinical applications.

A-274

Role of MR imaging

H.J. Lamb; Leiden/NL

Chronically hypoperfused and severely dysynergic myocardium in patients with chronic coronary artery disease (CAD) can maintain viability through a mechanism known as 'hibernation'. Reversal of myocardial dysfunction in patients with CAD improves long-term survival. However, revascularization is associated with a risk for complications and mortality. Therefore, it is clinically important to identify *a priori* those patients who may benefit from a revascularization procedure. Cardiovascular magnetic resonance imaging (CMR) is a new and highly reproducible technique allowing functional imaging and MR perfusion imaging of the heart at rest and during cardiac stress. For evaluation of myocardial viability, various approaches using MR imaging have been described, including assessment of end-diastolic wall thickness, assessment of contractile reserve using low-dose dobutamine and assessment of scar tissue using contrast-enhanced imaging. Recently, research has focused predominantly on these last 2 approaches. However, from a pathophysiological point-of-view, these 2 approaches do not reflect the same. While low-dose dobutamine is used to demonstrate the presence of contractile reserve in dysfunctional myocardium (and thus identifies viable myocardium), contrast-enhanced imaging identifies scar tissue. The precise relation between these 2 techniques will be explained and demonstrated in patient cases. Furthermore, prediction of therapy effect based on CMR viability imaging will be discussed. In addition, technical aspects of CMR viability imaging will be discussed.

Learning Objectives:

1. To learn about basic concepts of CMR viability imaging.
2. To obtain basic knowledge of CMR techniques for viability imaging.
3. To be able to decide what type of CMR exam answers what type of clinical question.

16:00 - 17:30

Room E1

Cardiac

RC 1203

Pericardial diseases

Moderator:

A.F. Kopp; Tübingen/DE

A-275

A. Clinical issues and US

M.R. Rees; Bristol/UK

Acute or chronic pericarditis may result from infection, malignancy, connective tissue disorders, trauma, myocardial infarction, drug therapy or AIDS where the pericarditis may be due to a fungal infection, Kaposi's sarcoma or tuberculosis. Acute pericarditis may be a result of acute myocardial infarction (Dressler's syndrome) in 10-15% of cases and may also be a cause of acute cardiac rupture resulting in haemopericardium, both syndromes usually occur within 10 days of a MI. Acute pericarditis also occurs with trauma and post pericardiectomy syndrome. Acute pericarditis often causes chest pain which usually is aggravated by thoracic motion, cough and respiration and relieved by sitting up and moving forward. The most significant finding is a pericardial rub. Fluid around the heart may muffle heart sounds. There may be characteristic ST elevation on ECG. Acute and chronic pericardial disease may also present with atrial arrhythmias particularly malignant pericardial disease. The heart may be enlarged on chest X-ray. Acute pericarditis is best diagnosed by cardiac ultrasound, detecting fluid around the heart.

Chronic pericarditis may be haemorrhagic, fibrous, adhesive, metastatic, chylous or calcific, it may follow connective tissue disease, trauma, infection or drug therapy or malignancy. Chronic pericarditis may be followed by constriction which causes raised systemic and hepatic venous pressures with signs of peripheral and hepatic congestion. The typical signs of pericardial tamponade may also be

Postgraduate Educational Programme

detected with right atrial collapse and right ventricular diastolic collapse but pericardial thickening is not easily diagnosed by ultrasound. Doppler echocardiography may help distinguish constrictive pericarditis from restrictive cardiomyopathy.

Learning Objectives:

1. To discuss symptoms and clinical relevance.
2. To review radiological investigations and evidence base.
3. To review limitations and indications of ultrasound.

A-276

B. CT and MR imaging of the inflammatory diseases

M. Midiri, M. Galia, T. Bartolotta; *Palermo/IT*

Inflammatory diseases of the pericardium are common disorders which present with pericardial thickening, with or without constrictive pericarditis, determined by multiple causes, including infection (viral or tuberculous), idiopathic conditions, uremia, rheumatic heart disease, rheumatoid arthritis, sarcoidosis and mediastinal irradiation. They are safely managed with various primary and secondary-care settings, which need accurate diagnostic evaluation.

Computed tomography (CT) and magnetic resonance (MR) imaging may provide accurate delineation of the pericardial anatomy and can aid in the precise localization and characterization of various pericardial pathological changes.

Multidetector CT enables motion-free imaging of the pericardium as well as multiplanar reformation images, allowing the detection of pericardial calcification, often associated to constrictive pericarditis, and contrast-enhancement of the inflamed thickened pericardium. Disadvantages of CT include the use of intravenously administered contrast material, ionizing radiation exposure and its occasional difficulty in differentiating fluid from thickened pericardial tissue.

MR imaging is able to distinguish pericardial effusions by pericardial thickening with the use of T1-W, T2-W and gradient-recalled echo (GRE) cine sequences. It provides depiction of the pericardium without the use of either iodinated contrast material or ionizing radiation, allowing to recognize the high signal intensity of the inflamed thickened pericardium and its enhancement after administration of gadolinium-based contrast material.

Both imaging techniques provide a large field of view, allowing the examination of the entire chest and detection of eventually associated abnormalities in the mediastinum and lungs.

Potential applications and limits of CT and MR imaging involved in the study of inflammatory diseases of pericardium will be discussed.

Learning Objectives:

1. To review aetiological classification.
2. To review patho-physiology and clinical symptoms.
3. To discuss the diagnostic possibilities of CT and MR.

A-277

C. CT and MR imaging of the neoplastic diseases

J. Bremerich; *Basle/CH*

Introduction: Neoplastic disease of the pericardium can be classified as benign, primary malignant, metastases and tumorlike lesions. Among the benign lesions are pericardial cysts and lipoma. Primary pericardial malignancies such as mesothelioma, liposarcoma, fibrosarcoma, and teratoma are rare. Metastatic disease from melanoma or cancer from breast, lung, and colon are more frequently encountered.

Methods and Results: Echocardiography is first line modality for imaging pericardial masses. But it can not characterize effusions, is limited in loculated effusions, and is unreliable in definition of pericardial thickening. Moreover, acoustic windows are not optimal in many patients.

CT is an excellent tool for morphologic assessment of pericardial masses, particularly when calcifications are present. Normal myocardium is visible as a thin line between the epicardial and pericardial fat, masses are readily identified. However, differentiation of thickened pericardium from exudative pericardial effusion with high protein content can be difficult.

Magnetic Resonance provides information on structure and function of the heart and pericardium. Free choice of imaging plane and excellent soft tissue contrast allow accurate characterization of masses, adjacent structures and cardiac function. Pericardial cysts often contain transudative fluid with low protein content and thus appear dark on T1- and bright on T2-weighted images. Lipomas will have characteristic high signal intensity on T1-weighted images. Mesotheliomas and other malignant masses will typically enhance after contrast administration.

Conclusion: Echocardiography is the first line imaging modality for pericardial masses. CT provides excellent definition of morphology, particularly when calcifications are present. MR imaging allows both specific characterization of pericardial masses and cardiac function.

Learning Objectives:

1. To understand the pathological classification and incidence of (para)cardiac neoplasms.
2. To understand the indication for various imaging modalities.
3. To understand the major differences between CT and MR imaging findings and their clinical impact.

16:00 - 17:30

Room F1

Chest

RC 1204

Multislice CT of the thorax

Moderator:

Y. Pallardó; *Alzira Valencia/ES*

A-278

A. Evidence-based optimisation of standard protocols

S.M. Ellis; *London/UK*

In radiology the optimisation of imaging using ionising radiation must always consider the reciprocal relationship between radiation dose to the patient and image quality. Multi-detector CT scanners are more dose efficient than their predecessors but, with the facility to reconstruct ever thinner contiguous slices, the temptation is to use that dose efficiency to improve image quality rather than lower the dose.

Standard multi-detector CT (MDCT) protocols are to some extent evidence based, in that they are derived from protocols that have become established in clinical use, and scanner-specific modifications are performed with reference to the preferences of authoritative radiologists in the field. Alterations to these standard protocols may have a significant impact on the patient outcome therefore any "optimisation" of protocols should be rigorous and evidence based; at present there is little published data on which to base optimisation of standard protocols, a situation that should improve as MDCT scanning becomes more widespread. MDCT, more than any previous CT technology, broadens the range of alterations that can be made to scanning parameters and therefore requires careful study into how this flexibility is best utilised. I aim to outline the range of optimising techniques available, comment on the existing literature and highlight some of the problems that may be encountered when trying to optimise protocols in an evidence based manner.

Learning Objectives:

1. To review the existing literature on evidenced based multislice CT protocols.
2. To consider the relevance of evidence based protocol optimisation to an MSCT design that differs to that on which the evidence is based.

A-279

B. Dose reduction in thoracic CT

D. Tack; *Baudour/BE*

The assertion that any radiation dose, no matter how small, can cause cancer is the basis for the linear no-threshold theory of radiation carcinogenesis. However, some health scientists consider the cancer risk from low-dose radiations as used in clinical practice for diagnostic procedures as being grossly exaggerated or even negligible. The European Commission has published precautionary measures in order to limit the radiation dose, in particular from CT, because the dose from a chest CT may be 100 times higher than that by a CXR. The influence of CT parameters (number of detector-rows, beam collimation, KVp, mAs, pitch, CT-Dlw), of patient parameters (height, weight, body mass index, age, gender, and underlying conditions) as well as of radiologist-dependant parameters on the effective dose are presented. Radiation dose levels from typical standard CT protocols with single and multislice technique are compared to those of a CXR. Low-dose HRCT and multislice CT protocols enable reduction of the radiation per examination by a factor of 10 as compared to standard acquisitions, mainly by decreasing the mAs or by increasing the pitch. Potential benefit in dose reduction by the use of low KVp is presented. Newly developed automatic dose reduction systems are promising because they adapt the tube conditions to the patient's geometry. Distinction has to be made between the radiation dose delivered to one single individual and the collective radiation dose because the effect of diagnostic strategies on the individual and the collective doses may be opposite.

Learning Objectives:

1. To discuss the risk of induction of cancer through radiation exposure at chest CT.

Postgraduate Educational Programme

2. To understand how CT and biometric parameters influence the effective radiation dose.
3. To learn methods to decrease radiation exposure at chest CT by varying examination parameters maintaining diagnostic image quality.

A-280

C. The application of post-processing

J. Rémy, M. Rémy-Jardin; Lille/FR

Image processing in thoracic disorders includes multiple operations aimed at improving the diagnostic capabilities of a CT examination. Isotropic imaging, short acquisition times and data explosion have triggered the development of post-processing. One can classify postprocessing contributions into morphologic and functional approaches. Whatever the disease, a morphologic reformatting approach can be used for: a) Selective visualization of bronchial and vascular lumina and walls along their main axis with their surrounding structures. b) Virtual angiography and bronchoscopy. c) Angiographic and bronchographic renderings before interventional procedures. d) Morphological evaluation of the heart. e) Quantification and follow-up of pulmonary nodules. The functional approach using postprocessing deals with: a) Perfusion and ventilatory imaging. b) Analysis of the right ventricle. c) Evaluation of the thoracic outlet. As opposed to the aorta or peripheral arterial occlusive disease, whose evaluation can be exclusively based on angiographic renderings, investigation of a pulmonary or systemic vascular disease implies a simultaneous examination of vascular and bronchopulmonary structures which are supplied by or which have generated the abnormal circulation.

Learning Objectives:

1. To review the usual techniques of post-processing in diseases of the chest.
2. To learn their main applications in routine clinical practice: Pulmonary embolism, preoperative management of bronchial carcinoma, hemoptysis and vascular anomalies of the lung.
3. To emphasize their growing indications in the technological context of multi-slice thoracic imaging.

16:00 - 17:30

Room F2

Neuro

RC 1211

Diffusion and perfusion MR imaging of the brain

Moderator:

M.M. Thurnher; Vienna/AT

A-281

A. Imaging technique and protocols, post-processing

L. Østergaard; Århus/DK

Perfusion and Diffusion weighted MR imaging are becoming important tools in the diagnosis of neurological disease. In order to insure images of maximum quality of the derived parametric maps (Cerebral Blood Flow -CBF, Cerebral Blood Volume - CBV, Mean Transit Time - MTT, Apparent Diffusion Coefficient - ADC) a number of precautions must taken in the acquisition and post processing of the images. These involve tracer injection speed, saline flush volume, image acquisition rate and choice of EPI sequence in relation to the pathology. Also, the information inferred from post-processed images must be related closely to the inherent methodological problems of perfusion MR imaging (delay, dispersion).

This talk will supply a framework for acquiring and analysing perfusion data and briefly discuss issues of importance in analysis of diffusion MR imaging, especially in the context of acute stroke.

Learning Objectives:

1. To understand the problems and merits of the most common imaging techniques in perfusion imaging.
2. To discuss necessary features for imaging protocols.
3. To understand the basics of perfusion postprocessing and its limitations.
4. To discuss various pitfalls that may lead to false interpretation of perfusion weighted images.

A-282

B. Clinical applications of diffusion and perfusion MR of the brain

P. Reimer, S. Arnold, Z. Puskas; Karlsruhe/DE

Over the past 10 years, considerable experience has been accrued using both diffusion and perfusion MR imaging by means of contrast agents to measure

cerebral hemodynamics and other cerebral diseases. Diffusion and perfusion MR imaging can be performed on nearly all up-to-date clinical scanners. Imaging technology is at a stage where, in addition to morphological information, the concomitant acquisition of functional and physiological information is possible. The previous speaker will explain the techniques in detail.

The most common clinical application of both techniques is within the field of stroke imaging where diffusion MR imaging can be considered a "must do it" and perfusion MR imaging is added to solve further questions. However, imaging of neoplasm, inflammation, or infection has gained considerable interest as well. Patients presenting with possible brain ischemia are routinely imaged with diffusion MR imaging and "lesions" are also further differentiated by means of ADC maps. The combination of diffusion and perfusion MR imaging is applied when tissue at risk needs to be detected. Unfortunately, mean-transit-time and other timing maps do not appear to do an adequate task of distinguishing between levels of hemodynamic compromise. That is, the feature that makes them easy to interpret - being normal or abnormal - does not allow for the gradation of abnormalities, the difference between blood flow decreases that are mild to moderate versus moderate to severe. Perfusion techniques appear not to be able to distinguish between acute hemodynamic compromise and chronic hemodynamic compromise. Fortunately, DWI can easily make this distinction.

Learning Objectives:

1. To learn about the most common clinical applications of diffusion imaging and perfusion imaging in neuro MR imaging.
2. To understand the rationale of adding diffusion imaging and perfusion imaging to morphological MR imaging.
3. To value diffusion imaging and perfusion imaging in the scenario of a comprehensive neuro MR imaging examination.

A-283

C. Diffusion tensor imaging and fibre tracking

C. Oppenheim, J.-F. Meder, D. Fredy; Paris/FR

Diffusion tensor imaging (DTI) is generating high expectations in the study of the central nervous system (CNS) because it is currently the only way to non invasively study the 3D architecture of white matter tracts. Using DTI, diffusion anisotropy effects can be extracted and used to characterize tissue microstructure. Several scalar parameters, such as mean diffusivity and anisotropic indices, can be obtained with DTI. Their potential over routine DWI for demonstrating subtle abnormalities and improving our knowledge of brain pathophysiology will be illustrated by means of clinical applications: stroke, multiple sclerosis, tumours, dementia, epilepsy, The methods for reconstructing axonal tracts using DTI will be presented. Clinical applications, validation issues and potential future improvements will also be discussed.

Learning Objectives:

1. To understand the concept behind DTI and fiber tracking.
2. To discuss the quantitative parameters derived from DTI.
3. To identify their potential uses in clinical studies.

16:00 - 17:30

Room G

Physics in Radiology

RC 1213

Safety considerations in MR

Moderator:

T.G. Maris; Iraklion/GR

A-284

A. MR safety, biophysical effects and the European legislation

J.M.L. Engels; Best/NL

Modern MR scanners approach the safety limits for patients for almost all relevant physical parameters for the MR scanner. More recently also legislation is accepted for the safety of MR workers (at the MR manufacturer and in the hospital). The applied dynamic gradient fields (which may create peripheral nerve stimulation), but also the acoustic noise produced by the gradients (which makes the use of ear protection essential) and the RF fields transmitted by the RF coils (which may heat up the human body), make it essential to implement safety measures on the MR scanner. Also the static magnetic field (known to create instantaneous effects such as nausea or dizziness or metal taste) may become a limiting factor for future scanners. The MR specific limits for these parameters for patients are described in the IEC 60601-2-33 international standard for safety of

Postgraduate Educational Programme

MR equipment. Recently, new European legislation is accepted which also limits these parameters for MR workers and thus has direct implications for the use of MR. Especially, high field systems and interventional MR are hindered by this new legislation and urgently call for more research, to determine the safety levels. In spite of all these potential dangerous situations MR scanners are still considered to be a most safe and patient friendly modality.

Learning Objectives:

1. To discuss the biophysical effects of static and dynamic magnetic fields.
2. To discuss the biophysical effects of RF power and related SAR.
3. To present the status of current international MR safety standards and legislation.

A-285

B. Clinical safety practice

J. de Wilde; London/UK

In MR imaging safety issues affect everyday clinical practice. Every patient and visitor to the MR suite has to be screened for implants, tattoos, eyeliner and clothing, i.e. anything which may move in the magnetic field or may heat up due to the radiofrequency field and cause injury. It is important to note that MR imaging burns are the most frequently reported incident within the UK. Patient set up within the bore of the magnet is an important safety issue, especially if there are monitoring devices involved. These issues will be reviewed in the talk. Another major cause of injury in MR is projectile hazards; ways in which to minimize the risk of this will be discussed in term of good practice within the MR suite. Currently there is a trend towards higher field strengths MR systems which means that patients and staff are likely to be exposed to higher noise levels. This talk will examine noise protection issues. Another important concern is that of pregnancy and MR imaging. The current state of play regarding imaging of pregnant patients and pregnant staff working in MR imaging will be addressed.

Learning Objectives:

1. To understand patient screening issues including implants in MR imaging.
2. To review patient monitoring issues in MR environment.
3. To understand how to minimize the projectile risk.
4. To review of acoustic noise issues.
5. To overview of MR imaging in pregnancy.

A-286

C. Interventional MR imaging: Safety considerations for patients and personnel

A. Bücker; Aachen/DE

Fast imaging sequence are a prerequisite for MR-guided interventions to speed up the procedure and allow even real-time imaging for guidance of vascular interventions. The main obstacle so far is not imaging speed but the development of interventional devices, which are MR-safe as well as MR-compatible. Using passive methods for device visualization one has to be aware of the artifact behaviour of interventional instruments in order to correctly localize the instrument tip. The artifact behaviour depends on the used imaging sequence (gradient versus spin echo) and sequence parameters like echo time and phase encoding direction. Active methods can overcome these potential problems and allow not only for device visualization but also for slice tracking. Drawbacks of active methods are more sophisticated hardware and software requirements. Furthermore safety issues concerning heating of long conductive wires have to be taken into account in order not to jeopardize the patient or interventionalist. First approaches are using fiberoptic means to achieve MR-safe active instrument visualization. While passive device visualization is sufficient for interventions like biopsies, vascular interventions will greatly profit from the possibility of slice and tip tracking of active means especially in the region of small and tortuous vessels. Performing interventions in the MR environment requires special awareness of all personnel involved in the procedure including anesthesiology. Consequently, a dedicated team should be set up in order to avoid accidents due to inexperienced handling of metallic patient support devices.

Learning Objectives:

1. To learn about imaging characteristics of interventional instruments.
2. To learn safety considerations for organizing an interventional MR suite and how to safely perform interventions.
3. To learn about safety problems of interventional instruments.

16:00 - 17:30

Room H

Interventional Radiology

WS 1209

Aortic stent grafts

Moderator:

C. Düber; Mannheim/DE

A-287

A. Thoracic

K. Ivancev; Malmö/SE

Stent-graft (SG) treatment of conditions in the descending thoracic aorta has its own merits and limitations depending on the indications for treatment.

Material and Methods: Complicated Type B dissections were treated in 33 patients, 23 of which on emergency basis. Median imaging FU was 12 months (1-61). Traumatic transections and pseudoaneurysms were treated in 4 patients. Fusiform atherosclerotic aneurysms were treated in 34 patients at high operative risk, 8 of which on emergency basis. Median imaging FU was 22 months (3-85).

Results: In the Type B dissection group 30-day mortality was 21% in the emergency subgroup, 0% in the elective subgroup. One patient developed paraplegia. Two patients died of erosion caused by the SG during follow-up. In the group with traumatic transections and pseudoaneurysms there were no complications. In the fusiform atherosclerotic aneurysm group 30-day mortality was 26% and paraplegia 6%. Eight patients succumbed to SG-related complications during FU: Migration 2 pts, SG separation 2 pts, aortic wall erosion by the SG 4 pts.

Conclusions: SG treatment is a truly valuable alternative to open surgery in patients with traumatic transections and pseudoaneurysms and in patients with complicated Type B dissections. Extensive fusiform atherosclerotic aneurysms continue to present a challenge for SG treatment.

Learning Objectives:

1. To briefly review the literature and present the results with stent-graft treatment in the descending thoracic aorta.
2. To highlight the advantages of stent-graft treatment over open repair in complicated type B dissections.
3. To stimulate radiologists to use their imaging skills in correctly planning for stent-graft placement in the descending thoracic aorta.
4. To emphasize the limitations of current stent-graft treatment in atherosclerotic descending thoracic aortic aneurysms.

A-288

B. Abdominal

J. Lammer; Vienna/AT

Purpose: Abdominal aortic aneurysms (AAA) with a diameter of more than 6 cm have a rupture risk of 25% per year. The purpose of stentgrafts is to prevent rupture.

Materials and Methods: The indications for treatment are:

- diameter of AAA > 5 cm
- growth > 0.5 mm/year
- symptomatic aneurysm
- rupture

Specific indications for endovascular treatment are:

- patient > 75 years
- ASA 3 and 4
- > surgical risk.

Stentgrafts can be placed under epidural and local anesthesia. Arteriotomy is required because delivery systems have a diameter of 12-22 F. The stentgraft is placed below the renal arteries under fluoroscopy. Suprarenal fixation usually does not cause renal artery thrombosis or embolization.

Stentgrafts have a self expandable stent structure covered by an ultrathin polyester or ePTFE fabric. Currently only bifurcated stentgrafts are used for treatment of AAA.

Results: According to the Eurostar registry (> 4,700 patients) technical successful stentgraft placement was achieved in > 99%. Conversion to open surgery was required in 0.7%. The in-hospital mortality rate was 2.2%. At completion angiography endoleaks were demonstrated in 15.7% (type 1-4.3%, type 2 -9.0%, type 3-2.4%). Life-table analysis revealed at 1 and 5 years a survival rate of 92.3%, and 78.8%, freedom from persistent endoleaks 93% and 91%, freedom from rupture 99.8% and 98.6%, respectively.

Conclusion: AAA's can be excluded by stentgrafts with a high technical success rate of 99%. Conversion to open surgery is rarely required. Freedom from rupture is 98% at 5 years.

Postgraduate Educational Programme

Learning Objectives:

1. To understand the indications of endovascular repair of AAA.
2. To learn the technique of stentgraft implantation.
3. To get the most recent results of longterm outcome after stentgraft treatment of AAA.
4. To learn the preliminary results of endovascular treatment of ruptured AAA.

A-289

C. Bifurcated grafts

M. Maynar; Santa Cruz de Tenerife/ES

Endovascular bifurcated grafts can offer an alternative treatment for patients with symptomatic non-aneurysmal aortoiliac lesions. Indications for treatment are aortoiliac occlusion, complex aortoiliac stenotic lesions and ulcerated plaques causing blue toe syndrome. To prevent adverse hemodynamic and pathologic changes, we opted to use the Excluder® prosthesis to rebuild the aortoiliac region as it offers features like high conformability due to the flexible endoprosthesis body, a low-profile delivery system and a smooth lumen surface without metal struts or sutures. In aortas with a small distal diameter that prevent expansion of the contralateral short leg, we used a combined femoral/brachial access as the guide wire can be advanced more easily through the non-expanded contralateral leg than from a contralateral femoral access. After a through and through wire has been established, the contralateral leg can then be deployed. An angioplasty with the kissing technique is subsequently performed to ensure total expansion of the graft at the level of the bifurcation up to the maximum aortic diameter. The aortobifemoral bypass graft remains the procedure of choice for the treatment of diffuse aortoiliac disease but it is associated with a relatively high morbidity and operative mortality. Aortic uni-iliac graft combined with a femoro-femoral bypass is only considered in case of failure of the endovascular treatment, as both surgical techniques offer suboptimal clinical results. The placement of bifurcated endoprostheses is technically feasible, effective, and safe in the management of aortoiliac lesions and offers an alternative to the conventional surgical techniques.

Learning Objectives:

1. To discuss indications and patient selection.
2. To discuss graft selection.
3. To know how to work in small abdominal aortic lumen.
4. To discuss bifurcated graft vs aortic uni-iliac graft and femoro femoral bypass.
5. To know tips and tricks.

16:00 - 17:30

Room I

Vascular

RC 1215

Vascular imaging

Moderator:

C. Catalano; Rome/IT

A-290

A. MRA: Basic principles and clinical applications

G.M. Bongartz; Basle/CH

MR-angiography (MRA) has evolved from cross-sectional imaging by converting artefactual flow signals into diagnostic information. So-called native techniques comprise Time-of-Flight and Phase-Contrast MRA. Today, most native MRA techniques are replaced by contrast-media enhanced MRA (CE-MRA) that combines fast imaging with high vascular contrast and easy post-processing.

CE-MRA depends on ultrafast techniques to "freeze" the arterial bolus following venous injection. The most challenging task is the timely exact coordination of the bolus and the signal collection. MR shows dedicated features during signal reading represented by the k-space. All alterations in k-space directly affect the MRA signal. Basic knowledge of k-space is therefore mandatory to achieve good results and to understand artefacts.

Bolus geometry directly affects MRA results. Especially in multi-volume imaging, the arterial bolus must remain on constant high level. The problem of conflicting venous signal is important for MRA of the lower extremities, requiring technical adaptation.

Hybrid techniques are helpful in several indications although they may suffer from decreased resolution. Recently, high speed acquisition while maintaining high contrast and high spatial resolution have been developed by using parallel imaging or ultra-high field strength and increased gradient's performance.

Learning Objectives:

1. To understand the underlying principles of the various forms of MR-angiography.
2. To learn about the physics and techniques for contrast-enhanced 3D MR-angiography.
3. To recognize and avoid common pitfalls in MR-angiography.
4. To recognize emerging applications of MR-angiography.

A-291

B. CTA: Basic principles and clinical applications

M. Prokop; Utrecht/NL

CT angiography (CTA) has been revolutionized with the advent of multislice scanning. While single slice CTA was mainly focusing on the aorta and pulmonary arteries, multislice CTA can now cover any vascular territory in the body because of a substantially increased scan coverage as well as spatial resolution. Spatial resolution is now good enough to see very small vessels like the central bronchial arteries or the arteries of the hand. This course will discuss how scanning parameters and contrast administration have to be adapted to multislice scanning. New challenges include the increased noise with thin-section imaging, the individual adaptation of radiation dose and contrast material depending on patient parameters, and the optimum timing of the scan. The course will discuss how to avoid new pitfalls introduced by the newest generation of 32 to 64 slice scanners. Postprocessing techniques will be reviewed, with a special focus on simple techniques that allow for quick and problem-oriented solutions for image display and evaluation. CTA can be used for stroke imaging, pulmonary embolism, aortic diseases, renal artery stenosis and mesenteric artery abnormalities. The latter can be examined as part of a standard arterial phase scan of the abdomen. Portal phase images allow for evaluation of portal hypertension, vascular occlusion or tumor involvement. Newer developments include CTA of the peripheral arteries of the lower and upper extremities as well as full body CTA. Compared to MRA, CTA has regained lost territory with the introduction of multislice scanning, but CTA should be used with care in young individuals and patients with impaired renal function.

Learning Objectives:

1. To learn how to adapt acquisition parameters for CTA to a specific clinical question.
2. To understand how contrast administration protocols have to be modified for multislice scanning.
3. To become familiar with the advantages and disadvantages of CTA for various clinical indications.
4. To comprehend the role of CTA relative to the other modalities.

A-292

C. Sonography: New directions

P. Landwehr; Hannover/DE

Sonography is the first procedure in the work-up of vascular disease in the majority of cases. Vascular ultrasound serves as a decision-maker in peripheral, carotid and renal arterial disease, in detection and follow-up of arterial aneurysms and in demonstration of venous thrombosis. Follow-up after therapy is mainly accomplished by ultrasound, too. CE-MRA and CTA compete with vascular ultrasound, and the results of this competition will influence clinical decision pathways under the scope of new reimbursement strategies.

This review focuses on the potential impact of new ultrasound techniques and deals with the role of signal enhancers. Transducer improvement, digital beam forming and signal processing, extended field and 3D/4D techniques, imaging modes like tissue harmonic imaging and excitation techniques (e.g., B-flow) improve resolution, spatial understanding and demonstrability. Contrast agents based on different microbubble designs are available for enhancing signals in greyscale as well as in Doppler studies. Contrast enhancers can be combined with bubble-specific modes for semi-selective demonstration of bubble location (e.g., contrast harmonic imaging).

Above all, the general technical improvements of US technology helped to improve US capabilities in vascular imaging. Many new techniques as well as contrast agents are supplementary tools (sometimes toys...) in weak signal situations like in renal arteries, tight carotid stenoses and transcranial Doppler. But: All new tools do not reduce the main challenges in vascular ultrasound: Training, standardization and establishment of cost-effective pathways for work-up of vascular disease. To underline this statement, clinical examples for the role of US in the decision-making process are demonstrated.

Learning Objectives:

1. To be familiar with all established and new techniques of vascular ultrasound.

Postgraduate Educational Programme

2. To get an overview on ultrasound signal enhancers and their limited role in vascular disease.
3. To include ultrasound in rational strategies for the diagnosis of vascular disease.

16:00 - 17:30

Room K

Pediatric

RC 1212

Chest imaging

Moderator:

M. Fujioka; Utsunomiya/JP

A-293

A. Multidetector CT of the chest: Guidelines and specificities in children

H. Ducou le Pointe, M. Lenoir, S. Ariche-Maman, J.-P. Montagne; Paris/FR

By combining both helical volumetric acquisition and thin slice thickness, Multidetector CT (MDCT) offers new applications in pediatric chest imaging. Concerning management of the exam, MDCT allows to reduction in numbers sedated, especially in patients older than 3. With MDCT faster coverage leads to reduction in the amount of IV contrast material. The injected quantity of contrast material is now 1 ml per kilogram of body weight. Concerning CT acquisition parameters: acquisitions are performed with 0.75 or 1.5 mm slice thickness. Isotropic viewing allows very good multiplanar reconstructions. Multiplanar reconstruction is used for all exams even in the axial plane: images are viewed with a thickness of 3 to 5 mm. Better signal to noise ratio allows lower scanning parameters to be chosen. For children under 10, lung parenchyma and airway CTs are performed with 90 kV and a tube current less than 90 mA. New applications are thoracic angiography and virtual bronchoscopy. Virtual bronchoscopy seems to produce images that correlate well with bronchoscopy.

Learning Objectives:

1. To conduct a multidetector CT exam of the chest.
2. To choose CT parameters acquisition.
3. To discuss the new applications (virtual endoscopy, angiography).

A-294

B. MR imaging of the lung

W. Hirsch; Leipzig/DE

MR imaging is not yet able to show the same precise pictures of the lung parenchyma as CT. First the principle problems that occur with imaging of the lung parenchyma in MR imaging are discussed.

Central bronchus lesions are detectable in MR imaging with the same reliability as in computer tomography. The visibility of intrapulmonary metastases depends on the size of the lesion. Peripheral metastases can be recognised from a size of 4 mm by using optimal investigation strategies. Interstitial processes show discrete findings: Fibrosis is better demonstrated on MR imaging since it shows a higher signal due to its cellular component in T2 and even in T1. Alveolar processes are very well imaged in proton MR imaging due to the high liquid content, even in small findings.

The possibilities of functional imaging by using proton MR imaging are demonstrated. Perfusion measures are the most common functional assessment in clinical use. With colour coded perfusion maps, perfusion defects are often very clear. Even the spatial resolution is much higher than in conventional perfusion scintigraphy. Imaging of the ventilation is still work in progress. Methods we used are oxygen enhanced imaging of the air space, volume estimation of the lung and imaging of trapped air by using expiration technique. A new possibility seems to be the estimation of the lung function diffusion by means of nebulized Gadobutrol. Between morphological and functional imaging MR imaging of the lung will find its place in Paediatric Radiology.

Learning Objectives:

1. To point out the principle problems that will occur when you image the lung in MR imaging.
2. To discuss what kind of morphologically lung lesions are visible reliable in MR imaging.
3. To show the present and future possibilities of functional lung imaging.

A-295

C. Cardiac MR imaging in children

A.M. Taylor; London/UK

Introduction: Cardiovascular magnetic resonance (MR) imaging is becoming commonplace in the assessment of grown-up congenital heart disease and more recently in neonates, infants and children. Not only can an accurate description of cardiac and vascular anatomy in relation to the other structures be performed, but MR can also provide accurate quantification of cardiac function and vascular flow.

Indications: In young children, cardiovascular MR is used as a second line investigation, when echocardiography cannot provide all the necessary information, and cardiac catheterisation can be avoided.

The indications for cardiovascular MR include assessment of:

- Right ventricular conduits, providing information about conduit function (stenosis and regurgitation), and the underlying RV function,
- Aortic pathology (coarctation and Marfan syndrome),
- Anomalous coronary arteries, and
- Complex congenital heart disease, where understanding the three-dimensional structure is paramount, and can be difficult with other imaging methods.

Imaging sequences: Imaging sequences can be broadly be divided into:

- 'Black-blood' spin-echo imaging - for accurate anatomical assessment,
- 'White-blood' gradient echo or SSFP imaging - for accurate anatomical and functional cine imaging (quantification of ventricular function),
- Phase contrast velocity mapping - for quantification of vascular flow, and
- Gadolinium contrast-enhanced MR angiography - for accurate assessment of thoracic vasculature.

All these sequences can be acquired in a single breath-hold, and importantly, contiguous isotropic volume datasets can be acquired enabling 3D volume rendering. Overall, cardiovascular MR can provide an accurate anatomical and functional assessment of the heart and great vessels in the majority of children with congenital and acquired heart disease.

Learning Objectives:

1. To discuss indications for cardiac MR in children.
2. To describe a MR protocol for imaging the heart in children.
3. To describe the diagnosis of congenital heart disease diagnosis using a sequential segmental analysis.

16:00 - 17:30

Room L/M

Radiographers

RC 1214

Pediatrics/Radiography

Moderators:

V. Donoghue; Dublin/IE

K. Eklund; Lund/SE

A-296

A. Radiographer's role in optimisation of child's radiation doses

A. Kettunen; Oulu/FI

The latest studies indicate that there may be some effects on the lower levels of radiation doses. Children are more sensitive than adults. Radiosensitive cell-forming bone marrow is present in most bones at birth. The developing breast, thyroid and gonads are sensitive to radiation detriment. The radiation doses to children must be at a minimum while the quality of the radiographic image is optimised. Wide variations have been found in techniques, equipment and radiation doses. Substantial dose reductions could be achieved without loss of image quality. Beam energy, filtration, collimation, use of grid, the anode heel-effect, low attenuation materials (carbon) in table tops, patient size, the screen-film combination and film processing conditions affect the patient dose in conventional and mostly in computed radiography. It seems that FPD gives a good resolution and no significant difference in diagnostic quality even with 50%-70% decrease in radiation dose. Lead-rubber shielding of the parts of the body next to the primary beam should always be used. A training programme, regular provision of dose information and collaboration between physicist, radiographers and radiologists can significantly reduce the doses received by children. Educated and trained staff should take X-ray examinations of children. It is important to assess image quality in relation to patient dose. The criteria for good radiographic technique must be also met. Because the weight of newborns varies widely (about 0.4 kg-6 kg), several reference levels should be set to X-ray examinations of newborns. The radiographer is in key position in dose optimisation of children.

Postgraduate Educational Programme

Learning Objectives:

1. To understand the factors effecting to the radiation risk and radiation dose of children in X-ray examinations.
2. To understand the role of the radiographer in the radiation dose optimization of children by patient care and imaging technique.

A-297

B. Radiographer reporting

D. Keane; *South Tyneside/UK*

Background: Accident and Emergency medicine brings together a complex patient group presenting with a wide diversity of pathology. The inexperience of junior doctors and emergency nurse practitioners in image interpretation can lead to inappropriate management and time delays. The introduction of a Consultant Radiographer who has undergone post graduate training in image interpretation has significantly improved the service to A&E patients and support given to A&E staff.

Procedure Details: Trauma images are 'hot reported' by the Consultant Radiographer during the normal working day. All radiographers have been given training and support in offering written opinions on trauma images out of hours, creating a 24 hour service to patients and A&E staff. All written opinions are checked and confirmed by the Consultant Radiographer during the next working day. Robust protocols, training, review and monthly audit enable the clinical governance of the process.

Conclusions: Audit results have demonstrated significant reduction in the incidence of missed fractures over the two years since the system was introduced. Other benefits include better working relationships between Radiology and A&E, improved job satisfaction and joint training initiatives to further develop practice.

Learning Objectives:

1. To identify the role of the reporting radiographer in developing A&E services.
2. To learn about new developments in the UK.
3. To identify the implications of the UK experience.
4. To identify the benefits to doctors, radiographers and patients.
5. To learn about the rationale for role development.

A-298

C. Pros and cons of radiographer reporting: A radiologist's viewpoint

P.A. Dubbins; *Plymouth/UK*

- Radiographer reporting is not a new issue - red dot reporting for A&E films in 1985, sonographers reporting ultrasound since the early 80's

- Why should radiographers report?
 - + Too few radiologists?
 - + Cheaper labour?
- Why should radiographers report?
 - + Because the service is enhanced
 - + Because the service is more timely
 - + Because they are the right individual to report the particular image
 - + Because they have the right skills for image reporting in the particular clinical environment (A&E for example)
 - + Because they understand the imaging modality and are aware of artefacts
- When should radiographers report?
 - + When they are part of a clinical team
 - + When they have clinical support from experienced radiologists
 - + When their work is carefully defined and is within defined protocols jointly developed
 - + When medical knowledge is not critical for the correct interpretation of an examination
 - + Or where this can be provided through the team
 - + Where medical support is not required for the performance of a procedure
 - + When it is cost effective, cost efficient and maintains or improves patient care within an environment that provides audit, feedback and quality improvement

Learning Objectives:

1. To learn about the nature of a clinical report and the modifications required dependant on the intended recipient.
2. To understand the responsibility of the reporter for quality and promptness.
3. To learn about the training issues affecting the nature of the report.
4. To identify the contribution of the team to quality of service and support of the individual.
5. To recognise your own limitations.

16:00 - 17:30

Room N/O

Primer: Molecular Imaging

PR 1219

Imaging of gene expression: Optical and nuclear techniques

Moderator:

R. Passariello; *Rome/IT*

A-299

A. Optical contrast agents for imaging genes and proteins

C. Bremer; *Münster/DE*

Optical imaging has emerged as a new imaging modality offering high sensitivity for detecting molecular structures *in vivo*. In the near infrared range sufficient tissue penetration is achieved for imaging small animal models as well as considerable volumes in human applications. Different absorbers such as hemoglobin, fat and water can be used to interrogate tissue characteristics (e.g. perfusion) non-invasively. Moreover, a variety of optical contrast agents are currently explored for non invasive detection of protein expression patterns *in vivo*. Fluorochromes can be linked to specific ligands (antibodies, antibody fragments or peptides) imparting probe selectivity for various targets of interest allowing e.g. the imaging of apoptosis or cancer related proteins (e.g. EGF receptor). Moreover, enzyme-sensing optical probes have been applied for the detection of protease expression *in vivo*. In these "smart" probes signal amplification is achieved by an enzyme-mediated dequenching mechanism.

For "upstream" imaging of gene (as opposed to protein) expression various fluorescent proteins (e.g. GFP, dsRed) are currently explored. Moreover, bioluminescence imaging exploiting luciferase genes can be used to sensitively detect transgene expression *in vivo*. Combined with novel 3-dimensional imaging techniques such as fluorescence mediated tomography (FMT) or surface weighted imaging tools such as fluorescence reflectance imaging these novel contrast agents will help to interrogate molecular structures *in vivo*.

Learning Objectives:

1. To elucidate the strength of optical imaging for molecular *in-vivo* diagnostics.
2. To explain different optical contrasting strategies including "intrinsic", "targeted" and "smart contrast agents".
3. To emphasize the clinical potential of this method.

A-300

B. Gene expression imaging using bioluminescence

C.W.G.M. Löwik; *Leiden/NL*

Now that the human genome project has come to completion most genes have been identified. However, the big challenge for the future is to try to discover where the genes are expressed, how they are regulated, and what their exact function is in the homeostasis of specific cell types or tissues. This will lead to a better understanding of the molecular, cellular, and biological processes involved in normal physiology and pathology in a variety of diseases. It will also allow us to find new drug targets and, consequently, better management of diseases.

In order to study the location and regulation of gene expression *in vitro* as well as *in vivo*, reporter genes (e.g. β -galactosidase, GFP, luciferase) have been widely used. They are also used for tracking the fate of cells injected systemically in small experimental animals. Until recently, the proteins translated from the reporter gene-constructs were either visualized in histological tissue sections or detected biochemically in tissue extracts after sacrifice of the animal. However, development of highly sensitive CCD camera's and bioluminescent imaging (BLI), in which luciferase is used as a reporter gene, currently allows very sensitive image recording of the topographical expression of this enzyme non-invasively and repetitively in the living animal.

In this presentation the following points will be discussed:

1. The basic principles and advantages of bioluminescent imaging.
2. How BLI can be used to image gene expression *in vivo*.
3. The broad application of the technology for other applications.

Learning Objectives:

1. To understand the basic principles and advantages of bioluminescent imaging.
2. To understand how it can be used to image gene expression *in vivo*.
3. To learn about other applications.

Postgraduate Educational Programme

A-301

C. Gene expression imaging: From bench to bedside

A.H. Jacobs, A. Winkeler, H. Li, A. Rüger, M. Klein, S. Vollmar, R. Graf, K. Wienhard, W.D. Heiss; Cologne/DE

Positron emission tomography (PET) allows a non-invasive assessment of physiological, metabolic and molecular processes in humans and animals *in vivo* (molecular imaging). With the developments in tracer technology a variety of endogenously expressed and exogenously introduced genes coding for membrane receptors and transporters or cellular enzymes can be analyzed by PET. The main and most intriguing advantage of molecular imaging is the *kinetic* analysis of a given molecular event in the same experimental subject over time. This allows a non-invasive characterization and "phenotyping" of animal models of human disease at various disease stages, under certain pathophysiological stimuli and after therapeutic intervention. Apart from *direct* detection and imaging of a certain gene product, *indirect* imaging technology is based on proportional coexpression of a PET marker gene (e.g. HSV-1-tk) with any gene of interest where specific probes are not available, yet. Moreover, certain genes can be used as *surrogate* markers, e.g. hexokinase gene expression as direct marker for glucose metabolism and as surrogate marker for cell density of a glioma or as surrogate marker for disease severity in Alzheimer's disease. The overall attractive goal of molecular imaging technology is the direct translation from *in vivo* animal data into clinical application (translations research) especially in the development of novel therapeutics.

Learning Objectives:

1. Imaging endogenous and exogenous gene expression by PET.
2. Principle of imaging-guided gene therapy of gliomas.
3. Introduction into universal HSV-1 vectors for imaging and gene therapy.

16:00 - 17:30

Room P

Computer Applications

RC 1205

Building an electronic patient record system

Moderator:

D. Caramella; Pisa/IT

A-302

A. Computer generated reports: A solution

P. Mildenberger; Mainz/DE

Reports are an essential part of all radiological procedures and relevant for active clinical patient management. Therefore reports should contain a description of findings and a clinical judgement. Conventional dictation has some inconveniences regarding costs, delays or strengths.

Furthermore developments like CAD, fMR imaging or fCT, Software tools for quantitative measurements using high-end workstations creates evident findings. These become part of the a complete report.

Therefore the creation of radiological reports has to incorporate different aspects like encoding or classifiers (e.g. based on ICD, LOINC, SNOMED, UMLS...), transmission and storage (e.g. XML, HL7 CDA or DICOM SR). Also structured reporting is relevant for evaluation of reports in different scenarios (scientific, economical, quality management).

Structured reporting is an important issue for Radiology, it can improve instructions for residents, turnaround time, content and interoperability with information systems outside the radiological department.

Learning Objectives:

1. To understand how a report could be partially generated on a modality or a workstation.
 - a. What are structured reports - different solutions.
 - b. How to build reports using the DICOM SR.
2. To understand how such solutions could help to solve daily issues.

A-303

B. Speech recognition

J.H. Thrall; Boston, MA/US

Speech recognition systems translate spoken words into digital text. Commercial speech recognition systems are typically tailored for specific applications with respect to vocabulary and ancillary functions such as the ability to use pre-set macros and templates. For radiology, the systems are interfaced to radiology information systems to maintain the integrity of patient demographics and information about the radiological studies.

The two most important advantages of using speech recognition are shortened cycle times for creating radiological reports and making them available for clinical use and significant cost reductions through reduced personnel requirements for transcription.

The single biggest hurdle in implementing speech recognition is overcoming the perception on the part of some radiologists that speech recognition increases the time it takes them to accomplish the interpretation/reporting process. The keys to overcoming this issue are full education of system users, full use of macros and templates, comprehensive voice training and adequate system technical support for users. Vendors should also completely integrate speech recognition systems with RIS and PACS systems to reduce work process steps.

Speech recognition reporting systems offer the rare opportunity of improving quality of care and quality of service while at the same time reducing cost. Departments of Radiology that successfully implement this technology have significant quality and cost advantages compared with departments that do not.

Learning Objectives:

1. To develop an understanding of how speech recognition works and how to incorporate speech recognition systems into the radiology interpretation workflow.
2. To learn factors that are associated with successful implementation versus failed implementation of speech recognition systems.
3. To understand the potential positive operational impact associated with implementation of speech recognition dictation of radiology reports.

A-304

C. Image distribution within the hospital and beyond

N.H. Strickland; London/UK

Electronic radiological image distribution within the hospital and beyond assumes that a PACS is in place. If non-radiological images are also to be distributed, these must be acquired in digital form, and must be entered onto the PACS (or similar system) via an electronic booking system equivalent to a RIS. Seamless integration with other hospital computer systems is an essential goal if workflow efficiency is to be improved. Requesting clinical details and previous reports must be available on the same system as the images displayed for reporting.

The purpose of image viewing at each access site in the distribution system must be precisely defined, since this dictates the appropriate technical requirements. Examples include: (1) The acceptable retrieval speed, and (2) the image viewing device: Diagnostic PACS workstation versus PC web browser verses hand-held device.

Security (firewalls and encryption) becomes an issue if public highways are used for image distribution.

Learning Objectives:

1. Electronic image distribution alone is insufficient: Seamless integration with other hospital computer systems (as part of the electronic patient record) is an essential goal.
2. A clear understanding is needed of the purpose of image viewing at every display node on the image distribution system.

Postgraduate Educational Programme

16:00 - 17:30

La Scala

Foundation Course - Chest Radiology

E3 1220

Wrapping it up ...

Moderator:

C.J. Zylak; Detroit, MI/US

A-305

A. The pleura and diaphragm

M. Maffessanti; Trieste/IT

A basic review of principal anatomical landmarks and variants of pleura and diaphragm will be offered not only to understand the images and to avoid avoidable misinterpretation of normal structures as abnormal, but also to acquire the ability to localize adjacent lesions correctly.

For the pleura, an overview of effusions and their radiological aspects, from their free fluid stage to the organized or loculated stage, will introduce the discussion of specific diseases, either focal, multiple or unique and diffuse, neoplastic or fibrotic.

For the diaphragm, the variations in shape of the muscle with the respiration have to be taken into account to fully understand the images, as well as when looking at it from the physiological point of view. This tiny structure not only can be affected by its own pathology, but often participates in adjacent disorders either indirectly or directly, giving passage to fluids, organs or other elements through openings either congenital (i.e., hernias) and acquired (i.e., trauma).

Different lesions may be located in contact, above or under the diaphragm, and somehow cause modifications of its shape: effusions, masses, abscesses, large bullae and emphysema, etc., either unilaterally or bilaterally.

A particular question that often arises on the chest film is: where is the diaphragm? Ultrasound and especially Computed Tomography are very helpful in answering this question. Several key signs and a few tips to give the answer to this question will be discussed.

Learning Objectives:

1. To familiarize the audience with the anatomy of pleura and diaphragm, in particular with reference to the structures that may simulate abnormalities.
2. To illustrate how anatomy can condition appearance of some diseases and how it is modified by the diseases.
3. To discuss selected clinical cases to enhance the recognition of specific entities.

A-306 ♀

B. Mediastinal disease

K. Malagari; Athens/GR

Imaging examinations of mediastinal space-occupying lesions aim to increase recognition of the abnormality, exact localization within the mediastinum, demonstration of the relationships with surrounding anatomic structures, and texture analysis based on CT and MR imaging data. The localization approach comprises the traditional diagnostic differential based on a list of common anterior, middle and posterior mediastinal masses. However, cross-sectional imaging today definitely offers a more detailed analysis that, if combined with epidemiologic characteristics such as age-related incidence and density-texture information, may narrow the differential diagnosis considerably. Density information leading to specific diagnosis includes recognition of cystic density or fat, while calcification patterns often overlap. Characterization of cystic lesions may be difficult if the lesion contains nonserous fluid since this may present high attenuation at CT, and they may be mistaken for solid lesions, especially when intravenous contrast material cannot be administered. MR imaging can be useful in showing the cystic nature of these masses because these cysts continue to have characteristically high signal intensity on T2-weighted sequences. Fat-containing lesions include benign lipomas, diaphragmatic hernias, fat-containing mesenchymal tumors, teratomas, thymolipomas, and mediastinal lipomatosis.

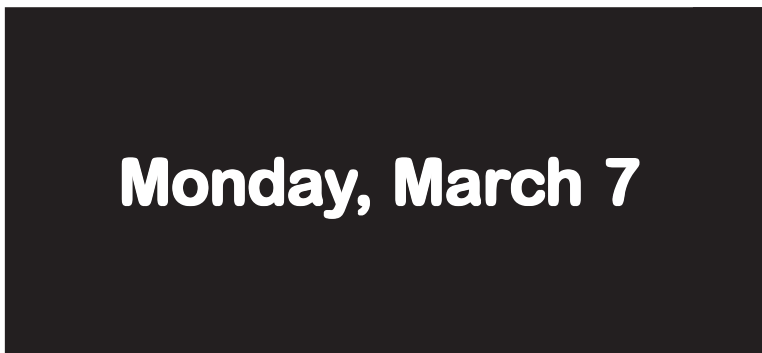
The borders of the lesion may suggest its nature, and signs of infiltration may suggest malignancy, unless inflammation or adjacent lung atelectasis coexist.

Learning Objectives:

1. To illustrate the anatomical mediastinal compartments as seen on plain films, CT and MR imaging, and discuss the concept and limitations.
2. To describe the anatomy, as well as the imaging findings of mediastinal lymph node enlargement.

3. To discuss imaging findings and differential diagnosis of space occupying lesions in the mediastinal compartments.
4. To familiarize with imaging findings of mediastinal neoplasms, pseudotumors and infectious processes of the mediastinum.
5. To promote an elaborate use of imaging modalities and interventional procedures in the diagnosis and treatment of mediastinal disease.

Postgraduate Educational Programme



Monday, March 7

Postgraduate Educational Programme

		room A 2nd level	room B 2nd level	room C 2nd level	room E1 entr. level	room E2 entr. level	room F1 entr. level	room F2 entr. level	room G lower level	room H lower level	
07:00											07:00
07:30											07:30
08:00											08:00
08:30											08:30
09:00		CC 1317 Essentials of Neuroradiology Craniocerebral and spinal trauma (p. 92)	RC 1310 Musculoskeletal Shoulder joint (p. 92)	SF 13 Special Focus Session MR imaging of the small intestine (p. 93)	RC 1302 Breast Digital mammography (p. 94)	RC 1301 Abdominal and Gastrointestinal Imaging of the pancreas: Key questions (p. 95)	RC 1306 Molecular Imaging and Contrast Media Molecular imaging (p. 96)	RC 1311 Neuro MR spectroscopy of the brain in clinical practice (p. 96)	RC 1307 Genitourinary Multislice CT of the urinary tract (p. 97)	RC 1309 Interventional Radiology Percutaneous tumor ablation (p. 98)	09:00
09:30											09:30
10:00											10:00
10:30		SA 14 State-of-the-Art Symposium Imaging of prostate cancer: Present and future (p. 102)	SS 1410 Musculoskeletal Imaging of the arthritis and periarthritis tissues (p. 262)	SS 1401a GI Tract MR imaging of the abdomen (p. 264)	ECR General Assembly	SS 1402 Breast Mammography and ultrasound (p. 266)	SS 1404 Chest Pulmonary embolism: Imaging technique and outcome (p. 268)	SS 1401b Abdominal Vissera (Solid Organs) Contrast enhanced US of the liver and spleen (p. 270)	SS 1407 Genitourinary CT imaging of the urinary tract (p. 272)	SS 1409a Interventional Radiology Thermal ablations in lung and liver (p. 274)	10:30
11:00											11:00
11:30											11:30
12:00											12:00
12:30											12:30
13:00											13:00
13:30											13:30
14:00		EM 3 "ECR meets" Japan "Oriental Pearls" in oncology imaging (p. 105)	SS 1510 Musculoskeletal Advanced MR imaging techniques (p. 287)	SS 1501a GI Tract CT colonography (p. 289)	SY 15 Satellite Symposium Open PET/CT imaging in diagnosis and treatment (p. 588)	SS 1504 Chest CT and MR imaging in emphysema and COPD (p. 291)	SY 16 Satellite Symposium Latest advances in musculo-skeletal and nerve ultrasound (p. 588)	SS 1501b Abdominal Vissera (Solid Organs) Focal liver lesions: MDCT, MR imaging and PET-CT (p. 293)	SS 1507 Genitourinary Lower urogenital tract (p. 295)	SS 1502 Breast Interventional procedures (p. 297)	14:00
14:30											14:30
15:00											15:00
15:30											15:30
16:00		CC 1617 Essentials of Neuroradiology Degenerative disorders, tumors and infection of the spine (p. 106)	EAR General Assembly	SF 16 Special Focus Session Pulmonary hypertension: All that the radiologist needs to know (p. 107)	RC 1602 Breast Radiopathological correlation (p. 108)		RC 1604 Chest Thoracic manifestations of extra-thoracic disease (p. 109)	RC 1610 Musculoskeletal Inflammatory joint disease (p. 109)	RC 1608 Head and Neck Imaging of skull base tumors: A practical approach for your daily practice (p. 110)	WS 1609 Interventional Radiology Percutaneous access to the abdomen (p. 111)	16:00
16:30											16:30
17:00											17:00
17:30											17:30
18:00											18:00
18:30											18:30
19:00											19:00

Postgraduate Educational Programme

	room I lower level	room K lower level	room L/M 1st level	room N/O 1st level	room P lower level	room W basement	room X 1st level	room Y 1st level	room Z entr. level	La Scala 2nd level	
07:00											07:00
07:30											07:30
08:00											08:00
08:30	ER 1326 Joint ECR/EAR sessions: Challenges for European Radiology Teleradiology: Threat or opportunity? (p. 99)	RC 1312 Pediatric Neonatal problems (p. 100)	RC 1314 Radiographers Professional matters (p. 100)	RC 1313 Physics in Radiology Quality control and dose reduction in digital radiology (p. 101)	WS 1321 Musculo-skeletal US "Hands-on" Workshop				WS 1324 Basic Life Support for Radiologists "Hands-on" Workshop	E³ 1320 Interactive Image Teaching Paranasal sinuses (p. 102)	08:30
09:00									WS 23D1 Screening Mammography Interpretation Test "Hands-on" Workshop		09:00
09:30											09:30
10:00									WS 23D2 Screening Mammography Interpretation Test "Hands-on" Workshop		10:00
10:30	SS 1409b Interventional Radiology Peripheral vascular interventions (p. 276)	SS 1412 Pediatric Neuro-imaging (p. 278)	SS 1403 Cardiac MR imaging of the coronary arteries (p. 280)	SS 1413 Physics in Radiology CT: Technical developments (p. 283)	SS 1406 Molecular Imaging Targeting and PET imaging (p. 285)		WS 1421 Musculo-skeletal US "Hands-on" Workshop	WS 1424 Basic Life Support for Radiologists "Hands-on" Workshop	E³ 1420 Diagnostic workstations: The new super-assistants of the radiologist and surgeon (p. 103)		10:30
11:00								WS 23D3 Screening Mammography Interpretation Test "Hands-on" Workshop			11:00
11:30											11:30
12:00								WS 23D4 Screening Mammography Interpretation Test "Hands-on" Workshop			12:00
12:30											12:30
13:00											13:00
13:30											13:30
14:00	SS 1506a Contrast Media Specific MR imaging contrast media (p. 298)	SS 1512 Pediatric Novel imaging approaches (p. 301)	SS 1511 Neuro Cerebrovascular disease: Endovascular treatment and non-invasive follow-up (p. 303)	SS 1513 Physics in Radiology Radiation protection/Image quality (p. 305)	SS 1506b Molecular Imaging Cellular and molecular imaging (p. 307)			WS 23E1 Screening Mammography Interpretation Test "Hands-on" Workshop	WS 1524 Basic Life Support for Radiologists "Hands-on" Workshop	E³ 1520 Interactive Image Teaching Cervical spine trauma (p. 106)	14:00
14:30								WS 23E2 Screening Mammography Interpretation Test "Hands-on" Workshop			14:30
15:00											15:00
15:30											15:30
16:00	WS 1615 Vascular Imaging of atherosclerotic plaques (p. 112)	RC 1612 Pediatric Emergencies in pediatrics (p. 113)	RC 1614 Radiographers CT (p. 113)	RC 1613 Physics in Radiology Justification and optimization of multislice CT (MSCT) examinations (p. 114)				WS 23E3 Screening Mammography Interpretation Test "Hands-on" Workshop			16:00
16:30											16:30
17:00											17:00
17:30											17:30
18:00											18:00
18:30											18:30
19:00											19:00

Monday

Postgraduate Educational Programme

08:30 - 10:00

Room A

Essentials of Neuroradiology

CC 1317

Craniocerebral and spinal trauma

Moderator:

P. Brennan; Dublin/IE

A-307

A. Craniocerebral trauma (1): General principles and maxillofacial trauma

B.F. Schuknecht; Zürich/CH

The sequelae of trauma to the skull and maxillofacial skeleton depends on a dynamic factor consisting of the nature of the force (energy, impact area) and a static factor which is determined by the anatomic disposition of the bone involved. A small impact area results in localized direct fractures such as a depressed skull fracture or deformation fractures of the midface. A force that is transmitted over a larger area of bone results in indirect fractures or "burst" fractures which are common at the skull base, the petrous bone, or involve the mandibular condyles bilaterally. Multirow spiral CT has increasingly replaced conventional images to depict the presence, location and deformity caused by fractures and - more importantly- reveals intracranial involvement in skull trauma. Cranial nerve and vascular complications related to osseous compromise are delineated by CT as well but may require MR to be adequately assessed. The classification of trauma is accomplished by multiplanar CT images and in case of deformity by 3D surface reconstructions. Classification of midface fractures distinguishes central (Le Fort I, II, naso-ethmoid fractures), lateral (trimolar) or combined centro-lateral (Le Fort III) fractures. Mandibular fractures are subdivided into those that affect the mandibula proper, the alveolar and condylar processes. Lateral skull base (petrous bone) fractures consist of longitudinal and transverse fractures, central skull base fractures are described as transverse and oblique fractures. While classifications in the past primarily reflected mechanism, CT and/or MR have redirected the focus on predominantly therapeutic implications and recognition of complications typical for a specific fracture type.

Learning Objectives:

1. To comprehend the two general principle pathogenic mechanisms in crano-facial trauma.
2. To learn the diagnostic procedure in isolated mandibular and midface fractures and combined cranio-facial and skull base trauma.
3. To become familiar with the classification of mandibular and midface fractures.
4. To become familiar with the classification of lateral and central skull base fractures.
5. To learn typical early and late complications in midface and skull base trauma and the principles of their diagnostic investigation.

A-308

B. Craniocerebral trauma (2): Intra- and extra-axial lesions, secondary lesions

P.M. Parizel; Antwerp/BE

Accurate radiographic diagnosis is a cornerstone in the clinical management and outcome prediction of the head-injured patient. New technological advances, such as multidetector CT scanning and diffusion-weighted MR imaging have influenced imaging strategies. In this article, we review the impact of these developments on the neuroradiological diagnosis of acute head injury. In the acute phase, multidetector CT has supplanted plain X-ray films of the skull as the initial imaging study of choice. MR imaging, including fluid attenuated inversion recovery, gradient echo T2* and diffusion-weighted sequences, is useful in determining the severity of acute brain tissue injury and may help to predict outcome. The role of MR imaging in showing diffuse axonal injuries is emphasized. We review the different patterns of primary and secondary extra- and intra-axial traumatic brain lesions, and integrate new insights. Assessment of intracranial hypertension and cerebral herniation are of major clinical importance in patient management. We discuss the issue of pediatric brain trauma, and stress the importance of MR imaging in non-accidental injury. In summary, new developments in imaging technology have advanced our understanding of the pathophysiology of brain trauma, and contributed towards improving the survival of patients with craniocerebral injuries.

Learning Objectives:

1. To document the impact of new imaging technologies on the management and outcome prediction of head-injured patients.

2. To demonstrate the growing role of MR imaging (including FLAIR, gradient echo T2*, and diffusion-weighted sequences) in acute and subacute craniocerebral trauma.
3. To discuss radiological manifestations of primary and secondary traumatic brain lesions, and integrate concepts regarding the pathophysiology of brain trauma.
4. To provide an overview of the most common extra- and intra-axial traumatic brain lesions.

A-309

C. Spine trauma

J.W. Van Goethem; Antwerp/BE

Because it may cause paralysis, injury to the spine is one of the most feared traumas, and spinal cord injury is a major cause of disability. Although the number of individuals sustaining paralysis is far less than those with moderate or severe brain injury, the socio-economic costs are significant.

Little controversy exists regarding the need for accurate and emergent imaging assessment of the traumatized spine in order to evaluate spinal stability and integrity of neural elements. Because clinicians fear missing occult spine injuries, they obtain radiographs for nearly all patients who present with blunt trauma. We are influenced on one side by fear of litigation and the possible devastating medical, psychological and financial consequences of cervical spine injury, and on the other side by pressure to reduce health care costs. Several criteria can be very useful in identifying patients who have an extremely low probability of injury and who consequently have no need for imaging. MDCT is the preferred primary imaging modality in blunt spinal trauma patients who do need imaging. Not only is CT more accurate in diagnosing spinal injury, it also reduces imaging time and patient manipulation. Evidence-based research has established that MDCT improves patient outcome and saves money in comparison to plain film.

The remainder of the text discusses the use, advantages and disadvantages of the different imaging techniques used in spinal trauma patients and the criteria used in selecting patients that do not need imaging. Finally an overview of different types of spinal injuries is presented.

Learning Objectives:

1. To learn the advantages, disadvantages and indications of different imaging modalities in spinal trauma and to be able to choose the right imaging algorithm for a particular patient.
2. To become familiar with the different types of lesions in spinal trauma.
3. To understand the pathophysiology of whiplash lesions and to know what to expect in imaging whiplash-injured patients.
4. To become familiar with traumatic spinal cord lesions.

08:30 - 10:00

Room B

Musculoskeletal

RC 1310

Shoulder joint

Moderator:

D. Weishaupt; Zürich/CH

A-310

A. Acute and chronic shoulder injuries: US and MR imaging

F. Kainberger, C. Krestan; Vienna/AT

The main anatomic structures involved in injuries of the glenohumeral joint are the rotator cuff, the labrocapsular complex and the surrounding bones. In the acromio-clavicular joint the fibrous structures may be disrupted.

Indications: Ultrasound (US) is useful for imaging lesions of the rotator cuff but is of limited diagnostic impact in case of other traumatic disorders. MR imaging is sensitive in displaying abnormalities due to instability and in detecting osseous lesions.

Investigation: US should be performed with paracoronal and parasagittal scans and should include a dynamic investigation under external and internal rotation. MR imaging is performed in paracoronal, parasagittal, and axial slice direction with T2-weighted fat-suppressed, T1-weighted, and gradient-echo sequences. MR arthrography is still regarded as gold-standard for the detection of labrocapsular lesions. Some institutions use additional ABER-position of the elevated arm to detect certain labral abnormalities. For the AC-joint, images with a high-resolution surface coil are valuable to detect intrinsic abnormalities.

Interpretation: Partial and full-thickness tendon ruptures should be differentiated

Postgraduate Educational Programme

from other causes that lead to edema (calcifying tendinitis, Parsonage-Turner syndrome). SLAP lesions may occur in various forms depending on anatomic variants. Osseous edema is indicative of bone bruises and fractures and should be differentiated from arthritis. AC joint disruptions are often associated with ruptures of the coraco-clavicular ligaments.

Learning Objectives:

1. To understand and appreciate the indications for performing US and MR imaging with view on the diagnostic impact of each of them.
2. To know the techniques of investigation and standards of documentation with focus on slice orientation and anatomic reference structures.
3. To recognize typical appearances and pitfalls in the diagnosis of lesions of the rotator cuff, of abnormalities due to instability, and of arthritis with focus on sports injuries.

A-311

B. Soft tissue mass in the shoulder region: US and MR imaging

P.W.P. Bearcroft; Cambridge/UK

The finding of a mass related to the shoulder girdle is a common clinical entity with a wide differential diagnosis. This presentation will start by identifying how the most common causes for a soft tissue mass depends on the patient's age. Conditions will include benign and malignant soft tissue masses, bone lesions, synovial conditions, arthritis, bursitis and infection with special emphasis on conditions specifically found in relation to the shoulder girdle such as elastofibroma dorsi.

An imaging strategy for a soft tissue mass will then be discussed with particular reference to MR imaging and ultrasound including the strengths and weaknesses of each technique. Finally an approach to imaging-guided percutaneous biopsy of masses in this region will be considered, including a discussion of when such masses are best left alone.

Learning Objectives:

1. To understand and recognise the various conditions that can present with a mass in the shoulder region.
2. To know the strengths and weaknesses of the various imaging modalities.
3. To appreciate when to perform an image-guided biopsy, and when not to.

A-312

C. Postoperative shoulder US and MR imaging

C. Faletti; Turin/IT

The first thing is to know both the kind of surgery performed and the symptomatology of the patient, bearing in mind that most common pitfalls are false positive and false negative.

Therefore, the evaluation carried out by means of imaging techniques varies along with the pathology and surgery.

In the post-operative shoulder operated for instability, an incomplete resolution of the problem must be studied by plain X-ray, so as to be able to study the gleno-humeral articular relationship and the correct position of the different devices. Capsular detachment or glenoid labrum avulsion after surgical reinsertion must be studied by CT-arthrography or MR-arthrography in order to determine precisely the site and the entity of the new lesions.

In impingement syndrome, the post operative imaging study is much more complicated due to the difficulty in pin-pointing the relationship between the symptomatology and the imaging finding.

Plain X-ray examination is useful to study the bone morphology and to demonstrate the atrophic alteration or the cortical discontinuity due to an undesirable post-surgical phlogistic reaction. US examination is also useful to show intra-articular fluid and offers some basic elements to diagnose the presence of post-surgical rotator cuff tendon pathology, such as a new tear or degenerative involution.

To study the various levels in which the different articular components are involved a more panoramic picture may be obtained by using MR imaging and MR-arthrography: Bone edema, muscle atrophy, tendon degeneration, etc.

Learning Objectives:

1. To understand the proper use of the various techniques (US, MRI, arthroMRI) in the study of the post-operative shoulder, taking into account the different imaging based on the surgery.
2. To offer protocols to be used based on a determined pathology which led to surgery.
3. To identify the possible pitfalls due to the specific imaging that may be observed in post-surgical examination of the rotator cuff and gleno-humeral complex.

08:30 - 10:00

Room C

Special Focus Session

SF 13

MR imaging of the small intestine

Moderator:

N. Gourtsoyiannis; Iraklion/GR

A-313

MR imaging of the small intestine (Introduction)

N. Gourtsoyiannis; Iraklion/GR

Recent advances in gradient technology and novel ultrafast pulse sequences made it possible to assess small intestinal diseases with MR imaging. Various pulse sequences, intraluminal contrast agents and administration techniques have been proposed. Since adequate luminal distention is considered as a major prerequisite for accurate diagnosis of even subtle intestinal lesions, MR enteroclysis was developed as a novel diagnostic method that combines the advantages of conventional enteroclysis (CE) with those of MR imaging. Clinical applications of MR imaging in the small intestine include assessment of Crohn's disease in adult and pediatric population, tumors, ischemia and obstruction. Initial results demonstrate the clinical impact of MR imaging of the small bowel and its potential limitations when applied in a clinical setting.

Learning Objectives:

1. To understand hardware and software requirements for MR imaging of the small intestine, to present an overview of the available oral contrast agents and to discuss tailored MR imaging examination protocols for specific indications in the small intestine.
2. To present clinical results of MR enteroclysis in patients with Crohn's disease, as compared with conventional enteroclysis.
3. To analyze imaging findings and clinical results of small intestinal disorders other than Crohn's disease.
4. To present imaging findings and clinical results of MR imaging applications in pediatric small intestinal diseases.
5. To analyze current limitations of different MR imaging approaches and present its future prospects in intestinal diseases.

A-314

Functional studies

D.J. Lomas; Cambridge/UK

Static imaging sequences: Modern MR imaging systems have several fast imaging sequences that allow imaging of the small bowel with either subsecond or breath-hold temporal resolution thereby reducing motion related artifacts. T1w imaging with gadolinium enhancement can delineate active inflammation in Crohn's disease but often requires anti-peristaltic agents to completely avoid motion artifacts. T2w imaging has also proven valuable in demonstrating wall thickening, but may suffer from intra-luminal motion artifacts with thin section images. Balanced T2/T1w imaging allows good delineation of wall and lumen as well as adjacent mesenteric vessels and nodes owing to the intrinsic chemical shift artifact but may suffer distortions at gas-tissue interfaces. Combining these sequences provides the ability to discriminate between artifacts and definite pathological lesions.

Interactive imaging & fluoroscopy: Currently MR systems do not have appropriate fluoroscopic capabilities and do not allow easy change of body position during an examination, unlike conventional X-ray exams. Prototype systems for interventional use may bring the required capability to allow interactive selection of contrast, imaging plane and fast switching of image acquisition type - analogous to a conventional X-ray study which combines fluoroscopy and "spot films". **Contrast media:** Intravenous gadolinium media have been used primarily with fat suppressed T1w imaging to demonstrate above normal enhancement of inflamed bowel wall. Intra-luminal contrast agents are predominantly water based with methyl cellulose widely used for nasojejunal tube studies. Orally based studies have used a wide range of agents to try and retain fluid within the lumen by osmotic or other means.

Learning Objectives:

1. To learn which imaging sequences are appropriate for imaging the small bowel, their advantages and related artifacts.
2. To learn how interactive MR fluoroscopy can be achieved and how this may be applied to small bowel examinations.
3. To understand the principles, advantages and disadvantages of the currently used intra-luminal contrast media.

Postgraduate Educational Programme

A-315

Clinical results in Crohn's disease

N. Papanikolaou; Iraklion/GR

MR enteroclysis is an emerging technique for SB imaging combining the advantages of conventional enteroclysis (CE) with those of cross-sectional imaging. MRE is equal to conventional enteroclysis in detecting, localizing and estimating the length of involved small bowel segments. Early lesions such as thickening and distortion of the valvulae conniventes and superficial type ulcers are clearly demonstrated on CE but they are not consistently depicted by MRE, due to its inadequate spatial resolution. The valvulae conniventes are shown in their best advantage and distortion of the mucosal folds are easily detected by MRE. The characteristic discrete longitudinal or transverse ulcers of Crohn's disease can be demonstrated on MRE, provided there is satisfactory distension and opacification of the bowel. Cobblestoning is caused mostly by a combination longitudinal and transverse ulceration and it is easily shown by MRE. Bowel wall thickening is clearly shown by all MRE sequences. Bowel wall thickness and length of small bowel involvement can be measured on MRE images. Narrowing of the lumen and associated prestenotic dilatation are easily recognized on MRE images by all sequences. Exoenteric manifestations of the disease are demonstrated in detail on true FISP images due to the high contrast generated from the bright mesenteric fat. Additionally, complications may be more accurately diagnosed on 3D FLASH images with fat saturation by the characteristic pattern of enhancement after gadolinium administration. The latter sequence may disclose disease activity by contrast uptake in the thickened SB wall and by mesenteric lymph nodes enhancement.

Learning Objectives:

1. To present a comprehensive MR enteroclysis imaging protocol.
2. To present clinical results of MR enteroclysis in patients with Crohn's disease, as compared with conventional enteroclysis.
3. To analyze MR enteroclysis current limitations and its future prospects in Crohn's disease.

A-316

Clinical results in non-inflammatory small intestinal disorders

H.-W. Umschaden; Wolfsberg/AT

The detection of subtle small-bowel lesions on MR imaging requires adequate distension, but there are many diseases that can be detected without distension, such as acute diseases associated with bowel wall edema, high grade small-bowel obstruction and diseases with pronounced bowel wall thickening, such as tumors or long standing Crohn's disease.

Recent technical developments facilitate MR imaging of acute diseases of the small bowel even in severely ill patients. The HASTE sequence provides adequate image quality in almost all patients and excellently demonstrates edema which is often associated with acute intestinal disorders, such as acute infectious or subacute ischemic diseases. Emboli in the superior mesenteric artery are more accurately depicted with MDCT due to the superior spatial resolution.

The demonstration of high-grade small bowel obstruction is easy with the HASTE sequence, since the loops are fluid filled and distended. The real time true FISP sequence allows functional imaging of the bowel loops proximal and distal to the obstruction and therefore a more accurate assessment of the degree of obstruction is possible.

The excellent soft tissue contrast of MR imaging is helpful in differentiating small-bowel diseases. Respiratory triggered T2-weighted TSE sequences provide more information of the bowel wall than other sequences and are therefore useful to differentiate between small-bowel diseases. In non-tumorous diseases the thickened bowel wall often shows a target pattern with high SI in the bowel wall in acute diseases and intermediate SI in chronic (Crohn's) diseases. Tumors produce asymmetric bowel wall thickening with homogeneous SI in T2.

Learning Objectives:

1. To comprehend the indications of MR imaging versus MR enteroclysis for small-bowel diseases.
2. To understand the advantages and limitations of the available sequences for small-bowel MR imaging.
3. To learn to use the superior soft tissue contrast of MR imaging for more accurate diagnosis of small-bowel diseases.

A-317

Clinical results in pediatric disorders

A. Laghi; Rome/IT

MR of the small bowel in paediatric patients requires intestinal distension, patient cooperation and the availability of fast imaging sequences. One of the major goals

of a paediatric examination is to be as minimally invasive as possible. For this reason, intestinal distension should be obtained using oral contrast agent trying to avoid naso-jejunal intubation. In the choice of the adequate oral contrast medium organoleptic properties, like taste and flavour, must be taken into consideration in order to improve patient compliance. Patients should be able to hold their breath for at least 20 sec; for this reason the examination is difficult in patients younger than six years.

The major clinical indication is represented by the work-up of children with suspected IBD. In paediatric patients the availability of a non-invasive tests for the identification of ileal inflammation is very useful in distinguishing between Crohn's disease and other gut inflammation and may represent a crucial tool in the diagnostic approach, patient selection for ileocolonoscopy and assessment of therapy response. A sensitivity of 85% and specificity of 100% for the identification of terminal ileum flogosis have been recently reported.

Another clinical indication is mainly represented by the work-up of patients with celiac disease.

The major drawback of MR imaging of the small intestine is represented by a 5% of non-diagnostic examinations due to low patient compliance and cooperation. This problem should partially be carried out from a specific preparation of both MR units suite and operator training for a better children hosting.

Learning Objectives:

1. To understand hardware and software requirements for MR imaging of the small intestine, to present an overview of the available oral contrast agents and to discuss tailored MR imaging examination protocols for specific indications in the small intestine.
2. To present clinical results of MR enteroclysis in patients with Crohn's disease, as compared with conventional enteroclysis.
3. To analyze imaging findings and clinical results of small intestinal disorders other than Crohn's disease.
4. To present imaging findings and clinical results of MR imaging applications in pediatric small intestinal diseases.
5. To analyze current limitations of different MR imaging approaches and present its future prospects in intestinal diseases.

08:30 - 10:00

Room E1

Breast

RC 1302

Digital mammography

Moderator:

R.C. Otto; Baden/CH

A-318

A. Technical aspects and future trends

R. Salvador; Barcelona/ES

All the aspects concerning the state of the art in full field digital mammography are reviewed, and presented, as well as the forthcoming changes and related techniques developed in the last years.

First of all, the basic physical aspects are reviewed to know how the different systems and devices work to obtain the image. How those images obtained, in so different ways, can be compared objectively is another issue. The technical differences between FFDM and SFM are also considered. Advantages and disadvantages, image management and new items appeared related to digital imaging, different displays and management of digital imaging in monitors. Resolution requirements of every component of the systems, etc..

The forthcoming technologies applied to FFDM are also reviewed. PACS, filmless diagnosis and the new technologies CAD, breast tomosynthesis, 3D imaging, telerradiology, digital subtraction mammography, dual energy mammography, etc. and all the new techniques on digital imaging are successively overviewed. Finally some recommendations when transition to digital has been decided for a big department or a small center. A final indication for QA aspects is also described.

Learning Objectives:

1. To present the different digital mammography technologies.
2. To describe the basics to manage (reading, storage, print) digital images.
3. To bear in mind recommendations while moving from SFM to FFDM.
4. To describe key-points for comparison of digital systems.
5. To report future research trends.

Postgraduate Educational Programme

A-319

B. Logistics and workflow
F. Diekmann; Berlin/DE

Digital mammography, and in particular "direct" digital mammography, may change the procedure and workflow in performing mammographies in many situations besides screening (e.g. in diagnostic workup). This is primarily attributable to the faster availability of the images without the necessity for film development and to the high dynamic range and good contrast resolution of digital mammography. Examples will be presented to illustrate the procedural changes associated with digital mammography in different situations and it will be shown how potential future applications can be integrated into the workflow. Special focus will be held to:

- a) Wire localization procedure - temporal gain, changed workflow
- b) Changed procedures using digital mammography:
- c) Additional views: Low-dose tangential views, low-dose galactography
- d) Workflow with CAD: CAD applications for assessment, software enhancement algorithms
- e) Contrast-enhanced mammography, automated ultrasound

Learning Objectives:

1. To understand the importance of viewing software for workflow with digital mammography.
2. To learn about the impact of digital mammography on workflow in special assessment procedures.
3. To learn about integration of different CAD systems for improvement of workflow in digital mammography.
4. To discuss logistics of assessment with advanced applications in digital mammography.
5. To discuss workflow with future applications like contrast medium mammography.

A-320

C. Screening with digital mammography
P. Skaane; Oslo/NO

Full field digital mammography (FFDM) has potential benefits in future breast cancer screening programs, including: Simplified archival, retrieval and transmission of images; elimination of technical failures; increased diagnostic accuracy especially in women with dense parenchyma; implementation of CAD; telemammography; and screening program reorganization. The true flexibility and the true benefit of FFDM are realized primarily in soft-copy reading.

Factors influencing diagnostic accuracy of FFDM with soft-copy reading include spatial resolution, reading environment, comparison with hardcopies, display system, reading protocol and efficient work station, learning curve effect (training) and CAD to reduce the challenge of interobserver variation.

Results from three large-scale comparisons of screen-film mammography (SFM) and FFDM with soft-copy reading in asymptomatic women ("screening") are so far available. The two earliest studies showed a slightly lower cancer detection rate for SFM although the difference between the two modalities was not statistically significant. The third study showed a higher cancer detection rate for FFDM approaching statistical significance for the age group 50-69 years. The first study revealed a lower recall rate on FFDM but the two other studies showed a higher recall rate for FFDM.

Learning Objectives:

1. To understand the challenge of soft-copy reading in a screening program.
2. To discuss aspects of false negative interpretations in soft-copy reading.
3. To discuss the interobserver variation of SFM and FFDM.
4. To discuss the use of FFDM and CAD within screening programmes.

08:30 - 10:00

Room E2

Abdominal and Gastrointestinal

RC 1301

Imaging of the pancreas: Key questions

Moderator:
L. Lincender; Sarajevo/BA

A-321

A. The choice: US/EUS, CT, MR imaging
D. Vanbeckevoort; Leuven/BE

The diagnostic flowchart in patients with suspected pancreatic disorders depends on many factors such as local expertise, interest and availability of equipment.

Most commonly, transabdominal ultrasound (US) is the first imaging technique. In some patients this technique may also be the final examination.

The addition of colour and pulsed Doppler sonography has contributed to assessing tumour involvement of vascular structures such as the portal and mesenteric system.

However, a sonographic diagnosis of suspected pancreatic disease depends on patient-related factors and is not always straightforward.

Endoscopic ultrasound (EUS) eliminates the problem of overlying bowel gas and allows for focussed high-resolution imaging. This technique is well suited to detect vascular invasion and EUS-guided fine-needle aspiration biopsy can further increase the diagnostic accuracy in pancreatic cancer.

When compared to US the performance of computed tomography (CT) is less operator and patient dependent. The value of helical CT in the management of acute pancreatitis and pre-operative staging of pancreatic neoplasms is well established. Moreover, multislice helical CT using narrow collimation and thin slices, provides excellent spatial resolution and three-dimensional reconstructions showing all relevant anatomical information.

Due to the introduction of (ultra-)fast MR sequences and the development of new, tissue specific contrast agents, magnetic resonance imaging (MRI) may currently be as accurate as spiral CT for depicting inflammatory and neoplastic pancreatic disease. Moreover MRI has the advantage of allowing simultaneous investigation of the pancreatic duct, pancreatic parenchyma and peripancreatic vessels ("all-in-one"). In other words MRI can provide all information required to differentiate resectable from unresectable tumours.

Learning Objectives:

1. To get an update on basic imaging techniques.
2. To enable someone to choose between different imaging techniques.
3. To learn to set up a logical approach of pancreatic disease (when is US enough; and if not, should we go to EUS, CT or MRI?)

A-322

B. What lesions are difficult at CT?
R.W. Prokesch; Vienna/AT

Detection and staging of pancreatic tumors remains a challenge for radiologists. Considering the poor prognosis of pancreatic cancer, accurate preoperative staging is the key to a possibly curative surgical treatment. Contrast-enhanced helical CT has been the most commonly used for evaluation of pancreatic cancer in many institutions, although it suffers from many limitations. With the fast pace of advances in multidetector CT (MDCT), and the implementation of multidetector-row scanners, improvements in spatial resolution in the z-axis with near isotropic imaging provide exquisite multiplanar reconstructions of pancreatic anatomy.

Learning Objectives:

1. To describe the characteristic features of pancreatic tumours.
2. To present imaging findings useful in the identification of subtle pancreatic cancers.
3. To supply CT/MR criteria which help to differentiate adenocarcinoma of the pancreas from chronic pancreatitis.

A-323

C. Uncommon pancreatic tumors
T.K. Helmerger; Munich/DE

Dependent on the three main cell lineages, pancreatic tumors may arise from the duct cells, the acinar cells or the endocrine cells. The "classic" ductal adenocarcinoma of the pancreas accounts for about 80% of all pancreatic tumors, important variants as mucinous noncystic carcinomas (1-3%), adenosquamous carcinomas (3-4%) and undifferentiated (anaplastic) carcinomas (2-7%) add another 10% to the ductal tumors. The latter ones together with endocrine tumors (2%), mucinous cystic tumors (2%), intraductal papillary-mucinous tumors (1%), serous cystadenomas (1%), acinar cell carcinomas (1%), solid-pseudopapillary tumors (1%), pancreaticoblastoma (< 0.5%) and other rare entities represent the "uncommon" pancreatic tumors.

Some of these uncommon tumors may mimic the clinical findings and appearance in imaging of ductal adenocarcinomas. Nevertheless, the knowledge of specific imaging features in tailored CT and MR imaging studies may help to differentiate uncommon pancreatic tumors from the classic ductal carcinomas. This can be especially crucial since some of these tumors hold a significantly better prognosis in comparison to the generally dismal prognosis of ductal adenocarcinomas of the pancreas, while other rare tumors do not need even therapy at all.

Learning Objectives:

1. To become aware of the variety of uncommon pancreatic tumors.
2. To identify the prognostic implications of uncommon pancreatic tumors.

Postgraduate Educational Programme

3. To identify clinical and imaging features, which distinguish between uncommon tumors and classic adenocarcinomas.

08:30 - 10:00

Room F1

Molecular Imaging and Contrast Media

RC 1306

Molecular imaging

Moderator:

O. Clément; Paris/FR

A-324

A. Molecular imaging with PET

G.K. von Schulthess; Zürich/CH

PET radiopharmaceuticals are by several orders of magnitude (10^5 - 10^8) more sensitive probes than contrast agents used in MR and CT. As a result, many radioactively labelled probes of molecular biological processes can be injected into a patient, which would be toxic when injected at doses required to produce contrast alterations in MR or CT. Consequently, PET together with conventional Nuclear Medicine methods currently represent the only forms of clinical molecular imaging.

The most frequent clinical application of PET is the use of FDG, a glucose analogue, which is an excellent probe to depict tumor glucose uptake and metabolism. Imaging this property of tissues has proven to provide an excellent tumor staging and therapy control modality, by far superior to anatomic imaging. Other molecular probes are in the pre-clinical testing phase, such as F-choline, F-thymidine, and F-tyrosine related compounds, which label cell membrane synthesis, cellular proliferation and amino acid uptake and metabolism as well as hypoxia markers. Many other PET-probes are evaluated in a research setting.

As many of the compounds show little anatomic information, fusion of images with an anatomic reference frame is becoming increasingly important. This is the reason, why PET-CT is currently the fastest growing imaging modality in the western hemisphere.

Learning Objectives:

1. To understand the essential advantages of PET over other imaging modalities.
2. To become familiar with the clinical and research potential of PET imaging.
3. To understand the advantages of PET-CT over PET imaging alone.

A-325

B. Cell targeting and cell tracking with MR imaging

H.E. Daldrup-Link; San Francisco, CA/US

New stem cell based therapies require to assess cell homing and engraftment quantitatively and qualitatively. MR imaging is well suited to depict and track transplanted stem cells in vivo, if the cells are labelled with MR contrast agents. Basic principles, capabilities and limitations of various labelling techniques will be presented.

Virtually any cell type can be labelled with MR contrast agents. Labelling techniques comprise simple incubation, receptor mediated uptake, transfection and electroporation techniques. Cells can be labelled with positive or negative MR contrast agents and can be subsequently depicted with clinical MR scanners. Iron oxide contrast agents are generally better suited than gadolinium or manganese contrast agents and SPIOs are better suited than USPIOs. However, each labelling procedure has to be tailored to the investigated cell type and target organ.

In vivo applications comprise MR based cell tracking studies of bone marrow transplantation and new cell based therapies, such as homing of mesenchymal stem cells in injured myocardium, homing and migration of neurologic stem cells in impaired brain tissue and accumulations of transplanted natural killer cells in tumors. In addition, labelled leukocytes may be used diagnostically to detect and characterize inflammation.

In conclusion, MR contrast agents can be used for labelling and in vivo tracking of various cell types with clinical MR scanners. The ability to provide in vivo cell tracking with non-invasive imaging techniques may improve our understanding of how stem cells mediate recovery of injured organs and may be ultimately applied clinically for safety assessments of transplantation procedures.

Learning Objectives:

1. To understand advantages and disadvantages of various currently available cell labeling techniques with MR contrast agents.

2. To be able to apply optimized and dedicated protocols for cell labeling purposes.
3. To get an overview of potential experimental and clinical in vivo applications.

A-326

C. Optical imaging

P. Wunderbaldinger; Vienna/AT

Molecular imaging has become one of the most exiting fields of research in radiology. In order to image on a cellular and even subcellular level new imaging techniques such as optical imaging have been developed. Optical imaging relies on either endogenous tissue contrast such as absorption and scattering (transillumination imaging), autofluorescence (spectroscopic techniques), reflectance (diffuse tomography), bioluminescence (luciferase imaging) or on optical contrast agents (fluorochromes, dye). These agents usually emit in specific bandwidths and can be used for targeted imaging by attaching them to peptides (e.g. VIP, Somatostatin), specific ligands (e.g. folate receptor), macromolecules (e.g. Transferrin). The main disadvantage of this approach is the direct dependence on receptor/binding affinity and a low signal-to-background ratio.

More promising is the use of activatable optical probes that are inactive in their native state (quenched) and following enzymatic activation start to strongly fluorescence in the near infrared light spectrum (basically no autofluorescence). These probes can be engineered to target specific enzymes (e.g. MMP-II, Cathepsin) and, thus, be used for specific tumor detection and differentiation, therapy monitoring, lymph node and plaque imaging, gene expression/therapy monitoring, etc. With the development of new imaging devices such as fluorescence mediated tomography allowing a combined optical and MR or CT imaging, endoscopic probes and hand held scanners initial problems such as low tissue penetration and poor anatomical resolution have been solved.

Based on recent observations optical imaging may soon be ready for clinical use, such as tumor detection/screening, intraoperative biopsy guidance, lymph node differentiation and therapy monitoring.

Learning Objectives:

1. To understand the basic principles of optical imaging.
2. To comprehend the different optical imaging strategies and applications.
3. To learn about different optical contrast agents/probes.
4. To hear about potential clinical applications of these new imaging techniques.

08:30 - 10:00

Room F2

Neuro

RC 1311

MR spectroscopy of the brain in clinical practice

Moderator:

N. Sener; Izmir/TR

A-327

A. Technique and protocols

E.R. Danielsen; Copenhagen/DK

Background: ^1H MRS is becoming an increasingly automated procedure, and will often add information to a negative or non-conclusive MR imaging study. Hypoxic, traumatic, toxic, or hypoglycaemic brain injuries, metabolic diseases, neurodegenerative diseases, or systemic diseases such as hepatic encephalopathy are typical pathologies with diffuse brain abnormalities calling for MRS. In focal brain diseases MRS should be considered in, abscess versus cystic necrotic tumor, differential diagnosis of lesions in HIV+ patients, recurrent tumor versus necrosis, tumor classification, guide for tumor biopsies, and lesions of unknown etiology.

Procedure Details: The concentrations of the metabolites, which MRS can detect in the human brain, are typically between 1 mM and 20 mM. N-acetylaspartate, total creatine, total choline, myo-inositol, glutamate, glutamine, lactate, glucose, and lipid are the most prominent detectable metabolites. It is possible to quantify the metabolites and obtain coefficient of variance between 5% and 18%, this however requires attention to methodological detail. It is crucial to know how to obtain good S/N and high resolution. Positioning and size of the selected volume, shimming, TE and TR, and even minor patient movement become important factors.

Conclusion: High quality and precise MRS results require a basic understanding of underlying methods including spatial selection methods, water suppression, shimming and how to acquire high S/N spectra. The rewards are low

Postgraduate Educational Programme

coefficient of variance, artefact-free spectra, and hereby the possibility to provide data that influence clinical decisions making for individual patients.

Learning Objectives:

1. To learn about choices of measurement protocols, and how they influence the result.
2. To understand procedures performed (automatically and manually) prior to acquisition.
3. To learn about single volume of interest versus multiple volume methods.
4. To learn about the MR spectrum, MRS visible metabolites and post processing methods.
5. To learn about normal values, reproducibility and how certain conditions unrelated to the clinical question may influence the measurement.
6. To get a brief recipe of how to use MRS to answer clinical questions.

A-328 ♀

B. Clinical applications of MRS: Focal lesions

I.M. Björkman-Burtscher; Lund/SE

MR spectroscopy allows the examination of tissue biochemistry, which adds to the diagnostic information obtained with other radiological modalities. As MRS techniques have become more user friendly and reliable, clinical *in vivo* MRS applications are increasing, more metabolites can be included in data analysis, and confidence of interpretation increases.

When investigating patients with focal brain lesions, it is advantageous to use single volume short TE methods combined with multiple volume methods adding spatial information. MRS can optimize the reliability of diagnostics and prognostics in focal brain lesions by depiction of subtle differences in complex metabolite profiles obtained by short TE studies and spatial correlation of MRS abnormalities to MR imaging features including normal appearing tissue.

This presentation will focus on differential diagnosis, spectral features and diagnostic pitfalls in brain disorders presenting with focal lesions: tumours and tumour like masses - including classification, grading and therapy response -, infectious and inflammatory diseases, and focal hypoxic and traumatic injuries.

Learning Objectives:

1. To learn about basic information on metabolites relevant for the interpretation of proton MR spectra in focal brain lesions.
2. To understand the typical spectral features of focal brain lesions.
3. To get some clues for differential diagnosis.
4. To understand the necessity to appreciate MRS as a complement to MR imaging and not a substitute for MR imaging for differential diagnosis.

A-329

C. Clinical applications of MRS: Diffuse lesions

P.J.W. Pouwels; Amsterdam/NL

Knowledge of normal regional and developmental metabolite patterns is mandatory, especially for MR examinations of a pediatric population with childhood white matter disorders. This broad field includes mitochondrial disorders and leukodystrophies, such as hypomyelinating, demyelinating, and cavitating disorders. These diseases are sometimes due to enzyme defects causing absence or accumulation of metabolites. First of all, it has to be ascertained that uncommon resonances are real and not due to artefacts. But when the presence or absence of those metabolites is recognized in the spectrum, MRS can be diagnostically specific. In most diseases however, the spectrum may only indicate processes which occur in many different diseases, such as neuronal loss, demyelination, or gliosis. Nevertheless, there are many differences between the leukodystrophies with regard to the severity, the location and the extent of spectroscopic abnormalities. And the spectra often also change during progression of the disease. Of course, conventional MR imaging is indispensable in addition to MRS for correct diagnosis of known leukodystrophies, and to recognize common patterns in as yet unspecified white matter disorders. Furthermore, other quantitative MR techniques, such as diffusion weighted imaging (yielding the apparent diffusion coefficient and fractional anisotropy), and magnetization transfer imaging (yielding the magnetization transfer ratio) add valuable information. In combination with MRS these techniques may help understand the pathology of white matter disorders.

Learning Objectives:

1. To understand normal regional and developmental metabolite patterns.
2. To understand spectral abnormalities in childhood inborn errors of metabolism, leading to white matter disorders.
3. To distinguish uncommon resonances due to accumulation of metabolites from artefacts.
4. To learn about the evolution of a spectrum after ischemia.

5. To compare MRS with other quantitative MR techniques for following disease progression.

08:30 - 10:00

Room G

Genitourinary

RC 1307

Multislice CT of the urinary tract

Moderator:

P. Pavlica; Bologna/IT

A-330

A. Multislice CT of urothelial tumors

N.C. Cowan; Oxford/UK

Multislice computed tomography (CT) allows fast acquisition of thin slices for large body volumes. Single breath-hold acquisition & faster table speeds reduce movement artefact. Thinner slices allow reduction in pixel size with improvement in spatial resolution. By adjustment of image matrix, reconstructed FOV and pixel size, isotropic voxels may be reconstructed providing the opportunity for 3D imaging techniques to be applied to multislice CT urography (CTU).

The principle indication for CTU is the detection of urothelial tumours, which present most commonly with haematuria or more rarely with unexplained hydronephrosis. Correct timing of the acquired series is critical and is best between 10-15 minutes post-injection of contrast medium. 2-series acquisition is possible using a split-bolus technique for administration of contrast medium. The effective dose for 2-series CTU is ~11.5 mSv compared with 2.5 mSv for intravenous urography (IVU). For CTU the risk of fatal cancer induction is calculated as 1 in 1,400 and for IVU 17,600. It is important to restrict CTU for appropriate population groups at high risk for cancer.

CTU signs for urothelial tumours are of a papillary or polypoid mass sometimes with invasion of adjacent structures.

Circumferential wall thickening is a lesser-known CT sign. CTU visualizes the entire urinary tract, which is an advantage for the detection of urothelial cancer, a multifocal process. Small tumours may be identified throughout the entire upper urinary tract and also within the bladder. Wide windowing is essential.

CTU compares favourably with other imaging modalities for the detection of urothelial cancer.

Learning Objectives:

1. To optimize the use of multislice CT (MSCT) for the investigation of urothelial tumors.
2. To review the radiological signs of urothelial tumors using MSCT.
3. To illustrate the diagnostic pitfalls of using MSCT for the investigation of urothelial tumors.
4. To compare the use of MSCT for investigation of urothelial tumors with other imaging modalities.

A-331

B. Multislice CT of renal cancer

U.G. Müller-Lisse; Munich/DE

Multislice computed tomography (MDCT) has widely increased the range of helical CT scanning, the speed of data acquisition, and the spatial resolution of image data along the z-axis (long axis of body). Current MDCT scanners allow for breath-hold scanning of the abdomen and pelvis or of the chest without motion-artifact. MDCT of the kidneys and urinary tract allows for multiplanar image reconstruction with meaningful interpretation and demonstration of the precise location, size, and extent of renal lesions in imaging planes that are other than axial. Postprocessing tools provide 2D- and 3D-impressions of renal lesions in relation to renal parenchyma, extrarenal fat, renal sinus, pyelocalyceal system, ureter, blood vessels, and surrounding organs. Nephron-sparing surgery is most feasible in small (T1a, TNM 2002 classification) renal cancers that do not extend into or immediately abut hilar or pyelocalyceal structures. High temporal resolution (now down to 0.33 s/rotation) of MDCT scans distinguishes arterial, corticomedullary, nephrographic (renal parenchymal), and excretory (urographic) phases of passage of intravenous contrast media through the kidneys. Limitation of radiation exposure requires tailoring of MDCT protocols to specific clinical needs. Detection, localization, and local (T-) staging of renal cancer by MDCT demonstrate 80-95% accuracy. Current MDCT and MR imaging techniques perform equally well in the staging of renal cancer.

Postgraduate Educational Programme

Learning Objectives:

1. To learn about advantages and disadvantages of different examination protocols in MSCT of renal cancer, particularly image information versus radiation exposure.
2. To learn about the influence of MSCT information on uro-surgical decision making, particularly in small renal tumors.
3. To learn about the diagnostic value of MSCT in view of other imaging techniques in the evaluation of renal cancer.

A-332

C. Multislice CT in trauma of urinary tract

M. Hellström; Gothenburg/SE

Injuries of the kidney by blunt or penetrating trauma include renal contusion, parenchymal laceration, fracture, "shattered kidney", subcapsular haematoma and injuries to the renal pedicle, including renal artery avulsion, laceration or occlusion, or renal vein thrombosis. Depending on the extent of injury, perirenal and pararenal haematoma and, if the collecting system or ureter has been injured, urinoma may ensue. The urinary bladder may suffer intra- or extraperitoneal rupture due to blunt or penetrating or trauma, sometimes due to pelvic fractures. Multislice CT (MSCT) of the kidney is superior to ultrasonography, urography, conventional and single slice CT due to its fast image acquisition, reducing motion artefacts and allowing imaging in several phases, and the availability of multiplanar reformats, which are very helpful in visualising the full extent of injury. MSCT in suspected injury of the urinary system should include the entire abdomen and pelvis, in order to detect injuries of other organs, and to reveal the full extent of haematomas and urinomas, which may otherwise be underestimated. MSCT in the corticomedullary phase allows detection of renal vessel injuries, active bleeding and defective parenchymal perfusion. Renal parenchymal injuries and non-perfused areas are also well depicted during the nephrographic phase. Delayed imaging, 8-15 minutes after contrast administration, is necessary to reveal the full extent of contrast leakage from rupture of the collecting system, ureter or bladder. Bladder rupture may require scanning after contrast filling via bladder catheter, but only after urethral injury has been ruled out, if necessary by a retrograde urethrogram.

Learning Objectives:

1. To provide an understanding of the mechanisms and types of traumatic injuries of the kidneys and urinary tract.
2. To provide an understanding on the role of MSCT, as related to other imaging modalities, in the work-up and follow-up of traumatic injuries of the kidneys and urinary tract.
3. To provide an understanding of the diagnostic appearances, as well as diagnostic pitfalls, of traumatic injuries of the kidney and urinary tract at MSCT.
4. To provide an understanding of the technical performance, role of contrast medium administration, role of post-processing and technical limitations of MSCT in diagnosing traumatic injuries of the kidney and urinary tract at MSCT.

08:30 - 10:00

Room H

Interventional Radiology

RC 1309

Percutaneous tumor ablation

Moderator:

M. Sato; Wakayama/JP

A-333

A. Liver

P.L. Pereira; Tübingen/DE

As an alternative to liver surgery, percutaneous thermotherapy has gained increasing importance within recent years. Different modalities of energy deposition have been developed: RF ablation has proven superior to other modalities as a cost-effective, efficient and safe treatment alternative. Current commercially available ablation electrodes include monopolar, bipolar, and multipolar devices. The shapes of these needles allow *in vivo* a nearly spherical ablation zone of up to 4 cm in diameter. Patients can be treated on either an outpatient or inpatient basis. The RF needle is placed into the lesion under US, CT or MR guidance. Exact navigation of the applicator into the tumour, and monitoring of the procedure are crucial factors for complete tumour coagulation. Targeting of applicator position and a near on-line monitoring of the ablation procedure are much facilitated since the introduction of MR-compatible RF-ablation devic-

es. Complications after RF ablation are infrequent (< 2%). For long term follow-up MR imaging of the liver every three months for one year, and every six months thereafter has been recommended by the Expert German Group for Radiofrequency Ablation (EGRA/AGIR/DRG). Results of multiple clinical series appeared to be very promising showing 52-98% complete ablation rates. The major determinate of success is initial tumor size, cut-off value seems to be 3.5 cm for colorectal metastases and 5 cm for encapsulated hepatocellular carcinomas. RF ablation may be favourably combined with chemotherapy or embolisation. If recurrence occurs at the ablation site, or new tumors occur outside of the treated area, additional treatments with RF ablation are potentially possible.

Learning Objectives:

1. To understand indication for RFA of the liver.
2. To know the mechanism of radiofrequency ablations for liver tumor.
3. To know different equipment and techniques.
4. To understand the results and follow-up.

A-334

B. Kidney

P.R. Mueller; Boston, MA/US

Increasingly, RCC's are detected as small incidental findings on cross-sectional imaging studies. Coupled with an aging population, the result is an increasing number of elderly people and/or people with comorbid conditions with small RCC. This population has been the impetus for development of minimally invasive percutaneous techniques to treat RCC. Because of the recent introductions of the techniques and the lack of large cohorts of patients with the gold standard 5-year survival data, ablative techniques for treatment of RCC have generally been limited to patients with one or more of the following conditions: solitary kidney, limited renal function such that surgical resection would result in dialysis, comorbid conditions rendering the patient a poor operative candidate, predisposition to multiple multifocal RCC's such as in von Hippel Lindau disease, and advanced age such that life expectancy is less than 10 years. The likelihood of achieving complete coagulation necrosis is influenced by tumor size and location. Tumors 3 cm or smaller can generally all be ablated successfully regardless of location, with a rare RCC requiring a second ablation session for complete treatment. Tumors 3-5 cm can be ablated completely, but up to 30% of these may require a second ablation session. Major complications are rare. Hemorrhage is the most common reported complication. Hemorrhage is the most common reported complication. Our experience with our 100 patients will be presented.

Learning Objectives:

1. To understand the "rationnel" for radiofrequency ablation of renal masses.
2. To know the indication for RFA of renal masses.
3. To understand the role of imaging.
4. To know the results of RFA.

A-335

C. Lung

R. Lencioni; Pisa/IT

Lung cancer is a leading cause of cancer death. Non-small cell lung cancer (NSCLC) comprises approximately 80% of primary malignant lung tumors. Lungs are also the second most frequent site of metastatic disease. Surgical resection is the treatment of choice for early-stage NSCLC and oligometastases from colorectal cancer. Unfortunately, because of the high prevalence of chronic respiratory disorders and atherosclerotic vascular disease, only 30% of patients with NSCLC are clinically operable. On the other hand, the high risk of recurrence and the need to remove functioning lung tissue along with the lesions limit the indications for surgery in patients with colorectal metastases. Image-guided radiofrequency ablation (RFA) is a minimally invasive technique used to treat solid tumors. Because of its ability to produce large volumes of coagulation necrosis in a controlled fashion, this technique has gained acceptance as viable therapeutic option for unresectable liver malignancies. Recently, investigation has been focused on the use of RFA for the treatment of lung tumors. Pilot clinical trials have shown that this technique can achieve effective and reproducible tumor destruction with acceptable morbidity and have suggested that it could represent a viable alternative or complementary treatment method for selected patients with NSCLC or lung metastases who are not candidates for surgical resection. However, further investigation in larger patient cohorts and longer follow-up will be needed to confirm these promising results and to establish the role of RFA in the clinical management of nonsurgical patients with lung malignancies.

Learning Objectives:

1. To discuss the rationale of percutaneous tumor ablation in the treatment of primary and secondary lung malignancies.

Postgraduate Educational Programme

2. To review the results of experimental animal studies.
3. To describe indications and contraindications, technical issues, results and complications emerged from clinical trials.
4. To have a good understanding of the current role of percutaneous tumor ablation in the multidisciplinary management of lung tumors and be aware of the different technical approaches by the end of the presentation.

08:30 - 10:00

Room I

Joint ECR/EAR sessions: Challenges for European Radiology

ER 1326

Teleradiology: Threat or opportunity?

Moderator:

B. Silberman; Paris/FR

A-336

Teleradiology professional issues: A new radiological service

P.M.T. Pattynama; Rotterdam/NL

Teleradiology allows one to read and report radiology images at a site distant from where the examinations have been performed. Its advantages are that it provides flexibility to a radiology practice allowing for temporary shortages in manpower, it brings radiology services to remote areas and it provides easy access to outside expert opinion to raise quality of care.

In teleradiology, a division is made between the various roles of the radiologist: on the one hand, his role on-site is as a consultant to his fellow clinicians with a critical importance in clinical management, and as the person who is responsible and accountable for the quality of the in-hospital radiology service. On the other hand, he has a role as the provider of a written radiology report.

Potential problems may arise because of this role separation. Reports made at a distance in relative clinical isolation may lack clinical relevance. Legal issues remain: who is responsible for errors in reporting? Will defensive reporting abound? There is also the financial issue. Conventionally, the radiologists' fee has been based on the written report as the unit of work output. This makes sense when all reporting is done on-site. But when radiology reports will be made at a distant site, this computation will not be valid anymore because the "clinical" part of the radiologist work will then not be accounted for. In this presentation, it is argued that the "clinical services" and "report writing" parts of the radiologist's work should be separately reimbursed.

Learning Objectives:

1. To discuss the separate roles of the radiologist as a clinician, the "imaging consultant" versus the provider of the radiology report.
2. To review advantages and disadvantages of teleradiology.
3. To discuss the potential impact of teleradiology on the radiology profession.

A-337

International consensus standards for clinical teleradiology

L. Lau; Brunswick, VIC/AU

Good quality clinical radiology may be defined as the timely access to an efficient, effective and integrated delivery of clinically appropriate and accurately interpreted, good quality imaging studies in a safe, service-orientated and sustainable practice environment. Teleradiology offers a new opportunity of service delivery to a range of clinical scenarios. However, when employing this 'new modality', we need to consider other important factors which may influence quality in addition to those related to the transmission and reporting of images.

The ACR, EAR and RCR have prepared position papers on the appropriate practice of teleradiology. The RANZCR is developing a teleradiology consensus statement. However, the practice of teleradiology is not constrained by national boundaries. To ensure consistency, minimum quality and safety, it is desirable to have an international set of practice standards/guidelines in this emerging field. These standards should cover the various aspects of good quality clinical radiology and not simply focus on the technical issues alone. It is important for our profession to lead proactively rather than to have this imposed upon us by third parties.

The International Radiology Quality Network (IRQN) is a network of national and international organisations. Its objective is to promote quality in radiology through collaboration, experience sharing and mutual assistance. One of its long term tasks is the development of a set of international accreditation standards in radiology. The IRQN is ideally placed to facilitate the radiology profession towards the drafting of a set of international practice standards/guidelines in clinical teleradiology.

Learning Objectives:

1. To learn the role and impact of teleradiology in the practice of good quality clinical radiology.
2. To learn why it is important and desirable to adopt an international set of clinical teleradiology standards and practice guidelines.
3. To learn the role of the International Radiology Quality Network (IRQN) in facilitating this development by proactively working with the profession and employing a consensus approach.

A-338

Report of the ACR task force: Legal aspect, US professional last guidelines and international issues

J.P. Borgstede; Colorado Springs, CO/US

Teleradiology is a valuable tool in providing access to timely, quality radiological interpretations. Today, teleradiology has facilitated a unique role in delivering quality interpretations to hospital emergency rooms and other health facilities that did not have access to a radiologist's contemporaneous interpretation in the past. While teleradiology has led to an improved level of care in the United States, the potential use of this technology abroad raises some significant potential challenges to the assurance of high-quality patient care in the future.

The American College of Radiology (ACR) Board of Chancellors, convened a Task Force on International Teleradiology to study legal, regulatory, reimbursement, insurance, quality assurance and other issues associated with this new and emerging practice. The ability of teleradiology to transmit images electronically from one location to another, outside the borders of the United States, has made this a prominent issue for the profession and the College.

Results of the task force include the following principles: international teleradiology must not reduce quality of patient care, it must be consistent with the ACR technical standard for teleradiology, appropriate licensure and medical liability insurance must be maintained, appropriate credentialing and medical staff privileging must be maintained, independent image interpretation is required by the physician signing their report as his/her own interpretation and signing reports as one's own without reviewing the images (ghosting of reports) is unethical. Regular participation in quality assurance, availability for emergency consultations, and assurance of privacy protection were also requirements of international teleradiology recommended by the task force.

Learning Objectives:

1. To understand the background resulting in the ACR task force on international teleradiology.
2. To understand the results of the ACR task force on international teleradiology.
3. To obtain a perspective on the future of international teleradiology.

A-339

First attempt for a European guidelines for the use of teleradiology

B. Silberman; Paris/FR

The daily practise of Radiology and the benefits to patients has significantly altered with advances in science and new technics in the last 25 years. Some examples include vascular imaging, ultrasound, CT, MR imaging and digital radiography.

Teleradiology is the latest development and has to be included in the new daily radiological service for patients.

In many countries around the world and within Europe, teleradiology is already an established service.

But many threatening questions are arising about the use of teleradiology without the real involvement and responsibility of local and accredited radiologists in order to assure a good quality clinical radiological service to patients.

ACR, Italian radiological society and RCR has already published documents or guidelines.

EAR Professional Organisation Committee and UEMS radiological section worked together closely in order to present guidelines for the good use of teleradiology in Europe. This work is to be formalised through EU official professional association, as it is for the UEMS training Charter.

Learning Objectives:

1. To understand the benefits of radiology and quality standards for the delivery of a quality clinical radiological service to patients.
2. To know potential pitfalls especially if teleradiology to become a general method of national and international radiological service delivery.
3. To discuss what should be European radiological guidelines for a good clinical use of teleradiology.

Postgraduate Educational Programme

08:30 - 10:00

Room K

Pediatric

RC 1312

Neonatal problems

Moderator:

M. Clauzon; Vandoeuvre/FR

A-340

A. Investigation of ano-rectal anomalies

M. Hiorns; London/UK

The term "ano-rectal anomalies" is often used synonymously with "imperforate anus" but more accurately encompasses a wide range of abnormalities including ectopic anus, imperforate anus, rectal atresia, and anal and rectal stenosis. The spectrum of anomalies is in part due to the complexity of the embryological development of the anorectal segment of the hind gut. Several classifications have historically been used to delineate these anomalies but the most simple distinction is into high and low malformations (depending on whether the rectum ends above or below the puborectalis sling), this having implications for both prognosis and treatment.

Presentation is either antenatal or at the immediate post natal check (absent anus). Occasionally presentation may be delayed until the infant has failed to pass meconium, or meconium is passed in the urine, or the infant becomes obstructed. If the lesion is unequivocally low it is usually managed by anoplasty or dilatation but most commonly a diverting colostomy is fashioned soon after birth with other imaging investigations being delayed.

Before definitive surgery a loopogram and cystogram are routinely performed to evaluate communications between the end of the hindgut and the genitourinary tract (a "fistula"). The range of findings will be illustrated. More accurate assessment of the position of the puborectalis sling can be made using MR imaging if required.

Due to the high association (up to 90%) with other abnormalities (part of the VACTERL syndrome) other imaging would normally include renal ultrasound and spinal ultrasound in the first few weeks of life.

Learning Objectives:

1. To understand the normal anatomy and normal development of the lower gastrointestinal tract.
2. To understand the range of anomalies of the lower GI tract.
3. To understand the range of investigation available and their applications.

A-341

B. Broncho-pulmonary foregut malformations: Antenatal and postnatal imaging

S. Puig; Vienna/AT

The foregut (FG) is defined as the anterior part of the alimentary tract leading from the mouth to the entrance of the bile duct. The human lung is a derivative of the primitive foregut and appears by 3 weeks of gestation as an enlargement of the caudal end of the laryngotracheal sulcus of the foregut. Further development of the pulmonary parenchyma includes 4 steps.

Structural and functional defects in lung development may lead to a number of abnormalities including bronchopulmonary foregut malformations (BPFM).

Routine US screening enables the visualization of fetal intrapulmonary malformations. Prenatal MR imaging, especially with ultra-fast sequences, is an important adjunct helping to differentiate different masses and/or to evaluate large or atypical masses. This is particularly useful for the planning of in-utero interventional procedures, delivery, and immediate postnatal surgery.

Prenatal US-examinations have been systematically performed for more than 30 years.

Prenatal MR imaging was introduced in 1983. Since the early 1990s single-shot rapid acquisition with refocused echos are available. This high quality fast T2-technique leads to freezing of fetal motion.

After birth, chest radiography is the primary image tool. For further evaluation, high spatial resolution of contrast enhanced multi-detector CT (MDCT) is recommended to visualize small anatomical structures to either confirm the diagnosis or to demonstrate the exact anatomy for the surgeon. Using low-dose protocols and dose modulation software in combination with multiplanar reformats lead to excellent image quality at low radiation exposure. Using new tube current modulation software, dose reductions of up to 90% were possible.

Learning Objectives:

1. To understand normal embryological development and possible developmental abnormalities, which lead to foregut malformations.
2. To describe the prenatal evaluation of foregut malformation using US and MR imaging.
3. To describe the postnatal clinical findings.
4. To describe the postnatal imaging features using radiography, US, MR imaging, and multidetector CT with special consideration of low-dose CT protocols.

A-342

C. Investigation of the dilated urinary tract

M. Riccabona; Graz/AUT

Aim: To present the common conditions and theories of paediatric UT dilation, to discuss the various imaging modalities, their potential and their importance, and to finally suggest modern imaging algorithms for typical clinical presentations and queries.

Background: We learned that dilatation itself is not a disease and does not equal obstruction; only a threat to the kidney has to be focused both clinically and by imaging. The advanced capabilities of modern imaging displays even physiologically fluid filled collecting systems, creating confusing terms such as "low degree hydronephrosis". Many conditions have to be considered: non-obstructive dilatation, megacalicosis, collecting system laxity, UPJO, MU, gross VUR, or dilatation due to tumors, clots, fungus balls and stones. The task of imaging is to depict those that may deteriorate prior to causing irreversible damage.

Imaging: Depending on the underlying condition, the presentation and age, and the availability of imaging facilities such as VCUG, US, scintigraphy, and MR imaging (with decreasing importance of IVU and CT) different imaging algorithms are used. Reliable assessment of obstruction is essential for therapy decisions - improper assessment may either lead to a diagnostic overkill or may cause permanent damage. In spite of the improved anatomical and functional assessment by modern imaging there still is no method that provides a reliable *a priori* pro futuro assessment; currently obstruction is defined by declining function, deteriorating drainage, increasing dilatation, or by indirect signs.

Conclusion: Advanced techniques have improved comprehensive imaging of the dilated UT. However, at present this is complimentary to the established "gold standard"; with only some variations of current imaging concepts.

Learning Objectives:

1. To know the common causes with its clinical implication for pediatric urinary tract dilatation and to understand their origin, pathophysiology, and future risks.
2. To refresh the knowledge on standard imaging techniques applied for investigating urinary tract dilatation, and to learn about the potential of modern imaging using modern US, scintigraphy and MRU.
3. To suggest updated imaging algorithms for the most common and typical clinical queries trying to avoid a diagnostic overkill without the risk to easily miss significant aspects that may influence therapy decisions or prognosis, based on established procedures and yet trying to include modern approaches.

08:30 - 10:00

Room L/M

Radiographers

RC 1314

Professional matters

Moderators:

S. Geers-van Gemenen; Utrecht/NL

M. Golebiowski; Warsaw/PL

A-343

A. Recruitment and retention of radiographic staff

T. O'Connor; Galway/IE

Recruitment and retention of radiographers in the Republic of Ireland has become a major issue of importance since 2001. In 2001 the normal recruitment practices were not able to sustain the level of radiography staffing required to meet service demand. The various factors that led to this situation were diverse and the impact on the remaining staff and service delivery only became obvious once the effect had reached a critical mass. Delays in making changes to the way the service was delivered meant that the staff who continued to work in the system ended up working under extreme pressure in an effort to ensure service

Postgraduate Educational Programme

delivery was not reduced. This became a factor in terms of retention of radiographers in an increasingly competitive employment market. The impact on service delivery took several different forms ranging from delays in opening new services, rotating service closures and reducing worklists on a daily basis. To address the issues a concerted overseas recruitment drive took place. A range of new recruitment methods were used by different organisations. Efforts were made to reduce delays in getting new staff on board. The ability to offer incentives to prospective employees was explored and implemented to varying degrees. The lessons of the recruitment and staffing issues from 2001 are still being learnt. Retention and incentivisation, both monetary and non-monetary, remain key to maintaining stable staff levels while in tandem reducing any delays in recruitment to ensure impact on service delivery is minimised.

Learning Objectives:

1. To understand why there is a staffing/recruitment issue, using the Irish experience.
2. To appreciate the effect of the problem on delivery of services to patients.
3. To identify different means of recruiting radiographers.
4. To identify delays in the recruitment process.
5. To learn what needs to be done to retain existing staff as well as new recruits.

A-344

B. HENRE (Higher Education Network for Radiography in Europe):

Education

A. Kettunen; Oulu/FI

The Higher Education Network for Radiography in Europe Sub Group 1 has performed an Educational Institute survey to ascertain Nature of Radiography Education across EU. The survey asks the level of education award on completion of programme, staff educational and working arrangements with clinical practice, course content, degree of multidisciplinary working, credit ratings and details about the modular system. In addition to ascertain the nature of radiographer education across the EU the survey aims to appreciate the differing capabilities of newly qualified radiographers and attempts to learn, through a competences tuning process aligned with the Bologna employment of radiographers educated in a non-host country. To date 14 countries have responded to the survey. A wide range of study options, hourage requirements/ECTS use and teaching delivery approaches have been identified. Commonalities exist amongst some countries with respect to the major comparison is the belief that a large clinical experimental component is necessary in all programmes. In conclusion it is evident that some differences need to be addressed to ensure free movement of personnel across the EU as there are national differences to the functionality of the post of radiographer. Harmonising should be done to reach an optimal level in all EU countries.

Learning Objectives:

1. To understand the nature of radiographer education across the EU.
2. To appreciate the differing capabilities of radiographers who have just qualified across the EU.
3. To learn about what further education may be necessary to employ radiographers educated in another country.

A-345

B. HENRE (Higher Education Network for Radiography in Europe):

Learning methods

J.J.M. Peeters; Eindhoven/NL

Background: Subgroup 2 of the HENRE project (3rd year) is dealing with the outcomes of a questionnaire concerning learning and teaching methods used in Radiography education in the EU. The questionnaire was developed and piloted in Austria in November 2003. Partners in the subgroup then revised it.

Findings: Analysis of the outcomes. One of the items is teaching and learning methods: subject learning - teacher centred versus Problem Based Learning (PBL), student centred learning. There are a variety of teaching and learning methods in use throughout Europe. PBL is not widely used. Furthermore the use of VLE tended to be a useful supporting technique and was being provided in a minority of the European countries. The technique enables institutions to provide education with a different didactical approach including flexibility of location. Side effect: the RLOs were developed in relation to student centred education.

Conclusion: Many countries are seeking alternatives to the teacher centred approach. Subgroup 2 has developed several RLOs being forwarded to all the participating countries. RLOs provide education, which is time-independent and interactive.

Learning Objectives:

1. To meet the similarities and differences in radiology education between the European partners development of Reusable Learning Objects (RLO) in the EU.
2. To describe the benefits of RLO in a European setting exploration and application of Virtual Learning Environment (VLE) in higher education in the EU.
3. To understand VLEs and the implementation in higher education.

A-346

B. HENRE (Higher Education Network for Radiography in Europe):

Continuous professional development (CPD)

G. Marshall; Lancaster/UK

Method: Members of the CPD subgroup of the Higher Education Network for Radiography in Europe devised a questionnaire to sample the CPD needs of radiographers in their countries. 437 questionnaires were distributed and 307 returned (70%).

Results: 92% of radiographers believed CPD was important or very important. Of those believing CPD was not important 83% had 11 or more years experience. 8% of radiographers were not prepared to spend any time on CPD, 44% 1-5 hours, 33% 6-10 hours and 15% 10 hours or more monthly. The majority 66% would prefer a combination of internet and paper based materials. 62% of radiographers would only use learning materials in their first language, with 38% being prepared to use other languages, the majority preferring English. 73% had facilities to use materials through the internet. The favored areas for CPD provision were CT 11%, MR imaging 10%, digital imaging 8% and image interpretation by 5%.

Conclusion: Most radiographers believe CPD is important, with 1-5 hours monthly being the preferred amount. A mix of paper and internet based materials in their own language would be most popular. Cross sectional imaging was the most popular area for CPD training although training in digital imaging and image interpretation were also required.

Learning Objectives:

1. To analyse the results of a questionnaire study (distributed in six languages) re. CPD requirements of radiographers.
2. To evaluate the implications of the findings.
3. To identify how CPD requirements can optimally be addressed.

08:30 - 10:00

Room N/O

Physics in Radiology

RC 1313

Quality control and dose reduction in digital radiology

Moderator:

G. Marchal; Leuven/BE

A-347

A. Principles of flat panel X-ray detectors and photostimulable plates

B. Geiger; Forchheim/DE

In contrast to inherently digital techniques, such as CT or MR imaging modalities, all digital projection radiography techniques result from the continuous development of conventional (i.e. analogue) techniques. There is a variety of different applications for digital techniques in the field of radiology, and each application has specific requirements for the X-ray equipment.

It is characteristic for any digital-radiography device that the X-ray detection stage, the final storage, and the means for displaying the image are physically separate components. This is of importance for a definitive understanding of the differences between analogue and digital-radiography systems for the practical application as well as for quality control.

From that perspective the principles of the most popular technological solutions for radiography applications (photostimulable plates, electro-direct flat panel detectors, opto-direct flat panel detectors) are discussed. The principles of X-ray detection and signal processing will be shown on a physical level as well as its impact on practical applications.

Learning Objectives:

1. To understand the basics of X-ray detection: What happens in the scintillators, what is the captured "signal" and which processes of signal deterioration exist (noise, flare etc.).

Postgraduate Educational Programme

2. To learn the principles of available technological solutions (photostimulable plates, electro-direct flat panel detectors and opto-direct flat panel detectors).
3. To understand the differences in physical imaging performance. Practical considerations with respect to application fields will also be discussed.

A-348

B. Managing patient dose in digital radiology

E. Vano; Madrid/ES

The International Commission on Radiological Protection (ICRP) has approved in 2003, the document on "Managing patient dose in digital radiology", published in 2004. The ICRP report is structured in four chapters and three appendices. Diagnostic information provided by modern digital detectors can be equal or superior to conventional film-screen systems, with comparable patient doses but with digital systems, an overexposure can occur without an adverse impact on image quality. Overexposure may not be recognised by the radiologist or radiographer. A tendency to increase doses can occur. The ICRP document summarizes actions that can influence image quality and patient doses and includes an assessment of the impact of each action. The document includes eight formal recommendations dealing with: 1) Training aspects; 2) review of diagnostic reference levels; 3) patient dose audits; 4) availability of the original image data to the user; 5) optimisation when new digital systems or new post-processing software are introduced; 6) procedures for quality control; 7) justification criteria; 8) role of the industry promoting tools to know and control the exposure parameters. It is expected that the ICRP report helps to profit the benefits of this important technological advance in medical imaging with the best management of radiation doses to the patients. It is also expected to promote training actions before the digital techniques are introduced in radiology departments and to foster the industry to offer enough technical and dosimetric information to radiologists, radiographers and medical physicists to help in the optimisation of the imaging.

Learning Objectives:

1. To realize that the International Commission on Radiological Protection (ICRP) has published recommendations on patient dose management in digital radiology.
2. To introduce the key points of the ICRP document specially those related with aspects influencing patient dose and image quality.
3. To highlight the role of the radiology industry to help in the protection of the patient for the new digital technologies.

A-349

C. Quality assurance in digital radiology: How we do it

H.-P. Busch, C. Schilz; Trier/DE

Background: The aim of all imaging methods is to answer the diagnostic question with sufficient quality and certainty. Decoupling of image acquisition, image processing and image documentation leads to new possibilities and risks for digital radiography. For digital imaging methods a suitable choice of parameters can lead to advantages in diagnostic information. An unsuitable choice can lead to harmful effect down to wrong diagnose.

Procedure Details: The aim of image quality optimisation should be to reach the necessary quality with the lowest possible dose. The following concept shows the strategy for optimization and quality assurance in the digital radiography.

1. Optimisation

Optimal post processing is not independent from the dose range. Therefore the necessity exists to optimise the quality depending on clinical criteria.

2. Objectivation

A strategy for quality management can be performed for each kind of examination in different reference centres. Afterwards the result will be objectivated by phantom exposures.

3. Standardisation

The range of results, which corresponds to a sufficient image quality, will be defined by these reference centres. For an unknown equipment image quality can determined by evaluation of similar phantom exposures.

Conclusion: Dose and quality management means, that in a broad range the dose and image quality can be optimized and adapted to the clinical questions. For the future optimisation, objectivation and standardisation will be necessary in the framework of European quality assurance program.

Learning Objectives:

1. To discuss European guidelines for quality assurance.
2. To explain new aspects for quality assurance especially for digital radiography.
3. To fit the concept of quality assurance into the new strategy of dose and quality management.

4. To describe experience and test phantoms for routine use. (Which parameters are controlled in detail? What are objective quality criteria for digital images?).
5. To give examples of optimisation of image quality.

08:30 - 10:00

La Scala

E³ - European Excellence in Education

E³ 1320

Interactive image teaching

Moderator:

T.J. Vogl; Frankfurt a. Main/DE

A-350

Paranasal sinuses

T.J. Vogl, M. Mack; Frankfurt a. Main/DE

With the advent of modern therapeutic procedures such as functional sinus surgery (FSS), cross-sectional imaging modalities have assumed major importance in diagnosis as well as treatment planning, especially in patients with chronic inflammatory diseases such as maxillary, ethmoid and frontal sinusitis. Today treatment planning is done with a CT examination, which affords maximum spatial resolution for defining key bony structures and aerated spaces. Several pathologic entities including inflammatory processes and benign or malignant tumors lead to the unspecific symptom of nasal obstruction. In general, disturbances of the epithelium in acute and chronic sinusitis lead to mucus retention and possible superinfection. In problem cases such as chronic inflammation or complete paranasal sinus obstruction, MR imaging makes an excellent adjunct for differentiating inflammatory and neoplastic processes. The understanding of normal anatomy, anatomical variations and physiology within the nasal cavity, the paranasal sinuses and its adjacent structures is a prerequisite for the radiological diagnosis of sinus disease. It will help to determine the location and nature of the ostomeatal obstruction in sinusitis and is necessary for accurate tumor staging in the paranasal region. The role of different imaging techniques will be discussed.

Learning Objectives:

1. To learn the normal anatomy and anatomical variations of the paranasal sinuses.
2. To understand the state of the art imaging technique in the paranasal region.
3. To review the most common imaging findings in patients with nasal obstruction.
4. To review typical radiologic features of benign and malignant tumors.
5. To recognize CT and MR appearance of chronic sinusitis. The typical imaging appearance of mucocele, sinonasal polyposis, and post-surgical infection will be presented.

10:30 - 12:00

Room A

State-of-the-Art Symposium

SA 14

Imaging of prostate cancer: Present and future

Moderator:

J.O. Barentsz; Nijmegen/NL

A-351

Imaging of prostate cancer: Present and future (Introduction)

J.O. Barentsz; Nijmegen/NL

This course will present the clinical role of current and new imaging techniques, such as US and MR imaging. The focus will be on how to apply these techniques and how they may influence therapy decisions. This will be presented by an expert team, including a clinician, an ultrasonographer and a MR specialist.

Learning Objectives:

1. To understand the clinical questions in patients with prostate cancer.
2. To show the role of US and MR imaging in this respect.
3. To learn how to use these techniques.

Postgraduate Educational Programme

A-352

Clinical questions

F. Witjes; Nijmegen/NL

Currently screening for carcinoma of the prostate is done with PSA pre-screening. In case with an elevated PSA, biopsies are performed, but only 20-25% of patients with a PSA between 3.0 and 10.0 actually have prostate cancer. To improve this detection rate, sometimes up to 20 biopsies per session are taken.

Question 1: Can imaging techniques improve the sensitivity of detection, and the accuracy of the biopsies without increasing the number of biopsies?

A substantial proportion of patients receive local treatment advice based on local staging done with imaging and Digital Rectal Examination. However, currently T2 tumours are understaged in 30-40% (dubious indication for surgery, screening could have been considered) and overstaged in 10% (curative option was withheld).

Question 2: Can imaging determine the T-stage?

Radiotherapy is very dependent on imaging to prevent damage outside the prostate. Future planning for an additional (salvage) boost on the (recurrent) tumour is also dependent upon imaging.

Question 3: Can imaging detect tumour (recurrence) within the prostate?

Recent reports indicate that extended lymph node dissection (LND) could cure 10-15% of N+ patients. Presence and localisation of abnormal nodes can guide a palliative approach with fine needle aspiration, preventing unnecessary surgery, or an extended LND, in patients that might profit from aggressive therapy.

Question 4: Can imaging detect nodes?

Learning Objectives:

1. To understand the therapeutic consequences of local staging of prostate cancer.
2. To understand the potential consequences of localisation of the tumour within a prostate cancer.
3. To understand the importance of imaging in recurrent prostate cancer after local treatment with curative intent (recurrence).
4. To understand the clinical consequences of proper lymph node imaging and localisation.

A-353

Ultrasound

F. Frauscher; Innsbruck/AT

The value of ultrasound in the diagnostic evaluation of prostate cancer has increased in importance in the past decade. This is mainly due to the increasing incidence of prostate cancer, the most common malignancy in men. Conventional grey-scale ultrasound has been extensively investigated, but this technique has shown a low sensitivity and specificity for prostate cancer detection. The additional use of color Doppler imaging has been shown to improve the positive predictive value only. With the introduction of ultrasound contrast agents, the role of ultrasound in prostate cancer detection has dramatically changed. Advances in ultrasound techniques were introduced to further increase the role of ultrasound contrast agents. These techniques use the interaction of the contrast agent with the transmitted ultrasound waves, and are very sensitive for the detection of microbubbles. Contrast-enhanced ultrasound investigations of blood flow within the prostate have shown that contrast-enhanced ultrasound adds important information to the conventional ultrasound technique. Early results from studies evaluating contrast-enhanced ultrasound suggest the use of ultrasound contrast agents to enhance ultrasound imaging of the prostate is feasible. Recently elastography (strain imaging), a technique which enables the visualisation of displacements between ultrasonic image-pairs under compression, has been shown to be of potential use for the detection of prostate cancer. Therefore the application of contrast-enhanced ultrasound and elastography for the detection and clinical staging of prostate cancer is promising. However, future clinical trials will be needed to ensure that the promise these new ultrasound techniques of the prostate have demonstrated evolves into clinical application.

Learning Objectives:

1. To demonstrate current new developments of ultrasound in prostate cancer.
2. To demonstrate the clinical relevance of these new techniques.
3. To demonstrate future prospects.

A-354

MR imaging

J.O. Barentsz; Nijmegen/NL

This paper describes the local staging performance and localization of prostate cancer in magnetic resonance (MR) imaging. Both a literature review and our

own results are presented. Additionally, potential ways to improve local staging performance and localization with MR imaging will be described. Various staging methods, including digital rectal examination, prostate specific antigen level (PSA), Gleason score, transrectal ultrasound and MR imaging are discussed.

Also new developments of MR in evaluating prostate cancer and its subsequent clinical role will be shown. The use of USPIO in detecting lymph node metastases in small (5 mm) nodes will be discussed. The role of endorectal coil MR imaging, dynamic MR imaging and MR-spectroscopy will be illustrated. Fusion of CT with functional MR images, allowing more precise radiotherapy will be shown. Finally advantages of 3 T endorectal coil MR imaging, being high spatial, spectral and dynamic resolution are presented.

Learning Objectives:

1. To show how state-of-the art MR imaging should be performed.
2. To present the clinical relevance of MR imaging.
3. To show new developments.

10:30 - 12:00

La Scala

E³ - European Excellence in Education

E³ 1420

Diagnostic workstations: The new super-assistants of the radiologist and surgeon

Moderator:

B.M. ter Haar Romeny; Eindhoven/NL

A-355



Diagnostic workstations: The new super-assistants of the radiologist and surgeon (Introduction)

B.M. ter Haar Romeny; Eindhoven/NL

In the medical sciences image acquisition and image interpretation play a crucial role. 80% of all diagnoses and surgery planning are based primarily on images. Many modalities exist, and new imaging techniques continue to appear, such as the recent molecular imaging techniques. Every major vendor has a gamut of workstation applications in its product range. 3D visualization, MIP and cine-view are currently the most frequently used modes, but there is much more to come into the daily routine, with great benefits for sensitivity and specificity, and serious reduction of workload.

The conventional visual interpretation of these images however is hampered by significant variations between the interpreters, and within one and the same interpreter. On the other hand, a semi-quantitative approach with manual contour tracing of the object of interest requires much concentration and time of the user, and also leads to significant observer variations.

In addition, the modern MR imaging and multi-slice CT scanners provide enormous amounts of 3D data to the extend, that software solutions on high speed workstations are required to visualize and present all the data to the medical specialist in a convenient manner.

The medical image processing developments are directed at the automated recognition (or segmentation) and subsequent measurement (i.e. quantification) of structures in medical images to support the clinical decision making processes for both diagnosis and therapy and the clinical research. Modern research and development in image processing attempt to include knowledge about the structures to be detected as much as possible in the segmentation process, in order to minimize the user interactions, to increase the accuracy, and optimize the degree of automation. To be able to apply this kind of techniques in clinical practice, requires extensive validation studies.

Three world renowned experts will highlight in this special educational session the developments in workstation applications, richly illustrated with examples.

Learning Objectives:

1. To have a good overview of the state-of-the-art in modern medical workstation applications.
2. To learn about modern applications of diagnostic workstations, for surgery, cardiology and computer aided diagnosis.

A-356

Workstations for computer aided diagnosis and surgery planning

H.-O. Peitgen; Bremen/DE

In this tutorial we will discuss new software assistants for the radiological work towards surgery planning in oncological and living-donor-liver surgery. For oncological surgery the issue at hand is to detect and quantify the lesions and evaluate

Postgraduate Educational Programme

ate the risks of, for example, a compromised liver function after resection. To that end the assistant permits the user to choose variable safety margins and determines the parenchyma at risk from the point of view of compromised branches of the hepatic vascular systems. Finally, the assistant supports the choice of optimal resection proposals.

For living-donor-liver transplantation the issue at hand is to quantify the risks when a graft or remnant lobe has critical volume; determine, quantify and visualize the risks when grafts or remnant lobes are left with compromised territories; and to determine the appropriate cutting lines interactively and associate these with resulting risks.

Software assistants that support analogous issues in oncological brain surgery (compromised axonal fibers) and lung surgery (compromised subsegments) will also be presented.

MeVis - Center for Medical Diagnostic Systems and Visualization at the University of Bremen - has established a new research and prototyping platform - MeVisLab (www.mevislab.de) - for medical image processing and visualization. Several software assistants have been developed for CAD problems such as for example diagnosis and therapy monitoring of neurological diseases; detection and quantification of stenoses; bone removal in CTA data; diagnosis of contrast enhanced dynamic MRT data - in particular for breast MR imaging - and therapy monitoring for tumors.

Learning Objectives:

1. To comprehend compromised liver function based on CT imaging in liver tumor surgery and living-donor-liver surgery.
2. To understand the radiological role of new preoperative planning tasks for oncological liver surgery, living-donor-liver transplantation, interventional ablation procedures.
3. To become familiar with new risk assessment strategies in the radiological work up for liver surgery and intervention planning.

A-357

Computer-aided quantitation and diagnosis in cardiovascular applications

J.H.C. Reiber; Leiden/NL

In all aspects of cardiovascular medicine, from the daily clinical decision making processes, to therapeutic interventions and the clinical research, imaging plays a dominant role, which will only increase and expand in the coming years. In addition, all existing imaging modalities are used from conventional X-ray imaging during catheterization procedures to multi-slice tomography (MSCT), echocardiography including intravascular ultrasound, nuclear cardiology with SPECT and PET, and magnetic resonance imaging (MRI). Applications include both organ (left and right heart chambers and atria) and vessel (coronary and peripheral vessels) imaging, as well as fusion approaches between the different modalities, such as PET and MSCT or MRI.

There is a continuous need for automated analysis of such data sets with minimal user interactions, and small systematic and random errors, to support the interventions, as well as to properly describe the baseline and follow-up situations, and the associated changes. This field is denoted computer-aided quantitation and diagnosis. Modern cardiovascular workstations should be able to acquire data sets from the equipment of different vendors from local and hospital-wide networks (PACS systems), display the data in an intuitive manner to the user, allow the quantitation of the data, provide appropriate and customized reporting, and be able to transfer the derived data to databases for subsequent statistical analyses.

In this presentation a number of widely used quantitation approaches will be described, such as the assessment of the severity of narrowings in coronary and peripheral vessels by conventional X-ray and MSCT, of wall motion, thickening/thinning and perfusion of the myocardial muscle by MRI and MSCT, of flow measurements in vessels by MRI, etc. Research towards the fully automated analysis of the 3D data sets have made clear that statistical models of the organs to be detected are required; these have been shown to be very promising and effective. It has also become clear that combinations of various segmentation techniques are often required to approach the (fully)-automated analysis in routine practice with widely varying imaging qualities. Finally, extensive validation studies are always necessary before such quantitation techniques can be used in clinical practice.

Learning Objectives:

1. To become familiar with the developments in the field of computer-aided quantitation and diagnosis in cardiovascular imaging.
2. To understand its possible implications in the daily workflow and in clinical research.
3. To understand the advantages and limitations of the computer-aided quantitation and diagnostic approaches.

A-358

Workstations for image guided interventions

P. Suetens; Leuven/BE

In 1947 the first image-guided intervention was applied to a human brain. At that time X-ray and ultrasonic images were the only imaging modalities. A stereotactic frame fixed to the patient's head was used to geometrically register the images and planning data with the surgical instruments. The introduction of computers and 3D imaging modalities boosted the use of stereotactic neurosurgery. Whereas in its early days (1950-1970) stereotactic interventions were primarily used to treat functional disorders, such as certain persistent pain syndromes, in the 1970s many tumors and other pathologies could be identified everywhere in the brain. In the past two decades, neurosurgical procedures have continuously been augmented and improved with new technical possibilities, such as frameless systems, multimodal image fusion (CT, MR imaging, MRA, PET), true 3D visualization, and navigation systems.

The technical improvements opened the way to new applications outside neurosurgery. This is for example the case in orthopaedics, traumatology, maxillofacial surgery and dentistry, where the same technology can be applied to rigid bony structures. Unlike in brain surgery, complex cutting planes require that more attention is given to 3D visualization and corresponding user interfaces. On the other hand, the (mathematically) complex shape of the bony structures gives the opportunity to use synthetic templates and personalized equipment and prostheses without the need for a navigation system. An overwhelming number of products and services is currently being offered by several companies for a diversity of applications, such as personalized dental implants and prostheses with immediate function, distraction osteogenesis and orthognathic maxillofacial surgery with soft tissue simulation, and knee replacement surgery with kinematic analysis for an optimally balanced leg alignment.

While surgery planning is mostly performed on pre-operative images, intra-operative imaging is not new. Examples are laparoscopy, endoscopy, angiography for vascular repermeabilization, fluoroscopy for osteosynthesis in traumatology, and ultrasound imaging for biopsies and for abscess drain. Computer-based interventional imaging, however, such as CT for stereotactic craniotomy and MR imaging for thermotherapy are more recent but already proved their relevance. Intra-operative imaging is particularly useful in case of expected tissue deformation between pre-operative imaging and surgery, which is the case for most interventions on soft tissue.

Besides for diagnosis, intra-operative imaging can also be useful for the registration of pre-operative images and planning data with the surgical instruments. Examples are the automatic fusion of pre-operative CT images with intra-operatively acquired fluoroscopic images for percutaneous localization of the spine, or with 2D portal images for accurate positioning of the prostate prior to radiotherapy. After registration, the intra-operative images can also be visualized together with the pre-operative images, planning data, and tracked instruments into a single integrated image, known as augmented reality.

It can be expected that interventional imaging will become increasingly important in the future.

Learning Objectives:

1. To become familiar with the opportunities of medical imaging for therapy and surgery.
2. To learn the principles underlying the techniques of image guided interventions.
3. To comprehend the capabilities and technical limitations of image guided therapy and surgery.

Postgraduate Educational Programme

12:15 - 12:45

Room B

Plenary Session

HL 3

Alessandro Vallobona - Honorary Lecture

Presiding:

A. Chiesa; Brescia/IT

A-359

Pulmonary circulation: From old to new imaging modalities

L. Bonomo; Rome/IT

The lung is the only organ where vessels (arteries and veins) are visualized without contrast administration.

Since the advent of spiral CT and MR the chest radiograph has been the only non-invasive imaging modality for evaluating the pulmonary vessels.

The gravitational distribution of pulmonary blood flow, a fundamental observation made in 1927 by Bjure and Laurell, represented and still represents the fundamentals of functional radiology.

Computed tomography and magnetic resonance, thanks to angiographic and functional techniques, have increased the potentials of non-invasive imaging of the pulmonary vessels.

Rapid technical developments of CT and MR allow the radiologist to achieve a qualitative morphologic and quantitative functional evaluation of pulmonary perfusion so that the role of angiography and V/Q scintigraphy can be significantly reduced.

Learning Objectives:

1. To get familiar with the different imaging modalities available for evaluating the pulmonary circulation.
2. To learn about the different roles of chest radiography, CTA, MRA in the diagnosis of pulmonary vascular diseases.

14:00 - 15:30

Room A

"ECR meets" Japan

EM 3

"Oriental Pearls" in oncology imaging: Imaging-pathologic correlation of early cancer in gastrointestinal tracts

Presiding:

A. Chiesa; Brescia/IT
T. Ishigaki; Nagoya/JP

A-360

"Oriental Pearls" in oncology imaging: Imaging-pathologic correlation of early cancer in gastrointestinal tracts (Introduction)

T. Ishigaki; Nagoya/JP

The number of cancer deaths in 2002 in Japan was 304,286, and the death rate per 100,000 was 241.5, accounting for 31.0% of the total number of deaths. Lung cancer is the most common, accounting for 22.0% of all cancer deaths for males, followed by stomach cancer with 17.8% and hepatic cancer with 13.0%, while stomach cancer is the most common for females with 14.8%, followed by lung cancer with 12.7% and colon cancer with 10.1%. The number of deaths from cancer of pancreas and biliary tract is also increasing. Stomach cancer and uterine cervix cancer which used to be major causes of death among the Japanese now show decreasing trends, indicating that the advance of medical technologies such as early detection and early treatment is also a relevant factor. In this session imaging-pathologic correlation of early cancer in upper abdominal organs is presented and efficacy of imaging modalities including CT and MR imaging is discussed. Four Japanese diagnostic radiologists will present excellent papers: Early gastric and colonic cancers, early hepatic carcinoma, early-stage pancreatic cancer and early cancer of the biliary tract. It is sure that remarkable progress of the diagnostic imaging of an early cancer can be introduced.

Learning Objectives:

1. To learn "What is early cancer?"
2. To learn the correlation between pathology and diagnostic imaging in early cancer of gastrointestinal organs.
3. To understand the role of CT, MR imaging, and other diagnostic imaging modalities for the detection and diagnosis of the gastrointestinal organs.

A-361

Early gastric and colonic cancers

Y. Imai; Isehara/JP

Though the mortality from gastric cancer has slightly decreased recently in Japan, the incidence of gastric cancer is still high. While the morbidity of colorectal cancer is increasing year by year, because of the change in eating habits to western style.

Cancer detection in the gastrointestinal tract is mainly performed by double contrast radiography (DCR) and optical endoscopy. Recently, virtual endoscopy (VE) from the data of multi-slice CT has also been utilized. In Japan, the key point for the reliable modality in cancer detection is how to pick up the superficial depressed cancer of the stomach and superficial type cancer of the colon. Recently developed multi-slice CT can evaluate such a superficial type tumor, which is even difficult to diagnose by optical endoscope.

Accuracy of the tumor staging in early gastric and colorectal cancers by DCR is more than 90%, however lower percentages are achieved in advanced staged tumor. MR imaging using an endorectal coil provides a more accurate preoperative assessment of tumor staging for rectal cancers. Intramural tumor invasion confined to the intestinal wall was best evaluated on T2-weighted images. In 45 out of 55 cases (81.8%) of rectal cancers including in both early and advanced stage, MR imaging led to the correct diagnoses on the extent of tumor infiltration. MR imaging findings correlated well with the pathological in terms of macroscopic growth pattern, depth of mural invasion and other histological features. Computer aided diagnosis (CAD) using the volume data of multi-slice CT for the detection of gastric and colorectal cancers will develop in near future.

Learning Objectives:

1. To comprehend the role of DCR, VE and MR imaging for the diagnosis of the early gastric and colorectal cancers.
2. To understand the clinical significance of superficial type cancer in the stomach and colon in Japan.
3. To learn the radiological findings of the superficial type early gastric and colorectal cancers obtained by DCR and VE.
4. To understand MR imaging findings of normal layering structure of the intestinal wall and the diagnosis of tumor staging.

A-362

Early hepatocellular carcinoma: Imaging of multi-step hepatocarcinogenesis

O. Matsui; Kanazawa/JP

In Japan, around 31 deaths/100,000/year due to hepatocellular carcinoma (HCC) are seen and around 95% of them are due to hepatitis C (80%) or B (15%) virus infection. By periodic imaging of high-risk patients it has become possible to detect small, early stage HCC. In addition, multi-step development of HCC from adenomatous hyperplasia (AH, low-grade dysplastic nodule), atypical AH (high-grade dysplastic nodule), early HCC (highly well-differentiated HCC), well-differentiated HCC, to HCC with ED.II or above (classical HCC) has been clarified.

The pathologic and imaging features of early HCC are a small nodule with indistinct margins, occasional fatty metamorphosis, arterial hypovascularity, internal portal tracts or portal flow and isointensity on T2-weighted images. However, because of the histological continuity among these nodules, the precise imaging diagnosis of early HCC is often difficult. Therefore, understanding the sequential changes of imaging features during hepatocarcinogenesis is important.

In the course of hepatocarcinogenesis, both arterial and portal supply decrease first due to decreased portal tracts (borderline lesion), then arterial supply returns to the equivalent of the surrounding liver due to newly formed abnormal arteries (early HCC), while the portal supply continues decreasing, and finally the portal supply vanishes and only arterial blood supplies the lesion (classical HCC). Signal intensity on T2-weighted images also shows sequential changes from hypointensity (borderline lesion), isointensity (early HCC) through to hyperintensity (classical HCC).

Because there was intense correlation between the imaging features and prognosis of the nodules, it has become possible to estimate the grade of malignancy of the nodules by imaging.

Learning Objectives:

1. To understand the screening system of small early-stage HCC.
2. To understand the concept of multi-step human hepatocarcinogenesis
3. To know the sequential changes of pathological and imaging features during multi-step hepatocarcinogenesis.
4. To understand the imaging features and their pathological background of early HCC.

Postgraduate Educational Programme

A-363 ♀

Early-stage pancreatic cancer

H. Mori; Oita/JP

During the past decades, the incidence of pancreatic cancers has increased in Japan, and it has become the 5th most common cause of death from cancer. About 18,000 new patients have been found every year. Only 10% to 15% of patients have resectable disease with negative surgical margin and postoperative median survival of 12 to 18 months was unfavorably short. The early-stage cancers may be defined as the margin-negative tumors when they underwent pancreatic resection. This means tumors with invasion to extrapancreatic nerve plexuses, to roots of peripancreatic mesenteries, and to the superior mesenteric-portal venous axis are excluded. The modern role of pancreatic imaging is to evaluate these criteria of local invasiveness as well as metastases to discourage unnecessary surgery. For the assessment of peripancreatic veins, contrast-enhanced CT including multiplanar images on multidetector CT is essential rather than angiography. Observation of peripancreatic veins such as the inferior pancreatic vein leads to diagnosis of cancerous involvement of extrapancreatic nerve plexuses and peripancreatic mesenteries. Differentiation from mass-like chronic pancreatitis or focal-appearing autoimmune pancreatitis became important because a fairly large number of pancreatic resections had been undertaken for these non-malignant diseases. There may be some characteristic contrast enhancement patterns over the time of pancreatic cancer and benign fibrosis that are recognizable on multiphasic CT, which are influenced by microvessel density and fibrosis. For future perspectives, the establishment of screening system such as fecal DNA analysis, clinical installment of new serum tumor marker, and image-guided pancreatic biopsy with p53/Ki-ras staining are essential for detection of the early-stage pancreatic cancer.

Learning Objectives:

1. To comprehend the role of CT including multidetector CT, and MR imaging for the diagnosis of the early-stage pancreatic cancers.
2. To learn the radiological findings of the early-stage pancreatic cancers obtained by CT.
3. To learn CT finding of invasion of pancreatic cancer to the extrapancreatic neural plexuses, roots of small bowel mesentery/ transverse mesocolon.
4. To learn normal anatomy of peri-pancreatic veins, peripancreatic lymphatic drainage pathways to understand the tumor staging.
5. To learn differential diagnosis between pancreatic cancer and focal pancreatic fibrosis or pancreatitis on multiphasic CT or MR imaging study.
6. To understand the recent development of gene/DNA level researches about tumor aggressiveness of pancreatic cancer and possibility of their clinical installment.

A-364

Early cancer in biliary tract

S. Hirohashi; Nara/JP

The early detection of gallbladder or bile duct carcinoma is considered to be difficult because it seldom shows any symptoms except for carcinoma of the papilla Vater. Although various kinds of non-invasive therapy have recently been developed for other carcinomas, complete resection as the classical surgical treatment is the only curative treatment available, and there is no effective evidence-based non-invasive therapy like radiotherapy or chemotherapy for gall bladder or bile duct carcinoma. However, a good prognosis can be expected if complete resection can be carried out, making early detection of these carcinomas by imaging diagnosis mandatory. In Japan, abdominal ultrasonography has become routine in medical checkup screening, and consequently early carcinoma, especially adenocarcinoma in adenoma, is being picked up increasingly frequently. In this lecture, I will talk about the pathology and tips on imaging diagnosis for three major early carcinomas (gall bladder carcinoma, bile duct carcinoma, and carcinoma of the papilla Vater) by various imaging modalities focusing on the practical radiological aspects.

Learning Objectives:

1. To understand the clinical significance of superficial type cancer in the gall-bladder and bile duct carcinoma in Japan.
2. To learn the EUS or IDUS findings of normal layering structure of the gall-bladder and bile duct wall and the diagnosis of tumor staging.
3. To understand the imaging features and their pathological background of early gallbladder and bile duct carcinoma.
4. To comprehend the role of EUS, IDUS and other imaging modalities for the diagnosis of early gallbladder and bile duct carcinoma.

14:00 - 15:30

La Scala

E³ - European Excellence in Education

E³ 1520

Interactive image teaching

Moderator:

D.J. Wilson; Oxford/UK

A-365 ♀

Cervical spine trauma

D.J. Wilson¹, C. van Kuijk²; ¹Oxford/UK, ²Nijmegen/NL

Cervical spine fractures are common and account for 65% of spinal fractures and occur in 3% of major trauma victims. The increased availability of fast helical CT and MR imaging have changed the sensitivity, accuracy and precision of imaging and now should be routine tools.

The role of screening is to detect or exclude both fractures of bone and ligament/disc injury that would lead to instability.

Different approaches to fracture detection using plain films, CT and MR imaging will be discussed covering the pitfalls, strengths and weaknesses of each protocol. Severe cord damage may be present with normal plain films and CT examinations. Most teams will await recovery of consciousness and reduction of pain before attempting to study for instability.

Whiplash injuries may show little on imaging despite the severity and chronicity of the symptoms.

MR is the primary technique in determining the nature of cord and neurological damage.

Fracture patterns include:

- Compression fractures
- Burst fractures
- Combined transverse and ligamentous fractures (Chance)
- Spinous process avulsion fractures (Clay Shoveler's)
- Odontoid peg fractures.
- Lateral mass dislocation due to C1 axial loading fractures (Jefferson)
- Facet fractures and dislocations.
- Avulsion fragments.

Imaging will have a role in planning treatment. CT is the best technique for most cases but MR will have a vital role when there is suspicion of cord damage.

Learning Objectives:

1. To recognise the need for screening for cervical spine injury.
2. To understand the role of imaging in the screening process.
3. To appreciate the benefits and limitation of plain films.
4. To be aware of the value of CT and MR imaging in screening for injury.
5. To recognise fracture and injury patterns.
6. To understand how imaging influences management and treatment.
7. To understand the pitfalls of imaging interpretation.

16:00 - 17:30

Room A

Essentials of Neuroradiology

CC 1617

Degenerative disorders, tumors and infection of the spine

Moderator:

M. Sasiadek; Wroclaw/PL

A-366

A. Degenerative disorders of the spine

M. Gallucci; L'Aquila/IT

The widespread prevalence of patients with back and neck pain makes the spine one of the most frequently radiologically investigated areas, having a significant impact on health care costs. Some authors estimate that up to 80% of all adults have low-back pain at some time in their lives and that a herniated nucleus pulposus is the cause of only a small percentage of these cases.

Pathology and imaging of degenerative spine disease will be discussed starting from normal age-related changes of the intervertebral disc and vertebral body. Interventional radiology also offers several possibilities in therapy, with percentage success rate ranging from 65 to 75%. Minimally invasive procedures such as CT or fluoroscopy-guided radiofrequency discoplasty, O₂-O₃ or corticosteroid in-

Postgraduate Educational Programme

tradiscal and periganglionic injection will be specially discussed. Differential diagnosis from other forms of back pain is also mandatory in order to discriminate further forms susceptible to interventional therapy, like facet syndromes treatable by peri-facet steroid injection, synovial cysts, by evacuation and steroid injection, sacro-ileitis, by intra-articular steroid injection.

The interventional approach can be also successfully widely proposed in cases of osteoporotic (or tumoral) vertebral fractures and vertebroplasty is a progressively growing therapeutic challenge.

Learning Objectives:

1. To understand pathophysiology and classification of normal aging and degenerative diseases of the spine.
2. To become familiar with diagnostic radiology main indications and techniques.
3. To discuss the usefulness of dynamic conventional exams and axial loaded dynamic MR and CT studies.
4. To introduce to interventional radiology in the management of disk and vertebral diseases.

A-367

B. Tumors of the spinal canal

D. Balériaux¹, J. Brotchi¹, I. Salmon¹, W. Fang²; ¹Brussels/BE, ²Shanghai/CN

Early diagnosis plays an important role in the management of tumors of the spinal canal and affects the prognosis and final outcome of the patient. Tumours involving the spinal canal are mostly epidural malignant lesions, predominantly metastases. Intracanalar extramedullary tumors are on the contrary mostly benign and consist of meningiomas and schwannomas. Their prognosis is excellent. Intramedullary tumors are rarer but should be diagnosed early as their prognosis depends largely not only on histology but also tumour size. MR imaging has definitely become the imaging modality of choice for the investigation of the content of the spinal canal. 3D CT on the contrary is the optimal modality for evaluating the bony components of the spine.

Spinal cord tumours occur at any age but are commonly seen in children and young adults. Clinical presentation of spinal cord tumours is poorly specific, with pain surprisingly being the most common and frequently the first symptom. According to tumour localisation, sensory and motor deficits, urinary and sexual disturbances occur, the latter developing usually late in the course of the disease. Astrocytoma, ependymoma and hemangioblastoma account for more than 75% of the lesions: the radiologist may play a key role in trying to differentiate these lesions as surgical approach and final prognosis are different. The differential diagnosis includes uncommon tumours (cavernoma, ganglioglioma, oligoastrocytoma, metastases) as well as inflammatory/infectious mass lesions that do not necessarily require surgery.

Learning Objectives:

1. To be able to perform optimal imaging procedures to diagnose rapidly and efficiently tumors of the spinal canal.
2. To make a differential diagnosis between extracanalar lesions versus intracanalar extradural and intracanalar intramedullary tumors.
3. To become familiar with the differential diagnosis of intramedullary space occupying lesions.

A-368

C. Infectious disease of the spine

E.T. Tali; Ankara/TR

Spinal infection is a significant cause of morbidity and mortality and has an increasing prevalence amongst the general population. Definitive diagnosis based solely on clinical grounds is usually not possible and radiological imaging is used in almost all patients. Spinal infections can be categorized into three groups according to the involved compartment:

1. Extradural infections (osseous spine, epidural space, facet joints, and paraspinal soft tissues)
2. Intradural extramedullary infections
3. Intramedullary infections

Spinal infections are pyogenic, granulomatous, parasitic, viral and, fungal in origin. The incidence is largely dependent on the involved compartment and immunological status of the patient. Epidural and intradural extramedullary infections are most often pyogenic, whereas intramedullary infections are usually caused by viral agents. Infections of each compartment have distinct imaging findings and differentiation can be made by the use of these characteristic imaging patterns. MR imaging has become the modality of choice with its higher sensitivity for the intradural infections than plain X-rays and CT. Contrast administration is essential for the diagnosis. Contrast administration increases the sensitivity but does not affect the specificity and is also useful for the treatment monitoring. Mass-like lesions are seen for epidural infections while different patterns of me-

ningeal contrast enhancement are characteristic for meningitis-arachnoiditis. Fusiform enlargement of the spinal cord with signal change on T1- and T2WI, with/without contrast enhancement is the usual imaging findings of the myelitis. Neoplasms, nonbacterial granulomatous diseases and acute ischemic cord lesions should be considered in the differential diagnosis.

Learning Objectives:

1. To learn briefly about the classification, prevalence, etiology and clinical features of spinal infections.
2. To become familiar with the algorithm and the latest imaging techniques.
3. To learn the basic imaging findings and also imaging hints and tips of epidural, intradural and intramedullary spinal infections.
4. To discuss the imaging findings of different causative agents.
5. To get an overview of differential diagnosis.
6. To get an idea of the latest researches on the spinal infections.

16:00 - 17:30

Room C

Special Focus Session

SF 16

Pulmonary hypertension:

All that the radiologist needs to know

Moderator:

D. Musset; Clamart/FR

A-369

Pulmonary hypertension: All that the radiologist needs to know (Introduction)

D. Musset; Clamart/FR

During the world symposium on PPH in Evian in 1998, a group of specialized physicians was selected by the WHA to make a more physiopathological classification of PPH than the preceding ones. My colleague, Prof. Gerald Simonneau, will explain to you this new classification which was revisited and simplified in 2003.

Among the different diseases included, major knowledges and improvements were done during the past few years for the diagnosis and treatment of two types of vascular entities.

Prof. Martine Rémy-Jardin will focus his talk on chronic thrombo-embolic disease and demonstrate the role of imaging methods for the diagnosis and pre operative staging of this disease.

Dr. Arnaud Resten on the sporadic unexplained PH. He will try to show you the difference of this last presentation with other clinically similar diseases which are the veno occlusive disease and the capillary hemangiomatosis because of the therapeutic implications.

Learning Objectives:

1. To learn the new classification of PPH from the WHO.
2. To understand the clinical presentations of the different types of this disease.
3. To comprehend the indications of imaging methods for the diagnosis and pre operative staging of the chronic thrombo-embolic disease.
4. To become familiar with the different radiological presentations of primary pulmonary hypertension and their consequences on prognosis and treatment of this entity.

A-370

Pulmonary hypertension: Classification, clinical data

G. Simonneau; Clamart/FR

In 1998, during the Second World Meeting on pulmonary hypertension held in Evian, a clinical classification of PH was proposed. The aim of the Evian classification was to individualize different categories sharing similarities in pathophysiological mechanisms, clinical presentation and therapeutical options. The Evian classification is now well accepted and widely used in clinical practice especially in specialized centers. In addition, this classification has been used by the Food and Drug Administration and European Agency for Drug Evaluation for the labeling of newly approved drugs in pulmonary hypertension. In 2003, during the Third World Symposium on PH held in Venice, it was decided to maintain the general architecture and philosophy of the Evian classification. However, some modifications have been proposed, mainly: To abandon the term "primary pulmonary hypertension" and to replace it with "idiopathic pulmonary hypertension", to reclassify pulmonary veno-occlusive disease and pulmonary capillary hemangiomatosis, to update risk factors and associated conditions for PAH, and to pro-

Postgraduate Educational Programme

pose some guidelines in order to improve the classification of congenital systemic-to-pulmonary shunts.

Learning Objectives:

To update and learn on clinical classification of pulmonary hypertension.

A-371

Chronic thromboembolic disease

M. Rémy-Jardin, J. Rémy; Lille/FR

Among the various causes of pulmonary hypertension, the recognition of chronic thromboembolic obstruction of pulmonary arteries resulting in pulmonary hypertension is important since this condition is potentially curable by pulmonary endarterectomy. Several mechanisms are postulated to be responsible for the development of chronic pulmonary hypertension including the recurrence of acute embolic events, the incomplete resolution of treated thrombi leading to variable degrees of residual vascular obstruction as well as *in situ* thrombus propagation into pulmonary branch vessels. Clinically, the disease manifestation is similar to that of primary, idiopathic pulmonary hypertension, a condition associated with a disappointing management despite advances in pharmacotherapy and transplantation. Although the CT diagnosis of chronic thromboembolic disease relies on precise vascular features, the distinction between thromboembolic pulmonary hypertension and primary pulmonary hypertension may be sometimes difficult as *in situ* pulmonary artery thrombosis in patients with primary pulmonary hypertension may mimic occlusions of pulmonary arteries caused by thrombotic material of embolic origin. The purpose of this presentation is to review the most characteristic features of chronic thromboembolic disease as well as newly recognized abnormalities at the level of vessels and lung parenchyma. Updated CT angiographic protocols will also be reviewed in order to emphasize the current trends in dose reduction and optimization of administration of contrast medium in this subset of patients.

Learning Objectives:

1. To describe and illustrate the transition between acute and chronic pulmonary embolism.
2. To review the characteristic CT features of chronic thromboembolic disease.
3. To discuss recent advances in multislice CT technology and their application in routine clinical practice when evaluating patients suspected of having thromboembolic pulmonary hypertension.

A-372

Primary pulmonary hypertension

A. Resten; Clamart/FR

Pulmonary hypertension (PHT) is defined as a mean pulmonary artery pressure above 25 mmHg at rest with a normal pulmonary artery wedge pressure (< 12 mmHg) measured by right heart catheterization. Primary pulmonary hypertension (PPH) is an idiopathic condition at the precapillary level that occurs in the absence of an embolic source or any other identifiable cause such as cardiac shunt, toxic insult or interstitial lung disease. It is a rare condition, with an estimated prevalence of 1-2 per million people. The natural history of PPH is usually progressive and fatal. Pulmonary arterial hypertension with associated conditions can be brought closer. Pathologic confirmation is rarely required and diagnosis is most often posed on the conjunction of an evocative clinical presentation, hemodynamic data and complementary examinations, intended to eliminate the great "causes" of pulmonary hypertension.

Imaging can show nonspecific aspects of pulmonary arterial hypertension, but its main interest is to eliminate secondary causes of hypertension. It is particularly helpful to eliminate a pulmonary venoocclusive disease (PVOD), contraindicating the medical treatment of PPH by prostacyclin, harmful and occasionally fatal in PVOD.

So, in a first part of this presentation, we will review imaging findings of PPH and pulmonary arterial hypertension with associated conditions, dominated by enlargement of pulmonary arteries. In a second part, we will review imaging findings of PVOD and particularly thin-slices CT findings, dominated by ground glass opacity, septal lines and adenopathy.

Learning Objectives:

1. To understand the role of imaging, and particularly CT in the management of primary pulmonary hypertension.
2. To become familiar with radiological findings of primary pulmonary hypertension.
3. To learn the principles underlying the techniques used by radiologists in the management of primary pulmonary hypertension.

16:00 - 17:30

Room E1

Breast

RC 1602

Radiopathological correlation

Moderator:

I.M. Ramos; Porto/PT

A-373

A. Tumoral growth

T. Tot; Falun/SE

Most pathologic processes in the breast originate in the terminal ductal-lobular units (TDLUs) of one sick lobe. The affected TDLUs are distended, distorted or destroyed by accumulation of fluid, mucin, cancer cells, necrotic debris or calcium in the lumina or by accumulation of collagen, glycoproteins or stromal cells in the intralobular stroma. All these processes lead to a considerable enlargement of the TDLUs. In neoplasia, the largest diameter of the largest invasive focus is considered to be the *tumor size*. If the pathologic process involves a single or a few neighboring TDLUs, a *unifocal* lesion develops. If the process simultaneously involves distant TDLUs, leaving uninvolved TDLU-s in between, a multiple (*multifocal*) lesion develops. Lesions developing from a large number of simultaneously involved TDLUs may exhibit a *diffuse* growth pattern, often losing their lobulocentricity in an advanced stadium. The entire area of the present invasive and *in situ* tumor foci is referred to as the *extent of the disease*. Within this area, a considerable *intratumoral and intertumoral heterogeneity* is often observed. All these morphological parameters are dynamically changing over time: The size increases, an initially multifocal lesion may become unifocal by coalescence of the tumor foci or an initially unifocal lesion may become multifocal as new independent foci develop. This *progression* is related to the age of the patient and to the histological type and grade of the tumor. The progression may also be altered by *dedifferentiation* of the tumors during their growth as well as by effective medical interventions.

Learning Objectives:

1. To discuss the different growths of breast tumors.
2. To discuss the tumoral growth timing (enhance problems linked to litigation) and its correlation to imaging (enhance mammography and ultrasound).

A-374

B. Size and vascularity

J. Teubner; Mannheim/DE

The tumor size is recorded as one of multiple prognostic data of breast carcinoma. Gold standard is the measurement on the excised specimen and that obtained on histological preparation. The invasive part, accompanying intraductal components, multifocal satellites and multicentric growth have to be documented, if present.

The nearest distance of tumorous spread towards the excision margin may be important in determining the risk of recurrence. Preoperative imaging is therefore essential for the surgeon's choice on an optimal pathway of excision. In this field mammography, ultrasound and magnetic resonance have specific strengths and limitations in cancer visualization. Since the methods provide complementary tissue information, a multimodal approach will give best results, even though in many cases one method alone presents already all diagnostic information which will not be gained by the others. Parameters affecting the diagnostic value are: Tumor size, histomorphological entity, macroscopic growth pattern, vascularity, presence of microcalcifications and tissue composition of the surrounding tissue. Major imaging differences become apparent in the evaluation of tiny tumors and the estimation of potentially extensive intraductal component in invasive (EIC) or *in situ* carcinoma (DCIS). Postoperative specimen sonography and/or thin sectioning with consecutive specimen radiography are helpful tools in the interdisciplinary approach on the evaluation of the "real" tumor size. Both methods invaluable assist the pathologist in the assessment of the specimen's margins.

Vessel density, permeability and perfusion characteristics differ from benign to malignant lesions. With upcoming contrast agents further tumor characteristics may be evaluated by Doppler sonography and contrast-enhanced MR imaging.

Learning Objectives:

1. To discuss which is the real size of breast cancer, including multifocality and multicentricity.
2. To discuss the potential of the imaging methods in assessing the "useful" tumoral size.
3. To discuss the vascularity of breast cancer as assessed by non radiological and imaging methods.

Postgraduate Educational Programme

A-375

C. Nodal invasion
G. Rizzatto; Gorizia/IT

The principal route whereby most carcinomas migrate to distant tissues, is via the lymphatics. Therefore nodal invasion is a very important determinant in breast staging.

This evaluation is mostly based on the sentinel node (SLN) concept: The efferent lymphatic channel draining a primary tumor leads directly to the first SLN in the regional lymphatic basin.

To better detect the SLN the use of a radiolabeled colloid at preoperative lymphoscintigraphy and intraoperative detection with gamma-ray detection probe have been incorporated into the traditional blue dye protocol. Actually this is the gold standard with a technical success rate of 88%, sensitivity of 93% and accuracy of 97%.

Based on these excellent results many centers perform the axillary dissection only if sentinel nodes are not found or if positive nodes are found at physical examination.

Incorporating ultrasound in the preoperative evaluation of nodal chains may avoid SLN procedure in over 20% clinically node-negative patients. Contrast agents allow perfusion studies that increase the sensitivity for small nodal metastases and allow useful monitoring in locally advanced breast cancers.

Recent studies show interesting potentials also for PET and MR lymphography. In the near future nodal staging will include also molecular imaging with optical and near-infrared probes.

Learning Objectives:

1. To discuss the pathways of nodal invasion.
2. To discuss the potential of the imaging methods in assessing nodal invasion.
3. To propose a cost-effective flow chart.

16:00 - 17:30

Room F1

Chest

RC 1604

Thoracic manifestations of extra-thoracic disease

Moderator:
L. Bonomo; Rome/IT

A-376

A. Lung nodules in patients with extra-thoracic neoplasia
S.R. Desai; London/UK

In patients with a known primary extrathoracic malignancy, staging investigations will commonly include an examination of the chest. Whilst most patients will be referred for a plain chest radiograph, there is a limit to the size (typically around 1 cm diameter) of pulmonary nodules detectable by conventional radiography. Because the contrast resolution of computed tomography (CT) is higher and there is no anatomical superimposition, small intrapulmonary nodules will frequently be identified; this is particularly true since the advent of spiral and now, multidetector-row CT machines. However, determining the significance of focal intrapulmonary nodules, in patients with a known malignancy, remains a vexing problem for the radiologist and clinician. The significance of imaging findings (specifically at CT) in patients with underlying malignancy will be discussed. The relevance of multiplicity, size of pulmonary nodules, the presence/absence of an underlying malignancy and the smoking history will be reviewed.

Learning Objectives:

1. To understand the capabilities and limitations of imaging studies in the detection of focal pulmonary lesions.
2. To determine the significance of intrapulmonary nodules in patients with underlying extrathoracic malignancy.
3. To appreciate the potential importance of the multiplicity and size of pulmonary nodules in patients with known extrathoracic malignancy.

A-377

B. Collagen vascular disease
T. Franquet; Barcelona/ES

The connective tissue diseases are a heterogeneous group of immunologically mediated disorders in which the lungs are an important target organ due to their abundant connective tissue. The most common form of diffuse pulmonary lung disease in patients with collagen vascular disorders is a chronic pulmonary fibro-

sis indistinguishable from other causes of usual interstitial pneumonia (UIP). Rarely, the chronic pulmonary fibrosis may precede the extrapulmonary manifestations of the disease. Other complications of the connective tissue diseases include esophageal dysfunction leading to recurrent aspiration and secondary infection (in scleroderma and mixed connective tissue disease), respiratory muscle weakness contributing to atelectasis and secondary infection (in systemic lupus erythematosus, polymyositis) and drug-induced lung disease (methotrexate and gold treatment in rheumatoid arthritis). Because the pathology of chronic interstitial pneumonia takes a limited number of forms, there are also a limited number of radiographic manifestations. Although of limited value in detecting early stages of disease, conventional chest radiography still remains an invaluable aid in documenting the presence of ILD. Currently, high resolution computed tomography (HRCT) is the imaging method of choice in evaluating patients with ILD.

Learning Objectives:

1. To summarize the HRCT features in collagen vascular diseases.
2. To describe some complications associated with collagen vascular diseases.
3. To learn key points in distinguishing collagen vascular disease from other infiltrative lung diseases.

A-378 ♀

C. Multisystem vasculitides
K. Malagari; Athens/GR

Multisystem vasculitides are a group of diseases characterised by chronic inflammation of the vessel walls. Clinical and immunological overlaps are very common, while the aetiology is unknown (primary). The dominant classification system today of primary non-infectious systemic vasculitides is based on the 1994 Chapel Hill International Consensus Conference, classifying vasculitides according to vessel size predominantly involved into: large-vessel vasculitis (Giant cell arteritis, Takayasu arteritis), medium-sized vessel vasculitis (polyarteritis nodosa, Kawasaki's disease), and small-vessel vasculitis. The latter group is further subclassified according to ANCA positivity into: microscopic polyangiitis arteritis, Wegener's granulomatosis, Churg Strauss syndrome (ANCA positive) and ANCA negative group including, Henoch Schonlein purpura, cryoglobulinemia and cutaneous leucoclastic angiitis.

Despite the considerable overlap, small vessel vasculitides are more often manifested by alveolar hemorrhage associated with increased permeability of the small lung vessels, while moving to larger vessel involvement, manifestations are associated with weakening and inflammation of the vessel walls forming aneurysms, stenosis, occlusion and infarcts.

HRCT features, criteria to establish the diagnosis and differential diagnosis will be discussed.

Learning Objectives:

1. To discuss about anatomic features of pulmonary microcirculation and differentiate between occlusive and inflammatory vasculopathies.
2. To review HRCT, and histologic features of entities in which pulmonary vasculitis is the central pathologic process including Wegener's granulomatosis, Churg-Strauss syndrome, and pulmonary capillaritis.
3. To describe HRCT manifestations of pulmonary involvement in other systemic vasculitides: Giant cell arteritis, Takayasu's arteritis and Behcet's disease.
4. To discuss the differential diagnosis of pulmonary haemorrhage, and anti-glomerular basement membrane disease.

16:00 - 17:30

Room F2

Musculoskeletal

RC 1610

Inflammatory joint disease

Moderator:
V. Jevtic; Ljubljana/SI

A-379

A. Plain film analysis
M. Cobby; Bristol/UK

Imaging studies may be performed in patients with suspected or definite arthritis to:

- determine the presence of an arthritis
- establish a diagnosis
- determine the extent of disease

Postgraduate Educational Programme

- assess disease activity
- evaluate progression
- select patients for surgery
- determine the type of surgical procedure

This talk will concentrate on the radiological differential diagnosis of an inflammatory arthritis. This is achieved most effectively by:

- determining what tissue within a joint is primarily affected
- identifying which joints are involved

For a radiological analysis there are essentially three sites of involvement within a joint that can be differentiated:

- the "bare" area, where synovium directly contacts bone
- hyaline cartilage and the immediate subchondral bone
- the enthesis

Once the principal site of involvement has been determined a series of further questions need to be asked:

- A. Synovial disease. Symmetrical or asymmetrical soft tissue swelling? Erosions: Well-defined, ill-defined, proliferative or non-proliferative?
- B. Cartilage disease. Loss of cartilage, thickening of cartilage or calcification of cartilage? Secondary bone changes?
- C. Enthesal disease. Non-erosive or erosive? Symmetrical or asymmetrical involvement?

Using this combination of binary analysis in conjunction with the distribution of joint involvement a specific diagnosis or short differential diagnosis of an arthritis can usually be made.

Learning Objectives:

1. To provide an overview of the radiographic features of the various inflammatory arthropathies.
2. To show how the changes within an individual joint enable the various arthropathies to be differentiated.

A-380

B. What's new in sero negative joint disease?

A.G. Jurik; Arhus/DK

The group of seronegative spondylarthropathies (SpA) encompasses ankylosing spondylitis, psoriatic, reactive, enteropathic, pustulotic and unclassifiable arthropathy. The prevalence of SpA is similar to that of rheumatoid arthritis, but they have not gained the same attention regarding imaging. The promising effect of new therapies, especially biological therapy, has made the need for accurate diagnosis and disease monitoring obvious.

The sacroiliac joints (SIJs) are involved in most forms of SpA, and an accurate diagnosis of sacro-ilitis is therefore important. MR imaging has proven valuable with regard to this, having a high sensitivity and specificity. However, the performance and interpretation of MR imaging of the SIJs demands knowledge about the normal joint anatomy and optimal technique. With such knowledge, it is possible to gain greater benefit from MR imaging. It can demonstrate both joint destruction and signs of disease activity, and is able to detect inflammatory SIJ pathology before it has resulted in osseous destruction visible at radiography and CT. Furthermore, MR imaging may be of help in differentiating between the different forms of SpA early in the disease, and provides the potential for monitoring disease severity during therapy. MR imaging can also be valuable with regard to the detection of early spinal lesions, in addition to evaluation of disco-vertebral or other lesions later in the disease. In the case of clinical signs indicating spinal cord compression, cross sectional imaging is always needed.

Learning Objectives:

1. To understand and recognise the features of normal sacroiliac joints (SIJ) at MR imaging and technical aspects.
2. To know the differentiation between SIJ involvement in the different forms of SpA.
3. To suggest a system for MR imaging grading of SIJ involvement to be used for monitoring disease.
4. To know the imaging features of spinal involvement in the different forms of SpA with emphasis on MR imaging.

A-381

C. What's new in rheumatoid arthritis?

P.J. O'Connor; Leeds/UK

MR imaging and ultrasound have an increasingly prominent role in the assessment of articular disease. Rheumatoid arthritis (RA) is a chronic inflammatory polyarthritis characterised by synovitis and joint destruction, particularly of the small joints. Studies have shown progression of joint destruction despite suppression of synovitis. Other studies indicate that despite no change in clinical

synovitis measures, certain therapies retard bone damage. More recently it has been demonstrated that the suppression of disease activity will slow or even halt progression of bone damage although there was poor correlation between clinical response and radiological change in these studies. Such clinical and radiographic observations, where synovitis and bone damage are seemingly independent processes, have been supported by experimental models of RA where joint damage may be uncoupled from synovitis. However, all studies have used either indirect or insensitive measures of synovitis and bone damage or have imaged complex joints such as the wrist which makes interpretation of any imaging findings difficult. An understanding of the inter-relationship between synovitis and bony damage is critical for the optimal management of patients, especially in determining a logical approach for drug treatment, and provides the model for all disease where chronic inflammation is a prominent feature.

This lecture focuses on the use of MR imaging and ultrasound in the assessment of rheumatoid disease with specific emphasis on the detection and potential impact of diagnosing sub-clinical synovitis, pre-radiographic erosion and complications. A list of relevant references will be provided.

Learning Objectives:

1. To appreciate the relationships between imaging abnormalities and the rheumatoid arthritis disease process.
2. To understand the diagnostic and therapeutic impact of imaging in the rheumatoid arthritis patient.
3. To understand potential pitfalls in employing new imaging modalities in inflammatory arthritis.
4. To be aware of the relevant literature regarding the use of MR and ultrasound in rheumatoid arthritis.

16:00 - 17:30

Room G

Head and Neck

RC 1608

Imaging of skull base tumors: A practical approach for your daily practice

Moderator:

H.B. Eggesbø; Oslo/NO

A-382

A. Anterior skull base

R. Maroldi; Brescia/IT

Assessment of anterior cranial fossa floor neoplastic invasion has a great impact on surgical planning. Bone destruction of the skull base and dura mater invasion are key information provided by imaging techniques. CT shows bone destruction better, whereas MR is more precise in *grading* dural invasion, which implies a worse prognosis. A proper assessment requires the careful analysis of the signal intensities that compose a "sandwich" of signals corresponding to the bony floor of anterior cranial fossa, the overlying dura mater, and the CSF. On enhanced sagittal and coronal SE T1, when a sinonasal neoplasm abuts the cribriform plate interface, without interrupting its hypointense signal, the lesion should be considered limited to the ethmoid/nasal fossa. Replacement of the hypointense signal by tumor implies bone penetration. In this case, a thickened enhancing dura mater usually borders the neoplasm. If uninterrupted, the neoplasm may be graded as intracranial-extradural. Conversely, focal or more extensive replacement of enhanced thickened dura mater by tumor signal indicate intracranial-intradural invasion. Cerebral invasion is suspected in the presence of edema. Resectability of tumors invading the brain does not depend only upon the assessment by imaging of the depth of tumor extent into the brain or on the detection of bilateral brain invasion. It requires a thorough evaluation of several other issues, the most important being the histotype and patient's performance status. Patients with limited brain invasion treated by craniofacial resection are reported to have a non-significant decrease in survival compared to those with dural invasion only.

Learning Objectives:

1. To become familiar with the CT and MR techniques and how to use them in patients with suspected anterior skull base tumors.
2. To know the basic anatomy of the anterior skull base and to be able to identify anatomic variants.
3. To know the characteristic aspect of a variety of anterior skull base tumors and be able to provide a differential diagnosis.
4. To be able to recognize characteristic patterns of tumor spread.
5. To be aware of the therapeutic implications.

Postgraduate Educational Programme

A-383

B. Central skull base

S. Köslin; Halle a.d. Saale/DE

Anatomy: The primary component of the central skull base (CSB) is the sphenoid bone (basisphenoid, greater and lesser wing) with its sinus. A smaller contribution comes from the clivus. Apertures (superior orbital fissure; foramen ovale, rotundum etc.) and adjacent structures as the pterygopalatine fossa and the cavernous sinus are integral parts of the CSB. A key point is the knowledge of cross-ways between the extracranial and intracranial spaces.

Imaging technique: Both CT and MR imaging are often needed to study CSB lesions exactly. In CT examinations, the following general guidelines are recommended: slice thickness ≤ 3 mm; axial and coronal planes (as reformations in multi-detector CT); bone algorithms. A routine MR imaging examination of this area should include axial, coronal and sagittal images such as T1-weighted and T2-weighted sequences with a slice thickness between 3 to 5 mm. Intravenous contrast medium is used to evaluate the cavernous sinus and potential tumours. Contrast enhanced T1-weighted images are helpful in the demonstration of perineural spread. Nowadays angiography is mostly performed in combination with interventions.

Diseases of the skull base: Diseases of the skull base can be divided into intrinsic lesions and lesions affecting the skull base from adjacent spaces. The latter one will only be mentioned. In intrinsic lesions, the volume of the lesion is centred in the skull base. These lesions are rare. Normal variants, congenital, inflammatory, traumatic lesions, tumours and tumour like lesions will be demonstrated on typical examples. The diagnostic possibilities and their influence on the therapeutic strategy are discussed.

Learning Objectives:

1. To know the basic anatomy of the central skull base.
2. To become familiar with CT and MR imaging protocols in imaging of the central skull base.
3. To be able to recognize common central skull base lesions and be able to provide a differential diagnosis.
4. To be able to depict characteristic patterns of spread and the relationship of lesions to important anatomic structures.
5. To be aware of the therapeutic implications of imaging findings.

A-384

C. Temporal bone

F. Veillon; Strasbourg/FR

MR imaging and CT are both necessary for evaluating temporal bone tumors. Injection of contrast medium is performed in most of the cases: Primitive cholesteatoma and cholesterol granuloma never enhance.

The following will be considered; in the external auditory meatus (EAM): Polyps, granulomatosis, carcinoma; in the middle ear (ME): Glomus tumors, neuroma of the VII and VIIIth nerves, granulomatosis, extension of lesions from the EAM, jugular foramen (JF) and apex; in the inner ear (IE): Papillary tumors of the endolymphatic sac, extension of lesions from the ME, JF and apex. Primitive cholesteatoma (PC) are found in the EAM, ME, IE.

Other lesions in the skull base are; in the jugular foramen: Jugular glomus tumor (JGT), meningioma, mixed nerve neuroma; in the apex: Cholesterol granuloma, PC, vascular dysplasia, chondrosarcoma (CS), neuromas of the V and VIII cranial nerves, mixed nerve neuromas, meningiomas, extension of carcinoma from the adjacent pharynx and lateral pharyngeal space, sphenoidal sinus, pituitary gland adenoma, JGT. Bony temporal bone lesions include: Osteoma (EAM), chondrosarcoma (apex), giant cell tumors (apex), myeloma (apex), osteoblastoma (mastoid), fibrous dysplasia, Pagets. Finally metastases can occur from the following primaries: Oropharynx, breast, prostate, lung.

In most of the cases the etiologic diagnosis is possible.

Learning Objectives:

1. To learn the imaging techniques needed to detect tumors of the temporal bone.
2. To be able to recognize the most common temporal bone tumors and be able to differentiate them from non-tumorous pathology.
3. To be able to assess characteristic patterns of tumor spread and involvement of important anatomic structures located in immediate vicinity of the temporal bone.
4. To be aware of the therapeutic implications of imaging findings.
5. To learn how to report the imaging findings to the clinical colleagues.

16:00 - 17:30

Room H

Interventional Radiology

WS 1609

Percutaneous access to the abdomen

Moderator:

I. Rozanes; Istanbul/TR

A-385

A. Biliary drainage

A. Adam; London/UK

Percutaneous biliary drainage has a high success rate and is preferable to endoscopic drainage in the case of hilar malignant strictures. Endoprostheses should be used in virtually all patients, in order to avoid the physical and psychological complications associated with external catheters. Self-expandable metallic biliary endoprostheses combine the advantages of a small track through the liver and a large lumen, which is less likely to become occluded by encrusted bile. Their insertion is less painful than that of plastic stents. The usual cause of obstruction is growth of tumor above or below the stent or through the stainless steel mesh, which forms the wall of the endoprosthesis. A very effective way of dealing with this problem is the insertion of a second stent overlapping with the first. Cost effectiveness analyses have shown that the cost of treatment is lower when using Wallstents than when using plastic endoprostheses, because of the lower rate of re-intervention. Benign biliary strictures should be treated with balloon dilatation, which often has to be repeated. Pigment stones often co-exist with benign strictures. They are best cleared with occlusion balloons or saline irrigation. Metallic stents should be used only as a last resort as they often become occluded by epithelial hyperplasia. Roux loops secured to the parietal peritoneum provide convenient access to the biliary tree in patients undergoing hepaticojejunostomy.

Learning Objectives:

1. To learn the indications for percutaneous biliary interventions.
2. To learn the principles of the main percutaneous radiological techniques used in the management of benign and malignant biliary strictures.
3. To understand the technical possibilities and limitations of biliary interventions.

A-386

B. Abscesses drainage

M. Bezzi; Rome/IT

Over the last 20 years, percutaneous abscess drainage (PAD) has evolved from revolutionary to routine, replacing surgical drainage in all but the most inaccessible cases. Even septated and viscous collections may be successfully treated, particularly with the use of lytic agents; however, the simpler the abscess, the more likely PAD will be rapidly successful. Pre-procedural work-up include evaluation of clinical conditions and imaging studies to make sure that percutaneous drainage is indicated and feasible. After consultation, further imaging may be indicated to differentiate abscess from other lesions or to assess the best approach. In our Institution US guidance is used in 80-85% of cases, while CT guidance is preferred in cases where US does not guarantee a safe access. Transperitoneal and extraperitoneal approaches as well as approaches through solid organs and abdominal viscera will be discussed. Post-procedural care include rounds every 2 days and sinograms every 3-4 days. Catheter removal should be performed after a sinogram has established abscess resolution. Strategies to enhance success will be discussed and consist of careful planning of best drainage site (most dependant portion, larger loculations, etc.), use of multiple catheters in complex conditions, use of fibrinolytic agents, mechanical removal of necrotic tissues from pancreatic collections, and establishment of permanent internal drainage in selected cases. Success rate is higher than 80-90%. Significant complications are rare and include bleeding and fistula formation with other viscera. The greatest complication risk for all catheter placement procedures remains catheter dislodgment and catheter occlusion due to poor post-PDA care.

Learning Objectives:

1. To understand the percutaneous approaches and imaging guidance techniques used in abscess drainage.
2. To discuss the follow-up strategies and the post-procedural care.
3. To critically analyze the results and the reason of an unsuccessful outcomes.

Postgraduate Educational Programme

A-387

C. Interventions in the renal pelvis and ureter

C. Allen; London/UK

Percutaneous renal tract interventions are carried out for a wide variety of indications, the most common being stone removal, relief of obstruction, tumour treatment and following trauma.

Successful and safe percutaneous access to the renal tract requires an appreciation of renal anatomy. Renal tract imaging using ultrasound and/or IVU [intravenous urogram] is acceptable for simple renal access but new MDCT [multidetector computed tomography] and MR [magnetic resonance] techniques are becoming necessary in order to plan complex interventions. The interventional anatomy of the kidney will be discussed along with the imaging features.

Simple access for temporary drainage of the renal tract will be briefly described followed by the indications and techniques for more complex access. This will include calyx selection and track dilatation using ultrasound and fluoroscopic guidance. Examples of renal access will be illustrated using cases of complex stone removal. The complications of such access and their treatment will be discussed.

Techniques of ureteric access will be described including access via conduits and the rendezvous procedure. Indications for and the technique of temporary and permanent stenting will be discussed. Cases illustrating ureteric interventions including the treatment of fistulas will be shown.

This lecture will review percutaneous intervention in the kidney and ureter. The important role of renal anatomy will be highlighted and various access techniques will be discussed including their limitations and complications. Each type of intervention will be illustrated using case presentations.

Learning Objectives:

1. To discuss the indications for complex percutaneous intervention of the kidney and ureter.
2. To describe the benefits of preoperative 3D imaging.
3. To describe the variety of techniques available.
4. To describe outcomes and complications.

16:00 - 17:30

Room I

Vascular

WS 1615

Imaging of atherosclerotic plaques

Moderator:

K.Y.J.A.M. Ho; Groningen/NL

A-388

A. CT and EBT for coronary plaque detection

F. Cademartiri; Rotterdam/NL

Electron beam tomography (EBCT) first and multislice computed tomography later (MSCT) have emerged as non-invasive diagnostic modalities that can quantify coronary calcium. The role of coronary calcium is well known, and in particular its association with cardiovascular risk and coronary plaque burden.

The most recent generations of MSCT scanners, able to scan 16 and up to 64 slices per rotation with high temporal and spatial resolution, allow non-invasive assessment of coronary plaques. This development creates an alternative to traditional plaque imaging modalities for in-vivo evaluation (e.g. intra-coronary ultrasound: ICUS).

MSCT has shown the ability to display, quantify, and characterize the various components of atherosclerotic plaque. Eventually, this could become the approach for the identification of vulnerable plaques.

A particular advantage of MSCT over ICUS is also related to its ability to visualise the entire coronary tree and its plaque (calcific and non-calcific) burden. This last concept could enter clinical practice as a predictor of outcome in several conditions.

In this scenario, though, several issues and limitations remain. The most important limitations are the ones that impair the successful completion of a MSCT coronary angiography (e.g. high and irregular heart rates). Additional limitations can be addressed regarding the radiation dose. In fact, thinking about extensive investigations of a population at high risk, for the purpose of plaque imaging the radiation dose currently necessary to obtain the information seems quite high.

Learning Objectives:

1. To understand the features of EBT and spiral CT images relevant for atherosclerotic plaque imaging.

2. To learn how to look and classify atherosclerotic plaques with EBT and CT.
3. To understand the potential use of EBT/CT based plaque imaging in clinical research.
4. To recognize the pitfalls of both techniques affecting plaque detection and characterization.

A-389

B. MR imaging of the vessel wall

R.H. Mohiaddin; London/UK

Cardiovascular disease is an important cause of worldwide mortality, accounting for almost 17 million deaths annually, predominantly through coronary and carotid artery disease. Cardiovascular magnetic resonance (CMR) provides quantitative assessment of plaque burden in a noninvasive manner. In addition, it provides tomographic assessment with consistent localization which enables identification of arterial remodeling over time. In this process, the external border of the artery expands and thickens well before luminal encroachment occurs, allowing tomographic vessel wall imaging to identify early atherosclerosis well before conventional luminal angiography. The main task of this talk is to introduce CMR as a non invasive tool for assessment of atheromatous vascular disease, describe the technical requirements for performing such studies including image resolution, sequence design and receiver coils, review common current applications and discuss advantages and limitations.

Learning Objectives:

1. To introduce MR imaging as an emerging non-invasive tool for vascular wall imaging.
2. To give an overview of the basic technical requirement and the MR imaging techniques commonly used for wall imaging.
3. To discuss advantages and limitations.
4. To review the current status for the main applications.

A-390

C. Molecular imaging of vulnerable plaques

I. Carrió; Barcelona/ES

Understanding of the biology of atherosclerotic plaques has led to the concept of plaque vulnerability. Such vulnerable plaques usually do not cause high-grade stenosis, they have a large lipid core and a thin fibrous cap that is often infiltrated by inflammatory cells. Rupture at the site of a vulnerable atherosclerotic plaque is the most frequent cause of acute coronary syndromes. Radionuclide imaging of vulnerable plaques is focused on targeting either the lipid cores, the macrophage infiltration or the proliferating smooth muscle cells. In vivo visualization of vulnerable plaques is feasible by SPECT and PET/CT.

Several components of the lipid pool have been radiolabelled for imaging of atherosclerotic plaques, including low-density lipoproteins, cholestry ester and apolipoprotein B, radiolabelled porphyrins, and antibody MDA2, which only recognizes oxidized LDL. Accumulation of radiolabelled porphyrins has also been demonstrated in the esterified cholesterol deposits.

Another important strategy for the imaging of vulnerable plaques is based on targeting of macrophages. Expression of scavenger receptors on plaque macrophages results in unlimited ingestion of modified LDL cholesterol. In addition, chemoattractant receptors and activation-dependent receptors are upregulated during diapedesis of monocytes. Iodinated monocyte chemotactic peptide MCP-1 has been used to evaluate the intensity of macrophage infiltration in experimental atherosclerotic lesions. Activation-dependent receptors such as Mac-1 may be targeted by radiolabelled LFA or ICAM or VCAM, and matrix metalloproteinase release can be targeted with radiolabelled inhibitors of metalloproteinases. Predicting outcome by plaque characterization should offer a new paradigm for the management of coronary artery disease.

Learning Objectives:

1. To understand the molecular targets in the atherosclerotic plaques.
2. To learn the different ligands for targeted imaging of atherosclerotic plaques.
3. To understand the potential role of PET and SPECT in imaging vulnerable plaques.
4. To review the current status of nuclear imaging of vulnerable atherosclerotic plaques.

Postgraduate Educational Programme

16:00 - 17:30

Room K

Pediatric

RC 1612

Emergencies in pediatrics

Moderator:

J.G. Blickman; Nijmegen/NL

A-391

A. Abdominal distension in the neonate

T. Berrocal; Madrid/ES

Radiological investigation is one of the most important sources of information in the evaluation of abdominal distension in the neonate, but the need for these examinations should be carefully weighed in order to avoid inconveniencing the patient, unnecessary exposure to radiation or delaying surgical correction. This lecture will present a general approach to neonatal abdominal distension and will discuss the most common specific causes, the indications as well as the diagnostic value of the commonly used modalities, giving some suggestions for an efficient imaging algorithm.

Intestinal obstruction is the most important cause of abdominal distension in the newborn period. The role of imaging may vary from helping to establish a diagnosis, to the evaluation of associated abnormalities, to surgical planning, or to therapy for some conditions like meconium ileus or meconium plug syndrome. Plain abdominal radiographs and sonography frequently can answer the most clinically important questions; however, in certain conditions contrast enema is mandatory. Only rarely is CT or MR imaging indicated.

Ultrasound is the best imaging modality to assess urinary tract dilatation causing abdominal distension, the result of this study guiding the selection of subsequent imaging modalities. Ultrasound is also suited to the screening of solid or cystic masses and organomegalias. CT and MR imaging are unsuitable techniques for general screening but they provide superb anatomic detail and add diagnostic specificity in the evaluation of complex anomalies and to plan surgery.

Learning Objectives:

1. To understand normal and abnormal gas distribution patterns in the neonatal gastrointestinal tract.
2. To discuss the embryological and pathological basis of conditions that cause abdominal distension in the neonate.
3. To describe the clinical manifestations and imaging features of selected abnormalities causing abdominal distension in the neonate and their differential diagnoses.
4. To describe the imaging appearance and to understand the merits and pitfalls of each imaging modality.

A-392

B. Imaging in neonatal distress

B. Smevik; Oslo/NO

Neonatal distress may be caused by a variety of different conditions related to the lungs, the heart, the diaphragm or the chest wall. Imaging procedures play an important role in diagnosing and monitoring respiratory distress, and although chest radiography is the most important diagnostic tool, sometimes additional imaging modalities like computed tomography, angiography, ultrasonography and magnetic resonance imaging may be needed. An overview of conditions causing neonatal distress will be given. Diseases typical of premature babies like idiopathic respiratory distress syndrome and conditions related to air leak, like pneumothorax and pneumomediastinum are explained. An open ductus arteriosus and persistent foetal circulation may be important factors in neonatal distress. Meconium aspiration, neonatal upper airway obstruction and pleural and pericardial effusions will be discussed. A special focus on the placement of the different tubes, catheters and drains needed for treatment is included. Chest wall abnormalities, abnormalities in lung development and in the diaphragm as well as important lung- and heart malformations responsible for neonatal distress are also presented. Imaging characteristics of the initial presentation as well as during and after treatment will be shown.

Learning Objectives:

1. To recognise the characteristic radiological presentations of the most important conditions resulting in neonatal distress.
2. To become familiar with the different types of air leak in the newborn.
3. To understand the influence of congenital heart disease on neonatal distress, and to comprehend the role of the adaption of the pulmonary circulation at birth.

A-393

C. The asphyxiated newborn: Role of new MR imaging techniques

E. Whithy; Sheffield/UK

Despite improvements in obstetric and paediatric practice and a major decline in neonatal death rate, neonatal asphyxia remains a significant problem.

Hypoxia/ischaemia is a significant cause of neurological damage arising in the pre and perinatal periods. Term infants with hypoxia/ischaemic brain injury have a better prognosis than the preterm infant. The pattern of brain damage depends on the maturity of the brain at the time of the insult, the severity of the insult and the duration of the damaging event. Selective vulnerability occurs in different parts of the brain depending on the gestational age.

MR imaging techniques allow accurate detection of the site of the lesion and pattern of damage. This is not only important for timing for the medico-legal environment but also for the understanding of the different aetiologies and future interventions.

Large prospective studies with consecutive scans and post-mortem data if appropriate will allow assessment of the newer novel MR techniques. Close collaboration of clinicians and radiologists is essential to obtain an accurate clinical history and examination findings to ensure any patterns of damage are appropriately attributed to the suspected aetiology.

Learning Objectives:

1. To clarify important issues about the timing of the MR examinations.
2. To understand that the clinical history helps predict the pattern of injury.
3. To understand the evolution of lesions with time.
4. To establish the optimum sequence and plane for identifying the recognised patterns of lesion.
5. To identify the clinical sequelae of each pattern of lesion.
6. To establish the role of newer techniques such as FLAIR, diffusion and perfusion weighted imaging in the examination of the asphyxiated neonate.
7. To discuss the effect of future developments on the choice of imaging sequences and their timing on lesion evolution and clinical outcome.

16:00 - 17:30

Room L/M

Radiographers

RC 1614

CT

Moderators:

N. Kolmannskog; Oslo/NO

S.K. Morcos; Sheffield/UK

A-394

A. CT multitrauma protocol

P. Beyer-Jørgensen, A. Hartvig Sode; Odense/DK

Working at a hospital which is a trauma center, means that the staff involved in the trauma situation is able to work close together, and every one is aware of their function in the team. We are going to describe the admission of the traumatised patient, and follow the patient from emergency to the CT trauma scan. Within the last three years we have CT scanned traumatised patients with a new scan technique, where the patient is positioned in a trauma pillow, which is specially designed for the scanning of the traumatised patient. This meant a new way of thinking, and a new protocol for the scan procedure.

We will show the new protocol, and go over the detail of our results.

The new protocol is clearly time reducing and gives information of the traumatised patient from the top of the head to bottom of the pelvis. This information is gathered without changing the position of the patient.

As an additional bonus to the trauma scan, we visualize the vessels of the neck, because we scan with I.V. contrast in this area.

We will show scans made with this protocol, and go through our intentions behind the admission of the I.V. contrast, considering the patients condition.

Learning Objectives:

1. Admission of the traumatised patient
 - 1.1. To understand the A-B-C-D-E principle.
 - 1.2. To identify the importance of the trauma coordinator.
 - 1.3. To identify the importance of the golden hour.
2. A new scan technique on a multislice CT scanner.
 - 2.1. To identify the pro and cons in development of the trauma pillow.
 - 2.2. To see the challenge in development of a new protocol for the trauma patient.

Postgraduate Educational Programme

- 2.3. To understand the i.v. contrast administration for this protocol.
- 2.4. To identify the parameters which give less quality for CT examination.
- 2.5. To learn the benefits of the protocol for the patient and the staff.
3. The challenges for the future.

A-395

B. Multislice CT: Introduction and application

A. Riemer; Neuss/DE

Because the parallel acquisition of up to 64 slices per rotation and a rotation speed of 400 msec per rotation, the multislice-CT is up to 128-times faster than a standard one-second-single-slice-CT-scanner. This high scan speed enables the scanning of large volumes with thin slices in one breath hold and gives multislice-CT the capability to acquire 3D-volumes in isotropic voxel geometry. This means that we can reformat the scanned volume in every plane without loosing spatial resolution. The high scan speed and the excellent spatial resolution of multislice-CT makes new diagnostic and functional applications possible. Multislice-CT enables us to adapt the scan-strategy and protocol to every patient very precisely and the combination of high speed isotropic scanning and a powerful bolus-tracking-software enables independent from the cycle time of the patient a very precise contrast timing.

In comparison with a single-slice-CT the multislice-CT has less limitations in scanning. So it could be very tempting to scan more than necessary and increase the X-ray dose. It is very important to use the scanner very conscientious. On principle the correct application of a multislice-CT in combination with optimised scan-protocols, quantum denoising filters and a software for X-ray modulation the patient dose can be extremely reduced.

Learning Objectives:

1. To understand the basic of multislice technologie (detector technology, fan-beam/conebeam, reconstruction algorithm, isotropic voxel geometrie, patient dose in multislice CT).
2. To learn new diagnostic and interventional applications (diagnostical advantages of isotropic imaging, cardiac applications, multislice angio applications, new concepts in trauma diagnostic).
3. To handle image data.

16:00 - 17:30

Room N/O

Physics in Radiology

RC 1613

Justification and optimization of multislice CT (MSCT) examinations

Moderator:
W. Bautz; Erlangen/DE

A-396

A. Justification of MSCT examinations

J. Geleijns, J.L. Bloem, J. Kievit, A. Spilt; Leiden/NL

The potential benefit of multislice CT (MSCT) depends on the appropriate selection of patients. Benefits based on accurate detection or exclusion of disease are appropriate treatment decisions such as starting, continuing, discontinuing or even withholding specific treatment, or additional diagnostic procedures. Decisions on proper indications for MSCT are even more relevant considering the radiation risk factor. Because the accuracy of diagnostic tests is not perfect, the second type of risk is an erroneous treatment decision based on an erroneous test result. The third type of risk is direct complication of the test itself, for MSCT these are predominantly adverse effects related to contrast agents. The balance between benefits and risks of MSCT should be in favour of the benefits. Justification of MSCT deserves special attention since recent technical progress caused an increase of the number of MSCT examinations and an expansion of the clinical indications for MSCT. Differences between the volumes of imaging tests, including MSCT, in European countries is large. This reflects differences in mortality attributable to diagnostic X-ray imaging and demonstrates that there is ample room for improving appropriate use of imaging, including MSCT. Appropriateness criteria such as those published by the American College of Radiologists and the UK Royal College of Radiologists serve as guidelines for the physician. Decision trees can be used to describe optimal patient flow through the diagnostic process. To resolve remaining problems further research, including meta-analysis and prospective studies, is required.

Learning Objectives:

1. To present justification of MSCT examinations in the context of radiation protection.
2. To present justification of MSCT examinations in the context of medical decision theory.
3. To learn about the practical clinical implementation of justification of MSCT examinations.

A-397

B. MSCT: Balancing image quality and dose

W.A. Kalender; Erlangen/DE

As an introduction the technical basis of MSCT will be reviewed briefly. The most important component is the detector which typically allows simultaneous scanning of 4 to 64 slices in today's MSCT scanners. In general, the geometric efficiency decreases and the collimation efficiency may increase as the detector pixel pitch becomes finer and the number of detector rows increases. The respective aspects are illustrated and discussed in detail. The X-ray source, the inherent and added filtration, the reconstruction algorithms can also influence dose efficiency; the respective factors will be reviewed.

Patient dose levels in MSCT can be assessed quite accurately today based on tabulations or based on scanner- and patient-specific calculations. Typical values range between 1 to 20 mSv per examination. The parameters which affect patient dose are above all the scan volume, the chosen X-ray parameter settings and, to some degree, the reconstruction algorithm. It is important to scan with parameters which allow maximum resolution, but to consider reconstructions with lower spatial resolution to limit pixel noise. The respective dependencies of spatial resolution and image noise will be explained and demonstrated interactively. Low-contrast detectability and soft tissue differentiation, the prime objectives in most CT examinations, are affected by image noise and contrast characteristics. The influence of the spectrum on contrast and on low-contrast detectability will be explained and demonstrated.

Learning Objectives:

1. To understand the technical basics of MSCT.
2. To know the patient dose levels and parameters affecting dose.
3. To understand the influence of dose on low-contrast detectability.

A-398

C. Optimization of pediatric MSCT examinations

S. Puig; Vienna/AT

The introduction of MSCT in 1998 was a breakthrough in CT technology. Recently, new 64-slice-CT scanners were introduced. However, a major disadvantage of MSCT scanning is the high radiation. Using unfavourable scanning parameters, exposure dose is substantially increased compared to single-slice scanning. A comparison of radiation exposure in multi- and single-slice CT showed that companies recommended MSCT protocols leading to a radiation dose eight times higher than with single slice CT! Furthermore, a small field of view results in a relative increase of the pixel size and so-called "noisy" images. Individual dose modulation and overlapping reconstructions provide a so-called "secondary raw-data set" which can be used for further image reconstructions. Software for tube current modulation is characterized by online monitoring of the attenuation and subsequent tuning of tube current. New software programs have been introduced, which enable tube current (mA) modulation according a predefined noise level along the z-axis. With this software called CARE Dose4D, a dose reduction of up to 66% are possible in adults and children using 16 row scanners. In a phantom study, a dose reduction of 90% was possible in neonates and small infant. Comparable mA modulation software was introduced by GE (AutomA) and by Toshiba (RealEC).

There are several programs available, which help to estimate the doses or the CTDI of different imaging protocols in different scanners, including WinDose, CTDOSE, CT-Dose, CTDosimetry or CT-Expo.

However, the most sufficient way to protect the patient from radiation exposure is to use radiation-free techniques.

Learning Objectives:

1. To learn how to develop low-dose protocols for pediatric MSCT of the chest and the abdomen.
2. To understand how image noise affects the image quality of low-dose scans.
3. To understand which impact the field of view has on image resolution.
4. To learn how to improve image quality of low-dose scans using to post processing techniques.
5. To learn how to reconstruct secondary raw data sets replacing original raw data sets which need large storage capacity in order to enable further 3D reformations.

Tuesday, March 8

Postgraduate Educational Programme

		room A 2nd level	room B 2nd level	room C 2nd level	room E1 entr. level	room E2 entr. level	room F1 entr. level	room F2 entr. level	room G lower level	room H lower level	
07:00	EPOSTM - scientific exhibition registration										07:00
07:30											07:30
08:00											08:00
08:30		CC 1717 Essentials of Neuroradiology Metastatic disease of the brain and spine (p. 118)	RC 1710 Musculoskeletal Knee joint (p. 118)	SF 17 Special Focus Session Fetal MR imaging (p. 119)	RC 1703 Cardiac Morphological and functional assessment of the heart (p. 120)	RC 1701 Abdominal and Gastrointestinal CT colonography and colon cancer (p. 121)	RC 1704 Chest HRCT in diffuse lung disease (p. 122)	RC 1711 Neuro Pediatric neuroradiology (p. 122)	RC 1708 Head and Neck How to investigate facial pain (p. 123)	RC 1709 Interventional Radiology Venuous occlusion (p. 124)	08:30
09:00											09:00
09:30											09:30
10:00											10:00
10:30											10:30
11:00		SS 1807a Genitourinary Female pelvis (p. 314)	SS 1810 Musculoskeletal Ultrasonography and videofluoroscopy (p. 315)	SS 1801a GI Tract Functional abnormalities of the GI Tract (p. 317)	SS 1803 Cardiac Technical advances in cardiac imaging (p. 320)	SS 1802 Breast Breast cancer screening (p. 322)	SS 1804 Chest New trends in chest imaging (p. 324)	SS 1801b Abdominal Viscera (Solid Organs) MR imaging and MDCT: Practical considerations (p. 326)	SS 1807b Genitourinary Urogenital lesions: Diagnosis and interventions (p. 328)	SS 1809 Interventional Radiology New developments in interventional radiology (p. 330)	11:00
11:30											11:30
12:00											12:00
12:30											12:30
13:00											13:00
13:30											13:30
14:00											14:00
14:30											14:30
15:00											15:00
15:30											15:30
16:00											16:00
16:30											16:30
17:00											17:00
17:30											17:30
18:00											18:00
18:30											18:30
19:00											19:00

Postgraduate Educational Programme

	room I lower level	room K lower level	room L/M 1st level	room N/O 1st level	room P lower level	room W basement	room X 1st level	room Y 1st level	room Z entr. level	La Scala 2nd level	
07:00											07:00
07:30											07:30
08:00											08:00
08:30											08:30
09:00	WS 1715 Vascular Planning issues in vascular radiological intervention (p. 125)	RC 1712 Pediatric Musculoskeletal imaging (p. 125)	RC 1714 Radiographers Breast imaging (p. 126)	WS 1718 Workshops on Interventional Radiology Chest intervention (p. 126)	WS 1721 Musculo-skeletal US "Hands-on" Workshop						09:00
09:30											09:30
10:00											10:00
10:30											10:30
11:00	SS 1806 Contrast Media Iodinated contrast media: Technical advances and side effects (p. 332)	SS 1812 Pediatric Thoracic and abdominal imaging (p. 334)	SS 1811a Neuro Non-invasive neurovascular imaging (p. 336)	SS 1813 Physics in Radiology Magnetic resonance/ Nuclear medicine (p. 340)	SS 1811b Neuro fMRI imaging and new MR imaging sequences (p. 342)					SS 1814 Radiographers Challenge and development in radiography (p. 338)	11:00
11:30											11:30
12:00											12:00
12:30											12:30
13:00											13:00
13:30											13:30
14:00											14:00
14:30											14:30
15:00											15:00
15:30											15:30
16:00											16:00
16:30											16:30
17:00											17:00
17:30											17:30
18:00											18:00
18:30											18:30
19:00											19:00

Tuesday

Postgraduate Educational Programme

08:30 - 10:00

Room A

Essentials of Neuroradiology

CC 1717

Metastatic disease of the brain and spine

Moderator:

L. van den Hauwe; Brasschaat/BE

A-399

A. Metastases in the brain parenchyma

G. Krumina; Riga/LV

Brain metastases are the most common manifestation of somatic primary tumours. The placement of tumour emboli in the brain depends on passive supply of tumour cells via blood circulation. Brain stem, cerebellar and hemispheric metastases arise proportionally to the weight of these structures and blood circulation. Deposition of metastases occurs at the points of turbulent flow where vessel calibre changes or at arterial end points. The most common neoplasms producing brain metastases, are lung, breast, melanoma, colorectal, and urogenital cancers. Clinical presentation and therapeutic options depend on dissemination of systemic malignancy, number and localisation of brain metastases. CT and MR imaging are the mainly used imaging modalities. Contrast-enhanced (CE) MR imaging is more sensitive than CE-CT. The lesions undetected on CT are less than 1-2 cm in diameter and located near to the convex and skull base. Visualisation of additional metastases on CT could be improved by administering double to triple contrast dosage and performing scans with 1-3 hours delay. In cancers that frequently seed brain metastases, MR imaging as a primary screening method is more reasonable and cost-effective. Routine contrast dose T1-WI with mt contrast improves detection of small lesions. In contrast to CT, delayed post contrast MR imaging does not improve lesion-to-brain contrast. The recommended basic MR imaging protocol and usefulness of additional functional MR sequences are described and disputed. Primary malignant glial tumour, brain abscess, primary CNS lymphoma, inflammatory granuloma and also spontaneous parenchymal haemorrhage are differential diagnoses for solitary brain metastases. Differential diagnoses for multiple metastases include abscesses, inflammatory granulomas, lymphoma, and demyelinating disease.

Learning Objectives:

1. To review the basic concepts of metastatic disease of the brain parenchyma: incidence, theories of the spread, general locations, tumours of origin, typical clinical presentations and treatment modalities.
2. To describe CT and MR imaging algorithms for patient's evaluation with suspected parenchymal brain metastases.
3. To present typical differential diagnostic features and possible diagnostic pitfalls for solitary and multiple parenchymal brain metastases.

A-400

B. Extra-axial metastases (skull, dura, leptomeningeal) and tumor spread

R. Maroldi; Brescia/IT

Extra-axial intracranial metastases may arise through several routes. Hematogenous spread to the meninges is the most frequent. Direct extension from contiguous extra-cranial neoplasms, secondary invasion of the meninges by calvarium and skull base metastases, and migration along perineural or perivascular structures are less common. The incidence of leptomeningeal metastasis seems to increase, probably because of the increment in survival of many systemic neoplasms. Leptomeningeal invasion gives rise to tumor cell dissemination by CSF, eventually leading to neoplastic coating of brain surfaces (neoplastic meningitis). The CSF exam is the most useful non-imaging based test. Contrast-enhanced MR imaging is complementary and can be invaluable, detecting up to 50% of false-negative lumbar punctures. MR findings range from diffuse linear leptomeningeal enhancement - following the gyri and extending into the sulci - to multiple enhancing extra-axial nodules. Obstructive communicating and non-communicating hydrocephalus may occur, due to obstruction of the ventricular system or CSF resorption. Both calvarial and epidural metastases infrequently transgress the dura, which acts as a barrier against tumor spread. Radionuclide bone studies are still a valuable screening test to detect bone metastases. On CT and MR, bone metastases extending intracranially and primary dural metastases show the characteristic biconvex shape, usually associated with brain displacement away from the inner table. Although CT is better in detecting bone erosion of the skull base, MR is more sensitive in demonstrating even subtle abnormalities of the meninges, providing more detailed information about dural involvement.

Perineural and perivascular spread from head and neck neoplasms require thin-section contrast-enhanced MR.

Learning Objectives:

1. To comprehend the mechanisms of extra-axial metastases to the skull base, the dura mater and leptomeninges, skull base invasion, and neoplastic intracranial spread.
2. To become familiar with the basic anatomy of the skull base, meninges, and how to use the imaging techniques to identify neoplastic involvement.
3. To recognize characteristic aspects of leptomeningeal, dural metastases, and to be able to provide a differential diagnosis.
4. To be able to recognize perineural and perivascular spread from head and neck neoplasms.
5. To be aware of the therapeutic applications.

A-401

C. Metastatic disease of the spine

C.F. Andreula; Bari/IT

Metastases of the spine occur in the spinal cord, in the extramedullary dura, in the epidural space and in the vertebral bodies.

Imaging modalities evaluate patients with symptoms; they can also be used to screen for lesions; assessing the localisation and the compartments involved (extradural, epidural, subdural, and paraspinal) and can help suggest a therapeutic strategy.

The suggested patients for screening of metastases are:

- asymptomatic patients suspected for metastases
- the patient with neurological symptoms.

Imaging modalities are indispensable in the differential diagnosis of non tumoral lesions mimicking metastases.

Learning Objectives:

To suggest the diagnosis criteria differentiates them between metastasis and other pathologies.

08:30 - 10:00

Room B

Musculoskeletal

RC 1710

Knee joint

Moderator:

M. Zanetti; Zürich/CH

A-402

A. Soft tissue structures of the knee with US and MR imaging

E.G. McNally; Oxford/UK

Meniscal tears can be divided into two groups, those that manifest as abnormal lines breaching an articular surface and those that cause abnormalities of meniscal morphology. The commonest tear patterns are usually easy to identify, but more subtle lesions, particularly those that involve more subtle derangement of normal meniscal morphology, are sources for diagnostic error. These and other common pitfalls will be reviewed. MR imaging also plays an important role in assessing the intra-articular ligaments. The extra-articular ligaments are also easily examined by ultrasound, though as many injuries occur in combination, MR imaging reserves the dominant role. An exception is the extensor mechanism where patellar tendinopathy is a common cause of anterior knee pain and is easily assessed using ultrasound. Cystic lesions around the knee are common, the majority are extra-articular and a firm diagnosis can usually be made by their location, ultrasound or MR imaging appearances. The diagnosis of intra-articular soft-tissue masses is more problematic, but an approach to differential diagnosis will be offered.

Learning Objectives:

1. To describe the common patterns of injury to the menisci.
2. To establish a methodology for detecting the more subtle avulsion meniscal tear.
3. To describe the common ligament abnormalities and comment on their important associations and patterns of multiple ligament injury.
4. To review the abnormalities that can be found in other intra and extra-articular soft tissue structures such as Hoffas fat pad, periarticular bursae and muscles.

Postgraduate Educational Programme

A-403

B. MR-based cartilage imaging in the knee prior and after transplantation

C. Glaser; Munich/DE

The motivation for MR imaging-based assessment of articular cartilage is the increasing availability of and experience with cartilage dedicated therapies, mainly on the background of acute trauma or osteoarthritis.

Yet, cartilage MR imaging still remains challenging due to its complex composition and small spatial dimensions. High spatial resolution, good SNR/CNR and reasonable imaging times are prerequisites for an accurate MR imaging assessment of articular cartilage. Fat suppression eliminates chemical shift artefacts and improves CNR of cartilage. Using selective water excitation (WE) contributes to further reduce imaging time. T2-/PD-w FS sequences are considered to be sensitive to focal intra-cartilaginous signal alterations and show a good delineation of the cartilage surface from effusion indicating even relatively small cartilage lesions. However, assessment of such small lesions is still problematic and suffers from low accuracy.

Clinical classification systems are based on evaluation of focal lesions, of diffuse thickness reduction and of intra-cartilaginous signal intensity changes as well as erosion of the subchondral bone plate and BMEP-like signal within the underlying bone. Usually, they are derived from arthroscopic grading scales. Although still not common place, there is increasing (short term) experience with MR imaging of OATS and ACI procedures underlining surface congruity, bony healing and development of subchondral cystic lesions to be important prognostic factors for graft ongoing/loosening.

First longitudinal volumetric studies indicate an annual rate of cartilage loss of 4-6% in OA. T2 has been associated with spatial arrangement and water content and focal alterations in T2 with cartilage degeneration.

Learning Objectives:

1. To outline basic patho-anatomic considerations for MR imaging-based cartilage imaging.
2. To describe MR imaging sequences for cartilage imaging in clinical routine including artifacts.
3. To discuss the evaluation of cartilage lesions.
4. To review MR imaging of cartilage repair procedures: OATS and ACI.
5. To give an outlook on advanced MR techniques for assessing the matrix of articular cartilage.

A-404

C. Postoperative knee

V.N. Cassar-Pullicino; Oswestry/UK

This lecture will focus on the imaging of the knee following operative procedures carried out to cruciate ligaments, menisci and articular cartilage. Accurate diagnosis requires a clear understanding of the clinical symptoms and signs which will help tailor the optimal imaging methods and protocols that are required. Accurate interpretation of the post-operative status also requires a thorough working knowledge of the surgical procedures employed, including familiarity with the expected post-operative imaging appearances following surgical repair, resection, replacement or transplantation. It is also essential to understand the individual strength and weaknesses of the imaging modalities with particular reference to radiography, CT, ultrasound and MR imaging with or without contrast enhancement.

Learning Objectives:

1. To discuss the relative merits of US, CT and MR imaging in the assessment of the post-operative knee.
2. To familiarise the delegates with the expected post-operative knee appearances.
3. To describe the role of CT/MR imaging in the symptomatic knee following anterior cruciate ligament reconstruction.
4. To describe the role of MR imaging and MR arthrography in assessing residual or recurrent knee symptoms following meniscal surgery.

08:30 - 10:00

Room C

Special Focus Session

SF 17

Fetal MR imaging

Moderator:

I.M. Björkman-Burtscher; Lund/SE

A-405

Fetal MR imaging (Introduction)

I.M. Björkman-Burtscher; Lund/SE

Although prenatal diagnosis of developmental disorders or in utero injuries is still dominated by the use of ultrasound, fetal MR imaging has been evolving continuously during the past few years. Fetal MR imaging offers the possibility to assess not only the fetus, but also intrauterine structures, such as the placenta and umbilical cord, and the uterus. The technique demands knowledge of normal fetal development, optimal techniques for fetal MR imaging studies and careful interpretation of pathologic findings. Many clinical strategies remain to be discussed, results are yet to be validated and standards have to be established. However, physicians are beginning to appreciate the capabilities of fetal MR imaging as a method to optimize the reliability of prenatal diagnostics and prognostics.

In three presentations at the cutting edge of technique and clinical application the speakers will share and discuss their experience in fetal MR imaging, offering the audience the opportunity to learn the essentials of this emerging field and allow patients to benefit from the technique even beyond major centres of prenatal care.

Learning Objectives:

1. To learn the choice of sequences/coils and specific safety issues.
2. To understand the symptomatology of MR imaging in cerebral malformation.
3. To discuss the correlation between fetal MR and postnatal imaging or neuro-fetopathology.
4. To learn the normal and pathological MR-appearance of the fetus, placenta, umbilical cord, and amniotic fluid.
5. To discuss imaging protocols of frequent clinical indications.

A-406

Technical considerations

P.A. Gowland; Nottingham/UK

The value of MR imaging in studying fetal congenital pathologies has been proved, but it also has potential applications in studying fetal development and physiology. MR imaging can be used to measure the fetal growth and has shown different patterns of brain growth compared to ultrasound in fetuses suffering fetal growth restriction. Similarly MR imaging is being used to study fetal brain development, anatomically as well as in terms of pre-myelination and myelination related changes. MR imaging can also be used to measure placental blood flow and preliminary data indicate that measures based on the intravoxel incoherent motion are able to distinguish pregnancies affected by pre-eclampsia.

Given the probable increase in fetal MR imaging over the next few years, it is important to consider the possible associated risks. Although no teratogenic effects are associated with clinical exposures to the various magnetic fields associated with MR imaging, there are some particular areas of concern. RF exposure limits are based on models of heat loss from the adult, but the fetus has reduced heat loss mechanisms. Similarly, acoustic noise exposure levels assume that an adult is wearing ear defenders. The maternal abdomen and the fluid-filled fetal ear will attenuate air borne noise, but mechanical vibrations of the bed will be coupled to the fetus through the maternal abdomen.

To enable dynamic studies for instance of cardiac function, it is necessary to monitor the fetal heart beat. At present this is generally carried out with fetal CTG, although some groups are investigating the use of ECG.

Learning Objectives:

1. To learn about novel measurements that MR imaging can provide in obstetrics.
2. To discuss technical pros and cons of MR imaging and ultrasound for quantitative assessment of fetal/placental growth/function.
3. To understand the specific safety issues relevant to fetal imaging (particularly acoustic noise, RF and 3 T).
4. To understand additional methods of monitoring the fetus within the MR environment (CTG).

Tuesday

Postgraduate Educational Programme

A-407

CNS malformations

C. Garel; Paris/FR

Background: The role held by fetal MR has grown in importance during the past few years and fetal MR plays now an essential part in major centres of antenatal diagnosis.

Procedure Details: The main advantages of MR over US are its ability to depict the surface of the brain and hence to delineate sulcation, and its higher contrast resolution which allows improved analysis of the cerebral parenchyma. Moreover, some structures (optic chiasm, olfactory bulbs, pituitary gland and stalk) can be visualised only with MR and not with US, so that some pathologies can be diagnosed only with MR. It must also be kept in mind that some *in utero* acquired cerebral abnormalities may be very difficult to differentiate from genetically determined malformations.

This talk will give a brief overview of the main fetal cerebral malformations, whose main highlights are the findings described above.

Conclusion: Cerebral malformations account for a large part of fetal anomalies and their detection constitutes a critical element of antenatal diagnosis. Fetal MR has become an indispensable adjunct to ultrasound in the diagnosis of such pathologies.

Learning Objectives:

1. To learn the symptomatology of MR imaging in cerebral malformations.
2. To understand the contribution of this technique compared to US.
3. To discuss the correlation between fetal MR and postnatal imaging or neurofetopathology for a better understanding of fetal MR images.

A-408

Body MR imaging

D. Prayer; Vienna/AT

Fetal body MR imaging is used to assess face, neck, thoracic and abdominal organs, and limbs. In addition, with any fetal indication, the placenta, umbilical cord, the amniotic fluid and the uterine wall should be examined too. T2-weighted contrast is acquired with single shot fast spin-echo (SSFSE) sequences, steady state free precession sequences or advanced gradient-echo sequences. T1-contrast, necessary to depict hemorrhage, fat, the thyroid gland, meconium and liver, can be achieved using 2D or 3D gradient-echo sequences, with or without fat suppression, or T1-weighted FLAIR sequences. Thick-slab SSFSE sequences create a 3D-like effect that is helpful with the assessment of body surface structures and limbs. Dynamic sequences allow visualization of intrinsic fetal movements, such as swallowing. In the fetal body diffusion-weighted sequences selectively display the kidneys, which may be important in assessment of suspect renal dysfunction, morphological abnormalities or oligohydramnios. Hallmarks of normal lung development are calculated volumes and T2-weighted and FLAIR hyperintensities increasing with gestational age. Bowel-development is assessed by using T2-weighted signal characteristics of fluid-filled intestines and meconium-based T1-weighted signal properties of the colon. The latter features help with the prognosis of pathologies involving both systems like congenital diaphragmatic hernias, where intrathoracic abdominal organs interfere with lung development and the amount of functional lung tissue determines postnatal survival. Complex pathological situations including intrauterine growth restriction, premature rupture of membranes and pathological umbilical cord Doppler values, underline the necessity of investigating the whole fetus and the extrafetal intrauterine structures regardless of the clinical indication.

Learning Objectives:

1. To learn the normal and pathological MR-appearance of the fetus, placenta, umbilical cord, and amniotic fluid.
2. To understand MR in intrauterine growth restriction, premature rupture of membranes, and pathological umbilical cord Doppler.
3. To discuss imaging protocols of frequent clinical indications and postnatal/postmortem controls to point out the contribution of prenatal MR imaging.

08:30 - 10:00

Room E1

Cardiac

RC 1703

Morphological and functional assessment of the heart

Moderator:
R. Fattori; Bologna/IT

A-409

A. Morphological assessment of the heart

V.E. Sinitsyn; Moscow/RU

Modern tomographic modalities like MR imaging and MSCT are more and more frequently used for morphological evaluation of the heart. Both these methods have several advantages over traditional cardiac imaging technologies, among them are large artefact-free field-of-view, high spatial and temporal resolution. Due to continuous and rapid movements of the heart, MR imaging and MSCT studies must be synchronized with the cardiac cycle.

Anatomical axes of the heart do not coincide with conventional orthogonal planes. It is important to evaluate the heart along anatomical axes and planes. Both MR imaging and MSCT give allow the possibility of creation of 3D reconstructions of heart chambers.

In the clinical setting the most common indication for MR imaging is further characterization of abnormalities discovered on echocardiography, nuclear cardiac studies or even on cardiac catheterization. It has been proven that they could be methods of choice in the following clinical situations:

- Complex congenital heart diseases
- Postoperative assessment of patients after heart surgery
- Aortic and pericardial pathology
- Arrhythmogenic dysplasia
- Hypertrophic cardiomyopathy (especially apical)
- Cardiac and paracardiac masses
- Quantification of heart chamber volumes, myocardial mass.
- Characterization of myocardium (areas of ischemia, inflammation, necrosis, scars)

Learning Objectives:

1. To discuss the principles and techniques of cardiac images.
2. To compare advantages and limitations of the different imaging modalities in the morphological assessment of the heart.
3. To describe anatomy by means of CT and MR imaging.

A-410

B. Assessment of the left heart function

N.L. Kelekis; Athens/GR

Echocardiography is currently the most commonly used modality in the assessment of LV function. It is widely available, cheap and easily combined with pharmacological stress-test. Recent advances include better delineation of endocardial border using harmonic imaging or contrast agents. There are, however, limitations, including poor acoustic windows in obese or postoperative patients, occasional difficulty in assessing postero-basal, postero-lateral and apical myocardial segments. Evaluation of global function relies on geometric assumptions, which may not be valid in several disease states such as LV remodeling post myocardial infarction or LV aneurysms.

SPECT and multidetector-row spiral CT provide objective volumetric assessment without geometrical assumptions, but both require contrast administration and exposure to ionizing radiation.

MR imaging offers objective reproducible quantitative volumetric and velocity/flow assessment, irrespective of ventricular shape and remodeling, as well as high contrast delineation of endocardial and epicardial borders. Its overall high anatomical detail permits excellent regional function evaluation, which may be boosted by quantification of 3-dimensional motion information from tagging techniques. It may also be combined with stress testing, studies of myocardial viability using delayed enhancement, and angiographic assessment of proximal coronary arteries in a comprehensive examination.

MR imaging is still expensive, with relatively limited availability, more time-consuming, needs breath-holding and effective cardiac synchronization. Latest developments, however, permit real-time cine imaging without the need of triggering with a quality superior to ultrasonography and comparable to today's state-of-the-art breath-hold cardiac-triggered SSFP cine sequences.

Postgraduate Educational Programme

Learning Objectives:

1. To compare advantages and limitations of the different imaging modalities in the functional assessment of the left ventricle.
2. To describe the method and clinical meaning of the global functional analysis.
3. To describe the method and clinical meaning of the regional functional analysis.

A-411

C. Assessment of the right heart function

M. Gutberlet, B. Spors, K. Klimes, M. Grothoff, R. Felix; Berlin/DE

The right ventricle has a complicated shape and therefore geometric assumptions can not be made for volumetric assessments like for the left ventricle. The left ventricle can be seen as an ellipsoid, so that a 2-dimensional calculation of ventricular volumes by area-length methods is possible. For the volumetric assessment of the right ventricle such easy and less time consuming methods are not available. Thus, the so called Simpson's rule, which uses a contiguous set of short axis slices covering the whole ventricle, has to be used for the volumetric assessment of the right ventricle. Hence, magnetic resonance imaging (MRI) is the optimal modality for the evaluation of right ventricular function, especially in patients in whom lifelong follow-ups are necessary, like in patients with corrected congenital heart diseases. Beside CINE-MRI with the use of steady state free precession sequences (SSFP) there are other MRI methods available to assess right ventricular function like myocardial tagging or phase velocity mapping, which will be addressed also. The different appearances of the right ventricle in patients with pressure or volume overload will be discussed.

Learning Objectives:

1. To compare advantage and limitations of the different imaging modalities in the functional assessment of the right ventricle.
2. To describe the method of functional analysis.
3. To discuss the clinical applications.

08:30 - 10:00

Room E2

Abdominal and Gastrointestinal

RC 1701

CT colonography and colon cancer

Moderator:

R.A. Frost; Salisbury/UK

A-412

A. Epidemiology and evidence for screening

S.A. Taylor; Harrow/UK

The colorectum is the fourth commonest site for cancer world wide, although the incidence is second only to lung cancer in Northern Europe and North America. There has been a marked increase in incidence amongst migrants adopting a Western lifestyle, and although a clear genetic predisposition exists, over 75% of cancers develop in people with no identifiable risk factors. Most colorectal cancer arises from precursor adenomatous polyps, with the adenoma-carcinoma sequence taking around 10 years. There is however an increasing realisation that progression of disease may be accelerated in flat or depressed adenomas, which could account for up to 25% of cancers. Good evidence exists that endoscopic polypectomy can prevent colorectal cancer and a clear relationship exists between cancer stage and prognosis. Colorectal cancer thus lends itself well to population screening, being prevalent, treatable and preventable by well-established techniques. The optimum screening strategy is not yet established. Many candidate tests exist, but only faecal occult blood testing (FOBT) has been shown to be both feasible and to reduce mortality in randomised control trials. Data from large-scale trials of flexible sigmoidoscopy are currently awaited. Emerging technologies such as CT and MR imaging colonography and DNA based stool tests may play future roles. Mass screening is not without risk with cardiac morbidity secondary to laxative use or sedation, and complications related to endoscopy such as perforation and haemorrhage all well described. Cost effectiveness compares well to more established programmes such as breast screening, but is heavily reliant on frequency and initial screening age.

Learning Objectives:

1. To demonstrate an understanding of the epidemiology of colon cancer.
2. To review the rationale of screening for colorectal cancer.
3. To discuss the disadvantages of screening.

A-413

B. Performance and technique of CT colonography

A. Laghi; Rome/IT

CT colonography is a noninvasive test for the examination of the colon. The technique is extremely easy. Following the same meticulous bowel preparation as conventional colonoscopy, the colon is inflated with air or carbon dioxide using a rectal tube. No sedation is required. Dual scanning with the patient respectively in a prone and supine position is obtained. A major technical advance in the procedure is represented by the introduction of multislice CT scanners, which provide higher resolution as well as faster acquisition. Low-dose protocols also minimize radiation exposure. The acquired volumetric dataset is post-processed on dedicated workstations using commercially available software programs. Image analysis is performed using a primary 2D or 3D approach (i.e. scrolling through axial slices and multiplanar reformatted images on the workstation and using 3D endoluminal views as problem-solving support, or using 3D endoluminal view as a primary approach for lesion detection).

To date, several studies have reported a high sensitivity and specificity of CT colonography in the detection of colonic neoplasms - not only large colonic carcinomas, but also polyps. In the polyp-rich population per-patient sensitivity for polyps 10 mm or larger is around 88%, for polyps between 6 mm and 9 mm is 84% and for polyps 5 mm or smaller is 65%; specificity is around 95%. In the screening population data are more controversial, with one large study (Pichard et al) showing similar results between CT colonography and conventional colonoscopy and others (Johnson et al; Cotton et al) demonstrating poor sensitivity as well as wide interobserver variability.

Learning Objectives:

1. To discuss patient preparation.
2. To teach the technique of CT colonography.
3. To teach the interpretation of CT colonography.

A-414

C. The practical application of CT colonography

J. Stoker; Amsterdam/NL

CT-colonography (CTC) is an accurate technique for the detection of colorectal cancer and significant polyps in symptomatic patients. CTC has replaced double contrast barium enema as the primary imaging technique in symptomatic patients and is important as an adjunct in incomplete colonoscopy examinations. Most series concern CTC after extensive bowel cleansing, but more recent series have demonstrated that accurate CTC after limited bowel preparation is feasible thus resulting in reduced burden to patients. Primary two-dimensional evaluation is commonly performed, but recent studies seem to indicate the advantage of primary three-dimensional evaluation.

The role of CTC in screening is currently extensively studied. Studies on CTC with extensive bowel preparation in low prevalence populations have demonstrated that high sensitivity and specificity can be obtained in such populations. However, factors such as reader experience and evaluation technique influence the results and require further study. Reduction of the burden of CTC (primarily extensive bowel preparation) is mandatory before the technique can be implemented. Modified bowel preparation and radiation exposure reduction are feasible and large series with this CTC-modifications are mandatory in low prevalence populations. Development of accurate automated polyp detection is important for cost effective screening programs.

Learning Objectives:

1. To discuss the role of CT colonography in the screening situation.
2. To discuss the role of CT colonography in the symptomatic patient.
3. To discuss the use of CT colonography as an adjunct to conventional colonoscopy.

Tuesday

Postgraduate Educational Programme

08:30 - 10:00

Room F1

Chest

RC 1704

HRCT in diffuse lung disease

Moderator:

S. Akyar; Ankara/TR

A-415

A. Nodular pattern

S.P.G. Padley; London/UK

This component of the refresher course will focus on nodular lung disease as depicted with HRCT. Pulmonary nodules are usually in the 1 millimetre to 1 centimetre size range. The nodular pattern is a relatively common HRCT finding that is often poorly characterised on conventional chest radiography. HRCT allows accurate assessment of distribution, outline, size, density and uniformity of pulmonary nodules and allows the presence of cavitation to be determined. This presentation will illustrate the range of these characteristics and then demonstrate how appreciation of these features may be used to arrive at a meaningful differential diagnosis. Whilst the presentation will concentrate on the more commonly encountered nodular disease processes it will also include rarer causes of a nodular pattern.

Learning Objectives:

1. To describe and illustrate the nomenclature for description of different HRCT findings.
2. To present typical HRCT manifestations of different pathologic conditions.
3. To discuss the impact of HRCT on diagnostic strategies in patients with diffuse infiltrative lung disease.

A-416

B. Reticular pattern

N.J. Screaton; Cambridge/UK

A reticular pattern consists of innumerable interlacing lines resembling a net and almost invariably indicates interstitial disease. It may result from inter- and/or intra-lobular septal thickening. Interlobular septal thickening is commonly associated with peribronchovascular and intralobular interstitial thickening. The latter is identified either by intralobular fine reticular pattern or, when below the resolution of HRCT, by diffuse ground-glass opacity. Occasionally peribronchiolar or perivascular interstitial fibrosis results in centrilobular nodules as in asbestososis. Fibrotic parenchymal distortion commonly causes traction bronchiectasis.

Extensive fibrosis associated with severe distortion of normal lobular architecture causes a coarse reticular pattern or, when characterised by the presence of irregular cystic spaces, a honeycomb pattern.

Clearly visible interlobular septa almost always indicate interstitial abnormality. Although interlobular septal thickening is seen in numerous interstitial diseases, when it is the predominant finding the differential diagnosis is limited. Although the division of interlobular septal thickening into smooth, nodular or irregular can be difficult, it may aid diagnosis. Smooth septal thickening is seen in pulmonary interstitial oedema, and alveolar proteinosis, nodular septal thickening in sarcoidosis and lymphangitic spread of tumour, while irregular septal thickening results from architectural distortion by interstitial fibrosis.

Several factors assist diagnosis of a reticular pattern on HRCT. These include character of the HRCT features such as the coarseness of the pattern and the presence and nature of interlobular septal thickening. The distribution of reticulation, ancillary imaging features and clinical features are also instrumental in refining the differential diagnosis.

Learning Objectives:

1. To describe and illustrate the nomenclature for description of different HRCT findings.
2. To present typical HRCT manifestations of different pathologic conditions.
3. To discuss the impact of HRCT on diagnostic strategies in patients with diffuse infiltrative lung disease.

A-417

C. Ground glass opacities

S. Diederich; Düsseldorf/DE

Ground glass opacity is defined as infiltration of the lung parenchyma which is not dense enough to obscure pulmonary vessels. Histologically, the key feature

is the preservation of air-filled alveoli in lung parenchyma with otherwise increased soft tissue attenuation.

It may be due to increase in the volume of the interstitium, partial filling of air spaces with cells or fluid, or both.

Ground glass opacity presenting as areas of increased density in otherwise normal density lung parenchyma needs to be differentiated from the apparent increased density of normal lung parenchyma in the presence of abnormal decreased attenuation either due to air-trapping or mosaic perfusion. Observation of the width of pulmonary vessels in areas of low density is helpful in deciding whether areas of increased or decreased density are abnormal in such circumstances. HRCT in expiration may also assist in this differential diagnosis. In many diseases, ground glass opacity corresponds to areas of active disease, prompting initiation of therapy. However, as it may also represent end-stage fibrosis. Secondary signs need to be recognized which can indicate irreversible fibrosis, such as traction bronchiectasis and bronchiolectasis and parenchymal distortion.

Ground glass opacity may be found in a variety of diseases. Examples will be presented including pneumonia (e.g. pneumocystis carinii pneumonia, viral and bacterial pneumonias, fungal pneumonia), pulmonary oedema, haemorrhage, collagen vascular disease, other diffuse infiltrative lung diseases and effects of therapy. Imaging protocols to assess and quantify the presence of ground glass infiltration and facilitate the differential diagnosis will be presented.

Learning Objectives:

1. To describe and illustrate the nomenclature for description of different HRCT findings.
2. To present typical HRCT manifestations of different pathologic conditions.
3. To discuss the impact of HRCT on diagnostic strategies in patients with diffuse infiltrative lung disease.

08:30 - 10:00

Room F2

Neuro

RC 1711

Pediatric neuroradiology

Moderator:

K.A. Vergesslich; Basle/CH

A-418

A. Congenital lesions of the brain

N. Girard; Marseille/FR

Congenital lesions of the brain is a vast chapter including: congenital malformations, congenital infections, inborn errors of metabolism and destructive brain lesions acquired in utero.

Malformations are described following embryological timing and include neural tube defects, disorders of diverticulation (holoprosencephaly spectrum, cystic malformations of the posterior fossa), commissural agenesis, malformations of cortical development that can involve cellular multiplication, differentiation, migration and organization. Malformations also include extracerebral cysts and vascular malformations. Although brain malformations are characterized by specific anatomical features, MR imaging features can change with time along with brain maturational changes, especially in cases of malformation of cortical development, but also in midline lipomas.

The most common congenital infections are CMV and toxoplasmosis and result in brain malformations and destructive lesions of the brain. Neonatal herpes encephalitis is less frequent and highly destructive.

Inborn errors of metabolism can be encountered in utero and in neonates, the most frequent seen being mitochondrial cytopathies that rarely display basal ganglia involvement (until the first year of life) compared to older children. Some metabolic disease are also known to give brain malformations (i.e. corpus callosal agenesis in pyruvate dehydrogenase deficiency). Other metabolic disease are known to lead to brain damage similar to cerebral lesions of hypoxic-ischemic origin.

Destructive brain acquired in utero of hypoxic origin can be encountered postnatally especially in the neonatal period such as stroke and necrosis. Acute events one to several days before birth also happen leading to brain damage sometimes difficult to differentiate from cerebral damage that have taken place pernatally.

Learning Objectives:

1. Listing of the different types of congenital lesions of the brain.
2. To recognize the different types of malformation.
3. To recognize the different features of a definite malformation depending on the age at the time of neuroimaging.

Postgraduate Educational Programme

4. To recognize anatomic markers of an etiology (i.e. congenital infection and brain lesions).

A-419

B. Non-accidental head injury/child abuse

O. Flodmark; Stockholm/SE

To the radiologist, neuroradiologist in particular, physical abuse of infants and babies are of greatest interest since neuroradiology is often the only means by which the diagnosis of abuse can be suspected and subsequently proven. Small infants are most often shaken while larger infants are more often submitted to shaken/impact injury. The resulting brain damage is devastating. The infant presents with most non-specific symptoms, making the clinical diagnosis of abuse extremely difficult.

The repeated accelerations and decelerations and rotations associated with repeated shaking of a small baby will cause venous haemorrhage into the subdural space, a very important marker indicating that the baby has been shaken. Repeated instances of abuse will cause haemorrhages of different ages. The same treatment will also cause tearing injuries seen in the white/grey matter interface, often with small haemorrhages as well as retinal haemorrhages. Hypoxic/ischaemic brain injury added upon the tearing injuries aggravates brain oedema.

The finding of subdural haemorrhages, brain oedema and retinal bleeds in combination provides as close to 10% proof for child abuse as is possible.

The most important method used to diagnose abuse of infants is CT-scanning. It is an effective way of showing subdural haemorrhage and can give an indication of the age of the haemorrhage. MR imaging has a superior sensitivity in detecting collections of haemorrhage in the subdural space. It has a superior ability to demonstrate brain injury. The only, but most important weakness of MR imaging is its inability to accurately show the age of a subdural haemorrhage.

Learning Objectives:

1. To learn about the incidence of child abuse.
2. To understand how a baby or child commonly is abused.
3. To understand the mechanisms behind skull fractures and brain injury following child abuse.
4. To know how these injuries can and should be imaged.
5. To understand how to interpret the imaging findings of skull and brain injury in child abuse.
6. To discuss briefly the role of the radiologist in the legal process often following on detection of child abuse.

A-420

C. Hydrocephalus

S. Cakirer; Istanbul/TR

Hydrocephalus is a condition in which there is increase in ventricular size due to an imbalance between the production of cerebrospinal fluid (CSF) and its drainage by the arachnoid villi. The result is increased intracranial pressure.

Three major mechanisms account for the development of hydrocephalus. The first mechanism is obstruction to CSF flow, usually secondary to congenital lesions as stenosis/web of aqueductus Sylvii, inflammatory conditions such as tuberculosis, meningitis, granulomatous infiltrations, blood clot, and various tumors. Second is decreased absorption of CSF by arachnoid villi, this is seen in subarachnoid and intraventricular bleeding, inflammatory conditions, and tumoral seeding to the subarachnoid spaces. Third is the overproduction of CSF, unique to infants and young children and caused by choroid plexus papillomas and carcinomas. While congenital anomalies, infections and hemorrhagic insults are leading causes in newborns and infants, infections and tumors are more common in older age groups. Hydrocephalus may be classified on the basis of level of obstruction as communicating (extraventricular) or noncommunicating (intraventricular) hydrocephalus. The situation might be compensated or noncompensated depending on the presence of transependymal CSF migration.

All of the above will be discussed during the lecture with their corresponding neuroimaging findings, including antenatal and postnatal transcranial ultrasound, computed tomography, magnetic resonance (MR) imaging and advanced techniques such as cine MR, fetal MR studies.

Differential diagnoses for neuroimaging findings and for age groups as well as neuroimaging findings following therapeutic shunting operations with their complications will be discussed briefly as well.

Learning Objectives:

1. To learn about the etiology and pathogenesis of the pediatric hydrocephalus.
2. To identify imaging modalities used in the study of hydrocephalus.
3. To learn about the potential of new MR imaging techniques in the study of hydrocephalus.

08:30 - 10:00

Room G

Head and Neck

RC 1708

How to investigate facial pain

Moderator:

K. Marsot-Dupuch; Le Kremlin-Bicêtre/FR

A-421

A. Neuralgia and uncommon causes

T.J. Vogl, S. Bisdas; Frankfurt a. Main/DE

Facial pain presents predominantly as unilateral pain and is caused by dental, neurological, vascular, temporomandibular, and atypical neuralgic conditions. Imaging techniques will be presented, including conventional X-ray (digital radiography), multislice computed tomography (MS-CT), and high-resolution magnetic resonance imaging (MR imaging techniques).

Imaging findings due to dental causes such as osteomyelitis and compression syndromes have to be evaluated. Temporomandibular joint disorders are evaluated by performing static and dynamic MR imaging techniques. The major cause of facial neuralgia is trigeminal neuralgia (TN). Here the evaluation has to include compression of the trigeminal nerve by vascular loops or other space-occupying lesions such as inflammatory diseases or primary and secondary tumors.

Plain radiographs and CT of the nasal cavity and paranasal sinuses are helpful for detecting sinus disease as a cause for facial pain. MR imaging is the elective method for neoplastic disease evaluation and pre-operative imaging.

In summary, clinical evaluation and other imaging techniques such as conventional X-ray, CT and MR imaging have to be used according to the clinical question and the evaluation has to follow exact topographic knowledge and detailed morphological findings of the radiological causes.

Learning Objectives:

1. To be become familiar with the causes of neuralgiform facial pain and the currently existing treatment modalities.
2. To be aware of the key anatomic structures that play a role in facial pain of neurogenic origin.
3. To be aware of the advantages and disadvantages of the imaging modalities to use and to know when to perform the most appropriate imaging technique.
4. To be able to recognize the most common causes of neuralgiform facial pain.
5. To be aware of rare diseases that may lead to facial pain.

A-422

B. Pain of dental origin

A. Gaheitner; Vienna/AT

Pain of dental origin is most frequently caused by the root canal or the periodontal ligament space. Inflammation, trauma or tumor in this region can easily spread into the surrounding soft tissue, sinus or jaw bone. Separate to this, a multitude of diseases occurring in the jaw can involve the teeth leading to pain as a first indicator of a lesion. While conventional imaging methods such as panoramic radiography and dental films are very useful in detection of these diseases, newer imaging methods as dental-CT and dental-MR have recently gained importance in diagnosing dentition-associated diseases of the mandible and maxilla. Unfortunately, most radiologists have had little experience in this area and many of the CT and MR findings remain undescribed.

This presentation will focus on the technique and usefulness of CT and MR in diagnosing pathologic conditions and complications as a cause for pain of dental origin. Furthermore the correct imaging technique and the most important error sources will be discussed. To enable a clear understanding of dental-CT and MR, clinical images and aspects will be added to facilitate the transition from the intraoperative situation to radiological presentation.

As a goal the radiologist should be aware of possible findings presenting as pain in the jaw region and should be able to communicate them to the clinician.

Learning Objectives:

1. To become familiar with the various causes of facial pain of dental origin.
2. To be aware of the advantages and disadvantages of the imaging modalities to use and know when to perform the most appropriate imaging technique.
3. To recognize the diagnostic features of the most common causes of odontogenic facial pain, such as, periapical granuloma, radicular cysts, osteomyelitis of the mandible and odontogenic tumors.

Tuesday

Postgraduate Educational Programme

A-423

C. Pain related to the temporomandibular joint and muscles of mastication

S. Robinson; Helsinki/FI

Facial pain related to the TMJ and masticator space can occur in both open and closed mouth positions and can be accompanied by a clicking noise on movement of the jaw, difficulties in opening the mouth, malocclusion, skin deviation, asymmetry of the muscles of mastication or a palpable mass.

The mandibular condyle and fossa are separated by the disk, which is attached to the upper belly of the lateral pterygoid muscle anteriorly and the elastic fibers of the bilaminar zone posteriorly.

Cortical changes are best depicted by CT; soft tissue including bone marrow is best visualized by MR imaging and OPG shows the relationship to the dentoalveolar system.

Common causes of pain are disk dislocation, osteoarthritis ("internal derangement"), rheumatoid arthritis, and trauma.

Imbalance of the muscles of mastication or masticator space tumours, as well as dysfunction of the cervical spine or sacroiliac joint are rare causes for facial pain.

Learning Objectives:

1. To become familiar with the clinical aspects of facial pain related to the TMJ and masticator space and to be aware of their therapeutic implications.
2. To know the key anatomic structures that play a role in facial pain related to the TMJ and masticator space.
3. To be aware of the advantages and disadvantages of the imaging modalities to use and to know when to perform the most appropriate imaging technique.
4. To be able to recognize the most common types of TMJ dysfunction, as well as common diseases that may affect the muscles of mastication and mandible.
5. To be aware of rare diseases that may lead to facial pain related to the TMJ and masticator space.

08:30 - 10:00

Room H

Interventional Radiology

RC 1709

Venous occlusion

Moderator:

N. Batakis; Athens/GR

A-424

A. Deep venous thrombosis

H. Bjarnason; Rochester, MN/US

Learning Objectives: To describe the sequelae of deep venous thrombosis, discuss incidence, distribution and pathophysiology. The different technical aspects of venous thrombolysis and use of mechanical thrombectomy devices as well as different thrombolytic agents will also be briefly discussed. The past literature and future developments will be discussed as well.

Background: Traditionally, deep vein thrombosis has been treated with anticoagulation alone. It has been estimated that up to 65% of patients who suffer acute deep vein thrombosis will develop post-thrombotic syndrome. In addition to dependent edema and chronic leg swelling, as many as 5% will develop venous ulcers. Early spontaneous lysis of the thrombus has been found to prevent damage to the valvular elements.

Outcomes: A number of small-randomized studies have demonstrated significantly increased clot lysis in patients treated with systemic thrombolysis compared to conventional anticoagulation. This treatment has though been found to be associated with a higher risk of bleeding complications which has lead to use of catheter directed thrombolysis. Two retrospective evaluations of catheter-directed venous thrombolysis have been performed. Major bleeding complications were encountered in 5% and 11% of patients respectively but more than 50% lysis was achieved in 83% and the 1-year primary patency rate was 60%. With the use of mechanical thrombectomy in combination with thrombolytics the treatment time has been reduced from over 50 hours to 2 to 24 hours with low rate of complications.

Conclusion: Long-term outcomes still need to be evaluated and there are studies ongoing where thrombolysis is randomized to anticoagulation alone.

Learning Objectives:

1. To give an insight into sequelae of deep venous thrombosis, frequency and pathophysiology.
2. To review past literature on systemic and catheter directed thrombolysis for iliofemoral deep venous thrombosis.

3. To discuss the current methods applied for mechanical and pharmacologic thrombolysis.
4. To discuss upcoming issues related to the topic.

A-425

B. Vena cava management

C.L. Zollinger; Winterthur/CH

Vena cava obstruction is caused by malignancies in 95% of the cases and only a minority are of benign origin and most commonly the sequelae of iatrogenic interventions such as central venous lines, hemodialysis fistulas or thrombotic occlusions such as deep vein thrombosis etc. Stenting of malignant central venous obstruction has become the method of choice for these mostly severely ill patients. A significant relief of symptoms within 12-24 hours can be expected in 70-100% with this low risk procedure. Long-term palliation including secondary interventions usually lies in the range of 85% or more, however, due to tumour progression additional stents may have to be implanted. Stent procedures for benign disease of the central veins have a very high success rate with an 90-100% overall initial and 80-100% longterm clinical success. Morbidity and complication rates are extremely low. Particularly for treatment of the May-Thurner syndrome stents are the method of choice. Central venous lesions related to hemodialysis fistulas are a further indication for primary stenting to improve the often unsatisfactory result of simple balloon dilatation. However, because of the high rate of intimal hyperplasia, usually occurring after 8-12 months, a close shunt surveillance is mandatory to install early reintervention. Indications, techniques and results will be discussed for the various clinical manifestations of central venous obstruction.

Learning Objectives:

1. To understand the indications and limitations for vena cava recanalisation and stenting.
2. To be able to select the appropriate patients with vena cava obstruction.
3. To be familiar with the techniques and possible complications of vena cava stenting.
4. To have a better understanding of the importance and techniques and results of vena cava recanalisation and stenting by the end of this presentation.

A-426

C. Pulmonary embolism: Protection and treatment

T. Schmitz-Rode; Aachen/DE

Despite prophylactic anticoagulation acute massive pulmonary embolism (PE) is still a common and often life-threatening entity. Survival of patients with right ventricular dysfunction depends on rapid recanalisation of the pulmonary arterial occlusion. Percutaneous catheter treatment represents an therapeutic option. Catheter devices include standard diagnostic catheters, balloon catheters, dedicated suction catheters (Greenfield vacuum cup catheter), rotating pigtail catheter, hydrodynamic thrombectomy catheter, and high-speed rotating tip catheters. The principles employed are extraction and/or fragmentation of the embolic material. Fragmentation of central emboli and dislocation of the fragments to the periphery result in a relative gain of non-obstructed cross-sectional area. The increased total surface area of the fragments accelerates the efficacy of an accompanying thrombolysis or of spontaneous intrinsic lytic activity. In the workshop pulmonary placement and navigation of the pigtail rotation catheter will be demonstrated as well as the mechanical action for recanalisation. The indications, safety, efficacy, the influence on hemodynamic parameters, possible complications, and pitfalls will be discussed. Percutaneous inferior vena cava (IVC) filter implantation represents a mechanical prophylaxis of PE. Absolute indications are recurrent PE despite sufficient anticoagulation and occurrence of PE in patients with contraindicated anticoagulation. The most common IVC filters will be presented. Implantation can be performed via femoral or jugular access. Temporary and facultative temporary filters can be removed within a certain duration after placement. Filter complications include misplacement, IVC thrombosis, perforation, migration, filter breakage, and recurrent PE. Therefore, diligent check of the indication for IVC filter implantation is advisable.

Learning Objectives:

1. To discuss indications, contraindications, and complications of catheter therapy of PE.
2. To discuss types of catheters and techniques.
3. To discuss selective vs systemic thrombolysis of PE.
4. To discuss indications and contraindications of IVC filter placement.
5. To discuss IVC filter placement techniques, filter removal, filter complications.

Postgraduate Educational Programme

08:30 - 10:00

Room I

Vascular

WS 1715

Planning issues in vascular radiological intervention

Moderator:

L.K.A. Tan; Singapore/SG

A-427

A. How to set up an endovascular centre

L.A. Jacob; Basle/CH

1. **Place:** Your new interventional center must be located at a hospital. The severity of illnesses and of the possible complications dictates an immediate availability of emergency facilities.
2. **Planning:** The planning is to be embedded into the hospital's strategy and profile: Patient referral patterns, interventional, OR- and ICU-facilities and other factors must be taken into account.
3. **Players (partner, opponents):** Besides the patient, the interventional radiologist and the technicians there are other people that have to be dealt with: vascular surgeons and/or internists (aka angiologists), other medical and surgical specialties, the hospital administration, insurances, political entities etc. Assign an attractive role for all important players to make them partners.
4. **Pliancy:** Adapt your plan to the local realities. If you cannot make a partner out of a particular player, or do not have the patients in a certain segment, you have to find a way around, leave the field out, or even cancel the whole plan.
5. **Patient access:** Normally an interventional radiologist has to rely on referrals from other clinicians. Direct patient access should be sought whenever possible: interventional rounds, a parlor, an outpatient clinic are all important means.
6. **Procedure rooms:** The physical configuration and equipment is less important than the other factors mentioned. You will solve these problems together with your partners. Again, local characteristics will strongly influence your choices.
7. **Patience and perseverance:** You will need some time to find your place among the other clinicians. Hang on!

Learning Objectives:

1. To impart information needed and issues to be discussed in setting-up an endovascular centre.
2. To understand the practical issues in setting-up such a service in conjunction with vascular surgery.
3. To know what equipment is needed e.g. CT, MR, interventional suite and theatre-time.
4. To be able to discuss working models with vascular surgeons.

A-428

B. Mapping peripheral vascular disease

M.G. Cowling; Stoke-on-Trent/UK

Assessment of peripheral vascular disease depends in the first instance on careful history taking and examination. Decisions about endovascular or open surgical intervention also depend on knowledge of the precise nature and location of stenotic or occlusive arterial disease.

Palpation of peripheral pulses is known to be unreliable in determining the presence and level of arterial disease. For example, the femoral pulse may be difficult to feel because of obesity, and the popliteal artery can be very difficult to palpate, even when normal. Severity of limb ischaemia is relatively easy to assess. The most commonly used technique for assessment of severity of arterial disease is the measurement of Doppler ankle pressures to derive the ABPI. In difficult cases the value of ABPIs may be enhanced by the use of exercise testing. Other techniques, such as plethysmography, transcutaneous oximetry and isotope blood flows are also available and will be discussed.

Non-invasive assessment of the location of arterial disease is more difficult. Segmental arterial pressures have been used, but are unreliable in the assessment of aortoiliac disease in the presence of femoropopliteal disease. Duplex ultrasound is a very valuable non-invasive tool, which allows analysis of the waveform and measurement of peak systolic velocity. Use of colour flow imaging allows relatively rapid assessment of an arterial segment. Areas of concern can then be examined in more detail. In many institutions, including our own this has become the mainstay of non-invasive arterial imaging.

Learning Objectives:

1. To understand the value and use of clinical examination.
2. To understand the role of clinic based non-invasive investigations.
3. To understand the optimal use of vascular laboratory investigations.

08:30 - 10:00

Room K

Pediatric

RC 1712

Musculoskeletal imaging

Moderator:

E. Sorantin; Graz/AU

A-429

A. Imaging of juvenile idiopathic arthritis

K.J. Johnson; Birmingham/UK

Juvenile idiopathic arthritis (JIA) is an inflammatory disorder of childhood that may affect any joint or organ system. JIA is a relatively recent classification for childhood arthritis and is an attempt to unify a disease that was previously described as Juvenile Chronic Arthritis (JCA) in North America and Juvenile Rheumatoid Arthritis (JRA) within Europe.

The purpose of this presentation is to illustrate the imaging findings of JIA. The different subgroups of JIA will be discussed including any of their unique imaging features. The presentation will highlight the very early and subtle radiographic appearances of JIA that may enable an early diagnosis of the disorder to be made.

The chronic features and complications of the disease will also be illustrated. A review of the differential diagnoses that need to be considered in childhood arthritis will also be made.

The value of both MR imaging and ultrasound in assessing the joint will be discussed. The most appropriate MR imaging sequence selection to allow visualisation of joint structures; articular cartilage and inflamed synovium will be detailed. In particular the use of post Gadolinium fat-saturated T1 weighted sequences for the detection of inflamed synovium will be emphasised.

There have been major advances in therapeutic options in the management of JIA. It is important that the diagnosis is arrived at as early as possible so that treatment can be optimised and the child maintain as normal function and mobility as possible.

Learning Objectives:

1. To increase awareness of the disease.
2. To show the imaging features (X-ray, US, MRI) of early disease.
3. To demonstrate chronic disease changes.
4. To show complications of the disease.
5. To describe other diseases that should be considered in the differential diagnosis in pediatric joint disease.

A-430

B. An approach to the diagnosis of skeletal dysplasias

A. Offiah; London/UK

During the course of their training programme, most radiology residents are taught systematic approaches to analysing plain radiographs of e.g. bone tumours and arthritic disease. We are all familiar with the approach to interpretation of a chest radiograph. However very little is taught on the approach to diagnosing skeletal dysplasias and other constitutional disorders of bone. The result is that many radiologists feel daunted when faced with a skeletal survey of a child with a possible dysplasia. The purpose of this talk is to present delegates with a simple but systematic method of diagnosing skeletal dysplasias.

Learning Objectives:

1. To highlight the radiographs obtained as part of a routine skeletal survey.
2. To discuss circumstances in which additional radiographs may be required.
3. To outline a simple approach to interpreting skeletal surveys in possible dysplasia.
4. To demonstrate this approach using radiographs from surveys of children with various skeletal dysplasias.
5. To discuss methods in which after having identified the abnormalities, the final diagnosis may be reached.

A-431

C. Imaging of malignant tumors of the long bones in children: What to do or not to do

H. Brisse; Paris/FR

Background: Osteosarcoma and Ewing's sarcoma represent more than 90% of all primary malignant bone tumours in children. The current treatment for local-

Tuesday

Postgraduate Educational Programme

ized forms is based on neoadjuvant chemotherapy designed to treat micrometastatic disease and reduce tumour volume to facilitate the surgical procedure. Surgery must be as conservative as possible, but must ensure complete resection. The role of imaging is to precisely evaluate the degree of local extension prior to surgery and to assess the response to chemotherapy. The current treatment protocols are still based on the gold standard of histological response.

Imaging findings: MR imaging is currently the best method to evaluate local extension prior to tumour resection, especially to assess the feasibility of conservative surgery. Morphological criteria on plain films and static MR imaging are insufficiently correlated with histological response. The contribution of dynamic MR imaging, diffusion-weighted MR imaging and nuclear medicine (¹⁸FDG-PET) to monitor tumoural necrosis are described.

Conclusion: The initial pre-treatment imaging actually remains the most important assessment. The first MR examination performed before treatment and initial biopsy constitutes the reference for follow-up during treatment and for local staging. Various nonspecific morphological and signal changes are induced by pre-operative chemotherapy, and assessment of response on the basis of these changes must be interpreted cautiously. Dynamic MR imaging can be used as a complementary technique for local staging and assessment of response for inoperable forms. Quantitative models in dynamic MR imaging and ¹⁸FDG-PET are currently being developed in order to demonstrate early prognostic criteria, which could be decisive in future protocols.

Learning Objectives:

1. To learn how to perform MR examinations of a malignant tumor of the long bones in children at diagnosis, during neoadjuvant chemotherapy and before surgery.
2. To learn how to precisely evaluate the degree of local extension and help the surgeon regarding the decision of conservative surgery.
3. To learn how to assess the response to neoadjuvant chemotherapy with imaging.

08:30 - 10:00

Room L/M

Radiographers

RC 1714

Breast imaging

Moderators:

A. Hartvig Sode; Odense/DK
P.F.G.M. van Waes; Amersfoort/NL

A-432

A. Breast cancer and imaging

D. Scutt, A. Nandi, L. Zhang, L.B. Jack; Liverpool/UK

We have combined 2 sources of information (mammographic reports and separately held questionnaire and nurse examination data from the Liverpool Breast Cancer Risk Factor study 1977-84; current diagnostic data from the Merseyside and Cheshire Cancer Registry). The secondary analysis on this combined data will allow a) an assessment of individual risk factors associated with subsequent diagnosis of breast cancer over a 30 year period and b) the development of a multifactorial risk model. We intend to subject the data to some comparatively recent machine learning algorithms, adopted and further developed at the Department of Electrical Engineering and Electronics. We will work with the main dataset of known outcome (cancer/no cancer). This will be split into two sets. One set will be used for learning (training) that could highlight risk factors. The other set will be used for testing to confirm its predictive accuracy. Subsequently we will undertake a prospective randomised controlled trial in patients with suspicion of, or at risk from breast cancer.

Learning Objectives:

1. To give an appreciation of the role of imaging in the diagnosis of breast cancer.
2. To raise awareness of the risk factors for breast cancer - results of a 30 year Liverpool study.
3. To give an overview of Liverpool developments in breast cancer imaging using microwave technology.

A-433

B. Softcopy display of mammograms

L. Costaridou; Patras/GR

Mammography is at present the dominant technique for early detection of breast cancer. However cancer signs, such as microcalcifications and masses, have often similar density to dense tissue, due to low inherent contrast, non-linear film

response to incident radiation exposures and tissue superimposition.

Full field digital mammography systems are characterized by improved contrast resolution compared to screen/film mammography, by decoupling image acquisition from display, while providing digital images to filmless- and tele-radiology environments. Softcopy display, i.e. interpretation of mammograms from electronic displays such as CRTs, is an essential part of such systems. Issues of software functionality and speed are of major importance to softcopy display. Meeting the technical challenge of matching display spatial resolution to acquisition resolution is an on going effort, partly fulfilled by the highest end display systems, not commonly available. Thus at present, a key issue of softcopy display is the treatment (processing) of display image intensities to benefit human image interpretation, also exploited in digitized mammography. Image processing methods, termed contrast enhancement methods, are targeted to fully utilizing the acquired intensity range as well as intensity differences (edges), conveying image structure. In such methods emphasis is given to locally adaptive ones, as well as in evaluating diagnostic performance efficiency by observer and quantitative means.

Learning Objectives:

1. To illustrate the basic principles of contrast- and edge-enhancement methods.
2. To provide application examples of major state-of-the-art enhancement methods on mammograms, with emphasis on difficult cases (e.g. dense tissue).
3. To discuss performance of enhancement methods and workstation issues (e.g. digitizer, display monitor, compression algorithms).

08:30 - 10:00

Room N/O

Workshops on Interventional Radiology

WS 1718

Chest intervention

Moderator:

D. Liermann; Herne/DE

A-434

A. Tracheobronchial stenting

T. Sabharwal; London/UK

Large-airway obstruction may be caused by intraluminal disease, stenosis, tracheobronchial collapse, or extrinsic compression. In benign strictures, surgical resection and anastomosis or various forms of tracheoplasty represent the standard approaches to the treatment of symptomatic tracheal stenosis. This method, however, is not always possible for long lesions (> 6 cm); in such cases, surgery is often debilitating, and the anastomosis can be the site of recurrent stenosis. In malignant strictures, palliative therapy is required, and a combined approach to treatment is often used, with alternative methods that include endoscopic debriement, brachytherapy, percutaneous balloon dilation, endoluminal splinting, percutaneous irradiation, and chemotherapy. Recent advances in interventional radiology techniques and materials have enabled the endoluminal use of tracheo-bronchial stents. Effective and immediate palliation of obstructive airway symptoms usually result in significant improvement in the functional status and quality of life of patients with benign and malignant airway problems. Balloon or self expanding metallic stents can be used (author prefers the latter group). Uncovered stents are deployed in the bronchus so that airway branches are not occluded and covered stents reserved when there is a fistula. In the trachea, covered or uncovered stents can be deployed. CT images are helpful to size the stents and for planning of the procedure. The stent insertion can be done under sedation and fluoroscopic guidance but in our institution we perform them using combined fluoroscopic and endoscopic guidance under general anaesthesia. The three major problems currently associated with airway stents are mucous impaction, the formation of granulation tissue, and migration.

Learning Objectives:

1. To be familiar with the principle and application of tracheo-bronchial stenting.
2. To learn the radiological technique for stent insertion and to know the different available stents.
3. To discuss the indications, contraindications and radiological placement of tracheobronchial stenting.
4. To understand potential complications and brief outline of literature review.

Postgraduate Educational Programme

A-435

B. Pulmonary vascular intervention

J.E. Jackson; London/UK

Massive haemoptysis, which is perhaps best defined as bleeding into the bronchial tree at a rate that poses a threat to life, is associated with considerable mortality unless treated aggressively. Common aetiologies include bronchiectasis, active tuberculosis (TB) and colonization by aspergillus species of a pre-existing pulmonary cavity. The majority of patients are not surgical candidates because of the presence of severe bilateral pulmonary disease. The primary vascular abnormality that occurs is the development of abnormal broncho-pulmonary shunts within peri-bronchial inflammatory tissue. The bronchial arteries, and other non-bronchial systemic arteries, dilate because of the resultant increased blood flow and the small fragile vessels within the inflammatory tissue are thus exposed to systemic arterial pressure. Bronchial arterial embolization is aimed at reducing the perfusion pressure to the fragile vessels within the inflammatory tissue by occluding systemic arterial inflow. A pulmonary source of haemorrhage in chronic lung disease may occur in as many as 10% of individuals. It most commonly arises from a pseudo-aneurysm caused by erosion of a pulmonary arterial branch by adjacent lung disease and should be considered in any patient who has a further large haemoptysis shortly after a technically successful embolization of bronchial and non-bronchial systemic arteries. The immediate control of haemorrhage will be achieved in between 75% and 90% of patients by bronchial embolization but at least 20% of these individuals will rebleed within the next six months and up to 50% may have further significant haemoptysis on longer term follow-up.

Learning Objectives:

1. To learn the indications for angiography and embolization in massive haemoptysis.
2. To be familiar with the angiographic abnormalities seen in patients with haemoptysis due to chronic inflammatory lung disease and understand why they develop.
3. To understand the importance of imaging and embolizing both the bronchial and non-bronchial systemic arterial supplies to the lung.
4. To be aware of the importance of a pulmonary arterial source of haemorrhage in some patients.
5. To understand the potential complications of bronchial angiography and embolization.

A-436

C. Thermal ablation of lung tumors

T.K. Helmberger; Munich/DE

The lung is a common site for primary or secondary malignancies, whereas pulmonary metastases present a significantly higher incidence than bronchial carcinomas. While radiotherapy +/- chemotherapy can provide sufficient tumor control dependent on the underlying tumor entity, in resectable patients surgical resection is considered the only curative therapy. Recently, percutaneous, minimal-invasive interventional methods as thermal ablation by radiofrequency or laser are competing with minimal - invasive surgical resection techniques as thoracoscopical surgery. In general, thermal ablation of pulmonary tumors is comparable to thermal ablation in other soft tissue tumor entities. Nevertheless, specific technical advisements, a different spectrum of indications and contraindications as in comparison to e.g. ablation in hepatic tumors, different types of tissue reactions and complications after thermal ablation, and specific thoughts regarding the follow-up have to be considered. The limited world wide available data are indicating that thermal ablation of pulmonary tumors might be a safe and effective treatment option. However, no long term data are yet available nor comparative studies to surgical minimal-invasive treatments. Therefore, specific attention has to be paid to the implementation of pulmonary thermal ablation into an oncological therapy regimen. The task of present and future research has to define the clinical significance of pulmonary thermal ablation especially in comparison to other evolving treatment techniques.

Learning Objectives:

1. To know the technique of pulmonary thermal ablation.
2. To assess the indications and contraindication for pulmonary thermal ablation.
3. To be familiar with the potential side effects and complications in pulmonary thermal ablation.
4. To understand the role of thermal ablation within a multidisciplinary concept in pulmonary tumor treatment.

12:15 - 14:00

Room A

Plenary Session

EAR Awards

Presiding:

N. Gourtsoyannis; Iraklion/GR

Presentation of the EAR - Boris Rajewsky Medal to:

M. Bléry; Le Kremlin-Bicêtre/FR

R. Riemmüller; Graz/AT

JIIS

Junior Image Interpretation Session

Moderator:

D. Farina; Brescia/IT

Panellists:

T. Laswed; Lausanne/CH

S. Morozov; Moscow/RU

A. Sélley; Szeged/HU

D.J. Tuite; Dublin/IE

M. Vernooy; Rotterdam/NL

Closing Ceremony

Presiding:

A. Chiesa; Brescia/IT

H.M.L. Carty; Liverpool/UK

Concluding Remarks

A. Chiesa; Brescia/IT

President ECR 2005

Address by the President of ECR 2006

A. Adam; London/UK

Tuesday

Postgraduate Educational Programme

B

Scientific Sessions (SS)

Friday.....	131
Saturday	187
Sunday	235
Monday	259
Tuesday	311

Scientific Sessions

Scientific Sessions

Friday, March 4

Scientific Sessions

		room A 2nd level	room B 2nd level	room C 2nd level	room E1 entr. level	room E2 entr. level	room F1 entr. level	room F2 entr. level	room G lower level	room H lower level	
07:00											07:00
07:30											07:30
08:00											08:00
08:30											08:30
09:00		CC 117 Essentials of Neuroradiology Ischemic stroke (p. 8)	RC 110 Musculoskeletal Sports injuries (p. 8)	SF 1 Special Focus Session Computer assisted diagnosis (p. 9)	RC 102 Breast Breast MR imaging (p. 10)	RC 101 Abdominal and Gastrointestinal MR of the colon and rectum (p. 11)	RC 104 Chest Smoking-related diseases (p. 11)	RC 111 Neuro Imaging of normal anatomy and function (p. 12)	RC 108 Head and Neck Salivary glands (p. 13)	ER 126 Joint ECR/EAR sessions: Challenges for European Radiology Harmonization of training programmes: Myth or reality? (p. 13)	09:00
09:30											09:30
10:00											10:00
10:30		SA 2 State-of-the-Art Symposium Whole-body imaging (p. 17)	SS 210 Musculoskeletal Imaging in orthopedic and traumatologic disorders (p. 134)	SS 201a GI Tract Upper GI tract cancer: Diagnosis and staging (p. 136)	SY 1 Satellite Symposium Real-time virtual sonography (RVS) (p. 578)	SS 202 Breast New developments in breast imaging (p. 138)	SS 204 Chest Pulmonary nodule: Detection and significance (p. 140)	SS 201b Abdominal Viscera (Solid Organs) Focal liver lesions: MR imaging contrast agents (p. 142)	SS 208 Head and Neck Salivary glands, mandible and thyroid imaging (p. 144)	SS 209a Interventional Radiology Intervention in the thoracic aorta (p. 146)	10:30
11:00											11:00
11:30											11:30
12:00		Opening Ceremony/ Inauguration Lecture/ Presentation of Honorary Members (p. 19)									12:00
12:30											12:30
13:00											13:00
13:30											13:30
14:00											14:00
14:30		SS 306 Contrast Media US contrast media (p. 159)	SS 310 Musculoskeletal Invasive and interventional procedures (p. 161)	SS 301a GI Tract Colorectal cancer and staging (p. 163)	SY 2 Satellite Symposium Advances in MR contrast media imaging (p. 578)	SS 302 Breast Digital mammography (p. 165)	SS 304 Chest Computer aided detection (CAD) and volumetry of pulmonary nodules (p. 167)	SS 301b Abdominal Viscera (Solid Organs) Benign biliary disease and liver transplantation (p. 169)	SS 308 Head and Neck Oncologic imaging (p. 172)	SS 309a Interventional Radiology Non-vascular interventional procedures (p. 174)	14:30
15:00											15:00
15:30											15:30
16:00											16:00
16:30		CC 417 Essentials of Neuroradiology Hemorrhagic stroke (p. 19)	SF 4a Special Focus Session Rectal carcinoma (p. 20)	SF 4b Special Focus Session Imaging of the lymphatic system (p. 21)	RC 401 Abdominal and Gastrointestinal Abdominal trauma (p. 22)	RC 403 Cardiac Cardiomyopathies (p. 23)	RC 411 Neuro Functional MR imaging (p. 23)	RC 408 Head and Neck Radiological approach to stage head and neck squamous cell carcinoma (p. 24)	SF 4c Special Focus Session History of contrast media (p. 25)	16:30	
17:00	registration										17:00
17:30	EPOS™ - scientific exhibition										17:30
18:00		ECR Opening Concert									18:00
18:30											18:30
19:00											19:00

Scientific Sessions

	room I lower level	room K lower level	room L/M 1st level	room N/O 1st level	room P lower level	room W basement	room R 1st level	room Y 1st level	room Z entr. level	La Scala 2nd level		
07:00											07:00	
07:30											07:30	
08:00											08:00	
08:30											08:30	
09:00	WS 118 Workshops on Interventional Radiology Abdominal intervention (p. 14)	RC 107 Genitourinary Imaging of the female pelvis (p. 15)	CC 116 Infection in the Adult Today Spinocranial infection (p. 16)	RC 106 Contrast Media Contrast media for MR imaging and US liver imaging (p. 16)						E ³ 120 Foundation Course: Chest Radiology Anatomy and basic signs in imaging (p. 17)	09:00	
09:30											09:30	
10:00											10:00	
10:30											10:30	
11:00	SS 209b Interventional Radiology Experimental interventions in models and animals (1) (p. 148)	SS 203 Cardiac MR imaging in cardiomyopathy (p. 150)	SS 211 Neuro Inflammatory, infectious and degenerative CNS disease (p. 153)	SS 205 Computer Applications Advanced image processing (p. 155)	SS 215 Vascular Plaque imaging/ Thrombo- embolic disease (p. 157)	WS 222 Vertebroplasty "Hands on" Workshop				E ³ 220a Radiology on the web (p. 18)	11:00	
11:30											E ³ 220b E-mail for the radiologist (p. 19)	11:30
12:00											12:00	
12:30											12:30	
13:00											13:00	
13:30											13:30	
14:00											14:00	
14:30	SS 309b Interventional Radiology Experimental interventions in models and animals (2) (p. 176)	SS 303 Cardiac MR imaging in myocardial infarction (p. 178)	SS 311 Neuro The young and the old brain (p. 180)	SS 305 Computer Applications New developments in PACS (p. 182)	SS 315 Vascular Peripheral circulation (p. 184)		WS 325 Tips and Tricks in Radiofrequency Ablation "Hands on" Workshop				E ³ 320 Interactive Image Teaching Acute abdomen (p. 19)	14:30
15:00											15:00	
15:30											15:30	
16:00											16:00	
16:30	WS 418 Workshops on Interventional Radiology Arterial and venous liver intervention (p. 26)	RC 407 Genitourinary Imaging problem lesions (tumors) (p. 27)	CC 416 Infection in the Adult Today Chest (p. 27)	PR 419 Primer: Molecular Imaging New imaging methods and technologies (p. 28)	RC 405 Computer Applications Tele-imaging in Europe today (p. 29)						E ³ 420 Foundation Course: Chest Radiology Interstitial and alveolar disorders (p. 30)	16:30
17:00											17:00	
17:30											17:30	
18:00											18:00	
18:30											18:30	
19:00											19:00	

Scientific Sessions

10:30 - 12:00

Room B

Musculoskeletal

SS 210

Imaging in orthopedic and traumatologic disorders

Moderators:

M. Crockford; G'Mangia/MT
J. Sprindrich; Prague/CZ

B-001 10:30

The measurement and evaluation of lumbar muscularity in lumbar degenerative kyphosis (LDK) patients: Comparison with non-LDK patients on MR imaging

C. Kang, M. Shin, J. Ryu, S. Lee, S. Kim; Seoul/KR

Purpose: To compare lumbar muscularity in lumbar degenerative kyphosis (LDK) patients and non-LDK patients.

Materials and Methods: The study comprised LDK group (54 women, aged 44-74, mean 60) and non-LDK group with low back pain (36 women, aged 45-73, mean 60). Patients with spinal fracture, tumor, infection or previous surgery were excluded. The cross-sectional area (Acs) of individual muscle (psoas, erector spinae and multifidus) and intervertebral disc was measured at L4-5 by MR imaging using 1.5 T magnetic resonance system. Lumbar muscularity was expressed by three ratios; the ratio between Acs of right psoas, erector spinae, multifidus and Acs of disc (P: disc, ES: disc, MF: disc). The degree of fat deposit in erector spinae and shape of fascia overlying erector spinae on L5-S1 were analyzed. The degree of fat deposit was estimated using four grades: normal, mild, moderate and severe. The shape of fascia overlying erector spinae was classified into one of concave, flat and convex.

Results: Lumbar muscularity was found to be significantly smaller ($p < 0.001$, t-test) in LDK (P: disc=0.39, SD 0.11; ES: disc=0.95, SD 0.33; MF: disc=0.27, SD 0.1) than non-LDK (P: disc=0.51, SD 0.11; ES: disc=1.33, SD 0.3; MF: disc=0.44, SD 0.12). The degree of fat deposit and shape of fascia overlying erector spinae were also statistically different in two groups ($p < 0.05$). LDKc showed more fat deposit in erector spinae and has a tendency of flat or concave fascia overlying erector spinae.

Conclusion: Patients with LDK have a smaller lumbar muscularity and more fat deposit in erector spinae. The flat or concave fascia overlying erector spinae is significant feature of LDK.

B-002 10:39

Degenerative changes of the intervertebral disc and facet joint of the adjacent motion segment in the pre-operative MR imaging: Can it be the predictable factor of post-operative instability after posterolateral fusion of lumbar spine?

J. Ryu, M. Shin, S. Kim, S. Lee, C. Kang; Seoul/KR

Purpose: To assess whether the degenerative changes of the intervertebral disc and facet joint of the adjacent motion segment seen in pre-operative MR imaging can be the predictable factor of post-operative instability after posterolateral fusion of lumbar spine, with comparison of post-operative MRI imaging.

Materials and Methods: We included 40 patients with pre and post-op MR imaging and divided them into two groups according to the presence of instability of adjacent motion segment. We assessed the presence of instability in the flexion-extension view, and the degeneration of the disc, facet joint change, and the size of osteophyte in the pre and postop MR imaging. We had tried to clarify the possibilities of the degenerative changes to predict future development of the adjacent motion segment instability.

Results: The sum of the increase of the grade of disc degeneration in the group of instability was a mean of 1.05/patient, and mean of 0.5/patient in the other. Those of the osteophyte were mean 0.75 and mean 0.55, each other. Facet joint fluid was developed in eight cases in the instability group, and only three in stability group. These showed the tendency of the occurrence of instability.

Conclusion: Instability in the failed back surgery syndrome could not fully explained with these degenerative changes. This suggests the possibility that other factors affects the instability in the failed back surgery syndrome, and the more subtle findings that were not included in the criteria of this study may contribute to the instability.

B-003 10:48

Steroid-induced femoral head osteonecrosis: Comparison of proximal femur marrow status at baseline MR imaging between patients who will develop and who will not develop femoral head osteonecrosis during corticosteroid-treatment

R. Gilon, F.A. Houssiau, B.C. Vande Berg, F. Lecouvet, J. Malghem; Brussels/BE

Purpose: To test the hypothesis that the development of steroid-induced femoral head osteonecrosis may be influenced by the femoral neck marrow status before treatment.

Materials and Methods: 20 consecutive untreated patients with a newly diagnosed rheumatic disease in whom a standardized GC regimen was planned were selected for this study. MR parameters obtained before the start of treatment included (a) determination of Index of marrow conversion (IMC; SI (neck)/SI (greater trochanter)*100) and proportion of surface area of femoral neck occupied by fatty marrow (on coronal T1W SE images) and (b) bulk T1 and T2 relaxation time values of femoral head and neck marrow (on a quantitative MR sequence). Presence of osteonecrosis was determined at follow-up MR imaging obtained 6 months after onset of treatment.

Results: Four patients (20%) developed femoral head osteonecrosis at follow-up MR. The mean IMC value was higher in ON-positive (83.2 ± 6.2) than ON-negative patients (75.8 ± 8.1) ($p = 0.09$). The mean percentage of fat marrow in the femoral neck was higher in ON-positive ($86.5 \pm 1.3\%$) than in ON-negative patients (31.7 ± 35) ($p = 0.0066$). Mean T1 relaxation time values of femoral neck were shorter in ON-positive (257 msec) than in ON-negative patients (307 msec) ($p = 0.0423$).

Conclusion: A high fat content in the proximal femur marrow as determined by MR imaging before CS-treatment is predictive for the development of femoral head ON in CS-treated patients.

B-004 10:57

Comparative study of post-operative and spontaneous pyogenic spondylodiscitis

A. Feydy, V. Dufour, L. Le Page, N. Belmatoug, B. Fantin, V. Vilgrain; Clichy/FR

Purpose: Post-operative spondylodiscitis are poorly characterized, partly owing to their rarity. The aim of this prospective study was to compare the clinical, biological, bacteriological and imaging features of post-operative and spontaneous spondylodiscitis.

Methods: A multidisciplinary spondylodiscitis cohort follow-up study was conducted between February 1999 and June 2003 in a 500-bed teaching hospital. All patients hospitalized in internal medicine, orthopedic and neurosurgery wards with a culture-proven diagnosis of pyogenic spondylodiscitis were included. Clinical and bacteriological data were collected. All patients underwent computed tomography and/or magnetic resonance imaging of the spine.

Results: 16 patients had spontaneous spondylodiscitis (SS) and 7 patients had post-operative spondylodiscitis (POS). Patients with POS tended to be younger (52 versus 69 y), with less frequent underlying diseases (29% versus 75%) and a more prolonged interval between symptom onset and diagnosis (16 versus 3.4 weeks) than patients with SS. Blood cultures were positive in 14% and 81% of cases in the POS and SS groups respectively, and invasive diagnostic procedures were therefore necessary in 86% of patients with POS and 19% of patients with SS ($p = 0.005$). Staphylococci were the more frequent isolates in both groups but were more frequently coagulase-negative in POS patients than in patients with SS ($p = 0.01$). Vertebral edema tended to be more frequent in POS and was located more posteriorly than in SS ($p = 0.023$).

Conclusions: POS are associated with specific clinical, microbiological and imaging features possibly related to pathophysiological characteristics. Knowledge of these characteristics should help reduce the current delay in the diagnosis of POS.

B-005 11:06



Investigation of a tightly collimated lateral view of the cervico-thoracic region as a alternative to Swimmers's view for trauma patients

D. O'Leary¹, A. O'Loughlin², ¹Dublin/IE, ²Cork/IE

Purpose: Radiographic visualisation of the lateral cervico-thoracic region is rarely easy and is the greatest cause of trauma patients being delayed in X-ray. The region is obscured by the trapezius muscle/ humeral heads depending on patient body habitus. Previous studies show non-demonstration in 26%-38% of patients.

"Swimmer's view" is commonly employed to image C7/T1; the success of which is unpredictable with high radiation dose. "Swimmer's" is contra-indicated in the presence of an unstable cervical spine fracture. CT scanning is higher dose but

Scientific Sessions

remains the gold standard. An alternative projection is proposed: a true lateral, tightly collimated projection of the cervico-thoracic region (CTL) involving no patient movement and low exposure factor settings. We compared via a prospective study the proposed CTL projection and "swimmer's" projection for diagnostic efficacy, time efficiency and patient dose reduction.

Method: Trauma patients presenting for cervical spine radiography were randomised into two groups, half imaged with "Swimmer's" and half with CTL. Entrance Surface Dose (ESD) and Thyroid Dose (TD) were recorded using thermoluminescent dosimeters.

Results: ESD for CTL was consistently below 11 mGy. ESD for "Swimmer's" ranged from 7 mGy to 320 mGy. Assessment by a team of radiologists, radiographers and emergency physicians indicated that CTL is comparable to "swimmers" in image quality and diagnostic efficacy, while the patient dose was reduced to 2% of that for "swimmers". Imaging time and number of repeats were reduced.

Conclusion: The CTL projection considerably reduces patient dose with comparable diagnostic efficacy while reducing the time spent in the X-ray department.

B-006 11:15

Multi-slice CT (MSCT) as an integral component in primary trauma resuscitation

M. Körner, K.-G. Kanz, U. Linsenmaier, K.-J. Pfeifer, W. Mutschler, M. Reiser; *Munich/DE*

Purpose: To evaluate the time needed for whole-body MSCT in the early phase of trauma resuscitation.

Methods and Materials: In a prospective series, 125 consecutive patients fulfilling criteria for major trauma were evaluated. Initial imaging is limited to abdominal sonography (FAST) and supine chest radiograms. MSCT examination is initiated as an adjunct to primary survey immediately after clearing of critical conditions (i.e. intubation, chest tube, bleeding control). It consists of cranial, thoracic and abdominal CT. All MSCT scans were evaluated for time (min) from admission to CCT completion, duration of CT examination, and MPR calculating time as well as complications from early MSCT scanning.

Results: Time from trauma room admission to completion of cranial CT scan was 21:12 min. (median, interquartile range (IQR) 18:13 - 27:52), duration of complete CT examination including planning and contrast media administration was 6:08 min. (median, IQR 4:40 - 8:27). All MPR data was calculated in 5:29 min. (median, IQR 3:26 - 8:14). By using multiple workstations, data processing, image calculation, multiplanar reconstructions (MPR), and image reading can be performed at the same time. By processing the raw data, which is acquired by scanning the thorax and abdomen with 5 mm slice thickness, reconstructions of the spine with 3 mm slice thickness can be provided. No life-threatening complication due to early phase CT scanning was observed (0/125 CI 95% 0-3).

Conclusion: Integration of MSCT in very early trauma care provides a high standard of imaging in very short time without endangering a patient.

B-007 11:24

Imaging scaphoid trauma: An international survey of hospital practice

A.M. Groves, I. Kayani, R. Syed, N. Nagabushan, P.J. Ell; *London/UK*

Purpose: The scaphoid is the most common carpal bone fracture. The fracture must be identified early, as immediate treatment is required to minimise the chances of non-union and avascular necrosis thereby avoiding disability. However the imaging and treatment of such fractures remain controversial. In order to assess the consistency and evidence base of scaphoid imaging strategies we performed a survey of hospital practice in suspected scaphoid fracture.

Materials and Methods: Trauma or imaging specialists were surveyed by email regarding the imaging strategy in their respective hospitals of patients with suspected scaphoid fracture with normal/equivocal radiographs. 30 hospitals were surveyed including 12 from Europe, 6 from North America, 3 from South America, 6 from Asia and 3 from Australia.

Results: Data was obtained from 18/30 hospitals surveyed. None of the 18 hospitals had the same scaphoid imaging strategy. Less than half had a fixed protocol. The number of views of scaphoid plain radiographs varied from 2-6. Repeat radiographs were performed in 15/18 institutions, whilst in 3/18 other imaging modalities were used without further radiography. The definitive investigation was clinical examination in 1/18, scintigraphy in 5/18, magnetic resonance imaging in 4/18, computed tomography (CT) in 3/18, both CT and scintigraphy in 1/18, both MR imaging and scintigraphy in 1/18 and no single recognised definitive investigation in 3/18.

Conclusion: Despite the importance of early diagnosis/treatment of scaphoid

fracture, there is a lack of consistency and evidence base in scaphoid trauma imaging protocols. Further research is being performed at our institution to address this.

B-008 11:33

MR imaging in thoracolumbar burst fractures

N.A. Ghanem, M. Schwarz, G. Pache, C. Müller, M. Uhl, T. Bley, M. Langer; *Freiburg/DE*

Purpose: Evaluation of the diagnostic value of MR imaging in trauma patients with thoracolumbar burst fractures.

Material and Methods: A prospective study with 71 trauma patients was performed on a 1.5 T Magnetom. The MR imaging using sagittal T1-W-SE and T2-W-TSE or TIRM sequences was performed in a time frame of 5.8 days (range 1-19) 110). The evaluation included injuries of the vertebral body, adjoining intervertebral discs, ligaments, spinal canal and cord and adjoining soft tissue.

Results: Vertebral fractures were mostly located in the thoraco-lumbar transition (70.1% from T11 to L3) as well as the affected intervertebral discs (72%, 70 discs from T11 to L4). Anterior part involvement (48 cases, 67.6%) and posterior part involvement (56 cases, 78.9%) are usual after spine trauma, double fractures (32.9%) and a retropulsion of the posterior bone fragment (40%) less frequent. A spinal canal stenosis was shown in 72 fractures, a myelon compression the myelon was seen in 21 cases (30%) and a prevertebral haematoma was detected in 19 cases (26.8%). Signal alterations appeared in 97 intervertebral discs. MR imaging detected in 60/97 cases intradiscal bleedings (61.9%), herniations in ventral position were seen in 29.9% (29 cases), in medial position 44/97 (45.4%) and 5/97 (5.2%) in dorsal position. Stripping of the anterior longitudinal ligament (ALL) was seen in 56.3%, the posterior longitudinal ligament (PLL) was stripped in 28.2%.

Conclusion: MR imaging as a non-invasive method detects fractures and associated traumatised discs and ligament injuries and is essential for surgical treatment.

B-009 11:42

Traumatic injuries of the pelvis and thoracic and lumbar spine. Does thin-slice multidetector-row CT increase diagnostic accuracy?

C. Herzog, M.G. Mack, S. Zangos, W. Schwarz, K. Eichler, L. Thomas, T.J. Vogl; *Frankfurt a. Main/DE*

Purpose: To evaluate different multidetector-row CT (MDCT) strategies for adequate classification of spinal and pelvic injuries.

Material and Methods: 70 intubated patients after multiple trauma underwent conventional radiography (CR) and MDCT. Examinations included the pelvis (P), the lumbar spine (LS) and the thoracic spine (TS). Conventional radiographs, 3-mm (CT5) and 5-mm scans (CT3) and 3-mm and 5-mm scans combined with MPR (CT3R/CT5R) were compared to surgery, autopsy and clinical course.

Results: MDCT led to significantly better results than CR ($p < 0.01$). Correlation coefficients were $r = 1.0$ (CT3R), $r = 0.96$ [TS] to $r = 1.0$ [P/LS] (CT5R), $r = 0.8$ [P] to $r = 1.0$ [TS] (CT3), $r = 0.80$ [P] to $r = 0.86$ [TS] (CT5) and $r = 0.3$ [TS] to $r = 0.69$ [P] (CR). Fractures were identified by CT3R in 100% of cases, by CT5R in 95%, by CT3 in 90% [P] - 100% [TS], by CT5 in 83.3% [LS] - 90% [P] and by CR in 57.1% [TS] - 87.2% [P]. Unstable fractures were identified in 100% by CT3R, CT5R and CT3, 85.7% [TS] - 100% [P/LS] by CT5 and 57.1% [TS] - 80% [P] by CR.

Conclusion: Only overlapping thin-slice multiplanar reformation allows for an adequate classification of spinal and pelvic injuries and thus is highly emphasized in patients after severe blunt trauma.

B-010 11:51

New technique to avoid an increase in CT radiation dose from metallic prostheses with automatic tube current modulation: Phantom and patient study

T. Dalal¹, S.M.R. Rizzo¹, M.K. Kalra¹, B. Schmidt², C. Suess², M.A. Blake¹, T. Flohr², S. Saini¹; ¹Boston, MA/US, ²Forchheim/DE

Purpose: To evaluate a new technique to avoid increase in CT radiation dose using automatic tube current modulation in patients with metallic prostheses.

Materials and Methods: A Plexiglas phantom with and without metallic prosthesis was scanned using fixed effective mAs (200) and combined automatic tube current modulation. In clinical evaluation, 500 abdominal-pelvic MDCT exams (Sensation 16, Siemens Medical Solution) using combined modulation were reviewed to identify 9 patients (mean age = 66 years, range = 35-86 years) with metallic prostheses. Scanning parameters included 140 kVp, image quality reference mAs

Scientific Sessions

160, 0.5 s rotation time, 16*1.5 mm detector configuration, 24 mm table feed/gantry rotation, and 5 mm reconstructed slice thickness images. Nine age- and abdominal transverse diameter-matched patients (Mean age = 56, range = 36-72) with no metallic prosthesis who underwent abdominal-pelvic CT using identical scanning parameters were included in control cohort. Two radiologists graded phantom and clinical images acquired with combined modulation on 3-point scale based on extent and severity of streak artifacts. Effective mAs were recorded for each slice in all studies. Statistical analysis included Student's t test and Wilcoxon signed rank test.

Results: No significant differences in CTDIvol and DLP values were noted with combined modulation in phantom studies with and without metallic prosthesis ($p > 0.05$). In patients, there was no significant difference in mean effective mAs and artifacts between study and control cohorts ($p = 0.49$). There was almost perfect inter-observer agreement between the two radiologists ($\kappa = 1$).

Conclusion: The new technique successfully avoids increase in CT radiation dose from metallic prostheses in both phantom studies and patients undergoing CT with automatic tube current modulation.

10:30 - 12:00

Room C

GI Tract

SS 201a

Upper GI tract cancer: Diagnosis and staging

Moderators:

A. Del Maschio; Milan/IT
K. Harris; Leeds/UK

B-011 10:30

Preoperative TNM staging of esophageal cancer: Comparison of 16-row multidetector CT (MDCT) with endoscopic ultrasonography (EUS) with correlation to the histopathological findings. Preliminary results

A. Ba-Ssalamah¹, W. Schima¹, S. Mehrain¹, A. Puespoeck¹, J. Zacherl¹, R. Sedivey¹, M. Prokop²; ¹Vienna/AT, ²Utrecht/NL

Purpose: To evaluate the preoperative staging of esophageal carcinoma with enhanced 16-row MDCT and compare the findings with results by EUS, in correlation with histopathological findings.

Materials and Methods: Twenty-three patients with esophageal carcinoma (proven by endoscopical biopsy) were preoperatively examined with a MDCT in a prone position. After distending the esophagus (gas granules) and stomach (1.5 l water) the thorax and neck were subjected to MDCT scanning with 16x0.5 mm, the abdomen with 16x1.5 mm and using an individualized contrast injection protocol based on a bolus tracking techniques. EUS were performed using a fibre-optic endoscopy with a 5-10 MHz electronic array and a 360° scanning angle. Our MDCT staging criteria were drawn from a careful review of literature and from personal experience and we used the TNM classification by the AJCC 1987.

Results: Both modalities detected all tumors with a sensitivity of 100%. T staging by MDCT and EUS reached accuracies of 79% and 89%. The diagnosis of local node involvement by MDCT was correct in 76% and in EUS in 82%. The evaluation of distant node involvement and other metastases reached an accuracy of 92% with MDCT and 65% with EUS.

Conclusion: Non-invasive MDCT does provide valuable information in the preoperative staging of esophageal carcinoma producing results which are comparable to EUS results.

B-012 10:39

Preoperative staging of gastric cancer: Value of hydro-enhanced multidetector CT in comparison to endoscopic ultrasound and surgical correlation

A. Ba-Ssalamah¹, W. Schima¹, S. Mehrain¹, J. Zacherl¹, A. Puespoeck¹, B. Happel¹, R. Sedivey¹, P. Pokieser¹, M. Prokop²; ¹Vienna/AT, ²Utrecht/NL

Purpose: To assess the utility of hydro-multidetector CT (HMCT) in the preoperative staging of gastric cancer in comparison to endoscopical ultrasonography (EUS) with post-operative histopathological correlation.

Material and Methods: HMCT and EUS examinations were performed in 57 patients with gastric cancer diagnosed by biopsy prior to surgery, on two different days. Distention of the stomach was achieved with 1 to 1.5 l of water. The HMCT- and EUS-findings were prospectively analyzed. Each case was staged according to the TNM classification and correlated with histopathological findings. HMCT scans were performed with a 16 channel scanner. EUS were performed using a fiber-optic endoscopy with a 5-10 MHz electronic array and a 360° scanning angle.

Accuracy of TNM-staging was calculated for each modality and findings of EUS and HMCT were directly compared to each other and correlated with histopathological findings.

Results: The accuracy for T staging with HMCT was 84%, for N staging 79% and for M staging 97%. The results of EUS were 90%, 69% and 43%. The correct classification was most difficult for CT in differentiating between T2 and T3.

Conclusion: Noninvasive HMCT of the stomach represents a valuable tool for the preoperative staging of gastric cancer. In cases of advanced gastric cancer the full extent of the disease is better visualized with CT than with EUS.

B-013 10:48

FDG PET/CT in staging of esophageal carcinoma

C. Thuerl, D.B. Husarik, G.K. von Schulthess, T.F. Hany; Zürich/CH

Purpose: To evaluate the diagnostic accuracy of FDG PET/CT in staging of esophageal carcinoma.

Material and Methods: Retrospective analysis of 16 patients (11 male/ 5 female, average age 58.5 years) with biopsy- proven carcinomas of the esophagus (EC) who underwent FDG PET/CT (standard dose of 370 MBq F-18 FDG, non-contrast enhanced low-dose CT for attenuation correction and image fusion) and conventional imaging studies for staging. Conventional imaging studies included endoscopic ultrasound (EUS) for T and N staging and contrast enhanced CT. PET/CT were read in consensus by two radiologists/nuclear medicine physicians blinded to the clinical information. Analysis included assignment to N- and M-stage.

Results: In all but one patient, FDG-PET/CT demonstrated the correct localization of the primary tumor. In all patients (n = 16) periesophageal lymph node metastases were suspected in EUS. In only three patients pathological periesophageal FDG-uptake in lymph nodes was observed and in five patients, distant metastases (M1a or M1b) were observed. 4 out of these 5 patients presented with pathological FDG-uptake in celiac lymph nodes (M1a). One patient showed pathological FDG-uptake in periportal lymph nodes.

Conclusion: Periesophageal lymph node staging cannot be improved by PET/CT in EC. Distant metastases, including celiac lymph node metastases, can reliably depicted by PET/CT.

B-014 10:57

The down staging evaluation of neo-adjuvant therapy for advanced esophageal cancer using volume rendered 3D-enhanced CT

S. Okazumi, K. Shuto, Y. Yoshinaga, H. Shimada, H. Matsubara, Y. Nabeya, Y. Gunji, T. Ochiai; Chiba/JP

Purpose: Using enhanced CT with full scale volume rendering analysis, the evaluation of the histological responses of neo-adjuvant therapy for advanced esophageal cancer were performed, and a diagnostic image for the evaluation of down staging was developed.

Methods and Materials: 53 cases of advanced esophageal cancer (pathologically diagnosed T3: 39, T4: 14) were examined. Contrast media (300 mg iodine/ml, 3 ml/kg) was administrated intravenously (3 ml/sec). CT (SIEMENS SOMATOM plus4) scans were performed (slice thickness: 2 mm) at 50 seconds delay. For creating the diagnostic image a SIEMENS 3D-VIRTUOSO was used as the workstation for image reconstruction and the area of complete response was expressed with specially selected colors and opacities. Simultaneous 3-dimensional images displaying inner esophageal or airway spaces, and outer solid organs were obtained. The diagnostic results were compared with the histological findings of specimens after surgery.

Results: The enhanced CT values significantly decreased after the therapies according to the histological responses ($p < 0.01$). As the result of the evaluation of down staging using the newly developed diagnostic image for the area of complete response, 100% of the positive predictive value, 97.4% of the negative predictive value and 98.1% of the overall accuracy were obtained. Especially, the estimation of invasion to the airway, pulmonary vein and pericardium, which were difficult with conventional methods, were markedly improved.

Conclusions: The qualitative diagnosis using an enhanced CT volume rendering method is useful to evaluate the histological response to neo- adjuvant therapy for advanced esophageal cancer.

Scientific Sessions

Friday

B-015 11:06

Computed tomography for assessing the resectability and restaging TNM classification of esophageal carcinoma treated with pre-operative radiotherapy

G. Guo, C.H. Zang, Z.X. Lin, X.G. Zhou, R.H. Wu; Shantou/CN

Purpose: To evaluate the resectability and restaging for patients with esophageal carcinoma treated by radiotherapy using CT scan.

Methods: CT scans of 46 patients with squamous cell esophageal carcinoma treated by pre-operative radiotherapy were analyzed before operation. The aortic invasion, tracheobronchial invasion and positive lymphatic nodes were assessed respectively and compared with the pathologic data. Twenty-six cases had both pre- and post-radiotherapeutic CT data. The changes in aortic invasion, triangle-space, tracheobronchial invasion and lymphatic nodes between pre- and post-radiotherapy were compared.

Results: The accuracy, sensitivity and specificity of CT assessment for patients with esophageal carcinoma treated by radiotherapy in aortic invasion was 80%, 70%, and 88%; in tracheobronchial invasion was 91%, 89% and 94%; and in thoracic positive lymphatic metastases was 86%, 67% and 94%, respectively. There was significant difference in T down-staging between pre- and post-radiotherapy, but no significant difference in N down-staging.

Conclusion: CT was very helpful in restaging TNM classification in pre-operative patients with esophageal carcinoma treated by radiotherapy. The T classification of patients with esophageal carcinoma would be down-staged after radiotherapy. However, the N classification would not. An interval of 3-4 weeks between completion of radiotherapy and operation was recommended.

B-016 11:15

Hydro-multidetector CT in patients with gastric and duodenal lymphoma: Correlation with histopathological results

M. Uffmann¹, A. Ba-Ssalamah¹, C. Schaefer-Prokop¹, S. Mehrain¹, M. Raderer¹, M. Prokop²; ¹Vienna/AT, ²Utrecht/NL

Purpose: To evaluate the performance of hydro-multidetector CT for the characterization of gastric and duodenal lymphoma.

Methods and Materials: We examined 21 patients with endoscopically detected lymphoma using hydro-CT technique. Immediately prior to the examination, the stomach was distended by 1-1.5 l flavoured methylcellulose, and a spasmolytic i.v. agent was administered. The upper abdomen was scanned first with 4x1 mm or 16x1 mm using an individualized contrast injection protocol, followed by a scan of the lower abdomen and the chest for staging of the entire trunk. Interactive multiplanar reformations were used for reading. CT findings were evaluated and correlated with histopathological results.

Results: 12 patients had aggressive lymphoma (9 with diffuse large cell lymphoma, DLCL; 2 with aggressive follicular lymphoma; 1 with T-cell lymphoma). In this group, the thickness of the affected gastric wall ranged from 1 to 17 cm (mean 4.6 ± 5.8 cm). The tumour growth pattern was nodular (n = 6), circular (n = 3) or diffuse (n = 3). In 7 out of the 12 patients, the corpus was affected. 9 patients had indolent lymphoma (7 with gastric MALT lymphoma; 2 with indolent follicular lymphoma of the duodenum). The tumor growth pattern was homogeneous (n = 4) or circular (n = 3), with subtle to moderate wall thickening (0.5 to 1.5 cm, mean 0.9 ± 0.4 cm). In 2 patients with MALT lymphoma, the gastric wall was unremarkable.

Conclusions: For evaluation of gastric and duodenal lymphomas, hydro-multidetector CT is a valuable addition to regular CT-staging. It does not allow the characterisation of different histopathological types, but may assist in the differentiation between aggressive and indolent lymphoma.

B-017 11:24

Lymphoma of the colon: The spectrum of radiological changes

R. Ananthasivan, S. Fataar, A. Derweesh; Muscat/OM

Objectives: Lymphoma of the colon constitutes less than 1% of large bowel malignancies and yet is the second most common malignant disease of the colon. The aim of this study is to present the spectrum of radiological findings in colonic lymphoma.

Materials and Methods: We retrospectively reviewed the radiological investigations in patients with lymphoma of the colon referred to our institution over five year period.

Results: Colonic lymphoma may be either focal or diffuse in form. Caecum and/or ascending colon was the most common site involved, followed by the rectum. Focal forms included gross mural circumferential thickening of the bowel wall, sometimes accompanied by aneurysmal/paradoxical dilatation of the bowel lumen,

polypoid mass, intussusception, annular "apple-core" sticture, mucosal nodularity and mucosal fold thickening. Diffuse forms manifested as irregular thickening of the folds, extensive mucosal ulceration or multiple polypoid protrusions of the entire colon mimicking polyposis. Concomitant enlargement of the aortic, coeliac or retroperitoneal lymph nodes or extension to the surrounding tissues suggests a poor prognosis. An attempt was made to represent pictorially the spectrum of radiological findings in colonic lymphoma.

Conclusion: The imaging findings of colonic lymphoma are quite variable and overlap with other colonic pathology, yet there are some characteristics which help in the radiological diagnosis. Biopsy is required both for confirming the diagnosis and for a more detailed pathological classification.

B-018 11:33

Differentiation of gastric wall thickness between normal and gastric cancer on hydro-multislice CT

Y. Jeong, J. Oh, J. Seo, J. Park, H. Kang; Gwang Ju/KR

Purpose: The purpose of this study was to evaluate the wall thickness of normal and gastric cancer on hydro-MSCT.

Materials and Methods: 122 patients with gastric cancer diagnosed by endoscopic biopsy were scanned by MSCT (Light Speed QXi, GE). The stomach was optimally distended by 1,000 ml water. After administration of 130 ml of nonionic contrast material at 3 ml/sec, arterial and portal venous phases were obtained at 2.5 mm slice thicknesses. One radiologist measured the thickness of normal fundal, body, antral and pyloric wall (n = 488) and the involved wall by gastric cancer (n = 122) on PACS monitor. Two radiologists reviewed the presence of layering and enhancement pattern of the gastric wall.

Results: The mean wall thickness of normal stomach is 2.4 mm (range, 0.5-7 mm). The mean wall thickness of EGC (n = 67) and AGC (n = 55) is 8.9 mm (range, 3.1-17.5 mm) and 11.9 mm (range, 5.6-29.5) respectively. The finding of gastric wall thickness of 5 mm or greater had sensitivity of 90% and specificity of 57% for EGC and a sensitivity of 100% and specificity of 98% for AGC. Although gastric wall thickness on EGC is less than 5 mm, focal or eccentric wall enhancement showed a specificity of 67% and a sensitivity of 94%.

Conclusion: Gastric wall thickness of 5 mm or greater on hydro-MSCT may be a useful indicator for diagnosis of AGC, but not for diagnosis of EGC. Focal or eccentric wall enhancement is more important than gastric wall thickening only in the detection of EGC.

B-019 11:42

High resolution MR imaging of oesophageal cancer with pathological correlation

A.M. Riddell, J. Hillier, D.M. King, A. Wotherspoon, G. Brown; London/UK

Purpose: Currently EUS has higher accuracy than CT for local staging of oesophageal cancer (at 60-80%), but has limitations; restricted sonographic view, reduced accuracy post chemotherapy and failure in up to 20% for stenotic tumours. High resolution MR imaging can potentially delineate tumour and surrounding anatomic structures. Our study aims were: (1) To determine whether anatomical structures and tumour are clearly depicted on MR imaging and (2) To validate accuracy by correlating MR imaging measurements with pathology.

Method: Ten patients with oesophageal carcinoma underwent MR imaging prior to surgical resection. High resolution T2W axial images through the oesophagus were acquired and images matched with histology sections. Three radiologists blinded to histology reports reviewed the MR images. For each image, tumour appearance and location, together with measurements of normal wall and tumour thickness were noted and correlated with histology. Interobserver variability was assessed by analysing repeatability of measurements between different readers.

Results: 50 images had corresponding histology. All readers correctly located tumour in 8 patients; pathology for the other 2 revealed only microscopic disease. Tumour returned intermediate signal intensity distinct from normal tissue. Mean difference between MR imaging and histology for measurements of wall and tumour thickness (in mm) was: 0.54 ($SD \pm 4.19$), 0.86 ($SD \pm 3.93$) and 1.01 ($SD \pm 4.11$) respectively for the 3 readers. Mean difference in measurements between readers ranged from 0.2 to 0.47 mm.

Conclusion: High resolution MR imaging of oesophageal cancer provides detailed imaging of the tumour and surrounding anatomical structures thus confirming the potential as an alternative method of local tumour staging.

Scientific Sessions

B-020 11:51

Efficacy of multidetector row CT in staging gastric cancer according to the Japanese classification of gastric carcinoma

M. Mazzei, D. Marrelli, E. Pinto, L. Pirtoli, L. Volterrani; Siena/IT

Purpose: To correlate high resolution multidetector row CT with pathological findings in T and N-staging gastric cancer according to the Japanese classification of gastric carcinoma.

Methods and Materials: 44 patients with gastric carcinoma underwent preoperative multislice-CT after drug induced hypotonia and gaseous distention of the stomach. Contrast-enhanced CT after i.v. administration of 160 ml of iodinated contrast media at 4 ml/s and 50-55 sec delay, were acquired at 2.5 mm of slice thickness, 0.8 mm reconstruction interval and a 0.6 s rotation time. The examination was performed from the diaphragmatic domes to the pubis. Precontrast scanning was not performed. Regional lymph nodes were considered involved when the short-axis diameter was > 5 mm for the lymph nodes of group 1 and > 8 mm for the lymph nodes of other groups according to location of the tumor and Japanese classification of gastric carcinoma. All patients underwent laparotomy resection of the primary gastric tumor with complete lymph node group dissection.

Results: Regarding T-stage, in 36/44 (81.8%) there was a good correlation with histological results. Regarding the N-stage a good correlation with pathologic results occurred in 38/44 (86.36%) patients.

Conclusion: Multidetector-row CT improves the accuracy of preoperative staging of gastric cancer according to the Japanese classification of gastric carcinoma and the results can be used to optimize the therapeutic strategy for each individual patient prior to surgery.

10:30 - 12:00

Room E2

Breast

SS 202

New developments in breast imaging

Moderators:

F. Diekmann; Berlin/DE
A. Tardivon; Paris/FR

B-021 10:30

Breast MR adding single-voxel proton spectroscopy to dynamic imaging

A. Fausto, F. Sardanelli; Milan/IT

Purpose: To evaluate feasibility and gain in specificity of breast proton MR spectroscopy (1H-MRS) added to dynamic MR imaging (D-MRI).

Methods and Materials: Thirty-seven patients underwent breast D-MRI (1.5 T) using 128 T1-weighted 3D gradient-echo coronal 1 mm partitions (1 mm³ voxel) with 0.1 mmol/kg Gd-DOTA and 120-s resolution (1 pre- and 4 postcontrast). Thereafter, water- and fat-suppressed spin-echo (TR/TE = 1500/136 ms) single-voxel 1H-MRS was obtained for 16 malignancies, 15 benign lesions and 10 normal glands. An intensity cholin peak (Cho) integral at 3.2 ppm equal or higher than 2.0 was considered as a marker of malignancy. D-MRI was interpreted integrating morphologic and dynamic parameters.

Results: Examination time: D-MRI, 10'; 1H-MRS, 7-19 minutes (adjustments, 6'; acquisition 1'36"-13'). No reliable spectrum (low signal-to-noise ratio) was obtained in 3 cases (2 IDCs and 1 benign enhancement). Acceptable spectra were obtained in 38 cases with a median voxel size of 2.2 cc (3.0 ± 2.3 cc). The only false negative at 1H-MRS was a DCIS (Cho 1.42). In the remaining 13 malignancies, median Cho was 3.2 (range 2.0-7.45); 3 false positive cases had a Cho of 12.6 (inflamed lymph node), 9.0 (dysplasia), and 2.3 (benign contrast enhancement); in 21 benign cases, Cho was not distinguishable from noise. Sensitivity was 93% (13/14) for both D-MRI and 1H-MRS, specificity 75% (18/24) and 88% (21/24), respectively, giving a 13% gain in specificity.

Conclusions: Single-voxel 1H-MRS can be performed as a final step after D-MRI and seems to give an interesting gain in specificity.

B-022 10:39

Influence of vascularization of breast lesions on electrical conductance and detection rate using EIS

A. Malich¹, M. Facius¹, J. Boettcher¹, M.G. Freesmeyer², B. Scholz³, W.A. Kaiser¹; ¹Jena/DE, ²Halle/DE, ³Forchheim/DE

Purpose: Currently electrical impedance scanning (EIS) despite its advantages (handling, applicability, no side effects, lack of radiation) is limited in its clinical

relevance due to high number of false positives. Whereas superficial artifacts play a major role inducing these FP, other factors do cause these FP-value furthermore. This study is aimed to analyze whether hypervascularization causes these focal enhanced electrical values as well.

Methods and Materials: All patients undergoing an EIS (TS2000, TransScan, USA) and a MRM-examination (ACSI, Philips, Netherlands), who finally were histopathologically verified or had a follow-up of > 1 year were included. Dynamic enhancement was scored: D1=strong; D2=moderate; D3=similar to glandular tissue; D4=no or subtle enhancement. Type of enhancement was correlated to histopathological outcome and EIS-performance (Chi-Square-Testing).

Results: 88/113 malignant and 107/182 benign findings were correctly detected in EIS (S = 79%; Sp = 59%). MRM was not possible due to contraindications in 17 cases. MR correctly detected 101/104 malignancies and 141/174 benign lesions (S = 97%; Sp = 81%). 22/55 benign lesions with D1 were correctly negative in EIS (44.4%), whereas this value was 82/119 for D2-4 (68.9%, p < .01), being highest in D4 (75%). Taking into account only fibrotic/fibroadenomatous tissue, 10/23 lesions with D1 were correctly unsuspicious and 29/37 lesions of same histology with D2-4 were correctly unsuspicious (43.5% vs. 78.4%, p < .01).

Conclusion: Although impedance scanning uses low frequencies up to 5 kHz, vascularization of the lesion influences the measurable conductance and, thus, induces false positive results in highly vascularized benign lesions.

B-023 10:48

The negative predictive value of electrical impedance scanning in BI-RADS IV breast lesions

M.H. Fuchsäger, D. Flöry, M. Philipp, C.C. Riedl, J. Sylvia, T.H. Helbich; Vienna/AT

Purpose: To assess the value of electrical impedance scanning (EIS) as negative predictor in breast lesions classified as probably malignant (BI-RADS IV) in mammography.

Methods and Materials: EIS (TransScan TS2000, TransScan Medical, Israel, Siemens-Elema, Sweden) was performed on 184 BI-RADS IV lesions in 169 women (51.5 ± 8.1 yrs) using the targeted mode after sonographic and / or mammographic localization. The current EIS-software 2.67 calculates a BI-RADS-like level of suspicion (LOS) on a 5-grade scale (1-negative, 2-benign finding, 3-probably benign finding, 4-suspicious abnormality, 5-highly suggestive of malignancy). LOS 1, 2 and 3 were considered as negative. LOS 4 and 5 were considered as positive. Histopathologic results were obtained in all lesions.

Results: Histology proved 57 lesions to be malignant, 127 benign. Sensitivity, specificity and accuracy rates, PPV and NPV were, respectively, 92.9%, 59.8%, 70.1%, 50.9% and 95.0%.

Conclusion: Our results suggest that EIS is an useful adjunct to mammography in the evaluation of BI-RADS IV breast lesions. With a NPV of 95%, EIS may reduce unnecessary interventions in benign lesions and therefore also minimize costs and patients morbidity, which could occur in a short-time follow-up.

B-024 10:57

Elastosonography of benign and malignant nodular breast lesions

A. Martegani, F. Clarizia, G. Rossini, C. Borghi, C. Del Favero, R. Campi; Como/IT

Purpose: To evaluate if elastosonography can play a significant role in the diagnosis of breast nodular lesions.

Methods: 76 patients, affected by a total of 89 nodular lesions (benign and malignant), were enrolled in our study from January 2004 to August 2004. Each patient was submitted to ultrasound examination followed by elastography, both performed by EUB-8500/Logos-Hitachi/Esaote-Japan, equipped with different linear electronic 7.5-13 MHz transducers. A dedicated device was applied to the transducer in order to improve the contact with skin. The elastographic scan required a short training for the operator; the entire elastographic scan acquisition required generally only few minutes to be performed (2-5 minutes). Breast nodules were classified according to the morphological elastographic Ueno scores. Cytohistologic biopsy, surgical specimen and follow-up were considered as gold standard.

Results: Some reproducible elastographic patterns were found both in cystic lesions and in large (> 2 cm) malignancies. Sensitivity, specificity, positive predictive value, negative predictive value and accuracy were respectively 82.2, 97.7, 97.3, 84.3, 89.8% considering 4-5 score as cut off values and 97.7, 86.4, 88, 97.4 and 92.2% considering 3-5 score as cut off value. A statistical analysis considering the reliability of the method according to lesion diameter (< 1 cm, 1-2 cm, > 2 cm) was performed as well. Elastographic behaviour of small benign and malignant nodules (up to 1 cm) was more uniform compared to those larger than 2 cm.

Scientific Sessions

Conclusion: Elastography demonstrates a high diagnostic accuracy in characterising breast nodular lesions, especially if smaller than 2 cm.

B-025 11:06 ♀

Real-time ultrasound elastography: Diagnostic tool or electronic gadget?

M. Locatelli, R. Chersevani, G. Rizzato; Gorizia/IT

Purpose: To assess the accuracy of in vivo ultrasound elastography in the evaluation of nodular benign and malignant breast lesions.

Methods and Materials: Ninety-seven breast lesions from 68 patients were studied with the EUB 8500 Logos ultrasonic unit (Hitachi, Japan) and a linear array transducer of 7.5-13 MHz. In 54% of lesions we obtained a pathologic diagnosis. All the other cases were well known benign lesions that we had monitored for at least two years. The elastic score was classified according a five-point color scale. The size of the lesions obtained by conventional B-mode was compared with the elastographic size.

Results: 25 lesions resulted as very stiff and 23 of them turned out to be malignant (92%). 19 masses were classified as soft-mixed areas and 16 were fibroadenomas (84%). Typical three-layered areas were found in 93% of cysts. In 21 cases the estimated diameter of the lesion was greater with elastography than with B-mode; most were tumoral masses with infiltrating pathological behaviour. The exam was hampered in 4 cases (5.8%) because of the extremely stiff breast or because the lesion was located in a marginal area with insufficient surrounding tissues.

Conclusions: Real-time elastography is a very quick and easy to perform diagnostic tool. Its online availability helps to increase the diagnostic confidence and to reduce unnecessary biopical procedures in benign masses. Its ability to compare a lesion with the surrounding tissues might also be tested in the evaluation of the therapeutic efficacy for both tumors and inflammation.

B-026 11:15

Multislice galacto-CT versus galactography in the evaluation of nipple discharge

L. Bacigalupo, D. Brizzi, G. Baio, C. Faedda, G. Gaggero, M. Calabrese; Genoa/IT

Purpose: To compare multislice galacto-CT (MSGCT) with galactography (GG) in the evaluation of single lactiferous duct discharge.

Methods and Materials: 16 patients have undergone GG (Siemens, Mammomat) with the intraductal injection of 2 ml of iodinated contrast media (CM). Then, with the iodinated contrast media still inside the duct, the 16 patients have undergone 1 contrast-enhanced MSGCT (Siemens, Somatom sensation 4) acquisition. All the MSGCT examinations have been post-processed with MIP and MPR reconstructions. Both procedures have undergone dosimetric controls.

Results: GG has individuated 5 single intraductal papillomas, 3 multiple papillomatosis, 7 stops to contrast media progression and 1 galactophoritis. MSGCT has confirmed the results of GG in 10 cases. In the remaining 6 cases it has modified the results of GG: 2 cases that appeared as single papillomas at GG (distal stop at CM progression), at MSGCT showed multiple papillomatosis; 3 cases that appeared as proximal stops at CM showed on MSGCT as 1 single papilloma and 2 multiple papillomatosis; in 1 case in which at GG we had observed a proximal stop at CM, at MSGCT showed 1 papilliferous carcinoma and a multiple papillomatosis in different quadrants. The mean glandular dose for the GG was 7.6 mGy, for the MSGCT 10 mGy.

Conclusion: From our preliminary experience MSGCT appears to be a valid alternative to GG, in particular in the evaluation of stops at GG. Furthermore MSGCT glandular mean dose appears comparable to the one of GG.

B-027 11:24

Complementary role of CT-laser-mammography (CTLM) to mammography and ultrasound in patients with breast lesions

D. Floery, C.C. Riedl, S. Jaromi, M.H. Fuchsjaeger, W.K. Matzek, G. Heinz-Peer, S. Leodolter, T.H. Helbich; Vienna/AT

Purpose: To assess the value of Computed Tomography Laser Mammography (CTLM) as an adjunct to mammography (MG) and ultrasound (US) in the detection of malignant breast lesions.

Methods and Materials: In a prospective study, CTLM scans (CTLM scanner Model 1020 by IMDS, Inc. FL), MG and US of 292 patients with 300 breast lesions were obtained. Histopathological diagnosis (biopsy and/or surgery) was performed in all cases. The CTLM images were read as an adjunct to MG and US.

Results: Of 300 lesions, 132 (44.0%) were malignant and 168 (56.0%) benign including 70 invasive ductal carcinoma (IDC), 18 invasive lobular carcinoma (ILC), 35 ductal carcinoma in situ (DCIS) and nine cancers of other types. CTLM achieved

a sensitivity of 64.4% (85/132 true positive) and a specificity of 55.4% (93/168 true negative). Positive and negative predictive value were 54.0%, and 65.6% respectively. Sensitivity, specificity, PPV and NPV were 92.8%, 40.4%, 56.2%, and 87.2% for MG and 65.4%, 53.0%, 53.0%, and 65.4% for US.

Conclusion: The present results indicate that CTLM may have potential adjunctive value to MG and US in the diagnosis of breast cancer.

B-028 11:33

The value of imaging angiogenesis in breast cancer: Is "benign" angiogenesis a diagnostic problem?

E.N.C. Milne; Plantation, FL/US

Purpose: Mammography is fundamentally a triage procedure to decide whether to biopsy. Its results are poor, 40 to 80% of biopsies being negative. Our aim is to reduce the percentage of negative biopsies.

Materials and Methods: Computed tomographic laser mammography, (CTLM), uses the same mechanical principles as X-ray CT. The laser, tuned to 808 nm, selectively visualises hemoglobin to demonstrate normal vessels and angiogenesis. Each of 700 patients received a mammogram, and a CTLM, and 445 were biopsied.

Results: 81 of 445 biopsies were positive. Adding CTLM to mammography did not change sensitivity but increased specificity by over 20% and reduced the percentage of negative biopsies by 42%. Of 351 benign cases with detailed pathology, 23% showed some evidence of angiogenesis as follows. Fibroadenomas (78) 27%, Mastitis (78) 25%, Fibrosis (26) 23%, Apocrine metaplasia (19) 21%, Normal Tissue *(39) 18%, Fibrocystic disease (108) 12%, Cysts (43) 9%, Adenosis (34) 9%. *The "angiogenesis" in 'normal' tissue was not related to hormonal effects but to involution of portions of the breast leading to 'redistribution' of blood flow to normal parenchyma. Benign angiogenesis is not of great clinical import. It does not result in false negatives but simply in a failure to save those cases from biopsy.

Conclusion: Imaging angiogenesis is a valuable approach to reducing negative biopsies but, to assist in the decision whether to biopsy, should be combined with prior imaging and clinical data.

B-029 11:42

Effect of acquisition geometry and radiation dose on lesion visibility in full field breast tomosynthesis

A.P. Smith, G. Hitzke, C. Ruth, B. Ren, Z. Jing, N. Gkanatsios, J. Stein; Bedford, MA/US

Purpose: Clinical use of breast tomosynthesis requires optimization of parameters such as view orientation, scan angles and dose. We have studied the effects of acquisition geometry and patient dose on the conspicuity of lesions and microcalcifications.

Methods and Materials: Patients referred for diagnostic mammography underwent tomosynthesis scans on a modified Selenia full field digital mammography system. Patients and phantoms were acquired with a variety of scan angles, number of views and total radiation dose. Reconstructions were evaluated and rated on feature conspicuity and overall image quality.

Results: Scans angles were varied from 10 to 30 degrees. Number of views ranged from 4 to 11. Doses for a 4.5 cm breast ranged from 1.5 to 5 mGy. For each case, images were reconstructed into 3D volumes with slice separation of 1 mm. Objects with non-zero thickness showed contrast improvement as the scan angle decreased, which also increased the depth of field. Shadows from out-of-plane objects increased as the scan angle decreased and decreased with more views for reconstruction. Individual microcalcification sharpness was mainly independent of scan angle, but cluster visualization improved at smaller scan angles. Similar to 2D digital mammograms, image noise is clearly a function of radiation dose. However, there appears to be a lesser effect of radiation dose on the visibility of lesions.

Conclusions: Many variables affect tomosynthesis acquisitions. Our preliminary results are directing clinical trials to further optimize the system. System design allows technique selection to favor either sharpness or contrast while keeping dose fixed.

B-030 11:51

Contrast-medium enhanced mammography: A twofold approach

P. Baldelli¹, A. Bravin², E. Fabbri¹, M. Gambaccini¹, M. Marziani¹, A. Sarnelli¹, A. Taibi¹; ¹Ferrara/IT, ²Grenoble/FR

Purpose: The aim of the work is to investigate the use of a contrast medium in mammography.

Methods and Materials: There are two different techniques to enhance the

Scientific Sessions

radiographic signal of contrast media. The first one - Contrast enhanced dual energy mammography (CEDEM) - is based on the acquisition of two images at different energies after the contrast medium injection. By combining these images, hybrid images are obtained in which the contrast of relevant structures is preserved while unwanted tissue contrast is largely removed. The second one - K-Edge Subtraction Mammography (KESM) - is based on the K-edge absorption of the contrast medium. Two images are obtained from those acquired at energies below and above the k-edge. The first one is the contrast-medium-concentration map and the second one is the distribution of all other tissues. Experiments have been performed using both conventional systems and monochromatic radiation. A three component phantom with iodine filled details has been developed. A simulation study has been carried out in order to study the relationship between the contrast medium concentration and the SNR achievable on the resulting image.

Results: The SNR (Signal-to-noise-ratio) as a function of the dose to the patient and of the contrast medium concentration has been taken as figure of merit for comparing CEDEM and KESM.

Conclusion: Results of simulations and radiographic tests are in good agreement and show the potential of the two techniques to improve the detection of small details.

10:30 - 12:00

Room F1

Chest

SS 204

Pulmonary nodule: Detection and significance

Moderators:

P. Armstrong; London/UK

N. Howarth; Chêne-Bougeries/CH

B-031 10:30

Incidental finding of primary lung cancer in patients with atherosclerotic disease: Single-centre retrospective evaluation of MDCT angiography studies over the past three years

A. Napoli, C. Catalano, P.G. Nardis, M. Cavacece, L. Bertoletti, F. Fraioli, R. Passariello; Rome/IT

Purpose: To retrospectively evaluate the incidence of primary lung cancer in patients with symptomatic atherosclerotic disease, undergoing multi-detector row CT (MDCT) angiography.

Materials and Methods: From January 2001 until May 2004, 832 CTA examinations were evaluated. Relevant atherosclerotic disease was observed in 712 patients (158 women and 554 men; age 35-92). CTA was required for carotid arteries stenosis (n = 277), thoraco-abdominal aortic aneurysm (n = 38), thoracic aortic aneurysm (n = 31), abdominal aortic aneurysm (n = 186) and lower extremity arterial disease (n = 180). Scan volume, depending on vascular region, always included: the lung apices and lung bases respectively in the examination of carotid arteries and the abdominal aorta and run off vessels and the entire lung when examining thoracic aorta. Biopsy was performed in each patient with suspected lung nodules. Study population incidence was compared with healthy subjects aged more than 65 years old.

Results: Lung cancer was found in 17 patients, 11 men and 6 women. The incidence of primary lung cancer in our study population was 2.4% with an increased relative risk, compared with healthy subjects, of as much as 8.6-fold for primary lung cancer. When considering each sex separately, we found 2.3% incidence in males and 3.8% in females, where the relative risk was as high as 3.5-fold and 64.6-fold respectively.

Conclusion: Our study showed a higher incidence of primary lung cancer in patients with symptomatic atherosclerotic disease, particularly in female patients. These results might suggest extending the CT scan for vascular patients to include the entire lung parenchyma by means of a very low dose.

B-032 10:39

Chest X-ray vs. multislice CT performed at identical radiation doses for detection and characterization of pulmonary nodules

U. Zaspel, V. Romano, P. Hein, B. Hamm, P. Rogalla; Berlin/DE

Purpose: To compare chest X-ray and multislice CT (MSCT) using identical radiation doses for detection and characterization of pulmonary nodules.

Material and Methods: 42 consecutive patients (age range: 22-87) underwent chest X-ray (pa and lat: 28, pa:14), followed by a minimized-dose chest MSCT (time interval ranged: 1-32 days), performed at 3.5 eff. mAs, 120 kV, collimation 16*1 mm (Toshiba Aquilion), resulting in a dose identical to chest X-ray (0.2 mSv).

Images were reformatted in axial, coronal and sagittal planes. Two experienced radiologists evaluated both studies in consensus (minimum time interval between X-ray and CT: 7 days) with regard to number, size, location, shape and characterization of nodules. Diagnostic confidence in detection and characterization was ranked along a scale from 1 (min) to 10 (max).

Results: Correlation for identifying patients with nodules was 0.43 (kappa) ($p = 0.05$). A total of 52 pulmonary nodules (mean 1.2 per patient, range: 0-10) were diagnosed with chest X-ray and 136 pulmonary nodules (mean 3.2 per patient, range: 0-20) using MSCT (paired Wilcoxon U-test $p = 0.001$). CT classified 59 nodules as benign, 74 as malignant and 3 as undetermined. Chest X-ray categorized 7 nodules as benign, 37 as malignant and 8 as undetermined. Confidence in detection was significantly higher on CT than on chest X-ray ($p < 0.001$) as was the characterization of nodules ($p < 0.001$).

Conclusion: MSCT of the chest performed with X-ray dose detects more nodules at higher diagnostic confidence than chest X-ray and may serve as alternative in patients with suspected pulmonary nodules without an increase in dose.

B-033 10:48

MR imaging of the lung: Comparison of turbo-spin-echo and 3D gradient-echo pulse sequences for the detection of pulmonary metastases

M. Bruegel, J. Gaa, K. Woertler, C. Ganter, S. Waldt, K. Marten, C. Engelke, E.J. Rummeny; Munich/DE

Purpose: Suitable MR pulse sequences for imaging of the lung have become important due to increasing interest in whole-body MR imaging for tumor staging in oncology. We compared different MR pulse sequences for imaging of the lung with respect to lesion detectability in patients with pulmonary metastases.

Material and Methods: 16 patients with pulmonary metastases detected by multislice CT (MSCT) underwent MR imaging of the lungs at 1.5 T. MR imaging included breath-hold T2-weighted TSE, IR-TSE, HASTE and IR-HASTE sequences, a respiratory- and pulse-triggered black-blood-prepared T2-IR-TSE sequence and T1-weighted volumetric interpolated breath-hold (VIBE) 3D-GRE sequences (pre- and post-Gd-DTPA). MR pulse sequences were analyzed quantitatively and qualitatively. MSCT served as the gold standard.

Results: Mean lesion-to-lung contrast-to-noise ratios were highest with T2-TSE (57 ± 12) and post-contrast-VIBE (41 ± 11) and lowest with T2-IR-HASTE (12 ± 4) and pre-contrast-VIBE (18 ± 5). Respiratory/pulse-triggered T2-IR-TSE and pre- and post-contrast-VIBE images showed the lowest rate of artifacts. Lesion conspicuity of 144 pulmonary nodules detected by MSCT was highest with respiratory/pulse-triggered T2-IR-TSE (sensitivity, 76%; PPV, 96%), followed by T2-TSE (sensitivity, 71%; PPV, 95%). With HASTE, IR-HASTE, pre- and post-contrast-VIBE significantly lower ($p < .05$) sensitivities (< 50%) were obtained. Breath-hold T2-IR-TSE produced the highest number of false-positive findings (sensitivity, 60%; PPV, 87%). Sensitivities using respiratory/pulse-triggered T2-IR-TSE were 94% and 100% regarding 5-10 mm-sized and > 10 mm-sized nodules, respectively; however, only 33% of < 5 mm-sized nodules were detected.

Conclusion: Compared to different turbo-spin-echo and 3D-gradient-echo pulse sequences for MR imaging of the lung, respiratory- and pulse-triggered T2-IR-TSE was most sensitive in the depiction of pulmonary metastases and allowed reliable detection of nodules ≥ 5 mm.

B-034 10:57

Detection of malignant pulmonary nodules: Determination of the optimal MR imaging sequence and evaluation of its performance

W. Luboldt, K. Eichler, C. Herborn, T.O.F. Wagner, H.-G. Fieguth, T.J. Vogl; Frankfurt a. Main/DE

Purpose: To determine the optimal MR imaging sequence for detecting malignant pulmonary nodules.

Materials and Methods: On the basis of 6 lung cancer, 46 metastases and one tuberculoma in 13 patients eight MR imaging sequences were compared in terms of contrast-to-noise ratio (CNR), sensitivity and quality in the visualization of pulmonary nodules. The following sequences were used: HASTE, IR-HASTE, fat saturated TrueFISP, STIR, VIBE_{ipat=2}, and contrast-enhanced (CE) VIBE with $ipat = 2, 0, 4$ and performed in high spatial resolution using parallel imaging with 12 coil elements.

Results: The STIR sequence significantly ($p < 0.01$) showed the highest CNR (mean: 22 ± 13) followed by the FS TrueFISP (CNR: 18 ± 18), CE VIBE_{ipat=0} (CNR: 17 ± 15), CE VIBE_{ipat=2} (CNR: 15 ± 17), HASTEIRM (CNR: 12 ± 10), HASTE (CNR: 9 ± 11), CE VIBE_{ipat=4} (CNR: 6 ± 7), and VIBE (CNR: 4 ± 6). The STIR sequence showed 25 of 28 nodules ≤ 5 mm and all nodules > 5 mm. The 19 mm benign nodule was nearly invisible on the STIR-sequences and showed the highest CNR on the TrueFISP, VIBE and HASTE.

Scientific Sessions

Conclusion: The STIR sequence is the optimal sequence for detecting malignant pulmonary nodules, promises not to display benign nodules, and thus, should be used in future studies comparing MR imaging with CT and PET for the early detection of pulmonary malignancies.

B-035 11:06

Evaluation of dynamic contrast enhancement pattern of solitary pulmonary nodules on 3D gradient-echo MR imaging

E. Yekeler, V. Saedi, F. Yildirim Donmez, A. Tunaci, M. Tunaci, G. Acunas; *Istanbul/TR*

Purpose: To evaluate the dynamic contrast enhancement pattern of solitary pulmonary nodules using a 3D-FLASH sequence and to investigate the predictive value of contrast enhancement features of the lesions in differential diagnosis.

Materials and Methods: 40 patients with solitary pulmonary nodules detected on CT underwent MR imaging using T1-W GRE, T2-W spin-echo, pre-contrast and 10 consecutive contrast-enhanced 3D-FLASH sequences obtained every 30 seconds. Using Mean-Curve software, a plot was drawn encircling the lesions and SNR (signal-to-noise) values were measured for each sequence. Final diagnosis of the solitary pulmonary nodules was obtained by CT-guided biopsy, operation or re-imaging after medical treatment.

Results: According to final diagnosis, 10 patients had tuberculoma (25%, size-range, 1-3 cm; mean size, 2.1 cm), 20 patients had lung cancer (50%, size-range, 0.7-7; mean size, 3.8 cm), 10 patients had round atelectasis (25%, size-range, 1-4 cm; mean size, 2.1 cm), and 3 patients had both cancer and atelectasis (7.5%, size-range, 2-4 cm; mean size, 3 cm). The contrast enhancement patterns of all the lesions were significantly different from each other. Tuberculomas had peripheral rim enhancement, round atelectasis had homogeneous intense enhancement, whereas lung cancers enhanced peripherally with slow progressive heterogeneous fill-in of the lesions on late images. Time-to-peak values were 1.6, 4, and 2 minutes for tuberculomas, round atelectasis and lung cancers respectively. Lung cancers showed wash-out after the peak on the curve, unlike the atelectasis and tuberculomas.

Conclusion: Rim contrast enhancement pattern is highly valuable in diagnosing tuberculomas. SNR values are useful in differentiating round atelectasis from other nodular lesions. Time to peak values of round atelectasis, tuberculomas, and lung cancers can be taken into consideration in differential diagnosis.

B-036 11:15

Resolving small pulmonary nodules: CT characteristics

J. Hansen¹, D. Wormanns², S. Diederich¹; ¹Düsseldorf/DE, ²Münster/DE

Purpose: Small non-calcified pulmonary nodules are common. As most of these lesions are benign, non-invasive classification is required, usually based on follow-up with CT. According to current recommendations, growing nodules should undergo biopsy, stable nodules should be followed with CT, whereas resolving nodules do not require further investigation. Our aim was to analyse CT morphology over time of resolving nodules in order seek morphologic features helpful in initial nodule classification.

Material and Methods: Imaging characteristics of 133 consecutive resolving pulmonary nodules detected in 56 subjects in a screening trial for early lung cancer with low-dose CT were retrospectively reviewed by two readers in consensus.

Results: Maximum diameter was ≤ 5 mm in 71/133 (53%), 6-10 mm in 52/133 (39%), and > 10 mm in 10/133 (8%) of resolving nodules, ranging from 1 - 45 mm; (mean 5.9 mm). Location was mainly peripheral with a mean distance to the costal pleura of 10 mm. There was no lobe predominance of nodules. 85% (113/133) of nodules were solid, 10% (14/133) were part-solid and 5% (6/13) were non-solid. 77% (103/133) of nodules were well-defined, and 23% (30/133) were ill-defined. 73% (97/133) were non-lobulated, and 27% (36/133) were lobulated. 80% (107/133) resolved completely within 14 to 1671 (mean 492) days; 20% (26/133) resolved incompletely with residual abnormalities within 51 to 1777 (mean 613) days.

Conclusion: Resolving pulmonary nodules are mostly ≤ 10 mm, peripherally located, solid, well-defined, and non-lobulated. Most resolve completely within a variable interval ranging from several days to years.

B-037 11:24

Pulmonary micronodules (< 5 mm): 3 year follow-up of 238 nodules in 165 smokers

E. De Fiori, S. Ferretti, C. Rampinelli, M. Bellomi; *Milan/IT*

Purpose: Aim of this study is the evaluation of the clinical impact of pulmonary micronodules (diameter < 5 mm) in asymptomatic smokers.

Materials and Methods: Between June 2000 and June 2001, 238 non-calcified pulmonary nodules with diameter < 5 mm, were diagnosed with low-dose CT (ldCT), in 165 subjects enrolled in the observational study for the early diagnosis of lung cancer. All nodules were followed up at 12, 24 and 36 months with ldCT.

Results: 123 subjects (74%) had a single nodule, 42 had 115 nodules. In 39 subjects (23.6%) nodules disappeared during the 3 following years. In 110 subjects (66.6%) nodules remained unchanged. 16 nodules (6.7% of nodules, 9.7% of subjects) grew: 9 in subjects with a single nodule and 7 in subjects with multiple nodules. Only 6/16 nodules (37.5%) grew larger than 5 mm and were biopsied: 3 turned out to be tumors (all T1NO, two adenocarcinoma and one large cell neuroendocrine carcinoma) and 3 were benign lesions (one hamartoma and 2 inflammatory nodules).

Conclusions: Pulmonary micronodules are present in 16% of smokers. Their risk for being a carcinoma is 0.12%, in high risk subjects; these are often slow-growing tumors (doubling time > 200 days) that should not be followed up at intervals of less than 12 months.

B-038 11:33

Detection performance of a portable, large area, indirect flat-panel detector compared with storage phosphor radiography at different exposures in a phantom study

T.M. Bernhardt¹, U. Rapp-Bernhardt¹, H. Lenzen¹, R. Esseling¹, F.W. Roehl², F. Beyer¹, A. Wall¹, W. Heindel¹; ¹Münster/DE, ²Magdeburg/DE

Purpose: To evaluate detection of catheters, pulmonary nodules, simulated interstitial lung disease, and exposure requirements of a portable, indirect flat-panel detector versus storage phosphor radiography.

Materials and Methods: Catheters, nodules and simulated subtle interstitial lung disease (miliary, reticular, linear, ground-glass patterns) were superimposed over an anthropomorphic chest phantom. Images were acquired at 109 kVp and different exposures corresponding to 400 and 800 simulated speed with a portable flat-panel detector (CXDI-50 G, 14*17 inch imaging area, 4.8 kg weight, pixel pitch: 160 µm, Canon Inc.) and printed on hard copies. Images were compared with storage phosphor radiography images (ADC Compact Plus, Agfa Inc.) at 400 simulated speed. Four board-certified radiologists recorded 43,200 observations subjected to an ROC-analysis. Significance level was p = 0.05.

Results: Catheters over obscured chest areas, nodules (\leq and $>$ 10 mm) over lucent lung and nodules \leq 10 mm over obscured chest areas, miliary and linear patterns over lucent lung showed higher areas under curves (Az) with the GadOX-aSi flat-panel detector at 400- and 800-digital speed compared with storage phosphor radiography ($p > 0.05$). Equal or smaller Az values were found for reticular and ground-glass patterns for the flat-panel detector. However, these results were not statistically significant ($p > 0.05$).

Conclusion: Detection performance of a portable flat-panel detector showed higher Az values for detection of catheters, nodules and almost all interstitial lung disease at equivalent and reduced speed compared with storage phosphor radiography. These results suggest the use of the portable flat-panel detector with reduced exposure dose in patients.

B-039 11:42

Potential benefit of computer-aided diagnosis: Detection of subtle pulmonary lung nodules on chest radiography

Z. Huo¹, D. Yankelevitz², C. Henschke², W. Kostis², J. Wandtke¹, N. Paul³; ¹Rochester, NY/US, ²New York, NY/US, ³Toronto, ON/CA

Purpose: To assess the potential benefit of computer-aided diagnosis for lung cancer on chest radiography.

Methods and Materials: Forty-six subtle nodules (avg. size = 20 mm) were selected from 80 consecutive computed radiographic (CR) chest images, each with a CT-documented lung nodule. These images along with 54 CT-confirmed normal chest images were presented on a high-resolution monochrome monitor to five chest radiologists. The radiologists were asked to mark the location of each lung nodule seen, and their confidence level (on a 100-point confidence scale) of the likelihood of the nodule actually being present. Subsequently, they were asked to retrospectively review images on which they had missed nodules in their initial readings. With the nodule locations now marked, they were asked to rate the visibility of the nodule on a 5-point scale, and were asked if their visibility warranted further evaluation with CT.

Results: In their initial readings, radiologists correctly marked, on average, 51% of the CT-determined lung nodules on chest radiographs. Upon re-review of CR images with the nodule locations marked, however, radiologists would recommend a CT exam for more than half of CT-documented nodules that they had missed in their initial reading. Further, one third of these missed nodules were thought to have fair visibility as a nodule.

Scientific Sessions

Conclusion: Radiologists miss both high- and low-visibility nodules. A computer-aided system that proposes these nodules to radiologists should influence their decision to order a CT scan. Thus, potential benefit of using a computer-aided diagnosis system to indicate possible nodule locations is suggested.

B-040 11:51

A study of inter-observer variation of small pulmonary nodule marking on DR by using an interactive computer analysis system

W. Song¹, L. Fan², Y. Xie¹, G.-Q. Wei², J. Xu¹, Q. Si¹, C.-C. Liang², J.-Z. Qian², Z. Jin¹; ¹Beijing/CN, ²Princeton Junction, NJ/US

Purpose: To assess inter-observer variations of marking small actionable pulmonary nodules (5 to 15 mm in diameter) on chest digital radiograph (DR) by using an interactive lung nodule analysis system.

Method and Materials: A total of 194 chest DR PA screening studies were selected. An expert panel of chest radiologists used a computer system (EDDA Technology, Inc.) to mark and characterize small actionable nodules in the data set with consensus. Two additional radiologists independently read the same studies and marked small actionable nodules in two passes: first without reference to the suspicious nodules suggested by the computer but using other analysis functions provided by the system; then with reference to the suspicious nodules suggested by the computer. The five sets of marking and characterizing results were analyzed and compared.

Results: There were 50 small actionable nodules marked by the expert panel. Without consulting the computer suggestions but with usage of other interactive analysis functions the system provided, the two radiologists' detection rates of small actionable nodules were 54% and 40%, respectively. After consulting the computer suggestions, the detection rates increased to 80% and 76%, respectively, with a reduced inter-observer variation. The computer system reached a sensitivity of 70%, with an average FP of 2.8 per study. Statistics of other inter-observer variations also showed clinical significance.

Conclusion: The interactive computer aided analysis system can help to reduce inter-observer variation and to improve detection rates of actionable nodules, especially small nodules which are more likely to be overlooked.

10:30 - 12:00

Room F2

Abdominal Viscera

SS 201b

Focal liver lesions: MR imaging contrast agents

Moderators:

S. Kakhadze; Tbilisi/GE

L. Martí-Bonmatí; Valencia/ES

B-041 10:30



Hepatocellular carcinoma missed on gadolinium enhanced MR imaging, discovered in liver explants: Retrospective evaluation

M.Y.K. Bilgili¹, K. Birchard², D. Gerber², Z. Firat², L. Braga², J. Woosley², R. Shrestha², R. Semelka²; ¹Ankara/TR, ²Chapel Hill, NC/US

Purpose: To determine if hepatocellular carcinomas (HCCs) missed in prospective MR study, but depicted in histopathologic analysis of explanted livers, could be identified in retrospective MR analysis. Also, to determine the cause for the misdiagnosis and MR imaging features of missed nodules.

Material and Methods: Patients with chronic liver disease that underwent liver transplantation between 1991 and 2004 were extracted from the transplant database. Amongst 555 patients, six patients revealed HCCs in explanted livers not depicted in prospective MR examination. From six patients, two were excluded due to the fact that time between prospective MR imaging and liver transplant exceeded 3 months. In total, four patients were analyzed. Liver nodules were characterized by MR imaging based on the signal intensity on T1- and T2-weighted, and degree of enhancement on early and late phase images.

Results: All HCCs missed on MR imaging before liver transplantation were depicted in retrospective analysis by both readers. Histopathologic analysis demonstrated five HCCs in four patients. The mean size of HCCs was 1.4-cm (range, 1 to 2.2 cm). The main cause of missed lesions were suboptimal image quality due to inability of patients to suspend respiration, followed by high-grade dysplastic nodule and HCC with atypical MR features on early phase image.

Conclusions: HCCs prospectively missed on MR examinations were retrospectively identifiable. Reasons for missing HCC include inability of patients to breathhold, categorizing lesion as high-grade dysplastic nodule and failure to

recognize that isovascular early enhancing lesions with subsequent washout and capsule enhancement were HCC.

B-042 10:39

Comparative assessment of Resovist-enhanced MR imaging and Magnevist in the detection and characterization of focal hepatic lesions

W. Cheng, M. Zeng, F. Yan; Shanghai/CN

Purpose: To compare Resovist-enhanced MR imaging with Magnevist in detecting and characterising focal hepatic lesions, and to further evaluate the efficacy of Resovist enhanced MR imaging in focal hepatic lesion diagnosis.

Methods and Materials: A total of 62 patients with suspected focal hepatic lesions (female21, male41) were evaluated. Serial MR imaging of the liver was initially performed using Magnevist, and followed by Resovist 48 hours later. All examinations were concluded with SE T1- and FSE T2-weighted with fat suppression, pre-contrast and contrast dynamic GRE T1 in 10 min, and accumulation-phase FSE T2 or T2* GRE only for the Resovist. All images were randomly analyzed by 2 experienced radiologists.

Results: A total of 105 solid lesions [among 24 micro-lesion (< 1.0 cm)] were verified at the standard-of-reference examinations. Comparison with the plain MR imaging (5/24) and Magnevist enhanced MRI imaging (14/24) in the detection of the micro-lesions, Resovist-enhanced MR imaging (24/24) was highly improved with statistical significance ($P < 0.05$). But there was no significant difference for the detection of the lesions (≥ 1.0 cm). Histopathologic specimens were available for 32 patients, those revealed 51 lesions [including hepatocellular carcinoma (n = 30), dysplastic nodules (n = 3), metastases (n = 9), hemangioma (n = 2), focal nodular hyperplasia (n = 3), inflammatory pseudotumor (n = 1), tuberculoma (n = 1), angiomyolipoma (n = 2)]. The specificity was not significantly different for both MR contrasts (Resovist 92% vs Magnevist 91%). The accuracy of diagnosis reaches 92% for Resovist-enhanced MR imaging which combined T1 GRE dynamic scanning and T2 FSE/T2* GRE in accumulation-phase.

Conclusion: The use of Resovist greatly improves detection of small, focal hepatic lesions (especially for < 1 cm). A combined protocol with dynamic scanning and subsequent accumulation-phase T2-weighted is recommended to enhance the diagnosis in both specificity and accuracy.

B-043 10:48

The added value of the hepato-biliary phase imaging in Gd-BOPTA magnetic resonance study (Gd-BOPTA-MR) of benign liver tumors and metastases in normally functioning livers

I. Sansoni, A. Laghi, M. Di Martino, C. Miglio, M. Celestre, L. Coletta, M. Rengo, R. Passariello; Rome/IT

Purpose: To determine the value of adding hepato-biliary phase imaging to triple-phase dynamic Gd-BOPTA-MR for detection and characterization of focal lesions in non-hepatopathic livers.

Methods and Materials: Fifty patients with liver lesions underwent MR-study on 1.5 T-scanner using the following acquisition protocol: Basal T2-weighted and T1-weighted; post i.v. administration of Gd-BOPTA (0.2 mM/kg), dynamic contrast-enhanced T1-weighted sequence was acquired at 15-seconds, 55-seconds and 135-seconds, and delayed T1-weighted hepato-biliary phase at 60 minutes. Dynamic-MR and Complete-MR study were reviewed independently by three radiologists assessing presence, number and characterization of lesions. Separate reading sessions were performed for images from only Dynamic-phases, and images from all dynamic and hepato-biliary phases, calculating related sensitivities and specificities. The value of Delayed-phase images in lesion characterization was also assessed. The number of lesions at final diagnosis was considered equal to detected lesions at Complete-MR study plus lesions detected by other imaging modalities (CT, US, MR with other specific c.m.). Lesion characterization was established by histopathologic examination after surgical resection or biopsy, or by follow-up imaging and treatment response.

Results: Diagnostic accuracy of MR-study with hepato-biliary phase was significantly higher than that of Dynamic-MR in benign lesions and metastases. Concerning benign lesion identification, the hepato-biliary phase of Gd-BOPTA-MR imaging allowed us to detect 9% more lesions compared to Dynamic-MR. Among lesions identified by both sets of images, delayed hepato-biliary phase images were helpful in lesion characterization in 5% of cases.

Conclusion: The addition of Delayed-phase imaging to dynamic Gd-BOPTA MR-study is valuable for detection and characterization of focal lesions in normally functioning livers.

Scientific Sessions

B-044 10:57

Detection and characterization of hepatocellular carcinoma (HCC): Value of adding the hepato-biliary phase imaging to dynamic Gd-BOPTA magnetic resonance imaging (Gd-BOPTA-MRI)

I. Sansoni, A. Laghi, M. Di Martino, M. Celestre, C. Miglio, L. Coletta, M. Rengo, R. Passariello; Rome/IT

Purpose: The purpose of our study was to determine the value of adding delayed hepato-biliary phase imaging to triple-phase dynamic Gd-BOPTA MR for detection and characterization of HCC suspected lesions.

Methods and Materials: Eighty-one patients with chronic hepatitis underwent MR study on 1.5 T-scanner using the following acquisition protocol: Basal T2-weighted and T1-weighted; post i.v. administration of Gd-BOPTA (0.2 mM/kg), dynamic contrast-enhanced T1-weighted sequence was acquired at 15-seconds, 55-seconds and 135-seconds, and delayed T1-weighted hepato-biliary phase at 60 minutes. Dynamic-MR and Complete-MR study were reviewed independently by three radiologists assessing presence, number and characterization of lesions. Separate reading sessions were performed for images from only Dynamic-phases, and images from all dynamic and hepato-biliary phases, calculating related sensitivities and specificities. Value of Delayed-phase images in HCC characterization was also assessed. The number of lesions at final diagnosis was considered equal to detected lesions at Complete MR study plus lesions detected by other imaging modalities (CT, US). Lesion characterization was established by histopathologic examination after surgical resection or biopsy, or by follow-up-imaging and treatment response.

Results: MR study with hepato-biliary phase and MRI without hepato-biliary phase had a comparable diagnostic accuracy. The percentage of identified HCC at Complete Gd-BOPTA-MRI (92%) was slightly higher than that at dynamic MR study (89.7%). HCC correct characterization of Delayed-phase images was not statistically different from Dynamic-study.

Conclusion: The addition of Delayed-phase imaging to dynamic Gd-BOPTA-MR study doesn't provide significant additional benefit for the detection and characterization of hepatocellular carcinoma, due to reduced liver function and subsequent inhomogeneous appearance.

B-045 11:06

Double contrast technique in MR imaging of liver: Differential diagnosis compared to histopathologic findings

R. Hammerstingl, S. Parmentier, W. Schwarz, T.J. Vogl; Frankfurt a. Main/DE

Purpose: To prospectively evaluate the value of double contrast-enhanced MR imaging for the differential diagnosis of focal liver lesions in correlation to histopathologic and clinical findings.

Methods and Materials: In this prospective, phase III, single-center clinical study 90 patients with known liver tumors (53 benign and 37 malignant) were investigated using a 1.5 Tesla MR imaging Scanner. Mono-contrast technique (Gd-enhanced MR imaging, 0.1 mmol Gd-DTPA i.v.) was performed from 4 weeks up to 24 h prior to inclusion. Study MR imaging was obtained using SPIO-enhanced imaging (SHU 555 A i.v.) as well as double-contrast technique (Gd-DTPA post SPIO). Sequence protocol included a dynamic evaluation of the complete liver using a high resolution 3D-protocol and static conventional and fat saturated T1-weighted sequences. Using ROI-technique signal intensities of liver parenchyma, liver lesions and vascular structures were measured. Percentage enhancement was calculated and verified using statistical analysis (Friedman and t-test).

Results: Double-contrast technique (DCT) was well tolerated compared to mono-contrast technique. Dynamic imaging using DCT was comparable to Gd-enhanced imaging regarding the flushing and characteristics of the diagnosed liver tumors. A statistically significant improvement in contrast to noise ratio was calculated for focal liver lesions in static DCT versus mono-contrast imaging. Five lesions (FNH n = 2, haemangioma n = 2 and HCC n = 1) were detected additionally in DCT compared to the other technique and evaluated using histopathologic and clinical follow-up. Using a five-point ranking system a statistically significant improvement was stated for diagnostic confidence levels regarding delineation and differential diagnosis.

Conclusion: The use of double contrast techniques is an excellent tool for the delineation and differential diagnosis of focal liver lesions and allows the acquisition of additional information compared to mono contrast technique in the pretherapeutic work-up.

B-046 11:15

Diagnostic work-up in the liver using SPIO-enhanced MR imaging:

Comparison with histopathologic and clinical findings

W.V. Schwarz, R. Hammerstingl, F. Marquardt, B. Götz, M. Heller, T.J. Vogl; Frankfurt a. Main/DE

Purpose: To prospectively evaluate the diagnostic potential of SPIO particles (SHU 555A, Resovist, Schering AG, Berlin, Germany) in MR imaging for the diagnostic work up of focal liver lesions and to evaluate classification and characterisation in correlation to histopathologic and clinical findings.

Materials and Methods: In a clinical phase III/IV study, MR imaging was obtained in patients with a suspicion of focal liver lesions diagnosed by biphasic Spiral-CT or Gd-enhanced MR imaging. 100 patients were investigated using a high field MR imaging scanner. Sequence protocol included T2-weighted HASTE/TSE-sequences as well as T1-weighted fat saturated GRE-protocols using unenhanced, dynamic, and SPIO-enhanced studies.

Results: Histopathology and clinical follow-up diagnosed malignant [HCC (n = 38), metastases (n = 29)] and benign liver lesions [FNH (n = 15), adenoma (n = 5), hemangioma (n = 9) and regenerating nodules (n = 4)]. Patients underwent liver resection, liver transplantation, biopsy or clinical verification using MR imaging as a follow-up examination.

Using SPIO-enhanced MR imaging a sensitivity of 91.5% and a specificity of 92.9% was calculated for malignant lesions. In benign lesions a sensitivity of 95.8% and a specificity of 93.5% was assessed. Benign liver tumors showed a significant loss in signal intensity using T2-weighted sequences ($p < 0.05$, Wilcoxon-signed rank test) compared to malignant primary lesions. For malignant tumors no significant decrease in signal was documented. The overall therapeutic decision (transplantation, resection or interventional procedures) changed statistically significantly using combined T2- and T1-weighted SPIO-enhanced studies compared to previous diagnostic imaging.

Conclusion: SPIO-enhanced MR imaging is an effective imaging tool for the diagnostic work up of focal liver lesions. Combined T2- and T1-weighted SPIO-enhanced imaging enable a sufficient classification and characterisation.

B-047 11:24

Evaluation of the detectability of HCC in patients with liver cirrhosis by means of Gd-EOB-DTPA: Results of a qualitative and quantitative phase III study

B. Schulte¹, P. Reimer¹, J. Kuehnen², E. EOB Study Group²; ¹Karlsruhe/DE, ²Berlin/DE

Purpose: To study whether the hepatobiliary contrast agent Gd-EOB-DTPA shows decreased uptake and detectability of hepatocellular carcinoma in patients with liver cirrhosis.

Methods and Materials: Within a prospective multicenter phase III trial, 20 patients with HCC (11 patients with cirrhotic liver - 9 patients with non-cirrhotic liver) proven by histopathology as a standard of reference were enrolled. Parameters of T1-W GRE pulse sequences were systematically varied for spatial resolution (128 phase x 256 frequency matrix versus 160 x 512) and fat saturation for the 128 x 256 matrix within all patients. All pulse sequences were measured before and 20 min post injection (p.i.) of 25 µmol Gd-EOB-DTPA/kg bodyweight. Data were quantitatively analyzed to calculate for relative signal change, signal to noise ratio (SNR) and lesion-liver contrast (CNR).

Results: Relative signal changes were 41% in liver and 16% in tumor for non-cirrhotic liver vs. 47% in liver and 13% in tumor in cirrhotic liver. SNR (18.80 in the non-cirrhotic and 16.05 in the cirrhotic group; FS T1 GRE with 128 x 256 matrix) and CNR (0.2281 vs. 0.2074) for both groups were not significantly different. At higher resolution (160 x 512), CNR significantly increased from 8 min p.i. to 20 min p.i. (0.137 vs 0.207) in the cirrhosis group.

Conclusion: Liver cirrhosis appears to have only a minor impact on the uptake of Gd-EOB-DTPA. Tumor-contrast and thus detectability of lesions can be achieved by proper pulse sequence selection and scanning after a sufficient long period of time (20 min) post injection.

B-048 11:33

Diagnostic imaging of primary liver tumors: Evaluation of the hepatocyte-specific contrast agent Gd-EOB-DTPA

R. Hammerstingl¹, W. Schwarz¹, J. Breuer², T. Balzer², T.J. Vogl¹;

¹Frankfurt a. Main/DE, ²Berlin/DE

Purpose: To prospectively compare the efficacy of the liver-specific hepatobiliary MR imaging contrast agent Gd-EOB-DTPA versus standard Gd-DTPA for the diagnosis of primary liver tumors within individuals.

Scientific Sessions

Methods and Materials: In a phase II trial, 57 patients with known focal liver lesions were prospectively investigated using a high field MR imaging scanner. The sequence protocol included T1-GRE weighted ultrafast sequences before, during, and post i.v. administration of Gd-EOB-DTPA. Within one week Gd-DTPA was performed in the same patient (0.1 mmol/kg b.w.).

Results: Histopathology/clinical follow-up (within 12 months) revealed the diagnosis of malignant primary tumors in 24 cases [HCC (n = 22), CCC (n = 2)] and benign primary lesions in 7 cases [FNH (n = 4), hemangioma (n = 3)]. Secondary infiltrations were detected in 26 patients. Dynamic Gd-EOB-DTPA-enhanced images revealed a biphasic dose-dependent enhancement in liver parenchyma with lower but diagnostic signal increase in liver cirrhosis. In the hepatobiliary phase a significant increase in liver signal with a plateau phase was evaluated. FNH-nodules provided a prolonged high signal intensity, whereas HCC documented a specific rim-enhancement in the early phase. In the hepatobiliary phase Gd-EOB-DTPA-enhanced imaging yielded an increased detection rate (HCC: 79% increase) compared to standard extracellular MR imaging (Wilcoxon-signed rank test: p < 0.05).

Conclusion: The liver specific MR imaging enables improved detection of primary hepatic lesions, especially HCC, when compared to standard MR imaging. Benign primary tumors have specific morphologic criteria for tissue characterization using hepatobiliary MR imaging.

B-049 11:42

MR with different liver specific contrast media in the evaluation of hepatic adenoma (HA) and liver adenomatosis (LA): Imaging and pathological findings in an intra-individual comparison group

L. Graziolii¹, G. Morana², L. Romanini¹, G. Mazza¹, M. Morena¹, G. Schneider³, ¹Brescia/IT, ²Verona/IT, ³Homburg a.d. Saar/DE

Purpose: To compare the imaging findings of different MR liver specific contrast materials (Gd-BOPTA, Mn-DPDP, and ferumoxides) in the diagnosis of hepatic adenoma.

Methods and Materials: 37 patients with either confirmed HA (n = 32) or LA (n = 9) were evaluated. MR imaging was performed in all patients before and after administration of Gd-BOPTA. In 21 patients T1W GRE pre and 1 h after Mn-DPDP and in 17 patients T2W TSE and T2W' pre and at 30 min post ferumoxides were acquired. The qualitative enhancement evaluation was assessed and compared after Gd-BOPTA administration in 122 HA, in 74 HA after Mn-DPDP administration, and in 61 HA after ferumoxides.

Results: The signal intensity on pre contrast T1 and T2W sequences didn't show a typical pattern. 99/107 lesions were either slightly hyperintense or isointense to the surrounding parenchyma on precontrast T2W images. A more varied behaviour was noted on precontrast T1W images. 94/122 lesions appeared isointense or slightly hypointense, and 21/107 slightly hyperintense. Dynamic evaluation after Gd-BOPTA in all cases showed homogeneous (118/122) or heterogeneous (4/107) hypervascularity. In the delayed hepatobiliary phase all 122 lesions after Gd-BOPTA appeared hyperintense, differently to that observed in FNH. All 74 HA after Mn-DPDP appeared iso or hyperintense similarly to the FNH. After ferumoxide administration 44/46 HA showed homogeneous signal drop.

Conclusion: Gd-BOPTA is a more appropriate contrast agent than ferumoxides and Mn-DPDP for the characterization of HA. The enhancement pattern on dynamic phase imaging provide information on the hypervascular nature. The hypointensity on the delayed hepatobiliary phase permits us to differentiate HA from FNH.

B-050 11:51

Does dual contrast MR imaging of the liver with ferucarbotran and gadolinium chelates improve the detection rate of focal liver lesions?

Results of an investigator initiated prospective multicenter study

C. Wirth¹, P. Reimer¹, W. Schima², T. Vestring³, S.O. Schoenberg⁴, C. Zech⁴, P.J. Robinson⁵, D. Study Group¹; ¹Karlsruhe/DE, ²Vienna/AT, ³Rotenburg/DE, ⁴Munich/DE, ⁵Leeds/UK

Purpose: To investigate whether dual contrast MR imaging with the new SPIO ferucarbotran (Schering AG, Berlin, Germany) and a gadolinium chelate improves the detection rate of focal liver lesions.

Methods and Materials: Following ethics committee approval, patients with focal liver lesions demonstrated by dual phase CT were enrolled. Within this study 74 patients with 202 liver lesions proven by standard of reference procedures were analysed. Following a precontrast MR imaging consisting of T1-W GRE, T2-W TSE, T2-W HASTE, and T2*-W GRE 1.4 ml ferucarbotran was IV-injected. The same pulse sequences were repeated > 10 min postinjection. Finally, a dynamic T1-W GRE gadolinium study (0.1 mmol/kg bw) was performed (30 s, 70 s, and

120 s). Images were qualitatively analysed on-site for the presence of focal lesions and quantitatively to calculate for lesion-liver-contrast. The non-parametric Wilcoxon test (p ≤ 0.05) was applied for statistical analysis.

Results: The detection rate of hypervascular lesions like HCC significantly increased by dual contrast MR imaging from 47 lesions precontrast, to 63 lesions post ferucarbotran, and 85 lesions post gadolinium. Within this group, contrast was highest during the arterial phase (0.236) and portalvenous phase (0.233) of the gadolinium-enhanced acquisition. The detection rate of hypovascular lesions like metastases did not improve with 33 lesions precontrast, 35 lesions post ferucarbotran, and 39 lesions post gadolinium. Within this group, contrast was lowest during the portalvenous phase (0.101) of the gadolinium-enhanced acquisition.

Conclusion: Dual contrast-enhanced MR imaging with a SPIO like ferucarbotran and gadolinium chelates significantly improves the detection rate of hypervascular liver lesions.

10:30 - 12:00

Room G

Head and Neck

SS 208

Salivary glands, mandible and thyroid imaging

Moderators:

D. Coutinho; Lisbon/PT

L. Jäger; Munich/DE

B-051 10:30



Functional imaging of parotid glands: Diffusion-weighted echo-planar MR imaging before and after stimulation

C.R. Habermann, M.C. Cramer, J. Graessner, P. Gossrau, F. Reitmeier, J. Fiehler, M. Jaehne, G. Adam; Hamburg/DE

Purpose: Investigate the feasibility of using diffusion-weighted (DW) echo-planar imaging (EPI) for measuring different functional conditions of the parotid gland and to compare different measurement approaches.

Methods and Materials: Parotid glands of 27 healthy volunteers were examined with a DW EPI sequence with a 1.5 T system before and after oral stimulation with commercially available lemon juice. The b factors used were 0, 500, and 1,000 sec/mm². ADC maps were transferred to MR imagingcro (Rorden, University Nottingham, Great Britain) and evaluated with a manually placed circular region of interest (ROI) consisting of 100-200 pixels. Additionally, ROIs including the entire parotid gland were placed bilaterally. For comparison of the results, the Student's t test was used. Comparing both measurement approaches the Pearson's correlation coefficient (r) was calculated.

Results: With use of ROIs containing 100-200 pixels, the median for both parotid glands prior to stimulation was 1.06×10^{-3} mm²/sec ± 0.07×10^{-3} mm²/sec. After stimulation, the median ADC for both parotid glands was measured at 1.15×10^{-3} mm²/sec ± 0.08×10^{-3} mm²/sec. For evaluating the entire parotid gland, the ADC prior to stimulation was 1.13×10^{-3} mm²/sec ± 0.05×10^{-3} mm²/sec, whereas after stimulation with lemon juice, the ADC increased to 1.22×10^{-3} mm²/sec ± 0.09×10^{-3} mm²/sec. For both measurement approaches, the increase in ADC after stimulation proved to be significant ($P < 0.001$). High correlations between measurement approaches were found ($r > 0.83$).

Conclusion: Diffusion-weighted echo-planar MR imaging allows quantification of functional changes in the parotid glands.

B-052 10:39

Dynamic contrast-enhanced MR imaging studies in parotid tumors

H. Greess, S. Alibek, J. Zenk, A. Bozzato, H. Iro, W. Bautz; Erlangen/DE

Purpose: To evaluate the value of dynamic contrast-enhanced MR imaging to differentiate several parotid tumor entities.

Methods: 110 patients with 113 parotid tumors were examined with dynamic contrast-enhanced MR on a 1.5-T Symphony over a period of 18 months. An axial T1-weighted SE sequence was performed to determine 5 selected slices for the dynamic study. Subsequently a T1-weighted FLASH sequence was used for the dynamic contrast study with 0.2 ml Gadolinium per kilogram bodyweight administered intravenously. Contrast agent application and the FLASH sequence were started simultaneously. 10 acquisitions of 10 seconds scan time were performed. Intensity versus time studies were performed in the region of interest. The examination was completed by axial T2 STIR and axial and coronal T1 SE FATSAT sequences.

Scientific Sessions

Results: Tumor entities were pleomorphic adenomas (40%), adenolymphomas (Warthin tumors) (21%), carcinomas (11%), lymph nodes (7%), oncocytomas (4%) and cysts (3%). Four typical intensity curves were observed: Pleomorphic adenoma showed a gradual increase in signal intensity, followed by a plateau phase on a low intensity level; cysts showed a vacillate course at a low signal intensity level; adenolymphomas as well carcinomas showed a rapid increase in signal intensity followed by a plateau phase, but peak values were strikingly different with > 500 in adenolymphomas versus > 1000 in carcinomas. Together with the other MR criteria (contrast enhancement, sharp or blurred border) and clinical criteria a differentiation between adenolymphomas and carcinoma was possible.

Conclusions: With dynamic contrast-enhanced MR studies, differentiation between the common parotid tumors before surgery is possible.

B-053 10:48

Ultrafast MR-sialography: Sequence optimization and evaluation of parallel acquisition techniques and different functional conditions of the salivary glands

M.C. Cramer¹, C.R. Habermann¹, J. Graessner², F. Weiss¹, K. Petersen¹, M. Jaehne¹, G. Adam¹; ¹Hamburg/DE, ²Erlangen/DE

Purpose: To develop a fast and reproducible sequence for MR-sialography requiring no post-processing, to compare parallel and non-parallel acquisition techniques, and to evaluate the effects of oral stimulation.

Methods and Materials: Examinations were performed on a 1.5-T system. The lower part of CP-head coil and standard two-element CP neck array coil were used. After developing a sufficient sequence for MR-sialography an ss-TSE with an acquisition time of 2.8 sec was used in transverse and oblique sagittal orientation, with and without parallel imaging techniques and oral sialogogue. Images were evaluated by four independent radiologists using a 1 to 5 visual scale. For statistical comparison of the results, an ANOVA with post-hoc comparisons was used. Inter-observer variability was computed with an intraclass correlation.

Results: Ducts were visualized with an overall rating for all ducts of 2.26 ($SD \pm 1.09$). Between the four raters a high correlation has been obtained (intraclass correlation = 0.948). For axial orientation the proximal Stensen duct showed best visualization (1.35-1.74; $SD \pm 0.72-1.17$), using an oblique sagittal orientation. The intra-glandular submandibular ducts showed best visualization (1.18-2.62; $SD 0.81-1.14$). Significant influence regarding the slice angulations could not be obtained ($p = 0.74$). Visibility of ducts improved significantly after oral application of a Sialogogue ($p < 0.001$; $\eta^2 = 0.049$). Using parallel imaging technique showed significant loss of image quality ($p < 0.001$; $\eta^2 = 0.049$).

Conclusion: The developed ss-TSE sequence is a fast and sufficient technique for visualization of ducts of main salivary glands, with no post-processing. To improve results of MR-sialography it is reasonable to use oral Sialogogue.

B-054 10:57



Effect of window settings of dental-CT images on visualization of the tooth tissues

A. Mangov, L. Dakhno; Kiev/UA

Purpose: To investigate the proper window settings for the tooth tissues on dental-CT images.

Methods and Materials: We investigated 43 jaws (24 maxillae and 19 mandibles) in 37 patients with various dental pathologies. Spiral CT in axial plane with low-dose dental protocol (120 kVp; 40 mAs; slice thickness: 1 mm; pitch: 1.3; rotation time: 1 sec; reconstruction interval: 0.8 mm) was performed on a spiral single-slice "Asteion VF" scanner (Toshiba Medical Systems, Japan). All axial images were reconstructed with a high spatial frequency algorithm and with five window settings: settings-1 - width = 2500, level = 500 HU; settings-2 - width = 4000, level = 750 HU; settings-3 - width = 5000, level = 1000 HU; settings-4 - width = 7000, level = 1000 HU; settings-5 - width = 18000, level = 3000 HU. Two observers assessed the teeth status; they estimated the quality of visualization of enamel, dentin and root of tooth, adjacent bone and artificial metal structures.

Results: We found that the tissues of a tooth were not differentiated on images performed with settings-1. Images obtained with settings-2 provided good visualization of the root, adjacent bone and dentin of the crown; enamel was intensively white and it was hard to distinguish a radiopaque filling from enamel. Settings-3 clearly depicted the dentinoenamel junction of the tooth. Settings-4 provided good visualization of a radiopaque filling in a pulp space. Metal artificial structures were well depicted with settings-5.

Conclusion: We suggest that the appropriate window settings (width, 5,000; level, 1,000 HU) should be applied to visualization of the tooth tissues and their pathologies.

B-055 11:06

Imaging cortical bone by MR imaging: A new approach to image-guided planning for reconstructive surgery of the face

S.J. Golding, R. Saeed, C. Alvey, I. Evangelou, A. McIntyre, S. Watt-Smith; Oxford/UK

Purpose: CT and 3D reformatting, are widely used for supporting reconstructive surgery of the face but incur absorbed radiation. We report a new approach using an MR imaging sequence to replace CT in the demonstration of cortical bone.

Methods and Materials: The characteristics of Gradient Echo imaging of cortical bone on MR imaging were manipulated to define a sequence in which contrast differences between soft tissues were suppressed and cortical bone was demonstrated with high resolution as a black image. The sequence is weighted to Proton Density, utilising a flip angle of 5 degrees and in-phase echo time. Post processing allows image data acquired with a matrix of 256 x 256 to be displayed at 512 x 512. Biomorphometric accuracy of the sequence compared to CT was achieved using a geometric test object and an anthropomorphic head phantom developed in-house. Comparison included caliper measurements from a variety of anatomical structures and this was repeated in a pilot study on 15 patients undergoing investigation for facial disease.

Results: The new sequence showed good definition and resolution of bone. Linear measurements between 8 anatomical landmarks showed less than 1 mm variance between CT and MR imaging, within surgical tolerance. Further, data from the MR imaging sequence were found to be compatible with 3D imaging processing software. Exploration of the clinical value continues.

Conclusion: The new MR imaging sequence offers a promising means of replacing CT in support for reconstructive surgery of the face, with acceptable accuracy and improved radiation protection for the patient.

B-056 11:15

Serial contrast-enhanced MR imaging in the assessment of the temporomandibular joint disorders

T. Otani, N. Tomura, T. Ohnuki, S. Takahashi, I. Sakuma, J. Watarai; Akita/JP

Purpose: To determine the usefulness of serial contrast-enhanced MR imaging (SCE-MRI) in the assessment of temporomandibular joint disorders (TMD).

Materials and Methods: SCE-MRI was performed in 114 patients (103 unilateral joint disease, 11 bilateral) with various TMD. For the control group, 50 asymptomatic joints of patients with unilateral clinical symptoms were included. SCE-MRI was performed in a total of 175 joints. Four series of SCE-MRIs using fat-suppressed SE-T1WI were bilaterally started at 0, 5, 10, and 15 minutes after bolus injection of contrast material. The peak of contrast enhancement (P-CE) was evaluated from SCE-MRIs, and maximum signal intensity ratio (MSIR) with the reference to the signal intensity of pre-contrast images was calculated in the region of the condyle (CON) and posterior disc attachment (PDA). The relationships among P-CE, MSIR, and clinical symptoms were studied.

Results: P-CE of the CON was seen in the first or second SCE-MRI in 123/125 of affected joints and 49/50 of asymptomatic joints, while P-CE of PDA was seen in the third or fourth SCE-MRI in 103/125 of affected joints and 40/50 of asymptomatic joints. In the affected joints, mean MSIR of the CON (1.41 ± 0.54) and PDA (0.97 ± 0.64) was significantly ($p < 0.001$) higher than that of asymptomatic joints (CON: 1.01 ± 0.42 , PDA: 0.60 ± 0.45). In patients with disc displacement without reduction, MSIR of the CON (1.49 ± 0.59) and PDA (1.07 ± 0.66) was significantly higher than patients without disc displacement (CON: 1.02 ± 0.39 , p < 0.01; PDA: 0.46 ± 0.27 , p < 0.005).

Conclusion: MSIR obtained by SCE-MRI reflects clinical symptoms and are of diagnostic value to assess various TMD.

B-057 11:24

Differential analysis of vascularization of thyroid nodules examined with volume rendered 3D power Doppler ultrasound

R.Z. Slapa, J. Slowinska-Szrednicka, W. Jakubowski, M. Serafin-Krol, K.T. Szopinski, M. Gietka-Czerniel, H. Jastrzebska, I. Kozicki, E. Stachlewska-Nastfeter; Warsaw/PL

Purpose: Analysis of vascularization of thyroid nodules with volume rendered three-dimensional power Doppler ultrasound and possible establishment of features characteristic for thyroid carcinoma.

Methods and Materials: Fifty-seven thyroid nodules (10 papillary thyroid carcinomas, 47 benign) were evaluated with 3D power Doppler ultrasound. A dedicated 3D ultrasound machine with automatic linear transducer 11.5-4 MHz was applied. PRF and color gain were set just above noise level (usually PRF = 0.9 kHz). Vessel configuration was evaluated interactively in volume mode within

Scientific Sessions

a thin slab of tissue. The pattern, regularity and density of vessels were evaluated.

Results: There were 3 cancers with no central vessels and in 5 cancers there were a few central vessels with a peripheral-central pattern. The vessels with spoke and wheel alignment were observed in 6 cancers. In one cancer chaotic vessels were observed with a central pattern; this configuration was not observed in benign nodules. In one follicular type papillary cancer that was devoid of classical B mode suspicious features, moderately increased peripheral-central vessels with spoke and wheel alignment were the only features suggesting FNA. Vessels with spoke and wheel alignment were observed in 82% of benign nodules.

Conclusion: 1. Papillary thyroid carcinoma can present with different patterns of vessels; in most cases peripheral-central and only rarely peripheral or central. 2. There is a large overlap of vascularity patterns between papillary carcinomas and benign nodules. 3. Vascularization of thyroid nodules can be a complementary criteria in indication of the nodule for FNA.

B-058 11:33

Thyroid nodules: Evaluation with color Doppler and duplex Doppler ultrasound

M. Chammas, R. Gerhard, O. Saito, I.R. Oliveira, A. Widman, G.G. Cerri; São Paulo/BR

Purpose: To study thyroid nodules with power Doppler and duplex Doppler ultrasound (US) in order to determine its' value in predicting malignancy.

Materials and Methods: 177 nodules were analysed by B-mode scanning, power Doppler and spectral analysis and were related to the cytological findings (FNAB obtained by US). The equipment is GE, Logiq 500. Nodular analysis with color Doppler was classified in 5 vascular patterns: I) no vascularization; II) peri-lesional vascularization; III) peri-lesional vascularization \geq central vascularization; IV) central vascularization > peri-lesional vascularization; V) only central vascularization. Spectral analysis considered resistive index (RI). Univariate and multivariate logistic regression analysis were performed.

Results: The echogenicity parameter did not present significant statistical association at the univariate analysis, therefore only at the multivariate analysis, was it really identified as significant. Malignant nodules without vascularization or only peri-lesional vascularization were not observed; 2 malignant nodules showed pattern III; 6 showed pattern IV and 5 showed pattern V. This showed that the incidence of malignancy is larger where the central vascularization is predominant. This parameter presented statistically significant correlation with cytological results. The spectral analysis demonstrated that nodules with RI > 0.77 are at high risk of malignancy.

Conclusions: The multivariate analysis showed that to select malignant nodules the vascular patterns and RI are enough and significant. The nodules with high risk showed patterns IV and V, independent of RI; the nodules with other vascular pattern (II/ III) demonstrated high risk when the RI > 0.77, this model had sensitivity = 92.3%; specificity = 88%.

B-059 11:42

Follow-up of thyroid nodules with inadequate cytologic diagnosis

C. Avigo, S. Carizzoni, M. Zampedri, M.R. Cristinelli, F. Pittiani, A. Marconi, E. Archiati; Brescia/IT

Purpose: To analyze the follow-up of patients with a thyroid nodule and an inadequate cytologic diagnosis.

Materials and Methods: From January 1999 to June 2003 we subjected 93 patients (67 females and 26 males) to FNAC of a thyroid nodule, in 2 sessions (at least 1 month apart) with inadequate cytologic diagnosis. They were followed-up by ultrasound (US) periodically (from 7 to 51 months, with an average of 24.06 months).

Results: 80 nodules remained unchanged in size and structure. The other 13 that increased in volume, were submitted to surgical operation or to FNAC repetitions (4/13 resulted benign for cytology). After surgical operation, 9 patients showed: 2 thyroiditis, 1 hyperplastic nodule, 2 follicular adenomas, 1 follicular carcinoma, 2 papillary carcinomas, 1 medullar carcinoma.

Conclusions: Of the 93 patients followed-up, 13 changed (increase of volume); of these 4 (30.7%) resulted in malignancy (15.53 months of follow-up). This demonstrated that the ultrasound follow-up in inadequate thyroid nodules is necessary.

B-060 11:51

Accuracy of CT-SPECT image fusion in the pre-operative detection of parathyroid adenomas

P. Kovacs, K. Rapf, R. Prommegger, C. Profanter, T. Sauper, R.J. Bale, W.R. Jaschke; Innsbruck/AT

Purpose: To determine the accuracy of multiplanar CT, MIBI-SPECT and image fusion (IF) of both data sets in the detection of parathyroid adenomas in comparison with intra-operative data.

Materials and Methods: In 43 patients (Age: 14-81) with primary hyperparathyroidism, parathyroid adenomas were found intra-operatively at the upper ($n = 5$) and lower pole ($n = 9$) of the right thyroid gland and at the upper ($n = 7$) and lower pole ($n = 13$) of the left thyroid gland. 6 glands were detected in ectopic positions without connection to the thyroid gland. 3 patients with multiple adenomas were excluded from the study. Accuracy of pre-operative detection was determined using intra-operative data as gold standard. In a retrospective study all data sets were reinterpreted alone in a blinded fashion. Sensitivity, specificity and correlation (Kappa) were calculated.

Results: Sensitivity, specificity and correlation increased from SPECT (0.71/0.87/0.84) to CT (0.76/0.96/1.00) to IF (0.82/0.93/0.92) in the detection of the side (ectopic glands excluded) and increased from SPECT (0.41/0.90/0.34) to CT (0.59/0.91/0.51) to IF (0.69/0.93/0.62) in the detection of the site of adenoma. In 16 patients SPECT and CT showed the identical result. Only CT detected 3 out of 5 ectopic glands, but also misinterpreted 6 to be ectopic glands.

Conclusions: Although less than half of the patients show exactly the same results in both methods, IF allows for a more accurate detection of parathyroid adenomas in patients with primary hyperparathyroidism than CT and SPECT alone. Ectopic glands are still difficult to detect exactly, especially if they are situated near the thyroid gland.

10:30 - 12:00

Room H

Interventional Radiology

SS 209a

Intervention in the thoracic aorta

Moderators:

D.K. Tsatsis; Iraklion/GR
I.P. Vulev; Bratislava/SK

B-061 10:30

Endovascular stent graft placement in patients with traumatic rupture of thoracic aorta

D. Monaco, P. Larini, C. Marcato, S. Saccani, A. Agostinelli, M. Zompatori; Parma/IT

Purpose: To evaluate the effectiveness of endovascular treatment in patients with traumatic rupture of thoracic aorta following vehicle accident.

Materials and Methods: Between March 1998 and September 2004, 16 patients (12 male, 4 female, mean age 40 years) were recovered for traumatic rupture of the thoracic aorta with associated visceral lesions and bone fractures. All cases were managed by endovascular means, implanting in the ruptured thoracic aorta one or more stent graft segments (Medtronic-Talent). Two patients required also concomitant procedures for associated cardiovascular or visceral lesions. One patients for concomitant traumatic pseudoaneurysm of brachiocephalic trunk was submitted to aortic and supraaortic vessel stenting.

Results: The endovascular procedure was technically successful in all cases. In a mean follow-up time of 2.5 years, 13 out of 16 patients are alive and in good health. In 2 patients death occurred respectively few hours and two days after stent graft implantation as consequence of post-traumatic multi organ failure, while another patient died for a not related cause (pulmonary cancer).

Conclusions: Our experience suggests that stent graft placement, a minimally invasive procedure, can be proposed in patients with traumatic rupture of thoracic aorta and impending risk of massive hemorrhage as an emergency procedure.

B-062 10:39

Emergency stent-graft repair for blunt thoracic aortic injury

P. Castelli, R. Caronno, G. Piffaretti, M. Tozzi, C. Lomazzi, D. Laganà, G. Carrariello; Varese/IT

Purpose: Blunt thoracic aortic rupture (BTAI) are highly lethal; up to 80% of patients with acute aortic rupture die at the scene of injury or before reaching the

Scientific Sessions

operating room. Of those that survive to reach medical attention, prognosis is still poor, with a 30% mortality rate within the first 6 hours and a 40% to 50% mortality rate within the first 24 hours after injury. In this series, we report our experience with the endovascular treatment of 7 patients treated with SG for BTAI in the acute phase.

Methods: Out of a series of 29 thoracic aortic stent-graft implantation, 8 patients (mean age: 27 ± 10 years, range 17-69) were treated on an emergency basis for blunt thoracic aortic injuries. 4 out of 8 patients (50%) were hemodynamically unstable. The mean ISS was 56 (range 33-75). Mean elapsed time among E.R. admission and emergency repair was 4 hours. All patients had regular follow-up with CT-angiography and chest X-ray.

Results: Primary technical success rate was 100%; in-hospital mortality rate was 0. We did not observe spinal cord ischemia events. We performed a spiral-CT follow-up at 1, 3, 6, 12 months from the procedure. Mean follow-up was 17 months (range 1-48): the complete exclusion of the injury was achieved in all the patients with no sign of stent-graft complication.

Conclusions: Our experience confirms that endovascular repair is a feasible, safe and effective timely treatment approach emerging as the preferred method of repairing blunt thoracic aortic injuries in trauma patients.

B-063 10:48

Endovascular repair of aneurysm after previous tube graft interposition due to coarctation or traumatic transection

M. Gawenda, J. Heckenkamp, K. Krüger, J. Brunkwall; Cologne/DE

Purpose: Despite primary success, nearly 10% of patients develop aortic aneurysm after open surgical tube-graft interposition due to coarctation of the thoracic aorta and graft interpositions due to traumatic transections at the aortic isthmus. Formation of the false aortic aneurysm carries a significant risk of rupture and lethal outcome. The repeat surgical procedure is associated with more or less 15% in-hospital mortality rate and morbidity from recurrent laryngeal nerve paralysis (~20%), phrenic nerve injury (~5%), or from bleeding. The potential of endovascular repair by the use of stent-grafts instead of redo surgery for post-surgical aortic isthmus aneurysm is unknown.

Methods: prospective clinical study.

Results: The concept of postsurgical endovascular stent-graft placement was evaluated with respect to feasibility and safety in 4 consecutive patients with late aneurysm formation after coarctation repair and traumatic transections at the aortic isthmus. All patients had aneurysm formation late after graft interposition. Patients' ages were 36, 38, 40, and 50 years. Transluminal placement of customized stent-grafts was successful, with no 30-day or 1-year intervention-related mortality or morbidity. Follow-up survey of 13 months in median (range, 1 to 28) revealed optimal reconstruction of the thoracic aorta; 1 case of type-I-endoleak was treated by proximal stent extension, 1 case of type-II-endoleak is still under observation.

Conclusions: Nonsurgical aortic reconstruction of postsurgical thoracic aneurysms forming late after coarctation repair or traumatic transection at aortic isthmus is safe and feasible; interventional stent-graft placement has the potential to avoid repeat surgery of postsurgical aortic aneurysm.

B-064 10:57

Early and mid-term results of endovascular stent-graft in the treatment of descending thoracic aorta diseases

L. Lovato, V. Russo, M. Renzulli, K. Buttazzi, G. Gavelli, R. Fattori; Bologna/IT

Purpose: To report our experience with stent-graft repair in the treatment of descending thoracic aorta diseases.

Methods and Materials: From July 1997 to September 2004, 117 patients underwent thoracic endovascular repair (aortic dissection 38 patients, atherosclerotic aneurysms 25 patients, post-traumatic aneurysms 35 patients, penetrating atherosclerotic ulcers 13 patients and pseudoaneurysms 6 patients). 24 patients, with clinical and/or imaging features of impending aortic rupture, were treated on an emergency basis. CT or MR imaging were performed before the procedure and at 1, 3, 6, 12 months and yearly thereafter.

Results: Successful stent-graft advancement and deployment occurred in 112/117 patients (95%). There was no intraoperative mortality. Complete aneurysm exclusion was obtained in 105/112 cases (6.5% of primary endoleak). In-hospital procedure-related complications consisted of left transient paraparesis (2 patients, 1.7%), bilateral cerebellar ischemia for left subclavian artery occlusion (1 patient) and extension of dissection (1 patient). Secondary endoleaks were observed in 11 cases, 8 successfully treated with secondary procedure. Long-term procedure failure (aortic rupture or conversion to surgery) occurred in 8 cases (7.1%). 13 patients deceased during follow-up for other than aortic causes. 96 patients are alive and well after a mean follow-up time of 27 months (range 1-86).

Conclusion: Endovascular stent-graft repair is technically feasible, highly effective and minimally invasive in the treatment of both acute and chronic descending thoracic aorta diseases. Accurate selection of cases and strict imaging follow-up are necessary to obtain reliable long term results.

B-065 11:06

Thoracic aorta diseases: Stent-graft repair

G. Piccoli, A. Marzio, M. Sponza, R. Frassani, U. Livi, A. Vit, D. Gasparini; Udine/IT

Purpose: Aim of the study is the review of our experience in order to assess the feasibility, safety and efficacy of this technique in acute and chronic aortic lesions.

Materials and Methods: 47 pts have been treated for acute (16 pts) and chronic (31 pts) aortic pathologies. The acute lesions includes 9 pts with aortic traumatic rupture, 4 pts with complicated acute type B dissection and 3 pts with rupture of atherosclerotic thoracic aneurysm. The second group (chronic lesions) includes 27 pts with thoracic or thoracic-abdominal aortic aneurysm and 4 pts with complicated chronic type B dissections.

Results: All patients were treated successfully; two of them needed a second procedure. One pt died of ICD following surgical reconstruction of abdominal aorta after implantation of thoracic stent-graft. There were an accidental rupture of the external iliac artery requiring surgical reconstruction and one major stroke 24 hours after the procedure. One pt suffered medullary ischemia. Two pts died 2 months after the procedure; in both, death was unrelated to the procedure but secondary to other complications of the original pathology. All survivors, at a mean follow-up of 12 months (range, 2 to 42) were asymptomatic: 6-month or 1-year CT controls demonstrate neither prosthesis dislocation nor leaks.

Conclusions: Surgical repair of both aneurysms and dissection of the descending thoracic aorta is often associated with considerable morbility and mortality. On the contrary, endovascular treatment seems to be a feasible, safe and reliable technique for both chronic and acute lesions.

B-066 11:15

Improving early and long term survival in the treatment of type B dissection: Comparison among medical, surgical and endovascular therapy

L. Lovato, K. Buttazzi, E. Angeli, V. Russo, M. Renzulli, G. Gavelli, R. Fattori; Bologna/IT

Purpose: The optimal treatment strategy for aortic type B dissection continues to be controversial.

Methods and Materials: 133 patients admitted to our hospital with type B aortic dissection from 1994 to 2004 and treated with medical or surgical or endovascular therapy, were retrospectively analysed with respect to clinical and imaging outcome. Clinical conditions and two series of CT/MR data (before the treatment and at the last control) were reviewed. Kaplan-Meier method's and the log-rank test were used to compare curves for survival analysis, Mann-Whitney and Kruskall-Wallis's non-parametric tests to compare non-continuous data.

Results: Survival at 30 days was 76% in surgical group and 100% between stent and medically treated patients. The actual cumulative survival estimated for stent-graft, surgical and medical patients were 96%, 67% and 92% at 1 year, 82%, 50%, and 67% at 5 years. Surgical and medical survival became more similar at 9 years (respectively 50% and 55%, p = 0.0098) Survival in stent group was high (93%) also for patients in ASA 4-5 (p = 0.021) or treated under emergency conditions (100% at 3 month vs 27% in surgical group; p = 0.0027). Thoracic aortic diameter reduced in average by 1.03 mm in stent group while increased by 4.25 mm in medical group. 80% of surgical patients developed post-prosthetic dilatation, compared with 22% of stent patients (p < 0.0001).

Conclusion: In the management of this catastrophic disease, stent-graft repair of type B aortic dissection confirms to be a safe and efficacious procedure, providing important alternative to surgical and medical treatment also in the long term.

B-067 11:24



Endoluminal repair of type B aortic dissection

J.P. Morales, N. Fotiadis, T. Sabharwal, R.E. Bell, M. Aukett, S. Thomas, P.R. Taylor, J.F. Reidy; London/UK

Purpose: Aortic dissection is a challenging clinical condition. Surgical resection carries a high risk of paraplegia and death. We have studied the safety and efficacy of endovascular stenting.

Materials and Methods: 27 patients (23 male), mean 66 years (42-86), presented with acute (15) and chronic dissection (12). Indications were increasing size (12), persistent pain (5), ruptured (8), and limb ischaemia (2). 41 stents were deployed

Scientific Sessions

(Gore 23, Talent 7 and Endofit 11) and the left subclavian was covered in 6. CT follow-up was at 3-6 months and yearly thereafter. Diameter change was considered significant if greater than 4 mm.

Results: Technical success was achieved in all patients. 1 patient with an acute MI died at 2 day (30 day mortality 3.7%). Paraplegia occurred in 1 patient and fully recovered after CSF drainage. Otherwise no significant complications. Follow-up in 26 patients was 3-60, mean 27 months. 5 patients (19.2%) were not measured (1 was lost to follow-up and 4 are awaiting CT). Diameter decrease was observed in 13 (50%), increase in 4 (15.4%) and no change in 4 (15.4%). 2 patients had late open repair for increasing size (1 died). Late mortality was 3.7%. False lumen thrombosis occurred in all except 1.

Conclusion: Endovascular repair of type B aortic dissection is associated with significantly lower morbidity and mortality compared with open surgery. The encouraging early results require long term follow-up.

B-068 11:33

Emergent endovascular stentgraft implantation for perforated acute type B dissections and ruptured thoracic aortic aneurysms

J.O. Balzer, M. Doss, A. Thalhammer, M.G. Mack, A. Moritz, T.J. Vogl; Frankfurt a. Main/DE

Purpose: To demonstrate the effectiveness of endovascular stent grafts in the treatment of acutely ruptured thoracic aortic aneurysms and type B dissections as an alternative to the conventional surgical approach in an emergency setting. **Materials and Methods:** From January 2001 to September 2004, we treated 47 patients with either ruptured aortic aneurysms ($n = 28$) or acutely perforated type B dissections ($n = 19$) with endovascular stentgraft implantation. Aortic rupture was confirmed preoperatively by spiral computed tomography. In all cases, hemothorax as well as periaortic hematoma was present. The mean interval from onset of symptoms to treatment was 18.5 hours. We used 58 Talent (Medtronic Inc.) and six Excluder (W.L. Gore Inc.) stent grafts. All interventions were performed in an angiographic suite in general anesthesia and cardiac arrest in 34 cases.

Results: Stentgraft implantation was successful in 45 patients. Access failure due to small caliber of iliac arteries was encountered in one case, and one patient died before endograft implantation could be achieved. Complications encountered were paraplegia ($n = 1$), primary endoleak ($n = 3$), temporary renal failure ($n = 1$), and prolonged mechanical ventilation ($n = 2$). All patients with endoleaks could be successfully treated by a second Stentgraft implantation. At the 12 months follow-up 1 patient had died due to multiorgan failure, and two patients needed conversion to conventional surgical repair. All other patients were alive and free of symptoms.

Conclusion: Our experiences with emergency endovascular stent grafting show that the procedure is technically feasible, with less morbidity and mortality than conventional open surgery, in high-risk patients.

B-069 11:42



Midterm results of the thoracic Excluder: Does it has the same problems as the infrarenal device?

J.P. Morales, P.R. Taylor, J. Deguara, R.E. Bell, M. Aukett, S. Thomas, T. Sabharwal, J.F. Reidy; London/UK

Purpose: Despite good technical results, the Excluder AAA device is associated with sac enlargement in 37% of patients. We have studied the efficacy of the Excluder for aneurysms of the descending thoracic aorta.

Materials and Methods: 30 patients (15 male), mean 70.2 years (44-90) were followed up with computed tomography (CT) at 3-6 months and yearly thereafter. Procedures were urgent in 4 and elective in 26 patients. Sac increase or decrease was considered significant if greater than 4 mm.

Results: 8 patients were not measured. 1 urgent patient died (30 day mortality 3.3%), 1 graft was removed for type I endoleak, 2 were lost follow-up and 4 are awaiting CT scans. Follow-up was 1/12 - 7 years, mean 35 months. Sac increase was observed in 7 (23.3%), decrease in 7 (23.3%), and no change in 8 (26.6%). Late mortality was 13.3% (4 patients) but none were stent related (cerebral infarct 1, MI 1, Bronchopneumonia 1, Haemoptysis 1). Endoleaks were seen in 3 patients (2 spontaneous closures).

Conclusion: The Excluder seems to have similar problems in the thoracic aorta with a significant number of patients having an increase in the aneurysm sac diameter. Careful follow-up is essential.

B-070 11:51

Impaired renal flow resulting from aortic dissection - What is the most effective endovascular treatment?

M. Januszewicz, O. Rowinski, K. Milczarek, M. Jaworski, R. Maciąg, J. Szmidt, Z. Galazka; Warsaw/PL

Purpose: To estimate the effectiveness of endovascular treatment in patients with aortic dissection and renal hypoperfusion.

Material: 56 patients with aortic dissection (33 acute and 23 chronic) of descending aorta and impaired flow in renal arteries. 21 patients showed poor management of hypertension and rise of serum creatinine level. 35 patients manifested only poor management of hypertension. Renal malperfusion was confirmed in Duplex Doppler Sonography. All patients were diagnosed by means of spiral CT and angiography. Depending on the type of renal artery involvement we diagnosed impaired flow in static mechanism (15 cases) or dynamic mechanism (29 cases). In 2 patients we diagnosed renal artery dissection with re-entry site within the branch. In 10 patients renal hypoperfusion was anticipated after stentgraft placement in cases of renal artery arising from the false lumen.

Methods: 36 stentgraft implantations, 3 stentgraft and fenestrations or renal stenting, 1 stentgraft and additional surgical treatment, 4 renal stenting, 2 covered renal stents, 4 fenestrations.

Results: In 54 cases improvement of renal perfusion has been achieved. In 20 cases renal function and hypertension management has been improved. In 1 case we encountered unsuccessful fenestration. In 1 case covered renal stent implantation has become complicated with renal artery occlusion.

Conclusions: In most cases successful closure of the entry tear by stentgraft is sufficient for restoring renal flow. Approximately 20% cases require additional intervention combining of fenestration, peripheral stenting or open surgery. In chronic and stable dissection fenestration or peripheral stenting may be sufficient methods of treatment.

10:30 - 12:00

Room I

Interventional Radiology

SS 209b

Experimental interventions in models and animals (1)

Moderators:

J. Ramón Fortuño; Sabadell/ES
R. Yamada; Osaka-Sayama/JP

B-071 10:30

Superabsorbent polymer microspheres: A new embolic agent. An experimental study with pig kidneys

E. De Luis¹, J.-I. Bilbao Jaureguizar¹, P. Martínez-Miravete¹, J.J. Noguera¹, A. Martínez-Cuesta¹, J.A. García de Jalón², ¹Pamplona/ES, ²Zaragoza/ES

Purpose: Superabsorbent Polymer Microspheres (SAPM) are a new embolic agent that adapts itself to the arterial wall. SAPM alter their shape and size depending on the contrast media in which they are diluted. These spheres induce an inflammatory reaction and local necrosis that depend on the contrast media used for the dilution and the particle size.

Methods and Materials: We performed a study with 19 pigs (38 kidneys) that were embolised with SAPM. We used two different sizes of particles (50 and 150 microns) and two contrast media (Iodixanol and loxaglate). These organs were extracted right after the procedure (4 pigs) or one-month later (15 pigs). Samples of the kidneys stained with hematoxylin-eosin were evaluated.

Results: SAPM do not induce thrombosis around particles. The necrosis resulting from the embolization is due to the plasticity of particles that perfectly adapt themselves to the arterial wall. This necrosis depends on the particle size and the contrast media used for the dilution, being more intense when 150 microns SAPM are used mixed with loxaglate.

Conclusion: This new embolic agent alters its properties and its therapeutic effect depending on the size of the particles and the type of contrast media in which they are mixed. Clinical applications should be evaluated with new studies.

Scientific Sessions

B-072 10:39

Influence of hepatic vessel size on volume and shape of percutaneous thermoablative lesions: In-vivo evaluation in a porcine model

B.B. Frericks, K.S. Lehmann, J.P. Ritz, S. Valdeig, H.J. Buhr, K.J. Wolf; Berlin/DE

Purpose: To investigate the effect of hepatic vessel size on volume and shape of percutaneous thermoablative lesions in an in-vivo model.

Methods and Materials: 10 pigs were examined and treated in general anesthesia. After contrast enhanced multiphasic 16-detector row CT (Sensation 16, Siemens; slice thickness 1 mm, RI 0.8 mm), CT-guided laser-induced thermotherapy (LITT) with a power setting of 28 W for an exposure time of 15 minutes was performed. The distal end of the applicator was positioned either in close contact to major hepatic vessels or centrally within liver parenchyma. Immediately after LITT a second CT-scan was obtained. After extraction and fixation the liver was cut in 2 mm slices and the volume and shape of the coagulation area was determined using a digital macro camera and subsequent image analysis. Distance and diameter of the adjacent vessels were measured. Results were compared to CT and histologic findings.

Results: The macro imaging system allowed the determination of vessel diameter and the according cooling effects. Depending on vessel size and the position of the laser applicator relative to the vessel, lesion sizes and shapes were significantly altered, leading to horse-shoe- or sand-glass-like lesions. If the LITT-catheter ran parallel to a large vessel an asymmetry of the thermal lesion was observed.

Conclusion: In this porcine model size and shape of thermal ablation lesions are influenced by larger portal and hepatic veins. Based on these results, a software tool for semi-automatic simulation of the expected lesion morphology is currently under investigation.

B-073 10:48

MR guided intramyocardial injection using an MR imaging compatible catheter: Feasibility and changes of T1 values after injection of extracellular contrast medium

G.A. Krombach, J.E. Pfeffer, S. Kinzel, R.W. Günther, A. Buecker; Aachen/DE

Purpose: To assess the feasibility of MR-guided intramyocardial injection of Gd-DTPA-BMA using real-time imaging and to quantify T1-values and the size of the enhanced region for different concentrations of contrast agent for 30 min.

Material and Methods: A catheter with a needle tip was advanced into the left ventricle of 7 pigs using real-time MR imaging (radial true-FISP). After intramyocardial injection of 2 ml Gd-DTPA-BMA solution at concentrations of 0.05 or 0.1 mmol/ml, local changes of T1 and size of enhanced region were measured 3, 15 and 30 min after injection, using the Look-Locker sequence.

Results: Catheter guidance and visualization of contrast medium distribution were feasible in all animals. Local changes in T1 values were significantly different for both concentrations (0.05 mmol/ml: 456 ± 5 ms; 0.1 mmol/ml: 228 ± 4 ; $p < 0.001$) measured 3 min after injection. T1 values increased significantly to 720 ± 7 ms for 0.05 mmol/ml Gd-DTPA-BMA and 445 ± 6 ms for 0.1 mmol/ml Gd-DTPA-BMA, 30 min after injection, but remained significantly lower than those of remote myocardium (879 ± 8 ms). The size of the enhanced region increased from 13 ± 2 mm^2 at 3 min to 30 ± 3 mm^2 at 30 min ($p < 0.05$).

Conclusions: MR-guided intramyocardial injection of Gd-DTPA-BMA is feasible using real-time imaging and passive delineation of the catheter. The resulting increase of signal intensity at the injection site allowed for delineation of distribution of the injected solution for the time of the intervention. Thus repeated injections into the same region can be avoided.

B-074 10:57

Initial in vivo results with flat panel detector C-arm CT

R. Fahrig, N. Strobel, J.C. Hellinger, J.K. Frisoli, H. Arakawa, M. Marks, H.M. Do, M. Kukuk, G.M. Glazer; Stanford, CA/US

Purpose: A new 3D C-arm CT system (Siemens Artis dTA DynaCT, 30x40 cm flat panel (3D-FD)) extends the capabilities of C-arm CT to soft-tissue imaging, allowing detection of low-contrast objects. We report initial experience in a porcine model for a range of *in vivo* imaging applications with comparison to conventional CT.

Methods and Materials: Five animal investigations compared 3D-FD image quality with conventional CT. Each animal was imaged using a Siemens Sensation-16 clinical scanner (80 kVp, 100-150 mAs, 1 mm slice) before and 70 s after an injection into the femoral artery (30 s injection, 3 ml/s, 300 mg/ml Iodine). The FD system was used to acquire 3D CT volumes (30 s rotation, 0.25-0.5 mm slice, 70 kVp, 190 views) of: 1.) liver during intravenous injection and during selective hepatic artery injection (3 ml/s, 30 s); 2.) brain after injection of 5 cc's autologous

blood (hematocrit ~18%); 3.) abdominal aorta after the placement of nitinol stent; 4.) thorax.

Results: In the liver 3D-FD images clearly depicted the major portal and hepatic veins to the 200 micron level comparable to conventional CT; 3D-FD images obtained during hepatic arterial injection showed vessels below 100 microns (partial volume). In the brain, autologous blood clot was visualized. Individual struts of the abdominal stent could be seen in 3D-FD images. Images of the thorax showed vascular and bronchial detail with excellent clarity.

Conclusions: C-arm CT with FD (Artis dTA DynaCT) has been demonstrated to possess sufficient soft-tissue contrast to support broad clinical applications in the brain, thorax and abdomen, and enables new capabilities for 3D guidance.

B-075 11:06

Effect of laser-induced thermotherapy (LITT) on liver metastasis of varying size

A. Maataoui, J. Qian, M.G. Mack, M.F. Khan, R. Straub, E. Oppermann, T.J. Vogl; Frankfurt a. Main/DE

Purpose: To assess the effect of laser-induced thermotherapy (LITT) of liver metastasis of varying size from colon carcinoma in an animal model.

Materials and Methods: Liver metastases were implanted in 20 Wistar Albino Glaxo (WAG) rats by sub capsular injection of cells from a colorectal strain (CC531) (day 0). The animals were divided into two groups having regard to the measured tumor size varying from $0.05 - 0.06 \text{ cm}^3$ (Group A) and $0.10 - 0.12 \text{ cm}^3$ (Group B). On day 14 after laparotomy and intratumoral placement of the laser applicator set tumors were exposed to 1064 nm Nd:YAG laser light at 2 watts for 5 minutes. The tumor volumes before (V1, at day 13) and after treatment (V2, at day 28) were determined by MR imaging and the mean tumor growth ratio (V2/V1) was calculated.

Results: The mean tumor volumes V1 and V2 were $0.05 \pm 0.003 \text{ cm}^3$ and $0.23 \pm 0.016 \text{ cm}^3$ in group A, $0.11 \pm 0.006 \text{ cm}^3$ and $0.68 \pm 0.037 \text{ cm}^3$ in group B, respectively. The mean tumor growth ratio (V2/V1) was 4.31 ± 0.19 in group A, 6.11 ± 0.14 in group B, respectively. The mean volume of the induced necrosis ($0.15 \pm 0.01 \text{ cm}^3$) was for both groups alike ($P > 0.05$). Compared to group B liver metastases of group A showed a significant slower tumor growth velocity (double side t-test, $P < 0.0001$).

Conclusion: The interventional treatment of big hepatic tumors with LITT leads to a faster tumor growth compared to smaller lesions.

B-076 11:15

Parallel wet bipolar radiofrequency ablation of the liver: In vivo and ex vivo experiments with perfused-cooled electrodes

J. Lee, J. Han, S. Kim, J. Lee, K. Shin, B. Choi; Seoul/KR

Objective: To compare the performance of wet bipolar radiofrequency ablation (RFA) with that of wet-monopolar RFA *ex vivo* in bovine liver and *in vivo* in canine liver.

Materials and Methods: RFAs were performed using a 200 W generator and a 15-gauge perfused-cooled electrode with infusion of 6% hypertonic saline at 2 mL/min. In *ex vivo* experiments, 20 thermal ablation regions were created in wet monopolar (group A), and in wet bipolar mode (group B) with a 3-cm inter-electrode spacing. In *in vivo* experiments, a thermal ablation region was created by wet bipolar RFA using two perfused-cooled electrodes in each of 8 dogs via laparotomy. The volumes of the RF-induced ablation regions were measured, and lesion shapes were evaluated by computing their isoperimetric ratios.

Results: No significant difference in mean current was observed in groups A and B: 1543 ± 53.7 mA, and 1520 ± 89.6 mA, respectively ($p > 0.05$). However, the mean volumes of the ablation regions produced in group A ($33.9 \pm 12.7 \text{ cm}^3$) were lower than those produced in group B ($54.0 \pm 16.5 \text{ cm}^3$) ($p = 0.007$). In *in vivo* experiments, the mean volume of the coagulation necrosis created by wet bipolar radiofrequency ablation was $39.4 \pm 15.6 \text{ cm}^3$, with an isoperimetric ratio of 0.75 ± 0.1 .

Conclusion: Parallel wet bipolar radiofrequency ablation showed better performance in terms of creating a larger region of coagulation necrosis than wet-monopolar ablation.

B-077 11:24

Combined radiofrequency tumor ablation and acetic acid-hypertonic saline solution injection in a rat N1S1 liver tumor model: Effects on tissue coagulation

J. Lee, J. Han, S. Kim, J. Lee, B. Choi; Seoul/KR

Purpose: To determine whether 15% acetic acid-hypertonic saline solution (AHS)

Scientific Sessions

instillation before radiofrequency ablation (RFA) can increase the extent of coagulation necrosis in a rat N1S1 liver tumor model compared to RFA alone or combined RFA and ethanol injection therapy.

Materials and Methods: N1S1 tumors were implanted in the livers of 50 rats. Rats were assigned to one of five groups: (a) RFA using an internally cooled electrode with a 1-cm tip (20 watt; 3 mins); (b) combined RFA with the instillation of 0.3 mL of 15% acetic acid diluted in a saturated NaCl solution; (c) combined RFA with 0.3 mL of 100% ethanol instillation; (d) 15% AHS injected alone; and (e) a sham operated control group. We compared the resultant coagulation achieved by these different ablative strategies and RF parameters, such as impedance, current, and power.

Results: The combination of RF ablation with AHS or ethanol resulted in greater coagulation than by either therapy alone: 14 ± 2 mm (group A), 25 ± 3 mm (group B), 19 ± 4 mm (group C), 10 ± 5 mm (group D) ($P < 0.05$). However, maximum coagulation was observed with AHS, which ablated the entire tumor in eight cases. Significantly greater current deposition was observed when the tumors were pretreated with 15% AHS than with ethanol: 411 ± 66 mA and 281 ± 88 mA ($P < 0.05$).

Conclusion: The combination of AHS instillation with RFA substantially increases tumor destruction compared with RF or injection therapy alone.

B-078 11:33

Radiofrequency ablation of hepatic malignancies: Percutaneous insertion of an MR imaging-compatible application probe

C. Rosenberg, C. Weigel, N. Hosten; Greifswald/DE

Purpose: To evaluate efficacy and advantages of a new MR imaging-compatible probe for radiofrequency ablation (RFA) of primary and secondary liver malignancies. CT for needle placement can not be used if lesions are not seen in plain CT. Results from an ongoing study are presented.

Materials and Methods: RFA was performed using a 17 G saline-cooled single probe (Cool-tip®, Radionics). Optimal conditions for cooling, energy and ablation time were retrieved testing the system in porcine liver. Patients were strictly evaluated for insufficient CT imaging. 19 Patients received ablative therapy in a standardized manner. Percutaneous insertion and therapy monitoring were performed in a closed high-field scanner using a breath-hold T1-weighted GRE sequence.

Results: Lesions were well visualized in plain or contrast-enhanced MR imaging. Ablation time of 15 minutes and energy elevation to a maximum 200 W were found suitable to achieve safe and sufficient ablation of targeted malignant tissue. Maximal induced coagulative necrosis was 15.7 ccm in a single application. Lesion ablation was technically and clinically successful. Miniaturized design and surface profile of the application probe benifited its handling. The needle was well visualized in TRUEFISP and 2dFLASH sequences with minimal imaging artifacts not limiting the intervention.

Conclusion: MR imaging-guided RFA of liver malignancies is a safe and feasible procedure in an interdisciplinary multimodal cancer therapy. Advantages are evident for lesions not seen in plain CT. Probe insertion and therapy can be performed in one setting using a single imaging modality. Safety and feasibility of critical positioning maneuvers are increased using multiplanar imaging.

B-079 11:42

Accuracy of combined PET/CT in image-guided interventions of liver malignancies: An ex-vivo study

P. Veit, C. Kuehle, C. Herborn, H. Stergar, T. Beyer, A. Bockisch, H. Kuehl, G. Antoch; Essen/DE

Objective: Positioning of interventional devices for biopsy or radiofrequency ablation of liver lesions is a challenging task if only morphological data are available. We investigated the potential benefit of co-registered PET/CT data in liver interventions.

Materials and Methods: 90 lesions were injected in 15 ex-vivo pig livers, two hypodense, two isodense, and two hyperdense lesions each per liver. Each lesion was composed of 20 mL gelatine, different amounts of an iodine-based contrast agent, and 0.5 MBq of [¹⁸F]-2-Fluoro-2-deoxy-D-glucose (FDG). RF-probes were placed in these lesions under CT-guidance. CT and PET/CT imaging were performed to all lesions after needle placement. The accuracy of CT and PET/CT for determining the needles' position within the lesion was assessed by measuring the distance of the needle tip from the lesions' margins on CT and PET/CT. Imaging findings were correlated with macroscopic measurements after lesion dissection which served as the standard of reference.

Results: In hypo- and isodense lesions PET/CT proved significantly more accurate in defining the position of the interventional device ($p < 0.05$) based on the

additional functional data. There was no statistically significant difference between the two imaging procedures when determining the needles' position in hyperdense lesions.

Conclusion: Combined PET/CT adds additional information to CT alone when assessing the position of interventional devices within iso- and hypodense liver lesions. PET/CT can be recommended for planning of liver interventions, but should be limited to potentially curative procedures based on its additional complexity and cost.

B-080 11:51

Development and experimental testing of a percutaneous temporary pulmonary stent device for severe pulmonary embolism

R.K. Verma, J.E. Pfeffer, R.W. Günther, T. Schmitz-Rode; Aachen/DE

Purpose: Development of a percutaneous temporary stent device with adequate steerability and quick placeability for recanalization of central pulmonary embolism.

Methods and Materials: After developing a self-expandable Nitinol-stent, which was mounted at the cathetertip and could be placed across the thrombotic occlusion, in-vitro tests were performed in a benchtop pulmonary circulation model. In-vivo tests followed in 6 sheep. Partially organized thrombus material was introduced via the right jugular vein to produce pulmonary embolism. The catheter device was inserted via the right femoral vein and the stent deployed bridging the thrombus. During stent placement pulmonary angiography was performed to image the extent of recanalisation. After the procedure the stent catheter was removed. **Results:** Stent placement was successfully tested in-vitro. In-vivo the catheter device could be placed quickly and navigated adequately in all 6 sheep pulmonary arteries by bridging the whole embolus. Angiography confirmed recanalization in all cases to a certain amount, depending on the stretching quality of the stent and the consistency of the thrombus. After the procedure the stent was gently removed into the catheter with no trouble. Macroscopically slight wall damages in the pulmonary trunk and the left descending artery were found in one case.

Conclusion: The newly developed self expandable and removable stent can be placed quickly and adequately in case of central pulmonary embolism and allows an instant partial pulmonary recanalization. After circulatory stabilization the device can be removed trouble-free.

10:30 - 12:00

Room K

Cardiac

SS 203

MR imaging in cardiomyopathy

Moderators:

Y.H. Choe; Seoul/KR
P. Croisille; Lyon/FR

B-081 10:30

MR imaging gadolinium enhancement in cardiac amyloidosis as potential expression of the disease severity

V. Russo, E. Perugini, L. Lovato, M. Renzulli, C. La Palombara, C. Rapezzi, G. Gavelli, R. Fattori; Bologna/IT

Purpose: The aim of this study was to investigate prevalence and distribution of MR imaging gadolinium enhancement in patients with cardiac amyloidosis (CA) and its possible associations with clinical, morphological and functional features.

Methods and Materials: Eighteen patients with definitely diagnosed CA underwent gadolinium Cardiac MR imaging (Gd-CMRI). In all patients a breath-hold cine MR sequence was performed, covering the whole left ventricle in short axis plane and in four-chamber view. A segmented inversion recovery fast gradient echo sequence (IR-FGE) was performed in the short-axis plane of the left ventricle and in four-chamber view after Gadolinium injection.

Results: Gd enhancement was detected in 14/18 (77%) patients. Fifty-four of 306 (16.7%) segments were enhanced, more often at mid-ventricular level. Transmural extension of enhancement within each patient significantly correlated with left ventricular (LV) end-systolic volume ($r = 0.53$). Number of enhanced segments correlated with LV end-diastolic volume ($r = 0.76$), end-systolic volume ($r = 0.6$) and left atrial size ($r = 0.58$). Patients with enhancement in > 50% transmural extension more often had severe hypokinesia or akinesia ($p = 0.0001$). Patients with > 2 enhanced segments showed significantly lower 12-lead QRS voltage.

Conclusions: Gd enhancement is common in CA, probably due to expansion of infiltrated interstitium. The segmental and transmural distribution of the

Scientific Sessions

enhancement is highly variable, and midventricular regions are more frequently involved. Enhancement appears to be associated with impaired segmental and global contractility and larger atrial size. Gd-CMRI provides a unique opportunity for non-invasive study of amyloid myocardial infiltration and its pathophysiological consequences.

B-082 10:39

Correlation between phosphocreatine (PCr) to ATP ratio (PCr/ATP) at cardiac ^{31}P -MR spectroscopy and fibrosis at delayed-contrast enhanced MR imaging in hypertrophic cardiomyopathy (HCM)

A. Esposito, F. De Cobelli, G. Perseghin, E. Belloni, M. Pieroni, C. Chimenti, A. Frustaci, A. Maseri, A. Del Maschio; *Milan/IT*

Purpose: Reduced PCr/ATP myocardial ratio has been described in patients with HCM. Also known in these patients is the presence of delayed-gadolinium enhanced regions representing areas of increased myocardial collagen. Our specific purpose was to determine the relationship between these two features. **Methods and Materials:** 13 HCM patients underwent cardiac ^{31}P -MR-Spectroscopy (^{31}P -MRS) and cardiac-MR imaging on a 1.5 T system (Gyroscan Intera, Philips Medical System). 13 normal subjects underwent cardiac ^{31}P -MRS as control group. ^{31}P -spectra were acquired by using 10 cm-diameter surface-coil and corrected for partial saturation effects and blood contribution. PCr/ATP was normalized for left ventricular (LV) mass. ECG-gated black-blood TSE sequences were acquired for morphologic evaluation and cine-balanced-FFE for wall motion and functional analysis. 15 minutes after gadolinium-DTPA (0.2 mmol/Kg) injection, delayed MR-images were obtained with 3D-T1w-TFE sequence, adjusting inversion time to null normal myocardium. All HCM patients underwent cardiac catheterization with LV endomyocardial biopsy to verify histological features of delayed enhanced tissue.

Results: PCr/ATP was lower in HCM patients compared to control subjects (1.05 ± 0.12 vs 1.63 ± 0.17 ; $P < 0.05$). Delayed-enhanced areas were found in 11 HCM patients. The biopsies obtained from these areas showed abnormal presence of fibrosis. The volume of enhanced tissue (range = $0.1\text{--}40.4 \text{ cm}^3$; mean value = $14.60 \pm 3.51 \text{ cm}^3$) was inversely related to LV ejection fraction ($R = -0.58$; $P < 0.05$). Strong negative correlation was found between the volume of enhanced tissue and PCr/ATP ($R = -0.76$; $P < 0.005$).

Conclusion: Delayed-contrast enhanced MR-images allow the identification of fibrotic areas in LV wall of HCM patients. The presence of fibrotic regions could partially explain the low PCr/ATP showed in HCM patients.

B-083 10:48

Magnetic resonance angiography and phase-shift velocity mapping of the pulmonary veins compared to transesophageal echocardiography before and after radiofrequency catheter ablation for atrial fibrillation

A. Koops, B. Lutovsky, A. Stork, S. Willems, C. Nolte-Ernsting, G. Adam; *Hamburg/DE*

Purpose: Pulmonary vein (PV) stenosis is a known complication of radiofrequency catheter ablation for the treatment of atrial fibrillation. The aim of this prospective study was the early detection of PV stenosis by MRA and TEE.

Methods and Materials: Twenty-five patients underwent MRA and TEE prior to catheter ablation; 6 months follow-up was accomplished in 9 patients. MRA involved contrast-enhanced, FLASH-sequences for angiography and ECG-triggered phase-shift velocity mapping orthogonal to the distal PV section for flow measurements. Likewise, during TEE the Doppler sample volume was positioned in the PV adjacent to the venoatrial junction.

Results: MRA allowed reliable visualization of the morphology of all PV, whereas TEE showed an unreliable depiction of the left inferior PV with inconsistent venous flow detection. Maximum flow values calculated by magnetic resonance measurement for the left superior, left inferior, right superior and right inferior PV were 37.3, 38.9, 41.4 and 34.6 cm/s, respectively. On average, the maximum flow values assessed by TEE were 27.5% higher. Mean flow was 10.4, 11.6, 10.0 and 10.2 cm/s, respectively, which measured 54.0% higher by TEE. Post-interventionally one PV stenosis of a left superior PV was detected by MRA with a maximum flow increase to 82.1 cm/s (90.0 cm/s by TEE).

Conclusion: Flow differences between MRA and TEE may be explained by superior anatomical depiction thus allowing more exact positioning for in-plane measurement. MRA is capable of visualisation of all PV, while TEE lacks depiction of the left inferior pulmonary vein, in which stenosis commonly occurs.

B-084 10:57

Utility of real-time cine-MR imaging in the differential diagnosis between constrictive pericarditis and restrictive cardiomyopathy: Preliminary results

M. Francone, M. Kalantzi, F. Rademakers, M. Herregods, S. Dymarkowski, J. Bogaert; *Leuven/BE*

Purpose: Since pericardial thickness is not unfrequently normal (< 2 mm) in patients with surgically-proven constrictive pericarditis (CP), this morphologic parameter may not be reliable to diagnose CP. Assessment of the functional impact of CP on ventricular filling with real-time MR imaging may be more reliable to differentiate CP from restrictive cardiomyopathy (RCM).

Materials and Methods: In 15 CP, 10 RCM patients and 15 normal subjects, real-time MR imaging using a SSFP sequence in the midventricular cardiac short-axis (temporal resolution: 60 ms) was performed during continuous breathing with deep in- and expiration. The influence of respiration on ventricular septal position and total septal excursion normalized to total biventricular diameter was evaluated.

Results: Inspiratory flattening/inversion was found in CP: 15; normals: 1; RCM: 0. Flattening/inversion during early ventricular filling was always most prominent during onset of inspiration. Total respiratory septal excursion was significantly large in CP ($18.7 \pm 1.2\%$) than in normals: ($7.1 \pm 2.4\%$) $p < 0.0001$ and RCM ($5.8 \pm 2.1\%$) $p < 0.0001$. A cut-off value of 11.9% (mean $\pm 2 \text{ SD}$) is useful to discriminate CP patients from normal subjects and RCM patients, even in the presence of a normal pericardial thickness on MR imaging (present in 33% of CP in this series).

Conclusions: Pathologic ventricular coupling, ie, abnormal ventricular septal flattening or inversion during onset of inspiration and increased total respiratory septal excursion, is a reliable criterium to differentiate CP from RCM patients.

B-085 11:06

Evolution of MR imaging findings of arrhythmogenic right ventricular cardiomyopathy at follow-up

N. Limbucci, V. Pupillo, L. Mancini, E. Stavroulis, E. Di Cesare, C. Masciocchi; *L'Aquila/IT*

Purpose: To assess the evolution of MR imaging findings of arrhythmogenic right ventricular cardiomyopathy (ARVC) after 5 year follow-up in patients with diagnosed ARVC.

Methods and Materials: We studied 26 patients with diagnosed ARVC according to the international criteria. All patients underwent cardiac-MR imaging 43-60 months (average 49.8 months) after a previous MR imaging suggestive for ARVC. All examinations were performed with the same 1.5 T GE unit, with black-blood morphologic sequences and bright-blood breath-hold cine sequences.

Results: 15 patients (57.7%) presented right ventricular dilation, fat infiltration and dyskinetic areas at first MR imaging. 12 of 15 cases (80%) showed similar findings at follow-up. In 3 of 15 patients (20%) we observed evolution of the previously described findings with extension of the infiltrated and dyskinetic areas. In one of these cases the outflow tract diameter increased from 37 to 41 mm. In 6 patients (24%) the first MR imaging showed fat infiltration and dyskinetic areas, in 4 of them (66.6%) follow-up MR imaging showed comparable findings, in 1 case (16.7%) the fat infiltration was not evident, in 1 patient (16.7%) the dyskinetic area extended. In 5 patients (19.2%) with isolated fat infiltration evidence, follow-up MR imaging confirmed the findings in 2 cases (40%) but in 3 cases (60%) the new MR imaging could not confirm the finding.

Conclusion: Most of patients with MR imaging findings of ARVC presented a stable pattern at follow-up, but in some cases MR imaging showed disease evolution. Fat infiltration was not always confirmed at follow-up, agreeing with previous studies about the low specificity of this finding.

B-086 11:15

Myocardial tissue characterization by magnetic resonance imaging (MRI) in Anderson-Fabry disease

M. Imbriacomo, G. Sica, S. Maurea, M. Quarantelli, A. Cuocolo, M. Salvatore; *Naples/IT*

Purpose: Anderson-Fabry disease (AFD) is a multisystem X-linked disorder of lysosomal metabolism frequently associated with left ventricular (LV) hypertrophy. This study aimed to assess whether myocardial T2 relaxation time (MT2RT), determined by a black-blood multi-echo MRI sequence could help to evaluate cardiac involvement in AFD.

Materials and Methods: Nine patients with AFD (M/F: 7/2; mean age: 35 ± 10 years) and nine age-matched healthy controls (M/F: 7/2; mean age: 34 ± 14 years) underwent MRI. MT2RT was calculated using a T2 weighted black-blood TSE sequence at different echo times (TE): 45, 60, 75 and 90 msec in the

Scientific Sessions

4-chamber horizontal long-axis. Regions of interest were placed along interventricular septum, apex and lateral walls on the first echo image and reproduced on the other echo images. MT2RT was calculated using a linear least-square fit applied on the logarithm of myocardial signal intensity versus echo time according to the formula $M(TE)=M e^{-TE/T}$. A balanced-fast field echo multiphase-multislice sequence covering the left ventricle with 9-10 slices across the biventricular short axis from apex to base was obtained for evaluation of LV mass; LV mass index (LVMI) was subsequently calculated.

Results: In patients with AFD, MT2RT was 75 ± 7 msec in the interventricular septum, 78 ± 11 msec in the apex and 77 ± 11 msec in the lateral wall vs 51 ± 7 msec, 54 ± 5 msec and 51 ± 6 msec of the controls ($p < 0.001$). LVMI was 120 ± 32 g/m² in patients with AFD and 63 ± 9 g/m² in the controls ($p < 0.001$).

Conclusion: MT2RT is significantly prolonged in patients with AFD compared to controls. MRI may be useful for characterization of myocardial tissue in such patients and for monitoring the effects of enzyme replace therapy.

B-087 11:24

MR planimetry in aortic valvular stenosis

M. Lederlin, P. Reant, M. Montaudon, O. Corneloup, S. Lafite, F. Laurent; *Pessac/FR*

Purpose: Measurement of aortic valve area (AVA) is essential to evaluate the severity of aortic stenosis. The objective of this study was to evaluate the reliability of direct planimetry by MR imaging to measure aortic valve area in aortic stenosis and to compare MR imaging measurements with values obtained by current diagnostic techniques ie. transthoracic echocardiography (TTE), transoesophageal echocardiography (TOE), and cardiac catheterization.

Methods and Materials: 45 consecutive patients with aortic stenosis (ranging from 0.4 to 1.9 cm²) underwent TTE, TOE, cardiac catheterization, and MR imaging. By TTE and cardiac catheterization, AVA was indirectly assessed by the continuity equation (Doppler velocity-time integral) and the Gorlin equation (available in 27 subjects), respectively. By TOE and MR imaging, absolute AVA was measured by direct planimetry. We used steady-state-free-precession (SSFP) sequences on a 1.5 T Siemens system to perform the MR planimetric quantification of the stenosis.

Results: Mean AVA was 1.19 ± 0.88 cm² by TTE, 1.13 ± 0.78 cm² by TOE, and 1.21 ± 0.85 cm² by MR imaging. No significant difference was observed between TOE and MR imaging measurements, with a strong correlation coefficient ($r = 0.94$). Bland-Altman analysis evaluating intraobserver and interobserver variability showed a very small bias for both absolute measurements.

Conclusion: Magnetic resonance planimetry of the aortic valve area can be used alternatively to TOE as a reliable and reproducible tool for assessing absolute measurements of aortic valve area in subjects with aortic stenosis.

B-088 11:33

Myocardial scarring in beta thalassemia major by late gadolinium-enhanced magnetic resonance imaging: Correlation with myocardial iron overload and ECG-changes

F. Sorrentino¹, A. Pepe¹, V. Borsellino¹, M. Galia¹, M. Midiri¹, M. Lombardi²; ¹Palermo/IT, ²Pisa/IT

Purpose: Aims of this study were a) to determine in patients (pts) with beta thalassemia major (TM) whether myocardial scarring (MS) can be detected by late gadolinium-enhanced magnetic resonance imaging (MRI); b) to correlate the presence of MS with myocardial iron overload (MIO) and ECG-changes.

Materials and Methods: 38 beta TM pts were enrolled. Myocardial fibrosis was determined by late gadolinium-enhanced MRI. Images were evaluated by a visual assessment of two independent observers and by a semi-automatic post-processing software tool for objective pixel quantification. MIO was determined by a gradient T2-star (T2*) multi-echo sequence on three parallel short axis views (basal-medium-distal) of left ventricle. Twelve lead ECG was performed in 30 patients before the MRI study.

Results: Scarring was present in 15 patients, and it was predominantly patchy. Out of the 15 pts, 11 had two or more foci of scarring. Out of the 36 areas of scarring, 19 involved the interventricular septum. Scarring did not follow coronary distribution. No asynergic segments were detectable. Myocardial fibrosis did not significantly affect the T2* value. A significant correlation was found between the presence of MS and ECG changes (atrio-ventricular block, right bundle-branch block, ST segment depression, T wave inversion, abnormal Q-waves or decreased R waves). The sensitivity, specificity, negative and positive predictive value of ECG in detecting MS were 90%, 63%, 92% and 58%, respectively.

Conclusion: MS is detectable in a significant percentage of patients with beta TM. MS did not correlate with MIO. ECG-changes showed a significant accuracy to predict MS.

B-089 11:42

T2* measurement in patients with beta thalassemia major: Effect of heterogeneity of myocardial iron overload, myocardial fibrosis and blood oxygenation

F. Sorrentino¹, A. Pepe¹, C. Lo Pinto¹, V. Di Salvo¹, M. Midiri¹, M. Lombardi²; ¹Palermo/IT, ²Pisa/IT

Purpose: Aims of this study were: 1) to assess tissue iron concentration using the T2* multiecho technique; 2) to determine whether T2* measurements are influenced by heterogeneity of iron distribution, presence of myocardial fibrosis (MF) and blood oxygenation (BO).

Materials and Methods: 43 regular transfused patients (pts) with beta thalassemia major were enrolled. Three parallel short axis views (basal-medium-distal) of left ventricle were obtained by a gradient T2* multiecho sequence. Segmentation into four regions (anterior, lateral, posterior, septal) and T2* values within them were automatically obtained in order to evaluate the heterogeneity of iron distribution. MF was assessed by late gadolinium-enhanced magnetic resonance imaging (MRI). The BO was assessed by the non invasive measurement of oxygen pressure (P_{O₂}) during MRI exam.

Results: We identified three groups: A) with an homogeneous myocardial iron overload (MIO); B) with no MIO and C) with an heterogeneity of iron distribution. A correlation between the average of T2* values in all the 12 segments and the T2* value in the mid-ventricular septum was found; the latter showed a significant difference between A and C group and between C and B group. The range of the T2* value in the mid-ventricular septum showed an overlap between A and C group and between C and B group. MF did not significantly affect the T2* mean value. The P_{O₂} did not correlate with the T2* value.

Conclusion: MIO showed an heterogeneous distribution in about 50% of pts. MF and BO do not effect T2* cardiac measurements.

B-090 11:51

Use of inversion recovery contrast-enhanced MR imaging (IR-CE-MRI) in the evaluation of patients with clinically suspected pericarditis

M. Francone, A. Taylor, M. Kalantzi, S. Dymarkowski, J. Bogaert; *Leuven/BE*

Purpose: Diagnosis of pericarditis with current imaging techniques is not always straightforward. As pericarditis is an inflammatory process, IR-CE-MRI (similar to late enhancement myocardial MRI) may be of value for detecting pericardial inflammation.

Materials and Methods: An MRI study that included late enhancement acquisitions after contrast-administration (0.2 mmol/kg bodyweight Gd-DTPA) was performed in 31 patients with clinical suspicion of pericardial disease (PD group), 22 patients with a recent history (< 3 weeks) of acute MI (AMI group), and 12 patients with no clinical evidence of pericardial disease (CON group). Images were analyzed for the presence of pericardial effusion, pericardial thickening and pericardial enhancement.

Results: Enhancement of the pericardial layers was found in 11/31 (moderate: 4, strong: 7) patients in the PD group, which was not related to the concomitant presence of pericardial fluid. Enhancement was helpful for demonstrating acute inflammation of the pericardial layers, differentiating inflammatory from fibrosing forms of chronic pericarditis, and defining the different components of pericardial thickening (e.g. pericardial layers vs pericardial effusion). Although in the AMI group minimal pericardial effusion was found in 12 patients, in only 4 was pericardial enhancement detected (moderate: 2, slight: 2). The two patients with moderate pericardial enhancement had clinical evidence of post-infarction pericarditis. In all 12 patients in the CON group, no pericardial thickening or enhancement was demonstrated.

Conclusions: The present study results suggest a more versatile use for IR-CE-MRI, enabling visualisation of pericardial inflammation in patients with clinical suspicion of pericardial disease and detection of post-infarction pericarditis in patients with recent acute MI.

Scientific Sessions

Friday

10:30 - 12:00

Room L/M

Neuro

SS 211

Inflammatory, infectious and degenerative CNS disease

Moderators:

M. Essig; Heidelberg/DE

A.D. Gouliamou; Athens/GR

B-091 10:30

Diffusion tensor imaging (DTI) in patients with multiple sclerosis (MS):

Correlation with perfusion imaging

E. Papadaki, N. Papanikolaou, S. Karampekios, M. Spilioti, T. Maris,

N. Gourtsoyiannis; Iraklion/GR

Purpose: To perform DTI and dynamic susceptibility contrast (DSC) techniques in MS patients and healthy volunteers and investigate possible correlation between diffusion and perfusion properties.

Methods and Materials: A T2SE-EPI sequence with 6 different diffusion gradients and a single shot T2*GRE-EPI sequence with 50 dynamic axial scans after a single dose of Gd administration were applied to 36 MS patients and 10 healthy volunteers on a 1.5 T scanner. 677 measurements of Apparent Diffusion Coefficient (ADC), Fractional Anisotropy (FA) and relative Cerebral Blood Volume (rCBV%) were performed concerning focal white matter lesions (213), "Dirty" White Matter (DWM=96), Normal Appearing White Matter (NAWM=288) and Normal White Matter (NWM=80). Possible linearity between ADC or FA and rCBV% values of the different white matter regions was evaluated by linear regression analysis.

Results: ADC and rCBV%, or FA and rCBV% values demonstrate poor to moderate correlation coefficient for NWM, NAWM and most of the focal white matter lesions, while a very good correlation between ADC and rCBV% ($r = 0.86$, $p = 0.04$), or FA and rCBV% ($r = -0.85$, $p = 0.01$) of DWM was evaluated. There is also an excellent correlation between ADC and rCBV% ($r = 0.98$, $p = 0.01$) of enhancing lesions (EL).

Conclusion: There is poor to moderate correlation between ADC or FA and rCBV% values for most of the white matter regions, with the exception of DWM and EL. These findings suggest that the combination of diffusion and perfusion imaging techniques may improve the characterization of white matter lesions in patients with MS.

B-092 10:39

Quantitative study of fractional anisotropy of the corticospinal tract and corpus callosum in patients with relapsing-remitting MS

C.S. Yu, K.C. Li; Beijing/CN

Purpose: To investigate the differences in fractional anisotropy (FA) of the corticospinal tract (CST) and corpus callosum (CC) between remitting-relapsing multiple sclerosis (RRMS) patients and normal volunteers and whether these indices correlate with EDSS or pyramidal scores.

Methods and Materials: Single shot echo-planar diffusion tensor imaging was performed in 36 volunteers and 64 patients with RRMS. Then the fibers of CST and CC were reconstructed and FA values of them were computed by using a tractography software package. Differences in FA of individual tracts between RRMS patients and normal volunteers were investigated, and correlation of these indices with EDSS was also determined.

Results: FA of CST is 0.497 ± 0.028 without sex or lateral difference ($p > 0.05$), and FA of CC is 0.506 ± 0.020 without sex difference either ($p > 0.05$). FA of CC (0.465 ± 0.033) and CST (0.472 ± 0.037) of RRMS are significantly lower than normal volunteers. FA of CC of cerebral type of RRMS (0.456 ± 0.036) prominently lower than that of spinal type (0.475 ± 0.025), but this phenomenon does not exist in CST. In RRMS patients, there exists no correlation of FA of CC with EDSS ($r = -0.104$, $p > 0.05$). FA of CST correlate with EDSS ($r = -0.193$, $p < 0.05$) and pyramidal score ($r = -0.218$, $p < 0.05$), and higher in pyramidal score. Among them, FA of CST of cerebral type of MS correlate with EDSS ($r = -0.273$, $p < 0.05$) and pyramidal score ($r = -0.268$, $p < 0.05$), but this correlation does not exist in spinal type.

Conclusion: FA of CC and CST of RRMS can reflect pathological status of MS. FA of CST can be used to evaluate functional status of cerebral type of MS patients.

B-093 10:48

Diffusion-weighted MR imaging of the spinal cord in multiple sclerosis

A. Dirisamer¹, R. Bammer², K. Vass¹, M. Thurnher¹; ¹Vienna/AT, ²Stanford, CA/US

Purpose: To evaluate diffusion characteristics of multiple sclerosis (MS) lesions in the spinal cord, and compare the results with findings on conventional MR sequences.

Material and Methods: Nine patients with proven MS and lesions in the spinal cord were included in the study. MR studies were performed on 1.5 T clinical scanner with the following imaging protocol: T2WI, T1WI pre and postcontrast, and DWI in sagittal and axial planes. For DWI multi-shot EPI with fat suppression and max b factor of 600 was used. Slice thickness was 5 mm, fold over direction AP and scanning time was 3:05 min. For axial images performed with a surface coil (14 x 17 cm) single-shot EPI with 40 slices and 4 mm slice thickness was used. Signal intensities on DWI were recorded and ADC measurements were performed in all patients.

Results: All MS lesions showed high signal on T2WI, marked enhancement was present in 3/9 patients, faint enhancement was observed in 3/9 patients. In 3 patients no enhancement was present on postcontrast scans. In 8 of 9 patients, high signal was observed on DWI with low ADC values consistent with restricted diffusion. One patient did not show a diffusion abnormality despite enhancement on the postcontrast image.

Conclusion: DWI may provide new structural information in relation to spinal cord pathology in MS. Further work with comparison between DWI/ADC and signal intensities on T1WI, the presence or absence of enhancement and MTR is needed.

B-094 10:57

Cerebral lesion load in neuropsychiatric systemic lupus erythematosus: A longitudinal study

B.J. Emmer, S.C.A. Steens, M.G. Steup-Beekman, F. Admiraal-Behloul, G.P.T. Bosma, S. Le Cessie, W.J.N. Ouwendijk, T.W.J. Huizinga, M.A. van Buchem; Leiden/NL

Purpose: Magnetization transfer imaging (MTI) analysis detects brain parenchymal abnormalities in patients with neuropsychiatric systemic lupus erythematosus (NPSLE). The aim of this study was to assess whether clinical changes in NPSLE patients are reflected in changes of MTI parameters.

Methods and Materials: 19 female patients (mean age 37.5 years; range 19-64) were subjected to MTI. Following segmentation, whole brain magnetization transfer ratio (MTR) histograms were generated. The peak height (Pht) of these histograms was used as an estimate of cerebral lesion load. MTI data were generated on at least two separate occasions (mean time between scans 25.4 months; range 5.4-52.3). 25 pairs of scans were available from 19 patients. Clinical course was defined as improvement, stable, or deterioration, based on an expert panel scoring. Change in clinical classification was compared with Pht change, between first and second MR imaging. Differences in Pht change between the three groups were compared using a linear mixed model with random person effect.

Results: 4 pairs deteriorated, 15 were stable, and 6 improved. Clinically deteriorated patients showed a relative Pht decrease of 8.1%, in stable disease the relative Pht increase was 0.3%, and clinically improved patients showed a relative Pht increase of 12.5% (p -value < 0.001). Pair wise comparison detected significant differences between all groups (p values < 0.05 , with Bonferroni correction).

Conclusion: These findings demonstrate that MTI correlates with changes in clinical status in individual patients. This suggests that MTI parameters could serve as markers of NPSLE activity and that cerebral damage in NPSLE is, in part, reversible.

B-095 11:06



Brain metabolism in HIV-infection assessed by proton and ³¹phosphorus magnetic resonance spectroscopy

E.Z. Kovacs¹, S. Buchthal¹, R. Shin¹, B. Shelton², B.A. Bush¹, M.J. Kilby¹, H. Zeng¹, J. den Hollander¹, D.J. Benos¹; ¹Birmingham, AL/US, ²Lexington, KY/US

Purpose: Impaired energy-metabolism has been implicated in the pathogenesis of HIV-associated dementia (HAD). We combined ³¹phosphorus magnetic resonance spectroscopy imaging (³¹PMRSI) to measure high-energy phosphates in the brain, and high resolution proton magnetic resonance spectroscopy (¹HMRS) of the cerebrospinal fluid (CSF) to better understand the metabolic processes occurring in HAD.

Materials and Method: 25 HIV+ and 20 HIV- subjects underwent ³¹PMRSI in a

Scientific Sessions

4.1 T whole-body MR imaging/MRSI system. Metabolite ratios from PCr, ATP and Pi were measured and calculated in six brain regions. Following $^{31}\text{PMRSI}$, CSF was obtained from 19 HIV+ and 10 HIV- subjects. Specimens of CSF were analyzed by $^1\text{HMRS}$ in a 500 MHz Bruker Magnet. Lactate, organic- and amino-acid concentrations were measured.

Results: No significant difference was found between HIV+ and HIV- subjects in PCr/ATP, Pi/PCr and Pi/ATP in any brain regions. In contrast: lactate ($p = 0.008$), alanine ($p = 0.002$), citrate ($p = 0.036$), creatine and creatinine ($p = 0.044$) concentrations were significantly elevated in the CSF of HIV+ subjects. Pyruvate also tended to be elevated in CSF of patients ($p = 0.052$).

Conclusion: Elevation of citrate, alanine, lactate and pyruvate in the CSF of HIV+ subjects suggest impaired energy metabolism and the inhibition of tricarboxy-acid cycle, despite normal values of high energy phosphate metabolite-ratios measured *in vivo*. Our results suggest that CSF composition assessed by high resolution $^1\text{HMRS}$ may be a more sensitive indicator of disturbance in energy metabolism than alterations of PCr/ATP, Pi/PCr and Pi/ATP in HAD. Supported by NIMH grant MH50421 and NCI grant CA-13148.

B-096 11:15

Clinical diagnosis of sporadic Creutzfeldt-Jakob disease: Reliability of MR imaging and comparison with EEG and 14-3-3 protein analysis

H.J. Tschampa¹, K. Kallenberg², I. Zerr², B. Meissner², H.A. Kretzschmar³, M. Knauth², H. Urbach¹; ¹Bonn/DE, ²Göttingen/DE, ³Munich/DE

Purpose: Technical investigations included in the clinical diagnosis of sporadic Creutzfeldt-Jakob Disease (sCJD) are EEG and CSF-analysis for 14-3-3 protein. MR imaging is not a criterion for the diagnosis of sCJD, although typical changes have been described. We investigated the reliability of MR imaging in the sCJD diagnosis, evaluated MR imaging sequences and compared MR imaging with EEG and 14-3-3.

Methods and Materials: This study includes 193 consecutive suspected sCJD patients who had been referred to the German CJD Surveillance Unit during 2001 to 2003. Three observers independently analyzed MR imaging scans, blinded to clinical data. MR imaging was rated as "typical for sCJD" if increased signal intensity was detected in the caudate nucleus and putamen.

Results: We analyzed 442 MR imaging scans (184 T2-, 132 FLAIR, 75 diffusion- and 51 proton-density weighted sequences). Inter-observer agreement was good (123/193 patients or 63.7%, overall $\kappa = 0.53$). Sensitivity of MR imaging in clinically probable or autopsy-proven sCJD was 59.7%, 58.3% and 70.8% (observers 1-3). Specificity was high (84.2%; 89.5%; 81.6%). Diffusion weighted sequences best showed the pathologic changes, followed by FLAIR. MR imaging results were in the range of EEG (sensitivity 32%, specificity of 94%) and 14-3-3 data (sensitivity 91%, specificity 44%).

Conclusion: We propose to incorporate MR imaging in the diagnostic criteria for sCJD, equivalent to EEG and 14-3-3 analysis.

B-097 11:24

High b value diffusion MR imaging of the brain and the spinal cord in patients affected by amyotrophic lateral sclerosis: Preliminary results

L. Manfrè¹, M. Bonetti², T. Piccoli³, C. Cristaudo¹; ¹Catania/IT, ²Brescia/IT, ³Palermo/IT

Purpose: To evaluate segmental ADC values of white matter at the level of the motor area and the internal capsule (Upper Motor Neuron - UMN), anterior and lateral spinal columns (UMN), spinal gray matter of the anterior horns (LMN) in patient affected by ALS.

Materials and Method: From October 2003 to April 2004, we examined 14 ALS patients. All the patients underwent brain and spinal cord MR imaging and diffusion MR imaging study: b value was 2500 for brain evaluation, and 450 for spine study. ADC values of motor strip area, internal capsule and white and gray matter of the spinal cord were calculated on caudo-cranial (ADCcc), left-right (ADCr) and antero-posterior (ADCap) DWI images, as for isotropic image (ADCi).

Results: No significant abnormalities of ADC values were detected at the level of subcortical pre-central white matter. On the contrary, when the ADC ratio between anterior 1/3 and posterior 2/3 of the posterior limb of the internal capsule was evaluated, significant decrease in ADC ratio occurred in caudo-cranial DWI, suggesting UMN disease. Patients showed statistically significant increase in ADC values along all the direction of the b gradient at the spinal cord. Anisotropic index demonstrated prevalent distraction of caudo-cranial fibers of white matter (UMN disease), and gray matter of anterior horn (LMN disease).

Conclusion: Diffusion-weighted imaging appears to be a very sensitive MR technique in depicting selective white matter tract destruction secondary to neuronal and axonal degeneration as occurs in ALS patients.

B-098 11:33

MR proton spectroscopy of the brain in Tourette syndrome

W. Szczkowski, M. Golebiowski, P. Janik; Warsaw/PL

Purpose: The aim of this study was to assess the use of MR proton spectroscopy (MRS) in the examination of patients with Tourette syndrome (TS).

Methods and Materials: 15 patients (5 women, 10 men) with TS diagnosed according to the clinical criteria were examined. 11 patients had moderate motor and phonic tics, the others were classified as patients with mild tics. A control group consisted of 17 healthy, age-matched volunteers (5 women, 12 men). Single-voxel spectroscopy was performed using PRESS sequences with parameters of 22/2000 ms (TE/TR). Voxels (15x15x15 mm) were located in the left and right globi pallidus and thalamus. The calculations were expressed and analyzed as ratios to Creatine (Cr). Statistical significance of any differences was assessed with the t test for unpaired data.

Results: A significant increase in Glx/Cr ratios for the left ($p < .00001$) and right thalamus ($p < .0001$) and increase in Lip level for both globi pallidus and thalamus ($p < .0001$) compared to the control group was found. The most pronounced increase of Cho and mI levels ($p < .05$) was observed in the thalamus. No statistically significant differences were found in NAA/Cr ratios between TS patients and healthy volunteers.

Conclusion: The statistically significant increase of Glx, Lip, Cho and mI levels could reflect the dysfunction within the basal ganglia, especially increased glutamate mediated thalamo-cortical and -striatal transmission and elevated metabolism in these structures. MRS seems to be helpful as a better explanation of TS pathogenesis.

B-099 11:42

X-linked Charcot-Marie-Tooth disease: MR imaging of brain changes

J. Lisy, R. Mazanec, M. Bojar, P. Seeman, J. Neuwirth; Prague/CZ

Purpose: X-linked Charcot-Marie-Tooth disease is the second most common hereditary demyelinating neuropathy. Casuistic reports about these patients in the literature describe ADEM-like changes in white matter and changes in the splenium of the corpus callosum. We attempted to identify the spectrum of brain changes on MR imaging examination in a larger group of patients.

Methods and Materials: All 15 patients (5 female:10 male) with genetically proven X-linked Charcot-Marie-Tooth disease underwent MR imaging examination of the brain.

Results: The splenium of the corpus callosum was involved in 9 patients. Diffuse T2 hyper intense changes in the parietal lobes were seen in 2 patients with the splenium of the corpus callosum the most severely involved. The corpus callosum had a normal appearance in 6 patients. Focal ADEM like changes were not seen in any patient.

Conclusion: The splenium of the corpus callosum is the most commonly involved brain structure; 60% of patients with X-linked Charcot-Marie-Tooth disease. Diffuse T2 hyper intense changes in the white matter of the parietal lobe are associated in some cases with a most severely involved splenium. Changes in the splenium of the corpus callosum likely represent chronic involvement, ADEM like changes can represent acute involvement.

B-100 11:51

A multimodal neuroimaging approach in patients with early diagnosis of Parkinson's disease: Correlations between f-MR imaging with fine motor tasks, EEG and clinical tests

A. Sias, A. Balestrieri, L. Barberini, M. Fraschini, M. Puligheddu, F. Marrosu, G. Mallarini; Cagliari/IT

Purpose: Our study introduces a systematic multi-modality approach to Parkinson's disease (PD), combining functional MR imaging and EEG, to evaluate cognitive and movement disease symptoms. The aim is to depict alterations in physiological responses in relation to disease development and treatment.

Methods and Materials: We have acquired brain cortical activation maps in 10 patients with early diagnosis of PD, and 10 normal individuals, using both EEG and functional MR imaging. Using statistical methods we have established an integrated database of the two investigations, which will be helpful in the diagnosis and monitoring of the disease, also correlating to the pharmacological treatment aiming to strengthen the dopaminergic system.

Results: Our results appear to show a contralateral hyper activation which correlates to the degree of disease development.

Conclusion: This approach seems to be a promising diagnostic tool in patients with Parkinson's disease.

Scientific Sessions

10:30 - 12:00	Room N/O
---------------	----------

Computer Applications
SS 205
Advanced image processing
Moderators:

J. Kettenbach; Vienna/AT
E. Neri; Pisa/IT

B-101 10:30

Accuracy of liver superimposition in different ways of whole body image fusion of CT and PET datasets

P. Kovacs, D. Putzer, T.B. Lang, M. Knoflach, C. Hinterleitner, R.J. Bale, W.R. Jaschke; Innsbruck/AT

Purpose: To determine accuracy of liver superimposition in whole body image fusion (IF) of CT and PET datasets using a navigation system which allows IF by means of external fiducials, anatomical landmarks and automatic detection of similar voxels.

Materials and Methods: In 18 patients (range 24-77 y) thoraco-abdominal CT (2.5 mm slice thickness) and whole body PET datasets were obtained in exactly the same posture using BLUEBAG immobilization devices (Medical Intelligence, Germany). IF was performed on TREON StealthStation navigation system (Medtronic, USA) using 4-6 anatomical landmarks, 4-6 external fiducials fixed to the immobilisation device and in an automatic fashion via pair-point-matching of similar voxels. In all IFs a cuboid was superimposed to the liver. The distances of their centers were measured in the x-, y- and z-axis and totally. These distances were compared in all three ways of IF.

Results: The mean distances of the centers were 8.1/9.0/50.9 mm in anatomical/fiducial based/automatic IF. No significant differences were found between the measurements in anatomical and fiducial based IF, whereas significant differences were found in comparison to automatic IF. Fiducial based IF was more accurate in x-axis and less accurate in z-axis. These distances ranged between 0.9 and 3.8 mm.

Conclusions: Automatic pair-point-matching is not suitable for accurate whole body IFs, yet. In comparison with anatomical landmarks external fiducials can be used in combination with immobilisation devices to gain highly accurate IFs. To our experience in routinely practice external fiducials are easier to detect in both datasets and allow for faster gained IFs on navigation systems.

B-102 10:39

Quality maps for automated phase unwrapping of MR images

S. Witoszynskyj¹, A. Rauscher², J.R. Reichenbach², M. Barth¹; ¹Vienna/AT, ²Jena/DE

Purpose: MR sequences acquire complex information at the same time. Usually, phase images are discarded due to phase wraps and only magnitude information is used. With the advent of MR imaging techniques that employ phase information for enhancement of anatomical and/or functional contrast the need for solving these ambiguities arises. The aim of the study was to investigate different criteria or optimizing phase unwrapping.

Methods: Based on a region-growing algorithm a 2D phase unwrapping program for MR images was developed and implemented in C. For automated seed finding and unwrapping the algorithm depends on local quality criteria of the images. The following measures were used and their performance compared: local coherence used by the original algorithm (LCC), the average of the complex signal (ACS), the average of the magnitude (AM), the variance of the complex signal (VCS) and the variance of the phase (VPH). The algorithm with these different measures was implemented in an in-house developed software package with an IDL (RSI,USA) interface and a GUI for ParaVision (Bruker,Germany) and tested on high-resolution brain data sets.

Results: Best performance (minimum number of remaining phase wraps) was obtained with AM, followed by ACS and LCC. VCS and VPH did not produce reasonable results. AM performed best in areas of steep phase topology. AM and ACS perform better than LCC due to usage of magnitude information which helps to better separate signal from noise.

Conclusion: For automated phase unwrapping using region growing quality maps should include magnitude information to obtain meaningful results.

B-103 10:48

How to determine the quality of unsupervised functional MR imaging data analysis methods?

A. Wismueller¹, O. Lange¹, G. Leinsinger¹, A. Meyer-Baese², D. Auer³, M. Reiser¹; ¹Munich/DE, ²Tallahassee, FL/US, ³Nottingham/UK

Purpose: Unsupervised fMRI imaging image processing methods, such as clustering, Principal or Independent Component Analysis (PCA, ICA) are increasingly used as an alternative to model-based (MB) methods, e.g. cross-correlation or statistical regression. The aim was to develop and apply a method for quantitative comparative evaluation of unsupervised fMRI imaging analysis algorithms.

Methods and Materials: Functional MR imaging was performed in 11 healthy volunteers on a 1.5 T system (GE-EPI sequence, TR/TE = 4000/66 ms, 64 scan photic stimulation experiment). fMRI imaging time-series were analyzed by several unsupervised techniques: Minimal Free Energy Vector Quantization (MFE-VQ), Self-Organizing Maps (SOM), Fuzzy C-Means clustering (FCM), PCA, and ICA, employing 36 component time-series each. Stimulus-induced neural activation was determined by cross-correlation, serving as MB gold standard reference for ROC curve analysis. The area under the ROC curve (AUC) was used to determine the ability of unsupervised methods to properly detect activated brain regions.

Results: MFE-VQ performed best (AUC=0.98 ± 0.01), and provided the advantage of hierarchical data analysis on different scales of resolution. SOMs were slightly inferior (AUC=0.96 ± 0.02). In contrast to the other methods, FCM results were highly dependent on initial conditions (AUC=0.97 ± 0.05). Clustering methods clearly outperformed the data projection methods PCA (AUC=0.82 ± 0.03) and ICA (AUC=0.83 ± 0.04) that may be useful for preliminary screening, dimensionality reduction, or noise filtering.

Conclusion: Quantitative ROC plot quality assessment of unsupervised fMRI imaging data analysis can be based on stimulus-induced brain activation, i.e. relevant physiological information extracted from conventional MB methods. It is a valuable tool for the radiologist to reliably evaluate unsupervised fMRI imaging analysis methods.

B-104 10:57

A novel non-rigid mono-modal registration algorithm reducing motion artifacts at CE MR investigations

T.W. Vomweg¹, C. Hintze¹, D. Mayer¹, H. Faber¹, E. Grossi², A. Teifke¹, T. Achenbach¹, O. Rieker¹, M. Thelen¹; ¹Mainz/DE, ²Milan/IT

Purpose: To reduce artifacts within subtraction series of dynamic contrast enhanced (CE) MR-investigations caused by patient movement without compromising lesion morphology.

Material and Methods: The algorithm calculates a quality called 'eigenvalue' based on three-dimensional analysis of each voxel and its neighbours in a given volume. Comparing and filtering all volume elements by means of 'eigenvalue' results in a set of features of a given volume. By tracking these features in timely consecutive series of the same 3d-block it is possible to calculate motion vectors. In a next step registration is done by vector based morphing of original image information into a new image volume. This approach was applied to consecutive 50 studies of dynamic, bilateral CE MR-investigations of the breast using statistical and subjective tests. The mean signal intensity of all pixels of subtraction series before and after the application of the registration algorithm was calculated and compared. Lesion morphology was assessed and compared visually.

Results: Movement artifact correction reduced mean signal intensity of subtraction images by 35.78% significantly (SSD: 24.9%), while CE lesions remained as bright as without registration. Contrast of defined structures was raised; morphological features of lesions remained unchanged.

Conclusion: Using 'eigenvalue' based morphed images in non-rigid registration of CE MR-Mammography leads to significant improvements in image quality by reducing motion artifacts. Subtracted series that were generated in this manner are superior to conventional, non-registered subtractions and could proof helpful in detection and characterization of lesions. This project is financed by Bracco Imaging, Milan, Italy.

B-105 11:06

A graphical user interface for SWI-reconstruction

A. Deistung¹, A. Rauscher¹, J. Sedlacik¹, S. Witoszynskyj², M. Barth², W.A. Kaiser¹, J.R. Reichenbach¹; ¹Jena/DE, ²Vienna/AT

Purpose: Although BOLD-MR-venography (also named susceptibility weighted imaging, SWI), has been established for the examination of tumors and for studying physiological processes, its evaluation has not been implemented routinely in

Scientific Sessions

MR scanners yet. Therefore, a platform independent easy-to-use graphical user interface (GUI) has been developed for fast generation and extensive analysis of SWI data.

Material/Methods: High-resolution 3D scans were acquired with a first-order, flow compensated gradient echo sequence on 1.5 T MR imaging scanner (Magnetom Vision, Siemens, Erlangen, Germany) (TR/TE/alpha=67 ms/40 ms/25°). The GUI was developed using IDL (RSI, Boulder, USA). The interface allows scanner independent reconstruction of complex raw-data. Interactive setting of parameters for zero filling, hamming filtering and algorithms for phase unwrapping (homodyne filtering or phase unwrapping in image-space) are available. After automatic creation of phase masks computed from phase images and their manifold multiplication with the corresponding magnitude images, the data are displayed by minimum intensity projections (mIP) over a freely selectable number of slices.

Results: The software tool allows to visualize image data computed from raw k-space data as well as image data in DICOM-format. With this user interface it is possible to quickly generate venograms in different orientations and to set reconstruction and analysis parameters in a flexible manner, thereby facilitating data analysis for physicians and medical technicians. Since the software is executed on the IDL-Virtual-Machine platform it can be used without having to purchase an IDL-license.

Discussion: The software helps to make the wide range of possible applications of SWI more accessible to a larger group of users.

B-106 11:15

Effect of new non-linear, three-dimensional, noise reduction filters on image quality and lesion characteristics to improve image quality of low-dose abdominal CT

M.K. Kalra¹, S.M.R. Rizzo¹, M.M. Blake¹, M.M. Maher¹, B. Schmidt², C. Suess², S. Saini¹; ¹Boston, MA/US, ²Forchheim/DE

Purpose: Acquisition of low-dose CT images is limited by image noise and compromised image quality. Previously reported two-dimensional noise reduction filters (NRF) decreased lesion conspicuity. Non-linear, 3D-NRF was developed to reduce image noise without decreasing lesion conspicuity. Our purpose was to assess the effect of 3D-NRF on image quality and lesion characteristics in low-dose abdominal-CT.

Materials and Methods: Low dose abdominal/pelvic CTs of 40 patients (age range = 28-86 years) acquired with reduced tube current (60-120 eff.mAs) at 5 mm (n = 20) and 2 mm (n = 20) reconstructed slice thickness were processed with 3D-NRF at three levels of noise reduction. Baseline low-dose and post-processed image series were randomized and evaluated by two radiologists for image noise, contrast and sharpness at porta hepatis and acetabulum using a 5-point scale. Images were assessed for lesion number, conspicuity, margins, attenuation and calcification, as well as for edge-enhancement and artifacts.

Results: Regardless of slice thickness, compared to baseline images, significant noise reduction was noted with all settings of 3D-NRF ($p < 0.0004$). Significant reduction in image contrast was noted with application of two 3D-NRF settings to 5 mm images ($p < 0.005$) and one 3D-NRF setting to 2 mm images ($p < 0.05$). Baseline and post-processed images identified 128 lesions. Although 3D-NRF with the strongest noise reduction was diagnostically unacceptable ($p = 0.006$), no significant differences between remaining 3D-NRF and baseline images were found.

Conclusion: 3D-NRF improves image noise without affecting lesion conspicuity and detection in low-dose abdominal/pelvic CT. Although 3D-NRF reduce contrast in 5 mm images, they are helpful in improving noise while maintaining sharpness and contrast in thinner slices.

B-107 11:24

Automatic quantification of carotid artery stenosis: Preliminary results of a new vascular software module

M. Celestre, I. Sansoni, M. Rengo, M. Di Martino, L. Coletta, A. Laghi, R. Passariello; Rome/IT

Purpose: To show the feasibility and usefulness of a new automatic vessel quantification software (Viatronix V3D-vascular module), to aid physicians to analyze carotid arteries stenosis.

Methods and Materials: We retrospectively analysed 2D MSCT angiography examinations of 15 patients, with carotid arteries stenosis, to compare the percentage of stenosis diagnosed by sight, on the basis of MSCTA 2D images, with the automatic quantification evaluated using this new kind of vascular software module in the post processing analysis. Both values was referred to NASCET criteria (calculated on 2D CTA images) assumed as the gold-standard.

Results: For the extracranial carotid artery, our experiences indicated that there is a good correlation between Viatronix automatic vessel quantification and MSCTA. Although this accuracy is heavily depending on the dimension and morphology of calcification, that limits the automatic measurements.

Conclusion: Viatronix V3D-vascular module provides excellent image quality and appears to be an accurate, non-invasive tool in the assessment of carotid lumen stenosis, but technical improvements could perfect this software and the accuracy of its analysis.

B-108 11:33

Accuracy of computer based measurements in endovascular stent-graft planning: Experimental in vitro evaluation in an aortic aneurysmal phantom

S. Klein, M.H. Hoffman, D.T. Boll, H.J. Brambs, A.J. Aschoff; Ulm/DE

Purpose: The aim of this study was to evaluate the accuracy of automated software applications in endovascular stent-graft planning of abdominal aortic aneurysms with multidetector row Computed Tomography.

Methods and Materials: A vascular phantom of the abdominal aorta including the iliac arteries with an infrarenal aortic aneurysm was constructed and filled with an iodine based contrast medium solution. CT scan was performed with different slice thickness and increment using a 16-slice scanner. After transferring CT data to a workstation 3D Volume renderings were generated. Diameter and distance measurements were performed at specific vessel points for endovascular stent-graft implantation using a manually and an automatically generated centerline. The results were compared with the known dimension of the phantom and mean fractional errors were calculated. Necessary time of postprocessing was evaluated for both methods.

Results: Using the automatic software the mean fractional error for all diameter measurements combined was 0.054 (Standard deviation 0.018), respectively 0.061 (SD 0.049) for the manual method. Regarding the distance the mean fractional error was 0.027 (SD 0.026) for the automatically respectively 0.034 (SD 0.038) for the manually generated results. Using the automated measuring method 34% shorter postprocessing time was necessary.

Conclusion: Automated software application enables accurate measurements of diameter and distance used for stent-graft planning of abdominal aortic aneurysms in shorter postprocessing time than manually performed measurements.

B-109 11:42

Improving reproducibility of small structure segmentation by isotropic resolution filtering

R.M. Lapp, M. Kachelrieß, W.A. Kalender; Erlangen/DE

Purpose: Reproducibility of small volume segmentation in CT examinations suffers from a strong dependence on the orientation of the object. This results from the often anisotropic spatial resolution observed in CT image stacks, depending on selected effective slice width and reconstruction kernel, and influences the quality of e.g. calcium scoring or vessel segmentations. We introduce an image post-processing technique that compensates for this effect.

Methods and Materials: We simulated CT rawdata of a set of cylinders (10 mm length, 2 mm diameter, 300 HU) at angular directions of 0°, 30°, 60° and 90° to the x/y-plane and reconstructed the volumes using a smooth reconstruction kernel. The volume of the cylinders was determined as the voxel volume after thresholding. Our post-processing technique performs an image filtering in z-direction compensating for differences in the in-plane and axial resolution of the images. The determination of the spatial resolution is performed by measuring the response to a delta impulse. All investigations were conducted using dedicated CT simulation and image reconstruction software (www.vamp-gmbh.de).

Results: Without the proposed filtering technique measured volumes for the cylinders differed from 20.9 to 24.0 mm³ as a function of the angular direction with a standard deviation of 1.35 mm³ at a 150 HU threshold. After isotropic filtering values differed from 19.8 to 20.5 mm³ with 0.29 mm³ standard deviation showing a significantly lower dependence on the spatial orientation.

Conclusion: Isotropic resolution filtering significantly reduces the influence of object orientation on volume segmentation results and can be used to increase reproducibility.

Scientific Sessions

B-110 11:51

Three-dimensional visualization and calculation of lesional volume in patients of multiple sclerosis. Fundamentals and preliminary results
E. Gomez-Gonzalez, J. Aguilera-Navarro, A. Castela-Murillo, M. Vera-Valencia, M. Dominguez-Marín, A. Cano-Rodríguez; Seville/ES

Purpose: To present a new method, implemented as a computer program to evaluate absolute and relative lesional volume in patients of multiple sclerosis (MS) by computerized measurement of hyperintense findings. To evaluate the possibilities of interactive segmentation and three-dimensional visualization of lesions in clinical applications.

Methods and Materials: Three-dimensional visualizations of segmented hyperintense lesions in MR-studies (1.5 T GE-Signa) of 20 patients with confirmed MS are generated. Each study comprises an average of 15 slices having 4.42 lesions/slice. Using developed computer program, i) bone is segmented and total cranial volume is calculated, ii) hyperintense lesions are segmented using a semiautomated tool (user selects to include/exclude findings) and iii) absolute and relative volumes of demyelinated parenchyma are calculated.

Results: Segmentation thresholds for delimitation of bone regions and ventricles were obtained. 5 different segmentations (varying thresholds) were performed to isolate hyperintense lesions. Total and relative volumes of damaged parenchyma were calculated. Intraobserver correlation is very high ($K=0.83$) and statistically significant ($p < 0.0001$). Definition of the lower limiting threshold is very important.

Conclusion: Proposed method allows for precise calculation of total and relative volumes of lesions in patients suffering from MS. Semiautomated processing is controlled by user. It presents a potentially useful application in follow-up of response to treatment. (As a representation of the Cooperative Group for Research in Multiple Sclerosis of Seville: Univ.Hospital "V.Macarena", Univ. Hospital "V.Rocío", Univ.Hospital "N.S.Valme" and E.S.Ingenieros-University of Seville. Method by EGG, patented by the University of Seville. Partial funding by Schering España S.A. and III-Andalusian Research Plan is acknowledged).

10:30 - 12:00

Room P

Vascular

SS 215

Plaque imaging/Thrombo-embolic disease

Moderators:

D. Bilecen; Basle/CH
J.L. Struyven; Brussels/BE

B-111 10:30

Microstructural imaging with optical coherence tomography: Comparison with intravascular ultrasound and histology in coronary artery specimens

O.A. Meissner¹, J. Rieber¹, M. Oswald¹, S. Reim¹, G. Babaryka¹, U.G. Mueller-Lisse¹, T. Redel², M. Kleen², M. Reiser¹; ¹Munich/DE, ²Forchheim/DE

Purpose: Optical Coherence Tomography (OCT) is a new intravascular imaging modality providing real time ultrastructural information of tissue with a resolution of 10 µm. Intravascular ultrasound (IVUS) as the current reference standard for in-vivo vessel characterization has limited spatial resolution. This study compared OCT, IVUS and histology of coronary arteries *in vitro*.

Methods and Materials: OCT (Lightlab Imaging Inc.) and IVUS images of 480 coronary artery specimens were obtained (normal [$n = 319$], moderate [$n = 75$] and severe atherosclerosis [$n = 86$]). Quantitative measurements comprised lumen area (LA), vessel wall area (VA), minimum and maximum wall thickness (T_{min}, T_{max}). OCT findings in fibrous, fibrocalcific and lipid-rich plaques were correlated with IVUS and histology as standards of reference.

Results: Paired (OCT, IVUS) LA measurements were in close agreement: the Bland-Altman mean bias in LA was 0.1 mm² with a precision of ± 1.7 mm² ($p = 0.9$). VA measurements correlated moderately ($r = 0.76$; $p < 0.0001$) with a trend towards lower values with OCT. T_{min} and T_{max} showed a good correlation for atherosclerotic coronary segments ($r = 0.89$; $p < .0001$); however, no significant correlation was observed in normal coronary segments ($r = 0.48$; $p < 0.06$). Overall sensitivity for plaque type characterization ranged from 75 to 98% for OCT and from 50-98% for IVUS when compared to histology.

Conclusion: Due to its superior resolution, OCT provides unique histology-like images of coronary arteries and accurately quantifies vessel dimensions *in vitro*. Concerning plaque components, high agreement was found between OCT, IVUS, and histology.

B-112 10:39

Determination of components in atherosclerotic plaques from human carotid endarterectomy specimens by multislice computed tomography imaging ex vivo

A. Trojanowska, A. Drop, B. Jarosz, T. Jargiello, J. Wronski; Lublin/PL

Aim: To evaluate if multislice computed tomography (MSCT) can help accurate characterization of atherosclerotic plaques.

Materials and Methods: 21 carotid endarterectomy specimens from 23 patients underwent MSCT examination (scanner GE Light Speed Ultra Advantage 8-row, 1.25 mm slices, 0.6 mm overlap, 120 kV, 140 mAs) in a specially designed phantom filled with water. Thereafter, all specimens were stained and examined histological at selected levels, corresponding to MSCT axial slices. Based on CT examination, plaque density was measured in Hounsfield units (HU) and colour-coding density maps were automatically created, using a dedicated software (GEMS). Observations were compared with histological findings at corresponding levels. Presence or absence of ulcerations was also noted. Data were analyzed with 2-sample t-test and ANOVA analysis of variance.

Results: Based on computer-created maps coding HU in colours, it was possible to distinguish 3 major areas of different HU density range. Comparing to histological findings, they represented lipid core, fibrotic tissue and calcifications. Sensitivity and specificity, respectively, were: lipid core 80% and 83%, fibrotic tissue 72% and 75%, calcifications 100% and 100%. Plaque ulcerations were detected with sensitivity of 65% and specificity of 76%.

Conclusions: MSCT evaluation of carotid endarterectomy specimens based on HU colour-coding program helps in determining the type of plaque and shows very good correlation with histological analysis for the visualization of calcifications, lipid core and fibrotic tissue. The results in identifying major components of plaque *ex vivo* suggest its value for these measurements *in vivo* as well.

B-113 10:48

Detection of atherosclerotic plaques with low dose Gadofluorine-enhanced MR imaging at 3 T

H. Ittrich¹, A. Priest¹, C. Jahntz¹, C. Weber¹, B. Misselwitz², G. Adam¹, ¹Hamburg/DE, ²Berlin/DE

Purpose: To determine of the lowest plaque-enhancing concentration of Gadofluorine M (GdF, Schering AG) in atherosclerotic aortic plaques, using a 3 T clinical MR imaging scanner.

Method and Materials: High resolution MR imaging of the aorta was performed on 9 WHHL (16-28 months) and 6 NZW rabbits (control, 16 months) before, after and 24 h post administration of GdF on a 3 T MR scanner (Philips Intera), using an 8-channel head array coil. 3 groups with injection dosages of 50, 25, 12.5 µmol GdF/kg BW were used (each of 3 WHHL/2 NZW). 3D MRA (TR/TE = 5.6/2.1 ms, FA25°, matrix256×179×70, resolution 0.7×0.7×0.7 mm) and 3D IR-TurboFLASH sequences (TE/TR = 2.2/7.2 ms, TI 120 ms, FA20°, matrix256×195×19, resolution 0.55×0.72×1.6 mm) were used to investigate luminal diameters and uptake of GdF in the aorta. SNR-measurements were performed by placing ROIs in the aortic wall. All WHHL/NZW groups were compared by Student's t-test.

Results: In all animals luminal diameters of the aortic arch showed no significant differences (6.7 ± 0.7 mm). Enhancement of aortic wall was detected in all WHHL of the 50 µmol/kg group (SNR before administration (ba): 2.6 ± 1.3 , post administration (pa): 14.4 ± 2.5) and of 25 µmol/kg group (SNR ba: 3.4 ± 1.7 , pa: 12.2 ± 1.4). No significant uptake was shown in 12.5 µmol/kg WHHL group (SNR ba: 3.2 ± 1.4 , pa: 4.0 ± 1.5) and in NZW rabbits (SNR ba: 3.6 ± 0.4 , pa: 3.4 ± 0.6). The 50 and 25 µmol/kg groups showed significant differences in SNR (WHHL to NZW) at a level of 5%.

Conclusion: Contrast enhanced MR imaging techniques at 3 T using low dose GdF are able to identify nonstenotic atherosclerotic plaques. This technique holds promise for detection of lipid plaques and long term evaluation of plaque progression in atherosclerosis in clinical practise.

B-114 10:57

MR vessel wall imaging of abdominal aorta at 3 T: Understanding and minimising plaque-mimicking flow artifacts

A.N. Priest, S. Hegerfeldt, C. Weber, G. Adam; Hamburg/DE

Purpose: To investigate black-blood imaging of abdominal aortic vessel wall, in particular the appearance of plaque-mimicking flow artifacts as a function of cardiac trigger-delay time.

Methods and Materials: The abdominal aortas of 4 healthy volunteers were imaged with a 3 T clinical scanner (Philips) using a 6-element array coil, at varying delay times following cardiac triggering by either vector-ECG or peripheral pulse

Scientific Sessions

(PP) oximetry. A turbo-spin echo sequence was used with TE/TR = 70 ms/3RR for a 3-slice interleaved package. Abdominal motion artifacts were reduced using respiratory phase-encode ordering and an anterior saturation band. Two blood-suppression methods were compared: double-inversion recovery (DIR) and out-of-slice saturation (OSS) using superior and inferior saturation bands.

Measurements were made of mean blood signal-to-noise ratio (MB-SNR), apparent vessel wall thickness (AVWT) and subjective quality of vessel wall visualisation (scale 0-5).

Results: Using OSS, MB-SNR was 3.4/1.9/2.8 and quality was 2.2/3.6/2.8 at trigger-delays 150/300/450-470 ms using ECG. Using DIR, MB-SNR was 2.6 with quality 2.1 at trigger-delay 450-470 ms. Corresponding mean AVWT were 1.04/1.12/1.06 (OSS) and 0.96 (DIR). Imaging during mid-late diastole, OSS gave poorer blood suppression and apparently broader vessel walls than DIR (e.g. MB-SNR 5.5/2.5, AVWT 1.52/1.17, quality 3.2/2.8 for delays 400-475 ms after PP trigger).

Conclusions: In this preliminary study, optimum image-quality occurred for ECG delay-time 300 ms, when DIR cannot be used but OSS blood suppression is effective in volunteers. However DIR must be used for mid-late diastolic imaging, as OSS does not always adequately suppress slow-flowing blood and gives artefactually increased AVWT, which could be erroneously interpreted as plaque.

B-115 11:06

Lower limb MR venography with true FISP for suspected deep venous thrombosis

C.P. Cantwell, J. Bruzzi, A. Cradock, S. Eustace, J.G. Murray; Dublin/IE

Purpose: To compare True FISP MR venography for suspected deep venous thrombosis with conventional venography.

Materials and Methods: This was a prospective study of 16 patients with a clinical suspicion of deep venous thrombosis of the lower limb. Standard contrast venography was performed and compared to MR venography using True FISP (TR 3.6 ms, TE 1.8 ms) sequences. MR imaging was performed from the inferior vena cava to the feet. Standard protocol was axial imaging at 6 mm slice thickness, at three stations. Total scan time was 8 minutes. Twenty venous segments on the MR studies were independently read by two radiologists unaware of venography findings. Low signal in a vein on multiple slices was regarded as thrombosis.

Results: MR venography identified the site and extent of acute thrombosis in the 5 cases with venous thrombosis on venography. The presence of secondary signs of vein distension, peri-venous swelling and fascial high signal aid diagnosis. MR imaging identified another cause for calf pain and swelling in 4 cases including 3 calf muscle tears and chronic venous insufficiency.

Conclusion: MR venography with axial true FISP allows non-invasive rapid diagnosis of acute deep venous thrombosis without the need for IV contrast. Demonstration of the central extent of the thrombus is possible to the inferior vena cava. In patients without a DVT it may show an alternative cause for patient symptoms.

B-116 11:15

3D-Gd-enhanced MR angiography (MRA) for diagnosing venous thromboembolic disease: One-stop-shop imaging of pulmonary arteries, vena cava, pelvic and both lower extremity veins in 30 minutes

M. Aschauer, A. Obernosterer, R.H. Portugaller, R. Stollberger, J. Raith, F. Ebner; Graz/AU

Background: Treatment of patients with acute pulmonary embolism depends also on the extent of venous thrombosis. An emergency diagnosis is made routinely by spiral-CT and bipedal i.v. conventional venography (CV), especially when Doppler-ultrasound of pelvic veins and IVC is uncertain. Performing both investigations takes more than 1 hour, including internal transportation.

Purpose: To assess the feasibility and image quality for diagnosis of PAE and venous thrombosis in a one-stop-shop after PAE has been diagnosed, with CT and/or V/Q scan, within the last 48 hours.

Material and Methods: 21 patients underwent a one-stop-shop MR pulmonary angiography and a repeated 3-station MR-angiography (MRA/MRV) using a moving-table technique in early arterial and equilibrium phase of the abdomen, pelvis and lower extremities.

Results: The examination was feasible in 19/21 patients. The thrombi we found confirmed diagnosis in 13/14 patients. One patient had fibrinolysis and the thrombi resolved completely within 48 hours. One patient showed no thrombi, and it was retrospectively confirmed that the patient was misdiagnosed on the initial CT. With MRV we found additional large thrombi in the internal iliac vein in 2 patients, and gastrocnemius vein thrombi in 3. The extent of pelvic thrombi was much more reliably assessed with MRV than CV. In two patients additional thrombi were found in the IVC.

Conclusion: The high sensitivity and specificity of MRA for detection of acute pulmonary emboli can be confirmed. MRV is feasible in the same session in the majority of patients. MRV detects more thrombi than conventional phlebography and Doppler-ultrasound, especially in the IVC and pelvic veins, which are clinically relevant sites.

B-117 11:24

Direct thrombus MR imaging: Preliminary experience at 3 Tesla magnetic field strength

D. Gibson, D.P. O'Regan, S. Allen, D. Larkman, J. Zeka, J. Allsop, S. Schmitz; London/UK

Purpose: Direct visualization of blood degeneration products with heavily T1-weighted techniques has shown promise for imaging deep venous thromboses at 1.5 Tesla magnetic field strength. MR imaging scanning at 3 Tesla may improve this approach owing to its potential for higher spatial resolution. However, T2* effects of organizing thrombus also increase with field strength. We therefore tested the feasibility of direct thrombus MR imaging at 3 Tesla.

Methods and Materials: We included 4 patients with deep venous thrombosis, 2 patients with thrombophlebitis and 9 healthy volunteers. The presence or absence of thrombus was assessed by compression ultrasound in all cases. MR imaging was performed at 3 Tesla (Philips Intera) using a fat-suppressed magnetization prepared rapid gradient echo sequence. Regions-of-interest were placed in muscle and thrombosed vein segments of patients, or in muscle and patent veins of volunteers to measure signal intensity (SI). In a qualitative analysis, a blinded reader assessed the presence of thrombus.

Results: The sequence allowed excellent suppression of flow, blood and fat, and thrombi were clearly visible as high signal intensity structures. The signal intensity ratio in thrombosed vessels, defined as SI(thrombus) / SI(muscle), was significantly higher than in patent vessels, defined as SI(blood) / SI(muscle): 2.6+0.6 vs. 0.6+0.1, p = 0.0005. The blinded reader correctly diagnosed all positive and negative cases, but overlooked a superficial thrombophlebitis in a small vein.

Conclusion: This preliminary study shows the feasibility of direct thrombus MR imaging at 3 Tesla. The contrast properties of thrombus at 3 Tesla are similar to those known at lower field strength.

B-118 11:33

The usefulness of 3-D sonography in the analysis of collateral circulation in the course of deep vein thrombosis

M. Myjor, P. Grzelak, L. Stefanczyk; Lodz/PL

Purpose: The inability to produce visual documentation has been the major obstacle to ultrasonography of the venous system becoming the gold standard diagnostic method. Introduction of three dimensional (3-D) sonography could change this situation. Our analysis of usefulness of 3-D sonography in the visualisation of collateral circulation in the course of deep vein thrombosis (DVT) is presented.

Methods and Materials: Examinations were performed using GE Logiq 500 Pro in Color Doppler mode. Convex 3-6 MHz probes for the lower abdominal region and 4-9 MHz linear probes for lower extremities were used. The consecutive images in transverse planes were collected and reconstructed into longer sequences using the popular graphic program Corel. A total of 104 3-D examinations were performed in 61 patients in both iliac and femoro-popliteal segments and in different phases of the disease - acute, chronic and the post-thrombotic syndrome.

Results: DVT creates favourable conditions for 3-D presentation - increased velocities and reduced pulsation of the venous flow. In the lower abdominal region the presentation is hindered by the bowel gas and motion artefacts (peristaltic movements and pulsation of great vessels), whereas in the femoro-popliteal segment lack of artefacts and superficial course of vessels result in images similar to those acquired by venography.

Conclusion: The 3-D reconstruction of venous collateral flow enables better interpretation of images by the examiner in some cases. However, the main advantage of this method is the creation of image documentation, which is more acceptable to clinicians than a written report and selected images.

B-119 11:42

Arterial remodeling: In vivo analysis of femoral arterial atherosclerosis using computed tomographic angiography (CTA)

A. Napoli¹, A. Pezeshkmehr², D. Fleischmann², G.D. Rubin²; ¹Rome/IT, ²Stanford, CA/US

Purpose: To assess the ability of CTA to characterize arterial wall remodeling in

Scientific Sessions

the presence of atherosclerosis and to assess the relationship of positive and negative remodeling to degree of luminal narrowing and patient age.

Material and Methods: 48 superficial femoral arteries from 25 patients referred for assessment of lower extremity arterial occlusive disease were analyzed by CTA (16-row CT, 1.25-mm thickness). The cross-sectional area of the arterial lumina and outer walls were measured every 10 mm sections reformatted orthogonal to the median centerline. In each arterial segment, the cross-section that contained the least amount of plaque was the reference site. Measurements were expressed relative to the reference values. Patient population was sub-divided according to age; remodeling indices were examined in locations that presented a > 50% stenosis.

Results: A total of 1403 cross-sections were analyzed (29 sections per artery). In the most stenosed parts arterial remodeling was present in 153 observations and it was positive in 60(40%), while it was negative in 93(60%). Reference vessel area was not significantly different between the age-related groups. Patients > 70 y.o. (n = 15) had a greater proportion of stenotic segments ($p = 0.003$) when compared to patients < 70 y.o. For regions with > 50% luminal stenosis, positive to negative remodeling was observed 4:1 in < 70 y.o. and 1:2 in > 70 y.o. patients - an 8-fold difference between the two groups ($p < 0.01$). These ratios were not significant in regions of < 50% stenosis.

Conclusions: CTA allows simultaneous measurement of luminal narrowing and arterial wall remodeling. Significant age-related differences in arterial wall remodeling behavior are observed in regions of > 50% luminal stenoses.

B-120 11:51

Multicenter weighted magnetic resonance imaging of atherosclerotic plaques at 3.0 and 1.5 Tesla: Comparison ex vivo and with histopathologic correlation

A. Koops, H. Ittrich, S. Petri, A. Priest, A. Stork, C. Weber, G. Adam;
Hamburg/DE

Purpose: The purpose of this study was to analyze the image quality and histological correlation of atherosclerotic plaque MR imaging at 3.0 and 1.5 Tesla.

Method and Materials: In analogy to a screening protocol, MR imaging of the abdominal aorta and the femoral artery was performed on seven cadavers using T1-weighted, T2-weighted, and PD-weighted sequences at 3.0 Tesla and at 1.5 Tesla. Cross-sectional images at the branching of the inferior mesenteric artery and the profunda femoris artery were rated with respect to their image quality in a blinded reading by three radiologists. In addition, the images and the exact match of histological cross sections were classified according to the criteria of the American Heart Association and analyzed for differences.

Results: Multicenter weighted MR imaging at 3.0 Tesla offers a superior depiction of the arterial wall composition in all performed sequences, as compared to imaging at 1.5 Tesla. While the highest differences were observed in the T2-weighted ($p = 0.00058$) and T1-weighted ($p = 0.00067$) techniques, the differences in the PD-weighted sequence ($p = 0.0344$) were still significant. In the comparison of the atherosclerotic plaque types, it was found that MR imaging overrates the calcified plaques (type Vb) in up to 21% of the cases.

Conclusions: In future atherosclerotic plaque screening of patients, magnetic resonance imaging at 3.0 Tesla field strength should be preferred for its superior depiction of arterial wall components.

14:00 - 15:30

Room A

Contrast Media

SS 306

US contrast media

Moderators:

O. Catalano; Naples/IT
M. Laniado; Dresden/DE

B-121 14:00

European Federation of Societies for Ultrasound in Medicine and Biology (EFSUMB) guidelines for contrast-enhanced US of the liver: Validation in characterization of incidental liver lesions

C. DellaPina, R. Lencioni, L. Crocetti, D. Cioni, J. Lera, S. Montagnani, C. Bartolozzi; Pisa/IT

Purpose: To validate European Federation of Societies for Ultrasound in Medicine and Biology (EFSUMB) guidelines for contrast-enhanced ultrasound (CEUS) of the liver in characterizing focal lesions of incidental detection.

Methods and Materials: A series 153 solid focal lesions 1.0-11.5 cm in diameter (mean $3.3 \text{ cm} \pm 2.2$) incidentally detected, but not characterized, by baseline US in 91 patients with neither history of malignancy nor chronic liver disease, were examined with CEUS by using real-time low MI (0.06-0.09) scanning (Contrast Tuned Imaging; Esaote Biomedica, Italy) after bolus injection of 2.4 ml of SonoVue (Bracco, Italy). Videotapes of CEUS studies were reviewed by three blinded readers who were asked to reach a consensus. The image interpretation was based on the enhancement patterns reported in EFSUMB guidelines for CEUS of the liver. Final diagnosis was established in 85/91 patients (132/153 lesions) by imaging findings (MR, CT, or both) in combination with clinical-laboratory data ($n = 75$) or US-guided biopsy ($n = 10$). Final diagnoses included hemangioma ($n = 71$), focal nodular hyperplasia ($n = 48$), metastasis from unknown primary malignancy ($n = 5$), hepatocellular adenoma ($n = 2$) and primary malignant tumors ($n = 6$).

Results: The application of EFSUMB guidelines allowed correct differentiation of benign versus malignant lesions in 128/132 cases (97%). No malignant tumor had a false benign diagnosis. Correct lesion characterization was achieved in 102/132 (77%) lesions, including 60/71 hemangiomas, 39/48 focal nodular hyperplasias and 3/5 metastases.

Conclusion: Characterization of incidental liver lesions can be obtained at a high level of probability by CEUS in combination with clinical and laboratory data if typical enhancement patterns are present.

B-122 14:09

Small nodules in liver cirrhosis: Correlation between contrast-enhanced US and pathologic examination of explanted liver

D. Cioni, R. Lencioni, A. Conti, J. Lera, D. Campani, F. Filipponi, S. Montagnani, C. DellaPina, C. Bartolozzi; Pisa/IT

Purpose: The purpose of this study is to evaluate the ability of contrast-enhanced US (CEUS) to characterize small nodules in cirrhotic livers detected during US surveillance.

Methods and Materials: A series of 34 small (3 cm or less) nodular lesions detected by baseline US in 51 cirrhotic patients were examined with CEUS as part of an on-going prospective clinical trial. CEUS examinations were performed by using continuous, low MI (0.06-0.09), real-time scanning (Contrast Tuned Imaging; Esaote Biomedica, Italy) after bolus injection of 2.4 ml of a second-generation contrast agent (Sonovue; Bracco; Italy). All patients underwent liver transplantation within 6 months of the US examination. Findings at CEUS were correlated lesion-by-lesion with pathology findings.

Results: At pathology examination, the 34 lesions were classified as HCC ($n = 24$), high-grade dysplastic nodule (HG-DN, $n = 4$), and low-grade dysplastic nodule (LG-DN, $n = 6$). CEUS studies showed arterial contrast uptake (within 30 sec after the start of contrast injection) in 19/24 HCCs and in 2/4 HG-DNs. No arterial enhancement was seen at CEUS in 5/24 HCCs, 2/4 HG-DNs and 6/6 LG-DNs. In the delayed phase (120-240 sec after the start of contrast injection) 16/24 HCCs, 4/4 HG-DNs and 6/6 LG-DNs were isoechoic (undetectable) with respect to liver parenchyma. Delayed lesion hypoechogenicity was observed in 8/24 HCCs and none of the DN.

Conclusion: CEUS findings overlap in small hepatocellular nodules in liver cirrhosis. Nevertheless, detection of arterial hypervascularity at CEUS appears to be a reliable indicator of either a malignant or a premalignant lesion.

B-123 14:18

Very small focal liver lesions appearing uncharacteristic at conventional US: Does it make sense to investigate with contrast-enhanced US in attempt to further characterize the lesions? Comparison with multi-phase spiral CT

T. Rettenbacher¹, A. Hollerweger², J. Hoflehner¹, D. zur Nedden¹;
¹Innsbruck/AT, ²Salzburg/AT

Purpose: To evaluate if it is reasonable to perform contrast-enhanced-US in cases of very small liver lesions appearing uncharacteristic at conventional-US.

Methods and Materials: In a prospective study, 166 liver lesions < 25 mm with uncharacteristic appearance at conventional US as first imaging modality, underwent additional contrast enhanced US and contrast enhanced CT to further characterize the lesions. The lesions were divided into 4 groups as follows: group 1: < 10 mm, group 2: 10-15 mm, group 3: 15-20 mm, group 4: 20-25 mm. Contrast enhanced US was performed continuously for 5 minutes after a 2.4-4.8 ml SonoVue (Bracco) bolus. CT exams were carried out in 4 phases after a 120-150 ml Ultravist 370 (Schering) bolus. The results of the exams were categorized as being either confidently diagnostic, probably diagnostic or uncharacteristic.

Results: In group 1 contrast US was confidently diagnostic in 50%(22/44),

Scientific Sessions

probably diagnostic in 14%(6/44) and uncharacteristic in 36%(16/44) whereas contrast CT was confidently diagnostic in 30%(13/44), probably diagnostic in 25%(11/44) and uncharacteristic in 45%(20/44). In group 2 the corresponding numbers for contrast US were 60%(30/50), 22%(11/50) and 18%(9/50) whereas the numbers for CT were 46%(23/50), 42%(21/50) and 12%(6/50). In group 3 we calculated 74%(32/43), 14%(6/43) and 12%(5/43) for contrast US and 63%(27/43), 28%(12/43) and 9%(4/43) for contrast CT. In group 4 we calculated 79%(23/29), 14%(4/29) and 7%(2/29) for contrast US and 62%(18/29), 28%(8/29) and 10%(3/29) for contrast CT.

Conclusions: In very small liver lesions the probability that contrast-enhanced-US is diagnostic is decreased markedly, however, it is superior to contrast-enhanced-CT. Nevertheless, in lesions < 10 mm contrast-enhanced-US can be recommended since it enables a reliable diagnosis in 50%.

B-124 14:27

Characterization of focal liver lesions with contrast-enhanced ultrasound:

Clinical utility in cancer patients

L. Romanini, M. Cristinelli, P. Cabassa, V. Portugalli, F. Venturelli, L. Grazioli; Brescia/IT

Purpose: To evaluate the impact on the clinical practice of the use of contrast-enhanced ultrasound with SonoVue in the characterization of focal liver lesions in cancer patients.

Methods and Materials: 71 cancer patients with at least one focal lesion, but less than three, were studied before, with base-line (B-Mode and color-doppler) ultrasound, and after with contrast-enhanced ultrasound. The resulted 73 lesions were confirmed by MR study and biopsy for metastasis and indeterminate lesions. **Results:** 35/73 lesions (47.9%) were benign and 38/73 (52.1%) were malignant. With baseline ultrasound 37/73 lesions (50.7%) were correctly characterized: 11/35 (31.4%) benign and 26/38 (68.4%) malignant. After dynamic study the characterization was correct in 69/73 lesions (94.5%): 31/35 (88.5%) benign and 38/38 (100%) malignant. The lesions wrong or indeterminate were: 1 hemangioma, 2 FNHs and 1 adenoma with atypical enhancement behaviour. All malignant lesions were correctly characterized. Diagnostic gain for the characterization after SonoVue was 57.1% for benign lesions and 31.5% for malignant.

Conclusions: In the oncological patients the differential diagnosis between benign and malignant lesions is crucial. In our group the benign lesions were about 50% and they were correctly characterized in the 88.5% of the cases after the SonoVue study, allowing the final diagnosis at the same time as the ultrasound discovery.

B-125 14:36

Contrast enhanced harmonic sonography (CEUS) of focal liver lesions:

Discordance with contrast enhanced CT or MR

V. Portugalli, E. Archiati, P. Cabassa, L. Grazioli, L. Romanini, M. Cristinelli; Brescia/IT

Purpose: To evaluate the type and causes of discordant enhancement patterns between CEUS and CT/MR during vascular phases.

Methods and Materials: Over a three year period, 280 patient had CEUS, spiral CT or gadolinium-enhanced MR (or both) for characterization of focal liver lesions. CEUS was performed with second generation contrast media (Sonovue, Bracco) at the standard dose of 2.4 ml with continuous real time scanning at low mechanical index. Arterial and portal phase enhancement patterns on each imaging modality were assessed by comparing the relative echogenicity/attenuation/intensity of a lesion relative to adjacent liver. Data recorded prospectively in a database was analyzed retrospectively. Delayed phase were not compared due to the different timing.

Results: 79 patients showed discordance with triphasic spiral CT or MR imaging. Lesions include 44 HCCs, 9 metastases, 6 colangiocarcinomas, 5 FNHs, 5 hemangiomas and 10 others. Discordant enhancement was founded especially during portal (64/79 patients; 79.5%) phase (11/79 had both different). 40/44 HCCs showed discordant pattern in portal phase, resulting isoechoic at CEUS and hypodense/intense on CT/MR. Differences during arterial phase were observed most frequently in metastases and cholangiocarcinomas. An explanation of most of these findings is that microbubbles are confined in the intravascular space whereas CT or MR agents can distribute in the extracellular fluid space. A discrepancy in timing may explain other cases.

Conclusions: Recognition of the potential for discordance of enhancement patterns with explanation of their cause helps in the characterization of focal liver lesions using CEUS.

B-126 14:45

Fundamental nonlinear imaging versus harmonic imaging with contrast medium sonovue in the evaluation of the hepatic focal lesions: Preliminary results

V. Migaleddu, A. Manca, D. Turilli, P. Luciano, N. Canu, G. Campisi, G. Virgilio; Sassari/IT

Purpose: To compare the results obtained with contrast medium (SonoVue) and ultrasonography using two different low mechanical index softwares (CCI and CPS).

Methods and Materials: Fifty one patients (28 males; mean age 57.2; age range 32-79 years) were included. 78 lesions examined: 33 HCC, 2 FNH, 1 adenoma, 20 haemangioma, 15 metastasis and 7 regenerative nodules. Fundamental nonlinear imaging (CPS) was compared with harmonic imaging (CCI); both softwares used low mechanical index. Exams were performed with Sequoia 512 (Acuson-Siemens) after venous bolus injection of SonoVue (Bracco-I) (2.5 ml/8 ml/ml). Penetration, detail and contrast resolution were evaluated independently on stored clips by two blinded observers using Wilcoxon sign sum rank test.

Results: CPS with nonlinear fundamental contrast imaging, in some cases associated with tissue fundamental response, permit to obtain more information than CCI harmonic contrast imaging considering penetration, detail and contrast resolution ($P < 0.0001$ at Wilcoxon sign rank test). In all the cases CPS render intensity response up to 30 dB higher than CCI. The differences between the two observers were negligible and non significant from the statistical point of view ($P > 0.05$).

Conclusion: Contrast nonlinear fundamental imaging gives us more information than contrast harmonic imaging. Coupled tissue and contrast responses present in this new modality of imaging, allow to obtain a higher diagnostic confidence.

B-127 14:54

Parametric perfusion imaging with contrast-enhanced ultrasound in thyroid gland focal lesions differential diagnosis

R. Lanocita¹, F. Calliada², F. Berton², G. Gola², A. Parisio², P. Arcuti²; ¹Milan/IT, ²Pavia/IT

Purpose: Sonography (US) and fine needle aspiration biopsy (FNAB) are common diagnostic procedures in thyroid gland examination which, if used in conjunction, are economic and accurate in differential diagnosis of solid thyroid masses. The presence of multiple nodules should reduce the tolerability of FNAB in multinodular goiter. Perfusion maps can be calculated from ultrasound harmonic imaging data after ultrasound contrast agent injection to analyze thyroid tissue perfusion to improve US differential diagnosis.

Method and Materials: Thirty consecutive patients, (23 women, 7 men) with solitary (13 patients) or multiple (17 patients) nodules were investigated with HDI 5000 scanner before and after 4.8 mg SonoVue® (Bracco, Italy) i.v. injection. Perfusion maps were calculated from the ultrasound data with a research software developed by Amid and R&D Bracco. Microvascular blood volume (A), microbubble velocity (β) and blood flow ($A\beta$) were calculated from signal intensity versus time curves. FNAB was performed on each single nodule.

Results: FNAB evidenced 38 hyperplastic nodules in 23 patients, 5 follicular adenoma in 4 patients and 3 papillary carcinomas in 3 patients. Mean value of A, blood volume values was 9 (± 3) in patients with papillary carcinoma, 11 (± 3) in follicular adenomas and 18 (± 4) in hyperplastic nodules. The mean value of the A differed significantly with hyperplastic nodular goiters and both carcinomas and adenomas patients ($p < 0.01$).

Conclusions: Amid/Bracco parametric software seems to provide an easy tool to evaluate quantitative microvascular blood volume and velocity data after SonoVue® injection with possible clinical value in thyroid nodules differential diagnosis.

B-128 15:03

Doppler ultrasonography with contrast agent injection and perfusion software to assess the efficiency of radio-frequency in recurrent breast cancer

M. Lamuraglia, J.R. Garbay, M.C. Mathieu, P. Opolon, S. Jaziri, A. Roche, J. Leclère, N. Lassau; Villejuif/FR

Purpose: To determine the efficiency of radiofrequency (RF Generator - Boston Scientific) (RF) treatment of the local recurrent breast cancer using Doppler-ultrasonography with Sonovue (Bracco) and perfusion software (Toshiba) (DUSSP).

Methods and Materials: Ten patients with locally recurrent breast cancer will be included in this prospective phase II study. To date, 8 patients have been included.

Scientific Sessions

DUSSP was performed before and after treatment by RF for each patient. The RF procedure was followed by a total mastectomy. Treatment efficacy was assessed according to the destruction of the tumor neovascularisation analysed with DUSSP. The results were compared to histopathological findings.

Results: Before treatment, DUSSP depicted vascularization in the 8 tumors. Contrast agent injection and the use of perfusion software enhanced the conspicuity of neovascularization in all cases. Immediately after RF, DUSSP allowed us to confirm that tumor vascularization had been totally eradicated. Results obtained in 10 patients will be presented.

Conclusion: DUSSP is a promising technique for the immediate evaluation of response to RF treatment of local recurrent breast cancer, in the operating room.

B-129 15:12

Value of contrast enhanced gray scale sonography in rheumatoid arthritis patients: A multicenter study

A. Klauser¹, J. Demharter², D. Sureda³, A. Barile⁴, C. Faletti⁵, C. Masciocchi⁴, M. Schirmer¹, K. Bohndorf²; ¹Innsbruck/AT, ²Augsburg/DE, ³Barcelona/ES, ⁴L'Aquila/IT, ⁵Turin/IT

Purpose: To evaluate, in a multicenter study, the feasibility of contrast enhanced gray scale ultrasound (US), for characterization of joint distension in patients with rheumatoid arthritis (RA) by 5 European centers.

Methods and Materials: We assessed 113 patients (44 men and 69 women; mean age 51 ± 14 years) with established RA in different stages, in different joints, by the continuous mode and low pressure technique of CnTI™ (Contrast tuned Imaging using a EsaTune or Technos MPX US unit, Esaote, Genoa, Italy) using 4.8 mL intravenous administration of SonoVue® (Bracco, Milan, Italy), flushed with 10 mL saline. Unenhanced US, power Doppler US and CnTI™ was evaluated for differentiation of the presence of active synovitis or effusion in the joint distension. Further measurement of maximal thickness of active synovitis and effusion was performed before and after contrast administration.

Results: Joint thickening could not be differentiated in 45/103 (40%) joints by the unenhanced US. In 42/45 joints after contrast administration a differentiation between effusion and active synovitis could be obtained (96%). Maximal thickness measurement of synovial thickness and effusion improved after contrast administration ($p < 0.001$).

Conclusion: Sonovue-enhanced CnTI™ in comparison to unenhanced US showed a better confidence in differentiation of effusion from synovitis and in measurement of thickness of active synovitis in patient with RA. Therefore, this technique has shown to be of value for assessment of disease activity in patient with RA and may be useful in monitoring therapeutic response.

B-130 15:21

Contrast-enhanced US in the assessment of sacroiliac joint vascularity

A. Klauser, M. Schirmer, D. zur Nedden, F. Frauscher; Innsbruck/AT

Purpose: To assess quantitative measurement of vascularity in the sacroiliac (SI) joints of patients with active sacroiliitis and of healthy volunteers using dynamic contrast-enhanced ultrasound (US).

Methods and Materials: Twenty-two patients with active sacroiliitis (15 women, 7 men) based on the clinical criteria described by Calin et al. (JAMA 1977; 237:2613-4), and 10 healthy volunteers (7 women, 3 men) were studied. All patients and volunteers were examined with gray-scale fundamental US and gray-scale harmonic US, before and after injection of intravenous US contrast agent (SonoVue, Bracco, Italy). Both SI joints were imaged in a single transverse scan at three different levels using a 2.5 MHz curved array transducer (Esaote Ultrasound Systems, Italy). Quantitative estimation of the vascularity of the SI joints was performed with time-intensity curves and calculation of the area under the curves. We correlated the contrast US findings with age and disease duration.

Results: Mean value of the area underlying the time-intensity curves was 242 (± 41) in patients with active sacroiliitis and 34 (± 35) in healthy volunteers. The mean value of the areas differed significantly between the patients with active sacroiliitis and the healthy control group ($p < 0.01$). No correlation was found with age and disease duration ($p = 0.2$).

Conclusion: Dynamic contrast-enhanced US is sensitive to the presence of increased vascularity associated with active sacroiliitis and might therefore be useful in the diagnostic evaluation of patients with inflammatory lower back pain.

14:00 - 15:30

Room B

Musculoskeletal

SS 310

Invasive and interventional procedures

Moderators:

G.B. Adam; Hamburg/DE
A. Chevrot; Paris/FR

B-131 14:00

US-guided percutaneous treatment of calcific tendinitis of the rotator cuff.

Results in 651 patients over 8 years

F. Pugliese¹, N.G. Gandoifo², L. Dogliotti², C. Martinoli¹, G. Serafini²; ¹Genoa/IT, ²Pietra Ligure/IT

Purpose: To evaluate the treatment of calcified tendinitis of the shoulder by using an ultrasonography (US)-guided large-needle aspiration-irrigation technique (NAIT).

Materials and Methods: 651 subjects (421 women and 231 men; age range 31-72 years) with acute or chronic shoulder pain were treated percutaneously by US-guided large-needle aspiration-irrigation technique from May 1996 to February 2004. Two 16 G-diameter needles were positioned within the tendon at the level of the calcification. Irrigation and aspiration were alternatively performed through the two needles until calcific deposits were completely cleared. After 1 month, subjective shoulder pain and functional Constant's score were evaluated and compared to those obtained before the treatment. According to these criteria, results were thus classified as excellent, satisfactory and unsatisfactory. At 3 months, a shoulder radiograph was also obtained in all patients.

Results: The mean Constant's score before treatment was 57.2. The mean value after treatment was 91.5, therefore an average increase of 34.3 in Constant's score was observed. 75% of the patients reported the treatment subjectively as beneficial (satisfactory) or extremely beneficial (excellent). At 3 months, 70% of the calcifications were not visible anymore, 23.4% had decreased at least 50% in diameter and 6.6% had decreased less than 50% in diameter. These results indicate a significant clinical response.

Conclusion: This modified US-guided technique for calcified tendinitis of the shoulder is less invasive than previously described percutaneous therapies and appears to be an effective treatment option.

B-132 14:09

MR-arthrography of the scapholunate ligament: Correlation with arthroscopy

H. Guerini, A. Feydy, J.-L. Drapé, A. Chevrot; Paris/FR

Purpose: To describe the normal and pathologic appearances, and the variants of the scapholunate ligament (SLL) at MR-arthrography. To evaluate the effectiveness of the MR-arthrography with arthroscopy as gold standard.

Materials and Methods: Multi-centre retrospective study of 70 arthrograms and MR-arthrograms in 70 patients. Correlation with arthroscopy was performed in 29 patients. The sequences carried out were 3D DESS, 3D FSPGR and FIESTA. Images were assessed for the presence of linear and diffuse signal abnormalities within the SLL.

Results: The sensitivity of combined standard arthrography and MR-arthrography for the lesions of the SLL was 69% and the specificity was 94%. The NPV for SLL perforation was 90%, and the PPV was 70%. The accuracy was 83%. The combination of a diffuse and linear signal abnormality within the SLL improved the sensitivity of MR-arthrography (92%), while preserving a good specificity (83%). The T2-weighted sequences included in our MR-arthrography protocol allowed detection of poorly-opacified cysts within the SLL. MR-arthrography pitfalls are related to the variable signal of the SLL depending on the MR sequence used. The variable bony or cartilaginous insertion of the SLL can also be a source of misleading images.

Conclusion: Combined standard arthrography and MR-arthrography is an accurate method for the diagnosis of SLL perforations. The diagnostic criteria of perforations should include linear and diffuse abnormalities.

Scientific Sessions

B-133 14:18

Three-compartment wrist MR arthrography: Impact on diagnostic thinking and treatment plan

D.V. Guntern, N. Favarger, P. Schnyder, N.H. Theumann; Lausanne/CH

Purpose: To determine if three-compartment wrist MR arthrography has an impact on the orthopedic surgeons diagnosis and treatment plan.

Materials and Methods: Three-compartment MR arthrography was performed in 30 wrists of 30 patients. All patients were addressed to us form a clinic for hand surgery. First three-compartment injection of diluted gadolinium was performed under fluoroscopic control. Then a sagittal and an axial T1-weighted sequence, a coronal T2-weighted fat suppressed sequence and a coronal FISP sequence were acquired with a dedicated wrist coil and a 1.5 T scanner. Before and after MR imaging the orthopedic surgeons had to complete a questionnaire, that evaluated their diagnoses and treatment plans. The pre- and post MR questionnaires were compared. Changes in diagnoses and treatment plan were noted.

Results: MR arthrography changed orthopedic surgeons diagnostic thinking in 21 of 30 cases (70%). Without MR arthrography the orthopedic surgeons would have done an arthroscopy in all patient. Knowing the results of MR arthrography arthroscopy was planned in only 12 patients corresponding to a reduction of 66%.

Conclusion: Wrist MR arthrography has an important impact on orthopedic surgeons diagnostic thinking and treatment plan. The number of arthroscopies was reduced significantly.

B-134 14:27

Evaluation of rotator interval pathology in athletes with MR arthrography

E. Genovese, A. Leonardi, L. Callegari, M. Angeretti, S. Indrinella, C. Fugazzola; Varese/IT

Purpose: Rotator interval is an important anatomic and functional region commonly subject to overuse injuries in athletes participating in repetitive overhead sports. The aim of this study was to assess the role of MR Arthrography in detecting rotator interval lesions in chronic overuse-type disorders.

Materials and Methods: 23 athletes (swimmers, tennis players, pitchers) with rotator interval syndrome (chronic shoulder pain and dysfunction) underwent MR Arthrography. All patients were investigated with SET1, 3DT1-FATSAT, FSE FATSAT PD/T2 sequences before and after intrarticular injection of 20 cc of diluted contrast medium.

Results: MR Arthrography revealed rotator interval lesions in 11 athletes (in 3 cases laxity of rotator interval, in 3 cases contractures of the rotator interval, in 2 cases rotator interval synovitis, in 2 cases coraco-humeral ligament lesions and in 1 case rotator interval calcification). In 3/11 cases MR Arthrography identified rotator interval pathology with a SLAP lesion and in 2/11 cases rotator interval lesion associated with anterior instability. All results were compared with arthroscopic and surgical findings.

Conclusion: MR Arthrography enables an accurate evaluation of rotator interval lesions in chronic overuse-type disorders in athletes.

B-135 14:36

Shoulder MR-arthrography in the follow-up after surgery repair: Inter-individual comparison of anterior palpitory and posterior US-guided access

M. Barini, A. Stecco, F. Bruculeri, P. Neri, P. Fornara, A. Carriero; Novara/IT

Purpose: To compare efficacy, procedure time and patient discomfort between anterior palpitory and posterior US guided approach for intra-articular injection in the shoulder after rotator cuff surgical repair.

Methods and Materials: Gleno-humeral injection of contrast solution was performed in 35 consecutive patients, all treated for rotator cuff surgical repair. The first 15 patients underwent palpitory-guided anterior access; while the other 20 had a posterior US-guided intra-articular injection. Efficacy, procedure time and patient discomfort were evaluated in all patients, and a statistical test (t-student) was applied to evaluate the significative differences.

Results: Anterior palpitory-guided glenohumeral approach resulted in 9/15 correct intra-articular injections and 6/15 extra-articular injection, with severe discomfort in 8/15, moderate discomfort in 5/15 and mild to nothing in 2/15. Procedure mean time was 1.5 minutes. Posterior US-guided injection provided an intra-articular access in 19/20 of patients, with severe discomfort in 1/20, moderate in 6/20 and mild to nothing in 13/20. The mean time of the procedure was 3.2 minutes. Statistical analysis of effective intra-articular injection rate, and procedural time between the two modalities resulted in a significative difference ($P < 0.005$) between the two modalities, with better efficacy in intra-articular injection for the US-guided approach and a longer procedure time for the US-guided protocol.

Conclusion: In the post-operative shoulder, due to the post-surgical anterior scar, the posterior US-guided access to perform the intra-articular injection results are more accurate, though more time consuming, with less pain or discomfort with respect to the anterior palpitory access.

B-136 14:45

Labral lesions of the hip: Assessment with MR arthrography in symptomatic patients

E. Wiener, K. Wörtler, H. Rechl, L. Gerdesmeyer, E. Rummey; Munich/DE

Purpose: To evaluate the accuracy of MR arthrography in the detection and classification of acetabular labral lesions in symptomatic hips.

Material and Methods: MR arthrography of the hip was performed in 32 symptomatic patients who underwent subsequent surgical exploration. Following intraarticular injection of 10-15 ml of gadopentetate dimeglumine solution (2.5 mmol/l) MR imaging was performed on a 1.0 T system using triplanar T1 weighted SE sequences and WE 3D-DESS sequence. Images were evaluated by two experienced radiologists (agreement by consensus) with regard to degeneration (grade I), tear (grade II) and detachment (grade III) of the anterior, lateral and posterior labrum. Articular cartilage surface irregularities (grade I) or full thickness defects (grade II) were also assessed. The results of the radiological evaluation were compared with intraoperative findings (gold standard).

Results: 49/56 surgically proven labral lesions were depicted by MR arthrography, and 33/40 intraoperatively normal labral parts were assessed correctly. 62% of grade I, 79% of grade II and 84% of grade III lesions were classified concordant with surgical findings. For detection of labral lesions MR arthrography showed a sensitivity of 87.5%, a specificity of 82.5% and an accuracy of 85.4%. Articular cartilage lesions were diagnosed with a sensitivity of 57% and a specificity of 67%.

Conclusions: MR arthrography enables accurate detection and classification of acetabular labral lesions but appears to be limited in the evaluation of articular cartilage of the hip.

B-137 14:54

New arthro-MR imaging technical approach in the evaluation of intra-articular structures of the postero-lateral corner of the knee

N. Limbucci, A. Barile, L. Zugaro, G. Bonanni, V. Calvisi, C. Masciocchi; L'Aquila/IT

Purpose: To assess the role of a new oblique sagittal scan plane to evaluate by arthro-MR imaging the anatomy and the pathological findings related to post-traumatic instability of the ligamentous structures of the posterolateral corner (PLC) of the knee.

Methods and Materials: 28 patients entered the study. 16 patients, already submitted to ACL reconstruction and still complaining of posterolateral instability, and 12 patients with acute post-traumatic instability (9 ACL and 3 PCL lesions) underwent arthro-MR imaging to evaluate the capsulo-ligamentous structures of the PLC. All patients underwent arthroscopy. We evaluated 5 more patients with no traumatic history, submitted to arthro-MR imaging for cartilage assessment, to study the anatomical setting; after that they underwent arthroscopy. Arthro-MR imaging was performed with a 1.5 T unit (Signa Horizon, GE) employing SE-T1W and SE-T1W fat-sat sequences on conventional scan planes. In all cases we acquired the same sequences on a new 45° oblique sagittal plane. We compared arthro-MR imaging and arthroscopic findings.

Results: In all patients complaining of posterolateral instability of the knee, arthro-MR imaging discovered a lesion of the inferior posteromedial menisco-popliteal ligament. In one case the popliteus tendon was also involved. In all patients studied for anatomical setting, it was possible to identify the ligamentous components of the PLC (lateral and medial menisco-popliteal ligaments, popliteus tendon). Arthroscopy confirmed arthro-MR imaging findings in all cases.

Conclusion: We consider arthro-MR imaging as the method of choice in the evaluation of the PLC of the knee. We propose a new 45° oblique plane that can add further information respect to standard arthro-MR imaging.

B-138 15:03

Histological changes at the bone cement interface after kyphoplasty - comparison of PMMA and CaP with histomorphometry and high resolution CT

M. Libicher, M. Vetter, C. Kasperk, P.J. Meeder, G. Nöldge; Heidelberg/DE

Purpose: To quantify formation of new bone at the bone cement interface of PMMA and CaP in a dog model. To quantify signs of resorption of biocompatible CaP cement with high resolution CT and dedicated software. To compare changes of CaP vs. PMMA during follow-up over a period of 12 months.

Material and Methods: Three osteopenic foxhounds received cement implants

Scientific Sessions

into 3 thoracic and 2 lumbar vertebrae under intubation anaesthesia. The dogs were sacrificed 5, 10 and 15 months. The number of osteonal structures was counted at the bone cement interface. In a clinical trial, 20 vertebrae (10 CaP, 10 PMMA) were examined with HR-CT-volumetry using an identical imaging protocol. CT scans were obtained after kyphoplasty and after 12 months (collimation 0.5 mm, slice thickness 1 mm, in plane resolution 0.5 mm). To quantify the volume in sub voxel resolution we analyzed each cement fragment with a density-weighted algorithm.

Results: Histomorphometric analysis revealed in CaP a significant increase of osteons at the bone cement interface within 15 months indicating formation of new bone. In PMMA no signs of cement resorption or bone formation were discernible. CT measurements showed a significant decrease of border density between 1.5-6% in CaP compared to PMMA ($p < 0.05$). CT data are confirmed by histomorphometric analysis.

Conclusion: There are signs of resorption in biocompatible CaP cement that can be quantified by histomorphometric measurement. These changes at the bone cement interface can be detected by high resolution CT and dedicated software.

B-139 15:12

Temperature changes in surrounding soft tissue during CT-guided radio frequency ablation (RFA) of osteoid osteoma in an ex vivo animal model

R.-G. Bitsch, M.D. Daniels, R. Rupp, L. Bernd, K. Ludwig; Heidelberg/DE

Purpose: Examination of the temperatures in soft tissue surrounding bone during radio frequency ablation (RFA) of osteoid osteomas in an ex vivo animal model.

Materials and Methods: Intra-cortical cavities were created in fresh bovine long bone specimens as models for osteoid osteomas. The thickness of the cortical bone lamella separating nidus from periosteum was set at 1/3/5 mm. Three temperature probes were inserted into soft tissue surrounding bone at 0/5/10 mm from the periosteum. Before RFA, the thickness of the cortical bone lamella was documented by CT. Specimens were heated in a basin to 37 °C. RFA was performed with a target temperature of 95 °C for six minutes. During RFA, the temperature was continuously monitored at all temperature probes. No simulation of vessel perfusion was used.

Results: For a cortical bone lamella between the nidus and periosteum of 1 mm, maximum temperatures of 69.1/51.3/42.5 °C, for a cortical bone lamella of 3 mm 59.2/46.5/41.1 °C and for a cortical bone lamella of 5 mm 50.6/44.8/40.0 °C were measured at 0/5/10 mm from the periosteum within surrounding soft tissue.

Conclusion: In our model of osteoid osteomas, soft tissue temperature during RFA was shown to be dependent on thickness of cortical bone lamella as well as on distance from periosteum. Results demonstrate that with a cortical bone lamella of at least 1 mm thickness, there is no severe risk of nerve damage at distances of more than 10 mm from the periosteum.

B-140 15:21

Arthro-MR imaging evaluation and incidence of supranequatorial gleno-humeral lesions in athletes affected by acquired instability of overstressed shoulder

C. Bultrini, N. Limbucci, R. Manetta, A. Barile, V. Calvisi, C. Masciocchi; L'Aquila/IT

Purpose: To assess the diagnostic accuracy of arthro-MR imaging in the evaluation of supranequatorial anatomical variations with respect to pathological findings in athletes clinically suspected of acquired instability of overstressed shoulder (AIOS) using arthroscopy as a gold standard.

Methods and Materials: 29 patients (18-35 years, mean age 23), all athletes, entered the study. All patients presented, clinically suspected non-traumatic shoulder instability due to overstrain related to sport activity. Before arthroscopy, all patients underwent arthro-MR imaging. We employed SE T1-w and FSE T2-w sequences for standard examination, after the intrarticular injection of 10-15 ml of contrast agent (obtained from the dilution of 0.6 ml of Gd-DTPA in 250 ml of saline) SE T1-w and fat-sat SE T1-w sequences were acquired.

Results: In 14 of 29 patients (48.2%) we found supranequatorial lesions. We detected anatomic variations in 5 of 14 cases (35.7%): in 3 patients arthro-MR imaging showed the presence of Buford complex; in one patient the presence of sub-labral foramen and in one patient a type II bicipital labral complex. In the remaining 9 of 14 patients (64.3%), arthro-MR imaging allowed the diagnosis of acquired abnormalities: 2 type II and 1 type III SLAP lesions, 2 paralabral posterior cysts, 4 rotator interval lesions. Arthroscopy confirmed arthro-MR imaging findings in all cases.

Conclusion: Arthro-MR imaging appears to be the method of choice in the pre-operative study of the supranequatorial lesions of the glenoid labrum, allowing the correct identification of anatomic variations: in our experience this technique is as accurate as arthroscopy.

14:00 - 15:30

Room C

GI Tract

SS 301a

Colorectal cancer and staging

Moderators:

M. Bachmann Nielsen; Copenhagen/DK

M.H. Fuchsäger; Vienna/AT

B-141 14:00

Double contrast barium enema: Critical analysis of reported performance in the era of virtual colonoscopy

J. Sosna, T. Sella, E. Libson; Jerusalem/IL

Objective: CT colonography and conventional colonoscopy may have similar efficacy for detection of polyps > 6 mm. In this era the role of double contrast barium, an accepted screening tool for colorectal cancer, might be in doubt. The purpose of this study is to use meta-analysis to assess the accuracy of double contrast barium enema for detecting colorectal polyps and cancers.

Materials and Methods: Prospective studies comparing double contrast barium enema with conventional colonoscopy/ flexible sigmoidoscopy or clinical follow-up were identified and a standard form was used to extract relevant study data. Fisher's exact test and the Cochran-Mantel-Haenszel test were used for pooling of data. A 95% confidence interval (CI) was selected to determine sensitivity. Meta analysis methods were used to test robustness of results. Comparisons were made for the percentage of cancers and polyps detected.

Results: Only ten studies published since 1980 fulfilled all the inclusion criteria. Eighteen other studies were excluded due to their retrospective design. The pooled sensitivity for colorectal carcinoma was 0.80 (95% CI: 0.69, 0.91) and for polyps greater than or equal to 10 mm it was 0.73 (95% CI of 0.65, 0.83). The sensitivity for polyps 1-9 mm in size could not be calculated as only 4 of the 10 studies published such data and pooling was not statistically justified.

Conclusion: The scientific data on the overall performance of double contrast barium enema is scarce. Its performance might not be accepted as a screening tool especially when CT colonography might perform better.

B-142 14:09

The role of computed tomography, magnetic resonance imaging and positron emission tomography in the diagnosis of liver metastases: A meta-analysis

S. Bipat¹, M.S. van Leeuwen², E.F. Comans¹, M.E. Pijl³, J. Stoker¹;

¹Amsterdam/NL, ²Utrecht/NL, ³Groningen/NL

Purpose: To obtain summary estimates on the diagnostic performance of Computed Tomography (CT), Magnetic Resonance Imaging (MRI) and Positron Emission Tomography (PET) in assessing colorectal liver metastases.

Materials and Methods: The MEDLINE, EMBASE, Web of Science, CANCERLIT and Cochrane databases from the beginning of 1990 till December 2003 were searched for relevant original articles. Articles were included based on following criteria: 1) CT, MRI or PET to identify and characterize colorectal liver metastases; 2) findings at surgery, biopsy, autopsy, intra-operative findings and/or follow-up used as reference standard; 3) data presented to calculate true-positive and false-negative values. A random effects model was used to obtain summary estimates of sensitivity (lesion-based) in assessing liver metastases.

Results: Of 165 identified relevant articles, 61 fulfilled all inclusion criteria. Sensitivity estimates for nonhelical CT, helical CT, MRI at 1.0 T, MRI at 1.5 T and PET were 52.3% (95%CI:52.2, 52.4), 63.5% (95%CI:54.3, 71.9), 66.1% (95%CI:66.0, 66.3), 64.3% (95%CI:57.7, 70.4) and 75.8%(95%CI:61.1, 86.2) respectively. The estimates for nonenhanced MRI, Gd-enhanced MRI, SPIO-enhanced MRI were 59.8% (95%CI:49.0, 69.7), 78.2%(95%CI:63.0, 88.3) and 73.2% (95%CI:62.3, 81.9) respectively. Sensitivity estimates for GD-enhanced MRI ($p = 0.0186$) and SPIO-enhanced MRI ($p \leq 0.0001$) were significantly higher compared to nonenhanced MRI.

Conclusion: The diagnostic accuracies of MRI with contrast agents and PET were higher compared to helical CT for assessing colorectal liver metastases (not significantly). However, the availability of MRI and PET scanners in daily practice is limited and therefore it is most likely that only selected cases will undergo either MRI or PET.

Scientific Sessions

B-143 14:18

Careful CT and MR serial imaging review with a defined reporting protocol in follow-up colorectal cancer patients and correlation with ¹⁸FDG-PET-CT findings

K.C. Potter, G. Brown, B. Sharma, S.L. Houghton, J.E. Husband; Sutton/UK

Purpose: To evaluate the added value of ¹⁸FDG-PET-CT imaging over careful serial CT and MR imaging review in follow-up colorectal cancer patients.

Methods: Colorectal cancer patients at high risk of recurrence undergo regular follow-up CT and/or MR imaging in our institution. Indications for ¹⁸FDG-PET-CT include suspicion of recurrence due to elevated tumour marker (CEA) or equivocal findings on CT/MR. Over 4.5 months, 17 such patients underwent ¹⁸FDG-PET-CT within 4 weeks of CT/MR. CT/MR imaging was reviewed in detail using a defined reporting protocol for all prior serial imaging including baseline imaging with detailed criteria for scoring. Interobserver agreement was measured. Reviewers were blinded to the original reports, ¹⁸FDG-PET-CT findings and follow-up. Diagnosis was established by follow-up, biopsy, surgery or response to treatment.

Results: 10/17(59%) patients with normal CEA levels underwent ¹⁸FDG-PET-CT imaging for equivocal findings on original CT/MR investigations. Detailed review reduced the number of equivocal scans to 3(30%) ($p < 0.05$). No false negatives for CT/MR were demonstrated by ¹⁸FDG-PET-CT imaging. Of the 7/17(31%) patients with elevated CEA, CT/MR imaging alone was correct in 5/7 patients. ¹⁸FDG-PET-CT provided additional diagnostic information in 2/7 patients. Thus, the presence or absence of recurrence was resolved by detailed review in 12/17 (70.6%, 95% CI 48.9%-92.2%) patients referred for ¹⁸FDG-PET-CT.

Conclusion: We recommend careful review of all previous imaging prior to undertaking ¹⁸FDG-PET-CT imaging since this significantly decreases the number of equivocal reports in patients with normal CEA and confirms the cause of CEA elevation in the majority of patients.

B-144 14:27

Colorectal hepatic metastases: Evaluation using Magafodipir Trisodium enhanced MR imaging and breath-hold single-shot echo-planar diffusion-weighted MR imaging

D.-M. Koh¹, G. Brown¹, A. Riddell¹, D. Collins², E. Scurr¹, N. Karanji³, J. Husband¹; ¹London/UK, ²Sutton/UK, ³Guildford/UK

Purpose: To determine the sensitivity and specificity of T1-weighted Magafodipir Trisodium (Mn-DPDP) enhanced MR imaging and diffusion-weighted MR imaging (DWI) in the detection of colorectal hepatic metastases.

Method and Materials: 20 patients with potentially resectable colorectal hepatic metastases were prospectively evaluated using pre-contrast T1-weighted, T2-weighted and DWI (breath-hold single shot echo-planar imaging with three b values) of the liver was performed. Following Mn-DPDP administration, axial/coronal T1-weighted MR imaging of the liver were acquired. Two readers independently assessed DWI images and Mn-DPDP T1-weighted images separately and in combination. Histopathology and follow-up imaging were used as gold standards.

Results: There were 47 metastases and 33 benign lesions as determined by our gold standard. 40/47 metastases were confirmed at histopathology. The mean sensitivity and specificity of Mn-DPDP MR imaging for detecting metastasis were 87% (95% CI 73 - 96%) and 85% (95% CI 67 - 96%). The mean sensitivity and specificity of DWI were 85% (95% CI 71 - 94%) and 77% (95% CI 55-92%). The lower sensitivity and specificity of DWI alone could be attributed to motion and susceptibility artefacts obscuring lesions within the left lobe. The use of a combination of Mn-DPDP enhanced MR imaging and DWI yielded a mean sensitivity of 89% (95% CI 76 - 96%) and specificity of 94% (95% CI 91 - 100%).

Conclusions: Mn-DPDP enhanced T1-weighted MR imaging of the liver has a high sensitivity and specificity in detecting colorectal hepatic metastases. However, the addition of DWI improves the sensitivity and specificity of lesion detection.

B-145 14:36

CT perfusion as index of angiogenesis of rectal cancer

G. Petralia, L. Funicelli, S. Ferretti, A. Sonzogni, M. Bellomi; Milan/IT

Purpose: The aim of this study was to evaluate the different Computed Tomography (CT) parameters, characterizing tissue perfusion by contrast medium in rectal carcinomas and to define their relation with angiogenetic activity.

Materials and Methods: 41 patients with rectal cancer (24 of them before and after neo-adjuvant Radio- and Chemo-therapy) were studied by dynamic CT (16 slice light-speed G.E., scanned every second for 150°, after i.v. 2 ml/sec injection of 40 ml of 350 mg/dl iodine contrast medium). Semi-automatic calculation of time to peak (TTP), positive enhancement integral (PEI), maximum slope of

increase (MSI), maximum slope of decrease (MSD), blood flow (BF), blood volume (BV), mean transit time (MTT) and permeability surface (PS) were performed. Value distributions in the normal and neoplastic wall, their variation after therapies and their relation to pathological vessel density (MVD) were evaluated.

Results: BF, TTP, PS were higher in tumor than in normal wall, respectively in 68, 76 and 100% of patients; PS was > 20 ml/min/100 g in 100% of patients. PS decreased in 78% of patients submitted to neo-adjuvant Radio-chemotherapy. Significant correlation between TTP and MVD was found ($R = 0.679$).

Conclusion: CT perfusion could be reliable in the study of the neo-angiogenetic process, characterized by an increase in vessel number, vascular permeability and flow into extravascular spaces, better than pathological MVD count. Imaging will gain a role in monitoring targeted therapies, in the assessment of different angiogenetic patterns in tumors and in the selection of patients eligible to be treated by antiangiogenic therapy.

B-146 14:45

Comparison of MR imaging and CT for staging of advanced rectal carcinoma

J.C. Stollfuss, F. Zimmermann, K. Wörtler, F. Auer, E. Rummeny; Munich/DE

Purpose: To compare Magnetic-Resonance-Imaging (MRI) and Computed-Tomography (CT) for pre-operative staging in patients with advanced rectal carcinoma ($\geq T3$) after combined radio-chemotherapy.

Materials and Methods: 136 patients (98 male, 38 female, mean age 61 ± 9 yrs) with $\geq T3$ tumors at initial presentation were included in the study. All patients received pre-operative combined radio-chemotherapy. Contrast-enhanced and T2W MRI was performed after adequate bowel preparation. CT was performed after i.v. and rectal contrast application using conventional ($n = 70$) and multislice techniques ($n = 66$). Images were analyzed by two radiologists (consensus reading) according TNM categories using local tumor invasion and the presence of lymph-node metastases as the main parameters. Histopathological correlation was available in all cases. The accuracy of T2W and contrast-enhanced T1W-images were compared in a subgroup of 91 patients.

Results: The overall accuracy for prediction of local tumor invasion ($\geq T3$) by MRI was significantly higher when compared to that of CT ($p < 0.01$). There was no significant difference between T2W and T1W images after gadolinium-DTPA administration (n.s.). Compared to MRI, CT tends to be more specific regarding the prediction of nodal status ($p < 0.05$).

Conclusion: MRI is superior to CT for the prediction of local tumor invasion in patients with advanced rectal carcinoma, and may replace CT as the primary staging modality. Intravenous contrast administration in MRI was not superior to T2W imaging.

B-147 14:54

CT colonography in the follow-up of patients with partial colectomy

E. Neri, P. Vagli, S. Picchietti, F. Vannozi, A. Bardine, C. Bartolozzi; Pisa/IT

Purpose: To evaluate the role of CT colonography in the follow-up of patients submitted to surgical resection of the colon and who are intolerant of conventional colonoscopy.

Method and Materials: Four-row CT colonography was performed in a series of 24 subjects who had a previous partial colectomy for diverticulitis ($n = 4$) and colorectal cancer ($n = 20$). Patients were submitted to CTC because of incomplete conventional colonoscopy, for intolerance to endoscope insertion or stenosis of the lumen. In 22 cases pneumocolon was achieved via a rectal tube and in 2 cases through a cutaneous anastomosis. Colectomy involved the rectum ($n = 6$), the right colon ($n = 6$), descending colon ($n = 5$) and sigmoid colon ($n = 7$). In all cases CTC analysis included the combined evaluation of 2D images, 3D volume rendering of the external colon and endoluminal views simulating colonoscopy.

Results: CTC detected 3 cases of stenosis of the anastomosis in the sigmoid colon (1 neoplastic and 1 fibrotic) and in the ileo-colic junction in the transverse colon (neoplastic). The study of the residual colon showed 3 polyps - 8, 6 and 5 mm respectively - confirmed by CTC. In all cases the residual colon was entirely visualized. In 2 patients fecal residuals were present at the level of the ileo-colic anastomosis. The post-surgical anatomy was correctly depicted. In all cases with right colectomy the pneumocolon also involved the ileum through the ileo-colic junction, leading to difficulties in image interpretation.

Conclusions: CT colonography is a valid alternative to CC in patients with partial colectomy and who are intolerant to the introduction of the endoscope into the colon.



Scientific Sessions

B-148 15:03

Preoperative TN staging of rectal carcinoma: Prospective comparison of transrectal US (TRUS) and endorectal MR imaging

M. Scialpi, V. Cenciarini, P. Landi, L. Regi, C. Galuppo, L. Lupattelli; Perugia/IT

Purpose: To compare the diagnostic potential of transrectal US (TRUS) and endorectal MR imaging (EMRI) in the preoperative assessment of the spread of rectal cancer and the nodal status in order to evaluate and recommend an appropriate imaging strategy.

Methods and Materials: 19 consecutive patients with proven carcinoma of the rectum were included in this prospective study. TRUS was performed with a 9-5 MHz transrectal probe. MR images were obtained with a 0.5-T superconducting magnet using an endorectal coil. In all patients FSE and TSE sagittal, axial and coronal T1 and T2-weighted images were performed.

Results: TRUS and EMRI accurately assessed the depth of rectal wall invasion by carcinoma. The results were correlated with histopathology in 18/19 cases (94.7%) and 1 case was understaged. Lymph nodes as small as 2-3 mm were identified by TRUS and EMRI, but benign from malignant lymph nodes were not differentiated.

Conclusion: TRUS and EMRI shows similar results in preoperative T staging of rectal carcinoma, however detection of nodal disease is still a diagnostic problem. TRUS and EMRI can be recommended for routine clinical application.

B-149 15:12

Colorectal cancer perfusion measurement using dynamic contrast

enhanced MDCT: Effect of acquisition time and implications for protocols

V.J. Goh¹, S. Halligan², J.-A. Hugill², L. Gartner², C. Bartram²; ¹Northwood/UK, ²Harrow/UK

Purpose: To determine the effect of acquisition time on colorectal cancer perfusion measurement using MDCT.

Material and Methods: 10 patients with histologically proven colorectal cancer were examined prospectively using 4-detector row CT (Lightspeed Plus, GE). A dynamic contrast enhanced scan was performed through the mid tumour (cine mode; 4 x 5 mm collimation) and tumour blood flow, blood volume, mean transit time and permeability recorded for acquisition times of 45, 65 and 130 seconds using commercial software (Perfusion 3.0, GE). Differences in the four perfusion parameters studied, for each of the three acquisition times, were determined using the paired T test after confirming parametric distribution.

Results: The mean (standard deviation, SD) for tumour blood volume, blood flow, mean transit time and permeability was 5.7 (1.3) ml/100 g tissue, 82.2 (31) ml/100 g tissue/min, 7.9 (3.4) seconds and 11.7 (2.2) ml/100 g tissue/min respectively at 45 seconds; 6.3 (1.6) ml/100 g tissue, 84.9 (36.5) ml/100 g tissue/min, 8.2 (3.9) seconds and 14.2 (2.4) ml/100 g tissue/min at 65 seconds; and 6.2 (1.5) ml/100 g tissue, 82 (30.6) ml/100 g tissue/min, 8.2 (3.4) seconds and 14.9 (3.1) ml/100 g tissue/min respectively for a 130 second acquisition. Significant differences in permeability was noted between acquisitions of 45 seconds, and 65 and 120 seconds respectively ($p = 0.02$; 0.007). There was no significant difference in blood volume, blood flow, and mean transit time measurements for any of the acquisition times.

Conclusion: Values for tumour permeability are contingent upon data acquisition time, which should be long enough so that measurements are accurate. Other perfusion parameters are unaffected.

B-150 15:21

Multislice spiral CT for the prediction of an involved circumferential resection margin in primary rectal cancer

S.V.R.C. Wolberink¹, R.G.H. Beets-Tan², D.F.M. de Haas-Kock², M. Oudkerk¹, T. Wiggers¹; ¹Groningen/NL, ²Maastricht/NL

Purpose: To determine accuracy of multislice CT scan (MSCT) in the preoperative prediction of the circumferential resection margin (CRM) in rectal cancer.

Methods and Materials: 200 patients with primary rectal cancer underwent a MSCT scan of the abdomen. Scans were scored for yes (R1=distance to mesorectal fascia ≤ 1 mm) or no (R0 = distance > 1 mm) involved CRM by two teams consisting of two specialist readers, reading in consensus. The teams were blinded for each other's and the histological results, the latter of which were taken as the gold standard.

Results: There were 2 T0Nx, 7 T1Nx, 43 T2Nx, 126 T3Nx and 22 T4Nx tumors. A total of 400 predictions were made, 44 incorrect (11%) and 356 correct (89%). Sensitivity for team A was 65.6% with a specificity of 93.7%. Sensitivity for team B was 81.3% with a specificity of 94.7%. Discrepancies occurred in 33 patients, 16 false positive and 14 false negative. 16 of these had an anteriorly located

distal tumor with a close CRM in the direction of the seminal vesicles or uterus. 7 had an distal tumor with the distal margin close to the anal sphincter. Interobserver agreement was high ($\kappa 0.69$).

Conclusion: MSCT can predict the CRM in rectal cancer with high accuracy and high interobserver variability. Overstaging errors mostly occurred in either anteriorly located distal tumors or in tumors with a distal margin close to the anal sphincter, indicating that caution is needed when predicting the CRM in these types of tumors.

14:00 - 15:30

Room E2

Breast

SS 302

Digital mammography

Moderators:

C.C. Riedl; New York, NY/US

P. Skaane; Oslo/NO

B-151 14:00

Is CAD/CAC performance affected by breast tissue composition?

R. Lederman¹, I. Leichter¹, S. Fields¹, S. Buchbinder², B. Novak¹, M. Sklar-Levy¹, P. Bamberger¹; ¹Jerusalem/IL, ²Staten Island, NY/US

Purpose: To compare the performance of a two-tiered system with computerized detection (CAD) and classification (CAC), in high-density and low-density breast tissue.

Methods and Materials: 222 cases with pathologically-proven mammographic lesions (140 malignant) were retrospectively interpreted using a two-tiered CAD/CAC system. The CAD scheme automatically detected suspicious findings on digitized mammograms. The CAC scheme calculated the level-of-suspicion based on automatically extracted features. The CAC scheme was applied whenever the finding was retrospectively considered suspicious, whether detected or not, and for each biopsied lesion detected by the CAD tier even if it was retrospectively considered benign by the radiologist. Independently, all cases were ranked by breast composition. Fatty breasts were combined with scattered fibroglandular densities (low-density), while heterogeneously dense cases were combined with extremely dense cases (high-density).

Results: High-density breasts were found in 115 cases (88 malignant). For malignant masses, the detection sensitivity was 96.0% (48/50) in low-density breast tissue and 89.5% (34/38) in high-density breast tissue. For malignant clusters the detection sensitivity was 100% (21/21) in low-density breast tissue and 96.9% (30/31) in high-density breast tissue. The CAC scheme, increased the sensitivity of classification from 94.2% to 97.1% in dense breasts, while in low-density breast tissue it decreased from 100% to 98.6%. The specificity of classification with CAC increased from 13.9% to 63.9% in low-density breast tissue and from 17.4% to 60.9% in dense breasts.

Conclusion: Overall the CAD/CAC device performed similarly in low-density and high-density breast tissue. In dense breast, the CAD/CAC device increased both sensitivity and specificity.

B-152 14:09

A new approach for adjunct computerized assessment of mammographic findings, using a CAC system

I. Leichter¹, S. Buchbinder², R. Lederman¹, S. Fields¹, B. Novak¹, P. Bamberger¹; ¹Jerusalem/IL, ²Staten Island, NY/US

Purpose: To test the diagnostic performance of an adjunct use of Computer-Assisted-Classification (CAC), which assesses breast lesions by a differential weighting of BI-RADS categories.

Methods and Materials: 171 cases of mammographic lesions, with proven pathology (88 malignant) were retrospectively interpreted in a conventional manner, each by four radiologists. After digitizing the films, findings were automatically classified by a CAC system, which calculated the level-of-suspicion of each lesion. This level-of-suspicion yielded a CAC-modified assessment by potentially modifying each conventional BI-RADS category by one step only, in either direction. Subsequently, a CAC-adjunct assessment was attained by allowing BI-RADS categories modifications by more than one, depending on the level-of-concern expressed by the radiologist and never swapping non-actionable categories ("2" and "3"). The radiologist's and the two different computerized assessments were compared.

Results: For each radiologist, the ROC curves of both CAC-modified and CAC-adjunct assessments showed higher AUC compared to conventional interpretation.

Friday

Scientific Sessions

While the ROC curves for the limited CAC-modified assessment crossed those of conventional interpretation, the ROC curves for the CAC-adjunct assessment were consistently higher. The mean area for both the CAC-modified and CAC-adjunct assessments (0.86) was significantly higher ($p < 0.005$) than for the conventional interpretation (0.77). The average specificity increased from 26.8% for conventional interpretation to 47.0% ($p < 0.001$) for both CAC-modified and CAC-adjunct assessments.

Conclusion: For the same improvement in sensitivity and specificity compared to the conventional interpretation, the diagnostic performance of a CAC-adjunct assessment is superior to that of a CAC-modified assessment because the CAC-adjunct ROC curves do not cross the conventional curves.

B-153 14:18

The evaluation of image quality and dose on computed radiography systems for mammography

C.P. Lawinski, H. Cole, P. Blake, A. Mackenzie, A. Pascoal; *London/UK*

Purpose: Following recent concerns raised in Europe regarding the use of computed radiography (CR) in mammography, a comparative evaluation of the systems currently offered in the UK has been performed. CR for mammography was initially based on systems for general radiography. More recently, dedicated mammography systems are available with improved imaging capability, particularly in terms of spatial resolution.

Methods and Materials: Image quality data was obtained using a range of test objects. All acquired images were scored both as softcopy and as hardcopy. Breast and receptor dose were also assessed. The results were compared to typical data for screen-film mammography and to recent UK guidance on the introduction of CR for mammography.

Results: All of the systems evaluated met the requirements of UK guidance for visibility of the TOR MAX details. All TOR MAM softcopy scores were at least as good as typical screen-film results and in all cases were better than the associated hardcopy values. CDMAM results showed that, in general, contrast detail detectability was better for softcopy presentation than hardcopy. For all of the systems evaluated, limiting resolution measurements were close to the theoretical values derived from the pixel pitch and poorer than for typical screen-film systems.

Conclusions: All of the CR systems for mammography evaluated met the current UK minimum levels of performance in terms of test object image quality and radiation dose. Therefore any of these systems can undergo clinical evaluation as described in this guidance. Softcopy reporting may offer significant benefits over hardcopy.

B-154 14:27

Number and reasons for additional views (mosaic) at full-field digital mammography (FFDM) with a 19x23 digital detector

R. Gullien, A. Haakull, S.J. Kristiansen, M. Loevstad, P. Skaane; *Oslo/NO*

Purpose: To determine the number and reasons for women in the randomized Oslo II study requiring more than two standard views (cranio-caudal and mediolateral oblique) of each breast at mammography with a 19x23 digital detector.

Methods and Materials: 7005 women underwent digital mammography with a Senograph 2000D (GE Medical Systems). The women were examined by any two radiographers employed in the screening program at that time. Each of the woman's breasts was positioned by a different radiographer. In an on-site protocol, the radiographers registered all women who had taken more than four views and the reason for this deviation. The reasons for deviation were classified as: Breast size incompatible with detector size, positioning failure/error or need for additional axillary views or other reasons. Disabled women, women with implants and women after mastectomy were excluded from analysis.

Results: Of the 7005 women examined, 6705 (95.71%) women required standard views, 135 (1.92%) 5 views, 84 (1.19%) 6 views and 81 (1.15%) 7 views or more. Of the 297 (4.23%) women requiring more than standard views, 234 (78.78%) women required additional views due to breast size incompatible with detector size, 46 (15.48%) due to positioning error or need for axillary views and 17 (5.72%) due to other factors.

Conclusion: Relatively few women (4.23%) in Oslo aged 50-69 required a mosaic examination at FFDM. A further reduction of this number could be achieved with improved positioning techniques.

B-155 14:36



Digital luminescence mammography (CR) versus full-field digital mammography (DR): A phantom study

R. Schulz-Wendtland, E. Wenkel, M. Lell, K. Imhoff, W. Bautz; *Erlangen/DE*

Purpose: The objective of this phantom study was to compare the high resolution digital phosphor storage plate system (18x24 cm²) (Siemens) with the full field digital mammography system (Fischer) in diagnostic mammography.

Method and Materials: RMI-mammography-phantom X-ray studies were acquired with two different systems. A set of digital acquired images (Mammomat 3000 N (Siemens), storage phosphor plate IP HR BD, image reader FCR 5000 MA (Fuji / Siemens), resolution 8-9 lp/mm, printer FM DP L (Fuji), resolution 12.9 lp/mm) (CR) were compared as hardcopies to full-field digital images (SenoScan (Fischer), CCD-detector, resolution 10 lp/mm, printer TM 8600 (Kodak), resolution 12.9 lp/mm) (DR) by using the same parameters and exposure data (standard crano-caudal position, 100 mAs, 28 kV) of the same objects. Five in mammography experienced radiologists read the images with regard to recognizability of details like grains of aluminum oxide (200 to 740 micrometers), threats of nylon (0.4 to 1.6 mm) and round lesions / masses (diameters 5 to 14 mm).

Results: 225 right positive decisions were possible to detect for every system. We found 193 right positive decisions for the digital phosphor storage plate system (CR) and the maximum of 225 for the full-field digital system (DR) (significance $p < 0.001$).

Conclusion: The results of this study demonstrate a higher detectability rate of lesions for full-field digital mammography with a CCD-detector (DR) in comparison to the high resolution digital phosphor storage plate mammography (CR) in an experimental setting.

B-156 14:45



Experimental investigations in comparison of full-field digital mammography (a-Se detector) with a Mo/Mo and W/Rh filter: Is a dose reduction possible?

R. Schulz-Wendtland, K.-P. Hermann, E. Wenkel, C. Böhner, M. Lell, M.-S. Dassel, W. Bautz; *Erlangen/DE*

Purpose: Experimental investigations of a full-field digital mammography system with the question of a possible dose reduction.

Methods and Materials: The digital mammography system Novation® (Siemens) is based on a a-Se detector with a Mo/W double anode and Mo/Mo resp. W/Rh filter: spatial resolution 7 lp/mm, effective quantum efficiency (DQE) (0) 65%, memory depth 12-bit. The object of investigation was the Wisconsin Mammographic Random Phantom, Model 152A (Radiation Measurements Inc., Wisconsin). The radiograms were acquired using the digital mammography system with the filter combination Mo/Mo (28 kV; 59.0 mAs; 1.4 mGy (MGD - median glandular dose)) as AEC (automatic exposure control) in comparison to W/Rh (28 kV; 40.1 mAs - 100.1 mAs resp. 0.6 mGy - 1.5 mGy) and W/Rh (29 kV - 35 kV; 54.0 mAs - 24.8 mAs resp. 0.9 mGy - 0.7 mGy).

Results: Equivalent results (219 of 225 possible details) were detected with Mo/Mo (28 kV; 59.0 mAs; 1.4 mGy) and W/Rh (28 kV; 61.8 mAs; 0.9 mGy).

Conclusion: Based on these experimental results, the W/Rh filter in combination with the full-field digital mammography system and a-Se detector seems to give the possibility to reduce the dose of up to 25% in comparison to the standard filter with Mo/Mo.

B-157 14:54



Image quality of a prototype full-field digital mammography system based on amorphous selenium

A. Fischmann¹, K. Nykänen², M. Esslinger¹, K.C. Siegmann¹, A. Wersebe¹, T. Xydeas¹, C.D. Claussen¹, S. Miller¹; ¹Tübingen/DE, ²Tuusula/FI

Purpose: To evaluate the image quality of a novel Full-Field Digital Mammography (FFDM) System.

Methods and Materials: Image quality of a prototype FFDM System with a detector based on amorphous selenium a-Se (Instrumentarium Diamond FFDM) was compared to a FFDM system based on amorphous Silicon a-Si (General Electric Senographe 2000D). Images of a contrast detail phantom (CDMAM 3.4, St. Randout, NL) were taken at 28 kVp and 16 to 125 mAs, with Mo/Mo and Mo/Rh anode-filter-combination. To simulate different breast thicknesses phantom thickness was set to 2.5 and 4.5 cm. Images were evaluated by three readers independently. Correct observation ratio (COR) and image quality figures were calculated.

Results: Both FFDM systems showed comparable image quality with COR between 38 and 78% with the aSe system and between 41 and 75% with the aSi

Scientific Sessions

system for the 2.5 cm phantom. For the 4.5 cm phantom COR ranged between 13 and 54% with aSe and between 24 and 57% with aSi. With Rh-filter COR ranged from 53 to 81% with the aSe system and from 48 to 77% with the aSi system for thin phantom. For the thick phantom ranges were from 29 to 60% with aSe and from 30 to 60% with. Inter-reader variability ranged from 0.88 to 0.95. Omission of the grid lead to a dose reduction of 10 to 30% depending on breast thickness and beam quality.

Conclusion: In conclusion the prototype FFDM system based on a-Se is equal to an established FFDM system in contrast-detail resolution.

B-158 15:03

Comparison of full-field digital mammography (FFDM) and CR mammography: Physical imaging properties and contrast-detail characteristics

T. Ideguchi¹, Y. Higashida¹, K. Himuro¹, M. Ohki¹, R. Takagi², H. Hatano², R. Kuwahara², I. Tanaka¹, F. Toyofuku¹; ¹Fukuoka/JP, ²Kumamoto/JP

Purpose: An amorphous silicon-based flat panel detector for full digital mammography and a new computed radiography (CR) system with a pixel size of 50im were compared with respect to physical imaging properties and contrast-detail characteristics.

Methods and Materials: The presampled modulation transfer functions (MTF) of the flat panel detector and the CR system were measured using the slit method. Their noise power spectra were determined under various X-ray exposures. Their contrast-detail curves were obtained from observation experiments using a contrast-detail phantom. Image quality figures (IQF) were also calculated from the individual observer performance tests.

Results: The MTFs of the flat panel digital mammography system showed significantly higher values than those of the new CR digital mammography system with a pixel size of 50 im. The flat panel system showed a lower noise level compared with the CR system under the same exposure conditions. The contrast-detail curves and the IQFs of the flat panel system were superior to those of the new CR system.

Conclusion: The full-field digital mammography system had superior physical imaging properties and contrast-detail characteristics compared to the new CR digital mammography system with a pixel size of 50 im.

B-159 15:12

Clinical study to evaluate the diagnostic value of AGFA CR system: Comparison of mammographic hardcopy images to screen-film mammographic images

C. Van Ongeval¹, A. Van Steen¹, V. Celis¹, M. Van Goethem², I. Verslegers², K. Joossens¹, G. Marchal¹; ¹Leuven/BE, ²Antwerp/BE

Purpose: To compare the diagnostic value of a full field CR based mammography system (CRM), AGFA CR750.0 & CRMM2.0 plates to screen-film mammography (SFM) with hard copy viewing.

Methods and Materials: A series of 100 patients, scheduled for a diagnostic mammography, underwent a SFM and a CRM (double exposure, without removing compression of the corresponding breast). The CR images were processed with dedicated Musica processing. The sets of hard copy images were read by 6 radiologists (3 on-site and 3 independent). The primary efficacy parameter was the overall diagnostic value. The secondary efficacy parameters are lesion conspicuity and details (for masses and calcifications), tissue visibility at chest wall and at skin line, axillary details, overall density, overall noise and sharpness impression.

Results: The proportion of subjects with an overall diagnostic value greater or equal to zero was 100%. Pooled analysis of the 10 features for image quality comparison demonstrated for all, but one feature (detail of the calcifications) that CR was equal to SFM. Wilcoxon's exploratory analysis showed for lesion conspicuity of masses ($p = 0.021$), lesion detail of masses ($p < 0.001$), tissue visibility at skin line ($p < 0.001$) and overall density impression ($p = 0.003$) CR was statistically, significantly more confident than SFM. The same analysis for lesion detail of calcifications ($p < 0.001$) showed that the observers felt less confident with CR than with SFM.

Conclusion: Non-inferiority of AGFA CR system compared to SFM images could be concluded. Only in evaluating the detail of microcalcifications did the observer feel less confident with the CR system.

B-160 15:21



First experiences with iodine-based contrast medium in digital full-field mammography

F. Diekmann¹, S. Diekmann¹, F. Jeunehomme², S. Muller², B. Hamm¹, U. Bick¹; ¹Berlin/DE, ²Buc/FR

Purpose: To evaluate the potential of dynamic intravenous administration of an iodine-based contrast medium in digital full-field mammography.

Methods and Materials: Ten patients with 12 suspicious lesions of the breast (2 benign, 1 borderline, 9 malignant) underwent mammography with an iodine-based contrast medium (Ultravist 370, Schering AG, Berlin, Germany). Three sequential images of the lesion-bearing breast were acquired 60, 120, and 180 sec after administration at a dose of 1 ml/kg body weight at a flow of 4 ml/sec with digital full-field mammography (GE Medical Systems, Milwaukee, USA). Subsequently, the precontrast image was logarithmically subtracted from the postcontrast images. Lesion enhancement was correlated with enhancement of the breast tissue. The subtracted images were evaluated for lesion depiction and enhancement kinetics were analyzed. The lesion size and enhancement kinetics were compared with the histologic findings.

Results: All malignant lesions were detected by contrast-enhanced digital mammography. Three of the tumors were depicted on the contrast-enhanced images but not on the standard mammography images. The contrast medium kinetics of benign and malignant tumors in contrast-enhanced digital mammography is comparable to that known from magnetic resonance imaging using gadolinium-based contrast medium. This is true in particular for comparison of tumor kinetics with the enhancement of normal breast tissue.

Conclusion: The results of this preliminary study suggest that contrast-enhanced digital mammography has a great potential in the detection and characterization of breast lesions.

14:00 - 15:30

Room F1

Chest

SS 304

Computer aided detection (CAD) and volumetry of pulmonary nodules

Moderators:

D. Revel; Lyon/FR

D. Wormanns; Münster/DE

B-161 14:00

Influence of the CT reconstruction kernel on the performance of a CAD system for the detection of pulmonary nodules

M. Salganicoff¹, G. Kohl², D.P. Naidich³, P. Herzog⁴, M. Wolf¹, P. Cathier¹, J. Stoeckel¹; ¹Malvern, PA/US, ²Forchheim/DE, ³New York, NY/US, ⁴Munich/DE

Purpose: To assess the performance of a computer aided diagnosis (CAD) system for the detection of pulmonary nodules on MDCT datasets with different CT-reconstruction kernels.

Methods and Materials: 20 MDCT datasets reconstructed with section thicknesses of 1.0 - 1.25 mm and a B60f (Siemens Somatom system) high frequency reconstruction kernel were reviewed by a chest radiologist and processed on a prototype CAD system. The images on the CAD system were evaluated first originally, then consecutively after applying an image smoothing tool with 3 increasing levels of smoothing.

Results: The chest radiologist identified a total of 56 nodules with diameters from 3 - 8 mm.

The robustness of the CAD system to different smoothing levels was assessed by comparing the average sensitivity and false positive (FP) rate for each group of filtered scans to the group of unfiltered scans. For the small filter setting (corresponding to a B50f kernel) there was no difference in sensitivity or specificity. A medium filter (corresponding to B45f kernel) also did not affect sensitivity, but the number of false positives increased from 2.5 to 4.6 FP/case. The strongest filter setting (corresponding to a B40f kernel) showed increased sensitivity by 10% but at the cost of doubling the FP rate to 5.7 FP/case.

Conclusion: Overall the CAD system performed well for the smoothed CT volumes. Although strong noise reduction slightly improved sensitivity it also caused an increase in the number of false positives. CT-protocol changes should always be considered as possible influences on performance of CAD tools.

Scientific Sessions

B-162 14:09

Comparison of two different algorithms for the detection of pulmonary nodules on MDCT datasets

M. Salganicoff¹, P. Herzog², D.P. Naidich³, J. Stoeckel¹, H. Shen⁴, G. Kohl⁵, A. Krishnan¹; ¹Malvern, PA/US, ²Munich/DE, ³New York, NY/US, ⁴Princeton, NJ/US, ⁵Forchheim/DE

Purpose: To compare the sensitivity and false positive rate of two computer-aided detection systems for pulmonary nodules on MDCT datasets: Nodule Enhanced Viewing (LungNEV) vs. computer aided detection (LungCAD) using artificial intelligence (AI) methods.

Methods and Materials: 20 MDCT studies with section thicknesses ranging from 1.0-1.25 mm were evaluated by a radiologist who initially marked all nodules greater than 3 mm using the LungCARE Software (Siemens, Forchheim, Germany) prior to processing the datasets with both CAD systems, the commercially available LungNEV and the prototype LungCAD.

Results: 56 nodules with diameters from 3 mm - 8 mm were identified of which 8.9% were groundglass opacities (GGOs), 16.1% were vessel-attached, 28.6% were pleural-based, 12.5% were adjacent to fissures and 64.3% were solitary. LungCAD had a small improvement in sensitivity of 10% compared to LungNEV. A distribution-analysis of the true positives of LungCAD compared to LungNEV showed that improvement in sensitivity resulted for vessel-attached and solitary nodules rather than for pleural-based nodules. LungNEV identified a mean of 8 FP/case (median 7.5) while LungCAD only identified a mean of 2.3 FP/case (median 2) which proved to be statistically significant. Interpretation times for LungNEV and LungCAD were equivalent.

Conclusion: AI methods can achieve a very small false positive rate for the detection of lung nodules from multi-slice CT studies while maintaining an equivalent sensitivity. The use of AI technologies has the potential to further improve the benefits to radiologists derived from CAD both for preventive care medicine as well as routine clinical practice.

B-163 14:18

Computer-aided detection of pulmonary metastasis: Influence of nodule characteristics on detection performance

K. Marten¹, T. Seyfarth², E.J. Rummeny¹, C. Engelke¹; ¹Munich/DE, ²Forchheim/DE

Purpose: To evaluate the influence of pulmonary nodule location, size and morphology on the performance of a computer-aided diagnosis (CAD) tool using multislice CT (MSCT).

Materials and Methods: MSCT scans of 20 patients were separately evaluated by a CAD system and two blinded chest radiologists for pulmonary nodules. Nodule presence, size, position, margin, matrix characteristics, vascular and pleural attachments were recorded and compared to an independent reference standard. Statistical analysis included chi-square, retrograde stepwise logistic regression with nodule detection proportion estimates (DPE), and ROC analysis.

Results: 135 nodules were included (median diameter = 4.4 mm; range = 1-30.6 mm). Detection rates for CAD and readers were 76.3%, and 52.6%, respectively. False-positive rates were 0.55 and 0.15-0.25 per scan, respectively. Reader detection rate improved in consensus with CAD (93.3%, p < 0.05); the false-positive rate decreased (0.1/scan). Absence of vascular attachment significantly predicted nodule detection by CAD ($p = 0.001-0.008$). Pleural and vascular attachments predicted reader nodule detection ($p = 0.0005-0.02$). Reader sensitivity was higher for vascular attached vs. non-attached nodules (sensitivities = 0.725 and 0.354, 95% CI=0.604-0.825 and 0.239-0.482, respectively). DPEs for nodules ≤ 5 mm were higher for ICAD than for the readers ($p < 0.05$).

Conclusion: CAD outweighs deficient reader performance in detection of smallest lesions and nodules without vascular or pleural attachment.

B-164 14:27

Clinical evaluation of a computer aided pulmonary nodule detection system

P. Herzog¹, S. Buhmann¹, D.P. Naidich², J. Stoeckel³, M. Wolf³, H. Shen⁴, M. Salganicoff³, A. Krishnan³; ¹Munich/DE, ²New York, NY/US, ³Malvern, PA/US, ⁴Princeton, NJ/US

Purpose: To evaluate the effect of a prototype computer aided detection system (LungCAD) on the sensitivity of a cohort of community radiologists for detecting pulmonary nodules on MDCT datasets.

Methods and Materials: 16 MDCT studies with section thicknesses ranging from 1.0-1.25 mm were evaluated by a cohort of 6 community level radiologists from two sites (NYU Medical Center and University of Munich). The cohort members were instructed to mark all nodules greater than 3 mm using the LungCARE

Software (Siemens, Forchheim, Germany). The datasets were then processed with a prototype version LungCAD. Community radiologists then reviewed and accepted or rejected computer identified nodules. Ground truth was defined as any nodule marked by one of the community readers or by CAD that was also validated by a single expert's blinded review.

Results: The mean sensitivity of community radiologists without LungCAD was 53.5% with 4.63 FP/case while the sensitivity assisted with LungCAD was 66.5% with a mean of 5.98 FP/case. The difference of sensitivity proved to be statistically significant ($p < 0.021$, t-Test) while the change in FP/case was not. Additionally, the spread of sensitivity (excluding best and worst performing outliers) within the LungCAD assisted community reader cohort was less than that for the unassisted readers (12.5% versus 7.5%), implying less inter-observer variability.

Conclusion: The CAD assisted method yielded a higher sensitivity among community radiologists with no significant change in FP. Equally importantly, the variation in sensitivity was reduced, leading to a more predictable detection rate across radiologists.

B-165 14:36

Computer-aided detection of pulmonary metastasis using multislice CT: Performance evaluation in consensus with experienced versus inexperienced chest radiologists

K. Marten¹, T. Seyfarth², E.J. Rummeny¹, C. Engelke¹; ¹Munich/DE, ²Forchheim/DE

Purpose: To evaluate the performance of experienced versus inexperienced radiologists in comparison with a computer-aided detection (CAD) system for pulmonary nodules using multislice CT (MSCT).

Materials and Methods: Eighteen consecutive patients (age range: 29-83 years) prospectively underwent 16-row MSCT. Four blinded radiologists (experienced: readers 1, 2; inexperienced: readers 3, 4) assessed image data against CAD for pulmonary nodules. Thereafter, consensus readings of readers 1+3, reader 1+CAD and reader 3+CAD were performed. Data were compared against an independent gold standard. Statistical tests used to calculate interobserver agreement, reader performance and nodule size were Kappa, ROC and Mann-Whitney U.

Results: CAD as well as experienced readers outperformed inexperienced readers ($Az = 0.72, 0.71, 0.73, 0.49$ and 0.23 for CAD, readers 1-4, respectively; $p < 0.05$). Performance of reader 1+CAD was superior to single readers' and reader 1+3 performances ($Az = 0.93, 0.72$ for reader 1+CAD and reader 1+3 consensus, respectively, $p < 0.05$). Reader 3+CAD did not outperform experienced readers or CAD ($Az = 0.72$ for reader 3+CAD; $p > 0.05$).

Conclusion: Consensus of reader 1+CAD significantly outperformed all other readings, demonstrating a benefit as an inexperienced reader replacement. Inexperienced observers did not perform adequately to justify routine replacement of an experienced radiologist by CAD.

B-166 14:45

Computer-assisted detection (CAD) of pulmonary nodules at MDCT: Can CAD be used as concurrent reader?

F. Beyer¹, L. Zierott¹, J. Stoeckel², W. Heindel¹, D. Wormanns¹; ¹Münster/DE, ²Malvern, PA/US

Purpose: CAD can improve the sensitivity of radiologists in detection of pulmonary nodules at MDCT when used as a second opinion. CAD is also reported to save reporting time when used as "concurrent reader" but the influence on sensitivity is not clear. Our study is aimed to compare sensitivity and reporting time of second and concurrent reading.

Material and Methods: Fifty MDCT scans of the chest were randomly selected from the clinical routine. Two radiologists independently read the CT scans using CAD as concurrent reader (CAD results were displayed at the time of reading). More than one week later the same cases were read again using CAD as second reader (cases were first read without CAD; CAD results were displayed after completing the reading). A prototype of Siemens LungCAD (Siemens, Malvern, USA) was used. Times needed for concurrent reading, for reading without CAD (as part of second reading) and for using CAD as second opinion were recorded.

Results: A total of 225 nodules were detected. Combined sensitivity of one radiologist and CAD for concurrent versus second reading was 52% vs. 57% for reader A (McNemar's test: $p = 0.07$) and 69% vs. 74% for reader B ($p = 0.13$). Average reporting time was 206 ± 97 s for concurrent and 251 ± 98 s for second reading (Wilcoxon test: $p < 0.001$).

Conclusion: CAD as concurrent reader can save reporting time with some but not significant loss of sensitivity. However, if the clinical setting requires highest sensitivity, the use of CAD as second opinion is recommended instead.

Scientific Sessions

B-167 14:54

Impact of a computer-aided detection system (CAD) on a lung cancer screening program with low-dose multislice CT (MSCT)

P. Domínguez Echávarri, G. Bastarrika Alemán, D. Cano Rafart, M. Pons Renedo, J. Larrache Latasa, A. Alonso Burgos, J. Zulueta Francés; Pamplona/ES

Purpose: To evaluate the utility of CAD in the detection of lung nodules in screening low-dose MSCT chest exams (I-ELCAP screening program), previously dual-read by an expert radiologist and a radiology resident.

Methods and Materials: 114 already reported low dose MSCT chest exams (120 kv, 20 mAs, 1.3 slice thickness, 1.2 mm reconstruction interval) were analysed with the CAD system (ImageChecker CT, R2 Technology Inc). I-ELCAP and clinical reports were evaluated. All exams were carefully reviewed again by both another expert CT radiologist and a resident, evaluating each nodule and detecting new nodules, using overall as the standard of reference. Evaluation was focused on the detection of solid non-calcified 5 mm or bigger nodules, as only these change clinical action.

Results: Total of 285 nodules, 183 non-calcified. CAD detected 136 total (S 0.47) and 93 non-calcified (S 0.51), radiologists 166 (S 0.58) and 104 (S 0.57) and both 242 (S 0.84) and 155 (S 0.85). If we focus on solid non-calcified 5 mm or bigger nodules there were 19 nodules in 14 patients. CAD detected 17 (S 0.89), radiologists 16 (S 0.84), and both detected 19 (all of them, S 1). CAD changes clinical action in 3 patients of 114 (3 months follow-up instead of 12 months follow-up). CAD marked 2.1 false positive results per nodule, 2.5 per exam.

Conclusion: This CAD system is a valuable aid in the detection of lung nodules in a low-dose MSCT screening program, notably increasing the sensitivity of radiologists alone.

B-168 15:03

Computer aided detection of incidental pulmonary nodules in emergency thoracic CT angiography

G. Bartal¹, J.M. Gomori², T. Gaspar³, E. Rivlin³, R. Goldenberg³, E. Walach³, N. Peled³; ¹Hadera/IL, ²Jerusalem/IL, ³Haifa/IL

Purpose: CT angiography for the detection of pulmonary emboli (PE) or aortic dissection is performed and reported in an emergency setting. This may distract the radiologist from detecting incidental pulmonary pathology. Our aim was to assess the sensitivity of pulmonary nodule detection by radiologists with the assistance of an automatic computer aided detection (CAD) system.

Materials and Methods: We retrospectively evaluated written reports and images of 114 patients with suspected PE and 30 patients with suspected pathology in the thoracic aorta. CT angiograms were performed on 16-slice Philips Mx8000 IDT CT scanner bolus-tracking contrast injection method, and scan parameters: 16x1.5, 2 mm reconstructed slice thickness, pitch 1.3. Five certified radiologists interpreted these studies as an emergency. CAD of lung nodules was performed using an automatic CAD system (Netzview, RCADIA Ltd., Haifa, Israel). We used the evaluation by CAD and two experienced radiologists (GB, NP) as the gold standard.

Results: GB+NP+CAD (gold standard) found lung nodules in 18 patients. Five reporting radiologists diagnosed lung nodules in 10/18(56%) cases in PE and in 2/2 (100%) cases in aorta with only 2.9 and 2.2 false positives per case respectively. CAD detection rate was 78% higher than the radiologists ($p < 0.003$). Results of the evaluation by the reporting radiologists and CAD reached a sensitivity of 100%.

Conclusions: Emergency pulmonary and aortic CT angiography detect potentially actionable lung pathology. CAD significantly improves incidental pulmonary nodule detection rates of radiologists in these patients.

B-169 15:12

Phantom evaluation and patient correlation of computer-aided volumetry of small pulmonary nodules in MDCT chest examinations

M. Das¹, G. Mühlenbruch¹, A.H. Mahnken¹, L. Gundel², O. Hauenstein², J. Eckert¹, R.W. Günther¹, J.E. Wildberger¹; ¹Aachen/DE, ²Forchheim/DE

Purpose: To evaluate volumetry of pulmonary nodules in a lung phantom for different CT parameter settings and to compare the results to patient pulmonary nodules.

Methods and Material: A lung phantom with five different categories of nodules (intraparenchymal, around a vessel, attached to a vessel, pleural, attached to the pleura) each category with different sizes (3-10 mm, total nodules: 40) were scanned on a MDCT scanner (Somatom 64, Siemens Medical). Scan protocol: 64*0.6 mm collimation, 120 kV, 120 mAs_{eff}/20 mAs_{eff}. Reconstruction: slice

thicknesses (0.6 - 5 mm), algorithms (B45f, B50f, B60f). Volumetry (volume and size measurements) was performed for all nodules and compared for the different settings. Reproducibility with different clicking points was tested. MDCT data (Somatom Sensation 16, Siemens) from a patient with multiple nodules was chosen and the nodules were correlated to the different categories of the nodules in the phantom and measurements were compared.

Results: Average relative volume error for the different parameters was 9.64% ($\pm 6.4\%$). Average relative diameter error for the different parameters was 7.6% ($\pm 5.4\%$). No differences of the measurements could be detected regarding varying dose, slice thickness, reconstruction algorithm and clicking points. The error remained constant for slice thicknesses between 30 and 50% of the diameter. The patient data showed the same results.

Conclusion: The algorithm tested showed highly reproducible results over different dose settings, at multiple measurements and with different reconstruction algorithms. Correlation with real patient data indicates highly accurate and reproducible measurements of the algorithm also for nodules in real patients.

B-170 15:21

Measuring lung nodules: Inter-observer variability

H.A. Gietsma, M. Prokop, W.P.T.M. Mali; Utrecht/NL

Purpose: In the NELSON-project (Dutch-Belgian lung cancer screening), discrimination between malignant and benign for nodules < 500 mm³ is done by assessing the presence of growth on follow-up CT. *Inter-observer variability* can be an important factor causing an increase in measured volume without growth of the nodule. In this study we have measured *inter-observer variability* for automatic volume measurements.

Materials and Methods: To determine *inter-observer variability* we collected 230 nodules < 500 mm³ for which a first and second reading was available and compared the volumes of both readings. Volume of the nodules was assessed on a Leonardo© workstation (Siemens AG, Erlangen, Germany) using Lungcare© software. The difference was calculated by subtracting the volume on second scan from the first one and given in mm³ and as percentage of the mean volume of each nodule.

Results: For 174 lung nodules no *inter-observer variability* was seen. Mean volume was 84.4 mm³, mean difference between first and second reading was 0.4 mm³ (± 6.2 mm³, range (-52.7) – 36.9 mm³) or 0.79% ($\pm 9.54\%$).

Conclusion: Automatic measurement of volume by Lungcare© is highly reproducible by a second reader. In 75% of the cases no difference was seen.

14:00 - 15:30

Room F2

Abdominal Visceria

SS 301b

Benign biliary disease and liver transplantation

Moderators:

D. Akata; Ankara/TR

D.E. Malone; Dublin/IE

B-171 14:00

MRCP in primary sclerosing cholangitis

C. Weber, G. Krupski, U. Seitz, R. Kuhlencordt, X. Rogiers, G. Adam; Hamburg/DE

Purpose: To evaluate MR-Cholangiopancreaticography (MRCP) as a low risk alternative to Endoscopic Retrograde Cholangiopancreaticography (ERCP) in diagnosing primary sclerosing cholangitis (PSC) and to compare diagnostic accuracy of different T2 W sequences.

Methods and Materials: Ninety-five patients (59 males and 36 females; mean age 41 years, range 16 to 71 years) with suspected PSC were examined in a 1.5 T MR unit using breath hold, transverse and coronal HASTE (TR/TE 4.4/90 ms), coronal-oblique RARE (TR/TE 5000/1100 ms) and thin-sliced HASTE (TS-HASTE; TR/TE 11/95 ms) sequences. Applying a five point scale, two investigators assessed the image quality blind. Morphologic criteria of PSC were documented and correlated with ERCP, which served as the gold standard, and sensitivity, specificity and diagnostic accuracy were calculated.

Results: PSC was confirmed in 69 of 95 patients (ERCP 95 of 95, liver biopsy 40 of 95). Qualitative analysis of the image quality showed no significant difference between RARE, HASTE and TS-HASTE sequences (3.4/3.5/3.2). The RARE sequence had the highest sensitivity (86%), specificity (78%) and diagnostic accuracy (84%) for the detection of PSC. The difference between HASTE and

Scientific Sessions

TS-HASTE was statistically significant ($p < 0.01$). A Klatskin tumor and a cholangiocellular carcinoma, which were misdiagnosed by MRCP, were diagnosed by brush biopsy in 2 of the 69 patients with confirmed PSC. Interobserver variability was adequate to good (kappa 0.4 to 0.7).

Conclusion: MRCP is proven as a reliable non invasive imaging method to diagnose and follow PSC. For a streamlined MRCP protocol the RARE sequence is mandatory and the HASTE sequence recommended.

B-172 14:09

Endoscopic ultrasound or MR cholangiography for bile duct calculi and strictures? An evaluation using 'evidence-based radiology' methods

C.J. McMahon, R.G. Gibney, D.E. Malone; Dublin/IE

Purpose: To evaluate the relative roles of endoscopic ultrasound (EUS) and MR cholangiography (MRC) in the diagnosis of common bile duct (CBD) calculi and in distinguishing malignant vs. benign extra-hepatic biliary strictures (EHBS).

Materials and Methods: Two focused clinical questions were constructed. A structured search of Pubmed and RSNA Index was performed. Retrieved studies were appraised for validity, strength and level of evidence (Oxford/CEBM scale: 1-5). Standard test properties and conditional probability graphs (CPG) were analysed. CBD calculi literature was divided into group A; MRC slice thickness ≥ 5 mm; group B; MRC slice thickness = 3 mm or 3D MRC sequences. Results expressed; sensitivity (95% confidence intervals), specificity (95% confidence intervals), positive likelihood ratio (LR+), negative likelihood ratio (LR-).

Results: CBD calculi:

Four studies merited inclusion (two level 1b, two level 3b).

Group A:

EUS: 0.80(0.45,1.15), 0.96(0.88,1.04), LR+ 18.4, LR- 0.21.

MRC: 0.40(-0.03,0.83), 0.96(-0.87,1.04), LR+ 9.2, LR- 0.63.

Group B:

EUS: 0.90(0.83,0.98), 0.99(0.97,1.01), LR+ 92.70, LR- 0.10.

MRC: 0.87(0.78,0.95), 0.95(0.91,0.99), LR+ 17.85, LR- 0.14.

EHBS:

Three studies merited inclusion (two level 3b, one level 4).

EUS: 0.80(0.63,0.97), 0.80(0.62,0.97), LR+ 4, LR- 0.25.

MRC: 0.90(0.77,1.029), 0.65(0.48,0.86), LR+ 2.51, LR- 0.15.

CPG analysis: with a pre-test probability > 60%, EUS or MRC can confirm, but neither can alone adequately exclude, a malignant obstruction.

Conclusion: CBD calculi: EUS and MRC are equivalent when 3 mm slices or 3D sequences are used. 5 mm MRC slice-thickness has poor sensitivity for CBD calculi. EHBS: Either EUS or MRC can confirm malignant EHBS. Neither test alone adequately excludes malignant EHBS; multi-modality imaging is required.

B-173 14:18

Value of magnetic resonance cholangiography in iatrogenic biliary

stenosis: Comparative study with surgery

P. Ottaviani, L. Menchini, F. Giulante, R. Manfredi, L. Bonomo; Rome/IT

Purpose: To determine the accuracy of Magnetic Resonance Cholangio-pancreatography (MRCP) in the assessment of iatrogenic biliary stenosis after laparoscopic cholecystectomy, compared to surgery.

Method and Materials: 28 patients (13M, 15W; median age 55.1 years; range 28-79) with clinically suspected iatrogenic bile duct stenosis were prospectively included. Magnetic resonance cholangiography was performed within six months before surgery and was considered to be the gold standard. Image analysis included site and length of the stenosis according to Bismuth classification and were independently determined by 2 radiologists. Discrepancies were resolved by consensus. MRCP/surgery concordance was assessed using K statistics.

Results: At MRCP 1/28 (3.6%) patients had type I stenosis, 5/28 (17.6%) type II, 18/28 (64.3%) type III and 4/28 (14.3%) type IV. Compared to surgery, MRCP correctly identified the level of biliary ductal obstruction according to Bismuth classification in (20/28) 71.4% patients. K-value was 0.82. MRCP overestimated level of biliary ductal obstruction in 5 patients and underestimated in 3 patients. Our purpose is to evaluate in which type of stenosis there is more discrepancy.

Conclusions: MRCP can accurately diagnose postoperative biliary strictures and can characterize and anatomically classify these injuries for the planning of reparative surgery.

B-174 14:27

Value of magnetic resonance cholangiography in sclerosing cholangitis:

Comparative study with ERCP

C. Liguori, L. Menchini, M. Mutignani, R. Manfredi, L. Bonomo; Rome/IT

Purpose: To evaluate the accuracy of magnetic resonance cholangio-pancreatography (MRCP) for the detection of sclerosing cholangitis (SC) and to compare MRCP findings to endoscopic retrograde cholangiography (ERCP) used as the gold standard.

Method and Materials: MRCP findings were evaluated in 27 patients with clinical symptoms and/or laboratory values as signs of cholestasis, who consecutively underwent magnetic resonance imaging. Two observers independently classified bile duct abnormalities and established the MRCP diagnosis in a consensus reading. The results of MRCP were compared with the definitive diagnosis based on the clinical history and laboratory and histological data and ERCP findings. The observers compared the biliary system seen with MRCP and ERCP in patients with confirmed SC to determine the main biliary obstruction.

Results: All exams were diagnostic (27/27). The diagnosis of SC was confirmed by clinical data and ERCP in 20 of 27 patients (74%). The sensitivity and specificity of MRCP were 95% (19/20) and 100% (7/7) respectively. Different bile duct abnormalities leading to the diagnosis of SC were depicted by MRCP and ERCP; more bile duct stenoses and pruning were seen with ERCP and more skip dilation with MRCP, which has been more useful in the localization of the main stenoses in the biliary tree.

Conclusions: In patients with SC, MRCP is a highly sensitive method and its diagnostic accuracy is comparable to that of ERCP. MRCP can be used as the preliminary non-invasive imaging modality for the diagnosis of SC.

B-175 14:36

"All-in-One" multislice computed tomography (MSCT) of potential living liver donors

T. Schroeder¹, A. Radtke¹, J.F. Debatin², M. Malago¹, E. Wembacher¹, S.G. Ruehm³; ¹Essen/DE, ²Hamburg/DE, ³Los Angeles, CA/US

Purpose: To assess parenchymal, vascular and biliary anatomy of potential living liver donors in a single diagnostic step.

Methods and Materials: 250 potential living liver donors underwent three-phase, dual-enhancement MSCT to delineate biliary, vascular and parenchymal morphology. For display of the biliary system the first image set was collected following the infusion of a biliary contrast agent. Subsequently, CT angiography was performed for display of the arterial as well as the portal and hepatic venous systems following automated injection of a conventional iodinated contrast agent. All data sets were reconstructed in 1 mm slices. Data analysis was based on source images, MPRs and 3D postprocessings, focussing on detection of biliary and vascular variants, exclusion of focal lesions in the liver and determination of hepatic volumes. Preoperative findings were correlated with intraoperative findings (available in 67 subjects).

Results: Technical failures were experienced in 7/250 examinations. 27 subjects presented with moderate adverse reactions on the biliary contrast agent. Incidental lesions were detected in 61 patients (59 x benign, 2 x malignant). The underlying biliary and vascular anatomy were displayed at least to the second intrahepatic branch in all but 7 cases. Detected anatomical variants involved the biliary (n = 121), the arterial (n = 101), the portal venous (n = 57) and the hepatic venous (n = 72) system. Correlation with intraoperative findings was excellent.

Conclusion: This outlined approach allows the reliable collection of all relevant pre-op data in a single diagnostic step. The comparatively high incidence of adverse reactions to the biliary contrast agent has to be considered.

B-176 14:45

Sonographic and histological liver changes induced by intraportal islet transplantation in diabetics

E. Angeli, M. Venturini, P. Maffi, F. Bertuzzi, A. Secchi, A. Del Maschio; Milan/IT

Purpose: No imaging modality can demonstrate islet presence, survival and function after intraportal transplantation in diabetics. Recently, we recognized at sonography liver echotexture abnormalities due to focal fatty changes (FFC) and related to islet survival. Our purpose was to determine prevalence and meaning of these abnormalities.

Methods and Materials: 30 diabetics submitted to 35 procedures of percutaneous intraportal transplantation of pancreatic islets had a regular sonographic follow-up. Liver sonograms and color Doppler of portal vasculature were performed before islet transplant, immediately after, at one month and every 6 months. Sonograms

Scientific Sessions

were evaluated for possible hyperechoic FFC and portal vein abnormalities. Liver biopsies were recently performed in 8 patients positive at sonographic evaluation. Results were correlated with serum liver enzymes, fasting C-peptide (fCP), glycated haemoglobin (HbA1c) and Exogeneous Insulin Requirement (EIR).

Results: No major alteration of liver enzymes and portal vein patency was observed. FFC consisting in micro (< 5 mm) or macro focal hyperechogenicity were found after 12/35 (34.3%) procedures, mostly with diffuse distribution. FFC were generally detectable at 6 months, lasting from 6 months to 7 years. FFC positively correlated with islet viability and function. Liver biopsies showed mild to moderate, mainly macrovesicular steatosis, focally and randomly distributed, and focal nuclear glycogen accumulation.

Conclusion: FFC are relatively frequent after intraportal islet transplantation. Clinical and histopathologic data show that FFC must be considered the expression of a prolonged islet over-working, determining the storage of fat in the liver cell, as already shown in the animal model.

B-177 14:54

Changes in splenic volume and correlation with platelet counts in healthy patients following hepatic resection for living liver donation

K. Khalili¹, S. Roach¹, M. Khalili²; ¹Toronto, ON/CA, ²San Francisco, CA/US

Purpose: To evaluate changes in splenic volumes (SV) in healthy living liver donors with correlation with splenic function through platelet values.

Materials and Methods: A retrospective review of 30 healthy adults undergoing right hepatectomy for living liver donation was undertaken. All patients had a preoperative and one post-operative CT scan performed and 10 patients had 2 post op CTs. The 1st scan was performed at a mean of 102 and the 2nd scan mean post-op day (POD) of 84 days. SV's were measured using previously validated techniques. Pre-op and all post-op platelet levels were also recorded and clinical charts reviewed.

Results: An increase in splenic volume (SV) was seen in 28/30 (93%) patients following liver donation. Overall, mean% SV rise was 45.9% (range -14.2 to 113.5%), the rise being significant ($p < 0.0001$, 95% CI 35.4 to 56.4%). In 5/10 (50%) patients of with 2nd post op CT, there was a continued rise in SV (mean 13.5%, range 2.9-23.8%, CTs obtained mean POD 56), in 5 patients there was a drop in splenic volume (mean 14.7%, range 7.0-30.2%, 2nd CTs obtained mean POD 133). We noted an inverse relationship between splenic volumes and number of days post-op. Calculated Correlation Coefficient (Pearson) for all CT scans ($r = -0.55$ (95% CI -0.74 to -0.30, $p < 0.0002$). There was no correlation between changes in platelet values and SV, ($r = 0.04$). No patient had evidence of hypersplenism.

Conclusion: The majority of liver donors undergo a *subclinical splenomegaly* which is greatest closer to the surgical date.

B-178 15:03

Prediction of the appropriateness of a donor liver with respect to hepatic macrosteatosis by phase-contrast MR imaging: Correlation with histopathologic findings

S. Kim, J. Lee, J. Han, J. Lee, B. Choi, K.-S. Shin; Seoul/KR

Purpose: To determine whether phase-contrast MR could reflect hepatic steatosis qualitatively and to analyze MR performance in predicting the appropriateness of potential liver donors in LDLT.

Materials and Methods: Fifty-seven candidates underwent 1.5 T-MR. A radiologist calculated mean hepatic and splenic signal intensity by 25 and three ROI measurements, respectively. The percent decrease (PD) in liver signal on the opposed-phase relative to in-phase was calculated. Linear regression analysis was used to correlate PD with degree of total, macro-, and microsteatosis. The distributions of PD in appropriate and inappropriate donors were compared. The accuracy for predicting the appropriateness of donor liver using PD was analyzed.

Results: Fifty-two and five of 57 candidates were categorized into appropriate and inappropriate groups for macrosteatosis by histology respectively. With linear regression analysis, PD was correlated with only the degree of total steatosis. There was a significant difference in PD between two groups. When the criteria of PD for inappropriateness was set to 20, PD correctly predicted the appropriateness as a liver donor in 53 of 57 cases. In 48 of 48 cases, PD below 20 correlated with < 30% macrosteatosis. In five of nine cases, PD above 20 correlated with > 30% steatosis. Three of remaining four cases with an overestimated degree of macrosteatosis by PD were revealed to have microsteatosis of various degrees.

Conclusion: Although MR reflects total steatosis regardless of its type, potential donors with normal PD may be exclusively appropriate for liver transplantation. However, core biopsy is necessary in donors with high PD to exclude the microsteatosis.

B-179 15:12

A novel method for analysis of postoperative liver regeneration in the adult live liver donor

C. Wald¹, H. Bourquin², J. Pomposelli¹, H.-O. Peitgen², E. Pomfret¹; ¹Burlington, MA/US, ²Bremen/DE

Aims: Novel image-analysis software conveys better understanding of the determinants and dynamics of liver regeneration after right lobe live donor hepatectomy which could lead to optimization of surgical technique and improve prediction of expected regeneration in an individual patient.

Methods: Dynamic spiral CT was performed preoperatively and 1 week, 1, 3, 6 and 12 months after right lobe liver donation. 60 datasets were analysed with Hepavision2 (© MeVis, Bremen, Germany). Quantification of total liver volume, portal venous territory volume, as well as portal venous branch length (PVBL) and diameter growth analysis in regenerating liver segments was performed.

Results: Most volume restoration occurred during the first 60 days postop with a continued significant increase throughout the first year. Female donors regenerated more slowly with a lesser end result, this difference was statistically significant at 6 and 12 months postop. Compromise in PV supply or HV drainage of the medial left lobe lead to asymmetric regeneration in 4 patients. PVBL consistently increased over time in all patients and the normalized volume to length growth ratio changed from 1.0 to 0.8 ($p = 0.005$) suggestive of an allometric growth pattern. Increase in PV branch diameter over time, though exceeded by growth of PVBL, suggests true vessel growth rather than passive stretching during liver regeneration.

Conclusions: Donor liver remnant regeneration is characterized by allometric growth. Compromise of the Segment IV vasculature may lead to asymmetric regeneration of the remnant lobe. Increase of both portal vein length and diameter suggests true vessel growth during regeneration rather than mere passive stretching phenomenon.

B-180 15:21

Sensitivity and specificity of multidetector spiral CT in the detection of hepatocellular carcinoma in patients undergoing transplant for cirrhosis

D. Cioni, R. Lencioni, J. Lera, A. Conti, C. DellaPina, D. Campani, F. Filipponi, L. Crocetti, C. Bartolozzi; Pisa/IT

Purpose: To assess the sensitivity and specificity of multidetector spiral CT (MDCT) in the detection of small hepatocellular carcinomas (HCC) in patients undergoing transplant for cirrhosis.

Materials and Methods: Eighty-three cirrhotic patients were examined with MDCT who proceeded to liver transplantation within 3 months. CT was performed with a LightSpeed Plus scanner (GE Medical System) by injecting 120 ml iodixanol (Vispaque, Amersham Health) at 5 ml/sec. Following a timing bolus (25 ml, 5 ml/sec), early arterial (pitch 6; 1.25 mm collimation), delayed arterial, and portal-venous phases (pitch 3; 5 mm collimation) were acquired. Two readers prospectively assessed number, location and size of HCC. CT findings were correlated lesion-by-lesion with findings at pathology examination.

Results: Pathology examination showed 69 HCCs ranging 0.5-5 cm in diameter (mean, 2.8 cm) in 36/83 patients. MDCT studies detected HCCs in 31/36 patients with 5 false-negative and 5 false-positive results (sensitivity, 86%; specificity, 89%; accuracy 88%; NPV, 89%; PPV, 86%). At lesion-by-lesion analysis, pathology examinations showed 13 HCCs < 1 cm, 35 HCCs ranging 1-2 cm, and 21 HCCs > 2 cm. MDCT detected 6/13 HCCs < 1 cm with 5 false-positives (sensitivity, 46%; PPV 54%); 25/35 HCCs ranging 1-2 cm with 10 false-positives and 20/21 HCCs > 2 cm with 1 false-positive. False-positives included dysplastic nodules (n = 7), fibrosis (n = 2), hemangioma (n = 1) and transient arterial enhancing pseudo-lesions (n = 6).

Conclusion: MDCT shows high sensitivity for detecting HCCs larger than 1 cm but is insensitive in depiction of sub-centimetre lesions. MDCT seems to have a substantial false positive detection rate, in particular in cases of 1-2 cm hyperenhancing arterial phase lesions.

Scientific Sessions

14:00 - 15:30

Room G

Head and Neck

SS 308

Oncologic imaging

Moderators:

T.F. Gotwald; Innsbruck/AT
L. Oleaga Zufiria; Bilbao/ES

B-181 14:00

Reassessing the MR signal findings of sinonasal adenocarcinoma versus (non-adenocarcinoma) epithelial malignancies

C. Ghirardi, R. Maroldi, D. Farina, B. Piazzalunga; Brescia/IT

Purpose: To evaluate MR signal on T2-weighted images in sinonasal adenocarcinoma versus non-glandular malignant tumors.

Materials and Methods: The pre-treatment MR images of 22 patients with histologically proved sinonasal malignancies examined from 1995 to 2004 were reviewed. Eleven cases were adenocarcinomas (10/11 intestinal-type adenocarcinoma, 1/11 a poorly differentiated adenocarcinoma); 11 tumors were non-glandular carcinomas (8/11 squamous cell carcinomas, 3/11 sinonasal undifferentiated carcinomas). Eight out of 9 males with adenocarcinoma were exposed to wood and leather dust, known as a carcinogen. Seven out of 11 adenocarcinomas arose within the nasoethmoid cavities. On T2-weighted images, the value of the most intense and the least intense tumor areas, and the intensity of a normal medial pterygoid muscle were recorded. To standardize measurements, the absolute values of tumor areas were related to the pterygoid muscle.

Results: The hyperintense components within adenocarcinomas were greater than those measured in non-adenocarcinomas (739.54 ± 267 vs. 459 ± 101 ; t-test, $p = 0.0039$). Standardized values (6.97 ± 1.27 vs. 4.16 ± 0.81 ; t-test, $p = 0.000091$), and the ratio between the greatest and the lowest signal value (RGL) within the tumor (1.86 ± 0.5 vs. 1.1 ± 0.08 ; t-test, $p = 0.000077$) differed significantly. If a threshold value of RGL equal or greater than 1.3 is chosen, sensitivity, specificity, positive predictive value, and negative predictive value for adenocarcinoma are 90.91%, 100%, 100% and 91.67% respectively.

Conclusion: Although tissue characterization is a challenge for imaging techniques, quantitative data provided by MR may help to differentiate adenocarcinomas from squamous cell carcinomas and sinonasal undifferentiated carcinomas.

B-182 14:09

Quantitative and qualitative characterization of vascularization and hemodynamics in head and neck tumors with a 3D magnetic resonance.

Time-resolved echo-shared angiographic technique (TREAT). Initial results
H.J. Michaely, K.A. Herrmann, H. Kramer, M.F. Reiser, S.O. Schoenberg;
Munich/DE

Purpose: To determine the additional diagnostic value of a 3D- time-resolved echo-shared angiographic technique (TREAT) for monitoring of dynamic contrast enhancement in the differential diagnosis of head and neck tumors.

Material and Methods: In 16 patients with head and neck tumors contrast agent administration was monitored with a 3D TREAT sequence on a 1.5 T MR-scanner using parallel imaging techniques (GRAPPA, factor 2). A frame rate of 1/2.3 sec was employed with a total of 20 frames. A regular 0.1 mmol/kg BW bolus of Gadolinium-DTPA was injected followed by a 20 ml flush of saline at a flow rate of 4 ml/sec. TREAT imaging was started 5 seconds after the bolus injection. Pre and post-contrast T1w GRE images were acquired. Two radiologists assessed the type of tumor vascularization, enhancement pattern and secondary effects (collaterals, early venous drainage). A semi-quantitative analysis was derived from software based signal intensity (SI) versus time curves of the tumor and the carotid arteries. SI measurements were also performed within the tumor on T1w GRE sequences for comparison.

Results: The high temporal resolution of the TREAT allowed visual and semi-quantitative differentiation of hypervasculated tumors (glomus tumor, nasopharyngeal fibroma) from hypovascularized tumors (squamous cell carcinomas). For different tumor types distinctive patterns of enhancement were found on SI measurements while post-contrast T1w GRE images showed no differences.

Conclusion: The application of TREAT imaging to monitor the passage of the contrast agent bolus yields additional information about the tumor vascularization and characterization without additional scan time or additional contrast media application.

B-183 14:18

Detection and delineation of laryngeal tumors using MR imaging with parallel acquisition technique (PPI MRI) and 16 row multidetector CT (MDCT)

W.H. Flatz, L. Jäger, M.J. Hempel, R. Brüning, R. Helmberger, S. Pfennig, S.O. Schönberg, M.F. Reiser; Munich/DE

Purpose: The aim of our study was to evaluate tumor detection and delineation of laryngeal tumors using parallel magnetic resonance imaging (MRI) acquisition methods (PPI) with GRAPPA reconstruction algorithm and 16-row multislice computed tomography (MDCT).

Materials and Methods: We examined prospectively 30 patients with suspected laryngeal carcinoma using both modalities. MDCT images were acquired at rest and during e-phonation using a 16 row MDCT. Axial and coronal reconstructed images with 1 mm slice thickness were obtained. T1-, T2-weighted, STIR and fat-sat images using Gd-DTPA were acquired on a 1.5 T MR scanner using a high resolution matrix of 512x384 and 3.5 mm slice thickness employing parallel MRI with GRAPPA reconstruction algorithm. Three radiologists evaluated the images. The imaging findings were compared with the clinical and histopathological details. For statistical analysis Crosstabs procedures and Kappa test were applied.

Results: The statistical evaluation of image interpretation shows sensitivity of 86%, specificity of 91% and negative predictive value of 96% for MRI. The corresponding values were 73%, 93% respectively 92% for the MDCT examinations.

Conclusion: Imaging of suspected laryngeal carcinoma using MRI with parallel imaging employing the GRAPPA reconstruction algorithm and 16 row MDCT are suitable for detecting and delineating laryngeal tumors.

B-184 14:27

Histological diagnosis of the endolaryngeal tumours through ultrasound-guided transcutaneous tru-cut biopsy

E. De Fiori, L. Preda, M. Ansarin, M. Bellomi; Milan/IT

Purpose: To evaluate the technical feasibility and the results of transcutaneous ultrasound-guided tru-cut biopsy of endolaryngeal lesions in patients with tumors impairing respiration and/or with relative contraindications to general anaesthesia, not suitable for laryngoscopic biopsy in the operating room.

Material and Methods: From August to December 2003, 7 patients (6 males/ 1 female, age range 53-78) with suspect endolaryngeal bulky neoplasm or recurrent disease were submitted to ultrasound-guided tru-cut biopsy. All had stress dyspnoea due to the tumoral airway stenosis associated with post-radiotherapy oedema in 5 patients treated previously by external beam radiotherapy. The diagnosis was based on clinical examination, with fibre optic laryngoscopy, and 16-slice CT examination.

Results: All biopsy specimens were obtained and were significant for diagnosis: In 6 cases the histological diagnosis confirmed the clinical hypothesis of malignant disease (invasive SCC). In one patient, previously treated by endoscopy and radiotherapy, the US biopsy specimen demonstrated granulomatous inflammatory tissue obstructing the laryngeal lumen at the glottic region. The patient underwent laser-assisted endoscopic therapy to alleviate the obstruction which caused a clinical deterioration and respiratory difficulties. Final pathologic examination confirmed biopsy diagnosis in all cases.

Conclusion: Our preliminary experience demonstrates the feasibility of the procedure in outpatient setting, with low costs and good accuracy. This procedure is indicated in patients with high risk for general anaesthesia and candidate for non-surgical treatment of laryngeal neoplasms.

B-185 14:36

Unexpected internal carotid artery (ICA) atherosclerotic stenoses at biphasic MDCT for neck cancer

N. Flor, G. Castellazzi, C. Missiroli, A. Curti, S. Soldi, G. Franceschelli, F. Sardanelli, G.P. Cornalba; Milan/IT

Purpose: To evaluate the frequency of unexpected atherosclerotic ICA stenoses in patients undergoing biphasic MDCT for neck cancer.

Materials and Methods: Fifty-seven patients (10 females, 47 males; age 64.4 ± 10.5 years, median 67; range 44-88) underwent four-row MDCT (LightSpeed Qx/i, General Electric) for neck cancer diagnosis, staging or follow-up. Protocol: 4x1.25 mm collimation, pitch 3, kVp 120, mAs 140, effective slice width 1.25 mm, reconstruction index 0.8 mm; 90-100 ml of non-ionic contrast agent at 2 mm/l, arterial (20-s) and late (50-s) phases. Postprocessing: multiplanar reconstruction; maximum intensity projection; volume rendering. Vessel stenoses were classed as severe (70-99%), moderate (30-69%), or mild (< 30%).

Scientific Sessions

Results: Atherosclerotic ICA with vessel stenosis was found in 38 patients (age 67.1 ± 9.8 , median 69) and 67 ICAs. Five patients (age 68.5 ± 3.8) had severe stenosis, bilateral ($n = 1$) or associated with contralateral moderate stenosis ($n = 4$). Seventeen patients had moderate stenosis (age 70.4 ± 9.8), bilateral ($n = 9$), associated with contralateral mild stenosis ($n = 5$), unilateral ($n = 3$). Sixteen patients had mild stenosis (age 64.8 ± 9.8), bilateral ($n = 10$) or unilateral ($n = 6$). Out of the 5 patients with unexpected MDCT-detected severe stenosis, four had a newly diagnosed neck cancer and in 2 of them the treatment planning was changed (one endarterectomy before neck tumor surgery, one combined oncologic/vascular surgery), while one patient with a previously treated neck cancer had carotid stenting.

Conclusions: Of 57 patients, 5 (9%) had unexpected severe ICA stenoses, three of them with a relevant impact on therapy. ICAs should be carefully evaluated for atherosclerotic disease during MDCT for neck cancer.

B-186 14:45 ♂

MR imaging of adenoid cystic carcinoma in the head and neck after carbon ion therapy

S. Kandatsu, R. Kishimoto, S. Komatsu, J. Mizoe, H. Tsujii;
Chiba-ken Chiba-shi/JP

Purpose: To evaluate the changes of MR imaging of head and neck adenoid cystic carcinoma after carbon ion therapy.

Materials and Methods: Follow-up MR imaging at 1.5 T was performed in 39 patients (17 men and 22 women; mean age 51 years; age range 27-80 years) with head and neck adenoid cystic carcinoma having received carbon ion therapy. The patients underwent T1-weighted and T2-weighted imaging including post contrast enhanced imaging. Perineural invasion was suspected if high signal intensity after contrast enhancement was seen along the cranial nerves. Size and signal changes in the tumor were observed for more than one year after the therapy.

Results: The mean tumor size before therapy was 36 mm (range 6-75 mm) in diameter. After one year of carbon ion therapy, the mean tumor size was 18 mm in diameter. Continuous reduction in size was recognized for more than one year. Low intensity areas on T2 weighted MR image became high intensity after therapy. Almost all of the local tumor sizes were reduced. In one case, new peripheral neural invasion which was not apparent before the therapy, occurred. Local recurrence within one year after the therapy was seen in one case.

Conclusion: Adenoid cystic tumors in the head and neck were quickly reduced after carbon ion therapy. Low intensity areas in the tumor became high intensity after the therapy on T2 weighted MR image, suggestive of tumor necrosis. Carbon ion therapy is effective even if perineural invasion is recognized.

B-187 14:54

Evaluation of local recurrence in re-staging of head and neck cancer: A comparison between PET and PET/CT

B.S. Halpern, M.A. Auerbach, K. Yeom, B.J. Fueger, W.A. Weber, O. Ratib, R.B. Lufkin, J. Czernin; Los Angeles, CA/US

Background: ^{18}F -FDG PET has a high accuracy in re-staging of head and neck cancer. The purpose of this study was to determine whether additional gains in diagnostic performance arise from the use of integrated PET/CT.

Materials and Methods: A total of 49 patients with a mean age of 59 ± 18 years were enrolled in our study. Histo-pathological verification served as the reference standard for tumor detection. This was defined as complete mass resection \pm radical lymph node dissection in 27 patients, direct endoscopical biopsy in 16 patients and sonography-guided biopsy in 6 patients. Two blinded reviewers analyzed in consensus all PET images and an experienced radiologist was also recruited to assess integrated PET/CT images.

Results: A total of 110 lesions were analyzed by histopathology and were therefore available for further evaluation. Of these, 67 sites (61%) were positive for malignancy and 43 (39%) negative for disease. PET and PET/CT showed an overall accuracy for lesion detection of 84% and 88% ($p = 0.06$), respectively. Sensitivity and specificity for PET were 78% and 93% vs. 84% and 95% with PET/CT. Values were similar when calculated on a patient-by-patient analysis. Accuracy, sensitivity and specificity for PET were 80%, 83% and 67% compared to 86%, 88% and 78% for PET/CT.

Conclusion: PET/CT tended to re-stage patients with recurrent head and neck cancer with a higher accuracy, sensitivity and specificity compared to PET alone.

B-188 15:03

Detailed ultrasound study of the angioarchitecture in superficial lymphomatous lymph nodes. Preliminary results

E.J. Bialek, W. Jakubowski, A.B. Szczepanik, R.K. Maryniak, R. Bilski, M. Prochorec-Sobieszek, K.T. Szopinski; Warsaw/PL

Purpose: To assess possible vascular patterns in lymph nodes confirmed on histopathologic evaluation to be affected by lymphoma, in order to obtain an adjunct to ultrasound differential diagnosis of lymph nodes diseases.

Methods and Materials: Prospective sonographic classification of angioarchitecture (power-Doppler) in 53 superficial lymph nodes intended for diagnostic excision was performed. Thirty seven patients with histopathologically recognized lymphoma were selected for this study (25 cervical lymph nodes, 11 axillary and 1 inguinal).

Results: The angioarchitecture regarded as characteristic for reactive lymph nodes was found in 41% of lymphomatous lymph nodes in this study; 32% showed the distribution of vessels described in metastases; others had angioarchitecture not previously classified or equivocal. A longitudinal vessel was found in 13 lymphomas: single (1) or branching (symmetric = 2; asymmetric = 7; irregular = 3). Multiple vessels, partially branching, entering the node in a few rows from its longitudinal side were present in 5. Short vessel segments ($n = 5$): regularly (1) or irregularly (4) distributed in the hilum area or centrally. Multiple vessels branching irregularly with avascular areas were visible in 4 nodes. Peripheral vessel distribution was found in 8 lymphomas: vessel segments (3); chaotically branching vessels (3); concomitant single central segments (2). Peripheral and central vessels were shown 2 lymphomas.

Conclusion: The angioarchitecture in lymphomatous superficial lymph nodes is diverse and difficult to classify. It may vary from patterns met in normal or reactive lymph nodes to patterns found in metastases. *Work was financially supported by grant from State Committee for Scientific Research.*

B-189 15:12

Improved sentinel node detection and pre-operative planning in oral cavity cancer by image fusion of CT and SPECT versus planar imaging

M. Nuyens, F.G. Fuechsel, P. Zbaeren, T. Krause; Berne/CH

Purpose: Sentinel lymph node (SLN) scintigraphy for oral cavity carcinoma is a recently described method, mainly done with planar scintigraphy (pISc) and γ -probe detection. Precise SLN localisation is difficult, particularly around the injection site. We aim to evaluate the feasibility of fusion imaging of CT and SPECT (FICT) in pre-surgical planning and the advantages over pISc only.

Materials and Methods: SLN scintigraphy (Technetium-99m nanocolloid) was performed in 30 patients (mean: 65 yrs, 16 male, 14 female) with oral cavity squamous cell carcinoma (cT1/cT2, cN0). All patients underwent pISc and 10 patients had pISc and FICT. SPECT/CT were overlain with commercially available software utilising body markers for co-registration. All patients underwent intraoperative SLN detection, frozen-section histology and neck dissection level I-III. Predicted number, side, and anatomical level were compared between pISc versus FICT and both with intra- and post-operative findings. SLN resection time was recorded.

Results: SLN dissection revealed metastases in 39%. Pre-operative pISc and FICT was feasible in all cases. All 90 SLN were identified and resected. The predicted number of SLN was correct in 68% with pISc and in 98% with FICT. Both methods predicted the side correctly in 100%. The level was incorrectly diagnosed by pISc in 16% of all SLN versus 9% by FICT. The mean resection time per SLN was 13 min after pISc reduced to 8 min after FICT.

Conclusions: FICT is a feasible and reliable tool in SLN localisation. Compared to pISc it allows better prediction of number and anatomical localisation and significantly improves SLN resection.

B-190 15:21

High resolution superparamagnetic iron oxide enhanced MR imaging for the diagnosis lymph node metastases in patients with head and neck cancer

M.G. Mack, J. Rieger, M. Baghi, J.O. Balzer, R. Knecht, M. Helbig, T.J. Vogl; Frankfurt a. Main/DE

Purpose: To evaluate the diagnostic accuracy of Sinerem® enhanced MR imaging compared to standard MR imaging for the detection of lymph node (LN) metastases in patients with head neck cancer using histology as a gold standard.

Methods: 35 patients (mean age 57 years, range 39-76 years) were examined with unenhanced and intravenous Sinerem®-enhanced (2.6 mg Fe/kg b.w.) MR imaging with T1w, high resolution TSE T2w and T2w MEDIC sequence to detect possible LN metastasis. Resected LNs were analyzed by a pathologist and results

Scientific Sessions

were compared with MR findings. Clinical evaluation included ultrasound and palpation.

Results: A total of 560 LN were histopathologically evaluated, of which 48 were determined to be metastatic based on histopathology. MR imaging demonstrated 44 of the 48 LN metastases. The sensitivity was 91.7% and the specificity 100%. Standard MR imaging classified 34 of 48 lymph node metastases correctly based on the evaluation of size using a cut off of 10 mm for the short axis diameter, resulting in a sensitivity of 71% and a specificity of 96%. Using a cut off of 7 mm on plain MR imaging the sensitivity was 89%, however the specificity dropped down to 67%. Clinical N-staging was correct in 46%, Sinerem enhanced MR imaging was correct in 94%. 4 of 14 histologically N0 patients were clinically staged as N0. MR imaging staged 13 patients correctly as N0. Clinical examination staged 4 patients, Sinerem MR imaging 12 of 13 patients with contralateral LN metastases correctly.

Conclusion: Sinerem MR imaging improves the N-staging of patients with head and neck cancer.

14:00 - 15:30

Room H

Interventional Radiology

SS 309a

Non-vascular interventional procedures

Moderators:

F. Orsi; Milan/IT

E.-P.K. Strecker; Karlsruhe/DE

B-191 14:00

Pancreatic mass biopsy: Comparison 20 G fine needle trucut biopsy (FNTB) with fine needle aspiration cytology (FNAC)

A.-M. O'Connell, M.C. Hurley, A.N. Keeling, M.J. Lee; Dublin/IE

Purpose: Historically, FNAC has varying sensitivity, specificity, and accuracy in diagnosing abdominal lesions. A 15-20% insufficient sampling rate is associated with FNAC. We compared 20 G FNTB with historic FNAC results.

Materials and Methods: A retrospective review of 37 patients (M:F=25:12, mean age 60.78 yrs) (39 biopsies) was performed (US guidance in 38 and CT guidance in 1). Masses were located in the head (58%), body (12%), tail (3%) and uncinate process (27%). The mass size ranged from 1.5-4 cm (mean 2.2). No cyologist was available on-site. Comparison was made between 20 G FNTB and historic FNAC results regarding positive diagnostic rate, insufficient sampling rate and complications.

Results: An average of 2.03 passes (range 1-3) was performed. An accurate diagnosis was made in 32 of 39 biopsies (82%). Malignant diagnoses consisted of primary adenocarcinoma (25), focal pancreatitis (2), metastases (1), and lymphoma (1). 8 patients had either benign diagnoses (3), insufficient sampling (2) or inflammatory pathology (3). Seven of these latter 8 patients had a laparotomy. Benignity was confirmed in 3 and malignancy found in 4. The remaining patient had a repeat biopsy which identified malignancy. No significant complications were encountered. Sensitivity of 86.48% and specificity of 100% for FNTB is observed.

Conclusion: 20 G FNTB under ultrasound-guidance yields a significantly higher diagnostic accuracy (82%) than FNAC (69-76%), without an increase in complication rate. A greater insufficient sampling rate for FNAC (15-20%) than for FNTB (5.1%) is observed. 20 G FNTB is the method of choice for biopsy of pancreatic tumours, especially where no onsite cytology is available.

B-192 14:09



Percutaneous drainage of infected pancreatic fluid collections

M. Navalho, F. Pires, A. Duarte, A. Gonçalves, P. Alexandrino, I. Távora; Lisbon/PT

Purpose: The objective of our study was to review and report the results of percutaneous drainage of infected pancreatic fluid collections in patients with severe acute pancreatitis.

Methods and Materials: A retrospective review was performed of 30 patients with infected pancreatic fluid collections from complicated acute pancreatitis that were drained percutaneously under sonographic guidance. The patients were managed between 1993 and 2003, in a gastroenterology intensive care unit, and had a mean age of 58.4 years old. Gallstones were the most common cause of the pathologic process. The diagnosis was based on imaging, laboratory and bacteriological findings.

Results: Of the 30 patients, 19 (63%) were cured with percutaneous drainage and antibiotic therapy. In this group the mean c-reactive protein (CRP) value at the beginning of treatment was 172.8 mg/L and 102.5 mg/L at the end. Of the patients who were not cured with percutaneous drainage, one died (3.3%) and 10 (33.3%) required surgery. In this last group the mean initial CRP value was 190.9 mg/L, and 145.4 mg/L when the catheter was removed and the patient sent to surgery. There were four hospital deaths (40%) on the patients submitted to surgery. The catheterization had a mean duration of 21 days, and cultures were positive in 29 (96.7%) patients at the beginning of drainage. The most frequently seen organisms were *Escherichia coli*, *Staphylococcus aureus* and *Enterococcus faecium*.

Conclusion: This study confirms that infected pancreatic fluid collections can be safely and effectively treated, in most patients, with percutaneous catheter drainage.

B-193 14:18



Percutaneous cysto-gastrostomy using a combined, 2 steps, sonographic-endoscopic procedure in the treatment of pancreatic pseudocysts

Z. Spirchez, M. Tantau, R. Badea; Cluj-Napoca/RO

Purpose: To evaluate the efficacy of a modified echoguided percutaneous catheter drainage (PECD) in the management of pancreatic pseudocysts.

Methods: 10 patients (8 men and 2 women, mean age 40) with symptomatic large (median diameter 8 cm, range 6-16 cm) pseudocysts were treated. The underlying diagnosis was acute (8) and chronic pancreatitis (2). PECD was performed using 8-10Fr pigtail catheters, which were placed into the PSC under ultrasound guidance using a transgastric approach. The catheters were left in situ for a few days (mean 4, range 3-6) until no residual pseudocyst was demonstrated on ultrasound. The amount and aspect of the drained fluid were noted. The external end of the catheter was then cut and pulled-in the stomach using upper endoscopy. The patients were followed-up for 6 weeks and in case of no recurrence, the catheter was removed from the stomach and PSC using endoscopy.

Results: The transgastric approach was successful in all but 2 patients, in which the catheter did not pass through the stomach. There were no procedure-related complications. During the follow-up (6-24 months) the drainage was successful in 9 cases, including those with transabdominal approach. One patient developed an abscess 1 week after the catheter was endoscopically removed and was operated.

Conclusions: PECD of pancreatic pseudocysts with endoscopic internalization of the external end is a safe, minimal invasive and simple procedure with good results at follow-up. Maintaining an external drainage for short period allows monitoring the patency of the catheter and the aspect of aspirate.

B-194 14:27

Percutaneous gastrostomy (PG) with T-fastener gastropexy: Reduction in complication rates with early removal of T-fasteners

A. Foster, M. Given, E. Thornton, M. Lee; Dublin/IE

Purpose: T-fastener gastropexy has been shown to prevent peritoneal leaks and the literature recommends removal at 10 days. We reviewed a series of patients in whom T-fasteners were removed at shorter time intervals after PG to see if there was a reduced complication rate.

Methods and Materials: 113 patients (M:F=68:45 age range 18-81; mean age 67 years) were reviewed. Indications for PG included oesophageal cancer, head and neck cancer, and a variety of neurological disorders. Four T-fasteners were inserted in each patient using standard technique. T-fasteners were removed at different time intervals depending on the procurement of nursing home beds. In our study we defined 'early' removal as less than 2 days and 'delayed' removal as 3 days or more.

Results: In the overall cohort, minor complications were recorded in 30/113 patients (27%) with no complications in the remaining 83 patients. In 10/30 patients local infection occurred requiring antibiotic therapy, and 20/30 patients experienced pain at the gastrostomy site. In 69/113 patients (61%) T-fasteners were removed within 2 days. There was a statistically significant reduction in complication rate with 'early' removal compared to 'delayed' removal [8/69 (12%) vs 22/44 (50%) p < 0.05]. In the early removal group 6 patients experienced pain and 2 infection. In the delayed group there were 22 minor complications- infection (n = 8) and pain (n = 14). No peritubal leaks or other major complications were seen.

Conclusion: Removing T-fasteners earlier than 10 days is feasible. Minor complications including local pain and infection, increase in incidence with longer T-fastener dwell times.

Scientific Sessions

B-195 14:36

Super selective percutaneous treatment of liver transplantation cholangitis (LTC). Technical aspects and biochemical parameters for graft salvage

R. Lopez-Benitez¹, H.M. Barragan-Campos², G.M. Richter¹, G. Kauffmann¹, T. Marinelli¹, P.J. Hallscheidt¹; ¹Heidelberg/DE, ²Paris/FR

Purpose: Cholangitis is a well known and common complication in liver transplantation, specially in those cases with prolonged intraoperative times. We present here a short series of cases treated percutaneously, with an radiologically interventional superselective approach, that clearly demonstrate the benefits of a prolonged and prompt treatment as an effective therapeutic option for the salvage of liver transplant.

Materials/Methods: A total of 570 patients had undergone partial related or total cadaveric liver transplantation in a 16-year period (1987-2003). A total of ten patients complicated with chronic colangitis where included in this study. Study patients where treated in a percutaneous technique, but only half of the group (study group) was treated with a superselective lavage of the biliary tree branches. Liver function parameters (ALT, AST, AP, GGT and bilirubin) and systemic inflammatory parameters (CRP, Leucocytes) where assayed, and correlated with the number of interventions and clinical status of the study group. When required, complications such as stone removal or stenosis dilatation where performed.

Results: At the time of this report, 80% of the cases treated with this technique had prolonged graft survival. Almost all of this cases were treated as ambulatory patients with clear improvement in their clinical and biochemical parameters. Those patients treated with conventional techniques had a 100% mortality in less than a year.

Conclusion: Despite the high mortality rate of conventional LTC percutaneous treatment, our technique demonstrated a significant higher survival rate. However, this approach requires prolonged treatment times with several minimally invasive interventions and multidisciplinary care.

B-196 14:45

Palliation of pancreatic cancer by combined biliary and duodenal stenting

S. Profili, C. Urigo, A. Manca, F. Meloni, L. Canalis, F. Salaris; Sassari/IT

Purpose: To assess usefulness of combined biliary and duodenal stenting for the palliation of inoperable pancreatic cancer.

Materials and Methods: We report our experience on 5 patients (2 men, mean age 61.8 years) with inoperable pancreatic cancer, causing stricture of the common bile duct and second portion of duodenum, treated by implantation of 9 self-expandable metal stents and one plastic prosthesis inserted exclusively under fluoroscopic view. All patients presented with dysphagia and jaundice. Percutaneous insertion of the biliary stent (3 Memotherm, 1 biliary Wallstent, 1 Carey-Coons) was performed immediately before or 2-3 days after the duodenal stent (2 AV-Wallstent, 2 enteral Wallstent, 1 Choo) which was placed perorally.

Results: Technical and clinical success were obtained in all cases. All patients had a rapid improvement of dysphagia and were able to resume a semi-solid diet; serum bilirubin regressed to normal values in about 10 days. Mean follow-up was 7 months. Duodenal stent migration occurred in 1 case after 18 days; urgent laparotomy revealed colonic perforation: stent removal and sigmoid resection were performed. One patient developed recurrent dysphagia because of tumor in- and overgrowth after 4 months; a second coaxial stent was inserted with only partial relief of symptoms.

Conclusion: Despite the limited number of cases treated and the complications observed, combined recanalization of biliary and duodenal strictures allowed good palliation of symptoms and should be considered an effective alternative to palliative resection for advanced pancreatic cancer.

B-197 14:54

Follow-up of percutaneous transhepatic biliary drainage for malignant obstructive jaundice

X. Qian, D.C. Dai, R. Zhai; Beijing/CN

Purpose: To investigate the therapeutic efficacy of percutaneous transhepatic biliary drainage (PTBD) for malignant biliary obstruction and its affecting factors.

Materials and Methods: A total of 233 patients with malignant biliary obstruction were treated in our hospital with PTBD by placement of the metallic stents and/or plastic tubes. The patients were followed up with clinical and radiographic evaluation. Meanwhile, the serum level of total protein, hemoglobin, ALT, HBDH, ALP, GGT, BUN, and Cr were determined. Procedure- and device-related complication were recorded. The patients' survival and stent patency rate were calculated with Kaplan-Meier survival analysis.

Results: PTBD were successfully performed in all the patients. Stent placement

were conducted in 136 cases. One hundred cases were treated with only 1 stent, 20 cases had 2 stents for bilateral drainage and 16 had 2 stents for long strictures, made stent in stent. The other 97 patients received plastic catheters. The serum level of total bilirubin reduced from 349.2 ± 155.6 mmol/l before to 178.9 ± 141.2 mmol/l after PTBD ($t = 17.90$, $p = 0.000$). Sixty-two patients had incorporate infection before procedure and 23 of them were cured after procedure. Twenty-nine patients got inflammation after procedure. Thirty cases died within 30days. The mortality within 30days was related to age and serum level of bilirubin, protein and BUN etc. After PTBD, the re-occlusion occurred in 51 patients, and catheters broke off in 7. The median survival time was 7.3 months and median patency time was 14 months.

Conclusion: PTBD can provide good palliative drainage. It can also improve other condition caused by biliary obstruction.

B-198 15:03

Role of covered stents in biliary intervention

A. Bruni, F. Fanelli, M. Bezzi, S. Vagnarelli, M. Corona, L. Di Reze, G. Orgera, P. Rossi, R. Passariello; Rome/IT

Purpose: Evaluate the efficacy of e-PTFE covered stent (VIABIL-Gore) in the treatment of malignant biliary strictures.

Material and Methods: From 2001, 65 patients (mean age 69.4 y) with malignant common bile stricture were treated with an e-PTFE covered stent-graft (Viabil-Gore). The Viabil is a self-expandable stent-graft with an inner ePTFE/FEP lining and an outer supporting a structure of nitinol wire. Biliary obstruction was secondary to pancreatic carcinoma (n = 38), cholangiocarcinoma (n = 10), gallbladder cancer (n = 6), metastatic lymphadenopathy (n = 11). The stricture was located in the upper third of the common bile duct in eight patients, in the middle portion in 43, and in the lower third in 14. Sixty-nine stent-graft were implanted: 20 with side holes and 49 without holes. In 62/65 patients the distal end of the device was deployed in the duodenum. Clinical evaluation and assessment of serum bilirubin and liver enzyme levels were done before stnt placement and at 1, 3, 6, 9 and 12 months.

Results: Stent-graft placement was successful in all cases. The 30-day mortality rate was 11%. The survival rates were 40% at 6 months and 20.2% at 12 months. The stent patency rate were 91%, 78% and 78% at 3, 6 and 12 months respectively. After a mean follow-up of 37.2 months we reported acute cholecystitis in 6 cases (9.2%). Complications other than stent occlusion occurred in 12 patients (18.4%). No migration of the stent-graft was observed.

Conclusion: e-PTFE covered stent-graft seems to be an effective tool in case of malignant strictures of the common bile duct.

B-199 15:12

Percutaneous treatment of urological complications occurring after renal transplant

D. Righi, A. Doriguzzi Breatta, S. Barbero, A. Ruffino, A. Calvo, G. Gandini; Turin/IT

Purpose: To value the efficacy of Interventional Radiology in the treatment of urological complications post renal transplant.

Materials and Methods: Between November 1981 and January 2004 in our Renal Transplant Unit surgeons performed 1637 transplants. The incidence of urological complications was 9.4% (154/1637); of these, 134 cases underwent percutaneous treatment: 71 ureteral obstructions, 37 urinary fistulas, 25 collections and 1 urinary incontinence. In all the obstructions and fistulas first we performed a percutaneous pyelostomy; 55 obstructions underwent uretheroplasty. The collections were treated by percutaneous drainage and aspiration.

Results: We achieved technical success in 128/134 cases (95.5%). The follow-up (median 57 months) showed clinical success in 79/128 cases (61.7%). The specific results in case of obstruction showed a complete success in 3 cases of clot obstruction an 1 mycetoma. The complication was solved by urotheroplasty in 37/55 cases (67.3%). We achieved complete success in 21/35 urinary fistulas (60%) and in 17/22 collections. The procedure related major complications were 2/134 (1.5%).

Conclusions: The immediate and late results of percutaneous treatment in the urological complications post renal transplant show the efficacy of Interventional Radiology procedures. Because of its poor traumaticity, low incidence of complications and mortality rate close to 0%, percutaneous approach could be considered as the first choice in the therapy of urological complications post renal transplant. Even in unsuccessful cases, Interventional Radiology allows a reliable diagnosis of the complication and to delay the surgical procedure in conditions of election.

Scientific Sessions

B-200 15:21 

Ultrasonography-guided intraneural injection for intractable limb contracture control

J. Lee, Y. Lee; Daegu/KR

Purpose: To evaluate the feasibility of ultrasonography-guided intraneural nerve block to control intractable contracture of extremity.

Materials and Methods: Thirty-two patients showing muscular contracture of their extremities were controlled by 50 intraneural injections of nerve conduction inhibiting drugs. Among the 32 patients, male and female were 28 and four, subsequently. The age of patients ranged from two to 75 years old with mean age of 21. The target nerves were sciatic ($n = 30$), tibial ($n = 7$), musculocutaneous ($n = 9$) and other nerves ($n = 4$). Injected drugs were 2–5 ml lidocaine or phenol. Lidocaine ($n = 41$) was used for temporary nerve block and Phenol ($n = 9$) was for permanent block. Ultrasonography was done using 7–15 MHz linear transducers. After identification of the nerve, 22-gauge needle was inserted into the nerve and the drug was injected until the target nerve expanded to double in its diameter. The success of intraneural injection was confirmed by checking the increased nerve size and immediate improvement of the muscular contracture. The follow-up study was performed until the recurrence of spasticity.

Results: In 50 injections, nerve expanded and immediate release of the contracture occurred. No complication occurred by intraneural injection. In Lidocaine injection group, the effective period ranged from one to 70 days (average = 13 days). In Phenol injection group, the effect lasted from 23 to 765 days (average = 297 days).

Conclusions: Ultrasonography-guided intraneural nerve block showed perfect success rate in extremities. Lidocaine injection showed favorable effect for temporary nerve block. Phenol injection was feasible to control muscular contracture of extremities in long-term follow-up.

14:00 - 15:30

Room I

Interventional Radiology

SS 309b

Experimental interventions in models and animals (2)

Moderators:

M. Szczero-Trojanowska; Lublin/PL

J. Tacke; Passau/DE

B-201 14:00

Passive guidewire tracking on road maps - a phantom study

R. Meckle, O. Bieri, C. Hashagen, K. Scheffler, D. Bilecen; Basle/CH

Purpose/Introduction: The purpose of this study was to overlay images obtained with fast MR imaging scans onto a previously acquired roadmap for the passive visualization of a guidewire/balloon catheter for MR-guided endovascular interventions.

Subjects and Methods: All examinations were performed on a whole-body MR scanner at 1.5 Tesla. A magnetization prepared 2D FISP sequence was used to generate a contrast-enhanced roadmap. The first images were averaged to generate a mask, subsequent time frames were complex subtracted. All complex subtracted images were added up to create a roadmap. For passive tracking of a new guidewire prototype, data were rapidly acquired using a balanced steady-state free precession (b-SSFP) sequence and images were overlaid in near real time onto the roadmap. The entire procedure was performed in a phantom study. A single high-grade stenosis was modeled in the phantom to allow balloon angioplasty.

Results: Preliminary results indicated sufficient contrast between the passive guidewire and a contrast-enhanced MR-roadmap. A near real-time guidance of the tip of the guidewire was feasible. Inflation and deflation of a conventional balloon catheter was also monitored at the level of the artificial stenosis.

Discussion/Conclusion: The information from fast b-SSFP acquisitions was successfully overlaid onto a roadmap to visualize the tip of a guidewire in phantom studies.

B-202 14:09

Validation of a fixed model as a method of training in interventional radiology

P.R. Healey, A.E. Healey, S. Johnson, T. How, D.A. Gould; Liverpool/UK

Purpose: Simulator models are increasingly being used in medical training. The

commonest type are fixed models. Few medical training models have been validated as a method to train. Quantitative appraisal and assessment has been suggested as a method for maintaining standards. At present no criteria for assessment and no method of reproducible testing has been formulated.

Materials and Methods: A transparent polymer model of a female vascular tree used with optical cameras, light through transmission and a plain radiograph back drop was used to simulate the appearances of fluoroscopy during an interventional radiological procedure. A range of volunteers of varying interventional radiological experience were set tasks to complete and were videoed using the model. Two cohorts of trainees, both groups trained conventionally, and one trained on the model were assessed on the model. The time to completion of tasks and assessment of the operator's ability by several independent blinded expert interventional radiologists were performed.

Results: There was a significant difference between experts and trainees ability to perform tasks on the model. A rapid improvement and then plateau in ability in both experts and trainees was seen. The model seems to be a valid training tool for the development of basic interventional radiological skills. An improvement in the confidence of the trainees in dealing with real world interventional radiological tasks was also demonstrated.

Conclusions: Fixed models of this type does show some benefit in training, however the model does lack inherent flexibility that is required for convincing simulation.

B-203 14:18

Minimally invasive close-chest method for creating myocardial infarction in swine

G.A. Krombach, S. Kinzel, A. Mahnken, R.W. Günther, A. Buecker; Aachen/DE

Objectives: To evaluate a closed-chest model for reperfused and occlusive myocardial infarction (MI) in pigs and to report experiences and pitfalls.

Material and Methods: In 44 pigs, a balloon catheter was advanced into the left coronary artery (LAD), under fluoroscopic guidance. The balloon was inflated and occlusion of the vessel angiographically confirmed, while ECG was monitored. If ventricular fibrillation occurred, direct current defibrillation was performed. In 6 animals, the balloon was left inflated, to obtain occlusive infarction. In all other cases, the balloon was deflated after 45 min. After the experiments were finished, the hearts were stained with TTC for assessment of infarct size.

Results: MI was successfully induced in 34 animals. Mean size of MI was $15.8 \pm 5.1\%$ of left ventricular surface area for reperfused and $21.5 \pm 8.7\%$ for occlusive infarcts. In one pig, TTC did not confirm infarction. In 26 pigs, ventricular fibrillation occurred. Defibrillation was successful in 17 pigs. Failure rate due to ventricular fibrillation decreased from 42% (6) in the first 14 to 10% (3) in the following 30 animals. One animal died due to technical failure of the ventilator. After initial experiences, we used balloon catheters with a diameter of 2 - 3 mm, instead of 4 mm. The smaller balloon sizes were used so as to decrease the incidence of fibrillation.

Conclusions: The described technique of LAD occlusion presents a less invasive alternative to open chest models. The major pitfall, causing fatal arrhythmia, was over-dilatation of the LAD.

B-204 14:27

Photodynamic therapy of arthritis: An in vitro feasibility study

I. Hilger, S. Graefe, A. Hansch, O. Frey, W.A. Kaiser; Jena/DE

Purpose: To investigate if arthritis could be treated minimal-invasively using photodynamic therapy and to elucidate the effects of 2 different photodynamic agents in different cell systems which are present in arthritic joints.

Materials and Methods: Endothelial cells, fibroblasts and macrophages from mouse were incubated with Foscarn® and Fospeg® (Biolitec, Jena) at different concentrations (0.01 to 100 microM) and incubation times (30 min to 48 h). Cytotoxicity was determined by measuring the activity of cellular dehydrogenases with and without application of laser light ($\lambda = 652$ nm; power density: 10 J/cm², 50 sec). The intracellular localization of the agents was determined using confocal laser scanning microscopy (CLSM), the mechanisms of cell death by FACS analysis after propidium iodide and annexin-V staining.

Results: All investigated cells showed a distinct decrease of cell viability with increasing concentration and incubation times with the photodynamic agent (e.g. no viable cells at concentrations higher than 10 microM and after more than 2 h incubation time). Moreover, compared to the dark cytotoxicity (no laser light), a distinctly higher cytotoxicity was observed after light application. CLSM showed an intracellular agent accumulation in cytoplasmatic regions in the proximity of the cell nucleus. Cell death was predominantly induced by necrosis.

Conclusions: Local concentrations of at least 10 microM photodynamic agent should be effective for the minimal-invasive treatment of arthritic joints.

Scientific Sessions

Friday

B-205 14:36

Efficacy of alternative embolisation devices in an experimental aneurysm model

C. Roth, I.Q. Grunwald, T. Struffert, B. Romeike, R. Eymann, W. Reith; Homburg a.d. Saar/DE

Purpose: The most commonly used embolization device for intracerebral aneurysms are GDC-Coils. Other embolization devices like Matrix-Coils or the liquid embolization system ONYX (EVOH) are not used in daily routine for the treatment of intracranial aneurysms because they seem to bare more risks like thrombembolic events (ONYX) or harder handling (MATRIX). The aim of the study was to evaluate the efficacy and safety of both alternative embolization devices under anticoagulation in comparison to GDC-Coils in an experimental aneurysm model in rabbits.

Materials and Methods: 35 aneurysms were induced. 5 Animals serve as a control group. 10 aneurysms were treated with GDC-Coils, 10 were treated with Onyx and 10 with Matrix-Coils. Heparine was administered during embolization. Aspirine was administered until sacrifice. Occlusion rate, recanalization rate und histologic evaluation are being analysed.

Preliminary Results: Excellent occlusion rates (100%) could be achieved in all embolized aneurysms so far. Radiologically determined recanalization rate is up to now low (0). Histologic evaluation of 2 animals from the Onyx group and one of the Matrix group did not show recanalization. Anticoagulation either during embolization or long-time anticoagulation doesn't seem to affect the occlusion or recanalization rate of aneurysms treated with GDC-Coils, Matrix-Coils or ONYX.

B-206 14:45

Restenosis inhibition by non-stent-based local drug delivery

U. Speck¹, B. Scheller², C. Abramjuk¹; ¹Berlin/DE, ²Homburg a.d. Saar/DE

Purpose: Drug-eluting stents have shown promising anti-restenotic effects in clinical trials. Their efficacy is believed to depend on the sustained release of antiproliferative drugs. Animal studies by our group indicate persistent efficacy of drugs even after very short exposure of the vessel wall.

Methods and Materials: Paclitaxel was dissolved in CM or coated on balloons. Stents were crimped on paclitaxel coated balloons. 5-6 pigs each received 2 coronary stents applying slight overstretch by using either (a) uncoated balloons, bare stents, and plain CM, (b) the same but paclitaxel in CM, (c) paclitaxel-coated PTCA balloons with premounted bare stents and plain CM, (d) commercial premounted Cypher stents and plain CM. Restenosis was assessed 4 weeks later by angiography and histomorphometry. Based on the results of comprehensive animal experiments clinical trials were initiated.

Results: Treatment was successful in all animals. No adverse events attributable to paclitaxel in the CM or balloon coating were observed. Reangiography indicated pronounced restenosis in the control group and least restenosis in the animals treated with a coated balloon. Histomorphometry confirmed the efficacy of the 3 routes of drug delivery with the most impressive effect of the coated balloons. The structure of clinical trials and first results will be presented.

Conclusions: Paclitaxel added to CM or coated on PTCA catheters is effective in inhibiting restenosis in the porcine coronary overstretch model. Non-stent-based drug delivery may overcome some problems associated with stent coating and provide additional flexibility in restenosis inhibition.

B-207 14:54

Evaluation of balloon expanded stents in a cone-beam flat-panel volumetric-CT (FP-VCT)

G. Heidrich, S. Wenzel, K.-P. Hermann, C. Dullin, E. Grabbe, M. Funke; Göttingen/DE

Purpose: An experimental study was preformed to compare the visualisation of balloon expanded stents using a cone-beam flat-panel volumetric-CT (FP-VCT) with high isotropic spatial resolution and an 8-row multidetector-CT (8-MDCT). **Methods and Materials:** Seven different balloon expanded stents from 2 to 5 mm diameter were implanted in a flexible plastic tube of a vessel phantom. This phantom was examined with the 8-MDCT and the FP-VCT applying different acquisition protocols. The datasets were postprocessed on a workstation including 3D-reconstructions in Volume-rendering-technique (VRT) with axial and sagittal projections and overviews. Based on an evaluation score data analysis was performed.

Results: The visualisation of the stents was substantial superior using the FP-VCT as with the 8-MDCT. The stents material as well as the stent lumen could be exactly depicted. The smallest commercial available stent with a diameter of 2 mm could be excellently illustrated.

Conclusion: In experimental preclinical setting FP-VCT is an excellent diagnostic tool for the evaluation of balloon expanded stents and their lumen. Due to the high isotropic spatial resolution FP-VCT could also clearly depict the smallest 2 mm commercial available cardiac stent.

B-208 15:03

Development and animal experimental testing of a percutaneous thrombectomy device

R.K. Verma, J.E. Pfeffer, R.W. Günther, T. Schmitz-Rode; Aachen/DE

Purpose: To develop a thrombectomy device which is adequately steerable, quickly placeable and allows removal of large thrombus amounts in cases of extensive pulmonary embolism or deep venous thromboembolism.

Materials and Methods: The developed device consists of a self-expandable plastic-coated basket, mounted at the catheter-tip, which allows to suck and extract thrombus material. A small metal probe is manually moved within the suction channel to prevent obstruction. In vitro-tests in a stationary pulmonary circulation model were performed, followed by experimental tests in 6 sheep. Consolidated thrombus material was introduced over the right jugular vein to produce pulmonary embolism. The extraction catheter was inserted over the right jugular and femoral vein, the basket was placed in contact to the head of the thrombus. After the extraction procedure pulmonary angiography was performed to document the extent of pulmonary recanalization.

Results: In in-vitro tests embolus material could be extracted by suction over the basket-channel system without obstruction due to the moving metal probe. In vivo pulmonary thrombus material could be extracted in all cases. However, the amount extracted varied between 30% and 100% according to angiographic findings. Limiting factors were steerability and positioning of the basket.

Conclusion: Extraction of pulmonary embolism with a self-expanding, plastic-coated suction-basket is possible. Yet the extent of recanalization is limited due to restricted catheter maneuverability in the pulmonary arterial system. Nevertheless, the device may have potential in deep venous thrombectomy (iliac and femoral veins), where steerability is less crucial.

B-209 15:12



Treatment of experimental saccular aneurysms of carotid arteries with three covered stents in canine models

Y.S. Cheng, M.H. Li, H.X. Zhang; Shanghai/CN

Purpose: To assess the effectiveness and safe of balloon-expanding stainless steel stents (SSS) system covered with polyurethane membrane (PUM) and expanding poly teflon ester membrane (ePTFEM) and biomembrane (BM) in the treatment of experimental saccular aneurysms of carotid arteries in canine models.

Methods: Experimental aneurysms were treated with covered stents. Altogether there were twelve PUM-SSS and ePTFEM-SSS and BM-SSS respectively, they were placed endovascularly in the common carotid arteries covering the orifice of the aneurysms. Control angiography was performed immediately after the procedure and after 2 weeks, 4 weeks and 12 weeks. All treated canines were given conventional anticoagulation. The animals were sacrificed according to grouping time. Stented arteries were removed for histopathological examination.

Results: 36 experimental saccular side-wall aneurysms of carotid arteries were opened. Model success rate is 90%. All stents were placed successfully in target arteries. The complete patency rates of PUM-SSS and ePTFEM-SSS and BM-SSS were 25.00% and 41.67% and 91.67% respectively. Histological analysis indicated that all treated aneurysmal pouches were almost filled with thrombus. Stent wires were found to be located deep within the vessel wall and encased by an extension of the tunica intima; Endothelialization of BM-SSS already began at 2 weeks which was earlier than that of PUM-SSS and ePTFEM-SSS; Various degree of degenerate cells were seen under the transmission electron microscopy. Surface erosion of stents was not found in this study.

Conclusion: Placement of covered stent endovascularly proved expedient, safe, and effective. BM-SSS has better mechanical behavior, physiochemical stability, anticoagulative ability and biocompatibility and open than PUM-SSS, ePTFEM-SSS.

B-210 15:21

Radiofrequency thermal ablation in canine femur: Evaluation of coagulation necrosis reproducibility and MR-histopathologic correlation

J. Lee, J. Han, S. Kim, J. Lee, B. Choi; Seoul/KR

Objective: To determine whether a single application of radiofrequency (RF) energy to normal bone can create coagulation necrosis reproducibly and to assess the accuracy of MR imaging at revealing the extent of RF-induced thermal bone injury.

Scientific Sessions

Materials and Methods: Using a 200 W generator and a 17gauge cooled-tip electrode, a total of 11 RF ablations were performed in the distal femurs of seven dogs under fluoroscopic guidance. RF was applied at 100 W for 10 minutes. MR imaging including, precontrast T1- and T2-weighted images and post-contrast fat suppressed T1-weighted images, was performed to evaluate ablation regions. After MR imaging, six dogs were killed on day 4 after the procedure and one dog on day 7.

Results: In all animals, RF ablation created a well-defined coagulation and no significant complications were noted. The mean long-axis diameter and the mean short-axis diameter of the coagulation zones produced were 45.9 ± 5.5 mm and 17.7 ± 2.7 mm. On MR imaging, the ablated areas showed multilayered zones with signal intensities that differed from normal marrow on precontrast images, and a perfusion defect on postcontrast T1-weighted images. The correlation between the diameter of coagulation necrosis and lesion size at MR imaging was strong, with correlation coefficients ranging from 0.89 for T1-weighted images and 0.97 for T2-weighted images, to 0.98 for postcontrast T1-weighted images ($P < 0.05$).

Conclusion: RF ablation created well defined coagulation necrosis in a reproducible manner, and MR imaging accurately determined the extent of the RF-induced thermal bone injury.

14:00 - 15:30

Room K

Cardiac

SS 303

MR imaging in myocardial infarction

Moderators:

F. De Cobelli; Milan/IT

M. Pasowicz; Krakow/PL

B-211 14:00

Contrast enhanced magnetic resonance imaging of acute myocardial infarction: Optimization of image contrast

K.-U. Walterling, T. Schlosser, K. Gaida, O. Bruder, P. Hunold, J. Barkhausen; Essen/DE

Purpose: Variable T1 times of normal and infarcted tissues require individual adjustment of the inversion time to optimize contrast of late enhancement images. However, the time course of T1 times after contrast administration has not been investigated yet. Aim of our study was to measure T1 values of normal and acutely infarcted myocardium after contrast injection using IR-SSFP sequences.

Methods and Materials: 38 patients (30 male, 8 female, mean age 56.0 ± 13.0 years) with first acute ST-elevation myocardial infarction were enrolled in the study. T1 values of non-infarcted myocardium, the area of late enhancement (LE) and the no-reflow zone were estimated 1, 3, 5, 10, 15, 20 and 25 minutes after Gadodiamide injection (0.2 mmol/kg BW, Omnipaque, Amersham) using an inversion recovery steady state free precession sequence (TR 2.5 ms, TE 1.1 ms, FA 50°) with incrementally increased inversion times. T1 values were obtained using the following equation: $T1 = T1_{(min)} / \ln 2$, where $T1_{(min)}$ is the inversion time of the image with the minimum signal intensity of the tissue.

Results: The T1 times of normal myocardium and LE showed a maximum difference 15 minutes after contrast administration (LE: 264 ± 38 ms; normal myocardium: 354 ± 33 ms). The maximum difference between the no-reflow zone and the surrounding tissues was found immediately after contrast administration (no-reflow T1=347 \pm 167 ms, normal myocardium T1=206 \pm 41 ms, LE T1=211 \pm 86 ms).

Conclusion: To optimize image contrast in acute myocardial infarction measurements of the no-reflow zone should be performed immediately after contrast injection, whereas the area of LE should be assessed about 15 minutes after contrast injection.

B-212 14:09

Evaluation of left ventricular (LV) remodelling after acute myocardial infarction with MR imaging: The role of no reflow

L. Natale, A. Porcelli, A. Bernardini, A. Meduri, A. Lombardo, L. Bonomo; Rome/IT

Purpose: LV remodelling is crucial after PTCA for acute myocardial infarction. Aim of the study is to assess using MR imaging the role of edema, no-reflow and myocardial viability in the remodelling process.

Methods and Materials: 25 pts with AMI and primary PTCA (21 LAD, 2 CX, 3 RCA; 22: TIMI 3, 4: TIMI 2) were studied by MR imaging to measure end-diastolic

(EDV) and end-systolic (ESV) volumes immediately and 1-month later. A $> 20\%$ increase of EDV and/or ESV was considered indicative of remodelling. Triple IR-FSE for edema evaluation, steady-state free precession cine (FIESTA) for contractile function, fast-gradient echo train (FGRET) for first-pass perfusion study and IR-prep fast GRE for delayed enhancement assessment were obtained. A score for edema, no-reflow and hyperenhancement was calculated in each segment (17-segments LV model) based on number of segments and transmural extension ($< 25\%$, $25\text{--}50\%$, $50\text{--}75\%$, $> 75\%$).

Results: 11 pts had remodeling. EDV and ESV increased from 106 ± 30 ml to 153 ± 36 ml and from 60 ± 17 ml to 91 ± 23 ml respectively in pts with remodelling. No-reflow was detected in 22 pts (88%). The scores for edema, no-reflow and hyperenhancement were 4.0 ± 1.6 , 2.4 ± 1.1 , 3.3 ± 1.6 respectively in pts with remodelling and 2.9 ± 2.2 (p:NS), 1.4 ± 0.9 (p:0.04), 2.6 ± 1.7 (p:NS) respectively in patients without remodelling.

Conclusions: First-pass MR imaging detects a high incidence of no-reflow after PTCA. Its extension was more significantly related to remodelling compared to edema and necrotic myocardium.

B-213 14:18

Value of T2-weighted-, first-pass-enhancement and delayed-enhancement-MR imaging to differentiate between acute and chronic myocardial infarction

A. Stork, G.K. Lund, K. Muellerleile, P.M. Bansmann, J. Kemper, G. Adam; Hamburg/DE

Purpose: Assessment of diagnostic accuracy of T2-weighted (T2w)-, first-pass-enhancement (FPE), delayed-enhancement (DE)-MR imaging and cine-MR imaging to differentiate acute (AMI) from chronic myocardial infarction (CMI).

Material and Methods: 50 patients were imaged at 1.5 T 5.0 ± 3.3 days and 7.9 ± 2.7 months after AMI using cine- and T2w-MR imaging. FPE- and DE-MR imaging were performed during and 10 minutes after injection of Gd-DTPA, respectively. Images were acquired in short-axis planes. In a blinded consensus-reading wall-thinning on cine-MR imaging, enhancement-defects on FPE-MR imaging, central hypointensities on DE-MR imaging and edema on T2w-MR imaging were graded as present or absent. Signal-intensity (SI)-ratios for infarcted/normal myocardium on T2w-MR imaging were assessed quantitatively. Sensitivity, specificity and accuracy for the imaging findings were calculated. SI-ratios were compared by a t-test.

Results: The sensitivity and specificity, respectively, for detecting AMI were 96% and 98% for edema on T2w-MR imaging, 58% and 80% for an enhancement-defect on FPE-MR imaging, 48% and 96% for a central hypointensity on DE-MR imaging and 92% and 40% for the absence of wall-thinning on cine-MR imaging. Edema on T2w-MR imaging was more sensitive to AMI than an enhancement-defect on FPE-MR imaging ($p < 0.0001$) and a central hypointensity on DE-MR imaging ($p < 0.0001$). Edema on T2w-MR imaging and a central hypointensity on DE-MR imaging were more specific for AMI than an enhancement-defect on FPE-MR imaging ($p < 0.0001$). The SI-ratios for T2w-MR imaging in the acute stage were 1.48 ± 0.21 and 1.08 ± 0.11 for the chronic stage ($p < 0.0001$).

Conclusion: T2w-MR imaging can reliably differentiate between AMI and CMI. A central hypointensity on DE-MR imaging is more specific for AMI than an enhancement-defect on FPE-MR imaging. Wall thinning has a high specificity for CMI.

B-214 14:27

Presence of Q waves on the ECG predicted by MR imaging

T.A.M. Kaandorp¹, J.J. Bax¹, H.J. Lamb¹, E. Viergever¹, E. Boersma², D. Poldermans¹, E.E. van der Wall¹, A. de Roos¹; ¹Leiden/NL, ²Rotterdam/NL

Purpose: Studies have demonstrated that Q wave infarctions frequently have non-transmural scar formation, whereas non-Q wave infarctions may have transmural scars. The precise pathophysiological substrate underlying the Q waves remains unclear. MR imaging is the preferred technique to evaluate patients with infarction, since information can be obtained on function, contractile reserve and scar tissue. Therefore, we used MR imaging to predict the presence of Q waves on the ECG.

Methods and Materials: Consecutive patients ($n = 69$) with coronary artery disease and history of myocardial infarction underwent MR imaging investigation. The protocol included resting-, low-dose dobutamine- and contrast-enhanced MR imaging. Parameters included: LVEF, LV volumes, end-diastolic wall thickness and contractile reserve in the infarct region, transmurality and spatial extent of scar tissue, total scar score and the quantified percentage of scar tissue of the LV. The MR imaging data were related to the presence/absence of Q waves on the ECG.

Scientific Sessions

Results: Q waves were present in 39 (57%) patients. Univariate analysis identified the transmurality, the spatial extent, the total scar score and the quantified percentage scar tissue as predictors of Q waves. Multivariate analysis demonstrated that quantified percentage scar tissue was the single best predictor. A cutoff value of 17% infarcted tissue of the LV yielded a sensitivity and specificity of 90% to predict presence/absence of Q waves. When the quantified percentage scar tissue was removed from the model, the spatial extent of infarction was the best predictor.

Conclusions: Q waves on the ECG are best predicted by the quantified percentage scar tissue on contrast-enhanced MR imaging.

B-215 14:36



3 Tesla MR for myocardial viability evaluation with emphasis on comparison with 1.5 Tesla

G. Ligabue, A. Barbieri, F. Fiocchi, S. Ferraresi, L. Rossi, M.G. Modena, R. Romagnoli; *Modena/IT*

Purpose: To compare 3 Tesla cardiac imaging with 1.5 Tesla for myocardial viability evaluation in nearly identical experimental conditions.

Methods and Materials: 35 patients (mean age 58; 71% male) underwent both 3 T and 1.5 T MR cardiac examination within 2 weeks. Comparison between both scanners was made on the basis of the same study protocol which includes: cine b-FFE 2 and 4 chamber views multiple short-axis views (every 1 cm throughout the entire LV). Perfusion is evaluated after Gadolinium injection (0.15 mmol/kg). Delayed Enhancement evaluation is performed after 15 minutes with a segmented inversion-recovery technique. Image quality was assessed measuring Signal-to-Noise Ratio and Contrast-to-Noise Ratio in four left ventricle points in a cine b-FFE end-diastolic mid-ventricular image.

Results: Measured functional parameters were as follows respectively for 1.5 T and 3 T: ejection fraction 48.3 ± 12 and 49.2 ± 11 , stroke volume 87.99 ± 22 and 89.45 ± 21 ml, cardiac output 6.6 ± 1.5 and 6.7 ± 1.3 l/min, end diastolic volume 182 ± 45.5 and 179.6 ± 46.7 ml, end systolic volume 94.01 ± 23.5 and 90.15 ± 22.9 ml. Qualitative viability parameters were as follows respectively: kinesis score 6.7 ± 2.1 and 6.1 ± 2.6 , perfusion score 7.9 ± 1.9 and 8.1 ± 2.2 , DE score 15.4 ± 3.9 and 16.2 ± 4.1 , percentage of left ventricular dysfunctional but viable 14.77% and 12.35% , summed scar score 3.9 ± 1 and 4.1 ± 0.9 . SNR and CNR were respectively 23.64 ± 4.94 and 80.8 ± 4.69 and 81.88 ± 12.3 and 185.13 ± 21.4 ($p < 0.005$).

Conclusion: 3 T showed high concordance with 1.5 Tesla regarding functional and viability parameters while measured SNR is 3.92 times higher. Measured CNR is 2.26 times higher that leads to better anatomical structural representation.

B-216 14:45

Assessment of coronary artery lesion by MR perfusion of the myocardium and pressure derived fractional flow reserve

A.M. Huber, M. Schweyer, J. Rieber, I. Erhard, K. Theisen, S. Schönberg, M. Reiser; *Munich/DE*

Purpose: To compare semiquantitative MR perfusion parameters with results from intracoronary pressure derived fractional flow reserve (FFR) in the functional evaluation of known coronary artery lesions for assessment of their hemodynamic relevance.

Materials and Methods: 21 patients with CAD underwent MR imaging (Siemens Sonata, Erlangen) conventional coronary angiography (CA) with intracoronary pressure wire examination for determination of fractional flow reserve (FFR) in 23 stenotic lesions. SI curves of the first pass MR perfusion imaging (IPAT SR-turboFLASH) were analysed at rest and under adenosine-induced hyperemia. A 0.5 mmol/kg Gd-DTPA bolus was applied at rest and during hyperemia (Adenosin) with a flow rate of 5 ml/sec. Time-to-peak (TTP), maximum signal intensity (MSI) and upslope (US) values were determined. A lesion < 50% diameter reduction was defined as normal, a lesion > 50% with $\text{FFR} > 0.75$ as intermediate and a lesion with diameter reduction > 50% and $\text{FFR} < 0.75$ as severe, respectively.

Results: TTP was not significantly different between the three groups (11 ± 3.4 ; 15 ± 5.7 ; 13 ± 5.1 ; ns). US at rest was comparable (0.08 ± 0.17 ; 0.10 ± 0.035 ; 0.07 ± 0.01 ; n.s.). During stress US increased and was significantly different between normal coronary arteries and severe coronary stenoses (0.28 ± 0.12 vs. 0.08 ± 0.01 ; $p < 0.05$). The ratio US at stress and rest was 3.4 ± 1.5 (2.0-6.3) for normal coronary arteries and 1.7 ± 0.3 (1.2-1.7) and 1.1 ± 0.1 (1.0-1.3) for intermediate and severe coronary lesions ($p < 0.04$ and $p < 0.03$).

Conclusion: MPRI (USStress/USRest) were significantly different between normal and hemodynamically relevant diseased coronary arteries. MR perfusion imaging can give important information about assessment of hemodynamic relevance of coronary artery stenoses.

B-217 14:54

Cine SSFP MR imaging after myocardial infarction: Impact of G-CSF stimulation of peripheral stem cells on cardiac function

B.J. Wintersperger, M.G. Engelmann, H. Theiss, M.F. Reiser, W.M. Franz, S.O. Schönberg; *Munich/DE*

Purpose: Purpose of this study was to monitor global and regional cardiac function in patients after MI treated with granulocyte colony stimulating factor (G-CSF) for peripheral blood stem cell stimulation compared to placebo.

Material and Methods: 12 study patients with ST segment elevation MI (STEMI) were included and underwent cine MR imaging at baseline, 4 and 12 weeks after coronary intervention on a 1.5 T scanner (Magnetom Sonata; Siemens). Cine SSFP was performed in short-axis orientation with a pixel size of 1.5×1.5 mm. LV-EDV, ESV and EF were evaluated as well as regional wall thickening parameters for the main infarct segment based on a 16 segment model. Results of G-CSF and placebo group were compared.

Results: LV-EF of both study groups did not differ significantly, neither at baseline nor at 4 and 12 weeks ($P > 0.05$). LV-EDV and ESV also did not show significant differences when comparing both groups at any time point ($P > 0.05$). LV-EDV of the G-CSF group changed from 158 ± 21 ml at baseline to 143 ± 33 ml at 12 weeks ($P > 0.05$), while within the placebo group it changed from 186 ± 86 ml to 184 ± 15 ml ($P > 0.05$). ESV measurements did not show significant longitudinal changes within both groups ($P > 0.05$). While systolic thickening within the placebo group did not show significant changes from baseline to 4 weeks (0.6 ± 0.4 mm vs. 0.01 ± 0.9 mm; $P > 0.05$), the G-CSF group showed significant improvement ($P < 0.03$).

Conclusion: High-resolution SSFP cine imaging allows monitoring of global and regional cardiac function in MI. Preliminary data shows that the use of G-CSF in patients with STEMI may improve regional wall motion.

B-218 15:03

Single shot and phasesensitive detection for assessment of myocardial infarction within a single breathhold

A.M. Huber, B. Spannagl, C. Hayes, S. Schönberg, M. Reiser; *Munich/DE*

Purpose: The aim of the study was to compare the diagnostic accuracy in viability imaging of the myocardium with a multislice Phasesensitive Inversions Recovery (PSIR) 2 D single shot (SS) TrueFISP sequence and an established IR turboFLASH sequence.

Material and Methods: 21 patients with myocardial infarction were examined at a 1.5 Tesla MR System (Sonata) 10 minutes after administration of contrast material with a single shot 2D multislice technique (IR TrueFISP), that allows imaging of the entire short axis during one breathhold, and with a segmented 2D single slice technique (IR turboFLASH), that requires one breathhold per slice. The inversion time was optimized with a CINE TI-Scout sequence for IR turboFLASH, the PSIR-SS TrueFISP sequence was used with a standard TI of 200 msec. The voxel size was $2.1 \times 1.6 \times 8$ mm 3 for both MR techniques.

Results: The PSIR-SS TrueFISP sequence has a similar contrast/noise ratio (CNR) as the IR turboFLASH sequence (mean values: $11.6.0$ vs. 12.3 , $p > 0.05$, n.s.) for differentiation of viable and non viable myocardium. The assessment of the area of infarction within one slice ($r = 0.96$, $p < 0.003$) and the volume of the entire infarction is possible with excellent correlation of both techniques ($r = 0.97$, $p < 0.002$).

Conclusion: PSIR-SS TrueFISP sequence allows for accurate determination of the area and volume of the infarction with high spatial resolution during data acquisition within a single breathhold without significant loss of CNR.

B-219 15:12

Functional recovery after acute myocardial infarction: Evaluation by MR imaging

L. Natale, A. Bernardini, A. Porcelli, A. Meduri, A. Lombardo, C. Liguori, L. Bonomo; *Rome/IT*

Purpose: To assess the role of contrast enhanced (CE) MR imaging in the prediction of functional recovery after acute myocardial infarction.

Methods and Materials: 43 consecutive patients with first AMI (64 ± 9 yrs., 36 anterior, 7 inferior, 37 primary PTCA, 6 thrombolysis) underwent cine- and CE-MR imaging (GE Signa Horizon Echospeed; GE Signa LX Excite) within the fifth day after onset. Cine-MR imaging was performed in short axis (6-8 slices, Fastcard and FIESTA sequences); first pass imaging (IR-prep FGRE and FGRE-ET with 0.075 mmol/kg Gd-DTPA, 3 mL/s) was obtained on three short axis slices (basal, mid-ventricular and apical); multi-slice short axis (6 slices) delayed T1 imaging (IR-prep FGRE) was obtained 20 min after double dose Gd injection. A total

Scientific Sessions

amount of 731 segments were classified as: 1) normal first-pass, absent or delayed hyperenhancement; 2) hypoenhancement at first-pass, delayed hyperenhancement; 3) hypoenhancement both at first-pass and delayed imaging. Segments from first-pass slices (total amount 774) were classified at delayed imaging as normal (= type 1), hyperenhanced (= type 2) and hypoenhanced (= type 3). Patterns 2 and 3 were considered non viable. At six months MR imaging assessed functional recovery.

Results: Pattern 1 was observed in 1262 segments, with functional recovery appreciated in 1195 (94.7%). Pattern 3 was present in only 31 segments, without recovery (100%). Pattern 2 was observed in 212 segments: of them, 39 showed recovery (18%).

Conclusions: Patterns 1 and 3 respectively identify viable and non viable tissue. Pattern 2 is less specific early after AMI, as it may also represent viable myocardium.

B-220 15:21

MR imaging prediction of β-blocker therapy effect in ischemic cardiomyopathy by assessment of LVEF using dobutamine stress

T.A.M. Kaandorp, H.J. Lamb, J.J. Bax, E. Boersma, E. Viergever, E.E. van der Wall, A. de Roos; Leiden/NL

Purpose: Since left ventricular ejection fraction (LVEF) does not improve in all patients with ischemic cardiomyopathy in response to β-blocker therapy, an investigation to predict the likelihood of a response is desirable. Therefore, we sought to evaluate the feasibility for prediction of β-blocker therapy effect on global LVEF, by measurement of global LVEF during low-dose dobutamine MR imaging, before therapy, in patients with severe ischemic cardiomyopathy.

Methods and Materials: In 20 patients with chronic coronary artery disease, MR imaging was performed at rest and during low-dose dobutamine stress before starting carvedilol therapy and at follow-up to assess global LVEF. Additionally, a NYHA classification was assessed by the patient's cardiologist before and after β-blocker therapy.

Results: Global LVEF at follow-up may be predicted by using the formula: β-blocker induced LVEF improvement = $0.66 \times (\text{LVEF}_{\text{stress}} - \text{LVEF}_{\text{rest}}) + 0.34$ ($R^2 = 0.67$, $P < 0.01$). Thus, an induced improvement in $\text{LVEF} \geq 7\%$ may predict a positive response $\geq 5\%$ at follow-up. This improvement was consistent with the NYHA classification before and after β-blocker therapy.

Conclusion: β-blocker therapy effect may be predicted at baseline by using the formula: β-blocker induced LVEF improvement = $0.66 \times (\text{LVEF}_{\text{stress}} - \text{LVEF}_{\text{rest}}) + 0.34$ ($R^2 = 0.67$, $P < 0.01$). MR imaging can be helpful to select patients who benefit from β-blocker therapy.

14:00 - 15:30

Room L/M

Neuro

SS 311

The young and the old brain

Moderators:

I.M. Björkman-Burtscher; Lund/SE
D. Prayer; Vienna/AT

B-221 14:00

Temporal lobe development investigated using fetal MR imaging

G.J. Kasprian, P.C. Brugge, D. Prayer; Vienna/AT

Purpose: The temporal lobe (TL) contains substructures which host main neuropsychological functions. To date fetal TL anatomy has been investigated only *in vitro*. Using fetal magnetic resonance imaging (MRI) we evaluated TL development in healthy and pathological conditions.

Methods and Materials: 60 fetuses with normal brain development, aged between the 18th and 37th gestational weeks (GW), and 35 cases with malformations or acquired conditions known to be associated with hippocampal pathology, underwent MRI. Different substructures of the fetal TL (hippocampus, parahippocampal gyrus, amygdala, temporal gyration) were evaluated at different developmental stages on T2-, T1- and diffusion-weighted sequences in 3 section planes.

Results: The hippocampus and amygdala were recognized by 22 GW, further intrinsic detail became evident with continuing growth. Following the 25th GW temporal sulci begin to appear in an orderly fashion. Occipito-temporal progression of superior temporal sulcus infolding correlated best with GW. Development of the parahippocampal gyrus relates to the inward positioning of the hippocampus. Altered TL morphology was a frequent finding in pathological cases. Hippocampal

malposition was characteristic to corpus callosum agenesis, migrational disorders, and hydrocephalus.

Conclusion: The morphology of the TL can be evaluated quite accurately with fetal MRI after the 24th GW. Hippocampal malposition can be detected from the 24th GW in fetuses with brain anomalies. Further follow-up of the postnatal clinical course of those fetuses will offer more information about the clinical impact of this finding.

B-222 14:09

Incidental findings on brain MR imaging in asymptomatic young adults

M.M.L. de Win, C.B.L.M. Majolie, G.J. den Heeten; Amsterdam/NL

Purpose: When reviewing brain MRIs it is important to know which abnormalities and normal variants can be prevalent in asymptomatic individuals. We determined frequency and nature of incidental findings on brain MR imaging in asymptomatic young adults.

Methods and Materials: Brain MRIs of 237 research volunteers (110 M, 127 F, mean age 22.5 ± 3.6) were reviewed by an experienced neuroradiologist. The scan protocol included axial and coronal PD and T2 weighted images and a high resolution post contrast T1-3D scan. Informed consent stated that relevant findings would be reported to the GP.

Results: 102 incidental findings, both abnormalities and normal variants, were diagnosed in 87 subjects. Multiple findings included pineal gland cyst (N = 15; 6.3%), wide peripheral CSF space (N = 12; 5.1%), wide or asymmetric ventricles (N = 12; 5.1%), white matter hyperintensity on T2 (N = 11; 4.6%), Rathke's cleft cysts (N = 9; 3.8%), wide perivascular spaces (N = 8; 3.4%), mega cisterna magna (N = 7; 3.0%), sinusitis (N = 6; 2.5%), venous angiomas (N = 6; 2.5%), cavum septum pellucidum (N = 4; 1.7%), partial empty sella (N = 2; 0.8%) and low position of the tonsils (N = 2; 0.8%). Findings in single subjects included heterotopic gray matter, choroid plexus cyst, arachnoidal cyst, thalamic lesion and low position of the tonsils. One subject with two contrast-enhanced skull tumors was referred for further examination (diagnosis after CT: fibrous dysplasia).

Conclusion: Incidental findings, most without clinical consequences, were diagnosed in 37% of the asymptomatic subjects. This emphasizes the importance of a protocol for management and reporting of incidental findings when performing brain MR imaging research in healthy volunteers.

B-223 14:18

DTI, perfusion MR imaging and ¹H-MR-spectroscopy of the brain: 'Normal-values' in a population of young healthy adults

M.M.L. de Win, E.J.P. Vlieger, C. Lavini, C.B.L.M. Majolie, E.M. Akkerman, G.J. den Heeten; Amsterdam/NL

Purpose: Use of Diffusion Tensor Imaging (DTI), perfusion imaging (PI) and ¹H-MR-Spectroscopy (¹H-MRS) has increased, but little is known about values and variation in the 'normal population'. We determined 'normal-values' of DTI, PI and ¹H-MRS in young healthy adults.

Methods and Materials: 189 volunteers (84 males, 105 females, 21.9 ± 3.2 yr) were included. MR imaging (1.5 T, Signa, GE) protocol: PD- and T2-weighted images, single voxel ¹H-MRS, DTI (DW-EPI, TE/TR = 90/8000, b = 1000, 12 directions, slice thickness 5 mm), PI (GE-EPI, slice thickness 5 mm), T1-3D scan. ADC, FA and CBV maps were registered to spatially normalized T1-3D scans. The thalamus, putamen, globus pallidus, caudate nucleus, parietal white matter, splenium and genu of corpus callosum, frontal and occipital gray matter were drawn as ROIs onto the normalized brain (both hemispheres) and resized to the original maps. rCBV-values were obtained by dividing mean $\text{CBV}_{(\text{ROI})}$ by mean $\text{CBV}_{(\text{white matter})}$. Spectra were analyzed using LC-Model. NAA, Cho and mI concentrations were calculated using Cr as reference. Mean values and Coefficients of Variation (CV; SD as percentage of the mean) were calculated.

Results: CV varied, depending of the region, between 4 and 18% for ADC, 9 and 22% for FA, 12 and 19% for rCBV and 14 and 22% for spectra.

Conclusion: FA, ADC, rCBV and ¹H-MRS values are dependent of scanner, scan-protocol and analyses. Although these were constant, we found large variations. Possible explanations for the large variations are inter-individual variation, physiological variation, analysis method or partial volume effects and these possibilities should be studied in future research.

Scientific Sessions

B-224 14:27

Phenylketonuria: Conventional MR imaging and spectroscopic assessment of cerebral PHE concentration with 3 T 1H-MRS

S. Pollici¹, T. Scarabino², V. Leuzzi³, M. Tosetti⁴, F. Carnevale⁵, A. Carriero¹; ¹Novara/IT, ²San Giovanni Rotondo/IT, ³Rome/IT, ⁴Pisa/IT, ⁵Bari/IT

Purpose: Previous research has attested the existence of individual features in the transport of Phe through the blood-brain barrier, as a possible influencing factor of the phenotypic expression of the disease. The objectives of this research were: correlation analysis between Phe emetic value and cerebral tissue concentration; correlation analysis between cerebral Phe value and clinical evolution; correlation analysis between Phe cerebral levels and white matter distortion.

Methods and Materials: We studied thirty-two PKU patients (17M and 15F) between the ages of 7 and 34 years, with no food restriction during the research. The MR imaging sequences used for the white matter examination were: axial FLAIR T1-W, coronal FSE T2-W and sagittal FSPGR T1-W. A score was given in function of the white matter compromise. Phe cerebral concentration was valued with single-voxel method by using a TE PRESS short sequence (TE: 35 ms). VOI was of 8 cc, localized in the peri-ventricular white matter. The morphological and biochemical analysis was made with 3 T MR equipment.

Results: White matter distortion was observed in 93.7% of patients; there was not a great difference in the white matter distortion gravity between early treated patients and late diagnosed and treated subjects; we did not find a significant correlation between white matter distortion grade and Phe cerebral concentration; in patients not being treated there was not a correlation between the cerebral concentration and the I.Q.

Conclusion: Blood and cerebral Phe concentration do not seem to have a direct correlation with clinical state and tissue distortion.

B-225 14:36

Normal ageing compared to alterations in CRPS related regions of the brain: A DTI study

L. Jäger, J. Lutz, R. Stahl, O. Dietrich, G. Schelling, S.O. Schönberg, M.F. Reiser; Munich/DE

Purpose: To compare DTI findings in patients with complex regional pain syndrome (CRPS) to those of normal subjects.

Methods and Materials: 20 healthy volunteers (mean age 28.5 years), 15 healthy volunteers (mean age 61.3 years) and 20 patients with a confirmed diagnosis of CRPS were examined using an 1.5 T MR System with a IPAT DTI EPI-sequence (TE 71 ms, TR 6000 ms, 36 Slices, 1.8x1.8x3.6 mm spatial resolution). Bilaterally the amygdala, hippocampus, anterior cingulate gyrus (AGC) and the superior temporal gyrus (STG) were evaluated with references in the frontal white matter. The fractional anisotropy (FA) and the relative anisotropy (RA) were determined. **Results:** There were no age related changes of RA and FA in the amygdala. A significant decline of RA and FA in the grey and white matter of the STG was found in the elderly control subjects. In the AGC and the hippocampus a decline was lateralized left and right respectively for the elderly healthy controls in comparison to the younger ones. The CRPS patients showed bilaterally increased RA and FA values ($p < 0.001$) in the amygdala, the hippocampus and the AGC in comparison to the younger and older healthy controls.

Conclusion: The results support the hypothesis that the amygdala, the hippocampus and the anterior cingulate gyrus play a major role in mental stress associated disease and second, that CRPS is a mental stress associated disease.

B-226 14:45

Normal ageing compared to alterations in fibromyalgia related regions of the brain: A DTI study

J. Lutz, L. Jäger, R. Stahl, O. Dietrich, G. Schelling, S.O. Schönberg, M.F. Reiser; Munich/DE

Purpose: Aim of the study was to compare DTI findings in patients with fibromyalgia to those of normal subjects.

Methods and Materials: 20 young healthy volunteers (mean age 28.5 years), 15 elderly healthy volunteers (mean age 61.3 years) and 20 patients with a confirmed diagnosis of fibromyalgia were examined using an 1.5 T MR System with an IPAT DTI EPI-sequence (36 slices, 1.8x1.8x3.6 mm spatial resolution). Bilaterally the amygdala, hippocampus, anterior cingulate gyrus (AGC) and the superior temporal gyrus (STG) were evaluated with references in the frontal white matter. The fractional anisotropy (FA) and the relative anisotropy (RA) were determined.

Results: There were no age related changes of RA and FA in the amygdala. A significant decline of RA and FA in the grey and white matter of the STG was found in the elderly control subjects. In the AGC and the hippocampus a decline

was lateralized left and right respectively for the elderly healthy controls in comparison to the younger individuals. The patients with fibromyalgia showed bilaterally increased ($p < 0.001$) RA and FA values in the amygdala, the hippocampus and the AGC in comparison to the younger and elderly healthy controls.

Conclusion: The results support the hypothesis that fibromyalgia is a mental stress associated disease. A decline in anisotropy in the frontal cortex which is associated with normal ageing, confirms the hypothesis that the process of ageing results in bifrontal atrophy. The unevenly distributed anisotropy changes in the hippocampus and the AGC underline their association in the ageing process.

B-227 14:54

A voxel-based morphometric study of Alzheimer's disease

J. Hao, K. Li; Beijing/CN

Purpose: Up till now, the study of regional gray matter atrophy in Alzheimer's disease (AD) has been assessed with regions of interest (ROI), but this method has many shortcomings. In this study we used the fully automated voxel-based morphometry (VBM) approach in order to provide a full-brain assessment of AD morphology.

Methods and Materials: 19 patients with AD and 15 healthy subjects of similar age and gender ratio were included in the study. Magnetic resonance imaging was performed on a 1.5 T Siemens Sonata MR imaging system (Siemens, Erlangen, Germany). Whole brain T1-weighted 3D MPRAGE (magnetization-prepared rapid-acquisition gradient echo) data sets were acquired in the sagittal plane (TR 1900 ms; TE 3.93 ms; slice thickness 1.7 mm; skip 0.85 mm; FOV 250 mm; Matrix 448x512; Flip Angle 15°). Data analysis was performed by Statistical Parametric Mapping software (SPM 99) in conjunction with MATLAB version 6.5 to generate gray matter density map.

Results: Our results confirmed earlier findings with traditional MR imaging measurement, but additionally we demonstrate global asymmetrical cortical atrophy with sparing of the sensorimotor cortex, occipital lobe and cerebellum. Moreover, atrophy of the right caudate head and left medial thalamus was shown.

Conclusion: Our results offer a comprehensive view of atrophy pattern in AD. The consistency of these findings with histopathological descriptions demonstrates the utility of the VBM technique for investigating the neuroanatomy of AD.

B-228 15:03

Visual attention deficits in Alzheimer's disease. A fMR imaging study

J. Hao, K. Li; Beijing/CN

Purpose: To investigate functional activation patterns during two types of visual search tasks in AD patients using fMR imaging.

Materials and Methods: 13 patients with AD and 13 healthy subjects of similar age and gender ratio were measured with functional magnetic resonance imaging (fMRI) while they performed tasks. The time series of fMRI data were acquired with T2*-weighted EPI sequence (TR 4500 ms; TE 40 ms; slice thickness 5 mm; skip 1 mm; FOV 220 mm; Matrix 64x64; Flip Angle 90°) on a 1.5-T Siemens Sonata MR imaging system (Siemens, Erlangen, Germany). Two visual search tasks were used. The first was a "pop-out" single feature task, detecting a vertical target among horizontal distractors. The second was a conjunction task, where the target is defined by a conjunction of features (color and orientation) and the performance depends on some shifting of attention. Data analysis was performed by Statistical Parametric Mapping software (SPM 99) in conjunction with MATLAB version 6.5.

Results: AD patients have a particular impairment in the conjunction task but not in the single-feature task. Although both groups revealed almost overlapping networks engaged in the conjunction tasks including the superior parietal lobule (SPL), frontal and occipito-temporal cortical regions (OTC), primary visual cortex and some subcortical structures. The most pronounced differences between them were found in the SPL (more activity in controls) and OTC (more activity in subjects).

Conclusion: AD particularly affects those mechanisms controlling spatial shifts of attention. Some additional remote activation (ventral visual stream and temporal lobe) can be interpreted as dynamic reallocating of brain functional resource.

B-229 15:12

Brain tissue damage in dementia with Lewy bodies: An in vivo diffusion tensor MR imaging study

M. Bozzali¹, A. Falini¹, F. Baglio¹, M. Cercignani², E. Farina¹, P. Vezzulli¹, G. Scotti¹, R. Nemni¹; ¹Milan/IT, ²London/UK

Purpose: Conventional MR imaging showed uncertain results assessing neuro-radiological features of dementia with Lewy bodies (DLB). In this study, the presence and the distribution of microscopic brain tissue damage from patients

Scientific Sessions

with DLB was assessed in vivo using Diffusion Tensor Imaging (DTI) by Region of Interest (ROI) analysis.

Materials and Method: Fifteen patients with DLB and 10 sex- and age-matched healthy subjects were studied using dual-echo and DTI imaging. After estimation of the diffusion tensor, mean diffusivity (MD) and fractional anisotropy (FA) maps were derived for every voxel. Several anatomical ROIs were selected, and the corresponding MD and FA regional quantities were measured from every subject.

Results: Patients with DLB compared to controls showed statistically significant, (after Bonferroni's correction, $p < 0.005$) higher MD and lower FA values in the white matter (WM) from parietal, frontal and occipital lobes, in the corpus callosum and pericallosal areas. DTI abnormalities were also found in the caudate nucleus, temporal lobe WM, and putamen. Several correlations were found between neuropsychological and regional DTI-derived metrics in DLB patients.

Conclusion: Microstructural abnormalities in regions (corpus callosum, pericallosal areas) with a high prevalence of long connecting fibre tracts suggests the presence of Wallerian degeneration secondary to neuronal loss in the associated cortices. The selective involvement of parietal, frontal and occipital lobes might explain some of the clinical and neuropsychological features of DLB, providing a possible distinctive marker for DLB. The abnormalities in the caudate nucleus and putamen suggest DLB and Parkinson's disease might share a similar nigro-striatal involvement.

B-230 15:21

1H MRS comparative study of cerebral metabolism in patients with mild cognitive impairment (MCI), vascular dementia (VD) and in normal elderly subjects (N)

V.A. Rogozhyn, Z.Z. Rozhkova, N.Y. Bachinskaya; Kiev/UA

Purpose: To characterize the metabolic changes in the brain of patients with MCI and VD in comparison to N using 1H MRS data.

Materials and Method: Three groups of patients were studied by 1H MRS with 1.5 T Magnetom Vision (SIEMENS). The 1st group included 25 patients (56-84 y) with MCI. The 2nd group consisted of 9 patients with VD (52-73 y). The 3rd group (N) consisted of 30 subjects (60-75 y). 1H spectra were recorded in the hippocampus (H), amygdala (A), frontal lobes (FL), in the entothinal cortex (EC) with the SVSSTEAM: TR/TE = 1500/135.30 ms.

Results: From the spectra in all sampled regions of the brain the peak areas of NAA, Cr, Cho and mInos were obtained. For the patients of the 1st versus the 3rd group a significant decrease of NAA and Cr and an increase of Cho peak areas in all regions and also a significant decrease of NAA/Cr, and Cho/Cr in H and FL were observed. In the 1st group (NAA/Cr = 1.01; mInos/Cr = 0.82; Cho/NAA=0.96), in the 2nd group (NAA/Cr = 1.14; mInos/Cr = 0.58; Cho/NAA=0.86), and in the 3rd group (NAA/Cr = 1.25; mInos/Cr = 0.62; Cho/NAA=0.53) were obtained. An increase in mInos/Cr (0.69) ratios in the patients of the 1st compared with the 2nd group (0.52) was noted. The ratios of Cho/NAA, mInos/NAA in H, FL and EC were the most accurate values for differentiation of MCI, VD and N.

Conclusion: 1H MRS data are useful in predicting the progression of MCI and VD and also for identification of cognitively normal subjects at risk for developing MCI.

14:00 - 15:30

Room N/O

Computer Applications

SS 305

New developments in PACS

Moderators:

G.D. Hurley; Dublin/IE
M. Kämmerer; Mainz/DE

B-231 14:00

Using speech recognition reduces time slot between imaging and final report

T. Kauppinen, O. Tolki, P. Korhonen, J. Ahovuo; Helsinki/FI

Purpose: HUS Helsinki Medical Imaging Center (HMIC) is a part of the hospital district of Helsinki and Uusimaa. HMIC products medical imaging services and it is working using infrastructure of PACS. HMIC is formed of the radiological imaging units in ten hospitals around Helsinki and it produces over 500.000 examinations annually. The purpose of this study was to demonstrate the effect of the Finnish radiological speech recognition system for dictation process.

Methods and Materials: Radiological dictation process was examined in two different units of HMIC in different hospitals. Examination period was one week in

both hospitals and all examinations were included except studies of emergency units. Process was evaluated by defining time of the whole dictation procedure and each step starting from request and ending to the final report. The departments in question are mainly doing ultrasound, normal X-ray (e.g. bone and thorax), computed tomography and fluoroscopy examinations.

Results: Procedure turnaround times were defined into following time slots 0-2 h, 2-4 h, 4-6 h, 6-12 h, 12-24 h, 24-48 h, 48-62 h, and over 62 h. Using this classification the distribution of the turnaround were determined. The mean turnaround time of traditional tape based system was 27 h and 23 h in both hospitals when all examinations were included. Respectively, when 5% of minimum and maximum was removed the mean values were 23 h and 21 h.

Conclusion: It was noticed by this study that speech recognition speeds up a dictation process. It will also change a whole workflow increasing the quality of the reports.

B-232 14:09

Improvement of hospital-wide radiology report availability by implementation of a fully PACS/RIS integrated speech recognition system

C.G. Trumm¹, C. Glaser¹, V. Paasche¹, P. Popp², B. Küttner¹, M.F. Reiser¹,

¹Munich/DE, ²Erlangen/DE

Purpose: To quantify the effect of speech recognition on report availability in a university hospital with an integrated PACS/RIS system and digital image and report distribution.

Methods and Materials: Prospectively, time-stamps of image acquisition and first report availability in RIS/HIS were documented for 240 cases of X-ray (CR) and Computed Tomography (CT) each. Time interval between both time-stamps was addressed as report turnaround time (RTT). Reports were created by 12 radiologists with conventional (CD) and speech recognition dictation (SR) respectively. Retrospectively, RTT for 11/02-02/03 (conventional dictation with transcription) and 11/03-02/04 (remote or online SR with transcriptionist (TC) or self correction (SC)) were calculated from the PACS/RIS database. RTT were classified in 3 categories: Reports delivered I) in less than one day, II) in 5 hours or less, III) in less than 1 hour.

Results: Prospectively, mean RTT was 21.1 h /25.1 h /8.9 h for CR with CD/SR (TC/SC) and 23.8 h /29.6 h /7.6 h for CT with CD/SR (TC/SC). In retrospect, 37898/39680 datasets were analysed. The number of reports delivered in less than one day was 3485/11453, in 5 hours or less was 2410/9710 and in less than 1 hour was 352/2050 for 2002-03/2003-04. This corresponds to an increase of reports delivered in less than one day by a factor of 3.1, in 5 hours or less by 3.9, and in less than one hour by 5.6.

Conclusion: The implementation of speech recognition within an existing PACS/RIS environment facilitates a significant improvement of report availability when online speech recognition and radiologist self-correction are used.

B-233 14:18

Hard disk caches in PACS archives: How big is beautiful?

S. Wirth, M. Treitl, J. Rieger, K.-J. Pfeifer, M.F. Reiser; Munich/DE

Purpose: To recommend appropriate sizes of fast image caches for large PACS installations.

Materials and Methods: In a large hospital Radiography, CT and MR imaging studies of in- and outpatients were included consecutively ($n = 1200$). All priors were accessed using AGFA Impax, R4.1 as PACS-System (10 years image coverage). Age, modality, body region as well as relevance for the interpretation of the current examination were analyzed.

Results: Priors existed in 59.7% (CR 62.2%, CT 54.5%, MR imaging 62.3%, inpatients 76.4%, out-patients 46.6%). Number of prior examinations was 7.6 in mean (82% same body region, 71% same modality as well). Age of relevant priors was 203 days in mean, distributed as follows: $56.2 \pm 9.2\%$ within 3 months, $72.0 \pm 4.5\%$ within 6, $84.6 \pm 3.2\%$ within 12, $91.4 \pm 2.5\%$ within 24 and $99.5 \pm 0.2\%$ within 60 months, respectively.

Conclusions: Best workflow requires access to every relevant prior from the fast PACS archive cache. A cache size covering actual images of at least 12 months should be minimum, provided that a working prefetching algorithm can identify the missing 15.4% of priors correctly (8.6% prefetching quota for 24 months coverage). However, falling hard disk prices make prefetching become superfluously since in the near future PACS archiving may be handled by harddisk RAID systems exclusively.

Scientific Sessions

B-234 14:27

Managing the CT data explosion: Initial experiences of archiving volumetric datasets in a mini-PACS

K. Lee¹, K. Lee¹, H. Lee¹, J. Kim¹, H. Kang¹, H. Hong², H. Lee¹, T. Kim¹; ¹Seongnam-si, Gyeonggi-do/KR, ²Seoul/KR

Purpose: To report our initial experiences of managing increased CT data, using a mini-picture archiving and communication system (PACS).

Methods and Materials: The volumetric dataset from 16-detector-row CT scanners was stored in a mini-PACS with a 271-gigabyte online and 680-gigabyte nearline storages and routed to radiologists' workstations, while another conventional thicker slice dataset was stored in the main PACS. During a sample period of two weeks, the impact on storage need of each dataset type (classified as volumetric, thick axial, standardized three-dimensional (3D) images routinely produced by technologists, 3D images added by radiologists, and scan planning) was assessed by measuring percentage data volume. Storage need of each PACS was analyzed over a five-month period.

Results: For the 867 CT examinations performed during the two-week period, the percentage data volumes of volumetric, thick axial, standardized 3D, additional 3D, and scan planning datasets were 74.4, 15.9, 7.0, 2.3, 0.5%, respectively. Over the five-month period, 278-gigabytes of CT data (8,976 examinations) were stored in the main PACS, and 738-gigabytes of volumetric datasets (6,193 examinations) were stored in the mini-PACS. The volumetric datasets formed 32.8% of total data for all modalities (2.20 terabytes) in the main PACS and mini-PACS. At the end of this period, volumetric datasets of 1,892 and 5,162 examinations were kept online and nearline, respectively.

Conclusion: Using a mini-PACS might be an effective method to archive every volumetric dataset and to deliver it to radiologists.

B-235 14:36



OsiriX: Open-Source 3D/4D DICOM viewer

A. Rosset¹, L. Spadola¹, O. Ratib²; ¹Geneva/CH, ²Los Angeles, CA/US

A multidimensional image navigation and display software was designed for display and interpretation of large sets of multidimensional and multi-modality images such as combined PET-CT studies. The software is developed in Objective-C on a Macintosh platform under MacOS X operating system using GNUstep development environment. It also benefits from the extremely fast and optimized 3D graphic capabilities of OpenGL graphic standard for taking advantage of any hardware graphic accelerator boards available. In the design of the software a special attention was given to adapt the user interface to the specific complex tasks of navigating through large sets of image data. An interactive jog-wheel device widely used in the video and movie industry was implemented to allow the users to navigate in the different dimensions of an image set much faster than with a traditional mouse or on-screen cursors and sliders. The program can easily be adapted for very specific tasks that only require a limited number of functions by adding and removing tools from the program's toolbar and avoiding the users to be overwhelmed by an excessive number of unnecessary tools and functions. The processing and image rendering tools of the software are based on the open source libraries ITK and VTK ensuring that all new developments in image processing that could emerge from other academic institutions using these libraries could be directly ported to the OsiriX program. OsiriX is provided free of charge under the GNU open source licensing agreement at <http://homepage.mac.com/rossetantoine/osirix>.

B-236 14:45



Diagnostic reading of radiology images on a wireless PDA: Fact or fiction?

Futuristic or foolish?

H.E. Gregersen; Aalborg/DK

Hypothesis: The wireless/mobile device that is becoming pervasive today is the PDA. Numerous healthcare sites are adopting large-scale PDA-based IT systems, and emerging technologies are allowing devices to access the full spectrum of radiology data. The hypothesis of this paper is whether PDAs can be used for diagnostic purposes by radiologists, and such use is desirable.

Methods: Aalborg University Hospital is implementing an Image and Data Management (IDM) system that provides RIS and PACS features together with innovative distribution possibilities. Wireless PDAs can be used by clinicians and radiologists to gain full access to radiology data, including all of the analysis tools available on standard workstations. To evaluate the IDM system, examinations were read on PDA as well as on workstations. The findings were compared, with assessment of the radiologists confidence of the diagnosis.

Results: The reading on the PDA matched the reading on the workstation in

most cases. The wireless PDA, together with the IDM software application, provided a diagnostic platform for orthopedic studies that was similar to that for a dedicated workstation.

Discussion: The reason, the combination of the IDM and the PDA technology works, is the unique

- Access to Full-Resolution DICOM Data
- Access to Window Center/Level Operations on Full-Fidelity DICOM Data
- Access to Volume Reconstructions

without sending or processing data on the PDA, but on a central server and send with streaming technology.

Conclusion: We prove the hypothesis that wireless PDAs can be used for primary diagnosis of most radiology data involving orthopedic examinations.

B-237 14:54

Dicom storage into PACS of out-hospital CD-ROMS

P.M.A. van Ooijen, P. ten Bhomer, M. Oudkerk; Groningen/NL

Purpose: With the introduction of digital imaging in radiology, patient studies are increasingly distributed between hospitals using CD ROMs. However, because of different conventions on patient numbers between hospitals digital storage is not easy. We investigated the application of a new software to integrate out hospital data into the local PACS archive for easy storage and reporting.

Materials/Methods: A one month trial was started to import CD ROMs from the radiotherapy and the radiology department. Patients were included into the HIS to obtain a valid patient number and an examination (EXTERNAL DATA or RE-EVALUATION) was entered into the RIS to obtain a valid accession number. All data was read from CD; patient ID and accession number were automatically replaced during transfer to the PACS using a DICOM worklist connection.

Results: 70 CD-ROMs were collected from 19 different hospitals (8 different modality types, 11 different software versions, and 8 different packages from different vendors). All CD-ROMs were successfully transferred into the PACS and could be easily reported. Some CD-ROMs with missing or corrupted DICOM directory files were first transferred to the local hard-disk and then sent to the PACS. This only occurred in older software versions from one vendor.

Conclusion: An easy way of introducing the out-hospital data into the PACS is provided. CD-ROMs can be destroyed after storage and no off-line storage of media is required anymore. Furthermore, all data can now be viewed and reported using the default viewers of the hospital and no additional training of staff is required.

B-238 15:03

Web based system for handling DICOM structured report documents from PACS for educational and research purposes

A. Delistamatis, M. Mantatzis, E. Kaldoudi, D. Ouzounis, P. Prassopoulos; Alexandroupolis/GR

Purpose: The standard DICOM Structured Report (SR) enables constructing and transferring medical reports as well as their storage along with images of each examination in the PACS. The purpose of the study is to develop a web-based system communicating with PACS, for extracting information from stored SR documents for educational and research purposes.

Material / Methods: This system consists of an interface communicating with PACS, made up of web service technologies. The interface extracts data from SR documents stored in the PACS and stores them in a local database of the system. The system database is administrated from an easy to use web user interface which enables viewing and analyzing the data, creating new SR documents for a study and offering full archiving capabilities.

Results: The proposed system gave the opportunity to add medical reports in a study, using web user interface. The stored reports in the system could be transferred towards PACS in the format of DICOM SR and vice versa. Complex queries can be applied by establishing a synchronization between the database of the proposed system and PACS i.e. applying keywords related to specific pathology or imaging findings to reports and analyze results according to time periods, body area and imaging modality, gender, patient's age etc.

Conclusions: Any PACS can use the proposed web-based system for create SR documents, administrate them and analyze data for educational or research purposes.

Scientific Sessions

B-239 15:12

Enterprise information management: Closing the loop for a complete clinical data repository

M.P. Kirk; Genoa/IT

Purpose: Digital information availability is changing the world and Clinical Data Repositories, e.g. Enterprise Information Management, are taking Healthcare to another level of digital information utilization. The incorporation of hardcopy clinical data into a softcopy CDR will offer significant benefits in customer care.

Methods and Materials: The consolidation of clinical data into a widely available data resource, improves the utilization of archive resources and infrastructure. The data availability across multi-functions and multiple locations releases valuable clinical resources for improved patient care.

Results: PACS utilization is increasing and many clinical disciplines have separate hardcopy and softcopy archives resulting in independent 'islands' of clinical data. Healthcare institutions are seeking to unite these 'islands' using enterprise-wide clinical data repositories for softcopy data sources, the innovation of ingesting hardcopy files will create a complete patient record. The integration of document scanners via the ingestion interface of a Enterprise Information Management solution results in a complete Clinical Data Repository of digital information linked to patient identities.

Conclusion: This presentation gives an overview on the integration of document scanners to an intelligent archive and storage solution for a complete CDR available across multiple sites and multiple functions within the enterprise wide clinical information environment. This results in an improved ROI for storage infrastructure supported by the consolidation of the hard and softcopy archives with the hospital and frees valuable clinical support resources for better patient care.

B-240 15:21

Report of a PACS migration

E. Kotter, D. Jaeger, G. Pache, U. Saueressig, M. Langer; Freiburg/DE

Purpose: Migration from an older model PACS (Philips ARCHIMEDIS) to a modern system (TIANI).

Methods and Materials: *Initial situation:* Old PACS-archive: Philips ARCHIMEDIS. Stored data volume approx. 15 TB, of those approx. 7 TB on RAID, another 9 TB on 12'' WORM. Data production at time of migration 13 GB/day. Connected modalities: 5 CT+5 MR+12 CR+4 RF+4 XA/DS/US. 25 diagnostic workstations (DWS) in Radiology.

Complex system for report and image distribution on the wards via the Electronic Patient Record and a web server using the dynamic access authorization concept developed at Freiburg University Hospital.

Results: With a PACS running routinely and a nearly filmless hospital, the major migration requirement was to ensure undisturbed running of both the DWS in Radiology as well as web based image distribution. To avoid interruption of service, the old and new PACS archive had to run parallel during a transition period. DWS were replaced one by one. The changeover from web based image distribution to the new system by contrary, will be without transitional arrangements. *Status so far:* High Availability PACS server with load balancing is running at two sites. All DWS in Radiology have been replaced. 7 TB of data (2 years) have been imported into the TIANI archive. All clinical presentations have been switched to TIANI software. Tests for the new image distribution are running.

Conclusion: Migration of PACS without interruption of service has been successfully achieved in our hospital. Radiologists' worklist facilitated by the high speed of the new PACS.

14:00 - 15:30

Room P

Vascular

SS 315

Peripheral circulation

Moderators:

S. Müller-Hülsbeck; Kiel/DE

L. Vlahos; Athens/GR

B-241 14:00

Sixteen-row CT angiography for assessment of the aortoiliac and lower extremity arteries in patients with peripheral arterial disease: Prospective comparison with digital subtraction angiography

J.K. Willmann, B. Baumert, T. Schertler, S. Wildermuth, T. Pfammatter, B. Marincek, T. Böhm; Zürich/CH

Purpose: To prospectively compare the accuracy of sixteen-detector row computed tomography angiography (CTA) with digital subtraction angiography (DSA) for assessment of the aortoiliac and lower-extremity arteries in patients with peripheral arterial disease (PAD).

Materials and Methods: Thirty-nine consecutive patients with PAD underwent both DSA and CTA. For data analysis, the arterial vascular system was divided into 35 segments. A total of 1365 arterial segments were analyzed by two independent blinded readers for arterial stenosis using a four-point grading system. A third independent, blinded reader assessed possible reasons for disagreements between CTA and DSA. Effective radiation dose was calculated for both imaging modalities.

Results: CTA and DSA were diagnostic for all 1365 vascular segments. Compared to DSA, the sensitivity and specificity of CTA with regard to detection of hemodynamically significant stenosis of all 35 arterial segments combined were both 96% for reader 1 and both 97% for reader 2. Reader 1 and 2 overestimated arterial stenosis in 42 (3%) and 34 (2.5%) arterial segments, respectively and underestimated arterial stenosis in 13 (1%) and 10 (0.7%) arterial segments, respectively. Interobserver agreement was excellent ($\kappa = 0.84-1.00$). Presence of an anteroposterior located luminal narrowing and extensive vascular wall calcification were considered main reasons for disagreements between both imaging modalities. Effective radiation dose was lower for CTA (1.6-3.9 mSv) compared to DSA (6.4-16 mSv).

Conclusion: Sixteen-detector row CTA is an accurate and reliable, non-invasive alternative to DSA for assessing the aortoiliac and lower-extremity arteries in patients with PAD.

B-242 14:09

Low-dose multidetector row CT (MDCT) angiography of the infrarenal aorta and lower extremity vessels: Comparison of different radiation dosages with standard DSA

F. Fraioli, C. Catalano, F. Venditti, L. Bertoletti, R. Passariello; Rome/IT

Purpose: To compare the effect of different radiation dosages in MDCT-Angiography with DSA in the evaluation of the infrarenal-aorta and lower-extremities vessels.

Materials and Methods: 75 patients, randomly divided into three groups of 25 patients each, were evaluated for atherosclerotic disease with MDCT (4x2.5 mm) and DSA. MDCT scanning parameters were kept constant, except for milliamperage (mAs) and scanning-time. Group A: 50 mAs, scanning time 32 s; group B: 100 mAs, scanning time 40 s; group C: 130 mAs, scanning time: 45 s. Images were analysed by two radiologists in consensus. Diagnostic value of MDCT (comparing with DSA) were evaluated for each data set. Total radiation exposure for each group was also calculated.

Results: The average total weighted CT dose index was 4.7 mGy for 50 mAs, 9.4 mGy for 100 mAs, and 12.21 mGy for 130 mAs. Dose reduction was 62% for group A and 23% for group B. The evaluation of the presence and degree of stenosis revealed a sensitivity of 99.1%, a specificity of 95.5%, an accuracy of 96.3%, a PPV of 86.7%, and a NPV of 99.7% for Group A (50 mAs). Sensitivity, specificity, accuracy, PPV, and NPV of Group B (100 mAs) were 99.2%, 97.2%, 97.7%, 92.2%, and 99.7% respectively. For the standard dose protocol (Group C 130 mAs), we found a sensitivity, specificity, accuracy, PPV, and NPV of 99.2%, 97.4%, 97.9%, 93.2%, and 99.7% respectively for all stenotic lesions.

Conclusion: Low-dose scanning is a feasible and accurate option for 4-channel MDCT angiography of the peripheral vessels. This technique provides substantial reduction of the radiation-dose delivered to the patient while maintaining optimal diagnostic accuracy.

Scientific Sessions

B-243 14:18

Dynamic time-resolved MRA compared with DSA in patients with limb threatening ischemia

O.A. Meissner¹, J. Rieger¹, C. Weber¹, U. Siebert², M.F. Reiser¹, S.O. Schoenberg¹; ¹Munich/DE, ²Boston, MA/US

Purpose: To compare a time-resolved echoshared MRA technique (TREAT) with DSA in patients with limb threatening ischemia.

Methods and Materials: TREAT (Magnetom Sonata, Siemens Medical Solutions) and DSA studies were obtained in 17 consecutive patients. The MRA protocol consisted of an initial time-resolved acquisition of the lower calf and a four-station bolus-chase MRA of the pelvis, thigh and proximal calf. TREAT with isotropic 1 mm³ voxel size was performed using parallel imaging techniques with in-built auto-calibration of the receiver coils in combination with 3D echo sharing. Each affected limb was divided into 11 segments; 165 (100%) arterial segments were available for comparison. Three blinded readers evaluated the amount of venous contamination (1 = none, 2 = mild, 3 = major - diagnostic evaluation not possible) and identified the target lesion. TREAT was compared with DSA as reference standard. The overall interobserver and intermethod comparison was expressed as percent agreement with 95% confidence intervals (95%CI).

Results: Venous contamination was graded 1 in 162/165 (98%) and 2 in 3/165 (2%) vascular segments, none was graded 3. Interobserver agreement was excellent for TREAT and DSA for identifying the target lesion (89% [61%, 100%] and 94% [73%, 100%] respectively). Intermethod agreement for TREAT and DSA was high (92% [71%, 100%]).

Conclusion: TREAT with dynamic image evaluation has the potential to significantly reduce venous contamination, one major problem inherent to standard MRA. With its high interobserver and intermethod agreement, TREAT is comparable to DSA in planning treatment for patients with limb threatening ischemia.

B-244 14:27

16-slice CT angiography vs gadolinium enhanced MR angiography in the evaluation of peripheral arterial occlusive disease: A work in progress

A. Cina, C. Di Stasi, T. Misciasci, F.M. Martina, R. Manfredi, B. Merlino, L. Natale, L. Bonomo; Rome/IT

Purpose: Multidetector-CT angiography (MDCTA) and gadolinium-enhanced magnetic resonance angiography (MRA) are replacing transcatheter-angiography in the diagnostic imaging of peripheral arterial obliterating disease (PAOD). Several studies have compared MDCTA or MRA to transcatheter-angiography, however no data are available about the comparison MDCTA-MRA in the femoro-popliteal and infrapopliteal regions. The purpose of this paper is the assessment of the accuracy of MDCTA vs MRA.

Materials and Methods: 15 consecutive patients with PAOD (Fontaine II-IV) underwent MDCTA (Lightspeed 16,GE) and (within 30 days) Gadolinium subtracted mobitrac MRA (Signa Echospeed 1.5 T,GE). Thirteen arterial segments per limb were evaluated: from common iliac to pedal. For each segment, the degree of stenosis (< 50%; 50-70%; > 70; 100%) and diagnostic confidence were assessed by a blinded observer. We arbitrarily defined as true-positive and true-negative cases of concordance between MDCTA and MRA, while in discordant segments, false positive and negative where identified by a selective Color-Doppler-US examination performed by an experienced operator.

Results: 152 segments were available for the analysis. Overall accuracy of MDCTA (92%) and MRA (89%) were similar. In the infrapopliteal segments, MDCTA was slightly more accurate (85% vs 79%) giving more confidence for the identification of significant stenosis. In infrapopliteal arteries with extensive calcified lesions (11% in our series), however, MDCTA gave poor results in terms of accuracy (65%) and confidence compared to MRA (78%).

Conclusion: In patients without contraindications to MRA and MDCTA, both techniques are accurate for the identification of significant stenosis. MDCTA, in patients with suspected infrapopliteal lesions, may be considered as first choice if previous examinations (i.e. Color-Doppler) do not reveal extensive calcified lesions.

B-245 14:36

MRA of the pedal arteries with MS-325, a blood pool contrast agent, and comparison with selective intraarterial DSA

K.-F. Kreitner, C. Nieswand, R. Kunz, K. Oberholzer, M. Thelen; Mainz/DE

Purpose: To compare MS-325 enhanced MRA of the pedal vasculature with selective intraarterial DSA.

Patients and Methods: 18 patients with peripheral arterial occlusive disease

and type I or II diabetes were prospectively examined at 1.5 T. For contrast enhancement, 0.03 mmol of MS-325 was administered. MR imaging consisted of dynamic imaging with acquisition of 6 consecutive data sets so as not to miss the bolus arrival, and of high-resolution steady state imaging. Selective DSA was performed within 24 hours and served as a standard of reference. Image analysis was performed by two observers and comprised assessment of image quality as well as the detection of patent segments of the distal calf and pedal vessels.

Results: There were no differences between MRA and DSA regarding overall image quality. MRA detected significantly more patent vessel segments than did DSA ($P < 0.001$, kappa = 0.46). Interobserver agreement of MRA was very good with respect to the detection of patent vessel segments and the assessment of hemodynamically significant stenoses (kappa = 0.97 and kappa = 0.89, respectively). SNR and CNR measurements returned high values during dynamic imaging after contrast arrival and during steady state imaging. Steady state imaging was hampered by venous superimpositions. There were no clinically significant trends in vital signs, laboratory tests or ECGs.

Conclusion: MS-325 enhanced MRA of the pedal vasculature proved to be superior to selective DSA. It demonstrated a long imaging time window, however, due to venous superimpositions, steady state imaging requires dedicated postprocessing techniques.

B-246 14:45

MDCT angiographic evaluation of radial artery in coronary artery bypass candidates

M. Karcaaltincaba, D. Akata, O.F. Dogan, U. Duman, E. Boke, A. Besim; Ankara/TR

Purpose: The radial artery (RA) is increasingly being used for coronary bypass grafting (CABG). The aim of this study is to demonstrate the usefulness of MDCT angiography for evaluation of RA as an alternative to conventional angiography.

Methods and Materials: Seventeen patients scheduled for CABG entered this study. 4-channel ($n = 13$) and 16-channel ($n = 4$) MDCT angiography was performed in cases with a normal Allen test. There was no selection of patients in relation to patient characteristics. Technical parameters for 4-channel and 16-channel MDCT angiography were: Pitch 1.75 and 1.5; slice thickness, 1.25 mm and 1 mm; detector collimation, 1 mm and 0.75 mm increment, 1 mm and 1 mm; table speed 14 mm/s and 36 mm/s. Contrast dose ranged from 50-140 ml and rate of injection was 4 ml/s.

Results: Bilateral forearm arteries were visualized in all patients. Technical success rate was 100%. Radial artery pathologies were noted in four patients (23.5%). Unilateral radial artery calcification was noted in three of the patients (17.6%) and occlusion was found in one patient with a normal Allen test. Radial arteries with calcification were not used for CABG. Anatomic variations of the upper limb arteries were seen in two of the patients (11.8%), which were: Persistent median artery with absent radial and ulnar arteries, and high bifurcation of radial artery from brachial artery. Patency of the radial arteries were confirmed in patients who underwent surgery.

Conclusion: MDCT angiography can be used for the detection of radial artery calcification and patency, assesment of forearm circulation and its anatomic variations to avoid inadvertent use of a diseased radial artery conduit.

B-247 14:54

Bilateral contrast-enhanced MR angiography of the hands at 3.0 Tesla versus 1.5 Tesla using parallel imaging: Intraindividual comparison of signal behaviour and image quality with angiological correlation in patients with severe ischemic hand disease

O. Moske-Eick, J.T. Winterer, N. Ghanem, K. Elsner, J. Leupold, R. Strecker, E. Kotter, M. Langer; Freiburg/DE

Purpose: Due to the small-sized target vessels, early venous contamination and variety of possible pathologic conditions, arteriography of the hand vasculature is still a challenge for MR-Angiography. The purpose of this study was to determine the benefits of contrast-enhanced MR angiography (ce-MRA) at 3.0 Tesla to signal-to-noise (SNR), contrast-to-noise (CNR) and diagnostic imaging quality compared with 1.5 Tesla technique in patients with severe ischemic hand disease.

Methods: Following administration of 17 ml Gadobenate Dimeglumine bilateral MRA of the hands was performed on a Sonata 1.5 Tesla and a Trio 3.0 Tesla scanner (Siemens, Erlangen, Germany) in 10 patients with severe ischemic hand disease. MRA was done with a timed ultrafast gradient-spoiled multiphasic elliptically reordered fast low angle shot (FLASH) sequence protocol equipped with parallel imaging (GRAPPA). Postprocessing included image subtraction, overlapping thin-slice MIPs and angulated targeted MIPs. Differences between 1.5 T and 3 T were evaluated intraindividually with a) ROI measurements of vessel

Scientific Sessions

SNR and CNR, b) multi-observer rating of diagnostic image quality c) assessment of artefacts and venous contamination.

Results: Multiphasic centric reordered acquisition provided high-resolution arterial-phase images with sufficient suppression of venous contamination and low incidence of artefacts.

Compared with 1.5 Tesla, SNR and CNR at 3.0 Tesla showed a marked increase of 100% / 121% resulting in a significant improvement of vessel delineation and image quality grading.

Conclusion: 3.0 T parallel MR imaging clearly improves ce-MRA of the hands, providing a twofold increase of SNR/CNR and a better delineation of the small-sized arterial hand vessels in microvascular diseases.

B-248 15:03

Optimisation of imaging parameters of MR angiography of the hand with subsystolic cuff-compression

T. Gluecker, J. Schwarz, G. Bongartz, D. Bilecen; Basle/CH

Purpose: To assess the impact of various injection rates on MR angiography of the hand with and without subsystolic cuff-compression.

Methods and Materials: 10 healthy individuals (mean age 24.4 years, range 20-27 years) underwent MR angiography of both hands. Starting 3 min prior to data acquisition, subsystolic upper arm compression was applied (value 30% below the brachial artery systolic pressure).

Imaging parameters were: 1.5. T whole-body scanner (Magnetom Sonata, Siemens, Erlangen, Germany), 3D GRE sequence (TR 4.45, TE 1.28, flip angle 25°). 7 data sets (20 sec) were obtained consecutively. Intravenous contrast injection of 0.1 mg/kg bodyweight Gadobutrol (Gadovist®, Schering, Berlin, Germany) was done with flow rates of 0.5 ml, 1.0 ml and 1.5 ml /sec. For both hands, quantitative data evaluation was performed with contrast-to-noise ratio (CNR) in the radial, ulnar, palmar and digital arteries. Qualitative assessment of arterial signal and venous contamination was rated by two experienced radiologists.

Results: The lowest amount of venous signal and contamination (CNR and readers' assessment) was observed with a flow rate of 0.5 ml/sec ($p < 0.05$). For the arterial vessels, no significant difference concerning CNR values and readers' assessment of data quality was observed between the 3 flow rates ($p = 0.08$). For all 3 flow rates, compression yielded significantly less venous contamination as compared to the non-compressed side ($p < 0.05$).

Conclusion: For all flow rates, image quality of hand MR angiography was better with cuff-compression. A flow rate of 0.5 ml/sec yielded good CNR ratio and significantly lower venous contamination.

B-249 15:12

Optimized whole-body cardiovascular magnetic resonance (MR) screening with parallel imaging: Experience in over 100 patients on a 32-channel MR imaging system

H. Kramer, S.O. Schoenberg, K. Nikolaou, A. Struwe, M.F. Reiser; Munich/DE

Purpose: To develop a whole-body cardiovascular MR examination without compromises compared to organ based routine exams and to present experience on a standard and a whole-body scanner in more than 100 individuals.

Material and Methods: We combined recent technical developments such as the whole-body matrix coil system, a scanner with a large range of table movement and the advantages of iPAT. This made it possible to perform MR angiography (MRA) of the entire arterial system together with a complete cardiac examination. 3D-Gd-MRA was performed at a spatial resolution of less than $1.4 \times 1.0 \times 1.5 \text{ mm}^3$. Due to the matrix coils and the large range of table movement, imaging of the entire body including functional and perfusion imaging of the heart, whole-body 3D-Gd-MRA, imaging of CNS, lungs and abdomen was possible within less than 75 minutes. Image quality and pathologic findings were rated by two readers blinded to each other's findings.

Results: Over 100 individuals were examined on two different MR scanners (standard / whole-body). We detected several myocardial (6) and vascular (10) pathologies. Mean scan time on the whole-body scanner (75 min) was significantly shorter than on the standard scanner. Image quality and detection of pathologies showed good to excellent inter-observer agreement ($\kappa 0.67 - 0.91$).

Conclusion: The recent technical improvements in cardiovascular imaging with high temporal and spatial resolution enable a combination of different morphologic and functional techniques in a whole-body scan within less than 75 minutes. The matrix coils together with iPAT offer the possibility of whole-body imaging instead of organ-based imaging.

B-250 15:21

Reduction of contrast agent dose in intraarterial 3D contrast enhanced MR-angiography of the upper and lower leg

C. Hashagen, G. Bongartz, W. Steinbrich, M. Aschwanden, K. Jaeger, R. Hügli, L. Jakob, D. Bilecen; Basle/CH

Purpose: To perform MR-guided interventions, intraarterial repetitive injections of contrast agent are necessary. We focus on a reduction of gadolinium based contrast agent dose, by reducing the injection duration during image acquisition in patients with peripheral arterial occlusive disease (PAOD).

Methods and Materials: Intraarterial gadolinium injection was performed to depict femoropopliteal/infrapopliteal arteries in six patients. Conventional 3D turbo flash sequence was applied on a 1.5 T whole-body MR scanner. Six measurements with an injection duration of 20, 30, 40, 60, 80 and 100% of the total acquisition time (TA = 27 s) were performed. Quantitatively, the intraluminal contrast-to-noise ratio (CNR) was determined. Qualitatively, a consensus reading of image quality was performed.

Results: CNR values comparable to full length injection (100%) were obtained at the femoropopliteal artery at $\geq 40\%$ of injection duration and for the infrapopliteal artery at $\geq 60\%$. In contrast, qualitative analysis demonstrated that injection duration of $\geq 80\%$ is necessary to obtain good diagnostic image quality.

Conclusion: Our data are in accordance with a recently published phantom study, where the CNR value of vessel enhancement is - within a certain range - only moderately affected by reduction of the injection duration (1). In contrast, the image quality itself is strongly affected by the reduction of injection duration and might therefore hamper the diagnostic quality. We conclude that reduction of injection duration is not a valuable method to reduce intraarterial gadolinium dosage. (1.) Hwang,KP, et al., J Magn Reson Imaging, 2002. 15(1):p.55-61.

Scientific Sessions

Saturday, March 5

Scientific Sessions

		room A 2nd level	room B 2nd level	room C 2nd level	room E1 entr. level	room E2 entr. level	room F1 entr. level	room F2 entr. level	room G lower level	room H lower level	
07:00											07:00
07:30											07:30
08:00											08:00
08:30											08:30
09:00		CC 517 Essentials of Neuroradiology Cerebral tumors and infections (p. 34)	RC 510 Musculoskeletal Osteoporosis and osteopenia (p. 34)	SF 5 Special Focus Session High-field body MR imaging: The new standard? (p. 35)	RC 502 Breast Open questions (p. 36)	RC 501 Abdominal and Gastrointestinal Liver imaging: Characterisation and pitfalls (p. 36)	RC 504 Chest CT angiography of the chest (p. 37)	EF 1 EFOOMP Workshop State-of-the-art in information technology (p. 38)	RC 508 Head and Neck Imaging in cochlear implant candidates (p. 39)	RC 509 Interventional Radiology Endovascular treatment in female pelvis (p. 39)	
09:30											09:30
10:00											10:00
10:30		EM 1 “ECR meets” Italy Imaging of focal lesions (p. 45)	NH 6 New Horizons Session Nanotechnology (p. 46)	SS 610 Musculoskeletal Bone structure imaging and quantification (p. 190)	SY 3 Satellite Symposium Implementation of clinical system solutions in an e-health environment (p. 580)	SS 602 Breast MR mammography (1) (p. 192)	SY 4 Satellite Symposium Work safety in the daily routine for technical staff in radiology (p. 580)	EF 2 EFOOMP Workshop How to get the best from information technology for patient care (p. 47)	SS 608 Head and Neck Acoustic pathway and base of the skull imaging (p. 194)	SS 609a Interventional Radiology Skeletal interventions (p. 196)	
11:00											11:00
11:30											11:30
12:00											12:00
12:30											12:30
13:00											13:00
13:30											13:30
14:00											14:00
14:30		SS 703a Cardiac MDCT of the coronary arteries (p. 208)	SS 710 Musculoskeletal MR imaging of the cartilage (p. 210)	SS 701a GI Tract Acute abdomen (p. 212)	SY 7 Satellite Symposium Ultravist: Two decades of partnership in CT: Answers to current topics (p. 582)	SS 702 Breast MR mammography (2) (p. 215)	SS 704 Chest Malignant tumors: Screening, staging and outcome (p. 217)		SS 707 Genitourinary Renal and adrenal tumors (p. 219)	SS 709 Interventional Radiology MR, CT and US guided procedures (p. 221)	
15:00											14:30
15:30											15:00
16:00											15:30
16:30		CC 817 Essentials of Neuroradiology Epilepsy, white matter diseases and ageing (p. 49)	RC 810 Musculoskeletal Bone marrow disorders as a manifestation of disease (p. 50)	SF 8a Special Focus Session Imaging ICU patients (p. 50)	RC 803 Cardiac Coronary vessels (p. 51)	RC 801 Abdominal and Gastrointestinal Crohn's disease of the intestinal tract: Advances in imaging (p. 52)	RC 804 Chest Imaging of lung cancer (p. 53)	RC 811 Neuro Orbit and visual system (p. 53)	SF 8b Special Focus Session Diagnostic and interventional radiology of transplants (p. 54)	RC 813 Physics in Radiology Special issues of radiation exposure in diagnostic radiology (p. 55)	
17:00	registration										16:00
17:30	EPOS™ - scientific exhibition										16:30
18:00											17:00
18:30											17:30
19:00											18:00
											18:30
											19:00

Scientific Sessions

	room I lower level	room K lower level	room L/M 1st level	room N/O 1st level	room P lower level	room W basement	room R 1st level	room Y 1st level	room Z entr. level	La Scala 2nd level	
07:00											07:00
07:30											07:30
08:00											08:00
08:30											08:30
09:00	RC 515 Vascular Venous imaging and intervention (p. 40)	RC 507 Genitourinary Imaging of the uterus (p. 41)	CC 516 Infection in the Adult Today Gastrointestinal infection: A changing scene (p. 42)	RC 514 Radiographers MR imaging/ Neuroimaging (p. 43)	ER 526 Joint ECR/EAR sessions: Challenges for European Radiology Assessment and accreditation in radiology in Europe (p. 43)				WS 23A1 Screening Mammography Interpretation Test "Hands-on" Workshop	E ³ 520 Foundation Course: Chest Radiology Airways and infection (p. 44)	09:00
09:30											09:30
10:00									WS 23A2 Screening Mammography Interpretation Test "Hands-on" Workshop		10:00
10:30									WS 624 Basic Life Support for Radiologists "Hands-on" Workshop	E ³ 620a Logistic implications of MSCT (p. 48)	10:30
11:00	SS 609b Interventional Radiology Abdominal aortic aneurysms (p. 198)	SS 603 Cardiac Coronary plaque imaging (p. 200)	SS 611 Neuro Stroke imaging (p. 202)	SS 605 Computer Applications Computer aided deduction and diagnosis (p. 204)	SS 615 Vascular Post therapeutic follow up and monitoring of disease (p. 206)	WS 622 Vertebraloplasty "Hands-on" Workshop			WS 23A3 Screening Mammography Interpretation Test "Hands-on" Workshop	E ³ 620b How to write a successful grant proposal (p. 48)	11:00
11:30											11:30
12:00											12:00
12:30											12:30
13:00											13:00
13:30											13:30
14:00									WS 23B1 Screening Mammography Interpretation Test "Hands-on" Workshop	E ³ 720 Foundation Course: Chest Radiology Vascular, emergency and ICU imaging (p. 48)	14:00
14:30	SS 701b Abdominal Visera (Solid Organs) Pancreatic and bile duct cancer (p. 223)	SS 703b Cardiac Cardiac function (p. 225)	SS 711 Neuro Epilepsy and brain tumors: Advanced diagnostic imaging (p. 227)	SS 713 Physics in Radiology CT: Radiation dose (p. 229)	SS 715 Vascular Carotid imaging (p. 231)				WS 23B2 Screening Mammography Interpretation Test "Hands-on" Workshop	WS 724 Basic Life Support for Radiologists "Hands-on" Workshop	14:30
15:00											15:00
15:30									WS 23B3 Screening Mammography Interpretation Test "Hands-on" Workshop		15:30
16:00											16:00
16:30	WS 818 Workshops on Interventional Radiology Pediatric intervention (p. 56)	RC 807 Genitourinary Pediatric intervention (p. 56)	CC 816 Infection in the Adult Today Musculoskeletal infection (p. 57)	PR 819 Primer: Molecular Imaging MR approaches to molecular imaging (p. 58)	JRF Highlighted Lectures				WS 820 Interactive Image Teaching Mediastinal masses (p. 59)		16:30
17:00											17:00
17:30											17:30
18:00											18:00
18:30											18:30
19:00											19:00

Scientific Sessions

10:30 - 12:00

Room C

Musculoskeletal

SS 610

Bone structure imaging and quantification

Moderators:

C. Krestan; Vienna/AT

T.M. Link; San Francisco, CA/US

B-251 10:30

Detection of osteoporosis-related spine fractures on routine lateral chest radiographs

D. Mueller¹, M. Isbary¹, H. Boehm¹, J. Bauer¹, E.J. Rummey¹, T.M. Link²;
¹Munich/DE, ²San Francisco, CA/US

Purpose: Vertebral fractures are the most common complication of osteoporosis but remain frequently undetected by radiologists on routine lateral chest radiographs. As these fractures lead to important health consequences and further fractures are preventable by appropriate medication, recognition is important. The purpose of this study was to investigate how frequently vertebral fractures were found in lateral chest radiographs, how frequently they were missed in the initial reports and to assess treatment for osteoporosis in the postmenopausal women with fractures.

Methods and Materials: 802 consecutive routine lateral chest radiographs of postmenopausal women (age \geq 50 years) were evaluated. The radiographs were chosen without knowledge of clinical findings and were independently reviewed by two radiologists. A validated semi-quantitative method (spinal fracture index = SFI) was used to assess the radiographs for vertebral fracture. In addition medical record notes and radiology reports were assessed to determine how many fractures were correctly identified and how frequently osteoporosis specific treatment was initiated.

Results: The mean age of the postmenopausal women was 68.2 years ($SD \pm 10.1$ years). Clinically relevant vertebral fractures (SFI > 1) were found in 115 patients (14.3%). Only 36/115 (31.3%) of those fractures were noted in the official radiology reports and in only 22/115 (19.1%) treatment was initiated.

Conclusion: As future osteoporotic fractures can be prevented by appropriate medication and chest radiography has the potential to serve as a tool to diagnose osteoporosis it is of great importance for the radiologist to focus on the spine in these radiographs.

B-252 10:39

Digital X-ray radiogrammetry (DXR-BMD) used in follow-up efficacy of alfacalcidol in postmenopausal osteoporosis

C. Galesanu, R.G. Galesanu, G. Melnic; Iasi/RO

Purpose: To estimate by DXR-BMD, the therapeutic efficacy of alfacalcidol in post-menopausal osteoporosis after two years of treatment. Osteoporosis and fracture risk represent a worldwide public health problem. Estrogen deficiency and declining calcium absorption due to reduced D hormone levels are important factors in the pathogenesis of bone loss. DXR-BMD system has shown to have a good correlation (> 0.90) to DXA.

Material and Methods: 2,475 healthy women addressed to the service of Bone Densitometry using DXR-BMD (Pronosco Xposure System™). From among these 1,741 were in post-menopausal. Using WHO criteria of osteoporosis diagnosis (T-score lower as -2.5), we found 687 women with osteopenia and 303 women with osteoporosis. The other 751 women were represented by the control group. 391 patients with osteopenia received 0.5 mcg alfacalcidol/daily. 165 patients with osteoporosis received 1 mcg alfacalcidol/daily. After 12 and 24 months all patients were evaluated for change in BMD by DXR.

Results: In the group with osteopenia the BMD increased by 3.4% and 2.3% after one and two years respectively. In the group with osteoporosis BMD increased by 1.8% and 2.4% after one and two years respectively. The decrease of BMD in the control group was between 1.8% and 3.4% in the first and second year.

Conclusion: DXR-BMD technology confirmed the therapeutic effect of Alfacalcidol in the abolition of loss of bone mass and the increase of bone mass density (BMD) compared with the control group.

B-253 10:48

Lumbar spine and hip bone mineral density discordance assessed by dual-energy X-ray absorptiometry (DEXA)

A. Fausto, L. Menicagli, A. Aliprandi, N. Ulgheri, F. Sardanelli; Milan/IT

Purpose: To evaluate concordance and discordance between lumbar spine and hip bone mineral density assessed by dual-energy X-ray absorptiometry (DEXA).

Materials and Methods: Three hundred ninety-seven outpatients (age 62 ± 10 yrs.) with lumbar spine (L1-L4) and hip evaluation of bone mineral density with DEXA (Hologic Delphi) were retrospectively reviewed. We used World Health Organization criteria for the diagnosis of normal, osteopenic, and osteoporotic bone. The information supplied by DEXA, T-score and Z-score of both districts, was compared and scored as follows: same results in both districts = concordance; normal/osteopenia and osteopenia/osteoporosis = grade 1 discordance; normal/osteoporosis = grade 2 discordance.

Results: Analysis showed 215 cases of concordance (54%), 159 grade 1 discordance (40%), and 23 grade 2 discordance (6%). Grade 1 discordances were 23 normal lumbar spine/osteopenic hip (14%), 56 osteopenic lumbar spine/normal hip (35%), 12 osteopenic lumbar spine/osteoporotic hip (8%), 68 osteoporotic lumbar spine/osteopenic hip (43%). Grade 2 discordances were all osteoporotic lumbar spine/normal hip. In all groups, no significant difference for age, menopausal age, weight, and height was observed.

Conclusions: About 46% of DEXA of lumbar spine and hip were discordant. In our series, grade 2 discordance (all osteoporotic lumbar spine/normal hip) suggest a lumbar spine selective involvement by the disease, confirmed by the prevalence (35%) of osteopenic lumbar spine/normal hip in grade 1 discordance. Bone mineral density loss affects the lumbar spine more often, and probably then spreads to other body regions.

B-254 10:57

Potential predictive factors of osteoporosis in young HIV-positive subjects

A. Fausto, M. Bongiovanni, L. Menicagli, P. Cicconi, F. Sardanelli; Milan/IT

Purpose: To evaluate vertebral and hip demineralization with dual-energy X-ray absorptiometry (DEXA) in naive and those treated with highly active antiretroviral therapy (HAART) human immunodeficiency virus (HIV) outpatients.

Materials and Methods: Thirty-one naive HIV patients (20 male, 11 female; age 39 ± 6 years) were age- and sex-matched with a group of HIV outpatients treated with HAART. In both groups, bone mineral density (BMD) was assessed with DEXA in both lumbar spine (L1-L4) and hip. Additional parameters: weight, smoking, risk factors for HIV (intravenous drugs abuse, homosexuality or heterosexuality), HCV sero-status, total treatment duration, CD4 counts, HIV-RNA serum levels, fasting metabolic parameters and biochemical markers of bone metabolism. A Cox multivariable model was used.

Results: Thirty-one patients showed osteopenia and osteoporosis; 20 were on HAART and 11 naive (RR: 1.37, 95% CI: 1.12-2.15, $p = 0.09$). Mean CD4 count and HIV-RNA levels were 471 ± 127 cell/mm 3 and 4.28 ± 2.33 Log10 copies/ml respectively. Osteopenia and osteoporosis affected 22 men (6 naive) and 9 women (5 naive) (RR: 2.70, 95% CI: 0.84-8.68, $p = 0.09$), low weight patients (RR: 0.96, 95% CI: 0.91-1.00, $p = 0.06$ for each kilos more); moreover, the probability of bone demineralization increased with the duration of treatment (RR: 1.02, 95% CI: 1.01-1.03, $p < 0.01$ for each month of treatment more). No significant difference was observed for other parameters. Biochemical markers of bone metabolism were in the normal range for all patients.

Conclusions: Careful surveillance of BMD should be given to HIV infected subjects treated with HAART, particularly if they are women, of low weight, and on long-term treatment.

B-255 11:06

The influence of posterior instrumentation on adjacent and transfixated facet joints in patients with thoracolumbar spinal injuries: A morphological in vivo study using computed tomography osteoabsorptiometry (CT-OAM)

S. Wagner¹, M. Müller-Gerbl¹, A. Weckbach²; ¹Munich/DE, ²Würzburg/DE

Purpose: To examine the influence of posterior instrumentation on content and distribution of subchondral mineralization as a correlate of a long-term load acting on adjacent and transfixated facets.

Materials and Methods: 23 patients with thoraco-lumbar fractures had CTs and received posterior fixation. Patients were divided into group A (second CT on an average of 7.3 days) and group B (second CT on an average of 17 months after implant removal). CT-OAM was performed. Facet joints were separated on each CT-slice and 3D-reconstructed. The subchondral bone plate in each slice was isolated and reconstructed. In the density image summarized HU were represented

Scientific Sessions

by false colors. Finally, the density images were projected onto the 3D images. The resulting pictures were used to evaluate intra-individual changes in mineralization of paired facets joints by visual and quantitative analysis.

Results: There were significant differences between groups A and B with an overall mineralization decrease in group A and an increase in group B. In group A no significant differences between adjacent and transfixated facets were found, in group B the suprarectal joints showed a significantly higher mineralization increase than the transfixated joints.

Conclusion: Decrease in subchondral mineralization indicates reduced load upon the facets. This finding in patients with early follow-up seems to be caused by reduced activity until implant removal. In patients with longer follow-up intervals higher loads are shown which might be caused by unphysiological long-term stress induced by stabilization. Whether these changes lead to spondylarthrosis has to be the subject of further studies.

B-256 11:15

3D structure analysis based on the scaling index method in relationship to DXA in postmenopausal women with osteoporotic spine fractures

D. Mueller¹, R. Monetti², S. Majumdar³, H. Boehm¹, C. Raeth², E.J. Rummel¹, T.M. Link³; ¹Munich/DE, ²Garching/DE, ³San Francisco, CA/US

Purpose: The scaling index method (SIM) is a non-linear technique to extract texture measures for the quantitative characterisation of trabecular bone structure. This new method, which is demonstrated to improve the diagnostic performance in differentiating postmenopausal women with and without osteoporotic spine fractures, was applied to high resolution magnetic resonance (HR-MR) images of the distal radius. The purpose of this study was to investigate the relationship between the SIM and dual energy X-ray absorptiometry (DXA) at different sides of the body of postmenopausal women with osteoporotic spine fractures.

Methods and Materials: Axial HR-MR images of the distal radius were obtained at 1.5 T in 58 women with osteoporotic spine fractures. A 3D-GE sequence was used with a voxel size of 500x195x195 µm³. After segmentation and normalization, trabecular structure analysis was performed using algorithms based on our new local 3D SIM. In addition BMD measurements of the distal radius, spine and proximal femur using dual energy X-ray absorptiometry (DXA) were obtained in all patients.

Results: Linear regression was applied to describe the relationship between the SIM and BMD using DXA at different sides of the body. However, there was no correlation found for any of the BMD values versus the 3D structure measure based on the local scaling index method.

Conclusion: The results of this study suggest that our recently developed algorithm based on a local 3D SIM determines different entities of trabecular bone that are important for the prediction of individual fracture risk and are not reflected by BMD.

B-257 11:24

Multislice-CT-derived trabecular bone structure of the proximal femur.

A comparison with BMD in the assessment of osteoporosis

J.S. Bauer¹, S. Kohlmann², D. Mueller², F. Eckstein³, E.-M. Lochmueller², E.J. Rummel², T.M. Link¹; ¹San Francisco, CA/US, ²Munich/DE, ³Salzburg/AT

Purpose: With the development of Multislice Spiral Computed Tomography (MSCT) the achievable spatial resolution for imaging of trabecular bone at central skeletal sites has increased significantly. The goal of this in-vitro study was to investigate, whether structure parameters measured with MSCT at the proximal femur were able to improve the prediction of osteoporotic vertebral fractures compared to bone mineral density (BMD) as a standard parameter.

Materials and Methods: Ninety-five left femur specimens were harvested from formalin-fixed human cadavers (mean-age 80 ± 10 years). BMD was determined using Dual X-ray Absorptiometry (DXA). Structure parameters were calculated in MSCT-derived images of the proximal femur obtained with three different high resolution reconstruction algorithms (kernels). Additionally, the fracture status of the spine was determined in lateral radiographs of the spine. Receiver-operator-characteristics (ROC)-analysis was performed to determine the diagnostic performance of BMD and structure parameters.

Results: DXA and structure parameters both showed significant differences ($p < 0.01$) between the group of donors with and without fractures. With ROC-analysis AZ-values of up to 0.70 and 0.73 were determined for BMD and structure measures, respectively. The highest AZ-values were found in the trochanteric region with both modalities. No significant differences were found between the different kernels as well as between structure and BMD measurements ($p > 0.05$).

Conclusion: Structure measurements obtained from MSCT images of the proximal femur can be used to separate individuals with and without osteoporotic spine

fractures. However, with the settings used, DXA still remains the preferable method to assess osteoporosis due to better standardization and lower radiation exposure.

B-258 11:33

High-resolution MR imaging of the trabecular bone structure at 3 T:

Comparison between 1.5 T and 3 T

C.M. Phan¹, R. Krug¹, F. Eckstein², D.C. Newitt¹, S. Majumdar¹, T.M. Link¹; ¹San Francisco, CA/US, ²Munich/DE

Purpose: High-resolution magnetic resonance imaging (MRI) is a promising technique to depict trabecular bone (Tb) architecture. However, one drawback is the limited spatial resolution and SNR, which can be improved, in a clinical setting with the advent of 3 T MRI. The purpose of this study was to compare Tb structure parameters obtained from human calcaneus at 1.5 T and at 3 T, and to correlate these measurements with bone mineral density (BMD) data.

Methods: Thirty calcaneus specimens were imaged at 1.5 T and 3 T with a Gradient Echo (SPGR) sequence, using identical parameters (TR/TE/flip angle/bandwidth= 19 ms/4.6 ms/20°/12.5 kHz). Spatial resolution (slice thickness/field of view/matrix= 0.5 mm/80x100 mm/512x384 pixels) was identical at 1.5 T and 3 T. After spatially co-registering images obtained at the two field strengths, structural parameters and SNR in corresponding sections were compared and correlated with BMD measurements.

Results: Qualitative analysis showed a better depiction of the trabecular structure at 3 T than at 1.5 T. Quantitative analysis demonstrated significantly ($p < 0.01$) higher values for apparent trabecular number (1.84 mm⁻¹ vs. 1.538 mm⁻¹), trabecular thickness (0.225 mm vs. 0.186 mm) and bone volume fraction (0.416 vs. 0.287) in the 3 T images. Apparent bone volume fraction at 3 T showed higher correlation with BMD than at 1.5 T ($r = 0.758$ vs. $r = 0.740$). SNR at 3 T was 23% higher than at 1.5 T.

Conclusion: These preliminary results show that consistent high quality MR images of calcaneus can be obtained at 3 T using a sequence similar to that used at 1.5 T. Imaging at 3 T may substantially improve the depiction of trabecular bone micro-architecture though susceptibility artifacts also increase.

B-259 11:42

Variants of the superior labrum and labro-bicipital complex: A comparative study in shoulder specimens using MR arthrography, multi-slice CT arthrography, and anatomic dissection

S. Waldt¹, K. Woertler, S. Metz, E.J. Rummel; Munich/DE

Purpose: To assess the anatomic variability of the superior labrum and to compare the value of MR arthrography and multi-slice CT arthrography in the diagnosis of variants of the labro-bicipital complex.

Material and Methods: 55 human shoulder specimens were examined with the use of MR arthrography and multi-slice CT arthrography prior to joint exploration and macroscopic inspection of the labrum and labro-bicipital complex. Two radiologists evaluated MR and CT arthrograms and the results were compared with macroscopic assessments.

Results: Anatomic dissection of all shoulder specimens revealed a sublabral recess in 39/52 (75%) of cases. The attachment of the superior labrum was categorized as type 1 in 12 (23%) cases, as type 2 in 9 (17%) cases, as type 3 in 12 (23%) cases, and as type 4 in 18 (35%) cases. One lesion was classified as a SLAP type 3 lesion. On MR arthrography and CT arthrography the attachment of the superior labrum at the glenoid was categorized in concordance with macroscopic assessments in 83% and 86% of cases, respectively.

Conclusion: The attachment of the superior glenoid labrum shows great variability. Thus, exact depiction of variants is essential in order to avoid the false positive diagnosis of a superior labral tear (SLAP lesion). MR arthrography and multi-slice CT arthrography both were highly effective in the detection and classification of sublabral recesses.

B-260 11:51

Evaluation of a method for digital definition of bone shapes

P. Peloschek¹, G. Langs², M. Urschler², J. Sailer¹, M. Uffmann¹, T. Schlager¹, F. Kainberger¹, H. Bischof²; ¹Vienna/AT, ²Graz/AT

Purpose: Recent developments in digital radiography raise interest in morphometric analysis as generated data can be used for reproducible and automated quantitative analysis of shape deviations as erosions, osteophytes or fractures. Aim of this study is to evaluate the accuracy of a method allowing almost user independent definition of bone shapes.

Material and Methods: The shape (bone contour) of 10 fifth metacarpal bones (MC) was defined by three radiologists for an estimation of inter- and intra-user

Scientific Sessions

agreement. The time and number of clicks needed per bone was recorded. The annotations of different radiologists were compared by the area between two curves to quantify the inter-user error. On a set of 256 landmarks lying on the bone contour the regional error distribution was analyzed.

Results: The digital definition of a MC shape takes 2-4 (avg. 3.2) minutes per bone, 4-6 (avg. 4, 3) clicks are needed. An average of 92.48% of the bone contour is identical on the manual segmentation of all 3 readers. The mean difference over all landmarks is 0.03 mm. Taking only regions into account where differences occur the mean difference is 0.34 mm. Inter-user differences occur mainly in regions where more control points have to be set manually.

Conclusion: A procedure for digital definition of bone shapes with excellent inter- and intra-user agreement is presented. Future applications include morphometric analysis and training of shapes for advanced computer vision algorithms. The high accuracy of this procedure indicates that consensus reading is not recommendatory in every anatomical region.

10:30 - 12:00

Room E2

Breast

SS 602

MR mammography (1)

Moderators:

J. Kramer; Linz/AT

I. Leconte; Brussels/BE

B-261 10:30

Differential diagnosis of up to 10 mm sized breast lesions using morphologic and dynamic features of MR-mammography

M. Dietzel, A. Malich, D.R. Fischer, C. Marx, C. Deicke, C. Reuchsel, F. Taher, W.A. Kaiser; Jena/DE

Purpose: To evaluate the MR-Mammographical differences of dynamic and morphologic patterns in small malignant vs benign lesions of ≤ 10 mm.

Methods and Materials: All histologically verified lesions ≤ 10 mm having had a MR-Mammography (1/2002-3/2004; n = 118; 39 malignant, 79 benign) were retrospectively evaluated by two experienced radiologists in consensus according to standard protocols and study design (2D-FFE sequences, 0.1 mmol/kg bw Gd-DTPA, T2-TSE). The prevalence of the following signs statistically was analyzed (Chi-Square-testing): Dynamic signs - fast initial wash-in (D1), wash out (D2), plateau (D3), fast initial continued signal intensity increase (D4), blooming (D5), segmental enhancement (lesion's surrounding; D6), homogeneity of contrast uptake (D7). Morphologic signs (T1) - hook-sign (M1), root-sign (M2), adjacent vessels (M3), skin thickening (M4), nipple line-sign (M5), inhomogeneity of lesions composition (M6), lesion's shape (round/lobular/linear M7), regular margins (M8), septations (M9). Morphologic signs (T2) - necrosis (M10); perifocal (M11), diffuse edema (M12); hypointensity of vital tumor parts (M13).

Results: Prevalence malignant/benign were: D1s = 49%/34% (n.s.); D2s = 46%/24% ($p = 0.02$); D3s = 31%/36% (n.s.); D4s = 23%/40% (n.s.); D5s = 36%/10% ($p = 0.001$); D6s = 18%/4% ($p = 0.015$); D7s = 36%/57% ($p = 0.03$); M1s = 8%/3% (n.s.); M2s = 69%/19% ($p = 0.001$); M3s = 26%/4% ($p = 0.001$); M4s = 10%/1% ($p = 0.04$); M5s = 3%/4% (n.s.); M6s = 77%/89% (n.s.); M7s = 67%/89% (0.02); M8s = 8%/41% ($p = 0.001$); M9s = 5%/8% (n.s.); M10 = 0%/1% (n.s.); M11 = 15%/3% ($p = 0.015$.); M12 = 3%/5% (n.s.); M13 = 8%/25% ($p = 0.02$).

Conclusion: Whereas there is no significant difference regarding fast initial wash-in, plateau, septations and necrosis, wash out blooming, homogeneity of contrast uptake, root-sign, hypointensity of vital tumor parts, lesion's shape and margins are vital in assessment of small breast lesions.

B-262 10:39

Ductal carcinoma in situ: MR mammographic appearance and pathological correlation

S. Ganau, X. Andreu, E. Sáez, L. Tortajada, A. Massuet, M. Sentís; Sabadell/ES

Purpose: To assess the value of contrast enhancement MR-mammographic (MRM) findings in Ductal Carcinoma in Situ (DCIS).

Methods and Materials: One hundred and twenty-one patients with pure DCIS without micro-infiltration or association to another infiltrating carcinoma (n = 126), selected from the pathology registry, were elected for the present study. MRM was performed on a 1.0 T unit, using T2-weighted SE sequences and dynamic T1-weighted FLASH-3D sequences before and after 0.16 mmol/Kg of Gd-DTPA iv. Normalized signal intensity enhancement, wash-out, speed of enhancement

and morphology was analyzed for all cases. Findings in MRM were compared to histologic and immunohistochemical results.

Results: In 117 lesions enhancement was found (92.86%). In all cases enhancement could be classified as a pathological, despite different curve morphologies. High grade DCIS showed significantly higher enhancement values than lower and intermediate grade, and a more characteristic signal intensity curve. Non-enhancing lesions were predominantly scored 1 point in Van Nuys size evaluation. Significant correlation was found between size in MRM and pathologic size.

Conclusion: MRM is able to visualize the extent of DCIS. Correlation between high-grade DCIS and signal intensity values are found.

B-263 10:48

Correlation of dynamic and morphologic patterns of pure DCIS cases in MR-mammography

M. Facius, A. Malich, S. Wurdinger, H. Neubauer, C. Marx, W.A. Kaiser; Jena/DE

Purpose: To describe characteristic kinetic and morphological patterns of pure DCIS on dynamic MRM.

Methods and Materials: In 74 patients having had a MRM between 1995 to 2001 histopathology revealed a pure DCIS. All patients were performed on a 1.5 T unit (Gyroscan S15 ACS II, Philips) using the same protocol: T1w coronal, TSE prior/post Gd-DTPA (0.1 mmol/kg bw), a dynamic 2D FFE, T2w TSE. Two observers evaluated the features in consensus. Enhancement was: C1 = similar to glandular tissue, C2 = slow-continuous, C3 = strong initial-slowly further, C4 = strong initial-plateau, C5 = strong initial-wash out. Morphological pattern included: M0 = no pattern, M1 = linear/ductal, M2 = segmental/reticular, M3=segmental/homogeneous, M4 = circumscribed.

Results: Grading distribution was as follows: 30/74 (40.5%;G1); 19/74 (25.7%;G2), 18/74 (25.7%;G3), 7/74 (9.5%;no available grading). Dynamic pattern were observed as: C1: 7/74 (9.5%); C2 14/74 (18.9%); C3 15/74 (20.3%); C4: 15/74 (20.3%) and C5: 23/74 (31.1%). Morphological pattern were described as: M0: 8/74 (10.8%); M1: 3/74 (4.1%); M2: 41/74 (55.4%); M3: 9/74 (12.2%); M4: 13/74 (17.6%). Whereas all G3 cases had a morphological pattern in MRM, only 23/30 G1 cases (76.7%) were in any extent visible. 17/18 G3 cases (94.4%) were characterized by M2-4 morphology. 10/18 G3-cases (55.6%) and 11/30 G1-cases (36.7%) were suspicious due to C4 or C5. 6/18 G3-cases (33.3%) and 11/30 G1-cases (36.7%) were characterized by C1 or 2.

Conclusion: There are typical morphological (M2-4) as well as dynamic signs (C4-5), which are especially helpful in the detection of the clinically most relevant G3 cases.

B-264 10:57

What a sensitivity of mammography and dynamic MR for in situ breast cancers if we use the whole breast as a pathologic gold standard? Results from a multicenter trial

F. Sardanelli¹, A. Fausto¹, P. Panizza¹, G.M. Giuseppetti², V. Lattanzio³, A. Del Maschio¹; ¹Milan/IT, ²Ancona/IT, ³Bari/IT

Purpose: To compare mammography and MR in detecting in situ breast cancers (ISBCs).

Methods and Materials: Ninety patients candidate to monolateral (n = 81) or bilateral (n = 9) mastectomy underwent mammography and MR (coronal 3D gradient-echo; 3 mm thickness or less; gadoteridol, Bracco, 0.1 mmol/kg). Pathology: 5 mm slices covering the whole breast. Off-site reading aware of the entry criterion (planned mastectomy).

Results: Out of 99 breasts, pathology revealed 30 ISBCs: Ductal (n = 26), lobular (n = 3), and mixed (n = 1). Diameter at pathology: less than 5 mm (n = 5), between 5 and less than 10 mm (n = 7), between 10 and less than 20 mm (n = 3), greater than 20 mm (n = 2), not assessed (n = 13). Sensitivity was 37% (11/30) for mammography and 40% (12/30) for MR (not significant, McNemar). Mammography recognized 13 lesions, but two of them (opacities) were diagnosed as benign, the remaining 11 as malignant: Opacity (n = 6); opacity and microcalcifications (n = 2); only microcalcifications (n = 2); architectural distortion (n = 1). MR recognized 12 lesions, all as malignant. Mammography and MR were agreeing true positive (TP) in 9 cases (pathological diameter, 20.0 ± 12.9 mm) and agreeing false negative (FN) in 16 (3.5 ± 2.1 mm, $p = 0.017$, Mann-Whitney), disagreeing TP mammography and FN MR in 2, FN mammography and TP MR in 3. Thus, 37% of ISBCs were mammography-detected and only 10% (3/30) mammography-undetected and MR-detected; 40% were MR-detected and only 7% (2/30) MR-undetected and mammography-detected. Only 47% of ISBCs were mammography- or MR-detected, 53% remaining undetected.

Conclusion: If we use the whole breast as a gold standard, both mammography and MR show low sensitivity for ISBCs.

Scientific Sessions

B-265 11:06

Mammary parenchymal distortions with benign characteristics: Diagnostic accuracy of magnetic resonance

L. Carra, S. Attanasio, F. Crinò, A. Giampietro, F. Bosurgi, A. Carrieri; Novara/IT

Purpose: The aim of this study was to evaluate the diagnostic accuracy of Magnetic Resonance (MR) in patients with a mammographic parenchymal distortion with a radiotransparent core.

Material and Methods: 32 consecutive asymptomatic patients (age range 34-62 years) with parenchymal distortion with a radiotransparent core at the mammographic examination were studied. All patients underwent mammography (craniocaudal and lateral oblique projections with targeted enlargements when necessary), MR and biopsic exams (gold standard). A 1.5 T superconductive magnet with dedicated breast coil was used. The MR images were examined jointly by two experienced radiologists blinded to mammographic results. A multiple choice questionnaire was completed for each patient and the following MR parameters were evaluated: Intensity/time curve (type 1 increasement of 10%, type 2 from 11% to 50%, type 3 over 51%) and vascular pattern.

Results: 10 (31%) out of 32 lesions resulted histologically malignant. Overall sensitivity, specificity and diagnostic accuracy of MR were 100%, 64% and 75%, respectively. A statistically significant correlation between MR enhancement patterns and lesion malignancy was not observed. The absence of enhancement or a "type 2" pattern always corresponded to lesions with a benign characteristic, while "type 3" pattern was aspecific. The enhancement curves observed in patients with sclerosing adenosis were variable and non-specific.

Conclusion: Our results indicate that when a mammographic parenchymal distortion with radiotransparent core do not show any enhancement or the intensity/time curve is "type 1 or 2", the negative predictive value of MR allows the diagnosis of benign epithelial proliferation with a fibro-elastic core. A "type 3" enhancement curve means that mammo-guided surgery should be performed for a conclusive diagnosis.

B-266 11:15

Role of breast MR in the pre-surgical management of invasive breast carcinoma

C. Del Frate, L. Borghese, C. Cedolini, F. Puglisi, C. Zuiani, M. Bazzocchi; Udine/IT

Purpose: Evaluate role of breast-MR in pre-surgical management of invasive breast carcinoma.

Methods and Materials: Two radiologists and one surgeon retrospectively evaluated 121 patients (histological diagnosis of invasive breast carcinoma), who underwent pre-surgical breast-MR. Mammograms, sonograms and histology were re-examined to identify patients theoretically eligible to conservative surgery, from those eligible to radical surgery. Breast-MR and surgery effectively performed were then evaluated to identify cases for which MR determined a change in management. Gold standard was final pathology. Two evaluations, for single patient and for single lesions, were performed.

Results: Breast MR determined an overall change in management in 21/121 patients (26.4%). For patients eligible to conservative surgery, breast-MR determined a change in management in 32/87 (36.8%), 22 T1 (30.6%) and 10 T2 (66.7%), due to size increase in 8/32 cases (25%), to multifocality/multicentricity respectively in 5/32 (15.7%) and in 13/32 (40.7%), to size increase and multifocality/multicentricity in 4/32 (12.6%) cases, to contra-lateral and multicentric foci in 1/32 (3%), and to suspicious pectoral muscle infiltration in 1/32 (3%) case. In the evaluation for single patients RM resulted true positive in 25/32 (78.1%) cases, and false positive in 7/32 cases (21.9%). In the evaluation for single foci RM resulted true positive in 29/39 (74.4%) foci, while MR did not detect 6/35 foci identified in final pathology (17.1%).

Conclusions: Breast MR determines a significant change in management of patients affected by invasive breast carcinoma, particularly in patients eligible to conservative surgery after standard breast examination. Nevertheless, significant over-treatment may be expected.

B-267 11:24

Contrast-enhanced magnetic resonance mammography for screening of the contralateral breast in patients with diagnosed breast cancer

F. Pediconi, C. Catalano, F. Venditti, A. Roselli, S. Padula, R. Passariello; Rome/IT

Purpose: Role of contrast-enhanced Magnetic Resonance Mammography (CE-MRM) for evaluation of contralateral breast in patients with diagnosed breast cancer.

Methods and Materials: Fifty patients with proven unilateral breast cancer and negative contralateral breast at any examination, were evaluated. CE-MRM performed in the axial plane at 1.5 T using a bilateral surface breast coil. CE-MRM protocol comprised a T2-weighted STIR sequence and a dynamic 3D Flash T1-weighted sequence acquired before and at 2, 4, 6, 8 and 10 min after the administration of Gd-BOPTA at 0.1 mmol/Kg. Mammographic parenchymal density evaluated according to the Breast Imaging Reporting and Data System lexicon as class 1 (fatty) to 4 (dense). Level of suspicion was reported on a scale of 0 to 5 according to the BI-RADS classification. Results were compared with histological findings.

Results: 14 of 50 patients (28%) had contralateral lesions identified on CE-MRM. 4 of 14 patients were classified as BI-RADS 4 and underwent lesion biopsy, while 10 patients were classified as BI-RADS 5, and underwent surgery. At histology, 11 lesions were found to be malignant (5 DCIS, 2 LCIS, 3 infiltrating ductal carcinomas and one invasive lobular carcinoma) and considered to be true positive lesions. Conversely 3 lesions were fibroadenomas and were considered to be false positive lesions. No false negative lesions were detected on CE-MRM and none of the patients with fibroadenomas were classified as BI-RADS 5.

Conclusion: Our results demonstrated very good accuracy of CE-MRM for the detection of synchronous contralateral cancer in patients with newly diagnosed breast cancer.

B-268 11:33

Role of breast MR imaging in determining breast as source of unknown metastatic axillary lymphadenopathy

A. Athanasiou, C. Balleguier, C. Dromain, S. Delaloge, R. Sigal; Villejuif/FR

Purpose: To evaluate the role of breast MR imaging in the detection and diagnosis of primary, occult breast tumours in women presenting with isolated axillary lymphadenopathy. Impact of MR imaging in treatment planning.

Methods and Materials: Between 1999 and 2004, 32 women with malignant axillary lymphadenopathy, negative mammography and physical examination underwent a breast MR imaging. Lymph node biopsy revealed in all cases an adenocarcinoma, with hormonal profile indicating a breast tumour. Other imaging and laboratory investigations were negative. Results were compared to surgery and pathology.

Results: In 36.6% (n = 11), breast MR imaging was negative and mastectomy was performed, followed by chemotherapy and radiotherapy. In 63.4% (n = 21) cases, MR imaging detected a suspicious lesion. A focused US examination depicted a corresponding abnormality in 19% (n = 7), confirmed by biopsy. For these patients, lumpectomy followed by chemotherapy and/or radiotherapy was performed. US was normal in 14 patients: A large quadrantectomy was performed in 13 cases and a CT-guided wire localisation lumpectomy in one case. Pathology revealed 18 IDC and 3 ILC. Mean tumour size was 7 mm (4-12). In all mastectomy cases, no primary tumour was found in the specimen.

Conclusion: Breast MR imaging can be very sensitive for the detection and characterization of occult primary breast cancers in patients with isolated axillary lymphadenopathy. In these patients, MR imaging has also a potential role for staging, guiding a focused US examination and allowing a more conservative surgical approach.

B-269 11:42

Feasibility of second look sonography in clarification of incidental enhancing lesions found on preoperative MR imaging for breast cancer

M. Bernathova, G. Bodner, M. Dünser; Innsbruck/AT

Purpose: Incidental enhancing lesions that have no mammographic or palpable correlate, cause potential problems in preoperative breast MR in breast cancer. Post MR imaging second look high resolution sonography directed toward the site of the incidental lesion is introduced as alternative method to MR-guided biopsies.

Methods and Materials: From August 2003 to August 2004, 162 patient (median age 57; age range 33-84) were referred to MR imaging for preoperative staging of breast cancer. In 14 patients, the MR imaging was inconclusive with finding of an additional suspect enhancing lesion, distant from the primary lesion. These patients underwent consecutive high resolution sonography directed toward the site of the incidental finding. The correlation between two imaging modalities was done. The patients with multicentric and multifocal disease diagnosed in mammography and first look sonography were excluded from the study.

Results: In 14 (8.6%) of 162 patients, preoperative MR imaging revealed 20 new suspect foci. In 12 patients a second look sonography found a corresponding lesion. In 3 patients the sonographic guided biopsy and in 2 patients the sonographic guided wire localisation, followed by excisional biopsy disclosed a

Scientific Sessions

malignant lesion. On the basis of second look sonographic findings, a multicentric breast cancer was found in 5 (35%) of 14 patients. The clinical management changed: In 1 patient a wider excision and in 4 patients mastectomy was performed.

Conclusion: Second look direct sonography is a feasible method to clear the incidental finding in preoperative breast MR imaging, if MR-guided biopsy is not available. A skillful operator is indispensable.

B-270 11:51

Value of dynamic breast MR using an open 0.2 T magnet and Gd-BOPTA as a contrast agent: Preliminary results

M. Calabrese¹, L. Bacigalupo¹, A. Fausto², F. Sardanelli²; ¹Genoa/IT, ²Milan/IT

Purpose: To test breast MR using a low field magnet and a high T1-relaxivity contrast agent.

Methods and Materials: Fifteen patients (24-82 yrs, median 43) underwent breast MR using a 0.2 T open permanent magnet (Open, Siemens) and the body coil, in prone ($n = 2$) or supine position ($n = 13$). A coronal ($n = 7$) or axial ($n = 8$) 3D FLASH sequence was used (TR/TE = 23/10 ms, FA 30°; thickness 3 mm; pixel 1.8x1.8 mm) with 0.1 mmol/kg of Gd-BOPTA (MultiHance, Bracco) flushed by 20 ml of saline solution (2 ml/sec). All patients had ultrasound examination with BI-RADS score 5 ($n = 9$), 3 ($n = 1$), or 2 ($n = 5$); 12 patients had mammography with BI-RADS score 5 ($n = 8$), 4 ($n = 1$), or 2 ($n = 3$). Ten patients were operated; 5 MR negative cases had a 1-year or greater negative follow-up.

Results: Pathology: 4 IDCs (mean diameter 22.5 mm, range 15-30 mm); 5 ILCs (33 mm, 10-55 mm); one fibroadenoma (45 mm). At MR imaging, 4/4 IDCs and 3/5 ILCs presented suspicious morphologic and dynamic features and were classified as BI-RADS 5; one ILC presented benign morphology but inhomogeneous enhancement and strong wash-in with wash-out (BI-RADS 4); one ILC presented suspicious morphology, inhomogeneous enhancement and moderate wash-in with plateau (BI-RADS 4). The fibroadenoma presented benign morphology, homogenous enhancement and moderate wash-in with continuous increase (BIRADS 1). No MR false positive or negative case was found in this preliminary series.

Conclusions: Gd-BOPTA allows a reliable detection and characterization of breast tumors at an open magnetic field as low as 0.2 T.

10:30 - 12:00

Room G

Head and Neck

SS 608

Acoustic pathway and base of the skull

Moderators:

E.J. Adam; London/UK

D. Cuzino; Bucharest/RO

B-271 10:30

Loudness dependency of the primary auditory cortex: Simultaneous fMR imaging and EEG recording

L. Jäger, C. Mulert, S. Propp, S. Karch, M.F. Reiser; Munich/DE

Purpose: The aim of the study was to compare the loudness dependency of the primary auditory cortex by means of fMR imaging and EEG to study the central serotonergic system.

Methods and Materials: 210 pure tones (1000 Hz, 200 ms duration) were presented to 14 healthy subjects at sound pressure levels of 60, 80 and 100 dB. The acoustic stimulation was performed with simultaneous EEG and fMR imaging recording and with EEG recording outside the MR scanner room. fMR imaging was performed using a 1.5 T MR system and a BOLD-EPI sequence. A multiple regression analysis and a Bonferroni correction was done with the Brain Voyager. 61-channel EEG was recorded with an EEG amplifier designed for the special requirements of the MR environment. Current source density analysis was performed with LORETA software.

Results: For all subjects the N1-amplitude was clearly identified in the EEG recordings performed simultaneously with fMR imaging and outside of the MR scanner room. The amplitude was significantly ($p < 0.05$) larger outside. There was a strong correlation ($p < 0.001$) between the amplitude increase of the N1-potentials and for the LORETA source density of the EEG recorded simultaneously with fMR imaging and the activated fMR imaging volume in Heschl gyrus. The activated fMR imaging volume, the N1-potential and the LORETA source density correlated with the sound pressure level.

Conclusion: The presented results indicate that simultaneous acquisition of event-

related fMR imaging and EEG is useful to study the serotonergic system in the primary auditory cortex.

B-272 10:39

Aging of the acoustic pathway: A DTI study

L. Jäger, F. Hemminger, J. Lutz, R. Stahl, O. Dietrich, M.J. Hempel, S.O. Schönberg, M.F. Reiser; Munich/DE

Purpose: The aim of the study was to evaluate aging of the acoustic pathway by the means of DTI.

Methods and Materials: 20 young healthy volunteers (mean age 28.5 years) and 15 elderly healthy volunteers (mean age 61.3 years) were examined using a 1.5 T MR System (Magnetom Sonata, Siemens) with a T1-weighted sequence (MPRAGE-Sequence, 1.1x1.1x1.1 mm) and an IPAT DTI EPI-sequence (TE 71 ms, TR 6000 ms, 36 slices, 1.8x1.8x3.6 mm spatial distribution). Ten subjects underwent two examinations, the second one two days later. Lateral lemniscus, inferior colliculus, medial geniculate body, auditory radiation, superficial temporal gyrus and transverse temporal gyrus were evaluated. The fractional anisotropy (FA) and the relative anisotropy (RA) were studied.

Results: There were no significant differences in FA and RA in the lateral lemniscus and medial geniculate body. However, FA and RA were reduced significantly ($p < 0.05$) in the inferior colliculus, the auditory radiation, the superficial temporal gyrus and the transverse temporal gyrus in the elderly subjects in comparison to the younger ones. There were no significant differences in anisotropy in the follow-up examinations.

Conclusion: Normal aging of the acoustic pathway is associated with a decline in anisotropy mainly in the cortical grey and white matter rather than in the subcortical regions. The normal aging process may be responsible for a reduced plasticity of the associated cortical regions and the involvement of the inferior colliculus in the pathogenesis of tinnitus. DTI results of the acoustic pathway are reproducible.

B-273 10:48

CT-MR fusion image guidance for navigated neurosurgery of temporal bone tumors

S.F. Nemec; Vienna/AT

Purpose: Presentation of CT and MR image data fusion for computer assisted navigated neurosurgery of tumors of the temporal bone.

Materials and Methods: 16 patients with temporal bone tumors underwent computed tomography (CT) and magnetic resonance imaging (MRI). CT was performed with a multi-detector CT (MDCT) using 4x 0.75 mm thick slices in high resolution bone window level setting in axial plane without inclination. MRI was performed in axial and coronal planes with T2-weighted turbo spin-echo sequences, unenhanced and contrast-enhanced T1-weighted spin-echo (SE) sequences, and coronal T1-weighted SE sequences with fat suppression and 3D T1-weighted gradient-echo (GE) contrast-enhanced sequences. The 3D T1-weighted GE sequence had a slice thickness of 1 mm in axial plane without inclination. Image data sets of CT and 3D T1-weighted GE sequences were merged on a workstation for interventional planning and intra-operative image guidance. MDCT and MR images were used to depict and to characterize lesions, the accuracy of the navigation unit and the intervention time were measured.

Results: Tumorous lesions of bone and soft tissue were excellently depicted and characterized by CT and MR images and image fusion. The images had a high diagnostic value and great impact on the surgical procedure as lesions could be differentiated into benign and malignant pathologies. The accuracy of the navigation unit was under 1 mm. The neuro-navigation reduced the surgical intervention time for 30% on average.

Conclusion: Computer assisted navigated surgery with CT-MR image data fusion helps the surgeon in planning and performing surgery and decreases intervention time.

B-274 10:57

Comparison of multislice CT (MSCT) cross-sectional source images with multiplanar 2D-, 3D- reconstructions and virtual endoscopy in the assessment of middle ear diseases

A. Trojanowska, E. Czekajska-Chehab, P. Trojanowski, W. Olszanski, W. Golabek, A. Drop; Lublin/PL

Purpose: Evaluation of cross-sectional images, multiplanar 2D- reformations, 3D- reconstructions and virtual endoscopy in the assessment of the middle ear in inflammatory diseases, trauma, otosclerosis and tumours. Comparison of each method and correlation with surgical findings.

Scientific Sessions

Material and Methods: Investigations were carried out in 150 patients with middle ear pathology. MSCT of the petrous bone was performed (GE Light Speed Ultra Advantage 8-row scanner). Additionally to cross-sectional axial scans, frontal and sagittal images were created using MPR reconstructions. 3D volume rendering (VR) and virtual endoscopy (VE) images were generated. Value of axial scans information, 2D, 3D reconstructions and virtual endoscopic views was assessed in comparison to intra-operative findings.

Results: MPR reconstructions achieved higher scores for diagnostic value ($p < 0.001$, t-test), but not for the image quality with regard to both 2D and 3D reconstructions in the assessment of skull base trauma, skull base tumors and in cases of chronic otitis media. Axial images proved to be the best for direct interpretation in case of otosclerosis. In case of stapes prosthesis assessment the most useful were 3D reconstructions. 3D- and virtual reconstructions indicated an improved representation and spatial orientation of the ossicular chain, therefore were a method of choice in the assessment of stapes prosthesis. These reconstructions also provided additional important information in some tumors regards invasion of the skull base or vascularity.

Conclusions: MSCT virtual endoscopy proved to be useful in evaluating post-traumatic and post-operative changes. In the majority of diseases axial images and MPR reformations were most useful.

B-275 11:06 ♀

CT diagnosis of otosclerosis: A review of 31 cases

E. Neri, S. Berrettini, F. Ravecca, C. Bartolozzi; Pisa/IT

Purpose: To review the CT criteria for the diagnosis of otosclerosis and to evaluate the sensitivity of high resolution spiral CT in the detection of signs of fenestral and cochlear otosclerosis.

Methods and Materials: The spiral CT data sets (13 single-row and 18 multi-row CT) of the petrous bone of 31 patients (62 ears) with otosclerosis were reviewed. A thickening of the stapes (crus anterior or posterior, or involving the footplate), or a focus in the fissula antefenestrata were considered signs of fenestral otosclerosis; the focus in the fissula antefenestrata was also divided in otospongiotic or otosclerotic. The extension of bone demineralization in the perilabyrinthine region was classified as unifocal, multifocal and diffuse; the location was classified as anterior (peri-cochlear) and posterior (peri-vestibular). Other signs of otosclerosis were considered the obliteration of the round window and cochlear ossification.

Results: Signs of otosclerosis were found in 31/62 ears (sensitivity 50%). Perilabyrinthine foci of otosclerosis were found in 18 ears; anterior foci in 18 ears, posterior in 2 (but associated with anterior); these were single in 5, multiple in 3, and diffuse in 10 cases. Foci in the fissula antefenestrata were found in 28 ears. Obliteration of the round window was detected in 2 ears and cochlear ossification in 4.

Conclusions: Our study has shown a low sensitivity of CT in the detection of otosclerosis, but identifies for CT an important role in demonstrating the extension of the disease.

B-276 11:15

Flat-panel based volume-CT could overcome current limitations of CT in cochlea implant imaging

S.H. Bartling¹, T. Stoever¹, T. Rodt¹, R. Gupta², T. Lenarz¹, H. Becker¹;

¹Hannover/DE, ²Boston, MA/US

Purpose: Current imaging methods are challenged by cochlea implant imaging. The limited resolution and metal artifact behavior of current CT scanners make it impossible to assess single implant electrodes in relation to the cochlea - information highly desirable for advanced post-implantation evaluations. Due to its high resolution and excellent metal artifact behavior flat-panel based Volume-CT could overcome these limitations.

Materials and Methods: Two ex-vivo temporal bones were implanted and were scanned in a 4-slice CT (GE Lightspeed Qx/i) (MSCT) using a standard temporal bone protocol. Furthermore, a scan in an experimental gantry and flat-panel based Volume-CT (Siemens VCT) (VCT) was performed (250 μm^3 big voxels at Nyquist's limit). To acquire a ground truth, the ears were fine grinded. The data sets were compared regarding the information about the implant, the inner ear and their relationship.

Results: A rough assessment of the insertion depth was possible using both CT. No single electrodes were circumscribable in the MSCT, but they were in VCT. The surrounding cochlea was much less compromised by metal artifacts in VCT than in MSCT. Actually, the spiral osseous lamina was visible in some slices. The comparison with fine grinds confirmed the conclusions that were drawn from the VCT images regarding the implant position within the cochlea.

Conclusion: VCT has the potential to give exact measurements of electrode positions within the cochlea and its relationship to the spiral osseous lamina. Further experiments, need to show how scanning of whole skull base changes the image quality of VCT.

B-277 11:24

Delineation of temporal bone anatomy: A comparison between low-dose 64-slice CT and conventional 4-slice CT technique

J. Lutz¹, L. Jäger¹, M.J. Hempel¹, S. Srivastav², M.F. Reiser¹; ¹Munich/DE, ²New Orleans, LA/US

Purpose: The aim of the study was to evaluate the depiction of anatomical landmarks of the temporal bone using a 64-slice and a 4-slice computed tomography (CT).

Methods and Materials: In 100 patients HRCT of the temporal bone was performed; in 50 using a 64-slice CT (Sensation 64, Siemens) with low-dose technique (0.6 mm collimation, 120 kV, 140 mAs, 250 μSv) and in 50 using a 4-slice CT (Sensation 4, Siemens) with conventional technique (0.5 mm collimation, 120 kV, 180 mAs, 600 μSv). Axial images were acquired and reformatted coronal images (1 mm slice thickness) were calculated. Two radiologists performed the evaluation in consensus. The visibility of 30 anatomical landmarks was scored using a five-point quality rating scale. The Fisher exact test and the Mann-Whitney U test were performed to statistically evaluate the visibility of anatomical landmarks with both imaging techniques.

Results: In delineating anatomical landmarks on the primarily acquired axial images as well as on the reformatted coronal images there was no significant difference in image quality between the low-dose 64-slice CT technique and the conventional 4-slice CT technique. This was particularly true for the delineation of the ossicles, the tegmen tympani, the labyrinth, the oval window and the canal of the cochlear nerve, vestibular nerve and facial nerve.

Conclusion: The new scan geometry of the 64-slice CT scanner facilitates imaging of the temporal bone in a low-dose technique; a good image quality can be obtained and radiation exposure can be reduced by approximately 60%.

B-278 11:33

True-FISP for inner ear imaging: Delineation of anatomical structures and pathologies

G.A. Krombach, L. Pani, B. Jung, E. DiMartino, E. Spuentrup, R.W. Günther, A. Buecker; Aachen/DE

Purpose: To compare true-FISP images with standard T2-weighted turbo spin-echo (TSE) images for delineation of anatomical details and pathologies of the inner ear.

Materials and Methods: In 58 patients (mean age 50 years, range 1-73 years) true-FISP (TR/TE 9.8/4.2 ms, 80°, matrix 512 x 512, FOV 230 mm², imaging time 4.19 min) and TSE images (TR/TE 2000/500 ms, matrix 128x128, FOV 90 mm², imaging time 5.46 min) were obtained. Two radiologists evaluated visualization of anatomical structures and pathologies using a 4-point non-parametric scale. In addition SNR and CNR were calculated and compared.

Results: Small structures such as modiolus, osseous spiral laminal, facial, vestibulocochlear, cochlear, superior and inferior vestibular nerve were significantly better delineated on true-FISP images ($p < 0.001$). There was no difference for delineation of large structures with high signal intensity (vestibule, semicircular canals). Pathological findings were encountered in 28 cases. Delineation of pathologies did not differ between both types of images. CNR was higher for bone/brain on true-FISP images.

Conclusions: True-FISP can be used for imaging of the inner ear. Compared to TSE images more anatomical details can be delineated, due to differences in the point-spread function. Signal characteristics due to T2/T1 weighting of the true-FISP images contribute to better CNR between brain and bone. This may help in the assessment of pathologies.

B-279 11:42

CT and MR imaging of lesions involving the pterygopalatine fossa

D. Haba, C.C. Aldescu; Iasi/RO

Purpose: To present a wide spectrum of usual and unusual lesions involving the pterygopalatine fossa (PPF) and to evaluate the efficacy of CT and MR imaging in the assessment and management of these lesions.

Methods and Materials: The CT and MR imaging examinations of 41 patients, 22 females and 19 men, aged between 12 and 72 years, were retrospectively reviewed considering the site, bony walls, fatty contents and intracranial extension.

Results: The PPF was involved in 40 cases by lesions located in paranasal sinuses

Scientific Sessions

(squamous cell carcinoma n = 19, lymphoma n = 5, fibromyxoma n = 2, fibrosarcoma n = 2, adenoid cystic carcinoma n = 1), nasopharynx (squamous cell carcinoma n = 6, juvenile angiomyxoma n = 2), masticator space (lymphoma n = 2) and middle cranial fossa (meningioma n = 1). Only one lesion (pleomorphic adenoma) originated in the pterygopalatine fossa. The fatty content of the pterygopalatine fossa disappeared in all patients in association with enlargement of the PPF (n = 9), erosion of bony walls (n = 31) and hyperostosis (n = 1). MR imaging was superior to the CT in delineating the lesion involving the PPF with secondary intracranial extension.

Conclusion: The lesions involving the PPF are commonly depicted on CT and MR imaging. MR imaging seems to be better than CT for any residual or recurrent lesion involving the PPF.

B-280 11:51

Influence of different mAs-products on image quality in MSCT of the head and neck region

U. Baum, M. Lell, K. Anders, H. Greess, W.A. Bautz; Erlangen/DE

Purpose: To determine the influence of tube current-time products on image quality and noise in MSCT of the head and neck region.

Methods: 20 patients suffering from head and neck malignancies were examined by MSCT using a high resolution protocol (4 x 1 mm). Image reconstruction was performed by means of a dedicated reconstruction software (Syngo Explorer, VAMP GmbH, Germany) consisting of a standard reconstruction algorithm with additional adaptive filtering. Surplus image noise was added to existing raw data sets in order to simulate different effective mAs values, and raw data sets were reconstructed with a slice width of 3 mm at 160, 120, 80 and 40 mAs at three pre-defined anatomical positions. Image noise was measured in all reconstructions, and image quality was rated on a five-point scale.

Results: The coronal diameter varied from 100 to 181 mm in the neck region and 362 to 500 mm at the thoracic inlet. In order to reach sufficient image quality, 80, 40 and 160 mAs were required at the hypopharynx, larynx and the thoracic inlet, respectively. Taking into account the varying body diameter at the thoracic inlet, a dose reduction down to 120 mAs should be possible in slim patients with a coronal diameter of 410 mm and less at the thoracic inlet.

Conclusion: This study demonstrates the feasibility of considerable dose reduction in CT scans of the head and neck region. The collected data may provide a basis for mAs adjustments.

10:30 - 12:00

Room H

Interventional Radiology

SS 609a

Skeletal interventions

Moderators:

M. Pavia; Brescia/IT
O. Tervonen; Oulu/FI

B-281 10:30

Pre-procedural MR based decision of needle tip placement in vertebroplasty

C.W. Ryu, S.J. Kim, D.H. Lee, C.G. Choi, D.C. Suh; Seoul/KR

Purpose: To investigate the effectiveness of vertebroplasty according to the target of needle tip base on pre-procedural MR.

Materials and Methods: Retrospective reviews were conducted in 162 sites of 81 vertebral compression fracture (VCF) performed vertebroplasty. All cases were undergone pre-procedural MR. We classified the MR finding of VCF into three types: type1, VCF with fracture cleft near endplate; type2, VCF with fracture cleft around mid-body; type3, VCF without fracture cleft. The location of needle tip was identified on the X-ray radiography taken during the procedure and matched on the sagittal MR images. Location of needle tip was classified as follow: into cleft, abnormal marrow, borderline between abnormal and normal marrow, and normal marrow. On post-procedural X-ray radiography, result of vertebroplasty was assessed as good, if bone cement was filled over 70% of total body height combined with cleft and trabecular opacification (if fracture cleft is present), and assessed as incomplete, if bone cement was filled under 70% of total body height. VCF type and needle tip location was correlated with the result of vertebroplasty.

Results: In type1(48%) groups, when needle tip was placed into cleft, the result was significantly incomplete compared to other placement of needle tip ($p < 0.05$). In type2 groups (21%), and type3 groups (31%), the difference between each needle tip placement was not statistically significant.

Conclusion: According to presence or location of the fracture cleft and the

placement of needle tip, the result of vertebroplasty was varied. MR based decision of needle tip placement would be helpful for effective treatment of vertebroplasty.

B-282 10:39

Vertebroplasty in patients with osteoporosis-related osteonecrotic intravertebral clefts

M. Krauss, H. Hirschfelder, D. Losert, I. Bär; Nürnberg/DE

Purpose: To assess the results of vertebroplasty in patients with intravertebral clefts compared to patients with normal osteoporotic fractures.

Material and Methods: Between March 2002 and September 2004 we performed 140 vertebroplasties in 84 patients with osteoporotic fractures. Prior to intervention all patients underwent physical examination, conventional X-rays and MR imaging of the spine. Preoperative pain was classified using VAS-Scoring. All vertebroplasties were performed with a biplane angiography system using a monopolar approach. Conventional X-rays and VAS-Scoring were repeated before discharge and at regular follow-ups.

Results: 28 vertebrae showed intravertebral clefts, in some cases mobility of the fragments was visible under fluoroscopy. All clefts were filled with PMMA (average amount 3.2 ml) no matter where the needle tip was placed in the vertebra, showing a typical filling pattern. Due to prone position of the patient during vertebroplasty a significant reduction of kyphosis angle was achieved in some patients. Cement leakage occurred in 17.8% of clefts and 52.3% of regular osteoporotic fractures. No cement-dependant complications were observed. Average VAS-Score was 9.2 preoperatively, 4.5 before discharge and 3.5 at follow-ups showing no significant difference between both groups.

Conclusion: Patients with intravertebral clefts have a significantly lower risk of cement leakage during vertebroplasty. Clefts are easy to fill with bone cement, sometimes with a good reduction of kyphosis angle. Pain reduction is comparable to patients with normal osteoporotic fractures.

B-283 10:48

Percutaneous vertebroplasty: A multicenter Italian experience in over 1000 patients

G.C. Anselmetti¹, F. Baruzzi², G. Bonaldi³, P. Carpegiani⁴, L. Manfré⁵, M. Muto⁶, S. Vallone⁷, D. Regge¹; ¹Candiolo/IT, ²Varese/IT, ³Bergamo/IT, ⁴Pisa/IT, ⁵Catania/IT, ⁶Naples/IT, ⁷Imperia/IT

Purpose: To retrospectively evaluate the results and complications of percutaneous vertebroplasty performed in a large series of patients in seven different Italian centers.

Method and Materials: Since August 2000, 1118 patients underwent percutaneous vertebroplasty (PV) in 7 Italian Centers for a total of 2191 procedures. 826 (73.8%) patients had osteoporotic vertebral fracture, 259 (23.1%) had neoplastic disease, 27 (2.4%) suffered from symptomatic angioma and the remaining 6 (0.5%) had a recent traumatic fracture. A monolateral approach, under fluoroscopic (lower dorsal and lumbar levels) or combined CT-fluoroscopic guidance (cervical and upper dorsal levels), was mostly employed. All procedures were performed in local anesthesia.

Results: 1035/1118 (92.5%) patients had significant pain relief within 48 hours: 98% of cases with osteoporosis patients, 70% with cancer, 100% in the angioma and the recent traumatic fracture groups. 86 patients (7.6%) were retreated for a new fracture, 32 (2.8%) patients in the contiguous vertebra. No major neurological complications were reported. 12/1118 (1%) had asymptomatic cement pulmonary embolism while in 438 patients (39.1%) a venous and disk leakage was observed. In 6/1118 (0.5%) a subcutaneous haematoma was reported, and 10/1118 (0.8%) referred symptomatic radiculopathy successfully treated with steroid local injection.

Conclusions: This large series of patients confirms that Percutaneous Vertebroplasty is a safe procedure especially if combined CT-fluoroscopic guidance is employed for the upper spine. Percutaneous Vertebroplasty is effective in the treatment of backpain due to osteoporosis, angioma and traumatic vertebral fracture while the rate of pain relief is lower in patients suffering from neoplastic vertebral lesions.

B-284 10:57

New vertebroplastic procedures: Besides the vertebral body

L. Manfré¹, M. Bonetti², L. Tomarchio¹, C. Cristaudo¹; ¹Catania/IT, ²Brescia/IT

Objective: We investigate the use of vertebroplastic procedures in the treatment of sacral neoplastic and osteoporotic fracture, in case of neoplastic involvement of the vertebral pedicles, and in patients affected by severe spinal cord compression and paresis.

Method: From October 2001 to August 2004, 184 patients underwent vertebroplastic procedures in our department. In 5 patients, neoplastic involvement

Scientific Sessions

of the pedicle occurred, with destruction of the lateral wall of the spinal canal. 8 patients had sacral neoplastic involvement and one patient suffered from osteoporotic sacral fracture. Two patients had paraparesis related to severe collapse of the 7th thoracic vertebral body. Both pedicle and sacral involvement were cementified using a CT-guided & PMMA microinjection technique. The two patients affected by paraparesis underwent intraoperative vertebroplasty in the operating theatre.

Results: After vertebroplasty, all the patients with sacral and pedicle involvement had reconstruction of the pedicle and the sacral bone, maintaining regular neural foraminal shape. No foraminal PMMA leakage was observed. They became painless in 24 h. In patients undergone to combination of surgery & vertebroplasty, reduction of severe kyphosis and restorage of the spinal curve was obtained, with pain resolution and reduction of spinal cord compression.

Conclusion: Using a CT-guided vertebroplastic technique and PMMA micro-injection, vertebroplasty procedure can be performed in pedicle and sacral reconstruction. In combination with spinal surgery, vertebroplasty can be useful in restoring a regular shape in case of vertebral body collapse and spinal cord symptomatic compression.

B-285 11:06

Risk of secondary fractures after percutaneous vertebroplasty.

A retrospective analysis and a review of the literature

J. Hierholzer¹, H. Fuchs¹, K. Westphalen¹, G. Anselmetti², ¹Potsdam/DE, ²Candiolo/IT

Background: The potential risk of secondary fractures after vertebroplasty (VTP) is discussed in the literature. We report about our experience and review the pertinent literature.

Materials and Methods: Since 1999, VTP was performed on 414 vertebral bodies in 270 patients for severe back pain. In 229/270 pts. malignancy was excluded and osteoporosis identified as the cause of fracture and pain in 364 further treated vertebral bodies. Results were compared and added to those published in the literature.

Results: 27/229 pts. returned for 46 secondary vertebral body fractures. Time interval ranged from 7-400 days (mean 105 days). 21 symptomatic fractures were found adjacent to and 25 distant to previously treated levels. Together with our date, the literature offers data on 451 pts. treated, with 48 patient returning with 78 secondary fractures. 44/78 were adjacent and 34/78 distant to pre-treated levels. Baseline risk for new fractures after initial fractures ranges around 20% per year for untreated osteoporosis.

Conclusion: Although retrospective and un-controlled, our data and data published do not suggest an increased risk for secondary fractures after VTP for osteoporotic vertebral fractures.

B-286 11:15

Percutaneous kyphoplasty: Preliminary results with the SKy-Bone

Expander a new polymer device

G.C. Anselmetti¹, G. Bonaldi², M. Muto³, P. Carpegnani⁴, L. Manfrè⁵, D. Regge¹; ¹Candiolo/IT, ²Bergamo/IT, ³Naples/IT, ⁴Pisa/IT, ⁵Catania/IT

Purpose: To evaluate feasibility and effectiveness of kyphoplasty in old vertebral fractures by means of a new device: The SKy-Bone Expander.

Method and Materials: 20 percutaneous kyphoplasty were performed in 19 patients (17 female, 2 male - mean age 64 years) using the SKy-Bone Expander (Disc-O-Tech Medical Technologies Ltd, Herzliya, Israel), a new polymer device. All the patients had osteoporotic vertebral fractures aged more than 3 months (from 4 months to 8 years). All the procedures were performed in local anesthesia under fluoroscopic or combined CT and fluoroscopic guidance.

Results: In all patients percutaneous kyphoplasty with SKy-Bone Expander was feasible. Even if the procedure was performed with local anesthesia no pain have been reported during procedures. Mean vertebral height increase was 4.1 mm and mean difference between the anterior and the posterior vertebral wall height was 55% before and 78% after the procedure. In five cases a small cement leakage in the disk space was reported. No neurological injury were observed. All the patients referred complete back pain regression.

Conclusions: These preliminary results show that percutaneous kyphoplasty is also feasible in old vertebral fractures with the new polymer device SKy-Bone Expander and a reduction of kyphosis can be achieved. The procedure, performed with local anesthesia, was painless and well accepted by the patients. This new device, if compared with balloon kyphoplasty, seems to have the advantages of a pre-defined expanded configuration creating a defined void even in old vertebral fractures, a directional mechanical expansion, a safe and complete device retraction.

B-287 11:24

Intradiscal O2-O3 vs. corticosteroid injection in the treatment of sciatica

N. Limbucci, S. Carducci, C. Fiumara, M. Di Bartolomeo, C. Masciocchi, M. Gallucci; L'Aquila/IT

Purpose: To assess the clinical efficiency of O2-O3 periganglionic and intradiscal injection (chemiodiscolysis) vs periganglionic and intradiscal injection of corticosteroids in the management of acute pain following root compression from acute disk herniation.

Methods and Materials: 96 patients with sciatic nerve root compression due to disk herniation (level L3-S1) entered the study. 49 patients (group A) underwent intradiscal and periganglionic injection of 80 mg of Triamcinolone-acetonide and Ropivacaine 2%, 2-4 cc. 47 patients (group B) underwent intradiscal and periganglionic injection of 5-7 ml of O2-O3 (concentration 0.28 ig) and Ropivacaine 2%, 2-4 cc. Patients were assigned randomly to group A or B. All procedures were performed under CT guide (axial scans, 3 mm thickness), in prone position, with 22G spinal needle. We always performed clinical evaluation and administered pain questionnaire (McNaab) before treatment and after 7-14 days (mid time 11 days) and 6 months. Patients and clinicians who tested them before and after treatment were unaware about the kind of therapy performed.

Results: Group A: after 3 months remission of symptoms was registered in 35 patients (72%), after 6 months good results were registered in 23 (48%). Group B: after 3 months symptoms remission was registered in 36 (78%) of patients, while at 6 months in 34 (72%). Clinical controls correlate to data obtained by pain questionnaire.

Conclusion: O2-O3 periganglionic injection and chemiodiscolysis is most effective than periganglionic injection of corticosteroids in the treatment of acute lumbar pain and sciatica caused by acute disk herniation, resulting a valid alternative to other treatments.

B-288 11:33

Lumbar disk nucleolysis by oxygen-ozone injection: Midterm results in 244 patients

B. Oder, M. Loewe, G. Gruber, W. Ilias, W. Lang, S. Thurnher; Vienna/AT

Purpose: To assess the potential benefit of oxygen-ozone injection for disc nucleolysis in patients with chronic low back pain due to disk disease.

Materials and Methods: 710 patients were treated with an intradiscal (4 mL) and periganglionic (6 mL) injection of a oxygen-ozone mixture at an ozone concentration of 30 µg/mL, followed by a periganglionic injection of long lasting corticosteroid and anesthetic. All patients suffered from chronic low back pain and showed degenerative disorders of the lumbar spine visualized by MR imaging. Exclusion criteria was a motoric deficit. Patients were divided into 5 groups according to morphological changes: group 1 bulging disc, group 2 protruding disk, group 3 postoperative disk, group 4 osteochondrosis, group 5 various findings. Questionnaires regarding the Oswestry disability score (ODS) and a visual pain scale were sent to the patients 2 and 6 months after treatment, respectively.

Results: Questionairs of 244 patients could be evaluated for a 6 months follow-up: Improvement was stastically significant, especially in group 2, concerning the ODS before (mean value, 48.35%) and after treatment (mean value, 33.1% - Wilcoxon Test p < 0.0001). Improvement was also stastistically significant (p < 0.0001) comparing the visual pain scale before (mean value 85%) and 6 months after therapy (mean value 52%). 62% of the patients were generally content and 69% would accept the procedure again.

Conclusion: Disk nucleolysis by ozone injection is an effective minimal invasive treatment in patients with chronic low back pain with failing response to noninvasive means especially with MR imaging proven protruding disk disorder.

B-289 11:42

Percutaneous nucleoplasty in the treatment of lumbar pain

S. Masala, A. Ursone, R. Fiori, F. Massari, G. Simonetti; Rome/IT

Purpose: To assess the effectiveness of Percutaneous Nucleoplasty in the treatment of lumbar pain due to contained discal herniation.

Methods and Materials: Fifty Patients with positive Visual Analogue Scale (mean score: 7.5) and lumbar pain were selected for treatment. In all patients lumbar MR imaging revealed a contained discal herniation (8 pts: L2-L3; 15 pts: L3-L4; 27 pts: L4-L5). All patients were refractory to medical and rehabilitative therapy for more than three months. The main physical principle of this procedure is a bipolar radiofrequency energy emitted by an electrode-needle, with consequent volumetric reduction of the nucleus polposus and elastic return of the anulus fibrosus. The treatment is performed under fluoroscopic visualisation in the AP and LL projections.

Scientific Sessions

Results: Postprocedural evaluation confirmed reduction of the VAS (mean score: 3.5). MR imaging performed 6 and 12 months after the procedure demonstrated complete resolution of the treated discal pathology in all patients. No post-procedural complications or recurrences of the disease were observed.

Conclusion: In our experience Percutaneous Nucleoplasty demonstrated to be an effective and feasible technique. This minimally invasive procedure is ideal for treatment of patients with pain refractory to conservative medical therapy and contained discal herniation, not suitable for surgical treatment.

B-290 11:51

Percutaneous radiofrequency thermoablation with cool-tip probe of osteoid osteoma

E. Mazza, L. Sali, C. Vannini, D. Beccani, F. Toccafondi, M. Zini, M. Acquafresca; *Florence/IT*

Purpose: To evaluate the efficacy of CT-guided percutaneous RadioFrequency (RF) thermoablation with cool-tip probe in the treatment of osteoid osteoma.

Methods and Materials: From June 1998 to February 2004, 72 RF thermoablation procedures were performed in 71 patients (range of age, 3-70; mean age, 28) with osteoid osteoma located in the inferior or superior limbs, pelvic bones, vertebrae and, in one case, in a rib. Percutaneous thermoablation was performed with Radionics Cool-tip RF Ablation System by using probes with 1 or 2 cm unprotected tip applied for 4 minutes in the centre of the lesion. At the beginning the osteoid osteoma was localized on CT images. Thereafter a Kirschner wire was inserted within the lesion, rigged on a hand-drill device. Once the nidus was engaged the Kirschner wire was exchanged for a RF probe and radio waves were emitted.

Results: At a mean follow-up of 41 months the treatment was considered effective in 94% of the cases. In four patients pain had recurred; one of these cases was treated for a second time with success. In two cases procedural complications of minor degree (limited cutaneous burns) have occurred.

Conclusion: In our experience CT-guided percutaneous RF thermoablation of osteoid osteoma proved to be effective in the large majority of the cases. Deprived of severe complications, it may represent a minimally invasive, rapidly effective procedure, alternative to the surgical treatment.

10:30 - 12:00

Room I

Interventional Radiology

SS 609b

Abdominal aortic aneurysms

Moderators:

R.W. Günther; *Aachen/DE*
A. Hatzidakis; *Iraklion/GR*

B-291 10:30

Intra-abdominal pressure influences endotension following endoluminal grafting of AAA: Experimental findings

M. Gawenda, S. Winter, G. Jaschke, G. Wassmer, J. Brunkwall; *Cologne/DE*

Purpose: It has been postulated that the intra-abdominal pressure (IAP) produce pressurization inside the aneurysm sac. The present study was designed to investigate whether, and to what extent, aneurysm sac pressure after ELG is influenced by the IAP.

Methods and Material: Experimental study, *in vitro*. Compliant Latex aneurysms (aneurysm diameter: 60 mm) were inserted into an circulation model. The systemic mean pressure (SP_{mean}) was varied from 50 to 120 mm Hg with pulse pressure of 40 mm Hg. The aneurysms were excluded by a latex sealed woven polyethylene graft. The systemic and aneurysm sac pressures (ASP) were measured simultaneously. The aneurysm models were placed inside a closed chamber, which was pressurized stepwise (0, 20, and 40 cm H₂O), simulating an increasing intra-abdominal pressure.

Results: In the *in vitro* model ELG created a closed cavity without any endoleak, but showed a relevant aneurysm sac pressure. At a systemic mean pressure of 80 mm Hg, the aneurysm sac mean pressure (ASP_{mean}) was 24 mm Hg at median. By simulating an increasing IAP, the aneurysm sac pressure increased as well. At an IAP of 20 cm H₂O the ASP_{mean} was 29 mm Hg, at 40 mm H₂O IAP the ASP_{mean} was 34 mmHg.

Conclusions: The presented *in vitro* model demonstrated that the aneurysm sac mean pressure is influenced by the intra-abdominal pressure; increasing intra-abdominal pressure resulted in increasing aneurysm sac pressures as well. These data need to be considered when studying endotension.

B-292 10:39

CT angiography evaluation of patients with abdominal aortic aneurysms:

How many are candidates for endovascular repair?

R. Iezzi, F. Quinto, A. Pierro, F. Spigonardo, A. Cotroneo, C. Colosimo; *Chieti/IT*

Purpose: To determinate how many patients with abdominal aortic aneurysms (AAA) are candidates for endovascular repair (EVAR) on the basis of clinical and CT findings.

Method and Materials: From January 2002 to June 2003, 182 patients with suspected abdominal aortic aneurysm underwent MSCT angiography (MSCTA) (4x1-mm collimation, pitch 6, 1.25-mm slice width). The number of patients who met inclusion criteria for EVAR were recorded as were the anatomical characteristics of each aneurysm. All patients treated with EVAR underwent MSCTA follow-up at 1, 6 and 12 months.

Results: Among 182 patients, 130 patients were jumped to be candidates for treatment: EVAR in 51 patients (39.3%) and surgical repair in 79 patients (60.7%). The primary anatomical reason for ineligibility for EVAR was a short or extremely tortuous or calcified infrarenal neck in 41 patients (51.9%), abdominal aortic aneurysm diameter > 7 cm in 13 patients (16.4%), extremely tortuous iliac arteries in 6 patients (7.6%). 17 patients (21.5%) were classified as non-candidates due to age (< 65 years). 2 patients (2.5%) refused EVAR. CTA follow-up showed a low rate of midterm complications.

Conclusions: In our experience unfavourable infrarenal neck anatomy was the primary exclusion criteria of endovascular repair. EVAR is a safe and reliable procedure for the treatment of abdominal aortic aneurysm.

B-293 10:48

Outcome of endovascular repair in patients with difficult aortic necks

G.J. Munneke, E. Choke, T. Loosemore, M. Thompson, A. Belli, R. Morgan; *London/UK*

Purpose: The principle anatomical contra-indication to endovascular aneurysm repair (EVAR) is an unfavourable proximal aortic neck. The aim of this study is to illustrate how aneurysms with unfavourable anatomic morphology may be treated with stent-grafts.

Materials and Methods: 100 patients who underwent EVAR were studied. Unfavourable morphological features in the aortic neck were defined as neck diameter more than 25 mm, neck length less than 15 mm, angulation more than 60° and circumferential thrombus exceeding 50%. Endoleak and mortality rates were determined for patients with 0, 1 and ≥ 2 adverse features, groups 1 (55 patients) 2 (37 patients) and 3 (8 patients) respectively.

Results: After initial graft implantation the incidence of intra-operative attachment site endoleak requiring re-intervention was 9.1%, 24.3%, and 25% in groups 1-3 (The re-intervention rate for patients with favourable anatomy is 13% in the EUROSTAR registry). The incidence of Type I endoleaks at 30 days was 3.6%, 2.7% and 25% for Groups 1-3. Both patients in Group 3 underwent placement of Palmaz stents to abolish the leak. 30 day mortality was 7.2%, 2.7% and 0% in the three groups. The number of patients with AAA sac regression or stable sac was 44 (98.2%), 34 (91.9%) and 6 (75%) in groups 1-3 respectively.

Conclusions: Patients with unfavourable neck anatomy who are unsuitable for open surgery may be treated with EVAR, although many patients require additional procedures. Early outcomes are encouraging in this group of patients. These data suggest that the indications for EVAR may be expanded.

B-294 10:57

Haemodynamic differentiation of type II lumbar endoleaks by contrast-enhanced ultrasound

V. Napoli, I. Bargellini, A. Pratali, P. Petrucci, S. Sardella, C. Bartolozzi; *Pisa/IT*

Purpose: To differentiate type II lumbar endoleaks (ELs) through dynamic features identified by contrast-enhanced ultrasound (CUS), and to identify its relationship with aneurysm enlargement rate ≥ 1 mL/month.

Materials and Methods: Eighteen patients (mean age 71.8 years) with type II lumbar EL underwent Computed Tomography Angiography (CTA), CUS and Digital Subtraction Angiography (DSA). On CTA, AAA volumes were calculated, and EL visualization and volume were assessed. At CUS, detection of contrast enhancement within the aneurismal sac (EL) was assessed, together with the time of EL wash-in and wash-out from the beginning of contrast injection, the visualization of inflow and outflow vessels, and the presence of cavity filling.

Results: All patients showed an EL at CUS. Median wash-in and wash-out times were 84 and 320.5 sec, respectively, and were significantly associated ($P < .01$). By Youden plots, the ELs were classified as hyperdynamic when wash-in was < 100 sec ($n = 10, 55.5\%$) and/or wash-out was < 520 sec ($n = 13, 72.2\%$). Slower wash-out was associated with non-visualized outflow and/or inflow arteries

Scientific Sessions

($P < .05$). Eight ELs were missed at CTA; it occurred in hypodynamic ELs, no detectable inflow or outflow vessels and absence of cavity filling ($P < .05$). Mean aneurysm volume increase was 1.1 ± 1.7 mL/month. Aneurysm enlargement ≥ 1 mL/month ($n = 8$, 44.4%) was significantly associated with hypodynamic ELs. Sensitivity, specificity, PPV, NPV and accuracy in identifying enlarging AAA were 62.5%, 100%, 100%, 76.9% and 83.3% for wash-out time ≥ 520 sec.

Conclusion: Type II lumbar ELs show different haemodynamic features at CUS, that might influence aneurysm enlargement, addressing the need for treatment.

B-295 11:06

Endoleakdetection after endovascular aneurysm treatment

M.B. Pitten, H. Schweitzer, S. Herber, W. Schmiedt, A. Neufang, P. Kalden, J. Schneider, M. Thelen; Mainz/DE

Purpose: To investigate the diagnostic accuracy of MR imaging and spiral CT for endoleak detection.

Material and Methods: 52 patients, 48 men and 4 women (age 71.1 ± 6.9) underwent endovascular aneurysm repair with nitinol stent grafts. Follow-up data sets included spiral CT (slice thickness of 3 mm, reconstruction interval 2 mm, unenhanced and biphasic contrast enhanced) and MR imaging (1.5 Tesla MR scanner, axial T2w-TSE, T1w-Flash 2D unenhanced, Flash 3D angio and T1w-Flash 2D contrast enhanced) within 48 hours postinterventionally, at 3, 6, and 12 months and every year. Consensus reading of CT and MR imaging was defined as the standard of reference.

Results: 141 of 252 data sets demonstrated evidence for endoleaks. The incidence of Type I, II, III endoleaks, and complex endoleaks was 3.2%, 40.1%, 8.7%, and 4.0%, respectively. Sensitivity for endoleak detection was 92.9%, 43.3%, 34.0%, and 37.6% for MR imaging, biphasic CT, uniphasic arterial CT, and uniphasic late CT, respectively. The corresponding negative predictive values were 91.7%, 58.1%, 54.4%, and 55.8%. Cases without endoleaks in CT and MR imaging showed better aneurysm shrinkage compared to those with positive MR imaging but negative CT (-4.3, -7.9, -7.6, -9.4 mm versus -3.1, -5.8, -5.9, -7.3 mm at 1, 2, 3, and 4 years). In 2 of 15 cases with reinterventions, the positive MR imaging findings alone demonstrated the source of endoleak and enabled reintervention.

Conclusion: MR imaging is significantly superior to biphasic CT for endoleak detection and rating of endoleak size and can help to clarify endotension. Endoleak rates reported after endovascular aneurysm repair substantially depend on the imaging modalities used.

B-296 11:15

Modalities of treatment of type II endoleaks after abdominal aorta endoprostheses deployment

R. Marcello, M. Castrucci, G. Assegnati, P. Costa, E. Serrao, N. Mangialardi; Rome/IT

Purpose: To evaluate the treatment modalities of type II endoleaks.

Method and Materials: From January 1998 to July 2004, 520 patients received endoprostheses treatment of abdominal aorta aneurysms. Over this number, 11 subjects aged from 66 to 87 (mean 77 yrs, 10 men and 1 woman) with type II endoleaks were treated with percutaneous coil embolization of IMA (3 cases), ileolumbar artery coil embolization (2 cases), laparoscopic clipping (3 cases) and aneurysm sac needle injection of clotting drugs (3 cases). The procedure was selected on the basis of imaging appearances. Follow-up was carried out with c.e. spiral CT in 30 days and six months following the procedure.

Results: All cases turned out successful. The two patients treated with translumbar needle injection of glue and coils had impossible endovascular approach due to inconsistent vessels network. Laparoscopy clipping was the treatment of choice when endoleak perfusion was provided only by IMA but its endovascular navigation was unfavourable.

Conclusions: Type II endoleaks management should be performed on the basis of endovascular procedure in all cases of a feasible vascular pattern. Alternative fluoro guided needle injection technique may be advocated in those cases with unclear vascular mapping.

B-297 11:24

Treatment of type II endoleaks by CT-guided translumbar puncture and injection of N-butyl-2-cyanoacrylate glue into the aneurysm sac

R. Cioni, I. Bargellini, M. Femia, C. Cappelli, F. Fontana, S. Sardella, C. Bartolozzi; Pisa/IT

Purpose: To evaluate the results of CT-guided translumbar N-butyl-2-cyanoacrylate surgical glue (Glubran 2) injection in the treatment of type II endoleaks after endovascular repair of abdominal aortic aneurysm (EVAR).

Materials and Methods: From March 2003 to April 2004, nine patients (all male,

mean age 76.2 years) with type II endoleak and increasing aneurysm diameter, underwent translumbar puncture of the aneurysm sac 1-3 years after EVAR, using a 20-22- Gauge needle under CT-guidance. A mixture of N-butyl-2-cyanoacrylate glue (Glubran 2, 1-2 cc) and Lipiodol (2:1 ratio) was slowly injected under fluoroscopic guidance. Patients were discharged 24 hours after treatment. CT angiography was performed at 1, 6 and 12 months follow-up.

Results: The procedure was technically successful in all cases, with no major complications. In one patient an abscess along the psoas muscle was detected and solved completely 1 month later. One patient required a second procedure two months after the initial treatment, whereas in 2 patients the procedure was repeated three times. On follow-up (range, 3-18 months), the endoleak reduced in 1 patient, whereas in the remaining 8 cases it completely disappeared. CT examinations showed progressive aneurysm diameter reduction in all cases.

Conclusion: Translumbar intrasac glue injection represents a safe and effective procedure to treat selected cases of type II endoleak after EVAR.

B-298 11:33

Emergency endovascular treatment of ruptured abdominal aortic aneurysms

D. Laganà, G. Carrafiello, R. Caronno, P. Castelli, F. Fontana, M. Mangini, C. Fugazzola; Varese/IT

Purpose: To verify the feasibility and effectiveness of endovascular treatment of ruptured abdominal aortic aneurysms (RAAA).

Materials and Methods: In the last 36 months we have treated, in emergency, with endovascular exclusion, 27 symptomatic RAAA. In 19 haemodynamically stable patients a pre-operative angio-TC was performed to confirm the diagnosis and to plan the treatment; 8 patients, with hemorrhagic shock, were evaluated with pre-treatment aortography performed in operating room. 19 Excluder/Gore® and 5 Zenith/Cook® stent-grafts (22 bifurcated devices and 5 aorto-uni-iliac were used). The follow-up was performed with angio-CT at 1, 3, 6 and 12 months.

Results: We have obtained 100% technical success with 11% mortality rate (1 cardiac failure and 2 MOF). The follow-up (mean 8 months, range 1-24) has showed: the complete exclusion of AAA in 22/27 cases; 1 iliac leg occlusion (treated with femoro-femoral bypass), 3 type II endoleaks with spontaneous thrombosis and 1 patient with type I and III endoleak. We observed a reduction of aneurismal sac in 6/27 patients and stability of the same one in the other patients.

Conclusion: In conclusion we can affirm that EVAR is a good option for treatment of RAAA, with a lower mortality rate than surgery. The team's experience allows a correct planning of the procedure also in emergency with immediate and late results comparable with elective repair. In our experience the bifurcated stent-graft is the chosen device in patients with suitable anatomy because the procedure is less time consuming than aorto-uni-iliac stent-grafting with surgical cross-over, allowing faster aneurysm exclusion.

B-299 11:42

Six-year experience in the percutaneous treatment of abdominal aortic aneurysms

M. Corona, F. Fanelli, F. Salvatori, A. Bruni, V. Dominelli, L. Di Rezze, A. Pucci, P. Rossi, R. Passariello; Rome/IT

Purpose: To report our six-year experience using a bifurcated endoprosthesis in the treatment of abdominal aortic aneurysms (AAA).

Methods and Materials: From September 1998, 133 patients with AAA (mean 50.2 mm) were treated using different type of stent-grafts: 25 Vanguard II (Boston-Scientific), 89 Excluder (WL-Gore), 9 Talent (World-Medical), 2 Anaconda (Sulzer-Medical), 1 Quantum (Cordis), 2 Endologix (Endologix), and 5 Zenith (Cook). Procedures were performed in angio-suite (51) and operating room (82) with patients under general, epidural or local anesthesia.

Results: Technical success with complete exclusion of the aneurysm was achieved in 132/133 patients, while in 1 case an immediate conversion was necessary. After a follow-up ranging from 1 to 69 months, 125 patients (94.6%) are alive while 7 dead. A progressive reduction of the aneurysmatic sac (mean value 2.3 mm) was observed in 42 patients (31.8%). The sac diameter remained stable in 67 patients (50.7%), and increased in 23 patients (17.4%). Endoleak was detected in 21 patients (15.9%): 3 type I, 15 type II, 1 type III, 2 type IV. Two late conversion were performed after 22 and 31 months respectively for multiple fractures of the stent-graft and for a persistent type II endoleak. In one case (0.7%) an occlusion of the right renal artery was observed after 4 months for stent-graft migration. Limb obstruction occurred in 5 patients (3.7%) successfully solved with a fem-fem by-pass.

Conclusions: Percutaneous treatment of AAA seems to be a feasible technique only in selective patients. However an accurate follow-up is mandatory to prevent and manage complications.

Scientific Sessions

B-300

11:51

Fenestrated abdominal stent-grafts: Preliminary results

M.J. Fischer, G. Maselli, P. Pozzilli, S. Mosca, T. Lupattelli, G. Scalera, L. Lupattelli; Perugia/IT

Purpose: To report the preliminary experience in the endovascular treatment of abdominal aorta aneurysm (AAA) with proximal neck less than 10 mm using fenestrated stent-grafts.

Methods and Materials: In 6 patients with suprarenal AAA an aortic-biiliac fenestrated endoprostheses (COOK, Australia) was positioned. Multidetector CT angiography provided to produce a custom-design endovascular stent-graft for each patient.

Results: in 6 patients (mean age, 81 years; range, 66-81 years) classified as ASA III (n = 5), and ASA IV (n = 1), the exclusion of the aneurysm sac and a good representation of the renal arteries (n = 4) was obtained. Stent-graft prosthesis was converted and implanted in infrarenal site and covered by extensive fenestrated stent-graft because a selective catheterism of the renal artery was impossible. 1 patient had renal acute transitory insufficiency with fatal hemoperitoneum after 2 months. The death rate was 33% (two patients) and occurred within 30 days.

Conclusion: An adequate choice of a device allows treating the patients with limited options for treatment as well as the patients noneligible for placement of infrarenal prosthesis. An accurate patient selection, an appropriate CT assessment and a high skill in endovascular procedure is needed.

10:30 - 12:00

Room K

Cardiac

SS 603

Coronary plaque imaging

Moderators:

R. Rienmüller; Graz/AT

P.M.A. van Ooijen; Groningen/NL

B-301 10:30

Coronary plaque imaging with MSCT: The characterisation of lipid and fibrous plaques is affected by intracoronary attenuation

F. Cademartiri, N.R. Mollet, G. Runza, M. Midiri, R. Hamers, N. Bruining; Rotterdam/NL

Purpose: To define the effects of intracoronary contrast on the density values of coronary plaques.

Material and Methods: MSCT protocol (Sensation 16, Siemens, Germany): slice/collimation 16/0.75 mm, rotation time 375 ms retrospective ECG-gating mode. MSCT was performed in 7 ex-vivo left coronary artery specimens set in oil and filled with 5 solutions with decreasing dilutions of contrast material: 1/∞, 1/200, 1/80, 1/50 and 1/20. In-vivo assessment was performed in 12 patients (males 9; mean age 59 ± 10) who underwent two subsequent scans (arterial and delayed) (MSCT-CA) after intravenous administration of a single bolus of contrast material (100 ml of iomeprol 400 mg/ml at 4 ml/s). The attenuation (HU) value of atherosclerotic plaques was measured in each solution at: lumen, plaque (non calcified thickening of the vessel wall), calcium and oil. The results were compared with one-way ANOVA-test and correlated with Pearson's test.

Results: The mean attenuation of the 5 solutions in the lumen (45 ± 38 HU; 85 ± 38 HU; 121 ± 38 HU; 322 ± 104 HU; 669 ± 151 HU) and plaque (11 ± 35 HU; 20 ± 38 HU; 34 ± 43 HU; 61 ± 65 HU; 101 ± 72 HU) was significantly different ($p < 0.001$). The attenuation of lumen and plaque of coronary plaques showed moderate correlation ($r = 0.54$; $p < 0.001$). The mean attenuation value in-vivo arterial/delayed for lumen (325 ± 70 HU; 174 ± 46 HU) and non-calcified plaque (138 ± 71 HU; 100 ± 52 HU) was significantly different ($p < 0.001$). The attenuation of calcium and oil was not effected by differences in lumen contrast both in ex-vivo and in-vivo measurements.

Conclusion: Non-calcific coronary plaque attenuation values are significantly modified by differences in lumen contrast densities.

B-302 10:39

Imaging and classification of atherosclerotic plaques in Watanabe heritable hyperlipidemic rabbits using 16-row multidetector-CT

C. Herzog, S. Zangos, D.N. Krug, K. Eichler, T.J. Vogl; Frankfurt a. Main/DE

Purpose: To assess whether multidetector-row CT (MDCT) allows for a reliable

differentiation between different types of non-calcified atherosclerotic plaques (AHA types I-Va).

Methods: Six Watanabe heritable-hyperlipidemic rabbits underwent contrast-enhanced 16-row MDCT of the entire aorta. Scanning / image reconstruction parameters were: 16x0.75 mm collimation, LTF = 20 lp/cm, 9 mm feed/rotation, 500 ms TI, 120 kV and 300 mAs, 1.0 mm slice-thickness, 0.5 mm increment and a 50 mm FOV. Maximum in-plane resolution was 0.3 mm². After subdividing of the aorta into equal stacks of 5 mm, each atherosclerotic lesions was assessed for their tissue attenuation. For histopathological correlation each rabbit's aorta was dissected en-bloc, likewise cut into 5 mm pieces and analyzed by an experienced pathologist.

Results: Correlation to the histological results was possible in 237 plaques. Mean CT attenuation values for plaque types AHA I-Va were: -3.1 ± 49.0 HU; -17.6 ± 45.1 HU, 9.9 ± 58.9 HU; 39.9 ± 49.8 and 66.4 ± 45.2 HU. Correlation coefficients for the subdivision into groups AHA I-VI were $r = 0.42$ ($p = 10^{-6}$) and $r = 0.34$ ($p < 10^{-4}$) for observers 1. and 2. Mean CT attenuation values for plaques types ≤ AHA III (preatheroma) were -0.33 ± 57.4 HU, for plaque types ≥ AHA IV (atheroma) 49.3 ± 43.7 HU. Sensitivity of CTA for the detection of plaques types ≥ AHA IV was 67.3 (54.81%, 76.45%), specificity 76.21% (70.13%, 81.60%), NPV 33.75% (23.55%, 45.19%) and PPV 23.79% (18.40%, 29.87%).

Conclusion: High resolution CTA was neither able to adequately differentiate between varying stages of atherosclerosis nor between atheromas and preatheromas. A large variability in tissue attenuation as observed for either plaque type, prevented from any reliable assessment of the predominant component.

B-303

10:48

The association of low-dose sex hormone replacement therapy and coronary artery disease as determined by multi-slice spiral computed tomography

Y. Wang, Z. Jin, L. Kong, J. Jiang, H. Xue, Z. Zhang, Q. Ge; Beijing/CN

Purpose: To investigate whether longtime low-dose sex hormone replacement therapy (HRT) has an effect on coronary calcifications and stenoses.

Methods and Materials: 122 postmenopausal women (PMW) were studied by ECG-gated MSCT (0.42 s-rotation time, 16 × 0.75 mm collimation), 54 of them (aged 68 ± 8) who took low-dose HRT for more than five years composed HRT group, the other 75 (aged 69 ± 8) who never took HRT composed contrast group. Patients with a heart rate above 65/min received β-blockers before the scan. Plain scans were performed for calcium scoring (three people with coronary stents didn't have calcium scores). Contrast-enhanced scan (100 mL contrast agent IV at 4 mL/s) was performed during an approximately 20 s breath hold for screening over 70% stenoses. The calcium scores and incidence rate of over 70% stenoses of HRT group were compared with contrast group.

Results: In the analysis of calcium scores, the mean score of HRT group was 29.6 ± 81.3, which of contrast group was 125.8 ± 305.8; a significant difference was found between two groups ($Z = -2.025$, $P < 0.05$). The incidence rate of over 70% stenoses of HRT group was 9.6% (5/52), while that of the contrast group was 24.3% (17/70); a significant difference was found between these two groups ($\chi^2 = 4.344$, $P < 0.05$). Logistic regression found that HRT had a significant effect on coronary over 70% stenoses, the regression coefficient beta being -1.104 ($P < 0.05$).

Conclusion: These findings suggest that longtime low-dose HRT may decrease coronary calcifications and significant stenoses in PMW.

B-304

10:57

Coronary calcinosis and statin therapy

M.B. Belkind, V.E. Sinitsyn, A.A. Lyakishev, V.G. Naumov, S.K. Ternovoy; Moscow/RU

Purpose: The purpose of our study was to estimate the dynamics of coronary calcium score measured by electron-beam computed tomography (EBCT) in hypercholesterolemic patients treated with inhibitors of HMG-CoA reductase.

Materials and Methods: 119 patients with hypercholesterolemia (total serum cholesterol (TC) > 5.2 mmol/L) and positive calcium score were included in the study. 69 patients took statins, 50 without statin therapy - made the control group. EBCT (3-mm slices, acquisition time 100 ms, threshold definition of coronary calcification at 130 HU in an area > 1 mm², Agatston calcium score) and TC assessment were performed prior and after 25 ± 11 months of statin treatment.

Results: The average decrease of TC in the statin group was 24.4%, in the control group - 0.5% ($p < 0.0001$). Absolute increase of calcium score in the statin group was 63 ± 84 units, in control group - 122 ± 180 units ($p = 0.044$). We discovered inverse correlation between range of lowering TC and increase of coronary calcium ($r = -0.243$; $p = 0.008$).

Scientific Sessions

Conclusion: Therapy with HMG-CoA reductase inhibitors slows down the process of coronary calcification. EBCT may be used for follow-up of lipid-lowering therapy.

B-305 11:06

Electron beam CT measurement of coronary artery calcium allows individual risk assessment of CHD in UK diabetic patients

S.J. Howling, C. Hare, C. Harvey, T. McArthur, M. Tighe, C. Salek, P.J. Jenkins; London/UK

Purpose: Statins have been advocated for all patients with diabetes for primary prevention of CHD. Measurement of coronary artery calcium score (CACS) in diabetic patients is reported to offer a superior prognostic assessment of an individual's risk of cardiovascular disease than the Framingham Risk assessment. To date, there have been no studies of CACS in the UK diabetic population.

Methods and Materials: CACS was assessed in 1571 male subjects who had no cardiovascular symptoms, of whom 84 had diabetes. CACS was performed on a GE C300 Electron Beam CT (EBCT) scanner using Agatston's method, and categorised as Group 1 = 0; 2 = 1-10; 3 = 11-100; 4 = 101-400; 5 ≥ 400.

Results: Overall, the prevalence of elevated CACS was significantly greater in diabetic subjects than non-diabetic subjects: Group 4 - 34.5% vs 13.1%, p < 0.0001; Group 5 - 28.6% vs 11.6%, p < 0.0001. However, 23.9% of diabetics were in Group 1 or 2, indicative of no or very mild cardiovascular disease. Categorizing by total cholesterol levels revealed that of diabetic subjects with a level < 5.2 mmol/l, 20.9% were in Group 1 or 2, 16.7% in Group 3, and 62.5% in Groups 4 or 5.

Conclusion: Asymptomatic UK male diabetics have a high prevalence of significant coronary atherosclerosis. However, the significant proportion of subjects with no or mild CHD suggests that statin therapy may not be appropriate for all patients but reserved for those in whom EBCT has demonstrated an increased individual cardiovascular risk.

B-306 11:15

Analysis of the atherosclerotic plaque and cross-sectional surface of coronary arteries by MSCT (Vessel View software) and ICUS (reference method)

M. Pasowicz, P. Klimeczek, A. Gackowski, T. Przewlocki, R. Banys, K. Zmudka, W. Tracz; Krakow/PL

Aim: The purpose of this blinded study was to compare ICUS and MSCT in the assessment of the plaque, diameter and internal surface of coronary arteries.

Methods: 14 pts (3F, 11M, mean age 46(SD8)) were included in the study. Overall, 19 proximal segments of coronary arteries were assessed: LM-6, LAD-6, Cx-2, RCA-5. Only the segments with luminal diameter > 2 mm were analyzed. MSCT was performed using 16-slice device (Sensation 16 Cardiac, Siemens). All patients were pretreated with a beta blocker, mean heart rate during the study was 51 (SD9) bpm. The slice thickness was 0.75 mm. Intracoronary examination was performed using the Jomed In Vision Plus V4.8.2 device. Avanar F/X probes were pulled back from coronary arteries with a constant speed of 1 mm/s. Side branches or large calcifications were used as the landmarks to orient the ICUS and MSCT images. Overall, we analyzed 119 coronary arterial cross-sections (MSCT vs IVUS).

Results: ICUS revealed atherosclerotic lesions in 86 cross-sections (overall 20 plaques); soft-46, intermediate-24, calcified-16. MSCT revealed and correctly identified the morphology of the plaque in 71 cross-sections: soft-36, intermediate-19, calcified-16. The correlation between MSCT and ICUS in the assessment of the internal area was 0.86, the least internal diameter 0.72. Internal area ICUS vs. MSCT (11.1 (SD4.5) vs. 9.2 (SD4.67)), least diameter ICUS vs. MSCT (3, 1 (SD0.98) vs. 3.9 (SD1.3)).

Conclusions: MSCT was found to be consistent with ICUS in the detection and assessment of plaque morphology, especially calcified. There was a high correlation between ICUS and MSCT in the measurements of luminal area and least diameter.

B-307 11:24

Noninvasive coronary artery plaque visualization and differentiation by contrast enhanced black blood MR imaging

D. Maintz¹, M. Ozgun¹, A. Hoffmeier¹, W. Heindel¹, R. Fischbach¹, R. Botnar²; ¹Münster/DE, ²Boston, MA/US

Purpose: To evaluate contrast enhanced black-blood coronary MR imaging for selective visualization and non-invasive differentiation of atherosclerotic coronary plaque in humans.

Method and Materials: Eight patients with coronary artery disease (CAD) as

confirmed by X-ray angiography and multi-detector CT (MDCT) were studied by T1-weighted black-blood-inversion-recovery coronary MR imaging before (N-IR) and after administration of Gd-DTPA (CE-IR). Plaques were categorized as calcified, non-calcified, and mixed based on their Hounsfield number derived from MDCT.

Results: With MDCT, 27 plaques could be identified, 6 of which were calcified (calcified nodules were not evaluated), 5 non-calcified and 16 mixed calcified/non-calcified. On N-IR, 6/6(100%) calcified plaques appeared dark, 3/5(60%) non-calcified plaques were dark and the remaining 2/5(40%) were bright. 2/16(13%) mixed plaques were bright and 14/16(87%) were dark. On CE-IR, all calcified plaques appeared dark, 2/5(40%) non-calcified plaques were dark and 3/5(60%) were bright; 10/16(63%) mixed plaques were bright and 5/16(31%) were dark. Of the 16 non-calcified and mixed plaques that appeared dark on N-IR, 1 non-calcified and 10 mixed plaques appeared bright on CE-IR (contrast uptake). There were no plaques with bright appearance on N-IR and dark appearance on CE-IR MR imaging.

Conclusions: We demonstrate the use of black-blood CE-IR coronary MR imaging for the detection of selective contrast uptake in non-calcified and mixed coronary plaque in patients with CAD. The observed contrast uptake may be associated with neovascularization, inflammation, endothelial dysfunction and/or markers for plaque vulnerability. We conclude that this method may have potential for noninvasive characterization of coronary plaque in patients with subclinical and advanced CAD.

B-308 11:33

Coronary artery atherosclerotic plaque burden evaluated with MSCT

coronary angiography: Stable vs. unstable angina with ICUS validation

F. Cademartiri, N.R. Mollet, C. van Mieghem, G. Runza, T. Baks, P.J. de Feyter, G.P. Krestin; Rotterdam/NL

Purpose: Evaluate the differences in coronary plaque burden between patients with stable and unstable angina using 16-row Multislice CT (MSCT).

Materials and Methods: Twenty-one patients with stable (17 male, mean age 59 ± 9 yrs) and twenty patients with unstable angina pectoris (15 male, mean age 60 ± 11 yrs) underwent MSCT coronary angiography (Sensation 16, Siemens) prior to diagnostic conventional coronary angiography (CCA). A subset of 15 patients underwent intra-coronary ultrasound (ICUS) of a vessel not targeted for intervention. To determine the MSCT coronary plaque burden, we assessed the extent (number of diseased segments), size (small or large), type (calcific, non-calcific, or mixed) of plaque and its anatomic distribution in all ≥ 2 mm coronary segments.

Results: The sensitivity and specificity of MSCT in the detection of significant coronary plaques (≥ 50% plaque area on ICUS) was 83% (25/30) and 87% (54/62). A total of 473 ≥ 2 mm coronary segments were included for the assessment of MSCT plaque burden. Plaques were present in 62% (292/473) of all segments. Plaques were classified as small in 53% (155/292) and large in 47% (137/292) of diseased segments. Thirty-two percent (93/292) were non-calcific, 25% (73/292) calcific, and 43% (126/292) mixed. Plaques were predominantly located in the proximal and mid-segments of the main coronary vessels. Plaque was found in one third of segments classified as normal on CCA. Patients with unstable angina had significantly more non-calcific plaques when compared to stable patients.

Conclusions: MSCT coronary angiography provides in-vivo information regarding the presence, extent, severity, and distribution of coronary atherosclerosis.

B-309 11:42

Coronary calcification characteristics on multidetector CT and accompanying stenosis severity

J.B. Houwers, J. Dorgelo, T.P. Willems, F. Zijlstra, M. Oudkerk; Groningen/NL

Purpose: Coronary calcifications often complicate the differentiation between significant and non-significant stenoses in coronary multidetector CT (MDCT) due to blurring artifacts. This often leads to false positive cases of coronary stenoses, compared to coronary catheter angiography (CAG). A study was performed to determine whether certain characteristics of calcified lesions on MDCT are related to the severity of an accompanying lumen reduction.

Material and Methods: Fifty-eight patients (44 male, mean age 62.0 ± 8.7) scheduled for coronary intervention, were examined with 16-slice MDCT. The latest CAG on which the PCI indication was made was used as reference standard. The mean time between CAG and MDCT was 28.0 ± 11.0 days. Of all segments, calcified lesions were described by shape and presence or absence of accompanying soft plaque. The characteristics were compared to the lumen reduction on CAG.

Results: A total of 211 calcified lesions were found. The majority, 149 (71%), was

Scientific Sessions

accompanied by soft plaque. Of the 62 purely calcified lesions, in only eight cases (13%) was there a true stenosis, whereas 42 out of 149 mixed lesions (28%) were related to true stenosis. This difference was significant ($p < 0.02$).

When looking at the shape of the eight pure calcified stenotic lesions, seven of these were of the spotty type.

Conclusion: A significantly lower occurrence of $\geq 50\%$ stenosis was found in purely calcified lesions, compared to mixed lesions. Only in cases of spotty pure calcified lesions one has to be aware of possible underlying stenosis of the coronary lumen.

B-310 11:51

Is coronary plaque morphology a useful predictive tool for the detection of severe coronary lesions? Analysis of 469 plaques as assessed by 16-slice computed tomography

A. Kuettner, A. Feyer, J. Rothfuss, M. Heuschmid, A.F. Kopp, S. Schroeder, C.D. Claussen; Tübingen/DE

Background: MDCT systems with retrospective ECG-gating permit visualization of the coronaries. Also, plaque composition of atherosclerotic lesions can be assessed. The purpose of this study was to investigate whether plaque composition can be a tool to identify or rule out severe coronary lesions.

Methods and Results: 60 patients (pts) underwent conventional coronary angiography (CCA). All patients were also studied by 16-slice-MDCT. All coronary plaques as assessed by MDCT were compared to CCA regarding degree of luminal obstruction $> 70\%$ and also classified as having one of the following 11 characteristics: 1: calcified nodule, 2: small wall adherent calcified plaque (cp), 3: cp at vessel bifurcations, 4: "obstructive" cp, 5: cp conglomerate, 6: small non-calcified plaque (ncp), 7: larger ncp, 8: "twin" ncp, 9: vascular occlusion by ncp, 10: mixed plaque, 11: mixed plaque with predominant calcifications.

Results: 469 plaques were detected in $n = 60$ pts. The distribution was as follows (number of severe lesions): 1: $n = 33(0)$, 2: $n = 85(1)$, 3: $n = 12(0)$, 4: $n = 11(1)$, 5: $n = 33(6)$, 6: $n = 89(0)$, 7: $n = 47(1)$, 8: $n = 45(9)$, 9: $n = 30(10)$, 10: $n = 74(29)$, 11: $n = 18(12)$. For groups 1, 2, 3, 4, 6 and 7 a predictive value to exclude severe coronary lesion was ≥ 0.98 , for groups 6, 8, 9, 10, 11 and 12 the predictive value was < 0.91 .

Conclusions: Our data suggest that the postulated plaque groups allow for reliable exclusion of severe coronary artery lesions independent of luminal assessment of a given plaque type. Prospective studies have to show whether these findings can be used in clinical routine practice to exclude significant CAD.

10:30 - 12:00

Room L/M

Neuro

SS 611

Stroke imaging

Moderators:

J.-F. Bonneville; Besançon/FR
L. Østergaard; Århus/DK

B-311 10:30

Prediction of the extent of cerebral infarction and assessment of the clinical condition using functional CT perfusion and diffusion-weighted MR imaging in hyperacute ischemic stroke

S. Bisdas¹, F. Donnerstag², K. Weissenborn², C. Herzog¹, M. Harth¹, B. Ahl², I. Bohrer², H. Becker², T. Vogl¹; ¹Frankfurt a. Main/DE, ²Hannover/DE

Purpose: To determine the accuracy of CT perfusion (CTP) and diffusion-weighted MR imaging (DWI) in assessing the admission and follow-up clinical condition and predicting the follow-up infarction in hyperacute stroke.

Methods and Materials: CTP and DWI were obtained in 27 patients untreated with thrombolysis within 4 hours of stroke onset. On the CTP-delivered cerebral blood flow (CBF) images 3 CBF cut-off values were used to discriminate between infarcted, non-infarcted, and penumbra areas. On the DWI areas of acute infarction were delineated on the base of apparent diffusion coefficient (ADC) values. The measured areas on CTP and DWI were correlated with the admission and follow-up (mean interval time 5 days) National Institutes of Health Stroke Scale (NIHSS) scores as well as with the areas of infarction on follow-up imaging.

Results: The volumes of the infarcted and ischemic (infarction and penumbra) tissue on admission CTP correlated with the NIHSS score ($p < 0.005$). At the time of follow-up imaging the infarcted tissue volume correlated with the initial CTP ischemic and infarcted tissue volumes ($r = 0.63$, $p < 0.01$ and $r = 0.71$, $p < 0.01$). A correlation was shown between the initial diffusion abnormality volume

and the follow-up infarcted tissue ($r = 0.74$, $p < 0.01$). The follow-up NIHSS score correlated only with the ischemic and infarcted lesion area on CTP ($p = 0.001$). **Conclusion:** Admission CTP and DWI in hyperacute stroke can accurately predict the short-term follow-up infarct size. Areas of ischemic and infarcted tissue on the CTP correlate with the admission clinical condition and allow the evaluation of clinical prognosis.

B-312 10:39

Role of MR perfusion-weighted images for predicting severe lesion growth in the hyperacute stage infarction

S.H.J. Seon, K.S.J. Kim; Seoul/KR

Purpose: To evaluate the diagnostic performance of each perfusion map of MR perfusion-weighted images (PWI) for predicting severe lesion growth in stroke patients.

Methods and Materials: We examined 43 patients with acute middle cerebral artery territory infarction in whom diffusion-weighted images (DWI) and PWI were obtained within 6 hours after symptom onset and follow-up MR imaging including DWI within 5 days. Infarct volume was measured on initial and follow-up DWI by using threshold technique in the workstation. Enlargement of the lesion more than 1.5 times on follow-up was defined as severe progression. Perfusion maps (relative cerebral blood volume; rCBV, mean time to enhancement; MTE, and relative cerebral blood flow; rCBF map) were created by using a commercial software program. We regarded the presence of mismatch in each map as an indicator for predicting lesion growth. We analyzed the sensitivities, specificities, positive predictive value, negative predictive value, and diagnostic accuracy of each perfusion map for predicting severe lesion growth.

Results: rCBV map showed the highest diagnostic accuracy (65.1%) and specificity (77.4%), but low sensitivity (33.3%). rCBF and rMTE map showed the highest sensitivity (75.0%), but low specificity (48.4% and 22.6%). All maps showed relatively high negative predictive value (rCBV: 75%, rCBF: 83.3%, and rMTE: 70%), but low positive predictive value (36.4%, 36.0%, and 27.3%).

Conclusions: Perfusion images provide important clues for predicting severe lesion growth in acute stage infarction, but also have limitations in applying to individual cases and should be used as a complementary tool.

B-313 10:48

CT perfusion in the acute stage of SAH: Relationship to the development of delayed cerebral ischemia

I. van der Schaaf, R. Hoff, G. Rinkel, G. van Dijk, B. Velthuis; Utrecht/NL

Purpose: To study the relationship between quantitative perfusion parameters and perfusion asymmetries of both hemispheres in the acute stage of SAH with the development of DCI.

Methods and Materials: CTP scans were performed in 32 patients within 48 hour after SAH. Regions of interest were drawn in the peripheral (cortical) and deep (basal ganglia) flow territories of the anterior cerebral artery and middle cerebral artery by two observers. Ratios of CBF and CBV values and differences of MTT and TTP values were calculated between hemispheres. The differences of quantitative perfusion values, in patients and locations with and without DCI were compared by means of the T-test statistics.

Results: Eight of 32 patients developed DCI (25%). Patients with DCI had significantly lower quantitative CBV and CBF values, lower CBV and CBF ratios and higher MTT and TTP differences between the left and right hemisphere (both ratios and differences indicating more asymmetry between hemispheres). Significantly lower quantitative CBV and CBF values, higher MTT values and lower CBV and CBF ratios between both hemispheres were present for locations with DCI. The lowest CBF and CBV and the highest MTT were always on the side of DCI.

Conclusion: Lower CBF and CBV values are present in the acute stage after SAH in patients who develop DCI. More asymmetry of perfusion values between hemispheres is present for all four perfusion parameters. This information might help in the development of a predictive model for patients with a higher risk of developing DCI.

B-314 10:57

Diffusion and perfusion weighted magnetic resonance imaging in patients with acute ischemic stroke: Can diffusion/perfusion mismatch predict outcome?

J. Ma, R. Bruening, D. Morhard, G.F. Hamann, H. Brueckmann; Munich/DE

Purpose: To investigate whether perfusion MR imaging hemodynamic parameters in mismatched regions were correlated with stroke severity and if they were useful for prediction of outcome.

Scientific Sessions

Saturday

Methods and Materials: Routine MR imaging, diffusion and perfusion weighted imaging was performed in 35 acute stroke patients, and the stroke severity assessment (National Institutes of Health Stroke Scale Score, NIHSS) at admission and the functional outcome (modified Rankin scale, MRS) at discharge was recorded. The perfusion maps were processed and the parameters were obtained by identifying regions of interest on both ischemic core and mismatched regions, and on the normal mirror region.

Results: *Hemodynamic parameters in relation to MRS outcome score:* In the mismatched region, relative cerebral blood flow (rCBF) change and time to peak (TTP) delay showed statistically significant regression to MRS ($p < 0.05$). The more the rCBF decreased and the longer the TTP delay, the higher the MRS (poor outcome) was. In ischemic core, rCBF change and mean transit time (MTT) delay was significantly related to MRS ($p < 0.05$). *Hemodynamic parameters in relation to NIHSS:* Only TTP delay in the mismatched region was related to NIHSS significantly ($p < 0.05$). No other hemodynamic parameters were found to correlate with NIHSS. No statistical significance was found in cerebral blood volume (rCBV) and bolus arrival time (T0) in relation to NIHSS or MRS.

Conclusions: The hemodynamic parameters derived from perfusion MR imaging may be a helpful adjunct to predict the outcome and severity in acute stroke patients. In the mismatched region, the rCBF reduction and TTP delay are statistically correlated to stroke outcome (MRS).

B-315 11:06 ♀

Voxel-based CT analysis for improved detection of early CT signs in cerebral infarction

C. Grimm¹, A. Hochmuth², H.-J. Huppertz²; ¹Basle/CH, ²Freiburg/DE

Purpose: In acute cerebral infarction early CT signs (e.g., attenuation of involved structures due to edema, loss of gray-white matter differentiation) may be difficult to detect within the first hours after symptom onset. Here, we present a novel technique for post-processing of CT scans to enhance these signs.

Methods and Materials: A cranial CT scan with 512x512 matrix and axial cuts of 5 mm through infra- and supratentorial space is interpolated to a volume data set and normalized to a customized CT template using standard algorithms of SPM2 (Statistical Parametric Mapping Software, Wellcome Department of Imaging Neuroscience, London). The distribution of gray and white matter is analyzed on a voxelwise basis and compared with a normal database consisting of the normalized CT scans of 30 healthy subjects. Based on this analysis, a 3-dimensional map is created which characterizes density loss of brain tissue as compared to the normal database.

Results: In a preliminary study this technique was applied to the CT scans of 12 patients with acute cerebral infarction (CT within 1-6 hours after symptom onset). The resulting feature maps displayed the infarction much more clearly than the original CT scans, even in 3 cases in which the lesion was initially not detected in the CT.

Conclusion: The novel technique for CT post-processing presented here may facilitate the interpretation of CT scans in acute cerebral infarction.

B-316 11:15

Treatment of stroke in rats with microplasmin: Magnetic resonance imaging evaluation

F. Chen¹, Y. Suzuki¹, N. Nagai¹, P. Peeters¹, X. Sun², W. Coudyzer¹, G. Marchal¹, Y. Ni¹; ¹Leuven/BE, ²Weifang/CN

Purpose: To evaluate Microplasmin (μ Pli) in a rat thrombotic stroke model with magnetic resonance imaging.

Methods and Materials: Rats ($n = 24$) were subjected to photochemical thrombosis of the middle cerebral artery (MCA) and randomized to 3 groups: controls (solvent, $n = 8$), low dose (7.5 mg/kg, $n = 8$) or high dose (10 mg/kg, $n = 8$) μ Pli, administered as an intravenous bolus 90 min after MCA occlusion. Cerebral ischemic damage was evaluated at 1 and 24 h after MCA occlusion by diffusion weighted imaging (DWI), and susceptibility contrast enhanced perfusion weighted imaging (PWI), and correlated with 2, 3, 5-triphenyl tetrazolium chloride (TTC) staining. The relative lesion size (RLS), PWI-DWI derived growth rate of RLS, relative cerebral blood volume (rCBV) and neurological signs were evaluated.

Results: The RLS measured with TTC staining at 24 h was $19 \pm 5.0\%$ in controls, and $12.1 \pm 2.5\%$ and $13.1 \pm 4.7\%$ in rats with 7.5 and 10 mg/kg μ Pli. The growth rate of RLS from 1 to 24 h was reduced from $18.1 \pm 7.1\%$ in controls to $2.5 \pm 9.5\%$ and $3.4 \pm 10.9\%$ with 7.5 and 10 mg/kg μ Pli respectively. The rCBV of ischemic areas at 24 h increased from $37 \pm 14\%$ in controls to $54\% \pm 15$ and $46\% \pm 16$ with 7.5 and 10 mg/kg μ Pli respectively. The neurological deficits improved from a Bederson score of 7(6-9) in controls to 4.5(3-8) and 4(3-6) with 7.5 and 10 mg/kg μ Pli respectively ($p < 0.05$ for each dose vs controls for all parameters).

Conclusion: As monitored with MR imaging and histomorphology, μ Pli reduced stroke size with improved neurological function in rats.

B-317 11:24 ♀

Metabolite profile in pyramidal tracts after ischemic brain stroke - 1H MRS study.

B. Kubas, J. Walecki, W. Kulak, J. Kochanowicz, E. Tarasow, W. Dzienis, J. Janica; Bialystok/PL

Purpose: To assess the role of 1H MRS in the detection of changes in cerebral metabolite levels in pyramidal tracts after cortical/ subcortical infarction and to compare metabolite alterations to clinical outcome (Barthel index, Scandinavian Stroke Scale).

Materials and Methods: 21 patients with supratentorial cortical/ subcortical infarction were studied, 1 month after the onset of clinical symptoms of ischemic stroke. The MR studies were performed on 1.5 T system. The results of spectra approximation (presented as metabolite ratios: NAA/Cr, Cho/Cr, lac/Cr, lip/Cr) were subjected to statistical analysis. MR spectra were recorded from normal appearing brain regions: contra and ipsilateral internal capsule and cerebral peduncles. Spectra from stroke patients were compared with a control group of 32 healthy volunteers.

Results: The statistical analysis revealed significant differences between data obtained from the various regions in the same patients who had undergone ischemic stroke and between the infarcted and control groups. Proton MR spectroscopy detects changes in cerebral metabolite levels in also apparently normal regions. In contralateral brain regions, as well as in the internal capsule we have noticed significant reduction of NAA and increase of Cho and lac; we found correlation between NAA level and Barthel Index and between lac/Cr and SSS.

Conclusions: Proton MRS is a very useful tool for evaluating major changes in metabolite levels in pyramidal tracts after brain stroke. Our preliminary results of 1H MRS, MR imaging and clinical data support the idea that metabolic lesions distant from the infarcted tissue can be responsible for the clinical course and have predictive value.

B-318 11:33

Cerebral vasospasm after subarachnoid haemorrhage: Multislice computerized tomography (MSCTA): A comparison with digital subtraction angiography (DSA) and contribution of perfusion CT in vasospasm management

M. Colleoni, A. Uské, R. Meuli, P. Maeder, L. Regli, P. Schnyder, S. Binaghi; Lausanne/CH

Purpose: To assess the diagnostic accuracy of MSCTA in detecting vasospasm following subarachnoid haemorrhage, on several intracranial arterial segments. To discuss the combination of MSCTA and perfusion CT in the management of vasospasm.

Methods: Twenty-six patients with clinical cerebral vasospasm underwent simultaneously DSA, MSCTA and perfusion CT. MSCTA consisted of 125-mm slice, reconstructed every 0.8 mm, pitch 0.75 and timing determined by a test bolus. Vasospasm was analysed by MSCTA and DSA on seven intracranial arterial locations and was categorized as none, mild, moderate or severe. Sensitivity, specificity, and accuracy of MSCTA in detection of vasospasm were calculated for each segment. Perfusion CT maps were performed in 17 patients, from which regional cerebral blood volume (rCBV), regional cerebral blood flow (rCBF) and mean transit time (MTT) values were calculated in 5 regions of interest on each hemisphere.

Results: 63 vasospasms were identified by means of MSCTA and DSA on 261 arterial segments. Accuracy of MSCTA was greatest for the A2 segment of the anterior cerebral artery (100%) and M2 segment of the middle cerebral artery (100%), whereas it was lowest for distal carotid siphon (45%). On perfusion CT, overall mean CBF values were significantly lower in segments with moderate to severe vasospasm ($P < 0.001$).

Conclusion: MSCTA can identify vasospasms even if located distally. MSCTA coupled with perfusion CT is a fast, accurate and non-invasive strategy to detect and evaluate intracranial vasospasms and their consequences on cerebral perfusion, allowing a time-saving selection of patients that will undergo endovascular treatment.

Scientific Sessions

B-319 11:42

MR digital subtraction angiography using parallel imaging in the diagnosis of vasospasm after subarachnoid hemorrhage

K. Tsuchiya, A. Fujikawa, K. Honya, M. Nakajima, T. Nitatori, S. Takemoto; Tokyo/JP

Purpose: MR digital subtraction angiography (DSA) visualizes vessels employing a rapid T1-weighted sequence in combination with a bolus injection of gadolinium. We assessed whether MR DSA using parallel imaging is effective in the diagnosis of vasospasm after subarachnoid hemorrhage.

Methods and Materials: On a 1.5-T imager, we used a three-dimensional fast field-echo sequence using parallel imaging (TR/TE/excitations = 3.1/0.9/1, flip angle = 20 deg, matrix = 128x256, field of view = 26x28 cm, reduction factor = 2) with intravenous injection of 7 ml of ProHance at a rate of 3 ml/sec. In 28 patients examined 5-20 days after clipping of a ruptured cerebral aneurysm, we reviewed MR DSA images comparing with images of diffusion-weighted imaging, dynamic susceptibility contrast (DSC) perfusion imaging, and 3D time-of-flight (TOF) MR angiography (MRA).

Results: Temporal resolution was as short as 0.8 sec. Vasospasm was noted in a total of 48 arterial segments on MR DSA and/or 3D-TOF MRA. In 19 of the 48 segments (40%), MR DSA was able to detect vasospasms but 3D-TOF MRA was not due to artifacts from a clip. In other 26 segments (54%), MR DSA and 3D-TOF MRA showed concordant findings. In 16 of the 28 patients, diffusion-weighted images showed new ischemic lesions. MR DSA was able to depict vasospasm leading to ischemia in 10 of the 16 patients (63%). Abnormalities on DSC perfusion imaging noted in eight patients were consistent with areas with vasospasm on MR DSA.

Conclusion: MR DSA using parallel imaging can be a tool to sensitively visualize vasospasm after subarachnoid hemorrhage.

B-320 11:51

Diffusion-weighted MR imaging in MELAS (mitochondrial myopathy, encephalopathy, lactic acidosis and stroke-like episode) syndrome

M. Lim¹, J. Kim², C. Suh¹; ¹Incheon/KR, ²Seoul/KR

Purpose: To investigate the nature of the infarct-like lesions on MR images during acute stroke-like episodes of the MELAS syndrome.

Materials and Method: We reviewed 11 MR images (including 10 diffusion-weighted images (DWI)), obtained within a week of the acute neurological event, and the medical records of 4 patients with MELAS syndrome to identify new edematous brain lesions. Visual assessment of the conventional MR images, DWI, and apparent diffusion coefficient (ADC) maps were performed for each lesion. In addition, the ADCs in normal and abnormal appearing areas were compared. The temporal evolution of the lesions on follow-up MR images was also analyzed.

Results: A total of 13 lesions during six acute episodes were identified. They appeared as acute infarct-like swelling in the cortex and subcortical white matter of the cerebral hemispheres. All 13 lesions gave a variable degree of high signal on DWIs, and among them, 7 lesions exhibited lower signal on ADC maps and decreased ADCs compared to those of the normal appearing white matter. The remaining 6 lesions produced ADCs that were not significantly different from or slightly higher than those of the normal regions on ADC maps. Five of 8 followed lesions evolved to localized tissue loss (hemorrhage occurred in 2 of them) corresponding to initial ADC decrease. The remaining 3 lesions resolved with or without small areas of residual abnormal signal.

Conclusion: Cytotoxic edema may occur either from vasculopathy or energy production failure during the acute stroke-like episodes of MELAS syndrome and they evolve to progressive tissue loss.

10:30 - 12:00

Room N/O

Computer Applications

SS 605

Computer aided detection and diagnosis

Moderators:

A. Rosset; Geneva/CH
B.B. Wein; Aachen/DE

B-321 10:30

Machine learning for computer-aided diagnosis in dynamic breast MR imaging: Can neural network analysis improve the diagnostic accuracy in suspicious lesions?

A. Wismueler¹, G. Leinsinger¹, A. Meyer-Baese², R. Wiegard¹, O. Lange¹, T. Schlossbauer¹, M.F. Reiser¹; ¹Munich/DE, ²Tallahassee, FL/US

Purpose: To develop, test, and evaluate a neural network machine learning approach for characterization of diagnostically challenging breast lesions in MR imaging.

Methods and Materials: 88 women with 92 indeterminate mammographic lesions (BIRADS III-IV, 41/51 benign/malignant lesions confirmed by histopathology) were examined by standardized dynamic contrast-enhanced breast MR imaging on a 1.5 T system. The machine learning approach is based on a 3-layer radial basis functions (RBF) neural network for automatic classification of 6-dimensional lesion-specific signal intensity time course vectors. For reference, interactive visual classification was performed by human experts using a standardized semi-quantitative evaluation score (Kuhl et al., Radiology 211:101-110). In addition, morphological criteria were included by a clinically approved scoring system. Classification performance was evaluated by a meticulous 25-run multiple leave-out cross-validation setup for test and training data. For quantitative assessment of diagnostic accuracy, areas under ROC curves (AUC) were computed for both machine learning and human expert classification.

Results: Neural network machine learning increased both sensitivity and specificity for classification between benign and malignant lesions, as confirmed by quantitative analysis of diagnostic accuracy: Neural network results (AUC=80 ± 4%) clearly outperformed human expert evaluation of SI time-series with (AUC=64 ± 5%) and without (AUC=59 ± 6%) consideration of lesion morphology. The increase in diagnostic accuracy for neural network classification proved to be statistically significant (Wilcoxon matched-pairs, two-sided, p < 0.05).

Conclusion: Automatic lesion classification in breast MR imaging by RBF neural networks is a powerful method for computer-aided diagnosis in suspicious lesions leading to a substantial improvement of diagnostic accuracy beyond the visual interactive classification by human experts.

B-322 10:39

Performance of an adaptive wavelet contrast enhancement method in interpretation of microcalcification clusters on dense parenchyma

L. Costaridou, S. Skiadopoulos, P. Sakellaropoulos, C. Kalogeropoulou, E. Likaki, G. Panayiotakis; Patras/GR

Purpose: To assess performance of a locally adaptive-wavelet (AW) contrast enhancement method in interpretation of microcalcification (MC) clusters on dense breast parenchyma. The method was compared to the manual intensity-windowing (IW) method, considered as the current standard.

Methods and Materials: The sample consists of 86 mammographic images corresponding to dense breasts, originating from the DDSM database. Specifically, it consists of 43 images containing MC clusters (29 malignant and 14 benign) and 43 images without abnormalities. The sample has been processed with the AW and the IW enhancement methods and reviewed by two experienced qualified radiologists, using two high-resolution display monitors. Comparative evaluation was performed between original plus AW-processed and original plus IW-processed images with respect to the detection (five-point rating scale), morphology characterization (four categories) and pathology classification (five levels of confidence) of MC clusters, according to BIRADS lexicon.

Results: Detection accuracy of the method based on original plus AW-processed images is higher according to ROC analysis (area under the ROC curve, $A_z = 0.98$), than those of the method based on original plus IW-processed images ($A_z = 0.94$). Morphology characterization accuracy of the method based on original plus AW-processed images is better (18.6% increase). For pathology classification accuracy, high performance (~70%) is achieved for both enhancement methods as compared to radiologists' assessments of DDSM database (~63%), according to Wilcoxon signed ranks test.

Scientific Sessions

Saturday

Conclusion: The AW contrast enhancement method demonstrates improved performance for detection, morphology characterization and pathology classification of MC clusters on dense breast parenchyma, as compared to IW contrast enhancement method.

B-323 10:48 ♀

Computer-aided diagnosis as a second reader for nodule detection in chest radiographs versus single and double reading

A.M.R. Schilham, B. van Ginneken; Utrecht/NL

Purpose: Instead of using Computer-Aided Diagnosis (CAD) only for generating prompts at suspicious areas, we assess the potential of a CAD system as an independent second reader for lung nodule detection in chest radiographs, compared to single and double reading.

Method and Materials: The public JSRT database was used, containing 154 chest radiographs with a single proven lung nodule and 93 normal cases. Five experienced radiologists and one resident participated. All cases were read by one radiologist and by the resident. A CAD system developed by the authors was used as an independent second reader, operating at 7 markers on average per case (marking 68% of the nodules). Observers marked regions suspect of being a nodule, and assigned a suspicion score, using a low threshold on confidence. Scores were scaled to make observers comparable. Independent double reading was simulated by averaging probabilities of matching regions, with zero probability for missing regions. Performance was assessed with localized ROC curves. Results are given as sensitivities at a clinically important, low false positive referral rate of 0.02.

Results: Single reading sensitivities of radiologists and resident were similar: 0.13. The JSRT database contains many subtle nodules which may explain these low sensitivities. With double reading, the sensitivity increased to 0.40. Using CAD as a second reader gave a sensitivity of 0.27.

Conclusions: Using CAD as an independent double reader outperforms single reading. The sensitivity at low false positive referral rate is doubled. Human double reading is superior to CAD double reading.

B-324 10:57

Clinical evaluation of the sensitivity and specificity of a software for automated detection of lung nodules in preliminary CT examinations

J. Gurung, A. Wetter, T.J. Vogl; Frankfurt a. Main/DE

Purpose: To evaluate the efficacy (sensitivity/specificity) of a software for automated detection of intrapulmonary nodules in multidetector CT examinations.

Materials and Methods: The "Nodule Enhanced Viewing" (NEV) algorithm of Siemens LungCare was applied to 16-row multidetector CT (MDCT) examinations in 20 patients [Somatom Sensation, Software VB10A; tube-voltage 140 kVp; tube-current 120 mAs ($n = 11$) and 80 mAs ($n = 9$); 5 mm slice thickness; 1.5 mm reconstruction increment; lung kernel B60f] with a total of 510 intrapulmonary nodules. The nodules were first evaluated by 2 experienced radiologists and taken as control. The nodules detected by NEV were evaluated and compared by the radiologists for their genuinity and specificity. A nodule was considered correctly detected when both radiologists agreed in concordance. Factors influencing detectability were evaluated like diameter, location, density and overlapping of intrapulmonary blood vessels.

Results: Of 539 nodules detected by NEV, 166 co-related with nodules detected by the radiologists with sensitivity rate of 66.13% and specificity rate of 30.77%. Detection was not affected by location or density of the nodules. Detection was however affected by diameter (nodules with diameter > 1 cm were not detected). Over detection by NEV was attributed to localisation of overlapping blood vessels as nodules. NEV detected 7 additional nodules that were missed by the radiologists. Via NEV, nodules were detected that were shadowed by partial volume effect from bones and soft tissues.

Conclusion: NEV as sole algorithm for detection of lung nodules is not a dependable instrument but it has its advantage in detecting nodules usually shadowed by soft tissues and bones.

B-325 11:06 ♀

A visualization-based method for pulmonary emboli identification within high-resolution CT images

A.P. Kiraly¹, D.P. Naidich², C.L. Novak¹; ¹Princeton, NJ/US, ²New York, NY/US

Purpose: Contrast-enhanced high-resolution CT provides an effective means for detecting pulmonary emboli (PE). However these large datasets require tedious evaluation. We propose and evaluate a visualization method for rapid PE detection with high sensitivity and acceptable false positive (FP) rates.

Methods and Materials: Interactive 3D visualization of pulmonary vessel trees with Hounsfield unit (HU) values determining rendering color is utilized. Preprocessing consists of vessel segmentation and path-based labeling. Each element of the vessel tree is rendered with the color determined by HU values along a path to the vessel centerline. As a result, the entire vessel tree may be visualized simultaneously, with dark regions pointing to potential PE inside specific arteries. Classification is further applied to reduce false positives. Evaluation was performed on 13 patients, including 10 positive cases containing 128 emboli. Each visualization was examined and dark regions were marked, requiring about 5 minutes per patient. These markings were compared against ground truth to evaluate sensitivity and FP rates.

Results: Sensitivity equaled 72% of 114 emboli within the vessel segmentation or 64% for all emboli. The segmentation occasionally missed the main and lobar pulmonary arteries and hence missed 14 (11%) emboli. However, radiologists are unlikely to miss centrally located emboli. The average FP rate was 9.2/patient. Many FPs stemmed from segmentation errors and could be trivially dismissed.

Conclusion: Our method demonstrated good sensitivity for segmental and sub-segmental emboli with an acceptable FP rate. This visualization may provide a powerful tool, specifically in the identification of smaller peripheral PE.

B-326 11:15 ♀

Large evaluation of fully automatic colon tracker for CT colonoscopy

R. Tryoen¹, M. Medved², G.A.F. Schoonenberg³, R.E. van Gelder⁴; ¹Best/NL, ²Ljubljana/SI, ³Eindhoven/NL, ⁴Amsterdam/NL

Purpose: To evaluate the performance of a fully automatic colon tracker on a large set of CT colon cases. This automated preprocessing is intended to further facilitate primary 3D inspection of CT colon exams.

Method and Materials: CT scans of 185 patients (prone + supine) were retrospectively identified out of a larger colon study (1). After patient preparation multi-detector CT scans were performed (Mx8000 Philips Medical Systems) with parameters: 120 kV; 25-100 mAs; collimation 4x2.5 mm; slice thickness 3.2 mm. Scans were automatically processed by using a prototype based on EasyVision/ViewForum functionality (Philips Medical Systems). After background and lung removal, all air-filled parts were tracked and connected using anatomical knowledge. After comparison to a centerline defined by an expert the sensitivity (percentage of expert centerline found) and positive predictive value (percentage of tracked parts that were colon) were calculated before and after anatomy-based connection.

Results: The colon had no obstructions in 33% of the cases, few in 56% and many (3 or more) obstructions in the remaining 11%. Before applying anatomy-based connection 94% of the expert centerline was found (sensitivity) while 71% of the found parts were colon (positive predictive value). Anatomy-based connection increased the positive predictive value to 95%, at the cost of a reduced sensitivity (88%) caused by few cases where the anatomy-based connection fails.

Conclusion: Without anatomy-based connections the full colon centerline was found.

Automatic connection is feasible and dramatically reduces overdetection, but can fail in some cases. (1) Van Gelder RE et al. Gastroenterology 2004;127:41-48.

B-327 11:24

Evaluation of an automated polyp measurements tool compared with experienced observers: A comparative study

A. Jerebko¹, S. Lakare¹, T. Mang², C. Mueller², D. Salovic³, W. Schima², J. Weßling⁴, L. Bogoni¹; ¹Malvern, PA/US, ²Vienna/AT, ³Tournai/BE, ⁴Münster/DE

Purpose: Polyp size assessment could be critical for decision on a patient management. This comparative study was performed to assess the quality of 3D automatic segmentation, reliability and accuracy of automatic polyp measurement versus experienced radiologists.

Methods and Materials: An automatic polyp measurement tool was designed to allow the measurement of a polyp, along largest axial slice across the polyp (given fixed window-level). 44 polyps ranging in size from small (< 6 mm, $n = 18$), medium (6-9.9 mm, $n = 20$) and large (> 10 mm, $n = 6$) were measured and segmented by five radiologists (each performing VC on regular basis).

Results: The median difference of automatic and median manual measurements across all radiologists was 0.4285 mm (less than the average voxel size in the participating studies). Accuracy of automatic measurement was found to be highest in polyps in the 4 to 8 mm range. Two polyps out of 44 were automatically measured smaller by more than 1 mm than any of participant measurements. One small polyp located on a very thin fold was over measured by 4 mm since portion of the fold was erroneously included in the automatic segmentation of the polyp.

Conclusion: 3D automatic segmentation provided accurate measurements within expert inter-observer variability boundaries in 93% of polyps.

Scientific Sessions

B-328 11:33

Automatic registration of multiphase dynamic contrast multidetector CT (MDCT) studies for the diagnosis of small hepatocellular carcinoma (HCC)
G.-Q. Wei¹, F. Yan², P. Xu², W. Cheng², X. Zeng¹, J.-Z. Qian¹, L. Fan¹, C.-C. Liang¹; ¹Princeton Junction, NJ/US, ²Shanghai/CN

Purpose: Automated accurate localization of the same HCC across multiphase MDCT scans is desirable for efficient evaluation of its enhancement pattern and for diagnosis. This work is to develop and evaluate an automatic method for accurately registering multiple phase CT liver images.

Methods and Materials: 35 contrast-enhanced MDCT studies were acquired at pre-contrast, arterial and portal venous phases. Three physicians marked suspicious small HCCs (< 30 mm) by consensus in each scan, resulting a total of 41 lesions (9-27 mm) to be used as reference. The liver volume is first extracted using a fuzzy-segmentation technique in each phase. An intensity weighting method is then applied to suppress non-liver anatomies. A cross-correlation method is employed to find corresponding slices among different phases. A correspondence is defined as 'hit' if the error in registered position falls within the nodule radius.

Results: The hit rate for all 41 small HCCs was 82.9% between pre-contrast and arterial phases, and 90.2% between arterial and portal venous phases. The hit rate for simultaneous hit across all 3 phases was 78%. The mean registration error was 0.4 slices (maximum 2 slices). The higher hit rate between arterial and portal venous phases was attributed to a more accurate segmentation of the contrast enhanced liver area than at the pre-contrast phase.

Conclusion: The proposed intensity-weighted cross-correlation method effectively achieves accurate registration of small HCCs across multiphase MDCT liver scans. This method offers a base on which efficient tools may be developed to aid physicians in the detection and diagnosis of small HCCs.

B-329 11:42

A 3D CAD tool for body fat identification

D. Illea¹, O. Ghita², K. Robinson², M. Lynch², P.F. Whelan²; ¹Brasov/RO, ²Dublin/IE

In recent years non-invasive medical diagnostic techniques have been used widely in medical investigations. The distribution of fat tissue in the body is an important measure of health and overall fitness and is not well quantified by the body mass index (BMI) which is currently the measure most widely used to quantify body fat content. The aim of this work is to present the development of a fully automatic CAD tool that can be applied to identify the actual fat mass in MR data. The MR acquisition protocol currently in use involves imaging the patient in a number of successive coronal sections in order to achieve a full body scan. As the grayscale in-homogeneities between adjacent sections are quite significant, to make this data suitable for automated CAD we have been forced to devise a procedure to alleviate as much as possible the discontinuities in the unprocessed data. The devised unsupervised segmentation algorithm that is applied to segment the fatty tissues has three main steps. The first step pre-processes the data using a feature preserving diffusion-based technique to improve the local homogeneity and reduce the level of image noise. The second step extracts the image areas representing fat tissues by using an unsupervised clustering algorithm. Finally, image refinements are applied to reclassify the pixels adjacent to the initial fat estimate and to eliminate outliers. The devised CAD tool has been tested on a database of 42 patients and the experimental data indicates that the proposed tool returns accurate results.

B-330 11:51

Development of white matter tractography using 3D density field in diffusion tensor (DT) MR imaging

S. Kumazawa, T. Yoshiura, F. Mihara, H. Honda, Y. Higashida, F. Toyofuku; Fukuoka/JP

Purpose: Conventional tractography algorithms fail to trace the path at the crossing or branching of the fiber tracts. Our goal was to develop a new white matter tractography algorithm in DT-MR imaging which permits fiber tracts crossing and branching.

Method and Materials: To express the distribution of tract density based on the geometric nature of the DT within a voxel, we defined a polarized metaball which had a 3D Gaussian distribution of positive or negative density. Using a self-organizing map, voxels in DT-MR imaging were classified into three clusters according to the geometric measures of DT as follows: 1) linear diffusion (LD) cluster, 2) planar diffusion (PD) cluster, and 3) spherical diffusion (SD) cluster. Positive and negative metaballs were generated on each voxel of LD cluster and SD cluster, respectively. No metaball was assigned to the PD cluster. By summat-

ing effects of all metaballs in the voxel space, a map of density field of tracts was generated. In this tract density field, our algorithm tracked voxels with a density larger than a certain threshold value. We tested the algorithm on human brain DT-MR imaging datasets. The human brain data consisted of 6 diffusion-weighted image volumes ($b = 800 \text{ s/mm}^2$) and an unweighted image volume ($b = 0 \text{ s/mm}^2$) with a 128x128 in-plane resolution.

Results: Our algorithm could track major white matter tracts beyond the fiber crossing in the human brain datasets.

Conclusion: We developed a new tractography algorithm which permits tracking through crossing and branching. Efficacy of our new method was demonstrated in human brain data.

10:30 - 12:00

Room P

Vascular

SS 615

Post therapeutic follow-up and monitoring of disease

Moderators:

A.A. Azarine; Paris/FR
N. Matsunaga; Ube City/JP

B-331 10:30

MR assessment of collateral blood flow and cardiac function in acute experimental aortic coarctation before and after self-expandable stent placement

C.B. Henk, M. Saeed, O. Weber, A. Martin, M. Wilson, C.B. Higgins; San Francisco, CA/US

Purpose: The purpose of this study was to determine the acute effect of aortic coarctation on collateral flow and LV function in a dog model before and after endovascular repair.

Methods: In seven dogs, the descending aorta (DAO) was dissected distal to the left subclavian artery and looped with a plastic band which was tightened to reduce distal pressure to 40-50 mmHg. Imaging / intervention was done in an XMR suite containing two systems; MR (1.5 T Intera) and X-ray fluoroscopy system (Integris V5000) (Philips Medical Systems) connected by a movable tabletop. The retrospectively-gated FFE (VEC-MR, TR/TE/flip = 8.3/5.1 ms/15°, 16/RR, VENC = 50-200 cm/s) and B-TFE (TR/TE/flip = 4/2 ms/70°, 18/RR) were used for flow measurement / cardiac function. Aortic flow measurements were obtained proximal and 1 cm distal to the coarctation and at the diaphragm level. A self-expandable nitinol stent was placed across the coarctation.

Results: DAO flow changed after creation of the coarctation (proximal = 0.84 l/min, distal = 0.28 l/min, diaphragm = 0.83 l/min) compared to baseline (at subclavian artery = 1.46 l/min, diaphragm = 1.29 l/min). The greater flow at the diaphragm suggests that development of collateral flow is a rapid process. Stent deployment increased aortic flow distal to the stent (0.76 l/min). Cine MR imaging showed increase in LV volumes with coarctation. Coarctation reduced mean blood pressure from 110 ± 10 to 45 ± 8 mmHg. Stenting restored phasic and mean pressure.

Conclusions: The left ventricle and major vessels adjust rapidly to acute aortic coarctation. MR imaging provides quantitative assessment of aortic blood flow and cardiac function as well as immediately demonstrating the success of the intervention.

B-332 10:39

Arteries arising from the aneurysmal sac as a cause of type 2 endoleak after endovascular treatment of abdominal aortic aneurysms: Study of 115 patients

M. Gola, R. Pacho, L. Bakoñ, L. Grabowska, P. Palczewski; Warsaw/PL

Purpose: To evaluate the role of arteries arising from the AAA sac in the development of type 2 endoleak in patients treated endovascularly with stentgrafts for AAAs.

Methods and Materials: 115 patients were treated endovascularly for AAAs. All patients had a CT examination prior to the endovascular treatment and follow-up CTs performed at 6 month intervals (max. time of follow-up: 3 yrs).

Results: On the CT examination prior to endovascular treatment, patent inferior mesenteric artery, lumbar arteries or medial sacral artery were visualized in 72 patients. On follow-up CTs, patent arteries arising from the AAA sac were found in 43 patients; in 9 patients type 2 endoleak was observed. In 1 case the endoleak resolved spontaneously. In 1 case the endoleak was increasing and embolization

Scientific Sessions

of the IMA was necessary. In the remaining 7 cases, symptoms of endoleak and diameter of AAA did not increase.

Conclusion: Prophylactic embolization of arteries arising from the AAA sac is not needed prior to endovascular treatment. We suggest that intervention should be carried out when there is an increase in the symptoms of endoleak and/or in the diameter of AAA.

B-333 10:48

Evaluation of experimental implanted occlusions in a stent-tube-model with a cone-beam flat-panel volumetric-CT (FP-VCT)

G. Heidrich, F. Melderis, C. Dullin, K.-P. Hermann, E. Grabbe, M. Funke; Göttingen/DE

Purpose: The aim of this experimental study was stenosis evaluation and plaque quality assessment in a stent-tube-phantom using a cone-beam flat-panel volumetric CT (FP-VCT).

Methods and Materials: Balloon catheters from 2 to 5 mm filled with substances of different densities and X-ray attenuations were implanted in a 7 mm stent-tube-phantom to simulate occlusions with air embolism, soft or hard plaques. This phantom was scanned in a FP-VCT with an isotropic spatial resolution of 200 imx200 im. Volume-rendered images, being postprocessed on a workstation, were analysed with respect to the visibility of the stenosis diameter, the plaque quality and the residual lumen. Data analysis was performed based on a five or seven point evaluation scale.

Results: An excellent assessment of the intraluminal conditions was demonstrated. Independent from the balloon position the residual lumen could be reliably visualised up to 100 im. Concerning the assessment of the media in axial reformations, 71% of the simulated soft and hard plaques and 100% of the simulated air emboli reached the highest level of the evaluation scale, in sagittal reformations 86% of the hard plaques. 86% of the soft plaques and 71% of the air emboli showed a good identification of the residual lumen, 57% of the hard plaques showed a good identification. 19% of the balloon catheters showed the claimed size by the company, 81% a deviation between 0.1 and 0.3 mm.

Conclusion: In experimental preclinical use FP-VCT is an excellent diagnostic modality for evaluation of vessel reocclusions after stent implantation. In addition the quality of the plaque material could be exactly determined.

B-334 10:57

Active bleeding in a physiological phantom: Detectability on digital subtraction angiography (DSA) versus multislice CT (MCT)

S.H. Roy-Choudhury, D. Gallacher, J. Pilmer, P. Woodburn, G. Fowler, J. Steers, P. Morales, S. Rankin, A. Adam; London/UK

Purpose: To establish the lower threshold of bleeding detectable with DSA and MCT and the relative sensitivity of these two imaging modalities.

Methods: A closed pulsatile cardio-pulmonary bypass circuit was connected to tubing that ran through a water bath. Three smaller interconnecting 4 mm perspex tubes (no holes, 100 µm hole and 250 µm hole) were used to mimic bleeding arteries. Leak rates were predetermined with a cardiac output of 4.0 l and 2.5 l and with mean arterial pressure (MAP) of 10 to 100 mm of Hg for each hole size. 16-slice-CT was performed using bolus tracking after 35 ml of intravenous contrast was injected into the venous limb. DSA was performed with a 4F straight catheter placed at the holes and with the catheter 10 cm proximal to the holes. Cine-loops of MCT and DSA were read by 2 blinded observers.

Results: The lower limit of MCT was 0.30 ml/min while that of DSA with the catheter 10 cm proximal to the holes was 0.78 ml/min. Detection improved with increasing MAP with CT failing to detect leaks below MAP of 30 mm Hg. DSA with the catheter at the site of the holes was more sensitive (0.25 ml/min or less) and was independent of MAP.

Conclusion: In vitro, MCT is more sensitive than DSA in detecting active haemorrhage unless catheter position is highly super-selective, especially in presence of a MAP of 40 mm Hg and above. Time permitting, CT should be used as initial modality in diagnosis of active haemorrhage.

B-335 11:06

Value of high resistance index - HRI calculated from Doppler spectrum of popliteal arteries in patients with systemic lupus erythematosus (SLE)

A. Walecka, M. Sawicki, M. Brzosko, L. Ostanek, K. Fischer, J. Kordowski; Szczecin/PL

Purpose: HRI is a new Doppler index calculated as a ratio between S - maximal systolic flow and D - maximal early diastolic reversed flow - HRI=D/S. The aim of the study is to evaluate the diagnostic significance of HRI calculated from the Doppler spectrum of popliteal arteries in patients with systemic lupus

erythematosus (SLE), with and without secondary antiphospholipid syndrome (SAPS), compared with healthy controls.

Methods and Materials: During a 9-month period (May 2003 - January 2004), 93 patients (81 women and 12 men) with SLE (including 24 patients with SAPS) and 30 healthy controls (24 women and 6 men) underwent bilateral duplex Doppler examinations of lower limb arteries. The examinations were performed using HDI 3500 (ATL) with 5-12 MHz linear transducer under standardized conditions: correct insonation angle and sample volume size, with the patient in a supine position, after 10 minutes rest.

Results: Mean HRI value obtained in the control group was 0.415 (range 0.305-0.555; median 0.402). In the group of SLE patients without SAPS, mean HRI value was decreased to 0.320 (range 0-0.584; median 0.334) and even lower - 0.283 in SLE patients with SAPS (range 0.106-0.545; median 0.291).

Conclusion: Small arteries, arterioles and capillaries are the main affected vessels in SLE. This chronic process probably stimulates circulation through lower resistance collaterals, decreasing HRI value. The Doppler HRI calculation can be valuable in early diagnosis and monitoring of lower extremity vascular changes in patients suffering from SLE with and without SAPS.

B-336 11:15



Alterations in ocular artery blood flow in patients with type II diabetes mellitus

S. Mylona, A. Kokkinaki, E. Gamvroula, L. Thanos, E. Karaxaliou, N. Mpatakis; Athens/GR

Purpose: To study blood flow alterations in the ocular arteries in patients with diabetes mellitus type II, with or without retinopathy, according to the duration of diabetes, using color Doppler ultrasound.

Material and Method: During a 6-month period we performed color Doppler ultrasound in 50 type II diabetic patients and compared them with a control group of 50 healthy individuals of similar age range. We measured peak systolic and end diastolic velocity in the ophthalmic artery (OA), the central retinal artery (CRA) and the common carotid artery (CCA). We classified patients according to the duration of diabetes (which ranged from 5 to 40 years), and whether retinopathy (of different grades) was present. The presence of systemic hypertension was noted. Patients with other ophthalmic diseases were excluded. In addition we measured glycosylated hemoglobin and serum ferritin, which are elevated in diabetic retinopathy.

Results: A decrease was observed in flow velocity in patients with sub clinical, initial, moderate, proliferative or severe retinopathy, whereas no decrease was observed in diabetics without retinopathy and in the control group. The mean velocity ratio of CRA/CCA was lower in diabetics with severe retinopathy. Ocular blood flow was significantly lower in diabetics without systemic hypertension than in controls.

Conclusion: In diabetic eyes, decreased ocular blood flow velocity and high levels of glycosylated hemoglobin and serum ferritin may indicate risk of progression of diabetic retinopathy.

B-337 11:24

Ultrasound assessment of endothelial dysfunction in obstructive sleep apnea hypopnea syndrome (OSAHS) before and after continuous positive airway pressure (CPAP) therapy

K. Pagonidis, I. Lambiri, D. Tsetis, S. Schiza, S. Yarmenitis, N. Siafakas, N. Gourtsoyannis; Iraklion/GR

Purpose: Epidemiological studies have implicated OSAHS as an independent comorbid factor in cardiovascular and cerebrovascular disease. We discuss the induction of endothelial dysfunction as a possible mechanism. We evaluated endothelial function by high-resolution ultrasonography in patients with OSAHS before and after CPAP therapy by measuring endothelium-dependent (flow-mediated dilatation, FMD) and endothelium-independent (nitroglycerin mediated dilatation, NMD) vasodilator function of the brachial artery.

Materials and Methods: We evaluated 13 pts with OSAHS and 12 control subjects with a mean age 50.08 ± 8.94 years and 39.17 ± 5.69 years respectively and BMI 36.39 ± 7.3 and 33.02 ± 4.87 respectively. FMD and NMD of the brachial artery were measured by high-resolution ultrasonography. In the patient group, measurements were repeated 24 hours and one month after CPAP therapy. The average of 5 consecutive cardiac cycles was used for all measurements. FMD and NMD were expressed as the percent increase in vessel diameter from baseline.

Results: Patients before treatment, compared with control subjects had lower brachial FMD ($4.39 \pm 1.61\%$ vs. $13.04 \pm 1.23\%$; $p < 0.0001$) and comparable NMD (14.04 ± 6.4 vs. $16.4 \pm 2.1\%$; $p = 0.1427$). After CPAP treatment the FMD

Scientific Sessions

increased and was significantly higher compared with FMD before treatment ($4.39 \pm 1.61\%$ vs. $6.23 \pm 2.28\%$; $p = 0.0017$ after 24 hours and $4.39 \pm 1.61\%$ vs. $9.52 \pm 1.5\%$; $p = 0.0002$ after one month). In contrast, the NMD was not significantly altered 24 hours and one month after treatment ($15.37 \pm 6.02\%$; $p = 0.583$ and $15.68 \pm 4.84\%$; $p = 0.326$, respectively).

Conclusion: Obstructive Sleep Apnea Hypopnea Syndrome is associated with an impairment of endothelial function, as assessed by high-resolution ultrasonography, which improves promptly even 24 h after CPAP therapy.

B-338 11:33

Dynamic contrast-enhanced MR imaging or diffusion-weighted MR imaging for monitoring the effect of a vascular targeting agent on rodent tumors?

H.C. Thoeny¹, F. De Keyzer², V. Vandecaveye², F. Chen², C. Boesch¹, Y. Ni², W. Landuyt², G. Marchal², R. Hermans²; ¹Berne/CH, ²Leuven/BE

Purpose: To compare dynamic contrast-enhanced MR imaging (DCE-MRI) and diffusion-weighted MR imaging (DW-MRI) for noninvasive evaluation of early and late effects of a vascular targeting agent in a rat tumor model.

Material and Methods: Thirteen rats with rhabdomyosarcomas in both flanks underwent DCE-MRI and DW-MRI in a 1.5 T MR unit, before and early (1 and 6 hours) as well as later (2 and 9 days) after intraperitoneal injection of Combretastatin A-4 phosphate (CA-4-P). Histopathologic correlation was obtained at each time point. To differentiate the influence of perfusion and diffusion, the ADC was calculated for low ($b = 0, 50, 100 \text{ sec/mm}^2$; ADC_{low}) and high b values ($b = 500, 750, 1000 \text{ sec/mm}^2$; ADC_{high}). An indicator for the influence of perfusion was arbitrarily defined as the difference between these two values (ADC_{perf}). DCE-MRI was quantified by the volume transfer constant k and the initial slope of the contrast-time-curve.

Results: Early after CA-4-P administration, k , initial slope as well as ADC_{perf} decreased significantly ($p < 0.001$), while ADC_{high} remained essentially unchanged; histology showed still viable tumor tissue. At two days the necrotic tumor fraction increased markedly, whereas at nine days regrowth at the tumor periphery was histologically confirmed. ADC_{high} increased at two days and decreased at nine days. In turn, k , initial slope and ADC_{perf} increased at nine days. Changes in ADC_{perf} correlated with changes in k ($R^2 = 0.46$) and in initial slope ($R^2 = 0.67$).

Conclusion: Both DCE-MRI and DW-MRI allow monitoring of tumor perfusion changes by vascular targeting agents and correlate directly. DW-MRI provides additional information regarding cell viability versus necrosis.

B-339 11:42

Multiphase multidetector-row CT in abdominal aortic aneurysm treated with endovascular repair (EVAR): Are unenhanced and delayed phase enhanced images really effective for the detection of endoleaks?

R. Iezzi, F. Quinto, A. Pierro, F. Di Fabio, A. Filippone, A.R. Cotroneo; Chieti/IT

Purpose: To determine the true usefulness of performing unenhanced (UNE) and delayed phase enhanced (DEP) in addition to arterial phase enhanced (HAP) Multidetector-Row CT (MDCT) images for detecting endoleaks after EVAR.

Method and Materials: Fifty patients with abdominal aortic aneurysms treated with EVAR underwent long-term follow-up MDCT (at 1, 6 and 12 months). Unenhanced CT-images were obtained with a 2.5-mm collimation and a 5-mm slice thickness; arterial and delayed CT-images were obtained using a 1-mm collimation and a 1.25-mm slice thickness. Two independent readers were asked to assess the presence of endoleak, according to a five-point confidence scale. At 1 month, CT images were evaluated in four reading sessions, as follows: A) HAP; B) UNE + HAP; C) HAP + DEP; D) UNE + HAP + DEP. At 6- and 12-month follow-up a fifth reading session was added, including pUNE (1-month unenhanced phase CT-images) + HAP (E). Sensitivity, specificity and diagnostic accuracy of each reading session were compared.

Results: Sensitivity, specificity and diagnostic accuracy of session B were significantly higher ($p > 0.05$) than those obtained with A and C reading sessions. No statistically significant differences were found between values obtained with session B and session D. At 6 and 12-months follow-up session E showed similar values than session B.

Conclusions: The addition of UNE to HAP is truly effective for detection of endoleaks only at 1-month follow-up. Delayed phase does not statistically increase diagnostic accuracy in detecting endoleak.

B-340 11:51

Peripheral artery stent visualization and in-stent re-stenosis analysis in 16-row computed tomography: An in-vitro evaluation

C. Herzog, J.O. Balzer, M.G. Mack, T. Lehnert, W. Schwarz, S. Zangos, K. Eichler, T.J. Vogl; Frankfurt a. Main/DE

Purpose: To assess the accuracy of 16-row multidetector CT in the visualization of different peripheral artery stents and the appraisal of in-stent re-stenosis.

Methods: Twenty-seven stents, made of different material (steel, nitinol) and size (6-10 mm) were analyzed in a barrel-shaped (130 HU) vascular model. Low-grade ($\leq 40\%$) and high-grade ($\geq 60\%$) in-stent re-stenosis was simulated by polyurethane sticks (70 HU) with a defined length and diameter (2-6 mm) placed inside each stent. Imaging was performed parallel and perpendicular to the stent axis (scanning parameters: $16 \times 0.75 \text{ mm}$ detector collimation, 130 mAs , 120 kV , 12 mm table feed/rotation, 1.0 mm slice thickness and 0.5 mm increment). Stent diameter, strut thickness, intraluminal attenuation values, degree and length of in-stent re-stenosis were evaluated.

Results: Nitinol stents showed significantly less stent lumen narrowing ($27.4\% \pm 8.9\%$ vs. $32.3\% \pm 6.5\%$; $p < 10^{-6}$) and artificial strut thickening ($1.48 \text{ mm} \pm 0.14$ vs. $1.58 \text{ mm} \pm 0.13$; $p < 10^{-4}$) than stainless steel stents, distinctly less in-stent attenuation changes, less underestimation of the degree and less overestimation of the length of the in-stent stenosis. Stent lumen narrowing and in-stent attenuation values were significantly lower in 10 mm stents than in 8 mm ($p < 10^{-4}$) or 6 mm ($p < 10^{-6}$) stents; artificial strut thickening and overestimation of in-stent re-stenosis was significantly lower in 10 mm ($p < 10^{-6}$) and 8 mm ($p < 0.04$) stents than in 6 mm stents. High-grade in-stent re-stenosis was significantly ($p = 0.01$) more overestimated than low-grade stenosis.

Conclusions: 16-row MDCT allows for the reliable detection of in-stent re-stenosis and the differentiation between low- and high-grade re-stenosis under in-vitro conditions. The effective degree of re-stenosis is still significantly overestimated, preventing an accurate distinction particularly between total stent occlusion and high-grade re-stenosis.

14:00 - 15:30

Room A

Cardiac

SS 703a

MDCT of the coronary arteries

Moderators:

R. Marano; Chieti/IT

I. Mastorakou; Athens/GR

B-341 14:00

64-slice coronary CT angiography: Heart rate dependency of image quality at 0.33 s/360° gantry rotation

B.J. Wintersperger¹, K. Nikolaou¹, C.R. Becker¹, F. Ziegler¹, T. Johnson¹, T. Flohr², C. Rist¹, A. Knez¹, M.F. Reiser¹; ¹Munich/DE, ²Forchheim/DE

Purpose: The purpose of this study was to evaluate the impact of a $0.33/360^\circ$ rotation on image quality of coronary CTA in relationship to the patients' heart rate (HR) using a 64-slice scanner.

Material and Methods: Coronary CTA data sets of 32 patients (HR 53-92) examined on a 64-slice scanner system (Sensation 64, Siemens) with a $0.33 \text{ s}/360^\circ$ gantry rotation were evaluated. A standardized protocol with $64 \times 0.6 \text{ mm}$ collimation and automated contrast injection (Spectris, Medrad) of iopromide (Ultravist 300, Schering) was implemented. Data was reconstructed in 50 ms intervals throughout the RR-Interval and reviewed by 2 observers. At $\text{HR} > 65$, single- and dual-sector reconstruction was performed and image quality rated using a 3-point scale from excellent (1) to non-diagnostic (3) for coronary segments. Quality was correlated to the HR and the benefit of multi-sector reconstruction evaluated.

Results: Diagnostic quality was achieved in all patients. Mean image quality for $\text{HR} \leq 65 \text{ bpm}$ was 1.16 compared to 1.57 in $\text{HR} > 66 \text{ bpm}$ ($P = 0.01$). Dual-sector reconstruction did not significantly improve quality in $\text{HR} > 66 \text{ bpm}$ (1.71 ± 0.43 vs. 1.65 ± 0.30 ; $P = 0.62$). While in $\text{HR} \leq 70 \text{ bpm}$ best quality was consistently found in diastole, in $\text{HR} > 75 \text{ bpm}$ best quality was achieved in systole. Overall, image quality did not significantly correlate with HR ($R = 0.22$; $P = \text{NS}$).

Conclusion: Improved temporal resolution at 0.33 s rotation allows for diagnostic image quality within a wide range of HR even when using single-segment algorithm. However, with increasing HR the time point of best image quality shifts from mid-diastole to systole. Further studies are required to evaluate whether coronary imaging within systole affects the diagnostic value.

Scientific Sessions

B-342 14:09

Diagnostic accuracy of non-invasive 64-slice CT coronary angiography

F. Cademartiri, N.R. Mollet, C. van Mieghem, G. Runza, M. Belgrano, T. Baks, P.J. de Feyter, G.P. Krestin; *Rotterdam/NL*

Purpose: Evaluate diagnostic accuracy for the detection of significant obstructive coronary artery stenosis with a new 64-slice CT scanner.

Materials and Methods: We studied 30 patients (18 men, mean age 57.5 ± 6.7 years) with stable angina or an acute coronary syndrome prior to diagnostic conventional angiography. Only patients in sinus rhythm, who had never undergone angioplasty or bypass surgery and were able to breath-hold for 15 s, were included. Patients with pre-scan heart rates ≥ 70 bpm received oral β-blockade. The heart was scanned after intravenous injection of 100 ml contrast material (Iomeprol 400 mg/ml) at 5 ml/s with a 64-slice CT scanner (Sensation 64, Siemens, Germany) with the following parameters: slices/width 64/0.6 mm, gantry rotation time 330 ms, 700-900 mAs, 120 kV. Images were retrospectively reconstructed at 350 ms prior to the next R wave. The CT datasets were analysed by 2 observers unaware of the results of invasive angiography and all main coronary arteries and ≥ 1.5 mm branches were included for comparison with quantitative coronary angiography.

Results: Eighty-seven percent of the included patients received a β-blocker. The mean heart rate was 58 ± 7 bpm and the total scan-time was 13 ± 1 s. There were 47 significantly obstructed vessels. Sensitivity, specificity, positive and negative predictive value for detection of significantly obstructed vessels were 96% (47/49, 95% CI 86-97), 89% (63/71, 95% CI 79-95), 85% (47/55, 95% CI 73-95), and 97% (63/65, 95% CI 89-99) respectively.

Conclusions: 64-slice CT coronary angiography reliably detects significant coronary stenoses in patients with stable angina pectoris or an acute coronary syndrome.

B-343 14:18

High-resolution ex vivo imaging of coronary artery stents using 64-detector-row computed tomography with a z-axis flying focal spot technology. Initial experience

C. Rist¹, K. Nikolaou¹, T. Flohr², B.J. Wintersperger¹, M.F. Reiser¹, C.R. Becker¹; ¹Munich/DE, ²Forchheim/DE

Purpose: To test the potential of the new 64DCT scanner for the depiction of coronary artery stents in an ex-vivo setting.

Method and Materials: Three ex-vivo porcine hearts have been examined. Coronary artery stents of 3.0 and 2.5 mm diameter were implanted in the proximal right coronary artery. Ex-vivo hearts were scanned with a 16DCT (Somatom Sensation16, Siemens Medical Solutions; minimal slice-thickness 0.75 mm), and a new-generation 64DCT (Somatom Sensation64), applying a z-axis flying focal spot technology (minimal slice-thickness 0.6 mm). In all ex vivo hearts, lumen enhancement (HU) has been measured outside the stent lumen and within the stent lumen, using a region-of-interest of 2 mm diameter, on both the 16DCT and 64DCT images. Additionally, stent diameters have been measured.

Results: Assessing the vessel lumen enhancement, no significant differences between the 16DCT and 64DCT data was found outside the stent lumen (258 ± 20 HU vs. 245 ± 17 HU, respectively). CT densities derived from the 64DCT images were significantly lower as compared to densities measured on the 16DCT images (345 ± 35 HU vs. 398 ± 43 HU, respectively). Also, stent diameters could be assessed more exactly on the 64DCT images. With a known stent diameter of 3.0 and 2.5, measured diameters were 3.1 and 2.6 for the 64DCT scanner, and 3.3/2.8 using the 16DCT system, respectively.

Conclusions: With the new 64DCT using a z-axis flying focal spot technology, assessment of vessel lumen opacification within a coronary artery stent and the true stent diameter can be assessed more accurately as compared to a 16DCT system, due to a significantly higher spatial resolution.

B-344 14:27

Evaluation of coronary artery by-pass: Multi-slice CT assessment of artery and venous surgery graft

M. Sperandio, A. Romagnoli, M. Tomassini, M. Di Roma, L. Pellegrino, G. Simonetti; *Rome/IT*

Purpose: Our aim was to investigate the accuracy of the multislice spiral computed tomography (MSCT) in the detection of significant obstruction in the artery and venous grafts in symptomatic patients, who have undergone coronary artery bypass grafting.

Methods and Materials: In 126 patients (105 male, mean age 58 ± 5 years) with suspected graft anastomosis obstruction or a possible coronary artery stenosis,

a MSCT (GE Light Speed-16, collimation: 16 x 0.625 mm) was performed 20 days before the coronary angiography (CAG) that was regarded as the standard of reference. In total we studied 350 by-passes (90 internal mammary artery grafts and 260 aortocoronary saphena grafts).

Results: In all patients the MSCT was carried out without complications. Of 350 by-passes we could analyze completely 320 grafts, the other grafts were excluded for the presence of artefacts due to rapid heart rate during the contrast scan. Considering only the segments judged evaluable, we calculated a sensitivity of 97% and specificity 100%.

Conclusion: Using a scanner with a collimation of 16 x 0.625 mm, our study confirms the potential role of MSCT in the detection of artery and venous graft disease with an important value of sensitivity and a very high specificity (100%), in particular in the detection of occlusions of the proximal anastomosis of venous grafts.

B-345 14:36

Multidetector-row cardiac CT before minimal invasive bypass surgery

C. Herzog, W. Schwarz, S. Zangos, J.O. Balzer, K. Eichler, M.G. Mack, T.J. Vogl; *Frankfurt a. Main/DE*

Objective: To evaluate the benefit of multidetector-row cardiac CT (MDCT) before totally endoscopic coronary bypass (TECAB) procedures.

Material and Methods: 72 patients preoperatively underwent MDCT and quantitative coronary angiography (QCA). 38 patients were examined on a 4-row MDCT and 38 on a 16-row MDCT. Scanning parameters were: 4x1 mm / 12x0.75 mm collimation, 500 mm / 420 ms TI, 1.25 mm / 1.0 mm SD, increment 0.6/0.5 mm). Assesment criteria were: myocardial course of the coronary arteries, localization/degree of stenoses and localization/quality of atherosclerotic plaques. Finally the most suitable region for distal bypass touchdown was recommended. All findings were correlated to QCA and surgery.

Results: 4-row MDCT allowed evaluation of 79.4% of all segments of surgical relevance and 80.4% of all coronary segments. Values for 16-row MDCT amounted to 87.2% and 89.2%, for QCA to 91.7% and 96.3%. Calcified plaques were detected by 4- and 16 row MDCT in 100%, in QCA in 81.6%. Stenoses > 75% were detected by 4-row MDCT in 76.4%, by 16-row MDCT in 85.1% and by QCA in 100%. Intramyocardial coronary segments were identified by 4-row MDCT in 75%, by 16-row MDCT in 100% und by QCA in 20%. The site of distal bypass touchdown was predicted correctly by 4-row MDCT in 75.1%, by 16-row MDCT in 87.3% and by QCA in 80.1%.

Conclusion: 4 and 16-row MDCT were able to provide extended information on the coronary target site and therefore should be regarded as valuable planning tools before complex minimally invasive procedures such as TECAB or MIDCAB.

B-346 14:45

64-detector-row computed tomography of the coronary arteries: Initial experience

K. Nikolaou¹, C. Rist¹, B.J. Wintersperger¹, T. Flohr², T. Johnson¹, F. von Ziegler¹, A. Knez¹, M.F. Reiser¹, C.R. Becker¹; ¹Munich/DE, ²Forchheim/DE

Purpose: To compare the diagnostic value of a 64-detector-row CT system (64DCT) with that of invasive coronary angiography in the diagnosis of coronary artery disease (CAD).

Materials and Methods: 33 patients with known or suspected CAD underwent both 64DCT of the coronary arteries and invasive coronary angiography. For coronary CT angiography, a recently introduced 64DCT system (SOMATOM Sensation 64, Siemens Medical Solutions, Forchheim, Germany) was employed, using the following parameters: 64x0.6 mm slices; spatial resolution, 0.75x0.6x0.6 mm; gantry rotation time, 330 ms; temporal resolution, 83-165 ms; contrast agent, 80 ml; flow rate, 5 ml/s; retrospective ECG-gating. The MDCT-scans were analysed for signs of significant CAD (stenoses > 75%) on a per-patient basis, blinded to results from invasive angiography. Sensitivity, specificity and diagnostic accuracy in the detection or exclusion of significant CAD were evaluated.

Results: 31 of 33 (94%) coronary CT angiograms were of diagnostic image quality (image quality: 6% non assessable, 30% sufficient, 64% excellent). In the 31 patients available for comparison, invasive coronary angiography demonstrated significant CAD in 71% (22/31) and non-significant disease or normal coronary angiograms in 29% (9/31). Sensitivity, specificity, and diagnostic accuracy of 64DCT for the correct detection or exclusion of significant CAD on a per-patient basis were 95%, 89% and 94%, respectively.

Conclusion: 64DCT coronary angiography provides an increased spatial resolution with an isotropic sub-millimeter voxel size and an improved temporal

Scientific Sessions

resolution of 83-165 ms. These benefits hold great promise for the reliable diagnosis or exclusion of significant CAD.

B-347 14:54 ♀

Coronary angiography with 16-slice spiral computed tomography: Results in 180 patients

Y. Wang, Z. Jin, L. Kong, Z. Zhang, S. Zhang, S. Lin; Beijing/CN

Purpose: To evaluate the image quality of coronary CT angiography (CTA) and to determine the diagnostic accuracy of CTA for the assessment of coronary artery stenosis.

Methods and Materials: 180 patients (95 male, aged 63 ± 12) with suspected coronary artery disease were studied by a 16-slice spiral CT scanner: 0.42 s-rotation time, 16×0.75 mm collimation.; 47 of them underwent conventional coronary angiography (CAG). Contrast-enhanced scan (100 mL contrast agent IV at 4 mL/s) was performed during an approximately 20 s breath hold. The left main, left anterior descending, left circumflex and right coronary artery were evaluated for image quality which was divided into three classes, and screened for the presence of over 50% stenosis.

Results: In the evaluation of image quality with VRT images, there were 610 branches (85%) in the first class, 81 branches (11%) in the second class, and 29 branches (4%) in the third class. Logistic regression found that both heart rate and CT density in the root of the aorta had significant effect on image quality, regression coefficient beta was 0.296 and -0.010, respectively, $P < 0.05$. In comparison with CAG, the sensitivity, specificity, positive and negative predictive values of CTA to identify over 50% stenosis was 93% (50/54), 92% (123/134), 82% (50/61), and 97% (123/127), respectively.

Conclusion: 16-slice spiral CT coronary angiography permits reliable non-invasive detection of coronary artery stenosis with high image quality which is affected by heart rate and CT density in the root of the aorta.

B-348 15:03

A new way of looking at cardiac CT - polar maps of the coronary arteries

F. Schoth, G. Mühlensbruch, A.H. Mahnken, G.A. Krombach, R.W. Günther; Aachen/DE

Purpose: Contrast enhanced cardiac computed tomography (CT) opens up non-invasive evaluation of the coronary arteries. Yet the visualization of the coronary arteries requires curved MPR images or VRT, which are time-consuming to produce. In this study we applied polar maps of the coronary arteries to visualize the information of the complete coronary artery system on one single image.

Methods and Materials: 10 subjects (9 male, mean age 62.2 years) underwent contrast enhanced retrospectively ECG-gated cardiac MSCT (Sensation 16; Siemens, Erlangen, Germany) applying a standardized examination protocol (120 kV, 550 mAs/eff). Image reconstruction was performed at 60% of the RR-interval providing a voxel resolution of $0.35 \times 0.35 \times 1$ mm. Using a newly-developed algorithm the polar maps then provided a maximum intensity projection of the myocardium including the coronary arteries in polar coordinates. Unfold to two dimensions as planar projection, the polar maps were provided for evaluation. Visibility of the coronary arteries was rated on a scale from 0 (not visible) to 3 (good visibility).

Results: The visibility was rated as follows: LAD proximal 2.4 ± 0.7 , medial 2.2 ± 0.6 , distal 1.4 ± 0.9 ; RCA proximal 2.1 ± 0.7 , medial 1.9 ± 0.8 , distal 1.3 ± 0.8 ; RCX proximal 2.4 ± 0.6 , medial 1.8 ± 0.6 , distal 1.3 ± 0.7 . Stents and coronary calcifications were displayed accurately.

Conclusion: Polar maps of the coronary arteries provide information regarding morphology and patency of the coronary arteries in a single image. Therefore using this technique may speed up evaluation of contrast enhanced cardiac CT examinations.

B-349 15:12

Flat-panel detector CT for assessment of coronary artery stents:

Comparison with 16-slice spiral CT

A.H. Mahnken¹, T. Seyfarth², T. Flohr², C. Herzog³, S. Stanzel¹, R.W. Günther¹, J.E. Wildberger¹; ¹Aachen/DE, ²Forchheim/DE, ³Frankfurt a. Main/DE

Purpose: Evaluation of coronary artery stents is a major limitation of cardiac multislice spiral CT (MSCT). Development of flat-panel detector computed tomography (FPCT) with truly isotropic spatial resolution may overcome this limitation. Thus, we evaluated the use of FPCT in comparison to MSCT for the assessment of coronary artery stents.

Material and Methods: Eight different coronary artery stents with a diameter of 3 mm each were placed in a static chest phantom. The phantom was positioned

in the CT gantry at an angle of 0° , 45° and 90° towards the z-axis and examined with the prototype of a FPCT (Siemens, Forchheim, Germany) and a commercially available 16-slice spiral CT scanner (Sensation 16, Siemens). Slice thickness was 0.25 mm with FPCT while for MSCT an effective slice thickness of 1 mm with a reconstruction increment of 0.5 mm was used. Image quality was assessed visually using a five point grading scale. Stent diameters were measured and compared using a repeated measure ANOVA.

Results: When compared to MSCT artificial lumen reduction was significantly less using FPCT. On average the visible stent lumen was reduced by 16.1% with FPCT, whereas the mean of the lumen reduction was 47.2% with 16-slice spiral CT. Visible lumen diameter significantly increased using FPCT ($p < 0.001$). Even delineation of the different stent struts became possible.

Conclusion: FPCT proved to be superior when compared to 16-slice spiral CT for the in-vitro assessment of coronary artery stents. Improved spatial resolution allows for a superior assessment of the coronary artery stent lumen.

B-350 15:21

Cardiac imaging: Coronary artery bypass grafting imaging of the proximal anastomoses created by nitinol implants. A retrospective two observer evaluation

M. Khan, C. Herzog, K. Landenberger, S. Martens, A. Maataoui, M. Dietrich, T.J. Vogl; Frankfurt a. Main/DE

Purpose: To investigate the proximal anastomosis of CABG grafts using an automated aortic connector with nitinol implants in a 1 year follow-up by using different reformations.

Methods: To evaluate graft patency 33 patients after receiving CABG underwent CT examination of the heart. On the same patients CT was performed on postoperative day 5 (4- row CT, group A) and again as a follow-up examination 1 year thereafter (16- row CT, group B). 23 ACVB to RCX and 27 ACVB to RCA grafts were included. Every automated anastomosis was reviewed under different reformations such as thin slab MIP, multiplanar reformation and volume rendering technique (VRT). Interobserver correlation was determined.

Results: 5 days postop 48 anastomoses were classified as patent, 2 not patent. 1 year postop 42 anastomoses were classified as patent, 8 not patent. In both groups the aortic connector could be visualized in good quality: 1.82 ± 1.10 (group A) and 1.93 ± 1.22 (group B) for ACVB to RCA and 1.86 ± 1.10 (group A) and 1.77 ± 1.23 (group B) for ACVB to RCX grafts (MPR). Image quality at the aortic connector site did not display a significant difference for any reformation between groups ($p > 0.05$). Within groups MPR displayed better visualization as compared to MIP and VRT ($p < 0.05$).

Conclusion: In the presence of metal implants CT provides reliable data in evaluation of the proximal anastomosis; but 16- row CT does not bring a significant benefit to image quality. MPR displayed the best visualization within both groups.

14:00 - 15:30

Room B

Musculoskeletal

SS 710

MR imaging of the cartilage

Moderators:

I. Boric; Zagreb/HR
M. Shahabpour; Brussels/BE

B-351 14:00

The magic angle phenomenon in MR imaging of ankle tendons: Prevalence and site in asymptomatic subjects and cadaveric specimens with histologic correlation

B. Mengiardi, C.W.A. Pfirrmann, P.B. Schöttle, B. Bode, J. Hodler, P. Vienne, M. Zanetti; Zürich/CH

Purpose: To evaluate the prevalence and site of the magic angle phenomenon (MAP) of ankle tendons in MR examinations.

Materials and Methods: MR imaging of the ankle in 30 asymptomatic volunteers (mean age 42.8 years) and in five cadaveric feet was performed both in standard supine body position (with neutral position of the foot) and in prone position (with plantar flexion of the ankle). MR images were evaluated separately by two radiologists in consensus for the site and the extent of increased T1-weighted signal of the ankle tendons. Histological evaluation of the posterior tibialis tendon (PTT) was performed by a pathologist unaware of the MR findings.

Results: MAP was noted in 6 (20%) vs. 1 (3%) (supine vs. prone body position)

Scientific Sessions

anterior tibialis tendons (ATT), in 30 (100%) vs. 0 extensor hallucis longus tendons, in 29 (97%) vs. 0 PTT, in 30 (100%) vs. 1 (3%) peroneus brevis tendons and in 24 (80%) vs. 1 (3%) peroneus longus tendons. In the cadaveric study in 19 of 25 sites of the PTT an increased signal was observed in the supine body position. Signal abnormalities in both body positions were seen in 9 of 25 sites corresponding to degeneration (4/9) and to the presence of fibrocartilage or a chondroid sesamoid (3/9) within the tendon substance.

Conclusion: In the standard supine position, the prevalence of MAP in all ankle tendons is high (80-100%) except in the ATT (20%). Contrarily, MAP is almost never observed in prone position with plantar flexion of the ankle.

B-352 14:09

Histological correlation of MR imaging cartilage imaging in the knee joint before total replacement

A. Cavallaro¹, W. Horger¹, B. Swoboda¹, W. Bautz¹, B. von Rechenberg², T.C. Mamisch³, ¹Erlangen/DE, ²Zürich/CH, ³Bochum/DE

Purpose: To determine the diagnostic quality of different standard cartilage sequences in MR imaging in correlation with histological data in patients for total knee replacement.

Methods and Materials: 6 patients with severe osteoarthritis of the knee joint and who had an indication for total knee replacement underwent 3D-Flash, 2D TSE, 3d-Medic and 3D-Dess MR imaging (resolution 0.5x0.5x0.5, Siemens 1.5 T Symphony). After intra-operative macroscopic evaluation and grading, the resected surface of the condyles was marked with pins and imaged with the same protocol. The sections were then fixed and semi-thick slices of 0.25 mm were made with Toluidin Blue staining. The histological data was staged by Mankin histopathological scale and registered by the pin location to the MR imaging data. The MR imaging images were analysed by Noyes classification and compared.

Results: There were comparable results for grade 3 and 4 osteoarthritis for all four sequences with the histological data. For grade 2 lesions with loss of cartilage volume 3D-Flash and 3D-Medic were more comparable, for lesions without loss 3D-Dess. For grade 1 lesions with superficial loss of staining, the 2D TSE sequence was most sensitive, for grade 1 lesions with loss of cartilage structure and increase of chondrocytes all sequences were highly false negative.

Conclusion: Our preliminary results show still a lack of diagnostic efficiency for early stages of osteoarthritis. Also it shows the limits of thickness measurement techniques, especially in detection of structural defects with intact surface.

B-353 14:18

Contrast enhanced high resolution MR imaging of autologous cartilage implants of the knee joint

C.M. Plank, K. Kubin, K. Friedrich, M. Weber, S. Marlovits, S. Trattnig; Vienna/AT

Purpose: To investigate if the enhancement of synovial fluid by intravenous administration of contrast agent improves the magnetic resonance (MR) evaluation of cartilage repair in the knee joint.

Methods and Materials: Eleven patients after matrix-based autologous cartilage transplantation in the knee joint were examined by proton-density fast spin echo sequence (PD-FSE) without and after intravenous administration of gadodiamide (indirect MR-arthrography). High-resolution MR imaging could be achieved by the use of a surface coil placed over the implant site. Implant thickness, surface and integration of implant to the adjacent native cartilage and subchondral bone were evaluated.

Results: Contrast enhanced MR imaging of matrix-based autologous chondrocyte implants was superior to non-enhanced cartilage imaging. In particular, incomplete integration of the cartilage implant to adjacent normal hyaline cartilage was better delineated with indirect MR arthrography. Implant thickness and surface abnormalities such as fibrillations and fissures were better visualized by filling of defects with contrast-enhanced synovial fluid. Each of these properties could be distinguished significantly better with contrast enhanced imaging ($p < 0.001$ for all 3 parameters).

Conclusion: Indirect MR arthrography is a promising technique for the evaluation of cartilage repair, since it allows one to combine the advantage of high-resolution PD-FSE imaging for subtle intrachondral abnormalities with a better delineation of cartilage implant surface and integration defects.

B-354 14:27

Patellar osteochondral autograft transplantation: Assessment with high-resolution MR imaging at 1.5 T

K. Woertler, M. Settles, V. Martinek, J. Stollfuss, E.J. Rummeny; Munich/DE

Purpose: To evaluate high-resolution MR imaging at 1.5 T in the assessment of osteochondral autografts of the patella in correlation with clinical outcome.

Materials and Methods: 24 patients (16-59 years) were examined by high-resolution MR imaging at 12-64 (mean 31.4) months after patellar osteochondral autograft transplantation. Examinations were performed on a 1.5 T system (loop-coil) with use of an "arthrographic" T1-weighted FSE sequence and a fat-suppressed PD-weighted FSE sequence, both combined with DRIVen Equilibrium pulses and obtained with a resolution of 0.2 x 0.4 x 2 mm. MR images were evaluated with regard to alterations of the transplants and their adjacent structures using a 20-point score system. MR-score values were correlated with Lysholm-Score and Visual-Analogue-Scale (VAS = pain score) values.

Results: MR-score values of 5-20 were assigned. Improvement of Lysholm-Scores and decrease of VAS values between pre- and post-operative clinical examinations ranged from -18 to 71 (mean 32.1) and from -2 to 7 (mean 3.5), respectively. The best correlations were observed between overall MR-score values and differences in clinical scores (0.79-0.81). Pathologic alterations of adjacent structures showed a higher correlation with poor clinical outcome (0.79-0.82) than suboptimal fit (0.70) or alterations of the transplants themselves (0.64-0.65).

Conclusions: In patients with patellar osteochondral transplants, findings at high-resolution MR imaging correlate well with clinical outcome. However, mid-term results appear more closely related to the status of adjacent joint structures than to that of the transplants themselves. Long-term studies have to be awaited to assess the prognostic significance of fit and integrity of the osteochondral plugs.

B-355 14:36

Quantitative relationship of normal cartilage in the hip joint based on isotropic 1.5 T MR imaging

H. Mestan¹, A. Cavallaro¹, J. Kordelle², R. Forst¹, W. Bautz¹, T.C. Mamisch¹; ¹Erlangen/DE, ²Gießen/DE

Purpose: To determine the variability of cartilage thickness and pattern in the hip joint of healthy volunteers in correlation to sex, body weight, height and side of the standing leg based upon MR imaging.

Methods and Materials: We examined 30 healthy volunteers (15 male and 15 female) with an age range from 21 to 29 years with a 3D-DESS sequence (resolution 0.84x0.84x0.84, Siemens Symphony 1.5 T). The cartilage thickness was analysed in a Carthesian view based on the centre of rotation corrected by the femoral anteversion in five radial areas coronal and sagittal. The grade of acetabular coverage was assessed and compared to cartilage distribution.

Results: The acetabular coverage was 159.5 degrees (std.1.39) for the coronal and 158.2 degrees (std.1.07) for sagittal view. There was a thinning in the mid ventral portion of 17.81 mm (std. 2.14) to a maximum thickness of 25.54 mm (std. 4.84) in the mid anterior-superior portion. For the other contact areas we found a cartilage thickness of 23.45 (std. 7.82) with wide variation but no significant changes. There were also no significant changes of cartilage thickness side or sex differences.

Conclusion: The results of our ongoing study shows wide variation of cartilage thickness in the different contact pressure areas of the hip joint. It is possible to assess cartilage in the hip joint and correlate it to the centre of rotation and the femoral anteversion. This leads to biomechanical analysis of cartilage pathology in patients with osteoarthritis.

B-356 14:45

In vivo correlation of gross pathology in osteoarthritis of the hip to MR imaging cartilage imaging

T.C. Mamisch¹, G.C. Welsch², A. Cavallaro², W. Horger², M. Menzel², F.F. Hennig², G. Muhr¹; ¹Bochum/DE, ²Erlangen/DE

Purpose: To determine the quality of articular cartilage detection in the hip joint of MR imaging by comparison of these findings with the resected femoral head.

Methods and Materials: 12 patients with advanced osteoarthritis of the hip before total hip replacement underwent 3 T MR imaging of both hips (resolution 0.5x0.5x0.5 mm). A cartilage quality assessment based on the Noyes classification was performed after resection of the femoral head. For the macroscopic classification the femoral head was divided into 8 anatomical portions correlating to the femoral neck position. Identical MR imaging was performed for the femoral head. The results of MR imaging classification were compared to the macroscopic findings and histology in the mid-sagittal plane. The analysis of the histology was based on the Mankin criteria.

Scientific Sessions

Results: It was possible to analyse the femoral and acetabular cartilage separately in 86% of the observed areas. The detection of moderate and severe osteoarthritis corresponded significantly with the macroscopic findings. There were false positive findings in contact pressure areas without macroscopic changes and false negative to early stages of macroscopic changes with cartilage fibrillation. False findings in MR imaging compared to all stages of histological changes in the mid sagittal plane.

Conclusion: MR imaging is useful for non-invasive detection of cartilage lesions in the hip. There are still limitations to detection of early stages of osteoarthritis, especially without cartilage thinning in MR imaging for diagnosis.

B-357 14:54

3 T MR imaging cartilage imaging of the hip: Cartilage pattern, lesions, biomechanical analysis and comparison to 1.5 T

T.C. Mamisch¹, A. Cavallaro², W. Horger², G. Muhr¹, R. Forst², W. Bautz²,
¹Bochum/DE, ²Erlangen/DE

Purpose: To evaluate the possibility of 3 T imaging in the hip joint for cartilage thickness measurement, cartilage quality analysis, separation of femoral and acetabular cartilage for diagnosis of early lesions and imaging of both hips for biomechanical analysis using isotropic resolution in MR imaging.

Methods and Materials: 18 volunteers and 7 patients with X-ray signs of moderate osteoarthritis underwent MR imaging on 1.5 T and 3 T systems. On the 1.5 T system both hips were imaged separately (3D-MEDIC, resolution 0.84x0.84x0.84, Siemens Symphony). On the 3 T system both hips were imaged in one slab (3D-Medic, 0.7x0.7x0.7, Siemens TRIO). Radial images based on the centre of rotation in the axis of the femoral neck, each of 30 degrees, were reconstructed and analysed for separation of femoral and acetabular cartilage, assessment of cartilage quality and inter-observer reproducibility for cartilage thickness measurement of three observers. Perpendicular reconstructions in the acetabular opening were used to determine the acetabular labrum.

Results: There was a significant improvement in the separation of acetabular and femoral cartilage, especially in the lateral portions of the hip joint. Positioning of the femoral anteversion was more reliable; also the inter-observer correlation was significantly higher for cartilage thickness on the 3 T system. Classification of cartilage quality by Noyes was improved by division between losses of cartilage less and more than 50%.

Conclusion: By using a 3 T system we found an improvement for all diagnostic criteria of early osteoarthritis. Histological and macroscopic comparison is necessary in future work to show the clinical importance.

B-358 15:03

Morphology of the acetabular labrum on MR imaging in comparison to the quality of corresponding cartilage

G. Welsch¹, A. Cavallaro¹, W. Horger¹, M. Menzel¹, W. Bautz¹, T.C. Mamisch²,
¹Erlangen/DE, ²Bochum/DE

Purpose: To assess the cartilage quality in comparison to the morphology of the acetabular labrum and correlate it with the portion of the labrum based on radial MR imaging.

Methods and Materials: 20 healthy volunteers with an age range from 21 to 36 and 12 patients with a minimum of 15 years after prophylactic pin treatment of Slipped Capital Femoral Epiphysiolysis underwent MR imaging and clinical hip examination. For MR imaging a DESS-3D Sequence (resolution 0.7x0.7x0.7, Siemens Avanto 1.5 T) and a radially sectioned PD-TSE sequence (resolution 0.4 x 0.4 x 5 mm) perpendicular to the acetabular labrum were performed. For planning of the radial sections the acetabular opening was used from the isotropic images. The acetabular labrum morphology was compared to the corresponding femoral and acetabular cartilage quality in the radial portions.

Results: In healthy volunteers a triangular shape was detected in 78%, a round shape in 18% and an irregular round shape in 4% not correlated with cartilage lesions in the corresponding contact area. For 7 patients we found in the anterior-superior portion an increase of signal intensity with irregular labrum and corresponding cartilage thinning. These were correlated with femoral neck remodelling.

Conclusion: It was possible to compare cartilage morphology to acetabular abnormalities by using an isotropic cartilage sequence for positioning of the acetabular opening and the radial section. We found in our ongoing study variations of the labrum without cartilage defects and defects with cartilage lesions based of femoral neck impingement.

B-359 15:12

MR imaging in sports related groin pain - prevalence of adductor dysfunction versus osteitis pubis

C.J. Johnston, P. Cunningham, D. Brennan, J. Moriarty, S.J. Eustace; Dublin/IE

Purpose: To identify the mechanism and cause of sports related groin pain using MR imaging.

Methods: 70 sportsmen with groin pain referred for MR imaging and 70 age- and sex- matched asymptomatic sportsmen undergoing MR imaging pelvis as part of an unrelated study were included as controls. In each case images were reviewed to determine the presence or absence of an adductor tear at the tendo-osseous junction on the basis of hemorrhage and oedema at the attachment with local bone oedema, and assessed to determine the presence or absence of osteitis pubis on the basis of symphyseal articular surface irregularity, disc herniation and para-articular bone oedema.

Results: Isolated adductor dysfunction was identified in 32 patients, both adductor dysfunction and osteitis pubis were identified in the same patients in 13 cases, whilst isolated osteitis pubis was identified in 7 patients. No significant abnormality was identified in 18 cases. Features of osteitis pubis were identified in 3 of the asymptomatic controls; the remainder of the images of the controls were normal.

Conclusion: Adductor dysfunction appears to be the commonest cause of groin pain in affected sportsmen. Its presence appears to precede the development of osteitis pubis in most patients. Isolated osteitis pubis is uncommon.

B-360 15:21

MR imaging of wrist cartilage: Comparison between imaging at 1.5 T, 3 T and anatomical section

N. Saupe, C.W.A. Pfirrmann, M.R. Schmid, T. Schertler, S. Wildermuth, M. Manestar, B. Marincek, D. Weishaupt; Zürich/CH

Purpose: To compare MR imaging of the wrist cartilage at 3 T and at 1.5 T in cadaveric wrists using the same imaging protocol and similar imaging parameters for both magnetic field strengths with gross pathology as standard of reference.

Materials and Methods: Coronal proton density (PD)-w, intermediate-w (TSE) and 3D FFE-weighted sequences were obtained in 10 cadaveric wrists (7 left, 3 right, age range: 46-99 years) at both 1.5 T and 3 T MR systems (Signa GE Medical Systems 1.5 T and Intera 3.0, Philips Medical Systems). All MR imaging at 3 T as well as at 1.5 T was performed with similar imaging parameters, using a surface coil at 3 T and a dedicated wrist coil at 1.5 T. Two observers analyzed and graded the cartilage defects on the distal carpal row, proximal carpal row and STT joint using a 4-point grading scale. The results were compared between images obtained at 3 T, 1.5 T and gross pathology, respectively.

Results: Sensitivity ranged from 20-43% (specificity 83-91%, accuracy 52-59%) for the proximal and distal carpal rows and 66-74% (specificity 65-66%, accuracy 65-66%) for STT joint. There was no significant difference in diagnostic performance between 3 T and 1.5 T in assessing cartilage abnormalities compared to the gold standard ($p = 0.12$). No significant inter-rater differences were noted ($p = 0.14-0.57$).

Conclusion: MR imaging in detection of articular cartilage abnormalities at the wrist depends on the location but there is no difference in diagnostic performance between 3 T and 1.5 T assessing cartilage abnormalities, however no dedicated wrist coil was used at 3 T.

14:00 - 15:30

Room C

GI Tract

SS 701a

Acute abdomen

Moderators:

H. Fenlon; Dublin/IE
J. Puig Domingo; Sabadell/ES

B-361 14:00

Imaging in appendicitis: Ultrasound, CT or neither?

R. Ananthasivan, S. Fataar, A. Derweesh; Muscat/OM

Purpose: To assess whether ultrasound and CT has reduced negative appendectomy rates in our institution.

Methods and Materials: The results of ultrasound (145 patients) and CT (57 patients) referred with a suspected clinical diagnosis of appendicitis over an eight month period 1/1/2004-31/08/2004 were reviewed. The results were compared to the operative findings and the histopathological report of the resected specimen

Scientific Sessions

or to the clinical outcome. All patients had an ultrasound of the abdomen and pelvis with graded compression sonography of the right iliac fossa as the first investigation. Patients with an inconclusive study (57/145) alone proceeded to a limited CT for appendicitis. Negative appendectomy rates during the period of study were compared to the rates in a similar period prior to the regular use of ultrasound and CT for appendicitis in our institute. (1/1/1995-31/08/1995). Negative appendectomy rates during the period of study were compared between patients who had surgery on clinical grounds alone to those who had surgery after radiological assessment.

Results: CT had a negative predictive value of 96% and a specificity of 91.6% both higher than ultrasound. There was a significant reduction in negative appendectomy rates in patients who had imaging compared to those who had surgery on clinical assessment alone.

Conclusion: Ultrasound should be the first radiological investigation in suspected appendicitis followed by CT in inconclusive studies. Radiological assessment reduces negative appendectomy rates. Further reduction in negative appendectomy rates can be achieved by referring more patients for imaging.

B-362 14:09 ♀

Thickness and features of the normal appendix at MDCT: Are diameter and appendicoliths misleading tools?

L. Huwart, M. El Khoury, B. Bessoud, A.-S. Rangheard, Y. Menu;
Le Kremlin-Bicêtre/FR

Purpose: To evaluate the features of the normal appendix with MDCT.

Methods and Materials: MDCT of 57 consecutive adult patients without symptoms suggesting appendicitis were prospectively studied. Most patients (41/47) had IV iodine injection, but no intraluminal contrast. Thick (5 mm) and thin (1 mm) slices were analyzed on a workstation. MPR were available. Localization of the appendix, overall diameter, wall thickness, intraluminal gas and appendicoliths were recorded.

Results: The appendix was visualized in 47/57 (82%). The location was retrocaecal (28%), mediocaecal (21%), subcaecal (19%) or pelvic (32%). The overall diameter of the normal appendix varied between 5.0 and 11 mm (mean 6.7 mm ± 1.2) and was larger than 6 mm in 70%. The overall wall thickness varied between 2.6 and 6.4 mm (mean 4.8 mm ± 1). Intraluminal gas was identified in 87%. An appendicolith was found in 13%.

Conclusion: Despite MDCT, 18% of normal appendices were not detected. The overall diameter of normal appendix may overlap the currently accepted threshold for appendicitis at CT. Appendicolith was found in a significant number of normal patients and may not represent a reliable sign for appendicitis.

B-363 14:18

Slivers of free fluid detected by screening abdominal sonography after blunt trauma: What does it mean?

M. Scaglione, A. Pinto, S. Romano, R. Farina, R. Grassi, L. Romano; Naples/IT

Purpose: To assess the clinical implication of small amounts of free fluid detected on screening abdominal sonography (US) after blunt abdominal trauma (BAT).

Methods and Materials: 5142 consecutive patients with BAT were evaluated with abdominal US performed by radiologists in the emergency room. Those patients in whom US showed a sliver of free fluid < 15 mm thick were selected, recorded and compared to the findings on computed tomography (CT), repeat US, angiography, laparotomy and clinical follow-up.

Results: of 5142 patients screened with abdominal US, 127 patients were found to have a sliver of fluid < 15 mm. 109/127 patients were subjected to subsequent CT, 11/127 had repeat US, 7/127 were followed clinically and underwent CT before discharge. 7 patients had angiographic embolization, 4 went on to laparotomy with repair of injuries. Injured organs included the spleen (n = 21), liver (n = 16), bowel/mesentery (n = 15), kidneys (n = 12), adrenal glands (n = 7) and 9 patients were found to have retroperitoneal hemorrhage.

Conclusions: Our data suggest that small amounts of fluid can be related to minor injuries that heal non-operatively in most cases. Nevertheless, in the appropriate clinical context, this finding warrants further investigation to exclude significant injury and to be managed appropriately.

B-364 14:27

MSCT with combined CT-angiography for diagnosis of suspected mesenteric ischemia or intestinal bleeding in patients presenting with acute abdominal symptoms

M. Dobritz, W. Weiss, J. Stollfuss, E.J. Rummeny; Munich/DE

Purpose: To evaluate the diagnostic performance of Multislice-Computed-

Tomography (MSCT), including CT-angiography, in patients with suspected gastrointestinal bleeding or mesenteric ischemia.

Materials and Methods: 43 consecutive patients presenting with symptoms suggestive for intestinal bleeding (n = 15) or mesenteric ischemia (n = 28) were investigated. MSCT was acquired including an arterial and porto-venous phase (120 ml iodinated contrast media, 4-5 ml/sec flow, 16×0.75 mm collimation, 0.7 cm reconstruction increment, 0.75 mm slice thickness). In conjunction to standard image reading image interpretation was done with respect to vessel structures using a 3D workstation. Intraoperative findings and/or conventional fluoroscopic angiography was used as the standard of reference in patients with suspected bleeding. Intraoperative findings were available in 14/28 patients with suspected ischemia.

Results: 5/6 patients with confirmed mesenteric ischemia were correctly diagnosed by MSCT (Sensitivity 83%). MSCT was able to demonstrate other potential causes for abdominal pain in 15 of the remaining 22 patients with suspected ischemia including mesenteric vein thrombosis, inguinal herniation, bowel perforation, pneumonia and tumors. 9/9 patients with confirmed gastrointestinal bleeding were correctly identified by MSCT (Sensitivity 100%). Other findings that were likely to explain bleeding were found in 5 of the remaining 6 cases (GIST 3, NHL 1, Hematoma 1).

Conclusion: MSCT in conjunction with CT-angiography is highly reliable in the diagnosis of patients presenting with suspected bleeding or mesenteric ischemia. MSCT also shows important other causes of abdominal pain without evidence of bleeding or ischemia and, thus, should be used as the primary diagnostic technique in the management of these patients.

B-365 14:36 ♀

Frequency of visualization of normal appendix at MDCT: Junior versus senior radiologist performance

L. Huwart, M. El Khoury, B. Bessoud, A.-S. Rangheard, Y. Menu;
Le Kremlin-Bicêtre/FR

Purpose: To evaluate the detection rate of the normal appendix by a junior and a senior radiologist at MDCT.

Methods and Materials: A junior (< 6 months training) and a senior radiologist (specialized in abdominal radiology), blinded to patient history, prospectively and independently reviewed abdominopelvic MDCT scans in 85 consecutive adult patients without symptoms suggesting appendicitis. 70/85 patients had iodine injection. No contrast material was orally or rectally administered. All slices (1 and 5 mm) and MPR were available on the workstation. Interobserver agreement and effect of adequacy of intraperitoneal fat in identification of the appendix were assessed.

Results: The prevalence of appendectomy was 32.9% (28 of 85 patients). The means for the sensitivity, specificity, positive and negative predictive values of visualization of normal appendix were 79%, 82%, 90% and 66% for the junior and 82%, 93%, 96% and 72% for the senior radiologist. For the two reviewers, the detection rate did not increase with amount of intraperitoneal fat ($p > 0.05$, Chi² test). The nonweighted κ value for interobserver agreement for normal appendix visualization was 0.78, which indicated excellent agreement.

Conclusion: There was no significant difference between a junior or a senior radiologist for the detection of normal appendix at MDCT. No relationship between the detection rate and the amount of abdominal fat was found.

B-366 14:45 ♀

CT or plain abdominal X-rays as primary examination of patients with acute abdomen?

J.G. Andersen, Å. Torvund, T. Tofte; Oslo/NO

Purpose: To assess the total time used in the diagnostic process if CT is used as the primary evaluation of patients with acute abdomen compared to plain X-ray.

Methods and Materials: Sixty-nine consecutive patients with suspected ileus or subileus admitted to the Radiology department of Ulleval University Hospital were included. The patients were above 40 years old, none had known contrast agent allergy or kidney failure. For the first 23 of these patients the primary examination was plain abdominal X-ray, as opposed to CT for the remaining 46 patients. Effect measure was the total duration of the diagnostic process (TDP), defined as the time from entrance into the hospital until the final diagnostic examination was performed. TDP was analysed by using Statistical Process Control.

Results: TDP varied markedly from above 1 hour to 60 hours in both groups. Further, TDP appeared to be fairly stable over time in both periods. Average TDP was 16.5 hours when plain abdominal X-ray was first choice, as opposed to 9 hours when CT was first choice (45% reduction). The prevalence of patients with TDP above 24 hours was 26% when X-ray was the first choice, as opposed to 6.5% when CT was first choice.

Scientific Sessions

Conclusion: This study indicates that the prevalence of a long TDP is markedly reduced if CT is used compared to plain abdominal X-ray as the primary examination of patients with acute abdomen. However, the results must be interpreted with care because of the low sample size.

B-367 14:54

Comparison between the site of multislice spiral computed tomographic signs of gastrointestinal perforation and the site of perforation detected at surgery in fifty perforated patients

A. Pinto, M. Scaglione, N. Gagliardi, R. Grassi, F. Lassandro, L. Romano; Naples/IT

Purpose: To compare the site of MSCT signs of gastrointestinal perforation and the site of perforation at surgery in fifty perforated patients.

Materials and Methods: Fifty patients (32 men and 18 women, age ranging from 21 to 86 years old) underwent surgery for gastrointestinal perforation. In all cases, plain abdominal film was integrated by MSCT. The following MSCT findings were evaluated: free air, free fluid and bowel wall discontinuity. The site of these MSCT findings were compared with the site of perforation at surgery.

Results: Free air was detected in 72% of cases, free intraperitoneal fluid in 94% of cases and bowel wall discontinuity in no cases. In 15/50 patients with gastroduodenal perforation, free air and free fluid were detected together and free air was observed in supramesocolic compartments in all cases; in 4/50 cases of ileal perforation, free air was observed in one patient and fluid in three (in two of them in inframesocolic compartment). In 8/50 patients with acute perforated appendicitis free fluid was always observed in inframesocolic compartments; in 6/50 patients with sigmoid perforation free air was observed in four cases (all in supramesocolic compartments) while free fluid was detected in both compartments.

Conclusions: In gastroduodenal perforations free air and free fluid are present together and free air is localized in supramesocolic compartments. In acute perforated appendicitis free fluid is present in inframesocolic compartments and in sigmoid perforations free air, when present, is detected in supramesocolic compartments, while free fluid is observed in both compartments.

B-368 15:03

Multislice-CT findings in patients with colonic-diverticulitis: Do they correlate with intraoperative and postoperative immunohistological findings

S. Bitschnau, S.M. Maksan, F. Bittinger, P. Mildenberger; Mainz/DE

Purpose: The diagnosis of diverticulitis is often accompanied by controversies between CT-findings, macroscopic intraoperative findings and histological findings. The expression of intercellular-cell-adhesion-molecule-1 (ICAM-1) has been shown to have potential significance in the diagnosis of the stages of appendicitis. This study is designed to correlate the expression of ICAM-1 in diverticulitis with intraoperative-findings and preoperative CT-findings.

Material and Method: MSCT-datasets of 79 patients with clinically suspected colonic-diverticulitis were analyzed retrospectively. All patients had rectal-filling with positive iodine contrast-media. Extent of diverticula, signs of inflammation (e.g. thickening of fascia, fatty stranding) and complications like perforation, abscess were evaluated. Correlation to results of intraoperative and histomorphological and immunohistological findings (ICAM-1).

Results: 56 of 79 patients went to operation. 51 of the 56 operated patients had signs of diverticulitis in MSCT, which was proven intraoperatively. 1 patient did not have diverticula but had signs of inflammatory-bowel-disease. 4 pts were proven to have diverticulosis without inflammation. 23 pts without signs of inflammation in MSCT had consequently not been operated on (CT showed diverticulosis 11 patients and neither diverticulosis nor -itis in 12 patients). No relevant complication was missed by MSCT. Perforation (contained/ free) was detected in 36 pts (28/8).

Conclusion: MSCT can readily detect presence and extent of inflammation in patients with colonic diverticulitis. MSCT therefore has a high impact on the choice of therapy and can precisely give the indication for operation.

B-369 15:12

Importance of attending scientific paper sessions in international radiology meetings

S.M.R. Rizzo¹, M.K. Kalra¹, M.M. Maher¹, S. Saini², M. Bellomi³, G. Cornalba³; ¹Boston, MA/US, ²Atlanta, GA/US, ³Milan/IT

Purpose: To determine proportion of scientific papers presented at the annual RSNA meeting, which are subsequently published in peer-reviewed medical journals and factors that impact their publication.

Materials and Methods: We evaluated abstracts of scientific papers (n = 217) presented in the gastrointestinal sessions of the 2000 RSNA Annual Meeting. This meeting was chosen to allow a four-year period (April 2000-April 2004) for subsequent publication in peer-reviewed journals. Name and number of imaging modalities, number of authors, continent, grant support, research subjects (human, animal or phantom), number of patients, presentation date and study outcome were recorded for all abstracts. A Medline search was performed to find scientific papers published in indexed journals over a period of 4 years. For each published paper, journal name, study outcome result (positive/negative) and date of publication were recorded. Statistical analysis was performed to determine proportion of published papers and to assess factors impacting their publication.

Results: 29.9%(65/217) of scientific papers were published in indexed journals over a 4 years-period with most publications in Radiology (8.7%;19/217) and with an average presentation-to-publication time of 547 ± 32 days. Interestingly, there was no significant difference between number of imaging modalities, continent of origin, type of research subjects, number of recruited subjects and study outcome for published and unpublished papers ($p > 0.1$).

Conclusions: Less than one-third of scientific papers presented in the gastrointestinal sessions of 2000 RSNA Annual meeting were published within 4 years. Contrary to general expectation, type of study, country of origin, number of research subjects and research modalities did not predict publication of scientific papers.

B-370 15:21

Path to publication of original research articles in major peer-reviewed radiology journals: An audit of time from initial submission to publication

S.M.R. Rizzo¹, M.K. Kalra¹, M.M. Maher¹, T. Roberts¹, S. Saini², M. Bellomi³;

¹Boston, MA/US, ²Atlanta, GA/US, ³Milan/IT

Purpose: To compare time to publication of original research articles from submission-date to date of publication, and to assess if subjective and Evidence Based Medicine (EBM) grading of validity and strength of articles affect time to publication in radiology journals.

Materials and Methods: Twenty-five consecutive original research articles were selected from 8 peer-reviewed, monthly radiology journals from North America (Radiology, AJR, Academic Radiology, Investigative Radiology) and Europe (European Radiology, European Journal of Radiology, BJR, Clinical Radiology) (n = 200 articles). Dates of initial receipt, acceptance and print publication were recorded along with number of authors, institution and country. Average duration of receipt-to-acceptance, receipt-to-print publication, and acceptance-to-print publication were calculated. Two radiologists blinded to journal, author and affiliation graded validity and strength of articles using Oxford Center for EBM scoring system based on levels of evidence (1a-5). Each article was also graded based on likelihood to change current practice, cost to society, need for immediate research and safety concerns (1-5). Statistical analysis was performed using appropriate tests.

Results: Significant difference in receipt-to-print publication and acceptance-to-print publication was found between journals ($p < 0.0001$). North American authors had longer time-to-acceptance and to-publication in European journals and vice-versa ($p < 0.005$). No significant correlation was found between EBM scores ($p > 0.2$) and subjective grading scores ($p > 0.3$) and publication times in the journals.

Conclusions: Time-to-acceptance and to-publication of original research articles in major radiology journals are not affected by likelihood to change practice or cost to society and safety concerns. These disturbing trends may be explained on low EBM levels (3b-5) for validity and strength of most radiology research articles (78%;156/200).

Scientific Sessions

14:00 - 15:30

Room E2

Breast

SS 702

MR mammography (2)

Moderators:

K. Kinkel; Chêne-Bougeries/CH
F. Pediconi; Rome/IT

B-371 14:00

Comparison of dynamic and morphologic MR features of small vs large breast cancer cases

M. Dietzel, A. Malich, D.R. Fischer, C. Marx, C. Reuchsel, C. Deicke, F. Taher, W.A. Kaiser; Jena/DE

Purpose: To evaluate the clinical relevance of dynamic and morphologic pattern of breast cancer in MR-Mammography depending on the tumor size.

Methods and Materials: All histologically verified breast cancer cases having had a MR-Mammography (1/2002-3/2004; n = 188) were retrospectively evaluated by two experienced radiologists in consensus according to standard protocols and study design (2D-FFE sequences, 0.1 mmol/kgbw Gd-DTPA, T2-TSE). Two groups were created related: Up to 10 mm largest diameter=group 1 (n = 39); > 11 mm=group 2 (n = 149). The prevalence of the following signs were statistically analysed (Chi-Square-testing): Dynamic signs - fast initial wash-in (D1), wash out (D2), plateau (D3), blooming (D4), segmental enhancement (lesion's surrounding; D5), homogeneity of lesion's contrast uptake (D6). Morphologic signs (T1) - hook-sign (M1), root-sign (M2), adjacent vessels (M3), skin thickening (M4), nipple line-sign (M5), inhomogeneity of lesions composition (M6), lesion's shape (irregular; M7), irregular margins (M8). Morphologic signs (T2) - necrosis (M9), perifocal edema (M10), diffuse edema (M11), iso/hyperintensity of vital tumor parts (M12).

Results: Prevalence were: D1=49%/62% (n.s.); D2=46%/57% (n.s.); D3=31/28% (n.s.); D4=36%/47% (n.s.); D5=18%/56% (p = 0.001); D6=36%/ 8% (p = 0.001). M1=8%/32% (p = 0.003); M2=69%/83% (p = 0.038); M3=26%/45% (p = 0.03); M4=10%/21% (n.s.); M5=3%/10% (n.s.); M6=77%/89% (p = 0.06); M7=18%/44% (p = 0.003); M8=70%/83% (n.s.); M9=0%/14% (n.s.); M10=15%/37% (p = 0.01); M11=3%/9% (n.s.); M12=92%/97% (n.s.).

Conclusion: Whereas no significant differences regarding dynamic features could be obtained, hook-sign, root-sign, perifocal edema and adjacent vessels are significantly more often associated with larger breast cancers and less typical for small lesions.

B-372 14:09

Clinical potential of various MR signs to discriminate malignant from benign breast lesions in MR-mammography

A. Malich, D.R. Fischer, S. Wurdinger, J. Boettcher, A. Hansch, W.A. Kaiser; Jena/DE

Purpose: To increase objectivity of MR-mammography use of rating points for MR-signs, which are weighted according to their discriminatory power was tested.

Methods and Materials: From 3583 MR-mammographies, 641 cases were evaluated by two radiologists in consensus retrospectively. In extension to already published MR-signs the following were rated according to their prevalences in malignant and benign lesions: T2 intensity (vital tumor), blooming-sign, hook-sign, lymph nodes, septations, nipple line interruption, edema, skin thickening. In a prospective double-blinded study, 3 radiologists evaluated all histologically verified 132 cases of MR-mammographies (6-12/03). Mean sum of rating points was calculated in order to define cut off values for benignity and malignancy of lesions.

Results: In 10 cases the extended rating did not yield a clarification due to an intermediate sum (6 pt.) (PPV and NPV 50%). In total 10 pure CIS cases were analyzed, having a value of at least 7 points in 6/10 (Sens.60%). Within the remaining 112 lesions, 63/66 invasive malignancies and 6/46 benign lesions had 7 or more rating points, 3/66 invasive malignancies and 40/46 benign had 5 or less points (S = 95.5%; Sp = 87.0%, Acc=91.2%, PPV=91.3%; NPV=93.0%).

Conclusion: The use of rating points for MR-features is helpful to accurately discriminate benign and invasive malignant findings using cut off values of 5 (benignity) and 7 (malignancy). Further studies on pure CIS cases are required for a better detection rate. Lesions having a sum of 6 are recommended to be histologically verified (high ratio of malignancies in this subgroup).

B-373 14:18

Observer variability and applicability of BI-RADS terminology for breast MR imaging

G. Marcelli, F. Pediconi, R. Occhiato, F. Venditti, G. Nardis, R. Passariello; Rome/IT

Purpose: To assess the validity of the terminology and categories of the Breast Imaging Report and Data System for breast lesions detected with MR imaging and to assess the inter- and intraobserver variabilities in the use of the descriptors and final assessment categories.

Methods and Materials: In 122 patients, 150 were evaluated independently by three radiologists and described by BI-RADS classification with respect to lesion morphology (mass, shape, margin and enhancement pattern), signal intensity parameters (time to peak enhancement, maximum slope of enhancement curve, washout) and BI-RADS final assessment categories. Two radiologists interpreted each case twice to evaluate intraobserver variability.

Results: The final assessment category was BI-RADS category 5 in 52 lesions (34.6%), category 4 in 26 lesions (16%), category 3 in 21 lesions (14%) and category 2 in 51 lesions (34%). Histo-pathologic results, obtained in BI-RADS categories 3, 4 and 5, revealed 67 invasive carcinomas, 24 in situ carcinomas and 8 benign lesions. The interobserver agreement was moderate ($k = 0.40-0.60$), while the intraobserver agreement was good ($k = 0.55-0.75$).

Conclusions: The BI-RADS lexicon has a positive impact value to describe features of breast lesions detected on MR imaging.

B-374 14:27

Cluster analysis of signal-intensity time course in dynamic breast MR imaging: Does neural network clustering help to find the correct diagnosis in unclear small lesions?

T. Schlossbauer¹, A. Wismueller¹, G. Leinsinger¹, O. Lange¹, M. Scherr¹, A. Meyer-Baese², M.F. Reiser¹, ¹Munich/DE, ²Tallahassee, FL/US

Purpose: To examine whether neural network clustering could support the characterization of diagnostically challenging breast lesions in MR imaging.

Methods and Materials: We examined 88 women with 92 breast lesions (detected by mammography and classified BIRADS III - IV, median diameter 12 mm) using dynamic contrast-enhanced MR imaging. The diagnoses (51 malignant, 41 benign) were confirmed by histology. Conventional analysis included initial signal increase and post-initial signal intensity (SI) time-course. Morphological criteria were evaluated according to a clinically approved score system. For neural network analysis, all pixels within lesions were divided into four clusters. For clustering we used minimal-free-energy vector quantization which assigns pixels presenting similar SI-time-courses to prototypical clusters. The cluster with signal-characteristics most typical of malignancy was used for lesion characterization.

Results: All lesions with initial signal increase > 50% and plateau or wash-out of post-initial SI-time-course were classified as malignant. Sensitivity increased from 70.5% (conventional method) to 82.3% (vector quantization); specificity was 68.3% with both methods. Accuracy increased from 70.0% to 76.1%. When including morphological criteria, maximum accuracy was 66.3% (conventional method) compared to 69.6% (vector quantization). SI-dynamics proved to be more relevant than morphology for lesion characterization. In addition, vector quantization improved the inter-observer agreement for classification of lesion dignity from 80% to 85%. All results proved to be statistically significant ($p < 0.05$).

Conclusion: Vector quantization proved to be a useful tool for the characterization of unclear breast lesions and could provide valuable contributions to computer-aided diagnosis in MR imaging mammography.

B-375 14:36

Color-coded automated signal intensity-curve for detection and characterization of breast lesion: Preliminary evaluation of a new software for MR based breast imaging

F. Pediconi, C. Catalano, F. Venditti, M. Ercolani, L. Carotenuto, A. Roselli, R. Passariello; Rome/IT

Purpose: To investigate the value of a new color-coded automated signal intensity-curve software package for CE Magnetic Resonance Mammography in patients with breast cancer and correlate results with histo-pathologic specimens.

Methods and Materials: Fifty women with proven breast cancer at pathology who preoperatively underwent CE-MRM were included in the evaluation. CE-MRM was performed with a 1.5 T magnet using a bilateral surface coil. T2-weighted STIR and dynamic 2D Flash Dynamic T1-weighted sequences in axial plane acquired pre and 2, 4, 6, 8 and 10 min post-contrast media administration were performed. 0.1 mmol/Kg of Gd-BOPTA was administered at a flow rate of 2 ml/s

Saturday

Scientific Sessions

followed by 10 ml of saline. Criteria for lesion evaluation included morphological enhancement patterns and signal intensity-time curves. Images were analysed both with a new software using a user-friendly interactive mechanism and separately with a standard display method. Bi-RADS scores of lesions obtained with and without software analysis were compared and correlated to histopathological results.

Results: At pathology, 11 DCIS, 6 LCIS, 16 invasive ductal, 12 invasive lobular, 2 medullar carcinoma, 3 intra-ductal papilloma, 3 ductal hyperplasia, 2 lobular hyperplasia and 6 fibroadenoma were evaluated. Perfect agreement was seen between Bi-RADS scores obtained with and without software evaluation. Good correlation between CE-MRM findings and histo-pathological specimens was obtained with both methods.

Conclusion: Novel color-coded signal intensity-curve software allows visualization of lesions with corresponding signal intensity-time curves in a false-color map and provides quickly and easily interpretable images for detection and characterization of breast lesions.

B-376 14:45

CADM RM: A prototype software for automatic computer aided detection and classification of lesions in contrast-enhanced MR-mammography

T.W. Vomweg¹, M. Buscema², E. Grossi³, D. Mayer¹, H. Faber¹, C. Hintze¹, M. Mattiuzzi³, S. Terzi², M. Intraligi², ¹Mainz/DE, ²Rome/IT, ³Milan/IT

Purpose: Further improvement and widespread availability of MR scanners increase the number of performed MR investigations of the female breast. Assessing the likelihood of malignancy of a contrast enhancing lesion is more difficult than in any other organ. Therefore evaluating MRM is a demanding task for any physician and shows a high inter-observer variability. A fully automatic software functioning as independent second opinion should improve the situation.

Methods and Materials: A software prototype evaluating MRM investigations fully automatically was programmed using C++. At first a non-rigid image registration algorithm reduces motion artefacts to improve overall image quality. Next, a threshold based algorithm detects contrast enhancing lesions followed by several algorithms assessing morphological as well as dynamic features. Lastly, an Artificial Neural Networks analyses all information and estimates the likelihood of malignancy of each detected lesion. The results of 54 lesions were compared with histology. Performance of the whole prototype was evaluated by ROC-statistics.

Results: The prototype functions without any user interaction. Registration improves image quality by motion correction without compromising contrast enhancing lesions. Sensitivity and specificity for detection and classification of malignant lesions were 81% / 80% and for benign lesions were 82%/79%.

Conclusion: A software prototype for Computer Aided Detection and Classification was successfully applied to MR-Mammography. The performance of the system must be improved by larger sample sets. Cooperation of Semeion Research Centre and University of Mainz is financed by Bracco Imaging, Milan, Italy.

B-377 14:54

Impact of different measurements techniques in the prediction of histological response, in patients with locally advanced breast cancer treated by primary chemotherapy

L. Martincich, F. Montemurro, D. Campanella, S. Debernardi, F. Russo, D. Regge; Candiolo/IT

Purpose: To compare different measurement techniques (unidimensional, bi-dimensional and volumetric) in the prediction of response, in patients with locally advanced breast cancer (LABC), undergoing primary chemotherapy (PCT) and monitored by Dynamic Contrast-enhanced MR imaging (DCE-MRI).

Methods and Materials: 30 patients underwent PCT and were monitored by DCE-MRI (1.5 T; 3DSPPGR sequence) performed at baseline, after 2 and 4 cycles of PCT. MIP reconstructions were used to define unidimensional (greatest diameter) and bidimesional (product of 2 major diameters) measurements, while dedicated software was used to define the tumoral volume. Histological response was assessed using a grade system; grade 4 (small cluster of dispersed cancer cells) and grade 5 (absence of invasive cells) were defined as major histopathological response (MHR). The tumor reduction during PCT (defined with different measurement criteria) was correlated with the histological response.

Results: Baseline DCE-MRI identified 30 lesions (mean major diameter 51 mm; mean product of the two major diameters 2193 mm²; mean volume 31 cc). MHR was achieved in 11 patients. After 2 cycles of PCT, using unidimensional criteria, tumor reduction > 30% was identified in 14 cases; 9 were MHR (sensitivity 82%, specificity 73%, PPV 64% NPV 87%). Using bidimensional criteria tumor reduction > 50% was detected in 16 cases; 10 were MHR (sensitivity 91%, specificity 72%,

PPV 63%, NPV 76%). Using volumetric criteria tumor reduction > 65% was identified in 13 cases; 10 were MHR (sensitivity 91%, specificity 88%, PPV 77%, NPV 94%).

Conclusion: In our series, the reduction assessed using volumetric criteria showed the highest specificity and NPV values, providing a possible early identification of non responder patients.

B-378 15:03

Accuracy of breast MR in the evaluation of the response to chemotherapy in 70 patients and accuracy of parametric images in a subgroup of 46 patients

J. Camps Herrero¹, M. Sentís Crivellé², L. Tortajada Giménez², V. Ricart Selma¹, C. Martínez Rubio¹, M. Ferrer Puchol¹, M. Lloret Martí¹, ¹Alzira/ES, ²Sabadell/ES

Purpose: To assess the accuracy of breast MR imaging in the evaluation of the response to neoadjuvant chemotherapy in 70 patients. In a subgroup of 46 patients we also compared the accuracy of parametric maximum enhancement speed (MES) images and parametric maximum enhancement (ME) images in the evaluation of the response to neoadjuvant chemotherapy and in the differentiation between ductal carcinoma in situ (DCIS) and infiltrating ductal carcinoma (IDC).

Methods and Materials: Seventy patients with core biopsy proven breast cancer underwent breast MR imaging prior to and 3-4 weeks after completion of chemotherapy. T1-weighted FLASH 3D pre- and post-contrast images were obtained. Morphologic and semi-quantitative analysis was done in all patients. Analysis of MES and ME parametric images in a subgroup of 46 patients was done with a dedicated software for breast MR imaging (Asymed®). UICC criteria for response were followed. Maximum diameters (MD) were compared in breast MR imaging exams after chemotherapy and in the final histopathological exams and a linear regression model was obtained. We also compared maximum diameter of MES and ME parametric images and obtained a Pearson correlation coefficient.

Results: The Pearson correlation between breast MR and pathology was $r = 0.75$. For pathologic complete response, breast MR sensitivity and specificity were 73% and 96%. In the subgroup of 46 patients the best correlation was obtained with ME images. ME parametric images were more accurate in all DCIS cases, with a correlation coefficient of 0.85 and MES images enabled differentiation between DCIS and IDC.

Conclusion: Breast MR can accurately predict response after neoadjuvant chemotherapy.

B-379 15:12

Monitoring response to neoadjuvant chemotherapy in locally advanced breast cancer: Efficacy of contrast-enhanced MR imaging to predict presence of residual disease

C.E. Loo, A.T.E.F. Schijf, E.E. Deurloo, S.M. Muller, M. vd Vijver, K.G.A. Gilhuijs; Amsterdam/NL

Purpose: To assess the efficacy of contrast-enhanced (CE) MR imaging to predict presence of residual tumor during and after completion of neoadjuvant chemotherapy in patients with locally advanced breast cancer.

Method and Materials: 53 patients (24-66 years) with locally advanced breast cancer were consecutively included between September 2000 and August 2004. Tumors (44 IDC, 9 ILC) were examined with 3 CE MR imaging scans: 1st before, 2nd during (two courses) and 3rd after completion (6 courses) of neoadjuvant chemotherapy. A combined MR imaging protocol was employed: Fast dynamic imaging in the first 45 s after contrast injection (Turbo-FLASH) followed by dynamic imaging in 5 consecutive series at 90 s intervals (FLASH-3D). MR imaging findings were correlated with postoperative pathology findings. Multivariate logistic regression with double cross-validation and ROC analysis was employed to identify MR imaging features that are predictive of tumor response after the second and after the sixth course of chemotherapy.

Results: Pathology revealed residual disease in 37(70%) of 53 patients (pCR17; 30%). During chemotherapy (2 courses), prediction of tumor response was best indicated by the change of largest washout diameter on scan 2 relative to scan 1(double-validated Az = 0.76). After completion of chemotherapy, the best predictor of tumor response is the initial enhancement combined with the change of largest washout diameter on scan 2 relative to scan 1(double-validated Az = 0.84).

Conclusions: MR imaging is accurate in predicting the presence of residual tumor after completion of neoadjuvant chemotherapy in both early as well as late stages of the treatment.

Scientific Sessions

B-380 15:21

Locally advanced infiltrating lobular carcinoma (LALIC): A histological subtype with poor correlation when MRM is used to monitor primary chemotherapy (PCT)

M. Sentís¹, E. Saez Artacho¹, F. Andreu Navarro¹, L. Tortajada Jimenez¹, S. Ganau Macias¹, J. Camps², M. Seguí Palmer¹; ¹Sabadell/ES, ²Alzira/ES

Purpose: To describe the differential behaviour of LALIC during primary chemotherapy and the limitations of MRM to monitor the tumor changes.

Methods and Materials: A prospective study of 50 consecutive patients diagnosed with LABC between 2002 and 2003 by large needle core biopsy (LNCB) (38 (76%) ductal 12 (24%) lobular. 4 cycles of epirubicina-cyclophosphamide, followed by 8-12 weekly doses of docetaxel. Surgery after PCT. Pathological assessment using Miller & Payne histological grading with five grades of local response and four grades of lymph node response. The MR studies were performed before, after the first cycle and after chemotherapy. Protocol including T2-w and dynamic FLASH ·3D sequences with 0.16 mmols/bwKg. Measurements: Tumor size, volumetry, distribution and multifocality. Normalization of signal intensity values. Signal intensity variation. Saturation and wash-in rate was calculated before and after treatment in order to stratify the responses. Parametric images for correlation with pathological response and immunohistochemical markers.

Results: Local response in the breast directly correlates with axillary response. Good correlations exists in ductal carcinoma between MR and pathology. Good correlation in 35 cases (68%), underestimation in 8 cases (16%) and overestimation in 7 cases (14%). LALIC has a poor response and MR overestimates the level of response. Good correlation on 3 (25%) and overestimation in 9 (75%).

Conclusions: MR imaging results for monitoring PCT in LALIC should be interpreted with caution due to the difficulties in exactly depicting the extent of residual disease. Good categorization of the histological type before PCT is mandatory to better evaluate the MR imaging findings.

14:00 - 15:30

Room F1

Chest

SS 704

Malignant tumors: Screening, staging and outcome

Moderators:

V. Ene; Bucharest/RO
F. Gleeson; Oxford/UK

B-381 14:00

Trial design and first screening results from the Dutch-Belgian trial on lung cancer screening by spiral CT (NELSON study)

R. Vliegenthart¹, C. van Iersele², D. Xu¹, Y. Wang¹, R.J. van Klaveren², H.J. de Koning², M. Prokop³, W.P.T.M. Mali³, M. Oudkerk¹, ¹Groningen/NL, ²Rotterdam/NL, ³Utrecht/NL

Purpose: The NELSON study is a randomized screening trial in current and former smokers, aimed at early detection of lung cancer by spiral CT, and designed to be large enough to show a 20% reduction in lung cancer mortality.

Materials and Methods: In the Netherlands and Belgium 16.000 male current or ex-smokers aged 50-75 with a history of at least 20 cigarette pack-years were randomised 1:1 to spiral CT screening versus usual care in a randomised controlled trial. In the four screening sites 16-detector multi-slice CT scanners and Siemens Lungcare® workstations were used. Automated measurement of solid lesions and manual measurement of non-solid lesions was performed. Nodules were divided into 3 categories: solid, non-solid and part-solid. Solid nodules with a volume between 50 and 500 mm³, and non-solid nodules larger than 8 mm in diameter were called significant nodules. In these cases, a follow-up scan was performed after 3 months. Larger solid nodules were referred to the pulmonologist without delay.

Results: Of the first 806 patients screened, 651 (72%) had no significant pulmonary nodules. In 239 cases (26%), significant nodules were found. Sixteen patients (2%) were referred to the pulmonologist with a strong suspicion of lung cancer. Up-to-date screening results will be presented.

Conclusion: In an elderly population of male current and ex-smokers, only a low percentage (2%) showed pulmonary lesions very suspicious of lung cancer on a baseline low-dose CT scan.

B-382 14:09

Lung cancer screening in asbestos-exposed high risk patients with low dose MDCT: Results of baseline screening and first year follow-up

M. Das¹, G. Mühlenbruch¹, A.H. Mahnken¹, M.K. Felten¹, T.G. Flohr², T. Kraus¹, R.W. Günther¹, J.E. Wildberger¹; ¹Aachen/DE, ²Forchheim/DE

Purpose: To assess the risk of lung cancer in a high-risk cohort with low-dose MDCT baseline screening and first year follow-up.

Methods and Material: 174 former power plant workers (mean age 66.6 y; range 55-77 y) who were characterized as high risk individuals for lung cancer according to the risk model of Doll and Peto [(age/50) 3 x asbestos exposure time x smoking habits] were entered into a prospective trial. Average asbestos exposure time was 29.65 y (range 16-45 y); 87% were smokers, 12% ex-smokers and 1% non-smokers. CT-screening was performed on a 16-slice MDCT (Somatom Sensation 16, Siemens), using a low dose technique (120 kV, 10/20 mAs_{eff}, dependent on patients weight, collimation: 16 x 0.75 mm, rotation time: 0.5 s, table feed/rotation: 18 mm). Images were reconstructed as 1 mm thick sections with reconstruction increment: 0.5 mm. As well as visual analysis on a workstation, a dedicated CAD-software was used for data analysis (LungCARE; Siemens).

Results: Diagnostic workup with CT-guided biopsy was performed in eight patients showing bronchial cancer in six patients. 353 additional small lung nodules ranging between 1.2 mm to 13.1 mm were found (mean 5.36 mm). 133 were between 5-10 mm and were followed with CT. Asbestos related changes (plaques, fibrosis) were visible in 48 patients. Within the first year of follow-up no additional lung cancer was found.

Conclusion: Lung cancer screening in this high-risk cohort revealed a malignancy rate of 3.4% at baseline screening. Within the first year of follow-up no additional lung cancer has been found to date.

B-383 14:18

Comprehensive pulmonary MR imaging in patients with bronchial carcinoma using parallel acquisition techniques

S.O. Schoenberg, O. Dietrich, K.A. Herrmann, T. Strauss, R. Hatz, M.F. Reiser; Munich/DE

Purpose: To assess the value of a morphologic and functional MR imaging protocol for staging of bronchial carcinoma including high-resolution 3D-Gd-MRA, perfusion and oxygen imaging and whole-body tumor staging using integrated parallel acquisition techniques (iPAT).

Material and Methods: 20 patients with stage III a bronchial carcinoma were imaged on a 32 channel whole-body MR imaging scanner (Magnetom Avanto). The protocol consisted of pulmonary 3D-Gd-MRA with isotropic spatial resolution of 0.9 mm using iPAT with an acceleration factor of 3. Oxygen-enhanced imaging of the lungs was carried out with a gated IR-HASTE sequence and iPAT. Time-resolved perfusion was performed with a fast 3D FLASH sequence during injection of 0.1 mmol/kg BW of gadobutrol (Gadovist). Assessment of tumor invasion into the heart and mediastinum was detected by time-resolved TrueFISP imaging. For detection of metastases, whole-body STIR images were obtained with iPAT within 12 minutes. The results are compared to scintigraphy, CT and intraoperative findings.

Results: The entire protocol was completed in under 60 minutes. In the case of arterial or bronchial invasion by the tumor, perfusion or ventilation defects were well visualized using oxygen and perfusion MR imaging. In cases of isolated arterial occlusion, a ventilation/perfusion mismatch was observed. Bone metastases were well seen on the whole-body STIR images. Assessment of tumor invasion into the mediastinum by MR imaging correlated well with intraoperative findings.

Conclusion: Using whole-body MR imaging scanners, comprehensive morphologic and functional staging of bronchial carcinoma by MR imaging is feasible. High-resolution MRA, perfusion and oxygen imaging benefit greatly from the acceleration of image acquisition using iPAT.

B-384 14:27

Presurgical staging of non-small cell lung cancer: A performance comparison between PET, hardware PET/CT and software image fusion

B.S. Halpern, C. Schiepers, W.A. Weber, T. Crawford, B.J. Fueger, O. Ratib, M.E. Phelps, J. Czernin; Los Angeles, CA/US

Purpose: ¹⁸F-FDG PET stages Non-Small Cell Lung Cancer (NSCLC) with high accuracy. The purpose of our study was to assess whether hardware PET/CT and software PET and CT image fusion raise the diagnostic accuracy.

Materials and Methods: Thirty-six patients (17 males and 19 females) with NSCLC underwent staging with a hardware PET/CT followed by mediastinal lymph

Scientific Sessions

node dissection and tumor resection in 30 patients. 25 of the 36 patients (69%) had separate CT studies within a maximum of 6 six weeks of the hardware PET/CT study. With these images, fully automated image fusion was performed, by using commercially available software. Two blinded reviewers in consensus analyzed all PET images and an experienced radiologist was subsequently added to assess hardware and software fused PET/CT images.

Results: Reviewers examining PET and hardware PET/CT classified T-stage accurately in 67% (20/30) and 97% (29/30) of patients, respectively ($p < 0.05$) and tended to be more accurate than PET alone for N-staging (78% vs. 69%). Interpretations based on hardware PET/CT correctly staged 83% (25/30), overstaged 3 (10%) and under-staged 2 patients (7%). The overall staging accuracy of PET/CT was significantly higher than that of PET ($p < 0.05$). Automatic software fusion of separately obtained PET and CT studies failed in 32% of the patients, most frequently in those with extensive and intense glucose metabolic abnormalities.

Conclusion: Hardware PET/CT compared with PET alone was associated with 26% greater overall diagnostic accuracy. The software fusion method failed to provide acceptable co-registration in 32% of the patients.

B-385 14:36

Value of integrated PET-CT versus CT and PET alone in the detection of lung metastases in patients with a known primary tumor: A retrospective study

W.F.M. De Wever, L. Meylaerts, L. De Ceuninck, J.A. Verschakelen; Leuven/BE

Purpose: The purpose of this study was to retrospectively evaluate the additional value of integrated PET-CT in comparison with CT or PET alone to detect lung metastases in patients with a known primary tumor.

Material and Methods: Fifty-six lung nodules were detected in 24 patients with a known primary tumor who underwent a PET-CT examination for staging of their primary tumor. The benign or malignant character of these nodules was determined by either an anatomical-pathological examination or a follow-up during at least 6 months. The CT scan was evaluated by a radiologist, the PET-scan by a specialist in nuclear medicine and the integrated PET-CT images by a different radiologist and specialist in nuclear medicine in consensus. The investigators were asked to search for lung nodules and to determine whether these nodules were metastatic or not. The specificity, sensitivity, PPV, NPV and accuracy were calculated for PET-CT, CT and PET.

Results: With PET-CT 53 nodules were detected, while CT and PET detected respectively 55 and 20 nodules.

Specificity, sensitivity, PPV, NPV and accuracy are respectively:

- PETCT: 92%, 93%, 93%, 92%, 93%
- CT: 22%, 100%, 58%, 100%, 62%
- PET: 48%, 88%, 61%, 82%, 68%

Conclusion: PET-CT has a higher specificity, sensitivity, PPV, NPV and accuracy in the detection and characterisation of lung nodules in comparison with CT and PET alone and seems to be the most adequate examination for evaluation of lung metastases.

B-386 14:45

Clinical value of CT-based, software-assisted preoperative prediction of postoperative pulmonary function after lung surgery

D. Wormanns¹, F. Beyer¹, P. Hoffknecht¹, J.-M. Kuhnigk², V. Dicken², T. Lange¹, M. Thomas¹, W. Heindel¹; ¹Münster/DE, ²Bremen/DE

Purpose: To evaluate a morphology-based approach for prediction of post-operative forced expiratory volume in one second (FEV₁) after lung resection from preoperative CT scans.

Material and Methods: Fifteen patients with surgically treated (lobectomy or pneumonectomy) bronchogenic carcinoma were enrolled. A preoperative chest CT (slice thickness ≤ 5 mm) and pulmonary function tests (PFT) before and after surgery were performed. CT scans were analyzed by prototype software: Automated segmentation and volumetry of lung lobes was performed with minimal user interaction. Determined volumes of different lung lobes were used to predict postoperative FEV₁ as a percentage of the preoperative values. Predicted FEV₁ values were compared to the observed postoperative values as the standard of reference.

Results: Patients underwent lobectomy in twelve cases (6 upper lobes; 1 middle lobe; 5 lower lobes; 6 right side; 6 left side) and pneumonectomy in three cases. Automated calculation of predicted postoperative lung function was successful in all cases. Predicted FEV₁ ranged from 54% to 95% (mean $75\% \pm 11\%$) of the preoperative values. Two cases with obviously erroneous PFT were excluded from analysis. Mean error of predicted FEV₁ was 7.5 ± 250 ml, indicating absence of systematic error; mean absolute error was $11.1 \pm 5.3\%$ respective 204 ± 130 ml/s.

The 200 ml reproducibility criterion for FEV₁ was met in 10 of 13 cases (77%).

Conclusion: Software-assisted prediction of postoperative lung function yielded a clinically acceptable agreement with the observed postoperative values. This method might add useful information for evaluation of functional operability of patients with lung cancer.

B-387 14:54

Oxygen-enhanced MR imaging: Correlation with postoperative lung function in lung cancer patients

Y. Ohno¹, M. Nogami¹, T. Higashino¹, D. Takenaka², H. Hatabu³, K. Sugimura¹; ¹Kobe/JP, ²Kasai/JP, ³Boston, MA/US

Purpose: To prospectively determine if oxygen-enhanced MR imaging correlates with post-operative lung function in patients with lung cancer, as compared with quantitative and qualitative CT and scintigraphy.

Materials and Methods: Thirty consecutive patients (16 men, 14 women; aged 44 to 81 years; mean age 65 years) considered candidates for lung resection underwent oxygen-enhanced MR imaging, CT, perfusion scintigraphy, and measurement of forced expiratory volume in 1 second (FEV1). A respiratory-synchronized inversion recovery half-Fourier single shot turbo spin echo sequence (TR 3200-5000 ms; TE 4 ms; TI 900 ms; ETS 4 ms) was used for data acquisition. Correlation of post-operative lung function (post-operative FEV1) as determined by oxygen-enhanced MR imaging (poFEV1_{MR}), quantitative assessment by CT (poFEV1_{Quantitative CT}), qualitative assessment by CT (poFEV1_{Qualitative CT}), and perfusion scintigraphy (poFEV1_{Perfusion scintigraphy}) was made with actual post-operative FEV1, and the limits of agreement of each was also determined by Bland-Altman analysis.

Results: Correlation between poFEV1_{MR} and actual post-operative FEV1 was excellent ($r^2=0.81$, $p < 0.0001$); better than that of poFEV1_{Qualitative CT} ($r^2=0.76$) and poFEV1_{Perfusion scintigraphy} ($r^2=0.77$), and similar to that of poFEV1_{Quantitative CT} ($r^2=0.81$). The limits of agreement of poFEV1_{MR} were between -9.9% and 10.9%.

Conclusion: Oxygen-enhanced MR imaging correlates with post-operative lung function in lung cancer patients, similar to quantitative CT.

B-388 15:03

Accuracy of multislice CT with multiplanar reformations in staging malignant pleural mesothelioma

B. Feragalli, M.L. Storto, A.G. D'Agostino, R. Sacco, M. Mereu, C. Colosimo; Chieti/IT

Purpose: To assess the value of Multislice CT (MSCT) with multiplanar reformations in staging Malignant Pleural Mesothelioma (MPM) and in predicting resectability of tumor for radical surgery.

Methods and Materials: Twenty-four patients with biopsy-proved MPM underwent MSCT of the thorax before surgery. MSCT was performed with the following protocol: 1 mm-collimation, 1 mm-slice width, 0.8 mm-reconstruction increment. Two radiologists assessed tumor resectability by consensus, focusing on local invasion of three separate regions: the mediastinum, diaphragm and chest wall. Results of all CT examinations were carefully correlated with intraoperative pathologic findings.

Results: 14 patients underwent extrapleural pneumonectomy and 10 had pleural decortication because the tumor was unresectable. The sensitivity and specificity of MSCT in predicting resectability were 93% and 90% at the mediastinum, 94% and 100% at the diaphragm and 94% and 86% at the chest wall. Accuracy was 92%, 96% and 92% at the mediastinum, diaphragm and chest wall respectively.

Conclusion: MSCT with multiplanar reformations has high diagnostic accuracy in predicting tumor resectability, and also in the assessment of diaphragmatic involvement. It is likely that MSCT can replace Magnetic Resonance in the preoperative assessment of patients with MPM.

B-389 15:12

Evaluation of the diaphragm in malignant pleural mesothelioma: Role of US L.L. Ciarpaglini, S. Pascoli, P. Regimonti, L. Portalone, G. Pedicelli; Rome/IT

Purpose: To evaluate the sensitivity and diagnostic accuracy of contrast echo in diaphragmatic invasion in malignant pleural mesothelioma.

Materials and Methods: From January 2003 to August 2004 we observed 14 patients with the diagnosis of malignant pleural mesothelioma. 7 patients that did not present invasion of pericardium or chest wall were evaluated with CT, MR and US with contrast media for the detection of diaphragmatic involvement.

Results: There was full agreement of CT, MR and US: 3 patients had infiltration of the diaphragm, and in 4 patients there was no involvement of this structure.

Conclusion: This study has showed that US with contrast media, revealing the

Scientific Sessions

neoangiogenesis of neoplastic foci, has a very high diagnostic accuracy and sensitivity in the diagnosis of diaphragmatic invasion.

B-390 15:21

Interobserver variability in the CT assessment of suspected mesothelioma without final histologic diagnosis

I. Moraschi, D. Farina, P. Maculotti, G. Battaglia, P. Barbieri; *Brescia/IT*

Purpose: To identify CT findings statistically correlated to mesothelioma (M1). To assess interobserver variability in defining, based on CT, the probability of mesothelioma in pleural lesions without histologic diagnosis (M2: possible; M3: probable).

Methods and Materials: Retrospective analysis of CT examinations of 40 patients (11 M1, 7 M2, 13 M3, 9 non-mesothelioma) included in Malignant Mesothelioma Register of Brescia performed by three blinded radiologists. Several CT parameters were assessed (pleural effusion, hemithorax retraction, mediastinal shift, calcified/solid pleural plaques, thickening of fissures, parenchymal consolidation/nodules/masses, infiltration of mediastinum/diaphragm/thoracic wall, lymphadenopathy, pericardial effusion, distant metastases). Each patient was finally assigned a score designating the probability of mesothelioma, ranging from 0 (slight) to 5 (elevated). Statistical correlation between each of CT parameters and M1 class was assessed.

Results: In 70% of patient the reviewers completely agreed on the score assigned to the patients. In 30% of cases, minor inconsistencies occurred, as one reviewer assigned a score in all cases just one figure different from the others. Classification in Malignant Mesothelioma Register of Brescia was retrospectively changed in 2/20(10%) of M2 and M3 patients. Statistically significant correlation was found between M1 class and the following CT parameters: hemithorax retraction ($p = 0.0005$); solid pleural plaques ($p = 0.004$) with circumferential distribution ($p = 0.01$) or involving either the mediastinal ($p = 0.0001$) or diaphragmatic pleura ($p = 0.0003$); infiltration of mediastinum ($p = 0.01$) or diaphragm ($p = 0.008$).

Conclusion: CT findings allow us to define the probability of mesothelioma in suspected cases lacking a final diagnosis. This may have crucial legal implications.

14:00 - 15:30

Room G

Genitourinary

SS 707

Renal and adrenal tumors

Moderators:

P. Aspelin; *Huddinge/SE*
M. Kekelidze; *Rotterdam/NL*

B-391 14:00

Functional radiogenomic identification of alterations in global gene expression in human solid renal tumors with conventional cross sectional imaging

M.D. Kuo¹, B. Chan¹, J. Buckley², B. Gooding³; ¹*San Diego, CA/US*, ²*Palo Alto, CA/US*, ³*San Francisco, CA/US*

Purpose: Genomics, the study of genome-wide gene expression, has led to important discoveries about cancer but requires cells to be obtained invasively. We sought to show proof of concept that computed tomography (CT) and magnetic resonance imaging (MRI) has potential for non-invasively identifying functionally relevant alterations in global gene expression in solid renal neoplasms.

Methods: 27 renal tumors in 27 patients imaged with contrast enhanced CT ($n = 20$) or MRI ($n = 9$) were reviewed by 2 radiologists in consensus. 4 independent imaging parameters were defined a priori (pattern of enhancement, necrosis, hemorrhage, tumor borders), and then evaluated and scored without knowledge of the genomic information. Imaging parameters were then evaluated across matched tumor cDNA microarray data representing ~17,000 genes. Supervised and unsupervised statistical and bioinformatic analyses were then performed to identify imaging-genomic correlations.

Results: 2/4 imaging parameters (pattern of enhancement and necrosis) showed statistically significant correlation ($P < 0.01$) with the corresponding gene expression data and revealed plausible insights into tumor biology based on the imaging. These genes were largely grouped into several well defined co-expressed gene clusters representing: immune infiltration (e.g. T cell and B cell), hypoxia/angiogenesis (e.g. VEGF, HIF, CD34, THY-1), extracellular matrix remodeling, and metabolic and cell signaling gene expression clusters.

Conclusions: We show preliminary evidence that conventional cross sectional imaging has potential to non-invasively characterize components of large-scale gene regulation in renal neoplasms into co-regulated functional gene clusters

representing biological processes based on imaging traits alone. Further study into this emerging area of functional radiogenomics is warranted.

B-392 14:09

Renal lesions too small to classify by CT; outcome study based on follow-up for 18-62 months (38 mean) by multiphasic helical CT or laparoscopy

E.K. Lang¹, B. Gayle², R. Macchia², R. Charafeddine¹, L. Meyers¹; ¹*New Orleans, LA/US*, ²*Brooklyn, NY/US*

Purpose: Establish significance and possibly, etiology of "renal lesions too small to classify by CT" by follow-up multiphasic helical CT, laparoscopy, biopsy or surgery.

Materials and Methods: 465 "renal lesions too small to classify by CT" and with follow-up studies for 18 - 62 months (38 mean) at three university medical centers were analyzed in this retrospective study. 72 lesions featured a lower than parenchymal density on pre-enhancement CT, 393 lack of enhancement on post-enhancement CTs. The lesions ranged in size from 0.4 to 1.0 cm (7 mm mean), were hypovascular and lacked enhancement. Outcome is based on multiphasic helical CT ($N = 440$), laparoscopy ($N = 19$), biopsy ($N = 4$) and surgery ($N = 2$).

Results: 335 of these lesions were no longer identifiable on follow-up examinations. However, 58 of these had been treated for urinary tract infections. 69 lesions had increased to greater than 1 cm in diameter and exhibited CT criteria of cysts. 51 had increased in size with CT findings consistent with medullary necrosis, renal abscess, or calyceal diverticula. Follow-up CTs suggested renal infarcts in 4. Four enlarging lesions proved to be metastatic neoplasms; 2 others angiomyolipomas.

Conclusion: Less than 1% of the lesions were malignant neoplasms, however, 51 (11%) were caused by inflammatory disease prone to progress to medullary necrosis, renal abscesses or calyceal diverticula if left untreated. 58 (12.5%) of the lesions were no longer identifiable possibly due to treatment of coexisting urinary infections. 277 lesions (60%) disappeared without treatment, likely due to normalization of a temporary ischemic process.

B-393 14:18

Tuberous sclerosis complex: Prevalence of minimal fat-containing angiomyolipoma (AML) and renal cell carcinoma

E. Simpson, U. Patel; *London/UK*

Purpose: Define prevalence of the various types of renal masses in Tuberous Sclerosis Complex (TSC).

Materials and Methods: A study group of 12 patients with TSC (ages 17-66 years) evaluated. All patients underwent two dedicated renal Computerised Tomography (CT) scans, 2 years apart. The prevalence of solid and cystic renal masses was defined. The solid masses were further divided into typical AML's [definition: region of interest (ROI) density < -10 units] and indeterminate masses [ROI density > -10 units].

Results: 200 masses identified (mean diameter 3.6 cm, range 8 mm -16 cm). 12 were simple (Bosniak type 1) cysts. Of the rest, 136/188 were typical AML with a ROI density < -10 units. The remainder (52/188 or 27% of all solid masses) could not be accurately categorised by CT as being minimal fat containing AML or renal cell carcinoma. Over a two-year follow-up period, 7/52 masses have undergone biopsy because of suspected renal cell carcinoma. 1/7 proved to be carcinoma. The rest were minimal fat AML's. The remainder (45/52) have not shown any substantial interval growth and are presumed to represent minimal fat AML's as well.

Conclusion: In TSC, over a quarter (27%) of renal masses will be diagnostically indeterminate on renal CT and indistinguishable from renal cell carcinoma. But on two year follow-up only 1 case of renal cell carcinoma was found (overall incidence = 0.5%).

B-394 14:27

Renal angiomyolipoma with no discernible fat on CT and chemical shift MR imaging

J. Lee, S. Lee, S. Kim, T. Moon; *Pusan/KR*

Purpose: To evaluate the imaging findings of renal angiomyolipoma with no discernible fat on CT and chemical shift MR imaging.

Materials and Methods: Five patients with 16 proved angiomyolipoma after partial nephrectomy were retrospectively reviewed. The main CT features analyzed are the presence of fat component, homogeneity, enhancement of mass. Qualitative analysis of the MR images was done on the basis of signal loss on out-of-phase images and signal intensity of mass on T2-weighted images. Quantitative analysis

Scientific Sessions

of MR images was performed by calculating the difference in signal intensity between in-phase and out-of-phase by use of regions of interest (signal intensity index and mass-spleen ratio) and signal intensity ratio between renal mass and parenchyma on T2-weighted images.

Results: Renal masses were ranged from 3 mm to 3 cm in size. All of masses showed no fat component, homogenous density, and good enhancement and washout on CT images. All of masses showed no loss of signal intensity on out-of phase images and lower signal intensity compared to that of renal parenchyma on T2-weighted images. Quantitatively, there were no discernible fat components in the mass (mean signal intensity index, 24.7; mean mass-spleen ratio, 1). Mean signal intensity ratio between renal mass and parenchyma was 67.3 on T2-weighted images.

Conclusion: In case of renal mass with no discernible fat component on CT and chemical shift MR imaging, MR image may have value in demonstrating abundant muscle and vessel tissue, which leads to the diagnosis of angiomyolipoma.

B-395 14:36

The angular interface sign: New sign for differentiation of renal cell carcinoma and angiomyolipoma on MR imaging of small renal masses

H. Sherif, A.E. Mahfouz; Doha/QA

Purpose: To assess the shape of the interface between renal masses and normal renal parenchyma as differentiating sign between renal cell carcinoma and angiomyolipoma.

Methods and Materials: Sixty eight patients with small solid renal masses (< 3 cm) have been examined at 1.5 T by T2-weighted half-Fourier turbo spin echo (HASTE), and T1-weighted gradient-echo (GRE) images of the kidney before and after fat saturation in transverse, coronal, and sagittal orientations during breathhold. Additionally, breathhold gadolinium-enhanced fat-saturated T1-weighted GRE images were obtained in the three orthogonal orientations. To avoid bias caused by signal intensity of fat in angiomyolipoma, only fat saturated images were evaluated collectively in the three orthogonal planes by blinded reader for the angularity or roundness of the lesion-kidney interface.

Results: The lesion-kidney interface was round in 44 out of 50 renal cell carcinomas (88%) and angular in the remaining 6 lesions (12%). On the other hand, the lesion-kidney interface was angular in 16 out of 18 angiomyolipomas (89%), and round in 2 lesions (11%). Difference between renal cell carcinoma and angiomyolipoma was statistically significant ($p < 0.001$).

Conclusion: Angiomyolipoma has angular configuration of the interface with the normal renal parenchyma more frequently than malignant renal neoplasm. This newly described sign may be used, in conjunction with other imaging features, for differentiation between small angiomyolipoma and renal cell carcinoma on MR imaging.

B-396 14:45

Morphologic characterization of subtypes of renal cell carcinoma by multislice CT

M. El-Azab, A. Mosbah, M. El-Baz, K. Shoier; Mansoura/EG

Purpose: The purpose of our study to differentiate subtypes of renal cell carcinoma on multislice CT scans.

Materials and Methods: We reviewed CT scans of three subtypes of renal cell carcinoma: 37 conventional (clear cell), 26 papillary and 24 chromophobe. Biphasic CT scans (unenhanced, cortico-medullary, excretory phase scans) were obtained in all patients. We compared patient age and sex; tumor size; degree and pattern (homogeneous, heterogeneous, predominantly peripheral) of enhancement; presence or absence of calcification; and tumor-spreading patterns including perinephric change, venous invasion and lymphadenopathy in three subtypes.

Results: Conventional renal carcinoma showed stronger enhancement than the other subtypes ($p < 0.05$): 138 ± 38 H (mean \pm SD) in the corticomедullary phase. No statistically significant difference between papillary and chromophobe renal carcinomas was detected in attenuation value or degree of enhancement in either the corticomedullary phase or the excretory phase ($p > 0.05$). Conventional (70.3%) and papillary (69.2%) renal carcinomas tended to show heterogeneous or predominantly peripheral enhancement, whereas chromophobe renal carcinoma (75%) usually showed homogeneous enhancement. Calcification was noted in conventional (21.6%), papillary (23.1%) and chromophobe (25%) renal carcinomas without statistically significant difference ($p > 0.05$).

Conclusion: For the differentiation of the subtypes of renal cell carcinoma, pattern and degree of enhancement is the most valuable parameter.

B-397 14:54



Correlation between radiologic and pathologic TNM using MDCT in staging of renal masses

F. Toso, M. Vergendo, G. Ciccarese, G. Como, C. Del Frate, M. Bazzocchi; Udine/IT

Purpose: To evaluate role of MDCT in renal masses staging and to correlate pre-surgical staging, with pathologic staging.

Material and Methods: 48 patients with renal mass detected by US or CT underwent MDCT (Aquilion-TOSHIBA), using a multiphase protocol after iodine-contrast media (400 gml/ml) injection (flow-rate: 4 ml/s) using Sure Start® software for bolus-tracking. Acquired data were processed to obtain coronal MPR and three-dimensional MIP and VR for angiographic, nephrographic, urographic assessment. Each renal mass was evaluated for location, size, relationship with surrounding structures, urinary-tract invasion, loco-regional lymphadenopathy, and vascular invasion. Each mass was classified following radiologic-TNM and correlated with pathologic-TNM after surgery.

Results: 45 suspicious renal masses were detected in 40/48 patients who underwent MDCT, while in 8 patients renal findings resulted to be benign. Considering TNM staging system we identified 34/45 masses with major diameter smaller than 7 mm (T1). Comparing radiologic staging with pathologic one in patients who underwent surgery we found two discordant cases (MDCT overstaged both, for renal fascia invasion in one and of renal capsule in second). Seven masses were classified by MDCT as T3a, due to invasion of peri-renal fat tissue (in one case involvement of adrenal gland was found) and 4 masses as T4, due to invasion of renal fascia. No masses were classified as T2, and we never found involvement of renal vein in our cases.

Conclusions: In our experience, MDCT seems to be gold-standard examination in staging of renal masses, thanks to high correlation found between radiologic and pathologic-TNM.

B-398 15:03

Preoperative staging of renal cell carcinoma with inferior vena cava thrombus using multi-detector CT and MR imaging: Prospective study with histopathological correlation

P.J. Hallscheidt, C. Fink, A. Haferkamp, G. Kauffmann; Heidelberg/DE

Purpose: To evaluate accuracy of multi-detector computed tomography and magnetic resonance imaging in staging and estimating renal carcinomas with caval thrombus.

Materials and Methods: Initially 23 patients with suspected caval thrombi were admitted into this prospective study. Triphasic CT imaging was performed using a multi-detector CT with a reconstructed slice thickness of 2 mm. 3D CT reconstructions were used. MR imaging protocol included: a transverse T1-weighted GE sequence with and without Gd-DTPA, a transverse T2-weighted respiratory-gated TSE and a coronal T1-weighted GE sequence with Gd-DTPA and fat saturation. In addition, multi-phase 3D angiography was performed after Gd-DTPA injection. Patients were divided into three groups: caval thrombus below the insertion of the hepatic veins, within the intrahepatic vena cava, and intra-atrial extension. The results of tumor thrombus extension and staging results by two independent readers were correlated with surgical and histopathological staging.

Results: Of the 23 patients admitted, CT and MR scans of 14/13 patients respectively were correlated with histopathological workup. CT thrombus detection sensitivity and specificity for both readers was 0.93 and 0.8 respectively. MR imaging sensitivity and specificity for both readers was 1.0/0.85 and 0.75. Readers I and II evaluated the uppermost extension of the tumor thrombus by both CT and MR imaging. CT and MR accuracy was 78% and 72%, 88% and 76% respectively.

Conclusion: In cases of a suspected tumor thrombus, MR imaging and multi-detector CT imaging showed similar staging results. Consequently, these staging modalities can be used to assess the extension of the tumor thrombus.

B-399 15:12



Multiphase multidetector CT (MDCT) in diagnosis and staging of transitional cell carcinoma of the renal pelvis and the ureter

G.A. Fritz, H. Schoellnast, B. Unger, H.A. Deutschmann, U. Stessel, M. Tillich; Graz/AT

Purpose: To evaluate the potential of MDCT in the diagnosis and staging of transitional cell carcinoma of the renal pelvis and ureter.

Methods and Materials: CT scans of 30 patients with transitional cell carcinoma (9 renal pelvic, 21 ureteral) were evaluated. In all patients the urinary tract was examined using MDCT performing unenhanced and contrast enhanced scans

Scientific Sessions

during the corticomedullary phase (scan delay 30 s) and the excretory phase (scan delay 180 s). All scans were obtained with 2.5 mm collimation, pitch 1.5, and reconstruction interval of 2 mm. The attenuation of the tumors was documented in Hounsfield units (HU) using ROI measurements. Tumor staging was performed according to the TNM classification. CT and histopathologic findings were correlated.

Results: All transitional cell carcinomas were visible on corticomedullary and excretory phase scans, mean attenuation was 73 ± 10 HU in the corticomedullary and 77 ± 16 HU in the excretory phase. There was no statistically significant difference in the attenuation of the tumor between both contrast enhanced phases ($p = 0.23$). CT correctly diagnosed a transitional cell carcinoma confined to the organ in 19/20 cases (95%). In the one false positive case chronic inflammatory changes of the renal pelvis and proximal ureter were found at histopathological examination. A differentiation between T1 and T2 stages was not possible with MDCT. A stage T3 was correctly diagnosed in 7/8 patients (87.5%), in one patient histological examination revealed a stage T4. In 2/2 patients (100%) T4 was correctly diagnosed. CT was accurate in predicting pathologic TNM stage in 27/30 patients (90%).

Conclusion: MDCT with its high spatial resolution is an accurate tool for diagnosis and staging of transitional cell carcinoma. However, a reliable differentiation of neoplastic and chronic inflammatory lesions is not possible.

B-400 15:21

Characterization of adrenal masses with MDCT and MR imaging

B.M. Happel¹, T. Mang, W. Matzek, D. Latzke, B. Niederle, K. Kaserer, G. Heinz-Peer; Vienna/AT

Purpose: To compare the diagnostic performance of MDCT and MR imaging in characterization of adrenal masses and to correlate imaging findings with histopathologic results.

Material and Methods: 38 patients (25 female, 13 male, median age 51 y) underwent MDCT and MR imaging for evaluation of adrenal masses. CT was performed on either a 4 or 16 row scanner (Siemens). CT protocol included an unenhanced scan, 1 min post contrast and 15 min delayed contrast series. All MR examinations were performed on a 1.5 T unit (Siemens). MR protocol included chemical shift and Gd-enhanced dynamic imaging with delayed contrast series. CT- and MR images were independently reviewed by two radiologists, experienced in adrenal gland imaging, and blinded to patients' history. CT and MR imaging findings were compared to histologic results in all cases.

Results: 39 adrenal masses (1 bilateral) were detected on MDCT and MR imaging (mean size 32 mm, range 8-86 mm). Histology revealed 17 adenomas, 10 pheochromocytomas, and 12 further lesions (4 metastases, 1 carcinoma, 1 primary lymphoma, 1 borderline tumor, 1 haematoma,...). On MR imaging 15/17 adenomas, 9/10 pheochromocytomas and 11/12 further lesions were correctly diagnosed. In two atypical adenomas MR imaging findings were indicative for malignant lesions. Overall sensitivity for MR imaging was 90%.

On MDCT 17/17 adenomas, 9/10 pheochromocytomas and 11/12 further lesions were correctly diagnosed. Overall sensitivity was 95%.

Conclusion: Both MDCT and MR imaging have high sensitivity in characterization of adrenal masses. MDCT seems to be more reliable in evaluation of atypical adenomas compared to MR imaging.

14:00 - 15:30

Room H

Interventional Radiology

SS 709

MR, CT and US guided procedures

Moderators:

M. Bezzu; Rome/IT
M.A. Funovics; Vienna/AT

B-401 14:00

A new cordless coil for MR-guided percutaneous biopsies in a low field system: First clinical experiences

S. Zangos¹, M.G. Mack¹, K. Eichler¹, C. Herzog¹, M. Heller¹, T. Vetter², T. Lehnert¹, T.J. Vogl¹; ¹Frankfurt a. Main/DE, ²Erlangen/DE

Purpose: To evaluate the safety and precision of MR-guided biopsies with a new cordless coil in an open low field system for different regions.

Materials and Methods: In 8 patients with uncertain tumors MR-guided biopsies were performed in a low field system (0.2 T, Magnetom Concerto, Siemens) with a new cordless coil (Siemens). The biopsies were performed in different organ

systems (5 liver, 2 abdomen and 1 hip). For the monitoring of the biopsy procedures T1-weighted FLASH sequences were used. The lesions were biopsied repeatedly through a G15 pencil tip with a G16 biopsy-handy. The visibility of the anatomy, the tumor and the needles as well as the handling of the coils were evaluated.

Results: The cordless coil can be easily handled for the biopsies with sufficient image quality for interventional procedures. Via MR-guidance the needle position could be easily visualized during the biopsy of soft tissue lesions using T1-weighted sequences.

The biopsy procedures could be performed successfully in all cases without any side effects or complications. The use of the cordless coil allows an increased patients comfort during the biopsy procedure.

Conclusion: MR-guided biopsies of soft tissue lesions with cordless coils can be performed safely and precisely with easy handling of the coil resulting in an reducing of the procedure time.

B-402 14:09

Cryotherapy of breast cancer under ultrasound-guidance

S.O.R. Pfeiferer, C. Marx, A. Malich, O. Camara, W.A. Kaiser; Jena/DE

Purpose: Cryosurgery has been used in the treatment of tumours of the liver and prostate for more than 25 years. The potential and feasibility of cryotherapy in breast cancer was evaluated.

Methods and Materials: 48 female patients (median age 61 years; range 38-81 years) with breast cancers (median tumor diameter 12 mm; range 5-37 mm) underwent argon-based cryotherapy. 32 patients had tumors which were smaller than 16 mm. After local anaesthesia the tip of a 3 mm cryoprobe was placed into the tumor under ultrasound guidance. Two freeze/thawing were performed. The size of the iceballs was measured sonographically in one-minute intervals. The patients underwent open surgery within 3 weeks and the specimens were evaluated histologically.

Results: During cryosurgery iceballs could be well delineated using ultrasound. The mean diameter of the iceball was 31 ± 4.5 mm after the second freezing cycle. No severe side effects were observed. In all 32 patients with tumours of smaller than 16 mm histological evaluation of the specimens removed by open surgery did not reveal remnant invasive tissue. 4 of these had ductal carcinoma *in situ* (DCIS) in the surrounding area. In 16 patients cryotherapy of tumours reaching diameters of more than 15 mm resulted in incomplete necrosis.

Conclusions: Tumours of less than 16 mm diameter are completely destroyed by cryotherapy with a 13% risk of leaving DCIS in the surrounding tissue. In tumors of more than 15 mm diameter the technique of cryotherapy must be locally extended.

B-403 14:18

MR-guided large core breast biopsy inside the bore of a 1.5 Tesla scanner using a robotic system (ROBITOM)

S.O.R. Pfeiferer¹, C. Marx¹, J.R. Reichenbach¹, J. Vagner², H. Fischer², W.A. Kaiser¹; ¹Jena/DE, ²Karlsruhe/DE

Purpose: The aim of this study was to investigate the feasibility of MR-guided large core breast biopsy (LCBB) using a robotic system (ROBITOM) which helps to localize lesions and operates at the isocentre of a 1.5 Tesla scanner.

Methods and Materials: 16 patients with MR-detectable breast lesions were biopsied by using the first prototype ROBITOM I to position the trocar, which was subsequently inserted into the breast in front of the lesion. Specimens were taken in coaxial technique using a 14 G core needle biopsy gun. In case of malignant histology open surgery was performed afterwards. In vitro experiments using the second prototype (ROBITOM II) which contains a high-velocity device to insert the trocar and a phantom containing vitamine E capsules (7 x 3 mm in size) serving as artificial lesions were performed.

Results: Evaluating ROBITOM I in 5 cases biopsy findings were confirmed by open surgery. In 3 cases two invasive cancers were missed and one invasive cancer was underestimated. 8 patients with benign findings are still in the follow-up period. Investigating ROBITOM II under in-vitro conditions capsule material in the specimen cylinders were detected in all 13 experiments. First clinical results of LCBB using the second prototype will be presented.

Conclusions: The patient study demonstrated the feasibility of manipulator assisted LCBB inside a whole body scanner using ROBITOM I. The missed cases are most likely due to lesion shifts. Implementing a high-velocity trocar setting unit in the second prototype shifting the lesion could be avoided in-vitro.

Scientific Sessions

B-404 14:27

Interventional MR angiography with no strings attached: Wireless active catheter visualization

H.H. Quick¹, M.O. Zenge¹, H. Kuehl¹, G.M. Kaiser¹, S. Aker¹, S. Massing¹, S. Bosk², M.E. Ladd¹; ¹Essen/DE, ²Erlangen/DE

Purpose: To develop and evaluate a wireless active catheter visualization strategy for interventional MRA that 1) provides high contrast instrument visualization; 2) avoids electrical conducting wire connections to eliminate the risk of RF heating; and 3) offers unhampered instrument handling through obviating any wire connection.

Materials and Methods: 6F catheters were designed containing 120-mm-long self-resonant RF single-loop coils to enable wireless active instrument visualization. Surface coils were employed for simultaneous visualization of the anatomy and inductive signal coupling of the instrument coils. Imaging was performed on a 1.5 T Siemens Sonata using real-time TrueFISP sequences. Instrument-to-background contrast-to-noise vs. the excitation flip angle was systematically investigated in phantom experiments. In vivo evaluation of the concept was performed on five pigs. Instruments were guided through the vasculature under real-time MR imaging. Following selective catheterization, time-resolved 3D contrast-enhanced (CE) angiograms were acquired.

Results: The distal curvature of wireless active catheters could successfully be visualized with robust signal. TrueFISP sequences allowed for simultaneous depiction of the instrument outline and morphology with up to 9 frames/second. Instrument-to-background contrast could be adjusted by varying the excitation flip angle. Best contrast was achieved with flip angles about 15°. Time-resolved CE selective angiograms were successfully acquired in the abdominal aorta, the renal, splenic, mesenteric, and hepatic arteries of the pigs.

Conclusion: Wireless active visualization of catheters with resonant loop RF coils enables reliable visualization of the instrument curvature to the very tip. Additionally, due to inductive signal coupling, no wire connection compromises instrument handling. Instrument RF heating is not expected.

B-405 14:36

MR-guided laser induced thermotherapy (LITT) of colorectal carcinoma metastases in the liver

M.G. Mack, K. Eichler, R. Straub, T. Lehnert, J.O. Balzer, S. Zangos, T.J. Vogl; Frankfurt a. Main/DE

Purpose: To evaluate MR-guided LITT for the treatment of colorectal liver metastases in a long-term follow-up study and to demonstrate why ablation is superior to resection under certain circumstances.

Material and Methods: MR-guided LITT was performed in 803 patients (mean age 61.2 years) with 2376 liver metastases of colorectal cancer between 1993 and 2004. Survival rates were calculated using the Kaplan-Meier method.

Results: The local hepatic tumor control rate at 6-month follow-up was 2.2% for metastases up to 2 cm diameter, 2.9% for metastases between 2 and 3 cm diameter, 0.4% for metastases between 3 and 4 cm diameter and 2.6% for metastases larger than 4 cm in diameter. The mean survival rate for all treated patients, starting the calculation at the date of diagnosis of the metastases which was treated with LITT, was 3.9 years (95% confidence interval: 3.6 - 4.2 years, 1 year survival 93%, 2 year survival 72%, 3 year survival 49%, 5 year survival 25%). The mean survival of patients who refused resection and were treated with LITT was 5.2 years, which is superior to data published for surgical resection. The mean survival of patients who had already partial liver resection before was 3.8 years, in patients with bilobar liver metastases the mean survival was 3.6 years. **Conclusion:** MR-guided LITT yields high local tumor control and survival rates in patients with liver metastases of colorectal carcinoma. LITT appears in surgical candidates to be superior to resection.

B-406 14:45

MR-guided percutaneous sclerotherapy of low-flow vascular malformations: Final qualitative and quantitative assessment of therapy and outcome

D.T. Boll¹, E.M. Merkle², J.S. Lewin³; ¹Ulm/DE, ²Durham, NC/US, ³Baltimore, MD/US

Purpose: To prospectively assess the therapeutic procedure and outcome of magnetic resonance (MR)-guided percutaneous sclerotherapy in low-flow vascular malformations.

Material and Methods: 76 percutaneous sclerotherapy treatments were performed under real-time MR guidance on 15 patients with vascular malformations in the head and neck (n = 64), spine (n = 5), and extremities (n = 7). Qualitative assessment analyzed success of the therapy and occurrence of complications. Quantitative evaluation assessed length of time of minimally

invasive MR-guided sclerotherapy in a regression analysis, the ability of MR imaging to depict post-interventional perfusion changes by calculating changes in the Contrast to Noise Ratios (CNR), and the detection of volume changes on follow-up examinations.

Results: All sclerotherapy procedures were successfully performed without complications. Induced vascular sclerosis successfully treated the individual predominant symptoms, such as hemorrhage, pain, cosmetic disfigurement, and functional impairment. Quantitative analysis focusing on the actual interventional length of time presented a significant acceleration over the investigated five-year time period, matching a cubic function in the regression curve fit, and taking 31.50 ± 14 min. Induced vascular thrombosis was identified in all treated portions on post-interventional studies by the statistically significant changes in CNR ($p < 0.05$) compared to pre-interventional imaging. On follow-up examinations (after 12 ± 6 weeks), a significant shrinkage was observed in the targeted portions ($67.2 \pm 18.9\%$).

Conclusion: MR imaging allows the safe guidance and monitoring of minimally invasive sclerotherapy and also permits the verification of therapeutic success post-interventionally and during follow-up examinations.

B-407 14:54

MR guided focussed ultrasound surgery (MRgFUS) in the treatment of uterine fibroids. Are there any predictors for treatment success

S.A. Hengst, T. Ehrenstein, A. Beck, I. Utz-Billing, H. Herzog, R. Felix, J. Riecke; Berlin/DE

Purpose: MRgFUS represents a new, non-invasive thermoablative treatment procedure for uterine fibroids. Aim of this study was to evaluate the shortterm influence of MRgFUS in symptom relief and size of fibroids.

Method: As part of a prospective multicentric study 19 patients suffering from uterine fibroid related symptoms where included. Pretreatment MR imaging scans were performed and evaluated regarding size, location and characteristics of the fibroids. Additionally the symptom-severity-score was assessed prior to and 3, 6 and 12 month after MRgFUS. MR follow-up was performed after 6 and 12 month. For statistical analysis Students t-test, Mann-Whitney-test and Wilcoxon test were performed.

Results: 19 patients were included in the intention to treat analysis, for 15 patients the treatment was performed technically successful. None of the patients experienced severe adverse effects. The symptom severity score decreased from $70.6 (\pm 10)$ to $52.5 (\pm 13.1)$; $p = 0.003$, $n = 13$ after 3, to $58.7 (\pm 14.9)$; $p = 0.014$, $n = 13$ after 6 and eventually to $51.9 (\pm 22.7$, n.s.; $n = 9$) points after 12 month. Whereas there was no significant shrinkage in the size of the uterine fibroids for all patients after 6 and 12 month a subgroup analysis for patients with homogenous and dark myomas (T2w-images) revealed an average decrease in size of 28.6% (± 24 ; $p = 0.02$) after 6 and 51.0% (± 11.9 ; $p = 0.02$) after 12 month.

Conclusion: MRgFUS is a safe and effective procedure for short term symptom relief in patients suffering from uterine fibroids. Patients with homogenous and dark myomas are more likely to profit from this treatment.

B-408 15:03

MR-guided laser induced thermotherapy (LITT) for retroperitoneal lymph nodal metastases

T.J. Vogl, J. Li, M. Mack, T. Lehnert, K. Eichler, H. Ghazy, Y. Wang; Frankfurt a. Main/DE

Objective: The aim this study was to evaluate the experience with percutaneous MR image guided laser induced thermotherapy (LITT) for retroperitoneal lymph nodal metastases.

Materials and Methods: Twenty-two retroperitoneal lymph nodal metastases underwent MR-guided laser induced thermotherapy (LITT) using a 0.5 T MR unit. There were 15 men, and 7 women (average age 72.3 years). MR-guided LITT was performed with a cooled power laser system (Nd:YAG-Laser). A fast low-angle shot 2D sequence for MR thermometry was used for monitoring of the treatment tumors. The average metastases diameter was 3.6 cm (range, 1.5-5.6 cm). The follow-up was with MR imaging at 1.5 T MR unit at 3 months then 6 months interval after laser treatment. Lack of enhancement with contrast material in ablated tumors on MR images was considered coagulation necrosis.

Results: No complications occurred during laser treatment in 22 patients. A total of 28 laser applicators were performed. The mean laser power was 28.2 W; Average laser treatment time was 10.7 minutes. Follow-up was in average 9.2 months (range, 3-24 months) after procedure. Follow-up with gadolinium enhanced Min 20 treated tumors, In two lesions (diameter > 5 cm), enhancement of residual tissue was demonstrated; No patient had recurrent tumor at the treated site, 18 tumors size did no change, 4 lesions decreased in size about 60%-80%.

Conclusion: MR-guided laser induced thermotherapy (LITT) is a safe, feasible

Scientific Sessions

for treatment of retroperitoneal lymph nodal metastases, and can produce total destruction or large areas of necrosis within tumors.

B-409 15:12

Use of multidetector-row CT for the evaluation of E-PTFE covered stent in tips

M. De Rubeis, F. Fanelli, M. Bezzi, M. Corona, A. Bruni, L. Petrucci, A. Pucci, V. Dominelli, R. Passariello; Rome/IT

Purpose: Assess the efficacy of multidetector-row CT (MDCT) in the detection of TIPS malfunction, performed with e-PTFE stent-graft, to avoid the difficulties of Ultrasound-Color-Doppler (USCD) in stent-graft evaluation.

Materials and Methods: Eighty-five patients underwent a TIPS procedure with a stent-graft (Viatorr-Gore). Patients were followed-up with USCD and MDCT at 3-6-12 months; in case of abnormal findings a portogram and intravascular ultrasound (IVUS) were performed. MDCT was done using a multidetector scan (Somatom Volume Zoom-Siemens) at the level of the upper abdomen with 5 mm slice thickness (2.5 mm collimation, 5 mm reconstruction interval); after intravenous administration of 150 ml of iodinated contrast media at 4 ml/s, arterial (30 sec-3 mm slice thickness-2.5 mm collimation-1 mm reconstruction interval) and venous (60 sec-1.25 mm slice thickness-1 mm collimation-1 mm reconstruction interval) phases were acquired.

Results: MDCT was successfully performed in all cases, analysing stent-graft position, shunt patency, hepatic veins and portal vein. Correlation of shunt patency or malfunction between MDCT and USCD was observed in 80/85 patients (94.2%). In 5 cases (5.8%) MDCT indicated the completely shunt patency, not correlate with USCD that showed a mild stenosis of the shunt. Conventional venography and IVUS were then performed confirming the patency of the stent-graft according to the MDCT. Stenosis of the hepatic vein ($n = 8$) and of the portal vein ($n = 4$) were correctly diagnosed and MDCT demonstrated the complete patency of the shunt in 66 patients and shunt occlusion in 2 cases; these data were also evidenced by USCD and venography.

Conclusions: MDCT seems to be a safe and accurate method in the evaluation of stent-graft patency.

B-410 15:21

"Lesions in necrosis phenomenon" in patients with liver metastases of neuroendocrine tumor after thermal ablation

K. Eichler, M.G. Mack, T. Lehnhert, S. Zangos, O. Söllner, C. Herzog, T.J. Vogl; Frankfurt a. Main/DE

Purpose: To analyze the imaging characteristics of the "lesions in necrosis phenomenon" in patients with liver metastases of neuroendocrine carcinoma post treatment via thermal ablation.

Materials and Methods: 28 patients with 102 lesions of neuroendocrine carcinoma were treated with the MR-guided laser-induced thermotherapy (LITT) using a Nd-YAG laser device, liquid irrigated power laser applicators and multiapplicator technique. Local control of tumor was evaluated by unenhanced and contrast-enhanced MR imaging follow-up using T1 and T2 weighted SE and GRE sequences at 3-month intervals following treatment.

Results: Post interventional T1-weighted SE sequence images revealed in 51 lesions an intralesional hypointense area with corresponded exactly to the preinterventional morphology of the liver metastases pre interventional regarding size, shape and morphology within the coagulated necrosis.

Contrast-enhanced T1 weighted image 3 months after laser intervention demonstrated a reduction in the volume of necrosis. Follow-up studies revealed no local recurrence in all treated lesions.

Conclusion: The phenomenon of lesions in necrosis after MR-guided laser-induced thermotherapy (LITT) in patients with liver metastases of neuroendocrine carcinoma should be not misinterpreted as a local recurrence.

14:00 - 15:30

Room I

Abdominal Viscera

SS 701b

Pancreatic and bile duct cancer

Moderators:

J.E. Husband; Sutton/UK

P.K. Prassopoulos; Alexandroupolis/GR

B-411 14:00

Liver metastases on serial contrast-enhanced MDCT examinations.

Retrospective analysis of the previous examination: Were they detectable?

S. Tresoldi, I. Borzani, C. Valsecchi, M. Midulla, N. Flor, F. Sardanelli, G.P. Cornalba; Milan/IT

Purpose: To verify the detectability of liver metastases on serial contrast-enhanced multidetector CT examinations.

Material and Methods: A series of 12 (age 63.8 ± 7.7 years) patients with known diagnoses of a primary cancer (colon=5; lung=2; pancreas=1; stomach=1; melanoma=1; small bowel=1; non-Hodgkin lymphoma=1) who had undergone at least 4 contrast-enhanced 4-detector MDCT examinations (100-130 ml of non-ionic iodined contrast agent at 3 ml/sec, precontrast and portal venous phases) entered a retrospective study. When a metastasis was prospectively first reported, a retrospective evaluation of the previous MDCT examination was done by two readers by consensus in order to define whether the lesion was detectable, detectable only for minimal signs, undetectable or misdiagnosed as benign lesion.

Results: A total of 88 hypovascular metastases (diameter 13.7 ± 8 mm) were analyzed. Evaluating the previous exam (performed 1-14 months before, mean 3.7 ± 1.8), we defined that the metastases were; detectable ($n = 8$); detectable only for minimal signs, ($n = 5$); undetectable ($n = 74$) or misdiagnosed as a benign lesion ($n = 1$). The minimal signs group was comprised of 4 small (< 5 mm in diameter) hypodense foci and 1 calcification. The benign misdiagnosis was a hemangioma.

Conclusions: An important fraction (13/88 = 15%) of liver metastases were prospectively not reported but retrospectively detectable (8/88 = 9%) or visible as minimal signs (5/88 = 6%), while only less than 1% (1/88) were misdiagnosed as a benign lesion. In patients with known primary cancer, attention should be paid not to miss lesions which are judged as detectable metastases at a retrospective analysis.

B-412 14:09



Prospective evaluation of multi-detector CT (MDCT) for treatment decision making in pancreatic adenocarcinoma

H. Furukawa, K. Uesaka, N. Boku; Shizuoka/JP

Purpose: The usefulness of multi-detector computed tomography (MDCT) in selecting the treatment for patients with pancreatic carcinoma was prospectively evaluated.

Methods and Materials: When a patient with a suspicion of pancreatic carcinoma was referred to our hospital, MDCT and laboratory tests were the first examinations to be done, followed by the "pancreatic disease conference" held by surgeons, medical oncologists, endoscopists, and diagnostic radiologists to discuss the treatment plan. When the tumor was classified stage III or higher it was considered "certainly unresectable". When the tumor classification was stage IIB or lower it was deemed "probably resectable". When the tumor included equivocal unresectable findings it was considered as "probably unresectable". When additional information was required at the conference, further examinations were performed. We verified whether the intended treatment was completed or not.

Results: Among 111 patients with pancreatic carcinoma who were enrolled between September 2002 and March 2004, 41 cases were classified as "probably resectable", 67 as "certainly unresectable" and 3 as "probably unresectable". Thirty-eight of 41 "probably resectable" tumors turned out to be resectable. Among 3 cases that were deemed "probably unresectable" unresectable findings were found during surgery. Nonsurgical treatment was selected for the 67 cases classified as "certainly unresectable". MRCP was recommended for the 53 cases for gathering additional diagnostic information. Both EUS and ERCP were performed in 10 cases and angiography in 1.

Conclusion: MDCT provides reliable information for staging of pancreatic carcinoma. This noninvasive technique will replace other staging methods that are more invasive.

Scientific Sessions

B-413 14:18

Heidelberg score of vascular invasion for pancreatic cancer

T. Marinelli¹, A. Filippone¹, L. Grenacher², G. Kauffmann², G.M. Richter²,
¹Chieti/IT, ²Heidelberg/DE

Purpose: To create a new score for venous invasion in patients with potentially resectable pancreas adenocarcinoma using Computed Tomography (CT) for better assessment of potential outcome.

Materials and Methods: 56 patients with pancreatic adenocarcinoma who underwent surgical therapy were included. All patients underwent CT-scan according to a standard protocol. Resection was curative (R0) in 37 patients (66%). Tumour involvement of the portal and superior mesenteric veins was retrospectively graded on a new four-point scale based on the following CT-criteria: length of venous tumour contact; circumferential venous involvement; degree of venous stenosis and tumour convexity towards the vessel. The four-point scale was divided as following: 1-definite absence of invasion; 2-probable absence of invasion; 3-probable presence of invasion; 4-definite presence of invasion.

Results: Our score achieved a sensitivity of 80%, specificity of 96% and an accuracy of 93% in the evaluation of portal vein and a sensitivity of 100%, a specificity of 94% and an accuracy of 95% in the evaluation of the superior mesenteric vein. Considering surgical results for the parameter of portal vein infiltration 76% of patients with score 1-2 underwent a curative R0-resection meanwhile only 21% of patients with score 3-4 had a curative operation. Similar data were obtained for superior mesenteric vein infiltration: 76% of R0-resections in patients with a score 1-2 and 40% of curative resections for patients with a score 3-4.

Conclusions: Our Heidelberg score can predict a high risk of invasion in potentially resectable pancreatic cancer and achieve a high probability of determining resectability vs. non-resectability.

B-414 14:27

Prospective comparison of multislice-CT versus MR imaging in the diagnosis and staging of pancreatic carcinoma

M. Klauß, L. Dukic, S. Delorme, H.-P. Knaebel, H.-U. Kauczor, M.W. Büchler, G.W. Kauffmann, G.M. Richter, L. Grenacher; Heidelberg/DE

Purpose: To investigate the value of multislice-CT versus MR imaging in diagnosis and staging (resectability) of pancreatic carcinoma in a prospective multireader-analysis.

Material and Methods: 50 patients suspected of having a pancreatic carcinoma underwent both multislice-CT (4-row, hydro-technique) and MR imaging (1.5 T). For both modalities examination times were recorded. Examinations were evaluated by two reader pairs for 1. Diagnostic quality, 2. Lesion detection, 3. Resectability in positive findings and 4. Diagnostic reliability. A Kappa analysis was made to determine the observer variations. The gold standard was either postsurgical histopathological findings or clinical follow-up (6 months).

Results: In a total of 28 patients a pancreatic lesion was detected. Group 1 achieved 100% sensitivity for lesion detection by CT (specificity 77%) versus 73% at MR imaging (specificity 77%). Group 2 achieved 89% sensitivity at both modalities (specificity 77% at CT, 73% at MRI). For the subgroup of pancreatic adenocarcinomas (n = 17) we found an overall sensitivity of 100% (specificity 67%) at CT versus a sensitivity of 82% (group1)/94% (group 2) at MR imaging (specificity 67%/61%). In determining resectability CT achieved a sensitivity of 91%/82% versus 90%/82% in MR imaging. The Kappa analysis showed a good correlation in CT (0.71) and a moderate correlation in MR imaging (0.49). The average examination time for CT was 15 minutes and for MR imaging 45 minutes respectively ($p < 0.001$).

Conclusion: MR imaging and multislice-CT performed equally well for lesion detection and in the assessment of resectability. Therefore, the preference of CT for patients suspected of having pancreatic cancer is supported because of its lower costs and shorter examination time.

B-415 14:36

Multidetector CT in the assessment of pancreatic malignant masses

C. Cappelli, S. Mazzeo, D. Caramella, A. Belcari, G. Caproni, D. Campani, U. Boggi, C. Bartolozzi; Pisa/IT

Purpose: To evaluate the role of multidetector CT in the assessment of pancreatic malignant masses.

Methods and Materials: The study includes 86 patients submitted to surgical resection or biopsy for pancreatic malignant mass. We retrospectively analysed the multidetector CT images to evaluate the enhancement of the pancreatic masses compared to normal pancreatic parenchyma. Results were correlated

with the histopathological finding. CT studies were done before and after 120 ml of highly concentrated contrast medium in pancreatic (35") and venous phases (70"). The post-contrast enhancement of the lesions was evaluated in the pancreatic phase and four CT patterns were identified: hypodense, hyperdense, isodense and mixed.

Results: The histopathological results demonstrated: 65 ductal adenocarcinomas, 5 neuroendocrine lesions, 6 mucinous carcinomas, 6 metastases (2 breast, 4 kidney) and 4 other lesions. The hypodense pattern was observed in 60/65 (92%) ductal adenocarcinomas, 2/6 (33%) mucinous carcinomas and 2/5 (40%) neuroendocrine lesions. Hyperdensity was present in 1/65 (1.5%) ductal adenocarcinomas, 3/5 (60%) neuroendocrine carcinomas and 5/6 (83%) metastases. Only 2 cholangiocarcinomas and 1 metastasis appeared isodense. The mixed appearance was demonstrated in 4/65 (6%) ductal adenocarcinomas, 4/6 (67%) mucinous carcinomas and 1 case of pseudopapillary solid carcinoma.

Conclusion: In our experience multidetector CT is accurate in characterizing pancreatic malignant masses, and the CT enhancement pattern can be related to the histopathological type. The hypodense pattern is not only observed in ductal adenocarcinomas. When a hyperdense appearance is observed, a neuroendocrine or metastatic lesion must be suspected, while the mixed presentation suggests a mucinous lesion.

B-416 14:45

Value of single-phase multidetector CT in patients with suspected pancreatic tumor

M. Imbriacò, S. Maurea, C. Mollica, S. Bortone, M. Volpe, G. Buono, M. Salvatore; Naples/IT

Purpose: To assess the diagnostic value of single-phase multidetector CT (MDCT) in patients with suspected pancreatic tumor (PT).

Materials and Methods: Seventy-one patients suspected of having PT underwent MDCT scanning. Scans were performed on a MDCT scanner with 0.5 sec gantry rotation and acquisition of 4 slices per rotation. The unenhanced scan was followed by one set of scans in the caudo-cranial direction from the inferior hepatic margin to the diaphragm with a scan delay of 60 sec after I.V. injection of 150 ml of contrast material delivered at 3 ml/sec. Two readers scored images in a blinded fashion for the presence of tumor and assessment of resectability. ROC analysis was performed.

Results: Final diagnosis was PT in 40 cases and chronic pancreatitis in 31. A_z values for the assessment of tumor detection were 0.97 for reader 1 and 0.95 for reader 2 ($p = n.s.$). A_z values for tumor resectability were 0.90 for reader 1 and 0.89 for reader 2 ($p = n.s.$). No statistically significant differences were observed between superior mesenteric artery and vein opacification with the hepatic parenchyma enhancing at a time closer to the peak hepatic enhancement optimizing the detection of hepatic lesion.

Conclusion: Single-phase MDCT is an accurate technique for the diagnosis and assessment of resectability of patients with suspected PT. This technique provides optimal tumor-to-pancreas contrast, maximal pancreatic parenchymal and peripancreatic vascular enhancement and allows us to explore the entire liver and the whole upper abdomen during the portal-phase for accurate identification of liver metastases and peritoneal seeding.

B-417 14:54

The role of FDG PET and PET/CT in differential diagnostics of pancreatic lesions

J. Votruba, O. Belohlavek; Prague/CZ

Purpose: The aim of our study was to evaluate the usefulness of fluorodeoxyglucose (FDG) PET and PET/CT in the differential diagnosis of pancreatic lesions.

Materials and Methods: Forty-one patients (14 men and 17 women) with a clinical suspicion of pancreatic carcinoma with/without history of chronic pancreatitis underwent FDG PET (21 patients) or PET/CT (10 patients) examinations.

Results: A series of 41 patients was examined in a retrospective study. Twenty-nine patients were confirmed histologically, the others by follow-up (USG, CT and MRI). In the group of patients, who underwent FDG PET examination three cancers showed no pathological FDG uptake and they were considered to be false negative. Two of them were proven as tubular adenocarcinoma by histology and one as non-differentiated carcinoma. There were no false negative findings by PET/CT. FDG uptake was present in 24 of 27 cancers in total (sensitivity 88.9%). In 14 patients with benign lesions no false positive FDG uptake was found by PET or PET/CT (specificity 100%). The overall accuracy of FDG PET and PET/CT was 92.7%. In the subgroup of 10 patients investigated by PET/CT neither false positive nor false negative finding were found.

Scientific Sessions

Conclusion: Our results indicate that FDG PET and PET/CT are both excellent in the differential diagnosis of benign vs. malignant pancreatic lesions. In agreement with previously published data, we registered some limitations of PET alone in detecting FDG non-avid pancreatic tumours. Due to the additional morphological information provided by CT the hybrid PET/CT imaging seems to be even more promising.

B-418 15:03

TNM staging for ampullary carcinoma using thin-section helical CT:

Pathologic correlation with dual-phase CT images

S. Lee, W. Lee, Y. Yim, J. Choi, D. Choi, H. Lim, J. Lim; Seoul/KR

Purpose: To analyze thin-section helical CT findings of ampullary carcinoma (AC) and correlating with pathologic findings for assessing its TNM staging.

Materials and Methods: During 6-years, we collected 50 patients with surgically proven AC who had preoperative dual-phase (arterial (AP) and portal (PP)) thin-section helical CT (M:F=26:24, age range; 35-80 years, mean age; 60 years). All CT images were analyzed retrospectively for the following parameters: the tumor size and shape, the T stage [T2; duodenal invasion, T3; pancreatic invasion, T4; peripancreatic invasion] and the N stage [N1; regional lymph node (LN) metastasis]. Diagnostic values of all parameters were obtained by correlating pathologic results, and overall TNM staging was assessed by using these parameters.

Results: All tumors except six (88%) were detected that ranged from 9.4-40.0 mm (mean, 17 mm) and 80%(40/50) were round in shape. The sensitivity (Se), specificity (Sp) and accuracy (Ac) were 86%, 33% and 58% at AP, and 84%, 31% and 53% at PP for duodenal invasion ($p > 0.05$), were 65%, 74% and 71% at AP, and 64%, 68%, and 67% at PP for pancreatic invasion ($p > 0.05$), and were 38%, 95% 86% at AP and 38%, 95% and 86% at PP for peripancreatic invasion ($p = 0.024$). There was no significant difference between AP and PP for all parameters. A total of 233 LNs [short-axis diameter (< 5 mm; n = 36, 5-10 mm; n = 150, ≥ 10 mm; n = 47)] were detected at CT and 51 LNs (22%) (< 5 mm; n = 1, 5-10 mm; n = 26, ≥ 10 mm; n = 24) have metastasis respectively ($p < 0.001$).

Conclusion: Thin-section helical CT is useful in detecting the primary tumor but has limitations in precisely depicting the pathological TNM stage for AC.

B-419 15:12

Two-phase CT findings of mass-forming intrahepatic peripheral cholangiocarcinoma in cirrhotic patients: Comparison with those in non-cirrhotic patients

S. Yoon, J. Byun, S. Park, H. Won, A. Kim, Y. Shin, P. Kim, H. Ha, M.-G. Lee; Seoul/KR

Purpose: To compare the two-phase CT findings of mass-forming intrahepatic peripheral cholangiocarcinoma (MIPCC) in cirrhotic patients with those in non-cirrhotic patients.

Methods and Materials: We reviewed the two-phase CT findings of MIPCC proven pathologically in 33 cirrhotic patients (range, 27-67 years) and compared with those in 35 non-cirrhotic patients (range, 44-75 years). We evaluated the morphology of the tumors (size, margin and satellite nodules), enhancement patterns and other ancillary findings (capsular retraction, bile duct dilatation, portal vein invasion, lymphadenopathy and extrahepatic metastasis). The enhancement patterns of the tumor were classified as follows: Type 1 - peripheral enhancement during hepatic arterial phase (HAP) and delayed enhancement during portal venous phase (PVP), Type 2 - no enhancement during HAP and PVP, Type 3 - homogeneous enhancement during HAP and wash-out during PVP. We statistically evaluated the difference of the CT findings between two groups using χ^2 test.

Results: There was no statistically significant difference ($p > .05$) between the morphology and ancillary findings in cirrhosis and those in non-cirrhosis. Also, there was no statistical difference ($p = .236$) in the enhancement patterns between cirrhosis (type 1 in 25 patients [75.8%], type 2 in four [12.1%], type 3 in four [12.1%], respectively) and non-cirrhosis cases (type 1 in 22 patients [62.9%], type 2 in 10 [28.6%], type 3 in three [8.6%], respectively).

Conclusion: MIPCC in cirrhotic patients represents the same features as those in non-cirrhotic patients and therefore typical CT features of MIPCC are helpful when we distinguish MIPCC from hepatomas in cirrhotic patients.

14:00 - 15:30

Room K

Cardiac

SS 703b

Cardiac function

Moderators:

D. Tscholakoff; Vienna/AT

T.P. Willems; Groningen/NL

B-420 14:00

Assessment of left ventricular volume and mass in endurance athlete's heart: A cardiac-MR (CMR) and 3D ultrasound study (D-US)

I. Carbone, M. Francone, S. Visconti, A. Ascarelli, S. De Castro, R. Passariello; Rome/IT

Purpose: Extensive endurance training leads to cardiac hypertrophy. The aim of this study was to evaluate the left ventricular masses (LVMs) and volumes (LVVs) of endurance athletes and healthy volunteers and to compare CMR results with 3D-US.

Materials and Methods: Sixteen trained rowers underwent CMR and 3D US within the same day. A control group of 10 healthy untrained volunteers was enrolled in the study. CMR was performed with a 1.5-T system. Nine to 14 short axis on CINE-GRE images, with a sl.thickness of 10 mm and without any interslice gap were acquired for the evaluation LVMs and LVVs. Quantitative analysis including end-diastolic and end-systolic volume (EDS, ESV), ejection fraction (EF), and LVM, was performed off-line using a dedicated software by two blinded radiologist. 3D-US LV measurements were assessed on short axis, and quantitative analysis was blindly performed by 2 cardiologists. The interobserver agreement and results of either CMR and 3D-US were compared.

Results: LV masses and volumes were increased in endurance athletes compared with the healthy volunteers ($40 \pm 6\%$ and $34 \pm 9\%$ respectively). The average athlete's cardiac mass and volumes assessed by MR and 3D-US were respectively: LVM 204.7 g (MR), 210.1 g (3D-US); EDV 209.9 ml (MR), 232.7 ml (3D-US); ESV 85.8 ml (MR), 91.6 ml (3D-US). The interobserver agreement was almost perfect for either MR ($K=0.92$) and 3D-US ($K=0.86$).

Conclusions: CMR have shown that endurance athlete's heart has increased volumes and masses, compared with an healthy volunteer. 3D-US seems to be an interesting modality in the evaluation of LVVs and LVMs.

B-421 14:09

Comparison of contraction pattern of the normal right ventricle using cine magnetic resonance imaging in transaxial plane versus long axis plane

J. Fritz¹, M. Solaiyappan¹, C. Bomma¹, H. Tandri¹, J.A.C. Lima¹, C.D. Claussen², D.A. Bluemke¹; ¹Baltimore, MD/US, ²Tübingen/DE

Purpose: Transaxial images of the right ventricle (RV) may be difficult to interpret due to the double oblique orientation of the heart. Differences and description of RV contraction pattern as visualized in transaxial plane versus horizontal long axis (HLA) plane, which is orientated to the heart axis are introduced.

Material and Methods: 30 normal volunteers (13 females, 27 ± 7 years) were imaged using cine MR imaging in axial and HLA plane. Contraction patterns of the RV were qualitatively assessed in cine mode by two observers and compared to the calculated subtended angle between corresponding axial and HLA planes. Multiplanar reformation was used to directly visualize detected differences between corresponding planes by continuous rotating transition.

Results: On axial images, focal outpouching in the apical third of the anterior RV free wall during systole (bulging) was seen in 17/30 (57%) cases compared to 3/30 (10%) on HLA images. In volunteers with subtended angles between 30° - 40° , bulging was diagnosed in 9/18 (50%) cases on axial images whereas HLA views were normal. In volunteers with subtended angle $> 40^\circ$, bulging was always identified on axial images. Multiplanar reformation revealed that the appearance of bulging were due to increased portions of the right ventricular outflow tract, that were increasingly visualized with increasing subtended angle on axial images compared to HLA images.

Conclusions: Contraction pattern of the normal RV is substantially different on axial compared to HLA view. HLA view can add valuable information in order to avoid misdiagnosis of functional RV variations as abnormalities by axial MR imaging only.

Scientific Sessions

B-422 14:18

Functional and metabolic evaluation of the left ventricle of sprinters, middle distance and endurance elite track runners in the resting state by magnetic resonance imaging (MRI) and ^{31}P -MR spectroscopy (^{31}P -MRS)

A. Esposito, F. De Cobelli, G. Perseghin, P. Scifo, T. Canu, A. La Torre, L. Luzi, G. Alberti, A. Del Maschio; Milan/IT

Purpose: Our aim was to test whether different exercise training habits may influence the functional and metabolic status of the left ventricle (LV) of elite track runners.

Methods and Materials: 7 sprinters (SR:100-200 m), 7 middle distance runners (MDR:400-800 m), 11 endurance runners (ER:marathon) and 13 normal control subjects (NCS) underwent cardiac-MRI and ^{31}P -MRS with a 1.5 T-magnet (Gyroscan Intera; Philips Medical System). LV mass, volume and systolic function were determined by cine-balanced-FFE sequence. The parameters of LV diastolic function were obtained by analysing the trans-mitral flow with 2D-cine Phase-Contrast sequence. Phosphocreatine (PCr) to ATP myocardial ratio (PCr/ATP) was calculated by ^{31}P -MRS, performed by means of 10 cm-diameter surface coil. PCr/ATP was normalized for LV mass.

Results: The LV mass (SR:157 \pm 17, MDR:159 \pm 28, ER:167 \pm 31 vs NCS:129 \pm 16 g; $P < 0.01$) and the end-diastolic volume (SR:158 \pm 24, MDR:157 \pm 12, ER:161 \pm 33 vs NCS:137 \pm 22 ml; $P < 0.05$) were significantly higher in the athletes compared to normal subjects. There were no differences between the four groups regarding the LV mass to volume ratio (SR:0.99 \pm 0.13, MDR:1.02 \pm 0.16, ER:1.07 \pm 0.26, NCS:0.95 \pm 0.12) and the LV ejection-fraction (SR:63 \pm 6, MDR:59 \pm 8, ER:60 \pm 8, NCS:64 \pm 5%).

Early-to-Atrial peak filling rate ratio (E/A) was apparently higher in sprinters compared to normal subjects and middle distance runners but not compared to endurance runners (SR:3.7 \pm 1.0, MDR:2.6 \pm 0.4, ER:2.9 \pm 0.9, NCS:2.6 \pm 0.7; $P = 0.05$). Deceleration time was not different among study groups (SR:176 \pm 34, MDR:173 \pm 25, ER:192 \pm 28, NCS:177 \pm 36 ms). PCr/ATP corrected for LV mass did not differ among groups (SR:1.48 \pm 0.42, MDR:1.24 \pm 0.14, ER:1.46 \pm 0.28, NCS:1.47 \pm 0.30).

Conclusions: Despite different exercise training programs and increased LV wall mass, elite track runners showed normal LV function and normal high-energy phosphates metabolism.

B-423 14:27

Evaluation of parameters that effect QRS duration in patients after surgical repair of fallot determined by magnetic resonance imaging (MRI)

M. Grothoff, B. Spors, H. Abdul-Khalil, R. Felix, M. Gutberlet, M. Gutberlet; Berlin/DE

Purpose: To evaluate those right and left ventricular parameters which have the greatest effect on genesis of cardiac arrhythmias in patients after surgical repair of tetralogy of fallot (TOF).

Methods: 67 pts. were studied using a 1.5 T Gyroscan (Philips). Mean age at surgical repair was 6.8 years. Valveless repair with patch was performed in 34 patients, in 33 patients a conduit was used. Volumetry was performed with a SSFP-sequence with breathhold or respiratory gating. We obtained left and right ventricular volumes, ejection fractions and myocardial masses. To quantify regurgitation fraction (RF) we performed a phase contrast measurement in the main pulmonary artery in a transverse section. Acquired data was evaluated in an univariate and multivariate regression analysis.

Results: Flow-measurement showed 42 mild to moderate and 12 severe cases of regurgitation. Significant correlation was found between RF and QRS duration ($r = 0.49$; $p < 0.01$). RV end-diastolic volume index was correlated to RF ($r = 0.46$; $p < 0.001$) and QRS-duration ($r = 0.29$; $p < 0.05$). A further correlation was found between right- and left-ventricular EF ($r = 0.54$; $p < 0.01$). In the multivariate data analysis QRS-duration showed close relation to: 1. RF, 2. time since surgical repair 3. left ventricular end diastolic volume index and 4. a negative correlation to age at first surgical repair.

Conclusion: Pulmonary regurgitation has a great effect on QRS-prolongation. MRI flow-measurement can quantify regurgitation fraction exactly and is therefore an ideal method for follow-up examinations. In addition to right ventricular parameters also secondary impairment of left ventricular function seems to affect prognosis after correction of TOF.

B-424 14:36



MR evaluation of cardiac function in one breath hold with real-time true fast imaging with steady-state precession and parallel acquisition techniques

X. Zhao, K. Li, Y. Li; Beijing/CN

Purpose: To evaluate cardiac function using a real-time cine technique with parallel imaging algorithms.

Methods: Ten healthy volunteers and ten patients with cardiac diseases were enrolled in the study group. The subjects underwent cardiac cine MR imaging using real-time multislice cine trueFISP with iPAT. Data acquisition was performed in a single breath-hold along the short axis. Evaluation of end-diastolic volume (EDV), end-systolic volume (ESV), stroke volume (SV), ejection fraction (EF) and myocardial mass was performed and results were compared to a standard segmented single-slice cine trueFISP. Combination of real-time cine trueFISP and iPAT provided a temporal resolution of 52.8 ms. Data acquisition of a 192 x 72 matrix was completed in 6.4-7.2 s. Ventricular volume and mass were evaluated by two observers independently with manual tracing.

Results: Real-time True-FISP cine quality was sufficient for contour detection in all 20 subjects. Measurements based on real-time True-FISP cine with iPAT correlated well with those based on single-slice cine True-FISP [left ventricular (LV) EDV: $r = 0.996$; LV ESV: $r = 0.918$; LV SV: $r = 0.970$; LV EF: $r = 0.929$; LV mass: $r = 0.999$. No significant differences could be found. The use of parallel acquisition techniques (iPAT) allow for a substantial improvement of temporal resolution in real-time cine MR imaging. Intra- and interobserver variability were sufficiently small in real-time True-FISP cine with iPAT.

Conclusion: Real-time True-FISP cine with iPAT techniques in one breath-hold has high reproducibility and is applicable to patients with severe cardiac dysfunction and/or arrhythmias.

B-425 14:45

Contribution of early systole to total forward flow volume in breath-hold phase-contrast flow measurements

R.P. Kunz, F. Oellig, F. Krummenauer, K. Oberholzer, M. Thelen, K.-F. Kreitner; Mainz/DE

Purpose: To evaluate the contribution of early systole in the assessment of antegrade aortic flow volume by breath-hold velocity-encoded MR flow measurements.

Materials and Methods: Expiratory breath-hold fast low-angle shot phase-contrast flow measurements (temporal resolution tRes 61 msec, shared phases) perpendicular to the proximal ascending aorta and short-axis true fast imaging with steady-state precession (TrueFISP) cine MR ventriculometry (tRes 34.5 msec) were performed in ten healthy male volunteers on a 1.5 T MR system. Antegrade aortic flow volume (AFV) and left ventricular stroke volume (LV-SV) were evaluated using Argus MR 2002B software (Siemens Medical Solutions). A beta release of Argus MR 2004A allowed interpolation of the flow up-slope during early systole to the preceding R-wave trigger. The respective intraindividual median differences between AFV of each flow evaluation and LV-SV and between both AFV measurements were calculated and compared using the sign test for paired samples.

Results: Non-interpolated AFV significantly deviated from LV-SV ($p = 0.002$) underestimating the latter by 13.1 mL. Interpolating aortic flow during early systole significantly increased AFV by 10.8 mL compared to the flow evaluation that did not take early systole into account ($p = 0.002$). AFV with interpolation of early systolic flow agreed well with LV-SV (median difference -3.0 mL), and no significant difference between these measurements was found ($p = 0.344$).

Conclusion: Flow during early systole contributes tremendously to total forward flow volume in the ascending aorta. Interpolation of the early systolic up-slope is therefore recommended for the evaluation of breath-hold phase-contrast flow measurements.

B-426 14:54

Automatic determination of quiescent cardiac motion phases for CT imaging: Initial experience

M.H.K. Hoffmann¹, J. Lessick², M. Robert³, F. Schmid¹, A. Aschoff¹, M. Grass³; ¹Ulm/DE, ²Haifa/IL, ³Hamburg/DE

Purpose: Temporal resolution of cardiac multi-detector row CT is limited. Therefore quiescent motion phases of the cardiac cycle have to be detected to succeed with artifact-free imaging. Currently, low-motion phases are detected manually in a time consuming user-dependent selection process. This study reports initial experience with a semi-automatic tool ("motion-map") to provide guidance for the selection process.

Scientific Sessions

Method and Materials: 20 consecutive patients were included in the study. Low motion phases of the coronary tree were determined by usual user-dependent selection. 20 phases equally distributed over the cardiac cycle were reconstructed. Manually determined phase selections were compared to semi-automatic phase selection on the basis of a motion map. The motion map is derived from similarity measures calculated on 50 different phases of low spatial resolution reconstructions. Low motion phases of the cardiac cycle can be detected with a minima search applied. Manual and semi-automatic selection were compared. A quantitative comparison was conducted with a Bland-Altman analysis. A qualitative comparison relied on a side-by-side analysis of images generated with the two methods. Images were assessed for accurate delineation of the coronary vessel lumen. Interobserver variability was evaluated by simple Kappa analysis.

Results: A high level of agreement was found for percentage phase selection achieved with the two methods (mean difference 1.07%; 95%CI: -3.6-5.8%). Side-by-side comparison of image quality showed matching results of the two methods in 85%(17/20) of the cases. Interobserver agreement was good (kappa = 0.8).

Conclusions: Similarity measures and derived motion maps allow semi-automated quiescent phase detection of the cardiac cycle.

B-427 15:03

Determination of right ventricular volumes and function using multidetector row CT. Comparison with MR imaging

A. Lembcke, C. Klessen, M. Dewey, T. Elgeti, B. Hamm, D. Kivelitz; Berlin/DE

Purpose: To validate right ventricular (RV) measurements obtained from multidetector row CT (MDCT) in comparison with MR imaging.

Methods and Materials: Prior to cardiac surgery, 25 patients (among them 12 subjects with compromised RV function) underwent standardized contrast-enhanced, electrocardiogram-gated 16-detector row CT (Aquilion, Toshiba; maximum rotation speed 400 msec, effective acquisition time per cardiac cycle 123.8 ± 37.4 msec using multisegmental reconstruction) and MR imaging (Magnetom Vision, Siemens, repetition time 80-100 msec resulting in an effective acquisition time of 40-50 msec) RV end-diastolic, end-systolic and stroke volume (EDV, ESV, SV), ejection fraction (EF), and mass were calculated using 5 mm axial slices according to the slice summation method. Measurements were compared using Pearson's correlation coefficient, paired Student's t-test, and Bland-Altman analysis.

Results: The RV was completely visualized with invariably acceptable image quality on all MDCT and MR images. For all parameters a close correlation between MSCT and MR imaging was found (EDV: $r = 0.93$; ESV: $r = 0.95$; SV: $r = 0.91$; EF: $r = 0.96$; mass: $r = 0.94$; $p < 0.05$ each) and limits of agreement were in an acceptable range (EDV: -30.6 to 32.2 ml; ESV: -17.5 to 22.5 ml; SV: -19.8 to 15.8 ml; EF: -9.6 to 6.8%; mass: -16.8 to 12.0 g). Mean SV and EF obtained from MDCT were slightly lower compared to MR imaging, however these differences were not statistically significant ($p > 0.05$ each).

Conclusions: Despite its lower temporal resolution, MDCT seems to be an adequate technique for evaluating RV parameters, when compared with MR imaging.

B-428 15:12

Validation of right ventricular systolic function using multislice CT

H. Dogan, L.J.M. Kroft, J.J. Bax, J.D. Schuijf, A. de Roos; Leiden/NL

Materials and Methods: Data from 15 patients (13 male, 2 female; mean age, standard deviation: 61 year, ± 11) with suspected coronary artery disease were evaluated. These patients had no signs of valvular disease or intra-cardiac shunting on 2D-echocardiography. All patients had undergone contrast-enhanced ECG-triggered cardiac CT by using a 16-slice MSCT scanner (Aquilion 16, Toshiba), without β -blocker preparation. Twenty cardiac phases were reconstructed retrospectively for each investigation. The end-diastolic and end-systolic endocardial ventricular border contours of the right and left ventricles were drawn on axial slices covering the entire right and left ventricles. Ventricular stroke volumes (SV) and the ejection fractions (EF) were calculated. The Pearson correlation coefficient was assessed between the right and left ventricular SV, and between the left ventricular EFs as assessed by MSCT and 2D-echocardiography.

Results: An excellent correlation was found between the right and left ventricular SV as determined by MSCT (Pearson correlation coefficient, $r^2: 0.95$; 2-tailed $p < 0.0001$). In addition, MSCT and echocardiographically derived left ventricular EF showed a good correlation (Pearson correlation coefficient, $r^2: 0.79$; 2-tailed $p < 0.0001$).

Conclusion: Right ventricular systolic function can be accurately assessed by multiphase MSCT.

B-429 15:21

High-resolution multi-slice evaluation of cardiac function with cine SSFP using a dedicated 32-element array-coil and parallel acquisition techniques (PAT)

B.J. Wintersperger¹, S.B. Reeder², S.O. Schoenberg¹, T. Lanz³, O. Dietrich¹, A. Huber¹, M. Nitka⁴, C. Hayes⁴, M.F. Reiser¹; ¹Munich/DE, ²Palo Alto, CA/US, ³Würzburg/DE, ⁴Erlangen/DE

Purpose: The purpose of this study was to implement a high-resolution multi-slice cine SSFP technique with PAT using a newly developed dedicated 32-element cardiac array coil on a 32 receiver channel MR scanner system.

Material and Methods: 6 volunteers and 12 patients underwent cardiac imaging on a 32-channel 1.5 T scanner (Magnetom Avanto; Siemens) using a dedicated 32-element array-coil (RAPID Biomedical). Retro-gated Cine SSFP (2.2/1.2; 75°) was performed in multiple axis acquiring 5 slices in a single breath-hold. Data sampling (PAT) used GRAPPA (Factor 4) and allowed a temporal resolution of 48 ms and a spatial resolution of 2.2x1.8 mm (matrix 192). For comparison, identical slice orientations at identical parameters were acquired using a single-slice retro-gated cine SSFP without PAT (nonPAT) in consecutive breath-holds. Image data was compared regarding SNR and CNR as well as data acquisition length.

Results: Acquisition time per slice was significantly shorter for PAT compared to nonPAT (3 vs. 7 hb; $P < 0.001$). Myocardial SNR (11.5 ± 3.0 vs. 16.2 ± 1.8 ; $P = 0.005$) and SNR of the LV cavity (49.7 ± 18.8 vs. 75.9 ± 21.2 ; $P = 0.001$) were significantly lower for PAT. Myocardium/cavity CNR was 38.2 ± 17.4 for PAT and 59.7 ± 21.6 for nonPAT ($P = 0.0015$). Visual evaluation of PAT images did not reveal significant artifacts.

Conclusion: PAT using a dedicated 32-element coil system allows for significant speed up of data acquisition in cine imaging using high acceleration factors. Although with high acceleration factors a significant decrease in SNR and CNR comes along, based on the intrinsic high SNR in SSFP techniques, image quality remains acceptable for evaluation of cardiac function.

14:00 - 15:30

Room L/M

Neuro

SS 711

Epilepsy and brain tumors: Advanced diagnostic imaging

Moderators:

F. Bonneville; Paris/FR
J. Labuscagne; Pretoria/ZA

B-430 14:00

Interictal patterns of perfusion MR imaging in temporal lobe epilepsy

I. Huynh¹, V. Bouilleret¹, P. Masnou¹, P. Charlier², P. Lajaunesse¹, D. Ducreux¹; ¹Le Kremlin-Bicêtre/FR, ²Lille/FR

Purpose: To evaluate interictal MR Perfusion Weighted Imaging (PWI) patterns in patients with refractory temporal lobe epilepsy.

Materials and Methods: We prospectively studied on a 1.5 T MR scanner 13 patients with refractory temporal lobe epilepsy and 10 healthy volunteers using conventional T2-weighted sequences and T2* EPI sequences with Gadolinium bolus injection. Maps of Cerebral Blood Volume (CBV) and Cerebral Blood Flow (CBF) were calculated in volunteers and patients on which Region of Interest (ROI) were drawn on the Centra Oval, Thalamus, Hippocampal grey and white matter. Statistical correlations were performed using Z score analysis between volunteers and patients ($|Z| > 2$, $p < 0.02$), and PWI results were correlated with the clinical and electronic data.

Results: CBV and CBF measurements in volunteers were similar to those previously reported in normal grey and white matters. All patients had abnormal perfusion areas of hypo (decreased CBV and CBF) and/or hyperperfusion (increased CBV and CBF) and/or stasis (increased CBV, normal or decreased CBF). Eleven patients (85%) had PWI abnormalities correlated to the clinical and electronic data. All these patients had ipsilateral hippocampal PWI abnormalities, either on the grey ($n = 7$) or white ($n = 10$) or both ($n = 5$) matters, and also on the contralateral hippocampus. Eight patients (73%) had stasis remote from the temporal lobe in centra ovale ($n = 8$) and in the thalamus ($n = 1$).

Conclusion: PWI highlighted interictal brain perfusion remodelling in refractory temporal lobe epilepsy that not only involves the hippocampal areas but also affects remote grey and white matter structures.

Scientific Sessions

B-431

withdrawn by authors

B-432 14:09



Improved detection and localization of focal cortical dysplasia by voxel-based 3D MR imaging analysis

H.-J. Huppertz¹, C. Grimm², S. Fauser¹, J. Kassubek³, J. Spreer¹, A. Schulze-Bonhage¹; ¹Freiburg/DE, ²Basle/CH, ³Ulm/DE

Purpose: Focal cortical dysplasia (FCD), i.e. neuronal derangement due to developmental malformation, is a frequent cause of pharmaco-resistant epilepsy and can be difficult to detect in MR imaging. We present three novel post-processing techniques which improve lesion detection by enhancing image properties not readily accessible by visual analysis.

Methods and Materials: Following the principles of voxel-based morphometry, a T1-weighted MR imaging volume data set is normalized and segmented using algorithms of SPM99 (Statistical Parametric Mapping Software). The distribution of gray and white matter is analyzed on a voxelwise basis and compared with a normal database. Based on this analysis, 3-dimensional maps are created which characterize different features of FCD, i.e. abnormal thickness of the cortical ribbon, abnormal extension of gray matter into white matter, and blurring of the gray - white matter junction. These methods were applied to the MR imaging data of 25 epilepsy patients with histologically proven FCD. In each feature map the locations of the maximum deviations from the normal database were automatically determined and compared with the sites of the lesions or - in case of cryptogenic epilepsy - with the subsequent resections in the conventional MR imaging.

Results: With all feature maps combined, this approach was able to identify 23 out of 25 dysplastic lesions, four of which had totally or partly not been recognized in conventional MR imaging despite acquisition and assessment in a tertiary epilepsy center.

Conclusion: The automated post-processing of MR imaging presented here facilitates the detection of FCD and increases the sensitivity of MR imaging.

B-433 14:18

Temporal lobe epilepsy - correlation analysis of MR imaging volumetry, ¹H MRS and PET

H. He, T. Shen, X. Feng; Shanghai/CN

Purpose: To discuss the etiology of temporal lobe epilepsy (TLE) and the mechanism of ¹H MRS and PET abnormality by correlation analysis of MR imaging volumetry, ¹H MRS and PET results of 20 patients.

Materials and Methods: 20 patients with hippocampal sclerosis verified by operation and pathology were studied. MR imaging volumetry, ¹H MRS and PET were performed before surgery. The asymmetry index (AI) of hippocampal volume of both sides, AI of NAA/(Cr+Cho) ratio and AI of glucose metabolism of both temporal lobes were calculated. Correlation analysis of them was made respectively.

Results: The AI of hippocampal volume of 20 patients was $-27.14\% \pm 24\%$ ($-77.81\% \text{--} 7.63\%$). The AI of NAA/(Cr+Cho) ratio was $-19.45\% \pm 10.37\%$ ($-41.86\% \text{--} 3.08\%$). The AI of glucose metabolism of the medial temporal region was $-6.39\% \pm 8.61\%$ ($-21.76\% \text{--} 7.65\%$). The AI of glucose metabolism of the medial temporal region was found to be statistically related to the AI of NAA/(Cr+Cho) ratio and the AI of hippocampal volume, respectively ($r = 0.50, p = 0.029; r = 0.56, p = 0.011$).

Conclusions: MR imaging volumetry, ¹H MRS and PET are different methods to evaluate TLE. They reflect the structural abnormality, pathophysiology and metabolic changes of the brain, respectively. The correlation of them helps to understand the etiology of TLE and the mechanism of ¹H MRS and PET abnormality.

B-434 14:27

MR imaging segmentation in diagnosis and clinical correlations of temporal lobe epilepsy

H. He, T. Shen, X. Feng; Shanghai/CN

Purpose: To study the different patterns of hippocampal atrophy by MR imaging segmental analysis and to investigate the etiology and pathogenesis of temporal lobe epilepsy.

Methods and Materials: Oblique coronal T1W images were obtained perpendicular to the long axis of the hippocampus. The mesial temporal structures are divided into four parts: the amygdala and the hippocampal head, body and tail. We investigated the MR imaging patterns of atrophy in 50 hippocampal

sclerosis patients by MR imaging volumetric measurement and segmental analysis and compared the clinical features and surgical outcomes of different groups.

Results: Diffuse hippocampal atrophy was found in 22 of 50 patients (44%), 5 of the 50 patients showed diffuse atrophy involving both the amygdala and hippocampus. 20 of 50 patients (40%) had hippocampal focal atrophy and 8 of 50 patients (16%) had no obvious atrophy. 76% of those with hippocampal sclerosis had atrophy in the hippocampal body, 58% had hippocampal head atrophy, 48% had hippocampal tail atrophy and the least involved part was the amygdala (16%). 10 patients who had normal hippocampal volume showed focal hippocampal atrophy by segmental analysis. Various patterns of hippocampal atrophy were found to be statistically related to the duration of epilepsy, the frequency of seizure and the outcome of surgery respectively ($P < 0.05$), but not related to the history of febrile convulsions, age of onset and the history of secondary generalized tonic-clonic seizures ($P > 0.05$).

Conclusion: MR imaging segmental analysis can improve the diagnostic sensitivity of temporal lobe epilepsy and help to investigate its etiology and pathogenesis.

B-435 14:36

Supratentorial intra-axial brain tumors: Physiological MR imaging in diagnosis and preoperative planning

C.-V. Salvan, J.L. Ulmer, W.M. Mueller, K.M. Schmainda, R.W. Prost; Milwaukee, WI/US

Purpose: To present the potential of physiological MR imaging techniques in the diagnosis and preoperative planning of supratentorial intra-axial brain tumors.

Methods and Materials: Physiological MR Imaging techniques; BOLD functional MR imaging (fMRI), Diffusion Tensor Imaging (DTI), Fractional anisotropy (FA), Perfusion MR imaging and MR Spectroscopy were used in addition to standard MR imaging in the diagnosis and preoperative planning of 15 patients with supratentorial intra-axial brain tumors. Cortex and white matter tracts as part of eloquent networks, tumor angiogenesis, normal and pathological metabolites were assessed and integrated in the diagnosis and the impact on preoperative planning was defined. Contingent surgical risks and postoperative neurological deficits were suggested as well.

Results: Functional MRI established the relationship between brain tumor and sensori-motor, language and/or visual cortex. The displacement, involvement or destruction of white matter tracts was specified by Fractional anisotropy and color-coded maps. Total and microvascular regional cerebral blood volume was predictive for tumor grade and intraoperative complications. MR Spectroscopy confirmed the distribution of high mitotic activity. At least one of the physiological characteristics was important in the preoperative planning and risk assessment in each case.

Conclusion: Physiological MR imaging data is complementary and integrative in the diagnosis and preoperative planning of supratentorial intra-axial brain tumors, yielding powerful information to neurosurgeons and optimizing postoperative outcomes.

B-436 14:45

Perfusion MR imaging of cerebral gliomas: Which contrast media and dosage to use

M. Essig¹, S.O. Schönberg², W. Reith³, M. Le-Huu¹, N. Dannenberg¹, K.-P. Lodemann⁴; ¹Heidelberg/DE, ²Munich/DE, ³Homburg a.d. Saar/DE, ⁴Konstanz/DE

Purpose: To compare image quality and signal characteristics of two new generation contrast media for perfusion measurements of cerebral gliomas.

Methods and Materials: 30 patients with histologically confirmed cerebral gliomas (grade II - IV) were examined in a randomized exploratory intraindividual comparative study with dosages of 0.1 mmol/kgbw of MultiHance (Bracco) and Gadovist (Schering). For perfusion MR imaging a multislice gradient-echo EPI sequence was found to be best suited. Imaging parameters, slice positioning and contrast media application were standardized. For the quantitative assessment rCBV and rCBF measurements of tumor, normal gray and white matter were performed. The T2* effect of the contrast agents and dosages was assessed in a ROI analysis. The percentage of signal drop, and the full width half maximum of the signal time curves were quantified. The qualitative assessment focused on the quality of rCBV and rCBF maps.

Results: All perfusion measurements were of good to excellent image quality. The quantitative assessment of the T2* effect presented no significant difference between the two agents. The percentage of signal drop and the FWHM was not different between the contrast agents. For both agents the single dose measurements were sufficient to achieve high quality perfusion maps and yield to good tumor delineation and additional clinical information.

Scientific Sessions

Conclusion: MultiHance proved to be a safe and valuable contrast agent for perfusion imaging in CNS pathologies. It achieved a comparable T2* effect as the higher concentration Gadovist and produces high quality perfusion maps at a cost effective 0.1 dosage.

B-437 14:54

How much can a negative FDG-PET be trusted?

S. Wang¹, K. Ericson², B. Jorgen²; ¹Guangzhou/CN, ²Stockholm/SE

Purpose: To investigate the factors that may affect FDG accumulation in irradiated brain tumour.

Materials and Methods: 10 patients with an initial negative positron emission tomography (PET) finding whose subsequent PET study after a very short time was positive (group I) and 6 surgically confirmed false-negative PET (group II) were traced in a ten year retrospective review. Tumour size, histological types, irradiation parameters and steroid effect were analysed. To define residual radiation effect on fluorodeoxyglucose (FDG) uptake, post-radiotherapy time (from radiotherapy to PET) of group I and II was compared with that of 24 surgically confirmed true-positive PET (group III) and 5 surgically confirmed true-negative PET (group IV).

Results: 80% of transformation (from negative to positive PET finding) in group I happened within 31 weeks. The smallest lesion had a maximal diameter of 1.5 cm on MR. Histological types were similar among groups. Post-radiotherapy times of groups I,II, III, IV were not significantly different ($P > 0.05$). Approximately the same number of patients in group I had steroid treatment close to the initial negative and the subsequent positive PET examination. 5 of 6 patients (group II) did not have steroid treatment before PET examination.

Conclusion: Tumour size, histology types, residual radiation effect or steroid medication was not the single, main cause of false-negative PET.

B-438 15:03

Whole body positron emission tomography (18FDG PET) in patients with brain metastases

M.B. Dolgushin, I.N. Pronin, T.P. Tissen, L.A. Radkevich, A.J. Zayceva, V.N. Kornienko; Moscow/RU

Purpose: Metastases account for a quarter (24%) of all brain tumors. CT and MR imaging are the main diagnostic methods used in the detection of brain lesions. However detecting the primary source of brain metastases with both these methods is difficult. The purpose of our study was to evaluate whole body 18FDG PET in the detection of the primary of brain metastases.

Materials and Methods: 42 patients with CT and MR imaging brains suspicious for metastases and treated surgically were assessed. The given diagnosis has been exposed for the first time at all patients. Diagnostic investigations include CT, CT+CE, MR imaging (T1, T2, T1+CE, FLAIR) and some patient underwent 1H MR spectroscopy and DWI. In all cases the tumor enhanced with contrast media, usually with a ring-like pattern of enhancement suggesting a necrotic component at the center of the lesion with peritumoral edema. Multifocal lesions were detected in 44% of all tumors, and in 22% three or less were detected.

Results: Whole body (PET 18FDG) detected the primary tumors in the following locations: lungs-26%, melanomas-21.5%, breast-10%, uterus-7%, intestinal tract and kidney-5% each, pancreas and stomach-2% each. In 21.5% cases there was no pathological accumulation of glucose in any organs. In these cases the disease was evaluated as a primary brain tumor. However histological examination has shown the metastatic nature in 7%. Such cases were evaluated as brain metastases from an undetected source.

Conclusions: Whole body 18FDG PET was efficient in the detection of primary tumors in 93%.

B-439 15:12

MR imaging guided feature evaluation of characteristic gene expression signatures in glioblastoma multiforme

M.D. Kuo¹, C. Nardini², D. Wang¹, S. Cha³, M. Diehn⁴; ¹San Diego, CA/US, ²Bologna/IT, ³San Francisco, CA/US, ⁴Stanford, CA/US

Purpose: Glioblastoma multiforme (GBM) is characterized by genetic instability and an extremely variable appearance on magnetic resonance imaging (MRI). We sought to determine whether characteristic imaging features of GBM seen on MRI could capture significant alterations in intrinsic gene expression signatures identified by gene expression microarrays.

Methods: 4 imaging parameters were defined *a priori* to reflect fundamental GBM-defining MRI characteristics (degree of contrast enhancement, necrosis, T2 signal, mass effect). MR images (T1, T2, contrast enhanced) of 20 GBMs in 20 patients

were evaluated and scored across these 4 parameters by 2 radiologists in consensus and without knowledge of the genomic information. Unsupervised and supervised analyses were performed for correlation of the imaging parameters against the corresponding matched GBM microarray data (each microarray containing 23,000 clones) to identify relationships between imaging traits and tumor gene expression.

Results: 4/4 imaging traits demonstrated statistically significant correlation with gene expression: degree of contrast enhancement ($P < .01$), necrosis ($P < .01$), T2 signal ($P < .01$) and mass effect ($P < .005$). Further, there was significant enrichment of genes identified by each of the imaging traits in several fundamental GBM gene expression signatures: degree of contrast enhancement was enriched for the hypoxia/angiogenesis ($P = 3.9 \times 10^{-43}$), extracellular matrix ($P = 1.6 \times 10^{-48}$), and immune infiltration ($p = 9.1 \times 10^{-56}$) signatures, and necrosis and mass effect were both enriched for the proliferation signature ($P = 1.6 \times 10^{-14}$ and $P = 3.2 \times 10^{-51}$ respectively).

Conclusion: Radiogenomic evaluation of GBM on MRI can potentially co-localize several characteristic imaging findings to fundamental GBM gene expression signatures and may provide plausible insights into GBM tumor biology based on imaging alone.

14:00 - 15:30

Room N/O

Physics in Radiology

SS 713

CT: Radiation dose

Moderators:

W.A. Kalender; Erlangen/DE
M. Mazonakis; Iraklion/GR

B-440 14:00

Low-dose cardiac imaging with volumetric CT

J. Hsieh, J. Londt, J. Li, B. Hoppel; Waukesha, WI/US

Purpose: Nearly all of the current cardiac CT imaging protocols utilize low-pitch helical scans in order to ensure a complete volume coverage over multiple cardiac cycles. Although this approach is effective, X-ray dose to patient is high. We present a step-and-shoot acquisition for VCT cardiac imaging.

Methods and Materials: On 16-slice scanners, the coverage of the detector is limited to 10 mm for sub-mm acquisition. Helical mode was selected to eliminate the inter-scan delays. For a heart size of 16 cm, the inter-scan delay could be as high as 21 s if a step-and-shoot acquisition is used. However, with 64-slice VCT coverage has been increased to 40 mm. For the same coverage, the inter-scan delay is reduced to 4.2 s. Because the table remains stationary within each data acquisition, the X-ray is turned on only during the desired phase of cardiac cycles. Unlike the low-pitch helical, overlapped regions of X-ray exposure is not present.

Results: The proposed acquisition allows a 67-83% dose reduction when compared to a helical acquisition at pitch 0.3:1 without tube current modulation (the percentage dose saving is higher for lower-helical pitches). Even with an optimal tube current modulation, the dose reduction enabled by the proposed technique is still well above 35%. When combined with advanced cone beam reconstruction techniques, superior image quality is obtained.

Conclusion: With VCT-64 scanners, step-and-shoot acquisition combined with the advanced EKG gating enables a significant dose reduction for cardiac imaging, as compared to the helical mode acquisition. Phantom and clinical studies have confirmed its superior image quality.

B-441 14:09

Clinical evaluation of an 'automatic exposure control' mechanism for dose optimization in multidetector computed tomography

T.H.E.J. Mulkens, P. Bellinck, M. Baeyaert, D. Ghysen, X. Van Dijck, E. Mussel, C. Venstermans, J.-L. Termote; Lier/BE

Purpose: Evaluate dose reduction and image quality of a new automatic exposure control system for multidetector CT (MDCT), based on both z-axis and angular (x-y axis) tube current modulation and compare it with an angular modulation system.

Methods and Materials: In 2 groups of 200 patients, 5 regions (thorax, abdomen-pelvis, abdomen-liver, lumbar spine and cervical spine) were scanned on a 6-MDCT (Somatom Emotion, Siemens, Erlangen, Germany) with this modulation system (CARE DOSE 4D) and compared with 200 patients scanned with an angular modulation system (CARE DOSE). Wilcoxon tests were used for statistical

Scientific Sessions

comparison of dose reduction (reduction of mean mAs level) in these 600 exams, noise level in 200 exams of each modulation system and subjective image quality scores in 100 exams of each modulation system.

Results: Mean dose reduction for the new and angular dose modulation system was respectively: Thorax 20% and 14%, liver 38% and 18%, pelvis 32% and 26%, lumbar spine 37% and 10%, and cervical spine 68% and 16%. These differences were statistical significant. There was no statistical difference in noise and image quality scores, except for cervical spine exams ($p = 0.0002$ and 0.0007), where the angular modulation system scored better. A good correlation between mean mAs level and the body-mass-index of patients was found with the new modulation system, not with the angular modulation system.

Conclusion: An automatic exposure control mechanism for CT, based on real time anatomy-dependent mAs modulation, delivers good diagnostic image quality at significantly reduced dose levels.

B-442 14:18

Organ dose reduction using CT automatic exposure control (AEC): TLD measurements in an anthropomorphic phantom

B.T. Schmidt¹, C.H. McCollough², R. Banckwitz³, M.R. Bruesewitz², C. Suess³, T. Flohr³; ¹Malvern, PA/US, ²Rochester, MN/US, ³Forchheim/DE

Purpose: To measure directly the dose reduction achieved in specific organs within an anthropomorphic phantom by using Automatic Exposure Control (AEC). **Methods and Materials:** An Alderson-phantom was scanned using a 16-slice CT system (Sensation-16, Siemens Medical Solutions). Fifty TLDs were placed in the phantom for each scan. Scans were acquired using our clinical chest (TX) and chest-abdomen-pelvis (CAP) scan parameters. For each protocol, scans were acquired without and with AEC (CareDose4D). After each of the scans, the TLDs were removed and organ doses determined. The dose-length-product (DLP) reported on the scanner console was also recorded.

Results: All dose reductions are reported relative to the dose for scans without tube current modulation. For TX scans, the DLP was reduced by 33% with AEC. The dose in the shoulder region (upper lung) was as much as 26% higher than with no modulation, but in the middle/lower chest region, it was as much as 45% lower. Dose reductions were 33%, 17% and 17% for the breast, thymus and liver, respectively. For CAP scans, AEC reduced the DLP by 38%. The average dose to the lungs, breast, liver, stomach and bladder was reduced by 47%, 63%, 45%, 43% and 14%, respectively. These measured dose reductions correlate well to the effective mAs reductions at the respective anatomic levels.

Conclusion: AEC provides a large dose reduction relative to no tube modulation. However, the dose reduction to specific organs depends strongly on the anatomic region, and may be estimated by the effective mAs value reported at that location.

B-443 14:27

Implementation of automated exposure control (AEC) in a large body CT

practice: Assessment of image quality and dose savings

C.H. McCollough, J.M. Kofler, M.R. Bruesewitz; Rochester, MN/US

Purpose: To compare the image quality and dose resulting from the use of patient-size technique charts and an automated exposure control (AEC) system.

Methods and Materials: Approximately 2200 patients were imaged using an AEC system to adjust the X-ray output according to patient size (CareDose 4D, Siemens Medical Solutions). The reference effective mAs used for thorax (TX) was 170 and for abdomen/pelvis (AP) was 240. Patients were imaged for body indications only. Technologists noted patient size, eff. mAs from our technique chart, average eff. mAs over the entire AEC scan and the eff. mAs for specific anatomic levels. Qualitative image quality (IQ) feedback was obtained from a large number of readers.

Results: Radiologist assessment of image quality of the AEC exams was overall positive. Increased image quality in large patients and streak-prone regions such as shoulders was noted. Concerns regarding an increased noise level at the top of the liver were resolved by a modification of the AEC algorithm by the manufacturer. Relative to our technique charts, average eff. mAs decreased globally by 21%, and 29.7%, 54.8%, 13.2% and 23.2% at the levels of the upper lung, breast, liver, and pelvis, respectively.

Conclusions: The AEC system delivered on average of 21% less dose relative to our technique chart. The AEC system relieved the technologist of the responsibility of measuring and adjusting for patient size. The image quality of the AEC images was judged to be unchanged or improved, relative to non-AEC exams.

B-444 14:36

Apparent discrepancy between image quality and dose (CTDI) in MSCT automatic modulation modality

D. Origgi, S. Vigorito, G. Villa, G. Tosi, M. Bellomi; Milan/IT

Purpose: In a GE Lightspeed 4.X multislice CT, used in the automatic z-modulation modality, we observed a great CTDI variability between similar configurations at fixed noise index (NI). We therefore investigated if a different image quality could justify these dose variations.

Methods and Materials: We acquired a RANDO phantom at fixed NI of 7 for the head protocol and of 11.57 for the thorax protocol at different detectors configurations (16x1.25, 8x2.5-20 mm; 16x0.625, 8x1.25-10 mm) and pitches. We chose the couples of similar configurations with the highest CTDI differences. For each image, tube current adjustments (mAs) were recorded and signal-to-noise ratio (S/R) was measured in a ROI of 841 mm² at the same position.

Results: Series performed at the same slice thickness, collimation and similar pitch, but different detector configurations, showed CTDI variations ranging from 8 to 38% for the thorax and from 9 to 44% for the head in agreement with mAs modulation. The Wilcoxon sign test, performed for each couple of series, has shown always statistically significant differences ($p < 0.005$) for mAs, but not for S/R.

Conclusion: Other studies have already shown dose reduction in the modulation mAs modality compared to the fixed mAs modality, but no investigation has yet been reported about CTDI in the automatic mode. Our results show that unexpected dose variations can be found. This is a very critical point in the choice of a clinical protocol, as a higher dose to the patient doesn't mean better image quality.

B-445 14:45

A tool for fast Monte Carlo-based patient and scanner-specific dose calculations for CT with arbitrary tube current modulation

C. Leidecker, P. Deak, M. Kachelriess, W.A. Kalender; Erlangen/DE

Purpose: To provide a tool for patient-specific estimates of organ dose and effective dose values for arbitrary scan parameters.

Methods and Materials: A Monte Carlo-based simulation tool which we developed in cooperation with VAMP (Moehrendorf, Germany) allows calculation of dose distributions for 3D voxel data sets, from either phantoms or acquired patient CT images. The user can fit the calculation to a specific scanner through specifying the prefiltration and scanner geometry. Additionally, scan-specific parameters can be read in, e.g., the actual tube current used in the scan as a function of projection angle and z-position for arbitrary tube current modulations. Tools for the user to derive dose values for selected volumes of interest are also provided. Thereby, organ doses and effective dose can be computed for arbitrary scan protocols. As an application example, we used ImpactMC to investigate the dose reduction of an automatic exposure control (AEC) in CT [European Radiology 14(2):247, 2004.]

Results: Patient-specific calculations of dose distributions can be performed for arbitrary scanners and scan protocols with ImpactMC. We investigated the effects of varying scan parameters and techniques on the patient dose. E.g., with AEC dose reductions of 10-50% (typically 10-20% higher than the mAs-reduction), depending on patient and scan region, are obtained when compared to a constant tube current.

Conclusion: Dosimetry is an essential element in the management of patient dose from CT in relation to optimization of patient protection. ImpactMC is a convenient tool for patient and scanner-specific calculations of dose distributions.

B-446 14:54

Estimating organ and effective dose from multidetector CT using Monte Carlo simulations: Initial results from voxelized patient models

J. DeMarco¹, C. Cagnon¹, D. Cody², J. O'Daniel², C. McCollough³, M. Zankl⁴, M.F. McNitt-Gray¹; ¹Los Angeles, CA/US, ²Houston, TX/US, ³Rochester, MN/US, ⁴Neuherberg/DE

Purpose: The overall goal of this work is to develop accurate estimates of patient radiation dose from multidetector CT (MDCT) scans using Monte Carlo based simulation methods. The purpose of this work was to use voxelized patient models to estimate organ and effective doses.

Methods and Materials: A detailed mathematical model was developed for an MDCT scanner. The model included a detailed description of the X-ray source (e.g. X-ray spectra and bowtie filter) and geometry factors (e.g. distance from focal spot to isocenter and source movement pattern in helical scans of any pitch). The patient model used was the voxelized adult female (Donna, GSF, Neuherberg, Germany). This model is based on an actual patient scan and has radiosensitive



Scientific Sessions

organs labeled on a voxel-by voxel basis. Simulations were performed using a method to tally dose deposited on an organ-by-organ basis. To obtain initial results, a scan of the thorax was simulated using different pitch values. For each condition, mean organ dose was tallied and used to estimate effective dose.

Results: For most large organs, the mean value varied as 1/pitch as expected. Effective doses were obtained that ranged from 5.23 mSv/100 mAs at pitch 1.0 to 3.48 mSv/100 mAs at pitch 1.5. Other results demonstrated that the effective dose also varied according to 1/pitch.

Conclusion: These initial results demonstrate the ability to perform Monte Carlo based simulations using detailed scanner models and established voxelized patient models to determine organ and effective doses. Future work will include other adult and pediatric models.

B-447 15:03

Extra tube rotations (Z-overscanning) in helical multislice computed tomography of the body: Relative effects on organ doses of the thyroid and testicles, and on effective dose

A.J. van der Molen, J. Geleijns; Leiden/NL

Purpose: To quantify Z-overscanning in multislice CT and to study the relative effects on organ doses and effective dose in dose-optimized protocols of the chest and abdomen.

Materials and Methods: Z-overscanning was quantified by dose measurements on four 16-slice scanners of different vendors. Overscan rotations were derived by varying the number of tube rotations for all collimations at clinically used pitch values. The effect of reconstructed slice width was analyzed at a constant number of tube rotations. Results were applied to dose-optimized volumetric imaging protocols of the chest and abdomen from clinical reference sites. As sensitive organs will lie in the primary radiation beam, relative contributions to organ doses of the thyroid and testes and to effective doses were assessed using the IMPACT dose calculator.

Results: The number of overscan rotations is highly dependent on the image reconstruction algorithm. They decreased with increasing pitch, ranging 2.18-4.37 at low pitch and 0.96-2.23 at high pitch. Collimation had little effect. To accommodate thin and thick slices from the raw data, overscans increase slightly with increasing slice width. In the analyzed protocols the average overscan length was 4.1 cm for chest CT and 4.4 cm for abdominal CT. Thyroid dose increased by $320 \pm 50\%$ while testes dose increased by $127 \pm 4\%$. Effective dose increased $16.5 \pm 0.03\%$ in chest CT and $15.3 \pm 0.04\%$ in abdominal CT.

Conclusion: Overscan number is highly vendor-specific but is lower at increased pitch. These overscans radiate radiosensitive organs and contribute significantly to organ and effective doses.

B-448 15:12

Dose in multislice computed tomography: A comparative study on five scanners and correlation to a recent field study

A.J. van der Molen, J. Geleijns; Leiden/NL

Purpose: Comparative dose measurements were employed to document changes in effective dose in multislice computed tomography (CT) with improvements in scanner technology.

Materials and Methods: Normalized CT dose indexes (CTDI) free-in-air and in 16- and 32 cm dose phantoms were measured on four 16-slice and one 4-slice CT scanners of all major vendors. All available collimation and kVp settings were analyzed. Automatic exposure control was not employed. Results were applied to dose-optimized volumetric imaging protocols from clinical reference sites. Protocols included brain, chest, pulmonary embolism (PE), abdomen and biphasic liver. Effective doses in miliSievert (mSv) were calculated using volumeCTDI, Dose-Length-Product and conversion factors. Results of the 16-slice scanners were correlated with the 2002 German field study on 4-slice scanners. In one hospital a direct comparison between a 16-slice scanner and a 4-slice scanner (Toshiba) could be made.

Results: Effective doses on the 16-slice scanners ranged: Brain sequential 0.8-1.7 mSv, brain helical 1.5-2.7 mSv, chest 3.3-4.5 mSv, PE 2.8-3.0 mSv, abdomen 4.7-6.4 mSv and biphasic liver 7.3-9.2 mSv. Average values were 25-45% lower than averages reported by the German study. In direct comparison with 4-slice CT, effective doses for 16-slice (4-slice) were: Brain sequential 1.6 (1.6) mSv, brain helical 2.0 (3.1) mSv, chest 3.5 (5.5) mSv, PE 3.0 (4.7) mSv, abdomen 5.7 (8.6) mSv and biphasic liver 8.0 (12.4) mSv. Here 16-slice showed a reduction in effective dose of 34-36%.

Conclusion: With improvements in scanner technology, there is a reduction of effective dose in routine CT examinations.

B-449 15:21

Radiation dose to the patient in MSCT: What is the impact in practice of moving to 16 slice scanners?

C. Alvey, S. Mutch, S.J. Golding; Oxford/UK

Purpose: CT is perceived to deliver an increasing collective radiation dose to patients. This has been claimed to be partly due to increasing flexibility of modern technology. Our longitudinal study was carried out to assess the effect of technological upgrade to different levels of MSCT in a typical hospital practice over five years.

Methods and Materials: A longitudinal study was conducted between 1999 and 2004 to assess average dose-length product for typical examinations carried out in a service which moved progressively from single slice systems through 4, 8 and 16 slices on one manufacturer's equipment. Examinations were grouped into categories dependent upon standard clinical applications and mean dose-length products calculated for each phase of technological upgrade.

Results: The study indicates that the improved image quality of MSCT is expressed in significant dose reduction in practice. Common examinations of the trunk show exposure reductions which range between 9 and 30%. Examination of the brain may achieve a dose reduction of 42%. However some examinations, notably CT pulmonary angiography, have shown rising mean exposure. Detailed information showing variability within common applications are presented. The study is ongoing.

Conclusion: Although concern has been expressed that the total collective dose due to CT is increasing significantly, our study indicates that the dose advantage of new technology is realised to a degree in practice. Variation between similar examinations remains a source of concern but some guidelines on further dose reduction may be drawn from our data.

14:00 - 15:30

Room P

Vascular

SS 715

Carotid imaging

Moderators:

F.P. Boudghène; Paris/FR
T. Jargiello; Lublin/PL

B-450 14:00

Assessment of the prevalence and severity of carotid artery disease in patients with peripheral arterial disease

A. Drelich-Zbroja, M. Elfurah, T. Jargiello, M. Rzeszowska-Sieczka, M. Szczero-Brojanowska; Lublin/PL

Purpose: The aim of our study was to assess the correlation between severity of peripheral arterial disease and severity of the co-existent carotid artery disease.

Material and Method: 60 patients admitted with peripheral arterial disease (PAD) were included in the study. In every patient lower extremity angiography examination and carotid artery ultrasound examination were performed. Ultrasound examination was done using "ultrasound biopsy" classification to evaluate plaques and using Doppler measurements to assess blood flow hemodynamic changes.

Results: The prevalence of PAD according to TASC was: 15.0% patients had type A, 66.7% patients had type B, 11.7% patients had type C, 6.6% patients had type D. The prevalence of carotid artery disease was: 1.7% patients with 0% ICA stenosis, 68.3% with 1-39% ICA stenosis, 16.6% with 40-59% stenosis, 5% with 60-79% stenosis, 1.7% with 80-99% stenosis and 6.7% had unilateral ICA occlusion. Concerning hemodynamically significant ICA stenosis, that is $\geq 50\%$ or occlusion, the prevalence was 18.3% patients, of these 3 patients had 50-59% ICA stenosis, 3 had 60-79% stenosis, 1 had 80-99% stenosis and 4 had occlusion. The prevalence of carotid disease according to "ultrasound biopsy" classification was: 1.7% for class I, 1.7% II, 35% III, 31.6% IV, 18.3% V, 5% VI, 6.7% VII.

Conclusions: A high prevalence of carotid artery disease had been detected in patients with peripheral arterial disease. No correlation was confirmed between severity of peripheral arterial disease and severity of the co-existent carotid artery disease.

Scientific Sessions

B-451 14:09

Grading of carotid artery stenosis: Should we use estimation or measurement?

A. Waaijer, M.S. van Leeuwen, M. Olree, W. Niessen, M. Prokop; Utrecht/NL

Purpose: To compare accuracy and reproducibility of visual assessment and various objective measurement techniques for determining carotid artery stenosis on multislice CTA.

Materials and Methods: We performed 16-slice CTA in 23 patients with symptomatic carotid stenosis and used selective angiography of 32 carotids as the gold standard. We evaluated four methods for stenosis quantification on CTA: (1) stenosis estimation using 10% intervals; (2) measurement with calipers, using subjectively optimized window settings; (3) measurement with calipers using the Full Width at Half Maximum (FWHM) principle, (4) automatic measurement. Methods 1-3 were performed by two observers and repeated by one. Method 4 was performed twice by one observer. On DSA, carotid stenoses were measured twice by one observer using calipers on the projection showing the narrowest lumen. A Bland-Altman analysis was performed to determine mean intra- and inter-observer differences (bias) and standard deviation of differences (SDD). The same analysis was performed to compare CTA and DSA measurements by using the mean of two observers for CTA and the mean of two DSA readings.

Results: Intra-observer bias and SDD for stenosis grading were -1.7% ± 8.3% for DSA, and 0.9% ± 7.1%, 2.8% ± 8.9%, 1.3% ± 11.3%, and -0.2% ± 9.7% for methods 1-4, respectively. Inter-observer bias and SDD for methods 1-3 were 0% ± 9.7%, 8.0% ± 15.0%, and 8.2% ± 23.8%, respectively. Bias and SDD for comparison of methods 1-4 to DSA readings were 8.3% ± 10.6%, 3.2% ± 11.8%, -6.8% ± 16.6% and -15.4% ± 13.2%, respectively.

Conclusion: Stenosis grading on CTA based on estimation or subjectively using calipers outperformed stenosis grading based on FWHM or automated measurements.

B-452 14:18

Optimization of CT angiography of the carotid artery with a 16-multidetector-row CT scanner: Craniocaudal scan direction reduces contrast material-related perivenous streak artifacts

C. de Monyé, T.T. de Weert, W. Zaalberg, J. Roose, D. Siepman, A. van der Lugt; Rotterdam/NL

Purpose: To compare the effect of a caudocranial and a craniocaudal scan direction on arterial enhancement and perivenous artifacts in 16-multidetector-row CTA of the supra-aortic arteries.

Materials and Methods: Eighty consecutive patients (51 male; mean age = 62; range 28-89 yrs) were scanned in caudocranial (group 1; n = 40) or craniocaudal direction (group 2; n = 40). All patients received 80 mL contrast material followed by 40 mL saline i.v. at 4 mL/sec. Bolus tracking was applied. The attenuation inside the arterial lumen was measured at intervals of 1 second throughout the data set. The attenuation in the superior vena cava (SVC) was measured. Contrast material-related perivenous streak artifacts were graded on a scale of 0 to 3 (0=no; 1=minor; 2=moderate and 3=extensive).

Results: The attenuation in the ascending aorta, carotid bifurcation and intracranial arteries were slightly lower in group 2 versus 1 (231 ± 64 HU, 348 ± 52 HU and 258 ± 48 HU versus 282 ± 43 HU, 381 ± 73 HU and 291 ± 77 HU, respectively; p < 0.05). Also the maximum and mean arterial attenuation were slightly lower in group 2 versus 1 (369 ± 58 HU and 303 ± 48 HU versus 401 ± 71 HU and 334 ± 58 HU, respectively; p < 0.05). The attenuation in the SVC was much lower in group 2 versus 1 (169 ± 39 HU versus 783 ± 330 HU, respectively; p < 0.001). Mean streak-artifact-score was much lower in group 2 versus 1 (2.5 ± 0.6 versus 1.3 ± 0.9, respectively; p < 0.001).

Conclusion: A craniocaudal scan direction results in a slightly lower attenuation of the carotid artery, though still high enough for good evaluation, and a much lower attenuation of the SVC. Streak artifacts are significantly lower. This allows a better evaluation of the ascending aorta and supra-aortic side branches.

B-453 14:27

Optimization of stenosis quantification using 16-row MDCTA in a phantom model simulating soft and calcified plaque material

M. Fruth, M. Finke, K. Schliephake, F. Brassel, K. Papke; Duisburg/DE

Purpose: Quantification of vessel stenoses in CTA is hampered by window dependent blooming of either the plaque material in hyperdense plaques or the vessel lumen in hypodense plaques. It was the aim of our study to optimize stenosis measurements using a window independent method.

Materials and Methods: 110 stenoses from 0.5 to 2.5 mm were placed in tubes

with a diameter of 5 mm, simulating stenoses from 50 to 90% (NASCET method). 55 stenoses consisted of hyperdense material, the other 55 of hypodense material. Tubes were filled with diluted contrast and examined with 16-row MDCTA. Three methods were compared: 1. visual stenosis estimation, 2. diameter measurement with callipers at fixed window setting and 3. window independent quantification with a density profile across the stenosis; the full width at half maximum was taken as the stenosis diameter in soft stenoses, the full width at half the relative minimum between the peaks of the vessel walls was taken in calcified stenoses.

Results: Method 3 had the highest correlation between measurement result and gold standard ($r = 0.93$), as compared to $r = 0.83$ for method 2 and $r = 0.87$ for method 1. The difference between the methods was higher in stenoses with hyperdense plaque material.

Conclusion: Window independent stenosis quantification by using density profiles proved to be significantly more precise than the measurement methods used in clinical routine. We conclude that this method should be applied if a precise determination of the stenotic degree is crucial for clinical decisions, e.g., concerning treatment of carotid artery stenoses.

B-454 14:36

High resolution magnetic resonance angiography with iPAT compared to color Doppler and power Doppler in the assessment of carotid artery stenosis

D.-A. Clevert¹, S. Schoenberg¹, E. Jung², H. Michaely¹, M.F. Reiser¹;

¹Munich/DE, ²Passau/DE

Purpose: To compare the diagnostic accuracy of 3D contrast enhanced MR angiography (MRA) with parallel imaging techniques (iPAT) using a 32-channel MR-system with color Doppler (CD) and power Doppler (PD) in the grading of high grade stenosis of the internal carotid artery (ICA).

Material and Methods: 21 patients with known or suspected ICA-stenosis were examined with a 32-channel 1.5 T MR System with head, neck and spine array coils (Magnetom Avanto, Siemens, Germany) using iPAT sequences. MRA was acquired with a 512 matrix in a 20 second breath hold. Patients received a single i.v. dose of 20 ml gadobutrol (Gadovist®, Schering). MRA were analyzed for caliber irregularities and intravascular thrombi. In CD and PD sonography (Logiq 9, GE), the degree of stenosis (NASCET-criteria), the maximum peak systolic velocity at the stenotic site and the poststenotic flow parameters were evaluated. The degrees of stenosis were compared in MRA, CD and PD.

Results: Using the parallel acquisition technique, excellent visualization of vessels could be obtained in almost all cases. MRA revealed 10/21 stenosis between 70-80%, 7/21 stenosis between 80-90% 4/21 stenosis greater than 90%, which were correctly graded in MRA and CD/PD.

Conclusions: CE MRA with iPAT and PD/CD are highly accurate in the detection and grading of stenoses of the internal carotid artery. While duplex sonography is an excellent screening modality for the internal carotid artery, MRA is helpful for preoperative planning for the carotid internal artery.

B-455 14:45

Internal carotid artery (ICA) stenoses: Color Doppler ultrasound (CDUS), multidetector computed tomography (MDCT), and digital subtraction angiography (DSA) versus intraoperative plaque evaluation

R. Meroni, N. Flor, S. Soldi, L. Caverni, M. De Monti, F. Sardanelli, G.P. Cornalba; Milan/IT

Purpose: To compare CDUS, MDCT, and DSA with an intraoperative gold standard for evaluating ICA stenoses.

Materials and Methods: Twenty-seven ICA stenoses in 24 patients were prospectively studied with CDUS, contrast enhanced 4-row MDCT, and DSA. The stenosis rate was calculated using: CDUS with diameter (CDUS-d) or area method (CDUS-a); MDCT with area method on multiplanar reconstructions perpendicular to the vessel axis; DSA with NASCET diameter rate (DSA-NASCET-d), or NASCET diameter rate mathematically converted in area rate (DSA-NASCET-a), or common carotid diameter rate (DSA-CC-d) method, or common carotid diameter rate mathematically converted in area rate (DSA-CC-a). All patients underwent eversion endarterectomy (EEA) to obtain a precise stenosis measurement. A 4-point score was assigned to the plaque calcium and lipids content on MDCT and on gross specimens. Two-tail Sign test and Chi-square were used.

Results: The stenosis rate for the different measurement methods were as follows: 74.6 ± 10.8 (CDUS-d); 82.9 ± 7.0 (CDUS-a); 82.6 ± 8.1 (MDCT); 48.6 ± 22.7 (DSA-NASCET-d); 68.6 ± 26.2 (DSA-NASCET-a); 70.8 ± 13.6 (DSA-CC-d); 89.7 ± 8.5 (DSA-CC-a); 82.4 ± 9.9 (EEA). Significant differences with EEA ($p < 0.05$) were observed for DSA-NASCET-d, DSA-CC-a, and DSA-CC-d. Two

Scientific Sessions

plaques was not scored at MDCT (artifact from calcium at bifurcation); MDCT and EEA were in complete agreement for the calcium scoring in 17/25 and for the lipid scoring in 18/25 ($p < 0.001$).

Conclusions: Considering the high standard deviation of DSA-NASCET-a, MDCT and CDUS give better stenosis measurements than DSA. Moreover, MDCT enables prediction of the calcium and lipid content of the plaque. High calcium deposition at the bifurcation is a limitation for MDCT.

B-456 14:54

Changes of blood flow during carotid endarterectomy evaluated by transit-time flowmeter measurement

M. Alekšić, V. Matoussevitch, J. Heckenkamp, K. Krüger, M. Gawenda, J. Brunkwall; Cologne/DE

Purpose: Carotid endarterectomy (CEA) may be complicated by a cerebral hyperperfusion syndrome which clinically presents with various symptoms ranging from postoperative headache to convulsions. An association with the degree of the underlying stenosis of the internal carotid artery (ICA) is presumed. Such an association should be verified by evaluating intraoperative blood flow changes.

Methods and Materials: In 104 patients undergoing CEA for unilateral high-degree ICA stenosis, a preoperative intraarterial digital subtraction angiography of the supraaortic vessels was performed. The degree of the stenosis was digitally assessed by using graphical computer software (Adobe Photoshop®) according to the ECST-Index. Blood flow was measured before and after CEA with an ultrasound flowmeter which is based on the transit-time principle. These findings were correlated to the degree of stenosis.

Results: Preoperative median blood flow in the ICA was 180 ml/min (range 443 ml/min) with a significant ($p < 0.0001$) postoperative increase to 245 ml/min (range 96–345 ml/min). The relative increase in flow (post flow - pre flow / pre flow) was 85%. However, no direct correlation between the degree of stenosis and flow increase was found ($r = 0.18$, $p = 0.068$).

Conclusions: The increase of blood flow does not seem to be related to the degree of ICA stenosis. To describe the hemodynamic conditions and changes which takes place in CEA more precisely, further investigations using a perfusion model are required.

B-457 15:03

Intermediate follow-up of stented carotid arteries: Is it possible to define reliable ultrasound velocity criteria?

A. Vit, A. De Candia, G. Piccoli, S. Smania, A. Marzio, M. Bazzocchi, D. Gasparini; Udine/IT

Purpose: To develop blood flow velocity criteria reliable in Doppler follow-up of carotid artery stenting (CAS) and to compare Doppler velocity measurements and power Doppler (PD) geometric evaluation in identifying in-stent restenosis and in quantifying the degree of restenosis proven angiographically.

Methods and Materials: Intermediate 6-month follow-up US examinations were performed in 114 stented carotid arteries. Peak systolic velocity (PSV) inside the stent and internal carotid artery to common carotid artery ratio (ICA/CCA) were measured. PD evaluation was also performed to determine the geometrical degree of in-stent restenosis (significant if 50% or greater). The degree of restenosis based on PD evaluation and blow flow velocity measurements were compared with angiographic results. Receiver operator characteristic (ROC) curves were generated to develop appropriate US velocity measurements in the detection of restenosis.

Results: One US showed complete occlusion of the stent, which was confirmed by CT-angiography. Six significant in-stent restenoses on US were angiographically confirmed, with excellent correlation between geometric PD degree of stenosis and angiographic degree. Corresponding PSV was 213.8 ± 71.11 cm/s, with one case of 55% restenosis and PSV of 95 cm/s. The remaining 107 cases with no evidence of restenosis showed a PSV of 103.4 ± 28.5 cm/s, with 11 cases (10.3%) with PSV > 130 cm/s.

The area under the ROC curves for PSV (0.88) and ICA/CCA (0.80) demonstrated a moderate discriminant ability, but we could not identify reliable Doppler velocity criteria.

Conclusion: Doppler velocity evaluation after CAS is unreliable and leads to false positive and false negative results. PD geometric evaluation seems reliable in quantifying degree of restenosis.

B-458 15:12

Prospective evaluation of a comprehensive MR-protocol in patients with suspected cervical artery dissection (CAD)

R. Bachmann, I. Nassenstein, C. Stehling, T. Niederstadt, R. Dittrich, W. Heindel, S. Kraemer; Münster/DE

Purpose: To assess the diagnostic efficacy of a comprehensive MR-protocol for the diagnosis of CAD.

Methods and Materials: 36 consecutive patients (19m, 17f, mean 42 yrs.) with suspected CAD underwent cervical 1.5 T-MR (Gyroscan Intera, Philips). Imaging protocol consisted of axial T1w-TSE, T2w-TSE and contrast-enhanced T1w-TSE (MRI) and CE-MRA. Images were assessed for the presence of specific (mural hematoma, increased external diameter, pseudoaneurysmen, string sign) and unspecific (occlusion, stenosis, hyperintense lumen, perivascular enhancement) signs for MRI and MRA separately. CAD was judged definite, if any one specific sign was present in MRI or MRA, undetermined if an unspecific sign and normal if no pathologic signs were present. MR-diagnosis was verified by follow-up.

Results: 17 pts with no sign for CAD were rated normal. None had evidence of CAD in follow-up. In 19 pts pathologic findings occurred (12x ICA, 7x VA), which were judged specific in 7 pts by MRA and MRI, in 5 pts by MRA only and in 1 pt by MRI only. Diagnosis of CAD was confirmed in 13 pts with specific findings. In 6 pts vessel occlusion was diagnosed by MRI and MRA, but the etiology remained undetermined.

Conclusion: The presence of specific signs in MRA or MRI yields a high positive predictive value for the diagnosis of CAD. Furthermore, CAD can be excluded confidently in patients with normal findings. Thus, the presented comprehensive MR-protocol is well suited as first line study in pts with suspected CAD, assessing both luminal patency and vessel-wall pathology in a combined approach.

B-459 15:21

Detectability of specific radiological signs in cervical artery dissection: Comparative analysis of helical-CT, MR imaging, MRA and DSA

S.C. Krämer, G. Kuhlenbäumer, I. Nassenstein, L. Conrad, W. Heindel, R. Bachmann; Münster/DE

Purpose: Cervical artery dissection (CAD) is the main cause of stroke in young patients. Our purpose was to analyse the potential of different imaging modalities to detect specific radiological signs in CAD.

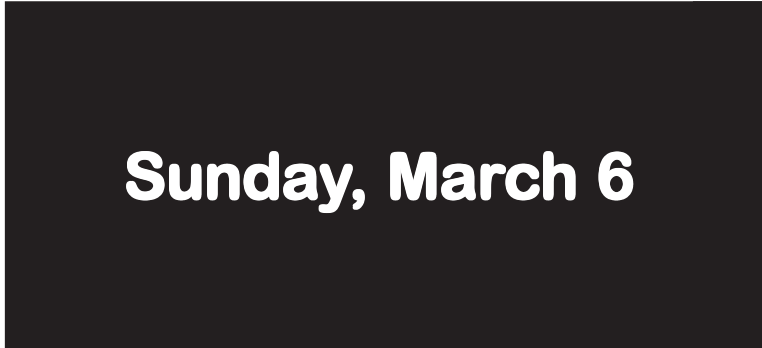
Methods and Materials: 46 clinically proven dissections of the carotid ($n = 29$) and vertebral ($n = 27$) arteries in 38 patients (female: 15, male: 23, mean age: 41 years) were retrospectively evaluated. Patients had at least one of the following imaging: Helical-CT, MR imaging (MRI), MR-angiography (MRA) or DSA. Specific signs such as mural hematoma, vessel diameter increase, string-sign or mural contrast deposit were defined for cross-sectional and angiographic imaging. Stenoses, occlusions and pseudoaneurysms were considered non-specific. Detection rates of specific and non-specific signs were compared by student's t-test.

Results: On cross-sectional imaging, specific signs could be detected in 11 of 19 cases (58%) with helical-CT and in 29 of 31 (95%) with MRI. Angiographic imaging was positive for specific signs in 7 of 29 cases (24%) with MRA and in 8 of 15 (53%) with DSA. Mural hematoma was seen in only 5 of 19 cases (26%) with CT whereas in 24 of 31 cases (77%) with MRI. Non-specific signs were present in 95% with helical-CT, 94% with MRI, 90% with MRA and 93% with DSA.

Conclusion: In cross-sectional imaging, MRI proved clearly superior to helical-CT in detecting specific signs of CAD. Although DSA is superior to MRA in angiographic imaging, the combined approach of MRI and MRA should be the modality of choice in patients with suspected CAD.

Scientific Sessions

Scientific Sessions



Sunday, March 6

Scientific Sessions

		room A 2nd level	room B 2nd level	room C 2nd level	room E1 entr. level	room E2 entr. level	room F1 entr. level	room F2 entr. level	room G lower level	room H lower level		
07:00											07:00	
07:30											07:30	
08:00											08:00	
08:30		CC 917 Essentials of Neuroradiology Three common neurological problems: Loss of vision, hearing loss, trigeminal and facial nerve palsy (p. 64)	RC 910 Musculoskeletal Wrist (p. 64)	SF 9a Special Focus Session Radiology of the elderly (p. 65)	RC 902 Breast Diagnostic highlights (p. 66)	RC 901 Abdominal and Gastrointestinal Impact of multislice CT on imaging of the upper abdomen (p. 67)	ER 926 Joint ECR/EAR sessions: Challenges for European Radiology European research network in biomedical imaging (p. 67)	RC 911 Neuro Radiological vascular interventions (p. 68)	SF 9b Special Focus Session PACS pitfalls (p. 69)	RC 909 Interventional Radiology Endovascular treatment of lower limb vascular occlusion (p. 70)		08:30
09:00											09:00	
09:30											09:30	
10:00											10:00	
10:30		EM 2 “ECR meets” Hungary The present and future of Hungarian radiology: Contribution of a new generation (p. 73)	NH 10 New Horizons Session Drug-eluting stents (p. 75)	SS 1010 Musculoskeletal Tumor imaging (p. 238)	SY 9 Satellite Symposium MDCT imaging: New challenges for scan and contrast optimisation (p. 584)	SS 1004 Chest CT and MR imaging of the pulmonary vessels and right heart (p. 239)	SY 10 Satellite Symposium Contrast-induced nephropathy (p. 586)	SS 1001 Abdominal Viscera Pancreas: MR imaging evaluation of pancreatic duct and pancreatic cystic lesions (p. 242)	SS 1007 Genitourinary MR imaging of the prostate (p. 244)	SS 1009a Interventional Radiology Hepatic interventions (p. 246)		10:30
11:00											11:00	
11:30											11:30	
12:00											12:00	
12:30											12:30	
13:00											13:00	
13:30											13:30	
14:00											14:00	
14:30											14:30	
15:00											15:00	
15:30											15:30	
16:00											16:00	
16:30		CC 1217 Essentials of Neuroradiology Base of the skull, hypophysis, supra- and parasellar region (p. 77)	SA 12 State-of-the-Art Symposium Multi-dimensional imaging for guiding therapy (p. 78)	SF 12 Special Focus Session Assessment of myocardial perfusion and viability (p. 79)	RC 1203 Cardiac Pericardial diseases (p. 79)	SY 12 Satellite Symposium Advances in head and neck imaging using CT and MR (p. 586)	RC 1204 Chest Multislice CT of the thorax (p. 80)	RC 1211 Neuro Diffusion and perfusion MR imaging of the brain (p. 81)	RC 1213 Physics in Radiology Safety considerations in MR (p. 81)	WS 1209 Interventional Radiology Aortic stent grafts (p. 82)		16:30
17:00	registration										17:00	
17:30	EPOS™ - scientific exhibition										17:30	
18:00											18:00	
18:30											18:30	
19:00											19:00	

Scientific Sessions

	room I lower level	room K lower level	room L/M 1st level	room N/O 1st level	room P lower level	room W basement	room X 1st level	room Y 1st level	room Z entr. level	La Scala 2nd level	
07:00											07:00
07:30											07:30
08:00											08:00
08:30											08:30
09:00	WS 918 Workshops on Interventional Radiology Urological intervention (p. 70)	RC 912 Pediatric Neuro-imaging (p. 71)	CC 916 Infection in the Adult Today Modern imaging of infective disease in the face and pelvis (p. 72)	RC 913 Physics in Radiology Medical image registration: Methods, applications and validation (p. 72)	WS 921 Musculo-skeletal US "Hands-on" Workshop				WS 924 Basic Life Support for Radiologists "Hands-on" Workshop	E ³ 920 Foundation Course: Chest Radiology Nodules and neoplasms (p. 73)	09:00
09:30											09:30
10:00									WS 23C2 Screening Mammography Interpretation Test "Hands-on" Workshop		10:00
10:30									WS 1024 Basic Life Support for Radiologists "Hands-on" Workshop	E ³ 1020 Errors in radiology (p. 76)	10:30
11:00	SS 1009b Interventional Radiology Carotid stenting (p. 248)	SS 1003 Cardiac MDCT in ischemic cardiomyopathy and myocardial infarction (p. 250)	SS 1011 Neuro Brain tumor evaluation with diffusion and perfusion MR imaging (p. 252)	SS 1013 Physics in Radiology Digital radiography/ Digital mammography (p. 254)	SS 1015 Vascular Imaging of stenosis, aneurysm and dissection in the abdominal vessels (p. 256)	WS 1022 Vertebraloplasty "Hands-on" Workshop	WS 1021 Musculo-skeletal US "Hands-on" Workshop	WS 23C3 Screening Mammography Interpretation Test "Hands-on" Workshop			11:00
11:30											11:30
12:00								WS 23C4 Screening Mammography Interpretation Test "Hands-on" Workshop			12:00
12:30											12:30
13:00											13:00
13:30											13:30
14:00											14:00
14:30											14:30
15:00											15:00
15:30											15:30
16:00											16:00
16:30	RC 1215 Vascular Vascular imaging (p. 83)	RC 1212 Pediatric Chest imaging (p. 84)	RC 1214 Radiographers Pediatrics/ Radiography (p. 84)	PR 1219 Primer: Molecular Imaging Imaging of gene expression: Optical and nuclear techniques (p. 85)	RC 1205 Computer Applications Building an electronic patient record system (p. 86)					E ³ 1220 Foundation Course: Chest Radiology Wrapping it up ... (p. 87)	16:30
17:00											17:00
17:30											17:30
18:00											18:00
18:30											18:30
19:00											19:00

Scientific Sessions

10:30 - 12:00

Room C

Musculoskeletal

SS 1010

Tumor imaging

Moderators:

S. Anderson; Berne/CH
G. Hadjidekov; Sofia/BG

B-460

withdrawn by authors

B-461 10:30

Osteoid osteoma: Role of dynamic MR imaging in detection of and definition of success after CT-guided radiofrequency ablation

V. Zampa¹, U. Albisinni², I. Bargellini¹, F. Odoguardi¹, R. Cioni¹, C. Bartolozzi¹; ¹Pisa/IT, ²Bologna/IT

Purpose: To evaluate the role of dynamic Gadolinium-enhanced MR imaging (D-MRI) in the nidus detection of osteoid osteoma (OO) and in the assessment of the results after radiofrequency (RF) thermal ablation.

Materials and Methods: Twenty-three patients with histologically proven OO underwent MRI before and 6 months after percutaneous CT-guided RF ablation. MRI protocol included a conventional study (C-MRI: SE-T1w, GRE-T2w and FSE-IR) and D-MRI (FastSPGR-T1w) after Gd injection. MRI images were evaluated by two blinded readers to assess bone edema and joint effusion on C-MRI, and degree of nidus contrast uptake on D-MRI.

Results: Pre-procedural C-MRI revealed specific abnormal findings in all cases, with clear nidus delineation only in 9; at D-MRI, early and high contrast uptake allowed accurate nidus identification in 20/23 cases. After treatment, 8 patients reported persistent pain. In these cases, where persistent edema and nidus contrast uptake was identified, patients underwent further treatment. In asymptomatic patients and in patients reporting residual discomfort not requiring medical therapy after treatment, D-MRI did not demonstrate residual nidus contrast uptake, and C-MRI showed reduction of bone edema and joint effusion, allowing definition of success. Moreover, in 6 cases of successful treatment, C-MRI showed an area of apparently normal bone marrow delineated by a rim (hypointense in T1-w and slightly hyperintense in T2-weighted images), recalling osteonecrosis in the site of previous RF ablation.

Conclusion: D-MRI allows nidus detection in OO. After RF ablation, MRI enables accurate assessment of results, and D-MRI is able to differentiate a persisting active nidus from bone edema.

B-462 10:39

Combined bipolar radiofrequency and cementoplasty in bone metastasis: Preliminary results in 8 patients

B.A.C. Kastler, H. Boulahdour, F.-G. Barral, P. Pereira, O. Saguet, P. Jacoulet, R. Lejoncour, R. Aubry, B. Fergane; Besancon/FR

Purpose: To evaluate the feasibility of combined bipolar radiofrequency and cementoplasty in the management of pain in bone metastasis. Cementoplasty is an already efficient and accepted method particularly when there is a risk of fracture. However the injection of acrylic glue has the potential drawback of spreading the disease as it may mechanically push out the malignant cells either in close proximity or at distance via the draining veins. Radiofrequency offers the possibility of a thermal ablation which can be optimized concerning the exact ablation size with a bipolar approach (Gelon generator). This is crucial when the lesion is close to major neural structures (motor nerves, spinal cord)

Method and Materials: 8 adult patients with bone metastasis in various locations (sternum, ribs, clavicle, vertebrae, iliac bone,) refractory to conventional pain treatment were included in the study. They first underwent RF ablation followed immediately by cementoplasty through the same Trocar, coaxially to optimize the intervention (namely reducing procedure time: range 30 to 90 min.). The trocar was placed under CT guidance.

Results: All patients had a significant pain relief persisting at 3 month.

Conclusions: This combined bipolar radiofrequency and cementoplasty approach appears to be an efficient alternative when other therapies provide no proper pain relief. Moreover it should reduce the risk of local recurrence and seeding at a distance, of the tumour. Thus it may have the potential of sterilizing lesions in unique locations. This novel combination deserves further investigation.

B-463 10:48

Benefit of peer-reviewed pathological examination of soft tissue tumors.

What is the role of radiology?

J.L.M.A. Gielen, A.M.A. De Schepper, E. Van Marck, P. Van Dyck, F. Vanhoenacker, P.M. Parizel; Edegem/BE

Purpose: The aim is to objectify the benefit of peer reviewed pathology of soft tissue tumors (STT) and to define the interaction between pathologist and radiologist.

Materials and Methods: Cases were selected from a multi-institutional prospective study on MR imaging of pathologically confirmed STT. Selected were all cases histologically diagnosed as malignant, cases with discrepancy between biopsy and resection histology and lesions with indefinite histology results, and cases with discrepancy between histology and MR imaging. 623 cases have a confirmed diagnosis. Of 173 cases, pathology slides are submitted to a peer review committee of 6 specialized pathologists.

Results: Initial histological diagnosis is confirmed in 124 cases, 41 malignant, 83 benign lesions. Diagnosis changed in 26 (39%) out of 67 malignant lesions and in 18 (17.5%) out of 103 benign lesions. Diagnostic accuracy of the referral pathologist concerning benign lesions (82.5%) is obviously better when compared with malignant lesions (61%). Histological phenotype changed in 11 (16.5%) out of 67 malignant cases and in 10 (9.5%) out of 103 benign lesions. Because of their therapeutic consequences cases with initially benign diagnoses, which became malignant diagnoses (8 out of 67) (false negatives) are of utmost importance, while the consequences of the vice versa situation (4 out of 103) (false positives) are not that significant.

Conclusion: The accuracy of the referring pathologist was calculated as follows, PPV 93.5%, NPV 92.5%, sensitivity 88%, specificity 96%. Discrepancy between MR imaging and pathology is an important selection criterion for pathological peer review optimizing the interaction between pathologist and radiologist.

B-464 10:57

MSCT versus MR imaging: Diagnostic sensitivity in the detection of spine metastases

A. Baur-Melnyk, S. Buhmann, A. Wieser, M.F. Reiser; Munich/DE

Purpose: The aim of the study was to evaluate the diagnostic sensitivity of Multi-Slice-computed tomography (MSCT) compared to the sensitivity of Magnetic Resonance imaging (MRI) concerning the detection of metastases in the spine.

Materials and Methods: In a retrospective clinical trial, 343 vertebral bodies of 27 patients with various primary malignancies, histologically attested, were analysed. The CT-images were acquired on a 16-row-MSCT (SIEMENS Sensation 16) with 120 kV, 100 mAs and 1 mm collimation. An image reconstruction in 3 mm axial slices and sagittal MPRs of the spine with an increment of 3 mm were performed. The MRI protocol consisted of STIR-sequences, T2-weighted SE-sequences and T1-weighted SE-sequences with and without application of contrast medium in all patients and was performed using a 1.5 Tesla-scanner (SIEMENS Symphony/Sonata). In a consensus reading the acquired CT and MRI images were evaluated by two experienced radiologists.

Results: 13% of the in MRI images detected metastases were not identified in MSCT-images. All osteoclastic metastases were detected in MSCT as well as in MRI due to the MSCT benefit of better evaluating bone structures. In our study, MRI reached a diagnostic accuracy of 100%. CT showed a sensitivity of 86% and a specificity of 100%.

Conclusion: 16-row-MSCT provides excellent image quality with high resolution but metastases at early stages of disease without bone destruction may only be visualized and detected with MRI.

B-465 11:06

Can 16-detector multislice CT rule out skeletal metastases whilst staging the soft tissues?

A.M. Groves, C.J. Beadsmoore, K.K. Balan, H.K. Cheow, H.M. Courtney, S. Kaptope, P.W.P. Bearcroft, A.K. Dixon; Cambridge/UK

Purpose: Presently in oncology, bone scintigraphy is used to stage the skeleton, whilst computed tomography (CT) stages the soft tissues. New CT technology has now, for the first-time, made it feasible to perform a whole-body bone CT and thus could save patients having to undergo duplication of investigations.

Methods and Materials: Over 6-months, 43 cancer patients presenting to the nuclear medicine department were recruited for additional whole body 16-detector multislice CT. Both studies were performed within six weeks of each other. CT was performed on a 16-detector multislice CT machine using 1.5 mm detectors and reconstructed in 2 mm slices from vertex to knee. Multiplanar reformatted

Scientific Sessions

images were then viewed interactively on a monitor. 4-hours after injection of 500 Mbq 99m Tc-MDP, whole-body planar images were taken using a dual-headed gamma camera. The findings were reported "blind" of each other. Discordant findings were reviewed at follow-up. The Newcombe-Wilson confidence interval method for testing equivalence of proportions was performed to determine if 16-detector multislice CT was statistically equivalent to skeletal scintigraphy in the detection of bone metastases.

Results: Skeletal scintigraphy detected bone metastases in 14/43 and CT in 13/43 patients. There were 7 discordances; 4 cases were positive on scintigraphy, but negative on CT. 3 cases were positive on CT and negative on scintigraphy. There was equivalence between scintigraphy and CT in detecting bone metastases within a $\pm 19\%$ equivalence limits.

Conclusions: Patients undergoing staging CT on a 16-detector multislice CT system may not always need additional skeletal scintigraphy to stage the bones.

B-466 11:15

Diagnostics of multiple myeloma using a 16-row-MSCT - low-dose whole body protocol

S. Buhmann, A. Baur-Melnyk, A. Wieser, M.F. Reiser; Munich/DE

Purpose: A comparison between a low-dose and a standard-dose protocol on a 16-row-multislice computed tomography scanner for the diagnosis of osteolytic bone lesions in patients suffering from multiple myeloma was the aim of our study.

Materials and Methods: In 30 patients with an attested diagnosis of multiple myeloma a whole-body MSCT (120 kV, 1.5 mm collimation, bone kernel) and consecutively a whole-body MR imaging (1.5 Tesla, Siemens Symphony, coronal/sagittal STIR and unenhanced T1-w SE sequences) serving as a gold standard was performed. The patients were divided into group A which was examined using 100 mAs compared to group B with 50 mAs. The images were reconstructed in 3 mm axial slices as well as the spine in 3 mm sagittal slices. The quality of MSCT images was evaluated by 2 experienced radiologists using a four-grade scaling reaching from 1=excellent to 4= not sufficient and the quantification was evaluated by ROI measurements (S/N+C/N ratio).

Results: The mean image noise value for groupA (12 HU) was significantly lower compared to groupB (24 HU) but the image quality for groupB was rated as excellent. The 100 mAs protocol resulted in an overall score of 1 while for the 50 mAs protocol a value of 1.3 was found. Mean radiation dose in groupA was 10 mSv, in groupB 5 mSv. All osteolytic lesions were identified using both modalities (MSCT, MRI).

Conclusion: Our low-dose whole-body MSCT reached similar dose values as X-rays of the skeleton and proved to be a valuable tool for the sensitive detection of osteolytic bone lesions in patients with multiple myeloma.

B-467 11:24

MR imaging of metastatic tumors in the spine: Are they different in signal intensity according to primary malignancy?

J. Koo, S. Hong, J.-Y. Choi, I. Lee, J. Lee, H. Kang, J.-A. Choi, Y. Koh; Seoul/KR

Purpose: The purpose of this study was to evaluate whether MR signal intensities of metastatic tumors are dependent on their primary malignancy.

Methods and Material: The T1-weighted images of 106 patients with spinal metastasis were reviewed retrospectively. Their primary lesions were hepatocellular carcinoma (HCC) ($n = 23$), lung cancer ($n = 31$), breast cancer ($n = 20$), GI malignancy ($n = 18$), and multiple myeloma ($n = 14$). The relative signal intensity of metastatic tumor was compared to adjacent intervertebral disc and spinal cord. We measured signal intensities of tumor, disc, and spinal cord and calculated signal ratios: tumor signal/disc signal (St/Sd) and tumor signal/cord signal (St/Sc).

Results: Both signal ratios St/Sd and St/Sc were significantly higher in HCC patients compared to patients with lung, breast, GI tract malignancies and multiple myeloma ($P = 0.00$, one-way ANOVA test). There was no signal difference amongst the other metastatic lesions. Six of 106 had hyperintense lesions compared with the spinal cord, all (100%) of which represented metastasis of HCC.

Conclusion: Metastatic tumors of HCC revealed significantly higher signal on T1-weighted MR images as compared to other metastatic tumors and multiple myeloma. Comparing with spinal cord signal, hyperintense lesions are highly suggestive of HCC metastasis.

B-468 11:33

Benign and malignant musculoskeletal masses: MR imaging differentiation with "maximum slope region"

K. Ishiyama, N. Tomura, R. Sashi, K. Okada, H. Nagasawa, K. Narita, J. Watarai; Akita/JP

Purpose: To evaluate the diagnostic potential of dynamic MR imaging in patients with musculoskeletal lesions.

Methods and Materials: Sixty-four patients with various musculoskeletal pathologies (37 benign lesions, 27 malignant lesions) were studied using dynamic MR imaging. Dynamic MR imaging was performed using a fast SPGR sequence (TR/TE = 90-200/4.2 ms). Dynamic images were transferred to an Advantage workstation 3.1 (GE) and analyzed using Functool. Functool can determine the location of strongest initial enhancement in the tumor (maximum slope region: MSR). MSR was categorized as peripheral, central, or absent. Progression of enhancement over time (time-signal intensity curve: TIC) was categorized as steep, steady or very low. Relationships between these parameters and histopathological findings were studied.

Results: For benign lesions, MSR was peripheral in 7 patients and central or absent in 30 patients. For malignant lesions, MSR was peripheral in 26 patients and central in 1 patient. For benign lesions, TIC was steep in 2 patients and steady or very low in 35 patients. For malignant lesions, TIC was steep in 19 patients and steady or very low in 8 patients. Differentiation between benign and malignant lesions was possible with 96.3% sensitivity, 83.8% specificity, 87.5% accuracy, 78.8% positive predictive value (PPV) and 96.8% negative predictive value (NPV) using MSR, and 70.3% sensitivity, 94.6% specificity, 84.4% accuracy, 90.4% PPV and 81.4% NPV using TIC.

Conclusion: Use of dynamic MR imaging to differentiate between benign and malignant lesions is feasible. MSR appears particularly useful as a new indicator of differential diagnoses.

B-469

withdrawn by authors

10:30 - 12:00

Room E2

Chest

SS 1004

CT and MR imaging of the pulmonary vessels and right heart

Moderators:

H. Hatabu; Boston, MA/US

G. Mostbeck; Vienna/AT

B-470 10:30

Velocity-encoded MR imaging with sensitivity encoding (SENSE):

Reproducibility and measuring agreement for quantitative assessment of pulmonary and systemic blood flow

M. Nogami¹, Y. Ohno¹, T. Higashino¹, D. Takenaka², M. Fujii¹, K. Sugimura¹;

¹Kobe/JP, ²Kasai/JP

Purpose: The purpose of our study was to assess the reproducibility and measuring agreement of velocity-MR imaging with SENSE and to determine the optimal scan parameters for quantitative assessment of pulmonary and systemic blood flow.

Materials and Methods: 10 healthy volunteers underwent velocity-MR imaging with SENSE and Doppler echocardiography (cardiac US). Flow rate in the pulmonary artery (Qp) and aorta (Qs) and flow ratio Qp/Qs in each subject were assessed by both velocity-MR imaging and cardiac US on two occasions. All velocity-MR imagings were performed by 2D Fourier method with SENSE technique at 1.5 T scanner. SENSE reduction factor was changed from 0 to 4, and R-R interval was divided into 10 to 40 frames. The total number of velocity-MR imaging sequence was 16. Differences between first and second velocity-MR imaging examinations were statistically compared. Qp/Qs of velocity-MR imaging obtained by determined optimal scan parameters and that of cardiac US were statistically compared. For assessment of the limits of agreement and reproducibility, Bland-Altman's analyses were adapted.

Results: The best coefficient of reproducibility for Qp/Qs (± 0.21) between first and second velocity-MR imaging examinations was obtained by SENSE reduction factor 4 and R-R interval divided into 30 frames. Qp/Qs between velocity-MR imaging and cardiac US had good correlation ($r = 0.81$, $p < 0.05$). The limits of

Scientific Sessions

agreement of Qp/Qs between velocity-MR imaging and cardiac US was less than ± 0.57 .

Conclusion: Velocity-encoded MR imaging with SENSE is useful for quantitative assessment of pulmonary and systemic blood flow. High SENSE reduction factor and high frame number of R-R interval provide good reproducibility, measuring agreement, and short breath-holding time.

B-471 10:39

Primary pulmonary hypertension: Quantitative analysis of regional pulmonary perfusion using 3D dynamic MR imaging

Y. Ohno¹, M. Nogami¹, T. Higashino¹, D. Takenaka², K. Murase³, H. Hatabu⁴, K. Sugimura¹; ¹Kobe/JP, ²Kasai/JP, ³Osaka/JP, ⁴Boston, MA/US

Purpose: To determine the capability of quantitative pulmonary perfusion parameters evaluated from 3D dynamic contrast-enhanced MR perfusion data for assessment of disease severity as indicated by pulmonary vascular resistance (PVR) in PPH patients.

Materials and Methods: 3D dynamic contrast-enhanced MR perfusion imaging (TR 2.7 ms/ TE 0.6 ms/ Flip angle 40°, 100-240 mm slab thickness, 10-12 partitions) was performed in 14 normal volunteers and nine consecutive PPH patients. All PPH patients underwent catheterization of the right side of the heart. From the signal intensity-time course curves, pulmonary blood flow (PBF), pulmonary blood volume (PBV) and mean transit time (MTT) maps were generated using deconvolution analysis, indicator dilution theories and the central volume principle on a pixel-by-pixel basis. From all pulmonary perfusion parameter maps, regional PBF, PBV and MTT of each lung field were determined in 6 spatially defined regions of interest (ROIs) in both lungs. PBF, PBV and MTT were statistically compared between normal and PPH subjects by Student's t-test. Pulmonary perfusion parameters with significant difference between the two groups were correlated with PVR.

Results: Regional PBF, PBV and MTT showed significant differences between normal and PPH subjects ($p < 0.0001$). PBF had excellent negative correlation with PVR ($r = -0.89$, $p = 0.002$). MTT had good positive correlation with PVR ($r = 0.78$, $p = 0.014$).

Conclusion: 3D dynamic contrast-enhanced MR imaging has the potential for assessment of disease severity as indicated by PVR in primary pulmonary hypertension patients.

B-472 10:48

Value of high spatial and high temporal resolution MR angiography for differentiation between primary and secondary pulmonary arterial hypertension

S. Ley¹, C. Fink¹, M. Borst¹, J. Zaporozhan¹, M. Puderbach¹, J. Meyer¹, E. Gruenig¹, K.-F. Kreitner², H.-U. Kauczor¹; ¹Heidelberg/DE, ²Mainz/DE

Objective: Differentiation between different forms of pulmonary hypertension (PH) is essential for correct disease management. Goal of this study was to elucidate the clinical impact of high spatial resolution MR angiography (SR-MRA) and high temporal resolution MRA (TR-MRA) to differentiate between patients with chronic thromboembolic PH (CTEPH) and primary PH (PPH).

Materials and Methods: 10 patients with PH and 5 healthy volunteers (V) were examined (1.5 T-MRI). 20 TR-MRA datasets ($3.5 \times 1.9 \times 4$ mm³, each TA 1.5 s) and SR-MRA ($1.2 \times 1.0 \times 1.6$ mm³, TA 23 s) were acquired after automatic injection of 0.1 mmol/kg BW of Gd-DTPA using parallel imaging. TR-MRA datasets were subtracted as angiography and perfusion images. Image evaluation comprised analysis of vascular pathologies on a segmental basis and detection of perfusion defects by 2 readers in consensus.

Results: Visualization of the pulmonary arteries down to a subsegmental (SR-MRA) and to a segmental (TR-MRA) level was possible. SR-MRA outperformed TR-MRA in direct visualization of intravascular changes. Patients with PPH predominantly showed a tortuous course while in CTEPH wall irregularities and abnormal proximal to distal tapering of the pulmonary arteries was found. Perfusion images showed a diffuse pattern in PPH and focal defects in CTEPH. TR-MRA (angiography and perfusion) and SR-MRA resulted in the same final diagnosis which was confirmed by further clinical evaluation.

Conclusion: Both MRA techniques allowed for differentiation between PPH and CTEPH. Therefore, TR-MRA can be used for clinical purpose, especially in dyspneic patients.

B-473 10:57

Contrast-enhanced 3D-MR imaging of lung perfusion in children with cystic fibrosis

M. Eichinger, M. Puderbach, C. Fink, S. Ley, J. Gahr, M. Wiebel, S. Tuengerthal, F.-M. Müller, H.-U. Kauczor; Heidelberg/DE

Purpose: Feasibility study of lung perfusion imaging using contrast-enhanced 3D-MR imaging. To assess the correlation of lung perfusion changes with structural abnormalities of the lung in children with cystic fibrosis (CF).

Methods and Materials: 11 CF-patients (9 female, 2 male; 12-18 years) were examined at 1.5 T (Magneton, Symphony). **Morphology:** HASTE sequence in coronal and transversal orientation (TR/TE/α: 600 ms/28 ms/180°, slice thickness 6 mm), breathhold 18 s. **Perfusion:** Time-resolved 3D-GRE pulse sequence (FLASH, TE/TR/α: 0.8/1.9 msec/40°), each using parallel imaging (GRAPPA, PAT factor 2). A total of 25 data sets were acquired after intravenous injection of 0.1 mmol/kg body weight of Gadodiamide at a rate of 3-5 ml/s. 198 lung segments were analysed by two radiologists in consensus and scored for morphological changes (1=normal, 2=mild, 3=severe) and perfusion changes (0=normal, 1=defect). Statistical analysis was performed by Mantel-Haenszel Chi square test.

Results: Segmental perfusion defects were observed in all patients and present in 80% of the upper, and 39% of the lower lobes. Normal lung parenchyma showed a homogenous perfusion in 86% of analysed lung segments ($p < 0.0001$), while in 97% severe morphological changes led to perfusion defects ($p < 0.0001$). Segments with mild morphological changes showed normal (53%) or impaired perfusion (47%).

Conclusion: In CF-patients, impaired ventilation causes perfusion defects due to hypoxic vasoconstriction. While the function is easy to judge in segments with normal parenchyma or severe changes, this is not possible in mildly damaged segments. Here, MR-lung perfusion measurement may help to better assess actual functional impairment.

B-474 11:06

Diagnosis of pulmonary arterial hypertension in patients with idiopathic fibrosing alveolitis

V.I. Osipenko, S.K. Ternovoy, A.I. Schekhter, I.A. Sokolina, E.N. Popova; Moscow/RU

Background: Idiopathic fibrosing alveolitis (IFA) is the most frequent variant of interstitial lung disease. Pulmonary hypertension (PH) in IFA is a strong predictor of patient prognosis, therefore its detection is of great clinical importance.

Purpose: Aim of the study was to assess the role of CT and high-resolution CT in early diagnosis of PH in IFA patients.

Materials and Methods: We studied 81 patient with IFA with spiral CT, high-resolution CT and linear filtration. Studies of pulmonary respiratory function and echocardiographic determination of pulmonary artery pressure were performed.

Results: Severe PH was found in patients with usual interstitial pneumonia (mean PAP 39 ± 2 Hg, area of interstitial fibrosis (S), measured on high-resolution CT scans = $45.6 \pm 3.6\%$). Moderate PH was typical for non-specific interstitial pneumonia (mean PAP 23.8 ± 8 Hg, S = 25.4 ± 3). In patients with desquamative interstitial pneumonia, PAP was normal (mean PAP 19 ± 9 Hg, S = 5.2 ± 2). We have found that PH in IFA patients develops when S > 27.3 ± 3.5 . For quantification of PH we have suggested pulmonary-thoracic ratio (PTI): transverse diameter of the chest/diameter of pulmonary trunk. Normal value of PTI was 11.7 ± 1.7 , in moderate PH its mean value was 8.1 ± 1.3 and in severe PH - 5.7 ± 2.1 .

Conclusion: Development of PH in IFA depends on the area of interstitial fibrosis. PTI helps to quantify severity of PH.

B-475 11:15

Pulmonary arteriovenous malformations: Could multi-detector row helical CT and angiographic reconstructions replace diagnostic angiography?

M. Memeo, A.A. Stabile Ianora, C. De Leo, P. Pignataro, M.C. Resta, A. Scardapane, G. Angelelli; Bari/IT

Purpose: To evaluate the possibilities of multi-detector row helical CT (MDCT) and angiographic reconstructions for diagnosis and characterization of pulmonary arteriovenous malformations (PAVMs) in comparison with pulmonary digital subtraction angiography (DSA).

Methods and Materials: 30 consecutive HHT patients with positive chest MDCT for pulmonary involvement were studied with DSA. MDCT was performed after injection of contrast medium and angiographic reconstructions were then obtained. DSA was performed with selective catheterization of pulmonary arteries and unilateral anteroposterior and oblique views; when necessary further views were

Scientific Sessions

added. The following were considered: 1. presence of PAVMs (nodular or tubular "serpiginous" lesions; afferent/efferent vessels identification; early visualization of efferent vessels); 2. number (isolated, multiple if < 15 or diffuse if ≥ 15); 3. location (intraparenchymal, subpleural); 4. aneurysmal dimensions (> or < 1 cm); 5. type (simple, complex); 6. afferent vessels diameter (≥ 3 mm).

Results: MDCT found 115 PAVMs. In 24/30 patients these were multiple and in 6 cases diffuse and bilateral. 80/115 PAVMs were subpleural; 68/80 had aneurysm < 1 cm and 73/80 were simple. Of the intraparenchymal PAVMs, 21/35 had aneurysm > 1 cm and 7/35 were complex. The afferent and efferent vessels were identified in all cases: afferent artery diameter was ≥ 3 mm in 27/115 cases. DSA identified 76 PAVMs: 29 intraparenchymal and 47 subpleural. For better identification of the aneurysmal sac and of afferent and efferent vessels, additional projections were required in 22/30 patients.

Conclusion: MDCT with angiographic reconstructions seems to be highly accurate for diagnosis of PAVMs and could be considered a valid alternative to angiography for their characterization.

B-476 11:24

Diagnosis of pulmonary arteriovenous malformations in patients with hereditary hemorrhagic telangiectasia: Multi-detector row helical CT versus contrast echocardiography. Preliminary results

M. Memeo, A.A. Stabile Ianora, C. De Leo, C. Memmola, C. Sabbà, A. Scardapane, G. Angelelli; Bari/IT

Purpose: To evaluate the possibilities of a non-invasive approach based on the association of contrast echocardiography (CEUS) and multi-detector row helical CT (MDCT) for diagnosis of pulmonary arteriovenous malformations (PAVMs) in patients with Hereditary Hemorrhagic Telangiectasia (HHT).

Methods and Material: 71 consecutive patients diagnosed with HHT according to clinical criteria were evaluated with CEUS and MDCT. CEUS was performed twice, first using as contrast medium a bolus of agitated saline (5 cc), then a bolus of agitated polygelin (3 cc). Chest MDCT was performed before and after contrast medium injection; multiplanar and angiographic reconstructions were then obtained. CEUS was considered positive if: 1. air bubbles were visible in the left heart within 3-6 cardiac cycles from their visualization in the right heart; 2. pulmonary veins were evident during contrast injection; 3. there was concordance between the two different contrast mediums. Contrast enhanced MDCT was considered positive in presence of: 1. nodular or tubular "serpiginous" lesions; 2. lesions with afferent/efferent vessels; 3. lesions enhancement; 4. early visualization of efferent veins.

Results: 19/71 patients were considered positive at CEUS while 22/71 patients had MDCT positive for PAVMs, therefore concordance was present in 19 cases (86%). In the 3 patients with negative CEUS, MDCT found some small fistulas with a diameter of less than 10 millimetres and a subpleural localization.

Conclusion: CEUS and MDCT seem to have good accuracy for detection of hemodynamically consistent PAVMs. CEUS/MDCT combination could be considered in the future for the screening of pulmonary involvement in HHT patients.

B-477 11:33

Multidetector-row CT of right ventricular function: Can it be integrated into a standard multislice CT angiogram of the chest?

A. Teisseire, D. Delhaye, J. Bruzzi, V. Delannoy-Deken, A. Duhamel, J. Rémy, M. Rémy-Jardin; Lille/FR

Purpose: To evaluate the possibility of assessing right ventricular function during a multidetector row CT angiographic examination of the chest.

Material and Methods: 44 consecutive patients known to have or suspected of having right ventricular dysfunction secondary to chest disorders underwent a 16-channel multidetector row CT angiographic examination of the chest with standard technique, completed by an ECG-gated examination of the heart.

Results: At the time of data acquisition: (a) the mean (\pm SD) heart rate of the study group was 81 (\pm 16.7) beats per minute (bpm) (range: 40 - 120); (b) the ECG tracing showed sinus rhythm in 27 patients (61%) and frequent extrasystolic beats in 17 patients (38%). The mean (\pm SD) attenuation value within the RV was 209.3 (\pm 42.4) HU (range: 126-312). Manual tracing of endocardial borders was possible for all patients. Assessment of the RV valvular borders mainly relied on the identification of the transitional zones between the interatrial and interventricular septa (n = 41; 93%) and between the RV myocardium and pulmonary trunk (n = 35; 79.5%) with no statistically significant difference according to the presence (n = 17) or absence (n = 27) of extrasystolic beats (p = 0.27; p = 0.78, respectively). All CT scans were graded as suitable for calculation of the RVEF.

Conclusion: Assessment of RV function during a multidetector row CT angiogram of the chest is feasible for all patients, including those with high heart rates and arrhythmia.

B-478 11:42

Multidetector-row CT of right ventricular function: Impact of the methodological approach in the determination of the right ventricular ejection fraction

A. Teisseire, D. Delhaye, J. Bruzzi, V. Delannoy-Deken, A. Duhamel, J. Rémy, M. Rémy-Jardin; Lille/FR

Purpose: To evaluate the impact of the methodological approach in the multidetector row CT estimation of the right ventricular ejection fraction (RVEF).

Material and Methods: In 33 patients, 16-channel multidetector row CT of the heart was performed after standard CT angiographic examination of the chest with determination of the RVEF by two readers. The reconstruction windows were determined (a) with the ECG (reader 1) or (b) on transverse test images obtained in 5% steps through the entire RR interval (reader 2). After manual segmentation of the ventricular cavity on diastolic and systolic short-axis reformations by each reader, the end diastolic and systolic RV volumes were calculated with determination of the RVEF. CT results were compared to those of equilibrium radionuclide ventriculography.

Results: An agreement between the two methods for selecting the reconstruction windows was observed in 51% of cases (n = 17) for the systole and 45% of cases (n = 15) for the diastole (variations ranging between 5% and 15% for discordant selections). No statistically significant difference was found in the determination of mean (\pm SD) end diastolic (reader 1: 172.33 \pm 46.43 mL vs reader 2: 172.33 \pm 46.43 mL; p = 0.29) and end systolic (reader 1: 85.12 \pm 31.13 mL vs reader 2: 80.59 \pm 30.22 mL; p = 0.23) volumes, suggesting the lack of operator-dependence in the manual contour drawing process. Good correlation was found between RVEFs obtained with CT by each reader and scintigraphy (p < .0001).

Conclusion: RVEF can be routinely assessed with ECG-gated multidetector row CT using commercially available analysis software.

B-479 11:51

Right ventricular function measured during ECG-gated MSCT of the whole chest: Intra-and inter-observer variability

E.E.J.G. Coche¹, R. de Crombrugge¹, A. Vlassenbroek²; ¹Brussels/BE, ²Best/NL

Purpose: To test the reproducibility of measurements to assess right ventricular function during ECG-gated chest CT.

Methods and Materials: Eighteen patients with suspected acute pulmonary embolism were enrolled in this prospective study. Multislice CT was performed on 16-slice CT (MX IDT, Philips Medical Systems, Cleveland, OH) with retrospective ECG-gating. Acquisition was performed from the lung apices down to the diaphragm with the following parameters: 16 x 1.5 mm, 420-msec gantry rotation time, 120 kV, 150 mAs. 120 mL of contrast media were injected at a rate of 3 mL/sec. Contiguous thin slices (2 mm) were reconstructed every 12.5% of the R-R interval and reviewed on a dedicated cardiac workstation. Time of CT acquisition and CTDI were systematically recorded. End-diastolic, end-systolic volumes of RV were measured by two independent observers from a dedicated three-dimensional software. Ejection fractions of the RV was calculated by using the Simpson's rule. Measurements were repeated twice by one of the 2 observers. Intra and interobserver variability of measurements were estimated by using the intra-class correlation coefficients.

Results: Acquisition time to cover the entire chest with ECG-gating was 18.7 sec (13.2-25.3 sec). CTDI was 10.13 mGy. The intraclass correlation of measurements for the two observers for RV end-diastolic volumes, end-systolic volumes and ejection fraction was 0.97. The intraclass correlation for one observer was 0.98, 0.98 and 0.94 for the same parameters.

Conclusion: Measurements of RV volumes and ejection fraction obtained during ECG-gated CT are highly reproducible.

Scientific Sessions

10:30 - 12:00

Room F2

Abdominal Viscera

SS 1001

Pancreas: MR imaging evaluation of pancreatic duct and pancreatic cystic lesions

Moderators:

T. Bader; Vienna/AT

B.I. Choi; Seoul/KR

B-480

withdrawn by author

B-481 10:30

Correlation of secretin MRCP derived quantification of exocrine function with faecal elastase 1 and urinary pancreoelastase tests

A.R. Gillams, S. Pereira, W. Lees; London/UK

Purpose: Secretin MRCP (sMRCP) provides a non-invasive, direct technique for quantifying pancreatic exocrine function. Our aim was to correlate sMRCP derived pancreatico-duodenal flow rates with indirect non-invasive tests of pancreatic function i.e. faecal elastase 1 (FE1) and/or urinary pancreoelastase (PL), in a group of patients with suspected or known chronic pancreatitis.

Methods and Materials: Standard, multi-slice, single shot fast spin echo sequences were obtained before and at 2 minute intervals following 0.1 ml/kg IV Secretin (Sanochemia, Germany). Change in fluid volume = mean signal intensity/ voxel x volume of the region of interest: Signal intensity in a 100% water voxel. Volume was plotted against time and the flow rate derived from the gradient, with a rate of < 4.5 ml/min being defined as abnormal. FE1 ± PL tests were performed in all patients.

Results: There were 34 patients, 21 male, median age 52 years (34-79). In 27 patients there was complete concordance between MR flow rate and FE1/PL, with 16 patients having normal values (mean flow rate 7.7 ± 2.5) and 11 abnormal (3.5 ± 0.8 ; ($p = 0.001$ by Students t test). Two patients had normal FE1 and abnormal flow rates, 5 had abnormal FE1 but normal flow rates. The exact Fisher test was highly significant ($p = 0.001$).

Conclusion: There was very good correlation between sMRCP flow rates and standard, non-invasive, indirect pancreatic function tests. sMRCP provides ductal, parenchymal and functional information in a single test.

B-482 10:39

Evaluation of pancreatic duct abnormalities using secretin-stimulated MR pancreatography

F. Donati, P. Boraschi, R. Gigoni, A. Auci, M.C. Cossu, F. Falaschi; Pisa/IT

Purpose: To determine the usefulness of Secretin-stimulated MR Pancreatography (SSMRP) for evaluating pancreatic duct abnormalities.

Method and Materials: A series of fifty-six patients with suspected pancreatic duct abnormalities at US and/or CT underwent MR imaging at 1.5 T (Signa Infinity, GE Healthcare). In order to suppress the signal intensity of overlapping fluid-containing organs, a super-paramagnetic suspension (Lumirem®, Guerbet) was orally administered. After the acquisition of axial T1W and T2W sequences, MR pancreatography was performed using a coronal breath-hold, thick-slab (40-60 mm), single-shot T2W fast spin-echo sequence. After the intravenous administration of Secretin (Secretlux®, Sanochemia; 1 cU/kg body/weight), single-slice image acquisition was repeated every 30 seconds up to 15 minutes. The presence of pancreatic abnormalities, the changes of the pancreatic ductal system and the filling of duodenum after Secretin-stimulation were evaluated by two observers in conference. Imaging results were correlated with ERCP, surgery, and/or follow-up.

Results: In patients with pancreatic cystic lesions ($n = 23$), SSMRP allowed the correct diagnosis of 14 cases of intraductal papillary mucinous tumor showing the communication with the pancreatic duct. In all cases of chronic pancreatitis ($n = 11$), SSMRP improved the identification of ductal stenoses and demonstrated a reduced pancreatic exocrine reserve. Twelve of fourteen congenital abnormalities were identified as complete pancreas divisum on SSMRP. Furthermore, in two patients with post-traumatic pseudocyst, SSMRP revealed the direct continuity between the lesion and the main pancreatic duct. No abnormality was observed in six cases.

Conclusion: Improvement in image quality after Secretin-stimulation increases the diagnostic value of MR pancreatography for evaluating pancreatic duct abnormalities.

B-483 10:48

Exocrine function of pancreatic transplants: Evaluation with dynamic MR pancreatography after secretin administration

P. Boraschi, F. Donati, R. Gigoni, F. Odoguardi, E. Neri, U. Boggi, F. Falaschi, C. Bartolozzi; Pisa/IT

Purpose: To evaluate the exocrine function of pancreatic transplants using dynamic MR pancreatography after Secretin administration.

Materials and Methods: Thirteen asymptomatic patients previously submitted to isolated pancreas ($n = 6$) or combined kidney-pancreas ($n = 7$) transplantation with enteric-portal pancreatic drainage underwent MR imaging at 1.5 T (Signa Infinity; GE Healthcare) using a phased-array coil. After the acquisition of axial and coronal T1W and T2W sequences, dynamic MR pancreatography was performed using a coronal breath-hold, thick-slab (40-60 mm), single-shot T2W fast spin-echo sequence. After the intravenous administration of Secretin (Secretlux®, Sanochemia; 1 cU/kg body/weight), single-slice image acquisition was repeated every 30 seconds up to 15 minutes. Two observers in conference estimated the calibre changes of the pancreatic ductal system and the filling of the donor duodenum on the basis of pancreatic secretion after Secretin-stimulation, also evaluated by using a mean signal intensity/time histogram in a chosen region of interest (ROI) including the transplanted pancreas and the connected small bowel.

Results: All patients tolerated the examination well and no side effects were reported after Secretin administration. In 12 out of 13 cases a significant increase (more than 1 mm) of the mean pancreatic duct was observed after Secretin-stimulation; in all patients a noticeable filling of the duodenum was demonstrated during dynamic MR pancreatography both on qualitative and quantitative analysis.

Conclusions: Dynamic MR imaging after Secretin administration allows non-invasive evaluation of exocrine function of the pancreatic transplants and could be used to differentiate patients with graft rejection from those with normal graft function.

B-484 10:57

Evaluation of the natural history of pancreatic branch duct IPMTs by follow-up with cross-sectional imaging

A. Guarise¹, M. Ferrari¹, S. Turchetta¹, L. Romano¹, R. Salvia², ¹Negrar/IT, ²Verona/IT

Purpose: To clarify the natural history of branch duct type IPMT by evaluating serial changes in the MRCP and CT findings.

Methods and Materials: Fifty-two Patients with a diagnosis of branch duct IPMT obtained with ERCP and/or MRCP were followed-up over a period of more than 12 months (range 12-108, mean 30.6). All imaging data were retrospectively reviewed by two Radiologists in order to evaluate serial changes in size and structure. The maximum diameter of the cystic lesion, the presence of associated MPD dilatation and filling defects were evaluated in order to establish the correlation between these findings and changes in size. Statistical analysis was performed using the Fisher exact probability test.

Results: Growth in size on follow-up MRCP was observed only in 7 cases, the remainder demonstrated no changes or size reduction in two cases. There was a significant correlation between enlargement of the cystic lesion and the following features: size more than 3 cm and presence of mural nodules. Only 2/37 cystic lesions less than 3 cm in size, without papillary proliferations and MPD dilatation increased in size. No cystic lesion showed changes in morphology and structure.

Conclusion: Branch duct IPMTs smaller than 3 cm, without filling defects and MPD dilatation can be monitored with MRCP thus sparing operation.

B-485 11:06

The usefulness of MR pancreatography in the evaluation of cystic lesions and their relationship to the pancreatic ductal system

F. Donati, P. Boraschi, R. Gigoni, A. Auci, F. Falaschi; Pisa/IT

Purpose: To determine the usefulness of MR Pancreatography (MRP) in the evaluation of cystic pancreatic lesions and their relationship to the pancreatic ductal system.

Method and Materials: Eighty-two patients with radiological diagnosis of cystic pancreatic lesions underwent MR imaging at 1.5 T device (Signa Infinity, GE Healthcare). After acquisition of axial T1W and T2W sequences, MRP was obtained using coronal, thin and thick-slab, single-shot fast spin-echo (SSFSE) T2W sequence. Secretin-stimulated imaging was performed in 25/82 patients using coronal breath-hold, thick-slab, SSFSE T2W sequence, repeated every 30 seconds up to 15 minutes after intravenous administration of Secretin (Secretlux®, Sanochemia; 1 cU/kg body/weight). MR examinations were evaluated in



Scientific Sessions

conference by two observers to identify pancreatic abnormalities and their relationship to the ductal system.

Results: The cystic lesions were classified into two types: a) Lesions related to the pancreatic ductal system (42 patients). On the basis of presence of septa and filling defects in the lesion, a preliminary diagnosis of intraductal papillary mucinous tumor was made in 40/42 cases, in 15 of them histological confirmation was obtained. In two patients with post-traumatic pseudocyst MRP revealed the continuity between lesion and main pancreatic duct. b) Lesions not related to the pancreatic ductal system (40 patients); serous cystadenoma ($n = 6$), mucinous cystadenocarcinoma ($n = 2$), cystic neuroendocrine tumor ($n = 1$), all confirmed at surgery. The remaining indeterminate (< 2 cm) cystic lesions ($n = 28$) and pancreatic pseudocysts ($n = 3$) underwent imaging follow-up.

Conclusion: Our study highlights the usefulness of MRP particularly after Secretin-stimulation to detect cystic pancreatic lesions and establish their relationship to the ductal system.

B-486 11:15

Assessment with secretin-enhanced MR hydrometry of pancreatic exocrine function in patients with obstructive chronic pancreatitis before and after treatment

M.A. Bali, A. Sztantics, M. Delhaye, T. Metens, J. Deviere, C. Matos;
Brussels/BE

Purpose: To evaluate with secretin enhanced MR hydrometry (S-MRH) patients with obstructive chronic pancreatitis, the pancreatic exocrine function before and after main pancreatic duct (MPD) drainage procedures, by quantifying pancreatic exocrine flow output and total excreted volume.

Methods and Materials: Eighteen consecutive patients with obstructive chronic pancreatitis and no previous endoscopic or surgical treatment underwent S-MRH before and 24 hours after treatment. The treatment consisted of extracorporeal shock-wave lithotripsy followed by endoscopic decompression procedures. S-MRH consisted of a dynamic multislice TSE, heavily T2-weighted sequence acquired in the coronal plane (acquisition time 12 sec/dynamic). 30 dynamic acquisitions were performed after secretin administration followed by 6 dynamic acquisitions after ingestion of known volumes of water, realized for calibration purpose. To calculate pancreatic exocrine output and total excreted volume a linear regression was computed between MR calculated volumes and time. MPD diameter was measured before and after treatment. Two readers performed all of the evaluations independently.

Results: In all but two patients a statistically significant improvement of pancreatic flow output and of the total excreted volume was observed after treatment ($P < .05$). In the two patients who presented with post-procedural acute pancreatitis, this was responsible for the reduced exocrine function. In all patients the MPD diameter was reduced after treatment ($P < .05$) but the kinetics during secretin stimulation did not change ($P > .05$). The inter-observer variability was good ($R^2 = 0.9$).

Conclusion: Pancreatic exocrine function improved significantly after MPD drainage procedures. Secretin-enhanced MR hydrometry is a feasible, non invasive technique that allows monitoring of exocrine pancreatic reserve after endoscopic treatment in chronic pancreatitis.

B-487 11:24

MR imaging assisted visualisation of flow changes in the pancreatic duct

J.C. Hellund¹, T. Storås¹, K. Gjesdal¹, J. Geitung²; ¹Oslo/NO, ²Bergen/NO

Purpose: To see if an MR imaging sequence could be used to visualize flow changes in the pancreatic (PD) and common bile (CBD) duct. Increased flow should be seen as the loss of viewable ducts on the flow sensitized MRCP images.

Methods and Materials: An in-house developed, flow-sensitive, single-shot turbo spin-echo (SS-TSE) MR imaging sequence was used (Ref: Eur Radiol. 2004 Sep; 14(9):1692-7). Flow directions along the y and z-axis were evaluated. Nine healthy volunteers were examined on a 1.5 T scanner. Images were obtained before and after the administration of first Glucagon (to reduce artifacts from bowel movement) and secondly Secretin (to increase fluid flow in the ducts). B-factors (s/m^2) of 0, 6 and 12, were used. A total of 845 images were obtained and examined.

Results: All images showed both the PD and CBD on B-factor = 0. The CBD showed no significant differences in visualisation either in flow directions or drugs given on $B = 6$ or $B = 12$. The PD had, after administration of intravenous Secretin, a significantly lower rate of identification on both B-factors and flow directions (Y-axis and $b = 6$: 57% vs. 31%; $b = 12$: 46% vs. 23%. Z-axis and $b = 6$: 55% vs. 24%; $b = 12$: 52% vs. 17%).

Conclusion: The method made it possible to visualise flow changes in the PD before and after the administration of Secretin.

B-488 11:33

Macrocytic neoplasms of the pancreas: Differentiation of serous oligocystic adenoma from mucinous cystadenoma and intraductal papillary mucin-producing tumor with CT

S. Kim; Seoul/KR

Purpose: To describe typical CT findings of serous oligocystic adenoma (SOA) of the pancreas and to find out differential points from other macrocytic neoplasms such as mucinous cystadenoma and intraductal papillary mucin-producing tumor of branch type (IPMT).

Materials and Methods: A total of 41 patients with histologically confirmed macrocytic neoplasms of the pancreas were enrolled in this study (SOA:10; mucinous cystadenoma:13; branch type IPMT:18). Two experienced radiologists reviewed CT findings of those patients in consensus. The location, longest dimension, shape, presence of mural nodule, presence of wall calcification and extent and degree of main pancreatic duct (MPD) dilatation were analyzed. The shapes were categorized into 7 groups as below: multicystic; lobulated contour with/without internal septation; smooth contour with/without internal septation; pleomorphic cystic; clubbed finger-like cystic. Comparative studies of three types of lesions were performed using Fisher's exact test and Mann-Whitney U test.

Results: There was a significant difference in the shape of the lesion between SOA and the other macrocytic neoplasms such as mucinous cystadenoma ($P < 0.05$) IPMT ($P < 0.05$). SOA showed a shape of multicystic or lobulated contour while mucinous cystadenoma showed a shape of smooth contour and IPMT showed either pleomorphic cystic or clubbed finger-like cystic. Upstream MPD dilatation was predominantly observed in SOA compared to the other two diseases while diffuse MPD dilation was noted in IPMT ($p = 0.025$).

Conclusion: SOA of the pancreas has typical CT findings differing from other cystic tumors. It appears as a multicystic or lobulated cystic lesion with septation and with up-stream MPD dilatation from lesion.

B-489 11:42



CT criteria for predicting survival of patients with potentially resectable pancreatic carcinoma

S.S.K.S. Phoa, E. Tilleman, O. van Delden, P. Bossuyt, D.J. Gouma, J.S. Laméris; Amsterdam/NL

Purpose: To establish the prognostic value of CT data obtained from a pre-operative CT in patients with potentially resectable pancreatic carcinoma.

Material and Methods: In 71 consecutive patients with pancreatic head carcinoma prognostic CT criteria were scored (e.g. tumor size, peripancreatic infiltration, grade of vascular encasement) as well as criteria for irresectability (> 180 degrees vascular involvement, tumor concavity towards a vessel and presence of peripancreatic infiltration). All patients underwent surgical exploration. CT criteria were correlated with surgical and histopathological findings. Prognostic factors were analysed in single and multi-factor analysis, separately for resected and unresected tumors.

Results: A resection was performed in 41/71 patient (in 24 radical). The sensitivity, specificity and positive predictive value of CT with respect to surgical irresectability were 0.67, 0.63, and 0.57 respectively. With respect to a nonradical resection these were 0.62, 0.75 and 0.83 respectively. The median survival was 21 months for resected tumors and 9.7 months for unresected tumors. For resected tumors survival was poor if the tumor diameter was > 3 cm (relative hazard of 3.8) and if signs of local unresectability were seen at CT. Median survival of resected tumors < 2 cm was nearly 20 months. Encasement of the superior mesenteric artery had a poor prognostic value for all tumors.

Conclusion: CT signs of local unresectability and a tumor diameter > 3 cm predict a poor survival for resected tumors.

Scientific Sessions

10:30 - 12:00

Room G

Genitourinary

SS 1007

MR imaging of the prostate

Moderators:

H. Hricak; New York, NY/US
G.M. Villeirs; Gent/BE

B-490 10:30

Staging and localizing prostate cancer using 3 T endorectal coil MR imaging

J.J. Fütterer, T.W.J. Scheenen, S.W.T.P. Heijmink,
C.A. Hulsbergen van der Kaa, F. Witjes, J.O. Barentsz; Nijmegen/NL

Purpose: To assess endorectal MR staging and localizing performance in prostate cancer at 3 T and to explore interobserver variability.

Methods and Materials: 3 T endorectal MR imaging was performed in 32 consecutive patients with biopsy proven prostate cancer, prior to radical prostatectomy. High resolution endorectal T2-weighted fast spin echo images (in plane resolution 0.18 x 0.18-mm) of the whole prostate in three planes were obtained. MR-images were prospectively evaluated by two experienced and one inexperienced radiologists with regard to local extent, prostate cancer localization and interobserver variability. Results were correlated with whole mount section histopathology.

Results: The local staging accuracy, sensitivity and specificity were respectively 94% (30/32), 88% (7/8) and 96% (23/24) for the experienced radiologists, and for the inexperienced radiologist 82% (26/32), 50% (4/8) and 92% (22/24). The localization accuracy was 79% for the experienced reader and for the inexperienced reader 64%, respectively. The interobserver variability between the readers showed substantial agreement ($\kappa = 0.68 - 0.79$) in staging and localizing prostate cancer. Two cases included minimal capsular invasion which were detected by both experienced radiologists.

Conclusion: Endorectal coil MR imaging at 3 T results in high staging and localization accuracies with substantial observer agreement ($\kappa = 0.68 - 0.79$). Minimal capsular invasion was detected. This may suggest a role in prostate staging at high fields.

B-491 10:39

MR imaging of prostate cancer: Comparison of imaging at 1.5 and 3 Tesla

D. Beyersdorff, C. Taymoorian, D. Schnorr, R. Felix, B. Hamm, H. Bruhn;
Berlin/DE

Purpose: To prospectively compare MR imaging of the prostate at 3 Tesla with MR imaging at 1.5 Tesla.

Materials and Methods: Twenty-four patients with histologically proven prostate cancer, PSA level of 2 to 14 ng/ml, underwent MR imaging comparing a phased-array body/endorectal coil at 1.5 Tesla with the body phased-array coil only at 3 Tesla. T2-weighted imaging was performed at both field strengths using axial and coronal TSE-sequences. Preoperative staging was done using all images acquired at 1.5-T and at 3-T. In a second, retrospective session, the images were evaluated separately for the two field strengths without knowledge of the histologic findings. The images were evaluated for image quality, delineation of zonal anatomy and prostate capsule, tumor detection, and presence of artifacts. MR imaging findings were compared with histologic results of prostatectomy specimens in 22 of the 24 patients. Wilcoxon test was applied.

Results: In the prospective analysis, the accuracy of staging was 73%. The retrospective analysis showed a better image quality ($p < 0.001$), a better delineation of zonal anatomy ($p = 0.003$), a better delineation of the prostate capsule ($p = 0.007$), and an improved tumor detection ($p = 0.012$) for endorectal MR imaging at 1.5-T. While there were no coil misplacements, also the incidence of artifacts was lower at 1.5-T ($p = 0.002$).

Conclusion: Endorectal coils will continue to be the gold standard of prostate MR imaging in future, most likely also at 3-T.

B-492 10:48



Comparison of 3 T body-coil MR imaging and endorectal-coil 1.5 MR imaging in evaluating prostate cancer

P. Torricelli, F. Cinquantini, G. Ligabue, F. Fiocchi, R. Romagnoli; Modena/IT

Purpose: To compare the results of body-coil 3 T MR imaging with endorectal-coil 1.5 T MR imaging in evaluating prostate cancer.

Methods and Materials: From November 2003 and August 2004, 30 consecutive patients, affected with pathological proven prostate cancer have been evaluated, in the same week, by both endorectal-coil 1.5 T MR imaging and cardiac-coil 3 T MR imaging. Two radiologists basing upon subjective criteria, independently scored the image quality focusing on the following items: cancer tissue conspicuity, capsule involvement, seminal vesicles involvement, neuro-vascular bundle involvement and apex involvement. The image-quality score ranged from 1 to 5 (1: invisible, 2: poorly visible, 3: fairly visible, 4: well visible with some artifacts, 5: well visible without artifacts). In 13/30 patients, who have undergone radical prostatectomy, the staging diagnostic accuracy was compared. Interobserver agreement (k value) and correlability in image quality (Spearman index) were calculated.

Results: The interobserver agreement was always good (k value higher than 0.7) and the image quality score was well correlateable for tumor conspicuity, capsule and apex involvement, (Spearman index higher than 0.3) while it was poorly correlateable for seminal vesicles and neuro-vascular bundle involvement (Spearman index lower than 0.3). The staging accuracy was 89% for endorectal-coil 1.5 T MR imaging and 87% for cardiac-coil 3 T MR imaging (the difference was not statistically significant).

Conclusions: The image quality of endorectal-coil 1.5 T MR imaging is fairly better than cardiac-coil 3 T MR imaging but in cancer staging cardiac-coil 3 T MR imaging can give almost the same diagnostic results of endorectal-coil 1.5 T MR imaging without any discomfort for the patients.

B-493 10:57

Differentiating prostate cancer from healthy prostatic tissue with dynamic contrast-enhanced MR imaging with an endorectal coil at 3 T

S.W.T.P. Heijmink, J.J. Fütterer, H.J. Huisman, T.W. Scheenen, C.A. Hulsbergen van der Kaa, J.A. Witjes, J.G. Blickman, J.O. Barentsz; Nijmegen/NL

Purpose: To evaluate prostate endorectal dynamic contrast enhanced MR imaging (DCE-MRI) at 3 Tesla (3 T) and determine characteristics that distinguish prostate cancer (PCA) from healthy prostatic tissue in PCA patients.

Materials and Methods: Ten patients with biopsy-proven PCA (mean age: 62 years, mean PSA level: 10.0 ng/ml) underwent 3 T endorectal DCE-MRI with subsequent radical prostatectomy. After administration of 15 ml of Gadolinium, T1-weighted 3D image volumes were acquired with a time resolution of 1 second (3D-turboflash, TR 34 ms, flip angle 10°, TE 1.6 ms) for two minutes. DCE-MRI analysis was performed with software developed at the institution. Whole-mount section pathology was used to determine the healthy and PCA regions of interest on MR images. The mean pharmacokinetic parameters of the regions were calculated. The parameters were: the start of enhancement, peak-enhancement, washout, vessel permeability and extracellular volume. PCA $< 0.5 \text{ cm}^3$ were considered beyond the limits of reliable correlation. For statistical analysis the paired Student t-test, ANOVA and ROC analysis were used.

Results: Twenty PCA foci (median Gleason score: 6) and 20 healthy segments were analyzed. The washout parameter (the disappearance of the contrast agent from PCA/healthy prostatic tissue at the end of the dynamic series) was a statistically significant predictor of PCA ($p < 0.05$) with a substantial area under the ROC curve (area under curve: 0.74). Other parameters were not statistically significant PCA predictors.

Conclusions: These preliminary results demonstrate that 3 T endorectal DCE-MRI shows promising results in distinguishing PCA from healthy prostatic tissue. The washout of contrast agent was a statistically significant predictor of PCA.

B-494 11:06

MR imaging and ^1H - MR spectroscopic imaging in the evaluation of prostate cancer

G. Manenti, E. Squillaci, M. Di Roma, S. Mancino, G. Simonetti; Rome/IT

Purpose: To determinate the accuracy of magnetic resonance (MR) imaging improved with proton magnetic resonance (MR) spectroscopic imaging in the detection and localization of human prostate cancer.

Materials and Methods: MR imaging and MR spectroscopic imaging examinations were performed in 38 patients with elevated prostate-specific antigen (PSA) levels or suspicious transrectal ultrasonography (TRUS). All patients underwent digital rectal examination (DRE) and the imaging results were proved with histopathologic examination findings. This population was examined with morphological sequences T2- weighted and T2 SPIR MR imaging at 1.5 T and PRESS spectroscopic sequence with C1-pelvic phased array. In the spectral data analysis, the ratios of choline (Cho) and creatine/phosphocreatine (Cr) to citrate (Cit) [Cho + Cr]/Cr, were compared in suspicious and control tissues, and the

Scientific Sessions

values obtained greater than 3 SDs were considered diagnostic for prostate cancer; conversely values at less than 2 SDs excluded the presence of cancer.

Results: At prospective analysis, MR imaging sensitivity and specificity, respectively, were 89% and 60%. The 3D MR spectroscopic imaging diagnosis of definite cancer had significantly higher sensitivity (97%) but lower specificity (83%).

Conclusion: The addition of proton magnetic resonance (MR) spectroscopic imaging to MR imaging provides better evaluation of prostatic pathologies and detection of prostate cancer than MR imaging alone.

B-495 11:15 ♂

Rapid therapeutic response from castration in prostate cancer demonstrated using ^1H -HRMAS NMR spectroscopy

J.R. Jones, K. Stenman, J. Hauksson, A. Bergh, A. Rydh; Umeå/SE

Purpose: To assess the value of high resolution magic angle spinning nuclear magnetic resonance spectroscopy (HRMAS NMR) in diagnosis of metabolic changes characteristic for prostate cancer.

Methods and Materials: Tumor specimens were achieved from highly differentiated Dunning R3327PAP experimental prostate tumors in rats. Samples were taken from four untreated tumors, and four tumors one, four and seven days each after castration. HRMAS NMR spectroscopy was performed on a NMR spectrometer operating at a ^1H NMR frequency of 500.13 MHz (11.7 T magnet). Regional integrals covering the chemical shift ranges corresponding to total choline, creatine and citrate were calculated.

Results: The characteristic high ratio of total choline to citrate in PCa was reduced already 1 day after castration. Total choline to citrate ratio for samples from castrated animals with induced PCa is highly variable, but tends overall to be significantly lower than for untreated animals, even as early as one day after castration.

Conclusion: HRMAS NMR spectroscopy can demonstrate early metabolic changes in PCa following endocrine therapy. These results could eventually be transferred to clinical practice using MR spectroscopy. Information about the effectiveness of castration treatment could thereby be achieved already within days from induction of endocrine therapy compared to serum prostate specific antigen testing, which demands up to three months waiting time.

B-496 11:24

Choline PET (-CT) and combined MR imaging+MR spectroscopy in the detection of intra-prostatic and pelvic lesions of prostate cancer

M.K. Scherr, B. Scher, M. Seitz, M.F. Reiser, U.G. Müller-Lisse; Munich/DE

Purpose: To determine if PET or PET-CT with C11-doted choline and combined MR imaging+MR spectroscopy (MRS) differ in the detection of intra-prostatic and pelvic lesions in patients with clinical suspicion of prostate cancer (PCA).

Material and Methods: Patients with clinical suspicion of PCA and previously negative biopsy ($n = 11$) or of recurrent PCA after radical prostatectomy/radiation therapy ($n = 4$), or biopsy-proven PCA ($n = 4$) underwent both PET ($n = 10$) or PET-CT ($n = 9$) with 800 MBq of C11-doted choline and combined MR imaging+MRS of the prostate within 1 week of each other. PET/PET-CT (skull base to proximal thigh) was analysed by two nuclear medicine physicians. MR imaging (T1ax, T2 ax, cor, sag) and 3D-SE-MRS of the prostate and pelvis was evaluated independently by two radiologists. Results were analysed as being positive or negative for PCA, PCA localization, and pelvic metastasis and validated by histopathology ($n = 15$) or follow-up imaging ($n = 4$).

Results: Sensitivity and specificity for PCA detection were 10/11 (91%) and 5/8 (63%) for PET/PET-CT, and 10/11 (91%) and 6/8 (67%) for MR imaging+MRS, respectively. MR imaging+MRS showed better per sextant localization of intra-prostatic PCA. All pelvic metastases (lymph nodes $n = 2$, osseous $n = 2$) were detected by both modalities, but PET/PET-CT provided additional metabolic information.

Conclusions: Results imply similarly high sensitivity for prostate cancer of PET/PET-CT with C11-doted choline and MR imaging+MRS. Both demonstrated pelvic metastasis. MR imaging+MRS was superior for intra-prostatic PCA localization, which may guide further biopsy in patients with previously negative biopsy.

B-497 11:33

Early detection of local prostate cancer recurrences after radiation therapy by means of endorectal dynamic contrast-enhanced MR imaging and 3D ^1H MR spectroscopy with biopsy confirmation

S.W.T.P. Heijmink, J.J. Fütterer, E. van Lin, T.W. Scheenen, C.A. Hulsbergen van der Kaa, J.A. Witjes, J.G. Blickman, J.O. Barentsz; Nijmegen/NL

Purpose: To determine the feasibility of early local prostate cancer (PCA) recurrence detection after radiation therapy using dynamic contrast-enhanced (DCE) endorectal MR imaging and ^1H MR spectroscopy followed by ultrasound-guided biopsy.

Methods and Materials: A cohort of 51 PCA patients that had undergone endorectal MR imaging prior to 3D conformal radiation therapy was followed up with half-yearly prostate-specific antigen (PSA) tests. Of this cohort, seven patients had three consecutive PSA rises (the ASTRO definition of biochemical recurrence). The mean PSA, PSA doubling time and PSA velocity were 3.4 ng/ml, 7.7 months and 3.1 ng/ml/year, respectively. Patients underwent MR imaging with an endorectal-phased array coil. T2-weighted FSE images in three directions, 3D ^1H MR spectroscopy (MRS) and T1-weighted postcontrast images were obtained. Three readers independently analyzed all MR images to determine recurrence localization and in consensus determined the spots for biopsy. Consequently, patients underwent ultrasound-guided biopsy. A sextant biopsy plus two transition zone cores were taken. Additionally, maximally four biopsies were taken based on MR/MRS findings.

Results: Two patients refused biopsy. A total of 40 sextant biopsy and 9 MR-guided biopsy cores were taken. On a core-by-core basis, the standard and MR/MRS-guided biopsies had positive biopsy rates of 23% (9/40) and 22% (2/9), respectively.

Conclusion: Using endorectal DCE MR and MRS imaging can importantly reduce the number of biopsy cores necessary with an equal detection rate for detecting early PCA local recurrence. MR-based biopsies needed only one-fifth (9/40) the number of cores that the standard biopsy used.

B-498 11:42

Retained seminal vesicles following prostatectomy: MR features

T. Sella¹, L.H. Schwartz², H. Hricak²; ¹Jerusalem/IL, ²New York, NY/US

Purpose: Seminal vesicle remnants following radical prostatectomy (RP) may present potential pitfalls in the interpretation of pelvic MR imaging. The purpose of this study is to define the frequency and the MR features of SV remnants, in patients following RP.

Materials and Methods: This retrospective review examined pelvic MR imagings of 126 consecutive post-RP patients between the years 1999–2003. The surgeon who performed RP, time interval between surgery and MR imaging, and presence of SV remnants on MR images were recorded. SV remnants were characterized for location, size, and signal intensity. Descriptive statistics were used for analysis.

Results: SV remnants were found in 72/126 patients (57%). These were bilateral in 57(79%) and unilateral in 15(21%). Complete SVs were seen in 6 patients (8%), partial SVs in 7(10%), and only tips of SVs in 59(82%). Overall, a total of 129 SV remnants were found in 72 patients. Fibrotic remnants were seen in 117/129(91%). 95/126 patients (75%) had surgery performed at a single institution, by 11 different surgeons. Average time from surgery to MR imaging was 39.5 months (range 2–156); 36.8 months (range 2–122; $n = 66$) for patients with fibrotic SV remnants, 41.8 months (range 6–84; $n = 8$) when SV remnants were intact.

Conclusion: Retained SV remnants are a common finding following RP. The majority are fibrosed distal tips. SV remnants must be recognized to avoid misinterpretation as local recurrences. We suggest reporting this finding as part of the standard report of a post-RP pelvic MR imaging, for the benefit of clinicians and radiologists involved in the patient's treatment.

B-499

withdrawn by author

Scientific Sessions

10:30 - 12:00

Room H

Interventional Radiology

SS 1009a

Hepatic interventions

Moderators:

R.D. García-Mónaco; Buenos Aires/AR
D.A. Kelekis; Athens/GR

B-500 10:30

MR-guided laser induced thermotherapy of liver metastases of gastric cancer

M.G. Mack, T. Lehnert, K. Eichler, R. Straub, J.O. Balzer, S. Zangos, T.J. Vogl; Frankfurt a. Main/DE

Purpose: To analyze the potential of LITT for the treatment of liver metastases of gastric cancer.

Methods and Materials: 25 patients (average age of 61 years, range 36 to 86 years) were treated. The total number of metastases was n = 53, ablated in 43 session. The mean number of lesions per patient was 2.1 (range 1 - 4). Survival rates were calculated using the Kaplan-Meier method. 9.1% of patients had recurrent metastases after surgery, 48.0% metastases in both liver lobes, 28.0% refused surgical resection, 8.0% had contraindications for surgery, and 8.0% had metastases at difficult localization.

Results: All ablations could be done on an out patient basis using local anesthesia. The mean survival was 2.2 years (95% CI 1.5 - 2.9 years, median survival 1.3 years, one year survival rate 67%, two year survival rate 43%) after the first LITT treatment and 2.6 years after the diagnosis of the metastases, which was treated with LITT (95% confidence interval 1.9 - 3.3 years, median survival 1.6 years, one year survival rate 79%, two year survival rate 49%, three year survival rate 42%). The mean size of the lesion was 2.7 cm (range 0.8 cm to 7 cm, mean volume 14.7 ml), the mean size of necrosis was 4.7 cm (range 2.0 to 8.0 cm, mean volume 31.3 ml). The mean applied energy was 99.2 kJ (range 33.1 to 258.8 kJ)

Conclusion: Local ablation of liver metastases of gastric cancer using LITT is a safe minimal invasive treatment option in well selected cases.

B-501 10:39

Preoperative chemoembolization in patients eligible for liver transplantation affected by hepatocellular carcinoma: Evaluation of antitumoral response on explanted livers and tumor recurrence

D. Leni, R. Corso, C. Zavaglia, A. Rampoldi, M. Castoldi, A. Vanzulli; Milan/IT

Purpose: To assess the antitumoral efficacy and the incidence of tumor recurrence in a cohort of cirrhotic patients, with hepatocellular carcinoma (HCC), who were treated preoperatively by transarterial chemoembolization (TACE) followed by liver transplantation (OLT).

Materials and Methods: 79 patients in transplantation list affected by unresectable solitary HCC nodule ≤ 5 cm or no more than 3 HCC nodules with none > 3 cm, underwent selective TACE infusing a mixture of epirubicin, lipiodol and gelatin sponge powder. Treatment response was assessed by histology on explanted livers.

Results: The median follow-up was 47 months (range 0-165). The median time between inclusion onto the transplantation list and OLT was 6 months (range 0.2-52). There were 10 deaths within 3 months of OLT that were considered postoperative complications. Overall 1-, 3-, 5- and 10-year survival were 80%, 69%, 64% and 55%, respectively. At the end of follow-up, 8 patients (10%) experienced tumor recurrence: among these, 7 patients had no response to treatment. An objective response was achieved in 36.7% of the patients. Complete necrosis of the tumor was observed in 15 patients (18.9%), 9 of them with monofocal tumor ≤ 3 cm. None of the patients who experienced a complete antitumoral response to treatment had recurrence of HCC after transplantation. Partial antitumoral response was observed in 14 patients (17.7%) with 1 recurrence of HCC observed in the follow-up.

Conclusion: Preoperative TACE induces a low rate of histological antitumoral response in patients with HCC who undergo liver transplantation. However, tumor recurrence is rarely observed in responders to treatment.

B-502 10:48

Selective internal radiation therapy with Yttrium-90 resin microspheres (SIRT-Y) in extended metastatic disease of the liver: Initial experiences

T.F. Jakobs, R.-T. Hoffmann, K. Tatsch, M.F. Reiser, T.K. Helmberger; Munich/DE

Purpose: In patients with extensive malignant hepatic disease non-responding to classic chemotherapy no effective therapeutical options are existing. Selective internal radiation therapy with Yttrium-90 microspheres (SIRT-Y) represents a novel treatment concept. Initial results regarding feasibility and efficacy in advanced hepatic metastases will be presented.

Methods and Materials: 18 patients with advanced metastatic disease of the liver non-responding to polychemotherapy qualified for SIRT-Y. If maintainable neo-adjuvant chemotherapy was continued. During follow-up by contrast enhanced MSCT, MR imaging, and FDG-PET hepatic tumor load, tumor markers, survival, and time to progress were recorded.

Results: One major adverse event was caused by the SIRT-Y procedure (gastric ulcer due to extrahepatic embolization). All patients are still alive. Mean follow-up time is 20 weeks (6 - 56). One patient presented enlarged abdominal lymphnodes 6 months after therapy, one patient underwent RF-ablation of a residual metastasis, and 2 patients presented new moderate progress of the residual tumor 7 and 12 months after SIRT-Y. According to RECIST criteria, the hepatic tumor load decreased substantially paralleled by a significant drop of tumor markers.

Conclusion: SIRT-Y has the potential of a powerful palliative therapy concept in patients with non-resectable, otherwise non-treatable or to chemotherapy non-responding hepatic metastases. Further studies are imperatively necessary to prove if the efficacy of SIRT-Y can be increased even more in a multimodality therapy regimen, e.g. in early stages of metastatic disease.

B-503 10:57

Percutaneous injection therapy by Holmium-166-chitosan complex in small hepatocellular carcinoma: Initial experience as a primary treatment

H.-K. Ko, K. Kim, J.-T. Lee, D.-Y. Lee, J.-Y. Won, S. Kim, J.-Y. Choi; Seoul/KR

Purpose: To evaluate local therapeutic efficacy, side effects and complications of percutaneous injection therapy of Holmium-166-chitosan complex (o-Chi-Com) in the treatment of small Hepatocellular carcinoma (CC) lesions as a primary treatment.

Materials and Method: 56 patients (mean age, 58.4; male 47; female 9) with 63 HCC lesions measuring 1.1-3.0 cm in diameter (mean, 2.4 cm) underwent percutaneous injection therapy of Ho-Chi-Com as a primary treatment. By ultrasonography-guided puncture of Multi-side hole fine needle in the center of tumor, 20 mCi/cm³ in tumor diameter of Ho-Chi-Com was injected for complete tumor necrosis. A single lesion was treated in 49 patients, and double lesion were treated in 7 patients. Follow-up with serial CT scan ranged from 1 to 43 months (mean, 14.5 months).

Result: Complete necrosis was achieved in 54 (85.7%) of 63 lesions. Among the 54 lesions, complete necrosis required a single treatment session in 47 lesions (87%), and two treatment sessions in 6 lesion (9.5%), three treatment sessions in 1 lesion (3.5%). Three major complication (Bone marrow suppression) were observed and required transfusion. Six minor complication (3 hypersensitivity to chitosan, 3 mild fever) was completely recovered after conservative treatment. There is no mortality related to treatment.

Conclusion: Percutaneous injection therapy by Ho-Chi-Com is an effective method to treat small HCC as a primary treatment.

B-504 11:06

Transarterial chemoembolization (TACE) in comparison to transarterial chemoperfusion (TACP) in patients with inoperable intrahepatic cholangiocellular carcinomas (ICC)

M. Heller, S. Zangos, W. Schwarz, J.O. Balzer, M.G. Mack, T.J. Vogl; Frankfurt a. Main/DE

Background: The ICC is one of the most chemotherapy-resistant tumors and it is mostly diagnosed in an advanced inoperable stage. In this study we compared the tolerability and efficacy of an intraarterial chemotherapy via TACE and via TACP.

Material and Methods: 40 patients were randomized in TACE (group A = 20 patients) and TACP (group B = 20 patients) arms. Both groups were given 2000 mg/m² Gemcitabine with additionally application of spherex in group A. Tumor response rates were evaluated via MR imaging.

Results: All patients of both groups were successfully treated with a mean of 5 courses. Partial response was noted in 6 patients of group A (30%) and 4 patients

Scientific Sessions

of group B (32%). Stable disease was assessed in 11 patients of group A (55%) and 8 patients of group B (40%) for at least 3 months. Median time to progression was 7.9 months in group A and 5.9 months in group B.

Conclusion: Both used outpatient treatment protocols are minimal invasive and seem to be an effective palliative treatment option. However the usage of Gemcitabine in a TACE regimen in comparison to a TACP regimen shows significantly better response rates.

B-505 11:15

Polyvinyl alcohol embolization adjuvant to oily chemoembolization in hepatocellular carcinoma with arterioportal shunt

H.G. Lee, Y.J. Kim, Y.S. Lim, M.H. Chung, M.S. Sung, W.J. Yoo, H.W. Lim; Buchon/KR

Purpose: This study was performed to assess the feasibility and safety of polyvinyl alcohol embolization adjuvant to oily chemoembolization (P-TACE) in hepatocellular carcinoma (HCC) with arterioportal shunt (APS).

Materials and Methods: We retrospectively reviewed 20 HCC patients with APS. Polyvinyl alcohol embolization was performed to block APS before routine TACE. Ten patients underwent P-TACE one time due to progression of liver cirrhosis and/or HCC. The rest 10 patients underwent the first P-TACE and the repeated TACE 2-3 times with PVA ($n = 6$) and without PVA ($n = 12$). Hepatic function test before and after P-TACE, and post procedural complication were evaluated for safety. Grade of APS and portal flow direction were observed for feasibility.

Results: Of 26 P-TACE, 7 developed transient hepatic insufficiency and 2 showed progressive deterioration of hepatic function (survival: 28 and 114 days, respectively). No major complication was occurred. APS and portal hepatofugal flow were improved after P-TACE on 1-5 months follow-up angiogram ($P < 0.05$). Eight patients improved APS grade and 2 patients did not changed on follow-up angiogram. Six patients with hepatofugal flow showed hepatopetal flow immediately after P-TACE and hepatofugal flow recurred in 2 patients on follow-up. The mean survival day was 207 days.

Conclusion: P-TACE is feasible and safe in HCC patients with APS.

B-506 11:24

Percutaneous, transfemoral implantation of an IA port system for locoregional chemotherapy in liver metastasis: Long term outcome

J.O. Balzer¹, N. Fleiter¹, M.G. Mack¹, E. Böcher², T. Hamm², T.J. Vogl¹; ¹Frankfurt a. Main/DE, ²Soest/DE

Purpose: To evaluate the primary technical success rate and long term outcome after percutaneous port implantation for IA chemotherapy of liver metastasis.

Methods: Between September 2001 and September 2004 69 patients with liver metastasis presented for percutaneous IA port system implantation. The IA port system was implanted via a transfemoral approach and placement of the port chamber above the Trochanter minor. The chamber was connected to a 5F diagnostic catheter which was placed in the hepatic artery. The patency rate was determined using the Kaplan Meier analysis.

Results: In 63.3% a successful port implantation could be achieved. Not successful implantations were due to anatomical variation of the celiac trunk (44%), accessory liver arteries with anatomical variation of arterial liver supply (33%) or catheter displacement during intervention (23%). The mean duration of port utilization was 207 ± 71.4 days. The catheter tip was located in 22.6% patients within the A. hepatica propria, in 74.2% in the common hepatic artery and in 3.2% in gastroduodenal artery. The periinterventional complication rate was 9.7%, mainly due to local bleeding complications. Postinterventionally the complication rate was 22.6% with catheter displacement or kinking of the diagnostic catheter (19.3%) and catheter thrombosis (3.2%). All complications could be managed interventional. The primary patency rate was 80.6% and the secondary patency rate 87.1%.

Conclusion: Percutaneous placement of an i.a. port via a transfemoral approach is feasible. This technique represents an alternative to surgical implantation in the locoregional treatment of liver metastases and opens new therapeutic possibilities for the local prolonged treatment.

B-507 11:33

Hepatic intra-arterial chemotherapy with gemcitabine: An ongoing phase II study in patients with liver metastases of breast cancer

K. Eichler, M.G. Mack, J.O. Balzer, A. Thalhammer, W. Schwarz, M. Heller, S. Zangos, T.J. Vogl; Frankfurt a. Main/DE

Purpose: To evaluate the efficacy and tolerability of hepatic intra-arterial chemoembolization with gemcitabine as a cytostatic agent in pts with inoperable liver metastases of breast cancer.

Material and Methods: Ongoing, open-label, single-center study design; pts had histologically confirmed breast cancer with inoperable liver metastases, adequate bone marrow reserve, sufficient liver/renal function, no active CNS metastases, KPS > 70%, and life expectancy > 12 weeks. A suspension of gemcitabine 1,200 mg/m², 10 ml/m² of iodised oil (Lipiodol), and 5 ml of a degradable starch microsphere (Spheraex) suspension, is administered intra-arterially up to 3 times every 4 wks. Dose-limiting toxicity (DLT) is defined as grade 4 thrombocytopenia, neutropenia, or nonhematologic toxicity > grade 3.

Results: 21 pts were enrolled (median 56 yrs, range 48-65). All pts tolerated the treatment well, with no DLTs. Tumor response was evaluated by magnetic resonance (MRT) and computed tomography (CT) imaging. Imaging revealed a decrease in the degree of vascularisation of the treated metastases, which was verified as a reduction in the Gd-DTPA enhanced T1-weighted transverse and sagittal MR imaging scans. Seven pts achieved a partial response, 10 stable disease, and 4 progressed. Progression was verified as an increase in size of the lesions or newly developing lesions.

Conclusion: Hepatic intra-arterial chemotherapy with gemcitabine is well tolerated and achieves encouraging response rates in pts with liver metastases of breast cancer.

B-508 11:42

PTFE-covered stent increases patency and clinical outcome in patients with TIPS for Budd-Chiari syndrome

R. Gandini, D. Konda, V. Pipitone, L. Maresca, A. Spinelli, E. Pampana, G. Simonetti; Rome/IT

Objective: to compare patency, re-intervention rate and clinical outcome of TIPS using uncovered and ePTFE-covered (VIATORR; W.L. Gore and Associates) stents in patients with Budd-Chiari Syndrome.

Materials and Methods: from January 1994 to November 2003 ten patients (mean age: 39 yrs, range: 17-65 yrs) affected by Budd-Chiari Syndrome underwent TIPS. In the first 5 patients TIPS was performed using uncovered Wallstents (group A). After April 2001, TIPS was carried out in 5 patients (group B) using an ePTFE-covered VIATORR stent-graft. Follow-up was performed with US at 7 and 30 days and subsequently every 3 months after the procedure. Liver function was evaluated every 3 months.

Results: All group A shunts underwent occlusion with a mean primary patency of 5.3 months (range: 7 days-10 months). During a 24.4-month mean follow-up (range: 7-37) an overall of 9 revisions with Wallstent and 20 balloon-angioplasty recanalizations were performed. The repeated re-occlusion of the Wallstents and worsening of liver function lead to one surgical mesocaval shunt, one orthotopic liver transplant and one death for liver insufficiency. One patient with re-occlusion of the shunt refused further treatment and was lost to follow-up. In one patient with re-occlusion, the shunt was revised with a VIATORR stent-graft and is still normally. In group B, a revision-free patency with persisting improvement of liver function was achieved in all patients with a mean follow-up of 22.0 months (range: 10-34).

Conclusion: ePTFE-covered VIATORR stent-graft significantly increases primary patency in TIPS for Budd-Chiari Syndrome with reduction of re-intervention rate and prolonged clinical improvement.

B-509 11:51

Porto-systemic shunt reduction for the treatment of hepatic encephalopathy after TIPS performed with E-PTFE covered stent-graft

G. Simonelli, F. Fanelli, F.M. Salvatori, M. Corona, D. Pepino, V. Dominelli, E. Boatta, P. Rossi, R. Passariello; Rome/IT

Purpose: To assess the rate of hepatic encephalopathy (HE) in patients who underwent a TIPS with PTFE covered stent-graft.

Materials and Methods: From January 2000, 98 TIPS were performed using an e- PTFE covered stent (Viatorr - WL Gore). In 10 cases the stent-grafts were 8 mm in diameter while in 88 patients a 10 mm diameter stent-graft was implanted. After a mean period of 1.2 months, 46 patients developed HE, not responding to medical care in 12 cases. In these cases a shunt reduction was performed with insertion inside the shunt of a balloon-expandable PTFE covered stent (Jostent-Jomed AG) with an hourglass shape.

Results: Technical success was achieved in all cases with immediate increase of the porto-systemic gradient and disappearance of symptoms. The mean pressure value increased from 7 to 14.8 mmHg. After a mean follow-up of 7.75 months 8 patients are alive without further episodes of HE or bleeding. In 1/12 pz (8%) a re-dilation of the shunt was necessary for reappearance of ascites. Three patients died after 6, 5 and 1 months for rebleeding ($n = 1$) and cardio-vascular failure ($n = 2$). No statistical correlations between shunt diameter and incidence of HE was observed.

Scientific Sessions

Conclusions: TIPS performed with the Viatorr stent-graft presented an increased rate of HE.

10:30 - 12:00

Room I

Interventional Radiology

SS 1009b

Carotid stenting

Moderators:

G. Napoli; Bologna/IT

S.A. Thurnher; Vienna/AT

B-510 10:30

Mid-term experience with intracranial stenting

F. Brassel¹, R. Raabe¹, C. Haupt¹, K. Papke¹, H. Becker²; ¹Duisburg/DE,

²Hannover/DE

Purpose: The aim of this study was to demonstrate the outcome and identify potential problems with intracranial stenting for different indications.

Methods and Materials: Between 1998 and 2004, 40 patients were selected for treatment with intracranial stents. There were 19 male and 21 female patients with ages ranging from 4 to 80 years. The treatment included patients with aneurysms ($n = 25$), dissecting aneurysms ($n = 4$), stenoses ($n = 9$) and arteriovenous fistulas ($n = 2$). 22 lesions were located in the internal carotid artery, 9 in the basilar artery, 5 in the middle cerebral artery, 3 in the vertebral artery and 1 in the posterior cerebral artery. 11 different types of stents were used (3 self expandable and 8 balloon expandable). 15 patients underwent combined endovascular stent implantation and coil placement.

Results: In 7 cases, it was not possible to reach the lesion with the stent catheter. Four patients died within a week after treatment. Good mid-term clinical outcome was achieved in the remaining 29 patients (72.5%). All patients who died were high-risk patients with stent placement during the acute phase of e.g. subarachnoid haemorrhage or cerebral infarction.

Conclusions: Advances in stent technology allow the treatment of the cerebral vasculature. The technique of using a stent on intracranial lesions shows good results in patients without preinterventional cerebral bleeding or infarction. The higher flexibility of so called neurostents improves the access to intracranial vascular lesions even in distal vessels and tortuous anatomy.

B-511 10:39

Carotid artery stenting under cerebral protection: Experience in 96 patients

R. Gandini, D. Konda, A. Spinelli, S. Fabiano, C.A. Reale, E. Pampana,

G. Simonetti; Rome/IT

Purpose: To assess efficacy and safety of CAS performed under cerebral protection.

Materials/Methods: 96 patients with 104 internal carotid artery stenoses (72 primary and 32 post-CEA) underwent CAS under cerebral protection (97 carotid Wallstents + EPI-filter protection device, 5 Acculink carotid stents + Accunet device, 2 Conformex stents + EPI-filter). Postprocedural follow-up was performed by Doppler US at 7 days, 3 months, 6 months and, subsequently, every 6 months.

Results: Technical success was achieved in 100% of the cases. Pre-dilation of the stenosis was required in 8 cases. During the procedure, two patients developed a TIA due to temporary blood flow interruption within the treated artery which resolved immediately after removal of the filter. One minor stroke was observed. Three autolimiting vagal reflexes occurred during balloon inflation. The post-procedural revision of the filters revealed embolic debris in 6 cases with primary stenosis. In all cases, the post-procedural DSA confirmed the optimal caliber of the treated artery and a physiological intracranial blood flow. At follow-up, all stents were patent and a mild intimal hyperplasia was observed in two patients at 6 months, 1 patient at 12 months and 1 patient at 18 months after the procedure. No late neurological complications occurred.

Conclusion: CAS performed under cerebral protection is safe, effective and reduces the risk of intra-procedural embolism.

B-512 10:48

Stenting of the carotid arteries: 4 years of experience

F. Fanelli, F.M. Salvatori, S. Vagnarelli, M. Corona, A. Bruni, L. Di Rezze,

A. Pucci, P. Rossi, R. Passariello; Rome/IT

Purpose: To evaluate the safety and efficacy of carotid artery stenting (CAS) performed with cerebral protection devices.

Methods and Materials: From February 2000, CAS with cerebral protection was performed in 105 patients with extracranial carotid artery stenoses (> 70%). The plaque was ulcerated in 21 cases, soft in 44 cases and calcified in 46 cases. Seventy-nine stenoses were primary, while 32 were secondary to TEA. 113 stents were implanted: 102 carotid wallstent, 8 Acculink, 3 Precise, were implanted in 111 carotid arteries. All procedures were performed using a cerebral protection device: Parodi system (4), EPI filter wire (99), Angioguard (2), NeuroShield (3), Spider embolic protection (2), Accunet (1). All patients had independent neurologic examination before and after the procedure. A cerebral MR examination with diffusion and perfusion sequences was also performed before and after the procedure to evaluate neurologic complications occurred during CAS.

Results: Technical success (residual stenosis < 30%) was achieved in all cases. No death occurred during the whole follow-up ranging from 1 to 47 months. Six complications (5.4%) were observed: 1 major stroke (0.9%) and 5 minor stroke (4.5%). In 7 cases (6.5%) embolic material was found inside the cerebral protection. In two cases (1.8%) a moderate in-stent restenosis was detected and treated with angioplasty ($n = 1$) and angioplasty with restenting ($n = 1$).

Conclusions: CAS represent a feasible procedure that can be performed in high-risk patients and it is associated with a low restenosis rate.

B-513 10:57

Protected carotid artery angioplasty and stenting: Acute and long term outcomes in 225 interventions

G. Piccoli, A. Marzio, A. Vit, M. Sponza, B. Bais, G. Gigli, D. Gasparini; Udine/IT

Purpose: The aim of our investigation was to evaluate the benefit of carotid angioplasty and stenting for prevention of cerebrovascular disease.

Materials and Methods: We treated 225 lesions using always protection device; 51 patient have 30 day follow-up and 151 have 6 month or more. We used NASCET to select patients; every candidate was previously clinically evaluated by Neurologist and Hagiologists.

Results: 65% of patients had neurological symptoms before the treatment, 41.30% of them had a previous stroke, 34.8% a previous T.I.A. and 23.9% a specific events like dizziness. The outcome was evaluated on a mean follow-up of 10.2 months (range 1-32). 3 patients had a minor stroke and 1 had a major stroke. One of the asymptomatic group had a major stroke 39 days after treatment, but on the contralateral hemisphere. One patient died because of pulmonary emboli and one because of fatal stroke. 3 more patients died after several months because of unrelated reasons. The 6 month follow-up showed 4.7% restenosis rate and a secondary patency of 99%.

Conclusion: Our findings demonstrate that carotid angioplasty is a safe procedure and the results are the same as of surgical ones reported in the literature. Global complication rate was 6 cases (2.7%), of these the neurological ones were 5 (2.2%). The restenosis rate was 7 (4.7%) using a cut off of 50% of stenosis. Our results are in line with those of recent randomised studies.

B-514 11:06



Primary carotid stenting: 2 years follow-up of the first 100 cases

R. Rostagno¹, R. Llorens¹, T. Zander¹, I. Zerolo¹, E. Sanabria¹, F. Barajas¹,

Z. Qian², M. Maynar¹, W. Castañeda-Zúñiga²; ¹Santa Cruz de Tenerife/ES,

²New Orleans, LA/US

Purpose: A local inflammatory response to arterial wall injury after PTA has been blamed as the main cause of intimal hyperplasia and later instant restenosis. We report the incidence of instant restenosis after primary carotid stenting without pre- or post balloon dilatation in patients with carotid stenosis.

Materials and Methods: Between May 2002 and August 2004, 100 carotid arteries in 87 consecutive patients were treated with primary Stent placement (Acculink, Guidant), without pre or post balloon dilatation. Following the initial stent procedure neurological examination, doppler ultrasound and plain film were perform at 24 hours, 1 month, 3 month and every 6 months thereafter. If restenosis was suspected by the Doppler ultrasound, arteriography was performed and the patients were subjected to endovascular intervention if a restenosis over 70% was confirmed at arteriogram.

Results: All patients were included in the follow-up. Initial residual stenosis after stenting was: mean 21% (from 0% and 50%). Restenosis was detected in 6 cases (6%) at 7.5 months (from 3 to 12 month). These patients had residual stenosis after stenting of 29% (from 0% to 40%). Balloon dilatation was perform with a balloon (Maverick, Boston Scientific) using a protection device (Accunet, Guidant). Technical success was achieved in all patients, defined as stenotic lumen less than 20%. No patient experienced any major or minor neurological complications.

Conclusions: In this short pool of patients, primary carotid stenting without pre or post dilatation shows reduction of instant restenosis.

Scientific Sessions

B-515 11:15

DW-MR imaging study after carotid stent placement with protection device (CASPD): Role of monitoring at 6 and 24 hours after procedure

I. Sansoni, A. Laghi, C. Miglio, M. Celestre, M. Rengo, M. Di Martino, L. Coletta, R. Passariello; *Rome/IT*

Purpose: To define the role of diffusion-weighted MR imaging performed within 6 hours from carotid angioplasty and stent placement with protection device (CASPD) in detecting new ischemic lesions.

Methods and Materials: We prospectively studied 34 consecutive patients (age range: 66-95 Ys, mean 75 ± 5.7) referred for CASPD procedure. Inclusion criteria were asymptomatic stenosis > 80% (30 pts) or symptomatic stenosis > 50% (4 pts). Patients underwent neurologic examination before, immediately after, and 1 day after CASPD. FLAIR and DW MR images were acquired immediately before (1-3 hours), within 6 and 24 hours after CASPD, in order to assess the number of symptomatic and silent new ischaemias. The pre- and post-intervention images obtained at b value of 1000 were examined by two independent blinded reviewers for new high-signal areas consistent with ischaemia. Total examination time was 5 minutes. We finally correlated positive results with risk factors, technical difficulties and plaque characteristics.

Results: Postprocedural (6 hours) DW-MR images showed one new symptomatic ischemic lesion (2.9%) on the opposite side of stent placement; the late (24 hour) DW-MR imaging detected recent ischaemic lesions on the side of stent placement in three more patients (8.82%), two symptomatic and one asymptomatic. All of them had at least two risk factors and fibrocalcified plaque.

Conclusion: CASPD may be associated with embolic events. The use of DW-MR imaging within 6 hours (early) confirm CASPD as a safe procedure, with few strictly procedure-related ischaemic complications. Twenty-four hour DW-MR imaging shows later embolization.

B-516 11:24

CT brain perfusion following carotid stenting

T. Jargiello, A. Trojanowska, J. Wojczal, A. Wolski, A. Drop, M. Szczero-Trojanowska; *Lublin/PL*

Purpose: The aim of our study was evaluation of brain CT-perfusion in patients undergoing CAS.

Material and Methods: CAS with filter neuroprotection was performed in 75 symptomatic patients (ICA stenosis > 70%). There were 59 patients with unilateral ICA stenosis and 16 with contralateral ICA occlusion or stenosis. CT examinations were performed using multidetector CT-scanner: non-contrast brain scans, dynamic perfusion imaging and CT-angiography. Maps showing absolute values of cerebral blood flow (CBF), cerebral blood volume (CBV) and mean transit time (MTT) were derived from brain tissue enhancement curves.

Results: CAS was successful in all patients. Among 59 patients with unilateral ICA stenosis, perfusion deficits were present in 54 (91%). MTT elongation was noted (average 6.6 s), together with decreased CBF (average 44 ml/100 g/min) and slightly increased CBV (average 3.4 ml/100 g). We observed perfusion improvement in all 54 patients after CAS. Normalization was found in 42 patients (77%) right after intervention, and after 6 months it was 49 (81%). In a group with contralateral ICA occlusion or stenosis, perfusion deficits were present in both hemispheres in all 16 patients (MTT average - 9.2 s; CBF average - 29 ml/100 g/min; CBV average - 3.7 ml/100 g). After CAS perfusion normalization was noticed in 9 patients (56%) and after 6 months in 4 more patients (13 - 81%).

Conclusion: CT-perfusion can assess brain perfusion before and after CAS. It helps to qualify patients for CAS and shows procedure's effectiveness.

B-517 11:33

Carotid stenting: Complications within 30 days using filter neuroprotection

T. Lupattelli, M.J. Fischer, S. Mosca, A. Maselli, P. Pozzilli, G. Scalera, L. Lupattelli; *Perugia/IT*

Purpose: To evaluate procedural complications using neuroprotection for carotid stenting.

Methods and Materials: 191 procedures for carotid stenting in patients with symptomatic or asymptomatic severe, and severe post-surgical restenosis were performed. For neuroprotection we used "TRAP" (Microvena, Italy) or "EPI-Filter" (Boston Scientific, USA) during primary stent with Carotid Wallstent (Boston scientific, USA).

Results: The TRAP and EPI-Filter device were used in 16% and 76% of the cases respectively. In the 8% of cases the filter device did not pass the stenosis. In 69 patients macroscopic debris in the filter device was revealed. Within 30 days neurological complications (n = 27), TIA (n = 11), and death due to ictus (n = 1) occurred.

Conclusion: Although filter neuroprotection reduces the risk of the intracerebral macroemboli due to carotid stenting, several peri- and postprocedural complications should be considered.

B-518 11:42

Occurrence of focal ischaemia after carotid artery stenting without using a neuroprotection device

A. Waaijer, T.H. Lo, T.H. Witkamp, M. Prokop; *Utrecht/NL*

Purpose: To identify the frequency of new focal ischaemic lesions after carotid artery stenting (CAS) without using neuroprotection.

Materials and Methods: Between October 2003 and June 2004, 24 patients with symptomatic stenosis of the internal carotid artery were consecutively treated with primary stent implantation. We did not use neuroprotection devices in any patient and focused on keeping the procedure time short and performing the intervention asatraumatic as possible. No additional procedures like rotational angiography or transcranial Doppler were performed during intervention. For the last 15 patients we performed DW-MR imaging before and within 24 hours after CAS. We obtained DW-MR imaging using a 1.5 Tesla system with a spin-echo sequence with b-values of 0-1000; the diffusion gradients were successively activated in the tree orthogonal space directions. Two neuroradiologists evaluated all MR images independently for the occurrence of new lesions by pair-wise comparison of pre- and post-images.

Results: All patients were treated successfully. Mean duration of the procedure was 54 minutes. Pre-dilatation was performed in most cases, post-dilatation only if necessary. Among the first nine patients one patient suffered from a TIA which lasted less than 2 minutes, and from which he recovered completely. In the next 15 patients no new lesions could be detected on DW-MR imaging.

Conclusion: Focal ischemia may be a rare event after carotid artery stenting without using a neuroprotection device if there is a focus on keeping the procedure as short and atraumatic as possible.

B-519 11:51

Use of covered stents in treatment of large neck internal carotid artery

R. Gandini, M. Chiocchi, M. Stefanini, V. Pipitone, G. Pendenza, G. Simonetti; *Rome/IT*

Purpose: To demonstrate efficacy and safety of the endovascular treatment of large neck internal carotid artery pseudoaneurysms, using covered stents.

Materials and Methods: Between 1999 and 2003 we treated 5 patients with large neck pseudoaneurysms. 4 pseudoaneurysms were post-traumatic and 1 was spontaneous. 4 patients were symptomatic, (headache, neck pain) while 1 was asymptomatic. The diameter of the pseudoaneurysms varied between 10 to 45 mm, with a wide neck between 8 and 25 mm. In all patients a 6Fr guiding catheter was positioned into the ICA. 3 Symbiot ePTFE covered stents, 1 JOSTENT, and 1 Advanta were deployed, using the monorail technique, over the neck of the pseudoaneurysms. During the procedure 1000 IU of Heparin were administered to all patients. Post procedurally all patients received an antiaggregant therapy (clopidogrel for six week and aspirin for six months).

Results: Post procedural DSA demonstrated, in all the patients, the complete exclusion of the aneurysms without complications. CT and ECD performed at 3, 9, 24 months confirmed the exclusion of the aneurysms and patency of ICA in 4 cases. In 1 case the controls revealed a rupture of the stent, in this patient a second stent graft was positioned.

Conclusion: Despite the limited experience with covered stents in the treatment of large neck internal carotid artery pseudoaneurysms, this technique seems very promising if combined with post-procedural anti-aggregant therapy.

Scientific Sessions

10:30 - 12:00

Room K

Cardiac

SS 1003

MDCT in ischemic cardiomyopathy and myocardial infarction

Moderators:

S. Tuma; Prague/CZ

B.J. Wintersperger; Munich/DE

B-520 10:30

16-detector row spiral CT versus MR imaging for the assessment of left ventricular function in acute myocardial infarction: An animal study

A.H. Mahnken, M. Katoh, P. Bruners, E. Spuentrup, J.E. Wildberger, R.W. Günther, A. Buecker; Aachen/DE

Purpose: To assess left ventricular (LV) function and regional wall motion using ECG-gated 16-slice computed tomography (MSCT) in comparison to magnetic resonance imaging (MRI).

Materials and Methods: In 15 pigs acute myocardial infarction was induced by occlusion of the left anterior descending coronary artery. Thereafter, MSCT and MRI were performed with standardized examination protocols. From manually drawn endo- and epicardial contours LV volumes (end-diastolic volume (EDV), end-systolic volume (ESV), stroke volume (SV)), ejection fraction (EF) peak filling rate (PFR), peak ejection rate (PER), time to PER (TPER), time from end-systole to PFR (TPFR) and myocardial mass were calculated. Regional wall motion was visually assessed from cine loops. LV function was analyzed using Bland-Altman method, Student's t-test and Pearson's correlation coefficient. Regional wall motion scores were compared with kappa-statistics.

Results: LV volumes as determined by MSCT correlated well with MRI with a mean ejection fraction (EF) of $46.1 \pm 6.5\%$ on MSCT and $46.8 \pm 5.9\%$ on MRI ($r = 0.97$). Bland-Altman plots revealed no systematic errors for EDV, ESV, SV and EF. PER, PFR, TPER and TPFR showed markedly worse results with a wide range of scattering and significant differences between MRI and MSCT for PER ($p = 0.04$) and TPFR ($p = 0.03$). Regional wall motion scores demonstrated a very high level of agreement between both modalities with $\kappa = 0.878$.

Conclusion: 16-slice CT allows for reliable assessment of LV volumes and regional wall motion at rest, but is not yet suited for the assessment of functional parameters, that directly depend on temporal resolution.

B-521 10:39

Evaluation of myocardial late enhancement using a low dose 40-slice CT protocol: A feasibility study

A. Rutten¹, S. de Vos¹, M.-J. Cramer¹, J. ten Berg², M. Prokop¹; ¹Utrecht/NL, ²Nieuwegein/NL

Purpose: To perform a feasibility study for the evaluation of late enhancement using a low dose protocol on a 40-slice CT scanner. The study group consisted of patients with hypertrophic obstructive cardiomyopathy (HOCM) who had undergone percutaneous transluminal septal myocardial ablation.

Methods: We included 10 patients with focal infarction of the interventricular septum induced by ethanol ablation (2-21 months post-ablation). We injected 100-120 ml contrast medium for cardiac CTA and performed an additional late scan 7-8 minutes after contrast injection. In order to keep dose to a minimum, we chose a non-gated protocol on a 40-slice scanner using 1.25 mm collimation, 1.25 pitch, 80 kVp and 120 mAs. Scan duration and dose were recorded. To assess late enhancement we used software to digitally subtract both image sets. Average CT numbers in non-enhanced and enhanced portions of the myocardium were determined on the late scan.

Results: The heart could be covered within an average of 0.84 s (0.78-0.96). Mean effective dose was 0.88 mSv (0.79-1.03). Digital subtraction appeared to be a useful aid for the assessment of late enhancement on low dose images. All regions of septal ablation showed higher CT numbers (average 132 HU (94-189)) than normal myocardium (average 82 HU (71-107)). In two patients we found patchy late enhancement in residual hypertrophic regions outside the infarcted area.

Conclusion: Even at a low effective dose of circa 0.9 mSv, evaluation of late enhancement with a 40-slice CT scanner appears feasible. This may be a useful tool in the non-invasive workup of patients with significant coronary artery disease.

B-522 10:48

Multislice spiral CT for assessment of myocardial viability: Comparison to contrast enhanced MR imaging

A.H. Mahnken, R. Koos, M. Katoh, J.E. Wildberger, E. Spuentrup, R.W. Günther, H.P. Kühl, A. Buecker; Aachen/DE

Purpose: To assess the value of arterial and late phase multislice spiral CT (MSCT) in the evaluation of acute myocardial infarction (MI) in comparison to magnetic resonance imaging (MRI).

Material and Methods: In 21 patients with reperfused MI contrast enhanced cardiac MSCT was performed. Images were acquired in the arterial phase and 15 minutes after administration of 120 ml contrast material. All patients underwent late enhancement MRI after administration of 0.2 mmol Gd-DTPA/kg/bodyweight. Area of MI was compared between the different imaging techniques using Bland-Altman method and multivariate analysis. Agreement of the contrast enhancement patterns was evaluated with a kappa test using a 16 segment model of the left ventricle.

Results: Mean infarct size on MRI was $36.8\% \pm 25.4\%$ of left ventricular area. Bland-Altman data showed a good agreement between MRI versus MSCT late enhancement (mean -2.3 ; lower and upper limits of agreement [LOA]: -12.4 ; 7.8). The corresponding values for MRI versus arterial phase MSCT were: 6.5 (-29.8 / 42.8). Comparing MSCT late enhancement with MSCT early perfusion deficit mean and LOA were: 8.8 (-28.7 / 46.3). Contrast enhancement patterns showed an excellent agreement between MRI and MSCT late enhancement ($\kappa=0.883$). The results were worse comparing MRI and early phase MSCT ($\kappa=0.613$) as well as early and late phase MSCT ($\kappa=0.592$). On early and on late phase CT density values of infarcted myocardium were significantly different from viable myocardium ($p < 0.0001$).

Conclusion: Contrast enhanced MSCT allows for the assessment of MI. MSCT late enhancement is as reliable as delayed contrast enhanced MRI in the assessment of infarct size.

B-523 10:57

Assessment of myocardial infarction with cardiac MSCT using model based heart segmentation and perfusion weighted color maps

A.H. Mahnken¹, E. Klotz², S. Lautenschläger², R. Koos¹, D. Fritz², M. Scheuerling², D. Rinck², R.W. Günther¹, J.E. Wildberger¹; ¹Aachen/DE, ²Forchheim/DE

Purpose: To optimize contrast-enhanced multislice spiral CT (MSCT) for detection of acute myocardial infarction (aMI) using perfusion weighted color maps and semi-automated assignment of infarcted areas to myocardial segments.

Material and Methods: First a model-based software tool for semi-automated detection of the long axis of the left ventricle and assignment of left-ventricular segments was developed using a region growing algorithm and a point distribution model. To visualize changes of the myocardial contrast enhancement pattern color coding was performed after low pass filtering and spreading of the attenuation values. 15 patients (12 men, mean age 57 ± 15 years) underwent cardiac MSCT (16x0.75 mm, 120 kV, 550 mAs_{eff}) after administration of 120 ml of contrast material. Contrast enhanced delayed enhanced magnetic resonance imaging (MRI) after administration of 0.2 mmol Gd-DTPA/kg/bodyweight was performed as reference standard. Areas of infarction were assessed from short axis reformats of routine MSCT images, post-processed MSCT images and MRI using a 17-segment model of the left ventricle.

Results: On MRI aMI was present in 78/255 myocardial segments. From routine MSCT images aMI was correctly detected in 58/255 segments (Sensitivity 74.4%; Specificity: 96.1%), while on post-processed images aMI was correctly diagnosed in 65/255 segments (Sensitivity 83.3%; Specificity: 96.0%). Agreement between MRI and routine MSCT images was $\kappa=0.76$. Using post-processed images agreement improved to $\kappa=0.81$.

Conclusion: Perfusion weighted color maps allow for an improved detection of aMI from cardiac MSCT data. On a segmental basis semi-automated assignment of infarcted areas to the left ventricular myocardium is feasible.

B-524 11:06

Determining treatment in patients with acute coronary syndrome using multidetector CT

J.B. Houwers, J. Dorgelo, T.P. Willems, C.H.C. Janssens, F. Zijlstra, M. Oudkerk; Groningen/NL

Purpose: Patients presenting with non-ST-elevation acute coronary syndrome (ACS) and evidence of myocardial ischemia are scheduled for diagnostic coronary angiography (CAG). In approximately 35% of patients no percutaneous coronary

Scientific Sessions

intervention (PCI) is performed. A study was designed to determine whether 16-slice multidetector CT (MDCT) in patients with ACS can predict the need for invasive therapy accurately and thus reduce the number of CAG's.

Material and Methods: Thirty patients with ACS (22 male, mean age 58.7 ± 11 years) were scanned prior to CAG. Data were observed in a blinded fashion. Scans were assigned a quality score, with segment, grade and composition of stenoses being recorded. Based on the MDCT data, a fictive treatment is proposed and compared to the real CAG based treatment.

Results: MDCT quality was good to excellent, with one exception, in the first 30 patients. Excellent accuracy was observed in the detection of significant stenoses using MDCT (sensitivity 91%, specificity 97%, PPV 78% and NPV 99%). In 48% of the cases, no PCI was performed during CAG, because of absence of or only slight coronary artery disease (27%) or severe coronary artery disease, demanding bypass graft operation (17%). MDCT predicted correct treatment in 79% of the cases. By using data obtained with MDCT, 27% of CAGs could have been avoided.

Conclusion: MDCT scanning prior to CAG in patients presenting with acute coronary syndrome can correctly determine the need for invasive treatment in a large majority of cases and leads to a reduction in diagnostic CAG's.

B-525 11:15

Assessment of myocardial bridging with 16-multidetector-row CT (16-MDCT)

P. Spagnolo¹, T. Khouri², M. Manfredi², M. Marks²; ¹Genoa/IT, ²Monza/IT

Purpose: To evaluate the ability of 16-MDCT coronary angiography to demonstrate myocardial bridging in the preoperative setting of patient candidates for coronary artery bypass.

Methods and Materials: 32 patients with coronary artery disease (CAD) and with a suspected diagnosis of tunneled course of the mid left anterior descending coronary artery (mid-LAD) on conventional coronary angiography (CA), underwent 16-MDCT coronary angiography. All examinations were performed with a 16-MDCT (Light Speed 16, GE Medical Systems) with retrospective ECG-triggering: 16x1.25 mm slice collimation, 0.5 s rotation time. Postprocessing methods included MPR, MIPs, and 3D volume rendering reconstructions. All patients underwent surgery bypass for CAD.

Results: In 12/32 patients 16-MDCT confirmed the diagnosis of myocardial bridging of the mid-LAD and allowed assessment of the location, length and thickness of the tunneled coronary segment. In 20/32 cases 16-MDCT correctly detected the epicardial course subsequently demonstrated by surgery.

Conclusion: Preoperative MDCT coronary angiography appears as a useful non-invasive method for identification and characterization of morphologic features of tunneled coronary artery, which may influence the choice of surgical modalities: myotomy versus CAGB.

B-526 11:24

Non-invasive assessment of drug-eluting coronary stents (DES) at 6-months follow-up: is there a role for multidetector-CT angiography (MDCTA)?

I. Carbone, M. Francone, M. Danti, K. Lanciotti, E. Doda, A. Granatelli, R. Passariello; Rome/IT

Purpose: DES are coated-stents capable of releasing bioactive agents into the bloodstream potentially reducing the incidence of restenosis. The aim of our study was to evaluate the feasibility of MDCTA in the evaluation of DES patency at 6-months follow-up.

Materials and Methods: Thirty-two patients who previously underwent coronary DES placement (27 Rapamycin-DES; 13 Paclitaxel-DES) were included in the study. After 6-9 months all patients were studied with MDCTA one week prior to SCA, in order to evaluate patency. ECG-gated MDCTA of the coronary arteries was performed with the following acquisition parameters: 4x1 mm collimation, 1.25 mm sl.thickness, 0.5 mm increment, 120 kV, 400 mAs. Images were analyzed by two radiologists on a dedicated workstation using a real-time interaction approach. Patency was evaluated qualitatively and quantitatively by measuring the attenuation values proximally, inside and distally to the stent. MDCT results were compared with SCA, considered the gold standard.

Results: In 6 cases stent patency was not assessable by MDCTA. Twenty-seven of 34 assessable DES were patent at SCA. MDCTA was able to detect in-stent re-stenosis in 6/7 cases by the first observer and in 5/7 cases by the second observer (overall Sensitivity 75%). One case of occlusion was detected by both observers. At MDCTA 25/27 stents were judged patent by the first observer and 24/27 by the second observer with an overall specificity of 88.6%. The interobserver agreement was substantial ($K = 0.72$).

Conclusions: MDCTA seems to be a reliable tool for assessment of DES patency. Faster CT scanners and "CT-dedicated" stents may improve detection of restenoses.

B-527 11:33

Multidetector-row spiral CT (MDSCT) angiography for the preoperative planning of minimally invasive coronary artery bypass (MICAB) grafting

M. Di Terlizzi, A. Puppi, R. Fossaceca, F. Caimmi, M. Sacco, A. Carrieri; Novara/IT

Purpose: To evaluate the capabilities of MDSCT in the assessment of vascular anatomy of the chest for patient selection and accurate planning of MICAB graft.

Materials and Methods: 20 consecutive patient candidates for MICAB for coronary artery disease underwent contrast-enhanced, ungated, MDSCT to obtain an accurate assessment of anatomy and to estimate availability of direct exposition of the structures involved in the surgical procedure. All the examinations were performed using a 4-row CT scanner (Lightspeed, GE, Milwaukee, USA) and the following protocol: collimation 4x1 mm, pitch 1.5, rotation time 500 msec, 120 kV and 300 mA. Images were analyzed both in the axial source view and after 3D reconstructions (MIP, VRT) using a dedicated workstation. Both internal mammary arteries (IMAs) were evaluated for the presence of anatomic variations, diameter, presence of wall calcifications and distance between IMAs and sternal margins.

Results: Both IMAs were clearly visualized in all 20 patients. 2/20 patients (10%) were excluded from the MICAB surgery due the presence of anatomical variations (anomalous origin and trifurcation). The remaining patients underwent successful, uneventful MICAB grafting.

Conclusion: Contrast-enhanced, ungated, MDSCT can be considered an optimal and minimally invasive tool for the preoperative planning in cardiac patients, (MDCT) giving robust and reliable information to surgeons in order to avoid complicated procedures.

B-528 11:42

MRA versus MSCT in the detection of coronary stenoses

M. Di Roma, A. Romagnoli, M. Sperandio, M. Tomassini, R. Cammarata, G. Simonetti; Rome/IT

Purpose: To assess the capability and clinical feasibility of the coronary MR angiography technique, comparing MR and MSCT results for detection of significant coronary artery stenoses.

Methods and Materials: MR and MSCT coronary angiographies were acquired from 26 patients. The MR protocol was performed using a 1.5 T whole-body unit (Philips Gyroscan; Best, The Netherlands) and included at least 2-3-dimensional navigator-echo-based respiratory-gated Balanced Turbo-Field-Echo sequences for the left and right coronary artery systems. MSCT coronary angiography was performed with a 16 slices scanner (Light Speed¹⁶, General Electric) with thin-slice collimation (0.625 mm). The MR and MSCT angiography results were compared with the DSA that was regarded as the standard of reference.

Results: Using an angiographic segmentation of coronary vessels, we analyzed 234 segments. 161 (69%) were judged evaluable by MRA and 213 (91%) by MSCT. In our series MSCT revealed significantly higher sensitivity (89%) and specificity (98%) than MR imaging (respectively 75% and 92% in the proximal branches).

Conclusion: The temporal and spatial resolution currently available with MRA cannot match MSCT results, still MRA does not expose the patients to radiation and potential nephrotoxic contrast. We believe MR will be the favourite non-invasive technique in patients with CAD, supplying morphological, kinetic and perfusional information about myocardial muscle and coronary anatomy.

B-529 11:51

MDCT coronary angiography in preoperative assessment of non-coronary cardiac surgery

V. Russo, L. Lovato, M. Renzulli, P. Bertaccini, G. Napoli, E. Pilato, G. Gavelli, R. Fattori; Bologna/IT

Purpose: To evaluate the clinical impact of MDCT coronary angiography as a preoperative screening test in patients candidate to major non-coronary cardiac surgery (heart valve replacement, aortic aneurysm, chronic aortic dissection), asymptomatic for ischemic heart disease.

Methods and Materials: 36 consecutive patients (29M-7F, years 43-74, mean 62.8) candidate to surgical treatment of non-coronary cardiovascular disease underwent MDCT coronary angiography (Somatom Sensation -16 Cardiac, Siemens, Forchheim, Germany; 0.75-mm collimation and 375-ms tube rotation), as preoperative assessment of the surgical risk. The left main (LM), left anterior descending (LAD), left circumflex (LCX), and right coronary artery (RCA), including

Scientific Sessions

2 mm side branches, were evaluated and screened for $\geq 50\%$ stenoses. All patients in whom MDCT detected a coronary lesion $\geq 50\%$ underwent catheter coronary angiography (CCA) while all patients without any coronary artery disease were submitted to surgery without any additional test.

Results: 12 patients presented coronary stenosis $\geq 50\%$ (RCA 5 pts, LCX 3 pts, LAD 1 pt, RCA+LCX 2 pts, LAD+LCX+RCA 1 pt), all confirmed by coronary angiography. Adjunctive by-pass surgery or PTCA were performed in 9/12 cases. 24 patients with no coronary artery disease at MDCT underwent surgery. None of the 36 patients presented any operative and/or post-operative cardiac complication, such as myocardial ischemia, myocardial infarction or cardiac failure.

Conclusions: MDCT coronary angiography is a reliable alternative to CCA in pre-operative assessment of non-coronary cardiac surgery avoiding the cost and the risk of an invasive procedure.

10:30 - 12:00

Room L/M

Neuro

SS 1011

Brain tumor evaluation with diffusion and perfusion MR imaging

Moderators:

E.-M.B. Larsson; Lund/SE
J. Stojanovska; Skopje/MK

B-530 10:30

DTI-based assessment of corpus callosum infiltration by primary brain tumors: A marker for contralateral growth

B. Stieltjes¹, M. Schlüter², M.-A. Weber¹, H.K. Hahn², J. Rexilius², O. Konrad-Verse², M.R. Essig¹; ¹Heidelberg/DE, ²Bremen/DE

Purpose: Delineation of gliomas and assessment of contralateral involvement is challenging using conventional imaging but of great importance for therapy decisions. Here we present a method for visualization and automatic quantification of white matter integrity/infiltration of the Corpus Callosum (CC) using DTI.

Methods and Materials: Ten patients with gliomas (5 with and 5 without contralateral lesions) were included. Five healthy age-matched volunteers served as reference. Imaging: T1/T2 conventional imaging, diffusion sensitized SSEPI 1.5 T, 50 slices, 2.5 mm isotropic voxels, 6 non-collinear diffusion directions, b-values 0/1000, 10 averages. Main diffusion directions and complete diffusion tensors were visualized using color maps and ellipsoids. Infiltration was quantified measuring Fractional Anisotropy (FA) along CC cross sections for patients and volunteers using a robust, user-insensitive method for automatic classification into fiber, mixture tissue and background.

Results: CC infiltration could be detected on DTI data as demonstrated in the combined visualization of anatomical and DTI data. Profiles of FA of patients with suspect lesions contralaterally all had a significant, clearly delineated FA decrease whereas patients with no contralateral lesions showed similar profiles when compared to healthy volunteers. DTI yielded additional information concerning tumor extent and delineation when compared to conventional imaging.

Conclusion: The proposed DTI based visualization of fiber tissue permits the visualization of CC infiltration by gliomas. The presented method for FA quantification proved to be robust, allowed for detailed assessment of CC infiltration and provides detailed information of contralateral involvement in patients with gliomas. This can improve pre-therapeutic decision making and planning.

B-531 10:39



Diffusion weighted imaging and diffusion tensor imaging in the evaluation of intra-axial tumors

X. Hong¹, D. Wang¹, T. Shen², X. Chen²; ¹Nanjing/CN, ²Shanghai/CN

Purpose: DWI has mainly been used to study hyperacute ischemia; it is also useful in various other diseases. Our purpose was to evaluate the usefulness of ADC, Trace D, FA value in differentiating tumor, edema, and normal brain tissue, and in grading the malignancy of intra-axial tumors.

Methods and Materials: Using a GE 1.5 T super conducting MR unit, 30 grade 1-2 and 40 grade 3-4 intra-axial tumors underwent conventional MR imaging, DWI and DTI. The ADC values, Trace D values, and FA values of ROIs were measured. These ROIs were manually placed over the areas of tumor, edema, and normal brain tissue. Comparisons were made by analysis of variance.

Results: When ADC values and Trace D values were analyzed as a group, significant differences were found between tumor, edema, and normal brain

tissues, but not between tumor and adjacent edema. Significant differences were also found between low-grade tumors and high grade tumors in ADC and Trace D values. FA maps depicted white matter features not typically seen on conventional MR images. Fiber mapping images showed the ipsilateral white matter as either discontinuous due to impaired anisotropy or compressed due to mass effect.

Conclusion: ADC values and Trace D values helped to distinguish tumor from normal tissue but could not be used to separate tumor from adjacent edema. Individually, ADC values overlapped considerably. Combined with conventional MR imaging, the ADC values and Trace D values may predict the degree of malignancy of intra-axial tumors.

B-532 10:48

Differentiation of benign subtypes of meningiomas by diffusion tensor imaging-based calculation of tensor shape

A. Tropine, J. Gawehn, P.D. Dellani, M. Glaser, J. Bohl, P. Stoeter; Mainz/DE

Purpose: Preoperative knowledge of the elasticity of tumours facilitates neuro-surgical treatment planning. Fibroblastic meningiomas are usually considered to be of a harder consistency during operation than other non-calcified benign subtypes of meningiomas. The purpose of this study was to assess the potential of preoperative DTI in the prediction of histopathological subtype of meningioma.

Methods and Materials: In 17 patients with benign non-calcified meningiomas, diffusion tensor imaging ($b = 900$ or $b = 1000 \text{ s/mm}^2$) was performed. Diffusion tensors, mean diffusivity (MD) and fractional anisotropy (FA) values were calculated and the geometrical shape of the tensor computed. All examinations were performed on a 1.5 T scanner.

Results: Histological analysis revealed 8 meningotheelial, 3 mixed and 6 fibroblastic meningiomas. Whereas meningotheelial meningiomas were represented by spherical tensors corresponding to isotropic diffusion, all fibroblastic meningiomas predominantly showed disc-shaped tensors indicating in-plane diffusion. This may be caused by the fascicular arrangement of long, spindle-shaped tumor cells and the high content of intra- and interfascicular fibers as shown by histology. In addition, a capsule-like rim of in-plane diffusion surrounded most meningiomas irrespective of their histological type. The other DTI parameters did not show significant differences between the subtypes.

Conclusions: DTI-based analysis demonstrates a one to one correlation of the shape of the diffusion tensor and the histopathological type of benign meningiomas. It is a promising method to differentiate between fibroblastic and other subtypes of benign meningiomas in order to obtain information about their "hard" or "soft" consistency prior to removal.

B-533

Preoperative perfusion CT of intracranial meningiomas compared with arteriography and microvessel density

M. Chouli¹, M. Colombe¹, M. Rodallec¹, M. Kalamardes¹, X. Paoletti², A. Feydy¹; ¹Clichy/FR, ²Paris/FR

withdrawn by authors

Scientific Sessions

B-534 10:57

Perfusion MR imaging in patients with non-enhancing brain gliomas:

A valuable tool to predict anaplasia and/or tumor progression?

M. Caudo¹, A. Tartaro¹, A. De Nicola¹, G. Maira², C. Colosimo¹; ¹Chieti/IT, ²Rome/IT

Purpose: To assess the relationship between MR perfusion patterns and tumor grading in non-enhancing gliomas.

Methods and Materials: 18 patients (mean age 50 years) with non-enhancing space occupying gliomas underwent perfusion MR imaging using a 1.5 T unit and EPI sequences (50 volumes, 10 preceding a single dose of contrast medium (1.0 mol/L Gadobutrol)). The standard outputs of the perfusion analysis included voxel-by-voxel maps of cerebral blood volume (CBV), cerebral blood flow (CBF) and mean transit time (MTT). Tissue segmentation was used in order to calculate the average CBV, CBF and MTT values in white (WM) and grey (GM) matter. The tumor was manually segmented and values of CBV, CBF and MTT were calculated from the tumor and the corresponding symmetrical contralateral volume (SCV) of normal brain from the hemisphere. Perfusion parameters of the tumors were compared with the segmented white and grey matter and with the SCV of brain tissue. 17 patients underwent surgery and 1 patient was inoperable.

Results: Pathology results revealed 6 high grade (Grade III WHO) and 11 low grade gliomas (Grade II). The inoperable patient did not have MR modifications at 30-month follow-up (non-anaplastic). All high grade gliomas had a higher CBV than segmented WM and SCV, but always lower than segmented GM.

Conclusion: Non-enhancing brain gliomas with a higher CBV than the segmented WM and the SCV are significantly correlated with anaplasia. Therefore, perfusion MR should be integrated in the diagnostic work-up of non-enhancing gliomas in order to predict grading and evolution.

B-535 11:06



Usefulness of diffusion/perfusion-weighted MR imaging in mouse gliomas: Correlation with histopathology

G. Fan, P. Zang, Q. Guo, Z. Wu; Shenyang/CN

Purpose: Diffusion/perfusion-weighted MR imaging (DWI/PWI) was performed to evaluate growth and vascularity of implanted C6 rat gliomas.

Methods and Materials: 36 Wistar rats were implanted with C6 glioma cells intracerebrally. Within 4 weeks, 8 to 10 rats were imaged with DWI/ PWI weekly. Apparent diffusion coefficient (ADC) values and maximal regional cerebral blood volume ($rCBV_{max}$) in both tumoral regions and peritumoral regions were calculated. After MR imaging, each rat brain was examined histologically using CD34 and assessment of tumor cellularity and microvascular density (MVD).

Results: Statistical differences of ADC values for both the solid tumor component and peritumoral region were present comparing 3-4 weeks with 1-2 weeks after implantation ($p < 0.01$). ADC value for the solid tumor was negatively correlated with tumor cellularity ($r = -0.682$, $p < 0.01$). Statistical difference of the $rCBV_{max}$ for the solid tumor components was present comparing 2-4 weeks with both 1 week after implantation and with contralateral white matter ($p < 0.01$). Native vessel dilatation in regions of normal brain at the periphery of the tumors at 1 week after implantation was observed, and $rCBV_{max}$ in these regions were elevated compared to the contralateral side ($p < 0.01$). Prominent positive correlation was present between $rCBV_{max}$ of the solid tumor component and MVD ($r = 0.716$, $p < 0.01$). **Conclusion:** Reduced ADC value for the solid tumor component is correlated with growth of C6 gliomas. $rCBV_{max}$ for the solid tumor component can evaluate tumoral microvessel in vivo, while those at the periphery may be useful for the differentiation between native vessel dilatation of normal brain and angiogenesis of the tumor.

B-536 11:15

Multiparametric MR assessment of cerebral gliomas at 3.0 Tesla:

Characterization of spatial heterogeneity and tumor malignancy

S. Pollici¹, T. Scarabino², A. Di Costanzo³, F. Troisi³, G. Giannatempo², F. Nemore³, U. Salvolini⁴, A. Carriero¹; ¹Novara/IT, ²San Giovanni Rotondo/IT, ³Naples/IT, ⁴Ancona/IT

Purpose: Characterize the spatial heterogeneity of metabolic, hemodynamic and diffusion features within gliomas and surrounding tissues.

Methods and Materials: Twenty-eight patients with different grade gliomas. Metabolic parameters were Cho, NAA, Cr and LL derived by 1H-MRSI; rCBV by PWI; ADC by DWI. ROI included tumor necrotic area, non-necrotic mass, margins, surrounding edematous areas and normal appearing tissue.

Results: In high-grade gliomas, necrotic ROIs of gliomas were divided in 2 groups: areas characterized by high ADC, no metabolites or high LL and no perfusion; areas characterized by low ADC, presence of Cho and LL, and low rCBV.

Apparently edematous ROI were divided in 3 groups: areas with very high Cho, abnormal Cho/NAA ratios, low ADC and high rCBV; areas with low metabolic signals, normal Cho/NAA ratios, high ADC and low rCBV; areas with Cho levels similar to normal, abnormal Cho/NAA ratios and intermediate ADC and rCBV values. In low-grade gliomas, cystic ROI presented low metabolite signals, high ADC, absent or low rCBV. In the differentiation of high-grade from low-grade gliomas, Cho was significantly higher in margins and NAA was significantly lower in mass and margins of high-grade gliomas. ADC was higher in masses of low-grade gliomas, although the difference was not significant. Mean rCBV of mass and margins were significantly higher in high-grade gliomas. LL peak were never detected in low-grade gliomas.

Conclusions: Multiparametric 3 T MR imaging discriminate high from low-grade gliomas; depict tissue heterogeneity within the tumor; provide useful information for stereotactic biopsies, surgical resection and radiotherapy.

B-537 11:24

Early postoperative diffusion-weighted MR imaging (DWI) of the brain parenchyma in the operative site following tumor resection

A. Ozturk, K. Karli Oguz, A. Cila, N. Akalan; Ankara/TR

Purpose: To evaluate diffusion changes in the brain parenchyma in the operative site of intracranial tumors in the first 24 hours following surgery.

Materials and Method: Seventeen patients (6 female, 11 male; 8-80 years) who underwent intracranial tumor surgery were included in the study. Postoperative MR imaging performed in the first 24 hours included DWI (TR/TE, 2800/78; b value of 0, 500, 1000; mtv:256x256) and routine cranial MR imaging including T2* imaging. Diffusion changes and any hemorrhage in the parenchyma that would interfere with diffusion abnormalities were noted. We also aimed to determine any effect of preoperative tumor size, tumor pathology and presence of residual tumor following surgery on these diffusion abnormalities.

Results: Pathological examination of the excised tissue revealed 2 oligodendrogiomas, 2 meningiomas, 1 medulloblastoma, 4 ependymomas, 2 hemangioblastomas, 1 pilocytic astrocytoma, 1 DNET, 2 PNET, 2 gangliogliomas. We found decreased diffusion in the parenchyma near the resection cavity of 11 patients. DWI showed increased ADC values in one patient and no diffusion abnormality in 3 patients. Among those 3 patients with no parenchymal diffusion change, 2 patients had signal abnormalities related to hemorrhage in the operation site. There was no relationship between diffusion abnormality and preoperative tumor size, pathology of the tumor or with the presence of residual tumor.

Conclusion: The most common abnormality in early postoperative DWI of the parenchyma in the operation site following surgery was restricted diffusion; suggesting cytotoxic edema probably resulting from ischemic damage to the tissue. Increased diffusion suggesting vasogenic edema and no diffusion abnormality may also be seen occasionally.

B-538 11:33

Diffusion changes in tumor and peritumoral brain regions following stereotactic irradiation for brain tumors

N. Tomura, J.-I. Izumi, T. Otani, I. Sakuma, S. Takahashi, J. Watarai; Akita/JP

Purpose: To evaluate the clinical role of diffusion-weighted MR imaging (DWI) in monitoring response of brain tumors to stereotactic irradiation (STI) by measuring changes in apparent diffusion coefficient (ADC) in tumor and peritumoral regions before and after STI.

Methods and Materials: MR studies including DWI were performed before and 2-4 weeks after STI in 19 patients with 20 brain tumors. The tumors comprised metastases ($n = 11$), glioblastomas ($n = 3$), meningiomas ($n = 2$), schwannoma ($n = 1$), chordoma ($n = 1$), malignant lymphoma ($n = 1$), and PNET ($n = 1$). Stereotactic radiosurgery was performed for 7 tumors, and fractionated stereotactic radiotherapy was performed for 13 tumors. Regions of interest (ROIs) were set on ADC maps in tumor and peritumoral regions. ADC values were normalized ($nADC$) by dividing ADC values for tumor by values for normal brain in the contralateral cerebral hemisphere. Follow-up MR imaging was performed 8-12 weeks following STI to evaluate the tumor response to STI.

Results: Mean $nADC$ values in tumor after STI was significantly higher after STI (1.91 ± 1.67) than before STI (1.40 ± 0.99) ($p < 0.05$). Mean $nADC$ values following STI were significantly higher in tumors with response to STI (2.5 ± 1.9) than in tumors without response to STI (1.0 ± 0.36) ($p < 0.05$). Increased $nADC$ levels of tumors suggested increased diffusivity due to tumor necrosis and interstitial edema.

Conclusion: Tumor ADC changes via STI-induced alterations in tumor diffusivity. Increased ADC at completion of STI can predict treatment effect. DWI is clinically valuable for evaluating treatment response to STI.

Scientific Sessions

B-539 11:42

Pre- and postoperative DTI examination in patients with brainstem cavernoma

T.F. Beyer, J. Iwinska-Zelder, T. Dukatz, H. Bertalanffy, B. Tackenberg, U. Sure, S. Bien; Marburg/DE

Purpose: Diffusion-tensor imaging (DTI) has a broad range of applications by creating MR imaging-based quantitative maps of molecular water displacement in brain tissues. This imaging tool allows the direct examination of white matter fiber tracts *in vivo*. The aim of our study was to examine pre- and postoperatively patients with brain stem cavernomas in order to picture the eventual distortion or dislocation of the nervous tracts.

Methods and Materials: Forty three patients with brain stem cavernomas were prospectively evaluated by MR imaging (1.5 T Signa Tomograph; GE). In addition to the standard sequences we used DTI fractional anisotropy measurement presented by gray-scale and colored images. 9 patients were examined with Tensor-application preoperatively, 29 patients postoperatively and 5 patients pre- and postoperatively.

Results: MR imaging generated anisotropy maps correlated very well with clinical neurological symptoms. In the majority of postoperative cases we could recognize the elasticity of the nervous tracts, which were dislocated by huge cavernomas. In 16 cases of bleeding cavernomas, anisotropy maps showed the damage of white matter tracts, which corresponded very well with neurological impairment.

Conclusions: DTI proved to be very useful for clinicians to examine and visualize nervous tracts, which provides the possibility of observing the trajectories of fibers and the connectivity of the human brain *in vivo*. Clinical, neuroradiological and pathological aspects of brain stem cavernomas make this entity demanding. According to our experiences DTI has increased already the diagnostic possibilities of MR imaging.

10:30 - 12:00

Room N/O

Physics in Radiology

SS 1013

Digital radiography/Digital mammography

Moderators:

R.W.R. Loose; Nürnberg/DE
N. Theocharopoulos; Iraklion/GR

B-540 10:30

Initial clinical evaluation of a monolithic passive-element direct digital (MOPEDD) radiography system for orthopedic imaging

G. Bartal¹, A. Breitgand¹, U. Soimu¹, R. Sebie¹, J.M. Gomori²; ¹Hadera/IL, ²Jerusalem/IL

Purpose: Orthopedic practices are reliant on use of screen/film radiography. Computed Radiography (CR) provides the orthopedic surgeon an intermediate solution. Digital Radiography (DR) has good workflow benefits but is currently very expensive with limited availability. Our aim was to compare diagnostic performance of a new flat panel technology, suitable for general radiography (retrofits and new systems) with that of a conventional screen-film in orthopedic patients.

Methods and Materials: Extremities and spine images produced by a retrofit MOPEDD Radiography system (Edge Medical Devices, Ltd., Raanana, Israel) were compared to reference conventional screen-film radiographs of the same patients taken consequently in the same room. The MOPEDD detector has an active imaging area of 17" x 17", pixel size 127μm and 200-speed sensitivity. Three certified radiologists and a certified orthopedic surgeon independently analyzed the digital and conventional images, and rated the diagnostic quality using a five-point scale. Digital images were rated twice: On a laser film and on a high-resolution grayscale monitor. The diagnostic quality of MOPEDD was assessed using Receiver Operating Characteristic (ROC) curves.

Results: The inter-observer reliability was 76% for the analog film rating, 77% for the laser-film rating and 81% for the grayscale monitor rating. MOPEDD ROC under-the-curve area was 0.594 for laser-film rating and 0.790 for grayscale monitor rating.

Conclusions: The diagnostic quality of MOPEDD technology printed on a laser imager provides orthopedic images slightly better than, or comparable to, conventional screen-film radiography. The digital display of MOPEDD images is significantly superior to films acquired using screen-film radiography.

B-541 10:39



Multiple photodiode sensor array digital receptor for radiographic and fluoroscopic applications

A.A. Nevhasymy, S.I. Miroshnichenko, A.A. Redchuk; Kiev/UA

Purpose: Digital X-ray receptor basic technical characteristics requirements for radiographic and fluoroscopic applications are contradictory. Fluoroscopic operating mode assumes image sequence acquisition at high frame rates; radiographic - separate frames acquisition at high resolution. Decreasing patient dose demands force the device to operate at quantum limited mode for both applications. The presented patented multiple photodiode sensors array (MPSA) technology allows developing single digital receptors implementing both operating modes.

Methods and Materials: MPSA receptor implements "virtual pixel" ideology. "Virtual pixel" is formed by the analog charge packets merging in the output matrix register. Until the total dark current noise exceeds read-out noise, the signal-to-noise ratio increases near proportionally to the merged cells number. "Virtual pixel" dimensions vary from 12.8x12.8 to 51.2x51.2 um² for each of 36 sensors at 8x11 inches field of view to fulfill the sensitivity and resolution requirements for operation modes.

Results: "Virtual pixel" mode along with real-time frames reconstruction ensures image acquisition at 12.5fps rate, 1.1 lp/mm resolution and 2% contrast sensitivity at 50uR/sec exposure dose while operating in fluoroscopic mode and 3 lp/mm image acquisition and below 1% contrast sensitivity at 1 mR exposure dose for radiographic mode. The fluoro-to-radiography mode switching time is below 0.3 sec. The acquired images spacial distortions are below 0.5% and essentially better comparing to Image Intensifiers.

Conclusion: Presented "virtual pixel" digital receptor technology provides high flexibility in constructing dual-mode receptors for real-time demanding X-ray applications.

B-542 10:48

Novel noise-reduction processing algorithm for digital radiography

K.N. Jabri, G.B. Avinash, N. Marinelli, T. Merisotis, G. Joglekar, C. Deodhar; Waukesha, WI/US

Purpose: To evaluate image quality improvement achievable by a novel noise-reduction algorithm for digital radiography. The algorithm is designed to reduce noise in highly attenuated (dense) regions of an image without affecting contrast and edge-sharpness in relatively low-attenuated regions.

Methods and Materials: The algorithm segments images into structures and non-structures; structures are anisotropically smoothed and sharpened, while non-structures are isotropically smoothed. A fraction of the original image is blended with the processed image to obtain an output image with improved noise characteristics. The blending fraction is spatially modulated by detector-signal level and image-structure content. Image quality was evaluated by reviewing adult chest radiographs without and with three different levels of noise-reduction filtering (none, *low*, *medium*, *high*) with 3 radiologists. Another radiologist rated (scale of 1 to 7) the noise level in 10 small (age 0-3) and 10 medium (age 3-8) pediatric chest radiographs, before and after *medium* noise reduction.

Results: For images that were originally low-noise, radiologists preferred, by consensus, the *low* or *medium* settings. For images that were relatively noisy to begin with, the *medium* setting was preferred. After noise reduction, ratings of pediatric radiographs improved by an average of 25% and 53% for small and medium pediatric patients, respectively.

Conclusion: We developed a novel noise-reduction algorithm that can improve image quality of low-dose digital radiographs. The algorithm can be used for image quality enhancement at nominal dose levels, or as a dose reduction technique by acquiring radiographs at lower doses and processing them to maintain image quality.

B-543 10:57

Image detail detectability in digital radiography: Comparison of new needle structured storage phosphor with a powder structured storage phosphor and a flat-panel detector

M. Körner, M. Treitl, C. Herrmann, S. Mair, M.F. Reiser; Munich/DE

Purpose: To compare image detail detectability of a needle structured image plate (NIP), a powder structured image plate (PIP) and a flat-panel detector (FPD).

Methods and Materials: 12 radiograms of 6 human foot specimens were obtained using a prototype NIP (AGFA, Belgium) and a FPD (Siemens, Germany). The reference image of each specimen (80 μGy entrance surface dose) was obtained using a PIP system. Entrance surface dose for all NIP and FPD images was

Scientific Sessions

63 µGy. NIP images were scanned with a newly developed ScanHead scanner (AGFA). Different post-processing software (NIP, PIP: AGFA, FPD: Siemens) was used. Hardcopies were evaluated on a standardized light box. Image evaluation was performed by 5 radiologists blinded to the imaging modality. Images were compared to the reference with respect to detail detectability of cortical bone, trabecular bone and soft tissue, and with respect to artefacts and noise, using a five-point scale (-2 clearly inferior, -1 inferior, 0 equivalent, +1 superior, +2 clearly superior to reference). Image quality was rated independently with marks 1-5.

Results: NIP images were rated superior to FPD and PIP concerning cortical bone (NIP: 1.267, FPD: 0.233), trabecular bone (NIP: 1.700, FPD 0.100), soft tissue (NIP: 0.867, FPD -0.233) and noise (NIP: 1.033, FPD: 0.767). Image quality of the was rated optimal (1.113) for NIP and good for FPD (1.900). Artefact rate of NIP images was slightly higher in the image background (-0.300).

Conclusion: Radiograms obtained with the new NIP were rated superior to both PIP and FPD for detail detection.

B-544 11:06

Radiation dose measurements and image quality evaluation in scoliosis radiography: Flat panel detector versus digital pulsed fluoroscopy

O. Heuga, O. Hauger, O. Bonnefoy, F. Diard, J.-F. Chateil; Bordeaux/FR

Purpose: To evaluate the radiation dose and the image quality of scoliosis radiography obtained with a flat panel detector versus digital pulsed fluoroscopy. **Methods and Materials:** Routine follow-up scoliosis evaluation was obtained from 120 consecutive patients using a digital pulsed fluoroscopy system (Siemens Iconos R 200, 60 patients) or a flat panel detector system (Siemens Aristos VX, 60 patients). Reconstructions were performed on a Leonardo Hardware System. Radiation dose was measured as kerma area-product and as entrance surface dose with three thermoluminescent dosimeters (TLD technology) placed on the thyroid, chest and gonads. Image quality was evaluated by two senior radiologists according to 19 specific items using a four point scale. An unpaired student t-test and a χ^2 test were respectively used for statistical comparison of entrance dose and qualitative assessment of both techniques.

Results: Dose measurements showed a statistically very significant ($p < .0001$) difference with the flat panel detector compared with the digital pulsed fluoroscopy with an estimated dose reduction of 72%. The image quality and visibility of anatomic structures obtained with the digital flat panel detector system were also rated significantly greater ($p < .01$) to those obtained with the digital pulsed fluoroscopy.

Conclusion: Compared to digital pulsed fluoroscopy, flat panel detector showed a major radiation dose reduction (72%) and a better image quality making it a very interesting technique in routine follow-up scoliosis.

B-545 11:15

A comparison of image quality and dose for digital flat panel detector and image intensifier fluoroscopy systems

C.P. Lawinski, H. Cole, A. Mackenzie; London/UK

Purpose: Many manufacturers now offer flat panel detectors for cardiac and other fluoroscopic applications in preference to image intensifiers. These offer certain advantages including compact design, improved geometric distortion and noise characteristics and the potential for improved image quality at lower dose levels. Comparative measurements of the imaging performance and dose characteristics were made on flat panel detector systems for cardiac applications from three major manufacturers. The results were also compared to those for cardiac image intensifier systems.

Methods and Materials: Image quality was assessed using typical threshold contrast detail detectability test objects under standard beam conditions at the recommended detector input exposure levels for each system. Detection index diagrams were plotted and, to aid comparison, the data was dose corrected to a mean exposure level. High contrast limiting spatial resolution was also measured.

Results: For fluoroscopy, the imaging performance of the flat panel systems was generally better than the equivalent image intensifier systems. In the digital acquisition mode the flat panel detectors again generally showed better performance. Unlike image intensifier systems, due to the pixelated nature of flat panel detectors, spatial resolution does not improve as the magnification is increased (field size reduced) but remains constant (depending on the pixel pitch). As expected, for all the flat panel systems geometric distortion and vignetting were insignificant. The detector input exposure levels were comparable for flat panel detectors and image intensifier systems.

Conclusions: In general, flat panel detector systems exhibit improved image quality over image intensifier systems at comparable exposure levels.

B-546 11:24

Scatter-to-primary evaluation in full field digital mammography

G. Gennaro¹, E. Bellan¹, M. Gambaccini², C. di Maggio¹; ¹Padua/IT, ²Ferrara/IT

Purpose: To quantify scatter radiation contribution in digital mammography and compare scatter-to-primary (SPR) ratios obtained by two different experimental methods.

Methods and Materials: SPR was evaluated as a function of both phantom thickness and beam energy, using the edge technique and the beam-stop method. Images were acquired without anti-scatter grid by a clinical digital mammography unit (GE Senograph 2000D). Both edge and beam-stops were obtained by a lead slab, 3 mm thick, absorbing the incident X-ray beam completely. The edge covered half of the field of view, whilst beam-stop diameters ranged between 4 and 40 mm. Grid absorption was also evaluated in terms of Bucky factor and contrast improvement factor.

Results: Images of phantoms with different thickness, acquired with and without grid, showed a Bucky factor greater than 2. SPR versus kV value, for phantoms 4 and 6 cm thick, revealed a weak dependence from beam energy; a quasi-linear trend of SPR versus phantom thickness was exhibited from 0.10 up to 0.75 for PMMA slabs between 1 and 8 cm. Scatter-to-primary ratios measured by edge and beam-stop techniques were comparable. Experimental results showed a good agreement with those published on literature.

Conclusions: Digital mammography permits proper quantification of the contribution of scatter radiation. The edge method appeared as reliable and preferable to the beam-stop method, but was more time consuming. There is a possibility of using the results to carry out a scatter correction algorithm; this could be applied to breast images acquired without grid, permitting a significant patient dose saving.

B-547 11:33

Physical characterization of the new FFDM system based on an a-Se detector

T. Mertelmeier, L. Bätz; Erlangen/DE

Purpose: To describe the physical performance of the new FFDM system Siemens Mammomat Novation^{DR} employing a large-area solid state detector based on direct conversion with amorphous selenium.

Methods and Materials: This detector is characterized by a usable area of 287 mm by 241 mm, and a pixel pitch of 0.07 mm corresponding to a Nyquist frequency of 7.1 lp/mm. For physical characterization we measured the gain factor, the linearity and the dynamic range. Spatial resolution is quantified by the modulation transfer function (MTF). The noise properties are described by the Noise Power Spectrum (NPS). From the X-ray spectrum and the measured quantities the Detective Quantum Efficiency (DQE) is determined as 2-D function of spatial frequency. The measurements are carried out according to the new IEC standard for DQE measurements.

Results: For example, the gain characteristic of the detector is strictly linear with entrance air kerma in a wide range of exposures. The MTF at Nyquist frequency turned out to be larger than 0.4. For a detector exposure of 60 microGy the DQE exceeds 0.6 at zero frequency and 0.15 at 7 lp/mm. The DQE is nearly independent of dose for exposure values larger than 30 microGy. Finally we present clinical images of early clinical installations.

Conclusion: The image quality of this detector can be considered as very satisfactory. Together with the unique features of the FFDM system, the selenium direct converting detection provides the potential to substantially reduce patient dose at superb image quality.

B-548 11:42

Characterization of CDMAM image observers

R. VanMeter¹, L. Fletcher-Heath²; ¹Washington, DC/US, ²Rochester, NY/US

Purpose: The "European Guidelines for Quality Assurance in Mammography Screening: Addendum on Digital Mammography" prescribes criteria for threshold contrast visibility based on images of the CDMAM phantom. The goals of this study were to: Quantify the performance of a group of CDMAM phantom observers; compare their performance with published scorings; compare visual scorings with software scorings generated by CDDCOM; analyze the performance of software scorings used as a prediction for visual observation; and understand the sources of variability associated with the prescribed protocols.

Methods and Materials: CDMAM phantom images downloaded from the EUREF website were compared using three scorings and two analysis methods. The scores included those of four expert readers from the EUREF website, 13 experienced observers from our laboratory, and those generated by the CDDCOM

Scientific Sessions

software. These were analyzed with the method described in the CDMAM-phantom 3.4 user manual and by a signal detection theory-based method.

Results: The average contrast sensitivity of our 13 observers and the published values were not significantly different. However, the 95% confidence limits for our observers averaged 38%, while those for the published data averaged 24.9% - with ANOVA showing significant interobserver variability. The software results were substantially different from both visual results, particularly for the small diameter targets. However, using the signal detection theory analysis significantly reduced these differences.

Conclusions: CDMAM scoring requires substantial time, and the results exhibit substantial variability. This suggests that further development of reliable software methods will be of considerable importance for practical implementation of threshold contrast visibility testing.

B-549 11:51

Dose reduction by technique optimization for FFDM based on an amorphous selenium detector

T. Mertelmeier¹, P. Bernhardt², M. Hoheisel², N. Palmberg¹; ¹Erlangen/DE, ²Forchheim/DE

Purpose: To optimize the radiographic technique for a new full-field digital mammography system based on an amorphous selenium detector by varying the anode/filter combinations.

Methods and Materials: The exposure parameters, i.e. anode material, tube voltage, filter material and thickness, are optimized by simulation and phantom experiments. Figure of merit (FOM) is the squared signal difference-to-noise ratio divided by the mean glandular dose. The simulations with both, monochromatic X-rays and real spectra, take into account the absorption properties of the new a-Se detector and scattered radiation, with and without grid, using Monte-Carlo methods. Breast equivalent phantoms (50% fat, 50% glandular; 30% fat, 70% glandular; 70% fat, 30% glandular) with breast thicknesses between 2 and 8 cm and additional lesion are used for simulations and measurements. The measurements are carried out with the FFDM system Siemens Mammomat Novation^{DR} employing a dual target (molybdenum (Mo) and tungsten (W)) anode with Mo and rhodium (Rh) filtration, respectively.

Results: We present results for constant image quality. The W/Rh combination gives a higher FOM than Mo/Mo or Mo/Rh for almost all cases investigated. With thick phantoms, up to 50% less dose is sufficient to maintain a constant image quality. The simulation results are confirmed by the phantom experiments.

Conclusion: For the specific a-Se-based system studied, a W anode with Rh filtration achieves higher image quality than Mo/Mo. Keeping the image quality constant, W/Rh allows to reduce dose by up to 50% compared to Mo/Mo.

10:30 - 12:00

Room P

Vascular

SS 1015

Imaging of stenosis, aneurysm and dissection in the abdominal vessels

Moderators:

M. Stajgis; Poznan/PL
J.K. Willmann; Zürich/CH

B-550 10:30

Diagnostic accuracy of multidetector-row CT angiography (MDCTA) using 4, 8 and 16-row CT scanners in diseases of the abdominal aorta and aortic major branches: Results of a European multicenter prospective clinical trial

M. Nonent¹, F. Thouveny², P. Simons³, O. Cappeliez⁴, M.F. Reiser⁵, V. Duddalwar⁶, L. Bonomo⁷, G. Liessi⁸, ¹Brest/FR, ²Angers/FR, ³Aalst/BE, ⁴La Louvière/BE, ⁵Munich/DE, ⁶Aberdeen/UK, ⁷Chieti/IT, ⁸Castelfranco Veneto/IT

Purpose: To assess the accuracy and utility of MDCTA compared to surgery, vascular intervention or digital subtraction angiography (DSA) in the diagnosis of aortic disease.

Methods and Materials: 173 patients with known/suspected abdominal aortic or aortic major branches disease (stenosis or aneurysm) were prospectively enrolled in 7 European countries (14 centres). Iso-osmolar iodixanol (Visipaque™) 320 mg I/ml was injected at mean flow-rate of 3.8 ml/s (2.4-5.0 ml/s) and mean volume of 120.5 ml (80-150 ml). Saline chaser was injected in 55 (31.8%) patients. Scan delay was determined by bolus tracking (98.3%) or test bolus (1.7%). Images

were acquired on 4 (n = 63), 8 (n = 24) and 16 (n = 86) detector-row CT scanners using the routine acquisition and reconstruction parameters at each centre. MDCTA and reference diagnoses were assessed on-site and compared.

Results: 136 patients had a referral diagnosis of aneurysm (n = 75) or stenosis (n = 61), established either on surgical findings (22.1%), angiography during vascular intervention (17.6%) or DSA (60.3%). Image quality of MDCTA was excellent (85.0%) or good (13.3%), with a mean aortic attenuation of above 300 HU. MDCTA diagnosis matched the referral diagnosis in 132 out of 136 patients, yielding an agreement rate of 97.1% (95% CI [92.6, 99.2]). The four non-matches were in patients with a referral diagnosis based on DSA. One patient reported pain upon injection of iodixanol.

Conclusions: MDCTA using iodixanol 320 mg I/ml showed high diagnostic accuracy and utility in patients with aortic or aortic major branch disease. Tolerability was good. This study indicates that MDCTA can replace DSA for this indication.

B-551 10:39



Non-rigid registration for subtraction CT angiography of the abdomen and evaluation of various regularization models

S. Drisis, D. Seghers, S. Srivastava, E. D'Agostino, F. Maes, G. Marchal; Leuven/BE

Purpose: Subtraction CT Angiography of the abdomen is affected by artifacts related to misalignment of corresponding high-intensity structures in the pre- and post-contrast images due to motion and local deformation. The use of non-rigid image registration using different regularization models was investigated to optimally align both images prior to subtraction.

Materials and Methods: Pre- and post-contrast CT images of the abdomen of 5 patients with voxel size of $0.72 \times 0.72 \times [0.5-1] \text{ mm}^3$ were acquired using a 16-slice multi-detector CT scanner (Sensation16, Siemens, Erlangen). Each image pair was first globally aligned by Rigid Registration (RR) and subsequently the post-contrast image was locally deformed to the pre-contrast by Non-Rigid Registration (NRR) using maximization of mutual information. Various regularization schemes for NRR were evaluated, imposing elastic, viscous fluid or curvature-based constraints on the deformation. To evaluate registration quality achieved with each regularizer, objects of interest, bones and plaques, were manually delineated in each data set and the percentage of overlap of 223 object pairs after NRR was computed.

Results: Overall overlap values for bone varied between 88.88% for RR to 89.66% for curvature NRR, but differences between methods were not significant. Overall overlap values for plaques varied between 63.35% for RR to 69.82% for viscous fluid NRR. Viscous fluid NRR performed significantly better than RR ($p < 6 \times 10^{-7}$) and curvature-based NRR ($p < 0.006$) and marginally better than elastic NRR ($p = 0.063$).

Conclusion: Viscous fluid NRR significantly improves the alignment of structures in SCTA. However further development of more effective algorithms is essential for clinical use.

B-552

withdrawn by authors

B-553 10:48

PET/CT in patients with acute aortic syndrome

H. Kuehl, H. Eggebrecht, P. Veit, G. Antoch, R. Erbel, J. Barkhausen; Essen/DE

Purpose: The acute aortic syndrome (AAS) is a potentially life-threatening disease. The aim of our study was to investigate whether PET-CT allows prediction of patients' outcome.

Methods and Materials: 20 patients with acute aortic syndrome (aneurysm TAA = 4, dissection TAD = 5, perforated aortic ulcer PAU = 6, intramural hematoma IMH = 5) were enrolled into this study. All exams were performed on a PET-CT scanner (Biograph, Siemens) 1 h after iv-administration of FDG and with iv-contrast. Follow-up CT exams were performed at 1, 3 and 6 months.

Results: 9 of 20 patients showed elevated tracer uptake in the aortic wall, whereas 11 patients were PET-negative. 7/9 PET-positive patients (78%) showed either progression from PAU or IMH to TAA or progression of the TAD. One of these patients with type-B dissection was treated by a stentgraft. 2/9 PET-positive patients showed a normalization of the glucose metabolism under anti-inflammatory therapy for inflammatory TAA. 6/11 PET-negative patients (55%) showed stable disease or regression of TAD-B or IMH during the follow-up period, whereas 5/11 (45%) patients showed progression of the AAS.

Scientific Sessions

Conclusions: In acute aortic syndrome PET-positive patients seem to be at higher risk for disease progression. The combination of morphologic and metabolic imaging might be able to predict patients' outcome. However, our results need to be confirmed in a larger patient cohort with acute aortic syndrome.

B-554 10:57 ♂

Demonstration of the sites of communication between true and false lumen in chronic aortic dissection with phase-contrast sequences

G.P. Spanos, I. Oikonomou, C. Kouskouras, A. Sarafopoulos, C. Giavroglou, I. Tsifountoudis, A.S. Dimitriadis; *Thessaloniki/GR*

Purpose: Our objective was to establish the sites of communication between true and false lumen, for assessment and planning of the intervention in patients with chronic aortic dissection.

Methods and Materials: During the last year, 9 patients with chronic aortic dissection (1 with dissection type A and 8 with type B according to the Stanford classification) were scanned at 1.5 T (Philips Intera and GE Infinity with EXCITE). Bright-blood sequences in three planes and contrast-enhanced 3D MR angiography were performed in all patients. A quick assessment of the angiography was followed by the use of multiplanar reformations in order to detect sites of communication. A localized phase-contrast sequence was used to confirm the site of the communication. An intraarterial DSA was performed in 7 patients after the MRA.

Results: Entry and re-entry tears were easily depicted with the 3D MR angiography. 15 sites of communication, apart from entry and re-entry sites, were found at 3D-MRA. 13 out of these 15 sites were demonstrated with phase-contrast sequence (sensitivity 100%- specificity 100% for phase-contrast technique, and sensitivity 100%- specificity 86% for 3D-MRA). All these sites were verified with DSA.

Conclusion: The use of focused phase-contrast sequences following 3D-MRA is an easily-applied, sensitive method for the evaluation of sites of communication in patients with chronic aortic dissection. Assessment of these sites is critical for planning intervention, especially those between the entry and re-entry tears, which are difficult to depict with intraarterial DSA.

B-555 11:06

Evaluation of aortic dissection: The role of ultra-fast three-dimensional dynamic contrast-enhanced magnetic resonance aortography

B. Jiang, Q. Meng, Y. Chen, B. Pan; *Guangzhou/CN*

Purpose: To assess the role of ultra-fast three-dimensional dynamic contrast-enhanced magnetic resonance aortography (UF 3D DCEMRA) in evaluating aortic dissection.

Methods and Materials: Twenty-four patients with aortic dissection underwent UF 3D DCEMRA in which the sequence of 3D Flash TurboMRA was used with the acquisition time at 8 sec and three consecutive phases of UF 3D DCEMRA images were obtained. The UF 3D DCEMRA were assessed for the detection of the intimal entrance tear and the origination of the celiac trunk (CT), superior mesenteric artery (SMA) and renal arteries (RA). The results were correlated with angiography.

Results: The tri-phasic display of the true lumen and false lumen of the aortic dissection were achieved in all 24 patients. 38 intimal entrance tears were detected on UF 3D DCEMRA in 24 patients, of which 21 were identified on the 1st phase, 13 on the 2nd phase and 4 on the 3rd phase. 41 intimal entrance tears were detected on angiography. The accuracy of intimal entrance tear-detection on UF 3D DCEMRA was 92.7%. 2 CT, 3 SMA and 5 RA were noted arising from the false lumen and the other 86 arteries from the true lumen on either UF 3D DCEMRA or angiography. The accuracy of the origination-detection by UF 3D DCEMRA of the 4 arteries was 100%.

Conclusion: UF 3D DCEMRA plays a vital role in the detection of the intimal entrance tear and the origination of aortic dissection.

B-556 11:15

MR evaluation of abdominal aorta: True-FISP versus Gd-enhanced MR angiography (Gd-MRA)

A. Iozzelli, G. D'Orta, T. Lupattelli, F. Sardanelli; *Milan/IT*

Purpose: To test true-FISP versus Gd-MRA for imaging abdominal aorta and major abdominal vessels.

Materials and Methods: Thirty-five consecutive patients (age 67 ± 11 years) with suspected abdominal and/or peripheral vascular disease underwent 2D true-FISP [TR/TE = 4.3/2.2 ms; FA 74°; NEX 2; thickness 3 mm (sagittal) or 5 mm (axial); 48 contiguous slices; pixel 1.4x1.4 mm; time 50 s (sagittal) or 73 s (axial) during

free breathing] and coronal 3D FLASH Gd-MRA (TR/TE = 3.3/1.2 ms; FA 25°; NEX 1; thickness 1.3 mm; pixel 1.4x0.8; breath-holding 24 s; 0.1 mmol/kg of Gd-DOTA at 2 ml/sec). We evaluated: suprarenal aorta, celiac trunk, superior mesenteric artery, right renal artery, left renal artery, infrarenal aorta, inferior mesenteric artery, aortic bifurcation/common iliac arteries, lumbar arteries, accessory renal arteries, collateral vasculature, aortic atheroma, and vascular prosthesis/stent. A quality score (0=non visible; 1=poor; 2=fair; 3=good) was assigned to each item on both sequences. Wilcoxon test.

Results: Main diagnosis: normal/atheromatous aorta (n = 26); aortic aneurysm (n = 4); patent vascular stent (n = 2); aneurysm of iliac arteries (n = 1); patent aortic prosthesis (n = 1); patent aorto-femoral bypass (n = 1). The score of true-FISP (25.9 ± 4.1 , median 27) was significantly greater than that of Gd-MRA (23.9 ± 3.6 , 24) ($p = 0.003$). True-FISP was better in visualizing inferior mesenteric artery (score 2.46 vs 1.00; $p < 0.001$) and detecting atherosomatic plaques (2.49 vs 1.23; $p < 0.001$). One collateral vasculature was demonstrated only with Gd-MRA.

Conclusions: True-FISP is a powerful and fast non-breath-hold sequence to be added to Gd-MRA, obtaining increased information. It can be used in non-cooperative patients and in cases of contraindication to contrast administration.

B-557 11:24

High-resolution (HR) renal magnetic resonance angiography (MRA): Prospective comparison of image quality and diagnostic value using integrated parallel acquisition techniques (iPAT) - factor 2 versus 3

H.J. Michaely, K.A. Herrmann, H. Kramer, M.F. Reiser, S.O. Schoenberg; *Munich/DE*

Purpose: To systematically compare the image quality and diagnostic value of renal HR-MRA using iPAT with acceleration factors of 2 and 3.

Material and Methods: 26 patients scheduled for renal MRA were included. All examinations were performed on a 32-channel whole body MR-scanner (Siemens Magnetom Avanto). For HR-MRA, a 3D GRE sequence with a spatial resolution of 0.9 mm x 0.9 mm x 1 mm and an iPAT factor of 2 (12 patients, acquisition time (TA) 28 sec) or an iPAT factor of 3 (14 patients, TA 19 sec) was applied. All other parameters were kept constant. Either 15 ml of gadobutrol or 25 ml of gadobenate dimeglumine were administered followed by a 30 ml saline flush, both at a flow rate of 2 ml/sec. Three independent radiologists analyzed the MRA images on 10 mm thin coronal MIPs regarding noise, artifacts and quality of depiction of the renal arteries (RA) using a three point rating scale. The RAs were assessed in four separate segments: ostium, proximal (until 1st division), segmental (until 2nd division) and sub-segmental portions.

Results: With iPAT factor 3, the noise increased significantly but the amount of motion artifacts was decreased significantly. Ostial and proximal portions of the RA were equally well delineated with both techniques. Segmental and subsegmental portions were significantly better depicted ($p < 0.001$) using an iPAT factor of 3.

Conclusion: The shorter scan time associated with iPAT factor 3 allows a better visualization of the peripheral segmental and subsegmental portions of the renal arteries. Increased noise seems not to be a diagnostic drawback.

B-558 11:33

Towards the identification of specific anatomic features of the renal artery influencing the results of renal artery percutaneous recanalization

I. Bargellini, M. Lazzereschi, C. Vignali, P. Petrucci, R. Cioni, V. Zampa, C. Bartolozzi; *Pisa/IT*

Purpose: To retrospectively identify the relationship between specific anatomic features of the renal artery and immediate and long-term results of renal artery percutaneous recanalization in patients with renovascular disease and atherosclerotic significant stenosis.

Materials and Methods: The study included 113 patients (134 lesions) with atherosclerotic significant (> 60%) renal artery stenosis and renovascular disease treated by PTCA (n = 44) or stenting (n = 90). Preprocedurally, MRA or CTA were performed in all patients. Images were retrospectively reviewed, to assess specific anatomical features of the stenosis such as site, grade, length, and presence of calcifications. Procedural data (balloon and stent length and diameters) were recorded, as well as immediate complications (residual stenosis, arterial dissection, distal embolization) and restenosis on follow-up.

Results: In the PTCA group, minor complications (not requiring further interventions) occurred in 7/43 (16.3%) patients and were significantly associated ($p < 0.05$) with higher stenosis grade, longer balloons, and smaller diameter balloons; restenosis on follow-up was observed in 7/43 patients (16.3%) and was more frequent when lower balloon oversizing was applied during the procedure.

Scientific Sessions

In the stent group, minor immediate complications were observed in 7/90 (7.8%) cases and in-stent restenosis on follow-up occurred in 14/90 (15.6%) cases. Immediate complications were significantly more frequent when longer stents were deployed ($P = .004$). No significant relationship was found between in-stent restenosis and morphological/procedural data.

Conclusion: The accurate assessment of lesion anatomy on MRA/CTA images could improve procedural planning, allowing selection of the proper devices to reduce the incidence of immediate complications.

B-559 11:42

Prevalence of renal artery stenosis in flash pulmonary oedema:

Determination using gadolinium-enhanced MRA

C.J. McMahon, M. Hennessy, G. Boyle, J. Feely, J.F.M. Meaney; Dublin/IE

Purpose: Flash pulmonary oedema, the association of recurrent acute onset pulmonary oedema in association with renal artery stenosis (RAS) is well known, as is the dramatic response to renal revascularization. However, the prevalence of RAS in patients with flash pulmonary oedema is unknown.

Materials and Methods: Contrast-enhanced MRA (CE-MRA) of the renal arteries was performed in patients with unexplained episodes of acute pulmonary oedema, to determine whether RAS could potentially be a contributory factor. Clinical parameters (blood pressure, serum creatinine, history of hypertension or hyperlipidaemia) were compared in patients with RAS and patients without RAS using an unpaired t-test. Results expressed; mean \pm SD.

Results: 20 eligible patients (4 male, 16 female, age 78.5 ± 11 years) underwent CE-MRA of renal arteries. 45% of patients had significant RAS ($> 50\%$ reduction of diameter). In two thirds of cases bilateral RAS was detected. Systolic BP was significantly higher in patients with RAS (191.9 ± 38.3 mmHg) than those without RAS (134.2 ± 29.6 mmHg) ($p < 0.005$). Diastolic BP was also significantly higher in patients with RAS (101.7 ± 22.8 mmHg) than those without RAS (76.1 ± 16.8 mmHg) ($p < 0.01$). All 11 patients with RAS and 5/9 patients (55%) without RAS had a history of hypertension. No significant differences in creatinine or hyperlipidaemia history were observed.

Conclusion: Renal artery stenosis causes flash pulmonary oedema and we recommend that renal artery stenosis should be actively excluded in all patients with unexplained recurrent pulmonary oedema. Contrast-enhanced MRA allows detection of renal artery stenosis without use of arterial catheterization, ionizing radiation or nephrotoxic iodinated contrast agents.

Scientific Sessions

Monday, March 7

Scientific Sessions

		room A 2nd level	room B 2nd level	room C 2nd level	room E1 entr. level	room E2 entr. level	room F1 entr. level	room F2 entr. level	room G lower level	room H lower level	
07:00											07:00
07:30											07:30
08:00											08:00
08:30											08:30
09:00		CC 1317 Essentials of Neuroradiology Craniocerebral and spinal trauma (p. 92)	RC 1310 Musculoskeletal Shoulder joint (p. 92)	SF 13 Special Focus Session MR imaging of the small intestine (p. 93)	RC 1302 Breast Digital mammography (p. 94)	RC 1301 Abdominal and Gastrointestinal Imaging of the pancreas: Key questions (p. 95)	RC 1306 Molecular Imaging and Contrast Media Molecular imaging (p. 96)	RC 1311 Neuro MR spectroscopy of the brain in clinical practice (p. 96)	RC 1307 Genitourinary Multislice CT of the urinary tract (p. 97)	RC 1309 Interventional Radiology Percutaneous tumor ablation (p. 98)	09:00
09:30											09:30
10:00											10:00
10:30		SA 14 State-of-the-Art Symposium Imaging of prostate cancer: Present and future (p. 102)	SS 1410 Musculoskeletal Imaging of the arthritis and periarthritis tissues (p. 262)	SS 1401a GI Tract MR imaging of the abdomen (p. 264)	ECR General Assembly	SS 1402 Breast Mammography and ultrasound (p. 266)	SS 1404 Chest Pulmonary embolism: Imaging technique and outcome (p. 268)	SS 1401b Abdominal Vissera (Solid Organs) Contrast enhanced US of the liver and spleen (p. 270)	SS 1407 Genitourinary CT imaging of the urinary tract (p. 272)	SS 1409a Interventional Radiology Thermal ablations in lung and liver (p. 274)	10:30
11:00											11:00
11:30											11:30
12:00											12:00
12:30											12:30
13:00											13:00
13:30											13:30
14:00											14:00
14:30		EM 3 "ECR meets" Japan "Oriental Pearls" in oncology imaging (p. 105)	SS 1510 Musculoskeletal Advanced MR imaging techniques (p. 287)	SS 1501a GI Tract CT colonography (p. 289)	SY 15 Satellite Symposium Open PET/CT imaging in diagnosis and treatment (p. 588)	SS 1504 Chest CT and MR imaging in emphysema and COPD (p. 291)	SY 16 Satellite Symposium Latest advances in musculo-skeletal and nerve ultrasound (p. 588)	SS 1501b Abdominal Vissera (Solid Organs) Focal liver lesions: MDCT, MR imaging and PET-CT (p. 293)	SS 1507 Genitourinary Lower urogenital tract (p. 295)	SS 1502 Breast Interventional procedures (p. 297)	14:30
15:00											15:00
15:30											15:30
16:00		CC 1617 Essentials of Neuroradiology Degenerative disorders, tumors and infection of the spine (p. 106)	EAR General Assembly	SF 16 Special Focus Session Pulmonary hypertension: All that the radiologist needs to know (p. 107)	RC 1602 Breast Radiopathological correlation (p. 108)		RC 1604 Chest Thoracic manifestations of extra-thoracic disease (p. 109)	RC 1610 Musculoskeletal Inflammatory joint disease (p. 109)	RC 1608 Head and Neck Imaging of skull base tumors: A practical approach for your daily practice (p. 110)	WS 1609 Interventional Radiology Percutaneous access to the abdomen (p. 111)	16:00
16:30											16:30
17:00											17:00
17:30											17:30
18:00											18:00
18:30											18:30
19:00											19:00

EPOS™ - scientific exhibition

Scientific Sessions

	room I lower level	room K lower level	room L/M 1st level	room N/O 1st level	room P lower level	room W basement	room X 1st level	room Y 1st level	room Z entr. level	La Scala 2nd level	
07:00											07:00
07:30											07:30
08:00											08:00
08:30	ER 1326 Joint ECR/EAR sessions: Challenges for European Radiology Teleradiology: Threat or opportunity? (p. 99)	RC 1312 Pediatric Neonatal problems (p. 100)	RC 1314 Radiographers Professional matters (p. 100)	RC 1313 Physics in Radiology Quality control and dose reduction in digital radiology (p. 101)	WS 1321 Musculo-skeletal US "Hands-on" Workshop				WS 1324 Basic Life Support for Radiologists "Hands-on" Workshop	E³ 1320 Interactive Image Teaching Paranasal sinuses (p. 102)	08:30
09:00								WS 23D1 Screening Mammography Interpretation Test "Hands-on" Workshop			09:00
09:30											09:30
10:00								WS 23D2 Screening Mammography Interpretation Test "Hands-on" Workshop			10:00
10:30	SS 1409b Interventional Radiology Peripheral vascular interventions (p. 276)	SS 1412 Pediatric Neuro-imaging (p. 278)	SS 1403 Cardiac MR imaging of the coronary arteries (p. 280)	SS 1413 Physics in Radiology CT: Technical developments (p. 283)	SS 1406 Molecular Imaging Targeting and PET imaging (p. 285)		WS 1421 Musculo-skeletal US "Hands-on" Workshop	WS 1424 Basic Life Support for Radiologists "Hands-on" Workshop	E³ 1420 Diagnostic workstations: The new super-assistants of the radiologist and surgeon (p. 103)		10:30
11:00							WS 1423 Screening Mammography Interpretation Test "Hands-on" Workshop				11:00
11:30											11:30
12:00								WS 23D4 Screening Mammography Interpretation Test "Hands-on" Workshop			12:00
12:30											12:30
13:00											13:00
13:30											13:30
14:00								WS 23E1 Screening Mammography Interpretation Test "Hands-on" Workshop			14:00
14:30	SS 1506a Contrast Media Specific MR imaging contrast media (p. 298)	SS 1512 Pediatric Novel imaging approaches (p. 301)	SS 1511 Neuro Cerebrovascular disease: Endovascular treatment and non-invasive follow-up (p. 303)	SS 1513 Physics in Radiology Radiation protection/Image quality (p. 305)	SS 1506b Molecular Imaging Cellular and molecular imaging (p. 307)			WS 1524 Basic Life Support for Radiologists "Hands-on" Workshop	E³ 1520 Interactive Image Teaching Cervical spine trauma (p. 106)		14:30
15:00								WS 23E2 Screening Mammography Interpretation Test "Hands-on" Workshop			15:00
15:30											15:30
16:00								WS 23E3 Screening Mammography Interpretation Test "Hands-on" Workshop			16:00
16:30	WS 1615 Vascular Imaging of atherosclerotic plaques (p. 112)	RC 1612 Pediatric Emergencies in pediatrics (p. 113)	RC 1614 Radiographers CT (p. 113)	RC 1613 Physics in Radiology Justification and optimization of multislice CT (MSCT) examinations (p. 114)							16:30
17:00											17:00
17:30											17:30
18:00											18:00
18:30											18:30
19:00											19:00

Monday

Scientific Sessions

10:30 - 12:00

Room B

Musculoskeletal

SS 1410

Imaging of the arthritis and periarticular tissues

Moderators:

M. Østergaard; Hvidovre/DK

H. Pettersson; Lund/SE

B-560 10:30

Heterotopic ossification in critically ill patients: Early diagnosis with MR imaging

E. Kostanti, A. Zikou, P. Kosta, D. Kastani, E. Galiatsou, A. Kitsakos, M.I. Argyropoulou, G. Nakos; Ioannina/GR

Purpose: Heterotopic ossification (HO) of the para-articular tissues is a potential complication in critically ill patients. We report a series of HO in the intensive care unit (ICU), which were diagnosed early with MR imaging.

Material and Methods: Thirty-one consecutive patients were included in the study. Sixteen had musculoskeletal or neurogenic trauma, while 15 had no recognized predisposing factor. Appropriate passive range-of-motion exercises were performed on a daily basis. Alkaline phosphate (ALP), Ca, P and CRP were measured on admission and every 4 days. Upon clinical suspicion of HO, conventional radiographs were performed in all patients and MR imaging in 8 of them. Three patients underwent a second MR imaging one month later.

Results: The most frequently involved joints were the knees (67.7%), the hips (64.5%) and the elbows (29%). ALP showed an acute elevation at 16.4 ± 7.7 days after admission, while the physical signs of HO became evident at 19.7 ± 7.2 days. MR imaging became positive for HO at 19.8 ± 7.3 days while conventional radiographs at 35 ± 7.7 days after admission. At early stage of HO, MR imaging of the knee joint depicted oedema of the subcutaneous fat and joint effusion associated with synovial enhancement. Moreover, the vastus medialis and lateral femoral muscles exhibited high signal on T2-weighted scans and intensive enhancement after intravenous contrast (Gadolinium-DTPA) injection. The follow-up MR imaging showed disappearance of the intra-articular fluid and synovial enhancement along with a decrease of muscular enhancement.

Conclusion: MR imaging is helpful in early detection of HO and may be included in the diagnostic work-up of these patients.

B-561 10:39

MR imaging involvement of the hands in early rheumatoid arthritis:

Comparison with systemic lupus erythematosus and primary Sjogren syndrome

N. Boutry, E. Hachulla, R.-M. Flipo, B. Cortet, A. Cotten; Lille/FR

Purpose: To compare magnetic resonance (MR) imaging involvement of the hands in patients with early rheumatoid arthritis (RA) with that of patients with lupus erythematosus (SLE) or primary Sjogren syndrome.

Method and Materials: Twenty-eight patients (16 women, 12 men; mean age, 42 years) with early RA and 19 patients (18 women, 1 men; mean age, 46 years) with SLE ($n = 14$) or primary Sjogren syndrome ($n = 5$) underwent MR imaging of both hands. They had presented with inflammatory polyarthralgia of the hands and no evidence of erosive changes on X-rays. Coronal STIR T2-weighted images, axial T1-weighted SE images, axial fat suppressed gadolinium-enhanced T1-weighted SE images, and axial gadolinium-enhanced 3D GE images were obtained. The following MR variables were assessed in the wrist and MCP joints: synovitis, bone lesions (erosion, defect, and edema) and tenosynovitis. Scoring of synovitis and bone lesions was done using the OMERACT RA-MR imaging score. Comparisons between patients with RA and those without RA were done using Mann-Whitney and Chi² tests.

Results: The only significant difference between the 2 groups was the presence of tenosynovitis of the right 4th extensor tendon in non-RA patients. There was no significant difference between RA and non-RA patients in terms of global scores for synovitis, bone lesions and tenosynovitis. However, in the MCP joints, bone marrow edema was seen most frequently in RA patients (71%), compared to non-RA patients (5%).

Conclusion: Distinction between early RA patients and non-RA patients using MR imaging may be impossible.

B-562 10:48

MR imaging of the phalangeal joints in cases of arthritis at 3 Tesla. Initial results

M.P. Lichy, C. Amberger, C. Müller-Horvat, I. Kötter, J. Schäfer, S. Lenk, C. Claussen, F. Schick, H.-P. Schlemmer; Tübingen/DE

Purpose: To evaluate the diagnostic potential of MR imaging at 3 Tesla for evaluation of arthritis.

Methods and Materials: High-resolution MR imaging was performed in 7 patients with arthritis with a 3 Tesla MR scanner (TRIO, Siemens), using a dedicated transmit-receive wrist-coil. The imaging protocol included: a) coronal TSE T2w (TR/TE = 4000/106 ms, 2 averages, 120 mm FOV, 384 matrix, fat suppressed) b) T1w MR imaging (TR/TE = 841/12 ms, 1 average, 120 mm FOV, 384 matrix, 1.5 mm slice thickness) c) multiphase angiography (T1w 3D FLASH; TR/TE = 4.3/1.29 ms, 20 mm FOV, flip angle = 20 degree, resulting voxel size = 1 mm³ [isotropic], time resolution = 12 s) d) coronal T1w MR imaging (fat suppressed). Signal-to-noise ratios (SNR) were calculated for volunteer examination at 1.5 and 3 Tesla MR imaging. Findings were compared with clinical, X-rays and ultrasound examinations. Evaluation of MR imaging was performed according to the OMERACT-criteria on high-resolution images. Image quality and diagnostic potential was also evaluated using recalculated images with lower resolutions (3 mm slice thickness, 256 matrix) by two radiologists.

Results: SNR and image quality of 3 Tesla MR imaging was significantly improved compared to 1.5 Tesla examinations. Synovial swelling and bone destruction were clearly visualized. Involved joints demonstrated intra-individual variations in degree and speed of contrast enhancement, indicating local variations in blood supply.

Conclusion: High-resolution MR-imaging of arthritic joints of the hand at 3 Tesla provides detailed information about bone destruction, synovial swelling and perfusion. This information can be used for early detection and therapy follow-up of arthritis.

B-563 10:57

Cervical spine involvement in rheumatoid arthritis: Correlation between neurologic manifestations and MR imaging findings

J.A. Narvaez, F.J. Narvaez, M. Serrallonga, J.M. Nolla, Y. Roca, J. Valverde; Barcelona/ES

Purpose: Our aim is to evaluate the correlation between neurological manifestations and MR findings in a series of patients with RA and involvement of the cervical spine.

Materials and Methods: Thirty-six RA patients were studied with MR imaging of the cervical spine from 1993 to 2002. All cases were symptomatic presenting neck pain not controlled with conservative management, symptoms or signs suggestive of cervical myopathy and/or atlanto-axial subluxation on radiographs. Clinical manifestations were categorized according to the Ranawat classification of rheumatoid myelopathy. MR imaging studies were interpreted in consensus by two radiologists. The spinal canal was graded as normal, stenosed without cord compression, and cord compression (with or without cord signal intensity changes), and evaluated at both atlanto-axial and sub-axial levels. At the atlanto-axial level, the presence of pannus, bone erosions, the cervico-medullary angle (normal > 135°), and anterior or vertical subluxation were evaluated. Multivariate Cox proportional hazards regression models were used to identify variables associated with the occurrence of neurological dysfunction (Ranawat class II or III).

Results: By Ranawat classification, 13 cases (36%) were in class I, 19 (53%) in class II, and 4 (11%) in class III. Only superior atlanto-axial subluxation, atlanto-axial stenosed spinal canal and cord compression at the atlanto-axial level showed a statistically significant risk of neurological dysfunction. The odds ratio were respectively 8.08 (95% IC: 1.23-53.25), 8.9 (95% IC: 1.48-54.78) and 21.25 (95% IC: 1.64-274.90).

Conclusion: In RA patients with symptomatic cervical spine involvement, neurological dysfunction correlates with MR identification of superior atlanto-axial subluxation, atlanto-axial spinal canal stenosis and atlanto-axial cord compression.

B-564 11:06

Longitudinal analysis of anti-citrulline (anti-CCP) antibodies during 5 years of follow-up in early rheumatoid arthritis: Anti-CCP status is a stable phenotype that predicts greater radiological progression and worse disease activity

M.C. Wick¹, J. Rönnelid², J. Lampa¹, S. Lindblad¹, B. Nordmark¹, L. Klareskog¹, R.F. van Vollenhoven¹; ¹Stockholm/SE, ²Uppsala/SE

Purpose: To study serum levels of anti-citrulline (anti-CCP) antibodies in patients with early rheumatoid arthritis (RA) during 5 years of follow-up, and relate this to

Scientific Sessions

radiological progression, disease course, and therapies in clinical practice.

Methods: 279 newly diagnosed early RA patients were prospectively followed with radiographs, clinical investigations, and measurements of anti-CCP antibodies up to 5 years. Radiographs were quantified using Larsen erosion score and the "X-ray RheumaCoach"-software. We utilized a novel method to estimate the expected radiological progression of untreated RA during the first years following diagnosis and to compare this rate to the observed progression under therapy.

Results: 57.3% (160/279) of patients were anti-CCP positive at baseline. The mean baseline Larsen score was 7.9 ± 9.1 , resulting in a mean pre-diagnosis progression rate of 15.5 ± 11.2 Larsen-units/year. All patients had similar disease activity at baseline, but during follow-up the anti-CCP-positive patients had worse clinical disease and greater radiological progression, despite equal anti-rheumatic therapies. Compared to the radiological progression predicted by the pre-diagnosis progression rates, in anti-CCP-negative patients the decrease in the rate of radiological progression was significantly greater compared to the reduction in progression-rates seen in anti-CCP-positive patients (-14.8 vs. -8.4 Larsen-units/year; $p < 0.01$).

Conclusion: Anti-CCP antibody status is a stable phenotype, suggesting that events before rather than after onset of disease determine this phenotype. The presence of anti-CCP antibodies at diagnosis predicts a greater radiological progression and less favorable disease-course despite anti-rheumatic therapy. These observations suggest that anti-CCP-positive RA is a distinct clinical and patho-physiological entity.

B-565 11:15

Relationship between bone marrow edema and cartilage degeneration assessed by high resolution MR imaging and clinical findings in patients with osteoarthritis

C.M. Phan, T.M. Link, G. Blumenkrantz, D.C. Newitt, S. Majumdar;
San Francisco, CA/US

Purpose: To assess the relationship between cartilage loss and bone marrow edema (BME) and to correlate these findings with the clinical Western Ontario and McMaster University Osteoarthritis (WOMAC) score in patients with advanced osteoarthritis over a 2-year period.

Methods: Seven females, seven males (44-76 years) with Kellgren-Lawrence scale ≥ 2 osteoarthritis were recruited. Baseline radiographs, 1.5 T MR imaging and WOMAC scores were obtained in all patients. MR imaging and WOMAC scores were repeated after one (FU1) ($n = 14$) and 2 years (FU2) ($n = 7$). Volume of femoral and tibial cartilage was calculated in fat suppressed spoiled gradient echo (SPGR) sagittal images. Nineteen BME volumes (BMEVo) were measured on T2-weighted images.

Results: At FU1, quantitative analysis showed an increase in BMEVo in 12/19 BME areas (mean increase: 199%) and a decrease in 7/19 areas (mean decrease: 66%). Patients showed a loss of cartilage volume of more than 60% at FU1 regardless of BMEVo variations. At FU2, an increase in BMEVo was found in 4/7 areas and a decrease in BMEVo in 3/7 areas. There was no significant correlation between WOMAC scores, cartilage loss and BME pattern ($p > 0.05$).

Conclusion: In this pilot study trends of decreasing cartilage volume in patients with osteoarthritis have been demonstrated regardless of changes in BME. Changes in BME patterns and size may be indicative of bone remodeling which may be linked to progression of osteoarthritis, but not necessarily to cartilage degeneration.

B-566 11:24



Importance of linear subchondral bone edema in MR imaging knee examination

B. Ciszewska-Lyson, Z. Czynny, R. Smigelski, A. Mioduszewski; Warsaw/PL

Purpose: To attempt to establish if the phenomenon of knee, subchondral linear bone edema of patellar, femoral and tibial surfaces is clinically important.

Materials and Methods: In the years 2003-2004 MR imaging of 759 knees were performed. Analysis was retrospective and included 25 MR imaging examinations in 24 (11-45 years old) patients with linear bone edema of patellar, femoral and tibial surfaces. Classic bone bruises were not a subject of this study. The examination was performed on 1.5 T unit with a dedicated extremity coil and included transverse and coronal STIR sequences. All patients from the group demonstrated linear subchondral edema of the patella or a combination: patella/femur/tibia. History, clinical examination, operational verification and control MR imaging were analyzed.

Results: Linear subchondral edema was found on patella in 25 knees, on femoral and tibial condyles in 11 knees. Prior to examination 23 patients encountered an injury (up to 90days) and/or 12 had knee operation. 18 patients presented with

knee pain (clinical symptoms of algodystrophy in 7). In arthroscopy: 7 patients revealed no macroscopic chondral lesions, 2 patients had osteochondritis dissecans of femoral condyles. In the control MR imaging study a total regression of changes was observed in three cases, transient osteoporosis in one case and transient osteoporosis followed with osteochondritis dissecans in one case. In 17 patients conservative treatment was sufficient.

Conclusion: Linear subchondral edema seems an important MR imaging examination feature, but the rarity of serious sequelae of this pathology indicates that aggressive treatment is not required based on this diagnosis.

B-567 11:33

Meniscal rim sign: Usefulness for evaluation of an extensive triangular or wedge-shaped signal in the meniscus on MR imaging of the knee

J.-Y. Choi, S. Hong, I. Lee, J. Lee, J. Koo, J.-A. Choi, Y. Koh, H. Kang;
Seoul/KR

Purpose: The purpose of our study is to define the meniscal rim sign on MR imaging and to assess the usefulness of this sign for evaluation of an extensive triangular or wedge-shaped signal in the meniscus on MR imaging of the knee.

Materials and Methods: Sagittal and coronal proton density MR images of 97 menisci showing triangular, wedge-shaped, extensive, or grade 2C signal in 74 patients who underwent arthroscopy were obtained, and were blindly reviewed by consensus of two musculoskeletal radiologists. Of 97 menisci, 46 meniscal tears were confirmed at arthroscopy. We grouped all 97 menisci as follows; type 1, intact meniscal rim (outline of the meniscus) with normal low signal intensity of the rim; type 2, intact meniscal rim, but with increased signal intensity of the rim; and type 3, loss of meniscal rim. Pearson χ^2 test was used to determine whether the types of meniscal rim on MR image and tears at arthroscopy were statistically significant.

Results: All menisci were grouped into type 1 in 38 (39.2%), type 2 in 27 (27.8%), and type 3 in 32 (33%). True meniscal tears were two (5.3%) in type 1, 16 (59.3%) in type 2, and 28 (87.5%) in type 3. Statistical analysis revealed significantly higher frequencies of meniscal tear in groups of type 2 and 3 than type 1 with linear by linear correlation ($P < 0.01$).

Conclusion: Meniscal rim sign was useful to evaluate an extensive triangular or wedge-shaped signal in the meniscus on MR imaging of the knee.

B-568 11:42

Calf muscle BOLD MR imaging: Comparison of healthy volunteers and grade II PAOD patients in a post-occlusive reactive hyperemia paradigm

H.P. Ledermann, A.C. Schulte, H.G. Heidecker, M. Aschwanden, K.A. Jäger, W. Steinbrich, D. Bilecen; Basle/CH

Purpose: To compare calf muscle BOLD measurements of healthy volunteers and patients with peripheral arterial occlusive disease (PAOD) grade II.

Patients and Methods: 17 healthy volunteers (mean age: 35 ± 9.2 years) and 17 patients (mean age: 63 ± 11.6 years) with PAOD grade IIA ($n = 8$) and grade IIB ($n = 9$) had BOLD MR imaging measurements of the calf muscles using an ischemia (6 min.) and reactive hyperemia (6 min.) paradigm with 50 mm Hg suprasystolic thigh compression. MR imaging was performed on a 1.5 T scanner (Sonata, Siemens) using a single-shot multi-echo GE-EPI sequence (TE ms: 16/38/61/83 TR: 1000 ms, flip angle: 90°, FOV: 380x238) with 1 measurement / sec in gastrocnemius muscle tissue. Comparison of both groups involved analysis of mean normalized and individual muscle BOLD curves, time to hyperemia-peak (TTP) after cuff deflation, hyperemia peak values (HPV) and slope of the initial 20 sec. of hyperemia (SL20) ($100 \times \Delta S_{20 \text{ sec.}} / 20 \text{ sec.}$).

Results: During ischemia progressive muscle BOLD signal decrease was similar for both groups with higher individual variation in the patient group. During reactive hyperemia the following mean values were calculated (volunteers / patients): TTP: 44.2 ± 8.2 sec / 103.1 ± 58.5 sec ($p < 0.001$), HPV: $19.7 \pm 5.5\%$ / $8.7 \pm 4.4\%$ ($p < 0.001$), SL 20: 41 ± 40 / 7 ± 18 ($p < 0.004$).

Conclusion: During reactive hyperemia PAOD patients have significantly slower BOLD signal ascents, decreased hyperemia peak values and a delayed time to peak compared to healthy volunteers. These BOLD signal alterations most probably reflect delayed reoxygenation of ischemic muscle tissue due to impaired calf perfusion.

B-569 11:51

High resolution imaging of the human wrist at 3.0 Tesla: A comparative study of carpal ligaments and TFCC in normal volunteers

V. Vieth¹, M. Langer¹, C. Stehling¹, S. Kraemer¹, H. Kooijmann², H. Kugel¹, W. Heindel¹, R. Bachmann¹; ¹Münster/DE, ²Hamburg/DE

Purpose: To assess the diagnostic capability of a new multi-contrast high

Scientific Sessions

resolution imaging protocol for the wrist at 3.0 T and to compare it to our standard 1.5 T protocol.

Methods and Materials: In 10 volunteers images were acquired at 1.5 T (standard surface coil) and 3.0 T (purpose build phased array coil) (Gyrosan Intera, Philips). Imaging protocols consisted of coronal T1-TSE, T2-TSE and PD-TSE-FS and sagittal T2-TSE and PD-TSE-FS sequences. Increased SNR at 3.0 T was used to reduce measured voxel size from 0.50 x 0.50 x 3.0 mm (1.5 T) to 0.20 x 0.20 x 1.5 mm (3.0 T). Total examination time was approximately 25 min. To compare the diagnostic capability of both protocols three observers assessed in consensus the visibility of 14 well-defined clinically important anatomical landmarks (origin and insertion of 5 intrinsic and extrinsic carpal ligaments, central portion of the TFCC and ulna, triquetral, and radial attachments). Image quality and artifacts were ranked qualitatively on a five-point scale.

Results: Out of a total of 140 detectable structures, 75 were detected at 1.5 T and 126 at 3.0. Overall image quality was significantly better at 3.0 T (3.8 vs. 4.9, $p = 0.002$), whereas artefact score did not differ significantly (4.3 vs. 4.5, $p = 0.317$).

Conclusion: Investing the higher SNR at 3.0 T into better spatial resolution, depiction of the normal anatomy of the wrist benefits significantly. We anticipate that increased spatial resolution at 3.0 T will also permit a more detailed analysis of pathologic findings.

10:30 - 12:00

Room C

GI Tract

SS 1401a

MR imaging of the abdomen

Moderators:

S. Schmidt; Lausanne/CH
R.C. Semelka; Chapel Hill, NC/US

B-570 10:30

Contrast enhanced dark lumen MR colonography in adenomatous versus hyperplastic colorectal polyps

B. Bassler, D. Hartmann, B. Pfeifer, D. Schilling, J.F. Riemann, G. Layer;
Ludwigshafen/DE

Purpose: To determine the influence of histology (adenomatous vs. hyperplastic intestinal mucosa) on the accuracy of contrast enhanced dark lumen MR colonography (MRC) for the detection of colonic polyps.

Materials and Methods: 100 consecutive patients with a clinical indication for colonic diagnostic workup were prospectively included in this study, undergoing MRC and subsequent conventional colonoscopy on the same day. All patients underwent standard preparation for colonoscopy. Two experienced readers interpreted each MRC, blinded to the results from CC, evaluating MPR's and virtual flight. In a second step, endoscopic and histologic results were compared to MRC.

Results: In 49 patients CC detected a total of 107 polyps: 82 adenomas, 25 hyperplastic polyps and 7 carcinomas. MRC could not detect any hyperplastic polyp which showed sizes ranging from 1 to 5 mm (22 polyps) and 6 to 9 mm (3 polyps). In adenoma the sensitivity was 18.2% in lesions up to 5 mm ($n = 22$), 84.2% from 6 to 9 mm ($n = 38$) and 100% larger than 9 mm ($n = 22$). Contrast uptake in adenomatous polyps was significantly higher than in normal mucous membrane.

Conclusion: Histology dependent mucous enhancement seems to be a size independent parameter for the detection of polyps by MRC. Contrast enhanced dark lumen MRC could not detect hyperplastic polyps, maybe because they don't develop a pathological wall enhancement due to their vascular architecture being similar to that of normal mucous membrane.

B-571 10:39

MR colonography without bowel purgation. Preliminary results of a new fecal tagging concept

C.A. Kuehle, W. Ajaj, S. Massing, J. Langhorst, M. Nuefer, S.C. Goehde,
J. Barkhausen, T.C. Lauenstein; Essen/DE

Purpose: For MR colonography (MRC) colonic cleansing has been unavoidable. However, the unpleasant bowel cleansing protocols reduce patient acceptance. This study was to evaluate the accuracy of a new MRC protocol without colonic cleansing.

Methods and Materials: 143 screening patients were included. In addition to their regular meals they ingested 2000 ml of a tagging solution starting 48 hours

prior to the MR examination. The solution contained 5% gastrografin, 1% barium and 0.2% locust bean gum. MRC was performed in conjunction with a rectal water enema on a 1.5 T MR System (Sonata, Siemens). A T1W 3D GRE sequence was acquired in a prone position pre- and 75 s after gadolinium administration. All patients underwent conventional colonoscopy within 3 weeks of the MR examination. MR data were analysed concerning image quality and the presence of colorectal masses. Additionally, patient acceptance was assessed for both methods.

Results: Image quality of fecal tagging based MRC was diagnostic in 87% of the examinations. Reasons for non-diagnostic examinations were related to motion artefacts and signal-intense stool in each of 8% of the procedures. Colorectal masses > 5 mm were detected with a sensitivity of 74% and a specificity of 97% compared to CC. Although MRC lacks therapeutic options 67% of the patients preferred MRC for future examinations.

Conclusions: Fecal tagging MRC is applicable for screening purposes. Major advantages are related to the high patient acceptance and the specific detection of colorectal masses. However, further investigations need to be performed to improve the detection rate for colorectal polyps.

B-572 10:48

Correlation of MR-hydrocolonography with endoscopic scores in inflammatory bowel disease

T. Robl, J. Raith, T. Hinterleitner, A. Ruppert-Kohlmayer, W. Petritsch, F. Ebner;
Graz/AT

Purpose: In a prospective series of patients with ulcerative colitis and Crohn's disease, MR-Colonography findings were correlated with endoscopic scores (0-3).

Method and Materials: MR-Hydrocolonography and Colonoscopy were performed in a series of 62 patients. MR examination took place after rectal filling of the large bowel with saline solution and including iv application of Gadolinium. MR findings were evaluated by 3 blinded radiologists and compared with the endoscopic scores (1-3).

Results: Series ($n = 56$, 32f/24m, mean 38 years): Crohn's disease ($n = 27$) colitis ($n = 29$), non-specific colitis ($n = 2$), colonoscopy incomplete ($n = 4$), MR not possible ($n = 1$). Global accuracy of MR imaging in the patient group with ulcerative colitis was 79% (rectum 69%, sigma 90%, descending colon 80%, transverse colon 83% and ascending colon 73%). The accuracy of MR imaging in the patient group with Crohn's disease was 69% (rectum 60%, sigma 70%, descending colon 63%, transverse colon 74% and ascending colon 78%). Endoscopic scores concerning the severity of disease (0-3) were established. In ulcerative colitis patients with score 0-1 ($n = 9$) MR imaging was positive in 72%; score 2 ($n = 7$) in 83% and score 3 ($n = 13$) in 82%. In Crohn's disease patients with scores of 0-1 ($n = 12$) MR imaging was positive in 62%, score 2 ($n = 7$) in 72% and score 3 ($n = 8$) in 78%.

Conclusion: MR was of higher diagnostic accuracy in patients with ulcerative colitis compared with Crohn's disease. The diagnostic accuracy of MR-Colonography increased with higher scores (2 and 3) and disease activity.

B-573 10:57

Blackberry and elderberry juice with high concentrations of manganese and iron ions as negative T2 and positive T1 contrast media: An in-vitro study

S. Puig, H. Redl; Vienna/AT

Purpose: To evaluate superparamagnetic and paramagnetic effects of blackberry (BB) and elderberry juice (EB) with high concentrations of manganese (Mn) and iron (Fe) ions as possible negative oral contrast agents.

Method and Materials: Two samples of unpreserved concentrates of BB and EB collected in Middle- and Eastern-European countries were analyzed for concentrations of Mn, Fe and other metallic ions (AAS, Phosyn Laboratories, Pocklington, York, GB). The juices were diluted with water 1:1, 1:2 and 1:4. Water served as control. Measurements were made with a 1.5 T scanner (Siemens, Symphony, Erlangen, Germany). Several T2 and T1 weighted sequences were used. We analyzed signal-to-noise ratio and relative contrast-to-noise ratio in relation to water and in relation to the background (BG).

Results: The undiluted BB and EB had Mn concentrations of 57 mg/l and 17.2 mg/l, and Fe concentrations of 13.3 mg/l and 52.8 mg/l, respectively. The lowest SNRs in T2W sequences were 2.68 and 28.2 for undiluted BB and EB, respectively. In T1W, juices showed a SNR of 44.72 and 60.71. The relative CNR of BB and EB in T2W sequences compared to BG was 3.60 (T2TSE) and 55.27 (T2TSE with fat saturation). The lowest CNR in T1W was -1.67 for BB (T1FLASH3D with fat saturation) and 382.15 for EB (T1FLASH2D with fat saturation).

Conclusions: BB has the potential to serve as a negative oral contrast agent in

Scientific Sessions

T2W and T1W sequences. EB can be used as a biphasic oral contrast agent, with negative signal effects in T2 and positive effects in T1W sequences.

B-574 11:06

Magnetic-resonance enteroclysis (MRE) in patients with Crohn's disease (CD): Complementary diagnostic value of additional retrograde large bowel filling

K.A. Herrmann, H.J.M. Michaely, C.J. Zech, J. Seiderer, T. Ochsenkuehn, S.O. Schoenberg, M.F. Reiser; *Munich/DE*

Purpose: To evaluate the complementary diagnostic impact of additional rectal water filling in MR-enteroclysis in patients with Crohn's disease (CD) and large bowel involvement.

Patients and Methods: From 12/2002 through 04/2004, 119 patients with proven CD underwent MRE with trans-jejunal intubation and instillation of iron-oxide containing contrast medium and additional retrograde rectal filling with water (extended(e) MRE). All examinations were performed on a 1.5 T MR-scanner (Magnetom Sonata, Siemens Medical Systems, Erlangen, Germany). eMRE images were reviewed by two board certified radiologists concerning large bowel involvement causing complications. Positive findings were correlated with colonoscopy and surgery.

Results: 15/119 (12.6%) patients were found to have significant involvement of the colon and the co-existing complication depicted with eMRE were; subtotal stenosis with sub-ileus (4), fistulae (3) and abscesses (7). One patient presented with adeno-carcinoma in a longstanding colonic stenosis. In 4/15 (26%) cases colonoscopy was refused by the patient (1) or incomplete (3) and MRE with rectal filling added conclusive information for appropriate therapy. 12/15 patients underwent surgery which confirmed eMRE diagnosis, one patient had percutaneous drainage of an abscess and 2 patients underwent conservative and medical treatment of stenosis due to its inflammatory character indicated by MRE. **Conclusion:** MRE combined with rectal filling is highly useful in the diagnosis of disease-related complications in CD with involvement of the large bowel.

B-575 11:15

Optimization of a new mixture of barium sulphate and sorbitol (Volumen) as oral contrast agent for MR of the small bowel in a pediatric population

P. Paolantonio, M. Rengo, A. Laghi, F. Lafrate, M. Di Martino, A. Guerrisi, R. Passariello; *Rome/IT*

Purpose: To evaluate the administration of barium sulphate and sorbitol mixture (Volumen; E-Z-EM, NY, USA) as an oral contrast agent for MR studies of the small bowel in a pediatric population.

Materials and Methods: We analyzed 20 paediatric subjects, ten with Crohn's disease and ten healthy subjects. Each patient underwent MR scan after oral administration of different amounts of Volumen (from 10 to 20 ml/kg/BW). MR protocol included HASTE T2W sequence, Tru-FISP sequence and FLASH T1W sequence acquired in coronal and axial planes every 5 minutes until the cecum was reached. Image analysis included a quantitative evaluation of small bowel distension by measuring small bowel caliber at 3 levels. A qualitative analysis of the signal properties of contrast media and of patients' compliance was also performed.

Results: Volumen has signal properties similar to water. An adequate small bowel distension after administration of 15 ml/kg/BW was observed. Optimal distension was observed for the proximal ileum in all subjects after 10 minutes from contrast agent administration. We observed some inter-individual differences in transit time of Volumen with an adequate distension of the terminal ileum after a mean time of 25 min. We did not observe any significant side effects except for mild diarrhoea for a dose of 20 ml/kg/BW.

Conclusions: Volumen is a safe and useful oral contrast agent for MR studies of the small bowel with biphasic properties in terms of signal intensity. Patient compliance during oral administration is high. The adequate dose in a pediatric population is of 15 ml/kg/BW.

B-576 11:24

MR-colonography in incomplete endoscopy of the colon: A prospective study

B. Bassler, D. Hartmann, B. Pfeifer, D. Schilling, J.F. Riemann, G. Layer; *Ludwigshafen/DE*

Purpose: The purpose of this study was the prospective segmental assessment of the colon using MR-colonography (MRC) in a dark lumen technique in incomplete endoscopy.

Material and Methods: 31 patients (21 female and 10 male, mean age 60.2 a

± 13.2 a) with an incomplete colonoscopy have been included in the study. All patients underwent standard preparation for colonoscopy. MRC protocol (1.5 T Magnetom Sonata, Siemens) included T1W 3D VIBE sequences before and 70 seconds after 0.2 mmol/kg bw Gd-BOPTA (Multihance™, Altana) in a prone position (rectal enema tube, approximately 3000 ml of water, 40 mg butylscopolamine i.v.). Evaluation for colonic distension, demonstration of morphologic stenoses, elongation /curvature was done by two experienced readers (one radiologist, one gastroenterologist) in consensus for six segments of the colon each.

Results: MRC demonstrated in 4 cases, that the inability of complete endoscopy was due to anatomical problems like elongation or curvature of colonic segments. Inflammatory stenoses were seen in 17 patients, stenotic tumors in 6 and postoperative adhesions in 1. MRC was diagnostically sufficient in 128 of 134 proximal prestenotic segments. Suboptimal distension was found in 5/134, stool artifacts in 6.5% and movement artifacts in 16.1%. Altogether 23 pathological findings could be detected in the endoscopically not evaluated 134 segments of the colon (8 polyps, 3 stenoses 4 inflammatory, 7 webs and 1 fistula).

Conclusion: MRC is a new diagnostic tool with excellent diagnostic performance to complete evaluation of the colon after incomplete colonoscopy. Compared with CT it has the advantage of no exposure to ionising radiation.

B-577 11:33

Crohn's disease: Comparison of MR enteroclysis with MR imaging using polyethylene glycol (PEG) solution as oral contrast medium

G. Masselli, L. Menchini, L. Minordi, A. Vecchioli, L. Bonomo; *Rome/IT*

Purpose: To compare the diagnostic value of MR enteroclysis (MRE) with MR imaging using Polyethylene Glycol (PEG) Solution as an oral contrast medium (MR imaging per OS).

Method and Materials: We undertook a prospective randomized trial of forty patients with known Crohn's disease who were examined with MRE ($n = 22$) or with MR imaging per OS ($n = 18$) on 1.5 T magnet. MRE was performed by injection of 1.5-2 l of PEG solution via a nasojejunal catheter, whereas MR imaging per OS was performed with orally administration of 700-1100 ml of PEG solution. Two radiologists reached a consensus about the following imaging findings: Small bowel filling and distension of the small bowel, bowel wall conspicuity and depiction of ulcer wall, bowel wall thickness and fistulas. Conventional enteroclysis was employed as a standard of reference. The imaging findings of the two procedures were compared using Mann-Whitney test, with $p < 0.05$ considered statistically significant.

Results: Good or excellent small bowel filling and distension was obtained in 21/22 patients (95%) examined with MRE and in 12/18 (66%) with MR imaging per OS ($p = 0.0001$) and bowel wall conspicuity was graded good or excellent in 21/22 (95%) and in 13/18 (72%) ($p = 0.02$) respectively. Ulcers of the bowel wall were statistically better delineated with MRE than MR imaging per OS ($p = 0.02$) whereas the specificity and sensitivity of detection of stenosis segments and fistulas although higher with MRE didn't reach statistical significance ($p > 0.05$).

Conclusions: Both MRE and MR imaging using per os PEG offer reliable information on superficial, mural and extramural abnormalities, however depiction of mural ulcers was statistically better with MRE.

B-578 11:42

Comparison of true-FISP MR imaging with and without i.v.-contrast-enhancement in patients with inflammatory bowel disease (IBD)

C. Hohl, G.A. Krombach, T. Schmidt, G. Staatz, R.W. Günther, P. Haage; *Aachen/DE*

Purpose: To evaluate the necessity of i.v.-contrast administration in the diagnosis of IBD with MR imaging using standard- and true-FISP sequences.

Materials and Methods: 40 patients aged 7-62 years with suspected or known IBD underwent MR imaging of the small bowel on a 1.5 T-scanner. 1 hour after 1 l mannitol-solution was given orally, MR imaging was performed using coronal HASTE-M2D, coronal fat-suppressed T2-TSE, axial dynamic T1-weighted GE-sequences before and after i.v.-contrast (Gd-DTPA) and true-FISP sequences before and after i.v.-contrast in coronal and axial planes. MR-images were correlated with endoscopy and clinical findings. The MR imaging sequences were evaluated for sensitivity and specificity regarding the detection of inflammatory bowel-wall changes by three experienced radiologists. Particularly the true-FISP sequences pre- and post-contrast were compared with one another using the Pearson-correlation.

Results: True-FISP MR imaging enabled an excellent assessment of inflammatory activity in IBD. With sensitivities of 95% (axial pre-contrast, coronal post-contrast) and 97.5% (axial post-contrast, coronal pre-contrast) the true-FISP sequences

Scientific Sessions

were superior to the other sequences (T1 = 85%, HASTE = 17.5% and T2-TSE = 55%). The comparison between true-FISP and contrast enhanced T1 showed no significant difference ($p = 0.21$). Pre- and post-contrast true-FISP sequences showed a good concordance of sensitivity values (correlation coefficient = 0.92). In one patient an ambiguous finding in the true-FISP could be confirmed as IBD by increased Gd-DTPA uptake in the T1-weighted dynamic.

Conclusion: I.V. contrast administration has no benefit for true-FISP sequences in bowel MR imaging. In most cases unenhanced true-FISP sequences in different planes are sufficient for diagnosis of IBD. In questionable cases Gd-enhanced T1-images can help to validate the true-FISP findings.

B-579 11:51

Outcome of patients with choledocholithiasis at MR cholangio-pancreatography

L.H. Bushby, A. Gimson, D.J. Lomas; Cambridge/UK

Purpose: To evaluate patient management following a positive diagnosis of choledocholithiasis at MRCP, associated presenting features and false positive rate.

Methods and Materials: Reports of 906 patients who underwent MRCP from 1996 to 2002 were reviewed retrospectively for positive diagnoses of choledocholithiasis. Imaging features were recorded by review of the examinations on a workstation. Presenting clinical features and subsequent therapeutic procedures were established by review of patient records.

Results: 100 MRCP examinations in 906 patients were reported positive for choledocholithiasis. 99 had medical records available for review, in whom 87 subsequent procedures were performed to confirm or refute the presence of choledocholithiasis. In 6 cases a procedure was attempted, but failed and in 12 cases no therapeutic procedure was attempted. Choledocholithiasis was confirmed in 65 of the 81 cases that underwent a successful procedure, giving a false positive rate of 19.8%. The likelihood of a false positive examination was not significantly associated with the presence of abdominal pain at presentation or the presence of multiple calculi at MRCP but was significantly inversely related to maximum stone diameter ($p = 0.002$). Whether or not a therapeutic procedure was performed was not significantly associated with patient age or the presence of comorbid disease or maximum stone diameter.

Conclusion: In the majority of patients with choledocholithiasis at MRCP a therapeutic procedure will be attempted. In our practice this is likely to confirm the diagnosis in at least 80% of cases. False positive diagnoses were significantly associated with small diameter calculi.

10:30 - 12:00

Room E2

Breast

SS 1402

Mammography and ultrasound

Moderators:

A. Fausto; Milan/IT

M. Müller-Schimpffle; Frankfurt a. Main/DE

B-580 10:30

Results of the radiology monitoring of breast in women with gynecological malignant tumors

V.B. Myakinkov; Kherson/UA

Purpose: There is contradictory data of breast cancer (BC) appearance frequency in women with gynecological malignant tumors (GMT). The purpose of this research is evaluation of BC appearance frequency in women with GMT depending on time passed after GMT detection, age when GMT were diagnosed, GMT types; definition of examination tactic.

Methods and Materials: Breast examination results of 2412 women with GMT were analysed (ovarian cancer - 442 patients; cervical carcinoma - 998; endometrial carcinoma - 972). During 5 years following the operation 868 women were being observed (36%); 6-10=699 (29%); 11-15=531 (22%); over 15=314 (13%). Mammography, ductography, pneumocystography and sonography were used.

Results: Breast cancer was revealed in 27 (1.1%) women; with ovarian cancer - 10 cases (2.2%); cervical carcinoma - 7 (0.7%); endometrial carcinoma - 10 (1.0%). During 5 years following the operation 7 cases (0.8%); 6-10=7 (1.0%); 11-15=7 (1.3%); over 15=6 (1.9%). The frequency of disease for BC at the moment of revealing the GMT before the age of 34=0.7%; 35-44=1.3%; 45-54=0.8%; 55-64=1.6%; 65 and older = 0.8%.

Conclusion: Frequency of BC appearance in women with GMT prevails morbidity in female population of region by 19 times and has 2 peaks. For breast monitoring the following tactic of using radiation methods of diagnosis was recommended: If GMT is detected under the age of 34 - mammography and sonography; 35-64 - annual mammography; over 65 - mammography every 2 years.

B-581 10:39

Benign breast diseases associated with cyclosporine A therapy in renal transplant recipients

Y. Seo, C. Choi, D. Yoon, E. Yun, S.-H. Lee, S. Park, J. Moon; Seoul/KR

Purpose: To determine radiologic characteristics of cyclosporine A induced benign breast diseases and to report clinical and pathologic findings.

Methods and Materials: The clinical, mammographic and ultrasonographic records of 33 female renal transplant recipients who received cyclosporine A were retrospectively reviewed. Eleven patients had 46 breast masses on ultrasonography. We performed core needle biopsies on 20 masses and reviewed pathologic findings.

Results: Among 33 female renal transplant recipients, 11 patients (33%) had 46 breast lesions on ultrasonography, which showed benign characteristics. We performed core needle biopsies on 20 out of 46 masses. On pathologic examinations, 12 were fibroadenomas, 6 were fibrocystic changes and 2 were dense fibrosis. Regardless of the final pathologic diagnosis, more than half of the lesions revealed severe lymphatic and venular swellings. Among 11 patients with breast lesions on ultrasonography, 10(91%) showed multiplicity, and 7(64%) showed bilaterality. Mammographically, patients with breast lesions revealed heterogeneously or extremely dense breast patterns and 8 of 11 patients showed positive findings, which were circumscribed masses. 22 patients without breast lesions showed scattered fibroglandular densities ($n = 7$), heterogeneously dense ($n = 11$) and extremely dense ($n = 4$) breast pattern, and 3 of 22 patients showed vague or asymmetric densities that needed further evaluation.

Conclusion: With the development of new breast lesions in patients after renal transplantation, the diagnosis of cyclosporine A induced benign breast diseases which are fibroadenoma, fibrocystic changes and dense fibrosis, should be considered. Also, understanding these entities will relieve the fear for the unexpected lumps in those who received transplantation.

B-582 10:48

Breast sonography in asymptomatic women with mammographically dense breasts

A. Memis Oktay, O. Oktay; Izmir/TR

Purpose: The sensitivity of mammography decreases in women with dense breast parenchyma. The objective of this study was to evaluate the efficacy of breast sonography (US) as an adjunct to mammography in screening asymptomatic women with dense breasts.

Methods and Materials: Between October 2000 - June 2004, 2821 asymptomatic women with dense breasts and negative mammograms were examined with breast sonography. In 59 women US showed solid lesions, and biopsy was performed with US guidance. The lesions were in BIRADS 3 category in 43 patients, and in BIRADS 4 category in 16. Within this group, histopathologic results were correlated with US findings.

Results: Histopathologic examination revealed 10 breast cancers in 59 patients who underwent biopsy. Cancer detection rate in 2821 women was 0.35%. All 43 BIRADS category-3 lesions were benign in histology (fibroadenoma, fibrocystic disease, etc.) and no cancer was detected in this group. Of 16 BIRADS category 4 lesions, 10 were diagnosed as malignant. All cancers were in stage T1.

Conclusion: Dense glandular tissue is the most important limitation of screening mammography. Breast sonography can detect small breast cancers in screening population that are not detected on mammography due to dense breast parenchyma. After a proper categorization of lesions by US, follow-up of the BIRADS category-3 lesions can reduce unnecessary biopsies and false positive results.

B-583 10:57

The value of normal mammographic and sonographic findings in evaluating palpable breast abnormalities

M.G. Skilakaki, I.V. Kalogeropoulos, B. Galina, E. Antipa, E.E. Maragaki, P.N. Piperopoulos; Athens/GR

Purpose: To retrospectively determine frequency of cancer in women with breast lumps and negative mammographic and sonographic findings.

Methods and Materials: 110 patients with a palpable abnormality at presentation

Scientific Sessions

and no corresponding mammographic or sonographic lesion were retrospectively identified from our mammography database. The study group consisted of 95 women who had a minimum mammographic and clinical follow-up of 3 years and 15 patients who underwent surgical biopsy. Evaluated parameters included the level of suspicion on physical examination, breast parenchymal density, mammographic and sonographic characteristics in the area of concern, whether there was any change in imaging and/or clinical findings at follow-up and biopsy results.

Results: Of the 110 women, 102 had radiographically dense breast tissue (Breast Imaging Reporting and Data System - BI-RADS - category 3 or 4) and only 8 had predominantly fatty breasts. All patients with histologically sampled lesions had a BI-RADS tissue pattern 3 or 4. No patient in the non-biopsy group developed carcinoma at the initial site of concern during a follow-up period of 3 years. Only one of the 15 women who underwent biopsy received a diagnosis of breast cancer in the area of palpable abnormality.

Conclusion: Results of this retrospective study suggest that if the mammogram and ultrasound depict normal breast tissue, the likelihood of a palpable abnormality being malignant is extremely low even in radiographically dense breasts.

B-584 11:06

Gray-scale and power Doppler US in the preoperative evaluation of axillary metastases in breast cancer patients with no palpable lymph nodes

G. Esen, B. Gurses, M.H. Yilmaz, S. Ilvan, S. Ulus, V. Celik; *Istanbul/TR*

Purpose: The purpose of this study is to evaluate prospectively the predictive value of gray scale and Doppler US findings for the preoperative detection of axillary metastases in breast cancer patients with no clinical evidence of axillary involvement.

Methods and Materials: 198 axillary lymph nodes detected in 83 women with breast cancer were evaluated. Each node was localized with peroperative US before full axillary dissection. Abscence of echogenic hilum, asymmetrical cortical thickening, and presence of peripheral flow on power Doppler US were considered signs of malignancy. The longest diameters and longitudinal/transverse axis ratios were also documented.

Results: Histopathologically 93 nodes were malignant, and 105 were benign. All three prospective criteria as well as a low longitudinal/transverse axis ratio were statistically significant for malignancy. Size was not a significant criterion. In lymph nodes smaller than 1 cm, only asymmetric cortical thickening ($p < 0.001$) and presence of peripheral flow ($p = 0.012$) were significant. The sensitivity, specificity, positive predictive value, negative predictive value and accuracy were 86.49%, 93.62%, 91.43%, 89.8%, 90.48% respectively. On patient basis, the positive and negative predictive values for the presence of axillary metastasis were 93.33%, and 88.57%.

Conclusion: US is successful and reliable in the preoperative determination of nonpalpable axillary metastatic lymph nodes. Sentinel node biopsy is the standard procedure for determining lymph node status in these patients. Inclusion of axillary US in the preoperative diagnostic evaluation, would be complimentary to and would also eliminate the need for sentinel node biopsy in those patients with positive US results.

B-585 11:15

Breast masses characterization: Use of ACR BI-RADS US lexicon in our experience

P. Belli, A. Magistrelli, R. Lombardi, G. Franceschini, M. Costantini; *Rome/IT*

Purpose: Ultrasound characterization of breast lesions improves the specificity of mammography in evaluating masses. Ultrasound is often the only diagnostic examination in detecting non palpable breast masses and is most often the imaging guide for percutaneous procedures. Our aim was to determine positive and negative predictive value (PPV and PNV) of each ultrasound descriptor and category of ACR BI-RADS US lexicon.

Methods and Materials: 178 breast masses were studied with a multifrequency 10-13 MHz linear-array probe. All lesions were classified by two breast imaging experienced radiologists using ACR BI-RADS US lexicon. Age, site, size, shape, orientation, margins, lesion boundary, echo pattern, posterior acoustic features, surrounding tissue and final assessment category were considered. All lesions underwent cytological/histological examination and results were compared to ultrasound features. PPV and PNV for descriptors and categories were calculated.

Results: Lesions were classified as: 2 class II, 24 class III, 73 class IV and 79 class V. PNV for class II and III was 100% and 83.3%. PPV for class IV and V was 46.6% and 84.8%. Irregular shape, spiculated and angular margins, non-parallel orientation, hypoechoic echopattern, echogenic halo and posterior shadowing were associated with the highest PPV. Mean horizontal diameter was 14.82 mm

(26.50 class II, 15.63 class III, 15.60 class IV, 13.57 class V). Mean vertical diameter was 11.14 mm (13 class II, 8.76 class III, 11.23 class IV, 11.73 class V).

Conclusion: ACR BI-RADS US lexicon is an important system to describe and to classify breast lesions and to determine the management of patients.

B-586 11:24

Comparison of BI-RADS categories and final diagnosis in case of second opinion assessment

J.H. Lorenzen, A.K. Wedel, B.W. Lisboa, G. Adam; *Hamburg/DE*

Purpose: To evaluate the value of second opinion assessment by using the BI-RADS system.

Methods and Materials: We analysed 374 diagnostic mammography and sonography examinations. All patients received mammography and sonography examinations at different outside facilities and all patients received an additional sonography examination at the university radiology department and if necessary supplemental mammographic views. Final diagnosis (Histology: 316; follow-up: 58) was ascertained and correlation of BI-RADS-assessment for mammography and sonography at both sides and final diagnosis was analysed.

Results: Final diagnosis yielded 146 benign lesions and 228 cancers (61%). Concordance of BI-RADS assessment was achieved in 62.8% of category 4 and 5 and only 10.7% of category 1,2 and 3. Overall agreement was documented in 73.5% of the cases. Correlation between the BI-RADS assessment and final diagnosis showed only a kappa value of 0.266 for the outside facilities, but a significant higher correlation of 0.753 ($p = 0.000$) for the second opinion rating at the university. Combination of mammography and sonography BI-RADS assessment reached the highest correlation of 0.838 for the radiology department and only 0.389 for the outside facilities, followed by mammography (0.727 versus 0.298) and sonography (0.683/0.358).

Conclusion: Second opinion leads to a significant improvement in the correlation of BI-RADS assessment and final diagnosis in case of diagnostic mammography and sonography.

B-587 11:33

The microcalcification matrix-system: A novel method to classify clusters of microcalcifications according to BI-RADS

A. Fischmann¹, R. Läufle¹, K. Siegmann¹, A. Wersebe¹, T. Xydeas¹, S. Miller¹, C.D. Claussen¹, M. Müller-Schimpffle²; ¹Tübingen/DE, ²Frankfurt a. Main/DE

Purpose: To evaluate a novel method to standardize the classification of breast microcalcifications according to the assessment categories of BI-RADS™.

Methods and Materials: A matrix system was developed to classify clusters of microcalcifications into the BI-RADS categories according to shape and distribution. In 75 clusters of microcalcifications with biopsy proven histology, the calcifications were classified according to the novel matrix system and with subjective malignancy estimation. Reading was done by 4 blinded readers with different experience in mammography (1 to 5 years), leading to a total of 300 readings. The negative and positive predictive values were calculated for each BI-RADS™ category. The relationship between BI-RADS™ assessment categories 2, 3, 4, and 5 with histological results was statistically evaluated with the χ^2 test.

Results: Using the microcalcification matrix, the prospectively classified BI-RADS™ 2/3/4/5 findings revealed a malignant histological diagnosis in 0%/38%/50%/78%, respectively. Conventional reading yielded malignant diagnosis in 27%/36%/53%/79% respectively. The relationship between BI-RADS™ categories 2 to 5 and histology was statistically significant ($p < 0.001$). No influence of the experience of the readers on the results with the matrix system could be found. Inter-reader variability was high with both methods, ranging from 0 to 0.78, as was intra-reader variability, ranging from -0.02 to 0.28.

Conclusion: The microcalcification matrix system allows for a standardized classification of microcalcifications, to enable especially less experienced readers to reliably classify microcalcifications according to BI-RADS™. High malignancy rates in BI-RADS™ category 3 could mainly be explained by a sampling bias, as only biopsy proven cases were evaluated.

B-588 11:42

Assessment of the image quality in a new mammography film-screen combination compared to a standard state of the art film-screen system

V.C. Romano, F. Diekmann, R. Juran, B. Hamm, U. Bick; *Berlin/DE*

Purpose: To compare image quality in a new film-screen combination and in a standard state of the art mammography film-screen system.

Methods and Materials: Investigations were performed with a new combination (KODAK Min-R EV 190 screen/Min-R EV Film= System-A) in comparison to a

Scientific Sessions

well known system (KODAK Min-R 2190 screen/MinR 2000 film= System-B) on a clinical setup and a mammography contrast-detail phantom (CDMAM 3.2, Med.Dept. Nijmegen, Netherlands). In 19 patients one of the views (CC/MLO) was randomly performed with system-A, the other with B. Three readers (I,II,III) compared the two in terms of sharpness, contrast and overall impression using a scale from -2 to +2. In addition, all readers evaluated five phantom studies performed with each system at following settings: 27 kVp with respectively 56, 80, 110, 160 and 280 mAs. The number of detected phantom fields was recorded.

Results: Subjective sharpness, contrast and overall impression of system-A was superior than in system-B (average score for contrast:0.91, sharpness:0.72, overall impression:0.51). The average number of detected fields for each reader was higher in the phantom studies performed with system-A than with B (System-A, I/II/III: 89.8/94.2/98.4; System-B: 89.6/89.2/95.8). The average amount of detected fields pooled for all readers was 94.13 with system-A and 91.5 with B. The difference was not statistically significant (Chi2-Test, p = 0.8939).

Conclusion: The results suggest that image quality obtained with system-A is equal or slightly better than with system-B, higher optical density and contrast at equal exposure was seen as the main advantage of the new combination.

B-589 11:51

Mammographic technique: Frontal oblique approach versus traditional lateral approach

M. Calabrese, C. Faedda, D. Brizzi, G. Baio, E. Bertoli, L. Bacigalupo;
Genoa/IT

Purpose: We try to demonstrate that a frontal oblique approach (FOA) permits visualization of more breast in comparison to the lateral approach (LA).

Methods and Materials: A mammographic system that permits the 2 different approaches (Giotto Image, IMS, Bologna, Italy) has been used. Each patient has undergone mammography (Mx) with FOA on the right side and LA on the left side or the opposite in a randomized mode, but in order to have equal number of left and right mammographies with the 2 approaches. One radiologist, after assessing that the examinations were qualitatively adequate and having excluded the presence of pathology (only Bi-Rads 1 patients were included in the study), has evaluated (blinded to the approach used) the presence of the pectoral muscle in the CC Mx, the presence of the whole pectoral muscle in the MLO Mx and in both projections the distance in mm between nipple and pectoral muscle or mammography image end in the absence of the pectoral muscle. 50 consecutive patients have been studied.

Results: The FOA showed better for the visualization of the pectoral muscle in the CC Mx (Mc Nemar test: p < 0.0001) and in the MLO Mx (Mc Nemar test: p = 0.0002); furthermore it improves (One sample t-test) the nipple-pectoral muscle distance in the CC Mx ($|Pr > |t| = 0.0020$) and in the MLO Mx ($|Pr > |t| < 0.0001$).

Conclusion: From the analysis of these data it seems that the FOA allows more breast to be examined with respect to the LA.

10:30 - 12:00

Room F1

Chest

SS 1404

Pulmonary embolism: Imaging technique and outcome

Moderators:

J. Chalaoui; Longueil, PQ/CA
B. Ghaye; Liège/BE

B-590 10:30

Optimization of enhancement in pulmonary CT-angiography using a 16 slice CT scanner: Influence of a scanning delay

J.C. Petersen¹, M.C. Freund¹, H. Jamnig², W.R. Jaschke¹; ¹Innsbruck/AT,
²Natters/AT

Purpose: To evaluate the physiological pressure-vacuum-pump-effect of inspiration resulting from mixing of unopacified blood from the inferior vena cava with well-opacified blood from the superior vena cava and right atrium, and subsequent insufficient enhancement of the pulmonary arteries.

Methods and Materials: 2 different groups of patients underwent CT-angiography of the pulmonary arteries utilizing a 16 slice CT (2.5 mm slice thickness, 13.75 table feed/rotation, 0.5 sec rotation period) with baso-apical scan direction during intravenous injection of 100-130 mL of non-ionic iodinated contrast media followed by 30 mL of sterile isotonic 0.9% saline using a power injector. The start of the CT

exam was automatically triggered by a smart-prep® function after sufficient enhancement of the right ventricle with a breathing command for deep inspiration. Scan delay was 0 sec. in group 1 (Dt1, 96 patients) and 10 sec. in group 2 (Dt1+10 sec, 29 patients) after deep inspiration and sufficient enhancement of the right ventricle.

Results: The enhancement of group 2 resulted in a significant higher density within the pulmonary artery system (e.g. segmental artery Dt1280 HU, SD ± 85 HU, Dt1+10 sec 342 HU, SD ± 87 HU; Mann Whitney, p below 0.002); additionally this resulted in a reduced influence of admixture of unopacified blood from the inferior vena cava within the pulmonary artery system (Fisher's exact test, p below 0.001).

Conclusion: Utilizing a 16 slice CT scanner for CT-angiography of the pulmonary arteries, a scan delay of 10 sec. after inspiration reduces the physiological pressure-vacuum-pump-effect and results in a higher enhancement within the pulmonary artery system.

B-591 10:39

16-slice multidetector CT angiography of the pulmonary circulation using gadolinium-based contrast agents: Prospective evaluation in 60 patients

M. Rémy-Jardin, J. Bahépar, J.-J. Lafitte, P. Dequiedt, O. Ertzbischoff,

J. Bruzzi, A. Duhamel, J. Rémy; Lille/FR

Purpose: To evaluate the safety and diagnostic value of gadolinium-enhanced 16-slice multidetector CT angiograms of the pulmonary circulation according to the dose administered.

Material and Methods: 60 patients with contraindications to the administration of iodinated contrast agents underwent a multislice spiral CT examination of the pulmonary circulation with a 0.5 mmol/L gadolinium contrast agent administered at 0.3 mmol/kg (n = 29; Group A) or 0.4 mmol/kg (n = 31; Group B) with a systematic evaluation of the clinical and biological tolerance of gadolinium.

Results: The mean (± SD) volume of gadolinium administered was 50.09 ± 8.45 mL, enabling one to obtain diagnostic CT angiograms in 55 (92%) patients with confident analysis of pulmonary arteries down to the subsegmental level in 26 patients (44%); and the segmental level in 21 patients (35%). In Group B: (a) the mean attenuation value within central and segmental pulmonary arteries was significantly higher compared with Group A patients; (b) the number of diagnostic CT angiograms was significantly higher than in Group A (n = 31; 100% vs n = 24; 83%; p = 0.02). Transient worsening of renal function was observed in one Group A patient with pre-existing marked chronic renal failure. A second Group A patient showed acute worsening of renal function in a context of multi-organ failure due to fulminant hepatic tumor.

Conclusion: (1) Diagnostic image quality was obtained in 92% of gadolinium-enhanced CT angiograms; (2) the doses administered did not alter renal function except in two cases.

B-592 10:48

80-kVp multislice CT of pulmonary arteries (msCTPA) to minimize contrast medium (CM) doses to diagnose pulmonary embolism (PE) in patients with decreased renal function

F. Holmquist, U. Nyman; Trelleborg/SE

Purpose: To report that 80 kVp msCTPA (increased iodine X-ray attenuation, reduced scanning time and bolus tracking) significantly reduces CM doses to diagnose PE in comparison with conventional 120 kVp single-slice CT often utilizing the 30-45 grams of iodine.

Methods and Materials: Eighteen patients (73-93 years; 38-79 kg) with an estimated GFR of 12-49 mL/min underwent msCTPA [80 kVp, 162-350 effective mAs (related to patient circumference), pitch 0.5-0.75, 16-detector row CT] for suspected PE using 40-80 mL 160-200 mg I/mL (6.4-14.7 g I), 4-5 mL/s, with an ROI in the PA for bolus tracking (100 HU threshold, 5 second delay). Contrast-to-noise ratio (CNR) in a central PA assuming a 70 HU-value for a fresh thrombus, subjective quality rating, follow-up of renal function and outcome of negative examinations were retrospectively analyzed.

Results: Mean CM dose per kg was 180 mg I/kg (12 mg I/kg/s). Mean PA density was 333 (range 250-694) HU, mean PA CNR 25 (range 19-40). Examination quality was judged as adequate or excellent in sixteen patients and suboptimal in two, but not related to CM enhancement (patient related artefacts). A transient 28 and 33% sCr increase was noted in two patients, respectively. Three patients were diagnosed with PE. Three months follow-up revealed a diagnosed DVT in one patient, one of whom had a suboptimal CTPA.

Conclusion: High quality 80 kVp msCTPA may be performed with significantly reduced CM doses in elderly patients with a reduced renal function, implying a lower risk for CM nephropathy.

Scientific Sessions

B-593 10:57

Evaluation of pulmonary artery flow with MR imaging in acute massive pulmonary thromboembolism

Y. Li; Beijing/CN

Objective: To investigate the value of MR imaging in evaluating pulmonary artery hemodynamics and pulmonary artery pressure in acute massive pulmonary embolism.

Methods: MR studies were performed in 21 patients with acute massive pulmonary embolism (diagnosed by contrast enhanced MR pulmonary angiography) and 20 healthy volunteers, to measure pulmonary artery hemodynamic parameters including the diameters of main and right pulmonary artery, peak velocity, average velocity, flow volume, flow patterns and ejection acceleration time in main pulmonary artery. The hemodynamic parameters in the patient group were correlated with mean pulmonary artery pressure acquired with right heart catheterization.

Results: The diameters of the main pulmonary artery (2.93 vs 2.52 cm) and right pulmonary artery (2.49 vs 1.92 cm) in patients and volunteers showed significant differences ($P < 0.01$, respectively); peak velocity (85.29 vs 100.63 cm/s), average velocity (11.00 vs 17.12 cm/s), flow volume (89.15 vs 98.96 ml/s) and ejection acceleration time (105.09 vs 163.85 ms) in the main pulmonary artery were significantly different between patients and volunteers (P values were 0.01, < 0.01 , 0.03 and < 0.01 , respectively). The peak velocity-time curve of the main pulmonary artery acquired with velocity encoded cine-MR demonstrated earlier and lower peak velocity in the patient group, as well as abnormal retrograde flow. In addition, linear correlations were seen between the mean pulmonary pressure and the diameter of main pulmonary artery ($r = 0.62$, $P = 0.01$), diameter of right pulmonary artery ($r = 0.63$, $P = 0.01$), and ejection acceleration time ($r = -0.55$, $P = 0.005$).

Conclusion: MR imaging is a promising technique not only for the detection of pulmonary thromboemboli but also for the evaluation of hemodynamic parameters in pulmonary hypertension.

B-594 11:06

Subsegmental pulmonary embolism: Comparison of 16row-CT and MR imaging

A. Kluge, G. Bachmann; Bad Nauheim/DE

Purpose: To assess the individual and combined value of three MR imaging techniques for the diagnosis of acute pulmonary embolism (PE) and to compare them to 16row-CT with an emphasis on subsegmental embolism.

Materials and Methods: Fifty-nine patients with symptoms indicating acute PE underwent both 16row-CT angiography with 0.75 mm collimation and a combined, step by step protocol progressing from Real-time MR imaging (RT-MRI) to MR perfusion and MR angiography (MRA)

Results: With CT, PE was diagnosed in 18 patients in 88 lobar, 240 segmental and 427 subsegmental arteries. CT imaged 97% of all subsegmental pulmonary arteries.

Sensitivity for acute PE for RT-MRI, MRA and MR perfusion was 85%, 76%, and 100%, respectively. Sensitivity for lobar PE was 78%, 62%, and 100%, while segmental PE was diagnosed with 87%, 83%, and 97% respectively. Subsegmental PE was diagnosed by MR perfusion with 93% sensitivity. Kappa values compared to CT were 0.85, 0.84, and 0.85 for RT-MRI, MRA and MR perfusion respectively.

Conclusion: The combined MRI protocol was both reliable in emergency diagnosis and as sensitive as the latest generation 16row-CT for diagnosing subsegmental pulmonary embolism. These results may contribute to a less reluctant use of MRI in suspected cases of PE.

B-595 11:15

Complete chest CTA versus a limited range CTA for the diagnosis of PE: What do we miss?

C. Schaefer-Prokop¹, A.A. Bankier¹, K. Janata¹, N. Riechling¹, M. Prokop²; ¹Vienna/AT, ²Utrecht/NL

Purpose: To examine how a reduction in scan range affects the detection of acute pulmonary emboli and other pulmonary findings relative to the radiation dose saved.

Methods: We retrospectively evaluated MD-CTAs of 58 outpatients suspected of having acute PE with positive D-dimer. We recorded the presence of PE and other chest abnormalities with respect to their location along the z-axis. We determined which findings would have been missed if the scan range was reduced to (a) between aortic arch and 2 cm below the lower pulmonary veins, and (b) between 2 cm above aortic arch and the lower hemidiaphragm.

Results: We found signs of acute PE on full chest CTA in 20/58 patients. With range (a), one patient would have been falsely classified as negative due to a subsegmental embolus. None of the patients would have been classified incorrectly with range (b). We found 67 additional chest abnormalities in 32 patients. 24 of these findings affected the clinical management in 18 patients. With range (a), 26/67 findings would have been missed and the management would have been different in 4 patients. With range (b), 11 findings would have been missed but none would have affected the patient's treatment. Relative to a full chest scan, scan dose would have been $45 \pm 8\%$ less with range (a) and $22 \pm 11\%$ less with range (b).

Conclusion: Preliminary results in this relatively small patient group suggest that for the majority of outpatients the scan range and thus the patient dose can be reduced by approximately 20% without affecting relevant diagnoses.

B-596 11:24

Acute pulmonary embolism: Predictive value of degree of arterial obstruction quantified with the CT obstruction index

G. Etechami, F. Doenz, A. Denys, J. Cornuz, P. Schnyder, S.-D. Qanadli; Lausanne/CH

Purpose: To evaluate the prognostic value of arterial obstruction quantification using a dedicated CT obstruction index (Io) in acute pulmonary embolism (PE).

Methods and Materials: The Io is defined as $\text{Io} = (n.d)/40 \times 100$, where n is the value of the proximal thrombus in the pulmonary arterial tree and d is the degree of obstruction. The study was derived from 1054 consecutive patients with clinical suspicion of PE. In 254 patients, PE was confirmed with CT angiography. Io index was calculated for each patient and correlated to one and 6 months follow-up, considering mortality and recurrence of thrombo-embolism (RTE). 40% was considered as the threshold value for group differentiation: group A with $\text{Io} < 40\%$ and group B with $\text{Io} > 40\%$. Predictive values of Io were calculated.

Results: The mean Io was $26 \pm 17\%$. Mortality rates at 1 and 6 months follow-up were 5.9% and 8.6%. At 1 month follow-up, 14 of 15 deaths were considered directly related to PE. Among these patients, 8 patients had pre-existing cardiopulmonary disease (CPD) with 7 in group A. Among 6 patients without CPD 4 were in group B. Regarding mortality in patients without CPD the negative predictive value of the Io was 98% and a significant difference was seen between groups A and B. No significant difference was observed regarding RTE.

Conclusion: The degree of arterial obstruction in PE may be quantified by this CT index. This index seems to provide a stratification of patient prognosis and to be predictive of mortality in patients without pre-existing CPD.

B-597 11:33

Acute pulmonary embolism: Correlation of computed tomography arterial obstruction index with blood gas values

Z.M. Metafratz, G. Maglaras, M. Vassiliou, S. Constantopoulos, S. Efremidis; Ioannina/GR

Objective: To investigate the relationship between the pulmonary arterial obstruction index assessed with Computed Tomography (CT) and the blood gases abnormalities in patients with acute pulmonary embolism.

Materials and Methods: Spiral CT pulmonary angiography was performed in 68 patients without prior cardiopulmonary disease suspected of having pulmonary embolism. Findings consistent with acute pulmonary embolism were observed in 32 patients. The severity was assessed by the pulmonary arterial obstruction index, defined as $\Sigma (n \times d)$ (n: number of segmental arteries occluded, d: degree of obstruction). The correlation of this index with PaO_2 , PaCO_2 and SaO_2 values was investigated by linear regression. Blood gases were comparatively evaluated below and above different index values (from 40% to 70%). PaCO_2 values of 25, 30 and 35 mm Hg were examined as possible indices of severity.

Results: Significant correlation was observed between obstruction index and PaCO_2 ($r = 0.46$, $p = 0.017$) and a marginally non-significant correlation between index and PaO_2 and SaO_2 ($r = 0.34$, $p = 0.057$). PaCO_2 differed significantly at above and below 40% ($p = 0.02$), 50% ($p = 0.02$) and 60% ($p < 0.001$) of obstruction. PaO_2 differed significantly at obstruction $> 60\%$ ($p = 0.001$). SaO_2 differed significantly at 60% ($p = 0.04$) and 70% ($p = 0.02$). A PaCO_2 value of 30 mmHg indicates an obstruction index higher than 50% with a sensitivity and specificity of 78% and 82% respectively.

Conclusion: PaCO_2 is a clinically useful predictor of pulmonary embolism severity, evaluated by obstruction index in patients with acute pulmonary embolism and without prior cardiopulmonary disease. An obstruction index, $> 50\%$ may be expected for $\text{PaCO}_2 \leq 30$ mmHg.

Scientific Sessions

B-598 11:42

Severity assessment and quantification of pulmonary embolism with CT pulmonary angiography as a predictor of patient outcome

S.K. Venkatesh, S. Wang; Singapore/SG

Purpose: To evaluate (a) whether quantification of pulmonary embolus (PE) with CT pulmonary angiography (CTPA) by using a standardized index is a predictor of clinical outcome; and (b) CT features which indicate severe pulmonary embolism (PE).

Materials and Methods: Multi-detector row CT was performed in 100 patients (mean age; 59.43 years, range; 27-94 years). The presence of PE was documented per vessel till the sub-segmental level. A pulmonary arterial obstruction index (PAOI) was derived for each patient based on embolus size and location using a standardized obstruction index. We also evaluated ventricular chamber sizes, chamber ratio and pulmonary artery diameter on CTPA for assessment of severity of PE. Patients were followed up for a minimum of 6 months and clinical outcome was compared. Ten patients died of pulmonary embolism, 13 patients due to other causes and 77 were alive at the time of data collection.

Results: Patients who died of PE had significantly higher PAOI (65.10 vs. 37.83, p = 0.03) and are likely to have significantly more central emboli (5.8 vs. 3.07, p = 0.047) as compared to those who die of other causes following PE. Patients who survive PE are likely to have lower PAOI (50.59, p = 0.09). The mean right ventricle chamber diameter is significantly higher in patients who die of pulmonary embolism as compared to others (58.80 vs. 52.98 and 41.12, p = 0.016).

Conclusion: High PAOI (> 65) is an important predictor of adverse outcome in cases of pulmonary embolism. Acute right ventricular dilatation and presence of more central emboli indicates severe pulmonary embolism.

B-599 11:51

Central pulmonary embolism in oncology patients: An underestimated phenomenon

A.J. Sebastian, A.J. Paddon; Hull/UK

Purpose: Incidental pulmonary embolism (PE) is often observed at staging or follow-up chest computerised tomography (CT) in oncology patients. A prospective study to determine the rate of such findings was undertaken.

Methods and Materials: 368 consecutive chest CTs were prospectively assessed during a 7 month period between October 2003 and April 2004. These were spiral acquisitions between 6 and 8 mm collimation acquired 25 seconds after intravenous contrast administration. PE was diagnosed if a filling defect was seen in the central pulmonary arteries on two or more consecutive slices.

Results: 2.5% (9/368) of patients had incidentally detected PE. 4% of patients with haematological malignancy had PE. This was not attributable to any specific chemotherapeutic regimen. These emboli were all central, between the main pulmonary artery and the lobar level. Though the significance of these findings in patients not suspected of having PE could be contentious, certainly these are not physiological. All our patients admitted to clinical features compatible with PE on direct questioning, though this information was not forthcoming during the routine oncological review. As a result all the patients received therapeutic anticoagulation.

Conclusion: One in forty oncology patients and up to one in twenty five patients with haematological malignancy have incidental central PE visible on the CT scans performed to assess their malignancy. This is a significant finding in this high-risk population. A more aggressive approach to diagnosing PE is required, the precise practice change should be debated, but screening CT pulmonary angiography is an option.

10:30 - 12:00

Room F2

Abdominal Viscera

SS 1401b

Contrast enhanced US of the liver and spleen

Moderators:

O. Lucidarme; Paris/FR

J. Tanus Hajj; Mexico/MX

B-600 10:30

Abnormal hepatic vein Doppler waveform in patients without liver disease

J.F. Pedersen, A.Z. Dakhil, D.B. Jensen, B. Soendergaard, P. Bytzer; Glostrup/DK

Purpose: In patients with liver cirrhosis Doppler ultrasound often detects absence of the retrograde (hepatopetal) flow phase in the hepatic vein, suggestive of an

increased stiffness of the liver parenchyma around the vein. This is rarely or never reported in healthy control persons. Our study examines the frequency of absent retrograde flow in unselected patients referred to abdominal sonography.

Methods and Materials: We studied a consecutive series of 139 patients referred for abdominal sonography. We used state-of-the-art ultrasound scanners, and placed the Doppler gate so that in non-forced end-expiration it would sample the right hepatic vein 4-6 cm from the vena cava.

Results: There was no association between the hepatic vein flow pattern and age, sex or body mass index. Forty-three of 139 studied patients showed absent retrograde flow. Review of the case records revealed liver disease in 26 patients: cirrhosis, 3; alcohol related liver disease, 14; non-alcoholic steatohepatitis 3, hepatitis 1, metastases, 4; hemangioma, 1. No liver disease could be suggested in 17 patients.

Conclusion: Absent retrograde flow in the hepatic veins may be seen not only in patients with overt liver disease but also in apparently liver-healthy patients.

B-601 10:39

Contrast-enhanced US imaging of splenic lymphomas

O. Catalano¹, F. Sandomenico¹, A. Nunziata¹, R. Lobianco², A. Siani¹;

¹Naples/IT, ²Pozzuoli/IT

Purpose: To illustrate our experience in the evaluation of splenic haematological malignancies with CE-US.

Methods and Materials: January to December 2003 we studied 45 patients (20 with Hodgkin disease and 25 with non-Hodgkin lymphoma): 24 M and 21 F aged 27-79 years. After a baseline exam, we injected 2.4-4.8 mL of contrast agent SonoVue (Bracco, Italy). Contrast-enhanced studies were carried out with a contrast-specific software (CnTi, Esaote, Italy) using continuous-mode, harmonic acquisition and low acoustic pressure. US studies outcome was correlated with standard tools, including CT (23 cases), MR imaging (3), US follow-up (16), FNAB (4) and splenectomy (1).

Results: Among 26 cases with focal involvement CE-US detected 67/72 lesions demonstrated altogether by reference tools. Conventional US recognised 55/72 lesions. Lesion extent defined by CE-US correlated with standard tools, being similar (80% of cases), underestimated (12%) and overestimated (6%). Baseline US defined lesion size correctly in 56% of cases, underestimating in 30% and overestimating in 14%. Lesion-to-parenchyma contrast of CE-US resulted low (12% of cases), intermediate (62%), and high (26%). Conspicuity at conventional US imaging was low (52% of cases), intermediate (35%), and high (13%). Lesions appeared as constantly hypoechoic (hypovascular) defects, better definable during intermediate-delayed phase of enhancement than on early phase. Arteries were visible around the lesion and perpendicularly entering along intralesional septa. Intralesional microcirculation was visible. Loss of microcirculation and marked hypoechogenicity were visible in case of response to chemotherapy.

Conclusion: CE-US is a simple and poorly invasive tool in morphological and functional imaging of lymphomatous splenic disease.

B-602 10:48



Contrast enhancement patterns and diagnostic confidence in splenic tumor characterization after microbubble-based contrast agent injection

E. Quaia, F. Degobbi, S. Rossi, M. Cova, R. Pozzi Mucelli; Trieste/IT

Purpose: To describe the different contrast enhancement patterns in focal lesions of the spleen after microbubble-based contrast agent injection and to evaluate whether diagnostic confidence in benign or malignant nature characterization is improved at contrast-enhanced US.

Methods and Materials: A series of 25 solid (10 splenic hemangiomas, 10 splenic metastases and 5 splenic nodular lymphomas) ≤ 4 cm from 25 consecutive patients (15 male and 10 female, age 65 ± 15) were assessed as indeterminate at baseline US by 2 on-site sonologists. Lesions were scanned by high (mechanical index: 0.9-1.1) or low (mechanical index: 0.08 - 0.12) transmit power after air-filled or sulphur hexafluoride-filled microbubble injection, during arterial (15-40 secs) and late (100-300 secs from injection) phase. Contrast enhancement patterns were assessed by 2 on-site sonologists in consensus. Off-site review of baseline and contrast-enhanced US scans was performed by 2 independent blinded readers who expressed a benign or malignant diagnosis according to reference criteria. The appearance at cross-sectional imaging (n = 20 tumours) or histologic findings (n = 5 tumours) were considered as the reference standards.

Results: Splenic hemangiomas revealed persistent rim-like peripheral contrast enhancement without (n = 8) or with (n = 2) progressive complete fill-in. Splenic metastases and nodular lymphomas revealed persistent hypovascular appearance. Diagnostic confidence in malignancy diagnosis improved after microbubble injection (area under ROC curve for observer 1/observer 2: 0.688/0.506 for baseline, 0.890/0.877 for contrast-enhanced scan; P < 0.05).

Scientific Sessions

Conclusion: Microbubble injection allows identification of different contrast enhancement patterns in focal lesions of the spleen and thus improves diagnostic confidence in the diagnosis of malignancy.

B-603 10:57

Vascularization of liver tumors: First results with coded harmonic angio (CHA), phase inversion imaging, 3-D power Doppler and contrast medium-enhanced B-flow with Optison®

E.M. Jung¹, D.-A. Clevert², R. Kubale³, K.-P. Jungius⁴, J. Tacke¹; ¹Passau/DE, ²Munich/DE, ³Pirmasens/DE, ⁴Brig/CH

Aim: To evaluate the possibility of successful evaluation of vascularization of liver tumors using harmonic imaging, 3-D power Doppler and B-flow after a bolus injection of Optison.

Materials and Methods: This prospective study was performed on 60 patients with 93 liver tumor foci. Comparative investigations were performed with multislice-CT and contrast medium-enhanced ultrasound. B-scan was performed with power Doppler followed by a bolus injection of Optison®. Arterial and capillary vascularization was then evaluated with coded harmonic angio (CHA). Portal venous vascularization was assessed with pulse inversion imaging with power Doppler, 3-D power Doppler and, in the late phase, (> 5 min.) with B-flow.

Results: In comparison to spiral-CT/MRT, only 72/93 (77%) of the lesions could be demarcated in the B-scan, 75/93 (81%) with CHA and 93/93 (100%) in the pulse inversion mode. Tumor vascularization was detectable in 43/93 (46%) of lesions with native power Doppler, in 75/93 (81%) of lesions after CM administration in the CHA mode, in 81/93 (87%) of lesions in the pulse inversion mode with power Doppler and in 77/93 (83%) of lesions with contrast-enhanced B-flow. Early arterial and capillary perfusion was best detected with CHA, particularly in 20/20 (100%) of the HCC lesions. Up to 20 min after CM injection, B-flow was capable of detecting increased metastatic tumor vascularization in 42/54 (78%) of cases and intratumoral perfusion in 17/20 (85%) of HCC cases.

Conclusion: Contrast medium-enhanced ultrasound investigation of liver tumors with Optison® allowed reliable detection of tumor foci and, in most cases, tumor vascularization.

B-604 11:06

Characterisation of focal liver lesions with SonoVue: Update with blinded off-site reading

T. Albrecht, J. Skrok, R. Basilico, M. Jenett, A. Oldenburg, J. Hohmann, K.-J. Wolf; Berlin/DE

Purpose: To investigate the ability of low MI real time phase inversion imaging with SonoVue® (Bracco) to characterize focal liver lesions in comparison to unenhanced B-mode and power Doppler sonography.

Methods: 99 patients with 53 malignant and 46 benign liver lesions were studied with unenhanced ultrasound (US) including B-mode and power Doppler, followed by SonoVue (2.4 - 4.8 ml) enhanced low MI real time US (phase inversion, contrast pulse sequencing) during arterial, portal-venous and delayed phases. Representative digital movie clips of each phase were reviewed off-site by a blinded reader with minimal clinical information available (age, sex, pre-existing diffuse liver disease). Findings obtained before and after contrast agent were compared with each other and with reference examinations (histology, imaging with follow-up).

Results: The number of correctly diagnosed lesions increased from 57 (58%) pre to 75 (76%) post contrast ($p < 0.05$). Correct differentiation of malignant from benign lesions improved from 69 (70%) to 88 (89%, $p < 0.05$). Most lesions were judged to have typical features as described previously. Common sources of error were incompletely filling haemangiomas misinterpreted as metastases (4 of 18) and FNH without a spoke wheel pattern or central scar misinterpreted as adenoma (3 of 16). Also 2 of 2 inflammatory lesions were interpreted as metastases.

Conclusion: Low MI real time US with SonoVue improves the characterization of focal hepatic lesions in comparison with unenhanced sonography. These results of blinded, off-site reading are less favourable than our own previous results with on-site reading of the same study population.

B-605 11:15

Blinded readers study of contrast-enhanced US in the characterisation of focal liver lesions (FLL): Impact on decision making

E. Leen, P. Ceccotti, C. Kalogeropoulou, W. Angerson, P. Horgan; Glasgow/UK

Purpose: The aim of the study was to assess the clinical value and potential impact of real time SonoVue-enhanced ultrasonography (CE-US) in the characterization of focal liver lesions (FLL).

Methods: 127 patients with 82 malignant and 52 benign lesions were studied

using unenhanced ultrasound (US) and CE-US. CE-US was performed using non-linear imaging modes at low mechanical index (0.1-0.3) to enable real-time visualization of arterial, portal and late phase contrast enhancement. Digital video recordings of the US and CEUS acquired were reviewed by two off-site blinded readers. Using histology and/or combined CT/MR as the standard of reference, the diagnostic accuracy of CEUS in identifying the lesion (a) as benign or malignant or indeterminate (b) as its actual tumour type, were compared with baseline US. The impact upon subsequent alteration in decision making was also documented.

Results: CE-US reduced the number of indeterminate diagnosis by 51-56% ($p < 0.001$); sensitivity and specificity significantly improved to 90.8-95.4% and 83.7-89.8% respectively ($p < 0.001$). CE-US eliminated observers' variability (kappa coefficient: 0.66-0.77) and there was no significant difference in all comparisons in the analysis of lesions measuring < 1.5 cm, 1.5-2.5 cm & all sizes combined. Diagnosis of metastases, HCCs, haemangiomas and FNHs were significantly improved on CE-US ($p < 0.0001$) with close correlation between the observers ($r = 0.87$). CE-US did not rely on availability of clinical history to enable diagnoses. There was a 23.7% to 90.4% reduction in the need for further imaging investigations following CE-US.

Conclusions: CE-US improves the characterization of focal liver lesions and may limit the need for further investigations.

B-606 11:24

Detection and characterization of focal liver lesions with the new RES penetrating US contrast agent BR14: First results of a phase II research

J. Hohmann, T. Albrecht, J. Skrok, C.W. Hoffmann, K.-J. Wolf; Berlin/DE

Purpose: BR14 (Bracco, Milano, Italy) is a new US contrast agent (CA) which is incorporated into the Kupffer cells a few minutes after injection. The microbubbles are composed of a gas phase of perfluorbutane (C_4F_{10}) encased by a phospholipid-stabilized membrane. We investigated focal liver lesions (metastases and HCC) during vascular and liver specific late phases to determine the detection and characterization of the lesions using phase inversion US (PIUS).

Methods: In all 12 patients we first conducted a baseline scan of the liver (grayscale and power Doppler). After three CA applications (0.25, 1.0, 4.0 ml, dosed 5 mg/ml) we scanned with PIUS (Accuson Sequoia, CCI) using low Mechanical Index (MI=0.2-0.4) in vascular (arterial and portalvenous) as well as in late phase (5-10 min p.i.). For each patient we conducted an MR imaging as a reference (in 9 patients with liver specific CA).

Results: In nine patients we found a total of 31 focal liver lesions (Baseline: 19; 0.25 ml: 11; 1.0 ml: 20; 4.0 ml: 26), and in three patients a disseminated disease of the liver. The MR imaging confirmed 20 of these focal lesions as well as the disseminated ones. In MR imaging, two additional lesions could be detected which had not been seen in PIUS. The lesions additionally found in PIUS were either < 11 mm ($n = 6$) or classified as benign ($n = 5$).

Conclusion: Detection and characterization of focal liver lesions with BR14 apparently provides results comparable to MR imaging. Additionally lesions detected in PIUS even seem to imply higher sensitivity and specificity.

B-607 11:33

Focal liver lesions: Malignant vs benign - the value of the sinusoidal phase of contrast-enhanced ultrasonography

M. D'Onofrio, B. Masinielli, S. Caffarri, R. Malago', G. Zamboni, R. Pozzi Mucelli; Verona/IT

Purpose: To evaluate the sinusoidal phase of contrast-enhanced ultrasonography (CEUS) in the study of solid focal liver lesions to distinguish malignancy from benignity.

Methods: 200 focal liver lesions, suspected for malignancy being hypoechoic and/or in high risk patients (cirrhotic or oncologic) were studied with contrast-enhanced ultrasonography (CEUS). The final diagnosis was obtained with spiral CT, MR, angiography, biopsy.

Results: 73/200 lesions were benign: 38 angiomas, 3 capillary angiomas, 19 FNHs, 7 areas spared by steatosis, 4 adenomas, and 2 necrotic nodules. All the benign lesions were followed-up. 127/200 lesions were malignant: 87 HCCs, 26 metastases, 10 endocrine metastases, 2 cholangiocarcinomas and 2 lymphomas. 108/127 (85%) malignant lesions resulted hypoechoic at CEUS in the sinusoidal phase. 68/87 (78%) HCCs resulted hypoechoic in the sinusoidal phase. 64/73 (88%) benign lesions resulted hyperechoic or isoechoic at CEUS in the sinusoidal phase. Hypoechoic aspect of the studied lesion in the sinusoidal phase of CEUS allowed diagnosis of malignancy with an accuracy of 86%, increasing the diagnostic confidence compared to basal US (receiver operating characteristic curve area increased from 0.536 for basal US to 0.902 for CEUS). Excluding HCCs, hypoechoic lesion aspect in the sinusoidal phase of CEUS allowed diagnosis of malignancy with an accuracy of 92%.

Scientific Sessions

Conclusions: Sinusoidal phase of CEUS can distinguish malignancy from benignancy during hepatic staging with an accuracy of about 90%.

B-608 11:42 ♀

Comparison of B-mode and contrast enhanced ultrasound of the liver in patients undergoing chemotherapy for known primary malignancy

S.D. Yarmenitis, A. Bakantaki, Y. Papantoniou, N. Gourtsoyiannis; Iraklion/GR

Purpose: To define the benefit of routine contrast enhanced ultrasound (CEUS) in the follow-up investigation of the liver in patients treated with chemotherapy for known primary malignant neoplasia.

Methods and Materials: Between January 2004 and July 2004, 283 patients were examined consecutively in our ultrasound unit during their routine follow-up to rule-out liver metastases. One hundred and eighty-six of them (breast:122, colorectal:32, endometrial:8, ovarian:5, gastric:5, prostatic:4, bladder:3, lung:2, renal:2, melanoma:2, thyroid:1) had a combined B-mode ultrasound (BMUS) and CEUS. Tissue Harmonic and Spatial Compounding techniques were used for the BMUS session. A second-generation ultrasound contrast agent was administered for the CEUS. Two independent radiologists examined, blindly, digital video-clips from each session. The presence and the characteristics of any focal lesions were recorded. MDCT, MR imaging and/or biopsy were used as reference. A correlation was not performed with these modalities in this study.

Results: Hepatic metastases were detected in 28/186 (15%) patients. BMUS missed 15/28 (54%) metastases which were successfully diagnosed by CEUS. Among them, 12 (43%) were solitary lesions. In 3 of the rest of the 13 cases that both techniques have diagnosed, CEUS depicted a more extensive spread of the disease. In 13/186 (7%) cases of atypical hemangiomas on BMUS, CEUS was diagnostic with certainty. Forty-three livers had heavy fatty infiltration and CEUS did not improve image quality.

Conclusion: CEUS may detect 50% more cases of hepatic metastases than BMUS in patients under chemotherapy for known primary malignant neoplasia. It is a promising routine technique in the follow-up investigation of the liver of these individuals.

B-609 11:51

Liver metastases treated with chemotherapy: Assessment of tumor vitality during arterial phase with contrast enhanced harmonic sonography (CEUS).

Work in progress

P. Cabassa, L. Romanini, L. Grazioli, V. Portugalli, M. Cristinelli, C. Avigo; Brescia/IT

Purpose: To evaluate the capability of Sonovue enhancement in the assessment of tumor response to chemotherapy.

Materials and Methods: To date, 17 liver metastases in 12 cancer patients (10 male, age range 42-74) were studied with CEUS before and after chemotherapy. CEUS was performed with second generation contrast media (Sonovue, Bracco) at the standard dose of 2.4 ml with continuous real time scanning at low mechanical index. The inclusion criteria are: At least one focal liver lesion visible at B-mode ultrasonography; biopsy proven pathologic specimen before treatment; at least one cross sectional examination (CT/MR) before treatment. The origins of disease were: Gastro-intestinal (n = 7), breast (n = 2), pancreas, lung and eye (n = 1 each). Pretreatment, the lesions mean maximum diameter was 25.1 mm (range 8-60 mm). Pre and post treatment maximum tumor diameter and pattern of enhancement were assessed lesion by lesion. We considered the arterial phase the most important phase to assess tumor necrosis.

Results: Before treatment 5/17 lesions in 5/12 patients enhanced homogeneously during the arterial phase. After therapy a reduction of intraleisonal enhancement was observed in all lesions. In 5/17 nodules the enhancement was totally absent and these lesions were considered completely treated. 4/5 of these decreased in size more than 30%. In the remaining 12/17 lesions the enhancement was persistent at the periphery (8/12 lesions) or inhomogeneous (4/12 lesions). 5/12 lesions decreased in size more than 30%.

Conclusions: CEUS during the arterial phase could be a valid and unique method to assess vitality (vascularization) of liver metastases. Further experience is mandatory to confirm these preliminary results.

10:30 - 12:00

Room G

Genitourinary

SS 1407

CT imaging of the urinary tract

Moderators:

L. Dalla Palma; Trieste/IT

R. Garcia Figueiras; Santiago de Compostela/ES

B-610 10:30

Delineation of upper urinary tract segments at multidetector CT urography:

Retrospective comparison of routine and low-dose protocols

U.G. Mueller-Lisse, T. Meindl, E.M. Coppenrath, U.L. Mueller-Lisse, C. Degenhardt, K. Rami, M.F. Reiser; Munich/DE

Purpose: CT urography (CTU), as an add-on to contrast-enhanced CT of the abdomen and pelvis, may replace excretory urography in patients with pelvic tumors. However, radiation exposure is a concern. We retrospectively compared upper urinary tract (UUT) delineation in low-dose and routine CTU.

Materials and Methods: CTU (1-2 phases) was obtained with 120 kV, 4x2.5 mm collimation, and pitch 0.875 after i.v. injection of 120 ml of non-ionic contrast media with 300 mg of iodine/ml with routine (14 patients, n = 116 UUT segments, average 175.6 mAs/slice, average delay 16.8 minutes) or low-dose (26 patients, n = 344 UUT segments, 29 mAs/slice, average delay 19.6 minutes) protocols. UUT segments included intrarenal collecting system (IRCS), upper, middle, and lower ureter (UU,MU,LU). Two independent readers (R1,R2) graded UUT segment delineation as 1-absent, 2-partial, 3-complete (noisy margins), 4-complete and clear. Chi square statistics were calculated for grades 1-2 vs. 3-4 (delineates course of UUT, may locate obstruction/dilation) and 1-3 vs. 4 (may locate intraluminal lesions).

Results: Delineation of UUT was equally good for all segments in routine and low-dose CTU (R1, chi²=0.0036-1.74, p > 0.15; R2, chi²=0.074-1.308, p > 0.2). IRCS, UU, and MU were as often clearly delineated in routine as in low-dose CTU (R1, chi²=0.074-1.013, p > 0.25; R2, chi²=0.919-2.159, p > 0.1). However, LU was more often clearly delineated in routine CTU (R1, 18/24 routine, 38/69 low-dose, chi²=2.178, p > 0.1; R2 18/24 routine, 21/69 low-dose, chi²=12.75, p < 0.05).

Conclusions: Low-dose CTU was sufficient to determine the course of UUT and perhaps locate obstruction/dilation, but would have been unlikely to locate intraluminal LU lesions.

B-611 10:39

CT-urography: Dose reduction in multidetector technique

E.M. Coppenrath, U.G. Mueller-Lisse, T. Meindl, P. Herzog, U. Mueller-Lisse, R. Khalil, M.F. Reiser; Munich/DE

Purpose: CT urography depicts ureter and bladder with distinct contrast to adjacent tissues. This allows for substantial dose reduction compared with standard dose abdomen CT. CT density values of ureter in clinical studies were compared with systematic dose variation in ureter phantom in order to find threshold of dose reduction.

Material and Methods: A novel contrast phantom consists of parallel plastic tubes (diameter 2.7 mm) filled with different dilutions of contrast media (1:10, 1:20, 1:40, 1:80, 1:160) embedded in a water-filled box (14 x 32 cm). Four row and sixteen row multidetector scanners were used with variation of tube current (15-100 mAs/slice), voltage (90, 100, 120 kV), pitch (0.875, 1.0, 1.25, 1.5, 1.75), slice thickness (1 mm, 2 mm, 3.2 mm). CT-density and signal-to-noise ratio of contrast-filled tubes were compared with patient studies in low and standard dose protocol.

Results: CT-density was dose-independent for different dilutions of contrast media in the phantom study, and could be matched with CT density values of patients' ureters. Signal-to-noise ratio as a parameter of image quality proved to be better with 90 kV than with 100 kV or 120 kV in the low dose range, whereas pitch and slice thickness did not show significant change.

Conclusions: The new contrast phantom seems to be suitable for further studies in CT urography. Initial results demonstrate favourable effects of low tube voltage (90 kV versus 100 and 120 kV) on signal-noise ratio in the low dose range. This may lead to substantial dose reduction in CT urography.

Scientific Sessions

B-612 10:48

Does ultralow-dose CT suffice for detecting urolithiasis?

E. Hein, C. Klüner, P. Hein, T. Elgeti, P. Rogalla, B. Hamm; Berlin/DE

Purpose: To evaluate the diagnostic yield of unenhanced multislice-CT with radically reduced radiation dose equivalent to that of a conventional radiograph (KUB) in assessing patients with renal colic.

Methods: 50 patients presenting with renal colic were prospectively examined with a CT scan (parameters: tube voltage 120 kV, 4.4 effective mAs, rotation time 0.5 s, pitch 23, collimation 16*1) and ultrasound. Radiation exposure was calculated using CT-EXPO V.1.3. The CT scans were randomly and independently evaluated by two radiologists blinded to the patients' data. Site, size, and number of calculi, and urinary-tract dilatation (UTD) were recorded. In addition, the readers rated their subjective diagnostic confidence on a 10-point scale. CT and ultrasound findings were compared statistically using the χ^2 -test.

Results: The mean effective whole body dose of the CT scan was 0.5 mSv in men and 0.7 mSv in women. These values are fairly equivalent to the dose of KUB (0.5-0.9 mSv). The incidence of renal calculi detected by CT was 69% in all cases, 78% in the presence of hematuria, and 54% without hematuria. All renal calculi identified by ultrasound were detected on CT. Significantly more ureteral calculi were identified on CT than on ultrasound ($p = 0.001$), whereas there was no significant difference in the diagnosis of renal calculi or UTD ($p > 0.05$). The readers' subjective diagnostic confidence in interpreting the ultralow-dose CT scans was 80% (range: 60-100%) for detection of calculi and 91% (range: 70-100%) for the diagnosis of UTD.

Conclusion: The ultralow-dose CT protocol presented here has a radiation dose comparable to one conventional radiograph and is reliable in detecting urolithiasis.

B-613 10:57



URO-CT vs IVU: Optimisation of URO-CT protocol with multislice CT (MSCT), comparing doses with conventional intravenous urography

M. Vergendo¹, F. Toso², C. Del Frate², C. Zuiani², R. Padovani², M. Bazzocchi²; ¹Spilimbergo/IT, ²Udine/IT

Purpose: Compare the dose of MSCT-URO-CT and IVU, and optimise URO-CT protocol in order to maintain high diagnostic power reducing as-much-as-possible the dose to the patient.

Materials and Methods: 30 patients underwent conventional-IVU; DAP, fluoroscopy-time and number-of-images acquired were recorded. Effective dose for average-procedure was estimated using MonteCarlo-conversion. Image quality and dose for CT were evaluated with a body phantom with high and low contrast-details, using 4 slices-MSCT with 2 uro-CT-protocols: 3 mm raw-thickness, pitch 0.75(Prot1) and pitch 1.4(Prot2) using decreasing values of mAs. Noise and image quality was estimated by two radiologists who compared standard-deviations of a constant ROI and degradation of high-contrast images at different milliAmperage. Effective dose to the patient for the different protocols were calculated using CTDIvol and DLP values and a selected conversion factors for abdomen and pelvic regions.

Results: Noise properties of images show significant increase under 150 mAs for both protocols. In particular image noise of Prot1 at 125 mAs was comparable to that of Prot2 at 200 mAs. Comparative study of high contrast-inserts in the test phantom shows a significant reduction of image quality under 150 mAs for both protocols and better spatial resolution of Prot1 at 100 mAs than Prot2 at 200 mAs. **Conclusions:** Image quality evaluation on test phantom would recommend a pitch 0.75 with 125 mAs for the basal phase (where there is mandatory high contrast resolution for stones) and a pitch of 1.4 with 150 mAs for the urographic-phase and the eventual nephrographic-phase. This three-phase protocol has total effective dose of 22 mSv that is 5 time greater than IVU.

B-614 11:06

Multislice-CT-urography (MSCTU): Experimental evaluation of low-dose protocols

J. Kemper, P.G.C. Begemann, M. Regier, A. Stork, G. Adam, C. Nolte-Ernsting; Hamburg/DE

Purpose: Experimental optimisation of MSCTU protocols for dose reduction with regard to image quality.

Material and Methods: MSCTU was performed in 8 healthy pigs under general anesthesia (weight \pm 70 kg). Examinations were performed with a gradual reduction of the tube current time product at 120 kV (100, 80, 70, 60, 50, 40, 30, 20 eff.mAs) and 80 kV (80, 50 eff.mAs). MIPs were postprocessed. Subjective image quality was rated for transverse images and MIPs using a five-point scale by two experienced radiologists. In addition, objective image noise was determined.

Image quality was correlated to radiation dose. Statistics included comparison of mean scores and calculation of multi-rater-kappa-coefficient.

Results: Adequate image quality for a detailed visibility of the upper urinary tract was obtained using a tube current time product of 70 eff.mAs and a voltage of 120 kV. Image noise did not impair image quality to a relevant degree using these parameters. There was a good agreement between the 2 observers ($\kappa > 0.75$).

Conclusion: In the experimental setting, image quality of low-dose MSCT-urography proved to be adequate at 70 eff.mAs and 120 kV offering advantageous reduction of radiation exposure. Systematic clinical studies are now required for the evaluation of the diagnostic potential and reliability of low dose MSCTU.

B-615 11:15

Systematic evaluation of optimal delay time for CT urography

T. Meindl, E. Coppenrath, R. Khalil, U. Mueller-Lisse, M.F. Reiser, U. Mueller-Lisse; Munich/DE

Purpose: To evaluate the optimal time delay between i.v. contrast-media application and CT urography (CTU).

Material and Methods: 31 patients underwent MDCT, including 1-2 CTU phases. After portovenous-phase CT and i.v. infusion of 250 mL of normal saline, CTU started at least 5 minutes after contrast-media administration. Individual upper urinary tracts (UUT) were divided into 4 segments: intrarenal collecting system (IRCS), proximal, middle and distal ureter. Two independent readers scored segmental opacification from none (1 point) to complete (5 points). Delay time between i.v. contrast and CTU was divided into 4 groups: 1=5-10 min, 2=11-20 min, 3 = 21-30 min, and 4 > 31 min.

Results: In all, 86 UUTs/344 segments were analysed (group 1, n = 15, 2, n = 43, 3, n = 14, 4, n = 14 UUTs). IRCS, proximal and middle ureter showed median opacification values > 4 in all groups. The distal ureter showed values of 4 and 3 in group 1, 3 in group 2, 1.5 in group 3, and 2 in group 4. In the IRCS and proximal ureter, > 90% of segments were completely opacified in each group. In the middle ureter, > 80% of segments were completely filled in groups 2 and 3. The distal ureter showed complete filling in 60% in group 1, 40% in group 2, and 36% and 11% in groups 3 and 4, respectively.

Conclusion: With respect to the distal ureter, CTU should be performed within 10 minutes after contrast-media injection. Delay times exceeding 30 minutes should be avoided.

B-616 11:24

Demonstration of ureteral calculus by thick planar reformation of multislice CT

M. Wehrscheutz¹, G. Fritz¹, G. Gallé¹, M. Tillich¹, A. Ruppert-Kohlmayr²; ¹Graz/AT, ²Leoben/AT

Purpose: This study evaluated optimal thickness of CPR of urinary tract to demonstrate it quickly and in an optimal quality.

Materials and Methods: In a prospective study MS-CT (coll. 3.75 mm, pitch 6, RI 3 mm, 120 kV, 100 mA) reconstructions of ureters of 75 patients with acute flank pain and suspected ureteral calculi were made. Curved planar reformation was performed with different slice thicknesses from 3 mm to 20 mm. Three radiologists evaluated quality of reformatted images using optimal visibility of all parts of ureter and correlated quality with slice thickness of CPR. Clinical impact was evaluated by urologists grading usefulness of CPR-images for therapeutic approach with a 10-point scale.

Results: Fifty-two patients of our cohort had urolithiasis. CPR could be made in all patients. We found reconstruction more difficult in thin patients and easier in obstructed ureter. Evaluation showed as optimal slice thickness 8 mm (7 mm was best in 5%, 8 mm in 65%, 9 mm in 15% and 10 mm in 15%). Acceptance of CPR-images was graded by urologists as very helpful for decision of therapeutic approach in 90% of patients.

Conclusion: Coronal reconstructed imaging is a feasible and quick useful tool with a good clinical impact. We recommend a 8-10 mm slice thickness for the optimal visualization of the whole ureter with or without calculi.

B-617 11:33

Multi-detector row CT urography in the evaluation of painless hematuria

A.C. Tsili, C. Tsampoulas, F. Katzioti, D. Giannakis, A. Silakos, N. Sofikitis, S.C. Efremidis; Ioannina/GR

Purpose: To assess multi-detector row CT urography in the evaluation of the urinary tract in patients with painless hematuria.

Methods and Materials: Forty-seven patients referred for painless hematuria underwent CT urography. Our CT protocol included unenhanced images obtained

Scientific Sessions

with a detector configuration of 16x1.5 mm and pitch 1.2. After intravenous administration of iodinated contrast material and 250 ml of saline solution nephrographic-phase and excretory-phase images were obtained, with collimation thickness 16x0.75 mm and pitch 1.2. Axial and coronal images were evaluated. Three-dimensional reformation of the excretory-phase images was performed using volume-rendering technique. The standard of reference included clinical and imaging follow-up, cystoscopic, surgical and histologic findings.

Results: In 16 of 47 patients (34%), no cause of hematuria was identified. In 31 of 47 patients (66%), the causes of hematuria were the following: urinary tract stones ($n = 14$), carcinoma of the urinary bladder ($n = 10$), carcinoma of the renal pelvis ($n = 4$), benign ureteral tumor ($n = 1$), acute pyelonephritis ($n = 1$), hyperdense renal cyst ($n = 1$).

Conclusion: Multi-detector CT urography is a highly accurate technique in the assessment of patients with painless hematuria. It can demonstrate a wide spectrum of diseases in these patients with a single study.

B-618 11:42 ♂

Multidetector CT of kidneys: Vascular collateral findings in pre-surgical management of renal masses

F. Toso¹, G. Ciccarese¹, M. Vergendo², R. Girometti¹, C. Del Frate¹, C. Zuiani¹, M. Bazzocchi¹; ¹Udine/IT, ²Spilimbergo/IT

Purpose: To evaluate the role of three-dimensional reconstruction MDCT in pre-surgical examination of renal masses, particularly in the precise definition of the vascular anatomy, due to the high percentage of anatomical variants, which may lead to a change in surgical approach.

Material and Methods: 48 patients with renal mass detected by US or CT, underwent MDCT (Aquilion, TOSHIBA) with multiphase protocol (pre-contrast, arterial, nephrographic and urographic phases). Iodine-contrast media (400 g/ml/ml) has been injected at flow-rate of 4 ml/s using an automated injection system and a Sure Start® software for bolus-tracking.

The acquired data after contrast media injection were processed to obtain coronal MPR and three-dimensional MIP and VR for angiographic, nephrographic and urographic assessment. Vascular collateral findings were classified as significant when they added information for surgical planning (laparoscopy or laparotomy).

Results: Anatomic variants of renal vascularization were found in 20/48 patients (40%): 16 arterial and 4 venous. Surgeon used these adjunctive information to pre-plan the surgery in 16/20 cases (75%) (polar arteries, proximal bifurcation of renal artery, renal artery calcification at the origin of the vessel), while he changed completely the surgical approach in 4/20 (25%) cases.

Conclusions: In our experience the multiphasic protocol used for pre-surgical evaluation of renal masses, permits the detection of vascular collateral findings which are relevant for the surgical planning.

B-619 11:51

Patients with acute flank pain: A stone and/or something else?

R. Studer, A. Spreng, A. Christe, G. Thalmann, P. Vock, H.C. Thoeny; Berne/CH

Purpose: To know whether CT performed for suspected renal colic provides additional information which may be relevant for the patient, either immediately or at a later stage.

Methods and Materials: Between July 1997 and July 2004 a consecutive series of 1100 patients with a median age of 50 years (range: 13-80) underwent spiral CT due to acute flank pain. The patients were examined on a single- or a multidetector spiral CT with continuous 5 mm slices from the upper pole of the kidneys to the symphysis without oral or i.v. contrast medium administration.

Results: Seventy-three patients had normal CT scans, 755 pts revealed urolithiasis (282 ureterolithiasis, 195 nephrolithiasis, 278 nephro-and ureterolithiasis), 272 pts had minor or major pathological findings, but no urolithiasis (22 acute pathologies, 31 findings with high importance, 82 with moderate and 137 with low importance were found). Of the pts with urolithiasis 535/755 had additional pathologies: 26 acute pathologies, 33 findings with high importance, 118 with moderate and 358 with low importance.

Conclusion: CT-scan in patients with acute flank pain is not only an excellent tool for the diagnosis of calcified and non calcified urolithiasis, but reveals additional pathologies which influences not only the management of the emergency situation but may also provide important diagnoses with therapeutic consequences.

10:30 - 12:00

Room H

Interventional Radiology

SS 1409a

Thermal ablations in lung and liver

Moderators:

C. Capontodi; Rome/IT

P.R. Mueller; Boston, MA/US

B-620 10:30

Sedation and analgesia in patients undergoing percutaneous liver radiofrequency ablation. Comparison of two protocols

S. Mylona¹, A.A. Hatzidakis², L. Thanos¹, E. Charonitakis², K.N. Chamalakis², N. Mpatakis¹; ¹Athens/GR, ²Iraklion/GR

Purpose: To compare two different protocols of intravenous sedoanalgesia for percutaneous radiofrequency ablation of metastatic liver nodules.

Methods and Materials: The study comprised 40 patients in two equal groups. Group A patients received initial dose of 0.02 mg fentanyl and 2 mg midazolam. If needed, maintenance dose of 0.01 mg fentanyl and 1 mg midazolam was administered. Forty-five minutes before the procedure, Group B patients received 3 mg bromazepam per os and 50 mg pethidine intramuscularly. During ablation, 2% lidocaine was injected through the side infusion-port. All patients were continuously monitored. In all cases RITA model 1500 was used. Following procedure, patient's pain score was recorded based on a 0 to 10 scale.

Results: All procedures were completed except one in group A, because of excessive pain. Average doses were 0.047 mg (0.03-0.09 mg) for fentanyl and 6.25 mg (3-8 mg) for midazolam. The pain-scale score points recorded were 1-7 (mean 4.5) in group A and 1-5 (mean 1.4) in group B. Three group A patients recorded pain score > 5 points, compared to one patient of group B with pain score 5. In group A, pain score was higher when lesion was close to the liver capsule, while in group B no such relation was found. No serious complications were noted.

Conclusions: Both protocols were safe under patient monitoring. Group B sedoanalgesia protocol seems to be more effective in controlling pain during liver ablation independent of the lesion localization.

B-621 10:39

MR-guided radiofrequency ablation of liver tumors using internally cooled electrodes: Clinical results in 28 patients

S. Clasen, A. Boss, D. Schmidt, J. Fritz, H. Graf, F. Schick, C. Claussen, P. Pereira; Tübingen/DE

Purpose: To evaluate effectiveness of MR-guided radiofrequency (RF) ablation of primary and secondary liver malignancies.

Methods and Materials: In 28 patients 38 primary ($n = 4$) or metastatic ($n = 34$) liver tumors (10-65 mm; mean: 26.7 mm) were treated with 41 sessions of RF ablation under guidance at an open 0.2 Tesla MR-Imager (Concerto, Siemens, Germany). MR-compatible internally cooled single or cluster electrodes (Cool-tip®, Valleylab, Boulder, CO) were used. Preinterventional MR-imaging was performed using non-enhanced T1w (TR:300 ms/TE:20 ms) and T2w (4400 ms/154 ms) sequences. Placement of the RF electrodes was performed under MR-fluoroscopy (45 ms/13 ms; acquisition-time: 2.3 sec.). T2w sequences were used to monitor therapy effects during a procedure. Follow-up (mean:12.9 months) was performed at a high-field MR-Imager (Magnetom, Sonata, Siemens).

Results: MR-guided RF ablations were technical successful in 82.9%. assessed at the end of each session. Clinical effectiveness, defined as complete ablation evidenced at MR-imaging within four months after RF ablation, was achieved in 32 of 38 liver tumors (84.2%). Intraoperative T2w sequences were accurate to near-online monitor the extend of induced coagulation and were helpful to guide the exact repositioning of the RF-electrode if overlapping coagulations were necessary. In seven of 32 tumours (21.9%), initially defined as effective RF ablation, a local relapse was detected more than four months after RF ablation. In 14 of 28 patients (50%) heterotopic liver tumors were detected at MR imaging follow-up.

Conclusion: MR-guided percutaneous RF ablation is a safe and effective therapy in the local treatment of primary and secondary liver tumors. Intraoperative T2w sequences are accurate to monitor acute effects of induced coagulation.

Scientific Sessions

B-622 10:48

Usefulness of SonoVue-enhanced ultrasound in the assessment of the efficacy of percutaneous ablation of hepatocellular carcinomas

C. Nicolau, R. Vilana, L. Bianchi, M. Varela, M. Garcia, M. Sanchez, C. Ayuso, J. Bruix, C. Bru; Barcelona/ES

Purpose: Spiral computed tomography (CT) is considered the gold standard imaging technique to assess the efficacy of percutaneous ablation of Hepatocellular Carcinoma (HCC). SonoVue®(Bracco, Italy) is a new microbubble contrast agent. The aim of this study was to assess the accuracy of Contrast-Enhanced Ultrasound (CEUS) using SonoVue in the evaluation of the response to percutaneous treatment of HCC, one month after treatment, compared with CT.

Methods: Forty-one early-stage untreated HCC (40 of them < 3 cm, mean diameter 22.5 mm) of 41 cirrhotic patients were treated with ethanol injection (36) or radiofrequency ablation (5). CT and CEUS were performed 1 month after treatment. CEUS was performed with Contrast Coherent Imaging software (ACUSON Sequoia™, Siemens Ultrasound), at a low mechanical index (< 0.2), after a bolus injection of 2.4 ml of SonoVue. The results of CEUS examination were compared with CT, which is considered the gold standard technique.

Results: The complete response at 1 month was achieved in 30/41 (73%) HCCs. CEUS was able to detect residual tumor in 10 out of 11 cases not completely treated (sensitivity of 91%), and correctly suggested the absence of residual tumor in 29 out of 30 tumors with complete response (specificity of 97%), with a 95% accuracy compared with CT.

Conclusion: CEUS using SonoVue has a very high accuracy at 1 month after treatment, and can be used as an alternative of CT in the assessment of treatment response.

B-623 10:57

Breast cancer hepatic metastases: Survival analysis by the tumor radiofrequency ablation Italian network (TRAIN)

R. Lencioni; Pisa/IT

Purpose: To determine the long-term results of percutaneous radiofrequency ablation (RFA) in the treatment of hepatic metastases from breast cancer.

Methods and Materials: One hundred and two breast cancer patients (mean age 53.8 years ± 12.1) with 153 hepatic metastases ranging 0.8-5 cm in diameter (mean, 2.4 cm ± 0.8) were treated with RFA at 12 centers that were part of the tumor radiofrequency ablation Italian network (TRAIN). Surgical option had been excluded or refused by the patient. RFA was performed percutaneously by using 50- or 150-W generators and 14-G expandable multitined electrodes with 4-9 prongs (RITA Medical Systems, Mountain View, CA). The follow-up period ranged 1-64 months (mean, 18.7 months ± 15.5).

Results: Complete tumor ablation was achieved in 93 (91.2%) of 102 patients after 121 treatment sessions. The primary effectiveness rate on a lesion-by-lesion basis was 86.9%. The 1-, 2-, 3-, 4- and 5-year overall survival rates by the Kaplan-Meier method were 95.2%, 77.3%, 49.6%, 39.7%, and 29.8% respectively. Median survival was 36 months. Analysis of proportional hazards showed that survival was significantly dependent on lesion size ($p = 0.0062$) and lesion multiplicity ($p = 0.039$). The 1-, 3-, and 5-year local tumor progression rates in a patient-by-patient analysis were 19.7%, 32.3%, and 32.3%, respectively. The 1-, 3-, and 5-year recurrence rates were 35.2%, 71.0%, and 85.0% for new hepatic lesions; and 24.8%, 44.0%, and 65.0% for extrahepatic disease.

Conclusion: RFA may be a viable complementary treatment method for selected patients with isolated breast cancer hepatic metastases.

B-624 11:06

Tumor radiofrequency ablation Italian network (TRAIN): Long-term survival outcomes in patients with stage 0 hepatocellular carcinoma

R. Lencioni; Pisa/IT

Purpose: Stage 0 hepatocellular carcinoma (HCC) defines a solitary tumor smaller than 2 cm in patients with well-compensated cirrhosis (Child-Pugh class A) and performance status of 0. Purpose of this study is to investigate the long-term results of radiofrequency ablation (RFA) in the treatment of stage 0 HCC.

Materials and Methods: We retrospectively analyzed a series of 96 consecutive patients (mean age, 63 years ± 12) with stage 0 HCC who received percutaneous RFA at 12 centers that were part of the tumor radiofrequency ablation Italian network (TRAIN). RFA was performed under US guidance by using 50- or 150-W generators and 14-G expandable multitined electrodes with 4-9 prongs (RITA Medical Systems, Mountain View, CA). The follow-up period ranged 8-84 months (mean, 33 months ± 23).

Results: Complete tumor ablation was achieved in 93/96 patients after 100

treatment sessions (primary effectiveness rate, 96.9%). The overall survival rates were 98.7% at 1 year, 95.7% at 2 years, 87.5% at 3 years, 78.1% at 4 years, 64.5% at 5 years, 57.3% at 6 years, and 45.9% at 7 years. The 1-, 2-, and 3-year local tumor progression rates were 1.1%, 5.0%, and 7.4% respectively. No later local tumor progressions were observed. The 1-, 3-, 5-, and 7-year recurrence rates with development of new HCC lesions were 3.5%, 37.6%, 70.2%, and 76.9% respectively.

Conclusion: RF ablation is an effective treatment for cirrhotic patients with stage 0 HCC. Long-term survival rates of RFA-treated patients are equivalent to those reported in Western patients who underwent resection.

B-625 11:15

Tumor radiofrequency ablation Italian network (TRAIN): Long-term results in hepatic colorectal cancer metastases

R. Lencioni; Pisa/IT

Purpose: To determine the long-term survival of patients with hepatic metastases from colorectal cancer who received percutaneous image-guided radiofrequency ablation (RFA).

Methods and Materials: From June 1996 to January 2004, 423 patients (mean age, 66 years ± 10) with 615 hepatic colorectal metastases (1-4 per patient) ranging 0.5-5 cm in diameter (mean, 2.7 cm ± 0.9) received RFA at 12 centers which were part of the tumor radiofrequency ablation Italian network (TRAIN). Surgical option had been excluded or refused by the patient. RFA was performed by using 50- or 150-W generators and 14-G expandable multitined electrodes with 4-9 prongs (RITA Medical Systems, Mountain View, CA). The follow-up period ranged 1-78 months (mean, 19 months ± 15).

Results: Complete tumor ablation was achieved in 373 (88.2%) of 423 patients after 503 treatment sessions. The primary effectiveness rate on a lesion-by-lesion basis was 85.4%. The 1-, 2-, 3-, 4-, and 5-year overall survival were 85.6%, 62.6%, 46.8%, 29.1%, and 24.1% respectively. Median survival was 33 months. Survival was significantly longer in patients with single lesion ≤ 2.5 cm (55.7% at 5 years) than in patients with single lesion > 2.5 cm (13.1% at 5 years) or multiple lesions (11.3% at 5 years) ($p = 0.0002$). The 1-, 3-, and 5-year local tumor progression rates in the patient-by-patient analysis were 21.5%, 32.0%, and 34.1% respectively.

Conclusion: Long-term follow-up data show that RFA is an effective treatment for hepatic colorectal cancer metastases. Results in patients with small solitary lesions are equivalent to those reported for resection.

B-626 11:24

Complications after radiofrequency thermal ablation (RFA) of abdominal tumors: A retrospective review

F.M. Danza, A. Crucitti, G. Pirulli, M. Cirillo, P. Magistrelli, E. Bock, L. Bonomo; Rome/IT

Purpose: We retrospectively reviewed a series of Patients with primitive and secondary abdominal neoplasms treated with RFA, in order to analyze complications related to this procedure.

Methods and Materials: From June 1998 to June 2004, 116 controlled Patients with hepatocellular carcinoma (HCC) or liver metastasis (LM) underwent to RFA; few cases concerned renal (11), adrenal (2) and bone (3) lesions. We performed percutaneously 130 US/CT-guided RFA procedures, using a cool-tip needle, single or cluster; 37 were performed during laparotomy, with US/direct control. Clinical records, symptoms, imaging and therapeutics data were reviewed.

Results: In our series a relatively low rate of complications was observed. We noted 15 complications out of 167 RFA procedures: 3 liver abscess in LM; 1 perihepatic abscess in HCC; 2 biliary duct stenosis, treated with biliary stenting, in LM; 2 acute colecystitis in HCC; 1 biliary-bronchial fistula in LM; 1 partial thrombosis of the left portal branch, spontaneously recovered; 1 duodenal perforation in LM.; 1 intrahepatic-FAV (without progression in 12 months) in LM; 1 liver fracture (7th p.o. day) in LM; 1 myocardial infarction in 3rd p.o. day (dead); 1 parietal seeding in LM, after laparotomic approach.

Conclusion: The biliary tree has an high sensibility to the thermal damage, due to its extremely slow flow. The heat diffusion into surrounding structures (gut, gallbladder) can lead to mild/severe complications. To avoiding them, an accurate treatment planning is mandatory (number and timing of applications, volume of necrosis), in one with a careful selection between percutaneous and open approach.

Scientific Sessions

B-627 11:33

Radiofrequency ablation of pulmonary tumors response evaluation (RAPTURE) trial

R. Lencioni¹, L. Crocetti¹, D. Glenn², D. Morris², R. Suh³, D. Regge⁴, T. Helmberger⁵, W. Lees⁶, C. Bartolozzi¹; ¹Pisa/IT, ²Sydney/AU, ³Los Angeles, CA/US, ⁴Candiolo/IT, ⁵Munich/DE, ⁶London/UK

Purpose: To determine the feasibility, safety, and effectiveness of percutaneous CT-guided radiofrequency ablation (RFA) of pulmonary malignancies.

Methods and Materials: One-hundred patients (35 females and 65 males; mean age, 64 years \pm 11) with 169 malignant lung tumors \leq 3.5 cm in diameter (mean, 1.6 cm \pm 0.8) were enrolled in a prospective, multicenter, single-arm clinical trial. Diagnoses included non-small cell lung cancer (NSCLC) in 33 patients, metastasis from colorectal adenocarcinoma in 52, and metastasis from other primary malignancy in 15. All patients were considered unfit for surgery. CT-guided RFA was performed by using a 150-200-W generator and expandable multi-tined needles (RITA Medical Systems, Mountain View, CA). Follow-up period ranged 1-18 months (mean, 6 months \pm 5).

Results: RFA was technically feasible in 99 (99%) of 100 patients. Overall, 168 lesions were treated in 124 treatment sessions. Major complications consisted of pneumothorax ($n = 18$) and pleural effusion ($n = 4$) requiring treatment, atelectasis ($n = 1$), and pneumonia ($n = 1$). Eighty-one (89%) of 91 lesions in 68 patients who were followed up for 6 months or more after RFA showed no tumor progression on CT. Complete ablation of treated lesions was confirmed by the absence of tumor re-growth over a follow-up period of 1 year or more in 48 (91%) of 53 lesions in 44 patients.

Conclusion: CT-guided RFA yields high local tumor control rates in patients with pulmonary malignancies, and is associated with acceptable morbidity. RFA may prove a viable alternate or complementary treatment for patients with NSCLC or metastases who are not candidates for surgery.

B-628 11:42

CT-guided percutaneous RF ablation of pulmonary neoplastic lesions

E. Mazza, L. Sali, C. Vannini, L. Bonasera, F. Toccafondi, E. Fabbri, M. Zini; Florence/IT

Purpose: To evaluate the effectiveness of percutaneous radiofrequency thermo-ablation (PRFTA) of inoperable primary and secondary pulmonary tumors.

Methods and Materials: From July 2002 to February 2004, 48 patients (age range, 42-82; mean age, 62) underwent PRFTA of malignant pulmonary lesions. Eleven patients were affected by primitive tumours and thirty-seven suffered from metastatic lesions. All nodules were equal to or smaller than 3 cm and were treated by means of Radionics Cool-tip Ablation System probes applied for 12 minutes in the centre of the lesions under CT guidance.

Results: Patients were hospitalized for 1 to 8 days. PRFTA resulted in complete necrosis in all cases as evaluated on CT and PET images. On follow-up at 3 and 6 months a reduction in diameter of pulmonary nodules was verified on CT images. In smaller lesions restitutio ad integrum of pulmonary parenchyma was observed. In 9 cases pneumothorax developed during the procedure. In 8 patients it was treated by positioning a pleural drainage under CT guidance at the end of thermoablation. In 1 case a hypertensive pneumothorax became clinically evident after 6 hours and was subsequently and equally dealt with percutaneous drainage.

Conclusion: PRFTA of primary and secondary pulmonary lesions demonstrated to be a straightforward, practically uncomplicated, low-cost procedure that allows the eradication of inoperable malignant nodules. Adequate follow-up studies are nevertheless necessary to determine the actual survival rate of these patients.

B-629 11:51

CT-guided radiofrequency ablation (RF) for lung metastases

T.J. Vogl, J. Li, T. Lehnert, Y. Wang, M. Mack; Frankfurt a. Main/DE

Objective: The purpose of this study is to evaluate experience and technical feasibility of percutaneous radiofrequency ablation (RF) for treatment of lung metastases.

Materials and Methods: Fifty-nine lung metastases (0.62-3.3 cm in largest diameter; mean, 2.64 cm) in 46 patients were treated with CT-guided percutaneous RF ablation. There were 29 men and 17 women (average age, 62.8 years). After the RF electrode was placed in tumor with computed tomography (CT) fluoroscopic guidance, RF ablation was performed by using a single internally cooled electrode. Follow-up was performed with CT and MR images; enhancement of the treated region on images were considered to indicate complete tumor necrosis.

Results: Average follow-up was 12.8 months (range, 1-28 months). The mean RF power was 22 W (range, 20-25 W), and the mean treatment time was 10.6 minutes

(range, 9.5-12.8 minutes). In follow-up, 52 (88.1% of 59) tumors were achieved total destruction with RF ablation. 2 (3.4% of 59) tumors were uncompleted ablation which enhancement of residual tissue was observed after treatment; 5 (8.5% of 59) tumors were difficult to definite ablation effect because of consolidation, no tumor regrowth at the treated site. Death occurred in 3 patients (6.5%, 3/46) during follow-up. Complications included pneumothorax 41 (69%, 41/59) during and after procedure (5 cases, 12% of 41 requiring pleural drainage), Pleural effusion 18 (30.5%, 18/59), subcutaneous emphysema 22 (37%, 22/59), intraparenchymal hemorrhage 28 (47.5% of 59), moderate pain 11 (18.6%, 11/59).

Conclusion: This study illustrates that CT-guided RF ablation is a promising minimally invasive, effective technique of treatment of small peripheral lung metastases.

10:30 - 12:00

Room I

Interventional Radiology

SS 1409b

Peripheral vascular interventions

Moderators:

J. Bigot; Paris/FR
A.E. Healey; Liverpool/UK

B-630 10:30

Impact of intravascular ultrasound (IVUS) on balloon sizing for interventional treatment of atherosclerotic superficial femoral artery (SFA) lesions

M. Treitl, J. Rieger, C. Weber, S. Wirth, K.-J. Pfeifer, M.F. Reiser; Munich/DE

Purpose: Intravascular Ultrasound (IVUS) represents the gold standard for balloon/stent sizing in coronary interventions. To reveal its impact on balloon sizing during peripheral percutaneous transluminal angioplasty (PTA) of the superficial femoral artery (SFA) we compared digital subtraction angiography (DSA) to IVUS to assess possible intermodality differences regarding selection of the balloon/stent size.

Methods and Materials: DSA and IVUS were carried out during interventional treatment of 32 patients with untreated short SFA lesions. Both modalities (32 examinations each) were randomly presented to 3 blinded readers, comprising of one interventional cardiologist (IC), radiologist (IR) and angiologist (IA) with > 10 years interventional experience. IC and IR were experienced IVUS users, IA was not. The collected data were analysed statistically.

Results: Mean balloon diameter was 4.73 mm ($SD \pm 0.67$ mm, 4-7 mm) for DSA and 5.77 mm ($SD \pm 0.75$ mm, 4-8 mm) for IVUS ($p < 0.0001$). Intramodality difference was significant for DSA and between IR (4.88 ± 0.55 mm, $p < 0.0001$) and IA (4.34 ± 0.48 mm) and IC (4.97 ± 0.78 mm) and IA ($p < 0.0001$), but not between IR and IC. There was no significant intramodality difference for IVUS (5.69 ± 0.84 mm, 5.88 ± 0.71 mm and 5.69 ± 0.72 mm). Intrareader intermodality difference was significant for all readers ($p < 0.0001$).

Conclusion: IVUS analysis is associated with a significant increase of the selected balloon diameter and improves interobserver agreement. Our study raises the question whether DSA may be misleading for correct balloon sizing in SFA stenosis.

B-631 10:39

Angio-seal vascular closure device for brachial artery access punctures

D. Bilecen¹, W. Ostheim-Dzerowycz²; ¹Basle/CH, ²Bad Saeckingen/DE

Introduction and aim: The feasibility of Angio-Seal vascular closure device in the brachial artery was investigated after transbrachial percutaneous transluminal angioplasty (PTA). The technique was modified to encompass the different anatomical skin condition of the cubital fossa.

Materials and Methods: After Transbrachial PTA, Angio-Seal vascular closure device (St. Jude Medical, Minnetonka, MN, USA) was applied in 36 patients (mean age 63.5 years). The procedure of arterial closure is demonstrated in the following in detail:

- Local anesthesia (2% procaine). Hump formation to increase the space.
- After arterial puncture subcutaneous pouch is created by a blade.
- Angio-Seal device is introduced via guide wire. The collagen stripe is pushed towards the artery and remains visible. The preformed pouch is used to cover the collagen stripe.
- Skin is taped by Leukostrip (Smith and Nephew, Largo, Florida, USA).

The patients were monitored clinically for pain, local bleeding and pulse status of the radial artery on day 1, 3, day of discharge and one year later.

Scientific Sessions

Results: In 65% of the patients the device deployed successfully without bleeding, pain or other complications, 19% of the patients experienced mild local bleeding within the cubital fossa, 9% of the patients reported mild transient pain during deployment of the device and 3% of the patient were diagnosed with mild phlebitis. **Conclusion:** Angio-Seal Vascular Closure Device is effective in sealing brachial artery access punctures. A dedicated protocol for closure is demonstrated.

B-632 10:48

Percutaneous treatment in iliac artery occlusion: Long-term results

R. Gandini, M. Chiocchi, S. Fabiano, E. Pampana, A. Spinelli, G. Simonetti; Rome/IT

Purpose: To evaluate long-term outcomes after recanalization of chronic iliac artery occlusion with primary stenting and to underline predictive factors of clinical success.

Materials and Methods: From January 1995 to August 2001, 128 consecutive patients (104 men, mean age 68.2 yrs), with occlusive iliac artery disease (12 bilateral occlusions), underwent recanalization with primary stenting. Pre-procedure evaluation was made according to Fontaine classification, ecocolor-Doppler, digital subtraction angiography (DSA) findings and ankle-brachial pressure index (ABI). The mean ABI at hospitalization was 0.52 (range: 0.23-0.72). Follow-ups included ABI measurements, vascular clinical control, ecocolor-Doppler, and, from September 2000, CT-multislice angiography at one, three, six months and every year thereafter. In case of significant ABI reduction (> 0.15) or worsening of clinical conditions, a DSA was performed. Length of occluded vessels ranged from 2 to 15 cm (mean, 10.5).

Results: Technical success was 98.5%. A clinical improvement was present in all patients in whom a technical success was achieved. Primary patencies were 91.2, 85, 80, 73.7 and 68% at one, two, three, four and five years; secondary patencies were 97, 94, 90.7, 85.9 and 80.4%, respectively.

Conclusion: Primary stenting is safe and effective in case of chronic occlusion, with long-term results of primary and secondary patencies similar to traditional surgery.

B-633 10:57

Cutting balloon angioplasty for the treatment of the stenosis of fistula due to haemodialysis, peripheral bypass, and stent

T. Lupattelli, G. Scalera, M.J. Fischer, F. Crusco, L. Lupattelli; Perugia/IT

Purpose: To present our experience in treating stenosis of arterial anastomosis of peripheral bypass, stent, native artery, and dialysis fistula by cutting balloon angioplasty (CBPTA).

Methods and Materials: From January 2003 to November 2003 we performed in 19 patients 24 CBPTA (4 prosthesis graft stenosis, 3 vein graft stenosis, 2 post PTA native arteries, 1 post-radiotherapy stenosis, 2 stent restenosis, and 12 haemodialysis fistulae. A cutting balloon of 4 mm/20 mm, 6 mm/20 mm, 8 mm/20 mm were used in 2, 12, and 10 lesions respectively. For each procedure we used before and post CBPTA a conventional PTA. The technical success was a residual stenosis less than 30% revealed by angiography or absence of pressure gradient. The follow-up of 15 patients (1-9 months) was performed by Doppler US.

Results: The procedure was technically successful in 84% of cases. The follow-up revealed: 2 restenosis, and 1 bypass occlusion. In the immediate post CBPTA, 2 patients had thrombosis of haemodialysis fistula. 4 restenosis (3 fistulae, and 1 bypass) were retreated with cutting balloon at 4 weeks and 12 months after primary procedure. The primary patency was 54% after 12 months, and 80% after 15 months in haemodialysis fistulae and peripheral bypass respectively.

Conclusion: CBPTA is a feasible and easy alternative treatment to conventional PTA.

B-634 11:06

The use of carbon coated stents (Carbostent) in aortoiliac stenosis. Our experience

M. Pomoni, K. Papadopoulos, A. Tsanis, S. Tanteles, D. Tzavoulis, A. Pagonas, N. Batakis; Athens/GR

Purpose: To present our preliminary results in the use of carbon coated stents (Carbostent) for the treatment of patients with aortoiliac stenosis.

Material and Method: During the last two years we treated 51 patients (46 men 5 women) with severe iliac stenoses. The majority of the patients were heavy smokers (60%), diabetics (30%), with high blood pressure (43%), hypercholesterolemia (22%) and presented with intermittent claudication or severe leg ischemia. Inclusion criteria were symptomatic ischemia, unilateral or bilateral

common or external iliac critical stenosis or occlusion, a limit of two stents to correct the lesion, and satisfactory outflow. 79 stents were placed. In 17 cases we used kissing stents because stenoses involved the aortoiliac bifurcation in 6 patients stenoses involved common and external iliac artery. In 5 patients we used the stent to stent technique in order to deal with long stenosis. Follow-up of the patient involves interview by phone on the first month and color Doppler ultrasound on the 3, 6, 9 and 12 month as well as every 6 months after the first year.

Results: In all cases the stent placement was successful and the patients reported improvement of the claudication. There were no immediate complications. Restenosis occurred in one patient 12 months after the stent placement and was treated with a new stent placement.

Conclusion: Carbon coated stents are easy and safe to use. Our results indicate that they are very promising for low restenosis and low intimal hyperplasia rate.

B-635 11:15

Subintimal angioplasty: Experience in 58 patients

R. Gandini, L. Maresca, V. Pipitone, E. Pampana, D. Konda, C. Reale, G. Simonetti; Rome/IT

Purpose: To evaluate indications, feasibility and results of subintimal angioplasty of long femoral-popliteal occlusions in patients with severe claudication and/or critical limbs ischaemia.

Materials and Methods: Fifty-eight patients (46 males and 12 females; mean age: 71 yrs) with long femoral-popliteal occlusion (> 15 cm) were included in our study. Thirty-four patients were symptomatic for claudication, 3 patients had rest pain and 21 patients presented with gangrene. All patients were studied with Angio-MR and Doppler-US. Recanalization of the superficial femoral artery was performed in all patients. A contemporary recanalization of limb arteries was carried out in 11 patients. In 54 cases recanalization was obtained by antegrade femoral approach, in 1 case by retrograde trans-popliteal approach and in 3 cases by combined femoral-popliteal approach. Follow-up was performed by physical examination and Doppler US 1, 3 and 6 months after the procedure and subsequently after every 6 months.

Results: Technical success was 96.5% with resolution of rest pain or claudication in 30/35 patients and complete resolution of gangrene in 19/21 patients. Two patients had a partial resolution of gangrene underwent only a minor amputation. A mean follow-up of 10.3 months (range: 3-18) demonstrated the patency of the treated vessels in 49/56 patients.

Conclusions: Subintimal angioplasty of long femoral-popliteal occlusions is a safe and effective technique that may be considered as a valid alternative to surgery.

B-636 11:24

Subintimal angioplasty of infrapopliteal vessel occlusions in the treatment of critical limb ischaemia

S. Tartari, L. Zattoni, A. Sacco; Rovigo/IT

Purpose: To evaluate the feasibility and results of subintimal angioplasty (SIA) of tibial occlusions in critical limb ischaemia (CLI).

Methods and Materials: From 2002 through June 2004 42 patients with tibial occlusions and rest pain or tissue loss underwent SIA: we treated 71 tibial vessel occlusions and 23 associated superficial femoral artery occlusions. Patients were followed for 6-21 months (mean 9 months); in all cases clinical and duplex examination was performed at 6 months.

Results: Technical success was obtained in 35 of 42 patients (83%); in this group 2 patient had below-the-knee amputation and 2 underwent surgical revascularization. Of the patients in whom complete recanalization of occluded vessel with SIA failed, 2 required major amputation. The 9-months limb salvage rate was 90% and the survival rate was 90%. Clinical recurrence occurred in 2 patients, who underwent a second successful treatment with SIA. There were 1 major and 5 minor complications; all of them were treated by endovascular procedures.

Conclusion: SIA is feasible and is effective for foot revascularization in patients with CLI. It offers a high rate of success and low complications rate. Clinical recurrence is infrequent. These results, plus SIA's many advantages, support an increasing role for SIA in the treatment of CLI.

Scientific Sessions

B-637 11:33

Giant cell arteritis of the upper extremities: Follow-up after treatment with percutaneous transluminal angioplasty

M. Both¹, P.M. Aries², S. Müller-Hülsbeck¹, T. Jahnke¹, H. Bolte¹, J. Biederer¹, W.L. Gross², M. Heller¹, M. Reuter¹; ¹Kiel/DE, ²Bad Bramstedt/DE

Purpose: To evaluate the feasibility and long-term outcome of upper extremity balloon angioplasty in stenotic and occlusive lesions due to giant cell arteritis.

Methods and Materials: 10 patients (10 female, mean age 66 years) with the diagnosis of extracranial giant cell arteritis underwent balloon angioplasty in 30 vascular territories (subclavian artery: n = 4, axillary artery: n = 11, brachial artery: n = 15) for treatment of symptomatic upper limb artery stenoses (n = 23) and occlusions (n = 1). Interventional therapy was accompanied with immunosuppressive therapy. In all patients, follow-up included imaging methods (Duplex ultrasound (n = 10), magnetic resonance angiography (n = 9)) and clinical examination.

Results: Initial technical success was achieved in all vascular lesions. During follow-up (mean 25 months), severe restenoses (vascular territories: n = 12) occurred in 4/10 patients (primary patency rate: 60%). Repeated PTA (lesions: n = 4, patients: n = 2) provided a secondary patency rate of 73% (22/30 lesions) and a clinical success rate of 80% (8/10 patients).

Conclusions: Despite a tendency to re-stenoses, upper extremity artery balloon angioplasty represents an efficient method for treatment of extracranial giant cell arteritis.

B-638 11:42

A prospective controlled trial on endovascular vs surgical treatment of stenosis in forearm arterious fistulae (AVF)

G. Mansueto, N. Tessitore, D. Cenzi, V. Bedogna, E. Baggio, A. Lupo, R. Pozzi Mucelli; Verona/IT

Purpose: to compare PTA versus surgery in the treatment of venous perianastomotic stenoses in forearm AVF.

Materials and Methods: A prospective controlled trial was performed in 62 forearm AVF. 40 AVF were treated by PTA and 22 by surgery. The two groups were comparable for subject and AVF age and for pre- and post-treatment QoL. Primary and assisted primary patency were reviewed at 6, 12, 24, 36 and 48 months. Endpoints for primary patency and assisted primary patency were restenosis and technique failure (reintervention by another technique or access loss). In surgery the two patencies corresponded, since restenosis was treated by PTA.

Results: Success rate at 6 months was 100% for surgery and $98 \pm 2\%$ for PTA assisted primary patency, while at 48 months success rate was $50 \pm 14\%$ for surgery and $64 \pm 12\%$ for PTA. The primary patency was lower in PTA than in surgery ($p = 0.02$) while assisted primary patencies were similar ($p = 0.22$) at Kaplan Meyer analysis. At multivariate Cox analysis PTA ad surgery have a similar risk of technique failure (HR 0.5; 95% CI 0.2-1.5; $p = 0.23$).

Conclusion: In our experience in forearm AVF the technique survival was similar for PTA and surgery. Even if restenosis rate after pre-emptive correction of perianastomotic stenosis is higher with PTA than surgery, PTA allows repeat intervention and primary assisted patency is better for PTA.

B-639 11:51



Percutaneous arm port device placement: Feasibility, efficacy and impact on quality of life in 1000 cancer patients using arm venography exclusively

P.-Y. Marcy¹, A. Chaturvedi¹, P. Brunner², P.-Y. Bondiau¹, O. Hericord¹, J.-C. Gallard³; ¹Nice/FR, ²Monaco/MC, ³Caen/FR

Purpose: To determine the feasibility and outcome of radiologically implanted arm port devices, the impact on quality of life in cancer patients and to select the specific indications for.

Methods and Materials: Arm port implantation was attempted in 1000 cancer patients. Ports were placed via the basilic vein under fluoroscopy guidance exclusively. Indications for port placement included chemotherapy (n = 861), blood transfusion (n = 78), other (n = 61). Feasibility and outcome were recorded. Quality of life was scored using a visual analogic score of 0 (worst imaginable pain) to 100/100 (no pain or discomfort) to evaluate interference with daily life (VAS1) and the practical aspects of chemotherapy (VAS2).

Results: Initial technical failures (6.3%) included inability to perform the venogram (1.9%), occurrence of a contrast medium hematoma (0.2%), inability to puncture/catheterize the veins (4.2%). Accidental puncture of the humeral artery occurred in four cases. Mean implantation duration was 255.9 days, the overall complications rate was 9.5%. 5.3% of the devices had to be removed prematurely. Complications included device related sepsis (n = 33), febrile neutropenia (n = 15), septicemia

(n = 7), port sepsis (n = 9), skin dehiscence (n = 11), deep venous thrombosis (n = 12), catheter occlusion (n = 7), drug extravasation (n = 2), embolization (n = 4), mechanical stimulation of the median nerve (n = 1), twist of the port (n = 2). VAS (1.2) mean scores were 0.87 and 0.92 respectively.

Conclusion: Specific indications for arm port implantation include young women (cosmetic aspect), patients who underwent previous radiation therapy of the chest or neck, patients who had previous upper extremity venous thrombosis, respiratory insufficiency, pacemaker, severe kyphosis.

10:30 - 12:00

Room K

Pediatric

SS 1412

Neuro-imaging

Moderators:

R. Gunny; London/UK

P.-L. Khong; Hong Kong/CN

B-640 10:30

Evaluation of lenticulostriate artery haemodynamics with color Doppler sonography (CDS) in infancy

S.P. Deftereos, I. Manavis, J. Sigalas, T. Giannoudi, P. Prassopoulos; Alexandroupolis/GR

Purpose: To measure lenticulostriate artery (LSA) haemodynamic parameters with CDS in neonatal brains and to establish normal data for LSA blood flow velocity (BFV), resistive index (RI) and pulsatility index (PI) to be used as reference in clinical practice.

Methods and Materials: The study comprised 132 consecutive neonates (47 preterm 85 term; 1 d to 8 m old) without any evidence of neurological abnormality or respiratory distress. Measurements of BFV, RI and PI were performed through the anterior fontanelle on the middle cerebral artery (MCA), its LSAs and the internal carotid artery (ICA), used as reference.

Results: The ICA, MCA and LSAs were invariably seen in all cases. Normal values of BFV, RI and PI were calculated for all measured arteries and corresponding tables were formulated for 9 age groups: 1 preterm and 8 month-groups for full-terms. BFV measurements showed progressive decrease with advancing age ($p < 0.01$) for LSAs, MCA and ICA. RI was also decreased with age for MCA and ICA ($p < 0.05$), but did not show age-related variations among the fullterm groups ($p > 0.10$) for LSAs. However, RI values of LSAs are significantly lower in preterm than in full-term neonates ($p < 0.05$). PI did not exhibit age-related differences for all arteries measured. BFV measurements for LSAs differ significantly ($p < 0.01$) from MCA with LSAs mean values being about half of the corresponding MCA values.

Conclusion: BFV, RI and PI measurements can be obtained from lenticulostriate arteries and narmal data established here may be useful in evaluating cerebral and basal ganglia abnormalities in neonates.

B-641 10:39

Hypertensive encephalopathy: Clinical and MR imaging findings

Y.-W. Kim¹, I.-O. Kim², W. Kim², K. Yeon²; ¹Busan/KR, ²Seoul/KR

Purpose: To investigate the MR imaging findings and associated clinical findings of hypertensive encephalopathy in children.

Methods and Materials: A retrospective study of 24 MR examinations was performed in 16 patients (M:F=9:6, age range: 2-17 yrs.) with clinically diagnosed hypertensive encephalopathy. Initial imaging was performed within 1 day of the attack and follow-up imaging was performed in 5 patients. The presence of underlying disease, BP, and neurological abnormalities at the time of imaging were recorded. We assessed the MR imaging findings and correlated with the clinical findings.

Results: 14 patients had abnormal MR imaging findings and two patients had negative MR imaging findings. MR images showed bilateral, nearly symmetrical areas of high signal intensity in the subcortical white matter of the occipital lobes. In five cases in which follow-up MR imaging was performed after the hypertension was corrected, there was either complete resolution or marked improvement of signal abnormalities on T2WI with contrast enhancement. Nine patients had suffered from renal disease; most frequently FSGS. The BP at the time was recorded as ranging from 103/50 to 170/120 in these patients. The clinical symptoms were headache in 10, seizure in 8, visual symptoms in 8, and focal neurological abnormalities in 8. Neurological symptoms and signs were correlated with the location of MR abnormalities.

Scientific Sessions

Conclusion: Characteristic MR imaging findings may be useful in establishing early diagnosis in the appropriate clinical setting, which allows timely initiation of appropriate therapy in hypertensive children.

B-642 10:48

Hypoxic-ischemic (HI) brain injury in neonatal rats: The relationship between early post HI apparent diffusion coefficient (ADC) and irreversible infarction

Y. Wang, P.-T. Cheung, G.X. Shen, E.X. Wu, G. Cao, P.-L. Khong; Hong Kong/CN

Purpose: Animal models are increasingly studied for the evaluation of neuro-protective interventions in perinatal HI brain injury. The significance of MR imaging findings at early time-points post HI is of interest because of the potential therapeutic window. We aim to study the relationship between early post-HI ADC, T2-weighted signal change and irreversible infarction.

Methods and Materials: Twenty-three 7-day-old rats underwent right common carotid artery ligation followed by hypoxia. MR imaging (MRI) was performed 1-2 hours post HI using diffusion-weighted imaging (DWI) and T2-weighted imaging (T2WI) (early MRI), and at day 4 post-HI using T2WI (late MRI). Lesion volumes relative to whole brain (LV) were measured on ADC maps at different relative ADC thresholds from 50%-80% of mean contralateral ADC, on T2WI and histopathology at day10 post-HI. Spearman's correlation was used to study the relationship between LV at various ADC thresholds, T2WI and histopathology.

Results: LV (mean \pm sd) at 50%, 60%, 70% and 80% ADC thresholds were $1.9\% \pm 4.9\%$, $7.4\% \pm 11.7\%$, $13.2\% \pm 14.0\%$ and $20.9\% \pm 14.5\%$ respectively. T2WI LV at early and late MRI were $2.8\% \pm 3.5\%$ and $23.3\% \pm 8.6\%$ respectively. Histopathology LV was $28.6\% \pm 7.8\%$. Significant correlation was found between LV at histopathology and 80% ADC threshold ($r = 0.466$, $p = 0.025$), but not with lower ADC thresholds or early T2WI. Significant correlation was also found between LV at histopathology and late T2WI ($r = 0.531$ and $p = 0.009$).

Conclusion: There is a weak correlation between LV at 80% ADC threshold early post HI and irreversible infarction. Reduced ADC thresholds do not strengthen this correlation.

B-643 10:57



Prediction of outcome of hypoxic-ischemic encephalopathy in term neonates with proton MR spectroscopy and diffusion weighted imaging

G. Fan, Z. Wu, Q. Guo; Shenyang/CN

Purpose: To evaluate Proton MR Spectroscopy (1HMRS) and diffusion weighted imaging (DWI) for outcome prediction of hypoxic-ischemic encephalopathy (HIE) in term neonates.

Methods: 42 HIE newborns were evaluated using DWI and 1HMRS. Follow-up MR examinations were performed after 6 months. Apparent diffusion coefficients (ADCs) were measured in the basal ganglia, subcortical white matter, and the cortex respectively. 1HMRS placed in the basal ganglia and thalamic areas. Long-term clinical outcome was classified as normal, abnormal and sequelae according to follow-up MR imaging findings. Logistic regression was performed to examine the predictive value of each ADC value and metabolite ratio relative to creatine (CR) for predicting clinical outcome.

Results: DWI showed a diffuse or symmetrical pattern of injury involving both the basal ganglia and the cortex or subcortical white matter in 12 cases (group 1); multifocal injury which was confined to single arterial territory in 17 (group 2); single lesion within periventricular white matter or basal ganglia was present in 13 (group 3). MR reexamination results showed that 57.14% of sequela were present in group2 (4/7) and 61.11% of abnormal present in group3 (11/18), while 58.82% of normal was present in group1 (10/17). Logistic regression confirmed that ADCs in basal ganglia could be used to differentiate normal from abnormal or sequela ($p < 0.01$), while lactate (LAC)/CR ratio could be used to differentiate normal from abnormal or sequela ($p < 0.001$). The probability of sequelae exceeded 97% for glutamate and glutamine (Glu-n)/CR ratio of 1.5.

Conclusion: Both DWI and 1HMRS play important roles in the quantitative prediction of worse clinical outcomes for HIE.

B-644 11:06

Contrast-enhanced MR imaging of pediatric CNS: Comparison of gadobenate dimeglumine and gadopentetate dimeglumine for lesion enhancement

C. Colosimo¹, G. Pirovano², M.A. Kirchin³, B. Hogstrom², A. Spinazzi²; ¹Chieti/IT, ²Princeton, NJ/US, ³Milan/IT

Purpose: To compare gadobenate dimeglumine (Gd-BOPTA), a contrast agent

with high T1-relaxivity ($9.7 \text{ mmol}^{-1}\text{s}^{-1}$) with gadopentetate dimeglumine (Gd-DTPA) for enhancement and visualization of central nervous system (CNS) lesions in pediatric patients.

Methods and Materials: 63 pediatric patients with CNS (brain and spine) lesions received 0.1 mmol/kg BW doses of Gd-BOPTA ($n = 29$; mean age 7.5 ± 4.8 years) or Gd-DTPA ($n = 34$; mean age 7.9 ± 4.7 years). Images were acquired before (T1-T2wSE) and within 10 minutes (T1wSE) of contrast agent injection. Blinded unpaired and paired qualitative assessment in 26 (Gd-BOPTA) and 32 (Gd-DTPA) patients compared pre- to post-dose changes in quality of lesion visualization (5-point scales for border delineation, visualization of internal morphology, contrast enhancement). Quantitative evaluation in 19 (Gd-BOPTA) and 23 (Gd-DTPA) patients compared changes in lesion-to-background ratio (L/B), contrast-to-noise ratio (CNR) and% enhancement (%En).

Results: Unpaired post-dose scores for lesion border delineation, visualization of internal morphology and contrast enhancement were 3.3 ± 0.6 , 3.4 ± 0.6 and 3.4 ± 0.6 for Gd-BOPTA and 3.1 ± 0.7 , 3.4 ± 0.6 and 3.1 ± 0.7 for Gd-DTPA. The pre- to post-dose changes were significantly superior for Gd-BOPTA for border delineation ($p = 0.018$) and contrast enhancement ($p = 0.006$) and equivalent for visualization of internal morphology ($p = 0.126$). Paired assessments revealed non-significant superiority for Gd-BOPTA for border delineation and visualization of internal morphology and significant superiority for contrast enhancement ($p = 0.04$). Mean post-dose values for L/B, CNR and%En were all superior for Gd-BOPTA (0.5 ± 0.4 vs. 0.3 ± 0.4 ; 9.1 ± 15.4 vs. 2.2 ± 9.9 ; 66.6 ± 47.4 vs. 42.8 ± 39.0 , respectively).

Conclusion: Gd-BOPTA demonstrates qualitative and quantitative superiority over Gd-DTPA for contrast enhancement of CNS lesions in pediatric patients.

B-645 11:15

Value of gadolinium administration in brain MR imaging examinations for developmental delay in children less than two years of age

B. Foerster, J. Ksar, M. Petrou, P. Eldevik, P. Maly, P.C. Sundgren; Ann Arbor, MI/US

Purpose: To review the radiological findings and associated clinical symptoms in the MR imaging work-up of developmental delay in children less than two years of age and evaluate the added utility of gadolinium administration.

Methods and Materials: During a 7.5 year period (1995-2002), 192 gadolinium enhanced brain MR imaging examinations were performed on children under two years of age at our institution for the evaluation of clinical developmental delay. We retrospectively reviewed the medical records, stated indications and MR imaging findings in all of these patients.

Results: Developmental delay was the primary clinical concern that prompted MR imaging examination in 117 studies (Group A). 75 patients (Group B) had other more significant clinical symptoms with developmental delay as a secondary concern. Out of the total 192 examinations, abnormal contrast enhancement was present in 16 cases (8%). In Group A, there were 4 cases (3%) with abnormal contrast enhancement, all of which represented incidental findings not related to the primary clinical question. In Group B, there were 12 cases (16%) with abnormal contrast enhancement. Gadolinium increased the confidence and/or clarified the diagnosis in 8 cases (4 neoplasms, 3 tuberous sclerosis, and 1 neurofibromatosis) with incidental findings in the remaining 4.

Conclusion: Administration of gadolinium in the MR imaging work-up of children under the age of 2 with developmental delay and no other symptoms does not help in the diagnosis of an underlying cause. Based on the results of this study, gadolinium is no longer administered in this population at our institution.

B-646 11:24

Magnetization transfer ratio in the brain of preterm subjects: Age related changes during the first 2 years of life

V.G. Xydis, A.G. Zikou, L. Astrakas, K. Pantou, S. Andronikou, M.I. Argyropoulou; Ioannina/GR

Purpose: Magnetization transfer (MT) imaging is a magnetic resonance imaging technique that has the potential for monitoring cerebral myelination in vivo. Our purpose was to study the progress of myelination in preterm born subjects by measuring the MT Ratio (MTR) from birth, up to 24 months of corrected age.

Methods and Materials: 125 preterm subjects (64 males, 61 females, of gestational age 33 ± 2.4 weeks, chronological and corrected age 9.3 ± 5.1 , 7.7 ± 5.1 months respectively) with normal brain MR using classic sequences, were further evaluated for MTR by using a three-dimensional gradient-echo sequence (TR = 32/TE = 8/ flip angle = 6° 4 mm/2 mm overlapping sections) without and with magnetization transfer prepulse. The magnetization transfer ratio was calculated as: $\text{MTR} = (\text{SI}_{\text{0}} - \text{SI}_{\text{m}}) / \text{SI}_{\text{0}} \times 100\%$, where SI_m refers to the signal

Scientific Sessions

intensity from an image acquired with a magnetization transfer prepulse and Slo the signal intensity from the image acquired without a magnetization transfer prepulse.

Results: MTR increased asymptotically in the white matter of frontal lobe ($R^2 = 0.91$), occipital lobe ($R^2 = 0.82$), genu ($R^2 = 0.85$), splenium of the corpus callosum ($R^2 = 0.85$), thalamus ($R^2 = 0.86$), putamen ($R^2 = 0.71$) and caudate nucleus ($R^2 = 0.67$), reaching a plateau at corrected age 1.3, 12.9, 18.7, 17.7, 10.4, 6.4, 9.2 months respectively.

Conclusion: This study in preterm subjects shows age related changes of the brain MTR and provides normal data that may be useful to assess disturbances in the progress of myelination.

B-647 11:33

Magnetization transfer imaging of the pituitary gland in patients with Prop1 gene mutations discloses a well-defined "mass" with normal secretory activity within the pituitary

A. Voutetakis¹, A. Sertedaki², M. Maniatzi-Christidi², D. Kiortsis³, I. Bossis¹, C. Dacou-Voutetakis², M.I. Argyropoulou³; ¹Bethesda, MD/US, ²Athens/GR, ³Ioannina/GR

Purpose: To apply Magnetization Transfer (MT) imaging in the evaluation of the pituitary enlargement observed in Prop1 deficient patients.

Methods and Materials: In 3 Prop1 deficient patients dynamic hormonal testing and genomic analysis of the Prop1 gene were performed using established methods. Classic MR and MT sequences were carried out. The MT phenomenon was quantified by the magnetization transfer ratio (MTR).

Results: All patients had low values of GH, TSH and Prl, whereas cortisol values were normal. The initial MR imaging of all three patients revealed an enlarged pituitary gland. The enlargement consisted of a "mass" interposed between the anterior and posterior lobes. MTR of the adenohypophysis was subnormal [patient A (male, 9 yrs): 37% vs 55.3% \pm 2.6 normal values, patient B (female, 3 yrs): 47.3% vs 57.6% \pm 2.68 normal values, patient C (male, 2.5 yrs): 48% vs 55.3% \pm 2.6 normal values], whereas the MTR of the "mass" was normal: patient B: 55.4%, patient C 58.5%.

Conclusion: MT indirectly reflects the secretory status of the tissue. The low MTR of the adenohypophysis reflects the low synthetic-secretory activity of the gland which is in agreement with the hormonal data. Conversely, the normal MTR of the well-defined "mass" causing the pituitary enlargement suggests the presence of tissue with normal synthetic-secretory activity. Cells normally residing in the intermediate lobe are Prop1 independent and could therefore expand, cause the enlargement and account for the normal MTR observed within the "mass". Our findings could help the differential diagnosis between enlargement from other causes and those associated with Prop1 mutations.

B-648 11:42



Diffusion tensor imaging of healthy neonates and children up to adolescence

U. Löbel, D. Güllmar, H.-J. Mentzel, J. Sedlacik, J.R. Reichenbach, W.A. Kaiser; Jena/DE

Purpose: Diffusion tensor imaging (DTI) provides a new diagnostic method for estimating myelination *in vivo*. We studied the development of the human brain using apparent diffusion coefficient (ADC) and fractional anisotropy (FA) in children and adolescents.

Methods and Materials: 133 subjects (68 females, 65 males; age-range 20 days to 25 years) without neuroradiological pathological findings were examined. MR imaging was performed on a 1.5 T MR scanner using a TRSE-epi-dti-sequence (6 directions; b=0/1000 sec/mm²; FOV=240; Matrix=128; in-plane resolution 1.8x1.8 mm²; 19 slices, 5 mm thick). ADC and FA were calculated and 20 bilateral ROIs were manually drawn into each brain.

Results: There was a significant decrease of ADC with age in 32 of 40 regions, most prominent in the frontal regions. FA increased with age significantly in 35 of 40 regions. A logarithmic function best fit the data. Spearman correlation coefficients (r) ranged from 0.188 to 0.688 for FA and from -0.182 to -0.817 for ADC. In the left frontal white matter ADC of all measured patients ranged from 139.8×10^{-5} mm²/sec to 51.0×10^{-5} mm²/sec with r = -0.785 (p < 0.01). Its FA ranged between 0.3077 and 0.8186 with r = 0.44 (p < 0.01). For the left caudate nucleus, ADC was highest with 112.8×10^{-5} mm²/sec, lowest with 56.4×10^{-5} mm²/sec, r = -0.72 (p < 0.01). FA ranged from 0.203 to 0.597, r = 0.195 (p < 0.05).

Conclusion: ADC and FA are able to describe the development of the human brain in most regions with ADC being more steady than FA. Our results suggest that water diffusion is dependent on subject age and brain region. The dimension of change in ADC and FA gives information about the stage of myelination.

B-649 11:51

Appropriate use and benefits of eye-lens bismuth shielding in pediatric head CT examinations

M. Raissaki, K. Perisinakis, A. Tzedakis, M. Daskalogiannaki, I. Damilakis, N. Gourtsoyiannis; Iraklion/GR

Purpose: To evaluate the optimal use of commercially available bismuth garments for eye-lens shielding in children undergoing head CT and to assess the resulting eye-lens dose reduction.

Methods and Material: We prospectively placed a bismuth shield over the eyelids of 27 consecutive children, aged 3 months-16 years (mean:7), referred for a CT scan that might involve lens exposure. Four thermoluminescent crystals were placed, two below and two above each shield, for the calculation of the shielded and unshielded eye-lens dose, respectively. The first 5 children were scanned with a distal shield, 3 cm over the eyes, to eliminate potential artifacts. Depending on the indication, 9 children were scanned with a total eye-sparing technique (Group A). In 11 children the eyes were partly exposed (Group B) and in 6 the eyes were entirely exposed (group C). Two independent readers assessed the scans for artifacts and their effect on the diagnosis.

Results: All but 1 child accepted the shield. Median dose reduction was 34% for group C, 20% for group B and < 2% for Group A.

Dose reduction was 5-30% less for children with distant shielding, compared to the reduction achieved for children in respective groups with direct shielding. Artifacts were noted in 1 scan, not considered to affect the diagnosis.

Conclusion: Direct eye-lens shielding should be applied in all children undergoing brain, sinuses, mastoid CT when the eyes are included entirely or partly in the scan. Resulting dose reduction is at least 20% reaching 43%. Shields are not of value when total eye-sparing technique is performed.

10:30 - 12:00

Room L/M

Cardiac

SS 1403

MR imaging of the coronary arteries

Moderators:

L. Natale; Rome/IT
E. Spüntrup; Aachen/DE

B-650 10:30

MR flow measurements in the coronary arteries before and after aortic valve surgery: Initial results

N.D. Abolmaali¹, M. Schiemann¹, V. Hietschold², A. Koch¹, P. Kleine¹, T.J. Vogl¹; ¹Frankfurt a. Main/DE, ²Dresden/DE

Purpose: To evaluate the velocity profiles in the coronary arteries before and after aortic valve surgery (AVS) in patients without coronary artery disease (CAD).

Material and Methods: 29 patients (median: 68 y) with angiographically excluded relevant CAD received MR-based coronary flow examinations of the LCA and the RCA (58 vessels) before and after AVS. Prospectively ECG-triggered breath hold phase-contrast flash sequences with high temporal resolution were used (1.5 T, Sonata). Noise reduction was done with the second order Savitzky-Golay equalization. Forward velocities and the foot of the curve related to the individual cardiac cycle time were analyzed.

Results: Before AVS, physiological velocity profiles were found in 38 CA (66%). Mean systolic/diastolic velocities were $14.8 \text{ cm/s} \pm 5.4$ / 23.5 ± 10.6 in the LCA and $12.1 \text{ cm/s} \pm 5.3$ / 13.9 ± 5.2 in the RCA. 20 CA showed non-physiological flow pattern pre-AVS, in part reverse flow was detectable. After AVS, 53 CA (91%) revealed physiological velocity profiles. Mean systolic/diastolic velocities increased significantly and were $20.8 \text{ cm/s} \pm 5.8$ / 27.4 ± 6.9 in the LCA and $15.5 \text{ cm/s} \pm 4.7$ / 17.6 ± 6.5 in the RCA. The foot of the heart cycle time of the velocity curves did not show significant differences before (LCA:34.0%; RCA:41.1%) and after (LCA:36.0%; RCA:42.9%) AVS. The velocity profiles of the remaining 5 CA showed steady forward velocities.

Conclusion: MR-based coronary flow measurements are capable of performing follow-up of aortic valve surgery. The increase in flow velocity after surgery, as well as the normalization of the velocity profiles can be quantified non-invasively. The MR-based detection of distorted flow patterns in the CA might add helpful information to the indication before aortic valve surgery.

Scientific Sessions

B-651 10:39

Accuracy of whole heart coronary magnetic resonance angiography for the detection of significant coronary stenoses in 92 patients with suspected coronary artery disease

H. Sakuma¹, Y. Ichikawa², K. Makino², S. Chino², T. Hirano², K. Takeda¹, M. VanCauteren³; ¹Tsu, Mie/JP, ²Matsusaka, Mie/JP, ³Tokyo/JP

Purpose: The purpose of this study was to evaluate the diagnostic accuracy of whole heart coronary MRA for the detection of significant stenoses in the coronary arteries in patients with suspected coronary artery disease.

Methods and Materials: Ninety-two patients with suspected coronary artery disease were evaluated. Three dimensional coronary MR images covering the entire heart were obtained with a navigator-gated, steady state free precession sequence with radial k-space sampling (TR/TE = 4.6/2.3 ms, SENSE factor = 2, FOV = 280x280x120 mm, acquisition matrices = 256x256x80, reconstruction matrices of 512x512x160). All subjects underwent coronary angiography within two weeks of MRA. All coronary arteries and side branches with a diameter of 1.5 mm or more on coronary angiography were evaluated by two blinded observers, and luminal diameter reduction of 50% or more on quantitative coronary angiography was considered to be significant.

Results: The averaged acquisition time of whole heart coronary MRA was 13.3 ± 4.4 minutes. High quality images (score 3 or 4 on 4-point scale) were observed in all segments of the coronary arteries in 75 (82.0%) of the 92 patients. The sensitivity, specificity, positive and negative predictive values, and accuracy of the whole heart coronary MRA for detecting patients having at least one coronary arterial stenosis was 85.3%, 90.2%, 87.9%, 88.1% and 88.0%, respectively. The sensitivity and specificity were 93.3% and 95.0% for RCA, 82.4% and 94.8% for LAD, and 84.6% and 93.1% for LCX, respectively.

Conclusion: Whole heart coronary MRA with a navigator-gated steady state sequence can provide noninvasive detection of coronary artery disease with high diagnostic accuracy.

B-652 10:48

Feasibility of balanced steady-state free precession and conventional gradient echo for coronary magnetic resonance angiography at 3 Tesla

M.G. Kaul, A. Stork, P.M. Bansmann, C. Nolte-Ernsting, G.K. Lund, C. Weber, G. Adam; Hamburg/DE

Purpose: To investigate the feasibility of coronary magnetic resonance angiography with balanced steady-state-free-precession (b-TFE, TrueFISP) and gradient-echo (TFE, turboFLASH) sequences at 3 Tesla.

Material and Methods: 15 volunteers were investigated with a 3 T MR-scanner. TFE and b-TFE were fat-suppressed, T2-prepared and respiratory-motion-compensated. First RCA was imaged with both sequences. Additionally, LM/LAD was examined in 10 volunteers with TFE. The images were analysed by two investigators. RCA was subdivided into three segments, LM/LAD into four. Visibility was graded on a five point scale (0=not visualized, 4=excellent). Contrast-to-noise-ratio (CNR), length, diameter in the first 4 cm and sharpness of the vessels were analysed.

Results: All 15 main and proximal segments of RCA were visualized with TFE and b-TFE. 14 distal segments were seen with TFE and 9 with b-TFE. The graded visibility for the three segments was higher for TFE (2.6/2.6/1.4) than for b-TFE (1.8/1.6/0.9). Kappa-interobserver variability was 0.75 for TFE and 0.8 for b-TFE. CNR was higher for TFE (10.1 ± 3.4) than for b-TFE (6.6 ± 2.2 , $p < 0.02$). Length, diameter and sharpness of RCA were for TFE (95 ± 22 mm, 2.4 ± 0.3 mm, $62\% \pm 6$) and b-TFE (80 ± 40 mm, 2.4 ± 0.3 mm, $60\% \pm 5$). All ten main and proximal segments of LM/LAD were visible with grade 2.5 and 2.1. Middle segments were visible in 7 cases with grade 1.3. In 3 cases distal segments were visible with grade 0.5. Length, diameter and sharpness were (78 ± 27 mm, 2.5 ± 0.3 mm, $64\% \pm 7$) and CNR 11.9 ± 2.4 .

Conclusion: The TFE sequence proved to be superior to the balanced-TFE at 3 T. It seems that the balanced-TFE suffers from offresonance effects.

B-653 10:57

Navigator-gated cardiac-triggered 3D SSFP coronary MRA: Improved image quality using a short RF-pulse

K.M. Ruhl¹, M. Katoh¹, R.M. Botnar², R.W. Günther¹, E. Spüntrup¹; ¹Aachen/DE, ²Boston, MA/US

Purpose: The investigation of the impact of a short RF-pulse on image quality in free-breathing navigator-gated and cardiac-triggered 3D steady-state-free-precession (SSFP) coronary MR angiography (cMRA).

Methods and Materials: cMRA was performed in six healthy volunteers on a

1.5 Tesla MR system (Gyroscan Intera, Philips Medical Systems, Best, The Netherlands) using four navigator-gated and cardiac-triggered SSFP sequences: standard SSFP (sSSFP), SSFP applying the short RF-pulse resulting in a shorter TR/TE and a decreased acquisition window (spSSFPshort), SSFP with the short RF-pulse maintaining the TR/TE of the standard SSFP sequence (spSSFPlongT) and SSFP with the short RF-pulse increasing the acquisition window by adapting the profiles/cardiac cycle (spSSFPlongAQ). Vessel border was analyzed using an edge detection tool. In addition, signal-to-noise-ratio (SNR) and contrast-to-noise-ratio (CNR) of the coronary vessel were assessed.

Results: Mean vessel sharpness was 41.0 ± 2.3 for the sSSFP, 44.6 ± 5.3 for the spSSFPshort, 43.1 ± 6.3 for the spSSFPlongT and 42.8 ± 8.3 for the spSSFPlongAQ. Mean SNR was 30.1 ± 5.8 (sSSFP), 31.8 ± 6.3 (spSSFPshort), 31.7 ± 12.1 (spSSFPlongT) and 31.6 ± 7.5 (spSSFPlongAQ). Mean CNR was 21.8 ± 5.1 (sSSFP), 24.6 ± 5.1 (spSSFPshort), 25.4 ± 9.2 (spSSFPlongT) and 22.2 ± 4.2 (spSSFPlongAQ).

Conclusion: Increased vessel sharpness can be obtained in free-breathing 3D SSFP cMRA by using a short RF-pulse. Consequently shorter TR/TE results also in a more brief acquisition window.

B-654 11:06

Coronary magnetic resonance angiography using parallel acquisition techniques and intravascular contrast media

K.-U. Waltering, K. Nassenstein, S. Massing, T. Schlosser, P. Hunold, J. Barkhausen; Essen/DE

Purpose: To investigate the use of a parallel acquisition technique (PAT) for breath-hold MRCA in increasing the overall coverage.

Methods and Materials: 12 healthy volunteers (6 male, 6 female, mean age 30 ± 5 years, range 22 - 40) were included in this study. All examinations were performed on a 1.5 T MR scanner (Magnetom Sonata, Siemens). MRCA was performed using an inversion recovery prepared fast low angle shot (IR-FLASH) sequence (TR/TE 3.8/1.6 ms, bandwidth 490 Hz/pixel, matrix 320) after i.v. administration of a Gadolinium-based intravascular contrast media (SH L 643A, Schering). Scans were performed without and with PAT in a single breath-hold. The use of GRAPPA with a PAT-factor of 2 and 37 reference lines allowed increasing spatial coverage. Signal-to-noise-ratio (SNR) and contrast-to-noise-ratio (CNR) values were calculated. Image quality was assessed based on a 5-point Likert scale ranging from 1=excellent to 5=non-diagnostic.

Results: The mean image quality score was higher for FLASH imaging without PAT (2.9 ± 0.8) compared to MRCA with parallel imaging (3.5 ± 0.9). Signal intensity measurements showed higher SNR for FLASH imaging without PAT (blood pool: 15.7 ± 2.8 versus 13.0 ± 3.6), whereas the CNR measurements showed no significant differences (12.2 ± 2.6 versus 10.4 ± 3.3).

Conclusion: Our results show that GRAPPA with a PAT-factor of 2 allows increasing spatial coverage without increasing the acquisition time. Although, overall image quality and SNR values were slightly reduced, delineation of the proximal and middle coronary segments was possible.

B-655 11:15

MR flow measurements in the coronary arteries: First results in patients without coronary artery disease

N.D. Abolmaali¹, M. Schiemann¹, V. Hietschold², A. Koch¹, P. Kleine¹, T.J. Vogl¹; ¹Frankfurt a. Main/DE, ²Dresden/DE

Purpose: To evaluate the feasibility of MR-based coronary flow measurements in patients without coronary artery disease (CAD) after aortic valve surgery.

Material and Methods: 70 patients (median: 67 y) with angiographically excluded relevant CAD received MR-based coronary flow measurements of the proximal segments of the LCA and the RCA (140 vessels). Using a prospectively ECG-triggered breath hold phase-contrast flash sequence (1.5 T, Sonata) with high temporal resolution, flow data were technically acquirable in 115 (82%) of the coronary arteries (CA). To reduce noise in the velocity quantification, the flow curves were filtered using the second order Savitzky-Golay equalization. Early and late forward velocities and the foot of the curve related to the individual cardiac cycle time were analyzed.

Results: Physiological velocity profiles were only found in 55 CA (48%). Mean systolic and diastolic velocities in these CA were significantly higher in the LCA ($21 \text{ cm/s} \pm 5.8$; $25 \text{ cm/s} \pm 8.0$) than in the RCA ($14.4 \text{ cm/s} \pm 5.4$; $16.1 \text{ cm/s} \pm 6.5$). The time of the foot of the heart cycle time of the velocity curves did not show significant differences (LCA: 37.5%; RCA: 40.9%). The velocity profiles of the remaining CA revealed severe alterations of the physiologic velocity profile with reduced flow undulations and steady velocities but forward flow was measurable in all CA.

Scientific Sessions

Conclusion: MR based coronary flow measurements were possible in most patients. Physiological velocity profiles were derivable from the acquired data sets. In the LCA, blood velocity is higher than in the RCA. Optimized MR flow measurements are feasible to evaluate the CA non-invasively in patients without CAD.

B-656 11:24

Comparison of conventional free-breathing coronary magnetic resonance angiography with affine motion compensated whole-heart MRA at 3 Tesla
M.G. Kaul, P.M. Bansmann, A. Stork, C. Nolte-Ernsting, K. Nehrke, G. Adam; *Hamburg/DE*

Purpose: To compare conventional free-breathing coronary magnetic resonance angiography (cMRA) with affine motion compensated whole-heart MRA (whMRA) at 3 Tesla.

Materials and Methods: Five volunteers were examined with a whole-body 3 T scanner (Philips Medical System, Netherlands) in combination with a vector-ECG and a six-element phased-array cardiac coil. Navigator driven prospective respiratory motion compensation for the segmented gradient-echo sequences was used. Double oblique scans of the RCA were performed with a gating window (GW) of 5 mm and a correlation of 0.6. The whMRA scan was performed with a 20 mm GW and a patient-specific affine motion compensation. CNR, visualized vessel length, diameter and vessel sharpness of the visualized coronaries were statistically analyzed.

Results: The mean scantime for whMRA was 12 min with a scan efficiency of 98% and 7 min for cMRA with a scan efficiency of 61%. In all volunteers, all major segments of the RCA were visualized. A significant increase in CNR with whMRA in comparison with cMRA was observed ($7.0 \pm 1.5 / 10.1 \pm 1.9 / p < 0.023$). The vessel length was measured longer for whMRA than for cMRA ($10.0 \pm 2.4 \text{ mm} / 11.6 \pm 1.8 \text{ cm} / p < 0.25$), while the vessel diameter was measured smaller for cMRA ($2.46 \pm 0.21 / 2.76 \pm 0.27 / p < 0.66$). A similar vessel sharpness ($0.59 \pm 0.6 / 0.60 \pm 0.02 / p < 0.76$) was estimated for cMRA and whMRA. For the whMRA also the left coronary arteries were visualized.

Conclusion: Comparable results for the affine motion compensated whMRA and the cMRA have been demonstrated. The whMRA shows up to be a time saving procedure because in a single scan information of all coronary arteries can be found.

B-657 11:33

Slice-selective inversion prepared steady-state free-precession (SSFP) MR angiography: Visualization of inflowing coronary blood

M. Katoh¹, E. Spüntrup¹, M. Stüber², A. Buecker¹, W.J. Manning³, R.W. Günther¹, R.M. Botnar³; ¹Aachen/DE, ²Baltimore, MD/US, ³Boston, MA/US

Purpose: Visualization of inflowing coronary blood by means of an inversion prepared bright-blood coronary MRA approach.

Materials and Methods: The right coronary artery (RCA) of seven volunteers (6 men, 1 woman, 39 years) was imaged on a 1.5 Tesla MR system (Gyroscan ACS-NT, Philips Medical Systems, Best, NL) using a navigator-gated cardiac-triggered 3D SSFP sequence with radial k-space sampling (TR/TE 6.3/3.2 ms, FA 120, FOV 360 mm², matrix 384 radial trajectories, spatial resolution 0.9x0.9x3 mm³). Imaging was performed a) with and b) without a slice-selective inversion prepulse, which was positioned along the main axis of the RCA. Hence, RCA and adjacent tissue included in the inversion volume are signal suppressed while unsaturated blood from the ascending aorta that subsequently enters into the coronary artery during an inversion delay appears with a bright signal. SNR, CNR, maximal visible vessel length, and vessel border definition were analyzed.

Results: The use of a selective inversion pre-pulse allowed for direct visualization of inflowing coronary blood. In addition, CNR between the RCA and right ventricular blood was increased (13 vs. 1; $p < 0.01$) and a tendency towards better vessel sharpness was found (68 vs. 60; n.s.). Blood SNR and CNR between RCA blood and epicardial fat were comparable in both sequences.

Conclusion: The combination of a free-breathing navigator-gated and cardiac-triggered 3D SSFP sequence with a slice-selective inversion pre-pulse allows for direct and directional visualization of inflowing coronary blood with the additional benefit of improved contrast between the RCA and right ventricular blood.

B-658 11:42

MR coronary vessel wall imaging: Comparison of radial and spiral k-space sampling

M. Katoh¹, E. Spüntrup¹, A. Buecker¹, W.J. Manning², R.W. Günther¹, R.M. Botnar²; ¹Aachen/DE, ²Boston, MA/US

Purpose: The aim of this study was to compare navigator-gated and cardiac-triggered 3D gradient-echo MR coronary vessel wall imaging using radial and spiral k-space sampling.

Materials and Methods: Right coronary artery vessel walls of eight healthy volunteers (6 men, 2 women; mean age: 37 years) were imaged on a 1.5 Tesla MR system (Gyroscan ACS-NT, Philips Medical Systems, Best, NL) using two double-inversion prepared black-blood gradient-echo sequences (radial: TR/TE 8.0/2.0 ms, FA 30, excitation/cardiac cycle 13; spiral: TR/TE 30.0/2.0 ms, FA 45/90, spiral interleaves 42, excitation/cardiac cycle 2) with identical spatial resolution (0.6 x 0.6 x 2.0 mm³). For data analysis, SNR, CNR and vessel wall definition were objectively analyzed. Furthermore, two investigators blinded to sequence parameters subjectively assessed image quality in terms of artifacts and vessel wall visualization.

Results: Radial k-space sampling demonstrated fewer artifacts and led to improved visualization of the coronary vessel wall compared to spiral imaging. In addition, significantly better vessel wall definition was found in radial imaging ($62 \text{ vs. } 56, p < 0.05$). However, a tendency towards increased SNR and CNR were found using spiral k-space sampling (n.s.).

Conclusion: Radial k-space sampling in free-breathing navigator-gated and cardiac-triggered MR imaging of the coronary vessel wall resulted in fewer motion artifacts and improved vessel wall definition compared to spiral k-space sampling.

B-659 11:51

Role of magnetic resonance angiography in coronary artery ectasia and Kawasaki disease

S.I. Mavrogeni, D.D. Cokkinos, A. Manginas, G. Papadopoulos, M. Douskou, S. Kaklis, S. Foussas, J. Seimenis, D.V. Cokkinos; *Athens/GR*

Purpose: Coronary artery ectasia (CAE) is defined as dilatation to a diameter at least 1.5 times of the normal. Differential diagnosis includes aneurysm due to Kawasaki Disease (KD). We compared each vessel's most ectatic/aneurysmatic diameter using quantitative coronary angiography (QCA) and MRA.

Methods and Materials: Twenty patients with isolated CAE 45-65 years old, 10 patients with KD 1-12 years y.o. and 5 controls with normal coronaries 45-55 y.o. were studied. Coronary MRA was performed using a 1.5 T Philips Intera CV MR scanner with two ECG-triggered pulse sequences, a 3-D segmented k-space GRE sequence (TE = 2.1 ms, TR = 7.5 ms, flip angle = 30°, eff. slice thickness = 1.5 mm) employing a T2W preparation prepulse and a frequency selective fat-sat prepulse to enhance "bright blood" coronaries' contrast. Data acquisition was performed in mid-diastole. We used a 2D real time navigator beam placed on the right hemidiaphragm. All patients underwent QCA. The diameter of the proximal/ middle most ectatic/ aneurysmatic part of each vessel was measured and compared to MRA.

Results: In CAE there was close correlation between MRA and QCA in the diameter ($r = 0.87, p < 0.001$) and length ($r = 0.82, p < 0.001$) of the most ectatic vessel part. In 7 patients with KD, aneurysms were identified. CAE alone was present in the remaining 3 patients. MRA-QCA differentiation of discrete aneurysms vs. ectasia showed complete agreement. In controls, no abnormalities were seen.

Conclusion: MRA is equivalent to QCA for coronary artery anatomy in patients with CEA and KD. It may prove of great value for serial noninvasive evaluation.

Scientific Sessions

10:30 - 12:00 Room N/O

Physics in Radiology

SS 1413

CT: Technical developments

Moderators:

A. Noel; Vandoeuvre-les-Nancy/FR
F. Schick; Tübingen/DE

B-660 10:30

Comparison of angular and combined automatic tube current modulation techniques with constant tube current CT scanning of the abdomen and pelvis

S.M.R. Rizzo¹, M.K. Kalra¹, M.A. Blake¹, T. Dalal¹, M.M. Maher¹, B. Schmidt², C. Suess², T. Flohr², S. Saini³; ¹Boston, MA/US, ²Forchheim/DE, ³Atlanta, GA/US

Purpose: To compare image quality and radiation dose associated with abdominal-pelvic CT using combined modulation, angular modulation and constant tube current.

Methods and Materials: Study cohort included 152 patients (mean age = 60 years, range = 25-101 years; M:F = 78:74) undergoing abdominal-pelvic CT with a 16-slice MDCT (Sensation 16, Siemens Medical Solutions) using either angular modulation ($n = 42$), combined modulation (weak decrease-strong increase type, $n = 42$, or average decrease-average increase type, $n = 37$; image quality reference mAs 160) or constant tube current ($n = 31$; effective mAs = 160-200). Remaining scanning parameters (held constant) included 140 kVp, 0.5 s rotation time, 16x1.5 mm detector configuration, 24 mm table feed per gantry rotation and 5 mm reconstructed slice thickness. Two radiologists assessed image noise, diagnostic acceptability, presence of streak artifacts and visibility of small structures at three levels (confluence of the hepatic veins, porta hepatis, and acetabulum). Quantitative image noise at the porta hepatis level, patients' weight, CTDIvol and DLP were recorded.

Results: Subjective noise and diagnostic acceptability in studies performed with angular modulation, combined modulation or constant tube current were acceptable. Compared to constant tube current, combined modulation resulted in 42% (weak decrease-strong increase type) to 44% (average decrease-average increase type) reduction in radiation dose ($p < 0.0001$), whereas angular modulation resulted in a 19% reduction ($p < 0.0001$). Significant correlation was found between patients' weight, CTDI-vol and DLP for combined modulation ($r = 0.6-0.8$, $p < 0.0001$) but not with constant tube current or angular modulation ($r = 0.01-0.19$, $p > 0.2$).

Conclusion: Compared to constant tube current scanning of abdominal-pelvic CT, combined modulation results in substantial reduction (42-44%) in radiation dose with acceptable image noise and diagnostic acceptability.

B-661 10:39

Impact of the z-flying focal spot (zFFS) on resolution and artifact behaviour for a 64-slice spiral-CT scanner

Y. Kyriakou, M. Kachelriess, M. Knaup, J.U. Krause, W.A. Kalender; Erlangen/DE

Purpose: To verify the effect of the zFFS by measurement with respect to resolution and artifact behaviour for a 64-slice spiral CT.

Methods and Materials: The Sensation 64 CT scanner (Siemens Medical Solutions, Forchheim, Germany) allows measuring of 64 overlapping slices of 0.6 mm thickness. The zFFS switches between two z-positions acquiring two slices per detector row which results in oversampling in the z-direction. We implemented a modified ASSR reconstruction (syngoeplorer, VAMP, Möhrendorf, Germany) that is able to obtain images as they would be without zFFS. A delta phantom equipped with a tiny gold disc was used to measure the slice sensitivity profiles (SSP). We evaluated the SSPs for standard spiral scan modes for various pitch values with and without the zFFS. A high-contrast bar phantom was used to quantify the resolution in the x/z-plane for both cases. Further, we performed cadaver and phantom measurements to determine the effect of the zFFS on spiral windmill artifacts.

Results: Applying the zFFS decreased the FWHM of the SSPs by a factor of about 1.4. The z-oversampling allowed the separation of 0.4 mm bars in the z-direction compared to 0.6 mm in the case of no zFFS. The zFFS reduced windmill artifacts in the reconstructed images while maintaining the transverse resolution even at the largest pitch value of 1.5.

Conclusions: Oversampling in the z-direction by means of the zFFS achieves a high spatial resolution in the z-direction of 0.4 mm, whilst diminishing the effect of spiral windmill artifacts.

B-662 10:48

Validating measures for temporal resolution on multi-slice CT scanners (MSCT)

K. Shanneik, M. Kachelrieß, S. Achenbach, W.A. Kalender; Erlangen/DE

Purpose: To evaluate the temporal resolution of modern MSCT scanners by introducing and validating numerical indicators for temporal resolution.

Methods and Materials: Computer simulations and a dynamic phantom assembly yielding a realistic 3D motion of the human heart were used to move a 100 μm tungsten bead. Heart rates were varied from 40-120 min⁻¹. Data were acquired from standard cardiac scans (pitch = 0.23, rotation time = 0.37 s) on a Sensation 64 CT scanner (Siemens Medical Solutions, Forchheim, Germany) and reconstructed with the ASSR algorithm at cardiac phases ranging from 0-90% R-R interval in 10% steps. We considered the full 3D properties of the point spread function to define the full volume at half maximum (FVHM). Correlation of the FVHM with visually assessed image quality, rated by 6 specialists, and also to the expected theoretical temporal resolution given by the phase contribution profile (PCP) were investigated.

Results: Simulations show that increasing the rotation speed from 0.5 s to 0.33 s improves FVHM results for heart rates between 105-120 min⁻¹ indicating better temporal resolution. Measurements for different reconstruction phases and gantry rotation times showed a good correlation of the FVHM with the PCP of the algorithm (Spearman's rank correlation $r = 0.85$). E.g. at an exemplary cardiac phase of 50% R-R, the FVHM ranged from 2.9 mm³ (no motion) to 9.8 mm³ over the range of heart rates.

Conclusion: The FVHM is an objective and reproducible measure of the temporal resolution, and correlates well with visual impression of image quality.

B-663 10:57

Large field-of-view ultrahigh-resolution flat-panel CT imaging system

J. Eberhard, W.R. Ross, S.K. Basu, P. Fitzgerald, M.A. Rumsey, A.M. Schmitz, B.D. Yanoff, C.J. Ritchie; Niskayuna, NY/US

Purpose: To develop an ultrahigh-resolution experimental clinical CT system, and evaluate the impact of ultrahigh-resolution CT on clinical applications.

Methods and Materials: Three 20 cm square (1024x1024, 200 μm pixels) flat panel detectors were integrated side by side in a clinical CT gantry, incorporating a vascular X-ray source (all components from GE Healthcare) to provide a 50 cm field-of-view (FOV). The detectors were modified to reduce gaps between them to 3.4 cm. Operating modes acquire 500-1000 projections of 180-360 detector rows, at 8 seconds per rotation. System magnification is 1.5; z-coverage per rotation ranges from 17-34 mm. A Beowulf cluster provides short reconstruction times.

Results: A cone-beam reconstruction algorithm that corrects for the gaps between detectors provides uniform image quality over the FOV. Spatial resolution of < 200 microns (MTF > 25 lp/cm, 10% modulation) is uniform over the central 35 cm of the FOV, in both the radial and azimuthal directions. Reconstruction times are 3 minutes for 512x512x180 voxels.

Conclusions: The first ultrahigh-resolution CT system capable of clinical imaging has been developed. Uniform image quality and ultrahigh isotropic spatial resolution have been achieved over a FOV covering the human thorax. The volumetric resolution, > 10X higher than current multi-slice CT systems, provides the ability to precisely quantify volumes on the order of a few mm³. This improved resolution may enable sufficiently precise lung tumor sizing to determine doubling times more quickly, potentially leading to earlier and more accurate diagnosis. In addition, this exceptional performance may enable new clinical CT applications, especially in the area of lung cancer detection.

B-664

withdrawn by authors

B-665 11:06

Cone beam filtered back projection algorithms for image reconstruction in volumetric CT

X. Tang¹, J. Hsieh¹, A. Hagiwara², R.A. Nilsen¹, C. Shaughnessy¹, E.C. Williams¹, E. Drapkin¹; ¹Waukesha, WI/US, ²Hino/JP

Purpose: With increased cone angle, maintaining reconstruction accuracy in volumetric CT becomes more challenging. To obtain well-balanced image qualities,

Scientific Sessions

we propose a novel CB-FBP reconstruction algorithm using 3D view weighting (3D-VW) for both helical and axial scanning geometries, along with a comprehensive experimental evaluation.

Methods and Materials: Through a row-wise fan-to-parallel rebinning, the filtering in the proposed algorithm is naturally carried out along the tangential direction of source trajectory. The 3D-VW is utilized to: (a) suppress artifacts at both axial and helical scanning geometries; (b) improve noise characteristics by allowing redundant projection data in reconstruction; (c) extend FOV at high helical pitches by maintaining data redundancy. Both simulated and scanned projection data (detector dimension: 64x0.625 mm) are used for algorithm evaluation.

Results: At helical mode, the 3D-VW enables the proposed algorithm to reach the reconstruction accuracy possessed by the exact CB-FBP algorithms while providing significantly improved noise characteristics, spatial resolution and temporal resolution. At axial mode, the 3D-VW is dependent on individual reconstruction plane and suppresses CB artifact substantially in comparison to the original FDK algorithm. Moreover, a comparison study shows that, the proposed algorithm outperforms other reconstruction algorithms, such as the titled-plane-based algorithms, in term of artifacts suppression even with large FOV at very high helical pitches.

Conclusions: It is the 3D-VW that assures the proposed algorithm to obtain optimal image qualities and the freedom in image quality controllability. It is believed that the proposed algorithm is applicable in and robust over diagnostic and functional CT imaging applications.

B-666 11:15

Conjugate cone beam back projection scheme for VCT thin slice imaging

J. Hsieh, X. Tang, J.-B. Thibault, C. Shaughnessy, E. Williams, D. Samsonov; Waukesha, WI/US

Purpose: One of the important CT performance parameters is the z-resolution. This parameter is impacted not only by the spot size, detector aperture, and geometry, but also by the reconstruction algorithm. We present a conjugate cone beam back projection approach that allows the reconstructed slice thickness comparable to the detector aperture.

Methods and Materials: One key step in the filtered back projection reconstruction algorithms is the three-dimensional back projection. The most widely used method is the row-to-row interpolation (interpolation takes place between two rows of the same view). The drawback of this approach is a degraded z-resolution. In this paper, we present a conjugate interpolation (CI) in which interpolation takes place between dynamically selected conjugate projection samples that are 180° apart. When appropriate helical pitch is selected, the conjugate rays form interlaced samples along z. For computation simplicity, a row-wise fan-parallel rebinning is first applied.

Results: Theoretical analysis has shown that CI enables a 30% improvement in SSP, as compared to the conventional back projection. This result is confirmed with a thin foil phantom. For a 64x0.625 mm acquisition, FWHM was measured at 0.6 mm, as compared to 0.84 mm for conventional back projection. The 0.4 mm air bars in the AAPM phantom insert can be clearly visualized with the proposed reconstruction.

Conclusion: Theoretical and phantom experiments have shown that CI algorithm enables a 30% improvement in SSP, as compared to the conventional method. It allows a simpler and more robust VCT system design.

B-667 11:24



Influence of increasing convolution kernels filtering on plaque imaging with multislice CT using an ex-vivo model of coronary angiography

G. Runza¹, F. Cademartiri², N.R. Mollet², M. Belgrano³, F. Barbiera⁴, M. Midiri¹, R. Hamers², N. Bruining²; ¹Palermo/IT, ²Rotterdam/NL, ³Trieste/IT, ⁴Sciaccia/IT

Purpose: To assess the variability in attenuation of coronary plaques with multislice CT-angiography (MSCT-CA) in an ex-vivo model with varying convolution kernels.

Methods and Materials: MSCT-CA (Sensation 16, Siemens) was performed in three ex-vivo left coronary arteries after instillation of contrast material solution (Iomeprol 400 mg/ml, dilution: 1/80). The specimens were put into oil to simulate the epicardial fat. Scan parameters: slices 16/0.75 mm, rotation time 375 ms, feed/rotation 3.0 mm, mAs 500, slice thickness 1 mm and FOV 50 mm. Datasets were reconstructed using 4 different kernels (B30f-smooth, B36f-medium smooth, B46f-medium and B60f-sharp). Each scan was scored for the presence of plaques. Once a plaque was detected, the operator performed attenuation measurements (HU) in coronary lumen, oil, calcified and soft plaque tissue using the same settings in all datasets. The results were compared with T-test and correlated with Pearson's test.

Results: Significant differences ($p < 0.05$) were found for the mean attenuation of lumen (B30f/B36f, B30f/B60f, B36f/B46f, B36f/B60f, and B46f/B60f), oil (B30f/B36f, B30f/B60f, B36f/B46f, and B46f/B60f), calcium (all kernels) and plaque (B30f/B36f, B30f/B46f, B30f/B60f, and B46f/B60f) using 4 different kernels. The attenuation values (mean \pm SD) within the lumen (246 \pm 6, 215 \pm 13, 248 \pm 5, and 270 \pm 7), oil (-123 \pm 3, -127 \pm 1, -121 \pm 6, and -127 \pm 4), calcified plaque tissue (703 \pm 334, 739 \pm 364, 817 \pm 381, and 1181 \pm 503) and soft plaque tissue (134 \pm 56, 111 \pm 49, 120 \pm 56, and 102 \pm 41) showed high correlation ($p < 0.01$). When attenuation of all structures were compared in different kernels.

Conclusion: Use of sharper convolution kernels significantly increases the attenuation of the calcium within coronary plaques and reduces the attenuation of soft plaque tissue.

B-668 11:33

Real-time prediction of the heart phase for tube current modulation (TCM) by kymogram detection from spiral CT scans of the heart

D. Ertel, M. Kachelriess, D.-A. Sennst, W.A. Kalender; Erlangen/DE

Purpose: To provide a rawdata-based synchronization signal alternative to the commonly used ECG as a basis for online heart-phase dependent TCM.

Method and Materials: The synchronization signal -the kymogram function- is generated by three different methods: A derivation of the projected mass with respect to the view angle, the difference of the projected mass after half a rotation and the published method [Med. Phys., 29 (7):1489-1503, 2002] based on a center-of-mass tracking of the scanned object. The technique to compute a kymogram is enhanced to be performed in real time. We used data of 12 patients scanned with a collimation of 12°*0.75 mm, a table increment of 2.8 mm/rotation, a rotation time of 0.42 s and a concurrent ECG recording (Sensation 16, Siemens, Forchheim, Germany). The signal extrapolation is performed on basis of the normalized least-mean-square algorithm by predicting the heart rate according to the prior values. The real-time capability of the kymogram calculation was verified by observing the time needed for signal processing with a standard PC.

Results: In 9 of 12 patient data-sets our method achieved a high correlation with the ECG. The derivation of the projected mass with respect to the view angle showed the least reliable results. All three methods satisfied the prerequisite of being able to perform in real time.

Conclusion: Sync peaks predicted on the basis of a kymogram correlated well with the ECG in most cases. We conclude that a kymogram-based tube current modulation for dose reduction in cardiac CT is feasible.

B-669 11:42

Assessment of automatic exposure control systems on CT scanners using a custom made phantom

N. Keat, M. Aplin, S. Edyvean, D.J. Platten, M.A. Lewis; London/UK

Purpose: Automatic exposure control (AEC) systems are now available on CT scanners from the four major manufacturers. These systems compensate for changes in attenuation of the X-ray beam by adjusting the tube current (mA). A phantom has been developed and used to test the capabilities of these systems to control image quality and radiation dose.

Method and Materials: A 300 mm long, cone shaped PMMA (Perspex) phantom with an elliptical cross section (major and minor diameters increasing from 61.2x40.8 to 428.7x285.8 mm) was constructed. The phantom was tested on four sixteen-slice CT scanners. The mA used by the scanner gave information on relative radiation dose with AEC on and off, and image quality was characterised using the standard deviation of the CT number values.

Results: Each AEC system used different methods for scan setup and implementation of exposure control. Selected results will be presented. For example, the GE scanner allows the user to set a required image noise level, which the AEC aims to achieve by setting the mA for each rotation. A helical scan (pitch 0.938, length 150 mm) with the noise index set to 8 gave measured noise values between 7.1 and 9.5 (mean of 7.9).

Conclusions: The elliptical cone phantom was capable of assessing the performance of AEC systems. All were largely successful in achieving their aims. Introduction of AEC systems into clinical use requires understanding of their operation so that the aims of consistent image quality and optimised patient radiation dose are achieved.

Scientific Sessions

10:30 - 12:00

Room P

Molecular Imaging

SS 1406

Targeting and PET imaging

Moderators:

A. Luciani; Creteil/FR

W. Semmler; Heidelberg/DE

B-670 10:30

Flare-up arthritis imaging with native Cy5.5 versus albumin bound Cy5.5

A. Hansch, I. Hilger, O. Frey, D. Sauner, A. Malich, J. Boettcher, R. Brauer, W.A. Kaiser; Jena/DE

Purpose: The aim of our study was to visualize arthritis with near-infrared fluorescence imaging (NIRF) in a murine arthritis model. The flare-up arthritis is an established arthritis model for human rheumatoid arthritis. NIRF was done for two preparations of the fluorochrome Cy5.5, one native, the other albumin conjugated. Albumin uptake is increased in arthritic joints.

Methods and Materials: Flare-up arthritis was induced in 8 mice. On day 7 after induction of flare-up arthritis, 4 mice received 50 nmol/kg Cy5.5 and 4 mice equimolar concentrations of the dye as albumin-dye conjugate intravenously. NIRF imaging was performed immediately before injection (baseline) and until 72 hours thereafter.

Results: NIRF imaging revealed higher fluorochrome uptake in all inflamed knees compared to contralateral ones. Cy5.5 labeled albumin uptake in arthritic joints was lower than native Cy5.5 uptake (e.g. mean signal intensity in arthritic knee joints 2 hours after application of Cy5.5 labeled albumin: 864a.u. \pm 89 and after application of Cy5.5: 1235a.u. \pm 102).

Conclusion: Imaging of flare-up arthritis with NIRF is feasible. Albumin conjugation prior injection does not improve the uptake of dye in arthritic joints. Therefore native dye seems to be favorable for arthritis imaging with NIRF.

B-671 10:39

Synthesis of a combined optical/MR imaging contrast agent for imaging endothelial E-selectin expression

M.A. Funovics¹, R. Weissleder², F. Reynolds², L. Josephson²; ¹Vienna/AT,

²Boston, MA/US

Purpose: Receptor-specific molecular imaging is limited by compartmental delivery barriers, lack of high affinity in monovalent receptor-probe interactions, and lack of efficient coupling chemistries to generate suitable multivalent systems. We attempted to overcome these problems by synthesizing a multivalent conjugate specifically targeting E-Selectin, which is upregulated on vascular endothelium in inflammation.

Methods and Materials: Two linear peptides containing DITWDQLWDLMK (sequence_1) and IELLQAR (sequence_2), which have been reported to bind to human E-selectin were synthesised and coupled to a nanoparticle consisting of an iron oxide core coated with cross-linked FITC-labelled aminodextran. Peptides were coupled C- and N-terminally using neutral or negatively charged spacer amino-acids by reacting the particle with N-hydroxysuccinimide esters to yield thioether- and disulfide-linkages, respectively, to the terminal cysteine of the peptide (@6-27_peptides/nanoparticle). The conjugates were incubated on stimulated and receptor negative unstimulated human umbilical vein endothelial cells. Amounts of bound conjugate were compared using a competitive anti-FITC immunoassay, FACS, and confocal microscopy.

Results: Particles containing sequence_1 showed no selective binding, the peptide containing sequence_2 with N-terminal attachment and negatively charged linker arm (S4) showed the specific affinity to e-selectin. During 4 h-incubations with 80-320fM conjugate, S4-binding was 80-1200x higher compared to neutral linker arm peptide, and 200-10000x higher compared to C-terminally attached peptide. Maximal uptake of S4-conjugate was 0.1 fmol/cell. Unstimulated cells showed at least 80x less uptake. Stimulated cells after incubation were brightly fluorescent due to receptor-mediated endocytosis of the conjugate.

Conclusion: A nanoparticle for receptor imaging of E-Selectin has been developed using a multivalent peptide-nanoparticle conjugate and has been used for imaging in vivo and in vitro.

B-672 10:48

MR imaging of Her-2/neu protein using high-affinity magnetic nanoparticles

C. Fritzsche, I. Hilger, R. Trost, J.R. Reichenbach, W.A. Kaiser; Jena/DE

Purpose: To detect Her-2/neu overexpressing tumor cells in vitro and in animal tumor models by MR imaging using high affinity magnetic nanoparticles.

Methods and Materials: High affinity magnetic nanoparticles (probes) were designed by coupling anti-Her-2/neu antibodies or gamma globulin (4 micrograms protein per milligram Fe). Her-2/neu overexpressing cells (SK-BR-3) were incubated with anti Her-2/neu (high affinity) and gamma globulin (non-affinity) labelled magnetic nanoparticles. Cell labelling was investigated MR imaging (1.5 T, Magnetom Vision, Siemens) using an inversion recovery sequence and verified by electron microscopy. Moreover, probes (high affinity or non-affinity, approximately 2 mg Fe) were injected into the tail vein from Her-2/neu over-expressing (SK-BR-3) and normal expressing tumor (MX-1) bearing mice (n = 8). Images were recorded before and 20 min, 6 and 24 hours after probe application using T1, T2 and PD spin echo sequences in coronal orientation. Signal intensity at the tumor region was analyzed in relation to normal tissue.

Results: In vitro, Her-2/neu overexpressing cells incubated with high affinity magnetic nanoparticles showed distinctly lower T1 relaxation times as compared to the treatment with non-affinity probes. Electron microscopic examinations were in agreement with MR imaging findings. In vivo whole body MR imaging showed a distinct relative decrease (-20%) in signal intensity in Her-2/neu overexpressing tumors after application of the high affinity probe as compared to controls (e.g. normal expressing tumors with high or non-affinity probes).

Conclusion: The whole body molecular detection of Her-2/neu overexpressing tumors using clinical MR imaging with high affinity magnetic nanoparticles is feasible.

B-673 10:57

The study of Gd-labelled liposomes with long circulation time

D. Zhang; Shanghai/CN

Purpose: To study Gd-labelled liposomes with long circulation time.

Methods and Materials: A 3/2/0.15(mole ratio) blend of HSPC (hydrogenated soy phosphatidyl choline), Chol (cholesterol) and mPEG-HSPE (methoxy poly ethylene glycol hydrogenated soy phosphatidyl ethanolamine) was employed for long circulating liposome preparation by the thin film hydration method. The blend was dissolved in chloroform. Then the solvent was rotary evaporated to dryness and the resulting film was further dried under vacuum over night. The lipids were hydrated with 0.5 mol/L Gd-DTPA. The lipid dispersion was allowed to swell for two hours and was then subjected to five freeze-thaw cycles in liquid nitrogen and warm water respectively. The liposomes was then passed through 0.08-0.1um polycarbonate membranes using a Lipex extruder, to give primarily vesicles of approx. 100 nm in diameter. Untrapped Gd-DTPA was removed by dialysis against isosmotic glucose solution. The effective Gd concentration within the liposome was determined by inductively coupled plasma atomic emission spectrophotometry. MR imaging scan was performed after the liposome was injected intravenously into rat with glioma.

Results: The mean intensity-weighted diameter of the liposome preparation ranged from 71 to 376 nm. The polydispersity index, a numerical expression of the breadth of the size distribution, varied from 0.13 to 0.22. MR imaging scan showed that the tumor had obviously contrast, but liver and spleen had no obviously contrast.

Conclusion: The Gd-labelled long circulating liposome can not be phagocytized by the cells of the reticuloendothelial system. It is possible to make targeted enhancement MR imaging by binding antibody or peptide to the surface of the liposome.

B-674 11:06

MR imaging of the Her2/neu and 9.2.27 tumor antigens using immunospecific contrast agents

M.A. Funovics, B. Kapeller, K. Macfelda; Vienna/AT

Purpose: Molecular imaging of tumor antigens using immunospecific MR contrast agents is a rapidly evolving field, which can potentially aid in early disease detection, monitoring of treatment efficacy, and drug development. In this study, we designed, synthesized, and tested in vitro, two novel monocrystalline iron oxide nanoparticles (MION) conjugated to antibodies against the her2/neu tyrosine kinase receptor and the 9.2.27 proteoglycane sulfate.

Methods and Materials: MION was synthesized by coprecipitation of iron(II) and iron(III) salts in 12 kD-dextran solution, antibody coupling was performed by reductive amination. The relaxivity of the conjugates was 24.1-29.1 mM-1sec-1,

Scientific Sessions

with 1.8-2.1 antibody molecules per nanoparticle. A panel of cultured melanoma and mammary cell lines was used for testing. The cells were incubated with the particles at 16-32 µg Fe/ml in culture medium for 3 h at 37 °C, and investigated with immune fluorescence, transmission electron microscopy (TEM), MR imaging of cell suspensions in gelatine, and spectrophotometric iron determination.

Results: All receptor-positive cell lines, but not the controls, showed receptor-specific immune fluorescence, and strong changes in T2 signal intensity at 1.5 T. The changes in 1/T2 were between 1.5-4.6 sec-1 and correlated with the amount of cell-bound iron ($R = 0.92$). The relaxivity of cell-bound MION increased to 55.9 ± 10.4 mM⁻¹sec⁻¹. TEM showed anti-9.2.27 conjugates binding to the plasma membrane, while the anti-her2/neu conjugates underwent receptor-mediated endocytosis.

Conclusion: We obtained receptor-specific T2 MR contrast with novel covalently bound, multivalent MION conjugates with anti-9.2.27 and anti-her2/neu to image tumor surface antigens. This concept can potentially be expanded to a large number of targets and to in vivo applications.

B-675 11:15

Whole-body MR imaging in staging cancer patients: A comparison with conventional CT and MR imaging

N.A. Ghanem, P. Franke, G. Pache, T. Bley, J. Winterer, M. Langer; *Freiburg/DE*

Purpose: Comparison of whole-body MR imaging and conventional CT and MR imaging in tumor detection and staging in cancer patients.

Methods and Materials: 103 patients were studied prospectively by whole-body MR imaging (WBM). The WBM examinations were performed using the rolling table platform "angiosurf" for unlimited field of view with a 1.5 Tesla system (Magnetom Sonata, Siemens, Erlangen, Germany). A coronal STIR-sequence was used for imaging of the different body regions. The findings of conventional CT and MR imaging and WBM were compared using region by region analysis evaluating the primary tumor, lymph nodes, bone and visceral metastases.

Results: In respect of tumor detection ($n = 64$), WBM and conventional CT and MR imaging concordantly revealed a tumor in 42 patients and in 15 patients both imaging techniques excluded a tumor. In 5 patients CT and MR imaging was positive, whereas WBM was false negative. In 2 patients WBM was superior to CT and MR imaging by detecting the primary tumor. In comparison to conventional CT and MR imaging, WBM detected only 39/50 lymph node metastases, 14/22 visceral metastases, 5/28 pulmonary metastases and 70/76 bone metastases. However, WBM revealed 163 new pathologies due to its band-width which were missed by conventional investigations.

Conclusion: WBM is an effective and fast method for examining cancer patients by the use of a rolling table platform. The wide range of WBM eases detection of new pathologies, but cannot reach accuracy of conventional CT and MR imaging.

B-676 11:24

Positron emission tomography can predict tumor response in prostate cancer gene therapy by oncolytic herpes simplex virus

C.C. Riedl, M. Mullerad, D.P. Eisenberg, T.J. Akhurst, P.S. Adusumilli, A. Bhargava, H. Hricak, P.T. Scardino, Y. Fong; *New York, NY/US*

Purpose: To assess if an enhanced response to oncolytic viral therapy in prostate cancer due to an androgen-induced increase in cellular metabolism can be predicted by Positron Emission Tomography (PET) scan.

Methods and Materials: Bilateral CWR22 flank tumors were implanted in seven athymic rats. Baseline ¹⁸FDG-PET scanning was performed after two weeks with an average tumor volume of 596 mm³. Subsequently, animals were randomized to undergo either orchietomy or sham-operation. ¹⁸FDG-PET imaging was then repeated at 108 hours. In a separate cohort, bilateral flank tumors were implanted in 14 rats. Seven days after tumor implantation, animals were again randomized to orchietomy or sham-operation. After two weeks, tumors were treated with a single intratumoral injection of NV1066 (1×10^7 plaque forming units). Viral replication was quantified 72 hours following infection by real-time quantitative PCR for the viral gene ICPO ($n = 14$).

Results: Decreased tumor metabolism induced by androgen withdrawal resulted in a significant decrease in FDG accumulation in the orchietomy group (32% decrease of maximum standardized uptake value, SUV_{max}) compared to hormonally intact animals (12% SUV_{max} increase) ($p = 0.002$). The presence of androgens in hormonally intact animals enhanced viral titer by a factor of 2.4 compared to orchietomized animals.

Conclusion: PET measured SUV_{max} predicted the enhanced efficacy of oncolytic herpes viruses in the treatment of androgen-sensitive prostate cancer cells. This proof-of-concept study provides the mechanistic basis for the selection of a subgroup of patients for oncolytic viral therapy by means of a non-invasive molecular imaging method.

B-677 11:33

Accuracy of whole-body FDG-PET/CT for tumor staging in oncology

P. Veit, N. Saoudi, L.S. Freudenberg, H. Kuehl, T. Beyer, A. Bockisch, G. Antoch; *Essen/DE*

Purpose: To assess the accuracy of PET/CT in staging different malignant diseases and to determine a potential benefit of PET/CT concerning the patients' management.

Methods and Materials: 260 consecutive patients with different oncological diseases underwent [¹⁸F]-2-Fluoro-2-deoxy-D-glucose (FDG) PET/CT for tumor staging. Image evaluation was performed for CT alone, PET alone, PET + CT viewed side by side, and fused PET/CT data. Histopathology and a clinical follow-up of 311 (± 125) days served as standards of reference.

Results: Fused PET/CT proved significantly more accurate in assessing the overall TNM stage compared to CT alone ($p < 0.05$), PET alone ($p < 0.05$), and side-by-side CT + PET ($p < 0.05$). Of all 260 patients 218 (84%) were correctly staged with PET/CT, 197 (76%) with side-by-side CT + PET, 166 (64%) with PET alone, and 163 (63%) with CT alone. No statistically significant difference could be detected between PET/CT and CT + PET when separately assessing M-staging. Combined PET/CT had an impact on the treatment plan in 6% of patients compared to side-by-side CT + PET, in 15% of patients compared to CT alone, and in 17% of patients compared to PET alone.

Conclusion: Dual-modality FDG-PET/CT is significantly more accurate than CT alone, PET alone, and side-by-side CT + PET when staging different malignant diseases. This diagnostic advantage translates into treatment plan changes in a substantial number of patients.

B-678 11:42

IV-contrast enhanced protocols for high-resolution whole-body PET/CT imaging: Optimization of CT-imaging

K. Brechtel¹, T. Beyer², S.M. Eschmann¹, M.S. Horger¹, M. Vogel¹, R. Bares¹, C.A. Pfannenberg¹, C.D. Claussen¹; ¹Tübingen/DE, ²Essen/DE

Purpose: PET/CT imaging requires the adoption of standard imaging protocols of standalone CT and PET examinations. We present strategies to optimize contrast enhanced CT protocols in high-resolution PET-CT imaging with a 16-row MD-CT scanner.

Methods and Materials: 45 patients were referred for 3 whole-body PET/CT scanning protocols, 1 h pi of 400 MBq FDG. IV contrast was administered as a single bolus of 100 ml followed by a 40 ml saline flush. Protocol A ($n = 15$) included a single-spiral CT scan during pv-enhancement in shallow breathing. In Protocol B ($n = 15$) the CT was divided into a multi-phasic study involving a pre-contrast liver, an arterial phase liver/thorax, and a pv-abdomen scan during breath hold in NormExp. Protocol C ($n = 15$) was similar to B with the patients being allowed to breathe shallowly.

Results: Protocols A and C resulted in the best alignment of CT and PET data. Overall misalignment of CT and PET was less than 10 mm in reference areas of maximum mobility (eg diaphragm) in all protocols. While B provided almost standard state-of-the-art diagnostic quality for multi-phase contrast enhancement, it was limited by the reproducibility of the NormExp state. A and C, however, resulted in a somewhat reduced diagnostic quality due to blurring effects caused by shallow breathing.

Conclusion: High resolution, whole body PET-CT imaging is feasible in clinical routine with optimized IV-contrast enhancement for nearly state-of-the-art multi-phase MD-CT examinations and without contrast induced artefacts on the corrected PET. However, an additional low-dose CT of the thorax may be required in full inspiration for the detection of small lesions.

B-679

withdrawn by author

Scientific Sessions

14:00 - 15:30

Room B

Musculoskeletal

SS 1510

Advanced MR imaging techniques

Moderators:

M. Mechrl; Brno/CZ

W.C.G. Peh; Singapore/SG

B-680 14:00



In-vivo ¹H MRS study of the vertebral body

V.A. Rogozhyn, Z.Z. Rozhkova, E.G. Pedachenko, A.R. Garmish; Kiev/UA

Purpose: Our goal is to describe the vertebral body state on the basis of ¹H MRS data of the vertebra.

Materials and Methods: Three groups of subjects are examined by ¹H MRS using 1.5 T MagnetomVision (Siemens). The 1st group (G1) includes 30 healthy volunteers (23-64 y). The 2nd group (G2) includes 30 patients (42-73 y) with vertebral osteoporosis. The 3rd group (G3) includes 45 patients (36-67 y) with vertebral hemangioma. The spectra are recorded with 2DCSI:TR/TE = 3000/20 ms.

Results: We consider the signals from water (4.7 ppm) and lipids: CH₃ (1.0 - 1.1 ppm), (CH₂)_n (1.5, 2.3 - 2.5, 5.4 ppm). We define the content A^M as peak amplitude (PA) and the concentration C^M=A^M/S, S = A^{Lip}+A^{Wat}. We describe the state of vertebra in each VOI by the pair T* = { A^{Wat}, A^{Lip} }, where A^{Lip} and A^{Wat} are the PA of the signals from water and lipids. The configuration 1* = { A^{Wat}> A^{Lip} } is observed in the spectra of young volunteers, in the spectra of G3 patients and in the spectra, overlying the intact tissue of vertebrae of those patients. The configuration 2* = { A^{Wat}< A^{Lip} } is observed in the spectra of elderly volunteers and in the spectra of G2 patients. In G1 and G2 the average values of A^{Lip} are equal to 0.793 and 0.639, in G3 in the tumor and in intact tissue these values are 0.131 and 0.178, respectively.

Conclusion: Quantitative classification of the state of vertebra according to the dyad spectral configurations allows us to differentiate vertebral pathologies.

B-681 14:09

Clinical application study of ¹H MRS on bone and soft tissue diseases in the lower limbs

C. Zhou, Q. Meng, M. Fan, B. Luo; Guangzhou/CN

Purpose: To investigate and analyze spectroscopic characteristics of ¹H MRS in benign and malignant bone diseases and in soft tissue tumors of the limbs.

Methods and Materials: 38 cases of bone diseases and 20 soft tissue tumors which were pathologically proven, and 24 normal bone marrows of the lower limbs were studied by a 1.5-T system and a ¹H MRS software package supplied by Siemens Company in Germany. Each had a routine MR imaging scan before ¹H MRS examination. SVS-STEAM was used. Parameters for ¹H MRS were TE 270 ms, TR 1500 ms, no. of acquisitions 256, and volumes of interests 2x2x2 cm³.

Results: 1. ¹H MRS of the normal bone marrow presented with a single wave peak. The single wave peak near 1.6 ppm was called lip1; the single wave peak near 0.9 ppm called lip2 in our study. 2. Increased Choline and Lactate signal, and decreased Lip1 signal in malignant bone and soft tissue tumors of the limbs, representing two higher peaks and one lower peak in wave shape, whereas, in benign lesions of the limbs, increased Lip1, decreased Choline and Lactate, presenting with two lower peaks and one higher peak in wave shape.

Conclusion: With ¹H MRS combining with routine MR imaging, the differentiation diagnostic accuracy between the benign and malignant bone lesions, as well as soft tissue tumors of the limbs should be elevated.

B-682 14:18

Validation of tMIX estimated T1-T2 values in correlation with relaxometry determined values in a phantom

I. Van Breuseghem¹, I.M. Van Mieghem¹, L. Vanderelst², H.T.C. Bosmans¹, S. Pans¹; ¹Leuven/BE, ²Mons/BE

Purpose: The turbo mixed T1 and T2 quantification sequence (tMIX) is used for cartilage mapping on a clinical 1.5 T system. In this study, we evaluated the correlation of T1 and T2 values determined with this tMIX sequence and with an accepted spectroscopic method in a phantom.

Materials and Methods: A phantom comprising 7 tubes with different gadolinium-DTPA/water solutions was made. T1 and T2 relaxation time of these solutions

were determined with relaxometry measurements on a Bruker minispec Mq 60. The tMIX sequence was run on a 1.5 T MR imaging system to determine the T1 and T2 relaxation times of the same solutions. The correlation between spectroscopy determined and tMIX estimated T1 and T2 values was calculated with Pearson correlation coefficient. Relative differences between both values were calculated.

Results: A high correlation between spectroscopy and tMIX obtained values is shown for T1 ($r = .99$) as well as for T2 ($r = .99$), but a broad range of relative differences exist (from 0.3 to 190.2%). The differences in the expected cartilage relaxation ranges however are low: for T1 in the interval 150 ms to 400 ms, relative differences vary between 15 and 20% (and can be linearly corrected), for T2 in the interval 20 ms to 100 ms, relative differences vary between 0.3 and 11.5%.

Conclusion: Obtained tMIX relaxation values correspond well in the expected cartilage relaxation times. However, errors need to be considered, but they can be corrected for.

B-683 14:27

Reduction of T2 relaxation times in articular cartilage after enzymatic proteoglycan depletion

C. Glaser, T. Mendlik, E. Rauch, S. Milz, S. Schulz, R. Putz, M.F. Reiser; Munich/DE

Purpose: To analyze changes of T2 relaxation times in human articular cartilage following enzymatic depletion of proteoglycans.

Material and Methods: Seven macroscopically intact human patellae were imaged within 48 hours of death in a clinical 1.5 T scanner before and after 6 hours of exposition of the medial patellar facets to 330 u/ml hyaluronidase. 20 transverse partitions/ sections (resolution: 0.6 x 0.6 x 3.0 mm³) were acquired with a 3D FLASH WE sequence (17.6/8.8 ms; 25°) and a multi echo sequence (TR/Temin = 3000/13.2 ms; 8 echoes). After segmentation of the cartilage (WE sequence) and superposition of the segmentation on the multi echo images, T2 values were calculated (pixel-by-pixel, monoexponential fit). Average T2 values were extracted for the medial and lateral patellar facets in both, the superficial and lower layers of the cartilage. Safranin O staining and Scanning Electron Microscopy (SEM) were performed on excised cartilage-on-bone samples from both facets.

Results: T2 values varied between 29 and 48 ms. Average T2 was decreased by 13% in the lower and by 23% in the superficial layer after hyaluronidase. NaCl controls showed but a small decrease of T2 in the superficial and no changes in the deep layers. There was good correlation between changes in staining intensity and T2 distribution after hyaluronidase. SEM showed an intact collagenous fibre architecture in all excised samples.

Conclusion: T2 relaxation times of articular cartilage are reduced after treatment by hyaluronidase. A possible explanation may be a reduced water content of cartilage consecutive to depletion of proteoglycans.

B-684 14:36

The value of three dimensional dual echo in steady state MR imaging (3D-DESS) as a standard technique in the evaluation of knee internal derangement

I.M. Van Mieghem, F. Frans, I. Van Breuseghem, S. Pans; Leuven/BE

Purpose: To correlate the diagnostic accuracy for evaluation of knee internal derangement using an optimised 3D-DESS MR imaging sequence with arthroscopy findings.

Methods and Materials: We retrospectively reviewed the MR examinations, MR reports and arthroscopy reports of 199 patients who were referred for assessment of internal derangement of the knee. All MR imaging was done with a 1.0 T MR imaging system where a 3D-DESS sequence was performed. The MR imaging interpretations were compared with the arthroscopy reports, being considered as the gold standard. Images were scored for the presence or absence of meniscal tear (medial/lateral), cruciate ligament tear (anterior/posterior) and morphological cartilage lesions. Per group sensitivity, specificity and diagnostic accuracy were calculated; the diagnostic value of the sequence was determined.

Results: At surgery, 41 lateral meniscus tears, 106 medial meniscus tears, 59 anterior cruciate ligament tears, 3 posterior cruciate ligaments tears and 96 cartilage lesions were observed. The sensitivity, specificity and accuracy was 93%, 96% and 95% for lateral meniscus tears; 99%, 92% and 96% for medial meniscus tears; 95%, 91% and 92% for anterior cruciate ligament tears; 100%, 100% and 100% for posterior cruciate ligament tears; and 89%, 79% and 85% for cartilage lesions, respectively. The overall sensitivity was 86%. For all sub-groups the technique is considered as highly diagnostic accurate ($p < .001$).

Conclusion: MR imaging with an optimised 3D-DESS technique is a highly accurate method in the evaluation of knee internal derangement.

Scientific Sessions

B-685 14:45

Fast magnetic resonance imaging of the knee using a parallel acquisition technique (mSENSE): A prospective performance study

K.-F. Kreitner, B. Romaneehsen, K. Oberholzer, F. Krummenauer, M. Thelen; Mainz/DE

Purpose: To evaluate overall image quality and performance of a magnetic resonance (MR) imaging strategy that uses multiple receiver coil elements for application of time saving integrated parallel imaging techniques (iPAT) in traumatic disorders of the knee.

Material and Methods: 90 patients with suspected traumatic derangements of the knee joint underwent MR imaging at 1.5 T. For signal detection we used a 6-channel body array coil that was wrapped around the knee joint. All patients were examined using a standard imaging protocol, which consisted of different turbo spin-echo sequences (PD-, T₂-weighted TSE with and without fat suppression). All sequences were repeated with an integrated parallel acquisition technique (iPAT) using modified sensitivity encoding (mSENSE) with an acceleration factor of 2. Overall image quality, artifacts as well as pathologic findings were evaluated by two radiologists using a four-point scale.

Results: There were no significant differences between standard imaging and imaging using mSENSE with inter- and intra-observer agreements ranging between 0.78 and 1.0 using Cohens' kappa test. All pathologic findings (occult fractures, meniscal and ligament tears, torn and interpositioned Hoffa's cleft, cartilage damages) were detected by both techniques. iPAT lead to a 48% reduction of acquisition time compared with standard technique. Additionally, time savings with iPAT can lead to a decrease of pain induced motion artifacts in selected cases.

Conclusion: The application of parallel imaging techniques proved to be an efficient and economic tool for fast musculoskeletal MR imaging of the knee joint as it revealed a comparable diagnostic performance to conventional techniques.

B-686 14:54



Computer-assisted quantitative analysis of bone marrow edema of the knee: STIR versus T1-weighted fat-suppressed contrast-enhanced MR imaging at 1.0 and 1.5 Tesla

M.E. Mayerhofer¹, M.J. Breitenseher², N. Aigner¹, S. Hofmann³, J. Kramer⁴; ¹Vienna/AT, ²Vienna / Horn/AT, ³Stolzalpe/AT, ⁴Linz/AT

Purpose: To compare STIR and T1-weighted contrast-enhanced fat-suppressed MR imaging of bone marrow edema of the knee (BME) using a new computer-assisted method of quantification.

Methods and Materials: For 59 patients with BME of the knee, STIR and T1-weighted Gadolinium-enhanced fat-suppressed MR images were obtained. 32 patients (group 1) were examined at 1.0 Tesla, with a contrast-media volume adapted to their body mass. The remaining 27 patients (group 2) were examined at 1.5 Tesla, with a fixed contrast-media volume regardless of their body mass. BME volume and signal contrast were assessed by computer-assisted quantification, based on calculation of a gray-scale threshold value between healthy and edematous bone marrow. MR sequences were compared through arithmetic means of BME volume and signal contrast and their correlation coefficients (r^2).

Results: In both patient groups, correlation was high between STIR and Gadolinium-enhanced images for both BME volume (r^2 : 0.96 to 0.99) and BME signal contrast (r^2 : 0.84 to 0.94). Whilst in group 1, mean BME volume was slightly larger on Gadolinium-enhanced images, the opposite was true for group 2. Gadolinium-enhanced images demonstrated higher BME signal intensity than STIR images in both groups.

Conclusion: STIR and Gadolinium-enhanced MR images depict almost identical BME volume. BME signal contrast, on the other hand, is significantly higher on Gadolinium-enhanced images. Factors like contrast-media volume, magnetic field strength and MR acquisition parameters also seem to affect apparent BME image pattern.

B-687 15:03

Evaluation of trabecular bone structure with high resolution MR imaging at 1.5 T. A comparison of spin echo and gradient echo sequences

J.S. Bauer¹, C.J. Roß², M. Settles², D. Mueller², F. Eckstein³, E.-M. Lochmueller², T.M. Link¹; ¹San Francisco, CA/US, ²Munich/DE, ³Salzburg/AT

Purpose: To compare spin echo and gradient echo sequences concerning trabecular bone structure analysis in the assessment of osteoporosis. Specific aims were to compare structure measurements derived from both MR sequences

with the corresponding true structure parameters obtained with Micro-CT (μ CT) in an in vitro study and to compare the ability of the individual structure measures to differentiate between donors with and without osteoporotic spine fractures.

Material and Methods: Fifty-six post-mortem distal forearm specimens were scanned with a 1.5 T MR scanner using a dedicated wrist-coil and optimized spin echo and gradient echo sequences. The contralateral radius specimens were scanned with μ CT. Structure parameters were calculated from μ CT and MR images analogous to standard bone histo-morphometry. Fracture status of the spine was classified on conventional radiographs. Diagnostic performance in differentiation of donors with and without vertebral fractures was assessed using receiver-operator-characteristics (ROC) analysis.

Results: All parameters obtained in the MR images correlated significantly with the corresponding μ CT-parameters. Highest correlation coefficients were found for apparent trabecular separation (Tr.Sp) with the spin echo sequence (up to $r^2=0.76$). For the spin echo sequence slightly higher ROC-values were also found compared to the gradient echo sequence (up to $Az = 0.75$ vs. $Az = 0.73$). These were lower than those for the μ CT (up to $Az = 0.81$), but the differences were not significant.

Conclusion: Spin echo sequences performed slightly better than gradient echo sequences in predicting true trabecular bone structure and in differentiating donors with and without osteoporotic fractures, but differences were not significant.

B-688 15:12



Imaging of advanced articular cartilage disease using 3D SPGR, 3D CISS and proton FSE imaging and arthroscopic correlation

R. Arunk, S. Gur, S. Aydogdu, M. Argin; Izmir/TR

Purpose: To determine the accuracy of 3D SPGR, 3D CISS and proton density FSE articular cartilage imaging in the identification of grades 3 and 4 chondromalacia of the knee.

Materials and Method: A prospective evaluation of 27 patients who underwent MR imaging and following 1-3 days arthroscopic evaluation was performed. The images were interpreted by an observer without knowledge of the surgical results. The medial and lateral femoral condyles, the medial and lateral tibial plateau, the patellar cartilage and trochlear groove were evaluated. Greater than 50% loss of cartilage thickness showed grade 3, and complete loss of cartilage thickness showed grade 4 chondromalacia. Comparison of the MR results with the arthroscopic findings was performed.

Results: 27 patients, 162 articular cartilage sites were evaluated with MR imaging and arthroscopy. Results of MR identification of grade 3 and 4 chondromalacia, all sites combined were: for 3D SPGR; sensitivity 85.3%, specificity 90.8%, positive predictive value 76%, negative predictive value 94.7% and overall accuracy 89.4%; for 3D CISS: sensitivity 65%, specificity 90.9%, positive predictive value 76.4%, negative predictive value 89% and overall accuracy 86.4%; for proton FSE; sensitivity 78.9%, specificity 91.9%, positive predictive value 75%, negative predictive value 93.4% and overall accuracy: 88.8%.

Conclusion: The results demonstrate that 3D SPGR, 3D CISS and proton FSE MR imaging can identify advanced chondromalacia. However, 3D CISS sequence is a new parameter for using in cartilage imaging and seems to be another useful sequence to image and evaluate articular cartilage.

B-689 15:21

Prospective analysis of the value of different MR imaging sequences for the detection of early stages of arthropathy in patients with hemophilia

M.G. Mack, K. Hochmuth, J.K.E. Müller, A. Thalhammer, M. Krause, A. Kurth, T.J. Vogl; Frankfurt a. Main/DE

Purpose: To analyse the value of different MR imaging sequences for diagnosis of early stages of arthropathy in patients with hemophilia.

Material and Methods: We evaluated 31 joints of 17 patients with hemophilia A (median age 42 years) with at least one intra-articular bleeding or a Pettersson Score of 8 or less. The sequence protocol included TIRM, Flash2D, Medic2D, PDw sequence, DESS, FLASH3D, T1SE and Vibe without contrast. Post-contrast fat saturated T1 SE sequence was repeated immediately and 1.5 hours later. We evaluated erosions, subchondral cysts, hyperplasia of the synovia, synovitis, hemosiderin depositions, joint effusion, focal cartilage defects, thickness of cartilage.

Results: The FLASH2D sequence was superior to regarding detection of hemosiderin depositions. For diagnosis of cartilage defects the best sequence was the DESS sequence with water excitation. The diagnosis of synovitis was best on enhanced T1SE FATSAT sequence. The diagnosis of bone marrow edema and joint effusion was best on the TIRM sequence. The PD sequence and T1SE sequence were optimal for the detection of ligaments and bony structures.

Scientific Sessions

FLASH3D, Medic2D, and Vibe sequence resulted not in additional information. Based on this evaluation we are recommending the following imaging protocol: TIRM, PD, DESS WE, standard and contrast enhanced T1 SE.

Conclusions: The optimised imaging protocol is suited for the diagnosis of early pathologies of the knee and ankle joint in patients with hemophilia. The early detection of synovial hyperplasia, synovitis and hemosiderin depositions may result in improved and prompt therapy in order to avoid further destruction of cartilage and joint.

14:00 - 15:30

Room C

GI Tract

SS 1501a

CT colonography

Moderators:

C.D. Claussen; Tübingen/DE
T. Glücker; Basle/CH

B-690 14:00

Time efficiency of CT colonography: 2D vs 3D visualization

E. Neri, F. Vannozzi, S. Picchietti, P. Vagli, A. Bardine, C. Bartolozzi; Pisa/IT

Purpose: To compare the time efficiency of 2D and 3D analysis in CT colonography.

Materials and Methods: Three visualization methods of CT colonography datasets were prospectively compared for time efficiency in a routine clinical work: Primary 2D image analysis with the use of 3D as problem solving tool, primary 3D viewing with manual navigation and primary 3D viewing with automated navigation (with the use of 2D as problem solving tool). Three radiologists were involved in the analysis, each performing separately the CTC evaluation of the same 20 cases consecutively.

Results: Time for 2D analysis ranged between 6 and 18 minutes (mean 12) for evaluation of both supine and prone decubitus with a synchronization method. In 3 cases a 3D integration was used, increasing time analysis from 6, 8 and 12, to 18 minutes, respectively. Time for manual navigation in supine + prone ranged between 9 and 24 minutes (mean 14) No time increase was caused by the 2D integration. Time for automated navigation ranged between 6 and 20 minutes (mean 12) for evaluation of both supine and prone decubitus. No time increase was caused by the 2D integration.

Conclusions: 2D and automated 3D navigation analysis have comparable time efficiency in a routine clinical setting. Manual navigation reduces the time efficiency.

B-691 14:09

Dose reduction and image quality assessment in multi-detector row CT virtual colonography by online z-axis tube current modulation

A. Graser¹, C.R. Becker¹, C. Suess², M.F. Reiser¹; ¹Munich/DE, ²Forchheim/DE

Purpose: To evaluate the effect of online attenuation-based X-ray tube current modulation (TCM) in virtual CT colonography of a screening population.

Materials and Methods: Eighty asymptomatic patients underwent virtual CT colonography for colon polyp screening. All patients were scanned using 16-detector row helical CT scanners (Sensation 16, Siemens Medical Systems, Forchheim, Germany). 40 pts were examined with a standard protocol with 120 kV tube current at 120 mAs in the supine and 40 mAs in the prone position. Another 40 pts were scanned using an on-line attenuation-based X-ray TCM that adjusts the tube current over the patient's z-axis (CareDose4D, Siemens Medical Systems, Forchheim, Germany). Individual patient radiation exposure was determined using the dose length product (DLP). To assess image quality, image noise was determined by Hounsfield unit measurements in the colonic lumen at four anatomic levels. The two-tailed Student's T-Test was used to test for statistically significant differences between these values.

Results: Radiation dose was significantly lower in the patient group scanned with TCM (supine position: 4.24 vs 6.55 mSv, p < 0.0001; prone position: 1.61 vs 2.38 mSv, p < 0.0001). Overall, radiation dose was reduced by 35% in the supine and 32% in the prone position. There was no statistically significant difference in image noise.

Conclusion: Attenuation-based on-line z-axis TCM leads to a significant reduction of radiation exposure in CT-based virtual colonography without loss of image quality. This is important in particular for patients examined for screening purposes.

B-692 14:18

Detection of colorectal polyps: Low-dose multi-detector CT (MDCT) colonography evaluated by back-to-back colonoscopies

R. Iannaccone, A. Laghi, C. Catalano, F. Mangiapane, D. Marin, R. Passariello; Rome/IT

Purpose: To prospectively evaluate the performance of low-dose MDCT colonography for the detection of colorectal polyps using back-to-back colonoscopies.

Methods and Materials: 88 patients underwent same-day MDCT colonography and an initial conventional colonoscopy. CT colonographic examinations were acquired using a low-dose MDCT protocol. Three observers interpreted the CT colonographic datasets separately and independently using a primary two-dimensional technique. Initial conventional colonoscopy was performed by one of two staff endoscopists unaware of CT colonographic findings. A second colonoscopy was performed within two weeks and served as reference standard. The sensitivities of CT colonography and initial colonoscopy were calculated both on a per-polyp and per-patient basis. For the latter, specificities, as well as positive and negative predictive values, were also calculated.

Results: Per-polyp sensitivity was 62% and 84% for MDCT colonography and initial colonoscopy, respectively. The sensitivity for detection of polyps ≥ 6 mm was 85.6% and 83.8% for MDCT colonography and initial colonoscopy respectively. Initial colonoscopy missed a total of 16 polyps; of these, six were correctly detected by MDCT colonography. With regard to per-patient analysis, MDCT colonography had a sensitivity of 80.4% (93.5% for initial colonoscopy); a specificity of 74.6% (100% for initial colonoscopy); a positive predictive value of 77.6% (100% for initial colonoscopy); and a negative predictive value of 77.7% (93.3% for initial colonoscopy).

Conclusion: Low-dose MDCT colonography compares favorably with colonoscopy for the detection of colorectal polyps ≥ 6 mm, with a marked decrease in performance for the detection of polyps ≤ 5 mm.

B-693 14:27

Prospective evaluation of extracolonic findings at contrast enhanced CT colonography in daily clinical practice

A. Spreng, P. Netzer, C. Quattropani, J. Mattich, H.-P. Dinkel, H. Hoppe; Berne/CH

Objective: To prospectively assess the frequency and clinical importance of extracolonic findings at contrast enhanced CT colonography in symptomatic patients in daily clinical practice.

Patients and Methods: CT colonography was performed in 102 symptomatic patients using contrast enhanced multidetector CT followed by conventional colonoscopy on the same day. Study analysis was embedded in clinical practice. Extracolonic findings were classified as of high, moderate, or low clinical importance. To determine the impact of extracolonic findings on further workup and patient treatment, patient records were reviewed.

Results: At CT colonography 89% (91/102) of patients had at least one extracolonic finding. In 32% (33/102) of all patients extracolonic findings of high clinical importance were detected, such as a hepatic lesion (n = 9), aortic aneurysm (n = 8), adrenal mass (n = 7) and enlarged lymph nodes (n = 7). Therefore, 40% (13/33) led to further workup or had an impact on therapy. In 45% (46/102) of patients findings of moderate importance were found such as gallstones (n = 14), pleural effusion (n = 11), ascites (n = 10) and cardiomegaly (n = 5). In 71% (72/102) of patients findings of low importance were seen, such as aortic sclerosis (n = 33), renal cysts (n = 27) and hepatic cysts (n = 15).

Conclusions: Using contrast enhanced CT colonography important extracolonic findings led to additional diagnostic or therapeutic considerations in 23% (23/102) of patients. In our study, the high number of patients with extracolonic findings is most likely due to IV contrast application and a symptomatic patient cohort.

B-694 14:36

CT colonography ("virtual colonoscopy"): Comparison of a new colon dissection software and a conventional endoluminal view software

M.S. Juchems¹, T.R. Fleiter², S. Pauls¹, S.A. Schmidt³, A.J. Aschoff¹, H.-J. Brambs¹; ¹Ulm/DE, ²Baltimore, MD/US, ³Stuttgart/DE

Purpose: To determine whether a new visualization software for CT colonography using a "colon dissection mode" has a better sensitivity and specificity in detection of colorectal lesions and is less time consuming.

Materials and Methods: We preselected 24 patients from our collective of whom 21 had either colon polyps or colon cancer. 3 patients were matched who had no findings. All patients received conventional colonoscopy after CT-colonography. CT-colonography was performed using a 4x- multi detector row (MDR) - CT (Philips

Scientific Sessions

MX 8000) in 13 cases and a 16x-MDR-CT (Philips MX 8000 IDT) in 11 cases. An experienced, blinded reader thereafter evaluated the data with both software systems on a dedicated CT workstation (Philips MxView).

Results: Conventional colonoscopy revealed 37 colonic lesions in 21 patients. 17 lesions were smaller than 5 mm, 16 lesions were 5-10 mm and 4 lesions were 10 mm or larger. The colon dissection software had an overall per-lesion sensitivity of 47.1% for lesions smaller than 5 mm, 56.3% (5-10 mm) and 75.0% for lesions larger than 10 mm. The endoluminal view software had an overall per-lesion sensitivity of 35.3% (< 5 mm), 81.5% (5-10 mm) and 100.0% for lesions larger than 10 mm. The average time consumption for evaluation with the colon dissection software was 10 min vs. 38 min with the endoluminal view software.

Conclusion: The "colon dissection" mode provides a significant time advantage during evaluation of CT colonography data sets. With "colon dissection" high sensitivities can be achieved. It is especially superior in detecting lesions smaller than 5 mm.

B-695 14:45

Value of multiplanar reconstruction in multidetector CT for preoperative staging of colorectal cancer: ROC analysis

K.-N. Jin¹, S.-H. Kim¹, J.-M. Lee¹, K.-S. Shin², J.-K. Han¹, B.-I. Choi¹, J.-Y. Lee¹;

¹Seoul/KR, ²Dae-Jeon/KR

Purpose: We hypothesized that multiplanar reconstruction (MPR) images have an additional role in preoperative staging of colorectal cancer.

Materials and Methods: Fifty-five patients with colorectal cancer underwent enhanced CT colonography using multidetector CT (MDCT). Interval reviews for both axial datasets without and with coronal and sagittal MPR images were performed independently by two radiologists. They were requested to determine the TNM-staging of colorectal cancer. Radiologists' performances in the context of identifying T4 versus ≤ T3, N0 versus ≥ N1, M0 versus M1 were evaluated by ROC analysis. Overall accuracy of the TNM-staging were calculated and compared between axial images only versus the combination of axial and MPRs. Interobserver agreement was also analyzed.

Results: By histology, pT2 in 5 patients, pT3 in 45, pT4 in 5, pN0 in 26, pN1 in 17, pN2 in 10, pN3 in 2, pM0 in 42 and pM1 in 13 were identified. When MPR images were added, ROC analysis revealed a significant improvement for differentiating N0 and ≥ N1 and marginal improvement for differentiating T4 and ≤ T3 for both reviewers. Overall accuracies were also significantly improved from 60% and 36.4% to 80% and 63.6% for T and N staging respectively. Accuracy for M-staging was improved in combined interpretation than in axial images alone, but the difference was not significant. Furthermore, for T-staging, good interobserver agreement was achieved for combined interpretation whereas fair agreement was achieved for axial images alone.

Conclusion: Combined interpretation of axial and MPR MDCT images for colorectal cancers significantly improves the local staging of the tumors.

B-696 14:54

Polyp measurement and size categorisation by CT colonography:

Agreement with colonoscopy and effect of observer experience

D. Burling, ESGAR CT colonography study GROUP investigators;

St. Mark's Hospital, London/UK

Purpose: To compare agreement between CT colonography and colonoscopy estimates for polyp size measurement and per-patient categorization, and to examine effects of observer experience.

Materials and Methods: 28 observers (3 groups: 9 experts, 9 radiologists, 10 technicians) from 9 European centres were asked to read 40 CT colonography cases from a dataset of 51 containing 12 large and 4 small polyp cases. Non-expert groups had no prior experience but were trained with 50 validated cases. Each observer categorised cases according to the largest lesion seen: cancer, large polyp, small polyp, normal. To distinguish large (≥ 1 cm) and small polyps (6 to 9 mm) observers measured the maximal 2D diameter using software callipers. Bland-Altman statistics were used to assess level of agreement between observer and colonoscopic reference measurement; differences between observer groups were assessed using Kruskal-Wallis and for polyp categorization using Chi-squared statistics.

Results: 375 (283 large, 92 small) polyp cases were read by 28 observers. Of these, 167 (45%) polyps were detected. The mean difference between observer measurements and colonoscopic reference size was -2.1 mm for experts (95% limits of agreement -9.4 to 5.2), -2.8 mm for radiologists (-13.3 to 7.7) and -2.2 mm for technicians (-11.1 to 6.6). There was no significant difference in either measurement variability ($P = 0.39$) or frequency of correct size categorization ($P = 0.28$) between the groups.

Conclusion: Training with 50 cases enabled inexperienced observers to measure and categorise polyps with a facility similar to experts. CT colonography appears to underestimate polyp size compared to a colonoscopy.

B-697 15:03

A multi-centre project of teaching CT colonography in Belgium: Work in progress

P. Lefere¹, S. Grayspeerdt¹, W. Roelandt², P. Van Wettere², L. Verhaeghe³, K. Ramboer³, P. Moons⁴, L. Djoa⁴, V. Herpels⁵, B. De Deurwaerder⁵, ¹Roeselare/BE, ²Oostende/BE, ³Bruges/BE, ⁴Tiel/BE, ⁵Kortrijk/BE

Purpose: To set up a teaching project in several radiology departments who are starting with CTC.

Materials and Methods: The teaching starts with a 4 hour-instruction course. The teaching period consists of performing 50 CTC followed by conventional colonoscopy. The colon is prepared by fecal tagging with barium and a reduced cathartic cleansing with magnesium citrate and bisacodyl. CTC is performed in the "novice" department. After smooth muscle relaxation the colon is inflated with CO₂ using an automated CO₂-injector. The colon is examined with multi-slice CT technique and with dual positioning. The data sets are read on a dedicated workstation by both the novice readers and the teachers. The preparation and colonic distention are graded by all readers. The detected polyps are recorded. The results of the novice readers are blinded to the teachers. The teachers give advise on the quality of the exam and on polyp detection and on how to avoid imperfections.

Results: Up to now 42 CTC were performed. At the time of the symposium more extensive results will be communicated. So far the preparation was adequate in all patients. Improvement of distention was possible in 15 patients. One patient presented with a lot of motion artefact. Fifteen lesions ≥ 6 mm were detected on conventional colonoscopy including one carcinoma. The teachers detected all lesions. The novices missed four 8 mm-polyps.

Conclusion: This multi-centre teaching project is an attempt to teach CTC to novice radiologists how to perform and read CTC using a standardized method.

B-698 15:12

Virtual colon dissection tool used in CT colonography: Comparison with conventional endoscopy results. A preliminary study

M. Cadi, R. Chollet, O. Lucidarme, P. Grenier; Paris/FR

Objective: The aim of this study was to determine the ease and accuracy of virtual colon dissection software to detect colonic polyps in CT colonography.

Methods and Material: To date, 60 patients, who underwent same day CT colonography and endoscopy, were studied using virtual colon dissection software. This commercially available software (Autodissection®, GEMS) dissects and unfolds the colon along its longitudinal axis to display the entire colonic surface with a 360° angle view. Hence, the entire inner surface of the colon can be studied at a glance without the need for navigation. Imaging findings were compared with conventional endoscopic results and the reading time of each examination was recorded.

Results: Four patients are excluded because of inadequate bowel preparation. Among the 56 remaining patients conventional endoscopy revealed 40 lesions. Using virtual colon dissection as primary tool to seek out polyps, the per-lesion sensitivities were 86.3%, 80.1% and 50.3% for polyps greater than 10 mm, 6-9 mm and smaller than 5 mm respectively. There was one false positive result for polyps greater than 10 mm as well as for polyps of 6-9 mm and 6 false positives for polyps smaller. Average time to display and analyse the entire inner surface of the colon was 14 minutes.

Conclusion: Virtual colon dissection software is a complementary tool to analyse CT colonography data that provides a good sensitivity for detection of colonic polyps in a short time.

B-699 15:21

Clinical impact and prevalence of incidental findings in a mixed population undergoing CT colonography

F. Iafrate, A. Laghi, M. Rengo, V. Panebianco, V. Martino, P. Paolantonio, M. Di Martino, R. Passariello; Rome/IT

Purpose: The aim of our study was to prospectively determine the frequency and clinical importance of extracolonic findings in patients undergoing CT colonography.

Material and Methods: 183 patients underwent CT colonography for several reasons. 133 patients (81 screening, 17 diverticulosis, 16 abdominal pain and cramping and 29 incomplete colonoscopy) performed the examination without

Scientific Sessions

i.v. administration of contrast agent. In 50 patients an additional i.v. contrast administration was performed based on the clinical indication for the examination (36: staging of neoplastic lesion, 14: follow-up). Helical CT from the diaphragm to the symphysis was performed in the supine and prone positions after rectal air insufflation. Two radiologists reviewed the CT images for extracolonic pathology and findings were classified as having major, moderate or minor clinical importance. **Results:** A total of 173 extracolonic findings were detected in 110 (60.1%) of the 183 patients. Of these, 43 (24.8%) were highly significant, 36 (20.8%) were moderately significant and 94 (54.33%) were of poor significance. In 72(39.34%) patients no extracolonic findings were observed. The most common highly significant lesions were mesenteric lymphadenopathy (n.18), aortic aneurysm and liver metastases (n. 6), peritoneal carcinomatosis and pulmonary nodules (n. 4). 32 of these 43 (74.4%) highly significant findings were new, and in 15 (34.88%) these abnormalities resulted in further diagnostic examinations.

Conclusions: CT colonography can detect highly significant extracolonic findings. Although extracolonic lesions were common, only a small proportion of patients required further diagnostic examinations. This finding must be considered when CT colonography is considered for routine workup or screening.

14:00 - 15:30

Room E2

Chest

SS 1504

CT and MR imaging in emphysema and COPD

Moderators:

S.R. Desai; London/UK
T. Petsas; Patras/GR

B-700 14:00

Hyperpolarized ^3He apparent diffusion coefficient MR imaging of the lung: Reproducibility, clinical correlation and safety

S. Diaz¹, P. Åkeson¹, I. Casselbrant¹, E. Pitulainen¹, G. Pettersson¹, P. Magnusson¹, P. Wollmer¹, B. Peterson², ¹Malmö/SE, ²Groton, CT/US

Purpose: The Apparent Diffusion Coefficient (ADC) reflects the size of the structures that compartmentalize the gas, in this case the size of the alveoli within the lung. The aim of this study was to examine the reproducibility of the ADC of hyperpolarized (HP) ^3He -inhalation MR imaging to assess emphysema and to verify its clinical application and safety.

Methods and Materials: 8 healthy volunteers and 16 emphysema patients (8 with Chronic Obstructive Pulmonary Disease (COPD) and 8 with alpha-1-antitrypsin deficiency (A1AT)) were imaged with HP ^3He -gas mixed with nitrogen. Each subject was imaged on 3 separate days with 5 different volumes of gas. Mean ADC per slice and per subject, histograms of the ADC values and ADC-maps were calculated. Comparison was made with lung function tests.

Results: The mean ADC values per subject showed very small intra-individual variation both in volunteers (mean 0.195-0.247 cm²/sec; SEM 0.000385-0.00516) and patients (mean 0.268-0.505 cm²/sec; SEM 0.001-0.006). The inter-individual variation was small in healthy volunteers (mean 0.210 cm²/sec; SD 0.020). A positional gradient was seen in all volunteers. Apical emphysema in COPD-patients, basal in A1AT-patients was seen. Comparison with Diffusion Capacity of Carbon Monoxide (DLCO) showed a good correlation ($R^2 = 0.626$). No correlation was found with FEV₁. No serious adverse events occurred.

Conclusion: The reproducibility over time was excellent in both groups. A difference in ADC between healthy volunteers and patients and between patient groups was found. The method seems to be sensitive and safe. Detection and monitoring of early emphysema and small changes should be possible.

B-701 14:09

Diffusion weighted ^3He -MR imaging in the assessment of pulmonary emphysema

K.K. Gast¹, T. Stavgaard², J.M. Wild³, A.E. Morbach¹, L. Vejby Soegaard⁴, A. Dahmen¹, H.-U. Kauczor⁵, E.J.R. van Beek⁶, C.-P. Heussel¹; ¹Mainz/DE, ²Copenhagen/DK, ³Sheffield/UK, ⁴Hvidovre/DK, ⁵Heidelberg/DE, ⁶Iowa, IA/US

Purpose: Diffusion weighted ^3He -MR imaging is a new method for quantitative assessment of lung microstructure. This study intends to investigate the usefulness of diffusion weighted ^3He -MR imaging in different forms of pulmonary emphysema in comparison with healthy volunteers.

Methods and Materials: In a European multicenter trial 79 patients with pulmonary emphysema and 37 healthy volunteers were included. All subjects underwent diffusion weighted ^3He -MR imaging, high resolution computed tomography (HR-

CT) and pulmonary function tests (PFT). Mean apparent diffusion coefficient (ADC) was calculated from diffusion weighted ^3He -MR imaging, emphysema index (EI) from HR-CT and the FEV1/VC ratio was determined by PFT.

Results: A total of 87 data sets from diffusion weighted ^3He -MR imaging were evaluable (patients, n = 58, volunteers, n = 29). Mean ADC showed higher values in patients (median, 0.28 cm²/s) than in healthy volunteers (median, 0.17 cm²/s, p < 0.001). Correlation between mean ADC and computed tomography was r = 0.52. Correlation between mean ADC and pulmonary function tests was r = -0.75. Correlation between PFT and HR-CT was r = -0.45 (n = 105).

Conclusion: Diffusion weighted ^3He -MR imaging differentiated well between volunteers and patients with pulmonary emphysema. Correlation of ^3He -MR imaging to HR-CT was fair. ^3He -MR imaging correlated significantly better with PFT compared with CT. The ADC determined from ^3He -MR imaging obviously does not simply describe morphology of the lung. Its good correlation to PFT emphasizes the functional character of ^3He -MR imaging. Diffusion weighted ^3He -MR imaging is an evolving method to quantitatively determine the extent and the regional distribution of pulmonary emphysema.

Acknowledgements: The ^3He project is supported by the European Commission ("PHIL") and the German Research Council (DFG, FOR474).

B-702 14:18

Quantitative analysis of regional airways obstruction using dynamic hyperpolarized ^3He MR imaging: Preliminary results in children with cystic fibrosis

P. Koumellis, E. van Beek, C. Hill, N. Woodhouse, S. Fichele, C. Taylor, J. Wild; ^{Sheffield/UK}

Purpose: Dynamic MR imaging of hyperpolarized ^3He can provide striking cine movies of lung ventilation in humans. This study aimed to examine the degree of pulmonary involvement and to quantitatively evaluate patterns of gas flow in lung regions in children with CF in comparison with spirometry.

Materials and Methods: The study population consisted of 8 children with CF aged 6-15 y (mean age 11.4 y). All of them had undergone recent spirometry. Imaging was performed on a 1.5 T whole body MR imaging system using a dynamic radial projection sequence described in [1]. A total of 7 ROI's were taken, three in each lung field and one in the trachea. Since all gas passes via the trachea, the tracheal signal intensity was used as a form of 'input function' to normalise for input flow effects.

Results: The low flow rate in the upper lobes was a pattern observed in all of the patients and is characteristic for CF, which has a preferential distribution in the upper lobes. When the flow measurements from the peripheral ROI's were averaged to give an index of flow in the peripheral lung these showed a good correlation (p < 0.005) with the forced expiratory volume (FEV1) from spirometry.

Conclusion: These results suggest that a quantitative measurement of localised airways obstruction in the early stages of CF may be obtained from dynamic ^3He MR imaging by using the slope of the signal rise as a measure of air flow in to the peripheral lung.

References: 1. Wild JM, et al. Magn Reson Med, Jun 2003; 49: 991-7.

B-703 14:27

Oxygen-enhanced MR imaging in the assessment of smoking-related pulmonary emphysema: Preliminary results

F. Molinari, O. Pantalone, G. Corbo, S. Valente, T. Pirroni, L. Bonomo; ^{Rome/IT}

Purpose: To demonstrate the capability of oxygen-enhanced MR imaging to assess smoking-related pulmonary emphysema.

Method and Materials: 12 consecutive patients (age range 39-58) with smoking-related bullous emphysema (DLCO/Va ratio < 70% of predicted value) and 10 healthy non-smoking volunteers (age range 24-36) underwent measurements of lung volumes, forced expiratory flows (FEV1%, FEV1%/VC, FEV1%/FVC), diffusing capacity of the lung (DLCO%) and oxygen-enhanced MR imaging. Arterial blood gases and cutaneous oxymetry during 6 min walking test were also obtained in the patient group. Oxygen-enhanced MR imaging was performed with a cardiac synchronized inversion recovery single-shot fast spin echo sequence (TE = 26 ms/ TI=1200 ms) using a 1.5 T MR scanner. Oxygen-enhanced MR images were obtained in the coronal planes. Oxygen-enhancement was determined on a pixel-by-pixel basis with parametric maps of correlation coefficient (CC-maps), with parametric maps of activation magnitude (AM-maps), and by averaging oxygen-enhancements in spatially defined regions of interest (ROIs) in both lungs (overall oxygen-enhancement). To evaluate the capabilities of oxygen-enhanced MR imaging for the assessment of smoking-related pulmonary emphysema, overall oxygen-enhancement was correlated with DLCO%, alveolo-arterial PO₂-difference, maximal arterial desaturation during exercise, and severity of obstructive impairment (FEV1%/VC). CC-maps, AM-maps and overall oxygen-

Scientific Sessions

enhancements of non-smoking subjects were also compared with those of emphysematous patients (Mann-Whitney's test).

Results: Overall oxygen-enhancement had good correlation with DLCO%, alveolo-arterial PO₂-difference, maximal arterial desaturation during exercise and FEV1%/VC ($r > 0.5$, $p < 0.01$). CC-maps, AM-maps and overall oxygen-enhancement results were statistically different between the two groups ($p < 0.05$).

Conclusion: Oxygen-enhanced MR imaging is a useful imaging technique for the assessment of smoking-related pulmonary emphysema.

B-704 14:36

Assessment of pulmonary hypertension by MR imaging in patients with severe obstructive lung disease: Correlation with pulmonary function test

S. Ley, J. Zaporozhan, R. Eberhardt, M. Eichinger, C. Fink, S. Yubai, S. Erdugan, F. Herth, H.-U. Kauczor; Heidelberg/DE

Purpose: Assessment of hemodynamic changes in patients with severe emphysema due to chronic obstructive pulmonary disease (COPD) using MR imaging and evaluation of a relationship between decrease in pulmonary function and decrease in pulmonary hemodynamics.

Material and Methods: 17 patients (4f, 13m; mean age 61 years) with severe emphysema (mean FEV1/VC=35%) underwent pulmonary function test (PFT; ITGV=intrathoracic-gas-volume; FEV1=forced-expiratory-volume-1 s; RV=residual-volume, VC=vital-capacity) and phase-contrast flow measurements in the aorta and pulmonary trunk (PT) using a 1.5 T MR imaging. Most PFT and MR imaging were performed on the same day (± 20 days). For correlation, 15 healthy volunteers (4f, 11m, mean age 26 years) were examined using MR imaging. Examinations were performed in inspiratory breath-hold and the following parameters were assessed: peak velocity[cm/s](PV), bloodflow/min, acceleration time (ACT), delta cross sectional area (systole vs. diastole), systemic to pulmonary shunt (SPS).

Results: Patients showed significant lower hemodynamic values in the PT than volunteers for PV ($p = 0.01$, 67 vs. 80 cm/s), bloodflow/min ($p = 0.04$, 4 vs. 5 l), delta area ($p = 0.004$, 1.6 vs. 2.8 cm²) and ACT ($p = 0.048$, 142 vs. 215 ms). The vessel area ratio between aorta and PT was significantly ($p = 0.006$) higher in patients (1.3) than in volunteers (1.0). There was no SPS in patients or volunteers. There were no linear correlations between PFT data and hemodynamic values of the patients ($r < 0.4$).

Conclusion: Patients with severe COPD showed a reduction of hemodynamics in the pulmonary vasculature indicating pulmonary hypertension, but without correlation to PFT values.

B-705 14:45

Influence of different emphysema size classes visualized by quantitative MDCT-analysis on MRA lung perfusion in patients with chronic obstructive pulmonary disease

J. Zaporozhan¹, S. Ley¹, R. Eberhardt¹, O. Weinheimer², C. Fink¹, F. Herth¹, H.-U. Kauczor¹; ¹Heidelberg/DE, ²Mainz/DE

Purpose: Severe emphysema due to COPD is associated with reduced oxygen uptake. Our aim was to examine which pattern of structural loss of lung parenchyma is most associated with a reduction in pulmonary perfusion.

Material and Methods: 13 patients (mean 61 years) with severe emphysema underwent inspiratory MDCT (slice thickness 1/0.8 mm) and MRA with high-temporal-resolution (1.5 T; 3.5x9x4 mm³; 20 phases, each TA 1.5 sec). CT data were analysed with a self-written software for detecting and quantifying emphysema. In each patient, four clusters of emphysema with different volumes (up to 2, 8, 65 and 120 mm³) were analysed and visualized by colour coding. On a double monitor system, the distribution of emphysema clusters and perfusion patterns were analysed for 3 lobes on each side. A 4-point-score was used (1: smallest to 4: large emphysema clusters) on CT and on MRA (1: normal to 4: no perfusion).

Results: 78 lobes were evaluated. With CT, the score was 1 for 6 lobes, 2 for 22, 3 for 31, and 4 for 19 lobes. With MRA, the score was 1 for 6 lobes, 2 for 22, 3 for 32, and 4 for 18 lobes. In 65 lobes, the score was identical for CT and MRA (weighted Kappa = 0.83). The score was higher on CT in 7, and higher on MRA in 6 lobes.

Conclusion: Large emphysema clusters are correlated with a severe reduction or a complete loss of perfusion. Moderate emphysema clusters presented perfusion defects of varying size. With small structural changes, perfusion is not or only moderately reduced.

B-706 14:54

Correlation between inspiratory and expiratory lung attenuation on HRCT, pulmonary function tests, and smoking history in healthy smokers

B. Rodríguez-Vigil, I. Torres, J. Echeveste, F. García Río, S. Serrano, M. Pardo; Madrid/ES

Purpose: To evaluate inspiratory and expiratory lung attenuation on high resolution CT in healthy smokers and to correlate these findings with pulmonary function tests (PFT) and smoking history.

Materials and Methods: Thirty-six healthy subjects, 30 smokers (12 mild, 18 heavy) and 6 non-smokers underwent HRCT following a standardised protocol. The mean number of cigarettes/day was 28 ± 7 (packs/year = 34 ± 12). Images were obtained during deep inspiration and expiration at two different lung levels. The mean expiratory increase in lung attenuation was measured. Air trapping was semiquantitatively calculated and visually classified into 4 degrees (none, lobular, mosaic, extensive). Smoking habit was assessed by the Brinkman index, Glover-Neelsen and Fagerström scores. Lung function was evaluated by spirometry, plethysmography and carbon monoxide transfer factor. Lung attenuation at the upper and lower lobes was compared to PFT and smoking history by the Mann-Whitney and Wilcoxon tests, and correlated by the Spearman coefficient.

Results: Healthy smokers showed a significantly lower inspiratory and expiratory attenuation both in upper and lower lobes compared to healthy nonsmokers. Heavy smokers showed a lower expiratory upper lobe attenuation compared to mild smokers ($p = 0.027$). A significant relationship between expiratory upper lobe attenuation and FEV1 ($r = 0.453$, $p = 0.039$), FEV1/FVC ratio ($r = 0.486$, $p = 0.026$), mesoexpiratory flows ($r = 0.521$, $p = 0.018$), residual volume/total lung capacity ratio ($r = -0.560$, $p = 0.046$) and diffusion capacity ($r = 665$, $p = 0.013$) was found in smokers.

Conclusion: A significant decrease in the expiratory upper lobes attenuation on HRCT is noted in healthy heavy smokers. This alteration is related to airflow calibre, static volumes and diffusion capacity of the lungs.

B-707 15:03

Low-dose MDCT in the evaluation of pulmonary emphysema: What is the minimum radiation dose?

A.R. Larici¹, M.L. Storto¹, A.G. D'Agostino¹, F. Palladino², A. Canadè², L. Bonomo²; ¹Chieti/IT, ²Rome/IT

Purpose: To determine the minimum radiation dose which does not impair the quality of MDCT examination in the quantitative and qualitative evaluation of pulmonary emphysema.

Methods and Materials: 24 patients with a clinical diagnosis of COPD underwent two consecutive MDCT scans of the chest (1-mm collimation, 5 and 1.25 mm slice thickness) at standard (100 mAs) and low dose (40 mAs in 12 patients and 20 mAs in the remaining 12). Lung volume and mean attenuation values as well as volume and attenuation values of emphysematous areas were calculated on both standard and low-dose 5-mm thick images using a commercial software. A chest radiologist and a third-year resident independently evaluated both standard and low-dose 1.25-mm thick images for the presence and extent of emphysema, according to a 4-point scale visual score.

Results: No significant differences were found between lung volume and density values automatically calculated on standard dose and low-dose images ($p > 0.05$). For the expert reader, the visual score results were significantly lower on 20 mAs images than on 100 mAs ($p < 0.05$). For the second reader, the visual score results were significantly lower on both 40 mAs and 20 mAs images ($p < 0.05$). Interobserver agreement was good on 100 mAs images ($K = 0.74$) and moderate on 40 mAs images ($K = 0.58$).

Conclusions: Although radiation dose does not affect the automatic quantitation of pulmonary emphysema by MDCT, it seems to impair the visual grading of emphysema when doses < 40 mAs are used. Less experienced readers may underestimate the extent of emphysema on low-dose images.

B-708 15:12

Instability of the central airways: Comparison of end expiratory to dynamic expiratory volumetric MDCT acquisitions

G.R. Ferretti, L. Aubaud, J. Pépin, N. Choury, M. Coulomb; Grenoble/FR

Purpose: To evaluate the role of dynamic expiratory imaging using multidetector CT (MDCT) in comparison to end expiratory imaging in patients with suspected tracheomalacia.

Material and Methods: 23 consecutive patients (15 men) were prospectively evaluated with MDCT. 3 acquisitions of the central airways were obtained (120 kV,

Scientific Sessions

40 mA): 1) end of inspiration; 2) end of expiration; 3) during dynamic expiration. (Mean acquisition time: 4.5 sec). Percentage changes in cross-sectional area at 3 levels in the trachea (upper, middle, and lower trachea), right and left main stem bronchus were calculated.

Results: 12 of 23 patients had instability of the central airways (localized, n = 4; diffuse, n = 8); maximum mean percent change in cross-sectional area during dynamic expiration was 78% as compared to 42% at the end of expiration ($p = 0.02$). In control patients, the figures were 21% and 16%, respectively (NS).

Conclusion: MDCT during dynamic expiratory acquisition is more effective than end expiration acquisition to demonstrate instability of the central airways.

B-709 15:21

Diagnosis of tracheal instability with dynamic CT

Y.V. Marchenkova, T.N. Vesselova, A.G. Chuchalin, T.L. Pashkova; Moscow/RU

Background: Cough is one of the most common symptoms of chronic obstructive pulmonary diseases (COPD). It is well known that severe cough can induce dynamic instability of trachea in COPD. Some studies have shown an important role of dynamic CT in diagnosis of dynamic instability of the upper respiratory tract (trachea) in COPD patients suffering from severe cough.

Aim of the study: To compare the diagnostic efficacy of different diagnostic methods (both imaging and functional ones) in assessment of dynamic tracheal instability in COPD patients.

Materials and Methods: Two groups of patients have been studied. Group 1 consisted of 20 COPD patients (14 females, 6 males, mean age 60.9 ± 7.9 years) with dynamic tracheal instability, diagnosed on fibrobronchoscopy. Group 2 consisted of 10 COPD patients (2 females, 8 males, mean age 55.2 ± 4.8 years) without bronchoscopic signs of dynamic tracheal instability. Stage of COPD, duration of smoking and body mass index were similar in both groups. Patients were studied with spirometry (flow-volume curve), impulse oscillometry, fibrobronchoscopy, and electron-beam tomography (EBCT). EBCT was performed in dynamic multislice cine mode. Tracheal cross-sectional area was measured across the whole respiratory cycle.

Results: Comparing with results of fibrobronchoscopy which was regarded as a gold standard, sensitivity and specificity of pulmonary function tests were, correspondingly, spirometry 55% and 90%, impulse oscillometry 85% and 60%, dynamic EBCT 90% and 80%.

Conclusion: EBCT has shown the highest sensitivity specificity in detection of dynamic tracheal instability in COPD patients comparing with impulse oscillometry and flow-volume curve.

14:00 - 15:30

Room F2

Abdominal Viscera

SS 1501b

Focal liver lesions: MDCT, MR imaging and PET-CT

Moderators:

N. Elmas; Izmir/TR
S. Fabiano; Rome/IT

B-710 14:00

Multislice-spiral computed tomography (MSCT) versus Gd-BOPTA-enhanced magnetic resonance imaging (Gd-BOPTA-MRI) in the detection and characterization of hepatocellular carcinoma

I. Sansoni, A. Laghi, M. Celestre, C. Miglio, M. Di Martino, L. Coletta, M. Rengo, R. Passariello; Rome/IT

Purpose: To compare diagnostic accuracy of tetraphasic multislice-spiral computed tomography (MSCT) and Gd-BOPTA-enhanced magnetic resonance imaging (Gd-BOPTA-MRI) in detecting and characterizing hepatocellular carcinoma (HCC) suspected lesions.

Methods and Materials: Sixty-five patients with chronic hepatitis were referred for CT and MRI hepatic evaluation. CT was performed using a 4-slice scanner with tetraphasic acquisition protocol (unenhanced phase, and contrasted arterial, portal venous and equilibrium phases). MR-study was performed on 1.5 T-scanner using the following acquisition protocol: pre-contrast T2-weighted and T1-weighted; dynamic Gd-BOPTA T1-weighted at arterial, portal, equilibrium phases; hepatobiliary (60 min) T1-weighted sequence. CT and MRI were evaluated for the presence, number and characterization of lesions. The number of lesions at final diagnosis was considered to be equal to CT plus MR detected lesions. Image data were compared with histopathological studies of surgical specimens and/or follow-up imaging.

Results: 5 patients were excluded from study because of claustrophobia in MR or allergy to contrast in CT. Among the remaining 60 patients, 17 were negative for HCC suspected lesions in both modalities and 43 were positive in at least 1 technique with 73 lesions (35 HCCs, 17 Dysplastic Nodules, 3 FNH, 18 Shunts). Both MSCT and Gd-BOPTA-MR imaging detected 66/73 (90.41%) HCC suspected lesions ($20 \geq 2$ cm, $46 < 2$ cm). Lesion characterization was correct in 52/66 (78.79%) cases at CT and in 58/66 (87.88%) at MR.

Conclusion: No statistically-significant difference between MSCT and Gd-BOPTA-MRI was observed in terms of lesion detection rate, independent of lesion size. Findings of MSCT and Gd-BOPTA-MRI in characterizing lesions were comparable. Both are valuable advanced techniques for cirrhotic liver screening.

B-711 14:09

Detection and characterization of focal hepatic lesions: Comparative study of MDCT and current MR techniques

H. Lee¹, J. Lee¹, S. Kim¹, K. Shin², J. Lee¹, J. Han¹, B. Choi¹; ¹Seoul/KR, ²Daejeon/KR

Purpose: To compare the diagnostic performance of MDCT and Gd-BOPTA-enhanced MR imaging for the detection and characterization of focal liver lesions.

Methods and Materials: We evaluated fifty-nine patients with 118 solid and 91 nonsolid lesions who underwent MDCT and MR imaging within a 1-month period (77 of malignant, and 132 of benign lesions). MR images were obtained as T2-weighted turbo spin-echo and T1-weighted gradient-echo before and after 0.1 mmole/kg Gd-BOPTA administration. Multiphasic multi-detector row helical CT was performed except ten cases of metastasis. In part I, two reviewers did a direct paired comparison of CT and MR images for the assessment of liver lesions in consensus. Differences in detection and characterization with CT and MR images were assessed with the two-sided Wilcoxon signed rank test. In part II, two independent and blinded reviewers assessed the CT and MR images separately and evaluated diagnostic performance of each image modality using ROC curve analysis.

Results: In a direct comparison of images, the reviewers showed better results in the performance of MR imaging than CT in solid lesion detection and lesion characterization (solid lesion detection, $p = 0.002$; lesion characterization, $p \leq 0.001$ and $p = 0.001$ for benign and malignant lesion). However, in the ROC analysis, areas under the ROC curves are not significantly different (solid lesion detection, $p = 0.862$ and $p = 0.281$ for each reviewer, non-solid lesion detection, $p = 0.916$ and $p = 0.284$, lesion characterization, $p = 0.125$ and $p = 0.426$).

Conclusions: In the detection and characterization of focal liver lesions Gd-BOPTA-enhanced MR and MDCT show a similar diagnostic performance.

B-712 14:18

Focal liver lesion detection and classification on multi detector-row computed tomography (MDCT) and SPIO-enhanced magnetic resonance imaging (MRI): Could awareness of the patients clinical history influence the reader's diagnosis?

R. Cianci, A. Filippone, E. Grassetto, F. Di Fabio, C. Colosimo; Chieti/IT

Purpose: To determine the influence of clinical data on reader's diagnostic accuracy in liver lesion detection and classification with MDCT and non-enhanced and ferucarbotran-enhanced MRI.

Materials and Methods: 87 oncology patients with focal lesions underwent MDCT and MRI within 1 week. Image analysis was performed for each diagnostic method by two experienced radiologists in two different reading sessions. The first session was carried out without knowledge of the clinical data and for the second one readers were aware of the data. The degree of diagnostic confidence was expressed according to a four point scale for detection (1: Certainly absent; 2: Probably absent; 3: Probably present; 4: Certainly present) or for classification (1: Certainly benign; 2: Probably benign; 3: Probably malignant; 4: Certainly malignant). The overall diagnostic accuracy and receiver operating characteristic curves analysis (ROC) for each reading session and each reader were calculated.

Results: Awareness of clinical data significantly improved the lesion detection rate ($p < .05$), mostly of small sized lesions (< 1 cm) for MDCT and for MRI. There wasn't any statistically significant difference between the two reading sessions regarding MDCT overall diagnostic accuracy and Az values because there was an associated increase in the number of false-positive findings with awareness of clinical data. Conversely, SPIO-enhanced MR diagnostic accuracy and Az values significantly increased with awareness of clinical data, thanks to a reduction in false negative cases without an increase in false positive cases.

Conclusions: Knowledge of clinical data does not influence the reader's overall accuracy for MDCT although it improves reader's overall accuracy for MRI in the diagnosis of focal liver lesions.

Scientific Sessions

B-713

withdrawn by author

B-714 14:27

Identifying resectable hilar cholangiocarcinoma: Mutidetector CT (MDCT) versus MR imaging

E.-S. Cho; Seoul/KR

Purpose: To compare the capability of MDCT and MR imaging in identifying patients who have resectable hilar cholangiocarcinoma.

Materials and Methods: Fourteen patients with suspected hilar cholangiocarcinoma underwent contrast-enhanced MDCT (using 4- and 16-slice scanners with a high resolution protocol and MPR reconstruction), MR imaging (with T1W axial, T2W axial, and MRCP images) and direct cholangiography. 7 of 14 patients underwent surgical resection. Two radiologists evaluated bile duct extension on MDCT and MR imaging according to the Bismuth classification and the results were correlated with pathologic findings (n = 7) or direct cholangiographic findings (n = 7). They evaluated lymph node metastasis and vascular involvement on MDCT and the results were correlated with pathologic findings (n = 7).

Results: In terms of bile duct invasion, the diagnostic accuracy of MDCT was 78.6% (11 of 14), whereas that of MR imaging was 42.9% (6 of 14). On MDCT, two cases were overdiagnosed and one was underdiagnosed. On MR imaging, six cases were overdiagnosed and two were underdiagnosed. On MDCT, the diagnostic accuracy of lymph node metastasis was 71.4% (5 of 7), that of hepatic arterial involvement was 85.7% (6 of 7) and that of portal vein involvement was 85.7% (6 of 7).

Conclusions: MDCT was superior to MR imaging in the evaluation of bile duct invasion. MDCT was accurate in the diagnosis of lymph node metastasis and vascular invasion. Therefore, MDCT provides more comprehensive preoperative information in hilar cholangiocarcinoma than MR imaging.

B-715 14:36

Comprehensive assessment of metastatic spread in patients with malignant melanoma by whole-body MR imaging with high-resolution

C. Müller-Horvat, P. Radny, J. Schäfer, C. Pfannenberg, S. Khorchidi, T. Nägele, C.D. Claussen, H.-P. Schlemmer; Tübingen/DE

Aim: Individual Therapy of patients with malignant melanoma considerably depends on information about tumor spread. Magnetic resonance imaging (MRI) has the distinct advantage to provide high resolution information, but state-of-the-art MRI of the whole body was so far impractical within one single examination. The aim was to investigate the clinical feasibility of a novel whole-body MRI system for comprehensive assessment of metastatic spread in clinical routine.

Methods: Initial feasibility study including 48 patients with malignant melanoma with known metastatic spread. MRI and conventional spiral CT of the whole body were performed between February 2, 2004 to August 8, 2004. Whole-body MRI and CT were assessed by two independent radiologist and findings were finally compared in consensus.

Results: Whole-body MRI was successfully performed in 48 subjects requiring a total room time < 60 min. Metastases not detected on CT were found in following locations (cerebral, n = 3; bone, n = 10; muscle, n = 4; subcutaneous metastases, n = 3; spleen, n = 2; liver, n = 2). In 3 patients therapy had to be modified. Pulmonary nodules smaller 5 mm were detected only on CT in 3 patients. Tumor spread to brain, abdominal and pelvic organs, lymph nodes and bone was otherwise correctly visualized compared to CT.

Conclusion: High-resolution whole-body MRI is feasible in clinical routine within one single examination and may have important impacts on management of patients with malignant melanoma.

B-716 14:45

The clinical impact of FDG PET on the management of patients with colorectal liver metastases and comparison with conventional imaging.

Evaluation with evidence based practice techniques

J.J. Sheehan, C.A. Ridge, E.V.M. Ward, S.E. Harte, G.J. Duffy, C.D. Collins, D.E. Malone, S.J. Skehan; Dublin/IE

Purpose: Using evidence based practice techniques we determined that PET with a sensitivity of 90% was the most sensitive imaging modality for detecting colorectal carcinoma liver metastases (CRCLM). All patients being considered for liver resection underwent a PET. This study retrospectively evaluated the clinical impact of using PET to stage colorectal liver metastases pre-operatively in our practice.

Materials and Methods: We selected consecutive patients with colorectal

carcinoma who had PET prior to liver resection. Radiologists reviewed PET images and compared these with conventional imaging (CT/MRI). Patients records were reviewed to establish surgical intentions before and after PET.

Results: From July 2002 to Dec 2003, 40 patients (M=25 and F=15) met the inclusion criteria. 95%(n = 38) had abnormal PET results. Of these, 47%(n=18) underwent hepatic resection. Diagnostic Impact: Discordance between PET and conventional imaging 64%(n = 24), which was predominately tumour upstaging (70%) by PET. Management Impact: Management change after PET 35% (n = 14), planned surgery cancelled 78% (n = 11). Surgical findings correlated with PET findings in 89% (n = 16). The discordances 11%(n = 2), (1 patient with tumour adherent to the diaphragm, 1 young patient with an equivocal PET result) were unresectable at laparotomy. 24%(n = 5) patients with limited extrahepatic disease on PET underwent laparotomy and CRCLM resection. Illustrative PET images will be shown and correlated with conventional imaging.

Conclusions: PET has a major impact on staging and surgical management of CRCLM. Extrahepatic metastases are not an absolute contraindication to liver resection.

B-717 14:54

Detection of tumor and metastatic disease by MR imaging vs PET-CT: Value of a new whole-body MR scanner

G.P. Schmidt, A. Baur-Melnyk, K. Hahn, M.F. Reiser, S.O. Schoenberg; Munich/DE

Purpose: To compare the accuracy for detection of malignant disease by whole body-MR imaging using parallel imaging and whole-body dual-modality PET-CT.

Materials and Methods: Preliminary results from a prospective study are presented, in which 20 patients with different oncological diseases underwent whole body dual modality-FDG-PET-CT screening for tumor staging or in case of suspected metastatic disease. All patients also underwent whole-body MR imaging with the use of parallel imaging. Coronal T1W- and STIR-sequences, axial T2W imaging of lung/abdomen (HASTE), contrast-enhanced dynamic and static T1W-sequences of liver, brain and abdomen were performed. Using a 32-channel MR imaging scanner with a total FOV of 205 cm and free table movement, complete patient anatomy was covered in one examination. Two experienced radiologists read the MR imaging-scans, one radiologist and nuclear scientist read PET-CT scans, each in consensus in a clinical setting. Presence of primary tumor, lymph node involvement and degree of metastatic disease was assessed using PET-CT as the gold standard for tumor staging.

Results: Metastasis from gastrointestinal tumor (25%) and breast cancer (25%) were the most common diagnoses. 4 patients had detectable primary tumor and 2 patients recurrent tumor. 124/140 malignant lesions were detected with MR imaging, resulting in a sensitivity of 89% and a specificity of 86%. In malignant lymph node detection sensitivity of MR imaging was 83% and specificity 85%.

Conclusion: Whole-body MR imaging is a reliable alternative in the detection of primary tumor and metastatic disease, although sensitivity in lymph node detection is impaired. With parallel imaging, high-resolution whole-body MR imaging is possible within reasonable scan times.

B-718 15:03

Preinterventional whole-body PET-CT in patients with malignant liver tumors: Influence on patient management to RF ablation therapy

H. Kuehl, G. Antoch, S. Rosenbaum, P. Veit, J. Barkhausen, A. Bockisch; Essen/DE

Purpose: Preinterventional imaging of patients with malignant liver tumors is mandatory to exclude extrahepatic tumor manifestation prior to RF ablation. The influence of whole-body PET-CT on management decision is evaluated.

Methods and Materials: 43 patients with hepatic malignancies (HCC 17, colorectal mets 14, other mets 12) were examined in PET-CT prior to planned intervention. CT was read alone by radiologists and the PET data evaluated by nuclear medicine physicians, each blinded to the others results. The PET-CT fusion data were read in consensus. The impact on the decision was analysed for the single imaging modalities as well as for the fusion data.

Results: 33 of 43 patients underwent RF ablation after whole-body PET-CT. The remaining 10 patients were not regarded as candidates for RF-ablation. In one patient CT showed complications of previous treatment and the patient was operated upon. In three patients negative PET results pointed to benign liver lesions which was then verified during follow-up. In the 6 remaining patients, whole-body scans revealed extrahepatic tumor spread, which was identified in 4 of 6 cases with CT and in all 6 cases with PET. PET/CT proved to be superior to PET alone in 5 of the 6 cases. Therapeutic regimen in 6 of the 10 patients not eligible for RF ablation was changed to systemic chemotherapy.

Scientific Sessions

Conclusions: The combination of whole body morphologic and metabolic imaging reliably identifies patients not suitable for local ablative therapy. PET-CT can be regarded as beneficial for patients planned for local ablative treatment with curative intention.

14:00 - 15:30 Room G

Genitourinary

SS 1507

Lower urogenital tract

Moderators:

S. Moussa; Edinburgh/UK
C. Roy; Strasbourg/FR

B-719 14:00

US-guided prostate biopsy: Is antibiotic prophylaxis necessary?

P. Bermudez Bencerray, J. Puig Domingo, A. Darnell Martin, A. Malet Munté, D. Gil Bello, A. Martin Olariz, M. Prieto Del Rei; Sabadell/ES

Purpose: To assess infectious complications in US-guided transrectal biopsy of the prostate comparing two groups of patients: one group with antibiotic prophylaxis and the other without prophylaxis.

Methods and Materials: A total of 1018 US-guided transrectal biopsies were performed in our centre from April 1996 to July 2003 with 16 G (n = 212) or 18 G (n = 806) core needles. Antibiotic prophylaxis was given in 404; the rest (614) received no antibiotics. Complications of the procedure were assessed at outpatient urologist visits between 1 week and one month after the procedure in the 212 first procedures and by telephone interview in the remaining 806.

Results: A total of 284 complications were found, including 41 major complications and 243 minor ones. Major complications were septic shock requiring admittance to the Intensive Care Unit (n = 3), sepsis (n = 3), Fournier gangrene (n = 1), urinary tract infection (n = 2), and fever requiring hospitalisation (n = 32). Minor complications were infection (n = 37), including 29 with fever that did not require admittance, prostatitis (n = 6), and epididymitis (n = 3). A total of 79.5% of all infectious complications occurred in patients without antibiotics and 20.5% in patients that received antibiotic prophylaxis. Of all major infectious complications, 73.2% occurred in the group without antibiotic prophylaxis, versus 26.8% in the prophylaxis group.

Conclusion: US-guided transrectal biopsy of the prostate has a statistically significant higher risk of infectious complications without antibiotic prophylaxis.

B-720 14:09

Comparison of the efficacy of three different anaesthetic regimens for transrectal ultrasound guided prostate biopsy (TUPB)

B.C. Anil Kumar, R.I. Doull; Dundee/UK

Purpose: TUPB is an increasingly common procedure performed using different anaesthetic techniques. This is a retrospective analysis of patient perceived pain during TUPB using three different regimens involving local intrarectal lignocaine gel (LILG) and Periprostatic lignocaine infiltration (PLI).

Materials and Methods: 241 patients who underwent TUPB between May 2001 and July 2004 were given a questionnaire to complete following their biopsy. Group A-(51 Patients, May 2001-December 2001) LILG 5 minutes before biopsy. Group B- (99 patients, January 2000-December 2002) LILG 5 minutes before and PLI 2 minutes before biopsy. Group C -(91 Patients, September 2003- July 2004) LILG 20 minutes prior and PLI 2 minutes before biopsy. Patients were asked about pain during the procedure, complications following the procedure and willingness to undergo repeat procedure if clinically indicated.

Results: 88% (45/ 51) in group A, 81%(81/ 99) in group B and 88% (80/91) in Group C responded. 88.5% in group A, 85% in group B and 96.2% in group C reported the procedure "easily tolerable" or "tolerable" which was statistically significant ($P < 0.018$). 11.5% in group A, 15% in group B and 4% in group C reported the procedure "barely tolerable" or "intolerable". Comparing groups A and B, there was no statistical difference in pain perception whereas there was significant statistical difference between Group B and C ($P < 0.046$).

Conclusion: LILG alone is as effective as LILG plus PLI for TUPB. LILG application 20 minutes before is more effective than application 5 minutes before the procedure.

B-721 14:18

Washout dynamic contrast enhanced versus T2 weighted MR imaging prior to transrectal ultrasound biopsy in patients at high risk for prostate cancer

M.A. Haider¹, A. Toi¹, J. Sweet¹, A. Kale¹, N. Bloch², J. Trachtenberg¹; ¹Toronto, ON/CA, ²Boston, MA/US

Purpose: Elevated PSA and prostatic intraepithelial neoplasia (PIN) are prostate cancer risk factors that can lead to repeated transrectal ultrasound biopsy (TRUSBx). The purpose of this study was to compare washout dynamic contrast enhanced MR imaging (WDCEMRI) to T2 weighted MRI for localization of prostate cancer in high risk patients.

Methods: In this prospective study, 33 patients with elevated PSA (> 4 ng/ml) and/or a prior diagnosis of PIN underwent WDCEMRI with an endorectal coil using a 1.5 T system (GEMS, Milwaukee, WI). Axial and coronal T2 weighted images and axial dynamic T1 contrast enhanced images were performed (3DFSPGR, 256x192, 3/0 mm, TR/TE 11.1/4.2 ms, flip angle 20deg, gadodiamide [Omniscan, Amersham, Princeton, NJ], 0.01 mg/kg at 4 ml/s, 9 phases, 7 post-contrast). Dynamis images were analyzed using a mono-exponential decay model. A washout decay constant threshold was used for cancer detection. Following MRI systematic TRUSBx biopsy was performed in 13 zones, 10 in the peripheral zone [PZ]. Pathologic diagnosis from the cores was used as a reference standard. Analysis was limited to the PZ.

Results: WDCEMRI accurately localized cancer in 11 of the 15 positive cores for a sensitivity of 73% versus 53% (8/15) for T2. Specificity was 73% (232/315) for WDCEMRI versus 79% (250/315) for T2. WDCEMRI was superior to T2 in providing useful localization for TRUSBx in 6/10 patients and T2 was superior in 0/10.

Conclusion: WDCEMRI has better regional sensitivity for prostate cancer than T2 weighted imaging and thus may be helpful in directing TRUSBx in patients who have had repeated negative biopsies.

B-722 14:27

Prostate biopsy in supine position in a standard 1.5 T scanner under realtime MR-imaging control using an MR-compatible endorectal biopsy device. First results

K. Engelhard¹, H.-P. Hollenbach², B. Kiefer², A. Winkel³, D. Engehausen², ¹Nürnberg/DE, ²Erlangen/DE, ³Schwerin/DE

Purpose: To investigate a biopsy device (MR imaging Devices Daum GmbH, Schwerin, Germany) for MR imaging-guided transrectal prostate biopsy.

Method and Materials: 20 patients with elevated PSA levels, negative tumor results in transrectal ultrasound (TRUS) and episodes of prior tumor negative prostate biopsies underwent MR imaging guided prostate biopsy in a 1.5 T scanner (Siemens Medical Solutions, Erlangen). After localisation of tumor suspected areas using a combination of an endorectal and two body-phased-array coils (one anterior, one posterior) the endorectal coil was replaced by the biopsy device. The needle guide was filled with a MR-visible fluid to control positioning of the needle using a real-time TrueFisp and a T2-TSE sequence observed with an in-room monitor. Core biopsies were taken manually in the magnet in supine position of the patient.

Results: The biopsy needle could be visualized and correctly positioned in all cases. Tumor suspected lesions with a diameter < 10 mm could be successfully punctured. In cases of histological confirmed cancer a good correlation was found between tumor location on the MR-images and tumor location at histology. The whole examination time was 60 minutes. No complications more than those associated with TRUS-guided biopsy were observed.

Conclusions: The demonstrated biopsy technique performed in a supine position of the patient can be a valuable tool for obtaining MR imaging-guided biopsies based on MR-images showing suspicious areas, which were not identified on TRUS-imaging.

B-723 14:36

Prospective evaluation of a routine protocol for combined magnetic resonance and ¹H-spectroscopic imaging of the prostate in patients prior to radical prostatectomy

A. Wetter, T. Engl, D. Nadjmabadi, T. Lehnert, W.-D. Beecken, D. Jonas, T.J. Vogl; Frankfurt a. Main/DE

Purpose: To prospectively evaluate a routine protocol for combined magnetic resonance and ¹H-spectroscopic imaging of the prostate in patients prior to radical prostatectomy.

Methods: 25 patients were examined prior to radical prostatectomy with our combined protocol, which consisted of T2-weighted turbo-spin-echo sequences

Scientific Sessions

and a transverse T2-weighted fat-sat TSE-sequence. For spectroscopy, we used a 3D-CSL-SE-sequence with a scan time of 10:45 minutes. Image reading was performed by two radiologists, tumors were classified in consensus according to the TNM classification. Voxels were classified as tumor-suspect, when the ratio of Cho+Crea/Cit was greater than 1.1, according to a previous work of our group. Imaging and spectroscopic results were compared and correlated to the results of the pathologic examination of the whole prostate.

Results: Examination time of the combined protocol was 20 minutes, a time feasible for routine use. Imaging alone resulted in a sensitivity and specificity regarding exact T-staging of 71% and 83%, respectively. Adding of spectroscopy could not enhance staging accuracy, in terms of a better differentiation between unilateral (T2a, T2b) and bilateral (T2c) involvement, as proved by comparison with the histological specimens. Also regarding T2 versus T3, the results of imaging and spectroscopy did not differ significantly. A disadvantage of spectroscopy was the long postprocessing time, taking in average 45 minutes per patient into account.

Conclusion: A combined examination with MR imaging and spectroscopy is possible in 20 minutes examination time and feasible for routine use, but cannot enhance sensitivity and specificity significantly.

B-724 14:45

Potential value of diffusion-weighted echo-planar magnetic resonance imaging in differentiating malignant from benign nodules in prostate cancer

S. Reinsberg, E. Scurr, J. Brewster, D. Dearnaley, A. Horwich, N.M. deSouza; Sutton/UK

Purpose: To determine the potential of diffusion-weighted magnetic resonance imaging (DW-MRI) in differentiating benign from malignant nodules by comparing the diffusion coefficients of low signal intensity nodules seen on T2-weighted images within the peripheral zone (PZ) with that of the central gland (CG).

Methods: Sixteen patients 48-80 years (median 71 years) with prostate cancer (Prostate Specific Antigen levels 11.3 ± 1.2 IU) were imaged using an endorectal receiver coil and echo-planar DW-MRI sequences with 4 diffusion values ($b = 0, 300, 600, 800$ s/mm 2). Image parameters were 2500/69 msec [TR/TE], 96x128 matrix, 200 mm field of view, 4 mm slice thickness. Apparent diffusion coefficients (ADC's) from regions of interest encompassing 20 nodules within the PZ (median ROI size 53 mm 2) with positive biopsies, and the whole CG (median ROI size 289 mm 2) were measured. In addition, patients in whom all three or four biopsies from one side were benign had ADC values measured in non-malignant PZ (median ROI size 63 mm 2).

Results: ADC values from CG were 1530 ± 110 (mean \pm sd) while those from malignant PZ nodules were 1310 ± 190 . Values from non-malignant PZ were 1690 ± 220 . Differences between all three regions were statistically significant. 95% confidence intervals of the means differences and p-values are 112 to 330 and $p = 0.0004$ (CG vs malignant PZ), 55 to 515 and $p = 0.02$ (malignant PZ vs non malignant PZ), 21 to 295 and $p = 0.03$ (CG vs non malignant PZ).

Conclusion: DW-MRI may be a useful adjunct to conventional T2-weighted sequences for increasing sensitivity of prostate cancer detection. Diffusion is restricted in malignant compared to benign prostatic nodules.

B-725 14:54

USPIO-enhanced T2* images at 1.5 T and 3 T: Initial results

R.A.M. Heesakkers¹, J.J. Futterer¹, A. Hövels¹, H.C. van den Bosch², T.W.J. Scheenen¹, J.O. Barentsz¹; ¹Nijmegen/NL, ²Eindhoven/NL

Purpose: To explore the ability to perform ultrasmall superparamagnetic particles of iron oxide (USPIO)-enhanced MR imaging at high field strengths (3 T) and to compare the image quality at 1.5 T and 3 T, in patients with prostate cancer.

Methods and Materials: 23 consecutive patients with prostate cancer were administered USPIO. 24 Hours after administration T2* images of the obturator area were acquired at 1.5 T and 3 T MR scanners, using a PPA coil, with an in-plane resolution of 0.56x0.56x3.00 mm and 0.50x0.50x2.50 mm, respectively. For both sequences 3 echo trains were used. Scanning parameters and type of scanner were not visible for the readers.

All images were evaluated on muscle-fat contrast, vessel-fat contrast, lymph node border, number of nodes and total image quality by 2 readers. All positive nodes were counted and compared.

Results: T-test showed significant difference in the results of the muscle-fat contrast, vessel-fat contrast, lymph node border and total image quality in the benefit of 3 T ($p < 0.05$). All positive nodes found at 1.5 T were also found at 3 T. In 3 patients an additional positive node was found at 3 T which was not visible on 1.5 T and which was outside of the usual resection area.

Conclusion: USPIO-enhanced techniques can be used at high field strengths and a high in plane resolution can be obtained. This may result in improved performance.

B-726 15:03

3D multiplanar TRUS with power Doppler in detecting prostatic fossa recurrences following radical prostatectomy

V. Gazhonova, A. Chepurov, A. Zubarev; Moscow/RU

Purpose: To identify the US features of local tumor progression with 3D PD TRUS in patients with rising PSA levels after radical prostatectomy (RP) for prostate cancer.

Methods and Materials: 14 pts with rising (more than 0.3 ng/ml) PSA following RP (range 3 to 10 years, mean 38 months) underwent 3D PDTRUS study for identification of local tumor recurrence. 3DUS images were evaluated for the presence of focal lesions, residual tissue volume, vascularity degree (VD) of the residual tissue. US finding were considered suspicious if any unusual hypoechoic tissue was present adjacent to the bladder neck, retro-trigone or perianastomotic site with an increase in the VD present.

Results: Of 14 pts, 9 had positive TRUS. Target biopsies revealed cancer in 8 of 14 pts (2-T2bNoMo, 4-T3aNoMo, 2-T3bNoMo). The mean volume of identified tissue in the prostatic fossa was higher in the cases with tumor recurrence than in normal cases ($p < 0.05$). There were significant differences for VD values between local recurrence areas than in non-cancerous zone ($p < 0.001$). The echogenicity was found to be lower in the region of malignancy ($p < 0.001$). Hyperechoic foci were characteristic of malignant tissue in 33% of cases. The overall accuracy, sensitivity and specificity of tumor recurrence detection after RP using 3D TRUS in were 93%, 89%, 83%, respectively.

Conclusions: 3D TRUS with PD appears to be clinically feasible and added anatomic information from the coronal plane for better detection of the recurrent tumor. Increase in the vascularity degree in the prostatic fossa could be used as criteria for diagnosis of tumor recurrence.

B-727 15:12

Multi-detector row CT cystoscopy in the evaluation of urinary bladder neoplasms

A.C. Tsili, C. Tsampoulas, F. Katzioti, D. Giannakis, A. Silakos, N. Sofikitis, S.C. Efremidis; Ioannina/GR

Purpose: To evaluate the utility of multi-detector row CT urography in the detection of urinary bladder tumors.

Materials and Methods: Twenty-one patients presented with hematuria and abnormal findings at conventional cystoscopy, underwent CT cystoscopy. The patients were examined in supine and prone positions, after bladder distention with room air. We used a detector configuration of 16x0.75 mm and pitch 1.2. We evaluated the transverse tomographic slices, the sagittal and coronal reformatted images. Virtual images were created using volume rendering technique. The results were compared to those of conventional cystoscopy, operative and pathology findings.

Results: CT cystoscopy detected all bladder lesions (43), as seen with conventional cystoscopy. The size of the lesions ranged from 0.3 to 8.2 cm in diameter (mean size: 2.4 cm). Fifteen lesions were smaller than 0.5 cm in diameter.

Conclusion: Multi-detector row CT cystoscopy is a highly accurate technique for the detection of urinary bladder neoplasms. With this technique the identification of lesions smaller than 0.5 cm seems promising.

B-728 15:21

Lymph node staging in patients with cervical cancer: Accuracy of integrated FDG PET/CT in correlation to histopathologic findings

S. Sironi, A. Buda, M. Picchio, C. Messa, F. Fazio; Monza/IT

Purpose: To prospectively determine the accuracy of integrated PET/CT for evaluating lymph node metastasis in patients with cervical cancer, using histopathologic findings as the reference standard.

Materials and Methods: Forty-eight women (mean age, 45.3 years) with clinical stage IA, IB, or IIA carcinoma of the uterine cervix were included in the study. All the 48 patients enrolled were scheduled for radical hysterectomy with pelvic lymph node dissection. Before surgical treatment, all of them underwent fluorodeoxyglucose (FDG) PET/CT imaging. At PET/CT studies, eight lymph node sites in the pelvis bilaterally were assessed for data analysis; paraaortic lymph node site was also evaluated. In all cases, imaging findings were compared with results of histopathologic examination. Fisher exact test and Cohen kappa test were used for statistical analysis.

Results: Ten (21%) of 48 patients had metastatic lymph nodes at histopathology, and thirty-eight (79%) of 48 had no histologically confirmed node metastasis. Of the total 864 lymph nodes sampled, 17 (2%) were found to be positive for malignant cells at histopathology, of which 15 were from pelvic and two from paraaortic

Scientific Sessions

sites. A good correlation was found between PET/CT and histopathologic diagnoses ($k = 0.67$). The overall lesion-based sensitivity, specificity, positive predictive value (PPV), negative value (NPV), and accuracy of PET/CT were 47%, 88%, 62%, 80% and 76%, respectively. The overall patient-based sensitivity, specificity, PPV, NPV, and accuracy of PET/CT were 50%, 95%, 71%, 88% and 85%, respectively.

Conclusion: PET/CT is accurate in depicting lymph node metastasis in cervical cancer.

14:00 - 15:30

Room H

Breast

SS 1502

Interventional procedures

Moderators:

W. Buchberger; Innsbruck/AT
R. Holland; Nijmegen/NL

B-729 14:00

Radiofrequency ablation of small breast cancer with a dedicated cooled tip needle electrode

G. Simonetti, G. Manenti, C. Pistolese, E. Cossu, O. Buonomo, A. Orlando; Rome/IT

Purpose: To evaluate the uniformity and reproducibility of thermal lesion ablation on selected breast tumors ≤ 2 cm and quantify the volume of tissue destruction induced with a new available radiofrequency ablation device and RF-generator.

Methods and Materials: A new cooled-tip electrode was realized to induce wide thermal lesions in eight swine breasts *in vivo* and in 12 resected pre and post-menopausal mammary glands from human surgical mastectomy. Five patients with biopsy proven non-palpable invasive breast carcinomas underwent sonographically guided RFTA of their breast tumors under general anesthesia followed by a 15 days delayed resection. Endpoints were technical success, completeness of tumor kill, marginal clearance, skin damage and patient reports of pain and procedural acceptability.

Results: In resected mammary glands the mean diameter of the radiofrequency-induced lesion was 3.7 ± 0.4 cm which correspond to approximate volume of 26.67 ± 9.59 cm^3 . *In vivo*, the mean diameter was 3 ± 0.4 cm corresponding to an approximate volume of 11.16 ± 3.65 cm^3 . The procedure was complete in all patients without any residual pathology and disease free margins histopathologically examined by using eosin hematoxilin and nicotinamide adenine dinucleotide diaphorase stains. The ablation procedure was well tolerated without skin and thoracic wall damages.

Conclusions: US-guided percutaneous ablation of small selected invasive breast carcinoma with dedicated device is a feasible and reliable technique because of the higher energy deposition due to the cooling of the needle electrode.

B-730 14:09

Galactography-guided stereotactic wire localization of intraductal lesions

M.H. Fuchsäger, R.S. Cárcilia, C.C. Riedl, M. Rudas, D. Flöry, T.H. Helbich; Vienna/AT

Purpose: Diagnostic galactography allows concise preoperative determination of number, location and extent of the lesions causing nipple discharge. Stereotactic targeting through galactography may provide further guidance to the surgeon and increase the likelihood of the causative lesion being found. The purpose of this study was to assess the feasibility of galactography-guided stereotactic wire localization in intraductal lesions.

Methods and Materials: 46 patients (mean age 58.7 years) with nipple discharge and galactographically verified intraductal lesions were included in this prospective trial. Galactography-guided stereotactic preoperative wire localization was performed in 47 lesions. Surgery and histologic work-up were performed in all cases.

Results: 14 (29.8%) lesions were malignant and 33 (70.2%) benign. 10 of 14 malignant lesions were ductal cancers *in situ*, three invasive ductal cancers and one invasive lobular cancer. 25 of 33 benign lesions were papillomas (five with atypia) and eight fibrocystic changes. In all patients nipple discharge ceased after open surgery (follow-up of at least 18 months).

Conclusion: Galactography-guided stereotactic wire localization is an accurate, safe, simple and time-saving method. This technique can be offered as an alternative to current surgical techniques in patients with galactographically verified intraductal lesions.

B-731 14:18

MR imaging guided localisation of breast lesion

J. Veltman, C. Boetes, J. Blickman, J.O. Barentsz; Nijmegen/NL

Purpose: To evaluate the accuracy of localisation wire placement using an open breast coil with mammography intervention aid and software (OBC, MIA&S).

Methods and Materials: Lesions only detectable on MR imaging were pre-operatively located using OBC and MIA&S (Machnet, Netherlands) and a double hook wire (DHW). Lesions were visualised using conventional FLASH3D pre and post gadolinium contrast subtraction images. DHW placement was done based on software output. Placement accuracy was evaluated by measuring the distance in three directions (AP, CC and LR) from the centre of the lesion and the tip of the DHW to the skin. Measurement differences were analysed. Time needed to perform a procedure was also recorded.

Results: 24 patients were included with a total of 26 lesions. Mean lesion size was 9 mm (range 4-35 mm). In AP direction the DHW was placed with a mean difference of 2.9 mm from the lesion centre (range 0-27 mm). In CC direction this was 1.2 mm (range 0-4 mm) and in LR direction 2.3 mm (range 0-5 mm). The largest difference in AP direction (27 mm) was due to technical limitations; the lesion was out of range for the device. Mean difference in AP direction, without this 1 problematic lesion, was 1.8 mm (range 0-4 mm). Procedure time varied between 25 and 50 minutes with an average of 33 minutes.

Conclusion: Localisation of breast lesions are accurate using the OBC with MIA&S and can be performed within acceptable time.

B-732 14:27

False-negative results after stereotactically-guided vacuum biopsy

D. Peter, J. Gruenhagen, R. Wenke, I. Schreer, M. Heller; Kiel/DE

Purpose: Detection of false-negative (FN) results after vacuum biopsy (VB) to differ retrospectively between misjudgement of a representative biopsy or an incidental occurrence of malignancy.

Methods and Materials: 343/668 patients, who underwent VB in our institution between 03/1999 and 12/2002 turned out to be benign. Those patients were followed to determine the FN rate of VB.

Results: The mean length of follow-up was 29.8 months for 1999 (25, 8 month for 2000, 23, 6 month for 2001 and 13 month for 2002). 44 patients (12.8%) were lost to follow-up. 7 cases (2%) showed progression, so that re-biopsy or open surgery had to be performed. 5/7 turned out to be malignant. Four cases must be considered retrospectively as not representative: One mass was obscured by hematoma on postinterventional mammography, three other cases with microcalcifications showed more than one lesion. These lesions remained because they were misinterpreted as being benign too.

Conclusion: The FN rate of 1.2% (4/343) is lower than the rate after needle localisation and open surgery. Correlation between histology and radiologic appearance is of highest importance, particularly if there is more than one group of microcalcifications. In 3 cases the diagnosis of malignancy was delayed because the remaining lesions were not removed. Furthermore patients must be strongly advised to take part in follow-up investigations for 3 years to finally exclude FN biopsy.

B-733 14:36

Vacuum-assisted breast biopsy (VAB): A study of cost-effectiveness

S.H. Heywang-Köbrunner¹, K. Bernerth², K. Rotter³, C. Perlet¹; ¹Munich/DE, ²Halle/DE, ³Leipzig/DE

Purpose: To examine cost effectiveness of percutaneous VAB.

Methods and Materials: The data of 244 patients with 288 single foci biopsied during 6 consecutive months were evaluated. 52 malignancies and 7 ADH were verified.

Results: Patients were split up into patients with single, two or 3 foci. Costs were calculated according to the diagnostic or therapeutic path which they had to follow based on their disease according to the usual treatment. The costs of vacuum biopsy were compared with the costs of open surgical biopsy (assuming that the lesions were too small or uncharacteristic for percutaneous biopsy (=correct selection)). Compared to surgical biopsy the costs for an average benign case were 67%, when VAB was used. For an average malignant case the costs using VAB also amounted to 67% of the costs of a merely surgical approach. Cost savings of malignant cases were due to the fact that fewer operations were needed to achieve clear margins and lymph node surgery, where needed.

Conclusion: With the correct selection (masses and larger lesions can undergo CNB) VAB is cost-effective.

Scientific Sessions

B-734 14:45

Clip migration after 11-gauge vacuum-assisted stereotactic breast biopsy with lateral approach: Retrospective review of 447 clips deployed after completion of breast biopsy

C. Chaveron, L. Ceugnart, F. Bachelle; *Lille/FR*

Purpose: To assess clip migration after vacuum-assisted breast biopsy with lateral approach and explain mechanisms of migration. We suggest options to localize the biopsy site before surgery in case of clip migration.

Methods and Materials: Retrospective review was performed of 447 lesions that underwent clip placement after stereotactic vacuum-assisted breast biopsy with an 11-gauge probe. The clip was placed when images obtained after biopsy suggested a complete removal. Postbiopsy mammography in two orthogonal planes was performed 8 days later.

We compared pre- and postbiopsy mammograms and measured the distance between the clip and biopsy site.

Results: The distance from clip to lesion site was more than 20 mm on at least one post-biopsy image in 60(13.4%) of 447 lesions that underwent clip placement. Marker clip misplacements are mainly attributed to an accordion effect along the axis of compression; in theory, this effect decreases with lateral approach of probe. Other mechanisms can explain: Delayed accordion effect, bleeding during or after the procedure, movement of the breast. A few options are suggested: Sonographically research of postbiopsy scar, sonographically clip placement a few days after biopsy....

Conclusion: Clip migration after vacuum-assisted breast biopsy does exist and is a practical concern. For surgical cases, repeat craniocaudal and 90° mediolateral mammograms should be obtained routinely on the day of pre-operative localization. We try to identify the percutaneous biopsy site in the excised specimen and to correlate histologic findings in the surgical specimen with those at vacuum-assisted biopsy to determine if the correct tissue was removed at surgery.

B-735 14:54

A new BiomarC tissue marker for breast biopsy: Clinical evaluation in ultrasound, mammography, cat scanning and breast MR imaging

M.T. Nelson, M. Garwood, S. Meisamy, P.J. Bolan, A. McIntosh; *Minneapolis, MN/US*

Purpose: To evaluate the clinical use of BiomarC tissue marker in image guided breast biopsies using MR imaging, mammography, and ultrasound.

Methods and Materials: Forty BiomarC breast markers were placed after breast biopsy using stereotactic mammography (11 markers), ultrasound (25 markers) and MR imaging placement (4 markers). The BiomarC tissue marker is a sterile, single patient use, pyrolytic carbon coated zirconium oxide discrete marker that is visible on standard radiographs (X-ray, mammography, stereotatic imaging and digital breast imaging) ultrasound and MR imaging at up to 4.0 Tesla field strength. All of the BiomarC tissue markers were placed through existing biopsy needles or through a 10 gauge trocar.

Results: All 40 BiomarC's were placed within 4 mm of the original biopsy site. Follow-up at 6 months on 10 benign biopsy patients showed no migration of the BiomarC tissue marker. The BiomarC was successfully placed under MR imaging guidance using a titanium trocar 140 mm. Four patients also had a 4 T MR imaging research study completed for follow-up neoadjuvant chemotherapy and the BiomarC tissue marker did not interfere with magnetic resonance imaging or magnetic resonance spectroscopy.

Conclusion: 40 BiomarC tissue markers were placed under image guidance using ultrasound, stereotactic mammography and MR imaging. All of the BiomarCs were in excellent position on post biopsy imaging and there is no evidence of breast marker migration on 6 month follow-up imaging. The BiomarC breast tissue marker does not interfere with magnetic resonance imaging or magnetic resonance spectroscopy studies.

B-736 15:03

A validation study for ultrasound guided 14-gauge large core breast biopsy

S. Jaromi¹, R. Mallek¹, M. Memarsadeghi¹, M. Fuchsjaeger¹, L. Liberman², T.H. Helbich¹; ¹*Vienna/AT*, ²*New York, NY/US*

Purpose: To determine the false-negative rate of ultrasound guided 14-gauge large core breast biopsy in a validation study of lesions that had subsequent surgical excision.

Methods and Materials: Retrospective review was performed of 722 lesions that underwent ultrasound guided 14-gauge large core breast biopsy and subsequent surgical excision. Biopsies were performed by five experienced radiologists. Medical records, imaging studies, and histologic findings were reviewed and

compared for agreement. A false-negative cancer case was defined as a pathologically proven cancer in which biopsy yielded benign results (except high-risk lesions).

Results: False-negative findings were encountered at ultrasound guided 14-gauge large core breast biopsy in 1.5% (7/468) of pathologically proven cancers. All false-negative findings could be prospectively identified due to imaging-histologic discordance. Ultrasound guided biopsy underestimated 46.4% (32/69) of the high-risk lesions. Ultrasound guided biopsy yielded benign results in 217 lesions. In ten of those 217 lesions (4.6%) the ultrasound guided benign biopsy result was not in agreement with the benign result of subsequent surgical excision.

Conclusion: Ultrasound guided 14-gauge large core breast biopsy had a false-negative rate of 1.5%. This 1.5% false negative rate is comparable to the previously published false-negative rate of needle localization and surgical biopsy.

B-737 15:12

Sonographically-guided percutaneous biopsy using two different vacuum biopsy systems

S.H. Heywang-Köbrunner¹, C. Perlet¹, A. Heinig², A. Bernhardt²; ¹*Munich/DE*, ²*Halle/DE*

Purpose: To evaluate the use of sonographically-guided percutaneous breast biopsy in lesions with uncertain histology and/or small size and to compare two vacuum-biopsy systems.

Methods and Materials: 34 patients were examined between July 2002 and August 2003. Patients were selected for large-volume percutaneous sonographically-guided vacuum assisted biopsy either by small size of the lesion or by its uncharacteristic features, which indicated a probably unspecific histology. Vacuum biopsy was performed with Mammotome HH (Ethicon) or Vacu Flash (BIP) through a coaxial needle.

Results: 2 invasive cancers (6, 10 mm) and one DCIS, 2 fibroadenomas, 1 papilloma, 1 fat necrosis, 1 inflammatory cyst and another 26 unspecific histologies resulted. 32/34 cases were considered representative due to removal of most of the lesion. One open biopsy and one MR imaging were recommended. The Vacu Flash system is handled easier, the Mammotome is faster but requires more skill. It shows advantages in case of bleeding.

Conclusion: Both systems are useful and reduce open biopsy in selected doubtful cases with unspecific histology. Study supported by Dt. Krebsliga and Dresdner Bank: Schleicher-Stiftung.

B-738

withdrawn by authors

14:00 - 15:30

Room I

Contrast Media

SS 1506a

Specific MR imaging contrast media

Moderators:

H.J. Lamb; *Leiden/NL*
E.J. Rummeny; *Munich/DE*

B-739 14:00

Comparison of ferumoxtran-10 and ferumoxytol for MR imaging of experimental arthritis

G.H. Simon, J. von Vopelius-Feldt, M.F. Wendland, Y. Fu, K.V. Berejnoi, H.E. Daldrup-Link; *San Francisco, CA/US*

Purpose: To detect and characterize inflammatory processes in an animal model of antigen-induced arthritis using MR imaging enhanced with two different USPIOs.

Methods and Materials: A monoarthritis was induced in the right knee of 12 Sprague Dawley rats by subcutaneous injections of Freund's adjuvant and intraarticular injections of methylated bovine serum albumin. Saline was injected into the left knee as a control. Both knees underwent MR imaging at 2 T before and 3-120 min and 24 h after injection of 200 micromolFe/kg Ferumoxtran-10 (n = 6) or Ferumoxytol (n = 6). Pulse sequences comprised T2-weighted multiecho-2D-SE 100/20, 40, 60, 80/90 (TR/TE/flipangle), T2*-3D-SPGR 100/15/38 and T1-3D-SPGR 50/1.7/60 sequences. USPIO induced signal intensity changes of arthritic and contralateral knees were determined. A paired t-test was used for statistical analyses. Joint specimens were processed for histopathologic correlation.

Results: The synovium of the arthritic joints showed a marked and progressive

Scientific Sessions

positive enhancement on T1-weighted images and a negative enhancement on T2-TSE and T2*-GE images after administration of either USPIO up to 120 min p.i. After 24 h, the T1-enhancement disappeared and a remaining negative T2-enhancement was observed. This enhancement in arthritic knees was significantly different from normal knees, which showed no or minimal enhancement ($p < 0.05$). No significant differences were observed between the two USPIOS ($p > 0.05$). Prussian blue histopathology confirmed iron oxide accumulation within the synovium of the arthritic joints, but not in the contralateral normal joints.

Conclusion: Inflammation in antigen-induced arthritis can be equally detected and characterized with Ferumoxtran-10 and Ferumoxytol. This imaging approach may prove clinically useful to target and grade inflammatory processes.

B-740 14:09

Evaluation of neck and body nodal metastases with ferumoxtran 10-enhanced MR imaging: Phase III safety and efficacy study

A. Saleh¹, F. Caseiro-Alves², C. Weber³, W. Schima⁴, ¹Düsseldorf/DE, ²Coimbra/PT, ³Roissy/FR, ⁴Vienna/AT

Purpose: To determine the safety and efficacy of magnetic resonance (MR) imaging with ultrasmall particles of iron oxide (USPIO) for nodal staging in oncologic patients.

Methods and Materials: 193 patients were examined by MR imaging before and after intravenous administration of the USPIO contrast agent ferumoxtran 10 (Sinerem®; Guerbet, Roissy, France and Combidex®; Advanced Magnetics, Boston, USA). 160 patients were evaluable for the efficacy analysis. The diagnostic accuracy for nodal staging of pre- and postcontrast MR imaging was compared with the use of McNemar's test. Imaging results were correlated with histopathological findings.

Results: The performance of ferumoxtran 10-enhanced MR imaging for nodal staging was significantly superior to non-enhanced studies ($p = 0.001$). In the patient-by-patient analysis, sensitivity, specificity and accuracy of precontrast MR imaging improved from 56%, 93%, and 70%, respectively, to 84%, 80%, and 83%, respectively, with ferumoxtran 10-enhanced MR imaging. In the node-by-node analysis sensitivity, specificity and accuracy were 23%, 99% and 63%, respectively, with precontrast MR imaging and 98%, 72% and 84%, respectively with ferumoxtran 10-enhanced MR imaging. Accuracies of ferumoxtran 10-enhanced MR imaging in patients with carcinomas of the head and neck (91), lung (25), breast (20) and the abdomino-pelvic area (24) were 88%, 76%, 80% and 54%, respectively. Back pain, increased sweating, nausea, rash and flushing each occurred in 2-3% of patients.

Conclusions: Ferumoxtran 10 is a safe and effective iron oxide contrast agent. Iron oxide-enhanced MR imaging is significantly more accurate compared to non-enhanced MR imaging for nodal staging in oncologic patients.

B-741 14:18

USPIO-enhanced GRE T2*W sequence versus TSE T2W sequence in T-staging evaluation of uterine malignancies: A comparison study with surgical and histological staging

P. Paolantonio, A. Laghi, C. Miglio, M. Rengo, V. Vergari, M. Di Martino, A. Guerrisi, R. Passariello; *Rome/IT*

Purpose: USPIO administration provides a significant decrease of SI of normal myometrium with higher C/N between neoplastic lesions and normal myometrium on GRE-T2*W sequences. The aim of our study was to compare the accuracy on T-staging of uterine carcinoma of USPIO-enhanced-GRE T2*W sequence versus TSE T2W sequence.

Methods and Materials: Thirty consecutive female patients referred for gynecological carcinomas, 19 with corpus uterine cancer and 11 with cervical carcinoma, underwent MR examination. TSE T2W sequence (TR/TE/matrix/acq. time: 3000 msec/132 msec/230x512/5.3 min) were acquired on axial and sagittal planes and GRE T2*W sequences (TR/TE/FA/matrix/acq. time: 1800 msec/15 msec/30°/230x512/13.51 min) were acquired on axial and sagittal planes before and 24 hours after iv administration of 2.6 mg/kg of body weight of USPIO (Sinerem, Guerbet, Paris, France). Image analysis was performed by consensus by two radiologists, assessing the T-staging of uterine malignancies on both USPIO-enhanced-GRE T2*W and TSE T2*W images and results were compared with the surgical and histological staging.

Results: No differences between the T-Staging obtained on USPIO-enhanced-GRE T2*W and TSE T2W images were observed. MR T-stage was confirmed in 28 cases after surgery. In two patients the T-stage obtained on both USPIO-enhanced-GRE T2*W and TSE T2W sequences resulted underestimated at histology.

Conclusions: T-stage of uterine malignancies obtained on USPIO-enhanced-

GRET2*W images was comparable with the one obtained on TSE T2W images. Therefore in patients with uterine malignancies that undergo iv USPIO administration for the N-staging assessment the T-stage may be obtained by only acquiring USPIO-enhanced-GRE T2*W sequence.

B-742 14:27

Whole body MR imaging in the evaluation of marrow disease employing intravenous iron contrast agent (Resovist)

C.J. Johnston, C. Gillan, J. Mc Hugh, P. O Gorman, S.J. Eustace; *Dublin/IE*

Purpose: To describe whole body MR imaging enhanced by intravenous superparamagnetic iron contrast agents (ferucarbotran) in the assessment of marrow based pathology: Preliminary experience.

Methods and Materials: 13 patients with proven marrow based disease (7 patients multiple myeloma, 6 patients metastatic disease) underwent whole body MR imaging. In each case patients underwent pre contrast, immediate and delayed (30 minutes) T2 weighted whole body scans with fat suppression after injection of 1.4 ml ferucarbotran (equivalent to 39.2 mg iron). Images were evaluated independently by 2 experienced readers and scored at a dedicated workstation.

Results: No difference in lesion detection was documented on pre- and immediate post-contrast scans. In 7 of 13 patients, documented marrow lesions were recorded as being more conspicuous on side by side comparison by both readers on the delayed (30 minute) scans. In 1 patient, additional lesions detected were detected.

Conclusion: Preliminary results using iron contrast agent enhanced whole body MR imaging shows promise for increasing lesion conspicuity in both myelomatous and metastatic marrow infiltration.

B-743 14:36

Experimental MRA investigations of atherosclerosis using ultra-small superparamagnetic particles of iron oxide at 3 T

A.N. Priest, H. Ittrich, C.L. Jahntz, H. Kooijman, C. Weber, G. Adam; *Hamburg/DE*

Purpose: To investigate the uptake by aortic plaques of an experimental USPIO contrast agent using MR imaging. Previous studies using a similar agent have demonstrated strong magnetic susceptibility effects impinging on the bright vessel lumen.

Methods and Materials: USPIOs (DDM43/34, Schering) were administered to six Watanabe rabbits at doses between 0.1 and 1.0 mmolFe/kg. Parasagittal MR angiography scans were acquired at 5 time-points during the subsequent 5 days. The contrast agent first reduced and then enhanced the blood signal over ~2 days following administration. At later time-points, additional bright-blood scans were acquired during gadopentate dimeglumine (Magnevist, Schering) infusion. Histological follow-up was performed for two animals, using HE, Prussian blue and RAM-11. MRA was performed with a 3 T clinical scanner (Philips) and head array-coil using two 3D gradient-echo sequences with acquired isotropic resolutions of 0.7 and 1.0 mm.

Results: Widespread susceptibility artifacts indicated USPIO uptake in bone marrow and liver. In the aorta, some one-sided lumen distortions were seen resulting from uptake in nearby ribs and spine, but surprisingly there were no artifacts suggestive of vessel wall uptake. Little USPIO uptake was seen in two animals histologically, despite the presence of active plaques.

Conclusions: Results of USPIO-enhanced scans of suspected atherosclerosis should be interpreted with caution. It is clear that the absence of susceptibility effects does not necessarily rule out the presence of plaque, even with the increased sensitivity to susceptibility at 3 T. The differing influences of USPIO agents and pulse sequences should be explored further by future studies.

B-744 14:45

Evaluation of CH3-DTPA-Gd (NMS60) as a new MR contrast agent: Early phase II study in brain tumors and dual dynamic contrast-enhanced imaging

M. Ito¹, H. Oshima¹, N. Shiraki¹, H. Ogino¹, Y. Shibamoto¹, H. Kasai¹, M. Mase¹, Y. Kawamura², T. Miyati³; ¹Nagoya/JP, ²Fukui/JP, ³Kanazawa/JP

Purpose: A newly developed contrast material CH3-DTPA-Gd (NMS60), a trimer containing 3 Gd³⁺ atoms per molecule has been shown to offer greater enhancement and longer vascular retention than Gd-DTPA in animals. We report on our experiences with an early phase II study on NMS60 in brain tumor patients together with our own additional investigations.

Methods and Materials: The longitudinal relaxation rate ($R_1=1/T_1$) and the transverse relaxation rate ($R_2=1/T_2$) of NMS60 and Gd-DTPA were determined at 20 °C in water at 1.5 T. An NMS60 dose of 0.1 or 0.2 mmolGd/kg was randomly

Scientific Sessions

assigned and administered to 10 patients (5 women, 5 men, mean age: 49 years) with brain tumors. Safety and contrast-enhancing ability of NMS60 were evaluated. Dual dynamic contrast-enhanced T₁ and R_{2'} studies (DUCE imaging) were also carried out in 2 patients.

Results: Regarding the relaxivity per Gd, R₁ and R_{2'} of NMS60 were 9.8 and 11.0 (mmol/L-s)⁻¹, respectively, compared to 4.9 and 8.0 (mmol/L-s)⁻¹ for Gd-DTPA. Although a transient slight increase of alanine aminotransferase was observed in 1 case, no other adverse reactions were observed after administration of NMS60. Contrast enhancement by NMS60 was excellent at both concentrations, and when tumor detectability was assessed with a 5-point scale, the diagnostic usefulness was 4 or higher in all cases. In DUCE imaging, NMS60 showed apparently higher signal intensity as compared with Gd-DTPA.

Conclusion: NMS60 had a stronger contrasting effect than Gd-DTPA in both fundamental and clinical studies, and thus is expected to be clinically useful.

B-745 14:54 ♀

Quantitative evaluation of SHU-555A (Resovist-Schering) enhancement in normal liver parenchyma and benign/malignant focal hepatic lesions

L. Santoro¹, S. Colagrande¹, A. Filippone², E. Grassedonio², G. Belli¹, N. Villari¹; ¹Florence/IT, ²Chieti/IT

Purpose: To quantify signal intensity (SI) enhancement (E) of liver parenchyma and focal lesions after bolus administration of contrast media (CM) Resovist in order to improve nodular masses characterization.

Methods and Materials: 10 normal subjects and 31 patients (16 male, age 58 ± 12) with definite nodular hepatic lesions (8 haemangiomas, 7 FNH, 18 metastases, 6 HCC; non haemangiomas have histological demonstration), underwent MR imaging examination on 1.5 Tunit (Gyrosan ACS NT, Philips). Axial 7 mm thick sections, respiratory gated TSE T2W, free breath SS T2W and breath-hold FFE T1W sequences were obtained. T1W sequences were repeated 20°, 50° and 180° after CM; both T1/T2W sequences were performed again at 10°. SI of normal liver and focal lesions were measured in each sequence and normalized to muscle in order to avoid rescaling phenomenon; E was calculated as (SI post-CM - SI pre-CM / SI pre-CM) × 100. Statistical analysis of E was performed by Anova/paired t-test.

Results: The only statistically significant SIE mean values were observed at T2/T1W 10° images: Respectively, normal liver -59 ± 9 and +2 ± 12%; haemangiomas -50 ± 15 and +70 ± 30%; FNH -45 ± 17 and -7 ± 19%; metastases -8 ± 14 and +10 ± 17%; HCC +13 ± 18 and +16 ± 18%. T2 SIE of benign lesions ranged from -30 to -70%, mean -46%, whereas T2 SIE of malignant from -20 to +15%, mean -3%. Haemangiomas had T1 SIE always higher than +40%; other lesions had T1 SIE always lower than +30%.

Conclusion: In our cases, after Resovist administration, we observed statistically significant differences in T2 SIE percentage of benign/malignant lesions without any overlap.

B-746 15:03

Hepatocellular carcinoma: Comparison of a macromolecular contrast agent vs gadobutrol and gadobenate dimeglumine in an experimental animal MR imaging study

S. Schindera¹, D. Semela¹, C. Redaelli¹, J. Fröhlich², P. Vock¹, C. Stoupis¹; ¹Berne/CH, ²Zürich/CH

Purpose: To compare MR imaging enhancement characteristics of a macromolecular blood-pool agent (Vistarem™) with those of gadobutrol and gadobenate dimeglumine for HCC detection.

Methods and Materials: 17 American Cancer Institute rats were implanted with HCC (1 mm³), using a subcutaneously grown Morris hepatoma cell line. Axial non-enhanced VIBE 3D T2 and T1 (contiguous slices: 1 mm) and dynamic contrast enhanced axial images were acquired on a 1.5 T system. Jugular vein injection of gadomelitol (Vistarem™, Guerbet, France) was performed in 11 animals, of gadobutrol (Gadovist®, Schering, Germany) in 3 animals and of gadobenate dimeglumine (MultiHance®, Bracco Imaging, Italy) in 3 animals. Signal intensity time curves and the contrast to noise ratio (CNR) were assessed for the centre and the rim zone of the tumor and normal parenchyma. MR findings were prospectively compared with histopathology.

Results: In all cases, compared to non-enhanced scans, a better tumor delineation after Vistarem™ administration was observed. Compared with gadobenate dimeglumine and gadobutrol, Vistarem™ showed a significantly higher ($p < 0.05$) and substantial stable CNR between parenchyma and HCC for all time points. Histology demonstrated reduced vascular structures within the tumor compared to the parenchyma, explaining the behaviour of Vistarem™. The long standing, constantly stable tumor-liver contrast of Vistarem™, compared to the extracellular

agents, demonstrates the little intratumoral vessel permeability of this agent through imaging time.

Conclusion: MR blood-pool agent Vistarem™ demonstrates an improved HCC delineation compared to extracellular agents, which suggests its potential for tumor characterization, targeting the differences in liver-lesion vascularization and permeability.

B-747 15:12

Delayed Gd-BOPTA MR imaging (Gd-BOPTA-MRI) phase: Different timing between normals and hepatopathics

I. Sansoni, A. Laghi, M. Celestre, C. Miglio, M. Di Martino, M. Rengo, L. Coletta, R. Passariello; Rome/IT

Purpose: The aim of our study was to assess the optimal timing of delayed phase of Gd-BOPTA-MRI of liver for patients with normal and impaired hepatic function.

Methods and Materials: Forty-one patients (28 hepatopathics, 13 normals) underwent MR examinations on 1.5 T-scanner using the following acquisition protocol: Basal T2-weighted HASTE sequence and T1-weighted FLASH sequence acquired before and after i.v. administration of Gd-BOPTA (0.2 mM/kg) at 15 seconds, 55 seconds and 135 seconds. Delayed T1-weighted FLASH hepatobilary phases were acquired at 40, 120 and 180 minutes after i.v. administration of Gd-BOPTA. Signal intensity (SI) measurements of hepatic parenchyma, bile and lesions were recorded for each Gd-BOPTA-enhanced acquisition. From the measured SI, liver and bile signal-to-noise ratio (SNR) and lesion to liver contrast-to-noise ratio (CNR) were calculated, and related behaviour curves were obtained. **Results:** Bile SNR in three delayed phases was progressively increasing in normal patients, whereas it was almost constant in hepatopathic patients, and this difference between the patient groups was statistically significant ($p < 0.05$). Concerning the liver SNR, the two curves have similar morphology, but cirrhotics one has lower values, related to reduced parenchyma functionality. Finally, in normal patients, the more delayed is the phase, the higher is the lesion/liver CNR value, while in hepatopathics, delayed phases don't allow significant increasing of lesion/parenchyma CNR, which moreover remains stable at three delayed phases.

Conclusion: Biliary excretion and delayed hepatic enhancement are decreased in cirrhotic patients. In hepatopathics, lesion/liver CNR is stable at three different delayed phases and is not statistically significantly different compared with the CNR of the equilibrium phase.

B-748 15:21

Imaging characteristics of hepatocellular carcinoma using the hepatobilary contrast agent Gd-EOB-DTPA

G. Jung¹, J. Breuer², U. Mödder¹; ¹Düsseldorf/DE, ²Berlin/DE

Purpose: To evaluate the ability of contrast-enhanced magnetic resonance imaging with Gd-EOB-DTPA in comparison with non-enhanced imaging and spiral computed tomography to provide additional information for classification and characterization of hepatocellular carcinoma.

Methods and Materials: 40 patients with histopathology proven hepatocellular carcinoma were selected for this subgroup analysis from a phase-III multicenter study in 235 patients with known or suspected liver lesions. The primary analysis was the comparison of the proportion of hepatocellular carcinoma correctly classified and characterized by combined pre-/post-contrast magnetic resonance imaging compared with pre-contrast magnetic resonance imaging alone or with spiral computed tomography. All images were evaluated on-site, and in a blinded reading by three independent readers off-site.

Results: In the on-site evaluation, the lesions were correctly classified as a malignant tumor with combined magnetic resonance imaging in 90.3%, with pre-contrast imaging alone in 82.9% and with spiral computed tomography in 87.8%. The proportion of correct characterization (lesion type diagnosis) with combined magnetic resonance imaging was 85.4%, 75.6% for pre-contrast imaging, and 77.5% for spiral computed tomography (n.s.), respectively.

In the blinded reading, one reader showed a significant increase in the proportion of correctly characterized lesions by 27% ($p < 0.05$). The other two readers showed a reduction in the proportion of correct characterization by 12% and 15%, respectively (n.s.).

Conclusion: Although the results of the blinded reading are equivocal, within a clinical setting Gd-EOB-DTPA seems to have a potential to improve the classification and characterization of hepatocellular carcinoma.

Scientific Sessions

14:00 - 15:30

Room K

Pediatric

SS 1512

Novel imaging approaches

Moderators:

H. Ringertz; Stanford, CA/US
G. Staatz; Aachen/DE

B-749 14:00

Visualization of the coronary arteries in children: A comparison between 2 MR sequences

N.D. Abolmaali¹, A. Esmaeili¹, M. Schmitt², R. Hofstetter¹, T.J. Vogl¹;
¹Frankfurt a. Main/DE, ²Erlangen/DE

Purpose: To compare conventional 2d T1-w SE sequences (T1SE) with 3d T2*-prepared true-FISP sequences (3dTfi) for the visualization of the main coronary arteries in children.

Methods and Materials: 8 children (1.5 to 10 years) with different cardiac diseases were examined in a 1.5 T system (Sonata). In addition to their routine imaging protocol they received either T1SE or 3dTfi for the visualization of the course of the main coronary arteries (CA). In three children, coronary anomalies were already suspected.

Results: As long as the sedation worked well, both sequence types produced adequate results. The proximal course of the main coronary arteries was visible with both techniques. Due to the small amount of epicardial fat in children, the CA were visualized more clearly and for a longer distance using the 3dTfi. Because of the higher spatial resolution, the CA were visible up to a length of 6.5 cm using 3dTfi. The following anomalies were visualized: Kawasaki disease, coronary course variants, and post-operative injury. The use of a minute amount of intravenous contrast material (Gd-DTPA) will increase the imaging quality of 3dTfi. **Conclusion:** For the visualization of the coronary arteries in children, 3dTfi offers higher quality than T1SE. Better and longer visualization is possible as compared with T1SE. The major prerequisite for both techniques is adequate sedation.

B-750 14:09

Contrast-enhanced low-dose 16-multislice CT (MSCT) in children with tracheal stenosis due to vascular compression: Initial results

D. Honnepf, J.E. Wildberger, A.H. Mahnken, M. Das, H. Schnöring,
J. Vázquez-Jiménez, R.W. Günther, G. Staatz; Aachen/DE

Purpose: To evaluate contrast-enhanced low-dose 16-MSCT in children for suspected vascular induced tracheal stenosis.

Methods and Materials: 8 children (1 newborn, 6 infants and 1 preschool child (13 days to 3 years, mean 0.8 years; 1.2 kg to 13.5 kg body weight; 6 male) with bronchoscopically suspected vascular tracheal stenosis were examined by contrast enhanced 16- MSCT (SOMATOM Sensation 16, Forchheim, Germany). Examination parameters were used as follows: beam collimation 16x1.5 mm resp. 0.75 mm, 120 kV resp. 80 kV, 18-50 effective mAs, tube rotation time 0.5 sec, i.v. contrast media application according to body weight (1.5 ml/kg body weight). In addition to conventional axial slices MPRs, VRTs and virtual bronchoscopy were additionally calculated.

Results: Dose adapted 16-MSCT revealed in all cases the cause of the bronchoscopically suspected vascular tracheal stenosis: double aortic arch (1), left main bronchus wedged between pulmonary artery stem and ascending aorta (1), compression due to brachiocephalic trunk (5), lusorian artery (1). In 3 patients further thoracic anomalies, such as tracheobronchial (2), vascular (1) and vertebral (1) anomalies were found. In 5 patients subsequent vascular surgery was performed due to the findings of the CT-examination.

Conclusion: Our preliminary data suggests that contrast enhanced low-dose 16-MSCT is favourable for the detection of vascular induced tracheal stenosis in newborns and infants.

B-751 14:18

Comparison of true FISP, HASTE, SSTSE and postcontrast T1w sequences in pediatric MR urography

M. Raissaki, N. Papanikolaou, V. Hatzimanoli, E. Drakonaki, M. Bitsori,
N. Gourtsoyiannis; Iraklion/GR

Purpose: To compare true FISP, HASTE and SSTSE sequences in delineating anatomical structures and identifying morphological abnormalities during MR

urography in neonates and children. To assess any additional diagnostic value on post contrast T1w sequences.

Methods and Materials: 19 consecutive patients, aged 4 days-9 years (mean 26.4 months) underwent MR urography in a 1.5 T unit. Coronal and/or axial true-FISP, HASTE sequences and projectional SSTSE images were acquired following intravenous administration of furosemide and were separately evaluated by 3 readers deciding by consensus. Depiction of morphology was assessed using a 5-point grading scale. The level of confidence for the presence and characterization of an abnormality was evaluated with a 3-point scale for each of the above sequences and for the turbo-FLASH sequence 0, 5, 15 minutes following intravenous contrast administration. Statistical analysis was performed using the Wilcoxon rank test.

Results: Renal parenchymal abnormalities were found in 7 renal units, ectopies and/or rotating anomalies in 5, agenesis in 3, duplicated systems in 5, dilatation in 17, and ureterocele in 1 unit. Visualization of the ureter was better with SSTSE compared to cross-sectional sequences, not reaching statistical significance. For pelvicalyceal systems and bladder, all T2-weighted sequences performed equally. Delayed post-contrast scans provided significantly higher ($p < 0.01$) diagnostic value compared to HASTE and true FISP sequences.

Conclusion: In pediatric MR urography, SSTSE sequences in combination with either HASTE or true FISP sequences provide excellent anatomical delineation of urinary tract collecting systems including the renal parenchyma. Delayed post-contrast T1w sequences may provide additional diagnostic information.

B-752 14:27

Contrast-enhanced MR cholangiography using mangafodipir trisodium for evaluation of neonatal jaundice

H.-K. Ryeom, B.-H. Choe, J.-Y. Kim; Taegu/KR

Purpose: To determine the feasibility and accuracy of contrast-enhanced magnetic resonance cholangiography (CEMRC) with Mangafodipir trisodium (Mn-DPDP) to exclude biliary atresia (BA) as the cause of neonatal jaundice.

Methods and Materials: Thirty-six jaundiced infants with suspected BA were prospectively evaluated using CEMRC and magnetic resonance cholangiopancreatography (MRCP) 1-5 days prior to ^{99m}Tc-DISIDA radionuclide scans. For the CEMRC, sequential magnetic resonance (MR) images were obtained one, two, and three hours after the administration of intravenous Mn-DPDP with a T1-weighted spoiled gradient-echo sequence. The possibility of biliary atresia was excluded if bowel excretion of the contrast material was noted in the CEMRC. The diagnostic specificity and accuracy of CEMRC was compared with those of conventional MR cholangiography, a ^{99m}Tc-diisopropyliminodiacetic acid (DISIDA) scan, and ultrasonographic triangular cord sign.

Results: The CEMRC was used to accurately distinguish biliary atresia ($n = 6$) from other cholestatic liver diseases ($n = 30$) without any false-positive results. Meanwhile, the conventional MR cholangiography, ^{99m}Tc-DISIDA scans, and ultrasonographic triangular cord sign showed 47% (14/30), 39% (11/28), and 7% (2/30) false-positive results in non-biliary atresia patients, respectively.

Conclusion: Accordingly, the current results suggest that CEMRC using Mn-DPDP is feasible and more accurate than MRCP, ^{99m}Tc-DISIDA scans, or ultrasonography for the exclusion of BA. As such, CEMRC using Mn-DPDP would appear to be a promising modality in the early exclusion of BA as the cause of neonatal cholestasis.

B-753 14:36

Diagnostic imaging in children with Crohn's disease: MR imaging with true-FISP as a new gold-standard?

C. Hohl, P. Haage, G.A. Krombach, T. Schmidt, M. Ahaus, R.W. Günther,
G. Staatz; Aachen/DE

Purpose: To evaluate the impact of MR imaging with true-FISP sequences in the evaluation of inflammatory bowel wall changes in children with Crohn's disease.

Materials and Methods: 24 children aged between 7 and 21 years with suspected or known IBD underwent MR imaging on a 1.5 T scanner. 1 hour after 1 l-mannitol solution was given orally, MR imaging was performed using coronal HASTE-M2D, coronal fat-suppressed T2-TSE, axial dynamic T1-weighted GE sequences before and after i.v.-contrast (Gd-DTPA) and true-FISP sequences before and after i.v.-contrast in coronal and axial planes. MR images were correlated with endoscopy and clinical findings. In 14 patients a recently performed conventional X-ray enteroclysis was available. The MR imaging sequences were evaluated by three experienced radiologists regarding sensitivity and specificity in the detection of inflammatory bowel wall changes. In addition the image quality was assessed regarding the different tissue contrasts and susceptibility to artifacts. Finally, patients' acceptance for the MR imaging examination was recorded.

Scientific Sessions

Results: With a sensitivity in the detection of inflammatory small-bowel changes of 93.3% and 100% the true-FISP outnumbers the other performed sequences (T1 = 80%, HASTE = 13.3% and T2-TSE = 53.3%). The true-FISP sequences revealed a significant superiority regarding soft-tissue differentiation in comparison to all other performed MR sequences. The distension of the bowel wall was good in all children. The patients acceptance of the MR imaging-examination was eminent.

Conclusion: Small-bowel MR imaging examination is appropriate for children and with use of true-FISP sequences it is a convincing method with an outstanding sensitivity in the diagnosis of IBD. MR imaging ought to replace conventional enteroclysis as a gold standard for IBD diagnosis in children.

B-754 14:45

Apparent diffusion coefficients of paediatric mass lesion with free-breathing diffusion-weighted MR imaging

O.E. Olsen, N.J. Sebire; London/UK

Purpose: To assess the distribution of apparent diffusion coefficients (ADC) within high and low cellularity mass lesions in the paediatric chest, abdomen and pelvis.

Methods and Materials: Thirteen children were scanned with a standard diffusion weighted MR sequence ($b = 0$ and 1000 s/mm^2). ADC maps were calculated. Subsequent histological specimens were categorised as high, intermediate or low cellularity. Lesion pixel values from the central three slices of the ADC maps were analysed and compared to histopathology.

Results: Median ADC for high cellularity lesions was 0.83 (25/75 centiles = 0.74/0.85) and low cellularity lesions 2.01 (25/75 centiles = 1.43/2.45) $\times 10^{-3} \text{ mm}^2/\text{s}$ (Kruskal-Wallis test, Chi-Square = 9.519; $p = 0.023$).

Conclusion: ADC mapping is feasible in imaging of paediatric mass lesions in the chest, abdomen and pelvis with standard clinical equipment. The distribution of ADC values within a mass lesion may be determined by its cellularity.

B-755 14:54

Functional MR imaging (BOLD) at 3 Tesla in the brain of fetal sheep: The relation to maternal blood oxygenation during hypoxia and methodological aspects

U. Wedegärtner, M. Tchirikov, S. Schäfer, A. Priest, H. Schröder, G. Adam; Hamburg/DE

Purpose: To quantify the dependence of the fetal brain BOLD signal on maternal blood oxygenation (MatSO₂) and to investigate the influence of position of Regions Of Interest (ROI).

Material and Methods: The brains of singleton fetuses of five anaesthetized (isoflurane/O₂/N₂O) sheep were subjected to rapid sequences (single-shot EPI) of BOLD measurements (3 T MR scanner). MatSO₂ and maternal heart rate were recorded continuously. After a normoxic phase, hypoxia was induced by reduction of oxygen in the ventilated gas mixture. ROI were placed in the cerebrum and in the cerebellum. BOLD SI% were calculated from mean values of steady state BOLD signal intensities (SI) of control and hypoxic plateaus: BOLD SI% = S_{hypoxia}/S_{control} × 100. BOLD SI% were correlated with MatSO₂, and linear regression analysis (slope) was performed. Additionally, ROI were varied slice level and position within the slice. Differences in BOLD SI% for ROI placements were calculated.

Results: Control MatSO₂ was 89%O₂ (80-96) [mean (95%CI)]. During hypoxia MatSO₂ was reduced to 62%(50-75) and fetal BOLD SI% decreased to 64% (44-85) in the cerebrum and significantly stronger to 56%(32-80) in the cerebellum. Correlation and regression ($p < 0.001$) between BOLD SI% and MatSO₂ were: cerebrum: $r^2 = 0.84$; slope = 1.27 SI%/MatSO₂ (1.17-1.36); cerebellum: $r^2 = 0.83$; slope = 1.54 (1.44-1.63). BOLD SI% was 4% less in the slice above. Variations of BOLD SI% for different ROI positions were in the range of 0-12%.

Conclusions: The depletion of oxygen supply is reflected by distinct decreases of fetal brain BOLD signal intensities which are faster in the cerebellum than in the hemispheres. BOLD SI% is influenced only slightly by ROI position.

B-756 15:03

Magnetic resonance imaging (MRI) of the perinatal thyroid gland

P.C. Brugger, D. Prayer; Vienna/AT

Purpose: As little information is available on the MRI signal characteristics of the normal perinatal thyroid gland (TG), we studied its signal characteristics in a series of fetuses, preterm neonates, term neonates and infants.

Methods and Materials: The series comprised 130 MRIs of fetuses imaged in utero (19th-38th gestational weeks), 100 term neonates and infants until the 5th month of postnatal life, and 25 preterm infants born between 24-33 weeks of

gestation which were imaged 8-200 days after delivery. Protocols included T2- and various T1-weighted sequences in frontal or sagittal planes. Signal intensity of the thyroid was measured.

Results: On T2-weighted images the TG was detectable only by its topographical relationships. In contrast, the fetal TG displayed T1-weighted hyperintensity from the 20th gestational week onwards which was also characteristic to term neonates. This hyperintensity then gradually disappeared to become isointense to muscle by the 3rd postnatal month (as in adults). In preterm neonates these signal changes took a similar temporal course, so no pronounced hyperintensity as was present at term. The relative and absolute signal intensities of the TG took the same course as the anterior pituitary.

Conclusion: T1-weighted hyperintensity of the TG is a normal finding in fetuses and neonates that disappears after birth following a temporary course, which parallels the decrease in signal intensity of the anterior pituitary gland. This is independent of gestational age at birth and may reflect changes associated with the maturation of the pituitary-thyroid axis in the postnatal period.

B-757 15:12

A new look at the fetus: Thick-slab T2-weighted sequences in fetal MR imaging

P.C. Brugger, C. Mittermayer, D. Prayer; Vienna/AT

Purpose: While magnetic resonance imaging (MRI) of the fetus may be considered as an established adjunct to fetal ultrasound, an overall impression of the fetus is hardly provided by stacks of slices alone. The present study evaluates the use of thick-slab T2-weighted images to obtain a three dimensional impression of the fetus using MRI.

Methods and Materials: A thick-slab T2-weighted sequence (TR: 8000/TE: 800-400) was added to the routine protocol in 100 fetal MRIs made for different clinical indications (19th-37th gestational weeks) on a 1.5 T magnet using a five-element phased-array surface coil. Slice thickness adapted to fetal size and uterine geometry varied between 25 and 50 mm, as did the field of view (250-350 mm). Acquisition of one image took less than one second.

Results: Thick-slab T2-weighted images visualize fetal anatomy in a more comprehensive way than is possible with a series of 3-4 mm thick slices. They facilitate the assessment of the whole fetus, surface structures, extremities and fetal proportions. Fetal pathology may be captured in one image. Lower TEs enhance the transparency of the skin and allow recognition of normal fluid-filled organs and pathologies associated with fluid accumulations.

Conclusion: Thick-slab T2-weighted imaging provides additional information that is difficult to gain from a series of images. It is a valuable adjunct to conventional 2D imaging and an alternative to three dimensional reconstructions. Moreover it facilitates communication with those not familiar with cross-sectional anatomy.

B-758 15:21

The use of magnetic resonance imaging in the evaluation of vascularization of porous ocular implants

A. Álvarez Luque, A. Royo, T. Berrocal, M. Fernández-Velilla, A. Fernández-Zubillaga, J. Abelairas; Madrid/ES

Purpose: To assess the utility of MR imaging in detecting fibrovascular tissue growth within porous implants used in orbital reconstruction following evisceration or enucleation.

Methods and Material: 39 children who had received a porous orbital implant (29 a hydroxyapatite, 10 a high-density polyethylene implant) were prospectively evaluated with MR imaging. T1-weighted sequences with fat saturation were acquired before and after Gd administration, and 3-mm thickness axial and sagittal reformations were obtained. MR imaging was evaluated for the degree of Gd-uptake by the implant (quantified as 0, 1/4, 1/4-2/4, 2/4, 2/4-3/4, 3/4, 4/4 enhancement); type of enhancement (homogeneous or heterogeneous); area of initial enhancement (anterior or posterior); extraimplant Gd-uptake indicating infection; and presence of lines in the prosthesis suggesting fissures. MR imaging findings were compared with the state of the implant during the surgical act of peg placement.

Results: The Gd-uptake was zero in three prosthesis, 1/4 in three, 1/4-2/4 in two, 2/4 in three, 2/4-3/4 in four, 3/4 in 12, and 4/4 in 12. The enhancement started in the posterior region in 22 cases (81.4%), was homogeneous in 21 (77.7%) and extraimplant enhancement occurred in 4 (18%). Lines suggesting fissures were observed in 4 prosthesis (14.8%), confirmed at surgery. The Gd enhancement on MR imaging and the surgically proven vascularization was similar in 34 implants (85%). MR was inconclusive in one case (3%). There was no correspondence between the MR findings and those of surgery in 5 cases (12%).

Conclusion: MR imaging is a reliable technique in detecting fibrovascular tissue growth within porous ocular implants.

Scientific Sessions

14:00 - 15:30

Room L/M

Neuro

SS 1511

Cerebrovascular disease: Endovascular treatment and non-invasive follow-up

Moderators:

A. Felber; Innsbruck/AT

A. Gholkar; Newcastle-upon-Tyne/UK

B-759 14:00

Endovascular treatment of brain AVMs using Onyx: Preliminary results of a prospective, multicenter study

C. Cognard¹, A. Januel¹, D. Herbreteau², X. Barreau³, J. Drouineau⁴, L. Pierot⁵; ¹Toulouse/FR, ²Tours/FR, ³Bordeaux/FR, ⁴Poitier/FR, ⁵Reims/FR

Purpose: To evaluate the safety and the efficacy of Onyx in the endovascular treatment of brain arteriovenous malformations (AVMs).

Methods and Materials: From May 2003 to July 2004, 38 patients (21 females/17 males; age: 16 to 64 years; mean: 30 years) harboring brain AVMs were treated using Onyx. Clinical presentation was intracranial hemorrhage in 19 cases, epilepsy in 10 cases, headaches in 5 cases, progressive neurological deficit in 1 case and other in 3 cases. AVMs were located in the cerebral hemispheres (33 cases), in the corpus callosum (3 cases), in the basal ganglia (1 case) and in the cerebellum (1 case).

Results: A total of 80 sessions of embolization was performed (1 to 8 sessions/patient; mean: 2.11). The technical way of using Onyx is described (selective catheterization, injection of Onyx and withdrawing of the microcatheter). The duration of injection was between 5 to 68 mn (mean: 35 mn) and the volume injected by session was between 0.3 and 5.5 ml (mean: 1.5 ml). Technical problems and clinical complications are reported. The final degree of occlusion and the complementary treatment, if needed, are described.

Conclusion: The preliminary results of this prospective, multicenter study demonstrate the great efficacy of Onyx in the treatment of brain AVMs. The technical way of using Onyx should be very precise to avoid some complications.

B-760 14:09

Endovascular treatment (EVT) in first intention in the management of ruptured intracranial aneurysm: Prospective consecutive series

C. Cognard, M. Mejdoubi, A. Januel, P. Tall, J. Albucher, F. Chollet, M. Gigaud, M. Tremoulet; Toulouse/FR

Purpose: Since January 1998 the neurovascular multidisciplinary team has decided to use embolisation as the first intention treatment of ruptured aneurysms. Our goal is to review the results of this therapeutic strategy.

Materials and Methods: From January 1998 to December 2002 (5 years), 401 patients were admitted with a subarachnoid hemorrhage (SAH). Seventy three patients had a sine materia hemorrhage (18%). Among the 328 patients with aneurysmal SAH, 28 were unexplored (8.5%), 28 untreated (8.5%), 272 had their ruptured aneurysm treated (83%). Embolization was performed in 222 of the 272 cases (82%) and surgery in 50 cases (18%). The reason why surgery was performed was: failure of EVT in 8 cases (2.9%), intracranial hematoma in 16 cases (5.7%), aneurysm morphology unsuitable for EVT in 15 cases (5.4%), absence of the interventional neuroradiologist in 11 cases (4%). EVT was successful in 96.8% of attempted procedures (243/251). Remodeling technique was used in 11.4% for broad based aneurysms. Clinical evolution was without any clinical complication in 69% of the cases. Thirty-two patients out of 222 (14%) died, 8 of them due to treatment complications (3.6%).

Conclusion: This series shows that embolization as a primary treatment in aneurysmal SAH is justified and can be performed routinely. Nevertheless, increasing the number of specialized neuro-interventionists and dedicated angiogram equipment is required. Patient and case selection must be discussed by a well-trained multidisciplinary neurovascular team. Creating hemorrhagic stroke centre recommendations is mandatory to promote global management of patients with intracranial bleeding.

B-761 14:18

Double microcatheter technique for endovascular coil embolization of large, wide-necked intracranial aneurysms

H.-J. Choo, T. Lee, H. Jeong, H. Choi, H. Kim, T. Moon, C. Choi, S. Lee; Pusan/KR

Purpose: To assess the feasibility, safety, and effectiveness of the double microcatheter technique in endovascular coil embolization of large, wide-necked intracranial aneurysms.

Methods and Materials: Between September 2002 and June 2004, 55 patients with 60 intracranial aneurysms were treated with endovascular coil embolization. The initial attempts at embolization failed in ten cases because evidence of coil instability within the aneurysm or significant impingement of coil loops on the parent artery were observed. Among these 10 cases, three were located in the anterior communicating artery, three in the middle cerebral artery bifurcation, two in basilar tip, one in the posterior communicating artery, and one in the superior hypophyseal artery. The 10 cases were treated with double microcatheter technique. Advancement of a second microcatheter into the aneurysm allowed two coils to be braced across the aneurysmal neck before the detachment of either coil. We retrospectively analyzed the feasibility and effectiveness of the technique.

Results: The double microcatheter technique permitted successful coil embolization in all 10 cases. The angiographic results were 6 complete, 2 small neck remnant, and 2 incomplete occlusion. There were no technique-related complications.

Conclusion: The double microcatheter technique might be feasible, safe, and effective when there is evidence of coil instability or parent vessel compromise during embolization of large, wide-necked aneurysms. The increased technical demands and potential for complications necessitate that clear indications be present before this adjunctive technique is considered.

B-762 14:27

Urgent recanalization using stents for acute internal carotid artery occlusion in progressive stroke syndromes with contralateral internal carotid stenosis or occlusion

H.-J. Choo, T. Lee, H. Jeong, H. Choi, K. Park, S. Sung, H. Kim, S. Lee; Pusan/KR

Purpose: To assess the feasibility, safety, and effectiveness of urgent recanalization using stents for acute internal carotid artery occlusion in the progressive stroke syndromes with chronic contralateral carotid stenosis or occlusion.

Methods and Materials: Between January 2004 and June 2004, urgent recanalization using stents for acute ICA occlusion was performed in 5 progressive stroke patients. Three patients had chronic occlusion and two patients had severe stenosis of the contralateral ICA. There were 3 men and 2 women with a mean age of 51.4 years. A 0.014-in microwire was placed into the distal ICA or middle cerebral artery, crossing the occluded segment. The stent was then advanced over the microwire and deployed in the lesion. We retrospectively analyzed the feasibility and effectiveness of the urgent recanalization using stents for acute ICA occlusion in the progressive stroke patients with chronic contralateral ICA stenosis or occlusion.

Results: We successfully completed recanalization using stents in all patients. All patients showed rapid improvement of neurological signs and favorable clinical outcomes. There were no procedure-related complications; patients were neurologically stable on clinical follow-up (mean 2 months, range 1-6 months). Angiographic follow-up after 3 months revealed no in-stent restenosis in 3 patients.

Conclusion: Urgent recanalization using stents for acute internal carotid occlusion may salvage the vessel and promise better clinical outcome in progressive stroke patients with contralateral chronic ICA stenosis or occlusion. Further studies are necessary to define the correct management of this catastrophic event.

B-763 14:36

MR angiography vs. digital subtraction angiography in the follow-up of clipped and coiled intracranial aneurysms

A. Hochmuth, U. Hubbe, S. Ziyeh, V. Vougioukas, A. Berlis; Freiburg/DE

Purpose: To evaluate the reliability of Time-of-Flight-MRA in comparison to digital subtraction angiography in the follow-up of endovascular and surgically treated ruptured intracranial aneurysms.

Methods and Materials: Between May 1998 and October 2003, in 62 patients with 73 treated aneurysms 96 MRA and 76 DSA examinations were performed to assess the occlusion rate and/or recurrence of coiled or clipped aneurysms. DSA and MRA were performed within one week.

Scientific Sessions

Results: 51/73 aneurysms were coiled (two of them later clipped and excluded from evaluation), 4 of them showed artifacts in MRA which hindered interpretation. 45/49 (91.8%) were well or sufficiently assessable. Residual flow was found or presumed in 20 and confirmed by DSA in 17 cases. Seven were partially thrombosed, which affected evaluation in 2. Sensitivity and specificity in detecting residual flow or persistent aneurysm neck were 90% and 93.5%, respectively. Of the 24 clipped aneurysms, only 2 were evaluable, 22 showed severe artifacts.

Conclusion: MRA is a valuable tool in the evaluation of coiled aneurysms, especially in rating residual flow or flow due to coil compaction. Problems may arise in partially thrombosed aneurysms due to hyperintense thrombus. Neurosurgical clips produce such intense artifacts, that MRA seems to be meaningless in the follow-up of clipped aneurysms.

B-764 14:45

Follow-up of coiled cerebral aneurysms: Comparison of 3D-TOF MRA at 3 T with 3D-TOF and contrast-enhanced MRA at 1.5 T

N. Anzalone, C. Righi, L.S. Politi, A. Iadanza, M. Cadioli, G. Scotti; Milan/IT

Purpose: To compare 3D-TOF-MRA of coiled aneurysms at 3 T with 3D-TOF-MRA and ultrafast contrast-enhanced MRA (CE-MRA) at 1.5 T.

Methods and Materials: Twenty-three patients treated with detachable coils for cerebral aneurysms underwent examinations at 3 T and 1.5 T separated by 24 hours. 3D-TOF-MRA at 3 T was performed with a head T/R coil and an axial acquisition (TR/TE = 23/3.2). At 1.5 T, a sensitivity encoding head coil was used; a 3D-TOF axial acquisition was performed first (SENSE factor 2, TR/TE = 23/3.6), followed by an axial 3D ultrafast (21 sec) gradient echo sequence (SENSE factor 2, TR/TE = 6.1/2.1) enhanced with 0.1 mmol/kg Gd-BOPA (MultiHance). Source images as well as MIP and SSD reconstructions targeted on the vessel of interest were evaluated.

Results: Twenty-four aneurysms were evaluated. The presence of coil artefact was equally evident on 3D-TOF at 3 T and 1.5 T but was not apparent on CE-MRA. The parent artery was identifiable in 22 cases after 3D-TOF-MRA at 3 T and CE-MRA at 1.5 T but in only 20 cases after 3D-TOF-MRA at 1.5 T. Patency of the residual aneurysm was demonstrated in 9 cases after 3D-TOF-MRA at 1.5 T, but in 12 cases after 3D-TOF-MRA at 3 T and CE-MRA at 1.5 T; in each case CE-MRA permitted superior demonstration of residual patency. Comparison of the 3D-TOF acquisitions revealed higher signal and a sharper definition of the parent vessel and residual patency at 3 T.

Conclusion: MRA follow-up of coiled aneurysms is feasible at 3 T and is better than at 1.5 T; nevertheless greater definition of residual patency is achieved with ultrafast CE-MRA at 1.5 T.

B-765 14:54

Multislice CT angiography (MSCTA): A comparison with digital subtraction angiography (DSA) in the postoperative evaluation of clipped aneurysms

S. Binaghi, M. Colleoni, A. Dehdashti, L. Regli, A. Uské; Lausanne/CH

Purpose: To evaluate the accuracy of MSCTA in the postoperative workup of clipped intracranial aneurysms compared to DSA.

Methods: Forty-two patients harbouring 52 aneurysms (34 ruptured, 18 unruptured) who underwent surgical clipping were included in this study. Postoperative MSCTA and DSA were simultaneously performed for each patient. Two independent neuroradiologists reviewed every DSA and MSCTA. The criteria that were applied were the occlusion of the aneurysmal dome, the presence of a residual neck, and the lack of stenosis on the parent vessels near the clip. The mean duration of MSCTA and DSA was respectively 15 and 45 minutes.

Results: The quality of MSCTA was good in 83% of cases, moderate in 9% and poor in 7%. MSCTA results were unclear in 7 patients (13%) due to clip-related artefacts in 5 patients, and to failed contrast injection in 2 patients. MSCTA showed complete exclusion of all treated aneurysms, whereas DSA revealed a residual neck in 2 aneurysms. Retrospectively, MSCTA identified these residual necks. The sensitivity of MSCTA was therefore 96% and the specificity was 100%.

Conclusion: MSCTA is a valuable and non-invasive method for postoperative control of clipped aneurysms. However, DSA should be performed when MSCTA results are doubtful or in presence of abnormalities which need further endovascular treatment.

B-766 15:03

Silent cerebral ischemic lesions revealed with diffusion weighted MR imaging (DWI) in patients submitted to thromboendarterectomy (CEA), protected and unprotected carotid artery stenting (CAS)

M.C. Michelassi, M. Cosottini, M. Puglioli, I. Trivelli, S. De Cori, G. Parenti, C. Bartolozzi; Pisa/IT

Purpose: Carotid endarterectomy (CEA) is a proven standard treatment of high-grade carotid artery (CA) stenosis. Carotid artery stenting (CAS) has gradually been established as an alternative method to CEA. Diffusion-weighted MR imaging (DWI) demonstrates new cerebral lesions during revascularization that is supposed to indicate the occurrence of cerebral microemboli. The purpose is to assess the prevalence of cerebral ischemic insults detectable with DWI during CEA and CAS and the role of cerebral protection during CAS as a method of reducing the number of cerebral ischemic events.

Materials and Method: We prospectively evaluated 76 unselected patients with high grade internal CA stenosis that underwent CEA (group I) and CAS (52 patients) with cerebral protection device in 30 patients (group II) and without in 22 (group III). All patients underwent to MR examination before and within 7 days after the procedure to assess the number of silent ischemic lesions.

Results: The incidence of new ischemic lesions in patients treated with CEA or CAS was 8% and 30% respectively. The total number of lesions and the lesions ipsilateral to the treated vessel were significantly higher in patients of group III compared to group II ($p = 0.02$ and 0.01). The number of lesions contralateral to the treated vessel was not different in the two groups.

Conclusion: Silent ischemic lesions are more frequent in patients treated with CAS than with CEA. The protection device during CAS seems to reduce the number of microembolic events. Contralateral lesions probably source from the procedural manoeuvres in the aortic arch.

B-767 15:12

MR imaging of brain embolism in patients with carotid stenosis before and after percutaneous angioplasty with distal protection

A. Koren; Ljubljana/SI

Purpose: To estimate the size, localization and incidence of brain embolism with MR imaging (MR) in 31 patients with hemodynamically important carotid stenoses discovered by ultrasound who were candidates for percutaneous transluminal carotid angioplasty with stenting and distal protection (PTAF).

Methods: The study was prospective and nonrandomized. We analyzed MR lesions in time windows of 24 hours before and after PTAF and describe correlations with clinical data and ultrasound properties of stenosis and plaques.

Results: 77.5% of lesions were smaller than 1 cm before PTAF. The number of lesions greater than 1 cm was statistically different between groups of asymptomatic and symptomatic patients for both hemispheres (R: $p < 0.05$, L: $p < 0.01$). We discovered new lesions after PTAF in 9.7% of all patients: 75% of lesions were smaller than 1 cm and in a site related to the treated carotid. No patients with embolism had new neurological symptoms after the procedure; most of them had lipid plaques and neurological deficit before PTAF.

Conclusions: Most patients with brain embolism had lipid plaques. We didn't discover any correlation between severity of stenosis or plaque type and morphology and site of brain lesions before PTAF. The majority of patients with new lesions after PTAF had stenoses greater than 90% and neurological symptoms before the procedure.

B-768 15:21

Changes in cerebral blood flow before and after carotid endarterectomy: Evaluation by acetazolamide-challenge ^{123}I -IMP SPECT

I. Sakuma, N. Tomura, S. Takahashi, T. Otani, T. Nishii, K. Sasaki, J. Watara; Akita/JP

Purpose: Hyperperfusion syndrome is now recognized as a disastrous complication after carotid endarterectomy (CEA). The present study investigated cerebral blood flow (CBF) changes after CEA.

Materials and Methods: In 16 patients (17 ICAs), CBF and cerebral vasoreactivity (CVR) were assessed before and 7-9 days after CEA using acetazolamide (ACZ)-challenge ^{123}I -IMP single photon emission CT (SPECT). CBF and CVR were measured by placing regions of interest (ROIs) in bilaterally symmetrical regions of the middle cerebral artery territory. Asymmetry index (AI) of CBF was also calculated in 12 patients without severe ICA stenosis on the contralateral side. To estimate presence or absence of hyperperfusion phenomena immediately after surgery, ^{99}mTc -HMPAO SPECT was also performed within 3 days after CEA.

Results: CBF of the ipsilateral hemisphere did not significantly change after CEA.

Scientific Sessions

However, CVR of the ipsilateral hemisphere was increased after CEA ($51.5 \pm 29.7\%$) compared to before CEA ($33.9 \pm 33.8\%$). Although no significant alteration of resting AI was seen, ACZ-challenge AI was significantly higher after surgery ($94.6 \pm 13.2\%$) compared to before CEA ($79.1 \pm 15.3\%$; $P < 0.05$). In 5 ICAs (29.4%), hyperperfusion of the ipsilateral hemisphere was seen on $^{99m}\text{Tc-HMPAO SPECT}$. Of these, severe stenosis of the contralateral ICA was present in 3 patients. Hyperperfusion after CEA was noted in 5 patients, and mean CVR before surgery was significantly lower in these patients ($18.1 \pm 23.9\%$) than in other patients ($40.5 \pm 36.0\%$).

Conclusion: CVR and ACZ-challenge AI improved after CEA. CVR before CEA can predict risk of hyperperfusion after CEA.

14:00 - 15:30 Room N/O

Physics in Radiology

SS 1513

Radiation protection/Image quality

Moderators:

D.J. Hawkes; London/UK

C. Leidecker; Erlangen/DE

B-769 14:00

Multi-centre study to assess patient doses in interventional radiology in Belgium

K. Smans¹, H. Bosmans¹, L. Struelens²; ¹Leuven/BE, ²Mol/BE

Purpose: The Euratom directive 97/43 and the Belgian Royal Decree of July 20, 2001 impose today, the application of the ALARA principle, in particular in rooms for interventional radiology. Within this framework, a multi-centre study is started to assess the patient doses in interventional radiology and to prepare from these data potential future auditing parameters.

Methods and Materials: 20 Centers, spread over Belgium, are participating in this ongoing project. The activities include an extensive interview with the interventionalist regarding the working procedures, the verification of the data in at least 10 (detailed) patient cases, the registry of DAP values during one year and physical/technical tests of the equipment. DAP values were corrected for patient weight and were then used to set National Diagnostic Reference Levels (DRL). The influence of different parameters on the DAP was studied.

Results: First results show that there is a large spread in the DAP-values per procedure. This is partly due to different system-parameters (e.g. dose levels at the image intensifier), but it is mainly due to the way of working. In particular, the number of frames and series taken during digital subtraction differs a lot between the participating centres. Averaged DAP-values of some centres largely exceed the (preliminary) DRL. A series of guidelines for the optimisation of interventional procedures could be derived.

Conclusion: It was possible to select a minimal data set for interventional procedures that allows a directed feedback or interaction/cooperation between interventionalist and medical physicist, and that may be used for future auditing.

B-770 14:09

A six year follow-up of patient dose values: Transition from conventional to digital in projection radiography

E. Vano, J.M. Fernandez, J.I. Ten, C. Prieto, L. Gonzalez, R. Rodriguez; Madrid/ES

Purpose: To report the evolution of patient doses in projection radiography during the last 6 years in a large University Hospital that has moved from film-screen to digital radiology.

Methods and Materials: Entrance surface air kerma for patients were calculated from the radiographic techniques using the measured X-ray tube outputs. After implantation of digital techniques in 1999 (computed radiography -CR- and flat panel -FP-), an automatic system to gather dosimetric data was designed and installed. The system, working in real time, allows to detect relevant changes on patient dose. A database with more than 100,000 patient dose data has enabled computing the evolution during the last 6 years.

Results: Mean values of entrance air kerma (with backscatter) for chest PA and LAT were respectively 0.20 and 0.60 mGy before digital, 0.27 and 1.27 mGy during the transition and 0.11 and 0.64 mGy in 2003 (CR). For FP these values have been: 0.15 and 0.74 mGy in 2003. No statistical significant difference exists between CR and FP. For lumbar spine AP and LAT values have been: 4.4 and 8.6 mGy during the transition and 3.2 and 8.6 mGy in 2003. Mean values for

abdomen images were 2.9 mGy during the transition and 2.2 mGy in 2003. Sample sizes were between 1,000 and 10,000 data.

Conclusion: Patient dose values for projection radiography showed an increase (35 to 110% for chest images) during the implantation of digital techniques and a relevant decrease (roughly by 30%) once the patient audit system was installed.

B-771 14:18

Embryo/fetal doses and risks from fluoroscopically assisted kyphoplasty during pregnancy

N. Theocaropoulos, J. Damilakis, K. Perisinakis, G. Papadokostakis, A. Hadjipavlou, N. Gourtsoyiannis; Iraklion/GR

Purpose: Inadvertent or emergency fluoroscopic exposures of the spine during pregnancy are reasonably suspected for delivering considerable radiation doses to the conceptus. The purpose of the study was to provide normalized data for the determination of conceptus dose specific to gestational stage and treated spinal level and to estimate the conceptus radiation dose and risk associated with typical kyphoplasty treatment.

Methods and Materials: Direct measurement of conceptus doses from simulated fluoroscopic projections involved in surgery at different spinal levels for the three trimesters of gestation with use of anthropomorphic phantoms and thermoluminescent dosimetry. The normalized data were used for the calculation of conceptus radiation dose from typical kyphoplasty procedure. The associated radiogenic risk of fatal cancer during childhood and congenital malformation to the progeny of the unborn child was derived.

Results: Normalized conceptus doses vary by a factor of 4000 with gestational stage, fluoroscopic projection and vertebral level. Conceptus doses from a typical kyphoplasty procedure are smaller than 4 mGy, provided that the conceptus lies outside the primarily irradiated region. The corresponding fatal cancer risk during childhood is from 2 to 160 times lower than the natural incidence rate. When the embryo is primarily irradiated, mean conceptus dose can be as high as 105 mGy from a non-optimized exposure. At least 35 minutes of fluoroscopy are required for the induction of deterministic effects. Optimization of fluoroscopy protocols may reduce conceptus dose by a factor of 40.

Conclusions: Low dose fluoroscopy protocols should be available for treatments in advanced pregnancy.

B-772 14:27

Optically stimulated luminescent (OSL) dosimeters for use in diagnostic and therapeutic radiology

C.A. Perks¹, J.E. Gray², C. Reft³, B. Markey², M. Salasky², J. Leppert⁴, R. Ford², D. Gress⁵, ¹Kidlington/UK, ²Glenwood, IL/US, ³Chicago, IL/US, ⁴Indianapolis, IN/US, ⁵Victor, NY/US

Purpose: To describe the dosimetric properties of OSL materials including energy sensitivity, linearity, angular dependence and ease of use.

Methods and Materials: Aluminum oxide doped with carbon ($\text{Al}_2\text{O}_3:\text{C}$) has been used for personal dosimetry for 10 years. The material is available in patch, dot or strip form, and can be read-out with a relatively inexpensive dosimeter-reader (inert gas is not required). $\text{Al}_2\text{O}_3:\text{C}$ elements were used to make measurements with beam qualities from mammography through megavoltage energies, including photons and electrons. Patches (1.5 cm square) and dots (6 mm diameter) were used to characterize the dosimetric properties of the material. Strips of material (6 mm x 15 cm) were used to measure CT dose and profiles.

Results: $\text{Al}_2\text{O}_3:\text{C}$ provides measurements with a precision of better than 1.5% (1 standard deviation) over the energy range evaluated and is capable of measurements down to 10iGy. It can be read multiple times with signal reductions of approximately 0.2% for each reading. Energy dependence is within 10% for energies from 22 to 120 kVp. CT dose profiles are possible with a 0.1 mm sampling interval. The signal does not fade with time and the material is not affected by environmental conditions, e.g., heat or humidity. The OSL response is similar to that of TLD in terms of dose and dose rate, and the response is independent of energy for 6 to 20 MeV electrons.

Conclusions: $\text{Al}_2\text{O}_3:\text{C}$ in the OSL mode is very promising for many applications in both diagnostic and therapeutic radiation dosimetry.

B-773 14:36

A novel method to manufacture anatomically correct phantoms for projection radiography

W. van der Putten, J. Gallagher, P. Woulfe; Galway/IE

Purpose: Appropriate use of medical radiography requires tools to assess image quality and radiation dose. Anatomically realistic phantoms can be expected to

Scientific Sessions

be useful for this purpose and this study reports on a novel way to obtain such phantoms.

Methods and Materials: The manufacturing process involves 1) the acquisition of a digital image and 2) conversion of the digital pixel matrix into an input file for a Rapid Prototyping machine. This uses previously obtained calibration factors which convert pixel grey scale values into appropriate polymer thickness. The type of polymer is chosen both for its suitability in the Rapid Prototyping process and appropriate radiological thickness. This raw model is then machined to improve its appearance and provide protection.

Results: Phantoms have been manufactured based on clinical X-rays obtained during normal clinical operation. In order to evaluate the range of imaging parameters a chest X-ray was used (acquired with Computed Radiography) and a mammography image obtained from a Full Field Digital System. Testing of the phantoms has been performed through comparison of the original images with those obtained from the phantom based on European Quality Criteria for diagnostic images.

Conclusion: It has been demonstrated that Rapid Prototyping is a convenient manufacturing method to obtain high quality phantoms which produce clinical images at relevant exposure levels. The phantoms are suitable for their intended task as test phantoms. Suggestions for improvement in the RP method are made. Phantoms can be easily manufactured and can include pathology if required.

B-774 14:45

Evaluation of a high-speed high-resolution film/screen system for medical radiography

R.E. Dickerson, P.C. Bunch; Rochester, NY/US

Purpose: This paper discusses the evaluation of a high-speed high-resolution film/screen system that provides improved image quality and opportunities for dose reduction. A description of the technical aspects of this system is given. The film features novel silver-halide microcrystals and is dual coated using a split E-layer coating format that features gradient crossover control. The system can be exposed with existing intensifying screens and provide significant dose reductions without sacrificing image quality.

Methods and Materials: This paper describes details of the system's design and performance. The film includes: 1) a dual layer structure that provides high-speed and high-resolution imaging of chest and orthopedic images, and 2) high-sensitivity silver-halide microcrystals that provide high contrast and high resolution. Modulation transfer function (MTF) measurements were used to describe the resolution of various film/screen combinations and they are compared to existing state-of-the-art film/screen systems.

Results: Inverse-square sensitometry and MTF measurements, as well as phantom and clinical radiographs using this film/screen system, demonstrate several benefits. A significant dose reduction is possible without reducing image quality using standard intensifying screens. In addition, significant image quality improvements are possible in orthopedic imaging using high-resolution extremity-intensifying screens at conventional radiation doses.

Conclusions: We have designed, built and implemented a novel film/screen system for general-purpose radiography that provides high-resolution images with a potential for dose reduction or MTF improvement. Initial clinical evaluation of the system demonstrates a 2X reduction in dose without sacrificing image quality. In addition, significant improvements in resolution are possible at the conventional radiation doses.

B-775 14:54

Improvement of X-ray image quality for medical applications using synchrotron radiation monochromatic X-rays

K. Hyodo, M. Ando, S. Ohtsuka, I. Yamaguchi, T. Takeda; Tsukuba/JP

Purpose: We have been developing two-dimensional imaging systems for intravenous coronary angiography and micro-angiography using synchrotron radiation monochromatic X-rays. To improve the image quality obtained by the systems, new techniques were introduced.

Methods and Materials: The first four patient examinations for intravenous coronary angiography were performed in May 1996 under collaboration between the University of Tsukuba and KEK using two-dimensional Imaging System I at the beamline AR-NE1. After improvement of the imaging system, Imaging System II has been employed for clinical examinations since 2000. Images were obtained at above the K-edge energy of iodine (33.2 keV) using an image intensifier-television (II-TV) system. The system has an advantage in producing dynamic two-dimensional images. To improve the image quality obtained by the system, preliminary experiments on stereo-imaging were performed using vessel phantoms to evaluate the three-dimensional structure of arteries by (1) rotating the object

and (2) using a Laue crystal. To further improve the image quality, image enhancement of the clinical images obtained by the Imaging System II was performed using a digital filter that used the value of mean density and standard deviation in a local area of the image.

Results: The possibilities of the image quality improvement by the stereo-imaging methods and the digital filter were confirmed.

Conclusion: Those improvements, along with the high current and the long lifetime of the electron beam obtained by efforts of the accelerator group, more practical examinations will be possible.

B-776 15:03

Combining deterministic and Monte-Carlo methods in the simulation of X-ray attenuation and scatter

Y. Kyriakou, P. Deak, T. Riedel, L.v. Smekal, W.A. Kalender; Erlangen/DE

Purpose: A new hybrid simulation approach which combines deterministic computation of X-ray attenuation and single-scatter contributions with estimates of multiple scattering via Monte-Carlo (MC) methods.

Methods and Materials: We employed mathematically defined objects in simulations of various scanner geometries. For the primary signal, X-ray attenuation was computed along the direct rays from the focus to each detector element using a prototype software (ImpactSim, VAMP, Möhrendorf, Germany). In addition, by summing single Compton or Rayleigh scattering inside the object over all paths from the focus to all detector elements, we calculated the corresponding single-scatter contribution to the signal. Standard MC simulations were used to validate the deterministic method and to quantify the single and the total scatter signal. The simulations were compared to measurements on a flat panel detector C-arm system (Axiom Artis dFC, Siemens Medical Solutions, Forchheim, Germany).

Results: Results for the calculated single-scatter signal were in agreement to within 1-3% with MC simulations. The structure in the scatter images was mainly determined by the single scatter signal; the total to single scatter difference images therefore show little or no structure and can thus be estimated efficiently by an adapted coarse MC simulation. Simulated and measured findings were in generally good agreement.

Conclusions: The new hybrid simulation method allows to assess scatter contributions at low computational expense as compared to standard MC. Thereby it provides a potential basis for systematic scatter corrections in X-ray tomography.

B-777 15:12

CT image quality performance of a flat-panel detector C-arm system

T. Riedel¹, Y. Kyriakou¹, D. Schäfer¹, T. Brunner², W.A. Kalender¹; ¹Erlangen/DE, ²Forchheim/DE

Purpose: To evaluate the achievable CT image quality of a commercial C-arm system equipped with a flat-panel detector.

Methods and Materials: A commercial Axiom Artis dFC C-arm system (Siemens, Forchheim, Germany) was available for the evaluation. The detector consists of a photodiode array of amorphous silicon (a-Si) providing 960x960 pixels with a pixel size of 184 µm coupled to a 600 µm thick phosphor layer of Thallium-doped cesium iodide (CsI:Tl) for X-ray absorption. The system offers a scan range of 240° of rotation with angular steps from 0.6° to 1.5° corresponding to 400 to 200 projections. For the measurements the source-to-detector distance was varied between 105 and 120 cm, thereby producing a magnification of 1.4 to 1.6. Several phantoms for spatial and low-contrast resolution as well as clinical specimens were measured. Scan times were 15 s and reconstruction was performed with prototype software (VAMP, Möhrendorf, Germany). Deterministic simulations (ImpactSim, VAMP) were applied for validation and tests.

Results: For a focal spot size of 0.4 mm an isotropic spatial resolution better than 200 µm was determined and was also demonstrated visually in specimen measurements. Phantom and specimen measurements indicated that low contrast details of 10 HU and diameters of 10 mm were recognized with air kerma values of about 100 mGy.

Conclusions: The evaluation confirmed the feasibility of CT imaging applications for commercial C-arm systems with flat-panel detectors. The evaluated system provided a high contrast resolution superior to standard CT imaging. Even details with contrasts of 10 HU are detectable but at the expense of high exposure levels.

Scientific Sessions

B-778 15:21

Imaging properties of a new dynamic large flat panel detector for DSA and 3D-rotational angiography (CT-mode)

R.W.R. Loose¹, M. Wucherer¹, B. Geiger², M. Mechtel¹, R. Adamus¹, E. Vano³; ¹Nürnberg/DE, ²Förchheim/DE, ³Madrid/ES

Purpose: To evaluate high- and low-contrast resolution of a dynamic CsI-aSi large flatpanel detector for DSA-mode and 3D-rotational angiography (CT-mode) for phantoms and clinical examinations.

Methods and Materials: Detail contrast detectability and high contrast resolution of a new DSA system with dynamic CsI-aSi flatpanel detector (FD) (AXIOM Artis-dTA) and an equivalent image intensifier (II) system (AXIOM Artis-FA) were compared with equivalent parameters (phantom dose and postprocessing). FD parameters are: detector size 30x40 cm, matrix 2480x1920, pixel size 154 µm. The diameter of the II was 40 cm. High contrast resolution was determined with a lead grid phantom at 42 cm/22 cm field of view (FOV) of the FD and 40 cm/20 cm of the II. Detail contrast detectabilities were determined with a CDRAD phantom and 20 cm PMMA with 20 different dose parameters for both systems. 3D-reconstructions (~400 slices, 0.3 mm thickness) were acquired with rotational angiography (CT-mode).

Results: The high contrast resolution of the FD was 25-38% better compared with the II (depending on magnification). For similar detail contrast detectability (51% of all objects) the Entrance Skin Air Kerma (ESAK) was 512 µGy for the FD and 818 µGy for the II. Reconstructed CT-images demonstrate a low contrast resolution of < 20 HU.

Conclusions: In comparison to an equivalent II, the FD demonstrates a significant higher contrast resolution and similar detail contrast detectability at 37% less dose. In clinical 3D-examinations a low contrast visualization of soft tissues is possible for the first time.

14:00 - 15:30

Room P

Molecular Imaging

SS 1506b

Cellular and molecular imaging

Moderators:

E. Canet Soulas; Bron/FR
E. Johansson; Malmö/SE

B-779 14:00

In vivo lymphocytes trafficking to tumor: A cellular magnetic resonance imaging approach for cell-based anticancer therapy

P. Smirnov¹, E. Lavergne¹, F. Gazeau¹, B. Doan², B. Gillet², C. Combadiere¹, B. Combadiere¹, O. Clement¹; ¹Paris/FR, ²Gif sur Yvette/FR

Purpose: Cellular imaging by MR imaging is potentially useful to track of injected cell-based therapy in vivo and estimate treatment efficiency against tumor growth. The aim of this study was the follow-up in vivo by MR imaging at 7 T of the infiltration of intravenously injected lymphocytes in implanted tumors in mice.

Methods and Materials: Cells were labelled with anionic nanoparticles, which are taken up by endocytosis pathway. OVA-specific lymphocytes (OT-1), labelled with 1.5 pg iron per cell, were adoptively transferred in C57BL/6 recipient mice with growing OVA-expressing EL-4 (EG-7) tumors. Injected OT-1 cells were tracked in vivo by 7 T MR imaging at 24, 48 and 72 h after transfer. Tumors were analyzed ex vivo by micro-MR imaging at 9.4 T.

Results: Images showed a significant negative enhancement of the spleen at 24 h. Between 48 and 72 h after labelled cells injection, a negative enhancement was observed in the tumor with heterogeneous signal. The presence of labelled cells in tumors was confirmed by ex-vivo studies on the 9.4 T high resolution imaging, and by iron histopathological staining. It suggests first the migration of lymphocytes into spleen followed by their recruitment by tumor site. Subsequently, we showed that labelled OT-1 lymphocytes kept their ability to induce in-vivo tumoral regression.

Conclusion: These results demonstrate that magnetic resonance tracking of lymphocytes is feasible. The ability to define the kinetics of CD8 antitumor migration is crucial for improving the efficiency of tumor rejection. Thus, high-resolution imaging method would have significant clinical and research applications.

B-780 14:09

In vitro cell labelling with SPIO and USPIO: A comparison

F.M.A. Kiessling¹, R. Sun¹, J. Bedke¹, R. Krueger¹, M. Bock¹, R. Huss², C. Seliger², H.-J. Gröne¹, W. Semmler¹; ¹Heidelberg/DE, ²Munich/DE

Purpose: The purpose of this study was to compare the labelling efficiency and toxicity of SPIO and USPIO for three cell lines.

Methods and Materials: Using human fibroblasts, immortalized rat progenitor cells and HEP-G2-hepatoma cells, dose- and time-dependency of SPIO and USPIO uptake were evaluated. The amount of intracellular SPIO and USPIO was monitored over two weeks by T2-magnetic resonance relaxometry, ICP mass spectroscopy (ICP-MS) and histology. Transmission-electronmicroscopy was used to specify the intracellular localization of the iron particles. Cell death-rate and proliferation-index were assessed as indicators of cell-toxicity.

Results: For all cell lines SPIO showed higher uptake rate than USPIO. With 3 mg Fe/ml growth medium highest uptake of SPIO was found in the HEP-G2 cells (110.1 ± 2.4 pg Fe/cell). However, intracellular iron contents in rat progenitor cells (13.7 ± 0.7 pg Fe/cell) and fibroblasts (7.2 ± 0.3 pg Fe/cell) were also capable of reducing T2-relaxation times in cell pellets below detection threshold after 5 h incubation with SPIO. While 4 days after re-cultivation of labelled cells a significant reduction of cellular iron oxide content was found by ICP-MS and histology for SPIO a strong MR-label was present for more than 6 days. For both particle types viability, apoptotic index and proliferation of labelled cells were not significantly different from unlabelled cells.

Conclusions: Our hematopoietic, mesenchymal and epithelial cell lines accumulated SPIO more efficiently than USPIO indicating SPIO to be better suited for cell labelling. Using SPIO labelled cells a suitable window of 6 days was available for in vivo MR tracking experiments.

B-781 14:18

Labelling of human mesenchymal stem cells with different iron oxide MR imaging contrast agents: Uptake, intracellular persistence and in-vitro imaging at 3 T

H. Ittrich, C. Lange, H. Dahnke, C. Nolte-Ernsting, G. Adam; Hamburg/DE

Purpose: In-vitro evaluation of cellular uptake and persistence of different types of superparamagnetic iron oxide nanoparticles ((U)SPIOs) in human mesenchymal stem cells (hMSC) as well as detection and quantification on MR imaging at 3 T.

Methods and Materials: hMSCs were incubated for 24 h with 4 dilutions of stock suspension (1:30-30.000) of 5 (U)SPIO contrast agents: Endorem, Resovist, citric acid coated magnetite cores of 7 nm (CMF3), 3 nm (CMF7) and cobalt ferrite cores (CoF) of 12 nm. Iron uptake, intracellular retention, detection and quantification in MR imaging were evaluated up to 5 weeks after incubation by histological analyses (Prussian blue), atomic absorption spectrometry (AAS) and T2*-MR-relaxometry (multiecho gradient echo sequence, 3 T Philips Intera) on homogenous solid gelatine phantoms of 5×10^4 labelled hMSCs/ml.

Results: An effective labelling of nearly all hMSCs was proven histologically by using Resovist, CMF7 and CMF3(1:30/1:300) with mean iron concentrations of 5.1/1.8, 1.9/1.4 and 1.5/1.0 pg/cell compared with 0.58/0.34 and 0.43/0.30 pg/cell (Endorem, CoF(1:30/1:300)) and 0.01 pg/cell for unlabelled control. Resovist showed best intracellular retention followed by CMF7 and CMF3. Detection of 5×10^4 labelled cells/ml in MR imaging was possible up the 5 weeks after incubation (Resovist, CMF7 and CMF3) with an increasing T2* time in contrast to Endorem and CoF-labeled cells (only 3 weeks). Correlation between cellular iron load and 1/T2* was shown ($R^2=0.76-0.98$).

Conclusion: Efficiency of labelling hMSCs with (U)SPIOs depends on coating, size and core compound of used particles. Long intracellular retention of (U)SPIOs offers the possibility of cell tracking and migration monitoring in a clinical 3 T Scanner and promising prospects for in vivo applications.

B-782

withdrawn by authors

B-783 14:27

Relaxation determination of magnetically labelled macrophages

R. Trost¹, J. Reichenbach¹, I. Hilger¹, M.-R. Lisy¹, D. Schueler², J. Sedlack¹, A. Rauscher¹, W.A. Kaiser¹; ¹Jena/DE, ²Bremen/DE

Purpose: In vitro MR relaxation times of magnetically labelled macrophages were determined on a 1.5 T clinical magnet.

Methods and Materials: Human macrophages (cell line J774) were incubated with bacterial magnetosomes (\varnothing 42 nm) which were covalently bound to fluorochrome Dy676 (Dyomics, Jena). Multiple cell samples (each 0.5 ml) with

Scientific Sessions

different numbers of incubated macrophages (range: 10^6 - 10^7) were measured with a small surface coil in a 1.5 T clinical scanner. IR- and multi-echo spin-echo sequences were used to determine T1 and T2 relaxation times, respectively, based on a ROI evaluation. In addition, a multi-echo gradient-echo sequence was used to determine T2*.

Results: Samples with the highest cell labelling caused severe signal loss and image distortions and were not further analyzed. Both T1- and T2-shortening was observed with increasing cell labelling with magnetosomes. T1 was shortened from approximately 2340 ms for pristine macrophages embedded in agar down to approximately 1500 ms for a sample containing 2.5×10^6 macrophages. Similarly, T2 decreased from 67 ms down to 30 ms. In contrast, T2* was strongly shortened (< 5 ms) and could not reliably be determined.

Conclusion: Magnetosomes are promising probes to label macrophages magnetically. Further MR imaging studies are needed to characterize their full potential for applications in molecular imaging.

B-784 14:36

Fast T2/T2*-mapping at 3.0 Tesla for quantification of cellular iron-uptake

L. Matuszewski¹, R. Kuhlpeter¹, H. Dahnke², T. Persigehl¹, A. Wall¹, B. Tombach¹, W. Heindel¹, T. Schaeffter¹, C. Bremer¹; ¹Münster/DE, ²Hamburg/DE

Purpose: To quantify cellular iron-uptake by T2/T2*-mapping using fast multi-echo sequences at 3.0-Tesla.

Methods and Materials: Human lung carcinoma cells (CLL-185) were labelled with superparamagnetic iron oxides (SPIO) by a previously established lipofection-protocol. MR imaging measurements were performed on a 3 T scanner (Philips Intera) using fast multi-echo readout sequences. Agarose gel-phantoms were prepared containing (a) 1×10^5 cells with increasing amounts of cellular SPIO (1.0-5.0 mg Fe/ml in the medium), (b) different amounts of identically labelled cells (5×10^3 - 2.5×10^5 cells/ml agarose) and (c) free SPIO at identical concentrations as measured in (a) and (b). Cellular iron-load was qualitatively analyzed by light microscopy (LM) and quantified by Atomic Emission Spectroscopy (AES).

Results: With increasing iron concentration in the medium LM and AES showed a dose dependent uptake of SPIO-particles (e.g. [1.00 mg Fe/ml]: $4.37 \pm 0.07 \mu\text{g}/10^5$ cells; [5.00 mg Fe/ml]: $18.65 \pm 1.38 \mu\text{g}/100,000$ cells; $p < 0.05$). While all MR phantom studies showed a strong dose-dependent decrease of T2*-relaxation time the decrease in T2-relaxation time was more subtle (e.g. [1.0-16.0 µg Fe/ 10^5 cells]: T2*: 59.2-9.7 ms; T2: 63.3-57.9 ms). Compared to phantoms containing free SPIO T2*-effects were significantly higher ($p < 0.01$) and T2-effects significantly lower ($p < 0.05$) for iron labelled cells. R2*-values were linearly correlated with cellular iron-load ($r = 0.99$; $p < 0.0001$) or cell number ($r = 0.99$; $p < 0.0001$) respectively.

Conclusion: Estimation of cellular iron load and/or number of iron labelled cells in vitro can be achieved by fast T2/T2*-mapping. The comparison of T2- and T2*-relaxation properties allows to differentiate between cell-bound and free SPIO. Further studies are warranted to elucidate if this method is applicable for cell quantification in-vivo.

B-785 14:45

Diffusion weighted imaging for monitoring of anti-angiogenic tumor treatment

T. Persigehl¹, L. Matuszewski¹, A. Wall¹, C. Wülfing¹, H. Kooijman², B. Tombach¹, R. Mesters¹, W. Heindel¹, C. Bremer¹; ¹Münster/DE, ²Hamburg/DE

Purpose: The aim of this study was to evaluate diffusion weighted imaging (DWI) for non-invasive assessment of anti-angiogenic tumor treatment efficacy.

Methods and Materials: Two different human cancer cell lines (HT-1080, KU-19-19) were implanted in nude mice. Tumor bearing animals were treated either with a vascular targeting agent (VTA, n = 11), an endothelin-A-receptor-inhibitor (ETAR; n = 9) or saline (control; n = 20). Diffusion weighted imaging (DWI) was performed after treatment initiation using a multi-shot EPI and a single-shot TSE DWI sequence. Apparent diffusion coefficient (ADC) maps were calculated and ADC values were correlated with the vascular volume fraction (VVF) measured by iron oxide enhanced MR imaging. Moreover, tumor volume and grade of tumor necrosis determined by MR imaging or histology, respectively, were correlated with the ADC values.

Results: In our models the VTA treatment of HT-1080 xenografts revealed a significant reduction of tumor size while ETAR therapy of KU-19-19 was inefficient. Effective tumor treatment (VTA) resulted in a significant increase of the ADC compared to control (e.g. MS-EPI: $1.45 \pm 0.23 \text{ } 10^{-3} \text{ mm}^2/\text{sec}$ versus $0.79 \pm 0.1 \text{ } 10^{-3} \text{ mm}^2/\text{sec}$; $p < 0.01$). Inefficient therapy (ETAR) showed no significant effects on the ADC compared to tumors treated with saline (MS-EPI: $0.65 \pm 0.038 \text{ } 10^{-3} \text{ mm}^2/\text{sec}$ versus $0.72 \pm 0.07 \text{ } 10^{-3} \text{ mm}^2/\text{sec}$). The grade of tumor necrosis and the VVF correlated well with the ADC changes.

Conclusion: DWI may allow non-invasive and early differentiation of effective versus ineffective anti-angiogenic tumor treatment. Further studies are warranted to elucidate the clinical potential of this imaging approach.

B-786 14:54

Diffusion weighted imaging: An early predictor for therapeutic efficacy

J. Stojanovska¹, B.A. Moffat², T.L. Chenevert², B.D. Ross², A. Rehemtulla², D.E. Hall²; ¹Skopje/MK, ²Ann Arbor, MI/US

Purpose: To assess diffusion weighted MR imaging as an early surrogate marker for evaluating the therapeutic-induced cellular changes of experimental gliomas.

Methods and Materials: Intracerebral 9L tumors were induced in Fischer-344 rats. Two groups ($n = 12$) were established. First group received intratumoral injection of either 67 mg/ml BCNU or ETOH at 50% of the tumor volume under stereotactic guidance. Second group received systemic IP injection of 6.65 mg/kg, 13.3 mg/kg and 26.6 mg/kg of BCNU. The protocol consisted of T2WI and DWI prior to treatment and post treatment at 24 hrs, 48 hrs, 72 hrs and 3 times a week thereafter on a 7 T Varian imaging system. Isotropic ADC maps were calculated and ADC pixel value histograms were generated from tumor ROIs.

Results: Diffusion changes can be detected at BCNU IT group after 48 hrs and the tumor shrinkage between 5 and 7 days post treatment with mean ADC value $1.49 \times 10^{-3} \text{ mm}^2/\text{sec}$. The ETOH group showed diffusion changes after 48 hrs and slowly tumor growing in comparison with Control. Diffusion changes and tumor shrinkage can be detected for groups 26.6 mg/kg and 13.3 mg/kg BCNU at day 7 post treatment in comparison with 6.65 mg/kg group. The cell Log Kill mean for BCNU groups (IT and 26.6 mg/kg) indicates no tumor tissue left in comparison with control and 6.65 mg/kg BCNU where tumor tissue was present confirmed by histology.

Conclusion: Diffusion MR imaging can monitor early changes in tumor cellularity caused by treatment response and can help the physician in tailoring treatment protocol if a tumor is resistant to first-line therapies.

B-787 15:03

In vivo imaging of protease activity and marker gene expression through a fiberoptic catheter-based fluorescence detection system

M.A. Funovics¹, H.S. Su², R. Weissleder², U. Mahmood²; ¹Vienna/AT, ²Boston, MA/US

Purpose: Design, construction, and evaluation in vivo of a fiberoptic catheter-based imaging sensor for the intravital monitoring of molecularly sensitive near infrared fluorescent (NIRF) probes and optical marker genes.

Methods: An imaging device based on a miniaturized fiberoptic sensor (MIFS) was built in which the image created by a 2.7F fiberoptic catheter is relayed through a dichroic mirror, bandpass filter and on two independent cameras, permitting simultaneous recording of white light and fluorescent images. Spatial resolution and spectral transmissions were measured, and sensitivity was determined on a dilution series of a near infrared (NIR) fluorophore. In vivo testing was performed on nude mice bearing intraperitoneal tumors expressing green fluorescent protein (GFP), and on a mouse model of ovarian carcinoma with enzyme-activatable NIR probes sensitive to tumoral activity of the protease cathepsin B.

Results: The 18 G catheter showed a resolution of 7 line-pairs per mm, and a detection limit for the fluorochrome Cy5.5 of 1-10 pmol. Detection of endogenous GFP gene expression was feasible in tumor nodules of < 1 mm in size, with tumor SI of 153.26 ± 26.45 (mean \pm SD) compared to SI from adjacent non-tumoral tissue of 36.73 ± 11.69 (mean \pm SD; $p < 0.008$). Similarly, activation of the NIR-probe by tumoral cathepsin B could be detected in the peritoneal tumor seeds of the ovarian cancer model with tumor SI of 246.33 ± 7.77 (mean \pm SD) compared to SI from adjacent non-tumoral tissue of 41.56 ± 18.64 (mean \pm SD; $p < 0.001$). Combined NIR/white light images consistently revealed more tumors than white light examinations alone.

Conclusion: The proposed minimally invasive optical imaging system offers a method to obtain simultaneous white light and fluorescent images at high sensitivity, allowing the superimposition of anatomic and molecular information in real time. In vivo MIFS imaging of gene expression, enzyme activity and potentially other molecular events is feasible using both a transvascular approach as well as direct interventional access to several organs and body cavities.

Scientific Sessions

B-788 15:12

In vivo assessment of gene expression ability after application of focused ultrasound

W. Hundt¹, S. Guccione², D. Mayer², M. Bednarski²; ¹Munich/DE, ²Stanford, CA/US

Purpose: Evaluation of gene expression changes of muscle tissue cells after treatment with focused ultrasound.

Methods and Materials: Muscle tissue of 25 Balb/c mice were transfected with a CMV_Luc plasmid. 10 days after the transfection focused ultrasound (Focus Surgery) using five different energy levels (4133 W/cm², 3067 W/cm², 2157 W/cm², 1401 W/cm², 802 W/cm²) was applied. After focused ultrasound application a MR imaging scan (1.5 T GE Signa) of all animals using a diffusion weighted steam sequence (TR = 6000 ms, TE = 30 ms, NEX=8, δ=9 ms, Δ=170 ms, b-values = 50, 250, 500, 750, 1000 (s/mm²)) was performed. The determination of the gene expression was done by an optical imaging system (Xenogen).

Results: At a intensity of 4133W/cm² the diffusion coefficients of the treated tissue was D=(0.30 ± 0.03) 10-3 mm²/s and the T2-time 117.49 ± 6.74 ms showing a 83% reduction of the Luciferase reporter gene activity. At an energy level of 2157W/cm² the diffusion coefficient was D=(0.78 ± 0.03)10-3 mm²/s and the tissue T2 time 63.91 ± 3.90 ms a 4 fold increase of gene expression was seen. At a intensity of 802W/cm² the mean diffusion coefficient was D=(0.74 ± 0.04)10-3 mm²/s and the T2= 46.34 ± 1.18 ms still leading to a higher gene expression of 2.5 fold compared to the reporter gene activity prior to the application of focused ultrasound (D=(0.68 ± 0.04)10-3 mm²/s; T2=(36.3403 ± 1.1827)ms).

Conclusion: Focused ultrasound can induce gene expression in muscle tissue. The diffusion coefficient D (mm²/s) and the T2 time (ms) of muscle tissue correlates with the reporter gene activity of the transfected muscle tissue.

Monday

Scientific Sessions

Scientific Sessions

Tuesday, March 8

Scientific Sessions

		room A 2nd level	room B 2nd level	room C 2nd level	room E1 entr. level	room E2 entr. level	room F1 entr. level	room F2 entr. level	room G lower level	room H lower level	
07:00	EPOSTM - scientific exhibition registration										07:00
07:30											07:30
08:00											08:00
08:30											08:30
09:00		CC 1717 Essentials of Neuroradiology Metastatic disease of the brain and spine (p. 118)	RC 1710 Musculoskeletal Knee joint (p. 118)	SF 17 Special Focus Session Fetal MR imaging (p. 119)	RC 1703 Cardiac Morphological and functional assessment of the heart (p. 120)	RC 1701 Abdominal and Gastrointestinal CT colonography and colon cancer (p. 121)	RC 1704 Chest HRCT in diffuse lung disease (p. 122)	RC 1711 Neuro Pediatric neuroradiology (p. 122)	RC 1708 Head and Neck How to investigate facial pain (p. 123)	RC 1709 Interventional Radiology Venuous occlusion (p. 124)	09:00
09:30											09:30
10:00											10:00
10:30											10:30
11:00		SS 1807a Genitourinary Female pelvis (p. 314)	SS 1810 Musculoskeletal Ultrasonography and videofluoroscopy (p. 315)	SS 1801a GI Tract Functional abnormalities of the GI Tract (p. 317)	SS 1803 Cardiac Technical advances in cardiac imaging (p. 320)	SS 1802 Breast Breast cancer screening (p. 322)	SS 1804 Chest New trends in chest imaging (p. 324)	SS 1801b Abdominal Viscera (Solid Organs) MR imaging and MDCT: Practical considerations (p. 326)	SS 1807b Genitourinary Urogenital lesions: Diagnosis and interventions (p. 328)	SS 1809 Interventional Radiology New developments in interventional radiology (p. 330)	11:00
11:30											11:30
12:00											12:00
12:30											12:30
13:00											13:00
13:30											13:30
14:00											14:00
14:30											14:30
15:00											15:00
15:30											15:30
16:00											16:00
16:30											16:30
17:00											17:00
17:30											17:30
18:00											18:00
18:30											18:30
19:00											

Scientific Sessions

	room I lower level	room K lower level	room L/M 1st level	room N/O 1st level	room P lower level	room W basement	room X 1st level	room Y 1st level	room Z entr. level	La Scala 2nd level	
07:00											07:00
07:30											07:30
08:00											08:00
08:30											08:30
09:00	WS 1715 Vascular Planning issues in vascular radiological intervention (p. 125)	RC 1712 Pediatric Musculoskeletal imaging (p. 125)	RC 1714 Radiographers Breast imaging (p. 126)	WS 1718 Workshops on Interventional Radiology Chest intervention (p. 126)	WS 1721 Musculo-skeletal US "Hands-on" Workshop						09:00
09:30											09:30
10:00											10:00
10:30	SS 1806 Contrast Media Iodinated contrast media: Technical advances and side effects (p. 332)	SS 1812 Pediatric Thoracic and abdominal imaging (p. 334)	SS 1811a Neuro Non-invasive neurovascular imaging (p. 336)	SS 1813 Physics in Radiology Nuclear medicine (p. 340)	SS 1811b Neuro fMRI imaging and new MR imaging sequences (p. 342)					SS 1814 Radiographers Challenge and development in radiography (p. 338)	10:30
11:00											11:00
11:30											11:30
12:00											12:00
12:30											12:30
13:00											13:00
13:30											13:30
14:00											14:00
14:30											14:30
15:00											15:00
15:30											15:30
16:00											16:00
16:30											16:30
17:00											17:00
17:30											17:30
18:00											18:00
18:30											18:30
19:00											19:00

Tuesday

Scientific Sessions

10:30 - 12:00

Room A

Genitourinary

SS 1807a

Female pelvis

Moderators:

M. Bekiesinska-Figatowska; Warsaw/PL
B. Hamm; Berlin/DE

B-789 10:30

In-vitro high-field (3 T) high-resolution MR imaging of the female pelvic floor anatomy in correlation with cadaveric cross-sections

K. Pinker, O. Preyer, M.C. Sora, A. Ba-Ssalamah, S. Trattning, V. Mlynarik, W. Umek; Vienna/AT

Purpose: The aim of this study was an anatomic-MR-comparison study using high resolution imaging of the regular female pelvic floor anatomy in-vitro with high-field MR imaging (3 T).

Methods and Materials: We isolated three female cadaveric pelvises of the Vienna Anatomy-Donation-program, cut to fit a standard MR headcoil. All MR images were acquired using a 3 T Bruker Medspec 30/80 Scanner and a head-birdcage transmit/receive coil with an actively shielded gradient system (maximum gradient strength 45 mT/m). A T2-RARE-sequence (TR/TE = 10.098/38.9 ms; matrix size 512x384; RARE factor=4, FOV 230x159 mm, TA 16 min) and a T2-MSME-sequence (TR/TE = 10.000/19 ms; matrix size 512x386; FOV 230x159 mm, TA 1 h 4 min, SI 2/4 mm) was used for high resolution axial images of the female pelvic floor anatomy. All images were carefully evaluated and compared with plastinated slices of the same orientation.

Results: High-field MR imaging depicted the female pelvic floor anatomy to anatomic detail. We could visualize the course and the fascicular structure of the levator ani muscle. The three layers of the urethra (two muscular, one endothelial) and the course of the muscle-fibres in the outer longitudinal and the inner circular layer of the urethra could be identified correctly. The neurovascular bundle was clearly visible.

Conclusion: High-field MR imaging depicts regular anatomy of the female pelvis to a level equal to plastinated macroscopic anatomic cross-sections.

B-790 10:39

Evaluation of female urethra and supporting ligaments with MR imaging

K.J. Macura, R.R. Genadry, D.A. Bluemke; Baltimore, MD/US

Purpose: One of the hypotheses for female stress urinary incontinence is that the sphincter deficiency results from decreased muscle volume and urethral hypermobility results from defects in the supporting ligaments. Our purpose was to evaluate the urethral sphincter in women with urinary incontinence and age-matched continent volunteers, and assess visualization of urethral ligaments with different MR techniques.

Methods and Materials: We evaluated urethral sphincter with intraurethral MR imaging in 10 incontinent women (mean age 59.7) and two groups of continent volunteers: 8 volunteers age-matched to the incontinent group (mean age 51.7), and 6 volunteers not age-matched, mean age 43.8. We measured the urethral sphincter muscle length and thickness and compared the sphincters between the incontinent patients and two groups of volunteers. We analyzed urethral support ligaments in 49 continent women. Twenty-patients (mean age 38.2) were imaged using 14 F endourethral MR coil, 29 women (mean age 40.1) were imaged using pelvic phased array coil. The visibility and symmetricity of three ligaments (periurethral, paraurethral, and pubourethral) were assessed.

Results: There was no significant difference in the urethral sphincter size when incontinent patients were compared to age-matched volunteers. The intact periurethral ligament was the most consistently visualized urethral support structure in continent population. With advancing age, urethral ligaments become thinner and asymmetric. Incontinent patients with urethral hypermobility have defects in periurethral ligaments.

Conclusions: Decrease in urethral sphincter volume is associated with normal aging. Defects in periurethral ligaments leading to urethral hypermobility can be well assessed with MR imaging.

B-791 10:48

Borderline tumors of the ovary: CT and MR features and tumor markers in differentiation from stage I disease

N.M. deSouza, R. O'Neill, R. Dina, W.P. Souter, G.A. McIndoe; London/UK

Purpose: To describe features of borderline ovarian tumours on CT and MR imaging in order to differentiate them from Stage I lesions.

Methods and Materials: We retrospectively reviewed preoperative CT and MR imaging of 38 ovarian tumours in 30 patients classified as borderline or Stage I at histopathology. Two radiologists in conference blinded to the histopathology noted tumour size, number and size of septations, nodules and vegetations, and presence of ascites.

Results: Nineteen borderline (17 patients) and 19 Stage I tumours (13 patients) were identified at histopathology. Borderline tumours were not significantly smaller than Stage I tumours (mean diameter 10.5 ± 5.4 cm versus 13.0 ± 5.3 cm). Although numbers of septations per mass were similar, there was a significant difference in their thickness between borderline and Stage I masses (mean \pm SD = 3.3 ± 1.5 mm vs. 5.1 ± 2.34 mm, $p = 0.04$). Also, although numbers of nodules/vegetations per mass were similar, borderline tumours had significantly smaller solid components than Stage I masses (mean \pm SD = 15.0 ± 9.8 mm vs. 32.0 ± 19.0 mm, $p = 0.003$). Areas under the Receiver Operating Characteristic curves were 0.75 and 0.68 respectively for these features, and a discriminant model resulted in correct classification of 78.6% of cases. Ascites was seen in 4 and 5 cases respectively. Tumour markers were marginally elevated in both groups with no significant differences.

Conclusion: Borderline ovarian tumours have imaging features similar to Stage I tumours. Although the thickness of septations and size of solid components may be helpful in predicting likelihood of Stage I disease, neither feature allows confident differentiation between these entities.

B-792 10:57



Comparison of clinical and MR imaging staging with pathologic evaluation in cervical carcinoma

T.M. Cunha, A. Félix, I. Cabral; Lisbon/PT

Purpose: To evaluate the accuracy of clinical and MR imaging staging in patients with cervical carcinoma.

Methods and Materials: 47 patients with histologically proven cervical carcinoma were included in this prospective study, between October of 1998 and April of 2004. The patients mean age was of 51.8 years (age range 30-77 years). All patients underwent preoperative pelvic MR imaging and MR imaging reports were revealed to the treating gynecologists. Clinical evaluation used FIGO staging. Clinical criteria for operability in our institution are: patients with stage \leq IB1 and IIA tumors \leq 4 cm with small vaginal invasion. Radical hysterectomy specimen histologic report was used as the gold standard of this study. MR imaging protocol: Axial T1- (TR/TE = 427/8), transverse, coronal and sagittal T2-weighted images (TR/TE = 5952/150), and a dynamic study (for small lesions) after 0.1 mmol/Kg Gd-DTPA intravenously in the sagittal plane were obtained with a Philips 1.0-T magnet, using a body coil. The mean elapsed time between MR imaging and surgery was of 36 days (Median = 33 days). MR imaging only found criteria for operability in 38 of the 47 cases. By pathological staging only 39 cases were eligible for surgical treatment accordingly with our protocol.

Results: In the 47 cases studied MR imaging obtained accuracy for surgical staging of 97.2%, and accuracy for staging of 97.5%. Clinical staging obtained accuracy for staging of 82.9%.

Conclusion: MR imaging is useful in the preoperative evaluation of early cervical carcinoma, especially when it is unclear from the clinical examination whether the choice of therapy is surgery or radiation therapy.

B-793 11:06

Pitfalls in MR imaging staging of cervical cancer

A. Sahdev, J.L. Hughes, R.H. Reznek; London/UK

Purpose: To appreciate potential errors and pitfalls in the interpretation of MR imaging during staging of cervical cancer. To learn strategies and techniques to avoid these potential errors.

Materials and Methods: MR scans of 132 women undergoing staging between 1994-2004 were retrospectively evaluated for potential pitfalls and errors. 81 patients underwent surgery allowing correlation of MR imaging and surgical findings.

Results: In 11 (14%) of 81 patients the tumour was not detected on MR imaging (false negatives). 8 of these 11 patients, had a pathological tumour less than 1 cm. In 2 patients residual tumour infiltrated the entire cervix without mass effect.

Scientific Sessions

or differential signal intensity. In the last patient co-existing endometriosis obscured the tumour. In 8(10%) patients MR tumour size was overestimated by 2-3 mm due to inflammatory changes. 4 (5%) patients had false positive MR diagnosis of parametrial invasion due to large exophytic tumours. In detection of nodal metastasis MR sensitivity was 63%, specificity 56% and accuracy 89%. Cystic change in metastatic nodes were a pitfall resembling ovarian tissue. Vaginal wall appearances are a further pitfall. Folding and post biopsy thickening lead to false impression of tumour invasion, upstaging the carcinoma.

Conclusions: We present pitfalls of staging MR in detection, size estimation of primary tumour and parametrial extension. These include technical inadequacies, anatomical variants, confusion by co-existent disease and effects of previous intervention. We describe alterations in MR techniques and protocols which avoid these pitfalls. Techniques and interpretation of lymph node specific contrast agents to assess nodal metastases are also discussed.

B-794 11:15

Uterine fibroids: Relationship between symptoms and MR imaging evaluation

Y. Fargeaudou¹, J.-P. Pelage², D. Jacob¹, M. Abitbol¹, O. Le Dref¹, R. Rymer¹; ¹Paris/FR, ²Boulogne/FR

Purpose: To determine the relationship between fibroid-related symptoms and fibroid volume/location evaluated using MR imaging.

Methods and Material: One hundred and sixteen consecutively seen women with symptomatic fibroids underwent pelvic MR imaging and clinical evaluation. Demographics and clinical presentation were recorded in all women who completed a questionnaire of fibroid-related symptoms. Special emphasis was given to heavy menstrual bleeding (duration of menses, presence of clots, number of pads/tampons used daily, hemoglobin level), bulk-related symptoms, pelvic pain and infertility precisely evaluated. All women had a pelvic MR imaging with axial and sagittal T1 and T2-weighted images. Location, number and volume of dominant uterine fibroids (submucosal, subserosal, intramural and full-thickness), uterine volume and the presence of adenomyosis were carefully recorded. Relationship between symptoms and fibroid volume/location was then computed.

Results: Black women were significantly younger and had multiple fibroid uterus more frequently than the others. Submucosal fibroids were associated with heavier menstrual bleeding than the other types (duration of periods, hemoglobin level, presence of clots). Women presenting with adenomyosis (with or without fibroids) had heavier menstrual bleeding than those with uterine fibroids only. Pelvic pain was more frequently observed in women with large uteri (> 500 cc) or in cases of intramural fibroids. There was a trend towards lower fertility in women with large uteri or multiple fibroids.

Conclusion: A significant relationship between menorrhagia and the presence of submucosal fibroids was found. Adenomyosis was also associated with bleeding symptoms.

B-795

withdrawn by authors

B-796 11:24

The effectiveness of MR imaging in the non-invasive diagnosis of endometriosis: Can laparoscopy be replaced?

C. Alvey, S. Kennedy, C. Ang, D. Barlow, S.J. Golding; Oxford/UK

Purpose: Retrospective study was carried out to determine the accuracy, sensitivity and specificity of MR imaging in detecting lesions of endometriosis, compared to the gold standard investigation of laparoscopy.

Methods and Materials: 100 women (age range 20 - 59 years; mean 37.03) underwent MR imaging using a standardised protocol in a 1.5 Tesla Sigma System (General Electric Medical Systems). Examinations were reported by one radiologist, blinded to the findings of laparoscopy. Imaging findings were compared retrospectively with the findings at surgical investigation to determine presence or absence of disease.

Results: Analysis showed that MR imaging in our study had an accuracy of 91.1%, sensitivity of 88.8% and specificity of 93.1%. This yields a positive predictive value of 92.3% and a negative predictive value of 90%. A Chi-squared test yielded a result of 37.79, indicating a high degree of conformity between the MR imaging and surgical findings. Moreover, findings in this study suggested that laparoscopy may have a false negative rate of 3%. It was notable that 30 patients failed to proceed to surgical investigation at the discretion of the clinician, as the MR imaging findings were deemed to be sufficiently positive for medical treatment to ensue.

Conclusion: MR imaging offers an efficient and effective means of diagnosing endometriosis before patients proceed to surgical investigation and can prevent

a significant number of patients from having invasive investigation. Our findings indicate strongly there is a case for detailed cost-effectiveness study.

B-797 11:33

CT features of adnexal torsion

T. Sella, D. Aharoni, N. Hiller; Jerusalem/IL

Purpose: The clinical presentation of adnexal torsion can at times mimic nongynecological causes of acute lower abdominal pain. In these cases, CT may be the initial imaging study performed. The purpose of this study is to define the CT characteristics of adnexal torsion.

Materials and Methods: This retrospective review examined pelvic CT findings in 35 patients with surgically proven adnexal torsion. CT findings were correlated with sonographic, surgical and pathologic findings.

Results: Localized abdominal pain was found in 79% of patients, with an acute onset in 60%. Torsion was clinically suspected only in 26% of cases. The time interval between admittance and CT ranged from the same day to 1 week (mean 1 day). On CT, the involved adnexa was misplaced in 65%; of these, 34% were midline and 31% were in the contralateral pelvis. The uterus was diverted to the side of the involved ovary in 47%. The size of the involved adnexa ranged from 3 - 20 cm (mean 9.5 cm). An underlying ovarian mass was noted in 71% (pathologically confirmed). All adnexal masses had smooth margins; 80% of them had a cystic component, 50% showed mural thickening. Pelvic ascites was seen in 40%, and effacement of the pelvic fat in 29%, pathologically correlating with adnexal necrosis. The uninvolved ovary was visualized and was normal in 74%.

Conclusion: A smooth adnexal mass which is abnormally located in the pelvis, with ipsilateral deviation of the uterus should raise the suspicion of adnexal torsion. Inflammatory signs on CT suggest necrosis.

B-798 11:42

Selecting postmenopausal patients with abnormal uterine bleeding (AUB) to invasive assessment by transvaginal ultrasonography (TVUS)

S. Ciatto, S. Cecchini, A. Landini, A. Benvenuti, M. Zappa; Florence/IT

Purpose: Abnormal uterine bleeding (AUB) is a common symptom in the menopause, is associated to increased risk of endometrial carcinoma (EC), and in the past did prompt immediate invasive diagnostic assessment (dilatation and curettage, endometrial biopsy, hysteroscopy). As most first AUB episode are spurious and are not associated to EC, risk-based selection to invasive assessment has been advocated for these patients. Measuring endometrial thickness by transvaginal ultrasonography (TVUS) has been suggested as a proper criterium.

Materials and Methods: A consecutive series of 2693 postmenopausal women referring for AUB and undergoing TVUS from 1993 to 2000 has been linked with the local cancer registry database. The adopted protocol foresaw hysteroscopy in presence of a) suspicion for EC at TVUS morphology, and/or b) persistent (> 2 episodes) AUB, and/or thickness (half layer) > 4 mm; 63 of 64 EC cases were correctly suspected according to these criteria.

Results: Endometrial thickness showed a significant association to EC: a cut off of 2 mm (half layer) was associated with a 94.9% sensitivity and a 68.2% specificity (68.2% of subjects could be spared unnecessary invasive assessment on this basis).

Conclusion: Endometrial thickness measured at TVUS is a safe criterium to select subjects at their first AUB episode to invasive assessment. A cut off of 2 mm (half layer) seems a reasonable and reliable clinical reference standard.

10:30 - 12:00

Room B

Musculoskeletal

SS 1810

Ultrasonography and videofluoroscopy

Moderators:

B. Forágás; Budapest/HU
S. Ostlere; Oxford/UK

B-799 10:30

An update on the use of ultrasound in osteomyelitis and the importance of power Doppler

A.K. Nath, A.U. Sethu; Muscat/OM

Purpose: An update study with 200 patients of our previously published paper from 1992 looking into the use of ultrasound in osteomyelitis.

Scientific Sessions

Materials and Methods: Plain radiographs of the affected area and sonography along with power doppler of the affected area and the opposite normal area was performed in 200 patients clinically suspected of having osteomyelitis. Sonograms were obtained using 7.5 to 11 MHz phased array linear transducer on Power vision 6000 Toshiba unit. Needle aspiration or surgery was performed to confirm diagnosis.

Results: 120 of the 200 patients had osteomyelitis, sonographically revealing fluid in contact with the bone with no intervening soft tissue. The fluid proved to be pus. 120 osteomyelitis patients had (a) radiograph and ultrasound positive - 50 patients (b) radiograph normal initially but ultrasound positive - 70 patients. 50 patients had following findings-30 patients had soft tissue abscesses, 10 patients had cellulitis and 10 were normal. Limitations of ultrasound in remaining 30 patients will be highlighted, as seen in sickle cell disease (10 pts), septic arthritis (10 pts), epiphyseal osteomyelitis (7 pts) and Brodie's abscess (3 pts). Color Doppler helped in showing increased blood supply to infected periosteum, adjacent infected bone and soft tissue.

Conclusion: Ultrasound and color Doppler is useful in 1) Predicting osteomyelitis 2) differentiating osteomyelitis from soft tissue abscesses 3) localizing the lesions 4) limitation of ultrasound in the disorders mentioned above help to resort to direct methods like aspirations to make the diagnosis of osteomyelitis 5) Power Doppler was useful as stated above.

B-800 10:39

Ultrasound of the reflection pulley of the long biceps tendon

L. Bacigalupo¹, C. Martinoli¹, Y. Morag², J.A. Jacobson², A.S. Miller², S. Bianchi³; ¹Genoa/IT, ²Ann Arbor, MI/US, ³Chene-Bougeries/CH

Purpose: To describe the US appearance of the coraco-humeral and superior gleno-humeral ligaments (forming the reflection pulley) in normal subjects and patients with pulley tears associated with rotator cuff pathology and biceps tendon instability.

Methods and Materials: A correlative US-anatomic study was performed on freeze-frozen cadaveric shoulders and correlated with the normal US appearance of the reflection pulley in 20 healthy volunteers. Then, 12-5, 15-7 and 17-5 MHz US images were obtained in n = 21 consecutive patients with pulley lesions confirmed on MR-arthrography. Patients with massive rotator cuff tears and biceps tendon rupture were excluded.

Results: High-resolution US was reliable to image the reflection pulley system in normal subjects. In the patients group, pulley lesions occurred in isolation (n = 1) or combined with either subscapularis (n = 11) or supraspinatus (n = 9) tendons tears. Main US signs of reflection pulley lesions included hypoechoic thickening (n = 3), discontinuity (n = 7) and non-visualization (n = 11) of the coraco-humeral ligament. Pulley thickening was associated with subscapularis tears but not with an abnormal biceps tendon position. Biceps tendon subluxation was observed over the subscapularis in patients with pulley rupture combined with anterior tears of the supraspinatus (n = 9) or superior tears of the subscapularis (n = 3). In complete tears of subscapularis (n = 5), the biceps was dislocated.

Conclusion: US is valuable in detecting lesions of the ligamentous structures forming the reflection pulley regardless of the associated cuff pathology. US allows differentiation of a pulley lesion from an isolated tear of the anterior border of the supraspinatus and superior border of the subscapularis.

B-801 10:48

Comparison of ultrasound and radiography in detecting tendon calcifications around the elbow, and differentiating them from enthesophytes

K. Motamed, L.L. Seeger, J. Kim, J.P. DiFiori; Los Angeles, CA/US

Purpose: To demonstrate the advantage of ultrasound over plain radiography in the detection of elbow calcific tendonitis, and in differentiation of elbow calcific tendinitis from enthesophytes.

Materials and Methods: A single sports medicine physician referred all patients for localized elbow pain. Ultrasound images and radiographs of 21 tendon attachment sites (olecranon, medial or lateral humeral epicondyle) in 13 elbows were reviewed by two musculoskeletal radiologists by consensus. A trained musculoskeletal sonographer performed dynamic ultrasound studies under the supervision of a musculoskeletal radiologist. The radiographic studies consisted of frontal, lateral and bilateral oblique views. The interpretations of the ultrasound images and radiographs were performed independently, and the radiologists were blinded to the results of the correlative studies.

Results: Ultrasound images revealed positive findings at 12 sites out of the possible 21 (57%). Of these positive cases six showed enthesophytes, and seven showed calcium deposits in the substance of the tendons at their attachment to bone (one site showed both). Radiographs demonstrated only four positive sites,

all felt to represent enthesophytes (19%). Two of these four were sonographically proven to be calcium deposits embedded entirely within the substance of the tendon at the attachment site.

Conclusion: Elbow ultrasound was shown to be superior to radiography in detecting elbow tendon calcifications, and differentiating them from enthesophytes.

B-802 10:57

Role of US in the evaluation of dorsal scapholunate ganglion cyst

M. Scialpi, C. Malaspina, B. Boranga, G. Scalera, F. Crusco, L. Lupattelli; Perugia/IT

Purpose: To assess the role of ultrasonography (US) in the demonstration of symptomatic occult dorsal scapholunate ganglion cysts.

Methods and Material: One hundred and forty-nine consecutive patients were examined over a period of 12 months with high-resolution US (13 MHz linear-array transducer). Validation of US findings was obtained with surgery in sixty-one patients and with MR imaging in the remaining ones. Topography of the lesion, evaluation of articular pedicle and the relationship with scapholunate ligament were recorded.

Results: In the detection of dorsal occult ganglion cysts, we reported a sensitivity of 98%, a specificity of 89% and a positive predictive value of 95.3%.

Conclusion: US is a useful diagnostic technique in the study of dorsal ganglion cyst. It is helpful in demonstrating occult cysts in symptomatic patients, in selecting treatment options and in post-operative follow-up.

B-803 11:06

Patients with suspicion of gout: Should the first metatarsophalangeal joints be additionally investigated if clinical symptoms are located in other regions? Evaluation with US

T. Rettenbacher, J. Hoflehner, M. Daniaux, M. Herold, D. zur Nedden; Innsbruck/AT

Purpose: Ultrasound (US) is a sensitive method to reveal urate deposits. The purpose of the study was to investigate, if US investigation of the clinical silent first metatarsophalangeal (MTP-I) joints in addition to the US investigation of the site of clinical symptoms can improve the detection rate of gout.

Methods and Materials: In a prospective study, 26 patients with clinical suspicion of gouty inflammation in a location other than the MTP-I-joints underwent high resolution US of the site of clinical symptoms and additionally of both MTP-I-joints. US-findings suggestive of urate deposits were stippled, bright foci and hyperechoic areas within joint effusions, within synovia, or around the joints. Definite diagnoses were established by microscopy of aspirates and/or by characteristic clinical and laboratory findings.

Results: Thirteen patients had gout, 9 were diagnosed having other types of arthritis, and 4 had a definite diagnosis of arthrosis. US revealed signs of urate deposits at the site of clinical symptoms in 9 of 13 patients with gout (69%) and at the clinical silent MTP-I-joints in 12 of those patients (92%). US investigation of the MTP-I-joints in addition to the site of clinical symptoms increased the US detection rate of urate deposits from 69% (9 of 13 patients) to 100% (13 of 13 patients) in our series.

Conclusions: US investigation of the clinical silent MTP-I-joints in addition to the regions of clinical symptoms markedly improved the detection rate of gout and should therefore always be additionally investigated.

B-804 11:15

US of the rotator cuff tendons in "pulse subtraction" mode: Are longitudinal intra-tendinous tears finally visible?

H. Guerini, A. Feydy, J.-L. Drapé, A. Chevrot; Paris/FR

Purpose: Intratendinous longitudinal tears remain the weakness of shoulder ultrasonography because they are considered invisible by this technique. Our purpose was to assess their visibility and to describe the pattern of longitudinal tears of the supra- and infraspinatus tendons using US with "pulse subtraction" mode.

Materials and Methods: Prospective study of 52 patients with a suspicion of tendinous lesions underwent US before a CT- or MR-arthrogram, or a CT-bursography. The examination was carried out with an 8-16 MHz probe in tissue harmonic mode ("pulse subtraction"). The diagnostic criterion for a longitudinal tear was an intratendinous hypoechoic line prolonging a partial or complete tendon tear. US images were correlated with CT and MR arthrograms findings.

Results: Ten cases of longitudinal tears were described at ultrasonography against 18 visible on the CT and MR arthrograms. The US false-negatives were related to poor patient echogenicity (4 cases), very retracted tendons (2 cases) or post-

Scientific Sessions

operative patients (2 cases). Sensitivity, specificity, positive predictive value and negative predictive value were 52%, 92%, 83% and 80%, respectively. Longitudinal tears accompanying complete tendon tears were more difficult to detect (5/11) than those accompanying partial tears (5/6). The "pulse subtraction" mode improved considerably the contrast between normal tendon and tears. Mobilization of the arm sometimes allowed a better visualization.

Conclusion: Contrary to the generally accepted idea, our results show that longitudinal tears can be detected with US. Nevertheless, the sensitivity remains insufficient, especially in cases accompanying full thickness tendon tears, in post-operative and poorly echogenic patients.

B-805 11:24



US morphology of the supraspinatus tendon in basketball players: Correlation with main pathologic models of impingement syndrome in young overhead athletes. Preliminary report

R. Girometti, A. De Candia, M. Sbuelz, F. Toso, C. Zuiani, M. Bazzocchi; Udine/IT

Purpose: To assess the normal and pathologic US morphology of supraspinatus tendon and its correlation with main pathologic models of secondary shoulder impingement syndrome in a population of young overhead athletes.

Methods and Materials: 10 basketball players, age range 19-22, professionals for at least 3 years, and a control group of 10 non-athlete patients of the same age range were investigated using a high resolution 5-12 MHz linear transducer. Static and dynamic standardized morphological study of supraspinatus tendon was performed. We evaluated tendon morphology, thickness of the subacromial bursa and width of the subacromial space.

Results: 6 of 10 players were asymptomatic for shoulder impingement and/or functional limitations, with no US evidence of impingement, except for 2 cases in which right subacromial space is reduced in comparison with contralateral, non-dominant side (6.0 vs. 7.4 mm and 6.6 vs. 7.9 mm). 4 of 10 players showed clinical and US findings of impingement syndrome: 2 players were symptomatic for right shoulder instability and present right (5.3 vs. 7.7 mm) or bilateral (5.2 vs. 6.0 mm) subacromial space reduction. 2 remaining players presented with moderate clinical impingement signs respectively at the left non-dominant shoulder (subacromial space: 6.8 vs. 7.4 mm) and at right shoulder (with bilateral US subacromial space reduction: 6.4 vs. 6.0 mm). Control group subjects were asymptomatic and presented normal tendon morphology according to selected US criteria.

Conclusion: These initial pathological findings seem to be due to different etiologies of secondary shoulder impingement according to the "continuum instability-impingement" model.

B-806 11:33

US diagnosis of talocalcaneal coalition

F. Pugliese¹, M. Valle¹, S. Bianchi², U. Rossi¹, P. Tomà¹, C. Martinoli¹; ¹Genoa/IT, ²Chene-Bougeries/CH

Purpose: To determine the value of high-resolution US in patients with talocalcaneal coalition.

Methods and Materials: A group of n = 10 patients with CT-proved talo-calcaneal coalition and n = 40 healthy subjects with no coalition used as controls underwent 12-5 MHz US of the medial ankle. In each examination, coronal scans over the medial aspect of the subtalar joint were obtained on each side keeping the patient's limbs in a frog-leg position. US images were reviewed by two observers who had neither prior knowledge of the cases nor access to previous radiographic examinations. Each observer reviewed the cases for signs of talo-calcaneal coalition and then decided if coalition was present.

Results: High-resolution US was reliable to image talo-calcaneal coalition based on an absent or markedly diminished subtalar joint space. US sensitivity and specificity for talo-calcaneal coalition ranged from 88% to 100% without false-positive results. The different type of coalition (synostosis, synchondrosis, syndesmosis) did not influence the US diagnosis. In 2/10 cases, the coalition was bilateral.

Conclusion: High-resolution US is valuable in detecting congenital talo-calcaneal coalition. It may help in the selection of patients with suspected disease to be submitted to other imaging modalities after an inconclusive radiographic study and may avoid axial and oblique views of the foot as part of the radiographic foot series. US may also be valuable in cases in which coalition might not be suspected clinically and in patients with atypical symptoms.

B-807 11:42

Feasibility and accuracy of US-guided sacroiliac joint injection: Preliminary experience

A. Klauser, B. Moriggl, M. Schrimmer, F. Frauscher, D. zur Nedden; Innsbruck/AT

Purpose: To assess the feasibility of ultrasound (US)-guided injections in the sacroiliac joint.

Materials and Methods: Twenty-two US-guided sacroiliac joint injections were performed in 11 human cadavers. US was performed with a 2.5 MHz curved array transducer (Esaote Technos MPX or Acuson Sequoia 512). 22-gauge spinal needles were used for injections. We injected 1 ml non-ionic contrast material (Iomeron, Bracco). Three different transverse scanning approaches for needle placements (1. level of L5; 2. level of S1, and 3. level of S2) were evaluated. Computed tomography (CT) was used to confirm the proper placement of the injections.

Results: Of 22 sacroiliac joint injections, 17 (77%) were intraarticular. The injections were repeated in 10 (45%) sacroiliac joints under CT guidance because of improper needle placement. The highest success rate was found using the most caudal (level of S2) approach.

Conclusion: Our preliminary findings suggest that US-guided injection using the most caudal located approach (level of S2) is an appropriate method for sacroiliac joint injection.

B-808 11:51

Dynamic videofluoroscopic assessment of the pseudoarthrosis of the scaphoid in decision making for surgical therapy

C.E.M. Hannig, P.H. Hellerhoff, A.C. Wuttge-Hannig, A. Schoppmann, K.-D. Werber, E.J. Rummey; Munich/DE

Purpose: In cases of pseudoarthrosis of the scaphoid (PAS) CT and MR imaging are excellent tools for the demonstration of bone structure and localisation of fragments. MR imaging can detect early stages of osteonecrosis. But for the surgeon it is of crucial interest to differentiate between stable fibrotic fixation, partially unstable fibrotic fixation and completely unstable pseudoarthrosis. The aim of our study was to find out how dynamic videofluoroscopy can contribute solutions for this problem.

Material and Methods: In the last 10 years we performed 1020 dynamic videofluoroscopic studies of carpal structures. 220 patients with PAS underwent dynamic videofluoroscopy. Radio-ulnar and dorso-palmar movements were registered. In 116 patients of them, arthroscopy and / or surgery were performed based on MR imaging and videofluoroscopic results. Arthroscopic and / or intraoperative findings were considered as gold standard. Mean age was 20.2 years, male: female ratio was 10:1.

Results: Distribution of videofluoroscopic findings was: stable fibrotic fixation n = 42; partially instable fibrotic fixation n = 22; complete instable n = 52. All cases of unstable fixation of PAS underwent surgery (Herbert-screw Matti-Russe intervention). Arthroscopic and intraoperative findings matched to 100% the videofluoroscopic diagnosis. The completely unstable PAS were frequently associated with other carpal instabilities like scapho-lunar dissociation, DISI or other ligamentous lesions.

Conclusion: Dynamic videofluoroscopy turned out to be a reliable tool in surgical decision making for the right functional therapy. Slow motion and frame-by-frame analysis allows a reliable diagnosis of the instability. Additional information is supplied by MR imaging.

10:30 - 12:00

Room C

GI Tract

SS 1801a

Functional abnormalities of the GI tract

Moderators:

E. Biscaldi; Genoa/IT
J. Pringot; Brussels/BE

B-809 10:30

Somatic findings in globus pharyngus: Results of a follow-up study before and after therapy

C.E.M. Hannig, P.H. Hellerhoff, A.C. Wuttge-Hannig, H. Stein, E.J. Rummey; Munich/DE

Aim of Study: To detect specific morphologic and functional alterations of the pharynx and esophagus in patients with the sensation of globus.

Scientific Sessions

Material and Methods: Between 1999 and July 2004, 668 patients were referred to our interdisciplinary consulting staff with the diagnosis of typical globus sensation. (Mean age 53.5 years, male:female ratio 1: 1.1) Diagnostic work-up was based on videofluoroscopy. Additional endoscopy, 24 h-pH-monitoring including manometry and ENT examinations were also performed. 450 patients showed up for follow-up study after therapy.

Results: 81.2% of the patients showed somatic findings. 61.2% suffered from gastro-esophageal reflux disease (GERD) proven by 24 h-pH-monitoring (gold-standard) and/or endoscopy. In 89.2% of these patients videofluoroscopy revealed a dysfunction of the upper esophageal sphincter (UES). Mostly we found delayed opening frequently associated with motor disturbances of the tubular esophagus. UES dysfunction was also responsible for the development of early Zenkers diverticula, oropharyngeal pouches due to an increase in intrapharyngeal pressure during deglutition with retention of saliva. The follow-up of the GERD group revealed a complete disappearance of UES dysfunction in patients sufficiently treated with anti-reflux medication or surgery. The remaining 20% with unproven GERD showed reduction of symptoms after treatment of the UES dysfunction (dilatation-therapy or UES myotomy). 18.8% showed no pathologic findings at first examination and in follow-up.

Conclusion: GERD was a predominant finding in our patient-population with globus pharyngus. Globus sensation disappeared in cases of adequate anti-reflux therapy. Videofluoroscopy is the method of first choice in the assessment of pharyngo-esophageal motor disturbances and could best demonstrate therapy effects.

B-810 10:39

Respiratory patterns associated with swallowing

O. Ekberg, M. Bülow, R. Olsson; *Malmö/SE*

Purpose: The pharynx is a common canal used for air during respiration and for food during swallowing. It is important that no part of the bolus reaches the airways. This is achieved by closure of the airways during swallowing and thereby by an interruption of respiration. We wanted to evaluate the timing of bolus transportation through the pharynx and apnea time during swallowing as well as the coordination between bolus transport and respiration.

Method and Materials: We used videofluoroscopy of the pharynx taken in a lateral projection during swallowing of thin liquids and paste. We simultaneously measured airflow through the nostrils with a silicon mask placed over the nose. The tracing of respiration was integrated on the fluoroscopy monitor. Therefore, bolus transportation and respiration could be assessed simultaneously. We examined 12 healthy adult volunteers. Each volunteer was examined during 6 swallows.

Results: We found that in 65% of the swallows expiration preceded pharyngeal swallowing, while in 35% an inspiration preceded. In 83% of the swallowings an expiration followed pharyngeal bolus transit. Pharyngeal transit time (PTT) of the bolus was less than 1 second. The apnea time during the bolus passage through the pharynx was also 1 second or less. There was no correlation between PTT and the apnea time.

Conclusions: In normal adults most swallowing occurs during expiration. However in about 20% of swallows an inspiration follows the swallowing. Pharyngeal transit time is short as is the apnea time during bolus transport.

B-811 10:48

Visualization of swallowing using real-time cineTurboFLASH sequence and a positive oral contrast agent: A feasibility study

P. Paolantonio, A. Laghi, M. Rengo, A. Guerrisi, V. Vergari, V. Panebianco, R. Passariello; *Rome/IT*

Purpose: The aim of this study was to evaluate the ability of cineTurbo FLASH sequence in depicting the oesophageal swallowing process using a positive oral contrast agent in healthy volunteers.

Methods and Materials: Ten healthy volunteers underwent MR imaging of the oesophagus during swallowing of a mixture of semolina pudding and Gd-DTPA as oral positive-contrast agent. All the examination were performed on 1.5 T magnet (Magnetom Vision; Siemens, Erlange, Germany) equipped with a phased-array coil. Single-slice imaging was performed in the median sagittal plane while subjects were in a prone position. Thirty serial images were obtained using cineTurbo FLASH (TR: 416 msec TE: 1.2 msec TI: 200 msec FA: 8° matrix: 90x128 acq. time: 0.57 sec) for an overall temporal acquisition time of 17 sec during swallowing. The images were reviewed by two gastrointestinal radiologists on a off-line console using a cine-view system.

Results: The semolina pudding and Gd-DTPA mixture showed optimal properties in terms of signal intensity, viscosity and density. The image quality was optimal

in all cases. The turbo-FLASH sequence provided optimal temporal resolution and sufficient spatial resolution during motion.

Conclusion: The depiction of swallowing using cine-turbo-FLASH sequence and oral positive contrast agent is a feasible technique representing a promising approach for the investigation of the oesophageal swallowing process and is expected to be of value for the documentation of functional disturbances in patients with dysphagia.

B-812 10:57

Outcome after endoscopic surgical therapy for Zenker's diverticula

A.C. Wuttge-Hannig, H. Feussner, C.E.M. Hannig; *Munich/DE*

Aim of the study: Myotomy of the upper esophageal sphincter (UES) in Zenker's diverticula is widely accepted in the surgical therapy for smaller diverticula of the type Brombart I-III. In stages III and IV myotomy was usually combined with diverticulectomy. Due to new developments in endoscopic equipment for minimally invasive surgical therapy, the dissection of the sphincter alone is now performed more in the higher stages of diverticula especially in the elderly. This leads to a new radiologic appearance of post-surgical cases.

Material and Methods: We examined 36 patients with advanced stages of Zenker's diverticula before and after minimally invasive endoscopic intervention. (Mean age: 67.7 yy, male:female = 25:9). Examination was performed by videofluoroscopy. Because of a high incidence of regurgitation and aspiration we used iso-osmolar lotrolan.

Results: Generally, the post-surgical appearance of the diverticula did not change very much due to the lack of resection. The neck of the diverticula appears much broader in the 21 cases with a good outcome. Also, the emptying of the diverticulum after therapy was faster with less retention. Preoperatively diagnosed regurgitation was not seen. In the 15 cases with poor outcome the leading finding was an incomplete dissection of the UES with retention, regurgitation and even aspiration. In the group, a high incidence of untreated GERD could be identified.

Conclusion: Videofluoroscopy is the best tool for the pre-/and postoperative assessment of Zenker's diverticula to identify a dysfunction, or incomplete dissection of the UES, sometimes caused by scarring.

B-813 11:06

Real-time high-resolution MR imaging for the assessment of gastric motility disorders

W. Ajaj¹, S.C. Goehde¹, C. Kuehle¹, N. Papanikolaou², M. Forsting¹, J. Barkhausen¹, T.C. Lauenstein¹; ¹*Essen/DE*, ²*Crete/GR*

Introduction: Disturbances of gastric motor function are believed to play a key role in the development of symptoms in patients with functional gastrointestinal disorders (FGID). Thus FGID represent a major burden to society and to affected patients. The aim of this study was to evaluate whether patients with increased or decreased gastric motility can be differentiated from healthy volunteers by means of real-time MR imaging.

Material and Methods: Ten healthy volunteers, ten patients with gastroparesis and ten patients with functional pylorospasm/peptic pyloric stenosis underwent real-time MR imaging. All patients were examined on two separate days one time prior to therapy and second time after adequate therapy. Antral motility was quantified by calculating a gastric motility index.

Results: Patients with gastroparesis showed a lower motility index (mean 1.5 mm²/s) compared to the reference volunteer group (mean 2.5 mm²/s), while the mean motility index of the patient group with pylorospasm was more than three times as high as the reference value of the volunteer group (mean 9 mm²/s). However, the gastric motility index in the patient group with gastroparesis increased and in the group with functional pylorospasm/peptic pyloric stenosis decreased statistically significantly after therapy.

Conclusion: Real-time MR imaging is a reliable tool for the assessment of gastric motion. Furthermore, the difference in gastric motility index in patients, whether with increased or decreased gastric motility, could be evaluated and quantified. Due to the non-invasive character of MR imaging, this imaging modality can be an attractive alternative to conventional invasive diagnostic tools for gastric motility disorders and therapeutic monitoring.

B-814 11:15

Sonographic comparison of gastric emptying of broth and water: Is there a promoting cephalic factor?

J.F. Pedersen, J.F. Pedersen; *Glostrup/DK*

Purpose: To examine the emptying times of broth and water, and explore the possibility of a cephalic influence on gastric emptying.

Scientific Sessions

Methods and Materials: On different days, each of twelve healthy volunteers had meals of either 350 ml water or 350 ml broth. The antral area was determined at sonography five times before the meal as a baseline, and every 1-4 minutes after the meal. The time until the antral area had decreased to 150% of baseline (T150) was determined and used as surrogate expression of gastric emptying time. In the second part of the study T150 was measured in ten volunteers who had meals of either water alone or water followed by sham feeding with broth.

Results: The mean T150 was for water 20.3 min (range 12-40), and for broth was significantly shorter at 12.6 min (5-21), $P = 0.0020$. In the subsequent series the mean T150 was 28.5 min (18-49) for water and significantly shorter for water followed by sham feeding, 22.8 (14-40), $P = 0.0078$.

Conclusion: Broth empties faster from the stomach than plain water, probably because of a "cephalic phase" stimulation of gastric motility via the vagus nerve.

B-815 11:24

Visualization and quantification of large bowel motility by the use of functional cine-MR imaging

S. Buhmann, C. Kirchhoff, C. Wielage, T. Mussack, M. Reiser, A. Lienemann; Munich/DE

Introduction: The aim of our study was to develop a method to visualize and quantify large bowel motility using MR imaging.

Material and Methods: 15 healthy individuals (8 male, 7 female, 25-40 years) were twice examined at 6 a.m. after a minimum starving phase of 8 hours. Two blocks of repeated measurements of the entire abdomen were performed using a 1.5 T MR imaging system with T2-weighted HASTE sequences (Matrix 256 + 207; FOV400 mm; 9-11 slices; SL6 mm) anatomically adjusted to the large bowel with a navigator technique for respiratory gating before and after the oral application of sennate versus intravenous erythromycin.

The diameter D (cm) of a bowel segment at 5 given positions in the ascending (AC), transverse (TC) and descending colon (DC) was set as the parameter for motility-measurement.

Results: D of the bowel lumen was estimated as median and the variance ratio as percentage before and after use of the prokinetics was calculated. After application of both drugs a significant ($p < 0.05$) increase of median D in all bowel regions was found. AC: 3.41 cm to 3.69 cm(ST); 3.52 cm to 3.59 cm(E). TC: 3 cm to 3.4 cm(ST); 3.3 cm to 3.42 cm(E). DC: 2.67 cm to 2.9 cm(ST); 2.86 cm to 2.97 cm(E). The variance ratio of the diameter 104%(AC), 69.1%(TC) and 103%(DC) was measured for ST while for E a ratio of 115.9%(AC), 90.4%(TC) and of 112%(DC) was calculated. Thus for E a greater variance and a greater bowel activity was considered.

Discussion: For the first time we developed an adequate non-invasive method to visualize and quantify large bowel motility. By comparing two prokinetic drugs to enhance motility, E was proofed to be the prepotent drug.

B-816 11:33

Functional cine MR imaging for the assessment of implanted synthetic mesh in patients after incisional hernia repair

T. Fischer, A. Ganghofer, S. Bensler, R. Ladurner, T. Mussack, A. Lienemann; Munich/DE

Purpose: The aim of our study was to develop a method that allows the visualization and evaluation of implanted meshes in patients after incisional hernia repair, with MR imaging. Furthermore we assessed problems typically related with mesh implantation like adhesions and muscular atrophy.

Methods and Materials: We enrolled 16 patients after incisional hernia repair, in each of 8 patients the mesh implantation was done by laparoscopy (ePTFE mesh) resp. laparotomy (polypropylene mesh). All patients had a clinical and ultrasound abdominal examination. Functional MR imaging was performed on a 1.5 T system in supine position. Sagittal and axial TrueFISP images of the entire abdomen were acquired with the patient repeatedly straining. Evaluation included: correct position and intact fixation of the mesh, visceral adhesions, recurrent hernia and atrophy of the rectus muscle.

Results: Time range between operation and examination was 6 to 36 months. In all patients with laparoscopy the ePTFE mesh was visible, the polypropylene mesh was not detectable in any case. In 5 of the 8 ePTFE meshes the fixation was not intact, 1 was crumpled, in 3 cases a recurrent hernia was detected. 13 of 16 patients had adhesions of the intestinum to the anterior abdominal wall, in 5 mobility of the abdominal wall was reduced, 8 showed an asymmetric atrophy of the rectus muscle.

Conclusion: Functional cine MR imaging is a suitable method for follow-up studies in patients after hernia repair. ePTFE meshes can be directly visualized and typical complications like intestinal adhesions and abdominal wall dysmotility can be assessed.

B-817 11:42

Pattern analysis of defecography in patients with chronic constipation: Analysis and its predictive value for the responsiveness of biofeedback therapy

H. Yang, A. Kim; Seoul/KR

Purpose: To determine diagnostic value of defecography in predicting the responsiveness of biofeedback therapy in patients with chronic constipation.

Materials and Methods: Over a two-year period, among patients medically diagnosed with chronic constipation (ROME II), 92 patients underwent defecography and biofeedback therapy. Two blinded readers analyzed and classified into five patterns; I = normal, II = hypertonic anal sphincter (poor opening of anus due to persistent contraction), III = dyskinetic puborectal sling (inadequate laxity), IV = spastic pelvic floor syndrome (persistent contraction of both puborectal sling and anal sphincter), V = unclassified. Also, the degree of rectal contraction during defecation was analyzed with scoring (grade0 to 3). Biofeedback therapy showed therapeutic response in 71 out of 92 patients (77%). In these two groups, responsive or non-responsive group to biofeedback therapy, we evaluated if the morphologic pattern of defecogram or the degree of rectal contraction predicts responsiveness of biofeedback therapy.

Results: On defecograms, type IV was most common (50 out of 92 patients, 54%), followed by II (21/92, 23%), III (12/92, 13%), and V (9/92, 10%). However, there was no significant difference in defecographic type between the responsive and non-responsive groups ($P = 0.630$). Defecograms showed rectal contraction in 78 patients (85%) and moderate to vigorous contraction (more than grade2) was seen in 66 patients. Most of the biofeedback-responsive group showed rectal contraction (66 out of 72 patients, 92%) with statistical significance ($p < 0.001$). **Conclusion:** There was no difference in morphologic types of defecogram between the responsive and non-responsive biofeedback groups. However, the presence of rectal contraction during defecation was highly associated with therapeutic response after biofeedback therapy.

B-818 11:51

Prospective assessment of interobserver agreement for defecography in fecal incontinence

A.C. Dobben¹, T.G. Wiersma², L.W.M. Janssen³, R. de Vos¹, M.P. Terra¹, C.G.M.I. Baeten⁴, J. Stoker¹; ¹Amsterdam/NL, ²Arnhem/NL, ³Utrecht/NL, ⁴Maastricht/NL

Purpose: Primary aim was to determine the interobserver agreement of defecography in diagnosing enterocele, anterior rectocele, intussusception and anismus in fecal incontinent patients. Subsidiary aim was to evaluate the influence of different levels of experience on reading defecographies.

Methods: Defecographies were performed in 105 consecutive fecally incontinent patients. Observers were classified by different levels of experience and were compared to the findings from an expert radiologist. Quality of the expert radiologist was evaluated by an intra-observer agreement procedure.

Results: Intra-observer agreement was good to very good except for anismus: incomplete evacuation > 30 seconds (kappa 0.55), puborectalis impression (kappa 0.54). Interobserver agreement for enterocele and rectocele were good (kappa both 0.66) and fair for intussusception (kappa 0.29). Interobserver agreement for anismus: incomplete evacuation > 30 seconds was moderate (kappa 0.47) and fair for puborectalis impression (kappa 0.24). Agreement in grading of enterocele and rectocele were good (kappa respectively 0.64 and 0.72) and for intussusception fair (kappa 0.39). Agreement separated by experience levels was very good for rectocele (kappa 0.83) and grading of rectoceles (kappa 0.83) and moderate for intussusception (kappa 0.44) at the most experienced level. For enterocele and grading different experience levels did not influence the reproducibility.

Conclusions: Reproducibility for enterocele, anterior rectocele and severity grading are good, while fair to moderate for intussusception. For anismus the diagnosis incomplete evacuation > 30 seconds is more reproducible than puborectalis impression. The level of experience seems to play a role in diagnosing anterior rectocele and its grading and in diagnosing intussusceptions.

Scientific Sessions

10:30 - 12:00

Room E1

Cardiac

SS 1803

Technical advances in cardiac imaging

Moderators:

T.-H. Lim; Seoul/KR

O. Stukalova; Moscow/RU

B-819 10:30

Estimation of radiation exposure in 16-detector row multislice computed tomography (MSCT) of the heart and comparison with calculation programs

C. Hohl¹, A.H. Mahnken¹, M. Das¹, C. Leinendecker², T. Schmidt¹, R.W. Günther¹, J.E. Wildberger¹; ¹Aachen/DE, ²Erlangen/DE

Purpose: To evaluate the defacto administered organ-dose in MSCT of the heart and compare it to calculated values.

Materials and Methods: A female Alderson-Rando-Phantom was equipped with thermoluminescent dosimeters (TLD) in five different positions to assess the organ-doses of five representative organs (thyroid, thymus, oesophagus, pancreas, liver). Radiation exposure was performed on a 16-row-MSCT scanner (Sensation 16, Siemens-Medical-Solutions, Forchheim, Germany) with seven different routine scan-protocols: Two 120 kV CT-Angiography-(CTA)-protocols with different collimation, a 100 kV CTA-protocol, two 120 kV Ca-Scoring-(CS)-protocols with different collimation and two 80 kV CS-protocols in different collimations. Each scanning-protocol was repeated five times. The ECG was simulated using a ECG-simulator (Laerdal Medical GmbH, Munich, Germany) with fixed heart rate of 80 bpm. The measured organ doses were compared with the values calculated by a commercially available computer program (ImpactDose, IMP, Erlangen, Germany).

Results: Directly irradiated organs such as thymus received organ-doses between 27 mSv (CTA 120 kV), 16 mSv (CTA 100 kV) and 7 mSv (CS 80 kV). Organs receiving only scattered radiation such as the thyroid collected organ-doses between 2.7 mSv (CTA 120 kV), 1.7 mSv (CTA 100 kV) and 0.6 mSv (CS 80 kV). The calculated values for the thymus were in good agreement with the measured doses. The calculation program underestimated depending on the scanning-protocol the measured organ doses by a factor between 1.8 and 3.5 for the thyroid. Due to different location of liver-dome and pancreas the measured organ-doses were 10 times higher than the calculated.

Conclusion: 100 kV-CTA-protocols lead to a 60% dose-reduction compared to 120 kV-CTA-protocols. Depending on the scanning protocol organ-doses are rather underestimated by the dose calculating program.

B-820 10:39

Measurements of spatial and temporal resolution for ECG-gated 16-row multidetector CT using a dynamic cardiac phantom

P.G.C. Begemann, U. van Stevendaal, R. Manzke, A. Stork, F. Weiss, C. Nolte-Ernsting, M. Grass, G. Adam; Hamburg/DE

Purpose: To measure spatial and temporal resolution for ECG-gated 16-row MDCT at various heart rates, pitches and rotation times using a beating heart phantom.

Methods and Materials: A resolution phantom with rows of cylindrical holes from 0.4-3.0 mm is mounted to a cardiac phantom, which simulates the motion of a beating heart. Stationary and moving data acquisition is performed at various heart rates (HR, 60-120 bpm), table pitches (0.15-0.30) and scanner rotation times (RT, 0.42 and 0.50 s for 70 bpm). Raw data are reconstructed using a multi-cycle real cone beam reconstruction algorithm at multiple phases of the RR-interval. Multi-planar reformations (MPR) are generated and analyzed. Temporal resolution and cardiac cycles used for image reconstruction are calculated.

Results: In 97.2% (243 / 250) of all data obtained with the stationary resolution phantom, the complete row of cylindrical holes with 0.6 mm in diameter is visible. These results are independent of heart rate, pitch, scanner rotation time and phase point of the reconstruction.

For the dynamic phantom, spatial resolution is determined during phases of minimal motion (116/250). In 40.5% (47/116), resolution is 0.6 mm and in 37.1% (43/116) 0.7 mm. Temporal resolution varies between 63 ms and 205 ms, using 1.5 to 4.37 cardiac cycles for image reconstruction.

Conclusion: With the stationary measurements, the stability of the cone-beam reconstruction algorithm can be proven. In the measurements during movement, the maximum spatial resolution is 0.6 mm, the maximum temporal resolution 63 ms. In phases of maximal motion, MPRs cannot be evaluated.

B-821 10:48



Dynamic cine-mode imaging of the mitral valve with 16-channel MDCT.

A feasibility study

H. Alkadhi, S. Leschka, B. Baumert, A. Plass, D.A. Bettex, B. Marincek, T. Boehm, S. Wildermuth; Zürich/CH

Objective: Our aim was to assess the feasibility and image quality of dynamic cine-mode imaging of the mitral valve using retrospectively electrocardiography-gated 16-channel MDCT.

Materials and Methods: Contrast material-enhanced MDCT was performed in 37 patients having a normal mitral valve, as demonstrated by transesophageal echocardiography. 20 CT data sets covering the valve apparatus were reconstructed every 5% step of the R-R interval. Multi-planar reconstructions were performed in the parallel short-axis and perpendicular long-axis of the left ventricle. Two independent, blinded readers evaluated the image quality for dynamic cine-mode visualization of the valve components in systole, diastole, and during transition phases in-between.

Results: Inter-observer agreements for image quality ratings of valve components in all cardiac cycle phases ranged from good to excellent. Image quality for visualization of valve leaflets, apposition zone, commissures, and mitral annulus (ranging from adequate to excellent) was significantly superior on perpendicular than on parallel planes for all cardiac phases ($p < 0.05$). Tendinous cords were visualized on both perpendicular and parallel planes with bad to adequate quality, whereas papillary muscle visualization was adequate to excellent on both imaging planes. Visualization of each valve component was superior in systole and diastole in both imaging planes as compared to the transition phases ($p < 0.001$).

Conclusions: Non-invasive cine-mode imaging of the mitral valve by using retrospectively electrocardiography-gated MDCT is feasible and allows an accurate visualization of the moving valve. Perpendicular long-axis reconstructions yield superior image quality when compared to the short-axis, and enable a determination of its functional morphology.

B-822 10:57

Assessment of left ventricular parameters using 16 slice computed tomography. Evaluation of a new software for endocardial and epicardial border delineation

T. Schlosser, K. Pagonidis, C.U. Herborn, P. Hunold, K.-U. Waltering, J. Barkhausen; Essen/DE

Purpose: To quantify left ventricular function and mass derived from 16 detector row computed tomography coronary angiography data sets using a new analysis software.

Materials and Methods: Multiplanar reformations in the short axis orientation were calculated from axial contrast enhanced CT images in 18 patients referred for CT coronary angiography. End-diastolic volume (EDV), end-systolic volume (ESV), ejection fraction (EF) and left ventricular mass (LVM) were analyzed with a recently developed imaging software (CT Mass, MEDIS, Leiden, The Netherlands) using an automated contour detection algorithm of left ventricular endo- and epicardial contours and by manual tracing. The data were compared to MR imaging measurements as standard of reference.

Results: EDV, ESV, EF and LVM derived from automated contour detection algorithm were not statistically significantly different compared to manual tracing (CT_{auto} vs. CT_{manual}: EDV = 137.1 ± 45.7 ml vs. 134.2 ± 39.9 ml, ESV = 58.8 ± 34.2 ml vs. 58.1 ± 30.1 ml, EF = $59.2 \pm 13.7\%$ vs. $58.1 \pm 12.0\%$, LVM: 130.9 ± 29.1 g vs. 133.7 ± 33.2 g; $p > 0.05$). However, EDV (118.7 ± 43.6 ml), ESV (50.1 ± 33.5 ml) and LVM (142.8 ± 38.4 g) as calculated based on MR data sets were statistically significantly different in comparison to CT ($p < 0.05$), whereas EF ($59.9 \pm 14.4\%$) did not differ significantly from both CT algorithms ($p > 0.05$).

Conclusion: Automatic and manual analysis of data acquired during CT coronary angiography using a 16 detector row-CT scanner allow for a reliable assessment of left ventricular ejection fraction and a rough estimation of left ventricular volumes and mass.

B-823 11:06

Time resolution and phase time resolution in ECG gated reconstruction using multislice CT

K. Tsujioka, N. Akino, Y. Takahashi, M. Niwa, Y. Uebayashi; Toyooka-city Aichi/JP

Purpose: Evaluating time resolution is important in ECG gated reconstruction methods using multi slice CT. However, in the past, evaluations were made according to the unit of time, even when changes in heart rate occurred. In practical terms, however, a higher heart rate means a shorter time between heartbeats,

Scientific Sessions

and motion artifact is more likely to occur in the time resolution. In this report we will propose the phase time resolution method to evaluate ECG gated reconstruction.

Method and Materials: We measured the time resolution of multi slice CT using our original rotating phantom, and also observed heart movement by an X-ray TV system excelling in time resolution. We determined the rate at which images are available within one heartbeat, and we regarded this outcome as the phase time resolution.

Results: A higher heart rate resulted in a shorter time resolution of CT images. However, the phase time resolution's performance improved when the heart rate was low.

Conclusions: Phase time resolution is an important factor in determining the image quality of ECG gated reconstruction. Even with a shorter time resolution, a shorter heartbeat time results in a larger value of the phase time resolution as well as occurrence of artifact. On the other hand, in the case of a longer time resolution, a longer heart beat time results in a smaller value of the phase time resolution, and thus causes no artifact to occur. From this investigation we obtained knowledge of the most appropriate parameter for scanning in clinical inspections.

B-824 11:15 ♀

Does thin slice multidetector CT (MDCT) improve stent patency and in-stent restenosis evaluation?

G. Ligabue, F. Fiocchi, S. Ferraresi, R. Rossi, L. Rossi, M.G. Modena, R. Romagnoli; Modena/IT

Purpose: To assess the value of 16 slice CT in non-invasive evaluation of stent patency.

Methods and Materials: We performed MDCT evaluation of stent patency in 88 patients (142 stents): 48 by means of 4 detector MDCT using 1.25 mm slice thickness, the remaining with 0.6 mm 16 detector MDCT. The comparison was based on: accuracy in stent patency assessment; accuracy in intra-stent restenosis detection and capability of visualization of the vessel lumen inside the stent. Coronary Angiography (CA) was considered gold standard.

Results: CA identified significant restenosis in 9/72 (12.5%) of stents evaluated with 1.2 mm protocol VS 8/70 (11.4%) with 0.6 mm protocol. Stent occlusion was detected respectively in 3/72 (4.1%) VS 4/70 (5.7%). Stent patency was correctly assessed in all cases with both techniques by means of detection of contrast material proximal and distal to the stent. Significant in-stent restenosis was never detected with 1.25 mm scanner while it was correctly diagnosed in 2/8 cases (25%) with 16 slice MDCT. Thin slice also allows a better visualization of the stent's lumen especially of the ones with < 3 mm diameter (12/14 [85.7%] VS 15/15 [100%]; p < 0.005) and the ones in the RCA (11/21 [52.4%] VS 14/18 [77.8%]; p < 0.005).

Conclusion: Although the stent lumen can be visualized in most stents with sub-millimeter MDCT, a reliable evaluation of in-stent restenoses is not feasible even if it is possible to detect this correctly in a few more cases. Nevertheless, for stent patency evaluation 16 slice MDCT might provide precious clinical information.

B-825 11:24

Cardiac imaging at 3 Tesla: Comparison of different sequences and the use of parallel imaging between 1.5 and 3 T

B. Spors, F. Patrick, K. Klimes, M. Grothoff, R. Noeske, M. Gutberlet, R. Felix; Berlin/DE

Purpose: To compare image quality, signal-to noise ratio (SNR), and contrast-to noise ratio (CNR) of different MR imaging sequences and the use of parallel imaging at 1.5 and 3 T in volunteers.

Method and Materials: We examined 20 volunteers (33 ± 8 years) with a 1.5 Twin Speed Excite and 3 T Signa V/I (GE Medical Systems) using a 4-element phase array surface coil. Fast Spinecho (FSE) T1 (Double-TR), T1-STIR (Triple-IR) and T2 sequences were performed in transverse orientation. Steady State Free Precession (SSFP) sequence was obtained in a 4-/2-chamber long and short axis view for functional analysis. At 3 T the flip angle used for the SSFP sequences was reduced from 45° to 30° . A Tagging sequence was performed in a 2-chamber short axis view. All sequence parameters apart from the flip angle remained constant for 1.5 and 3 T.

Results: Mean SNR was remarkably increased ($p < 0.05$) in all cardiac sequences at 3 compared to 1.5 T. At 3 T the SNR increased by 160% (T2), 123% (T1 STIR) and 91% (T1). CNR showed a similar increase. Mean SNR of SSFP sequences was more than doubled at 3 T (150%), without any significant effect on CNR. By using parallel imaging acquisition time, SNR and CNR was reduced by half. Using the tagging sequence, the grids were longer visible at 3 compared to 1.5 T.

Conclusion: Cardiac FSE sequences at 3 T demonstrated an increase of SNR

and CNR in comparison to 1.5 T without any major changes of sequence parameters. The increased SNR allows the use of parallel imaging with a reduction of imaging time.

B-826 11:33

MR evaluation of the anisotropic diffusion properties of human heart muscle in vivo using MRDTI with parallel acquisition techniques

X. Zhao, K. Li, Y. Li, C. Yu; Beijing/CN

Purpose: To evaluate the anisotropic diffusion properties of human heart muscle tissues with MR diffusion tensor imaging (MRDTI).

Methods: Ten healthy volunteers were enrolled in the study group. The subjects underwent cardiac MRDTI using singleshot EPI sequence with parallel acquisition techniques (iPAT). Data acquisition was performed along the midventricular short axis. The acquisition timing was performed at 100 ms, 200 ms, 300 ms, 400 ms, 500 ms, 600 ms, respectively representing different stages in the cardiac cycle. From the DTMR imaging images, the anisotropic diffusion parameters (FA, RA, VR) in different cardiac stages were calculated with post-processing tools.

Results: The cardiac MRDTI image quality was sufficient for processing in all 10 subjects. The measurements of FA, RA in 600 ms were significantly larger ($P < 0.001$) than those of the other cardiac stages; the measurements of VR in 600 ms were significantly smaller ($P < 0.001$) than those of other cardiac stages. There were no significant differences between the measurements of the other groups except 600 ms. No significant correlation between different groups could be found. The use of parallel acquisition techniques (iPAT) allowed for a substantial improvement in breath-related artifacts and image distortion. Intra- and interobserver variability were sufficiently small in the measurements of the anisotropic diffusion parameters.

Conclusion: Cardiac MRDTI techniques with iPAT can be used quantitatively to measure the anisotropic diffusion properties of human heart muscle tissues in vivo.

B-827 11:42

Multi-slice MR first-pass myocardial perfusion imaging: Impact of the receiver coil array

M.H.K. Hoffmann, F.T. Schmid, M. Jeltsch, A. Wunderlich, B. Schmitz, A.J. Aschoff; Ulm/DE

Purpose: Comparison of a new 12-element body phased-array coil with a conventional 4-element surface receiver coil array to provide increased signal-to-noise ratios for cardiac steady state free precession (SSFP) perfusion imaging.

Materials and Methods: 13 consecutive patients were included in the study. Patients were examined both with a 4-element surface coil array and a 12-element body coil array. First-pass myocardial perfusion imaging using saturation recovery SSFP was acquired during antecubital injection of Gd-DTPA. Imaging parameters: TR 2.8 ms/TE 1.3 ms, Flip Angle 50°, Bandwidth 960 Hz/pixel and Half-Fourier Acquisition. Signal-to-noise (SNR) ratio was calculated using 6 regions of interest (ROI) for the myocardial perfusion scans. Calculations of corresponding ROIs using the two different coil setups were compared using ANOVA analysis. Semi-quantitative perfusion parameters were calculated for both groups.

Results: The mean SNR in myocardial perfusion imaging increased by 21% using the 12-element coil setup ($p < 0.001$) when compared to the 4-element coil. ROI comparisons revealed an increased signal inhomogeneity with the 12-element coil when compared to 4-element coil experiments. Absolute normal range values of semi-quantitative perfusion parameters were consistently higher using the 12-element coil setup ($p < 0.001$).

Conclusions: The 12-element coil array provides higher SNR, but these improvements come with trade-offs in image homogeneity. Increased SNR translates into higher semi-quantitative perfusion values and offers the potential for improved detection of perfusion defects.

B-828 11:51

Quantification of aortic valve stenosis in MR imaging: Comparison of steady state free precession and fast low angle shot sequences

T. Schlosser, M. Jochims, M. Nasser, P. Hunold, K.-U. Waltering, T. Bartel, J. Barkhausen; Essen/DE

Purpose: To assess aortic valve areas by planimetry using two different MR sequences (steady state free precession (SSFP) and gradient-echo fast low-angle shot (FLASH)) in comparison to transesophageal echocardiography (TEE).

Methods: 27 patients with known aortic stenosis were imaged with MR and echocardiography. MR was performed on a 1.5 T MR scanner using a cine SSFP sequence (TR = 2.9 ms, TE = 1.3 ms, FA = 65°, temporal resolution = 19 ms,

Scientific Sessions

spatial resolution = 1.3 mm x 1.3 mm) and a cine FLASH sequence (TR = 8 ms, TE = 3.3 ms, FA = 20°, temporal resolution = 33 ms, spatial resolution = 1.9 mm x 1.3 mm). The imaging plane for planimetry was perpendicular to the aortic root. Planimetry was performed in cross-sectional images in systole by a radiologist blinded to the results of the TEE.

Results: MR planimetry could be performed in all patients. Mean aortic valve area measured by TEE was 0.97 mm², 1.00 mm² for SSFP and 1.25 mm² based on FLASH images. Good correlation was found between aortic valve areas measured on SSPF images and by TEE. The mean difference between the valve areas assessed based on SSFP and TEE images was 0.15 ± 0.13 cm² (FLASH vs. TEE: 0.29 ± 0.17 cm²).

Conclusion: Measurements of the aortic valve area based on SSPF images correlate better with TEE compared to FLASH images. The higher spatial and temporal resolution and the improved image contrast must be considered as major advantages of the SSFP images.

10:30 - 12:00

Room E2

Breast

SS 1802

Breast cancer screening

Moderators:

R. Given-Wilson; London/UK

M. Torres Tabanera; Logroño/ES

B-829 10:30

The impact of prior mammograms in mammography screening

A.J.J. Roelofs¹, N. Karssemeijer¹, N. Wedekind², S. van Woudenberg¹, C. Beck², J.H.C.L. Hendriks¹, M. Rosselli del Turco³, H. Junkermann², C.J.G. Everts²; ¹Nijmegen/NL, ²Bremen/DE, ³Florence/IT

Purpose: To investigate the impact of prior mammograms on mammography screening reading performance.

Methods and Materials: Twelve radiologists experienced in screening mammography each read 160 digitized screening cases twice on a soft-copy reading station (MeVis BreastCare), once with and once without previous-round mammograms. In half of the cases breast cancer was detected at a later stage; the other half were complicated normals, and benign cases. In about 50% of the positives the lesion was found in the next screening round, and in 50% during the screening interval. In retrospect all abnormalities were visible. For all cases mediolateral oblique images were available, for some also crano-caudal images. Readers annotated potential abnormalities, and estimated their likelihood of malignancy. Also, for every mammogram they assessed the priors as needed, helpful or not needed. CAD system markings for microcalcifications were accessible. Cases were displayed in a balanced order, regarding the availability of prior mammograms. Between the two readings of a case was a minimal period of two weeks. All readers participated in soft-copy reading training before starting the study. Effects of prior mammograms on detection performance were determined using LROC analysis.

Results: Reading performance was significantly better when prior screening mammograms were available. Results of displaying prior mammograms on request were significantly worse, but still better than when priors were not shown at all. With priors the referral rate can be reduced by 40% without loss of sensitivity.

Conclusion: The availability of prior mammograms has a significant effect on detection performance in screening mammography.

B-830 10:39

The impact of training on radiologists' performance in softcopy reading:

A study from the European SCREEN-TRIAL project

N. Wedekind¹, A.A.J. Roelofs², C. Beck¹, D. Boehm¹, J.H.C.L. Hendriks², P. Skaane³, N. Karssemeijer², C.J.G. Everts¹, H.-O. Peitgen¹; ¹Bremen/DE, ²Nijmegen/NL, ³Oslo/NO

Purpose: The purpose of this study was to evaluate the effect of appropriate training on radiologists' softcopy reading performance of FFDM.

Method and Materials: Eighteen radiologists from five different European countries participated in this 3-phase study. All of them were experienced in mammography screening, but novel to softcopy reading. In phase 1, participants received an initial training in operation and diagnostic reading skills on softcopy reading workstations before they read 150 FFDM cases (20% cancer) in hardcopy and softcopy, each with a time limit of 2 hours for 75 cases. During phase 2 of the

study, the radiologists read 500 to 1000 cases in softcopy during a six-months self-training period. Finally, in phase 3, the 150 cases were read again in softcopy. Sensitivity, specificity and reading speed were determined to allow for a quantitative comparison of the performance of softcopy and hardcopy reading as well as softcopy reading before and after the self-training period.

Results: After a short introductory training the radiologists' sensitivity and specificity for softcopy reading were already at a high level and were accordingly not significantly improved by training. Solely the initial reading speed was lower after the switch-over to softcopy reading. However, the average reading speed increased during the training, and was eventually on an equal or higher level as compared to hardcopy reading.

Conclusion: In conclusion, it is possible to increase the reading speed in softcopy reading by an appropriate training while keeping the sensitivity and specificity at a high level.

B-831 10:48



The imaging follow-up of ACR category 3 lesions in screening work-up

S.-Y. Ham¹, S. Chung¹, B.-K. Ko², I. Yang¹, H.-D. Kim¹; ¹Seoul/KR, ²Ulsan/KR

Purpose: To evaluate the imaging findings of ACR category 3 lesions, follow-up results and cancer incidence in screening breast evaluation. We aimed to analyze the percentage of women with a diagnosis of breast cancer 1 year after a short-interval follow-up recommendation.

Methods and Materials: We performed retrospective analysis of 6,901 screening mammograms and sonograms for last five years. The purpose of the evaluation is mostly asymptomatic screening in 73% (5,037/6,901) of the cases. Total 386 (5.6%) lesions had assigned to Breast Imaging Reporting and Data System (BI-RADS) category 3 for non palpable, probably benign lesions. At least six months follow-up imaging were reviewed and compared with the initial study.

Results: Ninety-four percent (363/386) were stable on follow-up sonography. Twenty-three lesions (6%) had minimal interval changes (ten were interval growth, seven were decreased dimension, six had disappeared). The number of breast cancers detected in category 3 was two (one ductal carcinoma in situ and one invasive ductal carcinoma). The frequency of cancer detection after a recommendation for short-term follow-up on subsequent examination was 2/386.

Conclusion: Most of the category 3 lesions (94%) are stable in follow-up imaging. However, the cancer detection rate is 0.52% (2/386) in category 3 lesions with at least six months follow-up study and is not trivial, so the recommendation for follow-up and patients compliance are important factors to increase the significance of screening.

B-832 10:57

A prospective study of computer aided detection in the United Kingdom

National Breast Screening Programme

L.A.L. Khoo, P. Taylor, R.M. Given-Wilson; London/UK

Purpose: We evaluated computer aided detection (CAD) prospectively in UK routine screening.

Methods and Materials: Films from 6,111 women, aged 50 and over, receiving three-yearly mammographic screening were analysed (R2 ImageChecker - V5.0). Films were independently double read. Readers recorded an initial evaluation, viewed CAD prompts then recorded a final evaluation. Assessment recall was decided following arbitration. Relative sensitivities were calculated for single reading, single reading with CAD and double reading.

Results: Total cancer detection rate 1.0% (62 cancers in 61 women). CAD prompted 84% (51/61) of detected cancers. Nine of 12 cancers missed on single reading were correctly prompted, but seven prompts were over-ruled by the reader. Sensitivity of single reading was 90.2% (95% CI: 85% to 95%), single reading with CAD 91.5% (95% CI: 86%-97%), double reading without CAD 98.4% (95% CI: 95%-100%). Acting on seven missed but prompted cancers would have given 97.5% sensitivity for single reading with CAD. Recall to assessment rate 6.1% with an increase of 5.8% due to CAD. Average time, per reader, to read a case was 25 seconds without CAD and 45 seconds with CAD.

Conclusion: Compared to single reading, CAD increases sensitivity by 1.3% and double reading by 8.2%. If all correct CAD prompts were actioned, sensitivity would be comparable to double reading. However, 78% of prompts on missed cancer were over-ruled. This may be because of low prompt specificity in the screening environment. Single reading with CAD increases radiologists' time required, compared to double reading, because of increased recall rates.

Scientific Sessions

B-833 11:06

Opportunistic breast cancer early detection in Tyrol, Austria 1996-2004. Do we really want or need a mammography screening program in Tyrol?
T.E. Frede; Innsbruck/AT

Purpose: Statements made in a recently published OeBIG feasibility study for a mammography screening program for Austria according to European Union guidelines commissioned by the Austrian Ministry for Health and Women have raised many questions.

Methods and Materials: This author has examined the state of breast cancer early detection in Tyrol. A comprehensive review of all available data and results based on 3,160 primary biopsy recommendations between 1996 and 2004 at our breast center was performed.

Results: Early detection has been improved by organizing the existing opportunistic screening through a true team approach, incorporating not only the clinic's specialties, but also the private radiologists and referring physicians. This year our center will make the definitive diagnosis in over 75% of the 340 primary breast cancers occurring yearly in Tyrol with 65% being discovered by routine examination. Over 75% stem from second-opinion examinations. About 94% of our primary biopsies are now performed minimally invasive with an overall 47.6% (1303/2740) malignancy rate. Pathological TNM-staging was obtained in over 96% of women under 70 years of age. 54.2% (61.8% in 2004) of all discovered cancers were TNM-stage 1 or better lesions (75.2% in our routine patients). With an overall participation of about 70% of our target group (women over 34 years), it is women under the age of 50, who most consistently follow our recommendations resulting in an above average rate of 57.9% TNM-stage 1 and better lesions.

Conclusions: A mammography screening program as proposed by the OeBIG would only represent one giant leap backwards for Tyrolean women-kind!

B-834 11:15

Screening US in mammographically normal dense breasts
H.-S. Choe, E. Ko, Y.-A. Bae, G.-H. Kim, Y. Lee, S.-Y. Chung; Anyang/KR

Purpose: To evaluate the value of additional US examination for screening in asymptomatic women who showed normal dense breast on screening mammography.

Materials and Methods: From January 1999 to June 2004, 513 women with normal mammographic findings and dense breast compositions underwent US examination. We analyzed the results of US examinations, and evaluated the cases that additional US examinations altered the managements of the patients.

Results: Age distribution of patients was from 26 to 70 (20 s: 19, 30 s: 148, 40 s: 275, 50 s: 58, over 60: 13). After the additional US examinations, final assessments were normal in 308 patients, changed to benign in 122 patients, to probably benign in 76 patients and to suspicious malignancy in 8 patients. Five out of 8 patients with suspicious malignant lesions underwent biopsy, and only one patient was diagnosed as mucinous carcinoma. Other four cases were fibrocystic changes, fibroadenomas(2), and focal ductal dilatation and sclerotic stroma. US examinations diagnosed additional category 3 or 4 lesions in 16% of all patients. Category 4 lesions were found in 2.6% of patients in 36 - 50 years old, and one 27 year-old woman. But breast carcinoma was diagnosed in only one case of total additional breast US examinations.

Conclusion: Additional US examination for screening can help the diagnosis of category 3 or 4 lesions, especially in late thirty and forties. But screening US examinations in all patients with normal dense mammography was not effective in the diagnosis of breast cancer.

B-835 11:24

Assessment of suspicious lesions in mammography screening by minimally invasive biopsy

H. Junkermann, I. Junkermann, M. Borowski, P. Hanisch, U. Bonk, W. Böcker; Bremen/DE

Purpose: Minimally invasive biopsies are standard for pathological assessment in the German model projects for mammographic screening. The results of this approach in the Bremen project are analyzed and compared to the standards of the European Guidelines for Mammographic Screening.

Methods and Materials: From June 2001 to 31st March 2004, 37574 women have taken part (34604 first round participants, FRP; 2967 second round participants, SRP). 5.6% of FRP and 4.5% of SRP have been invited for assessment. After clinical assessment, ultrasound and additional mammography, invasive assessment has been done in 591 FRP (=1.7%) and 36 SRP (= 1.2%).

Results: In 629 lesions, a minimally invasive biopsy and in 45 lesions, a primarily open biopsy was performed. 51% of the minimally invasive biopsies had a

malignant result. 359 lesions (=57%) had been biopsied under ultrasound guidance, 68% of these had been malignant. 34% of 140 stereotactically guided core biopsies and 22% of 130 stereotactically guided vacuum biopsies had been malignant. Routine use of minimal invasive biopsies allowed a preoperative diagnosis in 93% of malignant lesions (EU-guidelines optimal > 90%) and a low number of open benign biopsies (benign to malignant ratio 0.27:1; EU-guidelines optimal < 0.5:1).

Conclusion: The routine use of minimally invasive biopsies allowed preoperative diagnosis in carcinomas and a benign:malignant ratio according to optimal EU standards.

B-836 11:33

Core needle breast biopsy: An alternative to short-term follow-up in probably benign breast lesions (BI-RADS™ 3)?

S. Jaromi, G. Pfarl, D. Floery, C.C. Riedl, W.K. Matzek, M. Rudas, T.H. Helbich; Vienna/AT

Purpose: To assess if stereotactic or ultrasound-guided core needle breast biopsy (CNBB) can be used as an alternative to short-term follow-up in non palpable, probably benign breast lesions (BI-RADS 3™).

Methods and Materials: From 1994 to 2004, stereotactic or ultrasound guided CNBB were performed in 288 lesions which were prospectively assigned as BI-RADS™ 3. Stereotactic CNBB was performed with either spring loaded (needle size 14-g, n = 37) or directional vacuum-assisted biopsy devices (needle sizes 14-g; n = 85; 11-g, n = 90). Sonographically guided biopsies were performed with an automated gun and a 14-gauge needle (n = 76). Following CNBB, patients underwent either surgical excision (n = 204) or mammographic follow-up (n = 84) for at least 20 months. Histological results of CNBB were compared with those of surgical biopsy.

Results: There were 185 masses, 68 calcifications, 14 masses with calcifications, 16 asymmetric densities and five asymmetric densities with calcifications. A diagnosis of malignancy was found at CNBB in 1/288 (0.35%) [ductal carcinoma in situ (DCIS)]. Atypical ductal hyperplasia (ADH) was found at CNBB in 13/288 (4.5%) cases, of which 2 (0.75%) were underestimated. Thus, surgery revealed malignancy in 3/288 (1%) [3 cases of DCIS]. The remaining 285 lesions revealed a benign histology at surgery or were stable during follow-up.

Conclusions: The low number of carcinomas does not favor CNBB as an alternative to short-term follow-up in non palpable, probably benign breast lesions (BI-RADS 3™).

B-837 11:42

MR imaging breast tumor characteristics of BRCA1 and BRCA2 gene mutation carriers

J. Veltman¹, C. Boetes¹, T. Kok², I. Obdeijn³, R. Manoliu⁴, P. Besnard⁴, H. Zonderland⁵, J. Blickman¹, J. Barentsz¹; ¹Nijmegen/NL, ²Groningen/NL, ³Rotterdam/NL, ⁴Amsterdam/NL, ⁵Leiden/NL

Purpose: To evaluate breast tumors in gene mutation carriers (GMC) using MR imaging in order to detect potential misleading characteristics more frequently present in this group on mammography.

Methods and Materials: Retrospectively, MR imaging tumor characteristics of 25 GMC were evaluated. Results were compared with a control group (CG) of 25 breast cancer patients who underwent pre-operative breast MR imaging. Tumors were evaluated on lesion morphology, delineation, internal morphology and kinetics. Statistic comparison of characteristic spread between both groups was done using the Pearson Chi-Square test and multivariate analysis.

Results: 24 lesions were detected on MR imaging in the carrier group, 26 in the control group. In the GMC 19 cases had IDC, 5 DCIS, and 2 ILC. In the control group this was respectively 18, 5 and 3. Tumor size in the CG was significantly larger compared to the carrier group for both pathology and MR imaging measurements. The Pearson chi-square test resulted in $\chi^2 = 11.7$ ($p = 0.001$) for lesion morphology, $\chi^2 = 8.2$ ($p = 0.02$) for internal morphology, $\chi^2 = 5.0$ ($p = 0.08$) for delineation and $\chi^2 = 1.2$ ($p = 0.28$) for kinetics. Using the multi-variate analysis the most different characteristic was tumor shape.

Conclusion: Breast tumors in GMC often present as a rounded lesion with rim enhancement and a type 3 curve. On MR imaging detected rounded lesions in GMC should therefore closely be evaluated for rim-enhancement and kinetics. Both these parameters are essential in not evaluating these rounded lesions as benign.

Scientific Sessions

B-838 11:51

Mammographic, ultrasonographic, histologic and immunohistochemical features in patients with breast cancer and BRCA1 or BRCA2 gene mutation

C. Miro, M. Tomas, P. Pastor, E. Vazquez, A. Arjonilla, E. Ramiro, J. Contreras; Madrid/ES

Purpose: To analyze mammographic and ultrasonographic findings, morphology and immunohistochemical patterns in hereditary breast carcinomas in BRCA 1 and BRCA 2 mutation carriers.

Methods and Materials: Of 44 patients with hereditary breast carcinoma, BRCA 1 mutation was found in ten patients and BRCA 2 in seven. Fifteen of these seventeen patients were females aged 29 to 54 and two males that were 67 to 77 years old.

Results: The most common finding was a well defined nodule with size ranging from 0.5 to 3.5 cm in a dense breast (14 of 17 patients). In the other three cases microcalcifications were found. The most common histologic type was invasive ductal carcinoma (70% of cases in both groups). In two cases with BRCA 1 mutation histologic type was medullary carcinoma. One patient with BRCA 1 mutation showed bilateral involvement at the time of diagnosis. Three patients showed recurrences in the ipsi- or contralateral breast during follow-up. Two patients had also ovarian cancer. Two patients with BRCA 2 mutation were males. All of them were poorly differentiated carcinomas with an immunohistochemical pattern of poor prognosis. 50% of cases showed nodal involvement.

Conclusion: Patients with BRCA 1 mutation are relatively young women with nodules in dense breasts and aggressive immunohistochemical patterns. Bilateral involvement is common as well as early recurrences and association with ovarian cancer. Medullary carcinoma is more common (20%) in BRCA population than in sporadic breast cancer. In the BRCA 2 group the involvement of males stands out.

10:30 - 12:00

Room F1

Chest

SS 1804

New trends in chest imaging

Moderators:

J. Masterson; Dublin/IE
K. Steinke; Basle/CH

B-839 10:30

Real-time MR imaging of the thorax: Experience in 1100 examinations

A. Kluge, C. Mueller, G. Bachmann; Bad Nauheim/DE

Purpose: To assess the value of Real-time MR imaging (RT-MRI) in both emergencies and in dedicated cardiovascular questions.

Materials and Methods: From June 2001 to July 2004, 1132 RT-MRI examinations using TrueFisp sequences have been performed. Indications for this technique and its role in the diagnostic process have been evaluated retrospectively.

Results: 919 RT-MRI examinations did not apply either cardiac or respiratory gating. 180 sequences served for general anatomical overview of thoracic structures. 382 sequences were used as a first-line diagnostic technique in cases of suspected pulmonary embolism, and aortic dissection was suspected in 98 patients. 309 sequences served to assess suspected thoracic pathology, most of them after cardiac surgery. 163 RT-MRI were additionally applied to visualize incidental findings detected with other MRI techniques. RT-MRI was the sole MRI technique applied in 96 examinations. As most of the cases were non-emergencies, other sequences could be added, most of them being contrast enhanced MR angiography and T1-weighted non fat-saturated sequences. Retrospectively, the correct diagnosis could be established with RT-MRI alone in 86% of the examinations, and it shortened examination time in the other cases. 48 CT examinations were added to confirm and to further differentiate non-vascular thoracic RT-MRI findings.

Conclusion: RT-MRI was 100% reliable in emergencies and shortened the examination time in complex situations after cardiac surgery. The inherent T2-weighted contrast makes it well suited for vascular pathologies. Although 38 malignant neoplasms have been diagnosed, CT has to be used in these cases.

B-840 10:39

Comparison of whole-body PET/CT and whole-body MR imaging in patients with newly diagnosed non-small cell lung cancer: Initial results

F.M. Vogt, P. Veit, L. Freudenberg, S.G. Rühm, J. Barkhausen, G. Antoch; Essen/DE

Purpose: To assess the accuracy of whole-body PET/CT and whole-body MR imaging for staging non-small cell lung cancer (NSCLC).

Materials and Methods: 28 patients with newly diagnosed NSCLC underwent whole-body [¹⁸F]-2-Fluoro-2-deoxy-D-glucose (FDG) PET/CT and whole-body MR imaging for tumor staging. Images were evaluated by two different, blinded reader teams and diagnostic accuracies of both imaging procedures for assessing the TNM stage were compared. Histology and a mean clinical follow-up of 250 days served as standards of reference. Differences between both staging procedures were tested for statistical significance by McNemar's test.

Results: The overall TNM tumor stage was correctly determined in 23/28 patients (82%) with PET/CT and in 18/28 patients (64%) with MR imaging ($p = 0.1797$). PET/CT had a direct impact on patient management in 3 patients compared to MR imaging, while MR imaging did not change the therapy regimen compared to PET/CT. Separate assessment of the T-stage was limited to histologically verified cases ($n = 12$). PET/CT showed accurate T-staging in 12/12 of these patients (100%) whereas MR imaging allowed correct assessment of the T-stage in 7/12 of these patients (58%) ($p = 0.0625$). The N-stage was correctly determined in 27/28 of the patients (96%) with PET/CT and in 20/28 patients (71%) with MR imaging ($p = 0.0125$). Both imaging procedures showed a similar performance in detecting distant metastases.

Conclusion: Although no statistically significant difference was found for overall TNM-stage evaluation, there is a firm tendency for more accurate staging results with PET/CT. Assessment of larger patient cohorts will be required.

B-841 10:48

Can FDG-PET/CT replace mediastinoscopy or operative biopsy in patients with lung tumors?

P. Fencl, O. Belohlavek, J. Schutzner, P. Fiala, P. Pafko, P. Zatloukal; Prague/CZ

Purpose: FDG-PET/CT investigation enables exact anatomical localisation of hypermetabolic foci, thus it has the ability to evaluate neoplastic lymph node (LN) involvement with respect to topography. We performed a pilot study to determine whether this hybrid imaging modality could replace mediastinoscopy or per-operative biopsy.

Methods and Materials: 39 patients underwent FDG-PET/CT examination before planned lung surgery. LNs were classified as small (S, less than 10 mm) or large (L, larger than 10 mm) according to CT, and cold (C) or hot (H) according to PET. All primary tumours and 64 LNs in 32 patients were examined histologically after mediastinoscopy or thoracotomy. Only histologically confirmed specimens were included in the evaluation.

Results: There was one false negative and one false positive PET in diagnosis of primary tumours (sensitivity=96%, specificity=89%, accuracy=94%). In total 14 LNs were affected by neoplasm: 6 of 7 H/L LNs, 1 of 4 H/S LNs, 1 of 9 C/L LNs, 5 of 43 C/S LNs, and one LN was directly invaded by tumor. Assessment of LN involvement based separately on PET and CT, resulted in sensitivity of 50% and 50%, specificity of 92% and 82%, accuracy of 83% and 75%, respectively. Assessment of LNs based on FDG-PET/CT resulted in sensitivity of 43%, specificity of 96% and accuracy of 84%.

Conclusion: FDG-PET/CT is an accurate modality for differential diagnosis of primary lung tumours. Positive LN findings could reduce the number of patients for whom surgery is indicated. Negative LN findings, however, cannot replace mediastinoscopy or operative biopsy.

B-842 10:57

Multislice CT for detection pulmonary embolism after lung surgery for cancer

A. Lemmi, T. Lombardi, P. Corneli, M. Chiodi, M. Scialpi, L. Lupattelli; Perugia/IT

Purpose: The incidence of pulmonary embolism (PE) in patients undergoing lung surgery for cancer remains unclear. In these patients the risk for venous thromboembolism is potentially high due to the combination of prothrombotic effects of cancer, extensive surgery, prolonged immobilization and parietal or endothelial local alteration consequent to surgery. The aim of our study was to assess the incidence of PE after lung surgery for cancer using a multislice CT (MSCT).

Scientific Sessions

Materials and Methods: Thirty-four patients (mean age, 65 years; range, 48-78 years) undergoing major surgery for lung cancer were included in this study. Diagnosis of cancer was confirmed in all cases. Twenty-three patients underwent a lobectomy, 9 a pneumonectomy, and the remaining 2 a wedge resection. To detect PE we performed MSCT at 7-15 days after surgery. The diagnostic criteria for PE were a partial or total intraluminal filling defect. Patients were scheduled to receive pharmacological prophylaxis for venous thromboembolism at the discretion of the attending physician.

Results: MDCT showed PE in 7 out of 34 patients; of these two were asymptomatic. Of these 2 PE involved the stump of resection, 3 arteries (mainstream n = 1, lobar n = 1, and segmentary n = 1), and subsegmentary arteries" with "PE involved the stump of resection (n = 2), main artery (n = 1), lobar artery (n = 1), segmental artery (n = 1), and subsegmental arteries (n = 2).

Conclusions: Despite antithrombotic prophylaxis, PE is a common complication in patients undergoing lung surgery for cancer. MSCT is a reliable method to detect PE after lung surgery for cancer.

B-843 11:06

Does core lung biopsy with large needle (≥ 18 G) increase pneumothorax incidence?

A. Oikonomou, G. Patlakas, M. Mantatzis, L. Panagiotidou, D. Bouros, P. Prassopoulos; *Alexandroupolis/GR*

Objective: To evaluate the complication rate and diagnostic accuracy of core lung biopsy (CLB) with needles ≥ 18 G in patients with focal lung lesions.

Materials and Methods: Fifty-three consecutive patients with focal lung lesions (0.8-9.3 cm) underwent CT and CT-guided CLB (mean age: 65.7 yrs, range: 29-81 yrs) with the single-needle technique. 14 G, 16 G and 18 G needles were randomly selected for biopsy. The incidence of pneumothorax and catheter insertion was correlated with histology result, size and depth of the lesion, presence of emphysema, needle size and needle passes. The final diagnosis was established on histopathology after surgical resection or on follow-up and response to treatment.

Results: 14 G, 16 G and 18 G needles were used in 20, 40 and 21 passes, respectively. In 28 procedures two needle passes were performed including four cases where two different needle sizes were used. Pneumothorax occurred in 6 of 53 procedures (11.32%), 4 being in two passage procedures. Drainage was needed in 4 procedures (7.54%). Sensitivity, specificity and negative predictive value of CLB were 93.6, 100, and 63% respectively. None of the parameters examined were found to predict the incidence of pneumothorax ($p > 0.1$).

Conclusions: CLB with needles ≥ 18 G provide high diagnostic accuracy and a pneumothorax rate comparable with the best results reported in the literature for fine needle biopsy. This contradicts perceptions that the risk for pneumothorax increases with larger needles.

B-844 11:15

Modified CT-bronchoscopy as a guidance tool for bronchoscopic needle aspiration. A phantom study

G.M. Weiner¹, B. Geiger², K. Schulze¹, J. Bilger¹, P. Krebs¹, K.-J. Wolf¹, T. Albrecht¹; ¹Berlin/DE, ²Princeton, NJ/US

Purpose: During transbronchial needle aspiration, axial CT-slices are usually used for orientation. To improve the hit rate, a software tool was developed to visualize the target through a semitransparent wall in virtual bronchoscopy. This guidance tool was tested against the customary method in a phantom study.

Methods and Materials: To evaluate the software, an airway phantom with 16 "peribronchial" targets was scanned and examined by three bronchoscopists. In a first pass the targets were bronchoscopically punctured in the traditional way, with knowledge only of the axial CT images. In a second pass, the virtual bronchoscopy was used interactively in real time for guiding the intervention. In addition to the feature of three-dimensional display, measurements could be performed simultaneously to determine the puncture site. CT-scans with metal spots representing the puncture sites were used to analyze the number of hits or the distance and angle between puncture site and target.

Results: Using exclusively axial CT-sections for needle positioning, 14 out of 48 punctures hit the target. Guidance by virtual bronchoscopy increased the hit rate to 32 out of 48. Each investigator at least doubled the hit rate with the virtual guidance. When the target was missed the distance and angle between target and puncture site were significantly smaller applying the new method.

Conclusion: Despite its simplicity, the new virtual guidance tool shows a significant increase in yield, compared to the conventional type of orientation when performing TBNA. It could be a promising tool in clinical practice.

B-845 11:24

Evaluation of the bronchial suture in lung transplant recipients with virtual bronchoscopy

W.F.M. De Wever, I.M. Van Mieghem, I. Van Breuseghem, J.A. Verschakelen; *Leuven/BE*

Purpose: To compare virtual bronchoscopy (VB) with fiberoptic bronchoscopy (FB) in the evaluation of the bronchial suture in lung transplant recipients.

Material and Methods: 37 patients entered the study. Diameter and wall irregularity of the bronchial suture were graded independently using both techniques. Evaluation of VB was performed by 3 radiologists with consensus reading. Evaluation of FB was performed by the pulmonologist. The diameter was graded on a 4-point scale from 0=normal to 3=complete stenosis. Wall irregularity was scored between 0=normal and 2=severely irregular.

Results: There was a high correlation between VB and FB scores of the diameter ($r_s = 0.85$, $p < 0.05$); however the distribution of both scores was significantly different ($p < 0.05$) which was related to an overestimation of the constriction with VB in 29% cases. Correlation between VB and FB scores of wall irregularity ($r_s = 0.33$, $p < 0.05$) was moderate but significant; the distribution of both scores was not significantly different ($p = 0.6$) due to a high incongruence rate between VB and FB scores (48%).

Conclusion: VB can play an important role in the evaluation and follow-up of bronchial sutures in lung transplant recipients and is a very good alternative to the more invasive FB.

B-846 11:33

ECG gated 64 slice CT angiography for the differential diagnosis of acute chest pain

T.R.C. Johnson, C.R. Becker, B.J. Wintersperger, K. Nikolaou, C. Rist, S. Paul, A. Knez, M.F. Reiser; *Munich/DE*

Purpose: To evaluate the usefulness of an ECG-gated 64 slice CT angiography protocol for the assessment of pulmonary arteries, coronary arteries and the aorta in the differential diagnosis of acute chest pain.

Methods and Materials: ECG-gated 64 slice CTA was performed with a Siemens Somatom Sensation 64 CT scanner in 32 patients suffering from chest pain. Heart rates were 70.5 ± 12.2 /min. A Medrad Stellant dual head power injector was used for contrast media administration; volume and flow rate were adapted to the scan length, mean values were 143.1 ± 19.0 ml and 4.4 ± 0.5 ml/sec, respectively; scan time was 23.1 ± 3.3 sec. Bolus tracking in the ascending aorta was used with a delay of 6 seconds. Collimation was 64×0.6 mm, rotation time 0.33 sec; retrospective gating was used for reconstruction. Density measurements and visual assessment of motion artefacts were performed to evaluate image quality.

Results: Sufficient opacification of the pulmonary vessels, the coronary arteries and the aorta could be achieved in all individuals. There was minor blurring in seven patients and one examination with non-diagnostic images of the coronary arteries, whereas only slight motion artefacts of the pulmonary arteries were seen in two patients. Diagnoses included pulmonary embolism (n = 9), high grade coronary stenosis (n = 3) and aortic aneurysm (n = 4).

Conclusion: With current techniques, an ECG-gated CT angiography of the whole chest is feasible with very good image quality. The protocol proved to be helpful in the differential diagnosis of acute chest pain.

B-847 11:42

Endobronchial tuberculosis: Evaluation with multislice spiral CT

J.-Q. Yu¹, X.-H. Zhu², Z.-G. Yang¹; ¹Chengdu/CN, ²Shanghai/CN

Purpose: To explore the diagnostic value of multislice spiral CT with thin collimation, scanning the entire thorax with image post-processing, in endobronchial tuberculosis.

Materials and Methods: Ninety-eight patients with endobronchial tuberculosis diagnosed by bronchoscopy, microbiology and pathology were scanned using a multislice spiral CT, scanning the entire thorax with 3 mm collimation within one breath-hold. 3D image reconstructions including MIP, CVR and CTVE were used. The CT features, findings of fiberoptic bronchoscopy and pathology in these cases were evaluated.

Results: On CT images, bronchial abnormalities were found at 136 sites in 98 cases, including bronchial occlusion in 13(13/136, 9.6%) lesion sites, uniform stricture of bronchi in 27(27/136, 19.8%) and irregular stricture of bronchi in 96(96/136, 70.6%). Thirty-one lesions (31/136, 22.8%) were located in a main bronchus, 81 (81/136, 59.6%) in a lobar bronchus and 24 (24/136, 17.6%) in a segmental bronchus. Multiple lesions occurred in 56 (56/98, 57.1%) cases. Strictures of bronchi manifested as wall thickening (27/123, 22.0%) uniform or irregular stenosis

Scientific Sessions

(96/123, 78.0%). Using the results of fiberoptic bronchoscopy and pathology as diagnostic criteria, reviewers diagnosed endobronchial tuberculosis by the multislice spiral CT correctly in 84.6%, with 89.8% sensitivity, 63.2% specificity. **Conclusion:** Multislice spiral CT scan is a fast, effective and non-invasive diagnostic method. The use of thin section scans and 3D reconstruction will be useful in improving diagnosis of endobronchial tuberculosis.

B-848 11:51

CT-guided percutaneous radiofrequency ablation in patients with inoperable malignant lung tumors: Safety and efficacy

S.F. Lin, J.H. Chen, S.B. Wang; Shantou city Guangdong Province/CN

Purpose: To evaluate therapeutic safety and efficacy of percutaneous radiofrequency ablation (PRFA) for inoperable malignant lung tumors by contrast-enhanced dynamic CT.

Methods: CT-guided PRFA was performed on 81 patients with stage III or IV inoperable malignant lung tumors, in a total of 128 foci. Contrast-enhanced dynamic CT was performed before the PRFA, immediately after, 3 months and 12 months after the PRFA, respectively. The therapeutic safety and efficacy was evaluated by the complications of PRFA, CT scan, and survival rate. Fifty matched patients with a total of 75 foci were taken as the control group, undergoing chemotherapy but no PRFA.

Results: Immediately after PRFA, the margin of all foci were blurred; of 128 foci, density reduction was found in 73 (57%) foci; small air bubble signs were found in 64 (50%) foci. Of all foci at 3 months after PRFA, 4 (3%) foci were found to have almost completely disappeared; 68 (53%) foci had shrunk and 37 (29%) foci were expanded, while 19 (15%) foci remained unchanged. Continued follow-up in 67 patients in a total of 104 foci showed that 4 (4%) foci were found to have almost completely disappeared; 22 (21%) foci had shrunk and 63 (61%) foci were expanded; and 15 (14%) foci remained unchanged. Moreover, the median survival duration was significantly longer in PRFA group than in control group (15.2 months vs 8.7 months, $p < 0.01$).

Conclusion: CT-guided PRFA is a safe and effective treatment for inoperable malignant lung tumors. Contrast-enhanced dynamic CT is a useful modality for assessment of therapeutic efficacy.

10:30 - 12:00

Room F2

Abdominal Viscera

SS 180b

MR imaging and MDCT: Practical considerations

Moderators:

G.G. Karmazanovsky, Moscow/RU

K.A. Stringaris; Athens/GR

B-849 10:30

Quantification of hepatic iron by MR: Body or surface coil?

L. Martí-Bonmatí, M. Pastor Juan, F. Peñaloza, J. Olalla Muñoz, M. Martínez Pérez; Valencia/ES

Objective: The quantification of hepatic iron concentration from MR signal intensity (SI) measurements has a high predictive value for iron overload. The University of Rennes Web site (<http://www.radio.univ-rennes1.fr/Sources/EN/Hemo.html>) allows calculation of iron concentration by means of SI measurement obtained from MR sequences. The use of a volume body coil is mandatory in these calculations. The purpose of our study was to evaluate whether SI measurements from MR images obtained with the surface coil and parallel imaging have the same values as those obtained with the body coil.

Materials and Methods: A total of 10 patients (2 women and 8 men; mean age, 49 years) were prospectively included. MR imaging involved gradient-echo sequences with different weightings (120/4/90; 120/4/20; 120/14/20; 120/21/20). These sequences were obtained with both the body and a phase-array surface coil. SI measurements were obtained from each sequence by means of ROIs placed in the liver (3) and paraspinal muscle (2). Hepatic iron concentration is expressed in $\mu\text{mol/g}$.

Results: Seven patients had iron overload, between slight and moderate levels. There was no statistical difference (t student, $p = 0.3$) comparing quantifications obtained with the body coil (76 ± 72) and surface coil (79 ± 74). The correlation between measurements was excellent ($R^2=0.98$, $p = 0.000$). The mean difference between body and surface coil measurements per patient was -3 ± 9 (range, -9 to 3). No patient was classified in a different group of iron overload.

Conclusions: MR images with surface coils and parallel imaging allow an accurate quantification of hepatic iron concentration with shorter acquisition time and better resolution.

B-850 10:39

Diffusion-weighted MR imaging in differential diagnosis of adrenal masses.

Work in progress

V. Zampa, I. Bargellini, S. Ortori, F. Odoguardi, C. Bartolozzi; Pisa/IT

Purpose: To assess the usefulness of diffusion-weighted MR imaging (d-MRI) in providing an objective value to increase diagnostic accuracy in the differential diagnosis of adrenal masses.

Materials and Methods: Six patients (8 lesions) were enrolled with US or CT diagnosis of an adrenal mass (diameter range: 2.5-6 cm) and clinical and laboratory findings suggestive for pheochromocytoma. Conventional MR imaging (C-MRI, 1.5 T) was performed with: FSE-T2W with and without fat suppression (breath-holding or respiratory triggering), double-echo in- and out-of-phase GRE. d-MRI (single-shot echo-planar) was performed in breath-holding using two different b gradient factor values (500 and 1000 sec/mm²) in the three axes. Apparent diffusion coefficient (ADC) was calculated. All patients underwent surgical excision and histologic analysis of the mass. As a control group, d-MRI and C-MRI were performed in 10 patients (16 lesions) with adrenal adenoma ($n = 8$), hyperplasia ($n = 6$), myelolipoma ($n = 1$) and metastasis ($n = 1$), confirmed by clinical, laboratoristic and imaging follow-up.

Results: In all 6 patients the surgical specimens confirmed the diagnosis of pheochromocytoma. C-MRI was highly suggestive of pheochromocytoma in 5/8 lesions. Using $b = 500$, ADC was significantly higher ($P = .03$) in pheochromocytomas (mean ADC $2.26 \times 10^{-3} \text{ mm}^2/\text{sec}$) than in controls (mean ADC $1.69 \times 10^{-3} \text{ mm}^2/\text{sec}$); the difference was not statistically significant using $b = 1000$. By ROC curves (Area-Under-the-Curve = 0.734) an ADC cut-off value of $2.20 \times 10^{-3} \text{ mm}^2/\text{sec}$ (with $b=500$) was identified for the diagnosis of pheochromocytoma (specificity 87.5%, sensitivity 75%, PPV 75%, NPV 87.5%).

Conclusions: Although larger series are required, d-MRI using $b = 500 \text{ sec/mm}^2$ provides an objective value to distinguish pheochromocytomas from other adrenal masses with high diagnostic accuracy.

B-851 10:48

Black-blood-EPI sequences for the evaluation of focal liver lesion:

Comparison to a standard T2-weighted sequence

C.J. Zech¹, K.A. Herrmann¹, O. Dietrich¹, M.I. Menzel², M.F. Reiser¹, S.O. Schoenberg¹; ¹Munich/DE, ²Erlangen/DE

Purpose: To evaluate the feasibility of diffusion-weighted black-blood (BB)-EPI-sequences with parallel imaging for detection of focal liver lesions in comparison to a standard T2-weighted sequence.

Materials and Methods: 20 patients with known or suspected focal liver lesions underwent a diffusion-weighted fat-saturated BB-EPI-sequence (TR 2200 ms, TE 50 ms, b-value = 50 s/mm², 2 averages, 18 seconds breath-hold, Matrix 192x162) and a standard fat-saturated T2-W-sequence (TR = 2800; TE = 107, 1 average, 3 x 17 seconds breath-hold, Matrix 320x320) with 6 mm slice thickness on a 1.5 T MR imaging-system (Magnetom Avanto, Siemens Medical Solutions). Both sequences used parallel imaging with an acceleration factor of 2. Overall image quality and degree of artifacts were compared with help of a five-point scale with 5 being the most desirable score. The detection rate and the level of confidence with regard to lesion detection were evaluated for both sequences in comparison to a contrast-enhanced (gadolinium and /or SPIO) MR examination, which was used as a standard-of-reference.

Results: The diffusion-weighted BB-EPI-sequence showed significantly ($p < 0.05$) improved overall image quality (average score 4.1 versus 3.5) and fewer artifacts (average score 4.15 versus 3.3) in comparison to the T2-W-sequence. Lesion detection was 83% versus 61% superior in the BB-EPI sequence. The level of confidence for the detection of focal liver lesions was also superior for the BB-EPI-sequence.

Conclusion: Diffusion-weighted BB-EPI-sequences within a single breath-hold for liver imaging are feasible with parallel imaging and show excellent image quality. They might contribute to easy and confident lesion detection in comparison to T2-W-sequences.

Scientific Sessions

B-852 10:57

Diffusion-weighted MR imaging in the differentiation of benign and malignant focal liver lesions

C. DellaPina, R. Lencioni, D. Cioni, L. Crocetti, S. Montagnani, J. Lera, A. Conti, E. Batini, C. Bartolozzi; Pisa/IT

Purpose: To evaluate the ability of diffusion-weighted MR imaging to differentiate benign and malignant focal liver lesions.

Methods and Materials: Twenty-two patients 21-72 years old with 34 focal liver lesions were included in an on-going, prospective clinical trial. All patients were examined using a 1.5 T MR scanner and a phased-array torso coil. The MR protocol included T2-weighted FRFSE respiratory-triggered images, T2-weighted FRFSE breath-hold images, breath-hold diffusion-weighted echoplanar images ($b = 500$), breath-hold unenhanced and contrast-enhanced T1-weighted fat-suppressed FSPGR in the arterial (30 seconds), portal-venous (80 seconds) and delayed phase (180 seconds) after bolus injection of 0.2 ml/kg of paramagnetic contrast agent (MultiHance; Bracco, Milan, Italy). Apparent diffusion coefficient (ADC) values were evaluated. The t-test was used to compare the mean ADC values of benign and malignant liver lesions. The gold standard was provided by pathology ($n = 9$) or follow-up MR imaging for at least six months ($n = 13$).

Results: Final diagnoses included hemangioma ($n = 14$), focal nodular hyperplasia ($n = 9$), metastasis ($n = 6$) and hepatocellular carcinoma ($n = 5$). Lesion size ranged from 1.2-8.5 cm. Mean ADC value was 2.3×10^{-3} mm 2 /sec for hemangiomas, 1.6×10^{-3} mm 2 /sec for focal nodular hyperplasia, 0.8×10^{-3} mm 2 /sec for metastases and 1.1×10^{-3} mm 2 /sec for hepatocellular carcinoma. The difference between ADC values of benign and malignant liver lesions was statistically significant ($p < 0.05$).

Conclusion: Preliminary results suggest that diffusion-weighted MR imaging and ADC maps provide valuable information in the differentiation of benign and malignant liver lesions.

B-853 11:06

Diffusion weighted imaging of liver metastases: A study of the relative lesion conspicuity compared to conventional sequences

P. Cowley, J. MacLachlan, J. Tibballs, N. Davies, J. Bell; London/UK

Purpose: Little published data is available to support claims that diffusion weighted imaging (DWI) is highly sensitive for liver metastases. Since Aug 2003 we have included DWI in our standard MR liver protocol. This study retrospectively examines all cases involving liver metastases and quantitatively evaluates conspicuity on DWI compared to conventional sequences.

Method: Studies performed on one Tesla magnet with uniform protocol. Sequences evaluated are T2W TSE axial, STIR & DWI (b -factor 50). Lesion to liver signal intensity ratio (SIR) calculated on all sequences. Comparative analysis of data taking account of primary disease and size of deposits.

Results: 75 scans (59 cases) examined which identify 204 lesions. Primary diseases consist of carcinoid (106), colorectal (72), breast (10) and other (16). On average breast metastases DWI SIR is 62% greater than STIR (STD 0.69) and 86% greater than T2W (STD 0.67). Colorectal DWI SIR are 13% greater than STIR (0.29), 37% greater than T2 (0.37). Carcinoid DWI SIR are 6% greater than STIR (0.32), 25% greater than T2W (0.46).

Conclusion: DWI is indeed a highly sensitive sequence for liver metastases, in some cases indicating lesions otherwise overlooked. Lesions not visible on conventional sequences cannot be included in the quantitative comparison reducing the power of the study and the quantitative estimate of relative lesion conspicuity. Homogeneity of background liver is a further factor where DWI has advantages over STIR and T2W imaging.

B-854 11:15

Optimization of contrast enhancement for pancreatic CT imaging using multi-detector row CT: Effect of different scan delays on arterial, venous, pancreatic and hepatic enhancement

S. Lee, W. Lee, Y. Yim, J. Choi, D. Choi, H. Lim, J. Lim; Seoul/KR

Purpose: To evaluate the effect of different scan delays (SDs) on 3-phase pancreatic CT imaging; early arterial phase (EAP), pancreatic parenchymal phase (PPP), and portal venous phase (PVP), using multi-detector row CT (MDCT) for determining the optimal SDs for each phase.

Materials and Methods: During 8 months, 100 patients underwent 3-phase CT by using MDCT (8 and 16 slice CT). The SDs were determined as 5 s, 10 s and 15 s after the aortic initial enhancement (AIE) for EAP, as 20 s, 25 s and 30 s after the aortic peak enhancement (APE) for PPP and at 70 s, 80 s and 90 s postinjection for PVP. 120 mL of Ultravist 370 was injected at a rate of 4 mL/s. HU

of ROI was measured at the segment 8 for hepatic enhancement (HE), the pancreatic head for pancreatic enhancement (PE), the aorta, hepatic artery and SMA for arterial enhancement (AE), and the portal vein and SMV for venous enhancement (VE) at all three phases, and were compared for evaluating the effects of different SDs.

Results: During EAP, all of AE, PE, VE and HE revealed to be maximal at the 15 s-SD, but no significant difference between the 10 s- and 15 s-SDs in AE and between the 5 s-SD and 10 s-SDs in VE. During PPP, AE, PE, VE and HE were maximal at the 20 s-SD ($p = 0.001$), 25 s-SD ($p = 0.245$), 25 s-SD ($p = 0.037$) and 30 s-SD ($p = 0.001$), respectively. During PVP, AE, PE, VE and HE were maximal at the 70 s-SD ($p = 0.090$), 70 s-SD ($p = 0.657$), 80 s-SD ($p = 0.230$) and 70 s-SD ($p = 0.139$) postinjection, respectively. PE was maximal in PPP in SDs ($p = 0.000$).

Conclusion: The optimal SDs of EAP, PPP and PVP for pancreatic CT were 10 s SD after AIE, 25 s SD after APE and 70 s SD respectively.

B-855 11:24

Optimization of iodine concentration for the diagnosis of focal liver lesions in MDCT

R. Hammersting¹, P.J. Valette², D.M. Regent³, T.J. Vogl¹; ¹Frankfurt a. Main/DE, ²Lyon/FR, ³Vandoeuvre-les-Nancy/FR

Purpose: To optimise iodine concentration in multidetector CT (MDCT) of liver tumors.

Method and Materials: In this multicenter, double blind, randomised, parallel group comparison clinical Phase IV study, 91 patients with the diagnosis of abdominal tumors were included and 60 patients were suspicious of liver tumors. All patients underwent MDCT using a bi-phasic contrast-enhanced technique. Iomeprol was administered intravenously in three concentrations (300, 350, 400 mg iodine/ml). The overall iodine dose (36 g) was equal within the groups; administration of contrast was obtained in a dual mode [4 ml/sec for arterial, 2 ml/sec for portal venous phase imaging (equal for all three groups)]. The absolute contrast between lesions and surrounding tissue as well as contrast densities were analysed by summary statistics and an exploratory Kruskal-Wallis test.

Results: Contrast density of normal liver parenchyma was 61.3, 64.8 and 72.7 HU for Iomeprol 300, 350 and 400 ($p = 0.01$) in the arterial phase. The highest concentration led to higher densities for the enhancement of normal liver tissue. Median contrast density of lesion-surrounding tissue tended to be higher for Iomeprol 400 than for the other groups at arterial (74 HU versus 64 and 66) and portal-venous phase (113 HU versus 99 and 102). Higher contrasts of Iomeprol 400 were measured versus 300 and 350 for subgroups of patients with certain lesions: HCC (45, 48 and 71 HU), CCC (64, 65 and 84 HU).

Conclusions: High concentration contrast medium shows advantages in demarcation and delineation compared to lower iodine-concentrated contrast agents for the diagnosis of liver tumors especially of hypervascularized lesions.

B-856 11:33

Computer-assisted evaluation of small hepatocellular carcinoma (HCC) by multiphase dynamic imaging using multidetector helical CT (MDCT)

F. Yan¹, P. Xu¹, W. Cheng¹, G.-Q. Wei², X. Zeng², J.-Z. Qian², L. Fan²; ¹Shanghai/CN, ²Princeton Junction, NJ/US

Purpose: The increased data volume from MDCT poses challenges to clinical workflow. This work is to evaluate the feasibility of computer assistance for the diagnosis of small HCCs (< 30 mm) from MDCT scans, by employing tools of synchronized visualization of multiphase scans and automated quantification of lesion size and enhancement patterns.

Materials and Method: Tri-phase MDCT scans of 40 patients were acquired at pre-contrast, arterial and portal venous phases. The scans were evaluated for the diagnosis of small HCCs using a computer tool (EDDA Technology, Inc). The tool automatically finds corresponding locations of a marked lesion in scans at other phases, and allows synchronized scrolling and visualization of tri-phase scans. Lesion size and attenuation pattern are automatically quantified, with enhancement curve across tri-phases plotted together with that of the normal parenchyma.

Results: 80 small HCCs, ranging between 4.8-28 mm (mean, 15 mm), were diagnosed. With the registration tool, 66.3% of HCCs were quantified as having the "iso/hypo_hyper_hypo" attenuation pattern across the tri-phases. Their corresponding average differences in HU as compared to normal parenchyma were -13.7 ± 9.5 HU, $+22 \pm 9.7$ HU and -20 ± 13.8 HU respectively. 22.5% manifested the pattern of "iso/hypo_hypo_hypo". Their average differences in HU compared to normal parenchyma were -10.6 ± 5.8 HU, -10 ± 8.4 HU and -12 ± 4.6 HU respectively. The remaining HCCs had atypical attenuation patterns.

Scientific Sessions

Conclusions: The automatic registration of lesions across multiphase scans and the quantification of their enhancement patterns objectively reflected the contrast characteristics of small HCCs. The synchronized visualization and quantification tools improve the workflow efficiency and provide visual and quantitative information that aids diagnostic accuracy.

B-857 11:42

Quadruple-phase MDCT of the liver in patients with suspected HCC: Effect of contrast material flow rate

W. Schima¹, T.J. Vogl², C. Catalano³, L. Marti-Bonmatí⁴, E.J. Rummeny⁵, F. Tardagüila Montero⁶, ¹Vienna/AT, ²Frankfurt a. Main/DE, ³Rome/IT, ⁴Valencia/ES, ⁵Munich/DE, ⁶Priego/ES

Purpose: To evaluate the effect of contrast material flow rate (3 ml/s vs 5 ml/s) on the detection and visualization of HCC at MDCT.

Materials and Methods: In a prospective, randomized multi-center trial, 97 patients suspected of having HCC underwent quadruple-phase (double arterial, portal-venous, delayed phase) MDCT. Patients were randomized to receive the iso-osmolar contrast medium iodixanol 320 mg I/ml (1.5 ml/kg b.w.) at a flow rate of 3 or 5 ml/s (48 vs 49 patients). Qualitative (lesion detection, visualization, image quality) and safety assessment were performed.

Results: Overall, 100 and 145 HCC were detected in the 3 and 5 ml/s group, respectively ($p < .05$). More lesions < 1 cm were detected at 5 ml/s (33 vs 16 lesions). The late arterial phase showed significantly more lesions than the early arterial phase at both injection rates (133 vs 100 lesions and 96 vs 67 lesions, respectively, $p < .0001$). There was no difference between both groups in subjective visualization of HCC and in overall image quality, but hyperattenuating HCC were better visualized in the late arterial phase using the higher flow rate (excellent: 54% vs 27%). No differences between 3 ml/s and 5 ml/s were reported for the rate of patient discomfort ($p = 1.0$) and contrast media-related adverse events ($p = .62$). Most discomforts were of mild intensity and none was severe.

Conclusion: For detection of HCC with MDCT a higher flow rate of 5 ml/s is recommended. Visualization of small HCC is improved without increasing the rate of discomfort or the risk of adverse events.

B-858 11:51

Liver hemangiomas: Pattern-based classification scheme for enhancement speed at arterial phase CT

M. Scialpi¹, A. Rotondo², M. Scaglione², A. Ragazzino², L. Lupattelli¹, ¹Perugia/IT, ²Naples/IT

Purpose: To present a classification scheme for classifying liver hemangiomas on the basis of the enhancement speed patterns that they exhibit in the arterial phase on helical Computed Tomography (CT).

Methods and Materials: Triphasic helical CT scans in 54 non cirrhotic patients with 100 hemangiomas were retrospectively reviewed. On arterial phase enhancement the speed of all lesions were classified as follows: rapid (> 75% of tumor volume), intermediate (25%-75% of tumor volume), and slow (< 25% of tumor volume). Differences in mean size among the hemangiomas with slow, intermediate, and rapid enhancement were analysed. A P value of less than 0.05 was considered statistically significant.

Results: Slow enhancement was observed in 61 of the 100 hemangiomas (61%), intermediate enhancement was seen in 11 (11%), and rapid enhancement was seen in 28 (28%). A significant differences in mean size ($P < .001$) was seen among hemangioma with speed and intermediate enhancement. Temporal peritumoral enhancement was most frequently encountered in rapid enhancing hemangiomas (13 of 28 [46.4%]) than in those with intermediate (1 of 11 [0.9%]) and slow (0 of 61 [0%]) enhancement ($P < 0.001$).

Conclusion: Different phases of enhancement on helical CT facilitates the diagnosis of liver hemangiomas. Our classification scheme may be useful for the interpretation of the arterial phase on helical CT.

10:30 - 12:00

Room G

Genitourinary

SS 1807b

Urogenital lesions: Diagnosis and interventions

Moderators:

M. Bertolotto; Trieste/IT
A.J. Marcinski; Warsaw/PL

B-859 10:30

Natural history of incidental testicular masses ≤ 0.5 cm detected by US

L. Pallwein, H. Steiner, A. Klauser, F. Frauscher; Innsbruck/AT

Purpose: To evaluate the natural history of incidental testicular masses ≤ 0.5 cm detected with ultrasound (US).

Methods and Materials: Fifteen patients (mean age: 39.3 years; range, 27 - 61 years) with urological problems such as prostatitis, epididymitis, infertility, and lower abdominal pain but without suspicion of testicular tumor, underwent scrotal US using a transducer with a frequency of 12.0 MHz (Acuson Sequoia, Mountain View, Cal.). In the 15 patients 16 unilateral testicular masses were found. All patients underwent an organ-sparing frozen-section-guided approach. The US findings were compared with the histological findings.

Results: Tumor size varied from 0.15 - 0.5 cm (mean: 0.35 cm). Histological analysis revealed pure seminoma in 3 cases (18.8%), Leydig cell tumor in 9 cases (56.3%), Leydig cell hyperplasia in 3 cases (18.8%), and fibrotic pseudotumor in 1 case (6.6%). US findings showed in all cases a well-defined mainly hypoechoic mass with peripheral and central flow pattern on color Doppler US. Tumor markers were within normal range in all subjects.

Conclusion: US is highly sensitive in the detection of small testicular tumors. Since the majority of the tumors ≤ 0.5 cm were malignant, exploratory surgery remains the best therapeutic approach. Removal of a testicle can be avoided by an organ-sparing frozen section-guided approach.

B-860 10:39

Are renal perfusion parameters reliable without deconvolution analysis?

M.I. Dujardin, S.P. Sourbron, R. Luypaert, P. Van Schuerbeek, F. Deridder, D. Verbeelen, S. Makkat, T. Stadnik; Brussels/BE

Purpose: To investigate whether measures for renal blood flow, blood volume and mean transit time, obtained by T1-DCE perfusion MR imaging, are reliable without deconvolution analysis.

Materials and Methods: 12 normal patients underwent single-slice perfusion on a 1.5 T MR imaging. During the first pass of 20 ml Gadolinium (at 2 cc/s) one axial 4 mm slice was acquired using a Turboflash sequence (TR 4.4 ms, TE 2.2 ms, FA 50°, temporal resolution 0.3 s). Post-processing included conversion to tracer concentrations and deconvolution with an aorta AIF. Parametric maps (maximum time course, area under the curve and the ratio of both) were calculated before (rRBF, rRBV and rMTT) and after deconvolution (RBF, RBV and MTT). Average cortical values were obtained from whole cortex ROIs. Results were evaluated by visual image inspection and by non-parametric correlation analysis.

Results: Image inspection showed that in 4/12 patients rMTT values were lower in medulla than in cortex, contrary to expectations based on physiological considerations. For MTT and RBF no such discrepancies were observed. rRBV and RBV maps are essentially identical with proper scaling. Intersubject comparison of ROI data provided strong evidence for a complete lack of correlation between MTT and rMTT ($r = 0.16$, $p = 0.34$), and between RBV and rRBV ($r = 0.09$, $p = 0.54$). RBF and rRBF were weakly but negatively correlated ($r = -0.28$, $p = 0.056$).

Conclusion: Renal perfusion parameters are unreliable without a deconvolution analysis. Interpreting these parameters in terms of physiological quantities such as RBF or MTT may lead to erroneous conclusions.

B-861 10:48

Does a deconvolution analysis remove the dependency of renal perfusion parameters on injection dose?

M.I. Dujardin, S.P. Sourbron, R. Luypaert, P. Van Schuerbeek, C. Ernst, S. Makkat, T. Stadnik; Brussels/BE

Purpose: To determine whether a deconvolution analysis of T1-weighted dynamic contrast enhanced MR imaging produces values of renal blood flow (RBF), blood volume (RBV) and mean transit time (MTT) independent of injection dose.

Scientific Sessions

Materials and Methods: Perfusion measurements were performed on 14 normal humans using a 1.5 T MR imaging. During the first pass of Gadolinium, 4 mm single-slice axial images were obtained using a Turboflash sequence (180° preparatory pulse, TR 4.4 ms, TE 2.2 ms, FA 50°, matrix 128/256, acquisition time 0.3 s). A dose of 10 ml Gadolinium was injected in 6 patients (group 1) and of 20 ml in 7 patients (group 2). Injection rate was 2 cc/sec in both cases. Mean age was 52 years for group 1 and 51 for group 2. Using in-house built software, signals were converted to tracer concentrations and deconvolved with an AIF selected manually in the aorta. Whole cortical ROI measurements of RBF, RBV and MTT were obtained and compared between patient groups using non-parametric Mann-Whitney statistics.

Results: For group 1 we found mean cortical values for RBF (/ml/min/ml), MTT (/sec) and RBV (/ml/ml) of 1.7 ± 0.7 , 17 ± 9 and 0.5 ± 0.7 respectively. For group 2 the mean values were 1.3 ± 0.3 , 18 ± 4 and 0.4 ± 0.1 respectively. The difference between groups was not statistically significant ($p > 0.05$) for any of the parameters.

Conclusions: A deconvolution analysis of T1 weighted dynamic contrast enhanced MR imaging of the kidney leads to RBF, RBV and MTT values which are independent of injection dose.

B-862 10:57

Protective role of pancreas and successful islets transplantation on transplanted kidney of type I diabetic uremic patients: Clinical and color Doppler ultrasound (CDU) assessment in 234 patients

C. Losio, M. Venturini, P. Fiorina, E. Angeli, A. Secchi, A. Del Maschio; Milan/IT

Purpose: In type I diabetic uremic kidney-transplanted patients, diabetes and immunosuppression can reduce kidney-graft function. Simultaneous pancreas or successful-islets transplantation determine resolution of diabetes. Our purpose was to retrospectively evaluate the transplanted kidneys of Kidney-Alone (KA), Kidney-Pancreas (KP) and Successful-Kidney-Islets (KIS) transplanted patients.

Materials and Methods: From 1991 to 2004 the transplanted kidneys of 166 KP, 24 KIS and 44 KA patients were evaluated with CDU (Ansaldi-Esaote AU590/ATL-Philips HD15000); the mean resistance index (RI) of three intraparenchymal arteries and renal size (distance between the upper and lower poles) were measured. Urinary albumin excretion (UAE), Serum creatinine (SC) and glycated hemoglobin (HbA1c) were also evaluated. All data were recorded baseline, 2, 4 and 6 years from transplantation.

Results: The KP and KIS groups only showed a significant reduction of RI (KP-baseline: 0.74 ± 0.01 ; KP-6 years: 0.68 ± 0.01 ; KIS-baseline: 0.72 ± 0.02 ; KIS-6 years: 0.69 ± 0.02 , $p < 0.05$; KA-baseline: 0.76 ± 0.02 ; KA-6 years: 0.76 ± 0.04). Despite all groups showing an increase in graft size after the transplant, only in the KP group did renal hypertrophy persist at 6 years from transplantation. An increase of UAE was evident only among KA patients (KA-baseline: 31.4 ± 9.0 mg/L; KA-6 years: 82.9 ± 33.6 mg/L). A significant increase in SC was found at 6 years only in KA group, not in KP and KIS (KA-baseline: 1.58 ± 0.08 mg/dL; KA-6 years: 2.78 ± 0.44 mg/dL, $p < 0.05$). HbA1c levels at 6 years were significantly lower in KP than KA (KP-6 years: $5.9 \pm 0.1\%$; KD-6 years: $8.1 \pm 0.4\%$, $p < 0.05$).

Conclusion: CDU allows quantitative and reproducible measurements of transplanted kidney. Pancreas and successful-islets transplantation, restoring good glycometabolic control, exert a protective role on function, hypertrophy and microcirculation of kidney-graft.

B-863 11:06

Microscopic hematuria and pelvic congestion syndrome: A late sequela of cirrhosis

E.K. Lang, R. Thomas, M. Brammer, S. Joshi; New Orleans, LA/US

Purpose: To investigate the relationship of hematuria and pelvic congestion syndrome to collateral flow and pressure related changes in the left renal vein as consequence of cirrhosis and demonstrated on dynamic helical CT.

Methods and Materials: 40 patients, 29 male, 11 female, age 38-73 years, with the diagnosis of cirrhosis presented with microscopic hematuria ($n = 32$), pelvic congestion syndrome ($n = 8$) and varicoceles ($n = 2$). Patients were studied by multiphasic helical CT pre-enhancement, late arterial-early cortico-medullary, parenchymal and excretory phase sequences, 1.25 - 3.8 mm collimation.

Results: Advanced cirrhosis, hepatitis C, ($n = 14$) alcoholism or nutritional, ($n = 26$) was confirmed in all 40 patients. The early cortico-medullary and parenchymal phase CT demonstrated huge splenorenal shunts in all patients. In 17 of 18 patients elevated left renal vein pressure was confirmed by left renal vein catheterization. 8 of the female patients showed massive dilation of the ovarian vein communicating to dilated pelvic veins and causing a pelvic congestion syndrome, 2 male patients demonstrated left varicoceles, a consequence of retrograde flow in the dilated left gonadal vein.

Conclusions: Massive splenorenal anastomoses to the left renal vein cause elevation of left renal vein pressure and are likely responsible for microscopic hematuria. Retrograde flow from the left renal vein into the gonadal and ovarian veins cause pelvic vein congestive syndrome in the female and varicoceles in the male.

B-864 11:15

MR urethrography in complete posterior urethral stricture: Comparison with retrograde and/or voiding urethrography

D. Sung, S. Cho, Y. Kim, K. Chung, D. Moon, J. Kim; Seoul/KR

Purpose: The purpose of this study is to evaluate the usefulness of magnetic resonance (MR) urethrography in complete posterior urethral stricture.

Materials and Methods: Twelve patients with complete posterior urethral strictures were studied preoperatively with axial and sagittal TSE T2, sagittal T1 and contrast-enhanced sagittal T1-weighted images with 3 mm thickness covering the entire urethra by 1.5 T MR scanner. Before MR scanning, aseptic lubricant was infused through the external urethral meatus to dilate the distal urethra up to the stricture. To determine which method accurately estimate the stricture length, each imaging result was compared to surgical specimen or finding.

Results: At MR imaging, the strictured segment manifesting as low signal intensity on T1WI and T2WI was seen just proximally to the dilated distal urethra in all patients without contrast enhancement. MR imaging was able to show the periurethral extent of fibrosis and the prostatic displacement. Two patients with prostatic displacement and long strictures of 3 cm needed the combined perineal and transpubic approach at surgery. For MR versus retrograde and/or voiding urethrography, the mean measurement errors were 0.33 ± 0.26 cm and 1.69 ± 0.97 cm. MR measurement of the stricture length demonstrated significantly lower errors ($p < 0.05$) and better linear fit compared with the conventional urethrography ($R^2: 0.85$ vs 0.03).

Conclusion: MR imaging of the dilated urethra with aseptic lubricant, which we call "MR urethrography" is an effective tool in the evaluation of complete posterior urethral stricture. It can be particularly helpful in the surgical planning.

B-865 11:24

Diagnosis of epididymo-testicular disjunction on gadolinium-enhanced MR imaging in patients with cryptorchidism

A.E. Mahfouz, H. Sherif; Doha/QA

Purpose: To assess the value of magnetic resonance imaging in diagnosis of epididymo-testicular disjunction in patients with cryptorchidism.

Methods and Materials: Fifty children with cryptorchidism (44 unilateral and 6 bilateral) were examined by MR imaging. The patients were examined by coronal T2-weighted and proton density images as well as transverse T1-weighted images of the scrotum, inguinal region, and pelvis, followed by transverse and coronal fat-saturated T1-weighted GRE images before and after intravenous injection of Gd-DTPA. Maximum intensity projection (MIP) of the coronal gadolinium-enhanced fat-saturated T1-weighted images has been performed. All patients underwent surgical treatment. MR imaging and surgical findings were compared.

Results: Out of the 56 undescended testes included in the study, 52 testes could be identified on MR imaging, 30 intraabdominally and 22 within the inguinal canal. Epididymo-testicular disjunction could be demonstrated in 12 testes on MR images as enhancing soft tissue structure (representing the elongated epididymis) or vascular structures (representing the looping spermatic vessels) preceding the undescended testis through the inguinal canal into the scrotum. Compared to the gold standard of surgical exploration, MR imaging has sensitivity of 57%, specificity of 100%, negative predictive value of 80%, positive predictive value of 100%, and accuracy of 84% for the diagnosis of epididymo-testicular disjunction.

Conclusion: MR imaging has high specificity for the diagnosis of epididymo-testicular disjunction in patients with cryptorchidism.

B-866 11:33

An anatomical study of retro-renal peritoneal extension and implications for safe percutaneous renal intervention

R. Vikram, C. Ripley, I. Zealley; Dundee/UK

Purpose: Retro renal peritoneal reflections have been implicated in grave intraperitoneal complications following percutaneous renal interventions. We attempted to determine the prevalence and extent of this anatomical variant by studying CT scans on patients with ascites.

Materials and Methods: CT images of 105 consecutive patients with free intraperitoneal fluid were evaluated by two reader consensus. The angle between a horizontal line through the kidney and another line joining the most posterior

Tuesday

Scientific Sessions

extent of the peritoneal reflection and the epicentre of the infra-hilar portion of each kidney was measured.

Results: On the right (n = 105) the peritoneal reflection extended posteriorly to between 0° - 30° from the horizontal in 60.5%, between 31° - 60° in 24%, between 61° - 90° in 2% and beyond 91° in 1%. It did not extend posterior to the horizontal line in 12.5%. On the left (n = 88) it extended posteriorly to 0° - 30° in 48% and to 31° - 60° in 9% and did not extend posterior to the horizontal in 48%.

Conclusions: Retro-renal extension of the peritoneal reflection is surprisingly common and much more common on the right. During percutaneous renal interventions the kidneys are usually approached at an angle between 30° and 60° from the horizontal. Between these angles the likelihood of traversing the peritoneal cavity is substantially higher on the right (27% vs 9% p < 0.05). Where there is a choice, we suggest that percutaneous renal interventions be performed on the left side to minimize the risk of intraperitoneal hemorrhage.

B-867 11:42

Terminal stage pelvic malignancy with bilateral obstructive uropathy: Is there a role for percutaneous intervention?

D. Souftas, M. Mantatzis, P. Prassopoulos; *Alexandroupolis/GR*

Purpose: Patients with terminal stage pelvic malignancy and bilateral ureteric obstruction have a very short life expectancy. The purpose of this study is to evaluate the expediency of percutaneous nephrostomy (PN) -with or without ureteral stenting- in these cases.

Materials and Methods: PN was performed in 75 patients with obstructive uropathy, due to terminal stage pelvic malignancy, under imaging guidance. Percutaneous ureteral stenting was attempted in 38 patients, where guidewire passed through the obstruction, and was successful in 35. The patients' clinical improvement and quality of life after PN and/or stenting were objectively evaluated according to the Karnofsky-scale. Patients with painful bone metastases were not included in the study.

Results: In 60 (80%) of the patients urea and creatinine levels were restored to normal, in 9 (12%) there was improvement and in 6 (8%) no difference was noticed. Twenty-one (28%) patients could go back to usual personal activities, 11 (14.6%) needed minimal support, and 12 (16%) continued to need full support, despite clinical improvement. There was no clinical improvement in 31 (41.3%) patients (elderly, with ascites - limb edema and non painful metastatic bone disease). The patients died in a period between 48 h and 37 months post PN (median survival 7.2 months).

Conclusion: PN with or without stenting for management of obstructive uropathy in terminal stage pelvic malignancy is justified in terms of significant prolongation of survival, clinical improvement in the majority of cases and better quality of life in about half of the patients.

B-868 11:51

Percutaneous radiofrequency ablation (RFA) of small renal carcinoma D. Breen¹, B. Stedman¹, E. Rutherford¹, J. Cast²; ¹*Southampton/UK*, ²*Hull/UK*

Purpose: Small renal tumours are increasingly found incidentally in elderly patients. This group often have significant co-morbidity and may be unsuitable for major surgery. RFA offers a less invasive therapeutic option. This study aims to assess the safety, efficacy and medium term outcome of RFA in the management of small RCC.

Method and Materials: 41 patients (mean age 76.8 yrs, range 54-89) underwent RFA of 45 tumours (mean 3.5, range 1.5-6.8 cm) between November 1999-2004. 46 treatment sessions were performed, 32 under intravenous sedation and 14 under GA. Treatments lasted 12 to 24 minutes and were ultrasound (31) or CT (15)-guided. All patients were followed clinically, biochemically and with 6 monthly CT.

Results: Complete tumour necrosis was seen in 38 of the 45 tumours. Five tumours required further CT guided treatment for residual viable crescents of tumour. Two elderly patients (87, 88 years) have been treated conservatively despite traces of tumour on follow-up CT. Only minor complications have been identified. Self limiting macroscopic haematuria was seen with a large central tumour. No significant rise in mean serum creatinine has been noted (mean rise 5.8 mmol). One patient with VHL syndrome had 4 tumours treated in a solitary kidney with complete response, however metachronous nodules developed during follow-up and she died of metastatic renal carcinoma. Follow-up (mean 14.8 months, range 1-58 months) revealed no evidence of local or distant recurrence in 38 of 41 patients.

Conclusion: Medium term experience suggests RFA is a safe, well tolerated and minimally invasive therapy for small renal tumours.

10:30 - 12:00

Room H

Interventional Radiology

SS 1809

New developments in interventional radiology

Moderators:

F.G. Joffre; *Toulouse/FR*

M. Köcher; *Prague/CZ*

B-869 10:30



The early results of transhepatic hemodialysis catheters

C. Andic, S. Yilmaz, T. Sindel, E. Lüleci; *Antalya/TR*

Purpose: To assess the early results of transhepatic hemodialysis catheter placement in patients who have exhausted traditional sites of venous access.

Materials and Methods: Nine patients (seven men and two women aged 35-77 years; mean age, 56 years) underwent placement of 11 transhepatic hemodialysis catheters. Transhepatic catheters were placed in the absence of an available peripheral venous site (3 patients) or for preservation of the single remaining venous site for arteriovenous fistula and arteriovenous graft (6 patients). Patient follow-up was performed by reviewing dialysis records and maintaining communication between the patients and the radiologist.

Results: Technical success was achieved in all patients. The mean time of the catheters in situ was 34.6 days (range, 1-67 days). Because of catheter tip dislocation, two patients required catheter repositioning to achieve optimal blood flow in hemodialysis. Two patients required catheter exchange because of early device failure. There were three complications in the 11 catheter placements (%27.3) in 9 patients including unilateral (right) hemothorax (1 patient), venous-biliary-peritoneal fistula (1 patient) and massive intraperitoneal hemorrhage (1 patient). Catheters were removed after maturation of a functioning arteriovenous fistula (3 patients) and because of the complications (3 patients). One catheter dislodged prematurely due to pulling of the catheter by patient. Two patients still had functioning catheters in 42nd and 63rd days when this manuscript was submitted.

Conclusions: Despite the limited available literature and complications risks of the procedure, transhepatic hemodialysis catheters offer a viable option to patients who have exhausted traditional sites of venous access.

B-870 10:39

Treatment of renal cystic diseases: Use of minocycline hydrochloride as soft sclerosing agent

F.M. Danza, V. Marino, A. Magistrelli, A. Bernardini, S. Costanzi, E. Bock, L. Bonomo; *Rome/IT*

Purpose: To describe percutaneous treatment of renal cystic diseases, using a new sclerosing agent permitting a procedure with lower discomfort for patients and better handling for the operator.

Methods and Materials: 62 patients (54 simple cysts, 8 autosomic polycystic renal disease [APRD]) were treated with this soft method instead of classic alcoholization. After percutaneous extraction of half content of the cyst, a solution of minocycline hydrochloride (1 mg per ml of native volume of cyst) was introduced and left into the cavity (single-shot technique). For the absence of effects on excretory system of the sclerosing agent a previous opacification of cystic lumen is not required. Follow-up was performed at 3, 6, 9 and 12 month after treatment.

Results: In simple cyst the treatment was successful in 90% at 6 months (volume reduction over 50%). In 10% of cases a retreatment was needed, with a total success rate of 100%. No recurrence was noted. In APRD a significative reduction in renal volume was obtained, while no definitive signs of improvement of renal function or hypertension are demonstrated.

Conclusion: This method is superior to alcoholization: the discomfort for patient is minimal, results are better, without risks in accidental extravasation. The procedure is rapid and less expensive (catheter set not required). For simple cysts the method is superior to alcoholization. The application of this new kind of sclerosis in APRD has a promising, low cost role in reducing abdominal volume, but bigger experience and longer follow-up is needed.

Scientific Sessions

B-871 10:48

Partial endovascular embolisation of thyroid gland: Initial experience

K. Brzozowski, P. Zukowski, B. Jaron, P. Twarkowski; Warsaw/PL

Purposes: We have three current therapies for patients with hyperthyroidism: antithyroid drugs, radioiodine and surgery treatment, but it is exist a group of patients who cannot use these therapies. In this study we check the partial embolisation of thyroid gland as an alternative for patient who tolerate current therapies.

Material and Methods: Between January 2004 to August 2004 we perform partial embolisation of thyroid gland in six patients with hyperthyroidism. First we performed selective arteriography for evaluate the blood supply of thyroid gland and next we embolized two or three thyroid arteries by means of mixture of histoacryl and lipiodol. Next we use post embolisation angiography to evaluate the affectivity of embolisation.

Results: At the end of the follow-up period all six patients were euthyroid and the size of thyroid gland had decreased. We have no complication.

Conclusion: The clinical follow-up after embolisation suggest that this procedure is an effective, minimally invasive and safe method for the treatment for patients with hyperthyroidism.

B-872 10:57

Pregnancy outcome following uterine artery embolisation

W.J. Walker, T.T. Carpenter; Guildford/UK

Purpose: We present pregnancy course and outcome of 45 pregnancies in 37 women following Uterine Artery Embolisation. This being the largest reported series world wide of pregnancy post Uterine Artery Embolisation.

Materials and Methods: Cases identified by screening questionnaires and database, direct conversation and hospital delivery notes.

Results: 25 Live births, 5 Ongoing pregnancies (all past 2nd trimester), 2 Terminations, 10 Miscarriages, 1 Ectopic Pregnancy, 1 - 33 week still birth (True Knot in Cord), Uterine Volume on ongoing and successful pre-pregnancies varied from 59.95 cc - 1808.4 cc, 24 Successful deliveries after 24 weeks gestation, 18 by Caesarean section, Pre-term delivery rate 5/25 (20%), 2 Successful pregnancies complicated by bleeding first trimester, 2 Cases proteinuric hypertension, 2 Cases pre-term spontaneous rupture of membranes, 3 Cases primary post partum haemorrhage, Mean birth weight term babies 3.256 kg, One case of fetal growth restriction, Updated demographic and more detailed complication data will be presented.

Conclusion: When demographics of patient population in question is considered there does not appear to be an obvious excessive obstetric risk following Fibroid Embolisation.

B-873 11:06

Transcather embolization of male varicocele with Fibro-Vein mousse infusion: Experience with 260 patients

R. Gandini, V. Pipitone, M. Chiocchi, C. Reale, D. Konda, G. Simonetti; Rome/IT

Purpose: The aim of the study was to evaluate efficacy and safety of the Fibro-Vein mousse in the treatment of male varicocele.

Materials and Methods: From January 2000 to March 2004, 260 patients (mean age: 28.2 years; range 15-44) were treated by sclerotherapy of the pampiniform plexus venous dilatation. All patients had infertility, pain or both; the diagnosis was routinely obtained by physical examination and Doppler ultrasound. Phlebography was performed under local anesthesia with access through the basilic vein using 4 Fr Simmons II catheter. In all patients embolization was performed with mousse of Fibro-Vein 3% and air (ratio 1:4). Follow-up was routinely performed by Doppler ultrasound and clinical examinations.

Results: A technical success was obtained in all but 26 patients (10%); of the 73 patients (28.1%) with infertility 34 (46.6%) became again fertile; of the 153 (58.8%) patients with pain 132 (86.3%) had pain relief, of the 34 (13.1%) patients with pain and infertility, 27 (79.4%) had a pain relief and improvement of sperm count alteration, while 7 (20.6%) patients had relief of pain but still sperm count alteration.

Conclusion: Male varicocele treatment by Fibro-Vein mousse and air is safe and very effective technique that allows an easy pampiniform plexus sclerotherapy.

B-874 11:15

Bulbar urethral strictures treated with allium temporary covered stents:

First clinical experience

Z. Markovic¹, B. Markovic¹, D. Yachia², R. Levy², H. Maksimovic¹, O. Vojvodic¹; ¹Belgrade/YU, ²Hadera/IL

In August and October 2003, a new generation of urethral stents ALLIUM, produced in Israel, were inserted in 18 patients with chronic stricture of bulbar urethra. The indications for insertion were determined according to well-known and recognized therapeutic protocols. The stent is made of nitinol wire with polyurethane cover. Stent inserted under local anesthesia by a special self-expandable system that may be fixed or flexible. The stents are available in three lengths. Radioscopically-assisted insertion was performed over formerly placed metal guide. Balloon-catheter dilatation of stricture matching the stent width was carried out. Preinsertion urethrotomy was performed in one case. The insertion technique is simple presupposing the knowledge of interventional radiology and endoscopic urology techniques. The check-up was done according to a priori established protocol. Due to stent migration, the "stent over stent" technique was applied in one case, while reposition by balloon-catheter upward traction was performed in two cases of caudal migration. No irritative discomfort was reported in the first 4 months after stent dwelling. Uroflowmetric control verified at least four times better results than before the insertion. On behalf of flexibility, low radial force and conical shape of the posterior part of stent, no lesion of the external urethral sphincter were manifested. The stents withdrawn after 6-12 months by outward traction using the forceps. The first clinical experience are very favorable and ALLIUM stent may be expected to be the stent of choice for chronic bulbar strictures.

B-875 11:24

MR-guided galvano-therapy in patients with prostate cancer: Technique and first clinical results

S. Zangos¹, H. Mayer², F. Mayer¹, A. Wetter¹, K. Eichler¹, M.G. Mack¹, W. Schwarz¹, T.J. Vogl¹; ¹Frankfurt a. Main/DE, ²Regensburg/DE

Purpose: To examine the feasibility of MR-guided galvano-therapy (electrochemical treatment) in patients with prostate cancer.

Material and Methods: Sixteen patients (mean age 72 years) with histological proven prostate cancer were prospectively treated with galvano-therapy. Two MR compatible electrodes were positioned in the prostate under MR guidance with a transgluteal approach in an low field MR imaging-system (0.2 T, MR Concerto, Siemens). A maximum of 350 coulomb was applied with 3 treatments and an interval of 1 week. Follow-up was performed 3, 6 and 12 months with clinical examination, PSA values and MR-spectroscopy.

Results: The treatment was well tolerated by all patients. After the treatment 9 patients had a reversible urinary dysfunction and in 3 patients a hematuria emergent. One patient developed a prostatitis which had to be treated with antibiotics. In 9 patients a stable disease and in 2 patients a response could be observed in the follow-up. In 3 cases no success could be achieved. 3 patients died in the course of follow-up, whose dead could not be attributed to the prostate cancer or the treatment.

Conclusion: MR-guided galvano-therapy of the prostate gland is considered as a new and promising treatment option for prostate cancer.

B-876 11:33



Early experience with the self-expanding plastic stent (Polyflex) in oesophageal cancer

F.G. Irani, J.P. Morales, T. Sabharwal, R. Salter, R. Dourado, A. Adam; London/UK

Purpose: To present our early experience with the use of self-expanding plastic endoprosthesis (retrievable) in oesophageal cancer.

Material and Methods: A total of six stents (Polyflex) were placed in six patients (3 male, 3 female), mean age 64 years (range 48-77). Five had oesophageal cancer and required weight gain before surgical intervention. The remaining patient had a malignant fistula between the airway and the oesophagus. Stents were deployed using radiological guidance and conscious sedation in the interventional suite.

Results: In all patients successful deployment of stents was achieved (100%). No case of stent migration was noted. No major complications were seen. All the patients booked for surgical treatment improved their quality of life and dysphagia score at least in 1 grade. Weight gained was satisfactory prior to surgery. Immediate exclusion of the fistula was observed in the patient with the tracheo-oesophageal fistula.

Scientific Sessions

Conclusion: Our early experience would suggest that the use of the new self-expanding plastic stent is a feasible and safe option in palliative treatment for weight gain while awaiting surgery. Furthermore, the Polyflex should be considered a good option for the management of tracheo-oesophageal fistulae, and would also be suitable for use in refractory benign oesophageal strictures.

B-877 11:42

Human growth factor (HGF) evaluation before liver intervention:

A prognostic significance for liver regeneration

T. Lehnert, A. Gazis, A. Wetter, S. Zangos, R. Hammerstingl, A. Thalhammer, W.-O. Bechstein, T.J. Vogl; *Frankfurt a. Main/DE*

Purpose: To evaluate and compare the complexity of liver regeneration in correlation with the regeneration factor HGF, post liver resection and MR-guided laser induced thermotherapy (LITT).

Material and Methods: 40 patients were evaluated, 21 patients post surgical liver intervention and 19 patients post ablation (LITT). During a subsequent monitoring period of 12 months the effects of therapy on the cytokine HGF were evaluated and compared to the initial, pre-interventional HGF value. In addition, the effects on liver volume after surgical and interventional radiological procedure was evaluated using unenhanced and contrast enhanced MR imaging and CT. Volumetric examination (CT-volumetry) of liver parenchyma pre and post intervention was accomplished and the dynamics of liver regeneration and regional growth of liver segments were evaluated.

Results: A significant influence on the HGF process could be confirmed on loss of liver parenchyma resulting from surgery or LITT induction. Pre-interventional HGF-values < 1500 pg/ml (n = 23) led to a significant increase of liver volume (115-584 ml). Patients with initial HGF-values > 2000 pg/ml (n = 11) showed a decrease of liver volume (5-409 ml) after intervention. Pre-interventional HGF-values between 1501 pg/ml and 1999 pg/ml (n = 6) showed no definite reaction of liver parenchyma. All patients younger than 55 years showed stronger dynamics than 55+ year old patients.

Conclusion: Human growth factor (HGF)-value, pre-interventional, has a significant impact on the liver regeneration post MR-guided laser induced thermotherapy (LITT) and surgical resection. Pre-interventional low HGF-values correlate with increased liver regeneration and stronger regeneration dynamics.

B-878 11:51

Laser-induced thermal ablation of lung metastases: CT findings in a follow-up study

N. Hosten, C. Rosenberg, C. Weigel; *Greifswald/DE*

Purpose: Laser-induced thermal ablation of pulmonary metastases is a new option in multimodal cancer therapy. Preliminary results from patients of an ongoing study are presented.

Materials and Methods: 45 lesions in 34 patients were treated (CT fluoroscopy, Monocath 5.5 F water-cooled applicator, MeoMedical, Germany; maximal 14 W for up to 15 min, 1 to 3 applicators per lesion). Different primaries, mainly colorectal carcinomas (12 / 34 patients), had caused metastatic disease. Lesion size ranged from 6 to 64 mm, median 22 mm. Follow-up CT was performed the first 3 months each, then all 3 and 6 months, respectively. Median follow-up was 6 months (1 to 52 months).

Results: Ablative therapy was technically successful in 43 / 45 patients. In 5 cases therapy was completed after 2, in 3 cases after 3 sessions. An initial increase in size of the visualized correlate was seen in 13 cases, secondary cavity in 5 cases. 26 patients showed marked size reduction of the imaging correlate in further follow-up. These patients were diagnosed successfully treated. Residual CT findings were ground-glass opacity or cystic defects. Consecutive pneumothoraces (47%) needed drainage in 9% of the cases, hemorrhage (22%) was self-limited in all cases. Complications showed no significant difference to diagnostic lung biopsies.

Conclusion: Laser-induced thermal ablation is a promising option in multimodal therapy of non-resectable lung metastases. First results show differences in feasibility correlated to localization of the targeted lesion. Therapy success evaluation demands an interval of at least three months.

10:30 - 12:00

Room I

Contrast Media

SS 1806

Iodinated contrast media: Technical advances and side effects

Moderators:

A.N. Chalazonitis; *Athens/GR*
U. Erikson; *Uppsala/SE*

B-879 10:30

Nephrotoxicity after renal arteriography with "low" and "iso-osmolar" iodine and gadolinium contrast media (CM) in an experimental model

B.A. Elmståhl, U. Nyman, P. Leander, K. Golman, T. Almén, R. Pehrson, C.-M. Chai; *Malmö/SE*

Purpose: To compare the nephrotoxic effect of the "iso-osmolar" CM iodixanol (150 and 320 mg I/mL), "low-osmolar" CM iopromide (150 mg I/mL) and two gadolinium CM, 0.5M gadodiamide and 1.0 M gadobutrol, in an ischemic porcine model.

Methods and Materials: Following left-sided nephrectomy each test solution was injected in 8 animals at a rate of 20 mL/min (dose 3 ml per kg) into the right renal artery distal to an occluding balloon at the start of a 10-minute period of ischemia. The plasma half-life elimination times of the CM one to three hours post-injection were used to compare the effects of the different test solutions on glomerular filtration rate. Longer half-life means lower GFR.

Results: The median plasma half-lives following injection were: Iodixanol 150 mgI/mL - 144, iodixanol 320 mg I/mL - 142, iopromide 150 mg I/mL - 138, 0.5M gadodiamide - 237 and 1.0 M gadobutrol - 1583 minutes.

Conclusion: The "iso-osmolar" CM iodixanol and "low-osmolar" iopromide appeared less nephrotoxic than the two gadolinium CM. According to this experimental study iodixanol 320 mg I/mL is the agent of choice for renal arteriography and/or angioplasty procedures resulting in a far better X-ray attenuation than the other agents.

B-880 10:39

Effects of intravenous iomeprol on common carotid and brachial artery blood flow and shear stress

S. Tamburini, C. Irace, D. Barresi, S. De Franceschi, A. Gnasso; *Catanzaro/IT*

Purpose: Radiographic iodinated contrast media (CM) induce vascular tone and blood flow alterations. To evaluate hemodynamic modifications induced by CM, we measured blood flow and shear stress in the common carotid and brachial artery before and after intravenous iomeprol injection.

Methods and Materials: Thirty consecutive outpatients referred to our department of radiology for a thoracic or abdominal spiral CT scan were enrolled. The monomeric low osmolality iomeprol (iomeron 350) was injected. Common carotid and brachial arteries were studied by ultrasound and internal diameter and flow velocities were measured online. All subjects underwent a venous blood withdrawal for blood viscosity evaluation. Blood flow (BF), Pulsatility Index (PI) and shear stress (SS) were calculated.

Results: In the common carotid artery, no variation in vascular parameters was found. In the brachial artery, BF was significantly reduced (0.9 ± 0.4 vs. 0.6 ± 0.3 mL/s $p < 0.0001$) as well as SS (41.5 ± 13.9 vs. 35.3 ± 11.0 dynes/cm 2 $p < 0.002$), whereas PI significantly increased (5.0 ± 3.3 vs. 7.5 ± 5.3 $p < 0.001$).

Conclusion: The main finding of our study is that the intravenous injection of iomeprol causes a reduction in BF and SS at least in the brachial artery, but not in the common carotid artery. PI, a measure of peripheral vascular resistance, increases in the brachial artery and its change is related to BF. These modifications might be the consequence of the rigidification of erythrocytes following CM injection. Alternatively, endothelin release induced by CM, as described at renal level, might cause vasoconstriction of the small vessels distal to the brachial artery.

B-881 10:48

Contrast media inhibits oxygen consumption in proximal tubular cells from diabetic rats by inducing nitric oxide release

F. Palm, P.-O. Carlsson, A. Fasching, P. Hansell, P. Liss; *Uppsala/SE*

Purpose: Injection of iodinated contrast media (CM) is associated with increased risk for progressive renal dysfunction in diabetic subjects. The exact mechanism

Scientific Sessions

mediating the nephropathy is not known, but earlier studies have proposed alterations in the renal oxygen metabolism as a potential mediator. In this study, we compared the effect of ipromide on the oxygen consumption in isolated renal proximal tubular cells from normal and streptozotocin-induced (STZ)-diabetic rats. The involvement of nitric oxide (NO) was also studied, since the molecule interferes with oxygen consumption.

Methods and Materials: Renal proximal tubular cells were isolated from healthy and STZ-induced diabetic Sprague-Dawley rats weighing approximately 300 g. The in vitro oxygen consumption was measured in a sealed chamber. The influence of CM-induced NO-release was evaluated by pretreating the cells with the NO synthase inhibitor L-NAME.

Results: Iopromide decreased the oxygen consumption in the cells isolated from the diabetic animals, while no effect was seen in the cells from healthy normoglycaemic animals. Pretreatment of the cells obtained from diabetic animals with L-NAME did not effect the baseline oxygen consumption per se, but prevented the CM-induced decrease in oxygen consumption.

Conclusions: These observations suggest that CM selectively in renal tubular cells from diabetic subjects induce release of NO, which inhibits the cellular oxygen consumption. The consequence of intracellular ATP depletion in CM-induced nephropathy during diabetes remains to be established.

B-882 10:57

Evaluating the risk of contrast medium (CM) induced nephropathy (CIN) in relation to gram iodine dose and estimated glomerular filtration rate (eGFR)

U. Nyman¹, T. Almén², P. Aspelin³, M. Hellström⁴; ¹Trelleborg/SE, ²Malmö/SE,

³Stockholm/SE, ⁴Gothenburg/SE

Purpose: To make a preliminary meta-analysis of the risk of CIN in relation to CM-dose expressed as gram iodine (I) instead of simply volume and renal function as eGFR based on serum-creatinine (sCr), sex and weight instead of sCr alone.

Methods and Materials: A Medline search of reports containing definitions and frequencies of CIN, mean eGFR, mean dose of low-osmolality CM and using hydration as only prophylaxis identified ten randomised controlled trials and two cohort investigations, exclusively coronary examinations. The ratio "gram iodine/eGFR" (gram/mL x·min⁻¹) was correlated with the frequency of 1) unspecified CIN defined as rise of sCr of $\geq 44.2 \text{ } \mu\text{mol/L}$ or $\geq 25\%$ and 2) severe CIN defined as oliguria or need of dialysis.

Results: The linear correlation coefficient between the risk of CIN and the ratio "gram I-dose/eGFR" was 0.91 according to definition (1) and 0.84 according to definition (2). At a 1:1 ratio "gram I-dose/eGFR" the regression line indicated a 10% risk of unspecified CIN and a 1.5% risk of severe CIN. At a 3:1 ratio "gram I-dose/eGFR" the risk of unspecified and severe CIN increased to about 50% and 15%, respectively.

Conclusion: The ratio "gram iodine-dose/eGFR" may be an expedient way to predict the risk of CIN. Further studies are needed to define the safety of various ratios in relation to type of examination, type of CM, various risk factors and to reveal a possible exponential relation between CM dose, eGFR and the risk of CIN.

B-883 11:06

Development of water-soluble metallofullerenes as X-ray contrast media

A. Miyamoto, Y. Shibamoto, H. Okimoto, H. Shinohara; Nagoya/JP

Purpose: Although iodinated contrast media are very useful in diagnostic imaging, they can induce various side effects including allergic reaction. With the expectation to reduce the adverse effects, we tried to apply nanotechnology (especially, use of fullerene) to X-ray contrast media. Fullerenes have attracted much attention for various possibilities in recent years. We investigated whether fullerenes containing one or two atoms of heavy metals could be X-ray contrast media. By capsulating heavy metals in fullerene, it was expected to produce little side effects intrinsic to heavy metals.

Methods and Materials: Heavy metal atoms, such as Gd, Er and Eu were encapsulated into fullerene (C_{60}) and synthesized as polyhydroxyl forms ($Gd@C_{60}(OH)_n$, $n = 40$, Gd-fullerenols). They were dissolved in water at a maximum soluble concentration and subjected to CT number analysis. The CT numbers of the solutions were measured using a 16-row multidetector CT scanner. **Results:** The CT number of water-soluble metallofullerenes were 56.0 HU for $Gd@C_{60}(OH)_{40}$, 111.5 HU for $Er@C_{60}(OH)_{40}$, 100.9 HU for $Eu@C_{60}(OH)_{40}$ and 23.3 HU for $Gd_2@C_{60}(OH)_{40}$.

Conclusion: The CT numbers of the water-soluble metallofullerenes investigated in the present study were not high enough to be used clinically in place of iodinated contrast materials. However, if nanotechnology progresses in the near future, it may prove to have a possibility as an X-ray contrast material with little adverse effect.

B-884 11:15

Automatic injectors in magnetic resonance and computed tomography:

Pilot study on hygienic aspects

B. Buerke, A.-K. Sonntag, R. Fischbach, W. Heindel, B. Tombach; Münster/DE

Purpose: To evaluate hygienic conditions using automatic injectors in magnetic resonance (MR) and computed tomography (CT) during clinical routine.

Methods and Materials: Microbiological analysis of the surfaces of medical devices (e.g. control console) and the palm of technical and medical staff were performed by imprint before and after hygiene education. In addition, the microbiological contamination of spikes for contrast medium (CM) and saline following multiple (MR 14 h; CT 8 h) and single use and the potential of retrograde contamination along the tube by the patient were analysed separately.

Results: A bacterial contamination with typical dermal bacteria was documented for the analysed surfaces of medical devices, the palm of technical and medical staff and injections spikes following multiple use (MR: 10/10 CM spikes, 6/10 saline spikes; CT: 8/10 CM spikes, 5/10 saline spikes). Correct hand disinfection in combination with single use of spikes avoids bacterial colonization. Retrograde bacterial contamination from the patient was not observed.

Conclusion: Recurrent hygiene teaching sessions for technical and medical staff in MR and CT departments using automatic injectors are a matter of urgent necessity. Furthermore, multiple use of spikes has to be avoided until dedicated investigations on the potential of hygienical contamination of spikes in multiple clinical use according to time are performed.

B-885 11:24

High-concentration iomeprol in CT angiography: Aortic enhancement in anaesthetised swines

A. Napoli¹, C. Catalano¹, V. Lorusso², A. Morisetti², P.G. Nardis¹, F.A. Calabrese¹, R. Passariello¹; ¹Rome/IT, ²Milan/IT

Purpose: Iomeron® is a commercially available solution of iomeprol. Its highest marketed concentration is 400 mg iodine(I)/mL. However, it can be formulated in even more concentrated solutions. After positive cardiovascular safety assessment in rabbits, we tested the efficacy of a 500 mg (iodine)/mL formulation in a CT study in swines.

Material and Methods: Iomeprol formulations at 500 and 350 mg (iodine)/mL (Bracco SpA, Milan Italy) were injected at 3 mL/s in 8 female anaesthetised pigs (60-90 kg bw) at a dose of 0.5 g (iodine)/kg in a cross-over study design (at least 6 h elapsed time between the two administrations). CT examination (General Electric, HiSpeed DX) was performed with dynamic scans, starting 8 s after contrast medium administration; images were acquired every 3 s for 120 s. Each animal received 1 mL/kg of 500, and 1.43 mL/kg at 350 mgI/mL.

Results: Mean injected volume was 75 mL (60-86 mL range) for 500 and 107 mL (range 85-125) for 350 mgI/mL formulation. Mean aortic attenuation values achieved during 500 mgI/mL administration, across the arterial phase was significantly greater ($p < 0.03$) than that achieved during 350 contrast medium administration. Plotting enhancement over time, tests showed a contrast medium dynamic profile with a higher (mean arterial magnitude > 70 HU) and earlier arterial peak with iomeprol 500.

Conclusion: Iomeprol 500 favourably compares with lower concentrations, eliciting substantial HU enhancement, even in a small study population. Particularly, higher and earlier arterial peaks are promising features for small arterial imaging. Nevertheless, a further investigation with a larger study group is necessary.

B-886 11:33

Effect of iodine flow rate on parenchymal and vascular enhancement during contrast enhanced multiphasic abdominal multidetector row CT

H. Schoellnast, P. Brader, B. Georgieva, B. Oberdabernig, H.A. Deutschmann, M. Tillich; Graz/AT

Purpose: To assess the influence of iodine flow concentration on parenchymal and vascular enhancement during multiphasic abdominal multi-detector row CT (MDCT).

Methods and Materials: Fifteen patients underwent multiphasic abdominal MDCT with standard (group A) as well as with high concentration contrast media (group B) (paired study group), and 90 patients underwent abdominal MDCT either with standard (group A) or with high concentration contrast media (group B) (unpaired study group). In group A, 1.5 mL standard contrast media (300 mgI/ml) per kg was injected with a flow rate of 4 ml/sec while in group B 1.1 mL high concentration contrast media (400 mgI/mL) per kg was injected with the same flow rate. Measurements were performed for all groups in liver, spleen, pancreas, portal vein, inferior vena cava and abdominal aorta to compare enhancement.

Scientific Sessions

Results: Patients of group B showed higher aortal and pancreatic enhancement during the arterial phase than patients of group A. The mean difference in aortal enhancement was 60 HU in the paired and 70 HU in the unpaired study group ($p < 0.01$). The mean difference in pancreatic enhancement was 10 HU in the paired and 17 HU in the unpaired study group ($p < 0.05$ and $p < 0.01$, respectively). During the portal venous and hepatic venous phase no significant difference in parenchymal and vascular enhancement was observed between group A and B ($p > 0.05$).

Conclusion: A high iodine flow rate improves enhancement of the aorta and the pancreas during the arterial phase of multiphasic abdominal MDCT but does not influence later phases.

B-887 11:42

Influence of iodine flow concentration on vessel attenuation and visualization in multi-detector row CT angiography of the pulmonary arteries

H. Schoellnast, H.A. Deutschmann, G.A. Fritz, U. Stessel, G.J. Schaffler, M. Tillich; Graz/AT

Purpose: To assess the influence of iodine flow concentration on attenuation and visualization of the pulmonary arteries in thoracic multi-detector row CT angiography (MDCTA).

Methods and Materials: One hundred consecutive patients who were referred to our department with suspected acute pulmonary embolism underwent multi-detector row CTA of the pulmonary arteries either with 120 mL standard contrast media (300 mgI/mL) (group A) or with 90 mL high concentration contrast media (400 mgI/mL) (group B). The contrast media was injected with a flow rate of 4 mL/sec. The scan delay was determined using semiautomatic bolus tracking system in all examinations conducted with the same scanning parameters. Quantitative analysis was performed by region of interest measurements along the z-axis to compare the attenuation profile of both groups. Visual analysis of the attenuation of the fourth, fifth and sixth order arteries was performed to assess the difference in visualization of peripheral arteries between both groups.

Results: The mean enhancement along the z-axis was 268 ± 56 HU in group A and 344 ± 108 in group B. The difference of 77 HU was statistically significant ($p < 0.001$). The attenuation profile was similar in both groups. The detection rate of fifth and sixth order arteries was significantly higher in group B than in group A (94% compared to 91% and 72% compared to 60%, respectively, $p < 0.01$).

Conclusions: MDCTA of the pulmonary arteries with a high iodine flow concentration significantly increases the attenuation of the pulmonary arteries, thereby leading to an improved visualization of subsegmental pulmonary arteries.

B-888 11:51



Initial experience with the Artis dTA flat panel detector (FD) C-arm system: Optimizing hepatic contrast medium (CM) delivery

J.C. Hellinger, R. Fahrig, N. Strobel, D. Fleischmann, G. Glazer; Stanford, CA/US

Purpose: Three dimensional (3D) C-arm Computed Tomographic (CT) systems combine two dimensional (2D) angiographic imaging and 3D CT visualization. Streaming artifact can produce inhomogenous CT enhancement. The purpose of this work is to determine injection parameters which may be sufficient to overcome streaming artifact in the liver.

Methods and Materials: In a 36 kg porcine model, the common hepatic artery was selected using a Simmons 3 end-hole angiographic catheter. Conray 60(270 mgI/cc) was injected intra-arterially and angiographic (30 sec rotational acquisition, 70 kVp, 190 views) and CT (0.42 mm slice thickness) images were acquired with the FD system. Injection parameters included 1 cc/sec, 2 cc/sec and 3 cc/sec at 100% concentration and 4 cc/sec at 50% concentration. Image quality, enhancement values and signal to noise ratios (SNR) were recorded in right and left hepatic arteries as well as central and peripheral segmental arteries.

Results: Subjective image quality was highest with 3 cc/sec and 4 cc/sec injections. At 1 cc/sec, overall SNR was greater in right hepatic arteries as compared to the left (8 ± 4.6 vs 6 ± 2.7). Differential enhancement was observed in the right anterior (7 ± 4) and posterior segments (6 ± 2.8). Central SNR (7 ± 1.7) was greater than peripheral SNR (3 ± 1.3). 4 cc/sec injections at 50% concentration produced the greatest homogeneity for right (6 ± 3.0) and left (6 ± 2.4) lobes. Both 3 cc/sec and 4 cc/sec injections achieved more homogeneous SNR in right segmental anatomy. At 100% concentration, progressive increase in peripheral SNR was achieved with 2 cc/sec and 3 cc/sec injections.

Conclusion: With 3D C-arm CT systems, faster injection rates produce more homogenous vascular enhancement. At higher flow rates, lowering iodine concentrations can reduce the delivered iodine content without diminishing image quality.

10:30 - 12:00

Room K

Pediatric

SS 1812

Thoracic and abdominal imaging

Moderators:

M. Brzezski; Warsaw/PL

U.V. Willi; Zürich/CH

B-889 10:30

Morphology of congenital diaphragmatic hernias studied with fetal MR imaging

P.C. Brugge, G.J. Kasprian, U. Rauhofer, D. Prayer; Vienna/AT

Purpose: To define morphology of congenital diaphragmatic hernias (CDH) using fetal magnetic resonance imaging (MRI).

Methods and Materials: 21 fetuses (19-39 gestational weeks) with ultrasound diagnosis of suspected CDH underwent 1-3 fetal MRI studies (total 31) on a 1.5 T magnet using a five-element phased-array surface coil and no sedation. Imaging protocols included T2-, T1-weighted and balanced-angiography sequences in different section planes.

Results: Fetal MRI identified two right-sided and 19 left-sided CDHs. In all left-sided CDHs the herniated content included stomach, small intestine and colon except for the descending and sigmoid. With the left colonic flexure in place, the course of the colon corresponded to the lateral extent of the defect. Meconium filling of the intrathoracic colon was variable. The extent of an intrathoracic left hepatic lobe (13/19) situated on the ventral thoracic wall was variable, and associated with more dorsally positioned stomach. The ipsilateral lung was recognizable in only 3/19 cases. Contralateral lung size corresponded to mediastinal shift which was more pronounced in cases with intrathoracic liver and associated with left heart compression. Real hernias presented with fluid beneath the pleural cupula, low-positioned colon, or lung within the dorsal costodiaphragmatic recess. Marked progression of the pathology was observed in one case. Associated malformations included isolated palatal cleft and CAM.

Conclusion: Detailed morphological description of CDH is possible with fetal MRI which may have a bearing on prognosis as MRI can also identify real hernias. Possible progression of the pathology underlines the importance of intrauterine follow-up.

B-890 10:39

Logistic regression analysis of mortality and necessity of ECMO therapy in fetuses with CDH based on MR imaging lung volume measurement

A.K. Kilian, E.M. Schütz, T. Schaible, C. Düber, K.W. Neff; Mannheim/DE

Purpose: To calculate mortality rate and necessity of extracorporeal membrane oxygenation therapy (ECMO) in patients with congenital diaphragmatic hernia (CDH) using logistic regression analysis based on MR imaging fetal lung volume (FLV) measurement.

Methods and Materials: 38 fetuses with CDH, diagnosed on ultrasound examination prior to 32 weeks gestation, underwent MR imaging FLV measurement (3D HASTE-imaging) within 34-36 weeks gestation. Based on logistic regression analysis, mortality and necessity of ECMO therapy was calculated by estimating the prenatal FLV in MR imaging. 18 healthy age-matched fetuses served as normal controls.

Results: Mean FLV of all fetuses with CDH was 20.5 ± 11.8 ml (range 5.1-41.6 ml). Mean FLV of controls was 77.7 ± 25.5 ml. Mortality decreases with increasing FLV from 80% for neonates with 7 ml prenatal FLV to 1% for children with 30 ml FLV. Higher FLV was associated with improved survival. Children with FLV of 5 ml show a mortality rate of 86% in comparison to FLV of 25 ml with a mortality of 4%. Similar results were found for the necessity of ECMO therapy. Probability of ECMO therapy decreases with increasing FLV from 80% with 8.3 ml FLV to 1% with 76.6 ml FLV. Children with FLV of 5 ml have a probability of ECMO therapy of 84% compared to FLV of 45 ml with only 14%.

Conclusion: Logistic regression analysis based on MR imaging fetal lung volume measurement is a potential predictor for clinical time course including mortality and necessity of ECMO therapy in children with CDH. High risk infants can be identified prenatally.

Scientific Sessions

B-891 10:48

Comparison between single and multidetector CT in the reduction of sedation rates, conventional angiograms, and patient motion artifacts in young children following liver transplantation

A.A. Lemos, J.M. Sternberg, F. Somalvico, F. Ferrari, M.M. Castelnovo, P.R. Biondetti; Milan/IT

Purpose: To determine whether the use of multidetector-row helical CT (MDCT) can decrease the need for sedation, the number of conventional angiograms and patient motion artifacts compared with single detector CT (SDCT) in young children after liver transplantation.

Methods and Material: Between January 1993 and March 2004, 126 young children underwent liver transplantation at our institution. For detection of post-operative complications, 84 of the 124 studies were performed by using SDCT with either a step and shoot or helical mode acquisition (group 1), whereas the remaining 42 studies were performed with a four array MDCT (group 2). The mean age was 3.2 years in group 1 (range 8 months-17 years) and 2.4 years in group 2 (range 17 months-12 years). We retrospectively reviewed sedation records, the number of conventional angiograms additionally required to confirm the diagnosis, and patient motion artifacts before and after the introduction of MDCT at our institution. Statistical comparison among the two groups was determined by using the Mantel-Haenszel Chi-square test.

Results: In group 1, 60.7% (51 of 84) patients required sedation and/or catheter angiography, whereas in group 2, 28.5% (12 of 42) required sedation and/or catheter angiography. Patient motion artifacts were present in eight cases in group 1, and in four cases in group 2. Regarding sedation rates and the number of conventional angiograms; there was a significant statistical difference ($p < 0.001$). No statistical difference was found regarding patient motion artifacts ($p > 1$).

Conclusion: Sedation rates and the number of conventional angiograms were significantly reduced with MDCT. A real reduction of patient motion artifacts should be evaluated in a larger number of patients.

B-892 10:57

Virtual colonography of the fetal colon

P.C. Brugger, C. Mittermayer, C.J. Herold, D. Prayer; Vienna/AT

Purpose: To evaluate the power of fetal magnetic resonance imaging (MRI) in assessing fetal colon anatomy and pathology with virtual colonography.

Methods and Materials: 130 fetuses from 19 to 39 gestational weeks (GW) were imaged on a 1.5 T magnet using a five-element phased-array coil and no sedation. A variety of T1-weighted sequences were acquired in frontal or sagittal planes and maximum intensity projections (MIP) and three dimensional reconstructions were made.

Results: All T1-weighted sequences selectively visualized the hyperintense meconium within the fetal colon from the 19th GW onwards. By the 24th GW the whole colon was meconium filled and MIPs allowed virtual colonography. The topography, flexures and parts of the fetal colon including the variable sigmoid can be identified. Hastra became apparent with advancing age. Considerable variation in the total amount of meconium was observed in fetuses of comparable ages. The normal development could be followed *in vivo*, and colon pathologies (malrotation, congenital diaphragmatic hernias, atresia) were easily recognized. Due to the large field of view the whole colon (and terminal ileum) may be visualized in the frontal plane even in larger fetuses.

Conclusion: Using meconium as a natural contrast media, virtual fetal colonography is possible with fetal MRI. This method offers great potential in the prenatal diagnosis of colon pathologies and postnatal management. In addition to morphology, the pattern of meconium distribution within the fetal colon and small intestine may provide further clues to the location of intestinal stenosis or atresia.

B-893 11:06

Investigation of normal renal development with fetal magnetic resonance imaging

L. Witzani, M. Hoermann, G. Kasprian, C. Balassy, P. Brugger, D. Prayer; Vienna/AT

Purpose: Understanding urinary tract development is essential for the early detection of its abnormalities. Hence the aim of this study is to investigate the development of the normal fetal kidney with magnetic resonance imaging (MRI).

Methods and Materials: 426 fetal MRI examinations were carried out, 33 were excluded because abnormalities of the kidneys were detected and therefore a total of 393 examinations were evaluated between the 16th and the 39th gestational weeks. T2 weighted scouts in axial, coronal and sagittal planes were obtained on a 1.5 T superconducting unit using a phased array coil. Imaging protocol included

T2 weighted SSFSE, T2 weighted balanced angiography and diffusion weighted sequences. Renal size, signal intensity, lobulation, differentiation of the collecting system and function by means of signal intensity on diffusion weighted images were assessed.

Results: The mean length of the kidneys correlated well with gestational age and ranged from 13 to 45 mm. Lobulation was already detectable in the 16th gestational week. The collecting system appeared hyperintense on T2 weighted images from the 16th week. Renal parenchyma showed intermediate signal on T2 weighted images. The kidneys were hyperintense on diffusion weighted imaging during the course of pregnancy, suggesting normal renal function.

Conclusion: Fetal MRI appears to be an excellent tool in the assessment of morphological development of the kidneys and can provide information about intrauterine renal function, which is of great clinical importance in the early detection of abnormalities of the urinary tract.

B-894 11:15

Voiding urosonography combined with fluoroscopic voiding cystourethrography in the diagnosis of reflux: Does the order matter?

J. Tzovara, F. Papadopoulou, A. Anthopoulou, E. Siomou, E. Arkoumani, S. Efremidis; Ioannina/GR

Purpose: Diagnostic imaging for vesicoureteral reflux (VUR) in children includes both fluoroscopic voiding cystourethrography (VCUG) and contrast-enhanced voiding urosonography with harmonic imaging (CE VUS HI). Many studies have shown a higher sensitivity for VUS compared to VCUG. Some investigators however, argue that this might be due to that VUS usually precedes VCUG when performed at the same session. The purpose of our study is to assess if the order of the examination affects the detection of VUR.

Methods and Materials: Two hundred and two children with 402 kidney-ureter-units (KUU) of mean age 2.7 years were prospectively studied for possible VUR. In all children VUS with 1-2 ml of a 2nd generation contrast agent (sulfur-hexafluoride microbubbles, SonoVue, Bracco, Italy) and VCUG with the standard technique were performed. In group A (108 children, 214 KUU) VCUG preceded VUS, while in group B (94 children, 188 KUU), the sequence was reversed. McNemar test was used for statistical analysis.

Results: In group A VUS and VCUG revealed VUR in 65(30.4%) and 41(19.2%) KUU respectively. In group B VUS and VCUG depicted 75(39.9%) and 43(22.8%) refluxing KUU respectively. Concordance of findings regarding the presence of VUR between VUS and VCUG was found in group A in 179/214(83.6%) KUU and in group B in 154/188(81.9%) KUU, ($p = 0.48$). In group A VUS depicted 29/70(41.4%) more refluxing KUU and missed 5/70(0.07%) compared to VCUG. In group B VUS disclosed VUR in 33/76(43.4%) more KUU and missed 1/76(0.01) refluxing KUU. No significant difference was found between group A and B in the detection of VUR by the two modalities.

Conclusion: The order of the examination does not influence the detection of VUR by VUS and VCUG.

B-895 11:24

Voiding urosonography harmonic imaging with 2nd generation contrast agent for the diagnosis of reflux

F. Papadopoulou, J. Tzovara, A. Anthopoulou, E. Siomou, E. Evaggelidou, S. Efremidis; Ioannina/GR

Purpose: Contrast enhanced voiding urosonography harmonic imaging (CE VUS HI) has been introduced recently as a sensitive method in both the diagnosis and follow-up of vesicoureteral reflux (VUR). The purpose of our study is to evaluate the reliability of CE VUS HI in the diagnosis of VUR using a 2nd generation contrast agent.

Methods and Materials: We evaluated 70 children (mean age: 2.2 years) with 137 kidney-ureter-units (KUU) -3 children had single kidneys- for possible VUR performing C-E VUS HI after introduction of 1-2 ml of sulfur-hexafluoride microbubbles (SonoVue, Bracco, Italy) using low mechanical index and Fluoroscopic Voiding Cystourethrography (VCUG) with the standard technique on the same session. For the statistical analysis we used Mc Nemar test.

Results: VUS and VCUG revealed VUR in 47/137 (34%) and 23/137 (17%) KUU respectively. Concordance in findings regarding the presence of reflux between VUS and VCUG was found in 113/137 (82.4%). VUR was detected only by VUS in 25 KUU (19 grade II, 6 grade III) and missed in only 1 KUU (grade I) which was detected by VCUG. Consequently, VUS disclosed VUR in 25 KUU out of the 48 refluxing KUU (52%). VUS upgraded reflux in 6 KUU compared to VCUG and VCUG in 5 compared to VUS. The difference in the detection rate of reflux between VUS and VCUG was statistically significant ($p = 0.000006$).

Conclusion: CE VUS HI with 2nd generation contrast medium has improved the diagnosis of VUR in children compared to VCUG.

Scientific Sessions

B-896 11:33 ♂

Comparison of voiding urosonography harmonic imaging using 2nd generation contrast agent with direct radionuclide cystography for the diagnosis of reflux

A. Anthopoulou, A. Fotopoulos, J. Tzovara, J. Al Bokhrli, E. Siomou, I. Mantzios, F. Papadopoulou; Ioannina/GR

Purpose: The use of contrast-enhanced voiding urosonography harmonic imaging (CE VUS HI) for the diagnosis of vesicoureteral reflux (VUR) is gradually increasing. The purpose of this study is to determine the sensitivity of CE VUS HI using 2nd generation contrast agent in the diagnosis of VUR in children compared to direct radionuclide cystography (DRNC).

Methods and Materials: Twenty children (mean age: 3.3 years) with 41 kidney-ureter-units (KUU)-1 duplex kidney- were included in our prospective study for possible VUR, evaluated by CE VUS HI after introduction of 1-2 ml of sulfur-hexafluoride gas microbubbles (SonoVue, Bracco, Italy) using low mechanical index and DRNC using a maximum of 20 MBq of ^{99m}Tc DTPA. For the statistical analysis we used Mc Nemar test.

Results: VUS and DRNC detected VUR in 20/41 (49%) KUU and 11/41 (27%) KUU respectively. Concordance in findings regarding the presence of reflux between VUS and DRNC was found in 32/41 (78%). VUR was detected by VUS only in 9 out of the 20 (45%) refluxing KUU (8 grade II and 1 grade III). DRNC upgraded 1 KUU with grade I reflux into grade II. The difference in the detection rate of reflux was not significant ($p = 0.07$).

Conclusion: CE VUS HI with 2nd generation contrast medium has improved the diagnosis of VUR in children compared to DRNC. Our data seem to indicate a higher sensitivity of CE VUS HI compared to DRNC, although the number of our cases is still small.

B-897 11:42

Voiding cystourethrography versus low-dose contrast-enhanced harmonic voiding urosonography using the 2nd generation US contrast medium SonoVue

K. Darge, F. Schreiber, M. Beer, N. Gordjani, H. Riedmiller; Würzburg/DE

Purpose: To evaluate if low-dose contrast-enhanced voiding urosonography (VUS) using a 2nd generation US contrast medium (SonoVue®, Bracco, Italy) is comparable to voiding cystourethrography (VCUG).

Methods and Materials: In 40 patients (female = 30, male = 10; 1 month - 15 years), VUS was carried out. This comprised of a pre-contrast US of the urinary tract, catheterization of the bladder and administration of the US contrast medium, SonoVue®, at a volume of 1% of that of the bladder filling. This was followed by a repeat scan of the urinary tract including during voiding. The US study was conducted in fundamental and harmonic imaging modalities using a Sonoline Elegra® (Siemens, Germany) US machine. VCUG was subsequently performed in all patients.

Results: A total of 84 kidney-ureter units (4 duplex kidneys) were available for evaluation. In 25(30%) kidney-ureter units reflux was detected by one or both methods. In 76(90%) units the results were concordant. Discordance was present in 8(10%) kidney-ureter units as reflux was diagnosed in 5 and 3 units only with VUS and VCUG, respectively. Taking VCUG as the reference method the sensitivity and specificity of VUS were 85% and 92%, respectively.

Conclusion: The results of low-dose SonoVue® enhanced voiding urosonography point to a comparable diagnostic efficacy as that of VCUG. The volume of US contrast medium required for an examination is significantly less than that of the 1st generation US contrast medium, Levovist® (Schering, Berlin, Germany). This may bring about significant cost reduction for the examination.

B-898 11:51

Monitoring of Infliximab therapy in children with Crohn's disease (CD) with true-FISP MR-imaging

C. Hohl, M. Ahau, T. Schmidt, E. Berkemeier, R.W. Günther, G. Staatz; Aachen/DE

Purpose: Infliximab, as an Anti-TNF- α antibody agent, has been recently applied in children with severe CD. Because there is only little experience in treating children with Infliximab, short-term monitoring is essential. The purpose of our prospective study was to evaluate if true-FISP MR imaging is a suitable method for monitoring Infliximab therapy.

Materials and Methods: 5 children, aged 14-16 years, suffering from severe CD and not responding to corticosteroid therapy, were treated with Infliximab. Before and 1-2 weeks after Infliximab administration, all children underwent MR imaging of the small bowel on a 1.5-T-MR scanner. MR imaging was performed 1 hour

after 1 litre of a 2.5% Mannitol solution was given orally, with use of True-FISP sequences before and after i.v. contrast (Gd-DTPA) in coronal and axial planes. The activity of bowel inflammation was determined by assessment of bowel wall thickening and evaluation of extraintestinal inflammatory changes. The imaging findings were additionally correlated with the clinical symptoms of each child.

Results: True-FISP MR imaging enabled an excellent assessment of inflammatory activity in CD. 4 of 5 children showed a good response to Infliximab therapy with marked improvement of the inflammatory changes of the bowel wall and regression of extraintestinal inflammatory signs. The imaging findings of true-FISP MR imaging correlated well with the clinical findings and influenced the further therapeutic regimen.

Conclusion: True-FISP MR imaging of the small bowel enables short-term and precise monitoring of Infliximab therapy in children with CD.

10:30 - 12:00

Room L/M

Neuro

SS 1811a

Non-invasive neurovascular imaging

Moderators:

C. Manecke; Toulouse/FR
S. Wetzel; Basle/CH

B-899 10:30 ♂

CT angiography as a method of brain death confirmation

A. Pal, D. Ozretic, Z. Pavcec, H. Saghir, I. Zokalj, Z. Perhoc, B. Latin, M. Ozretic; Cakovec/HR

Purpose: After clinical diagnosis of brain death, Croatian legislature requires confirmation with one 'paraclinical' method (DSA, scintigraphy, TCD, evoked potentials, EEG). We explore the appropriateness of CT angiography, as a potential 'paraclinical' method.

Methods and Materials: From December 2002, 18 patients in coma after traumatic brain injury or nontraumatic SAH, aged 23-46, were evaluated as possible organ donors. Brain death was diagnosed according to clinical criteria (fixed dilated pupils, absence of bulbar reflexes, negative apnoea-test). Only 9 patients were later candidates for CT angiography. Exams were performed on single-slice scanner. An area from C1 to the lateral ventricle bodies was covered. Standard protocol was used: 100 mL of nonionic contrast medium (370 mg/mL) flow rate 4 mL/s, 1 mm slice thickness, pitch 1.5, scan delay up to 60 s. No visualization of great intracranial vessels and the absence of parenchymal attenuation increase after contrast administration due to cerebral circulatory arrest were criteria for brain death confirmation.

Results: In 7 patients there was no enhancement of vessels forming the Circle of Willis, and filling of ECAs and infracerebral ICAs was shown. In 2 patients there was slight enhancement of anterior circulation vessels (MCAs and ACAs) and in agreement with clinicians; exams were repeated 12 hours later when they were confirmatory. Eventually families allowed organ harvesting in 4 patients.

Conclusion: Rapid diagnosis of absence of intracranial arterial circulation is important for identification of potential organ donors. Results of CT angiography are comparable to other radiological 'paraclinical' methods, but further comparison studies are needed.

B-900 10:39

High resolution MR imaging of cervical artery dissection (CAD) at 3.0 T with a dedicated surface coil: New insights into the pathomorphology?

R. Bachmann¹, I. Nassenstein¹, H. Kooijman², H. Kugel¹, G. Kuhlenbaumer¹, S. Kraemer¹, W. Heindel¹; ¹Münster/DE, ²Hamburg/DE

Purpose: To assess in a prospective study the capability of high-resolution arterial vessel wall imaging at 3.0 T (HR-MRI) in pts with suspected CAD and to compare it to 1.5 T standard MRI.

Methods and Materials: 15 patients (5 m, 10 f, mean age 39 yrs) underwent cervical MRI at 1.5 T (T1w-TSE, T2w-TSE, CE-MRA) and HR-MRI at 3.0 T (Gyroscan Intera, Philips). HR-MRI was acquired using a phased array coil with four circular elements. HR-MRI-protocol consisted of: 1) bright blood 3D inflow MRA (TR/TE/FA = 25 ms/3.1 ms/16, 120 slices, reconstructed voxel size 0.3x0.3x0.8 mm); 2) black blood cardiac gated water selective T1w 3D spoiled GE (TR/TE/FA = 31 ms/7.7 ms/15, 36 slices, 0.3x0.3x1.0 mm); 3) black blood cardiac triggered fat suppressed T2w TSE (TR/TE/ETL = three heart beats/44 ms/7, 18 slices, 0.3x0.3x2 mm).

Scientific Sessions

Results: In 5 pts findings were normal at both studies. In 5 pts dissection diagnosed at 1.5-MRI was confirmed by HR-MRI. However, HR-MRI yielded much better delineation of internal and external vessel wall boundary and clearer distinction between intramural hematoma and thrombus. In 2 pts vessel occlusion was confirmed. In 2 pts an intramural hematoma was clearly visible at HR-MRI, not discernible at 1.5-MRI. In 1 pt a pseudoaneurysm of the vertebral artery was detected at HR-MRI, not visible at 1.5-MRI.

Conclusion: HR-MRI permitted excellent analysis of morphological features of CAD due to increased spatial resolution. Additional clinical relevant information could be gained in 3 pts. Thus, HR-MRI at 3.0 T is a promising tool for the assessment of vessel wall pathology in patients with CAD.

B-901 10:48

Comparison of stenosis quantification using 16-row MDCTA and contrast enhanced MRA in a phantom model simulating soft and calcified plaque material

K. Papke, K. Schliephake, M. Finke, M. Fruth, F. Brassel; Duisburg/DE

Purpose: To compare the precision of stenosis measurements using 16-row MDCTA and contrast enhanced MRA (ceMRA) in a phantom model simulating carotid artery disease with calcified and non-calcified stenoses.

Methods and Materials: 90 stenoses with lumens ranging from 0.5 to 2.5 mm were placed in tubes with a diameter of 5 mm, simulating stenoses from 50 to 90% according to the NASCET method. 45 stenoses consisted of PVC simulating calcified plaques, the other 45 of wax simulating plaques with high lipid content. The phantom tubes were filled with dilute contrast material and examined a) with a 16-row MDCT scanner (Siemens Somatom Sensation 16) and b) with a 1.5 T MR scanner (Siemens Magnetom Sonata), both with standard clinical examination protocols. With both methods, the stenotic residual lumen was measured independently of window settings using density profiles across the stenosis in a plane perpendicular to the vessel axis.

Results: Both methods demonstrated a high correlation between the measurement results and the gold standard with MRA performing slightly better than MDCTA ($r = 0.96$ for MRA vs. $r = 0.93$ for MDCTA, $p \leq 0.0005$). With MDCTA, the diagnostic precision was significantly lower in calcified stenoses ($r = 0.92$) as compared to soft stenoses ($r = 0.97$). In soft plaque stenoses, MRA and MDCTA did not differ significantly.

Conclusion: Although both methods provide excellent stenosis quantification, MRA is superior to MDCTA especially in calcified stenoses. Therefore, MRA should be used if precise stenosis quantification is crucial for therapeutic decisions, e.g., in carotid artery disease.

B-902 10:57

Imaging work-up in patients with suspected cervical artery dissection:

Diagnostic efficacy of a combined neck and head MR-imaging protocol

I. Nassenstein, T.-U. Niederstadt, S. Krämer, R. Dittrich, W. Heindel, R. Bachmann; Münster/DE

Purpose: To start immediate anticoagulant therapy the quick and reliable diagnosis of cervical artery dissection (CAD) and accompanying cerebral ischemia is of paramount importance. In this prospective study the diagnostic performance of a combined head and neck MR-imaging protocol in pts with suspected CAD was assessed.

Methods and Materials: 51 consecutive pts (24 m, 27 f, mean age 39.6 yrs) admitted to our stroke unit with suspected CAD and age < 56 yrs underwent a combined head and neck MR examination within 24 h (Gyrosan Intera 1.5 T, Philips). Neck-MR imaging consisted of ax T1w-TSE, T2w-TSE, contrast enhanced T1w-TSE and CE-MRA (imaging time 17 min). Head-MR imaging included DWI, Flair and TOF-angiography (12 min). Three radiologists assessed both studies in consensus with regard to the presence of CAD and acute ischemia.

Results: Mean time between onset of symptoms and scan was 7.3 days. In 18 pts neck and head MR imaging results were normal. In 15 pts acute ischemia was verified by head MR imaging, but neck MR imaging was normal. 6 pts presented with acute ischemia and specific findings of CAD. In 12 pts no acute ischemia was present but definite signs of CAD.

Conclusion: The proposed combined MR-protocol allows imaging work-up of pts with suspected CAD in approximately 30 min, giving conclusive information about the status of the intra- and extracranial vasculature and the presence of ischemia. The high incidence of pts with definite CAD lacking cerebral ischemia indicates the necessity of an early definite diagnosis in order to start timely anticoagulation to prevent development of stroke.

B-903 11:06

Improvement of CTA of the circle of Willis by using lower tube voltage

A. Waaijer, B.K. Velthuis, C.J.G. Bakker, G.A.P. de Kort, M.S. van Leeuwen; Utrecht/NL

Purpose: To compare using 90 kV for CT angiography (CTA) of the circle of Willis to the conventional 120 kV.

Materials and Method: Three patient groups were scanned: 30 with clipped cerebral aneurysms; 20 with acute subarachnoid hemorrhage (SAH) and 20 with a family history of cerebral aneurysms. Half of each group was scanned with 90 and half with 120 kV. Clipped patients were scanned with pitch 0.3 and effective tube current (mA_{eff}) was adjusted to keep radiation dose constant, resulting in 120 kV and 200 mA_{eff} or 90 kV and 450 mA_{eff}. The other groups were scanned with pitch 1, with 120 kV at 200 mA_{eff} and 90 kV at 330 mA_{eff} due to restricted tube load. Absolute CT values were measured in Hounsfield Units (HU) and contrast-to-noise ratio (CNR) was calculated. Two radiologists subjectively scored arterial visualization, detail visibility, noise, and hindrance from venous structures, SAH, or clip artifact on a five-point scale.

Results: Absolute vascular enhancement was significantly higher with 90 kV: mean 340 HU versus 247 HU ($p < 0.001$; 95% CI: 67.9-118.1). CNR increased with 20% in clipped and SAH patients, though insignificantly. Subjective analysis increased at 90 kV for arterial visualization with 0.9 points ($p < 0.001$) without increase in noise or venous enhancement. In SAH patients, hindrance of subarachnoid blood diminished at 90 kV with an increase of 0.6 points ($p < 0.01$).

Conclusion: This study shows that with 90 kV better image quality can be achieved for CTA of the circle of Willis at equal or lower radiation dose.

B-904 11:15

The application of MR perfusion-weighted imaging in patients with unilateral ICA stenosis or occlusion

J. Lu, K. Li; Beijing/CN

Purpose: To investigate the value of MR perfusion-weighted imaging (PWI) in patients who had unilateral ICA high-grade stenosis or occlusion and to assess the utility for evaluating cerebral hemodynamic changes before and after surgery or interventional therapy.

Methods: MR PWI (Siemens sonata) was performed on 62 patients with unilateral ICA high-grade stenosis or occlusion. rCBF, rCBV, rMTT and TTP were calculated. Surgery or interventional therapy was performed in 15 patients, among which 4 underwent STA-MCA anastomosis, 8 underwent PTAS and 3 underwent CEA. The perfusion findings before and after therapy were evaluated.

Results: The abnormal perfusion findings were depicted in 62 patients. The values of rCBV, rMTT and TTP of abnormal regions were statistically different between the affected and the contralateral side ($P < 0.01$). However rCBF was not statistically different ($P > 0.05$). There was a significant difference between the values of TTP, rCBV and rMTT and the degree of ICA stenosis. TTP and rMTT were higher in patients with ICA occlusion than stenosis ($P < 0.01$). Surgery or interventional therapy was performed in 15 patients; TTP and rMTT were decreased after therapy ($P < 0.01$). However, there was no statistical difference between rCBF and rCBV ($P > 0.05$).

Conclusions: PWI can objectively and clearly demonstrate the abnormal hemodynamic changes in patients with unilateral ICA high-grade stenosis or occlusion and can depict the improved situation of cerebral perfusion after surgery or interventional therapy.

B-905 11:24

Cerebral AVM: Hemodynamic characterisation by ultrafast contrast enhanced MRA and non-enhanced dynamic active tagging MRA

M. Essig, C. Fink, F. Giesel, J. Debus, M. Bock, H.-U. Kauczor; Heidelberg/DE

Purpose: To assess the hemodynamic characteristics of patients with angiographically proven cerebral AVMs we applied to 20 patients both an ultrafast, time resolved contrast enhanced MR-DSA technique (cMRA) as well as a non-enhanced dynamic tagging MR-DSA (dMRA).

Methods and Materials: The cMRA is based on an ultrafast 3D-FLASH acquisition after bolus injection of 10 cc of MultiHance® (Bracco Imaging, Milan, Italy) using parallel imaging techniques (IPAT) at a TR of < 2 ms and a TE of < 1 ms and a temporal resolution of about 250 ms. The dMRA sequence, with a temporal resolution of 100 ms, is based on the spin labeling sequence (STAR) in which a bolus of blood upstream from the AVM is tagged by an inversion pulse and imaged downstream at different time intervals after tagging (100 ms to 1200 ms) using also a 2D FLASH acquisition. For both techniques morphological and hemodynamic parameters were assessed and compared with the clinical presentation.

Scientific Sessions

Results: A hemodynamic assessment and a detailed analysis of the angiarchitectural of the malformation was possible with both techniques. Feeding arteries, AVM nidus, and draining veins were detected easily. The time resolution was better with dMRA, but suffers from a substantially longer acquisition. Artifacts are more pronounced on the dMRA while the cMRA proved to be robust.

Conclusion: Both cMRA and dMRA proved to be very helpful diagnostic tools in the assessment of the angiarchitectural and the hemodynamic changes of cerebral AVMs. The time resolved acquisition allowed interesting insights into the hemodynamics of such malformations.

B-906 11:33

CT and MR imaging features of cerebral cortical venous thrombosis

A. Stix, J. Simbrunner, A. Ruppert-Kohlmayr, G. Komatz, M. Feichtinger, G.E. Klein, F. Ebner, F. Ebner; Graz/AT

Purpose: Although thrombosis of the dural sinuses is increasingly recognised, the diagnosis of cortical venous thrombosis (CVT) remains challenging. The aim of this study was to describe the CT and MR imaging findings of CVT.

Methods and Materials: 15 patients (7 men and 8 women) with mean age 43 years (range 16-75) with CVT underwent CT and MR imaging. CTA was performed in 10, MRA in 11 and DSA in 4 patients. Scans were analysed by two radiologists retrospectively blinded for the diagnoses. The number of occluded cortical veins (CV) and sinuses was counted.

Results: 9 patients showed thrombosis of dural sinuses and CVT while 6 patients showed isolated CVT. CTA, MRA and DSA proved reliable in the detection of sinus thrombosis but MRA and DSA were inconclusive for CVT. Altogether unenhanced CT scans revealed 24 occluded CV, T1-weighted images 11 and T2-weighted images 2. T2-weighted gradient-echo images showed 32 occluded CV. Parenchymal lesions have been detected in 9 patients by CT and in 13 by MRT. **Conclusion:** Due to anatomical variations of cerebral cortical veins it is difficult to detect a CVT in MRA and DSA. Non-angiographic techniques are reliable in the diagnosis of CVT. Unenhanced CT scans and T2-weighted gradient-echo sequences have an especially high sensitivity in the detection of CVT.

B-907 11:42

Non invasive diagnosis with orbital color Doppler (OCD) of carotid cavernous sinus fistulas (CCSF): Personal experience in 20 cases

M. Venturini, F. D'Ascenzo, S. Bianchi Marzoli, F. Simonato, G. Scotti, A. Del Maschio; Milan/IT

Purpose: Several case reports have shown dilatation and modification of flow in the Superior Ophthalmic Vein (SOV) with OCD in CCSF. Our aim was to evaluate OCD in the diagnosis of CCSF, in a relatively large number of patients.

Methods and Materials: Both eyes of 20 patients with clinical suspicion of CCSF were examined with OCD (ATL-Philips HDI-5000 / 5-12 MHz linear-probe). Blood flow of the SOV, inferior ophthalmic veins (IOV), central retinal vessels and ophthalmic arteries was evaluated. The size of each vessel, the direction of blood flow and the following flow parameters were considered: maximum and minimum velocities for veins; peak systolic, end diastolic velocities and resistance indices (RI) for arteries. Positive diagnosis was based on the finding of SOV (and IOV) dilatation, with reversed, arterialized and low resistance (RI < 0.50) blood flow. Definitive diagnosis was based on digital angiography.

Results: CCSF was correctly diagnosed with OCD in 19/20 patients. SOV showed reversed, arterialized and low resistance blood flow in 19/20 cases, with bilateral orbital involvement in 4 cases. The SOV was dilated in 14/19 patients and not dilated in 5/19. The IOV was dilated with reversed and arterialized flow demonstrated in 8/20 cases (bilateral in 2 cases).

Conclusion: OCD provides an accurate and reproducible assessment of blood flow of retrobulbar vessels. An accurate and non invasive diagnosis of CCSF was obtained with OCD, due to SOV (and IOV) blood flow changes, and was also possible in non dilated orbital veins.

B-908 11:51

Application and efficacy of non-invasive spinal multidetector CT angiography in patients with suspected dural fistula with spinal drainage

P. Zabakis, C. Santosh, L.J. Walker, E. Teasdale; Glasgow/UK

Purpose: Multidetector CT has made a significant impact on intracranial vascular imaging. This study evaluates the technique and role of multidetector spinal CT Angiography (MDSCTA) in patients with possible spinal dural fistula.

Methods and Materials: 11 patients (9M) presenting with spinal symptoms and suspected by MR of harboring a fistula (DAVF) with spinal venous drainage, were studied by MDSCTA. All had spinal catheter angiography (DSA); 9 had contrast

enhanced spinal MRA; 5 had operative, 2 intravascular, and 1 combined treatment, while 3 had no intervention.

Results: DSA showed 5 typical spinal DAVFs; 2 cranial DAVFs with spinal drainage. In 2 cases it failed to demonstrate the fistula, and in 2 the results were equivocal. MDSCTA confirmed abnormal vessels in all cases and identified the DAVF level in 9 of the 11 patients. In 1 case MDSCTA failed to identify the level due to erroneous technique while in another case none of the imaging techniques (CTA, MRA, DSA) identified the level. MDSCTA identified the feeding vessel in 2 cases with negative/doubtful super-selective angiography (both were confirmed at surgery). Initial DSA failed to identify the level in 5 cases. In 3 of these cases, MDSCTA correctly guided the repeated DSA. In the 9 cases with both MRA and MDSCTA the DAVF level was correctly identified in 5 with MRA and 7 with MDSCTA.

Conclusion: MDSCTA is a feasible and effective diagnostic examination in DAVFs with spinal drainage, able to guide, limit and expedite DSA and surgery.

10:30 - 12:00

La Scala

Radiographers

SS 1814

Challenge and development in radiography

Moderators:

S. Huber; Munich/DE
C. Roche; Galway/IE

B-909 10:30

Radiographic role extension in fluoroscopy: The four tier structure in practice

S. Dyce, L.J. Abraham, G.P. Fitzgerald, C.J. Garvey; Liverpool/UK

Purpose: To illustrate the benefits of the four tier structure for radiographers providing a fluoroscopy service.

Methods: Rising demand and increased expectation have placed major pressure on radiology departments. A shortage of radiologists in the UK has resulted in existing radiologists devoting more time to cross-sectional imaging. Radiographers have assumed an increasingly important role in other areas, particularly in developing and running the GI fluoroscopy service. The four tier structure for radiographers currently being implemented in the UK offers significant opportunities for role redesign whilst ensuring appropriate competency and backfilling of more basic roles.

Results: Radiographers have become advanced practitioners through training in the performance of and, more recently, reporting barium enema studies, linked to local University programmes. Other developing areas include NG tube insertion, performing and interpreting contrast swallows and vetting requests for appropriateness. Backfilling of responsibilities has been done through the establishment of approved training programmes for assistant practitioners to perform basic duties including chest and extremity radiographs, venflon insertion and other duties previously performed by basic grade radiographers. Consultant radiographers are developing further skills including endoscopy along with research and audit programmes.

Conclusion: Role development for radiographers is advancing rapidly, especially in the area of GI fluoroscopy. Appropriate competency-based training programmes allow individuals to progress along assistant practitioner, practitioner and advanced practitioner grades. Roles for Consultant Radiographers in GI fluoroscopy are emerging and should be encouraged. Competency assessment is quite well advanced. More emphasis needs to be placed on research and audit.

B-910 10:39

Are digital images good enough? A comparative study of conventional film-screen vs digital radiographs on printed images of total hip replacement

K. Eklund, K. Jonsson, G. Lindblom, B. Lundin, J. Sanfridsson, M. Sloth, B. Sivberg; Lund/SE

Purpose: The aim was to evaluate the inter- and intra-observer variability and to find differences in diagnostic safety between digital and analog technique in diagnostic zones around hip prostheses.

Materials and Method: In eighty patients who had had a Total Hip Replacement (THR) for more than two years, a conventional image and a digital image were taken. Gruen's model of seven distinct regions of interest was used for evaluations. Five experienced radiologists observed the seven regions and noted in a protocol the following distances: stem-cement, cement-bone and stem-bone. All images were printed on hard copies and were read twice. Weighted kappa analyses has

Scientific Sessions

been used. The two most frequently loosening regions, stem-cement region 1 and cement-bone region 7, were closely analysed.

Results: In region 1 the five observers had an agreement of 86.75%-97.92% between analog and digital images in stem-cement, which is a varied weighted kappa 0.29-0.71. For cement-bone region 7 an agreement of 87.21%-90.45% was found, which is a varied weighted kappa of 0.48-0.58. All the kappa values differ significantly from nil.

Conclusions: The result shows that digital technique is as good as analog radiographs for diagnosing possible loosening of hip prostheses.

B-911 10:48

Strategy for redesigning workflow

R. Tjønneland, B. Lagesen, J. Andersen; Oslo/NO

Purpose: Presenting how we involved our staff to participate in redesigning the workflow, when changing our hospital RIS-PACS vendor.

Method and Materials: Reengineering of workflow was a highlighted topic and goal when purchasing RIS-PACS. The implementation process was established as a project task, with its own organisational team and leadership outside the department of Radiology. The project established a manager to organize user groups of different topics concerning workflow. These groups included employees of different occupations, who worked out executive principles. The management board of Radiology established reference groups to secure quality and anchor the suggested solutions among the users.

Results: *Strength:* The employees showed enthusiastic involvement in the process. The knowledge of our organization increased. This created an ownership among the employees to the workflow-solution and increased the power of accomplishment. *Weakness:* A big democracy process is time consuming. This kind of strategy might be difficult to manage, in order to find common solutions. *Possibilities:* The best solutions are made jointly. Where there were different interests of workflow solutions, the manager group decided to try out a common standard to continue process. No one could deviate from the decided standard before the manager group gave it's approval. *Treats:* Old well known solutions are presented. Loss of focus may occur. "The survival of the fittest" may be the result of choosing between old and new suggested solutions.

Conclusion: With this strategy of managing the implementing process, we have established a commitment to the solution.

B-912 10:57

The value of the radial head-capitellum view in the evaluation of patients with injury of the elbow

D. Koumarianos¹, E. Lavdas¹, N.I. Fezoulidis², I.V. Fezoulidis²; ¹Patras/GR, ²Larisa/GR

Although most radial head fractures are evident on AP and lateral views, additional projections are often necessary to demonstrate them. The radial head-capitellum view is a modified lateral view of the elbow joint accomplished by angling the tube 45° toward the shoulder.

Materials and Methods: A retrospective analysis of the radiographs of the elbow in 91 patients examined for acute trauma between January and August 2003 was undertaken. Each study included an AP, lateral and radial head-capitellum view and the data were analysed to determine the radiographic abnormalities detected by each view alone and if only AP and lateral views had been used.

Results: There were 31 abnormal studies; 11 studies with positive fat pad signs, but no evidence of bony injury and 20 studies with some radiographic evidence of bony injury. The radial head-capitellum view failed to demonstrate 8/20 (40%) of fractures and by omitting this view only one fracture would have been missed. The radial head-capitellum view proved to offer advantage over the diagnosis made by conventional views in 6 (30%) of all fractures.

Conclusion: The study suggests that the radial head-capitellum view should be considered a supplementary rather than a standard view in acute trauma of the elbow.

B-913 11:06

Follow-up of primary or secondary malignant liver tumors treated with radiofrequency ablation: Efficiency of PET/CT

H. Kuehl, G. Antoch, P. Veit, S. Rosenbaum, J. Barkhausen, A. Bockisch; Essen/DE

Purpose: Morphologic imaging can be seen as the standard for follow-up of patients with malignant liver tumors treated with radiofrequency ablation. The use of PET/CT in the surveillance of RF-ablation is evaluated in comparison to CT alone.

Methods and Materials: 26 patients with 37 liver tumors (HCC 14, metastases 23) were scanned with PET/CT (Siemens biograph) prior to RF ablation. FDG-PET/CT was only used for follow-up in patients with PET-positive tumors. Post-interventional PET/CT was performed within 48 h after ablation and repeated after 1, 3, 6 and 12 months. The accuracy of the different imaging modalities (CT, PET/CT) for detection of residual or recurrent tumor was assessed and compared with clinical follow-up.

Results: 13 of the 26 patients showed 17 liver tumors with elevated FDG uptake and were controlled with PET/CT. 34 PET/CT examinations were performed for follow-up. The mean time of follow-up was 10 months (min. 1, max. 24 months). 3 of 13 patients remained free of tumor during follow-up. 10 of 13 patients developed local, intrahepatic, or local and intrahepatic tumor recurrence. 5 recurrences were not detected with CT but with PET/CT. The sensitivity of CT alone for tumor detection was calculated to be 55%, the sensitivity of fused PET/CT data measured 89%. The accuracy of CT alone and PET/CT was 85%.

Conclusions: PET/CT proved to be superior to morphologic imaging with CT when assessing the liver after RF-ablation. Nevertheless very small areas of residual tumor may be missed on PET/CT.

B-914 11:15



Low-field open-MR imaging study of TMJ (temporomandibular joint)

L. Belli, M. Mentasti, R. Poletti Venegoni; Castellanza/IT

Purpose: Feasibility of the use of low-field open-MR imaging system to study temporomandibular joint (TMJ).

Materials and Methods: We studied TMJ in 55 patients (mean age 42 years) using an open-MR imaging system with a low field 0.3 T (AIRIS II, Esaote, Italy). We used brain-coil for comparative study; T1 and GET2 sagittal and coronal sequences have been performed at rest and during motion with progressive opening mouth. Condilar bone signal, presence of articular fluid and fibrocartilage were evaluated; motility was finally evaluated with dynamic images.

Results: Inflammatory distrophia was present in 22 cases, traumatic lesions of cartilage or ligaments in 12 cases, dynamic derangement or limitation in 10 cases.

Conclusions: Low-field rest and dynamic study of TMJ is useful to evaluate the status of the articulation especially in case of cartilage or adhesive pathology.

B-915 11:24

Comparative analysis of objective data and subjective impressions reported by patients related to iodinated oral contrast material administration

E. Fehér, A. Tökés, H. Tóth, Z. Mocsári, E. Turupoli, A. Bánkuti, A. Böröczki, A. Maléta; Budapest/HU

Aim: The study was the comparative evaluation of visual assessment of images and of patient's reports related to oral administration of two (partially) different iodinated oral contrast materials.

Materials and Methods: Two different contrast materials containing the same "Amidotrizoat" molecule in 60% Iodine concentration of 300 mg Iodine/ml were compared. The composition of additional vehicular materials were different: in one of them Sodium and Meglumin. In the other contrast material a physiological amino-acid, Lysin was the vehicular molecule. There are significant differences of water bounding, i.e. high osmotic effects of Sodium-Meglumin composition versus iso-osmotic behaviour of Lysin bound "Amidotrizoat" in the bowels. Other differences were related to added aromas (anis like versus fruit like). Statistical evaluation of questionnaires were done. Both undiluted (conventional G.I. studies) and diluted applications (for CT studies) were analysed in 200 patients.

Results: Contrast filling of bowel loops were equally intensive and homogenous in both materials. No physical reactions, like flocculation, crystallisation, sedimentation or inhomogeneous filling appeared. Significant differences in gastrointestinal reactions (nausea, retching, vomits, colic, diarrhoea) were observed, predominantly in diluted application (CT), and only smaller differences were if administered undiluted (conventional GI studies). Effects on bowel motility were significantly different, the Meglumin containing contrast material increased the bowel motility, but much less uncomfortable effects were reported by patients who got Lysin containing contrast material. Patients appreciated the offered choice of contrast materials with different tastes.

Conclusions: Image qualities didn't show significant differences. Different osmotic effects and different tastes can help the patient's comfort.

Scientific Sessions

B-916 11:33

Can we trust each other?

L. Forsyth, E.M. Robertson; Aberdeen/UK

Purpose: To survey the perceptions of the Scottish Radiology community in relation to Radiographer role development.

Materials and Methods: A postal questionnaire was sent to all Consultant Radiologists recorded on the NHS Scotland database of Consultants.

Results: Response rate 61%. (i) Respondents considered increased professional standing of Radiographers, best use of manpower resources, reduced pressure on the service and improved recruitment and retention, as positive advantages of Radiographer development. (ii) The potential impact on SPR training, lack of clear medico legal responsibilities and Radiographers recognising the limitations of their abilities were identified as the main areas of Radiologist anxiety. (iii) 57% did not consider current post registration Radiography education and training adequate to underpin the clinical skills requirement of developed roles. (iv) Barriers to Radiographer development were identified as lack of Radiologists and Radiographer staff, suitable education, financial constraints, traditional views and resistance to change. (v) 81% reported support for Radiographer role development and willingness to participate actively in developments.

Conclusion: Despite reservations, Scottish Radiologists are supportive of the development of Radiography colleagues, however guidance is required on the medico legal and accountability aspects of Radiographers assuming new roles. Radiologist involvement in education and training for new roles may increase confidence and trust in Radiographers to work within the limitations of their competency and training.

10:30 - 12:00

Room N/O

Physics in Radiology

SS 1813

Magnetic resonance/Nuclear medicine

Moderators:

M. Hájek; Prague/CZ
R. Wirestam; Lund/SE

B-917 10:30

Ultra-high-resolution whole-body MRA using parallel imaging on a 32-channel MR system and intravascular contrast agents: Protocol optimization for clinical applications

K. Nikolaou¹, S.O. Schoenberg¹, M. Hartmann², P. Chamberlin², M.F. Reiser¹;
¹Munich/DE, ²Cambridge, MA/US

Purpose: To optimize a whole-body MRA protocol with sub-millimeter spatial resolution and to assess its clinical utility for the evaluation of systemic atherosclerotic disease.

Methods and Materials: 10 healthy volunteers and 5 patients with proven atherosclerotic disease underwent whole-body MRA on a 32-channel 1.5 T MR imaging scanner with matrix coils and parallel imaging (Magnetom Avanto, Siemens Medical Solutions, Erlangen, Germany). For contrast-enhanced MRA, an albumin-binding Gadolinium chelate (MS 325, EPIX, Cambridge, MA and Schering AG, Berlin, Germany) was injected with a flow rate of 1 cc/s. In the dynamic phase, angiograms of the carotid arteries and calves were obtained during first pass of MS-325, with 1 mm³ isotropic spatial resolution. In the steady-state, a spatial resolution of up to 75 μm³ was realized. In patients, results were compared to state-of-the-art MRA protocols using conventional Gd-chelates.

Results: In the dynamic phase, MR angiograms with pure arterial contrast were consistently obtained without venous overlay. For the thorax and abdomen, MR angiograms were obtained with 1 mm³ isotropic spatial resolution within a single breath-hold during the steady-state phase of MS-325. In the thigh, knee and calf station of the lower extremity, the ultra-high resolution MRA datasets with voxel sizes between 75 and 130 μm³ revealed excellent vessel contrast and high signal-to-noise. In patients, MRA data obtained with this protocol showed excellent agreement with the conventional reference MR angiograms.

Conclusion: The combination of a whole-body MR imaging scanner and a blood pool imaging agent allows acquisition of a whole-body MR angiogram without compromises in spatial resolution or anatomic coverage.

B-918 10:39

Reduced angle double inversion recovery (RADIR): A flexible new pulse sequence for black-blood MR imaging

A.N. Priest, S. Hegerfeldt, G. Adam; Hamburg/DE

Purpose: To develop and demonstrate a new black-blood MR imaging preparation sequence with flexibility to choose the inflow time before signal nulling is achieved.

Methods and Materials: To achieve a net flip angle of zero within a slice-selective (imaging) region and α outside this volume (for $90^\circ < \alpha < 180^\circ$), a sequence of the following RF pulses was used: ($\alpha-180^\circ$), 180°, - α . Only the final - α pulse is slice-selective. The short interpulse delays were equal, so the central 180° pulse refocussed the transverse magnetisation. This prevented artefacts from phase dispersion off-resonance. To achieve nulling at delay TD, set $\alpha = \arccos((A-1)/(A-E))$ with $A = \exp(-TD/T1)$ and $E = \exp(-TR/T1)$. The abdominal aortas of four healthy volunteers were scanned using a 3 T clinical scanner (Philips) with an ECG-triggered turbo-spin echo sequence (TE/TR = 70 ms/3RR). The blood SNR from proposed sequence, with TD=100 ms, was compared with the standard black-blood methods 'double inversion-recovery' (DIR) and out-of-slice presaturation.

Results: The average blood SNR over 3 subjects, at trigger-delay 450-470, was 2.2 (RADIR), 2.6 (DIR) and 2.8 (presaturation). At trigger-delay 300 (where DIR was not applicable) SNR was 1.6 (RADIR) and 1.9 (presaturation). In another subject, RADIR at delay 200 ms and DIR at delay 1150 ms (= 200 ms+1RR) both achieved blood SNR 2.6.

Conclusions: The new preparation sequence achieves good blood suppression in these preliminary studies. RADIR will allow cardiac or vessel-wall imaging at shorter trigger-delays than standard DIR without limiting the suppression volume as with out-of-slice presaturation. This brings additional flexibility to black-blood imaging, for example triggering systolic acquisitions within the same heartbeat as the acquisition.

B-919 10:48



Outer volume saturation bands improve spatial signal homogeneity in MR 2D chemical shift imaging

R.H. Wu¹, D. Dureux², R. Lin¹, G. Guo¹, K. ter Brugge³, D.J. Mikulis³;

¹Shantou/CN, ²Le Kremlin-Bicêtre/FR, ³Toronto, ON/CA

Purpose: Many endeavors of improving chemical shift imaging (CSI) techniques have been made during last two decades. Good examples of two-dimensional CSI and three-dimensional CSI can be found in the literature. However, clinical CSI using available sequences is still not satisfactory. The purpose of this study was to assess the effect of outer volume saturation bands on signal homogeneity in MR 2D chemical shift imaging.

Methods and Materials: The 2D CSI scans were acquired using a point resolved spectroscopy (PRESS) CSI sequence on a phantom filled with brain metabolites. A single PRESS volume of interest was prescribed graphically. The acquisition matrix was 18x18 phase encodings over a 24 cm FOV. Identical acquisitions were obtained with and without outer-volume saturation bands. After initial acquisition was obtained, four more acquisitions were repeated for both studies with and without saturation bands. Identical five groups of voxels were compared for both studies. Standard deviations of ratios were calculated in each group for both studies.

Results: Spectra obtained without outer-volume saturation bands showed signal to noise gradient with higher concentration of signal within voxels at the center of the volume of interest. Outer volume saturation bands reduced this gradient. In general, standard deviations of metabolism ratios with saturation bands were smaller than those without saturation bands. Improved spatial homogeneity of spectra in voxels of CSI with saturation bands was obtained.

Conclusion: Outer-volume saturation bands improve spatial homogeneity of chemical shift imaging.

B-920 10:57

b-Matrix assessment in diffusion tensor imaging using a reference phantom

D. Güllmar, J. Haueisen, J.R. Reichenbach; Jena/DE

Purpose: In this study we try to establish a method to estimate the coefficients of the b-matrices in DTI experimentally. These coefficients are usually calculated by using a very simple equation which only takes into account the diffusion gradients. In this study we have determined the b-matrix analytically taking into account all gradients. The resulting system of equations with four unknown parameters can then be solved using a few measurements and an isotropic phantom with known diffusion coefficient.

Methods and Materials: All measurements were performed using a 1.5 T whole-body MR-Scanner. The diffusion coefficient of the phantom was determined by

Scientific Sessions

using a cross-term free diffusion acquisition method. To determine the full b-matrix we acquired a full diffusion tensor scan (six directions) and solved the corresponding system of equations.

Results: The individual elements of the experimentally determined b-matrix were different from the elements obtained by using the simplified b-value calculation. Depending on the actual b-value (100-1000 s/mm²) deviations of up to 30% (for low b-values) were observed for some of the elements. The experimentally determined b-matrix was in very good agreement with the fully analytically calculated b-matrix.

Conclusion: The presented experimental approach provides a simple way to assess the b-matrix in very good correlation to the analytically calculated b-matrix. For this approach only knowledge of the gradient scheme, the protocol parameter and the diffusion coefficient of the phantom is required. However, the accuracy of this method critically depends on the accuracy of the numerical value of the diffusion coefficient.

B-921 11:06 ♀

Caffeine-induced contrast enhancement in volunteers by using susceptibility-weighted imaging (SWI)

J. Sedlacik, A. Rauscher, A. Deistung, W.A. Kaiser, J.R. Reichenbach; Jena/DE

Purpose: Small susceptibility differences are only accumulated with phase with long echo times, which requires long measurement times. The aim of this work was to investigate the possibility of increasing SWI contrast with caffeine; thus reducing potentially measurement time.

Methods and Materials: High-resolution T2*-weighted images were acquired in four volunteers on a 1.5 T system using a velocity-compensated 3D-gradient-echo imaging sequence. Sequence parameters: TR/TE/FA = 67 ms/40 ms/15°, in-plane resolution = 0.5x0.75 mm², slice thickness = 1.75 mm, scan time 10 min. A native scan was performed first. Then the subjects drank a big cup of strong coffee (equivalent to 300 mg caffeine) directly in the scanner. The scan was repeated 5 times to cover a period of nearly one hour after drinking coffee. Complex images were reconstructed from the raw data and realigned. Maps of phase differences and relative signal changes were computed. SWIs were produced by combining phase and magnitude images.

Results: Maps of the relative signal change clearly visualized the caffeine-induced response of venous vessels. The signals in the veins decreased down to 50% compared to the native signal. Simultaneously, phase differences up to 90° were observed in the same vessels. The contrast could be increased impressively in the SWI, especially for the scans acquired up to one hour after coffee.

Conclusion: SWI contrast enhancement was demonstrated with caffeine. Maps of signal and phase changes showed most prominent effects in veins. It may therefore be possible to use the well-known vasoconstrictive effect of caffeine as a contrast-enhancer. Ultimately, acquisition time may be shortened while acquiring data after the intake of coffee.

B-922 11:15

Tmix imaging as alternative for femoro-tibial cartilage T2 mapping at 1.5 T

I. Van Breuseghem, I.M. Van Mieghem, R.R. Peeters, H.T.C. Bosmans, G.J. Marchal, S. Pans; Leuven/BE

Purpose: To evaluate the feasibility of T2 mapping of human femoro-tibial cartilage with tMIX imaging on a 1.5 T MR imaging system.

Methods and Materials: A turbo-mixed sequence was implemented on a 1.5 T MR imaging system. A standard knee coil was used. 25 healthy adult volunteers (male/female: 17/8; age range, 20.85-44.72 years; mean age 28.5 years) underwent MR imaging of either one or both knees after informed consent was obtained. The turbo mixed sequence was performed making 24 slices in a sagittal direction. T2 maps were calculated by using a built-in calculation tool. The images were transferred to a workstation for further post-processing to obtain colored quantitative T2 maps.

Results: A total of 46 knees were scanned. All areas demonstrate a similar pattern of spatial variation in cartilage T2 with longer values observed near the articular surface. 2 layers in T2 profile can be detected showing a first layer at the cartilage/bone interface (mean T2 relaxation value 36.8 msec - SD:1.4) and a second layer with T2 values progressively increasing towards the cartilage surface (mean T2 relaxation value 50.8 msec - SD:3.2).

Conclusion: To resolve technical challenges posed by the thin and curved femoro-tibial cartilage, we used a high resolution scan technique (in plane resolution of 270 µ) and post-processing (with color-encoding) for accurate T2 mapping of cartilage. As our results are in concordance with literature, the proposed tMIX technique can be used for T2 mapping of cartilage on a 1.5 T MR imaging scanner.

B-923 11:24 ♀

Complex data processing in dynamic MR-mammography

A. Rauscher, K.-H. Herrmann, J. Sedlacik, W.A. Kaiser, J.R. Reichenbach; Jena/DE

Purpose: Routine contrast-agent enhanced MR imaging uses a subtraction of the modulus of a native scan from one of several scans acquired after contrast agent administration. However, magnetic resonance images are complex (i.e. consisting of a real part and an imaginary part) by nature and processing of the modulus imposes limitations upon the information originally contained in the data sets. The purpose of this study was to evaluate the advantages of data processing in the complex domain.

Methods and Materials: For each of four patients (with invasive lobular carcinomas) four (1 pre-KM, 3 post-KM (0.1 mmol/kg bw Gd-DTPA)) T1 weighted 3D double-echo, gradient-echo scans (TR/TE1/TE2/FA = 7 ms/2.73/4.76 ms/15°) were acquired on a 1.5 T scanner using a double breast coil. Complex images were computed from the modulus images and the phase images and all operations such as subtraction or division of images were performed on the complex data and then the modulus of the resulting images was assessed.

Results: Contrast between the enhancing lesions and the healthy tissue is highly improved by complex processing. Complex division leads to a few pixels in noisy areas outside the breast where division by zero occurs. A simple thresholding of the resulting images eliminates the resulting spikes.

Conclusion: Complex processing preserves information and increases contrast-to-noise. Taking the modulus of the complex subtraction (instead of the subtraction of the modulus) may help to improve conspicuity of small lesions. More sophisticated calculations using combinations of in-phase and opposed-phase scans or the assessment of phase images are currently under evaluation.

B-924 11:33

Whole-body FDG-PET/CT with extended CT field-of-view for improved oncology imaging

T. Beyer¹, M.-J. Martinez², O. Sembritski³, F. Roberts⁴, S. Ziegler², H. Kuehl¹, A. Bockisch¹; ¹Essen/DE, ²Munich/DE, ³Forchheim/DE, ⁴London/UK

Purpose: We investigate the effect of CT-truncation in whole-body (WB) PET/CT-imaging of large patients and evaluate the efficacy of an extended field-of-view (e-fov) correction technique.

Methods and Materials: An 'arms-up'-phantom ('head': 20 cm-cylinder, 'arms': 1.5 l-plastic bottles) was filled with 10 kBq/mL FDG. A 'body'-phantom (40x30x20 cm³) was filled with 5 kBq/mL and contained 4 hot and 2 cold lesions. Both phantoms were positioned in the centre and with at least 10% of their volume beyond the transverse CT-fov. Phantoms were scanned on PET/CT tomographs with 2- and 16-row MD-CT (PET/CT-2.16). CT-based attenuation correction was performed using the CT-images reconstructed from truncated and extended projections to recover the truncated CT-information. The e-fov algorithm estimates full CT-projections from linear interpolation of the truncated projections. For clinical validation, we imaged 20 patients with significant truncation artefacts on PET/CT-2.16 with and without the extended CT-fov correction.

Results: PET tracer distribution was suppressed outside the transverse CT-fov in phantom and patient studies. Corrected PET activity concentration in the truncated regions of the 'arms-up' and 'body'-phantom was reduced to 40% and 10%, respectively but recovered within 7% of the true value through the use of the e-fov correction. With the e-fov correction visual distortion of lesions in the 'body'-phantom was reduced, and the body contour of patients was recovered to the anatomically-correct shape from the uncorrected emission images.

Conclusions: Truncation artefacts in WB-PET/CT imaging lead to a visual and quantitative distortion of the CT and corrected PET-images but can be corrected for through a simple algorithm for extended CT-fov reconstruction.

B-925 11:42

Does CT attenuation correction improve lesion conspicuity in nuclear medicine?

J.D. Birchall, R.H. Ganatra, R.M. Smith, K. Griffith, A.C. Perkins; Nottingham/UK

Purpose: Low dose CT for attenuation correction of SPECT studies improves the detection and localisation of activity deeper within the body and additionally the ability for the physiological NM image to be fused to an anatomical CT image. The CT dose is low being approximately 0.8 mSv.

Methods and Materials: We have used a dual headed gamma camera / CT system in our routine clinical practice over the last 12 months successfully on 44 of 45 occasions. In these studies, we have compared the effect of attenuation

Scientific Sessions

correction (AC) on count rate from the region of pathological interest. We have expressed this as a ratio of the AC counts to the non-AC counts (AC/NAC).

Results: Over all of the studies the effect of CT AC was to increase the AC/NAC ratio by a factor of 3.19 (Mann-Whitney U test $p < 0.0001$). For the 28 Tc^{99m} radionuclide studies the AC/NAC ratio increase was 3.64 ($p < 0.0001$). 36 SPECT studies were performed on the body trunk with an increase AC/NAC ratio 3.5 ($p < 0.0001$) and AC/NAC ratio increase of 2.19 (not significant) for 9 SPECT studies on the distal limbs. Not unsurprisingly, we found significant correlation between the AC/NAC ratio and depth of lesion from skin surface being for all radioisotopes ($r = 0.535$, $p < 0.0002$) and in particular for Tc^{99m} radionuclides ($r = 0.76$, $p < 0.0001$).

Conclusion: We conclude that SPECT with CT attenuation correction improves the NM image and will present clinical case vignettes highlighting the advantage of attenuation correction in SPECT/CT in the localisation of pathological lesions.

10:30 - 12:00

Room P

Neuro

SS 1811b

fMRI imaging and new MR imaging sequences

Moderators:

S. Sunaert; Leuven/BE

F.E. Zanella; Frankfurt a. Main/DE

B-926 10:30

What is different in a radiologist's brain?

S. Haller, E.W. Radü; Basle/CH

Purpose: The neuronal correlate of expertise of experienced radiologists was investigated using event-related functional magnetic resonance imaging (fMRI).

Methods and Materials: Radiographic (RI) and control images (CI) were presented to twelve experienced radiologists and twelve naive subjects. Half of images were artificially manipulated, e.g. a local shadow was introduced. Subjects had to indicate whether a visually presented image was original or manipulated, while neuronal activity was assessed using event-related fMRI.

Results: RI compared to CI evoked stronger activations exclusively in the group of radiologists, notably in bilateral Middle and Inferior Temporal Gyrus, bilateral Medial and Middle Frontal Gyrus and left Superior and Inferior Frontal Gyrus. Additionally, the visual processing of CI (i.e. non-radiographic images) significantly differs between experienced radiologists and naive subjects. Radiologists show strongest activation in left-dominant more posterior Superior and Inferior Parietal Lobule, while naive subjects show strongest activation in right-dominant and more anterior Superior and Inferior Parietal Lobule and Postcentral Gyrus.

Conclusion: Radiological experience modifies neuronal representation twofold. First, there is a selective enhancement for radiographic images, which might reflect the behavioral relevance of these specific images. Second, the visual system is modified in general, which might reflect the extensive usage of the visual system by experienced radiologists.

B-927 10:39

Verbal communication: A fMRI imaging - DTI study

C.-V. Salvan, J.L. Ulmer, L. Hacein-Bey, W.M. Mueller, R.W. Prost; Milwaukee, WI/US

Purpose: Verbal communication is a characteristic and a unique feature of the human being. Its substrate is considered intriguing in many scientific fields. Our goal is to present the underlying anatomical and functional networks as identified by functional MR imaging and Diffusion Tensor Imaging (DTI)-fractional anisotropy (FA). Secondly, we present the influence of lesions on these networks, as well as the capacity of plasticity in the brain.

Materials and Methods: BOLD functional MR imaging and DTI-FA data were obtained in normal subjects and 13 patients with lesions involving speech and language areas. Gray matter organization was studied with fMRI imaging and a cross-correlation analysis ($p < 0.01$) and white matter with DTI- FA and direction-sensitive maps. We also superimposed fMRI imaging data onto FA images for a better understanding of functional networks. In patients, WADA-testing, intraoperative mapping and/or postoperative outcome was used for functional assessments.

Results: Expressive and receptive language was mapped, together with important components of executive function, memory, planning, attention. Correspondence to known anatomical and physiological knowledge was obtained. Lateralization of language functions was also investigated and confirmed. In pathological cases,

depending on lesion type, localization, size and handedness, different models of language networks were obtained, and case scenarios were exemplified. Plasticity of language areas was suggested in 9 cases. WADA-testing, intraoperative mapping and/or postoperative outcomes supported our data in 10 cases.

Conclusion: The complexity of verbal communication and brain plasticity is difficult to understand, but fMRI imaging and DTI can contribute to our knowledge and can be used to optimize patient outcomes.

B-928 10:48

Time-resolved analysis of event related fMRI imaging during language comprehension at word and sentence level

S. Haller¹, J. Schwarzbach², M. Klarhöfer¹, E.W. Radü¹; ¹Basle/CH, ²Nijmegen/NL

Introduction: Neuronal activation during language comprehension at word and sentence level was assessed using event-related fMRI imaging. The effect of increasing task difficulty on the BOLD response was investigated based on time-resolved analysis of fMRI imaging.

Methods and Materials: Sixteen healthy participants performed three reading tasks of increasing linguistic difficulty during fMRI imaging. In the latency analysis, delay and duration of the BOLD response were estimated by fitting gamma functions used as hemodynamic model function to event-related average BOLD response for each single voxel. In the correlation analysis, single trial BOLD delay estimates were correlated with response time.

Results: The latency analysis revealed shortest BOLD response delay in the visual area, consistent with the visual stimulus presentation. Activations in left Inferior Frontal Gyrus (IFG), i.e. Brocas language area, showed later activation. Increasing task difficulty was paralleled by increasing BOLD response latency in left IFG, but not in the visual area. The duration of the BOLD response increased uniformly in all areas with increasing task difficulty. Additionally, the correlation analysis of estimated BOLD delay and response time revealed strongest correlation in motor area. Correlation in left IFG was smaller despite comparable BOLD response delay, consistent with the direct link between motor area and response button press.

Conclusions: The presented time-resolved analysis of er-fMRI imaging data illustrates the cascade of cognitive processes at high temporal and spatial resolution. The temporal information of this time-resolved analysis complements statistical information of general linear model analysis.

B-929 10:57

Differences in regional BOLD responses in the primary and secondary auditory cortex induced by mixed noise and speech like stimuli

M. Golebiowski, P. Bogorodzki, W. Szczeszkowski, E. Piatkowska-Jankó, T. Wolak, M. Orzechowski, R. Kurjata, A. Cieszanowski; Warsaw/PL

Purpose: The aim of the study was to investigate the hierarchical organization within the auditory cortex of humans with mixed noise and speech like auditory excitation using functional magnetic resonance imaging (fMRI) technique.

Methods and Materials: For each of 20 healthy subjects (16 males and 4 females, 19 right-handed and 1 left-handed) at age 23.6 ± 0.7 four functional sessions with block type speech like stimuli (15 repetitions of the BA-LU) and variable amount of noise were acquired. Statistical parametric maps were generated under SPM99 software and additionally, the raw Blood Oxygenation Level Dependent (BOLD) signal intensities from left and right primary (A1) and secondary (A2) auditory cortex regions were averaged to form a time series spanning the entire length of the experiment. The variation of resulting curves was described with percent signal change (PSC) measure.

Results: The random effect analysis shows strong activations in both A1 ($T = 10.59$ in left hemisphere and $T = 9.94$ in right hemisphere) and A2 ($T = 11.73$ in left hemisphere and $T = 8.75$ in right hemisphere) regions. Additionally, we noted substantial correlation of PSC measure with noise level in A1 ($R = 0.95$, $T = 13.4$) and practically no correlation in A2 ($R = 0.05$, $T = 0.2306$).

Conclusion: The experiment revealed auditory hierarchical architecture with the special emphasis on primary and secondary cortex function fields. An attenuation of noise at secondary cortex with good response for BA-LU stimuli.

B-930 11:06

Functional CNR as a fMRI imaging specific quality parameter for presurgical mapping in tumor patients

A. Geissler, M. Barth, R. Lanzenberger, A. Gartus, A.R. Tahamtan, G. Meller, T. Foki, D. Milakara, R. Beisteiner; Vienna/AT

Purpose: fMRI imaging has high potential for delineating eloquent brain tissue at risk and could possibly substitute complex procedures such as awake craniotomy

Scientific Sessions

or WADA test. To obtain significant fMRI activation the functional CNR has to be as high as possible to reduce false positive activation as, in the worst case, even a difference in the resection margin of only 1 mm may lead to subsequent irreversible functional deficits. We tested the hypothesis that besides SNR, CNR is an important indicator for fMRI stability.

Methods and Materials: 7 healthy subjects and 6 tumor patients were measured using a multi-slice, single-shot gradient-echo EPI sequence using a 3 T scanner. One run consisted of 4 resting and 3 movement phases with 20 s duration each, six runs were performed. Opening and closing of the dominant hand was used as the stimulus paradigm. A correlation analysis was performed and the rank of each run (RR) when the most reliable pixel was estimated unambiguously for the first time was assessed. Image SNR was obtained as a measure for data quality. The functional CNR in the most reliable pixel was calculated.

Results: The run-averaged SNR values were 32 ± 8.2 , the RR values 3.5 ± 2.3 . CNR values were 2.8 ± 0.8 . Correlation between SNR and CNR was 0.8, and -0.4 between RR and CNR.

Conclusion: The results indicate that CNR reflects both data quality and, to a lesser degree, fMRI stability. CNR can thus be used as a fMRI specific quality parameter.

B-931 11:15

BOLD functional MR imaging in simple motor tasks and equivalent motor imagery

E.J.M. Vandervliet, Ö. Özsarlak, M. Maes, J. Van Goethem, P.M. Parizel; Antwerp/BE

Purpose: To compare the amplitude and spatial distribution of BOLD responses of brain areas involved in simple motor tasks and equivalent motor imagery (imaginary motor performance, IMP).

Materials and Method: We recorded the BOLD response of distinct brain areas in 9 healthy volunteers (mean age 31 years) who performed self-paced bilateral fingertapping and IMP. For each condition we used a comparable block design in which the task of interest was alternated by periods of rest. All experiments were performed on a 1.5 T scanner with high-performance 40 mT/m gradients (Siemens Sonata, Erlangen, Germany). We used gradient-recalled multi-shot EPI sequences (TE 50 ms, TR 3000 ms) with 30 slices covering the whole brain. Voxels measured 3x3x3 mm. Data analysis was performed in BrainVoyager (Brain Innovation, Maastricht, The Netherlands).

Results: In all subjects highly significant activation of the primary motor cortex (M1), supplementary motor area (SMA) and premotor cortex (PMC) was observed in both conditions. Thalamic activation was seen in all subjects during fingertapping. The spatial distribution of BOLD responses did not differ in M1, SMA and PMC but the amplitude of BOLD responses of M1 and PMC was larger during fingertapping. Centers of gravity remained the same.

Conclusions: 1) IMP offers a robust alternative for fingertapping in identifying the motor cortex; 2) the actual performance of motor tasks is dictated only by the level of activation and not by its spatial distribution; 3) thalamic activation can be seen with simple motor tasks, even at 1.5 T.

B-932 11:24

Comparison of T1-weighted inversion-recovery, gradient-echo and spin-echo sequences for imaging of the brain at 3.0 Tesla

C. Stehling, T.-U. Niederstadt, S. Krämer, H. Kugel, W. Schwindt, W. Heindel, R. Bachmann; Münster/DE

Purpose: The increased T1-relaxation times at 3.0 Tesla lead to a reduced T1-contrast; therefore imaging protocols for high field examinations need to be adapted. This prospective study assessed the performance of three techniques for T1-weighted imaging (T1w) at 3.0 T with regard to gray/white differentiation and CNR.

Methods and Materials: 32 patients were examined at a 3.0 T system (Gyroscan Intera, Philips) with axial T1w Inversion Recovery (IR:TR/TE/TI = 9900/15/400 ms; scan-time 4:07 min), T1w Spin Echo (SE:TR/TE = 570/8 ms; 3:09 min) and T1w Gradient Echo (GE:TR/TE/FA = 214/2.4 ms/80°; 2:59 min) sequences; after contrast enhancement (CE) CE-SE and CE-GE were acquired. For qualitative analysis images were ranked with regard to artifacts, gray/white differentiation, image-noise and overall diagnostic quality. For quantitative analysis CNRs of cortex and basal ganglia to white matter were calculated. Statistical significance was determined by Student's t and Wilcoxon tests.

Results: In the qualitative analysis IR was judged superior to SE and GE for gray/white differentiation, image noise and overall diagnostic quality, but was inferior to GE with regard to artifacts. CE-GE proved superior to CE-SE in all categories. In the quantitative analysis CNR of the basal ganglia was highest for IR (10.9), followed by GE (4.9) and SE (2.7) ($p < 0.003$). For CNR of the cortex

no significant difference was found between IR (16.9) and GE (15.4) but both were superior to SE (9.4). Cortex-CNR of CE-GE was significantly higher than compared to CE-SE (12.7 vs. 7.6, $p < 0.001$), but basal ganglia CNR did not differ significantly.

Conclusion: For unenhanced T1w-imaging at 3.0 T the IR technique is, despite increased artefacts, the method of choice, due to its superior gray/white differentiation and best overall image quality. For CE studies GE sequences are recommended. SE sequences give unsatisfactory results at 3.0 T.

B-933 11:33

Diagnostic value of T1-weighted fluid-attenuated inversion recovery sequence with 3.0 T MR in the central nervous system (CNS)

S. Chen, X. Feng; Shanghai/CN

Purpose: To determine the clinical use of T1-weighted fluid-attenuated inversion recovery (T1 FLAIR) sequence with 3.0 T MR in the CNS by comparing results with those at pre-and postcontrast T1 and T2 FLAIR MR imaging.

Materials and Methods: During a 11-month period, 385 cases including 200 normal cases and 185 cases with brain tumors, were examined with T1SE, T1FLAIR and T2FLAIR using 3.0 T MR (GE signa 3.0 T VH/i MR). T2FLAIR was only done on plain MR scan. 185 cases with brain tumors were performed with pre-and post-contrast T1FLAIR and T1SE MR imaging. Qualitative measures of overall image contrast, lesion detectability and lesion conspicuity in addition to quantitative measures of lesion-to-background, lesion-to-cerebrospinal fluid, gray-to-white matter signal contrast and contrast-to-noise ratio (CNR) were used for evaluation of whether T1FLAIR improves lesion conspicuity.

Results: Lesion-to-background, lesion-to-cerebrospinal fluid, gray-to-white matter contrast and CNR were statistically superior in pre-and post-contrast contrast T1FLAIR. Qualitatively, the T1FLAIR sequence provided comparable lesion detection, improved lesion conspicuity, and superior image contrast compared with T1SE and T2FLAIR on both pre-and post-contrast images, especially in detection of lesions at the gray/white matter junction.

Conclusion: T1FLAIR MR imaging on 3.0 T MR is a potentially useful tool for diagnosis in the CNS; pre-and postcontrast T1 FLAIR could replace pre-and post-contrast T1SE MR imaging.

B-934 11:42

New MR sequences to detect the neurovascular conflict in cranial nerves

B.P.J. Kress, S. Siebert, M. Krause, C. Schwark, D. Rasche, G. Kolling, V. Tronnier, K. Sartor; Heidelberg/DE

Purpose: To show the options in MR imaging of the neurovascular conflict by newly developed T1 and T2 weighted imaging sequences.

Materials and Method: 85 patients (19 patients: facial hemispasm, 63 patients: unilateral facial pain, 1 patient: glossopharyngeal neuralgia, 1 patient: recurrent trochlear paresis, 1 patient: recurrent restriction of visual field) were examined by MR imaging to rule out a neurovascular conflict between an artery and a cranial nerve. (T1 FLASH 3D vibe, 0.9 mm isovoxel, coronal [before and after intravenous application of GdDTPA], T2-True FISP, 0.3x0.4x0.4 mm, coronal. The result of the MR imaging was compared to a preliminary examination of the same patient.

Results: In all patients with typical neurological symptoms it was possible to show a neurovascular conflict (all patients with trigeminal neuralgia, facial hemispasm, glossopharyngeal neuralgia) Also in the patient with trochlear nerve dysfunction and recurrent visual deficits a vessel was detected which had close contact to the nerve. In 13 of 24 patients with non neurological facial pain a vessel was found to have contact with the trigeminal nerve.

Conclusion: High resolution MR imaging can detect the adjacencies between vessel and cranial nerves. T2 TRUE FISP with an isovoxel of 0.3 mm in combination with high signal to noise ratio makes it possible to detect even small vessels, which are not seen on T2CISS images. Contrast enhanced T1 FLASH 3D vibe sequence makes it possible to differentiate between nerve and vessel confidently.

B-935 11:51

The value of high-field MR imaging (3 Tesla) in the assessment of sellar lesions

K. Pinker, A. Ba-Ssalamah, S. Wolfsberger, V. Mlynarik, E. Knosp, S. Trattnig; Vienna/AT

Purpose: The aim of this study was the evaluation of the normal sellar anatomy in-vitro and in-vivo with high-field MR imaging and its application in the diagnosis of sellar pathologies in comparison to standard MR imaging.

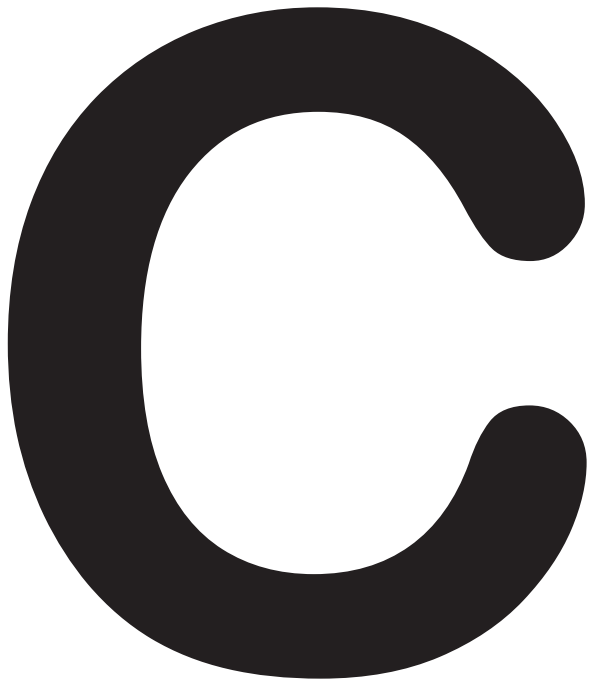
Methods and Materials: For high-field MR imaging we used a (3 T) Bruker Medspec 30/80 Scanner with a head birdcage transmit/receive coil and an actively

Scientific Sessions

shielded gradient system (maximum gradient strength 45 mT/m). We used a T2-weighted RARE sequence (TR/TE = 7790/19 ms; matrix size 512x512; FOV 200 mm) for coronal, axial and sagittal images and a T1-weighted-3D-MP-RAGE sequence (TR/TE/TI = 33.5/7.6/800 ms, matrix size 512x512; FOV 200 mm, SI 1.88 mm) for pre/post-contrast coronal images. 58 patients were enrolled in this study. Seven patients were examined for suspected microadenoma and in 51 patients 3 T MR imaging was used to obtain additional information about the sellar lesion already known to be present from standard MR imaging. In 21 cases the accuracy of the imaging findings was assessed by comparison with intraoperative findings.

Results: Infiltration of the medial cavernous sinus wall was suspected on standard MR imaging on 15 sides (47%), on high-field MR imaging on 9 sides (28%) and was verified by surgical findings on 6 sides (19%). Sensitivity of infiltration was 83% for 3 T MR imaging and 67% for standard MR imaging. Specificity was 84% for 3 T MR imaging and 58% for standard MR imaging. High-field MR imaging revealed microadenomas in 7 patients with a median diameter of 4 mm. The segments of the cranial nerves were seen as mean 4 hypointense spots on high-field MR imaging in contrast to 3 spots on standard MR imaging. This difference was statistically significant.

Conclusion: High-field MR imaging is superior to standard MR imaging for the prediction of invasion of adjacent structures in patients with pituitary adenomas and improves surgical planning.



Scientific and Educational Exhibits

☞ This icon indicates an exhibit scheduled for an electronic poster session (EPS) in one of the EPOS theatres on the second level.

☞ Electronic Poster Sessions (EPS)	346
Abdominal Viscera (Solid Organs).....	353
GI Tract	369
Breast.....	389
Cardiac	399
Chest	409
Computer Applications	425
Contrast Media.....	431
Molecular Imaging	435
Genitourinary	437
Head and Neck	458
Interventional Radiology	466
Musculoskeletal	483
Neuro	507
Pediatric	528
Physics in Radiology	538
Radiographers	547
Vascular	550
ECR Research Grant Winners	566

Electronic Poster Sessions

Friday, March 4

13:15 - 14:00

San Carlo

EPS 03

Cardiac

Moderator:

V.E. Sinitsyn; Moscow/RU

C-0227

MR and CT imaging of partial and total cavo-pulmonary connections: A guide to assessment of the Fontan circuit for the uninitiated

A. Crean, Y. Provost, N. Paul, N. Merchant; Toronto, ON/CA

C-0230

Noninvasive investigation of cardiac metabolism in patients with hypertensive heart disease (HHD) by ^{31}P -MR spectroscopy

R. Rzanny, J.-P. Heyne, A. Hansch, U. Leder, J.R. Reichenbach, W.A. Kaiser; Jena/DE

C-0257

ECG-gated 16-slice CT of coronary arteries: Assessment of image quality and accuracy in detecting stenoses

O. Luz, M. Heuschmid, A. Kuettner, S. Schroeder, A. Kopp, C.D. Claussen; Tübingen/DE

C-0259

Occlusive myocardial infarction on sixteen-slice multi-detector row helical CT in a rabbit model: Radiologic-pathologic correlation according to infarct age

J. Lee, Y. Kim; Seoul/KR

C-0260

Imaging of atrioventricular septal defect (AVSD) with multidetector-row CT angiography

R.L. Hallett, M.D. Hiatt, D. Fleischmann, J.C. Hellinger, G.D. Rubin, F.P. Chan; Stanford, CA/US

13:15 - 14:00

La Fenice

EPS 01b

GI Tract

Moderator:

B. Jamar; Ljubljana/SI

C-0080

The efficacy of CT-colonography for diagnosis and staging of colon cancer in symptomatic patients

P. Zdunek¹, A. Gmur¹, M. Wykret¹, R. Pacho², P. Wandzel¹; ¹Bielsko-Biala/PL, ²Warsaw/PL

C-0082

The correlation of endosonography versus peroperative and histopathological findings in a group of 350 patients with surgically treated anorectal tumor

Z. Chudáček¹, R. Sequens², M. Pechotová¹, J. Kuntscherová¹; ¹Plzen/CZ, ²Prague/CZ

C-0083

Integrated sonography of Crohn's disease by combining high-resolution B-mode techniques and contrast enhanced ultrasound (CEUS) perfusion studies of the involved bowel segments

S.D. Yarmenitis, G. Kolios, N. Papanikolaou, T. Maris, E. Kouroumalis, N. Gourtsoyiannis; Iraklion/GR

C-0168

The place of peritoneography in the evaluation of chronic groin pain compared with ultrasound and CT: A forgotten technique gets its due - a retrospective study of 112 patients

R.A. Salgado¹, M. Maes¹, P. Bellinck², B. Op de Beeck¹, J.-L. Termote², P.M. Parizel¹; ¹Edegem/BE, ²Lier/BE

C-0172

Normal anatomy and non-hernia pathology of the abdominal wall on cross-sectional imaging

J. Quintero¹, C. Pozuelo¹, C. Medrano¹, D. Mulattieri¹, S. Capurro², F. Tous³; ¹Badalona/ES, ²Barcelona/ES, ³Santa Coloma de Gramenet/ES

13:15 - 14:00

La Pergola

EPS 10

Musculoskeletal

Moderator:

O. Tervonen; Oulu/FI

C-0651

IVR techniques for bone tumor: A comprehensive review

T. Inaoka¹, K. Takahashi², T. Yamada¹, M. Mineta¹, W. Yamamoto¹, K. Nagasawa¹, H. Hirota¹, T. Yamaki¹, T. Aburano¹; ¹Asahikawa City/JP, ²Iowa City, IA/US

C-0652

The role of in-phase and out-of-phase magnetic resonance imaging and in vivo 1H single-voxel magnetic resonance spectroscopy in the differential diagnosis of monoclonal gammopathies

G. Bajzik, M. Egyed, E. Karadi, B. Kollar, G. Rumi, P. Rajnics; Kaposvar/HU

C-0678

High field magnetic resonance imaging of reconstituted articular cartilage: Evaluation of cartilage maturation for determination of optimal transplantation time

M.H. Fuchsberger, V. Mlynarik, S. Marlovits, M.O. Philipp, S. Trattnig; Vienna/AT

C-0713

High-resolution US to evaluate post-surgical peripheral nerve lesions

M. Aguilar, V. Gomez-Dermit, R. Landeras, P. Ruiz-Hernandez, P. Zubietta, M.A. Fernandez-Echevarria; Santander/ES

C-0738

Spectrum of cyst-like conditions found in and around the knee

M. Hjelt, A. Buzzi, M. Canedo, S. Gomez Zanetta, A. Mancini; Buenos Aires/AR

Electronic Poster Sessions

Saturday, March 5

13:00 - 13:45

La Fenice

EPS 01a

Abdominal Viscera

Moderator:

F. Caseiro-Alves; Coimbra/PT

C-0002

Value of imaging findings in the detection of recurrent primary sclerosing cholangitis after orthotopic liver transplantation

M.-F. Bellin, J. Duclos Vallee, I. Ewenzyk, E. Bigot, D. Azoulay, D. Castaing, C. Guettier, D. Samuel, L. Gilbert; Villejuif/FR

C-0010

Preoperative surgical estimation of the portal venous based territories compared to the surgical planning landmark to the right of the middle hepatic vein

T. Abe¹, B.B. Frericks², B. Nashan³, Y. Ohgiya¹, T. Gokan¹; ¹Tokyo/JP,

²Berlin/DE, ³Halifax, NS/CA

C-0012

Comparison between highly fat selective MR imaging and volume localized ¹H-spectroscopy of the liver for determination of intrahepatic fat accumulation

J. Machann, C. Thamer, B. Schnödt, H.-U. Häring, C.D. Claussen, A. Fritzsche, F. Schick; Tübingen/DE

C-0013

Double contrast MR imaging (DCMRI) of focal lesions in the cirrhotic and non cirrhotic liver: A problem solving technique

J.J. Sheehan, S.E. Harte, C.M. McKenna, D.E. Malone; Dublin/IE

C-0052

CT imaging based scores as predictors of severity in acute pancreatitis:

A comparative study with statistical evaluation

C. Triantopoulou, P. Maniatis, D. Lytras, I. Sifas, K. Manes, J. Papailiou, C. Dervenis, D. Chrysosvergis; Athens/GR

13:00 - 13:45

San Carlo

EPS 02

Breast

Moderator:

R. Chersevani; Gorizia/IT

C-0180

Radiological and histological features of mammography screen detected lesions undergone benign surgical excision

D.D. Manuel, S. Bose, D.D. Evans, R. Wasan, G. Ralleigh, M. Michell; London/UK

C-0185

Computer aided detection (CAD) results for mammography in a diagnostic center environment

R. Salvador, F. Ramírez, X. Martínez, M. Salvador, D. Coll, R. Salvador Jr; Barcelona/ES

C-0189

Locally advanced breast cancer: Magnetic resonance imaging versus clinical examination, mammography and ultrasonography in evaluation of residual disease after primary chemotherapy

M. Bodini, U.P. Marini, C. Fiorentino, L. Olivetti; Cremona/IT

C-0202

Differentiation of benign and malignant solid breast masses: Real-time spatial compound imaging versus conventional ultrasound

J. Cha¹, W. Moon¹, Y. Koh¹, J.-E. Cheon¹, J. Park², B.-K. Han¹, Y. Cheo¹;

¹Seoul/KR, ²Wisconsin, WI/US

C-0203

Differentiation of benign and malignant solid breast masses: Tissue harmonic imaging versus conventional ultrasound

J. Cha¹, W. Moon¹, Y. Koh¹, J. Cheon¹, J. Park², B.-K. Han¹, Y. Cheo¹;

¹Seoul/KR, ²Wisconsin, WI/US

13:00 - 13:45

La Pergola

EPS 09

Interventional Radiology

Moderator:

M. Sapoval; Paris/FR

C-0569

Contrast harmonic imaging with power mode and coded harmonic angiography using Optison for assessing vascularization during chemoembolization in HCC - First experiences

D.-A. Clevert¹, E. Jung², M. Reiser¹, N. Rupp²; ¹Munich/DE, ²Passau/DE

C-0610

Radiofrequency in the treatment of hepatocellular carcinoma. Multicenter study in Spain

M. Squarcia, R. Vilana, L. Bianchi, C. Nicolau, M. Sala, J.M. Llovet, J. Bruix, C. Bru; Barcelona/ES

C-0611

Radiofrequency ablation may activate the immune system and induce specific anti-tumoral immune responses in cancer patients

S. Haen¹, C. Gouttefangeas¹, A. Boss¹, S. Clasen¹, D. Schmidt¹, M. Kuczynk¹, A. Stenzl¹, H. Schild², P.L. Pereira¹, H.-G. Rammensee¹; ¹Tübingen/DE, ²Mainz/DE

C-0612

Presurgical transcutaneous MR imaging-guided marking of intramedullary tumors

J. Fritz, C.W. König, P. Böhm, F. Maurer, A. Badke, M. Müller-Schimpffle, C.D. Claussen, P.L. Pereira; Tübingen/DE

C-0613

Ureteral Implantation of Paclitaxel-eluting balloon-expandable metallic stents: An experimental study in the pig model

D. Siablis, N. Christeas, D. Karnabatidis, K. Katsanos, E.N. Liatsikos, N. Flaris, G.C. Kagadis; Patras/GR

Electronic Poster Sessions

Sunday, March 6

13:00 - 13:45

La Fenice

EPS 04

Chest

Moderator:
S.R. Desai; London/UK

C-0280

Staging of primary non-small cell lung cancer with CT, MR imaging and PET
S.A. O'Keefe, A. McGrath, S. O'Brien, R. McDermott, F. O'Connell,
J.F.M. Meaney; Dublin/IE

C-0326

Congenital and acquired anomalies of the pulmonary arteries in adults:
A radiologic overview.

D. Gil¹, E. Castaner¹, X. Gallardo¹, J. Mata¹, Y. Pallardo², J. Perendreu¹,
A. Massuet¹; ¹Sabadell/ES, ²Valencia/ES

C-0327

Role of D-dimer and pre-test probability scoring in suspected acute
pulmonary embolism

G. Annamalai, C. Campbell, P. Duffy; Glasgow/UK

C-0339

Microscopic findings in various lung diseases with peripheral lung imaging
using micro focus X-ray CT

H. Ikura¹, K. Shimizu², Y. Yasuhara¹, M. Miyagawa¹, T. Mochizuki¹, H. Ebara¹,
K. Ueno³, T. Nagareda⁴; ¹Ehime/JP, ²Kanagawa/JP, ³Tokyo/JP, ⁴Hyogo/JP

C-0348

F-18 FDG microPET imaging after percutaneous radiofrequency ablation
(RFA) in normal rabbit lung

T. Okuma, T. Matsuoka, T. Okamura, Y. Wada, A. Yamamoto, Y. Oyama,
K. Koyama, Y. Watanabe, Y. Inoue; Osaka/JP

13:00 - 13:45

San Carlo

EPS 11

Neuro

Moderator:
S. Cakirer; Istanbul/TR

C-0772

Epileptic mothers and their progeny in fMRI imaging assessment of
developmental dyslexia

A. Salagierska-Barwinska, B. Goraj, J. Wendorff, B. Wisniewska; Lodz/PL

C-0773

Correlation of diffusion tensor MR imaging with MR spectroscopy in
multiple sclerosis

R. Irwan, P. Sijens, M. Oudkerk; Groningen/NL

C-0774

Multidetector CT angiography: The method of choice to detect cerebral
venous thrombosis?

N. De Graaf, H.L.J. Tanghe, T.C. Leertouwer, H.Z. Flach, D.W.J. Dippel,
A. Van der Lugt; Rotterdam/NL

C-0778

Head and neck paragangliomas: Diagnostic and endovascular therapy

M. De Juan Delago, L. San Roman Manzanera, T. Salinas Yeregui,
C. Castaño Duque, E. Guardia Mas, J. Ruscalleda Nadal; Barcelona/ES

C-0779

Imaging of head and neck venous malformations: A pictorial review

C.M. Flis, S.E.J. Connor; London/UK

13:00 - 13:45

La Pergola

EPS 15

Vascular

Moderator:
J.F.M. Meaney; Dublin/IE

C-1017

Pseudo-occlusion of the internal carotid artery assessed by MRA: How to
avoid misinterpretation

J. Gasser, S. Celedin, K. Hausegger; Klagenfurt/AT

C-1018

Accuracy of magnetic resonance for identification and characterization of
carotid plaque constituents with histological correlation: A clinical
experience

G. Puppini, N. Cirola, F. Furlan, S. Quintarelli, G. Veraldi, S. Montemezzi,
G. Gortenutti; Verona/IT

C-1020

The pathophysiology of aortic-cardiac interaction in atherosclerotic disease
and the role of magnetic resonance imaging

Z.M. Metafratz¹, A. de Roos², A. Skopelitou¹, S.C. Efremidis¹; ¹Ioannina/GR,
²Leiden/NL

C-1037

Suspected entrapment syndrome of the popliteal vein: How to diagnose it.
Is it rare?

H. Minamiguchi, M. Sato; Wakayama/JP

C-1038

Radiological imaging of thoracic outlet syndrome

G. Bodner, H. Gruber, M. Schocke, M. Bernathova; Innsbruck/AT

16:00 - 17:30

La Fenice

EPS R&E

ECR Research Grant Winners

Moderators:
A.K. Dixon; Cambridge/UK, G.P. Krestin; Rotterdam /NL

C-1078

Characterisation of carotid atheroma in symptomatic and asymptomatic
patients using high-resolution gadolinium-enhanced MR imaging

J.M. U-King-Im¹, R.A. Trivedi, M.J. Graves, P.J. Kirkpatrick, N.M. Antoun,
J.H. Gillard; Cambridge/UK

C-1077

Technical optimization of diffusion tensor sequences: Evaluation of three
dimensional white matter tractography in various neurologic disorders

N. Papanikolaou; Iraklion/GR

C-1079

Automatic segmentation of airway wall area for quantitative assessment at
MDCT: Preliminary results in asthmatics

P.-Y. Brillet¹, C. Fetita², C. Beigelman-Aubry³, D. Perchet², F. Prêteux²,
P. Grenier³; ¹Bobigny/FR, ²Evry/FR, ³Paris/FR

Electronic Poster Sessions

C-1080

Proposal of an appropriate mathematical model to represent replenishment kinetic after microbubble destruction of an imaged renal volume to quantify renal perfusion

E. Quaia, L. Torelli; Trieste/IT

C-1081

The study of the human auditory system using combined fMRI imaging and DTI at 3T

S. Sunaert; Leuven/BE

Monday, March 7

13:00 - 13:45

La Fenice

EPS 08

Head and Neck

Moderator:

D. Farina; Brescia/IT

C-0522

The accessory oval foramen, so-called foramen of Vesalius: Anatomic CT study and clinical correlations

J. Renoux, K. Marsot-Dupuch, F. Benoudiba; Le Kremlin-Bicêtre/FR

C-0540

Ultrasound assessment of superficial lymph nodes (three-dimensional imaging, tissue harmonic imaging and panoramic imaging) intended for diagnostic excision

E.J. Bialek, W. Jakubowski, A.B. Szczepanik, R.K. Maryniak, M. Prochorec-Sobieszek, R. Bilski, M. Serafin-Krol; Warsaw/PL

C-0548

Role of multidetector CT in the evaluation of primary and secondary hyperparathyroidism

F. Ricci, S. Campagnano, A. Casale, M. De Vargas Macciucca, F. De Cristofaro, G. Panzironi; Rome/IT

C-0559

Endolymphatic sac tumors: A major criteria of Von Hippel-Lindau disease
K. Marsot-Dupuch, S. Richard, S. Bobin; Le Kremlin-Bicêtre/FR

C-0560

Imaging technique for obtaining optimal sections of the ossicular chain by high-resolution multiplanar reformation based on measurements of normal auditory ossicular angles

N. Fujii, K. Katada, S. Yoshioka, K. Takeuchi, A. Takasu, K. Naito; Toyoake/JP

13:00 - 13:45

San Carlo

EPS 12

Pediatric

Moderator:

T.A.G.M. Huisman; Zürich /CH

C-0887

Evaluation of [¹⁸F]FDG-PET and CT/MR imaging for monitoring therapy response in children with Hodgkin's disease

I. Sorge, A. Krausse, R. Kluge, C. Mauz-Körholz, D. Körholtz, W. Hirsch; Leipzig/DE

C-0888

MR imaging of the brain in Wilson's disease of childhood: Findings before and after treatment

J.-E. Cheon, I.-O. Kim, W. Kim, K. Yeon; Seoul/KR

C-0895

Significance of recurrent lung opacities in premature infants treated for respiratory distress syndrome: The SLOP study

S.P. Prabhu, S. Winterbottom, S. King; Bristol/UK

C-0898

Congenital deformities of the hand: Preoperative evaluation with multiple-detector row CT angiography

M. Rieger, A. Mallouhi, H. Piza, B. Czermak, M. Freund, W. Jaschke; Innsbruck/AT

Electronic Poster Sessions

C-0899

Uncomplicated versus torted testicular appendages in childhood:
Sonographic appearances with embryologic correlation

M. Vakaki, G. Pitsoulakis, V. Dermentzoglou, V. Begli, C. Koumanidou;
Athens/GR

13:00 - 13:45

La Pergola

EPS 13

Physics in Radiology

Moderator:
T.G. Maris; Iraklion/GR

C-0940

Synchrotron radiation microangiographic imaging of tumor-derived blood vessels in rabbit model of cancer for observation of angiogenic activity

K. Umetani¹, M. Kobatake², A. Yamamoto², T. Yamashita², S. Imai², Y. Kajihara²,

¹Sayo-gun, Hyogo/JP, ²Kurashiki-shi, Okayama/JP

C-0941

Age and gender related differences of adipose tissue compartments:

A whole body MR imaging study

J. Machann, C. Thamer, B. Schnödt, H.-U. Häring, C.D. Claussen, A. Fritzsche,
F. Schick; Tübingen/DE

C-0942

An elastic registration scheme for the alignment of thoracic CT data of patients with stage III non-small cell lung cancer during radiotherapy treatment

G. Matsopoulos¹, V.E. Kouloulias², N. Mouravliansky¹, P. Asvestas¹,
K. Delibasis¹, N. Uzunoglu¹, A. Kelekis², N. Kelekis²; ¹Athens/GR, ²Xaidari/GR

C-0943

Monte Carlo study on radiation absorption properties of Gd2O2S, CsI, LSO, CaWO4 phosphor screens for mammographic X-ray imaging

P. Liaparinos¹, I. Kandarakis², D. Cavouras², D. Nikolopoulos², G. Panayiotakis¹;

¹Patras/GR, ²Athens/GR

C-0944

Influence of rib structure on detection of subtle lung nodules

M. Ikeda, T. Ishigaki, S. Itoh; Nagoya/JP

16:00 - 16:45

La Fenice

EPS 05

Computer Applications

Moderator:
E. Bellon; Leuven/BE

C-0354

Towards standardization of hanging protocols for imaging display

E. Avraham; Plano, TX/US

C-0355

Computer-assisted diagnosis of thyroid nodules malignancy risk

S. Tsantis¹, D. Glotzos², I. Kalatzis², N. Pilouras², P. Spyridonos²,
N. Dimitropoulos², G. Nikiforidis², D. Cavouras²; ¹Patras/GR, ²Athens/GR

C-0356

Three-dimensional stereoscopic abdominal MR angiography as an educational tool for medical students

T. Yamagishi¹, K.H. Höhne², K. Abe¹; ¹Tokyo/JP, ²Hamburg/DE

C-0358

Virtual contrast injection: A software tool for selective visualization of vessel structures

A. Löfving¹, X. Tizon², A. Persson¹, G. Wiklund¹, Ö. Smedby¹; ¹Linköping/SE,
²Uppsala/SE

C-0359

EMIT: Digital multilingual medical radiation physics dictionary

M. Stoeva¹, S. Tabakov²; ¹Plovdiv/BG, ²London/UK

16:00 - 16:45

San Carlo

EPS 06

Contrast Media/Molecular Imaging

Moderator:
P. Wunderbaldinger; Vienna/AT

C-0386

Intraindividual comparison of 1.0M gadobutrol and 0.5M gadopentetate dimeglumine for time-resolved contrast-enhanced 3D magnetic resonance angiography of the upper torso

C. Fink, M. Puderbach, S. Ley, F. Risse, T.A. Kuder, M. Bock, J. Thaler,
C. Platow, H.-U. Kauczor; Heidelberg/DE

C-0389

Gd-IDa derivatives as potential hepatobiliary contrast media for MR imaging: Experimental studies on rats

M. Studniarek¹, E. Mikiciuk-Olasik², M. Retkowski¹, T. Wierzb¹, M. Sidorowicz¹;
¹Gdansk/PL, ²Lodz/PL

C-0391

A new MR findings: Decrease of signal intensity of myometrium after iV USPIO administration

P. Paolantonio, A. Laghi, C. Miglio, M. Rengo, V. Vergari, S. Ciccarelli,
A. Guerrisi, R. Passariello; Rome/IT

C-0405

Endothelial cell-targeted MR imaging using the anti-VEGFR2 and ICAM-1 antibody-conjugated Gd-DTPA

K.-H. Yoon, E.-A. Kim, J.-M. Hur, S.-H. Kim, Y.-H. Lee, K.-S. Choi; Iksan,
Jeonbuk/KR

C-0407

Human progenitor cells migrate into squamous cell carcinoma (SCC) xenografts

F.M.A. Kiessling, J. Dittrich, T. Moehler, M. Le-Huu, M. Bock, R. Schulz,
J. Peter, M. Mueller, W. Semmler; Heidelberg/DE

16:00 - 16:45

La Pergola

EPS 07

Genitourinary

Moderator:
L.H. Ros Mendoza; Zaragoza /ES

C-0468

MR imaging features of prostate carcinoma in local and nodal staging

J.J. Fütterer, S.W.T.P. Heijmink, R.A.M. Heesakkers,
C.A. Hulsbergen van der Kaa, F.A. Witjes, J.O. Barentsz; Nijmegen/NL

C-0493

Retroperitoneal anatomy: What could we learn from disease.

Part 1: Embryology

F.M. Danza¹, M. Scialpi², A. D'Amico¹, O. Pantalone¹, A. Bernardini¹, E. Bock¹,
L. Bonomo¹; ¹Rome/IT, ²Taranto/IT

Electronic Poster Sessions

C-0494

Retroperitoneal anatomy: What could we learn from disease.

Part 2: Pathway of spread of pathology

T.M. Scialpi¹, A. Magistrelli², M. Scaglione³, L. Lupattelli⁴, A. Rotondo³,
F.M. Danza², L.M. Bonomo²; ¹Taranto/IT, ²Rome/IT, ³Naples/IT, ⁴Perugia/IT

C-0495

Complications of urogenital non-vascular interventional procedures

Z.I. Siric, M. Radovanovic, M. Mrvic; Nis/YU

C-0496

Imaging of the ureter with multislice CT urography

A.F. Scarsbrook, N.C. Cowan, J. Willatt; Oxford/UK

Electronic Poster Sessions

Scientific and Educational Exhibits

Abdominal Viscera (Solid Organs)

Biliary tract

C-0001

MRCP findings of the choledochal cyst and anomalous pancreatico-biliary duct union: A comprehensive review with comparison to ERCP findings

M. Kim, J. Byun, H. Won, Y. Shin, A. Kim, P. Kim, H. Ha, M. Lee; Seoul/KR

Learning Objectives: To illustrate MR cholangiopancreatography (MRCP) and endoscopic retrograde cholangiopancreatography (ERCP) findings of various types of choledochal cysts and anomalous pancreatico-biliary duct union (APBDU). To assess diagnostic value with the benefits and pitfalls of MRCP compared with ERCP in evaluation of choledochal cysts and APBDU.

Background: The various types of choledochal cysts by Todani's classification are either associated with APBDU or not. The choledochal cyst is important to the patient because of the increased prevalence of malignancy or complications in the biliary tree. The presence of APBDU is helpful in diagnosis of choledochal cysts. We reviewed and classified MRCP images of 62 patients with choledochal cysts, with or without various APBDU. We also compared their MRCP findings with ERCP findings.

Imaging Findings: Of 62 patients with choledochal cysts the most common type was the type IVA ($n = 23$) and the second one was type IA ($n = 20$). Thirty-eight cases with choledochal cysts were associated with APBDU and the most common type was the type IIA ($n = 14$). Associated complications of choledochal cysts and APBDU were stone disease ($n = 14$), biliary malignancy proven pathologically ($n = 8$) and pancreatitis ($n = 52$).

Conclusion: MRCP provides equivalent information regarding choledochal cyst and APBDU to that provided with ERCP. MRCP should be considered as the first diagnostic modality for evaluation of the choledochal cyst and APBDU.

C-0002

Value of imaging findings in the detection of recurrent primary sclerosing cholangitis after orthotopic liver transplantation

M.-F. Bellin, J. Duclos Vallee, I. Ewenzyk, E. Bigot, D. Azoulay, D. Castaing, C. Guettier, D. Samuel; L. Gilbert; Villejuif/FR

Purpose: The aim of our study was to evaluate the role of imaging studies for the diagnosis of recurrent primary sclerosing cholangitis after liver transplantation.

Methods and Materials: 51 adult patients underwent liver orthoptic transplantation (LOT) between 1985 and 2004 for primary sclerosing cholangitis. Recurrent primary sclerosing cholangitis was histologically proven in 7 of these patients within 2-12 years following LOT. We reviewed the imaging studies [percutaneous cholangiography ($n = 6/7$), MR cholangiography ($n = 5/7$), Doppler ultrasonography ($n = 7/7$) and echoendoscopy ($n = 1/7$)] and compared the imaging findings with the biological and histologic results in these patients.

Results: The following aspects were observed on MR cholangiograms: non-anastomotic strictures ($n = 4$), segmental dilatation ($n = 3$) of intra or extrahepatic bile ducts, intrahepatic lithiasis ($n = 2$), irregular aspect of the bile ducts ($n = 3$), biliary abscess ($n = 1$) and normal aspect ($n = 1$). Percutaneous cholangiography confirmed the abnormalities observed with MR cholangiography in 4/7 patients and detected irregular walls of the intrahepatic bile ducts in one patient with normal MR cholangiography.

Conclusion: MR and cholangiographic abnormalities observed in patients with recurrent primary sclerosing cholangitis after LOT are identical to those observed in native livers. MR cholangiography may provide an excellent screening modality in patients with abnormal liver tests.

C-0003

Evaluation of biliary tract complications in hepatic transplantation with the use of magnetic resonance cholangiography

E. Maj, A. Cieszanowski, M. Golebiowski, K. Zieniewicz, E. Szwejda, B. Cieslak, M. Krawczyk; Warsaw/PL

Purpose: To assess the usefulness of magnetic resonance cholangiography (MRC) in the diagnosis of biliary complications after liver transplantation.

Methods and Materials: In 25 patients (17 women and 8 men) 29 MRC examinations were performed, from 1 to 56 months (mean=10) after liver transplantation. Indications for MR study were as follows: Suspected stenosis of biliary tree ($n = 16$), evaluation of intraductal stones ($n = 2$), abnormal biochemical tests ($n = 2$), recurrent biliary inflammations ($n = 1$) and other ($n = 8$). Studies were performed on a 1.5 T unit with the use of hydrographic TSE sequences: 2D, 3D and single-slice technique. The results were correlated with ERCP, percutaneous

cholangiography, ultrasound, clinical status and liver function tests. In 4 cases intraoperative confirmation was obtained during liver retransplantation.

Results: In 22 cases (76%) biliary strictures were diagnosed (10 at the anastomosis), in 18 (62%) marked dilatation of intrahepatic bile ducts was present and in 3 (10%) diffuse narrowing of biliary tree was identified suggestive of bile duct ischemia. In 4 patients (14%) stones or dense bile in the intrahepatic ducts were diagnosed and in 2 (7%) MRC revealed a bile leak at the anastomotic site. In 2 patients (7%) MRC was normal. In 27 cases (93%) there was concordance between MRC results and the standard of reference. Two remaining cases of bile duct ischemia and bile leak were not confirmed by other studies.

Conclusion: MRC is a noninvasive modality providing accurate assessment of biliary complications in patients after liver transplantation.

C-0004

Gall bladder wall thickening: An early sign of dengue fever

A.-L. Chang; Colombo/LK

Purpose of Study: To study whether the ultrasound findings of pseudo-thickening or oedema of gall bladder wall is a useful early sign of dengue fever in the recent epidemic in Sri Lanka.

Materials and Methods: A prospective study of 60 patients in the age group 10 to 65 years, with fever of 7 days or less with clinical suspicion of dengue fever, admitted to the medical ward or referred for assessment of fever and epigastric pain to our ultrasound practice were included in the study in the months of June and July 2004, during the peak of dengue fever epidemic in Colombo. Correlation with platelet count and serology for confirmation of presence of dengue antibodies was performed.

Results: Gall bladder wall thickening consisting of an echogenic inner wall and hypoechoic outer wall was demonstrated in the majority of patients with fever of 3-4 days. Only a small percentage of patients scanned on the 7th day of fever demonstrated gall bladder wall oedema. Majority of patients with marked gall bladder wall oedema scanned on day 3-4 of fever, demonstrated positive dengue IgM antibodies.

Conclusion: During an epidemic, sonographic finding of pseudo-thickening or oedema of the gall bladder in a febrile patient is an early sign of dengue fever. It suggests that the diagnosis of dengue fever can be strongly suggested by sonographic findings before antibody status is available. Other findings on ultrasound such as ascites and pleural effusion are helpful to the clinician in patient management.

C-0005

Usefulness of coronal multiple single slice mode balanced fast field echo MRCP with SENSE technique in the detection of choledocholithiasis

N.Y. Jung, S.K. Kim, H. Park, S.H. Hong, M.H. Lee, E.C. Chung; Seoul/KR

Purpose: The purpose of our study was to evaluate the usefulness of coronal multiple single slice mode (M2D) balanced FFE (fast field echo) MRCP with SENSE technique in the detection of choledocholithiasis by comparing observer performances with maximum-intensity-projection (MIP) of three-dimensional turbo spin echo (3D TSE) and single-shot turbo spin echo (TSE) MRCP.

Materials and Methods: MRCP was performed in 36 patients who were suspected having biliary calculi. Respiratory triggered MIP of 3D TSE, breath hold single shot TSE, and breath hold coronal M2D balanced FFE sequences with SENSE technique were compared. Image review was conducted for two anatomic compartments (upper biliary tract and common bile duct). Two independent radiologists reviewed a total of 72 compartments, including 13 bile duct calculi. The diagnostic accuracy of three sequences was assessed by means of receiver operating characteristic (ROC) analysis.

Results: Diagnostic accuracy of coronal M2D balanced FFE (96.5%) was higher than that of MIP of 3D TSE (89.6%, $p = 0.04$) and was similar to that of single shot TSE (95.1%, $p > 0.05$). Observer performance with coronal M2D balanced FFE ($Az = 0.956$) was higher than that with MIP of 3D TSE ($Az = 0.885$, $p = 0.12$) and was similar to that with single shot TSE ($Az = 0.970$, $p > 0.05$).

Conclusion: Coronal M2D balanced FFE MRCP is useful in the detection of choledocholithiasis as much as single shot TSE MR and MIP of 3D TSE MRCP.

C-0006

Acute cholecystitis: Helical CT findings

S. Quiroga, M. Sebastià, R. Boye, H. Cuellar, S. Roche, A. Alvarez; Barcelona/ES

Learning Objectives: To review and illustrate, as a pictorial essay, common and uncommon helical CT findings in acute cholecystitis, as well as a wide range of possible complications.

Scientific and Educational Exhibits

Background: Helical CT has become an important imaging technique for evaluating the acute abdomen. Although sonography is the method of choice to study the gallbladder when disease is suspected, the clinical signs and symptoms of acute cholecystitis are frequently nonspecific and helical CT is increasingly performed as the first-line technique in the evaluation of acute abdominal pain.

Imaging Findings: We review 79 cases of clinically unsuspected acute cholecystitis diagnosed with dual-slice or multidetector helical CT. The CT features of acute cholecystitis include gallstones, thickening of the gallbladder wall, pericholecystic inflammation or fluid, increased liver enhancement adjacent to inflamed gallbladder, hypertrophic cystic artery, air within the gallbladder lumen or wall, gallbladder rupture, hepatic or intraperitoneal abscess formation, extrahepatic bile duct obstruction (Mirizzi's syndrome), small bowel obstruction (due to abscess formation or gallstone ileus), portal vein thrombosis and gallbladder hemorrhage with or without haemoperitoneum.

Conclusion: Radiologists must be aware of the helical CT features of acute cholecystitis and its complications because of the widespread use of helical CT as the initial imaging technique for evaluating the acute abdomen.

C-0007

Primary sclerosing cholangitis: A spectrum of imaging findings with radiologic-histopathologic correlation

C. Belattar, A. Ayed, J. Duclos Vallee, I. Ewenzyk, C. Guettier, R. Adam, D. Samuel, D. Castaing, M. Bellin; Villejuif/FR

Learning Objectives: To become familiar with the broad spectrum of CT and MR characteristics of primary sclerosing cholangitis (PSC). To illustrate the typical and atypical aspects of CSP, as well as the complications after liver orthotopic transplantation (LOT). To correlate the pathological characteristics with the imaging findings and to discuss the key elements to be included in the differential diagnosis and to provide examples of them.

Background: PSC is an uncommon, chronic cholestatic disorder. Until recently diagnosis was based on percutaneous or retrograde cholangiography. Two experienced radiologists reviewed the ultrasound, CT, MR and cholangiographic studies in 50 patients with CSP who underwent LOT, and evaluated the presence of biliary strictures, segmental dilatations, biliary wall thickening, biliary stones, pseudodiverticula and associated parenchymal abnormalities.

Imaging Findings: The most common findings were diffuse and multifocal strictures. Long, confluent strictures were present in patients with long-standing disease. MR cholangiography proved useful as a suitable alternative method to radiological cholangiography. Extrahepatic involvement was observed in 15% of the cases. Diverticular protrusions were nicely depicted with MR and cholangiography. Recurrent PSC was observed after LOT in 7 patients.

Conclusion: The diagnosis of PSC may be difficult and is based on the association of clinical, biological and radiological abnormalities. MR imaging plays an increasing role for the diagnosis and follow-up of PSC. Early diagnosis of associated cholangiocarcinoma is essential and is based on subtle changes. MR and cholangiographic abnormalities observed in patients with recurrent PSC after LOT are identical to those observed in native livers.

C-0008

Radiologic findings of gallbladder adenomyomatosis: The importance of showing Rokitansky-Aschoff sinuses

J.-H. Yoon, S.-S. Cha, S.-S. Han, S.-J. Lee, M.-S. Kang; Busan/KR

Purpose: To demonstrate the radiologic characteristics of gallbladder adenomyomatosis (GADM) and emphasize the role of high-resolution ultrasound and MRCP.

Materials and Methods: We described 15 cases of GADM (eight males and seven females; 20-77 years old; mean age, 44.8) who underwent US (n = 11), helical CT (n = 8), PTC (n = 1) with MRCP and T2-weighted axial and coronal images (n = 8). All images were reviewed for the presence of GADM at three types (focal, segmental, diffuse), the involvement by compartment (fundus, body, neck), and radiological characteristics such as the presence of wall cystic spaces, intramural echogenic foci or hyperdense nodules and wall thickening.

Results: The types were as follows; focal (n = 9), combined focal and segmental (n = 4), segmental (n = 2). The compartments involved were as follows; fundus (n = 9), fundus and body (n = 4), body (n = 2). The sonographic appearances were as follows; intramural echogenic foci with or without associated acoustic shadows or reverberation artifacts (91%, 10/11), small anechoic cystic spaces, representing Rokitansky-Aschoff sinuses (73%, 8/11) and focal or diffuse thickening (73%, 8/11). The CT appearances were focal or diffuse wall thickening (50%, 4/8), hyperdense foci (50%, 4/8), focal cystic spaces (38%, 3/8), and the MRCP findings were as follows; focal or diffuse high-signal cystic structures, the so called pearl-necklace sign or diamond-ring sign (100%, 6/8).

Conclusion: GADM was commonly of focal type and usually involved the fundus with the most common radiological findings being intramural echogenic foci with acoustic shadows or reverberation artifacts and presence of wall cystic spaces. Sonography and MRCP has a higher sensitivity for visualization of Rokitansky-Aschoff sinuses in the differentiation of GADM from gallbladder carcinoma.

C-0009

MR cholangiography in the diagnosis and staging of extrahepatic cholangiocarcinoma

C. Juanco, F. González, R. Landeras, T. Piedra, P. Merino, M. Torres, M. Silván; Santander/ES

Purpose: To evaluate the role of MR and MR-cholangiography in the diagnosis and staging of extrahepatic cholangiocarcinoma.

Methods and Materials: We explored with a 1.5 MR unit (GE Genesis_Signa 1.5 T) 36 patients (22 women, mean age 23 y.o.) with a clinical onset and / or radiologic findings (CT or ultrasound) suggestive of a primary biliary tree neoplasm. All the examinations were performed with a phased array coil and T2-axial and coronal SSFSE sequences for the cholangiogram (thin and thick slab T2-SSFSE, radials) and in 17 cases (collaborative patients) we completed the examination with a dynamic 3D-FSPGR sequence before and after gadolinium injection and MR angiography using oblique and 3D-MIP vascular reformations to evaluate vascular involvement.

Results: MR examinations confirmed the presence of cholangiocarcinoma in 30 patients and assessed the exact location and tumoral extension. We classified the tumor pattern following the Bismuth scheme (7 cases Type I, 10 type II, 9 Type III and 4 Type IV). In 13 cases we diagnosed hilar vascular involvement with MR angiography (1 false negative and 2 false positive). Lymph node involvement was detected in 3 cases and satellite intrahepatic lesions were detected in 4 cases. We correlated MR findings with surgical excision or laparoscopic findings and also compared the MR with other diagnostic modalities (CT or ultrasound).

Conclusions: MR-cholangiography combined with a conventional and vascular MR examination is a complete, noninvasive diagnostic tool to confirm and stage biliary tree neoplasm. MR cholangiogram provides the surgeon with an exact biliary tree map that is necessary for surgical management.

Scientific and Educational Exhibits

Abdominal Viscera (Solid Organs)

Liver

C-0010

Preoperative surgical estimation of the portal venous based territories compared to the surgical planning landmark to the right of the middle hepatic vein

T. Abe¹, B.B. Frericks², B. Nashan³, Y. Ohgiya¹, T. Gokan¹; ¹Tokyo/JP,

²Berlin/DE, ³Halifax, NS/CA

Purpose: The purpose of our study was to evaluate the relationship between the surgical planning landmark of the middle hepatic vein (MHV) and the portal venous based avascular plane between the right and left liver lobe.

Methods and Materials: Contrast enhanced multi-detector row CT from 83 potential living donors were assessed. The patient group included 42 men and 41 women (mean age 39.4 ± 10.4 years). The data from the collimations of 2.5 mm and reconstructions at 2 mm were analyzed using the computer software "HepaVision 2" (MEVIS) for the portal venous based calculation.

Results: 76 adequate data were simulated. The anomalous portal venous branching were type I (with a short right common neck) in 57 cases, type II (trifurcation) in 10 (13%) cases, type III (right posterior portal branch division from the main portal branch) in 7 (9%) and type IV (the right anterior sectoral branches arose from left hepatic vein) in 2 (3%) cases. Based on portal venous territories, the avascular plane ran along the surgical plane, defined to the right of the MHV, in 23 donors. In 46 donors it ran to the left of the surgical plane (34 in type I, 8 in type II, 4 in type III) and it ran to the right of the surgical plane in 7 donors (4 in type I, 1 in type II, 2 in type IV).

Conclusion: When planning liver resection, knowledge of the shift of the portal venous based avascular plane is essential to estimate the ischemia of the portal venous territories.

C-0011

3D modelling of portal and hepatic venous analysis of the liver in living donor liver transplantation based on multi-detector row CT

T. Abe¹, B.B. Frericks², B. Nashan³, Y. Ohgiya¹, T. Gokan¹; ¹Tokyo/JP,

²Berlin/DE, ³Halifax, NS/CA

Purpose: The purpose of our study was to evaluate the portal and hepatic venous anatomy at the surgical plane to the right of middle hepatic vein, by using software in cases for living donor liver transplantation (LDLT).

Methods and Materials: Contrast enhanced multi-detector row CT (MDCT) from 83 potential LDLT were assessed. The patient group included 42 men and 41 women (mean age 39.4 ± 10.4 years). From the data from the collimations of 2.5 mm, reconstructions of 2 mm were analyzed using the computer software "HepaVision 2" (MEVIS, Bremen, Germany) for determining vascular anatomy. The prevalence of vascular variants for surgical planning was analyzed.

Results: A total of 76 venous data sets were considered technically adequate. A portal vein trifurcation was observed in 10 donors, an independent branch to the posterior sector from the main PV trunk in 7 donors and right anterior sectoral branches from the left portal vein in 2 donors. Segment VIII drained into MHV in 72 (95%) donors. In those cases, 44 MHV draining Segment VIII (diameter > 5 mm) occurred in 38 (50%) donors. Segment V draining into MHV occurred in 70 (92%) donors. In those cases, 43 MHV drained from Segment V (diameter > 5 mm) in 41 (54%) donors. 41 Small accessory right hepatic veins (ARHVs) (diameter ≤ 5 mm) were identified in 30 (39%) donors. 18 large ARHVs (diameter > 5 mm) were identified in 14 (18%) donors.

Conclusion: A wide range of anatomic variations is present which can be detected and visualized 3-dimensionally using the software and based on MDCT data.

C-0012

Comparison between highly fat selective MR imaging and volume localized 1H-spectroscopy of the liver for determination of intrahepatic fat accumulation

J. Machann, C. Thamer, B. Schnödt, H.-U. Häring, C.D. Claussen, A. Fritzsche, F. Schick; *Tübingen/DE*

Purpose: To test the feasibility of highly selective spectral-spatial fat selective MR imaging for determination of intrahepatic lipid content (IHL) and comparison with results from parallel proton MR spectroscopy (MRS) in healthy volunteers at an increased risk for type 2 diabetes.

Material and Methods: Fifty healthy volunteers were examined on a 1.5 T whole body unit (Magnetom Sonata, Siemens). MR imaging: single slice GE with spec-

tral spatial excitation, TR/TE 50 msec/16 msec, matrix 192x256 and an acquisition time of 16 sec in breathhold. Determination of hepatic lipids (HL) in ROI's of the posterior part (HL_P), anterior part (HL_A) and total cross-section of the liver (HL_T) referenced to subcutaneous fat. MRS: Single voxel STEAM, TE/TR 10 msec/4 sec, VOI 30x30x20 mm³ in the posterior part of segment 7 of the liver, 32 acquisitions. Determination of lipid/(lipid+water) ratio.

Results: MRS revealed reliable results in all volunteers with IHL in a range between 0.5 and 28.2% ($8.1 \pm 1.1\%$) using the water signal as internal reference. Fat selective MR imaging resulted in very similar data (HL_P: $1.52 \pm 0.18\%$, HL_A: $1.33 \pm 0.16\%$, HL_T: $1.36 \pm 0.16\%$) in different liver regions and correlated highly to spectroscopic results ($0.85 < r < 0.97$).

Discussion: Fat selective MR imaging of the liver within a single breathhold seems to be feasible even for determination of low amounts of hepatic lipids. However, the technique is more sensitive to breathing artifacts resulting in undesirable signal contaminations from subcutaneous fat. In healthy volunteers, lipids seem to be homogeneously distributed within the liver, but with a high interindividual variability in lipid content. Supported by a grant of the Deutsche Forschungsgemeinschaft (DFG, KFO 114/1).

C-0013

Double contrast MR imaging (DCMRI) of focal lesions in the cirrhotic and non cirrhotic liver: A problem solving technique

J.J. Sheehan, S.E. Harte, C.M. McKenna, D.E. Malone; *Dublin/IE*

Purpose: DCMRI synergistically combines unenhanced MRI with superparamagnetic iron oxide (SPIO), Gadolinium (Gd) enhancement and multiplanar, 3D imaging. We describe and illustrate our experience in cirrhotic and non-cirrhotic patients with focal liver lesions.

Methods and Materials: Consecutive patients presenting to a tertiary referral centre underwent DCMRI for characterisation of liver lesions first detected on US and/or CT. A GE 1.5 T magnet was used. Scan protocol included unenhanced sequences: (T1W GRE "in-phase/out of phase", T2W SSFSE, T2W FSE & Fat Saturation, T2*W GRE, T1W GRE 3D volumetric); SPIO-enhanced sequences: T2*W 10 minutes post SHU 555A (1.4 cc of 'Resovist'; 0.5 mmol of Fe/cc) followed immediately by the Gd-enhanced phase: (T1w GRE 3D volumetric: Gd-DOTA/Meg 20 cc @ 3 cc/sec by pump).

Results: 100 patients underwent DCMRI (M = 64, F = 36). 35 patients had cirrhosis. Diagnostic gold standards were applied. Illustrative US, CT and 3D DCMRI images will be shown from both groups. Cirrhotic Group: Solitary and multiple hepatocellular carcinomas, dysplastic nodules, siderotic nodules, transient hepatic attenuation defects, focal confluent fibrosis and portal vein thrombosis. Non-cirrhotic Group: Metastases, cavernous hemangioma, capillary hemangioma, cyst, focal nodular hyperplasia, adenoma, focal fatty infiltration and hamartomas. The added value of SPIO in terms of lesion conspicuity and characterisation will be illustrated. The benefit of 3D multi-planar imaging in terms of therapeutic planning will be shown.

Conclusion: DCMRI with 3D, volumetric acquisition is a valuable problem-solving and treatment planning technique. It is very useful for FLL characterisation and hepatic assessment in both cirrhotic and non-cirrhotic livers, especially when conventional imaging yielded indeterminate results.

C-0014

3D-CT angiography using 16-row multislice CT: Depiction of the feeding artery of hypervasculat HCCs

S. Kumano, H. Tanaka, H. Miki, T. Mochizuki; *Ehime/JP*

Purpose: Transcatheter arterial embolization (TAE) plays an important role in the treatment of hepatocellular carcinomas (HCCs). The purpose of this study was to evaluate the ability to depict the feeding artery of hypervasculat HCCs by 3D-CT angiography (3D-CTA) using 16-row multislice CT (MSCT) in the preoperative simulation of TAE for hypervasculat HCCs.

Method and Materials: Twenty patients with 35 hypervasculat HCCs underwent CT examination using 16-row MSCT (0.625-mm x 16) before TAE with digital subtraction angiography (DSA). In all patients 100 mL of contrast material was injected intravenously at a rate of 4 mL/sec. Timing for arterial phase scan was determined by a semiautomatic bolus tracking technique. Diagnostic scanning was started 10 seconds after the threshold was reached. 3D-CTA was produced using volume rendering and maximum intensity projection techniques.

Results: In all cases 3D-CTA demonstrated segmental branches of the hepatic artery, as well as hypervasculat HCCs. Feeding arteries of 18 HCCs were clearly identified. Fifteen of the 18 HCCs were fed by single segmental artery while the other three were fed by two different segmental arteries. Feeding arteries of the 13 HCCs were not clearly demonstrated but they could be predicted by the loca-

Scientific and Educational Exhibits

tion of tumors. Feeding arteries of the remaining four HCCs could not be identified or predicted because they were on the border between hepatic segments.
Conclusion: With 16-row MSCT 3D-CTA, segmental branches of the hepatic artery and feeding arteries of HCCs could be depicted. This technique is thought to be useful for the preoperative simulation of TAE.

C-0015

Differentiation of hemangiomas nonspecific at ultrasonography from malignant hepatic tumors: Comparison of the abilities of unenhanced and gadolinium-enhanced MR imaging and multiphase spiral CT
E. Szurowska, J. Pienkowska, E. Izycka-Swieszewska, R. Rzepko, M. Czarnowska, M. Studniarek; *Gdansk/PL*

Objective: To compare the abilities of unenhanced and gadolinium-enhanced MR imaging (MRI) and multiphase sCT in the differentiation of hepatic hemangiomas nonspecific at ultrasonography (US).

Materials and Methods: 183 patients with nonspecific, hypoechoic hepatic masses at US were examined with sCT and MRI. 77 hepatic hemangiomas in 38 patients and 416 malignant lesions in 145 persons were detected and confirmed pathologically or by clinical and imaging follow-up. Multiphase sCT included non-contrast scans, hepatic arterial-dominant, portal venous-dominant and equilibrium phase. Performed MR sequences included: SE, TSE, TFE-T1, double echo T2-weighted images, STIR and gadolinium dynamic study. The size of detectable lesions, their density, intensity, type of enhancement in CT and MRI (homogeneous, heterogeneous, nodular peripheral, ring, progressive fill-in) were prospectively analyzed by three radiologists.

Results: Moderately and heavily T2-weighted sequences correctly depicted 76 hemangiomas. Smaller hemangiomas (≤ 2 cm) more frequently (28/47) showed homogenous enhancement in three phases, but larger ones (22/30) showed nodular enhancement peripherally in HAP and progressive fill-in in PVP and EP. The sensitivity, specificity, PPV, NPV and accuracy of unenhanced versus gadolinium-enhanced MR and sCT imaging in the characterization of hemangioma were: 0.99 vs 0.84 vs 0.82; 1 vs 0.94 vs 0.93; 0.99 vs 0.70 vs 0.66; 1 vs 0.97 vs 0.97 and 0.99 vs 0.93 vs 0.91.

Conclusion: Unenhanced MRI is the most sensitive method for the characterization of hepatic hemangiomas which appear nonspecific in ultrasonography. There is no need for routine use of dynamic MR and CT exam in the differential diagnosis between hemangiomas and malignant tumors of the liver.

C-0016

Characterization of focal liver lesions appearing non-specific at ultrasonography: Comparison of usefulness of multiphase spiral CT and MR imaging
E. Szurowska, J. Pienkowska, E. Izycka-Swieszewska, B. Rutkowska, B. Balas, M. Studniarek; *Gdansk/PL*

Purpose: The purpose of the study was the evaluation of the utility of sCT and MR imaging in the characterization of HCC, metastases, hemangioma and FNH. **Materials and Methods:** Multiphase sCT and MR imaging was performed in 230 patients suspected (after ultrasonography) of having a hepatic tumor. 178 patients with an hepatic mass (confirmed pathologically or by clinical and radiological follow-up) were included in this study. Nonenhanced scans were performed in all cases along with HAP, PVP and EP. The following sequence MR imaging was obtained: SE, TSE, TFE T1- and T2-weighted images, STIR and dynamic study with administration Gd-DTPA. In statistical analysis, the sensitivity and accuracy of the methods were compared concerning the characterization of HCCs, metastases, hepatic hemangioma (HH) and FNH.

Results: 98 HCC foci, 316 liver metastases, 77 hemangiomas and 13 FNHs were detected in 178 patients. The lesions ranged in size from 5 to 140 mm (median value 20 mm). The sensitivity of MR imaging versus sCT for characterization HH was 0.99 vs 0.78 (significant difference). For HCC, the mean sensitivity of MR imaging (82%) was significantly higher than that of sCT study (66%). In characterization of FNH and metastases the sensitivity of both methods was as follows: 0.79 vs 0.82 and 0.92 vs 0.93.

Conclusion: The sensitivity of MR imaging seems similar to multiphase sCT study in the characterization of metastases and FNHs, but MR imaging is the most sensitive in characterization of hemangiomas and HCCs. MR imaging is superior to the routinely used methods (US and sCT) in the differentiation of focal liver lesions.

C-0017

Hepatic venous congestion in the anterior segment of the graft after living donor liver transplantation using right lobe: Characteristic findings at CT and Doppler ultrasound examination

S. Kim, K. Kim, T. Kim, S. Park, A. Kim, H. Won, J. Byun, Y. Shin, M.-G. Lee; *Seoul/KR*

Learning Objectives: To review the surgical techniques of middle hepatic vein reconstruction in living donor liver transplantation using a right lobe graft and to discuss the advantages and limitations of Doppler US and CT for the assessment of hepatic venous congestion of the graft.

Background: The recently increased incidence of living donor liver transplantation (LDLT) has led to increased demands on radiologists to educate themselves regarding the postoperative evaluation of these patients. Whereas LDLT using a donor's right lobe has been considered a safe and effective way in adult-to-adult LDLT to meet large metabolic demands of adult recipients, the graft usually does not contain the middle hepatic vein (MHV) because it is left in the donor for donor's safety. Therefore, the hepatic veins draining from the anterior segment of the graft are either ligated or anastomosed to the sidewall of the inferior vena cava using an interposition vein graft.

Imaging Findings: This operating method may result in variable degrees of hepatic venous congestion in the anterior segment of the graft, which produces several characteristic findings at CT and Doppler US examination.

Conclusion: In this exhibit, we illustrate a comprehensive pictorial review of the surgical techniques of middle hepatic vein reconstruction in LDLT using a right lobe graft, the CT and Doppler US demonstration of MHV tributaries and interposition vein graft, and various findings of hepatic venous congestion in the anterior segment of the right lobe graft at serial CT and Doppler US examination.

C-0018

Evaluating the relationship of the hepatic artery and portal vein using multi-detector row CT
H. Rikimaru, I. Kaneda, Y. Chiba, K. Igarashi; *Ishinomaki/JP*

Purpose: To investigate the relationship between the hepatic artery and portal vein near the pancreatic head using multi-detector row helical computed tomography (MDCT).

Materials and Methods: 1,160 patients underwent MDCT. Three-dimensional arteriograms and portograms were reconstructed to evaluate the relationship between the hepatic artery and portal vein, especially near the pancreatic head.

Results: In 984 (84.8%) patients, the common hepatic artery (CHA) arose from the celiac axis, crossed the portal vein immediately and then ran in front of the portal vein (type I). In 25 (2.2%), the CHA ran behind the portal vein before crossing it at the hepatic hilum (type II). The CHA arose from the celiac axis (IIa) in 6 (0.5%) and from the superior mesenteric artery (IIb) in the other 19 (1.6%). In 145 (12.5%) patients, the CHA ran in front of the portal vein and an aberrant right hepatic artery ran behind the portal vein (type III). The CHA arose from the celiac axis (IIIa) in 38 (3.3%) and from the superior mesenteric artery (IIIb) in the other 107 (9.2%). In 6 (0.5%) patients no CHA was found, and the hepatic inflow arose from the gastro-duodenal artery via the pancreatic arcade (type IV).

Conclusion: Six types of hepatic artery anatomy were seen in relation to the portal vein. Recognition of type IIa (0.5%) is clinically important for the preoperative evaluation of gastric malignancy, especially for video-assisted surgery.

C-0019

Hepatocellular carcinoma (HCC) suspected lesions: Detection and characterization at multislice-spiral computed tomography (MSCT) and Gd-BOPTA-enhanced magnetic resonance imaging (Gd-BOPTA-MRI)

I. Sansoni, A. Laghi, M. Celestre, C. Miglio, M. Di Martino, M. Rengo, L. Coletta, R. Passariello; *Rome/IT*

Purpose: To prospectively assess the diagnostic accuracy of MSCT versus Gd-BOPTA-MRI in the detection and characterization of HCC suspected lesions.

Methods and Materials: We studied forty-three patients with chronic hepatitis and HCC suspected lesions and they underwent CT and MRI liver evaluation. CT was performed using a 4-slice scanner with a tetraphasic acquisition protocol (unenhanced, contrasted arterial, portal venous and equilibrium phases). MR study was performed on 1.5 T-scanner using the following acquisition protocol: Pre-contrast T2-weighted HASTE and T1-weighted FLASH, dynamic Gd-BOPTA T1-weighted FLASH at arterial, portal venous and equilibrium phases and hepatobiliary (60 min) T1-weighted FLASH sequence. CT and MRI were blindly evaluated for presence, number and characterization of lesions. The number of lesions at final diagnosis was considered equal to CT plus MR detected lesions. Image

Scientific and Educational Exhibits

data were compared with histopathological studies of surgical specimens and/or follow-up imaging.

Results: Among the 43 patients, a total of 73 lesions (35 hepatocellular carcinoma, 17 dysplastic nodules, 3 focal nodular hyperplasia, 18 shunts) were detected in at least one technique. The detection rate of HCC suspected lesions was comparable for both MSCT and Gd-BOPTA-MRI (66/73; 90.41%). In particular 20 lesions were ≥ 2 cm and 46 were < 2 cm). MSCT offered a correct lesion characterization in 52/66 (78.79%) cases whereas Gd-BOPTA-MRI provided the correct diagnosis in 58/66 (87.88%) cases.

Conclusion: Concerning lesion identification, no statistically significant difference was observed between MSCT and Gd-BOPTA-MRI, independent of lesion size. They were also comparable for characterization. Both are valuable advanced techniques for hepatopathic liver screening and therefore they are interchangeable.

C-0020

Diagnosis of small hypervasculat hepatocellular carcinomas: Combined double phase CT during hepatic arteriography and CT during arterial portography versus dynamic CT with intravenous injection of contrast media, using multidetector-row CT scanner

T. Kamura, S. Yamamoto, T. Ozaki, T. Takano, K. Sasai; Niigata/JP

Purpose: Using a multidetector row CT scanner, we compared combined double phase CT during hepatic arteriography, CT during arterial portography (MD-DP-CTHA+MD-CTAP) and multiphase dynamic CT with intravenous injection of contrast media (IV-MDCT), for diagnosis of small hypervasculat hepatocellular carcinomas (HCC).

Materials and Methods: We reviewed 36 HCC nodules not more than 3 cm in diameter in 31 patients with chronic liver disease, who underwent both MD-DP-CTHA+CTAP and IV-MDCT. In all the nodules, increase of intranodular arterial blood flow was shown with at least one imaging modality. 29 nodules were diagnosed as HCC with surgical resection and 7 nodules were diagnosed with follow-up results. The findings of MD-DP-CTHA+CTAP were defined as confirmative of HCC when showing (a) Hyperdensity on 1st phase CTHA images, (b) Ringed enhancement on 2nd phase CTHA and (c) Hypodensity on CTAP. The findings of IV-MDCT were defined as confirmative of HCC when both (a) Hyperdensity on arterial dominant phase and (b) Visualization of the lesion besides arterial-dominant phase images were obtained.

Results: MD-DP-CTHA+MD-CTAP and IV-MDCT were confirmative in 32 nodules (89%) and in 27 nodules (75%), respectively. In all of 27 HCC nodules more than 1 cm in diameter, both MD-DP-CTHA+MD-CTAP and IV-MDCT were confirmative, without any false positive findings. In 9 HCC nodules less than 1 cm in diameter, MD-DP-CTHA+MD-CTAP confirmed 5 nodules and showed 1 false positive focus. IV-MDCT confirmed no nodules and showed no false positive findings.

Conclusion: MD-DP-CTHA+MD-CTAP may detect more hypervasculat HCC nodules less than 1 cm in diameter than IV-MDCT.

C-0021

Hepatic hemangiomas with arteriportal shunt in fatty liver: Atypical sonographic appearances by peritumoral sparing of fatty infiltration with CT and MR correlation

K. Kim, A. Kim, S. Kim, S. Park, H. Won, M.-G. Lee; Seoul/KR

Learning Objectives: To recognize spectrum of sonographic findings of hepatic hemangiomas with arteriportal shunt. To discuss the atypical sonographic appearance of hepatic hemangiomas with arteriportal shunt in fatty liver caused by peritumoral sparing of fatty infiltration, with CT and MR correlation.

Background: Hepatic hemangiomas are not uncommonly associated with arteriportal shunt. While several investigators focused on CT and MR findings of these tumors, relatively little attention has been paid to their sonographic appearances even though sonography has been considered the primary screening method for the evaluation of liver.

Imaging Findings: An associated arteriportal shunt may not influence sonographic appearances of hepatic hemangiomas in most cases. However, in the presence of fatty infiltration in liver, these tumors may occasionally exhibit atypical echo-poor appearance with peritumoral sparing of fatty infiltration, reflecting local hemodynamic alteration caused by associated arteriportal shunt. In this exhibit, we summarize and illustrate spectrum of sonographic appearances of hepatic hemangiomas with arteriportal shunt and correlate them with CT and MR findings.

Conclusion: Hepatic hemangioma with arteriportal shunt may show an atypical appearance in fatty liver by peritumoral sparing of fatty infiltration.

C-0022

Surgically important anatomical variations of the hepatic vasculature and intrahepatic bile duct in the evaluation of potential donor for living donor liver transplantation: A comprehensive pictorial review

S. Kim, K. Kim, A. Kim, S. Park, E. Chae, H. Won, J. Byun, Y. Shin, M.-G. Lee; Seoul/KR

Learning Objectives: To recognize the anatomical variations of the hepatic vasculature and intrahepatic bile duct that might influence surgical strategy of living donor liver transplantation (LDLT) and to determine their prevalence.

Background: Recently increasing performance of LDLT has led to increased demands on radiologists for an accurate assessment of the anatomy of the hepatic vasculature and intrahepatic bile duct in the evaluation of a potential donor for LDLT. A detailed understanding of their anatomy has become more important in living-donor evaluation, because the development of modified surgical techniques have allowed the use of grafts from donors with anatomical variation of these structures in some instances.

Procedure Details: Multi-detector row CT angiography, with three-dimensional volume rendering, maximal intensity projection and multiplanar reformation, is the most effective method for the evaluation of the hepatic vasculature. MR cholangiography or intraoperative direct cholangiography is used for the evaluation of intrahepatic bile duct anatomy. In this exhibit we illustrate a comprehensive pictorial review of the anatomical variations of the hepatic vasculature and intrahepatic bile duct that might influence surgical strategy of LDLT and discuss their prevalence.

Conclusion: Surgically important anatomical variations of the hepatic vasculature and intrahepatic bile duct are not infrequently seen in the evaluation of a potential donor for LDLT. A radiologic perspective in the evaluation of LDLT donors and an accurate assessment of these findings may help in establishing the surgical strategy.

C-0023

Computed tomography portography in the diagnosis of portal hypertension

S. Skrzewelski, J. Glowacki, R. Kachel, K. Gosek, W. Grzeszczak, S. Trzeszkowska-Rotkegel, H. Borowiak, Z. Jackowska; Zabrze/PL

Purpose: The aim of the study is an evaluation of computed tomography portography by spiral, multirow technique (MSCTP) in visualization of the anatomy of portal hypertension with special consideration to the portal vascular system and collateral circulations.

Methods and Materials: Biphasic MSCTP examination in 35 patients aged from 21 to 78 years with a clinical diagnosis of hepatic cirrhosis was performed. The received raw data underwent multiplanar reconstructions, maximum intensity reconstructions and three-dimensional volume reconstructions. The images of portal vessels, liver, spleen and other abdominal organs were assessed.

Results: Widening of portal and splenic veins and presence of a collateral circulation was found in 29 patients (82.9%). The observed anatomy included varicose coronary and short gastric veins, esophageal varices, retrogastric varices, perisplenic varices, retroperitoneal - paravertebral varices, collateral circulation through paraumbilical veins and abdominal wall varices and splenorenal shunts. There was no pathology within visible vessels in the remaining 6 patients (17.1%).

Conclusion: MSCTP in the diagnosis of portal hypertension allows fairly accurate, close to anatomical evaluation of the portal vascular system and collateral circulation vessels. The application of MSCTP can help the clinician to take a final decision about further clinical procedures. The use of a multirow spiral technique shortens the time of examination and decreases the dose of ionizing radiation. MSCTP, besides Doppler ultrasound examination, is in practice the only non-invasive method supporting the diagnosis of patients with portal hypertension. The limitation of MSCTP is a lack of the possibility to perform direct tension measurements and evaluate blood flow parameters in the portal system.

C-0024

Hemodynamic effects of a prostacyclin analog (Prostavasin) in systemic scleroderma patients

D. Salera, G. Argalia, G. Giuseppetti; Ancona/IT

Purpose: We examined the effects of a prostacyclin analog (Prostavasin) on the circulation of the upper extremities and visceral districts, portal vein, hepatic artery, superior mesenteric artery and interlobar renal artery in a group of scleroderma patients.

Methods and Materials: In an experimental group (EG) of 50 scleroderma patients without liver diseases or nephropathy, the peripheral vasculature was evaluated by brachial artery flow-mediated dilatation using high-resolution ultrasound

Scientific and Educational Exhibits

cross-sectional measurements. Splenic arterial pulsatility index (PI) and resistance index (RI) of the visceral arteries and portal vein flow were assessed by color Doppler sonography before and after 3 days of Prostavasin infusion. The control group (CG) consisted of 10 patients receiving no treatment.

Results: EG patients showed significantly ($p < 0.001$) increased brachial artery flow-mediated dilatation, portal vein velocity and splenic arterial PI after the infusion whereas the CG patients exhibited no significant changes. After treatment, interlobar renal artery, superior mesenteric artery and hepatic artery RI were reduced, though not significantly, in most EG patients.

Conclusions: The results indicate that Prostavasin has a powerful effect in improving the peripheral circulation of scleroderma patients. Prostavasin significantly increased portal vein flow but also splenic arterial PI, in contrast to the hypothesis of its direct and specific action on relaxation of hepatic micro-circulation.

C-0025

An algorithm-based approach to the sonographic diagnosis of focal liver lesions: A DVD-Rom teaching file with US image and video database

P.S. Zoumpoulis, I. Vafiadi, K. Pahou, E. Katsaounos, D. Dalakostas, I. Theotokas, S. Kyriazi; Athens/GR

Learning Objectives: 1. To teach the user to identify the principal sonographic features of a focal liver lesion. 2. To facilitate an accurate diagnosis by means of a simple algorithm employing sonographic characteristics. 3. To enable the comparison of the user's own US images to database images.

Background: This DVD-Rom is designed to aid the sonographic diagnostic approach of focal liver lesions by focusing on distinct ultrasonographic characteristics. The user provides US characteristics of a lesion by selecting key sonographic criteria. The system provides an algorithm leading to the differential diagnosis of all focal liver lesions pertaining to the criteria given. The user's US images can be compared to image galleries and videos of each diagnostic category. Interesting Cases with clinical, biochemical, imaging and histological findings highlight the overall profile of each diagnostic entity.

Procedure Details: The User can start using this teaching file by describing the US characteristics of a focal liver lesion that he has difficulty in characterizing (unilocular, hypoechoic, hypovascular). The system guides him through a specific algorithm of all possible liver lesions which fit the criteria. A large collection of US images and videos are available for comparison with the User's images. The User's image can also be linked to the contents of corresponding Interesting Cases, which are brief case reports with clinical, biochemical, imaging and pathological data.

Conclusion: This DVD-Rom establishes a diverse approach in the differential diagnosis of focal liver lesions.

C-0026

Digital subtraction MDCT (DS-MDCT): Impact in liver imaging

P. Tinazzi Martini¹, M. D'Onofrio², M. Pregraz¹, G. Zamboni², G. Mansueti²; ¹Peschiera/IT, ²Verona/IT

Purpose: To describe the digital subtraction, multidetector computed tomography (DS-MDCT) obtained with a double acquisition in a single breath-hold technique. This technique allows to subtract the pre-contrast from the contrast-enhanced acquisition obtaining a pure contrast-enhanced phase. The aim of this study is to discuss the possible applications of the DS-MDCT in liver imaging.

Methods and Materials: A 16 row CT (Sensation 16, Siemens, Erlangen) with standard software was used. The patients were asked to hold their breath for 22 seconds and, utilizing a 1.5 mm slice, this was enough to acquire two different phases in a single breath-hold. Later the pre-contrast enhanced acquisition, acting as a mask, was subtracted from the arterial phase thus obtaining images in the pure vascular phase in which the enhancing lesion were more clearly depicted (higher lesion conspicuity), since all the liver parenchyma having low or absent enhancement was erased.

Results: In our preliminary report we find this new technique useful and not time consuming, for example in HCC detection and follow-up after treatment with chemoembolization or radiofrequency ablation. In all cases the subtraction was possible thus obtaining the pure contrast-enhanced phase. The conspicuity of the studied lesions in the arterial and pure contrast phase was compared, being higher in the pure vascular phase than in the arterial phase due to a reduction of about 90% of the background liver parenchyma in terms of HU.

Conclusion: The DS-MDCT images in the pure contrast-enhanced phase obtained a better lesion conspicuity and improves the detection of HCC vascularization.

C-0027

Liver haemangiomas undetermined at grey-scale ultrasound: Contrast-enhancement patterns with SonoVue and pulse-inversion US

T.V. Bartolotta, M. Galia, G. Runza, G. Mamone, A. Comparetto, M. Midiri; Palermo/IT

Learning Objectives: To illustrate the spectrum of contrast-enhancement patterns of hepatic hemangiomas undetermined at grey-scale ultrasound (US) on SonoVue®-enhanced Pulse Inversion (PI) US.

Background: In about 20-40% of cases liver hemangiomas do not show typical features on B-mode US (homogeneous, hyperechoic mass with well-defined margins and posterior acoustic enhancement), thus making the correct diagnosis a difficult task. The introduction of contrast-specific US techniques, such as PI, has lead to a better depiction of both macro and microvascularization of liver tumors.

Procedure Details: Twenty patients with 35 hemangiomas (size range: 1-7 cm; mean: 3.1 cm) undetermined at baseline US underwent PI after i.v. injection of SonoVue®. All hemangiomas were confirmed by typical helical Computed Tomography and/or Magnetic Resonance Imaging findings. US examinations were videotaped and then reviewed by two experienced radiologists blinded to the final diagnosis. Readers evaluated by consensus the baseline echogenicity and the dynamic enhancement pattern of each lesion, in comparison with adjacent liver parenchyma.

Results: After administration of SonoVue®, 31/35 (88%) hemangiomas showed peripheral hyperechoic nodules in the arterial phase, followed by progressive centripetal fill-in, which was complete in 25/35 cases and incomplete in 6/35 cases. 3/35 (9%) hemangiomas showed rapid and complete fill-in in the arterial phase, which persisted in the portal and delayed phases. Finally 1/35 hemangiomas (3%) showed a rim of arterial contrast-enhancement with progressive and complete centripetal fill-in in portal-venous and delayed phases.

Conclusion: PI after the administration of SonoVue® enabled the depiction of typical contrast-enhancement patterns in haemangiomas undetermined at baseline US.

C-0028

Detection of hepatic metastases on ferucarbotran-enhanced MR imaging: Feasibility of 3D sensitivity-encoding water-excitation multi-shot echo-planar (3D-SWEEP) imaging

K. Mori, N. Takahashi, K. Matsueda, Y. Saida, M. Minami, T. Oda, N. Ohkohchi; Tsukuba/JP

Purpose: To evaluate the feasibility of ferucarbotran-enhanced 3D sensitivity-encoding water-excitation multi-shot echo-planar (3D-SWEEP) imaging for the detection of hepatic metastases compared with 2D gradient-recalled echo (GRE) sequence.

Materials and Methods: The study comprised 19 patients with surgically proven 65 hepatic metastases of which sizes ranged 3 to 90 mm (mean, 23.4 mm). The 3D-SWEEP sequence (TR/TE/Flip angle/EPI factor = 22/10/25/3) and 2D-GRE sequence (TR/TE/Flip angle = 148/9.2/30) were performed on a 1.5 T unit before and after administration of ferucarbotran. In the 3D-SWEEP sequence, 36 images of gapless 5-6.5 mm slice thickness covering the whole liver were acquired within a single breath hold of 23.4 seconds, whereas it took 27.2 seconds to acquire 18 images of 7-10 mm slice thickness with 0.7-3 mm inter-slice gaps in the 2D-GRE sequence. These two sequences were compared in terms of the percent signal intensity loss (PSIL), percent lesion-to-liver contrast (PLLC), lesion conspicuity and sensitivity. The lesion conspicuity was evaluated by consensus reading of two radiologists with the following 4 point scale.

Results: The mean values of PSIL, PLLC and lesion conspicuity were 66.7%, 46.6%, and 2.58 for the 3D-SWEEP and 64.3%, 41.6% and 2.42 for the 2D-GRE sequences, respectively. The sensitivity were 87.7% and 81.5% for the 3D-SWEEP and 2D-GRE sequences, respectively. Compared with the 2D-GRE, the 3D-SWEEP sequence showed significantly greater PSIL ($P = 0.036$) and depicted 4 more lesions.

Conclusion: The 3D-SWEEP sequence was clinically feasible and useful for the detection of hepatic metastases on ferucarbotran-enhanced MR imaging.

C-0029

MR imaging findings of focal eosinophilic infiltration of the liver

S. Kim, M.-J. Kim, J.-Y. Choi, J.-S. Lim, Y.-T. Oh, J.-H. Kim, K. Kim, J. Lee, H. Yoo; Seoul/KR

Purpose: To describe the MR imaging findings of focal eosinophilic infiltration (FEI) of the liver.

Scientific and Educational Exhibits

Methods and Materials: We retrospectively reviewed total of 70 FEIs of the liver in 15 patients (9 men and 6 women, mean age of 54 years), diagnosed by biopsy ($n = 6$) or clinically confirm ($n = 9$), and who had undergone MR imaging with unenhanced study, Gd-enhanced dynamic study, SPIO-T2WI and SPIO-T2'WI. The location, margin, shape, signal intensity (SI), enhancement pattern and size of FEI were evaluated. The margin and shape were evaluated on T2WI. Enhancement pattern was evaluated on delayed phase image. The size of FEI was measured three times on T2WI, SPIO-T2WI, SPIO-T2'WI, and the statistical significances of the size differences between T2WI and SPIO-T2WI, between T2WI and SPIO-T2'WI, and between SPIO-T2WI and SPIO-T2'WI were evaluated by the paired T-test.

Results: FEI of the liver more frequently showed a subcapsular location (61.4%), ill-defined margin (82.9%), non-spherical shape (81.4%) and homogeneous enhancement pattern (62.5%). FEI showed definite high SI on T2WI (50.0%), on SPIO-T2WI (58.6%), and on SPIO-T2'WI (82.9%). Therefore, FEI was the most conspicuous on SPIO-T2'WI. The average size of FEI was 13.3 ± 5.3 mm on T2WI, 10.5 ± 4.3 mm on SPIO-T2WI, and 10.8 ± 4.2 mm on SPIO-T2'WI. There were significant size differences ($p < 0.01$) between T2WI and SPIO-T2WI, and between T2WI and SPIO-T2'WI.

Conclusion: When a focal hepatic lesion with subcapsular location, an ill-defined margin, non-spherical shape, homogeneous enhancement pattern, and especially significant size decrease on SPIO-T2WI or SPIO-T2'WI in comparison with T2WI is found, the possibility of FEI of the liver should be considered.

C-0030

Thrombosis of the middle hepatic vein in living liver donors

A. García Criado¹, R. Gilabert¹, M. Vannoni², S. González¹, C. Brú¹; ¹Barcelona/ES, ²Porto Alegre/BR

Purpose: One of the most serious complications in liver donors after right hepatectomy for living donor liver transplantation (LDLT) is pulmonary embolism. Lower extremity venous thrombosis has been pointed out as the possible source of thrombi but sometimes the origin has remained unknown.

Methods and Materials: Thirty-two consecutive donors of right hepatic lobe for LDLT were included. The study protocol included abdominal Doppler sonography (DS) at 1, 2, 7 and 30 day after transplantation that assessed vessel patency (portal vein, hepatic artery, hepatic veins and cava vein). In the last 14 patients, the protocol included a DS of the lower extremities at 1 and 2 days after surgery looking for deep vein thrombosis.

Results: In three cases a partial thrombosis of the middle hepatic vein was detected by DS in the postoperative day 1 or 2. All thrombi began in a branch near of the edge of surgical resection and one of them extended to cava vein. These patients were treated immediately with heparin without serious hemorrhagic complications.

No cases of deep venous thrombosis were detected. There were no pulmonary emboli.

Conclusion: The middle hepatic vein must be carefully studied in living liver donors at the post-operative DS because partial thrombi after right hepatectomy is a possible complication that can be unseen in the imaging control. The cause of the thrombi could be related to surgical resection.

C-0031

The "C" sign: Sonographic assessment of hepatic hilar lymph node involvement

M.J. Sarrià Guzmán, X. Serres Créixams, S. Roche Vallés, M. Buti, A. Valdés, E. Castellà Fierro; Barcelona/ES

Learning Objectives: 1. To describe standard sonographic sections for the assessment of hepatic hilar lymph node (HLN) involvement. 2. To investigate the entities related with HLN. 3. To assess the degree of nodal involvement in these entities on the basis of the section area.

Background: HLN involvement has been described in CT, MR imaging and US studies. It is considered a non-specific manifestation, but has been related with the degree of liver inflammation activity. Nevertheless, evaluation of HLN involvement is not routinely performed.

Procedure Details: We studied 100 patients with chronic liver disease and HLN involvement (63 women and 37 men, mean age 57 years). The sonographic section we propose consists of a single oblique transversal plane through the left lobe that includes the HLN adjacent to the hepatic artery and those extending toward the portocaval region, forming a C-shaped configuration. Measurement of its section area gave the following values: 39 patients with hepatitis C virus (4.78 cm^2), 4 with hepatitis B (3.66 cm^2), 10 with enolic liver disease (2.05 cm^2), 6 with autoimmune liver disease (4.41 cm^2), 4 with primary liver disease (4.03 cm^2),

3 with pharmacological liver disease (2.65 cm^2), 2 with hemochromatosis (1.90 cm^2), 1 with non-enolic steatosis (1.50 cm^2), 16 associated with viral disease and other entities (4.45 cm^2) and 15 chronic liver disease of unknown origin (2.13 cm^2).

Conclusion: The "C-sign" is seen in various types of liver diseases and shows a higher area in processes of viral and immune origin and in primary biliary cirrhosis.

C-0032

Sonographic assessment of periportal hypoechoic halo

O. Persiva Morenza, X. Serres Créixams, S. Roche Vallés, H. Allende, C. Vilà Parera, R. Comet Segú; Barcelona/ES

Learning Objectives: 1. To describe the sonographic appearance of periportal hypoechoic halo. 2. To assess changes in this finding after i.v. contrast administration. 3. To investigate which entities are related with periportal hypoechoic halo.

Background: Periportal hypoechoic halo is a non-specific radiologic finding described in computed tomography and related with various hepatic alterations: trauma, transplant, biliary tract infections, tumoral process in the hepatic hilum and chronic liver disease. It has also been related with normal status.

Procedure Details: We studied 15 patients with generalized periportal hypoechoic halo, including ten women and five men with a mean age of 68 years. On ultrasound assessment, periportal hypoechoic was seen as a cuff around the portal vessels. On the transverse view, the portal vessels showed a target appearance and on the longitudinal view, the form of a rail. After contrast administration (4 patients), periportal hypoechoic halo demonstrated a slight delay in uptake as compared to hepatic parenchyma. At the onset of the portal phase the appearance became homogeneous and remained isoechoic also in the parenchymal phase. Among the 15 cases studied, eight had chronic hepatitis C infection, five primary biliary cirrhosis, one amyloidosis with pharmacological hepatotoxicity and in another case there was no apparent cause.

Conclusions: Periportal halo can be identified on ultrasound and shows characteristic features after administration of contrast material. This ultrasound finding may suggest a chronic underlying hepatic condition.

C-0033

Preoperative helical computerized tomography estimation of graft volumes: Experience in 150 living liver donors

S. Orguc, M. Zeytunlu, M. Kilic, U. Gurgan, Y. Yüzer, Y. Tokat; Izmir/TR

Purpose: The purpose of this study was to evaluate the accuracy of spiral computed tomography and 3D imaging models in measuring total and segmental liver volume in potential living donors.

Methods: A prospective study was undertaken to determine the correlation between the volumes of potential donor livers determined via helical CT and the actual volumes measured during operation. Left lateral segment (S2, 3) or left lobe (S2, 3, 4) transplantation was performed on 36 cases. In 96 recipients right lobe liver transplantation (S 5, 6, 7, 8) was done. Sixteen donor candidates were refused due to inadequate liver volumes.

Results: The regression analysis model showed a significant positive relation between the CT estimations of graft volumes and intraoperative weight measurements in living liver donors ($F:5525.37, p < 0.05$). 97.7% of changes in CT volume can be explained by the changes in the graft mass ($R^2:0.977$).

Conclusion: Preoperative estimation of segmental volumes of the donor livers is necessary to avoid donor-recipient size disparity and it has a major impact on the selection of the donor and type of surgical management. The accuracy of helical computerized tomography is very high in determining total and segmental liver volumes.

C-0034

Adding the hepato-biliary phase imaging to dynamic Gd-BOPTA magnetic resonance (Gd-BOPTA-MR): Its value in detection and characterization of hepatocellular carcinoma (HCC)

I. Sansoni, A. Laghi, M. Celestre, C. Miglio, M. Rengo, M. Di Martino, L. Coletta, R. Passariello; Rome/IT

Purpose: To assess if hepato-biliary phase imaging can supply triple-phase dynamic Gd-BOPTA-MR with adjunctive information for detection and characterization of HCC suspected lesions.

Methods and Materials: Eighty-one hepatopathics underwent MR-study on 1.5 T-scanner: Basal T2-weighted HASTE and T1-weighted FLASH; dynamic contrast-enhanced T1-weighted FLASH was acquired after i.v. administration of Gd-BOPTA (0.2 mM/kg) at 15-seconds, 55-seconds and 135-seconds; T1-weighted FLASH hepato-biliary phase was obtained 60 minutes after Gd-BOPTA administration.

Scientific and Educational Exhibits

Dynamic-MR and complete-MR study sets of images were reviewed for presence, number and characterization of lesions. Separate reading sessions were performed for dynamic-MR and complete-MR, calculating sensitivities and specificities. The value of delayed-phase images in characterization of HCC was finally assessed. The number of lesions at final diagnosis was considered equal to detected lesions at complete-MR study plus lesions detected by other imaging modalities (CT, US). Characterization of lesions was established by histopathologic examination after surgical resection or biopsy, or by follow-up imaging and treatment response.

Results: Diagnostic accuracy of MR study with the hepato-biliary phase was comparable to that of MR imaging without hepato-biliary phase, in particular, the percentage of identified HCC at complete Gd-BOPTA-MR imaging (92%) was slightly higher than that at dynamic-MR imaging (89.7%). Delayed phase images were not helpful in the characterization of suspected HCC lesions because the difference between the two set of images was not statistically significant.

Conclusion: Adding delayed phase imaging to dynamic Gd-BOPTA MR study does not provide significant additional benefit for the detection and characterization of hepatocellular carcinoma, probably in relation to reduced liver function and a subsequent inhomogeneous appearance.

C-0035

Benign liver tumors and metastases in normally functioning livers: The added value of the hepato-biliary phase imaging in Gd-BOPTA magnetic resonance imaging (Gd-BOPTA-MRI)

I. Sansoni, A. Laghi, C. Miglio, M. Celestre, M. Rengo, M. Di Martino, L. Coletta, R. Passariello; Rome/IT

Purpose: To verify if adding delayed hepato-biliary phase imaging to triple-phase dynamic Gd-BOPTA-MRI can provide further clues for detection and characterization of lesions in non-hepatopathic livers.

Methods and Materials: Fifty patients with liver lesions underwent Gd-BOPTA-MR study on 1.5 T-scanner: Basal T2-weighted HASTE and T1-weighted FLASH; dynamic contrast-enhanced T1-weighted FLASH acquired after i.v. administration of Gd-BOPTA (0.2 mM/kg) at arterial, portal venous and equilibrium phases; T1-weighted FLASH hepato-biliary phase obtained 60 minutes after Gd-BOPTA administration. Dynamic-MRI and complete-MR study were reviewed for the presence, number and characterization of lesions. Separate reading sessions were performed for images from both dynamic-MRI and complete-MR study, calculating sensitivities and specificities. The value of Delayed-phase images in the characterization of lesions was also assessed. The number of lesions at final diagnosis was considered equal to detected lesions at complete-MR study plus lesions detected by other imaging modalities (CT, US, MR with other specific c.m.). Characterization of lesions was established by histopathologic examination after surgical resection or biopsy, or by follow-up imaging and treatment response.

Results: Diagnostic accuracy of MR study with hepato-biliary phase was significantly higher than that of MRI without hepato-biliary phase in benign lesions and metastases. Hepato-biliary phase of Gd-BOPTA-MRI allowed us to detect 9% more lesions compared to dynamic MRI, whereas, considering lesions identified by both the set of images, delayed hepato-biliary phase images were helpful in the characterization of lesions in 5% of cases.

Conclusion: The addition of the delayed phase imaging to dynamic Gd-BOPTA MR study helps to detect and characterize focal lesions in normally functioning livers.

C-0036

Assessment of metastatic liver tumor burden on MR imaging: Validity of uni-dimensional and bi-dimensional measurements

M. Mazonakis¹, P. Prassopoulos², M. Mantatzis², J. Damilakis¹, N. Gourtsoyiannis¹; ¹Iraklion/GR, ²Alexandroupolis/GR

Purpose: Quantitative assessment of the extent of metastatic liver disease is an important parameter in the evaluation of anticancer treatment. The purpose of the study was to examine the validity of uni-dimensional and bi-dimensional measurements in the assessment of metastatic liver tumor burden on MR imaging.

Materials and Methods: Abdominal MR imaging examinations of 24 consecutive patients with liver metastases were analyzed. The size of each lesion was assessed using: (1) the maximum tumor diameter (d) according to RECIST guidelines, (2) the bidimensional tumor product, i.e. the product of maximum diameter and its longest perpendicular lesion dimension in accordance with WHO guidelines, and (3) the tumor volume planimetric measurement, based on manual tracing of lesion's boundaries, which was used as the gold standard. Lesions were categorized by maximum diameter as smaller than 1.5 cm (n = 41), between 1.5 and 3.0 cm (n = 26) and larger than 3.0 cm (n = 15).

Results: An excellent correlation was found between bi-dimensional tumor products and tumor volumes ($d < 1.5$ cm: $r = 0.90$, $p < 0.001$; $1.5 < d < 3$ cm: $r = 0.92$, $p < 0.001$; $d > 3$ cm: $r = 0.97$, $p < 0.0001$). Uni-dimensional measurements were strongly correlated with tumor volumes for lesions exceeding 1.5 cm in diameter ($1.5 < d < 3$ cm: $r = 0.89$, $p = 0.0034$; $d > 3$ cm: $r = 0.96$, $p < 0.001$). However, a weak correlation was observed between tumor diameters and planimetric measurements for lesions smaller than 1.5 cm ($r = 0.69$, $p = 0.0036$).

Conclusion: The validity of uni-dimensional measurements was dependent upon the size of the lesion. Bi-dimensional tumor product may be the preferred approach for assessing liver tumor burden on MR imaging due to its excellent correlation with tumor volume, irrespective of the size of the lesion.

C-0037

Role of contrast-enhanced sonography (CE-US) in percutaneous treatment for HCC

A. Nunziata, O. Catalano, F. Sandomenico, P. Vallone, A. Siani; Naples/IT

Learning Objective: To illustrate the CE-US findings during and after percutaneous ablation of HCC. To show the practical value of CE-US to help the ablation procedure and to assess results at early and late follow-up.

Background: Conventional US is the main tool in guiding percutaneous ablation therapies but fails to recognise residual viable tumour tissue during or after the ablation session. Contrast-enhanced, low-mechanical index US is being used with increasing frequency in the assessment of HCC during and after percutaneous ablation therapies.

Procedure Details: Cases are shown where CE-US is employed to guide percutaneous ablation of barely visible nodules, to demonstrate treatment complications, to depict incomplete treatment and need for retreatment, to assess tumour necrosis demonstrating viable tumour tissue persistence, to diagnose intra- and extrahepatic tumour seeding and to detect tumour recurrence after initially successful ablation therapy.

Conclusion: Real-time CE-US has several possible applications during percutaneous ablation therapies of HCC. It is also relevant after treatment, for short and long-term imaging follow-up.

C-0038

Detection of a hypervascular malignant focus in borderline lesions of hepatocellular carcinoma: Comparison of dynamic CT, dynamic MR imaging and SPIO-enhanced MR imaging

R. Shimura¹, O. Matsui¹, T. Gabata¹, K. Ueda²; ¹Kanazawa/JP, ²Shinshu/JP

Purpose: To assess the efficacy of dynamic CT, dynamic MR imaging, and superparamagnetic iron oxide (SPIO)-enhanced MR imaging in the detection of hypervascular foci in hypovascular borderline lesions of hepatocellular carcinoma (HCC).

Materials and Methods: 53 nodules in 33 patients showing hypodensity with internal hypervascular focus (or foci) on CT during hepatic arteriography (CTHA) and spotty hypodense area on CT during arterial portography (CTAP) were entered into the study (hepatitis B related 4, C 27, B and C 2). Dynamic CT was carried out using a helical CT system. Simultaneous multislice dynamic MR imaging was performed applying FMPSPGR technique after bolus intravenous administration of gadopentetate dimeglumine. SPIO-enhanced MR imaging was performed following intravenous injection of SPIO. Among these nodules, the detectability of hypervascular focus (sensitivity) and average size of the detected foci (AS) were analysed.

Results: Sensitivity and AS were 35.3% and 7.7 mm, respectively on dynamic CT, 25.5% and 8.2 mm on dynamic MR imaging, and 26.1% and 8.3 mm on SPIO-enhanced MR imaging. This difference between dynamic CT and MR imaging was not statistically significant. In 33 nodules (64.7%), malignant foci were not visualized on all three modalities, and the AS of them was 4.8 mm.

Conclusion: A hypervascular malignant focus in borderline hypovascular borderline nodules could be better visualized by dynamic CT than by MR imaging or SPIO-enhanced MR imaging without definite statistical significance, when it is larger than 7.8 mm. However, it was difficult to detect a malignant focus less than 5 mm by these non-invasive imaging modalities. Dynamic CT is recommended for the follow-up examination for hypovascular borderline lesions.

C-0039

Liver MR imaging with iron oxides: Is gradient-echo T2-weighted sequence always better?

L. Curvo-Semedo, F. Caseiro-Alves; Coimbra/PT

Objective: To compare the MR diagnostic performance of gradient-echo (GRE) T2-weighted to SE T2-weighted sequences (conventional and fast-spin-echo)

Scientific and Educational Exhibits

for liver lesion detection and/or characterization, after the administration of superparamagnetic iron oxide contrast agents (SPIO).

Material and Methods: From March 1996 to July 2004, 97 patients underwent MR imaging of the liver with administration of iron oxide particles (Endorem® or Resovist®) with pre- and post-contrast T2-weighted sequences, spin-echo (SE) or fast-spin-echo (FSE) and GRE sequences. Seventy-four patients had focal liver lesions that were retrospectively evaluated for signal intensity changes and conspicuity on SPIO-enhanced MR imaging for each T2-weighted sequence. Each sequence was evaluated regarding the ability to detect and characterize benign or malignant focal liver lesions, by consensus and by two observers.

Results: From the dataset there were three cases of patients with focal liver lesions, where detection or characterization of the nodules was better using the T2-weighted FSE sequence compared to the GRE T2-weighted sequence. There was a case of focal nodular hyperplasia in a male patient, a patient with liver metastases that underwent a previous surgical ligation of the right branch of the portal vein and a patient with simultaneous cysts and colorectal metastases that were not differentiated on the T2-weighted GRE sequence.

Conclusion: For SPIO-enhanced MR liver imaging the GRE T2-weighted sequence provides, in most instances, the best contrast for detection and characterization of focal lesions. However, to increase the overall MR accuracy, conventional SE T2-weighted sequences should also be routinely obtained.

C-0040

MR imaging assessment of radiofrequency liver tumor ablation

T.Y. Kudryavtseva, O.N. Sergeeva, A.V. Gavrilin, G.G. Karmazanovsky;
Moscow/RU

Purpose: Percutaneous US-guided radiofrequency ablation (RFA) of liver tumors is a widespread method nowadays, but US is unable to determine RFA margins. MR imaging was performed to assess the adequacy of tumor destruction.

Material and Methods: 18 patients (age range 32-66 years, 15 female, 3 male) have undergone percutaneous US-guided (Logiq-400, 3.5 MHz convex probe) RFA (Radionics Cool-Tip RF Ablation System, singe and cluster probes) of primary and metastatic liver tumors since January 2004. Pre- and post-procedural MR imaging was routinely performed in all patients (1 T Phillips Intera, using Synergy Body coil). The sequence protocol consisted of T1-weighted images (WI) and T2-WI in several planes, including fat-suppressed T2-WI STIR (TR = 1600 ms, TI = 155 ms, TE = 20 ms). Dynamic contrast enhanced (gadodiamide, dosage 0.2 mmol/kg, i.v. bolus, rate 2-3 ml/s) study (out-of-phase FFE (TR = 179 ms, TE = 3.5 ms, FA = 80°)) was performed. Arterial (25-30 sec), venous (60-70 sec) and late (3 min) phase images were analyzed.

Results: Real-time US assessed tumor destruction as complete in all patients, but post-procedural MR imaging revealed residual tumor at a periphery of the ablated regions in 6 (33.3%) patients. Non-damaged neoplastic tissue located at the posterior contour of the RFA-zone in 4 patients (66.6%), at the posterior superior contour in 1 patient (16.7%) and at the posterior lateral one in 1 patient (16.7%). Re-RFAs were required in all 6 cases and MR imaging verified their successes.

Conclusion: MR imaging accurately determines margins of the ablated areas. It allows to avoid incomplete tumor destruction in patients who have undergone RFA.

C-0041

withdrawn by authors

C-0042

Assessment of liver iron: Normal values

V. Belan, M. Srbecký, L. Pruzincová, B. Wlachovská, J. Moczová, J. Andrísová;
Bratislava/SK

Purpose: MR imaging has been proven to be clinically useful in determining liver iron concentration. In order to differentiate between mild overload and normal iron content, the best achievable knowledge of the distribution of normal values is necessary. The aim of the study was to choose the best sequences for different clinical situations.

Methods and Materials: The simplest quantitative method of the liver iron concentration estimation by MR imaging is to measure liver to muscle signal intensity ratio (SIR). We examined 39 men and women without liver disease on 1.5 T Magnetom Symphony (Siemens), in a whole body coil. The following sequences were used: SE T1/685/25 and GRE (PD/120/4/20, T1/120/4/90, T2/120/9/20, T2/120/14/20, T2/120/21/20). SIR values were estimated and analyzed for all sequences.

Results: Distribution of SIR values did not significantly differ from normal, there-

fore assessment of the normal limits were estimated as average \pm 2 SD. Estimated averages and limits (average - 2 SD) of SIR were:

SE T1/685/25: 1.45 1.05, GRE PD/120/4/20: 1.50 1.10, T1/120/4/90: 1.15 0.96, T2/120/9/20: 1.06 0.90, T2/120/14/20: 1.07 0.84, T2/120/21/20: 1.12 0.64, resp.

Conclusions: Assessment of normal values allows us to find iron liver overload without necessity to correlate SIR and liver iron concentration, and also to eliminate the differences between different equipment.

C-0043

Acquisition and postprocessing procedures for 3D CT modeling of hepatic vessel architecture and volume calculation in major liver resection and living donated liver transplantation

O. Lucidarme, P. Malzy, J.-C. Vaillant, M. Cadi, J. Taboury, L. Hannoun, P. Grenier; Paris/FR

Learning Objectives: Our objective is to present, discuss and illustrate the multi-detector row CT (MDCT) imaging techniques (including iodinated contrast media injection protocol) and the currently available postprocessing procedures that can optimize the 3D non-invasive preoperative visualization of the portal and hepatic veins anatomy and the volumetric assessment of the hepatic lobes.

Background: Injection protocols used in our last 60 patients, acquisition settings, as well as threshold, propagation, separation and fusion postprocessing techniques and shaded-surface or volume rendering display will be detailed and illustrated.

Procedure Details: 80 sec after injection of 120 ml of a contrast agent (350 mg iodine/ml, 4 ml/s) followed by 100 ml of physiologic serum (2 ml/s), a strong enhancement of both portal and hepatic veins occurs in all patients. The shortest procedure (15 min) is obtained mixing the propagation and the threshold techniques for, respectively, parenchyma and vessel extraction. The shaded-surface display allows a better visualization of the superficial marks of the liver while the volume rendering display permits a better analysis of the vessels due to the control of the parenchyma transparency. The calculated volumes are well correlated ($r^2 = 0.86$) with the weight of the resected specimen when the virtual resection is performed jointly with a surgeon.

Conclusion: MDCT with 3D shaded-surface and volume rendering display of liver, hepatic and portal veins is a fast procedure that may help the surgeon in planning major resections. Virtual resections are improved when performed by a radiologist jointly with a surgeon.

C-0044

Ultrasonography of diffuse and focal liver disease: A multimedia DVD-Rom based educational tool and database

P.S. Zoumpoulis, I. Theotokas, I. Bechrakis, S. Kyriazi, D. Schizas, K. Pahou, I. Vafiadi, P. Karavitis; Athens/GR

Learning Objectives: 1. To review the role of ultrasound in the diagnosis of chronic liver disease, portal hypertension and focal liver lesions by using educational text, selected images, case studies and video cases. 2. To help derive a sonographic diagnosis through correct algorithms. 3. To provide comparison of an US image of diagnostic difficulty to the database.

Background: The user-friendly interface provides the possibility of free navigation throughout multimedia data and a comparative database including images, text, videos and relevant bibliography.

Procedure Details: The educational DVD-Rom contains: Instructions on ultrasonographic techniques (including video with voice instructions), analytical commentary of liver diseases, archived ultrasound images with captions, discussion pertaining to the case, its ultrasonographic findings, interpretation of the findings, many interesting cases and bibliography links. The aim of this project, to teach US technique, is achieved mainly by a twofold video presentation. More specifically, in your environment you will view both a presentation of a) the examiner and his manipulations with the transducer and b) a real-time ultrasound examination. Each chapter contains articles with key words that correspond to ultrasound images. The Image Galleries contain a broad selection of ultrasound images and comments on sonographic findings. A database is included to aid the user in reaching the correct diagnosis of a lesion detected in the liver by comparing it to the sonographic images available.

Conclusion: This multimedia DVD-Rom familiarizes the radiologist with CD-ROM multi-media presentations and covers all major fields of US evaluation of focal and diffuse liver diseases as well as presenting US-guided procedures of various focal lesions.

Scientific and Educational Exhibits

C-0045

Role of contrast-enhanced sonography (CE-US) in transarterial chemoembolization treatment for HCC

A. Nunziata, O. Catalano, F. Sandomenico, F. Fiore, E. Montemarano, A. Siani; Naples/IT

Learning Objective: To illustrate the real-time CE-US findings during and after transcatheter embolization of HCC. To show the practical value of CE-US to help the embolization procedure and to assess results at early and late follow-up.

Background: Contrast-enhanced, low-mechanical index US is a recently introduced technique in the assessment of HCC treated with transcatheter intrarterial chemoembolization therapy.

Procedure Details: Cases are shown where CE-US is employed to assess HCC vascularity immediately before and immediately after chemoembolization, to demonstrate treatment complications, to depict incomplete treatment and need for retreatment, to assess tumour necrosis demonstrating viable tumour tissue persistence and to detect tumour recurrence after successful initial chemoembolization.

Conclusion: Real-time CE-US has several possible applications during transcatheter embolization therapy for HCC (via selective hepatic arteriography). It is also relevant after treatment, for short and long-term imaging follow-up (via IV peripheral injection).

C-0046

Temporal and blood-flow phase subtraction technique of the liver for detection of subtle hepatocellular carcinoma on abdominal CT images

E. Okumura¹, S. Sanada¹, M. Suzuki¹, Y. Tsushima², O. Matsui¹; ¹Kanazawa/JP, ²Gunma/JP

Learning Objectives: 1. To demonstrate the advantages of an automated image-matching technique for abdominal CT images. 2. To demonstrate the advantages of the temporal and blood-flow phase subtraction technique for diagnosis of hepatocellular carcinoma.

Background: It is difficult for radiologists to identify subtle hepatocellular carcinoma (HCC) because it is often difficult to achieve sufficiently sensitive enhancement in contrast-enhanced images for detection of these tumours. Therefore, we developed a new temporal and blood-flow phase subtraction technique to enhance isolated structures such as subtle HCC.

Procedure Details: The present study was performed using CT images from 18 subjects. First, to register current and previous images, we used template matching based on similarities in liver shape, etc., between current and previous images (non-enhanced, contrast-enhanced images) at the same position. Second, temporal subtraction images were then obtained by subtraction of current images from previous images taken at the same position of the liver, and the blood-flow phase subtraction images were obtained by subtraction of plain images from contrast-enhanced images taken at the same position of the liver. Our results indicated that approximately 90% of current images from these 18 cases were correctly matched with previous images taken at the same position of the liver. Visualization of the enhanced lesions in temporal and blood-flow phase subtraction images was increased, especially for detection of HCC.

Conclusion: Our subtraction technique may be useful in assisting radiologists in diagnosis of liver CT images.

C-0047

Differential diagnosis of multiple hyperintense lesions of the liver on T1WI of MR imaging with pathologic correlation

K. Matsuzaki, M. Takeuchi, H. Uehara, H. Nishitani; Tokushima/JP

Learning Objectives: To demonstrate the differential diagnosis of multiple hyperintense lesions of the liver on T1WI of MR imaging including various benign and malignant tumors and tumor-like lesions with pathologic correlation.

Background: Multiple hyperintense lesions of the liver on T1WI are rare and include various benign and malignant pathologies. Some characteristic imaging findings and enhancement patterns with positive and negative contrast media may be diagnostic.

Imaging Findings: The causes of T1 shortening are fat, hemorrhage, hyperproteinous materials (mucin etc.), melanin and other miscellaneous factors. Multicentric well differentiated hepatocellular carcinomas (wHCCs), dysplastic nodules, angiomyolipomas and round fatty infiltrations may be observed as hyperintense lesions on T1WI due to their fatty components, which show signal reduction on fat-suppressed images. Dysplastic nodules and wHCCs are hypovascular on dynamic study with positive contrast media reflecting ischemic fatty metamorphosis and show superparamagnetic iron oxide (SPIO) uptake reflecting their

residual Kupffer function. Angiomyolipomas are hypervascular on dynamic study reflecting abundant hamartomatous vascular components and do not show SPIO uptake. Other benign hyperplastic nodules without adipose tissue may show hyperintensity on T1WI, but the cause is still unclear. SPIO uptake and patients' background conditions (portal hypertension, alcoholism etc.) may helpful for diagnosis. Metastatic melanomas and mucinous adenocarcinomas show contrast enhancement on dynamic study and do not show SPIO uptake. Hyperproteinous or hemorrhagic cysts do not show either contrast enhancement on dynamic study or SPIO uptake.

Conclusion: To diagnose multiple hyperintense lesions of the liver on T1WI of MR imaging the adequate use of positive and negative contrast media is helpful.

C-0048

Hepatic VX2 carcinomas in rabbits: Detection with ferucarbotran-enhanced MR imaging and comparison of optimized sequences

S. Kim¹, H.K. Lim², D. Choi², M. Kim², K. Jang³, W. Lee², J. Lim²; ¹Wonju/KR, ²Seoul/KR, ³Choncheon/KR

Purpose: To compare the accuracy of a variety of ferucarbotran-enhanced MR imaging sequences for detection of multiple hepatic VX2 carcinomas in rabbits.

Materials and Methods: Fifteen rabbits with VX2 carcinomas in the liver underwent ferucarbotran-enhanced MR imaging using the following sequences: a fat-suppressed proton density- and T2-weighted images, T2*-weighted fast multiplanar gradient-recalled echo acquisition in the steady state (FMPGR) with different TE or flip angle setting (TEs with 9, 12, and 15 msec, flip angle with 20° and 80°, respectively), T2*-weighted fast multiplanar spoiled gradient-recalled echo sequence (FMPSPGR), T1-weighted FMPSPGR and unenhanced and dynamic enhanced T1-weighted FMPSPGR obtained with delays of 20 seconds, 1 minute, 3 minutes, and 5 minutes. Contrast-to-noise ratios (CNRs) of the tumors were calculated quantitatively and image qualities were assessed qualitatively. The diagnostic performance was assessed by using receiver operating characteristic (ROC) analysis on a tumor-by-tumor basis, which was correlated with histopathologic examination.

Results: Quantitatively, the CNR of the proton density-weighted sequence was significantly higher than those of the other sequences ($p < 0.05$). Quantitatively, image qualities of proton density- and T2-weighted sequences were significantly more excellent than those of the other sequences ($p < 0.05$). In diagnostic performance, T2-weighted, proton density-weighted, and T2*-weighted FMPGR with a TE of 12 msec and a flip angle of 20° sequences were higher than those of the other sequences.

Conclusions: T2- and proton density-weighted, and T2*-weighted FMPGR with a TE of 12 msec and a flip angle of 20° sequences showed higher accuracy for detection of multiple hepatic VX2 carcinomas.

C-0049

Multidetector CT imaging of common and uncommon large cystic hepatic masses

E. Dominguez-Franjo, M. Diez Perez de las Vacas, P. Ramos Lopez, L. Garcia del Salto, I. Salmeron, E. Fraile Moreno; Madrid/ES

Learning Objectives: To identify the clinical and pathologic features of large cystic hepatic masses. To describe the MDCT imaging techniques and features of various cystic hepatic masses.

Background: Cystic lesions of the liver in the adult are frequently found in routine clinical practice. Large cystic masses (> 5 cm) often imply a diagnostic challenge. Multidetector CT, with the possibility of real multiplanar reconstruction, constitutes an important tool to define intrahepatic origin and relationships of lesions, and it provides images in a format more familiar to many surgeons. Cystic lesions can be classified as congenital, neoplastic, inflammatory and miscellaneous. In this exhibit we illustrate the CT findings of several large cystic masses including neoplastic cysts (like cystadenoma, metastases...), congenital cyst (simple-bile cyst, polycystic liver disease, Caroli disease...), infectious diseases (pyogenic, amebic abscess, hydatid cyst) or traumatic lesions such as intrahepatic hematoma, bilioma.

Imaging Findings: There are no specific signs for each tumor type, but several MDCT features are very useful to characterize the lesion. Important imaging findings include size of the lesion, presence and thickness of the wall, presence of septum, calcifications, solid poles, and the enhancement pattern.

Conclusion: Although there are not pathognomonic features, the better spatial resolution on thin sections MDCT data sets allows the identification of fine septum and calcifications as well as solid poles, necessary to approximate to the etiologic nature of the masses.

Scientific and Educational Exhibits

C-0050

Value of MR imaging in the diagnosis of hemochromatosis

M. Lirola Cruz, M. Muñoz Beltran, E. Garcia Casado, M. Tuñón Gómez, J.M. Blazquez Ortiz; Madrid/ES

Purpose: To assess the role of magnetic resonance (MR) imaging in the detection of liver iron overload.

Materials and Methods: MR imaging at 1.5 T was prospectively performed on 49 patients (20 with iron liver overload and 19 without). In all patients the sequences used were GRE T1W, TSE T2W and GRE T2W. Ratios of signal intensities between liver and paraspinal muscle were calculated from images obtained with spin-echo and gradient-echo sequences. Correlation between ferritin serum levels and ratios of signal intensities were obtained.

Results: MR measurements showed a highly significant ($p < 0.001$, Mann Whitney test) decrease in the signal-to-muscle ratio of the liver in patients with iron overload as compared to non-iron overloaded patients with GRE T2W sequence. Correlation between the liver-to-muscle ratio and serum ferritin levels with GRE T2W sequence was significant ($\rho = -0.708$, $p < 0.016$, Spearman test).

Conclusion: Mr imaging is a useful tool in the diagnosis and management of liver iron overload. Gradient-echo T2W sequence is the most sensitive for iron overload and there is a correlation between the magnitude of signal intensity decrease and the degree of iron overload. However it is still necessary to evaluate the usefulness of MR imaging for the quantification of hepatic iron concentration in order to avoid hepatic biopsy for the diagnosis of hemochromatosis.

Abdominal Viscera (Solid Organs)

Pancreas

C-0051

Imaging spectrum and minimally invasive therapy in neuroendocrine tumours

P. Rajiah, A. Khan; Manchester/UK

Learning Objectives: A. To understand the role of imaging in diagnosis of neuroendocrine tumours. B. To illustrate the appearances of neuroendocrine tumours in various imaging modalities such as ultrasound, CT, MR imaging, PET and octreotide scanning. C. To suggest a diagnostic approach and to learn the common differential diagnosis. D. To learn the role of minimally invasive therapy (embolisation) in management of metastatic neuroendocrine tumours.

Background: Neuroendocrine tumours are rare neoplasms that arise from the small, neuroendocrine cells and these are divided into carcinoid and pancreatic neuroendocrine tumours. They can arise anywhere in the body. The systemic and local symptoms are myriad. Tremendous advances have been made in the diagnosis, localisation and management of these tumours. This review illustrates the role of imaging, the imaging spectrum of the tumours in USG, CT, MR imaging, contrast ultrasound, angiography, endoscopic ultrasound, In 111 DTPA octreotide scintigraphy and management of neuroendocrine tumours.

Procedure: All patients with suspected neuroendocrine tumours had ultrasound, multislice CT and MR imaging scans. Angiography, octreotide scintigraphy, contrast ultrasound, Endoscopic ultrasound and intraoperative ultrasound were performed in tumours that were difficult to localise. Hepatic artery embolisation was performed in metastatic neuroendocrine tumours in those who were not candidates for hepatic resection.

Conclusion: Radiology plays a vital role not only in the diagnosis and localisation of neuroendocrine tumours but also in management in the form of minimally invasive therapy.

C-0052

CT imaging based scores as predictors of severity in acute pancreatitis:

A comparative study with statistical evaluation

C. Triantopoulou, P. Maniatis, D. Lytras, I. Siafas, K. Manes, J. Papailiou, C. Dervenis; D. Chryssovergis, Athens/GR

Purpose: The aim of the study was to analyze the course of the disease in patients suffering from acute pancreatitis in conjunction with computed tomography (CT) evaluation of severity, using Balthazar and computed tomography severity index (CTSI) scoring systems.

Methods-Materials: 148 patients with acute pancreatitis were treated in the surgery department of our hospital. All data concerning etiology, Atlanta classification, CT findings, Apache score, CRP levels, stay in the intensive care unit (ICU), length of stay, treatment, complications and deaths were analyzed with Mann Whitney, Wilcoxon, Pearson and Spearman statistical tests. CT was performed within 96 hours of admission on a spiral unit, using 3-5 mm collimation after i.v. administration of iodinated contrast material in a total volume of 100-120 ml. Images were graded according to the Balthazar scoring system while, after measurement of the non enhanced necrotic pancreatic lesions using the "area" tool provided by the software, the CTSI was also calculated.

Results: A very good correlation was noticed between Balthazar-CTSI scores and local complications, while a not statistical significant correlation was found between CT scores and stay in the ICU. Among survivors and non-survivors there were no statistical significant differences as far as CT scores were concerned.

Conclusions: Although the extent of necrosis as defined on contrast-enhanced CT examinations is considered as a risk factor for a negative prognosis, our findings suggest that initially documented disease severity according only to imaging parameters is not highly important for the final patient outcome.

C-0053

Imaging findings after pancreas transplantation with enteric exocrine drainage: Posttransplantation anatomy and pathology

M.C. Freund, K.M. Unsinn, M. Rieger, W. Mark, H. Bonatti, R. Margreiter, W.R. Jaschke; Innsbruck/AT

Learning Objectives: 1. To illustrate the spectrum of imaging findings after pancreas transplantation with enteric exocrine drainage, utilizing different imaging modalities with regard to anatomy and pathology. 2. To be familiar with the different surgical techniques of pancreas transplantation with enteric exocrine drainage.

Background: Pancreas transplantation has emerged as an effective treatment

Scientific and Educational Exhibits

for patients with long-standing type 1 diabetes mellitus resulting in an insulin-independent euglycemic state and normalization of glycosylated hemoglobin levels. Knowledge of the transplantation procedure and postoperative imaging anatomy of the pancreas allograft are basic requirements for radiologists. Graft survival, among other factors, corresponds to early diagnosis and therapy for specific graft-related complications.

Imaging Findings: Interpretation of imaging studies after transplantation depends on familiarity of the surgical anatomy. For these reasons this pictorial essay schematically illustrates the intraoperative appearance during the various procedures of pancreas transplantation. Each procedure is supplemented by various examples of typical anatomy as shown by several imaging modalities including sonography, CT, MR imaging, gastrointestinal contrast examination and angiography. Additionally, this pictorial essay displays the spectrum of imaged pathology including vascular graft complications such as rejection (venous and arterial graft thrombosis), pancreatic graft complications including infection (pancreatitis, pseudocyst formation including expansion, infection with abscess formation, pseudoaneurysm formation, leakage of the enteric anastomosis or duodenal stump and small bowel obstruction) and other transplantation-associated complications (pseudothrombosis of the iliac vein and posttransplant lymphoproliferative disorder).

Conclusions: This pictorial essay displays the spectrum of imaging findings after pancreas transplantation with enteric exocrine drainage utilizing different imaging modalities with regard to anatomy and pathology.

C-0054

Vascular thrombosis in pancreatic transplantation: Multidetector CT in the evaluation of pancreatic vessels and parenchyma

C. Cappelli, E. Neri, A. Pratali, R. Cioni, U. Boggi, C. Bartolozzi; Pisa/IT

Purpose: The role of multidetector CT in the evaluation of pancreatic vessels and parenchyma in patients submitted to pancreas transplantation with arterial and/or venous graft thrombosis.

Methods and Materials: 22 patients submitted to pancreas transplantation were evaluated with multidetector CT because of Doppler-US suspicion of vascular thrombosis. CT study included unenhanced, arterial and portal phases with 1.25 mm collimation and 0.6 mm reconstruction interval. For the evaluation of vascular structures MPR and MIP reformats were performed. The pancreatic parenchyma was assessed both in unenhanced and post-contrast phases by evaluating morphology and parenchymal enhancement.

Results: The CT study demonstrated 4 cases of arterial thrombosis involving both the splenic and mesenteric branches. In such cases the pancreas appeared small and inhomogeneous (3) or completely atrophic and calcified (1). In 3 cases an arterial thrombosis of the mesenteric (2) or splenic (1) branch was found. In isolated mesenteric artery thrombosis, the parenchyma was normal, while in splenic artery thrombosis the tail of the pancreas was small and inhomogeneous. When a partial venous thrombosis (portal vein-1 case, splenic vein-5 cases) was demonstrated, the pancreas appeared normal. In complete venous thrombosis, isolated (3 cases) or associated with arterial thrombosis (6 cases) the parenchyma appeared hypodense and enlarged, suggesting a parenchymal necrosis.

Conclusion: Multidetector CT can accurately identify vascular thrombosis in patients with pancreatic transplantation. By assessing the morphology and enhancement of the parenchyma, it can be useful in the follow-up and therapeutic planning of such patients, in association with clinical findings.

C-0055

Perfusion CT of the pancreas in acute pancreatitis

S.D. Rud, G.E. Trufanov, O.F. Pozdniakova, V.S. Dekan, I.V. Pyanov; St. Petersburg/RU

Purpose: To assess the clinical significance of perfusion CT in evaluation of the pancreatic parenchyma of healthy adults and in acute pancreatitis (AP).

Materials and Methods: 17 patients with clinical signs of AP (10 men and 7 women, mean age 48.6) and 10 asymptomatic patients underwent dynamic MDCT (Somatom Volume Zoom™, Siemens). Measurements of perfusion index was performed using a maximum slope method and special software BasamaPerfusion 3.0.3.6. In all patients with AP, contrast-enhanced MDCT and calculation of Balthazar severity index were used. Patients with AP were divided into two groups: severe AP ($n = 10$, Balthazar score 3-10) and mild AP ($n = 7$, Balthazar score 0-3).

Results: Normal perfusion index calculated in patients without clinical and laboratory signs of pancreatic disease was 0.7-1.5 ml/min/cm³ and did not depend on the age of patient. In patients with AP the perfusion index was 0.8-0.4 ml/min/cm³ in mild pancreatitis and < 0.5 ml/min/cm³ in severe AP. Perfusion abnormalities of pancreatic parenchyma had as local as diffuse character. All results correlated with Balthazar severity index and further development of clinical signs.

Conclusion: Perfusion CT of pancreas seems to be a strong diagnostic tool for early detection of perfusion abnormalities in AP and prognosis of AP severity.

C-0056

How to reach the sonographic diagnosis of pancreatic lesions using a simple algorithm: A DVD-Rom based teaching file with US image and video database

P.S. Zoumpoulis, I. Theotokas, A. Plagou, D. Schizas, E. Tako, D. Leli, C. Beligiannis, K. Pahou; Athens/GR

Learning Objectives: To teach how to describe US characteristics of a *focal pancreatic lesion*. To facilitate diagnosis imaging through correct algorithms. To help compare a US image of diagnostic difficulty to US images with a proven diagnosis.

Background: The user may simply view the images, video cases and interesting case studies or compare his images to those of the database.

Procedure Details: The user has the option of viewing and comparing B-mode or color Doppler images. The user may enlarge any image whether it is from the image gallery or the interesting case studies and adjust the brightness if necessary so as to view it better. The user starts using this teaching file by describing the US characteristics of a focal pancreatic lesion that he has difficulty in diagnosing. The system guides him through a specific algorithm of all possible pancreatic lesions which fit the given description. A large collection of classified US image galleries and videos in each diagnostic category are available for comparison with the User's images. The user's image can also be linked to the contents of corresponding interesting cases, which are brief case reports with clinical, biochemical, imaging and pathological data.

Conclusion: The user can be aided in deriving a diagnosis of a pancreatic lesion by comparing it to other "similar" sonographic images, available in galleries, videos and interesting cases.

C-0057

Macrocystic neoplasms of the pancreas: Differentiation of serous oligocystic adenoma from mucinous cystadenoma and intraductal papillary mucin-producing tumor with CT

S. Kim; Seoul/KR

Purpose: To describe typical CT findings of serous oligocystic adenoma (SOA) of the pancreas and to find differential points from other macrocystic neoplasms such as mucinous cystadenoma and intraductal papillary mucin-producing tumor of branch duct type (IPMT).

Materials and Methods: A total of 41 patients with histologically confirmed macrocystic neoplasms of the pancreas were enrolled into this study (SOA:10; mucinous cystadenoma:13; branch type IPMT:18). Two experienced radiologists reviewed the CT findings of these patients in consensus. The location, longest dimension, shape, presence of mural nodule, presence of wall calcification and extent and degree of main pancreatic duct (MPD) dilatation were analyzed. The shapes were categorized into 7 groups as below: multicystic; lobulated contour with/without internal septation; smooth contour with/without internal septation; pleomorphic cystic; clubbed finger-like cystic. Comparative studies of three types of lesions were performed using Fisher's exact test and Mann-Whitney U test.

Results: There was significant difference in shape of the lesion between SOA and the other macrocystic neoplasm such as mucinous cystadenoma ($P < 0.05$) IPMT ($P < 0.05$). SOA showed a shape of multicystic or lobulated contour while mucinous cystadenoma showed a shape of smooth contour and IPMT showed either a pleomorphic cystic or clubbed, finger-like cystic shape. Upstream MPD dilatation was predominantly observed in SOA compared to other two diseases while diffuse MPD dilation was noted in IPMT ($p = 0.025$).

Conclusion: SOA of the pancreas has typical CT findings differing from other cystic tumors. It appears as a multicystic or lobulated cystic lesion with septation and with upstream MPD dilatation from the lesion.

C-0058

MR pancreatography and secretin enhanced MR pancreatography for the study of anatomical variants and developmental abnormalities of the pancreas

C. De Juan, M. Sanchez, S. Navarro, M. Pages, J.R. Ayuso, C. Ayuso; Barcelona/ES

Learning Objective: To describe and illustrate the use of magnetic resonance pancreatography (MRP) in the evaluation of the normal anatomy, anatomical variants and developmental abnormalities of pancreatic ducts, specially focused on the role of secretin enhanced MRP (S-MRP). MRP is being used increasingly as

Scientific and Educational Exhibits

a non-invasive technique to study the pancreas. However, due to the small diameter of pancreatic ducts in physiological conditions, in approximately 20% of patients the entire ductal anatomy can not be completely identified. In these cases, the administration of secretin clearly improves the visualization of the ducts. Secretin acts as an endogenous contrast agent which stimulates the pancreatic exocrine secretion and transiently distends the ducts displaying their full length. By filling non-visualized ductal segments, S-MRP increases diagnostic accuracy. Normal anatomy of pancreatic ducts varies greatly. It is important to be familiar with the different configuration types because they may be mistaken for pathologic conditions. Because of its complex embryologic development, the pancreas demonstrates multiple variations in ductal drainage pattern (E.g. persistent duct of Santorini, ansa pancreatica, pancreas divisum...) and different developmental abnormalities (E.g. agenesis of dorsal pancreas, annular pancreas, partial duplication or ectopic pancreas). Our objective is to describe the technique and diagnostic key facts to evaluate these conditions, specially focused on S-MRP. Images are provided from our series of patients and technical considerations based on our clinical experience. In conclusion, MRP combined with S-MRP can provide high quality images to identify the course and drainage pattern of pancreatic ducts and to diagnose congenital anomalies.

C-0059

Cephalic duodenopancreatectomy (Whipple's procedure): Assessment of complications with helical CT

C. Juanco, F. González, R. Landeras, J. Jordá, E. Ruiz, T. Piedra, M. Lopez, M. Silván; Santander/ES

We evaluate the role of helical CT to assess normal anatomy and to depict complications after Whipple's procedure (WP) (cephalic duodenopancreatectomy). Accurate interpretation of these examinations requires knowledge of the type of surgery performed and the normal appearance of the abdomen on CT following this complex surgery. The purpose of this pictorial essay is to illustrate the normal appearance of the bowel following a Whipple's procedure as well as some of the complications. We retrospectively review the findings in helical CT examinations performed after pancreatic surgery in 70 patients that underwent WP emphasizing normal anatomy and common postoperative changes (unopacified anastomotic bowel loops in the porta hepatis, perivascular cuffing, pneumobilia, dilated intrahepatic bile ducts, reactive lymphadenopathy and transient fluid collections) and describing the most frequent complications (abdominal abscess, bilomas, biliary obstructions, pancreatitis, pseudocyst, haemorrhage, pancreatojejunum anastomotic leak, ascitis, delayed gastric emptying and vascular complications). We illustrate these findings with examples. We also compare the advantages of helical CT with other diagnostic methods (sonography, MR, barium...). Helical CT examination is an accurate method to depict immediate and subacute postoperative complications in patients that undergo cephalic duodenopancreatectomy giving the surgeon essential information for the adequate management of the patient.

C-0060

Detection and differential diagnosis of benign and malignant pancreatic lesions by unenhanced and contrast enhanced MR imaging

G.K. Schneider, P. Fries, K. Altmeyer, B. Kramann, R.M. Seidel; Homburg a.d. Saar/DE

Learning Objectives: To teach the principles of unenhanced and dynamic contrast enhanced MR imaging in the differential diagnosis of benign and malignant pancreatic disease.

Background: Pancreatic tumors represent an entity that is often asymptomatic and incidentally found by abdominal cross sectional imaging. For the adequate therapeutic approach an exact delineation and differentiation of detected pathologies is crucial.

Imaging Findings: This exhibit reviews the most frequent pathologies of the pancreas with a major impact on MR imaging. Cases will be presented with patient history and correlation to other imaging modalities such as CT, ultrasound or nuclear medicine is demonstrated when appropriate. The topics to be covered include benign lesions (e.g. adenoma, serous cystadenoma, microcystic adenoma, glucagonoma, islet cell tumor and lymphangioma), malignant lesions (e.g. (cyst-)adenocarcinoma, IPMT, insulinoma, multiple endocrine neoplasia and lymphoma) as well as pseudotumors (e.g. edematous or hemorrhagic pancreatitis, chronic pancreatic disease, pseudocyst and duct ectasia). A special regard will be taken to local staging of pancreatic adenocarcinoma based on MR findings. Cases with characteristic patterns and diagnostic pitfalls are demonstrated to elucidate both the potential and limitations of MR imaging in the work up of pancreatic pathologies.

Conclusion: Diseases of the pancreas include a large variety of differential diagnosis with a major clinical impact on therapeutic strategies. MR imaging represents an adequate imaging modality revealing the diagnosis and local staging for the appropriate therapy to be planned.

C-0061

Imaging findings of biliopancreatic involvement by lymphomas and leukemias

B.R. Arenas, L. Del Campo, A. Barbosa, M.A. Llosa, M. Caraballo; Madrid/ES

Purpose: To illustrate the imaging findings on computed tomography (CT) and magnetic resonance (MR) of biliopancreatic involvement by lymphomas and leukemias.

Methods and Materials: We have reviewed 424 cases of leukemias and 350 of lymphomas diagnosed in our hospital between January 1999 and December 2003. We have found ten patients with radiological involvement of the pancreatic gland and/or the extrahepatic biliary tree. Imaging findings on CT were evaluated in all the cases and on MR in two cases. Biliopancreatic involvement was verified by histological examination after imaging-guided biopsy in two patients and by clinico-radiological evaluation post-chemotherapy in eight patients.

Results: We have found pancreatic gland involvement by lymphoma in five patients and by leukemia in three. The radiological patterns were: a big mass in the pancreatic head in two cases, a diffuse enlargement of the pancreatic gland with alteration of the density on CT or the signal intensity on MR in two cases and peripancreatic adenopathies which secondary infiltrated the gland in four cases. One patient developed an isolated granulocytic sarcoma of the choledochal duct that caused a concentric stenosis in the middle third. Another patient presented with invasion of the distal choledochal duct by a primary lymphoma of the Ampulla of Vater.

Conclusion: In our series, in accordance with the current literature, pancreatic involvement by lymphoma and leukemia usually appeared on CT and MR as peripancreatic adenopathies that secondary involved the pancreas. The isolated involvement of the extrahepatic biliary tree by lymphoma and leukemia was extremely rare.

Scientific and Educational Exhibits

Abdominal Viscera (Solid Organs)

Spleen

C-0062

Value of splenic artery resistive index in the differentiation between alcoholic and hepatitis B virus-related cirrhosis

J. Byun, J. Choi, D. Kim; Gwang-Ju/KR

Purpose: To assess the usefulness of splenic artery resistance index (RI) in the differentiation between alcoholic cirrhosis and hepatitis B virus-related cirrhosis.
Materials and Methods: Three groups with 109 subjects (28 controls, 38 hepatitis B virus-related cirrhosis patients, and 43 alcoholic cirrhosis patients) were included. Splenic artery RI and splenic size were compared in three groups. Splenic size, variceal bleeding episode and Child's score were compared in two cirrhotic groups. A cutoff value of splenic artery RI to differentiate two cirrhotic groups was defined as an RI of -2 SD. Sensitivity, specificity, accuracy, positive predictive value and negative predictive value for alcoholic cirrhosis were calculated.

Results: The mean splenic size (11.0 ± 1.6 cm) and mean splenic artery RI (0.58 ± 0.05) of controls were less than those of two cirrhotic groups ($p < 0.05$). Splenic size, variceal bleeding episode and Child's score were not different between two cirrhotic groups. In contrast, the mean splenic artery RI in patients with alcoholic cirrhosis was significantly higher than in patients with hepatitis B virus-related cirrhosis (0.72 ± 0.07 vs. 0.62 ± 0.06 , $p < 0.05$). The cut-off value of splenic artery RI for alcoholic cirrhosis was 0.7. If an RI was greater than 0.70 it suggested the possibility of alcoholic cirrhosis. Sensitivity, specificity, accuracy, positive predictive value and negative predictive value were 62.8%, 97.4%, 79.0%, 96.4% and 69.8% respectively.

Conclusion: A reasonable lower limit of alcoholic cirrhosis was an RI of 0.70, which appeared to be a specific parameter for differentiation between alcoholic and hepatitis B virus-related cirrhosis.

Abdominal Viscera (Solid Organs)

Miscellaneous

C-0063

Non-cutaneous peripheral T-cell lymphomas: Radiological-pathological correlation

X. Mallol, E. de Lama, E. Gonzalez, A. Fernández, E. Domingo, J. Narváez; Barcelona/ES

Learning Objectives: The aim of this exhibit is to illustrate the most common radiological patterns of peripheral T-cell lymphomas (PTCL), correlating them with clinical and histopathological manifestations. Differential diagnosis in each location is discussed.

Background: Most radiologists are unfamiliar with PTCL because it represents a relatively small proportion of lymphomas and has a low prevalence in Western countries. PTCL are an heterogeneous subgroup of lymphomas, being in their vast majority primarily cutaneous and which do not require imaging evaluation. The rest of them, represent specific clinicopathologic entities, with specific radiological imaging.

Procedure Details: Radiological images of patients with histologically proven non-cutaneous PTCL (classified according to the WHO classification) were retrospectively reviewed along with their clinical and pathological data. Our cases included: Precursor T lymphoblastic lymphoma/leukemia (n = 15), T-cell prolymphocytic leukemia (n = 4), T-cell granular lymphocytic leukemia (n = 29), Adult T-cell lymphoma leukemia (n = 2), Extranodal NK/T-cell lymphoma nasal type (n = 13), Enteropathy T-cell lymphoma (n = 4), Angioimmunoblastic T-cell lymphoma (n = 8) and peripheral T-cell lymphoma NOS (n = 35).

Conclusions: Non-cutaneous PTCL can present as a wide spectrum of disease involving different organs. There is a correlation between specific clinicopathological entities and the primary site of involvement, although findings in the disseminated stage of the disease do not allow differential diagnosis.

C-0064

Acute abdominal hemorrhage and its complications in hemophilic patients

K. Borbély, L. Nemes, A. Ceglédi, É. Cserepes, É. Bács, A. Laki, G. Székely, M. Barta, G. Forrai; Budapest/HU

Learning Objectives: To outline the forms of abdominal hemorrhage and its possible complications occurring in hemophilic patients with low coagulation factor levels.

Background: Spontaneous abdominal bleeding mostly occurs in severe hemophilia - patients with a plasma coagulation factor level as low as 1% of normal value. The frequently coexisting hepatic failure due to viral hepatitis acquired by transfusions worsens the coagulation disorder. Superinfection of hematoma is critical for immunocompromised patients just recovering from hypovolemic shock.

Imaging Findings: Characteristic types of abdominal hemorrhage occurring in hemophilic patients are demonstrated by CT and ultrasound images through the selected cases of the 128 severe hemophilic patients treated in the National Haemophilia Center between July 2003 and July 2004. Abdominal wall, intraperitoneal and retroperitoneal (iliopsoas muscle, pancreas) hematomas are presented giving rise to hypovolemic shock, abscess and fistula formation, sepsis, pancreatitis, peritonitis due to pseudocyst rupture, femoral nerve lesion, hip contracture and death. While ultrasound had a limited role, CT was required for the proper demonstration of abdominal status.

Conclusion: The knowledge of severe abdominal complications in hemophilic patients is essential. Cross sectional imaging (in emergencies, CT) is adequate for demonstrating abdominal status.

C-0065

The peripheral primitive neuroectodermal tumor in the abdomen and pelvis:

Imaging features of CT, MR, and ultrasound

M.-J. Kim¹, J. Byun², H. Won², Y. Shin², K. Kim², H.-S. Hong², A. Kim², P. Kim², H. Ha²; ¹Anyang, Kyungki-do/KR, ²Seoul/KR

Purpose: To evaluate the imaging features of the peripheral primitive neuroectodermal tumor (pPNET) in the abdomen and pelvis.

Method and Materials: Over a 9-year period, we found pPNET in 16 patients. There were 11 men and 5 women aged 5-80 years (mean age, 34.3 years). Histopathological proof was obtained by surgery in 10 patients and by percutaneous biopsy in six. Two abdominal radiologists reviewed the CT (n = 16), ultrasound (n = 8) and MR images (n = 4).

Results: The pPNET were located in the peritoneal cavity (n = 4), retroperitone-

Scientific and Educational Exhibits

um (n = 4), kidney (n = 3), abdominal wall (n = 1), liver (n = 1), GB (n = 1), CBD (n = 1) and jejunum (n = 1). Tumors appeared as solitary masses (n = 13, 81%) and multiple masses (n = 3). Tumors showed well-defined margin (n = 9, 56%) or clearly invasive margin (n = 7, 44%), internal necrosis (n = 14, 88%) and internal hemorrhage (n = 3, 19%). There was lymphadenopathy in six patients, ascites in another six, and omental and/or peritoneal nodules in five. The distant metastases were in the liver (n = 1) and the superior mediastinum (n = 1).

Conclusion: The pPNET should be included in the differential diagnosis of a large, solitary mass with internal necrosis and heterogeneous enhancement in the abdomen and pelvis.

C-0066

Melioidosis: A tropical disease with a spectrum of imaging features in different organ systems

S.-E. Lin¹, W.C.G. Peh¹, M. Muttarak², A.G.S. Tan¹, J. Euathrongchit², P. Lerittumongkun², S. Simarak², C. Sivasomboon², H.M.L. Oh¹; ¹Singapore/Singapore; ²Chiang Mai/Thailand

Learning Objectives: 1. To highlight the epidemiology, clinical patterns and management of patients with melioidosis. 2. To review the imaging features of melioidosis afflicting various organ systems, using multimodality illustrations.

Background: Melioidosis is an infectious diseases caused by Burkholderia pseudomallei, a bacterium endemic in South East Asia. We review the clinical and imaging features of 39 patients from 2 centers in Thailand and Singapore. Melioidosis was confirmed in all cases, mostly by culture. There were 19 Thais, 10 Chinese, 1 Indian and 9 Malays. All were adults (age range 20-77 years). 34/39 patient had fever, with other common symptoms being cough, dyspnoea, abdominal pain and pain/swelling due to local disease. 28/39 patients had co-morbid conditions, particularly diabetes mellitus (25) and renal failure (4).

Imaging Findings: Only 2 patients had localized infection (parotid and pseudoaneurysm) with the majority having pulmonary or systemic disease. Frequently-affected organs were the lung (18), spleen (18), liver (14), bone (9), superficial soft tissues (5), prostate (3) and kidney (2). 19/39 patients had multi-organ involvement.

Conclusion: Melioidosis infection can be localized or systemic. CT, ultrasound and MR imaging are useful for detecting deep lesions such as liver, splenic and prostatic abscesses and osteomyelitis. Melioidosis should be considered in patients with predisposing co-morbidities, whether the infection is localized or systemic, especially in an endemic area or with prior travel history to an endemic area.

C-0067

Posttransplant lymphoproliferative disease (PTLD): A pictorial review

L. Herraiz, A. Bermejo, M. Perez, S. Dieguez, S. Borruel, A. Arenas; Madrid/Spain

Learning Objectives: The purpose of this review is to summarize the clinical features of PTLD in liver, heart and kidney allograft recipients and the wide variety of imaging findings based on our experience in a tertiary hospital.

Background: PTLD occurs in patients who receive transplants in which chronic immunosuppression leads to an unregulated expansion of lymphoid cells. Risk factors affecting the incidence of PTLD include allograft type, Epstein-Barr virus infection and immunosuppression. Characteristics of PTLD include a proclivity toward extranodal involvement, affecting nearly any organ system including the allograft, and a variable response to treatment. We reviewed 2255 transplanted patients, finding 31 cases of PTLD.

Imaging Findings: Abdominal Imaging - The abdomen is the most common anatomic region involved. We report three patterns of hepatic PTLD: focal low-attenuation nodules, infiltrative hepatic lesions with hepatomegaly and porta hepatis involvement in liver transplant recipients. Gastrointestinal system (mostly the small bowel) is commonly involved. Splenic involvement by PTLD manifests as focal low-attenuation and/or splenomegaly.

We report also renal, adrenal, abdominal lymph nodes and mesenteric involvement. Thoracic Imaging - Pulmonary parenchymal disease presents as discrete nodules or masses with air-space pattern. We also report cardiac and pericardial involvement. Head and Neck - We present some cases of calvarian and brain parenchymal PTLD involvement. The neck involvement include cervical lymph nodes, sinonasal region and nasopharyngeal Waldeyer ring.

Conclusion: PTLD represents an increasing problem. Knowledge of the various appearances of PTLD is important because its clinical manifestations are non-specific and prompt diagnosis and appropriate treatment affects the outcome.

C-0068

Wisdom without answers: Patient care and medicolegal ramifications of incidental findings on thin-section body computed tomography

A. Kamaya, R.M. Hsu, R.B. Jeffrey; Palo Alto, CA/US

Learning Objectives: To illustrate the most common incidental findings in thin-section body computed tomography which are usually benign but have some finite probability to pose serious harm to the patient if not properly addressed. To enumerate the injurious potential of these findings. To review the evolving recommendations for clinical and radiological work-up and/or follow-up.

Background: As multidetector computed tomography allows the routine practical acquisition of thinner imaging sections with less partial-volume averaging, greater diagnostic accuracy can be achieved in many applications. However, with this power comes the burden to manage an increasing number of small incidental findings which hitherto may have been clinically and radiologically occult. From a patient care and medicolegal perspective, the proper analysis and workup of these findings is essential but in many cases still evolving.

Imaging Findings: Chest findings such as solid or ground-glass parenchymal nodules, apical pleuro-parenchymal changes and thyroid nodules. Abdominal parenchymal findings such as tiny hypodense foci in the liver, spleen, pancreas, or kidney, early enhancing foci in the liver or spleen, adrenal nodules and ovarian calcifications. Extrapancreatic findings such as small mesenteric nodes, misty mesentery, peritoneal calcifications, prominent bile ducts, subcutaneous nodules and lucent or sclerotic bone foci.

Conclusion: Increasing sensitivity for small incidental findings with small but finite probability for serious patient care and medicolegal ramifications requires the modern radiologist to stay abreast of evolving recommendations for clinical and radiological workup.

C-0069

Which assessment should be preferred for a polytrauma victim?

Y.K. Maratos, A. Kalai, O. Clément, T. Loeb, G. Frija; Paris/FR

Purpose: We compared the results of systematic use of whole-body-CT-scan in polytrauma exploration to the results of focused on-demand CT-scans performed after clinical evaluation of polytrauma and the resulting changes in patient assessment, care and survival.

Method and Material: 400 polytrauma victims (from January 2002 to September 2004) admitted at the level 1 Trauma Center European Hospital Georges Pompidou, Paris were reviewed retrospectively by experienced senior radiologists and clinicians. ISS (Index Severity Score), 24-hour mortality rate, number of surgical procedures and rate of delayed diagnosis were recorded. Our results were compared to those presented in the literature (multicentric studies) including 450 cases of polytrauma victims with comparable ISS assessed by focused, on-demand loco-regional scan after initial clinical evaluation.

Results: Patients assessed with whole-body-CT-scan had a better outcome: Percentage of delayed diagnosis was reduced from 24% to 7% by whole-body-CT (comparing patients with ISS > 20). Surgical procedures were reduced from 52 to 36%. 24-hour mortality is reduced from 16 to 9%.

Conclusion: Management of polytrauma victims by whole-body-CT-scan is highly recommended in order to enable prompt and early treatment of lesions and to ensure that the percentage of missed injuries is minimized, resulting in a better care of this patient group.

C-0070

US and CT in the detection and differentiation of peritoneal carcinomatosis and tuberculous peritonitis

F. Todua, L. Jvarsheishvili, G. Tsivtsivadze; Tbilisi/GE

Purpose: To determine the ability of US and CT in differential diagnosis of peritoneal carcinomatosis (PC) and tuberculous peritonitis (TP).

Methods and Materials: US and CT were performed in 36 patients with PC and TP. The cause of peritoneal damages was identified by radiological and histopathologic studies. We reviewed data about peritoneal, mesenteric and omental changes, the size and structure of lymph nodes and presence of calcifications.

Results: Mesenteric changes were more commonly seen in cases of TP (80.5%) than in PC (41.7%). The omentum appeared more irregularly infiltrated in PC. The "floating" omental cake on US was more frequently characterized for carcinomatosis. Various degrees of lymphadenopathy were observed in both pathologies but macronodules (> 5 mm) were much more frequently seen in cases of TP (63.9%) than in PC (22.2%). TP was characterized by "fatty" nodes on CT and had increased echogenicity relative to other enlarged nodes on US. The hypoechoic center within a node occurred in cases of caseation (38.9%) as well as in

Scientific and Educational Exhibits

necrosed metastatic nodes (16.7%). Simple ascites was more commonly associated with PC (83.3%) than TP (33.3%). In this group it contained fine, freely mobile septa and had latticelike pattern. In 52.7% of TP was revealed the "wet" type of ascites with high attenuation on CT. In 47.3% the "dry" type with caseous nodules and dense adhesions. In our series peritoneal calcification associated with calcified lymph nodes was more frequently seen in TP (41.5%) than in PC (13.8%).

Conclusion: Many of the patterns of peritoneal damage are nonspecific. The combination of US and CT findings in light of clinical findings increases the ability to diagnose and distinguish PC from TP.

C-0071

withdrawn by authors

C-0072

Computed tomography patterns of mesenteric and omental disease

S. García-Asensio, H. Gómez, L. Sarría, R. Cozcolluela, A. Forradellas, M. Martínez-Berganza, F. Monzón; *Tudela/ES*

Objectives: To review the CT patterns of the broad spectrum of mesenteric and omental abnormalities.

Methods and Material: The scans of 438 patients (243 males and 195 females) with mesenteric-omental involvement were retrospectively reviewed. Spiral CT was performed after oral and i.v administration of contrast material on model ProSpeed SX GE scan.

Results: Diagnosis included: Infectious and inflammatory (33.56%): 1 tuberculous peritonitis, 108 inflammatory changes, 12 fluid collections, 8 abscesses, 2 increased attenuation after radiotherapy and 16 after surgery. Neoplasm (24.88%): 99 secondary neoplasm, 8 primary tumors, 2 pseudomyxoma peritonei. Tumoral mesenteric involvement was classified in four patterns: rounded masses, cake-like masses, ill-defined masses and stellate pattern. The type of primary tumors was determined at histopathologic examination of surgical specimen from 3 cases, and on the basis of follow-up CT and clinical data from 5 patients. Tumorlike lesions (2.73%): 4 mesenteric cysts, 2 echinococcosis, 3 pseudotumoral lipomatosis, 3 retroperitoneal fibrosis. Vascular disease (1.41%): 2 SMA thrombosis, 1 mesentery venous gas, 2 venous dilatation. In addition CT showed lymphadenopathy (27.62%), ascites (24.88%), mesenteric injuries (2.73%), pneumoperitoneum (3.65%), edema or congestion (1.41%), idiopathic retractile mesenteritis (0.68%) and mesenteric torsion (0.22%). Imaging features and histopathologic correlation of disease processes are demonstrated in this pictorial essay.

Conclusions: Spiral CT is a reliable imaging method for revealing evidence of mesenteric and omental disease and may suggest the diagnosis and biopsy site when necessary. Knowledge of the spectrum of these abnormalities and the characteristic CT appearances of them is essential for improving the diagnosis of these conditions.

C-0073

Abdominal tuberculosis presenting with acute abdomen: CT findings

H. Sun, R. Bai, E. Wu; *Tianjin City/CN*

Learning Objectives: To illustrate and characterize the spectrum of abdominal tuberculosis that can present as an acute abdomen.

Background: Abdominal tuberculosis can present with a variety of nonspecific radiological findings. Clinically, it often manifests with chronic abdominal pain associated with systemic symptoms, however unusual cases may occasionally present with severe abdominal pain. CT is especially useful in the diagnosis of acute abdomen, and can depict abdominal tuberculosis.

Imaging Findings: Acute abdomen derived from tuberculosis can be divided into four pathologies: intestinal, genitourinary, peritoneal and lymphatic. The ileocecal region is the most commonly involved segment. Transmural ulceration may result in a fistula, pericecal abscess or can perforate resulting in peritonitis. A hypertrophic lesion, in contrast, may lead to bowel obstruction. CT features include depiction of the ulcer or the asymmetric thickening of the ileocecal valve. Ureteral involvement is seen in 50% of patients with genitourinary tuberculosis. The pattern of hydronephrosis depends on the site of the stricture. A ruptured caseous ovarian abscess can often mimic malignancy. Tuberculous peritonitis may result from ruptured lymphatics, hematogenous spread, or GI tract perforation. Acute abdomen is more often caused by the wet type, with high-density ascites as a characteristic feature. Lymphadenopathy is the most common finding of abdominal tuberculosis. Large and clustered peripancreatic lymph nodes may cause arterial erosion, resulting in visceral ischemia and splenic infarction.

Conclusions: Complications of abdominal tuberculosis can result in an acute abdomen. Although the CT findings are nonspecific, abdominal tuberculosis should be considered in the differential diagnosis of an acute abdomen.

C-0074

Celiac plexus and splanchnic nerve neurolysis via a posterior or anterior approach

B.A.C. Kastler, E. Rodière, J. Litzler, P. Sarlieve, D. Michalachis, E. Delabrousse, B. Fergane; *Besançon/FR*

Management of pain in tumors located in the upper abdomen extending to the celiac region is difficult and because they do not respond properly to high doses of opiates. We have undertaken 126 procedures over the last year, combining a celiac and a splanchnic neurolysis which we believe to be more efficient. The intervention can be performed either by means of a classical posterior approach (usually using a Trans-aortic approach) or, as has not yet been described when aiming at both the celiac and splanchnic sites, via an anterior approach (possibly avoiding the aorta). We will demonstrate step-by-step our technique of percutaneous neurolysis under CT-guidance. CT-guidance allows safe needle progression and precise positioning at target which reduces complications and optimizes procedure results. Advantages, drawbacks and results of each approach will be outlined and illustrated with drawings and pertinent CT-images and protocols.

C-0075

Comparison of tissue harmonic imaging with standard ultrasound mode, in the evaluation of abdomen and pelvic organs

M. Chalkia, A. Spanos, I. Kirimlidis, A. Papageorgiou, E. Chartabillas, N. Vougiouklis; *Thessaloniki/GR*

Purpose: The purpose of this study is to compare tissue harmonic imaging (THI) with conventional ultrasonography, regarding image quality and organ visualization.

Methods and Materials: 358 different organs and lesions of the abdomen and pelvis, were evaluated with both conventional ultrasonography and tissue harmonic imaging. Ultrasound was performed with frequencies 2-4 MHz. Two experienced radiologists, blind to the mode used and blind to each other, rated each image pair for resolution, detail, and total image quality. The images were evaluated as: (1) Insufficient, (2) Good and (3) Very good. For analysis of the results we used the statistical program SPSS Version 11, Chi Square method.

Results: Both the examiners considered the THI images very good in 33.2% of the cases, good in 43.6% and insufficient in 23.2%, while they considered the conventional ultrasonography images, very good in 19.1%, good in 52.8% and insufficient in 28.1% of the cases. More specifically, the two methods exhibit a statistically important difference in imaging of the liver parenchyma, the gallbladder, the kidneys, the urinary bladder, and the ovaries, with THI being superior than conventional ultrasonography. THI did not show any distinct superiority in imaging of the pancreas and the prostate gland.

Conclusion: THI proved to be superior than conventional ultrasonography regarding image quality and organ visualization in the evaluation of abdominal and pelvic organs.

C-0076

MDCT of the acute abdomen: A pictorial essay

M. Tzaloniou, Z. Athanasopoulou, M. Chatzopoulou, M. Papoudos, V. Polimeropoulos, V. Papadopoulos, K. Stringaris; *Athens/GR*

Purpose: The term "acute abdomen" is used in cases of acute abdominal pain and which can prove to be a true emergency situation. Radiologists quite frequently are asked to give specific answers regarding the cause of an acute abdomen.

Materials and Methods: We prospectively studied all cases of patients who presented with acute abdominal pain and underwent CT examination in our department. All examinations were performed on a 16-row detector CT-scanner (Siemens, Germany). Axial images were obtained and coronal and/or sagittal reconstructions were performed in all cases. Oral and IV contrast medium was administered when indicated and possible. Normal examinations were excluded from our study. The CT studies were reviewed by two independent board certified radiologists. If there was any disagreement in the study interpretation, images were reviewed once more by the same radiologists in order to reach a consensus reading.

Results: Peptic ulcer, perforation of hollow viscera, cholangitis, cholecystitis and lithiasis of the common bile duct, acute pancreatitis, renal colic and pyelonephritis, mesenteric lymphadenopathy, small or large bowel obstruction, intussusception, appendicitis, diverticulitis, inflammatory bowel disease, ovarian cysts, hydrosalpinx, ruptured abdominal aortic aneurysm, mesenteric ischemia, thrombosis of IVC or other major veins, air in the portal vein, abscesses, strangulated hernias, volvulus, hematomas and abdominal trauma are the causes of acute abdomen that we have studied with the use of MDCT.

Conclusion: Treatment planning of the acute abdomen needs the underlying cause to be revealed and MDCT is both sensitive and accurate in most of these cases. Image reformation also proves to be a useful tool in some of the cases.

Scientific and Educational Exhibits

C-0077

Hydatid disease revisited

A. Oikonomou, S. Deftereos, M. Mantatzis, V. Fotiadou, P. Sourailidis, P. Prassopoulos; *Alexandroupolis/GR*

Learning Objectives: To discuss the prevalence and imaging findings of hydatid disease (HD) in unusual anatomic locations and describe the atypical manifestations of hepatic HD.

Background: HD is a worldwide parasitic disease produced by the larval stage of Echinococcus. The liver is the most frequently involved organ and the typical imaging findings are well known. However, unusual anatomic locations and findings related to rare manifestations of HD are less frequently described.

Imaging Findings: Radiological findings range from purely cystic to almost completely solid lesions. HD can become quite large and can be solitary or multiple. Calcification is more common in HD of the liver, spleen and kidney but it is not seen in the pulmonary location. Gallbladder, biliary, adrenal, peritoneal and brain locations are very rare and may not exhibit findings similar to liver HD. Growth rate in atypical cases may overcome duplication in volume annually. Exophytic growth and transdiaphragmatic migration of liver HD is a rare manifestation. The coexistence of hydatid cyst and malignant neoplasms should be included in the differential diagnosis when clinical findings cannot be interpreted by presence of HD alone. The imaging method indicated depends on the organ involved and evolution stage of the disease. US most clearly demonstrates hydatid in purely cystic lesions, with floating membranes and daughter cysts. CT is preferable for detecting calcification and revealing chest HD. MR imaging is indicated for central nervous system HD diagnosis.

Conclusion: Familiarity with unusual locations of HD or atypical radiological manifestations enables accurate diagnosis of the disease.

C-0078

"Misty Mesentery": Multidetector row CT (MDCT) features and differential diagnosis

F. Di Fabio, R. Cianci, E. Grassedonio, A. Filippone; *Chieti/IT*

Learning Objective: To describe and to review the most common MDCT features of "Misty Mesentery" in different pathologies, with a special focus on differential diagnosis.

Background and Imaging Findings: The term "Misty Mesentery" means a pathologic increase in mesenteric fat attenuation at MDCT. It may diffusely involve the mesentery or it may present as a segmental finding. The distribution patterns may be useful in the assessment of a primary cause. Diffuse mesenteric alteration may be often observed in patients with inflammatory bowel disease, mesenteric bowel injury, cirrhosis, hypoalbuminemia or heart failure. On the other hand, segmental "Misty Mesentery" may represent a characteristic feature of pathologies such as portal or mesenteric vein thrombosis, focal inflammatory conditions (appendicitis, diverticulitis, epiploic appendagitis) and localized neoplastic infiltration. The diagnosis of sclerosing mesenteritis should always be considered because this rare disorder of unknown origin may manifest as a diffuse, localized or multinodular mesenteric alteration.

Conclusions: "Misty Mesentery" can be seen in various pathological conditions, such as vascular disorders, inflammation, fibrosis and neoplastic infiltrations. MDCT plays an important role not only in the differential diagnosis, but also in the follow-up, especially for those patients without a demonstrable underlying cause.

GI Tract

Gastrointestinal

C-0079

Preoperative staging of rectal cancer using magnetic resonance imaging:

Comparison with endosonography and histopathologic findings

R. Ciosci, G. Pompili, P. Bianchi, M. Montorsi, G. Cornalba; *Milan/IT*

Purpose: The aim of our study was to examine the accuracy of preoperative MR imaging and endosonography in the staging of rectal cancer.

Methods and Materials: 43 patients with biopsy proven rectal adenocarcinoma underwent MR imaging and endosonography. A group of 28 patients underwent MR imaging with a body-coil. A second group of 15 patients underwent MR imaging with external phased array coil and 6 also with an endocoil. Endosonography was performed in 39/43 patients. The results of examinations were compared with final histology. 33 patients directly underwent surgery, and 10 received neoadjuvant therapy.

Results: In the T staging, the best results were obtained with a phased array coil (accuracy 80% in 12/15) especially when used alongside a rectal endocoil (correct T and N staging in 6/6). MR imaging with a simple body coil had an accuracy of 50% (14/28). Endosonography correctly staged rectal cancer in 74.3% of cases. In N-staging accuracy was 74% for MR imaging and 51% for endosonography. MR imaging with phased-array coil was as accurate as endosonography in the T-staging of rectal cancer and far superior in the N-staging.

Conclusions: MR imaging, especially with phased-array and endocoil, is an accurate method of staging rectal cancer and it allows both better selection and assessment of patients undergoing preoperative therapy.

C-0080

The efficacy of CT-colonography for diagnosis and staging of colon cancer in symptomatic patients

P. Zdunek¹, A. Gmur¹, M. Wykret¹, R. Pacho², P. Wandzel¹; ¹*Bielsko-Biala/PL*, ²*Warsaw/PL*

Purpose: To evaluate the clinical value of CT-colonography for the diagnosis and staging of colon cancer in symptomatic patients.

Methods and Materials: From the group of 232 patients who underwent operations because of colon cancer between June 2000 and December 2003, we chose 56 patients (24%) who had diagnostic CT-colonography either as the first examination or after incomplete colonoscopy. Patients with rectal cancers were excluded. We reviewed retrospectively the findings of preoperative colonoscopy, intraoperative organ palpation and histopathologic outcome in this group and compared them with results of CT-colonography. 61 cancers (32 sigmoid, 29 proximal colon) were removed. In 5 cases synchronous cancers were found. Metastases to the lymph nodes, liver and peritoneum were assessed. Other colon pathologies, namely polyps, diverticulosis, intussusception and inflammatory infiltration were also evaluated.

Results: 59 cancers were correctly diagnosed at CT-colonography (96%) and 56 at colonoscopy (92%). Due to obstructive carcinoma complete CT-colonography was possible in 52 (92%) and colonoscopy in 27 cases (48%). The correct diagnosis for more than 4 liver metastases was made in 7/8 (sensitivity 87.5%, specificity 97%) and for less than 4 in 6/9 cases (sensitivity 66%, specificity 89%). Lymph nodes metastases were found in 9/15 (sensitivity 60%, specificity 90%) and peritoneal dissemination in 1/2 patients. 6/15 (40%) polyps were detected. Diverticulosis was disclosed in 13, intussusception in 1 patient and inflammatory complications in 4 patients.

Conclusion: CT-colonography is an effective method for diagnosing colon cancer, evaluating the entire colon preoperatively and disclosing any distant metastases.

C-0081

Gastric MALT lymphoma: CT findings

A. Roque, M. Sarrias, S. Quiroga, C. Sebastià, H. Cuéllar, A. Álvarez-Castells; *Barcelona/ES*

Learning Objectives: To identify helical CT features that could be useful for the imaging diagnosis in gastric MALT lymphoma.

Background: Lymphoma of the gastric mucosa-associated lymphoid tissue (MALT) is a process with characteristic anatomical and pathological features. Its prognosis is favorable with prompt, appropriate treatment and thus early diagnosis is important. In this exhibit we will describe CT findings that could help in the diagnosis of this disease. CT scans were retrospectively reviewed in 14 patients (6 men, 8 women; mean age 62.9 years) with histologically proven gastric MALT

Scientific and Educational Exhibits

lymphoma. The following findings were assessed; gastric wall thickness, visualization of vessels within tumor tissue, presence and distribution of lymphadenopathy and involvement or not of other organs.

Imaging Findings: The imaging technique was contrast-enhanced helical CT scanning, using 800-1000 ml of water as negative oral contrast agent. Mean gastric wall thickness was 3.7 cm. Significant intra-abdominal lymphadenopathy was found in 11 patients (78.6%), mainly in a perigastric location. Involvement of other organs was found in 3 of our patients. Vessels were identified within the gastric tumor tissue in 10 patients (71.4%).

Conclusion: Helical CT visualization of vessels within a gastric mass was found to be highly suggestive of MALT lymphoma, a finding that has not been previously described in the literature.

C-0082

The correlation of endosonography versus peroperative and histopathological findings in a group of 350 patients with surgically treated anorectal tumor

Z. Chudáček¹, R. Sequens², M. Pechotová¹, J. Kuntscherová¹; ¹Plzen/CZ, ²Prague/CZ

Purpose: Endosonography (EUS) is a well established method in the staging of anorectal tumors, indispensable especially before the decision on radical surgery. Modern equipment for EUS providing a circular image with the possibility of an end-firing display, supplemented with a high resolution linear-array electronic transducer and doppler imaging and combined with the examiner's experience are the basic prerequisite of good results when using the method. In a retrospective study the accuracy of EUS was evaluated by comparison with peroperative and histopathological findings. The sources of errors and diagnostic constraints were reviewed.

Methods and Materials: In a group of 350 surgically treated patients the correlation between EUS, surgery and histopathology was evaluated. In cases with contemporary CT or MR finding the evaluation was extended to these methods.

Results: The overall accuracy in tumor staging was 89%. In regional lymph nodes involvement only 70% overall accuracy was achieved. EUS overall accuracy exceeded the same by CT and MR.

Conclusion: The study confirmed a high sensitivity and specificity of EUS in the staging of anorectal tumors and the acceptability for a decision before radical surgery, but not however in staging of regional lymph node involvement. The second weakest point of the method represented an occasional difficult distinction between T2 and T3 stage, probably due to peritumoral inflammation.

C-0083

Integrated sonography of Crohn's disease by combining high-resolution B-mode techniques and contrast enhanced ultrasound (CEUS) perfusion studies of the involved bowel segments

S.D. Yarmenitis, G. Kolios, N. Papanikolaou, T. Maris, E. Kouroumalis, N. Gourtsoyiannis; Iraklion/GR

Purpose: The aims of this paper are: To describe the significance of CEUS in improving the assessment of qualitative findings from B-mode studies. To present the possible application of CEUS in quantifying inflammation in the involved intestinal segments.

Methods and Materials: Thirty-five individuals with Crohn's disease (CD), (active:21, remission:9, fibrostenotic:5) were examined by a combined technique including standard B-mode scans and CEUS perfusion studies at the sites of the involved bowel loops. A control group comprised 20 healthy individuals who underwent CEUS at the terminal ileum loop. In addition to B-mode findings, contrast illustrated the presence of hyperemic, enlarged mesenteric lymph nodes and of abundant hyperemic vasa recta at the mesenteric border. Perfusion throughout the full mural thickness was further recorded. Time to contrast intensity transit curves were built. The maximum inclination of the wash-in component of the curves was calculated for each individual.

Results: The maximum inclination mean value was 16.34 sec⁻¹ for the patients with active CD. Patients with inactive CD showed a mean value of 4.7 sec⁻¹. In the control group, the mean value was 6.67 sec⁻¹. Statistically significant differences were found between the values from the active CD patients, the non-active CD patients and the control group. The non-active CD individuals, although very few at present, showed similar perfusion values with those of the control group. Only patients with active CD showed hyperemia and increased number of the vasa recta.

Conclusions: CEUS broadens sonography of the bowel CD. Initial results are promising in the quantification of Crohn's disease activity.

C-0084

MR imaging of the small intestine in paediatric patients: An overview of technical features and clinical results

P. Paolantonio, A. Laghi, M. Rengo, F. Iafrate, V. Martino, A. Guerrisi, R. Passariello; Rome/IT

Learning Objectives: To illustrate the major clinical indications for MR imaging study of the bowel in paediatric patients. To show an overview of some technical issues of MR imaging of the small bowel with emphasis on bowel distension. To outline the advantages and limitations of the technique and to illustrate clinical results based on a series of 215 paediatric patients.

Background: In this exhibit we will describe the MR imaging of the small bowel performed with a biphasic oral contrast agent with the most suitable indications, the results, the advantages and the limits of this technique in a paediatric population. 215 paediatric patients with clinical suspicion of small bowel disorders underwent MR study of the small bowel. The major clinical indication was in the work-up of children with suspected IBD. Other clinical indications are mainly the work-up of patients with Celiac disease or other causes of intestinal malabsorption. MR findings of several small bowel disorders with emphasis on Crohn's disease and Celiac disease will be presented.

Procedure Details: Small bowel distension was obtained by means of oral administration of 10 ml/kg/BW of PEG solution immediately before the examination. MR examinations were performed using T2W HASTE, True-FISP and T1W FLASH sequences acquired after iv injection of Gd-DTPA in both axial and coronal planes.

Conclusion: MR studies of the small bowel represent a feasible and valid diagnostic tool for small intestine evaluation in a paediatric population.

C-0085

Transmesenteric internal hernias: CT findings

C. Polidura Arruga, I. De la Pedraja Gomez-Ceballos, J.L. Abades Vazquez, E. Huelga Zapico, J. Jimenez del Rio; Madrid/ES

Purpose: To describe the radiological features of transmesenteric internal hernias on CT.

Patients and Methods: Retrospective review of CT scans of 8 patients with radiological diagnosis of internal hernia. The abdomino-pelvic images were obtained in a helical CT GE, collimation of 7 mm and with both oral and intravenous contrast medium. Only one of the patients had previous abdominal surgery (Billroth II).

Results: The CT criteria that are evaluated were based on prior publications. In 7 patients, CT showed a cluster of small bowel loops and central displacement of the colon. On 6 cases, the lack of omental fat between the clustered small bowel and the abdominal wall was seen. 4 CT scans showed features of bowel obstruction and 3 of them findings of bowel ischemia. Surgical confirmation was obtained in 6 patients: 3 of them had transomental internal hernia and the other 3 had pericecal transmesenteric hernia.

Conclusion: The internal hernia, and in particular the transomental subtype, is an unusual cause of small bowel obstruction. The radiological CT findings of abdominal internal hernia are: clustered small bowel loops, especially those adjacent to the abdominal wall without overlying omental fat, central displacement of the colon and bowel obstruction and/or bowel ischemia. CT scanning allows a confident preoperative diagnosis, especially in patients with suspicion of small bowel mechanical obstruction and no previous surgical procedures.

C-0086

Sonographic diagnosis of acute intestinal anisakiasis

A. Alonso, B. Viñuela, J. Simal, A. Releja, M. Nieto, M. G. Urbón, C. Niño, A. Louredo, E. Robles; Palencia/ES

Learning Objectives: To study the utility of sonography and to illustrate the spectrum of ultrasound (US) findings in the early diagnosis of intestinal anisakiasis.

Background: The imaging findings, clinical data and simplex-specific serum IgE of 28 patients with proven acute intestinal anisakiasis between January 1999 and January 2004 were retrospectively reviewed.

Imaging Findings: Anisakiosis is a parasitic infection that follows consumption of raw or insufficiently pickled, salted, smoked or cooked wild marine fish infected with Anisakis species larvae. In this exhibit, ultrasound (US) showed markedly thickened bowel loops associated with luminal narrowing, including long segment disease, swelling of Kerckring's folds and local infiltrated mesentery fat with increased Doppler signal. A small amount of ascitic fluid around the bowel loops was found. The most common site was the distal ileum and cecum. All patients underwent treatment of symptoms without laparotomy, and their symptoms disappeared by the tenth day after onset.

Conclusion: Patients with acute abdominal symptoms should be asked about

Scientific and Educational Exhibits

the intake of raw or undercooked fish. If the above US features are found, the diagnosis of intestinal anisakiasis must be seriously considered and should be treated conservatively avoiding unnecessary laparotomy.

C-0087

Intestinal transplantation: Imaging findings of posttransplantation anatomy and pathology

K.M. Unsinn, M.C. Freund, M. Rieger, B. Czermak, A. Koenigsrainer, R. Margreiter, W.R. Jaschke; Innsbruck/AT

Learning Objectives: 1. To be familiar with the different surgical techniques of intestinal transplantation in adults. 2. To illustrate the regular postoperative situs and the spectrum of expected pathology in different imaging modalities.

Background: Intestinal transplantation represents a potential alternative to long-standing parenteral nutrition in patients with irreversible, chronic intestinal failure. The following techniques of intestinal transplantation can be performed: isolated intestinal transplant, combined intestinal and liver transplantation or multivisceral transplantation.

Imaging Findings: Knowledge of the regular postoperative anatomy after intestinal transplantation is of great importance for the proper interpretation of imaging studies and early detection of postoperative pathologies. In the first part of this pictorial essay the various operation procedures of intestinal transplantation performed in adults are illustrated schematically. Examples of the regular postoperative anatomy in several imaging modalities including CT, MR imaging, gastrointestinal contrast examination and angiography will be demonstrated. Part two of this pictorial essay displays the spectrum of imaged pathology including abdominal infections (e.g. abscess, peritonitis, fistula), vascular graft complications (e.g. arterial pseudoaneurysm), intestinal graft complications (e.g. anastomotic dehiscence and strictures, intestinal motility disorder) and other transplant-associated complications (pancreatitis, hematoma, lymphocele).

Conclusions: This pictorial essay displays the spectrum of imaging findings after different techniques of intestinal transplantation utilizing different imaging modalities with regard to anatomy and pathology.

C-0088

How to perform CT colonography: A case-based tutorial

P. Lefere, S. Gryspeert; Roeselare/BE

Learning Objectives: To teach how to perform CT colonography (CTC) with a case-based tutorial allowing interactive participation of the reader.

Background: Adequate colonic preparation, distention and reading of the data sets is essential to obtain good results of lesion detection in CTC. Preparations with and without faecal tagging are demonstrated with emphasis on patient compliance and faecal residue hampering diagnosis of polyps. The importance of adequate colonic distension using dual positioning, a CO₂ injector and smooth muscle relaxants is discussed. In the reading section, the use of primary 2D or 3D reading and the importance of dual positioning are discussed. Different imaging findings of tumoral lesions and false positive findings are also demonstrated. The need for close collaboration with the gastroenterologist is stressed.

Procedure Details: The tutorial consists of 10 CTC data sets controlled with conventional colonoscopy. Each data set addresses particular issues in CTC with particular emphasis on preparation, colonic distention and reading of the data sets. The reader can actively participate by scrolling through the images. In this way he is invited to make his diagnosis of each case. Each case ends with a discussion of the technique and diagnosis and concludes with pearls summarizing the essentials to be remembered.

Conclusion: This case-based tutorial provides the reader with essential information on how to adequately perform CTC.

C-0089

Ileocecal valve appearance on CT colonography

M. Cadi, R. Chollet, O. Lucidarme, P.A. Grenier; Paris/FR

Learning Objectives: Our purpose was to describe different CT appearances of the normal and pathologic ileocecal valve on virtual colonoscopy.

Background: CT virtual colonoscopy is a promising tool to depict colonic polyps. However, pitfalls in 3D endoscopic views are numerous. Among them, prominent ileocecal valve can be misdiagnosed as tumor and its normal appearances (well known by endoscopists) must be recognized by radiologists. We will display virtual colonoscopy views, and corresponding 2D images and endoscopic findings of various normal ileocecal valves obtained in our last 60 patients, as well as examples of lymphoma and lipoma involving the valve.

Imaging Findings: At virtual colonoscopy, prominent valves are seen in most

patients. They bulge into the caecum lumen along its medial side. Three main appearances can be isolated: 1) labial, in which the mouth of the valve is set between an upper and lower fold; 2) papillary, in which the valve appears as a domelike protrusion and 3) mixed. Following terminal ileum into the caecum on 2D images is helpful to confirm the diagnosis of normal ileocecal valve. Lymphoma of the ileocecal valve may induce intussusception of the terminal ileon into caecum lumen easily recognized in virtual colonoscopy. Lipoma increases the usual bulging of the valve and is easily recognized on 2D images.

Conclusion: Being familiar with the 2D and 3D virtual colonoscopy appearances of the normal, prominent ileocecal valve may help radiologists to avoid unnecessary complementary endoscopy.

C-0090

Un-prepped MR colonography in paediatric patients with inflammatory bowel disease (IBD)

P. Paolantonio, A. Laghi, M. Celestre, F. De Angelis, A. Guerrisi, M. Rengo, R. Passariello; Rome/IT

Purpose: To assess the feasibility of MR colonography performed without colonic cleasing, by means of fecal tagging using oral administration of barium sulphate in a pediatric population with inflammatory bowel disease.

Subjects and Methods: 10 paediatric patients (mean age 13.8 yrs) with known IBD assessed at colonoscopy with biopsy were enrolled in the study. Fecal tagging was performed by the oral administration of a fixed amount of 150 ml of highly-concentrated barium sulphate at major meals starting three days before MR examination. The colon was distended by a water enema. MR imaging protocol included T2W HASTE (TR, inf; TE, 90 msec; FA, 180°) and contrast enhanced T1W 3D VIBE (TR, 5.2 msec; TE, 2.6 msec; FA, 20°) and T1W 2D turboFLASH (TR/TE/FA/TI: 8.5 msec, 4 msec, 10°, 10 msec) sequences. Contrast enhancement was obtained by i.v injection of 0.1 mmol/kg b.w. ml of Gd-chelate.

Results: Image quality was judged to be optimal in all patients. Fecal material was completely tagged in all the cases and residual luminal air did not cause any significant imaging artefact. Patient tolerance was high. All the patients showed signs of IBD, Crohn's disease in three cases and ulcerative colitis in the remaining seven cases. MR correctly defined thickening of the colon and localization and extension of the inflamed bowel wall by means of contrast enhancement following Gd-chelate injection.

Conclusions: Unprepped MR colonography by barium fecal tagging is a promising and well tolerated diagnostic method in the evaluation of colonic involvement in pediatric patients with IBD.

C-0091

The use of contrast-enhanced ultrasonography in the diagnosis and follow-up of Crohn's disease

G. Runza¹, F. Cademartiri², F. Barbiera³, G. Salvaggio¹, T.V. Bartolotta¹, S. Pardo¹, G. Caruso¹, R. Lagalla¹; ¹Palermo/IT, ²Rotterdam/NL, ³Sciaccia/IT

Learning Objectives: The aim of this exhibit is to assess the potential role of contrast-enhanced ultrasonography (CEUS) in the diagnosis and follow-up of local complications in patients with Crohn's disease.

Background: Accurate detection and assessment of intestinal complications and activity signs is important for the clinical management and treatment follow-up in Crohn's disease. Small bowel enteroclysis and multidetector CT enterography (MDCT-enterography) can be performed but they inflict a significant amount of radiation. Therefore, they cannot be repeated on a regular base. CEUS, because of its non-invasive approach, can be repeated during the treatment of patients with Crohn's disease.

Procedure Details: In this exhibit we describe the protocol that allows proper imaging of Crohn's disease with CEUS. This technique, small bowel enteroclysis, and MDCT-enterography were compared in their ability to detect various pathological findings related to Crohn's disease: Definite stenosis, wall thickening (> 5 mm) and enhancement, mesenteric proliferation, enlarged mesenteric lymph nodes, abscess, fistulae and colonic involvement. A 1500-2000 mL solution of contrast isosmolar electrolyte was obtained by dissolving 18.5 g of polyethylene glycol (Macro P, Promefarm) in each 250 mL of water. This solution was administered perorally just before CEUS and MDCT-enterography to allow the distention and the optimal visualization of the entire small bowel. CEUS was performed after intravenous administration of ultrasound contrast agent (SonoVue, Bracco).

Conclusion: The usefulness of CEUS can be considered as a valuable tool for detecting, monitoring and follow-up treatment of local complications in patients with Crohn's disease.

Scientific and Educational Exhibits

C-0092

A pictorial review of the various extracolonic findings and their clinical impact on CT colonography examination

F. Jafrate, A. Laghi, P. Paolantonio, M. Rengo, A. Guerrisi, V. Martino, V. Panebianco, R. Passariello; *Rome/IT*

Purpose: To present a pictorial review of the various extracolonic findings on CT colonography examination. To underline the prevalence and clinical impact of these findings in patients undergoing CT colonography.

Background: CT colonography (virtual colonoscopy) is a new technique being offered to patients as a non-invasive method of imaging the colon. Potentially important extracolonic findings were revealed in 24.8% of the patients, leading to additional diagnostic or therapeutic considerations. Some of these findings were clinically important, whereas others were previously known or led to unnecessary workup. This finding must be taken into account when CT colonography is considered for routine diagnostic workup or screening.

Imaging Findings: A total of 173 extracolonic findings were detected in 110 (60.1%) of 183 patients that underwent CT colonography. Of these, 43 (24.8%) were highly significant, 36 (20.8%) were moderately significant and 94 (54.33%) were of poor significance. In 72 (39.34) patients no extracolonic findings were observed. The most common highly significant lesions were mesenteric lymphadenopathy (n.18), aortic aneurism and liver metastases (n. 6), peritoneal carcinomatosis and pulmonary nodules (n. 4). 32 of these 43 (74.4%) highly significant findings were new, and in 15 (34.88%) these abnormalities resulted in further diagnostic examinations.

Conclusion: Additional work-up of extracolonic CT colonographic findings was relatively infrequent but was often worthwhile when performed for lesions classified as highly important. The evaluation of extracolonic structures at CT colonography has definite limitations with regard to solid organs but can help detect serious disease without substantially increasing the cost per patient.

C-0093

Evaluation of pararectal lymph nodes in rectal cancer with a submucous injection of SPIO at colonoscopy and imaging by MR imaging

M. Shimada, K. Yoshikawa, K. Funahashi, T. Teramoto, M. Watanabe, Y. Inoue, T. Ookubo, J. Kojima, S. Hayashi; *Tokyo/JP*

Purpose: SPIO was administered, at colonoscopy via a paracentesis needle, into the submucosa around the tumor. We compared images before contrast media with images after contrast media for signal loss in pararectal lymph nodes (LN). We examined whether it was possible to recognize micrometastases to pararectal LN.

Methods: Five patients with rectal cancer became subjects (45-78 yrs). CT was performed on these patients to diagnose the presence of pararectal LN greater than 10 mm, and it was done when there was no metastasis. In the five patients SPIO (40 micromol/ml) was injected into four submucous places (0.4 mlx4) in the neighbourhood of the tumor. MR imaging images were taken before injection and at 24 hours after injection. The imaging sequence was a Fast Field Echo sequence (TR:12 msec, TE:5.0, TI:650). Images before enhancement and images after SPIO were examined and loss of signal intensity of the pararectal LN was examined.

Results: In all five rectal cancer patients, pararectal LNs (45 lymph nodes) of 1 cm or less were able to be depicted. In 3 of 5 patients, pararectal LN without deposition of SPIO were recognized. These LNs were diagnosed as metastatic LNs in the pathology. In short, it was diagnosed with the metastatic LN in the pathology without the deposition in LN of 12 of 45 LNs. In SPIO MR imaging, we were able to detect 9 metastatic LNs without deposits of 12 metastatic LNs which were diagnosed as metastatic LNs in pathologic studies. In short, the proper diagnosis rate was 75%.

Conclusions: SPIO injection into the submucosa under colonoscopy improves the diagnosis of metastatic pararectal LN.

C-0094

Alternative diagnoses of acute appendicitis on helical CT with IV and rectal contrast

A.R. Karam, M.J. Mehanna, G.A. Birjawi, G.E. Ishak, C.A. Sidani, M.C. Haddad; *Beirut/LB*

Learning Objectives: To illustrate the wide spectrum of diseases presenting as acute right lower quadrant pain and simulating acute appendicitis.

Background: Acute appendicitis is a frequently encountered disease in the young population presenting to an emergency room. Many entities can also present as febrile right lower quadrant pain and hence mimick acute appendicitis. These

require different and usually conservative treatment, thus rendering their recognition mandatory. In this exhibit we illustrate and describe the imaging findings of those diseases. Between December 2000 and March 2003, 75 patients were imaged with contrast enhanced CT scan for subclinical acute appendicitis. 24 had a normal appendix and an alternative diagnosis. We are reviewing the imaging pattern of these appendiceal mimickers.

Procedure Details: From December 2000 to March 2003, 75 consecutive patients presenting to the Emergency Unit with suspected appendicitis. Helical CT (Philips AV, Netherlands) was performed using 5 mm collimation at the level of the pelvis starting just above the iliac bone and 10 mm collimation at the level of the abdomen following administration of rectal and IV contrast.

Conclusion: The aim of this exhibit is to display the imaging findings of the alternative diagnosis of acute appendicitis identified in approximately 32% of patients investigated by CECT for clinical suspicion of atypical appendicitis.

C-0095

Intraoperative tumor localization using laparoscopic ultrasound for laparoscopic assisted tumor resection

J. Lim, M.-J. Kim, W. Hyung, K. Kim; *Seoul/KR*

Purpose: During the laparoscopic resection of tumor arising from stomach or small bowel, exact tumor localization is critical in laparoscopic surgery, especially when it is small or growing intraluminally. It is impossible to identify early gastric cancer (EGC) and small intraluminal submucosal or mucosal tumors arising from stomach or small bowel by laparoscopy only. The purpose of this study was to report our experience in 20 patients with intraoperative LUS for tumor localization.

Materials and Methods: Indications included EGC (n = 17), benign gastric submucosal tumor (n = 2) and benign small bowel tumor (n = 1, proximal ileum). In cases of EGCS, three endoscopic clips were placed just proximal to the tumor for sonographic detection during preoperative endoscopy. Clipping was not done in cases of gastric submucosal tumor and small bowel tumor. A laparoscopic ultrasound probe was inserted into the abdominal cavity via 12 mm port. The LUS examinations were performed at the the presumed site by intra-operative imaging evaluation for tumor localization.

Results: In all EGC patients, endoscopic clips were successfully detected in all 17 patients by the LUS. In all cases of gastric submucosal tumor and small bowel tumor, the masses themselves were detected by the LUS and the locations of lesions were marked with dye at the serosal surface of the lesions. In the resected specimens, the serosal surfaces marked with dye were always just above the clips or masses themselves.

Conclusions: Intraoperative LUS was an effective method for tumor localization for laparoscopic assisted tumor resection.

C-0096

Utility of multi-detector row CT angiography in cases of gastrointestinal hemorrhage

P.S. Goh, S.K. Venkatesh, A. Shabbir, L.K.A. Tan, S.C. Wang; *Singapore/SG*

Purpose: To describe the utility of multi-detector row CT angiography (CTA) in patients with gastrointestinal hemorrhage and incomplete/failed or non-diagnostic endoscopy.

Materials and Methods: Twelve consecutive patients presenting with acute gastrointestinal bleeding with incomplete, failed or non-diagnostic endoscopy were referred for CTA. CTA was performed on a 4-channel multi-detector row CT with 120 kV, 120 mAs, 1 mm collimation, pitch 1.5, rotation time 0.5 s with intravenous administration of 100 mls Omnipaque 350 at 3 ml/s. Bolus tracking triggered the scans. Maximum intensity projection images were processed on the Siemens Wizard console. The patients subsequently had repeat endoscopy or surgery and the site of bleeding was confirmed.

Results: CTA demonstrated the site of bleeding in all patients and localized the bleeding to the colon in 9 patients and small bowel in 3 patients. CTA suggested a cause in 4 patients: 3 patients with bleeding colonic diverticula and in one patient with bleeding from recurrent small bowel lymphoma. Ten patients underwent surgery (hemicolectomy 8, resection of Dieulafoy's lesion 1 and 1 patient had underrunning of a duodenal ulcer). Two patients stopped bleeding spontaneously after repeat endoscopy. Final pathological diagnosis was diverticular disease (6), angiodysplasia (1) iatrogenic colonic perforation (1), tubular adenoma (1), rectal ulcer (1), Dieulafoy's lesion (1), duodenal ulcer (1) and recurrent small bowel lymphoma (1).

Conclusions: Multi-detector row CT angiography is a useful, sensitive and accurate technique for evaluating patients with acute gastrointestinal bleeding. Demonstration of bleeding is possible with a non-invasive technique and precise demonstration of bleeding point may spare patients from extensive exploratory laparotomy.

Scientific and Educational Exhibits

C-0097

Imaging of duodenal disorders in children and adulthood

A. Bravo, M. Lamas, T. Berrocal, M. Allona, J. Larrauri, N. Gómez León; Madrid/ES

Learning Objectives: To understand the embryology, pathology, and imaging features of a wide spectrum of congenital and acquired alterations involving the duodenum in children and adults. To evaluate the efficacy of plain radiographs, barium studies, ultrasound, CT and MR imaging in the diagnosis and management of these conditions.

Background: We reviewed the imaging findings of patients with disorders involving the duodenum from our database of gastrointestinal pathology. Plain radiographs and barium studies were performed in all patients while ultrasound, CT or MR were performed in all tumours and whenever barium studies were not conclusive. The key findings at each imaging modality are shown and compared with the underlying pathologic features when available. Pitfalls, diagnostic difficulties and differential diagnoses are emphasised.

Imaging Findings: Specific topics addressed include congenital anomalies (duodenal atresia and stenosis, duodenal diaphragm or web, annular pancreas, duodenal duplication and diverticula), inflammatory diseases (Crohn's disease, tuberculosis, actinomycosis, eosinophilic granuloma, AIDS, Whipple's disease, radiation duodenitis), non inflammatory diseases (sarcoidosis, systemic sclerosis, celiac disease, hemophilia, Henoch-Schönlein purpura), diffuse infiltrative diseases (amyloidosis, eosinophilic enteritis, intestinal lymphangiectasia, lymphoid hyperplasia), duodenal ulcers, benign tumors (adenomatous polyp, lipoma, leiomyoma, angioma, lymphangioma, neurogenic tumors, Peutz-Jeghers syndrome), malignant tumors (villous adenoma, adenocarcinoma, leiomyosarcoma, lymphoma, carcinoid tumor, Kaposi's sarcoma, metastasis), duodenal trauma and postsurgical complications.

Conclusion: Evaluation of patients with duodenal disorders frequently requires multiple imaging modalities for diagnosis and planning treatment. Because many of these disorders have characteristic imaging appearances, this exhibit will help the practising radiologist to better understand and recognise pathologic processes affecting the duodenum.

C-0098

Histopathologic concordance of MR imaging findings in the local staging of rectal cancer: Is IV contrast administration needed?

P. Ramos Lopez, L. García del Salto, E. Domínguez Franjo, B. Ramos Moreno, A. Santana Acosta, E. Fraile Moreno; Alcalá de Henares/ES

Purpose: The preoperative assessment of the local staging of colorectal cancer is essential for the planning of optimal therapy. MR imaging has proved to be a reliable method for local staging of rectal carcinoma. The purpose of this study is to describe the MR imaging technique and protocol used in our hospital, to compare the imaging findings with histopathological results and to evaluate the usefulness of gadolinium-enhanced scanning.

Methods and Materials: From May-2003 to September 2004, twenty-five patients with colonoscopic biopsy-proven rectal cancer were preoperatively evaluated using 1.5 T MR imaging scanner with a phased-array coil. The protocol consists of T1 and T2-weighted turbo spin-echo and gadolinium-enhanced T1-weighted images with oriented in the three tumoral axis. Three radiologists, blinded to surgical result, evaluated the four most accurate signs described of local spread: depth of tumor growth in the colonic wall (T stage), circumferential resection margin (CRM), surrounding pelvic structures invasion and the nodal metastasis stage. The MR imaging findings were correlated with histological findings.

Results: The kappa values for depth of tumor growth in the colonic wall, circumferential resection margin, surrounding pelvic structures invasion and nodal metastasis stage were over 0.4. Contrast did not increase the kappa value in any of the categories.

Conclusion: We found excellent concordance between the MR imaging and histological findings. MR imaging showed to be an excellent method for local staging of rectal carcinoma. MR imaging without contrast administration is a reliable method to evaluate the local stage of rectal cancer, with both cost and time saved when compared with contrast-enhanced studies.

C-0099

Helical CT in the evaluation of acute bowel ischemia: Common findings, uncommon findings and pitfalls

S. García-Asensio, R. Cozcolluela, H. Gómez, L. Sarría, M. Martínez-Berganza, A. Forradellas, I. Alberdi, F. Monzón; Tudela/ES

Purpose: To illustrate the spectrum of imaging findings of various types of acute bowel ischemia, and potential pitfalls in interpretation of helical CT images.

Methods and Material: The imaging finding of patients with acute bowel ischemia demonstrated at surgery were reviewed from our database (1996-2004). Cases that mimic this entity at CT were also reviewed. These patients underwent evaluation with contrast enhanced spiral CT. In some cases reformatting images were obtained.

Results: The most frequent signs on CT in this study were: Bowel wall thickening, dilatation of small bowel loops, free intraperitoneal fluid, mesenteric arterial occlusion/stenosis, mesenteric or portal vein thrombosis, mesenteric edema, intramural bowel gas, infarction of other abdominal organs, gas filled portal or mesenteric veins, inhomogeneous enhancement of bowel wall, target sign, lack of bowel lack enhancement, thin bowel wall and hazy mesentery. The most common pitfalls in interpretation of images were: Pneumatosis, small intramural gas bubbles and pseudothickening of bowel wall. Other entities that can mimic acute bowel ischemia at CT were: infections and inflammatory bowel disease, bowel obstruction and intrabdominal sepsis. Correlation between CT results and pathological findings was shown.

Conclusion: This exhibit provides an overview of the spectrum of findings on CT in acute bowel ischemia. This entity is a high mortality pathology but usually presents with clinically non-specific manifestations. The knowledge of different CT findings and the conditions that can be misinterpreted for it produce an improvement in diagnostic suspicion and may even be helpful in determining the primary cause.

C-0100

Preoperative spiral CT in staging of colonic cancer

L. Sarría, R. Cozcolluela, S. García, H. Gómez, T. Martínez-Berganza, A. Forradellas, I. Alberdi, F. Monzón; Tudela/ES

Purpose: To evaluate the accuracy of helical computed tomography for preoperative T and N staging of colonic cancer.

Materials and Methods: Fifty-five patients with colonic carcinoma previously diagnosed by colonoscopy underwent preoperative helical CT. CT was performed with oral and intravenous contrast. Images were obtained in the portal venous phase (start delay of 70 seconds). Tumor invasion of colonic wall and local spread (T), and regional lymph node involvement (N) on transverse CT were evaluated in this study. CT findings were compared with pathologic findings. Patients with rectal carcinoma were excluded from this study because preoperative adjuvant radiation therapy could modify the histopathological findings. Patients diagnosed in the emergency room were also excluded. Sensitivity, specificity, accuracy, PPV and NPV values were assessed.

Results: Colonic wall thickening was shown in 4 of 6 T2 patients (60%), 39 of 41 T3 patients (95%) and 3 of T4 patients; a patient with gross vegetant T1 tumor was also shown by CT. In 50 patients without local complications stranding of pericolic fat was shown by CT in 8 of 10 patients with local tumor extension and all of 17 patients with inflammatory spread (Sensitivity 80%, specificity 49%, PPV 26%, NPV 92% and accuracy 54.5%). CT detected lymphadenopathy in 7 of 18 patients with regional nodal metastasis and in 6 of 37 patients without evidence of invasion (Sensitivity 39%, specificity 84%, PPV 54%, NPV 74%, accuracy 69.1%).

Conclusion: Helical CT is not an effective method in determination of T and N staging of colonic cancer.

C-0101

Small bowel traumatic injuries: A pictorial essay

M. Osorio, A. Maroto, G. Laguillo, J.I. Rodríguez, P. Ortuño, J. Pont; Girona/ES

Learning Objectives: To illustrate the different CT radiological signs of small bowel traumatic injuries. To underline the need of a careful search for these subtle CT signs in order to influence their surgical or conservative management.

Background: Injuries of the gastrointestinal tract are prevalent lesions in patients with blunt abdominal trauma. They are present in 3-7% of patients in different series. Bowel injuries are challenging to diagnose on CT. The knowledge of the spectrum of radiological presentation may allow a rapid detection of these serious lesions.

Procedure Details: Clinical reports of 165 poly-trauma patients admitted to our hospital during 2003 were retrieved. 25 of the 165 patients (15%) were diagnosed with bowel injuries. Abdominal CT scans of these patients were retrospectively reviewed. The most relevant CT signs associated with bowel injury are shown: Extravasation of vascular contrast agent, presence of free air, clot sign with or without associated bowel wall thickening and streaky mesenteric infiltration. Absence of pneumoperitoneum, or clot sign as the only finding and a small amount of free fluid were the radiological findings which permitted conservative management in a clinical setting of hemodynamic stability.

Scientific and Educational Exhibits

Conclusion: Bowel injury is frequent in abdominal blunt trauma and radiologists must be aware of this potentially life-threatening condition. A combination of clinical parameters and CT radiological findings are the clue to conservative management of these lesions.

C-0102

Imaging small bowel ischaemia: The role of multidetector CT

K. Burney¹, S.P. Prabhu¹, I. Lyburn², R. Hopkins²; ¹Bristol/UK, ²Cheltenham/UK

Learning Objectives: 1. Review pathogenesis and causes of acute small bowel ischemia. 2. To demonstrate the often subtle radiological signs of acute small bowel ischaemia. 3. To demonstrate contribution of CT in the diagnosis of this complex disease.

Background: Acute mesenteric ischaemia is caused by arterial, venous occlusion or mesenteric hypoperfusion. The patient can present with various clinical and radiologic manifestations, and the causative pathology can range from localised transient ischaemia to necrosis of the intestine. The underlying causes include thromboembolism (50% of cases), bowel obstruction, neoplasms, vasculitis, inflammatory conditions, trauma, chemotherapy, radiation, and corrosive injury. It has a high mortality rate between 70-90% and clinical diagnosis can be difficult due to non-specific nature of signs and symptoms.

Procedure Details: We reviewed the imaging of patients with surgically proven small bowel ischaemia treated at our hospital over the last 5 years and present a review of pathologies seen on radiological investigations. Multi-detector CT is being increasingly used in the evaluation of such patients with equivocal clinical signs. Apart from enabling direct visualisation of cause of ischaemia such as arterial or venous obstruction, CT can demonstrate changes resulting from ischaemic bowel and demonstrate important coexistent findings or complications. Secondary signs like portal venous gas, bowel wall thickening, and pneumatosis can help confirm the diagnosis.

Conclusion: Diagnosis of acute small bowel ischaemia is facilitated by radiological examination like MDCT, but often a combination of clinical, laboratory and radiologic signs that may lead to a correct diagnosis.

C-0103

MR imaging of the effects of neo-adjuvant radiotherapy on rectal carcinoma

J.L. Hughes, M. Alijani, J. Chin-Aleong, S. Babar, A. Rockall, R. Reznek; London/UK

Purpose: Neo-adjuvant radiotherapy reduces local recurrence in rectal cancer patients. MR imaging has been used after neo-adjuvant therapy to stage the tumour and aid surgical planning. We aimed to document the effect of radiotherapy on rectal carcinoma using MR imaging.

Methods and Materials: MR imaging was performed before and after neo-adjuvant therapy in 13 patients. Nine patients had short course radiotherapy and 4 had long course chemoradiotherapy. Axial and sagittal T2W images were supplemented with high-resolution oblique T2W images axial to the tumour. We assessed radiological stage and maximum tumour thickness, before and after neo-adjuvant therapy. MR imaging of the rectal tumour specimen was used to help correlate the tumour appearance with histology, the reference standard.

Results: Eleven patients were radiological stage T3 and 2 were stage T4 prior to neo-adjuvant therapy. The T stage accuracy was 85%. Two patients were overstaged from T3 to T4 and none was understaged. Overall there was a 17% reduction in tumour thickness (cm) post neo-adjuvant therapy, which was statistically significant ($p < 0.01$). Following short course radiotherapy, 2 tumours were downstaged, one from stage T3 to T2 and the other from stage T3 to T1.

Conclusion: We have shown that both neo-adjuvant chemoradiotherapy and short course radiotherapy result in a significant reduction in the size of rectal tumours prior to surgery. Short course radiotherapy resulted in downstaging of tumour in two patients, one of whom would have benefited from local excision surgery alone.

C-0104

Virtual colonoscopy: The way our department is beginning the change from barium enemas to virtual colonoscopy

M.J.F. Tapp, J.R. Ferrando; Birmingham/UK

Learning Objectives: To start using new techniques in the radiology department there needs to be a reason to change, as well as the commitment of team members to maintain the momentum of change. Having advance knowledge of why and how the introduction of virtual colonoscopy should be undertaken can help make the process go more smoothly.

Background: Although barium enemas have been performed for many years to image the large bowel, virtual colonoscopy is now starting to replace it. Not only

can the large bowel be well demonstrated, but the CT scan also has the added benefit of allowing imaging of the rest of the abdomen. As with all new techniques, there is a gradual process that takes place during its introduction.

Procedure Findings: We explain how we have initiated virtual colonoscopy into the daily routine of our radiology department. Certain techniques, such as performing both prone and supine scans help improve the diagnostic quality of the scan, whereas proper patient selection helps to keep the number of scans down. Although there are many benefits from changing from barium enemas to virtual colonoscopy, it is likely that both will be performed for the foreseeable future.

Conclusion: A well planned introduction of virtual colonoscopy into the department will help maintain good working relations with the clinicians, whilst both improving the service to patients and keeping workloads within achievable levels.

C-0105

Appendiceal CT: A prospective randomized controlled study comparing three different protocols

D. Fischer, N. Awad, D. Hershko, L. Goralnik, M. Krausz, A. Angel; Haifa/IL

Purpose: The important role of CT in the diagnosis of suspected acute appendicitis has recently been validated. Numerous CT protocols using different combinations of oral, rectal and intravenous contrast agents and studies without contrast materials are all commonly used in the diagnostic workup for this clinical presentation, yet the protocol of choice has not yet been determined. Here, we prospectively compare the diagnostic accuracy of three different CT protocols for the diagnosis of suspected acute appendicitis.

Methods and Materials: 222 consecutive patients with suspected acute appendicitis were randomly assigned to one of three focused CT protocols. In group A, non-contrast CT was performed; in group B, contrast material was administered rectally (PR); in group C, contrast material was administered both orally and intravenously (PO/IV).

Results: 104 patients had acute appendicitis. High accuracy rates were observed for both the PR and the PO/IV studies (94%). The accuracy rate of the non-contrast studies group was 70%, significantly lower than the other groups ($p < 0.01$).

Conclusions: High and similar accuracy rates were observed by PR and PO/IV contrast protocols. PR contrast examinations are quicker to perform than PO/IV and can lead to a prompt diagnosis. Non-contrast studies require a high level of expertise to evaluate. Therefore, we suggest that the PR contrast protocol may be the preferred initial CT examination in the diagnostic work-up of suspected appendicitis.

C-0106

Acute colonic disorders: CT findings

A. Buzzi, M. Figueiroa, V. Alarcon, F. Arredondo, M. Hjelt, A. Mancini; Buenos Aires/AR

Learning Objectives: To illustrate the spectrum of CT findings in acute pathologies of the colon. To understand the radiological findings on the basis of pathologic correlation. To demonstrate the efficacy of CT in the management of these diseases.

Background: Acute colonic disorders are represented by a large variety of entities such as inflammatory disease, intestinal obstruction, colonic ischemia, perforation and colorectal carcinoma complications. CT has the ability to show accurately the bowel wall, the pericolic soft tissues and the neighboring structures, being a very sensitive method for detection of mural penetration and extraluminal extension of the colonic disease.

Imaging Findings: The cardinal findings are mural thickening, surrounding mesenteric densities and fluid collections. A dilated and thickened appendix is suggestive of appendicitis; a fatty pericolic lesion with surrounding mesenteric inflammation is diagnostic of epiploic appendagitis; the presence of diverticula suggest diverticulitis; cecal distention with circumferential wall thickening suggests typhlitis; circumferential, symmetric wall thickening with fold enlargement suggests ischemic colitis and the "bowel-within-bowel" appearance is pathognomonic of intussusception. In infectious colitis the site and thickness of colon affected may suggest a specific organism. Crohn's disease and ulcerative colitis may be distinguished by the location of the involved segment and the extent and appearance of the wall thickening. CT may predict mechanical obstruction, determine the etiology and location and detect signs of complications related to strangulation. In radiation colitis, the clinical history is the key to suggesting the diagnosis.

Conclusion: CT is valuable for detection and characterization of acute conditions of the colon.

Scientific and Educational Exhibits

C-0107

The role of virtual colonoscopy in the evaluation of inflammatory disease

P.M. Carrascosa, C. Capuñay, R. Castiglioni, M. Ulla, J. Carrascosa; Buenos Aires/AR

Learning Objectives: To be familiar with the virtual endoscopic technique. To identify the typical findings of these diseases by virtual colonoscopy. To outline the best indications and results of the method.

Background: Virtual colonoscopy is used worldwide for the evaluation of the colon in the detection of elevated lesions. There is no experience in the study of inflammatory diseases. The improvement of CT technology gives the opportunity to scan the colon using thin collimation, up to 0.8 mm, and fine changes of the colon wall in early stages of the diseases can be diagnosed. The technique, indications and contraindications of the method are described. From the patients evaluated, 12 had ulcerative colitis (UC) and 8 Crohn's disease (CD). In UC, the findings were: Ulceration, pseudopolyps, a coarse granular appearance of the wall with haustral blunting and increase of the presacral space. In CD, the findings were: Thickening of the mucosal wall greater than 5 mm, filiform polyps and marked mesenteric thickening.

Procedure Details: CT studies were performed with a 16 row scanner using slices of 0.8 mm thickness. Patients performed a standard colonic cleansing the day before the exam. Conventional colonoscopy was carried out during the same day, with an E-P Fujimon colonoscope and the images were saved in a digital format. Findings of the two modalities were compared.

Conclusion: with 16-row CT scanners, virtual colonoscopy can detect early as well as advanced changes in both diseases and it can be considered as a potential modality to evaluate these patients in a non-invasive way.

C-0108

MSCT imaging of patients treated with surgery and/or Imatinib Mesylate therapy for gastrointestinal stromal tumors (GIST)

M. Lusic, R. Stern Padovan, D. Vrbanec, M. Kralik, K. Potocki; Zagreb/HR

Learning Objectives: To evaluate changes in MSCT presentation of GIST after surgery and/or Imatinib Mesylate treatment and to recognise response to therapy in patients treated with imatinib mesylate.

Background: GISTS are non-epithelial tumors which mostly occur in the stomach and small intestine. Because of tyrosine-kinase expression they could be treated with a KIT tyrosine-kinase inhibitor drug (Imatinib). We evaluated the imaging findings on MSCT in twenty patients treated with surgery and/or Imatinib in a two-year period. Morphology, size, number and sites of primary lesions and metastases were assessed on subsequent MSCT examinations.

Imaging Findings: GIST was found in the stomach and small intestine with metastatic disease in liver, peritoneum, mesentery, retroperitoneum, kidney, subcutis and subpleural regions. Reduction of tumor mass and cystic and necrotic transformation of metastases indicate good response to therapy. In resistant disease there was increase in tumor mass; metastases tended to increase in size and density, and new secondary lesions were found, especially in regions which were under surgical treatment.

Conclusion: MSCT imaging is the major diagnostic tool for diagnosis and follow-up studies of surgically treated, and recurrent and metastatic GIST patients treated with Imatinib Mesylate. Imaging findings correlate with the course of the disease and are used for planning further therapy. It is important to know the expected morphological changes on MSCT images for evaluation of response to therapy in patients treated with Imatinib Mesylate.

C-0109

Magnetic resonance imaging assessing the three-dimensional biomechanical properties of the human rectum

J.B. Frøkjær, D. Liao, A. Bergmann, B.P. McMahon, E. Steffensen, A.M. Drewes, H. Gregersen; Aalborg/DK

Purpose: In many gastrointestinal disorders the mechanisms behind the symptoms are poorly understood. A method to evaluate the three-dimensional (3-D) geometry of the human gastrointestinal wall may be valuable for understanding tissue biomechanics, mechano-sensation and function.

Methods: A special-designed bag inserted into the rectum was stepwise distended while magnetic resonance images, bag pressure and the sensory perception were recorded. Images from three healthy volunteers were analysed. The inner and outer edges of the rectal wall were identified semi-automatically. 3-D models of curvatures, radii, tension and stress were generated and the circumferential and longitudinal strains were calculated.

Results: The calculated bag volume based on the 3-D model corresponded to

the infused volume. During bag filling, a bag elongation and decrease in wall thickness was observed. The spatial distributions of the biomechanical parameters were distinctly different in individuals and non-homogeneous throughout the rectal wall due to its complex geometry. The average 3-D tension and stress increased as function of infused volume and circumferential strain. The sensory perception increased as function of infused volume, pressure, tension, stress and strain. The average tension based on 3-D models corresponded to the estimated tension based on the assumption of a spherical bag configuration.

Conclusion: The present study provides a method for characterizing the complex in-vivo 3-D geometry of the human rectum obtained from a clinical imaging modality. The non-homogenous spatial curvature distribution suggests that simple estimates of tension based on pressure and volume do not reflect the true 3-D biomechanical and mechano-sensory properties of the rectum.

C-0110

Magnetic resonance imaging of the small bowel in inflammatory bowel disease

J.B. Frøkjær, E. Larsen, E. Steffensen, A.H. Nielsen, A.M. Drewes; Aalborg/DK

Purpose: Magnetic resonance imaging (MRI) of small bowel disease has several advantages. The aims were to optimise the MRI examination technique and to evaluate the capabilities of MRI compared to conventional enteroclysis (CE).

Methods: MRI and CE were performed in 36 patients with suspected Crohn's disease. Based on 26 pilot studies optimal oral administration of plum juice and bulk fibre laxative was found. T2-weighted and gadolinium enhanced T1-weighted images were obtained using breath-hold technique and butylscopolamine. Virtual endoscopy was performed. Duodenal intubation with administration of barium and air was used for CE. Two radiologists evaluated the examination pathology and quality independently. Finally, each patient scored the degree of discomfort and the preference to either MRI or CE was found.

Results: The MRI technique ensured sufficient distension of the small bowel. MRI revealed small bowel pathology in 12 patients. In three patients it was not seen on CE. The CE revealed no pathology which was not seen on MRI. Pathological abdominal changes were revealed in 70% more patients during MRI than CE ($P < 0.001$). Endoscopic examination corresponded to the MRI findings. The examination quality decreased with increasing age ($P = 0.002$). The inter-observer agreement of the pathological changes was high ($P < 0.001$). Virtual endoscopy resulted in excellent demonstration of the mucosal surface. The examination discomfort scores obtained during the MRI were lower than during CE ($P < 0.001$).

Conclusions: MRI with the current technique is preferable to CE because of excellent demonstration of the entire small bowel pathology, low patient discomfort and absence of radiation exposure.

C-0111

Imaging findings of small bowel tumors on MR imaging enteroctysis

A.A. Alhajeri, D.A. McKenna, J. Murphy, C. Roche; Galway/IE

Learning Objectives: The aim of the study is to present the findings of small bowel tumors in MR imaging enteroclysis.

Background: Primary tumors of the small bowel are rare, making up only 3% of all GI tumors, and often have a nonspecific clinical presentation. Consequently, preoperative diagnosis remains the exception rather than the rule. With the advent of rapid MR imaging sequences, there has been increasing interest in the use of MR imaging for small bowel evaluation. This has been attributed to its inherent advantages such as the lack of radiation exposure, excellent soft tissue contrast and direct multiplanar capabilities.

Procedure Details: Fifty five patients underwent MR imaging enteroclysis over the past 24 months for variable clinical inductions. Patients received a positive oral contrast (Klean prep, Norgine, Middlesex) and were then imaged by MR imaging using breath hold protocol (T1-weighted fast low-angle shot and T2-weighted turbo spin echo). Within this group, 6 patients had small bowel tumors identified which included lymphoma, plasmacytoma and carcinoid. Furthermore, MR imaging allowed the identification of extraluminal complications such as perforation.

Conclusion: In this poster we demonstrate the imaging findings of a range of tumors of the small bowel on MR imaging.

Scientific and Educational Exhibits

C-0112

Assessment of patients with acute mesenteric ischemia (AMI):

Multidetector CT (MDCT) signs and clinical performance in a group of patients with surgical correlation

F. Zandriño, E. La Paglia, L. Benzi, F. Musante; Alessandria/IT

Purpose: To describe signs and clinical performance of MDCT in patients with AMI.
Methods and Materials: MDCT examinations of 26 patients with surgically proved AMI were retrospectively evaluated. Moreover, MDCT studies of 34 patients with a preoperative clinical diagnosis of acute abdomen and a surgical diagnosis excluding AMI were assessed. All MDCT studies were performed with arterial and portal venous phase scans, 2.5 slice thickness and 1.25 image interval, maximum intensity projection and multiplanar reconstructions. All MDCT studies were reviewed by two abdominal radiologists by consensus. In all patients signs suggesting AMI were recorded. Patients with thrombosis of the mesenteric artery or vein or pneumatosis or venous gas or bowel wall thickening associated with lack of bowel wall enhancement or venous thrombosis or parenchymal ischemic lesions were considered to be affected by AMI.

Results: AMI was due to arterial thrombosis in 19 patients and venous in 7. In 65% of patients arterial thrombosis was visualized, in 19% venous thrombosis; vascular gas was seen in 27% and pneumatosis in 38%; bowel wall thickening associated with other signs was found in 45%. Sensitivity was 96% (1 false negative) while specificity was 100%.

Conclusion: Thanks to its high temporal and spatial resolution MDCT allows an accurate assessment of the mesenteric circulation and of the bowel wall. This makes possible optimal visualization of signs of AMI resulting in a very good clinical performance.

C-0113

Spectrum of findings of celiac disease at MR imaging of the small bowel

P. Paolantonio, A. Laghi, M. Rengo, V. Martino, M. Di Martino, E. Tomei, R. Passariello; Rome/IT

Purpose: The aim of our study was to asses the intestinal findings at MR imaging of the small bowel perfomed using polyethylenglycol solution as oral contrast agent (PEG-MRI) in a population of patients with known celiac disease.

Materials and Methods: Twenty nine patients, 19 adults and 10 children, with known celiac disease underwent MR study of the small bowel. After an overnight fast, immediately before MR examination a fixed amount of 10 ml/kg of body weight of PEG solution was orally administered. MR study protocol included HASTE (TR/TE/acq.t.: inf/90 ms/18 s) and True-FISP (TR = 4.8 ms; TE = 2.3 ms; Flip Angle 50°) sequences obtained sequentially on axial and coronal planes.

Results: Image analysis showed alterations of mucosal pattern of ileal loops with an increased number of folds (5 or more folds per inch) ("ileal jejunalization") in 18 patients; reversal jejunum-ileal fold pattern in 6 patients; intestinal intussusception was observed in two patients and hypersplenism in one patient. MR was also able to identify mesenteric lymphadenopathy. No alteration of the small bowel loops was observed in five patients.

Conclusions: PEG-MR imaging is a feasible and reproducible imaging technique in both adult and paediatric populations. It may suggest a diagnosis of celiac disease as well as being able to identify potential intestinal complications together with extra-intestinal findings.

C-0114

Spectrum of findings of intestinal non-neoplastic disorders at MR imaging of the small bowel

P. Paolantonio, A. Laghi, R. Passariello; Rome/IT

Learning Objectives: To describe the findings of several intestinal disorders at MR imaging of the small bowel.

Background: Moving from the conventional barium studies of the small bowel to MR of the small bowel, radiologists are called to shift their attention from the evaluation of mucosal abnormalities and indirect signs of visceral wall pathology to the direct visualization of the small bowel wall. Using MR of the small bowel the major findings are represented by changes of small bowel thickness or in the enhancement pattern of the intestinal wall. Nevertheless, some evaluation of the intestinal mucosal layer is also possible using MR imaging. We show the typical MR findings of Crohn's disease and Coeliac disease and also several findings of intestinal infections like giardia intestinalis, taenia solium and tuberculosis. Some cases of congenital abnormalities like intestinal malrotation and small bowel involvement during vasculitis are also described.

Procedure Details: In the past 4 years we analized over 200 patients, from both the pediatric and adult populations, referred for intestinal disorders. All the MR

examination were performed acquiring HASTE and True-FISP sequence and Gd-DTPA-enhanced-FLASH T1W sequence after intestinal distension was obtained by means of oral administration of a fixed amount of 10 ml/kg of body weight of PEG solution 20 minutes before the MR examination.

Conclusions: PEG-MR imaging is a valid diagnostic tool in the identification of several intestinal findings and may help in the diagnostic process of several intestinal disorders.

C-0115

Advanced gastrointestinal stromal tumors (GIST) treated with Imatinib Mesilate: CT and MR tumor response assessment

A. Messina, C. Spreafico, P. Casali, D. Vergnaghi, F. Bianchi, A. Gronchi, R. Musumeci; Milan/IT

Purpose: To evaluate CT and MR patterns of tumor response to Imatinib Mesilate in advanced GIST.

Methods and Materials: 84 patients with abdominal advanced GIST, undergoing therapy with Imatinib Mesylate, were retrospectively reviewed. Liver lesions were detected in 69% of cases and peritoneal involvement in 59% of cases. CT (54 pts) and MR (30 pts) examinations were performed at baseline and than at 2, 4, 6, 8, 10 and 12 months during treatment.

Results: 84% of patients were judged to be responsive to therapy after 12 months. CT and MR patterns in responsive patients were: A) Tumor decrease in size (with an increase in tumor volume in 8% of cases at the first 2 months due to necrosis or bleeding), B) Hypovascularization of the lesions (due to the presence of degenerative tissue or necrosis), C) Presence of peritoneal fluid at the first month, reabsorbed in the following months and D) Hypointensity of the lesions on MR T1W images, hyperintensity of the lesions on MR T2W images and hypodensity on CE-CT images (correlating with presence of degenerative tissue or necrosis).

Conclusion: CT and MR are adequate to identify tumor response to Imatinib Mesylate in advanced GIST from the early months of therapy. Decrease in tumor size and increase in necrosis are held as early indicators of response. Nevertheless tumor volume should not be held as the only indicator of activity and in particular, volume increase should not be held as evidence of progression when associated with an increase in necrosis.

C-0116

Multiphase fusion technique of three-dimensional images using 16 MDCT for the preoperative simulation and intraoperative navigation of laparoscopic gastrectomy and colectomy

M. Matsuki, M. Tanikake, H. Kani, I. Narabayashi; Takatsuki/JP

Purpose: Recently, laparoscopic surgery has been attracting attention for its capability of improving the patient's QOL. However, this technique has the disadvantage that much time is required to deal with the arteries and veins, the pattern of which varies between patients, and the vessels are sometimes injured during dissection of lymph nodes along the arteries. We considered that the simultaneous assessment of arteries and veins by 3D CT angiography is helpful for the safe ligation of the vessels and dissection of lymph nodes. In this study, we evaluated the usefulness of the multiphase fusion technique for 3D images obtained using 16 MDCT for preoperative simulation and intraoperative navigation of laparoscopic surgery.

Methods and Materials: We performed contrast-enhanced examination at arterial and venous phase using 16 MDCT in twenty-five patients with gastric cancer and fifty patients with colorectal cancer. The slice data obtained from each phase were transferred to a work station, in which the data were individually converted into a 3D imaging format using the volume-rendering technique. Thereafter, the 3D arteriography and venography were fused together by multiphase fusion technique.

Results: In all the 75 patients, multiphase fusion images demonstrated clearly and simultaneously the arteries and veins around the stomach and the colon, which were correctly identified during surgery. We could utilize the multiphase fusion image for preoperative simulation and intraoperative navigation of laparoscopic gastrectomy and colectomy.

Conclusion: The utilization of multiphase fusion images contributed to the safe and prompt performance of laparoscopy.

C-0117

The evaluation of strangulation ileus using contrast enhanced ultrasonography

J. Koizumi; Isehara-city/JP

Purpose: To evaluate blood flow in strangulation ileus using contrast enhanced ultrasonography.

Scientific and Educational Exhibits

Materials and Methods : New Zealand white rabbits (approximately 3 kg) were incised under pentobarbital and medetomidine anesthesia. A small intestinal loop was extracted into the normal saline pool and observed using Coded Harmonic Angio by Logiq 700 (General Electric) under Levovist enhancement. A strangulation ileus was made by advancing a loop through a plastic syringe and compressing the bowel neck by the same diameter angioplasty balloon catheter inside in the syringe. For quantitative analysis the left carotid artery was cut down and the arterial pressure was monitored. The 'arterial' strangulation was made at higher balloon pressure than the systolic pressure, and the venous strangulation at lower one than the diastolic pressure. Enhancement was repeated approximately every thirty minutes after the previous injection.

Results: In the control, contrast enhancement distributes from the mesenteric artery to the bowel wall. In the arterial strangulation, contrast enhancement disappeared immediately after the compression. In the venous strangulation, contrast enhancement was delayed and diminished after the compression, and gradually disappeared in two hours.

Conclusions: Contrast enhanced ultrasonography can demonstrate vascular flow in the bowel and has efficacy in detecting strangulation.

C-0118

MR imaging of stomach cancer and ex vivo ^1H MR spectroscopy of the resected stomach

J.-H. Yoon, S.-S. Cha, S.-S. Han, S.-J. Lee, M.-S. Kang; Busan/KR

Purpose: To evaluate the usefulness of MR imaging and ex-vivo ^1H MRS to distinguish normal from tumor invasion of gastric wall.

Materials and Methods: Two specimens were examined with single-voxel ^1H MRS with 9.4 T equipped with custom-made surface coil. Fifty six surgical specimens were examined at 1.5 T MR imaging and ^1H MRS. Spectral measurements were done in the proper muscle layer and composite mucosa-submucosa layer. For all spectra, a PRESS technique with parameters of TR/TE = 2000/30 msec and 256 averages was used. Twenty one patients underwent preoperative MR imaging, and comparison to diagnostic T- and N-staging. High-resolution MR imaging was performed on resected specimens.

Results: The results at 9.4 T ^1H MRS showed metabolite peaks at 0.9 (lipid), 1.3 (lipid), 1.58 (Alanine), 2.03 (Sialic acid) and 2.25 ppm (glutathione) and with 1.5 T MRS, peaks are present at 0.9, 1.3, 2.0 and 2.2 ppm in normal gastric tissue. The peak levels of choline at 3.22 ppm were increased and peaks of lipid were decreased and split into 1.26 ppm and 1.36 ppm in gastric cancer tissues. Patients with gastric cancer showed various SI in MR imaging preoperatively, and overall accuracy was 80% (12/15) in T-staging and 86.7% (13/15) in N-staging. MR imaging of resected specimens clearly showed three different layers of normal gastric walls.

Conclusion: In evaluating the extent of gastric carcinoma, differentiation of up to three layers of the gastric wall was possible on ex vivo high resolution MR imaging. In the area of focal tumor invasion, the spectra obtained during ^1H MRS were useful, with the lipid peak decreasing and the choline splitting into two resonance peaks.

C-0119

Blood-borne metastatic tumors to the gastrointestinal tract: CT findings with clinicopathologic correlation

S. Kim, K. Kim, A. Kim, J.-S. Kim, H. Ha; Seoul/KR

Learning Objectives: To recognize the spectrum of CT findings of blood-borne metastases to the gastrointestinal tract from various malignancies and to discuss the characteristic CT findings of gastrointestinal metastases from each underlying primary malignancy, with clinicopathologic correlation.

Background: Although rare, blood-borne metastases to the gastrointestinal tract have been observed in patients with various malignancies. Most lesions are from malignant melanoma, carcinoma of the breast or lung, and hepatocellular carcinoma, and they most commonly involve the stomach and small bowel because of their rich blood supply. While most gastrointestinal metastases are encountered in patients with a known underlying malignancy and a widespread metastatic disease, they may occasionally occur as the initial manifestation of an occult primary lesion.

Imaging Findings: Although CT has played a key role in the evaluation of patients with a known or suspected malignancy, relatively little attention has been paid to the CT findings of gastrointestinal metastases. In this exhibit, we illustrate the spectrum of CT findings of gastrointestinal metastases, with clinicopathologic correlation.

Conclusion: A familiarity with this condition may ensure an accurate diagnosis and proper management in these patients.

C-0120

Branching patterns of the first jejunal vein: Evaluation using multi-detector row CT angiography

H. Kim, J. Lim, D. Lee, Y. Ko; Seoul/KR

Purpose: To evaluate branching patterns of the first jejunal vein using MDCT angiography in adults.

Materials and Methods: Two hundred twenty consecutive patients were enrolled in this study. Among 220 patients, 152 patients had no history of abdominal surgery. Branching patterns of the first jejunal vein were classified as follows: Type I, first jejunal vein crossed dorsal to the superior mesenteric artery (SMA) towards the left abdomen; Type II, First jejunal vein crossed dorsal to the SMA and abruptly turned towards the right abdomen; Type III, First jejunal vein crossed ventral to the SMA. Two radiologists classified branching patterns on PACS monitor using serial 5-mm thickness axial images of portal and delayed phase and MDCT angiography (volume rendering and maximum intensity projection technique).

Results: Of 220 patients, type I, II, and III branching patterns were identified respectively in 146 (66%), 38 (17%), and 36 (16%) patients. In the type II branching pattern, previous surgery or pathologic process that caused abrupt turning of first jejunal vein towards the right abdomen were as follows; biliary-enteric bypass surgery ($n = 7$), large hematoma in left abdomen ($n = 1$) and atrophy of the right kidney ($n = 1$). Of 152 patients who had no history of previous surgery, type I, II, and III branching patterns were identified respectively in 106 (70%), 22 (14%) and 24 (16%) patients.

Conclusions: We present the branching patterns of the first jejunal vein using MDCT angiography. The first jejunal vein, abruptly turning toward the right abdomen may be an anatomic variant or indirect finding of previous surgery such as biliary-enteric bypass.

C-0121

Imaging of non-tumoral disorders involving the small bowel in infancy and adulthood

M. Parrón, M. Lamas, T. Berrocal, E. Fernández, J. Gutiérrez, J. Fernández; Madrid/ES

Learning Objectives: To understand the embryology, pathology, and radiological features of disorders involving the jejunum and ileum. To know the utility of each imaging modality that can be applied to the management of these conditions. To show pitfalls, diagnostic difficulties and differential diagnoses.

Background: Non-tumoral disorders affecting the small bowel are a significant cause of morbidity in infants, children and adults, frequently requiring multiple imaging modalities to diagnose and plan treatment. This teaching exhibit analyses and illustrates practical aspects of a wide spectrum of usual, unusual and exceptional non-tumoral disorders affecting the jejunum and ileum, with particular emphasis on radiologic manifestations. The efficacy of the different imaging modalities in the diagnosis and management of these conditions will be evaluated.

Imaging Findings: Specific topics addressed include congenital anomalies (jejuno-ileal atresia and stenosis, Meckel's diverticulum, meconium ileus, anomalies of rotation and fixation, short bowel syndrome, duplication cysts), inflammatory diseases (Crohn's disease, therapy-induced enteritis, graft-versus-host disease, radiation enteritis), infective diseases (yersinia, salmonella, tuberculosi, actinomycosis, parasites, Whipple's disease), diffuse infiltrative diseases (amyloidosis, eosinophilic enteritis, intestinal lymphangiectasis, lymphoid hyperplasia), vascular disorders (acute and chronic ischaemia, vasculitis, necrotizing enterocolitis of newborn), intestinal obstruction (hernia, volvulus, intussusception, gallstone ileus), scleroderma, coeliac disease, diverticula, trauma and post-surgery complications.

Conclusions: This exhibit provides an overview of the small bowel disorders as well as the utility of the various imaging techniques available. Because many of these disorders have characteristic imaging appearances, this exhibit will help the practising radiologist to better understand and recognise pathologic processes affecting the small bowel.

C-0122

Ischemic colitis: Sonographic findings and differential diagnosis

M.R. Pastor-Juan, T. Ripollés, M.J. Martínez, J.R. Olalla-Muñoz, M.D. Monedero, A. Ruiz; Valencia/ES

Purpose: To describe the sonographic findings of ischemic colitis, and to differentiate this entity from other conditions that produce wall thickening of the colon.

Materials and Methods: A review was made of the histories of patients diagnosed with ischemic colitis over a period of 6 years and 4 months. Eighty patients had undergone sonographic examinations. The spectrum of sonographic find-

Scientific and Educational Exhibits

ings in ischemic colitis was based on the original imaging report, with an analysis of the presence of colonic abnormalities and their associated alterations.

Results: The prospective sensitivity of sonography for the characterization of colonic abnormalities was 95% (76 from 80 patients). Segmental involvement was detected in 75 of the 76 patients, with left-sided colitis in 61 (80%). The mean length of bowel involved was 20 cm with a mean wall thickness of 7.7 mm. Colon wall stratification was preserved in 50 patients (66%). Altered pericolic fat was observed in 24 patients (32%). Absent or barely visible color Doppler flow in the thickened bowel wall was recorded in 82% of cases.

Conclusions: Sonography is a valuable technique for the detection of colonic abnormalities secondary to ischemic colitis. However, there are other causes of colonic wall thickening, such as pseudomembranous colitis, Crohn's disease, ulcerative colitis, diverticulitis or malignancy. Knowledge of sonographic appearances of diseases that involve the colon may suggest a specific diagnosis based on the changes in the colonic wall and peri-enteric tissues.

C-0123

Intestinal perforation by fish bone: A radiologic diagnosis when not clinically suspected

F. Romero Cique, C. Martínez, E. Santos-Armentia, M. Fernández-Carrera, E. Chávarri, J. Táboas; Vigo/ES

Purpose: To describe CT findings in patients with intestinal perforation caused by fish bone (IPFB).

Patient and Methods: 14 patients with a surgically proven diagnosis of IPFB were retrospectively analyzed. Clinical symptoms, radiologic findings and presumption diagnosis with CT were variables recorded.

Results: 14 patients presented acute abdomen by IPFB. None was clinically suspected. CT showed subtle linear lesion with high density in 7 (50%) patients in whom a correct radiologic diagnosis was established. Other findings were; thickening of the bowel wall with stranding of mesenteric fat (3), extraintestinal bubble of gas (1), abscess (4), thumbprinting (1), mass in the middle line (1), focal thickened of bladder wall (1) and gas in the bladder(1).

Conclusion: The radiologist plays an important role in the diagnosis of IFPB because this entity is usually mistaken clinically in patients with acute abdomen. The presence of a linear and high-density lesion must suggest this diagnosis.

C-0124

Computerized analysis of abnormal areae gastricae on barium examination

S.M. Zangan, A.E. Gasparaitis, M.L. Giger; Chicago, IL/US

Purpose: Visualization of areae gastricae on double-contrast upper gastrointestinal tract examinations is related to technical, physiological and pathophysiological factors. Enlarged, irregularly shaped areae gastricae can be seen in patients with gastritis. A method utilizing computerized radiographic texture analysis to recognize abnormal areae gastrica is introduced.

Methods and Materials: Supine double contrast digital images of the stomach were acquired from 26 patients and regions of interest (ROI) 128 by 128 pixels in size were extracted. Computerized texture analysis was performed to assess the variation in the anatomic pattern. Individual texture features that describe the magnitude and spatial frequency content of the patterns were calculated. The area under the receiver operating characteristic (ROC) curve (Az) was used to assess the performance of the texture analysis in the task of distinguishing between patients with gastritis and normals.

Results: Computerized texture analysis performed favorably. ROC analysis yielded an Az value of 0.90 in accurately diagnosing gastritis based on the surface pattern of the areae gastricae.

Conclusion: Computerized radiographic texture analysis is capable of determining whether the areae gastricae is abnormal on double-contrast upper gastrointestinal barium examination. This technology has the potential not only to aid radiologists in assessing the gastric mucosa but also to objectively characterize the radiographic features of the areae gastricae in pathologic states.

C-0125

Radiographic imaging of normal anatomy and complications after gastric banding and gastric bypass surgery

H. Prosch, R. Tscherney, S. Kriwanek, D. Tscholakoff; Vienna/AT

Learning Objectives: To understand the normal radiographic findings after gastric banding and gastric bypass surgery and to recognize its most frequent complications.

Background: As the incidence of morbid obesity increases, bariatric operations to reduce body weight become more frequently performed. Among the wide vari-

ety of bariatric procedures, gastric banding and gastric bypass are the most common. Understanding the principles of these interventions is essential for the interpretation of resulting radiographic findings.

Procedure Details: Between 1.1.1998 and 1.9.2004 157 gastric banding and 107 gastric bypass operations were performed at our hospital. We report on the normal postoperative findings and observed complications in this patient population. Gastric banding aims to achieve an early sensation of satiety by dividing the stomach into two pouches with an adjustable silicone band. Fluoroscopy after gastric banding should reveal a small proximal pouch and a stoma with a diameter of approximately 3-4 mm. The most common complications after gastric banding are a slippage of the band, pouch enlargement and esophageal dilatation. Gastric bypass surgery is performed by creating a small gastric pouch that is anastomosed end-to-side to a Roux-en-Y limb. The most frequent complications are leaks at anastomoses, anastomotic strictures and small bowel obstruction. Fluoroscopy is performed as a routine radiological evaluation after both procedures. CT scans are performed to evaluate possible complications.

Conclusion: Radiologists play an important role in the evaluation of potential complications after bariatric surgery. The knowledge of surgical procedures and potential complications is essential for the correct interpretation of the findings.

C-0126

An illustrated history of gastrointestinal and abdominal medical imaging

D. Novak; Osijek/HR

Purpose: The aim is to show the early development of gastrointestinal radiology as the first step in the history of gastrointestinal and abdominal medical imaging.

Materials and Methods: In order to achieve an overview of the historical development of gastrointestinal radiology, the original publications were studied and systemized in chronological order. The biographies of pioneers of gastrointestinal radiology are illustrated with portrait photographs.

Results: The following historical landmarks are described and documented with corresponding illustrations: **1.** Upper gastrointestinal studies: W.BECHER (1896), W.B.CANNON (1896), J.-CH.ROUX and V.BALTHAZARD (1897), F.WILLIAMS (1901), G.HOLZKNECHT (1903), H.RIEDER(1904), H.HULST(1905), L.G.COLE(1905), M.KASSABIAN(1906), C.BACHEM and H.GUNTHER(1910), M.HAUDEK(1910), R.D.CARMAN(1917), G.FORSELL(1923); **2.** Examination of the colon: A.SCHUELE(1904), G.F.HAENISCH(1910), L.G.COLE(1910), M.EINHORN and H.LAUREL(1921), A.W.FISCHER(1923); **3.** Examination of the small bowel: H.RIEDER(1904), H.HULST(1905), L.G.COLE(1911), G.SCHWARZ(1924), G.S.PESQUERA(1929), E.P.PENDERGRASS(1935), J.GERSHON-COHEN(1939).

C-0127

CT in acute perforated sigmoid diverticulitis

C. Lohrmann, N. Ghanem, G. Pache, F. Makowiec, E. Kotter, M. Langer; Freiburg/DE

Purpose: To assess the value of computed in patients with acute perforated sigmoid diverticulitis.

Methods and Materials: 30 patients with acute perforated sigmoid diverticulitis underwent computed tomography prior to surgery (mean: approximately 4 days). Computed tomography scans were reviewed and subsequently compared with the surgical and histopathological reports in accordance with the Hinchen classification of perforated diverticular disease.

Results: Computed tomography correctly determined the Hinchen stage in 28 of the 30 (93%) patients examined. Computed tomography revealed 12 out of 14 (86%) patients with perforation sites and 3 out of 3 (100%) patients with contained perforation. In one (6%) patient a bowel wall discontinuity could be revealed on Computed tomography scans in 17 patients with surgically or histopathologically proven perforation or contained perforation. In 6 of the 17 (35%) patients with surgical or histopathological perforation or contained perforation, extraluminal contrast material was detected on Computed tomography. Computed tomography identified 23 out of 25 (92%) patients with pericolonic inflammation and 26 out of 28 (93%) patients with pericolonic oedema. Computed tomography detected 21 out of 23 (91%) patients with abscess formations and all 11 (100%) patients with free fluid collections in the mesentery root. 3 of the 30 (10%) patients successfully underwent Computed tomography-guided percutaneous abscess drainage before undergoing surgery.

Conclusion: Computed tomography is a valuable imaging tool for determining the degree of acute perforated sigmoid diverticulitis, by which means patients can be stratified according to the severity of their disease, and is therefore of assistance in surgical planning.

Scientific and Educational Exhibits

C-0128

Spectrum of CT colonography findings in colonic tuberculosis: A pictorial essay

V. Jain, S. Bandhu, S. Vashisht, M.S. Gulati, P.K. Garg; *Delhi/IN*

Learning Objective: To display and discuss the spectrum of findings in patients with colonic tuberculosis (TB) on CT colonography (CTC).

Background: Conventional barium studies are the most widely used modalities in patients with suspected colonic/abdominal TB. CT is frequently performed to investigate such patients when barium findings are equivocal. In addition to the mural aspect of the disease, CT helps in demonstrating the extracolonic findings of TB, thus adding specificity to the diagnosis. Although CTC has been extensively evaluated as screening modality for colorectal cancer, its role in patients with inflammatory bowel disease and particularly tuberculosis has not been examined.

Procedure Details: CT colonography (CTC) was performed in 12 patients with colonic TB, using a 4-slice CT scanner with a 3 mm slice width, 2.5 mm effective collimation, table feed 15 mm (pitch-6.0), 120 kVp, overlapping reconstruction at 2 mm intervals and 0.5 s rotation time, following intravenous contrast, in supine and prone positions. CT data were transferred to a remote 3D workstation where 2- and 3-D CTC were performed and findings compared with those of CC. A final diagnosis of colonic TB was based on positive histopathological report and/or a definite positive response to anti-tuberculosis treatment in all patients. We will display the comparable endoluminal images of CTC and CC in this patient group. Additional mural and extraluminal findings related to TB seen in these patients will also be demonstrated.

Conclusion: CTC gives comprehensive information regarding luminal, mural and extraluminal involvement in patients with colonic tuberculosis. Appearances at CTC are comparable to those seen at CC.

C-0129

Digital radiographs (DR) versus conventional screen films (SF) in small bowel follow-through: A prospective study

O.R. Brook, D. Fischer, A. Hirshenbaum, A. Engel; *Haifa/IL*

Purpose: We propose to perform in-between radiographs of SBFT with digital equipment. We prospectively compared subjective radiological quality and radiation dose of digital (DR) versus conventional screen film (SF) radiographs SBFT. Effect on workflow was also evaluated.

Methods: Five senior and four resident radiologists compared printed images from 11 SBFT examinations, when every patient has SF and DR images (Smart Rad®, CMT Medical Technologies, Ltd.). SF and DR images were done with same exposure data (102 kV and automated phototimer). Overall satisfaction, demonstration of mucosa and bone were graded 1-5, 5 being the best. The radiation doses and effect on workflow were compared between DR and SF.

Results: A total of 546 observations of image quality were made. DR produced images with significantly higher overall satisfaction (4.4 vs. 3.1, p < 0.001), better definition of mucosa (4.2 vs. 3.3, p < 0.001), and demonstration of bones (4.5 vs. 2.3, p < 0.001) compared to SF. The radiation dose with DR was 0.57 mGy, with SF - 0.86 mGy (p = 0.023). Production of DR image took 3.5 minutes; 5.5 minutes with SF.

Conclusion: Substituting conventional radiographs with DR combined with a PACS reading station in the SBFT examination results in significantly better image quality, lower radiation doses and speeds up the workflow.

C-0130

MR findings that may aid in the evaluation of Crohn's disease activity

S. Giusti, P. Giusti, L. Marchetti, C. Bartolozzi; *Pisa/IT*

Learning Objective: 1.To evaluate MR feasibility in the assessment of morphological bowel wall changes and mesenteric disease extension after the administration of a biphasic contrast agent. 2.To show the great variety of imaging findings detected with MR at early, advanced, and complicated stages.

Background: Thanks to higher performance gradient systems which allow ultra-fast sequences, MR examination has become a valid alternative to CT in the evaluation of Crohn's disease. Patients included in our series had advanced disease which had been diagnosed on small bowel follow-through studies. They underwent MR study to follow-up the disease and to detect eventual complications.

Procedure Details: MR was performed after the manual administration of 2 L of a biphasic contrast agent through a pediatric nasojejunal catheter, at a flow rate of 60 mL/min. Each patient was investigated in a prone position with a phased-array coil. Our protocol employed true FISP, HASTE and Gd-enhanced 3D FLASH fat sat sequences to evaluate each patient. In our experience, with true FISP we

were able to demonstrate all the different morphological changes found in Crohn's disease, with 3D FLASH sequences we succeeded in evaluating the severity of disease activity, mesenteric vascularity and lymph node enhancement. The use of HASTE sequences could be limited to the cases in which susceptibility artifacts, due to the presence of air, hamper true FAST images or when it is necessary to provide a more accurate quantification of the intestinal wall thickening.

Conclusions: MR examination is a promising technique and a valid alternative to CT in the evaluation of Crohn's disease, especially during the follow-up period.

C-0131

Appendiceal mucocele: Imaging with US and CT

F. Sandomenico, O. Catalano, A. Nunziata, M. Mattace Raso, A. Siani; *Naples/IT*

Learning Objectives: To illustrate the sonographic and CT findings in appendiceal mucocele with clues to differential diagnosis. To make the radiologist aware of the typical and atypical appearances of appendiceal mucocele as shown with US and CT. Knowledge of all possible appearances is necessary for adequate preoperative diagnosis.

Background: Appendiceal mucocele is an uncommon disorder of the ileocecal area. Sometimes it can create interpretation difficulties, especially in atypical or large-sized cases.

Procedure Details: Eight patients (5 M and 3 F, 51-78 years, mean 55) with surgically confirmed appendiceal mucocele (larger diameter 4-28 cm, mean 6 cm - volume 100-6000 mL) were evaluated with US, contrast-enhanced US, and CT. US and CT findings depend mainly on mucocele size. Smaller lesions appeared as thin-walled, cystic images close to the ileocecal area, sometimes showing mural calcification. Larger mucoceles were recognisable as large-volume masses filling the pelvis or even the abdomen and pelvis in a peritoneal or retroperitoneal location. Bowel loops were dislocated and, in the eventual absence of parietal calcification, the diagnosis of origin and nature was difficult.

Conclusion: Appendiceal mucocele may show various typical and atypical findings at sonographic and CT imaging.

C-0132

Histologic, surgical, endoscopic and imaging findings in gastrointestinal stromal tumors (GIST)

A. Nunziata¹, O. Catalano¹, E. De Lutio di Catelguidone¹, V. De Rosa¹, A. Prisco², L. Cipolletta², A. Siani¹; ¹Naples/IT, ²Torre del Greco/IT

Learning Objective: To illustrate all histologic, endoscopic, and radiological findings in GIST of stomach, small bowel and large bowel. To make the radiologist aware of clues to diagnosis because this outgrowing gastrointestinal tumour frequently mimics abnormalities arising in contiguous organs.

Background: GIST is the most common mesenchymal lesion of the alimentary tract, identified for expressing KIT-protein. This exhibit is a fulfilled essay of all typical and atypical histologic, endoscopic, and radiological aspects of GIST.

Procedure Details: Histological images are presented. Findings typical and atypical of GIST, with special references to clues to diagnosis and to suggest malignancy are provided. A review of GIST appearance with different tools is provided: transluminal conventional endoscopy (gastroscopy, enteroscopy, colonoscopy), capsule endoscopy, endoscopic sonography (US), transabdominal US, contrast-enhanced US (liver metastases), conventional gastrointestinal X-ray imaging, CT, virtual colonoscopy and MR imaging. Appearance of primary GIST, recurrence and metastasis is illustrated. Cases arising from stomach, small bowel, and colon are presented.

Conclusion: Current endoscopic and radiological techniques allow demonstration of all typical and atypical aspects of GIST.

C-0133

The role of spiral CT colonography in the pre-treatment staging of colorectal cancer

J.M. Pienkowska, E. Szurowska, J.M. Wierzbowski, I. Marek, B. Rutkowska, M. Studniarek; *Gdansk/PL*

Purpose: The aim of this study was the estimation of the role of spiral CT colonography (STC) in the pre-treatment staging of colorectal cancer.

Material and Methods: A total of 58 patients with a clinical suspicion of colorectal cancer underwent conventional colonoscopy and on the same day spiral CT colonography with a standard protocol. All results were compared with histopathologic examination. Pre-operative TNM staging was correlated with surgical/histologic staging.

Results: There were 32 colorectal cancers and 23 polyps identified in conven-

Scientific and Educational Exhibits

tional colonoscopy. SCTC detected all cancers (sensitivity 100%), as well as 16 of 23 polyps. In 7 patients liver metastases, in 21 patients local, pericolic fat extension and in 11 lymphadenopathy were detected. Additionally two synchronous tumours and five polyps located in the colon proximal to the stenosing lesion which could not be tranversed endoscopically were identified. Surgical excision was possible in 24/32 cases of colorectal cancer. SCTC correctly staged T in 19 (79.2%) cases, N in 13 (54.2%). T was overstaged in 3 (12.5%) cases and understaged in 2 (8.3%). SCTC overstaged N in 4 (16.7%) and understaged in 7 (29.2%).

Conclusion: SCTC is an accurate procedure for pre-operative staging assessment of colorectal cancer and can be used for treatment planning.

C-0134

Color Doppler of superior mesenteric artery in the semi severe form of Crohn's disease of the terminal ileum

L.V. Lukic-Kostic, S.Z. Sekulovic; Belgrade/YU

Purpose: To assess the value of color Doppler (CD) flow parameters in the superior mesenteric artery (SMA) in the semi severe form of Crohn's disease with disease activity index (CDAI) in the range 250-400.

Methods and Materials: 30 patients with CDAI in the range 250-400 and 10 healthy volunteers were examined with 3.5 MHz CD probe. We measured resistive index (RI) and maximum flow volume (MFV) in the SMA after overnight fasting and 15 minutes after a liquid meal in both groups.

Results: In the group with active Crohn's disease the value of RI after overnight fasting was 0.78 ± 0.02 and after the meal 0.70 ± 0.02 . In the group of volunteers it was 0.81 ± 0.04 on fasting and 0.67 ± 0.04 after the meal. We also measured MFV in both groups after fasting period and after the meal. In the group with active Crohn's disease, a marked increase in MFV was noted on fasting instead the healthy group: $1.549 \text{ ml/min} \pm 512$ versus $437 \text{ ml/min} \pm 152$. After the meal, MFV in the first group was $1.792 \text{ ml/min} \pm 576$ versus $672 \text{ ml/min} \pm 169$ for volunteers.

Conclusion: Results in this work support the fact that active Crohn's disease causes enormous increase of MFV in the SMA. Analyzing postprandial changes in RI and MFV in the SMA shows that these parameters are of more than physiological interest because they can focus attention on possible inflammatory disease which becomes apparent only during functional stress. We strongly suggest CD as a follow-up method in assessing the acute phase or regression of the semi severe form of Crohn's disease.

C-0135

Laparoscopic gastric bypass surgery in morbid obesity: Radiologic features and complications

J. Catala, D. Hernandez, M. Escobar, P. Veciana, S. Gispert, L. San Roman, J.I. Poves; Barcelona/ES

Purpose: To show the radiological anatomy and present our experience in post-operative complications after laparoscopic gastric bypass surgery in morbid obesity.

Methods and Materials: During a two-year period (January 2002 to January 2004) laparoscopic gastric bypass surgery was performed in 448 morbidly obese patients or as substitutive technique of previous bariatric surgery. In all patients, upper gastrointestinal radiography was performed within 48 h after surgery as part of a routine follow-up. CT was performed when an anastomotic leak was diagnosed on radiography or when the clinical outcome was not satisfactory and complications were suspected.

Results: We detected 43 complications (9.5%). They were classified as suture dehiscence (19 patients), gastrointestinal obstruction (8 patients): edema (2), torsion (2), clots (3), inappropriate anastomosis (1), miscellaneous (15 patients): abscess (5), paralytic ileus (3), other (7).

Conclusions: The particular characteristics of laparoscopic bypass surgery in morbid obesity makes necessary a proper knowledge of the radiologic anatomy as well as the imaging findings of the most common complications.

C-0136

Rectal carcinoma staging with MR imaging: The accuracy in the prediction of free tumour resection margins

C. Gonzalez¹, C. Garcia de Iturraspe², E. Fernandez¹, J. Alustiza¹, J. Ontañon¹, A. Arriillaga¹, M. Barrera¹, C. Gervás¹; ¹San Sebastian/ES, ²Bilbao/ES

Purpose: To identify patients with high risk for local recurrence after total mesorectal excision (TME) by predicting tumour involvement of circumferential resection margins.

Methods and Materials: In a prospective study of 42 patients with rectal aden-

carcina after colonoscopy and biopsy, preoperative MR imaging was performed with a phased-array coil and high resolution T2 weighted sequence. As we know from the literature a distance ≥ 5 mm from the mesorectal fascia in MR imaging, predicts at least 1 mm tumour-free resection margin at histology. We therefore separated tumours in two groups at staging. In one group tumours that affected only the rectal wall (T1 and T2), and tumours that extended to the perirectal fat but with a distance ≥ 5 mm to the fascia (T3 incipient). The second group included tumours with fat involvement with a distance < 5 mm to the mesorectal fascia (T3 advanced) and tumours that involved and crossed the fascia (T4). We compared our results with histology after EMT.

Results: MR imaging classified 32 tumours in the first group (T1, T2 and T3 incipient) and 10 in the second (T3 advanced and T4), with one false positive and 1 false negative. We found a sensibility = 88'8%, specificity = 96'9%, positive predictive value = 88'8% and negative predictive value = 96'9% of MR imaging to predict tumour-free circumferential resection margins.

Conclusion: MR imaging offers an excellent anatomic map of the rectum and tumor and its relation with mesorectal fascia, allowing the identification of patients at risk of local recurrence after surgery and to asses preoperative therapy.

C-0137

MDCT gastroscopy

A.M. Miranda, H. Cuellar, S. Quiroga, C. Sebastia, R. Boye, A. Alvarez; Barcelona/ES

Learning Objectives: To show the virtual gastroscopic evaluation of gastric tumoral pathology and to describe the advantages of gaseous gastric distension in MDCT gastroscopy in comparison to hidric distension.

Background: Virtual MDCT colonoscopy is an expanding technique that has established its sensitivity in the detection of colonic wall thickening. MDCT with gaseous gastric distension achieves a complete visualization of gastric and extragastric pathology, in contrast to gastroscopy and double-contrast studies of the stomach. Virtual navigation allows for mucosal mapping, clearly superior to double-contrast study. Multiplanar reformatted images depict local extension as well as regional lymphatic involvement. Preliminary results of virtual endoscopy after intravenous contrast injection show promise in identification of tumoral tissue through increased enhancement.

Procedure Details: 40 patients with gastric carcinoma underwent MDCT for staging of the disease. All the patients had fasted for a minimum of 6 hours. Scans were performed after oral administration of effervescent granules and intravenous injection of 20 mg of scopolamine. MDCT was performed before and after intravenous contrast injection using a 16 detector MDCT. Scan data were reconstructed using specially dedicated software for virtual colonoscopy.

Conclusion: MDCT with gaseous gastric distension is useful in the staging of gastric tumoral lesions, allowing for excellent mucosal mapping with virtual gastroscopy as well as tumoral delineation and extra-gastric extent of disease. Virtual gastroscopic study of tumoral enhancement after intravenous contrast injection might show advantages in tumoral characterization. MDCT with gaseous gastric distension might alter current diagnostic approaches to gastric tumor detection and staging.

C-0138

MR colonography versus conventional colonoscopy for the detection of colonic lesions

R. Haykır, S. Karaköse, A. Karabacakoglu, M. Sahin, E. Kayaçetin; Konya/TR

Purpose: MR colonography (MRC) based on MR imaging is a relatively new diagnostic modality for diagnosing colon pathology. The aim of this study was to evaluate its performance in detecting colonic lesions.

Material and Methods: 35 patients (22 men, 13 women; age range 2-85 years; mean age: 59.7) suspected of having colonic lesions because of rectal bleeding, positive fecal occult blood test results or altered bowel habit underwent MRC and subsequent conventional colonoscopy (CC). All patients underwent standard bowel preparation 24 hr before MRC. After placement of a rectal tube, the colon was filled with 1500-2000 ml of mixture 0.9% NaCl solution and 15-20 ml of 0.5 mmol/L gadopentetate dimeglumine solution. Once colonic distension was achieved 3D GRE MR colonography and complementary MR images were taken in all cases.

Results: Sensitivity of MRC for colon pathologies was 95.2% and specificity was 100%. The percentage of correct diagnosis of MRC was 97.1%. MRC was well tolerated without sedation or analgesia.

Conclusion: In detecting colonic lesions MRC achieved a diagnostic accuracy similar to CC. MRC is minimally invasive, has no need for sedation or analgesics during the investigation and has a lower percentage of perforation complications.

Scientific and Educational Exhibits

It can also demonstrate all colon segments due to multisectional imaging and intramural and extra-intestinal components of colonic lesions, metastasis and additional lesions can easily be seen. MRC is a new radiologic techniques that promises to be highly sensitive for colorectal screening.

C-0139

Look at what can be inserted into orifices

P. Rajiah, A. Khan; Manchester/UK

Learning Objectives: A. To illustrate the bewildering array of foreign bodies are inserted into different body orifices. B. To understand the role of imaging. C. To wonder why people have to insert these objects into their orifices.

Background: Some people insert foreign objects of all sizes and shapes into their orifices. This can be done for recreational or malvolent purposes such as smuggling contraband substances. It is more common in children and in psychiatric patients. Curiosity, sexual activities, non traditional medical treatments and instrumentation are other recognised causes. Rectum, vagina, urethra, nose, ear and mouth are the common sites of foreign body insertion.

Procedure: Plain X-rays are done in all cases of suspected foreign body insertion for confirmation and anatomical localisation. CT scans with oral or rectal and intravenous contrast may be required for accurate localisation and demarcation of the anatomical planes traversed by the foreign body. Most of the foreign bodies cause only minor injuries, but they can cause perforation, haemorrhage, sepsis or can migrate to distal places. The foreign bodies in our exhibit include nails, pins, needles, cups, cans, bottles, drug packets and wood.

Conclusion: Recognition of foreign bodies is important for prompt management and to prevent development of complications.

C-0140

16-Row CT colonography (MDCTC): Technique and pitfalls of 3D primary approach

D. Salovic; Tournai/BE

Learning Objectives: To understand the technique and pitfalls of 3D primary approach as an interpretation technique for the MDCTC with a 2D imaging reserved for problem solving.

Background: The 3D primary approach (endoluminal fly through) shows a greater ease of polyp detection owing to increased polyp conspicuity and better fold depiction. Inconveniently there is an elevated risk of false positive findings for the non experienced reader. The examples show the semiology of true (+) and true (-) lesions compared to the false (+) and a false (-) lesions. The importance of 3D global view (virtual double contrast) is also stressed.

Procedure Details: MDCTC was performed in 400 patients using the standardized technique: Bowel cleansing with phospho soda as a laxative (dry prep). Faecal tagging with 3% barium suspension. Electronically controlled CO₂ insufflations (PROTOCOL, E-Z-EM, Westbury, USA). Bowel hypotonia with 20 mg i.v. Buscopan (Hyoscine butylbromide). 16 row helical scanning in the prone and a supine position (Siemens Sensation 16, Forchheim, Germany) with 1.5 mm collimation, 1 mm increment, 120 kV and 50 mAs (effective). Interpretation on 3D endoluminal display for polyp detection (Leonardo work station, Siemens, Forchheim, Germany).

Conclusion: MDCTC is simply to perform. The primary 3D interpretation approach needs standardised technique and knowledge of the pitfalls for the detection of true(+) findings.

C-0141

Small and large bowel virtual colonoscopy in patients with Crohn's disease

G. Tóth, L. Tóth, B. Forgács, Z. Tarján, E.K. Makó; Budapest/HU

Purpose: Virtual enteroscopy is a new method for the assessment of inflammatory small bowel disease. Our goal was to assess the visualisation the small bowel and colon simultaneously by virtual colonoscopy.

Materials and Methods: In 42 patients with known Crohn's disease CT virtual colonoscopy was performed. We were searching for the typical CT features of inflammation by two radiologists by consensus.

After 2-5 days colonoscopy was performed. Results of CT colonoscopy were compared with colonoscopy and surgery. Colonoscopy and surgery were considered gold standard.

Results: Good small bowel distension was obtained in 35 cases, sufficient in 4 and insufficient in 3 cases. Large bowel distension was good in 39 cases, sufficient in 2 and insufficient in 1 cases. In 37 cases the thickness of the wall in all segments of the small and large bowel were correctly evaluated. In 8 cases we found a minimal, in 19 cases a medium and in 7 cases a strong small bowel wall

thickening. In 5 cases virtual enteroscopy did not show a small bowel wall thickening but colonoscopy showed aphthoid ulcerations in the terminal ileum. Virtual enteroscopy showed skip lesions in the small bowel in 9 cases.

Virtual colonoscopy detected 94% of mucosal abnormalities and all strictures in comparison with colonoscopy. Virtual colonoscopy showed 8 abscesses and 10 extraintestinal fistulas all confirmed at surgery.

Conclusion: Virtual colonoscopy can be a good tool in detecting intramural and complicated Crohn's disease in the small and large bowel, but we don't advise this in early Crohn's disease

C-0142

Use of Calogen® as an oral contrast medium in the evaluation of the gastric wall at MR imaging

D.G. Lohan, S.M. Walsh, P. McCarthy; Galway/IE

Purpose: Evaluation of gastric wall pathology using cross-sectional imaging has proved difficult, particularly in the imaging of early, localized disease. The properties of Calogen as a negative oral contrast agent for the evaluation of the upper gastro-intestinal tract and retroperitoneum in CT has been well described. We assess the suitability of this agent as an oral contrast medium for use in MR imaging examination of the gastric wall.

Materials and Methods: Multisequence, multiplanar acquisitions using a Siemens Symphony 1.5 T scanner were acquired following ingestion of 500 mL of either Calogen or a similar volume of water by 15 subjects, including healthy volunteers and patients with suspected mural abnormalities. Images were acquired in both supine and prone positions. These images were then blindly evaluated by 3 Consultant Radiologists and scored according to gastric distension, elimination of peristaltic artefact and homogenous distribution.

Results: The mean scores for Calogen and water with regard to gastric distension are 8.46 and 5.49, respectively ($p < 0.01$). Concerning obliteration of mucosal detail, the respective scores are 8.48 and 3.84 ($p < 0.01$). Calogen is also statistically superior to water with regard to prevention of peristalsis and homogeneity (mean scores 8.15 vs 5.74 and 8.69 vs 6.30 respectively). Oral Calogen, therefore, is superior to water as an oral contrast agent for MR imaging examination of the gastric wall.

Conclusions: Calogen preparation is a suitable oral contrast medium for assessment of gastric wall anomalies at MR imaging. While often poorly tolerated by patients, it is superior to water in the non-invasive assessment of potential mural lesions.

C-0143

A pictorial review of extra luminal findings on MR imaging of the small bowel

D.A. Mc Kenna, A. Alhajeri, C.J. Roche, J.M. Murphy, P.A. McCarthy; Galway/IE

Learning Objectives: MR imaging is a useful imaging modality in the investigation of small bowel pathology. MR imaging has been shown to be comparable to conventional enteroclysis in the detection of luminal involvement and superior in the detection of extramucosal extent. The aim of this paper is to present an atlas of extraluminal pathology found at MR imaging of the small bowel.

Abstract: Images were reviewed from 31 patients over a 2-year period to identify extra luminal pathology. The oral contrast used was Norgine (Klean-pep, Middlesex, UK) which is a balanced mixture of polyethylene glycol and electrolytes. MR imaging sequences were a T2* localiser and a true FISP sequence.

Results: In 68.5% of patients supplementary imaging was available, showing positive correlation with conventional imaging in 92.1%. Pathologies included Crohns, celiac disease, lymphoma, plasmacytoma and carcinoid. MR imaging allowed further characterisation of the extra luminal extent of the above pathologies and in 26.3% of patients showed additional unsuspected pathology such as hepatoma, colitis of the transverse colon, gallstones and primary biliary sclerosis.

Conclusions: Not only does MR imaging of the small bowel permit accurate assessment of the bowel but it also allows identification of extraluminal pathology in a quarter of patients, with no radiation.

C-0144

Contrast-enhanced transabdominal US with 2nd generation contrast medium and multislice CT in Crohn's disease: A preliminary report

M. Alabiso, I. Marano, F. Morace, N. Bonavolonta', G. Penza; Naples/IT

Learning Objective: The aim of the present study was to evaluate the diagnostic efficacy of Sonovue in differentiating active wall inflammation from fibrotic wall thickening in comparison to multislice CT with intravenous contrast medium.

Background: We enrolled 36 patients (20 M and 16 F, mean ages 34 and 7 y) with

Scientific and Educational Exhibits

Crohn's disease (CD) having a CDAI ranging between 80-470 (22 pts CDAI > 150). The location of CD was colonic in 20 patients, ileocolonic in 13, ileo-jejunal in 2 and colonic-jejunal in 1. All patients underwent colonoscopy and CT scan to evaluate extention and endoscopic score of the disease. These data were compared to US appearance of intestinal wall obtained after iv injection of 25 mg of Sonovue diluted in 5 ml of 0.9%NaCl and studied with a multifrequency convex-probe.

Procedure Detail: In all patients US showed an increased wall thickness (6.3 mm-range:2.8 mm). After injection of Sonovue all the patients with CDAI > 150 and 2 patients with CDAI < 150 had marked enhancement involving all wall layers, probably due to inflammatory hypervascularisation, similar to CT that, however, have a better visualisation of perivisceral inflammation. Furthermore, in 3 pts CT correctly detected a jejunal involvement which was undiagnosed by US. In the 14 pts with CDAI< 150 we found a mild increase of wall thickness (4.2 mm-range2.2 mm) but in 12 we did not record any enhancement after Sonovue.

Conclusions: The present study suggest that contrast enhanced US can improve the sonographic study of the intestinal wall and helps in detecting active wall inflammation in CD.

C-0145

Advanced abdominal gastrointestinal stromal tumors (GIST) treated with Imatinib Mesilate: MR tumor response assessment after 24 months follow-up

A. Messina, P. Casali, D. Vergnaghi, F. Bianchi, A. Gronchi, R. Musumeci; Milan/IT

Purpose: To evaluate MR imaging patterns of tumor response of advanced GIST treated with Imatinib Mesylate after a mid-term follow-up (24 months).

Methods and Materials: 26 patients with advanced GIST (83% with liver lesions and 75% with peritoneal involvement) underwent therapy with Imatinib Mesylate. All underwent a baseline MR imaging and then MR imaging every 2 months until 24 months after the treatment had started. MR imaging was performed with a 1.5 T system using morphologic GRE T1W, TSE T2W and CE dynamic GRE T1W sequences.

Results: 66% pts were judged to be responsive to therapy after 2 months and 84% after 12 months. Patients responsive to therapy showed: A) Tumor decrease in size (with an increase in tumor volume in 8% of cases due to necrosis or bleeding after 2 months of therapy). B) Hypointensity of the lesions on T1W images in 83% cases (hyperintensity in 17% cases for bleeding) and hyperintensity of the lesions on T2W images (correlating with degenerative tissue or necrosis), C) Hypovascularization of the lesions on CE-T1W images due to degenerative tissue or necrosis and D) Presence of peritoneal fluid in 30% cases at the first month, reabsorbed in the following months.

Conclusion: MR imaging is adequate to identify tumor response to Imatinib Mesylate in advanced GIST from the early months of therapy. Decrease in tumor size and increase in necrosis are effective indicators of response. Nevertheless, in the first months an increase in tumor volume should not be held as evidence of progression when associated with an increase in necrosis.

C-0146

CT Evaluation of the acute abdomen caused by colorectal carcinomas

K. Furuya¹, I. Sakino², N. Harada², K. Yasumori¹, T. Muranaka¹; ¹Fukuoka/JP, ²Kitakyushu-City/JP

Learning Objectives: To describe a wide variety of helical CT and multidetector-row CT images of acute abdomen in patients with colorectal carcinomas and to assess the diagnostic value of CT for such patients.

Background: Colorectal carcinomas cause a variety of acute abdominal conditions and sometimes an acute abdomen itself can be the first symptom for a patient with colorectal carcinoma. Thus, to detect hidden malignancies radiologists need to be familiar with various images of acute abdominal conditions.

Procedure Details: We reviewed the helical CT findings and medical records of 64 patients with colorectal carcinoma whose initial symptom was acute abdomen: large bowel obstruction in 30, perforation of the oral-sided intestine 7, acute appendicitis 6, abscess 3, intussusception 3, fistula formation and invasion to an adjacent organ 2, peritonitis 2, volvulus 1, obstructive colitis 1 and others 9. Pathological correlations were done with actual cases. CT with intravenous contrast media could well show these acute abdominal conditions and in many cases showed the tumors present. The modality presented hemodynamic conditions of affected bowel well. Multidetector-row CT provided additional precise information., although tumors were detectable by CT in many cases, some appendiceal and cecal carcinomas could not be shown because of accompanying acute appendicitis and/or abnormal cecal position.

Conclusion: Helical CT with intravenous contrast media provides detailed information for cancer diagnosis and management of patients suffering acute abdominal pains caused by colorectal carcinomas. Familiarity with the variety of acute abdominal conditions caused by colorectal carcinomas should improve diagnostic accuracy.

C-0147

Distributions of periods, sites and appearances of metastases from early and advanced gastric carcinomas

Y. Kobashi, Y. Imanishi, N. Tachizawa, M. Yanagihara, S. Sakaino, M. Yoshimatsu, N. Bhattacharai, K. Ishizuka, Y. Nakajima; Kawasaki/JP

Learning Objectives: To learn the appearances of metastatic lesions in various organs in conventional imaging modalities and distributions of metastatic periods and sites from early and advanced gastric cancers.

Background: It is very important in a long-range plan of follow-up examinations in a patient with gastric cancer for radiologists to know about distributions of metastatic periods of gastric cancers from first detection, metastatic sites and their frequencies. However, they have not been reported in detail.

Procedure: In 401 patients with gastric cancer, we investigated the distribution of periods from first detection, the sites and appearances of 494 metastatic lesions. Ninety-five percent of first metastases from advanced gastric cancers were seen within 4 years after primary tumor detection. However, early gastric cancers had three peaks of within a year, 3 and 7 years. The metastatic lesions were in 12 sites including liver, ovary, lung, bones, brain, adrenal glands and spleen. At primary tumor detection, both early and advanced gastric cancers showed the same distribution of metastatic sites, except for peritoneal and ovarian metastases in advanced gastric cancers. Adrenal metastases were prominent on the left side. Sixty-one percent of metastatic bone lesions were osteosclerotic and 11% of them showed beautiful bone scan.

Conclusion: Early and advanced gastric cancers were different in site and period of metastasis. Eight-year observation was necessary for an early gastric cancer although 4-year observation was enough for an advanced gastric cancer. In an early gastric cancer, follow-up examinations were necessary within a year, at 3-4 years and at 6-7 years from the detection.

C-0148

The imaging findings of primary gastric lymphoma in children

U. Zaleska-Dorobisz, J. Weclawek-Tompol, B. Kazanowska; Wroclaw/PL

Purpose: Primary gastric Non-Hodgkin Lymphoma (NHL) in childhood is rare. It was found in less than 2% of NHL pediatric patients. The aim was to illustrate the imaging findings of primary gastric lymphomas in children.

Material and Method: We reported four children with primary gastric lymphoma detected by ultrasound imaging. The imaging findings (US, Contrast-enhanced US, CT, MR) revealed large tumors of the stomach wall with markedly thickened gastric wall.

Results: Histologically three tumors were evaluated as Burkitt's lymphoma. One tumor was with histopathological diagnosis as lymphoblastic T-cell lymphoma. Clinical symptoms were nonspecific. Abdominal pain, anemia, vomiting, constipation and rapidly growing abdominal tumor were observed before admission. In 2 cases we had trouble obtaining remission after first cycle of chemotherapy. We decided to qualify these children to more intensive chemotherapy with second-look surgery. Two patients were qualified to autologous bone marrow transplantation. All patients are in complete remission.

Conclusion: Primary gastric lymphomas are a very rare tumor in children. This may cause diagnostic difficulties. US and CT is very important in the diagnosis and monitoring of treatment of gastric lymphomas. Contrast US and MR are useful to assess the tumor staging regarding invasion to the gastric wall, perigastric tumor involvement and neovascularisation.

C-0149

The role of spiral CT colonography as a routine method in patients after incomplete conventional colonoscopy

J.M. Pienkowska, E. Szurowska, J.M. Wierzbowski, M. Czarnowska, G. Rompa, M. Studniarek; Gdansk/PL

Purpose: The aim of this study was the estimation of the role of spiral CT colonography (SCTC) as a routine method in patients with incomplete conventional colonoscopy.

Material and Methods: A total of 28 patients with strong clinical suspicion of colorectal cancer underwent SCTC with the use of a standard protocol. Conventional colonoscopy was incomplete due to stenosing lesions in all cases in this study. All results were correlated with histopathologic findings.

Scientific and Educational Exhibits

Results: In all cases conventional colonoscopy was incomplete because of occlusive lesions which could not be transversed endoscopically. SCTC reached the cecum in all cases and correctly detected 19 cancers (sensitivity 100%), seen at conventional colonoscopy. Additionally, two synchronous tumours and five polyps located in the colon proximal to the stenosing lesion were identified. In 4 patients liver metastases and in 9 patients local, pericolic fat extension and in 7 lymphadenopathy were detected.

Conclusion: SCTC reaches the entire colon even in cases of occlusive colorectal carcinoma. Additionally the method is able to simultaneously assess other abdominal organs. It can be used as a routine method in patients with incomplete conventional colonoscopy for detection of colorectal cancer and for treatment planning.

C-0150

Barium contrast studies in Crohn's disease: Still fundamental?

M. Certo, R. Themudo, R. Santos, P. Varzim, A. Ferreira, A. Ribeiro; Porto/PT

Learning Objectives: To illustrate the importance of contrast study findings in classical and rare presentations of Crohn's disease.

Background: Crohn's disease is a condition of chronic inflammation potentially involving any location in the alimentary tract, but with a propensity for the distal small bowel and proximal large bowel. Nearly one half of all patients have disease affecting both ileum and colon. Another one third have disease confined to the small bowel, primarily the terminal ileum and in very rare cases the jejunum too. Gross involvement of the oesophagus, stomach and duodenum are rare. Clinical behaviour can be roughly divided in the two categories of penetrating and fibrostenotic. The diagnosis is established through a total assessment of the clinical presentation with confirmatory evidence from radiographic, endoscopic and, in most cases, pathologic findings. Barium studies accurately define the anatomic location of disease and can discern evidence of active inflammation.

Procedure Details: We reviewed the contrast barium studies (barium enemas, small bowel follow-through studies and enteroclysis) in 245 patients with Crohn's disease from our inflammatory bowel disease unit. In our series, most of the patients have disease affecting the terminal ileum and the ileocolon as is reported in the literature. The colon is affected in about 19% of our cases and upper gastrointestinal involvement affects about 3% of our patients. We present the classic radiographical features, such as cobblestoning, ulceration, fistulae, sinus tracks, different strictures, etc.

Conclusions: Barium contrast studies are still important in the diagnosis, location, behaviour and extension of Crohn's disease.

C-0151

Contribution of conventional radiology in adjustable gastric procedures for morbid obesity

N. Costa, H. Marques, P. Alves, R. Marques, J. Barros, J. Mauricio; Lisbon/PT

Learning Objective: To illustrate the conventional radiological findings in patients who underwent laparoscopic adjustable gastric banding procedure (LAGBP): - post surgical evaluation; - detection of early and late complications.

Background: Morbid obesity is associated with secondary health problems, having an important downsizing effect on life expectancy. LAGBP has gained importance due to low invasiveness and adjustability. Since 2001, LAGBP has been performed in the treatment of morbid obesity in our hospital in a total of 63 surgeries. The early and late post-surgical radiological evaluation was performed in our department. The main radiological evaluation items and the complications are reported and illustrated.

Procedure Details: In the early follow-up (first 48 h), we used water-soluble contrast agent to access the band position, size and morphology of gastric pouch, stomal width and presence of complications. Whenever complications were suspected we used the same contrast. In the late follow-up (6 to 8 weeks, 12 months) we used barium sulfate contrast agents, to access the stomal width and direct its adjustability. All of the parameters reported in the early follow-up were again investigated, paying particular attention to complications (pouch dilatation, slippage, system disconnection and transmural band penetration).

Conclusion: Single contrast conventional radiology is the method of choice for detecting the main complications as well as directing and monitoring band adjustment.

C-0152

Recurrence patterns after curative resection of colorectal cancer: Emphasis on comparison between colon cancer and rectal cancer

S. Shin, Y. Jeong, H. Kang, H. Lim, Y. Kim, J. Park, J. Oh; Gwang-Ju/KR

Background: Postoperative surveillance for colorectal cancer is focused on the early detection of potentially curable recurrent disease. Recurrence pattern of colorectal cancer can be reliably predicted based on the site of the primary tumor. In this exhibit, we will illustrate the recurrence patterns after curative resection of colorectal cancer with emphasis on distinguishing patients with colon cancer from those with rectal cancer.

Materials and Methods: Pathology records and 1127 CT studies of 437 patients with colorectal cancer were retrospectively reviewed. Overall median follow-up duration was 17.6 (range, 3-49) months. The recurrence pattern was determined based on the first site of recurrent disease after the initial operation.

Results: The most common site of recurrence was the liver in colon cancer. Recurrent disease was seen in the retroperitoneal lymph nodes, lung, and pelvic mass in decreasing order of frequency, whereas the pelvic mass or locoregional recurrence was the most frequent pattern in rectal cancer. Recurrent disease was seen in the lung, liver, and retroperitoneal lymph nodes in decreasing order of frequency.

Conclusion: It should be recognized that the common sites of recurrence are different in frequency according to the site of the primary tumor and postoperative surveillance must be focused on the most frequent site of recurrence.

C-0153

Immunoscintigraphy in the management of colorectal carcinomas

V. Artiko, V. Obradovic, N. Petrovic, M. Petrovic, Z. Krivokapic; Belgrade/YU

Purpose: The aim of the study is detection of the recurrences and metastases of colorectal carcinomas by immunoscintigraphy.

Materials and Methods: Fourteen patients were examined (13 with adenocarcinomas of caecum, colon and rectum and one with squamocellular colonic carcinoma) from 4 months till two years after surgery, two of them after two months after the end of radiotherapy. Planar scintigrams (tomography when necessary) of thorax, abdomen and pelvis were done after from 10 min till 96 h after i.v. injection of Oncoscint CR-103, containing monoclonal antibodies B72.3 labelled with 150 MBq 111-In.

Results: In 12 patients recurrences of carcinomas (5-12 cm), in 6 recurrences with liver metastasis, and in two only liver metastases were detected by immunoscintigraphy and confirmed by surgery. Planar immunoscintigraphy was positive in 8/8 patients with liver metastases and 9/14 patients with recurrences while in 5/14 recurrences were detected only by tomography. US was positive in all patients with liver metastases, CT finding was falsely negative in two patients with recurrence, while MR imaging in one. In three patients with recurrences, CEA blood level was not increased. In 4 patients intensive accumulation of labelled antibodies was observed in colostomas, in one with granuloma, as well as in one with recurrence of squamocellular carcinoma.

Conclusion: Oncoscint CR-103 can be useful in diagnosis of recurrences and metastases of colorectal carcinoma, viability assessment after radiotherapy and in the choice of adequate surgical treatment depending on the spread of the disease.

C-0154

withdrawn by authors

C-0155

Sonography and CT in duodenal pathology

E. Blanc, J. Cogollos, T. Ripollés, M. Martínez, M. Monedero, R. Pastor-Juan; Valencia/ES

Purpose: The duodenum is a segment of the gastrointestinal tract that due its intraperitoneal and retroperitoneal location and the proximity to other organs and structures, can be involved by a multitude of primary and secondary processes. The purpose of the study was to describe sonographic and CT findings of duodenal pathological conditions: congenital, traumatic, inflammatory, postsurgical and neoplastic disorders.

Methods and Materials: 58 patients with duodenal pathology diagnosed with sonography and CT were retrospectively reviewed from 1996 to 2003.

Results: We found the following pathologies: - *Developmental anomalies:* Congenital diverticula (some of them complicated with diverticulitis), intestinal malrotation and annular pancreas. - *Inflammatory conditions:* Duodenal ulcers (complicated with perforation or penetrating to the pancreas), secondary involve-

Scientific and Educational Exhibits

ment from pancreatitis (pancreatic pseudocyst in duodenal wall and intramural hematoma), groove pancreatitis, secondary inflammation of duodenum from cholecystitis, gallstone ileus with cholecystoduodenal fistula, Crohn disease and eosinophilic enteritis. - **Tumoral:** Benign primary neoplasms: lipoma, villous adenoma, leiomyoma and neurofibroma. Malignant primary neoplasms: adenocarcinoma, lymphoma and neuroendocrine tumor. Secondary duodenal involvement from other primary malignancies from stomach, pancreas, biliary tract and kidney. - Other more unusual pathologies found were: Traumatic duodenal perforation, intramural duodenal hematoma after surgery, foreign body (duodenitis from fish body ingestion), duodenal bezoar and aortoenteric fistula.

Conclusion: In this review of duodenal pathology we show how sonography and CT are reliable techniques in the study of this segment of gastrointestinal tract which can be involved in a multitude of primary and secondary diseases.

C-0156

Ultrasound of acute appendicitis: Spectrum of findings and role in the treatment planning

E. De Lama Salvador, C. Canas, M. de Albert, A. Guma, F.J. Garcia-Barriga, H. Aranda; Barcelona/ES

Learning Objectives: To describe the typical US findings of appendicitis, and to discuss the role of US in the clinical management. To describe the US findings of other entities that can mimic acute appendicitis

Background: Acute appendicitis is a common clinical problem. Accurate and prompt diagnosis is essential to minimize morbidity. The atypical presentations may result in diagnostic confusion and delay in treatment. US is a highly accurate means of establishing the diagnosis and it has now assumed a critical role in the treatment planning of patients suspected to have appendicitis. In addition, US can be used to guide abscess drainage treatment in patients with perforation.

Procedure Details: A retrospective review of medical charts and US of all cases of surgically proved appendicitis seen in our hospital in the last 2 years. US examinations were initially done using a broadband 4-7-MHz convex-array transducer, a broadband 5-10-MHz linear-array transducer and the graded-compression technique described by Puylaert. We illustrate the diagnostic findings of appendicitis, which were based on a set of eight criteria derived from reports in the literature and can be grouped into the two categories of appendiceal and periappendiceal findings. US findings of other entities mimicking appendicitis are also reviewed.

Conclusion: The effect of US on the management of acute appendicitis is considerable because it has decreased the rate of negative appendectomies and the number of appendiceal perforations. Moreover, the less severe disease observed indicated the earlier detection of appendicitis and the earlier initiation of treatment, which may explain the significant decrease in complications.

C-0157

Contrast-enhanced abdominal CT scan without bowel preparation for detection of colorectal polyps: A prospective comparative study

S.T. Bodewitz, M.H.J. Voormolen, J.M. Jansen, K.H. Schuur, W.N.H. Stuifbergen, A.W.M. van Milligen-de Wit, L.H. Visser; Tilburg/NL

Purpose: Virtual colonoscopy (VC) is as effective as conventional colonoscopy for detection of adenomatous polyps larger than 1 cm. However VC is time consuming, involves high radiation dose, requires bowel preparation and workstation processing. In order to develop a relatively simple screening method for colorectal polyps for both the radiologist and patient, the value of contrast-enhanced abdominal CT scan without prior bowel preparation was evaluated.

Methods: Prospective double-blind follow-up study in 53 patients with high risk for developing colorectal malignancy. Contrast-enhanced abdominal CT scan with air insufflation in prone position without prior bowel preparation. Independent interpretation of 2D images by three radiologists. Size and location of polyps were noted. Contrast-enhanced lesions were looked for. Final findings were scored upon corresponding interpretations by two or three radiologists. Colonoscopy ('gold standard') was used for reference without knowledge of CT findings.

Results: Thirteen patients were excluded because of incomplete colonoscopy or uncertain histology. In 40 included patients (mean age 60 (34-75 y), M:F = 28:12) colonoscopy showed adenomatous polyps in 16 patients (40%), CT in 10 patients (25%). CT showed 2 false positive findings (5%). Suboptimal interpretation due to faeces and/or bowel spasm in the entire or part of the colon in 1 (3%) and 10 patients (25%) respectively. Sensitivity, specificity, positive and negative predictive value of CT screening were 63%, 92%, 83% and 79% respectively. Interobserver variability was large ($\kappa < 0.5$).

Conclusions: We do not recommend contrast-enhanced abdominal CT scan without prior bowel preparation as screening method for colorectal polyps in high risk patients.

C-0158

Computed tomographic evaluation of serosal invasion and regional lymph node metastasis in colorectal adenocarcinomas

N. Tuncbilek, O. Okten, H. Sezer, F. Tokatli, M. Kaldir; Edirne/TR

Purpose: Tumor prognosis in colorectal carcinomas is determined by many factors. These prognostic factors may be used to choose suitable treatment and to develop new treatment strategies. We assessed the role of computed tomography (CT) in the presence of serosal invasion and regional lymph node metastasis of colorectal carcinomas.

Materials and Methods: The study group consisted of 39 patients (27 men, 12 female) aged between 29 and 82 (mean 59.9). Colorectal adenocarcinoma was diagnosed in all cases histopathologically. The cases were evaluated preoperatively with CT using oral and intravenous contrast material. The findings were correlated with CT features and histopathological data by using Kappa analysis.

Results: Serosal invasion and regional lymph node metastasis of tumor correlate well with CT scan and histopathologic findings and accuracy rates of 74% and 69% (sensitivity ratio: 96.2%, 94.4% and specificity ratio: 31%, 47.6%) (Cohen's kappa = 0.318; $p < 0.05$; 0.405; $p < 0.05$) were found respectively. The accuracy ratio of CT in TNM classification was found as 67% (26/39) (Cohen's kappa = 0.327; $p < 0.05$). The mean survival rate was 48.3 months. Survival rate for four years was 40.7% with regional lymph node metastasis and 62.5% without lymph node metastasis.

Conclusion: CT is reliable for confirming spread of advanced cancers through the bowel wall but is less useful in excluding such spread. A preoperatively performed CT enables the determination of the accurate treatment process by identifying serosal and regional lymph node metastasis and an indirect method of prognostic estimation in colorectal carcinomas.

C-0159

Staging of gastric cancers by computed tomography

N. Tuncbilek, O. Okten, H. Sezer, F. Tokatli; Edirne/TR

Purpose: Ultrasonography, CT and MR imaging can be used in preoperative staging of gastric cancers. The depth of the gastric wall invasion is one of the most important factors determining the prognosis in patients with gastric cancer. We evaluated the role of CT in determination of extraserosal invasion and staging in the preoperative assessment of gastric cancers.

Materials and Methods: We evaluated 21 patients (age range; 30-76; mean: 64.05) with gastric cancer using CT imaging in the preoperative period. The findings were correlated with CT features and histopathological data by using Kappa analysis.

Results: CT findings of extraserosal invasion of tumor correlate well with CT scan and histopathologic findings and accuracy rates of 85% (sensitivity ratio: 86.7% and specificity ratio: 83.3%) were found (Cohen's kappa = 0.667; $p < 0.05$). The accuracy ratio of CT in TNM classification was 66% (14/21) (Cohen's kappa = 0.491; $p < 0.001$). On the other hand, in classification of low and advanced stages, this ratio was 76% (Cohen's kappa = 0.483; $p < 0.05$).

Conclusion: Accurate diagnosis is now a highly specialized, intensive, multidisciplinary undertaking applicable both to early cancer and to less advanced stages of invasive cancer. CT imaging, performed preoperatively, is useful to evaluate the extraserosal invasion of gastric cancers with high accuracy rate so it can be used as a guiding method in treatment management and in estimation of prognosis. CT becomes useful to evaluate distant metastasis or regional spread when there is reason to consider avoiding or modifying plans for surgery. CT is clearly useful as both a baseline and assessment test when the physician contemplates chemotherapy.

C-0160

Reducing non-attendance rates for barium enemas through enhanced booking procedures

C.J. Garvey, L. Abraham, I. Furmidge, E. Holme; Liverpool/UK

Learning Objectives: To illustrate how enhanced booking procedures can reduce non-attendance rates for radiological investigations e.g. barium enemas, and to assess the impact on departmental efficiency.

Background: 10-15% is a typical non-attendance rate for barium enemas in the UK. Studies indicate poor patient satisfaction with current systems, largely due to lack of choice when scheduling appointments. Furthermore, many non-attenders will be referred again for investigation increasing demand. This has a detrimental effect on departmental efficiency.

Procedure Details: Following pilot work by the NHS Modernisation Agency, a new booking system was set up. A new referral form was designed in consultation with interested parties. Patients come directly from clinic with the form and

Scientific and Educational Exhibits

are greeted by a trained clerk. The test is explained and queries answered, preparation and instructions are supplied and a choice of appointments offered. Follow-up clinic appointments can be scheduled. Following these changes, non-attendance rates have dropped to 2-3% and this has been sustained over a 2 year period. Follow-up studies confirm improved patient satisfaction and further modifications have been introduced. Abolition of re-referral for non-attenders has reduced variation in demand and allowed better capacity/demand matching.

Conclusion: Improved booking procedures offering choice reduce non-attendance rates to an acceptable level, increase patient satisfaction and improve departmental efficiency. This model can be extended to many areas within a radiology department.

C-0161

Radiological review of lymphoma involving the gastrointestinal tract

P. Litter, C.J. Garvey; Liverpool/UK

Learning Objectives: Understand the radiological appearances and the complications of primary and secondary lymphoma involving the gastro-intestinal tract (GI tract). An educational text will accompany the images.

Background: Lymphomas involving the GI tract are predominantly of the non-Hodgkin's type (NHL) and are frequently on a background of immunosuppression. They may be primary, developing from lymphoid elements in the bowel wall or secondary, due to direct invasion of the bowel by locally involved lymph nodes. The commonest site of involvement is the stomach, followed by the small bowel and the colon (caecum and rectum). The oesophagus is rarely involved. Multi-site involvement in the GI tract is common. NHL usually presents with peripheral lymph node enlargement. Patients with low grade lymphoma may present with symptoms of marrow suppression such as anaemia or bleeding. Lymphoma affecting the GI tract may present with symptoms of obstruction, abdominal pain from intussusception or malabsorption due to small bowel involvement. If lymphoma affects the GI tract alone, it may mimic other pathology. Computerised tomography (CT) is very useful in the initial diagnosis, staging and follow-up of patients with lymphoma involving the GI tract.

Procedure Details: Multiplanar CT and barium studies will be used to illustrate the key radiological findings.

Conclusion: Lymphoma is an increasingly common malignancy and accurate diagnosis and treatment are crucial. This pictorial review will familiarise radiologists with the imaging appearances and complications of GI lymphoma.

C-0162

MR imaging staging of rectal carcinoma, pre and post chemoradiation, with histological correlation

S.D. Allen, A. Padhani, A.S. Dzik-Jurasz, R. Glynne-Jones; Northwood/UK

Purpose: To evaluate the accuracy of MR imaging staging of rectal carcinoma in patients undergoing chemoradiotherapy.

Methods: 24 patients with locally advanced rectal carcinoma were treated with chemoradiation and subsequently either had total mesorectal excision or abdominal-perineal resection. MR imaging was performed pre and 6 weeks post chemoradiation. Tumour morphology, extramural spread (including distance to mesorectal fascia, which forms the surgical circumferential resection margin, CRM), nodal presence and characteristics, overall TNM staging and post radiotherapy changes were recorded. Histopathology was subsequently examined for comparison.

Results: The majority of the patients in the study had extensive local disease. Prior to chemoradiation, MR staged 4.2% T2N0, 4.2% T2N1, 33.3% T3N0 and 58.3% T3N1+/T4. Different morphological subtypes were identified with annular and polypoid being the most common. Each subtype demonstrated different signal characteristics pre and post chemoradiation. Mucinous tumours were often difficult to stage as residual mucin pools were often indistinguishable from viable tumour or nodes. Post chemoradiation down staging was well demonstrated on MR in 12/14 cases (85.7%), with exact nodal staging shown in 16/24 cases (66.7%). 9/10 N0 patients remained N0 post chemoradiation, and 10/14 (71.4%) nodal positive patients became Nodal negative following treatment, indicating significant regression. CRM and post radiotherapy changes were also well predicted.

Conclusion: Preoperative chemoradiotherapy is standard treatment for locally advanced adenocarcinoma of the rectum. MR imaging can assess response to treatment and can often accurately predict histology. Mucinous tumours were less well assessed though, and certain types of post treatment fibrosis were indistinguishable from viable tumour.

GI Tract

Esophagus

C-0163

New method of evaluating pericardial invasion of esophageal cancer in 22 subjects using electrocardiogram-gated multislice computed tomography and compared with histological findings

K. Shuto, S. Okazumi, N. Yanagawa, T. Ochiai; Chiba/JP

Purpose: Evaluation of whether invasion of esophageal cancer (EC) stops at the adventitia or invades other organs is important because invasive EC is not amenable to surgery. Pericardial invasion, especially of the left atrium (LA), can be difficult to evaluate because of its pulsation. We tried to evaluate EC invasion to LA using ECG-gated enhanced multislice CT to eliminate the influence of pericardial pulsation.

Materials and Methods: Retrospective ECG-gated MSCT (Light Speed Ultra 16, General Electric) was performed in 22 subjects (17 male) with EC. Thirty seconds after intravenous injection of contrast, CT scanning was performed and images were reconstructed every 10% of the R-to-R interval (0-90%).

Results: In 21 subjects, in the 70% interval when the LA contracts, we could observe a low attenuation CT area between the LA and EC. But in the 40% interval, we could not observe a lower attenuation CT area between them. 4D movies using 10 phase data revealed the LA contracts separately from the EC, and we determined that the EC did not invade to the LA. All 21 subjects underwent surgery and none had EC invasion to the LA at histology.

Conclusions: ECG-gated MSCT can eliminate the influence of pericardial pulsation, and if there is no EC invasion of the LA, there is a low attenuation CT area between them during atrial contraction and in 4D images there is separate movement between them. This modality may become a useful tool to evaluate EC invasion of the pericardium.

C-0164

High resolution MR imaging of the anatomy of the oesophagus and surrounding posterior mediastinal structures

A.M. Riddell, C. Davies, A. Wotherspoon, G. Brown; London/UK

Purpose: Surgical resection for early stage oesophageal adenocarcinoma offers the longest disease free survival. Locoregional recurrence however remains the main cause of recurrent disease and tumour close to the circumferential resection margin (< 1 mm) has been shown to reduce survival. The aim of our study was to use high resolution MR imaging to: (1) Depict the oesophagus and its relationship to surrounding anatomical structures; (2) Identify fascial planes which could represent potential surgical resection margins and (3) Determine the importance of these structures in defining resectability.

Materials and Methods: High resolution T2W images of the thorax were performed on two cadaver specimens and patients prior to oesophageal resection. Comparison was made between structures identified on axial MR images of cadaveric and *in vivo* sections at corresponding anatomical levels with wholemount histological sections.

Results: High resolution MR imaging defined the layers of the oesophageal wall and clearly depicted surrounding structures such as the azygos vein and its tributaries, the prevertebral fascia and its attachments to the right oesophageal wall. Inferior to the level of the pulmonary trunk a band of connective tissue was identified arising from the aorta which encircled the lower oesophagus. Perioesophageal fat was situated beyond these fascial planes and extended to the parietal pleura laterally and the pericardium anteriorly. These structures were confirmed histologically.

Conclusion: High resolution MR imaging demonstrates detailed anatomy of the posterior mediastinum. Fascial planes described by the study will potentially be of importance for local staging of oesophageal cancer and surgical planning where indicated.

C-0165

Comparative observation on different interventional procedures in benign esophageal strictures

Y.S. Cheng, M.H. Li, K.Z. Shang; Shanghai/CN

Purpose: To determine the most effective interventional procedure in benign esophageal strictures.

Material and Methods: Different interventional procedures were used to treat benign esophageal strictures in 180 cases including pneumatic dilations (group A, n = 80), permanent (group B, n = 20) and temporary (group C, n = 80) placement of expandable metal stents.

Scientific and Educational Exhibits

Results: In group A, 160 dilations were performed (mean, 2.0 times per case). Complications in group A included chest pain (n = 20), reflux (n = 16) and bleeding (n = 6). Dysphagia relapse (DR) occurred in 24 (30.0%) and 48 (60.0%) cases respectively during 6-and-12 month follow-up periods in group A. In group B, 20 uncovered or partially covered or antireflux covered expandable metal stents were placed permanently, complications included chest pain (n = 9), reflux (n = 13), bleeding (n = 3), stent migration (n = 3) and DR occurred in 3 (15.0%) of 20 cases and 5 (31.3%) of 16 cases during the 6-and 12 month follow-up periods respectively. In group C, 80 partially covered expandable metal stents were temporarily placed in 80 cases and removed after 3-7 days via gastroscopy, complications including chest pain (n = 32), reflux (n = 10), bleeding (n = 13) and DR occurred in 8 (10.0%) of 80 cases and 12 (16.0%) of 75 cases during the 6-and-12 month follow-up periods respectively. The placement and withdrawal of stents were all successfully performed. The follow-up of all cases lasted for 6 to 103 months.

Conclusion: The effective procedures for benign esophageal strictures are pneumatic dilation and temporary stent. Temporary stent is one of the best methods for benign esophageal strictures.

C-0166

Barium esophagogram versus upper endoscopy for the screening of esophageal varices in patients with compensated cirrhosis: A blinded prospective study

D. Fischer, E. Farber, R. Eliakim, N. Beck-Razi, A. Angel, D. Gaitini, S. Linn, Y. Baruch; Haifa/IL

Purpose: To evaluate and compare the accuracy of barium esophagogram (BE) versus endoscopic gastroduodenoscopy (EGD) in diagnosing esophageal varices in patients with compensated cirrhosis and portal hypertension at an early stage. **Methods and Materials:** Sixty-one patients with liver cirrhosis were diagnosed by liver biopsy (62% postnecrotic, 14.5% NASH, 14.5% alcohol, 5% autoimmune hepatitis and 4% PBC. 87% were Child-Pugh's score A and 13% were Child-Pugh's B). They were subsequently evaluated by EGD using Japanese General Criteria as the gold standard, and BE for the presence and size (small, large) of varices. BE was performed within three weeks of endoscopy, with 98% barium sulfate (E-Z-HD), as suspension adjusted for double contrast studies and barium paste (E-Z, 60%, esophageal cream) for mucous coating.

Results: All large varices (F2-F3) were diagnosed by BE. Sensitivity declined with small varices (F1) to 71.5%. The overall sensitivity of BE was 89%, the overall positive predictive value was 89.2%. The correlation between EGD and BE was high, $r = 0.75$; $p < 0.0001$.

Conclusions: BE can be used as a non-invasive procedure for the screening of patients with varices and compensated liver disease at a minimal cost. Furthermore, using BE will preclude universal prophylaxis with beta-blockers.

C-0167

Digital cineradiographic study of swallowing in infants with neurologic disease: Our experience

G. Runza¹, F. Barbiera², F. Cademartiri³, M. Bellia¹, M. Galia¹, F. La Seta¹, M. Midiri¹; ¹Palermo/IT, ²Sciaccia/IT, ³Rotterdam/NL

Learning Objectives: To display the findings and clinical role of digital cineradiography in the evaluation of swallowing disorders in children with neurological or severe developmental disability. To determine the best feeding protocol and improve the nutritional status based on administration of oral contrast material with different consistency.

Background: Severe neurological and developmental disorders in children can determine recurrent respiratory infections, asthma and hospitalization in intensive care units for acute respiratory failure. The diagnosis of these disorders enables proper therapeutic solutions which will significantly improve the nutritional status of the patient while reducing the risk of lung infections. From March 2001 to July 2003 12 children (8 males, mean age 6.2 years) affected by severe neurological or psychomotor disorders were evaluated.

Procedure Details: The dynamic study of the swallowing was performed for recurrent pulmonary infections and/or dysphagia with weight loss. All the examinations were performed with radio-controlled equipment provided with a digital C arm. Using this technique, in all 12 patients it was possible to differentiate those with disorders of the oral and/or pharyngeal swallowing phase (9/12) from those without swallowing dysfunction (3/12). We will show the findings of digital cineradiography, the role of the radiological information relevant for clinical and therapeutic management and the different protocols that we use to address the problem of the type of food more suitable for optimal feeding.

Conclusion: The dynamic swallowing study with digital technique allows a clear-cut evaluation of the swallowing process with minimum discomfort for the patient.

GI Tract

Peritoneum

C-0168

The place of peritoneography in the evaluation of chronic groin pain compared with ultrasound and CT: A forgotten technique gets its due.

A retrospective study of 112 patients

R.A. Salgado¹, M. Maes¹, P. Bellinck², B. Op de Beeck¹, J.-L. Termote², P.M. Parizel¹; ¹Edegem/BE, ²Lier/BE

Purpose: To assess the usefulness of peritoneography in the evaluation of patients with chronic, indeterminate groin pain.

Materials and Method: 112 consecutive patients with groin pain who underwent a peritoneography during a four year period were retrospectively reviewed. The results were compared, when available, with the findings on CT, ultrasound and surgical exploration.

Results: Peritoneography showed an occult hernia in 40/106 (38%) patients with a negative or inconclusive clinical examination. 24/40 (60%) of these patients underwent laparoscopic exploration, which confirmed the hernia on all occasions (100% positive predictive value). In 9 patients peritoneography also revealed an asymptomatic hernia on the contralateral side. Of the 58/106 (54%) patients who showed no abnormality on peritoneography, 41/58 (70%) showed clinical improvement with time without surgical intervention. Eventually, no specific diagnosis could be found in 45/106 cases (42%). Three patients had a positive clinical examination for an inguinal hernia which was, on all cases, confirmed with peritoneography. Intraperitoneal injection could not be accomplished in two patients. One patient had injection of contrast into the colon, which required no significant intervention. An abdominal CT examination was performed in 22/112 (19.6%) patients, revealing an inguinal hernia on only one occasion. Thirty patients (26.7%) also underwent an ultrasound examination, clearly demonstrating an inguinal hernia in only three occasions.

Conclusion: Peritoneography is a safe and reliable technique in ruling out or demonstrating an occult hernia in patients with chronic unexplained groin pain. It is clearly superior in this respect to CT and ultrasound.

C-0169

Pictorial review of pneumoperitoneum: X-rays with CT correlation

P. Rajiah, A. Khan; Manchester/UK

Learning Objectives: A. To recognise the signs of pneumoperitoneum in a supine film. B. To correlate plain film findings of pneumoperitoneum with CT scan findings. C. To understand the role and limitation of CT in the diagnosis of hollow viscus perforations.

Background: Pneumoperitoneum is an important radiological sign which indicates perforation of a hollow viscus. Prompt recognition is vital for early surgical management. The findings in a supine film are often subtle and a beginner can be easily misled thus resulting in errors. The aim of this exhibit is to demonstrate the subtle findings of pneumoperitoneum in a supine film and to correlate this with appearances on the CT scan.

Procedure: Abdominal X-rays were obtained in both in erect and supine positions. CT scan was performed in subtle cases to confirm the presence of gas in the peritoneum or retroperitoneum. Multiplanar reconstruction and lung window settings were used for demonstrating small amounts of intra/retroperitoneal air. The signs described include the football sign, Rigler sign, urachus sign, cupola sign, tell tale triangle sign, visualisation of umbilical ligaments/falciform ligament/ligamentum teres, scrotal air, visualisation of diaphragmatic slips, air around the spleen, subhepatic gas, triangular collection in Morrison's pouch and gas in lesser sac/paraduodenal region/gall bladder.

Conclusion: Diagnosis of pneumoperitoneum in an erect X-ray of the abdomen is straightforward. The signs are more subtle in a supine film. Recognition of these subtle signs is essential for prompt diagnosis of perforations. CT scans are helpful in doubtful cases and can demonstrate the exact site of perforation.

C-0170

Diseases of peritoneum, mesentery, and omentum: Spectrum of helical and multidetector-row CT findings

K. Furuya¹, I. Sakino², K. Yasumori¹, T. Muranaka¹; ¹Fukuoka/JP, ²Kitakyushu-City/JP

Learning Objectives: To demonstrate miscellaneous CT findings of the diseases of peritoneum, mesentery, and omentum. To assess the role of CT for differentiating the nature of them.

Scientific and Educational Exhibits

Background: Peritoneum, mesentery, and omentum play important roles as pathways for the spreads of various inflammatory process and malignancies. Great improvements in CT have made it possible to determine these precisely. The purpose of this exhibit is to present their numerous features and to assess the diagnostic value of CT in these disease. Multidetector-row CT images will be also demonstrated.

Procedure Details: We reviewed the Helical CT findings of 105 patients who showed peritoneal, omental and mesenteric abnormalities on CT and had confirmed diagnosis. They included peritoneal dissemination 61, pseudomyxoma peritonei 3, malignant mesothelioma 3, malignant lymphoma 1, polycythemia vera 1, primary serous papillary tumor of peritoneum 1, desmoid tumor 1, abscess 19, peritonitis 10, mesenteric hematoma 2, tuberculous peritonitis 1 and mesenteric ischemia 2. The review was focused on 1) Smooth thickening of parietal peritoneum, 2) Nodules or masses, 3) Increased fat attenuation 4) Ascites, 5) Fixation or dislocation of intestinal loop, 6) Wall thickening of intestine and 7) Involvement of the abdominal wall. The relationship of these findings and the nature of the lesion were assessed.

Conclusion: Although some abnormalities, especially peritoneal tuberculosis, hematologic malignancy, malignant mesothelioma, and peritoneal dissemination, are difficult to differentiate the nature of by CT, CT provides precise information regarding peritoneal, omental, and mesenteric abnormalities and is useful for the differentiation their nature. Multidetector-row CT gives us additional information.

GI Tract

Miscellaneous

C-0171

Focal fat stranding in computed tomography as a diagnostic tool in the acute abdomen

E.M. Dieguez-Costa, J. Borrego-Gomez, P. Fernandez, B. Gonzalez, S. Novo; Madrid/ES

Purpose: CT has been proven a useful method to evaluate those patients with acute abdomen because of its ability to display both mural and extraluminal abnormalities. The purpose of this study was to assess the diagnostic value of computed tomography in those diseases with focal pericolonic fat stranding as a dominant sign (exceeding other findings).

Material and Methods: The CT scans of 260 patients who were admitted to our institution because of acute abdominal pain were retrospectively reviewed.

Results: We found 214 cases with focal fat stranding in CT. Among them, the following diagnosis were obtained by CT: Diverticulitis (97), appendicitis (39), ischemic bowel disease (14), epiploic appendagitis (4), bowel infection (17), trauma (5), recent surgery (7), omental infarction (2), pancreatitis (20) and cholecystitis (9). The CT findings were; focal fat stranding, segmental bowel wall thickening, pneumatosis intestinalis, pneumoperitoneum, fluid collections and abscesses, ascitis, diverticula and bowel obstruction. We found that in diverticulitis, appendicitis, epiploic appendagitis and omental infarction, focal fat stranding was greater than the degree of bowel wall thickening, being more obvious (although less specific) than other abnormalities.

Conclusion: Focal fat stranding as a prime finding is a valuable CT sign in patients with acute abdominal pain. It helps to narrow the broad differential diagnosis to four main entities; diverticulitis, appendicitis, epiploic appendagitis and omental infarction. The characteristic CT findings of each of these entities often leads to a final diagnosis.

C-0172

Normal anatomy and non-hernia pathology of the abdominal wall on cross-sectional imaging

J. Quintero¹, C. Pozuelo¹, C. Medrano¹, D. Mulattieri¹, S. Capurro², F. Tous³; ¹Badalona/ES, ²Barcelona/ES, ³Santa Coloma de Gramenet/ES

Learning Objectives: The purpose of this exhibit is to review normal anatomy of the abdominal wall by CT and to present the more usual non-hernia pathologies of the abdominal wall diagnosed in our institution.

Background: We revised all the reports for three years of abdominal CTs performed in our institution. We selected the cases where non-hernia pathology of the abdominal wall was present and they were read, retrospectively, by two radiologists who were unaware of CT findings. Usually the studies consisted of oral contrast, a 5-mm collimation, pitch: 1.5, 100 mL of contrast medium, rate: 2.5 mL/sec and with a delay of 70 sec. Since July 2001 from to July 2004 we found 6978 consecutive abdominal CTs. We encountered 87 cases (1.24% of the studies) of non-hernia pathology of the abdominal wall.

Procedure Details: To exhibit any cases of normal anatomy of the abdominal wall with their components: muscles, fascias layers, aponeurosis, ligaments, skeletal, vessels and nerves. The cases revisited were classified as: Congenital lesions: Urachal abnormalities (3) and omphalomesenteric duct abnormalities (1). Fluid collections: Hematoma (22), abscess and cellulites (10) and urinoma (3). Neoplasm: Primary malignancies (7), metastatic disease (10) and benign lesions (12). Miscellaneous: Vascular lesions (4), vascular grafts (7), calcifications (3) and subcutaneous gas (5).

Conclusion: Cross-sectional imaging provides an excellent, non-invasive means of evaluating pathologic processes of the abdominal wall. Specific observations on the nature, location, extent, and underlying causes of these lesions can be made, therapy planned and instituted, and follow-up accomplished.

C-0173

Multi detector CT in internal and external abdominal hernias:

A pictorial review

P. Rajiah, R. Sinha, J. Kirk, K. Irion, A. Khan; Manchester/UK

Learning Objectives: A. To illustrate the anatomy of normal peritoneal spaces and common sites of external and internal herniation, their pathogenic and demographic features. B. To learn the role and limitations of multi detector CT in diagnosis of abdominal hernias. C. To illustrate the imaging appearances of abdominal herniations, including Spigelian hernia. D. To recognise the CT features of complications of herniations.

Scientific and Educational Exhibits

Background: Abdominal hernia is a very common surgical problem. It can be external, internal or diaphragmatic. External hernia is herniation through a defect in abdominal wall. Internal hernias occur through peritoneal spaces. Diaphragmatic hernias occur through defects in the diaphragm, which can be congenital or traumatic.

Procedure: Abdominal X-ray is often the initial investigation in most patients who present with hernias and pain. CT scans were performed using a 4 slice GE scanner, after 1 L of oral contrast and 100 ml of i.v. contrast. Images were acquired from the dome of the diaphragm to just below pubic symphysis and were reconstructed in multiple planes. The hernias illustrated include midline defects (epigastric, hypogastric, umbilical), Spigelian, incisional hernias, inguinal, femoral, Littres, Richters, obturator, sciatic, perineal, lumbar and internal hernias.

Conclusion: Imaging plays an important role in diagnosing hernia, identifying the contents, demonstrating the anatomy, recognising complications such as incarceration, obstruction, strangulation, volvulus or underlying neoplasms and differentiating it from other similar conditions. Multi detector CT is the ideal method for elegant demonstration of the anatomy, especially with the multiplanar reconstructions. Early recognition of complications is an added advantage.

C-0174

Ultrasonographic visualisation of abdominal wall hernias

A. Djuric-Stefanovic, A. Ivanovic, D. Saranovic, D. Masulovic, B. Dobriserevic; Belgrade/YU

Learning Objectives: To exhibit the ultrasonographic appearance of different types of abdominal wall hernias. To show the possibilities of ultrasound in visualisation of hernial site, size, and contents of hernia sac. To correlate the ultrasonographic and surgical findings in 117 adult patients with different types of external abdominal hernias.

Background: Types of abdominal wall hernias are: ventral, umbilical, incisional, Spigelian hernia, lumbar, inguinal and femoral. Herniography, CT, barium studies and ultrasonography are the methods of possible diagnosis of hernia type, size and contents of hernia sac. Ultrasonographic examination of the abdominal wall enables visualisation of muscles and fascias of abdominal wall and consequently, the site, size and contents of hernia sac could be visualised. 117 adult patients with palpable suspected hernias underwent ultrasonographic examination between January 2003 and September 2004, and then they were operated upon. We will exhibit ultrasonographic appearance of different types of external abdominal hernias and correlate them with intraoperative findings.

Imaging Findings: Sonography was performed with a 7,5 MHz linear transducer, with the patient lying and with both relaxed and contracted abdominal muscles. The indication for ultrasonographic exam was a palpable mass of the abdominal wall which was clinically diagnosed as hernia. We will present the ultrasonographic appearance of two types of inguinal hernias: direct and indirect and criterions for their differentiation. Incisional, ventral and umbilical hernias of different sizes and contents will also be presented.

Conclusion: Ultrasonography of the abdominal wall is a convenient method for precise diagnosis of localisation, type, size and contents of abdominal wall hernias.

C-0175

High resolution ultrasound (HRUS) in small lesions of the abdominal wall

C.M.I. Brancaleone, C. Candia, C. Ambrogi, M. Blasetti, L. Tipaldi; Rome/IT

Pathology of the anterior abdominal wall is often overlooked in subacute/chronic abdominal pain. The purpose of this exhibit is to discuss the imaging findings of small abdominal wall lesions and present a pictorial comparative US and CT review of our findings. Twenty-six patients with subacute/chronic abdominal pain previously investigated by US and CT were evaluated by high resolution ultrasound (HRUS) of the anterior abdominal wall. Pathological lesions were revealed in 18 patients and included non iatrogenic (inflammatory, hernia, metastatic and neoplastic disease) and iatrogenic lesions (recent surgery, hematoma, incisional hernia, biopsic procedures). Good image quality was obtained with delineation of the rectus muscle, the three lateral abdominal muscles, the transverse fascia and the peritoneal line. Site of the lesions and extent of involvement was retrospectively compared to CT images. Dynamic scanning and repositioning were used in all cases. Contrast (Sonovue) harmonic imaging was used in 10 selected cases and compared to 10 normal subjects and this will also be depicted and discussed. HRUS appears to be a cost effective first line diagnostic tool for small unsuspected lesions of the abdominal wall. It requires meticulous technique and sound knowledge of HRUS anatomic-radiologic correlations and appears superior to CT in structure information.

C-0176

MDCT and MR imaging of abdominal inflammation: Beyond abdominal abscesses

J.L. Sancho¹, J.M. Vida², A. Luna³, R. Ribes², P. Ros⁴; ¹Andujar (Jaén)/ES, ²Cordoba/ES, ³Jaen/ES, ⁴Boston, MA/US

Learning Objectives: To describe the most important clinical and imaging findings of the different inflammatory conditions that may affect the abdominal cavity. To recognize and differentiate them from other entities by imaging. To evaluate the usefulness of the MR and MDCT in the diagnosis of abdominal inflammation.

Background: The spectrum of abdominal inflammatory conditions is extraordinarily ample. Although intraperitoneal abscesses represent a common cause of abdominal inflammation, especially in immunocompromised and postsurgical patients, many other entities such as pancreatitis, cholecystitis, appendicitis, epiploic appendagitis, inflammatory bowel disease, diverticulitis, radiation colitis, pelvic inflammatory disease, pyelonephritis, etc. must be taken into consideration.

Imaging Findings: We retrospectively review a group of patients with different abdominal inflammatory processes by MDCT and MR. This exhibition presents a comprehensive review of the distinctive features by MDCT and MR of the most clinically relevant abdominal inflammatory conditions, describing the key epidemiological, clinical and radiological features that may allow their diagnosis and differentiation from possible mimickers, especially neoplasms. A common imaging finding, although non-specific, is the presence of fat stranding that may help sometimes to differentiate them from other entities such as neoplastic processes.

Conclusion: MR and MDCT are valuable tools in the evaluation and characterization of the different inflammatory conditions that may affect the abdominal cavity.

C-0177

Anatomical considerations and imaging features of abdominal wall hernias: A pictorial review

R.R. Misra¹, P.J. Shorvon²; ¹High Wycombe/UK, ²London/UK

Learning Objectives: The aims of this poster are to review the indications for investigating potential hernias, to outline the important anatomical considerations for accurate diagnosis of hernias, to discuss the modalities available and their strengths in application, to illustrate the findings within the different modalities and to develop a suggested protocol for investigation.

Background: Radiology departments are increasingly being asked to diagnose potential abdominal wall hernias. A number of imaging modalities are available, all with their own strengths and weaknesses. High resolution near field ultrasound has taken a pre-eminent place in the detection of abdominal wall hernias. It can be performed in a dynamic manner asking the patient to cough or strain. Herniography is often considered the gold standard but requires injection of contrast into the peritoneal cavity. CT is good at identifying non-reducible hernias. MR imaging has the potential to replace CT and be used dynamically to identify hernias, which only occur during raised intra-abdominal pressure.

Imaging Findings: Ultrasound is the first line investigation but requires meticulous technique. Herniography may be negative in incarcerated hernias or those in concealed positions such as midline anterior hernias. To date, CT has not been able to demonstrate transient hernias which are only present during episodes of raised intra-abdominal pressure. Fast MR imaging techniques show promise in this latter regard, but the speed of herniation may still be too fast.

Conclusion: Radiologists and radiographers need to be familiar with both the anatomy of the abdominal wall and the appearances of hernias to allow accurate diagnosis.

C-0178

Detection and occurrence of retained surgical textilomas

R. Klaric-Custovic, N. Gotovac, I. Krolo, M. Marotti, N. Babic; Zagreb/HR

Learning Objectives: Retained surgical textile bodies are rare problem, but they occur at increased rate during stressful events. CT is the method of choice in diagnosing them. They are similar to several structures and processes, yet they have characteristics of their own.

Background: In our experience, textilomas are exceedingly rare. Several situations, such as war, natural catastrophes or terrorist attack can make the occurrence of textilomas more likely. Such situations happened in several hospitals during the war in Croatia, since they were in proximity to frontlines with large number of causalites. In all cases, acute textilomas resulted in a spongiform appearance, with a considerable amount of air trapped between textile fibres. Such air was the strongest diagnostic sign, together with a peripheral capsule and blood soaked rim. In most chronic cases calcifications were found and lesions did not enhance after administration of contrast media. We recorded 13 patients

Scientific and Educational Exhibits

that were admitted to CT for non-specific abdominal pain during period of 12 years. During one year of war, 9 cases of acute textiloma were found. Peroral contrast was given in six patients, while others were too weak or vomiting.

Conclusion: The procedure of choice is CT, where retained surgical material will be shown best due to entrapment of air inside textile material, while radio-opaque markers did not solve diagnostic problem completely. Calcifications are more common in chronic forms. There is no post-contrast enhancement. Despite precautions and care by surgical staff, textilomas are more likely to happen during war and similar events.

C-0179

Value of computed tomography in the follow-up of patients after laparoscopic repair of abdominal wall hernias

M. Moreno-Ramos, B. Vargas Serrano, E. Domínguez Ferreras, F. Castell Monsalve, M. Bustos Jiménez; Sevilla/ES

Learning Objectives: To illustrate the usefulness of CT in the follow-up of patients after laparoscopic repair of abdominal wall hernias in depicting normal findings as well as complications.

Background: Laparoscopic repair of abdominal wall hernias is a procedure that is replacing the open repair method because it is less invasive and has a lower rate of complications and recurrence. After surgery, CT is the procedure of choice to rule out complications or recurrence of hernias and to verify the normal appearance of the mesh. Within a 2 year period, 46 patients, 27 female (average age 57.25 years) and 19 males (average age 53.57 years) underwent laparoscopic repair of abdominal wall hernia in our hospital (43 ventral and 3 inguinal) and 28 abdominal CT were performed 10 to 304 days after surgery in the follow-up of 22 patients.

Procedure Details or Image Findings: 4 studies were not available. The other 24 CT examinations were reviewed with adequate visualization of the mesh in all cases. 8 cases were normal. CT detected recurrence of the hernia in 7 cases, fluid collections in 5 cases, fibrosis in 3 cases, wrinkling of the mesh in 3 cases and 1 abscess.

Conclusions: The laparoscopic approach is replacing conventional surgical repair for abdominal wall hernias. CT is a useful technique in the post-surgical follow-up of these patients, being able to detect recurrence of hernia as well as complications.

Breast

Biopsy

C-0180

Radiological and histological features of mammography screen detected lesions undergone benign surgical excision

D.D. Manuel, S. Bose, D.D. Evans, R. Wasan, G. Ralleigh, M. Michell; London/UK

Purpose: The development of modern image breast guided biopsy techniques including core biopsy and vacuum assisted core biopsy has improved the non-operative diagnosis for most screening mammography detected lesions, leading to a decrease in benign surgery. The aim is to describe the radiology and histology of benign screen detected lesions requiring surgical excision in our practice.

Methods and Materials: From April 1998 to March 2003, 155621 women were screened in the South East London Breast Screening Programme, 8836 women were assessed (5.7%), 182 benign lesions were surgically removed (0.1% of women screened). Radiological and histological features were recorded on a database.

Results: The primary histological diagnosis was: Fibrocystic change (FCC) (26%), radial scar/complex sclerosing lesion (CSL) (24%), fibroadenoma (FA) (14%), papilloma (11%), atypical ductal hyperplasia (ADH) (7%) and miscellaneous other (15%). The mammography features of benign lesions excised were well-defined mass (38%), microcalcifications (28%), stellate distortion (28%), asymmetry density (3%), other signs (4%). The commonest histology for each mammography sign was: Microcalcification: FCC (40%), papilloma (11%), FA (9%), ADH (8%), CSL (6%); well-defined mass: FA (28%), FCC (25%), papilloma (18%), CSL (10%); architectural distortion: CSL/radial scar (78%), only 16% in FCC with 6% in FA.

Conclusion: This study confirms that modern breast biopsy techniques decrease the need for surgery for benign lesions, particularly microcalcifications due to FCC. A further decrease in the need for surgical biopsy may be anticipated as techniques improve and data showing the effectiveness of non-operative diagnosis of such lesions as CSL/radial scar and papilloma becomes available.

C-0181

Controversial issues in atypia of the breast diagnosed by stereotactic 11-gauge vacuum-assisted biopsy: Systematic surgery or mammography assessment?

C.A.S. Labbe-Devilliers, P. Meingan, D. Loussouarn, L. Campion, M. Ricaud-Couprise; Nantes Saint-Herblain/FR

Purpose: To determine if some atypical lesions: Atypical ductal hyperplasia (ADH) and columnar cell with atypia (CCA), diagnosed at stereotactic 11-gauge vacuum-assisted biopsy (VAB) can avoid surgical excision and to define which patients may not need excision?

Methods and Materials: We reviewed retrospectively 570 patients who underwent VAB for breast microcalcifications, only 80 had atypical lesions alone ADH or CCA. We reviewed many characteristics for each patients about clinical presentation, mammography findings, histologic biopsy and the corresponding surgically excised tissue features. Because surgical excision was not performed or they were lost to follow-up, 26 patients were excluded.

Results: The 54 patients who subsequently underwent excision were the subject of this study. Data were statistically analyzed with the chi-2 test. Surgical excision of 54 atypical lesions revealed 19 missed carcinomas (35%). Four variables revealed higher-risk lesions on excision: Tumor size, number of specimens with microcalcifications, percentage of lesion removed and number of atypical foci. Whatever the combination of variable is, the rate of carcinoma involvement is still greater than 10%.

Conclusions: We recommend surgical excision for atypical lesions found after VAB.

C-0182

Can core biopsy be used instead of surgical biopsy in the diagnosis and prognostic factor analysis of nonpalpable breast cancer?

A. Özdemir, N.K. Voyvoda, N. Üzüm, A. Dursun; Ankara/TR

Purpose: To investigate the efficacy of US guided core biopsy (CB) in the diagnosis and prognostic factor analysis of nonpalpable breast cancer.

Materials and Methods: US guided CB was performed in 136 nonpalpable breast lesions, using 14 g semi-automatic needles. Mean number of core samples was 3.5 (range 3 to 6). Malignant lesions diagnosed with CB underwent therapeutic

Scientific and Educational Exhibits

surgical excision (SE). CB and SE results were compared for histological type, grade, estrogen and progesterone receptors (ER and PR), and c-erb-B2.

Results: Fifty-one lesions were malignant in CB (37.5%), with mean size of 17.8 mm (range 6 to 50 mm). Concordance between CB and SE was 83.9% (26/31) for histological type, 67.9% (19/28) for grade, 30.4% (7/23) for ER, 26.1% (6/23) for PR and 47.8% (11/23) for c-erb-B2. CB was insufficient to determine the histological type in four cancers (12.9%) which were reported as "infiltrating malignant." SE yielded positive (when negative on CB) or higher rates in 39.2% for ER, 34.8% for PR, 17.4% for c-erb B2 and 21.4% for grade. CB yielded positive (when negative on SE) or higher rates in 30.4% for ER, 39.1% for PR, 34.8% for c-erb B2 and 10.7% for grade.

Conclusion: Core and surgical biopsies demonstrated high concordance for histological type, moderate-to-high concordance for grade, moderate concordance for c-erb-B2 and low concordance for ER and PR. Relatively poor concordances may be related to tumor heterogeneity and may be decreased by increasing the sample number in core biopsy.

C-0183

SDAV percutaneous biopsy as an alternative to surgical biopsy in breast lesions with 12 G core biopsy disagreement

S. Sánchez, P. Martínez-Miravete, M. Sainz, M. Torres, E. Lag; Logroño/ES

Purpose: To show our experience with 11 and 8 gauge vacuum-assisted breast biopsy as an alternative to surgical biopsy, in breast lesions with 12 G core biopsy with disagreement result.

Methods and Materials: From January 2003 to August 2004, 607 core biopsies were performed. Rebiopsy with vacuum-assisted device was performed in 61 cases (10%): 6% with 8 G and 94% with 11 G. Fifty (90%) under ultrasound guidance and 6 (10%) with upright digital stereotactic device.

Results: Of the 61 lesions, the imaging finding were: 14 architectural distortion (23%); 8 asymmetric density (13%); 39 ultrasound nodules (64%). The degree of suspicious was: 1.5% BI-RADS™ 2; 41% BI-RADS™ 3; 56% BI-RADS™ 4 and 1.5% BI-RADS™ 5. Three cancers were diagnosed by SDAV (5%), just one was suspicious with core biopsy (1.5%), so there were two underestimations. Five lesions underwent surgical biopsy due to radio-pathologic disagreement. One new cancer was diagnosed (both systems were false negative). Fifty-three lesions were benign on percutaneous biopsy. After twenty months follow-up none of them required rebiopsy. There were 8 minor complications: 4 haematomas, 1 vasovaginal reaction, 1 traumatic skin lesion and 2 arterial bleeding.

Conclusion: 1. Vacuum-assisted breast biopsy is a valid alternative to surgical biopsy in lesions with radio-pathological disagreement at core biopsy. 2. It is a feasible technique with infrequent complications. False negatives and surgical biopsies can be avoided with a integrated radio-pathologic team approach.

C-0184

Psychological adjustment of stereotactic breast biopsy instrumentation procedures: About 73 cases

B. Barreau, S. Tastet, V. Picot, C. Henriquès, F. Valentin, R. Gilles, M.-H. Dilhuyd; Bordeaux/FR

Purpose: The objective was to investigate patient perceptions after stereotactic breast biopsy instrumentation, after the procedure and after the results.

Methods and Materials: From March 2002 to March 2003, a questionnaire (response type Likert) on stress was given to 73 patients who had breast biopsies procedures. The first time at the end of the procedure (T1) and after the histological diagnosis (T2). There are two groups of women: The first group (G1) corresponds to patients with a benign diagnosis ($n = 32$) and the group (G2) to patients with malignant diagnosis ($n = 32$).

Results: The questionnaire has been validated (analysis of principal component with varimax rotation). Three factors were identified: Procedure, quality of life, information and perception after biopsy. The responses were analysed with Chi-square. Only the "procedure" factor was different at T1 and T2 ($p = 0.022$). Compression was painful: 11% at T1 versus 21% at T2. Women were disturbed by local anaesthesia: 26% at T1 versus 21% at T2. Biopsy was painful: 6% at T1 versus 13% at T2. Examination is too long: 24% at T1 versus 35% at T2. The procedure is uncomfortable: 52% at T1 versus 54% at T2. Information satisfied patients in 90% cases. There was no statistically significant difference according to procedures and histological disease ($p = 0.0357$).

Conclusion: Information and medical empathy conditioned patients' perceptions. Patients tolerated the procedures well.

Breast

Digital mammography

C-0185

Computer aided detection (CAD) results for mammography in a diagnostic center environment

R. Salvador, F. Ramírez, X. Martínez, M. Salvador, D. Coll, R. Salvador Jr; Barcelona/ES

Purpose: The aim of this study is to review the results of a new CAD system applied to breast diagnosis.

Methods and Materials: We reviewed 48 patients consecutively sent to our institution for a core-biopsy sample on a BI-RADS 4 and 5 lesion found in a mammography previously obtained in our center. The CAD system was set at three different levels (high, medium and low threshold sensitivity) for each one of the two parameters evaluated (Tumor and Microcalcification clusters) were analyzed. All the marks were considered to obtain the NPV, PPV, sensitivity and specificity. The results were compared to the pathology analysis in the 22 infiltrating carcinomas (IC), 3 ductal carcinoma in situ (DCIS), 3 atypical ductal hyperplasias (ADH), and 20 benign conditions. A positive result was considered in three different scenarios, one IC, DCIS and ADH; two IC and DCIS; and three IC.

Results: The values for sensitivity at the higher level were 39.3%, 44% and 45.5% respectively for each scenario. Specificity 55%, 60.9% and 61.5%. PPV 55%, 55%, and 50%. NPV 39.3%, 50%, and 57.1%. Medium level values were sensitivity 39.3%, 44%, and 40.9%. Specificity 70%, 73.9% and 69.2%. PPV 64.7%, 64.7% and 52.9%. NPV 45.1%, 45.1% and 58%. And at the lower level sensitivity 53.6%, 60% and 59%. Specificity 55%, 60.9% and 57.9%. PPV 62.5%, 62.5% and 54.1%. NPV 45.8%, 58.3% and 62.5%.

Conclusion: The most advantageous setting was medium level of threshold and the scenario in which IC and DCIS were considered as a positive result.

C-0186

Clinical implication of phase contrast digital mammography using practical mammography equipment

T. Tanaka, K. Tsuchiya, N. Nitta, A. Furukawa, M. Takahashi, K. Murata; Otsu/JP

Purpose: To estimate clinical advantages of digital full-field phase contrast mammography (PCM) using a practical mammography equipment by comparing the digital mammograms printed in 25 micrometer pixels with conventional contact screen-film (S/F) mammography.

Methods and Materials: Our clinical tests have been conducted in a MLO direction on one side breast for PCM and S/F mammography. The mammography equipment used was customized for PCM so as to set an imaging plate of computed radiography away from an object by 49 cm, keeping the distance between a focal spot of X-ray tube and an object to be as 65 cm as in the conventional contact mammography. Focal spot size of molybdenum X-ray tube for PCM was 100 micrometers nominally, while focal spot size in S/F mammography was 300 micrometers. Each set of PCM and S/F mammograms for 38 patients was read independently by three qualified radiologists with expertise in mammography so as to evaluate each detectability of micro-calcification and nodules. The collected data was analyzed with ROC method.

Results: For micro-calcification, Az values are 0.9657 for PCM and 0.8874 for S/F. For nodule, those are 0.9651 for PCM and 0.9546 for S/F. Glandular architecture was depicted in PCM more clearly than in S/F.

Conclusions: Detectability for both micro-calcification and nodule in PCM are better than one in S/F. Clear depiction of glandular architecture in PCM suggests that PCM would be advantageous in dense breast mammography.

C-0187

Dose reduction and diagnostic accuracy in full-field digital mammography: A clinical study

G. Gennaro¹, H. Souchay², C. di Maggio¹, L. Katz², M. La Grassa¹, L. Pescarini¹, C. Alberelli²; ¹Padua/IT, ²Buc/FR

Purpose: Evaluate lesion classification changes with dose level in a diagnostic population undergoing direct digital mammography examinations.

Methods and Materials: A sample of 305 cases was collected, including 56 cancers, 153 benign lesions and 96 negative cases. Each patient had one view double-exposed with a full-field digital mammography unit (GE Senograph 2000D): One image at standard dose and another reducing dose. On basis of results from a previous phantom study, dose was reduced by 30% to 50% ac-

Scientific and Educational Exhibits

cording to breast thickness and composition. All images were anonymized for patient names and dose levels. Three experienced and independent radiologists using soft-copy reading, recorded findings of localization, type and confidence of presence. Images were classified using an extended 7-step BI-RADS scale. Lesion classifications were compared with the truth (histology or 2-years follow-up) and assessment differences between standard and reduced dose were evaluated.

Results: BI-RADS classifications at standard and reduced dose, referred to the truth, were not statistically different. P-values were 0.37 and 0.33, 0.69, 0.84 for overall and each individual radiologists, respectively. The applied dose reduction had no effect on false negatives, false positives, sensitivity and specificity.

Conclusion: Changes in lesion classification with FFDM dose reduction were not statistically significant in the population sample. The reader interpretation variability is much greater than the effect of dose reduction. Results support the opportunity of reducing dose in digital mammography without significant impact on clinical decision.

C-0188

Diagnostic pitfalls in digital mammography using a computerized assisted diagnosis (CAD) system

V. Annibale¹, F. Crinò¹, F. Bosurgi², A. Gambaro¹, F. Travaglini¹, A. Carriero¹; ¹Novara/IT, ²Siderno/IT

Purpose: To report our experience about diagnostic accuracy and CAD dependent pitfalls in a group of patients with breast cancer.

Methods and Materials: From January 2003 to August 2004, 83 consecutive patients with breast cancer, diagnosed by mammography and histologically confirmed, were studied both with digital mammography and with CAD. Patients were classified in three groups: Group A (CAD negative in both crano-caudal and oblique projections), group B (CAD negative either in crano-caudal or in oblique projection), group C (CAD positive in both projections).

Results: 71/83 (85%) of patients were considered positive by CAD system (group C), 9 (11%) partially negative (group B) and 3 (4%) completely negative (group A). 2 cases in group A presented as a nodule and 1 patient showed an area of parenchymal distortion. 5 patients in group B resulted negative in oblique projection and 4 resulted negative in crano-caudal projection. In the same group 4 cases presented as a nodule, 4 cases as nodules and calcifications and 1 case both parenchymal distortions and calcifications. In group C, 40 patients presented with mammary nodule, 7 microcalcifications, 17 parenchymal distortions and 6 combined lesions (ie. nodule with calcifications).

Conclusions: In our experience the use of CAD system in digital mammography resulted in uncertain help for the radiologist. In particular, the report of CAD assessed mammography can only be considered as a diagnostic aid and can not replace the complete clinical-diagnostic evaluation.

Breast

Magnetic resonance

C-0189

Locally advanced breast cancer: Magnetic resonance imaging versus clinical examination, mammography and ultrasonography in evaluation of residual disease after primary chemotherapy

M. Bodini, U.P. Marini, C. Fiorentino, L. Olivetti; Cremona/IT

Purpose: Primary chemotherapy (PC) is essential in the treatment of patients with locally advanced breast cancer. Magnetic resonance imaging (MRI) is the better tool for distinguishing fibrosis from richly vascularised neoplastic tissue and for evaluating tumour response to chemotherapy, namely tumour debulking and residual viability. The accuracy of MRI versus clinical examination, mammography and ultrasonography is evaluated.

Methods and Materials: Seventy-three patients with T2-T4, N0, M0 breast cancer were treated with 3-4 cycles of single agent epirubicin before definitive surgery. All patients were evaluated after PC with clinical examination and MRI. Forty out of 73 patients underwent also to mammography and ultrasonography. Size of any residual pathologic tissue was measured and the clinical and imaging dimension of the residual tumour were correlated with the pathologic specimen.

Results: Residual tumor assessed by MRI correlated with pathologic measurements (Spearman's $r=0.72$) better than residual tumor assessed by clinical palpation (Spearman's $r=0.58$). MRI attained better correlation to pathologic findings (Spearman's $r=0.74$; $p < 0.001$) than US ($r=0.55$; $p < 0.001$) and mammography ($r=0.32$; $p = \text{n.s.}$).

Conclusions: As compared to pathology specimens, MRI is able to represent the extent of cancer more accurately than clinical examination, mammography and ultrasonography. MRI is a promising technique in assessing the response of locally advanced breast cancer to PC. The current limit of MRI is the low specificity in predicting the nature of residual disease.

C-0190

Magnetic resonance imaging (MRI) in detecting early breast implant rupture: Report in 467 cases

S. Montemezzi, F. Fornasa, G. Barbazi, G. Puppini, A. Battistoni, A. Marchi, G. Gortenutti; Verona/IT

Purpose: To evaluate MRI accuracy in detecting early implant rupture as well as silicone gel bleeding.

Methods and Materials: From November 2000 to July 2004, 467 patients underwent MRI implant evaluation. MRI was performed by using Magnetom Symphony 1.5 Tesla (Siemens): The imaging protocol included Fast Spin EchoT2 weighted images and Turbo Inversion Recovery weighted images for silicone. 65/467 patients underwent surgery: MRI findings were correlated to surgical reports. 370/467 untreated patients were evaluated by clinical and/or MRI follow-up.

Results: MRI diagnosed implant rupture in 45 cases and gel bleeding in 7 cases. Surgery assessed implant rupture in 43/45 cases and gel bleeding in 7/7 cases; surgery showed a hematoma between the external shell and the capsule in 1/2 Patients who resulted MRI false positive for implant rupture. MRI did not assess implant rupture in 373/467 patients of whom 14 underwent surgery (negative in 11cases; early gel bleeding in 3cases): The retrospective analysis of those cases, detected as negative by MRI, showed a loose implant shell, assessed as radial fold, distinct from the capsule by a small silicone amount. MRI sensitivity, specificity, positive predictive value, negative predictive value and accuracy were respectively 94.3%, 99.4%, 96.1%, 99.1% and 98.8%.

Conclusion: In our experience, MRI has been effective in detecting early implant rupture. MRI diagnostic accuracy may be improved by assessing early silicone gel bleeding as well as differentiating between silicon gel bleeding and initial implant rupture, even if the latter is not clinically important because in both cases surgical removal of the implants is required.

C-0191

MR mammography of enhancing breast masses: Can MR predict carcinomas with a fibrotic focus?

M.L.A. Van Goethem¹, K. Schelfout¹, C. Colpaert¹, E. Kersschot², I. Verslegers¹, I. Biltjes¹, A. De Schepper¹, J. Weyler¹, P. Parizel¹; ¹Antwerp/BE, ²Aalst/BE

Purpose: To study whether dynamic MR mammography can predict the presence and the diameter of a fibrotic focus (FF) in breast carcinoma.

Methods and Materials: In a prospective study, 233 consecutive women with a

Scientific and Educational Exhibits

suspicious lesion underwent preoperative dynamic MR and 403 enhancing lesions were detected; 337 of them were masses. Enhancement pattern (homogeneous, non homogeneous, the presence of a less or later enhancing centre) and kinetic features of the masses were correlated with histopathological examination. **Results:** The prevalence of an FF in cancers with homogeneous enhancement, non homogeneous enhancement and cancers presenting with a centre was respectively 0%, 14.3% and 64.6%. Kinetic features did not help in the diagnosis of FF. Correlation of the diameter of the FF between MR and pathology was 0.616 (Spearman Rank) ($p < 0.0001$).

Conclusion: The presence of a less or later enhancing centre in a carcinoma on MR corresponds to FF in 64.6%. Assessment of the diameter of an FF on MR was good.

C-0192

Contrast enhanced magnetic resonance mammography (CE-MRM) in the evaluation of suspected microcalcifications at mammography

F. Pediconi, C. Catalano, F. Venditti, A. Roselli, E. Moriconi, R. Passariello; Rome/IT

Purpose: To evaluate the role of CE-MRM in the evaluation and characterization of breast lesions associated with microcalcification diagnosed by mammography.

Methods and Materials: Thirty women with suspected or unclear microcalcifications at mammography, underwent CE-MRM with a 1.5 T magnet using a bilateral breast surface coil. The CE-MRM protocol comprised a T2-weighted STIR sequence and 3D dynamic T1-weighted FLASH sequence before and after (four measurements) the administration of 0.1 mmol/Kg of Gd-BOPTA. At mammography microcalcifications were evaluated by LeGal and BI-RADS classifications. Criteria for lesion evaluation included site, number, morphological patterns, margins and dimensions of all enhancement areas at CE-MRM. All suspected lesions were classified according to BI-RADS classification. Bi-RADS scores of lesions detected at mammography and at CE-MRM were compared. All results were correlated with histopathological specimen.

Results: At histopathological examination, 17/30 lesions were invasive carcinomas, 9/30 were ductal carcinomas in situ and 4/30 were benign lesions. Almost perfect agreement was seen between Bi-RADS scores of lesions detected at mammography and at CE-MRM. A good correlation between CE-MRM findings and histopathological specimens was obtained.

Conclusions: CE-MRM showed high values of sensibility, specificity and accuracy in the evaluation and characterization of microcalcification.

C-0193

3 T-magnetic-resonance-elastography of the breast: Technical feasibility

K. Meyer, R. Sinkus, M. Kaul, J. Lorenzen, G. Adam; Hamburg/DE

Purpose: MR-elastography of the breast has been technically established at 1.5 T. At 3 T difficulties are encountered due to shortened T2-relaxation times and prolonged MR echo-times caused by increased pulse-duration (SAR). This leads to signal loss that is not compensated by the gain due to increased field-strength. The aim was to overcome these limitations.

Methods and Materials: Mechanical excitation frequency remains at 50 Hz, because higher values would lead to strong attenuation effects of the wave providing insufficient penetration. This frequency leads to a TE of about 60 ms for the motion-sensitised spin-echo-sequence. Shortening of this prohibitive long echo-time is achieved by running the sequence at twice the mechanical excitation frequency. Consequently, the sensitivity to detect motion is reduced by a factor of about two. Loss in SNR is compensated by introduction of an EPI-readout and a signal-average of two. 10 healthy volunteers were examined in a 3 T MR system in prone position with a four-element breast coil. Reconstruction of elasticity and viscosity was performed after.

Results: EPI-readout did not lead to any significant image distortions. The shortened TE (30 ms) led to sufficient SNR within the parenchyma. 50 Hz-oscillation provided a sufficient penetration of the wave into the breast. Reconstructed images of shear modulus did not show any suspect regions of enhanced elasticity.

Conclusions: MRE of breast at 3 T is technically feasible. An efficient insertion of the waves into breast was achieved. EPI-readout provided a successful data acquisition.

C-0194

Pre-operative MR imaging localization of breast cancer in supine position using a newly developed marking net

K. Oikado¹, H. Tsunoda-Shimizu¹, T. Kazama², S. Nakamura¹, H. Suzuki¹, M. Kikuchi¹, Y. Numaguchi¹; ¹Tokyo/JP, ²Chiba/JP

Purpose: To determine whether MR imaging in supine position with a newly developed marking net can be used reliably to localize preoperatively breast cancer with intraductal component.

Methods and Materials: Our study included 25 patients with breast cancer having intraductal components detected by mammography or ultrasound (mean age 50, 31-65). Breast conserving surgery was elected for these patients using a newly developed marking net filled with contrast media for precise localization of tumor extension. Twenty-six breast lesions of 25 patients underwent pre-operative localization in the supine position. Coronal fat-suppressed T1-weighted images with and without contrast enhancement were obtained and MIP reconstruction was performed. All patients underwent partial mastectomy and the range of resection was decided with the markings on MR imaging. Comparison of radiological and pathological findings was made using operated specimens.

Results: Twenty-two lesions were clearly defined on MR imaging and resection was relatively feasible with the use of a marking net. Evaluation of tumor extent was impossible in 4 patients due to enhancement of mastopathy or normal breast tissue. Eleven lesions of 22 showed tumor free on frozen section. The other 11 lesions showed tumor cells at the resected margin. However, in 10 of the 11 lesions, tumor cells were of non-invasive ductal component. Additional slightly wider resection was performed for these patients and no tumor cells were detected at resected margin.

Conclusion: Pre-operative MR imaging localization of breast cancer using a newly developed net may help pre-operative evaluation of tumor extent.

C-0195

Role of Gd-BOPTA-enhanced MR mammography in the evaluation of neoadjuvant chemotherapy response in patients with breast cancer

F. Pediconi, C. Catalano, F. Venditti, E. Moriconi, S. Padula, R. Passariello; Rome/IT

Purpose: Assess accuracy of MR mammography (MRM) for evaluation of size and changes in contrast agent uptake pattern in patients with invasive breast cancer after neoadjuvant chemotherapy.

Methods and Materials: Thirty women with core biopsy-confirmed invasive breast cancer underwent MRM prior to neoadjuvant chemotherapy and surgical excision. MRM protocol comprised a T2-weighted STIR sequence and a flash 3D T1-weighted sequence acquired before and at 2, 4, 6, 8 and 10 min after the administration of Gd-BOPTA at 0.1 mmol/Kg. Interval between pre-operative MRM examination and surgery was less than two weeks. Diameter of the tumor and pattern of dynamic contrast agent uptake on the MRM images after chemotherapy were evaluated against histological specimen.

Results: Four patients were excluded because surgery was performed more than two weeks after the last MRM; 26 patients were classified as either complete responders (n = 3), partial responders (n = 16) or non responders (n = 7) on basis of therapy response as indicated on the MRM images. Three complete responders and 3 of the 16 partial responders on MRM imaging showed no residual disease at pathology. Good correlation was found between tumor diameter measured on pre-operative MRM images and on the surgical specimen. MRM assessment had a slight tendency toward overestimation of lesion size compared with pathology. Reduction of tumor size after chemotherapy was associated with decreased contrast agent uptake and modification of dynamic uptake pattern.

Conclusion: MRM is appropriate to evaluate therapeutic effects of neoadjuvant chemotherapy in large breast tumors and permits an accurate assessment of residual breast tumor diameter.

C-0196

An advanced method of computer aided evaluation applied to breast MR imaging: A useful tool both for the radiologist analysis and for the diagnostic accuracy

J.C. Vilanova, J. Barcelo, M. Villalon; Girona/ES

Purpose: To analyze and compare a new method of computer aided evaluation for breast MR imaging and a standard MR imaging software analysis: For diagnostic accuracy, registration of data to correct patient movement-related artifact and the usefulness for the radiologist who interprets MR breast examinations.

Methods and Materials: We evaluated 36 subjects retrospectively from a consecutive series of breast cancer MR imaging patients (GE, Signa LX 1.5T). We

Scientific and Educational Exhibits

performed a comparative study between a commercially available automatic CAD system (CADstream) and standard software for MR imaging. We determined lesion size, morphology, kinetic enhancement, and additional lesions on MR imaging, quality of image correction of subtracted images by CAD and, time for study analysis on each system.

Results: CAD's automatic measurements showed higher tumor size correlation (0.92) with histologic analysis than with the manual standard software (0.86). The morphology and kinetic enhancement patterns did not show significant differences between CAD and standard MR imaging software. Both systems detected additional lesions in 10 patients (28%). Corrected subtraction series from CAD were chosen as better registered data for patient movement-related artifact than uncorrected subtraction images in 83% of cases. The mean analysis time for breast MR imaging on the CAD system was 12 minutes and for standard MR imaging software of 19 minutes.

Conclusion: The automatic CAD system shows an accurate diagnostic method for breast cancer MR evaluation with high histologic correlation. CAD system shows a significantly reduction in artifacts for the subtraction series and saves a substantial amount of time for the analysis and interpretation of MR processed images.

C-0197

MR imaging findings of breast implants complications

A. Roma, B. Ubeda, P. Nin, R. Rotger, R. Ramos, A. Palacio; *Barcelona/ES*

Learning Objectives: MR imaging features of normal breast silicone implants. MR imaging technique in the evaluation of breast implants. Description of the most common complications.

Background: Breast augmentation can be performed with the injection of foreign materials into the breast tissue, transplantation of autogenous tissue and use of prosthetic devices. Breast implants include silicone gel, saline, biocompatible gel, double-lumen and tissue expanders. The implant can be placed in a retroglandular or submuscular position. MR is an accurate technique to diagnose the type and extent of breast implants complications.

Imaging Findings: MR for breast implants evaluation is performed with a breast-dedicated coil with FSE T2, STIR, FSE T2 with silicone-suppressed and STIR with water-suppressed sequences in two or more planes. We describe the main features of normal breast silicone implants and the most common complications including capsule folds and contracture, herniation, fluid periprosthetic collections and intra and extracapsular ruptures.

Conclusion: MR imaging is an accurate technique for evaluation of breast implants and depicting its complications. Special sequences are useful for demonstration of extracapsular silicone. It also provides an overview of the breast, the axilla and the chest wall.

C-0198

A model for reporting dynamic breast MR imaging

A. Fausto, F. Sardanelli; *Milan/IT*

Learning Objectives: To propose a model for reporting breast MR imaging.

Background: High sensitivity and good specificity can be reached with dynamic breast MR, when integrating morphologic and dynamic criteria. The technique is mainly based on a predynamic unenhanced (2D T2-weighted fast spin-echo or STIR) and a dynamic 3D T1-weighted gradient-echo acquisition. Postprocessing: Image subtraction; MIP, MPR; percent enhancement versus time curves for targeted regions of interest. How to report the exam?

Procedure Details: Our model of report: *History* (2-4 lines). Hereditary predisposition to breast cancer; menarche age; oral contraceptives, pregnancy and lactation history; date of last menses or menopausal age; hormone replacing therapy. Breast symptoms; previous examinations (date and synthesis of findings). Clinical query for current MR exam. *Technique* (2 lines). Type/orientation of predynamic and dynamic sequences; type/dose of contrast agent; short description of postprocessing. *Results* (2-8 lines). Breast pattern (fatty, scattered fibroglandular, homogeneously glandular); possible diffuse signal alterations on predynamic scans. For any detected lesion: side/location (in correlation with previous examinations); size (mm in maximal diameter); signal intensity on predynamic scans; shape, margins, homogeneity and pattern of contrast enhancement; dynamics of percent enhancement (continuous increase, plateau, or wash-out); level of suspicion according to BI-RADS or similar score. *Conclusions* (1-3 lines). Synthesis of diagnosis and indications for further action (second look ultrasound; repeat MR; biopsy; surgery, etc.) or follow-up with conventional imaging or MR.

Conclusion: A standardized report can summarize in about 7-18 lines the information to be transmitted to other physicians not expert in breast MR.

C-0199

MR imaging in ductal carcinoma in situ (DCIS) with mammographic appearance of microcalcifications

A. Cilotti, C. Marini, C. Giacconi, D. Francesca, D. Mazzotta, A. Vaccaro, C. Della Pina, C. Bartolozzi; *Pisa/IT*

Purpose: To evaluate MR imaging performance in ductal carcinoma in situ (DCIS) with mammographic appearance of microcalcifications.

Methods and Materials: MR imaging examinations of 73 patients with histologic diagnosis of DCIS having microcalcifications were revalued. According to Fisher's score, MR imaging was classified in a 3-points scale for malignancy (BI-RADS).

Results: MR imaging revealed these types of enhancement: Dendritic (50 cases), nodular (23 cases), diffuse with sectorial shape (58 cases) and focal (15 cases). Time-intensity curves were type I (16 cases), type II (41 cases) and type III (16 cases). According to BI-RADS category MR imaging was classified as B3 (score 0-3) in 14 cases, B4 (score 4-5) in 37 cases and B5 (score 6-7) in 22 cases. Sensitivity was 84%. This data can increase if we contemplate Fisher's score 3 as suspect (BI-RADS B4).

Conclusion: The more available MR imaging findings in DCIS were: Dendritic enhancement (68%), quickly wash-in (78%), sectorial shape enhancement (79%), while contrast enhancement distribution is difficult to evaluate in small lesions, particularly if dendritic enhancement is present. On the contrary quickly wash-out, usually present in 90/95% of infiltrative cancer, was present only in 22% of DCIS. In score Fisher 0-3 category of DCIS, relative to False Negative at MR imaging, the most common data was the presence of more findings in a quadrant with diffuse/sectorial shape (incidence 75%). MR imaging is not a diagnostic technique in DCIS but the presence of reported findings as dendritic enhancement, quickly wash-in and sectorial shape can be suggestive of DCIS.

C-0200

Characterization of pure high grade DCIS on magnetic resonance imaging using the evolving breast MR lexicon terminology: Can it be differentiated from pure invasive disease?

A.M. Groves, R.M.L. Warren, S. Godward, P.S. Rajan; *Cambridge/UK*

Purpose: Magnetic resonance imaging (MRI) is now a recognized method of imaging the breast. Unfortunately, there is lack of standardization in the MRI terminology used to characterize the appearance of breast lesions. Moreover, cases of mixed histologies are often imaged. We retrospectively identified cases of pure high grade ductal carcinoma in situ (DCIS) and using the recently introduced Breast MRI Lexicon, characterized the lesions in order to try and identify features that might distinguish high grade DCIS from invasive disease.

Materials and Methods: A five-year review of our institution's database revealed 637 patients underwent gadolinium enhanced breast MRI examination. After excluding patients with previous chemotherapy or inadequate MRI examination, 13 patients with histologically proven high grade DCIS were analyzed and compared to the 13 most recent cases of pure invasive breast carcinoma. The morphological and dynamic features were then compared.

Results: DCIS cases were significantly more likely to show focal branching pattern ($P = 0.03$) and to have an irregular contour ($P = 0.03$), compared with invasive disease. Although of marginal statistical significance, DCIS lesions are more likely to have a lower morphological score than invasive carcinoma ($P = 0.06$), whilst the latter is more likely to show ring enhancement ($P = 0.07$).

Conclusions: Use of breast MRI for staging at our institution shows that pure high grade DCIS and pure invasive cancers are both rare entities. Despite the relatively limited numbers we identified features that would help to differentiate high grade DCIS from invasive carcinoma on MRI, as well as those characteristics that did not contribute.

C-0201

Magnetic resonance imaging of breast implant ruptures

A. Magistrelli, M. Costantini, M. Romani, R. Masetti, P. Belli; *Rome/IT*

Learning Objectives: To illustrate magnetic resonance imaging (MRI) findings of breast implant ruptures.

Background: The number of women with breast implants is estimated between 4 and 6 million of the world population. In these patients, mammography and sonography have a lower diagnostic accuracy. MRI plays a major role in breast implants evaluation, especially in diagnosis of complications. The incidence of silicon breast implant rupture varies with implantation time and type of implant. The rupture rate increased significantly with increasing implant age and double-lumen implants were associated with substantially lower rupture risk than single-

Scientific and Educational Exhibits

lumen implants. Implant rupture occurs in 15-20% of cases between the 3rd and 10th year after implantation. Both intracapsular (80-90%) and extra capsular (10-20%) rupture required explantation.

Procedure Details: From January 2000 to September 2004, we studied 47 asymptomatic women with implant rupture who subsequently had the implant surgically removed. We describe the most common MRI signs of rupture: "Linguine sign", "teardrop sign" and "C sign". For correct diagnosis, the radiologist should be familiar with all implant types. When a periprosthetic mass is associated with an undamaged implant, MRI allows the differential diagnosis between herniation, irregular fibrous capsule and breast cancer.

Conclusion: According to literature data, our study confirms the high MRI sensitivity and specificity in the evaluation of breast implant rupture. However an integration with clinical information and conventional imaging is useful to improve MRI diagnosis.

Breast

Ultrasound

C-0202

Differentiation of benign and malignant solid breast masses: Real-time spatial compound imaging versus conventional ultrasound

J. Cha¹, W. Moon¹, Y. Koh¹, J.-E. Cheon¹, J. Park², B.-K. Han¹, Y. Cheo¹;
¹Seoul/KR, ²Wisconsin, WI/US

Purpose: To compare the diagnostic performance of real-time spatial compound imaging (SCI) with that of conventional US in the differentiation of benign and malignant solid breast masses.

Methods and Materials: Seventy-five solid breast masses were prospectively evaluated using conventional US and SCI (ATL HDI 5000) with a 5-12 MHz transducer. Of 75 lesions, 21 were cancerous and 54 were benign masses, confirmed by surgical excision or percutaneous needle biopsy. Each image set was masked and randomized. Three experienced radiologists who had not performed the examinations independently analyzed the US findings of the lesion and provided a level of suspicion to indicate the probability of malignancy without information of physical examinations and mammograms. Results were correlated with histologic findings and evaluated with receiver operating characteristic (ROC) analysis.

Results: Regarding the description of US findings, punctate calcifications within the mass was mostly discordant between conventional US and SCI followed by echotexture, boundary echo, width/AP ratio, echogenicity, shape, margin and posterior acoustic transmission. Az and $\text{Az}_{0.90}$ of the conventional US and SCI for each reader were 0.79, 0.85 and 0.29, 0.29 for reader 1; 0.88, 0.88 and 0.69, 0.65 for reader 2; and 0.82, 0.89 and 0.39, 0.39 for reader 3. Diagnostic performance of the two techniques was not significantly different.

Conclusion: There was a remarkable difference in the description of US findings between conventional US and SCI. However, the performance of the radiologists in the characterization of solid breast masses did not change significantly with the use of SCI.

C-0203

Differentiation of benign and malignant solid breast masses: Tissue harmonic imaging versus conventional ultrasound

J. Cha¹, W. Moon¹, Y. Koh¹, J. Cheon¹, J. Park², B.-K. Han¹, Y. Cheo¹;
¹Seoul/KR, ²Wisconsin, WI/US

Purpose: To compare the diagnostic performance of tissue harmonic imaging (THI) with that of conventional US in the differentiation of benign and malignant solid breast masses.

Methods and Materials: Ninety-one solid breast masses were prospectively evaluated using conventional US and THI (LOGIQ 700; GE) with a 13 MHz transducer. Of 91 lesions, 30 were cancerous and 61 were benign masses, confirmed by surgical excision or percutaneous needle biopsy. Each image set was masked and randomized. Three experienced radiologists who had not performed the examinations independently analyzed the US findings of the lesion and provided a level of suspicion to indicate the probability of malignancy without information of physical examinations and mammograms. Results were correlated with histologic findings and evaluated with receiver operating characteristic (ROC) analysis.

Results: Regarding the description of US findings, echogenicity was mostly discordant between conventional US and THI followed by echotexture, margin, calcifications, posterior acoustic transmission, boundary echo, shape and width/AP. Az and $\text{Az}_{0.90}$ of the conventional US and THI for each reader were 0.8390, 0.8316 and 0.5889, 0.5886 for reader 1; 0.8677, 0.8979 and 0.7445, 0.7454 for reader 2; and 0.7682, 0.7838 and 0.2896, 0.2930 for reader 3. Diagnostic performance of the two techniques was not significantly different.

Conclusion: There was a remarkable difference in the description of US findings between conventional US and THI. However, the performance of the radiologists in the characterization of solid breast masses did not change significantly with the use of THI.

C-0204

US depiction and pathologic outcome of suspicious breast lesions additionally detected on MR imaging

J. Shin, B.-K. Han, Y. Choe, K. Ko; Seoul/KR

Purpose: The purpose of our study was to assess the feasibility of ultrasonographic (US) depiction of suspicious breast lesions additionally detected on magnetic resonance (MR) imaging of patients with breast cancer and to investigate their pathologic outcome.

Scientific and Educational Exhibits

Methods and Materials: We retrospectively reviewed 300 consecutive breast MR examinations with sagittal dynamic sequences performed for preoperative evaluation of patients with breast cancer from January 2002 to January 2004. We found 26 patients with 33 unexpectedly enhancing lesions on MR in addition to known focus of cancer and recommended to look for a US correlate amendable to biopsy or localization. These patients were reviewed for imaging findings and histopathologic findings from subsequent biopsy or surgery.

Results: Ninety one percent (30/33) of all additionally detected breast lesions on MR imaging were histologically confirmed. An US correlate was identified in 25 (75.8%) of all additionally detected lesions. Carcinoma was found in 17 (68%) of these lesions, of which 7 were invasive carcinoma and 10 were ductal carcinoma in situ (DCIS). Among 8 lesions without an US correlate, 3 (37.5%) yielded carcinoma, of which one was invasive carcinoma and two were DCIS.

Conclusion: Although additionally detected suspicious breast lesions on MR imaging were not evident on US, these had a higher possibility of carcinoma in those with underlying primary breast carcinoma. Additionally enhancing lesions with a US correlate were more prone to be malignant lesions.

C-0205

Possibility of the US-detection of clustered microcalcifications of female breast

H. Shevchenko; Moscow/RU

Purpose: To evaluate the US-changes in area of clustered microcalcifications (c.m.).

Methods and Materials: 147 patients (mean age = 58 y.o.) with cancer-suspicious c.m. detected mammographically have been examined with 7.5-12 MHz linear transducer (HDI-5000 ATL Philips) in B-mode and Sono CT. 90 cancers and 57 benign lesions were found. Mean diameter of calcifications was 1.7 mm (0.4-8 mm) and 0.15-0.8 mm when using X-ray. The diameter varied due to inability of US (even high-resolution) to detect c.m. as a group of microcalcifications, and not as a single one.

Results: C.m. were visualized with help of US only in 25% of all cases (37 patients). However, in X-ray-detected c.m., malignant lesions could be found only with help of US in 96% of all cases (86 cancers). X-ray-detected c.m. had intermediate concern or high probability of malignancy (cat. 4 and 5 BI-RADS). Their quantity varied from 1 to 30 per cm². US-detected calcifications were visible when their concentration lied in-between 5 and 20 per cm² (namely cat. 5 BI-RADS).

Conclusion: Detection of c.m. by US-scanning was possible only in 25% of all cases and only if their density was relatively high (> 5). Specificity of US-examination is 96%. The size and quantity of c.m. cannot be evaluated by means of X-ray. C.m. was seen as single big calcification in 25% of all cases.

C-0206

Is the echogenicity of a mass influenced by its morphology? An in vitro model

E. De Luis, J.J. Noguera, M. Pons, P.D. Domínguez, L.J. Pina, F. Martínez Regueira; Pamplona/ES

Purpose: Malignant hyperechoic masses are rarely found on breast ultrasound exams. These findings are frequently associated with infiltrating lobular carcinomas. Pathology of these lesions may show multiple layers of tumoral cells (Indian rows) mixed with normal adjacent fatty tissue. Our purpose was to evaluate if the echogenicity of a mass was influenced by its shape, using an in vitro model.

Methods and Materials: Two models of fatty breasts were created, using 500 ml of olive oil in hermetic plastic bags. Two beef pieces of meat (10 g each one) were used to simulate breast masses. Both pieces were introduced inside the bags. The morphology of both specimens was different. In model 1, the specimen was a round homogeneous mass, and in model 2 the specimen was mashed up and torn with a knife. Mammography and ultrasonography were performed.

Results: *Mammographic findings:* In model 1 the specimen appeared as a round, homogeneously dense mass with well-circumscribed margins. In model 2 the specimen was shown as an irregular heterogeneous mass, with small fatty densities inside. *Ultrasonographic findings:* In model 1 the specimen was shown as a hypoechoic well-circumscribed mass, while in model 2 it was shown as an irregular hyperechoic mass.

Conclusion: The echogenicity of a lesion may be influenced by its morphology. An heterogeneous mass with small fatty spaces inside is more echogenic than an homogeneous mass. This might justify the hyperechoic pattern of some infiltrating lobular carcinomas.

C-0207

withdrawn by authors

C-0208

Assessment of clinical outcomes and the sonographic criteria in benign and malignant solid breast masses

A. Özdemir, Z.Ö. Karadag, B. Coskun; Ankara/TR

Purpose: To assess the appropriateness of radiological diagnosis and the sonographic criteria in benign and malignant solid breast masses.

Methods and Materials: "Probably benign", "suspicious" or "probably malignant" 646 solid breast masses in 421 patients, biopsied or followed up between March 2000 and February 2004 were retrospectively analyzed. Radiological suspicion was based on mammographic and sonographic findings in 254 (39.3%) and only on sonographic findings in 392 (60.7%) lesions. Accordingly, 530 lesions (82%) were "probably benign", 55 lesions (8.5%) were "suspicious" and 61 lesions (9.4%) were "probably malignant".

Results: The final diagnosis was obtained through biopsy (30.9%) or periodic follow-up of at least 2 years (69.1%). Seventy-two lesions (11.2%) were malignant and 574 (88.8%) were benign. Ppv of the "probably malignant", "suspicious", and "probably benign" diagnoses were 91.8%, 21.8% and 0.75%, in order. Sensitivity, specificity, ppv and npv of US were 94.4%, 91.6%, 58.6% and 99.2%, respectively. Five cancers were diagnosed only with US (6.9%). The most useful US criteria in differential diagnosis were contour morphology (OR 26.9), transverse-to-anteroposterior diameter ratio (OR 5.4), shape (OR 4.2) and matrix echogenicity (OR 3.1). In retrospect, 3 of 4 cancers in the "probably benign" group could have been diagnosed by more strict use of the US criteria, providing a ppv of 0.19 instead of 0.75. Follow-up instead of biopsy saved 26,100 € and 55,500 €, compared to core and surgical biopsies, respectively.

Conclusion: Ppv for each diagnostic category was within best ranges. Strict use of US criteria can improve the diagnostic sensitivity.

C-0209

Elastosonography of benign and malignant nodular breast lesions: First experience review

A. Martegani, L. Aiani, L. Tufarulo, R. Campi, M. Ciancio, F. Mascheroni; Como/IT

Learning Objectives: Showing how to perform elastosonographic scan on breast nodules and provide a first image gallery based on Ueno's score.

Backgrounds: 121 nodular lesions (benign and malignant) in 89 patients were evaluated from November 2003 to August 2004 with an ultrasound examination followed by elastography, both performed by EUB-8500/Logos-Hitachi Japan, equipped with different linear electronic 7.5-13 MHz transducers with a dedicated device applied on the probe surface in order to improve the contact with the skin. The first 13 cases were propaedeutic.

A short, careful training is necessary for the operator to learn properly to perform the acquisition, that usually lasts only few minutes (2 - 5 minutes).

Breast nodules were classified according to the morphological elastographic Ueno scores. Cytohistologic biopsy, surgical specimen and follow-up were considered as gold standard.

Imaging Findings: A short demonstration showing how to perform the elastographic scan is provided. Some reproducible elastographic patterns found both in cystic lesions and in large (> 2 cm) malignancies are hereby proposed, with an image gallery of the most typical elastographic patterns based on Ueno's score. Elastographic behaviour of small benign and malignant nodules (up to 2 cm) seems to be more uniform compared to those larger than 2 cm. Some examples are shown.

Conclusion: A broadening of clinical studies is crucial for a definitive validation of the method. Our first experience demonstrates the diagnostic reliability of Elastosonography in characterising breast nodular lesions, especially if smaller than 2 cm.

Scientific and Educational Exhibits

C-0210

Real-time spatial compound ultrasound with XFOV imaging in the evaluation of breast lesions

K. Chatzimichael, G. Economou, M. Kampanarou, G. Dimitrakopoulou, D.A. Kelekis; *Athens/GR*

Purpose: To assess the diagnostic role of real-time spatial compound Ultrasound (US) with extended field of view (XFOV) imaging of breast lesions as compared with this of conventional B-mode US.

Methods and Materials: 30 women with breast abnormalities in screening or symptomatic mammography underwent both conventional high resolution B-mode US and real-time spatial compound XFOV imaging. Scans were performed with a SEQUOIA 512 ACUSON scanner under standarized examination settings. Subsequently images were evaluated independently by two radiologists experienced in breast US according to a multistage scoring system with regard to the presence of artifacts, margin definition, matrix definition and overall quality. We assessed also whether the compound XFOV images improved the localization of lesions and the demonstration of the large lesions.

Results: Our comparison of conventional US and compound XFOV imaging confirms a statistically significant reduction in speckle and clutter artifacts accompanied by improved definition of margins and matrix echotexture of both solid and cystic lesions. Compound XFOV technique was found to increase image quality and provide better information about lesion localization, as well as improve the demonstration of the large lesions.

Conclusion: For the time being our results have shown that compound XFOV imaging when compared with conventional US provides better information in localization and matrix characterization of breast lesions and may further improve the diagnostic role of breast US.

Breast

Miscellaneous

C-0211

Imaging of late recurrence in invasive breast cancer

P. Meingan, C. Labbe-Devilliers, I. Doutriaux-Dumoulin, C. Digabel-Chabay, M. Ricaud-Couprise; *Nantes Saint-Herblain/FR*

Purpose: 1) to describe the appearances of late recurrence (occurring more than 10 years after the initial diagnosis) in invasive breast cancer. 2) to evaluate the prevalence of the sites involved, local or distant. 3) to estimate the frequency of recurrences heralded by symptoms.

Method and Materials: The data of 2923 patients referred in our institution between 1982 and 1991 for a breast invasive carcinoma were reviewed. We noted for each patient the presence or not of late recurrence (occurring more than 10 years after the initial diagnosis with an interval free of disease). We evaluated the mode of detection of recurrences, clinical or on follow-up imaging. We describe the radiological features of these recurrences and evaluate the prevalence of the sites involved.

Results: 3% of patients developed late recurrence. 45% of these recurrences concerned the initially treated breast, 27% the contralateral breast and 28% affected a distant metastatic site. The most common sites involved were bone (18%), lung (10%), and pleura (4%). 66% of recurrences were heralded by symptoms and 34% were detected on follow-up imaging studies.

Conclusions: Late recurrences in breast carcinoma are rare but not uncommon and occur particularly in the initially treated breast or the opposite breast. Distant metastatic recurrences are observed in one third of the cases and consist mainly of bone metastases. Two-thirds of recurrences are heralded by clinical symptoms.

C-0212

Phyllodes tumors: Benign and malignant findings

W. Kwon¹, K.K. Oh², M.S. Kim¹; ¹Wonju/KR, ²Seoul/KR

Purpose: To characterize the mammographic and sonographic findings of pathologically confirmed benign and malignant phyllodes tumors.

Methods and Materials: Imaging findings were reviewed in 51 patients with 56 phyllodes tumors that were confirmed by histopathology. Fifty-one tumors (36 benign and 15 malignant) were reviewed using mammography and forty-two tumors (29 benign and 13 malignant) with sonography. The mammographic and sonographic features were analyzed.

Results: Sonography showed low-echoic cystic areas in 11 (84.6%) cases of malignant tumors and 5 (17.2%) cases of benign tumors with statistical significance ($p < 0.001$). Hypoechoic echogenicity ($p = 0.002$) and heterogeneous echotexture ($p < 0.001$) were seen in 13 cases (100%) of malignant tumors. Calcification within the tumor showed a higher frequency in malignant tumors (6 cases, 40%) than benign tumors (3 cases, 8.8%) with statistical significance ($p = 0.013$). Benign phyllodes tumors measured 3.25 cm and malignant tumors 5.57 cm in mean diameter ($p = 0.005$). The mean age of the malignant tumor patients (41 years old) was older than the benign tumor patients (33 years old) ($p = 0.007$). The benign and malignant phyllodes tumors showed a similar frequency of lobular shape in 61.1% and 73.3% ($p = 0.527$) and a circumscribed margin in 41.7% and 60% ($p = 0.356$), respectively.

Conclusion: Imaging cannot reliably separate malignant from benign phyllodes tumor. However, it appears that size, cystic areas, and a heterogeneous echotexture are associated with a higher likelihood of malignancy.

C-0213

Breast microcalcifications: Benign or malignant. Ready for a challenge?

A.R. Sever¹, S. Villan¹, F. Batmaz², N.A. Mounter¹, P. Mills¹, J.B. Schofield¹, S.E. Jones¹, P.A. Jones¹; ¹Maidstone/UK, ²London/UK

Learning Objectives: To study the spectrum of breast microcalcifications in the form of a self assessment test.

Background: Breast lesions consisting of microcalcifications only, with no accompanying mass, impose a challenge to breast radiologists in the decision making process. As these lesions are usually impalpable and rarely visible on ultrasound, an accurate mammographic evaluation is crucial in assessing the need of an immediate biopsy, follow-up or no follow-up. A programme is conceived as an interactive training session to practise with a set of mammograms designed for radiologists in training as well as breast screening radiologists.

Procedure Details: Maidstone Breast Unit has a large digital library of mammograms consisting of more than 600 cases with microcalcification only lesions which were biopsied using Vacuum-Assisted Mammatome device under stereo-

Scientific and Educational Exhibits

tactic guidance. In co-operation with GULEN Information Consultancy we designed a computer programme to review this teaching file in the form of a test. The test involves three sections. The first section is an introduction and a demonstration of the test consisting of three cases. Second section is the test itself consisting of 40 cases of mammograms including magnification views. The attendees will be asked to select a box indicating either benign or malignant for each case. The third section will give the statistical score of the test in terms of accuracy, sensitivity and specificity and the answers of each case including histopathology images and a brief explanation.

Conclusion: This test will be educational for residents in training and for radiologists to refresh their skills.

C-0214

Breast cancer in women 40 years of age and younger

J. Calbo, M. Castro, M. Carnero, L. Perez, N. Picazo, I. Gonzalez; Alicante/ES

Purpose: To review the clinical, radiological and histopathological findings, including biopathological parameters, in breast cancer diagnosed in women 40 years of age and younger.

Methods and Materials: We made a retrospective review of 71 cases. All the selected patients had radiologic studies (mammography and/or sonography) and histopathologic confirmation.

Results: A total of 1231 patients with breast cancer were studied, 71 of which were 40 years old or younger. In 89% a palpable mass was the clinical presentation. The most frequent mammographic finding was as a nodular lesion. Mammography did not find anomalies in 21% of the cases. By sonography, a hypoechoic nodule was the most frequent presentation (40%). Histologic findings revealed infiltrating ductal carcinoma in 82% of tumours, with a high incidence of poorly differentiated forms (GII - GIII). We observed lymphovascular invasion in 56% of the patients.

Conclusion: Breast cancer is a rare condition in adolescents and young adults. Invasive breast cancer occurring at a young age has more aggressive biological behaviour and is associated with a worse prognosis. In our series, we found a high incidence of poorly differentiated (GII-III) ductal carcinomas and more than 50% had lymphovascular invasion at diagnosis. Most of the patients had a positive clinical examination as a palpable mass. The accuracy of mammography is inferior in young women, who have denser breast tissue. In a fifth of our patients, mammography did not show the lesion, which was detected by sonography.

C-0215

Fat necrosis in TRAM flaps mimicking malignancy

A. Roditi, R. Arkun; Izmir/TR

Learning Objectives: To illustrate the mammographic spectrum of fat necrosis in patients with transverse rectus abdominis myocutaneous (TRAM) flaps and the challenge to differentiate these benign changes from malignancy.

Background: Fat necrosis in breasts with TRAM flaps has a wide spectrum of mammographic findings and these findings may occasionally mimic malignancy. With the use of mammography in TRAM flaps, radiologists are becoming aware of the different findings in these patients, and especially of fat necrosis. In a five year period of follow-up, the spectrum of fat necrosis changing from a bandlike increased density with accompanying pleomorphic calcifications to posttraumatic coarse heterogeneous calcifications are discussed.

Procedure Details: As part of the routine radiological workup of patients with TRAM flaps, mammography of the flap is being performed regularly in some institutions. The mammographic exam is performed with the routine projections used in screening mammography which are the craniocaudal (CC) and the mediolateral oblique (MLO) projections.

Conclusion: It is important to be aware of the reasons and frequent sites of complications occurring in TRAM flap patients and also the diversity of mammographic findings ranging from fat necrosis to malignancy. One should search diligently for all changes that may be a sign of early malignancy and all efforts should be used in the differentiation of fat necrosis from malignancy without compromising the cosmetic results.

C-0216

Diagnostic value of FDG PET-CT for detecting primary breast malignancy: Comparison with other image modalities and histopathologic correlation

N. Jung, J. Lee, S. Kim, B. Song, S. Jung, J. Byun; Seoul/KR

Purpose: To compare the diagnostic value of 18F-FDG PET-CT in detecting the primary breast malignancy with other imaging modalities and to determine whether detectability of PET-CT depends on any factors.

Methods and Materials: We retrospectively evaluated pathologically proven 36 lesions in 34 patients who underwent preoperative FDG PET-CT during the past 9 months. Other imaging modalities were also evaluated: Mammography (N = 32), US (N = 28) and MR imaging (N = 10) in the same population. Sensitivities of each modality were obtained. We also statistically analyzed PET-CT positive and negative groups in relation to SUV, size, nuclear grade and differentiation.

Results: 35 lesions among 36 were malignant breast lesions. Sensitivities of FDG PET-CT, mammography, US, and MR imaging for detecting malignant breast mass were 74% (26/35), 81% (27/33), 100% (29/29) and 91% (10/11) respectively. SUV(P) and SUV(M) in PET-CT positive group were significantly higher than those of PET-CT negative group [p < 0.0001 for SUV(P) and p = 0.0002 for SUV(M)]. The size of the mass in PET-CT positive group was also significantly larger than that in PET-CT negative group (p = 0.0090). Nuclear grade of the tumor was significantly different (p = 0.1265) between the two groups if the significance level of the test was set to 0.15. However, the tumor differentiation was not significantly different between two groups (p = 0.8507).

Conclusion: The sensitivity of the FDG-PET in detecting primary breast cancer is lower than those of other imaging modalities. The detectability of the FDG PET-CT might be degraded when the tumor is small in size and/or has a low nuclear grade.

C-0217

Breast manifestations in patients with systemic lupus erythematosus (SLE)

M. Kim¹, H. Kim¹, H. Yoon², S. Kim¹, W. Moon¹, S. Chung³, D. Kim¹, H. Shin¹, J. Park⁴; ¹Seoul/KR, ²Bucheon/KR, ³Bundang/KR, ⁴Madison, WI/US

Learning Objectives: To learn various radiological findings of the breast in patients with SLE. To understand the mechanisms of breast manifestations in patients with SLE.

Background: SLE may cause variable clinical presentations and pathologic patterns. Breast involvement with SLE is not frequent. We observed 15 patients with breast manifestations of SLE during the recent 5 years. In this exhibit, we will describe the breast manifestations in patients with SLE.

Procedure Details: Real-time ultrasonography of both breast and axilla and routine mammography (craniocaudal and mediolateral oblique view) were performed in these patients with SLE. Findings of breast manifestations of SLE included lupus mastitis and panniculitis with dystrophic calcifications (n = 3), bilateral or unilateral (dependent) breast edema due to heart failure or chronic renal failure (n = 3), benign tumors (n = 4), axillary lymphadenopathy (n = 2), breast cancer (n = 2) and infection due to steroid therapy (n = 1).

Conclusion: Various radiologic findings of breast manifestations of SLE including primary and secondary consequences of the disease will be exhibited with clinical and pathologic correlation.

C-0218

Male breast cancer: Retrospective analysis of 58 patients

D.N.D. Freitas¹, L. Orvalho²; ¹Funchal/PT, ²Lisbon/PT

Purpose: Male breast cancer is a rare cancer in men representing less than 1% of all breast cancer. A review of clinical aspects, risk factors, imaging, treatment and outcome was performed.

Methods and Materials: A 10 year list of male patients with breast cancer treated in Instituto Português de Oncologia de Lisboa was requested from ROR-Sul (Oncology registry). Clinical files were reviewed for relevant information.

Results: Average age on presentation was 66 years, (range 35-85). Most patients (75.9%) reported a nodule in the breast. Only 11% had family history of breast cancer. On mammography, a nodule was the most frequent finding, microcalcifications represented only 4%. The left breast accounted for 59% of cancers and the central region harboured 75% of cases. Staging revealed 36% of patients in stage II, 38% stage III, 7% stage IV and only 17% stage I. Invasive ductal carcinoma represented 86%. Treatment included modified radical mastectomy (65% of patients), radiotherapy (65%), hormone therapy (70%) and chemotherapy (48%). After treatment 52% remained cancer free, whereas 24% had distant metastases and 10.3% had another cancer. Most metastases were located in bone and lungs.

Conclusion: Male breast cancer is diagnosed in aged patients, mostly for a nodule in the breast. Neither family history nor risk factors were seen in the majority of patients. Male breast cancer is diagnosed in more advanced stages. Male breast cancer has a survival rate equal to breast cancer in women when adjusted for staging, but advanced staging implies worse prognosis in men.

Scientific and Educational Exhibits

C-0219

Evaluation of the use of MammoTool: An interactive, web-based, educational approach for the interpretation of mammographic studies
L. Bacigalupo¹, E. Soldi¹, P. Bonetto¹, G. Gozzi², A. Ganzetti², G.M. Conti³,
¹Genoa/IT, ²Como/IT, ³Parma/IT

Purpose: Among the causes of missed breast cancer there are lack of perception and incorrect interpretation. We designed MammoTool (MT), a web-based, interactive software for mammographic teaching files, aimed at training radiologists to correctly read mammograms. MT presents the user a set of cases. The user is expected to: Interpret each case (also with the use of a magnifying lens and other image manipulation tools), provide a grade of certainty with which he evaluates the image as being normal or abnormal and mouse-click on the possible lesion (only malignant lesions are considered in this study). We tested MT to evaluate the performance of a group of radiologists.

Methods and Materials: We tested MT on 67 radiologists. Each radiologist had to interpret 20 cases sorted randomly out of a database containing 68 cases (50% positive for malignancy and 50% negative for malignancy). Questionnaires were collected from these radiologists regarding their seniority, expertise and the use of MT.

Results: MT was user-friendly and no particular problems occurred during the test. We observed that the best results were obtained by radiologists who read more than 4000 mammographic studies every year. The years of expertise were less well correlated with the results.

Conclusion: The radiologist with MT can learn to interactively analyze mammographic teaching files with different image manipulation tools. After evaluating a series of cases, they will be able to assess their skills and performance, in terms of ROC and IROC curves. They may finally review the resolved cases and comprehend the errors.

C-0220

Radiologic evaluation of the inflammatory breast disorders
J. Sabate, M. Clotet, V. Villalba, T. Salinas, A. Gomez; Barcelona/ES

Purpose: To describe the radiological features in these entities that very infrequently involve the breast.

Methods and Materials: We include cases of: sarcoidosis, Wegener granulomatosis, amyloidosis, tuberculosis, Churg-strauss disease, Necrobiotic xantogranulomatosis and diabetes mastopathy. Image diagnostic Methods: mammography (M), ultrasound (US) and MR with pathological correlation have been obtained.

Results: Wegener granulomatosis may manifest as an irregular high-density mass simulating breast cancer. Sarcoidosis use to be a well-defined mass usually accompanied by lymph node enlargement. Amyloid tumor manifests as a calcified mass. Tuberculosis usually simulates malignancy. Churg-strauss disease manifests with diffuse and bilateral involvement. Diabetic fibrous mastopathy presents as a very dense breast tissue at M, suspicious of malignancy at US. Necrobiotic xantogranulomatosis of the breast manifest as a multiples ill-defined masses at M and hypoechoic at US. Granulomatous lobular mastitis presents as a mass suspicious of malignancy.

Conclusions: Radiologist should know the findings of these entities specially when malignant appearance is encountered.

C-0221

Use of macroaggregates of TC-99m labelled human serum albumin (MAA) for non palpable breast lesions marking. An easy new technique with minimum surgical invasion.

M. Ruiz, C. López, M. Valle, M. Cortés, R. Pardo, C. Pastor, T. Cañuelo, C. Martínez, C. Molino; Ciudad Real/ES

Purpose: Radioguided occult lesion localisation (ROLL) using MAA is proposed to replace standard techniques (wire hook localization) to biopsy non-palpable breast lesions. MAA is a radiotracer with large particles that cannot migrate rapidly by lymphatic and it is useful for marking.

Methods and Materials: From May 2003 to August 2004, 44 patients suspected to have occult breast carcinoma (BIRADS 4-5) were enrolled in the study. Three hours before surgery, 300-500 µCi in 0.1 ml of volumen were injected into the center of the lesion using stereotactic mammographic or ultrasound guidance. After that, anterior and lateral scintigraphy were obtained. All patients underwent open surgical biopsy guided by gamma probe and the specimen was radiographed to verify complete removal of the lesion.

Results: Radiological findings suspected of carcinoma were: Irregular cluster microcalcifications (21), nodules (5), spiculated lesions (17) and architectural distortion (1). We injected radiotracer under US guidance in 3 patients and under

stereotactic guidance in 41. Mammography and scintigraphy revealed that the radiotracer was correctly positioned in a small area in 42/43. The rate of confirmation of lesion removal was 100%. Pathological results were: 19 benign lesions, 3 atypical ductal hyperplasia and 22 infiltrating carcinoma.

Conclusion: ROLL with MAA is an alternative technique to be used for marking occult breast lesions that allows an easy and accurate removal with a directed surgical access avoiding displacement and migration associated with traditional methods.

C-0222

The role of CT in local staging of breast cancer

T. Uematsu, S. Yuen, H. Ikuma, A. Seki, T. Aramaki, N. Morimoto, M. Endou, H. Furukawa; Shizuoka/JP

Learning Objectives: 1) To describe the MDCT techniques used for local staging of breast cancer. 2) To illustrate the MDCT findings compared to MR imaging findings in breast cancer local staging. 3) To discuss the consequences of these findings on treatment and outcome. 4) To discuss both the additional value and the pitfalls of MDCT in breast imaging.

Background: The occurrence of local tumor recurrence after breast-conserving treatment is related to microscopic margin involvement. An adequate excision of the tumor may be necessary to obtain optimal local tumor control. CT can reveal the accurate determination of disease extent within the breast that is not detected on mammography, ultrasonography, or physical examination. Therefore, CT has become an important part of work up of these patients in some institutions. However, still uncertainty exists concerning the additional value of CT compared to MR imaging staging in determining tumor extent and the consequence of these findings on treatment choice and outcome.

Procedure Details: Based on our experience in over 100 patients with breast cancer, we will illustrate the CT findings compared the MR imaging findings in breast cancer local staging.

Conclusion: We discuss the consequences of the CT findings compared the MR imaging findings, with emphasis on the additional value and pitfalls of CT in local staging of breast cancer.

C-0223

Alternative utilities of a breast marking coil

J.J. Noguera, P.D. Dominguez, E. De Luis, L. Diaz, L.J. Pina, G. Zornoza; Pamplona/ES

Learning Objectives: To review the main indications for breast marking coils. To show alternative uses for breast marking coils.

Background: Breast markers have been widely used after vacuum-assisted biopsies if the lesion was completely removed. Also these markers have played an important role in marking breast tumours that undergo neoadjuvant chemotherapy, in order to localize the tumour bed if the lesion could not be macroscopically identified.

Procedure Details: We use the marker IDL-19.5-9.0-4-U-DM (Cook, Bjaevskov, Denmark). This marker may be guided by stereotaxis or ultrasound. The alternative utilities of this coil are: a) to mark an ultrasound detected lesion in order to correlate it with mammographic findings; b) to mark the tumour bed after breast conserving therapy in order to facilitate posterior interstitial radiation therapy; c) to mark a lesion only seen in one view in order to facilitate the most appropriate approach. Thirty markers were employed. One of them could not be properly delivered. The remaining cases were successfully performed. No displacement was observed in any case.

Conclusion: This procedure is effective in order to mark breast lesions, allowing posterior interventional procedures or to correlate ultrasonographic and mammographic findings.

C-0224

Concordance of the breast imaging reporting assessments and final diagnosis for diagnostic mammography and sonography.

J.H. Lorenzen, A.K. Wedel, B.W. Lisboa, G. Adam; Hamburg/DE

Purpose: To assess the final clinical outcome of BI-RADS categories for diagnostic mammography and sonography.

Methods and Materials: We analysed 632 mammography and sonography examinations from women with diagnostic indications (age: 23-100, mean 58) performed during 2001 and 2003. Final clinical outcome (Histology: 502; follow-up: 130) was ascertained in each case and concordance of BI-RADS-categories for mammography and sonography and final diagnosis were analysed.

Results: Final diagnosis yielded 231 benign lesions (37%) and 401 cancers (63%).

Scientific and Educational Exhibits

Concordance of BI-RADS Assessment and final outcome was documented in 542 cases (85.8%). There were 11 category 1 and 2 assessments and the positive predictive value was 0% (0 malignant lesion of 11 cases). 140 lesions were classified with BI-RADS 3. The PPV was 3% (5 of 140 lesions). There were 267 category 4 lesions (42%) with a PPV of 77% (186/267) and finally 214 BI-RADS 5 lesions with a PPV of 98% (210/214). Overall sensitivity of mammography was 93% with specificity of 72% and for sonography 86% and 74%. The highest correlation between BI-RADS category and final outcome was documented for the diagnostic combination of mammography and sonography with a kappa-value of 0.806 ($p < 0.001$), followed by mammography (kappa: 0.677) and sonography (kappa: 0.624). The overall correlation was 0.673 ($p=0.000$).

Conclusion: BI-RADS assessments of diagnostic mammography and sonography yields a higher cancer detection rate, especially for category 4, compared with screening examinations. Combination of mammography and sonography for diagnostic indications showed substantially the highest concordance of BI-RADS category and final diagnosis.

C-0225

Unusual breast lesions: Radiologic-pathologic correlation

M. Bernathova, M. Dünser, G. Retzl, G. Bodner, B. Zelger; Innsbruck/AT

Learning Objectives: To show the imaging findings in uncommon breast lesions and provide a radiologic-pathologic correlation.

Background: Unusual breast lesions can present a diagnostic challenge. Imaging findings in these entities are nonspecific, the benign lesion can clinically and radiologically mimic malignant tumour. The exact diagnosis is usually made by excisional biopsy.

Procedure Details: Retrospective review of radiologic findings in 20 patients with uncommon breast lesions examined during March 2000 and March 2004 was performed. Patients underwent diagnostic mammography, breast sonography and breast MR imaging. We chose 7 uncommon benign and malignant conditions (primary non-Hodgkin lymphoma of the breast, pseudolymphatic infiltration of the nipple, granular cell tumour, metastasis of the bronchial carcinoma to the breast, primary angiosarcoma of the breast, mucinous carcinoma with large cystic dilatation of the duct and tubular carcinoma) where the correct diagnosis was done by core needle biopsy and describe the radiological and pathological findings.

Conclusion: Learning the histological appearance helps to understand the radiological finding. Familiarity with variety of uncommon breast lesions is important for correct clinical management of disease.

C-0226

Unusual presentations of ductal carcinoma in situ: Radiological and pathological correlation

D.M. Duke, M.K. Kennedy, J. Kerr, E. Doyle, M.M. McNicholas, H.M. Fenlon, F. Flanagan; Dublin/IE

Learning Objectives: Our exhibit will review unusual clinical and radiological manifestations of breast ductal carcinoma in situ (DCIS) with the findings at mammography, sonography and magnetic resonance imaging being presented. Pathological correlation will also be outlined with particular reference to the incidence of concurrent carcinoma in situ.

Background: DCIS is heterogeneous in its mammographic, clinical and histological presentation and consequently its biological behaviour. It is most commonly diagnosed in asymptomatic women after the detection of micro-calcifications on screening mammograms. However, it may present as a palpable mass, spontaneous nipple discharge or Paget's disease. On mammography it may be detected as a noncalcified, macrolobulated mass with partially distinct margins, a spiculated mass, distortion or parenchymal asymmetry. This spectrum of DCIS manifestations presents a diagnostic dilemma for clinicians, radiologists and pathologists.

Procedure Details: Since its inception in 2000, the Eccles unit of the Irish National Breast screening programme has invited in excess of 70,000 women, aged 50-64, for mammography. 110 of these have been diagnosed with DCIS. We identified a subgroup of these patients who did not have the classical imaging features of microcalcifications on mammography. The imaging findings of these patients were correlated with pathological findings and clinical outcome. A pictorial review of our results will be displayed.

Conclusion: Unusual manifestation of DCIS causes a diagnostic dilemma for all involved in the management of breast cancer. It must be included as a differential diagnosis for a spectrum of mammography and clinical findings in order to correctly identify and treat these patients.

Cardiac

C-0227

MR and CT imaging of partial and total cavo-pulmonary connections: A guide to assessment of the fontan circuit for the uninitiated

A. Crean, Y. Provost, N. Paul, N. Merchant; Toronto, ON/CA

Learning Objectives: 1. To illustrate the range of cavopulmonary connections in existence. 2. To illustrate potential complications of the Fontan circuit. 3. To illustrate the relative merits of MR vs CT in this patient group.

Background: The Fontan procedure (cavo-pulmonary anastomosis) is used worldwide for the augmentation of pulmonary blood flow in the setting of tricuspid or pulmonary atresia. The original operation has been superceded by a number of variants which can confuse the uninitiated. Radiologists need to appreciate the diversity of cavopulmonary connections when planning and reporting studies in these patients. This exhibit reflects our experience with this patient population over the last 5 years.

Imaging Findings: We discuss: a) types of cavo-pulmonary connection. b) pitfalls in the assessment of Fontan (and/or pulmonary) thrombosis. c) what imaging sequences are most appropriate for full evaluation of the Fontan circuit, including how to quantitate cavopulmonary flow. d) how to recognise the "failing Fontan".

Conclusion: We aim to demystify the Fontan procedure for general radiologists and provide sufficient instruction to enable competent assessment of the functional status of the Fontan circuit.

C-0228

Feasibility of rapid-sequence ^{31}P -MRS of the heart in cardiac patients

K. Chida, H. Otani, H. Saito, T. Nagasaki, Y. Kagaya, M. Kohzuki, M. Zuguchi, S. Takahashi, K. Shirato; Sendai/JP

Purpose: The most critical element impeding the routine use of human cardiac phosphorus-31 magnetic resonance spectroscopy (^{31}P -MRS) is its low S/N ratio and consequent long examination time. The purpose of this paper was to determine the clinical feasibility of rapid-sequence ^{31}P -MRS of the heart in cardiac patients using a 1.5-Tesla clinical MR instrument.

Methods and Materials: The rapid-sequence ^{31}P -MRS procedure using a two-dimensional phosphorus chemical-shift imaging sequence in combination with 30-mm axial slice-selective excitation was phase encoded in arrays of 8x8 steps with an average of four acquisitions. Its acquisition time ranged from 3 to 5 minutes, depending on the heart rate. Twenty-three cardiac patients (dilated cardiomyopathy (DCM): 13 cases, hypertrophic cardiomyopathy: 3 cases, hypertensive heart diseases: 3 cases, aortic regurgitation: 1 case, and old myocardial infarction (OMI): 3 cases) were examined using rapid cardiac ^{31}P -MRS. The student's *t* test was used to compare phosphocreatine (PCr) / adenosine triphosphate (ATP) ratios from the cardiac patients with those of the control subjects ($n = 13$).

Results: The myocardial PCr/ATP ratio obtained by rapid ^{31}P -MRS was significantly lower ($p < 0.001$) in DCM patients (1.82 ± 0.33 , mean \pm SD), and in patients with global myocardial dysfunction (combined data for 20 patients (except OMI): 1.89 ± 0.32), than in normal volunteers (2.96 ± 0.59). These results are similar to previous studies. The anterior-septal myocardial PCr/ATP ratio was also lower (1.54) than in the patients with inferior infarction (3.17) and posterior infarction (2.31).

Conclusion: Rapid-sequence ^{31}P -MRS may be a valid diagnostic tool for patients with cardiac disease.

C-0229

Characteristics of myocardial enhancement in dilated cardiomyopathy with contrast-enhanced MR imaging

J. Nam, B. Choi, J. Seo, Y.-J. Kim, T. Kim, K. Choe; Seoul/KR

Purpose: With contrast-enhanced MR imaging (ceMRI), atypical patterned enhancement of myocardium has been reported in non-ischemic dilated cardiomyopathy (DCMP). We studied the characteristics of enhancement in DCMP by ceMRI.

Methods and Materials: Thirty nine patients (mean 59 ± 12 yrs) with DCMP and normal coronary arteries proven by conventional coronary angiography underwent ceMRI with 10-minute delay after contrast administration of Gd-DPTA at 0.2 mmol/kg. Thirty patients with myocardial infarction underwent ceMRI with the same protocol for comparison. The signal intensity of skeletal muscles on the chest wall (Slsm) was used as reference in the same patient. Sls of hyperenhanced infarcted myocardium (Slhm), remote myocardium (Slrm) from hyper-

Scientific and Educational Exhibits

hanced infarction, abnormally enhanced myocardium (SI_{em}) in DCMP, nonenhanced myocardium (SI_{nem}) in DCMP were measured and analyzed.

Results: Visual assessment of the myocardium in patients with DCMP resulted in no enhancement in 13 (33%) patients, and enhancement in 26 (67%), while all patients with infarction showed hyperenhancement on the infarcted region. The SI_{em}/SI_{nem} in DCMP was 4.02 ± 2.46 , SI_{nem}/SI_{em} 0.79 ± 0.67 , SI_{hm}/SI_{em} 6.73 ± 3.68 , SI_{re}/SI_{em} 0.79 ± 0.91 . Enhancement in DCMP was mild to moderate in 18 (70%), strong in 4 (15%) and both in 4 (15%). The most characteristic pattern were enhancement at base (42.3%), septum (42.3%), middle layer (34.6%), and enhancement with diffuse transmural pattern (46.2%). EF and EDV showed no significant correlation with the abnormal myocardial enhancement in DCMP.

Conclusions: The mild to moderate degree of diffuse transmural or middle layer enhancement especially on the basal septum is a frequent and characteristic enhancement pattern of myocardium in DCMP patients.

C-0230

Noninvasive investigation of cardiac metabolism in patients with hypertensive heart disease (HHD) by ^{31}P -MR spectroscopy

R. Rzanny, J.-P. Heyne, A. Hansch, U. Leder, J.R. Reichenbach, W.A. Kaiser; Jena/DE

Purpose: Hypertension with chronically increased blood pressure can induce left ventricular hypertrophy and fibrosis and is one of the most common risks for the development of a congestive heart failure. In this study the correlation between changes in the ^{31}P -metabolism and left ventricular end-systolic volume (LVEF) in patients with HHD was investigated non-invasively by ^{31}P -MRS.

Method/Materials: 36 patients with HHD and 20 volunteers without any symptoms of myocardial disease were examined at 1.5 T using a surface coil (300 mm \times 300 mm) and a ECG-gated ^{31}P -CSI sequence (voxel size measured: 40 x 40 x 100 mm³; reconstructed: 20 x 20 x 100 mm³). 24 patients had normal ventricle sizes and ejection fractions (EF) (compensated HHD), whereas 11 patients had a restricted EF (decompensated HHD).

Results: In all patients a decreased PCr/ γ -ATP ratio was observed. However in patients with a decompensated HHD the PCr/ γ -ATP ratio was lower than in patients with compensated HHD ($p = 0.012$). The PCr/ γ -ATP showed a linear correlation with the LVEF for all patients (Pearson coefficient: 0.39; $p = 0.025$). In addition, a decreased PDE/ γ -ATP ratio was observed in patients with decompensated HHD compared to volunteers.

Conclusions: The present results support the hypothesis of an altered energy metabolism in HHD. The small but significant linear correlation of our estimated PCr/ γ -ATP ratios with the LVEF supports the assumption that left ventricular dysfunction is related to impairments of the energy metabolism. The reduced PDE/ γ -ATP ratio in patients with decompensated HHD can be interpreted as a sign for hypertrophic growth.

C-0231

MR imaging for the diagnosis and follow-up of myocarditis

M.M. Huguet, J. Vila, N. Oller, C. Moure, P. Lozano, E. Delgado, G. Sabin; Barcelona/ES

Purpose: To evaluate the potential of ECG-gated breath-hold MR imaging in diagnosing acute myocarditis. Myocarditis is under-diagnosed with clinical criteria generally used for diagnosis. Diagnostic tools currently available are unsatisfactory. We tested the hypothesis that inflammation is reflected by signal changes in contrast-enhanced magnetic resonance imaging.

Material and Methods: We assessed 21 consecutive patients with symptoms of chest pain and altered ECG. Fifteen had elevated troponin I as indicator of myocardial damage. Coronary heart disease was excluded in 19 patients. One patient with coronary disease required a QCTP. MR images were performed at 1.5 T CVI (GE). Both cine and contrast-enhanced short axis CMR images were performed. Cine CMR was performed using a steady-state free-precession sequence. Contrast CMR images were acquired on average 5 to 10 minutes after contrast (0.2 mmol/Kg Gd-DTPA), using a segmented IR-GRE technique. Five patients were re-examined by MR imaging 3 months later.

Results: Contrast enhancement was present in 16 patients of 21 (76%). Regions of contrast enhancement has a subepicardial distribution and were most frequently located in the lateral wall (12 cases) and less frequently in the inferior wall (4 cases). No wall motion abnormalities were found. CMR at follow-up three months after the initial CMR, demonstrate a mild decrease in the average area of enhanced tissue.

Conclusion: Subepicardial enhancement is a frequent finding in cases of acute myocarditis. Contrast media-enhanced MR imaging visualizes the localization, activity, and extent of inflammation and may serve as a powerful noninvasive tool in the diagnosis and follow-up of myocarditis.

C-0232

Magnetic resonance imaging and non-compaction of the ventricular myocardium: Unusual or underdiagnosed disorder?

G. Garcia Continente, T.M. De Caralt, J.R. Ayuso, C. Pare, M. Sitges, C. Ayuso, R.J. Perea, J. Ramirez, A. Tomasello; Barcelona/ES

Learning Objectives: To illustrate typical morphological features by cardiac magnetic resonance imaging in non-compaction ventricular myocardium.

Background: Non-compaction of the myocardium is a rare unclassified congenital cardiomyopathy. The etiology is not clear but an arrest of intrauterine myocardial morphogenesis is the accepted basic mechanism. Early diagnosis is important in order to prevent the high incidence of cardiovascular complications such us heart failure, systemic embolism and arrhythmias. The increasing use of magnetic resonance in the study of cardiac diseases has lead to an increment in the recognized cases of this rare disorder. Therefore, to have knowledge of the imaging findings of this process is an important issue for radiologists working on cardiac magnetic resonance.

Imaging Findings: We report eight patients who were diagnosed of non-compaction left ventricle myocardium by contrast-enhanced echocardiography, and confirmed by cardiac magnetic resonance. T1-weighted spin-echo image (black blood) demonstrated two layer structure: a thin low intensity compacted epicardial portion and a thicker high intensity endocardial layer with prominent trabeculations and deep intertrabecular recesses which were filled with blood. Cine-MR gradient-echo sequences allow functional qualitative assessment: in all cases the prominent trabecular meshwork was more evident during diastole, and also revealed hypokinesia of the non-compacted ventricular wall.

Conclusion: Cardiac magnetic resonance imaging is a non-invasive method which provides high-resolution imaging of non-compaction myocardium, and permits us to confirm and evaluate the severity and prognosis of this cardiac disorder.

C-0233

CT and MR imaging of pericardial disease

S.P. Prabhu¹, A. Neelakantan²; ¹Bristol/UK, ²Hereford/UK

Learning Objectives: 1. To illustrate the utility of computed tomography (CT) and magnetic resonance (MR) imaging in the evaluation of pericardial disease. 2. To demonstrate the anatomy of normal pericardium and show how CT and MR imaging enable exquisite delineation of pericardial anatomy. 3. Illustrate examples where CT and MR imaging have assisted in noninvasive evaluation of loculated or hemorrhagic pericardial effusions, constrictive pericarditis and pericardial masses including congenital and neoplastic lesions. 4. Elaborate CT and MR imaging diagnostic criteria for pericardial constriction.

Background: Both CT and MR imaging are being increasingly used either as an adjunct or as a substitute to echocardiography as they provide a larger field of view and allow visualisation of the entire chest and associated abnormalities in the mediastinum and lungs. The main advantage of CT and MR imaging is the excellent soft-tissue contrast.

Procedure Details: Using examples from our tertiary care institution archives, we illustrate various examples of pericardial pathology investigated by CT and MR imaging. Anatomy of normal pericardium and associated cardiac structures are explained followed by description of pathological entities and criteria for their diagnosis on CT and MR imaging.

Conclusion: It is important to understand the normal anatomy and pathological appearances of the pericardium even for the general radiologist as there will be an increasing demand for imaging of the pericardium in the near future.

C-0234

Catheter deployed devices in adults with congenital heart disease:

A radiological perspective of normal appearances and complications

V.S. Warbey, M. Mullen, S.P. Padley; London/UK

Learning Objectives: To appreciate the range of catheter deployed devices available in the management of adults with congenital heart disease. To understand the indications for each device and the normal post-deployment radiological appearances. To recognise complications that may arise following device placement.

Background: Congenital heart disease (CHD) is common, occurring in approximately 0.8% of newborn infants. The success of paediatric cardiology programs has created a growing population of young adults who may require further intervention. Increasingly, these interventions may involve catheter deployment of a range of new devices. Radiologists should be able to recognise such devices and may be asked to perform additional cross-sectional imaging to evaluate device efficacy.

Scientific and Educational Exhibits

Procedure Details: Catheter interventions are undertaken to close abnormal vascular communications including atrial and ventricular septal defects, patent foramen ovale and ductus arteriosus. In addition, occlusion of coronary artery fistulae, postoperative fenestrations and aortopulmonary collaterals may be undertaken. Dilatation and stent placement is employed in conditions such as aortic coarctation and pulmonary artery stenosis, and to increase flow through surgical conduits and venous baffles. The indications for use, devices available and outcomes will be illustrated in each case.

Conclusion: The role of the chest radiograph is central to the management of adults who have undergone catheter intervention for congenital heart disease. Recognition of the normal and abnormal appearances following deployment of these devices is increasingly important as they become more frequently encountered in radiological practice.

C-0235

CT and MR imaging of benign primary cardiac neoplasms with echocardiographic correlation

F. Todua, M. Razmadze, G. Tsivtsivadze, S. Kakhadze; *Tbilisi/GE*

Purpose: Analyze the advantages and disadvantages of CT, MR imaging and transthoracic echocardiography (TE) in the assessment of heart neoplasms.

Material and Methods: 46 patients (age 8-68 years) with suspected heart neoplasms were examined with TE, CT and MR imaging. Examinations were performed under clinical indications in preparation for surgery or to obtain a precise diagnosis.

Results: In 37 patients the diagnosis of intracardiac tumor (21 myxomas, 6 rhabdomyomas, 5 lipomas, 3 fibromas, 2 cardiac echinococcosis) was confirmed pathologically. In 9 patients echocardiographic diagnosis was not confirmed. In these cases MR imaging and CT revealed an anatomic variant or other abnormality that had been interpreted as a probable mass on the echocardiogram.

Conclusion: All methods allow evaluation of tumor size, location and structure. TE is the primary modality for imaging of intracardiac disease. It provides high-resolution, real-time images, especially improved with the introduction of new ultrasonographic imaging techniques such as tissue harmonics. The resolution of CT and MR imaging is superior to that of TE, and both modalities proved to be useful for detection of the tumor, depiction of contour, relation with other cardiac structures, also allowing imaging of the entire mediastinum and evaluation of the extracardiac extent of disease. In comparison to MR imaging, CT is capable of detecting calcifications, which is an important variable in the differential diagnosis of cardiac neoplasms. In addition, CT is faster, easier to perform, and generally has more reliable image quality. MR imaging has better soft-tissue contrast than CT and allows much greater flexibility in the selection of imaging planes.

C-0236

Measurement of cardiac high-energy-phosphate metabolites in dilated cardiomyopathy (DCM) by ^{31}P -MR spectroscopy

A. Hansch, R. Rzanny, J.-P. Heyne, U. Leder, J. Reichenbach, J. Boettcher, W.A. Kaiser; *Jena/DE*

Introduction: Dilated cardiomyopathy (DCM) is accompanied by an impaired cardiac energy metabolism. The aim of this study was to investigate whether the PCr/ATP-ratio is reduced in patients with DCM by using spectroscopic chemical shift imaging (CSI). Additionally, we evaluated how this index correlates with the left ventricular ejection fraction (LVEF) as an established prognostic factor of heart failure.

Methods and Materials: This study involved 20 volunteers and 15 patients with severe symptoms and 10 patients with moderate symptoms of DCM. Cardiac ^{31}P -MR measurements were performed with a 1.5 T whole body scanner. Peak areas were evaluated for cardiac high-energy phosphates (PCr, ATP), as well as for 2,3-diphosphoglycerate (2,3-DPG) and phosphodiesters (PDE).

Results: PCr/ γ -ATP ratio was significantly decreased in patients with moderate and severe DCM (PCr/ γ -ATP in severe DCM 1.31 ± 0.38 , PCr/ γ -ATP in moderate DCM 1.63 ± 0.33 , PCr/ γ -ATP in volunteers 2.07 ± 0.17). PCr/ γ -ATP ratios showed a linear correlation with reduced left ventricular ejection fractions. PDE/ γ -ATP ratios were significantly increased in patients with severe DCM (mean PDE/ γ -ATP = 1.49 ± 0.56) as compared to volunteers (PDE/ γ -ATP = 1.07 ± 0.27).

Discussion: Applying ^{31}P -MRS with commonly available 2D-CSI sequences is a valuable technique to evaluate DCM by determining PCr/ATP ratios non-invasively. In addition to reduced PCr/ATP ratios observed in patients suffering from DCM, significantly increased PDE/ATP ratios were found in patients with severe DCM.

C-0237

MR imaging of cardiac and paracardiac masses: A pictorial review

G.K. Schneider, R. Seidel, P. Fries, I. Kindermann, M. Boehm, H. Winter; *Homburg a.d. Saar/DE*

Learning Objectives: Based on typical MR findings algorithms that include other diagnostic modalities like findings on catheter angiography or perfusion measurements will be presented to give the reader a maximum spectrum of findings to characterize cardiac and paracardiac masses.

Background: Although cardiac masses are most frequently detected on echocardiography, MR imaging is the method of choice to accurately evaluate and further characterize cardiac tumors. However the maximum information about a suspected cardiac mass is gained if all clinical information together with results of echocardiography, computed tomography, catheter angiography and endomyocardial biopsy are taken into consideration.

Imaging Findings: Case studies presented include common and rare benign and malignant tumors as well as tumor-like lesions with correlation to histology and surgical images. MR imaging results will be presented and discussed together with findings in other imaging modalities and typical and atypical manifestations of the different tumors will be discussed.

Conclusion: MR imaging has a major impact on the work up of cardiac and paracardiac masses as an accurate diagnostic tool for further characterisation and therapy planning.

C-0238

Utility of myocardial edema to differentiate between acute and chronic myocardial infarctions (MIs) and its correlation with the extension of necrosis: A T2-weighted and delayed enhancement (DE) cardiovascular-MR (CMR) study

M. Francone, I. Carbone, K. Lanciotti, E. Algeri, A. Ascarelli, M. Cavacece, F. Fedele, R. Passariello; *Rome/IT*

Purpose: Previous studies have shown that myocardial edema typically appears in the acute phase of MI after reperfusion and gradually resolves with infarct healing. Therefore, we intended to investigate the feasibility of T2-weighted CMR to discriminate acute from chronic MIs and to correlate the extension of edema with DE findings.

Materials and Methods: Forty-one patients with a previous history of MI were included in the study; 19 were studied in the acute phase (< 14 days) after MI, 22 had a chronic history of MI (> 30 days). In all patients a CMR protocol including T2-weighted black-blood and DE sequences was acquired using a 1.5-T CMR-system. In order to discriminate acute from chronic MI, the presence of edema and DE was visually assessed by two blinded observers. When detected, the volume of edematous myocardium was correlated with the extension of necrosis as shown by DE acquisitions.

Results: After images analysis, myocardial edema was detected as a transmural area of hyperintense T2-weighted signal in 19/19 patients with acute MI and 2/22 chronic patients. The combined assessment of T2-weighted and DE images yielded a specificity of 91% to differentiate acute from chronic lesions. The volume of edema was significantly larger than necrosis in all cases (mean +18.6%, p < 0.05) and a good correlation was found between edema and extension of MI ($r = 0.86$, p < 0.01).

Conclusions: Our study suggests that a combined approach of T2-weighted and DE CMR-sequences enables differentiation of acute from chronic MIs; T2-weighted images can depict the presence of edema in acute patients overestimating the extension of necrosis.

C-0239

Magnetic resonance for follow-up after orthotopic cardiac transplantation

G. Puppini, S. Quintarelli, L. Tomasi, M. Iafrancesco, G. Destro, S. Montemezzi, G. Gortenutti; *Verona/IT*

Purpose: Patients who underwent orthotopic cardiac transplantation (OCT) require several evaluations of myocardial function and of morphology of caval anastomosis (CA). The aim of this work is to determine whether magnetic resonance (MR) might be useful as a one-step technique to evaluate patients who underwent OCT.

Methods and Materials: 31 patients underwent MR evaluation (1.5 T) at least 12 months after OCT to assess cardiac morphology and function. We used T1-weighted sequences in order to analyze the morphology of anastomoses involving aorta, pulmonary artery and cava veins. We measured ejection fraction (EF) and regional function (RF) of left ventricle (LV), performing short-axis dynamic sequences. Segmental wall thickening was scored 0 if normokinetic, 1 if hypokinetic and 2 if dyskinetic. Data are expressed as mean \pm SD.

Scientific and Educational Exhibits

Results: Morphologic assessment was feasible for all vascular anastomoses, in particular for the caval ones which are not easily determined by either ultrasound or angiography. The diameter of postcaval anastomoses is 19.5 ± 4.2 mm (9 ± 1.7 mm/m²), while the diameter of precaval anastomoses is 16.6 ± 3.1 mm (9 ± 1.7 mm/m²). Out of 496 segments 487 (98.1%) are normokinetic, 9 (1.9%) hypokinetic and there are no dis/akinetik segments (mean score = 0.018 ± 0.13). We find a trend toward a correlation between the diameter of postcaval anastomosis and EF ($p = 0.05$), while there seems to be no link among EF, diameters of cavae, regional function in relation to the time from OCT.

Conclusions: We suggest that MR be considered as a potential one-step alternative tool for follow-up after OCT.

C-0240

MR assessment of nonischemic dilated cardiomyopathy: Correlation of left ventricular wall motion and delayed myocardial enhancement

J.-W. Lee, J. Seo, Y. Kim, B. Choi, K. Choe; Seoul/KR

Purpose: To evaluate and analyze the left ventricular (LV) wall motion in patients with nonischemic DCMP related to the presence of delayed myocardial enhancement.

Materials and Methods: Thirty-one consecutive patients (male: 20, female: 11, mean age: 54.1 years) with nonischemic DCMP and confirmed unobstructive coronary arteries were enrolled. MR imagings with short-axis myocardial tagging and delayed contrast enhancement were performed. With the myocardial tagging images, circumferential myocardial shortening (ECC) and radial myocardial thickening (ERR) were calculated by HARP analysis. The strains of ECC and ERR taken in every segments were analyzed related to myocardial enhancement.

Results: Fourteen patients revealed delayed enhancements of LV myocardium and seventeen patients did not. All patients showed marked regional heterogeneity of LV wall motion and regional paradoxical motion (19/31) by HARP analysis. Reduced wall motion of LV in septum and preserved wall motion in lateral wall were easily detected by HARP analysis. The LV myocardial wall motions by ECC and ERR at each segments were not significantly different in segments with and without delayed myocardial enhancement (ECC < mean p-value = 0.289 >, ERR < mean p-value = 0.455 >, $p < 0.05$) except for anterior wall at the middle and basal LV on ECC.

Conclusion: Short-axis tagged MR imaging and HARP analysis showed delicate regional heterogeneity and paradoxical motion in nonischemic DCMP patients. The tagged MR imaging and HARP analysis can be applied to analyze delicate and complex LV wall motion in nonischemic DCMP patients.

C-0241

Delay hyperenhancement by contrast-enhanced MR imaging: Clinical application of various cardiac disease

D. Kim, S.-I. Choi; Seoul/KR

Learning Objectives: The purpose of this study was to exhibit delayed enhancement of various cardiac diseases on MR imaging.

Background: Clinical applications of contrast-enhanced MR imaging in defining viability are evolving with the advantage of excellent spatial resolution. The value of delay hyperenhancement imaging is accurate identification of infarcted myocardium with resolution that allows the transmural extent of myocardial injury to be determined. Also, non-ischemic patterns of myocardial injury such as dilated or hypertrophic cardiomyopathy have been reported in other disease states. Delay hyperenhancement may have an additional role in guiding management or determining prognosis in diseases such as myocarditis.

Imaging Findings: In this exhibit, we will demonstrate clinical application of delay hyperenhancement in various cardiac diseases such as myocardial infarction including RV infarction, microvascular obstruction, non-ischemic cardiomyopathy such as dilated cardiomyopathy, and myocarditis on the basis of our experience.

C-0242

Use of positron emission tomography and [13N]-ammonia to estimate the relationship between regional myocardial blood flow and coronary artery stenosis severity in patients with coronary heart disease

D.V. Ryzhkova, M.I. Mostova, O.G. Zverev, L.A. Kofal, L.A. Tyutin; St. Petersburg/RU

Purpose: The purpose of this study was to determine the relationship between coronary artery stenosis (CAS) severity and regional myocardial blood flow (MBF) in patients with coronary artery disease (CAD).

Materials and Methods: 21 patients with angiographically confirmed CAD were included in the study. None of them had a clinical history or electrocardiographic

evidence of previous myocardial infarction, significant myocardial hypertrophy or valvular disease; no patient had evidence of complete coronary occlusion by angiography examination. 11 normal subjects served as controls. MBF at rest and during dipyridamole induced hyperemia was evaluated by [13N]-ammonia dynamic positron emission tomography ("HR+", Siemens). The coronary flow reserve (CFR) was defined as the ratio between MBF stress and MBF rest. Selective angiography of coronary arteries was performed according to the Judkins technique.

Results: MBF at rest was similar in the patients and controls (69.7 ± 15.4 mL/min/100 g. vs 71.7 ± 17.7 mL/min/100 g., NS). During hyperemia MBF significantly decreased in the regions supplied by diseased coronary vessels in the patients (76.6 ± 17.6 mL/min/100 g. vs 206.5 ± 63.5 mL/min/100 g., $P < 0.001$). It revealed a significant correlation between MBF during hyperemia and CAS degree ($r = -0.76$; $P < 0.05$). CFR began to decrease when CAS degree was equal 50 percent or more of the luminal diameter and approached unity (1.01 ± 0.17) when CAS was equal or greater than 80 percent.

Conclusion: MBF at rest remains constant despite increasing of CAS severity. Whereas, MBF during hyperemia begins to progressively decline if CAS degree is more than 50 percent. CFR approaches unity when CAS is 80 percent or greater.

C-0243

Tissue MR imaging of subacute myocardial infarction correlates with B-Type natriuretic peptide and tissue Doppler imaging

B.P. Paelinck¹, C.J. Vrints¹, J.J. Bax², J.M. Bosmans¹, A. de Roos², H.J. Lamb², ¹Edegem/BE, ²Leiden/NL

Purpose: B-type natriuretic peptide (BNP) is an amino acid protein released from the cardiac ventricles in response to myocyte stretch. BNP has been correlated to left ventricular (LV) filling pressures in patients with LV dysfunction and has been used to improve management of these patients. Combining Doppler assessed early diastolic mitral flow velocity (E) with early diastolic mitral annular velocity (Ea) has been correlated with both LV pressures and BNP. Phase-contrast MR imaging allows velocity encoding of both moving structures (tissue MRI) and blood. The study was aimed to investigate whether tissue MR Imaging assessed E/Ea correlates with BNP.

Methods and Materials: 14 patients in the subacute phase (5.9 ± 2.7 days) of Q-wave myocardial infarction (mass index: 83 ± 14 g/m², ejection fraction: $44 \pm 12\%$) underwent consecutive measurement of mitral inflow and mitral annular velocities with Doppler and phase-contrast MR imaging. The data were correlated with BNP.

Results: There was a strong relation between MR imaging (12.5 ± 6.3) and Doppler (12.6 ± 5.6) assessed E/Ea ($r = 0.89$, $P < 0.0001$) and between MR imaging (1.8 ± 0.8) and Doppler (1.5 ± 0.8) assessed E/A (A = late diastolic mitral velocity; $r = 0.92$, $P < 0.0001$). BNP ranged from 39.5 to 2380 pg/ml. E/A related strongly to BNP (MR: $r = 0.72$, $P = 0.004$ and Doppler: $r = 0.66$, $P = 0.014$). Best relation was found between E/Ea and BNP (MR: $r = 0.74$, $P = 0.002$ and Doppler: $r = 0.88$, $P < 0.0001$).

Conclusions: Tissue MR imaging has the ability to measure E/Ea. Tissue MR Imaging assessed E/Ea correlates with BNP in patients with subacute myocardial infarction.

C-0244

Comparison of delayed enhancement MR imaging and thallium SPECT for the assessment of myocardial viability

L. Klzo, M. Solar, J. Zizka; Hradec Kralove/CZ

Purpose: To compare delayed contrast enhancement MR imaging with thallium 201 single photon emission computed tomography (SPECT) in the evaluation of myocardial viability.

Methods and Material: Forty patients with ischemic cardiomyopathy (defined by significant coronary artery disease and systolic dysfunction with ejection fraction < 45%) were evaluated by both imaging techniques.

Results: Mean ejection fraction was $31.7\% (\pm 7.2\%)$. Totally, 1332 left ventricular segments were evaluated. An agreement in the assessment of myocardial viability was observed in 540 segments (41%): 415 segments were fully viable, 62 showed signs of impaired viability and 63 were non-viable. 285 segments (21%) with no signs of viability on SPECT showed some viable tissue on MR imaging: this finding was most common at the posterolateral left ventricular wall. 461 segments (35%) fully viable on SPECT showed non-transmural extent of enhancing scar on MR imaging. In 31 segments (2%) with impaired viability on SPECT, MR imaging did not reveal any non-viable tissue. 15 segments (1%) with signs of viability on SPECT were defined as non-viable on MR imaging.

Conclusion: When comparing delayed enhancement MR imaging with thallium

Scientific and Educational Exhibits

SPECT for the assessment of myocardial viability, MR imaging shows signs of viability in the segments that were defined as viable on SPECT. However, many segments (35%) with normal thallium uptake on SPECT show signs of irreversible myocardial injury on MR imaging. On the contrary, significant number (21%) of non-viable segments on SPECT shows signs of viability on MR imaging. Delayed enhancement MR imaging thus seems to be more accurate in the assessment of myocardial viability than thallium SPECT.

C-0245

Whole heart coronary MR-angiography: Presentation of a new technique and report of initial results

M. Ozgun, A. Hoffmeier, R.M. Botnar, W. Heindel, R. Fischbach, D. Maintz; Münster/DE

Purpose: To evaluate a new coronary MR angiography technique covering the whole coronary artery tree in one data set acquisition.

Material and Methods: 5 healthy volunteers and 15 patients with CAD were examined with navigator gated and corrected free-breathing 3D-balanced-gradient-echo sequence covering the whole heart (WH-MRA) (TR = 5.4, TE = 2.7, SENSE factor = 2, 160 slices, 0.75 mm reconstructed slice thickness, in-plane resolution = 0.99x0.99 mm, scan-time = 14 min and a vessel targeted 3D-balanced-gradient-turbo-field-echo (BTFE-MRA) sequence (TR = 5.6, TE = 2.8, 20 slices of 1.5 mm reconstructed slice thickness, in-plane resolution = 0.99 x 0.99 mm, scan-time = 7 min)). Subjective image quality (4 point scale) and objective image quality parameters including vessel sharpness, vessel diameter, SNR and CNR were calculated for WH-MRA and BTFE-MRA. In patients, accuracy for detection of stenoses larger than 50% was compared to X-ray coronary angiography, which was considered the goldstandard.

Results: WH-MRA demonstrated good vessel visibility in healthy subjects (100%) whereas in patients, vessel visibility was limited (78% in an 8 segment evaluation). Vessel sharpness was inferior to BTFE-MRA in patients (37% vs. 42%) but equal in healthy subjects (42%). Vessel diameters did not differ significantly between WH-MRA and BTFE-MRA. SNR and CNR were significantly reduced for the WH-MRA (SNR: 12.1 vs. 19, CNR 7.4 vs. 11.5). Diagnostic accuracy for the detection of CAD was inferior for WH-MRA (78%) when compared to CTA (84%) and comparable to BTFE-MRA (79%).

Conclusions: We successfully demonstrate the use of WH-MRA for coronary visualization in healthy subjects. In patients, subjective/objective image quality and accuracy for detection of CAD was inferior to BTFE-MRA.

C-0246

MR imaging evaluation of patients undergoing radiofrequency catheter ablation of atrial fibrillation: A preablation comprehensive approach

V. Katsiva, A. Katsivas, M. Douskou, C. Vasilopoulos, S. Mavrogeni, G.A. Michailidis, M. Tibshirani; Athens/GR

Learning Objectives: To briefly describe the use of radio-frequency catheter ablation (RFCA) of the distal pulmonary veins (PVs) and posterior left atrium in the treatment of atrial fibrillation. To define an optimized preablation MR imaging study protocol and analysis. To illustrate normal anatomy and anatomic variations of left atrium-PVs.

Background: Pulmonary vein (PV) isolation is considered the treatment of choice in patients undergoing RFCA of atrial fibrillation. Detailed knowledge of the left atrium-PVs anatomy is required for procedural success.

We investigated with MR imaging 26 patients with paroxysmal atrial fibrillation who were treated with catheter ablation. The protocol was designed to assess: patent foramen ovale, intraatrial thrombus and the anatomy of PVs-left atrium. The following anatomic features were described: number, size, location and shape of the PVs ostia, intervenous saddle distances, shape and orientation of the PVs trunks and branching pattern with emphasis on the presence of ostial branch.

Procedure Details: On a 1.5-T MR imager, a cine mode true-FISP sequence was acquired. Three-dimensional gadolinium-enhanced MR angiography was performed, in the coronal plane centered on the left atrium after intravenous bolus injection of gadolinium-based contrast material. Postprocessing of MRA data generated 2D multiplanar reformatted and 3D epicardial and intracardial images of the left atrium and distal PVs. A delayed contrast enhanced inversion recovery sequence was acquired 5 to 10 minutes following contrast administration.

Conclusion: Conventional PV anatomy was encountered in 14/26 patients. A common left PV, an additional PV, early branching pattern, ostium diameter > 25 mm or < 10 mm were the most important anatomic variants.

C-0247

Tc99m-Myoview and Ga-67-Citras combined SPECT imaging for diagnosis of cardiac sarcoidosis

A.N. Yalfimov, D.V. Ryzhkova, L.A. Tyutin, O.P. Baranova; St. Petersburg/RU

Purpose: Sarcoidosis is the multisystem disease of unknown etiology which is characterized long asymptomatic course. Cardiac sarcoidosis results in dilated cardiomyopathies, fatal ventricular tachyarrhythmia or blockade of conducting heart system. The aim of this study was to assess the diagnostic advantage of Tc99m-Myoview and Ga-67-Citras combined SPECT imaging for detection of myocardial involvement with sarcoidosis.

Methods and Materials: 24 patients with suspicion of cardiac sarcoidosis were included in the study. All the patients had no evidence of coronary artery disease and myocardial infarction history. Tc99m-Myoview and Ga-67-Citras SPECT (E. cam var, Siemens) were performed on different days. The intrabronchial myocardial biopsy was carried out in all cases.

Results: The patients were classified into two groups according the presence or absence of histological evidence of cardiac sarcoidosis. 11 patients with histologically proven cardiac sarcoidosis (the 1st group) had abnormal Ga-67-Citras uptake in the heart. The myocardial regions with abnormal Ga-67-Citras uptake corresponded with those with perfusion defects in all patients. Tc99m-Myoview SPECT revealed perfusion abnormalities in myocardial regions without high Ga-67-Citras uptake in 4 patients. Sarcoidosis lesions were not observed in those areas according the myocardial biopsy. 13 patients without histological evidence of cardiac sarcoidosis were classified into the 2nd group. In the 2nd group none had perfusion defects and abnormal Ga-67-Citras uptake.

Conclusion: Tc99m-Myoview and Ga-67-Citras combined SPECT imaging is a reliable protocol for cardiac sarcoidosis detection and allows avoidance of intrabronchial myocardial biopsy.

C-0248

Diagnosis of arrhythmogenic right ventricular cardiomyopathy: A modified magnetic resonance imaging scoring system

R. Maksimovic¹, T. Dill², G. Bachmann², P. Seferovic¹, S. Stankovic¹, H. Pitschner²; ¹Belgrade/YU, ²Bad Nauheim/DE

Purpose: Diagnostic value of magnetic resonance imaging (MRI) in patients with arrhythmogenic right ventricular cardiomyopathy (ARVC) has not been well established. This study aims to evaluate an MRI based scoring model formation and assess its diagnostic significance in patients with suspected ARVC.

Materials and Methods: 53 patients with myocardial abnormalities in the RV verified on MRI were included and divided into two groups: group 1 (17 patients) with ARVC and group 2 (36 patients) with other RV arrhythmias. Decision tree learning (DTL) and linear classification (based on a modified ARVC scoring model of major and minor criteria) were used to identify and assess MRI criterion information value, and to induce ARVC diagnostic rules.

Results: All major ARVC criteria were more frequent in group 1. Among minor criteria, regional RV hypokinesia, mild segmental RV dilatation and prominent trabeculae were more frequent in group 1 while mild global RV dilatation was more frequent in group 2. Diagnostic rules defined by DTL yielded a mean predictive accuracy of 76.8% and RV aneurysm emerged as a key criterion in the diagnosis of ARVC. Optimal diagnostic accuracy (sensitivity 93.3%, specificity 89.5%) was achieved when the value of the modified scoring model was equal to four, which corresponds to the following criteria combinations: two major, or, one major and two minor, or four minor criteria.

Conclusions: Accurate diagnostic rules based on MRI were derived with a RV aneurysm as the most important criterion. Combinations of major and minor criteria contributed to a statistically valid model for ARVC diagnosis.

C-0249

Cine-MR imaging: Morphologic analysis of congenital heart diseases

C. Barrera¹, C. Gervas¹, J. San Vicente¹, A. Cabrera², M. Izquierdo¹, E. Fernandez¹; ¹San Sebastian/ES, ²Bilbao/ES

Learning Objective: To illustrate the ability and contribution of cine-MR imaging sequences in the depiction of congenital heart diseases' morphologic alterations.

Background: Cine-MR imaging allows analysis of cardiac cavities, valves and blood flow in movement. In addition, high quality anatomic images with excellent contrast between blood flow (bright blood) and adjacent structures are obtained. These sequences help precise evaluation of the anatomy of congenital heart diseases (venoatrial and atrioventricular connections, ventriculoarterial alignment anomalies, atrial or ventricular septal defects, ...) and to obtain valvular information. They are very useful in the analysis of surgical conduits and anastomosis, as well as the presence of flow distal to a stent or valvular pathology.

Scientific and Educational Exhibits

Procedure Details: 102 cardiac MR imaging studies of 90 patients referred to our hospital for cardiac congenital anomaly analysis were retrospectively reviewed, 51 studies for the diagnosis and 51 after surgical treatment. 79 included cine fast gradient echo (GE) sequences, 34 magnetization prepared GE and 45 steady state coherent GE. The examinations which did not include cine-MR imaging sequences corresponded to pre and postsurgical aortic coarctation and pulmonary venous anomalous connections. We display different image examples where cine-MR imaging was useful for diagnosis.

Conclusion: In addition to the great value in functional analysis of congenital heart diseases, cine-MR imaging contributes to morphological evaluation of these pathologies because of the anatomic quality of the images, the excellent contrast and the ability to visualize the anatomical structures in movement.

C-0250

MR imaging of cardiomyopathies: A pictorial review

X. Merino-Casabiel, R. Dominguez-Oronoz, E. Castella-Fierro, V. Pineda, A. Evangelista; Barcelona/ES

Learning Objectives: To review and illustrate the MR imaging findings of cardiomyopathies.

Background: Cardiomyopathy is an important cause of morbidity and mortality. Myocardial diseases present clinically in a variety of forms ranging from a- or oligosymptomatic to fulminant cardiac failure. Diagnosis is based on patient's symptoms, cardiac imaging, laboratory test and endomyocardial biopsy. MR is well suited to evaluation of myocardial diseases and provides accurate and reproducible morphologic and dynamic images of the myocardium.

Procedure Details: Retrospective review of our cardiac MR exams database over last 5 years was made, selecting the most demonstrative examples of cardiomyopathies including primary cardiomyopathies (dilated, hypertrophic, restrictive and arrhythmogenic right ventricular dysplasia), specific cardiomyopathies (ischemic, valvular, infective inflammatory (myocarditis), noninfective inflammatory (connective tissue disorders), infiltrative (hemochromatosis), fibroplastic (Löfller disease) and unclassified cardiomyopathies.

Conclusion: MR imaging is a useful tool in the diagnosis and evaluation of severity of heart abnormalities in patients with cardiomyopathies.

C-0251

Using cardiovascular MR imaging to understand and simplify the chest radiograph for congenital heart disease

S.P. Prabhu, K. Burney; Bristol/UK

Learning Objectives: 1. Develop a systematic approach to the chest radiograph taken to evaluate congenital heart disease. 2. Narrow the differential diagnosis and guide further investigation. 3. Understand pathophysiology of common congenital heart disorders better using the help of MR imaging.

Background: The chest radiograph for congenital heart disease has always been seen by residents to be difficult to master. However, it is still the commonest investigation performed to investigate congenital heart disease throughout the world. With the advent of cross-sectional imaging modalities, it has become easier to understand pathophysiology of complex congenital heart disease. We have found that correlation of MR imaging images of patients with congenital heart disease are very useful to understand the chest radiographs. This review aims to elaborate on this correlation.

Imaging Findings: We reviewed data from patients who underwent MR imaging for congenital heart disease in our institution in the last 24 months. We obtained a chest radiograph taken as close to the date of the MR imaging as possible. We identified the pathology on these radiographs that could be illustrated in a three dimensional plane and correlated this to the chest X-ray findings. Normal cases are used to illustrate normal anatomical structures and accepted nomenclature in cardiac radiology. Case studies include both simple, isolated anomalies like coarctation of the aorta, septal defects and valvular stenosis and complex, multiple anomalies like tetralogy of Fallot and variants of transposition of the great arteries.

Conclusions: MR imaging can be used to enhance understanding of the chest radiograph for congenital heart disease.

C-0252

Fetal heart tumors

D. Elias, P. Marantz, M. Guerchicoff, A. Gutierrez, A. Villa, J. San Roman; Buenos Aires/AR

Purpose: To determine prevalence and natural history of heart tumors in patients referred for fetal echocardiography.

Methods and Materials: From May 1998 to December 2003, 7 fetuses with cardiac tumors have been sent to fetal echocardiography out of 9866 obstetric US studies.

Results: Four patients had multiple rhabdomyomas. Three of them had tuberous sclerosis (TS) with intracerebral tumors detected by MR imaging. Cardiac tumors regressed during first year of life and children were asymptomatic. Another fetus presented a single tumor with a rhabdomyoma appearance at US attached to the interventricular septum. At 5 months of life this mass became smaller. Another patient had a large left ventricular mass with US appearances of a fibroma, which required early surgery. This tumor was almost completely resected, and 4 years later a small residual mass has not grown. Histopathological exams revealed cardiac fibrosarcoma. The last fetus with a single intraseptal tumor with US appearances suggestive of a large fibroma, died at 7 months old with low cardiac output. MR imaging did not identify brain tumors. Autopsy was not authorized by parents.

Conclusion: (1) Prevalence of fetal cardiac tumors in our hospital was 0.05% and represented 7.5% of congenital heart disease in a 5-year period. (2) Rhabdomyomas were most frequent with spontaneous regression after birth. (3) Multiple rhabdomyomas were associated with TS. (4) No death occurred during fetal life in this series. (5) Fetal echocardiography provides an accurate diagnosis, allowing pregnancy follow-up and parental counseling.

C-0253

Characterization of acute and chronic myocardial infarcts by multidetector CT. Comparison with contrast-enhanced MR

B.L. Gerber, E. Coche, B. Belge, P. Lim, A. Pasquet, J.-L. Vanoverschelde; Brussels/BE

Background: Gd-DTPA contrast-enhanced (CE) MR imaging reveals patterns of hypoenhancement early and of hyper-enhancement late after contrast injection in myocardial infarction (MI). We evaluated whether the injection of iodated contrast at the time of non invasive coronary imaging might also allow infarct characterization by multidetector CT (MDCT).

Materials and Methods: Nineteen patients with acute MI and 14 patients with chronic dysfunction and suspected MI underwent MDCT and CE-MR imaging. CE patterns on short-axis tissue MDCT images acquired at the time of coronary imaging and 10 minutes after contrast injection were compared with MR.

Results: Early MDCT images demonstrated areas of reduced contrast enhancement in infarcted areas in 15 patients with acute infarct and in 4 patients with chronic infarct. The location of areas of early hypo-enhancement by MDCT was similar to those of MR. Size of early hypo-enhanced areas by MDCT and MR (4 ± 8 vs. $6 \pm 9\%$, $p = NS$) were similar and highly correlated ($r = 0.89$, $p < 0.001$). On late MDCT images all patients with acute infarcts and 10 patients with chronically dysfunctional myocardium had areas of increased contrast-enhancement (hyper-enhanced areas). Again, the location and size of late hyperenhanced areas by MDCT and CE-MR were similar (25 ± 18 vs. $22 \pm 16\%$, $p = NS$) and well correlated ($r = 0.78$, $p < 0.001$).

Conclusions: MDCT can characterize acute and chronic MI with similar contrast-enhancement patterns, i.e. hypoenhanced area on early images, and hyper-enhanced area on late images, as CE-MR. The technique can thus provide important information on tissue viability at the time of non-invasive coronary imaging.

C-0254

The complex of myxomas, spotty skin pigmentation and endocrine overactivity: Carney complex Imaging findings

N.A. Courcoutsakis¹, P. Prassopoulos¹, J.A. Carney², C.A. Stratakis³; ¹Alexandroupolis/GR, ²Minnesota, MN/US, ³Bethesda, MD/US

Learning Objectives: To illustrate the spectrum of the manifestations and corresponding imaging findings of "The Complex of Myxomas, Spotty Skin Pigmentation, and Endocrine Overactivity" or Carney Complex (CNC).

Background: CNC is a familial multiple neoplasia and lentiginosis syndrome. CNC is inherited by an autosomal dominant manner and it is genetically heterogeneous. CNC features overlapped with those of McCune-Albright syndrome and other multiple endocrine neoplasia (MEN) syndromes.

Imaging Findings: Spotty skin pigmentation is the major clinical manifestation of the syndrome, followed by multicentric heart myxomas, which occur at a young age and are the lethal component of the disease due to brain embolic episodes. Myxomas also occur in the skin (eyelid, external ear canal and nipple) and the breast. Breast myxomas, when present, are multiple and bilateral among female CNC-patients ("breast-myxomatosis"). Affected CNC-patients often present tumors in two or more endocrine glands, including primary pigmented nodular adren-

Scientific and Educational Exhibits

o cortical disease, growth hormone or prolactin producing pituitary adenomas, thyroid adenomas or carcinomas, testicular neoplasms (large-cell calcifying Sertoli cell tumor) and ovarian lesions. Infrequent but characteristic tumors in CNC patients include psammomatous melanotic schwannoma, breast ductal adenoma with tubular features, and osteochondromyxoma or "Carney bone tumor". Mammography or breast MR imaging, cardiac US or MR imaging, CT or MR imaging evaluation of the adrenals, pituitary gland, testicles or ovaries are important diagnostic tools for detecting tumors associated with CNC.

Conclusion: Patients with suspected CNC should undergo a thorough imaging evaluation to define to establish diagnosis and to disclose tumors associated with CNC.

C-0255

Magnetic resonance detection of subclinical cardiac impairment in patients with systemic sclerosis

E. De Cicco, S. Casanova, M. Gravano, G. Molinari; Genoa/IT

Purpose: Aim of our study was to assess myocardial involvement in patients suffering from Systemic sclerosis (SSc) with no apparent symptoms or instrumental detection of cardiac impairment.

Methods and Materials: Forty-six SSc consecutive patients, (55.5 ± 14.1 yrs; 40 females, 6 males) underwent cardiac MR imaging at 1.5-T (Magnetom Vision, Siemens). Ten healthy volunteers, matched for age and sex, were enrolled as control group. All patients with SSc were asymptomatic with an unremarkable physical examination and in sinus rhythm. A segmented ECG-gated breath hold cine gradient echo sequence (TR/TE = 100/6.1 msec; FA = 25°, thickness = 10 mm) to encompass both ventricles (from basis to apex) was used. Diastolic and systolic volumes as well as ejection fractions for both ventricles were evaluated.

Results: All patients had left ventricle ejection fraction (LVEF) ($61.5 \pm 6.1\%$) in the normal range and nobody presented left ventricle kinetic abnormalities. Thirty patients had a reduced right ventricle ejection fraction (RVEF) ($42.5 \pm 4.4\%$) with LVEF of $57.9 \pm 6.7\%$ and sixteen patients had normal RVEF ($55.2 \pm 4.1\%$) with a LVEF of $66 \pm 4.4\%$.

Conclusion: Impairment of RVEF was found in patients suffering from SSc, even if they were not symptomatic for cardiac involvement. Compared with control group, SSc patients had significative reduction in RVEF ($p < 0.05$). these preliminary data suggest that MR imaging could be a potentially predictive method in evaluating early myocardial damage in SSc.

C-0256

Assessment of right ventricular function with magnetic resonance.

Preliminary report

D. Piotrowska, L. Kownacki, M. Golebiowski, L. Krolicki; Warsaw/PL

Purpose: Magnetic resonance (MR) is a well established "golden standard" in the assessment of left ventricular (LV) function. However evaluation of function of the more complex-shaped right ventricle (RV) is still uncertain. We aim to determine the feasibility and accuracy of right ventricular volume, function, and mass measurements with MR in comparison with corresponding LV values.

Materials and Methods: 12 healthy volunteers, 4 patients with ventricular hypertrophy and 7 with history of MI (19M,4F;20-70 yrs. median 28) were examined. A ECG-gated cardiac CINE TFE sequence was used (TR = 9.5[ms], TE = 4.5[ms], Flip angle = 30[deg],matrix:256x256 [pixels],slice thickness:8[mm], phases:10-13, number of slices:8-10). The images obtained were analysed on workstation with MASS software.

Results: The global calculated values were: RVmass [g], RVEDV [ml], RVESV [ml], RVSV [ml], RVEF [%], LVmass [g], LVEDV [ml], LVESV [ml], LVSV [ml], LVEF [%]. RV analyses were successfully performed in all subjects. RVSV was nearly identical to LVSV ($R = 0.96$, $p < 0.0001$), with a mean difference between RVSV and LVSV of 1 ml in the whole group as well as in the subgroups. As expected the subjects with history of MI have significantly lower LVEF. However there were no differences in RVSV and RVEF. 6 subjects (body-builders) out of the 12 healthy volunteers have significantly higher LVmass, RVEDV (175.6 ml vs 136.7 ml) RVESV (91.8 ml vs 54 ml) and lower RVEF (48% vs 60%).

Conclusion: TFE cine MR imaging enables accurate quantification of RV function in healthy subjects, patients with HCM and patients with history of MI using MASS software.

Cardiac

Multidetector CT (MDCT)

C-0257

ECG-gated 16-slice CT of coronary arteries: Assessment of image quality and accuracy in detecting stenoses

O. Luz, M. Heuschmid, A. Kuettner, S. Schroeder, A. Kopp, C.D. Claussen; Tübingen/DE

Purpose: Aim of this study was to investigate image quality and diagnostic accuracy in detecting coronary artery lesions using a 16-slice multidetector CT scanner.

Material and Methods: 37 patients underwent non-contrast spiral scan and MDCT angiography of the coronary arteries. After oral beta-blockade, scans were obtained in a single breath-hold with a 16-slice scanner using ECG-gating. Image quality was assessed in terms of artifacts and segment visibility by two reviewers. Stenosis severity was compared with results of conventional coronary angiography.

Results: Data evaluation of image quality was based on 488 segments. 380 segments were considered to have diagnostic image quality. 108 segments (22.1%) could not be sufficiently evaluated because of severe calcifications (35 segments) and motion artifacts (73 segments). The mean calcium score (Agatston Score Equivalent, ASE) was 524.3 ± 807.6 . 28/37 (75.7%) patients had an ASE < 1000 (mean ASE: 90.8 ± 152.3) and 9/37 (24.3%) patients had an ASE ≥ 1000 (mean ASE: 1761.0 ± 637.6). For detecting lesions $\geq 50\%$, the overall sensitivity, specificity, positive predictive value and negative predictive value were 59%, 87%, 61% and 87%. When limiting the number of patients to those with a calcium score < 1000 ASE, the threshold-corrected sensitivity for lesions $\geq 50\%$ was 93%, specificity 94%, positive predictive value 68% and negative predictive value 99%.

Conclusions: In patients with no or moderate coronary calcification, MDCT of coronary arteries using 16-slice technology allows the reliable detection of coronary artery stenoses with high diagnostic accuracy. An initial non-contrast scan was found to be mandatory to avoid useless examinations in patients with severe calcifications.

C-0258

Low-attenuation of myocardium with contrast-enhanced multi-detector CT: Hypoperfusion or fat deposition?

J. Nam, B. Choi, J. Seo, Y.-J. Kim, T. Kim, K. Choe; Seoul/KR

Purpose: Recently, acute myocardial infarction has been reported to show low-attenuated myocardium due to hypoperfusion in contrast-enhanced CT. We investigated low-attenuation of myocardium in patients who underwent coronary artery angiography with multi-detector CT.

Methods and Materials: In total 655 patients (mean age 61 ± 10) underwent contrast-enhanced coronary CT angiography for evaluation of native coronary artery in suspicion of coronary artery disease (NCA group, n = 275) or patency of coronary artery bypass graft (CABG group, n = 380) with multidetector CT. They all underwent non-enhanced CT (NECT) with a protocol for coronary calcium scoring. If a low-attenuation region was detected in NECT, it was considered due to fat deposition. The degree of enhancement of the low-attenuation area was measured and compared to that of normally enhanced myocardium.

Results: Seventy two (11%) patients showed low-attenuation area of myocardium with CECT. Sixty patients (15.8%) in CABG group and 12 patients (4.4%) in NCA group showed low-attenuation area of myocardium in CECT. In NECT, fat deposition was noted in 61 (85%) of patients in the same areas as with CECT. In the 12 patients with low-attenuation areas in the NCA group, a history of previous myocardial infarction was present in 4 patients, but not in 8. CT attenuation value of low-attenuated myocardium in NECT and CECT was -24.1 ± 33.4 and -8.5 ± 33.9 HU and that of normal myocardium was 44.3 ± 15.4 and 111.9 ± 23.9 HU, respectively.

Conclusion: Chronic myocardial infarction or ischemia frequently shows low-attenuation in CECT by either hypoperfusion, fat deposition, or by both. Therefore, low-attenuated myocardium in CECT should be carefully interpreted.

C-0259

Occlusive myocardial infarction on sixteen-slice multi-detector row helical CT in a rabbit model: Radiologic-pathologic correlation according to infarct age

J. Lee, Y. Kim; Seoul/KR

Purpose: To evaluate imaging finding and diagnostic accuracy for myocardial infarct (MI) on sixteen-slice multi-detector row helical CT (MDCT) in rabbits with radiologic and pathologic correlation.

Scientific and Educational Exhibits

Materials and Methods: MI was induced in 20 rabbits by ligation of coronary arteries. MDCT was obtained at 1 minute (early) and 6 minutes (delayed) after intravenous contrast injection. Rabbits were sacrificed according to infarct age, acute or chronic. Sliced cardiac specimens were stained for gross and microscopic examination. Agreement of scored transmural extent of MI between MDCT and specimens was statistically analyzed.

Results: MI was demonstrated in 13 rabbits on specimens and MDCT. Infarcted myocardium was demonstrated as a low-attenuation area on early scan and a low-attenuation area with enhancement along periphery on delayed scans. There was excellent agreement in transmural extent of MI between specimens and MDCT in early phase and fair to good in delayed phase. Histopathologic examination revealed myocardial necrosis with granulation along periphery of necrotic myocardium, corresponding to low-attenuation area on early phase. Peripheral enhancement on delayed phase could correlate with the area of granulation. Granulation tissue in specimens and peripheral enhancement on delayed phase were increased with ageing of infarct.

Conclusion: MDCT was useful in the diagnosis of MI and the early phase was more accurate than delayed in evaluation of transmural extent. In histopathologic examination, infarcted myocardium consisted of myocardial necrosis with granulation along periphery of infarcted myocardium, which could match the low-attenuation area and peripheral enhancement on delay phase. Granulation and peripheral enhancement were increased with the ageing of infarcts.

C-0260

Imaging of atrioventricular septal defect (AVSD) with multidetector-row CT angiography

R.L. Hallett, M.D. Hiatt, D. Fleischmann, J.C. Hellinger, G.D. Rubin, F.P. Chan; Stanford, CA/US

Learning Objectives: To explain in detail our technique for acquisition of ECG-gated multidetector row CT (MDCT) angiography in children with congenital heart disease. To illustrate the spectrum of AVSD as depicted by MDCT angiography in infants through adolescents.

Background: ECG-gated MDCT has evolved into a viable problem-solving tool for the assessment of congenital abnormalities of the heart and great vessels. ECG-gated MDCT provides excellent spatial resolution and facilitates acquisition of volume data with acceptable temporal resolution, even at high heart rates. Short exam times, decreased anesthesia needs, and safe performance in patients with pacemakers are additional benefits. AVSD arises when the endocardial cushions fail to meet the septum primum, resulting in a spectrum of abnormalities from primum ASD to complete AVSD. Various AV valve abnormalities also coexist. The Rastelli classification of complete AVSD is useful for surgical planning. Diagnosis is often made by echocardiography, but MDCT angiography provides additional information including true 3D and 4D datasets for depiction of complex native and post-operative cardiac anatomy, mass, and function.

Imaging Findings: ECG-gated MDCT acquisition technique and contrast medium delivery methods will be described in detail. Dose-reduction techniques will be discussed. The anatomic structures important for characterization will be clearly demonstrated. A wide spectrum of AVSD including native and post-operative anatomy and associated cardiovascular anomalies will be presented.

Conclusion: AVSD is a spectrum of cardiac malformations. ECG-gated MDCT angiography is a useful problem-solving tool for evaluation of native and post-operative anatomy and function, and helps guide surgical planning and post-operative follow-up.

C-0261

Anomalous origin of coronary arteries: Demonstration with MSCT coronary angiography

Z. Wang, Z. Yang, J. Shen, H. Zhu, X. Zhou, W. Fang; Dalian/CN

Learning Objectives: To illustrate the ability of MSCT coronary angiography in the detection of anomalous origin of the coronary arteries. To demonstrate the ability of MSCT coronary angiography in the further evaluation of patients with chest pain in whom a coronary anomaly is suspected.

Purpose: To describe the value of multislice spiral CT (MSCT) coronary angiography in the detection of anomalous origin of the coronary arteries.

Materials and Methods: During three years, the 3010 subjects underwent MSCT coronary angiography (retrospectively ECG-gating; 0.5 s rotation; one-sector reconstruction algorithm; intravenous contrast agent).

Results: The anomalous origin of coronary artery was incidentally found with a multislice spiral CT in 22 patients (0.73%). There were 10 patients with an anomalously high origin of the right coronary artery. There were 9 patients with anomalous origin of the right coronary artery from left coronary sinus. In 2 patients, the

circumflex artery arises from the right coronary sinus and behind the aorta to reach the left atrioventricular groove. There was 1 patient with anomalous origin of the right coronary artery from posterior coronary sinus. These signs were better shown by MSCT coronary angiography.

Conclusions: MSCT coronary angiography is a useful adjunctive technique to invasive coronary angiography in the evaluation of anomalous origin of the coronary arteries.

C-0262

Assessment of mitral valvular replacement with chordal preservation using multidetector row computed tomography

D. Kim¹, S. Ryu², B.-H. Ahn²; ¹Seoul/KR, ²Gwang-Ju/KR

Background: The efficacy of multidetector row computed tomography (MDCT) for evaluating mitral valvular replacement (MVR) with chordal preservation has not been reported. The advanced diagnostic technique, MDCT may enable us to evaluate the cardiac function and morphology of MVR with chordal preservation. In this study, we demonstrated various MDCT images for the evaluation of MVR with chordal preservation in patients with mitral stenosis.

Materials and Methods: Twelve patients with MVR with chordal sparing or reconstruction were evaluated using MDCT. Nine patients underwent MVR with chordal reconstruction. Three patients underwent MVR with native chordal preservation. Four patients underwent partial preservation or reconstruction of chordae, two underwent preservation of the posterior leaflet chords only. Images of MDCT were recorded and measured according to echocardiographic view and criteria. Short-axis, two-chamber, four-chamber views, and three-dimensional images were processed for evaluating cardiac morphology and ventricular function.

Results: MDCT images were obtained successfully. Two-chamber and four-chamber views were useful in visualizing the papillary muscles and chordae. Short-axis view was most helpful in evaluating cardiac function. Three-dimensional images were used for evaluation of cardiac morphology.

Conclusion: MDCT can be another useful diagnostic modality for the cardiac function and morphologic evaluation of MVR with chordal preservation.

C-0263

Imaging of atrial septal defects (ASD) with multidetector-row CT (MDCT) angiography

S. Poplaw, J.C. Hellinger, M.D. Hiatt, F.P. Chan, D. Fleischmann; Palo Alto, CA/US

Learning Objectives: To review the embryology, anatomy and pathophysiology of atrial septal defects. To illustrate the MDCT findings, with echocardiographic and MR correlation.

Background: ASDs account for approximately 1% of congenital heart disease (CHD), but are the most common CHD in adults older than 20 years of age. MDCT acquisition speed has become so fast, that routine MDCT angiography (MDCTA) through the chest may depict ASD. It is paramount for the radiologist to detect and accurately classify these congenital abnormalities because of the associated complications (i.e. pulmonary hypertension, infective endocarditis, atrial dysrhythmias, and heart failure).

Imaging Findings: Ideal acquisitions require retrospective ECG-gated technique. However, as will be shown, routine MDCTA thin section technique can lead to the diagnosis. With robust technique MDCTA can demonstrate all anatomical types of ASD, associated congenital abnormalities, and the sequelae from ASD. At times, compared to echocardiography and MR imaging, MDCTA can more reliably depict ostium secundum, ostium primum, sinus venosus, and coronary sinus defects. At present, while complete volume acquisitions cannot demonstrate flow, identifying a CT shunt sign can localize a defect.

Conclusion: MDCTA is a valuable imaging modality for diagnosis of all types of ASD. Radiologist can play a significant role in minimizing the associated morbidity and mortality.

C-0264

Comparison between multi-detector CT and electro-anatomical mapping for evaluation of left atrium and distal pulmonary veins anatomy in atrial fibrillation patients

M. Centonze, M. Del Greco, M. Marini, S. Della Sala, P. Peterlongo; Trento/IT

Purpose: Aim of this study was to compare the results of left atrium (LA) and PVs reconstructions between CARTO™, an electro-anatomic navigation system used for atrial fibrillation (AF) radio-frequency catheter ablation (RFCA), and Multi-Detector 16 slices computed tomography (MDCT).

Method and Materials: 20 patients with drug refractory AF underwent PVs RFCA

Scientific and Educational Exhibits

guided by the CARTO™ maps of the LA and PVs ostia. MDCT examinations were performed after the procedure (> 1 month) for recognition of such potential complications as PVs stenosis. The following parameters were compared between MDCT and CARTO™: antero-posterior (AP), crano-caudal (CC) and late-ro-lateral (LL) axis of LA and number of right (RPVs) and left PVs (LPVs).

Results: The median values of LA axis were as follows: AP axis 37 mm CARTO™ versus 39 mm MDCT; CC axis 60 mm versus 65 mm; LL axis 81 mm versus 64 mm.

RPVs number concordance between CARTO™ and MDCT was found in 5/20 cases while in 13/20 cases CARTO™ overestimated the PVs number due to the presence in all of the cases of a branching less than 10 mm from the PVs ostium. Only in 2 cases CARTO™ failed to identify the PVs due to a small middle RPV. LPVs number was the same in 12/20 cases while in 8/20 cases CARTO™ overestimated due to the presence of a short common pulmonary trunk (7) or a branching less than 10 mm from the PV ostium (1).

Conclusion: MDCT defines the LA and PVs anatomy better than CARTO™ maps, providing useful information necessary for successful RFCA.

C-0265

The relationship between coronary calcium score and myocardial perfusion

I.E. Itsikovich, D.V. Ryzhkova, L.A. Tiutin, E.V. Rozengaouz, L.A. Kofal;
St. Petersburg/RU

Purpose: To estimate the relationship between coronary calcium score and myocardial perfusion in patients with coronary artery disease.

Materials and Methods: Full-scale examination was performed for 63 patients (47 males and 17 females; 37 - 75 years). Calcium score (CS) measurement was performed in 252 coronary arteries according to Agatstone's technique by Volume-Zoom CT scanner (Siemens) with retrospectively ECG-gating image reconstruction. 13N-ammonia PET scans were acquired at rest and during pharmacological test using "HR+" (Siemens) to assess the myocardial perfusion.

Results: All coronary arteries were divided in 4 groups depending on the value of CS. 198 coronary arteries with a low value of CS (10 units and less) were classified in the first group, 28 arteries with moderate CS (11 - 100 units) - in the second group, 13 arteries with mean CS (101 - 400 units) - in the third group and 7 arteries with high CS (over 400 units) - in the fourth group. Reversible perfusion defects were revealed in myocardial segments supplied by 18 (9.1%) coronary arteries of the first group, by 9 (32%) arteries of the second group, by 3 (23.1%) arteries of the third group, by 4 (57.1%) arteries of the fourth group. The flow-limiting stenoses (over 50%) were revealed in the mentioned arteries according MSCT coronary angiography.

Conclusion: Coronary artery calcification does not always result in myocardial ischemia. The perfusion abnormalities may be observed in territories supplied by coronary arteries with a low or zero CS.

C-0266

withdrawn by authors

C-0267

Visualisation of coronary artery stent patency with 64-slice computed tomography

F. Cademartiri, N.R. Mollet, G. Runza, M. Belgrano, M. Midiri, R. Pozzi Mucelli, G.P. Krestin; Rotterdam/NL

Learning Objectives: 1. Describe the technical features of a new generation of multislice CT scanner. 2. Describe the issues and the solutions adopted to improve the visualisation of coronary artery stents. 3. Provide cases that show the clinical impact of the technical improvements.

Background: 16-slice Computed Tomography (CT) has showed great potential in the visualization of significant stenosis in coronary artery. Coronary artery stents are difficult to image with CT because of their high density and the associated "blooming" effect due to volume averaging and interpolation. In addition, residual motion due to insufficient temporal resolution can deteriorate the image quality. For these reasons, the direct visualisation of stents is limited to large (> 3 mm diameter) stents with a relatively low attenuation. Based on this observation a better scanner should provide both improved spatial and temporal resolution.

Imaging Findings: We describe a multislice CT scanner able to scan 64 slices per rotation with a voxel size of 0.3x0.3x0.4 mm, and a rotation time of 0.33 s (effective temporal resolution up to 165 ms). Schemes of the main technical issues and solutions will be displayed as well as several clinical examples of coronary stents with conventional coronary angiography correlation.

Conclusion: The new 64-slice CT allows improved visualisation of coronary artery stents.

C-0268

16-row multidetector CT in the detection of coronary anomalies

P.M. Carrascosa, C. Capuñay, M. Ulla, P. García Merletti, E. Martín López, J. Carrascosa; Buenos Aires/AR

Learning Objectives: To illustrate the spectrum of coronary arteries anomalies. To outline the advantages of this non-invasive technique. To be familiar with these vascular findings to avoid diagnostic mistakes.

Background: Coronary artery anomalies (CAA) are anatomical variants that occur in 0.3-1.3% of patients. They can be related to syncope, dyspnea, ventricular fibrillation, angina, myocardial infarction, atrio-ventricular block or even sudden death. The purpose of this paper is to evaluate the usefulness of Multidetector CT (MDCT) in the evaluation of CAA. A total of 30 patients with CAA diagnosed by digital angiography (DA) were evaluated with CT coronary angiography between April and August 2004. There were 1 right coronary artery arising from main left coronary artery, 7 independent origins of the LAD and circumflex, 3 right side circumflex, 1 left coronary artery fistula into the pulmonary trunk, 14 intra-myocardial bridging and 4 intra-muscular coronary segments.

Procedure Details: CTs were performed with a 16-row CT scanner (Brilliance 16; Philips Medical Systems) with slices of 0.8 mm thickness, 0.4 mm reconstruction interval, gantry rotation time of 420 msec. An enhanced acquisition was performed with 120 ml of contrast. During the scan, the ECG's of the patients were recorded. The vascular analysis, the origin and cause of the CAA were performed using axial images, multiplanar reconstructions and volume rendering reconstruction.

Conclusion: Most anomalies are harmless but some of them require aggressive intervention. MDCT can accurately detect the origin and cause of CAA as well as the anatomical relationships to adjacent cardiac structures with high image resolution.

C-0269

Multidetector CT evaluation of congenital heart disease

M. Ledermann, V. Latrabe, M. Montaudon, O. Corneloup, F. Laurent; Pessac/FR

Learning Objectives: Based on the analysis of a series of 44 patients, the aim of this exhibit is to assess the capabilities of multidetector CT scan in exploring congenital heart diseases. The spectrum of congenital heart diseases will be reviewed and illustrated by numerous examples. Advantages and disadvantages of CT will be discussed.

Background: Echocardiography remains the initial imaging modality for diagnosis and follow-up of congenital heart diseases. However it suffers from some limits: operator-dependence, a small field of view, and problems relating to acoustic window. Multislice CT scan appears to be a valuable alternative for the morphologic evaluation of congenital heart disease.

Imaging Findings: 44 patients underwent multislice CT scan using a low-dose protocol. All these exams were performed after inconclusive echocardiography in exploring congenital heart diseases (tetralogy of Fallot, pulmonary atresia with ventricular septal defect, transposition of great vessels, tricuspid atresia, double-outlet right ventricle, partial anomalous pulmonary venous return, coarctation of the aorta, truncus arteriosus). All studies were requested to answer to specific anatomic questions, either prior to surgical management, or in the post-operative follow-up of these patients.

Conclusion: Multidetector CT scan is a useful noninvasive technique for evaluating congenital heart diseases. Compared with MR imaging, CT requires markedly decreased sedation time as it produces images with increased speed. Spatial resolution is clearly better, allowing valuable assessment of right outflow tract, coronary arteries, systemic artery collaterals, and surgical procedures. Finally, CT scan provides images of lung parenchymal structures.

C-0270

Evaluation of global left ventricular myocardial function using retrospectively ECG-gated 16-slice multidetector computed tomography: Comparison with magnetic resonance imaging

M. Heuschmid¹, J. Rothfuss¹, S. Schroeder¹, M. Fenchel¹, N. Stauber¹, A. Kuettner¹, M.D. Seemann², A.F. Kopp¹, C.D. Claussen¹; ¹Tübingen/DE, ²Munich/DE

Purpose: To assess the quantitative measurement of left ventricular functional parameters using retrospectively ECG-gated multidetector computed tomography (MDCT) and to compare the results with magnetic resonance imaging (MRI).

Methods and Materials: 52 patients (pts) with suspected coronary artery disease were included in the present study. 16-slice MDCT scans were performed using retrospective ECG-gating (0.75 mm collimation, 2.8 mm table feed/rota-

Scientific and Educational Exhibits

tion, 0.42 s rotation time). Based on the CT dataset, short axis reformats of the left ventricle were performed for the functional analysis. End-diastolic volume (EDV), end-systolic volume (ESV) and stroke volume (SV) as well as ejection fraction (EF) were calculated from MDCT data according the modified Simpson's method and compared to MRI results (1.5 T scanner).

Results: Comparing MDCT with MRI, the results for the determination of EDV, ESV, SV, and EF were as follows: EDV: MDCT 140.6 ± 40.0 ml vs. MRI 125.5 ± 29.4 ml, $r = 0.83$, [$p < 0.0001$], mean difference (MD) 15.1 ± 22.80 ; ESV: MDCT 75.0 ± 33.7 ml vs. MRI 64.4 ± 26.1 ml, $r = 0.90$, [$p < 0.0001$], MD 10.6 ± 15.5 ; SV: MDCT 65.6 ± 15.3 ml vs. MRI 61.1 ± 13.2 ml, $r = 0.66$, [$p = 0.008$], MD 4.5 ± 11.9 ml; EF: MDCT $48.0\% \pm 9.3\%$ vs. MRI $49.6\% \pm 9.6\%$, $r = 0.88$, [$p = 0.0072$], MD $-1.8\% \pm 4.7\%$.

Conclusion: Cardiac MDCT with retrospective ECG-gating displayed a high correlation of left ventricular functional parameters compared to MRI. Thus, important additional information with clinical and prognostic relevance can be achieved. However, although a high correlation was found, EDV, EVS and SV were overestimated and EF underestimated in MDCT which have to be taken into account when applying this technology in clinical practice.

C-0271

Whole heart coronary MR-angiography: Value for the detection of coronary artery stenoses in comparison to MSCT-angiography

D. Maintz¹, M. Ozgun¹, A. Hoffmeier¹, W. Heindel¹, R. Fischbach¹, R. Botnar²;
¹Münster/DE, ²Boston, MA/US

Purpose: To compare steady-state-free-precession whole heart coronary magnetic resonance imaging (MRI) with multidetector coronary computed tomography angiography (CTA) for the detection of coronary artery disease (CAD).

Material and Methods: Twenty patients with CAD were examined with navigator gated/corrected free-breathing 3D balanced-gradient-echo whole heart coronary MRI and coronary CTA. Subjective overall image quality (4 point scale, 1 = excellent), visibility of vessel segments and accuracy for the detection of significant coronary stenoses (> 50%) were compared to coronary X-ray angiography by two blinded readers.

Results: Average subjective image quality was 2.7 for MRI and 1.7 for CTA. Of a total of 209 segments, 67 segments (32%) had to be excluded from the evaluation by MRI (61 due to insufficient image quality and 6 due to stent artifacts). In CTA, 31 segments (15%) had to be excluded from the evaluation (12 due to insufficient image quality, 15 due to severe calcifications superimposing the vessel lumen and 4 due to stent artifacts). Within the evaluated segments, the prevalence of significant CAD was: MR imaging 23%, CTA 18%. Segment-based values for the detection of $\geq 50\%$ diameter coronary X-ray angiographic stenoses were: sensitivity: MRI 88%, CTA 95%; specificity: MRI 82%, CTA 84%; accuracy: MRI 87%, CTA 93%; positive predictive value: MRI 68%, CTA 77% and negative predictive value: MRI 94%, CTA 95%.

Conclusions: Coronary WH-MRI was inferior to coronary CTA regarding image quality and number of evaluable segments, but both had similar diagnostic value for the detection and exclusion of CAD when only evaluable segments were included.

C-0272

64-slice CT in coronary artery disease

B. Jankharia, P. Krishnan, K. Rajpal; Mumbai/IN

Learning Objectives: To illustrate the usefulness of 64-slice CT in the evaluation of coronary artery disease.

Background: Multi-slice CT is now a recognized modality for the evaluation of coronary artery disease. The faster the scanner, the easier it normally is to scan the coronary arteries. A new 64-slice CT (Sensation Cardiac, Siemens, Erlangen) has been recently introduced with a rotation time of 330 ms with an effective temporal resolution of 165 ms. The spatial resolution is 0.4 mm in the z-axis. This is a 32-detector row with double sampling in the z-axis with a flying focal spot. These improvements are expected to produce superior images of the coronary arteries, as compared to earlier 16-slice CT scanners.

Imaging Findings: Using a robust technique, diagnostic quality images can be obtained in the vast majority of patients. Normal studies exclude coronary artery disease with a high degree of confidence. Coronary artery lesions such as stenoses and plaques, both calcified and non-calcified can be seen well. Visualization of intra-stent pathology is also possible.

Conclusion: With a robust technique, coronary artery disease can be well appreciated using a 64-slice CT.

C-0273

Understanding ECG gated reconstruction by scanning diagram

N. Akino, K. Tsujikawa, Y. Takahashi, M. Niwa, Y. Uebayashi;
Toyoake-city Aichi/JP

Purpose: It is very difficult to understand the ECG gated reconstruction in multi slice CT scanning. In this report we would like to introduce a movie we have developed for educational use to help any operator easily understand what the ECG gated reconstruction is like.

Method and Materials: The scan diagram has X-ray revolving angles at the vertical axis and body axis direction's positions on the horizontal axis. The heart rate signals have been added to this in order for viewers to visually understand the ECG gated reconstruction. We performed a simulation on the time resolution, the space resolution and the image noise.

Results: We easily obtained understanding of the ECG gated reconstruction with help from the scanning diagram movie.

Conclusions: Understanding the ECG gated reconstruction is indispensable for performing best possible CT scanning inspections. We are sure that the educational movie of the reconstruction is helpful to radiologists and radiological technologists.

C-0274

Noninvasive assessment of in-stent restenosis of coronary artery with multi-detector row CT

J.-W. Lee, E. Yoo, B. Choi, J. Nam, J. Seo, Y.-J. Kim, K. Choe; Seoul/KR

Purpose: To assess the usefulness of 16-slice spiral CT for evaluation of restenosis of coronary artery stents.

Methods and Materials: 36 consecutive patients (mean 58 yrs) with coronary artery stents ($n = 48$) were enrolled. Sixteen-slice CT and invasive coronary arteriography were performed with interval from 1 to 22 days (mean 9 days) and were compared. All patients were pre-treated with propranolol (30-60 mg) prior to CT scan. Reconstruction window was tailored to individuals. Restenosis of in-stent lumen in CT was decided by presence of lower density of in-stent lumen than that of the proximal opacified vessel lumen with assessors being unaware of the results of invasive coronary arteriography.

Results: Three stents (6%) of total 48 stents could not be evaluated with CT because of motion artifact ($n = 2$) or complete obliteration of in-stent lumen by severe beam-hardening effect of stent ($n = 1$) and were excluded. Twelve (26%) of 45 stents revealed restenosis by invasive coronary arteriography. Nine of twelve restenosis were correctly diagnosed with CT (Sensitivity 75%). These 9 stents showed lower in-stent density ($n = 9$), severely degraded shape of stents ($n = 2$), and absence of distal segment enhancement ($n = 1$). One of 33 stents without restenosis was falsely diagnosed as restenosis with CT by equivocal lower density of in-stent lumen (Specificity 97%). The accuracy and positive and negative predictive value were 91% (41/45), 90% (9/10), and 89% (32/36), respectively.

Conclusions: Visual assessment with measurement of in-stent luminal density is useful to evaluate the restenosis of coronary artery stents with 16-slice spiral CT.

C-0275

Anomalous coronary anatomy using multi detector computed tomography

P.M.A. van Ooijen, J. Dorgelo, F. Zijlstra, M. Oudkerk; Groningen/NL

Purpose: The purpose of this study was to evaluate the usefulness of multi detector computed tomography (MDCT) for the evaluation of coronary anomalies.

Materials/Methods: MDCT was obtained in 13 patients (9 male, mean age 49.5 y.o.), following a standard protocol on a Sensation16 Cardiac (Siemens Medical Systems, Erlangen, Germany). All patients obtained the CT on clinical indication after a non conclusive conventional catheter angiogram. After acquisition of the data during recording of the ECG signal datasets were reconstructed retrospectively and transmitted to a special purpose visualization workstation (Vitrea, Vital Images, Plymouth, MN, USA).

Results: In the 13 patients, 6 different coronary anomalies were diagnosed (separate ostium of LAD and LCX (2), single vessel LCA (1), LCA from RCA (3) of which two followed a course between the RVOT and aorta, RCA from LCA (6), double LAD (1)). Two observers scored diagnostic quality at a 5 point scale (0 = non diagnostic, 5 = excellent quality) resulting in a mean quality of 3.73.

Conclusion: Multi detector computed tomography provides us with a high quality and accurate modality to visualize and diagnose coronary anomalies. Origin and course of all anomalous coronary arteries was visualized clearly with a high average diagnostic image quality. Shortcomings in conventional catheter coronary angiography, such as uncertainty of the proximal course and the inability to selectively catheterize the anomalous coronary artery are overcome by using contrast enhanced computed tomography.

Scientific and Educational Exhibits

C-0276

Study of CABG with MDCT: Something rather than patency, stenoses or obstruction!

C. Delgado Sánchez, G. Fernández, E. Santos-Armentia, C. Trinidad, M. Velasco, F. Tardáguila; Vigo/ES

Purpose: To learn other information present on MDCT angiography apart from the assessment of bypass graft patency that the radiologist must know and report.

Methods and Materials: 347 patients were studied with 16-MDCT coronary angiography. 21 patients with total of 54 bypass grafts (22 artery grafts and 32 venous grafts) were also evaluated.

Results: Calcified plaques in supraaortic branches must be reported because surgical cardioplegia predisposes to higher risk of cerebrovascular strokes. The location of coronary arteries close to the sternum is important to avoid injuries during the median sternotomy. Also, the surgeon needs to know if the aorta is free of atherosomatic plaques, calcium or other pathologies because this will be necessary to make an anastomosis in the wall of the proximal aorta. Radiological information regarding atherosomatosis within the distal coronary vessels or intramyocardial pathway of coronary vessels will be important. Description of the aortic valve will be appreciated in order to repair it in the same intervention. The radiologist must also be familiar with grafts used in CABG. Newer surgical techniques are also performed in CABG. Minimally invasive direct coronary artery bypass allow the practice of anastomoses with bypass particularly in the LAD. It can be performed with robotic instruments guided with endoscopic video.

Conclusion: The radiologist can provide very valuable information even in MDCT studies where patients may be candidates for surgery (information prior to surgery) and in relation to the surgical technique performed in CABG or what different grafts were used.

Chest

Lung

C-0277

Receptorial (Tc99m-Depreotide scintigraphy) and morphological (CT scan) imaging in the non-invasive characterization of lung nodules

P. Sullo, G. Mazzarella, E.M. Covelli, R. Cioffi, G. Belfiore; Caserta/IT

Purpose: Lung nodule (LN) assessment is based on CT, PET, bronchoscopy and histology. Malignant lung tumor cells overexpress somatostatin receptors (SSTR). Tc99m-Depreotide, a synthetic analog peptide which selectively binds to SSTR, has been proposed to differentiate indeterminate LN. We aimed to investigate Tc99m-Depreotide scintigraphy in the characterization of LN using morphological CT imaging and histology as reference.

Materials and Methods: Nineteen patients (16M, 3F; mean age 67 years) with CT-suspected malignant LN underwented Tc99m-Depreotide tomographic chest and whole-body scintigraphy 2 hours after tracer injection. Each study was considered positive for malignancy when significant uptake was present in CT-detected nodules. Conventional skeletal scintigraphy was also performed in 8 patient. All patients underwent CT-guided transthoracic needle and/or broncoscopic biopsy, and diagnosis was established by histology.

Results: Histologically proven lung cancer was diagnosed in 18 (95%) patients, 7 with squamous cell carcinoma, 5 adenocarcinoma, 5 poorly differentiated non-small cell cancer and 1 lymphoma. In 1 patient cancer was ruled out. Tc99m-Depreotide chest tomography correctly detected malignant LN in all patients with CT and histology suggestive for lung cancer (sensitivity 100%), and was negative in the inflammatory disease patient. Moreover, skeletal scintigraphy was positive in 4 patients detecting 21 metastatic bone lesions; Tc99m-Depreotide whole-body scintigraphy showed significative increased uptake in 12/21 (57%) bone metastases.

Conclusion: Tc99m-Depreotide imaging is an accurate method in the non-invasive diagnostic characterization of LN, complementary to CT scan. Therefore, it might be helpful in the management of LN, especially when invasive procedures are not indicated and/or PET is not available.

C-0278

CT-related prognosis in surgically treated bronchial carcinoid tumors

A. Bray; Rome/IT

Purpose: To define the CT findings at diagnosis and follow-up influencing the long-term survival of patients surgically treated for bronchial carcinoid tumors (BCT). To determine whether BCT show a favourable outcome.

Methods and Materials: A retrospective, single-centre review of 163 patients (86 men and 77 women with a mean age of 49.5 ± 11 years) surgically treated is reported. The cases were segregated into typical and atypical carcinoids. Symptoms were present in 29 patients (17.8%). Pre-operative radiological staging (chest X-ray and total body CT) was performed in all patients. Operations included 145 formal lung resection (89%), 10 wedge resections (6.1%) and 8 sleeve lobectomies (4.9%) plus radical mediastinal lymphadenectomy in all cases.

Results: Histology showed 121 (74.2%) typical carcinoids and 42 (25.8%) atypical carcinoids. Typical and atypical BCT have similar imaging features. The mass appear radiologically as a well-defined, round or ovoid (lobulated) lesion. Nodular calcification is a common CT finding. Atelectasis, air trapping, obstructing pneumonitis and mucoid impaction were usually associated with central BCT (80%). Peripheral BCT (20%) appeared as solitary nodules. Overall 5-year survival was 90.3% (mean 139 months): 100% of NO typical or atypical BCT, 90% in N1 typical BCT and 78.8% in N1 atypical BCT, 22.2% in N2 atypical BCT.

Conclusions: Prognosis in BCT is mainly related to nodal status rather than to histological subtype. In N0 and N1 BCT, no statistical significant difference has been found between typical and atypical subtypes. N2 BCT show a dismal prognosis. Accurate N staging with CT helps optimize surgical planning for BCT.

C-0279

Thoracic tumors and pseudo-tumors associated with interstitial lung diseases: HRCT findings with pathologic correlation

A. Giménez, T. Franquet, A. Hidalgo, T. Salinas, S. Valverde, R. Bordes; Barcelona/ES

Learning Objectives: To review the characteristic HRCT findings of a variety of malignancies and pseudotumors in patients with interstitial lung diseases. To understand the radiologic manifestations on the basis of the different histopathologic features.

Scientific and Educational Exhibits

Background: The purpose of this exhibit is to illustrate the spectrum of thoracic malignancies and non-malignant disorders (pseudotumors) related to a variety of underlying interstitial pulmonary diseases.

Imaging Findings: A wide spectrum of radiographic and CT findings of common and uncommon neoplasms are demonstrated including, among others: BALTo-ma and thymoma in Sjögren's syndrome; bronchioloalveolar cell carcinoma in progressive systemic sclerosis; squamous cell carcinoma in UIP and occupational lung disorders; non-Hodgkin's lymphoma in SLE; mesothelioma and rounded atelectasis in asbestosis; and focal amyloidosis in Sjögren's syndrome.

Conclusion: Because many of these diseases have a highly characteristic CT appearances, this exhibit will aid the practising radiologist in better understanding and recognition of these complications. The pathologic basis for the radiographic findings and correlation with gross or microscopic pathology will be discussed in appropriate cases.

C-0280

Staging of primary non-small cell lung cancer with CT, MR imaging and PET

S.A. O'Keeffe, A. McGrath, S. O'Brien, R. McDermott, F. O'Connell, J.F.M. Meaney; Dublin/IE

Learning Objectives: 1. To describe staging of primary non-small cell bronchogenic carcinoma with CT, MR imaging and PET scanning. 2. To describe an efficient pathway (CXR, CT, bone scanning and MRI) to allow most effective use of PET scanning. 3. To highlight the value of PET scanning in patients with solitary pulmonary nodules without a proven histological diagnosis of lung cancer. 4. To illustrate the role of CT in selecting patients for mediastinoscopy and for eliminating the need for mediastinoscopy in patients with obvious N3 disease. 5. To illustrate the features that designate Stage IIIB (irresectable by conventional criteria but eligible for radical radiotherapy) and Stage IV disease (distant metastases).

Background: The prognosis in patients with non-small cell lung cancer is poor. A primary aim of imaging is to eliminate unnecessary thoracotomy in patients in whom resection is not possible. Traditionally, stage has been determined by a combination of CXR, CT, MR imaging (occasionally) and mediastinoscopy. However, for CT sensitivity, specificity and negative predictive value are all approximately 60%. PET has significantly improved the staging of lung cancer, by enabling the detection of regional lymph node metastases, detecting spread in patients with apparently localized disease, and by demonstrating that a solitary pulmonary nodule probably represents a malignant lesion.

Imaging Findings: A comprehensive review of the findings on CXR, CT, MR imaging and PET scanning that differentiate resectable from irresectable disease is presented.

Conclusion: In this e-poster, we demonstrate combined modality imaging of lung cancer with CT, PET and MR imaging.

C-0281

Clinical validation of automated calculations of emphysema volumes

E. Dharaiya¹, R. Gilkeson², L. Ciancibello¹, K. Subramanyan¹, J. Durgan¹, S. Pohlman¹, A. Vlassenbroek¹; ¹Highland Heights, OH/US, ²Cleveland, OH/US

Purpose: This abstract compares the results of an automatic and manual method for calculation of emphysema.

Method: The study involved 17 patients. In the manual method a 3-D volume rendered image of the lung was created. The lung volume was calculated at a threshold of -750. Emphysema was calculated at a threshold of -950. A 3-D volume rendered image of the emphysema-affected tissue was obtained at the threshold. The automatic algorithm required no user interaction. It automatically aggregated the volumes in airway and lung tissue and labelled them accordingly. The high contrast vascular networks, myocardium, tissues in mediastinum, and lung walls were also labelled. The emphysema regions are characterised as small volumes of air trapping. By subtracting the airway out of lung volume, and subsequently summing all the air-trapped volumes, a total emphysema volume was determined. The algorithm also segmented the right and left lungs, displayed the emphysema distribution in each lung and calculated emphysema volumes in each lung separately.

Results: The emphysema values calculated manually and automatically at a threshold of -950 were 2850.34 ± 1448.55 and 2747.71 ± 1405.52 respectively. The coefficient of correlation between the two methods was 0.9997. The average emphysema volumes for right and left lungs were 1508.99 ± 716.24 and 1238.72 ± 721.47 respectively. The manual procedure takes approximately 10-15 mins while the automatic method takes about 1 min.

Conclusion: Emphysema quantification is very important in planning the surgical procedures for treatment of the disease. The automatic method provides a fast and close estimation of the emphysema and eliminates user variability.

C-0282

Qualitative and quantitative analysis of contrast enhancement maps for pulmonary nodule characterization

I. Petkovska, S.K. Shah, M.F. McNitt-Gray, H.J. Kim, J.G. Goldin, D.R. Aberle; Los Angeles, CA/US

Purpose: To determine whether quantitative and qualitative texture features derived from contrast enhancement maps, acquired on indeterminate lung nodules, can distinguish benign from malignant nodules.

Materials and Method: Thin section, contrast-enhanced CT (baseline and post-contrast series acquired at 45, 90, 180, and 360 seconds following IV contrast administration) was performed on 29 patients with lung nodules (14 benign, 15 malignant). A thoracic radiologist manually identified the boundary of each nodule and selected the axial slice with the greatest diameter on the baseline series. The post-contrast series with maximum enhancement was volumetrically registered to the baseline series. Corresponding axial images from the two series were subtracted and the difference voxels were quantized into 7 color-coded bins to create the contrast enhancement map. A thoracic radiologist visually scored each map for: magnitude, extent, and heterogeneity of enhancement on a 5-point scale. Also 14 quantitative texture features were calculated for each map. All features were analyzed for differences between benign and malignant nodules.

Results: Malignant nodules demonstrated a more heterogeneous pattern of enhancement ($p < 0.01$). Neither magnitude nor extent of enhancement was significant. A statistical analysis was performed to combine the 14 texture features to a single factor, which was significantly different between benign and malignant nodules ($p = 0.010$).

Conclusion: These maps may provide a richer understanding of nodule behavior giving information of contrast media spatial distribution. Heterogeneity may relate to the interplay between host stromal elements and neovascularity. Further studies are necessary to determine whether these patterns correlate with the biological behavior of neoplasms.

C-0283

CT findings of gefitinib-related interstitial pneumonitis in 65 patients: Multi-institutional analysis of West Japan Thoracic Oncology Group (WJTOG)

M. Endo¹, T. Johkoh², K. Kimura³, N. Yamamoto¹, ¹Shizuoka/JP, ²Osaka/JP, ³Kobe/JP

Purpose: To clarify the image characteristics of interstitial pneumonitis (IP) induced by the newly-developed molecular-targeting drug gefitinib.

Materials and Methods: In a total of 1,976 patients with non-small cell lung cancer, to whom gefitinib was administered from August to December 2002, 102 were suspected of having IP. 65 of these patients had undergone CT as well as chest roentgenogram at onset. Based on the findings of chest roentgenogram and CT, reviewed and analyzed by three radiologists, the final definitive diagnosis of gefitinib-related IP was determined, adding clinical data in the medical records. Moreover, CT findings were classified into four patterns: Pattern A: non-specific areas with ground-glass attenuation; B: multifocal areas of airspace consolidations; C: patchy distribution of areas with ground-glass attenuation accompanied by interlobular septal thickening, such as seen in acute eosinophilic pneumonia; and D: extensive bilateral areas with ground-glass attenuation or airspace consolidations with traction bronchiectasis, such as seen in acute interstitial pneumonia.

Results: Seventy patients were diagnosed as having gefitinib-related IP. The diagnostic images were classified as pattern A in 29 patients, B in 3, C in 7, D in 20 and others in 11. 24 patients with pattern A, 1 with pattern B, 7 with C and 12 with D were classified into a single pattern by CT findings. The patients dying due to gefitinib-related IP were significantly more frequent in pattern D.

Conclusion: Gefitinib is considered to induce IP in a certain proportion of patients, and the imaging findings are similar to drug-induced pneumonitis caused by conventional anticancer agents.

C-0284

Neuroendocrine proliferations of lung: Spectrum of diseases

A. Hidalgo, T. Franquet, A. Giménez, G. Sánchez, C. Blancas, R. Bordes; Barcelona/ES

Learning Objectives: To review the radiologic and pathologic appearance of neuroendocrine proliferations of the lung. To learn how to deal with problems related to diagnosis and classification of these tumors.

Background: Neuroendocrine proliferations of the lung are a heterogenous group of tumors of varying biological potential. The recent classification of these tumors includes 6 entities: Small cell lung carcinoma, Large cell neuroendocrine carcinoma,

Scientific and Educational Exhibits

noma, Carcinoid, Atypical carcinoid, Neuroendocrine hyperplasia and Tumorlet.

Procedure Details: We review the radiological findings of these processes including chest radiographs, CT and MR imaging. We correlate the images with bronchoscopic and pathologic findings. SCLC often present with bulky hilum and mediastinal lymph node masses. LCNC appears as a well-defined and lobulated tumor with no air-bronchograms or calcification. The differentiation between typical and atypical carcinoid tumor is based mainly on the mitotic count. Neuroendocrine hyperplasia and tumorlets are characterized by mosaic perfusion due to air trapping, airway wall thickening, and small nodules on HRCT.

Conclusion: Radiologists have to be aware of these tumors and to suggest a diagnosis based on imaging findings.

C-0285

Volumetric expiratory high-resolution CT of the lung: Basics and clinical applications

M. Nishino, M. Kuroki, V. Raptopoulos, J.F. Copeland, P.M. Boiselle, H. Hatabu; Boston, MA/US

Learning Objectives: To become familiar with 1) technical aspects of volumetric expiratory high-resolution CT (VEHRCT) 2) usefulness of contiguous scans, coronal and sagittal reformats, and 3) clinical application of VEHRCT in various diffuse lung diseases.

Background: Expiratory HRCT is a powerful adjunct to inspiratory HRCT in detecting various small airway diseases. We have developed a new VEHRCT which allows volumetric data acquisition of the lungs both at end-inspiration and end-expiration, with equivalent radiation dose compared to the standard non-contiguous expiratory HRCT. VEHRCT has been applied in patients with diffuse lung disease with small airway abnormalities.

Imaging Findings: The contiguous axial HRCT images enabled better identification of the conducting airway to the areas of air trapping ($p < 0.0001$). The coronal reformats provided added value by clearer visualization of the borders of air trapping over contiguous axial images ($p = 0.001$). Sagittal reformats provided significant additional information compared to axial images ($p = 0.004$). The volume rendering of the lungs at end-inspiration and end-expiration demonstrated changes in volume and attenuation after expiration in a three-dimensional manner, allowing for easy recognition of air trapping. In patients with emphysema, asthma, bronchiectasis or sarcoidosis, VEHRCT demonstrated representative findings in a multiplanar and 3 dimensional manner, providing added value over contiguous axial images.

Conclusion: VEHRCT with multiplanar reformats provides additional information in evaluating areas of air trapping and their conducting airways, and is clinically useful in evaluating diffuse lung diseases with small airway abnormalities. Further possibilities include quantitative analysis of lung biomechanics using computational analysis.

C-0286

Correlation between lymph node metastasis and the ratio of high attenuation area to tumor diameter by HRCT in adenocarcinoma of the lung of 3 cm or less

R. Nishio¹, S. Acata², N. Ikeda², K. Saito¹, H. Kotake¹, H. Kato², K. Abe²; ¹Ibaraki/JP, ²Tokyo/JP

Purpose: Limited resection of the lung can improve post-operative QOL, but it requires the absence of lymph node metastases. Early adenocarcinoma usually appears as ground-glass attenuation. We studied adenocarcinoma of the lung of 3 cm or less in diameter to determine whether or not there is a correlation between the ratio of high attenuation area to the tumor diameter (H/T ratio), and the presence of lymph node metastasis.

Method and Materials: From January 1996 to June 2004, we studied 281 patients with adenocarcinoma of the lung (≤ 3 cm) by pre-operative HRCT. The correlation between the H/T ratio and the presence of lymph node metastasis was evaluated. HRCT images were evaluated by two radiologists.

Results: None of the patients with tumors of ratios of 60% or less (33.5% of all cases) had lymph node metastasis. In contrast, tumors at H/T ratio of 100% had lymph node metastasis even if the diameter was only 6 mm. In tumors with H/T ratio greater than 60%, 16.6% had lymph node metastasis.

Conclusion: If the H/T ratio is around 60% or less, the likelihood of lymph node metastasis is nil, and prognosis may be considered to be extremely favorable. This data may be useful when considering limited resection.

C-0287

Spectrum of CT features in cavitary or cystic pulmonary metastases:

Correlation with primary and histologic types of the tumor

T. Koyama, S. Umeoka, T. Kubo, K. Tamai, H. Ueda, H. Kobayashi, H. Wada, T. Saga, K. Togashi; Kyoto/JP

Purpose: The purpose of this study is to investigate common histologic types and primary sites for cavitary and/or cystic pulmonary metastases, and to describe the spectrum of CT features in correlation with the primary and histology.

Methods and Materials: CT images in 57 patients with cavitary/cystic pulmonary metastases (age: 27-87, mean: 62.7) were retrospectively reviewed by two radiologists, for the size, margin of the largest lesion, the number of the cavitary/cystic lesions, and associated other CT findings. More than ten lesions were regarded as multiple. CT findings were correlated with histologic subtypes and primary.

Results: Histology included 32 adenocarcinoma (colon:13, pancreas:7, lung:5, biliary tract:4, others:3), 12 SqCC (head&neck:6, esophagus:3, others:3), 3 TCC (all urinary tract) and 10 sarcomas. Cystic metastases were seen in 9 patients, including one adenocarcinoma and 8 sarcomas, 5 of which were associated with pneumothorax. The remaining patients had cavitary metastases. The size of the largest lesions in adenocarcinoma, SqCC, sarcoma and TCC was 13.2 ± 10.2 cm, 28.6 ± 14.2 cm, 15.8 ± 4.1 cm and 23.7 ± 11.5 cm, respectively. The inner surface was irregular in 9 SqCC (75%), 3 TCC (100%), 11 adenocarcinoma (34%). The outer margin was smooth and round in 28 adenocarcinoma (81%), 9 SqCC (75%), 2 TCC (67%), and all sarcomas (100%). Multiple cavitations were seen in 21 adenocarcinoma, 1 SqCC and 7 sarcomas.

Conclusion: In cavitary and/or cystic metastases, adenocarcinoma of colon and lung, SqCC of head & neck, and sarcomas are common. Sarcomas commonly cause cystic metastases associated with pneumothorax. SqCC and TCC tend to form large cavitations with irregular inner surface, while adenocarcinoma tends to cause multiple small cavitation with smooth margin.

C-0288

Mediastinal disease of lymphatic tissue: Imaging findings with histopathologic correlation

T.U. Kim, Y.J. Jeong, K.-I. Kim, T.Y. Moon; Busan/KR

Learning Objectives: 1. To describe the categories of mediastinal disease of lymphatic tissue and their imaging findings with histopathologic correlation. 2. To provide the means of differential diagnosis between the various diseases.

Background: Mediastinal lymphadenopathy is a not uncommon radiologic finding on helical CT scan. Various diseases result in mediastinal lymphadenopathy, including neoplasms, infectious and inflammatory disease, and lymphoproliferative disorders. Differential diagnosis of mediastinal disease of lymphatic tissue is a challenging process, because radiographic appearances are variable and non-specific.

Procedure Details: Mediastinal diseases of lymphatic tissue are classified into three categories: neoplasms (lymphoma, bronchogenic cancer, metastasis), infectious and inflammatory disease (tuberculosis, sarcoidosis, amyloidosis), and lymphoproliferative disorders (Castleman's disease, angiolymphoblastic lymphadenopathy, infectious mononucleosis, Kikuchi disease). We describe the imaging findings of histologically proven mediastinal disease of lymphatic tissue in 275 patients, in terms of predominance of involved lymph node, nodal enhancement and morphology, and internal characteristics and correlate them with histopathologic findings.

Conclusion: Awareness of specific patterns of predominance of involved lymph node, nodal enhancement and morphology, and internal characteristics helps in the differential diagnosis and optimal treatment of mediastinal disease of lymphatic tissue.

C-0289

The spectrum of CT findings in pleural mesothelioma

A. Massuet, X. Gallardo, E. Castañer, J. Mata, D. Gil; Sabadell/ES

Learning Objectives: To describe the computed tomography (CT) features of malignant pleural mesothelioma (MPM). To illustrate the typical and atypical CT findings for this tumour. To describe the different ways that this tumour can spread.

Background: MPM is an uncommon neoplasm that arises from the pleura. Most cases are associated with prior asbestos exposure. Histologic evaluation is required to reach the definitive diagnosis. CT, MR and PET in combination are crucial in staging and determining the most appropriate treatment option for patients with this tumour. CT is the modality most frequently employed for the initial study; MR and PET are helpful in delineating the extent of disease.

Scientific and Educational Exhibits

Procedure Details: We reviewed the CT findings of 50 patients with pathologically confirmed MPM diagnosed at our center between 1990 and 2004. We present the most representative cases of typical MPM presentation with incipient signs that suggest the diagnosis. We also present selected cases of atypical presentation simulating pulmonary or chest wall lesions or a mediastinal mass. We show different kinds of local and distant dissemination, such as hilar and mediastinal adenopathies, pulmonary metastases, metastasis to the liver, to the brain and to the bone, as well as cases of carcinomatous lymphangitis and peritoneal carcinomatosis.

Conclusion: CT is usually the primary imaging technique used when this disease is suspected, so it is important to recognise how this tumour presents in this imaging modality. Although the definite diagnosis requires histopathologic evaluation, CT can be helpful in suggesting this malignant pleural disease.

C-0290

CT evaluation of non-malignant tracheal stenosis: What the surgeon needs to know

M.A. Molla Landete, F. Ferrando Valls, H. Benlloch, V. Tarazona Hervas, J. Palmero da Cruz; Valencia/ES

Learning Objectives: To demonstrate the application of MDCT with multiplanar and 3D reconstruction in the evaluation of non-malignant focal tracheal stenosis before surgical procedures. To describe the procedure and show its contribution to such surgical techniques.

Background: Benign tracheal stenosis is a rare condition, being mostly a complication of endotracheal intubation or placement of a tracheostomy tube. Bronchoscopy remains the primary procedure for the diagnostic work-up of this disease. However, evaluation with CT may aid in planning of surgical procedures particularly for tracheal resection with end-to-end anastomosis. Between Jan 1999 and Aug 2004, 18 patients with benign tracheal stenosis were diagnosed in our center. In all cases CT studies were performed before planning therapy.

Procedure Details: The scanned area was from 1-2 cm below carina to laryngeal ventricles in a caudo-cranial acquisition. Laryngeal cartilage integrity and vocal cord position were evaluated. Oblique axial images to the tracheal lumen assessed the shape, width and integrity of cartilaginous wall and submucous tissue. These images were the most accurate in measuring lumen diameter. Oblique coronal images along tracheal lumen are needed to measure distance from vocal cords to the most proximal altered tracheal wall and from distal end of the abnormality to the carina. Healthy tracheal length above and below the pathologic area must measure at least 7 cm.

Conclusion: MDCT can be helpful in determining the grade and extension of benign tracheal stenosis. Preoperative studies must include tracheal wall characteristics and exact length of healthy trachea from larynx to carina in order to allow surgical reconstruction.

C-0291

Lung nodule analysis software: Is what you see really what you get?

S.M. Ellis, M. Roddie, L. Honeyfield, J. Dehmeshki; London/UK

Purpose: To test the ability of 4 lung nodule analysis programs (3 commercially available) to accurately extract nodules from normal anatomical structures.

Materials and Methods: A lung phantom (QRM, Moehrendorf, Germany) was scanned on Phillips and Siemens 16 slice multislice CT scanners. The phantom contained 40 spherical nodules: 8 that were freestanding, 7 encasing and 9 adjacent to simulated vessels, 8 adjacent to and 8 arising from the chest wall. Analysis of each nodule yielded a 3D representation, which was used to determine the success or failure of the program under test to extract the nodule alone.

Results: All the nodule analysis programs successfully "extracted" the freestanding nodules. The commercial programs failed to exclude vessel or chest wall from those nodules adjacent to or intimately associated with these structures. The in-house software accurately extracted 40% of such nodules automatically and, with the ability to semi-automatically alter the detection algorithm, successfully extracted all but one.

Conclusion: Once a nodule analysis program has failed to exclude adjacent normal structures from a nodule, the resulting volume of that analysis will be flawed. There is certainly room for improvement in currently available nodule analysis software and the ability to semi-automatically alter the detection algorithm rendered a definite advantage to the in-house software.

C-0292

How many biopsies are necessary in pulmonary nodules to obtain an adequate diagnostic accuracy?

M. Wehrschaetz, H. Deutschmann, U. Aldrian, M. Tillich; Graz/AT

Purpose: To determine the frequency of biopsies in pulmonary lesions that is necessary to obtain adequate (the highest possible) accuracy in histological work up.

Materials and Methods: 260 patients suffering from thoracic lesions underwent computer tomography (CT)-guided core-cut biopsy using coaxial technique, from January 1999 to April 2004. These were evaluated retrospectively. Overall 669 adequate biopsies were taken (from one to five biopsies in each setting). The specimens were marked sequentially. Histological work up was performed on each biopsy. All biopsies were performed using a 19 gauge introducer needle and a 20 gauge core cut biopsy needle in all patients. The biopsy results were correlated to histology after surgery or autopsy. The number of biopsies was determined that is necessary to achieve the highest possible accuracy in diagnosing pulmonary lesions. Written informed consent was given by all patients.

Results: In 591 of 669 biopsies (88.3%) there were positive results. The accuracy was 87.4%. In 193 of 260 patients (74.2%), a suspected malignancy was confirmed. In 50 of 260 patients (19.2%), a benign lesion could be diagnosed. 17 (6.5%) patients were lost to follow-up. The first, second and third biopsy had an accuracy of 63.6%, 89.2% and 91.5%, respectively. More biopsies did not show any higher impact on accuracy.

Conclusion: To reach adequate diagnostic accuracy with CT-guided core cut biopsy, three adequate specimens are recommended.

C-0293

Cytomegalovirus pneumonia in immunocompromised patients with haematological disease: Correlation of HRCT findings with clinical outcome

M.S. Horger, C.A. Pfannenberg, H. Einsele, H. Hebart, R. Beck, C.D. Claussen; Tübingen/DE

Objectives: To assess correlation between HRCT findings of Cytomegalovirus (CMV) pneumonia in haematological patients and outcome.

Materials and Methods: We retrospectively evaluated the CT scans of 36 patients with CMV positive culture from broncho-alveolar lavage (BAL), with respect to CT morphology, and correlated these results with the outcome, also taking into consideration other risk factors including: underlying disease, CMV seropositivity, time of onset of antiviral therapy and presence of graft versus host disease (GvHD). The patients included 22 men and 14 women ranging in age from 26-80 years (mean age, 42 years). CT morphology of pulmonary infiltrates was classified into: ground-glass opacities (GGO), nodular, reticular or reticulonodular infiltrates and patchy areas of consolidation.

Results: 18 patients showed focal pulmonary abnormalities, whereas 18 patients had diffuse bilateral infiltrates. 19 patients demonstrated larger areas of GGO, 9 patients showed focal parenchymal consolidation, 7 patients presented with nodular opacifications and 1 patient showed only reticulation. 13 patients died during the acute episode of CMV pneumonia despite antiviral therapy. 12 of them belonged to the group showing either diffuse, or patchy GGO. 1 patient presented initially a small nodular CT pattern, which developed at follow-up into a patchy consolidation pattern as observed in the rest of the patients with fatal outcome, despite intensive ongoing antiviral therapy.

Conclusion: Initial HRCT findings in immunocompromised patients with CMV pneumonia seem to have an impact on patient outcome, being unfavourable in those forms of disease beginning as bilateral, diffuse or patchy ground-glass opacities followed by progressive consolidation, and in those where the CT morphology changes at follow-up to diffuse GGO and consolidation.

C-0294

Imaging of malignant pleural mesothelioma using morphological and functional MR imaging

C. Plathow, C. Fink, A. Sandner, M. Klopp, M. Puderbach, C. Thieke, A. Schmähl, H.-U. Kauczor; Heidelberg/DE

Learning Objectives: To introduce a routine state-of-the art protocol for morphological and functional MR imaging of pleural mesothelioma and illustrate typical findings.

Background: The interest in pleural mesothelioma has markedly increased in recent years because of the expected increase in incidence of more than 50% in the coming decade, and because of new therapeutic strategies that have become available. A correct and early histologic diagnosis, a complete and accurate staging of the tumor, and the differentiation between residual tumor and pleural fibrosis are essential to evaluate the efficacy of new therapeutic strategies.

Scientific and Educational Exhibits

Procedure Details: The imaging protocol at 1.5 T includes breathhold T1 and T2 weighted morphological MR imaging with and without ECG and respiratory gating. For the assessment of vascular invasion, contrast-enhanced 3D MR angiography with parallel imaging techniques is performed. Functional measurements include contrast-enhanced 3D perfusion with high temporal resolution as well as dynamic cine-MR imaging to assess infiltration of the diaphragm and the chest wall. The protocol takes about 30 minutes. Typical imaging findings are correlated to CT findings and discussed with regard to the TNM-classification.

Conclusion: While CT is the most frequently applied diagnostic tool, MR imaging using parallel imaging techniques gives more information, especially in terms of infiltration of the diaphragm and the spinal canal, but also in differentiating pleural mesothelioma from other malignancy or from benign pleural disease.

C-0295

The value of emergency room (ER) chest radiographs in patients with unsuspected thoracic pathology

M.G. Skilakaki, J.V. Kalogeropoulos, P. Galina, P. Polyviou, P.N. Piperopoulos; Athens/GR

Purpose: This study investigated the role of plain chest film in the evaluation of patients admitted to ER without any symptoms or clinical signs of thoracic pathology.

Methods and Materials: Conventional chest radiograph (PA or AP projection) was performed in 418 consecutive patients (age 32-96 years) without any history of respiratory disease (patients with fever and no other symptoms from the respiratory system were also excluded) and in 404 consecutive patients (age 37-89 years) in whom the possibility of the thoracic pathology was considered in their differential diagnosis.

Results: Of the subjects with no clinical signs of intrathoracic disease 86 (20.6%) had positive findings on their chest plain film: 62 patients (14.7%) had active disease of the lung parenchyma or/and the mediastinum, 18 patients had findings of old granulomatous disease or emphysema and 3 patients had metastatic bone lesions of unknown primary tumor. Further investigation in these cases included lateral chest radiograph (6 cases) and/or chest CT (46 cases). Of the subjects with possible thoracic pathology 224 had findings on chest radiograph and in 180 the plain chest film was normal.

Conclusion: Although positive history is statistically a very strong indication ($p < 0.001$) for performing chest radiograph, our study revealed a high percentage (20.6%) of positive findings in asymptomatic patients. We suggest that conventional chest radiograph (PA or AP projection) should be included in the investigation protocol of all patients admitted to ER.

C-0296

Multislice CT and SPECT-CT: Correlation in diagnosis of pulmonary nodules

G. Sergiacomi, M. Leporace, M. Cariani, F. Laviani, A. Bartolomucci, O. Schillaci, G. Simonetti; Rome/IT

Purpose: To demonstrate the validity and efficacy of ms-CT and Spect-CT in the assessment of pulmonary lesions.

Methods and Materials: 46 patients (34 males, 12 females; age range: 59-82 years) with solitary pulmonary nodules demonstrated on CT examination, underwent spect-CT after Tc-99m SESTAMIBI i.v. injection. Tc-99m SESTAMIBI is a lipophilic cation that is accumulated in areas where there is increased cellular metabolic activity. We used ms-CT LightSpeed 16 (GE Medical Systems) and a dual-head γ -camera Millennium (GE Medical Systems). To evaluate the diagnostic accuracy, a further ms-CT control was performed 4 months later.

Results: In 36 patients with 8-12 mm lesions at the first CT examination with positive scintigraphy, at the 4 months follow-up, CT demonstrated a volumetric increase, while histological examination revealed malignant lesions: 22 adenocarcinomas, 10 bronchogenic carcinomas, 2 large cell carcinomas and 2 metastases. Two false negative cases were adenocarcinomas with unclear CT characteristics, low tracer up-take at scintigraphy and a volumetric increase at the 4 month CT examination. Two false positive cases were granulomas with dubious CT characteristics and positive scintigraphy without significant volumetric increase (> 20%) at follow-up. 6 cases were diagnosed histologically as hamartomas, CT yielded dubious results with absence of radiotracer up-take and no significant volumetric increase at follow-up.

Conclusion: Scintigraphic evaluation revealed sensitivity of 0.95 and specificity of 0.75. Our study proposes a diagnostic protocol for the early diagnosis of pulmonary nodules with the aim of anticipating the surgical treatment of suspicious lesions at their first identification at CT.

C-0297

Multislice CT with retrospective ECG gating in the evaluation of central lung tumours

G. Sergiacomi, M. Cariani, M. Leporace, M. Sperandio, A. Romagnoli, G. Simonetti; Rome/IT

Purpose: To evaluate the efficacy of retrospective ECG gating in the assessment and diagnosis of central pulmonary tumours with possible hilar and parahilar structures involvement.

Methods and Materials: 50 patients (32 males and 18 females, age range 45-72) with central pulmonary tumours previously suspected on chest X-ray examinations (28 in the right lung and 22 in the left lung) were selected. Beta-blocker therapy was applied in 26 patients to reduce heart rate. The study was performed with a 16-row ms-CT with retrospective ECG gating after administration of contrast medium and saline flush. The axial images were reformatted using MPR, MIP and VR algorithms and evaluated independently by 2 experienced cardio-thoracic radiologists. Readers recorded their degree of diagnostic confidence for suspected involvement of the hilar and parahilar structures in each case on a 5 point scale. Twenty patients with central lung cancer studied without ECG gating were used as controls.

Results: Retrospective ECG gating significantly improves ($p < 0.05$) the assessment of hilar and parahilar tumour involvement. Without ECG gating the two readers recorded the maximum score on the confidence scale in 49% and 52% of cases respectively. With ECG gating the maximum score was recorded in 75% and 80% of cases respectively.

Conclusion: Retrospective ECG gating, thanks to reduced cardiac motion artefacts, allows a better evaluation of hilar and parahilar vascular and bronchial structures and optimal visualization of possible neoplastic pericardial and myocardial involvement, and can therefore be a valid tool in the evaluation of central pulmonary tumours and in planning a therapeutic approach.

C-0298

Characteristic high resolution computed tomography findings of pulmonary tuberculosis in patients with smear-positive sputum

N. Kosaka, T. Sakai, H. Uematsu, H. Kimura, M. Hase, M. Noguchi, H. Itoh; Fukui/JP

Purpose: To characterize the high-resolution computed tomography (HRCT) findings that can predict the infectivity of pulmonary tuberculosis.

Methods and Materials: HRCT images in 48 patients (age range: 21-92 years; mean age 58 years; 14 females, 34 males) with active pulmonary tuberculosis were retrospectively reviewed in this study. The 48 patients were divided into two groups: sputum-smear positive ($n = 25$) and negative ($n = 23$). HRCT (slice thickness: 2 mm) findings of these two groups were independently reviewed by two experienced radiologists, focusing on the presence or absence of nodular opacity, ground-glass opacity, cavitation, centrilobular opacity, bronchial wall thickening, and air-space consolidation.

Results: The frequency of air-space consolidation in the smear-positive group was significantly higher than that in the smear-negative group ($P < 0.005$), while its overall frequency was the lowest of the frequencies we measured. The frequencies of cavitation and ground-glass opacity in the smear-positive group were also statistically higher than those in the negative group ($P < 0.05$). The frequency of bronchial wall thickening, centrilobular opacity, and nodular opacities were not statistically significant between the two groups.

Conclusion: HRCT findings such as air-space consolidation, cavities, and ground-glass opacities have a significant correlation with smear-positivity in pulmonary tuberculosis. Therefore, HRCT may be useful to evaluate the infectivity of pulmonary tuberculosis, in addition to the establishing the diagnosis of active pulmonary tuberculosis.

C-0299

Computer-aided diagnosis: Differentiation between malignant and benign solitary pulmonary nodules using quantitative measures of shape

S. Iwano, T. Nakamura, Y. Kamioka, T. Ishigaki; Nagoya/JP

Purpose: To determine whether digital image analysis could differentiate between benign and malignant solitary pulmonary nodules (SPNs) based on morphological classification of high-resolution CT (HRCT) images.

Methods: HRCT images (0.5-mm or 1-mm slice thickness) of 97 solid SPNs were obtained. The diagnoses of these 97 cases (54 benign and 43 malignant) were determined from either radiological follow-up or pathological specimens. HRCT images were binarized with predefined threshold values (-300 HU), and the desired pulmonary nodules were extracted on image processing computer

Scientific and Educational Exhibits

software. From these binary image data, circularity ($= 4\pi \cdot \text{Area}/\text{Perimeter}^2$) and 2nd-moment of each nodule were calculated as quantitative measures of shape, to differentiate malignant and benign.

Results: Malignant nodules had lower measures in both circularity and 2nd-moment. Those nodules with circularity ≤ 0.75 and 2nd-moment ≤ 0.18 , had a high probability of malignancy, although several malignant nodules had high 2nd-moment measure because of emphysema, pleural indentation or air-bronchogram. Using these threshold values results in a sensitivity of 81.4%, specificity of 81.5%, positive predictive value of 77.8%, negative predictive value of 84.6%, and accuracy of 81.4%.

Conclusion: HRCT image analysis on a computer could differentiate between malignant and benign pulmonary nodules using quantitative measures of shape. This method could be applied to computer-aided diagnosis.

C-0300

Visualization of aberrant bronchial arteries and their anatomic course by CT bronchial angiography

S.M. Shin, Y.J. Jeong, K.I. Kim, C.W. Kim, T.Y. Moon; Busan/KR

Purpose: To evaluate the ability of multi-detector CT (MDCT) to identify aberrant bronchial arteries and their course.

Materials and Methods: Bronchial arteries (BA) were evaluated with MDCT bronchial arteriography (CTBA) in 83 patients with hemoptysis. CTBA was performed with 2.5 cc/sec injection rate of 100 cc non-ionic contrast agent and 1.25-2.5 mm collimation with a pitch of 6. Based on the original images and coronal reformats, two independent observers recorded the type of bronchial arteries (Classification of Cauldwell et al: type I-IV) and the presence of aberrant bronchial arteries. If aberrant bronchial arteries were present, the origins of the aberrant bronchial arteries were also recorded. Results on CTBA were compared with those of conventional bronchial arteriography (CBA).

Results: CTBA showed 61 (73%) type I, one (1%) type II, three (5%) type III, one (1%) type IV, seven (8%) common trunks of both BA, and nine (11%) aberrant bronchial arteries. Of nine aberrant bronchial arteries demonstrated on CTBA, three originated from the left internal mammary artery, two from the right subclavian artery, two from the aortic arch, one from the right bronchial artery, and one from the left thyrocervical trunk. The anatomic course of aberrant bronchial arteries on CTBA was correctly classified in nine of ten patients (90%) on CBA. Only one aberrant left bronchial artery, arising from the right bronchial artery, was not correctly identified on CTBA.

Conclusion: MDCT bronchial arteriography is a reliable, non-invasive technique to identify aberrant bronchial arteries and their course prior to arterial embolization in patients with hemoptysis.

C-0301

Differential CT features of focal pneumonia versus mucinous bronchioloalveolar carcinoma (BAC) mimicking pneumonia

T. Kim¹, S. Kim¹, S. Chung², B. Choi¹; ¹Seoul/KR, ²Yongin/KR

Purpose: To assess the characteristic CT findings of focal pneumonia versus mucinous BAC mimicking pneumonia, which were located at the lung periphery.

Methods and Materials: Two radiologists in consensus reviewed the thin-section CT findings in 47 patients with a focal area of parenchymal opacification, confirmed as a focal pneumonia or mucinous BAC, at the lung periphery. We evaluated presence of ground glass attenuation, marginal conspicuity, CT angiogram sign, air bronchogram sign, a bubble-like low-attenuation area, adjacent pleural thickening and retraction, pleural effusion, extra-pleural fatty hypertrophy, presence of bronchial wall thickening proximal to the lesions, and air-trapping in the adjacent normal lung. We used Chi-square test to evaluate the statistically significant differences between focal pneumonia and mucinous BAC mimicking pneumonia. A *p* value of < 0.05 was considered as being statistically significant.

Results: Twenty-nine patients had a focal pneumonia including pulmonary tuberculosis in 6 patients, and 18 patients were confirmed as a mucinous BAC or mixed adenocarcinoma with a predominant BAC pattern. The latter displayed the presence of a bubble-like low-attenuation area, whereas the former displayed bronchial wall thickening proximal to the lesions and adjacent pleural thickening surrounding the lesions. There were no significant differences in other CT findings.

Conclusion: A focal area of parenchymal opacification on the thin-section CT scans may suggest a focal pneumonia rather than a mucinous BAC when it shows bronchial wall thickening proximal to the lesions and adjacent pleural thickening surrounding the lesions.

C-0302

HRCT in differential diagnosis of types of interstitial pneumonia

A.L. Yudin, Y. Abovich; Moscow/RU

Purpose: To identify specific CT patterns of the different histologic types of interstitial pneumonias and create algorithms for differential diagnosis.

Methods and Materials: Between January 1998 and February 2004, 312 patients with diffuse infiltrative lung diseases were examined in our department. 137 patients had interstitial pneumonia, of whom 97 had idiopathic interstitial pneumonia with histologic verification (24 - UIP, 30 - NSIP, 17 - AIP, 14 - DIP, 12 - COP). HRCT features and their combinations were analyzed to reveal specific patterns.

Results: Different combinations of HRCT features determined positive predictive index for UIP - 100%, NSIP - 95%, AIP - 92%, DIP - 78%, COP - 67%. On the basis of specific patterns we created an algorithm for differential diagnosis of interstitial pneumonias. With the help of this algorithm independent experts were able to state true diagnoses in 88% of cases.

Conclusion: HRCT provides radiologists with ample opportunity to differentiate interstitial pneumonias without histologic verification.

C-0303

"Halo sign" on pulmonary CT: Radiologic-pathologic correlation

M. Parrón, M. Navarro, M. Pardo, I. Torres, M. Fernández-Veilla, J. Echeveste; Madrid/ES

Learning Objectives: To describe and illustrate the spectrum of diseases that can cause pulmonary nodules with the "halo sign" on thoracic computed tomography (CT). To show the correlation of the "halo sign" with pathologic findings.

Background: The "halo sign" consists of a halo of ground glass attenuation surrounding a pulmonary nodule. The "halo sign" has been demonstrated in a number of conditions associated with haemorrhagic nodules, and occasionally, with non-haemorrhagic pulmonary nodules. In the appropriate clinical setting, it is considered an early sign of pulmonary aspergillosis. The CT scans of patients with pulmonary nodules from our thoracic pathology database were reviewed and those with "halo sign" were selected. Diagnosis was always obtained by means of laboratory, cytologic, histological or microbiological tests. The pathology basis of this sign is discussed, and shown in appropriate cases.

Imaging Findings: The "halo sign" was found in association with four different pathological entities: haemorrhagic pulmonary nodules of infectious aetiology (invasive pulmonary aspergillosis, viral pneumonia, mucormycosis, cryptococcosis, candidiasis, tuberculosis, septic pulmonary embolism); haemorrhagic pulmonary nodules of non-infectious aetiology (Wegener granulomatosis, Kaposi sarcoma, haemorrhagic pulmonary metastasis); pulmonary nodules with halo due to neoplastic cell infiltration (bronchiolo-alveolar carcinoma, lymphoma, and other primary or secondary pulmonary tumours); and pulmonary nodules with halo due to non-haemorrhagic inflammatory injuries (sarcoidosis, inflammatory pseudotumor, organizing pneumonia, actinomycosis).

Conclusion: The "halo sign" is a non-specific but useful finding. A number of diseases can exhibit pulmonary nodules with a "halo sign" on the thoracic CT, displaying different pathological features, not only haemorrhagic nodules.

C-0304

Single versus four-level tumour perfusion measurement using dynamic helical contrast enhanced multi-detector computed tomography (MDCT):

Effect on measurement agreement and potential for whole tumour assessment

Q.S. Ng¹, V. Goh¹, E. Klotz², H. Fichte², D. Carnell¹, M. Saunders¹, P.J. Hoskin¹, A.R. Padhani¹; ¹Northwood/UK, ²Forchheim/DE

Purpose: To assess measurement agreement of single versus four level CT perfusion measurements using a novel dynamic helical technique.

Materials and Methods: Ten patients with lung cancer were examined using 16-detector row CT (Sensation 16, Siemens). 90 s dynamic acquisitions were obtained through the entire tumour following IV contrast infusion, and repeated within 24 hours. Median tumour permeability (0.5 ml/min/100 ml) and relative blood volume (0.1%) were determined (Patlak analysis; Functional CT, Siemens) on a pixel-by-pixel basis for a single 10 mm central axial image, and for three further adjacent slices. Measurement agreement was assessed using Bland-Altman statistics, following natural logarithmic transformation of values where necessary.

Results: Mean difference (95% limits of agreement) for permeability and blood volume were -0.07 (-0.74 to +0.60) and 20.2 (-39.7 to +80.1) respectively for one level, and 0.02 (-0.40 to +0.45) and 12.9 (-36.2 to +62.1) respectively for four levels. Intraclass correlation coefficients were 0.8 and 0.3 respectively for one

Scientific and Educational Exhibits

level, and 0.9 and 0.5 for four levels. Within subject standard deviation (within patient coefficient of variation) were 0.24 (27%) and 25.0 (40%) respectively for one level, and 0.15 (16%) and 19.2 (31%) respectively for four levels. For therapeutic response assessment, in a single patient, a permeability change of -48% to +92%, and blood volume of \pm 111% is required to be significant for a single level, compared with -33% to +50%, and \pm 86% respectively for four levels.

Conclusion: Perfusion CT measurement agreement is improved using multiple slices. We have established the degree of change required for therapeutic response.

C-0305

Pulmonary sequestration: A pictorial review

B.J. Op de Beeck¹, R. Salgado¹, L. Trappeniers², F. Vandenbroucke², K. de Jongh¹, P. Parizel¹; ¹Edegem/BE, ²Brussels/BE

Learning Objectives: To demonstrate the various appearances of pulmonary sequestration. To outline the advantages and limitations of HRCT, MDCT and MR imaging for differentiating intralobar from extralobar sequestration.

Background: A pulmonary sequestration is a portion of pulmonary tissue that does not have communication with the tracheobronchial system through a normal bronchus and is supplied by anomalous systemic arteries. Pulmonary sequestrations are anatomically divided into two categories, intralobar and extralobar. An intralobar sequestration lies within the pleural cavity of the normal lung. An extralobar sequestration has its own visceral supply. In this exhibit we will describe the diagnostic clues of the different imaging modalities.

Imaging Findings: Various parenchymal abnormalities have been observed, including cysts, soft tissue masses, emphysema surrounding the cysts or masses, and hypervascularity of a region of lung. Imaging findings depend on the volume and the presence or absence of infection. If infection is present, a fluid-filled pattern is seen. If cystic in nature, air trapping is seen on expiratory scans. When the sequestered lung becomes infected, it often appears to be a chronic pulmonary abscess. The caliber of the anomalous artery in intralobar sequestration is usually large, and venous drainage generally occurs through the pulmonary vein. The caliber of the anomalous artery is usually small; venous drainage is usually into a systemic vein, such as the azygous vein.

Conclusion: Meticulous vascular evaluation is mandatory. Diagnosis of pulmonary sequestration is related to the detection of an anomalous systemic artery. Different venous drainage is noticed in intra- and extralobar types.

C-0306

CT lung cancer screening supported by CAD system on Italian traffic policemen: One year preliminary results

F. Fraioli, C. Catalano, L. Bertoletti, P.G. Nardis, R. Passariello; Rome/IT

Purpose: To illustrate a one-year experience of lung cancer CT-screening on a large high risk population, supported by CAD.

Materials and Methods: Clinical study was approved by institutional review board and performed on 1000 traffic-policemen. Study-selection included people > 50 years, smokers and with 15 years working outside on the street. MDCT parameters were: 140 kVp; 20 mAs; sl.collimation: 1 mm; sl. Thickness 1 (kernel B60) and 5 mm (kernel B30). No i.v. contrast agent was administered. Algorithm for post HRCT classification includes 7 options: 1) inadequate examination; 2) negative examination; 3) negative examination for neoplastic lesion but with other benign findings; 4) < 5 mm suspicious solitary pulmonary nodules; 5) > 5 mm suspicious pulmonary nodule; 6) nodules found only by CAD; 7) multiple (> 7) nodules with diameter less than 5 mm. Categories 2-3-7 have been considered as non-neoplastic and will be recalled for a second screening after 2 years. Categories 4-5-6 will be recalled after 3-6 months.

Results: Preliminary results revealed 714 subjects in categories 2-3-7; 144 in category 4; 49 in category 5; 77 nodules in category 6; ten in category 1. 6 patients presented lung cancer; 4 with a well defined burden 3 cm lung cancer, and 2 neoplasms considered as 3b-stage.

Conclusion: Data are preliminary and need confirmation on the next follow-up study. Nevertheless, in a selected high risk population, a lung cancer screening programme can be applied to reduce mortality. In addition, because of high speed nodule detection of the CAD system, it can be used for diagnosis and can reduce false negative rates of the physicians.

C-0307

Cavitory lesions in the lung: Radiographic and CT findings

M. Mereu, F. Guido, B. Feragalli, A. Travaglini, C. Torrione, M. Storto; Chieti/IT

Learning Objectives: 1) To describe the radiographic and CT findings of the most common cavitary lesions in the lung. 2) To review the radiographic and CT

criteria most useful in the differential diagnosis between benign and malignant cavitory lesions.

Background: The term "cavity" is used to describe an air-containing lesion characterized by a > 4-mm thick wall or an air-containing lesion within a mass or a surrounding infiltrate. Cavitory lesions can be observed in patients with a number of pulmonary diseases including neoplasms, infectious processes, infarcts, septic embolism, congenital abnormalities, collagen vascular diseases, and progressive massive fibrosis occurring with pneumoconiosis.

Procedure Details: The most commonly encountered radiographic and CT findings of these different diseases will be illustrated and discussed together with some basic information that may help differentiate benign from malignant lesions.

Conclusion: Cavitory lesions of the lung are quite common and can be benign or malignant. Malignancy is commonly the first diagnosis to consider for a cavitory lesion, particularly in a middle-aged or older adult with a history of cigarette smoking. In contrast in patients with AIDS, cavitory lesions are usually caused by infections including bacteria, mycobacteria, *P. carinii* and other fungi, and cytomegalovirus. The clinical context is clearly of importance in prioritizing diagnostic possibilities.

C-0308

Peripheral lung cancer: Screening and detection with low dose helical CT. Toshima trial

H. Tajima, T. Kumazaki, S. Murata, K. Nakazawa, T. Fukunaga, J. Watari, M. Machida, K. Yamamoto, H. Fukasawa; Tokyo/JP

Purpose: To evaluate low dose helical CT for the screening and detection of small peripheral lung cancers at Toshima ward, Tokyo.

Methods and Materials: Low dose helical CT (Asteion, Toshiba) was obtained from May 2000 to Feb 2003 in 3953 participants. The parameters were 120 kVp, 50 mA, 10 collimation, and 2:1 pitch.

Results: Peripheral lung cancer was detected in 24 out of 3953 examinations (0.60%). Cell types were as follows: squamous cell tumor, 2; adenocarcinoma, 20; large cell tumor, 1; mucoepidermoid tumor, 1. The mean size of the lesions was 18.1 mm (range 7-40 mm). Twenty (83%) out of the 24 tumors were stage I.

Conclusion: Low dose helical CT can depict early-stage lung cancers.

C-0309

Recurrent lung cancer at the bronchial stump site: CT and bronchoscopic findings

W. Kwon, K. Sung, W.-Y. Lee, M. Kim; Wonju/KR

Learning Objectives: To illustrate the spectrum of recurrent lung cancer at the bronchial stump site after lung resection. To outline the advantages and limitations of CT and bronchoscopy. To promote awareness of careful evaluation of the bronchial stump site at CT.

Background: Recurrence at the bronchial stump was seen in 2.2% of all cases of resected lung cancer. There may be tumor recurrence at the bronchial stump, even when the resected margin is sufficiently distant from the tumor and the surgical margin of the resected specimen is negative for cancer. The recurrent mass is commonly located at the site of the bronchial stump. If the recurrent mass is small, not well defined, or does not displace adjacent structures, differentiation from postsurgical fibrosis is difficult.

Imaging Findings: Bronchoscopic findings such as endobronchial mass, ulceration, and submucosal infiltration were correlated with CT findings. The most common finding is endobronchial mass (10/14). Although submucosal infiltration is seen on bronchoscopy, definite recurrent lung cancer can be diagnosed compared with the previous CT scan.

Conclusion: Variable findings of CT and bronchoscopy for recurrent lung cancer are demonstrated. Correlation with bronchoscopic findings and CT findings is helpful in verifying the presence of a recurrent mass.

C-0310

Traumatic diaphragmatic hernia: Comprehensive evaluation using novel MR techniques and multislice CT

H. Yang, K.-H. Do, K.-S. Song, J. Seo; Seoul/KR

Learning Objectives: To know the CT findings of traumatic diaphragmatic hernia. To explain the technique of real-time respiratory dynamic MR imaging. To understand the advantage of the MR and MSCT in the evaluation of traumatic diaphragmatic hernia.

Background: Because the diaphragm is a thin and complex structure which is oriented transversely or obliquely, it is difficult to diagnose diaphragmatic pathology by conventional techniques. Early diagnosis of traumatic diaphragmatic inju-

Scientific and Educational Exhibits

ry is important because the pleuroperitoneal pressure gradient can cause the defects to enlarge over time. However, the diagnosis of diaphragmatic rupture or defect and its functional significance is difficult to assess by conventional techniques. The purpose of this exhibit is to illustrate the usefulness of MSCT and respiratory cine MR technique in the evaluation of traumatic diaphragmatic hernia.

Imaging Findings: We collected 35 cases of traumatic diaphragmatic hernia. Axial CT scans showed various direct and indirect signs suggesting a diaphragmatic defect. Reformatted sagittal or coronal images using MSCT are useful in detection of diaphragmatic defects. Using three dimensional real-time respiratory dynamic MR imaging, it is possible to assess the respiratory motion of the diaphragm and dynamic movement of herniated organs.

Conclusion: Diaphragmatic defects were well demonstrated on three dimensional real-time respiratory dynamic MR imaging and reformatted sagittal or coronal images from MSCT.

C-0311

Assessment of pulmonary nodules on multi-slice CT (MSCT) of the chest: Impact of computer-aided detection (CAD) in the management of oncology patients

G. Bastarrika, P.D. Domínguez, D. Cano, M.J. Pons, I. Vivas,
I. González-Crespo; Pamplona/ES

Purpose: To evaluate the role of a computer-aided detection (CAD) system in the detection and growth assessment of lung nodules on MSCT exams of patients with metastatic cancer.

Methods and Materials: MSCT data sets of 19 consecutive patients with known malignancy (38 exams) were acquired. Scan parameters: 120 kV, 165 mAs, 5 x 2.5 mm collimation, 1.5 mm reconstruction interval. Two experienced readers reviewed each study, considering in their analysis pulmonary nodules of any size. The standard of reference for each nodule was determined by a consensus double read. All studies were processed using a CAD system (ImageChecker CT, R2 Technology, Inc.) and findings were compared with the standard of reference. One radiologist confirmed or dismissed CAD detected lesions. The impact of the CAD in oncology patient management was also analysed.

Results: A total of 121 lung nodules were identified as the standard of reference (mean size: 5.18 mm; SD: 2.75). The CAD system detected 139 lesions - 52 lung nodules (sensitivity: 0.43) and 87 (62.4%) false positives - and did not detect 69 nodules (57%) (false negatives). The CAD detected a total of 2.29 false positives/case; the system did not detect 1.81 nodules/case (mean size: 4.08 mm; SD: 1.73). The CAD allowed assessment of nodule growth in three cases but was not capable of demonstrating progression of the disease in one patient (haematogenous metastatic spread).

Conclusion: Even if accurate and helpful, CAD should be considered as a second reading tool for radiologists in routine clinical MSCT interpretation.

C-0312

CT features of pulmonary hydatid disease

C. Hafsa, M. Golli, S. Kriaa, M. Zbidi, A. Gannouni; Monastir/TN

Purpose: To study the CT features of pulmonary hydatid disease and to specify when we realize the chest CT in hydatid disease?

Methods and Materials: A retrospective study of 250 children with pulmonary hydatidosis is presented. The 250 cases (145 boys and 105 girls aged from 18 months to 14 years) were studied during the period from January 1982 until December 2003. CT of the chest was obtained in 120 cases. Surgery was performed for all patients. Diagnosis was confirmed with serology tests and/or pathological study of resected cysts.

Results: Different sizes and shapes of hydatid cysts were encountered, 44 of them being ruptured. CT density of the cysts varied from -42 to 160 Hounsfield units (HU; median, 15.5 HU). Apart from the classically described features of pulmonary hydatid disease, a crescent-shaped rim of air at the lower end of the cyst (inverse crescent sign) was seen in 10 cysts, and a bleb of air in the wall of five as-yet unruptured cysts (signet ring sign). Thick wall (> 10 mm) was observed in thirty cysts, and each of them had associated evidence of infection.

Conclusions: Inverse crescent sign, signet ring sign, high CT density, and thick wall should be recognized as features of pulmonary hydatid cysts on CT. CT is useful for diagnosis of atypical or complicated lesions and to detect bronchiectasis.

C-0313

Imaging features of mediastinal hydatid cyst

C. Hafsa, M. Zbidi, S. Kriaa, S. Jerbi Ommezine, M. Golli, A. Gannouni; Monastir/TN

Purpose: Hydatid disease is a parasitic infestation caused by larvae of the echinococcus tapeworm. Mediastinal hydatid cyst is uncommon. We present the various radiological aspects of mediastinal hydatidosis based upon a series of 20 cases. The importance of Echocardiography and thoracic MRI and CT will be emphasized.

Methods and Materials: A retrospective study of 20 cases having mediastinal hydatid cyst is reported. Chest radiography, echocardiography and abdominal ultrasound were performed in all cases. CT was performed only in 10 cases. MRI was performed in three cases. Surgery was performed for all patients. Diagnosis was confirmed with serology tests and/or pathological study of resected cysts.

Resultat: Echocardiography showed a multivesicle cyst in the ventricular cavity in 6 cases. Thoracic computerised tomography (CT) and magnetic resonance imaging (MRI) also revealed a hypodense mass in the ventricular cavity. Only four cases have a cyst in the posterior mediastinum. A diagnosis of primary hydatid cyst was confirmed and total cystectomy was performed.

Conclusion: Echocardiography is the best diagnostic procedure for cardiac hydatid disease, although thoracic MR imaging and CT, and abdominal CT, are also necessary for detecting the exact location, size and number of disseminated hydatid cysts.

C-0314

A review of outpatient ventilation-perfusion scintigraphy

B.J. Holloway, P. Struhal; Wolverhampton/UK

Purpose: The aim of this review is to ascertain the outcomes of outpatient V/Q scans and their effect on management. Additionally there has been a more recent implementation of consistent vetting of requests in our institution. This has occurred following an improvement of staffing levels. This review provides an opportunity to analyse the consistency with which this is occurring.

Method: The information was compiled retrospectively for all outpatient V/Q scans performed between 01/01/2002 and 31/12/2003 inclusively. Once the total number was ascertained, the original request cards were obtained to check for vetting. The probability of pulmonary embolus was documented. In results of greater than low probability further information regarding relevant risk factors was sought.

Results: A total of 115 outpatient V/Q scans were performed within the two year time period specified. Documented evidence of vetting of the request cards was seen in 87 examinations (76%). 103 patients (90%) had a probability of pulmonary embolus reported as no greater than low. Of the 12 examinations with probabilities greater than low all had significant risk factors or had an abnormal chest radiograph.

Conclusion: Our review looks in depth at the frequency of, and outcomes in, outpatient ventilation perfusion scanning. We can conclude that in this population the chance of obtaining a high probability result in individuals with a normal chest radiograph and without risk factors such as malignancy and known thromboembolic disease is virtually nil. We have performed a review of the available literature on this subject.

C-0315

Ultrasound guided FNAC of impalpable cervical lymph nodes in lung cancer

L. Chandratreya, M. Cobby, R. Watura; Bristol/UK

Learning Objectives: We aim to demonstrate the anatomy, technique, indications and possible benefits of ultrasonography of impalpable cervical nodes and ultrasound guided fine needle aspiration cytology of these in lung cancer.

Background: The finding of an abnormal cervical lymph node in lung cancer is crucial to its staging and may radically alter management. Although routine scalene node biopsy is no longer performed in impalpable adenopathy by the surgeons in lung cancer, there has been resurging interest in ultrasonography of the neck with ultrasound guided FNAC of abnormal nodes in selected cases.

Technique: Using a 7.5 MHz linear probe we scan the neck from the suprascapular level to the submental and retroparotid regions, longitudinally and transversely, to include the Groups I to V of the cervical lymph node regions bilaterally. When lymph nodes are detected the most abnormal or the largest node is then aspirated by aseptic technique using a 22 G needle and smears are sent for cytological examination.

Conclusion: We have found this to be a safe and simple procedure, requiring no anaesthesia or preparation and can be easily performed on outpatients. This also accurately identifies lymph nodes differentiating them from thrombosed veins, fat

Scientific and Educational Exhibits

and thyroid masses. We firmly believe this is an important pre-treatment evaluation which may spare the patient more invasive and potentially more risky diagnostic procedures like percutaneous lung biopsy and mediastinoscopy.

C-0316

Rare primary mediastinal tumors: Helical CT features and pathological correlation

J.-Q. Yu, Z.-G. Yang, Z.-L. Li; Chengdu/CN

Learning Objectives: 1. To demonstrate the morphologic features of rare mediastinal tumors on helical CT. 2. To correlate the CT features with pathological findings of rare mediastinal tumors. 3. To learn how to differentiate the rare mediastinal tumors on the basis of location, size, shape, and particularly attenuation on un- or enhanced CT images.

Background: Primary mediastinal tumors comprise a diverse group of neoplasms. Some are rare and account for less 5% of primary mediastinal masses, therefore their morphological features are not easily recognized. We try to investigate the characteristics of these rare tumors on CT images.

Imaging Findings: Twenty-five cases with different types of rare mediastinal tumor were observed and analyzed retrospectively. Thymic cysts are round, uniloculated or multiiloculated thin-walled masses on helical CT. Thymic carcinoma and carcinoid show a large, poorly defined, infiltrative anterior mass, frequently associated with pleural and pericardial effusion or hemorrhage and necrosis. Hemangiomas are well-margined and heterogeneous masses on enhanced CT and have punctate or phlebolith calcification. Ganglia tumors are well-margined, homogeneous or heterogeneous, oblong masses with a broad base along the anterolateral aspect of the spine. Malignant fibrous histiocytoma, small cell undifferentiated sarcoma and angiomyolipoma are located in the posterior mediastinum and are heterogeneous masses, which manifest various densities due to different histologic components. The educational exhibit presents the helical CT features and pathology of these tumors.

C-0317

Invasive pulmonary aspergillosis: Significance and predictive value of the "hypodense sign" on unenhanced CT

M.S. Horger, C.A. Pfannenberg, C. Lengerke, H. Hebart, C.D. Claussen; Tübingen/DE

Purpose: To assess the diagnostic value of central hypointensity ("hypodense sign") in lung consolidation on unenhanced CT, in immunocompromised patients, suspected of having invasive pulmonary aspergillosis (IPA).

Material and Methods: Retrospective analysis of serial CT scans of the lung was performed in 43 patients with IPA in order to assess the hypodense sign using standard mediastinal and lung windowing settings, as well as narrower window setting (width, 110-140 HU; level, 15-40 HU). The time between the occurrence of early CT findings of IPA and the appearance of the hypodense sign, as well as between this and the occurrence of the crescent sign, cavitation or reduction in lesion size, was evaluated. In addition, we reviewed CT scans of immunocompromised patients with viral ($n = 45$) or bacterial ($n = 44$) pneumonia, with respect to the presence of the "hypodense" sign.

Results: Unenhanced CT scans revealed the hypodense sign in 13 (30.2%) patients. The mean time delay between the first manifestation of IPA and the hypodense sign was 7.8 days, while the time interval between the hypodense sign and the occurrence of crescent sign, cavitation, or decrease in the lesion's size was 8.3 days. The hypodense sign did not occur in any of the patients with viral or bacterial pneumonia, in the control series.

Conclusion: We consider the hypodense sign to be a supplementary tool in the diagnosis of IPA. Its sensitivity was low in our series, but the high specificity makes it valuable in predicting invasive pulmonary aspergillosis, preceding the occurrence of cavitation or crescent sign.

C-0318

CT diagnosis of pulmonary aspergilloses in hematological diseases

A. Varga, G. Forrai; Budapest/HU

Purpose: To review the spectrum of *Aspergillus*-related pulmonary disease focusing on the CT diagnosis of *Aspergillus* infections in patients with hematological diseases.

Procedure Details: 275 plain and contrast-enhanced helical chest CT examinations and high resolution CT examinations of hematology patients were performed between 1 January 2003 and 27 February 2004.

Background: *Aspergillus fumigatus*, a rare cause of pneumonia in the general population, has an important role in the immunocompromised group of patients,

particularly in patients with lymphoma or leukaemia. The pulmonary aspergilloses are a spectrum of diseases ranging from bronchopulmonary aspergillosis in the hyperimmune host, through pulmonary mycetoma formation in lung cavities of patients with normal immune status, to invasive pulmonary aspergillosis in immunocompromised hosts. The latter may be further categorised as angioinvasive and airway invasive pulmonary aspergillosis. Overlap between these entities occurs ("semi-invasive" pulmonary aspergillosis in chronic cavitary lung disease in patients with mild immunocompromise). In our study CT signs of pulmonary aspergillosis were established in 6.5% of cases (18/275). Differential diagnosis of pulmonary aspergillosis includes other opportunistic infections, pulmonary manifestation of hematological diseases, other neoplasms, drug or radiation induced lung disease. Definitive diagnosis can often only be established by biopsy.

Conclusion: Pulmonary aspergillosis is relatively common in immunocompromised patients with hematological diseases. Complications can result in serious life-threatening conditions, therefore easily accessible non-invasive imaging modalities are necessary. CT plays an important role in differential diagnosis, providing enough informations for most therapeutic decisions.

C-0319

Screening for lung cancer in a high risk population using spiral computed tomography: 3-year results

L. Cardinale, F. Ferraris, F. Perotto, P. Gollini, A. Priola, S. Novello, C. Fava; Orbassano/IT

Purpose: ELCAP and Japanese studies show low-dose-spiral-CT (sCT) detects early-stage lung cancer (LC) in high-risk populations. Our trial was designed to confirm these data, evaluating prevalence of LC at first sCT examination, and to assess the radiological detection during a 5-year follow-up. Our secondary aim was to determine overall resectability of detected LC.

Materials and Methods: We enrolled 519 asymptomatic volunteers, aged > 55 years, who smoked > 20 pack-years; we planned to perform an annual sCT for 5 years.

Results: Baseline sCT detected nodules > 5 mm in 22% of cases, < 5 mm in 25%; 53% were negative. At year 1, 18 patients dropped out: 14 due to personal decision, 4 due to diagnosis of other malignancies. During year 2 sCT detected nodules > 5 mm in 5% of cases. By year 2, 8 LC were diagnosed (5 at baseline, 3 at year 2): 6 stage I, 1 IIIB and 1 IV (adrenal metastases). During year 1, 2 additional cases were resected (1 atypical resection, 1 lobectomy) for bronchoalveolar adenoma. 3 year results are under evaluation.

Conclusion: In terms of LC prevalence/incidence, data from our feasibility trial are comparable to those previously reported and support the use of this screening tool in randomized studies.

C-0320

Virtual bronchoscopy: A new approach to facilitating endobronchial ultrasound-guided transbronchial needle aspiration biopsy

K. Nakatani, S. Morishita, K. Okino, T. Anayama, S. Sasaguri, S. Yoshida; Nankoku/JP

Purpose: Assessment of mediastinal lymph nodes (N2, N3) is one of the most important factors when planning therapy and estimating prognosis in thoracic malignancy. Recently, endobronchial ultrasound (EBUS) guided transbronchial needle aspiration biopsy has often been performed to ascertain lymph node status. The authors have constructed three dimensional images in order to help bronchoscopists.

Methods and Materials: Multidetector computed tomography (Aquilion, 1.0 mm x 16, helical pitch; 15, beam pitch; 0.94, Toshiba, Tokyo, Japan) was performed. Images were transferred to a workstation (Virtual Place Advance, AZE, Tokyo, Japan). Color images were reconstructed to distinguish between mediastinal lymph nodes and the great vessels. In this manner, movie images can be relayed to chest surgeons, enabling virtual bronchoscopy to "see through" the lymph nodes and vessels.

Results: EBUS-guided transbronchial needle aspiration biopsy requires considerable skill, as the bronchoscopist can only visualize 30 degrees in an upward direction and the ultrasound beam is very narrow. Moreover, anatomic position of great vessels differs greatly between individuals. The virtual bronchoscopy method reported herein could help bronchoscopists to gain an accurate understanding of the relationship between the bronchial tree, target lymph nodes, arteries and veins. These images could increase efficiency of the examination and allow it to be performed more safely.

Conclusion: We have developed a virtual bronchoscopy method that enables clinicians to "see through" the lymph nodes and great vessels. These images can help bronchoscopists understand the anatomic relationships and can expedite EBUS-guided transbronchial needle aspiration biopsy.

Scientific and Educational Exhibits

C-0321

CT-guided fine-needle aspiration biopsy in the diagnosis of focal pulmonary lesions

K. Bronisz, J. Wójcicka, P. Czyszkowski, C. Rybacki, T. Szylberg;
Bydgoszcz/PL

Background: The delay in the diagnosis of lung cancer makes the radical treatment of this disease impossible, leading to its becoming generalized. X-ray detection of focal pulmonary lesions ought to result in the establishment of the histopathological diagnosis. It is necessary to collect material from the lesion for microscopic investigation. The results determine the initiation of appropriate treatment. Many focal pulmonary lesions are inaccessible by bronchoscopy, and a biopsy through the chest wall is required.

Purpose: To show the possibilities created by the application of CT-guided FNAB in the diagnosis of focal pulmonary lesions.

Materials and Methods: 585 patients: 427 men (73%) and 158 women (27%). 592 fine-needle aspiration biopsies performed in CT Laboratory of the Radiology Department in the period between 1995 and 2003.

Results: Cytological diagnosis based on the obtained material was possible in 491 cases (82.9%). In 47 cases normal pulmonary cells were found in the material. Of the above-mentioned number of cases, as well as in 54 cases suspected of a tumor, where non-diagnostic material was obtained (blood, necrosis), 39 repeat biopsies were performed. Pneumothorax was the most serious complication after biopsy. It required surgical intervention in 37 cases (6.3%). Mild haemoptysis was observed in 30 cases (5%).

Conclusion: CT-guided FNAB of pulmonary focal lesions is an effective, minimally invasive diagnostic method, allowing establishment of the cytological diagnosis. This method substantially shortens the time between the X-ray detection of the lesion and the initiation of appropriate treatment.

C-0322

Distributional variations of thymic cysts in the mediastinum

T. Kim, S. Kim, S. Chung, B. Choi, K. Choe; Seoul/KR

Purpose: To retrospectively evaluate the distributional variations of thymic cysts in the mediastinum.

Methods and Materials: Twenty-seven patients (9 men, 18 women; mean age, 58.9 years; range, 24-82 years) with thymic cysts were included in this study. Two radiologists retrospectively reviewed the CT features in consensus, which included attenuation values, size and location of the tumors. The tumor location was classified as the anterior, middle, or superior mediastinum. The superior mediastinum was divided into either the anterior or middle compartment on the basis of the relationship with the vascular structures such as carotid and innominate arteries.

Results: The tumors were located in the anterior mediastinum in 22 patients (81.5%), in the middle mediastinum in 2 patients (7.4%), and in the superior mediastinum in 3 patients (11.1%), respectively. The superior mediastinal lesions were located in the anterior, pre-vascular compartment in 2 patients and in the middle, post-vascular compartment in one patient. The size of the tumors ranged from 2.2 to 12 cm (mean, 4.8 cm) at the axial longest diameter. The mean attenuation value was about 8.4 HU on the unenhanced scans and about 9.7 HU on the contrast-enhanced scans.

Conclusion: Thymic cysts are usually located in the anterior mediastinum, but some lesions occur in the superior or middle mediastinum. Therefore, we should include a thymic cyst in the differential diagnosis when cystic lesions are located in the superior or middle mediastinum.

C-0323

Quantitative multi-planar lung cancer perfusion measurement using multidetector row computed tomography (MDCT): Inter and intra-observer agreement

Q.S. Ng¹, V. Goh¹, H. Fichte², E. Klotz², D. Carnell¹, M. Saunders¹, P.J. Hoskin¹, A. Padhani¹; ¹Northwood/UK, ²Forchheim/DE

Purpose: Multi-planar perfusion measurement enables quantitative vascular assessment of an entire tumour, but inter and intra-observer measurement error has not been assessed to date.

Materials and Methods: 11 patients with lung cancer were examined prospectively using MDCT (Sensation 16, Siemens). 90 s helical dynamic acquisitions were acquired repeatedly through the entire tumour following intravenous contrast infusion. Mean tumour permeability (0.5 ml/min/100 ml) and relative blood volume (0.1%) in a central axial and reconstructed coronal plane were determined by two independent observers using prototype software (FunctionalCT,

Siemens). Measurements were repeated by each observer, and inter- and intra-observer agreement was assessed using Bland-Altman statistics.

Results: The mean difference (95% limits of agreement) for inter-observer agreement for permeability and relative blood volume was -0.6 (-6.9 to +5.8) and 1.2 (-10.3 to +12.7) respectively in the axial plane, and -2.1 (-8.6 to +4.4) and -6.5 (-44.4 to +31.5) respectively in the coronal plane. The mean difference (95% limits of agreement) for intra-observer agreement was 0.1 (-0.4 to +0.7) and -1.1 (-6.3 to +4) respectively in the axial plane, and 1.4 (-3.4 to +6.3) and 1.9 (-30.8 to +34.5) respectively in the coronal plane for observer one, and -0.2 (-6.5 to +6.1) and -0.2 (-6.3 to +5.8) respectively in the axial plane and -0.5 (-3.2 to +2.2) and 3.3 (-13.1 to +19.6) respectively in the coronal plane for observer two. Intraclass correlation coefficients ranged from 0.79 to 0.99.

Conclusion: Good agreement between and within observers was found in both planes, which is essential for reliable therapeutic assessment.

C-0324

An audit of percutaneous lung biopsy performed at University Hospitals of Leicester, UK

A. Donuru, V.V.R. Kandula, M. Kumaran, J. Entwistle; Leicester/UK

Learning Objectives: To assess the outcome of CT/USS guided lung biopsy. To determine the success, failure and complication rates of the procedure.

Background: Percutaneous transthoracic lung biopsy is a common procedure used mainly to elucidate the nature of pulmonary masses. Approximately 450 patients are newly diagnosed with lung cancer in Leicester, UK. Published complication rates vary widely. Only one meta-analysis was identified in thorax [1], which suggested local estimation of complication rates. A multidisciplinary team (MDT) should ensure the most appropriate approach to biopsy. Guidelines were published by British Thoracic Society in agreement with Royal College of Radiologists (RCR) in 2003[2]. **Guidelines:** Adequacy of sample should be over 90%. False positives should be < 1%. Sensitivity for malignancy should be 85-90% in lesions over 2 cms. All patients should be discussed at MDT prior to biopsy.

Imaging Findings: 50 patients audited prospectively (Nov'02 to Oct'03). 36 patients (day case), 13 (in-patient) and no record on 1 patient. Only 23 out of 50 patients had documented lung function tests. 94% CT guided and 6% USS guided. 86% lung biopsies and 14% pleural biopsies. 96% diagnostic and 4% non-diagnostic. Complications included pneumothorax (28%), haemoptysis (4%), haemorrhage (12%). No complications in 56%.

Conclusion: Pneumothorax was managed conservatively in all patients. Haemoptysis was mild - none required blood transfusion. No relationship between number of passes and associated complications. Lung function tests should be documented on all patients (as a part of overall risk assessment) prior to performing a biopsy.

C-0325

The thymus: A mediastinal mystery

M. Nishino, S.K. Ashiku, R. Thurer, O.N. Kocher, P.M. Boiselle, H. Hatabu; Boston, MA/US

Learning Objectives: To provide comprehensive understanding of various thymic pathologies, and to describe their characteristic CT and MR findings along with pathological findings.

Background: The thymus is a unique organ which plays an integral role in the immune response via its complex microenvironment. Reaching its maximum weight in puberty and subsequently undergoing fatty involution, the thymus is seldom an eye-catching structure on imaging studies in normal adults. However, once involved in a disease process, it shows a variety of clinical and radiological manifestations which require comprehensive understanding of each entity.

Imaging Findings: In this review, we describe CT and MR imaging findings of a variety of thymic pathologies, including thymoma, thymic carcinoma, thymic cyst, thymic hyperplasia, thymolipoma, etc. The useful imaging findings for differentiating these entities, including shape and location of the lesion, CT attenuation and MR signal intensity, the presence of mediastinal invasion, and pleural metastasis are discussed. Surgical and pathological findings are also presented and correlated with radiological findings, to enhance understanding of the underlying process reflected in the imaging.

Conclusion: The CT and MR imaging findings of the thymic diseases, in correlation with surgical and pathological findings, are useful in differentiating each entity, and enhance our understanding of the variety of thymic pathology.

Scientific and Educational Exhibits

Chest

Vascular

C-0326

Congenital and acquired anomalies of the pulmonary arteries in adults:

A radiologic overview

D. Gil¹, E. Castaner¹, X. Gallardo¹, J. Mata¹, Y. Pallardo², J. Perendreu¹, A. Massuet¹; ¹Sabadell/ES, ²Valencia/ES

Learning Objectives: To describe the signs that allow anomalies of the pulmonary arteries to be identified or suspected on chest radiographs. To show the usefulness of CT and MR imaging in confirming the suspected diagnosis. To illustrate a practical approach to anomalies of the pulmonary arteries. To warn of potential complications in some vascular diseases, or infectious settings.

Background: Evaluation of pulmonary arteries is mainly indicated in patients with suspected pulmonary thromboembolism. However, other acquired pathologies can affect pulmonary arteries in the setting of neoplasms, infectious diseases, or inflammatory vascular processes. Some congenital anomalies can also be suspected on chest radiographs.

Procedure Details: We show the most representative cases of pulmonary arteries anomalies, diagnosed at our centre between 1995-2004. First we described the congenital anomalies that can be seen in the adult patient, including idiopathic dilatation of pulmonary artery trunk, pulmonary artery sling, and agenesis of the pulmonary artery. Among the acquired entities that can affect the pulmonary arteries, we include neoplasms (primary pulmonary artery sarcomas and intra-vascular pulmonary metastases), anomalies associated with inflammatory vascular processes (Behcet's disease, Takayasu's arteritis), involvement secondary to infections, pulmonary thromboembolism (acute and chronic) and changes secondary to pulmonary hypertension.

Conclusion: CT angiography and MR angiography are useful in the evaluation of pulmonary artery anomalies. Radiologists should be aware of potential pulmonary artery complications in some vascular diseases or infectious settings. Some congenital anomalies can be suspected on the radiographic findings.

C-0327

Role of D-dimer and pre-test probability scoring in suspected acute pulmonary embolism

G. Annamalai, C. Campbell, P. Duffy; Glasgow/UK

Purpose: To determine the role of D-dimer and pre-test probability (PTP) scoring in the management of suspected acute pulmonary embolism (PE).

Methods and Materials: Prospective study of 70 consecutive patients with suspected acute PE. All patients had D-dimer (Vidas ELISA) and CT pulmonary angiography (CTPA) performed. Pre-test probabilities using validated scoring systems (Wells and Geneva) were categorised as low, intermediate or high. The Geneva PTP scoring system is an objective and therefore reproducible system. The Wells scoring system is more subjective, incorporating clinical judgement.

Results: Prevalence of PE in our study population was 16%. Sensitivity and specificity of D-dimer test were 80% and 28% respectively. Two of 17 patients (12%) with negative D-dimer (< 500 ug/l) had PE confirmed on CTPA. The Wells scoring system performed better at excluding PE. No patients with low Wells PTP score but 13% with low Geneva score had PE subsequently diagnosed. None of the patients with both low Wells PTP score and negative D-dimer had PE.

Conclusion: This study confirms that negative D-dimer alone does not exclude acute PE and D-dimer is not suitable as a routine screening test. However, negative D-dimer in combination with a low Wells PTP is useful in excluding the diagnosis, thus decreasing the need for further imaging for venous thromboembolism.

C-0328

Predictors on CT of hemodynamic improvement after pulmonary thromboendarterectomy

M. Heinrich¹, A. Grgic¹, D. Tscholl¹, B. Kramann¹, H.-J. Schäfers¹, M. Uder²; ¹Homburg a.d. Saar/DE, ²Erlangen/DE

Purpose: To correlate preoperative CT findings in patients with chronic thromboembolic pulmonary hypertension (CTEPH) with pulmonary vascular resistance (PVR) after pulmonary thromboendarterectomy (PTE) and to evaluate the use of CT in predicting hemodynamic improvement.

Methods and Materials: 60 patients who underwent PTE and helical CT were included in this retrospective study. Imaging findings in preoperative chest CT-scans were correlated with postoperative PVR. Patients with a postoperative PVR

higher than 500 dynes * s * cm⁻⁵ were considered to have insufficient hemodynamic improvement and not to have benefited from surgery. Univariate analyses were performed by Mann-Whitney test, Spearman's rank correlation and Fisher's exact test, as appropriate. Multivariate analysis was performed by multiple linear regression analysis.

Results: The presence ($p = 0.008$) and extent of central thrombi ($rs = -0.36$, $p = 0.007$) and the presence of dilated bronchial arteries ($p = 0.03$) was negatively correlated with postoperative PVR. 60% (3/5) of patients without visible central thromboembolic material on CT had an inadequate hemodynamic improvement, in contrast to 4% (2/51) of patients with central thrombi ($p = 0.003$). Preoperative PVR ($rs = 0.31$, $p = 0.018$) and the extent of a mosaic perfusion pattern ($rs = 0.37$, $p = 0.007$) and of peripheral scars ($rs = 0.32$, $p = 0.017$) were positively correlated with postoperative PVR.

Conclusion: Preoperative CT findings can help to predict hemodynamic improvement after PTE. The absence of central thromboembolic material, especially in combination with a mosaic perfusion pattern in all lobes, is a significant risk factor for inadequate hemodynamic improvement after surgery.

C-0329

Perfusion abnormalities in congenital and neoplastic pulmonary disease:

Comparison of ultrafast MR perfusion and multislice CT imaging

D.T. Boll¹, J.S. Lewin², A.J. Aschoff¹, R.C. Gilkeson³, ¹Ulm/DE, ²Baltimore, MD/US, ³Cleveland, OH/US

Purpose: To prospectively assess MR perfusion patterns of chronic, non-embolic pulmonary diseases and to compare the findings visualized with ultrafast MR perfusion imaging to those of pulmonary, contrast-enhanced multislice CT imaging.

Material and Methods: 25 patients underwent concurrent CT and MR evaluation of chronic, non-embolic pulmonary diseases of congenital ($n = 15$) or neoplastic ($n = 10$) origin. Analysis of MR perfusion and CT datasets was realized by defining pulmonary as well as vascular regions-of-interest. Utilizing MR imaging, time-intensity curves were plotted. Analogously, contrast-enhanced CT image datasets provided pulmonary signal-to-noise ratio measurements. Vessel centerlines of bronchial arteries were determined. Perfusion type was determined.

Results: Statistical analysis of pulmonary perfusion type detected 20 pulmonary artery perfusion patterns and five bronchial artery perfusion patterns. In patients with pulmonary artery perfusion, MR and multislice CT imaging differed in only four of twenty patients in not more than one lung segment per patient. In patients with systemic bronchial arterial supply, MR perfusion and multislice CT imaging differed in four of five patients in up to three segments per patient. Patients with systemic bronchial arterial supply had bronchial arteries ranging from 2.0 - 3.6 mm compared to the submillimeter diameters in pulmonary perfusion types.

Conclusion: Congenital and neoplastic pulmonary conditions require ultrafast MR imaging in order to successfully detect subtle and masked changes in lung perfusion patterns, especially in the systemic bronchial arterial supply. Presence of hypertrophied bronchial arteries indicated bronchial arterial perfusion with the subsequent need for high temporal resolution perfusion imaging of the pulmonary parenchyma.

C-0330

Multidetector CT of pulmonary vascular abnormalities in the adult

F. Triviño, A. Benito, G. Pérez, R. Ysamat, L. Zurera, M. Cara, M. Canis; ¹Cordoba/ES

Learning Objectives: To detail the anatomy and radiological features of unusual symptomatic vascular pulmonary lesions in the adult.

To emphasize the ability of multidetector CT in characterizing these lesions, guiding interventional therapy and avoiding unnecessary surgery.

Background: Multidetector CT is the modality of choice in depicting pulmonary vascular abnormalities, allowing their accurate characterization. High resolution enhanced 3D imaging provides a non-invasive method for the diagnosis of these lesions, avoiding the need for conventional angiography unless endovascular interventional procedures are required. Vascular pulmonary lesions in the adult are often symptomatic and can lead to dramatic situations requiring prompt diagnosis and treatment. Understanding the anatomy and radiological appearance of these lesions is essential in making the correct diagnosis.

Procedure Details: We reviewed all pulmonary vascular abnormalities detected in our department in the last four years. Multidetector CT led to the correct diagnosis in all cases. Angiography and interventional therapy was performed when necessary. Specific topics addressed include: intralobar sequestration, congenital pulmonary venolobar syndrome, pseudosequestration, pulmonary arteriovenous malformation, congenital and acquired occult main pulmonary artery, pulmonary

Scientific and Educational Exhibits

artery aneurysm, hematoma of pulmonary artery sheath, pulmonary venous varix, pulmonary vein anomalies and thromboembolic disease. Detailed anatomic-radiologic correlation and specific diagnostic criteria for each topic are revisited. Cross-sectional and 3D images are shown. Arteriography images are included when available.

Conclusion: Multidetector CT allows accurate diagnosis in vascular pulmonary lesions and facilitates optimal patient treatment. Knowledge of the radiological appearance of these entities is mandatory for its correct characterization.

C-0331

Identification of pulmonary vein variants by multidetector CT

C. Capuñay, PM. Carrascosa, M. Ulla, J. Carrascosa; Buenos Aires/AR

Learning Objectives: To illustrate a new application of 3D images in the evaluation of vein anatomy. To outline the advantages of this kind of non-invasive evaluation. To provide an overview of the spectrum of pulmonary vein variants.

Background: Anomalies in number and insertion of pulmonary veins (PV) are frequent in humans and their evaluation prior radiofrequency catheter ablation (RFCA) facilitates this anatomical based procedure.

Procedure Details: The anatomy of the PV were assessed in 110 patients admitted at the institution for coronary artery evaluation. CT scans were performed on a 16-row CT scanner (Brilliance 16; Philips Medical Systems) with the following parameters: 16x0.75 configuration, 1 mm slice thickness, 0.5 reconstruction interval, 140 kV, 450 mAs, pitch 0.24. ECG gated acquisitions were obtained at different moments of the cardiac cycle. Injection of 100 ml of iodinated contrast was performed by power injector.

Images were analyzed by 2D and 3D (volume rendering) reconstructions to assess the anatomy of the PV. Also the ostial diameters and branching patterns were determined.

Results: Sixty patients (54.5%) had two ostia for upper and lower lobe veins on the right side and 89 (81%) had two ostia for upper and lower lobe veins on the left side. 38 patients (34%) had three ostia and 12 patients (11%) 4 ostia on the right side. 18 patients (16.3%) has one ostium and 3 patients (2.7%) 3 ostia on the left side.

Conclusion: Multidetector CT is a valuable tool that allows detection of intra-patient and inter-patient anatomic variants of the PV.

C-0332

Detection of pulmonary embolism with unenhanced CT

R. Cobelli, M. Zompatori, E. Lombardo, C. Bnà, G. De Luca; Parma/IT

Objective: To evaluate the percentage of cases in which emboli can be detected in unenhanced scans and to identify the cases in which they appear hyperattenuating or hypoattenuating in comparison to the circulating blood.

Method: We performed an angio-CT before and after contrast injection on 140 consecutive patients, following clinical suspicion of pulmonary embolism. A radiologist analysed comparatively the examinations thus obtained. We analysed firstly the enhanced scan and, after detecting the thrombus, the unenhanced scan was evaluated.

Results: 51 exams were positive for pulmonary embolism; in 21/51 (41%) cases it was possible to identify the embolus even in the unenhanced scans; in particular in 10/21 (47.6%) cases the clots were hyperattenuating compared to the blood; in 5/21 (23.8%) cases hypoattenuating and in 6/21 (28.6%) cases were mixed hyper-hypoattenuating.

Conclusion: In a relatively high percentage of cases, above all those of central thromboembolism, it is possible to identify and characterize the clots, even in the unenhanced scans. The possibility of diagnosing pulmonary embolism without the use of contrast medium is of clinical importance as it could suggest the presence of pulmonary embolism in patients with non-specific cardiopulmonary symptoms and, through an analysis of the density and the morphology of the clot, similar to what may be observed via transesophageal ultrasound, it can provide information regarding the period in which the pulmonary embolism took place (acute or chronic pulmonary embolism).

C-0333

Evaluation of flow-related artefacts in the study of pulmonary embolism with multislice

R. Cobelli, M. Zompatori; Parma/IT

Objective: To evaluate the flow-related artefacts in CT exams performed to exclude pulmonary embolism.

Materials and Methods: We retrospectively analysed 98 CTs of the thorax performed for clinical suspicion of pulmonary embolism. In particular we analysed

the detection of flow-related artefacts that compromise the possibility of making a correct diagnosis of pulmonary embolism. All the exams were performed using bolus tracking and a collimation of 0.75 mm. The exam technique is described.

Results: Two type of artefacts are detected; the absence of contrast material in the pulmonary artery due to a transient interruption of contrast enhancement related to inspiration (present in 6/98 of the cases); and the second one (2/98) was created by the presence of poorly enhanced blood due to a local increase in vascular resistances (ie: atelectasis or pleural effusion). A complete iconography is illustrated.

Conclusion: In the first group, it was necessary repeat the scan to obtain correct opacification of the pulmonary vessels, while in the second group it is important to recognise the artefact to avoid the misdiagnosis of pulmonary embolism. In both cases it is necessary to repeat the scan to make a correct diagnosis.

C-0334

Elective bronchial artery embolisation for haemoptysis using spherical embolic agents

K. Malagari, D. Antonopoulos, J. Mitromaras, E. Alexopoulou, A. Sissopoulos, D. Shizas, D. Kelekis; Athens/GR

Purpose: To examine the efficacy of bronchial artery embolisation (BAE) with the use of newer embolic material.

Materials and Methods: Thirty-eight patients with a recent severe or massive haemoptysis (23 M, 15 F; mean age 48.3) underwent bronchial arteriography and were subsequently embolised electively. The underlying disease was cystic fibrosis (n = 5), bronchiectasis (n = 16), chronic fibrocystic lung disease (n = 9), complex hepatopulmonary infection (n = 1), postbullectomy (n = 2), and occult (n = 5). Embolic agents used included spherical embolic agents alone > 300 μ in 31 patients (Embospheres; Biosphere, Rockland, MA) combined with Gelatin sponge particles in 7 cases (Gelfoam; Upjohn, Kalamazoo, MI). A microcatheter was used in 9 of the patients while the remaining were catheterised with 4-5 F Cobra-shaped or Simmons catheters. Repeat bronchial arteriography was performed in 15 cases based on initial arteriography findings, extent of initial embolization and CT arteriography findings suggestive of bronchial artery dilatation. In 7 of these patients a repeat embolization was performed. No major complications were observed. Follow-up ranged from 5 to 44 months (mean: 26.2 months).

Results: On follow-up, relapse of haemoptysis was reported in 6 patients (2.3%), in two of whom it was severe. Recurrence after embolisation was correlated to chronic lung disease ($p = 0.04$) and active inflammation ($p = 0.005$).

Conclusion: Elective BAE with the use of newer embolic agents and superselective catheterization has very low intermediate recurrence rates. Active inflammation requires further treatment.

C-0335

Pre-test scores in patients suspected of having pulmonary embolism: Are they really useful before multidetector-CT examination?

A.A. Lemos, R. Castelli, D. Fortis, A. Guariglia, P. Biondetti, F. Porro; Milan/IT

Learning Objectives: To determine the usefulness of the most common clinical probability test performed before MDCT examination for pulmonary embolism.

Background: The high performance of multidetector-CT (MDCT) in the detection of pulmonary embolism (PE) has resulted in an increased workload at our department. In addition, several examinations are not justified because clinical indications are inadequate or insufficient.

Procedure Details: We evaluated 329 patients, 175 males and 154 females, ages 33-85 years (median 59 years) with an initial clinical work-up, which included: ECG, blood gas analysis, chest X-ray, and d-dimer levels. We performed the Wicki's, Well's, and Kline's scale of probabilities. We then obtained confirmation or exclusion of the diagnosis using MDCT and/or pulmonary scintigraphy. We divided the patients in two groups: Those with PE not confirmed (178 patients, group a), and those with PE confirmed (151 patients, group b). Our results were as follows: Wicki's scale: Low probability 29%, intermediate probability 44%, high probability 79%. Well's scale: Low probability 27%, intermediate probability 47%, high probability 82%. Kline's scale: Low probability 32%, high probability 61%.

Conclusion: None of the three scales yielded convincing results, because the percentage of confirmed PE was excessive in patients with low pre-test probability. The high demand for MDCT examinations may be justified in those patients with intermediate and high probabilities in which PE was confirmed.

Scientific and Educational Exhibits

C-0336

Thromboembolic complications after major orthopedic surgery: A 13-year register of 5607 patients

B. Bjørnarå, T. Gudmundsen, O. Dahl; Drammen/NO

Purpose: Our two recent studies examined "Late occurring clinical DVT in joint-operated patients" and "Risk of non-fatal pulmonary embolism after joint surgery in patients receiving in-hospital low molecular weight heparin prophylaxis". The present study examines the overall risk of venous thromboembolism after major orthopedic surgery.

Materials and Methods: A 13-year prospective registry of all patients undergoing major orthopaedic surgery (nailed hip fracture procedure, total hip and knee replacement surgery) at a Norwegian hospital between 1989 and 2001. Low molecular weight heparin was given routinely for about ten days. Patients with suspected pulmonary embolism underwent VP-scintigraphy or spiral CT. Patients with suspected DVT underwent ultrasonography and, if negative, venography.

Results: Out of 5607 operated patients, 64 had pulmonary embolism (incidence 1.1%) and 86 had DVT (incidence 1.5%). Only 7 patients had both pulmonary embolism and DVT. The overall incidence for thromboembolic complications was 2.6%. Average time to readmission for pulmonary embolism was 42 days after total hip replacement surgery, 25 days after nailed hip fracture procedure and 10 days after total knee replacement surgery. The average time to readmission for DVT was 32 days after total hip replacement, 37 days after nailed hip fracture and 26 days after total knee replacement.

Conclusions: For patients undergoing major orthopaedic surgery and only receiving in-hospital thromboprophylaxis, the incidence of pulmonary embolism and DVT remains elevated for 2-3 months. The different timing for developing pulmonary embolism and DVT suggests that these groups should be considered separately when determining the optimal thromboprophylaxis regimen.

Chest

Technical aspects

C-0337

Effective dose level from lung screening CT using auto exposure control

T. Koyama, M. Terada, M. Sato, M. Kobayashi, Y. Numaguchi, T. Horiuchi, J. Sekiguchi; Tokyo/JP

Purpose: The purpose of this study is to evaluate the effective dose level from Lung Screening CT using Automatic Exposure Control (AEC). AEC systems for CT are rapidly gaining widespread clinical use. These systems automatically adjust the tube current (mA) to improve dose utilization and/or to reduce variability of patient dependent image noise.

Materials and Methods: CT systems have recently implemented dose information display, such as CTDIvol and the DLP (dose-length product, in mGy.cm) on the operating consoles. The effective dose for CT examination is calculated from the DLP with the factor for converting into effective dose. We prospectively studied over 1,000 participants undergoing lung screening on 16-slice MDCT (Light-Speed16; GE Healthcare, Milwaukee, WI, USA). Each participant underwent scanning at Noise Index=30, single breath-hold, 1.25 x 16 mm detector configuration, 0.5 sec per rotation, pitch of 1.35: 1. Contiguous 2.5 mm thickness images were reconstructed.

Results: We confirmed the CT system provides various mA values along the z-axis during scanning, and maintains constant image noise. In screening exams, average effective dose was approximately 1.3 mSv, and was reduced by 30-40% as compared with fixed mA protocols. The same level of detectability for nodules in LSCT (Lung Screening CT phantom, Kyoto Kagaku) was confirmed with fixed mA and AEC protocols.

Conclusion: We conclude that AEC can achieve a significant reduction in dose without compromising diagnostic image quality. These results showed that AEC protocol produces sufficient diagnostic image quality compared with a conventional fixed mA technique.

C-0338

Diagnostic performance of a computer-aided diagnosis tool (CAD) for the detection of pulmonary nodules in low dose lung cancer screening CT

S. Giunta, S. Canitano, P.L. Ordonez, G. Vallati, M. Benassi, M. Crecco; Rome/IT

Purpose: To assess the diagnostic performance of a CAD system for automatic detection of pulmonary nodules using Multi Detector CT (MDCT) in lung cancer screening.

Materials and Methods: 80 dataset of MDCT (Somatom Plus 4\Volume Zoom, Siemens, Germany) low dose lung cancer screening from the Regina Elena I-ELCAP were submitted to an experimental CAD (syngo Lung Care CT, Siemens, Germany). The cases were reported independently by two chest radiologists in double blind report (DBR) and then in final version after the CAD evaluation. Each candidate nodule marked by CAD was analysed and evaluated as true positive (TP) or false positive (FP) by a consensus panel (CP). The CP was the DBR plus CAD analysis plus a second consensus reading by the two radiologists during the CAD analysis.

Results: The CP evaluated 369 nodules as TP. The CAD tool detected 1314 candidate nodules. 243 (18.50%) were classified as TP and 1071 as FP (81%). 12 nodules detected by CP (3.7%) were not detected by either the DBR or CAD. 67 nodules were detected both by CAD and DBR (18.1%), 176 were detected only by CAD (47.7%) and 114 were detected only by DBR (30.9%). DBR sensitivity was 50%, CAD sensitivity was 68% and system CAD-DBR sensitivity was 97%.

Conclusion: The CAD tool increases the number of pulmonary nodules detected, reducing the number of missed nodules. This method appears to play a supportive role, providing routine real-time clinical assistance to interpret chest MDCT studies of a lung cancer screening program.

C-0339

Microscopic findings in various lung diseases with peripheral lung imaging using micro focus X-ray CT

H. Ikura¹, K. Shimizu², Y. Yasuhara¹, M. Miyagawa¹, T. Mochizuki¹, H. Ebara¹, K. Ueno³, T. Nagareda⁴; ¹Ehime/JP, ²Kanagawa/JP, ³Tokyo/JP, ⁴Hyogo/JP

Purpose: Although synchrotron radiation (SR) CT can visualize fine structures of peripheral lung with approximately 10 µm of spatial resolution, it is difficult to access the largest SR facility. The objective of this study was to evaluate the potential of micro focus X-ray CT (MF-XCT), located in a corner of an ordinary laboratory, for peripheral lung imaging, comparing with pathology and SRCT imaging.

Scientific and Educational Exhibits

Methods and Materials: Postmortem human lungs with normal and pathologic states were inflated and fixed by Heitzman's method. Each specimen was cut down to small cylindrical shape with 6-mm diameter and 20-mm height for adaptation to the FOV of MFxCT system. The CT images were obtained using MFxCT system (MCT-CB100MF, Hitachi Medical Corp., Japan). Thereafter, microscopic sections were obtained with hematoxylin and eosin. Finally, MFxCT images were compared with the microscopic and SRCT images.

Results: MFxCT could clearly visualize the peripheral lung structures including alveolar walls with approximately 10 µm of spatial resolution as well as SRCT. MFxCT also demonstrated the pathologic features (destruction and enlargement of peripheral airspace in emphysema; destruction and micro honey-comb due to fibrosis in pulmonary fibrosis; apparent thickening of alveolar wall and filling within alveoli in pulmonary hemorrhage). Each MFxCT image of the normal and pathologic lung specimen correlated with the corresponding histopathologic and SRCT image, point to point.

Conclusions: MFxCT provided peripheral lung images with approximately 10 µm of spatial resolution non-invasively. Therefore, MFxCT could demonstrate the various diagnosable features in an ordinary laboratory to differentiate on microscopic order.

C-0340

Parallel imaging in lung MR

F. Molinari, S. Gaudino, D. Spina, T. Pirroni, L. Bonomo; Rome/IT

Learning Objectives: 1. To provide an extensive review of all the technical and methodological problems related to lung MR; 2. To illustrate strategies of optimization both for morphologic and functional imaging of lung; 3. To investigate the benefits of using parallel imaging in lung MR and fully explain the technical basis for it.

Background: MR imaging of lung is mainly limited by several technical and methodological problems, including a very weak signal of the lung tissue due to a low proton density, air-tissue interfaces, flow and diffusion, relaxation effects, cardiac and respiratory motion. Very short T2 values are therefore commonly observed, requiring optimised and dedicated sequences to perform both morphologic and functional studies.

Procedure Details: Single-shot Fast Spin Echo (SS-FSE) sequences, either with cardiac or respiratory triggering, are most effective in producing anatomic images of lung parenchyma. MR functional studies of lung, such as oxygen-enhanced MR imaging and non-invasive studies of lung perfusion, can be performed applying Inversion Recovery pulses to SS-FSE sequences. Parallel imaging (PI) represents a useful technical approach to speed up acquisition time and increase spatial resolution of MR images. An exhaustive explanation of potential advantages and limits of implementing PI on lung MR, in both morphologic and functional imaging, will be provided.

Conclusion: Parallel imaging in lung MR, as in other organs, improves image quality and reduces scan time. Despite some PI-related artefacts, this technical approach still provides advantages over conventional methods to overcome the many limitations of lung MR imaging.

C-0341

withdrawn by authors

C-0342

Automatic exposure control in low-dose chest CT with 16 slice MSCT

S. Gomi, M. Suzuki, S. Doi, H. Daisaki, T. Murano, K. Mayumi, Y. Muramatsu, S. Tsukagoshi, N. Moriyama; Tokyo/JP

Learning Objectives: To determine the optimal scan conditions for CT automatic exposure control (CT-AEC) and to understand how to use a phantom for Low-Dose Chest CT.

Background: Using 16-slice MSCT, Low-Dose Chest CT (scan conditions: 120 kV, 30 mA, 0.5 s/rotation, Pitch factor 11, 1 mm-slice) has been executed at our institution. Image quality depends on the individual patient and slice position. However, CT-AEC is not generally used in medical screening examinations because of the few changes of tube current in Low-Dose CT. Therefore, the present study was conducted to determine the optimal scan conditions for CT-AEC.

Procedure Details: A chest CT phantom (LSCT-001, Kyoto-Kagaku) was scanned to obtain the DLP (Dose Length Product) under routine scan conditions (DLP-routine). Scan conditions equivalent to DLP-routine were obtained using CT-AEC at 80, 100, and 120 kV with or without an additional filter. The phantom was scanned under these conditions to determine the minimum diameter of simulated tumors that could be visualized. And the maximum tumor was measured the CNR (Contrast-Noise Ratio). The minimum diameter of tumors visualized at the lung apex, tracheal bifurcation, and lung base was 4 mm for all scan conditions.

The CNR values in each region were 1.9, 2.6, and 2.9 using routine scan conditions, with high values obtained only with a filter at 100 or 120 kV.

Conclusion: Using CT-AEC, the optimal exposure dose can be obtained at 100 or 120 kV with a filter.

C-0343

Automated diagnosis of disease using texture analysis in CT of the lungs

S.P. Prabhu, J. Malone, L. Carrivick, J. Rossiter, P.R. Goddard; Bristol/UK

Purpose: To evaluate the feasibility of a computer-aided diagnosis (CAD) system to distinguish between normal lung and 5 patterns of disease commonly seen on MDCT scans of the lungs.

Method and Materials: Scans of 100 patients were gathered from daily practice and the lung fields identified using a fully automated segmentation algorithm where possible and semi-automated in the more unusual cases. Representative areas of normal tissue, various degrees of fibrosis, emphysema, consolidation and ground glass opacification were highlighted by radiologists. We used texture analysis to train 3 standard machine learner programmes. Each of the scans were classified in 3 different sized grids. The results from the block sizes of 16, 8 and 4 pixels were fused and a final classified image for each of the scans was produced. The results in each complete set of scans were combined to produce a bullet point report for each subject elaborating location and extent of the disease in question.

Results: We demonstrate 90% accuracy of the CAD programme in cases of normal tissue and severe disease when compared with large areas of selected scans labelled by experts. There is only a 62% agreement in more subtle and equivocal cases. We further compared computer generated bullet point reports to the actual reports and again achieved close to 90% correlation in the more clear-cut cases.

Conclusions: We demonstrate the feasibility of a fully automated system for diagnosis of lung disease on MDCT of the chest.

C-0344

Internet-based tool for differential diagnosis of HRCT findings in non-HIV patients with cancer presenting with lung diseases

C. de Bazelaire, S. Vignot, O. Mathieu, A.-M. Zagdanski, P. Bourrier, E. de Kerviler, J. Frijla; Paris/FR

Learning Objectives: To facilitate interpretation of lung HRCTs in patients with cancer presenting with lung disorders. To propose an internet-based tool for differential diagnosis, according to initial disease, treatments, HRCT patterns, and symptoms.

Background: Lung diseases are common in non-HIV patients under treatment for cancer. HRCT features lack specificity and differential diagnosis is tricky. Radiologists should correlate differential diagnoses (infection, non-infection), side-effects of treatments and clinical findings: gram-negative bacillus infection with potential septic shock occurs in the setting of transient neutropenia, while lymphopenia leads to *pneumocystis jiroveci* or viral pneumonias. HRCT findings should be interpreted carefully: Although nodules surrounded by ground-glass opacities suggest invasive aspergillosis in prolonged and severe neutropenia, halo sign also reflects intracellular bacterial infections (mycobacteria, *legionella*) in prolonged lymphopenia.

Procedure Details: HRCT findings were classified into alveolar consolidation, ground glass opacities, septal thickening, micro-nodules, nodules, and bronchiolar abnormalities. Patients with similar immune defects were pooled, based on type and duration of anticancer-therapy (induction, consolidation chemotherapies, intensification with autologous and allogeneic bone marrow transplants). Clinical course i.e. acute and sub-acute onset, or chronic evolution was also considered. For each subgroup, differential diagnoses seen in our institution or found in literature were recorded. This tool performed an analysis with patient's information and provided relevant diagnoses.

Conclusion: This internet-based educational tool is still evolving, along with inclusion of new patients. This may lead to the addition of new differential diagnoses and refinement of prevalence values. It helps young radiologists in our institution, to avoid uncommon differential diagnoses and to warn when life-threatening conditions are present.

C-0345

Time-resolved parallel 3D MRA of the lung: SNR improvement using correlation analysis

C. Fink, M. Bock, R. Buhmann, S. Ley, M. Puderbach, C. Plathow, H.-U. Kauczor; Heidelberg/DE

Purpose: Time-resolved parallel 3D MRA allows comprehensive imaging of the pulmonary vasculature and lung perfusion. A potential drawback of time-resolved

Scientific and Educational Exhibits

parallel 3D MRA, however, is the low inherent signal-to-noise ratio (SNR), which is further decreased by subtraction of a pre-contrast image. The aim of this study is to assess the SNR increase of a correlation analysis post-processing over conventional image subtraction.

Methods and Materials: 44 patients were examined with a time-resolved parallel 3D MRA (TR/TE/α: 0.8/1.9 msec/40°; GRAPPA; acceleration factor: 2; scan time per 3D data set: 1.5 sec; 0.1 mmol/kg b.w. Gd-DTPA). Pulmonary arteriograms, venograms, and perfusion-weighted data sets of the lung were calculated from the time-resolved MRA data using image subtraction and correlation analysis. In the correlation analysis the unnormalised correlation coefficient of the signal in each pixel and the signal from a manually selected target region (lung artery or vein, lung parenchyma) was calculated. For comparison, the SNR of the processed image data was measured.

Results: Correlation analysis achieved a significantly higher SNR than image subtraction: The mean SNR of the image data computed by correlation analysis and image subtraction was 484 vs. 266 for the arteriograms, 464 vs. 273 for the venograms, and 29 vs. 16 for the perfusion weighted data sets of the lung ($p < 0.0001$).

Conclusion: Correlation analysis is a useful algorithm for the processing of time-resolved parallel 3D MRA data. Compared to simple image subtraction, correlation analysis achieves a ~1.8-fold higher SNR.

C-0346

Correlation between automatic vs. manual lung nodule assessment

C. Capuñay, P.M. Carrascosa, M. Ulla, J. Vallejos, J. Carrascosa;
Buenos Aires/AR

Purpose: To determine the correlation between an automatic lung nodule assessment software and manual measurement.

Methods: Thirty patients with the suspected diagnosis of solitary pulmonary nodule were evaluated. CT exams were performed on a 16-row CT scanner (Brilliance 16; Philips Medical Systems) using 1 mm slice thickness and 0.5 mm reconstruction interval. The images were evaluated in the axial plane to identify the lung nodule and these selected images were then reprocessed on a workstation. Images were analyzed by two different operators. Operator 1 performed the measurement with an automatic nodule assessment software. Operator 2 performed the measurement using bi-dimensional and three-dimensional images. The volume of the nodule and its diameters (x, y, z axis) were determined. The correlation between the two measurements were assessed using the Spearman's rank correlation coefficient (Rho).

Results: Thirty-three nodules were diagnosed. For the volume assessment, Rho was 0.972 (0.945, 0.986). For the x, y and z nodule diameters, Rho was 0.953 (0.907, 0.977), 0.944 (0.888, 0.972) and 0.966 (0.931, 0.983) respectively.

Conclusion: There was good correlation between the manual and automatic lung nodule measurements.

C-0347

Intra-observer variability of automatic lung nodule assessment software

C. Capuñay, P.M. Carrascosa, M. Ulla, J. Vallejos, J. Carrascosa;
Buenos Aires/AR

Purpose: To determine the intra-observer variability of an automatic lung nodule assessment software.

Methods: Thirty patients with the suspected diagnosis of solitary pulmonary nodule were evaluated. CT exams were performed on a 16-row CT scanner (Brilliance 16; Philips Medical Systems) using 1 mm slice thickness and 0.5 mm reconstruction interval. The images were evaluated in the axial plane to identify the lung nodule and these selected images were then reprocessed on a workstation using an automatic nodule assessment software. The volume of the nodule and its diameters (X, Y, Z axis) were determined twice, on different days and by the same operator, using the same baseline parameters. The intra-observer variability of the software was assessed using the kappa coefficient.

Results: Thirty-three nodules were diagnosed. For the volume assessment, kappa was 0.853 (0.633, 1.072). For the x, y and z nodule diameters, kappa was 0.931 (0.716, 1.146), 0.910 (0.691, 1.128) and 0.894 (0.682, 1.106) respectively.

Conclusion: The automatic lung nodule assessment software evaluated was demonstrated to be a reproducible method, with low variability between the two measurements.

Chest

Miscellaneous

C-0348

F-18 FDG microPET imaging after percutaneous radiofrequency ablation (RFA) in normal rabbit lung

T. Okuma, T. Matsuoka, T. Okamura, Y. Wada, A. Yamamoto, Y. Oyama, K. Koyama, Y. Watanabe, Y. Inoue; Osaka/JP

Purpose: RFA has been recently used to treat unresectable lung cancer. RFA causes inflammatory change in surrounding normal tissue. Therefore we evaluated thermal effects of normal rabbit lung after RFA using FDG microPET which has a high resolution (1.85 mm).

Methods and Materials: Twenty-one Japanese white rabbits received CT-guided RFA. A LeVeen Needle Electrode was inserted and ablated until maximum impedance. Eleven rabbits underwent microPET scan on day 1, weeks 1, 2, 4, and 8, after RFA. The other 10 rabbits were followed by CT. For microPET, following transmission scan, emission data were acquired at early phase (40-60 min) after intravenous 18F-FDG injection. Ablated lesion-to-muscle (A/M) ratio was calculated to evaluate microPET images. We compared FDG uptake, CT image and pathological findings after RFA.

Results: A/M ratio on day 1, in weeks 1, 2, 4, and 8, after RFA was 2.7 ± 0.73 , 3.47 ± 0.09 , 3.37 ± 1.14 , 2.57 ± 0.42 , and 1.73 ± 0.01 , (mean \pm SD), respectively. A/M ratio at 1 and 2 weeks was significantly higher than at 4 and 8 weeks ($P < 0.05$). 1 and 2 weeks after RFA, ablated lesions showed rounded opacity on CT, and coagulation necrosis, hemorrhage, and inflammation on histology. 4 and 8 weeks after RFA, opacity decreased on CT and inflammation was reduced on histology.

Conclusion: Thermal damage of normal lung due to RFA affects FDG uptake 1 and 2 weeks after RFA. Decreases in FDG uptake on follow-up microPET correlated with pathological findings after normal lung RFA.

C-0349

CT-guided radiofrequency thermal ablation (RFA) of primary and metastatic lung tumours

L. Thanos, S. Mylona, N. Sakaridis, E. Karahaliou, A. Kokkinaki, N. Batakis; Athens/GR

Purpose: To present the technique, the effectiveness and the possible complications of RFA of primary and metastatic lung tumors.

Materials and Methods: During an eighteen-month period, we performed 65 RFA sessions under CT-guidance in 48 lesions (25 metastatic and 23 inoperable primary) on 35 patients with lung tumors. We used two different types of generators, RITA (hooked electrode) and MIRAS (spiral electrode). The ablation lasted 15-18 minutes.

The procedure was performed after analgesic treatment and local anaesthesia at the point of entry. Follow-up with dual-phase contrast enhanced spiral CT was performed immediately after the procedure and at 1-, 6- and 12-month intervals.

Results: Total necrosis was observed in 19 (82.6%) primary and in 19 (76%) metastatic lesions. In 4 (17.4%) patients with primary and in 6 (14%) with metastatic lesions that demonstrated partial necrosis, we proceeded to a second session. The 6-month CT follow-up demonstrated recurrence in 7 (14.5%) lesions (4 primary and 3 metastatic), which were treated with a new RFA session. We had minimal complications of two pneumothoraces and one hemorrhage. Two patients died after one year.

Conclusion: CT-guided RFA may provide a safe and effective alternative treatment as well as a good quality of life in patients with lung tumors.

C-0350

F-18 FDG-microPET evaluation after CT-guided radiofrequency ablation (RFA) in rabbit VX2 lung tumor model

T. Okuma, T. Matsuoka, T. Okamura, Y. Wada, A. Yamamoto, Y. Oyama, K. Koyama, K. Nakamura, Y. Watanabe, Y. Inoue; Osaka/JP

Purpose: To evaluate therapeutic effects of RFA for implanted lung VX2 tumor, using FDG microPET with a high resolution.

Methods and Materials: Six Japanese white rabbits received RFA for normal lung and underwent microPET on 1 day after RFA (group A). VX2 was implanted into 11 rabbits lung divided into 2 groups, 6 underwent microPET without RFA (group B), and 5 had microPET on day 1 after RFA (group C). For RFA, a LeVeen Needle Electrode was inserted and ablated until maximum impedance. For microPET study, dynamic emissions were acquired for 120 minutes after 18F-FDG

Scientific and Educational Exhibits

injection. Images were reconstructed at early (40-60 min.) and delayed phases (100-120 min.), and ablated lung-to-muscle (A/M), tumor-to-muscle (T/M), and ablated tumor-to-muscle (TA/M) ratios were calculated. FDG uptake and pathological findings were compared.

Results: In early phase, A/M, T/M, and RFA central and peripheral zone of TA/M ratios were 2.7 ± 0.73 , 6.05 ± 1.82 , 0.76 ± 0.33 , and 3.01 ± 0.79 , and in delayed phase, 2.9 ± 0.53 , 7.6 ± 2.26 , 0.84 ± 0.58 , and 3.54 ± 1.12 (mean \pm SD), respectively.

In groups A and C, histological findings were central coagulation necrosis, and peripheral inflammation, and A/M and TA/M ratios between early and delayed phases were not significantly different. A/M and peripheral zone of TA/M ratios were not significantly different. In group B, histology showed viable cells. T/M ratio of delayed phase was significantly higher than that of early phase. TA/M ratio of central zone was significantly lower than T/M ratio ($P < 0.05$).

Conclusion: Change in tumor FDG uptake on microPET was useful for evaluating early therapeutic effects after RFA.

C-0351

Chest MR imaging in post-mortem examinations: Autopsy imaging system

S. Kandatsu, R. Kishimoto, S. Komatsu, H. Ezawa, H. Tsuji; Chiba-ken Chiba-shi/JP

Purpose: To evaluate the diagnostic accuracy of chest MR and CT imaging performed immediately after death.

Materials and Methods: Twenty-five patients with malignant diseases underwent whole body MR and CT imaging within 24 hours after death. We autopsied them immediately after the examinations. They included 8 cases of hepatoma, 7 cases of lung carcinoma, 3 cases of head and neck melanoma, 2 cases of uterine carcinoma, 2 cases of pancreas carcinoma, one case of head and neck adenocarcinoma, one case of esophageal carcinoma, and one case of chondrosarcoma, respectively. We compared the images of MR and CT with the results of the autopsies.

Results: We precisely found pleural effusion, pulmonary nodules of more than 5 mm in diameter, hemorrhage, chest wall tumor invasion, mesenchymal thickening, and bone invasion on chest MR imaging. Almost all of abnormal lesions recognized on CT imaging were found on MR imaging. On MR imaging, we recognized more abnormal lesions which were not found on CT imaging.

Conclusion: Post mortem chest MR imaging in autopsy imaging system has diagnostic value and is superior to chest CT imaging.

C-0352

A comparative experimental study of the in-vivo efficiency of saline-enhanced bipolar versus monopolar pulmonary radiofrequency ablation

S.-H. Park, G.-Y. Jin, Y.-M. Han, H.-H. Park; Jeon-ju/KR

Purpose: To compare the in-vivo efficiency of a saline-enhanced bipolar radiofrequency (RF) system with monopolar RF by assessing the variable factor and dimensions of RF-created coagulation necrosis in rabbit lung.

Materials and Methods: In 15 rabbits, 15 RFA lesions were produced using a one or two 16-gauge open-perfused electrodes with a 1-cm active tip at an interelectrode distance of 1 cm. Rabbits were assigned to one of five groups: Group A ($n = 3$), 0.9% NaCl at a rate 30 cc/hr in monopolar mode; Group B ($n = 3$), 5.8% NaCl at a rate 30 cc/hr in bipolar mode; Group C ($n = 3$), 5.8% NaCl at a rate 15 cc/hr in bipolar mode; Group D ($n = 3$), the 0.9% NaCl at a rate 30 cc/hr in bipolar mode; Group E ($n = 3$), 0.9% NaCl at a rate 15 cc/hr in bipolar mode. RF energy was applied for 5 minutes and the temperature of the electrode tip was automatically measured. The dimensions of the thermal lesions in gross specimens were compared between the groups.

Results: The mean diameter of the thermal lesions was larger in the bipolar mode (30.9 ± 4.4 mm) than in the monopolar mode (22.5 ± 3.5) and the difference was statistically significant ($p < 0.05$). In bipolar mode, the dimensions of the thermal lesions was larger at a rate 15 cc/hr (34.2 ± 4.0 mm) than at a rate 30 cc/hr (27.6 ± 0.1 mm) and the difference was statistically significant ($p < 0.05$).

Conclusions: Using an open perfusion system, bipolar RFA more efficiently created larger area of thermal ablation than monopolar RFA.

C-0353

Saline-enhanced radiofrequency ablation for treating inoperable non-small cell lung malignancy

G.-Y. Jin, Y.-M. Han, Y.-C. Lee, C.-S. Kim, G.-H. Chung, S.-H. Chung, Y.-G. Kim; Jeon-ju/KR

Purpose: To assess the technical feasibility, safety, and complications of saline-enhanced radiofrequency (RF) ablation for treating inoperable non-small cell lung malignancy.

Materials and Methods: From December 2003 to February 2004, eleven patients (mean age, 73.5 years; range, 67-77 years) who had non-small cell lung malignancy ($n = 10$) or metastatic lung tumor ($n = 1$) underwent RF ablation with HiTT system (Berchtold®) under CT guidance. Patients were either non-surgical candidates because of advanced stage and/or co-morbid processes ($n = 10$), or refused surgery ($n = 1$). Tumor diameter ranged from 2 cm to 6 cm (4.1 ± 1.34 cm). The procedure was performed as palliative therapy for 11 patients. Contrast-enhanced CT was performed immediately, at 1 month, and at 3 months to evaluate response to RF therapy.

Results: The total duration of RF application ranged from 12 minutes to 70 minutes (mean: 32.5 ± 7.5 minutes) per each session. The mean numbers of needle electrode insertions through the mass was 1.9 (range: 1-3). The diameter of the treatment zone was larger (4.78 ± 1.30 cm) than that of the tumor, as ablated adjacent lung tissue had a similar appearance to the ablated tumor (initially 4.1 ± 1.34 cm). There were two major complications (2/11: 18.2%) including hemoptysis, and one hemothorax that required thoracostomy.

Conclusion: In this preliminary study, saline-enhanced RF ablation appears to be a safe and time-saving procedure for the treatment of inoperable non-small cell lung malignancy.

Scientific and Educational Exhibits

Computer Applications

C-0354

Towards standardization of hanging protocols for imaging display

E. Avraham; Plano, TX/US

Learning Objectives: To demonstrate limitations of current propriety hanging protocols (HP) for laying medical images on display workstations. To present the new standardization of "Hanging Protocols" for automatic layout of the medical Images based on user preferred methods, and display workstation capabilities. To demonstrate HP clinical use cases for chest X-ray and neurosurgery planning. To elucidate needs and opportunities to optimize the medical imaging reading workflow via standardized HP.

Background: Current propriety HPs aren't supporting all the user preferred layout methods. The supported HP varies among vendors, so there is no consistent imaging layout among different display workstations. The DICOM standard HP supplement resolves these HP limitations and optimizes automatically and consistently the medical imaging orientation and display positioning. The viewing methods are selected upon user layout preference and display device capability. **Procedure Details:** This educational exhibit includes but isn't limited to (1) demonstrating current propriety HP limitations, (2) presenting the DICOM standard HP supplement for automatic & consistent medical imaging layout, (3) demonstrating examples for X-ray imaging layout and Neurosurgery planning, (4) Proposing innovation for the current standard HP data model to support 3D imaging layout and orientation.

Conclusion: This HP standardization improves the medical imaging reading practice in several domains: 1. Orienting properly images before displaying. Lays out images automatically, based on user preferences, and displays device capabilities. 2. Standard HPs can be reused on different workstations (from different vendors) with similar capabilities, keeping the consistency on layout images on different display devices.

C-0355

Computer-assisted diagnosis of thyroid nodules malignancy risk

S. Tsantis¹, D. Glotso², I. Kalatzis², N. Piliouras², P. Spyridonos², N. Dimitropoulos², G. Nikiforidis², D. Cavouras²; ¹Patras/GR, ²Athens/GR

Purpose: To provide definite diagnosis of thyroid nodule malignancy risk factor, ultrasound scans are usually combined with the invasive Fine Needle Aspiration (FNA) examination. To prevent unnecessary invasive interventions, a computer-assisted diagnosis system is introduced for the automatic discrimination of low from high-risk thyroid nodules based solely on the quantitative analysis of ultrasound images.

Methods and Materials: Clinical material comprised of 120 ultrasound images from 120 pathologically confirmed cases of thyroid nodules (74 low-risk and 42 high-risk). An experienced physician (N.D) delineated the boundary of each nodule employing a custom developed in C++ software. Tumour malignancy was encoded in a set of 40 textural features, which fed a Probabilistic Neural Network classifier, designed to automatically discriminate low from high-risk cases.

Results: Maximum accuracy (96.7%) was obtained using three textural features (namely mean value, contrast and sum of squares variance) that describe nodule echogenicity, the presence or absence of calcifications and the intra-nodular vascular spots. Sensitivity (detection of high-risk cases) was 98.7% whereas specificity (discrimination of low-risk cases) was 92.8%.

Conclusion: The proposed system could be used as a second opinion tool to the radiologist for avoiding the risk of excessive FNA examination, thus decreasing the time/cost of diagnosis and the need for patients to undergo invasive examination.

Acknowledgements: The present research was carried for the project "Computer-based system for the automatic diagnosis of thyroid nodule cancer" co-funded by 75% from the European Union and 25% from the Greek Government under the framework of the Education and Initial Vocational Training Program "Archimedes".

C-0356

Three-dimensional stereoscopic abdominal MR angiography as an educational tool for medical students

T. Yamagishi¹, K.H. Höhne², K. Abe¹; ¹Tokyo/JP, ²Hamburg/DE

Purpose: It is important task for medical school lecturers to teach thorough knowledge of three-dimensional (3D) extent of the vascular structure. While in classical medicine, anatomical knowledge is represented in textbooks and atlases,

present-day computer assisted technique allows precise and realistic rendering of the morphological structure. We made use of MR angiography data of clinical cases and created stereoscopic images for the purpose of practical education.

Methods and Materials: Clinical image data of 10 examinees were obtained by routine abdominal 3D-VIBE (volumetric interpolated breath-fold examination) protocol (arterial phase after dynamic infusion of Gd-DTPA). A Siemens Avanto (1.5 T) scanner was used. Data sets were imported into the VOXEL-MAN program (Institute of Medical Informatics, University Hospital Eppendorf, Hamburg, Germany). Stereoscopic surface-rendered images were created from the segmented volume data. The panoramic sequential stereoscopic images of 3D angiography were evaluated for the value of educational benefits by a questionnaire survey, which was done by forty medical students.

Results: Ninety-three percent of the students evaluated the resulted images as excellent for medical education. The most advantageous benefit was getting a chance to know well about the 3D extent of the interested vascular structures. Most of them pointed out that these kinds of knowledge could hardly be grasped by non-stereoscopic image presentation.

Conclusion: Stereoscopic viewing yielded an exact 3D observation of the abdominal vascular structure. Real time rendering of the stereoscopic images could be performed by VOXEL-MAN. Using the data of clinical cases gave an impact on medical students. We could achieve improved educational outcome.

C-0357

withdrawn by authors

C-0358

Virtual contrast injection: A software tool for selective visualization of vessel structures

A. Löfväng¹, X. Tizon², A. Persson¹, G. Wiklund¹, Ö. Smedby¹; ¹Linköping/SE, ²Uppsala/SE

Learning Objectives: To understand the basic principle and potential clinical use of the virtual contrast injection algorithm (concurrent greyscale connectedness) for separation of overlying vessel structures from each other.

Background: When applying rendering methods like Maximum Intensity Projection (MIP) in both Computed Tomography Angiography (CTA) and Magnetic Resonance Angiography (MRA), a frequent problem is the superposition of adjacent vascular structures, e.g. arteries and veins in contrast-enhanced MRA or coronary arteries and heart chambers in CTA. The virtual contrast injection is a post-processing algorithm for such situations that allows unwanted vascular structures to be eliminated.

Procedure Details: The input data demonstrated here are high-resolution CTA images of the heart. In an interactive seeding step, the user marks with "seeds" in different colours, both coronaries, the heart chambers and surrounding structures. As the algorithm is started, the colours of the seeds are propagated between adjacent voxels, along with the grey-scale values of voxels passed on the way, until each voxel is labelled with the colour of the seed with which it is most strongly connected. Each vessel tree may then be displayed separately, and the most appropriate projection may be selected. In this exhibit, the viewer is able to interactively choose his/her favourite projection with the mouse (using Quicktime VR).

Conclusion: Virtual contrast injection can be used for display of vessels such as the coronaries in an angiographic format familiar from invasive angiography. The ability to interactively selecting optimal projections angles after the examination makes CTA an attractive alternative to invasive angiography.

C-0359

EMIT: Digital multilingual medical radiation physics dictionary

M. Stoeva¹, S. Tabakov²; ¹Plovdiv/BG, ²London/UK

Purpose: The main objective for the development of the Digital Multilingual Medical Radiation Physics and Engineering Dictionary was to provide a common tool for better understanding and improvement of the quality of the education and service in the field of Medical imaging.

Methods and Materials: Based on a case study, several thousand most common terms covering ionising and non-ionising radiation were collected by an interdisciplinary team. The further development of the software was conducted using MS Visual Basic 6. The Medical Physics Dictionary was developed under the European Medical Imaging Technology Training (EMIT) project, supported by Grant 308 of the EC program Leonardo da Vinci.

Results: The dictionary incorporates a large database of medical radiation terms in 5 European languages (English, French, German, Italian, Swedish). It also

Scientific and Educational Exhibits

provides tools for cross translation, sorting, typing prediction, analysis of coincidence, user's manual and help modules. The dynamic structure can easily be modified to broaden the range of the terms and languages. The Medical Physics EMIT Dictionary is now available on CD.

Conclusion: The ongoing process of development of common European standards for education and training in the field of medical radiation serves as a basis for the development of the Digital Medical Radiation Physics EMIT dictionary. The dictionary is now available throughout the world in all 65 countries using the EMIT training materials.

C-0360

Integration of electrical mapping and multi-detector CT imaging of left atrium and pulmonary veins for atrial fibrillation ablation

M. Centonze, A. Cristoforetti, F. Ravelli, M. Del Greco, F. Dalla Palma, G. Nollo; *Trento/IT*

Purpose: Correlation of electrical patterns and real anatomical structure of the atria remains an important challenge for successful radio-frequency ablation of atrial fibrillation. Aim of this study is the three-dimensional (3D) anatomic reconstruction of the left atrium (LA) and pulmonary veins (PVs) and its fusion with LA electrical maps.

Method and Materials: The LA and PVs of nine consecutive patients with atrial fibrillation (9 men, 56.9 ± 9 years) undergoing electrophysiological study for PVs ablation were previously examined with 16-slices spiral CT (MX 8000 IDT, Philips). Source images (0.75 mm slice thickness) were acquired by retrospective ECG-gating (75% of cardiac cycle) with temporal resolution = 210 ms. A specific method based on marker-controlled watershed segmentation was developed for 3D cardiac reconstruction. This allowed to separate the surface rendering of LA and PVs proximal branches from the other overlapping structures of the heart. Successively, electro-anatomic mapping (CARTO®, Biosense Webster) of LA and PVs ostia was performed.

Results: CARTO® maps were successfully registered on the 3D LA inner surface minimizing the residual error by a stochastic relaxation approach with a final error (distance of CARTO® coordinates to 3D LA surface) ranging from 2.03 to 3.00 mm. The fusion of the electrical maps with the 3D LA reconstruction was achieved by radial basis function interpolation.

Conclusion: Fusion of 3D anatomical images of LA and PVs with electrical maps is feasible. Pre-ablation procedure Multi-Detector CT examination may constitute a significant support for mechanism investigation and treatment of atrial fibrillation.

C-0361

Computed tomography angiography of the coronary arteries with virtual contrast injection

A. Löfving¹, X. Tizon², A. Persson¹, G. Wiklund¹, Ö. Smedby¹; ¹*Linköping/SE*, ²*Uppsala/SE*

Purpose: Computed Tomography Angiography (CTA) is an attractive non-invasive alternative to invasive angiography but has had limited use in the coronary arteries due to resolution and visualization difficulties. Maximum intensity projection (MIP) is frequently used in other domains but is difficult to apply in the heart with numerous overlying contrast-filled structures. The purpose of this feasibility study was to ascertain whether virtual contrast injection, originally proposed for MR angiography, can visualize the coronaries in CT datasets.

Methods: Ten patients were examined after i.v. contrast injection in a 16-detector CT scanner (Siemens Sensation 16) with collimation 16×0.75 mm, reconstructed slice thickness 1 mm and increment 0.5 mm. The virtual contrast injection (concurrent greyscale connectedness) was implemented in Java on a standard PC using the open-source ImageJ platform. Rendering of the right and left coronary separately was made with MIP and volume rendering (VRT).

Results: Images similar to invasive angiography were obtained in all 7 projections used in the clinical routine of our institution (3 for the right and 4 for the left coronary). In addition, the observer has the possibility to freely select an optimal projection (as demonstrated interactively in this digital poster). Typical time for interaction (vessel seeding) was 30 min and for processing 10-15 min.

Conclusion: CTA with subsequent virtual contrast injection can visualize coronary arteries in a mode similar to invasive angiography. After validation in larger materials, this may become a clinically useful non-invasive alternative for examination of coronary artery morphology. (Supported by Siemens Medical)

C-0362

Open source DICOM archive

V. Porod, J. Novotny, D. Vedlich, D. Kautznerova, M. Hajek; *Prague/CZ*

Purpose: This work describes building of the full-functional DICOM archive using open source applications.

Methods and Materials: All applications, which are necessary for DICOM files archiving are available as Open Source. The Open Source means, that you can download the source code of this applications. Having the source code, you can change the functionality of the application to fit your own requirements. For operating DICOM we used DICOM TOOLKIT from Oldenburger Forschungs- und Entwicklungsinstitute für Informatik-Werkzeuge und Systeme (OFFIS). To keep the database of pictures we used MySQL database server and for the web based pictures access we used Apache web server with PHP module. We also used the very popular open source operating system LINUX. The archiving software was running on DELL server with 2 Xeon (3 GHz) processors, 2 GB RAM and the external harddisk array with total capacity 3 TB. The source of DICOM data was CT SIEMENS SENSATION 16, with the output size approximately 180 000 GB per month. CT was connected with archive through 100 Mbit/s hospital network.

Results: All above mentioned applications were connected to build the DICOM archive with web based access. The time to archive 100 CT pictures was approximately 12 s and the download of 100 pictures to workstation took 9 s.

Conclusion: We presented the possibility of building Open Source DICOM archive. The fact, that we have the source code of all needed applications is useful for example to make a connection with hospital information system.

C-0363

Optimizing material management in interventional radiology departments through the introduction of a materials management system

D.-A. Clevert¹, N. Rupp², M.F. Reiser¹; ¹*Munich/DE*, ²*Passau/DE*

Objective: A cost analysis was performed to assess options of reorganizing material supplies and reducing radiology division costs through the introduction of a materials management system.

Materials and Methods: A materials management system (Piranha, Boston Scientific) was installed on an existing computer system. All consumables were inventoried and entered into the system. An ABC analysis determined further action. On the basis of order frequencies and availability requirements for emergencies, safety levels were agreed with physicians and other medical staff. Inventory costs were computed using these data. The interest rate for these calculations was 8% per year.

Results: The inventory showed that the capital tied up in stocks was 260,000 € in 2001 and 190,000 € in 2002. A change in supply strategy reduced inventory cost in 2001 and 2002. Annual interest expense was lowered by 18,420 €. Another saving of 2,700 € was achieved by a reduction in storage cost. Annual inventory turnover totaled 298,000 €. The total cost cut through improved inventory management was 21,120 € per year equivalent to 7% of annual expenses. Adding the decline in the cost of shelf time overruns equal to 5% of annual expenses, the saving was approximately 12% of total interventional radiology cost in 2001 and some 11% in 2002.

Conclusion: Flexible supply strategies and the introduction of a materials management program can help to reduce inventory costs in interventional radiology divisions without any impact on service levels.

C-0364

PACS in your pocket? The PDA as imaging tool of the future

C.P. Meehan, C.G. Cronin, D.J. Lohan, P.A. McCarthy; *Galway/IE*

Learning Objectives: To illustrate the emerging role for Personal Data Assistant technology in radiology practice. To enumerate technical challenges, hardware options and software developments which allow reporting of digital imaging via handheld computers.

Background: PACS technology is the favoured means of storing, viewing and archiving radiologic imaging data on a department-wide basis. However, this does present limitations. Workstations are costly and therefore of restricted access. Clinicians require access to imaging studies for review and for patient education at the bedside. Handheld computers, or Personal Data Assistants (PDAs) have been commercially available since the 1980s. However, from the late 1990s latter generations of these devices have undergone rapid development in terms of processing power, screen quality and user interface. There are now available software programs for viewing, manipulation and storage of medical imaging data, including the DICOM format. We have conducted a literature and internet search

Scientific and Educational Exhibits

to identify desired hardware specifications for effective image interpretation, and software currently available for this task.

Procedure Details: Several hardware criteria are important: screen dimensions and resolution, processor speed, storage capacity, battery life and interconnectivity using wireless communication standards. Commercially available software packages offer image storage and manipulation capabilities. We have illustrated the current state of the art, and point out technical challenges to the adoption of PDAs into everyday practice.

Conclusion: The current generation of PDAs already incorporates features well suited to interpreting medical imaging. As the technology evolves, more powerful dedicated handheld devices may be developed specifically for incorporation into a hospital-wide system.

C-0365

A multilingual radiological database on the web for medical students

J.C. Hellund, N. Kløw; Oslo/NO

Learning Objectives: To illustrate how a radiological database, founded on a problem-based learning model is made; including good image quality and integration of clinical and radiological data. To show how a monolingual text can be adapted into other languages.

Background: A no password limited radiological database, with images and readings, is for the medical students an opportunity to self-study and continuous education and distance learning. Multi-lingual editions give other nationalities a possibility to access the information.

Procedure Details: The images were digitized and metadata were appended to make search and retrieval possible. Each case was given a history, a examination description and a detailed reading. A case consists of images from one examination. The background data, thumbnails, text and metadata are stored in an Oracle database, the larger pictures are stored in the file system of the server. WebObjects, an object-oriented, java-programming tool for WWW applications, is used to access and display the data. The database is found at www.radiologi.net, where the Norwegian version has been translated to English during spring 2004, a Russian version is being made during the autumn of 2004. The translated text is uploaded during a common interface.

Conclusion: With a radiological database on the web, students report a high level of satisfaction with the educational method. During the 3 years with the Norwegian version, there were an average of 78.152 requests for pages/month with an average registrations of 423 distinct hosts servers. The programming tool makes the technical handling of translated text easy.

C-0366

SMARTDOC: A new system for real-time consultation and interaction of complex medical data over the internet on low end hardware

A. Persson, S. Palmberg, M. Ranlöf, M. Jern; Linköping/SE

Learning Objectives: Experience how to interact in a high quality medical 3D image incorporated in a Microsoft Word or PowerPoint document. Interact between PCs with voice communication over the Internet on standard software developed for collaborative games. The real-time interactivity and user-friendly interface will be demonstrated.

Background: The next decade will bring widespread, networked multimedia interpersonal computing into the Radiology world. Three-dimensional study has been increasingly used in medical diagnosis and treatment. We have developed web based application components for 2D and 3D visualization of medical data with support for peer-to-peer collaborative sessions on PC desktops and laptops. SMARTDOC's distributed architecture is based on "Application Component Sharing" and a network abstraction system for games providing real-time data interactivity and voice communication. SMARTDOC goes beyond the traditional hospital workflow management and allow the information integration, access and distribution which leads to a more effective patients' treatment.

Procedure Details: The technology and network infrastructure are based on available Microsoft technology. The distributed architecture is based on "Application Component Sharing" providing real-time data interactivity, reducing the load on the network and with zero administration client deployment. The innovation can be summarized as the integration of network technology used in collaborative games with 3D data navigation techniques.

Conclusion: SMARTDOC makes remote visualisation of medical 3D data over the Internet possible with low end computers with standard cost-effective software. The solution will assist in education and knowledge exchange regarding the interpretation of medical images.

C-0367

Context-enhanced detection of electrophysiology catheters in X-ray fluoroscopy images

E.M. Franken¹, M.A. van Almsick¹, P.M.J. Rongen², B.M. ter Haar Romeny¹; ¹Eindhoven/NL, ²Best/NL

Purpose: Cardiac catheter ablation is a minimal invasive medical procedure to treat patients with arrhythmias. For this purpose, special catheters are navigated through the patient's vascular system under continuous X-ray guidance. Our goal is to develop robust image analysis techniques that can detect catheters under fluoroscopy imaging conditions, and that may assist the doctor during the treatment.

Methods and Materials: Traditional image processing methods detect line structures with filters that utilize only small spatial neighborhoods, leading to bad performance in noisy images. Inspired by the biological visual system we use context filters, which enhance elongated structures in an image based on a model of line continuation. We use an adapted version of the tensor voting technique by Medioli et al. This technique makes the final extraction of the catheters easier and more robust.

Results: We compared the performance with and without the use of tensor voting on a test set consisting of 50 clinical images. The success rate of catheter tip extraction increased from 57% to 80% for low noise images. For high noise images the success rate improved from 43% to 72%.

Conclusion: Using tensor voting leads to an increased extraction performance. We expect that further refinement of context enhancement methods will improve existing methods for detecting elongated structures. These new developments in image analysis are applicable to a lot of other medical image analysis problems.

C-0368

Image compression in chest radiography: To the limit and beyond

C. Lefort, A. Merlin, O. Hurtier, P. Petitbon, G. Frija; Paris/FR

Purpose: To evaluate image quality after compression using the wavelet technique, in order to develop teleradiology.

Methods and Materials: 120 plain chest radiographies (60 normal, 60 pathological) were analyzed retrospectively by four radiologists. Each radiography was presented in six different formats: native, compressed with no loss of information, and four different levels of compression (20, 40, 60 and 80). The images were read on a 21-inch 1K cathodic screen, and were rated 'normal'/pathological'. Statistics were performed using the Cochran test.

Results: There was no statistically significant impact on diagnosis of the compression of the images, compared to native images. There was a good intra-observer correlation, independently of the level of compression. Specifically, the number of false negatives was identical for all types of images. However, there was a bias to the study, for example, the image was recognized the second time it was presented to the reader, pathology was not sufficiently diversified.

Conclusion: There was no statistical difference concerning diagnostic quality for the different levels of compression up to 80. These preliminary results need to be confirmed by a study on a larger population of images.

C-0369

Preoperative delineation of intracranial aneurysm's topography during surgery using CT angiography

M.T. Karamessini, G.C. Kagadis, D. Karnabatidis, D. Konstantinou, T. Petsas, G. Nikiforidis, D. Siablis; Patras/GR

Purpose: To describe a technique that tries to delineate intracranial aneurysm's topography during surgery, using volume rendering techniques (VRT) in spiral CT angiography data.

Methods and Materials: Thirty-four patients with ruptured intracranial aneurysms in the ACoA and MCA identified by both CTA and DSA, were included in our study group. The demonstration of the most important features of an aneurysm during surgery was efficient after rotation of the reconstructed image of the patient's head. Its optimal position was then recorded (standardized) by the implementation of a virtual three dimensional coordinate system. Each aneurysm possessed a unique orientation, given in degrees on each virtual axis. In the operating table the patient's head was fixated with the Mayfield device, applying the set of coordinates given in the three axes by the preoperative reconstructed VRT image.

Results: The application of the proposed technique was successful in all cases. Using standard anatomical landmarks in the head correspondingly to each virtual axis, the reproduction of the technique during surgery was easily feasible. In a total of 24 ACoA and 14 MCA aneurysms, we observed a range of rotation de-

Scientific and Educational Exhibits

grees around which our patients' optimum values ranged. There was a good correlation between the VRT reconstructed images and the intraoperative findings. **Conclusion:** The results of our study support the conclusion that the preoperative delineation of intracranial aneurysm's topography during surgery using CTA data is feasible and facilitates aneurysm surgery, especially for complex cases such aneurysms of the ACoA or MCA.

C-0370

Assessment of hip joint structural alterations in osteoarthritis using image texture analysis

I. Boniatis¹, L. Costaridou¹, D. Cavouras², E. Panagiotopoulos¹, G. Panayiotakis¹; ¹Patras/GR, ²Athens/GR

Purpose: Osteoarthritis is a condition characterized by structural and functional alterations of synovial joints. Radiographic Hip Joint Space (HJS) narrowing is regarded as the hallmark for monitoring of osteoarthritis progression. In this study, the potential capacity of computer-based texture analysis in evaluating structural alterations related to hip osteoarthritis was investigated.

Methods and Materials: Forty eight HJS ROIs were obtained from the digitized standing A-P pelvic radiographs of 24 patients with verified unilateral hip osteoarthritis. ROIs were obtained by means of a custom developed computer-aided cropping technique; first an adaptive wavelet enhancement algorithm was applied to emphasize the articular margins of the hip joint and next the HJS outline was manually delineated by an expert physician. A number of textural features regarding image pixel fluctuations were extracted from each segmented HJS region using first and second order statistics. Additionally, an index expressing textural differentiation between osteoarthritic and contralateral control HJS was computed for each patient and compared to a relative index reflecting HJS area decrease.

Results: Statistically significant differences ($p < 0.05$) between the osteoarthritic and the contralateral control Hip Joint were found for the HJS areas and the textural feature of Run Length Non Uniformity. The index expressing HJS narrowing correlated highly with the pathological HJS area ($r = -0.964$, $p < 0.001$), while the two indices (HJS narrowing and textural differentiation) were also highly correlated ($r = 0.976$, $p < 0.001$).

Conclusion: Texture analysis of the radiographic HJS has a potential value in evaluating structural changes associated with the progression of hip osteoarthritis.

C-0371

Web technology and wireless application in the management of radiological images and data

V. Panebianco, C. Catalano, A. Laghi, R. Ferrari, V. Campanella, P.G. Nardis, R. Passariello; Rome/IT

Objective learning: To increase productivity and make quickly radiological workflow and to cut in film and printing costs.

Background: Web technology in association with wireless application make the film-less enterprise a reality; our aim was currently satisfied by a recent project, which is an integrated system of multimedia different component for effectively managing electronic patient's images.

Details: System is composed by: - PACS and RIS system (Ferrania Imaging Technologies); - system for diffusion of images and data via Intranet (LAN) with wireless application (WLAN) and via Internet (web) technology; - high (2.5 k) and medium (standard PC) resolution workstations; - Laptops, Tablet PCs and pocket PCs; - Security systems: computer certification, VPN (virtual private network). A local area network (LAN) and a wireless local area network (WLAN), connected with the regular intranet, can grant network access practically everywhere. Laptops, Tablet PCs and pocket PCs, with embedded wireless card can be transferred everywhere in the same way as a film folder and gives immediate access to the PACS/RIS database. This system is able to manage electronically the complete exam workflow according to standard protocols (DICOM, HL7 and IHE) and to distribute the information through the web.

Conclusion: Web-applications are the most efficient to run over a wireless device. A web application is a program that have all the processing component at the server side and allows the access to each device, using simply the web browser.

C-0372

Improvement of visibility of the lentiform nucleus in CT images for diagnosis of acute middle cerebral artery infarction

N. Takahashi¹, Y. Lee², D.-Y. Tsai², S. Kamio¹; ¹Sendai-shi/JP, ²Niigata/JP

Purpose: The obscurity and partial disappearance of lentiform nucleus are early signs of acute middle cerebral artery infarction (AMCAI) in CT images. However,

the detection of obscure lentiform nucleus is considerably difficult. In this study, a method for improving the visibility and detectability of lentiform nucleus is presented. This approach is considered as the first step for computer-aided diagnosis in AMCAI

Method and Materials: Since the brain region of a head CT image is fairly rough, the contours of lentiform nucleus are generally obscure. In order to improve the visibility of lentiform nucleus, an image processing being able to reduce local noise while maintaining the contrast of contours and edges is desirable. To cope with this issue, an adaptive partial smoothing filter (APSF) was devised. The APSF is a specifically designed filter used to perform local smoothing using a variable filter size determined by the distribution of pixel values of contours or edges in the region of interest. By adjusting 3 major parameters which exist in the APSF, an optimal condition for image enhancement can be obtained.

Results: The APSF was applied to clinical CT images having AMCAI. Our preliminary results showed that the visibility of the lentiform nucleus is much improved. To validate the usefulness of the proposed method, a commonly used low-pass filter was also used for comparison. The results demonstrated the superiority of the APSF.

Conclusion: The APSF can improve the visibility of the lentiform nucleus resulting in the increase of detectability of AMCAI.

C-0373

Pulmonary nodule detection in CT images using ellipsoid models

S. Matsumoto¹, Y. Ohno¹, H. Watanabe², T. Higashino¹, K. Sugimura¹; ¹Kobe/JP, ²Akashi/JP

Purpose: To develop a new scheme for automatic nodule detection in chest CT images.

Methods and Materials: The scheme delineates nodule candidates utilizing deformable ellipsoid models and computes 7 newly devised features for each nodule candidate. After the number of nodule candidates is reduced using a cutoff value for each feature, nodule candidates are classified based on linear discriminant analysis (LDA). The scheme was evaluated using data sets of 52 cases each of which had 1-2 nodules suspected to be lung cancer. The data sets consisting of images of 5-mm slice thickness harbored 60 such nodules (effective diameter of 5-35 mm, mean 19 mm) of which 47 were pathologically proven to be primary lung cancers. LDA was carried out using the whole array of features as well as its subsets consisting of 2-6 features. Appropriate subsets were selected using scatter matrices. The performance of LDA was assessed by means of free-response receiver operating characteristic methodology. In addition, an individual feature itself was also evaluated as a final classifier using the same methodology.

Results: LDA gave similar performance whether it was based on the whole array of features or on one of its selected subsets, showing a sensitivity of 90% with 2.2-3.0 false positives per case. The performance of a single feature approached that of LDA, yielding 3.0 false positives per case at the same sensitivity.

Conclusion: These results indicate the feasibility of the new scheme. A high discrimination power of a newly devised feature was also demonstrated.

C-0374

Are small-matrix (256x256 pixels) images of emergency CT examinations good enough for teleradiology diagnosis?

A. Gmur¹, P. Zdunek², R. Pacho³; ¹Pszczyna/PL, ²Bielsko-Biala/PL, ³Warsaw/PL

Learning Objectives: To describe the method of shortening teleradiology data transmission time of emergency CT examinations with the use of small-matrix image reconstruction. To assess the diagnostic value of 256x256 pixels images in comparison with 512x512 pixels images.

Background: Teleradiology becomes an accepted method for distant consultations of difficult cases. However, the amount of data which has to be sent immediately remains a problem in emergency teleradiology. Instead of rising transmission speed, the reducing of data volume (e.g. image matrix size) can be done. Because small matrix affects quality we assessed the diagnostic value of 256x256 and 512x512 pixels images.

Procedure Details: 50 CT examinations of emergency patients were reconstructed on both matrixes. Two experienced radiologists evaluated the examinations independently: one of them assessed 512x512 images, the second - 256x256 images. In the next step, both radiologists reviewed all the examinations together to establish, whether differences in their diagnoses came from poor image quality or from overlooking.

Conclusion: Full compliance between both radiologist was noticed in 92% of examinations in the first step of assessment followed by 100% in the second. All clinically significant changes were visible on 256x256 pixels images, but the eval-

Scientific and Educational Exhibits

uation of these images was found to be more difficult. It was estimated that CT images reconstructed on 256x256 matrix can be used in after-hours emergency teleradiology for initial assessment, however, the examinations should be reviewed with the use of full-matrix images before making the final diagnosis (e.g. next day morning).

C-0375

Electronic thoracic atlas generated from high resolution computed tomography: Use in minimally invasive cardiothoracic surgery planning
A. Aziz, S.K. Venkatesh, G. Xiao, E.K.W. Sim, W.L. Nowinski, S. Wang;
Singapore/SG

Learning Objective: To develop a digital thoracic model using data from diagnostic high resolution CT for planning of minimal invasive cardio-thoracic surgery (MICTS).

Background: Successful MICTS depends on training of the surgeon and proper planning of the procedure. Surgeons select port locations using external anatomical landmarks as an estimate of patient's internal anatomy. The port location directly influences the access to surgical sites and maneuvering of the instruments. This clinical method is often inaccurate and external landmarks may not correspond to patient's internal anatomy. It is desirable to have digital thoracic model, which can be used for training and planning of MICTS.

Procedure Details: Data available with contrast enhanced high resolution CT is first segmented according to the tissues of interest into chest wall (bone and soft tissue) and mediastinum (blood vessels, heart and soft tissue). This process is done rapidly and semi-automatically using segmentation algorithm developed by us (patent pending). A 3D rotatable, deformable thoracic model is constructed that represents each segmented entity and is labeled in an atlas format. The system interface is well rendered and is easy to use. The port placement is then simulated considering the target internal anatomy.

Conclusion: A high-resolution digital thoracic model in atlas format can be readily obtained with segmentation algorithm and can be developed to form the basis for a virtual reality based simulation system for training and planning of MICTS.

C-0376

Network vulnerability management: Protecting a better view of life
D. Han, L. Van Nostrand; Plano, TX/US

Learning Objectives: To illustrate a network vulnerability management process suitable for medical system manufacturers to resolve malicious software (malware) and vulnerability issues.

Background: Malicious software (malware), in the forms of virus or worm, attacks vulnerabilities in operating systems and their bundled utility programs, and it can cause interruptions to smooth medical system operations. Medical system manufacturers are facing increasing challenges in trying to satisfy customer demands for the establishment of self-contained programs that will protect hospital enterprises from these threats, and, meanwhile, complying with the regulatory guidelines to validate medical software product. It has become imperative for every manufacturer to define an internal process to identify, evaluate, remediate system vulnerabilities, and prevent new threats before they materialize. In this exhibit, we will describe a network vulnerability management process that will help medical system manufacturers reduce the risk of new threats and improve customer satisfaction.

Procedure Details: This network vulnerability management process consists of three sub-processes: *Identification*, *Action*, and *Prevention*. These sub-processes work together to provide maximum protection against threats and vulnerabilities, and they construct a proper solution to secure medical systems.

Conclusion: This network vulnerability management process has been practiced within Kodak Health Imaging. It has proven effective in dealing with threats and vulnerabilities that affect Kodak Health Imaging products. A system like this is recommended to promote rapid-response and preventive activities to ensure the highest standard of quality and safety and to achieve customer satisfaction by testing and deploying appropriate patches in a timely manner.

C-0377

Towards an automatic segmentation of liver tumours in contrast enhanced ultrasound images

A.A. Kissi¹, L. Pourcelot¹, S. Cormier², F. Tranquart¹; ¹Tours/FR, ²Reims/FR

Doppler has been used for many years for cardiovascular exploration in order to visualize the walls and anatomical or functional diseases. The use of ultrasound contrast agents makes it possible to improve ultrasonic information. Nonlinear imaging is an application of this adaptation. It is a powerful technique which images perfusion of an organ. The visualization of flow and perfusion provides im-

portant information for the diagnosis of various diseases and for the detection of tumors. However, the images are buried in noise, the speckle, inherent in the image formation. Furthermore at portal phase, there is often an absence of clear contrast between the lesions and the surrounding tissues because the organ is filled with contrast agents. In this context, we propose a new method of automatic liver lesions segmentation in non linear imaging sequences for the quantification of perfusion. Our method of segmentation is divided into two stages. Initially, we developed an anisotropic diffusion step which raises the structural characteristics in order to eliminate the speckle. Then, a fuzzy competitive clustering process allows us to delineate liver lesions. This method has been used to detect focal hepatic lesions (focal nodular hyperplasia, adenoma). Compared to medical expert's report obtained on 15 varied lesions, the automatic segmentation allows to identify and to delineate the hepatic lesions during the portal phase. Our results show that the inclusion of this method makes it possible to improve the recognition of focal hepatic lesions.

C-0378

Teleradiology volume analysis of CT and MR imaging
D.J. Gardeur, C. Leprince, H. Baekeland; Paris/FR

Purpose: Volume analysis and MIP-CTA or MRA are now routinely performed with MDCT and 3D MR imaging. Teletransmission of hundreds of full DICOM images per exam is very long. As wavelet-JPEG 2000 is commonly used for teleradiology diagnosis, we have studied the feasibility and quality of post processing from the wavelet compressed volume images.

Method and Material: 200 exams-120 CT and 80 MR imaging-were loaded on a web based PACS server (DIAM GIOL) including both DICOM and wavelet images. Wavelet basic compression ratio was 15:1, optional 10:1 and 5:1. The software included an e-viewer with some volume analysis: MPR, MPVR (slab) with MIP, minIP and average slab processing; and volumeMIP. A comparison was performed between full dicom and wavelet-based volume analysis.

Results: In 89% of cases, the diagnostic quality was similar between dicom and wavelet-based post processing images, even for high resolution CT of lung and bones. Lesser diagnostic quality, with some blurring and bone related artifact was observed in posterior fossa CT, circle of Willis CTA, some supratentorial brain CT and FLAIR MR imaging. CTA of the circle of Willis is of good quality at a compression ratio of 10:1. For posterior fossa volume CT and FLAIR MR imaging a compression ratio of 5:1 must be used.

Conclusion: Using new generation web based PACS with wavelet compression and e-viewer, it is feasible to perform teleradiology volume analysis (MPR, MPVR, MIP) from MDCT, 3D MR imaging, CTA and MRA. A wavelet compression ratio up to 15:1 can be used without diagnostic loss of information in the majority of cases. For posterior fossa MDCT, CTA of the circle of Willis and some MR sequences, we recommend a compression ratio of 5:1.

C-0379

Image analysis of CT data of the paranasal sinuses for computer-assisted operational planning
D. Apelt¹, B. Preim², G. Strauss³, I. Hertel³; ¹Bremen/DE, ²Magdeburg/DE, ³Leipzig/DE

Purpose: Planning for endoscopic interventions of the paranasal sinuses (PNS) is supported by a patient-individual processing of the CT-data with image analysis and visualization methods. A segmentation procedure for separating the interesting anatomical and pathological structures was developed.

Methods and Materials: 7 CT datasets with different anatomical and pathological conditions were segmented (resolution between $0.275 \times 0.275 \times 1.000$ and $0.447 \times 0.447 \times 1.000 \text{ mm}^3$). For separating objects, barriers in the form of outlines are drawn by the user roughly around the object on selected slices. Outlines on layers in-between are generated by interpolation. Bone-segmentation is accomplished with the Interactive Watershed Transformation (IWT). For the segmentation of the soft parts an interval-based IWT is used. The segmentation-process is realized in the application RhinoVision (MeVis, Bremen). The visualization of the segmented objects is done with the InterventionPlanner (MeVis, Bremen).

Results: Segmenting the paranasal sinuses, optic nerves and soft parts was performed in less than one hour. In all cases the structures relevant for planning could be identified and delineated. In the examination of the different data sets a strong dependence of the work expended - particularly with the generation of the outline barriers - of the available CT data regarding the anatomical and pathological conditions of the patient showed up.

Conclusion: The procedure does not make assumptions about the shape of the objects and is therefore suitable for the coverage of all anatomical and pathological variations. A clinical evaluation of the prototype is accomplished currently.

Scientific and Educational Exhibits

C-0380

Psychophysical analysis of the DICOM grayscale standard display function

M. Yamaguchi¹, H. Fujita¹, T. Hirano², Y. Okura³, M. Matsumoto⁴, T. Johkoh⁴, Y. Asai⁵; ¹Habikino Osaka/JP, ²Sapporo Hokkaido/JP, ³Kurashiki-shi, Okayama/JP, ⁴Suita Osaka/JP, ⁵Sayama Osaka/JP

Purpose: Consistency in displaying the image over a wide variety of devices with different characteristics is essential for the DICOM Grayscale Standard Display Function (GSDF). The purpose of the present study was to evaluate the consistency of image display of GSDF with psychophysical analysis.

Methods and Materials: A monochromatic 3M Liquid Crystal Display (LCD) flat panel monitor with 8 bit visible gray shades (FC-2091, Eizo Corp., Ishikawa, Japan), which could be displayed with GSDF, CIELAB and gamma 2.2 functions, was used. The calibrated max luminance of this monitor was 480 cd/m². A photo sensor (Sequel Imaging Corp, USA) and calibration software (DR Kal) were used for monitor calibration. The procedure for this analysis was described as following four steps; (1) Calculation of physical gradient value (G) of each display function from characteristic curves after display calibration. (2) Calculation of psychophysical gradient (δ) from G. The psychophysical gradients obtained by $\delta = G/\Delta L_{min}$, where ΔL_{min} is the minimum perceptible luminance contrast as defined by the Barten model, and (3) Statistical analysis of δ regarding these display functions.

Result: δ value of GSDF was significantly greater than those of CIELAB and Exponential 2.2 ($P < 0.001$, by Wilcoxon Matched-Pairs Ranks test) in the range of digital driving level from 53 to 255 and almost constant (i.e., the mean of $\delta = 0.51$).

Conclusion: Although the psychophysical gradients of above three representative display functions were significantly different, from the viewpoint of image consistency, GSDF is considered to be superior.

C-0381

Real-time and interactive remote radiology/radiotherapy conference system using remote desktop software

Y. Baba, Y. Yamashita, S. Morishita, R. Murakami, E. Tomitaka; Kumamoto/JP

Purpose: To describe the implementation and use of a real-time radiotherapy conference system between university hospital and a regional hospital.

Materials and Methods: Remote desktop software was used to share the computer screen (desktop) and to operate the radiotherapy planning system in the regional hospital. Two hospitals were connected by the ADSL (12 Mbps) network. To secure the data, virtual private network (VPN) protocol was used. In the regional hospital, ECLIPSE (Varian Medical system) radiotherapy planning system and remote desktop server software was installed. In the university hospital, remote desktop viewer was installed in an Windows based PC; radiotherapy planning system was not installed. To reveal the usefulness of this system, the time to open a radiotherapy plan, and time to modify the plan was measured using 11 cases.

Results: Sharing the same computer screen between regional hospital and university hospital enabled real-time and interactive remote radiotherapy conference. Eight to 16 seconds was needed to send the computer screen data. The time to open a radiotherapy plan, 6.4 ± 2.5 minutes was needed. To modify the radiation plan, additional 3.8 ± 1.6 minutes /field was needed.

Conclusions: Remote radiotherapy conference system using the remote desktop software was a real time, easy to use, low-cost, and useful system. Using the relatively slow network system (ADSL 12 Mbps; up-word speed 512 kbps), the discussion was concluded within 20 minutes for a patient in most cases. We recommend the optical fiber network to reduce time lag.

C-0382

Computerized method for analysis of magnetic resonance (MR) cardiac perfusion images. Preliminary report

L. Kownacki, M. Orzech, D. Piotrowska, A. Cieszanowski, M. Golebiowski; Warsaw/PL

Introduction: Magnetic resonance (MR) plays a significant role in modern cardiac diagnosis. This method allows morphological and functional imaging as well as perfusion assessment of the heart. MR perfusion images are usually assessed qualitatively and thus the results can be operator-dependent.

Aim: To develop a semi-quantitative method for automatic assessment of MR myocardial perfusion images.

Material and Method: The method was developed for analysis of myocardial perfusion images obtained with Philips Gyroscan ACS 1.5 T system. ECG-gated TFE sequence was used for imaging (TR = 4.2[ms], TE = 2.1[ms], FlipAngle

= 15[deg], TI = 400[ms]). 3 crossections (short axis view) were imaged simultaneously during first-pass of injected contrast medium (Gd-DTPA). 10 series of T1 images were created and qualitatively assessed. Semiquantitative analyses were performed using custom written computer software working in MathLab environment. SVD algorithm was used for calculations. Mean signal intensity curve from left ventricular lumen was used as arterial input function (AIF). Color-coded maps and graphs were created for each image series.

Results: Ten maps were created representing crossections with normal and abnormal perfusion. All the results on maps matched the qualitative assessments performed by two operators.

Conclusion: The custom written computer software is useful for MR cardiac perfusion assessment, however its evaluation with more series of images must be performed.

C-0383

Precession measurement of angular and linear segmental lumbar motion by means of image registration

R. Irwan, L. Penning, M. Oudkerk; Groningen/NL

Purpose: Measurement of segmental lumbar motion by manual superimposition (MS) of flexion and extension radiographs is inaccurate due to differences in cortical outline of the corresponding vertebral bodies. A computerised superimposition ('matching') of digital vertebral body images by means of image registration (IR) is presented. By choosing the whole vertebral body image, and not only its cortical outline, as region of interest, more accurate matching and hence more precise measurement can be expected.

Methods and Materials: Five digital lumbar flexion-extension sets of five consecutive orthopaedic patients suspected of lumbar instability due to old L₁ fracture, spondylolytic spondylolisthesis and degenerative anterolisthesis, were used. Two computer experts A and B performed five IR measurements of each of the five lumbar motion segments in each of the sets. Both angular and linear motion were measured. For comparison a radiologist, experienced in the MS method, performed the same repeated measurements with the MS method. Measurement time for each single investigation was registered.

Results: Pooled SD with 95% CI for the IR method was 0.44 (0.39-0.51) degree, and 1.54 (1.35-1.78) degree for the MS method. Measurement time for the IR method (of angular and linear motion) was 2-3 minutes and for the MS method (of angular motion only) 3-6 minutes.

Conclusion: Measurement error of the IR method proved to be significantly smaller ($p < 0.005$) than that of the MS method. Additionally, the IR method is less time-consuming. We hope the new method will renew interest in diagnosis of abnormal segmental mobility and vertebral instability.

C-0384

A computer based examination for the assessment of reasoning skills in radiology

O. Dicle, M. Yazicioglu, M. Sevil; Izmir/TR

Purpose: Clinical reasoning is one of the most important practices of the radiologist. These kinds of professional skills should be assessed with the help of convenient assessment methods. Conventional assessment methods, like oral examinations have several limitations to make a valid, reliable and objective evaluation of these kinds of professional skills of the radiologists. In recent years clinically oriented reasoning examinations (CORE) have been developed to overcome the problems of conventional oral examinations. In our study we will explain the CORE and its use in radiology. We will also present a computer program that we have developed to perform such examinations by CORE type questions.

Method and Materials: A program was written to stimulate a CORE on a personal computer. Microsoft Office Excel was utilized as a base and several macros were prepared to run the program. Some text and JPEG type of files were used in the program. All the steps, including the timing and the evaluation was made automatically with the help of the program.

Results: The program was used in a simulation examination in four different stations. In all stations candidates those who had no previous knowledge about the program successfully ran the program and it worked without any problems. All the feedbacks from candidates were positive.

Conclusion: With the help of a simple program, interpretation, differential diagnosing and clinical reasoning skills of the radiologists can be successfully assessed. This program can also be used for self assessment processes.

Scientific and Educational Exhibits

C-0385

Transition to digital technology as method for enhancement of efficiency of screening radiographic systems using

N. Hnid¹, B. Tsvigun¹, Y. Kovalenko²; ¹Kamenec-Podolskiy/UA, ²Kiev/UA

Purpose: The purpose of this work was the comparative assessment of film and filmless technology using in preventive chest radiography of people that is the basic method for early revealing of pulmonary tuberculosis in adult population in the Ukraine.

Materials and Methods: The comparative analysis of the data received during preventive examinations of people in fluorography room at the municipal polyclinic in 2002-2003 was made. By the end of 2002, the fluorography room was put to numeral technology by means of additional equipping of 12F7 photofluorograph (Aktyubrentgen, Kazakhstan) with numeral receiver "Alpha" (Teleoptic, Ukraine) having resolving ability 2.5 line pair per millimeter.

Results: After transition to numeral technology, the number of examinations using of photofluorograph increased by 31.42%. On the one hand, it is achieved due to increased productivity of a room because the diagnostic image is available for analysis to radiologist in 15 seconds after exposure. As far as the self-descriptiveness of the digital image is comparable to survey on chest film radiography, and radiation-absorbed dose to the patient in digital radiography is less, the number of diagnostic X-ray inspections made together with phthisiotherapists, oncologists and other specialists rose 20 times. Thanks to that, in 2003 more than USD 9 thousand were saved on expendables only, and this is more than 17% of costs spent for transition to digital technology.

Conclusions: Transition to digital technology allows to lower the cost price of preventive X-ray examinations keeping the same quality of diagnostic images.

Contrast Media

C-0386

Intraindividual comparison of 1.0 M gadobutrol and 0.5 M gadopentetate dimeglumine for time-resolved contrast-enhanced 3D magnetic resonance angiography of the upper torso

C. Fink, M. Puderbach, S. Ley, F. Risse, T.A. Kuder, M. Bock, J. Thaler, C. Plathow, H.-U. Kauczor; Heidelberg/DE

Purpose: To compare the signal characteristics and bolus dynamics of 1.0 M gadobutrol and 0.5 M Gd-DTPA for time-resolved contrast-enhanced 3D MRA of the upper torso.

Methods and Materials: Ten healthy volunteers were examined with time-resolved contrast-enhanced 3D MRA (scan time per 3D data set: 0.86 sec; voxel size: 3.6x2x6.3 mm). Each volunteer underwent 8 individual exams after intravenous injection of 0.05 and 0.1 mmol/kg body weight (b.w.) of 1.0 M gadobutrol and 0.5 M Gd-DTPA using two injection rates (2.5 and 5 ml/sec). The data analysis included quantitative measurements of the peak signal-to-noise ratio (SNR) and bolus dispersion (full-width at half maximum) in the pulmonary artery, left atrium, thoracic and abdominal aorta.

Results: No significant differences of the peak SNR and bolus dispersion were observed between gadobutrol and Gd-DTPA for all dose levels and injection rates in any of the vascular segments. For both contrast agents a dose of 0.1 mmol/kg b.w. injected with 5 ml/sec achieved the highest SNR in all vascular segments.

Conclusion: Higher concentrated gadolinium chelates seem to offer no relevant advantages for time-resolved contrast-enhanced 3D MRA protocols of the upper torso.

C-0387

Incidence of contrast media induced nephropathy in different diagnostic procedures

M. Heinrich¹, A. Grgic¹, M. Heckmann¹, B. Kramann¹, M. Uder²;

¹Homburg a.d. Saar/DE, ²Erlangen/DE

Purpose: To compare the incidence of contrast media induced nephropathy (CIN) in different diagnostic procedures.

Methods and Materials: 17694 consecutive patients who underwent examination with X-ray contrast media (RCM) from 01/2003 to 05/2004 were retrospectively identified in the radiology information system. 6779 patients were excluded because of a lack of creatinine values (3002), repeated RCM-examinations within 4 weeks (3472) and a creatinine value ≥ 5 mg/dl before RCM-application (305). The examinations of the remaining 10915 patients consisted of 4854 cardiac catheterizations, 4742 contrast-enhanced CT scans, 753 intravenous pyelographies (IVP), 494 angiographies and 62 phlebographies. We used two definitions for CIN. Definition#1: Increase in serum creatinine ≥ 0.5 mg/dl or $\geq 25\%$ over baseline value to at least 1.0 mg/dl within 10 days after receiving RCM. Definition#2: Increase in serum creatinine ≥ 0.5 mg/dl or $\geq 25\%$ over baseline value to at least 2.0 mg/dl.

Results: According to definition#1, 1485 patients developed CIN including 19.8% of the patients who underwent cardiac catheterization, 16.4% of the patients who underwent angiography, 8.4% of the patients who underwent CT, 6.5% of the patients who underwent phlebography and 5.3% of the patients who underwent IVP. 421 patients were detected with CIN according to definition#2 including 6% of the patients who underwent cardiac catheterization, 6.1% of the patients who underwent angiography, 1.9% of the patients who underwent CT and 0.8% of the patients who underwent IVP.

Conclusion: Not only the definition of CIN but also the type of RCM-examination seems to influence the incidence of CIN.

C-0388

Microvascular imaging with contrast-enhanced ultrasound

M. Krix, H.-U. Kauczor, S. Delorme; Heidelberg/DE

Learning Objectives: To learn about the possibilities of contrast-enhanced ultrasound techniques for the visualization and quantification of tissue perfusion. Techniques and methods for microvascular imaging using contrast-enhanced ultrasound are presented and possible clinical indications are discussed.

Background: Functional imaging has gained critical importance in recent years. Perfusion, i.e. the blood flow per tissue unit including capillary flow, is an important functional parameter. Pathological changes of tissue perfusion can be found in various clinical diseases like in infarction, inflammation or neoplasia. Novel ultrasound contrast agents and low mechanical index ultrasound techniques al-

Scientific and Educational Exhibits

low for a sensitive detection of microvascularity in real-time. Furthermore, quantification of perfusion is achieved by analysing replenishment kinetics of the contrast agent.

Procedure Details: Technical requirements and examination protocols to use contrast-enhanced ultrasound in the detection of microvascularity are described. Procedures for quantification of perfusion are explained, in particular analysis of replenishment kinetics of ultrasound contrast agents. Fields of possible clinical applications for perfusion imaging with contrast-enhanced ultrasound are discussed.

Conclusion: Contrast-enhanced ultrasound allows sensitive detection and quantification of perfusion, and is a promising functional imaging method for various clinical applications.

C-0389

Gd-IDA derivatives as potential hepatobiliary contrast media for MR

imaging: Experimental studies on rats

M. Studniarek¹, E. Mikiciuk-Olasik², M. Retkowski¹, T. Wierzba¹, M. Sidorowicz¹, ¹Gdansk/PL, ²Lodz/PL

Purpose: Assessment of biodistribution of Gd-IDA (iminodiacetic acid) compound as a potential hepatobiliary MR imaging contrast agents. These substances are known to be specifically taken up by hepatocytes and excreted into bile.

Methods and Materials: Four rats were examined after i.v. injection of 10 mg Gd-IDA derivative (structural formula $C_{38}H_{66}GdN_4NaO_{10}$ and molecular weight 729.868). Continuous acquisition of T1 FSE and MTC sequences (in 2 min loops) before and immediately after c.m. administration was performed during 60 minutes in 2 min loops on 1.5 T MR imaging scanner. Percent of injected Gd dose accumulated in rat liver and enhancement were calculated and time/intensity curves were drafted for liver, kidney, heart, muscle and fat tissue.

Results: Enhancement in the liver reached the peak (100-150%) in 19-33 min p.i. which was followed by plateau with slight signal intensity decrease. The liver accumulation amounted to 60% of administrated Gd-dose. Time/intensity curve in the kidney was similar to typical renogram with the maximal enhancement of 19-39% in 4-6 min. That one for the heart presented exponential decrease of signal intensity when the curves for the muscle and fat tissue were flat.

Conclusions: Gd-IDA derivatives are the promising group of hepatotropic contrast media for MR imaging.

C-0390

Placental perfusion assessment with MR imaging using contrast agents in a mouse model

L.J. Salomon¹, N. Siauve¹, D. Balvay¹, C.A. Cuénot¹, C. Vayssettes¹, A. Luciani¹, G. Fréja¹, Y. Ville², O. Clément¹; ¹Paris/FR, ²Poissy/FR

Learning Objectives: To quantitatively analyze placental perfusion by using MR imaging with contrast agents in a mouse model.

Background: Thirty six Balb/c pregnant mice at 16 days of gestation were injected IV with either a conventional gadolinium chelate or a macromolecular gadolinium chelate and 1.5 Tesla single-slice T1-weighted 2D Fast SPGR sequential MR imaging was then performed for 14 minutes. Images were analyzed qualitatively and parametric map analysis were performed on the 25 mice finally included in the study. Signal intensity was measured in the maternal left ventricle (input function), the placenta and the fetus. After converting signal intensity into contrast agent tissue concentrations, a three-compartment model was developed. Placental perfusion was calculated for conventional ($n = 12$) and macromolecular gadolinium chelates ($n = 13$). Finally, placental and fetal gadolinium concentrations were assayed by means of atomic emission spectrophotometry ($n = 15$).

Imaging Findings: Based on a constant transfer parameter, estimated placental perfusion did not differ between procedures with conventional and macromolecular gadolinium chelates (0.99 ± 0.5 ml/min/g and 1.28 ± 0.6 ml/min/g, respectively, $p = 0.22$). Likewise, mean placental gadolinium concentrations did not differ after conventional and macromolecular chelates injection. In contrast, the mean fetal gadolinium concentration was $9.83 \pm 0.4 \mu\text{M}$ after conventional chelate injection and below the detection limit after macromolecular chelate injection.

Conclusion: Placental perfusion can be calculated by using dynamic contrast-enhanced MR imaging. If this approach is feasible and safe in humans, it may have potential for investigating the origin and course of intra-uterine growth restriction and for the management of compromised pregnancies.

C-0391

A new MR findings: Decrease of signal intensity of myometrium after iv USPIO administration

P. Paolantonio, A. Laghi, C. Miglio, M. Rengo, V. Vergari, S. Ciccarelli, A. Guerrisi, R. Passariello; *Rome/IT*

Purpose: To evaluate the diagnostic advantages of intravenous USPIO administration on T-staging of uterine carcinoma.

Methods and Materials: Seventeen female patients referred for gynecological carcinomas, 11 with corpus uterine cancer and six with cervical carcinoma, underwent MR scan of the pelvis on a 1.5 T magnet. GRE T2*W sequences (TR/TE/FA/matrix/acq. time: 1800 msec/15 msec/30°/230x512/13.51 min) were acquired on multiple planes before and 24 hours after iv administration of 2.6 mg/kg of body weight of Sinerem (Guerbet, Paris, France). Image analysis were performed by consensus by two radiologists and it included qualitative and quantitative analysis of signal intensity (SI) of both normal myometrium and neoplastic lesions before and after Sinerem administration. S/N and C/N were calculated. Modification of T-staging in images obtained after Sinerem administration was also evaluated. Statistical analysis was performed using Wilcoxon test ($p < 0.05$).

Results: Qualitative analysis showed a significant decrease of SI of normal myometrium after Sinerem administration leading to a better lesion conspicuity. Quantitative analysis showed a statistically significant difference between SI of myometrium on plain and Sinerem-enhanced MR images assessed by means of t-test. C/N between lesion and normal myometrium significantly increased following Sinerem administration. In 13 patients Sinerem-enhanced images provided additional information leading to more accurate T staging.

Conclusions: Intravenous injection of Sinerem provides a significant decrease of SI of normal myometrium with higher C/N between neoplastic lesion and normal myometrium increasing the conspicuity of neoplastic lesions.

C-0392

Small well-differentiated hepatocellular carcinoma and atypical adenomatous hyperplasia (≤ 2 cm) evaluated with contrast-enhanced dynamic CT and ferucarbotran-enhanced MR imaging

T. Touan¹, K. Fujimoto², S. Azuma¹, M. Uchida², N. Hayabuchi², N. Ono¹, S. Matsushita¹; ¹Chikugo city/JP, ²Kurume city/JP

Purpose: To compare between contrast-enhanced dynamic CT and ferucarbotran-enhanced MR imaging in the detection of small (≤ 2 cm) well-differentiated hepatocellular carcinomas (HCCs) and atypical adenomatous hyperplasias (AAHs) and to evaluate the signal intensity change of small HCCs and AAHs.

Methods and Materials: We identified 15 patients with pathologically confirmed 18 well-differentiated HCCs and 4 AAHs (median, 11 mm; range, 5-20 mm in the largest diameter) who underwent both dynamic CT and ferucarbotran-enhanced MR imaging. Conventional sequences of T2*-weighted gradient-echo (cT2*-GRE = TR280 ms/TE14 ms, FA: 60°) and specific sequences of T2-weighted gradient-echo (sT2-GRE = TR140 ms/TE8 ms, FA: 30°) images were obtained before and after administration of ferucarbotran. To assess the effect of ferucarbotran, the tumor-liver signal contrast-to-noise ratio (tumor-liver-CNR) was calculated.

Results: There was excellent interobserver agreement for the presence of nodules on each modality (kappa statistic, 0.9-1.0). The detection rates of nodules were 50% (11/22) on dynamic CT, 59% (13/22) on cT2*-GRE sequences with ferucarbotran and 68% (15/22) on sT2-GRE sequences with ferucarbotran. None of 4 AAHs were detected on dynamic CT; in contrast, 2 of 4 AAHs were detected on sT2-GRE sequences with ferucarbotran. There was no significant difference in the tumor-liver-CNR between HCCs and AAHs and 9 of 15 detected nodules revealed signal hypointensity compared to hepatic parenchyma on sT2-GRE sequences with ferucarbotran.

Conclusion: Small well-differentiated HCCs showed ferucarbotran uptake (presence of Kupffer cell phagocytic activity) as well as AAHs. In the detection of small well-differentiated HCCs and AAHs, sT2-GRE sequence with ferucarbotran is superior to dynamic CT and T2*-GRE sequence with ferucarbotran.

C-0393

Atherosclerotic plaque imaging of ApoE-deficient mice with gadofluorine M

M. Shimada¹, K. Yoshikawa¹, H.J. Weinmann², T. Tatebe¹, T. Morita¹, T. Ookubo¹, A. Senoo¹, Y. Inoue¹, S. Hayashi¹; ¹Tokyo/JP, ²Berlin/DE

Purpose: The study of atherosclerotic plaque using Watanabe rabbit was common. In our research, possibility as agents of new atherosclerotic plaque MR imaging of Gadofluorine M in apoE-deficient mice was examined.

Methods and Materials: Total 16 mice (BW:25 gr) were used. Items were apoE-deficient mice of high-cholesterol diet ($n = 8$) and apoE-deficient mice of normal

Scientific and Educational Exhibits

(n = 8). Femoral vein was exposed and catheter was inserted. Each 0.01 ml intravenous injection of Gadofluorine M (250 µmol/ml) was made. T1 WSE (TR:500 ms TE:15 ms) axial thin (2 mm slice) images and fat saturate T1 WSE (TR:500 ms TE:15 ms) were performed before and at 24 hrs after contrast media. Delineation of aortic wall atherosclerotic plaque was examined.

Results: In all apoE-deficient mice of high-cholesterol diet (8/8), enhanced atherosclerotic plaque which spread to whole tunica intima of aortic arch and to a dorsal part of tunica intima of thoracic descending aorta was clearly detected in T1 weighted SE sequence and fat saturate T1 weighted SE. Fat saturate T1 weighted SE sequence was more excellent in the delineation of the arteriosclerosis than T1 weighted SE. However, there were no plaques in abdominal aorta (8/8). In all apoE-deficient mice of normal diet, we can not detect contrast enhanced atherosclerotic plaque in aortic arch, thoracic aorta and abdominal aorta (8/8).

Conclusion: Using Gadofluorine M, we were able to perform good atherosclerotic plaque imaging in apoE-deficient mice of a high-cholesterol diet using fat saturate T1 weighted SE images. ApoE-deficient mice of high-cholesterol diet was a good new model of atherosclerotic plaque in MR imaging.

C-0394

Analysis of an automatic ultrasound image registration system to improve contrast quantification for hepatic perfusion assessment

E.A. Gardner¹, T.S. Sumanawera¹, M.N. Woelmer², R.W. Steins¹, E. Leen³;

¹Mountain View, CA/US, ²Ann Arbor, MI/US, ³Glasgow/UK

Purpose: To assess an ultrasound image registration method that uses nonaffine transforms in order to eliminate movement in the image.

Methods and Materials: Using a destruction/reperfusion technique, contrast-enhanced image sequences of the liver acquired from 14 patients with focal hepatic tumours using contrast pulse sequences (CPS) on a Siemens Sequoia(R) ultrasound system, were analyzed using an online quantification package (Autotracking Contrast Quantification). The quantification parameters, i.e. baseline intensity, enhancement amplitude and the wash-in constant (Bl, A, and β respectively) resulting from using the warping registration method on this system, were compared with those acquired without any motion compensation. The correlation coefficient of this parameterization was recorded as the goodness-of-fit (GOF). Manual image alignment was used as a standard of reference.

Results: There was significant difference in the β between no-alignment and automatic alignment as well as manual alignment (0.5 significance level). The GOF produced using automatic alignment was significantly better (0.5 significance level) than when no alignment was used but was significantly worse than when manual alignment was used. The GOF was never reduced by using automatic alignment and the percentage of cases with a GOF > 0.9 improved from 36% to 64% when using automatic alignment. 71% of manually aligned cases had GOF > 0.9.

Conclusions: The automatic alignment method tested provided consistent and significant improvement in contrast quantification for perfusion assessment. Whilst the performance of manual alignment was not matched, automatic alignment is quick and more practical clinically.

C-0395

Quantitative, contrast-enhanced ultrasound to detect pathologic skeletal muscle perfusion in patients with inflammatory myopathies: Initial results

M. Krix, M.-A. Weber, H.B. Huttner, U. Jappe, U. Meyding-Lamadé, M. Hartmann, M. Essig, H.-U. Kauczor, S. Delorme; Heidelberg/DE

Purpose: To evaluate whether contrast-enhanced ultrasound (CEUS) is able to determine pathologic muscle perfusion in patients with myositis and thereby non-invasively confirm the suspected diagnosis.

Methods and Materials: Skeletal muscle perfusion was quantified using contrast-enhanced (10 ml Levovist® i.v.), intermittent power-Doppler ultrasound applying a modified model analyzing replenishment kinetics of microbubbles. For validation, CEUS perfusion parameters of the right forearm flexor muscles at rest and after defined exercise were compared with venous-occlusion plethysmography (VOP) in 10 healthy volunteers. In 21 patients with suspected myositis, CEUS of the right biceps muscle was performed, and findings were compared with muscle biopsy, and MR imaging at 1.5 T using fat-suppressed T2w, STIR, and contrast-enhanced fat-suppressed T1w sequences.

Results: CEUS allowed for perfusion quantification in different skeletal muscle groups and was able to depict the physiological large variability of muscle perfusion at rest ($3.0 \pm 2.3[\sim\text{ml}/\text{sx}100 \text{ ml}]$) compared to the results after exercise ($22.9 \pm 11.0[\sim\text{ml}/\text{sx}100 \text{ ml}]$). VOP perfusion significantly correlated with the CEUS parameters perfusion ($r = 0.81$, $p < 0.001$) and blood volume ($r = 0.82$, $p < 0.001$). In 8 patients, myositis was confirmed histologically, and CEUS showed signifi-

cantly higher perfusion, blood volume and blood flow velocity values (all $p < 0.01$) than in non-myositis patients. In contrast, contrast enhancement in MR imaging was found in only 57% of the affected muscles, whereas an increased signal intensity on T2w images was found in all myositis patients.

Conclusion: CEUS is a sensitive, cost-saving method in a clinical setting to quantify skeletal muscle perfusion. CEUS is able to non-invasively demonstrate increased perfusion of involved muscle groups in patients with myositis.

C-0396

Everything you always wanted to know about iodinated contrast media interactions with other drugs, but you were afraid to ask

A.N. Chalazonitis, J. Tzovara, S. Velitsista, S. Giannou; Athens/GR

Learning Objectives: 1) To help the participant to understand why and when other drugs may increase the potential risk of adverse reaction to the administered iodinated contrast media. 2) To evaluate the risk of anaphylaxis or nephrotoxicity following interactions between iodinated contrast media and other medications given during hospitalization. 3) To provide guidelines for recommend precautions to prevent possible adverse iodinated contrast media reactions.

Background: Patients undergoing radiographic studies often have coexisting diseases or taking other drugs that increase the potential risk of adverse reaction to the administered iodinated contrast media. Drug interactions occur at varying rates in these patients. Unfortunately, the causative agents cannot be identified in all cases. Most of these drug interactions are pharmacokinetic and can be classified as alterations in absorption or elimination, protein-binding effects and changes in drug metabolism.

Procedure Details: The aim of this exhibit is to illustrate a list of the drugs that can potentially lead to interactions with administrated iodinated contrast media, to describe this pharmacokinetic mechanism after their initiation and to provide guidelines for necessary precautions and recommend actions.

Conclusion: The goal of radiologists and other personnel administering intravascular iodinated contrast material should be to utilize these agents appropriately and properly, so that imaging studies are optimized and risk to the patient is minimized.

C-0397

Basic examination of photoirradiation for possible control of angiogenesis by HP-denatured type IV collagen complex dissolution

M. Machida, K. Kameyama, A. Shimizu, N. Machida, H. Tajima, T. Kumazaki, N. Moriyama, Z. Naito; Tokyo/JP

Purpose: Hematoporphyrin (HP) accumulates selectively in cancer tissue and is used for photodynamic diagnosis and therapy. We have been focusing on HP present in the extracellular matrix between swollen collagen type IV (type IV) and lipid, and have previously reported a similarity between arteriosclerotic lesions and a lipid-protein complex model. Denatured type IV was recently shown to be an angiogenetic factor. In this study we observed the photoreaction of denatured type IV-lipid complex by using HP. We also examined the validity of this approach for the treatment of vascular matrix lesions and the control of angiogenesis.

Methods and Materials: We made a mixture of HP, type IV, and liposomes containing cholesterol, and examined the agglutination state of the collagen-lipid complex as follows. We first irradiated the complex with pulses of 680nm light from a LED source for one hour, then measured the circular dichroism (CD) spectrum and scattered light spectrum. We further inspected the complex using high-sensitivity CCD and electron microscopy.

Results: The structure of type IV collagen was confirmed by CD spectrometry. The denatured collagen was combined with HP. An increase in the scattered light spectrum was observed after light irradiation. The fluorescence spectrum of HP changed from a combined arteriosclerotic pattern to a solitary HP pattern after light irradiation.

Conclusion: The state of the type IV collagen-HP complex changes after weak light irradiation. Irradiation of HP with weak light may be useful for the diagnosis and treatment of angiogenetic lesions as well as vascular matrix lesions.

C-0398

Cytogenetic effects of diagnostic X-rays and contrast media in human peripheral blood lymphocytes

L. Popova¹, V.B. Hadjidekova¹, A. Karadjov¹, B.S. Rao², V.G. Hadjidekov¹; ¹Sofia/BG, ²Mumbai/IN

Purpose: To investigate the induction of cytogenetic damage as chromosomal aberrations and micronuclei formation in peripheral blood lymphocytes of patients undergoing cerebral and renal arteriography.

Scientific and Educational Exhibits

Methods and Materials: Peripheral blood samples were taken from 21 patients undergoing DSA-arteriography (11 male and 10 female, aged between 13-65 years) before the procedure, immediately after and 24 hours later. The skin dose obtained during the whole procedure X-ray exposure was measured by thermoluminescent dosimeters and varied between 0.04-0.30 Gy. Both low and high osmolarity contrast media were used. Cytogenetic analysis of chromosomal aberrations and micronuclei were applied for detection of genotoxic effects of angiographic procedures involving X-rays and iodinated contrast media. Aberrations were scored in 200-400 cells for each patient.

Results: The estimated frequencies of chromosomal aberrations and micronuclei show a significant increase of chromosomal damage after angiographic examination in comparison to the level before the diagnostic exposure. For all 21 patients, the mean frequency of cells carrying chromosomal aberrations after arteriography nearly double the value before X-ray and contrast media exposure, i.e. 1.48-2.54% and remained constant at 24 h analysis. There is no correlation between the increase in cytogenetic damage and entrance dose of X-rays nor the concentration of contrast medium.

Conclusion: Diagnostic procedures involving X-rays and iodinated contrast media as angiography cause a significant increase in cytogenetic damage in peripheral human lymphocytes. These results suggest the need of limitation of contrast media overdosing without compromising the image quality and further studying of their radiosensitivity property.

C-0399

The value of contrast enhanced US imaging in the reduction of TRUS-guided biopsies and minimization of complications: Impact on prostate cancer detection

D. Alexopoulos, A. Filippidou, I. Theotokas, A. Plagou, S. Faitaki, D. Leli, A. Stefanaki, P.S. Zoumpoulis; Athens/GR

Learning Objectives: To survey the physics and technology of US contrast agents and their role in the localization of prostate cancer. To demonstrate the procedure of contrast enhanced targeted biopsy of prostatic lesions. To compare USCA targeted biopsy with conventional TRUS guided biopsy in terms of cancer detection rates and incidence of complications.

Background: Prostatic cancer lesions are not always easily detected by TRUS. Contrast enhancement of these lesions aids in their detection and accurate sampling.

Procedure Details: The low sensitivity of B-mode and color Doppler TRUS in prostate cancer detection renders necessary the performance of systematic prostate biopsy with a frequently low yield. Contrast enhanced TRUS improves detectability of malignancy by revealing regions of increased vascularity, which may be targeted selectively to obtain biopsy specimens. In our study, contrast enhanced targeted biopsy was performed on 90 patients after IV administration of the US microbubble contrast agent SonoVue® (Bracco International). Comparison of cancer detection rates for USCA targeted biopsies and conventional systematic biopsies (control group) indicated improved yield with targeted biopsies. Furthermore, the frequency and severity of complications were reduced when the biopsy was performed under contrast enhancement direction. These initial results demonstrate the potential of contrast enhanced TRUS to decrease the number of biopsy cores and improve the sensitivity of prostate cancer diagnosis.

Conclusion: Despite certain restraints, USCA are most helpful in detecting prostate cancer lesions that are not easily visible on TRUS. This provides for a smaller number of samples and for precision sampling.

C-0400

Uncommon applications of contrast enhanced ultrasound

S.D. Yarmenitis, A. Bakantaki, C. Kourieraki, C. Fragos, T. Maris, N. Gourtsoyiannis; Iraklion/GR

Learning Objectives: To present clinical cases, beyond the established applications, in which contrast enhanced ultrasound (CEUS) proved to be helpful or decisive in the management of the patients.

Background: CEUS is an accepted technique that has entered the field of medical imaging with promising results. The vast majority of applications involve the focal lesions and trauma of the solid abdominal viscera, the study of renal transplants and the study of vesicoureteral reflux. However many other abnormalities may be diagnosed by CEUS. Between June 2003 and August 2004, 70 patients were examined with CEUS for conditions that are never or rarely investigated with this method. The techniques and the specific findings are illustrated.

Procedure Details: Our uncommon CEUS applications comprised cases of dissecting aneurysms of the abdominal aorta, uncertain diagnosis of abdominal and peripheral venous thrombosis, uncertain extent of arterial plaques or paten-

cy of arterial grafts, patency of TIPS, bowel inflammatory disease or bowel inflammatory masses, neoplastic bowel masses, ovarian or testicular torsion, neoplasms of the gallbladder, distal common bile duct and the papilla, neoplasms of the chest wall and studies of the urinary collecting system (UCS). Contrast was administered in standard dose intravenously in all applications except in these of the UCS where intervention route, already available, was used and the material was further diluted in saline.

Conclusions: CEUS is applicable in several uncommon conditions. It may solve the underlying problem, limit the use of more complicated procedures or successfully tailor-up further management of the patients.

C-0401

Effect of ultrasound contrast medium on human CD4⁺ lymphocytes in vitro culture

G. Caruso, G. Salvaggio, G. Fatta, N. Caccamo, C. La Mendola, F. Dieli; Palermo/IT

Purpose: Aim of this study was to investigate the effects of ultrasound contrast medium (SonoVue, Bracco, Italia), with and without ultrasound exposure, on normal release of Interferon-γ (IFN-γ) by human CD4⁺ T lymphocytes.

Methods and Materials: Cells were cultured in complete medium and split into 5 groups of samples as below: One exposed to ultrasound (2 minutes at 3.5 MHz) only, one to contrast medium (0.02 ml) only, one first to contrast medium and then to ultrasound, one first to ultrasound and then to contrast medium and the fifth as control. The supernatants were assayed for IFN-γ production by ELISA technique.

Results: CD4⁺ T cells exposed to ultrasound contrast medium with and without ultrasound exposure, after 48 h of in vitro culture, showed a decreased release of IFN-γ, with respect to cells exposed only to ultrasound and to control group.

Conclusion: Contrast medium ultrasound has a toxic effect on CD4⁺ T cell culture, independently to ultrasound exposure.

C-0402

Biliary strictures following orthotopic liver transplantation: Evaluation with mangafodipir trisodium-enhanced MR cholangiography

P. Boraschi, F. Donati, R. Gigoni, A. Volpi, L. Urbani, F. Falaschi; Pisa/IT

Purpose: To determine whether mangafodipir trisodium-enhanced MR cholangiography (MRC) could improve the diagnostic confidence provided by conventional T2w MRC in patients with suspected biliary strictures after liver transplantation.

Methods and Materials: Eleven liver transplant subjects with suspected biliary strictures underwent MR imaging and MRC at 1.5T device (Signa, GE Medical System) using a phased array coil. After the acquisition of axial T1w and T2w sequences, conventional MRC was performed through a respiratory-triggered, thin-slab (2 mm), heavily T2w fast spin-echo sequence and a breath-hold, thick-slab (10 and 40-50 mm), single-shot T2w sequence in the coronal plane. In each patient a further coronal T1w fat-suppressed breath-hold 3D gradient-echo imaging (FAME) was obtained 30-40 minutes after intravenous administration of mangafodipir trisodium (Mn-DPDP, Teslascan; GE Healthcare; 0.5-mL/Kg body weight). All source images and 3D reconstructions were reviewed in conference by two observers that were asked to determine presence and site of biliary tract strictures. Imaging results were correlated with surgery, direct cholangiography and/or follow-up.

Results: Patients were affected by non-anastomotic strictures (n = 8), anastomotic strictures (n = 3) and inflammatory ampullary stenosis (n = 1). Mangafodipir trisodium-enhanced MRC tended to outperform conventional MRC in delineating slight anastomotic stenoses and strictures involving the hepatic bifurcation and the biliary tree of the graft (ischemic-type biliary lesions).

Conclusion: Our preliminary results suggest that mangafodipir trisodium-enhanced MRC seems to improve the diagnostic performance of MRC in the evaluation of biliary strictures in liver transplant recipients.

C-0403

Comparison between concentration dependent relaxivity of gadopentetate dimeglumine (Magnevist®), gadobutrol (Gadovist®) and gadobenate dimeglumine (MultiHance®) in human blood plasma at 0.2 T, 1.5 T and 3.0 T

P. Martirosian¹, J. Pintaske¹, H. Graf¹, G. Erb², K.-P. Lodemann², C.D. Claussen¹, F. Schick¹; ¹Tübingen/DE, ²Konstanz/DE

Purpose: MR contrast media (CM) can interact with blood proteins leading to modified relaxivity. Effects of 3 different Gd-CM on T1 and T2 relaxation of blood were tested using in vitro human-plasma preparations at 37° C.

Methods: Samples containing Magnevist®, Gadovist® and MultiHance® were

Scientific and Educational Exhibits

prepared with concentrations in 14 logarithmic steps in a range between 0.01 mM and 64 mM. Measurements were performed at 0.2, 1.5, and 3.0 Tesla. T1 was measured by inversion recovery imaging with fast spin-echo readout (inversion time range: 23-8000 ms). Extremely short T1 of samples with high Gd-concentrations were assessed by measuring flip angle dependent signal intensities of a 3D gradient echo sequence with minimal echo time. T2 was assessed by multi-echo spin-echo sequences with equidistant TE between 8 and 256 ms, or 16 and 512 ms.

Results: Relaxivity data were nearly linearly dependent on CM concentrations for Magnevist® and Gadovist®. MultiHance® provided higher T1 and T2 relaxivity at all field strengths and for all concentrations than the other CM, but concentration dependence was not strictly linear. Smaller concentrations of MultiHance® led to most increased T1 and T2 relaxivity. For all three contrast media, T1 relaxivity decreased from 0.2 to 1.5 Tesla (21-29%) and from 1.5 to 3 Tesla (22-33%). T2 relaxivity decreased significantly from 0.2 to 1.5 Tesla for all three contrast media, whereas no further decrease from 1.5 to 3 Tesla was observed.

Conclusion: In human plasma MultiHance® was the most effective Gd-based CM for T1-imaging at field strengths from 0.2 to 3.0 Tesla.

C-0404

Hypervasculat focal liver lesions: A pictorial essay using SonoVue

C. Avigo, P. Cabassa, L. Romanini, L. Grazioli, M. Cristinelli; Brescia/IT

Learning Objectives: 1) to illustrate the range of focal liver lesions that enhance at CEUS. 2) to understand how to avoid the pitfalls. 3) to highlight the differences between CEUS and CT/MR.

Background: CEUS is very sensitive in the assessment of vascularization of focal liver lesions. This educational exhibit will show the wide range of lesions that enhance with the administration of SonoVue with a special focus on arterial phase. The spectrum of diseases include well known hypervasculat lesions at like HCCs, FNHs, hemangiomas and hypervasculat metastases as well as lesions that normally doesn't typically enhance at cross sectional imaging (CT/MR) like so called hypervasculat metastases and cholangiocarcinomas.

Procedure Details: CEUS was performed with second generation contrast media (SonoVue, Bracco) at the standard dose of 2.4 ml with continuous real time scanning at low mechanical index. Images and videos of each lesion pre and post contrast were recorded digitally.

Conclusions: Knowledge of the vascular patterns of enhancement could help in the differential diagnosis of focal liver lesions at CEUS.

Molecular Imaging

C-0405

Endothelial cell-targeted MR imaging using the anti-VEGFR2 and ICAM-1 antibody-conjugated Gd-DTPA

K.-H. Yoon, E.-A. Kim, J.-M. Hur, S.-H. Kim, Y.-H. Lee, K.-S. Choi; Iksan, Jeonbuk/KR

Objectives: We designed blood vessel endothelial cell-targeted MR contrast agents which were prepared with bioconjugation of gadolinium diethylenetriaminepentaacetic acid (Gd-DTPA) and anti-VEGFR2 or ICAM-1 antibody.

Methods and Materials: The anti-VEGFR2 and ICAM-1 antibodies were purified from the culture supernatant of rat hybridomas using the protein A/G-coupled affinity chromatography. The endothelial cell-specific contrast effect was assessed by the MR imaging of its differential contrast effects to human umbilical vein endothelial cells and non-endothelial cells (human fibrosarcoma cell line). The Gd-DTPA-antibody complexes (10 µg/ml) were added to the cell and placed at 4 °C for 4 hrs. MR image was obtained by the 1.5 T module with a microscopic coil. The endothelial cell-specific binding of the Gd-DTPA-antibody conjugates was also confirmed by immunofluorescence staining.

Results: The antibodies were conjugated with Gd-DTPA in an about 50% yield based on the protein content of the Gd-DTPA-antibody complex. The Gd-DTPA-anti-VEGFR2 antibody complex displayed endothelial cell-specific contrast effects in MR imaging. Immunofluorescence assay also showed that Gd-DTPA-anti-VEGFR2 antibody conjugates stained the endothelial cells but not fibrosarcoma cells. Gd-DTPA-anti-ICAM-1 antibody complex exhibited predominant binding to the endothelial cells which were stimulated with 2nM TNF-alpha, a potent inducer of ICAM-1 on endothelial cells.

Conclusion: We suggest that Gd-DTPA-anti-VEGFR2 antibody conjugates selectively detect the vessel endothelial cells and give endothelial cell-specific MR image. Moreover, Gd-DTPA-anti-ICAM-1 antibody complex appears to specifically bind the ICAM-1-expressing endothelial cells which is a typical characteristic of the inflammation, suggesting that Gd-DTPA-anti-ICAM-1 antibody is a useful MR contrast agent for the inflammatory tissue.

C-0406

In-vivo tracking of genetically engineered, anti HER2/neu directed natural killer cells to HER2/neu positive mammary tumors with magnetic resonance imaging

H.E. Daldrup-Link¹, R. Meier², M. Rudelius², G. Piontek², S. Metz², C. Uhreik³, W. Wels³, J. Schlegel², E.J. Rummeny²; ¹San Francisco, CA/US, ²Munich/DE, ³Frankfurt a. Main/DE

Purpose: To optimize labelling of human natural killer (NK) cells with iron oxide contrast agents and to monitor the in vivo distribution of genetically engineered NK cells, directed against HER2/neu receptors, to HER2/neu positive mammary tumors with magnetic resonance (MR) imaging.

Methods and Materials: Parental and genetically modified HER2/neu specific NK-92-scFv(FRP5)-zeta cells, expressing a chimeric antigen receptor specific to the tumor-associated HER2/neu antigen, were labelled with Ferumoxides and Ferucarbotran using simple incubation, lipofection, and electroporation. Labelling efficiencies were determined by spectrometry. Subsequently, Ferucarbotran-labelled NK-92-scFv(FRP5)-zeta or parental NK cells were intravenously injected into six mice with implanted HER2/neu positive mammary tumors. The tumor accumulation of the NK cells was monitored with MR before and 24 hours (h) after cell injection (p.i.). MR data were correlated with histopathology.

Results: Parental and genetically modified NK-92-scFv(FRP5)-zeta cells could be labelled with Ferucarbotran and Ferumoxides by lipofection and electroporation, but not simple incubation. The cytoplasmatic iron uptake was significantly higher after labelling with Ferucarbotran than Ferumoxides ($p < 0.05$). After injection of NK-92-scFv(FRP5)-zeta cells into tumor bearing mice, MR showed a significant signal decline in HER2/neu positive tumors 24 h p.i. Conversely, injection of parental NK cells, not directed against HER2/neu receptors, did not cause significant signal changes of the tumors. Histopathology confirmed an accumulation of the former, but not the latter cells in tumor tissue.

Conclusion: Human NK cells can be efficiently labelled with clinically applicable iron oxide contrast agents. The in vivo distribution and tumor accumulation of these labelled cells can be monitored in vivo with MR imaging.

Scientific and Educational Exhibits

C-0407

Human progenitor cells migrate into squamous cell carcinoma (SCC) xenografts

F.M.A. Kiessling, J. Dittrich, T. Moehler, M. Le-Huu, M. Bock, R. Schulz, J. Peter, M. Mueller, W. Semmler; Heidelberg/DE

Purpose: Progenitor cells participate in various repair processes, however, their role in tumor formation remains unclear. Purpose of this study was to evaluate, whether these cells migrate into human squamous cell carcinomas (SCC) in relevant amounts.

Methods and Materials: SCC were grown in the upper thigh of nude mice. An > 80% pure preparation of AC133+ human stem-cells was obtained from peripheral blood of G-CSF stimulated humans. Stem cells were labeled with 111In-oxine and SPIOs. Intracellular iron-concentrations were determined by mass-spectroscopy. The labeled cells were injected intravenously or subcutaneously in the lower thigh at the tumor side and tracked over 5 days by scintigraphy and MR imaging.

Results: Only the sessile fraction of human stem cells/progenitor cells showed high uptake rates of SPIO (12 pg/cell after 5 h incubation with 3 mg Fe/ml). Related to the quadriceps muscle of the contralateral side 5.1/4.0 times higher cell concentrations were found in tumors after subcutaneous/intravenous injection as determined by gamma counting. Independent of the injection route highest stem cell fractions were found in liver, spleen and kidney. In the bone marrow stem cell concentrations were 2.6/6.9 (subcutaneous/intravenous) fold higher than in the muscle. Accumulation of labeled cells in tumors was successfully monitored using MR imaging and confirmed by histology, where Prussian blue positive cells were detected along stromal components including blood vessels.

Conclusion: Thus, human stem cells accumulate in human SCC are located in the stromal compartment in particular the tumor blood vessels. The pathophysiological role of these cells in tumor progression and the mechanisms of incorporation into the tumor tissue are currently under investigation.

C-0408

Receptor-PET/CT of neuroendocrine tumors using the gallium-68 labelled somatostatin analog DOTA-NOC: First clinical results

R.P. Baum¹, M. Schmücking¹, A. Niesen¹, K.P. Zhernosekov², F. Rösch²; ¹Bad Berka/DE, ²Mainz/DE

The octapeptide [DOTA]-1-Nal3-octreotide (DOTA-NOC) has 3-4 times higher binding affinity to sstr2 than DOTA-TOC (Wild, EJNM 2003;30:1338). These promising preclinical data prompted us to use this radiopeptide for somatostatin receptor PET imaging in patients with neuroendocrine tumours (NET) after labelling with Gallium-68, a short-lived positron emitter ($t_{1/2}$ 68 min). Ga-68 was eluted from a 30 mCi Ge-68/Ga radionuclide generator. Following chemical and radiochemical purifications, Ga-68 was eluted into the labeling vial containing 50 µg DOTA-NOC. Radiolabeling yields of < 80% were achieved within 15 min. Ga-68-DOTA-NOC was purified and finally eluted using 0.5 ml ethanol into 4.5 ml of isotonic saline. Overall, 370 MBq of Ga-68-DOTA-NOC were obtained within 20 min. 34 patients with histologically proven NET (mostly carcinoids) and progressive metastases were studied before peptide receptor radiotherapy (PRRT). A mean of 74 MBq (65-140 MBq) Ga-68 DOTA-NOC was injected. Acquisition was started 20-110 min p.i. using an LSO-based PET/CT (biograph DUO, Siemens). Standardized uptake values (SUV) were determined for all tumour lesions and normal tissues. SUV in liver metastases was as high 44.3 whereas normal tissue was in the range of 0.4 (lung) to 31.5 (spleen). Sandostatin given s.c. reduced the specific uptake by a factor of 4. Brilliant PET/CT images of all known tumour lesions and in addition small lymph node metastases of less than 5 mm were easily visualized as early as 20 min p.i. Receptor PET/CT using Ga-68 labelled DOTA-NOC advances as the new gold standard for imaging of neuroendocrine tumours possibly allowing also tumour dosimetry.

C-0409

Combined MR- and NIR-targeting of macrophages using fluorochrome labelled magnetosomes *in vitro*

M.-R. Lisy¹, I. Hilger¹, R. Trost¹, J.R. Reichenbach¹, D. Schueler², W.A. Kaiser¹; ¹Jena/DE, ²Bremen/DE

Purpose: To label human cells with a bi-functional contrast medium for detection using near infrared optical imaging (NIR) as well as magnetic resonance tomography (MRT).

Methods and Materials: Fluorochrome Dy676 (Dyomics, Jena) has been covalently bound to bacterial magnetic nanoparticles (magnetosomes, particle diameter 42 nm). Cells from human macrophage cell line J774 were incubated with

the bi-functional contrast agent and examined by a whole body near infrared imaging system as well as by using a 1.5 T clinical MR system. T1 and T2 relaxation times were determined. Labelled cells were further characterized with fluorescence spectroscopy, fluorescence activated cell sorting (FACS) and confocal laser scanning microscopy (CLSM).

Results: Compared to non-labelled controls, macrophages that were incubated with our new contrast agent showed a significant fluorescence emission at 699nm using the whole body NIR imaging system, fluorescence spectroscopy, FACS and CLSM after excitation at 676nm. CLSM data showed highest fluorescence intensities within intracellular vesicles. The presence of magnetic nanoparticles caused a substantial signal decrease. Both T1 and T2 were shortened with increased labelling.

Conclusions: Human macrophages can be labelled by uptake of our new bi-functional contrast agent. The labelled cells can be detected by both 1.5 T MR scanner as well as by NIR fluorescence imaging.

C-0410

withdrawn by authors

C-0411

Non-invasive imaging of alpha-v-beta-3-expression in patients with malignant tumors using [¹⁸F]GalactoRGD

A.J. Beer¹, R. Haubner¹, M. Goebel¹, S. Luderschmidt¹, A. Grosu¹, W.A. Weber², E.J. Rummeny¹, M. Schwaiger¹; ¹Munich/DE, ²Los Angeles, CA/US

Purpose: The integrin $\alpha v\beta 3$ is of importance in angiogenesis and tumor metastasis. We tested the performance of [¹⁸F]GalactoRGD for non-invasive imaging of $\alpha v\beta 3$ -expression in patients with malignant tumors.

Methods and Materials: 17 patients with malignant tumors (melanoma n = 7; sarcoma n = 7; head/neck cancer n = 3) were examined on an EcateExact PET-scanner or a Sensation 16 biograph-scanner after injection of 144-200 MBq [¹⁸F]Galacto RGD. Multiple scans from the thorax to the pelvis between 0-100 min p.i. and delayed images up to 140 min p.i. were acquired. Results were correlated with morphologic imaging (n = 17) and with the results of histopathology (n = 14) and immunohistochemistry against $\alpha v\beta 3$ (n = 6).

Results: Analysis of metabolites in blood samples (n = 4) using RP-HPLC showed > 95% intact tracer up to 120 min p.i. [¹⁸F]GalactoRGD showed predominantly renal and to a lesser extent hepatobiliary excretion with rapid blood clearance. SUV measurements in normal organs were as follows (5 min and 60 min p.i.): Blood 2.8 ± 0.5 / 1.2 ± 0.5 ; liver 2.7 ± 0.5 / 2.3 ± 0.5 ; kidney 9.1 ± 3.8 / 6.9 ± 4.3 ; intestines 3.2 ± 0.7 / 2.9 ± 0.6 . Two patients with multiple melanoma metastases and one patient with a liposarcoma showed no significant tracer uptake. The SUV in patients with visible uptake ranged from 1.2 to 10.0 (mean 4.2; 60 min p.i.) with continuously rising tumor/blood ratio over time (mean 3.3 ± 2.6 ; 60 min p.i.). Immunohistochemistry confirmed the expression of $\alpha v\beta 3$ on tumor cells (n = 2/6) and endothelium of blood vessels (n = 6/6).

Conclusion: [¹⁸F]GalactoRGD allows non-invasive imaging of $\alpha v\beta 3$ -expression in humans with good contrast. This method could be used for analysis of biological activity of tumors and for monitoring pharmacotherapy with $\alpha v\beta 3$ -selective agents.

C-0412

An automated image-guided robot arm control system for transgenic and drug delivery studies

Y.H. Huang, C.L. Chen, T.H. Wu, M.H. Lin, C.C. Yang, J.J.S. Lee; Taipei/TW

Purpose: Biological discovery and molecular genetic techniques has made great progress in recent years, especially for malignant tumors, trying to figure out the most effective ways of treatment. Hence, the aim of this study is to establish an integration of image-guide automatic robot arm system, for transgenic or drug delivery onto animal tumor models.

Methods and Materials: This system is composed of three main parts, including image fusion technique, stereotactic frame system, and automatic robot arm system. (1) The image fusion technique combines the PET imaging with MR imaging, providing direct image registration of both functional and anatomical information. (2) the small animal stereotactic frame immobilizes the experiment animals and then employs the fiducial marker to pinpoint the transformation relationships between the imaging and physical coordinates. (3) the image-guide automatic robot arm system is set up upon a stereotactic frame device that can be well directed to the target positions, and in accordance with predefined delivery routes for achieving high precision of gene or drug delivery.

Results: The system successfully guided the micro-injection from image planned

Scientific and Educational Exhibits

delivery routes into practice. Consequently, the mean of registration errors in our system is less than 1.5 mm, that apply to achieve the effective drug delivery rate up to 85% and reduce the normal tissue uptake.

Conclusion: The main advantage of the system is that it can accurately provide relative location sites of tumors from high resolution imaging and also provide highly precise micro-injection to increase the feasibility and safety for gene (drug) delivery.

Genitourinary

Female

C-0413

Role of MR imaging and HSG in the evaluation of congenital uterine malformations

P. Nin Garaizabal, B. Ubeda Hernandez, A. Roma Dalfo, C. Traid Niella, R. Rotger Regi, A. Palacio Hermoso de Mendoza; *Barcelona/ES*

Learning Objectives: Describe the mean features of congenital uterine malformations with hysterosalpingography (HSG) and magnetic resonance (MR) imaging. Identify which imaging features at MR imaging are more specific for each entity for differential diagnosis.

Background: Congenital uterine malformations originate from nondevelopment or nonfusion of the Müllerian ducts, resulting in agenesis or doubling of the female reproductive organs, which are classified according to the American Society of Fertility. Anomalies of the urinary tract are frequently associated. Müllerian duct anomalies are often related to a broad variety of symptoms, including infertility and increased risk of miscarriages.

Imaging Findings: From January 2000 to December 2002, a total of 974 patients diagnosed of primary and secondary sterility underwent HSG at our institution, selecting those cases with congenital uterine malformations, according to the American Society of Fertility, correlating the findings with those found at MR imaging. The most frequent and illustrative cases of congenital uterine malformations are shown including unicornuate, septate, bicornuate and didelphys uterus, describing the HSG findings and making special emphasis in the role of MR imaging in the evaluation of the features that allow a differential diagnosis between the different entities.

Conclusions: HSG is the most commonly used technique in the diagnostic evaluation of infertility, often identifying Müllerian duct anomalies. MR is useful for documenting uterine morphology and is currently the most accurate technique for its diagnosis.

C-0414

Differential diagnosis of gynaecological solid masses on MR imaging-pattern approach and radiologic-pathologic correlation

S.P. Prabhu, T.V. Narayan, K. Prescod; *Bristol/UK*

Learning Objectives: 1. To define an algorithm for the differential diagnosis of gynaecological solid tumours on MR imaging. 2. To highlight features of gynaecological masses that suggest malignancy. 3. To illustrate the correlation of MR imaging appearances with histopathology. 4. Provide a desktop guide to the differential diagnosis of gynaecological tumours on MR imaging.

Background: There is a large variety of solid gynaecological tumors and this makes the diagnosis of these tumors challenging, even to experienced radiologists. Determining the organ of origin and then deciding if the mass could be malignant is the first step in the diagnostic algorithm.

Procedure Details: We reviewed MR imaging archives of two teaching hospitals in our area from Jan 2000 to Jun 2004 to identify cases of solid gynaecological tumours. We obtained clinical and histopathological data to compare with the radiology reports. Based on this data, we developed a desktop algorithm for the differential diagnosis of these tumours. We identified features of malignancy and invasive spread that are cornerstones of further management of these lesions. We also looked at and concurrent CT and ultrasound images in cases where these studies were useful. We elaborate findings of ovarian tumours and uterine tumours in this pictorial essay based on our research. In the final part of the essay, we present sample cases to show that our desktop algorithm is a practicable tool.

Conclusion: MR imaging is a useful investigation in the staging and differential diagnosis of solid gynaecological tumours, if clinical data is used in conjunction with radiological appearances.

C-0415

MR image characteristics during and after cryoablation of uterine fibroids

T. Shimizu, A. Sawada, Y. Kodama, Y. Watanabe, Y. Sakuhara, D. Abo, M. Funakubo, Y. Yoshida, K. Miyasaka; *Sapporo/JP*

Purpose: To demonstrate MR imaging characteristics of uterine fibroids during and after cryoablation.

Methods and Materials: Symptomatic uterine fibroids are cryoablated percutaneously using a MR compatible argon-based system under open MR imaging guidance. Follow up T1-weighted, T2-weighted and Gd-DTPA enhanced T1-weighted MR images are taken over at one day, two week, and six week intervals.

Scientific and Educational Exhibits

Results: Seven fibroids in 6 cases were treated. Five fibroids were intramural and two were submucosal. The maximum diameters of the fibroids ranged from 3.7 to 10 cm and the average was 7.4 cm. The maximum diameters of the frozen area ranged from 4.8 to 8.5 cm and the average was 6.5 cm. The average freezing time was 18.7 min. In four cases of intramural fibroids, the non-contrast enhanced areas in Gd-DTPA enhanced T1-weighted images at one day and 2-week intervals after cryoablation were larger than the frozen area. In two cases of submucosal fibroids, normal myometrium around the fibroids were frozen and the signal intensity of the MR images returned to normal in six weeks.

Conclusion: MR images after cryoablation indicate the necrotic area is larger than the frozen area in the uterine fibroid and we can expect spontaneous recovery of normal myometrium in the frozen area.

C-0416

Female genitalia on MR imaging: The comparison of premenopausal and postmenopausal women

D. Sung, K. Ahn, S. Cho, Y. Kim, K. Chung, J. Kim; Seoul/KR

Purpose: To describe normal anatomy and differences of the female genital organs on MR imaging between premenopausal and postmenopausal women.

Materials and Methods: A total of 19 premenopausal and 18 postmenopausal healthy women underwent 1.5 T MR imaging with a torso phased array coil. Axial T1, TSE T2 and fat suppressed Gd-enhanced axial T1-weighted images were obtained. Two radiologists measured the wall thickness of vagina, urethra and labium minora, the width of clitoral crura and vestibular bulb and the sectional dimensions of the clitoral glans.

Results: All genital structures were delineated more clearly on fat suppressed Gd-enhanced axial T1-weighted images than noncontrast axial T1 and TSE T2-weighted images. The separate three layers of vaginal wall were well visualized in premenopausal subjects but not clearly defined in postmenopausal subjects. The urethra had a target-like appearance with three layers in premenopausal and postmenopausal women. The clitoral crura were well delineated as a wishbone-shaped structure surrounding the urethra and vagina. The two vestibular bulbs were paramedian in location and lying just posterior to the clitoral crura as oval and elongated, enhanced structures. Postmenopausal subjects were observed to have smaller vaginal wall thickness (7.0 ± 0.9 mm versus 5.2 ± 0.7 , $p < 0.001$), urethral wall thickness (7.7 ± 0.8 versus 5.9 ± 0.9 , $p < 0.001$) and vestibular bulb width (5.6 ± 0.8 versus 4.9 ± 0.5 , $p < 0.05$) than premenopausal subjects.

Conclusions: The normal anatomy and differences of the female genital organs between premenopausal and postmenopausal women were well discernible on fat suppressed Gd-enhanced axial T1-weighted images. This study may provide valuable information for the future studies of female sexual function.

C-0417

Salpingitis isthmica nodosa (SIN) in female infertility

V.S. Gada, A. Hemingway, R. Williamson, G. Trew, S. Lavery, R. Margara; London/UK

Learning Objective: This study seeks to determine the incidence, distribution and clinical significance of salpingitis isthmica nodosa (SIN) diagnosed by hysterosalpingography (HSG) in women presenting with infertility.

Background: SIN, an uncommon disease of the fallopian tubes, is characterized microscopically by small diverticulae present in an irregularly hypertrophied myosalpinx.

Procedure Details: Between November 1996 and December 2003, 4464 women presenting to a tertiary referral centre with infertility were referred to two radiologists for an HSG. SIN was diagnosed in 100 examinations in 96 women, age range 21 to 47 years, (mean 35 years), accounting for 2.24% of the whole population studied and 10% of those with tubal pathology. Thirty two patients (33%) presented with primary and 64 patients (67%) with secondary infertility; 27 (28%) had one or more ectopic pregnancies. Other associated pathology included hydrosalpinges 23%, tubal occlusion 19%, tubal polyps 3%, uterine lesions (fibroids, adenomyosis, scar tissue) 20%. Fifteen patients had 46 previous IVF treatments elsewhere, 8 of which had been successful. Treatment options for SIN include resection of the diseased segment and tubal reanastomosis.

Conclusion: HSG is important not only in making the diagnosis of SIN but also in excluding other associated pathology which may dictate the success of the preferred management option. The strong association of SIN with ectopic pregnancy should also affect the early pregnancy management of women with this diagnosis.

C-0418

Patterns of recurrence in ovarian carcinoma

J.L. Hughes, A. Sadove, A. Rockall, R. Reznik; London/UK

Purpose: The aim of our study was to describe CT patterns of recurrent ovarian carcinoma after proven remission, to aid earlier recognition of recurrent disease which may facilitate successful treatment with second-line therapy.

Methods and Materials: We identified women with radiological relapse after complete remission, established by laparotomy and radiological assessment. CT imaging was retrospectively reviewed and site and patterns of recurrence were documented.

Results: Since 1985, 393 women were treated and 173 (44%) achieved complete remission. Of the 173, 79 (46%) had relapsed. Imaging was available in 60 patients. The most common site of relapse was in the pelvis (25 [42%]) which was seen alone in 12 (20%). 20 (33%) relapsed with enlarged lymph nodes, 13 (22%) had para-aortic or aorto-caval nodes. Five had para-cardiac nodes, and only three relapsed with pelvic or inguinal nodes. In 6 patients (10%) lymphadenopathy was the sole manifestation of recurrence. 15 (25%) presented had extra-peritoneal recurrence: 3 with splenic and 4 with hepatic metastasis and 2 with both; 3 with brain, 3 in skeletal muscles. 22 (36%) relapsed with peritoneal thickening. Median time to peritoneal relapse was 1.2 years (inter-quartile range 0.9-1.7) compared with 2.1 years (1.2-4.2) in those without radiological evidence of peritoneal relapse [$p < 0.001$].

Conclusion: Despite clinical complete remission, almost half relapse. The commonest mode of relapse is a recurrent pelvic mass or peritoneal disease. Extra-peritoneal disease may be the sole manifestation of recurrent disease in a significant number of women.

C-0419

Color Doppler and three dimensional ultrasound hystero-contrast-salpingography

B.M. Plavsic¹, S. Kupesic²; ¹New Orleans, LA/US, ²Zagreb/HR

Purpose: To demonstrate the efficacy of transvaginal color Doppler hystero-contrast-salpingography (Hy-Co-Sy) and 3D ultrasound Hy-Co-Sy in evaluation of patency of Fallopian tubes.

Methods and Materials: The findings of color Doppler Hy-Co-Sy in 152 patients and 3D ultrasound Hy-Co-Sy in 58 patients were compared to laparoscopic chromoperturbation. The contrast media used were isotonic saline or commercial echo contrast medium Echovist.

Results: Findings in 145 of 152 color Doppler Hy-Co-Sy were confirmed by chromoperturbation. Bilateral tubal patency was successfully detected by color Doppler Hy-Co-Sy in 64 of 67 patients (95%), while unilateral patency was shown in 36 out of 38 (95%). In 45 patients color Doppler Hy-Co-Sy showed bilateral tubal occlusion. Fifty six out of 58 (96%) 3D ultrasound Hy-Co-Sy findings were also confirmed by chromoperturbation. Transvaginal color Doppler Hy-Co-Sy had 98% sensitivity, 90% specificity, 95% positive predictive value and 96% negative predictive value respectively. Bilateral tubal patency was correctly detected by 3D ultrasound Hy-Co-Sy in each of 24 patients, while unilateral tubal patency was demonstrated in 17 out of 18 cases. In 15 patients 3D ultrasound Hy-Co-Sy indicated bilateral tubal occlusion. For 3D ultrasound Hy-Co-Sy the sensitivity was 97%, specificity 94%, positive predictive value 97% and negative predictive value 94%.

Conclusion: Transvaginal color Doppler Hy-Co-Sy is an efficacious and safe method to evaluate tubal patency without exposure to radiation and iodinated contrast media. Three dimensional ultrasound Hy-Co-Sy offers the possibility of simultaneous presentation of the uterine cavity and corresponding tube, shortening the procedure and discomfort.

C-0420

MR imaging of the urethral sphincter in incontinent women

K.J. Macura, R.R. Genadry, D.A. Bluemke; Baltimore, MD/US

Learning Objectives: 1. To review anatomic properties of the urethral sphincter, periurethral attachments, and pelvic floor that facilitate continence. 2. To discuss techniques for the evaluation of urethral morphology and function with MR imaging. 3. To review imaging findings in urinary incontinence, with a focus on dynamic pelvic floor evaluation and endocavitary MR imaging.

Background: Two generic conditions cause stress urinary incontinence in women: bladder abnormalities (detrusor overactivity and low bladder compliance) and sphincter abnormalities. Sphincteric incontinence is related to urethral hypermobility and intrinsic sphincter deficiency. MR imaging allows complete visualization of the urethral sphincter muscle and urethral support ligaments.

Scientific and Educational Exhibits

Imaging Findings: Dynamic MR imaging of the pelvic floor during straining allows evaluation of the urethral mobility, vesical neck insufficiency, and detection and grading of cystocele. Endocavitary MR imaging (intraurethral and endovaginal) provides higher spatial resolution imaging with smaller field of view, increased signal to noise, and improved depiction of the urethral sphincter morphology (striated and smooth muscles) and perirethral attachments (periurethral, paraurethral, and pubourethral ligaments).

Conclusions: MR imaging of the pelvic floor and urethral sphincter contributes to the evaluation of patients with urinary incontinence by allowing detailed assessment of the anterior pelvic floor compartment and urethral sphincter abnormalities related to urethral hypermobility and intrinsic sphincter deficiency.

C-0421

Three-dimensional power Doppler ultrasound in detection of early ovarian carcinoma

S. Kupesic¹, B.M. Plavsic²; ¹Zagreb/HR, ²New Orleans, LA/US

Purpose: To investigate the efficacy of different sonographic methods - 2D transvaginal grey scale ultrasound, 2D color Doppler ultrasound, 3D ultrasound, 3D power Doppler and contrast-enhanced 3D power Doppler ultrasound in preoperative evaluation of early ovarian carcinoma.

Methods and Materials: A five-year retrospective analysis of 43 patients with stage I ovarian carcinoma evaluated a week prior to surgery was performed. Sonographic assessment included examination of the ovarian volume, morphology and vascularity.

Results: Forty two of 43 early ovarian carcinomas were detected by combination of five complementary sonographic methods. 2D transvaginal ultrasound detected 28 (65%) cases of stage I ovarian carcinomas. By adding 2D transvaginal color Doppler ultrasound, 35 out of 43 early ovarian cancers (81%) were found. Morphological analysis by 3D ultrasound detected 31 of 43 ovarian carcinomas, reaching diagnostic sensitivity of 72%, yielding higher sensitivity than 2D transvaginal ultrasound alone. Qualitative analysis of the tumor neovascularity architecture by 3D power Doppler significantly improved the sensitivity to 93% and detected 40 cases of 43 stage I ovarian carcinomas. When morphological features obtained by 3D ultrasound were added to 3D power Doppler findings, diagnostic sensitivity of 95% has been achieved. Finally, the use of a contrast-enhanced 3D power Doppler sonography showed diagnostic sensitivity of 98% with only one false negative case.

Conclusion: Combined evaluations of morphology and neovascularity by 3D power Doppler ultrasound improve early detection of ovarian carcinoma. Contrast-enhanced 3D power Doppler imaging further contributes to the detection of the earliest features of ovarian carcinoma neovascularity.

C-0422

MR features of physiologic and benign conditions of the ovary

K. Tamai, T. Koyama, A. Kido, S. Umeoka, T. Fujiwara, T. Saga, S. Fujii, K. Togashi; Kyoto/JP

Learning Objectives: To review a spectrum of MR features in physiologic and benign conditions of the ovary.

Background: In reproductive women, various physiologic conditions can cause morphologic changes of the ovary, resembling pathologic conditions. Various benign diseases can also frequently simulate malignancies. In these conditions, MR imaging can play an important role in establishing accurate diagnosis and determining appropriate management. In this exhibit, MR and clinical features of various physiologic and benign conditions of the ovary are illustrated.

Imaging Findings: Various physiologic conditions cause ovarian cystic lesions. Corpus luteum cysts typically have a thick wall with increased intensity on T1WI. Endometrial cysts usually show specific pattern of signal intensity. In pregnant women, decidual change in endometrial cysts should not be confused with secondary malignancy. In peritoneal inclusion cysts, careful evaluation of the configuration may avoid confusion with neoplasms. Multi-cystic lesions simulating cystic neoplasms can be seen in hyperreactio luteinalis, ovarian hyperstimulation syndrome, and polycystic ovary syndrome. Recognition of clinical settings will help diagnose these conditions. Although ovarian torsion and massive ovarian edema may mimic solid malignant tumors, recognition of normal follicles and anatomic structures may help establish correct diagnosis. Many benign tumors, including teratoma, Brenner tumor, and sex-cord stromal tumor, frequently show characteristic MR findings. In inflammatory diseases, transfascial spread of the lesion should not be confused with invasive malignancy. Radiologic identification of abscess facilitates establishing diagnosis.

Conclusion: Knowledge of MR features in a variety of physiologic and benign conditions of the ovary facilitates establishing accurate diagnosis and determining treatment.

C-0423

Preoperative assessment of deep myometrial and cervical invasion in endometrial carcinoma: Comparison of magnetic resonance imaging and histopathologic evaluation

C. Vasconcelos, A. Félix, T.M. Cunha; Lisbon/PT

Purpose: This study aimed to evaluate the accuracy of magnetic resonance imaging (MRI) in the detection of deep myometrial invasion and cervical extension by endometrial carcinoma.

Methods and Materials: One hundred and one consecutive patients with histologically documented endometrial carcinoma were included in this prospective study, between July of 1998 and April of 2004. All patients underwent a preoperative pelvic MRI and the findings were compared with histologic diagnosis on surgical specimen. Axial T1, transverse and sagittal T2-weighted images and a dynamic study after the administration of 0.1 mmol gadolinium per kilogram of body weight in the sagittal plane were obtained with a 1-T superconducting magnet (model Gyroscan NT; Philips; Eindhoven, Netherlands), using a body coil.

Results: In the 101 cases studied by pelvic MRI, 43 were classified as deep myometrial invasion ($\geq 50\%$ of myometrium), 58 as superficial invasion ($< 50\%$). The pathologic evaluation confirmed those 43 cases as having deep myometrial invasion. Cervical extension in MRI study was found in 19 cases. Pathologic study found cervical extension and / or invasion in 31 cases, including all cases identified by MRI. The accuracy, sensitivity and specificity of MRI were 95%, 89%, and 100%, respectively, detecting deep myometrial invasion and 88%, 61%, and 100%, respectively, detecting cervical invasion.

Conclusion: MRI is an adequate method for determine the depth of myometrial invasion and cervical extension in endometrial carcinoma. The high accuracy achieved suggests that MRI is a reliable method for preoperative endometrial carcinoma "imaging staging".

C-0424

Posttreatment complications of gynecologic cancer

S. Vinhais, A. Félix, T.M. Cunha; Lisbon/PT

Learning Objectives: To review the imaging findings of complications related with the treatment of gynecologic cancer (GC).

Background: Curative procedures of GC can give rise to several complications, which can be separated into three categories: postsurgical, postirradiation and secondary to chemotherapy. Recognition of these complications is relevant, not only for their significant morbidity, and even mortality risk, as also because some may simulate tumoral disease, a critical situation for adequate clinical management.

Imaging Findings: Postsurgical complications of fluid nature comprise abscesses, hematomas, and more rarely, lymphoceles and urinomas, all these pathologic conditions being generally easy to diagnose. Difficulties arise in the identification of fistulas and unexpected entities such as gossypibomas.

The spectrum of postirradiation complications (fistulas, cystitis, stenosis of small bowel, thickening of uterosacral ligaments, hydro/hematometrocolpos, cases of hydrosalpinx, osteoradionecrosis and insufficiency fractures, among others) includes fibrotic changes and bone lesions, sometimes problematic of distinguishing from recurrent or metastatic disease. Imaging of chemotherapy complications is seldom depicted. Hepatic infarct is an example of a serious complication that may occur with specific drugs. Extensive knowledge of the possible effects of the chemotherapeutic agents is however crucial for a correct radiologic interpretation.

Conclusion: A careful clinical history comprising the previous therapeutics is essential for an appropriate radiological evaluation of patients with GC, allowing better orientation and interpretation of the exams. Computed tomography and magnetic resonance are the main imaging techniques to diagnose the posttreatment complications, but a multi-modality approach, including conventional radiographic studies, might be necessary.

C-0425

MR imaging spectrum of pelvic and extrapelvic endometriosis

A. Roma, P. Nin, B. Ubeda, J. Ares, C. Traid, A. Palacio; Barcelona/ES

Learning Objectives: - Describe the different manifestations of pelvic and extrapelvic endometriosis. - Outline MR imaging features of pelvic endometriosis. - Identify the MR imaging features that allow a differential diagnosis of endometriomas from other adnexal masses.

Background: Endometriosis is a gynaecologic disorder primarily affecting women during their reproductive years. Pathologically, it is the result of endometrium located outside the uterus and affects 5-10% of women. The most accepted etiologic theory is metastatic implantation from retrograde menstruation. Symptoms

Scientific and Educational Exhibits

do not necessarily correlate with severity of the disease. Patients may be asymptomatic or present with pelvic pain, infertility or adnexal masses. MR is a very useful and specific technique for the evaluation of endometriosis. Nevertheless, laparoscopy remains the mainstay for diagnosis, staging and treatment of the disease.

Imaging Findings: Pelvic endometriosis refers to lesions of the fallopian tubes, ovaries and local peritoneum. Extrapelvic endometriosis is defined as implants found elsewhere in the body, including the gastrointestinal tract, urinary tract and thoracic cavity. MR imaging is a very specific imaging technique for the diagnosis of endometriomas, more than the other non-invasive imaging techniques, due to the specific signal intensity of the lesions at the different sequences, depicting the presence of implants and adhesions and involvement of surrounding anatomic structures. Our protocol includes axial T1- and T2-weighted and T1 fat-suppressed, sagittal FSET2, and optional coronal FSET2 sequences.

Conclusion: This exhibit provides an overview of the pelvic and extrapelvic manifestations of endometriosis emphasizing the utility of MR imaging to diagnose and stage this entity.

C-0426

The effectiveness of MR hysterosalpingography in infertility

S. Karaköse, A. Karabacakoglu, E. Yalinkiliç, R. Haykir, H. Görkemli; Konya/TR

Purpose: In infertile patients the role of conventional hysterosalpingography (CHSG) and 3D MR hysterosalpingography (3D-MRHSG) were evaluated for detection of tubal, uterine, ovarian and paraovarian causes of infertility.

Material and Methods: 35 cases, their ages ranging between 19-39, clinically diagnosed as infertile (19 primary, 16 secondary) underwent CHSG and 3D-MRHSG. In examination, diluted paramagnetic and nonionic contrast material were injected into uterine cavity by 5F balloon catheter. Firstly 3D-MRHSG and then CHSG were performed in all cases. Also complementary MR images were taken during 3D-MRHSG.

Results: In 27 cases bilateral patent fallopian tubes were determined by CHSG, while bilateral tubal patency were determined in 25 of cases by 3D-MRHSG. Two tubal obstructions which has been demonstrated by 3D-MRHSG however were patent and patency was shown by CHSG. Congenital uterine anomalies were detected in 5 cases. Furthermore 4 cases with polycystic ovarian syndrome, 2 cases with ovarian cysts, a case of endometrioma, 5 cases with myoma were diagnosed by 3D-MRHSG but they were not shown by CHSG.

Conclusion: CHSG is used routinely in detection of uterine cavity pathologies and tubal patency, while CHSG remain insufficient in detection of myometrial pathologies, uterine congenital anomalies, ovarian and paraovarian pathologies. 3D-MRHSG is superior in the detection of internal and external borders of uterus, myometrial layers, ovarian and paraovarian pathologies. Also tubal patency and the uterine cavity can be examined by 3D-MRHSG. Due to these advantages of 3D-MRHSG it can be an effective alternative to CHSG.

C-0427

Imaging of endometriosis

G.C. Hargaden, M. Keogan; Dublin/IE

Learning Objectives: 1. To outline the classical appearances of endometriosis on ultrasound, barium enema and MR imaging. 2. To highlight the different imaging features of endometriomas and haemorrhagic ovarian cysts on ultrasound. 3. To show how the addition of fat saturation sequences on MR can improve diagnostic accuracy and help differentiate lipid-containing ovarian masses from endometriomas.

Background: Endometriosis is a common debilitating condition seen particularly in nulliparous women of child-bearing age in Europe and the USA. It is defined as the presence of functional endometrial tissue outside the endometrium and myometrium. Laparoscopy remains the gold-standard for diagnosis however many patients can be diagnosed on the basis of imaging findings in the correct clinical setting.

Procedure Details: Diagnosis of endometriosis remains a challenge to the radiologist although improvements in ultrasound and MR have led to improved diagnostic accuracy. We review the imaging findings of endometriosis on barium enema, the ultrasound appearances of endometriomas and highlight the differences between these and haemorrhagic cysts. We describe the optimal MR imaging sequences, illustrate how endometriomas can be confidently differentiated from lipid-containing dermoids and demonstrate the appearances of endometrial deposits in the bladder on MR imaging.

Conclusion: Although there are a wide range of imaging findings in endometriosis, familiarity with the more classical appearances as we describe in this educational exhibit can result in a high degree of diagnostic accuracy.

C-0428

Dynamic MR imaging in the assessment of female pelvic organ prolapse:

Baseline and post-surgical evaluation

A. Catalucci¹, L. Zugaro¹, M. Monina¹, A. Mancinotti¹, E. Di Cesare², C. Vicentini¹, C. Masciocchi²; ¹Teramo/IT, ²L'Aquila/IT

Purpose: To investigate the diagnostic role of MR imaging in the evaluation of female urinary incontinence and pelvic organ prolapse using dynamic MR imaging, in the baseline and after surgery using the "Patch and Plug" technique.

Material and Methods: 44 patients with a genuine stress urinary incontinence and genital prolapse were investigated by standard and dynamic MR imaging, using a 1.5 T unit. Patients were placed in a supine position with the legs slightly flexed and abducted; 250 ml of Gd-DTPA water solution were instilled into the bladder, 20 ml of Gd water-gel solution were injected into the vagina and 50 ml into the rectum. Dynamic images were obtained at rest and during Valsalva manoeuvre, using T1-FFE sequences on sagittal plane. Dynamic MR imaging was analyzed to determine the presence and extent of cystocele and vaginal vault prolapse.

Results: Dynamic MR imaging provided in all cases a good demonstration of genital prolapse during Valsalva manoeuvre; a good correlation with the clinical evaluation of both genital prolapse type and degree was found in the baseline and after surgery.

Conclusion: Dynamic MR imaging is a good aid in the evaluation of both kind and degree of the female pelvic organ prolapse. After surgery, it is useful to document both the disappear of the prolapse and the post-surgical evolution.

C-0429

Carcinosarcoma of the uterus: MR findings and the pattern of recurrence

S. Imai¹, T. Nakazono¹, Y. Matsuo², S. Kudo¹; ¹Saga/JP, ²Tokyo/JP

Purpose: To evaluate MR findings and the pattern of recurrence of uterine carcinosarcoma.

Material and Methods: We retrospectively reviewed clinical and radiologic findings of 10 women (ages 51-75, median age 65) with pathologically proven carcinosarcoma of the uterus. We evaluated preoperative MR findings, histopathological type, and surgical stage. We also evaluated the pattern of recurrence (rate, location, period after surgery), CT and MR findings of recurrence in 5 patients. The period of observation after the first diagnosis was 11-156 months (the mean 55.3 months).

Results: MR finding of primary uterine carcinosarcoma was a polyoid mass in the uterine cavity with inhomogeneous enhancement by contrast media. Five (50%) patients had recurrences within 12 months after the surgery. Locations of recurrences were at the stump of vagina, the pouch of Douglas, the retroperitoneum, and the pelvic wall. Extraabdominal recurrences were also seen in the lung and the thoracic vertebra. The majority of the abdominal and pelvic lesions were demonstrated as inhomogeneous solid masses similar to the primary lesions. All the patients with recurrence died within 10 months after the diagnosis of recurrence.

Conclusion: Uterine carcinosarcomas recurred in 50% of the patients within 12 months after the surgery, so they should be observed closely. In addition, uterine carcinosarcomas have no specific tumor marker, it is important to follow-up the patients radiologically.

C-0430

MR imaging features with pathologic correlation of uterine malignant mixed Mullerian tumors

E. Yamashita¹, T. Koyama², H. Kotani², A. Kido², S. Umeoka², T. Fujiwara², S. Fujii², Y. Imai¹, K. Togashi²; ¹Isehara-shi/JP, ²Kyoto/JP

Purpose: Malignant mixed Mullerian tumors (MMMTs) are rare but highly aggressive uterine tumor, though the role of MR imaging in this tumor have not been documented. The purpose of this study is to describe MR features of MMMTs in correlation with pathologic features, and to evaluate the accuracy of MR staging.

Methods and Materials: Preoperative MR images in 17 patients (age 50-82; mean 63.1) with pathologically confirmed MMMTs, including T1WI, T2WI and postcontrast-T1WI, were retrospectively reviewed for size, location, signal intensities and stage of the tumors. Pathologic specimens were reviewed for hemorrhage, necrosis, and the percentage of sarcomatous component. Pathologic stage was determined according to FIGO classification. Features and stages on MR imaging were compared with those in pathology.

Results: On MR, tumors were at least exophytic endometrial mass in all, with 10 lesions extending into the cervical canal. T1WI showed predominantly low intensity lesions in all, with focal high intensity (n=11). T2WI showed heterogeneous (n=13) or homogeneous high intensity lesion (n=4). Postcontrast-T1WI revealed

Scientific and Educational Exhibits

heterogeneous enhancement in all. Tumors with pathologic hemorrhage and necrosis corresponded to lesions with high intensity foci on T1WI. With increase of sarcomatous component, the size, the number of tumors with focal high on T1WI and heterogeneous appearance on T2WI increased. MR imaging provided correct staging in most of stage I lesions (8/10), but low accuracy for lesions over stage 2 (2/7).

Conclusion: MR features of MMMTs are variable according to pathological features. Although MR provides accurate staging in T1 disease, it frequently underestimates cervical involvement and extrauterine lesions.

C-0431

MR features of cervical adenocarcinoma with pathologic correlation

T. Koyama, S. Umeoka, A. Kido, K. Tamai, T. Saga, S. Fujii, K. Togashi; Kyoto/JP

Learning Objectives: To illustrate spectrum of MR features of cervical adenocarcinoma in correlation with pathologic findings, and to demonstrate problems and limitations in MR staging.

Background: In cervical cancer, the majority is squamous cell carcinoma (SqCC), while the incidence of adenocarcinoma is increasing. Histologically, cervical adenocarcinomas consist of several subtypes, which include mucinous carcinomas and carcinoma analogous to corpus cancer, such as endometrioid, serous, and clear cell carcinoma. The clinical and MR features differ according to histologic subtypes. Generally cervical adenocarcinomas are more resistant for chemotherapy and radiotherapy, and portends worse prognosis than SqCC. MR features in cervical adenocarcinoma have not been fully documented in radiologic literatures. In this exhibit, MR features in cervical adenocarcinoma are illustrated in correlation with pathologic findings. The problems in MR staging for adenocarcinoma are also discussed.

Imaging Findings: Cervical adenocarcinomas are typically demonstrated as infiltrative lesions of increased intensity on T2WI, arising from either cervical canal or lip. However, they can show variable appearance and signal intensity reflecting pathologic features. MR imaging occasionally fails in demonstrating invasive cancer confined within the cervical stroma. Although adenocarcinomas frequently infiltrate into the vaginal wall and parametrium, these extra-uterine extensions can be easily underestimated. As a result, the overall accuracy of MR staging in cervical adenocarcinomas is lower than that in SqCC.

Conclusion: The knowledge of MR features and clinical behavior of cervical adenocarcinomas helps accurate diagnosis and staging. The recognition of problems and limitations in MR staging encourages careful interpretation of MR findings.

C-0432

Ultrasound angiography in the assessment of cervical cancer treatment

E.A. Mikhailova, B.A. Minko, G.A. Ushakova, V.L. Vinokurov, K.V. Prozorovsky; St. Petersburg/RU

Purpose: To assess efficacy of 3D-ultrasound angiography (3D-UA) in the evaluation of cervical cancer (CC) treatment.

Materials and Methods: 25 patients (32-68 years old) with CC, stage II-III (FIGO classification) received combined radio- and chemotherapy including intra-arterial embolization (IAE) of internal iliac and uterine arteries. The treatment results were evaluated using 3D-UA. A digital color Doppler system SonoAce 8000 (Medison Co. Ltd., Korea) with transrectal transducers (3.5 and 7.5 MHz) was used at four different time points: before treatment; after chemotherapy with IAE; in the middle and after the completion of radiotherapy. Tumor characteristics, presence of metastasis, 3D image of tumor vascularisation were evaluated. The pulsatility, resistance index, and vascular index of tumor blood flow were measured.

Results: Out of the 25 patients, hypo- and hypervasculatized tumors were found in 3 and 15 patients, respectively. According to 3D-UA, in 16 patients, chemotherapy with IAE led to a 50% reduction in the tumor size and degree of vascularization. After completion of the radiotherapy, full deterioration of the tumor was found in 10 patients, substantial reduction (more than 50%) of tumor size and degree of vascularisation was found in 11 patients. Slight reduction (25%) of the tumor size was found in 4 patients, which can be explained by tumor resistance to the treatment. In these patients, changes in the treatment regimen were implemented.

Conclusions: 3D-UA provides accurate information during radiotherapy of CC by monitoring the tumor size and degree of vascularization and permits a more accurate selection of treatment options.

C-0433

Extrapelvic nodal metastases as the most frequent form of recurrence in uterine cervical carcinoma treated by radiation therapy

M. Castro Copete, J. Calbo Maiques, M. Carnero Ruiz, C. Crespo Martínez, M. Navarro Navarro, N. Picazo Escrivano, I. González Álvarez; Alicante/ES

Purpose: 1. To know the most frequent form of presentation and location of tumoral recurrences in patients with cervical cancer treated with radiation therapy. 2. To remember the importance of including an abdominopelvic CT in the following protocol of cervical carcinomas.

Materials and Methods: This is a retrospective evaluation of 121 patients with cervical carcinoma treated in our institution from 1994 to 2003. All patients had received radiation therapy, as unique or adjuvant therapy. We have reviewed CT images included in the follow-up protocol.

Results: Among 121 reviewed cases, we found tumoral recurrence in 21 patients: 5 local recurrences, 7 hematogenous metastases and 12 lymph node recurrence. In all lymph node recurrence cases, the nodal groups considered pathological at CT, were found above aortic bifurcation. There were no cases with pelvic lymph node recurrence.

Conclusion: Lymphatic involvement is the most frequent manifestation of recurrent disease in cervical carcinoma after treatment. There are three lymphatic pathways of spread of cervical carcinoma: external iliac nodes, internal iliac nodes and sacral nodes. All them converge at common iliac nodes and finally the tumor can arrive at paraaortic nodes. Pelvic radiation therapy includes only some of these nodal groups, and this results in a peculiar distribution of nodal recurrent that, definitively, "skip" radiated nodal levels. Radiologists and clinicians must become aware of the fact that the most frequent lymph node recurrence in patients with cervical cancer treated with pelvic radiation therapy occurs in extrapelvic lymph nodes and, as this way, far of primary tumor.

C-0434

Transvaginal sonography in postmenopausal bleeding. Sonographic findings in 200 cases. Endometrial carcinoma patterns

J. Morales Olaya, D. Dualde, T. Labrador, J. Cervera; Valencia/ES

Learning Objectives: To evaluate the utility of transvaginal ultrasound (TVS) in the diagnosis of postmenopausal bleeding.

Background: Prospective study of 200 women referred with abnormal vaginal bleeding. Mean age: 57.9 years. The period of amenorrhea surpassed one year in every case. The definitive diagnosis was established by means of hysteroscopy with or without biopsy. In cases of endometrial cancer TVS findings were compared with those obtained in the specimen after hysterectomy to evaluate the accuracy in determining the presence and the depth of myometrial invasion.

Imaging Findings: Endometrial atrophy: 98 patients (49%). Proliferative endometrium: 11 (5.5%). Endometrial hyperplasia: 37 (18.5%). Endometrial polyps: 32 (16%). Endometrial carcinoma: 22 (11%). 95.9% women with endometrial atrophy show an endometrial thickness less than 6 mm. Endometrial carcinoma pattern: endometrial thickness of over 6 mm (95.4%) (mean of 20.6 mm). Poorly defined margins (62.2%) heterogeneity (68.9%) and echogenicity (88.9%). 60% of cases presented myometrial invasion. The sensitivity of TVS in detecting deep invasion (more than 50% of the myometrial thickness) was 94.1%; specificity of 84.8%. Overall accuracy: 88%. Cervix was involved in 26.6%. The criteria to rule out a significant alteration was to consider 6 mm for normal endometrial thickness: Sensitivity: 95%. Specificity: 84%. Diagnostic safety: 90%.

Conclusion: We confirmed the value of TVS as the first test in postmenopausal vaginal bleeding, in ruling out significant disease when the endometrial thickness is less than 6 mm, avoiding more aggressive and costly tests.

C-0435

Prevalence of ovarian adrenal rest tumours and polycystic ovaries in females with congenital adrenal hyperplasia: Results of ultrasonography and MR imaging

H.M. Suliman¹, N.M.M.L. Stikkelbroeck², D.D.M. Braat², G.J. Jager², B.J. Otten²; ¹Amsterdam/NL, ²Nijmegen/NL

Purpose: The aim of the investigation was to assess the prevalence of ovarian adrenal rest tumours and polycystic ovaries in female patients with congenital adrenal hyperplasia (CAH).

Materials and Methods: Thirteen female CAH patients (median age 19.8 years, range 14.8-23.5 years) underwent transvaginal (n = 6) or transabdominal (n = 7) ultrasonography by a gynaecologist and MR imaging (n = 13) of the ovaries pre and post contrast-enhanced T1-and T2-weighted images.(Table.1). Ovarian adrenal rest tumours were defined as small hypoechoic and multifocal nodules on

Scientific and Educational Exhibits

ultrasound and iso-intense lesions on T1-and hypointense on T2-weighted MR images (derived from characteristics of testicular adrenal rest tumours). Polycystic ovaries were defined as the presence of > 10 follicles arranged peripherally around or scattered throughout increased stroma.

Results: No ovarian adrenal rest tumours were found either on ultrasound, or by MR imaging. Polycystic ovaries were found in 2 of the 13 patients (15.4%), both with ultrasound and MR (Fig.1). No ovarian adrenal rest tumours were detected in these female CAH patients, which suggests that ovarian adrenal rest tumours in CAH females are rare. The prevalence of polycystic ovaries corresponded to that in the general population.

Conclusion: From these results, we would suggest that routine ovarian imaging in CAH females is not indicated. However, when ovarian dysfunction is present, ovarian imaging is advised, first by ultrasonography, to detect ovarian adrenal rest tumours or polycystic ovaries.

C-0436

Pitfalls in MR imaging staging of carcinoma of the cervix

J.L. Hughes, A. Saddev, A. Rockall, R. Reznek; London/UK

Learning Objectives: 1.) To appreciate potential mistakes and pitfalls in the use and interpretation of MR imaging in the staging of cervical cancer. 2.) To learn strategies and techniques to avoid these potential errors.

Background: In patients with carcinoma of the cervix, accurate preoperative staging is key to determining management. MR imaging has gained wide acceptance for the staging of cervical cancer particularly in the detection of early parametrial invasion and nodal disease. Nevertheless the accuracy of the technique varies.

Procedure Details: We will present a range of pitfalls in the detection of the primary tumour and of parametrial spread including technical inadequacy, anatomical variants, confusion caused by co-existent disease and the effects of previous intervention. The limitations in sensitivity and specificity for detection of lymph node metastases are well known. We will however illustrate pitfalls in the identification of nodal metastases in the female pelvis such as confusion with physiological ovarian appearances.

Conclusion: Appreciation of pitfalls in the interpretation of MR imaging in cervical cancer can aid accurate diagnosis.

C-0437

MR imaging as an important tool in differentiating uterine adenomyosis from leiomyomas: A pictorial review

L. Chandratreya, S. Armstrong; Bristol/UK

Learning Objectives: MR imaging is an important imaging modality in the differentiation of adenomyosis and leiomyomas of the uterus, which are relatively common, but benign, myometrial conditions. We present a pictorial review of the MR imaging features distinguishing them.

Background: Adenomyosis is characterised by the invasion of the myometrium by endometrial tissue and hyperplasia of adjacent smooth muscle. Leiomyomas are well-circumscribed myometrial benign tumours containing mainly smooth muscle with some fibrous connective tissue. Adenomyosis is commonly a diffuse abnormality, or maybe focal as an adenomyoma. Presenting symptoms are similar.

Imaging Features: Sonographically adenomyosis may resemble leiomyoma, especially focal adenomyoma. MR imaging has a higher sensitivity and specificity in the differentiation of uterine adenomyosis from leiomyomas as compared to transvaginal ultrasound and this maybe due to better contrast and spatial resolution of MR imaging. The most pertinent feature of adenomyosis on T2 weighted MR imaging images is the widening of the junctional zone (JZ) and thickness of JZ over 12 mm is of high diagnostic accuracy. T2 weighted images also show areas of high intensity. Other features include myometrial nodules and cysts, linear striations and poor definition of the endomyometrial junction. Leiomyomas appear as well defined masses of low signal on T2 weighted images, which may enhance post Gadolinium. Appearances of degenerated leiomyomas vary.

Conclusion: The correct diagnosis is extremely important as the definitive treatment for adenomyosis is hysterectomy; whereas myomectomy can be performed for leiomyoma. MR imaging accurately detects leiomyomas and is useful in assessing the degree of myometrial penetration in adenomyosis.

C-0438

Magnetic resonance imaging in the characterization of ovarian masses

A.C. Tsili, C. Tsampoulas, F. Katzioti, E. Arkoumani, S. Tzioras, C. Mpougias, E. Paraskevaidis, S.C. Efremidis; Ioannina/GR

Learning Objectives: To describe the MR imaging features allowing differentiation between benign and malignant ovarian masses.

Background: Ovarian cancer accounts for nearly 4% of all cancer cases and it causes more deaths than any other cancer of the female reproductive system. The pretreatment characterization of ovarian masses is of outmost importance, since it can provide a basis for optimal preoperative planning, in cases of ovarian cancer. It can also reduce the number of unnecessary laparotomies in patients with benign disease. MR imaging has been shown to be useful in the characterization of ovarian masses.

Procedure Details: Sequences used were T1, T2 and fat-suppressed T1-weighted, before and after intravenous administration of gadolinium chelate. MR imaging due to its superb contrast resolution and its usefulness in tissue characterization, could accurately diagnose mature cystic teratomas, endometriomas or hemorrhagic cysts and tumors containing fibrosis or smooth muscle, in the majority of cases. The presence of entirely cystic lesions, with size less than 4 cm and wall or septal thickness less than 3 mm, were more suggestive of benignity. The presence of cystic lesions with wall or septal thickness more than 3 mm, with papillary projections, and the presence of solid components, with necrosis, all were suggestive of malignancy. The presence of lymphadenopathy, ascites and peritoneal metastasis were findings confirming malignancy.

Conclusion: MR imaging is a highly accurate technique in the differentiation between benign and malignant ovarian masses.

C-0439

Quantitative evaluation of ovarian tumors using Gd-dynamic contrast-enhanced MR imaging

K. Hayasaka, T. Saitoh, Y. Tanaka; Tokyo/JP

Objective: To conduct quantitative evaluation of ovarian tumors using Gd-dynamic contrast-enhanced MR imaging.

Materials and Methods: 78 ovarian tumors underwent Gd-enhanced dynamic MR imaging with a Siemens Magnetom Vision 1.5 T using 3D-FLASH (20 s) before and three times (30, 50, and 70 s) after a standardized bolus of Gd-DTPA. For quantitative MR imaging parameters, the following were examined by a consensus of two radiologists: ER (enhancement ratio) 1: (SI1-SI0)/SI0, ER2: (SI2-SI0)/SI0, ER3: (SI3-SI0)/SI0, ER2-1: ER2-ER1, and SAT: SI1/SI max. Analysis of variance was used to identify significant differences in quantitative parameters among ovarian tumors.

Results: The tumors were specified as benign [endometriosis (EM): 13, serous cystadenoma (SCA), fibrothecoma (FT): 2, mucinous cystadenoma (MCA), dermoid cyst (DC), cyst (CY): 7, other: 2], borderline: 2 and malignant group [serous cystadenocarcinoma (SCAC): 5, mucinous cystadenocarcinoma (MCAC): 12, clear cell carcinoma (CCC), endometrioid carcinoma (EMC): 7, immature teratoma (IMT): 2, other: 3]. In these ovarian tumors, there were statistically significant differences in various parameters between the following tumors ($p < 0.05$): benign vs malignancy (ER2, ER3, ER2-1, and ER3-1), CY vs. FT, FT vs. MCA, CY vs. EMC, EMC vs. FT, CCC vs. CY and MCA vs. SCAC (ER2-1, ER3-1), CCC vs. EM (ER1, ER2, ER3, ER2-1, ER3-1), CCC vs. MCA (ER3, ER2-1, ER3-1), DC vs. EMC, EM vs. SCAC and EMC vs. EM (ER2, ER3, ER2-1, ER3-1).

Conclusion: Analysis of various parameters using Gd-enhanced dynamic MR imaging with 3D FLASH technique was useful to determine the characteristics of ovarian tumors. Among various parameters analyzed, ER2-1 and ER3-1 were useful for differential diagnosis.

C-0440

Ancient schwannoma of the female pelvis: Radiologic-pathologic correlation

M. Takeuchi, K. Matsuzaki, H. Uehara, H. Nishitani; Tokushima/JP

Learning Objectives: To demonstrate characteristic imaging findings of ancient schwannoma in female pelvis with pathologic correlation based on ten patients. To describe the diagnostic clues of ancient schwannoma to differentiate from ovarian neoplasm.

Background: Schwannoma is a benign nerve sheath tumor which usually occur in the soft tissues of the head and neck and extremities. When the tumors are located in deep structures such as the mediastinum and the retroperitoneum, those tend to be larger masses with degenerative changes as ancient schwannoma. The majority of female pelvic masses arise from internal genital organs, but gastrointestinal, mesenteric, urinary, and primary extraperitoneal tumors also occur and may mimic gynecologic neoplasms. Especially masses with cystic nature may closely resemble ovarian neoplasm. Primary extraperitoneal neoplasms are rare and comprise various histologic origins. In the tumors, ancient schwannomas may tend to be mistaken for ovarian disease clinically, because the patients are usually asymptomatic and ultrasonography reveals as cystic masses.

Imaging Findings: On CT and MR imaging, centripetal displacement of the rec-

Scientific and Educational Exhibits

tum, the iliac vessels or the iliopsoas muscle are characteristic findings for its extraperitoneal origin and helpful to rule out ovarian disease. The characteristic location (presacral) is suggestive and detecting continuity to the nerve or neural foramen is diagnostic. Demonstration of formation of capsule, partial or total cystic degeneration and hemorrhagic change on MR imaging and calcification on CT reflected its pathologic features and suggestive of ancient schwannoma.

Conclusion: Diagnosis of ancient schwannoma mimicking ovarian neoplasm before surgical treatment is important for postoperative neurological difficulties often develop.

C-0441

The diverse ultrasonographic appearances of ectopic pregnancies: A pictorial review

S. Lam; Singapore/SG

Learning Objective: To review the ultrasonographic findings in ectopic pregnancies via illustrated examples.

Procedure Details: The ultrasonographic findings of ectopic gestations were retrospectively reviewed in a local women's hospital over a five year period.

Findings: The ultrasonographic findings depend largely on the different sites of implantations. An empty or near empty uterus with an intracavitory pseudosac or decidual cast is sometimes identified. Echogenic pelvic fluid suggests haemoperitoneum. A ring adnexal mass is considered the most predictive ultrasonographic finding. Associated risk factors (e.g. hydrosalpinx) may be detected adjacent to the ectopic gestation. A non specific adnexal mass due to haematoma surrounding the ectopic gestation and the ovary is sometimes seen. An adnexal mass containing a viable embryo is the only definitive diagnosis of an ectopic gestation. In interstitial ectopic pregnancy, the gestational sac bulges the cornua, thins the surrounding myometrium and disrupts the endometrium (interstitial line sign). In cervical pregnancy, the implantation causes cervical dilatation, giving an hourglass configuration. Peritrophoblastic blood flow can be identified on colour Doppler ultrasonography. Heterotopic pregnancies are very rare with both an intrauterine pregnancy and an ectopic gestation. This is seen in increasing frequency with assisted reproduction. A completely normal pelvic ultrasonogram may be present in up to 20% of patients.

Conclusion: Understanding that ectopic gestations can present in various forms can lead to an earlier diagnosis, reducing morbidity and mortality. Ultrasonography is widely available and remains the imaging modality of choice.

C-0442

Endometriosis or dermoid: Diagnostic dilemmas

S.A. Babar, E.K. Hughes, R. Willimason; London/UK

Purpose: To present the various diagnostic difficulties in MR imaging appearances of endometriomas versus dermoids and to determine the presence of associated pathology in these conditions.

Methods and Materials: We retrospectively reviewed 40 histopathologically confirmed cases of endometriomas and dermoids. MR scans were reviewed by two experienced radiologists to determine the cases with diagnostic difficulties. MR signal characteristics were identified in all cases and overlap in various imaging features determined. Our standard pelvic MR sequences include Coronal T1W, Sagittal and axial T2W and Coronal STIR. Fat saturation was used in some cases as a problem solving sequence.

Results: Of the total of 40 patients, we identified 16 (40%) cases with features resulting in some interpretative difficulty. This was seen in the form of signal loss on STIR sequence in endometriomas, various signal alterations of the blood products and the presence of various associated benign and malignant conditions. These associated conditions were seen in 5/16 (31.2%) cases of dermoids and 7/16 (43%) of endometriomas, which included adenomyosis, clear cell carcinoma, endometrial carcinoma and epithelioid angioma.

Conclusion: Although differentiation of endometriomas from dermoids should be straight forward this is not always the case. Use of fat saturation in addition to STIR can be used as extra sequence for problematic cases.

Genitourinary

Kidney

C-0443

An algorithm-based system to facilitate the sonographic diagnosis of renal disease: A DVD-Rom teaching file with US image and video database

P.S. Zoumpoulis, I. Theotokas, K. Pahou, D. Dalakostas, D. Schizas, V. Koratzinos, A. Filippidou, S. Kyriazi; Athens/GR

Learning Objectives: - To review the sonographic features of diffuse and focal renal diseases. - To provide a simple algorithm toward an accurate differential diagnosis. - To compare individual US images to image galleries of diagnostically confirmed cases.

Background: The purpose of this DVD-Rom is to promote accurate characterization of diffuse and focal renal lesions combining morphologic and hemodynamic criteria.

Procedure Details: The user can start using this teaching file by describing the US characteristics of a focal renal lesion that he has difficulty in diagnosing. The user designates the sonographic features of a specific renal lesion (echogenicity, border echogenicity, vascularity). The system guides him through a specific algorithm of all possible renal lesions that fit the characterization given. A large collection of classified US images and videos in each diagnostic category are available for comparison with the user's images. The user's image can also be linked to the contents of corresponding interesting cases, which are brief case reports with clinical, biochemical, imaging and pathological data. To outline the profile of each diagnostic category concise case reports are presented, correlating imaging findings with clinical, biochemical and histological data. This teaching file applies a dual approach to the differential diagnosis of renal disease, whereby a computer-based algorithm is complemented by the user's active and comparative assessment.

Conclusion: The user can be aided in the differential diagnosis of renal lesions by comparing his image to other "similar" sonographic images, which are available in galleries, videos and interesting cases.

C-0444

Renal perfusion abnormalities: Findings with multislice CT (MSCT)

A. Nunziata, O. Catalano, P. Mainenti, M. Salvatore, A. Siani; Naples/IT

Learning objective: To illustrate the MSCT findings in the wide spectrum of renal perfusion abnormalities. To show the practical value of MSCT findings in differential diagnosis of renal perfusion changes. To highlight the value of reformed, angiographic, and tridimensional MSCT images in this clinical setting.

Background: MSCT can recognise a wide spectrum of renal perfusion defects and abnormalities. In common clinical practice there is an overlap between different clinical scenarios capable of determining changes in the normal CT nephrogram.

Procedure Details: We illustrate several cases of renal perfusion defects, as seen on cortical, cortico-medullary, and/or excretory phase scans. These defects are segmental, multisegmental, total, or diffuse (non uniformly distributed) and can be unilateral or bilateral. Causes include dissection of abdominal aorta (so called malperfusion syndrome) hypovolemic/cardiogenic shock, avulsion or obstruction of arterial pedicle (blunt trauma, spontaneous thrombosis, aortic prosthesis placement or surgery, interventional renal procedures), severe stenosis of renal artery (atherosclerosis, neoplastic infiltration, or compression), acute urinary tract obstruction (ureterolithiasis).

Conclusion: MSCT transaxial and reformatted images have several applications in renal perfusion changes assessment. Knowledge of causes, related patterns, and clues to diagnosis allows proper categorization of these abnormalities.

C-0445

PCNL by numbers: A 7-year analysis of percutaneous nephrolithotomy in practice

C.P. Meehan, N. Gough, P.A. McCarthy; Galway/IE

Background: Percutaneous Nephrolithotomy is now an established string in the bow of the uroradiologist. In experienced hands and through careful patient selection, success rates above 90% can be achieved with minor complications. As this technique matures, innovative modifications promise to increase the variety of treatable calculi. We have reviewed our practice of PCNL.

Methods and Materials: We have undertaken a 7-year retrospective analysis of Percutaneous Nephrolithotomy practice at a university teaching hospital serving both rural and urban populations. A MS-Access database was compiled detailing

Scientific and Educational Exhibits

95 cases, performed between 1997 and 2004. Demographic data, clinical indications, indices of success, calculus characteristics and complications were compiled.

Results: 95 cases were documented involving 74 patients. Mean age was 49 years with slight female preponderance ($n = 55$). The majority of cases ($n = 56$) were idiopathic. Otherwise, PUJ obstruction ($n = 7$), ureteric stricture ($n = 3$) and patients post-urinary diversion surgery ($n = 3$) were predominant. The remainder ($n = 5$) comprised congenital structural malformation or metabolic derangements. 42 procedures were right sided. Of 112 calculi described, over half ($n = 60$) were located in either renal pelvis or lower pole. Successful retrieval, per initial objectives, was achieved in 80/95 cases, 67 being largely stone free or better post-PCNL. Complications were recorded in 14 cases, chiefly related to stone access, none proving serious.

Conclusions: PCNL is a well tolerated procedure with success rates up to and beyond 90% a realistic target. Lower pole calculi are especially amenable to retrieval. As experience continues to grow, further modifications will broaden the range of patients who may benefit.

C-0446

Renal tumours: Technical success and early clinical experience with radio-frequency ablation of 18 tumours

P. Vladica, R. Sabharwal; Sydney/AU

Purpose: To evaluate the safety and technical efficacy of image-guided radiofrequency ablation (RFA) for the treatment of small peripheral renal tumours and to report our early results with this treatment modality.

Materials and Methods: Thirteen RFA sessions for eighteen tumours were performed in eleven patients with renal tumours. Indications included coexistent morbidity, high surgical or anaesthetic risk, solitary kidney, and hereditary predisposition to renal cell carcinoma. Ten patients had CT-guided percutaneous RFA performed on an outpatient basis. One patient had open intra-operative ultrasound-guided RFA. Technical success was defined as elimination of areas that enhanced at imaging within the entire tumour. With the exception of one patient with renal insufficiency requiring a non-contrast enhanced CT, remaining patients underwent contrast enhanced CT for post treatment follow-up assessment. Follow up was performed after two to four weeks and then at three, six, twelve months, and every twelve months thereafter.

Results: Fourteen (78%) of eighteen tumours were successfully ablated with one treatment session. Three of the remaining four tumours required two treatment sessions for successful ablation. One tumour will require a third treatment session for areas of persistent enhancement. Mean patient age was 72.82 ± 10.43 years. Mean tumour size was 1.95 ± 0.79 cm. Mean follow-up time was 8.18 months. All procedures were performed without any major complications.

Conclusion: Percutaneous radiofrequency ablation of small renal tumours is well tolerated and minimally invasive. Our early experience with RFA demonstrates it to be a feasible, safe and effective treatment of small peripheral renal tumours.

C-0447

Cross-sectional imaging in the renal trauma: A trauma center experience

G. Regine, M. Atzori, V. Buffa, M. Galluzzo, V. Miele, L. Adami; Rome/IT

Purpose: To evaluate diagnostic accuracy of cross sectional imaging (ultrasound, ultrasound contrast agent, MDCT) in patients with renal trauma.

Material and Methods: Between September 2003 and August 2004, 265 patients, with abdominal blunt trauma, were evaluated. 25/265 showed renal lesions, the severity of renal injury was graded by the American Association for the Surgery of Trauma Organ Injury Severity Scale. All patients with hematuria (63) were evaluated with baseline ultrasound, after II generation (Sonovue) ultrasound contrast agent injection and multiphasic MDCT scan, integrated with vascular 3D reconstruction.

Results: 5/25 traumatic parenchymal lesions with perirenal fluid collection were identified at ultrasound baseline. 25/25 renal parenchymal lesions, with or without perirenal or retroperitoneal hematoma, were identified at contrast agent ultrasound. The MDCT multiphasic confirmed all positive cases at Ultrasound Contrast Agent, and moreover rated the lesions' grade, particularly the IV and V using 3D reconstruction in the vascular peduncle evaluation, the urinary excretory system lesion with urine leak was identified at delay phase scan integrated with MIP and V.R. reconstruction.

Conclusions: Our experience confirmed the diagnostic accuracy of the cross-sectional imaging both for correct diagnosis and for correct patient management. Specifically in our study we have noted the possibility of performing follow-up examination of renal lesions using ultrasound contrast agent which also reduces exposure to radiation (less MDCT examinations).

C-0448

Local staging in RCC: Is perinephric stranding and increased perirenal vascularity really helpful?

N. Kabakci, M. Secil, B. Tuna, A. Kefi, K. Yorukoglu, E. Igci, O. Dicle; Izmir/TR

Purpose: Preoperative staging of renal cell carcinoma has gained more importance after new techniques of nephron-sparing surgery. In this study, the aim was to investigate the accuracy of perinephric stranding and perirenal increased vascularity findings revealed by magnetic resonance imaging (MRI) in perinephric fat invasion.

Methods and Materials: The preoperative MR images of 40 patients who have received the diagnosis of RCC were retrospectively evaluated. MR examinations were performed by 1.5 T scanner (Gyroscan Intera, Philips, Netherlands) with fat-saturated TSE T2, WATS T1 and contrast-enhanced WATS T1 sequences. The patients who had renal vein thrombosis radiologically or pathologically were excluded from the study. Perinephric stranding and increased perirenal vascularity findings were investigated in the remaining 24 patients. The existence of this finding in any of the sequences was accepted to be positive for perirenal fat invasion. The RCCs were histopathologically staged according to the 1997 TNM classification. The results were compared with the pathological stages.

Results: Nineteen of 24 patients were pathologically stage 1; 3 were stage 2 and 2 were stage 3a. Perinephric stranding was seen in 14 of the 24 masses and perirenal increased vascularity was seen in 17 patients. These findings were not statistically consistent with stage 3a RCC.

Conclusion: Perinephric standing or perirenal increased vascularity findings do not reflect perirenal fat invasion in RCCs.

C-0449

withdrawn by authors

C-0450

Amyloid: Radiological manifestations from head to toe

S.P. Prabhu, K. Burney, A. Valencia; Bristol/UK

Learning Objectives: 1. To illustrate a few examples of biopsy-proven or post-mortem confirmed cases of amyloidosis seen on radiological investigations in our institutions over the last 10 years. 2. To demonstrate that radiological findings in amyloidosis are extremely variable and diverse

Background: Amyloidosis is a collective term for a group of diseases that are characterized by the widespread extracellular deposition of insoluble amyloid protein. The process is usually systemic, but localized forms are recognized.

Imaging Findings: We illustrate examples of biopsy-proven or post-mortem confirmed cases of amyloidosis seen on radiological investigations in our institutions over the last 10 years with radiologic-pathologic correlation. The usual sites of involvement in primary amyloidosis are kidneys, heart, lungs, gastrointestinal tract and skin, while the usual sites in secondary amyloidosis are kidneys, liver, spleen and adrenal glands. The focal form has been described in a number of entities including orbit, nasopharynx, larynx and tracheobronchial tree. Clinical manifestations are varied and are a result of organ dysfunction secondary to amyloid protein accumulation. Secondary causes include myeloma, solid malignancies, and chronic inflammatory conditions such as rheumatoid arthritis and tuberculosis.

Conclusion: Radiological findings in amyloidosis are extremely variable and diverse. It must be considered in the differential diagnosis in areas illustrated to enable appropriate patient management.

C-0451

Renal carcinoma: Therapeutic management with radiofrequency thermal ablation (RFA) under CT-guidance

L. Thanos, S. Mylona, M. Pomoni, A. Kokkinaki, E. Karahaliou, N. Batakis; Athens/GR

Purpose: To present the technique, the effectiveness and the possible complications of RFA in renal carcinoma.

Materials and Methods: In the last two years we applied RFA under CT-guidance on 49 patients with renal cancer. Thirty ablations were followed by surgical resection (24 nephrectomies and 6 tumor resections). Twelve patients were not candidates for surgery due to cardiorespiratory problems and seven patients had a recurrent tumor. We used RITA and MIRRAS generators with two different types of electrodes (hooked and spiral). The ablation lasted 15-18 minutes. The procedure was applied after analgesic treatment and local anaesthesia at the inlet. Follow-up with two-phase spiral CT after IV administration was made immediately after the procedure and 1, 6 and 12 months later.

Scientific and Educational Exhibits

Results: The histopathologic results in operated tumours were total necrosis in 28 and partial in 2. From the patients who underwent only RF ablation, we observed total necrosis in 13 tumours and partial necrosis in 6 (we proceeded to a second session). We had no complications. The 1- and 2-year survival was 100% and 91.83% respectively.

Conclusion: Radiofrequency thermal ablation is a safe and effective alternative method for the treatment of renal carcinoma.

C-0452

Comparison of tissue harmonic imaging with standard ultrasound mode, in the evaluation of the kidneys

M. Chalkia, I. Kirimlidis, A. Spanos, A. Papageorgiou, S. Spanidou, N. Vougiouklis; *Thessaloniki/GR*

Purpose: Our purpose is to compare tissue harmonic imaging (THI) with conventional ultrasonography (CU), regarding image quality and organ visualization during renal ultrasound examination.

Methods and Materials: 125 different kidneys were evaluated with both conventional ultrasonography and tissue harmonic imaging. Two experienced radiologists, blind the mode used and blind to each other, rated each image pair for resolution, detail and total image quality. The images were evaluated as: (1) insufficient, (2) good and (3) very good.

Results: Both the examiners considered the TH images very good in 34.4%, good in 45.6% and insufficient in 20% of the cases, while they considered the CU images very good in 15.6%, good in 49.2% and insufficient in 35.2% of them. More specifically, regarding imaging of renal cysts, the examiners considered the TH images very good in 38.39%, good in 45.53% and insufficient in 16.07% of the cases, while they considered the CU images, very good in 16.07%, good in 44.64% and insufficient in 39.28% of them. Regarding imaging of renal stones and nephroblastosis, THI shows superiority, since it was considered very good in 33.33% and good in 47.22% of the cases, while CU images were considered very good in only 5.5% and good in 38.88% of them. In imaging renal parenchyma THI shows a less distinct superiority, since it was considered very good in 29.76% and good in 45.23% of the cases.

Conclusion: THI proved to be superior than CU, regarding image quality and organ visualization in the evaluation of the kidneys.

C-0453

Laparoscopic cryoablation (LC) of small renal masses: Postoperative complications evaluation by magnetic resonance imaging (MRI)

G. Cardone, C. Iacobino, A. Cestari, L. Nava, P. Mangili, G. Balconi, G. Guazzoni; *Milan/IT*

Learning Objectives: To report the spectrum of post-operative complications in patients treated with laparoscopic renal cryoablation. To illustrate the MR findings of post-operative complications in patients treated with laparoscopic renal cryoablation.

Background: Laparoscopic renal cryoablation is a minimally invasive surgical technique for patients with small renal masses. MR is an effective tool for imaging follow-up of renal lesions treated with laparoscopic cryoablation.

Imaging Findings: 41 pts underwent LC of 43 renal masses. Patients were followed up clinically, biochemically and by MRI 24 hrs after surgery, and subsequently at 1, 3, 6, 12, 18, 24 and 36 months (mean 18). After surgery retroperitoneal and pleural effusions were found in all cases. Early post-procedure MR images showed incomplete ischemia of cryolesions in 10% of the cases, with small intraleisonal enhancement which afterwards disappeared in the following months. 21% of the cases showed a small intraleisonal haematoma which afterwards reabsorbed in the following months. In 11% of the cases a small perilesional haematoma was evident at 1 and 3 months after surgery, probably due to blood clot dissolution. No significant rise in creatinine was noted post-procedurally.

Conclusions: Our experience suggests that laparoscopic cryoablation is a safe, well tolerated and minimally invasive therapy for small renal masses, and MR is an effective imaging technique in the follow-up of renal lesions treated with laparoscopic cryoablation.

C-0454

Renal lesions treated with laparoscopic cryoablation (LC): Multi-detector row computed tomography (MDCT) imaging patterns

G. Cardone, D. Fiechi, A. Cestari, G. Guazzoni, P. Mangili, G. Balconi; *Milan/IT*

Learning Objectives: To report the spectrum of MDCT findings of renal lesions treated with LC. To show the evolution, as time passed, of the CT patterns of

renal lesions treated with LC. To illustrate the more significant MDCT criteria of absence of recurrence in the follow-up of renal masses treated with LC.

Background: Laparoscopic renal cryoablation is a minimally invasive surgical technique for patients with small renal masses. MR is an effective tool for imaging follow-up of renal lesions treated with LC, but in some cases CT can be a constrained choice.

Imaging Findings: 10 pts with 11 renal masses underwent renal LC. All patients underwent MDCT follow-up 24 hrs after surgery, and at 1, 3, 6 and 12 months. MDCT examinations were performed using unenhanced and post-contrast axial scans, associated to multiplanar reconstructions. Cryolesions were iso-dense on pre-contrast and hypo-dense on post-contrast images. 24 hrs after treatment all cryolesions were more than 1 cm larger than the original masses; cryolesions decreased in size of an average of 35%, 45%, 60% and 80% at 1, 3, 6 and 12 months respectively. Post-contrast MDCT images showed complete ischemia of cryolesions in all the cases. 50% of the cases showed a perinephric haematoma at 1, 3 and 6 months.

Conclusions: The more significant MDCT patterns in the follow-up of renal lesions treated with LC were the decrease in size as time passed and the complete ischemia of the cryolesions.

C-0455

Multislice CT (MSCT) features of renal and pelvic lesions: A pictorial review

P. Domínguez Echávarri, D. Cano Rafart, G. Bastarrica Aleman, J. Larrache Latasa, I. Vivas Perez, I. Gonzalez Crespo; *Pamplona/ES*

Learning Objectives: To review the MSCT appearance of renal and pelvic masses, benign and malignant. To illustrate MSCT features of local and advanced renal malignancy for staging purposes.

Background: Renal masses, cystic or solid represent a wide spectrum of diseases and constitute a common finding in radiological exams. MSCT is a valuable tool to characterise undetermined renal masses found after other diagnostic techniques, such as ultrasound. Furthermore, in many cases MSCT is the only imaging technique performed prior to surgery, and is the investigation of choice to stage renal carcinoma. MSCT renal imaging allows not only differentiation between benign and malignant lesions but also allows accurate delineation of the extent of the disease with multiphasic studies and high quality Multiplanar Reformations (MPR) and Maximum Intensity Projection (MIP).

Imaging Findings: We review and outline the most specific MSCT features of renal benign and malignant lesions including simple and complicated cysts, angiomyolipoma, adenoma, oncocytoma, cystic tumours, lymphoma, renal cell carcinoma, renal sarcoma, metastases and tumors of the renal pelvis.

Conclusion: MSCT is the technique of election to detect and characterise most renal masses, differentiating benign from malignant lesions. CT findings usually lead to an accurate diagnosis, allowing tumour staging in malignant tumours and adding precise anatomic information prior to surgery

C-0456

Angiogenesis assessment in renal cell carcinoma by echocontrast-enhanced power Doppler ultrasound

N. Kabakci, E. Igci, M. Seçil, U. Mungan, I. Celebi, Z. Kirkali, K. Yorukoglu, O. Dicle; *Izmir/TR*

Purpose: Tumoral growth is angiogenesis-dependent. Even if there are studies about the importance of histopathological angiogenesis in various malignancies, the assessment of the angiogenesis by radiological techniques, which is more practical to perform, is not well established. The aim in this study is to assess the efficiency of echocontrast-enhanced power Doppler ultrasound (PDUS) in determining the angiogenic status of RCC.

Materials and Methods: PDUS were performed before and after intravenous administration of the echocontrast agent, Levovist, in 43 renal lesions. The images were recorded in PACS. Twenty-one of these renal masses were diagnosed as RCC histopathologically. The images were analyzed by Photoshop 7.0 (Adobe Systems, San Jose, California), colored pixel ratios (CPR) of selected images were calculated using the ratio of the number of pixels showing power Doppler signals to the total number of pixels within the lesion. The results were compared with the histopathologic microvessel density (MVD), which is done by Chalkley method.

Results: A significant correlation was found between CPR and MVD values in both PDUS techniques. The use of echocontrast agent improved this correlation and p values (Spearman from $p = 0.436$ to 0.551 and from $p = 0.05$ to 0.01).

Conclusion: CPR values reflect the MVD in RCCs. Therefore, these results suggest that preoperative quantification of angiogenesis and therapy monitoring of antiangiogenetic agents could be possible by the help of PDUS in RCCs.

Scientific and Educational Exhibits

C-0457

Comparison of US and KUB for detecting renal calculi with nonenhanced multislice CT

K. Subramanian, A.K. Jain; Manchester/UK

Purpose: To compare the sensitivity and specificity of ultrasound (US) and plain radiograph abdomen (KUB) for detecting renal calculi with nonenhanced Multi-slice CT (NMSCT) as a reference standard. To compare their sensitivity in detection of calculi of different size.

Materials and Methods: US, KUB and NMSCT examinations of 42 consecutive patients presenting with renal colic and haematuria were compared retrospectively for detection of renal calculi. Their case notes, films and radiology reports were reviewed. Statistical analysis was performed using SPSS software.

Results: 21 male and 21 female patients with mean age of 51.8 years (range 21-78 years) were studied. US sensitivity was 68% with specificity of 50% (PPV 74%). However, the specificity for sonographers was 40% (62% for radiologists). KUBs sensitivity was 39% but specificity 100%. US sensitivity was 11% for calculi < 3 mm; 86% for 3-5 mm and 86% for > 5 mm. KUB sensitivity was 0% for < 5 mm and 68% for > 5 mm.

Conclusions: In comparison with previous studies, US sensitivity is comparable for calculi > 3 mm, but is low for < 3 mm. Furthermore, US specificity (50% vs. 90-95%) is poor. Commonest causes of false positive scans were misinterpretation of < 3 mm vascular, parenchymal calcification as intracalceal calculi. Focussed training in this regard could improve specificity. US is of limited value in assessing post-lithotripsy calculus burden (only 11% sensitivity for calculi < 3 mm). Such patients could be followed by NMSCT. With calculi > 5 mm, the specificity of KUB is very high, hence, KUB can be used to follow-up this group.

C-0458

Pictorial review of renal transplant imaging and complications

P. Rajiah, Y. Lim, N. Thomas; Manchester/UK

Learning Objectives: A. To illustrate the role and limitations of imaging in renal transplant recipients. B. To understand the normal ultrasound and Doppler appearances of renal transplant. C. To learn the imaging spectrum of pathological conditions affecting the renal transplant and the complications of immunosuppression. To demonstrate the role of interventional radiology in management of complications.

Background: The management of end stage renal disease has been revolutionized with the advent of renal transplantation, which offers good quality of life with low morbidity. The survival rates are very good due to excellent immunosuppressants. Imaging plays an important role in diagnosis and management of the complications arising in the renal transplant.

Imaging Findings: Ultrasound, Doppler and nuclear medicine are the main imaging modalities used in renal transplant recipients. CT scan, MR imaging and angiography are used in indeterminate cases. The various pathologies demonstrated in our pictorial review include rejection, ATN, Cyclosporine toxicity, infection, lymphocele, urinoma, haematoma, abscess, renal arterial stenosis, renal vein thrombosis, AV fistula and obstruction. Opportunistic infections and post transplant lymphoproliferative disorder are the complications of immunosuppression.

Conclusion: Ultrasound, Doppler, CT scan, nuclear medicine and MR imaging are vital investigations in diagnosing the complications of renal transplantation. Imaging guided interventional procedures are crucial in the management of complications such as collections, obstruction and vascular lesions.

C-0459

MR evaluation of renal cell carcinoma: Comprehensive protocol for determining venous extension

O. Mathieu, C. de Bazelaire, A.-M. Zagdanski, P. Bourrier, M. Albiter, J. Frija, E. de Kerviler; Paris/FR

Learning Objectives: To analyze renal and cava vena extension of renal cell carcinoma in MR imaging. A comprehensive protocol was performed using a black blood sequence (HASTE), a white blood sequence (TrueFISP), and a contrast-enhanced 3D T1-weighted sequence (VIBE).

Background: Preoperative staging of renal carcinoma relies on multi-slice CT. However, in patients in whom iodine injection is contraindicated, MR imaging becomes the method of choice for determining local tumour spread. Venous invasions represent one of main surgical concerns as it may lead to different surgical approaches. However, because of slowly flowing protons and numerous anatomical variants, MR examination of renal and cava veins could be tricky. The aim of this exhibit was to highlight specific advantages of 3 sequences based on dramatically different physics principles.

Procedure Details: MR imaging was performed on a 1.5 Tesla Siemens system, using three multiplanar breathold sequences: 1) Long TR/TE HASTE sequence i.e. black blood, 2) Short TR/TE steady state TrueFISP sequence i.e. white blood and 3) 3D contrast-enhanced VIBE sequence i.e. venography. Venous anatomy, normal signal and thrombus enhancement were evaluated.

Conclusion: Combining all three sequences took less than 10 minutes and lead to determine extension of renal tumour into the renal vein. HASTE was superior to other sequences in terms of contrast between thrombus and vascular lumen. Since TrueFISP uses a slice by slice acquisition, it was useful in uncooperative patients. The use of contrast enhancement with VIBE strengthens radiologist confidence in determining the nature of the thrombus.

C-0460

Imaging features of metastases and local recurrence in surgically treated kidney cancer

A. Guermazi¹, I. El-Hariry², Y. Miaux¹; ¹San Francisco, CA/US, ²Greenford/UK

Learning Objectives: To illustrate both typical and less typical ultrasound, CT and MR imaging appearances of metastases and local recurrence from renal cancers and to understand the mechanisms, risk factors, and clinical timing of recurrent disease in surgically treated renal cancer.

Background: Whole body spiral CT is currently the method of choice for evaluating the postsurgical nephrectomy site for the presence of recurrent lesions and for detecting the usual (common) anatomical sites of metastases. Administration of oral contrast material in CT is useful to differentiate these recurrent lesions from intestinal loops. In this study, we retrospectively review the radiological images of 120 patients with renal cancer who had been evaluated for the presence of recurrence or metastases.

Imaging Findings: Local recurrent lesions are usually detected as masses in the vacant renal fossa. Metastatic lesions are seen in the lung, pleura, pancreas, adrenal gland, liver, contralateral kidney, bone, lymph nodes, muscles, etc.

Conclusion: Knowledge of the mechanisms, risk factors, and clinical timing of recurrent disease in surgically treated renal cancer can assist the radiologist in understanding and detecting the patterns of recurrence observed on imaging. Ultrasound and MR imaging may be of interest when exploring particular organs such as liver, brain and spine.

C-0461

Imaging aspects of papillary renal cell carcinoma (RCC): Characterization and staging with pathological correlation

B. Sauer, S. El Ghali, X. Buy, H. Lang, C. Saussine, C. Roy; Strasbourg/FR

Learning Objectives: To recognize specific aspects of papillary type renal tumors. To define accurate criteria for local extension. To know and discuss main differential diagnoses.

Background: Papillary RCC is a subgroup (5-15%) of malignant renal epithelial neoplasms characterized by slower growth and a better prognosis. It represents a unique clinicopathologic entity which is morphologically and cytogenetically distinct from clear cell carcinoma. It is divided into basophilic type (I: most frequent, bilateral, multifocal) and eosinophilic type (II: unifocal, more aggressive with cystic aspect). It has been described as a hereditary tumor caused by a single gene mutation.

Procedure Details: MR imaging has been shown to be more accurate than CT in specific diagnosis and differential diagnosis for this tumoral type. On T2w, the specific aspect of papillary tumors is a low signal intensity, homogeneous pattern with delayed and low enhancement on dynamic Gd T1w compared to clear cell carcinoma. For local extension, identification of the pseudocapsule is an important and accurate feature to differentiate stage T1/T2 from T3a on MR, up to 95%. US is not pertinent enough. Multiple explanations are proposed to understand the hypointensity aspect. Several differential diagnoses of this pattern are discussed such as hemorrhagic cyst or tumor, lymphoma, fibroma.

Conclusion: Papillary renal tumors can be characterized on imaging findings, especially on MR, by an hypointense homogeneous pattern on T2w associated with low and late enhancement on Gd GET1w. Local extension is also sufficiently accurate on MR imaging to better select surgery type.

C-0462

Contrast-enhanced sonographic imaging of the kidney

A. Nunziata, O. Catalano, F. Sandomenico, M. Mattace Raso, A. Siani; Naples/IT

Learning objective: To illustrate the contrast-specific US findings in a wide spectrum of acute and nonacute disorders of the kidney. To show the practical value of

Scientific and Educational Exhibits

CE-US in renal differential diagnosis. To make radiologists aware of the typical and atypical appearance of renal disorders as shown with the novel, real-time, contrast-specific techniques.

Background: CE-US is used with increasing frequency in the evaluation of kidney. This is a highly vascularized organ, with a very rapid enhancement. These features make real-time, low mechanical-index US the ideal sonographic technique in imaging kidneys.

Procedure Details: A continuous-mode, low-mechanical index US technology is employed. A second-generation, sulfur-hexafluoride based contrast agent is used. The contrast agent, at a volume of 2.4 or 4.8 mL, is injected through a peripheral vein and a 20 G needle, using a three-way stopcock and 5-mL saline flushing. A wide spectrum of disorders are depicted: injury, infarction, abscess, acute pyelonephritis, small tumour (including differential diagnosis between angiomyolipoma and clear cell carcinoma), atypical cystic mass, and metastasis. Several potential pitfalls are also shown.

Conclusion: CE-US can recognise several findings useful in detection and characterisation of renal disease.

C-0463

Magnetic resonance imaging of pyelonephritis in renal transplantation

J. Maass, I. Tosetti, C.C. Bianchi, M. Stratta, C. De Feo, F. Barisone, M. Burdese, G. Gandini; Turin/IT

Learning Objectives: To illustrate the use of MR imaging in detecting acute pyelonephritis (APN) in patients with renal transplantation who have clinical signs of urinary tract infection.

Background: Urinary tract infections are common after renal transplant; APN is a critical disease which may cause permanent renal scar formation and sometimes result in allograft dysfunction and deteriorating renal function if prompt diagnosis and treatment are delayed. Between January 2003 and September 2004, 12 patients with clinical suspect of APN (fever, nausea, vomiting, pain in iliac fossa, leukocytosis) were evaluated with MR imaging; the procedure and its results are described and illustrated.

Imaging Findings: Ten out of 12 patients showed imaging signs of APN: among them, 5 had signs of focal APN in kidney poles, and other 5 showed diffuse APN signs. Three patients had also developed a renal abscess. Six patients came back for follow-up examination, where we were able to detect significant improvement or resolution of parenchymal lesions after antibiotic therapy; one patient developed a residual fibrotic scar following renal abscess. Two out of 12 patients had no signs of APN at all.

Conclusion: MR imaging is useful for detailed imaging of transplanted kidneys in order to diagnose APN and follow-up patients after treatment; it can also provide relevant information about evolution of parenchymal lesions.

C-0464

Focal hemorrhagic lesions of the kidney on MR imaging

A.E. Mahfouz, H. Sherif; Doha/QA

Objectives: To review the spectrum of focal hemorrhagic lesions of the kidney and to illustrate the MR imaging features of each of these lesions.

Background: Hemorrhagic lesions of the kidney are recognized on MR imaging by signal intensity of blood-degradation products. Signal intensity of hemorrhagic lesions differ widely according to age of the hemorrhagic process and the pulse sequence used. The most consistent of these signal intensity patterns is the high signal intensity on T1-weighted images which is not suppressed on fat saturation and the low signal intensity of the hemorrhagic lesion on T2-weighted images.

Procedure Details: Breathhold transverse, coronal, and sagittal half-Fourier fast spin-echo T2-weighted images (HASTE), transverse T1-weighted GRE images, and fat-saturated T1-weighted GRE images before and after intravenous injection of Gd-DTPA in the three orthogonal planes were performed for 100 patients with focal renal lesions. Among these, hemorrhagic lesions were selected to be presented in this educational exhibit. These lesions include traumatic injury, hemorrhagic cyst, hemorrhage in renal cell carcinoma, hemorrhage in angiomyolipoma, renal infarctions, and subcapsular hemorrhagic foci in cases of polyarteritis nodosa.

Conclusion: MR imaging is a useful imaging modality in detection of hemorrhagic focal lesions of the kidney and demonstration of certain imaging features which may help in reaching the diagnosis.

C-0465

Use of MR imaging for kidney evaluation after ESWL

P.V. Kuchuk, A.V. Arablinskiy, L.M. Rapoport, E.S. Belysheva, V.I. Rudenko, T.A. Uzhegov; Moscow/RU

Purpose: To use MR imaging for detection of possible renal complications after ESWL.

Materials and Methods: 15 patients with renal stones have been studied with MR imaging before lithotripsy, 1 and 9 days after ESWL. Renal perfusion was studied with fast spoiled gradient-recalled (FSPGR) sequences after Gd injection. Besides MR imaging, US Doppler and dynamic nephroscintigraphy with ^{99m}Tc-MAG₃ have been performed in all cases.

Results: After ESWL MR imaging detected some changes in kidneys in 14 of 15 patients. Perinephric oedema and perinephric fluid collection were revealed in 10 cases, subcapsular fluid collections in 4. Subcapsular haematoma was present in patient. Sites of intraparenchymal haemorrhage were detected in 3 patients and defects of cortico-medullary junction in 6. All changes, except for haematomas and intraparenchymal haemorrhage, regressed by 9 day after ESWL. Dynamic MR imaging found alterations of renal function in 9 patients, such as focal ($n = 2$) or total ($n = 3$) decrease of contrast enhancement and redistribution of renal blood flow ($n = 6$). US studies found morphological changes of kidneys in 3 patients.

Conclusion: MR imaging was more sensitive technique in revealing morphological changes of kidney impairment after ESWL, than US. At research of functional changes MR imaging has no important advantages over scintigraphy and ultrasound, except for an opportunity to reveal redistribution of blood flow between cortical and medullary substance. MR imaging should be used after ESWL in cases with high probability of complications.

C-0466

Evaluation of transplanted kidney function by the clearance of technetium-99m mercaptoacetyltriglycine: The comparison between two methods

S.L. Beatovic, E. Jaksic, R. Han; Belgrade/YU

Purpose: Our study aimed at evaluating the sensitivity of two methods for mercaptoacetyltriglycine (MAG3) clearance calculation in patients with transplanted kidney: single sample method and camera based method.

Methods and Materials: 62 patients were investigated. Group A consisted of 22 patients with well-functioning grafts, group B of 20 patients with suspected acute rejection and group C of 20 potential kidney donors. Single-sample method used the following formula: $CL = 512 \cdot e^{-0.00688 \cdot t} + 297 \cdot e^{-0.0135 \cdot t}$. In(dose/plasma counts). Camera-based method used counting rates from kidney region during the second minute of the study. The obtained value is expressed as clearance index (CI).

Results: Mean values of CL were: $187.8 \pm 39.2 \text{ ml} \cdot \text{min}^{-1}$ (group A), $64.3 \pm 22.6 \text{ ml} \cdot \text{min}^{-1}$ (group B) and $361.7 \pm 38.4 \text{ ml} \cdot \text{min}^{-1}$ (group C). The difference between groups A and B was statistically significant ($p < 0.05$). In groups A and B CL was significantly lower than in control group. Results of CI were: 50.9 ± 15.6 (group A), 27.9 ± 7.9 (group B) and 75.2 ± 9.5 (group C). Correlation between CL and CI was statistically significant. Results of CL correlated well with blood urea nitrogen (BUN), serum creatinine (Cr) and creatinine clearance (C_{Cr}): $BUN/CL r = -0.78$; $Cr/CL r = -0.69$; $C_{Cr}/CL r = 0.86$. Significant correlation between CI and kidney lab was not obtained.

Conclusion: CL is sensitive quantitative parameter of renal transplant function. CI could also reflect changes in kidney graft function, but is less sensitive than CL. Nevertheless, due to the simplicity of its calculation, CI merits further clinical evaluation as potential parameter of transplanted kidney function.

Scientific and Educational Exhibits

Genitourinary

Male

C-0467

Imaging findings of extratesticular scrotal masses

C. Pozuelo Segura, O. Pozuelo, Y. Roca, L. Mones, C. Medrano, A. Torremilans, J. Quintero, D. Mulattieri; Barcelona/ES

Learning Objectives: The aim of this study is to illustrate the distinguishing features of extratesticular scrotal masses and to analyse the role of US in the diagnosis.

Background: Sonography is the imaging modality of choice in detecting and characterizing pathologic conditions affecting the extratesticular space. Although most abnormalities are benign, many may simulate or represent malignant processes. Accurate diagnosis is therefore essential and must be based not only on the sonographic findings but also on accurate clinical history and physical examination findings. We performed a retrospective study from the database between January 2000-September 2004 at our institution. All different sonographic features of extratesticular masses we reviewed. All patients were evaluated with Toshiba power vision 6000 with the highest frequency transducer (5-10 MHz).

Procedure Details: Most extratesticular masses are benign. We divided the pathologic findings depend the anatomical region: 1) tunica vaginalis: fluid collections (hydroceles, spermatoceles, pyoceles) and tumors. 2) epididymis: epididymitis (acute or chronic), cysts, granulomas and tumors. 3) Spermatic cord: varicocele and tumors 4) paratesticular masses: hernia, calculi, ...

Conclusion: US is a valuable tool for screening of scrotal lesions. If the lesion is extratesticular and shows a cystic appearance, a specific diagnosis can often be made and can be reassured that the mass is benign. Solid extratesticular masses can be somewhat more problematic to diagnose.

C-0468

MR imaging features of prostate carcinoma in local and nodal staging

J.J. Fütterer, S.W.T.P. Heijmink, R.A.M. Heesakkers, C.A. Hulsbergen van der Kaa, F.A. Witjes, J.O. Barentsz; Nijmegen/NL

Learning Objectives: To illustrate the spectrum of MR imaging features of prostate carcinoma in local and nodal staging.

Background: Prostate cancer is the second most frequent cause of cancer related death in men. To diagnose prostate cancer, digital rectal examination and the determination of the blood level of prostate-specific antigen (PSA) are the first tools. If these findings are suspicious of cancer, an investigation of transrectal ultrasound (TRUS) will follow. Subsequently, TRUS-guided multiple histological biopsies will be performed to obtain histopathologic confirmation. However, TRUS-guidance may fail to detect cancer in the prostate. Other techniques such as MR imaging can be used to allow visualization of the prostate. MR imaging is important to non-invasively show cancer localization, the extent of cancer and in possibly the near future also aggression of the cancer. Recently new MR techniques have been developed, which do not only show prostate morphology but also function. These techniques are contrast enhanced MR imaging, MR spectroscopy and MR with a specific lymph node contrast agent. This last technique may replace pelvic lymph node dissection.

Imaging Findings: This educational exhibit illustrates the MR appearances of local tumours, local stages, and nodal metastasis in prostate cancer. We demonstrate in this pictorial essay the current value of MR imaging in prostate cancer and will illustrate new developments.

Conclusion: MR imaging of the prostate provides important pre-therapeutic information about local- and nodal staging.

C-0469

Testicular masses in association with congenital adrenal hyperplasia: MR features compared with sonographic findings

H.M. Suliman¹, N.M.M.L. Stikkelbroeck², G.J. Jager², J. Blickman², B.J. Otten², A.R.M.M. Hermus²; ¹Amsterdam/NL, ²Nijmegen/NL

Purpose: To evaluate and describe the imaging findings of testicular "adrenal rest tumors" in male patients with congenital adrenal hyperplasia (CAH).

Materials and Methods: Seventeen patients with CAH due to 21-OH deficiency were evaluated. All patients underwent scrotal ultrasound (US), with color Doppler, and in 16 patients MR was performed. T2W and T1W images pre and post contrast were obtained.

Results: In 6 of the 17 patients the lesions were palpable. US revealed lesions in 16 of 17 patients (94%). The size varied from 2 mm to 40 mm. In 10 patients the

lesions were hypoechoic and in 6 they were hypoechoic with hyperechoic reflections. All lesions were located against the mediastinum. Acoustic shadowing and well-defined margins was present in 16 cases (Fig. 1). Hypervascularity was seen in 4 lesions (Fig. 2). MR revealed lesions in 15 of 16 patients. All lesions were isointense on T1W, and hypointense on T2W images. The lesions were clearly defined, homogeneous and located adjacent to the mediastinum testis. After iv of Gadolinium all lesions demonstrated strong enhancement (Fig. 4 and Fig. 5). None of the lesions showed a capsule or pseudocapsule.

Conclusion: Testicular lesions are common in CAH and have characteristic US and MR features. They are often multifocal, bilateral and are found around the mediastinum testis. US monitoring will be adequate for diagnostic evaluation.

C-0470

Transrectal ultrasound (TRUS) of prostate cancer (PRCA): A multimedia DVD Rom-based educational tool and database: Sonographic-pathologic correlation

D. Alexopoulos, S. Papavassiliou, I. Mastorakou, D. Leli, E. Tako, S. Faitaki, P. Karavitis, P.S. Zoumpoulis; Athens/GR

Learning Objectives: - To demonstrate the role of TRUS in diagnosing prostate lesions. - To present TRUS prostate echoanatomy, semiology and haemodynamics of PrCa. - To reach a sonographic diagnosis using algorithms. - To provide comparison of an US image with images of the database.

Background: Since TRUS is the most efficient way to detect Prostate Cancer (PrCa) the main purpose of this e-book is to teach the TRUS procedure in detection and staging of PrCa and correlate it with the histological findings emphasizing the use and effectiveness of USCA and local anesthesia prior to biopsy sampling.

Procedure Details: This medical e-book is a multimedia DVD-Rom based teaching file featuring 2500 US prostate images, 150 US video demonstrations, 400 video cases presenting clinical data and detailed description of TRUS techniques; chapters on prostate anatomy, TRUS technique for the detection and staging of PrCa (based on over 10,000 cases), Color Doppler, the technique of US-guided biopsies. The proper TRUS technique is demonstrated step by step. Its educational role is based upon Video Cases and double video presentations. The latter consist of a simultaneous presentation of the real time ultrasound exam and the examiner's technique. A database is included aiding the user to reach the correct diagnosis and to compare his sonographic image to histologically proven images of the database.

Conclusion: User-friendly DVD-Rom based teaching file on the Prostate with chapters on Anatomy, Pathology, Ultrasound Physics, Sonographic Appearance of the Normal Prostate, TRUS Morphology, Detection and Staging of PrCa, Local Anesthesia, USCA and Comparative Database.

C-0471

Diagnostic imaging in the staging and evaluation of prostatic carcinoma

A.M. Camenzuli¹, S. Lea², C. Romanuk³; ¹Liverpool/UK, ²Upton - Wirral/UK, ³Bebington - Wirral/UK

Learning Objectives: 1. Provide examples of the anatomy and staging of prostate carcinoma using MR imaging. 2. Staging pitfalls in MR imaging - the influence of haemorrhage, surgery and medication on local staging. 3. The use of Partin Tables in MR imaging staging and image interpretation. 4. Compare the role of isotope bone scintigraphy versus MR imaging in the assessment of bone metastases 5. Illustrate uncommon appearances that are prevalent in post graduate examinations: The superscan effect, the solitary sclerotic bone and dural metastases.

Background: The management of prostatic carcinoma (radical curative surgery or radiotherapy versus controlled disease with hormones or symptom relief) largely depends on the staging. This presentation will provide insight to the radiologists' perspective.

Imaging Findings: This presentation will graphically illustrate the patterns of spread of disease on MR imaging and nuclear medicine, with an outline of factors that influence the accuracy of staging such as tumour location, haemorrhage, infection, medication or previous surgery. It will also highlight the use of Partin's tables to predict the degree of invasion and likelihood of nodal metastases to improve the degree of confidence in reporting staging scans. The roles of nuclear medicine versus MR imaging to assess the metastatic burden to bone and its complications will be presented graphically. The final section illustrates presentations of post graduate exam interest.

Scientific and Educational Exhibits

C-0472

The importance of the transitional zone at repeat transrectal ultrasound-guided prostate biopsy

N. Gough, C.P. Meehan, P.A. McCarthy; Galway/IE

Background: A significant number of patients attending for Transrectal ultrasound guided prostate biopsy are having repeat biopsy as Prostatic Specific Antigen levels remain high and/or digital rectal examination remains suspicious. Some patients may undergo several biopsies with negative results. 24% of prostate carcinoma occurs in the transitional zone, an area not traditionally biopsied.

Materials and Methods: Group A: 756 Transrectal ultrasound guided prostate biopsies were performed between Jan 00 and Jan 03. Of these 99 were being repeated in 87 patients. (Range 1-5 per patient). From Jan 03 we proposed to take repeat biopsies from the transitional zone. Group B: 279 biopsies were performed between Jan 03 and Jan 04. Of these 56 were being repeated in 52 patients. (range 1-2 per patient).

Results: Of the 99 repeated biopsies taken from the peripheral zone 21 patients (21.2%) had positive results. Of the 56 repeated biopsies from the transitional zone 19 patients (34%) had positive results.

Conclusion: In our experience, routine targeting of the transitional zone at repeat biopsy significantly increases the detection of prostate carcinoma.

C-0473

Color-Doppler sonography (US): A pictorial atlas of scrotal disorders

F. Sandomenico, O. Catalano, A. Nunziata, P. De Feo, A. Siani; Naples/IT

Learning objective: To illustrate the colour-Doppler US findings in a wide spectrum of acute and nonacute disorders of the scrotum. To show the practical value of colour-Doppler in differential diagnosis of scrotal disease. To make the radiologist aware of all typical and atypical appearances of scrotal disorders as shown with colour- and power-Doppler US.

Background: Colour and power-Doppler imaging techniques are currently used in addition to grey-scale imaging in the assessment of a variety of scrotal disorders.

Procedure Details: Optimal imaging technique and equipment setting is shown. A wide spectrum of scrotal acute and nonacute disorders is depicted: injuries, ischemia secondary to funicle torsion or inguinoscrotal hematoma (post-herniorrhaphy), testicular infarction, scrotal abscess, orchitis and orchiepididymitis, testicular and extratesticular cysts and tumours, varicocele, Fournier gangrene, undescended testis. Several potential interpretative pitfalls are also illustrated.

Conclusion: High-resolution colour-Doppler US is used with increasing frequency in the evaluation of the scrotum and can demonstrate several findings relevant for patient management. Radiologist should be aware of all colour-Doppler features of scrotal disorders.

C-0474

Sentinel lymph node assessment by ^{99m}Tc-colloid orchifuniculoscintigraphy in patients with testicular tumors

M.D. Sterpu, V.Y. Soukhov, L.A. Tyutin; St. Petersburg/RU

Purpose: To evaluate direct orchifuniculoscintigraphy used as method of clarifying the routes of lymphatic cancer spread for optimization of radiation therapy.

Materials and Methods: Orchifuniculoscintigraphy was performed in 31 patients 17 - 47 y.o. with tumors of the testis by administration of 37-74 MBq of ^{99m}Tc-colloid beneath the tunica albuginea of the tumor-affected testis prior to its surgical resection or in the stump of spermatic cord, if the patient had earlier undergone orchiectomy. Examinations were performed 45-60 minutes p.i. on gamma-camera "E.cam Var" (Siemens) in four projections. Intact lymph nodes were seen on scintigrams as foci of intensive accumulation of the radiopharmaceutical. Reduction or absence of tracer uptake in the lymph nodes projections with simultaneous imaging of lymphatic vessels was considered as potential lymphatic cancer spread required local irradiation of these regions.

Results: Data of orchifuniculoscintigraphy helped to determine the direction of lymph outflow from tumor-affected testis or the stump of spermatic cord to sentinel lymph nodes by normal or changed lymph collectors. Thus, orchifuniculoscintigraphy led to exact determination of fields' size and configuration for local radiation therapy.

Conclusions: Finding of the lymph outflow routes with ^{99m}Tc-colloid increases the validity of early lymphatic cancer spread detection, including cases without lymph node enlargement. Determination of the lymph outflow routes gave an opportunity to configure the radiation fields within sites of ^{99m}Tc-colloid accumulation.

C-0475

Feasibility of quadrature body coil in prostate spectroscopic MR imaging

M.C. Martinez-Bisbal¹, B. Celda¹, B. Martinez-Granados¹, C. San Juan², L. Martí-Bonmatí²; ¹Burjassot/ES, ²Valencia/ES

Purpose: PSA measurements, transrectal ultrasonography, CT, and MR imaging often cannot reliably differentiate early prostate cancer from BPH and normal tissue. Proton spectroscopic imaging (¹H-MRSI) can evaluate the prostate with an appropriate matrix size and field homogenisation. In most centres spectroscopic images are obtained with an endorectal coil. We present our results with ¹H-MRSI obtained using the quadrature body coil, ensuring faster and reliable clinical application and lower patient disturbances.

Materials and Methods: 25 male patients were studied (1.5 T system) with a sagittal and transverse T2W images orthogonal to the prostate central gland axis. Transverse images were used to localize 2 ¹H-MRSI slices (TE 272 ms, thickness 20x22 mm, ROI 65x65 mm) including both the central and peripheral glands. When necessary, a single volume (TE 136 ms) was also acquired in regions with abnormal ¹H-MRSI findings. Spectra were analysed with jMRUI and SiView. Only subjects with pathological data (surgery or biopsy) were included.

Results: Higher Choline and lower Citrate were found in those patients with cancer in all pathological areas. ¹H-MRSI allowed the location of higher cellular regions in the central and peripheral portions. The spatial resolution was considered adequate by radiologists and urologic surgeons.

Conclusion: ¹H-MRSI and single voxel MRS with a 1.5 T unit using the quadrature body coil is an easily accepted technique useful in the diagnosis of prostate cancer. Patient conformance is high; it is non-invasive; and allows patient follow-up.

C-0476

Sonographic features of intratesticular pathology

C. Pozuelo Segura, O. Pozuelo, L. Mones, Y. Roca, C. Medrano, J. Quintero, A. Torremilans, D. Mulattieri; Barcelona/ES

Learning Objectives: The aim of this exhibit is to present the imaging findings of the intratesticular scrotal pathology and to analyse the role of US in the diagnosis

Background: High-resolution sonography is a very sensitive imaging modality for detecting intratesticular pathology and is an accurate means of distinguishing intratesticular lesions (usually malignant) from extratesticular ones (usually benign). We retrospectively reviewed the imaging findings of intratesticular scrotal masses diagnosed by US seen in our centers between January 2000-September 2004. All patients were evaluated with Toshiba power vision 6000 and Toshiba Nemio with the highest frequency transducer (5-10 MHz).

Procedure Details: We divided the pathologic findings depending on the clinical presentation: 1) acute scrotum (testicular torsion, epididymo-orchitis), 2) trauma 3) undescended testes (cryptorchidism) 4) benign masses (cysts, ectasia rete testis, microlithiasis, varicocele, ...) 5) malignant masses.

Conclusions: US is the primary modality for imaging scrotal lesions. It provides excellent spatial resolution and it has been shown to be nearly 100% sensitive in the identification of scrotal masses. However, sonography does have limitations in distinguishing benign from malignant neoplasms or from some inflammatory lesions. The combination of clinical and US findings facilitated the differentiation between non-neoplastic and neoplastic testicular cysts.

C-0477

Analysis of suprapubic and transrectal measurements in assessing prostate dimensions and volume: Is transrectal ultrasonography really necessary for prostate volume measurement?

E. Özden, Ç. Göğüs, Ö. Kılıç, Ö. Yaman, E. Özdiğer; Ankara/TR

Purpose: The objective of this study is to evaluate the reliability of suprapubic ultrasonography (SU) in prostate volume measurement and determine the correlation of SU and transrectal ultrasonography (TRUS) in according to different prostate volume ranges.

Methods and Materials: 100 consecutive patients with benign prostatic hyperplasia (BPH) were examined by SU and TRUS in the same session. Patients were further divided into 2 subgroups according to prostate volumes measured by SPUS: < 60 cc and > 60 cc. The three dimension (anteroposterior, transverse and craniocaudal) and volume measurements performed by SU were compared with corresponding measurements performed by TRUS in order to determine the correlation of the measurements. Volumes were calculated using the ellipsoid formula.

Results: The mean prostate volume of the 100 patients, measured by SU and TRUS were 65.9 ± 35.8 cc and 62.5 ± 32 cc respectively and strongly correlated ($r: 0.94, p < 0.001$). Craniocaudal diameters had the strongest correlation among

Scientific and Educational Exhibits

dimension measurements ($r: 0.89, p < 0.001$). Correlation coefficients for antero-posterior and transverse measurements were $r: 0.86$ and $r: 0.79$ respectively. In accordance to volume ranges the strongest correlation of two techniques were determined for prostates with volumes > 60 cc ($r: 0.90, p < 0.001$). The equation that converts the volume measured by SU to TRUS was determined as; TRUS = $7.116 + (0.84 \times SU)$.

Conclusion: There is a strong correlation between SU and TRUS measurements of prostate. SU as a more comfortable and better tolerated technique, may be used reliably in the measurement of prostate volume.

C-0478

Diagnostic value of TRUS in patients with PSA values ≥ 20 ng/ml: Can only lesion biopsies be adequate for diagnosis?

E. Özden, A.T. Turgut, Ç. Göğüs, C. Yagci, S. Küpel; Ankara/TR

Purpose: To investigate the value of transrectal ultrasonography (TRUS) in patients with prostate specific antigen (PSA) values ≥ 20 ng/ml, in order to determine if only lesion biopsies can be adequate for the diagnosis of prostate carcinoma in these PSA ranges.

Methods and Materials: 51 consecutive patients with PSA values ≥ 20 ng/ml who underwent TRUS and TRUS guided prostate biopsy were included in the study. TRUS guided sextant + lesion biopsies were taken and TRUS findings of each biopsy location were correlated with histopathology results of the same site.

Results: In the analysis of 408 biopsy foci, calculated sensitivity, specificity, positive and negative predictive values of TRUS were 63.5%, 90.4%, 83.7% and 76.2% respectively. There were 65 (15.9%) biopsy foci in which cancer were identified histopathologically although TRUS detected no lesion. Four of the (7.84%) patients with nonsuspicious TRUS findings had prostate cancer. There were nine (17.64%) patients with cancer foci detected at the contralateral side of the lesion detected by TRUS.

Conclusion: Diagnostic value of TRUS is not sufficiently high even in high PSA ranges and we suggest that in addition to the lesion biopsies, systematic biopsies should also be performed in patients with PSA ≥ 20 ng/ml.

C-0479

Comparision of lateral-medial peripheral zone prostate biopsies: Analysis of 12 core locations in 160 patients

E. Özden, Ç. Göğüs, A. Zümrütbas, S. Baltaci, Y. Bedük; Ankara/TR

Purpose: To investigate the value of lateral peripheral zone prostate biopsies.

Methods and Materials: The study included 160 consecutive patients who underwent 12 core transrectal ultrasonography (TRUS) guided prostate biopsy with total serum prostate specific antigen (PSA) values between 4.0 - 19.9 ng/ml. Sextant + 6 core lateral biopsies have been performed. Each biopsy specimen was labelled according to location and sent for pathologic evaluation in separate containers. Percent of cancer for each core location was assessed according to PSA ranges.

Results: Prostate cancer was diagnosed in 43 of the 160 (26.87%) patients. By analysis of the 1920 cores 226 cancer foci were detected of which 117 (51.77%) were detected at lateral and 109 (48.23%) at medial locations ($p: 0.571$). The detection rates for lateral locations were 54.08% and 50% in 4-9.9 and 10-19.9 ng/ml PSA ranges respectively. There were also no statistically significant difference for cancer detection rates between lateral and medial biopsy locations for basal-middle and apical regions. The highest detection rate was for bilateral basal lateral locations (15%) and the lowest was for right apicolateral location (7.5%).

Conclusion: Although cancer detection rate at lateral biopsies are higher than medial locations, there is no significant difference between them.

C-0480

Pitfalls in MR staging of prostate carcinoma: A pathological correlation (or prognostic pitfalls of prostatic proton pictures)

S. Punwani, D.J. Hopster, R. Chaudhuri, D. Murray; London/UK

Learning Objectives: To raise the awareness of the pathological correlate of MR appearances encountered in the pre-operative staging of prostatic carcinoma.

Background: Prostate cancer is the most commonly diagnosed non cutaneous cancer diagnosed in males. Primary staging helps to select patients that are suitable for potential curative radical surgery. MR is now routinely used in pre-operative staging of prostate cancer, but is known to have only moderate sensitivity and specificity in detecting extracapsular spread. An audit conducted at our institution over 18 months directly compared post prostatectomy pathological staging with MR pre-operative staging ($n = 18$). The results of the audit are presented with a pictorial correlation of the pathological findings.

Procedure Details: Normal imaging findings of the prostate and seminal vesicles and the corresponding pathological interpretation is demonstrated. MR appearances mimicking extra-capsular disease such as fibrosis, haemorrhage and inflammation are individually illustrated with corresponding images of pathological sections. Also, pathological correlation for the various MR appearances of the seminal vesicles is shown.

Conclusion: Awareness of the underlying pathological processes resulting in the MR appearances allows a more informed interpretation of MR prostate imaging. A multi-disciplinary (clinical, radiological and pathological) approach in the management of patients is of great educational value in the accurate staging of prostate cancer.

C-0481

An efficient way to reach the correct diagnosis on prostate lesions with transrectal ultrasound: DVD-Rom based teaching file with ultrasound images, real-time video display and comparative data

P.S. Zoumpoulis, D. Alexopoulos, S. Kyriazi, C. Beligiannis, D. Dalakostas, K. Pahou, L. Kaklamanis; Athens/GR

Learning Objectives: - To teach a trainee to describe the US characteristics of Focal Prostate Lesions. - To aid and guide the user in reaching a sonographic diagnosis through correct algorithms. - To compare US images of diagnostic difficulty to those of the database.

Background: The purpose of this DVD-Rom is to suggest *diagnostic algorithms* in order to characterize *focal prostate lesions* seen by TRUS, starting from an US image and its main morphologic and haemodynamic features.

Procedure Details: The user can start using this teaching file by submitting the US characteristics of a focal prostate lesion, which he has difficulty in diagnosing. He is asked to describe the echogenicity, anatomical position, border shape, acoustic impedance and the vascularity of the lesion. The system guides him through a specific algorithm to all possible diseases that coincide with criteria given. A large collection of classified US image galleries and video galleries are available in each diagnostic category giving the user the capability of comparing his own image(s) to those of the database. The user's image can also be linked to the contents of corresponding "interesting cases", which are brief case reports with clinical, biochemical, imaging and pathological data.

Conclusion: Assistance in deriving a diagnosis of a prostate lesion by viewing or comparing images of diagnostic difficulty to sonographic images of the database.

C-0482

Local anaesthesia before TRUS-guided prostate biopsy: Performance, technical results and side-effects on image quality. Indications and side effects on patients

A. Plagou, D. Alexopoulos, I. Theotokas, P.S. Zoumpoulis, S. Prapavesis, A. Fousteris, A. Filippidou; Athens/GR

Learning Objectives: 1. To discuss the indications for the use of local anaesthesia prior to TRUS. 2. To demonstrate the procedure of TRUS guided local anaesthesia before prostate biopsy. 3. To estimate the efficacy of TRUS guided local anaesthesia before prostate biopsy.

Background: Administration of local anaesthesia prior to TRUS-guided biopsy efficiently eliminates patient discomfort allowing for greater number of biopsies. 1600 TRUS-guided prostate biopsies have been performed following local periprostatic anaesthesia from 2000-2004.

Procedure Details: The procedure begins by injecting 8-15 cc of Xylocaine and 2% adrenaline through the biopsy needle. The technique, its effects on the US image, complications and side effects were compared to 8500 US-guided biopsies performed between the years 1994-2004, without local anaesthesia. There was no significant difference between the number and severity of complications in the group with local anaesthesia compared to the group without anaesthesia. There were no significant side effects caused by the infusion of the anaesthesia drug. However, degradation of image resolution is noted since air bubbles are sometimes infused with the drug causing a "fuzzy" image, which results in a degree of difficulty in guiding the needle. A thorough TRUS examination of the prostate prior to the anaesthesia helps the radiologist guide the needle to the appropriate area, even through a "fuzzy" image.

Conclusion: US-guided local anaesthesia, before TRUS biopsy, assures patient cooperation and is essential for a large (more than 10) number of biopsies.

Scientific and Educational Exhibits

C-0483

Transrectal prostate biopsy: Does a role for neurovascular bundle local anaesthesia exist?

D.G. Lohan, N. Gough, S.M. Walsh, C. Roche, P. McCarthy; Galway/IE

Purpose: To evaluate the efficacy of neurovascular bundle local anaesthesia (LA) infiltration in decreasing the discomfort experienced by patients undergoing transrectal ultrasound (TRUS)-guided biopsy of prostate.

Materials and Methods: In a six month interval, 150 patients underwent transrectal ultrasound-guided prostate biopsy (TRUS). All biopsies were performed by two Consultant Radiologists using a similar technique in each case. These patients were randomized to one of two groups, one of which received 5 mL 1% lignocaine to the neurovascular bundles bilaterally prior to traditional sextant biopsies, the other group receiving no local anaesthesia whatsoever. Patients then completed 10-point pain scoring, using a visual analogue scale, for each biopsy during, then immediately after and one week following the procedure.

Results: Pain scores in the local anaesthesia group correlated almost exactly with those experienced by the no local anaesthesia group immediately after, and one week following, TRUS-guided prostate biopsies. In addition, no significant difference existed between the two groups regarding adverse effects following the procedures.

Conclusions: Local anaesthesia for TRUS biopsy is a simple and well tolerated intervention. However, it fails to significantly reduce the pain associated with this often uncomfortable procedure. It is not associated with an increased incidence of adverse complications and increases the duration of the procedure - therefore its adoption as a routine part of TRUS-guided biopsy cannot be recommended.

C-0484

Imaging of common and uncommon scrotal diseases

N.J. Khoury, M.J. Mehanna, A.R. Karam, M.C. Haddad; Beirut/LB

Learning Objectives: To present our experience in imaging scrotal diseases, both testicular and extratesticular, including the common and the uncommon pathologies.

Background: Scrotal disease processes are commonly symptomatic, manifested mainly by scrotal pain and/or swelling. Other causes of presentation include infertility and empty scrotum. Patients with scrotal complaints are frequently referred for imaging in particular sonography, which has high diagnostic accuracy. MR imaging may be a helpful adjunct in few cases.

Imaging Findings: In this scientific exhibit we present our experience in imaging a wide variety of scrotal diseases using mainly ultrasound. MR imaging, CT scan and nuclear studies were used in few cases for further assessment of sonographic findings. The disease processes include testicular and extratesticular pathologies. Testicular pathology include: tumors (germ cell tumors, seminomatous and non seminomatous, stromal tumors, and metastases), infections (orchitis, abscess), and miscellaneous conditions (torsion, trauma, tubular ectasia of the rete testis, benign cysts, supernumerary testicle, undescended testis). Extratesticular diseases include epididymitis, epididymal cysts and masses, varicocele, hydrocele, hematocoele, pyocele and scrotolith.

Conclusion: Scrotal diseases include a wide spectrum of pathologies commonly encountered by radiologist. This review enables us to be familiar with the radiological manifestations of these diseases.

C-0485

MR imaging of penis and pelvic floor in patients after perineal blunt injury

M. Sharia, O. Belichenko, S. Gamidov, A. Denisov; Moscow/RU

Purpose: To study the diagnostic possibilities of MR imaging in lesion assessing after blunt perineal injury.

Material and methods. 32 patients with blunt perineal injury (mean age 44 years) have been studied with 1.0 T MR imaging system (Magnetom Harmony, Siemens). 14 of them suffered from erectile dysfunction (ED). All the patients underwent examination which consisted of the pharmacological dopplerography, electromyography of the penis with pharmacological loading and MR imaging of the perineum and the penis.

Results: MR imaging was useful in identification of anatomic structures of the penis and pelvic fundus, pathological tissue processes (hematomas, damaged tissues, fibrous scars) after blunt injury of the perineum responsible for ED. Results of pharmacological dopplerography, electromyography of the penis with pharmacological loading showed arterial (in 100% patients), venous (in 33.3% patients) and neurogenic (in 11.1% patients) lesions. Algorithm for diagnostics of ED in patients after perineal blunt injury has been developed based on the received results.

Conclusion: MR imaging of the penis and pelvic fundus is objective and highly informative method for identification of anatomic structures and assessing of penis lesions in patients with blunt perineal injury.

C-0486

Can longer tissue samples be extracted by pressing the prostate with the probe during TRUS guided biopsy?

E. Özden, Ç. Göğüs, E. Dasdemirov, A.T. Turgut, K. Türkölmez, Ö. Tulunay; Ankara/TR

Purpose: Several authors reported that biopsy needles sometimes sample a longer tissue than their suggested core lengths during prostate biopsy, but no explanation for this has been proposed yet. This is important because a significant trend was reported for increased detection of prostate cancer as longer prostate tissue samples are obtained. We investigated whether pressing the prostate by the probe during biopsy enables extraction of longer tissue samples.

Methods and Materials: The study included 23 patients who underwent transrectal ultrasonography (TRUS) guided prostate biopsy. Randomly, left or right side of the prostate of each patient have been sampled by pressing the prostate by the tip of the probe, whereas other side of the prostate have been sampled without any pressure. Difference between the length of the samples extracted by each method have been analysed statistically.

Results: Although mean length of samples extracted during pressing by the probe (16.17 mm) was 3.12% longer than samples taken without pressure (15.68 mm), the difference was not statistically significant ($p = 0.232$). Mean sample lengths also showed no significant difference when analysed according to base- mid and apical locations. Two patients (8.7%) had high fever after biopsy.

Conclusion: Pressing the prostate with the probe is of no use for taking longer tissue samples. In addition, high fever rate noted in this study was higher than reported in the literature. We suggest that pressure should not be applied to the prostate during TRUS guided biopsy.

C-0487

The effect of gleason scores on TRUS detection rates and sonographic appearances of prostatic carcinoma

E. Özden, Ç. Göğüs, Z. Tokatlı, Ö. Yaman, O. Göğüs; Ankara/TR

Purpose: To evaluate the transrectal ultrasonography (TRUS) features and detection rates of prostatic cancers in accordance to gleason scores.

Materials and Methods: Histopathologic results of 246 peripheral zone prostate cancer foci detected in 61 patients who have undergone TRUS guided sextant + lesion biopsy were compared with the TRUS findings of the same biopsy location. Cancer detection rates of TRUS and differences in TRUS features were analyzed in according to gleason scores.

Results: Detection rates of TRUS were 29.5% for cancers with gleason scores less than 7, and 56.3% for cancers with higher scores ($p < 0.001$). Whereas the TRUS features regional decreased echogenicity and hypoechoic nodule were respectively defined at 67.85% and 32.15% of the cancers with gleason scores less than 7, these rates were respectively 62.35% and 23.54% for the cancers with higher gleason scores.

Conclusion: The detection rate of TRUS for prostate cancers with gleason scores 7 or more are significantly higher than cancers with gleason scores less than 7. The sonographic features defined by TRUS are not affected by the gleason scores.

C-0488

The effect of rectal enema before TRUS guided prostate biopsy on patient comfort and biopsy related complications

E. Özden, Ç. Göğüs, M. Akand, Ö. Yaman, O. Göğüs; Ankara/TR

Purpose: To evaluate the effect of rectal enema before transrectal ultrasonography (TRUS)-guided prostate biopsy on patient comfort and biopsy related complications.

Methods and Materials: A total of 100 men, who underwent TRUS-guided prostate biopsy were equally randomized into two groups. Rectal enema (1 packet of Fleet enema) was administered 1 hour before the procedure in the first group, no bowel preparation was performed in the second group. All patients had 12 core prostate biopsy. In both groups, pain scores during needle insertion and total procedure discomfort (including pre and postbiopsy phases) was assessed separately by a 11-pointed visual-linear scale. One week after the biopsy patients were questioned about complications.

Results: There was not a statistically significant difference in mean age, PSA level and prostate volume between groups. Mean biopsy pain score was 1.72 ± 1.26 in the first and 1.34 ± 1.0 in the second group ($p = 0.099$). Mean total

Scientific and Educational Exhibits

procedure discomfort was 2.18 ± 1.27 in the first and 1.44 ± 0.97 in the second group ($p = 0.003$). Complication rates were as follows in the first and second groups respectively: hematuria: 65.9%, 63.6% ($p = 1.0$); hematospermia: 53.7%, 56.8% ($p = 0.941$); rectal bleeding: 61%, 52.3% ($p = 0.555$); high fever: 4.9%, 2.3% ($p = 0.607$).

Conclusion: Although biopsy pain scores between groups were not significantly different, in the group that didn't receive enema total procedure discomfort was significantly lower than the other. We think that use of rectal enema before biopsy increases patient discomfort because of rectal irritation, and should not be used as it also doesn't reduce complication rates.

C-0489

The ability of serum prostate specific antigen and Gleason score to predict radionuclide bone scan findings in patients with untreated prostate cancer

H. Aw Yeang, R. Hurst, V. Jackson, D. Scutt, S. Vinjamuri; Liverpool/UK

Learning Objectives: This study sets out to determine whether there is a critical level of serum PSA and Gleason score below which routine bone scans may prove to be of minimal value in the diagnosis of skeletal metastases.

Methods and Materials: 268 patients with histologically proven prostate cancer underwent radionuclide bone scans over the 19-month study period. A retrospective review was performed on the cohort and data was compiled on serum PSA levels, Gleason score, TNM classification, prostatic biopsy histology findings and bone scan result. Patients who had received prostate cancer treatment before evaluation of their serum PSA were excluded.

Results: A significant statistical difference was observed ($p < 0.001$) for mean serum PSA values between patients found to be bone scan positive and bone scan negative for skeletal metastases. Of the 21 bone scan positive patients, none had serum PSA within the normal range of 0 - 4.0 ng/ml. One patient had a positive bone scan with a serum PSA below 10 ng/ml. The negative predictive value of a serum PSA below 20 ng/ml with a negative bone scan was 98.9%. A significant difference was found between the Gleason scores of bone scan positive and negative patients ($p < 0.001$).

Conclusion: Radionuclide bone scans have minimal diagnostic value for prostate cancer patients with a serum PSA level below 20 ng/ml and a low Gleason score (2-4). This criteria could be used to select patients who will benefit from a bone scan and could result in cost-savings and a reduction in waiting times.

C-0490

Audit of the use of testicular ultrasound

J. Brittenden; Harrogate/UK

Purpose: There are no guidelines governing the use of scrotal ultrasound in the investigation of testicular pathology.

Methods and Materials: The aim of our audit was to assess the clinical indication for imaging, results and outcome in 400 patients who had a scrotal ultrasound in our institution over a one year period (1st April 2003 - 31st March 2004).

Results: 62% of referrals were to investigate a clinically detected testicular swelling with one third of requests not specifying the location as being intra or extra-testicular. 30% of scans were normal. There was good correlation between the clinical and ultrasound findings in patients referred with an extra-testicular swelling but conversely there was poor correlation in patients referred with intra-testicular swelling. More than half of the patients referred with pain but no palpable mass had normal imaging. Of the patients referred with infection only 6% had associated complications that required intervention. Only 14% of patients with an abnormal scan underwent intervention (e.g surgery, aspiration and embolisation).

Conclusions: The lack of guidelines has resulted in 54% of scrotal ultrasounds being requested for patients with extra-testicular swellings and with normal testes, who are likely to undergo subsequent intervention. Analysis of the results of the use of testicular ultrasound in our hospital has resulted in the proposal of guidelines which have been issued to all family doctors and hospital consultants. The audit loop will be completed in one year's time to assess the effect of this action on the referral practice.

C-0491

Prostatic carcinoma (PC) treated with cryosurgical ablation (CA): Magnetic resonance imaging (MRI) patterns

G. Cardone, L. Nava, A. Losa, G. Guazzoni, P. Mangili, G. Balconi; Milan/IT

Learning Objectives: To report the spectrum of MR findings of prostate gland treated with cryotherapy. To show the evolution, as time passed, of the signal intensities of prostatic lesions treated with cryotherapy. To illustrate the more significant MR criteria of appropriate treatment of prostatic neoplasms by cryotherapy.

Background: Cryoablation is a minimally invasive surgical technique for early-stage prostatic carcinoma and MR is an effective imaging technique in the follow-up of lesions treated with cryoablation.

Imaging Findings: 12 pts with PC underwent cryosurgical ablation. All patients underwent MRI before and 24 hrs, 3, 6 and 12 months after surgery. MR examinations were performed using TSE T1w, TSE T2w and ce-FS TSE T1w sequences; ce-T1w images were also evaluated before and after digital subtraction. On T1w images the gland was iso-hyperintense 24 hrs after treatment and hypointense at 3, 6 and 12 months. On T2w images the gland was hyperintense at 24 hrs and hypointense at 3, 6 and 12 months. 24 hrs after treatment the prostate was 59% larger than the original volume of the gland; the treated gland decreased in size of an average of 41%, 52% and 65% at 3, 6 and 12 months respectively. Ce-FS TSE T1w and subtracted MR images showed complete ischemia of the gland in all cases, with periurethral zone sparing to preserve the urethra.

Conclusions: The more significant MR patterns in the follow-up of PC treated with CA were the decrease in size of the gland as time passed and the complete ischemia of the prostate, with periurethral zone sparing.

C-0492

Trauma-related erectile dysfunction: Spectrum of penile Doppler US findings

S. Kim¹, S. Kim¹, D. Yang²; ¹Seoul/KR, ²Incheon/KR

Learning Objectives: To illustrate the spectrum of Doppler US findings in trauma-related erectile dysfunction, categorizing them according to types of injuries.

Background: Erectile dysfunction can happen as a traumatic sequela, particularly with pelvic, vertebral, or straddle injuries. Penile Doppler findings in these patients are various, from normal to serious arterial impairment, according to types of injuries.

Imaging Findings: With neurogenic causes (e.g. vertebral injury), Doppler finding is usually normal or shows exaggerated response to vasoactive agent. Relatively or absolutely decreased peak velocity in unilateral cavernosal artery with anatomical variation (e.g. distal branches from contralateral cavernosal or dorsal artery) is a common finding in the patients with previous trauma or after major surgery in the pelvic region (e.g. radical cystectomy or prostatectomy). With trauma in the penis or perineum in straddle injury, distortion or reconstruction of vascular anatomy may be encountered in the penis, and arteriovenous fistula may be found in the corpus cavernosum in posttraumatic high-flow priapism. Dorsal vein thrombosis can be another cause of priapism after trauma or pelvic surgery.

Conclusions: Knowing this spectrum will help understand Doppler US findings in the patients with erectile dysfunction after trauma.

Scientific and Educational Exhibits

Genitourinary

Miscellaneous

C-0493

Retroperitoneal anatomy: What could we learn from disease.

Part 1: Embryology

F.M. Danza¹, M. Scialpi², A. D'Amico¹, O. Pantalone¹, A. Bernardini¹, E. Bock¹; L. Bonomo¹, ¹Rome/IT, ²Taranto/IT

Learning Objectives: To review abdominal embryogenesis for a better understanding of anatomy of the retroperitoneum (RP) and pathway of spread of pathology.

Background: The classical RP anatomy doesn't explain diffusion of fluid collections, as displayed in CT/MR exams.

Procedure Details: We retrospectively reviewed CT of patients without (200) and with (100) retroperitoneal diseases. Abdominal embryogenesis, rotations and adhesions of primitive gut/mesia were used to understand origin of retroperitoneal spaces and fascial planes (FP). We distinguish a true RP (perirenal space [PS] and posterior pararenal space [PPRS]) from acquired RP (anterior pararenal space [APRS], divided in two different compartments: supra-mesocolic APRS [smc-APRS], and under-mesocolic APRS [umc-APRS]), each resulting from different gastric/colic mesia. Adhesions generate virtual, potentially dissectible FP: the retromesenteric one cross the midline to the fascial trifurcation, communicating with two other planes, the retrorenal and lateroconal spaces. A long FP formed by inferior blending of anterior renal, posterior renal, and lateroconal fascia, continues into pelvis anterolateral to psoas muscle.

Conclusion: RP is composed of four compartments (PS, PPRS [true RP], smc-APRS, umc-APRS [acquired RP]) and multiple, potentially expandable FP; fluid collections can spread in compartments and open new spaces dissecting FP. Mesenteric root is the central way of communication between true/acquired RP and peritoneum through which diseases and fluid collections can spread bidirectionally. True RP is symmetric; acquired RP is asymmetric either in smc-APRS (on left reaches pelvis, on right stops under caecum) either in umc-APRS (smaller on right). Superiorly right PS communicates with the bare area of the liver.

C-0494

Retroperitoneal anatomy: What could we learn from disease.

Part 2: Pathway of spread of pathology

M. Scialpi¹, A. Magistrelli², M. Scaglione³, L. Lupattelli⁴, A. Rotondo³, F.M. Danza², L. Bonomo²; ¹Taranto/IT, ²Rome/IT, ³Naples/IT, ⁴Perugia/IT

Learning Objectives: To discuss the CT assessment of major retroperitoneal emergencies resulting in involvement of compartments and fascial planes (FP) of retroperitoneum, with radiologic and clinical implications.

Background: Radiologists base their diagnoses on retroperitoneal anatomy and its interconnection with the peritoneal cavity, identifying different spreads of diseases. The real way of diffusion of fluid collections in retroperitoneum has not ever been completely understood. The new sight of the retroperitoneal anatomy, previously proposed, is used to better evaluate retroperitoneal emergencies: four retroperitoneal compartments (supra-mesocolic anterior pararenal space, under-mesocolic anterior pararenal space, perirenal space and posterior pararenal space) and FP (retromesenteric, retro-renal, lateroconal planes; fascial trifurcation and combined interfascial plane that continues into pelvis).

Procedure Details: Between July 2001 and March 2004 CT of 124 patients with leaking abdominal aortic aneurysm (35), acute pancreatitis (42), renal trauma (39), and miscellaneous lesions (8) were reviewed. In all cases diagnoses were confirmed by surgery or autopsy or clinical or imaging follow-up. We evidenced an heterogeneous distribution of fluid collections and haematomas in the four retroperitoneal compartments and FP. The number of involved FP is calculated for each disease. Interconnections between retroperitoneum and peritoneal cavity were defined.

Conclusion: Helical CT increases the ability to diagnose and stage the retroperitoneal emergencies. It accurately defines spread of retroperitoneal collections, blood, pus or gas, in retroperitoneal lodges and interfascial planes. Along the anatomical interconnections with the peritoneal cavity and organs the anterior extension of some retroperitoneal diseases is easily depicted. Similar considerations can be applied to neoplastic spread in the retroperitoneum.

C-0495

Complications of urogenital non-vascular interventional procedures

Z.I. Siric, M. Radovanovic, M. Mrvic; Nis/YU

Purpose: To show the complications resulting from percutaneous interventional procedures in our patients as well as the treatment options.

Materials and Methods: During the period of the last ten years, we performed 1836 interventional non-vascular uroradiological procedures in 1650 patients (age between 10 months and 78 years). There were 970 (58.78%) female and 680 (41.22%) male patients. The performed interventions include 1269 PCN, 128 PCNL, 146 sclerosation of cysts, 88 abscess/urinoma drainages, 58 anterograde double-J stent placement, 70 biopsies, 28 stent placements, 45 ureteral dilatations and 4 anterograde extractions of encrusted double-J stents.

Results: In total we recorded 97 (5.28%) complications including 3 (0.16%) lethal complications. The complications which resulted directly from percutaneous procedures are: hemorrhage in 47 patients, lesions of the renal pelvis in 21, urosepsis in 9, urinoma formation in 8, lesions of the large bowel in 5, A-V fistula in 4 and penetration of the sclerosants into the kidney pelvis in 3 patients. Most of the complications were treated by interventional methods (5 renal artery embolizations, 12 compressions with balloon catheter, 8 urinoma drainage and 12 prolonged urine diversion). Surgical intervention was performed in 10 patients (in 8 due massive hemorrhage and 2 due lesion of large bowel).

Conclusions: Percutaneous, non-vascular interventional treatment of urogenital disorders resulted in less morbidity, shorter hospitalization and lower procedure-related complication rate. It is important that procedure should be performed by well trained radiologists who are capable of recognizing the complication and treating it percutaneously whenever it is possible.

C-0496

Imaging of the ureter with multislice CT urography

A.F. Scarsbrook, N.C. Cowan, J. Willatt; Oxford/UK

Learning Objectives: To review the anatomy and pathology of the ureter using multislice CT urography with retrograde ureteropyelographic (RP) correlation.

Background: Significant advances in computed tomography of the genitourinary system have been made since the advent of multislice technology. Multislice CT offers rapid thin slice acquisition with improved spatial resolution and the opportunity to reformat isotropic voxels for 2D & 3D image processing. CT is recognised as a method of choice for investigation of urinary tract stones and for detection and staging of renal masses. There is not yet consensus on the ability and use of multislice CT for detection and diagnosis of urothelial lesions and also small benign lesions of the ureter.

Imaging Findings: A pictorial review of the normal and pathological appearances of the ureter as demonstrated by multislice CT and RP is presented. Images were obtained from a series of > 1000 cases performed at our institution over a 6-year period. Illustrations of normal, normal variants and congenital anomalies of the ureter are included. Benign lesions such as retroperitoneal fibrosis, infection, drug induced strictures, stone disease, trauma and iatrogenic injuries are shown. Malignant pathology of the ureter and of adjacent structures is also featured.

Conclusion: This review demonstrates the radiological features of normal, normal variants and benign and malignant pathologies of the ureter using multislice CT.

C-0497

Strategy for self-directed learning of female pelvic floor anatomy from cadaver cross-sections and magnetic resonance images

W.H. Umek, O. Preyer, M.C. Sora, A. Ba-ssalamah, V. Mlynarik, S. Trattning, K. Pinker; Vienna/AT

Learning Objectives: To develop a strategy for interactive, self-directed learning of female pelvic floor anatomy using side-to-side comparison of macroscopic cadaver cross-sections and magnetic resonance (MR) images.

Background: Female pelvic floor anatomy is still little understood. Although modern imaging techniques provide high soft-tissue resolution, scientific comparisons of macroscopic anatomy with female pelvic floor MR images are still scarce.

Procedure Details: We isolated two female pelvis from cadavers of the Vienna Anatomy Donation Program, cut to fit a standard MR head coil. High-field MR images were obtained using a 3 Tesla Bruker Medspec 30/80 Scanner with a head birdcage coil and an actively shielded gradient system (maximum gradient strength: 45 mT/m). A T2-RARE sequence (TR/TE: 10.100/39 ms; acquisition time: 16 min) and a T2-MSME sequence (TR/TE: 10.000/19 ms; acquisition time: 64 min) were used for axial high resolution images (matrix size: 512x384; FOV: 230x159). Slice thickness was 2 mm with 4 mm interslice gap. The pelvis were then plastic-

Scientific and Educational Exhibits

nated, cut in 3 mm axial slices, and all slices scanned. MR and cross-sectional anatomic images were electronically arranged side-by-side. We labelled overlays to MR and anatomic images using the FreeForm AutoShapes function (Microsoft Powerpoint 2002©). These overlays allowed 1.) feedback to the viewer about their observations and 2.) tracking individual pelvic floor structures in several cross sections.

Conclusion: The presented method of interactive, self-directed learning from side-to-side comparison of macroscopic cadaver cross-sections with MR images is feasible and improves the understanding of female pelvic floor anatomy.

C-0498

CT imaging findings in primary pigmented nodular adrenocortical disease (PPNAD) in patients with Carney complex (CNC) and Cushing's disease

N.A. Courcoutsakis¹, P. Prassopoulos¹, J.A. Carney², C.A. Stratakis³,
¹Alexandroupolis/GR, ²Minnesota, MN/US, ³Bethesda, MD/US

Learning Objectives: To illustrate CT imaging findings with pathologic correlation in primary pigmented nodular adrenocortical disease (PPNAD) as they were presented in 20 patients with Carney complex (CNC) and Cushing's disease.

Background: PPNAD is the cause of a non-ACTH dependent Cushing disease. CT studies of 20 consecutive patients with CNC and PPNAD (15 familiar and five sporadic cases, mean age: 14.5 y.o.) were analyzed and compared with findings at pathology. Nineteen patients underwent bilateral and one unilateral adrenalectomy.

Imaging Findings: Pigmented micronodules - less than 3 mm in diameter- were demonstrated in all left adrenals (100%) and in 14 right adrenals (73.6%) of 19 patients who were cured with bilateral adrenalectomy. Pigmented macronodules -4 to 11 mm in size- were also observed in nine right and 10 left adrenals, being bilateral in eight (42.1%) patients. All nodules were hypodense comparing with the normal adrenal parenchyma and presented no contrast enhancement. Black or brown cortical nodules were seen on gross pathology while histology disclosed increased lipofuscin concentration within the pigmented nodules and the characteristic internodular cortical atrophy. CT of the adrenal gland revealed all pigmented macronodules but failed to demonstrate nodules when lesions were smaller than 3 mm and located in the right side in two patients.

Conclusions: 1) Patients with PPNAD demonstrate at least three small hypodense nodules on CT studies with the left adrenal invariably involved. 2) Young patients with non-suppressed hypercortisolism and adrenal nodularity demonstrated on CT studies should be evaluated for PPNAD and CNC.

C-0499

Diagnosing metastatic lymph nodes in urogenital cancers: The clinical impact and the role of radiologic imaging

N. Morisawa, T. Koyama, S. Umeoka, K. Tamai, T. Fujiwara, T. Saga, T. Itoh, K. Togashi; Kyoto/JP

Learning Objectives: To illustrate the clinical significance and the role of radiologic imaging in diagnosing metastatic nodes in urogenital cancers, showing their way of spread and frequency.

Background: Radiologic identification of metastatic nodes is crucial, since it significantly alters management of the patients. The clinical significance of metastatic nodes greatly differs according to the primary. The presence of metastatic nodes alters surgical procedure in renal and ureteral cancers, and management in vesical and prostatic cancers, i.e. palliative therapy instead of radical surgery. US and CT are common modalities for evaluating nodes. FDG-PET is also useful, but the role of MR imaging is under discussion. In this exhibit, diagnostic criteria for metastatic nodes at each modality are also reviewed. Understanding the merit and limitation of these modalities is also beneficial for planning radiologic evaluation.

Imaging Findings: The lymphatic spread and frequency of metastases depend on primary tumors and their histologic subtypes. In renal cancers, metastatic nodes are usually seen in the renal hilum, along the renal and ureteral vessels. In urinary tract cancers, metastatic nodes are seen along the major vessels nearby, with variable frequency according to the local stage of the primary. In vesical and prostatic cancers, metastatic nodes can affect variable regions, reflecting multidirectional lymphatic pathways. In testicular cancers, metastases initially occur in paraaortic nodes, which can result in systemic spreads.

Conclusion: The precise knowledge about the preferential sites and frequency of metastatic nodes facilitate radiologic evaluation, and the recognition of the clinical significance is beneficial in determining appropriate management.

C-0500

Is fluid ingestion really necessary before ultrasonography performed for detecting ureteral stones? A prospective randomized study

E. Özden, Ç. Göğüs, K. Türkölmez, C. Yagci; Ankara/TR

Purpose: Evaluation of ureteral stones with ultrasonography (US) is performed after fluid ingestion for filling the bladder. We hypothesized that water ingestion may decrease imaging quality of US by formation of intestinal artefacts and evaluated the value of US for detecting ureteral stones performed with or without fluid intake.

Methods and Materials: 150 consecutive patients who underwent US with suspect of ureteral stone were randomized into 2 groups. In order to distend the bladder, group A patients ingested 500 ml of water and examined by US after manifesting feelings of desired micturition. Group B patients were examined without any fluid intake. Diagnostic value of US was analyzed for all ureteral stones and also according to location of stones.

Results: US detected 35 of 52 stones (67%) in group A and 68 of 73 stones (93%) in group B ($p < 0.001$). Sensitivity and specificity of US were 67%, 82% for group A, and 93%, 94% for group B respectively. Accuracy of US for detecting ureteral stones was 71% in group A and 93% in group B.

Conclusions: Water ingestion before US decreases the detection rate of ureteral stones because of formation of intestinal artefacts. Patients with suspicion of ureteral stones should be examined by US without any fluid ingestion.

C-0501

withdrawn by authors

C-0502

Urinary tract neoplasms: Conventional and pyelo-urographic magnetic resonance (MR) patterns

G. Cardone, P. Mangili, L. Nava, G. Guazzoni, G. Balconi; Milan/IT

Learning Objectives: To illustrate conventional and pyelo-urographic MR patterns in urinary tract neoplasia evaluation. To evaluate the effectiveness of urographic and pyelographic MR sequences in the diagnosis of urinary tract neoplasia. To compare pyelographic and urographic MR sequences in the evaluation of urinary tract neoplasia.

Background: For many years conventional excretory Urography and Computed Tomography (CT) were considered the standard techniques used to examine patients with urinary tract neoplasia. Recently, the employment of MR using heavily T2w TSE sequences (MR-pyelography) such as gadolinium-enhanced 3D-GRE sequences (MR-Urography), have been described in patients with urinary tract disease.

Imaging Findings: 30 pts with 32 transitional cell carcinomas were analysed. All patients underwent MR-pyelographic, MR-urographic and conventional morphologic GRE T1w, TSE T2w and ce dynamic GRE FS-T1w sequences. Neoplastic lesions were visualised as solid papillomas in 58% of the cases, as thickening of collecting system walls in 33% of the cases and as solid tissue in the renal sinus in 9% of the cases. Lesions appeared more evident on TSE T2w, ce FS-GRE T1w and MR-urographic images. Lesions appeared quite vascularized. Urinary tract dilatation was evaluated in 85% of the patients. Dilatation was better estimated on both the TSE T2w and the MR-urographic images in the case of normal renal excretory function and on both the TSE T2w and the MR-pyelographic images in the case of functionally excluded kidneys.

Conclusions: Conventional MR images combined with uro-pyelographic techniques allow an accurate evaluation of urinary tract neoplasia.

C-0503

Primitive and recurrent liposarcoma of abdomen: What should we have to know for a correct CT and MR diagnosis

F.M. Danza, V. Marino, A. Magistrelli, M. Cirillo, P. Ottaviani, A.L. Valentini; L.Bonomo, Rome/IT

Learning Objectives: CT and MR appearance of liposarcomas is variable due to different stages of differentiation of their nodules. This exhibit shows examples of this variability, to learn how recognize real extent of disease at diagnosis or during follow-up, to reduce post-op residual disease or late diagnosis of recurrences.

Background: Liposarcomas are huge, multinodular masses with various appearances in radiological exams, due to their different histological differentiation, often coexistent in the same patient; the fat content of more differentiated nodules can determine their difficult detection. During follow-up surgical fibrosis and changing of the histological pattern complicate the diagnosis. Failure to recognize a

Scientific and Educational Exhibits

nodule at diagnosis or during follow-up affect significantly the survival, reducing the surgical radicality, with re-operations required, or inducing a diagnostic delay of recurrences.

Procedure Details: CT and MR of 35 cases of liposarcomas, surgically treated in the last 6 years, were reviewed to define their morphological and topographic appearance. Radiological follow-up to June 2004 was reviewed. Recurrences were high (20/35). Most early re-operations were related to residual diseases not recognized during surgery, instead of recurrences (12/20). In 15 patients recurrence occurred twice or three times. 22 patients died during follow-up, 3 were lost to follow-up and 10 are now disease-free (8 after surgical removal of residual nodules detected on imaging).

Conclusion: Prognosis of liposarcomas is directly related to complete surgical resection. Knowledge of CT and MR appearance of liposarcomas is crucial to recognize their real extent, residual nodules not resected at surgery and recurrences.

C-0504

Decreasing the radiation dose for renal stone CT

E. Eikefjord, N. Ulvik, D. Jensen, J. Rørvik; Bergen/NO

Purpose: To compare image quality and effective dose (ED) of different multidetector CT (MDCT) protocols from phantom measurements in order to optimize a low dose CT protocol for suspected ureteral stone.

Methods and Materials: A number of human ureteral stones were implanted in two porcine kidneys, fixed in a plastic tank filled with water. The number, size and density of the smallest and largest stone in each kidney, together with subjective image quality (noise, sharpness, contrast and artefact) ranging from 1 (poor) to 5 (best), were evaluated at 7 different protocols. The protocols differed in ED from the standard protocol (7.5 mSv at 4 x 3.75 mm collimation, 120 kVp, 200 mA and pitch 1.5) in a range of 40% reduction to an increase of 34%. Parameters differed in collimation, pitch and mA. Doses were computer-simulated, based on NRPB SR 250.

Results: The measurements showed no statistically significant differences in the detection of number of stones (right kidney: mean 12.75 ± 0.27), size (right kidney: 16.92 ± 0.49) and density between the 7 protocols. The protocol of the highest ED (11.25 mSv) scored 3.87 in image quality compared to 3 at the lowest dose protocol (4.5 mSv).

Conclusion: Image quality and effective dose did not correspond in a linear fashion. There exists a potential to reduce MDCT radiation dose for suspected ureteral stones. A low-dose protocol should be evaluated on patients for image quality before establishing MDCT for ureteral colic.

C-0505

Bilateral adrenal masses: Algorithmic approach for diagnosis

J. Lim, H. Kim, D. Lee, Y. Ko; Seoul/KR

Learning Objectives: To identify the variety of diseases that cause bilateral adrenal masses. To describe the appropriate radiologic work-up of bilateral adrenal masses. To differentiate bilateral adrenal masses based on CT and MR imaging features.

Background: Bilateral adrenal masses are uncommon and various causes have been reported. The most common causes are adenoma and metastasis. The rest includes hemorrhage, lymphoma, granulomatous infection, and pheochromocytoma. In this exhibit we will describe the radiologic findings of bilateral adrenal masses and present the appropriate algorithmic approach for the diagnosis of bilateral adrenal masses.

Procedure Details: Of various imaging modalities, CT and MR imaging play a major role in the evaluation of adrenal masses. Unenhanced CT is often the key study in characterization of adrenal masses by identifying high fat component, hemorrhage, or calcification. When unenhanced CT is indeterminate in characterization, contrast-enhanced dynamic CT is helpful by identifying enhancement patterns; early washout in adenoma, significant enhancement in pheochromocytoma, homogeneous enhancement in lymphoma, and poor enhancement in granulomatous disease or hemorrhage. If there is uncertainty in the diagnosis on CT examination, MR imaging may act as a problem solving method. MR imaging can demonstrate more sensitively and definitely fat component, hemorrhage, and necrosis. High signal intensity on T2-weighted image is also helpful for the diagnosis of pheochromocytoma or metastasis.

Conclusion: Various diseases may affect the adrenal gland, bilaterally. Systemic algorithmic approach to bilateral adrenal masses may be helpful for correct diagnosis and may reduce the efforts of radiologists.

C-0506

Imaging of urethral disease: Pictorial review

A. Kawashima¹, C.M. Sandler², A.J. LeRoy¹, N.F. Wasserman³, B.F. King¹, S.M. Goldman²; ¹Rochester, MN/US, ²Houston, TX/US, ³Minneapolis, MN/US

Learning Objectives: To review the anatomy and diseases of the urethra in adults to define the current role of imaging of the urethra and periurethral structure.

Background: We reviewed our case series and the literature on this topic. While we focus on conventional urethrography, cross sectional imaging modalities are also discussed as appropriate. The scope of this exhibit is as follows: 1) normal anatomy of the urethra, 2) urethrography technique, 3) traumatic injuries, 4) inflammatory diseases, 5) strictures, 6) acquired urethral diverticula, 7) urethral calculi, and 8) primary and metastatic tumors. The key imaging features of the urethral diseases on conventional contrast urethrograms and cross-sectional imaging studies are illustrated with representative cases.

Imaging Findings: Retrograde urethrography and voiding cystourethrography are imaging modalities of choice for the urethra while cross-sectional imaging modalities including ultrasound, MR imaging, and CT are useful in evaluating periurethral structures. Retrograde urethrography is a primary imaging modality of the male urethra for the evaluation of traumatic injuries, inflammatory and stricture diseases. Sonourethrography has an important role in assessing thickness and length of bulbar urethral stricture disease. Although voiding cystourethrography is frequently used to evaluate women with urethral diverticula, MR imaging is highly sensitive in demonstrating urethral diverticula. MR imaging is accurate in local staging of urethral tumors.

Conclusion: Imaging of the urethra based on urethrography is an integral component of the evaluation of patients with suspected urethral disease. The incorporation of cross-sectional imaging techniques, particularly MR imaging, yields additional information essential to diagnosis and therapy planning.

C-0507

Retroperitoneal sarcomas

E. Alonso, E. de Lama, J.A. Narvaez, Y. Roca, E. Merino, S. Ruiz Osuna, J.L. Lopez-Moreno; Barcelona/ES

Learning Objectives: - To describe the CT and MR imaging features of retroperitoneal sarcomas, with special emphasis in those which suggest a specific diagnosis. - To illustrate the usefulness of CT and MR imaging in the treatment planning of these lesions. - To describe the more important prognostic factors in retroperitoneal sarcomas.

Background: Retroperitoneal sarcomas are rare mesenchymal neoplasms. These tumors typically originate as large masses. They usually present with pain and a palpable abdominal mass. Liposarcomas and leiomyosarcomas were the most common tumors. Some histologic subtypes have specific patterns of growth and extension that aid in narrowing the differential diagnosis. Moreover, some tumor contents (fat, myxoid stroma, calcification, and necrosis) can be clearly demonstrated at CT and MR imaging and may provide strong clues that help narrow the differential diagnosis.

Procedure Details: A retrospectively review of the clinical charts, and CT and MR imaging studies of all histologically proven retroperitoneal sarcomas seen in a universitary hospital during 10 years retrieved 40 cases. Epidemiological characteristics (age, localization, size, type and grade histological, treatment, surgery margins, treatment complementary, recurrence and survival) were reviewed. CT and MR imaging studies were also reviewed in order to determinate specifically these components than can delineate the specific diagnosis.

Conclusion: Familiarity with the specific features of various retroperitoneal tumors often allows accurate histologic diagnosis and helps suggest proper management. Complete resection and low grade continue to be the most important prognostic factors for this tumor. Anatomic restrictions to wide resection and local recurrence were the most important factors determining survival.

C-0508

Adrenal glands in beta-thalassemia major: MR imaging features and correlation with iron stores

E. Drakonaki¹, O. Papakonstantinou¹, T. Maris¹, C. Koulieraki¹, A. Vasiliadou², A. Papadakis¹, N. Gourtsoyiannis¹; ¹Iraklion/GR, ²Chania/GR

Purpose: To describe the MR imaging features of the adrenal glands in beta-thalassemia major and investigate the relation between adrenal signal intensity (SI) and liver iron overload, as expressed by the SI ratio of liver to the right paraspinous muscle (L/M). Adrenals in beta thalassemia have not been previously studied with MR imaging.

Materials and Methods: Abdominal MR imaging studies of 64 patients with beta-

Scientific and Educational Exhibits

thalassemia major (mean age 27 ± 5 years old) were retrospectively studied for determining adrenal size and SI on T1 (120/4/90), PD (120/4/20) and T2' (120/15/20) GRE sequences and compared to those of ten healthy controls. L/M ratios on all MR sequences were calculated. Adrenal SI was graded on a 3-point scale: grade 0 indicated normal SI on all sequences, grade 1 hypointensity on T2* only and grade 2 hypointensity on all sequences. Ferritin levels of the patients were also recorded. The data were statistically analysed using one-way ANOVA. Statistical significance was set at $p < 0.05$.

Results: The size of adrenals in all patients was within normal limits. Adrenal hypointensity (grade 1 and 2) was noted in 24/35 (68.5%) patients. Hepatic siderosis, expressed by L/M ratios, correlated with ferritin levels ($p < 0.001$) and adrenal SI ($p < 0.003$) in all three sequences. Patients with grade 1 and grade 2 adrenal SI had decreased L/M ratios compared to those with grade 0 ($p < 0.003$).

Conclusion: Adrenal hypointensity without size alteration is a common finding in MR imaging of beta-thalassemic patients and correlates with the degree of liver siderosis.

C-0509

Bladder imaging using multidetector row CT: Techniques, applications and findings

T.G. Mang¹, B. Happel¹, C. Mueller¹, M. Prokop², H.C. Klingler¹, M. Suasn¹, G. Heinz-Peer¹; ¹Vienna/AT, ²Utrecht/NL

Learning Objectives: 1. To describe the spectrum of multidetector CT (MDCT) findings of common and uncommon diseases of the urinary bladder. 2. To demonstrate the usefulness of virtual cystoscopy in the evaluation of bladder lesions. 3. To illustrate MDCT signs and criteria for staging of bladder cancer.

Background: Multidetector CT offers new possibilities for imaging of the urinary tract. Using thin collimation, near isotropic imaging of the urinary tract is possible and provides high quality multiplanar reformations and 3D reconstructions of the organ including virtual cystoscopic views. Thus, MDCT seems to be a valuable tool in the evaluation of hematuria. Proper distension of the urinary bladder and optimum intravenous contrast timing is required for detecting and staging of bladder lesions. Compared to conventional cystoscopy, MDCT provides information about the extravesical extent of disease.

Procedure Details: We describe optimized CT protocols and the CT appearance of various urinary bladder lesions. Additionally, staging criteria of bladder neoplasms are demonstrated.

Conclusion: MDCT is an accurate tool for detection and evaluation of bladder lesions. With the benefit of 3D imaging further increase of the diagnostic performance is possible.

C-0510

Comparison between 3D CT and MR protocols in the detection of bladder lesions

V. Panebianco, D. Tancredi, T. Celano, P.G. Nardis, L. Di Rezze, P. Paolantonio, R. Passariello; Rome/IT

Purpose: To evaluate the value of 3D-protocol based on MR and CT-datasets in detection and T-staging of bladder lesions.

Methods: Thirty five patients with known bladder lesion underwent CT and MR. CT included a non contrast enhanced scan. Each patient received air distension by Foley catheter. A pre-contrast CT scanning was performed (Kvp120, mAs80 slice, slice coll. thk3 mm, image-recon 1-2 mm). Images were used for 3D reconstructions. An additional scan was performed after contrast-agents administration (slice coll. thk 5 mm, image recon 5 mm). MR examinations were performed on 1.5 T magnet with phased array coil and included 2D FSE sequence on axial plane (TR: 4300 msec, TE eff.:132 msec, ETL: 33, Matrix: 420x512); 2D FLASH sequence on axial plane pre and post Gadolinium administration and 3D-FLASH sequence (TR: 4.6 msec, FA: 30°, TE: 1.8 msec, Slice thk:2 mm, Matrix: 195x512, TA: 23 sec.) for 3D reconstructions. Images were analyzed on Workstation (Vitrea "Vital Images"). We analyzed site, size, depth of invasion, perivesical fat tissue and lymph nodes. All images were compared with histology.

Results: Concerning site, size, morphology and lymph node involvement CT and MR allowed a precise detection of 33 bladder lesions, two polypoid lesions of 5 mm were missed only by MR. 10% of T1 lesions were overestimated by MR while 20% of T2 lesion with muscle invasion were underestimated by CT.

Conclusions: MR allowed a more precise local staging of bladder neoplasms compared to CT protocols. On the other hand CT protocols demonstrate a better identification of smaller lesions (5 mm size).

C-0511

MR-urography in the evaluation of urinary tract obstruction

L. Zugaro¹, A. Catalucci¹, M. Monina¹, E. Di Cesare², C. Vicentini¹, C. Masciocchi²; ¹Teramo/IT, ²L'Aquila/IT

Purpose: To evaluate the diagnostic capability of MRU in case of urinary tract obstruction.

Methods and Materials: 72 patients suffering by obstructive uropathy underwent MR examination (1.5 T units). Saline solution was administrated about 10 min before. Unenhanced-MRU (heavily T2-w fat-sat seq.) was followed by enhanced-MRU (coronal 3DT1FFE seq. after Gd-BOPTA); diuresis was induced by i.v. administration of low-dose furosemide; standard MR imaging was also performed. All patients underwent US examination, 55 excretory urography, 21 CT. MRU was evaluated to detect urinary tract dilatation, cause and level of the obstruction. Excretory urography and the final clinical diagnosis were used as reference.

Results: The obstruction site and cause were detected in all cases by MR imaging. Unenhanced-MRU was capable of demonstrating 68/72 dilated urinary tracts, including 5 cases of non functioning kidneys. Twenty-four patients had urinary tract obstruction by urinary stones, 32 by neoplasms, 9 by ureteral benign stricture, 6 congenital ureteral stricture, 1 by iatrogenic cause.

Conclusion: MRU, providing both morphological and functional information, may replace conventional urography to determine the level of obstruction in cases where iodinated contrast is contraindicated or ionizing radiation should be avoided; in combination with standard MR imaging, it can detect the cause of urinary tract obstruction.

C-0512

Multi-detector row CT urography: Comparison of fluid administration protocols for depicting the urinary collecting system

H. Shinjo, T. Gokan, N. Takeyama, J. Suyama; Tokyo/JP

Purpose: To compare four different fluid administration protocols for depiction of the urinary collecting system with multi-detector row CT urography (MDCTU).

Method and Materials: 172 patients with hematuria underwent MDCTU, during which thinly collimated (1-mm) excretory phase scanning was performed 8 minutes after contrast medium injection. Patients were examined one of four techniques: (A) (N = 46) intravenous infusion of 250 ml normal saline; (B) (N = 39) oral administration of 350 ml green tea about 15 minutes before the examination; (C) (N = 52) oral administration of 350 ml water about 15 minutes before the examination; (D) (N = 35) no administration of fluid and no intravenous infusion (control). Two reviewers measured urinary tract opacification on MIP (maximum intensity projection) images. Scoring system was used to evaluate the opacification of ureter. 0,unopacified; 1,less than 1/3 of segment opacified; 2,1/3 to 2/3 of segment opacified; 3, 2/3 to less than 100% opacified.

Results: Mean opacification scores of each group were as follows: group A:3.23, group B:3.30, group C:3.16, group D:2.84. Group B had the highest mean opacification score. Mean opacification of the ureter in A, B and C was significantly improved over that in group D ($P < 0.001$). But there was no significant difference among the scores in group A, B and C.

Conclusion: MDCTU with supplemental oral administration of green tea significantly improves display of the urinary collecting system and is easier than and as useful as supplemental infusion of normal saline.

C-0513

Imaging of lymphoproliferative diseases involving urogenital system

S. Hwang, S. Kim, S. Kim, S. Jung; Seoul/KR

Learning Objectives: To illustrate and review the wide spectrum of radiological findings of lymphoproliferative diseases such as lymphoma, leukemia, castleman disease and posttransplantation lymphoproliferative disease that involve urogenital systems including kidney, uterus, ovary, testis, adrenal gland. And describe clues for differential diagnosis of these diseases.

Background: Lymphoproliferative diseases are diseases characterized by proliferation of lymphoid tissue. Lymphoproliferative disease includes lymphoma, leukemia, postlymphoproliferative diseases, and castleman disease. Primary involvements of urogenital system from lymphoproliferative diseases are uncommon. But the manifestation of lymphoproliferative diseases shows wide variability with potential involvement of multi-organ systems.

Imaging Findings: Lymphoproliferative diseases in urogenital system shows variable imaging findings. Preservation of normal anatomy, homogenous solid mass, rarity of necrosis or hemorrhage, and associated lymphadenopathy will be sometimes clues in diagnosis.

Conclusion: The manifestation of lymphoproliferative diseases shows wide var-

Scientific and Educational Exhibits

ability with potential involvement of multi-organ systems. Both clinical and radiological findings often mimic other disease processes, so the radiologist should be aware of this entity.

C-0514

withdrawn by authors

C-0515

Spectrum of imaging findings in genitourinary tuberculosis

F. Binokay, B. Soyupak, E. Akgul, S. Soyupak, M. Celiktas; Adana/TR

Background: The objective of this study is to describe the various diagnostic features of the genitourinary system as seen in our department.

Materials and Methods: A retrospective case review of all female and male cases of genitourinary tuberculosis imaged in our department over a six-year of period was done. A total of 16 cases of urogenital tuberculosis were reported during this time period. Only 21.4% of patients had a known history of tuberculosis. The age of the patients ranged from 26 to 54 years. The ratio of male to female patients was 1:1. Cystitis was the most frequent sign (74%), hematuria, nonspecific lumbar pain, genital signs and nephrologic signs are not rare.

Results: The series included three cases of renal, two adrenal, four bladder, two prostate, four endometrial and one tubo-ovarian tuberculosis. Patients were examined with intravenous pyelography (IVP), computed tomography (CT), ultrasonography (USG), color Doppler ultrasonography (RDUS) and hysterosalpingography (HSG). The radiological lesions most frequently encountered were renal calcifications (25.2%), destruction of calyces and pseudohydronephrosis (22.3%), atrophy and calcification in adrenal glands (9%), small-rigid tuberculous bladder (6.3%), tuberculous mass mimicking bladder carcinoma (4.2%), prostatic abscesses (3%), endometrial adhesions (6.5%), obliteration of the uterine cavity (2.1%), salpingitis isthmica nodosa and tubo-ovarian abscesses (8%).

Conclusions: Since tuberculous involvement in the genitourinary system may be confused with many other pathologies, both clinically and radiologically, radiologists should be aware of the different radiographic appearances of this protean but curable disease and should consider it in the differential diagnosis.

C-0516

Pheochromocytomas: Usual and unusual imaging findings

M.J. Pons, L. Diaz, A. Villanueva, P.D. Dominguez, M.A. Idoate, J.F. Boan, A. Benito; Pamplona/ES

Learning Objectives: To describe the different imaging findings in the study of adrenal pheochromocytomas.

Background: The great majority of adenomas, myelolipomas and adrenal gland cysts have typical radiological findings. The remaining pathological processes of the adrenals are a challenge for the radiologist. Adrenal pheochromocytomas are usually benign neuroendocrine tumors that very often show malignant behaviour on imaging studies.

Imaging Findings: 18 cases of pheochromocytomas diagnosed by a pathologist are illustrated. These cases were studied by intraoperative US, CT, PET and MR imaging. Pheochromocytomas appear as circumscribed round lesions, hyperintense in T2 weighted images, with early and prolonged contrast uptake. There are some aspects that still remain unclear about pheochromocytomas. In this study some of the most frequent and not so frequent findings of adrenal pheochromocytomas are shown. We included mixed pheochromocytomas, malignancy-associated pheochromocytomas and phaeochromocytoma involving the inferior cava vein and suprahepatic vein.

Conclusion: Even though their radiological appearance may be malignant, most cases of pheochromocytomas are benign lesions.

C-0517

Imaging of idiopathic retroperitoneal fibrosis

R. Cobelli, A. Vaglio, P. Greco, C. Buzio, M. Zompatori; Parma/IT

Learning Objectives: To illustrate the imaging with CT, MR of idiopathic retroperitoneal fibrosis and to described the differential diagnosis with other pathology of the retroperitoneum.

Background: Idiopathic retroperitoneal fibrosis is a rare pathology of the retroperitoneum. Its initial signs and symptoms are often nonspecific. For this reason it is important that the radiologist know the way of presentation, the differential diagnosis and the radiological criteria to establish the activity of this pathology.

Procedure Details: We retrospectively analysed 42 CT and 10 MR of 20 patient affected by idiopathic retroperitoneal fibrosis. We described the radiological pres-

entation, the natural history, the reactivation, the most frequent complication and the differential diagnosis through variegate and complete iconography.

Conclusion: Idiopathic retroperitoneal fibrosis is a rare pathology that can be manifested with different radiological pictures. The role of the radiologist is the detection, the evaluation of the effectiveness of the therapy and the identification of possible complications.

C-0518

Patient radiation dose at multidetector CT and conventional urography (IVU) for acute flank pain

E. Eikefjord, N. Ulvik, J. Rørvik; Bergen/NO

Purpose: To measure and compare patient effective doses (ED) from multidetector computed tomography (MDCT) and intravenous urography (IVU) for acute flank pain.

Methods and Materials: 117 patients with acute flank pain were included. Everyone underwent both MDCT (GE) with 4 x 3.75 mm collimation, 120 kVp, 200 mAs and pitch 1.5 and IVU with 70 kVp and automatic mA device (Canon DR) as standard parameters. The CT protocol included one volumetric acquisition of the abdomen and pelvis at standard parameters, mA varying due to patient size. The IVU protocol consisted of a standard acquisition of 3 AP images, total number varying. Effective doses were computer-simulated by using dosimetry programs for CT and conventional radiography, based on NRPB dose data sets from SR 250 and SR 262 respectively. Mean and SD of measured patient doses were calculated and compared.

Results: Mean patient ED for MDCT was $7.7 \text{ mSv} \pm 1.86$. The difference between men and women were 7.4 and 9.4 mSv respectively. Mean ED for IVU was $3.63 \text{ mSv} \pm 2.91$. Contrary to MDCT the ED was higher for men than for women, 3.93 mSv and 2.12 mSv respectively.

Conclusion: Standard protocol MDCT lead to approximately 50% higher ED than IVU. An optimized low-dose protocol should be considered before establishing MDCT for ureteral colic to minimize radiation induced cancer risk and secure adequate image quality. A low-dose MDCT protocol will be evaluated in a coming study.

C-0519

Dual time point [18F]-FDG PET for the differentiation between malignant and benign genitourinary lesions

D.V. Ryzhkova, L.A. Tyutin, N.A. Kostenikov, M.S. Tlostanova, S.V. Shatik, V.V. Zaytsev; St. Petersburg/RU

Purpose: The purpose of this study was to assess the advantage of dual time point [18F]-FDG PET imaging for the differentiation between malignant and benign genitourinary lesions.

Materials and Methods: We examined 31 patients (5 female, 26 male, aged 42 to 69 years) with genitourinary lesions proven by ultrasound, CT or MR imaging. Histological conformation of the diagnosis was performed in all patients. [18F]-FDG PET scans ("HR+", Siemens) were acquired in "Whole body" mode at 2 h and 4 h after injection of 370 MBq [18F]-FDG. During the time between injection and 2-h scans the patients were given 2 mg furosemide to remove excreted [18F]-FDG activity from the bladder. The patients were asked to void just before 2-h and 4-h scans. All images were evaluated visually and quantitatively calculating standard uptake value (SUV).

Results: We noted [18F]-FDG activity completely vanished from the bladder at 4-h, leading to good visualization of lower abdomen and pelvis areas. Benign lesions showed a low [18F]-FDG uptake (SUV < 2.5) at 2-h and had no significant [18F]-FDG uptake changes to 4-h. By contrast, malignant lesions showed more than 10-percent increase in [18F]-FDG uptake from 2-h to 4-h. Lesion-based diagnostic accuracy was improved from 71.4% to 95.2%, and patient-based diagnostic accuracy from 77.4% to 93.5%.

Conclusion: Dual time point [18F]-FDG PET imaging is a more reliable protocol for the differentiation of malignant from benign genitourinary lesions.

C-0520

The analytical value of the dynamic MR imaging semiquantitative parameters in detecting the stage and grade of bladder cancers

N. Tuncbilek, M. Kaplan, A. Semsi, O.O. Okten, I. Atakan, O. Inci; Edirne/TR

Purpose: So called "neoangiogenesis" is a new and an important prognostic sign that signifies the biological behaviour of solitary tumours. We investigated the role of semiquantitative contrast parameters of dynamic contrast enhanced magnetic resonance imaging (DCE-MRI) on tumour grade, stage and indirectly on neoangiogenesis in patients with bladder cancer.

Scientific and Educational Exhibits

Materials and Methods: A total of 17 patients are taken with bladder cancer aged between 49 and 78 (mean: 64.1) to dynamic investigate with 1 T magnet turbo-FLASH sequence parameters with the formed time signal intensity curves in the end, first (E_1), second (E_2) and third (E_3) minute contrasting values and time SI curve slopes are calculated. The findings were correlated with DCE-MRI features and histopathological data by using statistical.

Results: The differential analysis to detect the difference between the superficial and deep tumours was successful in a 70.6% rate by using E_1 , E_2 , E_3 and time SI curve slopes. A significant correlation found between time SI curve slope and E_1 values and tumour grade ($p < 0.05$). In a multivariation differentiation analysis, tumour grade detected 58.8% correctly by using the DCE-MRI semiquantitative parameters in combination ($p < 0.05$).

Conclusion: DCE-MRI parameters are the indirect determinants of tumour microcirculation and perfusion. According to our findings, the relationship between the preoperative DCE-MRI semiquantitative parameters and the tumour stage and grade will indirectly show the biological behaviour of the tumour and will give the chance to estimate the metastasizing ability. By using the DCE-MRI findings, discriminating analysis can be used additionally to the known treatment methods.

C-0521

Urinary tract abnormalities on bone scintigrams: Boosting the diagnostic yield

S.P. Prabhu¹, D. Dunlop², K. Prescod¹; ¹Bristol/UK, ²Bath/UK

Learning Objectives: 1. To highlight the importance of looking at the renal outline on bone scans. 2. To illustrate cases where renal abnormalities on bone scans either added to or led to diagnosis of pathology. 3. To demonstrate variants of renal anatomy and physiology that may be seen on bone scans. 4. To show correlative cross-sectional or planar imaging to prove the diagnosis obtained from the bone scan.

Background: Renal tract abnormalities are detected as incidental findings in 10-15% of isotope bone scintigrams. We present a series of patterns seen on review of more than 7500 scintigrams in our institution.

Imaging Findings: Bilateral, diffuse increased renal uptake is seen in patients undergoing chemotherapy, hyperparathyroidism, hypercalcemia and sickle cell disease. Bilateral diffuse decreased renal uptake is seen in patients with end-stage renal disease, widespread skeletal metastases and hematologic disorders. Focal increased activity is associated with postsurgical and radiation changes. Focal decreased uptake is caused by space-occupying lesions such as abscesses, cysts, and neoplasms either arising from the kidney or adjacent structures. Renovascular disease, nephrectomy and congenital anomalies can cause decrease in renal size, shape and position. Bladder anomalies are also discernible on many bone scans. We correlate bone scan findings with appearances on other modalities.

Conclusions: Urinary tract abnormalities are seen on 20% of bone scintigrams and can enhance diagnostic yield in many cases. In some cases, diagnoses not related to the skeletal system but causing patient's symptoms are recognised like hydronephrosis or renal cell carcinoma. So, don't forget the kidneys and bladder on bone scans!!

Head and Neck

Head

C-0522

The accessory oval foramen, so-called foramen of Vesalius: Anatomic CT study and clinical correlations

J. Renoux, K. Marsot-Dupuch, F. Benoudiba; *Le Kremlin-Bicêtre/FR*

Purpose: To define the prevalence and variants of the accessory oval foramen. We aimed to understand its significance and its correlation with clinical disorders.

Materials and Methods: We selected adult patients, without previous history of surgery. We examined prospectively one hundred ultra-high resolution CT studies of the skull-base performed in the same unit, with the same parameters, and read by the same team. Correlations with MR data were made when possible.

Results: The accessory oval foramen is an oblong hole with smooth walls, developed in the base of the pterygoid process. It has a tubular canal in sagittal and coronal views, coming from infra-temporal fossa to the temporal fossa. This canal is lateral to the pterygoid canal. Accessory oval foramen was depicted in 90%; in 70% it was well depicted and in 20% only multi-planar reconstruction could depict a very thin accessory oval foramen. It was bilateral in 70%, double in 2%. Presence of a bony dehiscence in the sphenoid sinus was found in 2%. In 4%, it was in continuity with a lateral canal, coming from the carotid canal, which contains the accessory meningeal artery. Accessory oval foramen was found to be larger than the foramen spinosum in 10%. This seems to be correlated with development factors, and not with pathological disorders.

Conclusion: Accessory oval foramen is a key route for dissemination of infections or tumors from the infra-temporal fossa to the cavernous sinus. Its anatomical characteristics can explain some sympathetic signs in sinus disorders.

C-0523

Greater occipital nerve infiltration under CT guidance: An anatomical and radiological study

B.A.C. Kastler, Z. Patay, Z. Boulahdour, E. Rodière, S. Aubry, J. Lerais, B. Fergane; *Besançon/FR*

Learning Objectives: To perform the infiltration one must first have a good understanding of the anatomical relationship of the greater occipital nerve (GON) and the surrounding structures, which determine the possible safe percutaneous pathways.

Background: Infiltration has been found helpful in the diagnosis and management of occipital neuralgia, particularly in patients resistant to specific medication. The purpose of this exhibit is firstly to depict the anatomy of the course of the GON. Anatomical studies suggest that there are two possible conflicting sites. The first site is at its origin (dorsal primary ramus of the second cervical nerve), located behind the C1 and C2 joint just medial to the vertebral artery. The second site is at its emergence where the GON pierces the fascia, just below the superior nuchal ridge along with the occipital artery.

Procedure Details: We will demonstrate step-by-step our technique of percutaneous infiltration of the nerve under CT-guidance.

Conclusion: CT-guidance allows safe needle progression and precise positioning particularly at the 1st target, which is not otherwise accessible. It allows reducing complications and optimizes procedure results.

C-0524

MR microimaging of human eye with a blinking-gated pulse sequence

T. Obata, H. Ikehira, M. Tamura, S. Tanada; *Chiba/JP*

Purpose: MR microimaging of the human eye is very difficult because of eye movement during the MR scan. To acquire high-resolution MR images, we developed a new blinking-gated pulse sequence with a surface coil specialized for microscopic imaging.

Methods and Materials: Four normal subjects were studied. Informed consent was obtained from all subjects prior to the experiment according to the guidelines of our institutional review board. To reduce eye movement, the eyes were kept open and fixated to a target in the MR gantry. To reduce motion artifact from blinking, images were obtained using the blinking-gated pulse sequences (T2 weighted fast spin echo, TR: 6 sec, TE: 100 ms, ET: 11, matrix: 256x128, FOV: 5 cm, slices: 1 mm x 30). Three scans (100 sec x 3) were obtained for each subject. They were added together after adjustment for location to make one high signal-to-noise-ratio (SNR) image set.

Results: T2 weighted MR images were acquired with high resolution and high SNR. Microscopic structures such as the iris and ciliary muscles were clearly

Scientific and Educational Exhibits

visualized. Since the whole eye can be covered by this method, 3D maps can easily be made from the obtained images.

Conclusion: The application of blinking-gated pulse sequences with surface coil for MR microimaging of the human eye might become a useful and widely adopted procedure.

C-0525

The role of radioimmunoscintigraphy in the diagnosis and follow-up of primary ocular melanoma

S.L. Beatovic, V. Obradovic, Z. Latkovic, E. Jaksic; Belgrade/YU

Purpose: Our study aimed at evaluating the role of immunoscintigraphy (IS) in the diagnosis and follow-up of patients with primary ocular melanoma.

Materials and Methods: IS was done in 17 patients: 9 patients with newly diagnosed choroidal melanoma (group A), 6 patients with choroidal melanoma treated by contact radiotherapy (group B) and 2 patients with melanoma conjunctivae (group C). F-(ab')-2 fragments of monoclonal antibody 225.28 S, directed against the high molecular weight-melanoma associated antigen (HMW-MAA) were used in our investigation. Planar scintigraphy was done 4 hours after injection of 270 MBq of labeled antibodies. 500000 counts static images were acquired in a 256x256 resolution matrix.

Results: All patients in group A showed positive finding of IS. The maximal diameter of these tumors, measured by ultrasound, was between 9 and 18 mm, with prominence between 5 and 10.5 mm. Both patients of group C showed negative IS finding, due to the small dimensions of the tumor (< 2.7 mm). In all 6 patients of group B, IS was negative, although the tumor dimensions were sufficiently visible by the scintigraphy (diameter between 8.3 and 17 mm and prominence between 5 and 10.3 mm).

Conclusion: IS is a useful diagnostic modality in detection of small intra-ocular tumors. Negative IS in patients with tumors treated by radiotherapy could be explained by the biological regression of tumor, that precedes regression in its volume. This finding indicates the potential usefulness of IS in the follow-up of conservatively or surgically treated patients with choroidal melanoma.

C-0526

Color Doppler US in the evaluation of Behcet's disease

B. Yagci, C. Isik, C. Yildirim, N. Sabir, S. Tatlipinar; Denizli/TR

Purpose: The purpose of the study was to detect prospectively the value of color Doppler US of orbital vasculature in the assessment of ocular involvement in patients with Behcet's disease without clinical ophthalmologic abnormalities.

Methods and Materials: Color Doppler US of the orbital vessels was performed on 26 eyes of 13 patients who were diagnosed as having Behcet's disease with ocular involvement (group1), 65 eyes of 33 patients who had Behcet's disease without ocular involvement (group2) and 40 eyes of 20 healthy volunteers (group3).

Results: The peak systolic (PSV) and end-diastolic (EDV) velocities of central retinal arteries (CRA) were significantly lower in both patient groups than in healthy control group ($p < 0.001$). When both patient and control groups were compared, slightly increase in the mean resistance indexes (RI) values of CRA in both patient groups were statistically significant (group1: $p = 0.027$, and group2: $p = 0.001$). In group2 a statistically significant decrease in the PSV and EDV, and a significant increase in the RI of the ophthalmic arteries (OA) were detected when compared with the control group ($p = 0.049$, $p < 0.001$, $p = 0.003$, respectively). In group1; the decrease in EDV of OA were statistically significant ($p = 0.041$). No significant differences between both patient groups were shown for the velocities and indexes of both arteries.

Conclusion: These results suggest that the detection of increased vascular resistance in the ophthalmic and central retinal arteries with color Doppler US analysis in patients with Behcet's disease without clinical ophthalmologic abnormalities might predict the pre-clinical diagnosis of ocular involvement in Behcet's disease.

C-0527

Role of radiology in the diagnosis and management of epiphora

K. Gopal, J. Tuck, R. Razzaq; Bolton/UK

Learning Objectives: Epiphora (watery eyes) is a common condition in ophthalmologic practice. In this pictorial review we present the common causes for the above and our role in the management of these patients.

Background: Epiphora is a common ophthalmologic problem, comprising 3% of clinical visits. It results most commonly from stenosis or obstruction of tear ducts in the majority of patients. Once over secretion of tear fluid has been ruled out, digital subtraction dacrocystography is performed to demonstrate obstruction of the lacrimal system. In stenosis or obstruction, interventional procedures such

as balloon dacrocystoplasty or stent implantation have become an alternative to surgical procedures in many cases.

Procedure Details: In this pictorial review we would like to highlight the anatomy of the lacrimal system, technique of dacrocystogram and balloon dacrocystoplasty. Both these procedures can ideally be performed in one sitting which obviates the need for a prior attendance for non-invasive imaging.

Conclusion: Dacrocystogram is a very quick and simple technique, which is able to demonstrate the cause of epiphora in most cases. In addition balloon dacrocystoplasty is a feasible non-surgical therapy in nasolacrimal duct obstructions with good clinical results that may be used as an alternative to surgical procedures.

C-0528

Imaging of head and neck vascular masses: A pictorial review

S.E.J. Connor, C.M. Flis; London/UK

Learning Objectives: To review the classification, radiological appearances and image guided treatment options of vascular masses of the head and neck.

Background: Vascular masses of the head and neck may be classified as congenital (vascular malformations and haemangiomas) or acquired (aneurysms and tumours). They may also be termed as low flow (venous, mixed and capillary malformations) or high flow (arteriovenous malformations, proliferating haemangiomas and aneurysms) and proliferative (haemangiomas or other tumours with secondary angiogenesis) or non proliferative (vascular malformations or aneurysms). Ultrasound or magnetic resonance imaging (MRI) are valuable in characterising these lesions on the basis of enhancement patterns, extent of parenchymal mass and flow characteristics. They can also delineate the deep extent and involvement of vital structures. Computed tomography (CT) may be reserved for the detection of bony involvement and the presence of phleboliths. Conventional angiography and percutaneous phlebography are performed as a precursor to radiological therapeutic procedures.

Imaging Findings: The ultrasound (including colour and duplex Doppler), CT, MRI and conventional angiographic appearances of venous and mixed low flow malformations, AVMs, aneurysms, haemangiomas (proliferating and involuting) and other vascular tumours (paragangliomas, juvenile angiobromas, haemangiopericytomas, vascular metastases) will be described and illustrated together with examples of radiological interventions. An approach to their radiological evaluation and the typical imaging features will be highlighted.

Conclusion: An understanding of the classification and imaging appearances of vascular masses of the head and neck is vital for the radiologist to propose an appropriate differential diagnosis and for the consideration of image guided therapy.

C-0529

Pictorial review of eye ultrasound with CT and MR correlation

D. Spitzer, J. Novák, M. Mrklovský, P. Jiricková, O. Spitzerová, V. Sloboda; Pardubice/CZ

Purpose: The objective of this exhibit is to review the normal and abnormal appearances of eye and orbit. Emphasis is placed on the use of state-of-the-art equipment and technique, including colour Doppler imaging.

Material and Methods: Over 30 different eye and/or orbit ultrasound (high definition high frequency linear probe) cases are demonstrated, including CT (double slice) and/or MR (1.5 T) imaging correlation.

Results: The cases include examples of normal anatomy, benign and malignant neoplasm, abscess, haematoma, simple and complex cyst, and both normal implants and implant complications, intraocular foreign bodies, cataract, vitreal pathology and ablation of the retina etc. We review the specific utility of ultrasound as it compares with other imaging modalities. We also demonstrate cases in which ultrasound was not useful.

Conclusion: Adequate knowledge of the anatomy of the eye and orbit is needed to correctly limit the differential diagnostic possibility of pathology of the eye and orbit. US is a readily available method for an accurate diagnosis within the eye, with CT and preferably MR, being reserved for cases which require additional information about deep structure, or those with which there is discrepancy between the sonographic and clinical diagnosis.

C-0530

withdrawn by authors

Scientific and Educational Exhibits

C-0531

Orbital MR imaging: A pictorial review

A.P. Dahir; Mumbai/IN

Purpose: To establish the importance of MR imaging in orbital imaging. To demonstrate MRI appearance of various orbital pathologies. To compare CT and MRI in diagnosis of orbital lesions.

Materials and Methods: 50 patients with orbital and visual complaints were studied on a 1.5 T MRI scanner. A comparative study between CT and MRI of 50 patients was performed. Contrast enhanced studies were performed to look for patterns and dynamics of enhancement.

Results: 20 out of 50 patients were identified as having neoplasms, 13 had inflammatory disease, and 8 had vascular abnormalities, 2 patient each had trauma, infection and congenital anomalies. In the comparative study between CT and MRI, MRI was found to be superior in 14 cases.

Conclusion: MRI is an excellent, non-invasive modality to diagnose and detect the extent of orbital pathologies and it is far superior to CT examination of the orbit.

C-0532

Post-radiation malignant tumors in head and neck: A review of the clinical and imaging features

S. Yamamoto, K. Motoori, T. Ueda; Chiba/JP

Purpose: The development of malignant tumors is a recognized complication of radiation therapy. Post-radiation malignant tumors are not rare but a long latency period, difficulty with long-term follow-up, and a failure to recognize and report cases of post-radiation tumors confound analysis of risk. We set out to retrospectively review the clinical and imaging features in patients with post-radiation sarcomas, especially in head and neck region.

Materials and Methods: 4 patients with post-radiation tumors in the head and neck were identified at a single institution. Computed tomography and/or magnetic resonance imaging were available for all patients. The medical records were reviewed for primary diagnosis, the radiation history, and the latency period prior to development of the malignant tumor.

Results: There were 2 male and 2 female with a mean age of 69 years. The mean latency period for the development of the malignant tumor was 10 years. The primary diagnoses were maxillary carcinoma, nasopharyngeal carcinoma, adenoid cystic carcinoma of oral floor and tonsillar tumor. The histopathologies were osteosarcoma of the jaw, spindle cell sarcoma, chondrosarcoma and malignant peripheral nerve sheath tumor. The common findings were an avidly-enhancing soft tissue mass and bone destruction.

Conclusions: Post-radiation malignant tumors, while uncommon, are not rare. The imaging findings are not pathognomonic, but an appreciation of the expected latency period may help to suggest the diagnosis. When radiotherapy is performed for a head neck neoplasm, even if the neoplasm is treated completely, periodical progress observation may be necessary at least for about ten years.

C-0533

Radiologic findings of variable diseases involving the orbital apex

I. Bae, S.-Y. Lee, K. Park, S. Kim, S. Cha, G. Han; Chungbuk/KR

Purpose: To illustrate the CT and MRI findings and to identify features that may differentiate between the benign and malignant diseases involving the orbital apex. **Materials and Methods:** We retrospectively reviewed the CT ($n = 3$) and MR ($n = 7$) findings in 7 patients with lesions involving orbital apex. The patients were 5 female and 2 male, aged between 33–63 years (mean: 52 years) who had visual disturbance, ptosis, CNIII palsy or eyeball pain. They underwent surgical mass excision, transphenoidal or endoscopic biopsy with pathological confirmation. We evaluated the lesions according to the location, gross appearance, signal intensity, contrast enhancement pattern, and associated bony change.

Results: Tumoral conditions included metastasis ($n = 2$), squamous cell carcinoma of the sphenoid sinus ($n = 1$), chondrosarcoma ($n = 1$), and meningioma ($n = 1$). Inflammatory conditions included mucocele of the pneumatized anterior clinoid process ($n = 1$) and aspergillosis of the posterior ethmoid air cell ($n = 1$). In metastasis, squamous cell carcinoma, chondrosarcoma, and aspergillosis, soft tissue mass formation with adjacent bony destruction were found. In mucocele and meningioma, soft tissue mass formation with bony remodelling were present. They could be differentiated by clinical history (metastasis), characteristic signal intensity (chondrosarcoma and mucocele), enhancement pattern (aspergillosis), and location (meningioma).

Conclusion: Awareness and knowledge of lesions of the orbital apex is important because there may be much confusion both clinically and radiologically. Familiarity with imaging findings of lesions of the orbital apex will facilitate accurate diagnosis and can help to avoid unnecessary radical surgery.

Head and Neck

Neck

C-0534

Utility of contrast-enhanced MR imaging with three-dimensional volumetric interpolated breath-hold examination (3D-VIBE) in preoperative staging of hypopharyngeal cancer

K. Tamai, T. Koyama, S. Tanaka, R. Asato, S. Umeoka, A. Kido, T. Saga, K. Togashi; Kyoto/JP

Purpose: To evaluate the value of contrast-enhanced (CE) MR imaging with 3D-VIBE in staging hypopharyngeal cancer (HPC), in comparison with T2-weighted images (T2WI).

Methods and Materials: 22 patients (18 male, 4 female) with histologically proven HPC underwent preoperative MR imaging. Following T2WI, CE 3D-VIBE images were obtained at 20 (1st-early-phase) and 60 seconds (2nd-early-phase) after injection of Gd-DTPA at a rate of 3 ml/sec. Two radiologists evaluated both T2WI and CE images independently, regarding T- and N-stage. Radiologic criteria for T-stage were as follows; T1: Limited to one subsite and < 2 cm; T2: More than one subsite or 2–4 cm without deviation of hemilarynx; T3: > 4 cm or with deviation of hemilarynx; T4: Invasion into the adjacent structures. The results were compared with pathologic findings. On CE images, SNR and CNR between the tumor and muscles were calculated for both phases and statistically compared.

Results: On CE images, 21 tumors were correctly staged (96%), while one was understaged (T3). On T2WI, 18 (82%) were correctly staged, while one was over-staged (T3), 2 understaged (T3 and 4), and one missed (T2). In 2 T2 tumors, involvement of posterocord region was missed on T2WI, whereas it was clearly demonstrated on CE images. N-staging was same on both T2WI and CE images ($n = 11$). SNR of 1st- and 2nd-early-phase was 45 ± 15 and 43 ± 12 , respectively ($P = 0.226$). CNR was 27 ± 13 and 21 ± 10 , respectively ($P = 0.002$).

Conclusion: CE 3D-VIBE is highly accurate in staging of HPC and superior to T2WI in delineating tumor extent. In 3D-VIBE images, 1st-early-phase can provide better conspicuity.

C-0535

CT-MR image fusion vs. CT and MR in the pre-surgical evaluation of laryngeal cartilage neoplastic invasion: Reliability in correlation with histopathology

F. Bruculeri, S. Santocino, A. Stecco, M. Dominietto, M. Brambilla, A. Carriero, G. Valente; Novara/IT

Purpose: To evaluate the diagnostic reliability of fusion image vs. CT and MR, on the identification of laryngeal cartilage neoplastic invasion, using the histological test as gold standard.

Methods and Materials: 5 patients with laryngeal carcinoma were submitted to contrast-enhanced CT and unenhanced MR scans. After surgical treatment, a pathologist evaluated the specimens. Image fusion was accomplished by mean of Syntegra Pinnacle software (version 1.2 B), fusion of MR SET1 images on MR SET2 and MR SET1 images on CT data set. Sensitivity, specificity and diagnostic accuracy were calculated, together with software elaboration time and feasibility.

Results: Image fusion was feasible in 100% of cases. Average fusion time for any patient was 10 minutes. Compared to histological test, fusion of MR SET1 images on MR SET2s showed a 100% sensitivity, 100% specificity, 100% diagnostic accuracy; whereas fusion of MR SET1 images on CTs has shown 67% sensitivity, 100% specificity, 80% diagnostic accuracy. MR alone had 100% sensitivity, 50% specificity and 80% diagnostic accuracy, while CT alone 67% sensitivity, 100% specificity and 80% diagnostic accuracy.

Conclusion: The assessment of laryngeal cartilage neoplastic invasion with MR on CT fused images and CT only gives similar results. The evaluation by mean of MR SET1 on MR SET2 fused images shows the same sensitivity of MR alone, but with improved the specificity.

C-0536

Image findings of idiopathic carotidynia in multiple modalities

N. Kosaka, H. Uematsu, T. Sagoh, S. Miyayama, M. Noguchi, H. Itoh; Fukui/JP

Learning Objectives: To familiarize participants with the clinical entity of idiopathic carotidynia. To teach participants to recognize the radiological features of idiopathic carotidynia in multiple modalities.

Background: Idiopathic carotidynia is a self-limited neck pain syndrome associated with tenderness over the carotid bifurcation. This entity is well known by otolaryngologists and neurologists, but not by radiologists. In this presentation,

Scientific and Educational Exhibits

we discuss five patients who met the clinical criteria established for the diagnosis of carotidynia by the International Headache Society Classification Committee. We also review the image findings of idiopathic carotidynia, including ultrasonography ($n = 5$), computed tomography ($n = 4$), and magnetic resonance imaging ($n = 4$).

Imaging Findings: Abnormally enhanced tissue surrounding the symptomatic carotid artery localized at the level of the distal common carotid and carotid bifurcation is supportive of the diagnosis. No associated narrowing of the vessel lumen was present in these patients. The lack of any other findings to suggest alternative diagnoses strongly supports the existence of carotidynia as a distinct clinical entity. In addition, follow-up imaging studies ($n = 3$) after resolution of symptoms demonstrated disappearance or improvement of the abnormal enhancing tissue.

Conclusion: These radiological findings may be helpful in the evaluation of patients with suspected carotidynia. To avoid unnecessary invasive examinations, the radiologist should be familiar with the clinical entity and radiological features of idiopathic carotidynia.

C-0537

Dental CT in the detection of periodontal lesions

P.M. Carrascosa, F. Sanchez, C. Capuñay, E. Martín López, M. Ulla, J. Carrascosa; Buenos Aires/AR

Purpose: To describe the CT characteristics of the periodontal lesions.

Methods: 72 patients with pre-implant studies were evaluated by CT. Their diagnoses were confirmed by clinical evaluation, plain films findings and in one case by histology. Studies were performed with slices of 1 mm width, 1 mm reconstruction interval. After acquisition, images were post-processed in a workstation with Dental CT software. Panoramic, axial, parasagittal and 3D images were obtained.

Results: There were 41 (24.1%) periapical lesions, 78 (45.8%) periodontal lesions, 1 (0.5%) condensant osteitis, 1 (0.5%) osteomyelitis, 37 (21.7%) diffuse atrophy, 1 (0.5) complicated odontogenic cyst and 11 (6.4%) maxillary sinusitis.

Conclusions: The high prevalence of periodontal and periapical lesions in patients who have a Dental CT carried out as a pre-implant study makes tomographic recognition of these lesions necessary, in order to allow the dentist to perform the right treatment and to prevent future complications.

C-0538

Basal cell adenoma of the parotid gland: MR imaging findings with pathologic correlation

M. Okahara, H. Kiyosue, S. Matsumoto, Y. Hori, S. Tanoue, D. Uchida, H. Mori, Y. Kondo; Oita/JP

Purpose: Basal cell adenomas (BAC) are rare parotid gland tumors. Few case reports describing MR imaging features of BAC have been published. The aim of this study is to describe and characterize the MR findings of BAC of the parotid gland.

Methods and Materials: We retrospectively reviewed MR images of BAC with pathologic correlation in 7 cases (2 men, 5 women; age range, 52-82 years) collected between January 1992 and August 2004 from our pathological database. All MR images were retrospectively evaluated with respect to the marginal morphology, signal intensity, and enhancement behavior by two experienced radiologists.

Results: Pathologically, 4 tumors were solid type, 2 tumors were trabecular type and one was membranous type. All the tumors were well-circumscribed with a smooth contour. Cystic changes were seen in 3 cases. On T1-weighted images, 6 tumors showed homogeneously low signal intensity (SI) equal to muscle and one showed inhomogeneously low SI. On T2-weighted image, all of them showed slightly lower SI than that of surrounding parotid tissue. On Gd-enhanced T1-weighted images, six tumors demonstrated moderate enhancement and one demonstrated avid enhancement (membranous type). Dynamic studies were performed in 4 cases. All showed rapid and prolonged enhancement.

Conclusion: MR imaging findings of basal cell adenoma were well-defined and smooth marginal morphology, contrary to lobulated contours seen in pleomorphic adenoma; relatively low SI on both T1 and T2-weighted images and rapid and prolonged enhancement on dynamic studies. Although BACs are rarity, BAC should be suspected when the tumor shows all of these characteristics.

C-0539

Development of the method of kinetic analysis for the temporomandibular joint using flat panel detector system: Verification by magnetic resonance imaging

Y. Ohtani, S. Sanada, K. Ueki, T. Miyati, T. Matsui, Y. Matsuura; Kanazawa/JP

Purpose: To verify the accuracy of the result of the kinetic analysis of the temporomandibular joint (TMJ) using flat panel detector (FPD) system by pseudo-dynamic MR imaging.

Methods and Materials: Axially positioned radiographs were obtained sequentially from opening to closing of the mouth by a modified dynamic FPD system. Pseudo-dynamic MR imaging of the TMJ was performed. The images were taken at seven mouth opening steps that started from a closed position to fully-opened mouth position. The images were taken for mouth closing steps with the same manner as mouth opening. The subjects were five symptomatic and asymptomatic volunteers. We analyzed the movement of the condyle. We also checked the movement and displacement of the temporomandibular articular disc by MR imaging. We compared both results of the TMJ kinetics by dynamic FPD and pseudo-dynamic MR imaging.

Results: Using an FPD system, we found that anteroposterior condylar movement ranged over a distance from 18.8 mm to 20.3 mm (average = 19.6 mm). There were deviations in the incisal path of the symptomatic volunteers, and the temporal changes in the maximum velocity of their condyles were asymmetric, unlike in those of healthy volunteers. These results were consistent with the diagnosis of an experienced maxillofacial surgeon by visual inspection and palpation. However, there are no asymmetric movements between right and left condyles and disc displacement with mild symptomatic volunteers by pseudo-dynamic MR imaging.

Conclusion: The kinetic analysis using FPD system is capable of analyzing the real entire motion of the TMJ in normal and pathologic stages, especially in those with mild pathology.

C-0540

Ultrasound assessment of superficial lymph nodes (three-dimensional imaging, tissue harmonic imaging and panoramic imaging) intended for diagnostic excision

E.J. Bialek, W. Jakubowski, A.B. Szczepanik, R.K. Maryniak, M. Prochorec-Sobieszek, R. Bilski, M. Serafin-Krol; Warsaw/PL

Purpose: To assess the usefulness of three-dimensional (3D), tissue harmonic (THI) and panoramic imaging in the ultrasound assessment of superficial lymph nodes intended for diagnostic excision.

Methods and Materials: Fifty-two lymph nodes (35 cervical, 16 axillary, 1 inguinal), scheduled for resection (clinical suspicion of lymphoma), in 52 patients were examined by ultrasound using 3D, THI and panoramic modes. Final histopathologic diagnoses included 36 lymphomas, 11 reactive lymph nodes, 3 metastases and 2 plasmacytoma infiltrations.

Results: THI improved visualization of borders and internal structure of lymph nodes in 96% and of surrounding tissue architecture in 92%. Intra-nodal artifacts were reduced after application of THI in 85% of lymph nodes. The appearance of hilum and lymph nodes as a whole changed in C-plane of 3D mode (as compared with 2D presentation) respectively in 28% and 36%. Panoramic imaging allowed for measurement of large lymph nodes, presentation of relations between the examined lymph node and surrounding tissues or other lymph nodes on one image, and demonstration of the arrangement and spatial relationships between lymph nodes within a group.

Conclusion: Application of THI, 3D and panoramic imaging may improve general quality of ultrasound images of examined lymph nodes, supply the examiner with new information in comparison to standard 2-D ultrasound, and allow for presentation of location, arrangement and spatial relationships between the examined node and other lymph nodes or tissues on one image. *The work was financially supported by a grant from the State Committee for Scientific Research.*

C-0541

withdrawn by authors

Scientific and Educational Exhibits

C-0542

Comparison of ultrasonography (US)-guided fine needle aspiration biopsy (FNAB) with histopathologic finding after thyroidectomy for thyroid nodules and the usefulness of follow-up US-guided FNAB

D.H. Kim, H.W. Oh, J.Y. Choi, J.N. Byun, Y.C. Kim, Y.S. Kim, J.H. Oh; Gwang-Ju/KR

Purpose: The purpose of this study was to compare of US-guided FNAB result with histopathologic finding after thyroidectomy for thyroid nodules and to assess the usefulness of follow-up US-guided FNAB.

Material and Method: US-guided FNAB was performed in 926 patients from 2002 to 2004. Thyroidectomies were performed in 96 of these patients. We compared the results for US-guided FNAB with post-operative histopathologic finding in these patients. All aspirations were performed with 21-gauge needles attached to a 10-mL syringe with a syringe holder. A high-frequency linear-array transducer was used for biopsies performed under ultrasound guidance.

Results: A comparison of US-guided FNAB results with histopathologic findings after thyroidectomies was interpreted as 2 (5%) false-positive and 7 (12%) false-negative results. 2 patients with non-diagnostic US-guided FNAB results were proven to be benign nodules on histopathologic findings after thyroidectomies. Cause of false negative results was mainly inadequate sampling due to very small size (infracentimetric). On follow-up FNAB or histopathologic findings after thyroidectomies, these nodular lesions were proven to be malignant nodules.

Conclusion: The main cause of false negative US-guided FNAB results was inadequate sampling due to very small nodule size. To improve the detection rate of malignant nodule, follow-up US-guided FNAB is necessary.

C-0543

The relationship between clinical outcome and detailed nodal features on initial and follow-up CT for cervical tuberculous lymphadenitis

B.-K. Je¹, S.-B. Kim², D. Park², T.-K. Kim¹, M. Kim², N. Lee²; ¹Kyungido Ansancy/KR, ²Seoul/KR

Purpose: The purpose of this study is to correlate the relationship between initial and follow-up CT features of cervical tuberculous lymphadenitis with clinical outcome.

Materials and Methods: Reviewing the medical records from March 2000 to March 2004, we selected 69 patients with cervical tuberculous lymphadenitis who underwent both initial and follow-up CT during scheduled chemotherapy. The outcomes of the patients were divided into favorable (n=41) and unfavorable groups (n=28) by clinical responses. On both initial and follow-up CT, we evaluated the features of the nodes in terms of calcification (no/punctuate/large), necrosis (no/eccentric/central), perinodal infiltration (no/localized/extensive), and enhancement pattern (no/peripheral/homogeneous).

Results: No detailed nodal feature on initial CT had a statistically significant relation with the clinical outcomes. However, some of detailed nodal features on follow-up CT showed statistical significance; the favorable group had more "no calcification" ($p=0.001$), but "punctuate calcification" was more frequent in unfavorable group ($p = 0.036$). There was more "no necrosis" with the favorable group ($p \leq 0.001$), but more "central necrosis" with the unfavorable group ($p \leq 0.036$). With regards to infiltration, "no infiltration" was more frequent in the favorable group ($p \leq 0.001$), but "localized infiltration" in the unfavorable group ($p = 0.002$). Enhancing pattern showed that "normal (no or homogeneous) enhancement" was related to the favorable group ($p = 0.005$), and peripheral enhancement to the unfavorable group ($p \leq 0.001$).

Conclusion: Cervical tuberculous lymphadenitis which showed punctuate calcification, central necrosis, localized infiltration, and peripheral enhancement on follow-up CT after scheduled medication is more likely to have an unfavorable outcome.

C-0544

Application of dynamic temporomandibular MRT in evaluating the effectiveness of orthodontal treatment

T.V. Bulanova, A.Y. Vasilyev, M.M. Antonik, N.S. Drobysheva; Moscow/RU

Purpose: To assess the dynamics of the TMJ condition in patients with occlusion disorders.

Material and Methods: MRT was performed on 270 occlusion disorder patients wearing brackets and occlusal splints. All patients (Age: 10-34; 178 female, 92 male), regardless of subjective and clinical manifestation, underwent bilateral TMJ examinations prior to treatment. The TMJ dynamics was examined in 56 patients (observation period 7-12 months). The MR-protocol included the following: in occlusion - T1 and T2WI in oblique sagittal projection, T1WI - in oblique

coronal projection; in mouth-open-position - T1WI in oblique sagittal projection; 5-phase imaging (from the mouth-closed to the maximal mouth-open position).

Results: The original asymmetric changes of TMJ were found in 251 patients (92.5%). The group for dynamic observation comprised of 56 patients with a complete or partial ventral dislocations of the disc. The dynamics did not reveal a full normalization of disc position, whereby in 44 patients the initial position of the disk remained unchanged, in 12 cases only the grade of dislocation became less distinctive. The appearance of fibrous changes in the bilaminar zone and the superior belly of the lateral pterygoid muscle during treatment was observed in 13 patients with a complete ventral disc dislocation. In patients with condyle hypermobility wearing occlusal splints, a normalization of the condylar motion despite the remaining disc dislocation was observed in 84% of cases.

Conclusion: The orthodontic occlusion treatment allows one to achieve a reduction of the condyle hypermobility, however, it barely corrects the ventral disc dislocation.

C-0545

Dynamic phono-articulation tract assessment by gated MR imaging

J.C. Vilanova, J. Barceló, J. Pujol, M. Villalón; Girona/ES

Learning Objectives: To illustrate the phono-articulation tract during repetitive speech using gated MR imaging, displaying 2D movies and outlining its applications in different fields.

Background: Current methods to evaluate the phono-articulation tract are video-nasendoscopy and video-fluoroscopy. Both methods are difficult to perform and non-objective. MR imaging is capable of producing images with excellent contrast and spatial resolution. However conventional MR imaging is limited to static structures as moving structures produce blurred images. New techniques could attempt to overcome these limitations.

Procedure Details: The phono-articulatory tract was imaged using a 1.5 T MR unit with a gated SPGR sequence. An external 1 Hz trigger was fed to the cardiac gate. Each acquisition of 16 phases/s was performed. All the vowels, selected consonants and several consonant-vowel syllables were acquired. Single slice FSE T1 was acquired as an anatomical image for each vowel and consonant. Single-slice data was displayed static and dynamically as a cine-loop. The relationship between the tongue, palate, lips, pharynx and epiglottis was depicted either from the single image as from the cine loop images, and from the gated images.

Conclusion: Dynamic gated MR imaging of the phono-articulation tract allows one to visualize the movement of all its anatomical structures. This method provides a very useful tool in the phonetic field from every speaking language in various aspects of logopedics such as diagnosis and rehabilitation regarding the speech pathology and in evaluating defects in the velum and palate; but also in other fields like teaching phonetics and other languages, physiologic speech, research or design synthesized voices.

C-0546

The role of computed tomography with aerial manoeuvres in the diagnosis of aerodigestive tract tumors

C. Gonzalez Gordaliza, J. Martinez San Millan, A. Vicente Bartulos, O. Sanz de Leon; Madrid/ES

Purpose: The aim of this study is to show the accuracy of helical multislice CT with aerial manoeuvres (inhalation, phonation and Valsalva) for detection, localization and exact extension of tumoral pathology in oral cavity, hypopharynx and larynx.

Material and Methods: Prospective study between May 2003 and August 2004 involving 42 patients (40 male and 2 female), mean age 61 years, with clinical suspicion of larynx (n = 21), pyriform sinus (n = 6), faucial tonsil (n = 5), buccal mucosa (n = 5), gingival mucosa (n = 1), tongue (n = 3) or lip (n = 1) tumors. All patients were examined using helical CT with neutral (inhalation), phonation and double Valsalva manoeuvres. The protocol was: matrix 512 x 512, thickness 3.2 mm, interval reconstruction 2.5 mm, pitch 1, 40 seconds after 80 cc intravenous iodinated contrast media.

Results: In our experience, morphologic assessment of the laryngeal, hypopharyngeal and oral cavity lesions was easier in CT with manoeuvres. In comparison with a baseline study (neutral CT), the use of manoeuvres better identified tumoral lesions in 15% cases (n = 6) and dismissed this pathology in 23% patients. In addition, in 26 patients (62%) we proved with manoeuvres more extension than without them.

Conclusion: CT with aerial manoeuvres showed more exactly presence and extension of tumoral lesions in aerodigestive tract.

Scientific and Educational Exhibits

C-0547

CT evaluation of neck masses: A pictorial review

A.P. Datar; Mumbai/IN

Purpose: (1) To assess the role of spiral CT in pre-operative characterization of neck masses and to evaluate the role of 3D reconstruction techniques in delineating the anatomical extent of neck masses. (2) To evaluate the imaging criteria in correlation with histopathological diagnosis.

Materials and Methods: 110 patients with palpable neck masses were studied by Multislice spiral CT Siemens Somatom volume access. 3D reconstruction techniques were performed to demonstrate the anatomical extent, and pre-operative findings were compared with FNAC/HP diagnosis.

Results: Review in the study group of 110 cases revealed specified age of presentation, anatomical location and CT imaging features of the pathological diagnostic categories. Metastatic lymphadenopathy (35%) predominated amongst the cases followed by malignant thyroid masses (20%). Inflammatory features were confirmed in 8%. Miscellaneous group included vascular masses, cystic masses, soft tissue tumors, etc (37%). The presence of fat, calcification, extension into extra-glandular spaces, hemorrhage, necrosis and cystic changes proved beneficial in CT characterization of neck masses and subsequent treatment planning.

Conclusions: Multislice spiral CT is an invaluable tool in the pre-operative evaluation of neck masses. The superior soft tissue discrimination and precise spatial resolution with respect to critical structures in the neck were beautifully depicted by various 3D reconstruction techniques. Although exact tissue diagnosis was not possible, careful analysis of imaging features in combination with clinical correlation provided a reasonably short differential diagnosis in nearly every case.

C-0548

Role of multidetector CT in the evaluation of primary and secondary hyperparathyroidism

F. Ricci, S. Campagnano, A. Casale, M. De Vargas Macchiucca, F. De Cristofaro, G. Panzironi; Rome/IT

Purpose: In primary and secondary hyperparathyroidism, accurate localisation of abnormal glands is essential in order to perform a minimally invasive surgery. The aim of this study is to evaluate the role of multidetector CT in primary, recurrent or persistent, and secondary hyperparathyroidism.

Methods and Materials: 25 consecutive patients with secondary hyperparathyroidism, due to chronic renal failure, and primary hyperparathyroidism, recurrent or persistent, or primary hyperparathyroidism with inconclusive scintigraphy and ultrasonographic examinations underwent multidetector CT (Somatom Volume Plus 4 Siemens). At surgery the location, number, size and histopathologic results of all identified parathyroid tissue was recorded and compared with CT results.

Results: At surgery, 11 adenomas and 35 hyperplastic parathyroid glands were detected in 12 cases of primary hyperparathyroidism, 1 primary, persistent and 2 primary, recurrent cases of hyperparathyroidism, 7 secondary and 3 secondary, recurrent cases of hyperparathyroidism. CT sensitivity was 57% because it does not detect small hyperplastic glands; most of them smaller than 1 cm (16/35 nodules). CT demonstrates a good accuracy in the localization of adenomas (91%) and of the 5 cases of ectopic glands (100%), all of them larger than 1 cm.

Conclusion: Multidetector CT is able to correct localize adenomas and ectopic parathyroid glands while it does not correctly detect hyperplastic multi-glandular involvement which is usually smaller in size. However CT is surgically useful in the selection of patients for minimally invasive procedures.

C-0549

Usefulness of the apparent diffusion coefficient in line scan diffusion-weighted Imaging for distinguishing between squamous cell carcinoma and malignant lymphoma of the head and neck

M. Maeda, H. Sakuma, K. Takeda; Tsu/JP

Purpose: Squamous cell carcinoma (SCC) and malignant lymphoma are common malignant tumors of the head and neck. The purpose of this study was to determine whether the apparent diffusion coefficient (ADC) in line scan diffusion-weighted imaging (LSDWI) is useful for distinguishing between SCC and malignant lymphoma of the head and neck.

Methods and Materials: LSDWI was prospectively performed for 39 patients with SCC and 14 patients with malignant lymphoma. Images were obtained with a diffusion-weighted factor (b factor) of 5 and 1000 sec/mm², and ADC maps were generated. ADC values were measured for the two types of tumors.

Results: The mean ADC values were $0.96 \pm 0.11 \times 10^{-3}$ mm²/sec for SCC and $0.65 \pm 0.09 \times 10^{-3}$ mm²/sec for malignant lymphoma, showing a statistically significant difference ($p < 0.001$). All but one of the patients with malignant lymphoma showed lower ADC values than the lowest ADC value (0.76×10^{-3} mm²/sec)

observed in SCC. When an ADC value of 0.76×10^{-3} mm²/sec was used for distinguishing between SCC and malignant lymphoma, an accuracy rate of 98% (52/53) was achieved.

Conclusion: The ADC value may be useful for distinguishing between SCC and malignant lymphoma in the head and neck.

C-0550

withdrawn by authors

C-0551

Color Doppler ultrasonography findings in hypothyroidism

A.T. Turgut, E. Cakal, P. Birincioglu, U. Kosar, B. Demirbas, Y. Aral; Ankara/TR

Purpose: To define the color Doppler ultrasonography (CDUS) characteristics of the thyroid gland and inferior thyroidal artery (ITA) in patients with hypothyroidism.

Materials and Methods: We investigated 42 patients with hypothyroidism clinically, by thyroid function laboratory tests and by CDUS concerning the estimation of the parenchymal color flow pattern (PCFP) of the thyroid and the measurement of the maximum systolic velocity (MSV) in the ITA.

Results: 8 of the 42 hypothyroid patients had PCFP 0, MSV of 23.4 cm/sec, TSH of 21.6 µIU/ml. In 34 patients different degrees of increased parenchymal vascularisation and MSV were detected (22 patients with PCFP I, MSV: 35.8 cm/sec, TSH: 21.8 µIU/ml, 9 patients with PCFP II, MSV: 44.9 cm/sec, TSH: 20.0 µIU/ml, 3 patients with PCFP III, MSV: 37.7 cm/sec, TSH: 82.5 µIU/ml). In regard to the PCFP, significant differences for TSH, glandular volume and MSV were detected ($p = 0.047$, $p = 0.007$ and $p < 0.001$ for each). Significant differences were detected by the comparison of each of the subgroups with PCFP 1, 2 and 3 and that with CFP 0 for mean MSV ($p < 0.001$, $p < 0.001$ and $p = 0.014$ for each) and of the subgroups with PCFP 0, 1 and 2 and that with PCFP 4 for mean TSH ($p = 0.024$, $p = 0.015$, $p = 0.012$ for each).

Conclusion: We conclude that MSV of the ITA, as well as PCFP, can be accepted as a reliable measure of increased vascularity in hypothyroidism, a state formerly attributed only to hyperthyroidism. Our findings suggest that thyroid stimulation mainly by TSH is responsible for the increased flow.

C-0552

A new parameter for the evaluation of the efficacy of medical treatment in hypothyroidism: Color Doppler measurement of blood flow in the inferior thyroidal artery

A.T. Turgut, E. Cakal, U. Kosar, P. Birincioglu, B. Demirbas; Ankara/TR

Purpose: To determine whether color Doppler ultrasonography (CDUS) of the thyroid gland and the inferior thyroidal artery (ITA) can be a reliable measure for the efficacy of the medical treatment for hypothyroidism.

Methods and Materials: 42 patients with hypothyroidism were evaluated clinically, by laboratory tests regarding the thyroid function and by CDUS concerning the estimation of the parenchymal color flow pattern (PCFP) of the thyroid and the measurement of the maximum systolic velocity (MSV) in the ITA both before and after medical treatment for 6 months.

Results: The number of patients with PCFP 0, I, II and III before and therapy were 8, 22, 9, 3 and 10, 23, 9, 0 respectively. Mean TSH and MSV values of the ITA which were noted before and after therapy as 25.7 ± 26.7 µIU/ml, 35.5 ± 10.1 cm/sec and 1.6 ± 0.8 µIU/ml, 31.0 ± 10.2 cm/sec respectively were significantly different from each other ($p = 0.02$, $p < 0.001$, for each). The PCFP did not change in 29 patients whereas in 14 patients it decreased and in 3 patients it became higher. By comparison of the patients without any change in PCFP and those with a change to lower grade, a significant decrease for TSH and MSV of the ITA was noted in the latter ($p = 0.026$ and $p = 0.017$, for each).

Conclusion: The decrease in the MSV of the ITA closely reflects the efficacy of the medical treatment in hypothyroidism and can be utilized for the follow-up as an alternative to laboratory tests.

C-0553

MR imaging of parotid gland tumours with radiologic-pathologic correlation

S.P. Prabhu, R. Davies, J. Luker, J. Kabala; Bristol/UK

Learning Objectives: To illustrate the role of magnetic resonance imaging in the diagnostic work-up of parotid tumours. To illustrate MR imaging findings of parotid tumours and demonstrate how these correlate with pathologic findings.

Background: Benign and malignant tumours of the parotid gland are being increasingly imaged on MR imaging before surgery. We elaborate our imaging protocols and algorithms to differentiate benign tumours, low-grade malignant tumours and high grade malignant tumours on MR imaging.

Scientific and Educational Exhibits

Procedure Details: We reviewed the MR imaging archives in our teaching hospital to identify cases of parotid tumours imaged preoperatively with MR imaging. We obtained the pathology reports of these cases and details of any follow-up imaging. We elaborate on the appearances of various types of parotid masses with radiologic-pathologic correlation. Difficulties faced in distinguishing various tumour types are highlighted and suggestions for overcoming these problems are elaborated. The various tumours illustrated include pleomorphic adenomas, adenolymphomas, monomorphic adenomas, mucoepidermoid carcinomas, adenoid cystic carcinomas, lymphomas, squamous cell carcinomas and acinic cell carcinomas.

Conclusion: MR imaging is often useful in differentiating benign and malignant tumours of the parotid gland, and can provide important clues in the diagnosis of their histology.

C-0554

Neck lumps and bumps: Ultrasound is the way forward

K. Satchithananda, H. Purushothaman, P.S. Sidhu; London/UK

Learning Objectives: 1. To understand the diverse disease processes that affect the soft tissues of the neck in both children and adults. 2. To learn how to use all aspects of ultrasound imaging (grey scale, colour Doppler and fine needle aspiration) to evaluate lesions. 3. To recognise the pattern of ultrasound features of the different pathological processes.

Background: The soft tissues of the neck lie in a superficial position, thus making them ideal for ultrasound examination. High frequency linear probes with new colour Doppler facilities make imaging of this region by ultrasound the optimal modality.

Procedural Details: Diseases of the thyroid, parathyroid, major salivary glands and lymph nodes are well characterised by ultrasound and a definitive diagnosis can often be made without needing to use CT or MR imaging. Ultrasound is also advantageous in imaging children with its use of non-ionising radiation and its ability to make the diagnosis with both congenital and acquired lesions. Image-guided tissue sampling with ultrasound allows accurate, real time aspiration of cells for immediate histological diagnosis.

Conclusion: This exhibit will illustrate the use of ultrasound in evaluating masses in the neck and demonstrate the vital role ultrasound plays in this clinical setting.

C-0555

Cancer of the posterior tongue: Contribution of MR imaging in staging and in therapeutic workup

A. Kalai, Brot, Y.K. Maratos, P. Halimi; Paris/FR

Purpose: We compared MR imaging findings to the initial staging after clinical examination of posterior tongue cancer. We evaluated the impact of MR imaging and the modification of the therapeutic workup.

Materials and Methods: 40 patients with cancer of the posterior tongue were examined by MR imaging. The following anatomic structures were analyzed by MR imaging, endoscopy and surgery: extension to the midline, lateral oropharyngeal wall, soft palate, posterior pillar, pterygo-mandibular area, anterior tongue, vallecula and pre-epiglottic space. Results of MR imaging were compared to the results of biopsy, surgery and follow-up of patients.

Results: MR imaging showed often that lesions were much larger than they were expected after clinical examination, particularly in relation to midline extension, the pterygo-mandibular area, the posterior pillar and deep extension. Evaluation with MR imaging prevented more than 30% of the operations that were planned after initial clinical evaluation.

Conclusion: MR imaging is better correlated to histological and surgical data than clinical findings. MR imaging evaluation is mandatory prior every curative surgical procedure.

C-0556

Nodal involvement of peripheral T-cell lymphoma in the neck: Two-phase CT findings

J. Choi¹, S. Kim², E. Kim¹, D. Na¹, J. Ryoo³, H.-J. Kim¹; ¹Seoul/KR,
²Chunchon/KR, ³Jinju-Si/KR

Purpose: To describe two-phase CT findings of nodal involvement of PTCL in the neck.

Methods and Materials: Enrolled were 27 patients (M:F = 20:7; mean age, 57.5 years) who had pathologically proven PTCL with nodal involvement in the neck. Patients consist of those with PTCL, not otherwise specified (NOS) (n = 20), natural killer (NK)/T-cell lymphoma (NKT) (n = 5), and angioimmunoblastic T-cell lymphoma (AITL) (n = 2). Early- and late-phase axial CT scans were obtained with

scanning delays of 30 and 180 seconds respectively, following administration of contrast medium in all patients. We retrospectively evaluated lymph nodes on CT images with special attention to central necrosis, extra-nodal extension, and enhancement patterns.

Results: Extra-nodal extension and central necrosis were seen in 19 of 27 patients (70.4%) and 11 of 27 patients (40.7%), respectively. Nineteen of 27 patients (70.4%) demonstrated heterogeneous enhancement of the enlarged lymph nodes on early phase, of whom heterogeneous enhancement on late phase is noted in 11 patients (57.9%). In 6 of 27 patients (22.2%) including 5 patients with PTCL NOS and one with NKT, homogeneous enhancement was seen on both early and late phases without extra-nodal extension or central necrosis. Heterogeneous enhancement on early phase, extra-nodal extension, and central necrosis were seen in 13, 13, and 6 patients with PTCL NOS, respectively; 4, 4, and 3 patients with NKT; and in all patients with AITL.

Conclusion: Heterogeneous enhancement on early phase, extra-nodal extension, and central necrosis of the lymph nodes are relatively common findings of PTCL.

C-0557

Differentiation of benign from malignant salivary gland tumors using color Doppler sonography

S.S. Petrovic; Nis/YU

Purpose: The aim of this study was to determine the color Doppler features of benign and malignant salivary gland tumors and their possible differentiation using color Doppler sonography.

Materials and Methods: This prospective study included 76 patients with salivary gland tumors examined using color Doppler sonography before surgery. Examinations were made by 7.5 MHz linear probe with Doppler imaging. The intratumor vascularity was graded on a four step analogue scale and the patterns of vascular distribution were characterized as peripheral (basketlike) or hilar (branching).

Results: Post surgical and histo-pathological verification revealed that 58 patients (76.32%) had benign and 18 patients (23.68%) had malignant salivary gland tumors. Of the benign tumors, 10 (17.24%) showed no color Doppler signal, 29 (50%) had first, 17 (29.31%) second, and 2 (3.44%) third grade of vascularization. Of the malignant tumors 1 (5.55%) had first, 5 (27.77%) second, and 12 (66.66%) third grade of vascularization. The peripheral pattern of vascularization was found in 34 (58.62%) and hilar in 14 (24.13%) benign tumors. On the contrary, only 2 (11.11%) malignant tumors had peripheral, and 16 (88.89%) hilar pattern of vascularization. A statistically significant difference was found in grade ($p < 0.001$) and pattern ($p > 0.05$) of vascularization between benign and malignant salivary gland tumors.

Conclusion: Our experience showed that color Doppler sonography is a sensitive method for the diagnosis of salivary gland tumors. On the basis of the grade and pattern of vascularity it is possible to distinguish benign from malignant salivary gland tumors with great certainty.

C-0558

The importance of cervical fascial planes and compartments in treatment and prognosis in life threatening deep neck infections

N. Erdogan, E. Inci, B. Dirim Vidinli, E. Uluç, A. Roditi, M. Dirik; Izmir/TR

Learning Objective: We aimed to emphasize the importance of radiological evaluation in cervical fascial planes and compartments in deep neck infections, which have a high morbidity and mortality.

Background: 15 patients who were thought to have deep neck infection were evaluated. The patients went through contrast-enhanced axial CT scan with routine neck protocol including the upper mediastinum.

Imaging Findings: In our study 15 patients (Age: 3-90, mean age 40.4; 4 Male; 11 Female) underwent enhanced axial neck CT scan. The location of infection (compartment), mediastinal infiltration, the characteristics (abscess, cellulitis), accompanying lymph nodes and primary cause which could not be diagnosed clinically were evaluated by radiologists. In 5 patients the primary cause could not be diagnosed. 6 patients had gingivitis and related illness. The rest had peritonsillar abscess, meningitis, burns in the neck and rheumatoid arthritis (amyloidosis and renal insufficiency).

Conclusion: The cervical region has a complex anatomical structure subdivided by fascial planes. Deep neck infections infiltrate by these routes into anatomical spaces and most often these infections require surgical procedure. Some invade the mediastinum which has a poor prognosis. Even though it is relatively easy to diagnose a deep neck infection clinically, it is very important to evaluate the fascial planes and compartments accurately for the treatment choice, for surgical planning and patient follow-up.

Scientific and Educational Exhibits

Head and Neck

Miscellaneous

C-0559

Endolymphatic sac tumors: A major criteria of Von Hippel-Lindau disease

K. Marsot-Dupuch, S. Richard, S. Bobin; *Le Kremlin-Bicêtre/FR*

Purpose: To analyze the characteristic findings of endolymphatic sac tumors (ELST) in VHL disease.

Materials and Methods: A consecutive series of 250 patients presented with VHL disease controlled by the same team of geneticist (S. Richard). All patients had an imaging survey consisting of a brain and spine MR imaging with focused images on the temporal bone if deafness, vertigo, tinnitus or facial palsy was present.

Results: 8% (20) of VHL patients had an endolymphatic sac tumor. In one case out of 250, the lesion was very suspicious but not proven as it was not operated upon. The lesion was always unilateral except in one case. In 20% ELST was the onset of the disease. In one case, the delay between the ELST and the disease was of 30 years. Deafness was always present except in one case. Hormonal impact on the tumor growth was evident in one patient. A cerebellar location of a metastasis of a kidney neoplasm mimicked an ELST.

Conclusions: The work depicts all aspects of the ELST, their spread and the follow-up to perform. Sporadic ELST should raise the suspicion of VHL disease and the patient should have a genetic screening.

C-0560

Imaging technique for obtaining optimal sections of the ossicular chain by high-resolution multiplanar reformation based on measurements of normal auditory ossicular angles

N. Fujii, K. Katada, S. Yoshioka, K. Takeuchi, A. Takasu, K. Naito; *Toyoake/JP*

Purpose: The angles of the ossicles relative to a reference plane were measured, and optimal sections for high-resolution multiplanar reformation (HR-MPR) of the ossicular chain were reconstructed.

Methods and Materials: The reference plane included the lower margin of the orbit and the external auditory canal. Using 3D-CT, the angles of the stapedial crus in the sagittal plane and the incudal long process and stapes in the coronal plane and rotation of the stapes relative to the incudal long process in the axial plane were measured in HR-MPR images of 50 normal ears with a 0.5 mm, 4-row multislice CT scanner (Toshiba).

Results: The section including the malleal head and manubrium was parallel to the incudal long process, vertical in the reference plane. The angle of the stapedial crus to the reference plane was similar (mean 6°). The incudal long process was approximately 90° to the stapes (mean 89°), and the stapes was approximately 45° to the reference plane (mean 44°). The stapes extended straight from the incudal long process in 80% of ears. The malleal head and incudal short process were easily seen in the axial plane. The malleus image including the malleal manubrium was reconstructed in the coronal plane. The incudal long process was seen immediately behind the malleus. The stapes image was reconstructed from the incudal long process image. These four sections are considered optimal for visualizing the ossicular chain.

Conclusion: This imaging technique for the ossicular chain is useful due to its reproducibility and ease of operation.

C-0561

Labyrinthitis ossificans: CT scan and MR imaging findings

C. Gonzalez Gordaliza, J. Martinez San Millan, A. Vicente Bartulos, O. Sanz de Leon; *Madrid/ES*

Purpose: Labyrinthitis ossificans (LO) is a pathologic ossification in the cochlea and labyrinth. It is usually caused by an infection that reaches inner ear via tympanogenic, meningeal or hematogenous route. Inflammatory injury results in fibrosis (fibrous stage), which is followed by formation of new bone (ossification stage). The aim of this study is to describe the CT and MR findings of LO, and to show their role in diagnosing each stage.

Material and Methods: Prospective study involving 26 ears (13 patients) with sensori-neural hearing loss. All patients were examined using helical CT and MR. CT imaging was performed with a high resolution protocol: contiguous 0.6 mm thick images obtained through the petrous bones with posterior reconstruction in axial, coronal and sagittal planes. MR imaging was performed on a Philips 1.5 T scanner, with fast spin echo T2-weighted study of temporal bones, 3D-CIIS acquisition and spin echo T1-weighted pre/post-gadolinium scans.

Results: We studied 26 ears, 15 with LO. 2 patients were bilaterally affected. In 13 ears, CT showed sclerosis, irregularity or obliteration of labyrinth (ossification stage). In 4 ears, MR could correctly demonstrate high signal of normal labyrinth replaced by low signal intensity (sclerosing tissue: Fibrous stage). However, in these 4 ears, CT failed to visualize sclerosing tissue. In 2 cases, there was a simultaneous stage: Endoluminal calcifications demonstrated in CT and sclerosing tissue showed in MR.

Conclusion: CT scan can precisely demonstrate ossification stage of LO, but MR better demonstrates the fibrous stage and the real extent of the disease.

C-0562

Embryological correlation of congenital labyrinthine abnormalities

S. Avula, A. Thimmarayappa, C. Yeong; *Warrington/UK*

Learning Objectives: This poster aims to illustrate the development of the inner ear and demonstrate the appearances of congenital labyrinthine abnormalities that occur as a result of arrests during the various stages of embryogenesis.

Background: The inner ear development starts at the 4th week and its ossification is complete by the 24th week of gestation. The basic structure of the bony labyrinth is formed by the 8th week. Genetic and non-genetic insults occurring during this period can arrest or cause aberration in the development, resulting in labyrinthine anomalies whose appearance resemble that of the inner ear at the corresponding stage of embryogenesis. These anomalies can be identified on CT or MR scans and are accountable for approximately 20% of patients with congenital sensorineural hearing loss.

Procedure Details: Labyrinthine anomalies noted in high resolution CT scans of the temporal bone in patients investigated for sensorineural hearing loss have been demonstrated with comparative images of the developing labyrinth between 4 and 8 weeks of gestation.

Conclusion: A clear understanding and application of labyrinthine embryogenesis will be helpful in the interpretation of CT or MR studies performed for the investigation of congenital sensorineural hearing loss.

C-0563

Magnetic resonance imaging in temporo-mandibular joint internal derangements

J. Kleinrok, T.K. Rozylo, M. Janczarek; *Lublin/PL*

Learning Objectives: To present the spectrum of imaging findings in internal derangements of the temporomandibular joint (TMJ) obtained by means of magnetic resonance imaging (MRI).

Background: An internal derangement is an abnormality in the position and sometimes the morphology of the TMJ disk that may interfere with normal function. MRI is a gold standard in TMJ disk imaging and therefore it is essential to know the range of possible findings.

Procedure Details: MRI examinations were performed in 216 patients aged 13-57. The examinations were performed by means of a 1.5 T machine. T1- and T2-weighted images were obtained in sagittal and coronal views. The examinations were performed in different positions of the mandible: maximum occlusion (closed mouth), maximum mouth opening, mandibular protrusion, mandibular retro position in occlusion as well as in therapeutic position with an individual silicone splint. This was presented as a pictorial review of the range of MRI findings and the impact of different mandibular positions on disk images was underlined.

Conclusion: Internal derangement is a common problem and therefore confident radiological diagnosis is essential. It is important to perform MRI studies in different positions of the mandible as this may enhance the sensitivity and specificity of diagnosis of causes of TMJ internal derangement.

C-0564

Three-dimensional reconstruction of spiral, multidetector images from computer tomography in diagnosing innate and acquired anomalies of facial skeleton

S. Trzeszkowska-Rotkegel, S. Skrzelewski, J. Glowacki, M. Tarnawski, A. Pisulska-Otremba, H. Borowiak, T. Legaszewski; *Zabrze/PL*

Purpose: Recognition of the type of anomaly, its size and character and the degree of deformation of the visible anatomic elements is vital in making the right decision about further clinical procedures. The usefulness of three-dimensional reconstruction of spiral computer tomography images in constructing virtual, three-dimensional models of the facial skeleton to show the deformations and to make planimetric measurements before a planned, surgical correction of the anomaly was evaluated.

Methods and Materials: A group of 35 patients with a clinical diagnosis of hemi-

Scientific and Educational Exhibits

hypoplasia of a face (22 persons) and with temporomandibular joint ankylosis (13 patients) was examined. The group consisted of 23 males (aged 7-23) and 12 females (aged 4-21). CT examinations were performed with a spiral, four-row apparatus. The data from this was then used for multiplanar and three-dimensional reconstructions. The obtained models were presented as bone (skeleton) and soft-tissue images. Our own modification of planimetric measurements was used for comparing chosen anatomic and topographic parameters of the right and left side of the face. In each case an image of the cervical part of the spine was evaluated.

Results: The performed examinations in all 35 patients allowed us to define the type of anomaly, its size and the degree of facial skeleton deformations.

Conclusion: A spatial visualization of the examined structures allows a better and more complex understanding of the anatomic anomalies present in a patient, as well as defining possibilities and tactics of further treatment pre-operatively and prognostically evaluating the operative treatment effectiveness.

Interventional Radiology

Vascular

C-0565

Virtual stenting (VS): A new modality for choosing a stent or a stent-graft by three-dimensional rotational angiography (3DRA)

F. Pozzi-Mucelli¹, D. Babic², A. Calgaro¹, R. Pozzi-Mucelli¹; ¹Trieste/IT, ²Best/NL

Purpose: VS is a new dedicated technique, recently implemented in the 3D rotational angio workstation and intended for virtual placement of stents on pathological vessel portions. The technique enables 3D assessment of stents and stent graft geometry on stenotic, obstructive or aneurysmatic vessel lesion to be treated.

Methods and Materials: 28 patients underwent 3DRA for stenotic or aneurysmatic lesions of thoracic or abdominal aorta (5 patients) and/or iliac arteries (23 patients: 30 lesions) and 3D vessel elaborations and VS was performed. The geometrical properties of the virtual stents (length, proximal/distal diameter) were compared with the geometry of the stents implanted in the patients or with CT scanner measurements (in cases of AAA not treated by endovascular approach).

Results: Iliac artery stenting was performed in 28/30 lesions; only 2 elongated iliac aneurysms were considered unsuitable for endovascular treatment. In treated cases a corresponding correlation between VS and real stenting was observed with a mean diameter of real stent of 8.72 mm compared to 8.61 mm of the virtual stent. Aneurysmatic aortic lesion underwent endovascular treatment in 2/5 cases with a good correlation to VS data while the 3/5 cases not endovascular treated VS showed a good agreement to CT scanner measurements.

Conclusions: The "virtual stenting" technique appeared effective, fast and objective in almost all cases. The technique provides the required geometrical information on the minimum stent diameter and optimal length. In cases of extreme vessel tortuosity associated with aneurysmatic disease a manual intervention is required in order to optimize the lumen path.

C-0566

Catheter fragmentation of acute massive pulmonary thromboembolism: Relationship between distal embolization and pulmonary arterial pressure elevation

K. Nakazawa, H. Tajima, S. Murata, T. Kumazaki, K. Ichikawa, T. Fukunaga, S. Onozawa, T. Yamamoto, T. Takano; Tokyo/JP

Purpose: To clarify the relationship between pulmonary arterial pressure and distal embolization due to catheter fragmentation for lifethreatening acute massive pulmonary thromboembolism.

Methods and Materials: 33 patients with hemodynamic impairment (10 men and 23 women; aged 27-82 years) were treated by mechanical thrombus fragmentation with a modified rotating pigtail catheter. After thrombus fragmentation, all patients received thrombolytic therapy, followed by manual clot aspiration using a large-lumen PTCA guide catheter. Serial pulmonary angiography was performed for the evaluation of the extent of thrombus formation. Pulmonary arterial pressure was also continuously recorded during the procedure.

Results: Distal embolization was confirmed by angiography in 13 out of 33 patients. A significant elevation in mean pulmonary arterial pressure occurred after thrombus fragmentation (pre 30 ± 8.3 mmHg, post fragmentation 33 ± 9.8 mmHg, $p < 0.005$), and a statistical decrease in mean pulmonary arterial pressure was found after thrombolytic therapy and thrombus aspiration in this group (post aspiration 22 ± 5.6 mmHg, $p < 0.001$). No distal embolization was seen in 20 of 33 patients, and a significant decrease in mean pulmonary arterial pressure was confirmed after thrombus fragmentation (pre 32 ± 6.2 mmHg, post fragmentation 27 ± 8.8 mmHg, $p < 0.001$), and after thrombolysis and thrombus aspiration (post aspiration 22 ± 4.6 mmHg, $p < 0.001$).

Conclusion: Distal embolization and a elevation in pulmonary arterial pressure might occur during mechanical fragmentation using a rotating pigtail catheter for the treatment of acute massive pulmonary thromboembolism. Thrombolysis and thrombus aspiration provided for a hemodynamic stabilization and partial recanalization.

C-0567

A new ischemic model using radiofrequency wire electrode in rabbit hind limb

H. Baik, B. Kwak, H. Shim, Y. Kim, J. Lee, I. Song, K. Kim; Seoul/KR

Purpose: To establish an ischemic limb model endovascularly made by radiofrequency (RF) wire electrode for the investigation of new treatment modality of limb-threatening ischemia.

Scientific and Educational Exhibits

Methods and Materials: Polytetrafluoroethylene coated 0.035 inch wire with 2 cm-exposed tip was inserted through left carotid artery into left femoral artery in 7 New Zealand white rabbits. RF ablation at 20 watt with RF generator (RF3000) was performed for 145 ± 7.97 seconds pulling it from distal superficial femoral artery up to proximal external iliac artery. We observed clinical changes and performed angiography. Blood pressure and tissue perfusion and permeability measured by the laser tissue blood flowmeter and CT were assessed up to 6 weeks and left to right (L/R) ratio were calculated. The degree of collateral formation and vascular reconstitution in angiography was graded from 0 to 6 as an angiogenic score.

Results: In all rabbits, the angiography demonstrated complete obstruction from proximal external iliac artery to distal superficial femoral artery. The angiogenic score gradually increased to a plateau at the sixth postoperative week ($R = 0.86$, $p < 0.05$). Blood pressure at left calf was too weak to be measurable before the fourth postoperative week. The L/R ratio of blood pressure at the fourth week was 0.68 ± 0.100 and increased to 0.71 ± 0.074 at the sixth week. The L/R ratio of the tissue perfusion and permeability was significantly reduced at the first and second week ($p < 0.05$), and gradually increased until the sixth week.

Conclusion: Endovascular RF ablation with wire electrode is a reproducible and measurable model of ischemic limb disease.

C-0568

The endovascular treatment of deep vein thrombosis

S.-H. Suh, J. Won, D. Lee; Seoul/KR

Purpose: To evaluate the effectiveness of endovascular treatment of deep vein thrombosis.

Materials and Methods: 80 patients (M:F = 35:45, mean 55 years) with deep vein thrombosis (DVT) were analyzed since Jan 1999. All patients had acute ($n = 56$) or chronic ($n = 24$) pain, swelling and color changes on lower extremity. Various methods of thrombus removal had been performed until patency of external iliac vein was restored. All patients underwent consecutive angioplasty and stent insertion. Placement of IVC filter before stenting was combined in 12 patients with risk factor of thromboembolism. Patients were followed up by ultrasound or venography.

Results: Procedures were successful in all but one patient in whom passage of the guide wire through the common iliac vein failed (technical success rate = 98%). There were complications of minor bleedings (gum, nasal bleeding and woozing at puncture site) in 4 patients. Immediately after treatment, complete or partial resolution of symptoms was achieved in all patients with technical success. 4 patient received secondary thrombolysis and angioplasty due to the rethrombosis of iliac vein and stent on venography taken 1 month after the initial treatment and patency of iliac vein and stent was restored. On the follow-up ($n = 45$, mean 18 months), all stents were proved patent, however, partial stenosis (< 50%) was noted due to the intimal hyperplasia on venography. The overall patency rate at 1, 2, 3 year was 100, 98, 95%. (2 - 43 months, mean = 14 month).

Conclusion: Endovascular treatment of DVT is effective and safe.

C-0569

Contrast harmonic imaging with power mode and coded harmonic angiography using Optison for assessing vascularization during chemoembolization in HCC. First experiences

D.-A. Clevert¹, E. Jung², M.F. Reiser¹, N. Rupp²; ¹Munich/DE, ²Passau/DE

Problem: To what extent does contrast enhanced ultrasound using Optison enable recording of intratumoral vessels in hepatocellular carcinoma as compared to selective DSA?

Materials/Methods: In 30 patients with 39 lesions caused by hepatocellular carcinoma, a perfusion assessment using vascular ultrasound (Logiq 700, Logiq 9, GE) was carried out immediately before and during a selective chemoembolization. Using multifrequency transducer, it was possible to assess blood flow using color duplex sonography (CDS), power mode (PM) and after a contrast agent injection intermittently using coded harmonic angiography mode (CHA) and contrast harmonic imaging with power mode (CHI+PM). An evaluation was performed comparative to selective intra-arterial DSA with probing of the segmental vessels perfusing the tumor.

Results: Using CDS it was only possible to record intratumoral perfusion in 15/39 HCC tumor lesions. Using power mode it was possible in 20/39 lesions, primarily at the tumor margins. A one-time injection of Optison via a peripheral indwelling cannula permitted recording of intratumoral vessels in 30/39 lesions using CHA mode and in all 39 cases using CHI + power mode. An assessment of capillary perfusion only succeeded in CHA mode, which permitted subtraction of the surrounding tissue. Using CHI+PM, it was possible in all cases to sonograph-

ically record the segmental vessels perfusing the tumor for performing the chemoembolization after contrast agent enhancement.

Conclusion: A one-time injection of Optison in small doses in CHA mode and in CHI with power mode enables a recording of intratumoral vessels in HCC with high diagnostic certainty before and during chemoembolization.

C-0570

Percutaneous treatment of pulmonary arterio-venous malformations (PAVM)

F. Volpini, D. Ghirardo, A. Scarrone, I. Mondino, M. Grosso; Cuneo/IT

Purpose: Rendu-Osler-Weber's disease is a rare autosomic dominant pathology; the main symptoms are epistaxis, teleangiectasia and visceral lesions. The prevalence in Europe in 1991 was 1-2 cases on 100,000; the incidence of Pulmonary Arterio Venous Malformations (PAVM) is 15-33%. Right to left shunt causes complications such as cyanosis with dyspnea on efforts, paradoxal embolization with TIA, stroke and cerebral abscess due to septic emboli. We report our experience about treating PAVM in Rendu-Osler-Weber disease, to show the benefits of percutaneous treatment of high flow lesions by embolization, saving the parenchyma.

Materials and Methods: Since 2001 until May 2004, in our hospital 11 patients (4 male and 7 female, from 20 to 74 years) suffering from Rendu-Osler-Weber disease were treated for an amount of 18 PAVM embolized. All our patients have been treated using non-magnetic coils.

Results: Clinical and radiographic involution of PAVM was immediately complete in all patients, with a meanful increasing of PAO₂. No early or late migration of the devices occurred; no significant complications were noted, except for a case of transitorial ischaemic brain attack solved in 72 hours.

Conclusions: Percutaneous embolization is an optimal treatment of PAVM in Rendu-Osler-Weber disease, allowing a selective occlusion saving pulmonary parenchyma. Indications are all fistulas with the afferent artery > 3 mm diam. Non-magnetic coils, particulary spiral shaped coils (VortX, Boston Scientific), are the best material because of their biocompatibility and the security of a definitive occlusion, preserving pulmonary parenchyma.

C-0571

Partial splenic embolization using microsphere

J. Koizumi; Isehara-city/JP

Purpose: To assess the effect of embolization of the splenic artery by various size of microspheres.

Materials and Methods: Four different size (100-300, 300-500, 500-700, 700-900 microns) of microspheres were infused into the main splenic artery of swines (about 40 kg) via 4 Fr. catheter under general anesthesia. Microspheres were infused incrementally under duplex ultrasound measurement until the splenic arterial flow ceased. Splenic arteriography was performed before and after embolization. Five hours later the swine was sacrificed and the spleen was harvested from the swine after the final duplex measurement and angiography.

Results: Total amount of microspheres to obtain an initial cease of the splenic arterial flow was 0.65, 0.30, 0.75, 1.0 mL, while the flow recovery ratio (final blood flow volume before sacrifice/initial blood flow volume before embolization) was to 41.6, 42.2, 61.2, 54.5% by 100-300, 300-500, 500-700, 700-900 microns correspondingly. The specimen showed mostly patchy distribution of ischemic changes in any size variation but the size of each ischemic focus was the smallest using 100-300 microns of microspheres.

Conclusions: The most effective size of microspheres for partial splenic embolization seems to be 300-500 microns although flow recovery was the least at 100-300 microns of microspheres.

C-0572

Endovascular treatment of cerebral arteriovenous malformation

K. Kordecki¹, J.R. Janica¹, A. Lewszuk¹, J. Kochanowicz¹, B. Kadzolek², M. Zabek², J. Walecki¹; ¹Bialystok/PL, ²Warsaw/PL

Purpose: We present our results of treatment of cerebral arteriovenous malformations by implementing percutaneous embolization.

Material and Methods: Between 2001-2003 34 patients had undergone endovascular embolization of cerebral arteriovenous malformation. Ten female and 24 male patients, aged 15 to 78 years. Angiographic DSA examination was performed to assess possibility of percutaneous embolization. Microcatheters 1.2f, 15f or 1.8f were used in accordance with the malformation dimensions. The tip of catheter was placed close to nidus of malformation.

Results: Cerebral arteriovenous malformations were localized mainly in temple

Scientific and Educational Exhibits

region - 38% or in parietal region - 27%. The primary embolization resulted in total occlusion in 41% of AVMs fed by up to three vessels. Repeated interventions led to occlusion of the additional hemangiomas up to 70.5% of all lesions. In case of AVMs fed by more than 4 vessels, the second embolization have not resulted in total occlusion of hemangiomas. The curative results have been obtained only in 12 patients (35%). Total or partial occlusion have resulted in the partial reduction in malformation diameter by 30 to 80%.

Conclusions: The best results of embolization were achieved in cases of small and medium malformations fed by 1-3 vessels - 70.5% cases. In our opinion, percutaneous embolization could be applied as independent curative method in adult patients with small and medium arteriovenous malformation, grade I or III in Spetzler-Martine score.

C-0573

Advantages of virtual 3D Digital Subtraction Angiography option and "cut" function for imaging of the neck of aneurysm of the Willis' circle with complicated morphology

W. Wawrzynek¹, J. Baron², S. Kasprowska¹, A. Siemianowicz¹, B. Koczy¹, H. Boldys²; ¹Piekary Śląskie/PL, ²Katowice/PL

Purpose: Purpose of the work is to show the usefulness of the new technique of 3D DSA and a simple "cut" function for: - Evaluation and imaging of the aneurysmal neck with complicated structure before planned endovascular embolization procedure. - Qualification to endovascular or clipping procedures.

Materials and Method: 21 patients with aneurysms with complicated morphology. Phillips DSA Allura apparatus with 3D station and virtual angi option (AVA) and "cut" function.

Results: For 9 out of 21 patients with aneurysms with complicated morphology virtual 3D option and "cut" function occurred to be the only methods to precise analysis of the aneurysmal neck and it was possible to image additional vessel from aneurysmal neck and its sac. Based on images acquired in virtual option there were six aneurysms rejected, qualified earlier after DSA and 3D DSA for endovascular embolization procedure. Two aneurysms were disqualified for any medical procedure and one was provided with endovascular GDC embolization coils.

Conclusions: Virtual 3D DSA (AVA) option and "cut" function of 3D DSA may be very helpful in some percent of diagnostically difficult aneurysms. For some cases these techniques are the only possible tools to describe morphology of the aneurysmal neck and its sac.

C-0574

Transcatheter arterial chemoembolization through left inferior phrenic artery in hepatocellular carcinoma

S.-H. Suh, J. Won, D. Lee, K.-M. Paik; Seoul/KR

Purpose: To evaluate radiological findings of Hepatocellular Carcinoma (HCC) supplied by extrahepatic collateral supply of left inferior phrenic artery (LIPA) and the efficacy of transcatheter arterial chemoembolization (TACE) through LIPA.

Materials and Methods: Among 1,508 patients who underwent hepatic angiography for the treatment of HCC from February 2003 to January 2004, we found 13 patients with HCC supplied by LIPA collateral (10 males and 3 females, mean age 52 years). TACE of all the LIPA collaterals was performed. We evaluated the radiologic findings of HCC with LIPA collaterals. The clinical outcome, complication and development of another collateral supplies were also evaluated.

Results: The radiological findings of HCC with LIPA were: multinodular HCC (82%), located in left lateral segment (56%), and defect in iodized oil retention or progression of HCC at right dome and left anterolateral segment (68%). The angiographic findings had shown history of TACE more than 4 sessions (60%), hypertrophied LIPA (56%) and isolated origin of LIPA above celiac trunk (73%). The follow-up angiogram showed persistent occlusion in 8 patients and development of other collateral supplies in 7 patients. Three patients complained of left shoulder pain and no other specific complications.

Conclusion: TACE through LIPA was safe and effective. LIPA collaterals developed in 0.8% of patients with HCC. The search for LIPA collaterals should be performed in treatment of such a HCC.

C-0575

Treatment of malfunctioning radial native haemodialysis fistulas:

Comparison between cutting-balloon PTA and standard PTA

J. García-Medina¹, C. Serrano-García¹, A. León-Hernández¹, A. Basile², V. García-Medina¹, R. Leal-Adán¹; ¹Murcia/ES, ²Catania/IT

Purpose: To compare the results of cutting-balloon (CB) angioplasty versus and

high pressure balloon (HPB) angioplasty in the treatment of radial native haemodialysis fistulas.

Methods and Materials: We prospectively evaluate 20 randomized patients (16 men and 4 women, with average age of 66 years), with post-anastomotic stenoses in 20 radial autogenous malfunctioning arterio-venous fistulas treated either with CB (n = 10) or with HPB (n = 10). Inclusion criteria was fistulas without any previous treatment either radiological or surgical. The follow-up finished at 12 months, and the last case at 6 months of the end of the surveillance.

Results: We treated 24 post-anastomotic venous stenoses with an average length of 4 cm (range: 1-8 cm). The average number of inflations was 3 for CB and 4 for HPB. The average inflation pressure was 8 atmospheres for CB (range = 5-10) and 17 for HPB (range = 10-20). Five patients treated with CB had no pain feeling during the inflation, versus only one patient treated with HPB. The Technical success was of 100% in both group. A burst cutting-balloon occurred at the inflation pressure of 5 atmospheres without any consequences. The patency rate at 6 and 12 months were 75% and 8% with the CB and 58% and 16% with the HPB.

Conclusion: In our experience the use of cutting-balloon angioplasty is not justified in the treatment of radial native fistulas with first dysfunction, due to its greater price. The only advantage is related to the less pain feeling experienced by patients during the inflation.

C-0576

Vascular complications in orthotopic liver transplantation (OLT): A pictorial essay

A. Alonso, J.J. Noguera, L. Díaz, P. Domínguez, A. Martínez-Cuesta, J.I. Bilbao; Pamplona/ES

Learning objectives: To review and illustrate the different findings and the role of the percutaneous interventional procedures in the treatment of vascular complications after orthotopic liver transplantation (OLT) in living and cadaveric donors. In this report, special attention to the interventional techniques and diagnostic procedures, as well as the results obtained, is given.

Background: Vascular complications occur in approximately 7% to 14% of liver transplant recipients and they are responsible for 10% of graft losses. The clinical relevance will be determined by the extent of the graft vascular compromise and these complications are associated with a higher risk of graft's dysfunction. The most representative cases in each type of vascular complication following OLT, since the beginning of the OLT program in our centre in 1990, as well as the diagnosis and percutaneous interventional treatment are illustrated and described.

Imaging Findings: Imaging findings from fluoroscopy, angiography (including 3D-angiography), multislice-CT and ultrasound obtained at the time of diagnosis, treatment and follow-up in different cases are illustrated and shown.

Conclusion: Percutaneous interventional procedures, including angioplasty, local thrombolysis and embolization, have gained worldwide acceptance for treatment of these complications, due to their minimal invasiveness as well as low complication and high success rates. A reduced blood loss and a low incidence of procedural complications allow for rapid recovery and to diminish the rate of retransplantation, however, an early diagnosis and correct patient selection are essential factors in order to obtain the best results.

C-0577

Head and neck paragangliomas: Imaging and embolization

A.M. Crespo, G. Hernandez, R. Barrena, A.B. Garcia, B. Izquierdo, E. Angulo; Zaragoza/ES

Purpose: 1. To determinate imaging features of head and neck paragangliomas and to study their value in the differential diagnosis and surgical planning. 2. To determinate the usefulness of pre-operative embolization.

Methods and Materials: From January 1994 to March 2004, 28 patients were found to have paraganglioma in our institution. They were imaged by US, CT, MR imaging and angiography and histopathologically confirmed. 19 patients underwent selective embolization.

Results: Jugulo-tympanicum tumors represented the most common paraganglioma, 15 patients (54%). 12 patients (43%) had carotid body tumors. One patient suffered from a vagal paraganglioma. One patient had bilateral carotid glomus, another one had family history and another patient had multicentric paraganglioma. Presentation was typically late in the course of the disease, with a pain-less slow-growing mass. 22 paragangliomas (79%) were surgically removed. 5 glomus (18%) were only surgically treated and 2 paragangliomas underwent embolization without surgery. 17 tumors (61%) underwent combined endovascular and surgical treatment. 2 patients were treated with pre-operative embolization, surgery and radiation therapy as palliative adjunct. Surgical complications were nerve paralysis in 6 patients (21%) and cerebrovascular accident in one case. A patient

Scientific and Educational Exhibits

had an inguinal hematoma, another one a facial paralysis and another one stroke due to pre-operative embolization.

Conclusions: 1. Imaging studies are essential to differentiate paragangliomas from other masses of the head and neck. 2. Imaging procedures depict location and extent of the paraganglioma, helping determinate the surgical approach and help predict post-operative morbidity. 3. Pre-operative embolization decrease intra-operative bleeding.

C-0578

Endovascular treatment of aortoiliac occlusive lesions using a bifurcated endoprosthesis

T. Zander¹, R. Llorens¹, R. Rostagno¹, I. Zerolo¹, V. Prieto¹, Z. Qian², M. Maynar¹; ¹Santa Cruz de Tenerife/ES, ²New Orleans, LA/US

Purpose: To report initial experience with bifurcated endoprostheses in the management of aortoiliac occlusion.

Patients and Methods: Five patients with diffuse aortoiliac occlusions were treated by the endovascular placement of bifurcated endoprostheses. Indications for treatment were severe claudication (n=3), rest pain (n=1) tissue loss (n=1). All these patients were considered as non-surgical candidates because of their high-risk factors, such as cardiac disease, hostile abdomen, or obesity. After the occlusive lesions were successfully recanalized by fibrinolysis and/or balloon angioplasty, bifurcated aortic endoprosthesis (Excluder®, W.L. Gore, Flagstaff, AZ) was placed to reconstruct the aortoiliac bifurcation. The patients were followed up clinically and ultrasonographically every 3 months during the first year and semiannually afterwards.

Results: Technical success was achieved in all patients. Endovascular aortoiliac bifurcation reconstruction restored iliac artery flow immediately in all cases. The mean post-grafting ABI was significantly improved from 0.66 ± 0.04 before the procedure to 0.94 ± 0.06 immediately after procedure ($P < 0.01$). The ABI remained stable during the follow-up period. There was no mortality nor amputation required in this series during the follow-up period. All patients have remained free of ischemic symptoms up to the last follow-up.

Conclusion: Endovascular placement of bifurcated endoprostheses is technically feasible, effective, and safe in the management of aortoiliac occlusive disease.

C-0579

Indications, diagnostic methods and radiologist's role in acute interventional stroke therapy

B. Schmitz, R. Huber, A.J. Aschoff; Ulm/DE

Learning Objectives: To learn about the role of the radiologist in acute interventional stroke therapy. To review the appropriate diagnostic strategies to identify tissue at risk. To illustrate educational cases in which (based on MR imaging criteria) local thrombolysis has been successfully performed beyond the 6 hour time window.

Background: Intravenous and local intraarterial thrombolysis is the only acute stroke therapy with evidence based improved outcome. However, time windows of 3 hours for intravenous and 6 hours for intraarterial therapy are still small. The rationale of thrombolysis is based on the penumbra concept that is reflected in a diffusion - perfusion (DWI/PWI) mismatch in MR imaging studies. MR imaging may justify even later local thrombolysis in selected cases based on thorough image interpretation.

Imaging Findings: To rapidly identify tissue at risk an immediate DWI/PWI MR imaging is desirable. The only other crucial task is the reliable exclusion of intracerebral hemorrhage as the major differential diagnosis. This can be done with MR imaging as well and a CT scan can be omitted even in the acute stage if a MR imaging scanner is available.

Conclusion: In this exhibit we describe the indications and possibilities for interventions in acute stroke. Radiologist's role, interventional methods and strategies are reviewed in detail. MR imaging is pointed out as the method of choice for the identification of tissue at risk. Additionally, educational cases with successful interventional treatment beyond the 6 hour time window based on MR imaging diagnosis are presented.

C-0580

Transplant renal artery stenosis (TRAS): Long-term impact on kidney function and blood pressure control of percutaneous transluminal angioplasty and stenting

R. Corso, R. Vercelli, A. Rampoldi, E. Minetti, D. Leni, A. Vanzulli; Milan/IT

Purpose: We assessed long-term effect on blood pressure control and renal graft function in the treatment of TRAS with PTA and/or stenting.

Materials and Methods: From 1996, 884 kidney transplants have been performed in our Institution. 12 of these were referred to angiographic suite for TRAS associated to refractory hypertension (6), renal function impairment (4), or both conditions (2). Four patients had end-to-end anastomosis while eight had end-to-side anastomosis. All cases underwent PTA and/or stent placement. Immediate outcome and follow-up data have been reviewed and analysed. Mean blood pressure, load in antihypertensive drugs and serum creatinine levels were considered before PTA and in the follow-up (1, 3 month and every 6 months after the procedure). The average follow-up was 42.8 months (range 21-102).

Results: The mean age of transplant at intervention was 11.7 months. Technical success was achieved in all patients, with no major complications. In 7 patients PTA alone was performed while 5 patients underwent stent placement after PTA (3 recurrence, 1 recoil and 1 for dissection). In the follow-up the mean blood pressure fell from 116.6 ± 8.4 to 100.9 ± 9.44 mmHg ($p < 0.01$) and in 7 patients (87.5%) we registered persistent normal blood pressure with reduction or suspension of load in antihypertensive drugs. Similarly, the serum creatinine levels fell from 1.78 ± 0.8 to 1.20 ± 0.6 ($p < 0.05$), being still stable in the follow-up for 5 patients (83.3%).

Conclusion: PTA and/or stent placement is effective and safe in the treatment of TRAS and it warrants a long-term benefit over blood pressure control and graft function.

C-0581

Coil embolization therapy of pulmonary arteriovenous malformations: Combination of 16-detector CT angiography and interlocking detachable coils

N. Hirai, N. Toyota, H. Kakizawa, M. Hieda, T. Tachikake, K. Ito; Hiroshima/JP

Purpose: Our goal was to establish the utility of CT pulmonary angiography (CTPA) and interlocking detachable coils (IDCs) for coil embolization therapy of pulmonary arteriovenous malformations (PAVMs).

Materials and Methods: Seven consecutive patients with PAVMs were performed both CTPA and coil embolization therapy using IDCs. CTPA were performed as pre-embolization survey using sixteen-detector CT scanner. CT scanning started at twenty seconds after starting injection of non-ionic contrast material via antecubital vein at the rate of 2.5 ml/sec. Acquired scanning data was reconstructed into 1.25-mm-thick axial images at every 1.25-mm interval. Volume rendering images were constructed using segmentation threshold at 130 HU. After the careful selection of pulmonary vessel trees, color coding were performed as feeding arteries into red, nidus into yellow, and drainage veins into blue to distinguish these structures easily. Using these volume rendering images, we considered the location and shape of PAVMs, and we shaped five-french sized strait catheter to fit to feeding arteries. We also studied about the best angle for fluoroscopy to select feeding arteries. Coil embolization of feeding arteries were performed using IDCs. Conventional microcoils were also used as additional embolization, if required.

Results: Eighteen PAVMs of seven patients were treated using these methods. In all eighteen PAVMs were completely embolized without coil migration and incidental pulmonary infarction. Using preparation CTPA and shaped catheters, fluoroscopic time and contrast material dose were reduced compared with our conventional methods.

Conclusion: CTPA and IDCs combination therapy is useful to treat PAVMs with lower invasion.

C-0582

Percutaneous transhepatic portal vein embolization using newly altered four-lumen balloon catheter: Preliminary clinical experience

M. Gibo, S. Murayama, T. Nakayama, T. Morita, S. Gibo; Okinawa/JP

Purpose: Percutaneous transhepatic portal vein embolization (PTPE) is effective to expand the residual liver volume and to avoid postoperative hepatic failure. The purpose of the present study was to assess the safety and technical success rate of PTPE using improved four-lumen balloon catheter by ipsilateral approach.

Methods and Material: To make better ipsilateral approach method, we used an improved four-lumen balloon catheter which has one lumen connected to the catheter tip for guide wire, one lumen connected to the balloon, and two other lumina connected to the side-hole open just proximal to the balloon. The right branch of portal vein was embolized in 6 patients, the left branch in one patient. We used fibrin glue with iodized oil as the embolic material and injected simultaneously through the separate side-hole lumina.

Result: Technical success was achieved in all cases. Complications related to the procedures did not occur. We could inject a large amount of fibrin glue with iodized oil (6.0-15.4 ml; mean 10.8 ml) and perform effective embolization.

Scientific and Educational Exhibits

Conclusion: Ipsilateral approach using triple-lumen balloon catheter without guide wire lumen previously reported. Our method is considered to be more easy and safe than that traditional ipsilateral approach because a guide wire is available for accessing targeted portal vein. In addition, use of our new catheter makes it possible to measure the portal vein pressure elevation following PTPE through guide wire lumen of the catheter tip.

C-0583

withdrawn by authors

C-0584

Giant liver hemangiomas: Results of transcatheter embolization

K. Malagari, D. Antonopoulos, J. Mitromaras, E. Alexopoulou, K. Hatzimichail, A. Nikita, A. Kelekis, M. Kampanarou, D. Kelekis; *Athens/GR*

Purpose: To evaluate the efficacy of transcatheter embolization in the management of giant liver hemangiomas.

Material and Methods: Twenty two patients with giant liver hemangiomas (mean diameter 8.9cm; range 5-18) were included in the study. Mean age was 43.6 yrs (32-67). Of them, 16 were symptomatic (consumption coagulopathy: n=2; abdominal pain: n=9, discomfort and abdominal fullness: n=5). Color Doppler evaluation with contrast enhancement and CT evaluation was available before and after embolization (one week and 6 months post procedure). Embolization was performed after selective arteriography in 21 cases with spherical embolic agents (Embospheres; Biosphere, Rockland, MA) alone or in 17 patients combined with Gelatin sponge particles in 4 cases (Gelfoam; Upjohn, Kalamazoo, MI). One patient was excluded because of extensive arteriovenous shunting.

Results: Embolization was successful in obliterating the vasculature of the lesions in all cases immediately post procedure. In the patients with Kasabach Merritt the coagulopathy reversed immediately and 24 h post embolisation platelet counts were above 150.000/mm³ and fibrinogen 244 µg/dl and 280 µg/dl respectively. Vascularity was significantly decreased on Doppler studies in all cases. Follow up showed relief of symptoms in 19 patients (90.47%). On six month follow-up, 17 patients showed revascularization on Doppler evaluation (80.95%). Nine patients underwent repeat embolization and angiography showed increased vascularity before embolization within the lesion. Six month follow-up in these cases also showed revascularization.

Conclusion: Embolization of giant liver hemangiomas is useful for relief of symptoms, however, in the long run the lesions are revascularized and may present a similar to preembolization clinical pattern.

C-0585

Carotid stenting with protection device (CASPD) and brain diffusion-weighted MR imaging (DWI-MRI): Control within 6 and 24 hours after stenting

I. Sansoni, A. Laghi, C. Miglio, M. Celestre, M. Rengo, L. Coletta, M. Di Martino, R. Passariello; *Rome/IT*

Purpose: The aim of this study was to assess if brain diffusion-weighted MRI monitorization should be performed within 6 or 24 hours from carotid angioplasty and stent placement with protection device (CASPD).

Methods and Materials: Thirty-four age range: 66-95 Ys, mean 75 ± 5.7 consecutive patients referred for CASPD procedure (inclusion criteria: asymptomatic stenosis > 80% in 30 cases or symptomatic stenosis > 50% in 4 cases) underwent neurologic examination before, within 6 hours and 1 day after CASPD. MR protocol (FLAIR and DWI images) were performed 1-3 hours before, within 6 and 24 hours after CASPD, in order to verify the number of new ischemies (symptomatic or silent). Total examination time was 5 minutes. The three set of images were examined by two independent blinded reviewers for new high-signal areas suggestive for acute ischaemic lesions. We correlated positive results with risk factors, technical difficulties and plaque characteristics.

Results: Within 6 hours DW-MRI images showed one new high signal intensity lesions (2.9%) on the opposite side of stent placement; 24 hour DWI detected three more cases of acute ischemic lesions in 8.82% of patients, two symptomatic and one asymptomatic; all four patients had two or more risk factors and a fibrocalcified plaque.

Conclusion: Embolic events may occur after CASPD, even if the use of early (within 6 hours) DW-MRI confirmed CASPD as a safe procedure, with few strictly procedure-related ischemic complications. On the other hand, late (24 hours) DW-MRI monitorization showed the possibility of later embolization.

C-0586

The effectiveness of magnetic resonance (MR) in diagnostic pattern prediction and follow-up of uterine fibroids embolization

R. Marcello, F. Anglana, P. Signorile, G. Assegnati, A. Di Blasi, M. Castrucci; *Rome/IT*

Purpose: To assess the value of MR imaging pattern in the planning and follow-up of uterine fibroids treated with percutaneous catheter embolization.

Methods and Materials: 29 patients (31-46 Y, mean 38), were evaluated with MR of the pelvis before uterine fibroid embolization and after 10 days, 6 months and 12 months the interventional procedure. MR examination was based upon FFE T1W, FFE T1W post Gad and TSE T2W sequences in coronal, sagittal and axial planes. The volume, location, number, vascularity appearance and the association with any other gynecologic abnormalities were evaluated. Volume decrease rate of fibroids and the possible symptoms persistence after embolization were assessed at follow-up.

Results: MR was useful in assessing the correct imaging pattern predicting the better clinical results of fibroid embolization. MR follow-up showed a volume decrease rate of uterine fibroids ranging from 50% to 65%. Any patient was retreated.

Conclusions: MR is to be considered the leading imaging modality in the assessment of uterine fibroids before embolization and in the follow-up. The early (10 days) post procedure MR examination is predictable of the further response to embolization treatment.

C-0587

withdrawn by authors

C-0588

Selective arterial emolisation in the management of massive obstetrics hemorrhagic complications

A. Álvarez Luque, I. Acitores, F. Ybáñez, G. Garzón, B. Marín, A. Bravo, M. Parrón; *Madrid/ES*

Learning Objectives: To describe the selective percutaneous arterial embolisation technique in the treatment of hemorrhagic obstetrics complications, outlining the advantages and limitations of the procedure.

Background: Massive obstetric hemorrhagic bleeding is a life-threatening complication of pregnancy and postpartum. Classically hemorrhage was treated conservatively with external compressive massage, internal packing and drugs. Hysterectomy and major vascular procedures were used to preserve life. Percutaneous vascular technique allows localising and selectively embolising the bleeding point. This challenging technique helps decreasing further complications and preserve the uterus.

Procedure Details: A serial of 41 ASE was carried out. Distal aortography including external iliac, femoral and hypogastric arteries with its pelvic branches was performed to localise any bleeding point. Hypogastric arteries were selectively catheterised by conventional diagnostic catheters as 4F or 5F renal catheters or 3F co-axial catheters. Bleeding points were embolised with polyvinyl alcohol or microspheric particles (700µ) and sealed with coils. An arteriography was then performed to rule out extravasation. After the procedure, arterial inducers were always kept to allow urgent intervention if any complication. None of the patients died although four were reembolised because of rebleeding. Endovascular procedures were performed at the internal pudendal artery in 12 patients, at the uterine artery in 9, hypogastric branches in 7, vaginal artery in 5, obturator artery in 4, and pelvic muscular branches in 3 patients.

Conclusion: Endovascular treatment of massive obstetrics bleeding should be considered as an effective alternative to surgery. This procedure allows preserving the uterus and the reproductive function, avoiding the surgical morbility.

C-0589

Endoluminal treatment of liver transplantation complications. Sixteen-year experience in 570 patients

R. Lopez-Benitez¹, H.M. Barragan-Campos², G.M. Richter¹, G. Kauffmann¹, T. Marinelli¹, P.J. Hallscheidt¹; ¹Heidelberg/DE, ²Paris/FR

Purpose: To retrospectively evaluate most frequent complications related to liver transplantation and how interventional radiology has contributed to improve survivals and outcomes in these patients.

Materials/Methods: From a total of 570 patients who had undergone partial or total liver transplantation in a 16-year period (1987-2003) those in whom one or several minimally invasive procedures were performed in our institution where included.

Scientific and Educational Exhibits

Results: Several variables were evaluated, including number of interventions, type of complication (vascular, portal, biliary or miscellaneous), morbidity and mortality, improvement of survival in every specific complication and outcomes. Seven percent of all transplanted patients underwent interventional procedures. Biliary and arterial interventions were most frequent and included stent insertions and biliary drainages.

Conclusion: There was an increase in the number of interventional procedures in the last years due to the improvement of materials and new devices. The survival of the transplanted patient has significantly improved.

C-0590

A 4-year experience in trans arterial chemo embolization of primary and metastatic liver tumors

A. Scarrone, F. Pedrazzini, G. Lingua, F. Testa, M. Grossi,
F. Groppo Marchisio; Cuneo/IT

Purpose: To report our experience using biocompatible hydrophilic microspheres (Embosphere, Biosphere medical), in hepatic Trans Arterial Chemo Embolization (TACE).

Materials and Methods: Since February 2000 until August 2004, 52 patients (50 HCC, 2 liver metastases; 38 male, 14 female) underwent a selective segmentary chemoembolization. We used a mixture of chemotherapeutic drug (Adriblastin or Doxorubicin 30-40 mg), Lipiodol (10 ml) and Embospheres (100-300 microns, 1-2 ml), opportunely emulsified. At the end of the infusion, if blood support remains, embolization is completed by using microspheres of larger diameter (300-500 microns), according to residual vascularization.

Results: Twenty-five patients had only 1 lesion, 14 had a maximum of 3 lesions, 13 had multifocal lesions. CT follow-up at 1, 6 and 12 months showed in most of cases good results with no contrast enhancement in treated lesions; any new lesions were furtherly treated with the same technique. No problems occurred versus the cases treated by TACE with Spongostan. Death rate at 30 days was about 8%, with survival rate at 6 months of 81%.

Conclusions: Our preliminary experience shows that the treatment with Embospheres is optimal in hepatic TACEs, because they can be emulsified with Lipiodol and a chemotherapeutic drug. It is possible to get a distal embolization and exclude the lesion from any blood support. Complication rate is lower than TACEs traditionally made. TACE with Embospheres does not exclude further chemoembolizations.

C-0591

Percutaneous revascularization of popliteal and infrapopliteal arteries

S. Tettoni, A. Scarrone, F. Pedrazzini, R. Priotto, G. Gallarato, M. Grossi;
Cuneo/IT

Purpose: To present 3-years experience results in percutaneous treatment of distal occlusions of lower limb arteries in patients with AOCP.

Material and Methods: Since May 2002 to September 2004, we treated 48 patients (20 female, 28 male, mean age 70 years), suffering from claudication and/or trophic lesions due to critical atheromasic stenosis of distal vessels of lower limb. 71 angioplasties were performed (30 in popliteal artery, 14 in posterior tibial artery, 9 in anterior tibial artery, 12 in interosseous artery, 5 in tibio-peroneal trunk, 1 in pedal artery). Technique consists of a wire-made recanalization followed by balloon dilatation, trough a percutaneous proximal access. Forty-six patients were treated by traditional technique, 2 by subintimal technique.

Results: Six months mean follow-up showed lower limb saving in 82.9%. Three patients underwent a minor amputation, 6 a major amputation; 4 patients died before radiologic follow-up for other causes not related to the procedure.

Conclusions: Percutaneous treatment of lower limb popliteal and infrapopliteal arteries critical stenosis is a safe technique which allows to preserve limb from amputation in most cases. Vessels treated develop compensatory collateral blood-streams, which remain even if mean artery re-occludes.

C-0592

Preoperative selective transarterial embolization therapy for diffuse plexiform neurofibroma of the skin: Our initial experiences

J. Tanaka, A. Kuramochi, N. Nishi, M. Yuasa; Iruma-gun/JP

Purpose: To evaluate the usefulness of transarterial embolization as a preoperative therapy to cutaneous diffuse plexiform neurofibroma of neurofibromatosis type 1 (NF-1). This disease of the skin sometimes grows to an enormous size and occasionally becomes malignant. Surgical reduction is desirable as far as possible but is usually very difficult to stop bleeding during surgery due to the abundance of vulnerable abnormal vessels within the tumor. Preoperative em-

bolization therapy has never been applied to this disease so far as we know, however.

Methods and Materials: Selective angiography and embolization have been carried out without any technical difficulties for four cases of NF-1 cutaneous diffuse neurofibromas up to 16 cm in maximum diameter, using gelatin sponge particles few days prior to reduction surgery. Amount of bleeding was recorded accurately at surgery.

Results: In all of the four cases, subtotal removal of the tumors have been done with less than 10 ml of total bleeding. Results of reduction surgeries were satisfactory in all of the cases.

Conclusion: Preoperative selective transarterial embolisation may be a preferable option for patients with cutaneous plexiform neurofibroma when surgical resection is planned.

C-0593

Development of collateral channels after successful transcatheter gastric variceal embolization: Assessment by CT and endoscopic examinations

Y. Watanabe¹, H. Sugimoto²; ¹Sapporo/JP, ²Yakushiji/JP

Learning Objectives: To describe how often and when new collaterals such as esophageal varices or splenorenal shunt develop or gastric varices recur after successful transcatheter gastric variceal embolization based on a series of 15 patients.

Background: Gastric varices due to portal hypertension are treated by endoscopic, surgical or interventional radiological procedures. Since its introduction in the mid-1990s, balloon-occluded retrograde transvenous obliteration (BRTO) has become a widely accepted transcatheter gastric variceal embolization method in Japan. This method is minimally invasive and highly effective. However, even after successful variceal treatment, development of collaterals or recurrences of gastric varices do occur due to the remaining portal hypertension. In this exhibits, we will describe the long term result after successful BRTO, especially regarding collateral development and gastric variceal recurrence.

Procedure Details: We retrospectively reviewed follow-up CT and endoscopic examinations of 15 patients with gastric varices due to portal hypertension. Gastric variceal embolization was successfully performed by balloon-occluded retrograde transcatheter obliteration (BRTO) method. The follow-up periods ranged from 12 to 66 months (average 33 months). We evaluated collateral vessels after BRTO using serial CT and endoscopic examinations.

Conclusion: Recurrence of gastric varices was rare and did not require any additional treatment. Esophageal varices occurred in 9 patients. The period of occurrence showed a bimodal peak for 4 months and 20 months in average after successful BRTO and they required additional treatment. Two developed spleno-renal shunt with no recurrence of gastric varices or esophageal variceal development.

C-0594

Interventional procedures of acute retroperitoneal hemorrhage, especially renal and pancreatic hemorrhage

Y. Watanabe¹, Y. Kodama¹, A. Sawada¹, Y. Sakuhara¹, D. Abo¹, M. Funakubo¹, H. Sugimoto², K. Miyasaka¹; ¹Sapporo/JP, ²Tochigi/JP

Learning Objectives: To illustrate the spectrum of acute retroperitoneal hemorrhage, especially renal and pancreatic hemorrhage, that could be treated by transcatheter embolization.

Background: Retroperitoneal hemorrhage is a clinical setting in which transcatheter embolization may prove useful. Transcatheter embolization for active bleeding is less invasive treatment than surgical intervention, and in certain clinical settings, such as postsurgical fields, it can become only alternative treatment because of the difficulty of surgery.

Procedure Details: We reviewed 18 cases of acute renal and pancreatic hemorrhage that underwent angiography between January 2000 and August 2004. Six renal cases included blunt renal trauma, rupture of renal angiomyolipoma, rupture of renal pseudoaneurysm due to polyarteritis nodosa, and rupture of aneurysmal type of renal AVM. Twelve pancreatic cases included aneurysm of the splenic artery, pseudoaneurysm of the celiac artery, postoperative psuedoaneurysm of the gastroduodenal artery stump after pancreatectoduodenectomy. Embolized materials were steel coils, microcoils, gelatin sponge particle, and absolute ethanol.

Conclusion: Transcatheter embolization is useful treatment for acute retroperitoneal hemorrhage.

Scientific and Educational Exhibits

C-0595

Is transcatheter therapy of renal artery stenosis choice in treatment of renal hypertension? Diagnostic value to detect restenosis in long-term follow-up
J. Saponjski, M. Ostojic, D. Masulovic, B. Beleslin, Z. Markovic; Belgrade/YU

Purpose: The aim of the study was to analyze in eight-year follow-up period the value of PTA (percutaneous angioplasty) in the treatment of renovascular hypertension.

Methods: In eight-year period (1996-04) selective arteriography of the renal arteries was performed in 93 patients (female 60, male 32; mean age 41 ± 7 years). Significant renal stenosis, defined as diameter stenosis $> 50\%$ was found in 43 (46%) patients (mean diameter stenosis $78 \pm 12\%$).

Results: PTA was done in all 43 patients, reaching successful result in 38 patients, while in 5 patients procedure was completed with stent implantation. Mean systolic and diastolic blood pressure before intervention was 180 ± 25 mmHg and 120 ± 15 mmHg, respectively. Immediately after the intervention, systolic and diastolic blood pressures were reduced to 130 ± 7 mmHg and 90 ± 5 mmHg, respectively ($p < 0.001$). In the follow-up period, control arteriography was performed in all patients disclosing restenosis of the renal artery in 12 patients (31%), and all of them had increased blood pressure (defined as higher than 140/90 mmHg). In 13/43 patients with normal blood pressure in the follow-up period, none of the patients had significant renal restenosis (sensitivity 100%). However, increased blood pressure was found in 30/43 patients, of whom in 13 patients elevated blood pressure was not accompanied by renal restenosis (specificity 46%).

Conclusion: Increased blood pressure in the follow-up period after PTA is not associated with renal restenosis, indirectly supporting the concept of reevaluation of the indications for PTA of the renal arteries.

C-0596

Communications between carotid and vertebrobasilar system via persistent primitive arteries

D. Mihajloski, G. Damjanoski; Skopje/MK

Learning Objectives: To present a very rare cases of persistent primitive arterial communications between carotid and vertebrobasilar system. To outline the necessity of detailed angiographic evaluation of cerebral arterial supply in such cases.

Background: Communication between carotid and vertebrobasilar system via persistent primitive arteries is very rare condition. Such primitive persistent arteries are: persistent primitive proatlantal intersegmental artery (PPPIA), primitive trigeminal artery, hypoglossal artery and otic artery. We present three cases with this type of primitive persistent communication. Two of them with primitive trigeminal artery and one with PPPIA and saccular aneurysm originating from PPPIA.

Imaging Findings: In all cases a detailed angiographic evaluation of cerebral arterial supply was performed. In two cases angiography revealed a primitive trigeminal artery originating from internal carotid artery. In one case 42-year old female patient was admitted for MR imaging study of the brain because of persistent headache. On MR imaging study basilar artery aneurysm was suspected. A detailed angiographic study of carotid and vertebrobasilar system was performed. A PPPIA was revealed originating from left internal carotid artery on the level of C1-C2. The vessel coursed dorsally and entered skull via the foramen magnum. A saccular aneurysm was also revealed originating from PPPIA. The basilar artery was originating exclusively from this vessel. Both vertebral arteries were hypoplastic.

Conclusion: Communications between carotid and vertebrobasilar system via persistent primitive arteries is very rare. In such cases a detailed evaluation of cerebral arterial supply is necessary.

C-0597

Stent placement in symptomatic middle cerebral artery stenosis

K. Karaman, L. Onat, C. Duran, M. Sirvanci; Istanbul/TR

Purpose: To report our experience with the stent placement for symptomatic middle cerebral artery stenosis in three patients.

Materials and Methods: We treated 3 patients with middle cerebral artery stenosis with primary stent dilatation ($n = 2$) and in combination with stent placement due to impaired balloon dilatation ($n = 1$). Two of the lesions were located in MCA M1 segment and the other in M2 segment. According to the NASCET criteria, all patients had high grade stenoses (70-90%). The indication for stent placement was acute ischemic stroke in all patients.

Results: Transient procedural complication was not detected. During clinical follow-up, no one had further ischemic symptoms. In one patient, balloon angioplasty was done at first. 1 month later, restenosis was seen and finally stent

placement was applied. The treatment was technically successful in all patients.

Conclusion: Endovascular revascularization of middle cerebral artery stenosis by stent placement is technically feasible, effective and safe. But for the best treatment modality, more clinical trials and much research are needed.

C-0598

Lipiodol flowing into portal vein after arterial embolization: The influential factors and clinical significance

H. Wu, G. Feng, H. Liang; Wuhan/CN

Purpose: To find out the factors correlated with lipiodol flowing into portal vein (LFPV) after arterial embolization and its clinical significance.

Methods and Materials: Total 274 times of LP-TACE procedures were performed to 147 cases of HCC (247 times) and 26 cases of hepatic hemangioma (27 times), who had no evidence of hepatic arterioportal shunt in conventional DSA. The sign of LFPV was observed and the relationship between it and multivariate factors (sex, age, tumor type, size, blood vessel abundant degree, procedure times, catheter location, lipiodol type, lipiodol dosage /tumor size) were analyzed by multivariate logistic regression model.

Results: The signs of LFPV were seen 78 times in 274 procedures (28.5%), 62/247 in HCC group and 16/23 in hemangioma group. In HCC group, single-variate analysis showed that LFPV was related to tumor type, size, catheter location, lipiodol type and lipiodol dosage/tumor size, and multivariate logistic regression analysis showed that it was related with lipiodol type, catheter location and tumor type. In hemangioma group, LFPV was only related with lipiodol type. The lipiodol in portal veins disappeared gradually within 1-3 days after TACE. The liver function changes were no different between LFPV positive and negative groups. Lipiodol accumulated better in LFPV positive group than in the negative groups.

Conclusion: It is suggested that the sign of LFPV was one of the markers of full dosage of lipiodol in TACE procedures. The LFPV sign easily appeared in hepatic hemangioma, using ultrafluid lipiodol, super-selective embolization and small-size tumor.

C-0599

Standard-protocol moving-bed MR angiography for planning of interventional procedures in patients with peripheral vascular occlusive disease

R. Drescher, T. von Rothenburg, O. Köster; Bochum/DE

Purpose: The aim of this study was to evaluate the usefulness of standard-protocol MR angiography for the planning of interventional procedures in the lower extremity vascular territory.

Methods and Materials: In this prospective study, patients with known or suspected peripheral vascular occlusive disease of the lower extremities underwent MR angiography for planning of interventional treatment. Contrast-enhanced MR angiography was performed using a three-step moving-bed technique on a 1.5 T scanner with a dedicated flex array. Digital subtraction angiography (DSA) was done in patients scheduled for interventional treatment and served as the standard of reference.

Results: 100 MR and digital subtraction angiographies of 83 patients (63 men, 20 women, mean age 65 years) were evaluated. MR angiography showed slight overestimation of stenoses compared to DSA (stenosis 55-99%, mean 81.1% versus 60-93%, mean 76.9%). 4 vessel occlusions were shown. 34 balloon angioplasties, 58 stent implantations and 3 recanalizations were performed. 92 interventions (92%) were correctly planned. One low-grade in-stent restenosis was not treated. In 4 cases balloon angioplasty was planned, but stent implantation was performed. In 3 cases endovascular treatment was not possible. In one patient a highly stenotic artery occluded before DSA could be performed. No complications occurred during MR angiography or DSA.

Conclusion: MR angiography of the lower extremities is a safe, noninvasive tool for preinterventional assessment of peripheral vascular occlusive disease. It allows exact planning of endovascular interventions despite a slight overestimation of stenoses on MR imaging compared with DSA. Artifacts due to stents can make evaluation more difficult.

C-0600

Estimating the maximum radiation skin dose during percutaneous coronary intervention using the fluoroscopic time, dose-area product, and body mass index

K. Chida, H. Saito, M. Zuguchi, H. Otani, H. Shimura, D. Ito, M. Nakada, S. Takahashi, K. Shirato; Sendai/JP

Learning Objectives: To understand that the skin dose of percutaneous coronary intervention (PCI) may occasionally exceed the dose causing erythema. To

Scientific and Educational Exhibits

understand the methods to obtain useful information for estimating the maximum radiation skin dose (MSD) in patients who underwent PCI.

Background: PCI can potentially result in high patient radiation doses. Since high doses cause potentially harmful radiation skin injuries, the MSDs should be recorded. However, real-time maximum dose monitoring of the skin is unavailable on many of the X-ray machines. Therefore in this exhibit, the correlations between the MSD and body mass index (BMI), fluoroscopic time, and dose-area product (DAP) were investigated to examine whether these factors could prove useful in estimating the MSDs during PCI.

Procedure Details: We measured the skin dose, fluoroscopic time, DAP, and BMI for 172 consecutive patients who underwent PCI. The patient skin dose and DAP were measured using Caregraph (Siemens) with skin dose mapping software. We found a poor correlation between the MSD and total fluoroscopic time ($r^2 = 0.395$, $p < 0.0001$). There was a significant correlation between the MSD and total DAP in PCI ($r^2 = 0.524$, $p < 0.0001$). We found reasonable correlations between the MSD and BFP (BMI \times fluoroscopic time, $r^2 = 0.494$, $p < 0.0001$) and BDAP (BMI \times DAP, $r^2 = 0.565$, $p < 0.0001$).

Conclusion: BDAP may be good predictor of skin injury risk in PCI. When DAP cannot be monitored, BFP may be reasonable predictors of skin injury risk. This study provides potentially useful information for estimating MSDs; this information could be used to help prevent patient skin injuries during PCI.

C-0601

Repeated transarterial chemoembolization for the treatment of advanced pancreatic cancer with superselective catheterization of the pancreas

S. Kawamura, T. Okuno, F. Ganaha, K. Hayakawa; Kanagawa/JP

Learning Objectives: To present the advantages and limitations of the transarterial chemoembolization for advanced pancreatic cancer. To describe the angiographic findings and the result of the treatment for a series of 25 patients.

Background: Pancreatic carcinomas still present poor prognosis because many of the cases are found at an advanced stages and are therefore non-resectable. When conventional chemotherapy is discontinued because of its ineffectiveness or its side effects, alternative therapies have been few. From January 1998 to June 2004, 25 patients with advanced pancreatic cancer received transarterial chemoembolization with superselective catheterization of the pancreas.

Procedure Details: Patients with stage III (n = 3) or IV (n = 22) pancreatic cancer were treated on an outpatient basis once a month. We superselected into dorsal pancreatic arteries (DPA) or inferior pancreaticoduodenal arteries (IPDA) to sufficiently supply chemotherapeutic reagent accompanied with molecules of hundreds-nanometer in diameter to the primary tumors. Metastatic lesions were treated in the same way.

Conclusion: Superselective catheterization was attained in 64% (16 patients). The mean survival period was 188 days. The seemingly short survival may be associated with the long latency period (137 days, Mean) before the initiation of the therapy. The procedure takes 65 minutes in average, so far has presented little complication and therefore may result in make better quality of life of the patients than chemotherapy or surgery. The superselective chemoembolization may make an alternative treatment for advanced pancreatic cancer when conventional therapy is discontinued or no longer indicated.

C-0602

Endovascular embolization of multiple arteriovenous fistulas of extremities

Y.A. Akhmetov, D.D. Potseluyev, V.A. Jakupov, D.T. Mussagalev, O.V. Gorgots; Almaty/KZ

Purpose: To improve the results of treatment of patients with multiple AVF of extremities through improvement of the tactics and methods of radio-endovascular surgical interventions.

Materials and Methods: 33 patients with AVF of extremities at the age from 7 to 31 had examination and treatment at SSC for the period from 1994 to 2004, which is 42.64% of the total number of patients with AVF of different localization. Lesion of 2 and more anatomic regions of extremities were reported in 27 cases (81.81%). Duplex scanning of main arteries, veins, and the zone of AVFs, CT, MRT of extremities, were used to assess the patients. The principal method of AVF diagnostic was selective, super-selective digital subtraction angiography, which was combined with the cure stage - endovascular embolization of AVF arteries. The number of stages of inpatient treatment of the patients was 2 to 7 and depended on the vessels involvement.

Results: Satisfactory results of treatment of multiple AVF of extremities (disappearance or reduction of pain intensity, volume of extremities, and pathological arteriovenous fistula) were received in 30 (90.91%) of patients. In 3 cases (9.09%), there was no any improvement in regional hemodynamic after RES.

Conclusion: Thus, multi-phased super-selective catheterization and emboliza-

tion of multiple AVF of extremities permit to receive satisfactory clinical results in majority of patients.

C-0603

Stent-assisted coil embolization of wide-necked aneurysms

M. Jaworski, O. Rowinski, R. Maciąg, M. Januszewicz; Warsaw/PL

Purpose: To present our initial experience in using stent to treat patients with broad-neck cerebral aneurysms.

Methods and Material: Material consists of 10 patients (F: 6, M: 4), age range: 28 - 54 years with intracranial aneurysms. Aneurysms location: Carotid cavernous n = 2, carotid ophthalmic n = 3, MCA n = 1, basilar tip with extension to P1 n = 4. Aneurysms architecture: neck length from 5 till 11 mm, aneurysms size from 4 till 31 mm. Qualification to procedure was done after angio CT by a neuro-radiologist and neurosurgeon. After appropriate anticoagulation was performed (Clopidogrel and Aspirin), microstent was delivered across the neck of the aneurysm via femoral route. Subsequent filling of the aneurysmal sac was done with GDC or/and Matrix coils through the stent interstices.

Results: Microstents were deployed in correct position in whole cases. After stent placement, total coil embolization was achieved in eight cases, subtotal in one case. One aneurysm was stented only; disappeared during the procedure. One patient experienced thromboembolic event, resolved after Abciximab (ReoPro) with no neurological deficit.

Conclusion: Intracranial stent is an important new tool in endovascular therapy, improving the occlusion of wide-neck aneurysms while protecting the proper lumen of the patent parent artery.

C-0604

Recovery of non-developed vascular accesses for hemodialysis

D. Coll, R. Vidal, M. Perez-Lafuente, M. Moreiras, A. Romero-Jaramillo, A. Segarra; Barcelona/ES

Objectives: To demonstrate the effectiveness of interventional techniques for the repair and recovery of non-developed arterio-venous dialysis fistulas as an alternative to surgery.

Methods and Materials: 62 patients were reviewed (42 men, 20 women), ranging in age from 37 to 81 years (mean age 60). The type of vascular access was native fistulas in 59 (43 radiocephalic, 11 brachiocephalic, 5 brachiobasilic) and synthetic grafts in 3. The clinical findings were: fistulas did not develop (45 patients), scant arterial flow (15 patients), elevated venous pressure during dialysis (8 patients), prolonged compression time (1 patient) and access occlusion (2 patients). All patients underwent fistulography of the vascular region before treatment. Therapy consisted of PCTA, PCTA + mechanical thrombectomy, PCTA + fibrinolysis or stent placement.

Results: Initial technical success was obtained in 58 accesses (93%). There were 15 relapses (12 patients); 9 of these responded to repeat percutaneous treatment. The complications were: 3 venous tears (with loss of the access in 1), 1 thrombosis that resolved with fibrinolytic treatment, 1 transient arterial spasm and 1 hematoma at the puncture site.

Conclusion: With the increased life expectancy of patients undergoing dialysis, viability of the vascular access and the quality of dialysis are of prime importance. In contrast to surgery, interventional techniques preserve the vein in its entire length and can be repeated as often as necessary during the life of the fistula. Percutaneous repair is the technique of choice for non-developed accesses, with surgical treatment being reserved for fistulas that cannot be recovered percutaneously.

C-0605

Life-threatening rectus sheath hematomas in patients undergoing anticoagulation. Management with selective arterial embolization

J. Rimola, J. Perendreu, J. Falcó, J.R. Fortuño, J. Branera, A. Massuet; Sabadell/ES

Learning Objectives: Rectus sheath hematomas due to inferior epigastric artery pseudoaneurysm are a recognized complication of anticoagulation therapy with a potential risk of hemodynamic collapse. The aim of this study is to review the vascular anatomy of the abdominal wall and evaluate the utility of embolization of the inferior epigastric artery in rectus sheath hematoma with hemodynamic collapse.

Background: We performed a retrospective review of ten patients with rectus sheath hematoma that caused hemodynamic collapse diagnosed with US and/or CT between January 2001 and April 2004. All patients were undergoing anticoagulation therapy when bleeding occurred.

Scientific and Educational Exhibits

Procedure Details: Selective angiography demonstrated active bleeding of the inferior epigastric artery in all cases and, in 2 cases, also from the deep iliac circumflex artery. In all patients, hemodynamic parameters (blood pressure and heart rate) stabilized shortly after embolization. Eight of the ten patients had good evolution, though two died a few days after the procedure due to multiple organ failure.

Conclusions: Embolization of active bleeding from the inferior epigastric artery using coils and gelfoam in patients is an effective and safe technique for restoring hemodynamic stability in anticoagulated patients. Knowledge of the vascular anatomy of the abdominal wall and the vessels that supply it is essential to ensure the success of embolization.

C-0606

Isolated iliac artery aneurysms: An infrequent pathology with effective endovascular treatment

M.I. Alegre, A. Talens, S. Ferrer, R. García, I. Artigues, A. Batista; Valencia/ES

Learning Objectives: Isolated iliac artery aneurysms are infrequent but entail a dangerous high risk of rupture and have been associated with high operative mortality rates. We describe our experience with the percutaneous placement of stentgrafts for endovascular repair of iliac artery aneurysms.

Background: Between January 1998 and October 2003 eight iliac artery aneurysms in seven patients (all males, mean age 75.5 years) were treated with 12 covered stentgrafts. CT preoperative and arteriography were performed to define the exact diameter and length.

Procedure Details: All the patients underwent initially successful treatment with immediate aneurysm exclusion. In three cases iliac aneurysm involve both common and hypogastric arteries, in two cases the common iliac artery and only the hypogastric artery in three. Eleven different types of stentgrafts were positioned in the external and/or common iliac artery using over-the-wire techniques under local anaesthesia in six cases; coil embolization of the hypogastric artery was performed in two patients. One iliac aneurysm was treated using a bifurcated prosthesis under epidural anaesthesia and femoral exposition. No procedural complications, acute or late graft thrombosis or further leakage occurred. The median follow-up period was 42 months.

Conclusion: Endovascular repair of iliac artery aneurysms is a safe and effective technique with satisfactory results in patients at standard and high operative risk.

Interventional Radiology

Non-vascular

C-0607

Covered, retrievable, expandable prostatic stent: Feasibility study in dogs

C. Yoon¹, H.-Y. Song², J. Shin²; ¹Seong Nam/KR, ²Seoul/KR

Purpose: To evaluate the feasibility of a covered, retrievable prostatic stent and to determine whether persistent dilation of the prostatic urethra can be achieved even after stent removal.

Materials and Methods : PTFE-covered retrievable nitinol stents were placed in the prostatic urethras of 13 dogs. The stents were removed with retrieval hook wires 8 weeks after placement. Five dogs were sacrificed just after stent removal, and the other eight dogs were sacrificed 4 weeks (n = 3) and 8 weeks (n=5) after stent removal. Retrograde urethrograms were obtained at 2-weeks interval after stent placement until sacrifice. The explanted prostate specimens were histologically examined.

Results: Stent placement was technically successful in all dogs. In two dogs, a second stent was placed because of complete migration of the first stent into the urinary bladder. Stent removal was successful in all dogs without complication. Follow up urethrograms showed persistent dilation of prostatic urethra until sacrifice, while filling defect due to granulation tissue gradually decrease after stent removal. Histologic examination revealed periurethral glandular atrophy and fibrosis, which were persistent until sacrifice. The papillary projection of the epithelium and inflammatory cell infiltration gradually decreased after stent removal. **Conclusion:** The covered, retrievable nitinol stent seems feasible for use in the prostatic urethra. The urethrographic findings and histologic changes obtained after stent removal suggest persistent dilation of the prostatic urethra can be induced.

C-0608

Complications of living donor liver transplantation: Image findings and interventional treatment strategies

N. Muraoka¹, H. Uematsu¹, K. Kinoshita², T. Takeda², H. Matsunami², E. Yamanouchi³, H. Itoh¹; ¹Fukui/JP, ²Gifu/JP, ³Tokyo/JP

Learning Objectives: To present representative image findings of fatal complications in living donor liver transplantation (LDLT) based on 24 recipients and to describe interventional treatment strategies for these complications.

Background: Liver transplantation is an accepted therapy for patients with end-stage liver disease. In Japan, LDLT is mainly performed instead of the orthotopic liver transplantation due to legal issues. Retransplantation is difficult after transplantation because of post-operative adhesion; in some cases, an interventional procedure may be useful for various vascular and biliary complications. In this exhibit, we present the representative image findings of fatal vascular and biliary complications based on 24 recipients in LDLT, and demonstrate the advantages of interventional treatment for the various complications.

Procedure Details: We demonstrate the successful percutaneous transluminal angioplasty (PTA) of various vascular types, including hepatic artery, portal vein, hepatic vein and inferior vena cava at the anastomosis. We also demonstrate successful stent placement in portal venous elastic stenosis at the anastomosis and covered stent graft placement for hepatic artery pseudo-aneurysm. Biliary stricture or occlusion at the anastomosis is one of the most common complications in LDLT; however, conventional percutaneous biliary treatment sometimes fails to re-canalize at the occlusion. Recently, our group has proposed a new therapy called "magnetic compression anastomosis development method," for biliary-enteric anastomotic stricture. We discuss the advantages and limitations of this method in this presentation.

Conclusion: Appropriate interventional procedures are invaluable in the management of LDLT complications.

C-0609

PTFE covered metallic stent in the treatment of nasolacrimal duct obstruction: Long-term results

M.D. Monedero, J.R. Olalla, J.J. Martinez-Rodrigo, A. Ruiz, E. Lonjedo, J. Vilar; Valencia/ES

Purpose: To evaluate the long-term efficacy of PTFE covered metallic stent placement as treatment in patients with nasolacrimal duct obstruction.

Methods and Materials: PTFE covered metallic stents (JOSTENT®) were placed under fluoroscopic guidance in 128 eyes of 110 patients (20 men and 90 women) with nasolacrimal duct obstruction (age range: 40-75 years; mean age: 58 years).

Scientific and Educational Exhibits

Patients with obstruction at the nasolacrimal duct and the junction between the lacrimal sac with the nasolacrimal duct were selected. All of them had severe epiphora according to Munk's scale (69.5% grade V and 30.5% grade IV). Slit-lamp exam, lacrimal irrigation and anterior rhinoscopy were performed in order to exclude lacrimal sac and endonasal tumors. Dacryocystography was performed in all patients before stent placement and in patients with recurrence of epiphora after the stenting. Follow-up examinations were scheduled for 1 week, 1, 3 and 6 months, 1, 2 and 3 years after stent placement. The clinical follow-up consisted on lacrimal irrigation and Munk's test to evaluate stent patency and clinical success.

Results: Stent placement was technically successful in all patients. Primary and secondary patency were 74.2% and 81.3% respectively. The overall clinical success rate was 78.1%. Stent patency was higher in women ($p < 0.05$) but it was not related to age.

Conclusion: PTFE covered metallic stents are an effective therapeutic option for treating epiphora.

C-0610

Radiofrequency in the treatment of hepatocellular carcinoma. Multicenter study in Spain

M. Squarcia, R. Vilana, L. Bianchi, C. Nicolau, M. Sala, J.M. Llovet, J. Bruix, C. Bru; Barcelona/ES

Purpose: To assess the therapeutic efficacy, survival rates and complications of Radiofrequency (RF) in the treatment of hepatocellular carcinoma (HCC) in a multicenter study in Spain.

Methods and Materials: Data of 10 Spanish hospitals were retrospectively (1998-2002) collected and reviewed. The study includes 249 patients (167 male/82 female), mean age 68 ± 8 years, with HCC, (uninodular = 203/multinodular = 46, mean tumor size = 29 ± 2 mm) that were treated with RF.

Results: Evaluation of tumoral necrosis was possible only in 233 patients. Initial Complete Response (CR) = 83% (single tumors < 2 cm, CR = 97.2%). Intratumoral recurrence was seen in 58 patients (25%) and distant recurrence was seen in 39 patients (17%). One, 2 / 3 and 4 years survival rates were 87%, 74%, 61% and 47% (mean follow-up = 19.5 months). Preserved liver function (Child-Pugh), and achievement of CR were observed to be predictors factors of longer survival. Tumor seeding was observed in 7 cases of subcapsular tumors treated in the initial period during which RF was performed. Others major complications accounted for 5%.

Conclusion: RF is an effective procedure for the treatment of HCC. Higher rates of CR and survival are obtained in patients with small tumors and preserved liver function. RF is a safe technique, however precautions should be taken while performing this procedure.

C-0611

Radiofrequency ablation may activate the immune system and induce specific anti-tumoral immune responses in cancer patients

S. Haen¹, C. Gouttefangeas¹, A. Boss¹, S. Clasen¹, D. Schmidt¹, M. Kuczyk¹, A. Stenzl¹, H. Schild², P.L. Pereira¹, H.-G. Rammensee¹; ¹Tübingen/DE, ²Mainz/DE

Purpose: Percutaneous radiofrequency (RF) ablation causes local coagulation necrosis of tumoral tissues. This could lead to the release of heat shock proteins (HSPs) and to the subsequent activation of an anti-tumoral immune response. Our purpose was to determine if an increased level of HSP70 was measurable in the blood of patients after RF ablation and if CD8⁺ T cells specific for tumor-associated antigens could then be detected.

Methods and Materials: 20 patients treated with RF ablation for liver metastasis (colorectal or breast carcinomas) or for primary carcinomas of the liver or the kidney were prospectively included in the study. Peripheral blood mononuclear cells (PBMCs) and serum were isolated from blood samples obtained at predefined time-points before and after RF ablation. We measured serum levels of HSP70 by specific ELISA. PBMCs of HLA-A2⁺ patients were stimulated with HLA class I-binding peptides derived from tumor antigens known to be expressed by most of the tumors. Specific IFN γ production was subsequently measured by real time RT-PCR.

Results: Preliminary results show a transient increase in HSP70 serum levels in several patients one day after RF ablation. Moreover, induction of tumor-antigen specific CD8⁺ T lymphocytes was detected at the earliest 3 months after treatment.

Conclusion: Production of HSP70 and increase in the activity of antigen-specific CD8⁺ T lymphocytes was observed in some patients after RF ablation. Thus, activation of the immune system might represent another beneficial effect of RF-ablation in addition to the local destruction of metastasis or primary carcinomas.

C-0612

Presurgical transcutaneous MR imaging-guided marking of intramedullary tumors

J. Fritz, C.W. König, P. Böhm, F. Maurer, A. Badke, M. Müller-Schimpffle, C.D. Claussen, P.L. Pereira; Tübingen/DE

Purpose: The extent of intramedullary tumor is intraoperatively difficult to assess. A new stereotactic method for presurgical transcutaneous coil-marking of intramedullary tumor using interventional magnetic resonance imaging (MRI) guidance is introduced.

Material and Methods: In 5 patients intramedullary tumor extent was preoperatively marked. Imaging and puncture guidance were performed using an open low-field MR-Scanner with horizontal access (Magnetom Open Viva®, Siemens, Erlangen, Germany). After imaging the extent of the tumor, MR imaging guidance was used to place MR-compatible titanium coils (MReye®, Cook, Bjaevskov, Denmark) parasagittally at the level of the upper and lower pole of the lesion. Postinterventional X-ray imaging of the puncture side documented coil position in all patients. Intraoperative X-ray fluoroscopy was used to confirm congruence of coil position. Coil placement was performed up to 58 hours prior to surgery. The inclusion of the tumor borders was examined by cross sectional pathology of surgical specimens.

Results: All lesions could be precisely evaluated by using MRI only. Intervention was successfully performed in all patients using MRI guidance only. Ten coils were used to preoperatively mark 5 lesions. Intraoperative X-ray fluoroscopy demonstrated no evidence of coil migration. Histological examination of the resection borders proved no residual tumor cells were present. No complications were observed. With a mean follow-up of 12 months, no recurrence occurred.

Conclusion: Presurgical MRI-guided coil-marking for exact delineation of the extent of intramedullary lesions is technically feasible and can readily demonstrate the full extent of tumors. It contributes to sufficient surgical exploration and total resection.

C-0613

Ureteral implantation of Paclitaxel-eluting balloon-expandable metallic stents: An experimental study in the pig model

D. Siablis, N. Christeas, D. Karnabatidis, K. Katsanos, E.N. Liatsikos, N. Flaris, G.C. Kagadis; Patras/GR

Purpose: Ureteral implantation of metallic stents suffers from low patency rates owing to urothelium hyperplasia and stent encrustation. Paclitaxel-eluting stents have portrayed auspicious results in inhibiting neointimal hyperplasia in the coronary vascular bed. The goal of our study was to evaluate the paclitaxel-eluting versus the conventional metallic stents in the pig ureter model.

Methods and Materials: The metallic stents under investigation were randomly balloon-expanded near the ureteropelvic junction of either the right or left ureter of 10 female pigs (weight 25-30 kgs), for a total of 20 stented ureters. Ten ureters received a 4x32 mm Paclitaxel-Eluting Coronary stent (Boston Scientific, USA), while the contralateral ureters were stented with a 4x18 mm R-Stent (Orbus Medical Technologies, Netherlands) serving as the control. Ureteral patency was assessed with nephrostomography 24 hours and 21 days following stent insertion. Subsequently, animals were sacrificed and the ureters were pathologically inspected.

Results: Uncomplicated stent delivery was accomplished in all ureters (20/20). Unobstructed urine flow was depicted 24 hours after implantation in all stented ureters. The 21-day nephrostogram revealed complete blockage of 5 ureters from the R-Stent group (5/10), whereas no obstructed ureter was detected in the Paclitaxel group (0/10). Pathologic inspection documented severe inflammation and urothelium metaplasia in the obstructed R-Stents, a polypoid reaction in the still patent R-Stents and only a mild ureteral inflammatory response in the Paclitaxel group.

Conclusion: Ureteral stenting with Paclitaxel-eluting stents inhibits tissue inflammation and urothelium hyperplastic response and improves ureteral patency. Long-term human trials are required in order to verify our results.

C-0614

Malignant biliary obstruction: Treatment with interventional radiology

F. Amodio, A. Pinto, R. Niola, G. Taliercio, M. Maglione; Naples/IT

Purpose: The authors report their experience in the palliative percutaneous treatment of malignant biliary obstruction.

Methods e Materials: 729 patients underwent transhepatic placement of metallic stents and/or plastic tubes. Obstruction predominantly involved both the right and left hepatic ducts in 324 and in 405 common bile duct or choledochus. All

Scientific and Educational Exhibits

stents were self-expanding flexible tubes made from woven stainless steel or nitinol wires. In its constrained state the stent has an outer diameter of 7-10 Fr. After deployment, it expands to a maximal lumen of 8-10 mm.

Results: In hilar obstructions we implanted Kissing stents in 51, 81 were treated with one stent and external drainage on the other side, 138 underwent catheter placement for two sided drainage and 54 required single-sided external drainage. For common bile duct or choledochus obstructions, 264 underwent stent placement and 141 catheter placement (8 external drainage). In 74 (10.1%) jaundice was not adequately reduced. Major complications occurred in 21 (2.9%) (9 severe septic events, 3 subcutaneous abscesses, 3 hepatic abscesses and 6 subcapsular hematoma). Minor complications involved 45 (6.1%) with self-limited bleeding into the drainage tube and 57 (7.8%) with fever less than 39° C. Average patency of stents was 7.5 months and average survival was 9 months.

Conclusions: Percutaneous transhepatic bile drainage as a palliative procedure is well tolerated by patients. Major complications are rare. Treatment (metallic stent or plastic tube) is based on the site of obstruction, nature of malignancy, life expectancy and ability to pass the stenosis.

C-0615

Early experiences of percutaneous radio-frequency ablation for unresectable small lung malignancies

T. Matsuoka¹, M. Toyoshima², A. Yamamoto¹, Y. Oyama¹, T. Okuma¹, K. Nakamura¹, R. Yamada¹, Y. Inoue¹; ¹Osaka/JP, ²Kobe/JP

Purpose: To assess technical and clinical success of RFA for unresectable lung metastases of less than 3 cm.

Materials and Methods: Fifty-nine secondary nodules (5-29 mm, mean 16.0 mm, from lung 18, others 41) in 31 patients were treated by RFA under CT guidance using LeVeen Needle from June 2000. The procedure was started at 10-30 watt by gradually increasing output until roll off (sudden rise of impedance meaning tissue coagulation) being achieved or 15 minutes. CT was performed every 2 or 3 months after the procedure and the largest diameter (LD) of ablated area consisting of the lesion and surrounding lung tissue was measured. It was judged as a recurrence when LD which had reduced with time turned in increase. Clinical success was assessed among nodules observed more than six months.

Results: All procedures were technically successful. In 40 nodules ablation was repeated to cover the whole lesion. Average ablation time per a nodule was approximately 40 minutes. Pain needing treatment was observed in 57%. Minor pneumothorax occurred in 30% except one case, which required a chest tube. Of 37 nodules which were observed during 6-43 months (mean 14.6 months), 9 were judged as a recurrence and an effective rate was 75.7% (28/37). The group in which roll off was achieved in the whole lesion had a significantly higher effective rate of 86.7% (26/30) than non roll off group of 28.6% (2/7).

Conclusion: Percutaneous RFA has the potential to become an effective and minimally invasive option for small lung metastases.

C-0616

Malignant duodenal obstructions: Palliative treatment using self-expandable nitinol stents

C. Yoon¹, H.-Y. Song², J. Shin²; ¹Seong Nam/KR, ²Seoul/KR

Purpose: To assess the efficacy and complications of self-expandable nitinol stents in the palliative treatment of malignant duodenal obstructions.

Materials and Methods: Under fluoroscopic guidance, 66 patients (44 male and 22 female, mean 63.0 years) with malignant duodenal obstructions were treated with per-oral placement of four types of self-expandable nitinol stents. All patients presented with severe nausea and recurrent vomiting, and their obstructions were inoperable.

Results: Technical success was achieved in 62 of 66 patients (93.9%). After stent placement, food intake capacity improved in 59 of 62 patients (95.2%). Stent migration occurred in one patient 4 days after stent placement. A covered stent was placed over ampulla of Vater in eight patients without external biliary drainage, of whom three patients (37.5%) became jaundiced. During the mean follow-up of 73.6 days (9-370 days), seven patients developed recurrent obstructive symptoms caused by tumor ingrowth (n = 2) and tumor overgrowth (n = 5), which were successfully treated with additional stent placement. The primary stent patency rates were 96.1%, 81.0%, and 37.8% at 1-, 3-, and 6-months, respectively.

Conclusions: Fluoroscopic peroral placement of self-expandable nitinol stents is an effective palliative treatment for malignant duodenal obstructions.

C-0617

Percutaneous vertebroplasty: Correlation between cement leakage into the disk and new fractures of adjacent vertebral bodies

M. Romero, A. Tomasello, J. Blasco, J. Pomés, J. Macho, M. Burrel, X. Tomàs; *Barcelona/ES*

Purpose: Patients successfully treated with vertebroplasty may return with pain caused by a new vertebral fracture that often affects vertebral bodies adjacent to the ones initially treated. We have analyzed the risk of subsequent fractures of adjacent vertebral bodies in relationship to cement leakage into the disk during initial vertebroplasty in a group of osteoporotic patients.

Methods and Materials: We have analyzed 44 patients treated with vertebroplasty between April 2002 and March 2004. Postprocedural CT scans were obtained in all cases to evaluate cement leakage. Patients who developed new pain after initial successful vertebroplasty were evaluated by repeat MR imaging. We documented the incidence of new fractures of adjacent vertebral bodies in relationship to cement leakage into the disk occurred during the initial vertebroplasty.

Results: Thirteen cases of cement leakage into the disk were detected. Five patients developed new fractures affecting adjacent vertebral bodies during the follow-up period, but only in 1 case this new fracture was associated with cement leakage into the adjacent disk. A secondary analysis showed that 7.7% of vertebral bodies adjacent to a disk with cement leakage fractured during the follow-up period, compared with 3.8% of the vertebral bodies adjacent to disks without cement leakage.

Conclusion: In our series, probably due to our low percentage of new fractures associated with adjacent disk cement leakage - only 1 case, there is not enough evidence to confirm or exclude this association.

C-0618

Ultrasound guided interventional procedures. A simple way of self-training

A.N. Chalazonitis, J. Tzovara, E. Protopapa, S. Giannou; *Athens/GR*

Learning Objectives: 1. To learn the general principles and advantages of ultrasonographic-guided interventions. 2. To learn the techniques and applications employed with ultrasonographic guidance. 3. To acquire the skill to direct a needle to a target with ultrasonographic guidance. 4. To anticipate common pitfalls to be avoided.

Background: Ultrasound-guided intervention offers the unique ability of real time imaging of both needle and the target. Low cost, speed and portability are further advantages of the method.

Procedure Details: This exhibit is a comprehensive and user-friendly educational tool for freehand ultrasonographic techniques of aspiration, core biopsy, cyst drainage and positioning of localization needles. Our presentation provides practical advice on current techniques mainly to residents and physicians with minimal or no experience on interventional procedures. Techniques and procedures are presented using versatile animal tissue models modified with a variety of implants to simulate solid or cystic lesions, as described above. Indications and contraindications, patient's preparation, possible complications and pitfalls are also analyzed.

Conclusion: Our tutorial, that consists of real time ultrasonography, live practical demonstrations, images and graphics presented audiovisual can be used to explore the general principles and advantages of ultrasonographic-guided interventions and to acquire the skills to perform a successful procedure.

C-0619

Non-liver metastases in patients with primary gastrointestinal carcinoma.

Treatment with radiofrequency thermal ablation

L. Thanos, S. Mylona, E. Karahaliou, M. Pomoni, A. Kokkinaki, N. Batakis; *Athens/GR*

Purpose: To evaluate the results of RFA on non-liver metastatic tumors from gastrointestinal carcinoma.

Materials and Methods: In a thirty-month period we performed 83 RFA sessions under CT-guidance on 61 metastatic lesions (10 from gastric and 51 from colorectal carcinoma) in 42 patients. The RFA was performed in 25 pulmonary, 23 osseous, 2 retrosternal and 3 painful perineal lesions, as well as in 4 supradiaphragmatic lymph nodes and in 4 local recurrences from rectal carcinoma. Each session lasted 13-17 min. We began the procedure after analgesic therapy and local anesthesia at the point of puncture. The follow-up with dual-phase spiral CT took place immediately after the ablation and at 1-, 3-, 6- and 12-month intervals.

Results: We succeeded total necrosis in 48 (78.68%) lesions and partial necrosis in 13 (21.32%). A new session was performed on all tumors with partial necrosis. Nine (14.7%) lesions that relapsed were treated with RFA. All patients with

Scientific and Educational Exhibits

osseous metastatic disease and perineal lesions had elimination of their pain symptoms. The one- and two-year survival was 100% and 78% respectively. We had no complications.

Conclusion: In our experience RFA provides a new alternative treatment in metastatic disease.

C-0620

Vascular complications of biliary interventional radiology

M. Acquafresca, E. Mazza, F. Toccafondi, M. Zini, L. Sali, C. Vannini, M. Falchini; Florence/IT

Purpose: To assess the incidence of vascular complications that occur during biliary interventional procedures and validate the effectiveness of the embolization treatment.

Methods and Materials: From January 1991 to February 2004, 2322 biliary interventional procedures were performed at our Interventional Radiology Unit of A.O. Careggi, in Florence, Italy. Nine cases of severe hemobilia represented the most relevant vascular complication. An angiographic examination was carried in all cases and demonstrated the presence of a pseudoaneurysm of the right hepatic artery in six cases; a pseudoaneurysm of the left hepatic artery in one case, an artero-portal fistula in one case and extravascular spread of contrast medium at the site of the right hepatic artery in one last case. All patients were treated by means of transcatheter embolization. Gianturco's coils were employed in four cases whereas gelatin sponge pledges (Gelfoam) were applied in five patients.

Results: In all cases, complete remission of the hemobilia was achieved after percutaneous embolization treatment. A limited hepatic septic ischemia occurred in one case in which Gianturco's coils had been used and we resolved it through percutaneous treatment.

Conclusion: Percutaneous interventional procedures represent a well established method to treat several cases of biliary disorders. They are rarely burdened with complications, mostly represented by hemobilia, which can be effectively treated and resolved through percutaneous procedures, without resort to the surgical intervention.

C-0621

The efficacy of "mini-perc" technique for the treatment of renal complete staghorn calculi, especially results in the upper pole

S.Y. Jeong, S.W. Choo, Y.M. Sung, S.S. Jeon; Seoul/KR

Purpose: To evaluate the effectiveness of "mini-perc" technique of the percutaneous nephrolithotomy in complete staghorn stones, especially those in the upper pole.

Materials and Methods: We retrospectively reviewed the records of 39 patients (10 males and 29 females, mean age 49) with complete staghorns, who had been treated with "mini-perc" technique between July 1999 and June 2004. Percutaneous tract formation was done via single lower-pole access with exception of two patients who had two tracts. A 14 Fr peel away sheath was then utilized for percutaneous access at the operating room. Lithotripsy was achieved using a Holmium: YAG laser by an experienced urologist. Initial stone free rate and final stone free rate after additional treatment were evaluated. Procedure-related complications also were evaluated. And postoperative intravenous urography was performed when intraoperative urinary tract injuries were suspected.

Results: Initial stone free rate and final stone free rate after additional treatment such as ESWL was 13% and 64% overall, and 41% and 90% respectively in the upper pole. Intravenous urography was done in 16 renal units postoperatively and revealed good function in all the units. Bleeding requiring transfusion occurred in 3 patients (7.6%), and one of them had an arterial embolization.

Conclusions: "Mini-perc" monotherapy for complete staghorn calculi resulted in a lower stone free rate, but when combined with additional treatment such as ESWL, it achieved better results. The stones located in the upper pole could be removed effectively via only single lower-pole access.

C-0622

MR imaging of radiofrequency (RF) induced coagulation in liver ex vivo: Histopathological correlation of different MR sequences between a low and a high field MR scanner

D. Schmidt, S. Clasen, A. Boss, J. Truebenbach, P. Pereira, F. Schick, C.D. Claussen; Tübingen/DE

Purpose: To compare MR sequences for the visualization and the determination of short axis diameter of coagulation following RF ablation between low and high field MR scanner.

Method and Materials: RF ablations ($n = 10$) were performed in bovine liver

tissue ex-vivo by using an internally-cooled cluster electrode. MR imaging of the coagulation were obtained by using two different spin echo sequences for the open low (0.2 T) and closed high (1.0 T) field MR scanner with following parameters: T1 weighted (TR 400 ms/TE 12 ms; matrix 256x256, 4 acquisitions) and T2 weighted (TR 4000 ms/TE 85 ms; matrix 256x256, 4 acquisitions). Both MR scans were evaluated by two observers for assessment of the zone of white coagulation with a score ranging between 1-5. The zone of white coagulation was determined histopathologically. Short axis diameters of the zone of white coagulation were measured and correlated with MR imaging.

Results: The white zone of coagulation necrosis was significantly better visualized in T2 weighted sequences using high field (1.0 T) MR imaging ($p < 0.001$). The short axis diameters of histopathologically determined white coagulation had the best correlation to with high field MR imaging ($r^2 = 0.97$). The differentiation of normal liver tissue and white coagulation was possible for both MR sequences and MR scanners.

Conclusion: T2w sequences are superior to T1w sequences for the visualisation of RF induced white coagulation in liver tissue ex-vivo. The short axis diameters measured with T2w sequences in high field MR scanner had the best correlation to histopathologically findings.

C-0623

MR-fluoroscopy-guided corticosteroid-infiltration of the sacroiliac joints:

Pain therapy of sacroiliitis in patients with spondylarthropathy

J. Fritz, C.W. König, S. Clasen, I. Günaydin, G. Tepe, I. Köller, C.D. Claussen, P.L. Pereira; Tübingen/DE

Purpose: To evaluate the efficacy and specific properties of MR-fluoroscopy-guided corticosteroid-infiltration of the sacroiliac joints (SIJ) in patients with therapy refractory sacroiliitis due to spondylarthropathy.

Material and Methods: In 20 patients MR-fluoroscopy-guided SIJ-Infiltration was performed using a fast imaging with steady precession (FISP) sequence. The entire intervention was performed by using a C-shaped open 0.2-T-MR-Scanner (Magnetom Open Viva®, Siemens, Erlangen, Germany). Puncture side evaluation and needle placement was performed with free-hand technique and continuous action control via in-room monitor. After needle placement two perpendicular MR images ensured successful articular needle placement and 40 mg triamcinolonacetone (Volon A, Bristol-Myers Squibb, München, Germany) were instilled. Inflammatory back pain was documented on a visual analog scale (VAS). Wilcoxon test was used to assess significant differences between VAS-Scores.

Results: MR-fluoroscopy-guided SIJ-Infiltration was feasible and technically successful in all patients. There was statistically significant ($p < 0.001$) improvement (-62.5%) of the VAS-Score from 8 (10-5) to 3 (0-6). FISP sequence was characterized by decreased resolution and decreased tissue contrast but did provide fast imaging of sufficient quality for save and exact needle placement. The average procedure time for puncture site evaluation was 2 (1-3) min and 4 (2-7) min for needle placement. The mean remission time was 11 (5-14) months.

Conclusion: MR-fluoroscopy-guided corticosteroid infiltration of the SIJ proved to be an effective therapy of inflammatory back pain with a long lasting effect in patients with therapy refractory sacroiliitis. MR-Fluoroscopy guidance proved to be a feasible modality that enabled exact and fast device placement with continuous action control.

C-0624

Percutaneous CT-guided drainage of abdominal and pelvic abscesses

L. Thanos, A. Nikita, G. Papaioannou, K. Malagari, D. Loggitsi, D. Kelekis; Athens/GR

Purpose: To assess the efficacy of percutaneous drainage of abdominal and pelvic abscesses under CT-guidance.

Materials and Methods: During a 6-years period, 641 patients with abdominal and pelvic abscesses underwent percutaneous CT-guided drainage using pigtail catheters 8-16F. Two hundred sixty-eight of them were liver abscesses, 21 splenic, 72 pancreatic or peripancreatic, 134 retroperitoneal (37 renal and perinephric and 97 iliopsoas abscesses) and 146 pelvic abscesses. In all the cases, for the insertion of the catheter we used the trocar technique. Aspiration of the lesions was performed in order to obtain material for culture and susceptibility testing.

Results: The length of time that catheters remained in place ranged from 6 to 25 days. Abscesses were successfully drained in 545 (85%) of 641 patients. In the remaining 96 (15%) cases, residual collection was noted indicating incomplete drainage of the abscess and an open surgical drainage was performed. No major complications were observed related to the procedure.

Conclusion: CT-guided percutaneous catheter drainage of abdominal and pelvic abscesses is an effective and safe treatment procedure and it may replace surgery in the majority of the cases.

Scientific and Educational Exhibits

C-0625

Radiofrequency ablation of liver tumors developed after hepatectomy

L. Thanos, A. Nikita, G. Papaioannou, D. Danassi-Afentaki, S. Kampanarou, D. Kelekis; *Athens/GR*

Purpose: To assess the effectiveness of radiofrequency ablation (RF) in the treatment of recurrent or new liver tumors developed after hepatectomy.

Materials and Methods: Twenty-six patients with liver tumors developed after hepatectomy (17 with hepatocellular carcinomas and 9 with metastatic lesions) underwent percutaneous RF ablation instead of repeated hepatectomy. Fourteen of them represented new lesions and the remaining 12 of them represented recurrent tumors. The mean diameter of treated tumors was 3.3 cm (range 1-5 cm). Electrodes of 7 or 9 active tips were advanced under CT guidance. Contrast enhanced CT was used to assess the therapeutic response immediately after the procedure and for the follow-up.

Results: In the CT scan immediately after the procedure 23 (88.4%) of 26 lesions presented complete necrosis. Incomplete local RF treatment was observed in the remaining 3 (11.6%) patients and a second RF session was performed resulting to complete necrosis of the tumors. The 1-year, 2-year and 3-year survival rates are 100%, 96% and 76% respectively. No deaths or major complications were observed related to RF ablation.

Conclusion: Percutaneous RF ablation is an effective method for treating liver tumors developed after hepatectomy, with satisfying survival rates.

C-0626

Radiofrequency thermal ablation coupled with hepatic arterial occlusion in treating large-size HCC

L.F. Frigerio, F. Garbagnati, G. Di Tolla, S. Rossi; *Milan/IT*

Purpose: To assess whether the RTFA coupled with the mechanical occlusion of the hepatic artery achieves necrosis 2 to 4 cm larger than RTFA alone (loose blood flow) in lesions with diameter up to 8.5 cm.

Methods: A single-session RTFA was performed together with i.a. hepatic embolization with Gelfoam in 132 patients with single HCC lesions ranging from 3.5 to 8.5 cm in maximum diameter, rejected to surgery.

Results: 100% of the lesions showed a partial reduction in size ranging from 40 to 80%. 22% of the patients had local recurrence at the site of the lesion, 43% had satellite nodules during follow-up from 3 months to 2 years after the initial treatment, the actual follow-up is 28 months.

Conclusion: The reduced thermal dispersion by convection and the modified tumoral tissue conductivity related to occlusion of the HCC blood supply as well as the single pass of the neoplastic capsule by the RTFA needle result in larger areas of coagulative necrosis while preserving the critical amount of residual liver intact

C-0627

Role of contrast-enhanced ultrasound in the radiofrequency thermal ablation treatment of malignant hepatic tumors

A. Orlacchio, S. Fabiano, A. Rotili, M. Stefanini, R. Pasquarelli, G. Simonetti; *Rome/IT*

Learning Objectives: To evaluate the role of contrast-enhanced ultrasound in the management of malignant neoplasms of liver treated by means of radiofrequency (RF) thermal ablation. To illustrate the patterns of contrast enhanced ultrasound in the recognizing of residual tumor or neoplastic recurrence. To show the method to guide a further ablative treatment to residual viable tumor.

Background: The traditional therapeutic option to treat primitive focal liver tumors is surgery. Liver resection is not always possible. The improvements in imaging technologies have permitted to guide better the percutaneous treatment of liver neoplasms.

Procedures Details: Many thousands of RF thermal ablation treatments have been performed during the last years. Usually RF thermal ablation treatment was performed by means of ultrasound guide. The immediate result of RF thermal ablation treatment is not detectable with conventional ultrasound because of intense sonolucency.

Conclusion: The recent introduction of contrast enhanced ultrasonography is a very promising tool to cross this limit of US and it shortened the length of treatment.

C-0628

Usefulness of three-dimensional rotational angiography following percutaneous vertebroplasty; with special interest on detectability of cement leakage

Y. Arisaka¹, M. Matsusako¹, A. Uemura¹, N. Kobayashi¹, M. Takase¹, M. Terada¹, R. Nakagawa², H. Komatsu², Y. Numaguchi¹; ¹Chuo-ku, Tokyo/JP, ²Shinagawa-ku, Tokyo/JP

Purpose: Imaging evaluation of cement leakage around vertebral bodies is crucial because it affects the postprocedural patient care. The goal of this study is to evaluate the usefulness of three-dimensional rotation angiography (3D-RA) following percutaneous vertebroplasty (PVP) in terms of detectability of cement leakage.

Methods and Materials: Thirty-eight patients (84 vertebral bodies) who underwent 3D-RA and multidetector CT (MDCT) were included in this study. 3D-RA was performed by using a rotational angiographic unit. Multiplanar reconstruction (MPR), maximum intensity projection (MIP) and gradient rendering images were created by using workstation. 3D-RA images and MDCT images were evaluated by two radiologists. The existence and location of cement leakage around the vertebral bodies was evaluated. 3D-RA findings were correlated with MDCT as a golden standard.

Results: MDCT revealed 52 leakages among 38 vertebral bodies. On 3D-RA, 53 sites among 39 vertebral bodies were diagnosed as cement leakage. Sensitivity, specificity, positive predictive value and accuracy of 3D-RA were 86.5%, 98.4%, 84.9% and 97.0% respectively.

Conclusion: 3D-RA is useful tool for evaluation of cement leakage during PVP and may replace postprocedural CT.

C-0629

MR imaging findings following radiofrequency ablation (RFA) of lung tumors

J. Yoshigi, J. Ishida, T. Nakamura, K. Izaki, S. Ando, T. Kajitani, T. Yoshizako, H. Kitagaki; *Izumo/JP*

Learning Objectives: 1. To describe MR findings within treated tumor and to recognize features of residual disease. 2. To review peritumoral findings following RFA on MR imaging.

Background: Therapy effect judgment by imaging for RFA of lung tumor is not established, because contrast enhancement of lung tumor is generally low and evaluation by ultrasound is difficult. On CT, visual evaluation of contrast enhancement and ablated area is difficult. Therefore we reviewed MR imaging findings following RFA of lung tumor to investigate potential of therapy effect judgment by MR imaging.

Procedure Details: MR imaging was performed before, 1 week and 1 month after RFA. MR imaging was performed with a 1.5 T system with torso phased array coil. T1 and T2-weighted image (WI) and 3D dynamic images were obtained. Subtracted images were also obtained by subtracting ordinary T1-WI from the enhanced T1-WI. The effectiveness of RFA was evaluated on the basis of the area of the enhanced components in the tumor on initial and follow-up images. Subtracted image was excellent to detect enhanced component. After 1 week, the diameter of tumor increased in size. Signal change of a tumor was unsettled on T1 and T2-WI. Peritumoral enhancement and slightly high signal intensity on T2-WI were also seen. Residual tumor was detected by only the subtracted image. After 1 month necrotic lesion decreased in size. Peritumoral enhancement and high signal intensity on T2-weighted image decreased in size.

Conclusion: MR imaging findings following RFA of Lung tumors has an impression to be useful in a therapy effect judgment.

C-0630

Development of animal model for solitary hepatic tumor: Operative intrahepatic transneedle inoculation of VX2 particles

J.H. Cho, B.H. Park, T.B. Shin, J.Y. Oh, J.H. Lee, S.K. Yoon, J.C. Choi, K.N. Lee, K.J. Nam; *Busan/KR*

Purpose: To develop a large animal model which has a proper solitary intrahepatic tumor and to evaluate tumor progression after intrahepatic inoculation of VX2 cells to New Zealand white rabbits

Materials and Methods: 21 NZ white rabbits were selected. We made a 1 mm³ VX2 tumor fragment and minced it to be mountable in a tuberculin syringe with normal saline. We injected the minced VX2 tumor onto the left hepatic lobe through 21 G needle. To prevent hemorrhage or leakage of VX2 tumor cells from the injected site, we tied around the suture site using black silk and covered the injection site with Surgicel® patch. Intrahepatic inoculated VX2 tumors were then

Scientific and Educational Exhibits

imaged with 16 channelled MDCT at every week interval. We sacrificed from 3 weeks bi-weekly, and correlated with CT and pathologic findings.

Results: Intrahepatic inoculated VX2 tumor was invisible on first week, and detectable on 2nd week by 66.7% (6/9). After 3rd week after inoculation, all tumors are detectable on CT scan. Tumor metastasis to extrahepatic organ increased according to time and size increase. In 3 cases (15%), early peritoneal seeding was detected within 3 weeks after inoculation. The other rabbits (85%) show successful inoculation to make a solitary hepatic tumor models without complication. **Conclusion:** Tumor metastasis to extrahepatic organs were detected from 4th week in period or more than 35 mm in diameter, after inoculation of tumors. Operative intrahepatic VX2 tumor particles injection method seems to be good for development of animal model with intrahepatic solitary tumor.

C-0631

Percutaneous treatment of hydatid cysts of the liver: Our experience

D.M. Masulovic, M. Milicevic, D. Saranovic, A. Djuric, A. Ivanovic, B. Dobriserevic; Belgrade/YU

Objective: The purpose of our study was to present our experiences in percutaneous treatment of liver hydatid cysts.

Materials and Methods: 21 male and 36 female patients, ranging in age between 17 and 67 years with 84 liver hydatid cysts underwent percutaneous treatment with albendazole prophylaxis. In 61 cases, PAIR were used for hydatid cysts smaller than 6 cm. Larger cysts (23) were treated by catheterization. CT and/or ultrasound guidance with or without fluoroscopy was used. Ultrasound was used in follow-up that has been performed every third month of the first year, every sixth month of the second year, and once a year thereafter.

Results: The mean reduction in volume at the time of the first follow-up was 82.0% in catheterization and 70% in PAIR patients. The immediate US changes after treatment were detachment of the endocyst and disappearance of the regular endocyst, with a decrease in the fluid component. Fifty three of fifty seven patients were cured, with four recurrences. No mortality, abdominal dissemination, or tract seeding occurred. Minor complications were urticaria and fever in three patients. Major complications were infection of the cyst cavity in (3) and development of biliary fistula (2). Average hospitalization time was 20 days for cases with complications and 2 days in uncomplicated cases.

Conclusion: Our experience shows that long-term results of percutaneous liver hydatid cyst treatment are in line with short-term results, indicating that the procedure is efficient and safe and offers complete cure in selected patients with a short hospitalization.

C-0632

CT guided therapeutic spine interventions

H. Brat¹, T. Bouziane², O. Cappeliez³; ¹Mons/BE, ²Tournai/BE, ³La Louvière/BE

Learning Objective: Teaching file for CT guided minimally invasive therapeutic spine interventions.

Background: CT fluoroscopic needle guidance has allowed decreasing risk and maximizing patient comfort in peri-spinal minimal invasive interventions. These techniques may represent alternative treatments to surgery in many cases.

Imaging Findings and Procedure Details: Indications, target, procedure details, potential hazards and complications are detailed and illustrated with images and CT fluoroscopy films for each type of intervention. Interventions are listed in green and red light procedures according to degree of difficulty. Perispinal infiltrations and neurolysis, treatment of disc herniation, vertebral metastasis and fractures are reviewed using a step by step teaching file.

Conclusion: CT fluoroscopic guidance for interventional procedures allows fast, safe and precise interventions with minimal risk and X-ray exposure to the patient.

C-0633

Changes in disc herniations after CT guided percutaneous laser disc decompression (PLDD): MR findings

H. Brat¹, T. Bouziane², O. Cappeliez³, L. Divano¹; ¹Mons/BE, ²Tournai/BE, ³La Louvière/BE

Purpose: To assess changes in disc herniations on MR imaging after PLDD.

Materiel and Methods: Follow-up MR imaging were obtained in 27 consecutive patients (M:F = 19:8, mean age: 43 years) who had been successfully treated by CT guided PLDD for persistent radiculopathy due to a lumbar disc herniation after 6 weeks of conservative treatment. Mean duration of symptoms before treatment was 39 weeks (6-200). Mean follow-up with MR imaging was 7.5 months (3-15). Size and signal of diseased disc and hernia has been assessed before and after treatment on MR examinations.

Results: Follow-up MR imaging showed no change in the decreased disc signal in T1 & T2WI. Conversely, the disc hernia, initially always of low signal on T1WI and T2WI, presented a high signal on T2WI in 59% (16/27 patients) and a low signal in 41%. Shrinking of the hernia with raise of nerve root compression has been observed in 18/27 patients (66%) on MR imaging. Height of discs remained stable in all patients.

Conclusion: MR imaging of disc hernia after PLDD shows appearance of a high signal on T2WI in the hernia in 59% and a shrinking of the hernia in 66%.

C-0634

Ultrasound of the liver to follow-up ablative therapy of liver malignancies: Detection of residual and recurrent tumor compared to CT and MR imaging

W. Kröger, V. Nauck, C. Rosenberg, N. Hosten; Greifswald/DE

Purpose: To evaluate the efficacy and potential of ultrasound as an alternative to CT and MR imaging, the gold standard in controlling hepatic tumor ablative therapy. Description of sonographic criteria to determine tumor tissue activity.

Materials and Methods: 25 liver lesions in 18 patients with non-resectable primary or secondary hepatic malignancies (1 gastric, 10 colorectal, 4 hepatocellular, 3 renal cell carcinomas) were examined before and after thermoablative therapy (laser or radiofrequency-induced) at days -1, +4, +120. Lesion size and perfusion were measured to determine tumor tissue activity (HDI 5000, Philips). Tumor perfusion was visualized using color Doppler, pulsed Doppler and contrast-enhanced (SonoVue, Altana Pharma) ultrasound. CT, MR imaging or histologic findings, if performed, were correlated with ultrasound.

Results: US visualized 19 out of 25 lesions before and after ablative therapy. On follow-up, in 17/19 patients the US diagnosis "no residual tumor" or "residual tumor" was correct when compared to CT/MR imaging/histology. 10 out of 17 hepatic tumors were found to be treated sufficiently. 7 lesions showed residual or recurrent tumor activity. Sufficient ablative therapy of liver malignancies resulted in missing tumor perfusion and a decreased or stable lesion size, whereas detectable perfusion on US and /or enhanced tumor size defined residual or recurrent tumor. In one case ultrasound led to a false-negative result; residual tumor was not detected. One residual tumor in ultrasound was shown as complete ablation in CT.

Conclusion: Contrast-enhanced ultrasound to follow-up thermoablative therapy of liver malignancies represents an alternative method to CT/MR imaging.

C-0635

Stenting of the tracheobronchial tree

D.G. Lohan, S.M. Walsh, G.J. O'Sullivan; Galway/IE

Learning Objectives: According to patient requirements, temporary or permanent endoluminal stents of various types are now available for use throughout the central tracheobronchial tree.

Background: Insertion of a cylindrical structure into the trachea to maintain its patency was first performed by Trendelenburg, in 1872. However, it was not until the 1980s that both flexible silicone rubber and rigid metallic endoluminal stents became commercially available for use in the management of subglottic tracheobronchial stenoses. Central airway stenosis, with resultant severe morbidity, patient distress and potential mortality, may occur secondary to a myriad of both benign and malignant endoluminal and extrinsic tracheobronchial conditions. Until recent times, existing therapeutic options were often quite limited, with poor patient general condition and multiple comorbidities often precluding open reconstructive surgery. By providing a non-invasive alternative to surgical techniques, endoluminal tracheobronchial stenting has revolutionized the management of airway stenoses of many aetiologies.

Imaging Findings: By way of a pictorial review, we explore the realm of tracheobronchial stenting including pre- and post-insertion studies of patients treated in our institute. In addition, we illustrate the complications of this procedure including a discussion on methods of prevention and management of these adverse outcomes.

Conclusion: Often surgical options may be limited due to underlying co-morbidities in patients with tracheobronchial pathology. In this instance endobronchial stenting may offer a rapid, relatively inexpensive, well-tolerated method of symptomatic relief suitable for physically poor patients.

Scientific and Educational Exhibits

C-0636

Transgastric drainage technique in pancreatic fluid collections and in traumatic lesions

E. Mazza, L. Sali, C. Vannini, D. Beccani, M. Falchini, M. Zini, M. Acquafresca; Florence/IT

Purpose: To evaluate modified transgastric drainage technique of acute fluid collections secondary to biliary or pancreatic surgery or to pancreatic trauma.

Methods and Materials: From January 1998 to February 2004, 11 patients with retrogastric fluid collections (post surgical fluid collections in 6 cases; infected collections from acute pancreatitis in 2 cases, post traumatic fluid collections in 3 cases) were treated with modified transgastric technique. Lesions were single in 7 cases and multiple in 4. In all patients multiple drainages (from 2 to 6) were positioned under CT guidance and left in place for a period of 10 to 30 days. Subsequently they were replaced under fluoroscopic and endoscopic guidance with cysto-gastrostomic double-mushroom prostheses, left in place for 4 to 6 months. Finally all endoprostheses were endoscopically removed, after remission of collections was ascertained on CT images.

Results: Resolution of fluid collections was achieved in all lesions. In post-traumatic lesions the procedure was repeated up to 3 times due to the development of new collections days to months after the first procedure. Due to isolation of a Vancomycin- and Fluconazol-resistant strain, in one case drainages were left in place for a prolonged time till the resolution was finally obtained.

Conclusion: Transgastric drainage technique, already validated for the treatment of pancreatic pseudocysts, may be successfully employed with a few adaptations to the treatment of acute, infected collections secondary to biliary or pancreatic surgery or to pancreatic trauma.

C-0637

Radiographic and clinical results of balloon kyphoplasty in the treatment of osteoporotic vertebral compression fractures

C. Doria, G.B. Meloni, P. Lisai, S. Profili, F. Meloni; Sassari/IT

Purpose: Aim of this study was to measure sagittal alignment of the spine in patients with osteoporotic vertebral compression fractures (VCFs), before and after treatment with balloon kyphoplasty.

Materials and Methods: 29 osteoporotic VCFs were treated during 21 balloon kyphoplasty procedures in 17 patients. The fractures, which occurred between T8 and L4, were sustained within a mean of 3.2 months of the procedure. The fracture was confirmed as the likely pain generator by correlating physical findings with the identification of edema in the fractured vertebra with Short Tau Inversion Recovery Magnetic Resonance Imaging. Under general anesthesia and biplanar fluoroscopy an 11-gauge Jamshidi needle was placed percutaneously into the posterior vertebral body through either a trans-pedicular approach. KyphX® Inflatable Bone Tamps (IBTs) were placed bilaterally into the vertebral body through a working cannula. The IBTs were inflated using visual fluoroscopic and manometric parameters. Once maximum fracture reduction and height restoration were achieved, both balloons were deflated and removed, leaving behind a cavity, which was then manually filled under low pressure with viscous, radioopaque polymethylmethacrylate cement. Standing radiographs centered on the treated level/s obtained prekyphoplasty and postkyphoplasty were analysed for improvement in sagittal alignment using the Cobb technique. Statistical analyses were done using paired simple t test and Wilcoxon signed-rank-test.

Results: Mean improvement in local sagittal alignment was 11.4° toward lordosis (range 0°-32°). Patients surveys revealed significant pain reduction within the first week after kyphoplasty.

Conclusion: Kyphoplasty improves physical function, reduces pain and may correct kyphotic deformity associated with vertebral compression fractures.

C-0638

Sacral cementoplasty using combination CT and fluoroscopic guidance: Technical approach

P.C. Young; Cleveland, OH/US

Learning Objectives: The radiologist will understand the indications for percutaneous sacral cementoplasty and become familiar with the technique of utilizing a combination of fluoroscopy and computed tomography for needle placement and cement injection.

Background: Vertebroplasty with injection of PMMA (bone cement) has become common in the treatment of osteoporotic compression fractures of vertebral bodies. Recently a similar procedure for treatment of sacral insufficiency fractures has been described. A few preliminary results have been published with favorable results in relieving pain from these fractures. Here, we describe a different technique for sacroplasty using CT and fluoroscopy.

Procedure Details: Patients are prone in the CT/fluoroscopy suite. The fluoroscopic tube is placed in an oblique orientation in a manner that profiles the sacroiliac joints. The needle is then placed in a location at the mid sacrum on the side of the sacral insufficiency fracture 1-2 cm medial to the SI joint. This approach allows a safe placement of the needle avoiding sacral nerve roots. Radioopaque PMMA is then injected and intermittent fluoroscopic and CT images are obtained allowing confirmation of appropriate location of the cement and prompt visualization of any extravasation. The procedure is otherwise similar to the technique of percutaneous vertebroplasty.

Conclusion: Percutaneous cementoplasty (sacroplasty) is a promising new therapy for the treatment of sacral insufficiency fractures. Using a combination of CT and fluoroscopy during needle placement and injection of PMMA improves visualization of the sacral neuroforamina thus decreasing the risk of extravasation and sacral nerve injury.

C-0639

Percutaneous tumor ablation in liver tumors causes a transient immunosuppression

C. Schmuckenschlager, M. Ploder, B. Wessner, F. Längle, E. Roth, J. Lammer, J. Kettenbach, A. Spittler; Vienna/AT

Purpose: Radio frequency ablation or ethanol instillation in patients with liver tumors are possibly accompanied by an activation of Kupffer cells which then produce a variety of inflammatory cytokines and cause an imbalance of the redox status. The aim of the present work was to determine the patients' immunological and oxidative status before and after percutaneous tumor ablation.

Methods: 0.5 h before, 0.5 h, 24 h and 5d after intervention human leucocyte antigen-DR (HLA-DR) expression on monocytes, ex-vivo LPS induced tumor necrosis factor-alpha (TNF-alpha) production, plasma interleukin (IL)-6, procalcitonin (PCT), peroxide levels and antioxidative capacity were measured.

Results: In this prospective study 25 patients (mean age 67.0 ± 10.6) were included. In all patients HLA-DR expression (24 h $p < 0.01$; 5d $p < 0.05$) and TNF-alpha production (1 h $p < 0.001$) were significantly diminished, IL-6 (24 h and 5d $p < 0.01$) and PCT levels (24 h $p < 0.05$) were significantly enhanced compared with pretreatment values. Interestingly, 5d after intervention peroxide levels were significantly higher ($p < 0.01$), whereas antioxidative capacity did not change. Significant differences between the two treatment groups were found in IL-6 (24 h $p < 0.05$), PCT (1 h $p < 0.05$, 24 h $p < 0.05$, 5d $p < 0.05$) and peroxide levels (1 h $p < 0.05$).

Conclusion: Although in all patients interventions were minimal invasive treatments, we assume that Kupffer cells were activated triggering a transient immunosuppression. In addition altered peroxide levels indicate the occurrence of oxidative stress.

C-0640

Computed tomography guided automated cutting needle biopsy of pulmonary lesions. Self assessment test

A. Grgic¹, M. Heinrich¹, M. Girmann¹, B. Kramann¹, M. Uder²;

¹Homburg a.d. Saar/DE, ²Erlangen/DE

Purpose: We evaluated the diagnostic accuracy and incidence of complications of transthoracic needle biopsy with an automated cutting 16-gauge core biopsy needle and gun using computed tomography guidance.

Patients and Methods: In a retrospective analysis diagnostic yield and complications of the needle biopsy with a 16 gauge needle in 44 patients (33m, 11f, 61 years, range 29 to 80 years) between May 2000 and August 2004 were analysed. Hard copy images, pathology reports and clinical reports were reviewed for the histopathological diagnoses and complications of the biopsy. The size of the lesions ranged from 1.8 cm to 8 cm in diameter.

Results: An adequate sample for histological diagnosis was obtained in all cases. There were 40 of 44 (90.9%) true positive biopsies for malignant lesions and a specific histopathological diagnosis was obtained in all benign and malignant lesions. Complications occurred in 11 patients (25%) and included 8 cases with a small pneumothorax, one case with a pneumothorax requiring drainage and 6 cases of local parenchymal hemorrhage with minor hemoptysis.

Conclusion: The transthoracic biopsy with an automated 16-gauge core biopsy needle and gun system provides a high level of diagnostic accuracy that effectively distinguishes benign from malignant diseases and allows an accurate distinction of malignant cell types with low complication rate.

Scientific and Educational Exhibits

C-0641

Management of pancreatic fluid collections with percutaneous drainage under CT guidance

G. Papaioannou, L. Thanos, A. Nikita, A. Sissopoulos, D. Antonopoulos, D. Kelekis; *Athens/GR*

Purpose: To assess the efficacy of percutaneous drainage of pancreatic fluid collections under CT-guidance.

Materials and Methods: During a 5-years period, 148 patients with pancreatic fluid collections (noninfected fluid collections, pseudocysts and abscesses) underwent percutaneous CT-guided drainage using pigtail catheters 12-16F. Indications for drainage were pain, sepsis and gastrointestinal or biliary obstruction. Forty-five cases required the use of multiple catheters.

Results: Percutaneous drainage was successful in 128 of 148 (86.4%) patients. Recurrence occurred in 20 of 148 (13.6%). Fifteen of them underwent repetition of the procedure. Overall, failure of the technique occurred in 18 out of 148 (12.1%) patients, requiring subsequent surgical drainage. No procedural complications were noted.

Conclusion: Percutaneous CT-guided drainage of pancreatic fluid collections is a safe and effective procedure and it may replace surgery in the majority of the cases.

C-0642

Percutaneous radiological gastrostomy: New modifications

M.C. Hurley, M. Given, S. Lyon, M. Lee; *Dublin/IE*

Learning Objectives: 1. To describe Percutaneous Radiological Gastrostomy (PRG). 2. To detail new developments in gastrostomy tube placement.

Background: Preshaw first described the fluoroscopic technique of PRG in 1981. The procedure was initially limited to standard foley or pigtail catheters. Because of difficulties with catheter clogging and displacement, recent trends include placing pull-type PEG tubes radiologically or placing gastrostomy button catheters de novo. Advantages of PEG-type tubes include their robust nature and good retention. Button advantages include lack of clogging and patient preference. PRG has advantages in patients with neurodegenerative disorders, due to poor respiratory function, aspiration risk, and high riding stomachs.

Procedure Details: To safely introduce a button tube de-novo, T-fastener gastropexy is routinely performed. Track length is measured to ensure a good fit. The button tube has a flush exterior, reducing the rate of dislodgement. To introduce a PEG-type tube, the stomach is punctured percutaneously, a guidewire is passed retrogradely up the esophagus and retrieved from the oropharynx. A snare catheter is then used to draw suture material along the same path. This is attached to the outer portion of the PEG tube which is pulled antegradely and into position. These robust tubes are ideal for long-term use.

Conclusion: Technical success rate is close to 100%, though a significant number require replacement. Complications include peritonitis, due to leakage or intraperitoneal siting of the tube, and puncture of colon or liver. These new techniques place the interventional radiologist at the forefront of enteral nutrition provision.

C-0643

Bleeding after US-guided percutaneous liver biopsy: Role of Doppler US examination immediately after the biopsy procedure

K. Kim, T. Kim, S. Park, M.-J. Kim, A. Kim, H. Ha; *Seoul/KR*

Learning Objectives: To illustrate predictive findings or evidences of bleeding after the percutaneous liver biopsy at Doppler US examination immediately after the biopsy procedure.

Background: The role of US-guided percutaneous needle biopsy has been well established in the diagnosis of both diffuse and focal hepatic diseases. Whereas it is considered a relatively safe procedure in patients with normal coagulation, the risk of bleeding after the procedure increases in patients with coagulopathy. Although Doppler US examination has been known to be a sensitive method in detection of post-biopsy complications such as arterial pseudoaneurysm and arteriovenous fistula, the efficacy of Doppler US in the detection of the bleeding immediately after the biopsy procedure has not been determined yet.

Procedure Details: We recently performed Doppler US examinations immediately after percutaneous liver biopsy in 114 patients and found several predictive findings of post-biopsy bleeding including flow signals along the needle tract. In this exhibit, we present a pictorial review of predictive findings or evidences of post-biopsy bleeding at Doppler US examination immediately after percutaneous liver biopsy.

Conclusion: Doppler US examination after percutaneous liver biopsy provides excellent screening for detection of post-biopsy bleeding. A patent tract sign,

which persists for five minutes after the biopsy, strongly predicts the possibility of subsequent occurrence of clinically significant post-biopsy bleeding.

C-0644

Percutaneous vertebroplasty in the treatment of metastatic spinal disease

S. Ristic, P. Bosnjakovic, M. Mrvic, A. Bojanovic, D. Ilic, D. Stojanov, M. Ilic; *Nis/YU*

Purpose: The objective of this study was to determine the efficacy and durability of percutaneous vertebroplasty for the treatment of back pain associated with metastatic vertebral body lesions.

Methods and Materials: Over the last 30-months period sixty four vertebrae (48 lumbar, 16 thoracic) were treated in 40 patients with spinal metastases. There were 36 female and 4 male patients (32 ambulatory, 8 hospitalized) in our group, mean age 52 years All patients suffered intractable spinal pain refractory to analgesic therapy. Pain intensity before and after the procedure was evaluated using a visual analog scale (VAS). Vertebroplasty was done under continuous fluoroscopy guidance, after pre-medication and under local anesthesia. Percutaneous puncture of the involved vertebral bodies was performed via transpedicular or intercostovertebral approach.

Results: All procedures were technically successful and resulted in significant pain relief and clinical improvement in all patients immediately after. Preoperative VAS score ranged 6.6-9.4 (mean 7.8) decreased to 0-3.8 (mean 2.3) postoperative. No major complications were noted. Paraspinal soft tissue leakages, that occurred in nine levels, eight epidural, five intradiskal and three venous leaks of methyl methacrylate had no clinical importance. Two patients experienced mild transient radiculopathy, which resolved after NSAID therapy. Beneficial effects were persisted in all of cases at follow-up, with mean duration 13.6 months (range 2-27 months).

Conclusion: Vertebroplasty is a minimally invasive outpatient procedure that provides immediate pain relief, spinal stabilization and mobility improvement in cancer patients. It is safe and highly efficacious therapy, and promising to have long lasting benefit.

C-0645

Vertebroplasty using transoral approach in vertebral fractures due to metastatic lesions at C2 level

M. Romero, A. Tomasello, J. Blasco, J. Macho, J. Pomes, M. Burrel, X. Tomas; *Barcelona/ES*

Learning Objectives: To illustrate our experience in vertebroplasty using the transoral approach in vertebral fractures due to metastatic lesions at C2 level.

Background: Percutaneous vertebroplasty is becoming the standard treatment of painful vertebral fractures associated with metastasis and osteoporosis. The Transoral approach allows a safe and effective access for the upper cervical spine.

Procedure Details: CT scan and MR imaging were used to confirm the diagnosis and the absence of any anatomical vascular variants around the oropharynx. The procedure was done under general anaesthesia and with the aid of a mouth retractor. Under fluoroscopy an appropriate access to C2 vertebral body was achieved. After placement of a 15 cm/15 G needle at the center of the vertebral body, the cement was injected by using a screw syringe. Feasibility of the technique as well as immediate and mid-term follow-up were analyzed. Cement distribution was optimal in both cases, without any vein or disk cement leakage. No medical or radiological complications appeared related with the procedure. Both patients experienced important pain relief within 24 hours after the procedure. One of the patients died during follow-up due to his primitive disease. Pain relief persisted 6 months after the procedure in the other patient.

Conclusion: Transoral approach is an effective and safe access for upper cervical spine vertebroplasty.

C-0646

Radiofrequency ablation in the management of colorectal liver metastases

A. Afag; *London/UK*

Learning Objectives: Essentials of technical considerations in Radiofrequency Ablation (RFA) of hepatic metastases. Current concepts in the role of RFA from a review of the literature. Suggestions for further research for optimizing management of colorectal liver metastases.

Background: Surgical resection is known as the gold standard of treatment, but most patients present with unresectable disease. RFA has been shown to be a safe and feasible alternative in unresectable tumours. This involves image guided placement of a needle electrode into the metastases allowing alternating current to cause localized thermal coagulative necrosis.

Scientific and Educational Exhibits

Imaging Findings: Follow up imaging of successful RFA should demonstrate an area of necrosis with no residual tumour. Of the few published studies, there is a greater proportion including reports from London, (5 year survival 30%), Bordeaux, (1 year survival 85%), and Busto Arsizio, (3 year survival 46%) promoting the role of RFA. However results from the largest study from Texas, were less favourable.

Conclusion: Most studies favour the use of RFA in unresectable disease and it has the advantage of being more easily repeatable so new tumours can be treated as they are detected. Unfortunately outcomes of studies can be difficult to interpret, with problems of variation of tumour biology likely to influence which metastases are unresectable, small cohorts and short follow-up. Although evidence for the role of RFA in combination with resection is growing, controversy remains and comprehensive clinical trials with comparable designs would help determine whether studies on potentially resectable metastases is the way forward.

C-0647

Vertebroplasty with volumetric CT guidance: Speed, precision and clinical efficiency

H. Brat¹, T. Bouziane², J. Lambert¹, O. Cappeliez³, L. Divano¹; ¹Mons/BE,
²Tournai/BE, ³La Louvière/BE

Learning Objective: Teaching file for volumetric CT guided vertebroplasty.

Background: Usually, vertebroplasty is performed under general anaesthesia and with a conventional C-arm fluoroscopy. Triple slice CT fluoroscopy allows a volumetric approach of the collapsed vertebra and highest precision in needle tip placement. Local anaesthesia alone allows one day stay in hospital.

Imaging findings and procedure details: Indications, technical aspects, advantages, procedure details, hazards and complications for volumetric CT guided vertebroplasty compared to conventional fluoroscopy and combined (conventional and CT) fluoroscopy are detailed and illustrated. Advantages in terms of speed of procedure, increase in security and precision, decrease in hospital stay are emphasized. Case reports are used for additional illustration.

Conclusion: Volumetric CT guidance makes percutaneous vertebroplasty under local anaesthesia an easy to perform procedure with maximum patient security and comfort.

C-0648

Benefits of triple slice CT fluoroscopic needle guidance in percutaneous laser disc decompression (PLDD)

H. Brat¹, T. Bouziane², O. Cappeliez³; ¹Mons/BE, ²Tournai/BE, ³La Louvière/BE

Purpose: To evaluate benefits of triple slice CT fluoroscopic needle guidance in PLDD.

Material and Methods: 40 consecutive patients (M:F = 21:9, mean age: 43 years) presenting a contained disc hernia (2 L3/L4, 15 L4/L5, 23 L5/S1) and corresponding radicular pain of more than 6 weeks have been treated with multislice CT guided PLDD. Mean duration of symptoms before treatment: 39 weeks (6-200). Patients were treated under local anaesthesia on a one-day treatment unit. All procedures have been achieved with a 2/4/2 mm collimation and at low dose (10-25 mAs). Evaluated criteria: mean duration of fluoroscopy, percentage of needle repositioning, confidence interval for needle placement and technical success rate of the procedure.

Results: Mean duration of fluoroscopy: 23 seconds (11-43). Percentage of needle repositioning: 5%. Confidence interval for needle placement: 3/3. Technical success rate of the procedure: 100%. Benefits of multislice fluoro-CT needle guidance: low X-ray exposure time, management of patient z-axis, central intradiscal needle placement, absence of technical failure and absence of radicular lesion.

Conclusion: Triple slice CT fluoroscopy allows a volumetric approach for fast, precise and efficient needle positioning, increasing patient's comfort and security. Main benefit seems to be due to management of patient Z-axis.

C-0649

Percutaneous image-guided lymph node biopsy in lymphoma: Tips and tricks

A. Guermazi¹, S. Guth², A. Gangi²; ¹San Francisco, CA/US, ²Strasbourg/FR

Learning Objectives: Our objectives are to describe thoracic and abdominal percutaneous image-guided lymph node biopsy in patients with lymphoma and to describe some alternatives, tips and tricks for when the procedure tends to be difficult.

Background: Open surgical biopsy has long been the gold standard for obtaining lymph node samples in patients with lymphoma. However, the procedure can

have significant complications. With advances in cytopathologic diagnostic techniques, percutaneous image-guided biopsy with its high overall accuracy has become the procedure of choice, and is taking a prominent place in the management of lymphoma. It is now considered a safe, low cost, and valuable tool for patients with suspected or recurrent lymphomas. Between January 1998 and December 2003, we performed 198 percutaneous image-guided lymph node biopsies in patients with non-Hodgkin lymphoma.

Procedure Details: We will describe the technique of abdominal and thoracic percutaneous image-guided lymph node biopsy and give some suggestions and tips and tricks for when the procedure tends to be difficult, especially in posterior and/or deep-seated lymph nodes.

Conclusion: A well-planned and executed biopsy provides an accurate diagnosis and facilitates treatment. CT, which is widely available, allows image-guided biopsy in a large majority of patients. US-guided biopsy is an alternative, and is the guidance technique of choice at some institutions.

Scientific and Educational Exhibits

Interventional Radiology

Miscellaneous

C-0650

A survey of radiation dose and image optimisation for cardiac

interventional procedures

C.S. D'Helft¹, A.M. Mc Gee¹, L.A. Rainford¹, S.L. Mc Fadden², C.M. Hughes², J.R. Winder¹, P.C. Brennan¹; ¹Dublin/IE, ²Belfast/UK

Purpose: Interventional radiological procedures are increasingly common because of their cost-effectiveness compared with surgical procedures. Prolonged fluoroscopic exposures, particularly those associated with cardiovascular studies are responsible for some of the highest patient and staff radiation doses. Such exposures increase the risk of stochastic effects and regularly cross the threshold dose above which, deterministic effects such as erythema, epilation and ulceration are experienced.

Method and Materials: Radiation levels using dose area product and fluoroscopy time are currently being determined and compared for coronary angiograms (CA), percutaneous coronary intervention (PCI) and permanent pacemaker insertion procedures (PPI) across 15 hospitals. Other factors such as operator grade, technique and equipment used are also recorded, and their potential effect on patient dose investigated.

Results: To date, the results demonstrate a mean dose for CA procedures of 74.26 Gy cm², for PCI procedures 107.44 Gy cm², for PPI procedures 37.05 Gy cm². However, large intra- and inter-hospital variations were noted. The screening time varied by a procedure-specific extent, and shows a strong relationship with radiation dose delivered. Other causal will be discussed.

Conclusions: Due to the risks associated with X-ray exposure, radiation doses should be kept as low as reasonably achievable, consistent with good image quality. However, significant variations in radiation dose and image quality for coronary interventional procedures have been shown within and between hospitals in Ireland for the first time. Possible areas of standardisation and potential Diagnostic Reference Levels will be proposed.

Musculoskeletal

Bone

C-0651

IVR techniques for bone tumor: A comprehensive review

T. Inaoka¹, K. Takahashi², T. Yamada¹, M. Mineta¹, W. Yamamoto¹, K. Nagasawa¹, H. Hirota¹, T. Yamaki¹, T. Aburano¹; ¹Asahikawa City/JP, ²Iowa City, IA/US

Learning Objectives: To review a variety of interventional radiologic (IVR) techniques of primary and secondary bone tumors. To describe indications, contraindications, efficacy and complications.

Background: A variety of interventional radiologic (IVR) techniques of primary and secondary bone tumors have been described. It is important for general radiologists to know a variety of IVR techniques of bone tumors for establishing an optimal patient management. The purpose of this exhibit is to demonstrate various IVR techniques with indications, contraindications, efficacy and complications.

Procedure Details: Topics are primarily divided into two categories by approaches, 1) transcatheter approach including transcatheter arterial embolization (TAE), trans-catheter arterial infusion (TAI), arterial infusion chemotherapy via arterial port-catheter system; and 2) percutaneous approach including US-guided or CT-guided bone biopsy, percutaneous vertebroplasty and percutaneous ablation therapy.

Conclusion: Essential knowledge of a variety of IVR techniques of primary and secondary bone tumors could make it possible to perform more effectively and safely, and to improve patient's quality of life.

C-0652

The role of in-phase and out-of-phase magnetic resonance imaging and in vivo ¹H single-voxel magnetic resonance spectroscopy in the differential diagnosis of monoclonal gammopathies

G. Bajzik, M. Egyed, E. Karadi, B. Kollar, G. Rumi, P. Rajnics; Kaposvar/HU

Purpose: In many cases it is difficult to separate multiple myeloma and monoclonal gammopathy of unknown significance (MGUS) by routine clinical and pathological examination and the appropriate therapy can be delayed. We investigated the potential role of in-phase and out-of-phase magnetic resonance imaging and in vivo ¹H single-voxel magnetic resonance spectroscopy in characterization of bone marrow tissue in patients with multiple myeloma and MGUS.

Methods and Materials: Twenty patients with clinically and pathologically confirmed monoclonal gammopathy were examined. We acquired in-phase and out-of-phase gradient-echo sagittal images of the lumbar spine using a 1.5 T magnet. Identical region of interests were placed on the body of the first to fourth lumbar vertebra and the difference in mean signal intensities were calculated. The voxel of the ¹H magnetic resonance spectroscopy (PRESS) sequence was placed on the body of the third or fourth lumbar vertebra. We calculated the ratio of the areas under the water and lipid peaks followed by logarithmic transformation. The Mann-Whitney test was used for statistical analysis.

Results: The signal intensity difference values for in-phase and out-of-phase images were significantly higher ($p = 0.0002$) in the MGUS group (Mean: 152.3, SD: 13.1), than in the myeloma group (Mean: 24.9, SD: 13.1). Values of logarithmic transformation of water/lipid ratios were significantly different ($p < 0.0001$) between the MGUS group (Mean:-0.29, SD:0.32) and the myeloma group (Mean:0.93, SD:0.51).

Conclusion: Our findings suggest that chemical shift imaging and magnetic resonance spectroscopy could be useful in differentiation myeloma from MGUS, therefore can help to decide the initiation of therapy.

C-0653

Investigation of trabecular bone structure by means of DTI techniques

S. Capuani, C. Rossi, F. Fasano, B. Maraviglia; Rome/IT

Purpose: An application of DTI techniques to trabecular bone marrow analysis to obtain structural information on spongy bone tissue was presented.

Methods and Materials: In trabecular bone tissue, molecular diffusion shows different properties along the different observation directions. In such anisotropic media it is necessary to introduce a diffusion tensor, D, that describes the mobility of Brownian particles. The set of all MR imaging techniques that enables us to determine the elements of such a tensor is known as Diffusion Tensor Imaging (DTI). In our study a PGSTE sequence was used to obtain a series of MR images from a bovine bone sample. The intensity of the gradient was varied for each of the seven directions of the diffusion sensitive-gradients and therefore, the experimental b-value varied as well. Starting from these images it was possible to

Scientific and Educational Exhibits

calculate the fractional anisotropy (FA) map, which measures the degree of anisotropy of the sample, and the mean diffusivity (MD) map, which allows monitoring of the general diffusion properties of the sample.

Results: The MD and FA images show different contrast with respect to conventional T2-weighted image, especially in trabecular bone region. In particular, the FA map appears more sensitive to orientated sample structures while MD provides information on mean pore size.

Conclusion: Our preliminary results show that MD and FA maps are more sensitive than conventional NMR imaging techniques to bone trabecular network microstructure. DTI maps might provide a powerful tool to improve diagnosis of bone diseases at an early stage.

C-0654

withdrawn by authors

C-0655

Effectiveness of ESWT (extracorporeal shock wave therapy) in treating pseudoarthrosis and delayed union

D. Rozzati, F. Cravero, A. Meni, G. Sessa, A. Stecco, A. Carrieri; Novara/IT

Purpose: To investigate the effectiveness of ESWT in the treatment of non-healed fractures of long bones or pseudoarthrosis, and which of these categories is more eligible to perform ESWT with a clinical success.

Methods and Materials: From March 2003 to March 2004, 10 female and 20 male (range 15-68 years) were treated. 15 patients had pseudoarthrosis and 15 delayed union of long bones. The fractures included diaphyseal fractures of femur, tibia, humerus, radius, ulna, scaphoid and metatarsus. Inclusion criteria were well assessed non-union of long bones fractures, defined as a failure to show bony union 6 months after initial closed or open treatment. Exclusion criteria were pregnancy, heart disease, neoplastic disease, coagulopathy, epiphyseal plate within the shock wave field, brain or spine within the shock wave field. The study was done with an HMT (High Medical Technologies) "Reflectron" ESWT system. An evaluation form to define the outcome of bony union was done for every patient. We applied the Mann Whitney U Test to evaluate statistically significant differences in percentage of success between the two groups.

Results: The treatment was successful in 8/30 patients (26%), 2/15 (13%) of the patients with pseudoarthrosis and 6/15 (40%) of patients treated for delayed healing of long bones fractures. We found a statistical significant difference between the percentages of success in ESWT in the two groups.

Conclusion: Results in our study show that ESWT can be considered a complementary therapy in the treatment of delayed union of long bones and pseudoarthrosis.

C-0656

Os trigonum syndrome: MR imaging findings in young athletes

A. Iovane, M. Galia, T. Bartolotta, F. Sorrentino, M. Midiri; Palermo/IT

Learning Objectives: To illustrate Magnetic Resonance (MR) imaging findings of the os trigonum syndrome.

Background: The os trigonum is an accessory bone of the foot, localized posterolateral to the lateral tubercle of talus. Even in the presence of os trigonum it is usually an asymptomatic condition; particular activities, such as ballet, running, soccer, football and volleyball may cause repeated stress and chronic micro-traumas to the hindfoot, resulting in the os trigonum syndrome, also called posterior ankle impingement syndrome (PAIS).

Procedure Details: Twenty-eight patients with a clinical diagnosis of PAIS, were submitted to MR, which was performed by using a 0.5 T superconductive MR unit with a dedicated extremities transmitter/receiver coil, and a 0.3 T dedicated MR unit. SE T1-w, GE T2*-w and STIR images were obtained in the axial, sagittal and coronal plane. Two experienced radiologists evaluated all MR studies in consensus. MR evaluation showed the following pathological changes: a) osteochondrosis changes of the os trigonum and neighboring bones, talus, calcaneus and tibia; b) soft tissue changes, represented by impingement between the os trigonum and the flexor hallucis longus tendon with distension of its sheath and distension of the posterior capsular recess consistent with presence of fluid or synovitis.

Conclusions: MR imaging allowed the correct identification of the os trigonum and characterization of the structural changes (osseous, cartilaginous, tendinous and capsular) taking place or associated with PAIS. Moreover MR may provide some important information concerning the biomechanics underlying disease development.

C-0657

Percutaneous radiofrequency ablation: Relationship between probe type, time of procedure and the extent of the osteonecrosis in a long bone dog model.

J. Martel¹, Á. Bueno¹, P. Domínguez¹, M. Nevado¹, P. Llorens², J. Quirós², C. Delgado²; ¹Alcorcón/ES, ²Madrid/ES

Purpose: We have been using radiofrequency ablation (RFA) for the percutaneous treatment of osteoid osteomas since 2001. Frequently, lesions are located near the joint surface, involve the vertebral body or are close to major nerves. We seek to determine whether RFA can be used safely in these cases.

Material and Methods: A total of 65 lesions were induced in 4 dogs. Each dog underwent RFA on the diaphysis of long bones, as well as femoral and humeral heads. Four different sessions were carried out by using 1 cm and 2 cm probes with or without a cool-tip system and varying the time procedure. Plain film, CT, and MR imaging were obtained. All bone samples were examined histologically.

Results: The activity of dogs after the procedure was normal. No complications were found. Cortical bone was respected. There was no damage to joint cartilage. Plain radiographs obtained *in vivo* demonstrated only the drill holes. CT showed a spherical lytic lesion with a sclerotic rim around the electrode tract. With MR imaging, the thermal lesions displayed low signal intensity with a sharp rim of high signal intensity and showed a good correlation with the pathologic measurement. There were no significant differences between lesion size, probe type and the duration of the procedure. The mean lesion diameter perpendicular to the electrode was 18.5 mm.

Conclusions: Our study confirms the insulative effect of cortical bone. RFA can be safely performed close to the joint surface without damaging the cartilage.

C-0658

Protocol optimization for analysis of trabecular bone structure with multislice spiral CT at the calcaneus for the assessment of osteoporosis

J.S. Bauer¹, P.V. Patel², S. Prevrhal¹, C. Phan¹, F. Eckstein³, E.-M. Lochmueller⁴, S. Majumdar¹, T.M. Link¹; ¹San Francisco, CA/US, ²North Chicago, IL/US, ³Salzburg/AT, ⁴Munich/DE

Purpose: With the spatial resolution of Multislice Spiral CT (MSCT) coming close to trabecular dimensions, visualization and analysis of trabecular bone structure becomes more feasible. The aim of this study was to optimize MSCT protocols for analysis of trabecular bone structure of the calcaneus and to compare these measures with bone mineral density (BMD) in their ability to differentiate donors with and without osteoporotic fractures of the spine.

Material and Methods: Forty-two formalin-fixed calcaneus specimens (mean age of donors: 81.2 ± 10 years) were imaged with a 16-detector MSCT system using four different scan protocols with varying spatial resolution ($400\mu\text{m}$ to $210\mu\text{m}$ in-plane) and radiation dose levels (90-120 kV and 150-300 mAs). Structure parameters of trabecular bone were derived from these images, and BMD of the calcanei was determined using dual energy X-ray absorptiometry (DXA). Fracture status of the spine was classified on conventional lateral post-mortem radiographs. Receiver-operator-characteristics (ROC) - analysis was performed to determine the diagnostic performance of BMD and structure parameters.

Results: Significant differences between both donor groups were found for structure parameters and BMD ($p < 0.05$). The highest ROC-values were found for the protocol with the highest spatial resolution and highest exposure dose. Apparent trabecular thickness was the structure parameter that obtained best results and stayed significant when corrected for BMD.

Conclusion: A high-resolution, high-dose MSCT protocol is required to sufficiently assess trabecular bone structure. Using such a protocol, structural parameters of trabecular bone of the calcaneus can be used to differentiate donors with and without osteoporotic vertebral fractures.

C-0659

MR imaging of bone tumors: A pictorial review

G.K. Schneider, R.M. Seidel, K. Remberger, D. Kohn, P. Fries; Homburg a.d. Saar/DE

Learning Objectives: To present MR imaging features of both benign and malignant tumors as well as tumor-like lesions. To demonstrate characteristics of benign and malignant tumors in MR imaging. To demonstrate important findings for staging and therapy planning.

Background: The therapy of bone tumors generally depends on the extent of the tumor, its growth behavior as well as its exact histological diagnosis. Although conventional X-ray is the basis of diagnosis, MR imaging today is the method of choice for evaluating the soft tissue components and extent of the tumor. Unlike

Scientific and Educational Exhibits

most of other imaging modalities MR imaging allows exact tumor staging, which generally is essential for treatment.

Imaging Findings: The aim of our exhibit is to show typical MR imaging patterns of malignant bone tumors such as osteosarcoma, Ewing sarcoma and metastases as well as benign tumors and tumor-like lesions (e.g. histiocytosis, aneurysmal bone cyst, chondroblastoma and others) and to explain important imaging findings for staging and therapy planning. Emphasis is laid on typical cases and special differential diagnosis by age specific algorithms. Additionally, the appropriate imaging technique is presented.

Conclusion: Adequate characterisation and staging is crucial for an optimal therapeutic approach to bone tumors. MR imaging reveals an excellent technique for the characterisation of bone tumors in addition to radiography.

C-0660

Comparison of DEXA, QCT and trabecular structure in beta-thalassaemia

M.D. Mylona, M. Leotsinidis, P. Andrikakos, A. Christopoulos, P.A. Dimopoulos; Patras/GR

Purpose: The assessment of β-thalassaemic spinal disease with DEXA and QCT, with emphasis on lumbar trabecular and cortical properties, assessed by HRCT.

Materials/Methods: Bone Mineral Densities (BMD) of 48 patients were expressed as Z scores, using values of sex- and age-matched controls and the results were correlated. The presence of hypogonadism, hypothyroidism, hypoparathyroidism, diabetes, backaches and fractures was recorded. The effect of age, sex, type of thalassaemia and hormonal factors on BMD was assessed. HRCT was performed in each vertebra with the lowest BMD, in order to estimate the cortex integrity and the number of trabeculae; the latter were classified to a three-grade scale.

Results: The overall prevalence of osteoporosis was 43.8% with DEXA and 6.3% with QCT. Both techniques revealed an inverse correlation between age and BMD and no difference between Thalassaemia Major and Intermedia (TM, TI) patients. Hormonal factors demonstrated associations with QCT and DEXA measurements. Patient's classification into normal, osteopenic and osteoporotic, using the number of trabeculae, was in better agreement with that of QCT's Z ($K = 0.209$, $p = 0.053$), than classification according DEXA's Z ($K = 0.145$, $p = 0.120$). Cortex evaluation by HRCT showed discontinuity in 15 patients (10 of 15 were TI).

Conclusion: Hormonal deficiency is associated with thalassaemic osteoporosis. Both methods indicate a progression of osteoporosis with age whereas the visual estimation of cortex indicates that TI could be more affected than TM. Regarding the number of trabeculae, as an indicator of osteoporosis, it seems that QCT may reflect osteopathy more accurately than DEXA.

C-0661

Computed tomography (CT) in monitoring of remineralization of bone metastases in patients treated with radiotherapy and ibandronate: Work in progress

C. Kalogeropoulou, V. Vassiliou, I. Tsota, D. Kardamakis, P. Sakellaropoulos, C. Katsarou, T. Petsas, I. Dimopoulos; Patras/GR

Purpose: To quantitatively evaluate the effect of external radiotherapy in conjunction with ibandronate on osteolytic bone metastases using CT and to correlate our results with the patient's clinical outcome.

Method: Eighteen patients with osteolytic bone metastases (11 males, 7 females; age range: 52 - 77) received radiotherapy with a 6-MV linear accelerator combined with a monthly infusion of 4 mg ibandronate. The total dose received was 30-40 Gy (1.8-2.0 Gy /fraction). CT scans were performed at the irradiated site before and 3 months after the treatment. Two radiologists contoured the osteolytic irradiated areas on the most representative CT slices (3-5 mm thickness). The same anatomical area was defined on the post treatment images. The delineated areas were analyzed as to density and the pre- and post-treatment values compared in ratios. The patient's clinical outcome was monitored by pain response, re-treatment rate, pathological fracture rate, spinal cord compression rate and quality of life.

Preliminary Results: The three months follow-up results were favorable since there was complete pain response in 15/18 patients. The re-treatment rate was 0/18, the pathological fracture rate was 1/18, and the spinal cord compression rate was 0/18. Quality of life was found to improve by an average of 3.94 out of 10 points (EORTC-QOL). CT density measurement changes in the region of bone metastases seemed to correlate with patient's clinical status.

Conclusion: CT-based bone density measurements could offer an objective method to assess the effect of treatment in patients with osteolytic bone metastases.

C-0662

Surface lesions of bone: A pictorial review

S. Takaø, M. Uetani, T. Yamaguchi, Y. Kawahara; Nagasaki/JP

Learning Objectives: To present an overview of imaging features of surface lesions of the bone with an emphasis on the plain radiographic findings. To describe the utility of other imaging modalities that assist in lesion characterization.

Background: A variety of tumor and tumor-like conditions originate from the surface of bone. They can arise within the cortex, between the cortex and the periosteum, within the periosteum, or in the tissues adjacent to the periosteum. Whilst some lesions have classical imaging features, many are nonspecific, and correlation with clinical information is often the key to the proper diagnosis.

Imaging Findings: Radiographic features are characterized by patterns of calcification, appearance of cortex and patterns of periosteal reaction. CT can assist in characterizing the origin, location and extent of the lesion. MR imaging is best for demonstrating soft tissue mass and bone marrow involvement and is therefore useful for pre-operative planning once a diagnosis is established.

Conclusion: Careful radiographic analysis with appropriate use of other imaging modalities is important to reach the proper diagnosis of surface lesions of the bone.

C-0663

Osteoid osteoma treated with percutaneous radiofrequency ablation: MR imaging follow-up

M. Lee¹, J. Ahn², J. Suh¹, H. Lim¹, E. Chung¹, N. Jung¹; ¹Seoul/KR, ²Iowa City, IA/US

Purpose: To assess the usefulness of MR imaging in follow-up evaluation of osteoid osteoma treated with CT-guided percutaneous radiofrequency (RF) ablation.

Materials and Methods: Fifteen patients with osteoid osteoma treated with RF ablation underwent MR imaging. The protocol required T1w, T2w and contrast-enhanced (CE) T1-weighted images with fat saturation at each visit, from immediately to 15 months after treatment (mean, 2.5 times; range of time interval, 1-7 months). MR images were evaluated by consensus of two reviewers, with regard to the appearance of treated areas including nidus, presence of abnormal findings such as fluid collection, and the best sequence for visualization of signal intensity (SI) changes. The therapeutic response was evaluated to be a clinical success with relief of pain.

Results: The treated areas had a characteristic "target" appearance at MR imaging: inner band (Z2), peripheral outer zone (Z3) surrounding central core (Z1). Z2 was hyperintense on T2WI with strong enhancement. Z3 was less hyperintense and less enhanced. Z1 was non-enhancing central zone with low SI on T2WI. All nidus were within Z1, showing low to intermediate SI on T1, T2WI. Target appearance became evident on MR images after 1 week following treatment. On follow-up, Z2 became thicker with fill-in enhancement into Z1, whereas Z1 was gradually decreased in size. Z3 showed diminishing enhancement and extent. No complications were found. CE-T1WI was best for visualizing SI changes. Clinical success was achieved in all patients.

Conclusion: MR imaging allowed accurate monitoring of treated areas for osteoid osteoma following RF ablation.

C-0664

Bone stiffness indices in patients having type I and type II diabetes mellitus based upon ultrasound osteometry of the calcaneum

V.D. Zavadovskaja, O.S. Shoulga, O.Y. Kilina, O.S. Tonkikh, E.S. Nigmatova; Tomsk/RU

Purpose: To assess bone stiffness in patients with diabetes mellitus of the 1st and 2nd type (DM 1-2) using ultrasound osteometry (UO) on the setting of peripheral flow disturbance.

Material and Methods: We studied 72 DM patients (18 males and 28 females aged 41.1 ± 6.7 years, 24 patients with DM-1 and 48 patients with DM-2). Angiopathy was revealed in 58% of DM-1 patients and in 36% of DM-2 patients. UO was performed using "Achilles Express" (Lunar, USA).

Results: Mean indices of SOS, BUA and STI (stiffness index) did not differ significantly in DM-1 and DM-2 patients. DM-1 patients revealed significantly higher osteoporosis frequency than DM-2 patients ($31 \pm 5\%$ versus $20 \pm 6\%$ respectively, $P = 0.001$). Frequency of osteopenia and osteometry normal indices did not differ in M-1 and DM-2 patients. STI indices of DM-1 patients with distal angiopathy were significantly lower than those of DM-1 patients without angiopathy ($P = 0.004$). Osteoporosis was revealed in 50% of DM-1 patients with distal angiopathy and was not revealed in those without angiopathy. Osteometry indices

Scientific and Educational Exhibits

and osteoporosis frequency did not depend on peripheral flow disturbances in DM-2 patients.

Conclusion: Based upon ultrasound osteometry, DM-1 patients reveal a higher frequency of osteoporosis compared to DM-2 patients. Bone metabolism disturbance is aggravated by distal angiopathy in DM-1 patients.

C-0665

Radiologic and magnetic resonance patterns of myeloma and differential diagnosis

J.J. Noguera, A. Alonso, E. De Luis, P.D. Domínguez, J.D. Aquerreta, O. Cosín; Pamplona/ES

Learning Objectives: To describe the four classical radiological patterns of myeloma on plain films. To correlate these four patterns with magnetic resonance imaging (MRI). To expose the main differential diagnosis of each pattern.

Background: Myeloma is a plasma-cell neoplasm with bone marrow affection, usually detected in the elderly population. The knowledge of MRI appearance of myeloma is needed due to the widespread use of MRI in the diagnosis and staging of myeloma.

Imaging Findings: Apart from the normal findings, four radiological patterns of myeloma have been typically described in plain films: a) Unique lytic lesion or plasmocytoma. b) Multiple lytic lesions or myelomatosis. c) Diffuse osteopenia and multiple vertebral fractures. d) Osteosclerotic myeloma, typically related with POEMS syndrome (very rare, 1%). Sensitivity of MRI is higher than plain film to detect osseous involvement by myeloma. In MRI myelomatous lesions appear as hypointense in T1 sequences and hyperintense in T2, in a poorly specific manner. Three MRI patterns are observed, with prognostic significance: a) Focal lesion, the most frequent appearance. b) Diffuse pattern. c) Variegated pattern, with multiple tiny foci of marrow affection and the best prognosis. These patterns in plain films and MRI are compared and illustrated.

Conclusion: MRI bone marrow surveys in patients with myeloma show a broad spectrum of involvement, with important prognostic significance. These patterns should be widely known by radiologists, as MRI will very probably be the diagnostic and staging tool of choice for myeloma instead of the plain film survey.

C-0666

Chondroblastoma: Radiographic and MR features

C. Blancas, J. Llauger, J. Palmer, E. Granell, N. Cañete; Barcelona/ES

Learning Objectives: To review and present the various imaging manifestations of chondroblastoma at different locations, emphasizing the role of MR imaging in its diagnosis.

Background: Chondroblastoma is an uncommon benign chondral tumor, which typically involves the epiphysis of long bones. 16 patients with histologically confirmed chondroblastoma were investigated with routine radiographs, MR imaging ($n = 13$), and CT ($n = 9$). The age and sex of the patient, location and size of the lesion, matrix calcifications, periosteal reaction, and signal characteristics were recorded.

Imaging Findings: Of the 16 patients with chondroblastoma, 12 were found in the epiphysis of the long bones, 3 around the hip, and one in the patella. Epiphyseal lesions were found in distal femur ($n = 6$), proximal humerus ($n = 4$), femoral head ($n = 1$), and proximal tibia ($n = 1$). The average size of the tumor was 3 cm in maximum diameter. Average age was 18.6 years. All lesions were well circumscribed. Mineralization was seen in 35% of lesions on radiographs or CT. On MR imaging, surrounding marrow edema was a prominent feature, as seen in 80% of the cases. Signal intensity on T2-weighted images was predominantly low to intermediate.

Conclusion: Chondroblastomas commonly manifest as well-defined epiphyseal lesions in young patients. MR imaging features of low to intermediate signal intensity on T2-W images and prominent surrounding edema are characteristic of this tumor.

C-0667

Added value of helical CT multiplanar reconstructions on the conventional transverse CT examination of the degenerative spine

S. Costa, L. Martí-Bonmatí, E. Arana, J. Forner, E. Mollá; Valencia/ES

Purpose: To analyse the diagnostic value of multiplanar sagittal and coronal reconstructions (MPR) in the CT evaluation of degenerative spine diseases, compared with CT axial slices.

Methods and Materials: A total of 170 patients were studied with helical CT (Phillips CT Aura). There were 50 cervical, 20 dorsal, and 100 lumbar spine examinations. Images were prospectively reconstructed in the transversal, sagittal

and coronal planes. The following variables were recorded: more affected disc abnormality, spondylolisthesis, spinal stenosis, degeneration of posterior articular facet joints, lateral foramina, and osteophytes. A global subjective comparison was established: axial better than MPRs, MPRs better than axial, or both of equal value. Statistical comparisons were obtained.

Results: Of the 170 patients, 125 showed discal pathology, with the transverse plane better analysing discal pathology with statistical significance. Conversely, all spondylolisthesis and most spondylolysis were undetected in the transverse images. Lateral foramina and osteophytes were better seen in the MPR images (which detected 29 foraminal stenosis and 32 osteophytes misdiagnosed in the axial plane) with statistical significance. On the contrary, there was good concordance in the evaluation of spinal canal stenosis and posterior facet joints. There were no differences between the different spinal segments.

Conclusion: Sagittal and coronal helical CT reconstructed images are quite useful in evaluating degenerative spinal diseases. The main additional valuable information is related to spondylolysis and spondylolisthesis, lateral foramina and osteophytes. A volumetric helical CT acquisition of the spine with posterior multiplanar reconstructions, at least in transversal and sagittal planes, is advocated.

C-0668

Standardization of BMD measurements in different DXA devices

M. Ucar, A. Özdemir; Ankara/TR

Purpose: To compare BMD values of AP lumbar and hip regions measured in two different DXA devices in one laboratory, and to investigate the efficiency of a standardization formula.

Materials and Methods: AP lumbar (L2-L4) and right hip BMD values were obtained in 100 women, consecutively in Lunar DPX-NT and Hologic QDR 4500 C DXA devices. Standardization of BMD values was done according to the method developed by ICSBM, using the European Spine phantom to obtain the specific constant value. Mean calculated sBMD values in two devices were compared with each other and with mean reported sBMD values, respectively.

Results: Mean lumbar BMD values were $0.950 \pm 0.117 \text{ g/cm}^2$ for Hologic and $1.068 \pm 0.135 \text{ g/cm}^2$ for Lunar ($p < 0.05$); mean sBMD values were $1.035 \pm 0.128 \text{ g/cm}^2$ for Hologic and $1.035 \pm 0.131 \text{ g/cm}^2$ for Lunar ($p > 0.05$). Mean hip BMD values were $0.798 \pm 0.114 \text{ g/cm}^2$ for Hologic and $0.895 \pm 0.111 \text{ g/cm}^2$ for Lunar ($p < 0.05$); mean sBMD values were $0.869 \pm 0.124 \text{ g/cm}^2$ for Hologic and $0.867 \pm 0.108 \text{ g/cm}^2$ for Lunar ($p > 0.05$). The difference between the mean values of BMD and sBMD were statistically important in each device ($p < 0.05$). Mean values of calculated and reported sBMD were also significantly different in each device ($p < 0.05$), which is probably related to manufacturers' references of ICSBM calculations based on models different from ours.

Conclusion: sBMD values should be used instead of BMD, whenever quantitative values are needed. However, reported sBMD values by DXA devices may not represent the model-specific sBMD values.

C-0669

Solitary bone lesions: Imaging approach and differential diagnosis

C. Mueller, T.G. Mang, W. Huber, H. Imhof, F. Kainberger; Vienna/AT

Learning Objectives: To demonstrate the imaging features of lytic and sclerotic solitary bone lesions. To recognize characteristic benign and malignant bone lesions on radiographs. To illustrate the optimal imaging work-up of indeterminate and malignant bone lesions.

Background: Radiographs are usually the first imaging modality in patients with bone pain. Therefore they play an important role in differentiating benign, so called "leave me alone" lesions from indeterminate or malignant bone lesions. To prevent unnecessary investigations or biopsies it is important to recognize the imaging criteria of benign bone lesions. Additionally it is essential to identify signs of malignancy on radiographs.

Procedure Details: We present the broad spectrum of benign and malignant solitary bone lesions on base of radiographs, CT and MR images. The imaging criteria that are helpful for differential diagnosis for these diseases will be discussed.

Conclusion: Radiographs are a useful diagnostic tool to identify characteristic benign bone lesions that need no further follow-up. If malignancy is suspected additional imaging studies with CT and MR imaging are needed for the subsequent diagnostic and therapeutic approach.

Scientific and Educational Exhibits

C-0670

3D structure analysis of the calcaneus using the scaling vector method in the prediction of osteoporotic spine fractures

D. Mueller¹, R. Monetti², S. Majumdar³, C. Raeth², E.J. Rummeny¹, T.M. Link³,
¹Munich/DE, ²Garching/DE, ³San Francisco, CA/US

Purpose: To investigate the trabecular bone structure of the calcaneus applying the new scaling vector method (SVM) on high resolution magnetic resonance (HR-MR) images. Using the SVM a 3D non-linear texture measure which takes into account the anisotropic nature of the trabeculae was extracted and compared with BMD in its diagnostic performance to differentiate post-menopausal patients with and without osteoporotic spine fractures.

Methods and Materials: Axial HR-MR images of the calcaneus were obtained in 76 women (40 postmenopausal women with osteoporotic spine fractures and 36 postmenopausal controls) at 1.5 T. A 3D-GE sequence was used with a slice thickness of 500 µm and in-plane spatial resolution of 195x195 µm². Structure analysis was performed using algorithms based on the anisotropic SVM, which respects the orientation of the trabeculae of the analyzed bone. In addition BMD measurements of the spine, calcaneus and proximal femur using dual energy X-ray absorptiometry (DXA) were obtained in all patients.

Results: Receiver operating characteristics (ROC) analyses were used to determine the diagnostic performance in differentiating both groups. In the comparison with BMD of the spine (AUC = 0.75), BMD of the calcaneus (AUC = 0.71) and BMD of the proximal femur (AUC = 0.84) the best results were found for the 3D SVM (AUC = 0.88).

Conclusion: The results of this study show that the new anisotropic algorithm based on a local 3D SVM which respects the orientation of the trabeculae may improve the diagnostic performance in differentiating postmenopausal women with and without osteoporotic spine fractures.

C-0671

Bone marrow invasion in patients with Hodgkin's disease: Prognostic value of scintigraphic data

S. Kanaev, S. Novikov, M. Gershovich; E. Shelkoplias, St. Petersburg/RU

Purpose: It has been demonstrated that in patients with Hodgkin's disease (HD) bone marrow (BM) scintigraphy (BMS) is significantly more sensitive and accurate than iliac crest biopsy. Prognostic value of scintigraphic data remains undetermined.

Materials and Methods: Since 1992 BMS was performed in 319 primary patients with HD. Whole body BM visualisation started 45-90 min after i/v injection of 8-10 MBq/kg of 99mTc-colloids. Scintigraphic signs of BM invasion (BMI) were classified as follows: localised lesions manifested by 1-2 focal defects, generalised involvement - by multifocal (3 and more) defects or diffusely diminished tracer uptake. BMI was confirmed by additional examinations (biopsy, MR imaging, bone scanning, X-ray). Patients with localised BMI underwent combined modality treatment: 6 cycles of chemotherapy and involved-field irradiation. Patients with generalised BMI received 6-8 cycles of chemotherapy without irradiation.

Results: From 1992 to 1998 BMS was performed in 319 primary patients with HD. BMI by HD was diagnosed in 56 (17.5%) cases: localised - in 39, generalised - in another 17 patients. For all 56 patients with BMI 5 year disease free survival was equal to 27% (15/56). Only 2 of 17 patients with generalised HD survived 5 years without HD: DFS - 11%. 5 year disease-free survival for patients with localised BMI by HD was equal to 33% ($p < 0.05$).

Conclusions: Scintigraphic pattern of BMI by HD has significant prognostic value: for localised BMI 5 year disease free survival it is 33%; for generalised BMI only 11%.

C-0672

Osteoid osteoma: A pictorial review

L.F. Foo, N. Raby, M. Sambrook; Glasgow/UK

Learning Objectives: To present the spectrum of imaging findings of osteoid osteoma.

Background: Osteoid osteoma is a painful benign bone-forming tumour, most frequently affecting children and young adults. Although typically a small lesion, rarely achieving a size greater than 1.5 cm, it has a tendency to incite marked peritumoural local tissue reaction. This may result in a wide spectrum of symptoms and imaging appearances, depending on the site of the lesion.

Imaging Findings: A pictorial review of imaging findings are presented, with an emphasis on the plain radiograph, isotope bone scan, CT and MR imaging appearances.

Conclusion: Osteoid osteomas display a wide spectrum of presentations. Most

lesions have characteristic imaging features. Those in unusual sites often present as diagnostic challenges, with atypical manifestations which may mimic and confuse.

C-0673

Imaging of spinal primary bone tumors in adults

M. Rodallec, L. Rillardon, M. Kalamardes, A. Feydy; Clichy/FR

Learning Objectives: To have an overview on the imaging findings of the most common primary bone tumors of the spine in adults. To be able to recognize the specific imaging features of some of these tumors.

Background: Primary bone tumors of the spine are relatively infrequent lesions compared with metastatic disease, multiple myeloma, and lymphoma. An accurate diagnosis is warranted, as the therapeutic approach differs between these two groups of tumoral lesions. A wide variety of benign bone neoplasms can involve the spine, including hemangioma, osteoid osteoma, osteoblastoma, aneurysmal bone cyst, giant cell tumor, enostosis, and osteochondroma. Common primary non-lymphoproliferative malignant neoplasms of the spine include chordoma and chondrosarcoma. The imaging features of these lesions of the spine are often characteristic and suggestive of the diagnosis.

Procedure Details: In this educational exhibit, we discuss and illustrate the most common benign and malignant primary bone tumors of the spine with radiographs, CT and MR imaging.

Conclusion: This educational exhibit provides a comprehensive review of the imaging findings of primary bone tumors of the spine. Radiologists should be aware of the typical imaging features of the most common of these tumors.

C-0674

Evaluation of the phenotype of an insertional mutation affecting the osteopontin (opt) gene in mice: A comparative pilot study using micro CT, radiography and histology

F.W. Roemer¹, M.L. Sohaskey², A. Mohr³, W.C. Skarnes², H.K. Genant⁴,
¹Augsburg/DE, ²Berkeley, CA/US, ³Kiel/DE, ⁴San Francisco, CA/US

Purpose: The *osteopontin (opt)* gene is a novel gene of undefined biochemical function. The aim of this study was the evaluation of micro CT and radiography for the morphologic assessment of the phenotype of *osteopontin (opt)* mutant mice in comparison to histology.

Material and Methods: 8 mice with insertional mutations in the *opt* gene and 4 wild-type controls (age 20 days) were evaluated radiographically, by micro CT and histologically. For the micro CT evaluation multiplanar reconstructions and 3D surface reconstructions were applied. The three modalities were compared regarding the detectability of bone pathologies.

Results: The *opt* -/- mice exhibited severe growth retardation in comparison to the *opt* +/- and +/+ mice. The radiographic examinations showed osteopenia and fractures with hypertrophic callus formation and pseudarthroses of the forelimbs and ribs. The radiographically detected fractures were verified by micro CT. Additional fractures not seen by radiography were detected by micro CT (radius and ulna n = 2, scapula n = 2, phalanges n = 11 artificial fractures n = 8, ribs n = 23). Histological analysis verified several of the micro CT-detected pathologies. Additionally, a disorganized non-columnar appearance of proliferating chondrocytes within the growth plates was observed histologically, as was reduced ossification in the -/- mice.

Conclusion: Micro CT is able to screen *opt* mutant mice for osseous pathologies and furthermore identify and classify these anomalies. The modality is superior to conventional radiography but is not able to identify cellular pathology or organization as could be shown by histology. However, histology is invasive and more time and material consuming than micro CT.

C-0675

The role of computed tomography examination with multiplanar and three-dimensional reconstructions in evaluation of cervical spine fractures

A. Siemianowicz¹, W. Wawrzynek¹, J. Baron², B. Koczy¹, S. Kasprowska¹,
¹Piekary Slaskie/PL, ²Katowice/PL

Purpose: To evaluate the role of CT examination including multiplanar and 3D reconstructions in the diagnosis of cervical spine fractures, especially in patients with false negative X-ray films and in patients whose X-ray films did not show all existing pathology.

Material and Methods: 71 patients aged 11-75 were admitted to hospital because of trauma, with suspicion of cervical spine injury. In all cases the CT examination was performed in the Radiology Department of Trauma Surgery Hospital in Piekary Slaskie. Helical CT scanner - Hi Speed CT^e GE Medical System was

Scientific and Educational Exhibits

used. The following examination conditions were applied: slice thickness 2 or 3 mm; reconstruction 2 mm; pitch 1.3; with automatic mAs selection. Multiplanar and three-dimensional reconstructions were performed. In some cases X-ray films were previously done in other hospitals.

Results: We often observed multi-level fractures and fractures of different parts of one vertebra. Fractures of C1 vertebra were observed in 10 patients, fractures of C2 in 21 patients, fractures of C3 in 12 patients, fractures of C4 in 15 patients, fractures of C5 in 27 patients, fractures of C6 in 17 patients, fractures of C7 in 8 patients. At levels C3-C7 in 20 cases we observed dislocation of bone parts into the vertebral canal with compression of the spinal cord. In some cases not all fractures were visible on X-ray films.

Conclusions: Application of CT examination technique with multiplanar and 3D reconstructions extends the possibilities of precise radiological diagnosis of cervical spine fractures ensuring the optimal choice of therapeutic method.

C-0676

The role of bone mineral density and risk factors with gonarthritis patients

J. Vasic-Vilic¹, N. Prodanovic¹, O. Jovanovic-Nikolic², S. Radovinovic-Tasic¹, B. Vukomancic¹, ¹Belgrade/YU, ²Podgorica/YU

Purpose: Recent findings showed connection of lower level of bone mineral density (BMD) and osteoarthritis stages. Obesity, general weakness, weakness of leg muscles, genetic factors and hormonal status influence the disease progress. The aim was to determinate BMD and compare them to gonarthritis radiographic stages, in female and to determinate percent of known risk factors.

Methods and Materials: Since October 2002 to April 2003 we carried out measurements, which included 86 women with gonarthritis, with average age of 66 with the 2nd, 3rd and 4th radiographic stages. We determined body mass index (BMI), physical activity. We established the percents of hormonal imbalance and investigated living environment. The BMD was measured on the femur with LumarDEXA2000.

Results: Knee joints radiographs confirmed osteoarthritis of the 2nd stage in 37 female patients (groupA), of the 3rd stage in 43 patients (groupB), and of the 4th stage in 16 (groupC). GroupA: 22 patients had a normal BMD, osteopenia BMD level, with an average Tscore-1.57SD was detected in 14 patients,osteoporosis was found in 1 patient,with an average Tscore-2.55SD. GroupB: 13 patients had a normal BMD, BMD at the osteopenia level, with an average Tscore-1.72SD was found in 22 patients, and osteoporosis was found in 8 patients,with an average Tscore-1.68SD. GroupC: normal BMD was detected in 5 patients,BMD at the level of osteopenia with an average Tscore-1.57SD was detected in 7 patients,while a lower BMD at the osteoporosis level, with average Tscore-2.74 was found in 4 patients. 22(A), 33(B) and 11(C) patients had lower muscles power, 20(A), 24(B), and 9(C) had the high BMI. In 9 (A), 12(B) and 7 patients (C) was detected hormonal imbalance. Planned physical activity was carried out by 7 patients (A), 12(B) and 8(C). 8 patients (A), 14(B) and 12(C) lived in villages. 18 patients (A), 21(B) and 10(C) had the positive genetic.

Conclusion: Research showed strong correlation between more severe radiographic stages of gonarthritis (3rd and 4th) and decreasing of BMD. This conclusion indicates the necessity for BMD measurement with gonarthritis patients. Muscle power, BMI and the physical activity are important for developing osteoarthritis; it is necessary to apply adequate physical therapy.

C-0677

Imaging of calcaneal tumours: Radiologic-pathologic correlation

B. Rodriguez-Vigil, D. Bernabeu, C. Martín Hervas, F. Lopez Barea, E. Fernandez Canabal, N. Gomez León; Madrid/ES

Learning Objectives: To analyse and illustrate a wide spectrum of bone neoplasms involving the calcaneus in infancy and adulthood. To understand the radiologic features on the basis of pathologic correlation.

Background: The incidence of calcaneal tumours is low. Bone tumours involving the calcaneus as the sole site constitute an uncommon finding, with few cases reported. Both benign and malignant neoplasms can be found. Since early diagnosis is crucial for prompt therapy, imaging plays an essential role. Plain radiograph is the primary modality in the diagnostic approach. Computed tomography (CT), magnetic resonance imaging (MRI) and bone scan may also help establish the diagnosis.

Imaging Findings: We retrospectively reviewed the imaging findings of all the bone tumours of the calcaneus from our musculoskeletal pathology database. Fourteen bone tumours affecting the calcaneus were found. Plain X-rays were performed in all the patients, CT in 9 cases, MRI in 8 cases, and bone scan in 4 patients to assess for metastasis. Findings were correlated with pathology (biopsy or surgery) in all the cases. Specific neoplasms addressed include benign

(intraosseous lipoma, chondromyxoid fibroma, benign fibrous histiocytoma, solitary bone cyst, benign schwannoma) and malignant tumours (Ewing's sarcoma, osteogenic sarcoma, malignant hemangioendothelioma, solitary calcaneal metastasis). Imaging and pathologic features are discussed. Diagnostic difficulties, as well as pitfalls and differential diagnoses are emphasised.

Conclusions: Bone tumours of the calcaneus are rare. Since we will show different types of neoplasms affecting the calcaneus, this exhibit will help the radiologist to better understand and recognise them.

Scientific and Educational Exhibits

Musculoskeletal

Joints

C-0678

High field magnetic resonance imaging of reconstituted articular cartilage: Evaluation of cartilage maturation for determination of optimal transplantation time

M.H. Fuchsjäger, V. Mlynarik, S. Marlovits, M.O. Philipp, S. Trattnig; Vienna/AT

Purpose: To assess growth and maturation in reconstituted articular cartilage in-vitro and to compare it with histology findings.

Materials and Methods: Six specimens, consisting of collagen matrix with autologous chondrocytes transferred on its surface, were examined on a 3 T-whole-body scanner using a micro-imaging gradient system. Specimens were cultivated in standard and simulated conditions. T1-weighted inversion recovery spin-echo and T2-weighted multiple spin-echo images of specimens were acquired with in-phase resolution of 0.27 mm. Diffusion maps were measured using the pulse gradient spin echo experiment. In-vitro cultivation for all specimens started the same day, measurements were obtained after 14, 28, 42, 56 and 70 days. Afterwards cell constructs were analyzed histologically and with molecular biology.

Results: Cultivated specimens demonstrated a slight increase of T1 and T2-relaxation times and apparent diffusion constants, followed by a drop in values after 70 days. Histological evaluation revealed a continuous increase of glycosaminoglycan until day 42. Total number of chondrocytes was constant under simulated conditions and showed a slight drop under standard conditions beginning after day 28. Apoptosis index showed a peak for both types of cultivation at day 56. The primary architecture of collagen membranes gradually dissolved over the study period. Decrease of relaxation times corresponded to degradation of specimens in histology.

Conclusion: MR-imaging of cartilage implants in vitro may help to determine optimal transplantation time.

C-0679

Pitfalls in MR arthrography of shoulder

F. Cravero, M. Barini, A. Puppi, M. Lovisolo, A. Stecco, A. Carriero; Novara/IT

Learning Objectives: The evaluation of MR arthrograms is complicated by several procedural, technical and anatomic pitfalls that can be confused with pathologic abnormalities; our objective is to review, illustrate, classify and eventually find solutions to avoid the most important of these.

Background: Shoulder MR arthrography is mandatory in evaluation of the glenoid labrum, glenoid cartilage, gleno-humeral-ligaments, rotator cuff lesions, and capsular and periosteal lesions that can be found in shoulder instability, traumatic injuries, overhead athletes and also in the evaluation of the postoperative shoulder.

Imaging Findings: Analyzing our electronic archives we grouped these findings into three classes: (1) "iatrogenic" artifacts; (2) technical artifacts and (3) anatomic variants. "Iatrogenic" artifacts include extra-articular injection of contrast media, presence of intra-articular gas and degradation of contrast material solution. The most important technical artifacts are the magic angle effect and the transitional zone that can be mistaken respectively for tendinosis or SLAP lesions. Anatomic variations include the three categories of capsular insertion, the variable morphology of the anterior and posterior parts of glenoid labrum, the sublabral recess, or sulcus; sublabral foramen, or hole; and Buford complex. For each type we have analyzed the main elements of differential diagnosis with similar pathological findings and we have tried to find the technical and methodological solutions.

Conclusion: Knowledge of the typical location and MR appearance of pitfalls aids the radiologist to avoid technical errors and in evaluating MR arthrography images of the shoulder.

C-0680

withdrawn by authors

C-0681

MR imaging of traumatic elbow injuries with arthrographic, sonographic, clinical and surgical correlation

J.S. Weaver, J.A. Jacobson, M. De Maeseneer, M. Kalume Brigido, Y. Morag, D.A. Jamadar; Ann Arbor, MI/US

Learning Objectives: The learning objectives are to describe the spectrum of MR imaging findings of common traumatic elbow injuries and to correlate these with arthrographic, sonographic, clinical, and surgical findings.

Background: A computerized database was searched to retrieve all elbow MR examinations performed from September 2003 to September 2004 at our institution. Images from MR examinations of the elbow of 43 patients were retrospectively evaluated and characterized. MR imaging findings were compared to arthrographic and sonographic findings where available. Clinical data and operative reports were also reviewed.

Procedure Details: 43 patients were identified (35 male, 8 female; mean age 35 years) with injuries sustained during sporting events, recreational activities, motor vehicle accidents, falls, and occupational over use. Injuries include ulnar collateral ligament tears/sprains, lateral and medial epicondylitis, ulnar neuropathy/edema, common flexor and extensor tears/tendinosis, loose bodies, osteochondral defects, biceps and triceps tears/tendinosis, and ganglion cysts. These injuries will be demonstrated with MR, as well as with MR arthrography and sonography where available. The utility of dynamic sonography in the diagnosis of ulnar collateral ligament pathology will be demonstrated. Pearls and pitfalls, and differential diagnoses will be discussed.

Conclusion: MR imaging can accurately identify the extent and location of elbow abnormalities following traumatic injury. MR arthrography and sonography also play an important role in post-traumatic imaging. Dynamic sonography can aid in the diagnosis of ulnar collateral ligament pathology, while arthrography can provide added sensitivity and specificity in detecting ulnar collateral ligament tears.

C-0682

MR arthrography of the shoulder joint: A pictorial review of technique, anatomy and expected range of pathology

R. Bhat, T.B. Oliver; Dundee/UK

Learning Objectives: To illustrate the technique of MR shoulder arthrography, demonstrating normal anatomy, common pathologies, normal variants and pitfalls.

Background: MR arthrography is the most accurate method of assessing internal derangement of the shoulder. It is minimally invasive. Although most commonly performed in patients with uni or multidirectional instability, it also has a role in evaluating the superior labrum (SLAP tears), intra-articular loose bodies and the rotator cuff. Good technique, knowledge of normal shoulder anatomy and its variations and an understanding of the various capsular, tendinous and labro-ligamentous abnormalities which are often subtle to the untrained eye allow accurate diagnosis and guidance of treatment in patients who are often young, active and have high therapeutic expectations.

Procedure Details: In our institution we perform direct MR arthrography for assessment of a range of shoulder disorders. Up to 20 ml of a gadolinium, iodinated contrast and saline mixture is injected into the shoulder under fluoroscopic guidance; the volume injected depending on the laxity of the capsule. T1 fat saturated sequences in three orthogonal planes are obtained using a 1.5 T MR system. A STIR sequence is performed to evaluate bone marrow oedema and a further T1 fat saturated sequence in abduction and internal rotation (ABER) may be added to evaluate subtle anterior labral tears.

Conclusion: MR arthrography is a very useful technique. A detailed knowledge of the anatomy and familiarity with the common abnormalities is essential for interpretation.

C-0683

MR features of ankle impingement syndromes

H. Aniq, S.A. Babar; Liverpool/UK

Learning Objectives: To illustrate MR features of various impingement syndromes around the ankle joint which can be a cause of chronic ankle pain.

Background: Soft-tissue and osseous impingement of the ankle is increasingly recognized as the cause of chronic ankle pain especially in a younger population. These conditions arise from initial ankle injuries leading to development of abnormal osseous and soft-tissue thickening within the ankle joint. Impingement syndromes have been well described in the anterolateral, anterior, and posterior ankle but recently anteromedial and posteromedial entities have also been described.

Procedure Details: We describe the MR appearances of all the impingement syndromes around the ankle. A brief anatomy of the ankle joint and its various compartments and ligaments is presented initially followed by key points in diagnosis; diagnostic difficulties and various differential possibilities are discussed. Conventional radiography is usually the first imaging technique performed and allows assessment of any potential bone abnormality, particularly in anterior and posterior impingement. CT scanning and isotope bone scanning has been superseded by magnetic resonance imaging (MR). MR can not only identify the relative contribution of both soft tissue and bony abnormalities but it is also quite accurate in assessing the capsular injuries.

Conclusion: Knowledge of the typical MR imaging appearances of various impingement syndromes is useful in determining the cause of chronic ankle pain.

Scientific and Educational Exhibits

C-0684

Acute knee trauma: Sonographic emergency?

B. Diris, O. Bonnefoy, O. Hauger, M. Moinard, F. Diard; *Bordeaux/FR*

Purpose: The purpose of this study was to determine the diagnostic accuracy of high spatial resolution ultrasonography (US) in the detection of lipohemarthrosis of the knee and to evaluate this sign as a criterion of intra-articular fracture.

Materials and Methods: Forty-five patients were prospectively examined for a possible knee fracture with clinical examination, conventional radiography, US and computer tomography (CT) imaging within 96 hours of trauma. Changes in the US appearance of the supra-patellar collection were evaluated without knowledge of the CT results and an intra-articular fracture was suspected if lipohemarthrosis with two or three layers was present.

Results: At CT, 65% of the patients with acute trauma have intra-articular fractures with visualization of a lipohemarthrosis in 96% of cases. At US, 93% of those patients with proven intra-articular fractures have positive results (lipohemarthrosis) with false-positive results in one case and false-negative results in two cases. The sensitivity, specificity, positive predictive value, negative predictive value of US in the diagnosis of lipohemarthrosis was respectively 96%, 100%, 100%, 94% compared with 55%, 100%, 100%, 55% obtained for conventional radiographs. Using lipohemarthrosis as a criterion of fracture, the sensitivity, specificity, positive predictive value and negative predictive value of US for early detection of intra-articular knee fractures were respectively 93%, 93%, 96% and 87%, compared with 85%, 87%, 92%, 76% obtained for conventional radiographs

Conclusion: High resolution US is a reliable and accurate method to evaluate intra-articular fractures of the knee. Lipohemarthrosis is the diagnostic key.

C-0685

Prognostic value of reactive interface in femoral head osteonecrosis on magnetic resonance imaging

I. Sedonja¹, V. Jevtic², M. Milcinski²; ¹Murska Sobota/SI, ²Ljubljana/SI

Purpose: The aim of our study was to assess prognostic value of reactive interface (RI) in femoral head osteonecrosis (FHO) on magnetic resonance imaging (MRI) in early stages of disease.

Patients and Methods: In 46 hips in 40 patients (29 M, 11 F, 20-64 y, mean 41 y) with radiographic stage 1 and 2 of FHO T1-weighted, STIR and fat-suppression T1-weighted images enhanced with gadolinium-DTPA in coronal plane were performed. Width of hypointensive line on T1 W MRI, hyperintensive part of RI on STIR and enhanced part of RI on Gd-enhanced images were measured on mid-coronal slice and expressed in % of femoral head diameter (%fhd). RI were classified into narrow RI - less than mean value of RI in all hips on same sequence and wide RI - mean value or more. 39 conservatively treated hips were evaluated for eventual FH collapse.

Results: In 12/46 hips (26.1%) border line was not seen on mid-coronal slice. Width of RI was different (SE T1 W MRI: 2.3 to 12.5%fhd, mean 4.6, SD 2.05; STIR: 2.2 to 12.5%fhd, mean 4.2, SD 1.75; Gd-enhanced MRI: 2.3 to 4.4%fhd, mean 3.2, SD 0.51). Heads with wide RI on MRI collapsed more frequently and earlier (SE T1 W MRI: no visible RI - 0/10; narrow RI - 2/17 (11.8%) in mean 8.3 months; wide RI - 8/12 (66.7%) in mean 3.4 months; chi square, p < 0.01).

Conclusion: Wide RI on MRI in early phase of FHO is bad prognostic factor for head collapse.

C-0686

Imaging features of tarsal coalition

Y. Roca Vanaclocha¹, J. Narvaez², E. De Lama², L. Mones¹, C. Pozuelo¹, C. Medrano¹, D. Mulattieri¹, A. Sanchez²; ¹Badalona/ES, ²Barcelona/ES

Learning Objectives: The aim of this exhibit is to illustrate the distinguishing features of tarsal coalition and emphasize the importance of the different imaging techniques. We will also discuss the adequate protocols.

Background: Congenital tarsal coalition represents the failure of normal segmentation between two tarsal bones. Coalitions may be osseous, cartilaginous, or fibrous. The usual symptoms, which appear when the abnormal union begins to limit inter-tarsal motion, are foot rigidity and pain, relieved by rest. Clinical diagnosis is sometimes difficult, especially in non-osseous types, which are difficult to detect on radiographs. We performed a retrospective study from records between 1994-2003, and 35 cases were found. Talo-calcaneal coalitions were mostly encountered. Images (radiographs, CT and/or MRI) were interpreted by consensus of two radiologists.

Imaging Findings: Conventional radiographs are essential for screening. They may be normal or show secondary indirect signs such us talar beaking, absent middle facet and C sign. Cross-sectional imaging with CT or MR imaging is indi-

cated to confirm the presence and extent of the coalition. CT clearly demonstrates any osseous coalition and fibrous coalition is characteristically shown as joint space narrowing with irregular cortical margins. MR imaging depicts non-osseous fibrous and cartilaginous coalitions. Bone marrow edema and associated joint and tendon abnormalities can be also visualized.

Conclusion: Congenital tarsal coalition is a frequent cause of foot pain and ankle sprains among young patients. Being a generally overlooked diagnosis, it is important to be familiar with the features on the different techniques, so that early adequate treatment can be considered.

C-0687

Long-term follow-up of total knee replacement: Role of high resolution ultrasound

E. Gallardo¹, R. García-Barredo², J.R. Prieto¹, J. García¹; ¹Santander/ES, ²Liencres/ES

Purpose: To describe the normal sonographic findings in long-term total knee replacement (TKR) and to emphasise the abnormalities that can be depicted in cases of painful prostheses.

Materials and Methods: We reviewed 75 TPK performed before 1993. Time since the surgical procedure ranged from 10 to 15 years (average time = 11.5 years). They were 55 patients, 43 women and 12 men (average age = 76.5 years). The radiological study included anteroposterior and lateral radiographs and a Merchant's view. The sonographic study was performed using a 7-10 MHz linear transducer in the supine position, evaluating: polyethylene thickness, bone-to-metal interface, extensor mechanism, joint effusion and synovial thickening.

Results: Thinning of the polyethylene liner was present in 80% of the cases, more severe in the medial compartment. In 30% of the knees we demonstrated an abnormal increase in the metal-to-bone interface. Synovial thickening was shown in 66% of the cases with characteristic findings of metallosis in 3 of them. Post-surgical patellar tendinitis was detected in all patients and heterotopic ossification in 30% of them.

Conclusion: Sonography is a useful method to evaluate peripheral polyethylene liner, metal-to-bone interface, extensor mechanism and synovial thickening. It is also a valuable technique in detection of late complications of TKR such as: polyethylene wear, aseptic loosening, synovitis and extensor mechanism dysfunction. Sonography can be recommended, especially in pre-operative planning of painful prostheses.

C-0688

Intra-articular fat tissue tumors of the suprapatellar recess: Magnetic resonance imaging with pathological correlation

E. Gallardo¹, J. Figols¹, E. Sanchez¹, R. García-Barredo², R. Landeras¹, M. Fernández¹; ¹Santander/ES, ²Liencres/ES

Learning Objectives: To describe the MR characteristic findings of fat tissue tumors affecting the suprapatellar recess of the knee. To emphasise the clues in the differential diagnosis between true tumors and fatty synovial proliferation.

Background: Lipoma is the most common soft-tissue tumor, accounting for up to one half of all subcutaneous tumors. However, intra-articular lipoma is exceedingly rare with a few reports in the literature. On the other hand, lipoma arborescens is currently recognised as a reactive process secondary to degenerative joint disease and not truly a neoplasm, consisting in the proliferation of fatty tissue in the subsynovial connective tissue of joints, most commonly found in the knee.

Procedure Details: 5 patients with lipoma arborescens affecting the suprapatellar recess of the knee were reported in our unit over a period of 2 years (3 female and 2 male). During the same period, we diagnosed 3 true fatty tumors in a suprapatellar location, 1 lipoma and 2 liposarcomas, all of them pathologically proven. All MR studies were performed in a high field scanner, 1.5 T (Signa GE), using T1- and T2-weighted sequences in three planes, and fat suppression images after gadolinium administration.

Conclusion: MR is an excellent method for the diagnosis of lipoma arborescens and true fatty tumors of the suprapatellar recess with an excellent correlation with the pathological findings. This distinction becomes clinically important because the treatment and surgical approach differs between the two entities.

Scientific and Educational Exhibits

C-0689

Clinical and radiological characteristics of spontaneous osteonecrosis of the knee

E. Pérez, A. Sanchez, J. Narváez, D. Martínez de la Haza, E. Merino, X. Mallol; Barcelona/ES

Purpose: To review the Spontaneous Osteonecrosis of the Knee (SONK) in terms of clinical and radiological characteristics and its MR imaging patterns.

Materials and Methods: A retrospective review was performed on all the patients diagnosed with SONK by MR imaging at our institution between June 1994 and June 2004. Clinical charts, plain radiographs (when available) and MR imaging were evaluated. In MR imaging location, morphology and signal pattern of the necrotic lesion and associated findings (bone marrow oedema, cartilage, articular affection, meniscus rupture or degeneration, synovitis, existence of stress fractures and arthropathy) were analysed.

Results: 84 patients underwent our study (48 women and 36 men), aged 50-86. The clinical diagnosis was of internal meniscopathy in more than 75% of cases and radiographs did not show osteonecrosis in more than 50%. Location was unilateral in all cases except from one, involving the internal femoral condyle in 91% and internal tibial plateau in 9%. In 55 patients (65%) oedema was observed, and in 73% of cases a subcondral well defined lesion, hypointense in all sequences. Evidence of meniscal degeneration or rupture was present in 73% of cases, arthropathy in 80% and stress fractures in 5 cases (6%). Differential diagnosis with other pathologies of the knee, including secondary osteonecrosis is discussed at this point.

Conclusion: SONK is a difficult clinical diagnosis that must be suspected in aging patients with acute knee pain. MR imaging provides a precise diagnosis, when radiographs are normal or not conclusive with a characteristic pattern, which was observed in the majority of our patients.

C-0690

MR imaging in assessing the changes of rheumatoid arthritis of hand

O.V. Mazurenko, Y.S. Babiy, E.A. Garmish; Kiev/UA

Purpose: To investigate diagnostics of rheumatoid arthritis (RA) in hand using MR imaging and to study the role of MR imaging for evaluating of treatment effectiveness by defining disease activity.

Methods: 24 patients who fulfilled 1987 American Rheumatologic Association (ARA) criteria for RA, with disease duration 6-37 months, mainly II degree of disease activity, (age: 19-62 yrs) were examined in this investigation. All patients (1st group) were observed by MR imaging and conventional radiography (CR) underwent clinical and laboratory measurements, 9 patients of them (2nd group) were examined by all methods before and 12 months after administering anti-rheumatic treatment. T1-SE, T1-GE axial and coronal images were obtained before and after contrast enhancement (Omniscan®, Nycomed Imaging AS, Norway). Each hand was divided into 11 regions of interest. The quantification assessment of erosions and subchondral cysts, synovial membrane hypertrophy, joint effusion and tenosynovitis were examined. A total number of 273 regions of interest were investigated.

Results: In the 1st group, 285 MR imaging-erosions and subchondral cysts, 106 CR-erosions, joint effusions in 16 patients, tenosynovitis in 19 patients, synovial membrane hypertrophy of different degrees in all patients were found. In the 2nd group, in the first investigation, 170 MR imaging-erosions, 50 CR-erosions were detected; in the second investigation, MR imaging visualized 175 erosions, 67 erosions were found by CR.

Conclusion: These data demonstrate that all components of synovitis complex in RA of hand can be determined by MR imaging, it is important for diagnosing RA and monitoring the effectiveness of treatment, particularly in early stages.

C-0691

SLAP lesions of the glenoid labrum: An imaging study with anatomical correlation

L. Meziti, J.-L. Drapé, A. Mirat, E. Pessis, C. Duffaut-André, H. Guerini, S. Malan, A. Chevrot; Paris/FR

Purpose: Superior labrum anterior-posterior lesions (SLAP lesions) are well described but their characterisation remains difficult given the presence of numerous anatomical variants of the glenoid labrum. Our purpose is to show the different SLAP lesion types and patterns at CT arthrography and MR-arthrography.

Materials and Methods: Retrospective study on 20 patients aged 20-40 years, including sports players (n = 15). All patients had either a multidetector CT-arthrography (n = 15) or an MR-arthrography (n = 5) for a superior labral lesion. All patients had an arthroscopic surgery with anatomical correlation.

Results: Based on the international arthroscopic classification from Snyder, we identified the following SLAP lesions: Type I (n = 4/20), Type II (n = 12/20), Type III (n = 2/20) and Type IV (n = 2/20). We submit a pictorial checklist, which should help to recognize the different lesion types, differentiate anatomical variants (sublabral recesses) from type II lesions and identify the differential diagnoses such as impingement, sublabral hole or Buford complex.

Conclusion: Unstable types II and IV lesions that need arthroscopic surgery and treatment (fixation) must be recognised at CT or MR-arthrography. CT-arthrography remains our preferred imaging modality.

C-0692

Rehabilitation and radiographic imaging of the joints in the post-electrical injury course

M.D. Mylona, M.T. Karamessini, P. Salonikidis, E. Mentzelopoulou, P.A. Dimopoulos; Patras/GR

Learning Objectives: To illustrate the radiographic findings of the joints in electrically injured patients admitted to our rehabilitation center, days to months after the original injury.

Background: Patients with electrical injuries have problems which are unique and they are subjected to two types of trauma: the insult caused by the acute event and complications which occur mostly because of poor positioning, bulky dressings, intramuscular injections and neurotoxic medications. In this exhibit we will describe and illustrate the radiographic findings of the joints in these patients.

Imaging Findings: The most common radiographic finding was bridging extra-articular heterotopic ossification (HO) with preservation of the underlying joint, developed in the elbow, shoulder, knee, hip, distal femur and fibula. It occurred most frequently about the elbow and it was not related to "entrance and exit" wounds; some patients eventually developed bilateral elbow disease. In some cases of HO spontaneous resolution occurred. In few patients with joint pain and normal X-rays, CT scans and ultrasound were performed and revealed soft tissue structures like blood vessels and nerves near the joint, findings which were attributed to HO of early stage. Another radiographic finding was intra-articular fusion and joint destruction due to associated fractures or necrotic tissues and osteoarticular changes, in joints close to "entrance and exit" wounds. Periarticular osteoporosis was also revealed in many cases.

Conclusion: In most cases, X-rays allow noninvasive diagnosis and follow-up of joint abnormalities in the rehabilitation course of electrically injured patients.

C-0693

Extracorporeal shock waves therapy (ESWT) of calcific tendinitis of the shoulder: Clinical and radiologic evaluation

F. Cravero, D. Rozzati, A. Meni, G. Sessa, A. Stecco, A. Carrieri; Novara/IT

Purpose: We present our experience in the evaluation of the effectiveness of extracorporeal shock waves therapy (ESWT) in patients with symptomatic calcifying tendinitis of the shoulder.

Materials and Methods: Between March 2003 and September 2003, 50 patients (21 men and 29 women) with an average age of 53 years, with painful shoulder calcifying tendinitis, were treated with shock waves using Reflectron (High Medical Technology, Kreuzlinger, Switzerland). All patients received four treatments of 600 shock waves per treatment in two weeks. Two criteria were used in the follow-up examination: subjective pain evaluation and X-ray analysis of calcareous deposits. Clinical follow-up of subjective pain was evaluated six and twelve weeks after the last treatment by comparing with the pre-treatment status. All patients had a radiological follow-up two months after ESWT.

Results: In the evaluation of subjective pain after 6 weeks the results showed that: 19 patients (38%) were pain free, 26 (52%) had improved symptoms and 5 (10%) experienced no change. After 12 weeks 20 patients (40%) were pain free, 26 (52%) had improved symptoms and 4 (8%) experienced no change. Radiological follow-up showed that: 12 patients (24%) were completely free of calcareous deposits, 26 (52%) had notable disintegration and 12 (24%) were unchanged.

Conclusions: ESWT can be considered an additional treatment for patients with calcifying tendinitis of the shoulder.

C-0694

Shoulder MR arthrography: Intra-individual comparison of two dimensional vs. three-dimensional with virtual arthroscopy pulse sequences

S. Nicolazzini, A. Puppi, M. Lovisolo, A. Stecco, P. Fornara, A. Carrieri; Novara/IT

Purpose: Aim of the present work is the demonstration of accuracy and sensitivity of 3D compared to multiplanar 2D multiple acquisition in MR arthrography (MR-art).

Scientific and Educational Exhibits

Methods and Materials: We evaluated 16 patients; after MR-art examination they underwent arthroscopic or surgical treatment (gold standard). MR-art has been conducted with percutaneous anterior palpation-guided access; all patients were evaluated with 3D standard MR-arthrographic sequences (SE T1, GRE T1 FATSAT), and supplemental 3DSpoiledGradientEcho T1 slab positioned in the coronal plane.

Results: The access was successful in 16/16 cases. No complications were recorded. Total scan time of 2D was 19 minutes, while 3D sequences required additional 9 minutes. 3DSPGR allowed up to 1 mm slice thickness, while 2D pulses thickness reduced only to 4 mm, to optimize S/N ratio and acquisition time. 31% patients showed Bankart or SLAP lesion at 2D MR, while 3D revealed 2 more (43.7%) patients with SLAP lesion, all confirmed arthroscopically. 56.2% revealed supraspinatus tendon tear at 2D MR evidenced one more case (62.5%), with small partial tendon tear; in one case we evidenced a medium gleno-humeral ligament (MGHL) was thickened. Affidability and sensitivity of 3D in detecting glenoid labrum tears were 87.5% and 93.7%, while 2D pulse had 81.2% and 62.5%; for tendon tear were 100%-100% vs. 93.7%-90%. Virtual Arthroscopy (VA) was performed in all cases, with 30 min mean workstation time for each patient, resulting able to depict correctly the labial tears, the MGHL and tendon ruptures in all cases.

Conclusion: VA images resulted helping in surgical planning but time-consuming.

C-0695

MR imaging vs. arthroscopy in the evaluation of tibio-talar joint impingement

E. Stavroulis, L. Zugaro, N. Limbucci, A. Barile, V. Calvisi, C. Masciocchi; L'Aquila/IT

Purpose: To assess MR imaging diagnostic accuracy in detecting pathological conditions leading to tibio-talar joint (TTJ) impingement, having arthroscopy as a gold standard.

Methods and Materials: 42 patients (aging 19-37 years) clinically complaining of ankle unsteadiness and swelling entered this study; 30 of 42 patients (71.4%) referred a history of ankle sprain. MR imaging examination was performed with both a 1.5 T whole-body (TSE-T2w and SE-T1w sequences) and a 0.2 T dedicated system (SE-T1w and T2w sequences). In 12 cases i.v. contrast agent was administered followed by SE-T1w sequences with fat saturation pulse. All patients underwent arthroscopy.

Results: MR imaging examination revealed the presence of TTJ synovial impingement in 15 patients (35.7%) and in only 5 of them, the presence of contrast enhancement revealed an acute inflammatory stage; arthroscopy always detected a thickened synovial lining. In 7 patients (16.6%) MR imaging showed the presence of tibio-peroneal tendon injury associated with synovial hypertrophy ("meniscoid syndrome"); in 1 of these cases contrast enhancement was evident. In 17 patients (40.7%) MR imaging documented the presence of a bony impingement due to talus and tibial osteophyte, and it was always possible to define if the osteophyte was intra- or extracapsular; in these cases arthroscopy confirmed MR imaging diagnosis. 3 patients (7.1%) had a negative MR imaging examination, one of them showing a 'meniscoid syndrome' on arthroscopy.

Conclusion: As a result of a good correspondence with arthroscopic findings, we consider MR imaging very accurate in the differential diagnosis of pathological conditions causing TTJ impingement. MR imaging is also able to detect extra-capsular causes of impingement.

C-0696

Emergency MR imaging of knee trauma with normal radiographic findings

M. Galluzzo, V. Buffa, A. Cortese, G. Regine, F. Pallotta, V. Miele, L. Adami; Rome/IT

Purpose: To evaluate the clinical impact and medico-legal significance of MR imaging, in acute knee sprain in patients with normal standard radiographs.

Materials and Methods: 128 patients (78 M, 32 F; age: 15- 59), from January 2003 to August 2004 with clinically suspected injuries were reviewed. All patients underwent plain radiographs (AP and LL views) which were negative, and within 5 days had MR imaging. Sagittal SE T1, STIR T2, coronal GE T2 and axial SE T2 weighted images were obtained, using a low field dedicated MR imaging (Arto-scan, Esaote, Italy)

Results: MR identified 48 bone bruises (36 lateral, 12 medial compartment); 12 MCL tears, 3 LCL tears; 5 ACL and 1 PCL isolated lesions; 2 internal derangements; 10 combined (MCL, ACL, internal meniscal) tears; 4 lateral patellar dislocations; 2 posterolateral corner lesions, 8 muscular lesions and 33 normal findings.

Conclusion: Actually, following acute knee trauma MR imaging is limited by availability, cost and time resources. Many lesions are subtle, and can lead to joint instability and early degenerative disease. Accurate diagnosis with MR imaging

allows appropriate treatment and classification of the lesions. Results are significant, and encourage more frequent use of MR imaging in acute orthopedics trauma. MR imaging is going to have a dramatic impact in assessing acute skeletal trauma.

C-0697

Rheumatoid arthritis (RA): The ABC's of hand-bone erosions imaging and management of disease

F. Priolo, A.P. Mancini, F.M. Martina, G. Savino, A. Magistrelli; Rome/IT

Learning Objectives: The aim of our study is to evaluate the role of MR imaging of the hand in detecting early erosions in patients with RA.

Background: The gold standard for joint damage in rheumatoid arthritis is currently the presence of radiological erosions. There is often a delay of 6 to 12 month before erosions can be confirmed by radiography. This fact is important if we consider that anti-rheumatic drugs are most effective in retarding progression of RA in the early stages of disease.

Procedure Details: 37 Patients affected by RA and with no radiological signs of hand/wrist involvement were studied with MR imaging. Signal intensity of pre-erosive lesions, sharply marginated areas of trabecular loss without a visible cortical break and bone defects with sharp margins with a cortical break were analysed. MR imaging ability to detect synovial hypertrophy and pannus formation before the onset of bony erosions has become more valuable with the advent of anti-rheumatic drugs.

Conclusion: MR imaging can reveal precocious erosions as well as synovitis and tendonitis in RA, giving a detailed picture of joint inflammation and damage. In fact, MR imaging of the wrist (carpal bones, distal radius, distal ulna, metacarpal bases) and of metacarpo-phalangeal joints (metacarpal head and phalangeal base) detects early erosions in RA and sharply marginated areas of trabecular loss without a visible cortical break (bone defect) and bone defects with sharp margins (erosion).

C-0698

Knee joint cartilage lesions treated with stem cells grafting

W. Dzienis, P. Jancewicz, E. Tarasow, J. Skowronski, J. Walecki, B. Kubas, J. Janica; Bialystok/PL

Purpose: The authors present clinical and radiological results of cartilage repair using stem cells grafting technique.

Materials and Methods: The studied group consisted of 30 patients suffering from clinically diagnosed and MR imaging confirmed osteochondritis dissecans or Grade IV degree of chondromalatias according to ICRS (International Cartilage Repair Society) score. The autologic marrow stem cell grafts, previously stimulated with growth factor, were applied under the periosteous interponat. Cancellous bone grafts were used simultaneously in case of large subchondral layer deficiency. An MR imaging examination was performed on 1.5 T Marconi Medical System using T1-w, T2-w, PD-w, T2*-w sequences and fat saturation sequences in sagital, coronal and axial plane, before and after operation.

Results: The clinic and radiological outcomes were estimated after 3 months. According to IKDC (International Knee Documentation Committee) score, 85% good and very good results were present, 15% of results were assessed as satisfactory. Poor results were not detected. Supervisory MR imaging demonstrated a solid coverage of the injured region with chondral tissue and good integration with booth surrounding cartilage and subchondral base layer. In 97% of cases the radiological evaluation provides an active remodeling process of subchondral bone.

Conclusion: In light of the presented results stem cells grafting is found to be an effective method of chondral defect repairs and MR imaging study is the method of choice in the evaluation of the clinical and radiological outcomes.

C-0699

Image findings of ruptured Baker's cyst

M. Park, S. Kwon, J. Ohm, B. Shin, Y. Kim; Daejeon/KR

Purpose: To evaluate the image findings of ruptured Baker's cysts.

Materials and Methods: We retrospectively evaluated the image findings of 16 patients with a ruptured Baker's cyst, nine patients with knee MR imaging, and 7 US. Surgical excision in 10 patients and aspiration in eight was done, respectively. We analyzed the direction of rupture, location of fluid collection, continuity between fluid collection and Baker's cyst, and margin of rupture site.

Results: Baker's cyst ruptured superiorly in 10 cases (63%), inferiorly in three, and posteriorly in three. Fluid was located in subfascial area in seven cases, between semimembranous and medial gastrocnemius tendon in six, subcutane-

Scientific and Educational Exhibits

ous in one, gastrocnemius muscle in one. One case showed fluid collection in both subfascial and subsoleus area. In four of 16 cases, fluid collection was far extended to mid-calf. The margin of rupture site was irregular and acute angle in 14 cases (88%). Septations in the cyst were noted in eight cases (50%). The ruptured fluid collection was continuous with main cyst except in three cases.

Conclusion: Most rupture of Baker's cyst occurred downward. The margin of ruptured Baker's cyst was irregular and septated, and showed acute angle.

C-0700

Comparing diagnostic efficacy of sonography and scintigraphy in the diagnosis of rheumatoid arthritis

V.D. Zavadovskaja, M.A. Zorkaltsev, O.Y. Kilina, N.L. Klimentenko, T.B. Perova, A.V. Khodashinskaja, O. Tjuleneva; Tomsk/RU

Purpose: To compare efficacy of scintigraphy with 99mTc-nanocis-labeled leukocytes (LC) and ultrasonography in rheumatoid arthritis (RA) diagnosis.

Material and Methods: We studied 21 RA patients (11 males and 10 females aged 42 ± 9 years). Clinical signs of knee joint injury were seen in 14 patients. LC ("Searle Scintiscan", 370 MBq) was performed 1 hour after indicator administration. Ultrasonography was performed using "Aloka 1700", "Siemens -450", transducers of 7.5-10 MHz.

Results: Local accumulation of a radiopharmaceutical was revealed in 32 knee joints (high accumulation - in 5, mean in 17 and low in 10 joints). Ultrasonography revealed synovitis signs in 15 joints. Accumulation of a radiopharmaceutical in the joints together with synovitis signs on ultrasound were seen in 14 joints (in 4 with high radiopharmaceutical accumulation, in 8 with mean and in 2 with low accumulation). Accumulation of a radiopharmaceutical in the joints without synovitis signs on ultrasound were seen in 18 joints: high accumulation was in 1 joint, mean one in 9 joints and low one in 4 joints. Both scintigraphic and ultrasound inflammation signs were absent in 9 joints. Synovitis ultrasound image did not show accumulation of a radiopharmaceutical in one joint. Radionuclide study showed 32 true-positive results, 9 true-negative ones and 1 false-negative result. Sonography showed 15 true-positive, 9 true-negative and 18 false-negative results.

Conclusion: Sensitivity of LC to reveal synovitis is higher (97%) than of sonography sensitivity (45%). High accumulation of a radiopharmaceutical is associated with presence of fluid and proliferation in 60% of knee joints.

C-0701

Radiological presentation of avulsion injuries of the shoulder, knee, ankle and foot

B. Dobriserevic, D.M. Masulovic, D. Saranovic, A. Ivanovic, A. Djuric; Belgrade/YU

Learning Objectives/Background: Avulsion injuries are common in sportsmen, especially in adolescents exerting the increased physical effort. Different radiological manifestations of both acute and chronic avulsion injuries of the shoulder, knee, ankle and foot enable their differentiation and differential diagnostics in relation to more serious and prognostically more severe diseases, such as neoplasm and infections.

Imaging Findings: Radiographically, the acute injuries, commonly resulting from the extreme, unbalanced, frequently eccentric muscle contractions, may be associated with the avulsion of bone fragments. Subacute injuries have more aggressive characteristics with the areas of mixed lysis and sclerosis. Chronic injuries, which are the result of repeated microtraumas or repeated over-exercise, as well as old inactive injuries, may be manifested as bulges and various growths on bones, and accordingly, may represent a great diagnostic dilemma being confused with neoplastic and infectious process. CT imaging is very beneficial in cases of dubious radiographical findings and injuries that were not radiologically treated in the acute phase. MR imaging is most valuable for the evaluation of muscle, tendon and ligament injuries.

Conclusion: Recognition of characteristics of imaging demonstration and specific pathologic manifestation as well as knowledge of osteomuscular anatomy is very helpful in frequently vague pathological bone conditions. In this study, involving 28 treated patients, the authors have made an attempt to clearly specify radiological criteria for differentiation of mechanical avulsion injuries of the shoulder, knee, ankle and foot from those lesions with similar radiological manifestation, but of more malignant nature.

C-0702

Diagnostic value of ultrasonography in ruptures of the posterior cruciate ligament of the knee

B. Dobriserevic, D.M. Masulovic, D. Saranovic, A. Ivanovic, A. Djuric; Belgrade/YU

Purpose: Based on our practical experience, we have made an attempt, by presenting ultrasonographic findings of the acute ruptures compared with the findings of the same region within physiological limits, to define the place and estimate the value of ultrasound diagnostics in the injuries of the posterior cruciate ligament (PCL) of the knee.

Material and Methods: Ultrasound examination was performed in 10 asymptomatic patients, who were the controls, and 27 patients clinically suspected of acute injury of the PCL of the knee. 21 of 27 patients were verified by MR imaging or MR imaging and clinical examination. Out of these 21 subjects, 8 had normal MR imaging and clinical results, while 13 demonstrated rupture of the PCL verified by MR imaging or surgery, or MR imaging and clinical examination.

Results: Normal ultrasound of the PCL was homogenous and hypoechoogenic, with a well-defined posterior margin. Rupture of the PCL of the knee was manifested as heterogeneous and hypoechoogenic in 10 of 15 patients, with indistinct posterior margin in 9. Ruptured PCLs of the knee were considerably thickened (12 to 20 mm) in relation to normal findings, when compared with the controls (3.7 - 6.2 mm).

Conclusion: The acute rupture of the PCL of the knee, over 10 mm thick, is manifested by the loss of sharpness of the posterior margin and its ultrasonogram is heterogeneous and hypoechoogenic. Ultrasonography may be valuable in patients suspected of the injury of the PCL of the knee.

C-0703

MR imaging of hip pain: Prevalence and mimickers of radiographically occult hip fractures

Y.Y. Ho; Singapore/SG

Learning Objectives: To evaluate the prevalence of radiographically occult hip fractures. To illustrate the MR imaging appearance of some of their mimickers.

Background: A 'hip fracture' is defined as fracture of the femoral neck region. 55 MR imaging studies were performed in 54 consecutive patients with hip pain and a negative radiograph. There was either a history of recent trauma or the study was requested because the patient's medical history suggested the possibility of an unexpected hip fracture.

Imaging Findings: 25% (14/55) studies showed an acute fracture. Of these, 8 had a hip fracture and 6 had fractures in the ischium, pubis and/or sacrum. 16% (9/55) studies had muscle strain or grade 1 muscle tear without a fracture. 15% (8/55) had other bone disease. 15% (8/55) had unrelated soft tissue disease. 31% (17/55) studies showed no cause for hip pain. In our series, the following mimickers were encountered: 5 avascular necrosis, 1 acute myeloid leukaemia, 1 lymphoma, 1 osteoarthritis, 1 trochanteric bursitis, 1 pyomyositis, 3 paralabral cyst, 1 transient osteoporosis of the hip, 1 injection site edema in the gluteal muscles, 1 non-specific hip effusion.

Conclusion: Not everyone with hip pain has a hip fracture. Apart from diagnosing subtle fractures, MR imaging is also useful to demonstrate other bone or soft tissue conditions which cause hip pain. Because of the locations of this wide range of mimickers, an imaging protocol, which extends from the pubic symphysis to the sacrum, is recommended.

C-0704

Evaluation of acromioclavicular joint with MR imaging

P. Calvillo Batllés, M. Graells Ferrer, M. Vega Martínez, F. Delgado Cordón, J. Ballestín Vicente, L. Martí-Bonmatí; Valencia/ES

Learning Objectives: To illustrate the anatomy, morphological variants, and pathology of the acromioclavicular (AC) joint. To quantify the prevalence of these entities in a large number of MR imaging studies of the shoulder.

Background: The AC joint disorders are a common finding on the MR imagings of the shoulder. We reviewed retrospectively the radiological reports of the MR imagings of the shoulder performed at our institution from April 2001 to September 2003 (n = 730). We selected the images with non-degenerative pathology in the AC joint and we assessed the following imaging aspects: 1) morphology and signal intensity of bone marrow 2) joint margins, joint space, capsular distension and fluid joint 3) ligaments and subacromial bursa. The images were obtained using a 1.5 T MR system, in oblique coronal, oblique sagittal and axial planes.

Imaging Findings: From the 730 MR imagings we excluded 15 patients with a history of AC surgery. We found osteoarthritis in 514 shoulders (72%). The other

Scientific and Educational Exhibits

cases (n = 28) were grouped, according to clinical criteria and imaging findings, in the following entities: 4 os acromiale, 5 AC dislocations, 4 posttraumatic or stress-induced distal clavicle osteolysis, 2 resorption of distal clavicle by hyperparathyroidism, 4 non-specific changes of bone marrow, 7 isolated subacromial bursitis and 2 septic arthritis. In 178 shoulders (25%) the acromion morphology corresponded to II and III types.

Conclusion: The radiologist must be conscious of the high prevalence of degenerative changes keeping in mind the other imaging patterns of AC pathology.

C-0705

The ultrasound and MR imaging appearances of the hand and wrist from a busy rheumatology practice: A pictorial review

J. Berry¹, Svasti-salee², K. Satchithananda¹, J.C. Wilkins¹, J. Totman¹, L. Pollard¹, E. Choy¹, D.A. Elias¹; ¹Camberwell/UK, ²London/UK

Learning Objectives: To illustrate the use of grey scale, colour Doppler with spectral trace analysis and the use of microbubble contrast agents to optimally image all the early and late changes of RA and also to show the pitfalls of the technique. To demonstrate how MR imaging and dynamic enhanced MR imaging can be used to both image and objectively monitor disease.

Background: Rheumatoid arthritis (RA) is a common autoimmune disease. It involves a sequence of antibody-mediated events leading from hyperaemia to synovitis and finally cartilage and bone destruction. Imaging is vital in diagnosing the changes early in the disease but also in monitoring response to treatment options available.

Procedure Details: The superficial anatomy of the hand and wrist makes ultrasound of this region ideal. Ultrasound imaging: grey scale images, colour Doppler imaging with spectral wave analysis and microbubble contrast enhanced ultrasound imaging allows all stages of RA including joint effusion, synovitis, tenosynovitis, tendon rupture, cortical abnormalities and erosions to be visualised. MR imaging allows excellent multiplanar imaging of the soft tissue changes (tendons, ligaments and synovium) in the small joints of the hand and wrist. MR imaging with dynamic contrast enhancement also helps to objectively assess hyperaemia and synovitis. MR imaging has the added advantage of imaging not only the osteochondral surface but also the important underlying bone marrow changes.

Conclusion: This exhibit will show all the changes that are seen in the hand and wrist in RA using all the newer ultrasound and MR imaging techniques available today.

C-0706

Clinically significant cases of wrist pathology: MR appearance. Correlation with surgical findings

M. Tzalonikou, A. Foteinos, Z. Athanasopoulou, C. Iliadis, G. Mpouchlis, K. Stringaris; Athens/GR

Purpose: The wrist joint is of complex anatomy. Imaging studies, MR imaging especially, are a necessary supplement in cases of suspected wrist pathology. The aim of this presentation is to review the clinically most significant pathologic entities that involve the wrist.

Materials and Methods: During the past four years 114 patients had MR imaging examinations of the wrist, 68 of whom had pathologic findings that required surgery. All MR imaging examinations were performed on a 1.5 T MR imaging Unit. Dedicated coils were used for imaging; micro-coils (43 mm in diam.) were additionally used in selected pathology. IV Gd was also administered in selected cases. The examinations were retrospectively reviewed by two board certified radiologists to reach a consensus reading. In the cases of surgery, correlation with the surgical findings was made.

Results: The MR imaging findings in cases of pathology of the triangular fibrocartilage and the scapholunate ligament, osteonecrosis of the scaphoid or the lunate bone (Kienbock's disease), instability syndromes, carpal tunnel syndrome, tendon abnormalities, arthritides of different etiologies and bone or soft-tissue tumors in the wrist are described. A case of osteomyelitis of the distal radius and of adjacent soft tissues is also presented. Surgical findings, in cases where surgery was done, are presented and compared to the imaging ones.

Conclusion: MR imaging proves to be a particularly useful means of non-invasive imaging of the wrist that provides important information regarding clinically significant pathology of the wrist.

C-0707

Shoulder MR arthrography: Evaluation of anterior access by palpatory guide

M. Barini, A. Stecco, P. Oronzo, T. Meloni, P. Fornara, A. Carrieri; Novara/IT

Purpose: To evaluate the efficacy and technical aspects of anterior palpatory access in shoulder MR arthrography.

Methods and Materials: 605 shoulders were examined in 11 months; in 242 cases we used intra-articular injection of Gadolinium because of instability, to detect partial lesions of the rotator cuff or to follow-up after surgical repair. Gadolinium injection was performed directly in the MR scan room, identifying an anterior "soft point" access, that corresponded to the anatomical space between external coracoid and medial aspect of the humeral head.

Results: Gadolinium injection was correctly performed in 219 patients (90.5%), while in 23 patients (9.5%) was extracapsular and in 1 patient (0.004%) we had a haematoma in the injection site. Average time to execution is about 3 minutes. All patients, except one, had pain resolution after 20 minutes from injection. We found 66 cases of glenoid labrum tears (30.1%), 89 partial lesions of the rotator cuff (40.6%) and 64 cases were normal (29.2).

Conclusions: We think that MR arthrography by palpatory guide is perfectly feasible and can be rapidly executed, with few periprocedural complications.

C-0708

Ossicle of the knee menisci: MR findings

S. Ortori¹, V. Zampa¹, F. Odoguardi¹, E. Batini¹, E. Ceretti², C. Bartolozzi¹; ¹Pisa/IT, ²Forte dei Marmi/IT

Learning Objectives: To report imaging findings of meniscal ossicle (MO).

Background: MO is an ossification area located inside the menisci usually found in young men. It represents a rare cause of knee pain and its origin is controversial. Commonly it is solitary, small (about 7-10 mm) and located in the posterior horn of the medial meniscus, although it can be placed in the anterior and posterior horn of both menisci. MO is defined as cortical bone containing fatty bone marrow surrounded by hyaline cartilage. Surgical excision is suggested in symptomatic patients.

Imaging Findings: Radiographically MO is an oblong or triangular formation with a rim of cortex and internal trabeculation projecting within the joint space. Spiral CT may be useful especially when two-dimensional reconstructions are performed and it appears as a trabecular bone fragment surrounded by a rim of cortex inside the menisci. MR images show the MO as an intra-meniscal lesion; it is a well-margined structure with a low signal intensity rim in all sequences. The internal part of the ossicle demonstrates the signal intensity of normal fatty bone marrow, high signal intensity on T1 WI that decreases on T2 WI associated with low signal on T2 WI with fat saturation.

Conclusions: MR imaging demonstrates the intra-meniscal location of the MO and allows one to differentiate it from intra-articular loose bodies, ossified osteochondral lesion, bone avulsion and chondrocalcinosis localised on the contrary outside the menisci, to permit an appropriate therapy.

C-0709

Juxta-articular bone marrow edema: Pattern approach on MR imaging

S. Takao, M. Uetani, T. Yamaguchi, Y. Kawahara; Nagasaki/JP

Learning Objectives: To describe various patterns of juxta-articular bone marrow edema on MR imaging. To discuss the differential diagnosis and its clinical significance based on these patterns.

Background: Bone marrow edema (BME) is demonstrated as an ill-defined area of hyperintensity on STIR and hypointensity on T1-weighted images without bone destruction. The lesion usually shows an enhancement effect after administration of Gd-DTPA. We present illustrative cases and discuss the differential diagnosis and clinical significance of juxta-articular BME on MR imaging.

Imaging Findings: The distribution patterns of juxta-articular BME were classified into following three types; type I - subchondral BME in only one side of the joint (e.g. osteochondral fracture, osteochondritis dissecans, subchondral insufficiency fracture, transient osteoporosis), type II - subchondral BME in both sides of the joint (e.g. various inflammatory or degenerative arthritis, bone bruise), type III - non-subchondral BME (e.g. avascular necrosis with collapse, stress fracture, juxta-articular bone tumors).

Conclusion: Juxta-articular BME can be associated with various bone and joint disorders and its distribution patterns could be a useful tool for differential diagnoses.

Scientific and Educational Exhibits

C-0710

Ultrasonography of ankle joint and foot in early diagnosis of rheumatoid arthritis

I. German, I. Dolgova, H. Andriyanicheva, A. Gordeev, A.V. Zubarev; Moscow/RU

Purpose: To compare the diagnostic utility of ultrasound in the diagnosis of early stages of rheumatoid arthritis (RA) of the ankle and foot with MR imaging.

Materials and Methods: 45 patients ages 20 to 55 years (20 men, 25 women) with suspected diagnosis of RA were investigated. All diagnosis were established on the basis of the clinical and laboratory data. All patients underwent US examination with Power Doppler. The structure and thickness of the tendons and ligaments of the ankle and foot joints were studied. US diagnoses were compared with MR imaging.

Results: In 80%, the presence of tenosynovitis of fibularis muscles and flexor muscles was revealed. Narrowing of the development of regional bone erosions were revealed in 60%. In 40% were marked early erosion changes of articulate surface in proximalis interphalanges, calcaneo-phalangeal joints. Sensitivity of the US method in comparison with MR imaging -97%, specificity -88% in detection of RA of ankle joint and foot. Vascularisation degree of the periarticular region correlated in 100% of cases with the laboratory data of the activity of RA.

Conclusion: US allows one to diagnose rheumatoid arthritis of an ankle joint and foot at early stages of the diseases. US may be useful as an additional modality for evaluation of the activity of rheumatoid arthritis.

Musculoskeletal

Soft tissue

C-0711

Quantitative assessment of diffusion in myxoid and non-myxoid soft tissue tumors by line scan diffusion-weighted imaging

M. Maeda, K. Takeda; Tsu/JP

Purpose: Diffusion-weighted imaging (DWI) may be potentially useful to characterize soft tissue tumors. Myxoid matrix is widely observed in various soft tissue tumors either in benign or malignant tumors. We hypothesize that myxoid matrix increases diffusion of soft tissue tumors. Our purpose was to evaluate apparent diffusion coefficient (ADC) of soft tissue tumors and compare ADC between myxoid and non-myxoid type tumors by using line scan DWI (LSDWI).

Methods and Materials: We prospectively studied 43 patients with pathologically proven various soft tissue tumors. The tumors were divided into two groups according to the presence or absence of myxoid. The one group consisted of myxoid-type soft tissue tumors (e.g. myxoid MFH) ($n = 23$), and the other group consisted of non-myxoid type soft tissue tumors (e.g. lymphoma) ($n = 21$). Forty-three patients were histologically divided into 26 with malignant soft tissue tumors and 18 with benign soft tissue tumors. The LSDWI was performed using b-factors of 5 and 1000 s/mm^2 . The ADC was measured for the solid appearing portions of tumors. ADC values were compared between myxoid and non-myxoid, and between benign and malignant tumors.

Results: The ADC (mean \pm S.D.) was $1.92 \pm 0.41 \times 10^{-3} \text{ mm}^2/\text{s}$ in myxoid type and $0.97 \pm 0.33 \times 10^{-3} \text{ mm}^2/\text{s}$ in non-myxoid type ($p < 0.001$). The ADC was $1.45 \pm 0.59 \times 10^{-3} \text{ mm}^2/\text{s}$ in malignant tumors and $1.50 \pm 0.64 \times 10^{-3} \text{ mm}^2/\text{s}$ in benign tumors (no significant difference).

Conclusion: Myxoid matrix significantly increases ADC of soft tissue tumors regardless of benign or malignant tumors.

C-0713

High-resolution US to evaluate post-surgical peripheral nerve lesions

M. Aguilar, V. Gomez-Dermit, R. Landeras, P. Ruiz-Hernandez, P. Zubieta, M.A. Fernandez-Echevarria; Santander/ES

Purpose: To assess the usefulness of HRUS to evaluate and localize post-operative lesions in peripheral nerves.

Materials and Methods: US were performed using a broadband linear transducer of 5.5-12 MHz. We examined 22 patients with post-operative peripheral nerve lesions confirmed by clinical examinations and electro-diagnostic tests (11 lesions after direct nerve surgery and 11 after orthopaedic surgery, usually fracture repair or focal lesions excision). Sonographic findings were correlated with electromyography examinations and surgical results.

Results: US visualized the injured nerve in 17 patients and failed to direct detection in 3 patients: 2 cases of accessory nerve lesions (in these patients atrophy of the trapezius muscle was present) and 1 patient with axillary nerve lesion (detecting deltoid atrophy). US depicted 4 cases of stump neuroma, 9 entrapment nerve cases caused by hypertrophied scar, 4 cases of nerve oedema with thickened nerve and abnormal fascicular pattern and 2 cases of nerve compression due to oedema or haematoma in the surrounding tissues.

Conclusion: HRUS can determine localization, extent and post-operative nerve damage; evaluate the continuity of the nerve in most patients, depicts a loss of the fascicular nerve structure and allows the evaluation of surrounding structures. US is a complementary tool to electro-diagnosis and the clinical findings and may be helpful to decide if surgical treatment is needed. In advanced cases atrophy is shown in denervated muscles. Finally sonography can be useful to follow-up the lesion when conservative treatment is the choice.

C-0714

Imaging of musculoskeletal fibromatosis

M. Bernathova, H. Gruber, G. Bodner, M. Schocke; Innsbruck/AT

Learning Objectives: To define the characteristic appearance of musculoskeletal fibromatosis and to propose a proper diagnostic work-up for this condition.

Background: Fibromatosis of the musculoskeletal system is a broad group of diseases of benign fibrous tissue proliferation with semi-malignant behaviour and potential for local recurrence after surgical resection. The group is divided into the subgroups of superficial fascial fibromatosis and deep musculo-aponeurotic fibromatosis. Whereas deep fibromatosis behaves locally aggressive, superficial fibromatosis typically remains small and less likely to recur despite essentially identical morphology. MR imaging is usually the modality of choice for evaluation

Scientific and Educational Exhibits

of these soft-tissue lesions. However, the specific diagnosis can be made with high resolution sonography as well.

Procedure Details: We retrospectively evaluated MR imaging and sonography images of 57 patients (35 patients with Morbus Ledderhose, 14 patients with Morbus Dupuytren, 1 patient with Morbus Peyronie and 7 patients with abdominal and extra-abdominal fibromatosis) from both subgroups. The definitive diagnosis was made by biopsy, in some patients by long term follow-up.

Conclusion: We could find some new characteristic sonographic features, which allow one to make a specific diagnosis.

C-0715

Radiographic features of heterotopic ossification: A pictorial essay

M.T. Karamessini, M.D. Mylona, P. Salonikidis, I. Vlahomitros, P.A. Dimopoulos; Patras/GR

Learning Objectives: We present a comprehensive review of the radiographic features of Heterotopic Ossification (HO) of patients in our rehabilitation center. **Background:** Heterotopic ossification is the abnormal formation of true bone within extraskeletal soft tissues and represents one of the most common conditions seen in long-term immobilized patients. Forty-five patients with HO were retrospectively studied during a 1-year period. The final diagnoses following admission were: Closed head injuries, spinal cord injury, stroke, orthopaedic injuries, brain tumors, electrocution, bacteraemia, subarachnoid haemorrhage, encephalitis and tuberculous arthritis. Plain radiography was the first imaging modality performed at request and imaging findings are illustrated and discussed.

Imaging Findings: A peripheral zone of early mineralization became apparent 7-10 days after the onset of symptoms and was followed by a mature mass of ossification. The hip was one of the most common sites of HO in patients with traumatic brain injury or spinal cord injury. The next most common sites of involvement in patients with traumatic brain injury were the shoulders and elbows, with the knees rarely affected. In contrast, knees were frequently involved in patients with spinal cord pathology. Other sites of HO occurrence are illustrated. Further investigation using other imaging modalities was not necessary for the diagnosis in the majority of the patients while, where resection of HO was needed computed tomography was performed. Differential diagnosis included the presence of haematoma, joint sepsis, osteomyelitis, local trauma, osteoblastic neoplasms and cellulitis.

Conclusion: HO seen in long-term immobilized patients can be diagnosed and followed-up using plain radiography.

C-0716

withdrawn by authors

C-0717

MR imaging of overuse tendon conditions

I. Kalaitzoglou, P. Papadopoulou, A.S. Dimitriadis; Thessaloniki/GR

Learning Objectives: To illustrate the MR imaging features, which help in the differential diagnosis of overuse tendon conditions.

Background: The classification and nomenclature of tendinopathies is an area of confusion in the literature. The most recent pathologic classification divides them into four categories: tendinosis, partial rupture or tendinitis, paratenonitis and paratenonitis with tendinosis. Over 3000 joint examinations were performed in two MR units from January to July 2004. Evidence of tendinopathy was present in approximately 250 cases. We selected and present some of the most characteristic ones.

Procedure Details: MR units used ranged from 1.0 to 1.5 Tesla and the examination protocols included T1 W and T2 W fat sat or STIR images in three orthogonal planes, while contrast enhancement was reserved for selected cases only. Dedicated extremity coils, which allow one to utilize a small FOV and thin slices, were used. We illustrate and discuss the imaging findings leading to diagnosis of various tendinopathies. We also present some of the commonest artifacts, which can lead to diagnostic pitfalls.

Conclusion: MR imaging is a very powerful tool in evaluating tendinopathy. Tendon abnormalities are rather easily identified but the distinction between various pathologies can be more challenging since some of them may often co-exist.

C-0718

MR imaging, ultrasonography and color Doppler in the assessment of palpable nodularities of the abdominal wall with post-partum onset

F. Prefumo¹, L. Derchi¹, N. Gandofo², L. Dogliotti², A. Maritano², M. Bazzocchi², L. Bacicalupo¹, G. Serafini²; ¹Genoa/IT, ²Pietra Ligure/IT

Purpose: To define the role of ultrasonography (USG) and magnetic resonance imaging (MRI) in the assessment of palpable nodularities with post-partum onset.

Materials and Methods: A series of 17 palpable lesion of the anterior abdominal wall with onset during the 12 months after delivery (12 vaginal, 5 caesarean) were excised. The pathological diagnoses were desmoid tumour in 7 cases, endometriosis in 7, suture granuloma in 2 and Merkel carcinoma in one. Before surgery, all cases were investigated by USG and 12 also underwent MRI.

Results: In the 7 desmoid tumours, USG showed solid nodules, less echogenic than adjacent fibromuscular structures, with margins clearly identified on a transverse plane, but irregular along the longitudinal plane, highly vascular at color Doppler. MRI documented homogeneous hypointense signals in all sequences due to the presence of fibrous tissue. In the 7 cases of endometriosis, USG revealed a dyshomogeneous structure with fluid areas and variable vascularity; MRI demonstrated the presence of haemoglobin degradation products. The 2 granulomas presented as dyshomogeneous and poorly vascularized hypoechoic nodules, showing small hyperechogenic spots internally. In the single case of Merkel carcinoma, USG showed its subcutaneous localisation, excluding any relationship with the muscles.

Conclusion: During the post-partum period, the USG finding of a solid homogeneous vascular lesion in the context of the muscle fibres of the abdominal wall, is suggestive of a desmoid tumour. Dyshomogeneous lesions with fluid areas and variably hypo- or hyper-vascular can suggest endometriosis on USG. MRI allows the identification of haemoglobin degradation products within these lesions.

C-0719

High resolution ultrasound of the leg

R. Podesta¹, F. Zuccarino¹, A. Picotti², G. Succio¹, S. Bianchi³, C. Martinoli¹; ¹Genoa/IT, ²Siena/IT, ³Geneva/CH

Learning Objectives: To provide an overview of the US aspects of diseases of the leg. To correlate them with clinical, radiographic and MR imaging findings. To emphasize the role of US in the management of these lesions to further delineate the nature and extent of the process.

Background: A wide spectrum of diseases in the soft-tissues of the leg are amenable to US examination.

Imaging Findings: This computer presentation will use schematic drawings, static US images and real-time video clips to illustrate the US appearance of normal leg anatomy and the spectrum of pathologic conditions for which US examination is indicated. Correlation of US findings with the results from other imaging modalities and open surgery will be provided in selected cases. US is able to diagnose several abnormalities affecting muscles (tennis leg, muscle hernias, compartment syndromes), fascial planes (shin splints), nerves (superficial peroneal neuropathy, sural neuropathy) and vessels (gemellary vein thrombosis, phlebitis of calf veins) of the leg. Dynamic US study is ideal to distinguish between partial and complete muscle disinsertions and to assess muscle hernias. In leg neuropathies, US provides useful information on level of compression, nature of constricting findings and continuity of the nerve.

Conclusion: US is able to identify and characterize a variety of diseases in the soft-tissues of the leg. Key advantages of this technique include cost-effectiveness, availability and ability to perform a dynamic examination.

C-0720

Abnormal US features of skeletal muscles of extremities: Correlation with MR images

S. Koh; Anyang/KR

Learning Objectives: To list various causes of abnormalities of skeletal muscles. To become familiar with US features of normal and abnormal skeletal muscles. To know advantages and limitations of US in the evaluation of skeletal muscles of the extremities

Background: In musculoskeletal US, confrontations with skeletal muscles are inevitable. US has many advantages as a first line modality in evaluation of skeletal muscles of extremities. The purpose of this exhibit is to become familiar with abnormal US features of skeletal muscles and to know the advantages and limitations of US in evaluation of skeletal muscles that lead to correct diagnosis, prompt and proper management, and the appropriate next step for further evaluation. We illustrate various US features abnormalities of skeletal muscles with MR correlation.

Scientific and Educational Exhibits

Imaging Findings: Complete and partial muscle tears, intramuscular hematoma, intramuscular pseudoaneurysm, pyomyositis, intramuscular abscess, myositis ossificans before and after ossification, rhabdomyolysis, polymyositis, disuse atrophy and tumors were all well demonstrated on US. US provided images of abnormalities of skeletal muscle of extremities with higher resolution than MR, but MR demonstrated adjacent bone lesions better.

Conclusion: In evaluation of skeletal muscle, US could be a useful imaging tool as a first line modality.

C-0721

Injury of the distal tibiofibular syndesmosis: Assessment with contrast-enhanced 3D-FSPGR MR imaging

Y.-M. Huh, S. Kim, J.-S. Suh, H.-T. Song, J.-W. Lee; Seoul/KR

Purpose: To determine the effectiveness of contrast enhanced (CE), fat suppressed, 3D-FSPGR MR imaging in the diagnosis of the tibiofibular ligament injury of the ankle, comparing to routine ankle MR imaging.

Materials and Methods: CE 3D-FSPGR and routine MR images were reviewed in 18 ankles with arthroscopically proven tibiofibular ligament injury and in 20 control subjects with diagnoses other than the tibiofibular ligament injury. Two sets of images were reviewed in random order: 1) CE 3D-FSPGR MR images (the CE set), 2) the routine MR images (the routine set). When the CE set revealed nodular synovial enhancement on the tibiofibular ligament and the routine set showed either ligament discontinuity or a wavy ligament or non-visualization of the ligament, the injury was regarded as a ligament disruption, respectively. Additionally 3 cadaveric dissections and histology, and 3 cadaveric transections were performed and correlated with MR image to ascertain the histology and anatomy of enhancing structure of syndesmosis.

Results: The CE set had an accuracy of 82% (31/38), sensitivity of 100% (18/18), and specificity of 65% (13/20) for the assessment of the tibiofibular ligament injury; whereas the routine set had an accuracy of 84% (32/38), sensitivity of 83% (15/18), and specificity of 85% (17/20). The CE set finding was well correlated with arthroscopic finding and cadaveric histology study suggesting syndesmotic synovial impingement.

Conclusion: CE 3D-FSPGR MR imaging of the ankle is more sensitive and objective, but less specific in assessing the distal tibiofibular syndesmosis injury of the ankle, comparing to routine MR imaging.

C-0722

Bright soft tissue masses of the extremities on MR imaging: The spectrum of diseases

J. Koo, S. Hong, J.-Y. Choi, I. Lee, J. Lee, Y. Koh, J.-A. Choi, H. Kang; Seoul/KR

Learning Objectives: To familiarize radiologists with bright soft tissue masses of the extremities on MR imaging. To provide distinguishing clues to differentiate amongst the bright masses.

Background: Since the MR imaging features of most soft tissue masses are non-specific; prediction of a specific histological diagnosis remains a challenge for the radiologists. However, there are certain specific lesions showing bright signal intensity on T2-weighted MR images.

Imaging Findings: We exhibit various bright soft tissue masses of the extremities on T2-weighted MR images. Illustrative cases include ganglion, bursitis, epidermal cyst, hemangioma, lymphangioma, intramuscular myxoma, neurogenic tumor, myxoid liposarcoma, and extraskeletal chondrosarcoma. Additional T1-weighted images and gadolinium-enhanced images provide helpful information to differentiate among them.

Conclusion: It is a prerequisite to be familiar with various spectrums of bright soft tissue masses for accurate interpretation of MR imaging and shortening the list of differential diagnoses.

C-0723

MR image findings of acute rhabdomyolysis

S. Kwon¹, K. Jung¹, I. Yang², Y. Kim³, Y. Choi², J. Cha⁴; ¹Daejeon/KR,

²Seoul/KR, ³Gwang-Ju/KR, ⁴Bucheon/KR

Purpose: To evaluate the MR image findings of acute rhabdomyolysis and correlate with clinico-pathological findings.

Materials and Methods: MR images in nine patients (7 men, 2 women; age range 15-45 years) with acute rhabdomyolysis were analyzed. Diagnosis of acute rhabdomyolysis was done by biopsy in two cases, clinical findings & follow-up imaging in 7 cases. The involved muscle, signal intensity and enhancement pattern of the lesion including in follow-up images, were assessed. Four cases with follow-up imaging were also analyzed with the same.

Results: Involved muscles were five cases in gluteal muscle, cervical and lumbar back muscle two, and leg (tibialis and gastrocnemius) & vastus muscle one, respectively. The T2 weighted images show heterogeneous high signal intensity in involved muscles, and central and peripheral rim enhancement pattern on gadolinium enhanced images in all cases. A decrease in initial high signal intensity and degree of enhancement of the involved area paralleled the clinical course in four follow-up cases.

Conclusion: The degree and pattern of signal intensity and contrast enhancement in involved muscle on MR images may contribute to the diagnosis of acute rhabdomyolysis and may parallel the clinical course.

C-0724

withdrawn by authors

C-0725

Radiological features of histologically proven post-traumatic fat necrosis

G. Raghuathan, S. McKie, G. Bourke, P. Robinson; Leeds/UK

Learning Objectives: 1. Pictorial illustration of fat necrosis by Ultrasound and Magnetic Resonance Imaging (MRI). 2. Correlation of imaging findings with proven histopathology.

Background: Fat necrosis most commonly occurs after trauma, and is well described in the breast. It is however less well documented in other anatomical sites. It can be seen in association with medical conditions such as pancreatitis, obstetric trauma, myeloproliferative and connective tissue disorders. Trauma is thought to cause vascular compromise resulting in necrosis that is propagated by both inflammatory and hormonal influences. The precipitating insult is however only recalled in one third of patients. It is a benign lesion that may be mistaken for malignancy and radiological differentiation is therefore important.

Procedure: The imaging features of fat necrosis are variable but Ultrasound is the primary investigation of choice with MRI used in indeterminate cases. This poster will illustrate the radiological features of 3 cases of fat necrosis with correlation of Ultrasound, MRI and histopathology (obtained with Ultrasound guided biopsy). All cases were referred with a high clinical suspicion for malignancy to the regional sarcoma centre.

Conclusion: The features of fat necrosis by MRI and Ultrasound are illustrated pictorially. A history of trauma is frequently not available and so the clinician relies on the imaging findings to aid diagnosis. Histological confirmation by Ultrasound guided biopsy may be required if clinical suspicion is high. However interpretation of the pathological features must be made in conjunction with the imaging features.

C-0726

The contribution of conventional and color Doppler ultrasonography in the estimation of musculoskeletal infections

C. Kontopoulos, A. Balanika, N. Economopoulos, G.A. Michailidis, N.L. Kelekis; Athens/GR

Purpose: The purpose of this study is to evaluate the role of conventional and color Doppler Ultrasonography in the detection of musculoskeletal infections.

Materials and Methods: Thirty patients (19 men/11 women), age 32-70 years were studied with Ultrasonography over a period of six months. Sonograms were obtained using a high resolution (7-12 MHz) linear transducer. The infection sites were: tibia (9), femur (7), hip joint (6), rib (2), clavicle (2), abdominal wall (2), elbow, (1) knee (1). They were results of contamination after surgical procedures, bone implants and abdominal wall mesh or spread of infections of contiguous site.

Results: The extension, the depth, the echomorphology and the vascularization of the infected tissues were studied. The osseous involvement was estimated by periosteal thickening or lifting, subperiosteal fluid collection, subperiosteal vascularization and presence of bone sequestrum. In seven patients there was suspicion of osteomyelitis, confirmed by MR imaging. In nine patients with abscess formation, aspiration and cytologic examination was performed. The cultured bacteria were *Staphylococcus* (2 MRSAs), *Pseudomonas* and *Proteus*.

Conclusion: Conventional and color Doppler Ultrasonography may contribute in the diagnosis of musculoskeletal infections, their extension and complications. It may also be used for the diagnostic aspiration and the following up of these patients.

Scientific and Educational Exhibits

C-0727

Real-time spatial compound sonography versus conventional US of the Achilles tendon in patients with heterozygous familial hypercholesterolemia
T.V. Bartolotta, M. Galia, G. Mamone, G. Runza, F. Sorrentino, M. Midiri; Palermo/IT

Purpose: To compare Real-Time Spatial Compound Sonography (CS) and conventional US in the evaluation of Achilles tendons in patients with heterozygous familial hypercholesterolemia (HFH).

Materials and Methods: Both Achilles tendons of 40 patients (19 men and 21 women; age range: 11-78 years; mean: 50.5 years) with HFH were studied with conventional US and CS by using a 7.5-10 MHz multifrequency linear-array transducer. Patients with previous history and/or clinical findings of tears and tendonitis were excluded from the study. Two experienced radiologists evaluated in consensus: a) tendon thickness, b) tendon echotexture, including the presence of calcifications and/or hypoechoic lesions (xanthoma). Structural changes were classified as follows: 1) no lesions; 2) unifocal or multifocal hypoechoic lesions, 3) diffuse abnormalities. Readers were also asked to evaluate the conspicuity of the lesions on a five-point scale: 1) definitely present, 2) probably present, 3) not assessable, 4) probably absent, 5) definitely absent.

Results: 7/80 tendons in 5/40 patients showed thickening (AP diameter > 7.1 mm) and abnormal echotexture. Ten xanthomas sized from 2.3 mm to 8.7 mm were identified in 5/80 tendons of four patients. In one patient bilateral, heterogeneous, hypoechoic tendon enlargement and calcifications were detected at US. No difference in the number of xanthomas detected at conventional US or CS was observed. The number of xanthomas classified as definitely present was statistically significant higher with CS than conventional US ($p < 0.05$).

Conclusion: CS is an effective tool in the assessment of Achilles tendons in patients with HFH, by improving xanthoma conspicuity.

C-0728

Myositis ossificans: What is the real diagnostic value of magnetic resonance?

S. Ortori, V. Zampa, F. Odoguardi, L. Marchetti, C. Cappelli, C. Bartolozzi; Pisa/IT

Learning Objectives: To describe the real diagnostic role of MR in the myositis ossificans.

Background: Myositis is an aberrant reparative process that causes benign heterotopic ossification in soft tissue. It is commonly associated with trauma, although in almost one-third of the cases there is no history of injury; usually the clinical presentation is a painful soft-tissue swelling that occurs within skeletal muscle of the extremities.

Imaging Findings: The radiologic diagnostic findings are dependent of the phase of the disease. Three different appearances of myositis ossificans are noted on MR: in the early phase before the appearance of calcification, MR shows a mass isointense to muscle on T1WI and hyperintense on T2WI with marked amount of adjacent edema. When the mineralization appears this is seen as a mineralized core, hypointense on T1 with hypointense rim both T1 and T2WI due to the surrounding rim of calcifications; in the mature phase, the lesion develops as well-defined calcified mass with a rim of decreased signal intensity both T1 and T2W representing the peripheral ossification. Highly diagnostic on radiographs and CT is the presence of calcification that develops between 4 and 6 weeks after the initial trauma.

Conclusion: Plain radiography and CT are superior to MR in demonstrating calcification and ossification, but MR is the best method for early detection and for differential diagnosis (that includes malignant process), and following the progression of changes.

C-0729

MR findings and pathologic correlation of subcutaneous soft-tissue lesions of dermatosis: A pictorial review

S. Otake; Toki, Gifu/JP

Learning Objectives: MR imaging and pathological correlation was performed in 55 subcutaneous soft-tissue lesions of dermatosis. This review includes epidermal cyst (epidermoid cyst, infundibular cyst), eccrine spiradenoma, trichilemmal cyst, porokeratosis, panniculitis, angiolioma, angioleiomyoma, verruca vulgaris, ossifying fibroma, calcifying granulation, neurofibroma, and angiosarcoma.

Background: Pre-operative MR study is useful in localization of soft-tissue lesions and the evaluation of their relationship with the surrounding tissues. However, MR findings of subcutaneous soft-tissue lesions of dermatosis have not been well documented.

Procedure Details: 1.5-T MR equipment and a surface coil were used. Conventional T1- and T2-weighted imaging and fat-suppressed imaging were performed in all the cases. A Gd-enhanced contrast study was performed in selected cases. Surgical resection was performed in all the cases. MR images and pathological findings were retrospectively reviewed. Location, shape, homogeneity, presence of the septa, signal intensity pattern, and degree of contrast enhancement of the lesions were analysed. Signal intensity patterns of the contents were correlated with pathological findings.

Conclusion: MR is useful in demonstrating subcutaneous lesions of dermatosis. Signal intensity patterns represent internal components and provide useful information in differential diagnoses.

C-0730

Soft-tissue vascular malformations: MR and MR angiographic imaging with pathologic correlation

J.C. Vilanova, J. Barceló, M. Villalón, J. Miró; Girona/ES

Learning Objectives: To review, be familiar with and differentiate the typical MR and MRA features of soft tissue vascular malformations with pathologic correlation.

Background: Soft tissue vascular malformations are relatively common. Different classifications separate vascular lesions of soft tissues into hemangiomas and vascular malformations on the basis of their natural history, location, cellular turnover, and histology.

Imaging Findings: These lesions can be categorized on MR imaging because of its typical appearance as multiple lobules with fat overgrowth and serpentine channels depending on the vascular flow. The combination of conventional MR and MR angiography (MRA) enable the differentiation between low flow and high flow vascular malformations and allows a non-invasive diagnostic strategy. Conventional MR sequences (T1, T2 WI and fat suppression techniques) and MR angiography (MRA) technique (3D FGRE-contrast enhanced) on a dynamic acquisition have been used to illustrate and characterize vascular malformations with pathologic correlation.

Conclusion: MR and MRA characteristics of vascular malformations allows one to perform more specific diagnosis and evaluation, to determine the extent of the anomaly and to classify appropriately. It provides a better overall assessment of vascular tumors.

C-0731

Usefulness of high-resolution sonography in the evaluation of soft tissue masses of the foot

V. Gomez-Dermit, R. Landeras, P. Merino, E. Sanchez-Salmon, M. Aguilar, M.A. Fernandez-Echevarria; Santander/ES

Purpose: Soft-tissue masses of the foot are an important clinical problem because of their high frequency and the severe functional importance that in most cases they imply. Our objective is to demonstrate the usefulness of ultrasound in the pre-surgical diagnostic approximation of these lesions.

Materials and Methods: We reviewed the sonographies of 55 patients (39 men, 16 women; with an age range of 17 to 80 years) remitted for the evaluation of tumours located in the foot. Examinations were carried out with two devices, Logiq500 (GE) and Aspen (Acuson), which had multifrequency linear arrays of 7.5-11 MHz and 5-11 MHz, respectively. The analysis of the tumours was focused on the following characteristics: location, size and shape, contours, echostructure and echogenicity, vascularization and relationships with adjacent structures. Excision or biopsy of the masses was practised in all cases with consequent pathological examination.

Results: The histological results contributed 4 lipomas, 12 neuromas, 4 angioleiomyomas, 1 chondroma, 1 synovial chondroma, 1 synovial sarcoma, 2 cases of bursitis, 6 plantar and 1 nodular fibromatosis, 15 cystic synovial lesions, 1 inclusion cyst, 1 giant cells tumour, 1 plantar papilloma and 5 abscesses. The ultrasound study of the tumours give us important details for orientation the possible nature of the lesions, i.e. if they were solid or liquid, pattern of vascularization, pattern of growth and their relationships with other structures.

Conclusion: High-resolution sonography is a technique that allows the radiologist to characterize soft-tissue masses, in most of the cases with an appropriate correlation with the pathological examination.

C-0732

Ultrasound investigation in differential diagnostics and treatment planning of soft tissues pathologies

T. Golovko, V. Medvedev; Kiev/UA

Purpose: We report our experience in ultrasound diagnostics and treatment planning of soft tissue tumors.

Scientific and Educational Exhibits

Methods and Materials: 710 patients with pathological formations of soft tissues were investigated: 240 - with sarcomas, 118 - with malignant disease of lymphoid tissues, 174 - with benign tumors, 92 - with non-neoplastic processes and 86 - with osteogenic sarcomas. Ultrasoundography (including color and energetic Doppler) was applied in all patients; traditional X-ray - in 569, CT - in 476, MR imaging - in 68 patients. 496 patients were surgically treated, 238 of them had neo-adjuvant chemotherapy. Results were compared with those of surgery and morphological investigation (volume part of vitality tumors tissues).

Results: US imaging characteristics of soft tissues pathological formations as well as typical neovascularity of tumors were elaborated. B-mode ultrasound can document the size and extension of tumor including lesion location, surrounding anatomical structure and US imaging characteristics of tumors. Power Doppler detected adjacent vessels, their correlation with tumor. Sensitivity, specificity and accuracy of ultrasound diagnostics were respectively 98%, 96% and 97%. The objectivity of complex ultrasound investigations for the evaluation of sarcomas neo-adjuvant therapy efficacy was proved.

Conclusion: The neoplasm localization is of decisive importance at soft tissues radiation investigation methods choice. The application of complex of methods ensures the most accurate results. Complex ultrasonography can be used for differentiation between potentially good and poor respondents for neo-adjuvant therapy and may be recommended for preoperative therapy effectiveness monitoring.

C-0733

Necrotising fasciitis: A pictorial essay with radiological correlation

A. Halka¹, R.R. Misra², M.C. Uthappa³, S. Kaniyur⁴, M.G. Berry¹,

¹Manchester/UK, ²High Wycombe/UK, ³Aylesbury/UK, ⁴Stevenage/UK

Learning Objectives: We present a pictorial review of several case of Necrotizing Fasciitis (NF) outlining the radiological changes seen with this aggressive condition.

Background: Necrotizing Fasciitis is an insidiously advancing soft tissue infection characterized by widespread fascial necrosis. It is a devastating condition with high mortality. NF may be thought of in three forms; type I, or polymicrobial; type II, or group A streptococcal (GAS); and type III gas gangrene, or clostridial myonecrosis. Type I is generally associated with immune compromise such as diabetes, malignancy, HIV, intravenous drug abuse and hepato-renal impairment. Type II tends to affect healthy patients who may be susceptible if they do not possess antibodies against GAS virulence factors. NF is frequently polymicrobial in children without pre-existing conditions.

Imaging Findings: The main role of imaging is to direct the extent of surgical debridement. CT is sensitive in detecting the changes associated with necrotizing fasciitis but lacks specificity. Several examples will be presented.

Conclusion: Necrotizing fasciitis is optimally managed in a multidisciplinary setting. Prompt imaging, radical debridement and reconstruction are required in order to reduce both the morbidity and mortality that result from this shocking condition.

C-0734

Soft tissues liposarcomas: Relationship between histopathologic features and CT/MR imaging findings

L. Zugaro¹, A. Catalucci¹, A. Barile², M. Monina¹, C. Masciocchi²; ¹Teramo/IT,

²L'Aquila/IT

Purpose: To evaluate MR imaging findings of liposarcomas subtypes and to correlate the histopathologic features with the MR imaging findings.

Material and Methods: Twenty-three patients examined in the last 9 years all underwent ultrasound and MR imaging; CTs were performed in twelve patients. All patients were submitted to biopsy and surgical resection.

Results: The study group had 9 well-differentiated, 10 myxoid, 3 pleomorphic and 1 round cell liposarcomas. Well-differentiated liposarcomas had a largely lipomatous appearance typically with septa and areas which were hyperintense on T2W SE MR images. Myxoid liposarcoma were mildly heterogeneous with high signal intensity on T2W images with lacy or linear septa of fatty tissue in six cases. Pleomorphic and round cell subtypes demonstrated marked heterogeneity indistinguishable from other high-grade sarcomas.

Conclusions: Well-differentiated liposarcomas may be differentiated from other types of the tumor by their largely lipomatous appearance. Myxoid subtypes may be distinguished on the basis of their homogeneous or mildly heterogeneous structure. On the basis of our experience and of literature, we believe that diagnostic criteria exist to distinguish the different liposarcomas subtypes, so allowing the correct differential diagnosis.

C-0735

Routine ultrasound diagnostic of the most frequently injured muscles of professional football players from the transfer list

W. Wawrzynek¹, B. Koczy¹, J. Widuchowski¹, S. Kasprowska¹,
A. Siemianowicz¹, R. Majer¹, J. Baron², A. Krol¹; ¹Piekary Slaskie/PL,
²Katowice/PL

Purpose: The purpose of this work was the confirmation of full fitness and prognosis as to physical efficiency of particular muscular groups for professional football players from the transfer list.

Materials and Method: 32 professional Polish I league football players and 9 foreign players from the transfer list were studied. A Siemens Antares machine with linear matrix head of 9-13 MHz was used. Based upon the experience of over 200 previous examinations, only the muscular groups that are most frequently injured: quadriceps and biceps of thigh and adductors, were examined.

Results: For 8 of 41 players there were fibrous and cicatricial changes in the examined muscles diagnosed. These changes could have an influence on the seasonal efficiency but despite that the transfers have been signed. For 3 foreign players the examination revealed massive cicatricial changes not reported by the players. For two cases the long head of quadriceps of thigh was not cured after sub-total rupture, for one case massive myositis ossificans calcification of long adductor and additionally right gono-arthrosis were diagnosed. For these three cases the transfer was not signed.

Conclusion: Ultrasound diagnostic of muscles of players being transferred in commercial sport disciplines is very important for estimation of the player's fitness and his future efficiency.

C-0736

Usefulness of sonography in diagnosis and postoperative evaluation of carpal tunnel syndrome

J. Cha, J. Park, S. Paik, J. Joh, H. Hong, H. Lee; Bucheon-Si/KR

Purpose: To evaluate the usefulness of the dimpling index on sonography of proximal carpal tunnel in the diagnosis of carpal tunnel syndrome (CTS) and post-operative evaluation.

Materials and Methods: Twenty patients suspected of CTS and control groups of 9 asymptomatic subjects underwent high-resolution sonography of the carpal tunnel. In addition, a comparison between pre and postoperative sonographic findings in six patients was made. Cross sectional area and dimpling index of proximal carpal tunnel, flattening ratio and swelling ratio of median nerve in proximal and distal carpal tunnel were measured between control groups and patients including 6 post-operative patients. We defined the depth of dimpling of median nerve on longitudinal view of sonography in proximal carpal tunnel as the dimpling index. We evaluated electrophysiologically the median nerve function of the affected wrists of all patients.

Results: Analysis revealed that a significant difference in the cross-sectional area of the median nerve and dimpling index on proximal carpal tunnel was found between patients' group and control group with a larger area than 0.09 cm² and a higher value of dimpling index than 0.07 being highly predictive of carpal tunnel syndrome. We also found a significant difference in swelling ratio and dimpling index between pre and postoperative patients.

Conclusion: In this study, we suggest that dimpling index and cross sectional area of median nerve on proximal carpal tunnel are effective value of confirming compression of median nerve and dimpling index and swelling ratio may be useful in the quantitative assessment of post-operative patients.

Scientific and Educational Exhibits

Musculoskeletal

Miscellaneous

C-0737

Imaging of diabetic foot

P. Rajiah, R. Whitehouse; Manchester/UK

Learning Objectives: To learn the role and limitations of imaging in diabetic foot. To illustrate the imaging spectrum of the different lesions in different imaging modalities. To learn the imaging protocol to be followed in different clinical scenarios.

Background: Diabetic foot is a major cause of morbidity in diabetic patients. It is seen in 25% of diabetics and is the common cause of prolonged hospitalisation, eventually ending in amputation in more than 10%. The pathological processes are a combination of neurological and vascular etiologies and include cellulitis, abscesses, sinuses, osteomyelitis, neuropathic joints, traumatic & stress fractures, peripheral vascular disease and gangrene.

Procedure Details: Good quality plain X-rays were obtained in all patients which identifies gross osteomyelitis, ulcerations, foreign bodies, antibiotic pellets, gas, neuropathic joints and fractures. Bone scan, white cell scan and gallium scan were useful in osteomyelitis, cellulitis and neuropathic joints. MR imaging was done for assessing the extent of lesion prior to surgery. MR imaging was performed in sagittal, coronal and axial planes. Gadolinium was administered in subtle lesions or small sinuses. Angiography or MR angiography was done in vascular disease.

Conclusion: Plain X-rays are the initial modality used in diagnosis of diabetic foot complications. Bone scan, white cell scan, gallium scans are helpful in differentiating osteomyelitis, cellulitis and neuropathic joints. CT scan identifies sequestra, periosteal reaction and cortical destruction. MR imaging with its superior soft tissue contrast is very helpful in assessing the exact extent of the disease, which is vital in management of osteomyelitis.

C-0738

Spectrum of cyst-like conditions found in and around the knee

M. Hjelt, A. Buzzi, M. Canedo, S. Gomez Zanetta, A. Mancini; Buenos Aires/AR

Learning Objectives: To recognize the different types of fluid filled structures (normal and abnormal) frequently found in the knee and in the surrounding soft tissues.

Background: There is a broad spectrum of cyst-like or water containing structures adjacent or within the knee. The purpose of this exhibit is to classify and describe these different fluid-filled structures.

Imaging Findings: Three types of fluid-filled structures can be found. Bursae, recesses and cysts. Bursae are synovial lined sacs found between structures that move against each other, whose main purpose is to reduce friction between these structures: the suprapatellar bursae, the subcutaneous pre-patellar bursae, the superficial and deep infra-patellar bursae, the pens anserine bursae, the gastrocnemius bursae and the medial collateral ligament bursae. Recesses are considered direct extensions of the articular cavity. They include Baker's cyst and distended hiatus popliteus. Cysts are liquid masses, including meniscal cysts and ganglion cysts (anterior and posterior cruciate ligament ganglions, intraosseous ganglion and proximal tibia fibular ganglion).

Conclusion: MR imaging is an excellent method to evaluate the different types of water containing structures that are frequently found in and around the knee.

C-0739

Ultrasonography of the musculoskeletal system: Principles of US physics and technology, examination technique, echoanatomy and sonographic features of musculoskeletal disease (a DVD-based teaching file)

C. Chatzimihail, P.S. Zoumpoulis, S. Kyriazi, A. Mihailidis, S. Faitaki, K. Pahou, I. Bechrakis, G. Adamakis, G. Delibasis, H. Tragea; Athens/GR

Learning Objectives: To outline basic US physics, technology and examination technique of the musculoskeletal system. To illustrate the main indications and limitations of the modality. To present normal echoanatomy and correlate abnormal sonographic findings with specific musculoskeletal disease.

Background: Modern high-resolution sonography is increasingly employed in the diagnosis of musculoskeletal injury and disease. The present DVD-Rom is based on a series of lectures focused on facilitating training and incorporates technical aspects of correct US examination with features of normal and diseased echostructure of the joints. Emphasis has been placed on delineating the

significance of appropriate transducer manipulation and selection of machine settings so as to optimize diagnostic results. "Real-time" video files are used to demonstrate correct technique through the simultaneous screen display of transducer positioning and obtained US images. Furthermore, these "hands-on" sessions elucidate the merits of dynamic scanning. A bilingual approach has been carried out by complementing the main Greek text with English subtitles.

Procedure Details: Individual topics include the fundamentals of US physics and technology, study of the shoulder (with particular focus on rotator cuff pathology), elbow, wrist and carpal tunnel syndrome, knee, as well as examination of the paediatric patient and US applications in non-traumatic musculoskeletal disease. Normal sonographic appearances are identified and juxtaposed to abnormal features associated with specific joint pathology. Relevant Doppler findings, aberrations during dynamic scanning and common artefacts are also discussed.

Conclusion: Sonography is a valuable modality for musculoskeletal imaging provided it is implemented meticulously and with consideration of its potentials and limitations.

C-0740

Animal signs in radiology

C.G. Cronin, D.G. Lohan, C.P. Meehan, C.J. Roche; Galway/IE

Learning Objective: To provide an educational and pictorial review of radiological signs, linked by the fact that they are named after and/or having a similar appearance to animals. Each radiological sign will be accompanied by a description of the sign/disease process involved.

Background: Radiologists have unique skills of observation and description. Descriptive signs in Radiology, as in all specialties are extremely useful. Signs aid characterization and classification of disease processes. They can allow confident radiological diagnosis on imaging grounds or help narrow a differential diagnosis.

Imaging Findings/Procedure Details: We will outline each particular sign, its etiology, where possible and provide a pictorial example from our department. These signs include Fish Vertebrae, Butterfly Vertebrae, Butterfly Fragment, Scottie Dog, Elephant Ears, Moth Eaten Bone, Seagull Configuration, Open Fish Mouth Sign of the skeletal system; Caterpillar Sign, Bulls Eye, Bird Beaking, Rat's Tail Sign of the gastrointestinal system; Bat Winging, Mickey Mouse Ears of CNS to name but a few.

Conclusion: This has provided an interesting and informative review of both common and uncommon radiological signs.

C-0741

Rheumatoid foot: Spectrum of imaging findings

E. de Lama, J.A. Narvaez, J. Narvaez, X. Mallol, J. Pellicer, V. Fabregas, C. Canas; Barcelona/ES

Learning Objectives: To review the main imaging features of the rheumatoid foot as seen at radiographs, US, CT and MR imaging. To correlate these imaging features with clinical symptoms, evaluating their usefulness in the clinical management of RA patients. To review the role of tibial posterior tendon dysfunction in the development (only or associated with other entities) of rheumatoid pes planovalgus.

Background: Foot and ankle involvement is common in rheumatoid arthritis (RA), leading to pain, functional impairment, and disability. Radiologic manifestations are predominantly the result of the synovial proliferation and inflammation that characterize the disease. MR imaging and US are valuable imaging methods for early evaluation. MR imaging is the preferred method for detecting early changes in RA. US is a valuable tool for evaluation of synovial arthritis and by facilitating the differentiation of tenosynovitis from articular inflammation and characterizing joint effusions.

Procedure Details: In this exhibit we review the main imaging findings in RA of the foot and ankle (joints, bursal, and tendon injuries as well as rheumatoid nodules) using multiple imaging modalities (radiographs, US, CT and MRI), and we will evaluate their usefulness in the everyday clinical management of these patients.

Conclusion: Knowledge of these imaging findings is important because feet are often affected earlier than hands, and may give a good overall impression of the joint damage, helping to plan the most adequate therapeutic strategy. Special emphasis is placed on imaging assessment of the role of the posterior tibial tendon and other structures in the development of rheumatoid pes planovalgus.

Scientific and Educational Exhibits

C-0742

A practical synopsis of knee cysts imaging

S. Bianchi¹, C. Martinoli², C. Gaingot¹; ¹Chene-Bougeries/CH,
²Largo Rosanna Benzi/IT

Learning Objectives: Musculoskeletal radiologists must be aware of the imaging appearance of cysts of the knee (KC) for their early detection and accurate assessment. Imaging has two crucial roles in the diagnostic work-up of KC. First, it must confirm the clinical suspicion of a KC and evaluate its size, borders, internal composition and relations with the adjacent structures. Second, it must investigate the internal knee structures to detect potentially associated disorders.

Background: KC are common clinical findings and are mainly related to synovial cysts and ganglia. The former are synovium lined, contain synovial fluid and when communicating with the joint cavity, result from a one-way valve mechanism that allows fluid only to pass from the joint space into the cyst. Ganglia are cysts with a fibrous wall and a thick, viscous content that result from a mucoid degeneration of connective tissue. They may or may not communicate with the joint cavity. Typical examples of knee ganglia are meniscal cysts, intramuscular and atypical popliteal ganglia and cruciate ligaments cysts.

Imaging Findings: The goals of this practical synopsis are to describe briefly the patho-mechanism and clinical findings of KC and to illustrate their imaging appearances on standard radiographs, arthrography, ultrasound, MR imaging, CT, CT and MR imaging arthrography. From our teaching file paradigmatic images of different types of KC will be presented. Schematic drawings will be used to clarify the imaging appearance. Special emphasis will be made on correlation among the different imaging modalities.

C-0743

Musculoskeletal manifestations of sickle cell disease. A pictorial review

M. Mashayekhi¹, R.R. Misra², A.L. Hine³; ¹Enfield/UK, ²High Wycombe/UK,
³London/UK

Learning Objectives: We would like to present a pictorial review of the varied musculoskeletal presentations of sickle cell anaemia.

Background: Haemoglobinopathies result from the presence of abnormal haemoglobin chains within haemoglobin (Hb). Sickle cell disease is characterised by the presence of haemoglobin S (Hb-S), which may result in sickle cell anaemia (Hb-SS), sickle cell trait (Hb-SA), or a hybrid Hb. Sickle cell disease is usually prevalent in those of African origin. About 7 percent of Blacks Americans and 40 percent of some African tribes carry Hb-S. Only 0.2 percent of Black Americans manifest Hb-SS. Clinical findings in Hb-SS are explained by the physical properties of the abnormal Hb. Sickle cells are fragile and cause vaso-occlusive crises, which are a striking feature of the disease. The incidence of Hb-SS is decreasing due to antenatal screening, but the disease still causes significant morbidity.

Imaging Findings: Conditions presented include marrow hyperplasia and reconversion, marrow ischaemia, osteomyelitis, muscle and soft tissue abnormalities, extra-medullary haematopoiesis, bone sclerosis, AVN, growth disturbances and changes to the axial skeleton.

Conclusion: We have the second largest population of sickle cell disease in the U.K. and regularly encounter the skeletal manifestations of Hb-SS. We hope that this poster will familiarise general radiologists with their varied appearances.

C-0744

Ilio-psoas compartment: A radiological approach

A. Buzzi, C. Garcia Pellegrino, C. Brizuela, M. Hjelt, M. Buzzi, A. Mancini;
Buenos Aires/AR

Learning Objectives: To show the important role of imaging in the diagnostic approach of ilio-psoas compartment disorders. To review the radiological techniques used in this type of patient. To illustrate the various imaging finding in ilio-psoas compartment diseases.

Background: Iliopsoas compartment disorders include infections, hemorrhage and neoplasms, and their symptoms are often subtle and non-specific. This results in delayed diagnosis and treatment. Anatomical knowledge is essential to understand the radiological findings and to correlate with clinical evidence. CT and MR provide a non-invasive highly precise evaluation of this area, and have led to early detection of pathology.

Imaging Finding: We show the complex anatomy of the region, and findings in pathologic conditions. Imaging can identify different primary disorders and spread of disease to this space.

Conclusion: Imaging plays a pivotal role in the diagnostic approach to ilio-psoas compartment pathologies. This compartment is an important pathway for spread of disease to remote areas.

C-0745

CT and MR imaging of spinal infections

A. Buzzi, V. Alarcon, F. Arredondo, M. Hjelt, M. Buzzi, A. Mancini;
Buenos Aires/AR

Learning Objectives: To review pyogenic and non-pyogenic infections of the spine. To understand the different imaging findings of spinal infections in several imaging modalities and to develop an approach to diagnosis based on these features.

Background: Infections of the spine involve primarily the disc space in children and the vertebral body in adults. Adults in the 6th to 7th decade of life are most frequently afflicted. The lumbar region is mostly involved. Pyogenic infections organisms included: Staphylococcus Aureus (60%), Enterobacter series 30% (Escherichia coli). Non-pyogenic infections organisms included: Coccidioides immitis and Mycobacterium tuberculosis.

Imaging Findings: CT and MR imaging permit both accurate detection and greater specificity in the diagnosis of infectious disease of the spine. The findings are irregularity and erosion of contiguous end plates with associated narrowing of the disc space, and diminished attenuation of the vertebral body. The posterior elements are rarely involved. The presence of marginal sclerosis permitted distinction between pyogenic and non-pyogenic infection.

Conclusion: An understanding of the mechanisms of contamination and the imaging features of spine infections usually lead to accurate diagnosis. MR imaging is the most sensitive technique for detection of osteomyelitis and discitis and is the technique of choice in the evaluation of patients suspicious for spinal infection. Even when all of the characteristic imaging features are not present, an awareness of the varied patterns with which infection may present allows early and accurate diagnosis.

C-0746

Tuberculosis of the spine: CT and MR imaging features

T. Van der Zijden¹, A.I. De Backer¹, F.M. Vanhoenacker², P.M. Parizel³;
¹Antwerp/BE, ²Duffel/BE, ³Edegem/BE

Learning Objectives: To present a comprehensive overview of the imaging features in vertebral tuberculosis (TB) illustrated with multiple cases.

Background: Vertebral TB is the most common site of musculoskeletal TB. Hematogenous spread of the tubercle bacillus is the cornerstone in the pathogenesis of tuberculosis of the musculoskeletal system, resulting in a typical anterior corner involvement of the vertebral body. Two distinct patterns of vertebral TB may be seen: The classic finding of spondylodiscitis, characterized by destruction of two or more contiguous vertebrae and opposed end plates, disk infection and commonly a paraspinal mass or collection. The second pattern is an atypical form of spondylitis without disk involvement. Early diagnosis and therapy is important in preventing severe spinal deformity.

Procedure Details: Plain radiographs are extremely insensitive for early detection of TB spondylitis. They do not detect vertebral involvement until at least 50% of a vertebra is destroyed. MR imaging is generally accepted as the imaging modality of choice for diagnosis and demonstration of both bony and soft tissue extent. Moreover, it may be very helpful in the differential diagnosis with pyogenic spondylodiscitis. Features in favour of TB spondylitis are anterior corner destruction, a relative preservation of the intervertebral disk, multi-level involvement with or without skip lesions and a large soft tissue abscess. CT is still superior in the demonstration of calcifications.

Conclusion: MR imaging is the imaging modality of choice for diagnosis, evaluation of disease extent and follow-up of spinal TB. Final diagnosis is based upon microbiological and/or histological examination.

C-0747

Lumbar foraminal injections: Two techniques under fluoroscopic control

C. Duffaut-Andreux, H. Guerini, A. Feydy, F. Bach, E. Pessis, A. Minoui,
L. Meziti, J.-L. Drapé, A. Chevrot; Paris/FR

Purpose: To report our experience in 54 lumbar foraminal injections performed in our institution over a 9-month period. To describe the two techniques we use for lumbar foraminal injections under fluoroscopic control. To report the indications of steroid injections

Materials and Methods: We retrospectively reviewed 54 lumbar foraminal injections performed in our institution over a 9-month period. Two approaches were used under fluoroscopic control: a strict posterior approach with a patient in procumbitus and a postero-lateral approach with a patient in an oblique ventral position. The good needle position was confirmed on 2 orthogonal views and after injection of 2 ml of contrast material, yielding a periradicular epidural opacification. Delayed-action-corticosteroids were then injected.

Scientific and Educational Exhibits

Results: Disk herniation with nerve root impingement was the most frequent indication for injection, which was performed most commonly at L4-L5 and L5-S1 levels. The injection reproduced the usual radicular pain. No immediate complications were reported.

Conclusion: We conclude that lumbar foraminal injection under fluoroscopic control is a mini-invasive procedure, which may be done on an outpatient basis.

C-0748

Stress MR imaging of the lumbo-sacral spine with an axial loading device. A pictorial essay

B. Jankharia, P. Krishnan, M. Ursekar; Mumbai/IN

Learning Objectives: To illustrate the usefulness and indications of stress MR imaging of the lumbar spine with an axial loading device.

Background: Many symptomatic patients with degenerative disease of the lumbo-sacral spine have normal or minimally abnormal findings on standard supine MR imaging studies. It is known from dynamic myelography that thecal sac and nerve compression is often unmasked only in the erect position. An axial loading device (Dynawell, Sweden) was used in 85 consecutive patients with suspected degenerative disease of the lumbar spine. All patients with obvious disc herniations that explained the patients' symptoms were excluded. All studies were performed on a 1.5 T scanner (Siemens, Erlangen) with pre- and post-stress T2W sagittal, axial and sagittal and coronal MR imaging myelogram sequences. This axial loading device applies a compressive force that is equal to half the body weight of the patient, distributed equally on both sides. This has been shown to simulate the effect of gravity.

Imaging Findings: Stress MR imaging showed significant findings mainly in patients with degenerative soft tissue canal stenosis, especially those with single level stenosis, often reproducing the symptoms as well. It was also helpful in post-operative patients and in patients with synovial cysts. It was rarely helpful in patients with predominantly disc herniations. MR imaging myelogram images were extremely useful in depicting the changes in thecal sac and nerve compression.

Conclusion: Stress MR imaging of the lumbo-sacral spine with an axial loading device is useful in degenerative diseases of the lumbo-sacral spine, mainly in single-level degenerative soft tissue canal stenosis.

C-0749

The spectrum of the failed back surgery syndrome: Radiological comprehension with emphasis on MR imaging

J. Ryu, M. Shin, S. Kim, S. Lee, C. Kang; Seoul/KR

Learning Objectives: 1.To assimilate the complex and various imaging findings of the failed back surgery syndrome, with accurate understanding of the surgical procedure, the post-operative anatomy, and the biomechanical nature of post-operative period. 2.To show the important role of MR imaging after lumbar surgery with or without instrumentation in failed back surgery syndrome.

Background: MR imaging is best suitable for demonstrating the anatomical details of the post-operative spine. With a thorough understanding about the post-operative spine, MR imaging can not only demonstrate the anatomical details of the lumbar disc and vertebra but also give information regarding the other causes of pain that is usually not seen on the other modalities.

Procedure Details: We tried to show the complex and various imaging findings of the failed back surgery syndrome, and the usefulness of MR imaging. Various conditions including usual post-operative findings, post-operative recurrence, infection, instrumentation failure, the changes of facet and disco-vertebral joint and adjacent segment instability, with explanation for the biomechanical nature of the post-operative spine will be included. The advantages and pitfalls of MR imaging in the evaluation of the post-operative lumbar spine will also be discussed.

Conclusion: MR imaging is suitable and useful method for demonstration of failed back surgery syndrome.

C-0750

Diagnosis of skeletal invasion by Hodgkin's disease: Bone versus bone marrow survey

S. Novikov, S. Kanaev, M. Gershovich; E. Shelkoplias, St. Petersburg/RU

Purpose: To compare the diagnostic accuracy of bone & bone marrow survey in patients with Hodgkin's disease.

Material and Method: Whole body bone marrow (BMS) & bone scanning (BS) were performed in 155 pts with Hodgkin's disease. Focal and diffuse changes of tracer uptake were considered as the signs of BM metastatic invasion. Forty-two "high risk" patients had unilateral bone marrow biopsy, which was obtained from the posterior iliac crest. Discordant results of examinations were settled on the

basis of additional survey (MR imaging, X-ray, CT) at presentation and during follow-up.

Results: Fifty-five patients had scintigraphic signs of bone marrow invasion: Focal changes were revealed in 61, multifocal and diffuse - in 25 cases. Positive results of BS were mentioned in 41 cases. Nine patients had BM invasion according to histological examinations of BM. False positive results were revealed in 5 patients - for BMS, 3 patients - BS. Biopsy was always considered correct. False-negative results were mentioned in 6 pts - for BMS, 29 patients - BS and 12 patients - BM biopsy. Sensitivity, specificity and accuracy were as follow: 91.4%, 94.8%, 92.9% - for BM scanning; 49.1%, 97%, 80.6% - for bone scanning, 36%, 100%, 70.7% - for BM biopsy.

Conclusion: In the evaluated patients with HD BM scanning was the most accurate and sensitive method of skeletal survey.

C-0751

Intravertebral vacuum cleft sign: Can we consider it a sign of benign vertebral collapse?

L. Herranz, A. Bermejo, M.A. Martin, R. Carrera, P. Manjon, J. Manrique; Madrid/ES

Learning Objectives: We present a pictorial review of the intravertebral vacuum cleft (IVC) sign and discuss the clinical and radiological features and the mechanism of formation of this cleft gas collection.

Background: The IVC sign appears on radiographs as a transverse, linear or semilunar radiolucent shadow that is located centrally within or adjacent to the endplate of a collapsed vertebral body and is exclusively seen in conjunction with vertebral fracture and collapse. The radiolucent or semilunar shadow represents gas (principally nitrogen) in the fracture line. The observation of IVC in a collapsed vertebral body on plain radiograph was considered virtually pathognomonic for osteonecrosis. Classically it was thought that the mechanism of formation of these gas collections in the vertebral bodies required that neither fluid nor tumor should occupy the cleft. So, almost every author had assured one that the intravertebral vacuum cleft sign militates against the diagnosis of infection and malignancy.

Imaging Findings: We illustrate this phenomenon with some examples including frontal and lateral lumbar column radiographs, CT scans and MR images of osteonecrosis and Kümmell disease (delayed posttraumatic collapse). We also report a case of intravertebral vacuum cleft in vertebral collapse from a metastatic renal cell carcinoma, being to our knowledge the first case described.

Conclusion: Almost all reported cases of intravertebral vacuum phenomena correspond to vertebral collapse of a non-neoplastic and non-infectious origin. However, IVC has been reported in a few cases of vertebral malignancy; therefore it can not be considered a pathognomonic sign of ischemic bone necrosis.

C-0752

Ultrasound-guided intervention in the musculoskeletal system

J.L. del Cura, R. Zabala, A. Legórburu, O. Gorriño, D. Grande; Bilbao/ES

Learning Objectives: To illustrate the different US-guided interventional procedures performed in the musculoskeletal system (MSS). To describe their technique, including the use of drugs when appropriate. To describe their complications and how to prevent and treat them. To discuss their indications and to describe the results.

Background: US allows exploring most of the MSS, including lytic bone lesions. Its flexibility, availability, and low cost makes it the best tool to guide interventional procedures in any MSS lesion visible on US. These techniques include percutaneous biopsy, drainages (abscesses, hematomas, muscular breaks, ganglions, Baker's cysts and bursitis), arthrocentesis and aspiration of calcific tendinitis.

Procedure Details: Percutaneous biopsy is performed using spring-loaded automatic guns that allow obtaining specimens available for histological exam from soft tissues and lytic bone lesions. The technique is highly accurate to distinguish between benign and malignant lesions. Drains can be performed using catheters or needles and avoid a more aggressive approach most of the time. Intracavitary urokinase helps when the aim is to drain clotted hematomas or fibrinous collections. Injection of corticoids is useful in the treatment of ganglions, Baker's cysts and in non-infected arthritis. Calcific tendinitis of the shoulder can be effectively treated using percutaneous "washing" with lidocaine. Calcifications usually disappear and symptoms improve in near 90% of the cases within a year. Most of these techniques are low cost and require only a moderate skill.

Conclusion: US-guided procedures are useful tools to diagnose and treat MSS diseases and should be routine in any imaging department.

Scientific and Educational Exhibits

C-0753

Spinal tuberculosis: Typical and atypical findings at MR imaging

F. Matute Teresa, A. Saiz Ayala, N. Santamaría; Madrid/ES

Purpose: To describe MR imaging findings of typical and atypical tuberculous spondylitis and compare the diagnostic yield of MR versus other radiological modalities.

Materials and Methods: Between January of 1998 and July of 2004, we studied and compare the radiological findings (MR, CT and plain films) of 29 patients (13 men and 16 women, aged 20 to 76 years) that had a final diagnosis of tuberculous spondylitis.

Results: Thoracic spine was the region most commonly affected, partial involvement was detected in the majority of the vertebral lesions. MR imaging evidence of disc space involvement is very infrequent. High signal intensity on T1-weighted images of previously affected vertebrae suggested healing. More typical findings of spinal tuberculosis include destruction of two adjacent vertebral bodies and opposing end plates, destruction of intervening disk space, collapse, and/or occurrence of paravertebral abscesses or extension into the epidural space. Depending on the stage of the disease, three different patterns of infection were revealed: osteitis, osteitis with an abscess and osteitis with or without an abscess plus discitis.

Conclusion: The ability of MR to detect tuberculous spondylitis earlier than other radiological techniques could reduce bone destruction and deformity and diminish the need for surgical intervention. Instability and deformity of the spine can result, mandating prompt diagnosis and treatment to prevent permanent neurological damage. Biopsy is recommended to confirm the diagnosis.

C-0754

Coronal ultra-thick CT reconstructions of the pelvis in the multiple trauma patient: An alternative for the initial conventional radiograph

S. Leschka¹, H. Alkadhi¹, T. Boehm², B. Marincek¹, S. Wildermuth¹; ¹Zürich/CH, ²Chur/CH

Purpose: Uncertainties of the initial conventional pelvic radiographs have questioned its usefulness in multiple trauma patients who will undergo abdomino-pelvic CT scan. Post-processing of axial CT datasets allows for generating coronal ultra-thick multiplanar reconstructions, which resemble conventional AP radiographs. This study was performed to evaluate the image quality and diagnostic accuracy of this reconstruction for pelvic fractures.

Methods and Materials: 33 multiple trauma patients with initial conventional pelvic radiographs and CT imaging were retrospectively reviewed by two radiologists regarding image quality, visualization of anatomical landmarks and diagnostic concordance. Statistics were performed using kappa statistics for inter-observer agreement, Wilcoxon signed-rank test for modality comparison and chi square test of contingency for diagnostic certainty.

Results: Ultra-thick multiplanar reconstructions were superior in terms of image adjustment ($p < 0.02$), absence of overlaying structures ($p < 0.05$), and overall image quality ($p < 0.01$). The ilio-sacral joint ($p < 0.05$) and the anterior and posterior acetabular line ($p < 0.01$ and $p < 0.02$, respectively) were more accurately depicted on reconstructions. Consequently, sensitivity for detection of fractures in the acetabular rear column and ilio-sacral joint were significantly improved. The visualization of all other anatomical landmarks and pathological findings did not differ significantly between both modalities.

Conclusion: If conventional pelvic radiography is omitted while abdomino-pelvic CT scan is performed, the reconstruction of thick anterior-posterior images of the pelvis may be a sufficient alternative to gain conventional radiography-like images.

C-0755

Clinical application of 16-slice multidetector row CT (MDCT) with 2D and 3D image processing in musculoskeletal trauma

J.Y. Hwang, S.W. Lee, H.Y. Choi; Seoul/KR

Learning Objectives: To illustrate the various images of 16-slice multidetector row CT (MDCT) with 3D volume rendering (VR) and multiplanar reformation (MPR) in musculoskeletal trauma of 105 patients. To describe the advantages and limits of MDCT with 3D image-processing and its clinical applications.

Background: With the revolution of MDCT, image quality of MPR and VR from 3D image processing approaches that of axial images from the raw data. The stair-step artifacts were reduced as compared with conventional helical CT owing to higher Z-axis resolution. This study included 105 patients with musculoskeletal trauma who underwent 16-slice MDCT from May 2004 to July 2004. MPR images and 3D volume rendering images were reformatted using a PC-based 3D reconstruction program. In this exhibits, we compared the diagnostic value of

MPR and 3D volume rendering images with axial CT images only.

Imaging Findings: MDCT with 3D VR was particularly helpful in evaluating fractures in the scapula including bony glenoid, elbow, wrist, acetabulum, and in evaluating fixation positioning after operation. Additional MPR CT images were useful in visualizing the spine in patients with kyphosis, scoliosis and severe compression, evaluating fractures in the talus, calcaneus, carpal bone, sacrum, pelvic bone, determining bony union of fractures after fixation, and evaluating post-traumatic complications on follow-up examinations.

Conclusion: MDCT with 3D volume rendering or MPR images clarify the areas of complex bony anatomy in patients with musculoskeletal trauma. It is valuable in operation planning as well as in postoperative follow-up imaging for fixation positioning, healing, and traumatic sequelae.

C-0756

Pelvic ring fractures: Advantages and pitfalls of MDCT

A. Lesavre, A. Miquel, C. Phan, Y. Menu; Le Kremlin-Bicêtre/FR

Learning Objectives: To review the MDCT imaging findings of the pelvic ring fractures. To determine whether they are stable or not with the help of the Tile's classification.

Background: Pelvic ring fractures occur as the result of high-energy blunt trauma, as in motor vehicle collisions. Patients with an unstable pelvic ring fracture require pelvic stabilisation. The approach to classifying pelvic fractures has evolved over the past several decades. Tile's classification into stable and rotational or multiplanar instability is most useful.

Imaging Findings: Conventional X-rays were the gold standard method. Due to the importance of trauma patients, pelvic ring images may be obtained with high quality reconstruction within short acquisitions. Axial slices, as well as coronal, sagittal and oblique reformatted images help the surgeon. 3D imaging may be a simple way to image major fractures in a radiographic manner, although reconstruction algorithm tend to alter fracture detection.

Conclusion: Helical CT should be the first-line imaging method in detection and evaluation of pelvic ring fractures, providing a good communication with the surgeon.

C-0757

MSCT in the postoperative follow-up of vertebral osteosynthetic procedures: Comparison with conventional radiography

M. Lorenzen, U. Wedegärtner, C. Weber, G. Adam, J. Lorenzen; Hamburg/DE

Purpose: Comparison of MSCT and conventional radiography in the evaluation of surgically treated vertebral spines.

Material and Methods: Our retrospective study included 30 patients with surgically treated spines (metastases 5, fractures 20, spondylolisthesis 3, scoliosis 2) who underwent both conventional radiography and MSCT during hospitalisation. MSCT of the operated spine was performed using the following parameters: 140 kV, 200 mAs, collimation 4x1 mm, pitch 0.75. We evaluated the in-situ position of the implanted osteosynthetic devices (OD) as well as the integrity and alignment of the vertebral column. Images were analysed in a consensus reading by two blinded radiologists.

Results: In 9/30 cases, MSCT detected an extraosseous screw tip compared to 5/30 patients by radiography. A displacement of OD into the spinal canal was diagnosed in 8/30 by MSCT and 4/30 by radiography. Bone fragments within the spinal cord were detected by MSCT alone (2/30) and missed on plain films. Based on MSCT findings, corrective surgery was necessary because of malpositioned OD in 1 patient. Fractured OD were detected in 3 cases with both methods equally.

Conclusion: MSCT proved to be superior to conventional radiography in the postoperative assessment of the vertebral column providing clear and relevant information for further therapeutic decisions.

C-0758

Early evaluation of the therapeutic effects of radiotherapy and/or hyperthermia in VX2 rabbit carcinoma using FDG-microPET

K. Ishii, M. Hosono, Y. Wada, S. Kondo, Y. Takada, T. Tada, M. Maeda, Y. Watanabe, Y. Inoue; Osaka/JP

Purpose: The aim of this study was to evaluate the early effect of local irradiation and/or hyperthermia on tumor bearing rabbits using FDG-microPET.

Methods and Materials: Twenty-eight VX2 xenografts in the thigh were divided into five groups; radiotherapy at dose of 10-30 Gy, hyperthermia (43 degrees C, 1 hour) and combination of radiotherapy and hyperthermia (10 Gy+43 degrees C, 1 hour). Primary effect was determined by a comparison of the tumor volume. Finally, all of the xenografts were divided into PR+NC group and PD group. For

Scientific and Educational Exhibits

the quantitative evaluation of FDG, tumor/muscle (T/M) ratios and time activity curve (TAC) were measured using microPET P4 system, at pre-treatment, 24 hours and 7 days after treatments.

Results: In PR+NC group, T/M ratios were 5.0 ± 1.3 , and 6.8 ± 1.9 at 24 hours and 7 days after treatments respectively. In PD group, T/M ratios were 8.0 ± 3.0 , and 8.8 ± 2.5 at each point. Compared to T/M ratios at pre-treatment (9.1 ± 1.9), T/M ratios in PR+NC group were remarkably decreased at 24 hours after treatments ($p < 0.05$). The patterns of TAC were also comparable to the quantitative evaluation of T/M ratios.

Conclusion: Our results suggest that early evaluation of FDG-PET, especially 24 hours after treatments, is useful to predict the primary effects of the treatments.

C-0759

Imaging of extraskeletal osteosarcoma

H. Yoshikawa, T. Ueda, A. Miyaji, N. Tamai, N. Araki, I. Kudawara; *Osaka/JP*

Purpose: Extraskeletal osteosarcoma is a unique and extremely rare neoplasm. In this study, we have analyzed radiologic findings of this tumor, especially focused on pattern of ossification by plain films, computed tomography (CT) and MR imaging.

Methods and Materials: 10 patients with extraskeletal osteosarcoma (7 male and 3 female), aged 49-74 years (mean 61), were reviewed radiologically. The tumors were located in the thigh in 3 patients, the upper arm in 3 patients, in the calf in 2 patients, and in other sites. All cases have been confirmed histologically, and studied radiologically with plain films, CT, and MR imaging.

Results: Plain films and CT revealed calcified or ossified materials in 8 out of 10 cases, but not in the remaining 2 cases. In 3 of the 8 cases with calcification/ossification, spicula formation, so-called 'sunburst appearance', was partly detected within the soft-tissue mass, and in the remaining 5 cases, only amorphous calcification/ossification was detected. All the tumors were heterogenous on MR imaging and demonstrated lower or iso-intensity to muscle on T1-weighted imaging and high signal intensity on T2-weighted imaging. The areas of calcification/ossification showed low signal intensity on both T1 and T2-weighted images.

Conclusion: The "sunburst" appearance, a distinctive periosteal reaction of conventional osteosarcoma, could be a characteristic finding, even in some extraskeletal osteosarcomas. The MR imaging findings are non-specific, but in elderly patients the differential diagnosis of a soft-tissue mass should include extraskeletal osteosarcoma, even in the absence of radiologically discernible calcification/ossification.

C-0760

The influence of oral glucose ingestion during a dynamic FDG-microPET study using a rabbit VX2 tumor model

K. Koyama, T. Okamura, Y. Hamazawa, T. Okuma, Y. Wada, K. Ishii, S. Kondo, Y. Watanabe, Y. Inoue; *Osaka/JP*

Purpose: Delayed images are reported to be useful for differentiating malignant from benign masses, but patients are required to fast for additional hours, which can be stressful. We investigated the influence of oral glucose ingestion during a study on tumor FDG accumulations in an animal tumor model using a small animal PET imaging system with a high spatial resolution (1.85 mm).

Materials and Methods: Japanese white rabbits, with eight transplanted VX2 tumors in their thighs, were employed. As a no-glucose-loading FDG-microPET study, after four hours fasting, dynamic emission data acquisition was performed until 2 hours after intravenous FDG injection. For glucose-loading FDG-microPET study, oral ingestion of 10 ml of 50% glucose solution at one hour after intravenous FDG injection was added to no-glucose-loading study using the same rabbits. Images, reconstructed every ten minutes using a filtered-back projection method, were analyzed visually. Time activity curves (TACs) and tumor-to-muscle ratios (T/M ratios) were also calculated after regions of interest were set in tumors and muscles.

Results: Blood glucose levels after two hours were significantly higher than those before oral ingestion. In visual analysis, tumor FDG accumulations increased with time in both studies. T/M ratios also increased with time and TACs showed increasing curves in both studies. Concerning the ratios of T/M ratios obtained at one hour to those obtained at 2 hours; there was no significant difference between both studies.

Conclusion: Tumor FDG accumulations in dynamic FDG-microPET are not influenced by oral glucose ingestion at one hour after intravenous FDG injection.

C-0761

Comparison of dynamic FDG-microPET study in a rabbit VX2 tumor model and that in a turpentine-induced rabbit inflammatory model

Y. Hamazawa, K. Koyama, T. Okamura, Y. Wada, T. Wakasa, T. Okuma, Y. Inoue; *Osaka/JP*

Purpose: We evaluated the differentiation of tumor from inflammation using FDG-microPET dynamic scans obtained by MicroPET P4 scanner in an animal tumor model and animal inflammation model.

Materials and Methods: Five Japanese white rabbits with 10 tumors, which were transplanted VX2 tumors and 3 Japanese white rabbits with 6 inflammations, which were induced by turpentine oil injection. Helical CT scans were done before the PET studies. In the PET study, after four hours fasting, and following transmission scans, dynamic emission data acquisitions were performed until two hours after intravenous FDG injection. Images, reconstructed every ten minutes using a filtered-back projection method, were analyzed visually. Time activity curve (TAC) and tumor-to-muscle ratio (T/M ratio) or inflammation-to-muscle ratio (I/M ratio) were calculated after regions of interest were set in tumors, inflammatory regions and muscles referring to CT images.

Results: The T/M ratio and the I/M ratio increased with time. Between after 1 hour and after 2 hours, TAC of tumor showed a linear rise, whereas TAC of inflammation showed a convex curve. The T/M ratio was significantly higher than I/M ratio at after 2 hours, although at after 1 hour there was no significant difference between them.

Conclusion: The differentiation of tumors from inflammations not possible using FDG-PET images obtained after 1 hour; on the other hand, it was easy and capable using FDG PET images obtained after 2 hours because of the differing rates of increase. The delayed images were thought to be useful for differentiation between those.

C-0762

High-resolution ultrasonography findings of peripheral nerve abnormalities

Y. Koh, J.H. Cha, D. Han; *Seoul/KR*

Learning Objectives: The object of the poster is to illustrate ultrasonographic findings of various peripheral nerve abnormalities.

Background: MR imaging is the most popular imaging modality in evaluation of peripheral nerve abnormalities. However, modern ultrasonography using high-resolution linear probes offers excellent images of superficial lesions. Therefore, peripheral nerves, except those in the brachial or sacral plexus are potential targets of ultrasonography. The author's experience shows that ultrasonography is a powerful imaging tool in evaluating many peripheral nerve abnormalities.

Procedure Details: All ultrasound examination was done using with ATL HDI 3000 system (Bortheil, WA, USA) with 5-12 MHz linear transducer and Accuson Secquoia (Mountain View, California, USA) with 8-15 MHz transducer. Ultrasonographic findings are correlated with MR imaging findings. This poster presents cases of carpal tunnel syndrome (cubital tunnel syndrome, tarsal tunnel syndrome, common peroneal nerve entrapment syndrome) and traumatic nerve injury (nerve traction injury after base ball pitching, median nerve laceration after elbow joint dislocation, superficial peroneal nerve lateral branch compression neuritis by boot, ulnar nerve neuritis after recurrent ulnar nerve dislocation at cubital tunnel, traumatic neuroma after neuropathy, axonal degeneration of radial nerve by compression by internal fixation after humerus fracture) nerve origin mass lesion (neurilemmoma, neurofibroma, nerve origin lymphoma).

Conclusion: High resolution ultrasonography is a promising tool in the evaluation of peripheral nerve abnormalities. Ultrasound is complementary to MR imaging; it is both faster and cheaper than MR imaging, and it sometimes demonstrates lesions not visualized at MR imaging. In conclusion, ultrasonography should be a major radiologic evaluation tool for evaluating peripheral nerve abnormalities.

C-0763

Intraneuronal ganglion cyst of the common peroneal nerve: MR imaging findings

S. Ruiz, A. Sánchez, J. Narváez, E. Andia; *Barcelona/ES*

Learning Objectives: To describe the MR imaging findings in intraneuronal ganglion cyst of the common peroneal nerve (CPN).

Background: Intraneuronal ganglion cyst is a rare disorder characterized by an accumulation of mucoid substance in one nerve, leading to pseudocyst formation. The CPN is the peripheral nerve most frequently affected. We retrospectively reviewed 5 examinations performed in 5 patients with progressive foot drop. Diagnosis was pathologically confirmed in 4 cases. MR imaging examinations were performed using a surface-coil. Spin Echo T1W and T2W, fat suppression

Scientific and Educational Exhibits

and STIR sequences were obtained. Contrast enhanced MR imaging images were obtained in 2 patients. Location, shape, size and signal intensity of the lesion and muscular oedema-like pattern were analysed.

Imaging Findings: All patients had difficulty in dorsiflexion of the foot and paraesthesia along the nerve's distribution. Palpable mass was present in 1 case and Tinel's sign in 2. MR imaging images showed in all cases, a well-defined round or tubular lesion with homogeneous signal intensity, low on T1-weighted images and bright on T2-weighted images, STIR and fat suppression sequences along the course of the CPN. Slightly peripheral enhancement was seen after gadolinium administration. Oedema-like pattern was observed in anterior or lateral muscular compartments. Intra-neuronal ganglion cyst was pathologically confirmed in 4 patients.

Conclusions: Although intra-neuronal ganglion cyst of CPN is a rare disorder, it should be considered in the differential diagnosis of progressive foot drop due to potential recovery after surgery. MR imaging demonstrated the cystic nature of the lesion, extension and anatomic relationship.

C-0764

High-resolution ultrasonography to evaluate the radial nerve

T. Piedra, V. Gomez-Dermit, R. Landeras, M. Aguilar, P. Zubietta, M.A. Fernandez-Echevarria; Santander/ES

Purpose: Our purpose is to describe the findings on high-frequency sonography of normal and pathologic radial nerve and determine whether sonography can help in the detection and characterization of the disease in these patients.

Materials and Methods: US studies were performed with a 5.5-12 MHz high-resolution linear array transducer. The utilization of Color-Doppler imaging allows the visualization of the artery adjacent to the radial nerve and the detection of hyperperfused areas especially in inflammatory, infectious and tumoral diseases. Patients were in a supine position and the elbow was flexed at 90° to access to the lateral part of the humerus.

Results: We describe the normal anatomy of the radial nerve through the middle and distal thirds of the upper extremity and of its sensory and motor branches. We illustrate different pathologic conditions like affection of the nerve secondary to humeral shaft fractures (5 cases), compression of posterior interosseous nerve (4 cases: 1 lipoma, 1 liposarcoma, 1 synovial cyst, 1 myositis) and superficial branch of the radial nerve (1 schwannoma).

Conclusion: US is an available, innocuous technique that allows identification of the radial nerve in normal and pathologic conditions, contributes to the decision on whether or not nerve exploration should be performed, provides important information about nerve damage especially when surgery is needed and can be used to monitor nerve regeneration in cases conservatively treated.

C-0765

Assessment of entheses by power Doppler technique in ankylosing spondylitis: A pilot study

A. Kiris, A. Kaya, S. Ozgocmen, E. Kocakoc; Elazig/TR

Purpose: Ankylosing spondylitis (AS), a chronic disease leads to progressive spinal ankylosis and deformity. Enthesitis is one of its' most prominent features. The aim of this pilot study is to validate a rationale for the value of power Doppler ultrasonography (PDU) in evaluation of entheses.

Method and Materials: Eleven patients (7M, 4F, mean age 34.3, disease duration 8.6 years) were included in the study. Patients were scrutinized for disease activity parameters, pain on entheses. B-mode and PDU was performed using 7-14 MHz multifrequency broadband linear array transducer. On B-mode examination changes on entheses were noted and power Doppler signals on entheses were graded (0-3). Ten entheses were examined in each patient.

Results: B-mode ultrasonography revealed pathological findings in 51/220 entheses (23%) examined. All patients had pathological changes in B-mode in at least two entheses. PDU revealed detectable flow in 31/220 entheses (14%) examined. Five patients had both flow signals and B-mode changes on entheses, whereas six had no flow signal on PDU although they had pathologic findings in B-mode. Pressure pain threshold was significantly lower in 31 entheses that had PD signals than entheses without PD signals (4.3 vs. 4.9, p = 0.006).

Conclusions: Consequently, B-mode ultrasonography is a valuable tool to examine entheses and a reliable method. Concomitant use of PDU with B-mode may enhance ultrasonographic features and may predict inflammation of enthesitis by means of hypervascularisation. In this regard, there may be a link between inflammation, hypervascularisation and pain on entheses. These results promote a rationale for further studies.

C-0766

MR imaging in spinal injury in patients with ankylosing spondylitis

G. Mantzikopoulos, K. Pikoulas, I. Staikidou, G. Giannikouris, K. Ioannidis, K. Dagiada; Athens/GR

Purpose: To present the imaging findings and the role of MR imaging in the investigation of spinal injuries in patients with ankylosing spondylitis.

Materials and Methods: We retrospectively reviewed the MR imaging studies of 9 patients (7 men & 2 women, 44-75 years of age) with ankylosing spondylitis who had sustained spinal injury and were admitted to our hospital during the last 4 years.

Results: 6 patients had Chance-type flexion-distraction injuries and 2 patients had compression fractures. 1 patient had vertical atlanto-axial subluxation. Involvement of cervical spine was seen in 3 cases and of thoracic spine in 6 cases. Contiguous vertebral injury was present in 4 cases and non-contiguous injury in 2 cases. 3 cases had displaced fractures with significant stenosis of the spinal canal. 1 patient had a fibrous union at the fracture site in a follow-up examination. Bone and soft tissue edema were clearly depicted and the fracture line was evident in all cases. Posterior ligamentous disruption was present in all Chance-type injuries. A horizontal fracture of the posterior neural arches producing a "sandwich sign" was seen in 2 cases.

Conclusion: MR imaging of spinal injuries in patients with ankylosing spondylitis allows a timely and confident diagnosis of the various types of bone and soft tissue injuries present as well as their possible neurological complications.

C-0767

MR imaging evaluation of tibialis posterior tendon: Assessment of its disorders and its role in determining coxa pedis syndrome

C. Bultrini, N. Limbucci, A. Barile, R. Manetta, G. Bonanni, C. Masciocchi; L'Aquila/IT

Purpose: To assess the role of MR imaging in the evaluation of the tibialis posterior tendon (TPT) and its influence in determining coxa pedis syndrome.

Methods and Materials: We retrospectively analysed 45 patients undergoing MR imaging because of the clinical diagnosis of coxa pedis syndrome. MR imaging examinations were performed with 1.5 T whole body and 0.2 T dedicated MR units. The sequences employed were SE-T1W, GE-T2W and SE-T2W with fat-saturation on sagittal and oblique-axial scan planes; the slice thickness was 3-4 mm. All patients were previously submitted to plain film. Five safe volunteers were previously submitted to MR imaging examination to optimize sequences, scan planes and anatomy.

Results: In all cases MR imaging allowed identification of TPT. In 36 of 45 patients (80%) MR imaging showed signal abnormalities suggestive of TPT degeneration with or without tenosynovitis; an associated condition of os tibiale was discovered in 14 of these 36 patients (38.9%). 10 of 36 patients (27.8%) had MR imaging signs of partial TPT tear, and in 4 cases (11.1%) we found complete TPT tear. In 6 of 36 cases (16.7%) we found talo-navicular chondropathy associated to TPT disease and in 2 cases (5.5%) spring ligament pathology.

Conclusion: MR imaging is very accurate in the evaluation of TPT and the other structures of the coxa pedis complex, allowing the diagnosis of TPT disease and the detection of possible associated abnormalities. According to our results, TPT disease is the main factor determining coxa pedis syndrome, this confirms that TPT is the main active stabilization structure of the coxa pedis complex.

C-0768

Bryan cervical disc prosthesis: A radiological study

G. Iannucci¹, R. Fossaceca¹, P. Cervellini², F. Causin², M.D. Marchi², V. Pinna¹, A. Carrieri¹; ¹Novara/IT, ²Vicenza/IT

Purpose: The Bryan Cervical Disc Prosthesis provides an innovative method of restoring mobility in patients with cervical disc degenerative disease. This study radiologically evaluated their stability and normal range of motion as well as the clinical evolution of patients 2 years from surgical implantation.

Methods and Materials: This prospective study included 15 patients. 13 patients with symptomatic cervical radiculopathy and 2 patients with myelopathy. We measured maximal flexion-extension (Cobb method) on plain films of the cervical spine in all cases with 1 and 2 years follow-up. We performed CT of the prosthesis at the same time. Effectiveness of the device was also characterized by evaluating each patient's pain, neurological signs and symptoms.

Results: There were no significant differences between the first and the second control in the follow-up period. The average range of motion of devices in flexion-extension at 1 year (mean flexion 31.1°, SD 9.8; mean extension 30.6°, SD 11.9) was demonstrated to be equal or decreased by ~ 2 degrees when compared to 2

Scientific and Educational Exhibits

years control (mean flexion 29.7°, SD 13.3; mean extension 32.8°, SD 12.4). CT scans of the prosthesis never showed fusion of adjacent vertebral bodies but in 2 cases marginal osteophytes were observed. We demonstrated clinical improvement in 14 patients; 1 patient showed no clinical change. None of the patients deteriorated from the baseline pre-operative assessment.

Conclusion: The two-year follow-up study based on neurological signs and symptoms showed a good assessment of the prosthesis function with relief of pain and improvement of cervical motion function.

C-0769

Advanced chordomas treated with imatinib mesilate: MR imaging tumor response assessment after 18 months follow-up

A. Messina, P. Casali, D. Vergnaghi, A. Gronchi, S. Stacchiotti, R. Musumeci;
Milan/IT

Purpose: To evaluate MR imaging patterns of tumor response to imatinib mesylate in advanced chordomas.

Materials and Methods: Following detection of PDGF-R expression in tumor samples, 12 pts with advanced disease (10 with sacral, one with clivus and one with vertebral chordomas) were treated with imatinib mesylate. Before medical treatment 9 patients underwent debulking surgery for a sacral chordoma. All patients were evaluated with MR imaging at baseline, and then every 1-3 months until 18 months from treatment start. MR imaging was performed with a 1.5 T system using morphologic GRE T1w, TSE T2w and contrast enhanced-GRE T1w sequences.

Results: 8 patients (66%) were judged to be responsive to therapy after 18 months. Pts responsive to therapy showed these hints of tumor response: A) minor and slow decrease in size in the pts with the longest follow-up (18 months), following a transient initial increase in size, which was seen in all pts; B) hypointensity of lesions on T1w and hyperintensity on T2w MR images; C) hypovascularity of lesions on CE-T1w MR images in comparison to baseline assessment. These signs supposed a tumor liquefaction, at least in a substantial portion of the tumor volume.

Conclusion: MR imaging may be useful to assess tumor response in patients affected by advanced chordomas treated with imatinib mesylate. Signs of response may be subtle, likely depending on changes in tumor tissue rather than (or before) decrease in size.

different from those who do, that usually have an acute or subacute course. Several bones affected by bone marrow edema, mottled-pattern edema or diffuse-confluent pattern of edema are findings of less chronic disease. Reticular pattern of signal changes, soft tissue atrophy, and even changes in trabecular configuration correlate better with a long-standing course

Conclusion: MR imaging shows findings that make the diagnosis of RSD possible, in certain kinds of patients with chronic pain around a joint or in a limb, not proportional to initial cause of events. Correlation between this set of imaging findings with clinical evolution is good in patients with a previous diagnosis of RSD, and in those without such a diagnosis but a clinical suspicion. In acute and subacute cases, often there are no conventional imaging findings (X-ray).

C-0770

Magnetic resonance findings in macromelia and macrodactyly

X. Merino-Casabiel, R. Dominguez-Oronoz, E. Castella-Fierro, V. Pineda,
F. Ramirez-Urbano; Barcelona/ES

Learning Objectives: To describe the etiologic spectrum and MR findings in macromelia and macrodactyly.

Background: Localized soft tissue and bone overgrowth may be the result of many different causes and will vary in severity, from involvement of a single digit to one half of the body. There are a variety of causes, including chronic lymphedema; lymphangiomatous malformations; neurofibromatosis; vascular malformations including the Klippel-Trenaunay-Weber syndrome; macrodystrophy lipomatosa; multiple enchondromatosis and Maffucci's syndrome.

Imaging Procedures: We reviewed MR images of all patients referred for clinical macromelia and macrodactyly over the last 10 years.

Conclusion: This review illustrates the importance of MR imaging in not only establishing an accurate diagnosis but also in defining the extent of the underlying abnormality.

C-0771

MR imaging findings in patients with a clinical diagnosis or clinical suspicion of reflex sympathetic dystrophy (RSD)

A. Ferreiro, A. Delgado, P. Muyor, A. Martinez de Aragon, R. Stefanova,
A. Ramirez; Madrid/ES

Materials and Methods: We collect imaging findings of 40 patients with a diagnosis of RSD previously reached by clinician, or patients coming with chronic pain around some joint with or without previous injury, not related with initial degree of harm. Most of the cases are related to knee or ankle, but also wrist and hip. All the studies are performed with a 0.65 T open MR imaging machine (FO-NAR corp.). We use Chi square statistics to set a correlation between clinical and imaging criteria.

Results: We compare chronicity of symptoms with imaging findings, and describe findings in patients without a definite diagnosis but with chronic pain in the joint or limb affected. In most of the patients that don't localize pain, findings are

Scientific and Educational Exhibits

Neuro Brain

C-0772

Epileptic mothers and their progeny in fMRI imaging assessment of developmental dyslexia

A. Salagierska-Barwinska, B. Goraj, J. Wendorff, B. Wisniewska; Lodz/PL

Purpose: Although much has been said about the occurrence of developmental dyslexia in families, this problem has not been studied in the group of epileptic parents and their progeny. In 40% of children of epileptic mothers there are specific difficulties in learning to write and read; this constitutes a significantly higher percentage than in the general population. This project assesses two of the important etiological factors of dyslexia, that is family history of disorders and abnormalities in the range of neuropsychological function.

Materials and Methods: fMRI imaging was carried out in 20 participants: 10 epileptic mothers and 10 of their healthy children. Our previous control study was performed in 30 dyslexic participants and 30 healthy participants. All subjects had normal mental development. MR examination with a 1.5 T Siemens Vision scanner equipped with echo-planar imaging software was performed. 21 contiguous brain slices were acquired. Data recording was performed alternating at rest and in task execution. Two different language problems were performed. Functional images were generated using statistical methods - SPM'99 software.

Results: Anatomical location of cortical activation in all participants was unusual comparing with our preceding research in control dyslexic and normal participants. During the tasks in children of epileptic mothers no significant activation in Broca's center (44.45 BA) in the left lobe was observed.

Conclusion: This research indicates the role of two of the most significant etiological factors in developmental dyslexia (family history and CNS functional changes). Our studies have shown deficit in the neural mechanisms underlying phonological processing in children of epileptic mothers.

C-0773

Correlation of diffusion tensor MR imaging with MR spectroscopy in multiple sclerosis

R. Irwan, P. Sijens, M. Oudkerk; Groningen/NL

Purpose: To compare the results of magnetic resonance spectroscopy (MRS) and diffusion tensor imaging (DTI) in multiple sclerosis (MS) patients.

Methods and Materials: Sixteen patients with MS were examined by MRS and DTI using a 1.5 Tesla MR system (Sonata, Siemens Medical Systems, Erlangen, Germany). Point resolved spectroscopy (PRESS, TE/TR = 135/1500) was used for chemical shift imaging applied on a supraventricular transverse volume of interest of 8x8x2 cm³. For the inner 6x6 = 36 voxels the peak areas of choline (Cho), creatine (Cr) and N-acetylaspartate (NAA) were determined by curve fitting. In DTI a segmental spin-echo sequence (TE/TR = 91/5500) was used with the following acquisition parameters: field of view 23 cm; matrix 128 x 128 with interpolated readout to 256 steps; 12 directions and two b-values ($b = 0$ and $b = 1000 \text{ sec/mm}^2$). Five slices of 4 mm each (non-overlapping) were stacked in order to reproduce the 20 mm slab used in MRS. Mean fractional anisotropy (FA) and apparent diffusion coefficient (ADC) were subsequently determined for the 36 voxels defined in MRS.

Results: Significant correlations between the spatial distributions of metabolites and DTI parameters in normal appearing white matter of MS patients were found, most notably that of NAA/Cr ratio and FA ($r = 0.65$ and $P < 0.0001$).

Conclusion: It has been known that MS patients have increased Cho levels, reduced NAA levels, reduced FA and increased ADC. This is the first association of neuronal loss indicated by MRS (NAA drop) with loss of structure as indicated by DTI (FA decrease).

C-0774

Multidetector CT angiography: The method of choice to detect cerebral venous thrombosis?

N. De Graaf, H.L.J. Tanghe, T.C. Leertouwer, H.Z. Flach, D.W.J. Dippel, A. Van der Lugt; Rotterdam/NL

Learning Objectives: To describe the multidetector computer tomographic angiography (CTA) scanning protocol for detection of cerebral venous thrombosis. To describe the postprocessing protocol for analysis of CTA data. To show the cerebral venous anatomy on CTA images. To illustrate the role of CTA in detecting cerebral venous thrombosis.

Background: Cerebral venous thrombosis (CVT) is a relatively rare, but potentially severe condition. Magnetic resonance angiography (MRA) is usually con-

sidered the gold standard to detect CVT. In our institution we have gained experience using CTA instead of MRA.

Procedure Details: This exhibit describes our scanning protocol (delay, scan direction, scan range, contrast volume, bolus chaser, pitch). Postprocessing is done by creating coronal, sagittal, and axial maximum intensity projections. In addition, volume rendering of the inner skull is performed to evaluate the cortical veins. The venous anatomy will be shown on CTA images. Examples of thrombosis of the superior sagittal sinus, transverse sinus, sigmoid sinus, and straight sinus are shown. In addition, an example of isolated cortical vein thrombosis is demonstrated. Pitfalls are also discussed: arachnoid granulations versus thrombosis, and aplasia of the transverse sinus versus thrombosis of the transverse sinus.

Conclusion: CTA can be used in the acute phase of patients suspected of having CVT.

C-0775

Pontine bright lesions: MR imaging findings and differential diagnosis

V.K. Katsaros, M. Mitropoulou, P. Lampropoulou, C. Mourtopoulos, D. Kolomodi, A. Nikolaou, C. Drossos; Athens/GR

Purpose: The aim of this study was to evaluate different MR imaging sequences for the diagnosis of neoplastic, vascular, inflammatory and miscellaneous pontine lesions.

Methods and Materials: 336 brain MR examinations with pontine lesions were performed by a 1.5 T MR unit (Magneton, Vision). The routine brain MR imaging protocol used included axial T1, proton density and T2-W and FLAIR (Dark-Fluid) and coronal, sagittal T2-W images. T2*-W in the axial plane was obtained in cases of suspected hemorrhage. If necessary enhanced T1-W images were obtained. Correlation with clinical and laboratory findings followed.

Results: A pontine volume increase or decrease was proved comparing the data of the normal and affected brain stem. The topography of lesions was clearly documented by MR imaging. Subacute hematomas were better outlined than by CT, while acute infarctions, foci of demyelination and pontine encephalitis were proved only by MR imaging. Small calcifications and vessels of arteriovenous malformations, however, caused the same MR signal patterns. Pathological hyperintensity in T2, T2*W and FLAIR (Dark Fluid) sequences and pathological enhancement in contrast-enhanced T1W images were found in the following lesions: 1) contusion: 1 2)hematoma: 8; 3)vascular malformations: 12; 4)ischemic lesions: 197; 5)infections: 4; 6)multiple sclerosis: 64; 7)central pontine myelinolysis: 2; 8)polyarteritis nodosa: 1; 9)Wilson's disease: 2; 10)neoplastic: 43; 11)radiation: 2.

Conclusion: MR imaging is of utmost importance in the diagnostic work-up of patients with pontine lesions and in correlation with clinical and laboratory findings the correct diagnosis is established.

C-0776

Transcranial color-Doppler sonography (TCDS) today: When and how to use it

A. Pedicelli, A. Bellitti, A. Cina, M. Rollo; Rome/IT

Learning Objectives: 1)To learn the technique and describe the state of the art of TCDS: probes, conventional and non-conventional acoustic windows (AW), morphological and flowmetric studies, common pitfalls, use of sonographic contrast agents and technical innovations. 2)To give an overview of clinical conditions where the method can be used for diagnosis, integration imaging a/o follow-up.

Background: Compared to traditional Doppler, TCDS permits direct visualization of the vessels (course and abnormalities) and precise positioning of sample volumes on vascular segments for selective flowmetric analysis. We report our experience from 1993 to 2004, discuss the present role, with technical improvements, and show the use of the method in assessment of: vasospasm after SAH, arterial stenosis/occlusion, cerebral embolism monitoring, diagnosis of brain-death. Moreover we report our results in diagnosis and follow-up of:cerebral aneurysms, AVMs (including DAVM and CCF with integration of non conventional facial AW). Initial studies of cerebral perfusion are also reported.

Imaging Findings: In the poster, vascular anatomy as demonstrated by the technique is reviewed. We describe AW (pterional, sub-occipital, trans-orbital), analyze the value and describe when to use quantitative and semi-quantitative flowmetric parameters (SPV, EDV, PI, RI) and finally describe pitfalls that occur by wrong parametric setting, calcium-related artifacts, etc.

Conclusion: At present TCDS is a non-invasive, cost-effective, rapid and bedside performable technique that is useful and has acquired a major role in diagnosis and follow-up for many clinical conditions. Limits of TCDS are due to poor AW and thecal bone thickness, which are overcome by sonographic contrast agents in 85% of cases, by power-Doppler modality and increased spatial resolution of new systems.

Scientific and Educational Exhibits

C-0777

Embolization of cavernous dural arteriovenous fistulas via superior ophthalmic vein approach

S.-H. Suh, D.-I. Kim, D.-J. Kim; Seoul/KR

Purpose: To present the results of treatment for cavernous dural arteriovenous fistulas (DAVFs) with transvenous or surgical approach through the superior ophthalmic vein (SOV).

Materials and Method: 10 patients (M:F = 2:8, mean age = 52 yrs) with cavernous DAVFs were treated via transvenous or surgical approach of SOV during a 4-year period. All patients had chief complaints of proptosis, chemosis and decreased visual acuity. Angiography showed preferential venous drainage of DAVFs to an enlarged ipsilateral SOV. 3 patients had surgical exposure of the SOV and 7 patients had a retrograde transvenous approach via the facial vein. Embolization with coil or polyvinylalcohol was performed through a microcatheter at the fistula site and into the root of the SOV and cavernous sinus, until there was complete angiographic closure. In the follow-up period, angiography or magnetic resonance angiography was performed 3 or 6 months after embolization.

Results: Catheterization and embolization was successful in all patients, with complete angiographic occlusion of the fistula. After successful occlusion of DAVFs, clinical symptoms and signs were completely resolved and no early or late complications had occurred. At follow-up (mean 37 months), all except one patient's embolized fistula was persistently occluded. No patients had recurrent symptoms and signs.

Conclusion: Coil embolization of cavernous DAVFs with retrograde transvenous or surgical approach through SOV is a safe and effective treatment, which are not acceptable to transarterial or other transvenous approach.

C-0778

Head and neck paragangliomas: Diagnostic and endovascular therapy

M. De Juan Delago, L. San Roman Manzanares, T. Salinas Yeregui, C. Castaño Duque, E. Guardia Mas, J. Ruscalleda Nadal; Barcelona/ES

Learning Objectives: To define and illustrate imaging features in CT, MR imaging and arteriography, utility and presurgical endovascular embolization techniques in the diagnosis and therapy of head and neck paragangliomas

Background: 25 paragangliomas were evaluated and included: jugulotimpanic, carotid and vagal glomus. All were evaluated with CT and MR imaging. A selective catheterization of the external carotid artery and their branches with presurgical embolization with PVA particles and coils was made in 14 patients.

Procedure Details: The most frequent initial symptom was a laterocervical painless growing mass. Other symptoms included instability, pulsatile tinnitus and cranial nerves palsies. CT and MR imaging showed typical characteristics of these tumors: well defined masses with important enhancement with intravenous contrast, vascular structures inside producing salt and pepper appearance in standard spin-echo magnetic resonance imaging. The angiography studies demonstrated the presence of hypervascular masses with the characteristic "blush". Also allowed a correct valoration of the venous return. Presurgical embolization obtained devascularization about 90% in all the cases, reducing the bleeding spectacularly in relation with the cases nonembolized previously.

Conclusion: We presented the location, the imaging characteristics and the endovascular presurgical treatment of 25 head and neck paragangliomas.

C-0779

Imaging of head and neck venous malformations: A pictorial review

C.M. Flis, S.E.J. Connor; London/UK

Learning Objectives: To review the classification of venous malformations in the context of head and neck vascular malformations and tumors. To describe and illustrate the imaging findings using ultrasound, magnetic resonance imaging (MRI), computed tomography (CT), conventional angiography and percutaneous phlebography and explain how to differentiate from other vascular/lymphatic malformations. To outline the specific role of these imaging techniques and image guided sclerotherapy.

Background: Venous vascular malformations are non proliferative low flow vascular lesions that consist of dysplastic venous channels. Ultrasound and MRI are the initial imaging modalities of choice with a supplementary role for CT. Characteristic appearances of venous malformations include the presence of phleboliths and markedly hyperintense lobulated lesions on T2-weighted MRI sequences. Image guided sclerotherapy is the first line treatment option in selected cases.

Imaging Findings: The plain film, ultrasound (including colour and duplex Doppler), CT and MRI as well as conventional angiographic appearances of head and neck venous malformations will be described and illustrated together with

examples of image guided sclerotherapy. A range of head and neck subtypes including orbit, oral cavity, superficial and deep facial space, supraglottic, intraosseous and intramuscular will be illustrated.

Conclusion: An understanding of the imaging characteristics of venous malformations of the head and neck is important to enable the correct diagnosis. The radiologist plays a pivotal role in selecting the most appropriate diagnostic and therapeutic modalities.

C-0780

fMRI imaging evidence of functionality in polymicrogyric cortex

D. Araújo, D.B. de Araújo, O.M. Pontes-Neto, S. Scorsi-Rosset, L. Wicher-Anna, J.P. Leite, A.C. Sakamoto, A.C. Santos; Ribeirão Preto/BR

Purpose: Malformations of cortical development (MCD) are one of the most common pathological findings in refractory extratemporal epilepsy. Magnetic resonance imaging (MRI) can reliably show these alterations and provide information for surgical resection. However, there is increasing evidence that neurons in MCD areas are functional and may show different organization patterns in comparison to normal brains. Our objective was to analyze patterns of plasticity and function in polymicrogyric cortex in epileptic patients by blood oxygenation level dependent functional MR imaging (fMRI).

Methods and Materials: Six adult patients (4 female), with clinical and neurophysiological evidence of extratemporal epilepsy, and a radiological diagnosis of polymicrogyria were scanned in a 1.5 T Siemens magnet with fMRI sequences according to language (word generation), and motor (finger tapping) protocols.

Results: Statistical maps showed significant activation of polymicrogyric cortex in the motor strip in the 5 cases in which it was present in that location. In two cases language tasks did not show any significant activation.

Conclusion: Functionality was shown in polymicrogyric areas. In some cases there was evidence of reorganization to ipsi and contralateral areas. Surgical resection may be performed but there is need for functional planning due to reorganization and functionality of polymicrogyric cortex.

C-0781

Perfusion CT imaging of angiogenesis in VX2 rabbit brain tumors

Y. Zhang, L.Q. Kang; Tianjin/CN

Purpose: To validate perfusion CT for reflection of angiogenesis in VX2 rabbit brain tumors.

Methods and Materials: The VX2 rabbit brain tumor model was established. 20 New Zealand White rabbits with tumor size over 3 mm in diameter were randomly divided into group 1 (≤ 3 weeks) and group 2 (> 3 weeks). Perfusion CT was performed with GE Hispeed CT/i scanner. 50 cine mode images were acquired before, during and after intravenous injection of 1.5 ml/kg Omnipaque (300 mg/ml) at a speed of 0.4 ml/s. CT measurements of BV, BF and PS from tumor, peritumor and contralateral normal tissue were obtained using GE perfusion-2 software. 2% Evans blue (2 ml/kg) was given intravenously one hour prior to sacrifice to detect breakdown of BBB. VEGF and MVD were evaluated in immunohistochemical examination of the specimens.

Results: Tumors had significantly higher BV, BF and PS ($P = 0.000$) than did peritumor and normal tissue. Tumor BV, BF and MVD in group 2 were significantly higher than those in group 1. We found a significant linear correlation between MVD and BV ($r = 0.915$, $P = 0.000$), MVD and BF ($r = 0.915$, $P = 0.000$), and MVD and PS ($r = 0.459$, $P = 0.042$). We also found a rank correlation between PS and blue stain of tumor ($r_s = 0.861$, $P = 0.000$).

Conclusion: Perfusion CT can distinguish tumor from peritumor and normal tissue clearly, reflect tumor angiogenesis accurately, and thus provide useful information for the evaluation of brain tumors.

C-0782

Diffusion tensor based analysis of the uncinate fasciculus in mesial temporal sclerosis

S. Rodrigo¹, C. Oppenheim¹, F. Chassoux¹, Y. Cointepas², F.-X. Roux¹, J.-F. Meder¹; ¹Paris/FR, ²Orsay/FR

Purpose: Diffusion tensor imaging (DTI) is a noninvasive technique that can assess the coherence of white matter bundles. Our aim was to evaluate the integrity of the uncinate fasciculus, one of the major bundles connecting the frontal and temporal lobe in mesial temporal sclerosis (MTS).

Methods and Materials: We compared 6 right handed patients with intractable epilepsy related to right hippocampal sclerosis (MTS) and 6 right handed healthy controls. DTI was acquired on a 1.5 T unit (41 directions, $b = 00$ s/mm², 60 contiguous, 2 mm-axial sections). We compared the right and left DTI measurements

Scientific and Educational Exhibits

(mean fractional anisotropy (FA) and mean diffusivity (MD)) measured along the uncinate fasciculus delineated by fiber tracking ("Brainvisa/Anatomist" software, <http://brainvisa.info>). Right/left asymmetry of DTI values were compared in each subject using a student T-test.

Results: Five patients had significantly ($p < 0.001$) higher MD in the right uncinate fasciculus, ipsilateral to the MTS, while all controls had higher MD in the left side ($p < 0.001$). One patient, with an atypical EEG pattern, showed a higher MD, contralateral to the MTS. Fractional anisotropy asymmetry did not significantly differ between patients and controls.

Conclusion: While right handed controls showed a MD asymmetry of the uncinate fasciculus (left superior to right), this pattern is inverted when a right MTS is present. This confirms the ability of DTI to depict microstructural abnormalities along the temporo-frontal white matter bundles, which may be involved during the ictal spread.

C-0783

Comparison of BOLD signal strength and susceptibility artifacts between 1.5 and 3.0 Tesla at different TE

B. Schmitz, G. Grön, A.J. Aschoff; Ulm/DE

Purpose: Blood oxygen level dependent (BOLD) signal for functional magnetic resonance imaging (fMRI) relies on changes in susceptibility. Susceptibility artefacts become stronger with increasing B_0 as well as with increasing echo time (TE). We compared BOLD signal strength for different TE at 1.5 and 3.0 Tesla (T).

Methods and Materials: 48 slices with 3.3 mm isotropic voxels covering the whole brain within an interscan interval (TR) of 4500 ms were acquired on a 1.5 T Symphony and 3.0 T Allegra (both Siemens) at echo times of 20, 30, 40, 50 and 60 ms. A blocked finger tapping within subject design was used with 54 volumes scanned, a stimulus onset asynchrony of 16 volumes, and an epoch length of 8 volumes. Beta values were computed from scaled EPI-series within the general linear model (SPM 99) as a quantitative measure of BOLD signal strength.

Results: Significant activation in the hand motor area was achieved in all sessions. BOLD signal increased with increasing TE. At every TE signal strength from 3.0 T was higher than from 1.5 T with a peak at 40 ms with a fourfold increase. Susceptibility artefacts at air-bone interfaces increased with increasing TE and B_0 strength.

Conclusion: The BOLD signal increase at higher B_0 allows shorter TE down to 20 ms, which in turn enhances temporal resolution and allows for scanning volumes at a higher frequency. This will augment statistical power for analysis of functional data. Susceptibility artefacts at the skull base from large B_0 can be overcome by using shorter TE.

C-0784

MR imaging patterns of hypoxic-ischemic encephalopathy in premature and term born infants

J. Nikas, C. Hadjigeorgi, A. Anagnostara, M. Theofanopoulou; Athens/GR

Purpose: To describe and attempt to classify the different MR imaging patterns of hypoxic-ischemic injury in preterm and term infants.

Materials and Method: We retrospectively reviewed the MR scans of 49 children with some type of cerebral palsy (21 preterm and 28 term) and history of perinatal injury.

Results: In all premature children MR imaging revealed lesions of periventricular leukomalacia of different severity. In term infants we observed 6 different MR patterns of ischemic lesions; either isolated or in combination: a)profound-selective lesions, b)parasagittal lesions, c)ulegryria, d)multicystic encephalomalacia, e)periventricular leukomalacia and f)arterial infarcts.

Conclusion: Hypoxic-ischemic brain damage in preterm infants is manifested with periventricular leukomalacia, while in term infants a variety of brain lesions can be found. We describe 6 different MR patterns of hypoxic encephalopathy, occurring in isolation or in combination, which are closely related to the perinatal history and the neurological deficits.

C-0785

Differential diagnosis of lesions involving the brain and spinal cord in patients with lymphoma

A. McGrath, C. Farrelly, N. Sheehy, J.F.M. Meaney; Dublin/IE

Learning Objectives: 1.To describe the spectrum of appearances in patients with primary CNS lymphoma. 2.To illustrate the spectrum of abnormalities in patients with disseminated disease. 3.To illustrate the differential diagnosis of lesions involving the brain and spinal cord in patients with known/treated lymphoma. 4.To highlight changes attributable to the effects of radiation and chemotherapy in patients treated for lymphoma.

Background: Lymphoma most commonly affects the brain as a result of disseminated disease in patients in whom the diagnosis has already been established. Primary CNS lymphoma is increasing in incidence, primarily due to an increasing incidence in patients with immunocompromise (most commonly HIV related). Intramedullary spinal lesions are also usually associated with disseminated disease.

Procedural details: Imaging features are non-specific, and biopsy is usually essential for diagnosis. However, findings that suggest a diagnosis of lymphoma include periventricular white/gray matter involvement, peri-vascular spread, tumour crossing the corpus callosum, low attenuation on CT, low signal intensity on T2W MR imaging and less oedema compared to other tumours. Findings in patients with known lymphoma include lymphoma masses, meningeal infiltration, infections, radiation changes and drug-induced leuco-encephalopathy. Lymphoma associated granulomatous vasculitis is a rare cause of multiple brain lesions.

Conclusion: This electronic poster illustrates the wide spectrum of imaging abnormalities in patients with primary and secondary CNS lymphoma. Treatment related complications are also presented.

C-0786

Cocaine and heroin abuse related to acute encephalopathy: Emergency MR imaging findings

V. Pupillo, E. Puglielli, C. Fiumara, R. De Amicis, C. Masciocchi, M. Gallucci; L'Aquila/IT

Purpose: Many studies have dealt with MR imaging patterns in relation to cocaine and heroin abuse but none concern pts studied in the emergency situation.

Methods and Materials: 12 patients (4 females and 8 males, average age 29.7) entered the study. All of them came from a first aid station and were suffering from an acute encephalopathy resultant from cocaine or heroin abuse. All patients underwent standard MR imaging examination, performed with 1.5 T MR scanner.

Results: In 3 patients Delayed Post-Hypoxic Leucoencephalopathy (DPHL) related to cocaine abuse and consequent to protracted cardiac dysrhythmia were found; in 3 patients with heroin abuse bihemispheric leucoencephalopathy involving also fronto-temporal cortex and basal ganglia were found; in 1 case of heroin and benzodiazepine abuse aspects compatible with a bilateral limbic encephalitis were registered; 1 case of anterior spinal artery ischemia was related to cocaine abuse; 2 cases of cerebellar ischemic lesion and 2 cases of supratentorial cerebral ischemia related to cocaine were registered.

Conclusion: Alterations due to cocaine abuse are usually caused by direct alterations that the drug induces on vessel walls while in the case of heroin, to toxic substances that are "cut" with the drug.

C-0787

Malignant lymphomas and carcinomas involving the cavernous sinus: Assessment with apparent diffusion coefficient

M. Maeda, K. Takeda; Tsu/JP

Purpose: Malignant tumors such as lymphoma and carcinoma can spread into the cavernous sinus. The purpose of this study was to evaluate apparent diffusion coefficient (ADC) of tumors involving the cavernous sinus by line scan diffusion-weighted imaging (LSDWI) and to determine the usefulness of it for differentiating between the two tumors.

Methods and Materials: Four patients with malignant lymphoma (mean maximum diameter, 19 mm) and five patients with carcinoma (mean maximum diameter, 25 mm) were studied. The MR study was performed prior to treatment in all patients. LSDWI was performed using b values of 5 and 1000 s/mm², and effective section thickness/gap of 3/0.5 mm. LSDWI images were obtained in the coronal plane focusing on the cavernous sinus. ADC values were calculated and compared between malignant lymphomas and carcinomas. Mann-Whitney U test was applied to detect any significant differences in mean ADC values.

Results: LSDWI could provide images free from susceptibility artifacts and permit measurements of ADC values in all cases. The ADC value (mean \pm SD) was $0.51 \pm 0.06 \times 10^{-3}$ mm²/s in malignant lymphomas and $1.01 \pm 0.06 \times 10^{-3}$ mm²/s in carcinomas. A significant difference in ADC values was found between the two ($p < 0.01$).

Conclusion: LSDWI enabled quantitative assessment of diffusion in malignant tumors involving the cavernous sinus. Malignant lymphoma showed significantly lower ADC value than carcinoma. This method appears to be useful for differentiating between malignant lymphoma and carcinoma involving the cavernous sinus.

Scientific and Educational Exhibits

C-0788

Cerebral blood flow in subclavian steal syndrome evaluated by arm exercise Tc-99m ECD SPECT

K. Kaneko, K. Yasumori, T. Matsumura, K. Hiraka, K. Furuya, S. Uehara, S. Fujimoto, Y. Okada, T. Muranaka; Fukuoka/JP

Purpose: To evaluate cerebral hemodynamic state in patients with subclavian steal syndrome, we investigated both arm exercise and arm hemostasis using Tc-99m ECD SPECT.

Methods and Materials: The subjects were ten patients with subclavian steal syndrome who had subclavian stenosis and systolic reversed vertebral flow. SPECT images were obtained using an equal-volume-split dual-injection single-day protocol [resting and vascular reserve (RVR) method]. Then we measured regional cerebral blood flow (rCBF), and automated ROI analysis using a three-dimensional stereotaxic ROI template (3DSRT) was performed in the cerebral cortices and cerebellum.

Results: Four patients showed a decrease of rCBF in posterior cerebral artery (PCA) territory (12.9%; mean) and cerebellum (12.4%) than those of arm hemostasis SPECT, and those of middle cerebral artery (MCA) and anterior cerebral artery (ACA) territory were also decreased. One of four patients who complained of vertigo during the examination showed over 20% decrease of rCBF in cerebral cortices and cerebellum. In other patients, rCBF were preserved in arm exercise SPECT.

Conclusion: Arm exercise may cause cerebral and/or cerebellar hypoperfusion in patients with subclavian steal syndrome. Arm exercise Tc-99m ECD SPECT could show these phenomena, and make it possible to evaluate their degree and distribution.

C-0789

Tractography of corticospinal tract stroke by diffusion tensor imaging:

Clinicotopographical correlation

J.-H. Kim, J.-S. Lee, S.-H. Kim; Seongnam-Si/KR

Purpose: Fiber tracking of the white matter using diffusion tensor imaging is a new imaging technique to visualize the integrity of the white matter. We investigated the capability of this technique in localizing lacunar infarctions, specifically with respect to the body parts affected.

Methods and Materials: Twenty-seven patients with acute lacunar infarctions in capsular and percapsular regions underwent diffusion tensor imaging and subsequent fiber tracking of the corticospinal tract (CST). According to lesion topography with regard to the CST, infarctions were categorized into four different types: 1)cranial type involving the anterior part of the CST, 2)central type involving the middle or whole part of the CST, 3)caudal type involving the posterior part of the CST, 4)intact type not involving the CST. Each type was correlated with the presence or absence of motor weakness of the specific body parts.

Results: Cranial type was found in 9 patients, central type in 9 patients, caudal type in 5 patients and intact type in 4 patients. Motor weakness of the face, upper extremity and lower extremity was found in 100%, 67% and 44%, respectively in cranial type, in 89%, 100% and 89%, respectively in central type, at 20%, 80% and 100%, respectively in caudal type. Intact type was not associated with motor weakness.

Conclusion: Fiber tracking of the CST enables specific localization of lacunar infarctions with regard to the body parts affected. Our results support strongly the topographical accuracy of the fiber tracking of the CST.

C-0790

Metronidazole induced encephalopathy: MR findings and clinical presentation

E. Kim¹, S. Kim², E. Kim¹, D. Na¹, J. Ryoo³, S. Lee¹; ¹Seoul/KR, ²Chunchon/KR, ³Inju-Si/KR

Purpose: To describe the clinical features and magnetic resonance findings of metronidazole induced encephalopathy.

Materials and Methods: Six patients with Crohn's disease (n = 2), pseudomembranous colitis (n = 1), brain abscess (n = 1), spontaneous bacterial peritonitis (n = 1), and intraabdominal abscess (n = 1) were enrolled in the study. They had been treated with metronidazole and subsequently presented with neurological signs and symptoms consisting of ataxia, dysarthria, and weakness or tingling sensation of both extremities. They underwent MR imaging with or without diffusion-weighted imaging (DWI) within 7-66 days after symptom onset. Follow-up MR was obtained in 4 patients after discontinuation of metronidazole.

Results: All patients showed high signal intensity in the splenium of the corpus callosum, red nucleus, and/or dentate nuclei on both T2-weighted and FLAIR

images. High signal intensity was also seen at the bilateral subcortical white matter in two patients; the basal ganglia, anterior commissure, and tectum in one patient. No enhancement was seen in the hyperintense lesions. DWI was obtained in four patients, and showed iso- or hyperintensity and variable ADC values on the corresponding areas. All patients rapidly improved clinically after discontinuation of metronidazole. Repeat MR imaging including DWI was obtained in four patients, and showed near complete resolution of the previous abnormalities.

Conclusion: Hyperintense lesions in the splenium of the corpus callosum, red nucleus, and/or dentate nuclei on T2-weighted and FLAIR images were noted in all patients with metronidazole-induced encephalopathy. They were also noted in the subcortical white matter, basal ganglia, anterior commissure, and tectum. Metronidazole-induced encephalopathy was reversible both radiologically and clinically.

C-0791

18 F-FDG PET in anxiety-obsessive disorders (AOD): Metabolic and clinical correlation study

A.A. Stanzhevsky, L.A. Tyutin, A.V. Korzenev, N.A. Kostenikov, V.A. Shustin, T.A. Skoromets, N.G. Neznanov; St. Petersburg/RU

Purpose: To evaluate metabolic involvement of limbicostrital system structures in patients with AOD before and after treatment.

Methods and Materials: 18F-FDG PET was carried out in 10 patients with AOD and 30 age-matched normal controls. In all cases of AOD the examinations were performed before and after the treatment with serotonin reuptake inhibitors and anxiolytic drugs. The 18F-FDG images of patients with AOD were assessed using statistical parametric mapping. Then PET results were compared with clinical state estimated according to standard scales (Y-BOCS and Spilberger Anxiety State Scale-SASS).

Results: The regional cerebral glucose metabolism was increased in the anterior cingulate before treatment in 5 cases of AOD. Hypometabolism in the head of the caudate in 6 cases and thalamus in 5 cases was observed before treatment. A significant improvement in obsessive-compulsive and anxiety symptoms on the Y-BOCS and SASS was observed after treatment in all patients. Follow up 18F-FDG PET examinations revealed a metabolism decrease in anterior cingulate, increase of metabolism in the head of the caudate and thalamus in these patients. Metabolic and clinical data significantly intercorrelated.(anterior cingulate - Spearman R = 0.68 (Y-BOCS), 0.51 (SASS), p < 0.05, caudate heads - Spearman R = -0.58 (Y-BOCS), -0.46 (SASS), p < 0.05, thalamus- Spearman R = -0.67 (Y-BOCS), -0.43 (SASS), p < 0.05).

Conclusion: This data proves participation of the limbicostrital system in the pathogenesis of AOD. Our results demonstrate the possibility of using 18F-FDG PET for estimation of treatment efficacy of AOD.

C-0792

Trigeminal neuralgia: Imaging of normal anatomy and pathological conditions

P. Bermudez Bencerray, A. Carvajal, M. Zauner, A. Rovira, D. Gil, M. Prenafeta, A. Lüttich; Sabadell/ES

Learning Objectives: 1. To explain and illustrate trigeminal nerve anatomy in its spinal root. 2. To describe the imaging findings for different pathologies involving the trigeminal nerve in its spinal root, based on its anatomical topography and its aetiology.

Background: Understanding the different pathologies that can affect the trigeminal nerve requires thorough knowledge of the anatomy of this cranial nerve, from its real origin in the brainstem through its apparent origin and along its pathways through the cisterns and parasellar region. The different intrinsic and extrinsic pathologies that can cause trigeminal neuralgia have particular characteristics depending on their topography and aetiology.

Imaging Findings: We present a pictorial review of the anatomical details of the trigeminal nerve, including the most significant cases of pathologies involving the trigeminal nerve at different points along its pathway (pons, cisternal and parasellar) from a retrospective review of the examinations carried out in our centre.

Conclusion: Knowledge of the anatomy and pathological states of the trigeminal nerve is essential to understand imaging findings in the different pathologies that affect this cranial nerve and enables a correct differential diagnosis among the different pathological entities.

Scientific and Educational Exhibits

C-0793

CT perfusion: Possible diagnostic applications

E. Sanchez, E. Marco de Lucas, V. Gomez, T. Piedra, P. Merino, M. Aguilar, P. Ruiz, E. Ruiz, A. Gonzalez; *Santander/ES*

Learning Objectives: CT perfusion is a relatively new technique useful in studying cerebral ischemia; we illustrate the usefulness of this method in the study of other brain lesions.

Background: 113 patients were examined in our department during last year, most of them due to an acute ischemic stroke in order to select possible candidates for fibrinolytic treatment. The other pathologies included were transient global amnesia, migraine attacks, inflammatory processes and infections (AIDS), and neoplasms to measure the permeability surface product area (metastasis, lymphoma, meningioma, glioma...). We consider that CT perfusion is very useful in all of these cases because it can be performed quickly and give additional information comparable to MR. Even in cerebral death it could be an ideal technique in the early diagnosis before the donation of organs.

Procedure Details: We analysed the CT perfusion findings and evaluated the correlation between these findings, the clinical evolution and other methods of diagnosis applied. We used protocol CT perfusion² from GE that allows evaluation of cerebral perfusion by generating maps of Cerebral Blood Flow, Cerebral Blood Volume, Mean Transit Time and Surface Permeability.

Conclusion: CT perfusion is an useful, easy and fast technique to study ischemic, neoplastic, degenerative or inflammatory pathology in the brain, with wide future prospects because of its accessibility; although it will be necessary to carry out further studies in the future to demonstrate these benefits.

C-0794

Cervical vessel dissection: Comparison of CT angiography with digital subtraction angiography and radiological findings

J.M. Martos Becerra, J.J. Espejo Herrero, R. Diaz Aguilera, M. Ramos Gómez, F. Bravo Rodriguez, F. Delgado Acosta, C. Landauro Comesña, E. Roldán Romero; *Cordoba/ES*

Purpose: Spontaneous dissection of cervical arteries is an uncommon but important cause of stroke because it usually occurs in young patients. We show the correlation between diagnosis with CT angiography and digital subtraction angiography (DSA), as well as the statistical association between cranial CT findings in the first 24 hours and the clinical outcome.

Methods and Materials: We analyzed prospectively 43 cases of spontaneous dissection of cervical vessels (32 carotid arteries and 11 vertebral arteries). All patients showed findings in angiography that were compatible with dissection of at least one cervical artery. A cranial CT was carried out in 41 patients and 29 were studied with CT angiography. We collected epidemiological data, radiological findings and three-month outcome (using Rankin modified scale). We performed Chi-square test and Cramer's V test to study the association between findings in CT angiography and DSA and between cranial CT findings and clinical outcome.

Results: The most frequent finding in angiography and angi CT was stenosis (25 patients). We found a correlation between findings in angiography (gold standard) and CT angiography (Chi-square: 0.8949 for p < 0.05; Cramer's V: 0.2483) and a bad prognosis in patients with pathological findings in cranial CT (Chi-square: 0.174 for p < 0.05 Cramer's V: 0.4603).

Conclusion: CT angiography gives a valid and minimally invasive choice for the early diagnosis of cervical artery dissection, showing a good correlation with DSA findings (gold standard). Findings in cranial CT in the first 24 hours are associated with the clinical outcome in those patients.

C-0795

CT angiography in cerebral aneurysms and beyond: A pictorial review

P. Rajiah, T. Patankar, A. Herwadker, N. Hoggard, R. Laitt, D. Hughes; *Manchester/UK*

Learning Objectives: 1. To review the indications, role and limitations of CT angiography (CTA) in neuroimaging. 2. To illustrate the spectrum of normal variants and abnormalities involving cerebral vessels with CTA. 3. To outline the technical difficulties, artefacts and diagnostic pitfalls in CTA.

Background: CTA has become a well established technique in the evaluation of subarachnoid haemorrhage. It is used as an effective alternative and frequently replaces cerebral angiography.

Procedure Details: All examinations were performed on a 4 slice CT scanner (GE Lightspeed). Timing scans were performed using 20 mls of iohexol injected at 4 ml/sec and main acquisition obtained during first pass of a 70 ml bolus [Slice thickness 4x1.25 mm, table speed 3.75 mm/sec, pitch ratio 0.75:1, 0° tilt, 0.5 sec

rotation, 5 mm collimation, 0.63 mm reconstruction interval, 25 cm FOV with a bowtie filter]. Multiplanar and 3D reconstructions were reviewed. Retrospective analysis of the role of CTA in a variety of pathological neurovascular conditions such as aneurysms (76), AV malformations (6), dural fistulas (3), & vertebral dissections (4), intracranial tumours (20) and trauma (5) was performed. We also illustrate the arterial and venous variants, artefacts due to venous contamination and coil and pitfalls due to lack of visibility of small arteries, infundibular dilatation, kissing vessel artefact, venous structures that stimulate aneurysms and inability to identify thrombosis/calcification on 3D images.

Conclusion: CT angiography is good technique in assessment of cerebral vasculature. It has almost completely replaced diagnostic catheter angiography in the evaluation of acute SAH. It is extremely useful in showing other conditions such as AV malformations and fistulas, dissections and planning tumour surgery.

C-0796

Which is the optimal sequence for the detection of hyperacute intracranial hemorrhage on multimodal stroke MR imaging?

C. Oppenheim¹, D. Hernalsteen², E. Touzé¹, A. Peeters², C. Lamy¹, J.-L. Mas¹, J.-F. Meder¹, G. Cosnard²; ¹Paris/FR, ²Brussels/BE

Purpose: MR imaging is increasingly used as the sole examination for imaging acute stroke patients. Although multisquence MR protocols seem to always be target like for the detection of intracerebral hemorrhage (ICH), the contribution of each single sequence to the diagnosis of ICH is still open to question. We evaluated the sensitivity and specificity of 5 MR sequences for depicting acute ICH.

Methods and Materials: MR images from 102 patients (43 ICH, 59 non-ICH), referred with suspicion of acute stroke and imaged within 6 hours from onset, were independently reviewed by two observers, blinded to clinical status. Reviewers searched for signs of acute ICH on T1- and T2-weighted gradient echo (GRE), FLAIR, T2-echo-planar (T2-EPI) and diffusion-weighted (DWI), each sequence being presented anonymously and singly.

Results: A perfect ($\kappa = 1$) inter-observer concordance for the identification of ICH was achieved for four pulse sequences (T2-EPI, DWI, GRE and FLAIR) and reached $\kappa_{T1} = 0.952$ for the T1-weighted sequence. All patients were correctly classified by both observers on T2-EPI, DWI and FLAIR sequences, while sensitivity_{T1} = 97.4-100%, specificity_{T1} = 97.7-100%, and sensitivity_{DWI} = 100% and specificity_{DWI} = 98%.

Conclusion: In the setting of hyperacute stroke, ICH can easily be identified on any combination of two or more of the 5 studied MR sequences, confirming that emergency MR can be used as the prime and sole screening modality for ultra-fast patient triage prior to treatment decision.

C-0797

Imaging of the cranial nerves

R. Puy¹, C. Boyer¹, B. Leloutre-Françon¹, V. Ben Amor¹, A. Capdevila², A. Geoffray¹; ¹Nice/FR, ²Barcelona/ES

Learning Objectives: Anatomical-radiological illustration of the 12 cranial nerves.

Background: Several imaging techniques have been used to demonstrate the cranial nerves: MR imaging images (GE 1.5 T) with high definition sequences T1-weighted SE with and without injection of gadolinium, T2-weighted SE and 3D T2 EG, CT images (GE 8 multidetector) with inframillimetric slices in bone windows with reconstructions, US cervical images (14 MHz linear probe GE Logiq 9) and conventional radiographs of the 12 cranial nerves at different levels.

Procedure Details: Images of the 12 cranial nerves are shown from their cerebral emergence to their extracranial pathways, including some osseous canals, foramina and main branches.

Conclusion: This poster will help in recognizing the cranial nerves in various imaging techniques.

C-0798

Assessment of different ischemic compartments using quantitative multi-slice CT perfusion imaging in patients with acute stroke

G. Bohner, H. Stiepani, H.-C. Bauknecht, R. Klingebiel; *Berlin/DE*

Purpose: Evaluation of CT Perfusion (CTP) in the diagnostic assessment of stroke patients to discriminate between different ischemic compartments.

Methods and Materials: Out of a group of 107 consecutive patients with clinically suspected acute cerebral ischemia in whom multislice CTP was performed on admission a subgroup of 17 patients was chosen. Selected patients had infarction confirmed by follow-up imaging and showed no recanalization. Parameter maps of cerebral blood perfusion (CBP), cerebral blood volume (CBV) and mean transit time (MTT) were generated. Perfusion values were calculated within are-

Scientific and Educational Exhibits

as of infarction as assessed by follow-up imaging and from adjacent areas of ischemia defined by MTT-prolongation. Each parameter was tested for efficiency to predict tissue outcome.

Results: Compared with areas of infarction those defined as ischemic showed significantly higher absolute values for CBP (19.4 ± 8.3 vs. 9.7 ± 5.1 ; $p < 0.01$) and CBV (2.7 ± 1.0 vs. 1.6 ± 0.7 ; $p < 0.01$), as well as significantly lower values for MTT (9.9 ± 3.2 vs. 13.1 ± 2.7 ; $p < 0.01$). Similar results were yielded by testing ratios normalized to mirrored contralateral areas. Normalized threshold values for infarction as derived by ROC analysis were found to be 0.31 for rCBP, 0.85 for rCBV and 2.9 for rMTT respectively. Efficiency to predict tissue outcome was more than 75%.

Conclusion: CT Perfusion might be a feasible method to predict tissue outcome in stroke patients. Our findings suggest that, based on quantitative analysis, efficient threshold levels to discriminate between tissue at risk for infarction and tissue with disturbed perfusion might be possible. However, further studies including successfully recanalized patients are needed.

C-0799

Exploring the continuum: 1H-MR spectroscopy in prodromal and first-episode patients with schizophrenia

G. Bohner, F. Forstreuter, J. Gallinat, H. Witthaus, H. Stiepani, Y. Gudlowski, A. Heinz, R. Klingebiel, G. Juckel; Berlin/DE

Purpose: Patients with schizophrenia are characterized by reduced levels of N-acetylaspartate (NAA) as assessed by 1H-MR spectroscopy (MRS) in schizophrenia-relevant areas. Our purpose was to explore a possible continuum of NAA changes, as a first sign of impaired neuronal integrity, from the prodromal phase to the first episode of schizophrenic psychosis.

Materials and Methods: We studied 13 patients in the early and late prodromal state of psychosis (in part patients of the European Prediction of Psychosis Study, EPOS), 10 first-episode patients with schizophrenia and 21 healthy controls matched by age and gender. Single voxel 1H-MRS (1.5 T, TR = 1500 ms, TE = 140 ms, VOI = 8 ml) was performed in the left hippocampus, the anterior cingulate cortex (ACC) and the medial prefrontal cortex. NAA/creatinine (Cr), choline (Cho)/Cr and NAA/Cho ratios were calculated.

Results: Analysis of the data revealed significantly elevated NAA/Cr and Cho/Cr ratios in the ACC of prodromal and first-episode patients compared to healthy controls. NAA/Cr ratios in the hippocampus of prodromal patients showed no significant difference compared to healthy controls. Reduced NAA/Cr ratios in the left hippocampus of first-episode patients were found; however the difference compared to healthy controls did not reach a level of significance.

Conclusion: In patients with first-episode schizophrenia expected reduction of NAA/Cr was found in the left hippocampus indicating impaired neuronal integrity. The joint elevations of NAA/Cr and Cho/Cr ratios in prefrontal areas of prodromal and first-episode patients could result from a decline in creatine indicating hypometabolism in these areas. Further studies using absolute quantification should be initiated to assess these metabolite alterations.

C-0800

Normal ageing of the brain: Assessment with quantitative MR diffusion tensor imaging

N. Papanikolaou, S. Karampekios, E. Papadaki, T. Maris, N. Gourtsoyiannis; Iraklion/GR

Purpose: To assess the distribution of microscopic brain tissue alterations related to normal ageing using magnetic resonance diffusion tensor imaging (DTI).

Methods and Materials: Axial FLAIR and DTI sequences were applied in 30 normal subjects (mean age: 33.7 years, min: 8, max: 72). Spatial normalization to the Talairach space of the non-diffusion weighted scans was performed using a standard EPI template. Transformation parameters were applied to the six diffusion weighted image sets and mean diffusivity (MD) and fractional anisotropy (FA) maps were reconstructed. A voxel based statistical analysis was performed to identify anatomical regions of the brain that correlated with age.

Results: Areas of statistically significant ($p < 0.001$) MD increase with age were located in the left and right inferior frontal gyrus gray matter, left and right insula gray matter, left middle frontal gyrus, left superior temporal gyrus white and gray matter, left and right inferior parietal lobule white matter, right inferior frontal gyrus white matter, right superior temporal gyrus, left superior frontal gyrus white matter and right superior frontal gyrus gray matter. Areas with statistically significant ($p < 0.001$) FA decrease with age were found in the right medial frontal lobe white matter, left middle frontal lobe white matter, right brainstem, right frontal lobe sub-gyral white matter, right middle temporal gyrus white matter and left frontal lobe sub-gyral white matter.

Conclusions: Diffusion tensor derived metrics are sensitive to the microscopic brain tissue alterations related to normal aging. MD changes are mainly located in the gray matter while FA changes in the white matter.

C-0801

Appearance of the meninges on contrast-enhanced MR imaging: Spectrum of normal and abnormal appearance in the brain and spinal cord

N. Sheehy, C. Farrelly, J. McCann, G. Boyle, J.F.M. Meaney; Dublin/IE

Learning Objectives: 1. To describe the normal appearance of the meninges on contrast-enhanced MR imaging within the crano-spinal axis. 2. To describe the findings in patients with cranio-spinal malignant meningeal infiltration. 3. To illustrate non-malignant causes such as sarcoidosis, infection, and post lumbar puncture and subdural-haematoma. 4. To demonstrate the potential benefits of using isotropic fat suppressed volumetric sequences.

Background: Detection of meningeal abnormality with CT and standard (non-contrast) MR is very limited. Contrast-enhanced MR Imaging affords the best opportunity to detect both dural and leptomeningeal involvement. However, dural enhancement is a normal finding and differentiation of normal from abnormal can be challenging.

Imaging Findings: A comprehensive review of the findings on contrast-enhanced MR imaging in normal subjects, and in patients with benign and malignant meningeal infiltration is presented. Correlation with other modalities is given where appropriate. The potential benefits of a T1 fat suppressed high-resolution volumetric sequence in the assessment of meningeal pathology are discussed.

Conclusion: Meningeal abnormality, most commonly due to malignant infiltration, is readily demonstrated by MR imaging but not easily identified on non-contrast MR imaging or CT.

C-0802

MR-spectroscopy in multiple sclerosis (MS) patients: Correlation between *in vivo* and *in vitro* analysis of CSF fluid

A. Sias, A. Balestrieri, L. Barberini, M. Puligheddu, M. Fraschini, F. Cesare Marincola, A. Lai, F. Marrosu, G. Mallarini, M.G. Marrosu, E. Cocco, E. Locci; Cagliari/IT

Purpose: Our study aims to find a role for MR spectroscopy, performed both *in vivo* and *in vitro* in the diagnosis of multiple sclerosis (MS), which may be helpful in those patients whose conventional MR findings might overlap those of other demyelinating diseases.

Methods and Materials: We have performed *in vivo* MR spectroscopy on 30 individuals (15 patients with known MS, and 15 healthy volunteers), and *in vitro* MR spectroscopy in the CSF of these two subgroups, on a spectrometer VARIAN 400 MHz with both solid and liquid state probes. Having performed ^1H (proton)-spectroscopy we were able to measure the concentrations of NAA, Cho, Cr, Gix, GABA, ml, and LA. Data obtained has been analyzed with software from the European Union project "Advanced Signal Processing for Medical Magnetic Resonance Imaging and Spectroscopy".

Results: The altered concentrations of the metabolites confirm the importance of MR spectroscopy and correlate with lesion development in MS patients. Our results show that MS is a diffuse white matter disease, not confined to the demyelinating plaques seen in conventional MR examinations, and the role of MR spectroscopy might be also to investigate the metabolic changes of neural pathways.

Conclusion: MR spectroscopy, both *in vivo* and *in vitro*, appears to be a highly sensitive technique in the evaluation of MS.

C-0803

Slow expressive language development in children: Typical MR imaging pattern? Critical review of 1880 cases

V. Pupillo, G. Gismondi, R. De Amicis, A. Splendiani, C. Masciocchi, M. Gallucci; L'Aquila/IT

Purpose: To assess the potential of MR imaging to study children with language impairment, through critical review of 1880 cases produced in our institute, in the hope of identifying typical MR imaging patterns. We analyzed possible alterations of morphology or signal intensity in late talking patients versus patients with different pathologies. We studied eventual relationships between language impairment and myelin development.

Methods and Materials: 1880 MR imaging examinations (age range from 1 to 8 years) have been reviewed. 60% of these examinations have been performed in children with clinically proven language impairment. All MR imaging examinations were performed with a 1.5 T GE magnet, using a head coil; T1 and T2-

Scientific and Educational Exhibits

weighted sequences were acquired on axial and sagittal planes and FLAIR on coronal plane. All pts had also been studied by means of 3D T-w FFE, with the aim of evaluating cerebral cortical architectural disorders.

Results: In 63% of cases MR imaging showed symmetrical and bilateral high signal intensity areas at a periventricular level; at 1 year MR imaging follow-up this signal alteration was not still visible in any case. In 78% cases we observed punctiform or line shape areas interpreted like dilated perivascular spaces; after 1 year, independent of clinical conditions, the MR imaging findings were not different.

Conclusion: Our experience, like other studies present in literature, suggests a possible correlation between late myelin development and language impairment.

C-0804

Advanced MR imaging in the surgical planning of intracranial tumors

G. Luccichenti¹, M. Salvati¹, A. Frati¹, C. Brogna¹, R. Delfini¹, S. Bastianello²; ¹Rome/IT, ²Pavia/IT

Learning Objectives: 1)To illustrate the rationale of the MR imaging of intracranial tumors by correlating the pathology and the neurosurgical approach with imaging principles of the MR examination. 2)To describe the advanced MR techniques (relaxometry, DWI, DTI, MT, MR spectroscopy and functional MRI) and the advantages of an integrated imaging approach.

Background: The treatment of intracranial tumors is difficult due to the combined necessities of performing radical excision of the lesion and preserving vital structures. Generally, conventional imaging does not allow the discrimination of neoplastic tissue from edema and normal surrounding structures, the accurate characterization of the lesion, and the precise location of the functional areas, which can be displaced by the lesion. This information is crucial in preoperative planning, and can be obtained through advanced imaging techniques.

Procedure Details: A method for imaging intracranial tumors with conventional and advanced techniques is provided. Simple criteria for differential diagnosis between primary and secondary, extra- and intra-cerebral lesions, and for lesion characterization with advanced techniques are provided. The features that are crucial for surgical planning are described. The integration of morphological and functional imaging into neuronavigation systems for image-guided neurosurgery is shown using clinical examples.

Conclusion: Integrating conventional morphological imaging with advanced functional and metabolic techniques is crucial for adequate preoperative planning of intracranial tumors and to enhance the performances of image-guided neurosurgery.

C-0805

T1 and T2 characterization in the brain during hyperoxia at 9.4 T

H. Uematsu; Fukui/JP

Purpose: The aims of this study were to characterize T1 and T2 changes in mice brain during hyperoxia at 9.4 T.

Methods and Materials: After T1 and T2 values of wild-type mice brain were measured on a 9.4 T MR system, the room air was changed to either 100% oxygen (N = 8) or carbogen (N = 8). Five minutes later, the same scan protocol was repeated. Statistical analysis of the data was performed using paired Students' t-test.

Results: During hyperoxia, the T1 value of the cerebral cortex significantly decreased (100% oxygen: 11% decrease, P < 0.05 and carbogen: 9% decrease, P < 0.05). No significant difference in% T1 changes were observed between the 100% oxygen and carbogen conditions. The T2 value of the cortex significantly increased during exposure to either 100% oxygen (cortex: 3.7% increase, P < 0.05) or carbogen (cortex: 5.4% increase, P < 0.05). No significant difference in% T2 changes was observed between 100% oxygen and carbogen conditions.

Conclusion: The increased dissolved oxygen may reduce the T1 during hyperoxia. The changes in T1 were not significantly different between the two types of gas. The reduced cerebral perfusion due to 100% oxygen may have little effect on T1. In the case of T2, the mechanism may be related to the BOLD effect. Carbogen is known to increase the cerebral perfusion, which may increase the T2. However, no significant difference in T2 was observed between the 100% oxygen and carbogen conditions. Therefore, the prolonged T2 during hyperoxia may be mainly caused by increased BOLD effect rather than by increased cerebral perfusion at 9.4 T.

C-0806

Brain activation in the differences game: A functional magnetic resonance imaging study

E. Fukuba, A. Wada, K. Uchida, T. Kajitani, A. Nagami, H. Kitagaki; Izumo/JP

Purpose: The differences game in which we find differences between two similar pictures is a popular game with children. Superior space recognition and concentration are needed to win this game. The radiologist also requires these skills in diagnostic imaging. We examined brain activation areas during the differences game using functional MR imaging.

Methods and Materials: Five right-handed volunteers were recruited with a mean age of 26. When the subjects looked for differences between two pictures which were side by side, we examined brain activation areas of the subjects. We applied the block design paradigm which repeated quiz presentation of 30 seconds and 30 seconds rest. In addition, we examined the second activation using the same quiz.

Results: Activation was recognized in the bilateral posterior prefrontal area, the primary visual area, and the intraparietal sulcus. In the second measurement when subjects knew the picture beforehand, activation of the right prefrontal area and the bilateral intraparietal sulcus increased.

Conclusion: In the differences game, the frontal, parietal and occipital lobe are activated. Activation of the frontal lobe reflects visual recognition, and activation of the parietal lobe reflects the three dimensional conversion of visual information and analysis. Repetition of a challenge to the game gives subjects adaptation. Re-challenge to the game that we experienced promotes the activation.

C-0807

Usefulness of proton magnetic resonance spectroscopy (¹H MRS) in the diagnosis of subclinical hepatic encephalopathy (SHE)

R. Banyś, A. Slowik, M. Pasowicz, I. Ciecko-Michalska, M. Irzyk, M. Motyl, A. Szczudlik, J. Bogdal; Krakow/PL

Purpose: SHE is a disorder of cognitive function in patients with liver cirrhosis, detectable only during neuropsychological examination, adversely affecting daily activity, and without any deficits during standard neurological examination. The disorder affects up to 70% of patients with liver cirrhosis. ¹H MRS is a fast developing, noninvasive method allowing the *in vivo* evaluation of biochemical changes in the human brain. The aim of the study was to assess the usefulness of *in vivo* ¹H MRS detection of metabolic abnormalities in brains of patients with SHE.

Methods and Materials: In this study we included 30 patients with the diagnosis of SHE and 32 healthy volunteers. ¹H MRS examination was performed on 1.5 T Magnetom Sonata (Siemens) scanner with single voxel PRESS technique (TR = 1500 ms, TE = 30 ms, 256 acquisition with the H O signal suppression). Three voxels of 8 cm³ were positioned in: 1) predominantly white matter in the posteromedial parietal cortex, 2) predominantly gray matter in the posterior occipital cortex 3) globus pallidus. Metabolite concentrations were calculated manually using integral Siemens software. Peaks from myo-inositol (ml), choline (Cho) and N-acetyl-asparatate (NAA) were normalized with respect to the creatine (Cr) peak (ml/Cr, Cho/Cr and NAA/Cr).

Results: Patients with SHE presented with significant reduction of the ml/Cr ratio as compared to controls (0.041 ± 0.011 vs 0.20 ± 0.071) and no significant changes between the two groups in Cho/Cr ratio (0.84 ± 0.15 vs. 0.85 ± 0.17) and NAA/Cr ratio (1.56 ± 0.26 vs. 1.67 ± 0.31).

Conclusion: (¹H MRS) detects *in vivo* neurometabolic changes in patients with SHE. The significant reduction of ml/Cr ratio suggests an alteration of glial function.

C-0808

The fMRI imaging study of hypnotic suggestion during pain stimulation

A. Urbanik, J. Aleksandrowicz, M. Binder, R. Chrzan, B. Sobiecka, J. Kozub; Krakow/PL

Purpose: The aim of the study was assessment of the influence of hypnotic suggestion on the patterns of neural activation during pain stimulation.

Materials and Methods: Twelve volunteers (5 men, 7 women; mean age 25) were examined on a 1.5 T MR scanner. Each subject underwent four subsequent experimental sessions with different conditions applied: 1) pain stimulation (PS), 2) PS and verbal analgesic suggestion (VAS), 3) PS and hypnotic induction (HI), 4) PS, HI and VAS. Nociceptive stimulation was performed by pricking the palmar side of the hand with a sharp piece of wood (avoiding skin puncture). To avoid pain adaptation stimulation was carried out in various points within the palmar region. Statistical analysis of the data was done using SPM2 and MarsBaR software. We assessed global patterns of neural activity and differences in the mean signal intensity within the selected ROI's (postcentral and cingulate gyri and insulae), participating in pain perception.

Scientific and Educational Exhibits

Results: In all sessions nociceptive stimulation evoked enhanced BOLD responses in postcentral gyri bilaterally (with stronger activation within contralateral gyrus), insular regions and cingulate gyri. We did not find any significant regional differences in patterns of activation in all four experimental sessions. However, ROI analysis yielded significant decrease of the signal correlated with conditions: 3)PS+HI and 4)PS+HI+VAS. These effects were strongest in the postcentral gyri and insular cortex.

Conclusion: We have observed that induction of hypnotic state and hypnotic suggestion can markedly reduce neural activity within regions responsible for pain perception.

C-0809

Fusion of MR imaging and SPECT images in the diagnosis of glioma recurrence

P. Grzelak, M. Gorska-Chrzastek, B. Goraj, J. Kusmirek, L. Stefanczyk; Lodz/PL

Introduction: In clinical practice patients with cerebral glioma are usually treated with the combination of surgery and radiotherapy. However, in the majority of patients recurrence of the disease occurs. The most essential requirement for further treatment is to diagnose the relapse as early as possible. In practice this means to differentiate active neoplastic growth from radiation induced changes and scars in the brain; the latter may mask the recurrent tumor.

Materials and Method: This study was performed on 33 patients who had had surgery and radiotherapy to a glioma of the brain. Follow-up MR imaging post gadolinium images of the brain were obtained using a 1.5 T scanner. SPECT was performed 15 min after iv administration of the 131 I-alfa-metyl-tyroline (131I-IMT). The 131I-IMT is a marker of brain tumors. Fusion of the images was performed by means of a three-dimensional technique using a PC work-station; the technique was based on statistical analysis of three-dimensional distribution of the voxels, using maximization of the statistical resemblance (mutual information).

Results: It is not technically possible to combine acquisition of the data from MR imaging and scintigraphy in one installation. In 27 patients MR imaging images demonstrated presence of a polymorphic focus, indicating recurrence of the tumor, in 4 individuals the result was equivocal due to post-operative and post-radiation changes.

Conclusions: MR imaging and SPECT fusion images enables confirmation of malignant growth at a site of morphological change in the brain, potentially corresponding to the recurrence of tumor. It helped to exclude the recurrence in a case with equivocal MR imaging images.

C-0810

Comparison of CT and diffusion-weighted MR imaging after reperfusion in a cat model of focal acute cerebral ischemia

J. Lee, D. Na, J. Park, S.-C. Hong, J. Yoon; Seoul/KR

Purpose: To determine if the early ischemic changes on CT are reversible after early reperfusion of MCA occlusion in a cat model, and to compare changes of CT attenuation with ADC change in ischemic tissue after early reperfusion.

Materials and Methods: We evaluated DWI, ADC, T2WI and CT obtained after 1 hour of right MCA occlusion and at 1 hr, 3 hr, 5 hr, and 24 hr after reperfusion, in 7 cats. Qualitative image review and quantitative ROI assessments were made.

Results: Two types of evolution of signal intensities were observed on DWI: Type 1, which showed persistent high SI, and Type 2, which showed reversal of high SI after reperfusion. Type 1 lesions were seen in all 7 cats, but type 2 lesions were seen in only 3 cats. In type 1, ADC values were relatively constantly low over time, but CT density showed a linear decline. In type 2, ADC values were reversed at either 3 hrs or 5 hrs after reperfusion, CT scans showed partly persistent low density and partly reversal of low density. Both type 1 and type 2 lesions revealed high SI on T2WI and low density on CT at 24 hrs, and pathologically proved as infarcts.

Conclusion: Subtle hypodensity of an early ischemic lesion on CT can be either reversible and not reversible after early reperfusion. The time course of ADC changes had a different pattern from that of CT density in both type 1 and 2 lesions.

C-0811

1H MRS and 18F FDG PET in patients with single epileptic seizure

A.V. Pozdniakov, L.A. Tiutin, D.E. Dyskin, A.A. Stanzhevsky, G.D. Rokhlin; St. Petersburg/RU

Purpose: To study the features of metabolic disorders in patients with repeated unprovoked epileptic seizures according to triennial follow-up.

Materials and Methods: 1H MRS and 18F FDG PET were carried out in 27 patients with single generalized tonic clonic seizure. The follow-up was performed during 3 years after 1H MRS and 18F FDG PET examinations.

Results: 1H MRS and 18F FDG PET revealed metabolic disorders in 9 of 27 patients and 7 of 27 patients respectively. Combined use of these methods showed metabolic disorders in 10 of 27 patients. The incidence of metabolic disorders was more in patients with repeated epileptic seizures (22 cases) than in patients with a single epileptic seizure (2 cases) according to triennial follow-up ($p < 0.05$). Decrease of N-acetylaspartate, creatine and choline increase, decrease of 18F FDG uptake were shown in patients with single epileptic seizure. The true positive results of combined PET and 1H MRS use were observed in 6 of 9 patients. As a rule metabolic disorders were revealed in the mediobasal part of temporal lobes. Combined 18F FDG PET and 1H MRS use showed metabolic disorders in 8 of 10 cases. According to PET data unilateral focal disorders predominated in comparison with focal bilateral disorders, whereas 1H MRS showed uni- and bilateral changes equally. The isolated focal neocortical changes in frontal lobes were found by 1H MRS only in 2 cases.

Conclusion: 1H MRS and 18F FDG PET are shown to be a feasible methods for follow-up of patients with single provoked and unprovoked seizures and prediction of epilepsy course.

C-0812

Enlarged temporal horns and transient amnesia after perimesencephalic haemorrhage

D.A. Stojanov, P. Bosnjakovic, M. Zivkovic, N. Stojanovic, S. Ristic; Nis/YU

Purpose: Many patients with perimesencephalic hemorrhage, a benign subset of subarachnoid hemorrhage, have an episode of amnesia. We studied the relation between the occurrence of amnesia and size of the ventricles, including the temporal horns.

Materials and Method: Thirty-seven consecutive patients (20 female, 17 male; mean age 51.81, SD 12.19) with perimesencephalic hemorrhage admitted to the Clinical Center Nis between January 1995 and December 2001 were asked about the occurrence of amnesia. The temporal horns were measured in three different directions: medio-lateral, antero-posterior, and oblique. Measurements were taken from the CT slice on which the temporal horns were best visible.

Results: Amnesia was reported in 13 (35.13%) of the 37 patients. The episode of amnesia started a few hours after the onset of the bleed and lasted for several hours or days. In these patients the mean size of the temporal horns was significantly larger than in patients without amnesia. Linear measurements of the temporal horns in patients with amnesia were larger in all three direction: antero-posterior (10.4 ± 5.9 mm vs. 4.1 ± 5.9 mm; $p < 0.01$), medio-lateral (11.9 ± 6.5 mm vs. 6.8 ± 5.8 mm; $p < 0.05$), and oblique (5.3 ± 3.0 mm vs. 2.7 ± 1.9 mm; $p < 0.05$).

Conclusion: Amnesia is present in about one third of patients with perimesencephalic hemorrhage shortly after the bleed. The occurrence is associated with enlargement of the temporal horns.

C-0813

MR and alterations of cortical development

J. Alvarez Linera-Prado, J. Escribano Vera, I. Garcia Morales, A. Perez Garcia, R. Martinez Alvarez, A. Gil-Nagel Rein; Madrid/ES

Learning Objectives: To review the classification of the malformations of cortical development and to demonstrate the different types, with greater emphasis on focal cortical dysplasias. The more advisable study protocols are recommended and we comment on new techniques, explaining their possible use.

Background: In the knowledge of alterations of cortical development, imaging techniques have contributed in a decisive way to their better handling and understanding. Morphological criteria are used for their classification; hence MR, especially the morphological techniques of high resolution, plays a fundamental role. We include imaging of the new techniques (Diffusion, DTI, Perfusion, BOLD and the Spectroscopy), which we assess to see if they add new information.

Procedure Details: Studies with a 3 T magnet have been made in most of the cases to obtain images with maximum spatial resolution. In each case the more advisable protocols of study are explained and their clinical correlation, with special attention to Diffusion, DTI, Perfusion, BOLD and Spectroscopy.

Conclusion: Diagnosis of the alterations of cortical development is based on the knowledge of its multiple manifestations. The use of a suitable protocol is important, since it increases the sensitivity, mainly in the case of cortical focal dysplasia. The new techniques can contribute with excellent information, although most of them are still in the early phase of development.

Scientific and Educational Exhibits

C-0814

Radiological atlas of central nervous system tuberculosis

F. Matute Teresa, A. Saiz Ayala, N. Santamaría; Madrid/ES

Purpose: To illustrate the broad spectrum of imaging findings (MR and CT) in patients with proven central nervous system tuberculosis (CNS).

Methods and Materials: We reviewed between January of 1998 and July of 2004, the imaging findings of 35 patients with proven tuberculosis.

Results: Tuberculosis can lead to localized or diffuse CNS involvement. 25 patients had meningitis, 13 patients had focal intra-axial tuberculomas: 13 brain masses and 1 intramedullary spinal lesion; 3 patients had focal extra-axial lesions: 2 lesions in pontine cistern, and one in the spine. MR showed diffuse thick, meningeal enhancement, on CT the lesions appeared hyperdense, with a characteristic pattern of basal cistern involvement. On MR tuberculomas showed low signal intensity on T1 weighted images. On T2 weighted images the signal intensity varied according to the stage of evolution of the lesion, incipient tuberculomas appeared as scattered areas of hypointensity surrounded by edema, mature tuberculomas had a necrotic center, surrounded by an isointense capsule, surrounded by edema. On CT tuberculomas are hypo or isodense lesions and they had ring or nodular enhancement.

Conclusion: A thorough knowledge of CNS tuberculosis is important because early diagnosis may prevent a permanent loss of function. MR and CT were equally sensitive in visualizing tuberculomas, but MR was slightly superior in demonstrating the extent of the lesion, and infarcts. CT is better than MR in evaluating meningeal sequelae with calcification.

C-0815

MR imaging based prospective longitudinal study on neurotoxicity of ecstasy in novice ecstasy users

M.M.L. de Win, L. Reneman, E.J.P. Vlieger, C. Lavini, W. van den Brink, G. den Heeten; Amsterdam/NL

Purpose: Ecstasy (3,4-methylenedioxymethamphetamine, MDMA) has been shown to be neurotoxic in heavy users. We studied potential neurotoxicity of a low dose of ecstasy in new users.

Methods and Materials: At baseline 200 ecstasy-naïve adults (18-35 y) with high risk for first-time ecstasy use were included. During follow-up the new ecstasy users ($N = 26$, 12M/14F, 21.5 ± 3.1 yr, 2.8 ± 5.7 tablets) were reexamined. We compared parameters of neurotoxicity measured with MR imaging techniques between baseline and follow-up sessions. MR imaging (1.5 T, Signa, GE) protocol included PD- and T2-weighted images, single voxel ^1H -MRS, DTI (DW-EPI, TE/TR = 90/8000, b = 1000, 12 directions), perfusion MR imaging (GE EPI), and a T13D scan. ADC, FA and rCBV maps were registered to the spatially normalized T13D scans. Regions of interests were drawn onto the normalized brain (both hemispheres) and resized to the original maps. rCBV-values were obtained by dividing mean CBV_(ROI) by mean CBV_(white matter). Spectra were analyzed using LC-Model. NAA, Cho and ml concentrations were calculated using Cr as reference. Wilcoxon signed ranks test was used with $P < 0.05$ as threshold for statistical significance.

Results: ml/Cr in frontal gray matter was significantly increased after ecstasy use. No significant differences in ADC, FA and rCBV values were found.

Conclusion: Increased ml probably indicates gliosis after ecstasy use, although absence of other parameters of neurotoxicity suggests that incidental use, in contrast to heavy use, does not lead to major brain damage. However, there are different factors that may play a role in individual vulnerability for acute and long-term effects of ecstasy.

C-0816

MR spectroscopic imaging for targeting in stereotactic brain biopsy

K. Karaman, L. Onat, M. Sirvancı, O. Barlas; Istanbul/TR

Purpose: To evaluate the role of MR spectroscopy in stereotactic brain biopsy.

Materials and Methods: 7 patients with intracranial tumors underwent MR imaging, proton MR spectroscopy, and stereotactic biopsy. Biopsy samples were taken from regions of maximally elevated levels of choline used by color-coded metabolite map.

Results: All patients showed elevated Cho/Cr and Cho/NAA levels. In all cases diagnosis was made by single biopsy. Low-grade astrocytoma in two cases, anaplastic astrocytoma in 3 cases, and glioblastoma multiforme in 2 cases were detected. Biopsy specimens from regions with maximally elevated Cho showed dense tumor infiltration.

Conclusion: Brain biopsy is still a necessary procedure in the diagnosis of brain lesions. MR spectroscopy supports conventional MR imaging in detecting and selecting the target area for stereotactic brain biopsy.

C-0817

Three-dimensional CISS sequence: Use in the evaluation of intra- and extra-axial brain masses

A. Tosun, A. Kartel, B. Cakir; Edirne/TR

Purpose: To assess and illustrate the value of a three-dimensional Constructive Interference in Steady State (3D-CISS) technique in different pathologies related to CSF spaces.

Materials and Method: 57 consecutive patients underwent both routine MR imaging as well as 3D-CISS examination. Parameters for the 3D-CISS images were 16.7/8.08/1 (TR/TE/excitations), flip angle 70°, matrix of 192 x 256; field of view 150-210 x 200-210, in-plain resolution, 0.82 x 0.82 mm. An axial 64-mm-thick slab with 32-64 partitions covered the target lesions based on conventional MR images. The phase-encoding direction was from right to left for every patient.

Results: There were cisternal and intraventricular lesions including arachnoid cysts ($n = 18$), choroidal fissure cysts ($n = 2$), choroid plexus cysts ($n = 4$), pineal cysts ($n = 2$), lipomas ($n = 2$), epidermoid cysts ($n = 1$), schwannomas ($n = 3$), meningiomas ($n = 7$), aneurysms ($n = 2$). Parenchymal lesions were porencephalic cysts ($n = 2$), encephalomalacia ($n = 4$), cortical dysplasia ($n = 2$), subependymal hamartoma ($n = 1$) and brain tumors ($n = 7$). 3D-CISS sequences produce high contrast between the CSF and solid structures. Cyst walls, extent and margins of tumors and small cystic components in the tumors were clearly shown on 3D-CISS images.

Conclusion: The 3D-CISS MR imaging provides superb spatial resolution and signal-to-noise ratio in the diagnosis of pathologies especially related to the CSF areas. 3D-CISS sequence is a complementary technique to conventional MR and makes accurate diagnosis easier.

C-0818

withdrawn by authors

C-0819

Brain tumors associated with chronic epileptic seizures: A pictorial review

S. Cakirer¹, B. Yagmurlu², B. Koklu¹, Y. Karagoz¹, N. Kahraman¹; ¹Istanbul/TR, ²Ankara/TR

Learning Objectives: To describe various tumoral processes which are associated with chronic epileptic disorders. To evaluate the role of conventional and advanced MR imaging studies in the chronic epileptic seizures developing secondary to tumors.

Background: Most histological types of brain tumors that are associated with chronic epileptic seizures are rare in neuro-oncological series. Between January 2000 and May 2004, cranial MR imaging findings of 233 patients with chronic epileptic seizures with an age range of 2-67 year-old were retrospectively studied, and 37 of them were found to have tumoral lesions as the underlying lesions.

Imaging Findings: The most frequent tumors that have been found as the underlying reasons of chronic epileptic seizures are dysembryoblastic neuroepithelial tumors (DNET), pleomorphic xanthoastrocytoma (PXA), ganglioglioma, oligodendroglioma, low-grade astrocytomas and other rare tumors. The above-mentioned tumors are presented with their distinct features on conventional and advanced MR imaging studies.

Conclusion: The underlying reasons for conventional and advanced MR imaging features, the role of additional sequences for their diagnosis, and the differential diagnoses between the lesions with similar appearances have been evaluated in the chronic epileptic cases associated with tumoral lesions.

C-0820

DWI and DTI in Creutzfeldt-Jakob disease

C. Romero, F.J. Meli, H. Lambre, G. Sevlever, S. Carpiniero, R.E. Salvatico, A.L. Taratuto; Buenos Aires/AR

Learning Objectives: To report four cases of sporadic Creutzfeldt-Jakob disease (sCJD) proved with brain biopsy. To illustrate the findings of diffusion-weighted imaging (DWI) and diffusion-tensor imaging (DTI) on two patients.

Background: sCJD has an incidence of about one per million annually. In 1996, a new and clinicopathologically distinct form of CJD was described and named variant CJD. Routine MR imaging sequences may show abnormalities in the basal ganglia and cerebral cortex. However, 21% of patients with sCJD have normal MR imaging. DWI is more sensitive to the pathological changes of CJD than T2. Regions of abnormally restricted DWI have been shown both in cortex and in deep gray matter structures. We report four cases of histologically proved sCJD. All cases had DWI and two patients had DTI. We also report apparent diffusion coefficient measurement (ADC) and fractional anisotropy (FA) values in patients with DTI.

Scientific and Educational Exhibits

Procedure Details: Conventional sequences of MR imaging and DWI were done in all patients. In two cases we also did DTI. We used a 1.5 T clinical MR scanner with echo planar imaging. ADC values were measured in head caudate and lentiform nuclei in all patients. The regions were compared with data from corresponding areas in four normal age and gender-matched subjects. We also obtained FA values for the same regions. For the processing, we used a commercial software provided by the manufacturer.

Conclusion: DWI and DTI could be useful sequences within the clinical setting of presumptive CJD, and together with conventional MR imaging, they add additional information before biopsy diagnosis.

C-0821

Anatomical atlas of pig's brain by MR imaging and CT in stereotactic conditions

M.A. Pietrani, J. Zaloff Dakoff, A. Rabadan, J. San Roman, F. Eleta, R. Rosler, P. Argibay; *Buenos Aires/AR*

Learning Objectives: Present a pictorial comparing pig's brain anatomical specimens with CT and MR imaging brain slices in stereotactic conditions and emphasize potential applications for brain research.

Background: Brain research requires high resolution imaging studies with CT and MR imaging in animal models to guide biopsy and implants. Pigs are particularly useful in neuroscience research because of the similarity with human brain anatomy and physiology. Although there are several pig's brain atlases, to our knowledge no one has actually correlated with CT and MR imaging brain images.

Procedure Details: Using inhalatory anesthesia five pigs 3 month old and 20 kg weight were scanned with CT and MR imaging and then sacrificed. Three mm slice thickness axial images with helical CT and 4 mm slice thickness axial, coronal and sagittal slices with 1.5 T MR imaging were obtained using T1, T2 and MRA sequences. Anatomical specimen slices and imaging were carefully compared to identify anatomic landmarks and precisely locate specific targets with non ferromagnetic stereotactic device. This device was designed to be adjustable to animals of different age and size and also to be useful with CT or MR imaging.

Conclusion: The anatomical structures of a pig's brain can be identified by CT and MR imaging. Stereotactic procedure including biopsy and implants may be guided with CT and MR imaging for research purposes.

C-0822

Wernicke's encephalopathy: Typical and atypical MR imaging findings

A. Buzzi, C. Garcia Pellegrino, M. Hjelt, E. Paez de la Torre, P. Balcarce, A. Mancini; *Buenos Aires/AR*

Learning Objective: To recognize the typical and atypical MR imaging findings of Wernicke's encephalopathy.

Background: Wernicke's encephalopathy is a neurological disorder due to nutritional deficiency of vitamin B₁ (thiamine), characterized by a classic triad (ophthalmoplegia, ataxia and an apathetic confusional state). It occurs most often in alcoholics, however is observed in non-alcoholic patients with infectious-febrile conditions, carcinoma, hyperemesis gravidarum, small-bowel obstruction, anorexia nervosa, etc.

Imaging Findings: Typical findings of Wernicke's encephalopathy are symmetrical hyperintense lesions on T2-WI and FLAIR images in the paraventricular regions of the thalamus and hypothalamus, periaqueductal regions of the midbrain, floor of the fourth ventricle, midline structures of the cerebellum and mammillary body atrophy. Unusual finding include symmetrical hyperintense lesions in the cerebral cortex, especially along the central and paracentral sulci.

Conclusions: Wernicke's encephalopathy is caused by a large variety of clinical conditions and its characterized by typical and atypical imaging findings. The knowledge of these findings allows the correct diagnosis with MR imaging in patients without the classical clinical triad or in patients in coma. This early diagnosis allow the early indication of the proper treatment, modifying the prognosis of this disease.

C-0823

Preliminary study on the mechanism of reading recovery in a pure alexia by using functional MR imaging

L. Ma, X. Weng, W. Sun; *Beijing/CN*

Purpose: To observe the changes of brain function during reading recovery by using functional MR imaging (fMRI), and to provide the experimental data in elucidating the mechanism on the recovery of reading and language function.

Methods and Materials: fMRI was performed in a native Chinese patient with pure alexia on the 45th and 130th day after the onset, respectively. Three kinds of

Chinese characters were presented during the scan and the patient was asked to judge whether he could recognize the characters or not. The brain activation maps were acquired after postprocessing, and the activated location and volume were compared between the first and second experiments.

Results: In both experiments, Broca area, Wernicke area, and the right extrastriate were significantly activated, while the left extrastriate around the lesion was markedly activated only in the second experiment, and the volume of activation in the right extrastriate in the second experiment was about 3 times as large as that in the first experiment.

Conclusion The left extrastriate cortex is one of the key areas responsible for reading function in the brain. The recovery of reading function can be compensated for in a contralateral corresponding cortical area, or it can be the result of reorganization in ipsilateral peri-lesion cortex. Both mechanisms may simultaneously play important roles in reading recovery.

C-0824

How many diffusion gradient directions will be adequate for the clinical applications of diffusion tensor imaging and tractography in cerebral tumors at 3 T MR imaging

H.H. Fu, F. Feng, Z.Y. Jin, W. Tao, R.Z. Wang, Y. Yang, H. You, X.Z. Li, F. Sun; *Beijing/CN*

Purpose: To investigate how many directions acquired in diffusion gradient imaging will be adequate for diffusion tensor imaging (DTI) and tractography (DTT) of cerebral tumors. To demonstrate abnormalities distally and detect occult white matter (WM) tract invasion by tumors on DTI and DTT images.

Materials and Method: MR imaging was performed in 8 patients with histologically confirmed tumors or metastases using a GE Signa VH/3.0 T scanner and T1WI, T2WI and DTI sequences. The diffusion gradient directions of DTI were logically selected at 55, 33, 25, 15, and 6; and b value = 1200, 128x128 matrix. Regions of interest (ROI) were drawn within the tumor, the Ratio Anisotropy (RA), Fractional Anisotropy (FA), Average DC (ADC), and other parameters were calculated for these ROI on all DTI sequences. DTT images in direction sequence were reconstructed by post processing.

Results: The relationship of tumor to WM tracts was uniquely depicted by DTT images compared to that seen on T1WI and T2WI. Four major patterns (deviated, infiltrated, edematous and destroyed) in affected WM tracts were identified and are discussed. In the high-grade tumors, the average values of RA and FA in areas of WM disruption with normal appearance was reduced significantly; by comparison, ADC was increased remarkably.

Conclusion: WM disruption can be identified clearly using the values of RA/FA/ADC and DTT images which were not affected in different acquired diffusion gradient directions (more than 6) in patients with a high-grade tumor. Detecting the other potential patterns of WM fiber tract alteration by cerebral tumors may have to increase the diffusion gradient directions.

C-0825

Radiological manifestations of suicide attempt. A multisystem and multimodality approach

E. Testempski, V. Vantali, N. Kartakis, D. Chondros; *Athens/GR*

Purpose: The purpose of this exhibit is to illustrate various types of injuries in patients after having committed a suicide attempt and to be aware of usual and unusual imaging findings related with suicide attempt.

Methods and Materials: Self-injured patients are not rarely seen in the Emergency Department and may have a variety of head and neck injuries, body and abdominal viscera injuries and also injuries of the extremities. Plain radiographs, US, CT and MR imaging are used in various combinations to evaluate the extent of these injuries. After reviewing the data of our Department, we present a pictorial multisystem and multimodality approach of common and some uncommon self-inflicted injuries.

Results: Esophageal stenosis and rupture after ingestion of caustic agents and esophageal foreign bodies in prisoners and psychiatric patients are depicted. Brain CT and MR images in patients after hanging and after receiving sedatives, anesthetics poisons and other kinds of medications are also shown. A variety of injuries of the head, of the spine, of viscera and extremities in patients having jumped intentionally from a great height are also presented. Head and body injuries in suicides with guns are also demonstrated.

Conclusion: A complete radiological assessment is necessary in these patients in poor clinical condition in order to avoid significant morbidity. The role of imaging modalities in the investigation of self-inflicted injuries is helpful in the diagnosis and management of these critically ill patients and in the differentiation from criminal injuries.

Scientific and Educational Exhibits

C-0826

Primary brain lymphomas: Distinctive imaging features

E. Xinou, G. Boulogianni, D. Chourmouzi, I. Dedes, A. Drevelegas;
Thessaloniki/GR

Purpose: To describe and compare CT and MR features of primary cerebral lymphoma (PCL) and to define its imaging characteristics.

Materials and Method: CT and MR studies of 16 patients with histologically proven PCL were reviewed (6 men, 10 women, 19-76 years, median age 50 years). Ten patients underwent CT-guided stereotactic biopsy and in five patients an open surgical intervention was performed. CT was performed in 6 cases, whereas all patients underwent MR (axial SE PD/T2, axial T1 and triplanar T1+gadolinium). The radiological evaluation included location, number of lesions, measurement of the edema, T1-T2 signal intensity and enhancement characteristics.

Results: A total of 43 lesions (0.5-5.5 cm diameter) were present in 16 patients; 11 patients (69%) had multiple lesions. Most lesions (50%) were in the periventricular areas, appearing as multiple well-defined masses with minimal surrounding edema. The most frequent locations were in descending order: Cerebral hemispheres (50%), cerebellum (25%), basal ganglia (12.5%), pons (12.5%), third ventricle (12.5%) and leptomeninges (12.5%). The hypothalamus ($n = 1$) and the corpus callosum ($n = 1$) were rare locations. On CT scan, most lesions (85%) were isointense or hyperintense. On MR, all lesions were isointense or hypointense compared to the gray matter on T1-weighted images and 62.5% were isointense on T2-weighted images. Dense homogeneous enhancement was observed on both CT and MR studies in 87.5% of the lesions; rim enhancement was depicted in one AIDS patient with multiple lesions. Diffuse leptomeningeal enhancement was demonstrated in two and subependymal enhancement in one case.

Conclusion: Periventricular location, iso- or hyperdense appearance on CT, T1 and T2 isointensity on MR and dense homogeneous enhancement are imaging characteristics that can suggest the diagnosis of PCL.

C-0827

Granulomatous angiitis of the central nervous system. A pictorial review

N. Sheehy, M. Farrell, P. Brennan, J. Thornton; Dublin/IE

Learning Objectives: 1. To describe imaging findings in granulomatous angiitis of the central nervous system (GANS). The findings on CT, MR imaging, MRA and DSA are included. 2. To demonstrate how GANS can mimic a number of pathologies including vascular, inflammatory, infectious and neoplastic aetiologies. 3. To demonstrate the use of imaging modalities in guiding biopsy.

Background: GANS is an idiopathic, isolated cranial vasculitis that may occur in association with infectious agents such as varicella or neoplastic diseases such as Hodgkin's disease. It may present with a variety of clinical events such as encephalopathy, coma, seizures and stroke. Diagnosis is hampered by the absence of a specific clinical, laboratory or radiological investigation. Frequently a brain biopsy is necessary to confirm the diagnosis. Because of its protean clinical and radiological manifestations, GANS is frequently included in the differential diagnosis of patients with neurological disorders.

Imaging Findings: A comprehensive review of the imaging findings in 6 cases of biopsy-confirmed GANS is illustrated.

Conclusion: In this e-poster, we demonstrate the multiple imaging findings of GANS.

C-0828

Detection of brain hyperintensities on fluid-attenuated inversion-recovery (FLAIR) images in multiple sclerosis (MS): In-plane high resolution (HR) versus standard low resolution (LR) matrix

F. Sardanelli, A. Fausto, B. Cotticelli; Milan/IT

Purpose: To compare the detection of brain hyperintensities on fast FLAIR images using a HR or a standard LR matrix in MS patients.

Methods and Materials: Ten consecutive MS patients (9 females, aged 22-64) underwent (1.5 T) a fast FLAIR paraaxial sequence (TR/TE/TI = 8300/135/2500 ms; ETL = 21; one excitation; FoV 230 mm; 20 no-gap slices, 5-mm thickness; 256x256 (LR) matrix; pixel = .90x.90 mm; time 3' 36"). The sequence was repeated using a 512x512 (HR) matrix with a 0.45x0.45-mm pixel and 7' 46" time. Patient-by-patient, for each slice, brain hyperintensities were counted, grading them as certain (C) or probable (P). Signal-to-noise ratio (SNR) was calculated for both sequences in each patient. Wilcoxon test.

Results: A total of 1179 hyperintensities (C/P = 1069/110) using LR matrix and of 983 (891/92) using HR matrix were counted, C/P ratio remaining unchanged (9.7) for both matrices. C hyperintensities ranged 32-to-351 (median = 117) and

23-to-282 (93), respectively; P hyperintensities 5-to-27 (10) and 2-to-26 (8), respectively. The number of total and C hyperintensities was significantly larger with LR matrix and mean SNR was 49.2 (LR matrix) and 18.5 (HR matrix), with a significant drop of about 60% ($P < .01$); no significant difference was found for P hyperintensities.

Conclusion: The lower SNR of FLAIR with HR matrix reduces significantly the number of total and certain hyperintensities in brain imaging of MS patients, probably due to the heavy reduction of voxel (only a fourth of LR voxel). The level of certainty in detecting brain hyperintensities remain unchanged, confirming the high sensitivity of FLAIR sequence.

C-0829

3 T 1H-MRSI assessment of spatial distribution of metabolites in cerebral gliomas

S. Pollici¹, A. Di Costanzo², G. Giannatempo³, T. Popolizio³, A. Carrieri¹, T. Scarabino³; ¹Novara/IT, ²Naples/IT, ³San Giovanni Rotondo/IT

Purpose: This research aims to characterize the spectrum of metabolites in tumour and surrounding tumour tissue by using 1H-MRSI.

Methods and Materials: We studied twenty-eight patients with histologically verified cerebral glioma. Region of interest (ROI) were positioned on necrotic areas, non-necrotic areas, lesion edges and on apparently normal or edematous surrounding tissues. The Cho, NAA, Cr, and LL signal in the ROI were compared with the signal of the same metabolite in the corresponding region of the opposite non-pathological hemisphere.

Results: The metabolite distribution in high and low grade gliomas was correctly characterized in the examined areas. Cho, NAA and LL, in our experience, have a different distribution in high and low grade tumor tissue, and in surrounding edematous regions with and without tumour infiltration.

Conclusions: 3 T 1H-MRSI is a non-invasive technique that allows recognition of the grade of the tumour, differentiation of the proliferating neoplasm from normal tissue, necrotic areas and edematous tissue; both secondary to neoplastic infiltration and from radiation. This research shows that the different spatial distribution of metabolites in a glioma allows distinction of high grade gliomas from low grade gliomas and highlights the heterogeneity and characteristics of these lesions. 3 T 1H-MRSI supplies useful information for the stereotactic biopsy, surgical resection and for radiotherapy planning.

C-0830

Tips and tricks in cerebral perfusion CT: Classification and literature review

A. Littera, A. Ferrari, A. Stecco, A. Boccardi, C. Civardi, A. Carrieri; Novara/IT

Learning Objectives: The exhibit allows the technician and radiologist to know the artifacts and pitfalls which can be found in each step of perfusion CT of the brain. Solutions for improvement in the quality of examination are shown.

Background: Dynamic Perfusion Computed Tomography is a well assessed technique to evaluate brain perfusional parameters in patients with ischemic stroke, in order to perform thrombolytic therapy.

Procedure Details: There are several technical aspects that can affect the perfusional data evaluation and the final report of the examination. We analyze and classify all these aspects, to allow the technician and the radiologist to know exactly what to avoid and what to choose, and we indicate when possible the way to improve the quality of the examination. The pitfalls can be divided into two major groups, related to technique and to elaboration. Among technical pitfalls we include: type of scanning (spiral/continuous mode, non-spiral/discontinuous mode), slice thickness choice, anatomic coverage, gantry tilting, Kv choice, infusion rate, prep delay. Data elaboration pitfalls include: movement software correction, artery/vein choice to begin the analysis, evaluation of the artery time/intensity curve morphology.

Conclusion: Knowing the type of artifacts or technical errors and the way to avoid them is mandatory to obtain satisfactory perfusional color maps, and correct CBV, CBF and MTT values.

C-0831

Multislice computed tomography (MSCT) and magnetic resonance imaging (MRI) in the evaluation of cerebrospinal fluid (CSF) fistulae with rhinorrhea

A. Bellussi, M. Cristofaro, L. Rovighi, A. De Santis, C. Bibbolino; Rome/IT

Learning Objectives: To illustrate the high sensitivity and accuracy of msct in association with MR, in identifying dural osseous defects with CSF leak, complicated by bacterial meningitis.

Background: From September 2002 to May 2004 we observed 7 cases of CSF fistulae in patients affected by bacterial meningitis. 4 cases were secondary to

Scientific and Educational Exhibits

trauma, 1 due to a congenital malformation and 1 due to a bone defect in the clivus (a very rare location as far as we know). The last was subsequent to ethmoidal surgery.

Procedure Details: CT examinations were performed with a 4 row scanner (GE Lightspeed QX I) at 4x1.25 mm detector collimation, 120 kv, 200 mA, 0.8 sec, table speed 3.8 mm (pitch 0.75). Data reconstruction interval was 0.62 mm. Images were reformatted on coronal and sagittal planes. MR images were obtained using a Philips Gyroscan 05 NT device. T1 SE and T2 TSE multiplanar sequences were performed and when necessary suitable decubitus imaging was obtained. In selected cases T2 TSE 3D images were acquired.

Results: We found that msCT examination was able to demonstrate the precise location and size of CSF fistulae in all cases, even when MR was not reliable in imaging the definite site of the bone breach. Four patients were successfully operated on and recovered.

Conclusions: In the evaluation of patients affected by CSF leak, msCT should be considered an indispensable integration to MR findings.

C-0832

Acute demielinating tumor-like disease: Multiple sclerosis Marbourg's variant

G. Iannucci¹, A. Stecco¹, D. Danieli², F. Causin², M.D. Marchi², V. Pinna², A. Carrieri¹; ¹Novara/IT, ²Vicenza/IT

Purpose: There are a few cases of Marbourg's disease reported in the medical literature. Marbourg's disease is described as a fulminant, monophasic, malignant multiple sclerosis that can result in death from severe disseminated demyelination within a few weeks. The MR imaging shows tumor-like lesions with large and confluent demyelination, without specific characteristics.

Methods and Materials: Case 1: 41 year old man, who was healthy until admission when he developed a headache, hemiparesis and a stupor. Two weeks after admission he became unconscious and underwent emergency neurosurgery with frontal left lobectomy. Case 2: 39 year old woman, who was healthy until admission when she developed headache and aphasia. Two days after admission she developed hemiparesis and stupor and a week later died. MR imaging scans, laboratory and clinical examinations were obtained from each of the two patients.

Results: MR imaging scans from each patient showed a frontal lobe tumor-like lesion. Conventional MR imaging sequences didn't allow us to better characterize the lesions. The histological findings were identical in each patient, corresponding to myelin loss with numerous macrophages, myelin breakdown products and a subtle perivascular infiltration of lymphocytes. Histological specimens were obtained from the frontal lobe in case 1 and from the whole brain in case 2.

Conclusion: Our study describes two cases of Marbourg's disease MS with large focal cerebral demyelinating lesions. They showed the same lesions in the frontal lobe with clinical and radiological characteristics typical of brain tumor but different in clinical evolution. The relevance of this study is about the rare recognition of Marbourg's disease in the medical literature.

C-0833

The body representation in the first somatic sensory area of human brain: An fMR imaging study

G. Polonara, M. Fabri, C. Mabiglia, T. Manzoni, U. Salvolini; Ancona/IT

Purpose: The present research aims at studying with fMR imaging the body representation in the first somatic sensory area of human brain.

Materials and Methods: Nine healthy volunteers were examined using a 1.5 T MR system. Tactile stimulation was applied by rubbing various cutaneous regions with a rough sponge (palm and back of the hand, foot, forearm, arm, shoulder, leg, thigh) or with a soft cotton pad (face, medial or lateral trunk) at a frequency of 1 Hz. Two 5-min protocols were used: one consisted of ten 30-sec alternating periods of rest and stimulation, the other of sixteen 18-sec alternating periods of rest and stimulation, followed by a 12-sec rest period. With the first protocol, a single body region was rubbed in all 5 stimulation periods, with the second, two body regions were alternately rubbed during the 8 stimulation periods.

Results: Cortical activation was found in the post-central gyrus (PCG) of the contralateral hemisphere. Stimulation of different body regions activated topographically different cortical regions: foci evoked by foot, leg, trunk, arm, hand and face stimulation were arranged medial to lateral throughout PCG, indicating a somatotopic map whose general features are in agreement with previous human functional (PET and MEG) and monkey recording studies. Proximal body and hand activation foci were also present in the posterior part of ipsilateral PCG.

Conclusion: Definition of the cortical cutaneous map with fMR imaging with an MR magnet commonly used for diagnostic purposes may be useful in pre-operative functional studies.

C-0834

Highly active antiretroviral therapy (HAART) and MR imaging of progressive multifocal leukoencephalopathy

E. Busi Rizzi, V. Schininá, M.L. Giancola, L. Rovighi, D. Larussa, A. Antinori, C. Bibbolino; Rome/IT

Purpose: To evaluate whether highly active antiretroviral therapy (HAART) modifies MR imaging appearances of progressive multifocal leukoencephalopathy (PML) among patients with HIV infection and whether MR imaging pattern and survival correlate.

Methods and Materials: We retrospectively reviewed MR imaging of 31 HIV+ patients with histological or clinicovirological diagnosis of PML, 18 with positive JCV-DNA in cerebral spinal fluid (CSF). 12 patients were naive for antiretrovirals and 8 were taking HAART at diagnosis. Median CD4: 69 x cells/ml, median plasma HIV-RNA: 4.89 x log₁₀ copies/ml. MR examinations were performed on a 0.5 T system, axial T1 spin-echo images before and after administration of contrast material, T2 fast spin-echo and T2 FLAIR images were obtained in all patients. Number, size, location, distribution, scalloping, signal intensity and contrast enhancement of the lesions were evaluated.

Results: Patients with positive or negative JCV-DNA in CSF displayed a similar pattern, except for a higher risk of pons involvement in JCV-DNA positive PML (OR 1.50 (1.08-2.08), P = 0.028). Analysing differences according with antiretroviral exposure no significant differences were observed in naive compared to experienced patients or between HAART-treated or not treated patients at diagnosis. Bulb involvement (p = 0.030) and mass effect were associated with higher risk of death (p = 0.009). MR findings were unrelated to immunological status.

Conclusions: MR PML pattern was not influenced by antiretroviral exposure. JCV positive and JCV negative PML presented similar MR imaging findings and these features are very relevant to distinguish PML with negative JCV-DNA in CSF from other leukoencephalopathy.

C-0835

Atypical multiple sclerosis: MR imaging findings and differential diagnosis

G. Lucchienti¹, M. Spadaro¹, P. Bramanti², C. Colonese¹, U. Sabatini¹, C. Uggetti³, S. Bastianello³; ¹Rome/IT, ²Messina/IT, ³Pavia/IT

Learning Objectives: 1)To illustrate the diagnostic criteria of MS and the findings of atypical MS phenotypes with conventional MR imaging. 2)To describe the differential diagnosis of atypical MS with other diseases of the CNS. 3)To propose a diagnostic algorithm, including advanced MR techniques, laboratory and clinical evaluations, for diseases that appear similar to MS.

Background: Atypical forms of Multiple Sclerosis and other diseases of the central nervous system may show similar patterns in MR. The differential diagnosis includes: vascular diseases (CADASIL), vasculitis (polyarteritis nodosa, systemic lupus erythematosus, Sjogren's syndrome, Behcet disease, giant cell arteritis and small single brain infarcts), secondary demyelinating diseases (Progressive Multifocal Leukoencephalopathy, Acute Disseminated Encephalomyelitis (ADEM)), multiple metastases or malignant brain tumor, inflammatory diseases (sarcoidosis), infectious diseases and metabolic diseases (Metachromatic Leucodystrophy).

Procedure Details: For each of the differential diagnoses a clinical case is demonstrated. A diagnostic algorithm that is useful for differential diagnosis in the clinical setting is presented. For correct diagnosis, the MR findings are correlated with the clinical and laboratory findings.

Conclusion: An accurate differential diagnosis is crucial to enable the appropriate therapy to be initiated without delay.

C-0836

Assessment of tissue characterization of gliomas: Comparison of tumor blood volume by perfusion-weighted MR imaging and TI-201 SPECT

H. Uematsu, T. Tsuchida, H. Kimura, M. Toyooka, H. Itoh; Fukui/JP

Purpose: TI-201 uptake is useful for evaluating the degree of glioma malignancy. Increased vascular leakage is considered to be a contributor to TI-201 uptake in early scans; however, studies on the contribution of tumor blood volume in the TI-201 accumulation are sparse. Perfusion-weighted magnetic resonance (MR) imaging can provide quantitative tumor blood volume values. The aim of this study was to clarify the contribution of tumor blood volume in TI-201 uptake in gliomas.

Methods and Materials: We evaluated 10 patients with glioblastoma multiforme. After the injection of TI-201 (74 MBq), early (15 min later) and delayed (3 hrs later) SPECT scans were acquired. TI-201 uptake ratios of tumors to contralateral normal white matter (T/N ratio) were calculated for both the early and delayed scans. Perfusion-weighted MR imaging with a gadolinium contrast agent can provide the tumor blood volume values. For the quantitative analysis, TI-201

Scientific and Educational Exhibits

uptake (T/N ratios) in the early and delayed scans were compared with tumor blood volume.

Results: In visual assessment, the tumor blood volume on the parametric map was concordant with the TI-201 early and delayed SPECT images. In the quantitative analysis, T/N ratios in the early scan were well correlated with tumor blood volume ($r^2 = 0.61$, $p < 0.01$). In the delayed scan, there was also significant correlation between T/N ratios and tumor blood volume ($r^2 = 0.53$, $p < 0.05$).

Conclusion: Tumor blood volume may contribute to greater TI-201 uptake seen on both the early and delayed scans.

C-0837

Head/neck CT angiography and CT perfusion in the assessment of patients with carotid occlusion

R. Takagi, H. Sato, H. Hayashi, N. Hidaka, H. Yoshihara, T. Kumazaki; Tokyo/JP

Purpose: To demonstrate the value of the combination technique of Head/neck CTA and CTP in a clinical study of patients with carotid occlusion.

Methods and Materials: 13 patients who were shown to have carotid occlusion by MRA underwent both head/neck CTA and CTP using 16-slice MD-CT. Initially, a dynamic perfusion series was acquired, head/neck CTA was performed from the origin of the aortic arch to the circle of Willis. The regional cerebral blood flow (CBF), cerebral blood volume (CBV) and mean transit time (MTT) maps were calculated. The head/neck CTA images were reconstructed. The MRA, neck CTA, head CTA and CTP images were reviewed. The interpretation of each of the 4 modalities was compared with the other results.

Results: MRA showed total ICA occlusion in 10 and distal occlusion in 3 patients, and did not depict ipsilateral MCA in 3 patients. Neck CTA revealed total ICA in 2 patients. Head CTA showed ipsilateral MCA in all patients. Head CTA showed ICA occlusion at supraclinoid segment in 4, narrowed ICA in 8, and normal in one patient. CTP showed increased CBV, decreased CBF and prolonged MTT at ICA territory in 2 patients. The other 11 patients were shown normal CBV and prolonged MTT at MCA territory. CBF map showed decreased CBF at MCA territory in 5, basal ganglia in 3 and normal in 3 patients.

Conclusion: In the assessment of patients with carotid occlusion, CTP represents various ischemic changes according to auto-regulation and collateral circulation. The combination diagnosis of head/neck CTA and CTP provides valuable information.

C-0838

Paracavernous sinus venous structures: Anatomical variations and pathological conditions evaluated on fat suppressed 3D fast-gradient-echo MR imaging

S. Tanoue, H. Kiyosue, Y. Hori, M. Okahara, Y. Sagara, J. Kashiwagi, H. Mori; Oita/JP

Learning Objectives: To know the anatomical variations of paracavernous sinus venous structures. To describe the usefulness of fat-suppressed 3D fast-gradient-echo MR imaging in evaluating venous structures of the skull base.

Background: The cavernous sinus (CS) communicates with several paraCS venous structures; receiving blood flow from superficial middle cerebral vein, sphenoparietal sinus, superior ophthalmic vein, and draining into superior and inferior petrosal sinuses, pterygoid and basilar plexuses. Anatomical variations of these veins have been previously reported, however some details such as the relationship between the sphenoparietal sinus and the superficial middle cerebral vein, are still controversial. The anatomical variations of paraCS veins, especially drainage patterns of superficial middle cerebral vein, were evaluated on MR imaging.

Procedure Details: Thirty cases, including patients without any lesions affecting CS or paracavernous veins and patients with carotid cavernous fistulas, were examined by using fat-suppressed, contrast-enhanced, 3D fast-gradient-echo MR imaging. Two neuroradiologists evaluated the images on a viewer, with regard to normal anatomy and any pathological findings of the paraCS veins.

Conclusion: Fat-suppressed 3D fast-gradient-echo MR imaging clearly depicts the paraCS venous structures in normal and pathological conditions. There were several variations in the drainage pattern of the superficial middle cerebral veins, e.g. draining into the sphenoparietal sinus, the CS, and other paracavernous veins. Knowledge of the variations is important for diagnosis and endovascular treatment of the CS lesions.

C-0839

Early diagnosis of postoperative empyema in brain and spine: Use and pitfalls of MR imaging

A. Wada¹, T. Hayashi², T. Katsume¹, E. Fukuba¹, M. Matsuo², H. Kitagaki¹; ¹Izumo, Shimane/JP, ²Tenri City, Nara/JP

Learning Objectives: Diffusion weighted MR imaging is a useful method to diagnose pyogenic empyema. In the post operative state, there are several conditions which reveal similar findings to pyogenic pus on diffusion-weighted images. We exhibit the use and pitfalls of MR diagnosis of postoperative empyema.

Background: Epidural and subdural empyemas are one of the most serious complications after brain and spine surgery. Postoperative empyema is not frequent, but has a high fatality rate, especially in compromised patients. Early diagnosis and treatment affects the patient's prognosis. We experienced five cases of post-operative epidural or subdural empyema and two cases of post operative reaction which showed similar MR findings to empyema. We noticed that there were some pitfalls in the MR diagnosis of postoperative empyema.

Procedure Details: Diffusion weighted MR imaging was performed in all seven cases. Content of the empyema (pus) showed remarkably high signal intensity and this finding contributed to the early diagnosis and treatment of the empyema. The high signal intensity of pus decreased after treatment (surgical resection or antibiotic therapy). There are other factors which show high signal intensity on DW images such as an inserted metal device, bleeding and an air collection.

Conclusion: Diffusion weighted MR imaging is useful in the early diagnosis of postoperative empyema with awareness of some pitfalls.

C-0840

Metallic artifact reduction techniques for MR imaging of the brain: Evaluation of fast-inversion-recovery T1-weighted images (fast-IR-T1WI)

M. Kawanishi; Chiba/JP

Purpose: In magnetic resonance (MR) imaging of the brain, magnetic fields can be locally distorted by ferromagnetic implants, such as fillings in teeth or aneurysmal surgical clips. In this study fast-IR-T1W imaging was performed and the ability of metallic artifact reduction was evaluated.

Methods and Materials: 10 patients with ferromagnetic implants were the subjects of this study. Fast-IR-T1WI were obtained with the following parameters: TR/TE/TI 2789/22/410 msec; echo train length 9; FOV 24 cm; matrix 256x192 and scan time 33.5 sec. Standard Spin-Echo-T1-weighted images (SE-T1WI) were also performed and were compared with fast-IR-T1WI. Reduction ability of metallic artifacts was evaluated.

Results: In all cases fast-IR-T1WI was superior to reduce metallic artifacts to standard SE-T1WI.

Conclusion: Fast-IR-T1WI is useful for patients with ferromagnetic implants. Fast-IR-T1WI is considered a good technique to reduce metallic artifacts in brain MR imaging.

C-0841

Normalization of CNS metabolite disturbances in clinically asymptomatic HIV patients after HAART treatment. MRS study

E. Tarasow, A. Wiercinska-Drapalo, J. Jaroszewicz, J. Walecki, A. Alathiaki; Bialystok/PL

Purpose: MR proton spectroscopy (1H MRS) enables early detection of metabolic changes, which occur in the course of AIDS Dementia Complex Syndrome (ADC). The goal of the study was the evaluation of highly active antiretroviral therapy (HAART) and its influence on the character and intensity of metabolic changes in brain 1H MRS spectra in clinically asymptomatic HIV-infected patients as well as search for correlation between the treatment and 1H MR spectroscopy results and immune deficit degree.

Methods and Materials: In the group of 20 HIV+ patients, the examination of the central nervous system (CNS), MR and 1H MRS were conducted twice: Before HAART treatment and during the therapy; on average after 6 months (4-9 months of treatment).

Results: The levels of NAA/Cr in the control MRS examination were close to the values observed before treatment. However, a statistically significant increase in the NAA/Cho ratio ($p < 0.05$) was noticed. The control examination showed a decrease of Cho/Cr and ml/Cr ratios, though statistically insignificant ($p > 0.05$). NAA and Cr contents in reference to the signal of non-suppressed water increased insignificantly in the follow-up examination. However, a statistically significant decrease in Cho/H₂O and ml/H₂O levels ($p < 0.05$) was observed.

Conclusion: The therapy with HAART affects normalization of metabolite levels in the central nervous system in clinically asymptomatic HIV+ patients and di-

Scientific and Educational Exhibits

minishes the risk of ADC occurrence. Myoinositol and choline levels estimated in 1H MRS may act as indices for antiretroviral treatment efficacy.

C-0842

MR imaging manifestation of central nervous system lesions in von Hippel-Lindau disease

L. Cyrylowski, G. Zaborowski, M. Sawicki, K. Krzystolik, C. Cybulski, L. Sagan, A. Walecka, J. Lubinski; Szczecin/PL

Purpose: The aim of the study was to evaluate localization, type, and MR appearance of the central nervous system (CNS) lesions in von Hippel-Lindau disease (vHL).

Methods and Materials: The study group comprised 42 patients from 34 Polish families (26 women, 16 men; mean age 34.5 years) with diagnosed vHL. MR imaging of the head and the spine was performed with 1.5 T unit, using dedicated coils. T2w, precontrast T1w, and postcontrast T1w sequences were obtained.

Results: One hundred and eleven lesions in 30 (71%) patients were detected, including 53 (47%) subsellar lesions [47 (42%) in the cerebellum, 6 (5%) in brain-stem], 2 (3%) suprasellar, and 56 (50%) in the spinal cord. Eighty seven solid (78%), 17 cystic-solid (15%), and 7 (7%) cystic lesions were found. Multiple lesions were diagnosed in 8 (26%) patients in the spinal cord, 12 (40%) in the cerebellum, and 1 (3%) in the brainstem. Multifocal lesions have been observed in 16 (53%) cases. Almost all solid lesions were isointense both in T1w and T2w. They were detected only with postcontrast imaging. Nineteen lesions were resected in 11 patients; pathological examination revealed hemangioblastomas in all cases.

Conclusion: Postcontrast T1w images are of the most value in the detection of CNS lesions in vHL patients. Proper prophylactic and diagnostic management can possibly identify asymptomatic carriers of germline vHL mutations. Early detection and treatment of small lesions can probably prolong survival of the patients and limit complications of the disease.

C-0843

MR CSF-flow examination in children with a ventriculo peritoneal shunt: The differentiation of shunt dependent and shunt independent hydrocephalus

M. Szafirska, A. Urbanik, A. Swierczyna, S. Kwiatkowski, S. Sztuk, I. Herman-Sucharska; Krakow/PL

Purpose: The aim of the study is the presentation of the value of MR examination of CSF flow through the cranial part of the ventriculo peritoneal shunt in the evaluation of shunt dependent hydrocephalus.

Methods and Materials: Thirteen patients 8-18 years of age in the course of longterm treatment using ventriculo-peritoneal shunts were examined. The examinations were performed with the use of Signa Horizon 1.5 T (GEMS) unit with 2D CINE/GR/PC sequence in the plane perpendicular to the direction of CSF-flow in the shunt. Flow parameters were calculated using the Flow Analysis program (the presence or absence of CSF-flow through the shunt as well as the flow velocity in ml/min were evaluated). No clinical manifestations of shunt obstruction had been observed in any of the patients prior to MR examination.

Results: In 5 children no CSF-flow was noted indicating shunt independent hydrocephalus. In 7 children CSF-flow was present (the flow velocity of 0.1-1.3 ml/min) indicating shunt dependent hydrocephalus.

Conclusion: MR examination allows the determination of the absence or presence of CSF-flow as well as its direction and velocity. This examination enables the differentiation between shunt dependent and shunt independent types of hydrocephalus, which is of great significance in the clinical management of patients after shunt implantation.

C-0844

Differences in regional BOLD responses in the primary and secondary auditory cortex by mixed noise and speech like stimuli

M. Golebiowski, P. Bogorodzki, E. Janko-Piatkowska, T. Wolak, M. Orzechowski, R. Kurjata, W. Szeszkowski; Warsaw/PL

Purpose: The aim of the study was to investigate the hierarchical organization within the auditory cortex of humans with mixed noise and speech like auditory excitation using functional magnetic resonance imaging (fMRI) technique.

Materials and Method: For each of 20 healthy subjects (16 males and 4 females, 19 right-handed and 1 left-handed) at age 23.6 ± 0.7 four functional sessions with block type speech like stimuli (15 repetitions of the BA-LU) and variable amount of noise were acquired. Statistical parametric maps were generated under SPM99 software and additionally, the raw Blood Oxygenation Level Dependent (BOLD) signal intensities from left and right primary (A1) and secondary (A2)

auditory cortex regions were averaged to form a time series spanning the entire length of the experiment. The variation of resulting curves was described with percent signal change (PSC) measure.

Results: The random effect analysis shows strong activations in both A1 ($T = 10.59$ in left hemisphere and $T = 9.94$ in right hemisphere) and A2 ($T = 11.73$ in left hemisphere and $T = 8.75$ in right hemisphere) regions. Additionally, we noted substantial correlation of PSC measure with noise level in A1 ($R = 0.95$, $T = 13.4$) and practically no correlation in A2 ($R = 0.05$, $T = 0.2306$).

Conclusion: The experiment revealed auditory hierarchical architecture with the special emphasis on primary and secondary cortex function fields. An attenuation of noise at secondary cortex with good response for BA-LU stimuli was noted.

C-0845

Single voxel ^1H MR spectroscopy of cerebral gliomas at 3.0 T: Comparison of short and long TE sequences in tumor grading

J.-h. Kim, K.-H. Chang, M. Han, D. Na, B. Kwon, I. Song; Seoul/KR

Purpose: To investigate the usefulness of short and long TE sequences at 3.0 T single voxel proton MR spectroscopy (^1H -MRS) in the grading of cerebral gliomas.

Methods and Materials: Single voxel ^1H -MRS was performed at 3.0 T in 27 patients with cerebral glioma. Pathological diagnosis included 5 WHO grade II tumors, 11 grade III tumors and 11 grade IV tumors. ^1H -MRS spectra were obtained with TR of 2000 msec and with both short TE (35 msec) and long TE (144 msec) PRESS sequences at the possible homogenous solid area in the brain tumors. Choline (Cho)/creatinine(Cr), Cho/N-acetylaspartate(NAA), and (lipid(Lip) + lactate(Lac))/Cr ratios were measured at the both spectra and compared among those three grades of the gliomas.

Results: (Lip + Lac)/Cr ratios of grade II, III and IV tumors at short TE were 0.82 ± 0.41 , 4.2 ± 7.5 and 11.1 ± 11.4 , respectively ($p < 0.001$ between grade II and IV). The Cho/Cr ratios of grade II, III and IV tumors at long TE were 1.90 ± 1.01 , 2.37 ± 1.27 , and 4.68 ± 4.49 , respectively ($p < 0.05$ between grade II and IV). (Lip + Lac)/Cr ratio at long TE, Cho/Cr ratio at short TE, and Cho/NAA ratio at both TEs also tended to be greater with higher grades but there were no significant differences among the grades.

Conclusion: Both short and long TE sequences of 3.0 T single voxel ^1H -MRS are complementary in the grading of the cerebral gliomas because of their own advantages.

C-0846

Assessment of small vessel stents for intracranial angiography by 16-slice CT angiography

H.-J. Choo, K.S. Choo, T. Lee, S. Kim, H. Jeong, T. Moon; Pusan/KR

Purpose: To determine whether 16-slice CT angiography is suitable for the evaluation of luminal patency and visibility of intracranial stents.

Methods and Materials: Twelve stents (7 middle cerebral arteries, 4 intracranial vertebral arteries, 1 pterocavernous internal carotid artery) of two different types were evaluated in 12 patients. CT was performed on a 16-slice scanner (detector collimation 12×0.75 mm; table feed 2.8 mm/rotation; 300 mAs; 120 kVp; reconstruction with standard and optimized sharp kernel). Longitudinal multiplanar reformations were evaluated for stent patency and visible lumen diameter by two experienced radiologists who were blinded to the reports from the conventional angiography.

Results: Evaluation of stent patency using CT angiography was correctly correlated with those using conventional angiography. On average, 65% of the stent lumen diameter was visible using optimized sharp kernel. Significant improvement of lumen visualization (20%, $P < 0.01$) was observed using the optimized sharp kernel compared with the standard sharp kernel.

Conclusion: 16-slice CT using the dedicated sharp kernel might provide useful information for evaluation of patency of stent and lumen diameter of intracranial stents.

C-0847

SPECT with HMPAO-Tc99m application to measure the cerebellar blood flow in patients with Chiari malformations

A.N. Yalfimov, L.A. Tyutin, A.V. Pozdniakov; St. Petersburg/RU

Purpose: The purpose of this study was to investigate the cerebellar blood flow in patients with Chiari malformations (CM).

Methods and Materials: 45 patients with CM were included in the study. To assess the cerebellar blood flow SPECT with HMPAO-Tc99m (Ceretec) was performed in all patients.

Scientific and Educational Exhibits

Results: Significant flow heterogeneity in the cerebellum and reduction of cerebellar blood flow in 15-20% of 25 patients was observed. 3 of them had symptoms of hydrocephaly. All 25 patients underwent surgical treatment. SPECT with Ceretec revealed significant cerebellar blood flow improvement a month after surgical treatment.

Conclusion: SPECT with Ceretec is a feasible method for measuring cerebellar blood flow and monitoring of surgical treatment in patients with Chiari malformations.

C-0848

Possibilities of PET with ^{11}C -Sodium Butyrate (^{11}C -SB) for morpho-functional estimation of brain malignant tumors (BMT)

N.A. Kostenikov, L.A. Tyutin, N.P. Fadeev, V.E. Savello, R.M. Zhabina; St. Petersburg/RU

Purpose: To define the role and significance of PET with ^{11}C -SB in the diagnosis of BMT.

Methods and Materials: 2D-PET scans (Ecat Exact HR+) were performed in 85 patients with BMT (glioblastomas, meningosarcomas, medulloblastomas, anaplastic astrocytomas and cancer metastases). 30 min dynamic scans were carried out immediately after intravenous administration of 450-750 MBq ^{11}C -SB by bolus. The diagnoses had been verified histologically & morphologically. The T/NT ratio and fatty acid (FA) metabolism were obtained in both tumors and unchanged cerebral cortex parts by the time/activity curve. The following parameters were determined: A T/NT ratio, the tumor vascularization degree (VD), the FA uptake rate (UR), the FA metabolization (washout) rate (MR), the oxygenation index (OI).

Results: The obtained results showed that ^{11}C -SB allows not only the visualization of BMT, but also enables definition of their VD (angiogenesis). It is noted that increased VD, high UR & MR are characteristic for BMT, such as glioblastomas and meningosarcomas. IO, calculated on the quantitative analysis of the time/activity curves, allows evaluation of the degree of tumor hypoxia that has an important role in prognosis. Moreover, this method allows the possibility of evaluating the influence of peritumoral edema on tumor vascularization and metabolism.

Conclusion: The performed studies showed that dynamic PET investigation with ^{11}C -SB allows precise visualisation of BMT of various histological subtypes and the estimation of their morphological state. This new data using ^{11}C -SB on FA metabolism in BMT supplements our knowledge about tumour biology.

C-0849

Technetium-99m-MIBI SPECT and image fusion with CT or MR imaging for the assessment of primary brain tumors and brain metastases

V.S. Dekan, G.E. Trufanov, S.D. Rud, V.A. Fokin, I.V. Boikov; St. Petersburg/RU

Purpose: To assess the value of ^{99}Tc -MIBI SPECT images and fused images with CT or MR in the diagnosis of brain tumors or metastases.

Materials and Method: 18 patients with CT or MR findings of brain neoplastic lesions underwent SPECT (E.Cam Variable, Siemens) with ^{99}Tc -MIBI after CT (Somatom Volume Zoom, Siemens) or MR (Magnetom Symphony, Siemens). 13 patients underwent CT or MR and SPECT after operation or chemotherapy. The digital workstation of the SPECT gamma-camera was used to make fused images. Quantitative analysis of native SPECT images was performed by comparing uptake indices in tumors and intact brain tissue.

Results: All 18 patients were histologically proven by biopsy or at operation and by SPECT as malignant lesions. One of them was shown to be the metastasis from a lung cancer, six were glioblastomas, 11 patients had differing grades of astrocytoma. The fused images helped to increase sensitivity of SPECT from 78% to 97% and specificity of CT and MR imaging from 68% to 83%.

Conclusion: ^{99}Tc -MIBI brain SPECT is an effective diagnostic tool for evaluation of brain malignant lesions and estimation of their malignant grade. Fused images with CT or MR imaging can increase the specificity of tumor detection.

C-0850

Long-term brain MR follow-up in patients with neurological form of Wilson's disease

D. Kozic¹, I. Petrovic², M. Svetel², M. Lucic¹, J. Ostojic¹, V. Kostic²;

¹Sremska Kamenica/YU, ²Belgrade/YU

Purpose: To evaluate the degree of pathological substrate regression within the brain parenchyma during a chronic course of chelating therapy in patients with Wilson's disease (WD).

Materials and Method: Brain MR reexamination was performed in 13 patients with the neurological form of WD after 3.5-7 years of treatment. MR was also performed in 1 patient who discontinued therapy for several months.

Results: Complete reversal of putaminal T2W signal alteration was noted in 38% of patients, partial regression in 15%, while more prominent signal alteration was present in 1 patient. Complete or near complete regression of T2W signal alteration was evident in the caudate nuclei, midbrain, pontine base and pontine tegmentum in 60%, 71%, 85% and 83% of patients, respectively. Paramagnetic deposition in the globus pallidus and substantia nigra was significantly less prominent in 80% of patients. Complete regression of lesions was seen in both patients with thalamic involvement. New lesions in the thalamus, putamina and pontine base and worsening of the T2W hyperintense signal in midbrain tegmentum were found in a patient who temporarily discontinued treatment.

Conclusion: Compared to previous reports in which MR reexamination was performed after 6-12 months, our long-term follow-up study showed gradual resolution of T2W signal alteration within the brain parenchyma in the majority of patients with neurological presentation of WD. Our results suggest that T2W signal elevation, particularly in the brain stem, is most likely consistent with chronic, but reversible inflammatory changes due to the toxic effect of copper, rather than with gliosis, necrosis and cavitation. Rapid deterioration is evident after chelating therapy discontinuation.

C-0851

Perfusion CT: Patterns of presentation in acute stroke

J. Munuera, A. Rodríguez, X. Perich, A. Solano, M. Gomis, N. Calvo, A. Ois, J. Roquer; Barcelona/ES

Purpose: To describe the perfusion CT (PCT) findings in acute stroke patients and to establish a classification based on the different observed patterns.

Methods and Materials: 19 patients with symptoms lasting less than 6 hours were prospectively evaluated: 11 territorial infarcts, 2 lacunar infarcts and 6 transient ischemic attacks (TIA). The protocol was: Brain CT scan plus angio-CT and a PCT. We evaluated the acute ischemic signs; findings of cerebral flow, volume and time to peak (TTP); and angiographical findings. The whole study lasted 10 minutes. A transcranial doppler was performed during the acute phase in all patients. The results were correlated to the clinical data and in 8 cases with a brain MR imaging performed 48 to 72 hours later.

Results: In 9/11 patients with territorial infarcts the PCT showed an infarct pattern; associated in four of them with a penumbra area. In one patient a hyperflow pattern was observed; and the only patient with a normal PCT was affected by a vertebrobasilar stroke. The PCT was also normal in the two patients suffering a lacunar stroke. Among the patients suffering a TIA the PCT was normal in five, showing in one case a hypoperfusion area.

Conclusions: 1. PCT is an alternative to diffusion-perfusion MR imaging in acute stroke patient evaluation, with easy application in the daily practice. 2. Using the combination of TTP with cerebral volume and flow findings it is possible to delineate the different acute ischemic patterns. 3. More studies are necessary to associate these patterns with different types of stroke.

C-0852

Malignant vs benign cystic brain masses: Role of perfusion MR imaging in the differential diagnosis

B. Yagmurlu, H. Tuna, I. Erden; Ankara/TR

Purpose: To determine the role of MR perfusion imaging in the differential diagnosis of cystic brain masses with similar appearances on conventional series and therefore challenging the radiologist.

Materials and Method: Thirty-one patients with single or multiple cystic brain masses (total of 40 lesions) were enrolled in the study. Of these, 12 were high grade gliomas, 18 were metastases and 10 were pyogenic abscesses. All patients had conventional MR scans with additional perfusion studies performed by using contrast enhanced T2* dynamic susceptibility imaging technique preoperatively. rCBV (cerebral blood volume) maps were used for multiple sampling from the mural component of the masses. A ratio analysis was made by comparing the data obtained from the lesion wall (L) with the normal appearing white matter (WM) and the difference between the two groups (malignant vs benign) as well as three subgroups (glioma, metastasis and abscess) were evaluated. Pathological confirmation was made for each patient postoperatively.

Results: Ratio of L/WM was 5.89 ± 2.8 in malignant lesions where benign lesions indicated a value of 1.76 ± 0.8 ($p < 0.01$). A significant difference was found between metastatic lesions and abscesses as well ($p < 0.05$). Assessment among the malignant lesions themselves showed an overlap between glial tumors and metastatic lesions with values of 6.8 ± 2.0 and 5.45 ± 3.1 respectively ($p = 0.08$).

Conclusion: MR perfusion imaging seems very effective in determining whether a cystic brain mass is benign or malignant but a slight overlap between the tumors of glial origin and metastasis was found.

Scientific and Educational Exhibits

C-0853

Diffusion-weighted MR imaging in intracranial infections

A. Tosun, I. Serifoglu, A. Kartel, B. Cakir; Edirne/TR

Purpose: To describe the MR findings of intracranial infections and assess the value of diffusion-weighted imaging in the diagnosis.

Methods and Materials: A total of 20 patients, twelve having meningoencephalitis, five with brain abscesses, two with cerebral tuberculomas and a single case of PML, were evaluated at a 1.0-T unit. We analysed conventional images and compared them with diffusion-weighted images. In all patients, diffusion-weighted echo-planar sequence with parameters 6600/160/1 (TR/TE/AC), a high b value ($b = 1000 \text{ s/mm}^2$) were obtained and fifteen patients pre and post contrast turbo FLAIR images were examined. The final diagnosis was made on the basis of clinical features, laboratory findings including CSF studies, and histopathological examination.

Results: In all cases except the meningitis abnormally hyperintense lesions of varying extent and location were noted on T2-weighted and precontrast FLAIR images. Encephalitis lesions and tuberculomas are characterized by variable hyperintensity on diffusion-weighted images. Cerebral abscesses, subdural empyemas and cholesteatomas complicated with meningitis or cerebral abscess ($n = 4$) were markedly hyperintense on diffusion-weighted sequences. Patients with meningitis without parenchymal involvement did not exhibit any abnormality of diffusion. Diffusion-weighted imaging demonstrated the parenchymal lesions as areas of restricted proton diffusion more clearly than conventional imaging.

Conclusion: Diffusion-weighted imaging is assuming an increasingly important role in the evaluation of intracranial infections and has assumed an essential role in the detection of parenchymal lesions such as encephalitis, abscess and empyema with respect to restriction of movement of water molecules.

C-0854

MR imaging findings of the craniocervical junction in Morquio's disease

N. Danchaivijitr, D. Thompson, A. Vellodi, D.E. Saunders; London/UK

Purpose: To establish the clinical and radiological criteria for timing of surgical intervention in children with Morquio's disease.

Materials and Methods: A retrospective review of patient's notes and serial neuroimaging studies of the craniocervical junction of all children with Morquio's disease currently under the care of Great Ormond Street Hospital was carried out. Plain films (flexion and extension views), CT and MR imaging of the cervical spine were studied for atlanto-axial (AA) subluxation and instability, cord compression, odontoid peg abnormalities and compressive soft tissue mass.

Results: Fourteen children were identified (8 boys, mean age 3.4 years, range 1 to 6 years). All patients had an abnormal odontoid peg, narrow cervical spinal canal and foramen magnum. Eight patients had AA subluxation with associated cord compression in seven cases; six had a posterior fixation and two are awaiting surgery. Three patients had no evidence of AA subluxation but had neurological deficit; one from cord compression from retro-odontoid soft tissue mass. The other three had no AA subluxation or cord compression and were clinically stable. Eleven children were referred for surgery. Mean age at surgery was 6.2 years, range 4 to 9 years. Indications for surgery include cord compression with or without AA subluxation and progressive neurological deficit.

Conclusion: In Morquio's disease, cord compression at the cranio-cervical junction can occur in the absence of AA subluxation. A combination of multimodality serial imaging and clinical monitoring are crucial in order to optimize the timing for surgery.

C-0855

Cerebral proliferative angiopathy: A distinct subgroup of brain AVMs?

A single centre experience

P. Zabakis, S. Lamin, S. Jenkins, V. Papanastassiou, J. Bhattacharya; Glasgow/UK

Purpose: Brain arteriovenous malformations (BAVM) show wide phenotypic variation. Diffuse AVMs represent a distinct and uncommon subtype for which Lasjaunias has proposed the term cerebral proliferative angiopathy (PA). We present our experience of this rare form of AVM.

Methods and Materials: From our departmental database and AVM clinic, 8 patients with PA were identified. We reviewed case records and imaging studies. All patients had angiography and MR imaging. Age and mode of presentation are described as well as clinical course and angioarchitecture of the malformations.

Results: There were 4 males and 4 females with mean age of presentation of 25 years. None of the patients initially presented with haemorrhage. The radiological features included large size lesions, diffuse-pattern nidus with presence of brain

parenchyma within the abnormality, absence of large AV shunts, relatively slow flow, arterial occlusive disease pattern and sprouting angiogenesis. In contrast, typical BAVMs present later (mean 45 years), most commonly with haemorrhage, have no intervening brain parenchyma and show no evidence of sprouting angiogenesis. Most of the lesions were deemed incurable although some underwent partial treatment.

Conclusion: Proliferative angiopathy, having specific angioarchitectural characteristics and probably a different aetiology, represents a distinct subgroup of cerebral arteriovenous malformations and follows a different clinical course.

C-0856

Brodmann's cortical areas revealed by fMRI imaging

C.-V. Salvan, J.L. Ulmer, E.A. DeYoe, D.L. Daniels, R.W. Prost, L.P. Mark; Milwaukee, WI/US

Learning Objectives: Our objective is to reveal Brodmann's areas using fMRI imaging and to create a functional brain map, and consequently to obtain a new perspective in understanding the human brain and its pathological processes.

Background: Brodmann's cortical areas were established based on local differences in the arrangement of nerve cells (cytoarchitecture). From anatomical, physiological and pathological data it is known that they are related to different brain functions.

Imaging Findings: BOLD functional MR imaging data of sensori-motor, language, auditory and/or visual systems were acquired in normal subjects and eloquent cortices were mapped using a 1.5 T scanner (GE-EPI, TR/TE-2000/40 or 3000/50, flip angle 90, FOV 240, 64/64 matrix, 18 or 28 slices with 4 or 5 mm thickness depending from task) and a cross-correlation analysis with a $p < 0.01$. Using a variety of tasks (sensori-motor, language, visual, auditory) we mapped eloquent cortical areas and determined the relationship to Brodmann's areas, as well as the "talk" of these areas for specific brain functions. Implications for pathology are also discussed.

Conclusion: Functional MR imaging can reveal Brodmann's areas and help us understand cortical organization, as well as physiological and pathophysiological mechanisms of the brain.

C-0857

Toxoplasmosis encephalitis after bone marrow transplantation: CT and MR features

C. Mueller, T.G. Mang, P. Kalhs, M.M. Thurnher; Vienna/AT

Purpose: Toxoplasmosis encephalitis is a rare but severe complication in patients following bone marrow transplantation (BMT), requiring immediate therapy. The aim of this work is to describe the CT and MR features of toxoplasmosis encephalitis after BMT.

Material and Methods: We present two cases of pathologically confirmed cerebral toxoplasmosis after allogeneic BMT and compare them to cases from the literature. The imaging studies of our patients included unenhanced CT ($n = 4$), post contrast CT ($n = 2$) and unenhanced and post contrast MR imaging ($n = 3$) and were evaluated for lesion location and size, presence of edema and hemorrhage, enhancement and findings on diffusion-weighted imaging (DWI).

Results: In both patients CT and MR imaging revealed more than 20 lesions in the cerebellum and both hemispheres. In one patient all lesions were hyperdense on unenhanced CT and hyperintense on unenhanced T1-weighted MR images. On DWI the lesions showed low signal with a hyperintense rim, representing acute hemorrhage. In the second patient the lesions were hypodense on unenhanced CT and hyperintense on T2-weighted MR images. Most of the lesions showed high signal on DWI with reduced apparent diffusion coefficient (ADC), consistent with restricted diffusion. In both patients the lesions were non-enhancing and showed no significant edema.

Conclusion: Toxoplasmosis encephalitis in patients after BMT has unique features on CT and MR images, appearing as multiple intracerebral lesions with lack of enhancement. MR imaging findings differ from those described in AIDS patients.

C-0858

Detection of intracranial aneurysms with multislice CT: Comparison with digital subtraction angiography

F. Saccardy, J. Drouineau, C. Hardit, J.-C. Ferrié, J.-M. Charonnet, P. vandermark, J.-P. Tasu; Poitiers/FR

Purpose: To assess the diagnostic performance of multislice CT (MSCT) in the detection of intracranial aneurysms, by comparing the results to digital subtraction angiography (DSA) which is the standard method.

Scientific and Educational Exhibits

Methods and Materials: 28 patients with non traumatic acute subarachnoid hemorrhage or unruptured intracranial aneurysms were included and underwent both MSCT and DSA within 12 hours. CT angiography was performed on a sixteen slice CT using collimation of 16x0.75 mm, with a minimal longitudinal spatial resolution of 0.6 mm. A neuroradiologist blinded to DSA results reviewed CT data at a computer workstation, by using multiplanar volumetric reformats (MPVR), maximum intensity projections (MIP), and volume rendering technique (VRT).

Results: DSA detected 20 intracranial aneurysms in 18 patients. Sensitivity, specificity, positive predictive value and negative predictive value for CT angiography were respectively 100%, 83%, 90.9% and 100%. The smallest aneurysm detected with MSCT was 3 mm (3-18 mm, mean 9 mm). All the aneurysms were located on the anterior circulation, except one on cerebral posterior artery.

Conclusion: MSCT with sixteen detector-rows is equivalent to DSA for detection of intracranial aneurysms. MSCT seems be useful in the early diagnosis of the cause of a subarachnoid hemorrhage, replacing DSA.

C-0859

Radiation dosage in pituitary surgery: Comparison between conventional and computer assisted methods

E. Schulz, U.H. Melchert, A.F. Haude, U.R. Krause, B.M. Stoeckelhuber, S. Ulmer; Lübeck/DE

Purpose: Comparison of the radiation dosage to the patient's lens in pituitary surgery using intraoperative computer assisted navigation system (CAS) based on computed tomography (CT) and intraoperative conventional fluoroscopy.

Methods and Materials: In pituitary surgery, the patient's head is positioned between the C-arm array for intraoperative fluoroscopy to enable mapping of the location of the dissectors. This technique is very effective in terms of speed, costs, and availability; however it has the disadvantage of a 2-dimensional projection. Newer technologies such as CAS based on CT offer 3-dimensional information. Using the Alderson-Rando head phantom, thermoluminescence dosimeters (TLD) were placed on the temporal bone and on the phantom's lens on either side. Continuous fluoroscopy focused on the sella was performed. For CAS, the range of the CT image stack included the maxilla bone up to the frontal bone to cover the entire surgical approach and the floor of the sella.

Results: In CAS, each TLD was displayed on the two CT slices. Radiation dosage in CAS was approximately 6800 nC on each side. In conventional fluoroscopy, radiation dosage at the radiation entrance side was 400 nC and at the opposite side 50 nC measured for a 1-minute fluoroscopy time.

Conclusion: Radiation dosage was significantly increased in CAS; however, CAS supplies more detailed and multiplanar information. The decision which modality to use remains case specific (age and sex of the patient, cumulative dosage for the surgeon).

C-0860

Correlation of repeated brain CT-scan findings with intracranial pressure catheter (IPC) values in intensive care unit (ICU) patients: Preliminary report

M. Michalakou, E. Astrinaki, M. Kokkinaki, N. Mourkogiannis, E. Psarakis, M. Gargoulaki, R. Kourgeraki, G. Vrouhos, L. Triantafillou; Iraklion/GR

Purpose: To examine the extent that intracranial pressure (ICP) can be determined by head CT and whether there is a good correlation between ICP changes and evolution of findings in CT follow-up.

Materials and Method: We retrospectively reviewed 227 head CTs and the charts of 45 ICU head-trauma patients 18-57 years old, recording the GCS on admission, APACHE II scale and ICP values. Initial head CT was performed on admission, the second 24-48 h after, or 24 h postoperatively and the third 48-72 h thereafter. CT was also performed whenever there was a sudden change in ICP. CTs were evaluated by two radiologists, unaware of clinical data at the time of the examination, based on Marshall CT classification of head trauma.

Results: The reason for ICP monitoring included GCS less than 8, and/or abnormal CT findings. Initial CT classified 17 patients as DI II, 13 as DI III, 4 as DI IV, 9 as NEML and 2 as EML. In patients with stable ICP, 13% had CT changes. Change in CT follow-up associated in 83% with ICP alterations. In four patients uncorrelated ICP monitoring values to CT findings raised the suspicion of functional impairment thus a second ICP catheter was required; revealing monitor malfunction, showing higher pressure than actually applied.

Conclusion: ICP monitoring is a safe procedure for monitoring brain damage in ICU patients. Frequent head CTs without alteration of ICP do not add more information required for patient management. Limiting their use as a monitoring method for these patients is cost-effective, time preserving and carries a smaller transportation risk for ICU patients

C-0861

Aicardi syndrome: MR imaging and clinical findings

C. Hadjigeorgi, J. Nikas, G. Pitsoulakis, M. Theofanopoulou; Athens/GR

Purpose: Aicardi syndrome is an X-linked congenital disorder associated with early-onset infantile spasms, EEG abnormalities and severe developmental delay. It consists of multiple anomalies of the brain, eye and axial skeleton. We report the clinical and neuroradiological findings in three cases.

Materials and Method: 3 girls (3, 11 and 4 months old) with no family history of neurological disease, presented with psychomotor retardation and the first 2 with infantile spasms. The electroencephalogram was abnormal in all cases (burst-suppression patterns) while ophthalmological examination revealed chorioretinopathy in all children and microphthalmia in 1. The patients underwent MR imaging.

Results: MR imaging demonstrated corpus callosum agenesis in all three cases. In 2 this was associated with interhemispheric cysts and cortical dysplasia; polymicrogyria and subependymal heterotopia.

Conclusion: The diagnosis of Aicardi syndrome is based on characteristic clinical, electroencephalographic and imaging findings. MR is the imaging modality of choice, as it reveals agenesis of the corpus callosum, but can also demonstrate associated anomalies in the spectrum of cortical dysplasias.

C-0862

The role of perfusion CT in acute stroke

G. Katona; Budapest/HU

Purpose: To evaluate perfusion CT (PCT) capability in predicting reversibly damaged brain tissue and outline its advantages and limits.

Methods: The patients were examined using multirow CT (8 row multidetector LightSpeed Ultra, GE) for suspected acute cerebral ischaemia. Initially non-enhanced CT (NCCT) images were acquired. Then a dynamic perfusion series was acquired over a 50 s period using 50 ccm contrast bolus (300 mg/ml). For evaluation dedicated perfusion software was applied. On the color-coded parameter maps hypoperfused brain tissue was identified then its regional cerebral blood volume (rCBV), flow (rCBF) and mean transit time (MTT) values were calculated in part compared with abnormalities identified on diffusion weighted MR images performed additionally.

Results: All areas of ischaemia visible on NCCT were also identified by perfusion mapping. The areas revealed reduced CBF and prolonged MTT. Furthermore areas of hypoperfused brain tissue discovered by PCT analysis were identified which remained indiscernible on review of the NCCT series.

Conclusion: NCCT has a clearly defined role in the current management of acute stroke. The additional information supplied by PCT can be rapidly obtained without removing the patient from the scanner table. In spite of some limitations and the disadvantages compared to MR (PWI, DWI) and other perfusion techniques PCT may be useful in identifying reversibly ischaemic tissues because it can be performed quickly and safely on critically ill patients. Integration of PCT into the diagnostic workup of stroke is a promising approach which may reinforce the role of CT in the management of acute stroke.

C-0863

Brain MR spectroscopy in the evaluation of Wilson's disease: Correlation with clinical status and response to therapy

A. Sias, A. Balestrieri, L. Barberini, M. Puligheddu, M. Fraschini, A. Murru, L. Demelia, F. Marrosu, G. Mallarini; Cagliari/IT

Purpose: The aim of our study is to correlate the presence of signal intensity alterations in the brain of patients affected by Wilson's disease, through MR-spectroscopy.

Methods and Materials: We have examined 20 adult individuals (10 patients with a known diagnosis of Wilson's disease and 10 healthy volunteers) with single-voxel spectroscopy performed on a 1.5 T magnet. We have placed a total of four VOIs (each VOI measuring 20 mm³) bilaterally in the basal ganglia and white matter, with TR/TE 2000/136 ms. We have also performed the same study with a decrease of TE, to establish if there is any alteration in the amount of metabolites other than NAA.

Results: Our results show a correlation between the therapy and the results obtained, in patients undergoing treatment, while untreated patients show classical Wilson's disease brain alterations, but the limited preliminary data available does appear to overlap the same findings of other encephalopathies.

Conclusion: MR spectroscopy appears to be a highly sensitive diagnostic tool in a distinct neurological condition such as Wilson's disease. Further work will be needed, in a larger patient sample, to narrow the interpersonal variables that might be obtained through this approach, and to better characterize the MR spectroscopy signals obtained.

Scientific and Educational Exhibits

C-0864

Evaluation strategies of multiple sclerosis with conventional and advanced techniques

G. Luccichenti¹, E. Giugni¹, A. Paolillo¹, F. Cademartiri², A. Pichieccchio³, S. Bastianello³; ¹Rome/IT, ²Rotterdam/NL, ³Pavia/IT

Learning Objectives: 1)To illustrate the standard and the advanced (MT, relaxometry, DWI, DTI, MRS) imaging techniques for the assessment of multiple sclerosis 2)To describe the MR imaging patterns of multiple sclerosis and the diagnostic criteria. 3)To learn the strategies for the quantification of the disease progression of different MS phenotypes that can be carried out in clinical routine.

Background: Multiple Sclerosis (MS) is a demyelinating disease of the CNS of unknown origin, with a relapsing and remitting, primary or secondary progressive course. The diagnosis is made by combining the clinical examination, the laboratory tests of the CSF and the MR imaging findings. The quantification of disease progression and the assessment of therapy response can be performed through visual or automated segmentation with estimation of lesion volume or of advanced indicators (MTR, FA, metabolite)

Procedure Details: conventional and advanced MR imaging techniques are described. MR findings are shown and the differential diagnosis is illustrated using clinical cases. Diagnostic criteria are discussed. Quantitation techniques for follow-up are described using examples.

Conclusion: The knowledge of imaging findings, differential diagnosis, and the quantitation techniques of conventional and advanced MR imaging is useful to optimize the examination and to integrate the quantitation techniques into clinical routine.

C-0865

Central nervous system involvement in limited forms of Wegener's granulomatosis: CT and MR imaging findings

G. Zuccoli, B. Tumiati, F. Nicoli; Reggio Emilia/IT

Learning Objectives: To illustrate the CT and MR findings of CNS involvement in patients with limited forms of Wegener's granulomatosis (WG).

Background: WG is a systemic necrotising granulomatous vasculitis of unknown cause that typically involves the upper and lower respiratory tracts and the kidneys. Limited forms have been described in which some features of the disease may be absent. Nervous system involvement (peripheral neuropathy) is frequent, but it has been found that CNS involvement is rare occurring in less than 10% of patients. CNS lesions with or without contrast enhancement, thickening of the dura, infarcts, pituitary gland and infundibulum involvement may be found in patients affected by WG. The three patients subject of this educational exhibit belong to a larger group of 37 patients with WG. They are affected by limited forms of the disease. MR or CT examinations were performed to investigate suspected CNS involvement.

Imaging Findings: In one patient CT showed thickening of the right tentorial edge associated with right venous sinus thrombosis. In the second patient MR showed abnormal contrast enhancement of the nasal fossa extending upwards to the surface of the anterior cranial fossa with nodular thickening and mass effect of the dura mater. In the third patient both dura mater thickening and enhancement and pituitary axis involvement were found. In the second and third patient regression of the CNS involvement was demonstrated after therapy.

Conclusions: We demonstrated various patterns of CNS involvement in limited form of WG by using MR or CT imaging.

C-0866

Role of MR spectroscopy in patients with temporal lobe epilepsy (TLE)

A. Sias, A. Balestrieri, L. Barberini, M. Puligheddu, M. Fraschini, F. Marrosu, G. Mallarini; Cagliari/IT

Purpose: To characterize with MR spectroscopy the brain anomalies in patients suffering with temporal lobe epilepsy (TLE).

Materials and Methods: We examined 10 patients with a known diagnosis of TLE. The patients underwent MR spectroscopy and high density EEG. MR examinations were performed on a Philips 1.5 T magnet, using PRESS sequences with TR/TE = 2000/136 and 2000/31, 1024 samples, 128/256 averages. Epileptic foci were preliminarily localized through automatic analysis with a specific software (Curry).

Results: MR spectroscopy confirmed the lateralization data obtained through EEG in all patients. Concentrations of NAA, Cho, Cr, ml, obtained using short TR/TE sequences allowed evaluation of altered hippocampal function even in patients with a normal conventional MR examination.

Conclusion: MR spectroscopy, combined with high density EEG, is a promising

diagnostic tool which will be helpful to monitor disease development and response to therapy.

C-0867

Cerebral perfusion measurements using continuous arterial spin labeling (CASL): Transit time measurements of normal subjects

H. Kimura¹, H. Kabasawa², H. Uematsu¹, Y. Koshimoto¹, Y. Yonekura¹, H. Itoh¹; ¹Fukui/JP, ²Hino/JP

Purpose: Arterial perfusion imaging (ASL) provides a quantitative measurement of cerebral blood flow (CBF). The most concerning parameter for ASL technique for quantification is the transit time problem. The nature of low signal to noise ratio (SNR) of the method makes transit time measurements difficult and time consuming. The continuous ASL (CASL) on 3.0 T can produce the better SNR of perfusion signal due to both higher Lamor frequency and prolonged T1 times. We present the theoretical framework of two compartment model including transit time as well as CBF.

Method and Materials: CASL Perfusion imaging was implemented on 3.0 T MR system (GE, Signa 3 T, LX) using multi slice single shot echo planar imaging. For the calculation of arterial transit time, we also changed the post label wait time from 300 ms to 1800 ms. We applied the model with transit time and CBF to CASL perfusion data obtained from six normal subjects.

Results: CBF and arterial arrival time maps were successfully created using two-parameter fitting procedure. The averaged values of transit time ranged from 474 to 712 ms from lower to upper slice in gray matter, whereas those ranged from 732 to 1179 ms in white matter. The overall gray and white matter CBF value was 44.6 ± 10.6 and 13.0 ± 3.9 ml/min/100 g, respectively. The CBF values calculated using the model showed the trend of low values relative to those in previously reported in 1.5 T data.

Conclusion: CASL imaging using two-compartment model provides a means of assessment both of arterial transit time and CBF.

C-0868

Cerebral vascular malformations and developmental anomalies in patients with extracranial carotid stenosis in CTA

K. Gruszcynska¹, J. Baron¹, Z. Zieliński²; ¹Katowice/PL, ²Tychy/PL

Learning Objectives: Presentation of cerebral vascular malformations, Circle of Willis normal variants and developmental anomalies visible in CTA, which can alter cerebral blood flow in patients with extracranial arterial stenosis.

Background: Although Circle of Willis anatomical variants usually have no clinical significance, they can become the cerebral ischemic infarction risk factor in patients undergoing carotid endarterectomy or stent placement. Cerebral vascular malformations or aneurysms visible on CTA in these patients may require earlier treatment than stenosis itself.

Procedure Details: Cerebral artery variants, developmental anomalies and vascular malformations which were diagnosed on CTA, (Twin, Marconi CT unit), in 70 patients with extracranial carotid stenosis will be presented. MIP, MPR and 3D reconstructions will depict detailed Circle of Willis anatomy highlighting those anomalies which can alter cerebral blood flow during the surgical or interventional procedure. CTA results were compared with a control group; 34 patients without extracranial stenosis. Posterior or anterior cerebral artery hypoplasia or aplasia were seen in 37% examined and 35% of control patients. In 12 cases they coexisted with intracranial stenosis. In 4% of examined patients cerebral aneurysms were found, multiple in two cases. Arterial dolichoectasy was seen in 4 patients and DVA in 1.

Conclusion: Cerebral artery developmental anomalies can be found in equal frequency in patients with and without extracranial carotid stenosis. The knowledge of Circle of Willis possible vascular variants and anomalies can help to select patients with increased risk of cerebral blood flow alteration during endarterectomy or stent placement.

C-0869

Fusion of MR imaging and SPECT images as a method of planning spectroscopy of recurrent brain tumors

P. Grzelak, M. Gorska-Chrzastek, K. Tybor, W. Gajewicz, J. Kusmirek, B. Goraj, L. Stefanczyk; Lodz/PL

Purpose: The essential modalities for morphological imaging of the brain are magnetic resonance imaging (MRI) and (for metabolic imaging) single photon emission tomography (SPECT). By using image fusion of different modalities, the location of areas exhibiting functional changes can be more easily identified. This study compares the results of iodine-131-alpha-methyl-tyrosine SPECT (IMT-

Scientific and Educational Exhibits

SPECT) with MRI in recurrent brain tumor detection. We used fusion images as the method of planning 1H-MRS and verifying the metabolic content of the regions.

Materials and Method: We investigated 27 patients post neurosurgical treatment, 25 of them were also following radiation therapy. IMT-SPECT and MRI were performed during the same week. Iodine-131-alfa-methyl-tyrozin (131-IMT) is a marker of brain tumors. Fusion of the images was done in a three-dimensional technique using a PC work-station; the technique was based on a statistical analysis of three-dimensional distribution of the voxels, using maximization of the statistical resemblance (mutual information). Regions of the highest accumulation of the 131-IMT were found by using subtraction method. In the result these areas were then subject to 1H-MRS (SVS or CSI).

Results: In all tumors the area of accumulation of 131-IMT was smaller when compared with the Gd-enhanced MR images. The concentration of IMT within brain tumors was heterogenous and the delineation of the highest metabolic area was possible. This allowed planning of H1-MRS. In 25 patients a good quality of 1H-MRS spectra were obtained.

Conclusion: The fusion images optimize selection of a site for spectroscopy investigation in recurrent tumors.

C-0870

Can unsaturated fatty acid emulsion technique be used as a model for research on BBB disruption?

H.J. Kim, Y.W. Kim; Pusan/KR

Purpose: The authors investigated whether fatty acid emulsion affects the BBB, whether disrupted BBB is reversible and whether this technique may be a model for BBB research.

Materials and Methods: The fat emulsion was made with 0.1 ml of oleic acid or linoleic acid and 20 ml of saline. The carotid artery was infused with oleic acid emulsion in 14 cats (Group 1) and with linoleic acid emulsion in 12 cats (Group 2). Gd-enhanced T1-weighted (Gd-T1WI), diffusion-weighted (DWI) and apparent diffusion coefficient (ADC) map MR imaging was obtained at one hour and one day after infusion. Qualitative analysis was performed. Quantitative analysis of the signal intensity ratio (SIRs) of the lesion to the contralateral hemisphere was performed on Gd-T1WIs. SIRs were analyzed statistically with t-test. The brain tissue was removed for light and electron microscopic examination.

Results: The lesions appeared as contrast enhancement on Gd-T1WIs, as isointensity or mild hyperintensity on DWIs and as isointensity on the ADC maps at 1 hour in both groups. On day 1, contrast enhancement was much decreased or absent in both groups and ADC maps showed isointensity. SIRs on Gd-T1WIs were significantly higher in Group 1 than in Group 2 at 1 hour ($p < .05$). SIRs were nearly 1.0 on day 1 in both groups. Histological findings showed minimal changes.

Conclusion: Infusion of unsaturated fatty acid emulsion revealed vasogenic edema of the brain and reversible changes. This unsaturated fatty acid emulsion model may be used as a model for research on BBB disruption.

C-0871

The assessment of early neurorehabilitation effectiveness with MR imaging

R.M. Umarova, M.V. Krotenkova, M.M. Tanashyan, L.A. Chernikova, R. Konovalov; Moscow/RU

Purpose: To evaluate the influence of early repetitive neuromuscular stimulation (NS) with MR imaging on brain infarct evolution in stroke patients.

Methods: Twenty two patients were studied with serial magnetic resonance imaging (T2WI, T1WI, DWI and PWI study) within the first 48 hours of ischemic stroke onset and again at periods of 5, 21 days and 3 months. The lesion expansion between acute and outcome studies was assessed. 15 patients (basic group) were started with NS of the paretic upper limb immediately after MR imaging examination, NS was continued during 3 weeks.

Results: Subjects from the basic group had better recovery of motor function versus the control group ($p < 0.05$). Two MR imaging patterns among all patients were obtained. Acute PWI>DWI lesion volume mismatch predicted brain lesion expansion, and was seen in ten patients, six of them were from the basic group. At the same time the expansion volume in the basic group didn't exceed the same volume of the control group and the acute PWI lesion. In DWI>PWI group there were not diffusion lesion expansion in basic group. So in spite of early beginning of NS in basic group the infarct evolution didn't worse.

Conclusion: We didn't find any deterioration of the diffusion and perfusion lesions in basic group with NS. Our study indicates that MR imaging data may be useful in evaluating the effectiveness and safety of early rehabilitation therapy.

C-0872

Quantitative assessment of brain perfusion by MR imaging in patients with arterial hypertension

D. Ustuzhanin, M. Kozhuhova, V. Sinitsyn, T. Pustovitova, O. Stukalova, I. Chazova, S. Ternovoy; Moscow/RU

Purpose: To evaluate quantitative values of brain perfusion in patients with arterial hypertension.

Materials and Method: Thirty patients (mean age 55 years) with arterial hypertension and one or more cerebrovascular events in anamnesis were included in the study. The control group consisted of fifteen healthy volunteers (mean age 42 years). For each person time-intensity curves were calculated. Relative cerebral blood flow (CBF), relative cerebral blood volume (CBV), time to peak (TTP), mean transit time (MTT) parametric maps were calculated for 4 slice levels in the brain (convex, central part of lateral ventricles, basal ganglia, cerebellum). CBF, CBV, MTT, TTP values were determined in two regions of interest (left and right hemispheres) for each slice level.

Results: CBV and CBF values did not differ significantly between the two groups. MTT was significantly shorter in healthy controls than in patients with arterial hypertension (5.2 ± 1.2 s vs. 6.6 ± 1.6 s, $p < 0.05$) only in one slice level (convex). TTP was significantly shorter in healthy controls in three slice levels: 6.2 ± 1.7 s vs. 9.8 ± 2.9 s, $p < 0.01$ (convex), 6.7 ± 1.7 s vs. 9.0 ± 2.6 s, $p < 0.04$ (basal ganglia), 7.3 ± 1.5 s vs. 9.6 ± 2.4 s, $p < 0.03$ (cerebellum).

Conclusions: Our study suggests that whereas CBF and CBV values did not differ significantly one can find some differences in TTP and MTT between normals and hypertensives. So MTT and TTP parameters can be useful for determining a group of patients at high risk.

C-0873

Comparison of detectability of endocranial lesions in multiple sclerosis at 1.0 and 3.0 Tesla.

T. Stosic-Oncincal, V. Peric, S. Lavrnici, M. Gavrilov; Belgrade/YU

Purpose: To estimate the relative sensitivity of MR examination for brain lesions in multiple sclerosis at 1.0 Tesla (T) and 3.0 T using identical acquisition conditions.

Methods and Materials: 19 patients with multiple sclerosis were examined both at 1.0 T (Siemens Impact Expert) and 3.0 T (Philips Intera) using T1-weighted spin echo (T1W-SE) with and without gadolinium contrast injections, T2W SE and fluid attenuated inversion recovery (FLAIR) imaging. Images were examined independently by three experienced neuroradiologists using focal lesion counting.

Results: 3.0 T scans compared with 1.0 T scans demonstrate a 26.5% increase in the number of detected contrast enhanced lesions and an 11.3% increase in the number of detected lesions on FLAIR MR tomograms.

Conclusion: High-field 3.0 T MR imaging demonstrates better sensitivity in the detection of focal brain lesions in multiple sclerosis. This improvement is more apparent in contrast enhanced lesion detection and less noticeable in FLAIR detected lesions.

C-0874

Benefits of early endovascular treatment of ruptured intracranial aneurysms: Clinical outcome and vasospasm incidence

R. Diaz Aguilera, J.M. Martos Becerra, J.J. Espejo Herrero, D. Bautista Rodriguez, F. Bravo Rodriguez, F. Delgado Acosta, A. Cano Sanchez, G. Perez Ortega; Cordoba/ES

Purpose: Endovascular embolization of ruptured intracranial aneurysms is a treatment option which is increasingly being used. The aim of this prospective study was to compare the incidence of vasospasm and the clinical outcome of patients who were treated with coils early after the hemorrhage (SAH) (< 48 hours) with those treated later.

Methods and Materials: We reviewed 49 patients (36 women and 13 men) who underwent endovascular treatment for aneurysmal SAH between June 2001 and June 2004 in our institution. 19 patients were treated within 48 hours of ictus. We collected epidemiological data, angiographic findings, CT findings (Fisher scale) and clinical outcome (Hunt and Hess and Rankin scales)

Results: Mean age was 57.2 years (range 26-81). 22 patients had a Hunt and Hess grade I-II subarachnoid hemorrhage. According to the Fisher classification, 14 patients were grade I-II and 20 were grade III-IV. 44 patients had aneurysms of the anterior circulation and 5 were on the posterior circulation. One (5.26%) of the nineteen patients treated within 48 hours after SAH showed vasospasm and in those treated later, twelve (40%) suffered from vasospasm.

Conclusion: Early endovascular treatment is a feasible and safe procedure in

Scientific and Educational Exhibits

the management of SAH after ruptured intracranial aneurysm. There was less incidence of vasospasm within the first 48 hours.

C-0875

New brain lesions at diffusion-weighted MR after carotid angioplasty and stent placement

J. Gil, J. Guijarro, J. Palmero, A. Vera, D. Dualde, R. Dosdá; Valencia/ES

Purpose: To evaluate with magnetic resonance imaging (MR) the incidence and clinical significance of cerebral ischemic lesions after carotid angioplasty and stent placement (CAS).

Materials and Method: Eighteen consecutive CAS procedures were performed in seventeen patients (for high-grade carotid stenosis). The patients underwent neurological examination before and 1 day and 3 months after CAS. Diffusion-weighted MR imaging (DW1) of the brain was performed before and after stent implantation. Any hyperintense signal was interpreted as a postprocedure ischemic lesion.

Results: Thirteen patients (72.2%) had unchanged postprocedure brain DW1. New ipsilateral lesions were found in five cases (27.7%) and in one, lesions were also found in the contralateral side (5.5%). In four patients, the lesions were clinically silent and one patient had a minor stroke.

Conclusion: CAS is associated with new areas of cerebral ischemia. The majority of new lesions are clinically silent.

C-0876

Value of the apparent diffusion coefficient in the differential diagnosis of brain glial tumors

A. Martínez de Aragón, C. Pérez López, J. Echeveste, A. Bravo, B. Rodríguez-Vigil, B. Marín; Madrid/ES

Learning Objectives: To show the role of diffusion weighted magnetic resonance imaging added to conventional MR imaging sequences in the diagnosis of the type and grade of malignancy of brain glial tumours.

Background: High sensitivity and specificity of diffusion weighted magnetic resonance imaging in the diagnosis of acute cerebral infarction and abscesses has been reported. This sequence also provides information about certain tumours like epidermoid cysts; however its usefulness in other brain tumours has still to be determined.

Imaging Findings: MR imaging and diffusion studies performed in 38 patients with brain gliomas, confirmed at surgery, were retrospectively reviewed. ADC value and diffusion signal intensity from different areas of the lesion were measured and compared. Presence of necrosis, macroscopic peritumoral areas, and areas that enhanced with paramagnetic contrast were specifically evaluated. Every value was compared to the diffusion weighted signal intensity value of the contralateral normal specific tissue.

Conclusion: Areas with high cellularity, necrotic areas, and bleeding areas have signal diffusion intensity and ADC values different from that of the normal brain. Together with conventional MR imaging, these values can guide in the diagnosis of the type and grade of glial brain tumours. Diffusion magnetic resonance imaging, due to its short duration, should be performed, together with more conventional sequences, on patients with brain tumours because it provides more thorough information regarding histology and grade of malignancy of the primary tumours. This sequence is especially useful when perfusion and spectroscopy is not available and in non-cooperative patients.

C-0877

MRS and DTI of two siblings with Hallervorden-Spatz syndrome

C. Lee, W.-H. Lee, C.-M. Ling, P.-S. Yen, P.-N. Chong, S.-K. Lee; Hualien/TW

Learning Objectives: To demonstrate brain lesions and show how state of art MR imaging techniques help clinical assessment in PANK2 disease.

Background: Hallervorden-Spatz syndrome is an autosomal recessive disorder characterized by dystonia, parkinsonism, and iron accumulation in the brain. Many patients with this disease have mutations in the gene encoding pantothenate kinase 2 (*PANK2*); they are said to have pantothenate kinase-associated neurodegeneration. Typically, T₂-weighted magnetic resonance imaging (MRI) of the brain shows a specific pattern of hyperintensity within the hypointense medial globus pallidus (tiger-eye sign). Two Chinese siblings (female aged 5 and her brother aged 9) were found with typical symptoms and signs of PANK2 syndrome. We present their detailed MRI studies including T₂-weighted MRI, FLAIR, multi-voxel MRS and diffusion tensor imaging (DTI).

Imaging Findings: T₂WI showed decreased signals in bilateral basal ganglia predominantly in the hypointense medial globus pallidus. The Tiger-eye sign was found in the sister only. Multiple voxel MRS demonstrated neuron loss not only in

the basal ganglia but also in the thalamus, especially in NAA/Choline ratio map. In particular, NAA/Choline ratio demonstrated more neuron loss in the sister that was compatible with clinical presentation. Widespread decrease of white matter fractional anisotropy (FA) were shown in the DTI images; compatible with generalized axon swelling in pathology reported in the literature.

Conclusion: MRS and DTI images may be useful in the evaluation of PANK2 disease neuron degeneration.

C-0878

The diagnostic utility of perfusion-weighted MR imaging, diffusion-weighted MR imaging and MR spectroscopy in mesial temporal sclerosis

S. Cakirer¹, B. Yagmurlu², B. Koklu¹, Y. Karagoz¹, N. Kahraman¹; ¹Istanbul/TR, ²Ankara/TR

Purpose: To determine the lateralizing value of perfusion-weighted MR (PWI), diffusion-weighted MR (DWI) and MR spectroscopy (MRS) in cases of mesial temporal sclerosis (MTS), and to detect correlation between conventional MR imaging and PWI, DWI, and MRS.

Methods and Materials: We evaluated ten patients with MTS in the interictal period, and ten normal control participants on a 1.5 T MR scanner. The protocol included coronal FLAIR, SS EPI T₂*-weighted PWI with mesial temporal rCBV measurements, DWI with coronal trace ADC map generation, and single voxel MRS for hippocampal gyri in both patients and controls. Regions of interests (ROI) were drawn on each hippocampal gyrus for calculation of rCBV, mean ADC values, and MRS. Absolute ADC asymmetry indices, perfusion asymmetry indices, average NAA/(Cr+Cho) ratio asymmetry indices were calculated.

Results: rCBV values, mean ADC values, and average NAA/(Cr+Cho) ratio of hippocampal gyri were more asymmetric in patients compared to normal controls ($p < 0.001$ according to Wilcoxon). rCBV values for MTS sides in patients were significantly lower than normal sides ($p < 0.001$). Mean ADC values for MTS sides in patients were significantly greater than normal sides ($p < 0.001$). Average NAA/(Cr+Cho) ratio for MTS sides in patients were significantly lower than normal sides ($p < 0.001$). rCBV values, mean ADC values, and NAA/(Cr+Cho) ratio for both sides of normal controls were not significantly different. Lateralization using absolute ADC asymmetry indices significantly correlated with lateralization based on rCBV asymmetry indices, and NAA/(Cr+Cho) ratio asymmetry indices (according to Spearman).

Conclusion: PWI, DWI, and single voxel MRS may detect interictal asymmetries, and concordant lateralization of the abnormal hippocampal gyri in patients with MTS.

C-0879

A pictorial review of the radiological imaging findings in III, IV and VI cranial nerve palsies using CT and MR imaging techniques

M. Khanna, R.L. Preston, K. Tonge; London/UK

Learning Objectives: 1. Learn the anatomy of the intracranial course of the III, IV and VI cranial nerves. 2. Learn to interpret the radiological appearances and findings of pathology along the course of the III, IV and VI cranial nerves. 3. Understand the use of different CT and MR imaging techniques to highlight abnormal pathology

Background and Imaging Findings: The III, IV and VI cranial nerves arise in the dorsal midbrain and pons, traversing anteriorly through the posterior and middle cranial fossae to exit at the superior orbital fissure. Their long intracranial course renders them susceptible to a wide range of focal and diffuse pathologies. They can be subtle and to maximise imaging potential requires correlation with neurological findings to localise the lesion. CT and MR imaging techniques can be tailored to the precise anatomical location with additional contrast enhancement or specialised sequences as required.

Conclusion: This exhibit will illustrate, using the most suitable CT and MR imaging techniques, the radiological appearances of pathology affecting the III, IV and VI cranial nerves in adult and paediatric images. They will be divided into mid-brain, subarachnoid space, cavernous sinus and superior orbital fissure locations. Examples will include vascular lesions, primary brain tumours, infection and multisystem disorders.

C-0880

Brain diffusivity in patients with neuropsychiatric systemic lupus erythematosus and acute neurological symptoms

M. Hughes, B. Foerster, R.C. Welsh, H. Rahbar, P.C. Sundgren; Ann Arbor, MI/US

Purpose: To investigate whether diffusion-weighted imaging (DWI) using apparent diffusion coefficient (ADC) histograms can depict statistically significant cer-

Scientific and Educational Exhibits

bral abnormalities in patients with acute symptoms of neuropsychiatric systemic lupus erythematosus (NPSLE) versus normal controls.

Methods and Materials: Conventional MR imaging of the brain and diffusion-weighted echo-planar imaging (DWI) was performed on a 1.5 T scanner (GE Medical Systems) in 9 female NPSLE patients, aged 35-59 years, mean 44.4 years, and in age matched healthy controls. Whole brain ADC histograms were constructed on each patient. The histogram results of each group were compared. P-value < 0.05 was set for statistical significance using the Students t-test.

Results: Eight of the nine patients (89%) had abnormal findings on MR imaging. The most common findings were focal areas of increased signal on T2-weighted and FLAIR images in the white matter without associated pathological contrast enhancement. Other abnormal findings included infarcts, brain atrophy and meningeal enhancement. The NPSLE patients had a mean ADC value of 1041×10^{-6} mm²/sec and the control had a mean ADC value of 946×10^{-6} mm²/sec. The mean ADC values were significantly higher ($p < 0.0002$) in the NPSLE patients compared to the controls.

Conclusion: ADC histogram analysis demonstrated increased general diffusivity in the brain in NPSLE patients with acute symptoms compared to healthy normal controls. These results suggest a loss of tissue integrity in the brain parenchyma of NPSLE patients occurs which facilitates motility of free-water protons. Larger studies are in progress to further evaluate this method and determine potential use in monitoring disease progression and treatment efficacy.

Neuro

Spine

C-0881

Diffusion tensor fraction anisotropy in the cervical spinal cord:

Reproducibility in 10 normal subjects

N. Abdala, R.D. Nascimento, H. Carrete Jr., R.G. Nogueira, S.M. Goldman, J. Szeinfeld; São Paulo/BR

Purpose: To quantify anisotropic water diffusion through variables like Apparent Diffusion Coefficient (ADC) and Fraction Anisotropy (FA) using Diffusion Tensor Imaging (DTI), in the cervical spinal cord of normal subjects.

Methods and Materials: Ten healthy volunteers were recruited (6M, 4F), mean age 29.5 years. DTI images of the cervical cord were acquired in a 1.5 T magnet. The imaging protocol consisted of axial Multi-Shot Echo Planar sequences, gradients sensitized to diffusion in 6 directions, TR 3500 ms, TE 70 ms, $b = 0$ and 800 s/mm², 20 excitations. Slabs of twenty-six 3 mm interpolated slices were obtained. Three ROI measurements were performed in three cord segments, with calculation of ADC/FA mean values.

Results: Overall means and SD for ADC and FA values of cervical cord were 1.549×10^{-3} mm²/s $\pm 0.596 \times 10^{-3}$ mm²/s, and 0.517 ± 0.207 , respectively.

Conclusion: The FA values of the cervical spinal cord obtained in this initial experience are within the standard deviations of a previous report. Conversely, ADC values are in discordance with other authors' experience, possibly due to the method employed. Factors to explain the variability of ADC/FA values observed throughout the cervical cord remain to be established. The validation of normal ADC/FA value limits becomes mandatory as the experience employing ADC and DTI in the spinal cord is mounting up. Standardization of imaging protocols, post-processing software and ROI measurement, could potentially lead to statistically significant thresholds which may correlate with the maintenance or loss of normal anisotropic water diffusion.

C-0882

The craniocervical junction (CVJ): Anatomy, bony variants and acquired pathology

A. Bermejo, L. Herraiz, M. Martin, J. Benito, M. Miralles, A. Ramos; Madrid/ES

Learning Objectives: To summarize the normal embryological development and anatomy of the CVJ and the craniometric measurements used in the radiological assessment of the region. To illustrate the spectrum of bony anomalies of the occipital bone, atlas and axis. To describe traumatic lesions of the CVJ, with emphasis on the mechanisms of injury and appropriate imaging techniques that lead to proper management.

Background: Congenital, developmental and acquired anomalies of the CVJ may result in atlantoaxial instability or may affect the vertebral vascular system. Evaluation of CVJ disorders can be challenging, and management depends on the correct radiological diagnosis. We retrospectively reviewed CT studies of 651 patients with upper cervical injury admitted to our Hospital between 2001 and 2003.

Imaging Findings: Imaging procedures included lateral radiographs, flexion and extension films, CT with multiplanar reformatting and MR. Anomalies were divided into congenital and acquired, including trauma. Occiput anomalies include basilar invagination, condylar tertius, basiocciput hypoplasia and atlanto-occipital assimilation. Atlas anomalies include aplasia, hypoplasia, and clefts. The axis may present fusion abnormalities or dysplasias of the odontoid process. Many acquired processes may also affect the CVJ. Fractures were classified attending to each affected segment.

Conclusion: The CVJ is a common site for anatomic variants and acquired pathology. Knowledge of the normal anatomy as well as the spectrum of bony variants, acquired anomalies and fractures of this region is vital for the emergency radiologist for correct image interpretation and ultimate management.

C-0883

CE-MRA in the diagnosis of spinal DAVF

P. Zabakis, I. McDonald, D. Hadley, C. Santosh; Glasgow/UK

Purpose: Accurate pre-treatment localization of the level of a spinal dural arteriovenous fistula (SDAVF) is very important. Pre-operative selective DSA is considered to be the gold standard in pre-treatment mapping of these lesions. However it is invasive, time consuming and sometimes non-diagnostic. The purpose of this retrospective analysis was to evaluate the use of CE-MRA in DAVFs with spinal drainage.

Scientific and Educational Exhibits

Methods and Materials: 9 patients (7M, 2F) (age range 44-77 years old, mean 67) with suspected spinal vascular lesions were evaluated with MR Angiography. In 7 patients a SDAVF was present and 2 had an intracranial dural AV fistula with spinal drainage. 3D CE-MRA studies were performed with a 1.5 T Signa NV/I system (GE medical systems) using a phased array spine coil. Seven patients were imaged using a first pass elliptic centric ordered technique. In two cases an ECTRICKS (Elliptic Centric Time Resolved Imaging of Contrast Kinetics) technique was used. Selective spinal angiography was also performed in all patients. **Results:** MRA showed abnormal draining vessels in all cases and accurately identified the level of the fistula in 5/9 cases. In another case it proved to be a valuable tool in detecting the fistula level. MRA failed to identify both the feeding arteries and the fistulous connection of the intracranial fistulae with spinal drainage. **Conclusion:** CE MRA proved to be an effective, quick, non-invasive and ionizing radiation-free technique for the diagnosis of spinal dural AVFs. The recent CE-MRA technique (EC-TRICKS) which provide dynamic information was successful in both cases in which it was used

C-0884

MR imaging and US value in myelomeningocele experimental surgical sheep model

D. Elias, G. Izbizky, S. Medina Portillo, M. Pietrani, P. Farias, J. San Roman, F. Eleta; Buenos Aires/AR

Purpose: To evaluate the role of US and MR imaging in the assessment of an experimental animal model of myelomeningocele (MM).

Materials and Method: A surgical MM-like lesion was created in 32 fetal lambs. In 21, the defect was repaired before delivery (cases); 11 fetuses were used as controls. All procedures were monitored during surgery with US. The lambs were clinically evaluated after delivery. MR imaging studies were performed in 8 cases. Complete Central Nervous System (CNS) scans were performed in order to find associated anomalies. Fourteen (14) lambs had histological evaluation.

Results: Intrauterine MR imaging was performed in 5 cases. MM like defects and kyphosis were clearly characterized by this method. Associated CNS malformations were ruled out (including Arnold Chiari). We also performed MR imaging in three new born lambs in which intrauterine surgery to correct defects had been done. In this group one tethered cord was delineated. All 11 fetal sheep with unrepairs MM developed motor sequelae. Eight (8) lambs with defects corrected before birth walked independently without any difficulty. During corrective surgery, the lesions resemble MM on visual macroscopical inspection. In those animals without correction, histological sections of spinal cord showed severe damage.

Conclusions: The use of US and MR imaging is adequate for monitoring this experimental model. Although ultrasound is the method of choice for prenatal diagnosis and follow-up of myelomeningocele, MR imaging is an useful technique for accurate diagnosis of associated anomalies (brain migration disorders, tethered cord)

C-0885

Evaluation of the effects of sildenafil citrate (Viagra) on vertebral artery blood flow of patients with vertebro-basilar insufficiency

Z. Bozgeyik, E. Kocakoc, S. Berilgen, H. Ozdemir, A. Tekatas, E. Ogur; Elazig/TR

Purpose: Sildenafil is used widely for the treatment of erectile dysfunction. This substance induces relaxation of smooth muscle in the corpus cavernosum. Although it is widely used, there are limited number of studies about the effects of sildenafil on major vascular structures. The effects of sildenafil citrate on vertebral artery blood flow are also unknown. The aim of this study was to investigate effects of sildenafil citrate on vertebral artery blood flow of patients with vertebro-basilar insufficiency (VBI) using color duplex sonography (CDS)

Materials and Methods: Twenty-one patients with VBI (aged 31-76; mean 61.0 ± 10.5) were included into this study. Peak systolic velocity, end diastolic velocity, resistance index (RI), pulsatility index (PI), diameter, area, and flow volume of vertebral arteries were measured before the administration of sildenafil citrate; 45, and 75 minutes after the administration of sildenafil using CDS.

Results: The significantly changed parameters were as follows; significant increase in post drug values of bilateral vertebral artery diameters, areas, and flow volumes compared to before drug administration values. There were no statistically significant changes of other measured parameters.

Conclusion: Sildenafil citrate causes an increase in vertebral artery diameter and flow volume. This effect may reduce symptoms of VBI in patients and sildenafil may be used for the treatment of these patients in the future. This theory needs to be investigated further with detailed, multi-center studies on the long-term effects of chronic sildenafil administration on different VBI patient groups.

Pediatric

C-0886

Imaging of pediatric liver transplantation

M. Parrón, T. Berrocal, C. Prieto, P. Cortés, I. Pastor, R.R. Lemos; Madrid/ES

Learning Objectives: To illustrate the different modalities of liver transplantation performed in children. To provide an imaging overview of early and late complications following pediatric liver transplantation. To evaluate the efficacy of conventional and Doppler US, CT, MR imaging and interventional procedures in the diagnosis and management of these complications.

Background: 349 liver transplants have been performed in 277 children in our institution (204 cadaveric whole-liver transplants, 112 cadaveric reduced-size grafts, 26 reduced-size grafts from living-related donors, 3 hepato-renal and 4 hepato-intestinal transplants). The imaging studies of those with any complications were reviewed. B-mode and Doppler ultrasound were performed in all the cases, while CT, MR imaging, or vascular studies were performed depending on the complication and whenever US and Doppler images were not conclusive.

Imaging Findings: Specific topics addressed include vascular complications (stenosis and thrombosis of the hepatic artery, portal vein, inferior vena cava and hepatic veins), biliary complications (strictures, stenoses, perforation and stones), abdominal fluid collections (hematomas, bilomas, ascites), infections, rejection, and lymphoproliferative disorders. The different modalities of liver transplantation performed in children will be shown. The key findings at each imaging modality will be discussed and compared with the surgical findings or underlying pathological features when available. Pitfalls, diagnostic difficulties and differential diagnosis will be emphasized.

Conclusion: Evaluation of patients with liver transplant frequently requires multiple imaging modalities for diagnosis and planning treatment. Because many of these disorders have characteristic imaging appearances, this exhibit will help the practising radiologist to better understand and recognise complications involving the transplanted liver.

C-0887

Evaluation of [^{18}F]FDG-PET and CT/MR imaging for monitoring therapy response in children with Hodgkin's disease

I. Sorge, A. Krausse, R. Kluge, C. Mauz-Körholz, D. Körholtz, W. Hirsch; Leipzig/DE

Purpose: To compare CT/MR imaging with PET with respect to its potential in monitoring the effect of chemotherapy in children with Hodgkin's disease (HD). Adults with HD who undergo adequate therapy have a low risk of relapse even if they still have residual masses on cross sectional imaging, i.e. the positive predictive value (PPV) is only 20%. For [^{18}F] FDG-PET the PPV is known to be substantially higher (about 80%).

Methods and Materials: Within the scope of the international GPOH-HD Pilot 2002 study in 43 HD-children CT/MR imaging was paralleled by PET imaging. In consensus conferences CT/MR imaging as well as PET findings were documented in 21 regions for each patient. Complete remission (CR) was defined as residual masses < 2 ml and > 90% regression of all initially involved lesions in follow-up CT/MR imaging and as normal FDG uptake in all regions in follow-up PET.

Results: In initial imaging 222 and 247 positive lesions were detected by CT/MR imaging and PET respectively. In follow-up imaging 81 regions were found to be still positive in CT/MR imaging but only 30 in PET. Out of 19 children with low stages ($\leq \text{IIa}$) only 2 were classified as CR in CT/MR imaging but 10 by PET.

Conclusion: Cross sectional imaging does not seem to be sufficient in recognising complete remission of Hodgkin's disease. A systematic use of PET for therapy monitoring should be warranted also in childhood HD. This might contribute to reducing over-treatment and drug side effect without a loss of treatment efficacy.

C-0888

MR imaging of the brain in Wilson's disease of childhood: Findings before and after treatment

J.-E. Cheon, I.-O. Kim, W. Kim, K. Yeon; Seoul/KR

Learning Objectives: To illustrate the MR findings of the brain in Wilson's disease in children at initial stage and follow-up after treatment, and to correlate MR manifestations with clinical response to treatment.

Background: Wilson's disease is an uncommon, autosomal recessive disorder involving copper metabolism that results in abnormal accumulation of copper in various tissues, mostly in the liver and the brain. Copper chelating agents are believed to improve the neurological symptoms. In this study we will illustrate the changes of MR findings before and after treatment of Wilson's disease.

Scientific and Educational Exhibits

Procedure Details: The study included 50 children with Wilson's disease (M:F = 26:24, mean age, 10.2 years). All patients had been treated with copper chelating agents since the diagnosis of Wilson's disease had been established. T1WI and T2WI MR images were obtained. Fifteen patients underwent a total of 20 follow-up MR scans during follow-up period (12-63 months). MR findings were divided into three groups; group I revealed normal MR findings, group II had increased signal in the basal ganglia and the midbrain on T1WI, and group III had increased signal in the globus pallidus, basal ganglia, thalamus, midbrain and pons on T2WI. High signal intensity areas on T2WI reflected cerebral involvement of Wilson's disease, and showed good correlation with neurological symptoms and clinical response after treatment.

Conclusion: MR imaging findings of Wilson's disease could be categorized into distinct groups. MR imaging could be helpful in assessing the clinical response to treatment in patients with Wilson's disease.

C-0889

withdrawn by authors

C-0890

Imaging of hip disorders in pediatric patients: A pictorial review

M. Parrón, T. Berrocal, A. Álvarez, D. Bernabeu, R.R. Lemos, N. Gómez-León; Madrid/ES

Learning Objectives: To understand the embryology, pathology, and imaging features of a wide spectrum of congenital and acquired alterations involving the hip in children. To know the utility of each imaging modality that can be applied to the management of these conditions. To emphasize pitfalls and differential diagnoses of these entities.

Background: We retrospectively reviewed the imaging findings of patients with disorders involving the hip from our database of musculoskeletal pathology. Plain radiographs were performed in all patients. Ultrasound, CT or MR were performed whenever plain radiographs were not conclusive. The embryology and pathological basis of the radiographic findings are discussed. The key findings at each imaging modality are shown and compared with the underlying pathological features when available.

Imaging Findings: Specific topics addressed include congenital and developmental abnormalities (hip dislocation, coxa vara, femoral capital dysplasias), femoral head necrosis of unknown (Legg-Perthes disease) and known etiology (Gaucher disease, hemoglobinopathies, corticosteroid therapy, and post-traumatic), infectious and inflammatory diseases (synovitis, arthritis, osteomyelitis, osteochondritis), synovial chondromatosis, slipped capital femoral epiphysis, benign and malignant neoplasms (osteoid osteoma, osteosarcoma, Ewings tumor, lymphoma) and trauma. Pitfalls, diagnostic difficulties and differential diagnoses are emphasized.

Conclusion: Evaluation of patients with hip disorders frequently requires multiple imaging modalities for diagnosis and planning treatment. Because many of these disorders have characteristic imaging appearances, this exhibit will help the practising radiologist to better understand and recognise pathology affecting the paediatric hip.

C-0891

High-resolution susceptibility weighted imaging (SWI) as a new diagnostic tool in children

H.-J. Mentzel, A. Rauscher, J. Böttcher, C. Fitzek, U. Brandl, J.R. Reichenbach, W.A. Kaiser; Jena/DE

Purpose: To evaluate the diagnostic potential of high resolution susceptibility weighted imaging (SWI) in children with vascular malformations. This blood oxygen level dependent (BOLD) method is based on susceptibility-induced phase contrast and is sensitive not only to the oxygen content of intravascular blood but also to breakdown products such as hemosiderin, due to increased signal dephasing.

Methods and Materials: We studied children with suspected vascular malformations on a 1.5 T MR unit (Siemens, Vision plus) using a standard head coil. Conventional MR imaging consisted of T1- and T2-weighted SE sequences, FLAIR and susceptibility sensitive EPI sequences (slice thickness 6 mm). 2D TOF-MR angiography was performed. A high-resolution 3D highly T2*-weighted gradient echo sequence with first-order flow compensation, and radiofrequency spoiling was used for SWI (TR 67 ms, TE 40 ms, flip angle 25°, FOV 256 mm, 512 matrix). Magnitude and phase images were reconstructed.

Results: With SWI highly detailed information about the veins was obtained in all patients. In a patient with Sturge-Weber syndrome early detection of vascular anomaly was possible; in patients with cavernoma more lesions could be detect-

ed compared to the conventional scans. In other patients developmental venous anomalies could be diagnosed clearly.

Conclusion: In children high-resolution SWI may be of special importance in the early detection and assessment of vascular malformations which are difficult to diagnose with other MR methods.

C-0892

Ultrasound in the diagnosis of acute abdominal pain in children during oncological treatment

U. Zaleska-Dorobisz, B. Jankowski, J. Kurcz, K. Moron; Wrocław/PL

Purpose: To assess the use of 2D and Doppler ultrasonography in children with acute abdominal symptoms during oncological therapy.

Methods and Materials: We analyzed 249 abdominal ultrasound examinations of 133 children with neoplasms and acute abdominal symptoms. Examinations were performed during chemotherapy, radiotherapy and after hematopoietic stem cell transplantation. All the patients were under routine hematological control. Based on the clinical symptoms and the laboratory tests we analysed two groups of children; a) 111 with neutropenia and b) 22 without neutropenia. In patients who underwent surgery the final diagnosis was established on histopathology. In the other cases diagnosis was based on clinical, laboratory and ultrasound findings.

Results: In the group of 133 children with acute abdominal symptoms most (69%) had acute lymphoblastic leukaemia (ALL), 12% had acute myeloblastic leukaemia (AML), Ewing sarcoma 2.2%, osteosarcoma 2.2%, NHL 6.0%, HL 3%, nephroblastoma 3%, neuroblastoma 2.2%. Clinical symptoms were very severe. Nonspecific gastrointestinal inflammation and typhilitis were the main cause of the acute abdominal pain in 71 children; perforation of the gastrointestinal tract (11), intestinal occlusion (10), acute pancreatitis (7), appendicitis (12), abscess (14), acute cholecystitis (6), peritoneal fluid was found in 45. The accuracy of ultrasound findings verified intraoperatively and by histopathological examination was 84%. In all cases the morphological changes were directly related to the duration of signs and symptoms.

Conclusion: High-resolution US is the first imaging method in the diagnosis of abdominal symptoms in children with neoplasms and neutropenia. US could be used for monitoring of treatment. Proper diagnosis can be established only with clinical information.

C-0893

Ultrasonographic findings of the fecally impacted appendix: Differentiating from acute appendicitis

N. Park, C. Park, E. Lee, M. Kim, S. Song; Koyang/KR

Purpose: To identify the ultrasonographic findings of the fecally impacted normal appendix in order to prevent unnecessary surgery due to its misdiagnosis as acute appendicitis.

Methods and Materials: 126 patients underwent ultrasonography between January 2004 to June 2004 for right lower quadrant pain. 8 cases including 3 pathologically confirmed cases and 5 clinically and follow-up ultrasonographically confirmed cases were diagnosed as a fecally impacted normal appendix. The criteria that we used to distinguish the fecally impacted appendix from acute appendicitis included preservation of normal wall layering of the appendix, absence of periappendiceal fat infiltration and lack of increase in blood flow of the appendiceal wall on color Doppler study.

Results: Fecal material within the appendix was seen as heterogeneous hyper-echoic intraluminal content without posterior shadowing. Fecal impaction was confined to the distal segment of the appendix in all cases. The AP diameter of the distended appendix was measured as 5.5-10.3 mm, while the mean diameter was 6.5 mm. The normal wall layers of the appendix were preserved and there was no evidence of periappendiceal fat infiltration in any of the cases. No demonstrable increase in blood flow in the appendiceal wall was seen.

Conclusion: Fecal impaction increases the outer transverse diameter of the normal appendix, thereby frequently leading to misdiagnosis of the fecally impacted appendix as acute appendicitis. Recognition of preservation of normal layering of the appendiceal wall, no periappendiceal mesenteric infiltration and no demonstrable increased blood flow in the appendiceal wall is expected to help prevent unnecessary surgery.

Scientific and Educational Exhibits

C-0894

Prenatal assessment of lung hypoplasia in congenital diaphragmatic hernia (CDH): Correlation between volumetric MR imaging and biometric ultrasound measurements

M. Fit  , G. Enriquez, A. Castellote, E. Gratac  s, J. Delgado, J. Piqueras, E. Carreras, J. Lucaya; *Barcelona/ES*

Purpose: To investigate the correlation between the relative fetal lung volume (RFLV) values measured with MR imaging planimetry and lung-to-head ratio (LHR) determined by ultrasound in fetuses with CDH.

Methods and Materials: Nineteen fetuses with an ultrasound diagnosis of CDH (16 left and 3 right) underwent MR imaging using single-shot rapid acquisition with relaxation enhancement and T1-weighted sequences. A total of 22 MR imaging exams were performed; fetal lung volume and liver volume were measured using planimetry. The RFLV was calculated according to a standard formula using the liver volume as a reference and expressed in percentage. The LHR was measured by ultrasound. Spearman correlation analyses were performed in the total group and in the cases of left hernias with ipsilateral apical cap.

Results: Among the 16 left-sided hernias, an ipsilateral pulmonary apical cap was identified by MR imaging in nine cases, seven in the first study and two after intrauterine tracheal plugging. The correlation coefficients (*r*) between the values obtained with the two methods were 0.60 (*p* < 0.005) for the total group of 19 and 0.13 (*p* > 0.5) for left hernias with ipsilateral apical cap.

Conclusion: There was a good overall correlation between the two methods. However, the correlation was poor in the subgroup of patients with apical cap. Presence of an apical cap may explain the prognostic variability reported for cases with borderline LHR values. Addition of volumetric MR imaging may improve the accuracy of current algorithms for determining pulmonary hypoplasia, indicating intrauterine treatment in borderline cases and predicting postnatal survival in patients with CDH.

C-0895

Significance of recurrent lung opacities in premature infants treated for respiratory distress syndrome: The SLOP study

S.P. Prabhu, S. Winterbottom, S. King; *Bristol/UK*

Purpose: To determine the significance of recurrent opacities on chest radiographs of neonates treated with surfactant for RDS after an initial period of improvement.

Methods and Materials: In this prospective study, serial chest radiographs on 61 premature infants (gestational age < 32 weeks) with RDS were analyzed pre- and post-surfactant at 3 days, 10 days, 36 weeks post conceptional age and at 3 months. The pattern of chest radiographic response was classified as (a)progressively clear, (b)recurrent opacification and (c)no response. Clinical characteristics including type of surfactant, mode of ventilation, presence of patent ductus and intraventricular haemorrhage were also recorded.

Results: In 23 infants (37%), RDS changes cleared within 3 days. 16 infants (26%) developed recurrent opacities within 10 days after an initial period of improvement. 22 infants (36%) failed to respond to surfactant. The corresponding mean birth weights for the three groups were 1.5, 1.12, and 0.82 kg and mean gestational ages 32, 27, and 25 weeks. The incidence of chronic lung disease was highest amongst infants with recurrent lung opacities.(63% vs. 51% in non responders, *p* < 0.001). The pattern of chest radiographic response in premature infants was primarily affected by gestational age and birth weight.

Conclusion: Recurrent lung opacities after initial improvement in neonates with RDS is an adverse factor in development of bronchopulmonary dysplasia. Recurrent lung opacities after surfactant may be a predictor of chronic lung disease in the preterm infant and necessitate reporting of neonatal films as a series in the first 2 weeks to avoid missing this important pattern.

C-0896

withdrawn by authors

C-0897

withdrawn by authors

C-0898

Congenital deformities of the hand: Preoperative evaluation with multiple-detector row CT angiography

M. Rieger, A. Mallouhi, H. Piza, B. Czermak, M. Freund, W. Jaschke; *Innsbruck/AT*

Learning Objectives: To demonstrate the usefulness of multislice CT examination in the preoperative evaluation of congenital deformities of the hand in children.

Background: Congenital hand deformities are relatively rare and vary greatly in appearance. Preoperative diagnostic work-up usually depends on conventional radiography. However, osseous deformities may be accompanied by abnormal vessels, muscles, tendons, and joints. For corrective surgery of congenital hand deformities, all its components and morphological characteristics should be precisely recognized. Multiple-detector row CT allows not only the visualization of osseous structures in three-dimensional perspective but also provides important information about tendons and arteries. The morphological changes found in cutaneous and osseous syndactyly, hypoplasia, symbrachdactyly, macrodactyly, cleft and club hand, mirror hand, and various numerical and metrical variations of the fingers will be discussed and analyzed as well as their impact on treatment planning. Syndromes like Apert, Schnueiring, Poland and Larsson that are associated with hand deformities will also be demonstrated.

Procedure Details: High-resolution multislice CT angiography (GE, LightSpeed QX/i; LightSpeed 16) of the forearm was preoperatively performed in 32 children under general anaesthesia. Contrast medium was applied by a power injector through a cubital or foot vein. The vascular, osseous and ligamentous conditions were reconstructed by means of an advantage windows workstation (GE, AW 4.0; AW 4.2).

Conclusion: Multislice CT angiography as the only preoperative work-up in children with congenital hand deformities is sufficient to demonstrate all abnormalities, which were important for corrective operation

C-0899

Uncomplicated versus torqued testicular appendages in childhood:

Sonographic appearances with embryologic correlation

M. Vakaki, G. Pitsoulakis, V. Dermentzoglou, V. Begli, C. Koumanidou; *Athens/GR*

Learning Objectives: To familiarize Radiologists and especially Pediatric Radiologists to the presence of more than the one well-known (appendix testis) testicular appendages and to highlight the significance of the correct sonographic diagnosis in the boy with an acute scrotum.

Background: Five testicular appendages, representing remnants of the degenerating mesonephric and paramesonephric ducts, have been identified microscopically. The appendix testis (hydatid of Morgagni) and appendix epididymis are the most common and have various sonographic appearances. Everyone of the above 5 appendages is liable to torsion, an important differential diagnosis versus testicular torsion, in the boy who presents with an acutely painful scrotum. Previous sonographic studies have mainly focused on Morgagni's torsion. Nowadays, high-resolution sonography with high-frequency transducers has made it possible to visualize the other normal or torqued testicular appendages, also.

Imaging Findings: In this exhibit, the embryology and anatomy, as well as the varying sonographic appearances of the testicular appendages are described and illustrated. Sonographic features of appendiceal torsion are also demonstrated. The differential diagnosis, including testicular torsion and acute epididymo-orchitis, is discussed.

Conclusion: The correct sonographic diagnosis is of utmost importance, as the clinical symptoms are often misleading, considering that appendiceal torsion is a self-limiting condition and can be managed conservatively, acute epididymo-orchitis also needs medical treatment, whereas testicular torsion requires urgent surgical intervention to save the testis.

C-0900

Range of sonographic appearances of the normal breast in children and young adolescents

M. Vakaki, G. Pitsoulakis, V. Dermentzoglou, V. Manoli, C. Koumanidou; *Athens/GR*

Learning Objectives: To present the changing sonographic appearance of the normal breast parenchyma in young children from birth to adolescence. To familiarize pediatric radiologists with normal variations of growing breast, to avoid misdiagnosis of normal as abnormal, and to emphasize the role of sonography in the imaging investigation of breast masses.

Scientific and Educational Exhibits

Background: Although the sonographic features of normal breast parenchyma in adults are well-known, similar data are lacking in children. On the other hand, sonography is the imaging method of choice in the evaluation and characterization of breast masses in childhood. The spectrum of breast diseases in children is different from that in adults and most of them are benign.

Imaging Findings: The sonographic characteristics of normal breast development and normal variations from birth to adolescence are described. Their differential diagnosis from pathological conditions is discussed and their correlation with Tanner grading system of breast development is presented.

Conclusion: Knowledge of the variable sonographic appearances of normal developing breast is quite important for successful use of breast sonography in imaging of the pediatric and adolescent breast.

C-0901

Contrast enhanced ultrasound in evaluation of pediatric blunt abdominal trauma

V. Miele, V. Buffa, A. Cortese, M. Galluzzo, G. Regine, L. Adami; Rome/IT

Purpose: To evaluate contrast enhanced US (CEUS) in the diagnosis of pediatric traumatic hepatic and splenic lesions when compared to conventional US.

Methods and Materials: In years 2002-2003 73 pediatric patients (age 5-16 ys) with blunt abdominal trauma (isolated or in polytrauma) were studied with conventional US and US with second generation contrast agent (Sonovue, Bracco, Italy). 18 patients were studied with angio-CT. We evaluated the presence of hepatic or splenic lesions and the size, echopattern and capsular involvement of the traumatic lesion.

Results: Conventional US revealed traumatic splenic and hepatic lesions in 7 and 8 patients respectively. CEUS revealed other hepatic and splenic lesions in 4 and 3 patients. Traumatic lesions with CEUS were hypoechoic with respect to enhanced hyperechoic parenchyma and size and margins were better defined. Capsular envelopment of the liver (3 cases) and spleen (2 cases), not identified with conventional US was demonstrated with CEUS. CEUS correlated well with CT. All hepatic lesions were treated conservatively; in 2 patients splenectomy was performed.

Conclusion: CEUS is more accurate when compared to conventional US in the detection and classification of hepatic and splenic traumatic lesions. In the pediatric age-group CEUS can substitute for CT and is preferable for follow-up. CT should be reserved for polytrauma.

C-0902

High-resolution ultrasound of angled buckle fractures in children

M. Valle¹, L. Bacigalupo¹, F. Pugliese¹, P. Toma¹, S. Bianchi², C. Martinoli¹; ¹Genoa/IT, ²Geneva/CH

Learning Objectives: To provide an overview of the most common angled buckle fractures in children. To familiarize radiologists with the appearance of these fractures. To emphasize the role of US for the identification of radiographically occult fractures in children.

Background: Angled buckle (torus) fractures are very common in children and derive from the application of axial loading to the involved bone, causing an impaction fracture, in combination with lateral forces leading to the angulation of the cortex. Although pediatric radiologists are familiar with the appearance of these subtle fractures on plain films and with the typical sites where they occur, angulated buckle fractures are frequently missed radiographically.

Imaging Findings: This exhibit will provide an overview of the US appearance of a series of radiographically occult fractures involving the metaphysis of the long bones of the hand (phalanges) and foot (bunk bed fracture), the wrist (distal radius) and the elbow (radial head, supracondylar). In most cases, angled buckle fractures present sonographically with a curved or fragmented appearance of the metaphysis compared with the contralateral side. The appropriate US scanning technique for detecting these subtle fractures and potential pitfalls in the interpretation of pathology will be discussed.

Conclusion: US is helpful to detect radiographically occult angled buckle fractures in children, especially in the case of multiple bone involvement. This technique may avoid the need for oblique or contralateral views, limiting the X-ray exposure to the patient.

C-0903

Changes of sonographic features of peripheral lymph nodes in Hodgkin's disease during specific therapy

V.P. Khartchenko, P.M. Kotlyarov, E.V. Abbasova, R.A. Parkhomenko; Moscow/RU

Purpose: To investigate changes of sonographic features of lymph nodes (LN) during therapy for Hodgkin's disease (HD).

Methods and Materials: 160 children with HD were examined (apparatus Logiq-7 GE). The following parameters of the LN were evaluated: diameters, shape, index of roundness, echogenicity, differentiation of the cortex and medulla, matting, vascular pattern, RI, spectrum of blood flow velocity. More than 400 LN were evaluated with B-mode, of which 100 were additionally examined using Color flow (CF) and Power Doppler (PDI), and Pulse-wave modes.

Results: The LNs affected by HD were enlarged, with a tendency of matting, the index of roundness approached 1, the outline was uneven, the general echogenicity was low, corticomedullary differentiation was not clearly seen. CF and PDI showed predominantly mixed chaotic vascular pattern (central + peripheral). RI was 0.55-0.71. During specific therapy the size and number of the LN decreased, their echogenicity increased, symmetrical corticomedullary differentiation appeared, vascular pattern became hilar with its gradual reduction. In some LN signs of micro- and macrocalcifications were seen. RI decreased (0.51-0.55), with no change in peak velocity.

Conclusion: Modern sonographic techniques objectively reflect changes of the peripheral LN affected by HD during therapy. One of the most informative parameters is change of RI and should be considered together with the reduction of the size, number of LN and normalization of the echo-structure. RI is increased in the specifically affected LN and decreases after effective treatment. The absolute values of peak blood flow velocity are not informative to assess the effect of treatment.

C-0904

Association of isolated preauricular skin tags and renal anomalies in the local UK population

T.A. Szyszko, Z. Stetina, C. Ward, D. Lindo; London/UK

Purpose: To look at the association of isolated preauricular skin tags and renal anomalies in the local population. Ear and renal anomalies are seen in multiple congenital anomaly syndromes; however, the principle evidence for the specific association of isolated preauricular skin tags and renal anomalies is a paper from Israel showing an 8.6% incidence in 70 infants. There is no European data for any such association.

Methods and Materials: We looked at the indications and outcomes of 151 renal ultrasounds requested on infants born in Kingston Hospital in 2003. The indications were categorised as: two vessel cord; preauricular skin tags; antenatal abnormality and "other" (including UTI). The outcomes were categorised as "normal"; "abnormal" or "did not attend".

Results: 141 (93%) of the 151 infants attended renal ultrasound examination. 100% of the infants with isolated preauricular skin tags had a normal renal ultrasound examination. 100% of the infants with two vessel umbilical cords had a normal renal ultrasound. 60% of infants with abnormal antenatal renal scans and 87% of the "other" indications also had normal scans. A telephone survey revealed that 30% of all units with delivery suites in the UK routinely referred infants with isolated preauricular skin tags for postnatal renal ultrasound assessment.

Conclusion: In the local population there were no renal anomalies found in infants with isolated preauricular skin tags and no renal anomalies found in infants with two vessel umbilical cords suggesting that there is no association and no need for routinely referring these infants for postnatal renal ultrasound examination.

C-0905

A pictorial review of pineal region masses and pathologies in children

J.L. Babar, L.K.R. MacPherson; Birmingham/UK

Learning Objectives: To illustrate the spectrum of pathologies that may affect the pineal gland and parapineal structures in children. To outline certain imaging characteristics that are associated with specific tumours and non-neoplastic lesions.

Background: Pineal tumours constitute approximately 3-8% of paediatric brain tumours. Pineal region lesions fall broadly into two categories; tumours arising from the pineal gland, and masses extending into the pineal region from adjacent structures. Clinically, children may present with abnormal eye movements (Parinaud's syndrome), symptoms related to hydrocephalus and neuroendocrine dysfunction, or as an incidental finding on cross-sectional imaging. The role of imaging

Scientific and Educational Exhibits

is to attempt to differentiate these lesions by identifying their origin, recognising different imaging characteristics, and noting any associated complications, concurrent tumours or disseminated disease.

Imaging Findings: The radiological appearance, particularly with reference to CT and MR imaging, of pineal gland tumours, including pineal cell and germ cell neoplasms are reviewed. Other parapineal tumours and non-neoplastic masses encountered, including cysts and vascular malformations are described. A pattern-based approach depending on the anatomical site affected and radiological appearance, in conjunction with clinical details is used to provide an aid to the diagnosis.

Conclusion: Neuroimaging has achieved a marked improvement in the preoperative delineation of benign and malignant pineal masses, and in distinguishing true pineal tumours from other parapineal pathologies in children.

C-0906

True FISP versus HASTE MR imaging in the diagnosis of non-cerebral foetal anomalies

B.J. Op de Beeck¹, P. Ramaekers¹, R. Salgado¹, F. De Ridder², L. De Catte², F. Vanhoenacker¹, P. Parizel¹; ¹Edegem/BE, ²Brussels/BE

Learning Objectives: To illustrate the most common non-cerebral foetal anomalies. To compare the image quality of two ultra-fast sequences (True FISP and HASTE) in prenatal MR imaging. To outline the advantages and limits of the technique compared with foetal ultrasonography.

Background: Foetal MR imaging provides the potential advantage of superior soft tissue characterization with better differentiation of tumour from normal tissue compared with US. The HASTE technique has been widespread in foetal MR imaging. True FISP offer some advantages: a better signal-to-noise ratio at a short TR, a high T1/T2 contrast, and a lower specific radiofrequency absorption rate. In this exhibit we will describe the use of both ultra-fast sequences in the diagnosis of non-cerebral foetal anomalies, the advantages and the limits compared with foetal ultrasonography.

Procedure Details: We included 15 patients with a suspicion of non-cerebral foetal abnormalities on ultrasound. Imaging was performed on Magnetom Vision and Sonata 1.5 T scanners (Siemens, Erlangen, Germany). HASTE and True FISP sequences were used in the 3 anatomical planes. Diagnostic confirmation was obtained with foetal ultrasound and post-partum imaging. The indications were: meningocele, sacrococcygeal teratoma, diaphragmatic hernia, cystic adenomatoid malformation, pulmonary hypoplasia, gastroschisis, meconium peritonitis, Potter syndrome and campomelic dysplasia.

Conclusion: True FISP images demonstrated superior contrast resolution and less blurring of the lesions despite the higher susceptibility to band-like artefacts. Ultra-fast MR imaging may further aid our understanding of developmental anatomy, help characterize congenital lesions, delineate associated findings, and ultimately assist in the management of both foetus and mother.

C-0907

Pediatric MRA with Gd-BOPTA

G.K. Schneider, P. Fries, M. Gruber, B. Kramann, R. Seidel; Homburg a.d. Saar/DE

Purpose: Vascular malformations in pediatric patients often present complex anatomy and implicate the need for an adequate imaging modality to correctly diagnose and subsequently plan therapy. This study reviews different congenital vascular malformations visualized by contrast enhanced MRA with the use of Gd-BOPTA, a high relaxivity contrast agent.

Methods and Material: MRA was performed on a 1.5 T magnet in a total of 38 patients (2 days to 8 years). MRA was performed either with sedation or after intubation and controlled ventilation corresponding to the age of the patient and the vascular territory imaged. For MR angiography Gd-BOPTA was applied intravenously at a dose of 0.1-0.2 mmol/kg body weight with injection by hand during ongoing sequence acquisition without the use of a test bolus.

Results: At the injected dose Gd-BOPTA produces excellent and homogeneous delineation of the aorta and the supra-aortic branches even in newborn babies in which vessel diameters of < 3 mm have to be considered. Long breath-hold intervals due to controlled ventilation allow for dynamic whole body imaging of the arterial and venous system in one imaging session and thus may give a complete overview of the vasculature.

Conclusion: Gd-BOPTA in contrast enhanced MRA of pediatric patients produces excellent delineation of even very small vessels and thus allows a diagnostic workup of even newborn or premature babies. Increased relaxivity as compared to other gadolinium chelates may result in better vessel demarcation making Gd-BOPTA favorable in contrast enhanced MRA of pediatric patients.

C-0908

Intraarticular osteoid osteoma in children

M. Hasiotou, E. Manoli, G. Pitsoulakis, N. Petras, I. Anastopoulos, E. Evangelidakis; Athens/GR

Purpose: To demonstrate and discuss the imaging findings of intraarticular osteoid osteoma (OO) in childhood.

Methods and Materials: The medical files of 35 patients (22 males and 13 females) with intra-articular osteoid osteoma were retrospectively studied. Patients' age ranged from 4 to 15 years and in all cases the final diagnosis was established histologically. We studied the imaging findings on plain films, computed tomography, magnetic resonance imaging and bone scintigraphic studies. The disease was located in the hip, spine, knee, ankle, heel, metatarsal bone and in the elbow.

Results: In 9 cases the plain films were unremarkable due to the absence of sclerosis and the projection of articular structures. Computed tomography, bone scintiscan and magnetic resonance imaging study were indicative for the disease in all cases, contributing to the localization of the lesion. The typical findings of the radiolucent nidus and of surrounding sclerosis were not present in all cases. Atypical imaging findings were also observed; joint effusion, cortical disruption, soft tissue swelling, marrow oedema, osteophyte formation, distal periosteal sclerosis, soft tissue mass, regional osteopenia and muscle wasting and fat obliteration.

Conclusion: In cases of intra-articular localization of OO, diagnosis may be challenging. Clinical presentation is often misleading. Bone scintigraphy and CT are important diagnostic tools for accurate and prompt diagnosis. MR imaging, especially after intravenous introduction of gadolinium helps in cases with vague symptoms or nonspecific findings on CT.

C-0909

Sonographic analysis with second-generation ultrasound contrast agents in pediatric liver transplantation

R. Nani, S. Placidi, G. Pezzotta, M. Gaffuri, A. Tomasoni, G. Bonini, R. Agazzi; Bergamo/IT

Purpose: To investigate the use of second generation sonographic contrast in sonographic follow-up of pediatric liver transplantation.

Methods and Materials: The pediatric liver transplantation center of OORR of Bergamo, from October 2002 to November 2003, performed in 40 patients, 44 liver transplantations (34 split-liver, 10 whole liver). All patients were studied with US-color-Doppler. 30 patients were studied with harmonic imaging US (ATL 5000) and sonographic contrast agent (SonoVue) before the use of invasive techniques (angiography, CT, PCT) in suspected vascular and biliary complications.

Results: 11 vascular complications were demonstrated (9 thromboses and 2 stenoses); 5 in the hepatic artery, 4 in the portal vein and 2 in the sovrahepatic v. 8 biliary complications were demonstrated: 3 stenoses, 3 fistulae, 2 bilomas. 15 fluid collections in split livers close to the surgical resection were found (cut surface of the liver). The enhancement pattern of hepatic vessels in the subsequent vascular phases (portal and late) confirmed the suspicion of vascular steno-trombosis, while the parenchymal phase was better for biliary duct detail.

Conclusion: Sonographic analysis with SonoVue contrast agent is a useful, non-invasive technique that improves the accuracy of traditional US in pediatric liver transplantation. The use of ultrasound agents has significantly improved the diagnosis and characterization of intrahepatic and extrahepatic lesions (necrosis, abscess, bilomas).

C-0910

Imaging of back pain in children and adolescents

N.J. Khoury, M.M.S. Arabi, F. Abi-Fakher, M.H. Hourani, M.C. Haddad; Beirut/LB

Learning Objectives: To present the imaging findings of the wide spectrum of musculoskeletal diseases causing back pain in children and adolescents.

Background: Back pain in children is a rare condition but may denote a serious health problem, hence full clinical history, physical examination and appropriate laboratory studies should be obtained.

Imaging Findings: In this scientific exhibit, we present the imaging findings of the variable musculoskeletal diseases that are associated with back pain in children and adolescents. These disease processes include: scoliosis of various causes, spondylolisthesis, spondylolisthesis, traumatic injuries, disc degeneration and herniation, Scheuermann's disease, spondylodiscitis, tumors (primary, secondary, hematogenous), and miscellaneous conditions (e.g. metabolic disorders, sickle cell disease, osteoporosis). The imaging modalities used include plain radiographs, CT scan, MR imaging and nuclear studies.

Scientific and Educational Exhibits

Conclusion: A wide spectrum of diseases causing back pain in children is presented. Radiologists should be aware of the imaging findings of this rather uncommon entity.

C-0911

Contrast enhanced versus baseline ultrasonography in characterization of enlarged peripheral lymph nodes in children

U. Zaleska-Dorobisz, B. Kazanowska, K. Moron; Wroclaw/PL

Purpose: To compare contrast enhanced ultrasonography to conventional US in the characterization of benign and malignant enlarged peripheral lymph nodes in children.

Methods and Materials: Ninety seven enlarged superficial lymph nodes in 40 children (18 girls and 22 boys; age range, 1- 16 years) were evaluated using color Doppler (CD), power Doppler before and after contrast (Levovist) agent administration(CEUS). The patterns of intranodal flow were identified. Hilar vessels with branches running in the long axis of the lymph node with branches to the cortex indicated lymphadenitis (sensitivity 94%, specificity 100%). Of the neoplastic lymph nodes, 90% showed predominantly peripheral vessels. Histologically, lymphadenitis was found in 62 nodes, metastases in 24 nodes, HL in 6 and NHL in 5 cases. Geometric dimension, architecture, and margin of the node and detection and localisation of vessels were evaluated. The ultrasound diagnoses were compared to the final diagnoses based on clinical tests, surgical and histological examination.

Results: The transverse- to longitudinal diameter ratio in combination with architecture and margin analysis resulted in a correct diagnosis in only approximately 80% of the nodes. With contrast enhanced CD and PD, 90% of nodes showed vessels, and 30% of nodes demonstrated vessels with this technique exclusively.

Conclusion: Enlarged peripheral lymph nodes in children can be categorized as inflammatory or neoplastic with high diagnostic accuracy on the basis of their vascular patterns as seen on contrast enhancend color Doppler US.

C-0912

Evaluation of the abnormal anatomy in infants with double outlet right ventricle with MR imaging

L. Bokeriya, A. Ivanitsky, V. Makarenko, L. Urpolskaya, I. Rychina; Moscow/RU

Purpose: To define the possibilities of cardiac MR imaging in the diagnosis of double outlet right ventricle (DORV) in infants.

Methods and Materials: 16 infants (13m 3f, weight 6.9 ± 2.9 kg, growth 67.9 ± 8.58 sm) with DORV were investigated by MR. MR images were acquired on a Signa GE system, field strength was 1.0 T. To reduce flow and motion artefacts ECG triggering and respiratory compensation and sedation were used in all patients. We used multislice spin-echo and gradient-echo technique. The selected slice thickness was 3-4 mm. Images were analyzed off-line on an Advantage Windows workstation. For the analysis of abnormal anatomy we used a segmental approach.

Results: For the evaluation of morphology, ECG-gated spin-echo images are optimal. In all patients we could define situs, atrioventricular connections, type of ventricular loop, the orientation of the great arteries to each other and ventricular arterial connections. Twelve patients had situs solitus, two patients right isomerism, one patient left isomerism and one infant had situs inversus. In all cases both vessels were located in the right ventricular out flow tract. The best images were oblique coronal and sagittal. The position of ventricular septal defect (VSD) and orientation and size of the outlet septum and the relation between the VSD and the arterial valves were defined by transverse and oblique MR images. MR imaging findings were confirmed by echocardiographic, angiographic and surgical findings.

Conclusion: MR imaging is excellent in depicting the details of DORV and it may obviate cardiac catheterization and angiography; it may be used in infants with DORV.

C-0913

The abdominal plain film in the newborn: How much can we obtain?

A. Bermejo, F. Ballenilla, L. Herraiz, M. Perez, M. Miralles, A. Martinez; Madrid/ES

Learning Objectives: To encourage a systematic reading of the newborn thoracoabdominal plain film in order to distinguish the normal radiological abdominal appearance from congenital or acquired abnormalities. To obtain the optimal information for accurate diagnosis and management, focused on gastrointestinal pathology.

Background: We reviewed 5,200 radiographs performed in 4,000 patients admitted to the Neonatology Department from 1998 to 2003.

Imaging Findings: Abdominal pain, distension, vomiting, mass and delayed/absent meconium passage were the usual requirements for radiological assessment. Reading of the film should include the analysis of intestinal gas pattern, solid organs, lung and diaphragms, catheter location, skeleton and soft tissues. We focused on intestinal gaseous pattern (location, distribution, bowel loop morphology, distension and wall thickening) and correlated it with symptomatology, physical exam and final clinical, surgical or pathological diagnosis. Only in 20% of the cases gas pattern distortion was secondary to organic gastrointestinal problems that required surgery. The other causes were non-surgical, systemic or extraabdominal pathology.

Conclusion: A systematic plain film analysis may lead to an accurate diagnosis in intestinal neonatal pathology and/or proper orientation for further management.

C-0914

Bronchopulmonary foregut malformations presenting as mass lesions in children

M. Kocaoglu¹, D.P. Frush², M.S. Ugurel¹, I. Somuncu¹; ¹Ankara/TR, ²Durham, NC/US

Learning Objectives: The objects of this presentation are to review the embryology, discuss the clinical presentation and to illustrate the imaging findings of bronchopulmonary foregut malformations (BFMs) presenting as mass lesions in the pediatric population. The role of the radiology in the evaluation and the management of this condition will be emphasized.

Background: The BFMs have embryologic similarities eventually involving lung parenchyma, conducting airways, vessels, or the esophagus. These malformations also may present with heterogeneous imaging features, including mass or mass-like lesions. This grouping of BFMs includes congenital cystic adenomatoid malformation, pulmonary sequestration, congenital lobar emphysema, foregut cysts, arteriovenous malformation and benign lung cysts. BFMs mostly demonstrate a single histopathology, however hybrid malformations, combination of different bronchopulmonary structures, have been reported. These disorders may manifest in various ways from incidental findings on radiography, to life threatening respiratory compromise.

Procedure Details: Imaging features of congenital cystic adenomatoid malformation, pulmonary sequestration, congenital lobar emphysema, foregut cysts, arteriovenous malformation and benign lung cyst with the hybrid malformations are discussed and appropriate imaging strategies consisting of radiography, CT, MR imaging and sonography are provided.

Conclusion: Familiarity with the presentation and imaging features of bronchopulmonary foregut malformations presenting as a congenital mass or mass-like lesion comprising is important. Moreover, imaging plays a central role in the evaluation of these lesions. Selection of the appropriate modality and technique is fundamental in this evaluation. With this, the presence and type of lesion can be defined and appropriate management determined.

C-0915

MR imaging assessment of fetal lung volume

J. Po, R.A. Barth, H. Ringertz, R. Bammer; Stanford, CA/US

Purpose: 1)To measure fetal lung volumes on MR images and quantify normal volume range. 2)To determine whether T2 signal intensity of fetal lungs correlates with development.

Methods and Materials: T2 weighted SSFSE images of 33 fetuses from 2001 to 2004 were analyzed. Regions-of-interest (ROIs) were traced around the lung parenchyma. Fetal lungs were characterized as normal ($n = 25$) and abnormal ($n = 7$) based on the radiology report. Volumes were calculated by summing the approximate volume of each slice [ROI surface area * (slice thickness + gap)]. Average total lung volume for each fetus was plotted against gestational age. A linear regression line was plotted through the normals, and 95% prediction intervals were calculated. ROIs were drawn over liver, amniotic fluid, CSF, stomach, bladder, and maternal psoas muscle to calculate lung signal intensity ratios. Signal intensity ratios were plotted against gestational age.

Results: Lung volumes were strongly correlated with gestational age. Lung volumes of 4 fetuses with thoracic abnormalities (27.7-36.3 weeks) fell outside the 95% prediction intervals defined by the normals. Lung volumes of 3 abnormal fetuses (19.4-24 weeks) fell within the intervals. Signal intensity ratios did not correlate significantly with gestational age.

Conclusion: At gestational ages greater than 25 weeks, MR imaging may distinguish abnormally developing fetuses based on lung volume. A graph of 95% prediction intervals would be a clinically useful tool to guage appropriate fetal lung

Scientific and Educational Exhibits

development. To address contradicting reports in the literature, we did not find significant evidence of lung T2 signal intensity increase with maturity.

C-0916

Incidence, clinical presentation, MR imaging and histological findings of intracranial neoplasms in children under the age of two and added utility of gadolinium in their initial diagnosis

M. Petrou, B.R. Foerster, P. Eldevik, P. Maly, P.C. Sundgren; *Ann Arbor, MI/US*

Purpose: To evaluate the incidence, clinical presentation, MR imaging findings and histology of intracranial neoplasms in children under the age of two, and to assess the added utility of gadolinium in their initial MR imaging work-up.

Materials and Methods: After completing a retrospective review of all the brain MR imaging examinations performed at our institution between 1995-2002 we concluded that the added utility of gadolinium in this set of exams is very limited. It does, however, provide valuable information in cases of newly diagnosed or known neoplastic disease. We then investigated how many exams were conducted for the initial work-up of intracranial neoplasms, and reviewed their clinical presentation and histological diagnoses.

Results: Out of a total of 1466 brain MR imaging examinations performed, only 17 were performed for initial work-up for intracranial tumors. All of these patients had significant neurological deficits and/or definite evidence of increased intracranial pressure on clinical exam. None of the patients presented with nonspecific symptoms. 11 of the 17 patients underwent a CT exam prior to MR imaging, and in all 11 cases the tumors were detected on CT. In all 17 patients, the tumors were easily identified on the MR noncontrast images, and contrast was only helpful to characterize the tumor further and assess for meningeal involvement.

Conclusions: We conclude that not using contrast for brain MR imaging in this age group would not result in a missed diagnosis of new intracranial malignancy. In the absence of significant neurological deficits, the clinical concern for an intracranial tumor can almost be excluded.

C-0917

Three-dimensional ultrasound (3DUS) of the neonatal brain: Clinical application in patients of the neonatal intensive care unit (NICU)

G.A. Fritz, M. Riccabona, H. Deutschmann, C. Weitzer, B. Resch; *Graz/AT*

Purpose: To prospectively evaluate the clinical value of 3DUS of the neonatal brain.

Methods and Materials: 60 patients from the NICU (gestational age: 25-42 weeks, mean: 31.6 weeks, age: 0 to 90 days, median: 10 days) underwent 2d- and 3d-neurosonography. Both studies were evaluated independently by two observers for comparison. Inter- and intraobserver variability was calculated.

Results: All 3DUS were of diagnostic quality and could be performed without sedation. 3DUS missed no essential diagnosis as established by 2DUS. Diagnoses included normal or physiologically immature neonatal brain sonograms ($n = 21$), plexus cysts ($n = 4$), plexus bleedings ($n = 10$), intraventricular haemorrhages grade I-III ($n = 8$), periventricular pathology such as periventricular echodensities ($n = 4$) and periventricular haemorrhages or cerebral infarctions ($n = 6$), hydrocephalus ($n = 4$), widened subdural spaces ($n = 2$) and one cerebral tumour. 3DUS imaging time (4.8 ± 2.6 min) was significantly shorter than for 2DUS (9.1 ± 6.1 min). The additional axial plane improved the sonographic potential for differential diagnosis. 3DUS allowed an improved standardisation and documentation especially valuable for follow-up. No statistically significant differences in intra- and interobserver variabilities were noted compared to 2DUS. Restrictions of 3DUS that have to be considered are the lack of duplex sonography and the lower resolution compared to conventional ultrasound.

Conclusion: 3DUS of the neonatal brain at the intensive care unit is feasible with diagnostic quality without sedation. 3DUS improves comparison during follow-up, as well as standardisation and documentation, and can be considered a useful adjunct in neonatal 2D-neurosonography.

C-0918

withdrawn by authors

C-0919

Spontaneous air leaks in the neonate: Imaging appearances and clinical significance

M. Raissaki, E. Drakonaki, E. Hatzidaki, C. Giannakopoulou, N. Gourtsoyiannis; *Iraklion/GR*

Learning Objectives: To underscore the occurrence and significance of spontaneous air leaks in neonates. To present and discuss the imaging features and

differences in types of air leaks in the neonatal chest radiograph. To demonstrate the complementary role of CT.

Background: Air leaks in neonates comprise pneumothorax, pneumomediastinum, pneumopericardium, pulmonary interstitial emphysema (PIE) and usually occur during assisted ventilation. Spontaneous air leaks are considered rare. During a 6-year-period, 21 neonates, (7 preterm, 14 full term), presented with respiratory distress and a pre-intubation abnormal chest radiograph, indicating an air-leak. 62 radiographs and 4 CTs were reviewed. Two neonates had undergone IPPV for 3-6 hours and were successfully extubated 12 and 24 hours prior to symptoms.

Results: Spontaneous air leaks detected were pneumomediastinum (7 patients, anterior in 6, infra-azygous in 1, coexisting with pneumothorax in 2), pneumothorax (17 neonates, in 2 bilaterally, coexisting with PIE in 3) and no case of spontaneous pneumopericardium. Perithymic lucency with/without elevation and peripheral radiolucency were the most sensitive signs for pneumomediastinum (85.7%) and pneumothorax (94.1%), respectively. Three neonates were successfully treated with oxygen therapy. A pleural tube was placed in 14 neonates and an endotracheal tube in 5. CT delineated the exact location of air, associated pressure effect and resolution.

Conclusion: Air leaks in preterm and full term neonates may occur spontaneously and are treated conservatively, or with endotracheal and/or chest tube placement. Chest radiography usually suffices for the diagnosis, especially when the thymus is outlined and/or elevated. Confusing appearances are confidently delineated with CT.

C-0920

Radiation dose and image quality in neonatal radiography

E. Dougeni¹, H. Delis¹, A. Karatza¹, C. Kalogeropoulou¹, S. Skiadopoulos¹, G. Malatara¹, E. Efstatopoulos², G. Panayiotakis¹; ¹Patras/GR, ²Athens/GR

Purpose: Neonates, especially the premature, frequently undergo a large number of chest and abdominal radiographs during the first days of their life. Their increased radiosensitivity, due to the highly mitotic state of their cells, plus their longer life expectancy, highlight the importance of minimizing dose while maintaining diagnostically acceptable imaging. A study of radiation dosimetry and image quality carried out in the Special Baby Care Unit of the University Hospital of Patras is presented.

Methods and Materials: Neonates were categorized depending on their birth-weight into 4 groups. Exposure parameters (kVp, mAs, field size) of 190 radiographs, performed with the same mobile unit, were recorded. Entrance Surface Dose (ESD) was estimated and Dose-Area Product (DAP) was measured directly. Interpretation of the images was performed by two independent observers in random order, based on the visibility of certain anatomical features and catheters, assessed in a 5-grade scale.

Results: ESD values increased with weight and ranged from 15.2 to 60.3 μ Gy. DAP measurements also demonstrated a wide variation among groups, from 0.23 to 0.92 μ Gym². The evaluation of image quality revealed the feasibility of achieving a high total image quality score, using both low and high kVp techniques.

Conclusion: The majority of the ESD values were below the dose reference levels proposed by the National Radiological Protection Board. However the results show that use of high kVp techniques could result in further reduction in neonatal dose, without degrading image quality. Wide dose variations highlight the need for developing examination protocols for neonatal radiography.

C-0921

Incomplete obliteration of canal of Nuck and processus vaginalis:

Sonographic diagnosis with embryological correlation

M. Vakaki, G. Pitsoulakis, C. Kosmas, P. Christopoulos, C. Koumanidou; *Athens/GR*

Purpose: Failure of complete closure of processus vaginalis (PV) (males) or canal of Nuck (females) during fetal life results in a spectrum of abnormalities. The purpose of this study was to evaluate the role of sonography in the diagnosis and differentiation of the various abnormalities, to highlight the clinical significance of the prompt and proper sonographic diagnosis and to correlate the sonographic findings with embryology.

Methods and Materials: The medical data of 161 boys (1 day to 14 years) and 6 girls (20 days to 14 years) with abnormal closure of the PV or canal of Nuck, respectively, were reviewed. The children were examined due to painful/painless, inguinal/inguinoscrotal swelling, without known underlying disease. Sonographic examination of the inguinal and scrotal areas was performed with high-frequency transducers, supplemented by color Doppler and abdominal sonogram, when necessary.

Scientific and Educational Exhibits

Results: The sonographic examination of the boys revealed: 30 communicating hydroceles, 14 incarcerated and 28 non-incarcerated inguinal/inguinoscrotal hernias, 43 testicular hydroceles, 13 funicular spermatic cord hydroceles and 33 encysted spermatic cord hydroceles. The sonographic examination of the girls showed: 3 noncarcerated inguinal hernias, involving bowel loops and the ipsilateral ovary, one case of ovarian inguinal herniation and 2 Nuck cysts. The embryology, sonographic patterns and sonographic differential diagnoses are presented. **Conclusion:** Sonography is the imaging method of choice in the diagnosis of all types of PV or Nuck canal abnormal closure. To the best of our knowledge, they represent rare and little-known developmental disorders. The pediatric radiologist's awareness is essential for an accurate sonographic diagnosis and determination of timely appropriate management.

C-0922

CT multislice in pediatric tracheopulmonary malformations

V. Buffa, M. Galluzzo, G. Regine, M. Atzori, V. Miele, L. Adami; Rome/IT

Purpose: To evaluate the usefulness and potential of multislice CT (MSCT) in the diagnosis and preoperative evaluation of pediatric tracheobronchopulmonary malformations.

Methods and Materials: 12 children (8:4 m/f, 2-15 months) with tracheomalacia (7 cases), pulmonary sequestration (3), adenomatoid cystic malformation (2) were studied with an 8-channel multislice CT (LightSpeed Ultra, GE, USA) using i.v. contrast media (slice thickness 1.25 mm, reconstruction interval 0.6 mm, 100 kV, 80 mA). Image processing was performed with an Advantage 4.1 workstation (GE, USA). Multiplanar and 3D images were related to bronchoscopy and surgery. **Results:** All cases of focal areas of tracheal stenosis/compression were diagnosed with accurate demonstration of vascular malformations. In pulmonary sequestration MSCT depicted abnormal vessels allowing differential diagnosis with adenomatoid cystic malformations. The procedure was fast, non-invasive and without complications.

Conclusion: MSCT is highly accurate for the detection and characterization of pediatric tracheopulmonary malformations, depicting the anatomical details relevant for surgery.

C-0923

The application of high frequency sonography in the diagnosis and monitoring of inflammatory bowel disease in children

U. Zaleska-Dorobisz, A. Stawarski, T. Pytrus, F. Iwanczak, K. Moron; Wroclaw/PL

Purpose: To present the usefulness of high frequency standard and color Doppler sonography in the diagnosis and therapy monitoring of nonspecific inflammatory bowel diseases (IBD) in children.

Methods and Materials: We studied 48 boys and 40 girls with nonspecific IBD: 35 with Crohns disease (CD), 37 with ulcerative colitis (UC), 16 with other non-specific IBD. We performed high resolution 2D sonography to evaluate the bowel wall thickness. Vascularity was assessed with color Doppler. The superior and inferior mesenteric artery flow; mean velocity, RI and PI were measured. We correlated with the clinical activity of the disease, colonoscopy and histology.

Results: CD predominantly involved the small intestine. The bowel wall was greatly thickened more than 8-10 mm. Mucosal ulcerations penetrated into the wall in 22 children, in 11 we found fistulas and peritoneal abscesses. The mesentery and fat around the bowel was thickened in all children. UC was limited to the left colon. The colon wall was thickened more than 5-9 mm. Mural inflammation was located on the mucosal surface with superficial ulceration and pseudopolyps (45%). Color Doppler revealed hyperemia with increased vascularity of the involved bowel wall. The RI and PI were significantly lower in active disease. After treatment RI and PI values increased significantly ($p < 0.005$).

Conclusions: High resolution and Doppler sonography is able to detect bowel wall abnormalities of most IBD in children. Doppler flow parameters in mesenteric arteries correlated strongly with disease activity. Doppler US could be used for monitoring treatment efficacy.

C-0924

Imaging evaluation of paediatric thoracic cystic lesions

V.M.V.T. Mascarenhas, L. Lobo, J. Fonseca-Santos; Lisbon/PT

Learning Objectives: To describe the imaging features of paediatric cystic thoracic lesions (CTL) and outline their main differential diagnostic pitfalls. To emphasise the role of imaging evaluation in treatment and guiding follow-up.

Background: CTL (defined as either fluid- or air-filled spaces separated from normal lung by an identifiable boundary) are common incidental or pathological

findings in the pediatric age group. A more precise diagnosis is essential to an adequate orientation in treatment and follow-up. In this regard, imaging evaluation particularly with chest radiography, sonography (especially in younger patients) and CT as the main techniques, undertake a pivotal role. We describe diagnostic imaging features, differential diagnosis problems and a systematic age-dependent framework approach to CTL among selected cases studied in our department.

Imaging Findings: Referred cases were reviewed based on age as the main factor, location (including single/multiple and uni/bilateral lesions) and morphological features. The main diagnostic entities considered were congenital lesions presenting in the newborn (congenital diaphragmatic hernia; cystic adenomatoid malformation; sequestration; congenital lobar overinflation and lymphangioma) or after the newborn period (parenchymal, bronchogenic and thymic cysts) and acquired lesions presenting in the perinatal period (pulmonary interstitial emphysema; bronchopulmonary dysplasia) or in children/young adults (pneumatoceles; abscess; systemic diseases).

Conclusion: Although there is a wide range of entities presenting as CTL in infants and children, a framework based on an age-dependent algorithm allows a more precise diagnosis or at least a considerable narrowing of diagnostic possibilities in the majority of cases, which is essential for therapeutic orientation.

C-0925

Parenchymal cyst-like lesions in tuberous sclerosis

C. Eun, Y.-W. Kim, S. Choi, S. Lee; Busan/KR

Purpose: To investigate the presence of small cyst-like lesions in the cerebral white matter on MR imaging of patients with tuberous sclerosis.

Methods and Materials: MR images were reviewed retrospectively in 15 patients in whom a clinical diagnosis of tuberous sclerosis had been made during the past 5 years. The incidence, MR findings, and possible pathogenesis of cyst-like lesions of the white matter were evaluated.

Results: Cyst-like lesions in the cerebral white matter were found in three of the 15 patients. The signal intensity of these lesions was isointense with CSF on T1-, T2-, and FLAIR sequences. The cystic lesions ranged in number from 1 to 6 per patient and were usually 1 to 2 cm.

Conclusion: Cyst-like lesions in the cerebral white matter were seen on the MR images of 20% of 15 patients with tuberous sclerosis. Cystic lesions are a rare but typical cerebral manifestation of tuberous sclerosis and tuberous sclerosis should be taken into consideration in patients with such lesions.

C-0926

Proton MR spectroscopy and MR imaging in childhood hypomyelinating disorders

K.M. Koprivsek, M. Spirovski, D. Kozic, R. Semnic, M. Lucic, N. Prvulovic, J. Ostojic; Sremska Kamenica/YU

Purpose: Hypomyelinating disorders (HD) are rare childhood leucoencephalopathies, characterized by a permanent deficit in myelin deposition in the brain. The purpose of our study was to define possible MR imaging and spectroscopy patterns, which could help distinguish subtypes of HD and HD from other leucoencephalopathic forms.

Methods and Materials: We have examined 42 children, at a 1.5 T unit, with suspected leucoencephalopathies, as well as 30 age-matched controls. HD was suspected in 12/42 children. After conventional brain MR imaging and single-voxel proton-MRS (SE135/STEAM20), patients were divided into subgroups according to biochemical profiles and predominant features of white matter abnormalities. Corresponding laboratory/clinical data were matched and reviewed. The correlation between MR and clinical diagnosis was tested by Spearman-rank test.

Results: Pathological MR imaging/MRS findings were detected in 34/42 patients. Six children had normal brain MR imaging with abnormal biochemical profiles. In 2/42 MRS were normal, despite diffuse pathology detected on MR imaging. In HD-group MR imaging demonstrates: cerebral/cerebellar atrophy (9 and 6 pts), white matter lesion (diffuse 4, supra- and infratentorial 12 and 4 pts, respectively), capsula interna abnormalities (2 pts) and basal ganglia lesion (3 pts). Corresponding MRS revealed: normal findings (2/12), decrease in all metabolites (2/12), mild elevation of myoinositol and creatine levels (6/12). Using detected MR imaging/MRS patterns we made final MR diagnoses for the HD-group: Pelizaeus-Merzbacher disease (2 pts), Salla disease (2 pts), H-ABC-syndrome (4 pts), Cockayne-syndrome (1 pts) and unknown origin (3 pts). Spearman-rank value confirmed correlation between MR and clinical diagnoses ($P < 0.05$).

Conclusion: MR imaging combined with MR spectroscopy can facilitate the diagnosis of HD. Detectable pattern could be specific for some subtypes.

Scientific and Educational Exhibits

C-0927

Imaging of disorders involving the stomach in pediatric patients: A pictorial review

A. Álvarez Luque, T. Berrocal, L. de Pablo, J. Gutiérrez, L. Martín, N. Gómez León; Madrid/ES

Learning Objectives: To understand the embryology, pathology, and imaging features of a wide spectrum of congenital and acquired alterations involving the stomach in children. To understand the utility of each imaging modality that can be applied to the management of these conditions. To emphasise pitfalls and differential diagnoses of these entities.

Background: Congenital and acquired disorders affecting the stomach are a significant cause of morbidity in infants and children, frequently requiring multiple imaging modalities to diagnose and plan treatment. This teaching exhibit analyses and illustrates practical aspects of a wide spectrum of usual, unusual, and exceptional disorders affecting the stomach, with particular emphasis on radiological manifestations. The efficacy of the different imaging modalities in the diagnosis and management of these conditions will be evaluated.

Imaging Findings: Specific topics addressed include congenital and developmental abnormalities (pyloric atresia, microgastria, antral web, situs inversus, diverticula, duplication cysts, ectopic pancreas in the gastric antrum), volvulus, hypertrophic pyloric stenosis, inflammatory diseases (gastric ulcer, eosinophilic gastroenteritis, Menetrier disease, gastric tuberculosis, gastric involvement in chronic granulomatous disease, emphysematous gastritis, corrosive gastritis), Zollinger-Ellison syndrome, foreign bodies, bezoars, varices, hernias, benign tumors (hamartoma, adenoma, teratoma, hemangioma and lipoma); malignant tumors (leiomyosarcoma, leiomyoblastoma, stromal tumor, lymphoma), and postsurgical complications.

Conclusion: This exhibit provides an overview of the pathological processes affecting the stomach in pediatric patients as well as the utility of the various imaging techniques available. Because many of these disorders have a characteristic appearance, this exhibit will help the practising radiologist to better understand and recognise these entities.

C-0928

Pediatric urolithiasis: High-resolution sonography and clinical review

V. Garriga, N. Roson, S. Medrano, M. Zarcero, X. Pruna, M. Cuadrado, A. Marin, S. Carbó, S. Vizcaya, M. Català; Granollers-Barcelona/ES

Learning Objectives: To describe high-resolution sonography (HRUS) of pediatric renal stone disease including nephrolithiasis and nephrocalcinosis. To emphasize the usefulness of high-resolution sonography in the evaluation of underlying cortical or urinary tract abnormalities, complications and follow-up of renal stone disease. To review the anatomical, clinical and epidemiological factors in pediatric urolithiasis.

Background: Urolithiasis is usually considered a disease of adults, but it certainly occurs in the pediatric age group. The clinical presentation in children differs from the acute renal colic in adult, being less specific and difficult to identify. In addition, the increase in our immigrant population has lead to a high prevalence of the disease. On the other hand, unenhanced computed tomography has been widely used to demonstrate renal stone disease, but the high radiation dose, higher cost and sedation are still disadvantages when studying children.

Procedure Details: We performed a retrospective review of all pediatric sonographic studies with urolithiasis. Description of size, location, number of lithiasis, urinary tract abnormalities or signs of infection were recorded. Clinical, analytical and epidemiological data were reviewed in each patient. Later complications and follow-up studies were also analyzed.

Conclusion: The HRUS is able to well characterize lithiasis, to detect its association with anomalies of urinary tract, and to follow-up calculus disease. This non-invasive technique may avoid the use of CT, especially in young children and those with greater risk of recurrence. The HRUS of a child with urolithiasis gives not only diagnostic information but also defines the medical or surgical management of the patient.

C-0929

Ultrasonographic measurements of the adrenal and thyroid dimensions and their correlation with length, gestational age and birth weight of healthy neonates

F. Golpinar, C. Ozer, M. Nass Duce, A.H. Turhan, T. Akbas, G. Sert, E. Kara, A. Atici; Mersin/TR

Purpose: The aim of this study is to create normal standards by measuring the dimensions of the thyroid and adrenal glands in healthy newborns and to correlate these measurements with their gestational age, birth weight and height.

Methods and Materials: The dimensions of thyroid and adrenal glands of 218 healthy newborns were measured. The transverse dimension of the isthmus and transverse, sagittal and anteroposterior dimensions of the two lobes were noted. Then, the volume of each lobe was calculated. Two dimensions for each adrenal gland were measured. The newborns were classified into thirteen groups according to their gestational ages, four groups according to their height and six groups according to their weight. The thyroid volumes, dimensions of thyroid glands and dimensions of adrenal glands were correlated with each of these parameters.

Results: The mean value of the right thyroid lobe was 238 mm³, that of the left lobe was 222 mm³. The length and thickness of the right and left adrenal glands were 12.2 mm and 2.6 mm; 11.3 mm and 2.33 mm, respectively. There was a positive correlation between thyroid volume and length, gestational age and birth weight, but we could not find any correlation between adrenal measurements and these parameters.

Conclusion: Evaluation of dimensions is as important as hormone levels in diagnosing disorders of the thyroid and adrenal glands. It is thus crucial to correlate the average volumes and dimensions with length, gestational age and birth weight of newborns.

C-0930

Prenatal fetal lung volume measurement using magnetic resonance imaging (MRI) in pairs of twins with congenital diaphragmatic hernia (CDH)

A.K. Kilian, M. Schröder, T. Schaible, C. Düber, K.W. Neff; Mannheim/DE

Purpose: To compare fetal lung volume (FLV) based on magnetic resonance imaging (MRI) in healthy and affected twins with congenital diaphragmatic hernia (CDH).

Methods and Materials: Three pairs of twins with CDH in one fetus of each pair and 11 age-matched normal control fetuses were evaluated using prenatal fetal MR imaging at 34 weeks gestation. MRI was performed on a 1.5 T Magnetom Sonata (Siemens, Erlangen, Germany). Diagnosis of CDH and FLV evaluation was based on T2-weighted HASTE imaging in coronal, transverse and sagittal direction. FLV of the affected and the healthy fetuses was calculated by semiautomatic segmentation of the fetal lungs followed by 3D volumetry.

Results: MRI confirmed the diagnosis of CDH in one fetus of each pair, all left-sided. All three affected twins showed significant reduction of FLV compared to the healthy twin. FLV was found to be 12.5 ml for the affected twin and 56.2 ml for the healthy twin for the first pair of twins, 15.4 ml (twin with CDH) vs. 55.3 ml (healthy twin) for the second pair of twins and 13.2 ml (CDH) vs. 49.1 ml (healthy) for the third pair of twins. Age-matched normal control fetuses demonstrated a mean FLV of 65.6 ± 16.9 ml at 34 weeks gestation.

Conclusion: MRI fetal lung volume measurement of twins with CDH offers the most effective correlation between lung volumes of healthy children and children with CDH because of the very similar conditions. The FLV of healthy twins is also reduced compared to normal controls.

C-0931

CT findings of non-odontogenic tumors of the jaw in childhood

M. Hasiotou, E. Manoli, M. Ioannidou, M. Zarifi, E. Evangelidakis; Athens/GR

Purpose: Tumors of the bones of the jaw are classified as odontogenic and non-odontogenic. The latter are additionally characterized as benign or malignant depending on their mitotic and pathological behavior. This study intends to demonstrate the CT imaging characteristics of non-odontogenic tumors of the mandible and the maxilla in children.

Methods and Materials: We retrospectively studied the CT examinations of 31 children (20 females and 11 males) aged 3 to 15 years that were examined in our department. The underlying disease was histologically confirmed in all cases; Langerhan's cell Histiocytosis (7), non-Hodgkin's lymphoma (6), acute lymphoblastic leukemia (1), fibrous dysplasia (5), metastatic neuroblastoma (3), osteosarcoma (2), aneurismal bone cyst (2), hemangioma (2), Ewing sarcoma (1), primitive neuroectodermal tumor (1), osteoma (1).

Results: The radiological CT findings were described according to the site (mandible, maxilla), the type of the bone lesion (lytic, osteoblastic, periosteal reaction, cortical disruption, internal diaphragms) and the participation of the adjacent soft tissues (soft tissue mass, "floating" teeth) and finally correlated to the histological reports.

Conclusion: Today's modern imaging modalities provide important information about not only the type of a mass lesion in the jaw, but also useful details concerning the extent of the disease and the potential invasion in surrounding soft tissues. This becomes a major advantage when referring to children given the exceptional difficulty in the performance of diagnostic biopsy sampling.

Scientific and Educational Exhibits

C-0932

Abdominal sonographic examination in the pediatric emergency room and incidental findings

M. Vakaki, G. Pitsoulakis, V. Dermentzoglou, C. Kosmas, C. Koumanidou; Athens/GR

Purpose: Sonography is the initial imaging method of choice in almost every acute abdominal problem in childhood. It usually provides valuable diagnostic information. Rarely, however, the sonographic findings are unexpected and significant for the child's health or even life. The purpose of this retrospective study was to determine the prevalence and significance of incidental findings detected on the abdominal sonogram for trauma and acute abdominal pain.

Methods and Materials: During a 6-year period, 6124 sonograms were performed in our radiology department in children with blunt abdominal trauma or acute abdominal pain of unknown aetiology. Those in which incidental findings had been recorded were assessed.

Results: Incidental findings were detected in 257 (4%) cases. Some were benign requiring further investigation and others more serious or even malignant: 8 hepatomegalias, 68 splenomegalias, 20 hyperechogenic livers, 16 cholelithiasis, 3 situs inversus, 4 renal ageneses, 5 renal ectopies, 6 significantly small kidneys, 6 horseshoe kidneys, 8 nephrolithiasis, 4 dilatations of the renal collecting systems, 4 renal cysts, 5 multicystic dysplastic kidneys, 4 autosomal recessive kidney disease, 40 simple or hemorrhagic ovarian cysts, 4 ovarian teratomas, 3 uteri didelphys associated with unilateral renal agenesis, 8 enteric duplication cysts, 3 mesenteric cysts, 1 cystic teratoma, 1 splenic dermoid cyst, 18 nephroblastomas (one associated with contralateral nephroblastomatosis), 14 neuroblastomas and 2 with hepatic metastases and 1 hepatoblastoma.

Conclusion: In the emergency setting the pediatric radiologist has to be particularly careful in order to avoid missing a significant diagnosis which may have important implications for the young patient.

C-0933

Soft tissue swelling of the hand or foot in childhood: The role of sonography

M. Vakaki, G. Pitsoulakis, V. Dermentzoglou, M. Tsianta, E. Emmanouil, C. Koumanidou; Athens/GR

Purpose: Soft-tissue swelling of the wrist, hand, ankle or foot, except in the case of trauma, represents an uncommon pediatric clinical problem. Until recently the imaging approach was not easy as the plain radiograph is not usually diagnostic. MR imaging is unsuitable as the routine imaging method due to the need for sedation and the high cost. The aim of our study is to present the role of sonography in the imaging investigation of this clinical problem.

Methods and Materials: 35 children (44 days to 14 years old) were sonographically examined due to wrist/hand/ankle/foot soft-tissue swelling. The clinical history and presentation varied. Children with a recent history of fall or trauma were excluded. The sonographic examination (gray-scale/color Doppler) was performed with high-frequency transducers.

Results: The sonographic findings included: periarticular ganglions (n = 8), tendon sheath ganglions (n = 4), tendinitis (n = 1), tenosynovitis (n = 4), bursitis (n = 2), coexistence of periarticular ganglion and neurofibroma (n = 1), cystic lymphangioma (n = 2), hemangioma (n = 4), neurofibroma (n = 3), foreign bodies (n = 4). Sonographic appearances were more or less characteristic. In 2 children a solid soft-tissue mass with non-specific features was sonographically depicted. CT and MR imaging followed. Histological examination established the diagnosis of benign xanthoma and malignant sarcoma, respectively. All remaining cases were confirmed surgically or by clinical follow-up.

Conclusion: The well-known advantages of sonography are of utmost importance during childhood. Nowadays, with high-definition modern equipment, the sonogram can provide an accurate diagnosis in the majority of hand/foot soft-tissue swellings, indicating the proper management. Further imaging investigation (plain radiograph, CT or/and MRI) should be performed only in selected cases with negative or indeterminate sonographic findings.

C-0934

Imaging evaluation of pediatric patients with peritoneal malignancies

G. Pitsoulakis, M. Vakaki, M. Zarifi, C. Hadjigeorgi, M. Xasiotou, I. Nikas, N. Evlogias; Athens/GR

Purpose: Peritoneal involvement by malignancy is rare in childhood and its spectrum is different from that in adulthood. The aim of this study is to present the imaging findings (US, CT, MR) in a variety of different cases of peritoneal malignancy.

Methods and Materials: The radiological studies (US, CT, MR) of 21 patients,

aged 1 month to 13 years, with peritoneal malignancies were retrospectively evaluated.

Results: The US, CT and MR appearances of 7 cases of leukemia, 5 cases of lymphoma (4 of them Burkitt's lymphoma), 3 cases of histiocytosis, 2 cases of intraabdominal desmoplastic small cell tumor, 2 cases of neuroblastoma gr IV, one case of congenital rhabdomyosarcoma and, finally one case of intraperitoneal metastases of a malignant rhabdoid tumor. All the above cases were histologically confirmed. The differential diagnosis and the characteristic findings are discussed.

Conclusion: Although rare and, in the majority without specific imaging features, most cases of peritoneal malignancy allow a narrow differential diagnosis, as long as the pediatric radiologist is aware of their existence and their imaging findings.

C-0935

Atypical presentations of pediatric osteomyelitis

N. Ruscalleda, R. Huguet, J. Ribo, J. Blanch, A. Capdevila; Esplugues de Ll./ES

Purpose: This pictorial essay shows some cases of pediatric osteomyelitis observed in our radiology department in which diagnosis proved to be difficult. We also describe some changing aspects related to the diagnostic approach.

Methods and Materials: Over the past ten years, we have diagnosed 152 cases of osteomyelitis; these have been subject to different imaging and microbiological techniques.

Results: Although pediatric osteomyelitis is usually located in long bones, we have observed an increase in the number of cases of osteomyelitis located in axial skeletal and small bones. Of the 152 cases 41 of were located in axial skeletal or small bones and 15 were multicentric. Although in the majority of cases the presentation is acute, we also observed an increase in the number of subacute forms in which clinical diagnosis is more difficult. This could be associated with an increase in atypical pathogens such as *Kingella kingae*.

Conclusion: Osteomyelitis is a serious disease that requires swift diagnosis in order to prevent or minimize consequences. The typical appearances of pediatric osteomyelitis in different imaging techniques is well established and diagnosis is therefore usually simple. However, there are some cases that are extremely difficult to differentiate from other entities.

C-0936

Utility of the posterior fontanelle approach in cranial sonography

R.M. Lorente-Ramos, Y. del Valle-Sanz, M.J. Alcaraz-Mexía; Madrid/ES

Purpose: To assess the utility of adding posterior fontanelle imaging to the anterior fontanelle approach in routine neonatal cranial sonography.

Methods and Materials: From 20th February to 30th June 2004, 136 consecutive transcranial sonograms were performed in 90 newborn patients. All patients underwent a US study within 72 hours from birth and follow-up sonograms were performed when needed. The sonographic sections were obtained, first through the anterior fontanelle in coronal, sagittal and oblique planes, and then through the posterior fontanelle when it was possible or otherwise through the posterior region of the sagittal suture, in sagittal, axial and oblique planes.

Results: We performed 1 sonogram in 69 patients, 2 sonograms in 12 patients, 3 in 5 patients, 6 in 2 and 12 in 1 patient. Low-birth-weight was the most frequent indication for sonography with 10 patients weighing less than 1500 g. Thirty-four sonograms were abnormal in 21 patients. In 19 patients findings were similar both with anterior and posterior fontanelle imaging (one primary choroid plexus hemorrhage, one posterior fossa cyst, one extensive intraparenchymal hemorrhage, and periventricular hyperechogenicity in 16 patients). In two patients hemorrhages within choroid plexus were suspected at anterior fontanelle views and lobular choroid plexus were diagnosed with posterior fontanelle imaging. In normal sonograms posterior fossa structures were better depicted through the posterior fontanelle.

Conclusion: Although our preliminary results do not support routine examination through the posterior fontanelle it is useful in selected cases as a complementary tool and helps in depicting posterior fossa structures.

C-0937

withdrawn by authors

C-0938

withdrawn by authors

Scientific and Educational Exhibits

Physics in Radiology

C-0939

Superficial melanoma and its metastases in the eyes of skin electrophysiological imaging (SEI)

Y.F. Babich, M.A. Nuzhdina; Kiev/UA

Purpose: A new functional imaging modality SEI enables non-invasive dynamic imaging of skin and underlying tissues in a complex of electrophysiological parameters. Our current work consists in lab-clinical investigation of the Skin Electrical Landscape' (SEL) dynamics in normals and pathology with the purpose of finding out early distinguishing features between malignant and benign lesions at the background of normal SEL.

Methods and Materials: SEI enables to monitor the SEL simultaneously in 6 electrical parameters. Proliferating nevus (7) and nodal melanoma (6) were chosen as model objects of investigation. In order to bring to light functional heterogeneities of the imaging region, non-thermal millimeter EMF (1 min, 0.5 mcW/sq.sm) and static MF (1+1 min of reversed orientation, ~20 mT) were used as stimulant factors. Through -SEL-frame-sequence-analysis resulted in detailed dispersion maps (DM). Subsequent phase plane analysis was applied to the distinctive DM points.

Results: New phenomena of the SEL dynamics have been discovered, specifically: Its spontaneous cluster character, which appeared to be noticeably correlated with the skin lesions' topology; hyperactive zones at the visible melanoma boundary; multilevel quasi-stationary character of the SEL abnormal points; high-speed MF-induced processes (presumably of enzyme origin). The SEL analysis revealed detailed, visually indistinguishable, pattern of primary melanoma, which was confirmed histologically. Remote (invisible) areas with similar SEL characteristics were determined.

Conclusion: SEI seemingly enables detailed metabolic mapping and monitoring of superficial tumours and their invisible metastases but further joint research with the additional use of appropriate functional imaging modalities is needed.

C-0940

Synchrotron radiation microangiographic imaging of tumor-derived blood vessels in rabbit model of cancer for observation of angiogenic activity

K. Umetani¹, M. Kobatake², A. Yamamoto², T. Yamashita², S. Imai², Y. Kajihara²,
¹Sayo-gun, Hyogo/JP, ²Kurashiki-shi, Okayama/JP

Purpose: To investigate the microangioarchitecture of tumor-derived angiogenic vessels, in vivo imaging experiments were carried out for depicting small blood vessels in a VX2 carcinoma transplanted into a rabbit auricle.

Methods and Materials: A microangiography system with spatial resolution in the micrometer range was developed using a high-resolution detector and a third generation synchrotron radiation source at SPring-8. Monochromatic synchrotron radiation X-rays transmitted through an object were detected by the X-ray direct-conversion type detector incorporating the X-ray SATICON pickup tube. In two real-time imaging modes, input fields of view were 9.5 mmx9.5 mm and 4.5 mmx4.5 mm, and pixel sizes were 9.5 and 4.5 microns in the case of the 1024x1024-pixel format, respectively.

Results: After contrast agent injection to the auricular artery, the microangiography system could provide images of immature vascular networks in the malignant tumor transplanted into the rabbit auricle. Small blood vessels of around 10 microns in diameter and the distribution of abnormal staining were observed and analyzed for the prediction of the level of angiogenic activity.

Conclusion: The microangiography system using the nearly parallel synchrotron radiation beam presents advantages over light microscopes for clarifying internal angioarchitecture of centimeter-sized objects with spatial resolution in the micrometer range. Using the imaging system, anti-angiogenic responses in preclinical drug testing can be assessed by observing changes in the angioarchitecture and perfusion characteristics of the tumor in animal studies.

C-0941

Age and gender related differences of adipose tissue compartments:

A whole body MR imaging study

J. Machann, C. Thamer, B. Schnödt, H.-U. Häring, C.D. Claussen, A. Fritzsche, F. Schick; Tübingen/DE

Purpose: Quantification of all major adipose tissue compartments by MR imaging in a large cohort of healthy volunteers at an increased risk for type 2 diabetes. Analysis of body fat distribution with respect to gender and age and metabolic data.

Methods and Materials: One hundred and thirty healthy volunteers (80 females, 19-69 years, 50 males, 21-65 years) underwent whole body MR imaging on a 1.5 T whole body unit (Magnetom Sonata, Siemens). A T1-weighted fast spin-echo technique was applied for fat-water discrimination. Parameters: TE/TR 12 ms/490 ms, slice thickness 10 mm, interslice gap 10 mm, acquisition time 12 s. Post-processing: segmentation of adipose tissue (AT) and quantification of total (TAT), subcutaneous (SCAT) and visceral adipose tissue (VAT). Determination of insulin sensitivity (ISI) by glucose clamp.

Results: Females are characterized by significant higher%TAT compared to males (f:33.5 ± 7.4%, m:22.8 ± 5.7%, p < 0.0001). On the other hand,%VAT is significantly higher in males (f:2.3 ± 1.0%, m:3.8 ± 1.3%). Furthermore,%VAT significantly increases with age in both gender groups (p < 0.001) whereas the other AT compartments are nearly unchanged (n.s.). ISI shows strong correlations with%VAT in both gender groups, but is independent on age (n.s.) in our study population.

Conclusion: Reliable quantification of different adipose tissue compartments in the human body is possible by common MR techniques. Especially the amount of visceral adipose tissue which is thought to be directly involved in the pathogenesis of insulin resistance markedly depends on gender and age. Those dependencies must be considered in cross-sectional metabolic studies. Supported by a grant of the Deutsche Forschungsgemeinschaft (DFG, KFO 114/1).

C-0942

An elastic registration scheme for the alignment of thoracic CT data of patients with stage III non-small cell lung cancer during radiotherapy treatment

G. Matsopoulos¹, V.E. Kouloulias², N. Mouravliansky¹, P. Asvestas¹, K. Delibasis¹, N. Uzunoglu¹, A. Kelekis², N. Kelekis², ¹Athens/GR, ²Xaidari/GR

Purpose: The establishment of an automatic three-dimensional (3D) non-rigid registration scheme for the alignment of thoracic computed tomography (CT) data of patients with stage III non-small cell lung cancer (NSCLC) during radiotherapy.

Methods and Materials: Initially anatomical set of points are automatically segmented slice by slice from the two CT scans of the same patient in order to serve as interpolant points. A rigid-body transformation is then applied to provide a pre-registration of the data. The novel application of the Self Organizing Maps (SOMs) is adopted. Then, Radial Basis Functions (RBFs) using the shifted log function is subsequently employed for elastic warping of the image volumes. Fifteen patients have been selected in this study having lung tumors and undergoing radiotherapy treatment.

Results: All CT data has been successfully registered by the proposed methodology as it has been revealed by detailed observation of the results by experienced radiologists. The proposed elastic registration scheme resulted in an average accuracy of around 6 mm against a surface-based registration method resulting an average accuracy of around 11 mm.

Conclusions: An automatic elastic registration scheme is proposed applied on thoracic CT data of patients diagnosed with NSCLC. The scheme can recover deformations occurred due to inspiration and/or any physiological movements during acquisition. This scheme could provide objective measurements of target volumes during radiotherapy treatment planning.

C-0943

Monte Carlo study on radiation absorption properties of Gd2O2S, CsI, LSO, CaWO4 phosphor screens for mammographic X-ray imaging

P. Liaparinos¹, I. Kandarakis², D. Cavouras², D. Nikolopoulos², G. Panayiotakis¹,
¹Patras/GR, ²Athens/GR

Purpose: The quantum detection efficiency (QDE) of the most commonly used CaWO4, Gd2O2S, CsI phosphor screens was compared with the recently introduced high efficiency Lu2SiO5 (LSO) powder scintillating phosphor under mammographic conditions using Monte Carlo methods.

Methods and Materials: A Monte Carlo program was developed for the simulation of X-ray interactions within the aforementioned phosphor materials in order to investigate their efficiency to detect radiation. Radiation absorption properties of phosphor screens were examined assuming molybdenum spectrum X-ray beam in the tube voltage range 20-30 kV. Phosphor coating thickness was chosen to vary from 25 up to 35 mg/cm². X-ray spectra and mass attenuation coefficients were taken from published tabulated data. A large number of photons (107 histories) were applied giving a statistical error less than 0.5%.

Results: Results obtained from Monte Carlo simulation showed that CsI exhibits highest radiation absorption properties in the whole voltage and thickness range. The detection efficiency of 30 mg/cm² CsI screen was found to vary from 93% down to 78% in the range of tube voltages from 20 kVp up to 30 kVp. For a corre-

Scientific and Educational Exhibits

sponding LSO screen the detection efficiency was found to vary from 78% down to 62%.

Conclusion: Considering the intrinsic columnar structure of CsI crystals which reduces light spreading and improves image resolution, CsI is significantly better to mammographic imaging systems although it has lower effective atomic number and density than LSO as well as than Gd₂O₂S, CaWO₄. Acknowledgments: This work was financially supported by EPEAEK program 'Archimidis'.

C-0944

Influence of rib structure on detection of subtle lung nodules

M. Ikeda, T. Ishigaki, S. Itoh; Nagoya/JP

Purpose: To access the influence of anatomic noise on the detectability of subtle lung nodules depicted on chest radiographs, focusing on the relationship between rib structures and nodule positions.

Methods and Materials: From the normal chest radiography images, 132 square regions were extracted, and the centers of these square images were on the upper margin of a rib, the inside of a rib, the lower margin of a rib and the central region between two adjoining ribs. Simulated nodules were digitally superimposed on the centers of these extracted square images. 12 radiologists viewed 50 soft-copy images including these 792 processed images, including the noise-added images. The observer's confidence level for the nodule-added square image was used as an index of observer performance.

Results: Results indicated a statistically significant effect of the relationship between rib structures and nodule positions on the detection performance ($P < 0.001$). The nodule detectability on the images with a center located between two adjoining ribs was significantly the best, whereas it was significantly the worst on the noise-added images with a center located between two adjoining ribs. Further, the detectability of the nodules located on ribs showed a tendency to decrease in the order of the upper margin, the inside and the lower margin of a rib. However, these differences were small.

Conclusion: The rib structure overlying a subtle lung nodule on chest X-ray images will have a detrimental effect on nodule detection performance as anatomic noise, regardless of the nodule location on ribs.

C-0945

Tutorial on physical principles of MR imaging: Spin behavior study

L. Chaustre-Mendoza, D. Moratal-Pérez, L. Martí-Bonmatí, Y. Flórez-Ordóñez, J. Millet-Roig; Valencia/ES

Learning Objectives: This tutorial shows to radiologists the spin behavior in the presence of a magnetic field and under the excitation of a RF pulse. It graphically animates and displays the precession movement of the spins and their behavior in a slice under the application of phase and frequency encoding gradients.

Background: The spin precession of the nucleus around its own axis acts as a small magnetic moment that behaves as a magnet. After applying an external main magnetic field, the small magnetic moment tends to align with it describing a precession movement. The encoding gradients generate a variation of the main field based on the position.

Procedure Details: The graphical user interface was developed under MATLAB 6.5. First, the user chooses some input parameters (main magnetic field strength, type of nucleus, applied RF excitation pulse flip angle). Then, the user will observe the precession movement of the selected nucleus and the amplitudes of the longitudinal and transverse magnetizations during the relaxation step, being able to analyze T1 and T2 relaxation times. The user will graphically evaluate the spins behavior of a slice under the application of a frequency and a phase encoding gradients.

Conclusion: The graphical study of the spin behavior under a RF pulse excitation in a magnetic field is, in general, a very useful way to explain the origin of the MR signal. This is a very important step in order to clarify how the MR image is obtained. It will be very well appreciated by radiologists.

C-0946

Performance evaluation of a clinical 64-slice spiral CT scanner

Y. Kyriakou, M. Kachelriess, J.U. Krause, W.A. Kalender; Erlangen/DE

Purpose: To evaluate a 64-slice cone-beam CT system with respect to image quality and susceptibility to cone-beam artifacts.

Methods and Materials: Our 64-slice CT scanner (Sensation 64, Siemens Medical Solutions, Forchheim, Germany) acquires 64 overlapping slices of 0.6 mm thickness. A z-flying focal spot (zFFS) switches between two z-positions and thereby allows one to acquire two slices per detector row. We used a thin wire phantom and a delta phantom (50µm gold disc) to quantify the spatial resolution. We

evaluated the 0.5 s standard spiral scan mode for pitch values ranging from 0.5 to 1.5 in steps of 0.1. Further, a high contrast spatial resolution phantom consisting of rows of small holes oriented along x/y and along x/z was measured. Additionally we used a water phantom to assess image noise and an artifact phantom to search for spiral windmill artifacts.

Results: Neither image noise nor spatial resolution (0.7 mm FWHM in-plane and 0.65 mm FWHM in the z-direction) were dependent on the pitch value. The 0.4 mm holes holes were separated both along x/y and x/z, documenting an isotropic resolution. Image noise was constant in the rotation center but showed a sinusoidal dependency off-center. Spiral windmill artifacts, which predominantly appear for higher pitch values, remained low due to the zFFS even for the largest pitch value.

Conclusions: The zFFS technology provides an isotropic resolution of 0.4 mm and achieves considerable windmill artifact suppression.

C-0947

Optimising scan protocols and assessing image quality in clinical MR imaging

G. Lucchicenti¹, F. Cademartiri², U. Sabatini¹, E. Giugni¹, M.G. Egito³, S. Bastianello³; ¹Rome/IT, ²Rotterdam/NL, ³Pavia/IT

Learning Objectives: 1) To illustrate the fundamentals of MR imaging through basic concepts which can be universally applied to imaging sequences, examination protocols and image interpretation. 2) To provide the basic criteria to assess image quality. 3) To provide simple criteria to optimise MR scan protocols for clinical radiology.

Background: The development of MR scanners and advanced techniques makes the scan protocol increasingly difficult to be optimised for clinical use. For this reason, the deep knowledge of the MR basis is crucial to perform a diagnostic examination within reasonable times and costs, considering the MR workflow. The clinical MR imaging can be summarised in these three aspects: 1) the generation of the signal (the magnetization), 2) the signal encoding and 3) the image contrast. The knowledge of the relationships between these aspects is crucial for optimising the scan protocol.

Procedure Details: The fundamentals of the MR imaging acquisition technique are described through a simple visual based approach using graphs, phantoms and clinical cases. The algorithm for the optimisation of the scan protocol is provided. The major artifacts of MR imaging are shown using phantoms and clinical examples.

Conclusion: The basic concepts of MR imaging are crucial for the optimisation of the imaging sequence, the examination protocol and for image interpretation.

C-0948

Reliability of contrast-detail (C-D) diagrams deduced from a Markov chain and reduction in the number of observation times

T. Niimi¹, K. Imai¹, M. Ikeda¹, H. Maeda¹, A. Mano¹, Y. Enchi²; ¹Nagoya/JP, ²Osaka/JP

Purpose: Contrast-detail (C-D) diagrams are being used to evaluate image quality in medical diagnostics. To improve the accuracy of C-D analysis, observers must interpret many phantom images. This process in image quality evaluation requires a lot of time and labor. In this study, we devise a C-D analysis method which can reduce the number of observation times effectively using information theory called Markov chain.

Methods and Materials: A commercially available Burger phantom was employed as a test object and 20 phantom radiographs with 0.8 background densities were prepared. Examinees were 29 radiological technicians and 6 radiologists. The observers interpreted all phantom radiographs independently of each other with the room lights off. Assuming that the observer's interpretation of the phantom radiographs involve a simple Markov process, the contrast detectability for each signal diameter was calculated using data obtained from interpretations of two phantom radiographs and a C-D curve was constructed based on this result. Reproductions of the C-D curve were also investigated using some arbitrary set of two phantom radiographs. In addition, a normal C-D curve was constructed using arithmetical averages of contrast detectability obtained from interpretations of all phantom radiographs.

Results: All C-D curves deduced from the Markov chain agreed well with each other. Furthermore, these C-D curves were in excellent accord with the normal C-D curve obtained from interpretations of all phantom radiographs.

Conclusions: C-D curves deduced from the Markov chain are reliable and introduction of the Markov chain makes it possible to reduce the number of observation times.

Scientific and Educational Exhibits

C-0949

The strict meaning of the area under a contrast-detail (C-D) curve

K. Imai¹, T. Niimi¹, M. Ikeda¹, H. Maeda¹, A. Mano¹, Y. Enchi²; ¹Nagoya/JP, ²Osaka/JP

Purpose: A receiver operating characteristic (ROC) analysis and a contrast-detail (C-D) analysis are being used for image quality evaluation in medical diagnostics. A quantitative index describing a ROC curve is the area under it and is useful in image quality evaluation. In contrast, a C-D analysis does not have a proper index. Intuitively, the area under a C-D curve may be a useful index in image quality evaluation. The purpose of this study is to clarify the meaning of the area under a C-D curve using information theory.

Methods and Materials: A commercially available Burger phantom was employed as a test object and 20 phantom radiographs with 0.8 background densities were prepared. 17 radiological technicians interpreted all phantom images independently of each other. A C-D curve was constructed based on this interpretation. Furthermore, image information $I(y)$ received by observers was calculated from detective probability $P(y)$ corresponding to the contrast detectability for each signal diameter ($I(y) = -\log_2 P(y)$). Image information $I(x)$ of the test object was calculated in a similar way ($I(x) = -\log_2 P(x)$, $P(x)$: generating probability of image signals).

Results and Conclusion: A small area dS under the C-D curve decreased with a signal diameter: the contrast detectability increased with it. The increase in the contrast detectability means the reduction in the image information loss. The information losses are given by $I(x)-I(y)$. The information loss calculated from this equation reduced with the signal diameter. Therefore, the area under a C-D curve given by integrating dS is equivalent to the total information loss.

C-0950

Preliminary studies on a quantum noise reduction filter in 16-slice multislice CT (MSCT)

T. Ishihara, T.S.S.R. Ishihara; Kashiwa, Chiba/JP

Learning Objectives: 1) To perform filter processing to reduce image SD and improve CNR while maintaining acceptable resolution. 2) To describe a new quantum noise reduction filter and confirm its clinical usefulness. 3) To compare images acquired at full dose and filter-processed images acquired at half dose.

Background: MSCT has higher resolution but also higher image noise. Noise varies with the target, and density resolution and target size cannot be ignored. We developed a 3-axis nonlinear quantum noise reduction filter and compared the spatial and density resolution of source and filtered images.

Imaging Findings: At a filter setting of 144, high contrast resolution fell. All 9 teeth (0.6 mm) of a comb were seen. The filter was set to improve granularity and low contrast resolution while maintaining high contrast resolution to improve image quality at full dose and for exposure compensation in low-dose areas. The teeth were not seen when resolution was reduced by > 60%. Image quality was similar at half and full dose for the same resolution. The higher SD and lower resolution due to patient size were compensated.

Conclusion: Filter processing reduces resolution slightly but is clinically useful. In the future, filter settings at each target size and for low-dose compensation may be set automatically.

C-0951

Development of a new three-dimensional image reconstruction algorithm to reduce cone-beam artifacts

T. Gomi¹, K. Koshida², T. Miyati²; ¹Nagano/JP, ²Kanazawa/JP

Purpose: An image reconstruction algorithm to reduce cone-beam artifacts in cone-beam CT was investigated.

Methods and Materials: Beeze sphere numerical phantom were arranged at different positions on the longitudinal direction and a computer simulation was performed. Due to differences in projection angle, data projected onto the detector surface were projected along trajectories exhibited as different periodic functions depending on the distance and position from the center of rotation. Therefore, projection in several detector channels by several projection data resulting from periodic functions is considered responsible for the increase in cone-beam artifacts with reconstruction planes at positions further from the center of rotation. We present here a new algorithm: 1) Weighting with respect to projection data at individual projection angles is changed. 2) The correction coefficient is distributed so as to be larger in the vicinity of the center of the detector with respect to individual channel data for a detector and smaller in the vicinity of the edges. 3) Corrected projection data were 3D back-projected. Evaluation and analysis of a new algorithm and the thorax numerical phantom were used.

Results: The effect of decreasing cone-beam artifacts of an object located at the edges was markedly increased in reconstruction planes at positions further from the center of rotation. Computer simulations showed that the spatial resolution (modulation transfer function) is improved by 14-20%, image noise (standard deviation) is improved by 10-18%.

Conclusions: We confirmed that this algorithm decreases cone-beam artifacts and generates high-quality reconstruction images.

C-0952

Fat suppression in MR imaging: Techniques and clinical applications

S.M. Dias, C. Pina Vaz, M. Gouvêa; Porto/PT

Learning Objectives: To review the most widely used fat signal suppression techniques in Magnetic Resonance Imaging and illustrate the main clinical applications. To describe the basic physical principles, advantages and limitations of each method.

Background: Fat signal suppression is a routinely used tool in Magnetic Resonance Imaging. It improves sensitivity for lesion detection and provides invaluable information in tissue characterization. Minimizing signal from fat in Magnetic Resonance can be achieved with different techniques: Selective fat saturation, selective water excitation, inversion-recovery imaging and opposed-phase imaging, among others.

Procedure Details: The authors present a review of the most common techniques of fat signal suppression and their physical principles based on the experience of our tertiary care hospital. The clinical applications, indications and disadvantages of the different methods are discussed and illustrated thoroughly.

Conclusion: There are several fat suppression techniques in Magnetic Resonance Imaging, which work by exploiting particular characteristics of the radio-frequency signals from fat and water. Understanding the mechanisms of each method provides insight into appropriate applications and anticipation of potential pitfalls.

C-0953

Measurement of carotid artery specimens comparing two CT imaging modalities using a 64-slice clinical CT scanner and a flat-panel detector

C-arm system

T. Riedel, Y. Kyriakou, D. Schäfer, M. Lell, W. Lang, W.A. Kalender; Erlangen/DE

Purpose: To assess CT image quality of carotid artery specimen measurements on a C-arm system equipped with a flat-panel detector in comparison to a 64-slice clinical CT scanner.

Methods and Materials: Carotid specimens were measured on a commercial C-arm system (Axiom Artis dFC, Siemens, Forchheim, Germany) and a clinical CT scanner (Sensation 64, Siemens, Forchheim, Germany). The C-arm is equipped with a flat-panel detector consisting of a photodiode array of amorphous silicon (a-Si) providing 960x960 pixels with a pixel size of 184µm coupled to a 600µm thick phosphor (CsI:TI) for X-ray absorption. The system offers a scan range of 240° of rotation with angular steps of 0.6°. The clinical 64-slice CT scanner acquires 64x0.6 mm overlapping slices.

Results: The structure of small calcifications and of the carotid artery wall was detected in both CT imaging systems. The C-arm provided a higher spatial resolution (better than 200µm) compared to the clinical CT scanner (400µm). Multiplanar reformations of the reconstructions confirmed the resolution isotropy in axial, coronal and sagittal. Especially the higher spatial resolution of the C-arm system allowed for a precise determination of the sizes of the artery lumen and of the single calcifications.

Conclusions: CT imaging of carotid artery specimens in air using C-arm systems equipped with flat-panel detectors demonstrated the possibility of accurate delineation of the artery wall and calcifications. Since it provides real 3D data it may be a fast alternative to histology in morphological analysis.

C-0954

Dose and low contrast detectability of new anode materials in mammography: Monte Carlo simulation studies

H. Delis¹, G. Spyrou², L. Costaridou¹, G. Tzanakos², G. Panayiotakis¹; ¹Patras/GR, ²Athens/GR

Purpose: Mammography is currently the technique with the highest sensitivity for early detection of breast cancer. As screening mammography refers to asymptomatic women, the task of optimization between image quality and radiation dose is critical. A way towards optimization is the introduction of new anode materials. Two new materials were evaluated, in terms of dose and low contrast detectability, using Monte Carlo simulation.

Scientific and Educational Exhibits

Methods and Materials: Several materials with characteristic energies inside the useful range of mammography were evaluated for their mechanical and thermal suitability as anode materials. The materials fulfilling the requirements were ruthenium (Ru) and silver (Ag). Using an analytical model, theoretical spectra were derived for these anode materials, for a number of tube voltages and filters. A recently developed and validated Monte Carlo simulation model was used to derive the dose and the low contrast detectability of these spectra.

Results: Ru/Ru (ruthenium anode / ruthenium filter) spectra demonstrate similar performance compared to Mo/Mo spectra, increasing slightly (2.1%) the Entrance Surface Dose, while providing increased low contrast detectability. In the case of harder spectra, Ag/Al-W spectra demonstrate analogous performance with W/Al spectra, for both dose and low contrast detectability.

Conclusion: New anode materials, such as Ru or Ag, could alternatively be used in mammography. Although further study is required, Monte Carlo simulation results demonstrate that dose and low contrast detectability of new theoretical systems are comparable, and in some cases improved, with respect to commonly used systems.

C-0955

The importance of detector type, detector material, reconstruction filter and reconstruction algorithm in simulated computed tomography breast imaging

A. Gaitanis¹, I. Kandarakis¹, D. Cavouras¹, N. Kalivas¹, N. Dimitropoulos¹, D. Nikolopoulos¹, G. Panayiotakis²; ¹Athens/GR, ²Patras/GR

Purpose: The aim of this work was to investigate the quality of an image produced by a Computed Tomography Breast Imaging (CTBI) system, taking into consideration the effect of detector type, material, reconstruction algorithm and reconstruction filter.

Methods and Materials: Software simulating a CTBI system was created. The simulated CTBI system consisted of: a) an X-ray source, b) the subject (software phantom including simulated glandular, carcinomas and calcifications structures), c) the detector array and d) the reconstruction software. Molybdenum target X-ray tube with voltages ranging from 20 to 40 kV was considered. The detector array was considered to be a linear one. The Quantum Detection Efficiency (QDE) of various scintillator materials such as CsI:Tl, Gd2O2S:Pr(UFC), Y1.34, Gd0.60O3(Eu,Pr)0.06 (Hilight) etc in several thicknesses were calculated. Also, the conversion of detected photons into the light was taken into consideration. To reduce noise energy weighted detector function was introduced. The reconstruction process was performed using Filtered Back-Projection (FBP) algorithm and several reconstruction filters such as Shepp-Logan, Hanning, etc for 360 projections. Calculated image characteristics were Signal to Noise Ratio (SNR) and Relative Contrast (RC).

Results: For carcinomas and calcifications highest SNR was obtained by a combination of Hilight scintillator, 160 mg/cm² thickness, 360 projections and Hanning reconstruction filter, while the highest RC was obtained by the same combination but for Ram-Lak reconstruction filter.

Conclusion: Detector type, detector material and reconstruction filter affect the detectability of carcinomas and calcifications in a computed tomography breast image. Acknowledgments: This work was financially supported by EPEAEK program 'Archimidis'.

C-0956

Influence of liquid crystal display (LCD) monitors on observer performance for detection of nodular lesions on chest radiographs

H. Usami, M. Ikeda, T. Ishigaki, H. Fukushima, K. Shimamoto; Nagoya/JP

Purpose: To access the influence of liquid crystal display (LCD) monitors on the detectability of nodular lesions depicted on chest radiographs, by comparing with a high-resolution cathode ray tube (CRT) monitor.

Methods and Materials: Ten radiologists observed 247 soft-copy images on LCD monitors with a pixel array of 1280×1024, 1600×1200, 2048×1536, 2560×2048 and a CRT monitor with a pixel array of 2560×2048, and were asked to indicate his or her confidence level regarding the presence of a nodule by using a continuous rating scale. These images were the chest radiographs with and without a lung nodule from "Standard Digital Image Database" created by the Japanese Society of Radiological Technology. The luminance distributions of all monitors were adjusted to the same and the ambient illumination was 200 lux in all image reading sessions. Observer performance was analyzed in terms of the receiver operating characteristics (ROC), and the statistical analysis of the differences among the five monitors comprised the analysis of variance of pseudovalue of the area under the binormal ROC curve computed by the jackknife analysis method.

Results: No statistical significant differences of nodule detection performance were found among the four LCD monitors and the CRT monitor, and there was no significant difference of the observer's confidence level for the image with a nodule among them.

Conclusion: The nodule detection performance on the LCD monitor with a higher spatial resolution than a matrix size of 1280×1024 is equivalent to the one on the high resolution CRT monitor.

C-0957

Proton MR imaging spectroscopy and fMR imaging changes associated to simple and complex movement in clinically isolated syndromes suggestive of multiple sclerosis

F. Preoteasa, I. Lupescu, R. Capsa, N. Cimpeanu, S. Georgescu, A. Cimpeanu; Bucharest/RO

Purpose: We conducted a pilot study to characterize plaques of multiple sclerosis (MS) using MR Spectroscopy and to put in evidence by fMR imaging that brain plasticity in MS can limit the clinical consequences of the structural brain damage associated with MS.

Methods and Materials: The study was performed on a 1.5 T GE Signa LX system. The fMR imaging and MR Spectroscopy data were acquired from 12 right-handed patients with established multiple sclerosis (MS) and 12 right-handed healthy subjects (the control group). The fMR imaging data were acquired during the performance of simple and complex motor tasks and the data were analyzed using statistical parametric software (SPM2).

Results: We found the N-Acetylaspartate (NAA)/Creatinine (Cr) ratio is correlated with the level of physical disabilities and, compared with control group, the patients showed, especially, more significant activations of the contralateral primary sensory cortex.

Conclusions: The pilot study that we conducted showed that Magnetic Resonance Spectroscopy (MRS) can add valuable information about the metabolic changes that occurs in multiple sclerosis (MS) and fMR imaging might quantify the efficiency of brain plasticity in response to MS injury.

C-0958

How do CT doses depend on patient size and radiographic techniques?

W. Huda, A. Vance; Syracuse, NY/US

Purpose: To investigate how patient size and radiographic techniques affect organ (local) doses and effective doses in MDCT imaging.

Method and Materials: Patients ranging from the newborn to oversized adults were modeled as equivalent cylinders of water. Monte Carlo techniques were used to estimate energy imparted to these water cylinders by MDCT systems. Energy imparted was converted to the average dose in the directly irradiated region, as well as to the corresponding effective dose. Patient doses were determined per 100 mAs for representative scan lengths, assuming an X-ray tube voltage of 120 kV and a helical pitch ratio of 1.

Results: The water cylinder diameter of patient heads ranged from 112 mm (newborn) to 182 mm (adult), whereas patient bodies ranged from 98 mm (newborn chest) to 352 mm (oversized adult abdomen). Head doses were 14 to 19 mGy/100 mAs, whereas body doses were 7 to 25 mGy/100 mAs, with the smallest patients receiving the highest doses. Head effective doses were 0.3 to 2.3 mSv/100 mAs, whereas body effective doses were 1.4 to 6.6 mGy/100 mAs. Increasing the tube voltage from 120 to 140 kV increased patient doses by 50%, whereas reducing the tube voltage to 80 kV reduced average doses threefold.

Conclusion: Patient doses undergoing any type of CT examination MDCT systems have been quantified for patients ranging from the newborn to oversized adults. At the same techniques (kV/mAs), newborns have effective doses approximately five times higher than those of oversized adults.

C-0959

An assessment of the performance of PACS workstation monitors in Ireland

C.K. Wade, M.F. McEntee, P.C. Brennan; Dublin/IE

Purpose: As workstation monitors are used increasingly in medical imaging, quality control programmes become vital to track variations in their performance. This study examined the performance of workstation monitors used for soft-copy reporting in Ireland, comparisons were made to standards where available and guidelines were drawn up for a quality assurance programme.

Methods and Materials: Initially, the calibration of each monitor was assessed using the IHE test plan or other equivalent software programme. Using the SMPTE test pattern the maximum luminance, spatial uniformity of luminance, temporal luminance stability, geometry and sharpness were assessed. Veiling glare and

Scientific and Educational Exhibits

spatial resolution was assessed using a selection of the AAPM TG18 test patterns.

Results: 97% of monitors were calibrated correctly to the DICOM GSDF standard. All monitors attained the guideline level for maximum luminance as set by the ACR (1999), 94% of monitors had acceptable levels of non-uniformity of luminance, whilst only 52.9% of monitors had acceptable levels of geometrical distortions. The results from the TG18 test patterns evaluation demonstrated that all monitors were affected by veiling glare and none of the monitors examined reached the standard for spatial resolution.

Conclusions: The results of this work demonstrate that regular assessment of workstation monitor performance is necessary as part of the radiology department's quality control programme. Using the results a quality control programme has been drawn up outlining the necessary image quality parameters to assess, intervals for testing, equipment required and personnel necessary. The TG18-QC test pattern can facilitate the testing of all relevant parameters.

C-0960

Retrospective patient dose analysis of digital radiography systems in routine clinical use

A. Schuncke, U. Neitzel; Hamburg/DE

Purpose: According to the European Medical Exposure Directive 97/43 patient dose values observed in clinical practice shall be compared to the Diagnostic Reference Levels (DRL). We investigated the use of examination logfiles, containing the exposure parameters of all images produced in an examination room, for determining average patient doses and their distribution.

Methods and Materials: The log files generated in flat-panel detector based digital radiography systems (Philips Digital Diagnost) at 11 different hospitals were used to acquire data regarding the dose-area product and the entrance air kerma as well as the detector exposure for all X-ray examinations performed in clinical routine. A retrospective statistical analysis of the data with respect to the average dose levels (kerma-area-product, entrance air kerma) was performed for several examination types and compared to the DRL.

Results: While dose values for individual patients vary widely due to different patient size, median values for ten or more examinations of the same type are rather stable and can be used for comparison to the DRL. We found rather large differences in median dose level for the same type of examination at different hospitals. However, almost all values were far below the DRL. Correlation of median patient dose for chest examinations with the level of detector exposure was only moderate ($R^2 = 0.70$ for pa and $R^2 = 0.56$ for lat)

Conclusion: Examination log files can be used for retrospective dose analysis in clinical routine. Median dose values determined in this analysis can be used for correlation with diagnostic reference levels.

C-0961

The exposure index: Definition of "speed" in digital radiography

U. Neitzel; Hamburg/DE

Learning Objectives: To compare the concept of film speed in conventional radiography with the definition and properties of the exposure index in digital radiography.

Background: In contrast to conventional screen-film systems, digital detectors do not have a fixed sensitivity or speed. Due to their large latitude they can be used at widely varying dose levels, while the displayed image exhibits a constant density or brightness because of signal normalization. The exposure index is used as a means to give feedback to the user about the actual dose level applied for imaging.

Procedure Details: Different definitions for the exposure index exist in digital radiography systems today. The exposure index is commonly determined from the pixel values of the actual image, which means that, unlike film speed, it is a property of the image and not of the detector. Besides the dose level, the value of the exposure index can be influenced by the type of the image, the radiation quality, and in some digital detectors also by the image processing.

Conclusion: The exposure index can be used as a feedback tool for radiation protection purposes. When comparing it to film speed care has to be taken because of different influencing factors. A standardization of exposure index definitions and scales seems appropriate to facilitate comparison between different digital imaging systems.

C-0962

The effect of patient weight on image noise in thoracic and abdominal CT:

Dosimetric analysis and clinical applications

V. Tsapaki, C. Triantopoulou, P. Maniatis, I. Siafas, D. Chrysostomou, P. Koukkou, E. Koulentianos, J. Papailiou; Athens/GR

Purpose: The purpose of the study was to investigate the influence of patient weight on image noise and radiation dose in routine CT examinations, during the International Atomic Energy Agency Research Co-ordination Project on *Dose Reduction in CT while maintaining Diagnostic Confidence*.

Methods and Materials: 50 patients were scanned using the routine abdomen protocol and 50 using the thorax protocol. Patients were divided into 5 categories according to weight. Noise (N) measurements were performed on 3 image levels, the median value of which was set as N. Dose measurements were performed in terms of the Computerized Tomography Dose Index (CTDI) using a special pencil-shaped ionization chamber. Total patient doses were assessed by estimating the Dose Length Product (DLP).

Results: Thoracic CT: No correlation was found between N and weight. Therefore, patient dimensions do not seem to affect image noise. Abdominal CT: N correlated well with weight ($R^2 = 0.62$), thus the amount of noise in the image was largely affected by patient size. Mean CTDI and DLP were 19.5 ± 3.5 mGy and 540.4 ± 201.2 mGycm for thoracic CT and 19.5 ± 2.3 mGy and 739.7 ± 182.2 mGycm for abdominal CT. These values were lower than the European reference dose levels.

Conclusions: Radiation doses using current technical parameters are satisfactory. For thoracic CT the parameters could be changed so as to lower even more radiation dose to the patient. On the contrary for abdominal CT, alterations of parameters in heavy patients in an effort to lower radiation dose should be performed cautiously, as the effect on image noise is more prominent.

C-0963

Image processing techniques for the manipulation, processing and storage of mammography radiological data

V.E. Kououlia¹, G. Matsopoulos², N. Mouravliansky², P. Asvestas², K. Delibasis², N. Uzunoglu², A.D. Kelekis¹, E. Efstatopoulos¹, N. Kelekis¹; ¹Xaidari/GR, ²Athens/GR

Purpose: The development of advanced image processing techniques for the manipulation, processing and storage of mammography radiological data.

Methods and Materials: The image processor includes the following tools: Image enhancement based on filters for the histogram equalization, the unsharp masking and the contrast limited adaptive histogram equalization, image segmentation to provide regions of interest (ROIs), classification tool and image registration and fusion. In particular, the segmentation tool consists of an automatic method based on mathematical morphology operations and a manual method, the classification tool consists of two sub-modules: The feature extraction module and the classifier, classifying normal from pathological cases, and the registration tool based on an automatic and a manual methods.

Results: The results of segmenting ROIs showed that the proposed automatic method outperforms the top hat filtering method and the watershed transformation, both qualitatively and quantitatively. The classification based on the Second Order Statistics, as feature extraction technique and a multilayer feedforward Artificial Neural Network produce a classification rate of 97% for the normal cases, 86% for the pathological and an overall performance of 93%. Finally, the registration methods of mammographic images acquired at different times by the automatic method based on the extraction of the external breast boundaries and the manual method have shown no statistical difference in terms of performance.

Conclusions: The developed image processing tools have been incorporated within a www-based system for managing patient data from mammography in a very user-friendly manner, requiring only basic knowledge of the Windows-type environment from the user-medical experts.

C-0964

Evaluation of the dose efficiency index compared to receiver operating characteristics for assessing CT low contrast performance

T. Ishida¹, S. Tsukagoshi², M. Okumura², K. Kainuma², K. Kondo²; ¹Fukui/JP, ²Tochigi/JP

Purpose: The dose efficiency index (DEI) is a dose invariant measure that quantifies the low contrast performance of CT scanners. The purpose of this study is to compare the DEI method with ROC analysis.

Method and Materials: A diluted contrast medium phantom comprised of low contrast targets of variable size and concentration was scanned at 80 to 135 kV

Scientific and Educational Exhibits

on a MSCT scanner. Eight radiologists reviewed the images and identified discernable targets. The likelihood of detection was measured as a function of target size and scan condition. Both DEI and ROC analysis were then performed, and the correlation between the two methods was calculated.

Results: When a difference in low-contrast resolution was seen under a certain condition using the ROC method, the difference under the same condition was also seen using the DEI method. The work efficiency of the DEI method is 6 times that of the ROC method. Both the ROC method and the DEI method showed significant differences between 120 kV and 80 kV when the phantom was scanned using the abdominal conditions. A possible cause is the energy-dependence of the contrast medium. The coefficient of correlation between DEI and ROC analysis was 0.985.

Conclusion: We investigated the relationship between the ROC method and the DEI method. The DEI method is an effective alternative to ROC analysis for characterizing the low contrast performance of CT scanners. It is much simpler to calculate than ROC and is useful in comparing scanners from different manufacturers or as part of ongoing quality assurance.

C-0965

Image degradation and pseudo-lesions from inappropriate use of post-processing techniques

T. Yamaoka, N. Inamoto, K. Ike, H. Nakagawa; Kyoto/JP

Learning Objectives: To review various post-processing techniques and recognize factors affecting post-processing images.

Background: Multi-detector CT (MDCT), which provides images with more information than those of single helical CT, is now seen as a standard clinical CT scanner. Appropriate post-processing of MDCT images can give much more information than evaluations of thin source images. However, incorrect use of these processing techniques can hide important information. Additionally, several factors affecting source images may influence post-processing images. Post-processing of inappropriate source images might even simulate pathological conditions. Such factors can be divided into three categories. First is related to source image quality: Slice thickness, slice interval, reconstruction algorithm, tube current and helical pitch are included in this category. Second relates to post-processing parameters and includes slab thickness, window setting (opacity curve) and softening filter. Third relates to artifacts of source images and includes beam hardening, motion and ring artifacts.

Procedure Details: MDCT scanners with a 4 detector row system were used to obtain source images, which were calculated with changing thickness, interval and algorithm. Post-processing images were made on a commercially available workstation. Maximum and minimum intensity projections, variable thickness viewing, volume rendering and virtual endoscopic images were made. We will demonstrate inappropriate post-processing images in comparison with acceptable images.

Conclusions: Radiologists and technologists should pay attention to several factors affecting post-processing images to enable the best images to be available.

C-0966

Clinical experience of a multifunctional image-guided therapy room

Y. Iwasaki, Y. Hama, T. Kaji, S. Kosuda; Tokorozawa/JP

Learning Objectives: To know the concepts of multifunctional image-guided therapy room. To know the implementation strategies of multifunctional image-guided therapy room. To review a comprehensive approach combining emergency care and elective computer-assisted therapy.

Background: Since minimally invasive therapy is essentially image-guided therapy, a new physical place for these activities has to be devised: The multifunctional therapy room integrates sophisticated imaging and image guidance modalities together with life support equipment.

Procedure Details: We developed, and started to clinically use, a multifunctional image-guided therapy room with a unified multidetector CT/fluoroscopy DSA system and US. A significant impact on the care of vitally threatened patients is given by using this room not only for elective image-guided therapy but also for emergent one-stop diagnosis and treatment.

Conclusion: The use in one-stop emergent diagnosis and treatment can possibly have a profound impact on corresponding patient pathways and outcomes. It may also further enhance the cost-benefit ratio. Motivation, technology, implementation strategies and funding of this image-guided, integrated and interdisciplinary therapy room, as well as a comprehensive approach combining emergency care and elective computer-assisted therapy, are discussed in this paper.

C-0967

Radial tomography: From acquisition lines to image grid

N.E. Myridis; Thessaloniki/GR

Purpose: We promote herein the approximation of irrational lines by broken lines (line segments), in radial techniques applied in MR imaging or other tomographic fields. The advantages are time and complexity reduction in reconstruction.

Methods and Materials: *Problem.* Given an irrational line (α, β) -i.e. a line with irrational slope- we wish to approximate that line by a sequence of pairs of rational numbers, i.e. by discrete line segments. The substitution sequences are Sturmian sequences (Jacobi-Perron (J-P) algorithm). The significance is the assignment of irrational spectral lines to line segments on the image grid, during the reconstruction procedure. *Algorithm:* 1. The algorithm is defined on unit square and uses maps defined by known equations. 2. For the line (α, β) a sequence $F(\phi^r(\alpha, \beta))$ is associated. 3. A sequence of pairs of rational numbers can be generated, thus approximating the initial line.

Results: A majority of tomographic techniques deals with radial lines, usually irrational. An interpretation of radial continuous lines in discrete grids might be considered. Focusing on a microscale, a spectral line is indeed a broken line (e.g. due to transitions of gradients etc). In radial trajectories algorithms, irrational lines (i.e. not passing from grid nodes) can be approximated by broken lines according to a Sturmian substitution algorithm. A couple of lines can be omitted. The number of required lines in reconstruction could be reduced at least by 25%.

Conclusion: The impact of J-P algorithm is critical for several known reconstruction techniques. Data burden and reconstruction time reduction of at least 25% results.

C-0968

Evaluation of the performance of two digital "flat panel" cardiac imaging systems using the NEMA cardiac benchmarking phantom

B. Tuohy, E. Keavey, L. Finlay, A. McGarrigle, K. Daly, J. Crowley, W. Van Der Putten; Galway/IE

Purpose: Until recently all cardiac angiography equipment availed of a conventional Image Intensifier-TV chain for image capture and display. However, many new cardiac catheterisation laboratories are being installed utilising an all-digital flat panel (FP) imaging design, which replaces the conventional analog image intensifier based imaging approach. This paper investigates the claim made by Manufacturers of this technology that considerable improvements in image quality, and reduced radiation exposure to staff and patients are achieved by this design.

Methods and Materials: By using the NEMA Cardiac Benchmarking phantom, entrance dose rates at varying levels of attenuation, static and dynamic spatial resolution, and contrast resolution were assessed on two modern recently installed digital "flat panel" cardiac systems from different manufacturers.

Results: Image quality findings for both FP systems are similar and are a significant improvement over conventionally designed systems. For average sized patients, entrance doses in fluoroscopic mode are approximately 25 mGy/min, however for larger patients, the equivalent dose rate reached 122.7 mGy/min. In addition, doses as large as 1.12 mGy/frame are reached during digital acquisition serial "runs" on "large" patients.

Conclusion: Image quality shows a marked improvement on modern FP cardiac imaging systems over conventionally designed systems. Entrance doses are similar between FP based systems and conventional technology in the case of average sized patients. However in the case of large patients, our findings suggest the FP approach delivers significantly higher doses, and therefore serious consideration should be given to reducing the dose for this patient population.

C-0969

An evaluation of the accuracy and precision of DEXA systems in the west of Ireland using the european spine phantom

E. Keavey, B. Tuohy, W. van der Putten; Galway/IE

Purpose: Over the past decade, Dual-Energy X-ray Absorptiometry (DEXA) has established itself as the most widely used method of measuring Bone Mineral Density (BMD). However, there is no uniformity in reporting results and in presenting reference data. This leads to difficulties in clinical practice when patients are followed up on different machines. Here the accuracy and precision of DEXA devices in the west of Ireland was assessed using the European Spine Phantom (ESP). This is composed of three semi-anthropomorphic hydroxyapatite vertebrae of varying densities surrounded by soft tissue equivalent plastic. Hence the ESP resembles human bone and soft tissue when scanned on bone densitometers. A total of 7 DEXA machines were evaluated.

Scientific and Educational Exhibits

Methods and Materials: The ESP was used to measure BMD on each machine using standardized protocols. Reproducibility and accuracy was assessed on each unit by determining projected areas, bone mineral content (BMC) and BMD for each vertebra. A further, long-term study was also carried out on some of the units to include the day-to-day variation in instrument performance.

Results: Initial findings indicate surprisingly large variations of up to 3.5% BMD between different machines of the same manufacturer. This was shown to depend on the type of vertebra scanned. Long term stability of each machine was found to be good.

Conclusion: The European Spine Phantom is an essential tool to audit typical bone densitometry systems. Differences are found between units and the implications for cross-calibration of DEXA units will be discussed.

C-0970

Objective assessment of image quality in conventional and digital mammography

P. Monnin, D. Lepori, F.R. Verdun; Lausanne/CH

Purpose: To compare in terms of NEQ and DQE a digital mammography system (GE) with the most recent Kodak, Fuji and Agfa screen-film systems.

Methods and Material: The characterization of the mammography systems were performed using a 28 kV Mo/Mo beam. Air kerma values were measured using a 6 cc ionizing chamber. The assessment of spatial resolution was performed by the determination of the modulation transfer function (MTF) of the detector. Noise power spectra were measured with homogeneous images acquired at three exposure levels that cover an air kerma range at the entrance of the detector of 10. The NEQ and DQE of these mammography detectors were obtained from these data.

Results: The constant contrast due to the linear response and the lower intrinsic noise of the digital system translates into a better image quality over a larger dynamical range than screen-film systems, especially when dealing with the detector of low contrast lesions.

Conclusion: Digital mammography systems have a high potential of image quality over a large dynamical range and a low intrinsic noise. They appear to be superior than conventional screen-film systems when dealing with the detection of low contrast lesion especially in the most glandular part of the breast.

C-0971

Computer analysis for the respiratory changes in X-ray translucency on chest radiographs using a dynamic flat-panel detector (FPD) system

R. Tanaka¹, S. Sanada¹, N. Okazaki², T. Kobayashi¹, M. Suzuki¹, T. Matsui¹, N. Hayashi¹, O. Matsui¹; ¹Kanazawa/JP, ²Arizona, AZ/US

Purpose: Recently developed dynamic flat-panel detector (FPD) with a large field of view, make it possible to obtain breathing chest radiographs, which provide respiratory kinetics information. The purpose of this study was to analyze the change of X-ray translucency in each local lung area on breathing chest radiographs and then investigate their relationship with the respiratory physiology.

Methods and Materials: Breathing chest radiographs in normal subjects were obtained using a dynamic FPD system in posteroanterior (PA) standing position and the right and left decubitus position. Images were sequentially obtained 30 frames within 10 seconds in the maximum voluntary respiration. We measured the change of X-ray translucency in each local lung area.

Results: Our method could detect the changes of X-ray translucency in each local lung area resulting from breathing phase. In the PA standing position, the changes of X-ray translucency in the lower lung fields was larger than those in the upper lung fields, and those in the right and left lung field were almost same. In the decubitus position, the changes of X-ray translucency in the upper area were smaller than those in the lower area. The results were consistent with well-known properties in respiratory physiology.

Conclusion: Chest radiography using a dynamic FPD combined with our computerized methods could detect the respiratory changes in each local lung area in the normal subjects, which resulted from the ventilation. We think that breathing chest radiography could be effective for diagnosing pulmonary diseases, such as chronic obstructive pulmonary disease and restrictive pulmonary disease.

C-0972

Precision of densitometric assessment of bone mass in mens' age-related bone loss: A comparison between DXA, pQCT and QUS

S. Petcu, G.D. Pop, C.E. Georgescu; Cluj-Napoca/RO

Purpose: Due to gender and disease-specific differences, a different approach to assessing BMD in men could be taken into account. We compared some diag-

nostic methods of osteoporosis in men who have the advanced age as a major risk factor.

Methods and Materials: The purpose of the study was to calculate and compare the short-term precision (CV%) of different osteodensitometric techniques and at different sites, assessing men aged 50 to 70, and to evaluate sensitivity (Se) and specificity (Sp) of radial pQCT and calcaneal QUS in detecting spinal bone loss defined by DXA AP spinal measurement. We selected a population of 75 men without secondary causes of osteoporosis, divided into three groups of 25 according to their BMD as measured by DXA: Osteoporotic, osteopenic and normal. The patients had their bone mineral density measured by three means: QUS using Achilles Express, DXA using DPX-PRO and pQCT using Stratec XCT 900.

Results: CV% of each technique and for each site was calculated, showing the best reproducibility for pQCT, followed by DXA. QUS had a very good Sp at T-score -2.5 (91.3%), but poor Se (28%), while pQCT showed a quite opposite feature, with low Sp but high Se. We obtained good correlations between measurements at different sites.

Conclusions: In conclusion, there are no significant differences between the values assessed by us when comparing to literature data about women. This study recommends again pQCT as the most suitable follow-up technique in detecting early changes in trabecular bone, changes preponderantly observed in this age group.

C-0973

Diagnostic efficacy of the twinkling-artifact in detection of calcifications

A.I. Gromov, A.Y. Vasilyev, B.I. Zykin, S.Y. Kubova, V.V. Kapustin; Moscow/RU

Purpose: To improve the sonographic detection of calculi.

Methods and Materials: We analyzed 417 cases of the twinkling-artifact in hyperechoic structures of inner organs and studied its appearance in 52 calcifications revealed CT.

Results: The Doppler twinkling-artifact was visualized in all organs, except liver and splenic calcifications: 61% of gallstones, 83% urinary stones, thyroid calcifications 65%, breast 71%, uterus 39%, ovary 72%, prostate 81%, scrotum 75%. The experiment determined that the artifact appeared in 86% gallstones with particles of calcium, detected by CT, and only 36% cholesterol gallstones (density < -30 HU). Use of color Doppler improved the efficacy of the detection of urinary stones in 15%, in the middle part of ureter in 38%. In 11 cases, we revealed renal stones 1-3 mm without any visualization in gray-scale imaging due to the artifact (CT confirmed). The artifact permitted determination of the nature of hyperechoic structures with reverberation within the renal parenchyma: "Milk of calcium" in calyceal diverticulum (was showed in 91% with maximum intensity). Using the artifact we detected breast calcifications of 1-2 mm (17 from 24 cases), which hadn't been visualized in gray-scale imaging. In B-flow imaging we determined this artifact, appeared as a twinkling white vertical line behind calcifications.

Conclusions: The twinkling-artifact is an additional diagnostic sign, improving the efficacy of the detection of urinary stones and breast calcifications. It visualizes in all organs, except liver and spleen. Frequency of the artifact's visualization depends on X-ray density of stones. The effect determines in B-flow imaging.

C-0974

Improvement of spatial and temporal resolution in 64-slice CT coronary angiography

F. Cademartiri, N.R. Mollet, G. Runza, M. Belgrano, M. Midiri, R. Pozzi Mucelli, G.P. Krestin; Rotterdam/NL

Learning Objectives: 1. Describe the technical features of a new generation of multislice CT scanner. 2. Describe the issues and the solutions adopted to improve spatial and temporal resolution. 3. Provide cases that show the clinical impact of the technical improvements.

Background: Coronary arteries can be studied reliably in a selected population of patients with relatively low and regular heart rate using 16-row multislice CT angiography. The clinical role of this technique is yet not well defined and several limitations to its widespread implementation remain. In particular, the effective temporal and spatial resolutions are still insufficient when the scan is applied to higher and irregular heart rates and to high-density structures such as large calcified plaque and stents. For this reason the technical developments are focused towards hardware improvements that can widen and strengthen the fields of application of multislice CT.

Imaging Findings: We describe a multislice CT scanner able to scan 64 slices per rotation with a voxel size of 0.3x0.3x0.4, and a rotation time of 0.33 s (effective temporal resolution up to 165 ms). Schemes of the main technical achievements will be displayed as well as clinical examples with conventional coronary angiography correlation.

Scientific and Educational Exhibits

Conclusion: The new 64-slice CT allows improved non-invasive coronary artery imaging.

C-0975

Metallic stents in MR imaging: Signal reduction in the lumen caused by RF effects

H. Graf, G. Steidle, U.A. Lauer, C.D. Claussen, F. Schick; *Tübingen/DE*

Purpose: The principles of radio frequency (RF) induced MR signal reduction in the lumen of metallic stents were examined theoretically as well as experimentally at 0.2 T and 1.5 T using tube models.

Methods and Materials: For the theoretical approach, the stent was assumed as tube, its axis along a linearly polarized RF excitation field. Calculations were performed with the transformer theory to obtain the RF amplitude in the tube lumen. The dependence on the electrical parameters of the tube, electrical resistance R and reactance $Y = wL$ (L : inductance, w : angular frequency) was determined. The obtained results were verified experimentally using carbon fibre tubes in the size of peripheral/coronary stents. Spin-echo imaging was applied at both field strengths.

Results: The calculations predicted, that > 90% of the RF-field amplitude can be reached in the tube lumen at a ratio $R/Y > 2$, with a rapid drop at lower ratios. RF shielding effects reduce at lower frequency (field strength) and for tubes with smaller diameter d . For the carbon fibre tubes with solid wall, resistance was high enough to confirm the theoretical predictions. For the $d = 8$ mm diameter tubes, lumen visualization ($R/Y > 2$) could be achieved at 0.2 T but not at 1.5 T. At 1.5 T, the lumen of the $d = 3$ mm tube could be visualized also.

Conclusion: RF shielding inside electrically conducting stents reduces, if the stent is small and displays high electrical resistance (material conductivity, strut arrangement). For enlarged field strength, shielding effects increase.

C-0976

Effect of a multislice scanner on patient effective dose: A Monte Carlo study

A. Tzedakis, J. Damilakis, K. Perisinakis, J. Stratakis, N. Gourtsoyannis; *Iraklion/GR*

Purpose: To assess the percentage differences in patient effective dose between 16-slice spiral and sequential CT scanning.

Methods and Materials: The MCNP(4C2) Monte Carlo code was used for simulation of a Siemens, Somatom Sensation 16 scanner. A mathematical anthropomorphic phantom was used, to calculate the effective dose. Patient effective doses were normalized to air kerma on the scanner axis of rotation. Four regions of the phantom body were scanned by 16-slice spiral and sequential mode. These regions are described as trunk, abdomen and pelvis, chest and head and neck.

Results: The percentage differences in effective dose between spiral and sequential mode for corresponding studies were ranged from 1.9 to 11.9%, 3.7 to 35.8%, 5.2 to 29.1% and 2.9 to 21.5% for head and neck, chest, abdomen and pelvis, and trunk examinations, respectively. Greater dose is always delivered to patients from spiral CT in comparison to that from sequential scanning. This is due to additional exposure of tissue, on both edges of the scan field that is needed for spiral mode. Patient effective dose from multislice spiral CT depends on slice thickness and beam collimation.

Conclusion: Multislice spiral CT delivers a considerable higher radiation dose to patients in comparison with sequential CT scanning.

C-0977

Art appreciation through radiology

C.G. Cronin, A. Alhajeri, C.J. Roche; *Galway/IE*

Learning Objective/ Background: To describe the non-medical adaptations of radiology in the World of Art. In this pictorial review we will illustrate the interesting uses of radiographic techniques in: 1. Detecting Art Forgeries. 2. Creating Original Art. 3. In Advertising.

Procedure Details: Art dealers claim that greater than 15% of all art sold at auctions are fake. X-ray fluorescence can detect fake paintings that had been forged on old canvases or over some other painting. Famous forgeries over the years include a work of art alledged to have been done by Picasso titled "Absinthe Drinker." Radiographs revealed an abstract painting underneath, which was a historical impossibility. Radiographs revealed faces and hunting scenes under paintings on canvases (which could not have been removed) and extra layers of paintings on forgeries carried out by Hans Van Meegeren of Veneers work. Art has progressed from famous paintings of Picasso to the fine art of X-ray Photography. These initially were mainly Floral Radiographs. This technique uses an industrial type generator, mammography film or graphic art film for

higher contrast, high resonance digital scanner and computer systems for contrast, coping and image adjustments. Recently in Ireland, the Advertising Industry has effectively used an interesting series of radiograph pictures in a sports advertising campaign.

Conclusion: This poster outlines radiology's impact on art. It illustrates a number of interesting radiological investigations and adaptations in the field of art/art history. Undoubtedly, radiology will continue to grow and diversify in both medical and non-medical areas.

C-0978

Optimisation of patient doses in angiography and interventional radiology: Proposal for auditing structure

L. Struelens¹, F. Vanhavere¹, H. Bosmans², R. Van Loon³, K. Smans¹; ¹*Mol/BE*, ²*Leuven/BE*, ³*Brussels/BE*

Purpose: The optimization principle, keeping doses as low as possible, without jeopardizing image quality is not straightforward for interventional radiology (IR). It is obvious that quantitative data about radiation exposures are of great interest for optimization purposes. In Belgium, there is lack of data concerning patient doses for IR examinations and no auditing structure to gain these data is determined.

Methods and Materials: The study started with the measurement of patient doses in 7 different hospitals, using thermoluminescent and dose-area-product meters. These results were entered into a database for analysis, together with the procedure and technical parameters (kVp, mAs, fluoroscopy time, number of frames, etc.).

Results: The measurements delivered us average dose values for angiography of the lower limbs, angiography of the carotid arteries and cerebral embolisations. These doses were analyzed against the different procedure and technical factors and guidelines were deduced from these observations. Practically, we propose, as part of a dose audit protocol, to register total DAP, total number of frames and/or fluoroscopy time, patient data and average kVp. Such audit protocol is illustrated for the procedure angiography of the lower limbs on the measured DAP data and recorded parameters for 111 patients.

Conclusions: If doses to patients are to be reduced, radiologists should be aware of their performance and how it relates to patient's dose. Hence, the results of this study were presented to all radiologists of the contributing hospitals. Through questionnaires they gave feedback on the different proposed guidelines for optimization of patient dose in IR.

C-0979

Investigation of magnification in digital radiography and validation of an automatic magnification calibration method

G. Ahuja¹, L. White¹, X. Wang², D.H. Foos²; ¹*Toronto, ON/CA*, ²*Rochester, NY/US*

Purpose: To investigate the distribution of femoral head magnification factors in digital radiography and to validate an automatic magnification calibration method for orthopedic surgical planning.

Methods and Materials: Thirty eight images of post-operative patients with prosthetic femoral heads (PFH) of documented sizes were acquired with computed radiography (CR). A radio-opaque sphere of 1.0inch in diameter was positioned on each patient adjacent to the hip during imaging. The actual magnification factor (G_{actual}) was calculated based on the measured PFH diameter and the known true dimension. An algorithm was developed that can automatically detect the radio-opaque sphere and determine its diameter in the image, from which the magnification factor of the sphere (G_{sphere}) was calculated. The measured PFH diameter was corrected with G_{sphere} and with the default magnification factor (15%) used in the conventional screen/film technique for orthopedic surgical planning. The two results were compared against the true size of the PFH.

Results: The value G_{actual} has a median that is 2.9% greater than default and deviates significantly for very large and small patients. With the automatic method, the median of the error in measuring the PFH diameters reduces to 0.51 mm from 0.70 mm.

Conclusion: Using the default magnification error of 15% when making PFH measurements, introduces significant magnification errors for very large and small patients. This error can lead to inappropriate PFH selection in the preoperative planning of reconstructive orthopedic procedures. The automated method corrected this error and would play a significant role in preoperative planning.

Scientific and Educational Exhibits

C-0980

Optimization of an algorithm for the arterial input function evaluation in CT brain perfusion

U. Anselmi¹, F. Saiani², L. Mascaro¹, R. Gasparotti¹, D. Mardighian¹; ¹Brescia/IT, ²Milan/IT

Purpose: In brain perfusion CT, an accurate evaluation of perfusion parameters needs an optimization of the AIF function suitable for the Central Volume theory. Aim of the study is to setup a strategy to best fit, through the Gamma Variate function, the temporal signal of the bolus passage in brain vessels.

Methods and Materials: A dynamic sequence of 50 CT images (temporal resolution 1.1 s, 80 kVp, 124 mAs) monitoring the bolus passage were collected for 4 patients. The anatomical identification of cerebral veins and arteries was performed by a neuroradiologist and the signal curve analysed for the pixel with the highest CT value, generally the central pixel of the vessel. A minimization routine provided by the CERNLIB was used. The optimization algorithm consisted of many iterative steps, including filtering of tail points, in order to cancel recirculation effects, and erosion of the first points, not yet involved in bolus passage. At every step the goodness of fit was compared with the previous one by means of normalized chi-square and Global Correlation of the four parameters of the Gamma-Variate model.

Results: Best normalized chi-square value and best Global Correlation parameters to stop the iteration process resulted to be respectively 0.02 and 0.90 and 30-45% of analysed curves were rejected using this strategy.

Conclusion: A strategy was set up to best fit CT signals from a bolus passage in brain vessels. Our results can be used to write an automatic program for the AIF mapping of perfusion brain studies.

(mean \pm standard deviation) in crano-caudal direction, 4.2 ± 3.4 mm in right and left direction, and 4.8 ± 3.0 mm in antero-posterior direction. The difference of the most unmatched margin was 28 mm, probably due to the respiratory motion. The average differences of center point of the 38 lesions was 8.2 ± 3.7 mm.

Conclusion: Although our manual fusion technique caused more larger misregistration compared to PET/CT studies, it was considered clinically acceptable. This simple technique could be helpful in clinical setting when a PET/CT device is not available.

C-0981

Measurement of MTFs for liquid crystal displays by rectangular waveform analysis

A. Horii¹, A. Chihara², M. Takamura¹, K. Ichikawa¹, Y. Kodera¹, M. Ikeda¹, T. Ishigaki¹; ¹Nagoya/JP, ²Kumamoto/JP

Purpose: To investigate the characteristics of liquid crystal displays that the numbers of pixels differ.

Methods and Materials: We measured MTFs of liquid crystal displays by rectangular waveform analysis. This is the method of taking a picture of the bar pattern on the monitor surface with a digital camera and analyzing the picture with a personal computer. The monitors used are the liquid crystal displays of 1M (about 1 million of the number of pixels), 2M, 3M and 5M, and a CRT display of pixel number of 5M. The display of 2M used two kinds (IPS system and VA system) from which liquid crystal operation mode differs.

Results: In the liquid crystal displays except the display of 1M, MTFs became high as the pixels increased. For the liquid crystal displays, MTFs in horizontal direction was higher than MTFs in perpendicular direction except 2M VA system. For the liquid crystal display of 2M VA system, MTF in horizontal direction became equal to MTF in perpendicular direction. For the monitors of the same number of pixels (5M), MTF of a liquid crystal display was high compared with MTF of a CRT display.

Conclusions: MTFs of liquid crystal displays are influenced on the form of a pixel, composition of pixels and the liquid crystal operation mode.

C-0982

Accuracy of manual fusion of CT and PET images using a fixation device

E. Minota, Y. Nakamoto, K. Matsumoto, S. Sakamoto, T. Okada, M. Senda; Kobe/JP

Purpose: Clinical usefulness of a combined PET/CT scanner has been recognized in oncology, because accurate image fusion can be easily obtained, yielding higher diagnostic confidence and accuracy. Manual fusion of PET and CT may cause more misregistration when compared to PET/CT. However, this could be acceptable in clinical in terms due to cost-effectiveness. The purpose of this study was to evaluate the differences in the positions between PET and CT images obtained separately, using a fixation device for positioning.

Methods and Materials: The study population comprised 30 patients referred for evaluation of known or suspected cancer, including lung cancer ($n = 14$), malignant lymphoma ($n = 11$) and colorectal cancer ($n = 5$). The patient was positioned using a vacuum cushion, and median and bilateral lines were marked on the surface of the skin. PET and CT scans were performed using the same fixation device and markers for positioning. Difference in the position between the two images was measured on a workstation.

Results: The absolute differences in the positions of the liver were 9.1 ± 7.4 mm

Scientific and Educational Exhibits

Radiographers

C-0983

Evaluation of virtual endoscopy at extremely low exposure dose

Y. Hirano¹, Y. Miyatani², H. Matsuya³, M. Iriyama³, S. Honma³, D. Ohura³, H. Sasaki³, N. Ohmi³, K. Sasaki³, Y. Takada³, ¹Otaru-city, Hokkaido/JP, ²Tokyo/JP, ³Sapporo-city/JP

Learning Objectives: To employ CT virtual endoscopy (VE) for screening examinations of the gastrointestinal tract. To minimize exposure dose in CT screening examinations. To evaluate the detectability of lesions in the gastrointestinal tract.

Abstract: In CT VE for gastrointestinal tract screening, exposure dose must be minimized. The usual exposure dose is intended for the visualization of lesions in solid organs, but the ideal exposure dose for VE of the stomach or large intestine has not been determined. The present study addressed the following three points in achieving extremely low-dose scanning.

Procedure Details: 1. Evaluation of changes in detection of elevated and depressed lesions due to noise. 2. Evaluation of image filter to achieve extremely low exposure dose. 3. Evaluation of clinical images obtained by extremely low-dose scanning.

Conclusion: By employing a scanning technique intended for VE only and by using the exposure dose reduction function provided in the CT system, the conventional scan exposure dose (CTDIw) of 16 mGy could be reduced to 1.7 mGy (i.e., 1/10th) while ensuring high detectability for elevated and depressed lesions. (Conventional method: 120 kV, 300 mA, 0.5 s/rot., Super-low-dose method: 120 kV, 30 mA, 0.5 s/rot.). Although multislice CT meets the basic requirements for 3D imaging of the gastrointestinal tract, extremely low-dose scanning must be achieved before screening examinations are performed.

C-0984

Impact of different flip angles on in-stent signal intensity in contrast-enhanced MR-angiography (CE-MRA) of current self-expanding stents

D. Blondin, B. Fritz, Y. Rado, A. Saleh, U. Mödder, M. Cohnen; Düsseldorf/DE

Purpose: Experimental study to evaluate the influence of different flip angles (FA) and stent orientations in the main magnetic field (B_0) on intraluminal signal intensity (SI) of modern self-expanding stent types in CE-MRA at a 1.0-T-scanner.

Materials/Methods: 12 stents of different diameters (8, 10, 12 mm, 2 stainless steel, 10 nitinol) were released in tubes filled with gadopentetate dimeglumine (Magnevist®, Schering) diluted in physiological saline (1:25) and immersed in a water-filled phantom parallel and transverse to B_0 . 6 stents were deployed at 10 mm diameter, 2 at 8 mm, and 4 at 12 mm, respectively. Imaging was performed with a T1-weighted three-dimensional gradient-echo sequence, using different FA (10°, 40°, 70°, 100° and 130°). After transfer to a remote PC-workstation, SI (relative units) within the stents, outside the stents (within the contrast filled tube), and background noise was determined using ROI-measurements. The perceivable stent diameter was measured using electronic calipers.

Results: Maximum SI was observed at a FA of 130° with an increase of approximately 100 relative SI-units per 30° resulting in a doubling of SI from 10° to 130°. Best signal-to-noise ratio yielded a flip angle of 100°. Apart from two stents (steel), in-stent diameter accounted for 80-95% of tube diameter without dependence on FA.

Conclusions: SI inside the stents increased significantly with increasing FA. Highest SI was reached at 130° FA, however, signal-to-noise ratio was worse than at 100° FA. In conclusion, CE-MRA at 1.0-T should be performed at higher FA to increase in-stent signal intensity.

C-0985

Registration and fusion of CT and MR 3D models in patients with brain tumours

G. Tezapsidis, A. Manolitsas, L. Tarazi, I. Tsitouridis; Thessaloniki/GR

Purpose: To describe two registration techniques, landmarks based and surface matching, of CT and MR imaging scans in patients with brain tumor and evaluate the utility of the fused 3D models.

Methods and Materials: 11 patients with various brain tumours were examined with both CT and MR images. CT and MR images were registered using two techniques, landmark based and surface matching. The images from CT were segmented and three-dimensional models of the bone structures were produced. The images from MR were segmented and three dimensional model of brain only and tumor only were produced. The three dimensional models were fused in one model which included bone structures from CT and brain and tumor from MR.

Results: In 10 patients the registration and fusion of 3D models was completed

successfully. In one patient the registration was unsuccessful due to movement artifacts in MR images. The fused 3D models were better at depicting the relationship between bone, brain and lesion than conventional display of different imaging modalities alone.

Conclusion: Registered 3D models from CT and MR images from patients with brain tumours can give information more clearly and accurately than single modality images alone. This information's can be used in daily clinical practice such as radiotherapy treatment planning or surgery or in basic clinical research.

C-0986

Optical index of the diaphragmatic motion during breath holding

T. Katsuda; Okayama-City/JP

Purpose: Lung computed tomography (CT) images for lung volume measurement have been obtained during full inspiration breath holding (B-H). It is, however, known that the lung volume changes due to diaphragmatic motion occurring both in cranial and caudal direction during B-H. To obtain appropriate CT images, it is necessary to consider the diaphragmatic motion. This study investigated the optical index of the moving direction of patient's diaphragm before imaging.

Methods and Materials: Forty patients underwent helical chest CT and immediately scanned sequential dynamic upper abdominal CT of which had been obtained for their clinical necessity, were used for this study. The relation between discrepancy of the antero-posterior dimension (Height) or lateral dimension (width) and discrepancy of right lung volume at almost the same plane position on CT images around the xiphoid process obtained in the same patient at different intervals after initiating B-H were evaluated by Spearman rank correlation test. In addition, the data distribution charts were evaluated.

Results: Discrepancy of heights at 4 cm in the caudal position from the xiphoid process showed the greatest correlation to right lung volume ($r = -0.770$; $p = 0.0021$). In 15 of 17 cases, the heights were correlated to the right lung volumes. There was no correlation between widths and lung volumes.

Conclusion: The optical index of the diaphragmatic motion could be identified by the abdominal wall motion. Abdominal thickness is increased when the patient inhales air and the diaphragm moves in a cranial direction during B-H.

C-0987

Lead coats as vectors of nosocomial infection

O. Mc Donnell, M. Hyland, J. Britten, R. Graham; Belfast/UK

Learning Objectives: This audit was undertaken to determine whether lead coats may act as vectors for nosocomial infection in the radiology department.

Background: Nosocomial infections are hospital acquired infections that occur 48 hours after admission to hospital. They are a significant cause of morbidity and mortality in the hospitalised patient. It is a significant problem particularly with the advent of MRSA. Its source may be from the patients own body or from contact with others. The hands of medical and nursing staff are most frequently responsible. However many articles of hospital workers' clothing and equipment have been identified as vectors of harmful organisms including pens, stethoscopes, neck ties, white coats, and ultrasound probes.

Procedure Details: A standard of 100% sterile cultures was established. Fifteen lead coats were identified. A dry swab was soaked in sterile saline and wiped across the surface of each coat. The swabs were cultured and details of flora examined at 48 hours. All coats grew skin commensals to include coagulase negative staphylococcus, micrococcus species and bacillus species. Three of fifteen coats cultured streptococcus viridans. One of fifteen coats cultured methicillin sensitive staphylococcus aureus.

Conclusion: The target was therefore not met. We therefore recommend cleaning each coat after each use with an alcohol based wipe. In cases where heavy contamination may occur the use of a disposable plastic apron is suggested. Re-audit is planned in 1 year after institution of the above changes.

C-0988

X-ray examinations of women of reproductive age in Finland

A.O. Kettunen¹, A. Servomaa²; ¹Oulu/FI, ²Helsinki/FI

Purpose: According to the Med.Dir (97/43/Euratom) special protection requirements are needed in childhood and during pregnancy. This study was focused on finding out the current practice of pelvic X-ray examinations of woman in fertile age.

Material and Methods: A questionnaire was sent to all radiation safety officers (290) in Finland; 173 questionnaires were returned. The questionnaire included questions about the number of pelvic X-ray examinations performed on a pregnant women, practice involved if the embryo or fetus has been exposed, practice

Scientific and Educational Exhibits

of excluding the possibility of pregnancy, practice of fetus dose estimation and guiding a pregnant woman after fetal expose.

Results: European recommendations for pregnant women X-ray examinations are not totally fulfilled in Finnish practice. The hospitals do not in general document the X-ray examinations of pregnant women. The most common way of excluding the possibility of pregnancy was to ask a woman whether she was pregnant by the physician and radiographer. Radiologists and referral physician were the main estimators (85%) of the fetal dose based mostly (61%) on the literature. Physicians and radiographers were the main explainers to the expectant mother about the radiation risk to the fetus.

Conclusions: To improve the practice, a guide to 'good practice' in the pelvic and lower abdomen X-ray examinations of a woman of reproductive age is needed. It should include guidelines on how to exclude and document the pregnancy of a woman of reproductive age coming for a pelvic X-ray examination and guidelines for fetal dose estimation and documentation.

C-0989

Virtual endoscopy: An additional imaging tool for the depiction of regions that the actual endoscopy cannot approach

A. Manolitsas, G. Tezapsidis, L. Tarazi, I. Tsitouridis; Thessaloniki/GR

Purpose: The purpose of our study is to demonstrate the applications of virtual endoscopy in regions where the actual endoscopy cannot be applied.

Methods and Materials: We studied 23 virtual endoscopies, (16 with SCT and 7 with MRI). In particular, 11 virtual angiographies, 4 virtual otoscopies, 3 virtual endoscopies of the upper urinary tract and 5 virtual endoscopies in closed cavities as the sphenoidal or frontal sinus. The examinations were performed using a Picker 5000 Spiral CT scanner, a Siemens Expert 1 T MR scanner, a Picker Voxel Q visualization workstation and Analyze version 5.0 software.

Results: The imaging findings were always in agreement with those of original CT and MR scans. We studied the results of the method and described the advantages and disadvantages.

Conclusion: Virtual endoscopy is a useful approach for assessment of volumetric CT and MR data, which can provide precise and realistic information for the inner surface of each examined structure. Moreover it is an additional, non-invasive, imaging method that can be applied in regions that the actual endoscopy cannot approach.

C-0990

Comparison of clinical evaluation of a flat-panel detector system and a computed radiography system for digital chest radiography

M. Ogawa, H. Kobayashi, K. Masuyama; Bunkyo-ku/JP

Purpose: Although a flat-panel detector digital chest radiography system (FPD system) has recently been introduced in a clinical setting and is in the limelight, a computed radiography system (CR system) is also evolving day by day. At present, a new CR system, which can detect emissions of lights from both sides of the imaging plate and has a flexible noise control (FNC) function as a new image processing, has been developed and introduced in some facilities. There are not a few facilities which use these two digital chest radiography systems under mixed conditions. We expected that the quality of images of both systems is not necessarily equal. Therefore we compared the difference of clinical utility between FPD system and CR system using postprocessed hard-copy images by conducting observer performance tests.

Methods and Materials: First, we studied the visual detectability of low contrast simulated nodules using a chest phantom. Observer performance data were analyzed by receiver operating characteristic (ROC) analysis. For statistical analysis, we used the jackknife method. In addition, we conducted observer performance tests with a contrast-detail (C-D) phantom and the method of paired comparisons using PA chest images.

Results: The result of the evaluation with ROC analysis and the method of paired comparisons indicated that a new CR system was equal or superior to FPD system. As for study of C-D phantom, both systems were almost equal.

Conclusion: As for observer tests with postprocessed hard-copy images, the quality of images of both systems is almost equal.

C-0991

Radiodiagnostics for hip and shin prosthesis after mine explosion and gunshot wounds

A.Y. Vasilyev, M.V. Vykhlyuk, I.N. Gipp; Moscow/RU

Purpose: To define the optimal extent of radiological examinations in evaluation of hip and shin stumps before prosthesis.

Methods and Materials: 60 patients with hip stumps and 18 patients with shin stumps were examined after mine explosions (81.0%) or after gunshot wounds (19.0%). All patients underwent the following examinations: routine radiography, microfocus radiography with the magnification factor of 5, high resolution ultrasoundography, helical computed tomography.

Results: The semiotics of changes in hip and shin stumps was defined with the help of radiological data. Doppler ultrasonography is recommended for determining the condition of soft tissues of the stump. Microfocus radiography has advantages when compared with the routine radiography in detecting small structural changes at their early stages and therefore is recommended for determining the condition of osseous structures. Both of those methods are sufficient for shin and hip stump evaluation during the preparation for prosthesis of the amputation stump. Computed tomography is recommended in difficult cases with grave general condition of the patient and vast wounds.

Conclusion: The application of up-to-date high resolution radiological methods allows to obtain reliable information about soft tissues and osseous structures of amputation stump. The application of radiological examinations in compliance with the suggested algorithm is necessary during the preparation of the stump for prosthesis.

C-0992

Guide, instruct and encourage. Radiographers' views on tutoring

T. Holtinkoski, A. Niemi, A. Kettunen; Oulu/FI

Purpose: The purpose of this study was to describe the tutoring of clinical practice from the viewpoint of the radiographers. Answers were sought to the following questions: 1) How the curriculum and the objectives of the students guide the tutoring given by the radiographers? 2) What is the tutoring like from the viewpoint of the radiographers? 3) How is the clinical practice evaluated? 4) On what kind of matters related to the tutoring would the radiographers want further information?

Methods: The data was collected quantitatively by means of a structured questionnaire. The target group for the study was the tutoring radiographers (N = 130). The structured questions were analyzed with SPSS/PC-software.

Results: The formulated practical objectives are carried out during the clinical practice of the students. One third of the tutors gave sufficient instruction in formulating students training objectives. Over half of the tutors knew what the student should learn during the training period. Tutors considered themselves to be able to sufficiently take into account the initial level of the student. Tutoring was generally considered demanding but not strenuous. The main opinion of the tutoring was that evaluation supports and encourages learning. It is guided by objectives, the student has an active role in it and the evaluations are usually correct.

Conclusion: This study increases knowledge of the tutoring of clinical practice. The results can be utilised in developing the tutoring both in radiological departments and polytechnics.

C-0993

Improved MR imaging of the extremities using a flexible multiple element phased array body coil

B. Schmitz, A.J. Aschoff; Ulm/DE

Learning Objectives: To learn how to improve MR image quality by using commercially available phased array body coils for imaging of the extremities.

Background: The advent of parallel MR imaging techniques gave rise to the development of multi-channel phased array coils. These coils were primarily designed for improvements in cardiac or abdominal imaging. Besides improved parallel imaging capabilities signal to noise ratio (SNR) is substantially enhanced. However, as a by-product this new coil design is very flexible which allows the extension of the application. Imaging of the extremities becomes possible by wrapping the coil around knee, shoulder, wrist or ankle. This ad hoc improves SNR and moreover transfers all parallel imaging possibilities to extremity imaging.

Procedure Details: Siemens Symphony 1.5 T scanner was extended with a commercially available package to allow 8 channel imaging with a 12 element phased array coil. Besides routine use in cardiac and abdominal examinations, the coil was used as a replacement of the regular flexible extremity coil. Images showed an immediately obvious improvement in SNR and image quality without artefacts.

Conclusion: In this exhibit we show how to replace regular flexible extremity coils with newer commercially available flexible multi-element phased array body coils for an improved imaging of the extremities.

Scientific and Educational Exhibits

C-0994

Lens dose reduction in paediatric CT brain scan using the supra-orbitomeatal baseline technique

K.K. Fung, K.H. Choi; Hung Hom/HK

Purpose: The increasing collective dose from CT scans has been a great concern in recent years. The aim of this study was to determine the effect of using two different scan planes in routine CT brain on lens dose reduction and resulted image quality in paediatric patients.

Methods and Materials: Fifty-two paediatric patients aged 1-12 years were selected for this study. They were randomly divided into two equal groups to receive the CT brain scans. One group underwent scanning with a modified technique using the supra-orbitomeatal (SOM) baseline and the other group with the conventional orbitomeatal (OM) baseline. Lens dose measurements were made using LiF:Mg,Ti TLD pellets. The resulted image quality and overall diagnostic value were also evaluated by 5 radiologists using the 5 point confidence scales. An adult head phantom was also scanned with the use of these two scan planes and the corresponding lens doses were measured.

Results: By using the SOM baseline instead of the OM baseline, the eye lenses were avoided from direct irradiation of the X-ray beam. Results showed that the measured lens dose can be reduced on average by 81%. The degree of lens dose reduction was nearly the same in the adult phantom (84%) experiment. Results also showed that the image quality and overall diagnostic value were similar using either scanning plane. Reliability tests showed consistent results.

Conclusion: It is recommended to use the SOM baseline in routine CT brain scan to reduce the lens dose for both adult and paediatric patients.

skills. In addition, the study indicated that students learned through an increased awareness of their own learning processes. Moreover, learning was found to improve social interaction with the Radiographers, Radiologists and Teachers. For better results, attention should be paid to support the learning process of plain X-ray examinations through increased awareness which enables students to monitor and review their progress in the key components of plain X-ray examinations.

C-0995

Reduction of skin exposure in interventional radiology

A. Kawabe, Y. Nakagiri, T. Katsuda, A. Matsushita, T. Maruyama, H. Wakasa, S. Kadohisa; Okayama-city/JP

Purpose: Radiation injury is one of most common problem in Interventional Radiology. One of reasons is scattered radiation from catheter table. To reduce the scattered radiation, polystyrene foam is placed between phantom and catheter table as an air gap. In this study, adequate thickness of polystyrene foam is decided for clinical practice.

Material and Methods: The polystyrene foams (2 cm thick, 28 kg/m³) are used instead of the air gap. Vinyl chloride foam (3 cm thick) is inserted into carbon plates (1 mm thick) for which substitute the catheter table. To measure surface dose and depth dose in each thickness of polystyrene foams from 0 cm to 20 cm. Twenty centimeter of Mix-DP plates are used as an object. X-ray tube voltages are 70-90 kVp.

Results: Surface doses were decreased 16% and 22% (80 kVp) at the thickness of 6 cm and 10 cm polystyrene foams, respectively. Depth dose at 14 cm Mix-DP was similar as compared to the dose without polystyrene foams.

Conclusion: The polystyrene foam as the air gap is able to decrease surface dose by the scattered radiation from catheter table without any deterioration of image quality. This method is easy to set and less expensive. Thickness of polystyrene foams 2 cm to 10 cm are useful for clinically to reduce surface dose.

C-0996

Student descriptions of learning how to perform plain X-ray examinations during practical studies

A. Holmström, A. Kettunen; Oulu/FI

Learning Objectives: To describe the experiences of radiography students learning how to make plain X-ray examinations during their practical studies.

Background: Plain X-ray examinations are patient's basic radiological examinations in Finland. Radiographers are responsible for making those examinations properly. During radiography studies the students study plain X-ray examinations both in academic and practical studies. There is a rather small number of research concerning students' learning of plain X-ray examinations during their practical studies.

Procedure Details: This study was qualitative in nature. The data comprised 21 learning diaries provided by radiography students during their 3rd and 7th term when they were practising plain X-ray examinations. The diaries were analysed by means of content analysis and quantifying expressions.

Conclusion: The study showed that the key components of the process of learning to conduct plain X-ray examinations were patient care, technical expertise and decision-making skills. Students in the 3rd term emphasized technical expertise, while students in the 7th term underlined the importance of patient care. Both student groups brought attention to the significance of learning decision-making

Scientific and Educational Exhibits

Vascular

CT

C-0997

Quantitative analysis of carotid artery atherosclerosis by micro-CT

A. Mohr¹, F.W. Roemer², A. Guermazi², C. Heiss³, C. Schmidt¹, P.J. Schaefer¹, H.K. Genant²; ¹Kiel/DE, ²San Francisco, CA/US, ³Giessen/DE

Purpose: To evaluate micro computed tomography (micro-CT) for two- and three-dimensional analysis of carotid artery atherosclerosis.

Methods and Materials: Micro-CT scans (STRATEC 0.125 mA, 40 keV) were performed on 10 carotid arteries (63 - 73 years) at 60 µm isotropic resolution. Image evaluation included the analysis of multiplanar reconstructions and volume renderings based on constant threshold levels for air (-140), soft tissue (430) and calcifications (750), which were identified by histogram analysis with interactive density thresholding. The following morphological parameters were calculated: Two-dimensional: original lumen perimeter (LP), original lumen area (OA), plaque area (PA), residual lumen area (RA), calcified area (CA), gross sectional area reduction (GSAR); three-dimensional: total tissue volume (TTV), the soft tissue volume (STV), calcified tissue volume (CTV).

Results: Micro-CT depicted the typical anatomy of the arteriosclerotic carotid artery, with high contrast between calcifications, soft tissue and air. Calcifications demonstrated variable internal densities, differences within the soft plaque were less obvious and ulcerations and/or fissures could not be detected. The two- and three-dimensional analysis yielded the following

Results: LP 25.29 ± 1.3 mm, OA 45.33 ± 5.5 mm², PA 21.9 ± 7.2 mm², RA 22.9 ± 9.9 mm², CA 3.7 ± 4.7 mm², GSAR $50.3 \pm 19.3\%$, TTV 1034.7 ± 80.8 mm³, STV 1007.2 ± 55.3 mm³, CTV 31.2 ± 8.9 mm³

Conclusion: Micro-CT as a time efficient, non-destructive, high-resolution tool for the volumetric evaluation of carotid atherosclerosis. It cannot replace histology if detailed information is needed, but offers advantages when samples need to remain intact, only gross morphological features are being evaluated, calcifications are of specific interest or entire samples or specific sample volumes have to be analyzed.

C-0998

Evaluation of the Vesselness and Laplacian of Gaussian filter for vessel enhancement in CT images

S.C. Saur, S. Großkopf; Forchheim/DE

Purpose: To evaluate the Vesselness and Laplacian of Gaussian (LoG) filter for the enhancement of vessel structures in CT images.

Methods and Materials: The filters were applied on CT coronary, aortic and carotid datasets coming from Siemens Sensation 16 and Sensation 64 scanners. syno® VesselView segmentation was taken as the gold standard. Voxels smaller than -125 HU values were excluded to speed up calculation. Filter parameters were adapted to the expected vessel diameter (coronary ~3 mm, carotid ~10 mm, aorta ~30 mm). Sensitivity (sens) and positive predictive value (pdv) were chosen as evaluation criteria. The segmentation threshold for the Vesselness filter responses was determined regarding discrimination analysis, entropy analysis and percentage-based approaches. For the LoG filter, a 15x15x1 minimum filter was used. Besides this global statistical approach, the general capability of the Vesselness filter is regarded using the a priori knowledge of the segmented vessels.

Results: Best results for vesselness filter achieved with entropy analysis (sens 0.8-36.2%, pdv 3.6-9.5%) followed by discrimination analysis (sens 1.2-47.3%, pdv 3.7-8.7%) and 95%-quantile (sens 0.1-30.3%, pdv 3.5-10.1%). LoG in combination with minimum filter attained positive predictive values not exceeding 1.1%. Using a seed point region growing, the Vesselness filter outperformed the gold standard in some cases but had weaknesses on certain bifurcations and stents.

Conclusion: Both Vesselness and Laplacian of Gaussian filter provide inadequately results for the purpose of vessel enhancement in a global application with no knowledge of the vessels position. Locally, the Vesselness filter can be applied to support the segmentation process.

C-0999

MDCT of collateral venous circulation in the retroperitoneum

H. Cuéllar i Calàbria, S. Quiroga, C. Sebastià, R. Boyé, A. Miranda, A. Álvarez-Castells; Barcelona/ES

Learning Objectives: To outline the venous anatomy and embryology of the retroperitoneum. To show MDCT cases of collateral retroperitoneal veins and discuss their pathologic and physiologic causes. To describe the advantages and limitations of the MDCT technique in the study of retroperitoneal vessels.

Background: The retroperitoneal space is traversed by several venous networks characterised by their variability as well as by multiple anastomoses among them and other vascular territories. Thus, blood may be diverted through the retroperitoneum in various patterns suggestive of a number of physiologic and pathologic conditions. MDCT has improved spatial resolution with an almost isometric voxel as well as temporal resolution with faster scanning velocity allowing for precisely timed vascular studies of high quality.

Imaging Findings: MDCT studies of collateral circulation through capsular, adrenal, lumbar-azygous, ureteral, gonadal, uterine and inferior mesenteric veins, as well as direct and indirect portosystemic shunts are shown, with emphasis on MDCT technique and volume rendering. MDCT patterns are illustrated and discussed in cases of congenital variants, anterior and posterior nutcracker phenomenon, incompetent gonadal veins, inferior vena cava tumoral invasion, hepatic cirrhosis, thoracic venous thrombosis, acute ovarian arterial hemorrhage as well as arteriovenous fistulae and idiopathic varices. Computed animations illustrating flow routes are included.

Conclusion: MDCT angiography depicts retroperitoneal venous circulation in detail, yielding diagnostic information of great utility in the differential diagnosis among pathologic vascular conditions, physiologic phenomena and anatomic variants.

C-1000

Endograft placement for aortic aneurysms and dissections: Pre and post evaluation using MDCT angiography: How to do it

H. von Tengg-Kobligk, M. Ganter, D. Boeckler, C. Fink, J. Zaporozhan, F.L. Giesel, S. Delorme, H.-U. Kauczor; Heidelberg/DE

Learning Objectives: 1. Evaluation of aortic aneurysms and dissections based on typical MDCT findings. 2. Relevant scanning and post processing techniques to meet the requirements for therapeutic decision. 3. Imaging findings of typical complications after endograft placement.

Background: MDCT-Angiography can play a decisive role for the pre-procedural planning and post-procedural follow-up of endovascular repair of aneurysms and dissections. An optimal visualization of the vascular anatomy and therapeutic material is crucial for decision making and assessment of therapeutic results or even complications.

Procedure Details: The suggested protocol for patients with aortic aneurysms or dissections using a 16 row CT (e.g. Aquilion 16, Toshiba, Japan) with the following parameters: 120 kVp, 120-150 mAs, 1 mm collimation, pitch 15, ≤ 0.5 s rotation time, bolus triggering, 100-120 ml of high-concentration iodinated contrast media such as Imeron 400 (Bracco ALTANA Pharma, Germany), 4-5 ml/s flow rate and saline flush. Post processing (MPR, surface rendering, vessel tracking) is preferential on a capable workstation (e.g. Vitrea, Vital Images, USA). Typical quality criteria are: Max. contrast in the aorta: ≥ 400 HE, no/little venous enhancement, visualization of Adamkiewicz artery, entries and re-entries. Crucial post endograft findings include leakage, residual perfusion of the aneurysmal sac, endograft rupture.

Conclusion: For an optimal evaluation of complex aortic aneurysms and dissections with MDCT, thin collimation with overlap, high-concentration iodinated contrast agents, a power injector enabling high flow rates and a workstation allowing for MPR of the spinal vasculature, vessel tracking for true vessel diameter and surface rendering for surgical planning are recommended.

C-1001

Multi-detector CT angiography in the evaluation of hemodialysis access failure

N. Hongo, H. Mori, S. Matsumoto, R. Shuto; Oita/JP

Purpose: To evaluate the utility of whole arm CT angiography (CTA) obtained by multi-detector CT in stenosis or occlusion of hemodialysis access.

Materials and Methods: Seventeen patients (7 males, 10 females, mean age 62.9) underwent DSA of their hemodialysis access and multi-detector CTA within 2 weeks. 63 stenoses or occlusions were detected on DSA. For CTA, 100 ml, 300 mg/ml nonionic iodinated contrast medium was injected intravenously at the rate of 3 ml/sec in the contralateral arm, and the whole arm was scanned with 1.5 mm collimation by a 16-detector row CT scanner. Maximum intensity projection 3D images acquired from 2 mm thickness CTA images were evaluated by two radiologists and stenoses were graded as follows: 25-50% (mild), 51-70% (moderate), 71-99% (severe), 100% (occluded). These findings were compared to DSA, which served as the standard of reference.

Results: Sensitivity / specificity of multi-detector CTA for detecting > 50% stenosis were 0.94/0.98 for reader 1, and 0.91/0.94 for reader 2. Sensitivity / specificity for detecting > 70% stenoses were 0.90 / 0.88 for reader 1 and 0.90/0.79 for

Scientific and Educational Exhibits

reader 2. The rate of stenosis agreement between CTA and DSA was 87.3%. Interobserver agreement of CTA was excellent ($\kappa = 0.915$)

Conclusion: Multi-detector CT Angiography can adequately detect hemodialysis access failure. It is a less invasive tool and provides useful information about the site and degree of hemodialysis access stenosis, which can lead to successful percutaneous transcatheter angioplasty.

C-1002

Ruptured abdominal aortic aneurysm: MSCTA imaging

R. Stern-Padovan, M. Lusic, I. Sjekavica, M. Hrabak, K. Potocki, B. Oberman, J. Marinic; Zagreb/HR

Learning Objectives: 1. To describe the imaging protocol in patients with suspected leaking abdominal aortic aneurysm. 2. To present various radiological findings after rupture of abdominal aortic aneurysm.

Background: Leaking abdominal aortic aneurysm is a life-threatening condition manifested as acute flank or epigastric pain and signs of hemorrhagic shock. To avoid unnecessary delay in surgery, the correct diagnosis must be provided as quickly as possible. Due to its speed and accessibility, MSCTA is the modality of choice before emergency treatment of ruptured abdominal aortic aneurysm. An unenhanced CT scan depicts abdominal aortic aneurysm and retroperitoneal hematoma, while MSCTA accurately delineates the actual site of bleeding.

Procedure Details: MSCTA was performed using SmartPrep feature after a bolus of 80-120 ml intravenous nonionic contrast medium with 4 ml/s flow rate. Axial images were transferred to a workstation and postprocessed using maximum intensity projection (MIP), multiplanar reconstruction (MPR) and 3D volume rendering (3D VR) protocols.

Conclusion: As well as visualization of retroperitoneal hemorrhage, abdominal aortic aneurysm and pseudoaneurysm formation, MSCTA also depicts mural thrombus, aneurysm length and width, its extension into aortic branches, as well as other morphological and blood flow changes in visceral and pelvic arteries. Considering the extension of retroperitoneal hemorrhage into different anatomical compartments (periaortic, perirenal, pararenal spaces, pelvis) and retroperitoneal organs (aortoduodenal fistula), the radiologist must determine the exact location of bleeding. MSCTA is the fastest, very safe and minimally invasive radiological procedure, which gives optimal information for urgent interventional or surgical repair of a ruptured abdominal aortic aneurysm.

C-1003

Multidetector row CT angiography of the abdominal aorta and lower extremities: Post-processing and arterial wall calcification removal

J.-M. Treutenaere, T. Bernasconi, C. Renard, M.-A. Auquier, A. Remond; Amiens/FR

Purpose: To describe post-processing techniques of multidetector row CT angiography (MDCTA) of the abdominal aorta and lower extremities, in particular methods to remove arterial wall calcifications in 3D Maximum Intensity Projections (MIP).

Methods and Materials: In 2003, 534 patients with symptomatic lower extremity peripheral arterial disease underwent MDCT angiography of aortoiliac and lower extremity arteries (Lightspeed Ultra and Lightspeed 16, GEMS). Post-processing was carried out on ADW 4.1 and 4.2 workstations. Vascular mapping was obtained in 3D MIP reconstruction. We present a method to remove arterial wall calcifications by segmentation starting vascular lumen density. Quantification of vascular diameter and study of the arterial wall are analyzed in 2D projections.

Results: Complementary Digital Subtraction Angiography (DSA) was necessary in only five patients: in 2 diabetic patients distal arteries were too heavily calcified and in 3 patients with acute lower extremity ischemia, CT acquisition was made before the arrival of contrast material distally. These techniques would thus be reliable, reproducible and fast. MDCT angiography with post-processing methods presented here makes it possible to decrease the quantity of contrast material injected and to avoid complications of DSA in nearly all patients.

Conclusion: Thanks to these methods of simple post-processing realizable on any workstation, MDCT angiography facilitates pre-therapeutic assessment of lower extremity peripheral arterial disease. A prospective study of MDCT angiography versus Digital Subtraction Angiography would allow the validation of this technique.

C-1004

Role of spiral CT in detection of intramural aortic hematomas and in selection of treatment tactics

F. Todua, M. Razmadze, G. Tsivtsivadze; Tbilisi/GE

Purpose: To evaluate the clinical significance of intramural hematoma in the thoracic aorta and the role of spiral-CT in determination of treatment tactics in patients with this pathology.

Materials and Methods: 34 patients with clinical suspicion of acute aortic dissection and CT findings of a thickened aortic wall were evaluated. CT examinations were performed within 24 hours of onset of symptoms and as a regular follow-up within 3-6 months. The technique used was contrast-enhanced spiral-CT with 3-5 mm slice thickness.

Results: 15 patients had intramural hematoma in the ascending aorta. 9 underwent acute surgery and a ruptured intima was determined as the cause of the hematoma. 3 died before operation and autopsy showed intimal dissection. In 3 patients the significance of the hematoma was not appreciated in the acute phase, but was discovered later. Follow-up CT showed regression of the hematoma. 19 patients had intramural hematoma in the descending aorta and were treated conservatively. At follow-up 13 showed normalization, 4 developed aneurysm and 1 developed a small ulcer-like saccular aneurysm. In one patient the findings were unchanged.

Conclusion: Intramural hematomas in the ascending aorta are usually caused by an intimal tear and represent true dissections. Detection of intramural hematomas is of great importance in the management of patients with aortic dissection, which includes evaluation of localization and spread of the hematoma, therefore selecting the patients for surgical treatment. In cases of descending aorta intramural hematoma, conservative treatment often leads to normalization of the aortic wall.

C-1005

Evaluation of MDCT in detection of atherosclerotic plaques in WHHL animals

H. Ittrich, P. Begemann, C. Jahntz, C. Weber, A. Priest, G. Adam; Hamburg/DE

Purpose: Evaluation of native and contrast-enhanced (CE) CT in detection of atherosclerotic plaques in 16 row multidetector CT (MDCT) scanner in an animal model.

Method and Materials: Native and CE-CT was performed on 25 WHHL (12-31months) and 11 New Zealand White (NZW,control,16 months) covering the aorta. Scans were performed before and during continuous administration of iopamidol (Solutrust 300) in a MDCT scanner (Philips) using 16x0.75 mm collimation with a standard protocol (120 kV,321 mA,rotation time 0.4 sec., automated injection: 5 cm³ iopamidol diluted in 5 cm³ NaCl, flow: 1 cm³/sec, contrast optimization: automated bolus tracking option, threshold 130 HU, slice reconstruction: 2 mm thickness, 1 mm increment). The degrees of calcification, measurements of the luminal diameter in 3 regions of the aorta (ascending part, arch and descending part) and visibility of aortic wall and anatomical layering (intima, media, adventitia) were estimated by two independent investigators (IH,BP) according to a five-point-scale, ranging from 0 (not visualised) to 4 (excellent).

Results: Only 5 of 25 WHHL animals showed calcifications in the aorta (mass:4.2 ± 5.8 mg (0.4-14.4 mg), volume:30.4 ± 42.2 mm³ (3.3-104.6 mm³)). No calcifications were detected in NZW. Luminal diameter of all animals showed no significant differences or severe stenosis (7.1 ± 1.3 mm). In all animals neither wall thickness (0.7 ± 0.5) nor differentiation of layers of the wall could be estimated (0.5 ± 0.4).

Conclusion: Native MDCT is able to detect and to quantify calcified plaques of atherosclerosis in the aortic wall (WHHL). Neither native nor CE-MDCT was able to identify anatomical layers of the aorta or to detect early stages of atherosclerotic plaques (lipid plaques) in this animal model.

C-1006

Multislice CT in the determination of suitability for endovascular aortic stent grafting

D.G. Lohan, S. Walsh, C. Meehan, I. Davidson, G.J. O'Sullivan; Galway/IE

Learning Objectives: Patient selection for endovascular stent grafting of abdominal aortic aneurysms depends upon numerous measurements, obtained at the time of multislice aortic CT. We explore and explain each of these measurements in turn, and consider the potential complications of stent grafting should these criteria not be obeyed.

Background: The popularity of covered stent grafting for abdominal aortic aneurysms has greatly increased in recent years due to a combination of low intra-

Scientific and Educational Exhibits

operative morbidity and mortality, coupled with often excellent medium-term patient outcomes. However, suitability of patients for this procedure depends upon high-quality imaging, with resultant accurate quantitative measurements. No longer is maximal aneurysm diameter an exclusion criterion for this procedure, rather neck length, and diameters of proximal and distal landing zones hold greater importance.

Imaging Findings: Using images obtained from conventional angiography, where available, as well as source and Maximum-Intensity-Projection images from multislice CT, we consider the relevant exclusion criteria for endovascular stent grafting of aortic aneurysms. By way of pictorial review we present cases in whom successful stenting was performed, with pre- and post-operative imaging. In addition, we consider images of cases in whom this technique was not suitable, explaining the reason for rejection of potential candidates in each case.

Conclusion: Using images from our institute, we explain the relevant measurements and considerations on pre-operative multislice CT with regard to endovascular AAA stent grafting.

C-1007

Utility of triple channel injection of contrast material with mixture of saline, with upward acquisition for arterial trees using multislice computed tomography

N. Yanagawa, F. Morita, S. Ochi, N. Funabashi; Chiba/JP

Purpose: If contrast material is injected into the cubital vein, high computed tomographic (CT) values in the vein hamper evaluation of the aorta and major branches. We describe a new protocol employing a combination of triple channel contrast material injection and a mixture of saline (Dual Shot, Nemoto) with upward acquisition in multislice CT.

Materials and Methods: 40 subjects underwent thoracic CT (Light Speed Ultra 16, GE). 20 subjects were injected with 60 ml contrast material. Scanning was then started with upward acquisition during the injection of contrast material diluted 50/50 with saline, followed by the injection of 30 ml of saline (new protocol). The other 20 subjects were injected with 100 ml contrast material at a rate of 3 ml/sec, with scanning in the downward direction (ordinary protocol).

Results: In the new protocol, the aorta measured an average of 290 HU which was no different from the ordinary protocol, but the injection side vein and superior vena cava measured 220 and 200 HU which were lower than in the ordinary protocol. The aorta and major branches could be observed easily without artifact and we were able to construct clear three-dimensional images of arterial trees.

Conclusions: We describe a new acquisition protocol in which the aorta and major branches can be evaluated without artifact due to high CT values in veins. This modification was achieved by rapid acquisition of multislice CT. In the future, CT scans can perform faster acquisition and the protocol using contrast material diluted with saline can be modified to provide more useful.

C-1008

Multidetector spiral CT renal angiography in the diagnosis of renal artery fibromuscular dysplasia

P. Vladica, R. Sabharwal; Sydney/AU

Introduction: The aim of the study was to evaluate the role and detection rate of Multidetector Spiral CT-Renal Angiography (CTRA) as compared with Conventional Renal Angiography (CRA) in the diagnosis of renal artery fibromuscular dysplasia (FMD).

Materials and Methods: Over a three year period three hundred and sixty eight patients with suspected renovascular hypertension were screened with CTRA. Clinical indications for referral included resistant hypertension (requiring greater than three anti-hypertensive medications), labile hypertension, hypertension in combination with renal impairment, and the presence of abdominal bruits in the context of systemic hypertension. CTRA demonstrated lesions suggestive of FMD in twenty eight patients. Twenty three of those twenty eight patients underwent CRA for further evaluation. The findings of CRA in those twenty three patients were compared to CTRA. Patients with haemodynamically significant lesions on CRA underwent balloon angioplasty.

Results: Mean patient age was 62.48 ± 13.66 years. CTRA identified all 46 main renal arteries (100%) and all 10 accessory renal arteries (100%) visualized on CRA. In the diagnosis of fibromuscular dysplasia with haemodynamically significant ($> 50\%$) stenosis, the sensitivity and specificity of CTRA were 100% and 96%, respectively.

Conclusion: Our experience suggests that CTRA is a safe, reliable and accurate method for the diagnosis of FMD. Moreover, CTRA has many advantages as a diagnostic tool over CRA, including accessibility, speed, lower complication profile, versatility and cost effectiveness. CTRA shows great potential as a guiding tool for directing subsequent procedures such as CRA \pm balloon angioplasty.

C-1009

Subclavian vein thrombosis secondary to thoracic outlet syndrome: CT and CT angiography evaluation

C. Kokkinis¹, N. Makris¹, S. Stathopoulou¹, A. Peteinelli¹, M. Vlychou², K. Vassiliou², P.J. Papadaki¹, G.M. Zavras¹, J.B. Fezoulidis²; ¹Athens/GR, ²Larissa/GR

Purpose: The aim of this study was to evaluate the diagnostic usefulness of CT and CT angiography for the detection of thoracic outlet syndrome in cases of subclavian vein thrombosis.

Methods and Materials: 11 patients with subclavian vein thrombosis (non catheter-related), diagnosed by Triplex or phlebography, were examined with CT and CT angiography after contralateral contrast medium injection in neutral and abducted positions. The evaluation included axial images, 2D MPR (Multiplanar Reformation) and MIP (Maximum Intensity Projection), 3D SSD (Surface Shaded Display) and VRT (Volume Rendering Technique) images.

Results: CT and CTA depicted thrombosis of the subclavian vein in all cases. In seven of the 11 patients (64%) the examination demonstrated thoracic outlet syndrome with significant narrowing of the costoclavicular space after abduction and compression of the vein. In 3 of them a cervical rib was found. 2D MPR, MIP and 3D SSD, VRT were very useful for the detection of subclavian vein compression.

Conclusion: CT and CT angiography can be used in patients with subclavian vein thrombosis suggestive of thoracic outlet syndrome, as it can confirm or exclude it, thus aiding planning of therapy.

C-1010

CT evaluation of congenital vena cava anomalies

M. Inal, S. Leblebisatan, F. Binokay, E. Akgül, E. Aksungur, M. Oguz, S. Soyupak, K. Biçakci, M. Çeliktaş; Adana/TR

Learning Objectives: Because of having complex developmental stages, the venous system shows numerous different congenital anomalies. 13 patients with vena cava (VC) anomalies were reported here as they are rare and have different variations. It is important to detect the anomalies of either superior (SVC) or inferior (IVC) in order to prevent fatal complications during surgery or catheterization.

Background: Anomalies of IVC are seen in 0.3% of the general population and in 0.6-2% of patients with congenital heart disease (CHD). Double SVC is the most common anomaly (0.3%), reaching over 11% in patients with CHD. We report 13 cases of VC anomalies detected with CT. Two patients had double IVC, 2 with double SVC, 4 with left IVC, 1 with left IVC with hemiazygous continuation, 1 with intrahepatic segmental atresia of IVC, 1 with azygos continuation of IVC, 1 with double SVC with hemiazygous continuation and 1 with double IVC with azygos continuation. None of the patients had CHD.

Procedure Details: Between 1997-2004, 13 patients who had complaints unrelated to their venous anomalies were analyzed with CT and congenital VC anomalies were detected. Diagnoses were confirmed by venographic studies in 3 patients. CT scans were performed in helical mode with a pre-delay of 55 seconds and a pitch of 1.2.

Conclusion: VC anomalies are generally asymptomatic and detected during surgical or diagnostic procedures. Catheterization or surgical intervention may result in life-threatening complications if the physician is unaware of the anomaly.

C-1011

Failing arteriovenous hemodialysis fistulas: Assessment with multidetector CT angiography and three-dimensional (3D) techniques

E. Karadeli, N.C. Tarhan, E.M. Kayahan, N. Tutar, O. Basaran, M. Coskun; Ankara/TR

Purpose: To evaluate failing hemodialysis arteriovenous fistulas and complications with multidetector CT angiography (MDCTA) and 3D reconstruction techniques.

Methods and Materials: Between September 2003 and July 2004, 30 patients (16 M and 14 F-aged between 27-79 years old), with suspected hemodialysis access dysfunction who were referred to our radiology department for diagnostic fistulography, had 31 MDCTA (Sensation 16, Siemens, Erlangen, Germany). All fistulas were in the upper extremity. Contrast was administered from a peripheral vein of the contralateral arm as a bolus of 150-200 cc at a flow rate 5 cc/s. Transverse scans were viewed in the arterial phase with reconstruction at 1 mm intervals. Transverse and coronal MIP, and VRT images were constituted. AV fistula sites, arterial, venous system and complications were evaluated. Fistulography served as the gold standard for comparison in all patients.

Results: 14 fistulas were at wrist level, 17 fistulas were at antecubital fossa level.

Scientific and Educational Exhibits

There were 27 native and 4 graft fistulas. There were 57 venous pathologies detected with MDCTA: Cephalic venous stenoses (n = 7, 22%), subclavian venous stenoses (n = 2, 6%), cephalic occlusion (n = 3, 9%), subclavian occlusion (n = 6, 19%), axillary occlusion (n = 2, 6%), venous aneurysms (n = 21, 67%), collaterals (n = 16, 51%). 10 arterial and fistula site complications were: Stenoses in subclavian artery (n = 2, 6%), stenoses in axillary artery (n = 2, 6%), stenoses in brachial artery (n = 2, 6%), aneurysm of brachial artery (n = 1, 3%) stenoses at the anastomosis site (n = 3, 9%).

Conclusion: MDCTA is a noninvasive, effective imaging method to evaluate hemodialysis vascular access and complications. Arterial vascular pathologies that cannot be detected with conventional fistulography can also be demonstrated with MDCTA.

C-1012

Spiral CT angiography: A valuable decision-making tool for carotid endarterectomy

C. George¹, M. Titi², D. Bhattacharya², P.M. Woodhead², W.J. Stevenson², A. Pillai², D.F. Ettles¹, H. Al-Khafaf², ¹Hull/UK, ²Burnley/UK

Purpose: To compare results of duplex ultrasound scan (DUS) and spiral CT angiography (CTA) in patients with suspected carotid artery stenosis and to evaluate its impact on decision making for carotid endarterectomy.

Materials and Methods: Data were collected retrospectively in patients who had undergone both DUS and CTA for the evaluation of suspected internal carotid artery stenosis. St Mary's criteria were used for estimation of severity by DUS while direct measurement of stenosis was made from multi-planar CT reformats. Degree of agreement between these modalities was assessed, along with limitations of both.

Results: 107 patients were evaluated over a two year period (Jan 2002 - March 2004). 27 of the 214 carotid arteries scanned were excluded because of technical imaging difficulties or inadequate source data. Concordance in severity of stenosis between the imaging modalities was found in 148/187 arteries (79.14%, 95% CI 0.72 - 0.83). DUS under-estimated and over-estimated the degree of stenosis in 26/187 (13.91%, 95% CI 0.09 - 0.19) and 13/187 (6.95%, 95% CI 0.04 - 0.12) respectively, which related to difficulties encountered during DUS including high carotid bifurcation, dysrhythmias and extensive calcification. When CTA was considered in conjunction with DUS, the decision regarding operative treatment was changed in 29/187 (15.51%, 95% CI 0.11-0.21) cases.

Conclusion: While DUS remains the first line non-invasive imaging technique for carotid artery stenosis, it is subject to several limitations. CTA provides an excellent non-invasive adjunctive technique in the preoperative assessment of carotid disease and may significantly affect the decision regarding operative treatment.

C-1013

Upper extremity (UE) multidetector-row CT angiography (MDCTA):

Evaluation of arterial disease

J.C. Hellinger, A. Kamaya, A. Napoli, E. Williamson, G.D. Rubin, D. Fleischmann; Stanford, CA/US

Learning Objectives: 1. To provide MDCTA techniques for evaluating UE arterial disease. 2. To illustrate UE arterial anatomy and pathology with MDCTA.

Background: The differential diagnosis for UE arterial disease is diverse. Atherosclerosis, thromboembolism, thoracic outlet syndrome, fibromuscular dysplasia, and large and small vessel vasculitis all warrant consideration depending on the clinical history and physical examination. With optimal technique and accurate interpretation, these pathologies can be depicted with UE-MDCTA. Radiologists can therefore play a significant role in reducing the risk of cerebral and/or digital thromboembolism, which may occur during conventional UE angiography.

Imaging Procedure: Complete UE coverage includes from at least the aortic arch through to the hand, ranging between 800-1000 mm. Given the requirements for high resolution datasets, this volume may yield 1000-1500 images, potentially limiting image reconstruction time, transfer, viewing, and storage. Volume coverage, however, can be targeted to the vascular segments of interest. Patients are placed supine or prone, with the affected extremity raised above their head into the scanner. Patients can be rotated into a modified swimmers position, to ensure the extremity is as close to the gantry isocenter as possible. As will be reviewed, optimizing contrast medium delivery is essential for depicting stenoses, occlusions, dissections, and vessel wall thickening, not to mention extra-vascular structures.

Conclusion: MDCTA is a robust modality to evaluate UE arterial disease and provide alternative diagnoses. Clinical success is dependent on an understanding of the technical challenges and image findings.

C-1014

Abdominal virtual angiography

P.M. Carrascosa, C. Capuñay, M. Ulla, E. Martín López, J. Carrascosa; Buenos Aires/AR

Learning Objectives: To illustrate a new application of virtual endoscopy in the evaluation of the abdominal vessels. To be familiar with virtual endovascular images. To provide an overview of the spectrum of abdominal CTA findings.

Background: Virtual techniques have been applied to the evaluation of the gastrointestinal tract, especially the evaluation of the colon. New multidetector CT technology allows one to perform vascular CT studies of excellent quality, and the improvement of 3D and endocavitory post-processing software gives the option of introducing this technique in the evaluation of vascular structures.

Procedure Details: The CT exams were performed using a 16-row CT scanners (Brilliance 16; Philips Medical Systems) with the following parameters: 16x1.5 configuration; 2 mm slice thickness; 1 mm reconstruction interval; 120 kV; 300 mAs. The iodinated contrast material was injected using a power injector at 3 ml/sec. The vascular analysis was performed using multiplanar reconstructions, 3D images and virtual angiography.

Imaging Findings: A total of 400 abdominal CT exams were reviewed. In 93 patients, an aneurysm was diagnosed. Nine cases of aortic dissection and 2 cases of mesenteric artery dissection were found. A total of 7 partial thrombosis of the stent-graft, 5 total thrombosis of the graft limbs and 10 leaks were diagnosed. In 8 patients, portal venous thrombosis was diagnosed.

Conclusion: CTA is a non-invasive technique to evaluate the abdominal vessels. Virtual angiography allows better definition of anatomical details and clearly depicts the intraluminal vascular anomalies. Current 3D postprocessing software allows the reconstruction of good quality virtual angiography images.

C-1015

Usefulness of CT angiography in the planning and follow-up of abdominal aortic aneurysm endovascular treatment

C. Capuñay, P.M. Carrascosa, M. Ulla, E. Martín López, J. Carrascosa; Buenos Aires/AR

Purpose: To determine the usefulness of CT Angiography (CTA) in pre- and post-treatment evaluation of abdominal aortic aneurysm.

Methods: A total of 200 CTA scans were retrospectively evaluated. 122 scans were performed as a pre-treatment assessment; 78 scans were carried out as a post-treatment control. CTs were performed on 4-row and 6-row CT scanners (MX8000 and Brilliance 16; Philips Medical Systems) with slices of 2.5 mm and 2 mm thickness, every 1.3 mm and 1 mm reconstruction interval respectively, and 120 ml of contrast material were injected using a power injector. Post-processing volume rendering, MPR and MIP images were obtained.

Results: In the pre-treatment group, the measurements of the aneurysm neck, its length and diameters were determined. The iliac artery diameters and angulation were also evaluated. In the post-treatment group, 24 complications were detected: a) periprosthetic hematoma (n = 2); b) neointimal hyperplasia (n = 2); c) partial stent-graft thrombosis (n = 4); d) total stent-graft thrombosis of an iliac branch (n = 7); e) endoleak type II (n = 4); f) endoleak type III (n = 4), separation of the stents' components (n = 1).

Conclusion: CTA is an accurate, fast and minimally invasive imaging method in the pre-treatment evaluation and also in the evaluation of complications after abdominal aortic aneurysm repair.

C-1016

Evaluation of thoracic aortic pathology by MSCT (16-slice) before and after endovascular treatment

D.N. Exarhos, H. Testembasi, F. Karkantzia, D. Chondros, D. Farsaris, I. Kaskarelis; Athens/GR

Purpose: To describe the CT findings of the thoracic aorta in patients treated by endovascular stents, and assess stent deployment.

Materials and Methods: Twenty-one male patients were examined before and after stent deployment, eight with acute aortic dissection, seven with an aortic rupture and six with an aneurysm. Diagnosis and postinterventional follow-up was performed with a 16-slice multislice scan (Toshiba Aquilion), reconstructions were done on a Vitrea workstation. Scanning parameters were: SC1 mm, SW/RI4/3 mm, MPR SW/RI 3/3cor-sag. Pre- and post-contrast scans were performed in the postinterventional series. Bolus triggering was used, CM370 mg/ml, 120 ml/4 ml per sec, trigger threshold 250 HU. The biphasic protocol in the postinterventional series was optimized individually. Twenty-nine Talent stents were deployed. **Results:** Diagnosis was confirmed by aortography in all cases. Detailed preinter-

Scientific and Educational Exhibits

ventional evaluation of the extent and morphology of pathology was achieved in all patients. Stent deployment was successful. Two patients died from unrelated causes. Follow-up of nineteen patients revealed progression of a dissection in one patient, two patients had endoleaks and were treated (one surgically, one with a stent).

Conclusion: MSCT is an essential tool for the diagnosis of thoracic aortic pathology. The good access to patients, its high spatial resolution, fast data acquisition and excellent quality multiplanar 3D reconstructions allow noninvasive detailed evaluation of aortic lesions. Intraluminal stent graft interposition is an alternative to surgical graft interposition for the treatment of certain aortic lesions. MSCT is the primary diagnostic modality used for pre and postinterventional assessment of the thoracic aorta.

Vascular

MR imaging

C-1017

Pseudo-occlusion of the internal carotid artery assessed by MRA: How to avoid misinterpretation

J. Gasser, S. Celedin, K. Hausegger; Klagenfurt/AT

Learning Objectives: 1. How to deal with pseudo-occlusion of the Internal Carotid Artery (ICA) with various MR-angiographic techniques. 2. How to detect minimal residual flow in a nearly occluded ICA with MRA.

Background: Minimal residual flow in a nearly occluded ICA can be missed with contrast enhanced (CE) MRA and a false positive diagnosis of ICA-occlusion can be made. This pitfall might exclude patients from potential surgical or endovascular correction of high grade ICA-stenosis. Over the last 2 years we examined 280 patients with carotid artery disease with a combination of CE-MRA and TOF-MRA. With CE-MRA 3 false positive diagnoses of ICA-occlusion were made. We will illustrate these cases and demonstrate how MRA with different techniques can help to make the correct diagnosis.

Procedure Details: Our CE-MRA protocol was performed with random central k-space segmentation in a centric filling order (CENTRA). The 3D-TOF sequence covered a FOV from the base of the skull up to the circle of Willis. In 3 cases the CE-MRA showed a carotid "occlusion", whereas TOF-MRA showed residual flow in the ICA. We repeated the CE-MRA in these cases without CENTRA at a slower contrast infusion rate and the correct diagnosis could be made.

Conclusion: In nearly occluded carotids CE-MRA with CENTRA can be false positive for occlusion. Additional 3D-TOF-MRA is helpful to depict minimal flow in subtotally occluded ICA. CE-MRA with conventional k-space filling at a slower contrast infusion rate is more sensitive for residual flow in the carotids than CE-MRA with CENTRA.

C-1018

Accuracy of magnetic resonance for identification and characterization of carotid plaque constituents with histological correlation: A clinical experience

G. Puppini, N. Cirotta, F. Furlan, S. Quintarelli, G. Veraldi, S. Montemezzi, G. Gortenutti; Verona/IT

Purpose: To identify and characterize, using Magnetic Resonance (MR), carotid plaque constituents, such as lipid-rich necrotic core and intraplaque hemorrhage and fibrous cap integrity, among patients treated with carotid endarterectomy (CEA), matched with histological evaluation.

Methods and Materials: 15 patients (9 male and 6 female), with a total of 16 lesions, scheduled for CEA between March and August 2004, were imaged on a 1.5 T Magnetom Symphony scanner. The protocol included 4 types of sequences (T1, T2, proton density and 3D-TOF). Images were reviewed considering integrity of fibrous cap, presence of lipid-rich necrotic core and intraplaque hemorrhage. Signal intensity was compared with reference to the adjacent sternocleidomastoid muscle. 4 cross sections per lesion were compared with the corresponding histologic specimens and independently reviewed by two radiologists and one pathologist.

Results: MR identifies loss of integrity of fibrous cap, presence of lipid-rich necrotic core and intraplaque hemorrhage with a global accuracy of 90%. MR detects lipid-rich necrotic core without intraplaque hemorrhage with a sensitivity and specificity of 88.5% and 91.6% respectively, while it can define intraplaque hemorrhage alone with a sensitivity and specificity of 80% and 97.3%. Loss of integrity of fibrous cap was identified with a sensitivity and specificity of 88% and 100%.

Conclusions: MR is able to identify signs of instability of carotid plaque with high sensitivity and specificity. Therefore it may be useful to evaluate hemodynamically insignificant stenosis with a potential embolic risk, in order to choose the best treatment.

C-1019

Effect of stent orientation and flip angle on subjectively visible stent lumen in contrast-enhanced MR at 1.0 Tesla

D. Blondin, Y. Rado, B. Fritz, A. Saleh, U. Mödder, M. Cohnen; Düsseldorf/DE

Purpose: Intravascular prostheses cause susceptibility artifacts on MR images, impairing complete visualization of the stent lumen. This in-vitro study was aimed at assessment of subjective visibility of modern self-expanding stents.

Materials and Methods: 12 different stents (2 stainless steel, 10 nitinol) were released in plastic tubes completely filled with gadopentetate dimeglumine (Mag-

Scientific and Educational Exhibits

nevist®, Schering) diluted in physiological saline (1:25) and immersed in a water-filled phantom positioned parallel and transverse to the main magnetic field (B_0). 6 stents were deployed at 10 mm diameter, 2 at 8 mm, and 4 at 12 mm. Imaging was performed at 1.0 Tesla with a T1-weighted three-dimensional gradient-echo sequence, using changing Flip angles (FA: 10°, 40°, 70°, 100°, and 130°). Stent lumen visibility was subjectively assessed by three independent and blinded investigators.

Results: In 9 prostheses (all nitinol), the stent lumen was visible to a moderate extent using a FA greater than 40. In general, visibility of stent lumen increased with higher FA resulting in a good visibility at FA of 100, and 130°, respectively ($p < 0.05$). Subjective assessment of transversely orientated stents was generally graded better by all three investigators ($p < 0.05$). Six stents - 3 with a diameter of 12 mm and 3 with 10 mm - proved a good quality in the subjective rating.

Conclusion: In this in-vitro study, 9 of 12 investigated stents showed a visible lumen on contrast-enhanced-MRA at 1.0-Tesla. 6 nitinol-type stents reached a good subjective assessment of lumen visibility. Best results were observed using high flip angles and transverse orientation to B_0 .

C-1020

The pathophysiology of aortic-cardiac interaction in atherosclerotic disease and the role of magnetic resonance imaging

Z.M. Metafratzil¹, A. de Roos², A. Skopelitou¹, S.C. Efremidis¹; ¹Ioannina/GR, ²Leiden/NL

Learning Objectives: 1. To review the histochemical structure and the biophysical properties of the aortic wall. 2. To understand the role of these properties in the pathogenesis of cardiovascular disease and normal aging. 3. To describe the techniques that are used in Magnetic Resonance Imaging (MRI) to assess the changes in aortic wall distensibility.

Background: One of the main functions of the aorta is to maintain a steady blood flow throughout the capillaries by transforming the pulsatile flow generated by ventricle contraction into a continuous flow. This function minimizes the load imposed on the left ventricle during systole and keeps the flow steady in the coronaries. For this effect to be maintained, the aortic wall has to be compliant. However, elastin fibers fracture at low stresses and contribute to the decrease of the aortic compliance and thus to the increase of the pulse pressure, a risk factor for cardiovascular disease. Early detection of a decrease in the compliance can identify early cardiovascular disease in asymptomatic subjects and monitor the results of medical interventions.

Procedure Details: MRI can estimate the arterial wall compliance either by measuring the regional compliance using ECG SE and GRE sequences or by measuring the pulse wave velocity through the aorta using the phase contrast technique.

Conclusion: MRI can assess the elastic properties of the aorta noninvasively and in an accurate and reproducible way. Thus, it provides a challenging tool to identify early cardiovascular disease and monitor subtle changes of wall elasticity in response to therapeutic manipulations.

C-1021

Pulmonary vein mapping with contrast-enhanced MR venography of the pulmonary veins prior to ablative therapy

G.C. Hargaden, D. Rea, S. O'Brien, D. Keane, J.F. Meaney; Dublin/IE

Learning Objectives: 1. To describe the technique of contrast-enhanced MR venography of the pulmonary veins. 2. To highlight the issue of appropriate timing to ensure adequate demonstration of the venous anatomy. 3. To illustrate the technique of "selective" venous enhancement by subtraction of the peak arterial phase. 4. To emphasise the common anatomical arrangement of the pulmonary veins. 5. To illustrate the common variants, particularly of the lingular and middle lobe veins. 6. To emphasise that the optimal imaging plane for catheter venography can be predicted from the 3D MR data-sets.

Background: The most common arrangement of the pulmonary veins is a single superior and single inferior pulmonary vein on each side, each with a separate ostium. The lingular and middle lobe veins usually drain into the upper lobe pulmonary vein. Under- or over-incorporation of the common PV into the left dorsal atrium during embryonic development results in anatomic variations in the number, branching patterns, and length of pre-ostial pulmonary veins.

Procedural details: At least two post-contrast acquisitions, centred over the proximal pulmonary circulation and tailored to the patient's breath-hold capability, are acquired in the coronal plane. Targeted reformat images of the left atrium and pulmonary veins are constructed to optimally demonstrate the anatomy.

Conclusion: Contrast-enhanced MRA/V in the coronal plane adequately visualises the pulmonary veins and left atrium. The number and size of pulmonary veins, size of the ostium and optimum plane for imaging during catheter ablation are clearly documented.

C-1022

Gadolinium-enhanced MR venography of the venous compression syndromes

A.E. Mahfouz, H. Sherif; Doha/QA

Objectives: To describe the imaging findings of the different venous compression syndromes on gadolinium-enhanced MR venography

Background: Venous compression syndromes are caused by compression of veins at certain anatomical locations between arteries and bones or between two arteries. Examples of these syndromes include left innominate vein compression syndrome caused by compression of the left innominate vein between the sternum and aortic arch, nut-cracker syndrome caused by compression of the left renal vein between the aorta and the superior mesenteric artery, retroaortic left renal vein which may be compressed between the spine and the aorta, and May-Thurner syndrome caused by compression of the left common iliac vein between the right common iliac artery and the spine.

Procedure Details: Gadolinium-enhanced MR venography has been performed by three-dimensional T1-weighted gradient-echo images performed before and repeatedly after intravenous injection of Gd-DTPA, followed by image subtraction and maximum intensity projection. The technique has been applied to different parts of the body where venous compression syndromes have been suspected. This educational exhibit illustrates the imaging features of the different venous compression syndromes with discussion of their clinical impact.

Conclusion: Gadolinium-enhanced MR venography may be helpful for diagnosis of venous compression syndromes.

C-1023

Chronic aortic dissection: Contribution of velocity-encoded cine MR imaging and multiphasic MR angiography

V. Pineda, R. Dominguez-Oronoz, X. Merino, E. Castellà, A. Evangelista, R. Vidal; Barcelona/ES

Learning Objectives: To describe the patterns of aortic flow in the false and true lumens in chronic aortic dissection, comparing them with morphologic and functional findings in multiphasic contrast-enhanced MR angiography (MRA).

Background: Multiphasic contrast-enhanced MRA provides morphologic and functional information in the dissected aorta. Velocity-encoded cine MR imaging can determine flow velocity and flow volume noninvasively in any desired plane, using phase-contrast sequences. The evaluation of flow patterns in the false lumen may be useful for predicting enlargement of the dissected aorta, considering that aneurysm formation is an important prognostic factor in patients with chronic aortic dissection. The flow patterns are influenced by communications between the true and false lumens, and the presence of arteries originating from the false lumen.

Imaging Findings: Morphologic and functional MRA findings are correlated with hemodynamic patterns obtained by velocity-encoded cine MRI imaging measurements. Flow patterns through the false and true lumens are illustrated in different cases of aortic dissection depending on the location, size and number of communications between both lumens. Analysis of blood flow in patients with and without arteries originating from the false lumen are shown.

Conclusion: Different hemodynamic patterns are found in chronic aortic dissection. There is a relationship between the flow characteristics in velocity-encoded MR imaging measurements and multiphasic MRA morphologic findings and enhancement patterns of both lumens.

C-1024

Evaluation of Takayasu arteritis with MR imaging and contrast enhanced magnetic resonance angiography (CEMRA)

A. Beresnak, E. Gomez, S.E. Rombolá, A. Simoncini; Buenos Aires/AR

Learning Objectives: To show the usefulness of a combined study (MR imaging and CEMRA) for evaluating the arteries in patients with Takayasu arteritis.

Background: Digital subtraction angiography (DSA) is the method generally used for the evaluation of patients with Takayasu arteritis, but it only allows the evaluation of the lumen. MR imaging combined with CEMRA allows us to evaluate both the lumina and the walls of the arteries. We studied 6 patients with Takayasu arteritis, observing the vessels involved, and the involvement of the lumen and the wall.

Procedure Details: We used a 1.5 T unit, using a body coil. We applied axial T2 FSE and axial T1 SE sequences in thoracoabdominal regions and CEMRA was performed using coronal FFE 3D with a double dose of gadolinium, and the delay time was determined through MR fluoroscopy. According to the *Numano classification* we detected 1 case of type I (17%), 2 type IV (33%), 3 type V (50%). In 5

Scientific and Educational Exhibits

patients we found luminal involvement (83%) and 1 had involvement of both lumen and wall (17%).

Conclusion: MR imaging together with CEMRA allows us to evaluate patients with Takayasu arteritis in a minimally invasive manner, delineating the disease extension and detecting both luminal and wall compromise. It does not use iodine contrast agents and the contraindications are those inherent to MR imaging.

C-1025

Evaluation of Gd-DTPA in detection of atherosclerotic plaques at 3 Tesla in WHHL animals

H. Ittrich¹, A. Priest¹, C. Jahntz¹, C. Weber¹, J. Meding², G. Adam¹;
¹Hamburg/DE, ²Berlin/DE

Purpose: To estimate the ability of Gd-DTPA (Magnevist) to enhance lipid atherosclerotic plaque on a clinical 3 T MR Scanner in an animal model.

Material and Methods: High resolution MR imaging of the aortic arch was performed on 6 WHHL (14-29 months) and 3 NZW rabbits (control, 16 months) before and at 10-minute-intervals up to 1 hour after injection of 200 µmol/kg Magnevist on a 3 Tesla MR scanner (Philips Intera), using an 8-channel head array coil. IR-TurboFLASH-Sequences (TE/TR = 2.6/7.8 ms, TI 120 ms, FA 20°, shot repetition time 300 ms, 15 excitations per shot, matrix 256x179, resolution 0.55x0.55x2.5 mm) of different parts of the aorta (perpendicular to wall) and in parasagittal orientation (cover whole aorta) were used to detect uptake of Gd-DTPA. SNR-measurements were performed by placing ROIs in the aorta. For each time point the groups were compared by Student's t-test.

Results: Measurements of luminal diameters showed no significant differences or severe stenosis (6.5 ± 0.6 mm). Significant increased uptake in aortic wall and delayed wash-out could be detected in the WHHL-group (SNR pre administration 2.6 ± 1.4 , 10 min.post admin. 5.2 ± 3.2 , 20 min.p.a. 4.2 ± 2.1 , 30 min.p.a. 3.6 ± 1.9 , 40 min.p.a. 3.1 ± 1.7 , 50 min.p.a. 2.9 ± 1.6 , 60 min.p.a. 2.7 ± 1.5) in comparison to the NZW-group (SNR pre admin. 2.5 ± 1.3 , 10 min.p.a. 3.3 ± 2.0 , 20 min.p.a. 2.9 ± 1.6 , 30 min.p.a. 2.7 ± 1.5 , 40 min.p.a. 2.5 ± 1.3 , 50 min.p.a. 2.4 ± 1.3 , 60 min.p.a. 2.4 ± 1.3). At the first 3 time points after administration the groups showed significant differences in SNR at a level of 5%.

Conclusion: Contrast enhanced MR imaging techniques at 3 T using clinically applicable dosages of Gd-DTPA are able to differentiate between wall segments with and without atherosclerotic changes in animals. This approach may also be suitable for detection of early stage atherosclerosis in humans.

C-1026

The correlation between the magnetic resonance imaging of clots and thromboaspiration in vitro

J. Koizumi; Isehara-city/JP

Purpose: To obtain the correlation between the direct MR imaging of clots and thromboaspiration in vitro.

Materials and Methods: Venous blood from the same human was clotted in vitro by addition of thrombin and calcium chloride. The clots in vitro were positioned between the two legs of the same human and the MR images were obtained immediately after clotting up to one month at 37°C of incubation. Each clot was then aspirated using the same thromboaspiration catheter. T1- and T2-values were calculated based on the mixed sequence with multiecho spin echo and multiecho inversion recovery, and proton density ratio was obtained on proton density images (TR 8000, TE 9.0) using 1.5 tesla GYROSCAN (Philips). The clots were aspirated by 8Fr. OASIS (Boston Scientific) at 2.5 mL/sec of normal saline, and the aspiration time was measured.

Results: The T1-value became shorter than that of muscle (660 ms) around one week after clotting and lasted to 257 ms at day 28, while the T2- value elongated from 31 ms to 117 ms correspondingly. Both T1- and T2- values were significantly ($p < .05$) correlated with the time after the clotting, but not with the aspiration velocity from 2.790 to 1.200 mL/sec or the proton density ratio from 763 to 630 correspondingly.

Conclusion: In vitro experiment suggests that the clots from one week to one month after clotting reveal higher signal intensity than muscle on T1-weighted image and respond well to thromboaspiration.

C-1027

Zero-filling interpolation processing (ZIP) technique can effectively suppress segmental stenosis artifact in small arteries in anatomical phantoms

R. Lin¹, R.H. Wu¹, Z.W. Xiao¹, G.R. Liu¹, K.M. Kong¹, Z.J. Lang²;

¹Shantou, Guangdong/CN, ²Dalian/CN

Purpose: The purpose of this study was to evaluate the zero-filling interpolation processing (ZIP) technique for contrast-enhanced MR angiography (CE-MRA).

Methods and Materials: Phantoms of arteries were made with different lumen diameters. Gadolinium-enhanced three-dimensional MR angiography was performed on a GE 1.5 T scanner. The parameters of FSPGR pulse sequence were: flip angle 30°, TR 6 ms, TE 1.4 ms, bandwidth 31.25 kHz, slice thickness 1.2 mm, matrix 256x256. These sequence parameters were kept constant for the studies, whereas one of four additional selections was chosen: (1) with ZIP1024 and ZIPx4 techniques; (2) only with ZIP1024 technique; (3) only with ZIPx4 technique; (4) without ZIP technique. For image quality evaluation, MR maximum intensity projection (MIP) images were created. Signal-to-noise ratio (SNR) was measured on MIP images. Vessel edge was determined using full width at half maximum (FWHM) for lumen diameter calculation.

Results: The FWHM results of lumen measurements for all ZIP techniques were more accurate than conventional technique in all phantoms, no matter what size the artery was. The vessel edge with ZIP1024 technique was more distinct than conventional technique ($P < 0.01$). The segmental stenosis artifacts in small arteries in phantoms were only effectively suppressed with ZIPx4 technique.

Conclusion: ZIP technique is excellent for CE-MRA to obtain high quality MR angiography. ZIPx4 technique can effectively suppress segmental stenosis artifact in small arteries in phantoms.

C-1028

Role of CE-MRA in studying vascular complications after kidney transplantation

C. Quirico, A. Stecco, P. Oronzo, G. Marano, D. Rozzati, F. Crinò, C. Borracini, A. Carriero; Novara/IT

Purpose: To assess accuracy of CE-MRA in patients with vascular complications after kidney transplantation.

Methods and Materials: 30 patients suspected of having renal artery stenosis after kidney transplantation, underwent ce-MRA. The imaging was performed on a 0.5 T (GE), using a body-flex coil and a 3D fast gradient echo sequence with and without contrast enhancement (GD-BOPTA 2.0 ml/sec). The MRA and post-processing images (reformat MIP) were evaluated by two radiologists.

Results: In 18 out of 30 patients (60%) ce-MRA showed a RA stenosis. Diagnostic accuracy of ce-MRA in the detection of renal artery stenosis was 100% compared to DSA.

Conclusion: ce-MRA imaging allows a complete anatomic and functional evaluation of patients with impaired graft function or vascular complications after kidney transplantation, and is associated with low nephrotoxicity. Ce-MRA shows high sensitivity in detection of significant renal artery stenosis.

C-1029

Non-renal artery incidental findings in a renal artery stenosis MR protocol: A pictorial essay

P. Bermudez Bencerrrey, J. Fortuño Andrés, J. Falcó Fages, J. Perendreu Sans, A. Darnell Martin, J. Branera Pujol; Sabadell/ES

Learning Objectives: To describe the spectrum of extra-renal artery incidental findings that it is possible to find in a renal artery stenosis MR protocol. The presentation emphasizes the necessity for a systematic review of all morphologic and angiographic MR pulse sequences in a renal stenosis MR protocol in order to identify clinically relevant incidental findings.

Background: Magnetic resonance is a widely accepted technique for the evaluation of renal artery stenosis. Although 3D T1 gradient-echo is the most important sequence to evaluate renal artery stenosis, non-vascular morphologic T1 and T2 MR weighted images are useful to evaluate renal size, parenchymal anatomy and to identify incidental neoplastic renal lesions.

These extra-renal artery incidental findings are common in patients undergoing MR study for the detection of renal artery stenosis. Most of these findings are inconsequential and do not require additional interventions, but in a minority of patients it is possible to demonstrate clinically relevant findings.

Procedure Details: In this pictorial issue we review high, moderate and low significance extra-renal artery vascular and non-vascular incidental findings in our renal artery stenosis studies from 1998 to 2003.

Scientific and Educational Exhibits

Conclusion: Systematic review of all morphologic and angiographic MR pulse sequences in a renal stenosis MR protocol permits the identification of clinically relevant incidental findings.

C-1030

Three dimensional cine phase contrast MR imaging: Evaluation of ascending aortic aneurysms

J.C. Hellinger, M.T. Draney, M. Markl, M. Alley, R.J. Herkens; Stanford, CA/US

Learning Objectives: 1. To review the flow patterns of ascending aortic aneurysms. 2. To demonstrate the use of three dimensional CINE phase contrast MR imaging for depicting ascending aortic aneurysm flow dynamics.

Background: Ascending thoracic aortic aneurysms generate variable flow patterns. These include circumferential flow, right handed helices in early systole, vortical retrograde flow during end-systole / early diastole, and "corkscrew" flow during the early diastolic phase. In a single acquisition, time-resolved, three-dimensional CINE phase contrast MR imaging (3D PC-MRI) can provide characterization of these complex flow dynamics four dimensionally (4D). In this exhibit, we illustrate our early experience with 3D PC-MRI to evaluate ascending aortic aneurysms.

Procedural Details: During 3D PC-MRI acquisitions, ECG and respiratory gated data are acquired throughout the cardiac cycle. Noise filtering and eddy current correction techniques are applied. To generate the 4D displays, cut-planes are first placed at selected levels in the 3D dataset. The data is then processed with visualization tools (EnSight, CEI), including vector fields, streamlines, and / or transient particles. 4D displays can be processed reliably and efficiently, providing invaluable information for planning surgical repair of ascending aortic aneurysms.

Conclusions: 3D PC-MRI is a promising imaging technique to noninvasively evaluate flow patterns in aneurysms of the ascending thoracic aorta. Continued application will determine its role in clinical decision making.

C-1031

MR angiography of lower extremities with moving-table infusion-tracking technique

A. Beresnak, E. Gomez, S.E. Rombolá, A. Simoncini; Buenos Aires/AR

Learning Objectives: To show the usefulness of lower extremity MR angiography with a moving-table infusion-tracking technique in the evaluation of arterial disease.

Background: Arterial pathology of lower extremities is usually evaluated with invasive methods such as digital subtraction angiography and with Doppler ultrasound, which is non-invasive but operator-dependent. This poster describes the technique, image findings, limitations and advantages of contrast-enhanced MR angiography (CEMRA). 39 patients with suspected pathology in the lower limbs were studied between 2001 and 2004.

Procedure details: A 1.5 T unit with a moving table feed was used, with a coronal FFE 3D sequence and a double dose of gadolinium. Leg and pelvic regions were imaged. Unenhanced images were subtracted from gadolinium-enhanced ones, and MIP projection images were generated with different rotation angles. 13 patients had stenosis or vascular occlusion (33%); in 10 of these, vascular encasement by a tumor was diagnosed (26%); 8 were normal (20%), 5 showed vascular malformations (13%), 2 pseudo-aneurysms (5%) and 1 aneurysm (3%). **Conclusion:** CEMRA with automatic table feed allows us to obtain in one single study images from the aorta, iliac and lower limb arteries in a quick and minimally invasive manner, with excellent image definition, which allows us to evaluate the different pathologies. It does not use iodinated contrast agents and is not operator-dependent. Its limitations are the contraindications inherent to any MR imaging procedure and the low resolution at the level of the lower third of the leg and foot.

C-1032

Renal artery fibromuscular dysplasia: Findings on contrast-enhanced MRA

S. O'Brien, C. Farrelly, N. Sheehy, G. Hargadon, S. O'Keeffe, J.F.M. Meaney; Dublin/IE

Learning Objectives: 1. To highlight the features of FMD of the renal arteries. 2. To present the imaging findings in 5 patients with FMD demonstrated on CE-MRA. 3. To emphasise the spatial resolution limitations of current CE-MRA techniques in the diagnosis of FMD. 4. To highlight advances in technology that will improve the ability to detect mild grades of FMD.

Background: Fibromuscular dysplasia (FMD) of the renal arteries is a relatively uncommon disorder which may be responsible for up to 10% of cases of reno-

vascular hypertension. The disorder is more common in females between 15 and 50 years but may present for the first time after the age of 60 years. Although CE-MRA is a proven modality for detection of atherosclerotic renal artery stenosis (which typically affects the ostium and proximal renal artery), the beaded appearance of FMD is more difficult to detect due to the fact that it typically occurs more distally where the artery is smaller, where more motion artefact is present, and where resolution constraints are more marked.

Imaging Findings: The findings on CE-MRA are presented in 5 patients with FMD who underwent 3D CE-MRA at 1.5 T using bolus detection to ensure correct timing.

Conclusion: FMD of moderate severity can be detected with CE-MRA despite significant challenges. Detection of milder degrees of FMD requires higher resolution imaging than is routinely available at present.

C-1033

Virtual MR endoscopy of aortic aneurysms and dissection

E. Squillaci, M. Speradio, M. Di Roma, S. Fabiano, V. Fiaschetti, G. Simonetti; Rome/IT

Learning Objectives: To report technique and pitfalls of MR Virtual Endoscopy (VE) of the aortic lumen. To understand the role of VE in MRA of aortic aneurysms. To compare VE vs MIP and Volume Rendering (VR) images.

Background: The potential advantages of VE have not yet been considered in the MR evaluation of aortic aneurysms and dissection.

Procedure Details: 22 patients affected by aneurysm in the thoracic (n = 9) or abdominal aorta (n = 13) with 7 dissections underwent contrast-enhanced MRA (0.2 mMol/kg) at 1.5 T (Philips Gyroscan Intera, Best The Netherlands) with a phased array body coil. MR protocols, including new pulse sequences (SENSE, SS-SE-EPI), are discussed as well as more common artifacts and pitfalls. Methods to obtain VE images on an external workstation are described. Aneurysm extension and involvement of aortic branches, intimal flap evidence and aortic dissection extension was considered as well as time for post-processing. Good imaging quality was obtained in all patients. A comparison with MIP and VR images is performed and comparative case are presented. MIP images allow a more precise detection of the intimal flap compared with VR. VE provided better results compared with VR and MIP for the evaluation of aortic branches involvement.

Conclusion: In our experience VE can be a helpful diagnostic tool in the evaluation of aortic aneurysms and dissections.

C-1034

High-speed 2D MR cerebral venography using spiral spoiled gradient-echo sequence

K. Uchida¹, K. Oda², T. Kajitani¹, E. Fukuba¹, A. Wada¹, H. Kitagaki¹; ¹Enya, Izumo, Shimane/JP, ²Miwa, kurashiki, okayama/JP

Purpose: We quantitatively compared 2D MR venography with both spiral SPGR (spoiled gradient-echo) and the SPGR in a phantom study and clinical study.

Methods and Materials: All images were acquired on a 1.5 T MR machine. In the phantom study, a plastic tube with pulsatile flow was used to simulate the cerebral venous system. Using fast SPGR and spiral SPGR sequences, the contrast-to-noise ratio (CNR) and Full Width Half Maximum (FWHM) of the plastic tube phantom were evaluated while altering flow velocities inside the phantom and the angle between the phantom and acquisition plane (tilt angle). In the clinical study, fifteen healthy volunteers were examined with both fast SPGR and spiral SPGR sequences following informed consent. The CNR of veins and sinuses were measured and evaluated.

Results: In the phantom study, the CNR of both the fast SPGR and the spiral SPGR were reduced with a decrease in tilt angle. The reduction in the CNR for the spiral SPGR were smaller than those of the fast SPGR, indicating that the spiral SPGR is a more consistent technique. In the clinical study, the CNR of the spiral and the fast SPGR were almost equal for each cerebral vessel. However, the scan time of cerebral venography with the spiral SPGR was only twenty percent of that with the fast SPGR sequence.

Conclusion: The temporal resolution for 2D MR cerebral venography is better with the spiral SPGR sequence than with the fast SPGR sequence, without loss of image quality.

Scientific and Educational Exhibits

C-1035

Nonenhanced peripheral MR angiography using peripheral pulse-triggered three-dimensional half-Fourier fast spin-echo in patients with chronic kidney disease

N. Yanagimachi¹, Y. Imai¹, M. Higashi²; ¹Isehara/JP, ²Yokohama/JP

Learning Objectives: To demonstrate the clinical usefulness of nonenhanced peripheral MR angiography in patients with chronic kidney disease.

Background: MR angiography using peripheral pulse-triggered three-dimensional half-Fourier fast spin-echo provides selective visualization of arteries or veins by diastolic and systolic subtraction without contrast media. Although this technique is more effective in fast-flow vessels, appropriate flow-spoiled gradient pulses in the readout direction permit distinction of arteries from veins even in slow-flow peripheral vessels in the hand and foot. This noninvasive technique is useful in evaluating peripheral vascular disease in patients with reduced renal function and in vascular mapping before creation of hemodialysis access fistulas in patients with end-stage renal disease. The possible applications of this technique in evaluation of hemodialysis access fistula complications are discussed.

Imaging Findings: In healthy volunteers, the peripheral vessels are depicted in good quality. In patients with chronic kidney disease, various arterial and venous diseases, such as arteriosclerosis obliterans and deep vein thrombosis are depicted. On preoperative MR angiography of the forearm for a hemodialysis access fistula, radial and ulnar arteries and superficial veins are well demonstrated. Images of hemodialysis access fistulas show only flow voids on this technique.

Conclusion: Nonenhanced peripheral MR angiography is useful in evaluating various vascular diseases in patients with chronic kidney disease.

C-1036

Diagnosis of abdominal aortic aneurysms

M.A. Aliev, V.A. Jakupov, Y. Akhmetov, A.M. Tayev, B.Z. Kassymov, S.E. Serikova; Almaty/KZ

Purpose: To evaluate magnetic resonance (MR) imaging accuracy in the characterization of mural thrombi in abdominal aortic aneurysms (AAA).

Material And Methods: 25 patients (22 men, 3 women; mean age - 68 years) with an AAA with mural thrombus thicker than 1 cm at sonography underwent T1- and T2-weighted spin-echo MR imaging. The thrombi were prospectively classified as one of three signal intensity (SI) categories: category 1 corresponds to low SI on both T1- and T2-weighted images; category 2, high SI on T1-and T2-weighted images; and category 3, inhomogeneous SI with hyperintense areas on both T1- and T2-weighted images. During surgery, thrombi were classified as organized, unorganized, and partially organized. MR imaging and surgical findings were compared.

Results: SI category 1 corresponded to organized thrombi in 15 of 15 patients. Category 2 corresponded to unorganized thrombi in 6 of 6 patients. In category 3, focal hyperintense areas corresponded (both for presence and location) to unorganized portions of partially organized thrombi in 4 of 4 patients.

Conclusion: MR imaging is accurate method in AAA thrombus characterization.

Vascular

Peripheral

C-1037

Suspected entrapment syndrome of the popliteal vein: How to diagnose it. Is it rare?

H. Minamiguchi, M. Sato; Wakayama/JP

Learning Objectives: To demonstrate and understand the entrapment syndrome of the popliteal vein.

Materials and Methods: From October 2003 to March 2004, we examined 42 patients (84 limbs) with chronic leg symptoms (calf numbness, calf swelling without redness) or with the history of pulmonary embolism. We evaluated venous diameter and flow rate of the popliteal vein in three positions: (neutral {N}, dorsal flexion{DF} and plantar flexion{PF}) with ultrasound sonography and/or venography.

Results: Twenty-four patients (57%) and 35 limbs (42%) were diagnosed as entrapment syndrome of the popliteal vein. Eleven patients had the syndrome in both limbs, 7 in left and 6 in the right limb. Twenty-six limbs showed entrapment syndrome in PF, 14 in DF and 2 in N. Two had an anomaly of the gastrocnemius muscle and 7 had obvious compression by gastrocnemius muscle during the movement.

Conclusion: Entrapment syndrome of the popliteal vein is not rare, and it may cause calf deep vein thrombosis and/or pulmonary embolism.

C-1038

Radiological imaging of thoracic outlet syndrome

G. Bodner, H. Gruber, M. Schocke, M. Bernathova; Innsbruck/AT

Learning Objectives: The purpose of this exhibit is to review radiological imaging appearance of TOS.

Background: Thoracic outlet syndrome (TOS) is a compression of the neurovascular structures at the thoracic outlet region. It can be caused by anatomical abnormalities or acquired changes in the soft tissues and bony structures in the region. The brachial plexus is the most frequently affected structure, followed by the subclavian vein and artery. Diagnosing and treating thoracic outlet syndrome can be challenging and time consuming, hampering patients quality of life.

Procedure Details: We present a series of 16 cases reviewing the imaging manifestations of TOS from MRT, MSCT, sonography and arteriography. Other causes mimicking a TOS are also presented.

Conclusion: The clinical suspicion of TOS can be supported by specific imaging findings without the need for interventional procedures.

C-1039

Sonographic approach for imaging calf veins: An anatomic study

M. Bernathova, H. Gruber, M. Pavelka, G. Bodner; Innsbruck/AT

Learning Objectives: To propose a valid sonographic approach to identify the posterior tibial veins, peroneal veins and the muscle veins (gastrocnemius and soleus veins) from the lateral and medial sides.

Background: Compression sonography is currently the method of choice to diagnose deep venous thrombosis of the femoral and popliteal vein. Controversially discussed, however, is the value of compression sonography in detecting a venous thrombosis in the calf. This may be due to lack of knowledge regarding the sonographic compartmental anatomy of the calf.

Procedure Details: We performed a cadaveric study comparing transverse sonographic images and corresponding cryosections from both calves of a cadaver specimen. Important sonographic landmarks to identify calf veins are the shape of the tibial and fibular bone, the gastrocnemius and soleus muscle and the different crural fascias. In addition we present selected cases of patients with calf vein thrombosis with special regard to sonographic landmarks.

Conclusion: The anatomic landmarks visible in sonography are helpful in identifying the main calf veins.

C-1040

Peripheral arterial blood flow and intima-media thickness in patients with predialysis stage chronic renal failure

Z. Serafin, B. Sobociński, P. Strzesniewski, W. Lasek, P. Strozecki, A. Kapala, J. Manitius, S. Dabrowski; Bydgoszcz/PL

Purpose: Progression of atherosclerosis in hemodialysis patients with end-stage chronic renal failure (CRF) has been demonstrated by increased carotid artery

Scientific and Educational Exhibits

intima-media thickness (IMT). The aim of this study was to evaluate the condition of the peripheral artery system in patients at the predialysis stage of renal failure. **Methods and Materials:** 35 patients at the predialysis stage of CRF and 15 healthy volunteers were included in the study. IMT was measured in the brachial artery using B-mode ultrasonography. Flow spectra were evaluated with duplex-scan mode and flow parameters were calculated for the brachial artery, and for distal parts of the radial and ulnar arteries.

Results: Brachial artery diameter and IMT were significantly higher in CRF patients than in controls (mean 4.1 vs. 3.4 mm, $P < 0.001$, and 0.46 vs. 0.37 mm, $P < 0.05$, respectively). Brachial blood flow volume was also larger in CRF patients (mean 179.5 vs. 145.5 ml/min.), but the difference was not statistically significant. In peripheral arteries, blood flow volume was significantly lower in CRF patients than in controls (22.3 vs. 34.2 ml/min., $P < 0.04$). There was a positive correlation between patients' age and IMT ($P < 0.01$), and a negative correlation between brachial flow volume and pulsatility and resistive indices ($P < 0.02$) in both groups. In CRF patients, age correlated with PI and RI ($P < 0.01$) in all arteries.

Conclusion: The results indicate that peripheral circulatory changes in early-stage CRF patients include alterations of the brachial artery wall and a decrease of blood flow volume in distal forearm arteries.

C-1041

The brachial artery reactivity in patients with metabolic syndrome

G.E. Roytberg, E.A. Artamonova, T.I. Ushakova; Moscow/RU

Purpose: Insulin resistance is one of the main risk factors for atherosclerosis, causing endothelial dysfunction, an early event in the disease process. The aim of this study was to determine whether vascular reactivity is associated with insulin resistance (IR) and metabolic syndrome.

Methods: We studied 131 non-diabetic clinically healthy men. 2-hour oral glucose-tolerance test (OGTT) was performed, anthropometrical measurements and serum lipids were analyzed. IR was estimated by HOMA-IR model. Endothelium-dependent (flow-mediated) vasodilatation was assessed in the brachial artery by ultrasound Doppler in two groups: with metabolic syndrome according to WHO criteria ($n = 70$), and controls ($n = 61$), mean age 42.5 ± 0.9 and 41.9 ± 0.8 respectively.

Results: The two groups were similar with regard to the brachial artery diameter and brachial blood-flow velocity and volume at baseline. As compared with the controls, the patients with metabolic syndrome had less flow-mediated brachial artery reactivity ($9.0 \pm 0.4\%$ vs. $11.9 \pm 0.4\%$, $p = 0.047$). A significant correlation was found between brachial artery reactivity and HOMA-IR ($r = 0.25$, $p = 0.041$), the inverse correlation was between body mass index ($r = -0.43$, $p < 0.001$), hypertension ($r = -0.29$, $p = 0.014$), triglycerides ($r = -0.28$, $p = 0.020$).

Conclusion: The results indicate that brachial artery reactivity was significantly lower in patients with metabolic syndrome and could be used as early marker of atherosclerosis.

C-1042

Duplex imaging in quantification of peripheral arterial disease: Is it reliable?

A. Krnic, N. Vucic, Z. Sucic, S. Schmidt, F. Jelavic-Kojic; Zagreb/HR

Purpose: To assess the correlation and the measure of agreement between duplex imaging and angiography in detecting arterial disease of lower limbs. Most of the performed studies assessed accuracy in detecting lesions, but correlation has not yet been established.

Materials and Methods: 84 legs in 42 patients were studied (25 men, 17 women, median age 67) with peripheral arterial disease. Each patient had duplex ultrasonography and conventional intra-arterial angiography. Each leg was divided into 7 arterial segments, and the disease in each segment was quantified as normal, mild (< 20% diameter reduction), moderate (20-< 50% reduction), severe (50-99% diameter reduction), or occlusion. For statistical purposes, these were scored as 0, 1, 2, 3 and 4, respectively. Pearson correlation and Kappa measure of agreement were applied.

Results: For each segment correlation and the Kappa value were statistically significant at the 0.01 level. However, the highest correlation coefficients were found for popliteal, distal and proximal superficial femoral arteries ($r = 0.77$, $r = 0.76$, and $r = 0.75$, respectively); the lowest for calf arteries and common femoral arteries ($r = 0.59$, $r = 0.43$). Kappa values ranged from 0.29 for anterior tibial to 0.65 for distal superficial femoral arteries. The most severely affected segment was distal superficial femoral and least severely, the common femoral arteries (mean score ranged from 3.24 ± 1.10 to 1.55 ± 1.03 , one-way ANOVA, $p < 0.01$)

Conclusion: Duplex ultrasonography is, up to a certain degree, reliable in detecting arterial lesions, particularly in segments which are most often bypassed

and most severely affected (superficial femoral, iliac). One must be aware of its shortcomings and possible pitfalls, and rely on it rationally.

C-1043

MDCT angiography in the preoperative evaluation of peripheral arterial disease: Comparison with catheter based DSA

A. Napoli, C. Catalano, P.G. Nardis, M. Francone, F.A. Calabrese, R. Passariello; Rome/IT

Purpose: The aim of this study was to evaluate the usefulness of multidetector-row spiral computed tomography angiography (MDCTA) compared with catheter-based digital subtraction angiography (DSA) as a preoperative tool in surgical decision making.

Materials and Methods: 74 patients with peripheral obstructive arterial disease were evaluated with MDCTA and catheter-based DSA. Computed tomography angiography was performed using a multidetector-row spiral scanner with 0.5 s gantry rotation time with the following parameters: slice collimation 4×2.5 mm, slice thickness 3 mm, slice interval 1.5 mm, feed/rotation 15 mm. A 28 second standard delay time was used in all patients. A volume of 140 mL of iodinated contrast agent was administered at 4 mL/s in all patients. Three blinded readers independently evaluated DSA and MDCTA. Agreement on one of 8 different treatment options was based on a consensus decision. Intra- and inter-observer agreement was obtained with Cohen k statistical analysis.

Results: Interobserver agreement among the three readers for treatment recommendation with MDCTA and DSA was almost perfect (k value = 0.931). Intraobserver agreement for treatment selection based on DSA and MDCT angiography was almost perfect for the three readers (observer 1, k value = 0.929; observer 2, k value = 0.957; observe 3, k value = 0.942).

Conclusion: MDCT angiography can replace catheter based DSA in preoperative evaluation of patients with obstructive arterial disease

C-1044

Relationship between serum C-reactive protein levels and angiographic findings in patients with peripheral arterial occlusive disease

M. Bustamante, E. Sánchez-Salmón, P. Ruiz-Hernández, P. Merino, M. Aguilar, I. Sampredo, A. González-Tutor; Santander/ES

Purpose: Inflammatory processes are recognized as playing a central role in the pathogenesis of atherosclerosis. Several inflammatory markers have been associated with cardiovascular risk. Acute-phase C-reactive protein (CRP) has been shown to be a predictor of future cardiovascular events. In this study we analyzed the relationship between serum CRP levels and angiographic findings in patients with peripheral arterial occlusive disease (PAOD).

Methods and Materials: 33 consecutive patients (28 male, 5 female) (aged 33-87, mean 69) with PAOD submitted for angiographic examination and without previous vascular surgery were included in the study. A high sensitivity test for CRP was performed. Digital subtraction angiography of the lower limbs or MR imaging angiography findings were analyzed and scored based in the presence of stenosis or obstruction of the iliac and femoral arteries (0 = normal, 1 = stenosis, 2 = obstruction).

Results: We found statistically significantly higher values of CRP ($p < 0.05$) in patients with complete obstruction of the superficial femoral artery when compared with those with a normal or stenotic artery. There where no significant differences in serum CRP levels related to the severity of angiographic findings in the iliac arteries.

Conclusion: Serum CRP levels appear to be related to severity of arterial damage in patients with peripheral arterial occlusive disease with superficial femoral artery involvement.

Scientific and Educational Exhibits

Vascular

Visceral

C-1045

Non-rigid image registration for subtraction CT angiography of the abdomen is significantly more effective when the post-contrast image is deformed to match the pre-contrast image

S. Drisis, D. Seghers, S. Srivastava, E. D'Agostino, F. Maes, G. Marchal; Leuven/BE

Purpose: Subtraction CT Angiography (SCTA) of the abdomen is affected by artifacts related to motion and local deformation. This leads to misalignment of corresponding high-intensity structures in the pre- and post-contrast images such as bones and plaques. We investigated the effectiveness of pre-to-post versus post-to-pre contrast non-rigid image registration (NRR) to optimally align both images prior to subtraction.

Materials and Methods: Pre- and post-contrast CT images of 5 patients (Sensation16, Siemens, Erlangen, voxel size $0.72 \times 0.72 \times [0.5-1] \text{ mm}$) were non-rigidly aligned with an automated image-processing algorithm (maximization of mutual information using a viscous fluid model), which either deformed the pre-contrast image to match the post-contrast image (Mode1) or vice versa (Mode2). To evaluate registration quality achieved with each mode, objects of interest, bones and plaques, were manually delineated in each data set and the percentage of overlap of 223 object pairs after NRR was computed.

Results: Overall overlap values for bone were not significantly different between Mode1 (90.14%) and Mode2 (89.74%). However, for plaques the overlap values were significantly larger ($p < 10^{-10}$) for Mode2 (69.82%) than for Mode1 (54.98%). Visual inspection showed that Mode1 NRR wrongly enlarged the plaques in the pre-contrast image to match the contrast-enhanced vessel in the post-contrast image. On the contrary in Mode2 NRR the deformation forces applied on the enhanced vessel in order to match the plaques in pre-contrast data set didn't distort the shape of this structure.

Conclusion: The order in which the images are considered for NRR significantly influences the registration result.

C-1046

Evaluation of left kidney function in patients who have undergone abdominal aortic aneurysm (AAA) surgery with renal vein ligation

P. Terlecki, J. Wronski, T. Zubilewicz, W. Kobusiewicz, A. Stepien, S. Przywara, M. Feldo, S. Mocarski, W. Krupski; Lublin/PL

Purpose: The anatomical location of AAA sometimes necessitates ligation of the left renal vein in order to gain safe access to the infrarenal aorta. This access seems to be quite safe for the patient, however opinions about its impact upon kidney function are mixed. The aim of this study is to evaluate retrospectively the long-term results of this treatment.

Materials and Methods: The retrospective analysis embraced 12 patients, aged between 56-85 (average 69.4), operated on for AAA, who had had the left renal vein ligated. Kidney function was analysed by means of urine analysis, creatinine and urea concentration, Doppler ultrasonography and, in selected cases, urography. The difference in particular dimensions was considered to be significant if it exceeded 20%.

Results: The observation period was from 8 months to 6 years. In all cases the urine analysis was normal, in 3 cases the creatinine level was increased (on average 0.31 mg%). The longitudinal dimension of the left kidney was decreased in comparison with the right side in 3 patients. The difference was not statistically significant. The Doppler examination revealed normal flow in all cases. There was no evidence of venous hypertension in the left kidney. Patients who underwent urography had normal micturition and urine concentration.

Conclusions: Left renal vein ligation does not significantly influence the kidney function and may be used as a safe surgical strategy.

C-1047

Patterns of disease in the mesenteric arteries in patients with significant renal artery stenosis as an indicator of atherosclerosis

C.J. Johnston, J. McCann, S. Ford, J.F.M. Meaney; Dublin/IE

Purpose: To use CE-MRA to assess the incidence of mesenteric artery stenosis in patients with significant renal artery stenosis, as a marker for generalized atherosclerosis

Methods: Asymptomatic patients presenting for assessment of RAS over 18 months were also evaluated for the presence of significant mesenteric artery

stenosis. Studies were performed at 1.5 T. Patients received 30 ml of gadolinium chelate via automated injector at 2 cc/s. Scan parameters included: TR 5.1 ms, TE 1.7 ms, flip angle 35°, matrix 200*512, RFOV 280-320*400 mm. Source images and operator-defined 3D reformats targeted to the region-of-interest were evaluated independently by two experienced radiologists for presence or absence of mesenteric and renal artery narrowing according to a graded scale.

Results: 108 patients with significant RAS were identified (41 bilateral, 67 unilateral). Significant (> 50%) celiac artery, SMA and IMA stenoses were identified in 19.5%, 4.9% and 29.2% patients with bilateral RAS. Figures for the unilateral RAS group were 7.5%, 3.0% and 20.8% respectively. No significant relationship existed between age or sex and degree of mesenteric or renal artery stenosis. > 50% reduction in luminal diameter of at least 2 of 3 mesenteric arteries was seen in 9.8% patients with bilateral RAS, and in 1.5% patients with unilateral RAS ($p < 0.05$, Pearson coefficient). Increasing severity of mesenteric artery stenosis correlated with worsening degrees of RAS.

Conclusion: Although mesenteric vascular disease is common in patients with renal artery stenosis, symptomatic mesenteric ischaemia was absent even in patients with multivessel disease. Mesenteric artery narrowing worsened with increasing RAS.

C-1048

Coeliac trunk and its variants: Demonstration with CT

S.K. Venkatesh, G.B.H. Lau, S. Wang; Singapore/SG

Learning Objectives: To present a pictorial essay of CT appearances of normal coeliac trunk anatomy and its variants, to familiarize interventional and abdominal radiologists

Background: Recognition of a variant coeliac artery has important diagnostic and therapeutic implications. The surgical strategy needs to be changed to prevent arterial aberrations interfering with major abdominal surgical techniques such as liver transplantation and resection, gastrectomy and pancreaticoduodenectomy. Aberrant arterial branches may also interfere with interventional radiological procedures. Before chemoembolization can be performed, a full understanding of the potential variations is necessary to facilitate selective cannulation, allowing complete treatment in chemoembolization. Careful manipulation of catheters is required to prevent spasm/dissection of the target artery. Spasm may result in inadequate flow to carry chemoembolization material into the lesion, and there may be an increase in reflux of chemoembolization material into other arteries.

Imaging Findings: The anatomical variations of the coeliac trunk are of three types: a) complete coeliac trunk with a branch arising proximally and the trunk bifurcating distally; b) incomplete coeliac trunk with a branch arising directly from the aorta and c) common origin of the main branches of the coeliac trunk with the superior mesenteric artery. We present the CT appearances of coeliac trunk variations, CT angiographic appearances and wherever possible angiographic correlation. Embryological explanation of the variations will also be presented.

Conclusion: Knowledge of coeliac artery variations should result in the accurate interpretation of disease in diagnostic imaging, as well as the optimum elective procedure in surgical or interventional radiological management.

C-1049

Aneurysms of the intra- and extra-hepatic portal vein: Helical CT demonstration.

S. Quiroga, M. Sebastià, H. Cuellar, R. Boye, A. Miranda, A. Alvarez; Barcelona/ES

Learning Objectives: To review portal venous system embryology, focussing on anomalous dilatation of the intra- and extrahepatic portal vein and related complications. To illustrate the helical CT appearance leading to the diagnosis.

Background: Portal vein (PV) aneurysms are rare, representing only 3% of all venous system aneurysms. They may be congenital or secondary to portal hypertension, and often occur at branching sites, usually in the extrahepatic PV. Aneurysms of the intrahepatic PV are less frequent, and can be located in the umbilical portion or in any portal branch. PV aneurysm complications include chronic portal hypertension, occlusion due to recurrent thrombosis, portosystemic shunt with a hepatic vein, bile duct obstruction, and rupture.

Imaging Findings: We retrospective reviewed 14 cases of PV aneurysm studied with dual-slice or multidetector helical CT. Five cases were extrahepatic and nine were intrahepatic (5 in the umbilical portion and 4 in portal branches). In five patients with intrahepatic PV aneurysm, a portosystemic shunt was also present (2 without associated liver cirrhosis). These aneurysms were occasionally associated with anatomic variations of intrahepatic portions of the PV. Partial thrombosis was demonstrated in three aneurysms of the umbilical portion of the PV.

Conclusion: Although most PV aneurysms are asymptomatic, it is important to

Scientific and Educational Exhibits

recognize them, thereby avoiding misdiagnoses such as hypervascular liver tumors, and to exclude complications such as thrombosis, rupture, local pressure effects, or development of portosystemic shunts. Contrast-enhanced helical CT can easily depict PV aneurysms and differentiate them from liver tumors by tracing the portal branches.

C-1050

CO₂ wedged hepatic venography in patients with portal hypertension:

Our experience

G. Alabau, J. Irurzun, S. Gil, F. De España, P. De la Iglesia, J. Verdu; Alicante/ES

Purpose: To describe the findings and utilities we have found in patients with liver cirrhosis in whom we have performed CO₂ wedged hepatic venography (WHV) in addition to measurement of hepatic venous pressure gradient (HVPG) or during the placement of transjugular intrahepatic portosystemic shunts (TIPS).

Methods and Materials: 39 patients were included, range 35-74 years, all of them with portal hypertension secondary to liver cirrhosis. 24 were referred for measurement of hepatic venous pressure gradient and 15 to perform TIPS. In the first group, CO₂ wedged hepatic venography was compared with direct portography with iodinated contrast (gadolinium-DTPA in an allergic case) made after portal canalization. Two of the portal hypertension cases also underwent indirect arterial portography.

Results: Good correlation was shown between CO₂ wedged hepatic venography and direct portography when performing a TIPS. CO₂ demonstrated varices during measurement of hepatic venous pressure gradient and may assess permeability of the portal vein, although it depends on the presence of collateral hepatic veins.

Conclusion: CO₂ wedged hepatic venography is an easy and safe procedure, allowing assessment of portal flow and a full radiological mapping of the portal venous system, very valuable when performing a TIPS, and it is very useful in the detection of varices and shunts during hepatic venous pressure gradient measurement.

C-1051

Preoperative evaluation of hepatic arteries in living-related liver transplantation donors with MDCT angiography

O. Ozbek, E.M. Kayahan, N.C. Tarhan, B. Cakir, C. Aytekin, M. Coskun, M. Haberal; Ankara/TR

Purpose: To assess the value of multidetector computed tomography angiography (MDCTA) in depicting hepatic arterial vascular variations in living-related liver transplantation donor candidates.

Materials and Methods: MDCTA was carried out using a 16-row CT (Sensation 16 Siemens Germany) in 32 living-related liver transplantation donor candidates in a 16-month period. Arterial phase images (0.75 mm collimation, 1 mm slice thickness, table speed of 7.8 mm per gantry rotation) were obtained after 150 ml IV contrast at a rate of 4 ml/s. Maximum intensity projection (MIP) and volume rendered (VRT) images were produced from axial raw data. All findings were compared with DSA.

Results: Excellent arterial opacification was achieved by MDCTA in all patients. Among 32 donor candidates, classic vascular anatomy of the hepatic arteries was seen in 16 patients (50%) and hepatic arterial vascular variants in 16 patients (50%) by MDCTA. The most common arterial variants were accessory left hepatic artery arising from left gastric artery ($n = 5$) and trifurcation of the common hepatic artery to gastroduodenal, right and left hepatic arteries ($n = 5$). Only a branch of the hepatic artery originating from the superior mesenteric artery, supplying the posterior segment of the right lobe, could not be identified on MDCTA.

Conclusion: Preoperative evaluation of hepatic vascular anatomy is crucial for surgical planning in living-related liver transplant donors. MDCTA is useful in depicting hepatic arterial anatomy with high accuracy in these patients. In the past, DSA was used to assess vascular anatomy; however, MDCTA is now replacing DSA to demonstrate hepatic arterial variations in living-related liver transplant donors.

C-1052

withdrawn by authors

C-1053

Pre- and postinterventional evaluation of abdominal vascular diseases using 16/64 row MSCT angiography

S. Leschka, H. Alkadhi, B. Marincek, S. Wildermuth; Zürich/CH

Learning Objectives: To describe an optimised scanning protocol for abdominal 16 and 64 row MSCT-angiography. To familiarize the radiologist with the pre- and postinterventional imaging features of different abdominal vascular diseases and surgical procedures. To highlight the role of post-processing in their evaluation.

Background: Multislice computed tomography angiography (CTA) has proved feasible for the pre- and postinterventional assessment of vascular anatomy. While the faster scanning speed increases volume coverage during a single breath-hold and improves the exploitation of contrast-medium, the better spatial resolution results in nearly iso-tropic voxels allowing reconstruction of high-resolution three-dimensional images with different algorithms. Burgeoning new surgical techniques often result in complex anatomic structures which are difficult to visualize with axial slices alone.

Imaging Findings: We present axial CT findings and post-processed images in 10 pre- and postinterventional vascular cases including acute mesenteric ischaemia, segmental mediolytic arteriopathy and complex vascular anatomy after different surgical interventions.

Conclusion: Multislice CT angiography is an excellent tool to assess a wide variety of abdominal vascular disease and offers a non-invasive imaging method for pre- and postinterventional evaluation. VR images in particular provide excellent visualization of pathologic conditions and their anatomic relationship with adjacent structures, that often cannot be confidently assessed by axial CT images alone.

C-1054

CT findings and clinical features of portomesenteric thrombosis

T. Yamaoka, A. Kurita, H. Azechi, Y. Endo, H. Nishikawa, M. Noguchi, Y. Nakano; Kyoto/JP

Learning Objectives: To summarize the CT findings and clinical features of portomesenteric venous thrombosis and demonstrate representative cases.

Background: Portomesenteric venous thrombosis is a rare condition; however, symptoms vary from "asymptomatic" to "severe acute abdomen", and thus may be difficult to correctly diagnose in cases with mild symptoms. Between April 1994 to August 2004, 8 patients were radiologically or pathologically diagnosed with portomesenteric venous thrombosis; cases with tumor thrombosis were excluded. We evaluate these cases from CT findings (density of thrombus, bowel wall thickening, enhancement of the bowel loop in the arterial phase, ascites, development of collateral veins, edema of the mesentery, and dilatation of the distal mesenteric vessels). We also review clinical presentation and past history, as this can affect presentation.

Image Finding: Dynamic CT was performed in 7 and plain CT in 1. On plain CT, venous thrombi were slightly high density in 4/8 cases. Bowel wall thickening, poor enhancement of the involved bowel loop in the arterial phase, ascites and collateral veins were found in 5/8, 4/7, 6/8, and 7/7 cases, respectively. Edema of the mesentery and dilatation of the distal mesenteric vessels were found in all 8 cases, however, in 2, these findings had been found in a previous study without venous thrombosis.

Conclusions: When bowel wall thickening and ascites are found in patients with an acute abdomen, attention should be paid not only to the mesenteric arteries but also to the portomesenteric vein. Dynamic CT of the whole abdomen may be helpful in making a diagnosis.

Scientific and Educational Exhibits

Vascular

Miscellaneous

C-1055

B-flow and color-coded-B-flow in sonographic diagnosis of filiform stenosis of the internal carotid artery

D.-A. Clevert¹, Jung², N. Rupp², M. Reiser¹; ¹Munich/DE, ²Passau/DE

Purpose: To evaluate diagnostic results of ultrasound B-flow in filiform (> 90%) stenosis or occlusion of the internal carotid artery (ICA) and to compare with other modalities.

Method and Materials: 60 patients with suspected occlusion or filiform stenosis of the internal carotid artery (ICA) on Doppler-ultrasound, were examined using the ultrasound B-Flow, either in color-coded or brightness mode. The pre-, intra- and poststenotic flow phenomena were all compared with color-coded duplex (CCD) and power Doppler (PD). In 18 cases contrast agent (Optison) was injected additionally. Results were compared with those of selective intraarterial DSA, and in 18 cases additional MR-angiography.

Results: Diagnosis of ICA occlusion was correct in all 27 cases using CCD, PD and B-flow. A filiform ICA-stenosis was correctly seen in all 34 cases using B-flow and contrast-enhanced power Doppler, but only in 15 cases using CCD. All 11 of 34 cases of ulcerated plaques with appositional thrombi were only detected when B-flow was used, but only 5 cases when CCD was used. Pre-, intra- and poststenotic flow phenomena in the longitudinal scan were demonstrated simultaneously using color-coded B-Flow in 33 of 34 cases, but only in 20 cases using CCD and in 27 cases using PD. In B-flow there was no overwriting of vessel walls in the intra- and poststenotic area, in the 18 cases where contrast agent was given.

Conclusions: B-flow is more reliable in ultrasound diagnosis of filiform stenosis of the ICA than other ultrasound modalities, displaying no vessel overwriting and better simultaneous intra- and poststenotic flow detection.

C-1056

All that the radiologist should know about color-Doppler US in chronic venous insufficiency

A. Cina, A. Pedicelli, C. Di Stasi, V. Lo Schiavo, A. Fiorentino, G. Cina, L. Bonomo; Rome/IT

Background: At present, color-Doppler US (CDUS) is the gold standard for diagnosis and patient screening for chronic venous insufficiency (CVI). While deep venous system disorders are well-known to radiologists, the diagnosis of superficial system disorders in most institutions remains the territory of angiologists or vascular surgeons. In recent years percutaneous endovenous technique for CVI are become available and are now also performed by interventional radiologists. **Learning Objectives:** To acquire an overview of the pathophysiologic principles of CVI. To review lower limb superficial vein anatomy, its most frequent variations and differences between perforating, communicating and collateral veins. To become familiar with CDUS findings in CVI. To be able to provide the surgeon and/or the interventional radiologist with the information necessary to select the best surgical approach and perform an adequate follow-up. To illustrate the main surgical and interventional techniques for CVI and the specific question for CDUS. To provide the interventional radiologist with the anatomical and pathophysiological background necessary to perform percutaneous procedures for CVI.

C-1057

Behcet's disease: Rare cardiovascular manifestations

N. Ben Achour, S. Bouomrani, R. Braham, S. Hammami, R. Salem, S. Mahjoub, A. Gannouni; Monastir/TN

Learning Objectives: To illustrate the spectrum of rare cardiovascular involvement patterns in Behcet's disease (BD), which have been misleading in presentation, with emphasis on pathologic associations, based on a series 17 patients among a total number of 141 BD patients.

Background: Arterial lesions are a rare but serious complication in BD. Cardiac lesions are even rarer and have the peculiarity of being the first presenting symptom in more than a third of cases. In this exhibit we describe rare cardiac, pulmonary and peripheral lesions diagnosed from 1976 to 2004. Peripheral ultrasound (US) coupled to Doppler, helical CT, angiography, scintigraphy and cardiac trans-thoracic and trans-esophageal-US findings are described and illustrated.

Imaging Findings: In our series we illustrate 3 cases of intra-cardiac thrombosis (ICT), all of them right-sided. Pulmonary aneurysms (PA) (4cases) were multiple in 3 cases (2 bilateral, 1 unilateral). Pulmonary embolism (PE), more typical but

still uncommon, were noted in 11 patients who were asymptomatic in 4 cases. Extra-pulmonary aneurysms were ruptured in two patients, in tibio-peroneal trunk (1 case) and primitive iliac artery (1 case, lethal), or unruptured in the distal superior mesenteric artery (1case), the latter being the rarest found in our series. Lesions were associated in 4 patients (ICT and PE, ICT with PE and PA, PA and extra-pulmonary aneurysms, PE and PA).

Conclusion: Although rare, arterial and cardiac BD manifestations should be well known because of their poor prognosis if untreated. Lesion association should urge a wider use of "total body" angio-screen especially following the advent of multi-row-detector-CT.

C-1058

Evaluation of endothelial function of normotensive and hypertensive subjects with flow mediated dilatation

O.O. Okten¹, N. Tuncbilek¹, M.H. Karakas², Y. Ince¹, S. Sen¹; ¹Edirne/TR, ²Malatya/TR

Purpose: Endothelial dysfunction is the inability of vascular structures to respond satisfactorily to vasodilator and vasoconstrictor agents. In this study the differences between endothelial function of normotensive (NT) and hypertensive (HT) subjects were evaluated using flow mediated dilatation (FMD) method.

Materials and Methods: 15 (10 male and 5 female) NT subjects with ages between 28-56, and 30 (19 male and 11 female) HT subjects with ages between 32-58 formed the study groups. HT subjects did not have target-organ damage and were not receiving medical treatment. All subjects were investigated in 24°C temperature and after 48 h of alcohol, 10 h of tobacco, and 8 h of food abstinence. Endothelium-dependent and sublingual nitroglycerine induced endothelium-independent FMD methods were employed under brachial artery ultrasonography. Relevant measurements were statistically compared.

Results: Average basal endothelium-dependent FMD values were 0.097 l/min in NT and 0.0714 l/min in HT subjects ($p < 0.05$). Average reactive phase endothelium-dependent FMD values were 0.1447 l/min in NT and 0.1004 l/min in HT subjects. A significant difference was found between NT and HT subjects regarding basal FMD that reflects endothelium-dependent FMD ($p < 0.001$) and reactive phase hyperemic FMD ($p < 0.05$). However no difference existed between groups regarding endothelium-independent FMD.

Conclusion: Although traditionally evaluated with biochemical indices, endothelial dysfunction, an early physiological result of atherosclerosis, may also be evaluated by the FMD method. This evaluation is critical in hypertensive subjects, who are at increased risk of cardiovascular disease, for early diagnosis of such disease and evaluation of treatment.

C-1059

Carotid artery blood flow and wall properties in patients with early stage renal insufficiency

Z. Serafin, P. Strozecki, W. Lasek, J. Manitus, B. Sobocinski; Bydgoszcz/PL

Purpose: Atherosclerosis is accelerated in hemodialysis patients with end-stage chronic renal failure (CRF), as shown by increased carotid artery intima-media thickness (IMT). However, less is known about carotid artery wall properties and carotid artery blood flow in the early stages of CRF.

Methods and Materials: Ultrasound duplex-scan of carotid arteries was performed in 31 patients in the predialysis stage of CRF and 18 healthy controls. IMT and distensibility were measured in both common carotid arteries (CCA). Blood flow spectra and were obtained in right and left CCAs, and in internal carotid arteries (ICA); mean flow parameters were then calculated. In CRF patients, results were correlated with clinical data.

Results: Mean IMT did not differ between the groups, whereas CCA distensibility was lower in CRF patients than in controls (0.53 vs. 0.76 mm, $P < 0.04$). In CRF patients, IMT correlated with age, systolic blood pressure, pulse pressure and plasma glucose level ($P < 0.001-0.02$). Duration of hypertension negatively correlated with mean velocities (TAVM, MN), and end-diastolic velocity in both carotids ($P < 0.05$). Pulse pressure correlated with pulsatility index (PI) and RI in ICA ($P < 0.03$). Total cholesterol correlated negatively with PI and RI in CCA, while HDL cholesterol correlated negatively with PI and RI in both CCA and ICA.

Conclusion: In patients in the predialysis stage of renal insufficiency, subtle carotid wall alterations are expressed by loss of distensibility. Blood pressure and cholesterol level are the main factors related to IMT and flow indices in this group.

Scientific and Educational Exhibits

C-1060

Evaluation of antibiotic therapy efficacy in patients with asymptomatic abdominal aortic aneurysm (AAA) and serological markers of chronic C. pneumoniae infection: Preliminary report

P. Terlecki, E. Mazur, J. Niedzwiedek, T. Zubilewicz, S. Przywara, M. Feldo, M. Koziol-Montewka, W. Krupski, J. Wronski; Lublin/PL

Introduction: The frequent finding of *C. pneumoniae* in atheroma and not in normal artery tissue by different methods and numerous investigators suggests that the organism may play a role in clinical manifestations of atherosclerosis, including AAA.

Material and Methods: 30 patients with AAA and serological markers of chronic *C. pneumoniae* infection were included in this study. They were treated with doxycycline at a dose of 100 mg daily for 3 months. Blood samples were collected to evaluate: serum concentrations of IgG and IgA anti-*C. pneumoniae*; C-reactive protein concentration; WBC count; lipid profile; the presence of *C. pneumoniae* DNA and RNA in blood monocytes (using PCR methods). Currently we are presenting the preliminary report: the results obtained after 2 months of antibiotic therapy received by 11 patients.

Results: Serological signs of chronic *C. pneumoniae* infection ($IgG \geq 1:128$, $IgA \geq 1:32$) were present in all patients prior to beginning the study. No significant changes were observed in specific IgG and IgA concentrations after 2 months of antibiotic therapy. 9 patients (82%) had the increased concentrations of C-reactive protein (mean concentration: 13.42 mg/l) before initiating antibiotic therapy. After 2 months of treatment the concentrations of C-reactive protein decreased significantly in all patients (mean concentration 7.37 mg/l). In 2 patients a decrease of AAA diameter was observed. The other patients showed no increase of AAA diameter.

Conclusions: Our preliminary results suggest that antibiotic therapy can be useful in the treatment of selected patients with asymptomatic AAA

C-1061

Congenital anomalies of the inferior vena cava: Cross-sectional imaging findings

J. Quintero¹, C. Pozuelo¹, Y. Roca¹, L. Monés¹, M. Torné², M. Pérez²;

¹Badalona/ES, ²Santa Coloma de Gramenet/ES

Learning Objectives: To review the normal anatomy of the retroperitoneum and to describe the congenital anomalies of the inferior vena cava (IVC) with computerized tomography (CT). We present our experience in the study and description of anomalies of the IVC with helical CT.

Background: We reviewed all the reports of abdominal CTs performed in our institution over three years. We selected the cases where congenital anomalies of the IVC were present and these were retrospectively reviewed by two radiologists who were unaware of the CT findings. The usual study protocol was: oral contrast, 5-mm collimation, pitch: 1.5, 100 mL of IV contrast medium, rate: 2.5 mL/sec, delay: 70 sec. From July 2001 to July 2004 we found 6978 consecutive abdominal CTs. We encountered 78 cases (1.11% of the studies) of congenital anomalies of the IVC.

Procedure Details: The cases reviewed were classified into: - Absence of the hepatic segment of the IVC with azygos/hemiazygos continuation (14); - Circum-aortic left renal vein (7) and retro-aortic left renal vein (43); - Double inferior vena cava (12); - Circumcaval ureter (2).

Conclusion: Congenital anomalies of the IVC have become more commonly recognized in asymptomatic patients and have been known to anatomists since 1793. Knowledge of these anomalies is essential to avoid diagnostic pitfalls. Some of these anomalies have significant clinical implications. Although vascular structures can usually be readily identified on contrast-enhanced CT scans, identification of unusual venous arrangements may be difficult in some cases. MR imaging may be used to distinguish aberrant vessels from masses.

C-1062

A pictorial review of anomalies of the thoracic aorta with embryological correlation

D.R. Bakshi, Gould, S. Powell, H. Yeang, H. Fewins; Liverpool/UK

Learning Objectives: To provide a comprehensive educational exhibit demonstrating the numerous anomalies of thoracic aortic development with embryologic correlation to attempt to achieve a better understanding.

Background: The development of the thoracic aorta is a complex process which is intimately associated with the development of the endocardial tube and which lends itself to a variety of congenital variants. The formation of the thoracic aorta takes approximately 3 weeks to complete, beginning in the presomite stage, about

20 days after fertilization. A review of this process is helpful in understanding normal variations and congenital anomalies of the thoracic aorta.

Procedural Details: An attempt is made to simplify the great number of anomalies by using Edwards' hypothetical double aortic arch model. Using CT/MR imaging, echocardiography, angiography and diagrams, we will illustrate both normal and abnormal thoracic aorta development such as aberrant subclavian arteries, double aortic arch, aortic stenosis and coarctation. These will be correlated with current embryologic understanding to provide a detailed overview.

C-1063

12 year follow-up of patients with type B aortic dissection

N. Limbucci, G. Gismondi, V. Pupillo, M. Ciriello, E. Di Cesare, C. Masciocchi; L'Aquila/IT

Purpose: To study long term evolution of type B aortic dissection with MR imaging during 12 years follow-up.

Methods and Materials: From 1992 May to 2004 May we studied 24 patients with type B aortic dissection (total 188 examinations). All MR imaging was performed with a 1.5 T unit (GE), using gated SE and Cine-MR imaging sequences until March 1998 and using contrast-enhanced 3D-FSPGR with a phased array coil from March 1998 to May 2004. We retrospectively analyzed the following parameters: maximum aortic dilatation, true/false lumen ratio, false lumen thrombosis, involvement of aortic branches and dissection extension.

Results: 1 patient (4.17%) underwent surgery because of wide false lumen dilatation (72 mm). 2 cases (8.33%) presented increase of maximum diameter (average 5.5 mm). In 6 patients (25%) MR imaging showed a variation of the false/true lumen ratio (average 0.4). In 2 subjects (8.33%) we observed partial thrombosis of false lumen and in 2 patients (8.33%) total thrombosis during early follow-up. Only in 10 patients (41.7%) was there no involvement of aortic branches. No patients had extension of dissection. 6 patients (25%) died during follow-up (mean time 3.7 years after first examination); 1 patient died from aortic rupture but the remaining 5 patients died from extravascular causes.

Conclusion: This survival study showed a very good outcome for the patients, confirming the efficacy of medical treatment and the important role of follow-up in patients with type B dissection in the identification of surgically manageable complications. MR imaging appears very effective because it is repeatable, not invasive and allows comparative measurements.

C-1064

Improved diagnosis of vessel dissections by ultrasound B-flow imaging

D.-A. Clevert¹, E. Jung², N. Rupp², M. Reiser¹; ¹Munich/DE, ²Passau/DE

Purpose: A study was completed to evaluate the efficiency of different ultrasound sound techniques (color-coded duplex sonography, power mode imaging and B-flow imaging) in vessel dissection diagnosis.

Methods and Materials: The study compared flow representation by color-coded duplex sonography, power-mode imaging and the recently developed B-flow imaging method in cases of dissection of the carotid artery (13 cases), the vertebral artery (10 cases), the abdominal artery (13 cases), the iliac artery (12 cases) and the femoral artery (25 cases). Reference standards were provided by contrast-enhanced MRA in 24 cases, CTA in 10 cases and intra-arterial DSA in the remaining cases.

Results: Boosted reflector signals provided by B-flow imaging facilitated the identification of the dissection membrane. Unlike intra-arterial DSA, CTA and MRA, B-flow imaging detected all 68 dissections. The comparative detection rates for color-coded duplex sonography, power-mode imaging and B-flow imaging were 10, 12 and 13 for 13 carotid artery dissections, 7, 8 and 10 for 10 vertebral artery dissections, 11, 11 and 13 for 13 abdominal artery dissections, 8, 9 and 12 for 12 iliac artery dissections and 20, 21 and 24 for 24 femoral artery dissections. The absence of overwriting in B-flow imaging produces more exact residual flow records, particularly for the false lumen. The reduced effect of angles facilitates the representation of fissures and membranes and enhanced near-wall flow recording improves the identification of low-reflection wall deposits.

Conclusion: B-flow imaging allows the primary diagnosis of dissection membranes, shows hemodynamic effects and facilitates the representation of membranes and any windowing.

C-1065

The role of echo enhanced ultrasonography in the investigation of extracranial vertebral arteries

A.A. Kotis, G. Chatzakis, A. Marinou, S. Karatapanis, P. Brestas; Rhodes/GR

Purpose: Evaluate the usefulness of ultrasound contrast agents on extra cranial vertebral arteries

Scientific and Educational Exhibits

Material and Methods: 15 pts performed colour Doppler sonography to investigate insufficiently detected extracranial vertebral arteries without and with echo enhancing agent I-vist 4 g, bolus concentration 16 ml. (average age 58 years). All examinations performed through Aspen Acuson scanner and head transducer 5-7 MHz. Were analyzed by two readers, with intraobserver agreement and estimated B-mode quality imaging, colour flow signal, blooming blood flow artifacts.

Results: There was increase assessment of VA by 37% and 25% according the two readers. After ultrasound contrast injection hypoplasia estimation raised in 49% vs. 45%, extra cranial occlusion 56% vs. 45%, and color flow signal in 52% vs. 34%. Only 5% of vertebral arteries showed no improvement in imaging quality after application of Levovist. Analysis of side-to-side differences of peak systolic and end-diastolic systolic blood velocities of VA showed no significant differences of flow velocities in all subjects and between men and women in CBF volume after I-vist injection. Echocontrast enlarged in each vessel segment the length that could be visualized.

Conclusion: Our study demonstrates that echocontrast provides effective Doppler signal enhancement and considerably increases the diagnostic gain in the extracranial vertebral vasculature.

C-1066

Follow up of aortic percutaneous endoprostheses with contrast enhanced ultrasound (CEUS) performed at low mechanical index (MI) and with a second generation contrast agent

L. Aiani, C. Ballarati, M. Soprani, T. Frattini, G. Belloni, A. Martegani; Como/IT

Purpose: To evaluate the accuracy of CEUS at low MI combined with low MI color Doppler (CEUS/CD low MI) in detecting endoleak after endovascular repair of aortic aneurysm. To evaluate the accuracy of CEUS/CD low MI in identifying the cause of endoleak

Materials and Methods: 28 patients diagnosed with aortic aneurysm and treated with a percutaneous endovascular approach underwent a conventional ultrasound and color Doppler (US/CD) evaluation and, in the same session, CEUS/CD low MI. Each patient underwent a spiral angioCT examination within one week.

Results: US/CD evaluation was burdened with 6 false negatives, due to the extremely low flow velocity, and 3 false positives, related to the presence of movement artefacts. CEUS/CD low MI detected 8 endoleaks, confirmed by the gold standard. No false positives were identified. The direction of blood inflow in the aneurysmal sac was correctly detected in every case, leading to the diagnosis of the endoleak type.

Conclusion: In our experience, CEUS/CD low MI has proved to be a valid, non-invasive, repeatable diagnostic technique in the diagnosis of endoleak after endovascular repair of aortic aneurysm, and can play a role in the follow-up protocol of these patients.

C-1067

3D image of Adamkiewicz artery: Preoperative assessment of thoracoabdominal aortic aneurysm

H. Yokoyama¹, S. Sanada¹, T. Ohno²; ¹Kanazawa/JP, ²Sapporo/JP

Learning Objectives: To assess the ability of multi detector 4-row computed tomography for depicting a 3D image of Adamkiewicz artery.

Background: The Adamkiewicz artery supplies most of the blood to the anterior spinal artery, which perfuses the anterior two thirds of the spinal cord. During operation for thoracoabdominal aortic aneurysm, detailed anatomic knowledge of the Adamkiewicz artery and its correlation with the intercostal and/or lumbar arteries is important to prevent postoperative paraplegia.

Procedure Details: Images were obtained with the following parameters: 0.5 sec/r, 1 mm collimation, H.P 3.5, 120 kV, 300 mA, with 40 seconds breath-hold during scanning after inhalation of oxygen. 100 ml of contrast material containing 350 mg iodine/ml was injected with a power injector (dual-shot type) into an antecubital vein at a rate of 3.5 ml/sec (70 ml). The remaining 30 ml plus the same volume of saline were then infused at a rate of 1 ml/sec simultaneously. Twenty-five seconds after the injection, the scan was performed from the level of L2 to T5 vertebrae. Transverse sections were reconstructed with a 1 mm thickness at 0.7 mm intervals.

Conclusion: In 141 patients, 107 (76%) Adamkiewicz arteries were visualized from the intervertebral foramen to the hairpin-shaped union with the anterior spinal artery. Seventy-nine arteries of Adamkiewicz (73%) originated from the left side. Sixty-eight (63%) originated between T9 and T12. Imaging was usually done with multiplanar and curved planar reformations. In cases of vertebral deformity, however, 3D images were useful to depict the Adamkiewicz arteries.

C-1068

Relation between the intrarenal arterial resistance, the carotid artery wall thickness and endothelial dysfunction (ultrasound study)

L.A. Krasilnikova, L.A. Tyutin; St. Petersburg/RU

Aim: To assess the relationship between intrarenal arterial resistance (IAR), carotid artery wall thickness (CAWT) and vasoactive dysfunction of the endothelium (VDE).

Methods: 31 male patients (mean age 55.1 ± 2.3 years) with essential hypertension were examined using ultrasound (SONOLINE OMNIA; Siemens). All vasoactive drugs were stopped one day before the study. We measured the maximal thickness of the "intima-media" complex in both the common carotid arteries. The study was also concerned with the VDE (ultrasound analyses of the brachial artery diameter response to compression or nitroglycerine). As markers of renal angiopathy we assessed the indices of IAR (PI and RI) which were measured at three points of arcuate arteries from both kidneys.

Results: In the patients (8 men) who had nitroglycerine-induced VDE (endothelium independent dysfunction) the CAWT was more than 1.0 mm and in 4 of these patients PI and RI were increased (PI > 1.4; RI > 0.8). In the 11 patients with compression-induced VDE (endothelium dependent dysfunction) only 6 patients had CAWT more than 1.0 mm and only 5 of them had high range of PI and RI. 12 patients had no signs of VDE. We observed CAWT of more than 1.0 mm in 4 patients without VDE, and only 2 of them had increased range of PI and RI.

Conclusion: VDE and abnormal CAWT range are not reliable markers of renal angiopathy in patients with essential hypertension. Nitroglycerine-induced VDE is often associated with CAWT more than 1.0 mm.

C-1069

Atherosclerosis as an inflammatory disease: Implications for the interventional radiologist

K.T. Tan¹, H.W. Aw-Yeang², D. Bakshi²; ¹Bristol/UK, ²Liverpool/UK

Learning Objectives: To understand the concept of atherosclerosis as an inflammatory disease and to be aware of the potential implications for vascular intervention.

Background: Recent advances in vascular biology have shown that inflammation plays an important part in the development and progression of atherosclerosis. Indeed, it has been demonstrated that the degree of inflammatory response can be correlated with the risk of developing adverse cardiovascular events.

Procedure Details: Of more relevance to the radiologist is the fact that an increased inflammatory response can also be related to the risk of recurrent disease following angioplasty. Indeed, it has recently been shown that peripheral artery angioplasty can elicit a strong inflammatory response. In this exhibit, we review the basic science behind the vascular inflammatory response as well as the possible mechanisms by which we can attenuate this response for potential therapeutic gain.

Conclusion: Advances in elucidating the causes of the vessel wall inflammation may be translated into therapeutic gain in the near future.

C-1070

Carotid intima-media thickness is associated with inflammation and endothelial cell adhesion molecules in end stage renal disease (ESRD)

M. Kalovoulos, A. Papagianni, K. Tsinoglou, C.A. Dimitriadis, G. Terzis, S. Dovas, D. Kirmizis, G. Grollios, D. Memmos; Thessaloniki/GR

Aim: To investigate adhesion molecule ICAM-1 and VCAM-1 levels in ESRD patients and their probable association with atherosclerotic disease as assessed by measuring intima-media thickness (IMT) of the common carotid arteries using an ultrasound scanner.

Methods and Materials: Eighty-five ESRD patients on conservative treatment, 91 haemodialyzed (HD) patients and 65 normotensive controls were enrolled.

Results: Compared with controls, ESRD and HD patients had significantly increased serum CRP and adhesion molecule ICAM-1 and VCAM-1 levels (each $p < 0.0001$), as well as IMT values (each $p < 0.001$). Moreover, compared with ESRD, HD patients had increased serum CRP, ICAM-1 and VCAM-1 ($p < 0.001$, $p < 0.001$ and $p < 0.0001$ respectively) and IMT ($p < 0.05$). In univariate analyses, IMT was correlated with age, systolic blood pressure (SBP), history of cardiovascular disease (CVD), logCRP and ICAM-1 levels in ESRD ($p = 0.0001$, $p = 0.01$, $p = 0.03$, $p = 0.02$ and $p = 0.004$ respectively) and HD patients ($p = 0.0001$, $p = 0.01$, $p = 0.02$, $p = 0.02$ and $p = 0.001$ respectively). Multivariate analyses showed that ICAM-1 was a strong independent correlate of IMT in ESRD and HD patients ($p = 0.001$ and $p = 0.001$ respectively). In addition, compared with patients with normal IMT, ESRD and HD patients with increased IMT (≥ 0.82 mm) had increased ICAM-1 ($p < 0.01$ and $p < 0.001$ respectively).

Scientific and Educational Exhibits

Conclusion: Increased endothelial cell adhesion molecule levels and advanced atherosclerosis are present in ESRD patients before starting HD treatment. The latter appeared associated with further activation of the inflammatory response and acceleration of the atherogenic process. In patients with ESRD, both on conservative treatment and on haemodialysis, ICAM-1 levels are potentially a useful surrogate marker of atherosclerosis.

C-1071

Emergency extracranial Doppler in diagnosis and monitoring the progress of primary cervicocerebral artery dissection

V. Bizimi, E. Manopoulou, P. Brestas, A. Tsikkini, E.S. Antipa, K. Bilas, P. Noti, M. Tsouroulas, C. Drossos; Athens/GR

Learning Objectives: Analyze the findings and value of extracranial ultrasonography, as the first noninvasive imaging approach, to establish a probable diagnosis and follow-up of cervicocerebral artery dissection.

Background: Cervicocephalic arterial dissection has been recognized as a neurological emergency because of an increased risk of cerebral infarction. Dissections have nonspecific symptoms, such as neurological deficits. The classic presentation is that of a headache and they occur at a relatively young age. They often occur in previously healthy individuals, developing either spontaneously or following various degrees of trauma.

Procedure Details: 152 patients with acute cerebral circulatory disturbances or cervical trauma, were examined with extracranial pulsed Doppler ultrasound, over a 3-year period (2001-2003). Twenty eight patients had dissection of the internal carotid artery, and 5 had vertebral artery dissection. All of them had their diagnosis confirmed by another reference method (digital angiography or MRA angiography). The presence of an intramural hematoma, echogenic thrombus, intimal flap, imaging of both true and false lumen in the absence of an atheroma plaque, in B-mode sonography, were considered to be positive signs. Doppler findings were variable, depending on the degree of stenosis caused by intramural hematoma (absence of flow or high resistance signal, damped wave form in the ICA, or wave form asymmetry between ICAs). The findings for vertebral artery dissection included absence of arterial flow signal or low blood flow velocities.

Conclusion: Extracranial ultrasonography substantiated clinically suspected cervicocranial artery dissection and showed efficacy to monitor evolution in the majority of cases (95%).

C-1072

CT and MR imaging aspects of superior vena cava pathologies

I. Lupescu, R. Capsa, S. Georgescu; Bucharest/RO

Aim: The purpose of our study is to create a comprehensive CT and MR imaging overview of superior vena cava (SVC) pathologies.

Material and Methods: We have reviewed 35 cases explored by spiral CT and MR imaging, with clinical signs of superior vena cava syndrome, over a period of 4 years. In addition, we have reviewed 5 cases of cardiac malformations associated with anomalies of the SVC.

Results: Amongst the 35 patients with signs or suspicion of SVC syndrome, 26 had mediastinal tumors (thymoma-6 cases, goiter-4 cases, malignant lymphomas-16 cases), 8 cases had bronchopulmonary carcinomas and 1 case nontumoral SVC thrombosis.

We also analysed the presence of collateral pathways. Congenital anomalies such as persistent left SVC were found in 5 patients: isolated (1 case) or in association with inferior vena cava pathology (4 cases).

Conclusion: Using spiral CT and MR imaging, it is possible to evaluate very accurately all the pathological lesions located in the course of the SVC and its tributaries.

C-1073

Early ultrasound characteristics of angiopathy in patients receiving antitumor therapy

L.A. Krasilnikova, L.A. Tyutin; St. Petersburg/RU

Purpose: To reveal the early ultrasound characteristics (UC) of angiopathy in patients receiving antitumor therapy.

Method: The UC of arterial walls were assessed in 82 young and middle-aged male (45) and female (37) cancer patients (mean age 30.1 ± 0.9 years) receiving radiation or polychemotherapy for less than 1 year. To reveal the angiopathy we used quantitative and qualitative analyses detecting the changes in the "intima-media" complex in the different peripheral arteries (arteries of upper and lower limbs, carotid and vertebral arteries, abdominal aorta). Also we estimate the va-

soactive dysfunction of the endothelium (VDE) as the response of the brachial artery diameter to compression and nitroglycerine.

Results: We noted the early changes in the "intima-media" complex were seen more frequently in patients who underwent radiation therapy, being more pronounced in the arteries localized in the irradiation areas. VDE was observed in patients who received polychemotherapy. However, these patients did not have visible changes in the "intima-media" complex in the peripheral arteries in early stages of treatment.

Conclusion: The lesions of arterial walls evoked by radiation therapy and polychemotherapy are different. The patients should be prescribed vascular protective treatment in depending on type of antitumor therapy.

C-1074

Follow-up of the aneurysm neck diameter after endovascular repair of abdominal aortic aneurysms

A. Bravo, M. Martí, G. Garzón, A. Alvarez Luque, B. Rodriguez-Vigil, M. Allona; Madrid/ES

Purpose: To assess aneurysm neck diameter change after endovascular repair (EVR) of abdominal aortic aneurysms.

Methods and Materials: 95 patients with abdominal aortic aneurysm who underwent EVR were studied with multislice CT following a standardised protocol. A preoperative study, an immediate postoperative, and a six month and one year follow-up were always performed. The volume of interest comprised from the supraceliac aorta to the femoral artery bifurcation, and 120 ml of contrast was administered at 3 ml/sec. A 3 mm collimation, table speed of 16 mm per rotation, pitch of 4, and 2 mm reconstruction interval were used. The images were post-processed and multiplanar reformations obtained on a workstation. The aneurysm neck was measured from adventitia to adventitia, 6 mm below the lowermost renal artery, in planar images performed perpendicular to the vessel axis (real axial section). For the statistical analysis a one-way ANOVA with repeated measures was used.

Results: The average neck diameter was 22.38 mm (16-32.5) on the preoperative study, 23.35 mm (17-33.9) on the immediate postoperative, 24.35 mm (18.2-34.5) on the 6 month, and 24.36 mm (18-34.5) on the one year follow-up. A statistically significant increase in the average neck diameter between the preoperative, immediate postoperative control, and the six month follow-up was observed. There was no significant increase in the average neck diameter between the six month and the one year follow-up.

Conclusions: An enlargement of the infrarenal aneurysm neck occurs during the first six months after EVR. No significant variation in the neck diameter occurs between the six month and the one year follow-up.

C-1075

The diagnosis and endovascular treatment of carotid artery and vertebral artery dissections

C.M. Flis, H.R. Jager, P.S. Sidhu; London/UK

Learning Objectives: To describe the clinical presentation of extra-cranial arterial dissections. To illustrate and describe the imaging findings on angiography, ultrasound, computed tomography (CT) and magnetic resonance imaging (MRI) and to emphasize the advantages and limitations of each modality. To describe the various management options and the current opinion on each form of treatment.

Background: Extra-cranial arterial dissections are a recognised cause of stroke in young adults. Clinical diagnosis may be difficult. The classic triad of presentation occurs in less than 1/3 of patients and so there must be a high degree of suspicion for the diagnosis not to be missed. Conventional angiography has been the reference standard for diagnosis. It will demonstrate stenosis, occlusion or a pseudoaneurysm. Other imaging modalities are now available. MR techniques provide a useful overview of the extent of a dissection and document cerebral ischaemia. Ultrasound gives haemodynamic information. CT angiography allows excellent visualization of the carotid arteries and allows data to be displayed using a MIP algorithm, providing angiography-like images. Surgery has a limited role in the management, whilst endovascular stent insertion and embolisation is the treatment of choice in failed medical management. Anticoagulation, however, remains the mainstay of medical treatment.

Conclusion: A combination of MRI is the most useful adjunct to diagnosis, but ultrasound provides a practical method for follow-up of arterial patency. Angiography is reserved for cases where endovascular management is considered. Endovascular management should be considered when medical treatment fails or there is disease progression.

Scientific Exhibits - ECR Research Grant Winners

C-1076

Deep venous thrombosis of the lower limb on screening with colour Doppler: Incidence and correlation with clinical history

M. Chalkia, I. Kirimlidis, A. Spanos, A. Mountzouoglou, P. Chalkia, N. Vougiouklis; Thessaloniki/GR

Purpose: Our purpose is to study the incidence and location of Deep Venous Thrombosis (DVT) of the lower limbs on screening with colour Doppler and to correlate it with the clinical history.

Methods and Materials: We performed colour Doppler examination of lower limb veins in 535 consecutive patients, 349 women and 186 men, (10- 84 years old, mean age = 55). Bilateral screening was performed in 260 patients and unilateral in 275.

Results: DVT was found in 126 patients (23.46% of the examined patients), 57 were women (45.23%) and 69 men (54.74%). DVT was unilateral in 122 patients (85 on the left and 37 on the right), while it was bilateral in four patients (3.14% of the patients with DVT). DVT was confined to the calf veins in two patients only (1.5% of the patients with DVT). Eleven patients (2% of the examined patients) had superficial vein thrombosis, while in one patient DVT and SVT coexisted. Forty-eight of the 126 patients with DVT (38%) had a predisposing factor for thrombosis; pregnancy-puerperum:13, neoplastic disease:8, varices:6, recent surgery:6, bedridden:5, fracture:3, contraceptive pills:2 and IV drug abuse:1.

Conclusion: DVT of the lower limbs is a common finding during examination with colour Doppler ultrasonography. The possibility of DVT confined to the calf veins is small, so screening of them can be avoided if examination of the more central veins is negative. A predisposing factor for thrombosis was present in 38% of the patients with DVT, pregnancy and neoplastic disease being the most commonly encountered.

ECR Research Grant Winners

C-1077

Technical optimization of diffusion tensor sequences: Evaluation of three dimensional white matter tractography in various neurologic disorders

N. Papapanikolaou; Iraklion/GR

Non-invasive in-vivo visualization of white matter fiber tracts is nowadays feasible by means of diffusion tensor imaging (DTI) techniques. Technical optimization of diffusion tensor sequences including signal to noise ratio and spatial resolution was performed. Parameters that were optimized for white matter tractography included b-value, slice thickness, scan matrix, number of slices and acquisition time. Two different DTI protocols applied on 20 normal subjects were compared in terms of signal to noise ratio, spatial resolution and scan time while fractional anisotropy (FA) and apparent diffusion coefficient (ADC) maps were reconstructed. A voxel based statistical analysis was made to reveal any potential regions with statistically significant differences between FA and ADC maps generated by the two different DTI protocols. Additionally, cortico-spinal tracts and the splenium of corpus callosum were reconstructed by using fiber-tracking algorithms and a qualitative comparison was performed. The optimized diffusion tensor sequence was applied in 10 patients with various brain tumors, 8 patients with multiple sclerosis, 7 patients with stroke and 2 patients with dementia. Examples of white matter tractography reconstructions along with its current limitations are presented.

C-1078

Characterisation of carotid atheroma in symptomatic and asymptomatic patients using high-resolution gadolinium-enhanced MR imaging

J.M. U-King-Im, R.A. Trivedi, M.J. Graves, P.J. Kirkpatrick, N.M. Antoun, J.H. Gillard; Cambridge/UK

Purpose: Risks of stroke secondary to carotid atheroma may be better predicted using plaque characteristics rather than luminal stenosis. The aim of this study is to explore plaque morphology in symptomatic and asymptomatic patients using high-resolution MR imaging and histology.

Materials and Methods: 9 patients (mean age 71, 3 women) with carotid artery territory symptoms within the previous 6 months and 8 asymptomatic patients (mean age 68, 1 woman), enrolled in the Asymptomatic Carotid Surgery Trial, were prospectively recruited to have high-resolution (0.39 x 0.39 mm) MR imaging prior to surgery. Imaging protocol consisted of a T2-W, PD-W, STIR, TI-W and post-gadolinium T1-W sequences using a 4-channel phased array coil (Flick Engineering Solutions) at 1.5 Tesla. Histological analysis of excised carotid specimens was independently performed using EVG, H&E and CD 31 (vascular endothelial marker) stains.

Results: MR imaging analysis show that 5 out of 8 asymptomatic plaques were mainly fibrous in composition with no evidence of necrotic lipid core while all 9 symptomatic plaques showed complex patterns with relatively large lipid cores separated from the lumen by fibrous caps (which were either thin or ruptured in 5 cases). Findings were confirmed on histological analysis. Visible patterns of enhancement post-gadolinium were observed in 12 out of 17 cases but appear confined to fibrous regions.

Conclusions: Symptomatic and asymptomatic carotid plaques show different morphological characteristics. Current work is under way to quantify fibrous cap thickness and lipid core areas as well as correlate histological areas of neovascularisation to regions of enhancement on MR imaging.

C-1079

Automatic segmentation of airway wall area for quantitative assessment at MDCT: Preliminary results in asthmatics

P.-Y. Brillet¹, C. Fetita², C. Beigelman-Aubry³, D. Perchet², F. Prêteux², P. Grenier³; ¹Bobigny/FR, ²Evry/FR, ³Paris/FR

Objective: We developed a CT lung analysis software based on mathematical modeling to provide automatically: 1) 3D segmentation of the bronchial lumen, 2) extraction of the central axis of the airway tree, 3) cross sectional image reconstruction orthogonal to the bronchus axis, 4) 2D segmentation of the outer contour of the bronchus for quantification of the luminal and wall (WA) areas. The objective was to determine the number of segmental and subsegmental bronchi correctly segmented by the software and to define criteria for accurate measurement of WA.

Methods and Materials: Eighteen thin collimation MDCT examinations (16 x 0.6 mm), performed in mild persistent asthmatics were retrospectively used for analysis of the airways. Acquisitions were performed at spirometrically controlled lung volume (65% TLC). Reconstructions were targeted on the right middle and

Scientific Exhibits - ECR Research Grant Winners

lower lobes (reconstruction interval: 0.3-mm, FOV: 18-20 cm) and all segmental and subsegmental bronchi were included for analysis. A confidence index (CI) defined as the percentage of the bronchus surrounded by lung parenchyma without apposition of vessels or soft tissue was calculated.

Results: The software correctly segmented 349/396 (88%) of bronchial lumen and correctly extract the central axis of 347/349 (98%) of the bronchi. By imposing a CI > 55% on 10 contiguous cross sectional images as a condition for an accurate segmentation of the outer contour, the software selected 48% of the segmented bronchi. B10b was the most frequently (87%) selected bronchi.

Conclusion: The developed software allows an adequate segmentation of the airways for quantitative assessment of WA at a segmental and subsegmental level.

C-1080

Proposal of an appropriate mathematical model to represent replenishment kinetic after microbubble destruction of an imaged renal volume to quantify renal perfusion

E. Quaia, L. Torelli; Trieste/IT

Purpose: To propose a mathematical model representing the replenishment kinetic of renal parenchyma after microbubbles destruction.

Methods and Materials: For this problem the biological models theory about diffusion and progressive volume filling was employed and *in vitro* and *in vivo* models were analysed. After sulfur hexafluoride - filled microbubbles injection (1 ml/min infusion rate), microbubbles filling the imaged volume were destroyed by high transmit power (8 pulses; mechanical index: 1.2-1.5) and the progressive volume replenishment was assessed by low transmit power (mechanical index: 0.02-0.08). The US video-intensity was measured by one region of interest encompassing entirely the kidney. Through mathematical approximation, renal flow was related to the slope of the first ascending tract of the obtained curve, while renal fractional blood volume was related to plateau intensity.

Results: The imaged renal volume (thickness of the US beam = 5 mm) was considered as the not conservative variable of state (volume replenishment is dependent from the grade of filling), while microbubbles velocity entering the volume (bi-compartmental model) were considered as bi-directional variable of control. After converters (equations transforming input in output values) and constants addition, a system of partial differential equations was derived including the velocity of volume replenishment, time, the volume percentage occupied by microbubbles, the percentage of microbubbles destroyed in the volume and of microbubbles leaving the volume and not replaced.

Conclusion: A system of partial differential equations was proposed to represent replenishment kinetic of renal parenchyma. Mathematical parameters are derived from this model through approximation procedures.

C-1081

The study of the human auditory system using combined fMR imaging and DTI at 3 T

S. Sunaert; Leuven/BE

Purpose: The combined fMR imaging and DTI study of the auditory system in normal and pathological conditions.

Methods and Materials: Fifteen normal subjects and 43 patients with non-pulsatile tinnitus (12/19 with right/left unilateral, 12 with bilateral) were enrolled. Imaging was performed on a 3 T imager using BOLD fMR imaging (GE-EPI, TR/TE = 5000/33 ms, 3x3x3 mm) with sparse temporal sampling to minimize interaction between auditory stimuli and scanner noise. A DTI dataset (SE-EPI, b = 800, 15 directions) was acquired in the normal volunteers. Auditory fMR imaging consisted of a blocked design with binaural musical stimulation and an event-related presentation of sinusoidal tones, either unattended or attended (1-back discrimination task). Analyses were performed using SPM2 (FIL, London) and PRIDE software (PMS, Best, NL).

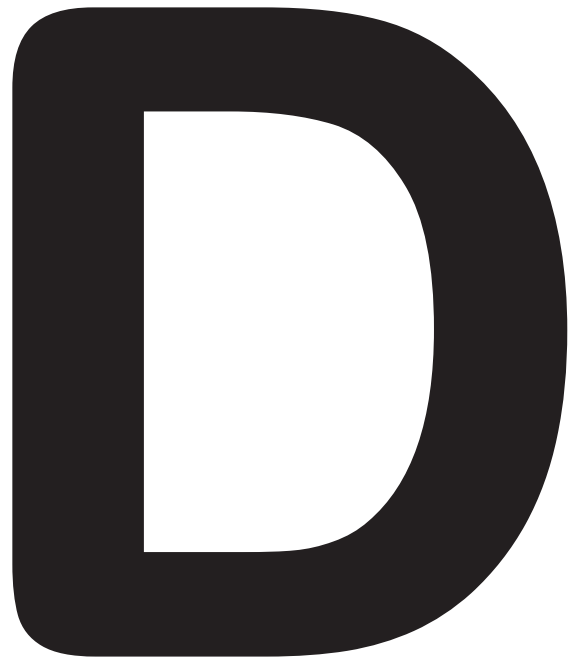
Results: 1. Significant ($p < 0.05$ corrected) (sub)cortical activity was present bilaterally in A1, A2 and the inferior colliculus in all subjects and in > 70% of subjects in medial geniculate body and superior olivary complex. 2. Tonotopy: within A1 an anterolateral to posteromedial tonotopic organisation was clear for low to high frequency stimuli (sinusoidal tones of 120, 800, 2000, 4000 and 6000 Hz); in A2, this organisation is reversed. 3. Task effects: A 1-back pitch discrimination task enhances activity in A2, but not in A1. 4. In patients with unilateral tinnitus a significant decrease of activity was found in the contralateral inferior colliculus, medial geniculate body and A1. A significant correlation exists between the reduced activity in A1 and the perceived loudness of the phantom sound. 5. DTI fiber tracts were identified from subcortical to cortical areas.

C-1083

Diagnostic accuracy of gadolinium-enhanced MR-angiography vs. contrast-enhanced helical CT in the diagnosis of pulmonary embolism in the presence of lung infiltrate: An animal study

T. Franquet¹, S.E. Kaloger², A. Oikonomou², S.L. MacDonald², E.M. Baile², J.R. Mayo²; ¹Barcelona/ES, ²Vancouver, BC/CA

Ten female juvenile pigs were used. Human sub-segmental sized pulmonary emboli were introduced by injecting 4.5 mm methacrylate beads into the external jugular vein. Lung infiltrates were simulated by intra-bronchial injection of 100 ml of human plasma. Animals were imaged in the supine position at suspended inspiration with 15 cm H2O PEEP. Contrast media was injected via brachial vein. Dual gradient (TwinSpeed) 1.5 T MR images were acquired using a 3 dimensional spoiled gradient-echo time of flight sequence; TR 4.8 msec, TE 1.2 msec, 45° flip angle, 6 mm section thickness, 32 cm FOV, 256x160 matrix, one average. Two MRA sets, pulmonary arterial and venous, were acquired in 39 seconds. Contrast enhancement was provided by 20 mL of Gd dimegloamine followed by 20 ml of normal saline, injected at 2 mL/sec. Non-contrast and contrast enhanced CT images were obtained using an 8 track spiral CT; 1.25 mm detector aperture, 90 ml contrast at 3 ml/sec. Subtraction perfusion images were calculated by subtracting contrast enhanced from non-contrast CT images. After imaging the pig was euthanized and a methacrylate cast of the pulmonary vasculature was obtained and used as a "gold-standard". All images were independently interpreted by two observers in a blinded fashion. No significant difference ($p > 0.05$) was seen between CTA, CTA with subtraction perfusion images and MR for sensitivity (86%, 88%, 68%) or specificity (94%, 94% 73%), respectively. No significant difference ($p > 0.05$) was seen in sensitivity or specificity between pigs with and without infiltrates.



IMAGINE
The Intelligent Department

IMAGINE - The Intelligent Department

D-01

B-ROB II: A robotic system for percutaneous interventions

J. Kettenbach¹, G. Kronreif², M. Figl¹, M. Fuerst², W. Birkfellner¹, R. Hanel¹, J. Hummel¹, H. Bergmann¹; ¹Vienna/AT, ²Seibersdorf/AT

We developed a robotic system (B-Rob II) in order to assist ultrasound (US)- and CT-guided percutaneous interventions such as biopsies and to provide the physician with a needle guidance tool that enables very stable access to lesions even difficult to reach. The robotic system will be cost-effective, has a plug-and play design and can be used with all currently available imaging modalities used for interventions.

Preliminary phantom tests so far demonstrated that with only one needle pass necessary a successful biopsy of peas (mean diameter 9.3 ± 0.1 mm) was performed using US-, and CT-guidance. In the first experiment positional data of an US transducer was recorded by an optical tracking system while targeting peas embedded within a custom-made gel-phantom. In the second experiment the same phantom was used and peas were localized using a spiral-CT scanner. The average radial distance between the needle tip and the center of the target was 1.9 ± 1.1 mm using US-guidance, and was 1.3 ± 0.9 mm using CT-guidance. So far we have proven that robotic assisted biopsies using US-, or CT-guidance were feasible with high accuracy. The visitor of IMAGINE will be able to perform US-guided roboter-assisted biopsies of a phantom on-site.

D-02

Unified patient: A medical media database supporting surgical planning and interdisciplinary meetings

P. Pokieser¹, J. Brandstätter², M. Wernig¹, J. Berger¹; ¹Vienna/AT, ²Wr. Neudorf/AT

The Unified Patient (UP) system is a web based software and database in order to provide as a multimedia storage for medical imaging data as well as for patient records. Available with a standard web-browser by the hospital's intranet radiological and clinical data are integrated into a "time-line". Thus patient data are demonstrated chronologically - every medical event is enhanced by radiologic, endoscopic, histopathologic, surgical or other relevant images, movies, sound files, laboratory findings as well as complementary text files and tables, approximated to a one stop shopping fashion for the use in routine, education and science.

Data collection starts at various stations of patient care: UP workstations in the operation theatre allow easy handling of images obtained during surgery, a PACS interface allows to export relevant images to UP.

At our institution UP is currently used to "submit" patients for weekly interdisciplinary oncologic meetings, as well as for plastic surgery and emergency medicine (www.univie.ac.at/interdis, www.unifiedpatient.org). At these meetings selected images of various tumor sites stored earlier are compared with current follow-up images obtained from PACS. Thus, large imaging files from MR imaging, MSCT, PET etc. can be reduced to relevant images from tumor sites treated by surgery, oncology, radiation therapy or interventional radiology.

Furthermore, relevant clinical information and the decision how to proceed with treatment are added to each patient's record in the UP system, which can be accessed anytime by authorized group members. We will further demonstrate how to submit teaching files from remote hospitals into the UP system and will offer remote-control instructions using a client-server TCP/IP software to improve radiologic service for clinicians located at distant sites such as intensive care units or operation theatre.

D-03

A novel navigation systems for percutaneous interventions

R.J. Bale¹, R. Petzold¹, M. Nagel¹, M. Voegeli², W.A. Kalender³, W. Jaschke¹;

¹Innsbruck/AT, ²Schwabmünchen/DE, ³Erlangen/DE

A novel immobilization and registration device (CAPPA® IRAD) for image-guided percutaneous interventions is presented. In addition novel registration algorithms for accurate fusion of various pre-operative imaging modalities such as CT, MR, SPECT, PET and ultrasonography will be shown. After planning of the pathway, the targeting device will be calibrated and adjusted according to the most accurate and safest access to a lesion (target) anywhere in the body. Next, our immobilization- and autoregistration device will be used to match the lesion coordinates with the adjusted targeting device without using any imaging modality. Once the targeting device is in place, puncture of the lesion for diagnostic or therapeutic

purpose can be performed quickly and safely. For safety reason, the position of the needle tip can be then confirmed by intraoperative imaging. Our system provides accurate guidance of an instrument along the desired trajectory to the target with minimal computational effort and time. Image fusion, planning, adjustment of the targeting device and puncture will be simulated using a phantom during the IMAGINE exhibition.

D-04

The virtual liver surgery planning system

E. Sorantin¹, G. Werkgartner¹, R. Beichel¹, A. Bornik¹, B. Reitinger¹, M. Riccabona¹, R. Wegenkittl², A. Fuhrmann², M. Sonka³, A. Koll¹; ¹Graz/AT, ²Vienna/AT, ³Iowa, IA/US

In patients suffering from liver tumours, the operability and choice of a surgical approach depends on the correct interpretation of preoperative imaging data. In particular, the correct assessment of the involved liver segments, the topographic relationship of the tumour to vessels, and the residual liver volume following liver surgery play a major role in patient outcome. Since cross sectional imaging such as CT or MR imaging represents an integral part of the preoperative assessment a virtual liver planning system was developed, which provides visualization of the underlying anatomy, pathology. Using a head mounted display (HMD) and passive registration tools (Polaris tracker) interactive 3D visualization as well as virtual planning of liver surgery is achieved. The semi-automated segmented tumour, liver segments and portal vessels can be evaluated from any direction including a pre-defined safety margin around the planned tumor resection. Moreover, distance measurements within the 3D-space as well as volumetric analysis of individual liver segments and the tumour itself can be obtained. Essential components of this project will be demonstrated at the exhibition.

D-05

Patient-specific computational analysis of transvenous defibrillation

D. Mocanu¹, J. Kettenbach², M.O. Sweeney¹, R. Kikinis¹, B.H. Kenknight³, S.R. Eisenberg¹; ¹Boston, MA/US, ²Vienna/AT, ³St. Paul, MN/US

The goal of this project is to assess the predictive capacity of computational models of transvenous defibrillation by comparing the results of patient-specific simulations to clinical defibrillation thresholds (DFT). Nine patient-specific models of the thorax and *in situ* electrodes were created from segmented CT images taken after implantation of the cardioverter-defibrillator.

The defibrillation field distribution was computed using the finite volume method. The DFTs were extracted from the calculated field distribution using the 95% critical mass criterion. The comparison between simulated and clinical DFT energy resulted in a rms difference of 12.4 J and a 0.05 correlation coefficient (cc). The model-predicted DFTs were well matched to the clinical values in four patients (rmsD1 1.5 J; ccD0.84). For the remaining five patients the rms difference was 18.4 J with a ccD0.85. These results suggest that computational models based solely on the critical mass criterion and a single value of the inexcitability threshold are not able to consistently predict DFTs for individual patients.

However, inspection of the weak potential gradient field in all nine patients revealed a relationship between the degree of dispersion of the weak field and the clinical DFT, which may help identify high DFT patients.

D-06

Computer aided diagnosis (CAD) in rheumatoid arthritis

P. Peloschek¹, G. Langs¹, F. Kainberger¹, H. Bischof², W.G. Kropatsch¹, H. Imhof¹; ¹Vienna/AT, ²Graz/AT

The aim of this project is to develop an automated analysis software of serial hand radiographs in patients with rheumatoid arthritis.

All software calculations are performed on a commercially available laptop using digital radiographs (DICOM). No manual initialisation is required for the localisation procedure. The training of the contour delineation algorithm was performed on two training sets T 15 and T 30 consisting of n = 15 and n = 30 sample radiographs. Statistical analysis for the localizer procedure was done on the CMC-, MCP- and DIP-joints of 10 subjects. Evaluation of the automated bone contour delineation was done using 42 landmarks per metacarpal bone on 10 different radiographs leading to a sample data set of 420 measurements.

Automated joint localization was found to be sufficiently robust (mean position error 2.7 mm) by means of further processing. The bone contour was found with high accuracy. Median error orthogonal to the contour was 0.113 mm, 74.6% of the landmarks in the test set lie within a 0.25 mm error corridor. Features extracted from the algorithm show good discriminative properties for the automated detection of bone erosions.

We conclude that our software provides an interactive robust automated quantification of bone lesions and an automated estimation of the bone contour is proposed. The software can be used interactively at the *IMAGINE* exhibition.

D-07

Advanced clinical applications for the digital hospital

J. Peters¹, R. Truyen¹, M. Quist¹, P. Ermes¹, R. Habets¹, M. Breeuwer¹, H. de Blieck¹, L. Spies², S. Deckers¹, F.A. Gerritsen¹; ¹Best/NL, ²Aachen/DE

This IMAGINE exhibit will be a 'behind-the-scenes' of our current research and advanced development activities in new clinical applications for medical imaging. A selection of innovations will be highlighted, where the common theme is our drive towards automated analysis and intelligent integration of clinical and image information. Work at various stages of the research and development cycle will be presented in the form of live demonstrators.

Digital osteotomy planning is a first in a range of orthopaedic tools that run as an advanced PACS application: starting from a worklist images are retrieved from the PACS, the tool starts and the orthopaedic surgeon can plan his procedures, subsequently the planned and simulated osteotomies are stored to the PACS where the orthopaedic surgeon can view and use the documented plan in his further procedure.

Fast and reliable methods are required for the comprehensive visualization and quantification of cardiac MRI images. We have developed software that has a simple and intuitive user interface enabling fast 3D visualization of the complete coronary-artery tree together with the heart that will work in concert with the new ViewForum software for the semi-automatic quantification of myocardial 1st-pass perfusion and myocardial viability.

Important drivers for innovation in virtual colonoscopy are patient compliance, dose-hygiene, time efficiency, sensitivity and specificity. Several validation prototypes addressing these issues are demonstrated: no-click automated path-tracking, matching of prone and supine paths, electronic cleansing of tagged stool, computer aided detection and quantification and XML based automated reporting for easy transfer of results.

Pulmonary embolism is a widespread and often deadly condition that is increasingly assessed using contrast enhanced CT. Although this method is successful in emboli detection, reading the large MD-CT volumes is still a laborious and time-consuming task. We will present detection and advanced visualization algorithms aimed at a more efficient and reproducible detection and delineation of pulmonary emboli.

In our Patient-specific hemodynamic modelling for diagnosis & therapy project we investigate how modern cardiovascular imaging can be combined with the latest techniques in hemodynamic modelling. Highlights will be shown for the recently started validation for modelling the prediction of the risk of rupture of abdominal aorta aneurysms.

Finally we will share the Philips vision on how software intelligence together with targeted imaging agents can convert multi-modality imaging equipment into molecular information, where we have created a molecular imaging toolbox that offers ease of use and seamless integration with the clinical workflow.

D-08

IMAGINE: Your heart - ONE-STOP-SHOP - in digital cardioradiology

R. Rienmüller, J. Teubl, T. Rienmüller, K. Kovaleva, G. Reiter, H. Mächler, M. Zink, W. Klein; Graz/AT

The present state of digital tomographic imaging methods as CT and MR enables to image complete cardiac morphology and function simultaneously. It means nowadays we can answer cardiac questions like in an ONE-STOP-SHOP replacing previous diagnostic methods and improving the quality of medical information. This however makes it necessary to be aware and to use the present understanding of the anatomy, patho-anatomy, physiology and patho-physiology of the cardio-vascular system inclusively the aorta and its central neuro-humoral regulation.

As permanent adequate myocardial perfusion is required for the heart as cardiac pump - the meaning of direct and derived key-factors of myocardial perfusion will be explained and discussed in the relationship to coronary morphology and function. The methods of myocardial perfusion measurements and of the evaluation of coronary vessel resistance will be extensively elucidated.

The goal of the exhibition is to demonstrate and to discuss with the visitors the results of a multi-variant-analysis of morphological and functional cardiac images and parameters and their meaning for the daily clinical diagnostic, therapy and as approach to evidence based medicine.

These results are based on more than 3000 patients studied by CT and above 500 studied by MR.

All studies were performed by standardized protocols evaluating the coronary and myo-, peri- and endocardial morphology, myocardial perfusion (ml/100 g/min) and cardiac functional parameters as EDV, ESV, EF, LVM, contractility and aortic compliance. Additionally in all patients the heart rate and the blood pressure were measured and the rate pressure product calculated.

Intracardiac, -coronary and -aortic blood flows were measured by MR whenever possible.

All images were digitally archived and integrated in a digital data bank with all morphologic, functional and clinical data as age, sex, blood pressure, pulse rate, ECG etc.

It means this data bank contains about 100 data per patient. A data bank is a prerequisite of a suitable understanding and interpretation of individual cardiac function and represents the basis for development of new strategies in risk stratification.

The structure of this data bank enables to perform any statistical evaluation with respect to age, sex, disease entity, and additionally a multi-variant-analysis of interrelationship of the various functional parameters as myocardial perfusion, blood pressure, pulse rate, stroke volume, myocardial wall tension, aortic compliance etc.

This multi-variant-analysis enables to recognize cardiac abnormalities (functional and morphologic deviation) in a very early stage of a disease and to classify a variety of cardiac diseases in a new digital quantitative manner.

This results in a better understanding of the control mechanisms of cardiac function and in direct concrete therapeutic recommendations.

The studied and digitally completely archived group of patients consists of:
Healthy volunteers, coronary heart disease (before and after bypass surgery or dilatation), congenital and acquired cardiac diseases, valvular diseases (before and after surgery), cardiomyopathies, hypertension, diabetes mellitus, renal failure with haemodialysis, pericardial disease, cardiac tumours, and cardiophobia.
The visitor of the IMAGINE exhibition will learn:

A

1. Past, present and future of digital cardio-radiology
2. The characteristics of the heart in young, adult and older people
3. The characteristics of woman heart
4. The characteristics of cardiac function at rest, at stress and in active sports-men.

B

1. How to use the CT- and MR-technology for cardiac imaging
2. How to perform morphologic image analysis
3. How to perform quantitative functional image analysis
4. How to organize and handle a data bank
5. How to perform multi-variant-analysis.

D-09

Computer aided image based diagnosis and therapy planning

S. Behrens, T. Boskamp, L. Bornemann, H. Bourquain, V. Dicken, J. Drexl, H.K. Hahn, A. Hennemuth, M. Hindennach, S. Kohle, S. Krass, B. Kümmelken, S. Kuhagen, J.-M. Kuhnigk, M. Lang, F. Link, G. Pausche, T. Preusser, R. Rascher-Friesenhausen, J. Rexilius, A. Schenk, M. Schlüter, A. Weihusen, S. Zidowitz, H.O. Peitgen; Bremen/DE

The research and development institute MeVis - Center for Medical Diagnostic Systems and Visualization - is dedicated to computer assistance for image based diagnosis in medicine. All applications described below are based on the software platform MeVisLab and result from various projects with more than 50 clinical and a number of industrial partners.

Software Platform MeVisLab: We present a software platform for rapid prototyping in R&D for computer aided image based diagnosis and treatment planning. It provides efficient image processing and visualization tools. MeVisLab allows a highly flexible software development on various levels (C++, graphical programming, application development with JavaScript) and offers substantial DICOM integration. MeVisLab is used by more than 40 partners. It is available for Windows and Linux.

Radiological and surgical interventions: We present projects for planning and preoperative risk assessment in oncological liver surgery (e.g., functional remaining volume), for living donor liver transplantation (e.g., functional graft volume), for percutaneous thermoablation of liver tumors (e.g., risk of incomplete tumor destruction), and for surgery of primary lung cancer (e.g., degree of impaired postoperative lung function based on CT data).

Distant service for surgical interventions: In this project, MeVis offers a distant service for the preoperative planning in liver surgery. Preoperative CT data are transmitted to MeVis, analyzed and the results are returned to liver centers worldwide where the computer aided surgery planning is performed. The service

has been used by more than 35 clinics in Asia, Europe and the US for more than 600 cases and is now part of the standard procedure for preoperative planning of LDLT in leading centers.

Neurological diseases: We present software applications to support diagnosis, intervention planning, and therapy monitoring in neurology, neuroradiology, and neurosurgery. Diagnosis and intervention planning are supported by multidimensional fusion of anatomical (MR imaging, CT), functional (Gd-MR imaging, fMRI), and structural (DTI, DWI, MTR) information. To assess brain atrophy, e.g., in AD or MS, we present fast, reproducible, and accurate volumetry of total brain, gray and white matter, cerebellum, cerebral ventricles, and temporal horns. Visualization and quantification of diffusion tensor characteristics facilitate the assessment of both tumor infiltration and white matter degeneration.

Oncological diseases: We present software applications for morphological and functional analysis of tumors. The morphological analysis is based on CT data and includes exact and reproducible tumor volumetry for chemotherapy of metastatic diseases. Functional assessment of tumor vitality is performed based on contrast enhanced dynamical MRI.

D-10

MARVIN: A modular image archive; ASENA: A web based RDE-tool, and secure DICOM-communication

D. Emmel, A. Haderer, N. Yakan, M. Gutberlet, K. Klimes, M. Werk, J. Ricke;
Berlin/DE

Purpose: The remote data entry (RDE) system ASENA together with the modular image archive MARVIN allows clinics and hospitals to establish digital image archiving and remote data collection including secure exchange of DICOM images. By using standard protocols for data transfer ASENAs and MARVIN integrate seamless into existing network infrastructures. MARVIN offers an everything online (EOL) DICOM image archive with an integrated web interface for image retrieval. The implementation of secure DICOM protocol allows image communication over insecure networks like the internet. ASENAs enables users to setup customized web based applications for RDE. Users enter data into the central ASENAs database using standard web browsers. Through the integration of MARVIN archiving components into ASENAs a seamless integration of DICOM image data and RDE is realized. This approach brings together textual and numerical information with DICOM images.

Methods and Materials: *DICOM image archive MARVIN:* MARVIN is set up as a modular EOL DICOM image archive. All image data is stored on mirrored hard-disks. EOL guarantees immediate access to all stored image data without delay, as there is no need to move image data between different storage media. By exchanging the hardware modules after three years of use, expensive and complicated migration of image can be avoided. Users access MARVIN either via web browser or by DICOM query/retrieve.

Remote data entry system ASENAs: ASENAs creates web applications out of customized HTML-forms for data entry into a central database. To realize a first step validation constraints can be attached to form elements. Fine granulated permissions can be given to individual users for role based access rules. Through the integrated MARVIN archiving component DICOM images can be attached directly to the database records. The database contents can be downloaded in a standardized format for further statistical evaluation with common analyzing tools.

Results: MARVIN realizes the storage and image distribution infrastructure for the department of radiology at Charité Campus Virchow-Klinikum in Berlin-Germany. Growing by 20 GB/day MARVIN currently stores 15 terabyte of image data (Sept. 2004) accessed by more than 300 users. The integrated secure DICOM protocol allows image exchange with external partners over insecure networks. Using ASENAs successful projects are established within the Charité as well as with external partners. The integration of DICOM images together with textual information in a central database system is a major feature of ASENAs.

Conclusion: ASENAs and MARVIN are well accepted and reliable systems. The growing importance of inter-hospital data exchange can be achieved by using the communication abilities of ASENAs and MARVIN. Using standard protocols makes integration into existing infrastructures easy.

D-11

Atlas-assisted analysis of brain scans

W.L. Nowinski¹, Q. Hu¹, B. Prakash¹, I. Volkau¹, G. Qian¹,
A. Thirunavukarasu¹, J. Liu¹, A. Aziz¹, R. Baimouratov¹, Z. Hou¹, S. Huang¹,
S. Luo¹, S. Minoshima², V. Runge³, N. Beauchamp²; ¹Singapore/SG, ²Seattle,
WA/US, ³Texas, TX/US

Two trends are observed in radiology: 1) the number of scans is increasing dramatically (e.g. 50% by 2010 in the US) while at the same time the number of radiologists will be growing much slowly (e.g. 20% in the US); and 2) about 65% of the world is radiologically void and another 30% has only basic technologies. Therefore, new approaches for facilitating and speeding up the interpretation of scans as well as reducing the learning curve of radiologists are needed. In our opinion, model-enhanced radiology may be one of solutions.

Our exhibit contains three computer demos: 1) Rapid and automatic atlas-based interpretation of MR imaging normal brain scans, 2) Assistance in interpretation of stroke images by means of anatomical and blood supply territories atlases, and 3) Atlas-assisted interpretation of PET/SPECT brain images.

Interpretation of normal brain scans is achieved by using a deformable anatomical atlas with a fast method of overlaying the atlas onto the scan. An electronic version of the Talairach-Tournoux (TT) brain atlas, fully segmented and labelled, was developed earlier [1,2]. The TT atlas is interpolated to provide a high resolution volume. A fast transformation of the TT atlas to the scan is developed based on the modified Talairach landmarks [3]. This transformation is done in five steps: extraction of the midsagittal plane [4], identification of the anterior and posterior commissures [5], extraction of the cortical landmarks [6], interpolation of the scan along the intercommissural plane, and overlaying the warped atlas images on the scan.

Assistance in interpretation of stroke scans is achieved by using both the TT atlas and a deformable atlas of blood supply territories with a fast method of overlaying them into the scan. The blood supply territories atlas is derived from a 3D vascular atlas constructed from MRA images [7].

The TT atlas with a fast technique for atlas-scan warping is used for assisting interpretation of PET and SPECT brain images.

D-12

The Cerefy Atlas of Brain Anatomy in Chinese

W.L. Nowinski¹, A. Thirunavukarasu¹, Y. Fu², M. Xin¹, Z. Lin², S. Wang²,
¹Singapore/SG, ²Harbin/CN

About 65% of the world is radiologically void and another 30% has only basic technologies (*Diagnostic Imaging*, special edition, 2003). One of major reasons of this situation is the lack of expertise and resource to interpret scans. This may be improved by providing tools affordable and acceptable in terms of cost, user-friendliness, and language. The most prevalent language on earth is Chinese. This work aims at development of a Chinese version of our neuroeducational bestseller *The Cerefy Atlas of Brain Anatomy* (CABA) [1].

Electronic brain atlases provide means for learning neuroanatomy. However, their common limitation from a radiology standpoint is the lack of radiological images. The CABA overcomes this limitation by providing MRI images which are co-registered spatially with an electronic atlas of gross anatomy. The CABA contains more than 1500 individual structures on 100 images. The anatomical index has 135 names of subcortical structures and cortical areas. The application runs on personal computers and provides functions for atlas-based labeling of MRI images with structure's name and description; testing against location and name of cerebral structures; triplanar image display and manipulation on axial, coronal, and sagittal orientations; mensuration useful to study spatial relationships; structure searching; and saving of labeled images useful to prepare teaching materials.

The CABA works in two modes: *explore* and *test*. In the explore mode, the atlas and data are explored on the triplanar images. In the test mode, the user is tested against either location or name of atlas structure.

The CABA is a useful tool for students and residents as well as teachers and researchers. For students it provides testing and scoring capabilities for exam preparation, while for teachers it helps in preparation of teaching materials.

The Chinese anatomical index and the descriptions of all anatomical structures have been compiled. These materials have substituted the English ones in the CABA. In addition, all textual information in the user interface has been translated into Chinese.

D-13

New applications for computed tomography

D. Rinck, L. Gündel, A. Bakai, E. Klotz, H. Fichte, H. Ditt, C. Süß, F. Trappe, T. Flohr; *Forchheim/DE*

We present new and innovative applications for computed tomography. The colonography application visualizes the entire colon in both 2D (MPRs) and 3D (endoluminal view) modes. It supports the search for polyps and detection of colon cancer. Prone and supine data sets can be displayed and the detection results can be documented in the integrated reporting tool. The colon CAD tool (under development) searches suspicious structures in the colon and lists them in addition to the lesions marked previously by the radiologist. The cardio-vascular evaluation application consists of a robust vessel segmentation and a stenosis quantification tool with plaque visualization and quantification, including color-coding of the different plaque compartments and sub-volume calculation. Cardiac function parameters such as ejection fraction and stroke volume are calculated. Using an advanced active shape model regional myocardial wall thickening is determined. A myocardial enhancement tool is integrated, which isolates the myocardium and visualizes ischemic regions by color-coding techniques. The fast detection of pulmonary embolism (PE) is supported with a new visualization tool using contrast enhanced CT data of the lung. The HU values of the vessels are mapped onto an interactive 3D vessel structure. Regions with suspicious PE can be examined on the original CT data, rendered CT planes, or by visualization of a simplified subtree or subtree analysis. For ground glass opacities (GGOs) common segmentation methods cannot be applied because of their small size and poorly defined boundaries. Enhanced algorithms, however, can be used for accurate and reproducible measurements of GGO size and doubling time. The fast volume acquisition capabilities of multislice CT scanners also allow scanning whole volumes repeatedly in relatively short scan times. Using dedicated organ adapted registration and post processing techniques we currently investigate 3D perfusion assessment of brain, lung, and liver based on multiple volume acquisition. Another important application is bone subtraction CTA of the cerebral vasculature. It is based on co-registration of an additional low dose plain CT scan in order to remove the complex bone structures of the skull base. This significantly simplifies and improves the analysis of pathologies such as aneurisms. A prototype platform allows the assessment of perfusion changes of organs, such as liver and pancreas, and tumors based on a three dimensional tracking of relevant object structures during multislice data acquisition. Dynamic volume data sets are evaluated with the 'maximum slope' model to quantify the perfusion of tissues and whole organs, including dedicated modelling of the complex blood flow dynamics of the liver. The implementation of the 'Patlak model' allows to measure permeability and blood flow of various tumors. Combining the body perfusion models with a 3-D volume registration allows to extend the application to the diagnosis of lung disorders and lung tumors. First clinical results are promising.

D-14

Advanced 3D image rendering and multi-level, clinically-focused PACS integrations

C. Chin, G. Jones, J. Archer, J. Field, M. Dimmock, P. Papageorgiou, R. Moffett; *Edinburgh/UK*

Modality advances are driving the need to routinely visualize and analyze high-resolution images using MPR and 3D volumetric software. This is placing a new demand on PACS to visualize and analyze studies containing over 1000 images. Radiologists need to rapidly load and manipulate these studies using advanced MPR and 3D tools within an integrated PACS diagnostic workflow. This provides unlimited user access to full MPR and 3D functionality, wherever you need it. Radiologists also need to offer the best possible service to referring physicians who are intensive users of radiological images.

Barco will present its latest MPR and 3D toolsets and, specialized clinical application modules designed for, and integrated into, a PACS environment. The company will also demonstrate performance advances made in software-and hardware-based 3D rendering using high-performance graphics accelerators.

Multi-level MPR and 3D software integrations for PACS: It is critical that the advanced post-processing MPR and 3D tools, which are required for the rapid and effective analysis of large volume image studies are seamlessly embedded into the PACS application software. Barco will demonstrate its 3D integrations for a range of PACS architectures, which benefit radiologists by providing a single streamlined diagnostic workflow. Barco will demonstrate its 3D integrations for a range of PACS architectures, which benefit radiologists by providing a single streamlined diagnostic workflow.

Cost-effective, advanced 3D clinical applications for PACS: Advances in modality technology are driving the development of new clinical applications. Some are

now a routine part of a radiologist's daily work list. Barco's new clinical software modules provide radiologists with effective methodologies for using advanced MPR and 3D functionality to read specific types of clinical studies, including:

- Vessel analysis
- CT colonography
- PET/CT fused image display

Optimizing user performance and functionality: MPR and 3D rendering performance is significantly improved using high-performance graphics accelerators. Using new 3D accelerated graphics processing units (GPUs), Barco can display slab MPR images at a very fast cine frame rate. This is extremely beneficial for efficient and accurate diagnosis. Barco will demonstrate a number of concepts for optimizing user performance and diagnostic effectiveness with this enhanced MPR frame rate capability.

D-15

Exploiting the power of GPUs in medical imaging

F. Wessels; *Bilthoven/NL*

3mensio Medical Imaging will be showing 3viseon, a next generation workstation based on the latest and most powerful GPUs. GPUs (graphics processing units) are chips found on the latest graphics cards which are quickly becoming commodity components of the PC-platform. They are dedicated to delivering high-quality high-resolution 3D graphics at interactive frame rates and have their origins in the computer games industry.

By shifting the medical visualization from the "traditional" CPU to the GPU new levels of performance can be offered. In addition new functionality can be developed by exploiting the programmability of the GPUs which allows ever more sophisticated algorithms to be run on the GPU at very high speeds. This can be extended beyond visualization to areas such as advanced image processing. Given the larger datasets in radiology due to trends such as multi-slice CT scanners, the "traditional" slice by slice reading of datasets is becoming more cumbersome. As such new ways of handling these vast amounts of information need to be found for which the processing power of the GPUs is ideally suited. Likewise users outside the radiology department are finding more and more needs for visualization which can now be offered to them at interactive speeds on commodity PC hardware.

D-16

Towards hysteroscopy simulation: Interactive simulation components for deformable tetrahedral meshes

M. Teschner, B. Heidelberger, M. Müller; *Zurich/CH*

This project focuses on the development of interactive methods and algorithms for surgery simulation and training. We investigate approaches to tetrahedral mesh generation, deformable modeling, deformable collision handling, fluid simulation, and the simulation of surgical instruments. Based on these components, it is intended to implement a generalized real-time surgical simulator, which processes anatomical models represented with tetrahedral meshes.

Hysteroscopy simulation is a first application for the developed components. Within this hysteroscopy training project we collaborate with numerous partners of the Swiss National Center of Competence in Research on Computer Aided and Image Guided Medical Interventions (NCCR Co-Me).

Our software demonstration shows a first prototype of a hysteroscopy training tool where we focus on efficient deformable modeling and deformable collision handling using complex tetrahedral meshes with up to 10000 tetrahedrons.

In contrast to existing simulation environments, our approaches are not restricted to specifically designed models but process any anatomical structure which is represented as a tetrahedral mesh. Thus, the simulation components can potentially be applied to many training scenarios.

While existing environments only handle collisions between deformable structures and rigid surgical tools, our simulation detects and resolves all collisions even among deformable structures. Further, the deformable modeling approach is stable under all user interaction and provides interactive update rates for geometrically complex models. Details regarding the deformable model, deformable collision detection and response have been published in various papers.

In our first prototype, a user can navigate a camera inside the cavity of a uterus and interact with all deformable structures such as cavity and several polyps. Deformation, deformable collision detection, and visualization are performed at interactive rates for models of up to 10,000 tetrahedrons using a standard PC with Intel Pentium 4, 2 GHz.

D-17

Interoperability solutions for an integrated imaging and information system

G. Venturi¹, S. Selvaggio¹, A. Fiumicelli¹, A. Budge², C. Bull², R. Shaw³, P. Wilson³, A. Chippendale³; ¹Cairo Montenotte/IT, ²Bracknell/UK, ³Newcastle upon Tyne/UK

The purpose of the demonstration is to highlight the importance of interoperability and data portability of a complex medical imaging and information system inside the healthcare enterprise and to show the solutions adopted by the LifeWeb suite. The demonstration is subdivided into three exhibits, each of them dedicated to a specific key task for the interoperability: single access point, cross enterprise data portability and security.

Exhibit one: Enterprise PACS single access point

This exhibit will show how a large enterprise PACS, made by multiple, heterogeneous data repositories, can be arranged as a single virtual collaborative system where the user can retrieve data wherever they are with a single query. Peculiarity of an enterprise PACS is to include all the images produced by the healthcare enterprise and goes beyond radiology. It can be designed as a single virtual archive or a cluster of distributed archives, departmental specific, eventually designed by different vendors. We will demonstrate how it is possible, through the implementation of proxy services, to add any type of data repositories to the system from any vendor, and make the data instantly available to the user completely transparently. The user does not need to know where data is but simply queries the system and it is the system's engine that looks for the data on the repositories, checks for consistency, prepares the presentation.

The same engine can be used to perform data migration from end-of-life systems destined to be turned-off.

Exhibit two: Cross Enterprise Data Portability

This exhibit will show the implementation of new data coding to allow cross-enterprise data portability, including images, report and diagnostic documentation. Import, export and interchange of data will be demonstrated.

Data can be stored on removable media, according to the PDI (portable data for imaging) IHE profile to be delivered to the patient and/or can be queried automatically to the central system by a remote host according to the IHE XDS (Cross Enterprise Clinical Document Sharing) profile.

An "in-progress" demonstration of an Electronic Healthcare record implementation, made according to the HL7 EHR-CR and EHR-LR model, will be presented.

Exhibit three: Secure distribution and visualisation of images and data through the web.

This exhibit will show the use of secure web technology to distribute and visualize images and in a heterogeneous network environment made by a local intranet, the internet and wireless network. Information and images can be accessed according to routing tables that, together with user's profile, set the privileges, i.e. the functions, that can be used locally at the department, inside the distributed healthcare enterprise or remotely in any place of the world.

This demonstration will cover security issues in the broadest way, including transmission security, wireless network security, access control, data preservation and error disaster policies. Moreover it will cover privacy issues, data integrity issues and data consistency issues. Finally, it will demonstrate how to solve the patient identifier issues to reconstruct a healthcare record merging data from different institution.

D-18

Fused deposition modeling for operation planning, multimodal matching of functional and anatomical data and development of a lung atlas/model

M. Verius, R. Huttary, W. Recheis, W. Eisner, S. Felber, D. zur Nedden; Innsbruck/AT

Our research field reaches from planning and construction of fused deposition models (FDM) which are used for operation planning in oral and plastic surgery, to datafusion of preoperative CT and MR-datasets, preoperative functional MR-data and by means of a 3D-digitizer scanned intra-operative cortical stimulation points (ICS).

1. On the basis of CT or MR data a corresponding virtual model in stl-format (stereolithographic file format) is calculated and by means of a "3D-printer" a plastic model is built layer by layer. The so originated model can be treated by the surgeon like sawing, drilling etc. to plan the optimal operation and access technique.
2. The project 'Planning of minimally destructive neuro-surgical operations: Correlation of functional magnetic resonance tomography and intra-operative cortical stimulation' is a data fusion project which is supported by a grant of the Austrian National Bank (No. 9044). Therefore datasets of MR, CT, functional MR and intraoperative cortical stimulation points are superposed in

one volume dataset. It should be determined if and in what way corresponding functional MR data agree with the intra-operative cortical electrostimulation points. The patient has to execute specific paradigms within the MR-scanner (for example motor paradigms as fingertapping, arm bending, biceps contraction or similar paradigms) to monitor the active areas. During the neuro-surgical operation the patient is electrical stimulated by means of a bipolar stimulation tweezers at previously marked points and the physiological answer of the patient (finger movements, biceps contractions etc.) is registered. These functional data are overlaid with the anatomical datasets performed with ANALYZE© and CURRY© software package. After 7 patients we conclude that a good correlation between ICS and functional MR imaging can be observed but still inaccuracies due to brainshift and low spatial resolution in the fMR imaging data occur. The goal of this project is a shortening of operation time and on the other side to establish a patient friendly operation method by avoiding the patients alertness during neuro surgery.

3. A third research project in cooperation with the University of Iowa is the building of a model or atlas of the normal human lung based upon X-ray CT scanning. This atlas includes the lungs, lobes, sublobar segments and airway and vascular branching structures of the lung and attached to each level of this structure will be the normal range of the CT-based measures of regional lung physiology including ventilation, perfusion, and specific compliance. This model/atlas of the normal human lung, developed for three decades of adult age, is providing the comparative basis for detecting and quantitating pulmonary pathology.

D-19

AngioVis: Computer graphics for clinical visualization of peripheral arterial occlusive disease

D. Fleischmann¹, M. Straka², M. Sramek², A. La Cruz², A. Koechl², A. Kanitsar², T. Rakshe¹, S. Napel¹, J. Lammer², E. Gröller²; ¹Stanford, CA/US, ²Vienna/AT

Purpose: The 'AngioVis' exhibit illustrates the 'bench-to-bedside' research equivalent in the field of computer aided diagnostic imaging, exemplified by the development of visualization tools for CT angiography of peripheral arterial occlusive disease (PAOD).

Background: Continuously evolving multiple detector-row CT (MDCT) technology allows the acquisition of large, high-resolution volumetric CT angiographic datasets of the entire lower extremity arterial tree. The development of adequate tools to extract and visualize the clinically relevant complex manifestations of peripheral arterial occlusive disease requires both, knowledge of disease morphology and therapeutic options, as well as expertise in computer sciences, image segmentation and computer graphics.

Methods and Materials: Several interconnected topics - ranging from clinical background and image acquisition technique, over different methods of image segmentation and visualization, to finally image evaluation and interpretation of routine clinical datasets - will be part of this interdisciplinary exhibit:

Imaging technique:

- CT acquisition and contrast medium injection: Strategies to optimize the spatial resolution of the CTA datasets, and to achieve adequate opacification of the peripheral arterial tree in patients with sometimes severely altered flow dynamics will be presented.

Visualization technique:

- Bone segmentation is an important pre-processing step when maximum intensity projections (MIP) are used for vessel visualization. We present a semiautomated density based technique, and a statistical approach using a bone atlas. One limitation of MIP is, that vessel wall calcifications, calcified plaque, and also endoluminal stents obscure the clinically relevant flow channel of a diseased artery.
- Another key pre-processing step is the definition of the medial axis of the branching vessel tree. We present a density/gradient based 'vessel-tracking' algorithm to identify the peripheral arterial tree from the aorta down to the crural and pedal arteries.
- Because automated vessel tracking may fail in severely diseased and occluded arterial segments, we will demonstrate the initial results obtained from a Knowledge based vessel tracking algorithm, which estimates the course of an occluded arterial segment based on a statistical comparison with reference datasets.
- In the presence of atherosclerotic change (plaque, calcifications, stenoses), it is difficult to accurately identify the vessel centerline. Several algorithms (ray-casting, block matching, template matching, fitting of elliptical cylinders) will be presented and their performance in normal versus diseased arteries of variable size will be illustrated.

- Curved planar reformations are longitudinal cross-sections through a vessel centerline, and allow the clinical evaluation of the flow-channel of a diseased arterial segment. We will present several variants of CPRs (thin/thick, projected-stretched-straightened). One disadvantage of CPRs in the setting of PAOD is the limited spatial perception. This can be overcome by creating 'MultiPathCPRs', which simultaneously display multiple longitudinal cuts through the entire peripheral arterial tree in a single image. This technique is currently our preferred visualization technique for percutaneous treatment planning.
- The vessel glyph: represents an abstract notation of combining different visualization techniques for focus & context rendering in the same image. This allows, for example, to display diseased arterial segments ('focus') as CPRs, while rendering the anatomically relevant 'context' using direct volume rendering.

Clinical integration:

- The AngioVis toolbox is the software platform which hosts the above algorithms as separate plug-ins. In the clinical environment, it also connects to the CT scanner and the PACS system, using DICOM communication software. This allows 'online' evaluation of new techniques and algorithms on a large spectrum of clinical cases.
- Interpretation of clinical datasets, using the above visualization techniques will be demonstrated with angiographic correlation.

Conclusion: Close interdisciplinary collaboration between clinical and computer scientists is an effective platform for both, basic image processing research as well as for the development of dedicated clinical applications in the field of medical imaging.

IMAGINE



Satellite Symposia

Satellite Symposia

Friday, March 4, 2005

10:30 - 12:00

Room E1

organised by **HITACHI**

SY 1

Real-time virtual sonography (RVS)

Moderator:

F. Frauscher; Innsbruck/AT

E-01

Technical principles of RVS

H. Frey; Zug/CH

Ultrasound imaging is a convenient and non-invasive examination method. However it is sometimes difficult to acquire the image of organs and lesions through bones or gas in gastrointestinal tract. The ultrasound probe is manipulated by freehand during examinations, so its cross section is less objective compared with other modalities. The real-time virtual sonography combines the advantages of CT and ultrasound. The system is able to display multi-planar reconstruction images (MPR) which indicate the same cross section as the live ultrasound image from the CT volume data set in real-time. The real-time virtual sonography is available for the HITACHI EUB-8500 digital ultrasound scanner. The CT volume data set is received via DICOM network or CD/DVD by the ultrasound unit. A magnetic positioning unit detects the position of the probe during the examination. The system processor of the ultrasound scanner calculates MPR images from CT volume data and displays them side by side with the ultrasound image. MPR image can be visualized in more than 10 frames per second as 256 by 256 pixels image. As a result, it becomes possible to compare ultrasound images with MPR image in real-time.

E-02

Real-time virtual sonography is not only a novel navigation tool in radiofrequency ablation, but also a novel evidence-based imaging for hepatocellular carcinoma

T. Iwasaki; Miyagi/JP

Because ultrasound is simple, noninvasive and real-time, percutaneous radiofrequency ablation of hepatocellular carcinomas is usually performed under ultrasound guidance. However, it is often difficult to detect residue or recurrence after ablation. To solve the problem without spoiling the advantages, utilizing virtual reality technology and multi-detector row CT, which acquires volume data and shows any MPR images, we developed real-time virtual sonography (RVS). This lecture is to demonstrate the clinical value of the RVS system. The RVS system is composed by magnetic motion tracking device, image-processing workstation and ultrasound equipment. The magnetic sensor mounted on the ultrasound probe registers and transmits the spatial location and orientation of the probe to the workstation which possesses CT volume data. The workstation computes and displays the MPR image corresponding to the ultrasound image in more than 10 frames per second. When starting RVS, the position adjustment is performed at the xiphoid process. Discrepancy by respiration is rectified by adjust system. RVS was performed in 62 hepatocellular carcinoma patients. MPR image of target tumor was displayed under good position correspondence with ultrasound image in all the patients. Ablation was successfully performed. RVS was useful for the identification of residue after ablation. The real-time existence of virtual MPR imaging, which must be the most convincing evidence imaging, enabled us to perform safe and definite ablation at ease. RVS is not only a novel and effective navigation tool in percutaneous radiofrequency ablation, but also a novel and persuasive evidence-based imaging for hepatocellular carcinoma.

E-03

RVS: Interventional applications in oncology

R. Lanocita; Milan/IT

E-04

Feasibility and clinical utility of real-time virtual sonography (RVS) for percutaneous radiofrequency ablation of renal tumor

O. Ukimura; Cleveland, OH/US

14:00 - 15:30

Room E1

organised by **SCHERING**

SY 2

Advances in MR contrast media imaging

Moderator:

J.F.M. Meaney; Dublin/IE

E-05

Impact of detection and characterization of liver lesions

R. Hammersting¹, J. Breuer², T.J. Vogl¹; ¹Frankfurt a. Main/DE, ²Berlin/DE

Introduction: Staging of malignant tumours is getting more and more important, especially because of new therapeutic strategies. Metastatic involvement of the liver in extrahepatic malignant disease alternates the therapeutic approach significantly in many cases and has to be ruled out with high confidence. Detection of focal liver lesions is determined by conspicuity and is related to the degree of tumour-to-liver contrast. As known tumour characterization is mainly based on the lesion contrast uptake at the different enhancement phases. Magnetic resonance imaging has proved to be a reliable diagnostic tool for the work-up of patients suffering from liver tumours. The use of different contrast agents enables good detection and precise characterisation of focal liver lesions, especially when liver-specific contrast agents are used.

New hepatobiliary contrast agent Primovist® for MR imaging of the liver: Gd-EOB-DTPA (Primovist®) is a new liver-specific magnetic resonance contrast agent for T1-weighted imaging. It consists of a gadolinium derivate linked to lipophilic ethoxybenzyl combining good hepatocellular specificity with excellent T1-relaxivity. After intravenous injection the new liver-specific Gd-Chelate is taken up by the hepatocytes via an organic anion-transporting polypeptide. It is excreted unmetabolized up to 50% via the kidneys and 50% via the bile. Renal excretion can be substituted by the hepato-biliary excretion and vice versa. The substance is a ready-to-use contrast agent which is administered intravenously in a concentration of 0.25 mmol/ml and a dosage of 0.1 ml/kg b.w. or 25 µmol/kg b.w.

Contrast mechanisms: After intravenous bolus injection of Gd-EOB-DTPA dynamic imaging (arterial, portal venous and equilibrium phase) as known from standard gadolinium-chelates can be performed. In the liver-specific phase (around 20 minutes post injection) the agent is taken up by normal liver parenchyma and hepatocyte-consisting liver lesions e.g. FNH or adenoma. Tumours without hepatocellular elements of the liver e.g. metastases do not show any hepatocyte uptake.

Results from the clinical development programme: The contrast agent has shown good safety properties in phase I - III clinical trials in up to now more than 1500 persons. In the detection study (European phase III clinical trial) 302 lesions were detected in the 131 patients (included in the final efficacy analysis). Histopathologically 215 lesions were malignant and 80 lesions were benign. 7 lesions could not be classified by histopathology. Gd-EOB-DTPA-enhanced MR imaging (EOB-MRI) was equivalent to spiral computed tomography in detection of focal liver lesions in the overall analysis. Lowest rate of false positive and false negative lesions was documented for EOB-MRI compared to CT and pre-contrast MR imaging. Highest rate of correctly detected lesions with a diameter below 1cm was achieved by EOB-MRI. A change in surgical therapy was documented in 14.5% of patients post EOB-MRI. In the characterization study (European phase III clinical trial) 176 patients with known or suspected focal liver lesions were included. The number of lesions correctly diagnosed by combined MRI (pre-contrast and EOB) was higher than for pre-contrast MRI in the on-site evaluation. The proportion of correctly characterized lesions was significantly higher for combined MR imaging compared to biphasic CT. In the overall analysis, sensitivity, specificity and accuracy for lesion classification improved with combined MRI by 3-14%. The proportion of lesions with a correct classification was superior for liver-specific MRI compared to CT, but not statistically significant.

Conclusion: Primovist® is a safe and well tolerated contrast agent for the diagnostic work-up in patients with focal liver lesions. It enables dynamic non-specific and hepatocyte phase imaging with improved detection and characterization of liver tumours.

E-06

Performance of high-concentrated contrast in MR imaging

B. Tombach; Münster/DE

The 1.0 molar Gd-chelate gadobutrol (Gadovist®, Schering AG, Germany) offers the potential to be injected as a more compact bolus for contrast-enhanced MR compared to other commercially available 0.5 M formulations. Modern MRA sequences using central k-space acquisition, half-fourier and parallel imaging techniques as well as MR perfusion techniques may therefore profit from the increased intraarterial Gd concentration during first pass. Our experience in clinical routine using conventional 1.5 T clinical MR systems (Gyroscan Intera, Philips Medical Systems, Best, The Netherlands) covers more than 7000 injections of Gadovist® for any indications and 1500 injections of gadobutrol for CE-MRA of the arterial vasculature from the cranial base to the run-off vessels of the lower extremities during the last 3 years.

Due to our experience Gadovist® can be safely applied in clinical routine for any indication offering excellent imaging properties. Fast imaging techniques, e.g. brain perfusion studies and CE-MRA seem to profit mostly from the higher concentrated agent. With respect to the small injection volume a manual bolus timing (1 ml) procedure is recommended to adapt the single dose injection precisely to central k-space data acquisitions for high resolution 3D-GE sequences in a single station MRA. For multi station bolus chase techniques like peripheral or whole body MRA a fixed volume of 20 ml result in diagnostic image qualities using biphasic injection protocols. Using modern high resolution keyhole techniques for MRA of the run-off vessels, and even for intracranial CE-MRA, 1 M gadobutrol offers the potential to separate precisely the arterial and venous phase combined with excellent imaging properties.

E-07

An important step forward in the evolution of MRA techniques

T. Grist; Madison, WI/US

Widespread dissemination of the gadolinium-enhanced MRA technique is limited by several factors, including the fact that the methods involve an off-label use of MR contrast media, complexities associated with acquisition of the images, and limited spatial resolution/coverage of the imaging sequences. The emergence of MS-325 (Schering AG/ EPIX) offers to overcome many of these limitations in clinical practice, and represents a significant potential step forward in the diagnosis of vascular disease.

First, MS-325 demonstrates higher relaxivity than conventional gadolinium contrast agents, resulting in a greater signal enhancement for a given dose of the agent. The greater degree of signal enhancement has important implications for contrast-enhanced MRA, since the increased signal may be translated into better image quality or a lower dose of the contrast media relative to conventional agents.

Second, MS-325 demonstrates protein binding to human serum albumin immediately upon injection, and this contributes to the long blood pool phase of the contrast agent. The long vascular half-life allows for prolonged image acquisitions of several minutes or more, as compared to the relatively short (30 second) acquisitions for conventional gadolinium contrast agents. In addition, the long blood half life allows for steady-state imaging of vascular territories that may be inadequately imaged on the initial first-pass MRA exam.

In summary, MS-325, an MRA-specific contrast agent, is a welcome advance in the diagnostic imaging of patients with vascular disease. MS-325 offers several potential advantages, including high relaxivity (greater signal enhancement), prolonged blood pool retention, and documented safety and efficacy for bolus injection MRA.

E-08

A new generation of contrast agents meets brand new MR imaging technology

S.O. Schönberg; Munich/DE

Numerous diseases affect multiple vascular territories in various regions of the body requiring diagnostic imaging with large anatomic coverage for comprehensive evaluation of the disease manifestations. Examples of such diseases include diabetes, vasculitis, and systemic manifestations of atherosclerosis. MR angiography has established its role for the diagnostic evaluation of almost all vascular territories as the primary modality of choice. However, different requirements for temporal and spatial resolution may exist for different vascular territories. In this situation accurate first pass contrast-enhanced MRA with global coverage is difficult because numerous bolus injections of extracellular contrast agents would be required. The recent introduction of multi-channel MR imaging

scanners with greater than 30 channels and capabilities for whole body imaging can now resolve these conflicts by accelerating the image acquisition with parallel acquisition techniques, providing high signal-to-noise ratio in all vascular territories. In combination with a new class of intravascular contrast agents, that can be used both for first pass imaging and imaging in the steady state, high resolution first pass imaging of a critical target area such as the carotid arteries or the arteries of the lower leg can be obtained. These acquisitions can be combined with steady state imaging of the remaining vascular areas, possibly even coronary arteries. Imaging in the steady-state has the potential to provide accurate evaluation of critical vascular structures with ultra high resolution, less than 100 µm³, gaining insight into pathologic changes of small arteries. This approach could be used to evaluate distal microangiopathy in diabetes or inflammatory changes in diseases such as vasculitis. In addition, up to ten fold decreases in voxel size with steady-state imaging would facilitate artery-vein-separation. Due to the high relaxivity of intravascular agents compared to standard gadolinium chelates, in combination with the dedicated surface coils excellent SNR performance can be preserved. In conclusion, the combination of new scanner technology and bolus injectable intravascular contrast agents allows comprehensive assessment of vascular disease manifestations by addressing different requirements for temporal and spatial resolution.

Satellite Symposia

Saturday, March 5, 2005

10:30 - 12:00

Room E1

organised by **KODAK**

SY 3

Implementation of clinical system solutions in an e-health environment

Moderator:

H. Pohjonen; Espoo/FI

E-09

Cross-border eRadiology

J.G. Blickman; Nijmegen/NL

As part of the eHealth initiative and action plan of the European Commission, procurement and implementation of healthcare IT systems is undergoing radical change.

As the entire imaging field can be seen as a microcosm of this process, it is useful to review the added value of the digital data movement/management and its changes: where are we in eRadiology?

We will review how building the infrastructure consisting of PACS, RIS towards an EPR in a major academic teaching hospital can gain valuable insight as to how cross-border radiology services might be conceived and executed. Ingredients such as the shortage of radiologists/radiographers, low reimbursements by national health insurers and the increasing part-time medical profession are drivers for change. Efficient workflow practices, long present in the business world, can be implemented and made 'profitable' in most of the medical world as well. The digital workplace knows no boundaries: remote reporting, off-hour coverage, the 'virtual' staff radiologist are all ways to offer imaging services in a non-traditional way.

These developments need to be balanced against legal, quality control and insurance issues, as well as cultural, language and protocol differences between locales.

This discussion will make the listener review, understand and learn from the above named concepts and experiences.

E-10

Electronic medical record: The distribution of patient-based e-health information in a regional context. The Legnano experience

V. Lombardo; Legnano/IT

The move from single-department architecture, based on stand alone systems, to the need for integrated communication between multi-modality legacy systems, in order to create an EPR-based hospital information system, has led to a significant reappraisal of organisational and technological choices at the Legnano Hospital in Milan, Italy.

The 1600-bed hospital, which covers four linked sites (with high capability WAN) in the north east of the city, employs some 4000 staff and has an annual turnover of around €250 million. Each site is linked by LAN (Gb Ethernet) which connects all clinical and administrative units.

The solution adopted at Legnano is based on a solid architecture of centralised, MPI-oriented patient demographics and on the implementation of a clinical/health data repository which is dynamically integrated with systems within individual departments, such as the LIS, RIS, Booking Centre, ADT and First Aid, through the use of specific HL7 compliant middleware.

The application of interoperability standards such as HL7 and DICOM has led to the creation of an on-line data base, directly accessible both by patients and authorised professionals.

Since September 2004, the new technology at Legnano has allowed the hospital to integrate with the CRS-SISS health project created by the Lombardy Region of Italy, designed to enable the accessibility of patients' clinical information between the hospitals, general practitioners, clinics and laboratories within the regional network.

E-11

UK national programme for IT: Delivering diagnostic imaging for the north west and west midlands in England

G.D. Larson; Hemel Hempstead/UK

In May 2004, Kodak participated in a CSC-led alliance that was awarded a 10-year contract with the UK National Health Service (NHS) for delivering diagnostic imaging services for a substantial portion of England. Under the contract, the alliance is designing, building, delivering and operating new Picture Archiving and Communications System (PACS) across the North West and West Midlands cluster.

The system is being established as part of the Department of Health's £6 billion National Program for IT (NPfIT) that will help millions of patients receive treatment more quickly and efficiently. There are four primary goals of the programme: an electronic appointment booking system, an electronic care records system, electronic transmission of prescriptions, and a fast, reliable underlying IT infrastructure.

This presentation will concentrate on some of the unique aspects of this programme that differentiate it from the delivery of a more traditional PACS. Together with other participants in the alliance, we are delivering a managed service for diagnostic imaging that is tightly coupled with the overall core services in the NPfIT. Using KODAK DIRECTVIEW Versatile Intelligent Patient Archive (VIPArchive) technology, we are delivering a single, data center-based archive for a population of approximately 12 million patients. Finally, in addition to KODAK DIRECTVIEW CR and DRYVIEW printing solutions, KODAK RIS 2010 is being used to electronically integrate the radiology workflow across hospitals in the cluster to optimize the utility of their assets in the delivery of patient care.

10:30 - 12:00

Room F1

organised by **GE HEALTHCARE**

SY 4

Work safety in the daily routine for technical staff in radiology

Moderator:

H. Kolmannskog; Oslo/NO

E-12

Contrast media side effects in the daily routine of a radiographer H. Harries-Jones, A. Holden; London/UK

E-13

Radiation safety in radiology

M. Jökel; Essen/DE

E-14

Safety in the MR imaging suite, little things to be aware of S. Massing; Essen/DE

E-15

Work safety features for technologists introduced by the industry W.-D. Rakut¹, R. Klausz²; ¹Amersham/UK, ²Paris/FR

Satellite Symposia

12:15 - 13:45

Room E2

organised by BRACCO

SY 5

High relaxivity contrast agents: A new gold standard for MRA?

Moderator:

G.M. Bongartz; Basle/CH

E-16

CE-MRA of intracranial vessels

N. Anzalone; Milan/IT

Despite the possibility to perform high quality and diagnostically useful examinations of the intracranial vasculature using time-of-flight (TOF) and phase contrast (PC) MR angiography (MRA), there are still some intrinsic technical problems that limit the application of these techniques. With TOF techniques the main problems are related to saturation effects and to spin dephasing, while for PC acquisitions the appropriate choice of the velocity encoding gradient can be crucial. Moreover, both techniques are limited by the lack of adequate spatial and temporal resolution which is essential for appropriate diagnostic evaluation of cerebral vascular malformations. Many of these problems, particularly those related to flow effects, can be avoided by the use of a suitable contrast agent. However, while the use of contrast agent can raise the signal-to-noise ratio, a major problem, particularly in conjunction with TOF acquisitions, is the superimposition of venous structures. To avoid this problem, ultrafast gradient echo MRA techniques with very short TR and TE have been developed. These sequences are designed to enable the acquisition of either small volumes with almost isotropic voxels in few seconds or larger volumes with longer scan times, and permit high quality images with good spatial resolution and high signal-to-noise ratio to be obtained. Alternatively, dynamic acquisitions with high temporal but low spatial resolution may be acquired. Although the precise sequence parameters vary between different manufacturers, the CE-MRA techniques are basically similar. It is important to target the arrival of the contrast bolus and again, different bolus timing methods are available for different makes of MR equipment.

The choice between a time resolved or high spatial resolution CE MRA technique is dependent upon the precise clinical application. The most common applications include the study of cerebral aneurysms, arterio-venous malformations, dural arterio-venous fistulas and dural venous sinus diseases. This presentation will focus both on the technical aspects of CE MRA for clinical applications concerning the intracranial vessels, and on the clinical application of different imaging techniques.

E-17

MRA of the carotid arteries

S.A. Thurnher; Vienna/AT

Magnetic resonance angiography (MRA) of the carotid arteries has undergone a long period of evolution to become a routine imaging modality. Contrast-enhanced (CE) MRA, which combines fast 3D spoiled gradient echo sequences with the intravenous bolus administration of paramagnetic contrast materials, has proven a highly capable replacement for conventional MRA techniques for the evaluation of extracranial carotid artery disease.

CE-MRA of the carotid arteries is uniquely challenging because the very short arterial-venous recirculation time in the brain leads to rapid jugular venous enhancement and hence the possibility of obscured visualization of the adjacent carotid arteries. Fortunately, improvements in CE-MRA technique such as randomly segmented centric k-space encoding, allow longer scans with higher spatial resolution without jugular venous contamination. Thus, the divergent demands of high spatial resolution, wide anatomic coverage, and arterial phase imaging have been reconciled.

Despite improvements in technique, CE-MRA has generally been considered to overestimate the degree of carotid artery stenosis compared to conventional DSA. Thus, in certain settings there may be questions as to whether the measured extent of carotid artery disease is sufficiently accurate as to meet surgical criteria. On the other hand, recent studies suggest a better correlation of CE-MRA with multiplanar rotational DSA than with conventional DSA in two or three planes. Compared with standard gadolinium contrast agents, high relaxivity contrast agents, e.g. gadobenate dimeglumine (Gd-BOPTA), have a substantially higher intravascular T1-relaxativity. This has been demonstrated in studies comparing Gd-DTPA and Gd-BOPTA enhanced MRA of the carotid arteries. Qualitative eval-

uation showed equivalent arterial contrast enhancement and vessel conspicuity with low-dose Gd-BOPTA compared with high-dose Gd-DTPA. Quantitative evaluation demonstrated an improvement in both signal intensity and contrast-to-noise ratio with Gd-BOPTA. Thus, the greater relaxivity of Gd-BOPTA, at lower doses, provides high intravascular signal and may permit improved accuracy in the depiction of carotid artery stenosis. In conclusion, high relaxivity contrast agents appear to be optimal for contrast enhanced MRA of the carotid arteries.

E-18

MultiHance in MRA of peripheral vasculature

P.C. Douek; Lyon/FR

Standard contrast-enhanced MRA of the peripheral vasculature employs a bolus-chase continuous infusion of gadolinium-based contrast agent at 0.3-0.5 ml/s, with a total contrast agent dose of 0.2 mmol per kilogram body weight, combined with moving table.

Recent technological advances in MRA, especially pertinent to imaging the peripheral vasculature, now permit "volume positioning", i.e. the acquisition of images of the body in three overlapping segments oriented to the natural angles of the torso and lower limbs. Other technological approaches to improving image quality include the adoption of a) dedicated coils, e.g. a phased-array coil for imaging the peripheral vasculature and a head coil for imaging the feet, b) tourniquets to reduce venous return, and c) time-resolved MRA sequences, e.g. sensitivity encoding (SENSE), two-dimensional (2D) projections, and 3D time-resolved imaging of contrast kinetics (TRICKS). A fourth approach involves use of the gadolinium-based contrast agent Gd-BOPTA (gadobenate dimeglumine, MultiHance; Bracco Imaging, Milan, Italy) since this agent offers greater imaging efficacy compared to conventional gadolinium chelates, because identical results can be obtained at lower doses: only 20-30 ml Gd-BOPTA are necessary to perform MRA of the entire peripheral vasculature, compared to 40-60 ml of a standard agent. The indications of contrast-enhanced MRA with MultiHance for the peripheral vasculature include: endovascular and surgical treatment planning, post-treatment follow-up, and emergency evaluation (when MR imaging equipment is available in emergency departments).

E-19

MRA in pediatrics

G.K. Schneider; Homburg a.d. Saar/DE

It is particularly important that vascular imaging in the pediatric age group be noninvasive without utilizing ionizing radiation or potentially nephrotoxic iodinated contrast media while at the same time providing precise anatomic and functional information. In children this can be achieved in part by ultrasound. However, to gain a complete overview of the anatomy and of accompanying vascular abnormalities in, for example, complex congenital heart disease, MR angiography (MRA), with its high spatial resolution and free choice of image orientation, is increasingly considered the noninvasive imaging modality of choice. Although unenhanced MRA still plays an important role, contrast enhanced (CE) 3D MRA has largely replaced spin-echo sequences and TOF-angiography for depiction of the vascular anatomy in pediatric subjects.

Vascular abnormalities may be found anywhere in the body although most clinically relevant malformations are found in the thoracic vasculature, comprising the thoracic aorta and its branching vessels, and the pulmonary vasculature.

The imaging protocol in newborns should include T2w and T1w sequences for the cross sectional anatomy and CINE imaging to evaluate flow effects, to quantify the maximum velocity in the great vessels or to evaluate concomitant congenital heart disease. To depict the vasculature with fast 3D gradient-echo sequences the application of Gd-contrast agents is mandatory, despite the fact that such an application is off-label. A principal advantage of Gd-BOPTA in pediatric patients is the potential to obtain high quality images using only a standard dose of 0.1 mmol/kg bodyweight. Moreover, the high relaxivity of this agent is known to be beneficial for the depiction of smaller vessels which is especially important in newborns whose vessels of interest are frequently ≤ 2 mm in diameter.

CE MRA in pediatric patients is a safe, non-invasive and accurate imaging modality for anatomical evaluation of vascular malformations and abnormalities. While sonography, echocardiography and plain film radiography are economic and widely available screening tools, MR imaging is superior in leading to a definitive diagnosis and for pre-therapeutic evaluation of malformations.

Satellite Symposia

12:30 - 15:30

Room F2

organised by GE HEALTHCARE

SY 6

Total imaging solution: Steps toward personalised healthcare

Moderator:

J.G. Blickman; Nijmegen/NL

E-20

New trends in body MR imaging

D. Weishaupt; Zürich/CH

E-21

Contrast enhanced MRA and perfusion imaging (1) Non invasive assessment of carotid stenosis: MRA and perfusion imaging

C. Walter; Trier/DE

E-22

Contrast enhanced MRA and perfusion imaging (2) Optimization of injection rates and sequence parameters in contrast-enhanced MRA

E. de Kerviler; Paris/FR

E-23

Clinical benefits for cardio-vascular acquisition with volume computed tomography (VCT)

J.L. Sablayrolles; St. Denis/FR

E-24

Tomosynthesis: 3D digital radiography

H.P. McAdams; Durham, NC/US

E-25

Breast cancer screening with full-field digital mammography

P. Skaane; Oslo/NO

E-26

Advanced 3D X-ray angiography on large digital flat panel: Clinical benefits during interventional procedures

F.G. Joffre¹, P. Gobert²; ¹Toulouse/FR, ²Buc/FR

14:00 - 15:30

Room E1

organised by SCHERING

SY 7

Ultravist: Two decades of partnership in CT. Answers to current topics

Moderator:

M.F. Reiser; Munich/DE

E-27

The milestones of X-ray contrast media development

U. Speck; Berlin/DE

Past important steps in the development of contrast media (CM) are easily recognised and will be briefly summarised:

1. The concept of enhancing contrast of body cavities and soft tissues by introducing either gas or dense materials which absorb X-rays more efficaciously than natural body constituents immediately after the discovery of X-rays and their use in medical diagnosis.
2. Selection of dense materials like barium, thorium, tantalum, iodine and search for suitable routes of administration.
3. Consideration of tolerance, preference for barium and iodine, first selective angiographic procedures.
4. Development of iodinated organic molecules such as lipiodol as well as the first oral cholecystographic agents and other substances for special indications.
5. Discovery of Uroselectan for intravenous urography.
6. Development of Urograffin, an almost universal CM applied in urography, selective angiography including cardiac and cerebral angiography and finally CT; development of a variety of additional CM for IV cholangiography and myelography.
7. Almost complete substitution of ionic and specific CM by nonionic CM, ongoing substitution of specific contrast-enhanced diagnostic procedures (angiography, urography, myelography, cholangiography) by CT, MR imaging or sonography.

To identify current and future directions of CM development is more difficult. Improvements of the existing nonionic CM will be welcome but won't change the practice of radiology. New CM must result in significant advantages over the currently used products that are efficacious, well tolerated and have very broad indications. The potential benefit of metal chelates, CM with different specificity and CM supporting image-guided therapy will be discussed.

E-28

Higher concentrations: Where does it make sense

J.E. Wildberger; Aachen/DE

Optimized contrast injection is an important issue for good attenuation and high contrast within a CT data set. Contrast media delivery becomes even more important, when using multidetector-row helical CT technique. A shorter imaging time permits a reduction in overall contrast volume; however, adequate total iodine levels must be preserved for certain applications. The faster data acquisition allows for optimization of organ-specific and vascular territory-specific enhancement patterns. Examinations of whole organs in dedicated contrast phases is now technically feasible (e.g. early- and late-arterial phase of the liver). A precise separation of different enhancement phases can be extremely helpful for tumor detection and characterization, especially for hypervasculär parenchymal lesions. To achieve this goal, numerous pharmacokinetic and physiologic parameters have to be considered. The relationships of contrast medium concentration, injection flow rates, injection protocols (mono-, bi-, and multiphasic injection protocols), and injection duration have to be addressed.

A high arterial enhancement is proportional to the flux of iodine: A high iodine injection rate (milligrams of iodine per second) can be realized by a high-concentration contrast medium (milligrams of iodine per milliliter) in combination with high flow rates (milliliters per second) which may be limited by viscosity as iodine concentration surpasses an optimum. The use of double-power injectors has been advocated for automated saline-flushing at the injection site. This issue becomes even more important using fast CT scanning techniques.

Accurate timing of the scanning delay, however, will also be closely linked to individual patient parameters. Therefore, test-bolus methodology and automated bolus triggering are widely used prior to the underlying CT-scan.

CT angiographies, in particular, will benefit from a comprehensive and compact

Satellite Symposia

bolus geometry. High and constant iodine contrast should be maintained throughout the whole data set for uniform vascular enhancement.

The same holds true for dedicated arterial phase CT-imaging of the body.

E-29

Multidetector CT of the kidneys and urinary tract

G. Heinz-Peer; Vienna/AT

Multidetector CT (MDCT) has expanded the utility of CT by improving longitudinal resolution and acquisition speed. In addition, MDCT technology allows for acquisition of different image thicknesses from the same acquisition data set. With MDCT it is possible to subdivide the enhancement phases of the kidney into appropriate time intervals to detect vascular and parenchymal abnormalities. Thin slice thickness in combination with multiplanar reformats and virtual endoscopy techniques is used for detection of small focal lesions of the urinary tract and bladder tumors.

This presentation will emphasize acquisition techniques and circulation characteristics to improve renal and urinary tract lesion detection and characterization. Additionally the utility of MDCT in evaluation of vascular abnormalities of the kidneys and virtual endoscopy techniques of the bladder and urinary tract will be addressed.

E-30

Cardiovascular imaging: First results on a 64 slice scanner

C.R. Becker; Munich/DE

The new 64 slice CT scanner has an improved temporal and spatial resolution compared to any former CT scanner generation. The temporal resolution and the isotropic spatial resolution are now at 165 ms and 0.4 mm, respectively. The investigation of the entire heart lasts about 10 s.

All of these parameters lead to any overall high success rate to perform a cardiac study. The investigation of the coronary arteries is possible with low and high heart rates. However, in patients with high heart rates images reconstructed in the systolic phase are superior to images reconstructed in the diastolic phase. As diagnosis is best been made in the diastolic phase, it is desirable to have a low heart rate when the investigation of the coronary arteries is performed. To achieve this, any patient without contra indications is receiving beta blocker before the investigation.

The short scan time together with a saline chaser bolus allows targeting the administration of contrast media for a selective enhancement of the left ventricular system and the coronary arteries.

Clinically the benefit of coronary CT angiography is the investigation of patients suspected for coronary anomalies and atypical chest pain. In patients with acute chest pain CT angiography may help to rule out pulmonary embolism, aortic dissection and coronary thrombosis.

With the improved spatial resolution it seems to be possible to investigate even patients with extensive calcified atherosclerotic disease and also holds promise to rule out in-stent-stenosis.

E-31

Safety of X-ray contrast agents

A.F. Kopp; Tübingen/DE

X-ray contrast agents are widely used and often the basic requirement of many imaging modalities. They are among the medicinal products with a good safety profile.

Since the introduction of non-ionic X-ray contrast media the rate of adverse drug reactions was reduced. Several substantial large contrast media studies show the better tolerance and safety non-ionic contrast agents with regard to pseudoallergic as well as organotoxic reactions. It remains difficult to determine mortality rates and the incidence of severe contrast media reactions because of the rarity of these events and the difficult assessment of the causal relationship. Adverse reactions to intravascular X-ray contrast agents can be classified into two categories; predictable reactions and unpredictable anaphylactoid reactions.

There are several important risk factors for the intravascular use of iodinated contrast media: e.g. thyroid disease, renal impairment, allergic diathesis, former CM-reaction, dehydration, diabetes mellitus. There are also different prophylactic measures and premedications which are suitable to prevent adverse reactions.

17:45 - 19:15

Room E1

organised by OREX

SY 8

Distributed Computed Radiography (CR): A flexible solution for digital imaging in any radiological environment

Moderator:

D. Devir; Yokneam/IL

E-32

Distributed CR everywhere

J. Koren; Yokneam/IL

E-33

ASCR: Application specific CR

U. Feldman; Auburndale, MA/US

E-34

Revolutionising radiology workflows with CR

J. Sapir, M. Hillit; Yokneam/IL

E-35

Battlefield CR: (M-CR, military CR?)

J. Tucker; Houston, TX/US

E-36

Mammo-CR

V. Gotfried; Yokneam/IL

E-37

Massively scalable PACS

U. Feldman; Auburndale, MA/US

Sunday, March 6, 2005

10:30 - 12:00

Room E1

organised by BRACCO

SY 9

MDCT imaging: New challenges for scan and contrast optimisation

Moderators:

L. Bonomo; Rome/IT

M.F. Reiser; Munich/DE

E-38

New challenges in MDCT: From 16 to 64 slices

M. Prokop; Utrecht/NL

E-39

Scan and contrast administration principles of MDCT

J.P. Heiken; St. Louis, MO/US

The markedly reduced scan durations of multi-detector CT examinations have made scan timing more critical than for single detector CT. At the same time, these short scan times have provided radiologists with an opportunity to improve contrast enhancement with MDCT. It is therefore important for radiologists and technologists to 1) understand the factors that determine both the magnitude and timing of arterial and parenchymal contrast enhancement for CT, and 2) identify the modifications needed to optimize contrast enhancement for 4-row to 64-row MDCT.

Scan Timing

Technical factors: The most important technical factor that affects scan timing is the contrast medium injection duration (1-3), which is determined by the contrast volume and the rate at which it is administered. In patients with normal cardiac output, peak arterial contrast enhancement is achieved shortly after the termination of a contrast medium injection (4). As the contrast medium volume increases, the time it takes to reach the peak of arterial or parenchymal contrast enhancement also increases (5). Conversely, an increase in injection rate results in a shorter time to peak enhancement (5). Therefore, a short injection duration (i.e., low volume and/or high injection rate) protocol results in earlier peak arterial and parenchymal enhancement, which requires a short scan delay. A long injection duration (i.e., high volume and/or low injection rate) protocol results in later peak enhancement, requiring a long scan delay.

Patient-related factors: The most important patient-related factor that affects scan timing is cardiac output (6). Decreased cardiac output results in delayed arrival of the contrast bolus in the aorta, which results in delayed arterial and parenchymal enhancement. Because of variation in cardiac output among patients, it is important to individualize the scan delay for CT angiography studies, in which scan timing is critical. Scan delay can be individualized by using a test bolus (7, 8) or a bolus tracking software program (9). When using the test bolus method, calculation of the scan delay must be modified depending on the speed of the MDCT scanner being used. With 8- and 16-row MDCT, an additional delay must be added to the contrast arrival time in the aorta, if no change is made to the contrast administration protocol. The shorter the scan duration, the longer the additional delay needed to insure that imaging takes place during the peak of aortic enhancement. With 8- and 16-row MDCT, however, one can take advantage of the very short scan durations by reducing the volume of contrast medium administered.

Contrast Enhancement Magnitude

Technical factors:

Arterial enhancement:

The magnitude of arterial enhancement is determined by the rate of iodine delivery into the vascular system. The iodine delivery rate depends upon three factors: 1) contrast medium concentration, 2) injection rate, and 3) contrast medium volume (primarily through recirculation). Increases in contrast medium concentration (10), injection rate (1, 11) and volume (10) all result in increased arterial enhancement. Use of higher iodine concentration contrast material produces greater magnitude of aortic contrast enhancement, even if total iodine dose and injection rate are unchanged, by virtue of increasing the rate of iodine delivery into the

vascular system. When contrast medium volume is reduced for CT angiography with 8- and 16-row MDCT, increased injection rate and high contrast medium concentration can compensate for the somewhat decreased magnitude of aortic enhancement achieved with the smaller contrast medium volume.

Hepatic parenchymal enhancement:

Hepatic parenchymal enhancement is determined by the total iodine dose administered (3, 12-18), which in turn is determined by the contrast medium volume and concentration. Use of higher iodine concentration contrast material improves hepatic parenchymal enhancement to the extent that it increases overall iodine dose (19). Injection rate plays a much more limited role in the magnitude of hepatic parenchymal contrast enhancement.

Although a rapid injection rate (e.g., 5 ml/sec) does not increase the magnitude of hepatic parenchymal enhancement compared with an intermediate injection rate (e.g., 2-3 ml/sec), use of a rapid injection rate increases the magnitude of hepatic arterial enhancement and separates the peaks of hepatic arterial and hepatic parenchymal enhancement (1), thus improving detection of hypervascular liver masses (20). Similarly, a rapid injection rate increases pancreatic parenchymal enhancement (21, 22). Therefore a rapid injection rate is useful for dedicated hepatic and pancreatic imaging protocols. Use of higher concentration contrast material increases tumor to liver contrast of hepatocellular carcinomas during the arterial phase of enhancement, and therefore also is useful for detecting hypervascular liver masses (23).

Patient-related factors: The most important patient-related factor that affects the magnitude of both arterial and hepatic parenchymal contrast enhancement is body weight (14, 24), which is related inversely to the magnitude of enhancement. In larger patients, less contrast enhancement is achieved for a given administered contrast dose compared with smaller patients. Therefore, when imaging large patients, one should consider modifying the contrast administration protocol by increasing the contrast medium concentration, volume or injection rate.

Saline Flush

Use of a saline flush immediately after contrast medium injection has several advantages. It increases peak aortic enhancement by 1) pushing into the cardiovascular system contrast material that otherwise would be left in the injection tubing and 2) improving bolus geometry by limiting contrast medium dispersion. Thus when a saline flush is employed, one can achieve an equivalent magnitude of contrast enhancement with a smaller contrast medium volume (25-27). An additional advantage of saline flush is that it minimizes streak artifact from dense contrast material in the brachiocephalic vein and superior vena cava on thoracic CT examinations (25, 26).

E-40

How to design injection protocols for MDCTA

D. Fleischmann; Stanford, CA/US

Continuous evolution of MDCT technology requires that contrast medium (CM) injection strategies for MDCT are regularly adopted to the increasingly faster acquisition speeds. The foundation for the development of optimal injection protocols is knowledge of the physiologic and pharmacokinetic principles of arterial enhancement.

The key-rules of early arterial contrast medium dynamics are: (§1) arterial enhancement is directly proportional to the iodine administration rate (iodine flux), and can be controlled by the injection flow rate and the iodine concentration of the contrast medium. (§2) arterial enhancement continuously increases over time with longer injection durations, due to the cumulative effects of bolus broadening and recirculation. Thus, increasing the injection duration also improves vascular opacification. (§3) the strength of an individual's enhancement response to intravenously administrated CM is controlled by cardiac output and central blood volume, and correlates with body weight.

In CTA, any of the following strategies can be employed alone or in combination to achieve adequate arterial enhancement in spite of short acquisition times: Increasing the injection rate, using higher concentration CM, or increasing the injection duration (and scanning delay) relative to the scan time. For long scan times (~30 s) biphasic injections - with initially increased flow-rates - improve the uniformity of arterial enhancement over time. Both, injection volumes and flow rates should be adjusted to body weight, at least for patients ≤ 60 kg and ≥ 90 kg BW.

Rationally designed injection protocols based on physiologic concepts allow optimal CM utilization and taking full advantage of the technical capabilities offered by modern MDCT scanners.

E-41

Optimized imaging of pulmonary embolism

M. Tillich; Graz/AT

Pulmonary embolism (PE) is a common disease with considerable mortality. Therefore, early and accurate diagnosis is important. There are no specific signs or symptoms of PE, the diagnosis relies on imaging tests. The development of multi-row-detector computed tomography has led to an improvement in the diagnosis of PE due to faster scanning and improved spatial resolution along the longitudinal axis of the patient. Aside from fast scanning and thin collimation, optimal arterial attenuation remains one of the most crucial determinants of sufficient depiction of the pulmonary arteries. Arterial attenuation over time is generally determined by iodine flow concentration, which may be increased either by raising the contrast material flow rate, and/or by using a high iodine concentration contrast material.

Currently four-to sixty-four-row detector scanners are available. The scan duration necessary for imaging the whole thorax ranges from about 20 seconds with a four-row detector scanner to about 5 seconds with a sixty-four-row detector scanner. The collimation ranges from 0.5 mm to 1 mm depending on the scanner used. This enables the most detailed display of the pulmonary arteries.

The data acquisition is obtained during the plateau phase of contrast material enhancement. Bolus triggering devices are a valuable tool for accurate timing of scanning. The administration of the contrast material bolus is performed using a power injector at a flow rate of about 4 mL/sec. A saline flush immediately after contrast material administration avoids pooling of the contrast material in the arm veins and in the injection system and reduces perivenous artifacts in the superior vena cava. Based on the findings of a study we have recently performed, the use of a high concentration contrast material (such as Iomeprol 400 mgI/mL) significantly improves attenuation of the pulmonary arteries leading to a better visualization of subsegmental and lower order pulmonary arteries in multi-row-detector-CTA of the pulmonary arteries. In addition, the higher attenuation may improve the conspicuity of emboli within the pulmonary arteries.

E-42

Advances in imaging protocols for cardiac MDCT

A.F. Kopp; Tübingen/DE

Examination of the function, perfusion, and viability of the heart muscle as well as of the morphology and function of the coronary arteries is of utmost importance in the diagnostic assessment of coronary artery disease. The current gold standard to assess the degree of stenotic artery disease is coronary angiography. In Germany alone, the total number of angiographic procedures rose by 45% from 1995 to 2000, while the fraction of interventional procedures remained almost constantly low at about 30%. Although coronary angiography has become a safe procedure with only a small risk associated, the inconvenience for the patient as well as the economic burden have fueled the quest to find an alternative, non-invasive method to visualize and assess coronary arteries. The results of MDCT coronary angiography in the detection and quantification of coronary lesions with 4-row and 16-row technology obtained so far from different centers are encouraging: CTA of the coronary arteries yielded a sensitivity of 75-90%, a specificity of 90-95%, a positive predictive value of 0.7-0.9, and a negative predictive value of 0.8-0.9 for detection of hemodynamically significant stenoses in the major segments of the coronary arteries.

Ropers et al. analyzed coronary stenoses in 16-row coronary MDCTA with a reference diameter down to 1.5 mm, thus covering all lesions that may be potential targets for revascularization. Both motion and calcification rendered fewer arteries (12%) unevaluable than in most previous studies and a high sensitivity (92%) and specificity (93%) for the detection of coronary stenoses was achieved. Nieman et al. demonstrated similar results with a sensitivity, specificity, and negative predictive value of 95, 86 and 97%, respectively, in a comparable patient population using the same 16 slice CT technology. However, their analysis was restricted to the major branches with a vessel size > 2 mm. Striking about this study was that only 7% of all coronary branches were poorly assessable.

Recently new 64-slice scanners became available. With this technology a comprehensive view of the heart and coronary arteries with submillimeter resolution in 5 seconds is now feasible. The coverage possible helps reduce beat-to-beat variability resulting in more robust, repeatable procedures, greater vessel visualization and shorter breath holds for sick patients. The increased scan speed allows to rule out (or in) the three most life-threatening critical conditions in chest pain in one single scan - aortic dissection, pulmonary embolism and coronary artery disease by acquisition of an entirely ECG-gated thorax study.

E-43

Abdominal MDCT: Protocols and contrast considerations

T.J. Vogl, R.M. Hammerstingl; Frankfurt a. Main/DE

Abdominal imaging in MDCT: Since its clinical introduction in 1991, volumetric CT scanning has resulted in a revolution for diagnostic imaging. Spiral CT has improved over the last years with faster gantry rotation, more powerful X-ray tubes, and improved interpolation algorithms, but the greatest advance has been the recent introduction of multi-detector computed tomography (MDCT). Currently capable of acquiring 64 channels of helical data simultaneously, MDCT scanners have achieved the greatest incremental gain in scan speed. Fundamental advantages include substantially shorter acquisition times, creation of thin sections on a routine basis in a single-breathhold technique, retrospective calculation of thinner or thicker sections from the same raw data, and improved 3D-postprocessing techniques.

This results in an improved detection as well as depiction of tumorous tissue, relating to aspects of tumor size and to tumor/surrounding tissue contrast ratio. Enhancement characteristics described with multiphasic scanning as well as thinner reconstructed sections allow an improved diagnosis in MDCT imaging of the abdomen.

Protocols in MDCT of the abdomen: Detection of lesions of the abdomen is determined by conspicuity and is related to the degree of tumor-to-tissue contrast. As known tumor characterization is mainly based on the lesion contrast uptake at the different enhancement phases and scanning in sufficient phases is absolutely mandatory.

During the early arterial phase (20 sec post start of injection) there is avid enhancement in the arterial vessels but relatively little enhancement of the parenchyma or hypervascular lesions. Accurate CT-angiography with optimal vessel opacification can be performed in presurgical evaluation.

In the late arterial phase or portal vein inflow phase, which occurs approximately at 30-35 sec post injection, solid neoplasms will be maximally enhanced, whereas the parenchyma will be only minimally enhanced due to predominantly portal venous supply. Therefore this phase is optimal for detection of hypervascular primary liver tumors and metastatic infiltration. The pancreatic parenchymal phase begins at 40-45 sec post injection and provides highest rates of enhancement of the pancreatic parenchyma.

The phase of portal venous dominance, the hepatic venous phase or portal venous phase or hepatic parenchymal phase occurs 60-70 sec post start of injection with maximum enhancement of the hepatic and still high values in pancreatic parenchyma. The detection of relatively hypovascular tumors, such as colorectal metastases or adenocarcinoma of the pancreas, is permitted, which may be unsuspected and in some cases poorly imaged during the other two phases.

For an elective diagnosis of the colon cleansing, distension, endoluminal contrast and spasmolytics are mandatory. A very thin-sliced protocol starting appr. 60 sec post injection with medium flow velocity is the optimal imaging protocol. Post scanning the colon can be assessed in 3D by using multiplanar reconstruction combined with endoscopic views.

Contrast considerations: Having early contrast dynamics in mind it is obvious, that the traditional concept for abdominal imaging, where the injection duration equals the scanning duration cannot be used without modifications. To ensure adequate vessel opacification as well as soft tissue imaging with fast MDCT acquisitions, the iodine administration rate needs to be increased. This can be achieved either by an increase of injection flow rate or -more conveniently- by using a higher iodine concentration of the contrast medium (400 mgI/mL). Data from several clinical trials provided higher contrast densities values of vascular structures as well as hepatic and pancreatic tissue enhancement and moreover of hypervascular tumors in arterial phase imaging using a high concentration contrast medium.

Conclusion: MDCT scanning times may vary substantially in daily clinical routine use depending on the scanner type and therefore acquisition parameters have to be modified. To ensure adequate vessel opacification as well as optimal detection as well as classification of depicted abnormal soft tissue with fast MDCT acquisitions, the iodine administration rate needs to be increased. This can be achieved either by an increase of injection flow rate or -more conveniently- by using a higher iodine concentration of the contrast medium. These agents produce better enhancement of vascular structures and improved overall display of soft tissue tumors.

Satellite Symposia

10:30 - 12:00	Room F1	16:00 - 17:30	Room E2
organised by GE HEALTHCARE		organised by SIEMENS	
SY 10 Contrast-induced nephropathy: Prevalence, consequences, and practical strategies for risk reduction in clinical practice <i>Moderator: P. Aspelin; Huddinge/SE</i>		SY 12 Advances in head and neck imaging using CT and MR <i>Moderator: B. Montag; Erlangen/DE</i>	
E-44 Contrast-induced nephropathy: Patient demographics and risk <i>M. Tepel; Berlin/DE</i>		E-52 Head and neck imaging with 64 slices <i>E.P. Lindell; Rochester, MN/US</i>	
E-45 Primary prevention of CIN <i>N.H. Lameire; Gent/BE</i>		E-53 Subtraction CTA in head and neck imaging <i>B.F. Tomandl; Erlangen/DE</i>	
E-46 Algorithms for prevention and management of CIN <i>T. Gleeson; Dublin/IE</i>		E-54 Clinical applications of isotropic high resolution 3D imaging with SPACE <i>G. Leroux; Liège/BE</i>	
E-47 Strategies and protocols for managing high-risk patients <i>M. Downes; Canterbury/UK</i>		E-55 Clinical applications of high resolution spectroscopy imaging <i>E.-M. Law; New York, NY/US</i>	
12:15 - 13:45	Room E2	17:45 - 19:15	Room F1
organised by PHILIPS		organised by IMAGING DIAGNOSTIC SYSTEMS	
SY 11 Breakthrough applications in CT/MR imaging <i>Moderator: G. Winkels; Best/NL</i>		SY 13 CT and 3D absorption and fluorescence optical molecular imaging of human breast cancer <i>Moderator: E.N.C. Milne; Plantation, FL/US</i>	
E-48 3.0 Tesla cardiac imaging <i>G. Ligabue; Modena/IT</i>		E-56 CTLM and mammography <i>T.H. Helbich; Vienna/AT</i>	
E-49 Panorama 1.0 T open MR and its clinical outcome <i>F. de Graaf; Best/NL</i>		E-57 CTLM and MR imaging <i>A. Pöllinger; Berlin/DE</i>	
E-50 CT colonography: Are we ready for clinical routine? <i>A.J. Aschoff; Ulm/DE</i>		E-58 Contrast enhanced optical imaging of the breast: Status and future prospects <i>C. Bremer; Münster/DE</i>	
E-51 New challenges in MDCT from 16 to 64 channels <i>M. Prokopp; Utrecht/NL</i>		Optical imaging techniques, particularly in the near infrared (NIR) range, offer high signal to noise ratios and efficient tissue penetration in the breast. With the advent of new optical contrast agents sensitive tumor detection can now be envisioned. Perfusion type fluorochromes can help to visualize tumor physiology such as angiogenic activity. Moreover, with the increasing understanding of the molecular basis of diseases a variety of new targets have been unravelled which may help in the future to (a) detect breast cancer earlier, (b) non-invasively grade breast cancer and (c) help monitoring of treatment response. 'Target-specific' contrast agents consisting of an affinity ligand (e.g.: antibody fragment, peptide) linked to a fluorochrome can help to detect these structures non- invasively <i>in vivo</i> . The imaging of apoptosis or cancer related antigens (e.g. EGF- receptor) can thus be achieved. 'Smart' contrast agents have been developed which undergo enzyme mediated activation and thus offer better SNR's. These 'smart' probes can be exploited to detect cancer related protease activity (e.g. cathepsin-B). Three-dimensional optical imaging technologies will help to resolve these new 'molecular beacons' <i>in vivo</i> .	

Satellite Symposia

E-59

Benign angiogenesis

E.N.C. Milne; *Plantation, FL/US*

Monday, March 7, 2005

12:15 - 13:45

Room E2

organised by BRACCO

SY 14

Highlights on contrast ultrasound in clinical practice

Moderator

T. Rettenbacher, *Innsbruck/AT*

E-60

Our experience using contrast enhanced ultrasound for uncharacteristic focal liver lesions

T. Rettenbacher; *Innsbruck/AT*

Gray-scale US is usually the first imaging modality, if diffuse or focal liver disease has to be confirmed or ruled out. It is a highly accurate method in characterizing focal liver lesions, especially if the lesions are small hemangiomas or cysts which usually have a specific appearance. However, quite frequently focal lesions appear uncharacteristic at gray-scale US, especially in steatotic livers. In such cases the established subsequent procedure is contrast-enhanced multi-phase Spiral CT or contrast-enhanced MR imaging. If conventional US of focal liver lesions fails to show specific patterns, contrast-enhanced US would be of great interest for several reasons. The lesions dynamic contrast behaviour could be evaluated for further characterization saving additional CT or MR imaging. The topographical correlation of lesions from US to CT or MR imaging would not be necessary. Furthermore, it would be convenient for patients, gaining the definite diagnosis at once.

We could show that contrast-enhanced US with SonoVue® (Bracco Imaging SpA) in cases of uncharacteristic focal liver lesions was confidently diagnostic in 72% in comparison to 56% in multi-phase Spiral CT. Even in cases of very small liver lesions (< 10 mm) contrast-enhanced US proved to be superior to CT - 50% in US versus 30% in CT.

Our experience shows that in the majority of cases of uncharacteristic focal liver lesions contrast-enhanced US may replace additional CT or MR imaging. Several studies performed by other investigators showed that contrast-enhanced liver US can reveal significantly more metastases in patients with known malignancies than conventional US. Even metastases not detected on multi-phase Spiral CT could quite often be demonstrated. However, it still remains controversial if CT or MR imaging can be replaced entirely if liver metastases have to be ruled out.

Finally, another well examined indication of contrast-enhanced US with SonoVue is chronic liver disease with hepatocellular carcinoma before treatment, after ablation and for follow-up.

E-61

Ultrasound contrast agents: The impact of EFSUMB guidelines in clinical practice

R. Lencioni; *Pisa/IT*

Worldwide, ultrasound is the most commonly used liver imaging modality. Unfortunately, it has limited sensitivity in the detection of small tumor nodules. In addition, ultrasound findings are often nonspecific, as there is enough variability and overlap in the appearance of benign and malignant liver lesions to make a definite distinction problematic. Recently, the introduction of microbubble contrast agents and the development of contrast-specific techniques have opened new prospects in liver ultrasound. Over the past few years, several reports have shown that contrast ultrasound can substantially improve detection and characterization of focal liver lesions with respect to baseline studies. The advent of second-generation agents and low mechanical index real-time scanning techniques has been instrumental in improving the easiness and the reproducibility of the examination. With the publication of the guidelines for the use of contrast agents in liver ultrasound by the European Federation of Societies for Ultrasound in Medicine and Biology (EFSUMB), contrast ultrasound enters into clinical practice. The guidelines define the indications and recommendations for the use of contrast ultrasound in focal liver lesion detection, characterization, and follow-up after tumor ablation procedures. In this presentation, the impact of EFSUMB guidelines into diagnostic protocols currently adopted in liver imaging will be discussed with regard to the following clinical situations: (1) characterization of focal lesions of

Satellite Symposia

incidental discovery; (2) early diagnosis of hepatocellular carcinoma in patients with hepatic cirrhosis; (3) detection of liver metastases in oncology patients; and (4) assessment of the local effect of percutaneous tumor ablation procedures.

E-62

Quantification of enhancement in contrast ultrasound: A tool for monitoring of therapies in liver metastases

M. Krix; Heidelberg/DE

Ultrasound techniques are presented using the contrast agent SonoVue® (Bracco, Italy) for microvascular imaging of liver metastases and for the detection of treatment-related changes in tumour perfusion.

Technical requirements and examination protocols for contrast-enhanced ultrasound (CEUS) in the detection of microvascularity are described. Procedures for the quantitative analysis of perfusion in follow-up examinations are explained. Compared to contrast-enhanced computed tomography, low-MI (mechanical index) CEUS with SonoVue® better reflected the arterial perfusion of liver metastases. Changes of tumour perfusion after stereotactic radiotherapy or chemotherapy of liver metastases could be sensitively detected using CEUS. In addition, possible changes of the liver perfusion after therapy could be assessed. Replenishment kinetics of the contrast agent allowed for a quantitative analysis of the arterial and portal venous perfusion in the tumour and the liver tissue. CEUS is a promising method to non-invasively monitor systemic or local-ablative therapies of liver metastases by sensitively detecting changes of tumour perfusion.

E-63

The use of contrast enhanced ultrasound in renal transplants: First results and potential clinical benefit

T. Fischer; Berlin/DE

Purpose: We performed a study to investigate whether it is possible to adequately diagnose rejection after kidney transplant by evaluating the arterial inflow of an echo enhancer.

Patients and methods: So far, 50 patients underwent US examination with an echo-enhancer (1.6 ml SonoVue, Bracco-Altanapharma) 5 to 7 days after kidney transplantation. The examinations were performed using the Aprio US system (Toshiba) with a 3.5-MHz transducer and contrast harmonic imaging (MI 0.1). Contrast medium (CM) inflow was determined by means of the time-intensity curve (TIC) software. An acute rejection quotient (ARQ) was defined as: slope interlobar artery / slope renal cortex. Findings in patients with large perirenal hematoma ($n = 6$), were compared with the results in the remaining patients.

Results: In 28 patients with an uneventful clinical course US demonstrated a uniform inflow of the CM. The slopes were comparable for the interlobar artery and renal cortex with an ARQ of 1.1 ± 0.5 (nonrejection group, NRG). In fourteen patients with histologically confirmed acute rejection on day 5 to 7 after transplantation (rejection group, RG) the slopes of the CM inflow curves were comparable to those of the NRG for the interlobar artery (9.4 ± 3.6 intensity units/sec vs 11.4 ± 5.6 intensity units/sec) and less pronounced for the renal cortex (4.4 ± 3.4 vs 9.8 ± 4.7 intensity units/sec).

The ARQ was twice as high in the RG (2.1 ± 0.4 , $p < 0.05$) as in the NRG (1.1 ± 0.5). The 6 patients of the hematoma group likewise had a higher ARQ (1.5 ± 0.5 , $p > 0.05$).

Conclusions: The use of echo enhancers has a potential for the early and standardized diagnosis of acute kidney graft rejection. US not only identifies perfusion loss but also provides information on the effect of a large perirenal hematoma on kidney perfusion.

E-64

Value of contrast enhanced ultrasound in rheumatic disease

A. Klauser; Innsbruck/AT

Purpose: Ultrasound (US) has proven to enable earlier detection of inflammatory changes in rheumatic disease than radiography, by delineation of synovial proliferation and early erosions. Color/Power Doppler US is further of value in the assessment of disease activity by depiction of vascularity. Contrast enhanced US (CEUS) is known to improve detection of vascularity by improving the signal to noise ratio. Sensitive detection of vascularity has impact in disease activity assessment in rheumatic diseases. Aim of this presentation is to demonstrate the value of CEUS for detection of inflammatory activity in rheumatic joint and tendon disease.

Methods and Materials: CEUS is performed by intravenous administration of 4.8-mL of SonoVue® (Bracco, Milan, Italy), flushed with 10 mL saline. For Color/

Power Doppler CEUS, continuous infusion (1 ml/min) is preferable to reduce blooming artifacts and allowing for 15 -20 minutes examination time. For gray scale CEUS, which further improves contrast and spatial resolution, bolus administration allows objective quantitative assessment of different parameters (time intensity curves, maximum peak enhancement,) when techniques such as "contrast tuned imaging" CNTI™ (Contrast Tuned Imaging) and CTET™ (Contrast Tissue Enhancement Imaging) (Esaote Biomedica, Genoa, Italy) are used.

Results: Using CEUS improved detection of vascularity can be obtained in early disease and in therapeutic follow-up compared to unenhanced US.

Conclusion: CEUS opens new horizons in rheumatological imaging allowing for sensitive detection of disease activity with a good availability in daily routine. Sensitive monitoring of decreasing vascularity is mandatory in therapeutic follow-up, as full remission is a definite aim in treating rheumatic disease.

Keywords: Contrast enhanced ultrasound - ultrasound contrast agent - rheumatic disease - inflammatory activity.

14:00 - 15:30

Room E1

organised by PHILIPS

SY 15

Open PET/CT imaging in diagnosis and treatment

Moderator:

M. Egger; Geneva/CH

E-65

PET/CT: A major advance

G. Cook; Surrey/UK

E-66

Diagnostic multimodality imaging of cancer beyond PET/CT

H. Hendl; Copenhagen/DK

E-67

Using Gemini PET/CT information to optimise radiotherapy treatment planning with Pinnacle

F. Jacobs; Gent/BE

E-68

Recent advances in molecular imaging technologies

Y. Haemisch; Böblingen/DE

14:00 - 15:30

Room F1

organised by PHILIPS

SY 16

Latest advances in musculoskeletal and nerve ultrasound

Moderator:

J. Walchenbach; Böblingen/DE

E-69

Ankle/foot ultrasound and ultrasound guided musculoskeletal interventions

A. Grainger; Leeds/UK

E-70

Nerve ultrasound: A new application

G. Bodner; Innsbruck/AT

F

Authors' Index

Authors' Index

A

Abdala N., Nascimento R.D., Carrete Jr. H., Nogueira R.G., Goldman S.M., Szeinfeld J.
Diffusion tensor fraction anisotropy in the cervical spinal cord. Reproducibility in 10 normal subjects, C-0881

Abe T., Frericks B.B., Nashan B., Ohgiya Y., Gokan T.
Preoperative surgical estimation of the portal venous based territories compared to the surgical planning landmark to the right of the middle hepatic vein, C-0010

Abe T., Frericks B.B., Nashan B., Ohgiya Y., Gokan T.
3D modelling of portal and hepatic venous analysis of the liver in living donor liver transplantation based on multi-detector row CT, C-0011

Abolmaali N.D., Schiemann M., Hietschold V., Koch A., Kleine P., Vogl T.J.
MR flow measurements in the coronary arteries before and after aortic valve surgery: Initial results (SS 1403), B-650

Abolmaali N.D., Schiemann M., Hietschold V., Koch A., Kleine P., Vogl T.J.
MR flow measurements in the coronary arteries: First results in patients without coronary artery disease (SS 1403), B-655

Abolmaali N.D., Esmaeili A., Schmitt M., Hofstetter R., Vogl T.J.
Visualization of the coronary arteries in children: A comparison between 2 MR sequences (SS 1512), B-749

Acquafresca M., Mazza E., Toccafondi F., Zini M., Sali L., Vannini C., Falchini M.
Vascular complications of biliary interventional radiology, C-0620

Adam E.J.
Radiological approach to stage head and neck squamous cell carcinoma: A. What the clinician needs to know and why (RC 408), A-072

Adam A.
Percutaneous access to the abdomen: B. Biliary drainage (WS 1609), A-386

Adams J.E.
Osteoporosis and osteopenia: A. Acquired osteoporosis (RC 510), A-101

Afaq A.
Radiofrequency ablation in the management of colorectal liver metastases, C-0646

Aguilar M., Gomez-Dermitt V., Landeras R., Ruiz-Hernandez P., Zubietta P., Fernandez-Echevarria M.A.
High-resolution US to evaluate post-surgical peripheral nerve lesions, C-0713

Ahuja G., White L., Wang X., Foos D.H.
Investigation of magnification in digital radiography and validation of an automatic magnification calibration method, C-0979

Aiani L., Ballarati C., Soprani M., Frattini T., Belloni G., Martegani A.
Follow-up of aortic percutaneous endoprostheses with contrast enhanced ultrasound (CEUS) performed at low mechanical index (MI) and with a second generation contrast agent, C-1066

Ajaj W., Goehde S.C., Kuehle C., Papanikolaou N., Forsting M., Barkhausen J., Lauenstein T.C.
Real-time high-resolution MR imaging for the assessment of gastric motility disorders (SS 1801a), B-813

Akhmetov Y.A., Potseluyev D.D., Jakupov V.A., Mussagaleev D.T., Gorgots O.V.
Endovascular embolization of multiple arteriovenous fistulas of extremities, C-0602

Akino N., Tsujioka K., Takahashi Y., Niwa M., Uebayashi Y.
Understanding ECG gated reconstruction by scanning diagram, C-0273

Alabau G., Irurzun J., Gil S., De España F., De la Iglesia P., Verdu J.
CO₂ wedged hepatic venography in patients with portal hypertension: Our experience, C-1050

Alabiso M., Marano I., Morace F., Bonavolonta' N., Penza G.
Contrast-enhanced transabdominal US with 2nd generation contrast medium and multislice CT in Crohn's disease: A preliminary report, C-0144

Albrecht T.
Contrast media for MRI and US liver imaging: C. Bubbles for US liver imaging (RC 106), A-041

Albrecht T., Skrok J., Basilico R., Jenett M., Oldenburg A., Hohmann J., Wolf K.
Characterisation of focal liver lesions with SonoVue: Update with blinded off-site reading (SS 1401b), B-604

Alegre M.I., Talens A., Ferrer S., García R., Artigues I., Batista A.
Isolated iliac artery aneurysms: An infrequent pathology with effective endovascular treatment, C-0606

Aleksic M., Matoussevitch V., Heckenkamp J., Krüger K., Gawenda M., Brunkwall J.
Changes of blood flow during carotid endarterectomy evaluated by transit-time flowmeter measurement (SS 715), B-456

Alexopoulos D., Filippidou A., Theotokas I., Plagou A., Faitaki S., Leli D., Stefanaki A., Zoumpoulis P.S.
The value of contrast enhanced US imaging in the reduction of TRUS-guided biopsies and minimization of complications: Impact on prostate cancer detection, C-0399

Alhajeri A.A., McKenna D.A., Murphy J., Roche C.
Imaging findings of small bowel tumors on MRI enteroctysis, C-0111

Aliev M.A., Jakupov V.A., Akhmetov Y., Tayev A.M., Kassymov B.Z., Serikova S.E.
Diagnosis of abdominal aortic aneurysms, C-1036

Alkadhi H., Leschka S., Baumert B., Plass A., Bettex D.A., Marincek B., Boehm T., Wildermuth S.
Dynamic cine-mode imaging of the mitral valve with 16-channel MDCT. A feasibility study (SS 1803), B-821

Allen C.
Percutaneous access to the abdomen: C. Interventions in the renal pelvis and ureter (WS 1609), A-387

Allen S.D., Padhani A., Dzik-Jurasz A.S., Glynn-Jones R.
MRI staging of rectal carcinoma, pre and post chemoradiation, with histological correlation, C-0162

Almén T.
History of contrast media: The development of the non-ionic contrast agents (SF 4c), A-079

Alonso A., Viñuela B., Simal J., Relea A., Nieto M., G. Urbón M., Niño C., Louredo A., Robles E.
Sonographic diagnosis of acute intestinal anisakiasis, C-0086

Alonso E., de Lama E., Narvaez J.A., Roca Y., Merino E., Ruiz Osuna S., Lopez-Moreno J.L.
Retroperitoneal sarcomas, C-0507

Alonso A., Noguera J.J., Díaz L., Domínguez P., Martínez-Cuesta A., Bilbao J.I.
Vascular complications in orthotopic liver transplantation (OLT): A pictorial essay, C-0576

Alvarez Linera-Prado J., Escribano Vera J., García Morales I., Pérez García A., Martínez Alvarez R., Gil-Nagel Rein A.
MR and alterations of cortical development, C-0813

Álvarez Luque A., Royo A., Berrocal T., Fernández-Velilla M., Fernández-Zubillaga A., Abelairas J.
The use of magnetic resonance imaging in the evaluation of vascularization of porous ocular implants (SS 1512), B-758

Álvarez Luque A., Acitores I., Ybáñez F., Garzón G., Marín B., Bravo A., Parrón M.
Selective arterial embolisation in the management of massive obstetrics hemorrhagic complications, C-0588

Álvarez Luque A., Berrocal T., de Pablo L., Gutiérrez J., Martín L., Gómez León N.
Imaging of disorders involving the stomach in pediatric patients: A pictorial review, C-0927

Alvey C., Mutch S., Golding S.J.
Radiation dose to the patient in MSCT: What is the impact in practice of moving to 16 slice scanners? (SS 713), B-449

Alvey C., Kennedy S., Ang C., Barlow D., Golding S.J.
The effectiveness of MRI in the non-invasive diagnosis of endometriosis: Can laparoscopy be replaced? (SS 1807a), B-796

Amendolia S.R.
State-of-the-art in information technology: Use of the GRID in medical imaging data management (EF 1), A-119

Amadio F., Pinto A., Niola R., Taliercio G., Maglione M.
Malignant biliary obstruction: Treatment with interventional radiology, C-0614

Ananthasivan R., Fataar S., Derweesh A.
Lymphoma of the colon: The spectrum of radiological changes (SS 201a), B-017

Ananthasivan R., Fataar S., Derweesh A.
Imaging in appendicitis: Ultrasound, CT or neither? (SS 701a), B-361

Andersen J.G., Torvund Å., Tofte T.
CT or plain abdominal X-rays as primary examination of patients with acute abdomen? (SS 701a), B-366

Authors' Index

- Andersson T.**
PACS pitfalls: PACS implementation pitfalls: How to avoid a staff revolt! (SF 9b), A-231
- Andic C., Yilmaz S., Sindel T., Lüleci E.**
The early results of transhepatic hemodialysis catheters (SS 1809), B-869
- Andre J.**
Radiology of the elderly: Dyspnea (SF 9a), A-213
- Andreula C.F.**
Spinocranial infection: A. Cranial viral infection (CC 116), A-036
- Andreula C.F.**
Metastatic disease of the brain and spine: C. Metastatic disease of the spine (CC 1717), A-401
- Angeli E., Venturini M., Maffi P., Bertuzzi F., Secchi A., Del Maschio A.**
Sonographic and histological liver changes induced by intraportal islet transplantation in diabetics (SS 301b), B-176
- Anil Kumar B.C., Doull R.I.**
Comparison of the efficacy of three different anaesthetic regimens for transrectal ultrasound guided prostate biopsy (TUPB) (SS 1507), B-720
- Aniq H., Babar S.A.**
MR features of ankle impingement syndromes, C-0683
- Annamalai G., Campbell C., Duffy P.**
Role of D-dimer and pre-test probability scoring in suspected acute pulmonary embolism, C-0327
- Annibale V., Crinò F., Bosurgi F., Gambaro A., Travaglini F., Carriero A.**
Diagnostic pitfalls in digital mammography using a computerized assisted diagnosis (CAD) system, C-0188
- Anselmetti G.C., Baruzzi F., Bonaldi G., Carpeggiani P., Manfré L., Muto M., Vallone S., Regge D.**
Percutaneous vertebroplasty: A multicenter Italian experience in over 1000 patients (SS 609a), B-283
- Anselmetti G.C., Bonaldi G., Muto M., Carpeggiani P., Manfrè L., Regge D.**
Percutaneous kyphoplasty: Preliminary results with the SKy-Bone Expander a new polymer device (SS 609a), B-286
- Anselmi U., Saiani F., Mascaro L., Gasparotti R., Mardighian D.**
Optimization of an algorithm for the arterial input function evaluation in CT brain perfusion, C-0980
- Ansloow P.L.**
Spinocranial infection: B. Cranial bacterial infection (CC 116), A-037
- Anthopoulou A., Fotopoulos A., Tzovara J., Al Bokhrli J., Siomou E., Mantzios I., Papadopoulou F.**
Comparison of voiding urosonography harmonic imaging using 2nd generation contrast agent with direct radionuclide cystography for the diagnosis of reflux (SS 1812), B-896
- Anzalone N.**
CE-MRA of intracranial vessels (SY 5), E-16
- Anzalone N., Righi C., Politis L.S., Iadanza A., Cadioli M., Scotti G.**
Follow-up of coiled cerebral aneurysms: Comparison of 3D-TOF MRA at 3 T with 3D-TOF and contrast-enhanced MRA at 1.5 T (SS 1511), B-764
- Apelt D., Preim B., Strauss G., Hertel I.**
Image analysis of CT data of the paranasal sinuses for computer-assisted operational planning, C-0379
- Araújo D., de Araújo D.B., Pontes-Neto O.M., Scorsi-Rosset S., Wichert-Anna L., Leite J.P., Sakamoto A.C., Santos A.C.**
fMRI evidence of functionality in polymicrogyric cortex, C-0780
- Arenas B.R., Del Campo L., Barbosa A., Llosa M.A., Caraballo M.**
Imaging findings of biliopancreatic involvement by lymphomas and leukemias, C-0061
- Arisaka Y., Matsusako M., Uemura A., Kobayashi N., Takase M., Terada M., Nakagawa R., Komatsu H., Numaguchi Y.**
Usefulness of three-dimensional rotational angiography following percutaneous vertebroplasty; with special interest on detectability of cement leakage, C-0628
- Arkun R., Gur S., Aydogdu S., Argin M.**
Imaging of advanced articular cartilage disease using 3D SPGR, 3D CISS and proton FSE imaging and arthroscopic correlation (SS 1510), B-688
- Armstrong P.**
Nodules and neoplasms: B. Staging of non-small cell and small cell lung cancer (E³ 920), A-248
- Artiko V., Obradovic V., Petrovic N., Petrovic M., Krivokapic Z.**
Immunoscintigraphy in the management of colorectal carcinomas, C-0153
- Aschauer M., Obernosterer A., Portugaller R.H., Stollberger R., Raith J., Ebner F.**
3D-Gd-enhanced MR angiography (MRA) for diagnosing venous thrombo-embolic disease: One-stop-shop imaging of pulmonary arteries, vena cava, pelvic and both lower extremity veins in 30 minutes (SS 215), B-116
- Aschoff A.J.**
Virtual endoscopy in MDCT (SY 11), E-50
- Athanasiou A., Balleyguier C., Dromain C., Delalage S., Sigal R.**
Role of breast MRI in determining breast as source of unknown metastatic axillary lymphadenopathy (SS 602), B-268
- Avigo C., Carizzoni S., Zampedri M., Cristinelli M.R., Pittiani F., Marconi A., Archiati E.**
Follow-up of thyroid nodules with inadequate cytologic diagnosis (SS 208), B-059
- Avigo C., Cabassa P., Romanini L., Grazioli L., Cristinelli M.**
Hypervascular focal liver lesions: A pictorial essay using SonoVue, C-0404
- Avraham E.**
Towards standardization of hanging protocols for imaging display, C-0354
- Avula S., Thimmarayappa A., Yeong C.**
Embryological correlation of congenital labyrinthine abnormalities, C-0562
- Aw Yeang H., Hurst R., Jackson V., Scutt D., Vinjamuri S.**
The ability of serum prostate specific antigen and Gleason score to predict radionuclide bone scan findings in patients with untreated prostate cancer, C-0489
- Azavedo E.**
Open questions: A. Technology assessment (RC 502), A-108
- Aziz A., Venkatesh S.K., Xiao G., Sim E.K.W., Nowinski W.L., Wang S.**
Electronic thoracic atlas generated from high resolution computed tomography: Use in minimally invasive cardiothoracic surgery planning, C-0375
-
- B**
- Ba-Salamah, Schima W., A., Mehrain S., Puespoek A., Zacherl J., Sedivey R., Prokop M.**
Preoperative TNM staging of esophageal cancer: Comparison of 16-row multidetector CT (MDCT) with endoscopic ultrasonography (EUS) with correlation to the histopathological findings. Preliminary results (SS 201a), B-011
- Ba-Salamah, Schima W., A., Mehrain S., Zacherl J., Puespoek A., Happel B., Sedivey R., Pokieser P., Prokop M.**
Preoperative staging of gastric cancer: Value of hydro-enhanced-multidetector CT in comparison to endoscopic ultrasound and surgical correlation (SS 201a), B-012
- Baba Y., Yamashita Y., Morishita S., Murakami R., Tomitaka E.**
Real-time and interactive remote radiology/radiotherapy conference system using remote desktop software, C-0381
- Babar S.A., Hughes E.K., Willimason R.**
Endometriosis or dermoid: Diagnostic dilemmas, C-0442
- Babar J.L., MacPherson L.K.R.**
A pictorial review of pineal region masses and pathologies in children, C-0905
- Babich Y.F., Nuzhdina M.A.**
Superficial melanoma and its metastases in the eyes of skin electrophysiological imaging (SEI), C-0939
- Bachmann R., Nassenstein I., Stehling C., Niederstadt T., Dittrich R., Heindel W., Kraemer S.**
Prospective evaluation of a comprehensive MR-protocol in patients with suspected cervical artery dissection (CAD) (SS 715), B-458
- Bachmann R., Nassenstein I., Kooijman H., Kugel H., Kuhlenbaeumer G., Kraemer S., Heindel W.**
High resolution MRI of cervical artery dissection (CAD) at 3.0 T with a dedicated surface coil: New insights into the pathomorphology? (SS 1811a), B-900
- Bacigalupo L., Brizzi D., Baio G., Faedda C., Gaggero G., Calabrese M.**
Multislice galacto-CT versus galactography in the evaluation of nipple discharge (SS 202), B-026
- Bacigalupo L., Martinoli C., Morag Y., Jacobson J.A., Miller A.S., Bianchi S.**
Ultrasound of the reflection pulley of the long biceps tendon (SS 1810), B-800
- Bacigalupo L., Soldi E., Bonetto P., Gozzi G., Ganzetti A., Conti G.M.**
Evaluation of the use of Mammotool: An interactive, web-based, educational approach for the interpretation of mammographic studies, C-0219

Authors' Index

Bae I., Lee S., Park K., Kim S., Cha S., Han G.
Radiologic findings of variable diseases involving the orbital apex, C-0533

Baik H., Kwak B., Shim H., Kim Y., Lee J., Song I., Kim K.
A new ischemic model using radiofrequency wire electrode in rabbit hind limb, C-0567

Bajzik G., Egyed M., Karadi E., Kollar B., Rumi G., Rajnics P.
The role of in-phase and out-of-phase magnetic resonance imaging and in vivo ¹H single-voxel magnetic resonance spectroscopy (1H MRS) in the diagnosis of subclinical hepatic encephalopathy (SHE), C-0807

Bakshi D.R., Gould , Powell S., Yeang H., Fewins H.
A pictorial review of anomalies of the thoracic aorta with embryological correlation, C-1062

Baldelli P., Bravin A., Fabbri E., Gambaccini M., Marziani M., Sarnelli A., Taibi A.
Contrast-medium enhanced mammography: A twofold approach (SS 202), B-030

Bale R.J., Petzold R., Nagel M., Voegele M., Kalender W.A., Jaschke W.
A novel navigation systems for percutaneous interventions (IM 1), D-03

Balériaux D.
Spinocranial infection: C. Spinal and spinal cord infection (CC 116), A-038

Balériaux D., Brotchi J., Salmon I., Fang W.
Degenerative disorders, tumors and infection of the spine: B. Tumors of the spinal canal (CC 1617), A-367

Bali M.A., Szantics A., Delhaye M., Metens T., Deviere J., Matos C.
Assessment with secretin-enhanced MR hydrometry of pancreatic exocrine function in patients with obstructive chronic pancreatitis before and after treatment (SS 1001), B-486

Balleyguier C.S., Kinkel K., Perrot N., Morice P., Sigal R.
Imaging of the female pelvis: C. Adnexal lesions characterization and staging (RC 107), A-035

Balzer J.O., Doss M., Thalhammer A., Mack M.G., Moritz A., Vogl T.J.
Emergent endovascular stentgraft implantation for perforated acute type B dissections and ruptured thoracic aortic aneurysms (SS 209a), B-068

Balzer J.O., Fleiter N., Mack M.G., Böcher E., Hamm T., Vogl T.J.
Percutaneous, transfemoral implantation of an IA port system for locoregional chemotherapy in liver metastasis: Long term outcome (SS 1009a), B-506

Bankier A.A.
Smoking-related diseases: A. Emphysema: State-of-the-art (RC 104), A-017

Bankier A.A.
Diagnostic and interventional radiology of transplants: Lung (heart and lung) (part 1) (SF 8b), A-187

Bankier A.A.
Nodules and neoplasms: A. Solitary and multiple pulmonary nodules (E³ 920), A-247

Banys R., Slowik A., Pasowicz M., Ciecko-Michalska I., Irzyk M., Motyl M., Szczudlik A., Bogdal J.

Usefulness of proton magnetic resonance spectroscopy (1H MRS) in the diagnosis of subclinical hepatic encephalopathy (SHE), C-0807

Barentsz J.O.

Imaging of prostate cancer: Present and future:
Imaging of prostate cancer: Present and future (Introduction) (SA 14), A-351

Barentsz J.O.

Imaging of prostate cancer: Present and future:
MRI (SA 14), A-354

Bargellini I., Lazzereschi M., Vignali C., Petrucci P., Cioni R., Zampa V., Bartolozzi C.
Towards the identification of specific anatomic features of the renal artery influencing the results of renal artery percutaneous recanalization (SS 1015), B-558

Barini M., Stecco A., Bruculeri F., Neri P., Fornara P., Carriero A.

Shoulder MR-arthrography in the follow-up after surgery repair: Inter-individual comparison of anterior palpatory and posterior US-guided access (SS 310), B-135

Barini M., Stecco A., Oronzo P., Meloni T., Fornara P., Carriero A.

Shoulder MR Arthrography: Evaluation of anterior access by palpatory guide, C-0707

Barkhausen J.

Assessment of myocardial perfusion and viability:
Role of multidetector CT (SF 12), A-273

Barkhof F.

Radiology of the elderly: Aging and dementia (SF 9a), A-212

Barreau B., Tastet S., Picot V., Henriquez C., Valentin F., Gilles R., Dilhuydy M.

Psychological adjustment of stereotactic breast biopsy instrumentation procedures: About 73 cases, C-0184

Barrera C., Gervas C., San Vicente J., Cabrera A., Izquierdo M., Fernandez E.

Cine-MRI: Morphologic analysis of congenital heart diseases, C-0249

Barsi P.

The present and future of Hungarian radiology:
Contribution of a new generation: Epilepsy patient: The complex neuroradiological approach (EM 2), A-251

Bartal G., Gomori J.M., Gaspar T., Rivlin E., Goldenberg R., Walach E., Peled N.

Computer aided detection of incidental pulmonary nodules in emergency thoracic CT angiography (SS 304), B-168

Bartal G., Breitgand A., Soimu U., Sebie R., Gomori J.M.

Initial clinical evaluation of a monolithic passive-element direct digital (MOPEDD) radiography system for orthopedic imaging (SS 1013), B-540

Bartling S.H., Stoever T., Rodt T., Gupta R., Lenarz T., Becker H.

Flat-panel based volume-CT could overcome current limitations of CT in cochlea implant imaging (SS 608), B-276

Bartolotta T.V., Galia M., Runza G., Mamone G., Comparetto A., Midiri M.

Liver haemangiomas undetermined at grey-scale ultrasound: Contrast-enhancement patterns with SonoVue and pulse-inversion US, C-0027

Bartolotta T.V., Galia M., Mamone G., Runza G., Sorrentino F., Midiri M.

Real-time spatial compound sonography versus conventional US of the Achilles tendon in patients with heterozygous familial hypercholesterolemia, C-0727

Bartolozzi C.

Multi-dimensional imaging for guiding therapy:
Multi-dimensional imaging for guiding therapy (Introduction) (SA 12), A-267

Bartram C.I.

Rectal carcinoma: Staging (SF 4a), A-057

Bassler B., Hartmann D., Pfeifer B., Schilling D., Riemann J.F., Layer G.

Contrast enhanced dark lumen MR colonography in adenomatous versus hyperplastic colorectal polyps (SS 1401a), B-570

Bassler B., Hartmann D., Pfeifer B., Schilling D., Riemann J.F., Layer G.

MR-colonography in incomplete endoscopy of the colon: A prospective study (SS 1401a), B-576

Bastarrika G., Domínguez P.D., Cano D., Pons M.J., Vivas I., González-Crespo I.

Assessment of pulmonary nodules on multi-slice CT (MSCT) of the chest: Impact of computer-aided detection (CAD) in the management of oncology patients, C-0311

Battyány I.

Arterial and venous liver intervention: B. Chemoembolization (WS 418), A-082

Bauer J.S., Kohlmann S., Mueller D., Eckstein F., Lochmueller E., Rummeny E.J., Link T.M.

Multislice-CT-derived trabecular bone structure of the proximal femur: A comparison with BMD in the assessment of osteoporosis (SS 610), B-257

Bauer J.S., Roß C.J., Settles M., Mueller D., Eckstein F., Lochmueller E., Link T.M.

Evaluation of trabecular bone structure with high resolution MRI at 1.5 T. A comparison of spin echo and gradient echo sequences (SS 1510), B-687

Bauer J.S., Patel P.V., Prevrhal S., Phan C., Eckstein F., Lochmueller E., Majumdar S., Link T.M.

Protocol optimization for analysis of trabecular bone structure with multislice spiral CT at the calcaneus for the assessment of osteoporosis, C-0658

Baum U., Lell M., Anders K., Greess H., Bautz W.A.

Influence of different mAs-products on image quality in MSCT of the head and neck region (SS 608), B-280

Baum R.P., Schmücking M., Niesen A., Zherosekov K.P., Rösch F.

Receptor-PET/CT of neuroendocrine tumors using the gallium-68 labelled somatostatin analog DOTA-NOC: First clinical results, C-0408

Baur-Melnyk A.

Whole-body imaging: Metastases (SA 2), A-046

Authors' Index

- Baur-Melnyk A., Buhmann S., Wieser A., Reiser M.F.**
MSCT versus MRI: Diagnostic sensitivity in the detection of spine metastases (SS 1010), B-464
- Bax J.J., Poldermans D.**
Assessment of myocardial perfusion and viability: Ultrasound and nuclear medicine (SF 12), A-272
- Bearcroft P.W.P.**
Shoulder joint: B. Soft tissue mass in the shoulder region: US and MRI (RC 1310), A-311
- Beatovic S.L., Jaksic E., Han R.**
Evaluation of transplanted kidney function by the clearance of technetium-99m mercaptoacetyltriglycine: The comparison between two methods, C-0466
- Beatovic S.L., Obradovic V., Latkovic Z., Jaksic E.**
The role of radioimmunoscintigraphy in the diagnosis and follow-up of primary ocular melanoma, C-0525
- Becker M.**
Salivary glands: B. The value of MR sialography today (RC 108), A-024
- Becker C.D.**
Assessment and accreditation in radiology in Europe: Appraisal and assessment of trainees during training (ER 526), A-139
- Becker C.D.**
Impact of multislice CT on imaging of the upper abdomen: B. Bile ducts and pancreatic ducts (RC 901), A-219
- Becker C.R.**
Coronary vessels: C. MDCT of the coronary arteries (RC 803), A-174
- Becker C.R.**
Cardiovascular imaging: First results on a 64 slice scanner (SY 7), E-30
- Beer A.J., Haubner R., Goebel M., Luderschmidt S., Grosu A., Weber W.A., Rummeny E.J., Schwaiger M.**
Non-invasive imaging of alpha-v-beta-3 expression in patients with malignant tumors using [¹⁸F]GalactoRGD, C-0411
- Beer M.J.**
Neuro-imaging: C. Pediatric MR spectroscopy: Current applications and future prospects (RC 912), A-240
- Beets-Tan R.G.H.**
MR of the colon and rectum: C. MR staging of rectal tumors, problems and pitfalls (RC 101), A-016
- Begemann P.G.C., van Stevendaal U., Manzke R., Stork A., Weiss F., Nolte-Ernsting C., Grass M., Adam G.**
Measurements of spatial and temporal resolution for ECG-gated 16-row multidetector CT using a dynamic cardiac phantom (SS 1803), B-820
- Behrens S., Boskamp T., Bornemann L., Bourquin H., Dicken V., Drexel J., Hahn H.K., Hennemuth A., Hindennach M., Kohle S., Krass S., Kümmelen B., Kuhagen S., Kuhnigk J., Lang M., Link F., Praise G., Preusser T., Rascher-Friesenhausen R., Rexilius J., Schenk A., Schlüter M., Weihusen A., Zidowitz S., Peitgen H.O.**
Computer aided image based diagnosis and therapy planning (IM 1), D-09
- Belan V., Srbecký M., Pruzincová L., Wlachovská B., Moczová J., Andrísová J.**
Assessment of liver iron: Normal values, C-0042
- Belattar C., Ayed A., Duclos Vallee J., Ewenzczyk I., Guettier C., Adam R., Samuel D., Castaing D., Bellin M.**
Primary sclerosing cholangitis: A spectrum of imaging findings with radiologic-histopathologic correlation, C-0007
- Belkind M.B., Sinitsyn V.E., Lyakishev A.A., Naumov V.G., Ternovoy S.K.**
Coronary calcinosis and statin therapy (SS 603), B-304
- Belli P., Magistrelli A., Lombardi R., Franceschini G., Costantini M.**
Breast masses characterization: Use of ACR BI-RADS US lexicon in our experience (SS 1402), B-585
- Belli L., Mentasti M., Poletti Venegoni R.**
Low-field open-MRI study of TMJ (temporomandibular joint) (SS 1814), B-914
- Bellin M., Duclos Vallee J., Ewenzczyk I., Bigot E., Azoulay D., Castaing D., Guettier C., Samuel D., Gilbert L.,**
Value of imaging findings in the detection of recurrent primary sclerosing cholangitis after orthotopic liver transplantation, C-0002
- Bellomi M.**
Imaging of the lymphatic system: The lymphatics: Clinical considerations (SF 4b), A-060
- Bellussi A., Cristofaro M., Rovighi L., De Santis A., Bibbolino C.**
Multislice computed tomography (MSCT) and magnetic resonance Imaging (MRI) in the evaluation of cerebrospinal fluid (CSF) fistulae with rhinorrhea, C-0831
- Ben Achour N., Bouomrani S., Braham R., Hammami S., Salem R., Mahjoub S., Gannouni A.**
Behçet's disease: Rare cardiovascular manifestations, C-1057
- Bermejo A., Herraiz L., Martin M., Benito J., Miralles M., Ramos A.**
The craniocervical junction (CVJ): Anatomy, bony variants and acquired pathology, C-0882
- Bermejo A., Ballenilla F., Herraiz L., Perez M., Miralles M., Martinez A.**
The abdominal plain film in the newborn: How much can we obtain?, C-0913
- Bermudez Bencerrey P., Puig Domingo J., Darnell Martin A., Malet Munté A., Gil Bello D., Martin Olariz A., Prieto Del Rei M.**
US-guided prostate biopsy: Is antibiotic prophylaxis necessary? (SS 1507), B-719
- Bermudez Bencerrey P., Carvajal A., Zauner M., Rovira A., Gil D., Prenafeta M., Lüttich A.**
Trigeminal neuralgia: Imaging of normal anatomy and pathological conditions, C-0792
- Bermudez Bencerrey P., Fortuño Andrés J., Falcó Fages J., Perendreu Sans J., Darnell Martin A., Branera Pujol J.**
Non-renal artery incidental findings in a renal artery stenosis MR protocol: A pictorial essay, C-1029
- Bernathova M., Bodner G., Dünser M.**
Feasibility of second look sonography in clarification of incidental enhancing lesions found on preoperative MRI for breast cancer (SS 602), B-269
- Bernathova M., Dünser M., Rettl G., Bodner G., Zelger B.**
Unusual breast lesions: Radiologic-pathologic correlation, C-0225
- Bernathova M., Gruber H., Bodner G., Schocke M.**
Imaging of musculoskeletal fibromatosis, C-0714
- Bernathova M., Gruber H., Pavelka M., Bodner G.**
Sonographic approach for imaging calf veins: An anatomic study, C-1039
- Bernhardt T.M., Rapp-Bernhardt U., Lenzen H., Esseling R., Roehl F.W., Beyer F., Wall A., Heindel W.**
Detection performance of a portable, large area, indirect flat-panel detector compared with storage phosphor radiography at different exposures in a phantom study (SS 204), B-038
- Berrocal T.**
Emergencies in pediatrics: A. Abdominal distension in the neonate (RC 1612), A-391
- Berry J., Svasti-salee , Satchithananda K., Wilkins J.C., Totman J., Pollard L., Choy E., Elias D.A.**
The ultrasound and MRI appearances of the hand and wrist from a busy rheumatology practice: A pictorial review, C-0705
- Bertolotto M.**
Imaging of focal lesions: Kidney (EM 1), A-148
- Beyer F., Zierott L., Stoeckel J., Heindel W., Wormanns D.**
Computer-assisted detection (CAD) of pulmonary nodules at MDCT: Can CAD be used as concurrent reader? (SS 304), B-166
- Beyer T.F., Iwinska-Zelder J., Dukatz T., Bertalanffy H., Tackenberg B., Sure U., Bien S.**
Pre- and postoperative DTI examination in patients with brainstem cavernoma (SS 1011), B-539
- Beyer T., Martinez M., Sembritzki O., Roberts F., Ziegler S., Kuehl H., Bockisch A.**
Whole-body FDG-PET/CT with extended CT field-of-view for improved oncology imaging (SS 1813), B-924
- Beyer-Jørgensen P., Hartvig Sode A.**
CT: A. CT multitrauma protocol (RC 1614), A-394
- Beyersdorff D., Taymoorian C., Schnorr D., Felix R., Hamm B., Bruhn H.**
MRI of prostate cancer: Comparison of imaging at 1.5 and 3 Tesla (SS 1007), B-491
- Bezzi M.**
Percutaneous access to the abdomen: A. Abscesses drainage (WS 1609), A-385
- Bhat R., Oliver T.B.**
MR arthrography of the shoulder joint: A pictorial review of technique, anatomy and expected range of pathology, C-0682
- Bialek E.J., Jakubowski W., Szczepanik A.B., Maryniak R.K., Bilski R., Prochorec-Sobieszek M., Szopinski K.T.**
Detailed ultrasound study of the angioarchitecture in superficial lymphomatous lymph nodes. Preliminary results (SS 308), B-188

Authors' Index

Bialek E.J., Jakubowski W., Szczepanik A.B., Maryniak R.K., Prochorec-Sobieszek M., Bilski R., Serafin-Krol M.

Ultrasound assessment of superficial lymph nodes (three-dimensional imaging, tissue harmonic imaging and panoramic imaging) intended for diagnostic excision, C-0540

Bianchi S., Martinoli C., Gaignot C.

A practical synopsis of knee cysts imaging, C-0742

Bilbao Jaureguizar J.

Harmonization of training programmes: Myth or reality?: Specific issues for training in a subspecialty (ER 126), A-028

Bilbao Jaureguizar J., Martínez-Cuesta A.

Arterial and venous liver intervention: C. Budd Chiari syndrome (WS 418), A-083

Bilecen D., Ostheim-Dzerowycz W.

Angio-seal vascular closure device for brachial artery access punctures (SS 1409b), B-631

Bilgili M.Y.K., Birchard K., Gerber D., Fırat Z., Braga L., Woosley J., Shrestha R., Semelka R.

Hepatocellular carcinoma missed on gadolinium enhanced MR imaging, discovered in liver explants: Retrospective evaluation (SS 201b), B-041

Binaghi S., Colleoni M., Dehdashti A., Regli L., Uské A.

Multislice CT angiography (MSCTA): A comparison with digital subtraction angiography (DSA) in the postoperative evaluation of clipped aneurysms (SS 1511), B-765

Binokay F., Soyupak B., Akgul E., Soyupak S., Celiktaş M.

Spectrum of imaging findings in genitourinary tuberculosis, C-0515

Bipat S., van Leeuwen M.S., Comans E.F., Pijl M.E., Stoker J.

The role of computed tomography, magnetic resonance imaging and positron emission tomography in the diagnosis of liver metastases: A meta-analysis (SS 301a), B-142

Birchall J.D., Ganatra R.H., Smith R.M., Griffith K., Perkins A.C.

Does CT attenuation correction improve lesion conspicuity in nuclear medicine? (SS 1813), B-925

Bisdas S., Donnerstag F., Weissenborn K., Herzog C., Harth M., Ahl B., Bohrer I., Becker H., Vogl T.

Prediction of the extent of cerebral infarction and assessment of the clinical condition using functional CT perfusion and diffusion-weighted MR imaging in hyperacute ischemic stroke (SS 611), B-311

Bitsch R., Daniels M.D., Rupp R., Bernd L., Ludwig K.

Temperature changes in surrounding soft tissue during CT-guided radio frequency ablation (RFA) of osteoid osteoma in an ex vivo animal model (SS 310), B-139

Bitschnau S., Maksan S.M., Bittinger F., Mildenberger P.

Multislice-CT findings in patients with colonic-diverticulitis: Do they correlate with intraoperative and postoperative immunohistological findings? (SS 701a), B-368

Bizimi V., Manopoulou E., Breitas P., Tsikkini A., Antipa E.S., Bilas K., Noti P., Tsouroulas M., Drossos C.

Emergency extracranial Doppler in diagnosis and monitoring the progress of primary cervicocerebral artery dissection, C-1071

Bizzi A., Blasi V.

Functional MRI: C. fMRI for evaluation of brain plasticity in multiple sclerosis, stroke and trauma (RC 411), A-071

Bjarnason H.

Venous occlusion: A. Deep venous thrombosis (RC 1709), A-424

Björkman-Burtscher I.M.

MR spectroscopy of the brain in clinical practice: B. Clinical applications of MRS: Focal lesions (RC 1311), A-328

Björkman-Burtscher I.M.

Fetal MR imaging: Fetal MR imaging (Introduction) (SF 17), A-405

Bjørnarå B., Gudmundsen T., Dahl O.

Thromboembolic complications after major orthopedic surgery: A 13-year register of 5607 patients, C-0336

Blanc E., Cogollos J., Ripollés T., Martínez M., Monedero M., Pastor-Juan R.

Sonography and CT in duodenal pathology, C-0155

Blancas C., Llauger J., Palmer J., Granell E., Cafete N.

Chondroblastoma: Radiographic and MR features, C-0666

Blickman J.G.

Cross-border eRadiology (SY 3), E-09

Blondin D., Fritz B., Rado Y., Saleh A., Mödder U., Cohnen M.

Impact of different flip angles on in-stent signal intensity in contrast-enhanced MR-angiography (CE-MRA) of current self-expanding stents, C-0984

Blondin D., Rado Y., Fritz B., Saleh A., Mödder U., Cohnen M.

Effect of stent orientation and flip angle on subjectively visible stent lumen in contrast-enhanced MR at 1.0 Tesla, C-1019

Blum A.

Wrist: A. Plain films revisited with MSCT and MRI (RC 910), A-208

Bodewitz S.T., Voormolen M.H.J., Jansen J.M., Schuur K.H., Stuifbergen W.N.H., van Milligen-de Wit A.W.M., Visser L.H.

Contrast-enhanced abdominal CT scan without bowel preparation for detection of colorectal polyps: A prospective comparative study, C-0157

Bodini M., Marini U.P., Fiorentino C., Olivetti L.

Locally advanced breast cancer: Magnetic resonance imaging versus clinical examination, mammography and ultrasonography in evaluation of residual disease after primary chemotherapy, C-0189

Bodner G.

Nerve ultrasound: A new application (SY 16), E-70

Bodner G., Gruber H., Schocke M., Bernathova M.

Radiological imaging of thoracic outlet syndrome, C-1038

Bogaert J.

Cardiomyopathies: A. Hypertrophic cardiomyopathy (RC 403), A-066

Bogner P.

The present and future of Hungarian radiology: Contribution of a new generation: What do we see on diffusion MR images? A lesson learned from model experiments (EM 2), A-250

Bohdorf K.

Musculoskeletal infection: B. Infection in the appendicular skeleton (CC 816), A-199

Bohner G., Stiepani H., Bauknecht H., Klingebiel R.

Assessment of different ischemic compartments using quantitative multi-slice CT perfusion imaging in patients with acute stroke, C-0798

Bohner G., Forstreuter F., Gallatin J., Witthaus H., Stiepani H., Gudłowski Y., Heinz A., Klingebiel R., Juckel G.

Exploring the continuum: 1H-MR spectroscopy in prodromal and first-episode patients with schizophrenia, C-0799

Bokeriya L., Ivanitsky A., Makarenko V., Urpolskaya L., Rychina I.

Evaluation of the abnormal anatomy in infants with double outlet right ventricle with MRI, C-0912

Bolia A.

Endovascular treatment of lower limb vascular occlusion: C. Infrapopliteal lesions (RC 909), A-234

Boll D.T., Merkle E.M., Lewin J.S.

MR-guided percutaneous sclerotherapy of low-flow vascular malformations: Final qualitative and quantitative assessment of therapy and outcome (SS 709), B-406

Boll D.T., Lewin J.S., Aschoff A.J., Gilkeson R.C.

Perfusion abnormalities in congenital and neoplastic pulmonary disease: Comparison of ultrafast MR perfusion and multislice CT imaging, C-0329

Bongartz G.M.

Vascular imaging: A. MRA: Basic principles and clinical applications (RC 1215), A-290

Boniatis I., Costaridou L., Cavouras D., Panagiotopoulos E., Panayiotakis G.

Assessment of hip joint structural alterations in osteoarthritis using image texture analysis, C-0370

Bonneville J., Cattin F.

Base of the skull, hypophysis, supra- and parasellar region: B. Pituitary lesions (CC 1217), A-265

Bonomo L., Urbanik A.

Harmonization of training programmes: Myth or reality?: Examples from the West and the East (ER 126), A-027

Bonomo L.

Imaging of focal lesions: Imaging of focal lesions (Introduction) (EM 1), A-144

Bonomo L.

Alessandro Vallebona - Honorary Lecture: Pulmonary circulation: From old to new imaging modalities (HL 3), A-359

Authors' Index

Boraschi P., Donati F., Gigoni R., Odoguardi F., Neri E., Boggi U., Falaschi F., Bartolozzi C.
Exocrine function of pancreatic transplants: Evaluation with dynamic MR pancreatography after secretin administration (SS 1001), B-483

Boraschi P., Donati F., Gigoni R., Volpi A., Urbani L., Falaschi F.
Biliary strictures following orthotopic liver transplantation: Evaluation with mangafodipir trisodium-enhanced MR cholangiography, C-0402

Borbély K., Nemes L., Ceglédi A., Cserepes É., Bács É., Laki A., Székely G., Barta M., Forrai G.
Acute abdominal hemorrhage and its complications in hemophilic patients, C-0064

Borges A.
Salivary glands: A. Choice of imaging technique in patients presenting with salivary gland problems (RC 108), A-023

Borges A.
Three common neurological problems: Loss of vision, hearing loss, trigeminal and facial nerve palsy: C. Facial nerve paralysis and trigeminal neuralgia (CC 917), A-207

Borgstede J.P.
Teleradiology: Threat or opportunity?: Report of the ACR task force: Legal aspect, US professional last guidelines and international issues (ER 1326), A-338

Both M., Aries P.M., Müller-Hülsbeck S., Jahnke T., Bolte H., Biederer J., Gross W.L., Heller M., Reuter M.

Giant cell arteritis of the upper extremities: Follow-up after treatment with percutaneous transluminal angioplasty (SS 1409b), B-637

Boutry N.
Sports injuries: C. Trauma of the appendicular skeleton (RC 110), A-006

Boutry N., Hachulla E., Flipo R., Cortet B., Cotten A.

MR imaging involvement of the hands in early rheumatoid arthritis: Comparison with systemic lupus erythematosus and primary Sjogren syndrome (SS 1410), B-561

Bogzeyik Z., Kocakoc E., Berilgen S., Ozdemir H., Tekatas A., Ogur E.
Evaluation of the effects of sildenafil citrate (Viagra) on vertebral artery blood flow of patients with vertebro-basilar insufficiency, C-0885

Bozzali M., Falini A., Baglio F., Cercignani M., Farina E., Vezzulli P., Scotti G., Nemni R.
Brain tissue damage in dementia with Lewy bodies: An in vivo diffusion tensor MRI study (SS 311), B-229

Brady A.P.
Assessment and accreditation in radiology in Europe: Revalidation and re-certification of radiologists in Europe (ER 526), A-141

Brancaleone C.M.I., Candia C., Ambrogi C., Blasetti M., Tipaldi L.
High resolution ultrasound (HRUS) in small lesions of the abdominal wall, C-0175

Brassel F., Raabe R., Haupt C., Papke K., Becker H.
Mid-term experience with intracranial stenting (SS 1009b), B-510

Brat H., Bouziane T., Cappeliez O.
CT guided therapeutic spine interventions, C-0632

Brat H., Bouziane T., Cappeliez O., Divano L.
Changes in disc herniations after CT guided percutaneous laser disc decompression (PLDD): MR findings, C-0633

Brat H., Bouziane T., Lambert J., Cappeliez O., Divano L.
Verteboplasty with volumetric CT guidance: Speed, precision and clinical efficiency, C-0647

Brat H., Bouziane T., Cappeliez O.
Benefits of triple slice CT fluoroscopic needle guidance in percutaneous laser disc decompression (PLDD), C-0648

Bravo A., Lamas M., Berrocal T., Allona M., Larrauri J., Gómez León N.
Imaging of duodenal disorders in children and adulthood, C-0097

Bravo A., Martí M., Garzón G., Alvarez Luque A., Rodriguez-Vigil B., Allona M.
Follow-up of the aneurysm neck diameter after endovascular repair of abdominal aortic aneurysms, C-1074

Bray A.
CT-related prognosis in surgically treated bronchial carcinoid tumors, C-0278

Brechtl K., Beyer T., Eschmann S.M., Horger M.S., Vogel M., Bares R., Pfannenberg C.A., Claussen C.D.
IV-contrast enhanced protocols for high-resolution whole-body PET/CT imaging: Optimization of CT-imaging (SS 1406), B-678

Breen D., Stedman B., Rutherford E., Cast J.
Percutaneous radiofrequency ablation (RFA) of small renal carcinoma (SS 1807b), B-868

Bremer C.
Contrast enhanced optical imaging of the breast: Status and future prospects (SY 13), E-58

Bremer C.
New imaging methods and technologies: What molecular imaging actually is (PR 419), A-089

Bremer C.
Imaging of gene expression: Optical and nuclear techniques: A. Optical contrast agents for imaging genes and proteins (PR 1219), A-299

Bremerich J.
Pericardial diseases: C. CT and MRI of the neoplastic diseases (RC 1203), A-277

Brillet P., Fetita C., Beigelman-Aubry C., Perchet D., Prêteux F., Grenier P.
Automatic segmentation of airway wall area for quantitative assessment at MDCT: Preliminary results in asthmatics, C-1079

Brisse H.
Musculoskeletal imaging: C. Imaging of malignant tumors of the long bones in children: What to do or not to do (RC 1712), A-431

Brittenden J.
Audit of the use of testicular ultrasound, C-0490

Bronisz K., Wójcicka J., Czyszkowski P., Rybacki C., Szylberg T.
CT-guided fine-needle aspiration biopsy in the diagnosis of focal pulmonary lesions, C-0321

Brook O.R., Fischer D., Hirshenbaum A., Engel A.
Digital radiographs (DR) versus conventional screen films (SF) in small bowel follow-through: A prospective study, C-0129

Bru C.

Crohn's disease of the intestinal tract: Advances in imaging: A. US and Doppler (RC 801), A-175

Bruculeri F., Santocono S., Stecco A., Dominietto M., Brambilla M., Carriero A., Valente G.

CT-MR image fusion vs. CT and MR in the pre-surgical evaluation of laryngeal cartilage neoplastic invasion: Reliability in correlation with histopathology, C-0535

Bruegel M., Gaa J., Woertler K., Ganter C., Waldt S., Marten K., Engelke C., Rummeny E.J.
MR imaging of the lung: Comparison of turbo-spin-echo and 3D gradient-echo pulse sequences for the detection of pulmonary metastases (SS 204), B-033

Brugger P.C., Prayer D.
Magnetic resonance imaging (MRI) of the perinatal thyroid gland (SS 1512), B-756

Brugger P.C., Mittermayer C., Prayer D.
A new look at the fetus: Thick-slab T2-weighted sequences in fetal MRI (SS 1512), B-757

Brugger P.C., Kasprian G.J., Rauhofer U., Prayer D.

Morphology of congenital diaphragmatic hernias studied with fetal MRI (SS 1812), B-889

Brugger P.C., Mittermayer C., Herold C.J., Prayer D.
Virtual colonography of the fetal colon (SS 1812), B-892

Brunelle F.

Pediatric intervention: B. Treatment of vascular malformations outside the central nervous system (WS 818), A-193

Brunelle F.
Neuro-imaging: A. Large infant heads: What do we do - and when? (RC 912), A-238

Bruni A., Fanelli F., Bezzi M., Vagnarelli S., Corona M., Di Rezze L., Orgera G., Rossi P., Passariello R.

Role of covered stents in biliary intervention (SS 309a), B-198

Brzozowski K., Zukowski P., Jaron B., Twardowski P.

Partial endovascular embolisation of thyroid gland: Initial experience (SS 1809), B-871

Bückler A.

Safety considerations in MR: C. Interventional MRI: Safety considerations for patients and personnel (RC 1213), A-286

Buerke B., Sonntag A., Fischbach R., Heindel W., Tombach B.

Automatic injectors in magnetic resonance and computed tomography: Pilot study on hygienic aspects (SS 1806), B-884

Buffa V., Galluzzo M., Regine G., Atzori M., Miele V., Adami L.

CT multislice in pediatric tracheopulmonary malformations, C-0922

Buhmann S., Baur-Melnyk A., Wieser A., Reiser M.F.

Diagnostics of multiple myeloma using a 16-row-MSCT - low-dose whole body protocol (SS 1010), B-466

Authors' Index

Buhmann S., Kirchhoff C., Wielage C.,
Mussack T., Reiser M.F., Lienemann A.
Visualization and quantification of large bowel
motility by the use of functional cine-MRI
(SS 1801a), B-815

Bulanova T.V., Vasilyev A.Y., Antonik M.M.,
Drobysheva N.S.
Application of dynamic temporomandibular MRT
in evaluating the effectiveness of orthodontal
treatment, C-0544

Bultrini C., Limbucci N., Manetta R., Barile A.,
Calvisi V., Masciocchi C.
Arthro-MRI evaluation and incidence of
supraequatorial gleno-humeral lesions in athletes
affected by acquired instability of overstressed
shoulder (SS 310), B-140

Bultrini C., Limbucci N., Barile A., Manetta R.,
Bonanni G., Masciocchi C.
MRI evaluation of tibialis posterior tendon:
Assessment of its disorders and its role in
determining coxa pedis syndrome, C-0767

Burling D.
Polyp measurement and size categorisation by
CT colonography: Agreement with colonoscopy
and effect of observer experience (SS 1501a),
B-696

Burney K., Prabhu S.P., Lyburn I., Hopkins R.
Imaging small bowel ischaemia: The role of
multidetector CT, C-0102

Bushby L.H., Gimson A., Lomas D.J.
Outcome of patients with Choledocholithiasis at
MR Cholangio-pancreatography (SS 1401a),
B-579

Busi Rizzi E., Schininá V., Giancola M.L.,
Rovighi L., Larussa D., Antinori A.,
Bibbolino C.
Highly active antiretroviral therapy (HAART) and
MR imaging of progressive multifocal
leukoencephalopathy, C-0834

Bustamante M., Sánchez-Salmón E.,
Ruiz-Hernández P., Merino P., Aguilar M.,
Sampedro I., González-Tutor A.
Relationship between serum C-reactive protein
levels and angiographic findings in patients with
peripheral arterial occlusive disease, C-1044

Buzzi A., Figueroa M., Alarcon V.,
Arredondo F., Hjelt M., Mancini A.
Acute colonic disorders: CT findings, C-0106

Buzzi A., Garcia Pellegrino C., Brizuela C.,
Hjelt M., Buzzi M., Mancini A.
Ilio-psoas compartment: A radiological approach,
C-0744

Buzzi A., Alarcon V., Arredondo F., Hjelt M.,
Buzzi M., Mancini A.
CT and MRI of spinal infections, C-0745

Buzzi A., Garcia Pellegrino C., Hjelt M.,
Paez de la Torre E., Balcarce P., Mancini A.
Wernicke's encephalopathy: Typical and atypical
MRI findings, C-0822

Byrne J.V.
Hemorrhagic stroke: C. Cerebrovascular
malformations (CC 417), A-054

Byun J., Choi J., Kim D.
Value of splenic artery resistive index in the
differentiation between alcoholic and hepatitis B
virus-related cirrhosis, C-0062

C

Cabassa P.
Abdominal intervention: A. Thermal ablation of
liver tumors (WS 118), A-030

Cabassa P., Romanini L., Grazioli L.,
Portugalli V., Cristinelli M., Avigo C.
Liver metastases treated with chemotherapy:
Assessment of tumor vitality during arterial phase
with contrast enhanced harmonic sonography
(CEUS). Work in progress (SS 1401b), B-609

Cáceres J.
Anatomy and basic signs in imaging: A. Normal
anatomy (E³ 120), A-042

Cáceres J., Vilar J.
Interactive image teaching: Mediastinal masses
(E³ 820), A-204

Cáceres J.
Radiology of the elderly: Radiology of the elderly
(Introduction) (SF 9a), A-211

Cademartiri F.
Imaging of atherosclerotic plaques: A. CT and
EBT for coronary plaque detection (WS 1615),
A-388

Cademartiri F., Mollet N.R., Runza G., Midiri M.,
Hamers R., Bruining N.
Coronary plaque imaging with MSCT: The
characterisation of lipid and fibrous plaques is
affected by intracoronary attenuation (SS 603),
B-301

Cademartiri F., Mollet N.R., van Mieghem C.,
Runza G., Baks T., de Feyter P.J., Krestin G.P.
Coronary artery atherosclerotic plaque burden
evaluated with MSCT coronary angiography:
Stable vs. unstable angina with ICUS validation
(SS 603), B-308

Cademartiri F., Mollet N.R., van Mieghem C.,
Runza G., Belgrano M., Baks T., de Feyter P.J.,
Krestin G.P.
Diagnostic accuracy of non-invasive 64-slice CT
coronary angiography (SS 703a), B-342

Cademartiri F., Mollet N.R., Runza G.,
Belgrano M., Midiri M., Pozzi Mucelli R.,
Krestin G.P.
Visualisation of coronary artery stent patency
with 64-slice computed tomography, C-0267

Cademartiri F., Mollet N.R., Runza G.,
Belgrano M., Midiri M., Pozzi Mucelli R.,
Krestin G.P.
Improvement of spatial and temporal resolution in
64-slice CT coronary angiography, C-0974

Cadi M., Chollet R., Lucidarme O., Grenier P.
Virtual colon dissection tool used in CT
colonography: Comparison with conventional
endoscopy results: A preliminary study
(SS 1501a), B-698

Cadi M., Chollet R., Lucidarme O., Grenier P.
Ileocecal valve appearance on CT colonography,
C-0089

Cakirer S.
Pediatric neuroradiology: C. Hydrocephalus
(RC 1711), A-420

Cakirer S., Yagmurlu B., Koklu B., Karagoz Y.,
Kahraman N.
Brain tumors associated with chronic epileptic
seizures: A pictorial review, C-0819

Cakirer S., Yagmurlu B., Koklu B., Karagoz Y.,
Kahraman N.
The diagnostic utility of perfusion-weighted MR
imaging, diffusion-weighted MR imaging and MR
spectroscopy in mesial temporal sclerosis,
C-0878

Calabrese M., Bacigalupo L., Fausto A.,
Sardanelli F.
Value of dynamic breast MR using an open 0.2 T
magnet and Gd-BOPTA as a contrast agent:
Preliminary results (SS 602), B-270

Calabrese M., Faedda C., Brizzi D., Baio G.,
Bertoli E., Bacigalupo L.
Mammographic technique: Frontal oblique
approach versus traditional lateral approach
(SS 1402), B-589

Calbo J., Castro M., Carnero M., Perez L.,
Picazo N., Gonzalez I.
Breast cancer in women 40 years of age and
younger, C-0214

Calvillo Batllés P., Graells Ferrer M.,
Vega Martínez M., Delgado Cordón F.,
Ballestín Vicente J., Martí-Bonmatí L.
Evaluation of acromioclavicular joint with MR
imaging, C-0704

Camenzuli A.M., Lea S., Romaniuk C.
Diagnostic imaging in the staging and evaluation
of prostatic carcinoma, C-0471

Camps Herrero J., Sentís Crivellé M.,
Tortajada Giménez L., Ricart Selma V.,
Martínez Rubio C., Ferrer Puchol M.,
Lloret Martí M.
Accuracy of breast MR in the evaluation of the
response to chemotherapy in 70 patients and
accuracy of parametric images in a subgroup of
46 patients (SS 702), B-378

Cantwell C.P., Bruzzì J., Cradock A.,
Eustace S., Murray J.G.
Lower limb MR venography with true FISP for
suspected deep venous thrombosis (SS 215),
B-115

Cappelli C., Mazzeo S., Caramella D.,
Belcaro A., Caproni G., Campani D., Boggi U.,
Bartolozzi C.
Multidetector CT in the assessment of pancreatic
malignant masses (SS 701b), B-415

Cappelli C., Neri E., Pratali A., Cioni R.,
Boggi U., Bartolozzi C.
Vascular thrombosis in pancreatic transplantation:
Multidetector CT in the evaluation of pancreatic
vessels and parenchyma, C-0054

Capuani S., Rossi C., Fasano F., Maraviglia B.
Investigation of trabecular bone structure by
means of DTI techniques, C-0653

Capuñay C., Carrascosa P.M., Ulla M.,
Carrascosa J.
Identification of pulmonary vein variants by
multidetector CT, C-0331

Capuñay C., Carrascosa P.M., Ulla M.,
Vallejos J., Carrascosa J.
Correlation between automatic vs. manual lung
nodule assessment, C-0346

Capuñay C., Carrascosa P.M., Ulla M.,
Vallejos J., Carrascosa J.
Intra-observer variability of automatic lung nodule
assessment software, C-0347

Authors' Index

- Capuñay C., Carrascosa P.M., Ulla M., Martín López E., Carrascosa J.**
Usefulness of CT angiography in the planning and follow-up of abdominal aortic aneurysm endovascular treatment, C-1015
- Caramella D.**
Radiology on the web: Radiology on the web (E³ 220a), A-048
- Caramella D.**
How to get the best from information technology for patient care: PACS and teleradiology in Europe (EF 2), A-154
- Carbone I., Francone M., Visconti S., Ascarelli A., De Castro S., Passariello R.**
Assessment of left ventricular volume and mass in endurance athlete's heart: A cardiac-MR (CMR) and 3D ultrasound study (D-US) (SS 703b), B-420
- Carbone I., Francone M., Danti M., Lanciotti K., Doda E., Granatelli A., Passariello R.**
Non-invasive assessment of drug-eluting coronary stents (DES) at 6-months follow-up; is there a role for multidetector-CT angiography (MDCTA)? (SS 1003), B-526
- Cardinale L., Ferraris F., Perotto F., Gollini P., Priola A., Novello S., Fava C.**
Screening for lung cancer in a high risk population using spiral computed tomography: 3-year results, C-0319
- Cardone G., Iabichino C., Cestari A., Nava L., Mangili P., Balconi G., Guazzoni G.**
Laparoscopic cryoablation (LC) of small renal masses: Postoperative complications evaluation by magnetic resonance imaging (MRI), C-0453
- Cardone G., Fiechi D., Cestari A., Guazzoni G., Mangili P., Balconi G.**
Renal lesions treated with laparoscopic cryoablation (LC): Multi-detector row computed tomography (MDCT) imaging patterns, C-0454
- Cardone G., Nava L., Losa A., Guazzoni G., Mangili P., Balconi G.**
Prostatic carcinoma (PC) treated with cryosurgical ablation (CA): Magnetic resonance imaging (MRI) patterns, C-0491
- Cardone G., Mangili P., Nava L., Guazzoni G., Balconi G.**
Urinary tract neoplasms: Conventional and pyeloureographic magnetic resonance (MR) patterns, C-0502
- Carra L., Attanasio S., Crinò F., Giampietro A., Bosurgi F., Carriero A.**
Mammary parenchymal distortions with benign characteristics: Diagnostic accuracy of magnetic resonance (SS 602), B-265
- Carrascosa P.M., Capuñay C., Castiglioni R., Ulla M., Carrascosa J.**
The role of virtual colonoscopy in the evaluation of inflammatory disease, C-0107
- Carrascosa P.M., Capuñay C., Ulla M., García Merletti P., Martín López E., Carrascosa J.**
16-row multidetector CT in the detection of coronary anomalies, C-0268
- Carrascosa P.M., Sanchez F., Capuñay C., Martín López E., Ulla M., Carrascosa J.**
Dental CT in the detection of periodontal lesions, C-0537
- Carrascosa P.M., Capuñay C., Ulla M., Martín López E., Carrascosa J.**
Abdominal virtual angioscopy, C-1014
- Carrió I.**
Imaging of atherosclerotic plaques: C. Molecular imaging of vulnerable plaques (WS 1615), A-390
- Caruso G., Salvaggio G., Fatta G., Caccamo N., La Mendola C., Dieli F.**
Effect of ultrasound contrast medium on human CD4⁺ lymphocytes in vitro culture, C-0401
- Cassar-Pullincino V.N.**
Knee joint: C. Postoperative knee (RC 1710), A-404
- Casselman J.-W.**
Imaging of normal anatomy and function: B. Brain stem and cranial nerves (RC 111), A-021
- Casselman J.-W.**
Imaging in cochlear implant candidates: B. Pre-implant imaging (RC 508), A-122
- Casselman J.-W.**
Base of the skull, hypophysis, supra- and parasellar region: A. The skull base (CC 1217), A-264
- Castelli P., Caronno R., Piffaretti G., Tozzi M., Lomazzi C., Laganà D., Carrafiello G.**
Emergency stent-graft repair for blunt thoracic aortic injury (SS 209a), B-062
- Castro Copete M., Calbo Maiques J., Carnero Ruiz M., Crespo Martínez C., Navarro Navarro M., Picazo Escribano N., González Álvarez I.**
Extraperitoneal nodal metastases as the most frequent form of recurrence in uterine cervical carcinoma treated by radiation therapy, C-0433
- Catala J., Hernandez D., Escobar M., Veciana P., Gispert S., San Roman L., Poves J.I.**
Laparoscopic gastric bypass surgery in morbid obesity: Radiologic features and complications, C-0135
- Catalano C.**
Impact of multislice CT on imaging of the upper abdomen: C. Liver (RC 901), A-220
- Catalano O., Sandomenico F., Nunziata A., Lobianco R., Siani A.**
Contrast-enhanced US imaging of splenic lymphomas (SS 1401b), B-601
- Catalucci A., Zugaro L., Monina M., Mancinotti A., Di Cesare E., Vicentini C., Masciocchi C.**
Dynamic MRI in the assessment of female pelvic organ prolapse: Baseline and post-surgical evaluation, C-0428
- Caulo M., Tartaro A., De Nicola A., Maira G., Colosimo C.**
Perfusion MR imaging in patients with non-enhancing brain gliomas: A valuable tool to predict anaplasia and/or tumor progression? (SS 1011), B-534
- Cavallaro A., Horger W., Swoboda B., Bautz W., von Rechenberg B., Mamisch T.C.**
Histological correlation of MRI cartilage imaging in the knee joint before total replacement (SS 710), B-352
- Celestre M., Sansoni I., Rengo M., Di Martino M., Coletta L., Laghi A., Passariello R.**
Automatic quantification of carotid artery stenosis: Preliminary results of a new vascular software module (SS 205), B-107
- Centonze M., Del Greco M., Marini M., Della Sala S., Peterlongo P.**
Comparison between multi-detector CT and electro-anatomical mapping for evaluation of left atrium and distal pulmonary veins anatomy in atrial fibrillation patients, C-0264
- Centonze M., Cristoforetti A., Ravelli F., Del Greco M., Dalla Palma F., Nollo G.**
Integration of electrical mapping and multi-detector CT imaging of left atrium and pulmonary veins for atrial fibrillation ablation, C-0360
- Certo M., Themudo R., Santos R., Varzim P., Ferreira A., Ribeiro A.**
Barium contrast studies in Crohn's disease: Still fundamental?, C-0150
- Cha J., Moon W., Koh Y., Cheon J., Park J., Han B., Cheo Y.**
Differentiation of benign and malignant solid breast masses: Real-time spatial compound imaging versus conventional ultrasound, C-0202
- Cha J., Moon W., Koh Y., Cheon J., Park J., Han B., Cheo Y.**
Differentiation of benign and malignant solid breast masses: Tissue harmonic imaging versus conventional ultrasound, C-0203
- Cha J., Park J., Paik S., Joh J., Hong H., Lee H.**
Usefulness of sonography in diagnosis and postoperative evaluation of carpal tunnel syndrome, C-0736
- Chalazonitis A.N., Tzovara J., Velitsista S., Giannou S.**
Everything you always wanted to know about iodinated contrast media interactions with other drugs, but you were afraid to ask, C-0396
- Chalazonitis A.N., Tzovara J., Protopapa E., Giannou S.**
Ultrasound guided interventional procedures. A simple way of self-training, C-0618
- Chalkia M., Spanos A., Kirimlidis I., Papageorgiou A., Chartabilas E., Vougiouklis N.**
Comparison of tissue harmonic imaging with standard ultrasound mode, in the evaluation of abdomen and pelvic organs, C-0075
- Chalkia M., Kirimlidis I., Spanos A., Papageorgiou A., Spanidou S., Vougiouklis N.**
Comparison of tissue harmonic imaging with standard ultrasound mode, in the evaluation of the kidneys, C-0452
- Chalkia M., Kirimlidis I., Spanos A., Mountzouoglou A., Chalkia P., Vougiouklis N.**
Deep venous thrombosis of the lower limb on screening with colour Doppler: Incidence and correlation with clinical history, C-1076
- Chammas M., Gerhard R., Saito O., Oliveira I.R., Widman A., Cerri G.G.**
Thyroid nodules: Evaluation with color Doppler and duplex Doppler ultrasound (SS 208), B-058
- Chan O.**
Abdominal trauma: B. How to image the trauma patient (RC 401), A-064

Authors' Index

- Chan O.**
Errors in radiology: Pitfalls in emergency radiology (E³ 1020), A-261
- Chandratreya L., Cobby M., Watura R.**
Ultrasound guided FNAC of impalpable cervical lymph nodes in lung cancer, C-0315
- Chandratreya L., Armstrong S.**
MRI as an important tool in differentiating uterine adenomyosis from leiomyomas: A pictorial review, C-0437
- Chang A.**
Gall bladder wall thickening: An early sign of dengue fever, C-0004
- Chatzimichael K., Economou G., Kampanarou M., Dimitrakopoulou G., Kelekis D.A.**
Real-time spatial compound ultrasound with XFOV imaging in the evaluation of breast lesions, C-0210
- Chastrue-Mendoza L., Moratal-Pérez D., Martí-Bonmatí L., Flórez-Ordóñez Y., Millet-Roig J.**
Tutorial on physical principles of MR imaging: Spin behavior study, C-0945
- Chavan A.**
Diagnostic and interventional radiology of transplants: Kidney and pancreas (part 2) (SF 8b), A-186
- Chaveron C., Ceugnart L., Bachelle F.**
Clip migration after 11-gauge vacuum-assisted stereotactic breast biopsy with lateral approach: Retrospective review of 447 clips deployed after completion of breast biopsy (SS 1502), B-734
- Chen F., Suzuki Y., Nagai N., Peeters P., Sun X., Coudyzer W., Marchal G., Ni Y.**
Treatment of stroke in rats with microplasmin: Magnetic resonance imaging evaluation (SS 611), B-316
- Chen S., Feng X.**
Diagnostic value of T1-weighted fluid-attenuated inversion recovery sequence with 3.0 T MR in the central nervous system (CNS) (SS 1811b), B-933
- Cheng W., Zeng M., Yan F.**
Comparative assessment of Resovist-enhanced MRI and Magnevist in the detection and characterization of focal hepatic lesions (SS 201b), B-042
- Cheng Y.S., Li M.H., Zhang H.X.**
Treatment of experimental saccular aneurysms of carotid arteries with three covered stents in canine models (SS 309b), B-209
- Cheng Y.S., Li M.H., Shang K.Z.**
Comparative observation on different interventional procedures in benign esophageal strictures, C-0165
- Cheon J., Kim I., Kim W., Yeon K.**
MR imaging of the brain in Wilson's disease of childhood: Findings before and after treatment, C-0888
- Chersevani R.**
Diagnostic highlights: C. Physician-patient relationship (RC 902), A-217
- Chida K., Otani H., Saito H., Nagasaki T., Kagaya Y., Kohzuki M., Zuguchi M., Takahashi S., Shirato K.**
Feasibility of rapid-sequence ³¹P-MRS of the heart in cardiac patients, C-0228
- Chida K., Saito H., Zuguchi M., Otani H., Shimura H., Ito D., Nakada M., Takahashi S., Shirato K.**
Estimating the maximum radiation skin dose during percutaneous coronary intervention using the fluoroscopic time, dose-area product, and body mass index, C-0600
- Chin C., Jones G., Archer J., Field J., Dimmock M., Papageorgiou P., Moffett R.**
Advanced 3D image rendering and multi-level, clinically-focused PACS integrations (IM 1), D-14
- Cho E.,**
Identifying resectable hilar cholangiocarcinoma: Multidetector CT (MDCT) versus MR imaging (SS 1501b), B-714
- Cho J.H., Park B.H., Shin T.B., Oh J.Y., Lee J.H., Yoon S.K., Choi J.C., Lee K.N., Nam K.J.**
Development of animal model for solitary hepatic tumor: Operative intrahepatic transneedle inoculation of VX2 particles C-0630
- Choe H., Ko E., Bae Y., Kim G., Lee Y., Chung S.**
Screening US in mammographically normal dense breasts (SS 1802), B-834
- Choi J., Hong S., Lee I., Lee J., Koo J., Choi J., Koh Y., Kang H.**
Meniscal rim sign: Usefulness for evaluation of an extensive triangular or wedge-shaped signal in the meniscus on MR imaging of the knee (SS 1410), B-567
- Choi J., Kim S., Kim E., Na D., Ryoo J., Kim H.**
Nodal involvement of peripheral T-cell lymphoma in the neck: Two-phase CT findings, C-0556
- Choo H., Lee T., Jeong H., Choi H., Kim H., Moon T., Choi C., Lee S.**
Double microcatheter technique for endovascular coil embolization of large, wide-necked intracranial aneurysms (SS 1511), B-761
- Choo H., Lee T., Jeong H., Choi H., Park K., Sung S., Kim H., Lee S.**
Urgent recanalization using stents for acute internal carotid artery occlusion in progressive stroke syndromes with contralateral internal carotid stenosis or occlusion (SS 1511), B-762
- Choo H., Choo K.S., Lee T., Kim S., Jeong H., Moon T.**
Assessment of small vessel stents for intracranial angiography by 16-slice CT angiography, C-0846
- Chudácek Z., Sequens R., Pechotová M., Kuntscherová J.**
The correlation of endosonography versus perioperative and histopathological findings in a group of 350 patients with surgically treated anorectal tumor, C-0082
- Cianci R., Filippone A., Grassedonio E., Di Fabio F., Colosimo C.**
Focal liver lesion detection and classification on multi detector-row computed tomography (MDCT) and SPIO-enhanced magnetic resonance imaging (MRI): Could awareness of the patients clinical history influence the reader's diagnosis? (SS 1501b), B-712
- Ciarpaglini L.L., Pascoli S., Regimenti P., Portalone L., Pedicelli G.**
Evaluation of the diaphragm in malignant pleural mesothelioma: Role of US (SS 704), B-389
- Ciatto S., Cecchini S., Landini A., Benvenuti A., Zappa M.**
Selecting postmenopausal patients with abnormal uterine bleeding (AUB) to invasive assessment by transvaginal ultrasonography (TVUS) (SS 1807a), B-798
- Ciliotti A., Marini C., Giacconi C., Francesca D., Mazzotta D., Vaccaro A., Della Pina C., Bartolozzi C.**
MRI in ductal carcinoma in situ (DCIS) with mammographic appearance of microcalcifications, C-0199
- Cina A., Di Stasi C., Misciasci T., Martina F.M., Manfredi R., Merlini B., Natale L., Bonomo L.**
16-slice CT angiography vs gadolinium enhanced MR angiography in the evaluation of peripheral arterial occlusive disease: A work in progress (SS 315), B-244
- Cina A., Pedicelli A., Di Stasi C., Lo Schiavo V., Fiorentino A., Cina G., Bonomo L.**
All that the radiologist should know about color-Doppler US in chronic venous insufficiency, C-1056
- Cioni D., Lencioni R., Conti A., Lera J., Campani D., Filippini F., Montagnani S., DellaPina C., Bartolozzi C.**
Small nodules in liver cirrhosis: Correlation between contrast-enhanced US and pathologic examination of explanted liver (SS 306), B-122
- Cioni D., Lencioni R., Lera J., Conti A., DellaPina C., Campani D., Filippini F., Crocetti L., Bartolozzi C.**
Sensitivity and specificity of multidetector spiral CT in the detection of hepatocellular carcinoma in patients undergoing transplant for cirrhosis (SS 301b), B-180
- Cioni R., Bargellini I., Femia M., Cappelli C., Fontana F., Sardella S., Bartolozzi C.**
Treatment of type II endoleaks by CT-guided translumbar puncture and injection of N-butyl-2-cyanoacrylate glue into the aneurysm sac (SS 609b), B-297
- Ciosci R., Pompili G., Bianchi P., Montorsi M., Cornalba G.**
Preoperative staging of rectal cancer using magnetic resonance imaging: Comparison with endosonography and histopathologic findings, C-0079
- Ciszkowska-Lyson B., Czerny Z., Smigelski R., Mioduszewski A.**
Importance of linear subchondral bone edema in MRI knee examination (SS 1410), B-566
- Clasen S., Boss A., Schmidt D., Fritz J., Graf H., Schick F., Claussen C., Pereira P.**
MR-guided radiofrequency ablation of liver tumors using internally cooled electrodes: Clinical results in 28 patients (SS 1409a), B-621
- Cleverd D., Schoenberg S., Jung E., Michaely H., Reiser M.F.**
High resolution magnetic resonance angiography with iPAT compared to color Doppler and power Doppler in the assessment of carotid artery stenosis (SS 715), B-454
- Cleverd D., Rupp N., Reiser M.F.**
Optimizing material management in interventional radiology departments through the introduction of a materials management system, C-0363

Authors' Index

Clevert D., Jung E., Reiser M.F., Rupp N.

Contrast harmonic imaging with power mode and coded harmonic angiography using Optison for assessing vascularization during chemoembolization in HCC. First experiences, C-0569

Clevert D., Jung E.M., Rupp N., Reiser M.F.

B-flow and color-coded-B-flow in sonographic diagnosis of filiform stenosis of the internal carotid artery, C-1055

Clevert D., Jung E., Rupp N., Reiser M.F.

Improved diagnosis of vessel dissections by ultrasound B-flow imaging, C-1064

Cobby M.

Inflammatory joint disease: A. Plain film analysis (RC 1610), A-379

Cobelli R., Zompatori M., Lombardo E., Bnà C., De Luca G.

Detection of pulmonary embolism with unenhanced CT, C-0332

Cobelli R., Zompatori M.

Evaluation of flow-related artefacts in the study of pulmonary embolism with multislice, C-0333

Cobelli R., Vaglio A., Greco P., Buzio C., Zompatori M.

Imaging of idiopathic retroperitoneal fibrosis, C-0517

Coche E.E.J.G., de Crombrugghe R., Vlassenbroek A.

Right ventricular function measured during ECG-gated MSCT of the whole chest: Intra-and inter-observer variability (SS 1004), B-479

Cognard C.

Radiological vascular interventions: C. Carotid stenting (RC 911), A-227

Cognard C., Januel A., Herbreteau D., Barreau X., Drouineau J., Pierot L.

Endovascular treatment of brain AVMs using onyx: Preliminary results of a prospective, multicenter study (SS 1511), B-759

Cognard C., Mejdoubi M., Januel A., Tall P., Albucher J., Chollet F., Gigaud M., Tremoulet M.

Endovascular treatment (EVT) in first intention in the management of ruptured intracranial aneurysm: Prospective consecutive series. (SS 1511), B-760

Coll D., Vidal R., Perez-Lafuente M.,

Moreiras M., Romero-Jaramillo A., Segarra A. Recovery of non-developed vascular accesses for hemodialysis, C-0604

Colleoni M., Uské A., Meuler R., Maeder P., Regli L., Schnyder P., Binaghi S.

Cerebral vasospasm after subarachnoid haemorrhage: Multislice computerized tomography (MSCTA): A comparison with digital subtraction angiography (DSA) and contribution of perfusion CT in vasospasm management (SS 611), B-318

Colosimo C., Pirovano G., Kirchin M.A., Hogstrom B., Spinazzi A.

Contrast-enhanced MR imaging of pediatric CNS: Comparison of gadobenate dimeglumine and gadopentetate dimeglumine for lesion enhancement (SS 1412), B-644

Connor S.E.J., Flis C.M.

Imaging of head and neck vascular masses: A pictorial review, C-0528

Cook G.

PET/CT: A major advance (SY 65), E-66

Coppenrath E.M., Mueller-Lisse U.G., Meindl T., Herzog P., Mueller-Lisse U., Khalil R., Reiser M.F.

CT-urography: Dose reduction in multidetector technique (SS 1407), B-611

Cordonnier E.

How to get the best from information technology for patient care: Industry, integrating solutions towards a better practice (EF 2), A-156

Cornud F.

Urological intervention: A. Nephrostomy and ureteric stenting (WS 918), A-235

Corona M., Fanelli F., Salvatori F., Bruni A., Dominelli V., Di Reze L., Pucci A., Rossi P., Passariello R.

Six-year experience in the percutaneous treatment of abdominal aortic aneurysms (SS 609b), B-299

Corso R., Vercelli R., Rampoldi A., Minetti E., Leni D., Vanzulli A.

Transplant renal artery stenosis (TRAS): Long-term impact on kidney function and blood pressure control of percutaneous transluminal angioplasty and stenting, C-0580

Costa N., Marques H., Alves P., Marques R., Barros J., Mauricio J.

Contribution of conventional radiology in adjustable gastric procedures for morbid obesity, C-0151

Costa S., Marti-Bonmati L., Arana E., Forner J., Mollá E.

Added value of helical CT multiplanar reconstructions on the conventional transverse CT examination of the degenerative spine, C-0667

Costaridou L.

Breast imaging: B. Softcopy display of mammograms (RC 1714), A-433

Costaridou L., Skiadopoulos S., Sakellaropoulos P., Kalogeropoulos C., Likaki E., Panayiotakis G.

Performance of an adaptive wavelet contrast enhancement method in interpretation of microcalcification clusters on dense parenchyma (SS 605), B-322

Courcoutsakis N.A., Prassopoulos P., Carney J.A., Stratakis C.A.

The complex of myxomas, spotty skin pigmentation and endocrine overactivity: Carney complex Imaging findings, C-0254

Courcoutsakis N.A., Prassopoulos P., Carney J.A., Stratakis C.A.

CT imaging findings in primary pigmented nodular adrenocortical disease (PPNAD) in patients with Carney complex (CNC) and Cushing's disease, C-0498

Cowan N.C.

Multislice CT of the urinary tract: A. Multislice CT of urothelial tumors (RC 1307), A-330

Cowley P., MacLachlan J., Tibballs J., Davies N., Bell J.

Diffusion weighted imaging of liver metastases: A study of the relative lesion conspicuity compared to conventional sequences (SS 1801b), B-853

Cowling M.G.

Planning issues in vascular radiological intervention: B. Mapping peripheral vascular disease (WS 1715), A-428

Cramer M.C., Habermann C.R., Graessner J., Weiss F., Petersen K., Jaehne M., Adam G.

Ultrafast MR-sialography: Sequence optimization and evaluation of parallel acquisition techniques and different functional conditions of the salivary glands (SS 208), B-053

Cravero F., Barini M., Puppi A., Lovisolo M., Stecco A., Carriero A.

Pitfalls in MR arthrography of shoulder, C-0679

Cravero F., Rozzati D., Meni A., Sessa G., Stecco A., Carriero A.

Extracorporeal shock waves therapy (ESWT) of calcific tendinitis of the shoulder: Clinical and radiologic evaluation, C-0693

Crean A., Provost Y., Paul N., Merchant N.

MR and CT imaging of partial and total cavo-pulmonary connections: A guide to assessment of the Fontan circuit for the uninitiated, C-0227

Crespo A.M., Hernandez G., Barrena R., Garcia A.B., Izquierdo B., Angulo E.

Head and neck paragangliomas: Imaging and embolization, C-0577

Cronin C.G., Lohan D.G., Meehan C.P., Roche C.J.

Animal signs in radiology, C-0740

Cronin C.G., Alhajeri A., Roche C.J.

Art appreciation through radiology, C-0977

Cuéllar i Calabria H., Quiroga S., Sebastià C., Boyé R., Miranda A., Àlvarez-Castells A.

MDCT of collateral venous circulation in the retroperitoneum, C-0999

Cunha T.M., Félix A., Cabral I.

Comparison of clinical and MRI staging with pathologic evaluation in cervical carcinoma (SS 1807a), B-792

Curati-Alasonatti W.

Radiology of the elderly: Abdominal pain (SF 9a), A-214

Curvo-Semedo L., Caseiro-Alves F.

Liver MR imaging with iron oxides: Is gradient-echo T2-weighted sequence always better?, C-0039

Cyrlowski L., Zaborowski G., Sawicki M., Krzystolik K., Cybulski C., Sagan L., Walecka A., Lubinski J.

MRI manifestation of central nervous system lesions in von Hippel-Lindau disease, C-0842

Czerny C., Baumgartner W.D., Gstöttner W.

Imaging in cochlear implant candidates: C. Post-implant imaging (RC 508), A-123

D

D'Helft C.S., Mc Gee A.M., Rainford L.A., Mc Fadden S.L., Hughes C.M., Winder J.R., Brennan P.C.

A survey of radiation dose and image optimisation for cardiac interventional procedures, C-0650

D'Onofrio M., Masinielli B., Caffarri S., Malago' R., Zamboni G., Pozzi Mucelli R.

Focal liver lesions: Malignant vs benign - the value of the sinusoidal phase of contrast-enhanced ultrasonography (SS 1401b), B-607

Authors' Index

Dalal T., Rizzo S.M.R., Kalra M.K., Schmidt B., Suess C., Blake M.A., Flohr T., Saini S.
New technique to avoid an increase in CT radiation dose from metallic prostheses with automatic tube current modulation: Phantom and patient study (SS 210), B-010

Daldrup-Link H.E.

Molecular imaging: B. Cell targeting and cell tracking with MR imaging (RC 1306), A-325

Daldrup-Link H.E., Meier R., Rudelius M., Piontek G., Metz S., Uherek C., Wels W., Schlegel J., Rummeny E.J.

In-vivo tracking of genetically engineered, anti HER2/neu directed natural killer cells to HER2/neu positive mammary tumors with magnetic resonance imaging, C-0406

Damilakis J.

Special issues of radiation exposure in diagnostic radiology: C. Pregnant employees working in diagnostic radiology (RC 813), A-191

Danchaivijitr N., Thompson D., Vellodi A., Saunders D.E.

MR imaging findings of the craniocervical junction in Morquio's disease, C-0854

Danes J.

Breast MR imaging: A. When and how (RC 102), A-011

Danielsen E.R.

MR spectroscopy of the brain in clinical practice: A. Technique and protocols (RC 1311), A-327

Danza F.M., Crucitti A., Pirulli G., Cirillo M., Magistrelli P., Bock E., Bonomo L.

Complications after radiofrequency thermal ablation (RFA) of abdominal tumors: A retrospective review (SS 1409a), B-626

Danza F.M., Marino V., Magistrelli A.,

Bernardini A., Costanzi S., Bock E., Bonomo L.
Treatment of renal cystic diseases: Use of minocycline hydrochloride as soft sclerosing agent (SS 1809), B-870

Danza F.M., Scialpi M., D'Amico A., Pantalone O., Bernardini A., Bock E.m., Bonomo L.

Retroperitoneal anatomy: What could we learn from disease. Part 1: Embryology, C-0493

Danza F.M., Marino V., Magistrelli A., Cirillo M., Ottaviani P., Valentini A.L., Bonomo L.

Primitive and recurrent liposarcoma of abdomen: What should we have to know for a correct CT and MR diagnosis, C-0503

Darge K., Schreiber F., Beer M., Gordjani N., Riedmiller H.

Voiding cystourethrography versus low-dose contrast-enhanced harmonic voiding urosonography using the 2nd generation US contrast medium SonoVue (SS 1812), B-897

Das M., Mühlenbruch G., Mahnken A.H., Gündel L., Hauenstein O., Eckert J., Günther R.W., Wildberger J.E.

Phantom evaluation and patient correlation of computer-aided volumetry of small pulmonary nodules in MDCT chest examinations (SS 304), B-169

Das M., Mühlenbruch G., Mahnken A.H., Felten M.K., Flohr T.G., Kraus T., Günther R.W., Wildberger J.E.

Lung cancer screening in asbestos-exposed high risk patients with low dose MDCT: Results of baseline screening and first year follow-up (SS 704), B-382

Datir A.P.

Orbital MR imaging: A pictorial review, C-0531

Datir A.P.

CT evaluation of neck masses - A pictorial review, C-0547

de Bazelaire C., Vignot S., Mathieu O., Zagdanski A., Bourrier P., de Kerviler E., Frija J.

Internet-based tool for differential diagnosis of HRCT findings in non-HIV patients with cancer presenting with lung diseases, C-0344

De Cicco E., Casanova S., Gravano M., Molinari G.

Magnetic resonance detection of subclinical cardiac impairment in patients with systemic sclerosis, C-0255

De Fiori E., Ferretti S., Rampinelli C., Bellomi M.

Pulmonary micronodules (< 5 mm): 3 year follow-up of 238 nodules in 165 smokers (SS 204), B-037

De Fiori E., Preda L., Ansarin M., Bellomi M.
Histological diagnosis of the endolaryngeal tumours through ultrasound-guided transcutaneous tru-cut biopsy (SS 308), B-184

de Graaf F.

Panorama 1.0T open MR and its clinical outcome (SY 11), E-49

De Graaf N., Tanghe H.L.J., Leertouwer T.C., Flach H.Z., Dippel D.W.J., Van der Lugt A.
Multidetector CT angiography: The method of choice to detect cerebral venous thrombosis?, C-0774

de Haen C.

History of contrast media: The classical ionic contrast media (SF 4c), A-078

De Juan C., Sanchez M., Navarro S., Pages M., Ayuso J.R., Ayuso C.

MR pancreatography and secretin enhanced MR pancreatography for the study of anatomical variants and developmental abnormalities of the pancreas, C-0058

De Juan Delago M., San Roman Manzanera L., Salinas Yeregui T., Castaño Duque C., Guardia Mas E., Ruscalleda Nadal J.

Head and neck paragangliomas: Diagnostic and endovascular therapy, C-0778

de Kerviler E.

Contrast enhanced MRA and perfusion imaging (2) Optimization of injection rates and sequence parameters in contrast-enhanced MRA (SY 6), E-22

de Lama E., Narvaez J.A., Narvaez J., Mallol X., Pellicer J., Fabregas V., Canas C.

Rheumatoid foot: Spectrum of imaging findings, C-0741

De Lama Salvador E., Canas C., de Albert M., Guma A., Garcia-Barriga F.J., Aranda H.

Ultrasound of acute appendicitis: Spectrum of findings and role in the treatment planning, C-0156

De Luis E., Bilbao Jaureguizar J., Martínez-Miravete P., Noguera J.J., Martínez -Cuesta A., García de Jalón J.A.

Superabsorbent polymer microspheres: A new embolic agent. An experimental study with pig kidneys (SS 209b), B-071

De Luis E., Noguera J.J., Pons M., Domínguez P.D., Pina L.J., Martínez Regueira F.

Is the echogenicity of a mass influenced by its morphology? An in vitro model, C-0206

de Monyé C., de Weert T.T., Zaalberg W., Roose J., Siepmann D., van der Lugt A.

Optimization of CT angiography of the carotid artery with a 16-multidetector-row CT scanner: Craniocaudal scan direction reduces contrast material-related perivenous streak artifacts (SS 715), B-452

de Roos A.

Coronary vessels: B. MRA of the coronary arteries (RC 803), A-173

de Roos A.

Assessment of myocardial perfusion and viability: Assessment of myocardial perfusion and viability (Introduction) (SF 12), A-271

De Rubeis M., Fanelli F., Bezzini M., Corona M., Bruni A., Petrucci L., Pucci A., Dominelli V., Passariello R.

Use of multidetector-row CT for the evaluation of E-PTFE covered stent in tips (SS 709), B-409

De Wever W.F.M., Meylaerts L., De Ceuninck L., Verschakelen J.A.

Value of integrated PET-CT versus CT and PET alone in the detection of lung metastases in patients with a known primary tumor: A retrospective study (SS 704), B-385

De Wever W.F.M., Van Mieghem I.M., Van Breuseghem I., Verschakelen J.A.

Evaluation of the bronchial suture in lung transplant recipients with virtual bronchoscopy (SS 1804), B-845

de Wilde J.

Safety considerations in MR: B. Clinical safety practice (RC 1213), A-285

de Win M.M.L., Majoe C.B.L.M., den Heeten G.J.

Incidental findings on brain MRI in asymptomatic young adults (SS 311), B-222

de Win M.M.L., Vlieger E.J.P., Lavini C., Majoe C.B.L.M., Akkerman E.M., den Heeten G.J.

DTI, perfusion MRI and ¹H-MR-spectroscopy of the brain: "Normal-values" in a population of young healthy adults (SS 311), B-223

de Win M.M.L., Reneman L., Vlieger E.J.P., Lavini C., van den Brink W., den Heeten G.

MRI based prospective longitudinal study on neurotoxicity of ecstasy in novice ecstasy users, C-0815

Debatin J.F.

Wilhelm Conrad Röntgen - Honorary Lecture: Would W.C. Röntgen get along with hospital managers? (HL 1), A-159

Deftereos S.P., Manavis I., Sigalas J., Giannoudi T., Prassopoulos P.

Evaluation of lenticulostriate artery hemodynamics with color Doppler sonography (CDS) in infancy (SS 1412), B-640

Authors' Index

- Deistung A., Rauscher A., Sedlacik J., Witoszynskyj S., Barth M., Kaiser W.A., Reichenbach J.R.**
A graphical user interface for SWI-reconstruction (SS 205), B-105
- Dekan V.S., Trufanov G.E., Rud S.D., Fokin V.A., Boikov I.V.**
Technetium-99m-MIBI SPECT and image fusion with CT or MR imaging for the assessment of primary brain tumors and brain metastases, C-0849
- Del Cura J.L., Zabala R., Legórburu A., Gorriño O., Grande D.**
Ultrasound-guided intervention in the musculoskeletal system, C-0752
- Del Frate C., Borghese L., Cedolini C., Puglisi F., Zuiani C., Bazzocchi M.**
Role of breast MR in the pre-surgical management of invasive breast carcinoma (SS 602), B-266
- Del Guerra A.**
State-of-the-art in information technology:
Welcome address (EF 1), A-117
- Delgado Sánchez C., Fernández G., Santos-Armentia E., Trinidad C., Velasco M., Tardáguila F.**
Study of CABG with MDCT: Something rather than patency, stenoses or obstruction!, C-0276
- Delis H., Spyrou G., Costaridou L., Tzanakos G., Panayiotakis G.**
Dose and low contrast detectability of new anode materials in mammography: Monte Carlo simulation studies, C-0954
- Delistamatis A., Mantatzis M., Kaldoudi E., Ouzounis D., Prassopoulos P.**
Web based system for handling DICOM structured report documents from PACS for educational and research purposes (SS 305), B-238
- DellaPina C., Lencioni R., Crocetti L., Cioni D., Lera J., Montagnani S., Bartolozzi C.**
European Federation of Societies for Ultrasound in Medicine and Biology (EFSUMB) guidelines for contrast-enhanced US of the liver: Validation in characterization of incidental liver lesions (SS 306), B-121
- DellaPina C., Lencioni R., Cioni D., Crocetti L., Montagnani S., Lera J., Conti A., Batini E., Bartolozzi C.**
Diffusion-weighted MR imaging in the differentiation of benign and malignant focal liver lesions (SS 1801b), B-852
- DeMarco J., Cagnon C., Cody D., O'Daniel J., McCollough C., Zankl M., McNitt-Gray M.F.**
Estimating organ and effective dose from multidetector CT using Monte Carlo simulations: Initial results from voxelized patient models (SS 713), B-446
- Denys A., Doenz F., Qanadli S., Bessoud B., Schnyder P.**
Abdominal intervention: B. Management of gastrointestinal bleeding (WS 118), A-031
- Desai S.R.**
Imaging ICU patients: Imaging sequelae of acute lung injury (SF 8a), A-171
- Desai S.R.**
Thoracic manifestations of extra-thoracic disease:
A. Lung nodules in patients with extra-thoracic neoplasia (RC 1604), A-376
- deSouza N.M., O'Neill R., Dina R., Souter W.P., McIndoe G.A.**
Borderline tumors of the ovary: CT and MR features and tumor markers in differentiation from stage I disease (SS 1807a), B-791
- Dharaiya E., Gilkeson R., Ciancibello L., Subramanyan K., Durgan J., Pohlman S., Vlassenbroek A.**
Clinical validation of automated calculations of emphysema volumes, C-0281
- Di Cesare E.**
Cardiomyopathies: C. Arrhythmogenic right ventricular cardiomyopathy (RC 403), A-068
- Di Fabio F., Cianci R., Grassedonio E., Filippone A.**
"Misty Mesentery": Multidector row CT (MDCT) features and differential diagnosis, C-0078
- Di Roma M., Romagnoli A., Sperandio M., Tomassini M., Cammarata R., Simonetti G.**
MRA versus MSCT in the detection of coronary stenoses (SS 1003), B-528
- Di Salle F.**
Imaging of normal anatomy and function: A. Brain morphology and function (RC 111), A-020
- Di Terlizzi M., Puppi A., Fossaceca R., Caimmi F., Sacco M., Carriero A.**
Multidetector-row spiral CT (MDCT) angiography for the preoperative planning of minimally invasive coronary artery bypass (MICAB) grafting (SS 1003), B-527
- Dias S.M., Pina Vaz C., Gouvea M.**
Fat suppression in MR imaging: Techniques and clinical applications, C-0952
- Diaz S., Åkeson P., Casselbrant I., Piitulainen E., Pettersson G., Magnusson P., Wollmer P., Peterson B.**
Hyperpolarized ³He apparent diffusion coefficient MRI of the lung: Reproducibility, clinical correlation and safety (SS 1504), B-700
- Diaz Aguilera R., Martos Becerra J.M., Espejo Herrero J.J., Bautista Rodriguez D., Bravo Rodriguez F., Delgado Acosta F., Cano Sanchez A., Perez Ortega G.**
Benefits of early endovascular treatment of ruptured intracranial aneurysms: Clinical outcome and vasospasm incidence, C-0874
- Dickerson R.E., Bunch P.C.**
Evaluation of a high-speed high-resolution film/screen system for medical radiography (SS 1513), B-774
- Dicle O., Yazicioglu M., Secil M.**
A computer based examination for the assessment of reasoning skills in radiology, C-0384
- Diederich S.**
HRCT in diffuse lung disease: C. Ground glass opacities (RC 1704), A-417
- Dieguez-Costa E.M., Borrego-Gomez J., Fernandez P., Gonzalez B., Novo S.**
Focal fat stranding in computed tomography as a diagnostic tool in the acute abdomen, C-0171
- Diekmann F.**
Digital mammography: B. Logistics and workflow (RC 1302), A-319
- Diekmann F., Diekmann S., Jeunehomme F., Muller S., Hamm B., Bick U.**
First experiences with iodine-based contrast medium in digital full-field mammography (SS 302), B-160
- Dietzel M., Malich A., Fischer D.R., Marx C., Deicke C., Reuchsel C., Taher F., Kaiser W.A.**
Differential diagnosis of up to 10 mm sized breast lesions using morphologic and dynamic features of MR-mammography (SS 602), B-261
- Dietzel M., Malich A., Fischer D.R., Marx C., Reuchsel C., Deicke C., Taher F., Kaiser W.A.**
Comparison of dynamic and morphologic MR features of small vs large breast cancer cases (SS 702), B-371
- Diris B., Bonnefoy O., Hauger O., Moinard M., Diard F.**
Acute knee trauma: Sonographic emergency?, C-0684
- Dirisamer A., Bammer R., Vass K., Thurnher M.M.**
Diffusion-weighted MR imaging of the spinal cord in multiple sclerosis (SS 211), B-093
- Dixon A.K., Housden B.**
Logistic implications of MDCT: Logistic implications of MDCT (E³ 620a), A-157
- Djuric-Stefanovic A., Ivanovic A., Saranovic D., Masulovic D., Dobriserevic B.**
Ultrasonographic visualisation of abdominal wall hernias, C-0174
- Dobben A.C., Wiersma T.G., Janssen L.W.M., de Vos R., Terra M.P., Baeten C.G.M.I., Stoker J.**
Prospective assessment of interobserver agreement for defecography in fecal incontinence (SS 1801a), B-818
- Dobriserevic B., Masulovic D.M., Saranovic D., Ivanovic A., Djuric A.**
Radiological presentation of avulsion injuries of the shoulder, knee, ankle and foot, C-0701
- Dobriserevic B., Masulovic D.M., Saranovic D., Ivanovic A., Djuric A.**
Diagnostic value of ultrasonography in ruptures of the posterior cruciate ligament of the knee, C-0702
- Dobritz M., Weiss W., Stolfuss J., Rummeny E.J.**
MSCT with combined CT-angiography for diagnosis of suspected mesenteric ischemia or intestinal bleeding in patients presenting with acute abdominal symptoms (SS 701a), B-364
- Dogan H., Kroft L.J.M., Bax J.J., Schuijf J.D., de Roos A.**
Validation of right ventricular systolic function using multislice CT (SS 703b), B-428
- Dolgushin M.B., Pronin I.N., Tissen T.P., Radkevich L.A., Zayceva A.J., Kornienko V.N.**
Whole body positron emission tomography (¹⁸FDG PET) in patients with brain metastases (SS 711), B-438
- Domínguez Echávarri P., Bastarrica Alemán G., Cano Rafart D., Pons Renedo M., Larrache Latasa J., Alonso Burgos A., Zulueta Francés J.**
Impact of a computer-aided detection system (CAD) on a lung cancer screening program with low-dose multislice CT (MSCT) (SS 304), B-167

Authors' Index

Domínguez Echávarri P., Cano Rafart D., Bastarrika Alemán G., Larrache Latasa J., Vivas Perez I., Gonzalez Crespo I.
Multislice CT (MSCT) features of renal and pelvic lesions: A pictorial review, C-0455

Dominguez-Franjo E., Diez Perez de las Vacas M., Ramos Lopez P., Garcia del Salto L., Salmeron I., Fraile Moreno E.
Multidetector CT imaging of common and uncommon large cystic hepatic masses, C-0049

Donati F., Boraschi P., Gigoni R., Auci A., Cossu M.C., Falaschi F.
Evaluation of pancreatic duct abnormalities using secretin-stimulated MR pancreatography (SS 1001), B-482

Donati F., Boraschi P., Gigoni R., Auci A., Falaschi F.
The usefulness of MR pancreatography in the evaluation of cystic lesions and their relationship to the pancreatic ductal system (SS 1001), B-485

Donoso L.
Tele-imaging in Europe today: A. Introductory lecture on teleradiology (RC 405), A-093

Donuru A., Kandula V.V.R., Kumaran M., Entwistle J.
An audit of percutaneous lung biopsy performed at University Hospitals of Leicester, UK, C-0324

Doria C., Meloni G.B., Lisai P., Profili S., Meloni F.
Radiographic and clinical results of balloon kyphoplasty in the treatment of osteoporotic vertebral compression fractures, C-0637

Douek P.
MultiHance in MRA of peripheral vasculature (SY 5), E-18

Dougeni E., Delis H., Karatza A., Kalogeropoulou C., Skiadopoulos S., Malatara G., Efstatopoulos E., Panayiotakis G.
Radiation dose and image quality in neonatal radiography, C-0920

Downes M.
Strategies and protocols for managing high-risk patients (SY 10), E-47

Drakonaki E., Papakonstantinou O., Maris T., Koulieraki C., Vasiliadou A., Papadakis A., Gourtsoyiannis N.
Adrenal glands in beta-thalassemia major: MR imaging features and correlation with iron stores, C-0508

Drellich-Zbroja A., Elfurah M., Jargiello T., Rzeszowska-Sieczka M., Szczero-Trojanowska M.

Assessment of the prevalence and severity of carotid artery disease in patients with peripheral arterial disease (SS 715), B-450

Drescher R., von Rothenburg T., Köster O.
Standard-protocol moving-bed MR angiography for planning of interventional procedures in patients with peripheral vascular occlusive disease, C-0599

Develegas A.
Cerebral tumors and infections: A. Extra-axial brain tumors (CC 517), A-098

Drisis S., Seghers D., Srivastava S., D'Agostino E., Maes F., Marchal G.
Non-rigid registration for subtraction CT angiography of the abdomen and evaluation of various regularization models (SS 1015), B-551

Drisis S., Seghers D., Srivastava S., D'Agostino E., Maes F., Marchal G.
Non-rigid image registration for subtraction CT angiography of the abdomen is significantly more effective when the post-contrast image is deformed to match the pre-contrast image, C-1045

Dubbins P.A.
Pediatrics/Radiography: C. Pros and cons of radiographer reporting: A radiologist's viewpoint (RC 1214), A-298

Ducou le Pointe H., Lenoir M., Ariche-Maman S., Montagne J.
Chest imaging: A. Multidetector CT of the chest: Guidelines and specificities in children (RC 1212), A-293

Duffaut-Andreux C., Guerini H., Feydy A., Bach F., Pessis E., Minoui A., Meziti L., Drapé J., Chevrot A.

Lumbar foraminal injections: Two techniques under fluoroscopic control, C-0747

Dujardin M.I., Sourbron S.P., Luypaert R., Van Schuerbeek P., Deridder F., Verbeelen D., Makkat S., Stadnik T.

Are renal perfusion parameters reliable without deconvolution analysis? (SS 1807b), B-860

Dujardin M.I., Sourbron S.P., Luypaert R., Van Schuerbeek P., Ernst C., Makkat S., Stadnik T.

Does a deconvolution analysis remove the dependency of renal perfusion parameters on injection dose? (SS 1807b), B-861

Duke D.M., Kennedy M.K., Kerr J., Doyle E., McNicholas M.M., Fenlon H.M., Flanagan F.
Unusual presentations of ductal carcinoma in situ: Radiological and pathological correlation, C-0226

Dyce S., Abraham L.J., Fitzgerald G.P., Garvey C.J.

Radiographic role extension in fluoroscopy: The four tier structure in practice (SS 1814), B-909

Dymarkowski S.

High-field body MRI: The new standard?: Cardiovascular (SF 5), A-105

Dzienis W., Jancewicz P., Tarasow E., Skowronski J., Walecki J., Kubas B., Janica J.
Knee joint cartilage lesions treated with stem cells grafting, C-0698

E

Eberhard J., Ross W.R., Basu S.K., FitzGerald P., Rumsey M.A., Schmitz A.M., Yanoff B.D., Ritchie C.J.
Large field-of-view ultrahigh-resolution flat-panel CT imaging system (SS 1413), B-663

Efremidis S.C.

Imaging of the lymphatic system: Imaging of the lymphatic system (Introduction) (SF 4b), A-059

Efremidis S.C.

Imaging of the lymphatic system: Normal lymphatic drainage (SF 4b), A-061

Eichinger M., Puderbach M., Fink C., Ley S., Gahr J., Wiebel M., Tuengerthal S., Müller F., Kauczor H.

Contrast-enhanced 3D-MRI of lung perfusion in children with cystic fibrosis (SS 1004), B-473

Eichler K., Mack M.G., Lehnert T., Zangos S., Söllner O., Herzog C., Vogl T.J.
"Lesions in necrosis phenomenon" in patients with liver metastases of neuroendocrine tumor after thermal ablation (SS 709), B-410

Eichler K., Mack M.G., Balzer J.O., Thalhammer A., Schwarz W., Heller M., Zangos S., Vogl T.J.
Hepatic intra-arterial chemotherapy with gemcitabine: An ongoing phase II study in patients with liver metastases of breast cancer (SS 1009a), B-507

Eikefjord E., Ulvik N., Jensen D., Rørvik J.
Decreasing the radiation dose for renal stone CT, C-0504

Eikefjord E., Ulvik N., Rørvik J.
Patient radiation dose at multidetector CT and conventional urography (IVU) for acute flank pain, C-0518

Ekborg O., Bülow M., Olsson R.
Respiratory patterns associated with swallowing (SS 1801a), B-810

Eklund K., Jonsson K., Lindblom G., Lundin B., Sanfridsson J., Sloth M., Sivberg B.
Are digital images good enough? A comparative study of conventional film-screen vs digital radiographs on printed images of total hip replacement (SS 1814), B-910

El Bagi M.E.A.
Gastrointestinal infection: A changing scene: C. Gastrointestinal parasite infestation (CC 516), A-135

Ei-Azab M., Mosbah A., El-Baz M., Shoier K.
Morphologic characterization of subtypes of renal cell carcinoma by multislice CT (SS 707), B-396

Elias D., Marantz P., Guerchicoff M., Gutierrez A., Villa A., San Roman J.
Fetal heart tumors, C-0252

Elias D., Izbizky G., Medina Portillo S., Pietrani M., Farias P., San Roman J., Eleta F.
MRI and US value in myelomeningocele experimental surgical sheep model, C-0884

Ellis S.M.
Chest: C. The spectrum of tuberculosis and non-mycobacterial tuberculous infection (CC 416), A-088

Ellis S.M.
Multislice CT of the thorax: A. Evidence-based optimisation of standard protocols (RC 1204), A-278

Ellis S.M., Roddie M., Honeyfield L., Dehmeshki J.
Lung nodule analysis software: Is what you see really what you get?, C-0291

Elmaleh M.
Neuro-imaging: B. Imaging of sensorineural hearing loss: A practical approach in children (RC 912), A-239

Authors' Index

Elmståhl B.A., Nyman U., Leander P., Golman K., Almén T., Pehrson R., Chai C.
Nephrotoxicity after renal arteriography with "low" and "iso-osmolar" iodine and gadolinium contrast media (CM) in an experimental model (SS 1806), B-879

Emmel D., Haderer A., Yakan N., Gutberlet M., Klimes K., Werk M., Ricke J.
MARVIN: A modular image archive; ASENA: A web based RDE-tool, and secure DICOM-communication (IM 1), D-10

Emmer B.J., Steens S.C.A., Steup-Bekkeman M.G., Admiraal-Behloul F., Bosma G.P.T., Le Cessie S., Ouwendijk W.J.N., Huizinga T.W.J., van Buchem M.A.
Cerebral lesion load in neuropsychiatric systemic lupus erythematosus: A longitudinal study (SS 211), B-094

Endo M., Johkoh T., Kimura K., Yamamoto N.
CT findings of gefitinib-related interstitial pneumonitis in 65 patients: Multi-institutional analysis of West Japan Thoracic Oncology Group (WJTOG), C-0283

Engelhard K., Hollenbach H., Kiefer B., Winkel A., Engehausen D.
Prostate biopsy in supine position in a standard 1.5 T scanner under realtime MR-imaging control using an MR-compatible endorectal biopsy device. First results. (SS 1507), B-722

Engels J.M.L.
Safety considerations in MR: A. MR safety, biophysical effects and the European legislation (RC 1213), A-284

Erdogan N., Inci E., Dirim Vidinli B., Uluç E., Roditi A., Dirik M.
The importance of cervical fascial planes and compartments in treatment and prognosis in life threatening deep neck infections, C-0558

Ertel D., Kachelriess M., Sennst D., Kalender W.A.
Real-time prediction of the heart phase for tube current modulation (TCM) by kymogram detection from spiral CT scans of the heart (SS 1413), B-668

Esen G., Gurses B., Yilmaz M.H., Ilvan S., Ulus S., Celik V.
Gray-scale and power Doppler US in the preoperative evaluation of axillary metastases in breast cancer patients with no palpable lymph nodes (SS 1402), B-584

Esposito A., De Cobelli F., Perseghin G., Belloni E., Pieroni M., Chimenti C., Frustaci A., Maseri A., Del Maschio A.
Correlation between phosphocreatine (PCr) to ATP ratio (PCr/ATP) at cardiac ^{31}P -MR spectroscopy and fibrosis at delayed-contrast enhanced MRI in hypertrophic cardiomyopathy (HCM) (SS 203), B-082

Esposito A., De Cobelli F., Perseghin G., Scifo P., Canu T., La Torre A., Luzi L., Alberti G., Del Maschio A.
Functional and metabolic evaluation of the left ventricle of sprinters, middle distance and endurance elite track runners in the resting state by magnetic resonance imaging (MRI) and ^{31}P -MR spectroscopy (^{31}P -MRS) (SS 703b), B-422

Essig M., Schönberg S.O., Reith W., Le-Huu M., Dannenberg N., Lodemann K.
Perfusion MR imaging of cerebral gliomas: Which contrast media and dosage to use (SS 711), B-436

Essig M., Fink C., Giesel F., Debus J., Bock M., Kauczor H.
Cerebral AVM: Hemodynamic characterisation by ultrafast contrast enhanced MRA and non-enhanced dynamic active tagging MRA (SS 1811a), B-905

Estenne M.
Diagnostic and interventional radiology of transplants: Lung (heart and lung) (part 2) (SF 8b), A-188

Etechami G., Doenz F., Denys A., Cornuz J., Schnyder P., Qanadli S.
Acute pulmonary embolism: Predictive value of degree of arterial obstruction quantified with the CT obstruction index (SS 1404), B-596

Eun C., Kim Y., Choi S., Lee S.
Parenchymal cyst-like lesions in tuberous sclerosis, C-0925

Evans A.
Open questions: C. Screening planning (RC 502), A-110

Everse L.
How to write a successful grant proposal: How to write a successful grant proposal (E³ 620b), A-158

Exarhos D.N., Testembasi H., Karkantzia F., Chondros D., Farsaris D., Kaskarelis I.
Evaluation of thoracic aortic pathology by MSCT(16-slice) before and after endovascular treatment, C-1016

F

Facius M., Malich A., Wurdinger S., Neubauer H., Marx C., Kaiser W.A.
Correlation of dynamic and morphologic patterns of pure DCIS cases in MR-mammography (SS 602), B-263

Fahrig R., Strobel N., Hellinger J.C., Frisoli J.K., Arakawa H., Marks M., Do H.M., Kukuk M., Glazer G.M.
Initial in vivo results with flat panel detector C-arm CT (SS 209b), B-074

Faletti C.
Shoulder joint: C. Postoperative shoulder US and MRI (RC 1310), A-312

Fan G., Zang P., Guo Q., Wu Z.
Usefulness of diffusion/perfusion-weighted MRI in mouse gliomas: Correlation with histopathology (SS 1011), B-535

Fan G., Wu Z., Guo Q.
Prediction of outcome of hypoxic-ischemic encephalopathy in term neonates with proton MR spectroscopy and diffusion weighted imaging (SS 1412), B-643

Fanelli F., Salvatori F.M., Vagnarelli S., Corona M., Bruni A., Di Rezze L., Pucci A., Rossi P., Passariello R.
Stenting of the carotid arteries: 4 years of experience (SS 1009b), B-512

Fargeaudou Y., Pelage J., Jacob D., Abitbol M., Le Dref O., Rymer R.
Uterine fibroids: Relationship between symptoms and MRI evaluation (SS 1807a), B-794

Fausto A., Sardanelli F.

Breast MR adding single-voxel proton spectroscopy to dynamic imaging (SS 202), B-021

Fausto A., Menicagli L., Aliprandi A., Ulgheri N., Sardanelli F.

Lumbar spine and hip bone mineral density discordance assessed by dual-energy X-ray absorptiometry (DEXA) (SS 610), B-253

Fausto A., Bongiovanni M., Menicagli L., Cicconi P., Sardanelli F.

Potential predictive factors of osetoporosis in young HIV-positive subjects (SS 610), B-254

Fausto A., Sardanelli F.

A model for reporting dynamic breast MR imaging, C-0198

Fehér E., Tökés A., Tóth H., Mocsári Z., Turupoli E., Bánkuti A., Böröczk A., Maléta A.
Comparative analysis of objective data and subjective impressions reported by patients related to iodinated oral contrast material administration (SS 1814), B-915

Feldman U.

ASCR: Application specific CR (SY 8), E-33

Feldman U.

Massively scalable PACS (SY 8), E-37

Fencí P., Belohlávek O., Schutzner J., Fiala P., Pafko P., Zatloukal P.

Can FDG-PET/CT replace mediastinoscopy or operative biopsy in patients with lung tumors? (SS 1804), B-841

Feragalli B., Storto M.L., D'Agostino A.G., Sacco R., Mereu M., Colosimo C.

Accuracy of multislice CT with multiplanar reformations in staging malignant pleural mesothelioma (SS 704), B-388

Ferreiro A., Delgado A., Muyor P., Martínez de Aragon A., Stefanova R., Ramírez A.

MRI findings in patients with a clinical diagnosis or clinical suspicion of reflex sympathetic dystrophy (RSD), C-0771

Ferretti G.R., Aubaud L., Pépin J., Choury N., Coulomb M.

Instability of the central airways: Comparison of end expiratory to dynamic expiratory volumetric MDCT acquisitions (SS 1504), B-708

Ferrucci J.T.

Inauguration Lecture: Quantitative imaging: The next paradigm (IL), A-050

Feydy A., Dufour V., Le Page L., Belmatoug N., Fantin B., Vilgrain V.

Comparative study of post-operative and spontaneous pyogenic spondylodiscitis (SS 210), B-004

Fink C., Bock M., Buhmann R., Ley S., Puderbach M., Plathow C., Kauczor H.

Time-resolved parallel 3D MRA of the lung: SNR improvement using correlation analysis, C-0345

Fink C., Puderbach M., Ley S., Risse F., Kuder T.A., Bock M., Thaler J., Plathow C., Kauczor H.

Intraindividual comparison of 1.0 M gadobutrol and 0.5 M gadopentetate dimeglumine for time-resolved contrast-enhanced 3D magnetic resonance angiography of the upper torso, C-0386

Authors' Index

Fischer T.

The use of contrast enhanced ultrasound in renal transplants: First results and potential clinical benefit (SY 14), E-63

Fischer M.J., Maselli G., Pozzilli P., Mosca S., Lupattelli T., Scalera G., Lupattelli L.

Fenestrated abdominal stent-grafts: Preliminary results (SS 609b), B-300

Fischer T., Gangkofner A., Bensler S.,

Ladurner R., Mussack T., Liemann A.

Functional cine MRI for the assessment of implanted synthetic mesh in patients after incisional hernia repair (SS 1801a), B-816

Fischer D., Awad N., Hershko D., Goralnik L., Krausz M., Angel A.

Appendiceal CT: A prospective randomized controlled study comparing three different protocols, C-0105

Fischer D., Farber E., Eliakim R., Beck-Razi N., Angel A., Gaitini D., Linn S., Baruch Y.

Barium esophagogram versus upper endoscopy for the screening of esophageal varices in patients with compensated cirrhosis. A blinded prospective study, C-0166

Fischmann A., Nykänen K., Esslinger M., Siegmann K.C., Wersebe A., Xydeas T., Claussen C.D., Miller S.

Image quality of a prototype full-field digital mammography system based on amorphous selenium (SS 302), B-157

Fischmann A., Läufle R., Siegmann K., Wersebe A., Xydeas T., Miller S., Claussen C.D., Müller-Schimpffle M.

The microcalcification matrix-system: A novel method to classify clusters of microcalcifications according to BI-RADS (SS 1402), B-587

Fité M., Enriquez G., Castellote A., Gratacós E., Delgado J., Piquer J., Carreras E., Lucaya J.

Prenatal assessment of lung hypoplasia in congenital diaphragmatic hernia (CDH): Correlation between volumetric MRI and biometric ultrasound measurements, C-0894

FitzGerald R.

Errors in radiology: Uncertainty, discrepancy, and errors in radiology (E³ 1020), A-260

Fitzmaurice D.

Nanotechnology: Basic tools and concepts (NH 6), A-151

Flatz W.H., Jäger L., Hempel M.J., Brüning R., Helmberger R., Pfennig S., Schönberg S.O., Reiser M.F.

Detection and delineation of laryngeal tumors using MRI with parallel acquisition technique (PPI MRI) and 16 row multidetector CT (MDCT) (SS 308), B-183

Fleischmann D.

How to design injection protocols for MDCTA (SY 9), E-40

Fleischmann D., Straka M., Sramek M.,

La Cruz A., Koehl A., Kanitsar A., Rakhs T., Napel S., Lammer J., Gröller E.

AngioVis: Computer graphics for clinical visualization of peripheral arterial occlusive disease (IM 1), D-19

Flis C.M., Connor S.E.J.

Imaging of head and neck venous malformations. A pictorial review., C-0779

Flis C.M., Jager H.R., Sidhu P.S.

The diagnosis and endovascular treatment of carotid artery and vertebral artery dissections, C-1075

Flodmark O.

Pediatric neuroradiology: B. Non-accidental head injury/child abuse (RC 1711), A-419

Floery D., Riedl C.C., Jaromi S.,

Fuchsjaeger M.H., Matzek W.K., Heinz-Peer G., Leodolter S., Helbich T.H.

Complementary role of CT-laser-mammography (CTLM) to mammography and ultrasound in patients with breast lesions (SS 202), B-027

Flor N., Castellazzi G., Missiroli C., Curti A., Soldi S., Franceschelli G., Sardanelli F., Cornalba G.P.

Unexpected internal carotid artery (ICA) atherosclerotic stenoses at biphasic MDCT for neck cancer (SS 308), B-185

Foerster B., Ksar J., Petrou M., Eldevik P., Maly P., Sundgren P.C.

Value of gadolinium administration in brain MRI examinations for developmental delay in children less than two years of age (SS 1412), B-645

Foo L.F., Raby N., Sambrook M.

Osteoid osteoma: A pictorial review, C-0672

Fork F.

Rectal carcinoma: Diagnosis (SF 4a), A-056

Forstner R.

Imaging of the uterus: B. Abnormal gynecological bleeding: What the gynecologist wants to know (RC 507), A-131

Forsyth L., Robertson E.M.

Can we trust each other? (SS 1814), B-916

Foster A., Given M., Thornton E., Lee M.

Percutaneous gastrostomy (PG) with T-fastener gastropexy: Reduction in complication rates with early removal of T-fasteners (SS 309a), B-194

Fraioli F., Catalano C., Venditti F., Bertoletti L., Passariello R.

Low-dose multidetector row CT (MDCT) angiography of the infrarenal aorta and lower extremity vessels: Comparison of different radiation dosages with standard DSA (SS 315), B-242

Fraioli F., Catalano C., Bertoletti L., Nardis P.G., Passariello R.

CT lung cancer screening supported by CAD system on Italian traffic policemen: One year preliminary results, C-0306

Francone M., Kalantzi M., Rademakers F.,

Herregods M., Dymarkowski S., Bogaert J.

Utility of real-time cine-MRI in the differential diagnosis between constrictive pericarditis and restrictive cardiomyopathy: Preliminary results (SS 203), B-084

Francone M., Taylor A., Kalantzi M., Dymarkowski S., Bogaert J.

Use of inversion recovery contrast-enhanced MRI (IR-CE-MRI) in the evaluation of patients with clinically suspected pericarditis (SS 203), B-090

Francone M., Carbone I., Lanciotti K., Algeri E., Ascarelli A., Cavacece M., Fedele F., Passariello R.

Utility of myocardial edema to differentiate between acute and chronic myocardial infarctions (MIs) and its correlation with the extension of necrosis: A T2-weighted and delayed enhancement (DE) cardiovascular-MR (CMR) study, C-0238

Franken E.M., van Almsick M.A.,

Rongen P.M.J., ter Haar Romeny B.M.

Context-enhanced detection of electrophysiology catheters in X-ray fluoroscopy images, C-0367

Franquet T.

Anatomy and basic signs in imaging: B. Basic findings and signs in imaging (E³ 120), A-043

Franquet T.

Chest: B. Infection in AIDS and the immunocompromised patient (CC 416), A-087

Franquet T.

Thoracic manifestations of extra-thoracic disease: B. Collagen vascular disease (RC 1604), A-377

Franquet T., Kaloger S.E., Oikonomou A., MacDonald S.L., Baile E.M., Mayo J.R.

Diagnostic accuracy of gadolinium-enhanced MR-angiography vs. Contrast-enhanced helical CT in the diagnosis of pulmonary embolism in the presence of lung infiltrate: An animal study., C-1083

Frauscher F.

Welcome and introduction (SY 1)

Frauscher F.

Imaging of prostate cancer: Present and future: Ultrasound (SA 14), A-353

Frede T.E.

Opportunistic breast cancer early detection in Tyrol, Austria 1996-2004. Do we really want or need a mammography screening program in Tyrol? (SS 1802), B-833

Freitas D.N.D., Orvalho L.

Male breast cancer: Retrospective analysis of 58 patients, C-0218

Freling N.J.M.

Salivary glands: C. Differential diagnosis in major and minor salivary gland tumors (RC 108), A-025

Frericks B.B., Lehmann K.S., Ritz J.P., Valdeig S., Buhr H.J., Wolf K.J.

Influence of hepatic vessel size on volume and shape of percutaneous thermoablative lesions: In-vivo evaluation in a porcine model (SS 209b), B-072

Freund M.C., Unsinn K.M., Rieger M., Mark W., Bonatti H., Margreiter R., Jaschke W.R.

Imaging findings after pancreas transplantation with enteric exocrine drainage: Posttransplantation anatomy and pathology, C-0053

Frey H.

Technical principles of RVS (SY 1), E-01

Freysschmidt J.

Assessment and accreditation in radiology in Europe: Delivering a national continuing medical education programme (ER 526), A-140

Frigerio L.F., Garbagati F., Di Tolla G., Rossi S.

Radiofrequency thermal ablation coupled with hepatic arterial occlusion in treating large-size HCC, C-0626

Fritzsche C., Hilger I., Trost R., Reichenbach J.R., Kaiser W.A.

MR imaging of Her-2/neu protein using high-affinity magnetic nanoparticles (SS 1406), B-672

Fritz G.A., Schoellnast H., Unger B., Deutschmann H.A., Stessel U., Tillich M.

Multiphase multidetector CT (MDCT) in diagnosis and staging of transitional cell carcinoma of the renal pelvis and the ureter (SS 707), B-399

Authors' Index

Fritz J., Solaiyappan M., Bomma C., Tandri H., Lima J.A.C., Claussen C.D., Bluemke D.A. Comparison of contraction pattern of the normal right ventricle using cine magnetic resonance imaging in transaxial plane versus long axis plane (SS 703b), B-421

Fritz J., König C.W., Böhm P., Maurer F., Badke A., Müller-Schimpffle M., Claussen C.D., Pereira P.L.

Presurgical transcutaneous MRI-guided marking of intramedullary tumors, C-0612

Fritz J., König C.W., Clasen S., Günaydin I., Tepe G., Köller I., Claussen C.D., Pereira P.L. MR-fluoroscopy-guided corticosteroid-infiltration of the sacroiliac joints: Pain therapy of sacroiliitis in patients with spondylarthropathy, C-0623

Fritz G.A., Riccabona M., Deutschmann H., Weitzer C., Resch B.

Three-dimensional ultrasound (3DUS) of the neonatal brain: Clinical application in patients of the neonatal intensive care unit (NICU), C-0917

Frokjær J.B., Liao D., Bergmann A., McMahon B.P., Steffensen E., Drewes A.M., Gregersen H.

Magnetic resonance imaging assessing the three-dimensional biomechanical properties of the human rectum, C-0109

Frokjær J.B., Larsen E., Steffensen E., Nielsen A.H., Drewes A.M.

Magnetic resonance imaging of the small bowel in inflammatory bowel disease, C-0110

Fruth M., Finke M., Schliephake K., Brassel F., Papke K.

Optimization of stenosis quantification using 16-row MDCTA in a phantom model simulating soft and calcified plaque material (SS 715), B-453

Fu H.H., Feng F., Jin Z.Y., Tao W., Wang R.Z., Yang Y., You H., Li X.Z., Sun F.

How many diffusion gradient directions will be adequate for the clinical applications of diffusion tensor imaging and tractography in cerebral tumors at 3 T MRI, C-0824

Fuchsäger M.H., Flöry D., Philipp M., Riedl C.C., Sylvia J., Helbich T.H.

The negative predictive value of electrical impedance scanning in BI-RADS IV breast lesions (SS 202), B-023

Fuchsäger M.H., Cáccilia R.S., Riedl C.C., Rudas M., Flöry D., Helbich T.H.

Galactography-guided stereotactic wire localization of intraductal lesions (SS 1502), B-730

Fuchsäger M.H., Mlynarik V., Marlovits S., Philipp M.O., Trattnig S.

High field magnetic resonance imaging of reconstituted articular cartilage: Evaluation of cartilage maturation for determination of optimal transplantation time, C-0678

Fujii N., Katada K., Yoshioka S., Takeuchi K., Takasu A., Naito K.

Imaging technique for obtaining optimal sections of the ossicular chain by high-resolution multiplanar reformation based on measurements of normal auditory ossicular angles, C-0560

Fukuba E., Wada A., Uchida K., Kajitani T., Nagami A., Kitagaki H.

Brain activation in the differences game: A functional magnetic resonance imaging study, C-0806

Fung K.K.-., Choi K.H.-.

Lens dose reduction in paediatric CT brain scan using the supra-orbitomeatal baseline technique, C-0994

Funovics M.A., Weissleder R., Reynolds F., Josephson L.

Synthesis of a combined optical/MRI contrast agent for imaging endothelial E-selectin expression (SS 1406), B-671

Funovics M.A., Kapeller B., Macfelda K.

MR imaging of the Her2/neu and 9.2.27 tumor antigens using immunospecific contrast agents (SS 1406), B-674

Funovics M.A., Su H.S., Weissleder R., Mahmood U.

In vivo imaging of protease activity and marker gene expression through a fiberoptic catheter-based fluorescence detection system (SS 1506b), B-787

Furukawa H., Uesaka K., Boku N.

Prospective evaluation of multi-detector CT (MDCT) for treatment decision making in pancreatic adenocarcinoma (SS 701b), B-412

Furuya K., Sakino I., Harada N., Yasumori K., Muranaka T.

CT Evaluation of the acute abdomen caused by colorectal carcinomas, C-0146

Furuya K., Sakino I., Yasumori K., Muranaka T.

Diseases of peritoneum, mesentery, and omentum: Spectrum of helical and multidetector-row CT findings, C-0170

Fütterer J.J., Scheenen T.W.J.,

Heijmink S.W.T.P.,

Hulsbergen van der Kaa C.A., Witjes F., Barentsz J.O.

Staging and localizing prostate cancer using 3 T endorectal coil MR imaging (SS 1007), B-490

Fütterer J.J., Heijmink S.W.T.P.,

Heesakkers R.A.M.,

Hulsbergen van der Kaa C.A., Witjes F.A., Barentsz J.O.

MR imaging features of prostate carcinoma in local and nodal staging, C-0468

G

Gada V.S., Hemingway A., Williamson R., Trew G., Lavery S., Margara R.

Salpingitis isthmica nodosa (SIN) in female infertility, C-0417

Gahleitner A.

How to investigate facial pain: B. Pain of dental origin (RC 1708), A-422

Gaitanis A., Kandarakis I., Cavouras D., Kalivas N., Dimitopoulos N., Nikolopoulos D., Panayiotakis G.

The importance of detector type, detector material, reconstruction filter and reconstruction algorithm in simulated computed tomography breast imaging, C-0955

Galanski M.

Diagnostic and interventional radiology of transplants: Diagnostic and interventional radiology of transplants (Introduction) (SF 8b), A-183

Galesanu C., Galesanu R.G., Melnic G.

Digital X-ray radiogrammetry (DXR-BMD) used in follow-up efficacy of alfalcalcidol in postmenopausal osteoporosis (SS 610), B-252

Gallardo E., García-Barredo R., Prieto J.R., García J.

Long-term follow-up of total knee replacement: Role of high resolution ultrasound, C-0687

Gallardo E., Figols J., Sanchez E., García-Barredo R., Landeras R., Fernández M. Intra-articular fat tissue tumors of the suprapatellar recess: Magnetic Resonance imaging with pathological correlation, C-0688

Gallucci M.

Degenerative disorders, tumors and infection of the spine: A. Degenerative disorders of the spine (CC 1617), A-366

Galluzzo M., Buffa V., Cortese A., Regine G., Pallotta F., Miele V., Adamí L.

Emergency MR imaging of knee trauma with normal radiographic findings, C-0696

Ganau S., Andreu X., Sáez E., Tortajada L., Massuet A., Sentís M.

Ductal carcinoma in situ: MR mammographic appearance and pathological correlation (SS 602), B-262

Gandini R., Konda D., Pipitone V., Maresca L., Spinelli A., Pampana E., Simonetti G.

PTFE-covered stent increases patency and clinical outcome in patients with TIPS for Budd-Chiari syndrome (SS 1009a), B-508

Gandini R., Konda D., Spinelli A., Fabiano S., Reale C.A., Pampana E., Simonetti G.

Carotid artery stenting under cerebral protection: Experience in 96 patients (SS 1009b), B-511

Gandini R., Chiocchi M., Stefanini M., Pipitone V., Pendenza G., Simonetti G.

Use of covered stents in treatment of large neck internal carotid artery (SS 1009b), B-519

Gandini R., Chiocchi M., Fabiano S., Pampana E., Spinelli A., Simonetti G.

Percutaneous treatment in iliac artery occlusion: Long-term results (SS 1409b), B-632

Gandini R., Maresca L., Pipitone V., Pampana E., Konda D., Reale C., Simonetti G. Subintimal angioplasty: Experience in 58 patients (SS 1409b), B-635

Gandini R., Pipitone V., Chiocchi M., Reale C., Konda D., Simonetti G.

Transcatheter embolization of male varicocele with Fibro-Vein mousse infusion: Experience with 260 patients (SS 1809), B-873

Garcia Contiente G., De Caralt T.M., Ayuso J.R., Pare C., Sitges M., Ayuso C., Perea R.J., Ramirez J., Tomaselio A.

Magnetic resonance imaging and non-compaction of the ventricular myocardium: Unusual or underdiagnosed disorder?, C-0232

García Criado A., Gilabert R., Vannoni M., González S., Brú C.

Thrombosis of the middle hepatic vein in living liver donors, C-0030

García-Asensio S., Gómez H., Sarría L., Cozcolluela R., Forradellas A., Martínez-Berganza M., Monzón F.

Computed tomography patterns of mesenteric and omental disease, C-0072

García-Asensio S., Cozcolluela R., Gómez H., Sarría L., Martínez-Berganza M., Forradellas A., Alberdi I., Monzón F.

Helical CT in the evaluation of acute bowel ischemia: Common findings, uncommon findings and pitfalls, C-0099

Authors' Index

- García-Medina J., Serrano-García C., León-Hernández A., Basile A., García-Medina V., Leal-Adán R. Treatment of malfunctioning radial native haemodialysis fistulas: Comparison between cutting-balloon PTA and standard PTA, C-0575
- Gardeur D.J., Leprince C., Baekeland H. Teleradiology volume analysis of CT and MRI, C-0378
- Gardner E.A., Sumanaweera T.S., Woelmer M.N., Steins R.W., Leen E. Analysis of an automatic ultrasound image registration system to improve contrast quantification for hepatic perfusion assessment, C-0394
- Garel C. Fetal MR imaging: CNS malformations (SF 17), A-407
- Garriga V., Roson N., Medrano S., Zarcero M., Pruna X., Cuadrado M., Marin A., Carbó S., Vizcaya S., Català M. Pediatric urolithiasis: High-resolution sonography and clinical review, C-0928
- Garvey C.J., Abraham L., Furdridge I., Holme E. Reducing non-attendance rates for barium enemas through enhanced booking procedures, C-0160
- Gasparotti R. Hemorrhagic stroke: B. Intracranial aneurysms (CC 417), A-053
- Gasser J., Celedin S., Hausegger K. Pseudo-occlusion of the internal carotid artery assessed by MRA: How to avoid misinterpretation, C-1017
- Gast K.K., Stavngaard T., Wild J.M., Morbach A.E., Vejby Soegaard L., Dahmen A., Kauczor H., van Beek E.J.R., Heussel C. Diffusion weighted ³He-MRI in the assessment of pulmonary emphysema (SS 1504), B-701
- Gattinoni L. Imaging ICU patients: Imaging ICU patients (Introduction) (SF 8a), A-168
- Gattinoni L. Imaging ICU patients: Structure-function correlations in acute lung injury (SF 8a), A-169
- Gawenda M., Heckenkamp J., Krüger K., Brunkwall J. Endovascular repair of aneurysm after previous tube graft interposition due to coarctation or traumatic transection (SS 209a), B-063
- Gawenda M., Winter S., Jaschke G., Wassmer G., Brunkwall J. Intra-abdominal pressure influences endotension following endoluminal grafting of AAA: Experimental findings (SS 609b), B-291
- Gazhonova V., Chepurov A., Zubarev A. 3D multiplanar TRUS with power Doppler in detecting prostatic fossa recurrences following radical prostatectomy (SS 1507), B-726
- Geiger B. Quality control and dose reduction in digital radiology: A. Principles of flat panel X-ray detectors and photostimulable plates (RC 1313), A-347
- Geissler A., Barth M., Lanzenberger R., Gartus A., Tahamtan A.R., Meller G., Foki T., Milakara D., Beisteiner R. Functional CNR as a fMRI specific quality parameter for presurgical mapping in tumor patients (SS 1811b), B-930
- Geleijns J., Bloem J.L., Kievit J., Spilt A. Justification and optimization of multidetector CT (MDCT) examinations: A. Justification of MDCT examinations (RC 1613), A-396
- Gennaro G., Bellan E., Gambaccini M., di Maggio C. Scatter-to-primary evaluation in full field digital mammography (SS 1013), B-546
- Gennaro G., Souchay H., di Maggio C., Katz L., La Grassa M., Pescarini L., Alberelli C. Dose reduction and diagnostic accuracy in full-field digital mammography: A clinical study, C-0187
- Genovese E., Leonardi A., Callegari L., Angeretti M., Indirinella S., Fugazzola C. Evaluation of rotator interval pathology in athletes with MR arthrography (SS 310), B-134
- George C., Titi M., Bhattacharya D., Woodhead P.M., Stevenson W.J., Pillai A., Ettes D.F., Al-Khaffaf H. Spiral CT angiography: A valuable decision-making tool for carotid endarterectomy, C-1012
- Gerber B.L., Coche E., Belge B., Lim P., Pasquet A., Vanoverschelde J. Characterization of acute and chronic myocardial infarcts by multidetector CT. Comparison with contrast-enhanced MR, C-0253
- German I., Dolgova I., Andriyanicheva H., Gordeev A., Zubarev A.V. Ultrasonography of ankle joint and foot in early diagnosis of rheumatoid arthritis, C-0710
- Ghanem N.A., Schwarz M., Pache G., Müller C., Uhl M., Bley T., Langer M. MRI in thoracolumbar burst fractures (SS 210), B-008
- Ghanem N.A., Franke P., Pache G., Bley T., Winterer J., Langer M. Whole-body MRI in staging cancer patients: A comparison with conventional CT and MRI (SS 1406), B-675
- Ghiasas A.A. Modern imaging of infective disease in the face and pelvis: C. The spectrum of pelvic infection (CC 916), A-243
- Ghirardi C., Maroldi R., Farina D., Piazzalunga B. Reassessing the MR signal findings of sinonasal adenocarcinoma versus (non-adenocarcinoma) epithelial malignancies (SS 308), B-181
- Gibo M., Murayama S., Nakayama T., Morita T., Gibo S. Percutaneous transhepatic portal vein embolization using newly altered four-lumen balloon catheter: Preliminary clinical experience, C-0582
- Gibson D., O'Regan D.P., Allen S., Larkman D., Zeka J., Allsop J., Schmitz S. Direct thrombus MRI: Preliminary experience at 3 Tesla magnetic field strength (SS 215), B-117
- Gielen J.L.M.A., De Schepper A.M.A., Van Marck E., Van Dyck P., Vanhoenacker F., Parizel P.M. Benefit of peer-reviewed pathological examination of soft tissue tumors. What is the role of radiology? (SS 1010), B-463
- Gietema H.A., Prokop M., Mali W.P.T.M. Measuring lung nodules: Inter-observer variability (SS 304), B-170
- Gil D., Castaner E., Gallardo X., Mata J., Pallardo Y., Perendreu J., Massuet A. Congenital and acquired anomalies of the pulmonary arteries in adults: A radiologic overview, C-0326
- Gil J., Guijarro J., Palmero J., Vera A., Dualde D., Dosdá R. New brain lesions at diffusion-weighted MR after carotid angioplasty and stent placement, C-0875
- Gillams A.R. Multi-dimensional imaging for guiding therapy: Real-time monitoring of interventional procedures (SA 12), A-269
- Gillams A.R., Pereira S., Lees W. Correlation of secretin MRCP derived quantification of exocrine function with faecal elastase 1 and urinary pancreoaural tests (SS 1001), B-481
- Gilon R., Houssiau F.A., Vande Berg B.C., Lecouvet F., Malghem J. Steroid-induced femoral head osteonecrosis: Comparison of proximal femur marrow status at baseline MR imaging between patients who will develop and who will not develop femoral head osteonecrosis during corticosteroid-treatment (SS 210), B-003
- Gimenez A., Franquet T., Hidalgo A., Salinas T., Valverde S., Bordes R. Thoracic tumors and pseudo-tumors associated with interstitial lung diseases: HRCT findings with pathologic correlation, C-0279
- Girard N. Pediatric neuroradiology: A. Congenital lesions of the brain (RC 1711), A-418
- Girometti R., De Candia A., Sbuelz M., Toso F., Zuiani C., Bazzocchi M. US morphology of the supraspinatus tendon in basketball players: Correlation with main pathologic models of impingement syndrome in young overhead athletes. Preliminary report (SS 1810), B-805
- Giunta S., Canitano S., Ordonez P.L., Vallati G., Benassi M., Crecco M. Diagnostic performance of a computer-aided diagnosis tool (CAD) for the detection of pulmonary nodules in low dose lung cancer screening CT, C-0338
- Giusti S., Giusti P., Marchetti L., Bartolozzi C. MR findings that may aid in the evaluation of Crohn's disease activity, C-0130
- Glaser C. Knee joint: B. MR-based cartilage imaging in the knee prior and after transplantation (RC 1710), A-403
- Glaser C., Mendlik T., Rauch E., Milz S., Schulz S., Putz R., Reiser M.F. Reduction of T2 relaxation times in articular cartilage after enzymatic proteoglycan depletion (SS 1510), B-683

Authors' Index

Gluecker T., Schwarz J., Bongartz G.,

Bilecen D.

Optimisation of imaging parameters of MR angiography of the hand with subsystolic cuff-compression (SS 315), B-248

Gleeson, T.

Contrast-induced nephropathy: Patient demographics and risk (SY 10), E-46

Gmur A., Zdunek P., Pacho R.

Are small-matrix (256x256 pixels) images of emergency CT examinations good enough for teleradiology diagnosis?, C-0374

Gollbiowski M., Bogorodzki P.,

Szeszkowski W., Piatkowska-Jankó E.,

Wolak T., Orzechowski M., Kurjata R.,

Cieszanowski A.

Differences in regional BOLD responses in the primary and secondary auditory cortex induced by mixed noise and speech like stimuli (SS 1811b), B-929

Goffette P.

Abdominal trauma: C. The role of intervention (RC 401), A-065

Goh V.J., Halligan S., Hugill J., Gartner L.,

Bartram C.

Colorectal cancer perfusion measurement using dynamic contrast enhanced MDCT: Effect of acquisition time and implications for protocols (SS 301a), B-149

Goh P.S., Venkatesh S.K., Shabbir A.,

Tan L.K.A., Wang S.C.

Utility of multi-detector row CT angiography in cases of gastrointestinal hemorrhage, C-0096

Gola M., Pacho R., Bakon L., Grabowska L., Palczewski P.

Arteries arising from the aneurysmal sac as a cause of type 2 endoleak after endovascular treatment of abdominal aortic aneurysms: Study of 115 patients (SS 615), B-332

Golding S.J., Saeed R., Alvey C., Evangelou I., McIntyre A., Watt-Smith S.

Imaging cortical bone by MRI: A new approach to image-guided planning for reconstructive surgery of the face (SS 208), B-055

Golebiowski M., Bogorodzki P.,

Jankó-Piatkowska E., Wolak T.,

Orzechowski M., Kurjata R., Szeszkowski W.

Differences in regional BOLD responses in the primary and secondary auditory cortex by mixed noise and speech like stimuli, C-0844

Golovko T., Medvedev V.

Ultrasound investigation in differential diagnostics and treatment planning of soft tissues pathologies, C-0732

Goldpinar F., Ozer C., Nass Duce M.,

Turhan A.H., Akbas T., Sert G., Kara E., Atici A.

Ultrasonographic measurements of the adrenal and thyroid dimensions and their correlation with length, gestational age and birth weight of healthy neonates, C-0929

Beresnak A., Gomez E., Rombolá S.E., Simoncini A.

Evaluation of Takayasu arteritis with MRI and contrast enhanced magnetic resonance angiography (CEMRA), C-1024

Beresnak A., Gomez E., Rombolá S.E.,

Simoncini A.

MR angiography of lower extremities with moving-table infusion-tracking technique, C-1031

Gomez-Dermit V., Landeras R., Merino P.,

Sanchez-Salmon E., Aguilar M.,

Fernandez-Echevarria M.A.

Usefulness of high-resolution sonography in the evaluation of soft tissue masses of the foot, C-0731

Gomez-Gonzalez E., Aguilera-Navarro J.,

Castela-Murillo A., Vera-Valencia M.,

Dominguez-Marín M., Cano-Rodríguez A.

Three-dimensional visualization and calculation of lesional volume in patients of multiple sclerosis. Fundamentals and preliminary results (SS 205), B-110

Gomi S., Suzuki M., Doi S., Daisaki H.,

Murano T., Mayumi K., Muramatsu Y.,

Tsukagoshi S., Moriyan N.

Automatic exposure control in low-dose chest CT with 16 slice MSCT, C-0342

Gomi T., Koshida K., Miyati T.

Development of a new three-dimensional image reconstruction algorithm to reduce cone-beam artifacts, C-0951

Gonzalez C., Garcia de Iturraspe C.,

Fernandez E., Alustiza J., Ontañón J.,

Arrillaga A., Barrera M., Gervás C.

Rectal carcinoma staging with MRI: The accuracy in the prediction of free tumour resection margins, C-0136

Gonzalez Gordaliza C., Martínez San Millán J.,

Vicente Bartolos A., Sanz de Leon O.

The role of computed tomography with aerial manoeuvres in the diagnosis of aerodigestive tract tumors, C-0546

Gonzalez Gordaliza C., Martínez San Millán J.,

Vicente Bartolos A., Sanz de Leon O.

Labyrinthitis ossificans: CT scan and MRI findings, C-0561

Goodman L.R.

Imaging ICU patients: Clinical correlation in the imaging of ARDS (SF 8a), A-170

Gopal K., Tuck J., Razzaq R.

Role of radiology in the diagnosis and management of epiphora, C-0527

Gotfried V.

Mammo-CR (SY 8), E-36

Gough N., Meehan C.P., McCarthy P.A.

The importance of the transitional zone at repeat transrectal ultrasound-guided prostate biopsy, C-0472

Goulão A.

Ischemic stroke: C. Carotid and vertebral artery disease (CC 117), A-003

Bakshi D.R., Gould , Powell S., Yeang H., Fewins H.

A pictorial review of anomalies of the thoracic aorta with embryological correlation, C-1062

Gourtsoyannis N.

MR imaging of the small intestine: MR imaging of the small intestine (Introduction) (SF 13), A-313

Gowland P.A.

Fetal MR imaging: Technical considerations (SF 17), A-406

Graf H., Steidle G., Lauer U.A., Claussen C.D.,

Schick F.

Metallic stents in MRI: Signal reduction in the lumen caused by RF effects, C-0975

Grainger A.

Ankle/foot ultrasound and ultrasound guided musculoskeletal interventions (SY 16), E-69

Grampp S.

Osteoporosis and osteopenia: B. How to measure and monitor it (RC 510), A-102

Graser A., Becker C.R., Suess C., Reiser M.F.

Dose reduction and image quality assessment in multi-detector row CT virtual colonography by online z-axis tube current modulation (SS 1501a), B-691

Grazioli L.

Imaging of focal lesions: Liver (EM 1), A-147

Grazioli L., Morana G., Romanini L., Mazza G., Morena M., Schneider G.

MR with different liver specific contrast media in the evaluation of hepatic adenoma (HA) and liver adenomatosis (LA): Imaging and pathological findings in an intra-individual comparison group (SS 201b), B-049

Greess H., Alibek S., Zenk J., Bozzato A., Iro H., Bautz W.

Dynamic contrast-enhanced MRI studies in parotid tumors (SS 208), B-052

Gregersen H.E.

Diagnostic reading of radiology images on a wireless PDA: Fact or fiction? Futuristic or foolish? (SS 305), B-236

Grenier P.A.

Harmonization of training programmes: Myth or reality?: Objectives for the future (ER 126), A-029

Grenier P.A.

Interstitial and alveolar disorders: B. Alveolar lung disease and atelectasis (E³ 420), A-097

Grgic A., Heinrich M., Girmann M., Kramann B., Uder M.

Computed tomography guided automated cutting needle biopsy of pulmonary lesions. Self assessment test, C-0640

Grimm C., Hochmuth A., Huppertz H.

Voxel-based CT analysis for improved detection of early CT signs in cerebral infarction (SS 611), B-315

Grist T.

An important step forward in the evolution of MRA techniques (SY 2), E-07

Gromov A.I., Vasilyev A.Y., Zykin B.I., Kubova S.Y., Kapustin V.V.

Diagnostic efficacy of the twinkling-artifact in detection of calcifications, C-0973

Grothoff M., Spors B., Abdul-Khalil H.,

Felix R., Gutberlet M., Gutberlet M.

Evaluation of parameters that effect QRS duration in patients after surgical repair of fallot determined by magnetic resonance imaging (MRI) (SS 703b), B-423

Groves A.M., Kayani I., Syed R., Nagabushan N., Ell P.J.

Imaging scaphoid trauma: An international survey of hospital practice (SS 210), B-007

Groves A.M., Beads Moore C.J., Balan K.K., Cheow H.K., Courtney H.M., Kaptoge S., Bearcroft P.W.P., Dixon A.K.

Can 16-detector multislice CT rule out skeletal metastases whilst staging the soft tissues? (SS 1010), B-465

Authors' Index

Groves A.M., Warren R.M.L., Godward S., Rajan P.S.

Characterization of pure high grade DCIS on magnetic resonance imaging using the evolving breast MR lexicon terminology: Can it be differentiated from pure invasive disease?, C-0200

Gruszcynska K., Baron J., Zielinski Z.

Cerebral vascular malformations and developmental anomalies in patients with extracranial carotid stenosis in CTA, C-0868

Grzelak P., Gorska-Chrzastek M., Goraj B., Kusmierenk J., Stefanczyk L.

Fusion of MRI and SPECT images in the diagnosis of glioma recurrence, C-0809

Grzelak P., Gorska-Chrzastek M., Tybor K., Gajewicz W., Kusmierenk J., Goraj B., Stefanczyk L.

Fusion of MRI and SPECT images as a method of planning spectroscopy of recurrent brain tumors, C-0869

Guarise A., Ferrari M., Turchetta S., Romano L., Salvia R.

Evaluation of the natural history of pancreatic branch duct IPMTs by follow-up with cross-sectional imaging (SS 1001), B-484

Guerini H., Feydy A., Drapé J., Chevrot A.

MR-arthrography of the scapholunate ligament: Correlation with arthroscopy (SS 310), B-132

Guerini H., Feydy A., Drapé J., Chevrot A.

US of the rotator cuff tendons in "pulse subtraction" mode: Are longitudinal intra-tendinous tears finally visible? (SS 1810), B-804

Guermazi A., El-Hariry I., Miaux Y.

Imaging features of metastases and local recurrence in surgically treated kidney cancer, C-0460

Guermazi A., Guth S., Gangi A.

Percutaneous image-guided lymph node biopsy in lymphoma: Tips and tricks, C-0649

Gullien R., Haakull A., Kristiansen S.J., Loevstad M., Skaane P.

Number and reasons for additional views (mosaic) at full-field digital mammography (FFDM) with a 19x23 digital detector (SS 302), B-154

Güllmar D., Haueisen J., Reichenbach J.R.

b-Matrix assessment in diffusion tensor imaging using a reference phantom (SS 1813), B-920

Guntern D.V., Favarger N., Schnyder P., Theumann N.H.

Three-compartment wrist MR arthrography: Impact on diagnostic thinking and treatment plan (SS 310), B-133

Guo G., Zang C.H., Lin Z.X., Zhou X.G., Wu R.H.

Computed tomography for assessing the resectability and restaging TNM classification of esophageal carcinoma treated with pre-operative radiotherapy (SS 201a), B-015

Gurung J., Wetter A., Vogl T.J.

Clinical evaluation of the sensitivity and specificity of a software for automated detection of lung nodules in preliminary CT examinations (SS 605), B-324

Gutberlet M., Spors B., Klimes K., Grothoff M., Felix R.

Morphological and functional assessment of the heart: C. Assessment of the right heart function (RC 1703), A-411

H

Haba D., Aldescu C.C.

CT and MRI imaging of lesions involving the pterygopalatine fossa (SS 608), B-279

Habermann C.R., Cramer M.C., Graessner J., Gossrau P., Reitmeier F., Fiebler J., Jaehne M., Adam G.

Functional imaging of parotid glands: Diffusion-weighted echo-planar MRI before and after stimulation (SS 208), B-051

Hadjigeorgi C., Nikas J., Pitsoulakis G., Theofanopoulou M.

Aicardi syndrome: MRI and clinical findings, C-0861

Haemisch Y.

Recent advances in molecular imaging technologies (SY 15), E-68

Haen S., Gouttefangeas C., Boss A., Clasen S., Schmidt D., Kuczyk M., Stenzl A., Schild H., Pereira P.L., Rammensee H.

Radiofrequency ablation may activate the immune system and induce specific anti-tumoral immune responses in cancer patients, C-0611

Hafsa C., Golli M., Kriaa S., Zbidi M., Gannouni A.

CT features of pulmonary hydatid disease, C-0312

Hafsa C., Zbidi M., Kriaa S., Jerbi Ommezine S., Golli M., Gannouni A.

Imaging features of mediastinal hydatid cyst, C-0313

Haider M.A., Toi A., Sweet J., Kale A., Bloch N., Trachtenberg J.

Washout dynamic contrast enhanced versus T2 weighted MRI prior to transrectal ultrasound biopsy in patients at high risk for prostate cancer (SS 1507), B-721

Halka A., Misra R.R., Uthappa M.C., Kaniyur S., Berry M.G.

Necrotising fasciitis: A pictorial essay with radiological correlation, C-0733

Haller S., Radü E.W.

What is different in a radiologist's brain? (SS 1811b), B-926

Haller S., Schwarzbach J., Klarhöfer M., Radü E.W.

Time-resolved analysis of event related fMRI during language comprehension at word and sentence level (SS 1811b), B-928

Hallett R.L., Hiatt M.D., Fleischmann D., Hellinger J.C., Rubin G.D., Chan F.P.

Imaging of atrioventricular septal defect (AVSD) with multidetector-row CT angiography, C-0260

Hallscheid P.J., Fink C., Haferkamp A., Kauffmann G.

Preoperative staging of renal cell carcinoma with inferior vena cava thrombus using multi-detector CT and MRI: Prospective study with histopathological correlation (SS 707), B-398

Halpern B.S., Auerbach M.A., Yeom K., Fueger B.J., Weber W.A., Ratib O., Lufkin R.B., Czernin J.

Evaluation of local recurrence in re-staging of head and neck cancer: A comparison between PET and PET/CT (SS 308), B-187

Halpern B.S., Schiepers C., Weber W.A., Crawford T., Fueger B.J., Ratib O., Phelps M.E., Czernin J.

Presurgical staging of non-small cell lung cancer: A performance comparison between PET, hardware PET/CT and software image fusion (SS 704), B-384

Ham S., Chung S., Ko B., Yang I., Kim H.

The imaging follow-up of ACR category 3 lesions in screening work-up (SS 1802), B-831

Hamazawa Y., Koyama K., Okamura T., Wada Y., Wakasa T., Okuma T., Inoue Y.

Comparison of dynamic FDG-microPET study in a rabbit VX2 tumor model and that in a turpentine-induced rabbit inflammatory model, C-0761

Hammerstingl R., Breuer J., Vogl T.J.

Impact of detection and characterization of liver lesions (SY 2), E-05

Hammerstingl R., Parmentier S., Schwarz W., Vogl T.J.

Double contrast technique in MRI of liver: Differential diagnosis compared to histopathologic findings (SS 201b), B-045

Hammerstingl R., Schwarz W., Breuer J., Balzer T., Vogl T.J.

Diagnostic imaging of primary liver tumors: Evaluation of the hepatocyte-specific contrast agent Gd-EOB-DTPA (SS 201b), B-048

Hammerstingl R., Valette P.J., Regent D.M., Vogl T.J.

Optimization of iodine concentration for the diagnosis of focal liver lesions in MDCT (SS 1801b), B-855

Han D., Van Nostrand L.

Network vulnerability management: Protecting a better view of life, C-0376

Hannig C.E.M., Hellerhoff P.H., Wuttge-Hannig A.C., Schoppmann A., Werber K., Rummery E.J.

Dynamic videofluoroscopic assessment of the pseudoarthrosis of the scaphoid in decision making for surgical therapy (SS 1810), B-808

Hannig C.E.M., Hellerhoff P.H., Wuttge-Hannig A.C., Stein H., Rummery E.J.

Somatic findings in globus pharyngus: Results of a follow-up study before and after therapy (SS 1801a), B-809

Hansch A., Hilger I., Frey O., Sauner D., Malich A., Boettcher J., Brauer R., Kaiser W.A.

Flare-up arthritis imaging with native Cy5.5 versus albumin bound Cy5.5 (SS 1406), B-670

Hansch A., Rzanny R., Heyne J., Leder U., Reichenbach J., Boettcher J., Kaiser W.A.

Measurement of cardiac high-energy-phosphate metabolites in dilated cardiomyopathy (DCM) by ³¹P-MR spectroscopy, C-0236

Hansell D.M.

Interstitial and alveolar disorders: A. Diffuse infiltrative lung disease (E³ 420), A-096

Hansen J., Wormanns D., Diederich S.

Resolving small pulmonary nodules: CT characteristics (SS 204), B-036

Hansson B.

MRI/Neuroimaging: A. 3 Tesla whole body system MRI: Experiences from Lund University Hospital (RC 514), A-136

Authors' Index

- Hao J., Li K.**
A voxel-based morphometric study of Alzheimer's disease (SS 311), B-227
- Hao J., Li K.**
Visual attention deficits in Alzheimer's disease. A fMRI study (SS 311), B-228
- Happel B.M., Mang T., Matzek W., Latzke D., Niederle B., Kaserer K., Heinz-Peer G.**
Characterization of adrenal masses with MDCT and MRI (SS 707), B-400
- Hargaden G.C., Keogan M.**
Imaging of endometriosis, C-0427
- Hargaden G.C., Rea D., O'Brien S., Keane D., Meaney J.F.**
Pulmonary vein mapping with contrast-enhanced MR venography of the pulmonary veins prior to ablative therapy, C-1021
- Harisinghani M.**
Nanotechnology: Nanotechnology and diagnostic imaging (NH 6), A-153
- Harries-Jones H., Holden A.**
Contrast media side effects in the daily routine of a Radiographer (SY 4), E-12
- Hashagen C., Bongartz G., Steinbrich W., Aschwanden M., Jaeger K., Hügli R., Jakob L., Bilecen D.**
Reduction of contrast agent dose in intraarterial 3D contrast enhanced MR-angiography of the upper and lower leg (SS 315), B-250
- Hasiotou M., Manoli E., Pitsoulakis G., Pettas N., Anastopoulos I., Evangelidakis E.**
Intraarticular osteoid osteoma in children, C-0908
- Hasiotou M., Manoli E., Ioannidou M., Zarifi M., Evangelidakis E.**
CT findings of non-odontogenic tumors of the jaw in childhood, C-0931
- Hawkes D.**
Medical image registration: Methods, applications and validation: B. Applications (RC 913), A-245
- Hayasaka K., Saithoh T., Tanaka Y.**
Quantitative evaluation of ovarian tumors using Gd-dynamic contrast-enhanced MRI, C-0439
- Haykir R., Karaköse S., Karabacakoglu A., Sahin M., Kayaçetin E.**
MR colonography versus conventional colonoscopy for the detection of colonic lesions, C-0138
- He H., Shen T., Feng X.**
Temporal lobe epilepsy - correlation analysis of MRI volumetry, ¹H MRS and PET (SS 711), B-433
- He H., Shen T., Feng X.**
MRI segmentation in diagnosis and clinical correlations of temporal lobe epilepsy (SS 711), B-434
- Healey P.R., Healey A.E., Johnson S., How T., Gould D.A.**
Validation of a fixed model as a method of training in interventional radiology (SS 309b), B-202
- Heesakers R.A.M., Futterer J.J., Hövels A., van den Bosch H.C., Scheenen T.W.J., Barentsz J.O.**
USPIO-enhanced T2* images at 1.5 T and 3 T: Initial results (SS 1507), B-725
- Heidrich G., Wenzel S., Hermann K., Dullin C., Grabbe E., Funke M.**
Evaluation of balloon expanded stents in a cone-beam flat-panel volumetric-CT (FP-VCT) (SS 309b), B-207
- Heidrich G., Melderis F., Dullin C., Hermann K., Grabbe E., Funke M.**
Evaluation of experimental implanted occlusions in a stent-tube-model with a cone-beam flat-panel volumetric-CT (FP-VCT) (SS 615), B-333
- Heijmink S.W.T.P., Fütterer J.J., Huisman H.J., Scheenen T.W., Hulsbergen van der Kaa C.A., Witjes J.A., Blickman J.G., Barentsz J.O.**
Differentiating prostate cancer from healthy prostatic tissue with dynamic contrast-enhanced MR imaging with an endorectal coil at 3 T (SS 1007), B-493
- Heijmink S.W.T.P., Fütterer J.J., van Lin E., Scheenen T.W., Hulsbergen van der Kaa C.A., Witjes J.A., Blickman J.G., Barentsz J.O.**
Early detection of local prostate cancer recurrences after radiation therapy by means of endorectal dynamic contrast-enhanced MR imaging and 3D ¹H MR spectroscopy with biopsy confirmation (SS 1007), B-497
- Heiken J.P.**
Scan and contrast administration principles of MDCT (SY 9), E-39
- Hein E., Klüner C., Hein P., Elgeti T., Rogalla P., Hamm B.**
Does ultralow-dose CT suffice for detecting urolithiasis? (SS 1407), B-612
- Heinrich M., Grgic A., Tscholl D., Kramann B., Schäfers H., Uder M.**
Predictors on CT of hemodynamic improvement after pulmonary thromboendarterectomy, C-0328
- Heinrich M., Grgic A., Heckmann M., Kramann B., Uder M.**
Incidence of contrast media induced nephropathy in different diagnostic procedures, C-0387
- Heinz-Peer G.**
Multidetector CT of the kidneys and urinary tract (SY 7), E-29
- Heinz-Peer G.**
Imaging of stones: A. Plain film, IVU and ultrasound (RC 807), A-195
- Helbich T.H.**
CTLM and mammography (SY 13), E-56
- Helbich T.H.**
Breast MR imaging: B. MR guided interventional procedures (RC 102), A-012
- Heller M., Zangos S., Schwarz W., Balzer J.O., Mack M.G., Vogl T.J.**
Transarterial chemoembolization (TACE) in comparison to transarterial chemoperfusion (TACP) in patients with inoperable intrahepatic cholangiocellular carcinomas (ICC) (SS 1009a), B-504
- Hellinger J.C., Fahrig R., Strobel N., Fleischmann D., Glazer G.**
Initial experience with the Artis dTA flat panel detector (FD) C-arm system: Optimizing hepatic contrast medium (CM) delivery (SS 1806), B-888
- Hellinger J.C., Draney M.T., Markl M., Alley M., Herfkens R.J.**
Three dimensional cine phase contrast MRI: Evaluation of ascending aortic aneurysms, C-1030
- Hellinger J.C., Kamaya A., Napoli A., Williamson E., Rubin G.D., Fleischmann D.**
Upper extremity (UE) multidetector-row CT angiography (MDCTA): Evaluation of arterial disease, C-1013
- Hellström M.**
Multislice CT of the urinary tract: C. Multislice CT in trauma of urinary tract (RC 1307), A-332
- Hellund J.C., Storås T., Gjesdal K., Geitung J.**
MRI assisted visualisation of flow changes in the pancreatic duct (SS 1001), B-487
- Hellund J.C., Kiow N.**
A multilingual radiological database on the web for medical students, C-0365
- Helmberger T.K.**
Imaging of the pancreas: Key questions: C. Uncommon pancreatic tumors (RC 1301), A-323
- Helmberger T.K.**
Chest intervention: C. Thermal ablation of lung tumors (WS 1718), A-436
- Hendel H.**
Diagnostic multimodality imaging of cancer beyond PET/CT (SY 15), E-66
- Hengst S.A., Ehrenstein T., Beck A., Utz-Billing I., Herzog H., Felix R., Ricke J.**
MR guided focussed ultrasound surgery (MRgFUS) in the treatment of uterine fibroids - Are there any predictors for treatment success (SS 709), B-407
- Henk C.B., Saeed M., Weber O., Martin A., Wilson M., Higgins C.B.**
MR assessment of collateral blood flow and cardiac function in acute experimental aortic coarctation before and after self-expandable stent placement (SS 615), B-331
- Hermans R.**
Radiological approach to stage head and neck squamous cell carcinoma: D. Laryngeal cancer (RC 408), A-075
- Herold C.J.**
Chest: A. Community-acquired and nosocomial infections (CC 416), A-086
- Herold C.J.**
Airways and infection: B. Pneumonia and disorders in the immunoincompetent host (E³ 520), A-143
- Herraiz L., Bermejo A., Perez M., Dieguez S., Borruel S., Arenas A.**
Posttransplant lymphoproliferative disease (PTLD): A pictorial review, C-0067
- Herraiz L., Bermejo A., Martin M.A., Carrera R., Manjon P., Manrique J.**
Intravertebral vacuum cleft sign: Can we consider it a sign of benign vertebral collapse?, C-0751
- Herrmann K.A., Michael H.J.M., Zech C.J., Seiderer J., Ochsenkuehn T., Schoenberg S.O., Reiser M.F.**
Magnetic-resonance enteroclysis (MRE) in patients with Crohn's disease (CD): Complementary diagnostic value of additional retrograde large bowel filling (SS 1401a), B-574
- Herzog P., Becker C.R., Reiser M.F.**
Computer assisted diagnosis: CAD of the chest (SF 1), A-010

Authors' Index

Herzog C., Mack M.G., Zangos S., Schwarz W., Eichler K., Thomas L., Vogl T.J.

Traumatic injuries of the pelvis and thoracic and lumbar spine. Does thin-slice multidetector-row CT increase diagnostic accuracy? (SS 210), B-009

Herzog P., Buhmann S., Naidich D.P., Stoeckel J., Wolf M., Shen H., Salganicoff M., Krishnan A.

Clinical evaluation of a computer aided pulmonary nodule detection system (SS 304), B-164

Herzog C., Zangos S., Krug D.N., Eichler K., Vogl T.J.

Imaging and classification of atherosclerotic plaques in Watanabe heritable hyperlipidemic rabbits using 16-row multidetector-CT (SS 603), B-302

Herzog C., Balzer J.O., Mack M.G., Lehnert T., Schwarz W., Zangos S., Eichler K., Vogl T.J.

Peripheral artery stent visualization and in-stent re-stenosis analysis in 16-row computed tomography: An in-vitro evaluation (SS 615), B-340

Herzog C., Schwarz W., Zangos S., Balzer J.O., Eichler K., Mack M.G., Vogl T.J.

Multidetector-row cardiac CT before minimal invasive bypass surgery (SS 703a), B-345

Heuga O., Hauger O., Bonnefoy O., Diard F., Chateil J.

Radiation dose measurements and image quality evaluation in scoliosis radiography: Flat panel detector versus digital pulsed fluoroscopy (SS 1013), B-544

Heuschmid M., Rothfuss J., Schroeder S., Fenchel M., Stauder N., Kuettner A., Seemann M.D., Kopp A.F., Claussen C.D.

Evaluation of global left ventricular myocardial function using retrospectively ECG-gated 16-slice multidetector computed tomography: Comparison with magnetic resonance imaging, C-0270

Heywang-Köbrunner S.H., Bernerth K., Rotter K., Perlet C.

Vacuum-assisted breast biopsy (VAB): A study of cost-effectiveness (SS 1502), B-733

Heywang-Köbrunner S.H., Perlet C., Heinig A., Bernhardt A.

Sonographically-guided percutaneous biopsy using two different vacuum biopsy systems (SS 1502), B-737

Hidalgo A., Franquet T., Giménez A., Sánchez G., Blancas C., Bordes R.

Neuroendocrine proliferations of lung: Spectrum of diseases, C-0284

Hierholzer J., Fuchs H., Westphalen K., Anselmetti G.

Risk of secondary fractures after percutaneous vertebroplasty: A retrospective analysis and a review of the literature (SS 609a), B-285

Hilger I., Graefe S., Hansch A., Frey O., Kaiser W.A.

Photodynamic therapy of arthritis: An in vitro feasibility study (SS 309b), B-204

Hiorns M.

Neonatal problems: A. Investigation of ano-rectal anomalies (RC 1312), A-340

Hirai N., Toyota N., Kakizawa H., Hieda M., Tachikake T., Ito K.

Coil embolization therapy of pulmonary arteriovenous malformations: Combination of 16-detector CT angiography and interlocking detachable coils, C-0581

Hirano Y., Miyatani Y., Matsuya H., Iriyama M., Honma S., Ohura D., Sasaki H., Ohmi N., Sasaki K., Takada Y.

Evaluation of virtual endoscopy at extremely low exposure dose, C-0983

Hirohashi S.

"Oriental Pearls" in oncology imaging: Imaging-pathologic correlation of early cancer in gastrointestinal tracts: Early cancer in biliary tract (EM 3), A-364

Hirsch W.

Chest imaging: B. MRI of the lung (RC 1212), A-294

Hjelt M., Buzzi A., Canedo M., Gomez Zanetta S., Mancini A.

Spectrum of cyst-like conditions found in and around the knee, C-0738

Hnid N., Tsvigun B., Kovalenko Y.

Transition to digital technology as method for enhancement of efficiency of screening radiographic systems using, C-0385

Ho Y.Y.

MRI of hip pain: Prevalence and mimickers of radiographically occult hip fractures, C-0703

Hochmuth A., Hubbe U., Ziyeh S., Vougioukas V., Berlis A.

MR angiography vs. digital subtraction angiography in the follow-up of clipped and coiled intracranial aneurysms (SS 1511), B-763

Hoffmann M.H.K., Lessick J., Robert M., Schmid F., Aschoff A., Grass M.

Automatic determination of quiescent cardiac motion phases for CT imaging: Initial experience (SS 703b), B-426

Hoffmann M.H.K., Schmid F.T., Jeltsch M., Wunderlich A., Schmitz B., Aschoff A.J.

Multi-slice MR first-pass myocardial perfusion imaging: Impact of the receiver coil array (SS 1803), B-827

Hohl C., Krombach G.A., Schmidt T., Staatz G., Günther R.W., Haage P.

Comparison of true-FISP MRI with and without i.v.-contrast-enhancement in patients with inflammatory bowel disease (IBD) (SS 1401a), B-578

Hohl C., Haage P., Krombach G.A., Schmidt T., Ahaus M., Günther R.W., Staatz G.

Diagnostic imaging in children with Crohn's disease: MRI with true-FISP as a new gold-standard? (SS 1512), B-753

Hohl C., Mahnken A.H., Das M., Leinendecker C., Schmidt T., Günther R.W., Wildberger J.E.

Estimation of radiation exposure in 16-detector row multi slice computed tomography (MSCT) of the heart and comparison with calculation programs (SS 1803), B-819

Hohl C., Ahaus M., Schmidt T., Berkemeier E., Günther R.W., Staatz G.

Monitoring of Infliximab therapy in children with Crohn's disease (CD) with true-FISP MR-imaging (SS 1812), B-898

Hohmann J., Albrecht T., Skrok J., Hoffmann C.W., Wolf K.

Detection and characterization of focal liver lesions with the new RES penetrating US contrast agent BR14: First results of a phase II research (SS 1401b), B-606

Höhn M.

MR approaches to molecular imaging: B. Imaging of cell migration (PR 819), A-202

Holloway B.J., Strouhal P.

A review of outpatient ventilation-perfusion scintigraphy, C-0314

Holmquist F., Nyman U.

80-kVp multislice CT of pulmonary arteries (msCTPA) to minimize contrast medium (CM) doses to diagnose pulmonary embolism (PE) in patients with decreased renal function (SS 1404), B-592

Holmström A., Kettunen A.

Student descriptions of learning how to perform plain X-ray examinations during practical studies, C-0996

Holtinkoski T., Niemi A., Kettunen A.

Guide, instruct and encourage. Radiographers' views on tutoring, C-0992

Hong X., Wang D., Shen T., Chen X.

Diffusion weighted imaging and diffusion tensor imaging in the evaluation of intra-axial tumors (SS 1011), B-531

Hongo N., Mori H., Matsumoto S., Shuto R.

Multi-detector CT angiography in the evaluation of hemodialysis access failure, C-1001

Honnef D., Wildberger J.E., Mahnken A.H., Das M., Schnöring H., Vázquez-Jiménez J., Günther R.W., Staatz G.

Contrast-enhanced low-dose 16-multislice CT (MSCT) in children with tracheal stenosis due to vascular compression: Initial results (SS 1512), B-750

Horger M.S., Pfannenberg C.A., Einsele H., Hebart H., Beck R., Claussen C.D.

Cytomegalovirus pneumonia in immunocompromised patients with haematological disease: Correlation of HRCT findings with clinical outcome, C-0293

Horger M.S., Pfannenberg C.A., Lengerke C., Hebart H., Claussen C.D.

Invasive pulmonary aspergillosis: Significance and predictive value of the "hypodense sign" on unenhanced CT, C-0317

Horii A., Chihara A., Takamura M., Ichikawa K., Kodera Y., Ikeda M., Ishigaki T.

Measurement of MTFs for liquid crystal displays by rectangular waveform analysis, C-0981

Hosten N., Rosenberg C., Weigel C.

Laser-induced thermal ablation of lung metastases: CT findings in a follow-up study (SS 1809), B-878

Houwers J.B., Dorgelo J., Willems T.P., Zijlstra F., Oudkerk M.

Coronary calcification characteristics on multidetector CT and accompanying stenosis severity (SS 603), B-309

Houwers J.B., Dorgelo J., Willems T.P., Janssens C.H.C., Zijlstra F., Oudkerk M.

Determining treatment in patients with acute coronary syndrome using multidetector CT (SS 1003), B-524

Authors' Index

- Howling S.J., Hare C., Harvey C., McArthur T., Tighe M., Salek C., Jenkins P.J.**
Electron beam CT measurement of coronary artery calcium allows individual risk assessment of CHD in UK diabetic patients (SS 603), B-305
- Hsieh J., Londt J., Li J., Hoppel B.**
Low-dose cardiac imaging with volumetric CT (SS 713), B-440
- Hsieh J., Tang X., Thibault J., Shaughnessy C., Williams E., Samsonov D.**
Conjugate cone beam back projection scheme for VCT thin slice imaging (SS 1413), B-666
- Huang Y.H., Chen C.L., Wu T.H., Lin M.H., Yang C.C., Lee J.J.S.**
An automated image-guided robot arm control system for transgenic and drug delivery studies, C-0412
- Huber A.M., Schweyer M., Rieber J., Erhard I., Theisen K., Schönberg S., Reiser M.F.**
Assessment of coronary artery lesion by MR perfusion of the myocardium and pressure derived fractional flow reserve (SS 303), B-216
- Huber A.M., Spannagl B., Hayes C., Schönberg S., Reiser M.F.**
Single shot and phasesensitive detection for assessment of myocardial infarction within a single breathhold (SS 303), B-218
- Huda W., Vance A.**
How do CT doses depend on patient size and radiographic techniques?, C-0958
- Hughes J.L., Alijani M., Chin-Aleong J., Babar S., Rockall A., Reznek R.**
MR imaging of the effects of neo-adjuvant radiotherapy on rectal carcinoma, C-0103
- Hughes J.L., Sadhev A., Rockall A., Reznek R.**
Patterns of recurrence in ovarian carcinoma, C-0418
- Hughes J.L., Sadhev A., Rockall A., Reznek R.**
Pitfalls in MRI staging of carcinoma of the cervix, C-0436
- Hughes M., Foerster B., Welsh R.C., Rahbar H., Sundgren P.C.**
Brain diffusivity in patients with neuropsychiatric systemic lupus erythematosus and acute neurological symptoms, C-0880
- Huguet M.M., Vila J., Oller N., Moure C., Lozano P., Delgado E., Sabin G.**
MRI for the diagnosis and follow-up of myocarditis, C-0231
- Huh Y., Kim S., Suh J., Song H., Lee J.**
Injury of the the distal tibiofibular syndesmosis: Assessment with contrast-enhanced 3D-FSPGR MR imaging, C-0721
- Huisman T.A.G.M.**
Hemorrhagic stroke: A. Intracranial hemorrhage (CC 417), A-052
- Hundt W., Guccione S., Mayer D., Bednarski M.**
In vivo assessment of gene expression ability after application of focused ultrasound (SS 1506b), B-788
- Huo Z., Yankelevitz D., Henschke C., Kostis W., Wandtke J., Paul N.**
Potential benefit of computer-aided diagnosis: Detection of subtle pulmonary lung nodules on chest radiography (SS 204), B-039
- Huppert P.**
Abdominal trauma: A. The radiologist's role in the trauma team (organisation and triage) (RC 401), A-063
- Huppertz H., Grimm C., Fauser S., Kassubek J., Spreer J., Schulze-Bonhage A.**
Improved detection and localization of focal cortical dysplasia by voxel-based 3D MRI analysis (SS 711), B-432
- Hurley M.C., Given M., Lyon S., Lee M.**
Percutaneous radiological gastrostomy: New modifications, C-0642
- Hussain S.M.**
High-field body MRI: The new standard?: Abdomen (SF 5), A-106
- Huwart L., El Khoury M., Bessoud B., Rangheard A., Menu Y.**
Thickness and features of the normal appendix at MDCT: Are diameter and appendicoliths misleading tools? (SS 701a), B-362
- Huwart L., El Khoury M., Bessoud B., Rangheard A., Menu Y.**
Frequency of visualization of normal appendix at MDCT: Junior versus senior radiologist performance (SS 701a), B-365
- Huynh I., Bouilleret V., Masnou P., Charlier P., Lajaunias P., Ducreux D.**
Interictal patterns of perfusion MR imaging in temporal lobe epilepsy (SS 711), B-430
- Hwang S., Kim S., Kim S., Jung S.**
Imaging of lymphoproliferative diseases involving urogenital system, C-0513
- Hwang J.Y., Lee S.W., Choi H.Y.**
Clinical application of 16-slice multidetector row CT (MDCT) with 2D and 3D image processing in musculoskeletal trauma, C-0755
- Hyodo K., Ando M., Ohtsuka S., Yamaguchi I., Takeda T.**
Improvement of X-ray image quality for medical applications using synchrotron radiation monochromatic X-rays (SS 1513), B-775
-
- I
- Iafrate F., Laghi A., Rengo M., Panebianco V., Martino V., Paolantonio P., Di Martino M., Passariello R.**
Clinical impact and prevalence of incidental findings in a mixed population undergoing CT colonography (SS 1501a), B-699
- Iafrate F., Laghi A., Paolantonio P., Rengo M., Guerrisi A., Martino V., Panebianco V., Passariello R.**
A pictorial review of the various extracolonic findings and their clinical impact on CT colonography examination, C-0092
- Iannaccone R., Laghi A., Catalano C., Mangiapane F., Marin D., Passariello R.**
Detection of colorectal polyps: Low-dose multidetector CT (MDCT) colonography evaluated by back-to-back colonoscopies (SS 1501a), B-692
- Iannucci G., Fossaceca R., Cervellini P., Causin F., Marchi M.D., Pinna V., Carriero A.**
Bryan cervical disc prosthesis: A radiological study, C-0768
- Iannucci G., Stecco A., Danieli D., Causin F., Marchi M.D., Pinna V., Carriero A.**
Acute demielinating tumor-like disease: Multiple sclerosis Marbourg's variant, C-0832
- Ideguchi T., Higashida Y., Himuro K., Ohki M., Takagi R., Hatano H., Kuwahara R., Tanaka I., Toyofuku F.**
Comparison of full-field digital mammography (FFDM) and CR mammography: Physical imaging properties and contrast-detail characteristics (SS 302), B-158
- Iezzi R., Quinto F., Pierro A., Spigonardo F., Cotroneo A., Colosimo C.**
CT angiography evaluation of patients with abdominal aortic aneurysms: How many are candidates for endovascular repair? (SS 609b), B-292
- Iezzi R., Quinto F., Pierro A., Di Fabio F., Filippone A., Cotroneo A.R.**
Multiphase multidetector-row CT in abdominal aortic aneurysm treated with endovascular repair (EVAR): Are unenhanced and delayed phase enhanced images really effective for the detection of endoleaks? (SS 615), B-339
- Ikeda M., Ishigaki T., Itoh S.**
Influence of rib structure on detection of subtle lung nodules, C-0944
- Ikura H., Shimizu K., Yasuhara Y., Miyagawa M., Mochizuki T., Ebara H., Ueno K., Nagareda T.**
Microscopic findings in various lung diseases with peripheral lung imaging using micro focus X-ray CT, C-0339
- Ilea D., Ghita O., Robinson K., Lynch M., Whelan P.F.**
A 3D CAD tool for body fat identification (SS 605), B-329
- Imai Y.**
"Oriental Pearls" in oncology imaging: Imaging-pathologic correlation of early cancer in gastrointestinal tracts: Early gastric and colonic cancers (EM 3), A-361
- Imai S., Nakazono T., Matsuo Y., Kudo S.**
Carcinosarcoma of the uterus: MR findings and the pattern of recurrence, C-0429
- Imai K., Niimi T., Ikeda M., Maeda H., Mano A., Enchi Y.**
The strict meaning of the area under a contrast-detail (C-D) curve, C-0949
- Imbriaci M., Sica G., Maurea S., Quarantelli M., Cuocolo A., Salvatore M.**
Myocardial tissue characterization by magnetic resonance imaging (MRI) in Anderson-Fabry disease (SS 203), B-086
- Imbraci M., Maurea S., Mollica C., Bortone S., Volpe M., Buono G., Salvatore M.**
Value of single-phase multidetector CT in patients with suspected pancreatic tumor (SS 701b), B-416
- Inal M., Leblebisatan S., Binokay F., Akgül E., Aksungur E., Oguz M., Soyupak S., Biçakci K., Çeliktaş M.**
CT evaluation of congenital vena cava anomalies, C-1010
- Inaoka T., Takahashi K., Yamada T., Mineta M., Yamamoto W., Nagasawa K., Hirota H., Yamaki T., Aburano T.**
IVR techniques for bone tumor: A comprehensive review, C-0651
- Iovane A., Galia M., Bartolotta T., Sorrentino F., Midiri M.**
Os trigonum syndrome: MR imaging findings in young athletes, C-0656

Authors' Index

Iozzelli A., D'Orta G., Lupattelli T., Sardanelli F.
MR evaluation of abdominal aorta: True-FISP
versus Gd-enhanced MR angiography (Gd-MRA)
(SS 1015), B-556

Irani F.G., Morales J.P., Sabharwal T., Salter R.,
Dourado R., Adam A.
Early experience with the self-expanding plastic
stent (Polyflex) in oesophageal cancer (SS 1809),
B-876

Irwan R., Penning L., Oudkerk M.
Precision measurement of angular and linear
segmental lumbar motion by means of image
registration, C-0383

Irwan R., Sijens P., Oudkerk M.
Correlation of diffusion tensor MR imaging with
MR spectroscopy in multiple sclerosis, C-0773

Ishida T., Tsukagoshi S., Okumura M.,
Kainuma K., Kondo K.
Evaluation of the dose efficiency index compared
to receiver operating characteristics for assessing
CT low contrast performance, C-0964

Ishigaki T.
*"Oriental Pearls" in oncology imaging: Imaging-pathologic correlation of early cancer in gastrointestinal tracts: "Oriental Pearls" in
oncology imaging: Imaging-pathologic correlation of early cancer in gastrointestinal tracts
(Introduction)* (EM 3), A-360

Ishihara T., Ishihara T.S.S.R.
Preliminary studies on a quantum noise reduction
filter in 16-slice multislice CT (MSCT), C-0950

Ishii K., Hosono M., Wada Y., Kondo S.,
Takada Y., Tada T., Maeda M., Watanabe Y.,
Inoue Y.
Early evaluation of the therapeutic effects of
radiotherapy and/or hyperthermia in VX2 rabbit
carcinoma using FDG-microPET, C-0758

Ishiyama K., Tomura N., Sashi R., Okada K.,
Nagasawa H., Narita K., Watarai J.
Benign and malignant musculoskeletal masses:
MR imaging differentiation with "maximum slope
region" (SS 1010), B-468

Ito M., Oshima H., Shiraki N., Ogino H.,
Shibamoto Y., Kasai H., Mase M., Kawamura Y.,
Miyati T.
Evaluation of CH3-DTPA-Gd (NMS60) as a new
MR contrast agent: Early phase II study in brain
tumors and dual dynamic contrast-enhanced
imaging (SS 1506a), B-744

Itskovich I.E., Ryzhkova D.V., Tiutin L.A.,
Rozengaouz E.V., Kofal L.A.
The relationship between coronary calcium score
and myocardial perfusion, C-0265

Ittrich H., Priest A., Jahntz C., Weber C.,
Mittelwitz B., Adam G.
Detection of atherosclerotic plaques with low
dose Gadofluorine-enhanced MRI at 3 T
(SS 215), B-113

Ittrich H., Lange C., Dahnke H.,
Nolte-Ernsting C., Adam G.
Labelling of human mesenchymal stem cells with
different iron oxide MRI contrast agents: Uptake,
intracellular persistence and in-vitro imaging at
3 T (SS 1506b), B-781

Ittrich H., Begemann P., Jahntz C., Weber C.,
Priest A., Adam G.
Evaluation of MDCT in detection of
atherosclerotic plaques in WHHL animals,
C-1005

Ittrich H., Priest A., Jahntz C., Weber C.,
Meding J., Adam G.
Evaluation of Gd-DTPA in detection of
atherosclerotic plaques at 3 Tesla in WHHL
animals, C-1025

Ivancev K.
Aortic stent grafts: A Thoracic (WS 1209), A-287
Iwano S., Nakamura T., Kamioka Y., Ishigaki T.
Computer-aided diagnosis: Differentiation
between malignant and benign solitary
pulmonary nodules using quantitative measures
of shape, C-0299

Iwasaki T.
Real-time virtual sonography is not only a novel
navigation tool in radiofrequency ablation, but
also a novel evidence-based imaging for
hepatocellular carcinoma (SY 1), E-02
Iwasaki Y., Hama Y., Kaji T., Kosuda S.
Clinical experience of a multifunctional image-
guided therapy room, C-0966

J

Jabri K.N., Avinash G.B., Marinelli N.,
Merisotis T., Joglekar G., Deodhar C.
Novel noise-reduction processing algorithm for
digital radiography (SS 1013), B-542

Jackson A.
*How to get the best from information technology
for patient care: Quantitative image processing*
(EF 2), A-155

Jackson J.E.
*Chest intervention: B. Pulmonary vascular
intervention* (WS 1718), A-435

Jacob L.A.
*Planning issues in vascular radiological
intervention: A. How to set up an endovascular
centre* (WS 1715), A-427

Jacobs A.H., Winkeler A., Li H., Rüger A.,
Klein M., Vollmar S., Graf R., Wienhard K.,
Heiss W.D.
*Imaging of gene expression: Optical and nuclear
techniques: C. Gene expression imaging: From
bench to bedside* (PR 1219), A-301

Jacobs F.
Using Gemini PET/CT information to optimise
radiotherapy treatment planning with Pinnacle
(SY 15), E-67

Jäger H.
*Three common neurological problems: Loss of
vision, hearing loss, trigeminal and facial nerve
palsy: A. Loss of vision: Imaging the visual
pathways* (CC 917), A-205

Jäger L., Lutz J., Stahl R., Dietrich O.,
Schelling G., Schönberg S.O., Reiser M.F.
Normal ageing compared to alterations in CRPS
related regions of the brain: A DTI study
(SS 311), B-225

Jäger L., Mulert C., Propp S., Karch S.,
Reiser M.F.
Loudness dependency of the primary auditory
cortex: Simultaneous fMRI and EEG recording
(SS 608), B-271

Jäger L., Hemminger F., Lutz J., Stahl R.,
Dietrich O., Hempel M.J., Schönberg S.O.,
Reiser M.F.
Aging of the acoustic pathway: A DTI study
(SS 608), B-272

Jain V., Bandhu S., Vashisht S., Gulati M.S.,
Garg P.K.

Spectrum of CT colonography findings in colonic
tuberculosis: A pictorial essay, C-0128

Jakobs T.F., Hoffmann R., Tatsch K.,
Reiser M.F., Helmberger T.K.
Selective internal radiation therapy with Yttrium-
90 resin microspheres (SIRT-Y) in extended
metastatic disease of the liver: Initial experiences
(SS 1009a), B-502

Jankharia B., Krishnan P., Rajpal K.
64-slice CT in coronary artery disease, C-0272

Jankharia B., Krishnan P., Ursekar M.
Stress MRI of the lumbo-sacral spine with an
axial loading device. A pictorial essay, C-0748

Januszewicz M., Rowinski O., Milczarek K.,
Jaworski M., Maciąg R., Szmidt J., Galazka Z.
Impaired renal flow resulting from aortic
dissection - What is the most effective
endovascular treatment? (SS 209a), B-070

Jargiello T., Trojanowska A., Wojczal J.,
Wolski A., Drop A., Szczerbo-Trojanowska M.
CT brain perfusion following carotid stenting
(SS 1009b), B-516

Jaromi S., Mallek R., Memarsadeghi M.,
Fuchsjaeger M., Liberman L., Helbich T.H.
A validation study for ultrasound guided 14-gauge
large core breast biopsy (SS 1502), B-736

Jaromi S., Pfarl G., Floery D., Riedl C.C.,
Matzek W.K., Rudas M., Helbich T.H.
Core needle breast biopsy: An alternative to
short-term follow-up in probably benign breast
lesions (BI-RADS™ 3)? (SS 1802), B-836

Jaworski M., Rowinski O., Maciąg R.,
Januszewicz M.
Stent-assisted coil embolization of wide-necked
aneurysms, C-0603

Je B., Kim S., Park D., Kim T., Kim M., Lee N.
The relationship between clinical outcome and
detailed nodal features on initial and follow-up CT
for cervical tuberculous lymphadenitis, C-0543

Jeong Y., Oh J., Seo J., Park J., Kang H.
Differentiation of gastric wall thickness between
normal and gastric cancer on hydro-multislice CT
(SS 201a), B-018

Jeong S., Choo S., Sung Y., Jeon S.
The efficacy of "mini-perc" technique for the
treatment of renal complete staghorn calculi,
especially results in the upper pole, C-0621

Jerebko A., Lakare S., Mang T., Mueller C.,
Salovic D., Schima W., Weßling J., Bogoni L.
Evaluation of an automated polyp measurements
tool compared with experienced observers: A
comparative study (SS 605), B-327

Jevtic V.
Musculoskeletal infection: A. Vertebral infection
(CC 816), A-198

Jiang B., Meng Q., Chen Y., Pan B.
Evaluation of aortic dissection: The role of ultra-
fast three-dimensional dynamic contrast-
enhanced magnetic resonance aortography
(SS 1015), B-555

Jin K., Kim S., Lee J., Shin K., Han J., Choi B.,
Lee J.
Value of multiplanar reconstruction in
multidetector CT for preoperative staging of
colorectal cancer: ROC analysis (SS 1501a),
B-695

Authors' Index

Jin G., Han Y., Lee Y., Kim C., Chung G., Chung S., Kim Y.

Saline-enhanced radiofrequency ablation for treating inoperable non-small cell lung malignancy, C-0353

Joffre F.G., Gobert P.

Advanced 3D X-ray angiography on large digital flat panel: Clinical benefits during interventional procedures (SY 6), E-26

Johnson K.J.

Musculoskeletal imaging: A. Imaging of juvenile idiopathic arthritis (RC 1712), A-429

Johnson T.R.C., Becker C.R.,

Wintersperger B.J., Nikolaou K., Rist C.,

Paul S., Knez A., Reiser M.F.

ECG gated 64 slice CT angiography for the differential diagnosis of acute chest pain (SS 1804), B-846

Johnston C.J., Cunningham P., Brennan D., Moriarty J., Eustace S.J.

MRI in sports related groin pain - prevalence of adductor dysfunction versus osteitis pubis (SS 710), B-359

Johnston C.J., Gillan C., Mc Hugh J.,

O Gorman P., Eustace S.J.

Whole body MRI in the evaluation of marrow disease employing intravenous iron contrast agent (Resovist) (SS 1506a), B-742

Johnston C.J., McCann J., Ford S., Meaney J.F.M.

Patterns of disease in the mesenteric arteries in patients with significant renal artery stenosis as an indicator of atherosclerosis, C-1047

Jökel M.

Radiation safety in radiology (SY 4), E-13

Jones J.R., Stenman K., Hauksson J.,

Bergh A., Rydh A.

Rapid therapeutic response from castration in prostate cancer demonstrated using ¹H-HRMAS NMR spectroscopy (SS 1007), B-495

Juanco C., González F., Landeras R., Piedra T., Merino P., Torres M., Silván M.

MR cholangiography in the diagnosis and staging of extrahepatic cholangiocarcinoma, C-0009

Juanco C., González F., Landeras R., Jordá J., Ruiz E., Piedra T., Lopez M., Silván M.

Cephalic duodenopancreatectomy (Whipple's procedure): Assessment of complications with helical CT, C-0059

Juchems M.S., Fleiter T.R., Pauls S.,

Schmidt S.A., Aschoff A.J., Brambs H.

CT colonography ("virtual colonoscopy"): Comparison of a new colon dissection software and a conventional endoluminal view software (SS 1501a), B-694

Jung E.M., Clevert D., Kubale R., Jungius K., Tacke J.

Vascularization of liver tumors: First results with coded harmonic angio (CHA), phase inversion imaging, 3-D power Doppler and contrast medium-enhanced B-flow with Optison® (SS 1401b), B-603

Jung G., Breuer J., Mödder U.

Imaging characteristics of hepatocellular carcinoma using the hepatobilary contrast agent Gd-EOB-DTPA (SS 1506a), B-748

Jung N.Y., Kim S.K., Park H., Hong S.H., Lee M.H., Chung E.C.

Usefulness of coronal multiple single slice mode balanced fast field echo MRCP with SENSE technique in the detection of choledocholithiasis, C-0005

Jung N., Lee J., Kim S., Song B., Jung S., Byun J.

Diagnostic value of FDG PET-CT for detecting primary breast malignancy: Comparison with other image modalities and histopathologic correlation, C-0216

Jung , Clevert D., Rupp N., Reiser M.F.

B-flow and color-coded-B-flow in sonographic diagnosis of filiform stenosis of the internal carotid artery, C-1055

Junkermann H., Junkermann I., Borowski M., Hanisch P., Bonk U., Böcker W.

Assessment of suspicious lesions in mammography screening by minimally invasive biopsy (SS 1802), B-835

Jurik A.

Inflammatory joint disease: B. What's new in sero negative joint disease? (RC 1610), A-380

K

Kaandorp T.A.M., Bax J.J., Lamb H.J., Viergever E., Boersma E., Poldermans D., van der Wall E.E., de Roos A.

Presence of Q waves on the ECG predicted by MRI (SS 303), B-214

Kaandorp T.A.M., Lamb H.J., Bax J.J., Boersma E., Viergever E., van der Wall E.E., de Roos A.

MRI prediction of β-blocker therapy effect in ischemic cardiomyopathy by assessment of LVEF using dobutamine stress (SS 303), B-220

Kabakci N., Sevil M., Tuna B., Kefi A., Yorukoglu K., Igci E., Dicle O.

Local staging in RCC: Is perinephric stranding and increased perirenal vascularity really helpful?, C-0448

Kabakci N., Igci E., Sevil M., Mungan U., Celebi I., Kirkali Z., Yorukoglu K., Dicle O.

Angiogenesis assessment in renal cell carcinoma by echocontrast-enhanced power Doppler ultrasound, C-0456

Kainberger F., Krestan C.

Shoulder joint: A. Acute and chronic shoulder injuries: US and MRI (RC 1310), A-310

Kalai A., Brot , Maratos Y.K., Halimi P.

Cancer of the posterior tongue: Contribution of MRI in staging and in therapeutic workup, C-0555

Kalaitzoglou I., Papadopoulos P.,

Dimitriadis A.S.

MR imaging of overuse tendon conditions, C-0717

Kalender W.A.

Justification and optimization of multidetector CT (MDCT) examinations: B. MDCT: Balancing image quality and dose (RC 1613), A-397

Kalogeropoulos C., Vassiliou V., Tsota I., Kardamakis D., Sakellaropoulos P.,

Katsarou C., Petsas T., Dimopoulos I.

Computed tomography (CT) in monitoring of remineralization of bone metastases in patients treated with radiotherapy and ibandronate: Work in progress, C-0661

Kalovoulos M., Papagianni A., Tsinoglou K., Dimitriadis C.A., Terzis G., Dovas S.,

Kirmizis D., Grollios G., Memmos D.

Carotid intima-media thickness is associated with inflammation and endothelial cell adhesion molecules in end stage renal disease(ESRD), C-1070

Kalra M.K., Rizzo S.M.R., Blake M.M.,

Maher M.M., Schmidt B., Suess C., Saini S.

Effect of new non-linear, three-dimensional, noise reduction filters on image quality and lesion characteristics to improve image quality of low-dose abdominal CT (SS 205), B-106

Kamaya A., Hsu R.M., Jeffrey R.B.

Wisdom without answers: Patient care and medicolegal ramifications of incidental findings on thin-section body computed tomography, C-0068

Kamura T., Yamamoto S., Ozaki T., Takano T., Sasai K.

Diagnosis of small hypervascular hepatocellular carcinomas: Combined double phase CT during hepatic arteriography and CT during arterial portography versus dynamic CT with intravenous injection of contrast media, using multidetector-row CT scanner, C-0020

Kanaev S., Novikov S., Gershovich M., Shekloprias E.

Bone marrow invasion in patients with Hodgkin's disease: Prognostic value of scintigraphic data, C-0671

Kandatsu S., Kishimoto R., Komatsu S., Mizoe J., Tsujii H.

MR imaging of adenoid cystic carcinoma in the head and neck after carbon ion therapy (SS 308), B-186

Kandatsu S., Kishimoto R., Komatsu S., Ezawa H., Tsujii H.

Chest MR imaging in post-mortem examinations: Autopsy imaging system, C-0351

Kaneko K., Yasumori K., Matsumura T., Hiraka K., Furuya K., Uehara S., Fujimoto S., Okada Y., Muranaka T.

Cerebral blood flow in subclavian steal syndrome evaluated by arm exercise Tc-99m ECD SPECT, C-0788

Kang C., Shin M., Ryu J., Lee S., Kim S.

The measurement and evaluation of lumbar muscularity in lumbar degenerative kyphosis(LDK) patients: Comparison with non-LDK patients on MRI (SS 210), B-001

Karadeli E., Tarhan N.C., Kayahan E.M., Tutar N., Basaran O., Coskun M.

Failing arteriovenous hemodialysis fistulas: Assessment with multidetector CT angiography and three-dimensional (3D) techniques, C-1011

Karaköse S., Karabacakoglu A., Yalinkılıç E., Haykın R., Görkemli H.

The effectiveness of MR hysterosalpingography in infertility, C-0426

Karam A.R., Mehanna M.J., Birjawi G.A., Ishak G.E., Sidani C.A., Haddad M.C.

Alternative diagnoses of acute appendicitis on helical CT with IV and rectal contrast, C-0094

Karaman K., Onat L., Duran C., Sirvanci M.

Stent placement in symptomatic middle cerebral artery stenosis, C-0597

Karaman K., Onat L., Sirvanci M., Barlas O.

MR spectroscopic imaging for targeting in stereotactic brain biopsy, C-0816

Authors' Index

- Karamessini M.T., Kagadis G.C.,**
Karnabatidis D., Konstantinou D., Petsas T.,
Nikiforidis G., Siablis D.
Preoperative delineation of intracranial aneurysm's topography during surgery using CT angiography, C-0369
- Karamessini M.T., Mylona M.D., Salonikidis P., Vlahomitros I., Dimopoulos P.A.**
Radiographic features of heterotopic ossification: A pictorial essay, C-0715
- Karampekios S.**
Cerebral tumors and infections: C. Cerebral infections (CC 517), A-100
- Karani J.B.**
Diagnostic and interventional radiology of transplants: Liver (SF 8b), A-184
- Karantanas A.H.**
Harmonization of training programmes: Myth or reality?: Current status from a survey (ER 126), A-026
- Karantanas A.H.**
Bone marrow disorders as a manifestation of disease: C. Non-neoplastic marrow disorders (RC 810), A-167
- Karcaaltincaba M., Akata D., Dogan O.F., Duman U., Boke E., Besim A.**
MDCT angiographic evaluation of radial artery in coronary artery bypass candidates (SS 315), B-246
- Karssemeijer N.**
Computer assisted diagnosis: CAD of the breast (SF 1), A-008
- Karssemeijer N.**
State-of-the-art in information technology: Advances in CAD for cancer detection (EF 1), A-118
- Tosun A., Serifoglu I., Kartel A., Cakir B.**
Diffusion-weighted MR imaging in intracranial infections, C-0853
- Kasprian G.J., Brugge P.C., Prayer D.**
Temporal lobe development investigated using fetal MRI (SS 311), B-221
- Kastler B.A.C., Boulahdour H., Barral F., Pereira P., Saguet O., Jacoulet P., Lejoncour R., Aubry R., Fergane B.**
Combined bipolar radiofrequency and cementoplasty in bone metastasis: Preliminary results in 8 patients (SS 1010), B-462
- Kastler B.A.C., Rodière E., Litzler J., Sarlieve P., Michalachis D., Delabrousse E., Fergane B.**
Celiac plexus and splanchnic nerve neurolysis via a posterior or anterior approach, C-0074
- Kastler B.A.C., Patay Z., Boulahdour Z., Rodière E., Aubry S., Lerais J., Fergane B.**
Greater occipital nerve infiltration under CT guidance: An anatomical and radiological study, C-0523
- Katoh M., Spüntrup E., Stuber M., Buecker A., Manning W.J., Günther R.W., Botnar R.M.**
Slice-selective inversion prepared steady-state free-precession (SSFP) MR angiography: Visualization of inflowing coronary blood (SS 1403), B-657
- Katoh M., Spüntrup E., Buecker A., Manning W.J., Günther R.W., Botnar R.M.**
MR coronary vessel wall imaging: Comparison of radial and spiral k-space sampling (SS 1403), B-658
- Katona G.**
The role of perfusion CT in acute stroke, C-0862
- Katsaros V.K., Mitropoulou M., Lampropoulou P., Mourtopoulos C., Kolomodi D., Nikolaou A., Drossos C.**
Pontine bright lesions: MRI findings and differential diagnosis, C-0775
- Katsiva V., Katsivas A., Douskou M., Vasilopoulos C., Mavrogeni S., Michailidis G.A., Tibshirani M.**
MRI evaluation of patients undergoing radiofrequency catheter ablation of atrial fibrillation: a preablation comprehensive approach, C-0246
- Katsuda T.**
Optical index of the diaphragmatic motion during breath holding, C-0986
- Kaul M.G., Stork A., Bansmann P.M., Nolte-Ernsting C., Lund G.K., Weber C., Adam G.**
Feasibility of balanced steady-state free precession and conventional gradient echo for coronary magnetic resonance angiography at 3 Tesla (SS 1403), B-652
- Kaul M.G., Bansmann P.M., Stork A., Nolte-Ernsting C., Nehrke K., Adam G.**
Comparison of conventional free-breathing coronary magnetic resonance angiography with affine motion compensated whole-heart MRA at 3 Tesla (SS 1403), B-656
- Kauppinen T., Tolki O., Korhonen P., Ahovuo J.**
Using speech recognition reduces time slot between imaging and final report (SS 305), B-231
- Kawabe A., Nakagiri Y., Katsuda T., Matsushita A., Maruyama T., Wakasa H., Kadohisa S.**
Reduction of skin exposure in interventional radiology, C-0995
- Kawamura S., Okuno T., Ganaha F., Hayakawa K.**
Repeated transarterial chemoembolization for the treatment of advanced pancreatic cancer with superselective catheterization of the pancreas, C-0601
- Kawanishi M.**
Metallic artifact reduction techniques for MR imaging of the brain: Evaluation of fast-inversion-recovery T1-weighted images (fast-IR-T1WI), C-0840
- Kawashima A., Sandler C.M., LeRoy A.J., Wasserman N.F., King B.F., Goldman S.M.**
Imaging of urethral disease: Pictorial review, C-0506
- Keane D.**
Pediatrics/Radiography: B. Radiographer reporting (RC 1214), A-297
- Keat N., Aplin M., Edyvean S., Platten D.J., Lewis M.A.**
Assessment of automatic exposure control systems on CT scanners using a custom made phantom (SS 1413), B-669
- Keavey E., Tuohy B., van der Putten W.**
An evaluation of the accuracy and precision of DEXA systems in the west of Ireland using the european spine phantom, C-0969
- Kelekis N.L.**
Morphological and functional assessment of the heart: B. Assessment of the left heart function (RC 1703), A-410
- Kelleher D.**
Nanotechnology: Implications for medicine and health (NH 6), A-152
- Kemper J., Begemann P.G.C., Regin M., Stork A., Adam G., Nolte-Ernsting C.**
Multislice-CT-urography (MSCTU): Experimental evaluation of low-dose protocols (SS 1407), B-614
- Kettenbach J., Kronreif G., Figl M., Fuerst M., Birkfellner W., Hanel R., Hummel J., Bergmann H.**
B-ROB II: A robotic system for percutaneous interventions (IM 1), D-01
- Kettunen A.**
Pediatrics/Radiography: A. Radiographer's role in optimisation of child's radiation doses (RC 1214), A-296
- Kettunen A.**
Professional matters: B. HENRE (Higher Education Network for Radiography in Europe): Education (RC 1314), A-344
- Kettunen A.O., Servomaa A.**
X-ray examinations of women of reproductive age in Finland, C-0988
- Khalili K., Roach S., Khalili M.**
Changes in splenic volume and correlation with platelet counts in healthy patients following hepatic resection for living liver donation (SS 301b), B-177
- Khan M., Herzog C., Landenberger K., Martens S., Maataoui A., Dietrich M., Vogl T.J.**
Cardiac imaging: Coronary artery bypass grafting imaging of the proximal anastomoses created by nitinol implants. A retrospective two observer evaluation (SS 703a), B-350
- Khanna M., Preston R.L., Tonge K.**
A pictorial review of the the radiological imaging findings in III, IV and VI cranial nerve palsies using CT and MRI techniques, C-0879
- Khartchenko V.P., Kotlyarov P.M., Abbasova E.V., Parkhomenko R.A.**
Changes of sonographic features of peripheral lymph nodes in Hodgkin's disease during specific therapy, C-0903
- Khoo L.A.L., Taylor P., Given-Wilson R.M.**
A prospective study of computer aided detection in the United Kingdom National Breast Screening Programme (SS 1802), B-832
- Khoury N.J., Mehanna M.J., Karam A.R., Haddad M.C.**
Imaging of common and uncommon scrotal diseases, C-0484
- Khoury N.J., Arabi M.M.S., Abi-Fakher F., Hourani M.H., Haddad M.C.**
Imaging of back pain in children and adolescents, C-0910

Authors' Index

- Kiessling F.M.A., Sun R., Bedke J., Krueger R., Bock M., Huss R., Seliger C., Gröne H., Semmler W.**
In vitro cell labelling with SPIO and USPIO: A comparison (SS 1506b), B-780
- Kiessling F.M.A., Dittrich J., Moehler T., Le-Huu M., Bock M., Schulz R., Peter J., Mueller M., Semmler W.**
Human progenitor cells migrate into squamous cell carcinoma (SCC) xenografts, C-0407
- Kilian A.K., Schütz E.M., Schaible T., Düber C., Neff K.W.**
Logistic regression analysis of mortality and necessity of ECMO therapy in fetuses with CDH based on MRI lung volume measurement (SS 1812), B-890
- Kilian A.K., Schröder M., Schaible T., Düber C., Neff K.W.**
Prenatal fetal lung volume measurement using magnetic resonance imaging (MRI) in pairs of twins with congenital diaphragmatic hernia (CDH), C-0930
- Kim S., Lee J., Han J., Lee J., Choi B., Shin K.**
Predicting the appropriateness of a donor liver with respect to hepatic macrosteatosis by phase-contrast MR imaging: Correlation with histopathologic findings (SS 301b), B-178
- Kim S.**
Macrocystic neoplasms of the pancreas: Differentiation of serous oligocystic adenoma from mucinous cystadenoma and intraductal papillary mucin-producing tumor with CT (SS 1001), B-488
- Kim Y., Kim I., Kim W., Yeon K.**
Hypertensive encephalopathy: Clinical and MRI findings (SS 1412), B-641
- Kim M., Byun J., Won H., Shin Y., Kim A., Kim P., Ha H., Lee M.**
MRCP findings of the choledochal cyst and anomalous pancreatico-biliary duct union: A comprehensive review with comparison to ERCP findings, C-0001
- Kim S., Kim K., Kim T., Park S., Kim A., Won H., Byun J., Shin Y., Lee M.**
Hepatic venous congestion in the anterior segment of the graft after living donor liver transplantation using right lobe: Characteristic findings at CT and Doppler ultrasound examination, C-0017
- Kim K., Kim A., Kim S., Park S., Won H., Lee M.**
Hepatic hemangiomas with arterioportal shunt in fatty liver: Atypical sonographic appearances by peritumoral sparing of fatty infiltration with CT and MR correlation, C-0021
- Kim S., Kim K., Kim A., Park S., Chae E., Won H., Byun J., Shin Y., Lee M.**
Surgically important anatomical variations of the hepatic vasculature and intrahepatic bile duct in the evaluation of potential donor for living donor liver transplantation: A comprehensive pictorial review, C-0022
- Kim S., Kim M., Choi J., Lim J., Oh Y., Kim J., Kim K., Lee J., Yoo H.**
MRI findings of focal eosinophilic infiltration of the liver, C-0029
- Kim S., Lim H.K., Choi D., Kim M., Jang K., Lee W., Lim J.**
Hepatic VX2 carcinomas in rabbits: Detection with ferucarbotran-enhanced MR imaging and comparison of optimized sequences, C-0048
- Kim S.**
Macrocystic neoplasms of the pancreas: Differentiation of serous oligocystic adenoma from mucinous cystadenoma and intraductal papillary mucin-producing tumor with CT, C-0057
- Kim M., Byun J., Won H., Shin Y., Kim K., Hong H., Kim A., Kim P., Ha H.**
The peripheral primitive neuroectodermal tumor in the abdomen and pelvis: Imaging features of CT, MR, and ultrasound, C-0065
- Kim S., Kim K., Kim A., Kim J., Ha H.**
Blood-borne metastatic tumors to the gastrointestinal tract: CT findings with clinicopathologic correlation, C-0119
- Kim H., Lim J., Lee D., Ko Y.**
Branching patterns of the first jejunal vein: Evaluation using multi-detector row CT angiography, C-0120
- Kim M., Kim H., Yoon H., Kim S., Moon W., Chung S., Kim D., Shin H., Park J.**
Breast manifestations in patients with systemic lupus erythematosus (SLE), C-0217
- Kim D., Choi S.**
Delay hyperenhancement by contrast-enhanced MRI: Clinical application of various cardiac disease, C-0241
- Kim D., Ryu S., Ahn B.**
Assessment of Mitral Valvular Replacement With Chordal Preservation Using Multidetector Row Computed Tomography, C-0262
- Kim T.U., Jeong Y.J., Kim K., Moon T.Y.**
Mediastinal disease of lymphatic tissue: Imaging findings with histopathologic correlation, C-0288
- Kim T., Kim S., Chung S., Choi B.**
Differential CT features of focal pneumonia versus mucinous bronchioloalveolar carcinoma (BAC) mimicking pneumonia, C-0301
- Kim T., Kim S., Chung S., Choi B., Choe K.**
Distributional variations of thymic cysts in the mediastinum, C-0322
- Kim S., Kim S., Yang D.**
Trauma-related erectile dysfunction: Spectrum of penile Doppler US findings, C-0492
- Kim D.H., Oh H.W., Choi J.Y., Byun J.N., Kim Y.C., Kim Y.S., Oh J.H.**
Comparison of ultrasonography (US)-guided fine needle aspiration biopsy (FNAB) with histopathologic finding after thyroideectomy for thyroid nodules and the usefulness of follow-up US-guided FNAB, C-0542
- Kim K., Kim T., Park S., Kim M., Kim A., Ha H.**
Bleeding after US-guided percutaneous liver biopsy: Role of Doppler US examination immediately after the biopsy procedure, C-0643
- Kim J., Lee J., Kim S.**
Tractography of corticospinal tract stroke by diffusion tensor imaging: Clinicotopographical correlation, C-0789
- Kim E., Kim S., Kim E., Na D., Ryoo J., Lee S.**
Metronidazole induced encephalopathy: MR findings and clinical presentation, C-0790
- Kim J., Chang K., Han M., Na D., Kwon B., Song I.**
Single voxel ¹H MR spectroscopy of cerebral gliomas at 3.0 T: Comparison of short and long TE sequences in tumor grading, C-0845
- Kim H.J., Kim Y.W.**
Can unsaturated fatty acid emulsion technique be used as a model for research on BBB disruption?, C-0870
- Kimura H., Kabasawa H., Uematsu H., Koshimoto Y., Yonekura Y., Itoh H.**
Cerebral perfusion measurements using continuous arterial spin labeling (CASL): Transit time measurements of normal subjects, C-0867
- Kinkel K.**
Imaging of the female pelvis: B. Endometriosis (RC 107), A-034
- Kiraly A.P., Naidich D.P., Novak C.L.**
A visualization-based method for pulmonary emboli identification within high-resolution CT images (SS 605), B-325
- Kiris A., Kaya A., Ozgocmen S., Kocakoc E.**
Assessment of entheses by power Doppler technique in ankylosing spondylitis: A pilot study, C-0765
- Kirk M.P.**
Enterprise information management: Closing the loop for a complete clinical data repository (SS 305), B-239
- Kissi A.A., Pourcelot L., Cormier S., Tranquart F.**
Towards an automatic segmentation of liver tumours in contrast enhanced ultrasound images, C-0377
- Klaric-Custovic R., Gotovac N., Krolo I., Marotti M., Babic N.**
Detection and occurrence of retained surgical textiomas, C-0178
- Klauser A.**
Value of contrast enhanced ultrasound in rheumatic disease (SY 14), E-64
- Klauser A., Demharter J., Sureda D., Barile A., Faletti C., Masciocchi C., Schirmer M., Bohndorf K.**
Value of contrast enhanced gray scale sonography in rheumatoid arthritis patients: A multicenter study (SS 306), B-129
- Klauser A., Schirmer M., zur Nedden D., Frauscher F.**
Contrast-enhanced US in the assessment of sacroiliac joint vascularity (SS 306), B-130
- Klauser A., Moriggl B., Schirmer M., Frauscher F., zur Nedden D.**
Feasibility and accuracy of US-guided sacroiliac joint injection: Preliminary experience (SS 1810), B-807
- Klauß M., Dukic L., Delorme S., Knaebel H., Kauczor H., Büchler M.W., Kauffmann G.W., Richter G.M., Grenacher L.**
Prospective comparison of multislice-CT versus MRI in the diagnosis and staging of pancreatic carcinoma (SS 701b), B-414
- Klein S., Hoffman M.H., Boll D.T., Brambs H.J., Aschoff A.J.**
Accuracy of computer based measurements in endovascular stent-graft planning: Experimental in vitro evaluation in an aortic aneurysmal phantom (SS 205), B-108

Authors' Index

- Kleinrok J., Rozylo T.K., Janczarek M.**
Magnetic resonance imaging in temporo-mandibular joint internal derangements, C-0563
- Klempnauer J., Lehner F.**
Diagnostic and interventional radiology of transplants: Kidney and pancreas (part 1) (SF 8b), A-185
- Klose K.**
Computer assisted diagnosis: Computer assisted diagnosis (Introduction) (SF 1), A-007
- Kluge A., Bachmann G.**
Subsegmental pulmonary embolism: Comparison of 16row-CT and MRI (SS 1404), B-594
- Kluge A., Mueller C., Bachmann G.**
Real-time MRI of the thorax: Experience in 1100 examinations (SS 1804), B-839
- Klzo L., Solar M., Zizka J.**
Comparison of delayed enhancement MRI and thallium SPECT for the assessment of myocardial viability, C-0244
- Ko H., Kim K., Lee J., Lee D., Won J., Kim S., Choi J.**
Percutaneous injection therapy by Holmium-166-chitosan complex in small hepatocellular carcinoma: Initial experience as a primary treatment (SS 1009a), B-503
- Kobashi Y., Imanishi Y., Tachizawa N., Yanagihara M., Sakaino S., Yoshimatsu M., Bhattacharji N., Ishizuka K., Nakajima Y.**
Distributions of periods, sites and appearances of metastases from early and advanced gastric carcinomas, C-0147
- Kocaoglu M., Frush D.P., Ugurel M.S., Somuncu I.**
Bronchopulmonary foregut malformations presenting as mass lesions in children, C-0914
- Koh D., Brown G., Riddell A., Collins D., Scurr E., Karanjia N., Husband J.E.**
Colorectal hepatic metastases: Evaluation using Magafodipir Trisodium enhanced MR imaging and breath-hold single-shot echo-planar diffusion-weighted MR imaging (SS 301a), B-144
- Koh S.**
Abnormal US features of skeletal muscles of extremities: Correlation with MR images, C-0720
- Koh Y., Cha J.H., Han D.**
High-resolution ultrasonography findings of peripheral nerve abnormalities, C-0762
- Kohl G., Salganicoff M., Naidich D.P., Herzog P., Wolf M., Cathier P., Stoeckel J.**
Influence of the CT reconstruction kernel on the performance of a CAD system for the detection of pulmonary nodules (SS 304), B-161
- Koizumi J.**
The evaluation of strangulation ileus using contrast enhanced ultrasonography, C-0117
- Koizumi J.**
Partial splenic embolization using microsphere, C-0571
- Koizumi J.**
The correlation between the magnetic resonance imaging of clots and thromboaspiration in vitro, C-1026
- Kokkinis C., Makris N., Stathopoulou S., Peteinelli A., Vlychou M., Vassiou K., Papadaki P.J., Zavras G.M., Fezoulidis J.B.**
Subclavian vein thrombosis secondary to thoracic outlet syndrome: CT and CT angiography evaluation, C-1009
- Kontopoulou C., Balanika A., Economopoulos N., Michailidis G.A., Kelekis N.L.**
The contribution of conventional and color Doppler ultrasonography in the estimation of musculoskeletal infections, C-0726
- Koo J., Hong S., Choi J., Lee I., Lee J., Kang H., Choi J., Koh Y.**
MR imaging of metastatic tumors in the spine: Are they different in signal intensity according to primary malignancy? (SS 1010), B-467
- Koo J., Hong S., Choi J., Lee I., Lee J., Koh Y., Choi J., Kang H.**
Bright soft tissue masses of the extremities on MR imaging: The spectrum of diseases, C-0722
- Koops A., Lutomsky B., Stork A., Willems S., Nolte-Ernsting C., Adam G.**
Magnetic resonance angiography and phase-shift velocity mapping of the pulmonary veins compared to transesophageal echocardiography before and after radiofrequency catheter ablation for atrial fibrillation (SS 203), B-083
- Koops A., Ittrich H., Petri S., Priest A., Stork A., Weber C., Adam G.**
Multicortical weighted magnetic resonance imaging of atherosclerotic plaques at 3.0 and 1.5 Tesla: Comparison ex vivo and with histopathologic correlation (SS 215), B-120
- Kopp A.F.**
Advances in imaging protocols for cardiac MDCT (SY 9), E-42
- Kopp A.F.**
Safety of X-ray contrast agents (SY 7), E-31
- Koprivsek K.M., Spirovski M., Kozic D., Semnic R., Lucic M., Prvulovic N., Ostojevic J.**
Proton MR spectroscopy and MR imaging in childhood hypomyelinating disorders, C-0926
- Kordecki K., Janica J.R., Lewszuk A., Kochanowicz J., Kadziolek B., Zabek M., Walecki J.**
Endovascular treatment of cerebral arteriovenous malformation, C-0572
- Koren J.**
Distributed CR everywhere (SY 8), E-32
- Koren A.**
MRI of brain embolism in patients with carotid stenosis before and after percutaneous angioplasty with distal protection (SS 1511), B-767
- Körner M., Kanz K., Linsenmaier U., Pfeifer K., Mutschler W., Reiser M.F.**
Multi-slice CT (MSCT) as an integral component in primary trauma resuscitation (SS 210), B-006
- Körner M., Treitl M., Herrmann C., Mair S., Reiser M.F.**
Image detail detectability in digital radiography: Comparison of new needle structured storage phosphor with a powder structured storage phosphor and a flat-panel detector (SS 1013), B-543
- Kosaka N., Sakai T., Uematsu H., Kimura H., Hase M., Noguchi M., Itoh H.**
Characteristic high resolution computed tomography findings of pulmonary tuberculosis in patients with smear-positive sputum, C-0298
- Kosaka N., Uematsu H., Sagoh T., Miyayama S., Noguchi M., Itoh H.**
Image findings of idiopathic carotidynia in multiple modalities, C-0536
- Kösling S.**
Imaging of skull base tumors: A practical approach for your daily practice: B. Central skull base (RC 1608), A-383
- Kostanti E., Zikou A., Kosta P., Kastani D., Galatsou E., Kitsakos A., Argyropoulou M.I., Nakos G.**
Heterotopic ossification in critically ill patients: Early diagnosis with MRI (SS 1410), B-560
- Kostenikov N.A., Tyutin L.A., Fadeev N.P., Savello V.E., Zhabina R.M.**
Possibilities of PET with 11C-Sodium Butyrate (11C-SB) for morpho-functional estimation of brain malignant tumors (BMT), C-0848
- Kotis A.A., Chatzakis G., Marinou A., Karatapanis S., Brestas P.**
The role of echo enhanced ultrasonography in the investigation of extracranial vertebral arteries, C-1065
- Kotter E., Jaeger D., Pache G., Saueressig U., Langer M.**
Report of a PACS migration (SS 305), B-240
- Kouloulias V.E., Matsopoulos G., Mouravliansky N., Asvestas P., Delibasis K., Uzunoglu N., Kelekis A.D., Efstatopoulos E., Kelekis N.**
Image processing techniques for the manipulation, processing and storage of mammography radiological data, C-0963
- Koumarianos D., Lavdas E., Fezoulidis N.I., Fezoulidis I.V.**
The value of the radial head-capitellum view in the evaluation of patients with injury of the elbow (SS 1814), B-912
- Koumellis P., van Beek E., Hill C., Woodhouse N., Fichele S., Taylor C., Wild J.**
Quantitative analysis of regional airways obstruction using dynamic hyperpolarized ³He MRI: Preliminary results in children with cystic fibrosis (SS 1504), B-702
- Kovacs P., Rapf K., Prommegger R., Profanter C., Sauper T., Bale R.J., Jaschke W.R.**
Accuracy of CT-SPECT image fusion in the pre-operative detection of parathyroid adenomas (SS 208), B-060
- Kovacs E.Z., Buchthal S., Shin R., Shelton B., Bush B.A., Kilby M.J., Zeng H., den Hollander J., Benos D.J.**
Brain metabolism in HIV-infection assessed by proton and ³¹phosphorus magnetic resonance spectroscopy (SS 211), B-095
- Kovacs P., Putzer D., Lang T.B., Knoflach M., Hinterleitner C., Bale R.J., Jaschke W.R.**
Accuracy of liver superimposition in different ways of whole body image fusion of CT and PET datasets (SS 205), B-101

Authors' Index

- Kownacki L., Orzech M., Piotrowska D., Cieszanowski A., Golebiowski M. Computerized method for analysis of magnetic resonance (MR) cardiac perfusion images. Preliminary report, C-0382
- Koyama T., Umeoka S., Kubo T., Tamai K., Ueda H., Kobayashi H., Wada H., Saga T., Togashi K. Spectrum of CT features in cavitary or cystic pulmonary metastases: Correlation with primary and histologic types of the tumor, C-0287
- Koyama T., Terada M., Sato M., Kobayashi M., Numaguchi Y., Horiuchi T., Sekiguchi J. Effective dose level from lung screening CT using auto exposure control, C-0337
- Koyama T., Umeoka S., Kido A., Tamai K., Saga T., Fujii S., Togashi K. MR features of cervical adenocarcinoma with pathologic correlation, C-0431
- Koyama K., Okamura T., Hamazawa Y., Okuma T., Wada Y., Ishii K., Kondo S., Watanabe Y., Inoue Y. The influence of oral glucose ingestion during a dynamic FDG-microPET study using a rabbit VX2 tumor model, C-0760
- Kozic D., Petrovic I., Svetel M., Lucic M., Ostojic J., Kostic V. Long-term brain MR follow-up in patients with neurological form of Wilson's disease, C-0850
- Kramer H., Schoenberg S.O., Nikolaou K., Struwe A., Reiser M.F. Optimized whole-body cardiovascular magnetic resonance (MR) screening with parallel imaging: Experience in over 100 patients on a 32-channel MRI system (SS 315), B-249
- Krämer S.C., Kuhlenbäumer G., Nassenstein I., Conrad L., Heindel W., Bachmann R. Detectability of specific radiological signs in cervical artery dissection: Comparative analysis of helical-CT, MRI, MRA and DSA (SS 715), B-459
- Krasilnikova L.A., Tyutin L.A. Relation between the intrarenal arterial resistance, the carotid artery wall thickness and endothelial dysfunction (ultrasound study), C-1068
- Krasilnikova L.A., Tyutin L.A. Early ultrasound characteristics of angiopathy in patients receiving antitumor therapy, C-1073
- Krauss M., Hirschfelder H., Losert D., Bär I. Vertebroplasty in patients with osteoporosis-related osteonecrotic intravertebral clefts (SS 609a), B-282
- Kreitner K., Nieswand C., Kunz R., Oberholzer K., Thelen M. MRA of the pedal arteries with MS-325, a blood pool contrast agent, and comparison with selective intraarterial DSA (SS 315), B-245
- Kreitner K., Romaneehsen B., Oberholzer K., Krummenauer F., Thelen M. Fast magnetic resonance imaging of the knee using a parallel acquisition technique (mSENSE): A prospective performance study (SS 1510), B-685
- Kress B.P.J., Siebert S., Krause M., Schwark C., Rasche D., Kolling G., Tronnier V., Sartor K. New MR sequences to detect the neurovascular conflict in cranial nerves (SS 1811b), B-934
- Krestin G.P., Marincek B. *Interactive image teaching: Acute abdomen (E³ 320)*, A-051
- Krestin G.P. *Imaging problem lesions (tumors): A. Adrenal imaging (RC 407)*, A-084
- Krestin G.P. *High-field body MRI: The new standard?: High-field body MRI: The new standard? (Introduction) (SF 5)*, A-104
- Krestin G.P. *European research network in biomedical imaging: Towards an European institute of biomedical imaging research (ER 926)*, A-224
- Krix M. Quantification of enhancement in contrast ultrasound: A tool for monitoring of therapies in liver metastases (SY 14), E-62
- Krix M., Kauczor H., Delorme S. Microvascular imaging with contrast-enhanced ultrasound, C-0388
- Krix M., Weber M., Huttner H.B., Jappe U., Meyding-Lamadé U., Hartmann M., Essig M., Kauczor H., Delorme S. Quantitative, contrast-enhanced ultrasound to detect pathologic skeletal muscle perfusion in patients with inflammatory myopathies: Initial results, C-0395
- Krnic A., Vucic N., Sucic Z., Schmidt S., Jelavic-Kojic F. Duplex imaging in quantification of peripheral arterial disease: Is it reliable?, C-1042
- Kröger W., Nauck V., Rosenberg C., Hosten N. Ultrasound of the liver to follow-up ablative therapy of liver malignancies: Detection of residual and recurrent tumor compared to CT and MRI, C-0634
- Krombach G.A., Pfeffer J.E., Kinzel S., Günther R.W., Buecker A. MR guided intramyocardial injection using an MRI compatible catheter: Feasibility and changes of T1 values after injection of extracellular contrast medium (SS 209b), B-073
- Krombach G.A., Kinzel S., Mahnken A., Günther R.W., Buecker A. Minimally invasive close-chest method for creating myocardial infarction in swine (SS 309b), B-203
- Krombach G.A., Pani L., Jung B., DiMartino E., Spüntrup E., Günther R.W., Buecker A. True-FISP for inner ear imaging: Delineation of anatomical structures and pathologies (SS 608), B-278
- Krumina G. *Metastatic disease of the brain and spine: A. Metastases in the brain parenchyma (CC 1717)*, A-399
- Kubas B., Walecki J., Kulak W., Kochanowicz J., Tarasow E., Dzienis W., Janica J. Metabolite profile in pyramidal tracts after ischemic brain stroke - 1H MRS study. (SS 611), B-317
- Kuchuk P.V., Arablinskiy A.V., Rapoport L.M., Belysheva E.S., Rudenko V.I., Uzhegov T.A. Use of MRI for kidney evaluation after ESWL, C-0465
- Kudryavtseva T.Y., Sergeeva O.N., Gavrilin A.V., Karmazanovsky G.G. MRI assessment of radiofrequency liver tumor ablation, C-0040
- Kuehl H., Eggebrecht H., Veit P., Antoch G., Erbel R., Barkhausen J. PET/CT in patients with acute aortic syndrome (SS 1015), B-553
- Kuehl H., Antoch G., Rosenbaum S., Veit P., Barkhausen J., Bockisch A. Preinterventional whole-body PET-CT in patients with malignant liver tumors: Influence on patient management to RF ablation therapy (SS 1501b), B-718
- Kuehl H., Antoch G., Veit P., Rosenbaum S., Barkhausen J., Bockisch A. Follow-up of primary or secondary malignant liver tumors treated with radiofrequency ablation: Efficiency of PET/CT (SS 1814), B-913
- Kuehle C.A., Ajaj W., Massing S., Langhorst J., Nuefer M., Goehde S.C., Barkhausen J., Lauenstein T.C. MR colonography without bowel purgation: Preliminary results of a new fecal tagging concept (SS 1401a), B-571
- Kuettner A., Feyer A., Rothfuss J., Heuschmid M., Kopp A.F., Schroeder S., Claussen C.D. Is coronary plaque morphology a useful predictive tool for the detection of severe coronary lesions? Analysis of 469 plaques as assessed by 16-slice computed tomography (SS 603), B-310
- Kuginuki Y., Tonami H., Matsubara J., Hida K., Matsuzawa T., Watanabe M. 3D animation with numerical simulations of blood flow in aortic aneurysms using multi-detector CT images (SS 1015), B-552
- Kumano S., Tanaka H., Miki H., Mochizuki T. 3D-CT angiography using 16-row multislice CT: Depiction of the feeding artery of hypervascular HCCs, C-0014
- Kumazawa S., Yoshiura T., Miura F., Honda H., Higashida Y., Toyofuku F. Development of white matter tractography using 3D density field in diffusion tensor (DT) MRI (SS 605), B-330
- Kunz R.P., Oellig F., Krummenauer F., Oberholzer K., Thelen M., Kreitner K. Contribution of early systole to total forward flow volume in breath-hold phase-contrast flow measurements (SS 703b), B-425
- Kuo M.D., Chan B., Buckley J., Gooding B. Functional radiogenomic identification of alterations in global gene expression in human solid renal tumors with conventional cross sectional imaging (SS 707), B-391
- Kuo M.D., Nardini C., Wang D., Cha S., Diehn M. MRI guided feature evaluation of characteristic gene expression signatures in glioblastoma multiforme (SS 711), B-439
- Kupesic S., Plavsic B.M. Three-dimensional power Doppler ultrasound in detection of early ovarian carcinoma, C-0421
- Kwon W., Oh K.K., Kim M.S. Phyllodes tumors: Benign and malignant findings, C-0212

Authors' Index

Kwon W., Sung K., Lee W., Kim M.
Recurrent lung cancer at the bronchial stump site: CT and bronchoscopic findings, C-0309

Kwon S., Jung K., Yang I., Kim Y., Choi Y., Cha J.
MR image findings of acute rhabdomyolysis, C-0723

Kyriakou Y., Kachelriess M., Knaup M., Krause J.U., Kalender W.A.
Impact of the z-flying focal spot (zFFS) on resolution and artifact behaviour for a 64-slice spiral-CT scanner (SS 1413), B-661

Kyriakou Y., Deak P., Riedel T., Smekal L.v., Kalender W.A.
Combining deterministic and Monte-Carlo methods in the simulation of X-ray attenuation and scatter (SS 1513), B-776

Kyriakou Y., Kachelriess M., Krause J.U., Kalender W.A.
Performance evaluation of a clinical 64-slice spiral CT scanner, C-0946

L

Labbe-Devilliers C.A.S., Meingan P., Loussouarn D., Campion L., Ricaud-Couprie M.
Controversial issues in atypia of the breast diagnosed by stereotactic 11-gauge vacuum-assisted biopsy: Systematic surgery or mammography assessment?, C-0181

Laganà D., Carrafielo G., Caronno R., Castelli P., Fontana F., Mangini M., Fugazzola C.
Emergency endovascular treatment of ruptured abdominal aortic aneurysms (SS 609b), B-298

Laghi A.
Multi-dimensional imaging for guiding therapy: 3D imaging in therapy planning (SA 12), A-268

Laghi A.
MR imaging of the small intestine: Clinical results in pediatric disorders (SF 13), A-317

Laghi A.
CT colonography and colon cancer: B. Performance and technique of CT colonography (RC 1701), A-413

Laghi A., Sansoni I., Di Martino M., Celestre M., Miglio C., Coletta L., Rengo M., Passariello R.
Detection and characterization of hepatocellular carcinoma (HCC): Value of adding the hepato-biliary phase imaging to dynamic Gd-BOPTA magnetic resonance imaging (Gd-BOPTA-MRI) (SS 201b), B-044

Lam S.
The diverse ultrasonographic appearances of ectopic pregnancies: A pictorial review, C-0441

Lamb H.J.
Assessment of myocardial perfusion and viability: Role of MRI (SF 12), A-274

Lameire N.H.
Primary prevention of CIN (SY 10), E-45

Lammer J., Kopp C., Cejna M., Rand T., Minar E.
Drug-eluting stents: Drug-eluting stents in SFA (NH 10), A-258

Lammer J.
Aortic stent grafts: B. Abdominal (WS 1209), A-288

Lamuraglia M., Garbay J.R., Mathieu M.C., Opolon P., Jaziri S., Roche A., Leclère J., Lassau N.
Doppler ultrasonography with contrast agent injection and perfusion software to assess the efficiency of radio-frequency in recurrent breast cancer (SS 306), B-128

Landwehr P.
Vascular imaging: C. Sonography: New directions (RC 1215), A-292

Lang E.K., Gayle B., Macchia R., Charafeddine R., Meyers L.
Renal lesions too small to classify by CT; outcome study based on follow-up for 18-62 months (38 mean) by multiphasic helical CT or laparoscopy (SS 707), B-392

Lang E.K., Thomas R., Brammer M., Joshi S.
Microscopic hematuria and pelvic congestion syndrome: A late sequela of cirrhosis (SS 1807b), B-863

Lanocita R.
RVS: Interventional applications in oncology (SY 1), E-03

Lanocita R., Calliada F., Berton F., Gola G., Parisio A., Arcuti P.
Parametric perfusion imaging with contrast-enhanced ultrasound in thyroid gland focal lesions differential diagnosis (SS 306), B-127

Lapp R.M., Kachelrieß M., Kalender W.A.
Improving reproducibility of small structure segmentation by isotropic resolution filtering (SS 205), B-109

Larici A.R., Storto M.L., D'Agostino A.G., Palladino F., Canadè A., Bonomo L.
Low-dose MDCT in the evaluation of pulmonary emphysema: What is the minimum radiation dose? (SS 1504), B-707

Larson G.D.
UK national programme for IT: Delivering diagnostic imaging for the north west and west midlands in England (SY 3), E-11

Lau L.
Teleradiology: Threat or opportunity?: International consensus standards for clinical teleradiology (ER 1326), A-337

Lauenstein T.C.
MR of the colon and rectum: B. Clinical applications and results of MR colonography (RC 101), A-015

Laurent F.
Imaging of lung cancer: A. Screening for lung cancer: Update on results of current trials (RC 804), A-178

Law E.
Clinical applications of high resolution spectroscopy imaging (SY 12), E-55

Lawinski C.P., Cole H., Blake P., Mackenzie A., Pascoal A.
The evaluation of image quality and dose on computed radiography systems for mammography (SS 302), B-153

Lawinski C.P., Cole H., Mackenzie A.
A comparison of image quality and dose for digital flat panel detector and image intensifier fluoroscopy systems (SS 1013), B-545

Lázár I.
The present and future of Hungarian radiology: Contribution of a new generation: Interventional radiology in portal hypertension (EM 2), A-253

Le Bihan D.
European research network in biomedical imaging: Fundamental biomedical imaging research in Europe (ER 926), A-221

Lecouvet F.
Bone marrow disorders as a manifestation of disease: B. Tumors (RC 810), A-166

Lederlin M., Reant P., Montaudon M., Corneloup O., Lafite S., Laurent F.
MR planimetry in aortic valvular stenosis (SS 203), B-087

Lederlin M., Latrabe V., Montaudon M., Corneloup O., Laurent F.
Multidetector CT evaluation of congenital heart disease, C-0269

Lederman R., Leichter I., Fields S., Buchbinder S., Novak B., Sklair-Levy M., Bamberger P.
Is CAD/CAC performance affected by breast tissue composition? (SS 302), B-151

Ledermann H.P., Schulte A.C., Heidecker H.G., Aschwanden M., Jäger K.A., Steinbrich W., Bilecen D.
Calf muscle BOLD MRI: Comparison of healthy volunteers and grade II PAOD patients in a post-occlusive reactive hyperemia paradigm (SS 1410), B-568

Lee M.J.
Nanotechnology: Nanotechnology (Introduction) (NH 6), A-150

Lee J., Han J., Kim S., Lee J., Shin K., Choi B.
Parallel wet bipolar radiofrequency ablation of the liver: In vivo and ex vivo experiments with perfused-cooled electrodes (SS 209b), B-076

Lee J., Han J., Kim S., Lee J., Choi B.
Combined radiofrequency tumor ablation and acetic acid-hypertonic saline solution injection in a rat N1S1 liver tumor model: Effects on tissue coagulation (SS 209b), B-077

Lee J., Lee Y.
Ultrasonography-guided intraneural injection for intractable limb contracture control (SS 309a), B-200

Lee J., Han J., Kim S., Lee J., Choi B.
Radiofrequency thermal ablation in canine femur: Evaluation of coagulation necrosis reproducibility and MR-histopathologic correlation (SS 309b), B-210

Lee K., Lee K., Lee H., Kim J., Kang H., Hong H., Lee H., Kim T.
Managing the CT data explosion: Initial experiences of archiving volumetric datasets in a mini-PACS (SS 305), B-234

Lee J., Lee S., Kim S., Moon T.
Renal angiomyolipoma with no discernible fat on CT and chemical shift MR imaging (SS 707), B-394

Lee S., Lee W., Yim Y., Choi J., Choi D., Lim H., Lim J.
TNM staging for ampullary carcinoma using thin-section helical CT: Pathologic correlation with dual-phase CT images (SS 701b), B-418

Authors' Index

- Lee H.G., Kim Y.J., Lim Y.S., Chung M.H., Sung M.S., Yoo W.J., Lim H.W.**
Polyvinyl alcohol embolization adjuvant to oily chemoembolization in hepatocellular carcinoma with arterioportal shunt (SS 1009a), B-505
- Lee H., Lee J., Kim S., Shin K., Lee J., Han J., Choi B.**
Detection and characterization of focal hepatic lesions: Comparative study of MDCT and current MR techniques (SS 1501b), B-711
- Lee S., Lee W., Yim Y., Choi J., Choi D., Lim H., Lim J.**
Optimization of contrast enhancement for pancreatic CT imaging using multi-detector row CT: Effect of different scan delays on arterial, venous, pancreatic and hepatic enhancement (SS 1801b), B-854
- Lee J., Seo J., Kim Y., Choi B., Choe K.**
MR assessment of nonischemic dilated cardiomyopathy: Correlation of left ventricular wall motion and delayed myocardial enhancement, C-0240
- Lee J., Kim Y.**
Occlusive myocardial infarction on sixteen-slice multi-detector row helical CT in a rabbit model: Radiologic-pathologic correlation according to infarct age, C-0259
- Lee J., Yoo E., Choi B., Nam J., Seo J., Kim Y., Choe K.**
Noninvasive assessment of in-stent restenosis of coronary artery with multi-detector row CT, C-0274
- Lee M., Ahn J., Suh J., Lim H., Chung E., Jung N.**
Osteoid osteoma treated with percutaneous radiofrequency ablation: MR imaging follow-up, C-0663
- Lee I., Choi J., Kang H., Hong S., Choi J., O J., Koo J.**
Comparison of CT arthrography using 16 slice MDCT and MR arthrography with arthroscopic correlation,
- Lee C., Lee W., Ling C., Yen P., Chong P., Lee S.**
MRS and DTI of two siblings with Hallervorden-Spatz syndrome, C-0877
- Leen E., Ceccotti P., Kalogeropoulou C., Angerson W., Horgan P.**
Blinded readers study of contrast-enhanced US in the characterisation of focal liver lesions (FLL): Impact on decision making (SS 1401b), B-605
- Lefer P., Gryspeerdt S., Roelandt W., Van Wettere P., Verhaeghe L., Ramboer K., Moons P., Djoa L., Herpels V., De Deurwaerdeer B.**
A multi-centre project of teaching CT colonography in Belgium: Work in progress (SS 1501a), B-697
- Lefer P., Gryspeerdt S.**
How to perform CT colonography: A case-based tutorial, C-0088
- Lefort C., Merlin A., Hurtier O., Petitbon P., Frija G.**
Image compression in chest radiography: To the limit and beyond, C-0368
- Lehnert T., Gazis A., Wetter A., Zangos S., Hammerstingl R., Thalhammer A., Bechstein W., Vogl T.J.**
Human growth factor (HGF) evaluation before liver intervention: A prognostic significance for liver regeneration (SS 1809), B-877
- Leichter I., Buchbinder S., Lederman R., Fields S., Novak B., Bamberger P.**
A new approach for adjunct computerized assessment of mammographic findings, using a CAC system (SS 302), B-152
- Leidecker C., Deak P., Kachelriess M., Kalender W.A.**
A tool for fast Monte Carlo-based patient and scanner-specific dose calculations for CT with arbitrary tube current modulation (SS 713), B-445
- Lembcke A., Klessen C., Dewey M., Elgeti T., Hamm B., Kivelitz D.**
Determination of right ventricular volumes and function using multidetector row CT. Comparison with MR imaging (SS 703b), B-427
- Leemmi A., Lombardi T., Cornelii P., Chiodi M., Scialpi M., Lupattelli L.**
Multislice CT for detection pulmonary embolism after lung surgery for cancer (SS 1804), B-842
- Lemos A.A., Sternberg J.M., Somalvico F., Ferrari F., Castelnovo M.M., Biondetti P.R.**
Comparison between single and multidetector CT in the reduction of sedation rates, conventional angiograms, and patient motion artifacts in young children following liver transplantation (SS 1812), B-891
- Lemos A.A., Castelli R., Fortis D., Guariglia A., Biondetti P., Porro F.**
Pre-test scores in patients suspected of having pulmonary embolism: Are they really useful before multidetector-CT examination?, C-0335
- Lencioni R.**
Ultrasound contrast agents: The impact of EFSUMB guidelines in clinical practice (SY 14), E-61
- Lencioni R.**
Percutaneous tumor ablation: C. Lung (RC 1309), A-335
- Lencioni R.**
Breast cancer hepatic metastases: Survival analysis by the tumor radiofrequency ablation Italian network (TRAIN) (SS 1409a), B-623
- Lencioni R.**
Tumor radiofrequency ablation Italian network (TRAIN): Long-term survival outcomes in patients with stage 0 hepatocellular carcinoma (SS 1409a), B-624
- Lencioni R.**
Tumor radiofrequency ablation Italian network (TRAIN): Long-term results in hepatic colorectal cancer metastases (SS 1409a), B-625
- Lencioni R., Crocetti L., Glenn D., Morris D., Suh R., Regge D., Helmberger T., Lees W., Bartolozzi C.**
Radiofrequency ablation of pulmonary tumors response evaluation (RAPTURE) trial (SS 1409a), B-627
- Leni D., Corso R., Zavaglia C., Rampoldi A., Castoldi M., Vanzulli A.**
Preoperative chemoembolization in patients eligible for liver transplantation affected by hepatocellular carcinoma: Evaluation of antitumoral response on explanted livers and tumor recurrence (SS 1009a), B-501
- Leodolter W.**
PACS pitfalls: Pitfalls when integrating HIS with PACS (SF 9b), A-230
- Leroux G.**
Clinical applications of isotropic high resolution 3D imaging with SPACE (SY 12), E-54
- Lesavre A., Miquel A., Phan C., Menu Y.**
Pelvic ring fractures: Advantages and pitfalls of MDCT, C-0756
- Leschka S., Alkadhi H., Boehm T., Marincek B., Wildermuth S.**
Coronal ultra-thick CT reconstructions of the pelvis in the multiple trauma patient: An alternative for the initial conventional radiograph, C-0754
- Leschka S., Alkadhi H., Marincek B., Wildermuth S.**
Pre- and postinterventional evaluation of abdominal vascular diseases using 16/64 row MSCT angiography, C-1053
- Ley S., Fink C., Borst M., Zaporozhan J., Puderbach M., Meyer J., Gruenig E., Kreitner K., Kauczor H.**
Value of high spatial and high temporal resolution MR angiography for differentiation between primary and secondary pulmonary arterial hypertension (SS 1004), B-472
- Ley S., Zaporozhan J., Eberhardt R., Eichinger M., Fink C., Yubai S., Erdogan S., Herth F., Kauczor H.**
Assessment of pulmonary hypertension by MRI in patients with severe obstructive lung disease: Correlation with pulmonary function test (SS 1504), B-704
- Li Y.**
Evaluation of pulmonary artery flow with MRI in acute massive pulmonary thromboembolism (SS 1404), B-593
- Liaparinos P., Kandarakis I., Cavouras D., Nikolopoulos D., Panayiotakis G.**
Monte Carlo study on radiation absorption properties of Gd2O2S, CsI, LSO, CaWO4 phosphor screens for mammographic X-ray imaging, C-0943
- Libicher M., Vetter M., Kasperk C., Meeder P.J., Nöldge G.**
Histological changes at the bone cement interface after kyphoplasty - comparison of PMMA and CaP with histomorphometry and high resolution CT (SS 310), B-138
- Lichy M.P., Amberger C., Müller-Horvat C., Kötter I., Schäfer J., Lenk S., Claussen C., Schick F., Schlemmer H.**
MR imaging of the phalangeal joints in cases of arthritis at 3 Tesla: Initial results (SS 1410), B-562
- Ligabue G.**
3.0 Tesla cardiac imaging (SY 11), E-48
- Ligabue G., Barbieri A., Fiocchi F., Ferraresi S., Rossi L., Modena M.G., Romagnoli R.**
3 Tesla MR for myocardial viability evaluation with emphasis on comparison with 1.5 Tesla (SS 303), B-215

Authors' Index

- Ligabue G., Fiocchi F., Ferraresi S., Rossi R., Rossi L., Modena M.G., Romagnoli R.**
Does thin slice multidetector CT (MDCT) improve stent patency and in-stent restenosis evaluation? (SS 1803), B-824
- Liguori C., Menchini L., Mutignani M., Manfredi R., Bonomo L.**
Value of magnetic resonance cholangiography in sclerosing cholangitis: Comparative study with ERCP (SS 301b), B-174
- Lim M., Kim J., Suh C.**
Diffusion-weighted MR imaging in MELAS (mitochondrial myopathy, encephalopathy, lactic acidosis and stroke-like episode) syndrome (SS 611), B-320
- Lim J., Kim M., Hyung W., Kim K.**
Intraoperative tumor localization using laparoscopic ultrasound for laparoscopic assisted tumor resection., C-0095
- Lim J., Kim H., Lee D., Ko Y.**
Bilateral adrenal masses: Algorithmic approach for diagnosis, C-0505
- Limbucci N., Pupillo V., Mancini L., Stavroulis E., Di Cesare E., Masciocchi C.**
Evolution of MRI findings of arrhythmogenic right ventricular cardiomyopathy at follow-up (SS 203), B-085
- Limbucci N., Barile A., Zugaro L., Bonanni G., Calvisi V., Masciocchi C.**
New arthro-MRI technical approach in the evaluation of intra-articular structures of the postero-lateral corner of the knee (SS 310), B-137
- Limbucci N., Carducci S., Fiumara C., Di Bartolomeo M., Masciocchi C., Gallucci M.**
Intradiscal O2-O3 vs. corticosteroid injection in the treatment of sciatica (SS 609a), B-287
- Limbucci N., Gismondi G., Pupillo V., Ciriello M., Di Cesare E., Masciocchi C.**
12 year follow-up of patients with type B aortic dissection, C-1063
- Lin S.F., Chen J.H., Wang S.B.**
CT-guided percutaneous radiofrequency ablation in patients with inoperable malignant lung tumors: Safety and efficacy (SS 1804), B-848
- Lin S., Peh W.C.G., Muttarak M., Tan A.G.S., Euathrongchit J., Lertrumngont P., Simarak S., Sivasomboon C., Oh H.M.L.**
Melioidosis: A tropical disease with a spectrum of imaging features in different organ systems, C-0066
- Lin R., Wu R.H., Xiao Z.W., Liu G.R., Kong K.M., Lang Z.J.**
Zero-filling interpolation processing (ZIP) technique can effectively suppress segmental stenosis artifact in small arteries in anatomical phantoms, C-1027
- Lindell E.P.**
Head and neck imaging with 64 slices (SY 12), E-52
- Link T.M.**
Osteoporosis and osteopenia: C. Juvenile osteopenia (RC 510), A-103
- Lirola Cruz M., Muñoz Beltran M., García Casado E., Tuñón Gómez M., Blazquez Ortiz J.M.**
Value of MRI in the diagnosis of hemochromatosis, C-0050
- Lisý J., Mazanec R., Bojar M., Seeman P., Neuwirth J.**
X-linked Charcot-Marie-Tooth disease: MRI of brain changes (SS 211), B-099
- Lisy M., Hilger I., Trost R., Reichenbach J.R., Schueler D., Kaiser W.A.**
Combined MR- and NIR-targeting of macrophages using fluorochrome labelled magnetosomes in vitro, C-0409
- Littera A., Ferrari A., Stecco A., Boccardi A., Civardi C., Carriero A.**
Tips and tricks in cerebral perfusion CT: Classification and literature review, C-0830
- Littler P., Garvey C.J.**
Radiological review of lymphoma involving the gastrointestinal tract, C-0161
- Livadas G.**
History of contrast media: History of contrast media (Introduction) (SF 4c), A-076
- Löbel U., Güllmar D., Mentzel H., Sedlacik J., Reichenbach J.R., Kaiser W.A.**
Diffusion tensor imaging of healthy neonates and children up to adolescence (SS 1412), B-648
- Locatelli M., Chersevani R., Rizzato G.**
Real-time ultrasound elastography: Diagnostic tool or electronic gadget? (SS 202), B-025
- Löfving A., Tizon X., Persson A., Wiklund G., Smedby Ö.**
Virtual contrast injection: A software tool for selective visualization of vessel structures, C-0358
- Löfving A., Tizon X., Persson A., Wiklund G., Smedby Ö.**
Computed Tomography Angiography of the coronary arteries with virtual contrast injection, C-0361
- Lohan D.G., Walsh S.M., McCarthy P.**
Use of Calogen® as an oral contrast medium in the evaluation of the gastric wall at MRI, C-0142
- Lohan D.G., Gough N., Walsh S.M., Roche C., McCarthy P.**
Transrectal prostate biopsy: Does a role for neurovascular bundle local anaesthesia exist?, C-0483
- Lohan D.G., Walsh S.M., O'Sullivan G.J.**
Stenting of the tracheobronchial tree, C-0635
- Lohan D.G., Walsh S., Meehan C., Davidson I., O'Sullivan G.J.**
Multislice CT in the determination of suitability for endovascular aortic stent grafting, C-1006
- Lohrmann C., Ghanem N., Pache G., Makowiec F., Kotter E., Langer M.**
CT in acute perforated sigmoid diverticulitis, C-0127
- Lomas D.J.**
Crohn's disease of the intestinal tract: Advances in imaging: C. MR imaging (RC 801), A-177
- Lomas D.J.**
MR imaging of the small intestine: Functional studies (SF 13), A-314
- Lombardi V.**
Electronic medical record: The distribution of patient-basede-health information in a regional context. The Legnano experience (SY 3), E-10
- Loo C.E., Schlieff A.T.E.F., Deurloo E.E., Muller S.M., vd Vijver M., Gilhuijs K.G.A.**
Monitoring response to neoadjuvant chemotherapy in locally advanced breast cancer: Efficacy of contrast-enhanced MRI to predict presence of residual disease (SS 702), B-379
- Loose R.W.R., Wucherer M., Geiger B., Mechtel M., Adamus R., Vano E.**
Imaging properties of a new dynamic large flat panel detector for DSA and 3D-rotational angiography (CT-mode) (SS 1513), B-778
- Lopez-Benitez R., Barragan-Campos H.M., Richter G.M., Kauffmann G., Marinelli T., Hallscheidt P.J.**
Super selective percutaneous treatment of liver transplantation cholangitis (LTC). Technical aspects and biochemical parameters for graft salvage (SS 309a), B-195
- Lopez-Benitez R., Barragan-Campos H.M., Richter G.M., Kauffmann G., Marinelli T., Hallscheidt P.J.**
Endoluminal treatment of liver transplantation complications. Sixteen-year experience in 570 patients, C-0589
- Lorente-Ramos R.M., del Valle-Sanz Y., Alcaraz-Mexía M.J.**
Utility of the posterior fontanelle approach in cranial sonography, C-0936
- Lorenzen J.H., Wedel A.K., Lisboa B.W., Adam G.**
Comparison of BI-RADS categories and final diagnosis in case of second opinion assessment (SS 1402), B-586
- Lorenzen J.H., Wedel A.K., Lisboa B.W., Adam G.**
Concordance of the breast imaging reporting assessments and final diagnosis for diagnostic mammography and sonography, C-0224
- Lorenzen M., Wedegärtner U., Weber C., Adam G., Lorenzen J.**
MSCT in the postoperative follow-up of vertebral osteosynthetic procedures: Comparison with conventional radiography, C-0757
- Losio C., Venturini M., Fiorina P., Angeli E., Secchi A., Del Maschio A.**
Protective role of pancreas and successful islets transplantation on transplanted kidney of type I diabetic uremic patients: Clinical and color Doppler ultrasound (CDU) assessment in 234 patients (SS 1807b), B-862
- Lovato L., Russo V., Renzulli M., Buttaffi K., Gavelli G., Fattori R.**
Early and mid-term results of endovascular stent-graft in the treatment of descending thoracic aorta diseases (SS 209a), B-064
- Lovato L., Buttaffi K., Angeli E., Russo V., Renzulli M., Gavelli G., Fattori R.**
Improving early and long term survival in the treatment of type B dissection: Comparison among medical, surgical and endovascular therapy (SS 209a), B-066
- Löwik C.W.G.M.**
Imaging of gene expression: Optical and nuclear techniques: B. Gene expression imaging using bioluminescence (PR 1219), A-300
- Lu J., Li K.**
The application of MR perfusion-weighted imaging in patients with unilateral ICA stenosis or occlusion (SS 1811a), B-904

Authors' Index

Luboldt W., Eichler K., Herborn C., Wagner T.O.F., Fieguth H., Vogl T.J.
Detection of malignant pulmonary nodules: Determination of the optimal MRI sequence and evaluation of its performance (SS 204), B-034

Luccichenti G., Salvati M., Frati A., Brogna C., Delfini R., Bastianello S.
Advanced MR imaging in the surgical planning of intracranial tumors, C-0804

Luccichenti G., Spadaro M., Bramanti P., Colonnese C., Sabatini U., Uggetti C., Bastianello S.
Atypical multiple sclerosis: MRI findings and differential diagnosis, C-0835

Luccichenti G., Giugni E., Paolillo A., Cademartiri F., Pichieccchio A., Bastianello S.
Evaluation strategies of multiple sclerosis with conventional and advanced techniques, C-0864

Luccichenti G., Cademartiri F., Sabatini U., Giugni E., Egitto M.G., Bastianello S.
Optimising scan protocols and assessing image quality in clinical MR imaging, C-0947

Lucidarme O., Malzy P., Vaillant J., Cadi M., Taboury J., Hannoun L., Grenier P.
Acquisition and postprocessing procedures for 3D CT modeling of hepatic vessel architecture and volume calculation in major liver resection and living donated liver transplantation, C-0043

Lukic-Kostic L.V., Sekulovic S.Z.
Color Doppler of superior mesenteric artery in the semi severe form of Crohn's disease of the terminal ileum, C-0134

Lupattelli T., Fischer M.J., Mosca S., Maselli A., Pozzilli P., Scalera G., Lupattelli L.
Carotid stenting: Complications within 30 days using filter neuroprotection (SS 1009b), B-517

Lupattelli T., Scalera G., Fischer M.J., Cruso F., Lupattelli L.
Cutting balloon angioplasty for the treatment of the stenosis of fistula due to haemodialysis, peripheral bypass, and stent (SS 1409b), B-633

Lupescu I., Capsa R., Georgescu S.
CT and MRI aspects of superior vena cava pathologies, C-1072

Lusic M., Stern Padovan R., Vrbanec D., Kralik M., Potocki K.
MSCT imaging of patients treated with surgery and/or Imatinib Mesylate therapy for gastrointestinal stromal tumors (GIST), C-0108

Lutz J., Jäger L., Stahl R., Dietrich O., Schelling G., Schönberg S.O., Reiser M.F.
Normal ageing compared to alterations in fibromyalgia related regions of the brain: A DTI study (SS 311), B-226

Lutz J., Jäger L., Hempel M.J., Srivastav S., Reiser M.F.
Delineation of temporal bone anatomy: A comparison between low-dose 64-slice CT and conventional 4-slice CT technique (SS 608), B-277

Luz O., Heuschen M., Kuettner A., Schroeder S., Kopp A., Claussen C.D.
ECG-gated 16-slice CT of coronary arteries: Assessment of image quality and accuracy in detecting stenoses, C-0257

M

Ma J., Bruening R., Morhard D., Hamann G.F., Brueckmann H.
Diffusion and perfusion weighted magnetic resonance imaging in patients with acute ischemic stroke: Can diffusion/perfusion mismatch predict outcome? (SS 611), B-314

Ma L., Weng X., Sun W.
Preliminary study on the mechanism of reading recovery in a pure alexia by using functional MRI, C-0823

Maass J., Tosetti I., Bianchi C.C., Stratta M., De Feo C., Barisone F., Burdese M., Gandini G.
Magnetic resonance imaging of pyelonephritis in renal transplantation, C-0463

Maataoui A., Qian J., Mack M.G., Khan M.F., Straub R., Oppermann E., Vogl T.J.
Effect of laser-induced thermotherapy (LITT) on liver metastasis of varying size (SS 209b), B-075

Machann J., Thamer C., Schnödt B., Häring H., Claussen C.D., Fritzsche A., Schick F.
Comparison between highly fat selective MR imaging and volume localized 1H-spectroscopy of the liver for determination of intrahepatic fat accumulation, C-0012

Machann J., Thamer C., Schnödt B., Häring H., Claussen C.D., Fritzsche A., Schick F.
Age and gender related differences of adipose tissue compartments: A whole body MRI study, C-0941

Machida M., Kameyama K., Shimizu A., Machida N., Tajima H., Kumazaki T., Moriyama N., Naito Z.
Basic examination of photoirradiation for possible control of angiogenesis by HP-denatured type IV collagen complex dissolution, C-0397

Mack M.G., Vogl T.J.
Radiological approach to stage head and neck squamous cell carcinoma: B. Nasopharynx (RC 408), A-073

Mack M.G., Rieger J., Baghi M., Balzer J.O., Knecht R., Helbig M., Vogl T.J.
High resolution superparamagnetic iron oxide enhanced MRI for the diagnosis lymph node metastases in patients with head and neck cancer (SS 308), B-190

Mack M.G., Eichler K., Straub R., Lehnert T., Balzer J.O., Zangos S., Vogl T.J.
MR-guided laser induced thermotherapy (LITT) of colorectal carcinoma metastases in the liver (SS 709), B-405

Mack M.G., Lehnert T., Eichler K., Straub R., Balzer J.O., Zangos S., Vogl T.J.
MR-guided laser induced thermotherapy of liver metastases of gastric cancer (SS 1009a), B-500

Mack M.G., Hochmuth K., Müller J.K.E., Thalhammer A., Krause M., Kurth A., Vogl T.J.
Prospective analysis of the value of different MRI sequences for the detection of early stages of arthropathy in patients with hemophilia (SS 1510), B-689

Macura K.J., Genadry R.R., Bluemke D.A.
Evaluation of female urethra and supporting ligaments with MR imaging (SS 1807a), B-790

Macura K.J., Genadry R.R., Bluemke D.A.
MR imaging of the urethral sphincter in incontinent women, C-0420

Maeda M., Sakuma H., Takeda K.

Usefulness of the apparent diffusion coefficient in line scan diffusion-weighted Imaging for distinguishing between squamous cell carcinoma and malignant lymphoma of the head and neck, C-0549

Maeda M., Takeda K.

Quantitative assessment of diffusion in myxoid and non-myxoid soft tissue tumors by line scan diffusion-weighted imaging, C-0711

Maeda M., Takeda K.

Malignant lymphomas and carcinomas involving the cavernous sinus: Assessment with apparent diffusion coefficient, C-0787

Maffessanti M.

Wrapping it up A. The pleura and diaphragm (E³ 1220), A-305

Magistrelli A., Costantini M., Romani M., Masetti R., Belli P.

Magnetic resonance imaging of breast implant ruptures, C-0201

Mahfouz A.E., Sherif H.

Diagnosis of epididymo-testicular disjunction on gadolinium-enhanced MR imaging in patients with cryptorchidism (SS 1807b), B-865

Mahfouz A.E., Sherif H.

Focal hemorrhagic lesions of the kidney on MR imaging, C-0464

Mahfouz A.E., Sherif H.

Gadolinium-enhanced MR venography of the venous compression syndromes, C-1022

Mahnken A.H., Seyfarth T., Flohr T., Herzog C., Stanzel S., Günther R.W., Wildberger J.E.
Flat-panel detector CT for assessment of coronary artery stents: Comparison with 16-slice spiral CT (SS 703a), B-349

Mahnken A.H., Katoh M., Bruners P., Spüntrup E., Wildberger J.E., Günther R.W., Buecker A.

16-detector row spiral CT versus MR imaging for the assessment of left ventricular function in acute myocardial infarction: An animal study (SS 1003), B-520

Mahnken A.H., Koos R., Katoh M., Wildberger J.E., Spüntrup E., Günther R.W., Kühl H.P., Buecker A.

Multislice spiral CT for assessment of myocardial viability: Comparison to contrast enhanced MR imaging (SS 1003), B-522

Mahnken A.H., Klotz E., Lautenschläger S., Koos R., Fritz D., Scheuring M., Rinck D., Günther R.W., Wildberger J.E.

Assessment of myocardial infarction with cardiac MSCT using model based heart segmentation and perfusion weighted color maps (SS 1003), B-523

Maintz D., Ozgun M., Hoffmeier A., Heindel W., Fischbach R., Botnar R.

Noninvasive coronary artery plaque visualization and differentiation by contrast enhanced black blood MRI (SS 603), B-307

Maintz D., Ozgun M., Hoffmeier A., Heindel W., Fischbach R., Botnar R.

Whole heart coronary MR-angiography: Value for the detection of coronary artery stenoses in comparison to MSCT-angiography, C-0271

Authors' Index

- Maj E., Cieszanowski A., Golebiowski M., Zieniewicz K., Szwejda E., Cieslak B., Krawczyk M.**
Evaluation of biliary tract complications in hepatic transplantation with the use of magnetic resonance cholangiography, C-0003
- Makó E.K.**
Crohn's disease of the intestinal tract: Advances in imaging: B. CT and CT enteroclysis (RC 801), A-176
- Maksimovic R., Dill T., Bachmann G., Seferovic P., Stankovic S., Pitschner H.**
Diagnosis of arrhythmogenic right ventricular cardiomyopathy: A modified magnetic resonance imaging scoring system, C-0248
- Malagari K.**
Wrapping it up ...: B. Mediastinal disease (E³ 1220), A-306
- Malagari K.**
Thoracic manifestations of extra-thoracic disease: C. Multisystem vasculitides (RC 1604), A-378
- Malagari K., Antonopoulos D., Mitromaras J., Alexopoulou E., Sissopoulos A., Shizas D., Kelekis D.**
Elective bronchial artery embolisation for haemoptysis using spherical embolic agents, C-0334
- Malagari K., Antonopoulos D., Mitromaras J., Alexopoulou E., Hatzimichail K., Nikita A., Kelekis A., Kampanarou M., Kelekis D.**
Giant liver hemangiomas: Results of transcatheter embolization, C-0584
- Malich A., Facius M., Boettcher J., Freesmeyer M.G., Scholz B., Kaiser W.A.**
Influence of vascularization of breast lesions on electrical conductance and detection rate using EIS (SS 202), B-022
- Malich A., Fischer D.R., Wurdinger S., Boettcher J., Hansch A., Kaiser W.A.**
Clinical potential of various MR signs to discriminate malignant from benign breast lesions in MR-mammography (SS 702), B-372
- Mallol X., de Lama E., Gonzalez E., Fernández A., Domingo E., Narváez J.**
Non-cutaneous peripheral T-cell lymphomas: Radiological-pathological correlation, C-0063
- Mamisch T.C., Welsch G.C., Cavallaro A., Horger W., Menzel M., Hennig F.F., Muhr G.**
In vivo correlation of gross pathology in osteoarthritis of the hip to MRI cartilage imaging (SS 710), B-356
- Mamisch T.C., Cavallaro A., Horger W., Muhr G., Forst R., Bautz W.**
3 T MRI cartilage imaging of the hip: Cartilage pattern, lesions, biomechanical analysis and comparison to 1.5 T (SS 710), B-357
- Manenti G., Squillaci E., Di Roma M., Mancino S., Simonetti G.**
MRI and ¹H - MR spectroscopic imaging in the evaluation of prostate cancer (SS 1007), B-494
- Manfrè L., Bonetti M., Piccoli T., Cristaudo C.**
High b value diffusion MR imaging of the brain and the spinal cord in patients affected by amyotrophic lateral sclerosis: Preliminary results (SS 211), B-097
- Manfrè L., Bonetti M., Tomarchio L., Cristaudo C.**
New vertebral procedures: Besides the vertebral body (SS 609a), B-284
- Mang T.G., Happel B., Mueller C., Prokop M., Klingler H.C., Suasn M., Heinz-Peer G.**
Bladder Imaging using multidetector row CT: Techniques, applications and findings, C-0509
- Mangov A., Dakhno L.**
Effect of window settings of dental-CT images on visualization of the tooth tissues (SS 208), B-054
- Manolitsas A., Tezapsidis G., Tarazi L., Tsitouridis I.**
Virtual endoscopy: An additional imaging tool for the depiction of regions that the actual endoscopy cannot approach, C-0989
- Mansueto G., Tessitore N., Cenzi D., Bedogna V., Baggio E., Lupo A., Pozzi Mucelli R.**
A prospective controlled trial on endovascular vs surgical treatment of stenosis in forearm arterious fistulae (AVF) (SS 1409b), B-638
- Mantzikopoulos G., Pikoulas K., Staikidou I., Giannikouris G., Ioannidis K., Dagiada K.**
MR imaging in spinal injury in patients with ankylosing spondylitis, C-0766
- Manuel D.D., Bose S., Evans D.D., Wasan R., Ralleigh G., Michell M.**
Radiological and histological features of mammography screen detected lesions undergone benign surgical excision, C-0180
- Maratos Y.K., Kalai A., Clément O., Loeb T., Frija G.**
Which assessment should be preferred for a polytrauma victim?, C-0069
- Marcelli G., Pediconi F., Occhiato R., Venditti F., Nardis G., Passariello R.**
Observer variability and applicability of BI-RADS terminology for breast MR imaging (SS 702), B-373
- Marcello R., Castrucci M., Assegnoti G., Costa P., Serrao E., Mangialardi N.**
Modalities of treatment of type II endoleaks after abdominal aorta endoprosthesis deployment (SS 609b), B-296
- Marcello R., Anglana F., Signorile P., Assegnoti G., Di Blasi A., Castrucci M.**
The effectiveness of magnetic resonance (MR) in diagnostic pattern prediction and follow-up of uterine fibroids embolization, C-0586
- Marchenkova Y.V., Vesselova T.N., Chuchalin A.G., Pashkova T.L.**
Diagnosis of tracheal instability with dynamic CT (SS 1504), B-709
- Marcy P., Chaturvedi A., Brunner P., Bondiau P., Hericord O., Gallard J.**
Percutaneous arm port device placement: Feasibility, efficacy and impact on quality of life in 1000 cancer patients using arm venography exclusively (SS 1409b), B-639
- Marinelli T., Filippone A., Grenacher L., Kauffmann G., Richter G.M.**
Heidelberg score of vascular invasion for pancreatic cancer (SS 701b), B-413
- Markovic Z., Markovic B., Yachia D., Levy R., Maksimovic H., Vojvodic O.**
Bulbar urethral strictures treated with allium temporary covered stents: First clinical experience (SS 1809), B-874
- Maroldi R.**
Imaging of skull base tumors: A practical approach for your daily practice: A. Anterior skull base (RC 1608), A-382
- Maroldi R.**
Metastatic disease of the brain and spine: B. Extra-axial metastases (skull, dura, leptomeningeal) and tumor spread (CC 1717), A-400
- Marshall G.**
Professional matters: B. HENRE (Higher Education Network for Radiography in Europe): Continuous professional development (CPD) (RC 1314), A-346
- Marsot-Dupuch K.**
Modern imaging of infective disease in the face and pelvis: A. Cervicofacial infection in the immunocompromised patient (CC 916), A-241
- Marsot-Dupuch K., Richard S., Bobin S.**
Endolymphatic sac tumors: A major criteria of Von Hippel-Lindau disease, C-0559
- Martegani A., Clarizia F., Rossini G., Borghi C., Del Favero C., Campi R.**
Elastosonography of benign and malignant nodular breast lesions (SS 202), B-024
- Martegani A., Aiani L., Tufarulo L., Campi R., Ciancio M., Mascheroni F.**
Elastosonography of benign and malignant nodular breast lesions: First experience review, C-0209
- Martel J., Bueno Á., Domínguez P., Nevado M., Llorens P., Quirós J., Delgado C.**
Percutaneous radiofrequency ablation: Relationship between probe type, time of procedure and the extent of the osteonecrosis in a long bone dog model., C-0657
- Marten K.**
Smoking-related diseases: B. Smoking-related interstitial diseases (RC 104), A-018
- Marten K., Seyfarth T., Rummery E.J., Engelke C.**
Computer-aided detection of pulmonary metastasis: Influence of nodule characteristics on detection performance (SS 304), B-163
- Marten K., Seyfarth T., Rummery E.J., Engelke C.**
Computer-aided detection of pulmonary metastasis using multislice CT: Performance evaluation in consensus with experienced versus inexperienced chest radiologists (SS 304), B-165
- Marti-Bonmati L., Pastor Juan M., Peñaloza F., Olalla Muñoz J., Martínez Pérez M.**
Quantification of hepatic iron by MR: Body or surface coil? (SS 1801b), B-849
- Martincich L., Montemurro F., Campanella D., Debernardi S., Russo F., Regge D.**
Impact of different measurements techniques in the prediction of histological response, in patients with locally advanced breast cancer treated by primary chemotherapy (SS 702), B-377
- Martinez de Aragón A., Pérez López C., Echeveste J., Bravo A., Rodriguez-Vigil B., Marín B.**
Value of the apparent diffusion coefficient in the differential diagnosis of brain glioma tumors, C-0876
- Martinez-Bisbal M.C., Celda B., Martinez-Granados B., San Juan C., Martí-Bonmati L.**
Feasibility of quadrature body coil in prostate spectroscopic MR imaging, C-0475

Authors' Index

Martinoli C., Podestà R., Succio G., Gauglio C., Zuccarino F.

Imaging of focal lesions: Muscles and tendons (EM 1), A-149

Martirosian P., Pintaske J., Graf H., Erb G., Lodemann K., Claussen C.D., Schick F.

Comparison between concentration dependent relaxivity of gadopentetate dimeglumine (Magnevist®), gadobutrol (Gadovist®) and gadobenate dimeglumine (MultiHance®) in human blood plasma at 0.2 T, 1.5 T and 3.0 T, C-0403

Martos Becerra J.M., Espejo Herrero J.J., Díaz Aguilera R., Ramos Gómez M., Bravo Rodriguez F., Delgado Acosta F., Landauro Comesaña C., Roldán Romero E.

Cervical vessel dissection: comparison of CT angiography with digital subtraction angiography and radiological findings, C-0794

Masala S., Ursone A., Fiori R., Massari F., Simonetti G.

Percutaneous nucleoplasty in the treatment of lumbar pain (SS 609a), B-289

Mascarenhas V.M.V.T., Lobo L., Fonseca-Santos J.

Imaging evaluation of paediatric thoracic cystic lesions, C-0924

Masciocchi C.

Sports injuries: B. Sports-related degenerative disease of joints (RC 110), A-005

Mashayekhi M., Misra R.R., Hine A.L.

Musculoskeletal manifestations of sickle cell disease. A pictorial review, C-0743

Masselli G., Menchini L., Minordi L., Vecchioli A., Bonomo L.

Crohn's disease: Comparison of MR enteroclysis with MRI using polyethylene glycol (PEG) solution as oral contrast medium (SS 1401a), B-577

Massing S.

Safety in the MRI suite, little things to be aware of (SY 4), E-14

Massuet A., Gallardo X., Castañer E., Mata J., Gil D.

The spectrum of CT findings in pleural mesothelioma, C-0289

Mastantuono M.

Wrist: C. Dynamic studies: MR and US clinical applications (RC 910), A-210

Masulovic D.M., Milicevic M., Saranovic D., Djuric A., Ivanovic A., Dobriserevic B.

Percutaneous treatment of hydatid cysts of the liver: Our experience, C-0631

Mathieu O., de Bazelaire C., Zagdanski A., Bourrier P., Albiter M., Frija J., de Kerviler E.

MR evaluation of renal cell carcinoma: Comprehensive protocol for determining venous extension, C-0459

Matsopoulos G., Kouloulias V.E.,

Mouravliansky N., Asvestas P., Delibasis K., Uzunoglu N., Kelekis A., Kelekis N.

An elastic registration scheme for the alignment of thoracic CT data of patients with stage III non-small cell lung cancer during radiotherapy treatment, C-0942

Matsui O.

"Oriental Pearls" in oncology imaging: Imaging-pathologic correlation of early cancer in gastrointestinal tracts: Early hepatocellular carcinoma: Imaging of multi-step hepatocarcinogenesis (EM 3), A-362

Matsuki M., Tanikake M., Kani H., Narabayashi I.

Multiphase fusion technique of three-dimensional images using 16 MDCT for the preoperative simulation and intraoperative navigation of laparoscopic gastrectomy and colectomy, C-0116

Matsumoto S., Ohno Y., Watanabe H., Higashino T., Sugimura K.

Pulmonary nodule detection in CT images using ellipsoid models, C-0373

Matsuoka T., Toyoshima M., Yamamoto A., Oyama Y., Okuma T., Nakamura K., Yamada R., Inoue Y.

Early experiences of percutaneous radiofrequency ablation for unresectable small lung malignancies, C-0615

Matsuzaki K., Takeuchi M., Uehara H., Nishitani H.

Differential diagnosis of multiple hyperintense lesions of the liver on T1WI of MRI with pathologic correlation, C-0047

Matuszewski L., Kuhlpeter R., Dahnke H., Persigehl T., Wall A., Tombach B., Heindel W., Schaeffer T., Bremer C.

Fast T2/T2*-mapping at 3.0 Tesla for quantification of cellular iron-uptake (SS 1506b), B-784

Matute Teresa F., Saiz Ayala A., Santamaría N.

Spinal tuberculosis: Typical and atypical findings at MR imaging, C-0753

Matute Teresa F., Saiz Ayala A., Santamaría N.

Radiological atlas of central nervous system tuberculosis, C-0814

Maubon A.J.M., Caire-Gana B., DeGraef M., Piver P., Aubard Y., Rouanet J.

Imaging of the female pelvis: A. Infertility (RC 107), A-033

Mavrogeni S.I., Cokkinos D.D., Manginas A., Papadopoulos G., Douskou M., Kaklis S., Foussas S., Seimenis J., Cokkinos D.V.

Role of magnetic resonance angiography in coronary artery ectasia and Kawasaki disease (SS 1403), B-659

Mayerhoefer M.E., Breitenseher M.J., Aigner N., Hofmann S., Kramer J.

Computer-assisted quantitative analysis of bone marrow edema of the knee: STIR versus T1-weighted fat-suppressed contrast-enhanced MR imaging at 1.0 and 1.5 Tesla (SS 1510), B-686

Maynar M.

Aortic stent grafts: C. Bifurcated grafts (WS 1209), A-289

Mazonakis M., Prassopoulos P., Mantatzis M., Damilakis J., Gourtsoyiannis N.

Assessment of metastatic liver tumor burden on MR imaging: Validity of uni-dimensional and bi-dimensional measurements, C-0036

Mazurek O.V., Babiy Y.S., Garmish E.A.

MRI in assessing the changes of rheumatoid arthritis of hand, C-0690

Mazza E., Sali L., Vannini C., Beccani D., Toccafondi F., Zini M., Acquafranca M.

Percutaneous radiofrequency thermoablation with cool-tip probe of osteoid osteoma (SS 609a), B-290

Mazza E., Sali L., Vannini C., Bonasera L., Toccafondi F., Fabbri E., Zini M.

CT-guided percutaneous RF ablation of pulmonary neoplastic lesions (SS 1409a), B-628

Mazza E., Sali L., Vannini C., Beccani D., Falchini M., Zini M., Acquafranca M.

Transgastric drainage technique in pancreatic fluid collections and in traumatic lesions, C-0636

Mazzei M., Marrelli D., Pinto E., Pirtoli L., Volterrani L.

Efficacy of multidetector row CT in staging gastric cancer according to The Japanese classification of gastric carcinoma (SS 201a), B-020

Mc Donnell O., Hyland M., Britten J., Graham R.

Lead coats as vectors of nosocomial infection, C-0987

Mc Kenna D.A., Alhajeri A., Roche C.J., Murphy J.M., McCarthy P.A.

A pictorial review of extra luminal findings on MRI of the small bowel, C-0143

McAdams H.P.

Tomosynthesis: 3D digital radiography (SY 6) E-24

McCall I.W.

Assessment and accreditation in radiology in Europe: Assessment and accreditation of training centres in Europe (ER 526), A-138

McCollough C.H., Kofler J.M., Bruesewitz M.R.

Implementation of automated exposure control (AEC) in a large body CT practice: Assessment of image quality and dose savings (SS 713), B-443

McGrath A., Farrelly C., Sheehy N., Meaney J.F.M.

Differential diagnosis of lesions involving the brain and spinal cord in patients with lymphoma, C-0785

McLaren C.

Pediatric intervention: C. Angioplasty and arterial stenting in children (WS 818), A-194

McMahon C.J., Gibney R.G., Malone D.E.

Endoscopic ultrasound or MR cholangiography for bile duct calculi and strictures? An evaluation using "evidence-based radiology" methods (SS 301b), B-172

McMahon C.J., Hennessy M., Boyle G., Feely J., Meaney J.F.M.

Prevalence of renal artery stenosis in flash pulmonary oedema: Determination using gadolinium-enhanced MRA (SS 1015), B-559

McNally E.G.

Knee joint: A. Soft tissue structures of the knee with US and MRI (RC 1710), A-402

Meaney J.F.M.

Venous imaging and intervention: B. MR venography (RC 515), A-128

Meckle R., Bieri O., Hashagen C., Scheffler K., Bilecen D.

Passive guidewire tracking on road maps - a phantom study (SS 309b), B-201

Authors' Index

- Meehan C.P., Cronin C.G., Lohan D.J., McCarthy P.A.**
PACS in your pocket? The PDA as imaging tool of the future, C-0364
- Meehan C.P., Gough N., McCarthy P.A.**
PCNL by numbers: A 7-year analysis of percutaneous nephrostolithotomy in practice, C-0445
- Meindl T., Coppenrath E., Khalil R., Mueller-Lisse U., Reiser M.F., Mueller-Lisse U.**
Systematic evaluation of optimal delay time for CT urography (SS 1407), B-615
- Meingan P., Labbe-Devilliers C., Doutriaux-Dumoulin I., Digabel-Chabay C., Ricaud-Couprise M.**
Imaging of late recurrence in invasive breast cancer, C-0211
- Meissner O.A., Rieber J., Oswald M., Reim S., Babaryka G., Mueller-Lisse U.G., Redel T., Kleen M., Reiser M.F.**
Microstructural imaging with optical coherence tomography: Comparison with intravascular ultrasound and histology in coronary artery specimens (SS 215), B-111
- Meissner O.A., Rieger J., Weber C., Siebert U., Reiser M.F., Schoenberg S.O.**
Dynamic time-resolved MRA compared with DSA in patients with limb threatening ischemia (SS 315), B-243
- Memeo M., Stabile Ianora A.A., De Leo C., Pignataro P., Resta M.C., Scardapane A., Angelelli G.**
Pulmonary arteriovenous malformations: Could multi-detector row helical CT and angiographic reconstructions replace diagnostic angiography? (SS 1004), B-475
- Memeo M., Stabile Ianora A.A., De Leo C., Memmola C., Sabbà C., Scardapane A., Angelelli G.**
Diagnosis of pulmonary arteriovenous malformations in patients with hereditary hemorrhagic telangiectasia: Multi-detector row helical CT versus contrast echocardiography. Preliminary results (SS 1004), B-476
- Memis Oktay A., Oktay O.**
Breast sonography in asymptomatic women with mammographically dense breasts (SS 1402), B-582
- Mengiardi B., Pfirrmann C.W.A., Schöttle P.B., Bode B., Hodler J., Vienne P., Zanetti M.**
The magic angle phenomenon in MR imaging of ankle tendons: Prevalence and site in asymptomatic subjects and cadaveric specimens with histologic correlation (SS 710), B-351
- Menzel H., Rauscher A., Böttcher J., Fitzek C., Brandl U., Reichenbach J.R., Kaiser W.A.**
High-resolution susceptibility weighted imaging (SWI) as a new diagnostic tool in children, C-0891
- Menu Y., Rangheard A.**
Liver imaging: Characterisation and pitfalls:
C. Vascular abnormalities (RC 501), A-113
- Mereu M., Guido F., Feragalli B., Travaglini A., Torrione C., Storto M.**
Cavitary lesions in the lung: Radiographic and CT findings, C-0307
- Merino-Casabiel X., Dominguez-Oronoz R., Castella-Fierro E., Pineda V., Evangelista A.**
MRI of cardiomyopathies: A pictorial review, C-0250
- Merino-Casabiel X., Dominguez-Oronoz R., Castella-Fierro E., Pineda V., Ramirez-Urbano F.**
Magnetic resonance findings in macromelia and macrodactyly, C-0770
- Meroni R., Flor N., Soldi S., Caverni L., De Monti M., Sardanelli F., Cornalba G.P.**
Internal carotid artery (ICA) stenoses: Color Doppler ultrasound (CDUS), multidetector computed tomography (MDCT), and digital subtraction angiography (DSA) versus intraoperative plaque evaluation (SS 715), B-455
- Mertelmeier T., Bätz L.**
Physical characterization of the new FFDM system based on an a-Se detector (SS 1013), B-547
- Mertelmeier T., Bernhardt P., Hoheisel M., Palmberg N.**
Dose reduction by technique optimization for FFDM based on an amorphous selenium detector (SS 1013), B-549
- Messina A., Spreafico C., Casali P., Vergnaghi D., Bianchi F., Gronchi A., Musumeci R.**
Advanced gastrointestinal stromal tumors (GIST) treated with Imatinib Mesilate: CT and MR tumor response assessment, C-0115
- Messina A., Casali P., Vergnaghi D., Bianchi F., Gronchi A., Musumeci R.**
Advanced abdominal gastrointestinal stromal tumors (GIST) treated with Imatinib Mesilate: MR tumor response assessment after 24 months follow-up, C-0145
- Messina A., Casali P., Vergnaghi D., Gronchi A., Stacchiotti S., Musumeci R.**
Advanced chordomas treated with imatinib mesilate: MRI tumor response assessment after 18 months follow-up, C-0769
- Mestan H., Cavallaro A., Kordelle J., Forst R., Bautz W., Mamisch T.C.**
Quantitative relationship of normal cartilage in the hip joint based on isotropic 1.5 T MRI (SS 710), B-355
- Metafratz Z.M., Maglaras G., Vassiliou M., Constantopoulos S., Efremidis S.**
Acute pulmonary embolism: Correlation of computed tomography arterial obstruction index with blood gas values (SS 1404), B-597
- Metafratz Z.M., de Roos A., Skopelitou A., Efremidis S.C.**
The pathophysiology of aortic-cardiac interaction in atherosclerotic disease and the role of magnetic resonance imaging, C-1020
- Meyer K., Sinkus R., Kaul M., Lorenzen J., Adam G.**
3 T-magnetic-resonance-elastography of the breast: Technical feasibility, C-0193
- Meziti L., Drapé J., Mirat A., Pessis E., Duffaut-Andreux C., Guerini H., Malan S., Chevrot A.**
SLAP lesions of the glenoid labrum: An imaging study with anatomical correlation, C-0691
- Michaely H.J., Herrmann K.A., Kramer H., Reiser M.F., Schoenberg S.O.**
Quantitative and qualitative characterization of vascularization and hemodynamics in head and neck tumors with a 3D magnetic resonance. Time-resolved echo-shared angiographic technique (TREAT). Initial results (SS 308), B-182
- Michaely H.J., Herrmann K.A., Kramer H., Reiser M.F., Schoenberg S.O.**
High-resolution (HR) renal magnetic resonance angiography (MRA): Prospective comparison of image quality and diagnostic value using integrated parallel acquisition techniques (iPAT) - factor 2 versus 3 (SS 1015), B-557
- Michalakou M., Astrinaki E., Kokkinaki M., Mourkogiannis N., Psarakis E., Gargoulaki M., Kourgeraki R., Vrouhos G., Triantafillou L.**
Correlation of repeated brain CT-scan findings with Intracranial pressure catheter (IPC) values in intensive care unit (ICU) patients: Preliminary report, C-0860
- Michelassi M.C., Cosottini M., Puglioli M., Trivelli I., De Cori S., Parenti G., Bartolozzi C.**
Silent cerebral ischemic lesions revealed with diffusion weighted MR imaging (DWI) in patients submitted to thromboendarterectomy (CEA), protected and unprotected carotid artery stenting (CAS) (SS 1511), B-766
- Midiri M., Galia M., Bartolotta T.**
Pericardial diseases: B. CT and MRI of the inflammatory diseases (RC 1203), A-276
- Miele V., Buffa V., Cortese A., Galluzzo M., Regine G., Adami L.**
Contrast enhanced ultrasound in evaluation of pediatric blunt abdominal trauma, C-0901
- Migaleddu V., Manca A., Turilli D., Luciano P., Canu N., Campisi G., Virgilio G.**
Fundamental nonlinear imaging versus harmonic imaging with contrast medium sonovue in the evaluation of the hepatic focal lesions: Preliminary results (SS 306), B-126
- Mihajloski D., Damjanoski G.**
Communications between carotid and vertebralbasilar system via persistent primitive arteries, C-0596
- Mikhailova E.A., Minko B.A., Ushakova G.A., Vinokurov V.L., Prozorovsky K.V.**
Ultrasound angiography in the assessment of cervical cancer treatment, C-0432
- Mildenberger P.**
Building an electronic patient record system:
A. Computer generated reports: A solution (RC 1205), A-302
- Milne E.N.C.**
Benign angiogenesis (SY 13), E-59
- Milne E.N.C.**
The value of imaging angiogenesis in breast cancer: Is "benign" angiogenesis a diagnostic problem? (SS 202), B-028
- Minamiguchi H., Sato M.**
Suspected entrapment syndrome of the popliteal vein: How to diagnose it. Is it rare?, C-1037
- Minota E., Nakamoto Y., Matsumoto K., Sakamoto S., Okada T., Senda M.**
Accuracy of manual fusion of CT and PET images using a fixation device, C-0982
- Miranda A.M., Cuellar H., Quiroga S., Sebastia C., Boye R., Alvarez A.**
MDCT gastroscopy, C-0137

Authors' Index

- Miro C., Tomas M., Pastor P., Vazquez E., Arjonilla A., Ramiro E., Contreras J.**
Mammographic, ultrasonographic, histologic and immunohistochemical features in patients with breast cancer and BRCA1 or BRCA2 gene mutation (SS 1802), B-838
- Misra R.R., Shorvon P.J.**
Anatomical considerations and imaging features of abdominal wall hernias: A pictorial review, C-0177
- Miyamoto A., Shibamoto Y., Okimoto H., Shinohara H.**
Development of water-soluble metallofullerenes as X-ray contrast media (SS 1806), B-883
- Mocanu D., Kettenbach J., Sweeney M.O., Kikinis R., Kenknight B.H., Eisenberg S.R.**
Patient-specific computational analysis of transvenous defibrillation (IM 1), D-05
- Mohiaddin R.H.**
Imaging of atherosclerotic plaques: B. MRI of the vessel wall (WS 1615), A-389
- Mohr A., Roemer F.W., Guermazi A., Heiss C., Schmidt C., Schaefer P.J., Genant H.K.**
Quantitative analysis of carotid artery atherosclerosis by micro-CT, C-0997
- Molinari F., Pantalone O., Corbo G., Valente S., Pirroni T., Bonomo L.**
Oxygen-enhanced MRI in the assessment of smoking-related pulmonary emphysema: Preliminary results (SS 1504), B-703
- Molinari F., Gaudino S., Spina D., Pirroni T., Bonomo L.**
Parallel imaging in lung MR, C-0340
- Molla Landete M.A., Ferrando Valls F., Benlloch H., Tarazona Hervas V., Palmero da Cruz J.**
CT evaluation of non-malignant tracheal stenosis: What the surgeon needs to know, C-0290
- Monaco D., Larini P., Marcato C., Saccani S., Agostinelli A., Zompatori M.**
Endovascular stent graft placement in patients with traumatic rupture of thoracic aorta (SS 209a), B-061
- Monedero M.D., Olalla J.R., Martinez-Rodrigo J.J., Ruiz A., Lonjedo E., Vilas J.**
PTFE covered metallic stent in the treatment of nasolacrimal duct obstruction: Long-term results, C-0609
- Monnin P., Lepori D., Verdun F.R.**
Objective assessment of image quality in conventional and digital mammography, C-0970
- Montemezzi S., Fornasa F., Barbzeni G., Puppini G., Battistoni A., Marchi A., Gortenuti G.**
Magnetic resonance imaging (MRI) in detecting early breast implant rupture: Report in 467 cases, C-0190
- Moonen C.**
New imaging methods and technologies:
A. Parametric and molecular MR techniques (PR 419), A-090
- Morales J.P., Fotiadis N., Sabharwal T., Bell R.E., Aukett M., Thomas S., Taylor P.R., Reidy J.F.**
Endoluminal repair of type B aortic dissection (SS 209a), B-067
- Morales J.P., Taylor P.R., Deguara J., Bell R.E., Aukett M., Thomas S., Sabharwal T., Reidy J.F.**
Midterm results of the thoracic Excluder: Does it has the same problems as the infrarenal device? (SS 209a), B-069
- Morales Olaya J., Dualde D., Labrador T., Cervera J.**
Transvaginal sonography in postmenopausal bleeding. Sonographic findings in 200 cases. Endometrial carcinoma patterns, C-0434
- Morana G.**
Contrast media for MRI and US liver imaging:
A. Non-specific and liver-specific paramagnetic contrast media (RC 106), A-039
- Moraschi I., Farina D., Maculotti P., Battaglia G., Barbieri P.**
Interobserver variability in the CT assessment of suspected mesothelioma without final histologic diagnosis (SS 704), B-390
- Moreno-Ramos M., Vargas Serrano B., Domínguez Ferreras E., Castell Monsalve F., Bustos Jiménez M.**
Value of computed tomography in the follow-up of patients after laparoscopic repair of abdominal wall hernias, C-0179
- Mori H.**
"Oriental Pearls" in oncology imaging: Imaging-pathologic correlation of early cancer in gastrointestinal tracts: Early-stage pancreatic cancer (EM 3), A-363
- Mori K., Takahashi N., Matsueda K., Saida Y., Minami M., Oda T., Ohkohchi N.**
Detection of hepatic metastases on ferucarbotran-enhanced MR imaging: Feasibility of 3D sensitivity-encoding water-excitation multi-shot echo-planar (3D-SWEEP) imaging, C-0028
- Morisawa N., Koyama T., Umeoka S., Tamai K., Fujiwara T., Saga T., Itoh T., Togashi K.**
Diagnosing metastatic lymph nodes in urogenital cancers: The clinical impact and the role of radiologic imaging, C-0499
- Moske-Eick O., Winterer J.T., Ghanem N., Elsner K., Leupold J., Strecker R., Kotter E., Langer M.**
Bilateral contrast-enhanced MR angiography of the hands at 3.0 Tesla versus 1.5 Tesla using parallel imaging: Intraindividual comparison of signal behaviour and image quality with angiographical correlation in patients with severe ischemic hand disease (SS 315), B-247
- Motamedi K., Seeger L.L., Kim J., DiFiori J.P.**
Comparison of ultrasound and radiography in detecting tendon calcifications around the elbow, and differentiating them from enthesophytes (SS 1810), B-801
- Mueller P.R.**
Urological intervention: B. Thermal ablation of renal tumors (WS 918), A-236
- Mueller P.R.**
Percutaneous tumor ablation: B. Kidney (RC 1309), A-334
- Mueller D., Isbary M., Boehm H., Bauer J., Rummery E.J., Link T.M.**
Detection of osteoporosis-related spine fractures on routine lateral chest radiographs (SS 610), B-251
- Mueller D., Monetti R., Majumdar S., Boehm H., Raeth C., Rummery E.J., Link T.M.**
3D structure analysis based on the scaling index method in relationship to DXA in postmenopausal women with osteoporotic spine fractures (SS 610), B-256
- Mueller C., Mang T.G., Huber W., Imhof H., Kainberger F.**
Solitary bone lesions: Imaging approach and differential diagnosis, C-0669
- Mueller D., Monetti R., Majumdar S., Raeth C., Rummery E.J., Link T.M.**
3D structure analysis of the calcaneus using the scaling vector method in the prediction of osteoporotic spine fractures, C-0670
- Mueller C., Mang T.G., Kalhs P., Thurnher M.M.**
Toxoplasmosis encephalitis after bone marrow transplantation: CT and MR features, C-0857
- Mueller-Lisse U.G., Meindl T., Coppenrath E.M., Mueller-Lisse U.L., Degenhardt C., Rami K., Reiser M.F.**
Delineation of upper urinary tract segments at multidetector CT urography: Retrospective comparison of routine and low-dose protocols (SS 1407), B-610
- Mulkens T.H.E.J., Bellinck P., Baeyaert M., Ghysen D., Van Dijck X., Mussen E., Venstermans C., Termote J.**
Clinical evaluation of an "automatic exposure control" mechanism for dose optimization in multidetector computed tomography (SS 713), B-441
- Müller-Forell W.**
Orbit and visual system: B. Imaging of optic chiasm and visual tract diseases (RC 811), A-182
- Müller-Horvat C., Radny P., Schäfer J., Pfannenberg C., Khorchidi S., Nägele T., Claussen C.D., Schlemmer H.**
Comprehensive assessment of metastatic spread in patients with malignant melanoma by whole-body MRI with high-resolution (SS 1501b), B-715
- Müller-Lisse U.G.**
Multislice CT of the urinary tract: B. Multislice CT of renal cancer (RC 1307), A-331
- Munneke G.J., Choke E., Loosemore T., Thompson M., Belli A., Morgan R.**
Outcome of endovascular repair in patients with difficult aortic necks (SS 609b), B-293
- Munuera J., Rodríguez A., Perich X., Solano A., Gomis M., Calvo N., Ois A., Roquer J.**
Perfusion CT: Patterns of presentation in acute stroke, C-0851
- Muraoka N., Uematsu H., Kinoshita K., Takeda T., Matsunami H., Yamanouchi E., Itoh H.**
Complications of living donor liver transplantation: Image findings and interventional treatment strategies, C-0608
- Mussel D.**
Pulmonary hypertension: All that the radiologist needs to know: Pulmonary hypertension: All that the radiologist needs to know (Introduction) (SF 16), A-369
- Myakinkov V.B.**
Results of the radiology monitoring of breast in women with gynecological malignant tumors (SS 1402), B-580

Authors' Index

- Mylona S., Kokkinaki A., Gamvroula E., Thanos L., Karaxalio E., Mpatakis N.**
Alterations in ocular artery blood flow in patients with type II diabetes mellitus (SS 615), B-336
- Mylona S., Hatzidakis A.A., Thanos L., Charonitakis E., Chamalakis K.N., Mpatakis N.**
Sedation and analgesia in patients undergoing percutaneous liver radiofrequency ablation. Comparison of two protocols (SS 1409a), B-620
- Mylona M.D., Leotsinidis M., Andrikakos P., Christopoulos A., Dimopoulos P.A.**
Comparison of DEXA, QCT and trabecular structure in beta-thalassaemia, C-0660
- Mylona M.D., Karamessini M.T., Salonikidis P., Mentzelopoulou E., Dimopoulos P.A.**
Rehabilitation and radiographic imaging of the joints in the post-electrical injury course, C-0692
- Myridis N.E.**
Radial tomography: From acquisition lines to image grid, C-0967
- Mysior M., Grzelak P., Stefanczyk L.**
The usefulness of 3-D sonography in the analysis of collateral circulation in the course of deep vein thrombosis (SS 215), B-118

N

- Nakatani K., Morishita S., Okino K., Anayama T., Sasaguri S., Yoshida S.**
Virtual bronchoscopy: A new approach to facilitating endobronchial ultrasound-guided transbronchial needle aspiration biopsy, C-0320
- Nakazawa K., Tajima H., Murata S., Kumazaki T., Ichikawa K., Fukunaga T., Onozawa S., Yamamoto T., Takano T.**
Catheter fragmentation of acute massive pulmonary thromboembolism: Relationship between distal embolization and pulmonary arterial pressure elevation, C-0566
- Nam J., Choi B., Seo J., Kim Y., Kim T., Choe K.**
Characteristics of myocardial enhancement in dilated cardiomyopathy with contrast-enhanced MRI, C-0229
- Nam J., Choi B., Seo J., Kim Y., Kim T., Choe K.**
Low-attenuation of myocardium with contrast-enhanced multi-detector CT: Hypoperfusion or fat deposition?, C-0258
- Nani R., Placidi S., Pezzotta G., Gaffuri M., Tomasoni A., Bonini G., Agazzi R.**
Sonographic analysis with second-generation ultrasound contrast agents in pediatric liver transplantation, C-0909
- Napoli A., Catalano C., Nardis P.G., Cavacece M., Bertoletti L., Fraioli F., Passariello R.**
Incidental finding of primary lung cancer in patients with atherosclerotic disease: Single-centre retrospective evaluation of MDCT angiography studies over the past three years (SS 204), B-031
- Napoli A., Pezeshkmehr A., Fleischmann D., Rubin G.D.**
Arterial remodeling: In vivo analysis of femoral arterial atherosclerosis using computed tomographic angiography (CTA) (SS 215), B-119
- Napoli V., Bargellini I., Pratali A., Petrucci P., Sardella S., Bartolozzi C.**
Haemodynamic differentiation of type II lumbar endoleaks by contrast-enhanced ultrasound (SS 609b), B-294
- Napoli A., Catalano C., Lorusso V., Morisetti A., Nardis P.G., Calabrese F.A., Passariello R.**
High-concentration iomeprol in CT angiography: Aortic enhancement in anaesthetised swines (SS 1806), B-885
- Napoli A., Catalano C., Nardis P.G., Francone M., Calabrese F.A., Passariello R.**
MDCT angiography in the preoperative evaluation of peripheral arterial disease: Comparison with catheter based DSA, C-1043
- Narvaez J.A., Narvaez F.J., Serrallonga M., Nolla J.M., Roca Y., Valverde J.**
Cervical spine involvement in rheumatoid arthritis: Correlation between neurologic manifestations and MR imaging findings (SS 1410), B-563
- Nassenstein I., Niederstadt T., Krämer S., Dittrich R., Heindel W., Bachmann R.**
Imaging work-up in patients with suspected cervical artery dissection: Diagnostic efficacy of a combined neck and head MR-imaging protocol (SS 1811a), B-902
- Natale L., Porcelli A., Bernardini A., Meduri A., Lombardo A., Bonomo L.**
Evaluation of left ventricular (LV) remodeling after acute myocardial infarction with MRI: The role of no reflow (SS 303), B-212
- Natale L., Bernardini A., Porcelli A., Meduri A., Lombardo A., Liguori C., Bonomo L.**
Functional recovery after acute myocardial infarction: Evaluation by MRI (SS 303), B-219
- Nath A.K., Sethu A.U.**
An update on the use of ultrasound in osteomyelitis and the importance of power Doppler (SS 1810), B-799
- Navalho M., Pires F., Duarte A., Gonçalves A., Alexandrino P., Távora I.**
Percutaneous drainage of infected pancreatic fluid collections (SS 309a), B-192
- Neitzel U.**
The exposure index: Definition of "speed" in digital radiography, C-0961
- Nelson M.T., Garwood M., Meisamy S., Bolan P.J., McIntosh A.**
A new BiomarC tissue marker for breast biopsy: Clinical evaluation in ultrasound, mammography, cat scanning and breast MRI (SS 1502), B-735
- Nemec S.F.**
CT-MR fusion image guidance for navigated neurosurgery of temporal bone tumors (SS 608), B-273
- Neri E., Vagli P., Picchietti S., Vannozzi F., Bardine A., Bartolozzi C.**
CT colonography in the follow-up of patients with partial colectomy (SS 301a), B-147
- Neri E., Berrettini S., Ravecca F., Bartolozzi C.**
CT diagnosis of otosclerosis: A review of 31 cases (SS 608), B-275
- Neri E., Vannozzi F., Picchietti S., Vagli P., Bardine A., Bartolozzi C.**
Time efficiency of CT colonography: 2D vs 3D visualization (SS 1501a), B-690
- Nevhasymy A.A., Miroshnichenko S.I., Redchuk A.A.**
Multiple photodiode sensor array digital receptor for radiographic and fluoroscopic applications (SS 1013), B-541
- Ng Q.S., Goh V., Klotz E., Fichte H., Carnell D., Saunders M., Hoskin P.J., Padhani A.R.**
Single versus four-level tumour perfusion measurement using dynamic helical contrast enhanced multi-detector computed tomography (MDCT): Effect on measurement agreement and potential for whole tumour assessment, C-0304
- Ng Q.S., Goh V., Fichte H., Klotz E., Carnell D., Saunders M., Hoskin P.J., Padhani A.**
Quantitative multi-planar lung cancer perfusion measurement using multidetector row computed tomography (MDCT): Inter and intra-observer agreement, C-0323
- Nicholson A.**
Endovascular treatment in female pelvis: B. Ovarian varicocele (RC 509), A-125
- Nicolau C., Vilana R., Bianchi L., Varela M., Garcia M., Sanchez M., Ayuso C., Bruix J., Bru C.**
Usefulness of SonoVue-enhanced ultrasound in the assessment of the efficacy of percutaneous ablation of hepatocellular carcinomas (SS 1409a), B-622
- Nicolazzini S., Puppi A., Lovisolo M., Stecco A., Fornara P., Carriero A.**
Shoulder MR arthrography: Intra-individual comparison of two dimensional vs. three-dimensional with virtual arthroscopy pulse sequences, C-0694
- Niimi T., Imai K., Ikeda M., Maeda H., Mano A., Enchi Y.**
Reliability of contrast-detail (C-D) diagrams deduced from a Markov chain and reduction in the number of observation times, C-0948
- Nikas J., Hadjigeorgi C., Anagnostara A., Theofanopoulou M.**
MR imaging patterns of hypoxic-ischemic encephalopathy in premature and term born infants, C-0784
- Nikolaou K., Rist C., Wintersperger B.J., Flohr T., Johnson T., von Ziegler F., Kneze A., Reiser M.F., Becker C.R.**
64-detector-row computed tomography of the coronary arteries: Initial experience (SS 703a), B-346
- Nikolaou K., Schoenberg S.O., Hartmann M., Chamberlin P., Reiser M.F.**
Ultra-high-resolution whole-body MRA using parallel imaging on a 32-channel MR system and intravascular contrast agents: Protocol optimization for clinical applications (SS 1813), B-917
- Nin Garaizabal P., Ubeda Hernandez B., Roma Dalfo A., Traid Niella C., Rotger Regi R., Palacio Hermoso de Mendoza A.**
Role of MR imaging and HSG in the evaluation of congenital uterine malformations, C-0413
- Nishino M., Kuroki M., Raptopoulos V., Copeland J.F., Boiselle P.M., Hatabu H.**
Volumetric expiratory high-resolution CT of the lung: Basics and clinical applications, C-0285
- Nishino M., Ashiku S.K., Thurer R., Kocher O.N., Boiselle P.M., Hatabu H.**
The thymus: A mediastinal mystery, C-0325

Authors' Index

- Nishio R., Acata S., Ikeda N., Saito K., Kotake H., Kato H., Abe K.**
Correlation between lymph node metastasis and the ratio of high attenuation area to tumor diameter by HRCT in adenocarcinoma of the lung of 3 cm or less, C-0286
- Nogami M., Ohno Y., Higashino T., Takenaka D., Fujii M., Sugimura K.**
Velocity-encoded MR imaging with sensitivity encoding (SENSE): Reproducibility and measuring agreement for quantitative assessment of pulmonary and systemic blood flow (SS 1004), B-470
- Noguera J.J., Domínguez P.D., De Luis E., Díaz L., Pina L.J., Zornoza G.**
Alternative utilities of a breast marking coil, C-0223
- Noguera J.J., Alonso A., De Luis E., Domínguez P.D., Aquerreta J.D., Cosín O.**
Radiologic and magnetic resonance patterns of myeloma and differential diagnosis, C-0665
- Nolte-Ernsting C.C.A.**
Imaging of stones: B. CT(U) and MRU (RC 807), A-196
- Nonent M., Thouveny F., Simons P., Cappeliez O., Reiser M.F., Duddalwar V., Bonomo L., Liessi G.**
Diagnostic accuracy of multidetector-row CT angiography (MDCTA) using 4, 8 and 16-row CT scanners in diseases of the abdominal aorta and aortic major branches: Results of a European multicenter prospective clinical trial (SS 1015), B-550
- Novak D.**
An illustrated history of gastrointestinal and abdominal medical imaging, C-0126
- Novikov S., Kanaev S., Gershovich M., Shelkoplias E.**
Diagnosis of skeletal invasion by Hodgkin's disease: Bone versus bone marrow survey, C-0750
- Nowinski W.L., Hu Q., Prakash B., Volkau I., Qian G., Thirunavukarasu A., Liu J., Aziz A., Baimouratov R., Hou Z., Huang S., Luo S., Minoshima S., Runge V., Beauchamp N.**
Atlas-assisted analysis of brain scans (IM 1), D-11
- Nowinski W.L., Thirunavukarasu A., Fu Y., Xin M., Lin Z., Wang S.**
The Cerefy Atlas of Brain Anatomy in Chinese (IM 1), D-12
- Ntziachristos V.**
New imaging methods and technologies:
B. Optical imaging (PR 419), A-091
- Nunziata A., Catalano O., Sandomenico F., Vallone P., Siani A.**
Role of contrast-enhanced sonography (CE-US) in percutaneous treatment for HCC, C-0037
- Nunziata A., Catalano O., Sandomenico F., Fiore F., Montemarano E., Siani A.**
Role of contrast-enhanced sonography (CE-US) in transarterial chemoembolization treatment for HCC, C-0045
- Nunziata A., Catalano O., De Lutio di Catelguidone E., De Rosa V., Prisco A., Cipolletta L., Siani A.**
Histologic, surgical, endoscopic and imaging findings in gastrointestinal stromal tumors (GIST), C-0132
- Nunziata A., Catalano O., Mainenti P., Salvatore M., Siani A.**
Renal perfusion abnormalities: Findings with multislice CT (MSCT), C-0444
- Nunziata A., Catalano O., Sandomenico F., Mattace Raso M., Siani A.**
Contrast-enhanced sonographic imaging of the kidney, C-0462
- Nuyens M., Fuechsel F.G., Zbaeren P., Krause T.**
Improved sentinel node detection and pre-operative planning in oral cavity cancer by image fusion of CT and SPECT versus planar imaging (SS 308), B-189
- Nyman U., Almén T., Aspelin P., Hellström M.**
Evaluating the risk of contrast medium (CM) induced nephropathy (CIN) in relation to gram iodine dose and estimated glomerular filtration rate (eGFR) (SS 1806), B-882
-
- O**
- O'Brien S., Farrelly C., Sheehy N., Hargadan G., O'Keffe S., Meaney J.F.M.**
Renal artery fibromuscular dysplasia: Findings on contrast-enhanced MRA, C-1032
- O'Connell A., Hurley M.C., Keeling A.N., Lee M.J.**
Pancreatic mass biopsy: Comparison 20 G fine needle trucut biopsy (FNTB) with fine needle aspiration cytology (FNAC) (SS 309a), B-191
- O'Connor T.**
Professional matters: A. Recruitment and retention of radiographic staff (RC 1314), A-343
- O'Connor P.J.**
Inflammatory joint disease: C. What's new in rheumatoid arthritis? (RC 1610), A-381
- O'Keffe S.A., McGrath A., O'Brien S., McDermott R., O'Connell F., Meaney J.F.M.**
Staging of primary non-small cell lung cancer with CT, MRI and PET, C-0280
- O'Leary D., O'Loughlin A.**
Investigation of a tightly collimated lateral view of the cervico-thoracic region as an alternative to Swimmers's view for trauma patients (SS 210), B-005
- Obata T., Ikehira H., Tamura M., Tanada S.**
MR microimaging of human eye with a blinking-gated pulse sequence, C-0524
- Oder B., Loewe M., Gruber G., Ilias W., Lang W., Thurnher S.**
Lumbar disk nucleolysis by oxygen-ozone injection: Midterm results in 244 patients (SS 609a), B-288
- Offeciers F.E.**
Imaging in cochlear implant candidates: A. What the clinician needs to know and why (RC 508), A-121
- Ogawa M., Kobayashi H., Masuyama K.**
Comparison of clinical evaluation of a flat-panel detector system and a computed radiography system for digital chest radiography, C-0990
- Ohno Y., Nogami M., Higashino T., Takenaka D., Hatabu H., Sugimura K.**
Oxygen-enhanced MR imaging: Correlation with postoperative lung function in lung cancer patients (SS 704), B-387
- Ohno Y., Nogami M., Higashino T., Takenaka D., Murase K., Hatabu H., Sugimura K.**
Primary pulmonary hypertension: Quantitative analysis of regional pulmonary perfusion using 3D dynamic MR imaging (SS 1004), B-471
- Ohtani Y., Sanada S., Ueki K., Miyati T., Matsui T., Matsuura Y.**
Development of the method of kinetic analysis for the temporomandibular joint using flat panel detector system: Verification by magnetic resonance imaging, C-0539
- Oikado K., Tsunoda-Shimizu H., Kazama T., Nakamura S., Suzuki H., Kikuchi M., Numaguchi Y.**
Pre-operative MRI localization of breast cancer in supine position using a newly developed marking net, C-0194
- Oikonomou A.**
Smoking-related diseases: C. Sites of airflow obstruction in cigarette smokers (RC 104), A-019
- Oikonomou A., Patlakas G., Mantatzis M., Panagiotidou L., Bouros D., Prassopoulos P.**
Does core lung biopsy with large needle (=18 G) increase pneumothorax incidence? (SS 1804), B-843
- Oikonomou A., Deftereos S., Mantatzis M., Fotiadou V., Sourailidis P., Prassopoulos P.**
Hydatid disease revisited, C-0077
- Okahara M., Kiyosue H., Matsumoto S., Hori Y., Tanoue S., Uchida D., Mori H., Kondo Y.**
Basal cell adenoma of the parotid gland: MR imaging findings with pathologic correlation, C-0538
- Okazumi S., Shuto K., Yoshinaga Y., Shimada H., Matsubara H., Nabeya Y., Gunji Y., Ochiai T.**
The down staging evaluation of neo-adjuvant therapy for advanced esophageal cancer using volume rendered 3D-enhanced CT (SS 201a), B-014
- Okten O.O., Tuncbilek N., Karakas M.H., Ince Y., Sen S.**
Evaluation of endothelial function of normotensive and hypertensive subjects with flow mediated dilatation, C-1058
- Okuma T., Matsuoka T., Okamura T., Wada Y., Yamamoto A., Oyama Y., Koyama K., Watanabe Y., Inoue Y.**
F-18 FDG microPET imaging after percutaneous radiofrequency ablation (RFA) in normal rabbit lung, C-0348
- Okuma T., Matsuoka T., Okamura T., Wada Y., Yamamoto A., Oyama Y., Koyama K., Nakamura K., Watanabe Y., Inoue Y.**
F-18 FDG-microPET evaluation after CT-guided radiofrequency ablation (RFA) in rabbit VX2 lung tumor model, C-0350
- Okumura E., Sanada S., Suzuki M., Tushima Y., Matsui O.**
Temporal and blood-flow phase subtraction technique of the liver for detection of subtle hepatocellular carcinoma on abdominal CT images, C-0046
- Olsen Ø.E., Sebire N.J.**
Apparent diffusion coefficients of paediatric mass lesion with free-breathing diffusion-weighted MRI (SS 1512), B-754

Authors' Index

Op de Beeck B.J., Salgado R., Trappeniers L., Vandenbroucke F., de Jongh K., Parizel P.
Pulmonary sequestration: A pictorial review, C-0305

Op de Beeck B.J., Ramaekers P., Salgado R., De Ridder F., De Catte L., Vanhoenacker F., Parizel P.
True FISP versus HASTE MR imaging in the diagnosis of non-cerebral foetal anomalies, C-0906

Oppenheim C., Meder J., Fredy D.
Diffusion and perfusion MR imaging of the brain: C. Diffusion tensor imaging and fibre tracking (RC 1211), A-283

Oppenheim C., Hernalsteen D., Touzé E., Peeters A., Lamy C., Mas J., Meder J., Cosnard G.
Which is the optimal sequence for the detection of hyperacute intracranial hemorrhage on multimodal stroke MRI?, C-0796

Orguc S., Zeytunlu M., Kilic M., Gurgan U., Yüzer Y., Tokat Y.
Preoperative helical computerized tomography estimation of graft volumes: Experience in 150 living liver donors, C-0033

Orrigi D., Vigorito S., Villa G., Tosi G., Bellomi M.
Apparent discrepancy between image quality and dose (CTDI) in MSCT automatic modulation modality (SS 713), B-444

Orlacchio A., Fabiano S., Rotili A., Stefanini M., Pasquarelli R., Simonetti G.
Role of contrast-enhanced ultrasound in the radiofrequency thermal ablation treatment of malignant hepatic tumors, C-0627

Ortori S., Zampa V., Odoguardi F., Batini E., Ceretti E., Bartolozzi C.
Ossicle of the knee menisci: MR findings, C-0708

Ortori S., Zampa V., Odoguardi F., Marchetti L., Cappelli C., Bartolozzi C.
Myositis ossificans: What is the real diagnostic value of magnetic resonance?, C-0728

Osborn A.G.
Marie Curie - Honorary Lecture: The brain perivasculär spaces in health and disease: 2005 update on anatomy, pathophysiology, advanced neuroimaging (HL 2), A-263

Osipenko V.I., Ternovoy S.K., Schekhter A.I., Sokolina I.A., Popova E.N.
Diagnosis of pulmonary arterial hypertension in patients with idiopathic fibrosing alveolitis (SS 1004), B-474

Osorio M., Maroto A., Laguillo G., Rodriguez J.I., Ortuño P., Pont J.
Small bowel traumatic injuries: A pictorial essay, C-0101

Østergaard L.
Diffusion and perfusion MR imaging of the brain: A. Imaging technique and protocols, post-processing (RC 1211), A-281

Otake S.
MR findings and pathologic correlation of subcutaneous soft-tissue lesions of dermatosis: A pictorial review, C-0729

Otani T., Tomura N., Ohnuki T., Takahashi S., Sakuma I., Watari J.
Serial contrast-enhanced MRI in the assessment of the temporomandibular joint disorders (SS 208), B-056

Ottaviani P., Menchini L., Giulante F., Manfredi R., Bonomo L.
Value of magnetic resonance cholangiography in iatrogenic biliary stenosis: Comparative study with surgery (SS 301b), B-173

Ozbek O., Kayahan E.M., Tarhan N.C., Cakir B., Aytekin C., Coskun M., Haberal M.
Preoperative evaluation of hepatic arteries in living-related liver transplantation donors with MDCT angiography, C-1051

Özdemir A., Voyvoda N.K., Üzüm N., Dursun A.
Can core biopsy be used instead of surgical biopsy in the diagnosis and prognostic factor analysis of nonpalpable breast cancer?, C-0182

Özdemir A., Karadag Z.Ö., Coskun A.
Assessment of clinical outcomes and the sonographic criteria in benign and malignant solid breast masses, C-0208

Özden E., Göögüs Ç., Kılıç Ö., Yaman Ö., Özdipler E.
Analysis of suprapubic and transrectal measurements in assessing prostate dimensions and volume: Is transrectal ultrasonography really necessary for prostate volume measurement?, C-0477

Özden E., Turgut A.T., Göögüs Ç., Yagci C., Küpeli S.

Diagnostic value of TRUS in patients with PSA values > 20 ng/ml: Can only lesion biopsies be adequate for diagnosis?, C-0478

Özden E., Göögüs Ç., Zümürütbas A., Baltaci S., Bedük Y.

Comparision of lateral-medial peripheral zone prostate biopsies: Analysis of 12 core locations in 160 patients, C-0479

Özden E., Göögüs Ç., Dasdemirov E., Turgut A.T., Türkölmez K., Tulinay Ö.

Can longer tissue samples be extracted by pressing the prostate with the probe during TRUS guided biopsy?, C-0486

Özden E., Göögüs Ç., Tokatlı Z., Yaman Ö., Göögüs O.

The effect of gleason scores on TRUS detection rates and sonographic appearances of prostatic carcinoma, C-0487

Özden E., Göögüs Ç., Akand M., Yaman Ö., Göögüs O.

The effect of rectal enema before TRUS guided prostate biopsy on patient comfort and biopsy related complications, C-0488

Özden E., Göögüs Ç., Türkölmez K., Yagci C.
Is fluid ingestion really necessary before ultrasonography performed for detecting ureteral stones? A prospective randomized study, C-0500

Ozgun M., Hoffmeier A., Botnar R.M., Heindel W., Fischbach R., Maintz D.
Whole heart coronary MR-angiography: Presentation of a new technique and report of initial results, C-0245

Ozturk A., Karli Oguz K., Cila A., Akalan N.
Early postoperative diffusion-weighted MR imaging (DWI) of the brain parenchyma in the operative site following tumor resection (SS 1011), B-537

P

Padhani A.R.

MR approaches to molecular imaging: A. Imaging of angiogenesis (PR 819), A-201

Padley S.P.G.

HRCT in diffuse lung disease: A. Nodular pattern (RC 1704), A-415

Paelinck B.P., Vrints C.J., Bax J.J.,

Bosmans J.M., de Roos A., Lamb H.J.

Tissue MR imaging of subacute myocardial infarction correlates with B-type natriuretic peptide and tissue Doppler imaging, C-0243

Pagonidis K., Lambiri I., Tsetis D., Schiza S., Yarmenitis S., Siafakas N., Gourtsoyiannis N.

Ultrasound assessment of endothelial dysfunction in obstructive sleep apnea hypopnea syndrome (OSAHS) before and after continuous positive airway pressure (CPAP) therapy (SS 615), B-337

Pal A., Ozretic D., Pavcev Z., Saghir H.,

Zokal I., Perhac Z., Latin B., Ozretic M.
CT angiography as a method of brain death confirmation (SS 1811a), B-899

Palkó A., Lombay B.

The present and future of Hungarian radiology: Contribution of a new generation: The present and future of Hungarian radiology: Contribution of a new generation (Introduction) (EM 2), A-249

Pallwein L., Steiner H., Klauser A.,

Frauscher F.

Natural history of incidental testicular masses ≤ 0.5 cm detected by US (SS 1807b), B-859

Palm F., Carlsson P., Fasching A., Hansell P., Liss P.

Contrast media inhibits oxygen consumption in proximal tubular cells from diabetic rats by inducing nitric oxide release (SS 1806), B-881

Panebianco V., Catalano C., Laghi A., Ferrari R., Campanella V., Nardis P.G., Passariello R.

Web technology and wireless application in the management of radiological images and data, C-0371

Panebianco V., Tancredi D., Celano T., Nardis P.G., Di Rezze L., Paolantonio P., Passariello R.

Comparison between 3D CT and MR protocols in the detection of bladder lesions, C-0510

Paolantonio P., Rengo M., Laghi A., Iafrate F., Di Martino M., Guerrisi A., Passariello R.

Optimization of a new mixture of barium sulphate and sorbitol (Volumen) as oral contrast agent for MR of the small bowel in a pediatric population (SS 1401a), B-575

Paolantonio P., Laghi A., Miglio C., Rengo M., Vergari V., Di Martino M., Guerrisi A., Passariello R.

USPIO-enhanced GRE T2*W sequence versus TSE T2W sequence in T-staging evaluation of uterine malignancies: A comparison study with surgical and histological staging (SS 1506a), B-741

Paolantonio P., Laghi A., Rengo M., Guerrisi A., Vergari V., Panebianco V., Passariello R.

Visualization of swallowing using real-time cineTurboFLASH sequence and a positive oral contrast agent: A feasibility study (SS 1801a), B-811

Authors' Index

- Paolantonio P., Laghi A., Rengo M., Iafrate F., Martino V., Guerrisi A., Passariello R.**
MR imaging of the small intestine in paediatric patients: An overview of technical features and clinical results, C-0084
- Paolantonio P., Laghi A., Celestre M., De Angelis F., Guerrisi A., Rengo M., Passariello R.**
Un-prepped MR colonography in paediatric patients with inflammatory bowel disease (IBD), C-0090
- Paolantonio P., Laghi A., Rengo M., Martino V., Di Martino M., Tomei E., Passariello R.**
Spectrum of findings of celiac disease at MRI of the small bowel, C-0113
- Paolantonio P., Laghi A., Passariello R.**
Spectrum of findings of intestinal non-neoplastic disorders at MRI of the small bowel, C-0114
- Paolantonio P., Laghi A., Miglio C., Rengo M., Vergari V., Ciccarelli S., Guerrisi A., Passariello R.**
A new MR findings: Decrease of signal intensity of myometrium after iv USPIO administration, C-0391
- Papadaki E., Papanikolaou N., Karampekios S., Spilioti M., Maris T., Gourtsoyiannis N.**
Diffusion tensor imaging (DTI) in patients with multiple sclerosis (MS): Correlation with perfusion imaging (SS 211), B-091
- Papadopoulou F., Tzovara J., Anthopoulos D., Siomou E., Evangelidou E., Efremidis S.**
Voiding urosonography harmonic imaging with 2nd generation contrast agent for the diagnosis of reflux (SS 1812), B-895
- Papaioannou G., Thanos L., Nikita A., Sissopoulos A., Antonopoulos D., Kelekis D.**
Management of pancreatic fluid collections with percutaneous drainage under CT guidance, C-0641
- Papakonstantinou O.**
Sports injuries: A. Ligamentous injuries of the knee revisited (RC 110), A-004
- Papanikolaou N.**
MR of the colon and rectum: A. Contrast agents and sequences in MR colonography (RC 101), A-014
- Papanikolaou N.**
MR imaging of the small intestine: Clinical results in Crohn's disease (SF 13), A-315
- Papanikolaou N., Karampekios S., Papadaki E., Maris T., Gourtsoyiannis N.**
Normal ageing of the brain: Assessment with quantitative MR diffusion tensor imaging, C-0800
- Papanikolaou N.**
Technical optimization of diffusion tensor sequences. Evaluation of three dimensional white matter tractography in various neurologic disorders, C-1077
- Parizel P.M.**
Craniocerebral and spinal trauma: B. Craniocerebral trauma (2): Intra- and extra-axial lesions, secondary lesions (CC 1317), A-308
- Park S., Jin G., Han Y., Park H.**
A comparative experimental study of the in-vivo efficiency of saline-enhanced bipolar versus monopolar pulmonary radiofrequency ablation, C-0352
- Park M., Kwon S., Ohm J., Shin B., Kim Y.**
Image findings of ruptured Baker's cyst, C-0699
- Park N., Park C., Lee E., Kim M., Song S.**
Ultrasonographic findings of the fecally impacted appendix: Differentiating from acute appendicitis, C-0893
- Parrón M., Lamas M., Berrocal T., Fernández E., Gutiérrez J., Fernández J.**
Imaging of non-tumoral disorders involving the small bowel in infancy and adulthood, C-0121
- Parrón M., Navarro M., Pardo M., Torres I., Fernández-Velilla M., Echeveste J.**
"Halo sign" on pulmonary CT: Radiologic-pathologic correlation, C-0303
- Parrón M., Berrocal T., Prieto C., Cortés P., Pastor I., Lemos R.R.**
Imaging of pediatric liver transplantation, C-0886
- Parrón M., Berrocal T., Álvarez A., Bernabeu D., Lemos R.R., Gómez-León N.**
Imaging of hip disorders in pediatric patients: A pictorial review, C-0890
- Pasowicz M., Klimeczek P., Gackowski A., Przewocki T., Banys R., Zmudka K., Tracz W.**
Analysis of the atherosclerotic plaque and cross-sectional surface of coronary arteries by MSCT(Vessel View software) and ICUS (reference method) (SS 603), B-306
- Pastor-Juan M.R., Ripollés T., Martínez M.J., Olalla-Muñoz J.R., Monedero M.D., Ruiz A.**
Ischemic colitis: Sonographic findings and differential diagnosis, C-0122
- Pattynama P.M.T.**
Urological intervention: C. Renal arterial intervention (WS 918), A-237
- Pattynama P.M.T.**
Teleradiology: Threat or opportunity?: Teleradiology professional issues: A new radiological service (ER 1326), A-336
- Pedersen J.F., Dakhil A.Z., Jensen D.B., Soendergaard B., Bytzer P.**
Abnormal hepatic vein Doppler waveform in patients without liver disease (SS 1401b), B-600
- Pedersen J.F., Pedersen J.F.**
Sonographic comparison of gastric emptying of broth and water: Is there a promoting cephalic factor? (SS 1801a), B-814
- Pedicelli A., Bellitti A., Cina A., Rollo M.**
Transcranial color-Doppler sonography (TCDS) today: When and how to use it, C-0776
- Pediconi F., Catalano C., Venditti F., Roselli A., Padula S., Passariello R.**
Contrast-enhanced magnetic resonance mammography for screening of the contralateral breast in patients with diagnosed breast cancer (SS 602), B-267
- Pediconi F., Catalano C., Venditti F., Ercolani M., Carotenuto L., Roselli A., Passariello R.**
Color-coded automated signal intensity-curve for detection and characterization of breast lesion: Preliminary evaluation of a new software for MR based breast imaging (SS 702), B-375
- Pediconi F., Catalano C., Venditti F., Roselli A., Moriconi E., Passariello R.**
Contrast enhanced magnetic resonance mammography (CE-MRM) in the evaluation of suspected microcalcifications at mammography, C-0192
- Pediconi F., Catalano C., Venditti F., Roselli A., Moriconi E., Passariello R.**
Role of Gd-BOPTA-enhanced MR mammography in the evaluation of neoadjuvant chemotherapy response in patients with breast cancer, C-0195
- Peeters J.J.M.**
Professional matters: B. HENRE (Higher Education Network for Radiography in Europe): Learning methods (RC 1314), A-345
- Peh W.C.G.**
Errors in radiology: Pitfalls in musculoskeletal MR imaging (E³ 1020), A-262
- Peitgen H.**
Computer assisted diagnosis: CAD and intervention planning of the liver (SF 1), A-009
- Peitgen H.**
Diagnostic workstations: The new super-assistants of the radiologist and surgeon: Workstations for computer aided diagnosis and surgery planning (E³ 1420), A-356
- Pelage J.**
Endovascular treatment in female pelvis: C. Post-partum haemorrhage (RC 509), A-126
- Peloschek P., Langs G., Kainberger F., Bischof H., Kropatsch W.G., Imhof H.**
Computer aided diagnosis (CAD) in rheumatoid arthritis (IM 1), D-06
- Peloschek P., Langs G., Urschler M., Sailer J., Uffmann M., Schlager T., Kainberger F., Bischof H.**
Evaluation of a method for digital definition of bone shapes (SS 610), B-260
- Pereira P.L.**
Percutaneous tumor ablation: A. Liver (RC 1309), A-333
- Pérez E., Sanchez A., Narváez J., Martínez de la Haza D., Merino E., Mallol X.**
Clinical and radiological characteristics of spontaneous osteonecrosis of the knee, C-0689
- Perisinakis K.**
Special issues of radiation exposure in diagnostic radiology: B. Topics in radiation protection to be learned by radiologists (RC 813), A-190
- Perks C.A., Gray J.E., Reft C., Markey B., Salasky M., Leppert J., Ford R., Gress D.**
Optically stimulated luminescent (OSL) dosimeters for use in diagnostic and therapeutic radiology (SS 1513), B-772
- Pero H.**
European research network in biomedical imaging: Structuring the European research area: Possibilities for biomedical research in Europe (ER 926), A-223
- Persigehl T., Matuszewski L., Wall A., Wülfing C., Kooijman H., Tombach B., Mesters R., Heindel W., Bremer C.**
Diffusion weighted imaging for monitoring of anti-angiogenic tumor treatment (SS 1506b), B-785
- Persiva Morenza O., Serres Créixams X., Roche Vallès S., Allende H., Vilà Parera C., Comet Segú R.**
Sonographic assessment of periportal hypoechoic halo, C-0032
- Persson A., Palmberg S., Ranlöf M., Jern M.**
SMARTDOC: A new system for real-time consultation and interaction of complex medical data over the internet on low end hardware, C-0366

Authors' Index

Petcu S., Pop G.D., Georgescu C.E.

Precision of densitometric assessment of bone mass in mens' age-related bone loss: A comparison between DXA, pQCT and QUS, C-0972

Peter D., Gruenhagen J., Wenke R., Schreier I., Heller M.

False-negative results after stereotactically-guided vacuumbiopsy (SS 1502), B-732

Peters J., Truyen R., Quist M., Ermes P., Habets R., Breeuwer M., de Blieck H., Spies L., Deckers S., Gerritsen F.A.

Advanced clinical applications for the digital hospital (IM 1), D-07

Petersen J.C., Freund M.C., Jamnig H., Jaschke W.R.

Optimization of enhancement in pulmonary CT-angiography using a 16 slice CT scanner: Influence of a scanning delay (SS 1404), B-590

Petkovska I., Shah S.K., McNitt-Gray M.F., Kim H.J., Goldin J.G., Aberle D.R.

Qualitative and quantitative analysis of contrast enhancement maps for pulmonary nodule characterization, C-0282

Petralia G., Funicelli L., Ferretti S.,

Sonzogni A., Bellomi M.

CT perfusion as index of angiogenesis of rectal cancer (SS 301a), B-145

Petrou M., Foerster B.R., Eldevik P., Maly P., Sundgren P.C.

Incidence, clinical presentation, MRI and histological findings of intracranial neoplasms in children under the age of two and added utility of gadolinium in their initial diagnosis, C-0916

Petrovic S.S.

Differentiation of benign from malignant salivary gland tumors using color Doppler sonography, C-0557

Petrow P.

Imaging of the uterus: C. Staging and follow-up of cervical cancer (RC 507), A-132

Pfleiderer S.O.R., Marx C., Malich A.,

Camara O., Kaiser W.A.

Cryotherapy of breast cancer under ultrasound-guidance (SS 709), B-402

Pfleiderer S.O.R., Marx C., Reichenbach J.R.,

Vagner J., Fischer H., Kaiser W.A.

MR-guided large core breast biopsy inside the bore of a 1.5 Tesla scanner using a robotic system (ROBITOM) (SS 709), B-403

Phan C.M., Krug R., Eckstein F., Newitt D.C., Majumdar S., Link T.M.

High-resolution MR imaging of the trabecular bone structure at 3 T: Comparison between 1.5 T and 3 T (SS 610), B-258

Phan C.M., Link T.M., Blumenkrantz G.,

Newitt D.C., Majumdar S.

Relationship between bone marrow edema and cartilage degeneration assessed by high resolution MRI and clinical findings in patients with osteoarthritis (SS 1410), B-565

Phoa S.S.K.S., Tilleman E., van Delden O.,

Bossuyt P., Gouma D.J., Laméris J.S.

CT criteria for predicting survival of patients with potentially resectable pancreatic carcinoma (SS 1001), B-489

Piccoli G., Marzio A., Sponza M., Frassani R., Livi U., Vit A., Gasparini D.

Thoracic aorta diseases: Stent-graft repair (SS 209a), B-065

Piccoli G., Marzio A., Vit A., Sponza M.,

Bais B., Gigli G., Gasparini D.

Protected carotid artery angioplasty and stenting: Acute and long term outcomes in 225 interventions (SS 1009b), B-513

Pienkowska J.M., Szurowska E.,

Wierzbowski J.M., Marek I., Rutkowska B., Studniarek M.

The role of spiral CT colonography in the pre-treatment staging of colorectal cancer, C-0133

Pienkowska J.M., Szurowska E.,

Wierzbowski J.M., Czarnowska M., Rompa G.,

Studniarek M.

The role of spiral CT colonography as a routine method in patients after incomplete conventional colonoscopy, C-0149

Piedra T., Gomez-Dermat V., Landeras R.,

Aguilar M., Zubia P.,

Fernandez-Echevarria M.A.

High-resolution ultrasonography to evaluate the radial nerve, C-0764

Pietrani M.A., Zaloff Dakoff J., Rabadian A.,

San Roman J., Eleta F., Rosler R., Argibay P.

Anatomical atlas of pig's brain by MRI and CT in stereotactic conditions, C-0821

Pineda V., Dominguez-Oronoz R., Merino X.,

Castellà E., Evangelista A., Vidal R.

Chronic aortic dissection: Contribution of velocity-encoded cine MRI and multiphasic MR angiography, C-1023

Pinker K., Preyer O., Sora M.C.,

Ba-Ssalamah A., Trattning S., Mlynarik V.,

Umek W.

In-vitro high-field (3 T) high-resolution MRI of the female pelvic floor anatomy in correlation with cadaveric cross-sections (SS 1807a), B-789

Pinker K., Ba-Ssalamah A., Wolfsberger S.,

Mlynarik V., Knosp E., Trattning S.

The value of high-field MRI (3 Tesla) in the assessment of sellar lesions (SS 1811b), B-935

Pinto A., Scaglione M., Gagliardi N., Grassi R., Lassandro F., Romano L.

Comparison between the site of multislice spiral computed tomographic signs of gastrointestinal perforation and the site of perforation detected at surgery in fifty perforated patients (SS 701a), B-367

Pinto Pabón I.

Endovascular treatment in female pelvis:

A. Leiomyomata (RC 509), A-124

Piotrowska D., Kownacki L., Golebiowski M., Krolicki L.

Assessment of right ventricular function with magnetic resonance. Preliminary report, C-0256

Pitsoulakis G., Vakaki M., Zarifi M.,

Hadjigeorgi C., Xasiotou M., Nikas I.,

Evlogias N.

Imaging evaluation of pediatric patients with peritoneal malignancies, C-0934

Pitton M.B., Schweitzer H., Herber S.,

Schmid W., Neufang A., Kalden P.,

Schneider J., Thelen M.

Endoleakdetection after endovascular aneurysm treatment (SS 609b), B-295

Plagou A., Alexopoulos D., Theotokas I.,

Zoumpoulis P.S., Prapavesis S., Fousteris A., Filippidou A.

Local anesthesia before TRUS-guided prostate biopsy: Performance, technical results and side-effects on image quality. Indications and side effects on patients, C-0482

Plank C.M., Kubin K., Friedrich K., Weber M., Marlovits S., Trattning S.

Contrast enhanced high resolution MR imaging of autologous cartilage implants of the knee joint (SS 710), B-353

Plathow C., Fink C., Sandner A., Klopp M., Puderbach M., Thieke C., Schmähl A., Kauczor H.

Imaging of malignant pleural mesothelioma using morphological and functional MRI, C-0294

Plavsic B.M., Kupesic S.

Color Doppler and three dimensional ultrasound hystero-contrast-salpingography, C-0419

Po J., Barth R.A., Ringertz H., Bammer R.

MRI assessment of fetal lung volume, C-0915

Podesta' R., Zuccarino F., Picotti A., Succio G., Bianchi S., Martinoli C.

High resolution ultrasound of the leg, C-0719

Pokieser P., Brandstätter J., Wernig M., Berger J.

Unified patient: A medical media database supporting surgical planning and interdisciplinary meetings (IM 1), D-02

Polidura Arruga C.,

De la Pedraja Gomez-Ceballos I.,

Abades Vazquez J.L., Huelga Zapico E., Jimenez del Rio J.

Transmesenteric internal hernias: CT findings, C-0085

Police S., Scarabino T., Leuzzi V., Tosetti M., Carnevale F., Carrero A.

Phenylketonuria: Conventional MR imaging and spectroscopic assessment of cerebral PHE concentration with 3 T 1H-MRS (SS 311), B-224

Police S., Scarabino T., Di Costanzo A.,

Troisi F., Giannatempo G., Nemore F., Salvolini U., Carrero A.

Multiparametric MR assessment of cerebral gliomas at 3.0 Tesla: Characterization of spatial heterogeneity and tumor malignancy (SS 1011), B-536

Police S., Di Costanzo A., Giannatempo G., Popolizio T., Carrero A., Scarabino T.

3 T 1H-MRSI assessment of spatial distribution of metabolites in cerebral gliomas, C-0829

Pöllinger A.

CTLM and MRI (SY 13), E-57

Polonara G.

Imaging of focal lesions: Brain (EM 1), A-145

Polonara G., Fabri M., Mabiglia C., Manzoni T., Salvolini U.

The body representation in the first somatic sensory area of human brain: An fMRI study, C-0833

Pomoni M., Papadopoulos K., Tsanis A., Tantaleas S., Tzavoulis D., Pagonas A., Batakis N.

The use of carbon coated stents (Carbosent) in aortoiliac stenosis. Our experience (SS 1409b), B-634

Authors' Index

Pons M.J., Diaz L., Villanueva A., Dominguez P.D., Idoate M.A., Boan J.F., Benito A.
Pheochromocytomas: Usual and unusual imaging findings, C-0516

Poplaw S., Hellinger J.C., Hiatt M.D., Chan F.P., Fleischmann D.
Imaging of atrial septal defects (ASD) with multidetector-row CT (MDCT) angiography, C-0263

Popova L., Hadjidekova V.B., Karadjov A., Rao B.S., Hadjidekov V.G.
Cytogenetic effects of diagnostic X-rays and contrast media in human peripheral blood lymphocytes, C-0398

Porod V., Novotny J., Vedlich D., Kautznerova D., Hajek M.
Open source DICOM archive, C-0362

Portugalli V., Archiati E., Cabassa P., Grazioli L., Romanini L., Cristinelli M.
Contrast enhanced harmonic sonography (CEUS) of focal liver lesions: Discordance with contrast enhanced CT or MR (SS 306), B-125

Potter K.C., Brown G., Sharma B., Houghton S.L., Husband J.E.
Careful CT and MR serial imaging review with a defined reporting protocol in follow-up colorectal cancer patients and correlation with ¹⁸FDG-PET-CT findings (SS 301a), B-143

Pouwels P.J.W.
MR spectroscopy of the brain in clinical practice: C. Clinical applications of MRS: Diffuse lesions (RC 1311), A-329

Pozdniakov A.V., Tiutin L.A., Dyskin D.E., Stanzhevsky A.A., Rokhlin G.D.
1H MRS and 18F FDG PET in patients with single epileptic seizure, C-0811

Pozuelo Segura C., Pozuelo O., Roca Y., Mones L., Medrano C., Torremilans A., Quintero J., Mulattieri D.
Imaging findings of extratesticular scrotal masses, C-0467

Pozuelo Segura C., Pozuelo O., Mones L., Roca Y., Medrano C., Quintero J., Torremilans A., Mulattieri D.
Sonographic features of intratesticular pathology, C-0476

Pozzi-Mucelli R.
Imaging problem lesions (tumors): B. Renal imaging (RC 407), A-085

Pozzi-Mucelli F., Babic D., Calgaro A., Pozzi-Mucelli R.
Virtual stenting (VS): A new modality for choosing a stent or a stent-graft by three-dimensional rotational angiography (3DRA), C-0565

Prabhu S.P., Neelakantan A.
CT and MRI of pericardial disease, C-0233

Prabhu S.P., Burney K.
Using cardiovascular MRI to understand and simplify the chest radiograph for congenital heart disease, C-0251

Prabhu S.P., Malone J., Carrivick L., Rossiter J., Goddard P.R.
Automated diagnosis of disease using texture analysis in CT of the lungs, C-0343

Prabhu S.P., Narayan T.V., Prescod K.
Differential diagnosis of gynaecological solid masses on MRI- pattern approach and radiologic-pathologic correlation, C-0414

Prabhu S.P., Burney K., Valencia A.
Amyloid: Radiological manifestations from head to toe, C-0450

Prabhu S.P., Dunlop D., Prescod K.
Urinary tract abnormalities on bone scintigrams: Boosting the diagnostic yield, C-0521

Prabhu S.P., Davies R., Luker J., Kabala J.
MRI of parotid gland tumours with radiologic-pathologic correlation, C-0553

Prabhu S.P., Winterbottom S., King S.
Significance of recurrent lung opacities in premature infants treated for respiratory distress syndrome: The SLOP study, C-0895

Prayer D.
Fetal MR imaging: Body MRI (SF 17), A-408

Prefumo F., Derchi L., Gandolfo N., Dogliotti L., Maritano A., Bazzocchi M., Bacicalupo L., Serafini G.
MRI, ultrasonography and color Doppler in the assessment of palpable nodularities of the abdominal wall with post-partum onset, C-0718

Preoteasa F., Lupescu I., Capsa R., Cimpeanu N., Georgescu S., Cimpeanu A.
Proton MRI spectroscopy and fMRI changes associated to simple and complex movement in clinically isolated syndromes suggestive of multiple sclerosis, C-0957

Priest A.N., Hegerfeldt S., Weber C., Adam G.
MR vessel wall imaging of abdominal aorta at 3 T: Understanding and minimising plaque-mimicking flow artifacts (SS 215), B-114

Priest A.N., Ittrich H., Jahntz C.L., Kooijman H., Weber C., Adam G.
Experimental MRA investigations of atherosclerosis using ultra-small superparamagnetic particles of iron oxide at 3 T (SS 1506a), B-743

Priest A.N., Hegerfeldt S., Adam G.
Reduced angle double inversion recovery (RADIR): A flexible new pulse sequence for black-blood MRI (SS 1813), B-918

Priolo F., Mancini A.P., Martina F.M., Savino G., Magistrelli A.
Rheumatoid arthritis (RA): The ABC's of hand-bone erosions imaging and management of disease, C-0697

Profili S., Urigo C., Manca A., Meloni F., Canalis L., Salaris F.
Palliation of pancreatic cancer by combined biliary and duodenal stenting (SS 309a), B-196

Prokesch R.W.
Imaging of the pancreas: Key questions: B. What lesions are difficult at CT? (RC 1301), A-322

Prokop M.
MDCT imaging: New challenges for scan and contrast optimisation: New challenges in MDCT: From 16 to 64 slices (SY 9), E-38

Prokop M.
New challenges in MDCT from 16 to 64 channels (SY 11), E-51

Prokop M.
CT angiography of the chest: C. Current role of CT in the evaluation of aortic diseases (RC 504), A-116

Prokop M.
Vascular, emergency and ICU imaging: A. Vascular disease and lung edema (E³ 720), A-160

Prokop M.
Impact of multislice CT on imaging of the upper abdomen: A. Technical advances (RC 901), A-218

Prokop M.
Vascular imaging: B. CTA: Basic principles and clinical applications (RC 1215), A-291

Prosch H., Tscherney R., Kriwanek S., Tscholakoff D.
Radiographic imaging of normal anatomy and complications after gastric banding and gastric bypass surgery, C-0125

Pugliese F., Gandolfo N.G., Dogliotti L., Martinoli C., Serafini G.
US-guided percutaneous treatment of calcific tendinitis of the rotator cuff. Results in 651 patients over 8 years (SS 310), B-131

Pugliese F., Valle M., Bianchi S., Rossi U., Tomà P., Martinoli C.
US diagnosis of talocalcaneal coalition (SS 1810), B-806

Puig S.
Neonatal problems: B. Broncho-pulmonary foregut malformations: Antenatal and postnatal imaging (RC 1312), A-341

Puig S.
Justification and optimization of multidetector CT (MDCT) examinations: C. Optimization of pediatric MDCT examinations (RC 1613), A-398

Puig S., Redl H.
Blackberry and elderberry juice with high concentrations of manganese and iron ions as negative T2 and positive T1 contrast media: An in-vitro study (SS 1401a), B-573

Punwani S., Hopster D.J., Chaudhuri R., Murray D.
Pitfalls in MR staging of prostate carcinoma: A pathological correlation (or prognostic pitfalls of prostatic proton pictures), C-0480

Pupillo V., Puglielli E., Fiumara C., De Amicis R., Masciocchi C., Gallucci M.
Cocaine and heroin abuse related to acute encephalopathy: Emergency MRI findings, C-0786

Pupillo V., Gismondi G., De Amicis R., Splendiani A., Masciocchi C., Gallucci M.
Slow expressive language development in children: Typical MRI pattern? Critical review of 1880 cases, C-0803

Puppini G., Quintarelli S., Tomasi L., Iafrancesco M., Destro G., Montemezzi S., Gortenuti G.
Magnetic resonance for follow-up after orthotopic cardiac transplantation, C-0239

Puppini G., Cirotta N., Furlan F., Quintarelli S., Veraldi G., Montemezzi S., Gortenuti G.
Accuracy of magnetic resonance for identification and characterization of carotid plaque constituents with histological correlation: A clinical experience, C-1018

Puy R., Boyer C., Leloutre-Françon B., Ben Amor V., Capdevila A., Geoffray A.
Imaging of the cranial nerves, C-0797

Authors' Index

Q

Qian X., Dai D.C., Zhai R.

Follow-up of percutaneous transhepatic biliary drainage for malignant obstructive jaundice (SS 309a), B-197

Quaia E., Degobbis F., Rossi S., Cova M., Pozzi Mucelli R.

Contrast enhancement patterns and diagnostic confidence in splenic tumor characterization after microbubble-based contrast agent injection (SS 1401b), B-602

Quaia E., Torelli L.

Proposal of an appropriate mathematical model to represent replenishment kinetic after microbubble destruction of an imaged renal volume to quantify renal perfusion, C-1080

Quick H.H., Zenge M.O., Kuehl H., Kaiser G.M., Aker S., Massing S., Bosk S., Ladd M.E.

Interventional MR angiography with no strings attached: Wireless active catheter visualization (SS 709), B-404

Quintero J., Pozuelo C., Medrano C., Mulattieri D., Capurro S., Tous F.

Normal anatomy and non-hernia pathology of the abdominal wall on cross-sectional imaging, C-0172

Quintero J., Pozuelo C., Roca Y., Monés L., Torné M., Pérez M.

Congenital anomalies of the inferior vena cava: Cross-sectional imaging findings, C-1061

Quirico C., Stecco A., Oronzo P., Marano G., Rozzati D., Crinò F., Borracini C., Carriero A.

Role of CE-MRA in studying vascular complications after kidney transplantation, C-1028

Quiroga S., Sebastià M., Boye R., Cuellar H., Roche S., Alvarez A.

Acute cholecystitis: Helical CT findings, C-0006

Quiroga S., Sebastià M., Cuellar H., Boye R., Miranda A., Alvarez A.

Aneurysms of the intra- and extra-hepatic portal vein: Helical CT demonstration., C-1049

R

Radü E.

Epilepsy, white matter diseases and ageing: B. White matter diseases (CC 817), A-163

Rafaelsen S.

Rectal carcinoma: Rectal carcinoma (Introduction) (SF 4a), A-055

Raghunathan G., McKie S., Bourke G., Robinson P.

Radiological features of histologically proven post-traumatic fat necrosis, C-0725

Raissaki M.

Special issues of radiation exposure in diagnostic radiology: A. Minimizing radiation doses to pediatric patients (RC 813), A-189

Raissaki M., Perisinakis K., Tzedakis A., Daskalogiannaki M., Damilakis I., Gourtsoyiannis N.

Appropriate use and benefits of eye-lens bismuth shielding in pediatric head CT examinations (SS 1412), B-649

Raissaki M., Papanikolaou N., Hatzimanoli V., Drakonaki E., Bitsori M., Gourtsoyiannis N.
Comparison of true FISP, HASTE, SSTSE and postcontrast T1w sequences in pediatric MR urography (SS 1512), B-751

Raissaki M., Drakonaki E., Hatzidakis E., Giannakopoulou C., Gourtsoyiannis N.
Spontaneous air leaks in the neonate: Imaging appearances and clinical significance, C-0919

Rajiah P., Khan A.
Imaging spectrum and minimally invasive therapy in neuroendocrine tumours, C-0051

Rajiah P., Khan A.
Look at what can be inserted into orifices, C-0139

Rajiah P., Khan A.
Pictorial review of pneumoperitoneum: X-rays with CT correlation, C-0169

Rajiah P., Sinha R., Kirk J., Irion K., Khan A.
Multi detector CT in internal and external abdominal hernias - a pictorial review, C-0173

Rajiah P., Lim Y., Thomas N.
Pictorial review of renal transplant imaging and complications, C-0458

Rajiah P., Whitehouse R.
Imaging of diabetic foot, C-0737

Rajiah P., Patankar T., Herwadker A., Hoggard N., Laitt R., Hughes D.
CT angiography in cerebral aneurysms and beyond: A pictorial review, C-0795

Rakut W., Klausz R.
Work safety features for technologists introduced by the industry (SY 4), E-15

Ramos Lopez P., Garcia del Salto L., Dominguez Franjo E., Ramos Moreno B., Santana Acosta A., Fraile Moreno E.
Histopathologic concordance of MRI findings in the local staging of rectal cancer: Is IV contrast administration needed?, C-0098

Ranschaert E.R.
E-mail for the radiologist: E-mail for the radiologist (E³ 220b), A-049

Rauscher A., Herrmann K., Sedlack J., Kaiser W.A., Reichenbach J.R.
Complex data processing in dynamic MR-mammography (SS 1813), B-923

Reeders J.W.A.J.
Gastrointestinal infection: A changing scene: A. Gastrointestinal infection in the immunocompromised patient (CC 516), A-133

Reekers J.A.
Endovascular treatment of lower limb vascular occlusion: A. Thrombolysis (RC 909), A-232

Reekers J.A.
Drug-eluting stents: Drug-eluting stents (Introduction) (NH 10), A-255

Rees M.R.
Pericardial diseases: A. Clinical issues and US (RC 1203), A-275

Regine G., Atzori M., Buffa V., Galluzzo M., Miele V., Adami L.
Cross-sectional imaging in the renal trauma: A trauma center experience, C-0447

Reiber J.H.C.
Diagnostic workstations: The new super-assistants of the radiologist and surgeon: Computer-aided quantitation and diagnosis in cardiovascular applications (E³ 1420), A-357

Reimer P., Arnold S., Puskas Z.

Diffusion and perfusion MR imaging of the brain: B. Clinical applications of diffusion and perfusion MR of the brain (RC 1211), A-282

Reinhardt E.

European research network in biomedical imaging: Role of industry in sustaining European biomedical imaging research (ER 926), A-222

Reinsberg S., Scurr E., Brewster J., Dearnaley D., Horwich A., deSouza N.M.
Potential value of diffusion-weighted echo-planar magnetic resonance imaging in differentiating malignant from benign nodules in prostate cancer (SS 1507), B-724

Reiser M.F.

Whole-body imaging: Whole-body imaging (Introduction) (SA 2), A-044

Remsei G.

Musculoskeletal imaging: B. Avascular necrosis of the capital femoral epiphysis in children (RC 1712), A-430

Rémy J.

Multislice CT of the thorax: C. The application of post-processing (RC 1204), A-280

Rémy-Jardin M., Rémy J.

CT angiography of the chest: A. Technique for imaging the great vessels (RC 504), A-114

Rémy-Jardin M., Rémy J.

Pulmonary hypertension: All that the radiologist needs to know: Chronic thromboembolic disease (SF 16), A-371

Rémy-Jardin M., Bahépar J., Lafitte J., Dequiedt P., Ertzbischoff O., Bruzzi J., Duhamel A., Rémy J.

16-slice multidetector CT angiography of the pulmonary circulation using gadolinium-based contrast agents: Prospective evaluation in 60 patients (SS 1404), B-591

Renoux J., Marsot-Dupuch K., Benoudiba F.
The accessory oval foramen, so-called foramen of Vesalius: Anatomic CT study and clinical correlations, C-0522

Reponen J.

Tele-imaging in Europe today: B. The mobile teleradiology (RC 405), A-094

Resten A.

Pulmonary hypertension: All that the radiologist needs to know: Primary pulmonary hypertension (SF 16), A-372

Rettenbacher T.

Our experience using contrast enhanced ultrasound for uncharacteristic focal liver lesions (SY 14), E-60

Rettenbacher T., Hollerweger A., Hoflehner J., zur Nedden D.

Very small focal liver lesions appearing uncharacteristic at conventional US: Does it make sense to investigate with contrast-enhanced US in attempt to further characterize the lesions? Comparison with multi-phase spiral CT (SS 306), B-123

Rettenbacher T., Hoflehner J., Daniaux M., Herold M., zur Nedden D.

Patients with suspicion of gout: Should the first metatarsophalangeal joints be additionally investigated if clinical symptoms are located in other regions? Evaluation with US (SS 1810), B-803

Authors' Index

- Riccabona M.**
Neonatal problems: C. Investigation of the dilated urinary tract (RC 1312), A-342
- Ricci F., Campagnano S., Casale A., De Vargas Macciucca M., De Cristofaro F., Panzironi G.**
Role of multidetector CT in the evaluation of primary and secondary hyperparathyroidism, C-0548
- Riddell A.M., Hillier J., King D.M., Wotherspoon A., Brown G.**
High resolution MRI of oesophageal cancer with pathological correlation (SS 201a), B-019
- Riddell A.M., Davies C., Wotherspoon A., Brown G.**
High resolution MRI of the anatomy of the oesophagus and surrounding posterior mediastinal structures, C-0164
- Riedel T., Kyriakou Y., Schäfer D., Brunner T., Kalender W.A.**
CT image quality performance of a flat-panel detector C-arm system (SS 1513), B-777
- Riedel T., Kyriakou Y., Schäfer D., Lell M., Lang W., Kalender W.A.**
Measurement of carotid artery specimens comparing two CT imaging modalities using a 64-slice clinical CT scanner and a flat-panel detector C-arm system, C-0953
- Riedl C.C., Mullerad M., Eisenberg D.P., Akhurst T.J., Adusumilli P.S., Bhargava A., Hricak H., Scardino P.T., Fong Y.**
Positron emission tomography can predict tumor response in prostate cancer gene therapy by oncolytic herpes simplex virus (SS 1406), B-676
- Rieger M., Mallouhi A., Piza H., Czermak B., Freund M., Jaschke W.**
Congenital deformities of the hand: Preoperative evaluation with multiple-detector row CT angiography, C-0898
- Riemer A.**
CT: B. Multislice CT: Introduction and application (RC 1614), A-395
- Rienmüller R., Teubl J., Rienmüller T., Kovaleva K., Reiter G., Mächler H., Zink M., Klein W.**
Your heart – ONE-STOP-SHOP - in digital cardioradiology (IM 1), D-08
- Rienmüller R.**
Coronary vessels: A. Clinical issues and anatomy of the coronary vessels (RC 803), A-172
- Righi D., Doriguzzi Breatta A., Barbero S., Ruffino A., Calvo A., Gandini G.**
Percutaneous treatment of urological complications occurring after renal transplant (SS 309a), B-199
- Rikimaru H., Kaneda I., Chiba Y., Igarashi K.**
Evaluating the relationship of the hepatic artery and portal vein using multi-detector row CT, C-0018
- Rimola J., Perendreu J., Falcó J., Fortuño J.R., Branera J., Massuet A.**
Life-threatening rectus sheath hematomas in patients undergoing anticoagulation . Management with selective arterial embolization, C-0605
- Rinck D., Gundel L., Bakai A., Klotz E., Fichte H., Ditt H., Süß C., Trappe F., Flohr T.**
New applications for computed tomography (IM 1), D-13
- Rist C., Nikolaou K., Flohr T., Wintersperger B.J., Reiser M.F., Becker C.R.**
High-resolution ex vivo imaging of coronary artery stents using 64-detector-row computed tomography with a z-axis flying focal spot technology. Initial experience (SS 703a), B-343
- Ristic S., Bosnjakovic P., Mrvic M., Bojanovic A., Ilic D., Stojanov D., Ilic M.**
Percutaneous vertebroplasty in the treatment of metastatic spinal disease, C-0644
- Rizzatto G.**
Radiopathological correlation: C. Nodal invasion (RC 1602), A-375
- Rizzo S.M.R., Kalra M.K., Maher M.M., Saini S., Bellomi M., Cornalba G.**
Importance of attending scientific paper sessions in international radiology meetings (SS 701a), B-369
- Rizzo S.M.R., Kalra M.K., Maher M.M., Roberts T., Saini S., Bellomi M.**
Path to publication of original research articles in major peer-reviewed radiology journals: An audit of time from initial submission to publication (SS 701a), B-370
- Rizzo S.M.R., Kalra M.K., Blake M.A., Dalal T., Maher M.M., Schmidt B., Suess C., Flohr T., Saini S.**
Comparison of angular and combined automatic tube current modulation techniques with constant tube current CT scanning of the abdomen and pelvis (SS 1413), B-660
- Robinson P.J.A.**
Contrast media for MRI and US liver imaging: B. Superparamagnetic contrast media for liver imaging (RC 106), A-040
- Robinson S.**
How to investigate facial pain: C. Pain related to the temporomandibular joint and muscles of mastication (RC 1708), A-423
- Robl T., Raith J., Hinterleitner T., Ruppert-Kohlmayer A., Petritsch W., Ebner F.**
Correlation of MR-hydrocolonography with endoscopic scores in inflammatory bowel disease (SS 1401a), B-572
- Roca Vanaclocha Y., Narvaez J., De Lama E., Mones L., Pozuelo C., Medrano C., Mulattieri D., Sanchez A.**
Imaging features of tarsal coalition, C-0686
- Roche A.J.**
Arterial and venous liver intervention: A. Portal venous embolization (WS 418), A-081
- Rodallec M., Rillardon L., Kalamardes M., Feydy A.**
Imaging of spinal primary bone tumors in adults, C-0673
- Roditi A., Arkun R.**
Fat necrosis in TRAM flaps mimicking malignancy, C-0215
- Rodrigo S., Oppenheim C., Chassoux F., Cointepas Y., Roux F., Meder J.**
Diffusion tensor based analysis of the uncinate fasciculus in mesial temporal sclerosis, C-0782
- Rodriguez-Vigil B., Torres I., Echeveste J., García Río F., Serrano S., Pardo M.**
Correlation between inspiratory and expiratory lung attenuation on HRCT, pulmonary function tests, and smoking history in healthy smokers (SS 1504), B-706
- Rodriguez-Vigil B., Bernabeu D., Martín Hervas C., Lopez Barea F., Fernandez Canabal E., Gomez León N.**
Imaging of calcaneal tumours: Radiologic-pathologic correlation, C-0677
- Roebuck D.**
Pediatric intervention: A. Oesophageal interventions in children (WS 818), A-192
- Roelofs A.A.J., Karssemeijer N., Wedekind N., van Woudenberg S., Beck C., Hendriks J.H.C.L., Rosselli del Turco M., Junkermann H., Evertsz C.J.G.**
The impact of prior mammograms in mammography screening (SS 1802), B-829
- Roemer F.W., Sohaskey M.L., Mohr A., Skarnes W.C., Genant H.K.**
Evaluation of the phenotype of an insertional mutation affecting the osteopontin (opt) gene in mice: A comparative pilot study using micro CT, radiography and histology, C-0674
- Rogozhyn V.A., Rozhková Z.Z., Bachinskaya N.Y.**
1H MRS comparative study of cerebral metabolism in patients with mild cognitive impairment (MCI), vascular dementia (VD) and in normal elderly subjects (N) (SS 311), B-230
- Rogozhyn V.A., Rozhková Z.Z., Pedachenko E.G., Garmish A.R.**
In-vivo 1H MRS study of the vertebral body (SS 1510), B-680
- Roma A., Ubeda B., Nin P., Rotger R., Ramos R., Palacio A.**
MR imaging findings of breast implants complications, C-0197
- Roma A., Nin P., Ubeda B., Ares J., Traid C., Palacio A.**
MR imaging spectrum of pelvic and extrapelvic endometriosis, C-0425
- Romanini L., Cristinelli M., Cabassa P., Portugalli V., Venturelli F., Grazioli L.**
Characterization of focal liver lesions with contrast-enhanced ultrasound: Clinical utility in cancer patients (SS 306), B-124
- Romano V.C., Diekmann F., Juran R., Hamm B., Bick U.**
Assessment of the image quality in a new mammography film-screen combination compared to a standard state of the art film-screen system (SS 1402), B-588
- Romero M., Tomasello A., Blasco J., Pomés J., Macho J., Burrel M., Tomàs X.**
Percutaneous vertebroplasty: Correlation between cement leakage into the disk and new fractures of adjacent vertebral bodies, C-0617
- Romero M., Tomasello A., Blasco J., Macho J., Pomés J., Burrel M., Tomàs X.**
Vertebroplasty using transoral approach in vertebral fractures due to metastatic lesions at C2 level, C-0645
- Romero C., Meli F.J., Lambre H., Sevlever G., Carpintiero S., Salvatico R.E., Taratuto A.L.**
DWI and DTI in Creutzfeldt-Jakob disease, C-0820
- Romero Cique F., Martínez C., Santos-Armentia E., Fernández-Carrera M., Chávarri E., Táboas J.**
Intestinal perforation by fish bone: A radiologic diagnosis when not clinically suspected, C-0123

Authors' Index

Roque A., Sarrias M., Quiroga S., Sebastià C., Cuéllar H., Álvarez-Castells A.
Gastric MALT lymphoma: CT findings, C-0081

Rose J.
Drug-eluting stents: General introduction drug-eluting stents (NH 10), A-256

Rosenberg C., Weigel C., Hosten N.
Radiofrequency ablation of hepatic malignancies: Percutaneous insertion of an MRI-compatible application probe (SS 209b), B-078

Rosset A., Spadola L., Ratib O.
OsiriX: Open-Source 3D/4D DICOM viewer (SS 305), B-235

Rostagno R., Llorens R., Zander T., Zerolo I., Sanabria E., Barajas F., Qian Z., Maynar M., Castañeda-Zúñiga W.
Primary carotid stenting: 2 years follow-up of the first 100 cases (SS 1009b), B-514

Roth C., Grunwald I.Q., Struffert T., Romeike B., Eymann R., Reith W.
Efficacy of alternative embolisation devices in an experimental aneurysm model (SS 309b), B-205

Rovira-Cañellas A., Grivé E., Rovira-Gols A., Alvarez-Sabin J.
Ischemic stroke: B. Cerebrovascular distribution territories (CC 117), A-002

Roy-Choudhury S.H., Gallacher D., Pilmer J., Woodburn P., Fowler G., Steers J., Morales P., Rankin S., Adam A.
Active bleeding in a physiological phantom: Detectability on digital subtraction angiography (DSA) versus multislice CT (MCT) (SS 615), B-334

Roytberg G.E., Artamonova E.A., Ushakova T.I.
The brachial artery reactivity in patients with metabolic syndrome, C-1041

Rozzati D., Cravero F., Meni A., Sessa G., Stecco A., Carriero A.
Effectiveness of ESWT (extracorporeal shock wave therapy) in treating pseudoarthrosis and delayed union, C-0655

Rud S.D., Trufanov G.E., Pozdniakova O.F., Dekan V.S., Pyanova I.V.
Perfusion CT of the pancreas in acute pancreatitis, C-0055

Rueckert D.
Medical image registration: Methods, applications and validation: A. A tutorial on algorithms and methods (RC 913), A-244

Ruehm S.G.
Whole-body imaging: Vascular imaging (SA 2), A-047

Ruehm S.G.
Imaging of the lymphatic system: Imaging of lymph vessel disease (SF 4b), A-062

Ruhl K.M., Katoh M., Botnar R.M., Günther R.W., Spüntrup E.
Navigator-gated cardiac-triggered 3D SSFP coronary MRA: Improved image quality using a short RF-pulse (SS 1403), B-653

Ruiz M., López C., Valle M., Cortés M., Pardo R., Pastor C., Cañuelo T., Martínez C., Molino C.
Use of macroaggregates of TC-99m labelled human serum albumin (MAA) for non palpable breast lesions marking. An easy new technique with minimum surgical invasion., C-0221

Ruiz S., Sánchez A., Narváez J., Andia E.
Intraneuronal ganglion cyst of the common peroneal nerve: MRI findings, C-0763

Runza G., Cademartiri F., Mollet N.R., Belgrano M., Barbiera F., Midiri M., Hamers R., Bruining N.
Influence of increasing convolution kernels filtering on plaque imaging with multislice CT using an ex-vivo model of coronary angiography (SS 1413), B-667

Runza G., Cademartiri F., Barbiera F., Salvaggio G., Bartolotta T.V., Pardo S., Caruso G., Lagalla R.
The use of contrast-enhanced ultrasonography in the diagnosis and follow-up of Crohn's disease, C-0091

Runza G., Barbiera F., Cademartiri F., Bellia M., Galia M., La Seta F., Midiri M.
Digital cineradiographic study of swallowing in infants with neurologic disease: Our experience, C-0167

Ruscalleda J.
Base of the skull, hypophysis, supra- and parasellar region: C. Supra- and parasellar lesions (CC 1217), A-266

Ruscalleda N., Huguet R., Ribo J., Blanch J., Capdevila A.
Atypical presentations of pediatric osteomyelitis, C-0935

Russo V., Perugini E., Lovato L., Renzulli M., La Palombara C., Rapezzi C., Gavelli G., Fattori R.
MRI gadolinium enhancement in cardiac amyloidosis as potential expression of the disease severity (SS 203), B-081

Russo V., Lovato L., Renzulli M., Bertaccini P., Napoli G., Pilato E., Gavelli G., Fattori R.
MDCT coronary angiography in preoperative assessment of non-coronary cardiac surgery (SS 1003), B-529

Rutten A., de Vos S., Cramer M., ten Berg J., Prokop M.
Evaluation of myocardial late enhancement using a low dose 40-slice CT protocol: A feasibility study (SS 1003), B-521

Ryeom H., Choe B., Kim J.
Contrast-enhanced MR cholangiography using mangafodipir trisodium for evaluation of neonatal jaundice (SS 1512), B-752

Ryu J., Shin M., Kim S., Lee S., Kang C.
Degenerative changes of the intervertebral disc and facet joint of the adjacent motion segment in the pre-operative MRI: Can it be the predictable factor of post-operative instability after posterolateral fusion of lumbar spine? (SS 210), B-002

Ryu C.W., Kim S.J., Lee D.H., Choi C.G., Suh D.C.
Pre-procedural MR based decision of needle tip placement in vertebroplasty (SS 609a), B-281

Ryu J., Shin M., Kim S., Lee S., Kang C.
The spectrum of the failed back surgery syndrome: Radiological comprehension with emphasis on MRI, C-0749

Ryzhkova D.V., Mostova M.I., Zverev O.G., Kofal L.A., Tyutin L.A.

Use of positron emission tomography and [13N]-ammonia to estimate the relationship between regional myocardial blood flow and coronary artery stenosis severity in patients with coronary heart disease, C-0242

Ryzhkova D.V., Tyutin L.A., Kostenikov N.A., Tlostanova M.S., Shatik S.V., Zaytsev V.V.
Dual time point [18F]-FDG PET for the differentiation between malignant and benign genitourinary lesions, C-0519

Rzanny R., Heyne J., Hansch A., Leder U., Reichenbach J.R., Kaiser W.A.
Noninvasive investigation of cardiac metabolism in patients with hypertensive heart disease (HHD) by ³¹P-MR spectroscopy, C-0230

S

Saarenmaa I., Salminen T.

Diagnostic highlights: A. Increased lifetime risk (RC 902), A-215

Sabate J., Clotet M., Villalba V., Salinas T., Gomez A.

Radiologic evaluation of the inflammatory breast disorders, C-0220

Sabharwal T.

Chest intervention: A. Tracheobronchial stenting (WS 1718), A-434

Sablayrolles J.L.

Clinical benefits for cardio-vascular acquisition with volume computed tomography (VCT) (SY 6), E-23

Saccardi F., Drouineau J., Hardit C., Ferrié J., Charonnet J., vandermark P., Tasu J.

Detection of intracranial aneurysms with multislice CT: Comparison with digital subtraction angiography, C-0858

Sahdev A., Hughes J.L., Reznek R.H.

Pitfalls in MRI staging of cervical cancer (SS 1807a), B-793

Sakuma H., Ichikawa Y., Makino K., Chino S., Hirano T., Takeda K., VanCauteren M.

Accuracy of whole heart coronary magnetic resonance angiography for the detection of significant coronary stenoses in 92 patients with suspected coronary artery disease (SS 1403), B-651

Sakuma I., Tomura N., Takahashi S., Otani T., Nishii T., Sasaki K., Watarai J.

Changes in cerebral blood flow before and after carotid endarterectomy: Evaluation by acetazolamide-challenge ¹²³I-IMP SPECT (SS 1511), B-768

Salagierska-Barwinska A., Goraj B., Wendorff J., Wisniewska B.

Epileptic mothers and their progeny in fMRI assessment of developmental dyslexia, C-0772

Saleh A., Caseiro-Alves F., Weber C., Schima W.

Evaluation of neck and body nodal metastases with ferumoxtran 10-enhanced MR imaging: Phase III safety and efficacy study (SS 1506a), B-740

Salera D., Argalia G., Giuseppetti G.

Hemodynamic effects of a prostacyclin analog (Prostavasin) in systemic scleroderma patients, C-0024

Authors' Index

Salgado R.A., Maes M., Bellinck P., Op de Beeck B., Termote J., Parizel P.M.
The place of peritoneography in the evaluation of chronic groin pain compared with ultrasound and CT: A forgotten technique gets its due. A retrospective study of 112 patients, C-0168

Kohl G., Salganicoff M., Naidich D.P., Herzog P., Wolf M., Cathier P., Stoeckel J.
Influence of the CT reconstruction kernel on the performance of a CAD system for the detection of pulmonary nodules (SS 304), B-161

Salganicoff M., Herzog P., Naidich D.P., Stoeckel J., Shen H., Kohl G., Krishnan A.
Comparison of two different algorithms for the detection of pulmonary nodules on MDCT datasets (SS 304), B-162

Salomon L.J., Siauve N., Balvay D., Cuénod C.A., Vayssettes C., Luciani A., Frija G., Ville Y., Clément O.
Placental perfusion assessment with MRI using contrast agents in a mouse model, C-0390

Salovic D.
16-Row CT Colonography (MDCTC): Technique and pitfalls of 3D primary approach, C-0140

Salvador R.
Digital mammography: A. Technical aspects and future trends (RC 1302), A-318

Salvador R., Ramírez F., Martínez X., Salvador M., Coll D., Salvador Jr R.
Computer aided detection (CAD) results for mammography in a diagnostic center environment, C-0185

Salvan C., Ulmer J.L., Mueller W.M., Schmainda K.M., Prost R.W.
Supratentorial intra-axial brain tumors: Physiological MR imaging in diagnosis and preoperative planning (SS 711), B-435

Salvan C., Ulmer J.L., Hacein-Bey L., Mueller W.M., Prost R.W.
Verbal communication: A fMRI - DTI study (SS 1811b), B-927

Salvan C., Ulmer J.L., DeYoe E.A., Daniels D.L., Prost R.W., Mark L.P.
Brodmann's cortical areas revealed by fMRI, C-0856

Sánchez S., Martínez-Miravete P., Sainz M., Torres M., Lag E.
SDAV percutaneous biopsy as an alternative to surgical biopsy in breast lesions with 12 G core biopsies disagreement, C-0183

Sanchez E., Marco de Lucas E., Gomez V., Piedra T., Merino P., Aguilar M., Ruiz P., Ruiz E., Gonzalez A.
CT perfusion: Possible diagnostic applications, C-0793

Sancho J.L., Vida J.M., Luna A., Ribes R., Ros P.
MDCT and MRI of abdominal inflammation: Beyond abdominal abscesses, C-0176

Sandomenico F., Catalano O., Nunziata A., Mattace Raso M., Siani A.
Appendiceal mucocele: Imaging with US and CT, C-0131

Sandomenico F., Catalano O., Nunziata A., De Feo P., Siani A.
Color-Doppler sonography (US): A pictorial atlas of scrotal disorders, C-0473

Sansoni I., Laghi A., Di Martino M., Miglio C., Celestre M., Coletta L., Rengo M., Passariello R.

The added value of the hepato-biliary phase imaging in Gd-BOPTA magnetic resonance study (Gd-BOPTA-MR) of benign liver tumors and metastases in normally functioning livers (SS 201b), B-043

Laghi A., Sansoni I., Di Martino M., Celestre M., Miglio C., Coletta L., Rengo M., Passariello R.
Detection and characterization of hepatocellular carcinoma (HCC): Value of adding the hepato-biliary phase imaging to dynamic Gd-BOPTA magnetic resonance imaging (Gd-BOPTA-MRI) (SS 201b), B-044

Sansoni I., Laghi A., Miglio C., Celestre M., Rengo M., Di Martino M., Coletta L., Passariello R.
DW-MR imaging study after carotid stent placement with protection device (CASPD): Role of monitorization at 6 and 24 hours after procedure (SS 1009b), B-515

Sansoni I., Laghi A., Celestre M., Miglio C., Di Martino M., Coletta L., Rengo M., Passariello R.

Multislice-spiral computed tomography (MSCT) versus Gd-BOPTA-enhanced magnetic resonance imaging (Gd-BOPTA-MRI) in the detection and characterization of hepatocellular carcinoma (SS 1501b), B-710

Sansoni I., Laghi A., Celestre M., Miglio C., Di Martino M., Rengo M., Coletta L., Passariello R.

Delayed Gd-BOPTA MR imaging (Gd-BOPTA-MRI) phase: Different timing between normals and hepatopathics (SS 1506a), B-747

Sansoni I., Laghi A., Celestre M., Miglio C., Di Martino M., Rengo M., Coletta L., Passariello R.

Hepatocellular carcinoma (HCC) suspected lesions: Detection and characterization at multislice-spiral computed tomography (MSCT) and Gd-BOPTA-enhanced magnetic resonance imaging (Gd-BOPTA-MRI), C-0019

Sansoni I., Laghi A., Celestre M., Miglio C., Rengo M., Di Martino M., Coletta L., Passariello R.

Adding the hepato-biliary phase imaging to dynamic Gd-BOPTA magnetic resonance (Gd-BOPTA-MR): Its value in detection and characterization of hepatocellular carcinoma (HCC), C-0034

Sansoni I., Laghi A., Miglio C., Celestre M., Rengo M., Di Martino M., Coletta L., Passariello R.

Benign liver tumors and metastases in normally functioning livers: The added value of the hepato-biliary phase imaging in Gd-BOPTA magnetic resonance imaging (Gd-BOPTA-MRI), C-0035

Sansoni I., Laghi A., Miglio C., Celestre M., Rengo M., Coletta L., Di Martino M., Passariello R.

Carotid stenting with protection device (CASPD) and brain diffusion-weighted MR imaging (DWI-MRI): Control within 6 and 24 hours after stenting, C-0585

Santoro L., Colagrande S., Filippone A., Grassettonio E., Belli G., Villari N.

Quantitative evaluation of SHU-555A (Resovist-Schering) enhancement in normal liver parenchyma and benign/malignant focal hepatic lesions (SS 1506a), B-745

Sapir J.

Revolutionizing radiology workflows with CR (SY 8), E-34

Saponjski J., Ostožić M., Masulovic D., Beleslin B., Markovic Z.

Is transcatheter therapy of renal artery stenosis choice in treatment of renal hypertension? Diagnostic value to detect restenosis in long-term follow-up, C-0595

Sapoval M.

Endovascular treatment of lower limb vascular occlusion: B. Uncovered stents vs covered stents (RC 909), A-233

Sardanelli F., Fausto A., Panizza P., Giuseppetti G.M., Lattanzio V., Del Maschio A.
What a sensitivity of mammography and dynamic MR for *in situ* breast cancers if we use the whole breast as a pathologic gold standard? Results from a multicenter trial (SS 602), B-264

Sardanelli F., Fausto A., Cotticelli B.

Detection of brain hyperintensities on fluid-attenuated inversion-recovery (FLAIR) images in multiple sclerosis (MS): In-plane high resolution (HR) versus standard low resolution (LR) matrix, C-0828

Sarria L., Cozcolluela R., García S., Gomez H., Martínez-Berganza T., Forradellas A., Alberdi I., Monzon F.

Preoperative spiral CT in staging of colonic cancer, C-0100

Sarrias Guzmán M.J., Serres Créixams X., Roche Vallés S., Buti M., Valdés A., Castellà Fierro E.

The "C" sign: Sonographic assessment of hepatic hilar lymph node involvement, C-0031

Satchithananda K., Purushothaman H., Sidhu P.S.

Neck lumps and bumps: Ultrasound is the way forward, C-0554

Sauer B., El Ghali S., Buy X., Lang H., Saussine C., Roy C.

Imaging aspects of papillary renal cell carcinoma (RCC): Characterization and staging with pathological correlation, C-0461

Saupe N., Pfirrmann C.W.A., Schmid M.R., Schertler T., Wildermuth S., Manestar M., Marincek B., Weishaupt D.

MR imaging of wrist cartilage: Comparison between imaging at 1.5 T, 3 T and anatomical section (SS 710), B-360

Saur S.C., Großkopf S.

Evaluation of the Vesselness and Laplacian of Gaussian filter for vessel enhancement in CT images, C-0998

Scaglione M., Pinto A., Romano S., Farina R., Grassi R., Romano L.

Slivers of free fluid detected by screening abdominal sonography after blunt trauma: What does it mean? (SS 701a), B-363

Authors' Index

Scarrone A., Pedrazzini F., Lingua G., Testa F., Grosso M., Groppo Marchisio F.
A 4-year experience in trans arterial chemo embolization of primary and metastatic liver tumors, C-0590

Scarsbrook A.F., Cowan N.C., Willatt J.
Imaging of the ureter with multislice CT urography, C-0496

Schaefer-Prokop C., Bankier A.A., Janata K., Riechling N., Prokop M.
Complete chest CTA versus a limited range CTA for the diagnosis of PE: What do we miss? (SS 1404), B-595

Schäfers M.
New imaging methods and technologies:
C. Nuclear imaging including PET (PR 419), A-092

Scherr M.K., Scher B., Seitz M., Reiser M.F., Müller-Lisse U.G.
Choline PET (-CT) and combined MRI+MR spectroscopy in the detection of intra-prostatic and pelvic lesions of prostate cancer (SS 1007), B-496

Schilham A.M.R., van Ginneken B.
Computer-aided diagnosis as a second reader for nodule detection in chest radiographs versus single and double reading (SS 605), B-323

Busch H.-P., Schilz C.
Quality control and dose reduction in digital radiology: C. Quality assurance in digital radiology: How we do it (RC 1313), A-349

Schima W., Vogl T.J., Catalano C., Marti-Bonmati L., Rummeny E.J., Tardaguita Montero F.
Quadruple-phase MDCT of the liver in patients with suspected HCC: Effect of contrast material flow rate (SS 1801b), B-857

Schindera S., Semela D., Redaelli C., Fröhlich J., Vock P., Stoupis C.
Hepatocellular carcinoma: Comparison of a macromolecular contrast agent vs gadobutrol and gadobenate dimeglumine in an experimental animal MRI study (SS 1506a), B-746

Schlemmer H.
Whole-body imaging: Modalities (SA 2), A-045

Schlossbauer T., Wismueller A., Leinsinger G., Lange O., Scherr M., Meyer-Baese A., Reiser M.F.

Cluster analysis of signal-intensity time course in dynamic breast MRI: Does neural network clustering help to find the correct diagnosis in unclear small lesions? (SS 702), B-374

Schlosser T., Pagonidis K., Herborn C.U., Hunold P., Walterling K., Barkhausen J.
Assessment of left ventricular parameters using 16 slice computed tomography: Evaluation of a new software for endocardial and epicardial border delineation (SS 1803), B-822

Schlosser T., Jochims M., Nasser M., Hunold P., Walterling K., Bartel T., Barkhausen J.
Quantification of aortic valve stenosis in MRI: Comparison of steady state free precession and fast low angle shot sequences (SS 1803), B-828

Schmidt B.T., McCollough C.H., Banckwitz R., Bruesewitz M.R., Suess C., Flohr T.

Organ dose reduction using CT automatic exposure control (AEC): TLD measurements in an anthropomorphic phantom (SS 713), B-442

Schmidt G.P., Baur-Melnyk A., Hahn K., Reiser M.F., Schoenberg S.O.
Detection of tumor and metastatic disease by MR imaging vs PET-CT: Value of a new whole-body MR scanner (SS 1501b), B-717

Schmidt D., Clasen S., Boss A., Truebenbach J., Pereira P., Schick F., Claussen C.D.
MR imaging of radiofrequency (RF) induced coagulation in liver ex vivo: Histopathological correlation of different MR sequences between a low and a high field MR scanner, C-0622

Schmitz B., Huber R., Aschoff A.J.
Indications, diagnostic methods and radiologist's role in acute interventional stroke therapy, C-0579

Schmitz B., Grön G., Aschoff A.J.
Comparison of BOLD signal strength and susceptibility artifacts between 1.5 and 3.0 Tesla at different TE, C-0783

Schmitz B., Aschoff A.J.
Improved MR imaging of the extremities using a flexible multiple element phased array body coil, C-0993

Schmitz-Rode T.
Venous occlusion: C. Pulmonary embolism: Protection and treatment (RC 1709), A-426

Schmuckenschläger C., Ploder M., Wessner B., Längle F., Roth E., Lammer J., Kettenbach J., Spittler A.

Percutaneous tumor ablation in liver tumors causes a transient immunosuppression, C-0639

Schneider G.K.
MRA in pediatrics (SY 5), E-19

Schneider G.K., Fries P., Altmeyer K., Kramann B., Seidel R.M.

Detection and differential diagnosis of benign and malignant pancreatic lesions by unenhanced and contrast enhanced MR imaging, C-0060

Schneider G.K., Seidel R., Fries P., Kindermann I., Boehm M., Winter H.
MRI of cardiac and paracardiac masses. A pictorial review, C-0237

Schneider G.K., Seidel R.M., Remberger K., Kohn D., Fries P.

MR imaging of Bone tumors - A pictorial review, C-0659

Schneider G.K., Fries P., Gruber M., Kramann B., Seidel R.
Pediatric MRA with Gd-BOPTA, C-0907

Schnyder P.
Vascular, emergency and ICU imaging:
B. Trauma, emergency and ICU imaging (E³ 720), A-161

Schoellnast H., Brader P., Georgieva B., Oberdabernig B., Deutschmann H.A., Tillich M.
Effect of iodine flow rate on parenchymal and vascular enhancement during contrast enhanced multiphasic abdominal multidetector row CT (SS 1806), B-886

Schoellnast H., Deutschmann H.A., Fritz G.A., Stessel U., Schaffler G.J., Tillich M.
Influence of iodine flow concentration on vessel attenuation and visualization in multi-detector row CT angiography of the pulmonary arteries (SS 1806), B-887

Schoenberg S.O., Dietrich O., Herrmann K.A., Strauss T., Hatz R., Reiser M.F.
Comprehensive pulmonary MR imaging in patients with bronchial carcinoma using parallel acquisition techniques (SS 704), B-383

Schönberg S.
A new generation of contrast agents meets brand new MRI technology (SY 2), E-08

Schoth F., Mühlensbruch G., Mahnken A.H., Krombach G.A., Günther R.W.
A new way of looking at cardiac CT - polar maps of the coronary arteries (SS 703a), B-348

Schroeder T., Radtke A., Debatin J.F., Malago M., Wembacher E., Ruehm S.G.
"All-in-One" multislice computed tomography (MSCT) of potential living liver donors (SS 301b), B-175

Schuknecht B.F.
Craniocerebral and spinal trauma:
A. Craniocerebral trauma (1): General principles and maxillofacial trauma (CC 1317), A-307

Schulte B., Reimer P., Kuehnen J., EOB Study Group E.
Evaluation of the detectability of HCC in patients with liver cirrhosis by means of Gd-EOB-DTPA: Results of a qualitative and quantitative phase III study (SS 201b), B-047

Schulz E., Melchert U.H., Haude A.F., Krause U.R., Stoeckelhuber B.M., Ulmer S.
Radiation dosage in pituitary surgery: Comparison between conventional and computer assisted methods, C-0859

Schulz-Wendtland R., Wenkel E., Lell M., Imhoff K., Bautz W.
Digital luminescence mammography (CR) versus full-field digital mammography (DR): A phantom study (SS 302), B-155

Schulz-Wendtland R., Hermann K., Wenkel E., Böhner C., Lell M., Dassel M., Bautz W.
Experimental investigations in comparison of full-field digital mammography (a-Se detector) with a Mo/Mo and W/Rh filter: Is a dose reduction possible? (SS 302), B-156

Schumacher M.
Imaging of normal anatomy and function:
C. Spine, spinal cord and circulation of cerebrospinal fluid (RC 111), A-022

Schuncke A., Neitzel U.
Retrospective patient dose analysis of digital radiography systems in routine clinical use, C-0960

Schwarz W.V., Hammerstingl R., Marquardt F., Götz B., Heller M., Vogl T.J.
Diagnostic work-up in the liver using SPIO-enhanced MRI: Comparison with histopathologic and clinical findings (SS 201b), B-046

Scialpi M., Cenciarini V., Landi P., Regi L., Galuppo C., Lupattelli L.
Preoperative TN staging of rectal carcinoma: Prospective comparison of transrectal US (TRUS) and endorectal MR imaging (SS 301a), B-148

Scialpi M., Malaspina C., Boranga B., Scalera G., Crusco F., Lupattelli L.
Role of US in the evaluation of dorsal scapholunate ganglion cyst (SS 1810), B-802

Authors' Index

Scialpi M., Rotondo A., Scaglione M., Ragozzino A., Lupattelli L.
Liver hemangiomas: Pattern-based classification scheme for enhancement speed at arterial phase CT (SS 1801b), B-858

Scialpi M., Magistrelli A., Scaglione M., Lupattelli L., Rotondo A., Danza F.M., Bonomo L.
Retroperitoneal anatomy: What could we learn from disease. Part 2: Pathway of spread of pathology, C-0494

Screaton N.J.
HRCT in diffuse lung disease: B. Reticular pattern (RC 1704), A-416

Scutt D., Nandi A., Zhang L., Jack L.B.
Breast imaging: A. Breast cancer and imaging (RC 1714), A-432

Sebastian A.J., Paddon A.J.
Central pulmonary embolism in oncology patients: An underestimated phenomenon (SS 1404), B-599

Sedlack J., Rauscher A., Deistung A., Kaiser W.A., Reichenbach J.R.
Caffeine-induced contrast enhancement in volunteers by using susceptibility-weighted imaging (SWI) (SS 1813), B-921

Sedonja I., Jevtic V., Milcinski M.
Prognostic value of reactive interface in femoral head osteonecrosis on magnetic resonance imaging, C-0685

Seitz J.
Abdominal intervention: C. Percutaneous gastrostomy/Gastrojejunostomy (WS 118), A-032

Sella T., Schwartz L.H., Hricak H.
Retained seminal vesicles following prostatectomy: MR features (SS 1007), B-498

Sella T., Aharoni D., Hiller N.
CT features of adnexal torsion (SS 1807a), B-797

Sentis M., Saez Artacho E., Andreu Navarro F., Tortajada Jimenez L., Ganau Macias S., Camps J., Segui Palmer M.
Locally advanced infiltrating lobular carcinoma (LALIC): A histological subtype with poor correlation when MRM is used to monitor primary chemotherapy (PCT) (SS 702), B-380

Seo Y., Choi C., Yoon D., Yun E., Lee S., Park S., Moon J.
Benign breast diseases associated with cyclosporine A therapy in renal transplant recipients (SS 1402), B-581

Seon S.H.J., Kim K.S.J.
Role of MR perfusion-weighted images for predicting severe lesion growth in the hyperacute stage infarction (SS 611), B-312

Serafin Z., Sobocinski B., Strzesniewski P., Lasek W., Strozecki P., Kapala A., Manitius J., Dabrowiecki S.
Peripheral arterial blood flow and intima-media thickness in patients with predialysis stage chronic renal failure, C-1040

Serafin Z., Strozecki P., Lasek W., Manitius J., Sobocinski B.
Carotid artery blood flow and wall properties in patients with early stage renal insufficiency, C-1059

Serafini G.
Imaging of the uterus: A. Ultrasound imaging techniques (RC 507), A-130

Sergiacomi G., Leporace M., Cariani M., Laviani F., Bartolomucci A., Schillaci O., Simonetti G.
Multislice CT and SPECT-CT: Correlation in diagnosis of pulmonary nodules, C-0296

Sergiacomi G., Cariani M., Leporace M., Sperandio M., Romagnoli A., Simonetti G.
Multislice CT with retrospective ECG gating in the evaluation of central lung tumours, C-0297

Sever A.R., Villan S., Batmaz F., Mounter N.A., Mills P., Schofield J.B., Jones S.E., Jones P.A.
Breast microcalcifications: Benign or malignant. Ready for a challenge?, C-0213

Shanneik K., Kachelrieß M., Achenbach S., Kalender W.A.
Validating measures for temporal resolution on multi-slice CT scanners (MSCT) (SS 1413), B-662

Sharafuddin M.J.
Venous imaging and intervention: C. DVT and interventional therapy: Fact or fiction (RC 515), A-129

Sharia M., Belichenko O., Gamidov S., Denisov A.
MRI of penis and pelvic floor in patients after perineal blunt injury, C-0485

Sheehan J.J., Ridge C.A., Ward E.V.M., Harte S.E., Duffy G.J., Collins C.D., Malone D.E., Skehan S.J.
The clinical impact of FDG PET on the management of patients with colorectal liver metastases and comparison with conventional imaging. Evaluation with evidence based practice techniques (SS 1501b), B-716

Sheehan J.J., Harte S.E., McKenna C.M., Malone D.E.
Double contrast MRI (DCMRI) of focal lesions in the cirrhotic and non cirrhotic liver: A problem solving technique, C-0013

Sheehy N., Farrelly C., McCann J., Boyle G., Meaney J.F.M.
Appearance of the meninges on contrast-enhanced MRI: Spectrum of normal and abnormal appearance in the brain and spinal cord, C-0801

Sheehy N., Farrell M., Brennan P., Thornton J.
Granulomatous angiitis of the central nervous system. A pictorial review, C-0827

Sherif H., Mahfouz A.E.
The angular interface sign: New sign for differentiation of renal cell carcinoma and angiomyolipoma on MR imaging of small renal masses (SS 707), B-395

Shevchenko H.
Possibility of the US-detection of clustered microcalcifications of female breast, C-0205

Shimada M., Yoshikawa K., Funahashi K., Teramoto T., Watanabe M., Inoue Y., Ookubo T., Kojima J., Hayashi S.
Evaluation of pararectal lymph nodes in rectal cancer with a submucosal injection of SPIO at colonoscopy and imaging by MRI, C-0093

Shimada M., Yoshikawa K., Weinmann H.J., Tatebe T., Morita T., Ookubo T., Senoo A., Inoue Y., Hayashi S.
Atherosclerotic plaque imaging of ApoE-deficient mice with gadofluorine M, C-0393

Shimizu T., Sawada A., Kodama Y., Watanabe Y., Sakuhara Y., Abo D., Funakubo M., Yoshida Y., Miyasaka K.
MR image characteristics during and after cryoablation of uterine fibroids, C-0415

Shin S., Jeong Y., Kang H., Lim H., Kim Y., Park J., Oh J.
Recurrence Patterns after Curative Resection of Colorectal Cancer: Emphasis on Comparison between Colon Cancer and Rectal Cancer, C-0152

Shin J., Han B., Choe Y., Ko K.
US depiction and pathologic outcome of suspicious breast lesions additionally detected on MR imaging, C-0204

Shin S.M., Jeong Y.J., Kim K.I., Kim C.W., Moon T.Y.
Visualization of aberrant bronchial arteries and their anatomic course by CT bronchial angiography, C-0300

Shinjo H., Gokan T., Takeyama N., Suyama J.
Multi-detector row CT urography: Comparison of fluid administration protocols for depicting the urinary collecting system, C-0512

Shimura R., Matsui O., Gabata T., Ueda K.
Detection of a hypervascular malignant focus in borderline lesions of hepatocellular carcinoma: Comparison of dynamic CT, dynamic MRI and SPIO-enhanced MRI, C-0038

Shuto K., Okazumi S., Yanagawa N., Ochiai T.
New method of evaluating pericardial invasion of esophageal cancer in 22 subjects using electrocardiogram-gated multislice computed tomography and compared with histological findings, C-0163

Siablis D., Christeas N., Karnabatidis D., Katsanos K., Liatsikos E.N., Flaris N., Kagadis G.C.
Ureteral implantation of Paclitaxel-eluting balloon-expandable metallic stents: An experimental study in the pig model, C-0613

Sias A., Balestrieri A., Barberini L., Fraschini M., Puligheddu M., Marrosu F., Mallarini G.
A multimodal neuroimaging approach in patients with early diagnosis of Parkinson's disease: Correlations between f-MRI with fine motor tasks, EEG and clinical tests (SS 211), B-100

Sias A., Balestrieri A., Barberini L., Puligheddu M., Fraschini M., Cesare Marincola F., Lai A., Marrosu F., Mallarini G., Marrosu M.G., Cocco E., Locci E.
MR-spectroscopy in multiple sclerosis (MS) patients: Correlation between in vivo and in vitro analysis of CSF fluid, C-0802

Sias A., Balestrieri A., Barberini L., Puligheddu M., Fraschini M., Murru A., Demelia L., Marrosu F., Mallarini G.
Brain MR spectroscopy in the evaluation of Wilson's disease: Correlation with clinical status and response to therapy, C-0863

Sias A., Balestrieri A., Barberini L., Puligheddu M., Fraschini M., Marrosu F., Mallarini G.
Role of MR spectroscopy in patients with temporal lobe epilepsy (TLE), C-0866

Authors' Index

- Siemianowicz A., Wawrzynek W., Baron J., Koczy B., Kasprowska S.**
The role of computed tomography examination with multiplanar and three-dimensional reconstructions in evaluation of cervical spine fractures, C-0675
- Sigal R.C.**
Radiological approach to stage head and neck squamous cell carcinoma: C. Oral and oropharyngeal cancer (RC 408), A-074
- Silberman B.**
Teleradiology: Threat or opportunity?: First attempt for a European guidelines for the use of teleradiology (ER 1326), A-339
- Simon G.H., von Vopelius-Feldt J., Wendland M.F., Fu Y., Berejnoi K.V., Daldrup-Link H.E.**
Comparison of ferumoxtran-10 and ferumoxytol for MR imaging of experimental arthritis (SS 1506a), B-739
- Simonelli G., Fanelli F., Salvatori F.M., Corona M., Pepino D., Dominelli V., Boatta E., Rossi P., Passariello R.**
Porto-systemic shunt reduction for the treatment of hepatic encephalopathy after TIPS performed with E-PTFE covered stent-graft (SS 1009a), B-509
- Simonetti G., Manenti G., Pistolese C., Cossu E., Buonomo O., Orlandi A.**
Radiofrequency ablation of small breast cancer with a dedicated cooled tip needle electrode (SS 1502), B-729
- Simonneau G.**
Pulmonary hypertension: All that the radiologist needs to know: Pulmonary hypertension: Classification, clinical data (SF 16), A-370
- Simpson E., Patel U.**
Tuberous sclerosis complex: Prevalence of minimal fat-containing angiomyolipoma (AML) and renal cell carcinoma (SS 707), B-393
- Sinitsyn V.E.**
Morphological and functional assessment of the heart: A. Morphological assessment of the heart (RC 1703), A-409
- Siric Z.I., Radovanovic M., Mrvic M.**
Complications of urogenital non-vascular interventional procedures, C-0495
- Sironi S., Buda A., Picchio M., Messa C., Fazio F.**
Lymph node staging in patients with cervical cancer: Accuracy of integrated FDG PET/CT in correlation to histopathologic findings (SS 1507), B-728
- Skaane P.**
Digital mammography: C. Screening with digital mammography (RC 1302), A-320
- Skaane P.**
Breast cancer screening with full-field digital mammography (SY 6), E-25
- Skilakaki M.G., Kalogeropoulos I.V., Galina B., Antipa E., Maragaki E.E., Piperopoulos P.N.**
The value of normal mammographic and sonographic findings in evaluating palpable breast abnormalities (SS 1402), B-583
- Skilakaki M.G., Kalogeropoulos J.V., Galina P., Polyviou P., Piperopoulos P.N.**
The value of emergency room (ER) chest radiographs in patients with unsuspected thoracic pathology, C-0295
- Skrzelewski S., Glowacki J., Kachel R., Gosek K., Grzeszczak W., Trzeszkowska-Rotkegel S., Borowiak H., Jackowska Z.**
Computed tomography portography in the diagnosis of portal hypertension, C-0023
- Slapa R.Z., Slowinska-Szednicka J., Jakubowski W., Serafin-Krol M., Szopinski K.T., Gietka-Czernel M., Jastrzebska H., Kozicki I., Stachlewska-Nasfeter E.**
Differential analysis of vascularization of thyroid nodules examined with volume rendered 3D power Doppler ultrasound (SS 208), B-057
- Sluming V.**
MRI/Neuroimaging: B. Neuroimaging and analysis techniques for research into brain structure and function (RC 514), A-137
- Smans K., Bosmans H., Struelens L.**
Multi-centre study to assess patient doses in interventional radiology in Belgium (SS 1513), B-769
- Smevik B.**
Emergencies in pediatrics: B. Imaging in neonatal distress (RC 1612), A-392
- Smirnov P., Lavergne E., Gazeau F., Doan B., Gillet B., Combadiere C., Combadiere B., Clement O.**
In vivo lymphocytes trafficking to tumor: A cellular magnetic resonance imaging approach for cell-based anticancer therapy (SS 1506b), B-779
- Smith A.P., Hitzke G., Ruth C., Ren B., Jing Z., Gkanatsios N., Stein J.**
Effect of acquisition geometry and radiation dose on lesion visibility in full field breast tomosynthesis (SS 202), B-029
- Song W., Fan L., Xie Y., Wei G., Xu J., Si Q., Liang C., Qian J., Jin Z.**
A study of inter-observer variation of small pulmonary nodule marking on DR by using an interactive computer analysis system (SS 204), B-040
- Sorantin E., Werkpartner G., Beichel R., Bornik A., Reitinger B., Riccabona M., Wegenkittl R., Fuhrmann A., Sonka M., Kolli A.**
The virtual liver surgery planning system (IM 1), D-04
- Sorantin E., Kettenbach J., Bale R., Kronreif G., Werkpartner G., Beichel R., Bornik A., Reitinger B., Sonka M.**
Multi-dimensional imaging for guiding therapy: Image-guided therapy and robotic applications (SA 12), A-270
- Sorge I., Krausse A., Kluge R., Mauz-Körholz C., Körholz D., Hirsch W.**
Evaluation of [¹⁸F]FDG-PET and CT/MRI for monitoring therapy response in children with Hodgkin's disease, C-0887
- Sorrentino F., Pepe A., Borsellino V., Galia M., Midiri M., Lombardi M.**
Myocardial scarring in beta thalassemia major by late gadolinium-enhanced magnetic resonance imaging: Correlation with myocardial iron overload and ECG-changes (SS 203), B-088
- Sorrentino F., Pepe A., Lo Pinto C., Di Salvo V., Midiri M., Lombardi M.**
T2* measurement in patients with beta thalassemia major: Effect of heterogeneity of myocardial iron overload, myocardial fibrosis and blood oxygenation (SS 203), B-089
- Sosna J., Sella T., Libson E.**
Double contrast barium enema: Critical analysis of reported performance in the era of virtual colonoscopy (SS 301a), B-141
- Sosnowski P.**
Orbit and visual system: A. Imaging of orbital pathology (RC 811), A-181
- Souftas V.D., Mantatzis M., Prassopoulos P.**
Terminal stage pelvic malignancy with bilateral obstructive uropathy: Is there a role for percutaneous intervention? (SS 1807b), B-867
- Spagnolo P., Khouri T., Manfredi M., Marks M.**
Assessment of myocardial bridging with 16-multidetector-row CT (16-MDCT) (SS 1003), B-525
- Spanos G.P., Oikonomou I., Kouskouras C., Sarafopoulos A., Giavroglou C., Tsifountoudis I., Dimitriadis A.S.**
Demonstration of the sites of communication between true and false lumen in chronic aortic dissection with phase-contrast sequences (SS 1015), B-554
- Speck U.**
The milestones of X-ray contrast media development (SY 7), E-27
- Speck U., Scheller B., Abramjuk C.**
Restenosis inhibition by non-stent-based local drug delivery (SS 309b), B-206
- Sperandio M., Romagnoli A., Tomassini M., Di Roma M., Pellegrino L., Simonetti G.**
Evaluation of coronary artery by-pass: Multi-slice CT assessment of artery and venous surgery graft (SS 703a), B-344
- Spirchez Z., Tantau M., Badea R.**
Percutaneous cysto-gastrostomy using a combined, 2 steps, sonographic-endoscopic procedure in the treatment of pancreatic pseudocysts (SS 309a), B-193
- Spitzer D., Novák J., Mrklovský M., Jiricková P., Spitzerová O., Sloboda V.**
Pictorial review of eye ultrasound with CT and MR correlation, C-0529
- Spors B., Patrick F., Klimes K., Grothoff M., Noeske R., Gutberlet M., Felix R.**
Cardiac imaging at 3 Tesla: Comparison of different sequences and the use of parallel imaging between 1.5 and 3 T (SS 1803), B-825
- Spreng A., Netzer P., Quattropani C., Mattich J., Dinkel H., Hoppe H.**
Prospective evaluation of extracolonic findings at contrast enhanced CT colonography in daily clinical practice (SS 1501a), B-693
- Squarcia M., Vilana R., Bianchi L., Nicolau C., Sala M., Llovet J.M., Bruix J., Bru C.**
Radiofrequency in the treatment of hepatocellular carcinoma. Multicenter study in Spain, C-0610
- Squillaci E., Sperandio M., Di Roma M., Fabiano S., Fiaschetti V., Simonetti G.**
Virtual MR endoscopy of aortic aneurysms and dissection, C-1033

Authors' Index

Stäbler A.

Bone marrow disorders as a manifestation of disease: A. How to image bone marrow (RC 810), A-165

Stacul F.

Imaging of stones: C. Radiation issues and economic aspects (RC 807), A-197

Stanzhevsky A.A., Tyutin L.A., Korzenev A.V., Kostenikov N.A., Shustyn V.A., Skoromets T.A., Neznanov N.G.

18 F-FDG PET in anxiety-obsessive disorders (AOD): Metabolic and clinical correlation study, C-0791

Stavroulis E., Zugaro L., Limbucci N., Barile A., Calvisi V., Masciocchi C.

MRI vs. arthroscopy in the evaluation of tibio-talar joint impingement, C-0695

Stepling C., Niederstadt T., Krämer S., Kugel H., Schwindt W., Heindel W., Bachmann R.

Comparison of T1-weighted inversion-recovery, gradient-echo and spin-echo sequences for imaging of the brain at 3.0 Tesla (SS 1811b), B-932

Stern-Padovan R., Lusic M., Sjekavica I., Hrabak M., Potocki K., Oberman B., Marinic J.

Ruptured abdominal aortic aneurysm: MSCTA imaging, C-1002

Sterpu M.D., Soukhov V.Y., Tyutin L.A.

Sentinel lymph node assessment by ^{99m}Tc-colloid orchifuniculoscintigraphy in patients with testicular tumors, C-0474

Stieljes B., Schlüter M., Weber M., Hahn H.K., Rexilius J., Konrad-Verse O., Essig M.R.

DTI-based assessment of corpus callosum infiltration by primary brain tumors: A marker for contralateral growth (SS 1011), B-530

Stippich C.

Functional MRI: B. Clinical applications of fMRI for intracranial tumors and epilepsy (RC 411), A-070

Stix A., Simbrunner J., Ruppert-Kohlmayr A., Komatz G., Feichtinger M., Klein G.E., Ebner F., Ebner F.

CT and MR imaging features of cerebral cortical venous thrombosis (SS 1811a), B-906

Stoeva M., Tabakov S.

EMIT: Digital multilingual medical radiation physics dictionary, C-0359

Stojanov D.A., Bosnjakovic P., Zivkovic M., Stojanovic N., Ristic S.

Enlarged temporal horns and transient amnesia after perimesencephalic haemorrhage, C-0812

Stojanovska J., Moffat B.A., Chenevert T.L., Ross B.D., Rehemtulla A., Hall D.E.

Diffusion weighted imaging: An early predictor for therapeutic efficacy (SS 1506b), B-786

Stoker J.

CT colonography and colon cancer: C. The practical application of CT colonography (RC 1701), A-414

Stollfuss J.C., Zimmermann F., Wörtler K., Auer F., Rummery E.

Comparison of MRI and CT for staging of advanced rectal carcinoma (SS 301a), B-146

Stork A., Lund G.K., Muellerleile K.,

Bansmann P.M., Kemper J., Adam G.

Value of T2-weighted-, first-pass-enhancement and delayed-enhancement-MRI to differentiate between acute and chronic myocardial infarction (SS 303), B-213

Størmer J.

Tele-imaging in Europe today: C. Results in practice: The Norwegian experience (RC 405), A-095

Storto M.L.

CT angiography of the chest: B. Normal and variant anatomy (RC 504), A-115

Storto M.L.

Imaging of focal lesions: Chest (EM 1), A-146

Stosic-Opincal T., Peric V., Lavrnec S., Gavrilov M.

Comparison of detectability of endocranial lesions in multiple sclerosis at 1.0 and 3.0 Tesla., C-0873

Stoupis C.

Liver imaging: Characterisation and pitfalls: A. Calcifications (RC 501), A-111

Strickland N.H.

PACS pitfalls: PACS pitfalls (Introduction) (SF 9b), A-228

Strickland N.H.

Building an electronic patient record system: C. Image distribution within the hospital and beyond (RC 1205), A-304

Struelens L., Vanhavere F., Bosmans H., Van Loon R., Smans K.

Optimisation of patient doses in angiography and interventional radiology: Proposal for auditing structure, C-0978

Studer R., Spreng A., Christe A., Thalmann G., Vock P., Thoeny H.C.

Patients with acute flank pain: A stone and/or something else? (SS 1407), B-619

Studniarek M., Mikiciuk-Olasik E.,

Retkowski M., Wierzba T., Sidorowicz M.

Gd-IDSA derivatives as potential hepatobiliary contrast media for MRI: Experimental studies on rats, C-0389

Subramanian K., Jain A.K.

Comparison of US and KUB for detecting renal calculi with nonenhanced multislice CT, C-0457

Suetens P.

Diagnostic workstations: The new super-assistants of the radiologist and surgeon:

Workstations for image guided interventions (E³ 1420), A-358

Suh S., Won J., Lee D.

The endovascular treatment of deep vein thrombosis, C-0568

Suh S., Won J., Lee D., Paik K.

Transcatheter arterial chemoembolization through left inferior phrenic artery in hepatocellular carcinoma, C-0574

Suh S., Kim D., Kim D.

Embolization of cavernous dural arteriovenous fistulas via superior ophthalmic vein approach, C-0777

Suliman H.M., Stikkelbroeck N.M.M.L.,

Braat D.D.M., Jager G.J., Otten B.J.

Prevalence of ovarian adrenal rest tumours and polycystic ovaries in females with congenital adrenal hyperplasia: Results of ultrasonography and MRI imaging, C-0435

Suliman H.M., Stikkelbroeck N.M.M.L.,

Jager G.J., Otten B.J., Blickman J.,

Hermus A.R.M.M.

Testicular masses in association with congenital adrenal hyperplasia: MR features compared with sonographic findings, C-0469

Sullo P., Mazzarella G., Covelli E.M., Cioffi R., Belfiore G.

Receptorial (Tc99m-Depreotide scintigraphy) and morphological (CT scan) imaging in the non-invasive characterization of lung nodules, C-0277

Sun H., Bai R., Wu E.

Abdominal tuberculosis presenting with acute abdomen: CT findings, C-0073

Sunaert S.

Functional MRI: A. Technique, protocols and stimulation equipment (RC 411), A-069

Sunaert S.

The study of the human auditory system using combined fMRI and DTI at 3 T, C-1081

Sung D., Cho S., Kim Y., Chung K., Moon D., Kim J.

MR urethrography in complete posterior urethral stricture: Comparison with retrograde and/or voiding urethrography (SS 1807b), B-864

Sung D., Ahn K., Cho S., Kim Y., Chung K., Kim J.

Female genitalia on MR imaging: The comparison of premenopausal and postmenopausal women, C-0416

Sutton L.

PACS pitfalls: A typical PACS implementation: More than just the image! Organisational and infrastructural considerations (SF 9b), A-229

Szafirska M., Urbanik A., Swierczyna A.,

Kwiatkowski S., Sztuk S., Herman-Sucharska I. MR CSF-flow examination in children with a ventriculo peritoneal shunt: The differentiation of shunt dependent and shunt independent hydrocephalus, C-0843

Szentgyörgyi R.

The present and future of Hungarian radiology: Contribution of a new generation: Radiological diagnosis and treatment of carotid artery stenosis (EM 2), A-252

Szeszkowski W., Golebiowski M., Janik P.

MR proton spectroscopy of the brain in Tourette syndrome (SS 211), B-098

Sziklai I.

Radiological vascular interventions: A. Aneurysms and vascular malformations (RC 911), A-225

Szurowska E., Pienkowska J.,

Izycka-Swieszewska E., Rzepko R.,

Czarnowska M., Studniarek M.

Differentiation of hemangiomas nonspecific at ultrasonography from malignant hepatic tumors: Comparison of the abilities of unenhanced and gadolinium-enhanced MR imaging and multiphase spiral CT, C-0015

Authors' Index

Szurowska E., Pienkowska J., Izycza-Swieszewska E., Rutkowska B., Balas B., Studniarek M.

Characterization of focal liver lesions appearing non-specific at ultrasonography: Comparison of usefulness of multiphase spiral CT and MR imaging, C-0016

Szyszko T.A., Stetina Z., Ward C., Lindo D.

Association of isolated preauricular skin tags and renal anomalies in the local UK population, C-0904

T

Tack D.

Multislice CT of the thorax: B. Dose reduction in thoracic CT (RC 1204), A-279

Tajima H., Kumazaki T., Murata S., Nakazawa K., Fukunaga T., Watari J., Machida M., Yamamoto K., Fukasawa H.

Peripheral lung cancer: Screening and detection with low dose helical CT. Toshima trial, C-0308

Takagi R., Sato H., Hayashi H., Hidaka N., Yoshihara H., Kumazaki T.

Head/neck CT angiography and CT perfusion in the assessment of patients with carotid occlusion, C-0837

Takahashi N., Lee Y., Tsai D., Kamio S.

Improvement of visibility of the lentiform nucleus in CT images for diagnosis of acute middle cerebral artery infarction, C-0372

Takao S., Uetani M., Yamaguchi T., Kawahara Y.

Surface lesions of bone: A pictorial review, C-0662

Takao S., Uetani M., Yamaguchi T., Kawahara Y.

Juxta-articular bone marrow edema: Pattern approach on MR imaging, C-0709

Takeuchi M., Matsuzaki K., Uehara H., Nishitani H.

Ancient schwannoma of the female pelvis: Radiologic-pathologic correlation, C-0440

Tali E.T.

Degenerative disorders, tumors and infection of the spine: C. Infectious disease of the spine (CC 1617), A-368

Tamai K., Koyama T., Kido A., Umeoka S., Fujiwara T., Saga T., Fujii S., Togashi K.

MR features of physiologic and benign conditions of the ovary, C-0422

Tamai K., Koyama T., Tanaka S., Asato R., Umeoka S., Kido A., Saga T., Togashi K.

Utility of contrast-enhanced MR imaging with three-dimensional volumetric interpolated breath-hold examination (3D-VIBE) in preoperative staging of hypopharyngeal cancer, C-0534

Tamburini S., Irace C., Barresi D., De Franceschi S., Gnasso A.

Effects of intravenous iomeprol on common carotid and brachial artery blood flow and shear stress (SS 1806), B-880

Tan K.T., Aw-Yeang H.W., Bakshi D.

Atherosclerosis as an inflammatory disease: Implications for the interventional radiologist, C-1069

Tanaka T., Tsuchiya K., Nitta N., Furukawa A., Takahashi M., Murata K.

Clinical implication of phase contrast digital mammography using practical mammography equipment, C-0186

Tanaka J., Kuramochi A., Nishi N., Yuasa M.

Preoperative selective transarterial embolization therapy for diffuse plexiform neurofibroma of the skin: Our initial experiences, C-0592

Tanaka R., Sanada S., Okazaki N., Kobayashi T., Suzuki M., Matsui T., Hayashi N., Matsui O.

Computer analysis for the respiratory changes in X-ray translucency on chest radiographs using a dynamic flat-panel detector (FPD) system, C-0971

Tang X., Hsieh J., Hagiwara A., Nilsen R.A., Shaughnessy C., Williams E.C., Drapkin E.

Cone beam filtered back projection algorithms for image reconstruction in volumetric CT (SS 1413), B-665

Tanoue S., Kiyosue H., Hori Y., Okahara M., Sagara Y., Kashiwagi J., Mori H.

Paracavernous sinus venous structures: Anatomical variations and pathological conditions evaluated on fat suppressed 3D fast-gradient-echo MR imaging, C-0838

Tapp M.J.F., Ferrando J.R.

Virtual colonoscopy: The way our department is beginning the change from barium enemas to virtual colonoscopy, C-0104

Tarasow E., Wiercinska-Drapalo A., Jaroszewicz J., Walecki J., Alathiaki A.

Normalization of CNS metabolite disturbances in clinically asymptomatic HIV patients after HAART treatment. MRS study, C-0841

Tardivon A.

Breast MR imaging: C. Future trends: Technique, indications, contrast media (RC 102), A-013

Tarján Z.

The present and future of Hungarian radiology: Contribution of a new generation: Results of the virtual colonoscopy CAD project (EM 2), A-254

Tartari S., Zattoni L., Sacco A.

Subintimal angioplasty of infrapopliteal vessel occlusions in the treatment of critical limb ischaemia (SS 1409b), B-636

Taylor A.

Chest imaging: C. Cardiac MRI in children (RC 1212), A-295

Taylor S.A.

CT colonography and colon cancer: A. Epidemiology and evidence for screening (RC 1701), A-412

Teisseire A., Delhayé D., Bruzzi J.,

DElannoy-Deken V., Duhamel A., Rémy J., Rémy-Jardin M.

Multidetector-row CT of right ventricular function: Can it be integrated into a standard multislice CT angiogram of the chest? (SS 1004), B-477

Teisseire A., Delhayé D., Bruzzi J.,

Delannoy-Deken V., Duhamel A., Rémy J., Rémy-Jardin M.

Multidetector-row CT of right ventricular function: Impact of the methodological approach in the determination of the right ventricular ejection fraction (SS 1004), B-478

Tepel M.

Contrast-induced nephropathy: Patient demographics and risk (SY 10), E-44

ter Haar Romeny B.M.

State-of-the-art in information technology: Designing image analysis algorithms for molecular imaging (EF 1), A-120

ter Haar Romeny B.M.

Diagnostic workstations: The new super-assistants of the radiologist and surgeon: Diagnostic workstations: The new super-assistants of the radiologist and surgeon (Introduction) (E³ 1420), A-355

Terlecki P., Wronski J., Zubilewicz T., Kobusiewicz W., Stepien A., Przywara S., Feldo M., Mocarski S., Krupski W.

Evaluation of left kidney function in patients who have undergone abdominal aortic aneurysm (AAA) surgery with renal vein ligation, C-1046

Terlecki P., Mazur E., Niedzwiadek J., Zubilewicz T., Przywara S., Feldo M., Koziol-Montewka M., Krupski W., Wronski J.

Evaluation of antibiotic therapy efficacy in patients with asymptomatic abdominal aortic aneurysm (AAA) and serological markers of chronic C. pneumoniae infection: Preliminary report, C-1060

Teschner M., Heidelberger B., Müller M.

Towards hysteroscopy simulation: Interactive simulation components for deformable tetrahedral meshes (IM 1), D-16

Testempassi E., Vantali V., Kartakis N., Chondros D.

Radiological manifestations of suicide attempt. A multisystem and multimodality approach, C-0825

Tettoni S., Scarrone A., Pedrazzini F., Priotto R., Gallarato G., Grossi M.

Percutaneous revascularization of popliteal and infrapopliteal arteries, C-0591

Teubner J.

Radiopathological correlation: B. Size and vascularity (RC 1602), A-374

Tezapsidis G., Manolitsas A., Tarazi L., Tsitouridis I.

Registration and fusion of CT and MR 3D models in patients with brain tumours, C-0985

Thanos L., Mylona S., Sakaridis N., Karahaliou E., Kokkinaki A., Batakis N.

CT-guided radiofrequency thermal ablation (RFA) of primary and metastatic lung tumours, C-0349

Thanos L., Mylona S., Pomoni M., Kokkinaki A., Karahaliou E., Batakis N.

Renal carcinoma: Therapeutic management with radiofrequency thermal ablation (RFA) under CT-guidance, C-0451

Thanos L., Mylona S., Karahaliou E., Pomoni M., Kokkinaki A., Batakis N.

Non-liver metastases in patients with primary gastrointestinal carcinoma. Treatment with radiofrequency thermal ablation, C-0619

Thanos L., Nikita A., Papaioannou G., Malagari K., Logitsi D., Kelekis D.

Percutaneous CT-guided drainage of abdominal and pelvic abscesses, C-0624

Thanos L., Nikita A., Papaioannou G., Danassi-Afentaki D., Kampanarou S., Kelekis D.

Radiofrequency ablation of liver tumors developed after hepatectomy, C-0625

Theocharopoulos N., Damilakis J., Perisinakis K., Papadokostakis G., Hadjipavlou A., Gourtsoyiannis N.

Embryo/fetal doses and risks from fluoroscopically assisted kyphoplasty during pregnancy (SS 1513), B-771

Authors' Index

- Thoeny H.C., De Keyzer F., Vandecaveye V., Chen F., Boesch C., Ni Y., Landuyt W., Marchal G., Hermans R.**
Dynamic contrast-enhanced MRI or diffusion-weighted MRI for monitoring the effect of a vascular targeting agent on rodent tumors? (SS 615), B-338
- Thomas A.M.K.**
History of contrast media: The early years of contrast media (SF 4c), A-077
- Thrall J.H.**
Building an electronic patient record system: B. Speech recognition (RC 1205), A-303
- Thuerl C., Husarik D.B., von Schultheiss G.K., Hany T.F.**
FDG PET/CT in staging of esophageal carcinoma (SS 201a), B-013
- Thurnher S.A.**
MRA of the carotid arteries (SY 5), E-17
- Thurnher M.M.**
Ischemic stroke: A. Imaging in acute stroke (CC 117), A-001
- Tillich M.**
Optimized imaging of pulmonary embolism (SY 9), E-41
- Tinazzi Martini P., D'Onofrio M., Pregarz M., Zamboni G., Mansueti G.**
Digital subtraction MDCT (DS-MDCT): Impact in liver imaging, C-0026
- Tjønneland R., Lagesen B., Andersen J.**
Strategy for redesigning workflow (SS 1814), B-911
- Todd-Pokropek A.**
Medical image registration: Methods, applications and validation: C. Strategies for validation (RC 913), A-246
- Todua F., Jvarsheishvili L., Tsvitsivadze G.**
US and CT in the detection and differentiation of peritoneal carcinomatosis and tuberculous peritonitis, C-0070
- Todua F., Razmadze M., Tsvitsivadze G., Kakhadze S.**
CT and MR imaging of benign primary cardiac neoplasms with echocardiographic correlation, C-0235
- Todua F., Razmadze M., Tsvitsivadze G.**
Role of spiral CT in detection of intramural aortic hematomas and in selection of treatment tactics, C-1004
- Tomandi B.F.**
Subtraction CTA in head and neck imaging (SY 12), E-53
- Tombach B.**
Performance of high-concentrated contrast in MR imaging (SY 2), E-06
- Tomura N., Izumi J., Otani T., Sakuma I., Takahashi S., Watarai J.**
Diffusion changes in tumor and peritumoral brain regions following stereotactic irradiation for brain tumors (SS 1011), B-538
- Torreggiani W., Browne R.**
Modern imaging of infective disease in the face and pelvis: B. Urinary infection (CC 916), A-242
- Torricelli P., Cinquantini F., Ligabue G., Fiocchi F., Romagnoli R.**
Comparison of 3 T body-coil MRI and endorectal coil 1.5 MRI in evaluating prostate cancer (SS 1007), B-492
- Toso F., Vergendo M., Ciccarese G., Como G., Del Frate C., Bazzocchi M.**
Correlation between radiologic and pathologic TNM using MDCT in staging of renal masses (SS 707), B-397
- Toso F., Ciccarese G., Vergendo M., Girometti R., Del Frate C., Zuiani C., Bazzocchi M.**
Multidetector CT of kidneys: Vascular collateral findings in pre-surgical management of renal masses (SS 1407), B-618
- Tosun A., Kartel A., Cakir B.**
Three-dimensional CISS sequence: Use in the evaluation of intra- and extra-axial brain masses, C-0817
- Tot T.**
Radiopathological correlation: A. Tumoral growth (RC 1602), A-373
- Tóth G., Tóth L., Forgács B., Tarján Z., Makó E.K.**
Small and large bowel virtual colonoscopy in patients with Crohn's disease, C-0141
- Tounan T., Fujimoto K., Azuma S., Uchida M., Hayabuchi N., Ono N., Matsushita S.**
Small well-differentiated hepatocellular carcinoma and atypical adenomatous hyperplasia (= 2 cm) evaluated with contrast-enhanced dynamic CT and ferucarbotran-enhanced MR imaging, C-0392
- Treitl M., Rieger J., Weber C., Wirth S., Pfeifer K., Reiser M.F.**
Impact of intravascular ultrasound (IVUS) on balloon sizing for interventional treatment of atherosclerotic superficial femoral artery (SFA) lesions (SS 1409b), B-630
- Tresoldi S., Borzani I., Valsecchi C., Midulla M., Flor N., Sardanelli F., Cornalba G.P.**
Liver metastases on serial contrast-enhanced MDCT examinations. Retrospective analysis of the previous examination: Were they detectable? (SS 701b), B-411
- Treutenaere J., Bernasconi T., Renard C., Auquier M., Remond A.**
Multidetector row CT angiography of the abdominal aorta and lower extremities: Post-processing and arterial wall calcification removal, C-1003
- Triantopoulou C., Maniatis P., Lytras D., Sifas I., Manes K., Papailiou J., Dervenis C., Chrysostomou D.**
CT imaging based scores as predictors of severity in acute pancreatitis: A comparative study with statistical evaluation, C-0052
- Triviño F., Benito A., Pérez G., Ysamat R., Zurera L., Cara M., Canis M.**
Multidetector CT of pulmonary vascular abnormalities in the adult, C-0330
- Trojanowska A., Drop A., Jarosz B., Jargiello T., Wronski J.**
Determination of components in atherosclerotic plaques from human carotid endarterectomy specimens by multislice computed tomography imaging ex vivo (SS 215), B-112
- Trojanowska A., Czekajska-Chehab E., Trojanowski P., Olszanski W., Golabek W., Drop A.**
Comparison of multislice CT (MSCT) cross-sectional source images with multiplanar 2D-, 3D-reconstructions and virtual endoscopy in the assessment of middle ear diseases (SS 608), B-274
- Tropine A., Gawehn J., Dellani P.D., Glaser M., Bohl J., Stoeter P.**
Differentiation of benign subtypes of meningiomas by diffusion tensor imaging-based calculation of tensor shape (SS 1011), B-532
- Trost R., Reichenbach J., Hilger I., Lisy M., Schueler D., Sedlack J., Rauscher A., Kaiser W.A.**
Relaxation determination of magnetically labelled macrophages (SS 1506b), B-783
- Trumm C.G., Glaser C., Paasche V., Popp P., Küttner B., Reiser M.F.**
Improvement of hospital-wide radiology report availability by implementation of a fully PACS/RIS integrated speech recognition system (SS 305), B-232
- Truyen R., Medved M., Schoonenberg G.A.F., van Gelder R.E.**
Large evaluation of fully automatic colon tracker for CT colonoscopy (SS 605), B-326
- Trzeszkowska-Rotkiewicz S., Skrzewski S., Glowacki J., Tarnawski M., Pisulski-Otremba A., Borowiak H., Legaszewski T.**
Three-dimensional reconstruction of spiral, multidetector images from computer tomography in diagnosing innate and acquired anomalies of facial skeleton, C-0564
- Tsantis S., Glotsos D., Kalatzis I., Piliouras N., Spyridonos P., Dimitropoulos N., Nikiforidis G., Cavouras D.**
Computer-assisted diagnosis of thyroid nodules malignancy risk, C-0355
- Tsapaki V., Triantopoulou C., Maniatis P., Sifas I., Chrysostomou D., Koukkou P., Koulentianos E., Papailiou J.**
The effect of patient weight on image noise in thoracic and abdominal CT: Dosimetric analysis and clinical applications, C-0962
- Tschampa H.J., Kallenberg K., Zerr I., Meissner B., Kretzschmar H.A., Knauth M., Urbach H.**
Clinical diagnosis of sporadic Creutzfeldt-Jakob disease: Reliability of MRI and comparison with EEG and 14-3-3 protein analysis (SS 211), B-096
- Tsili A.C., Tsampoulas C., Katzioti F., Giannakis D., Silakos A., Sofikitis N., Efremidis S.C.**
Multi-detector row CT urography in the evaluation of painless hematuria (SS 1407), B-617
- Tsili A.C., Tsampoulas C., Katzioti F., Giannakis D., Silakos A., Sofikitis N., Efremidis S.C.**
Multi-detector row CT cystoscopy in the evaluation of urinary bladder neoplasms (SS 1507), B-727
- Tsili A.C., Tsampoulas C., Katzioti F., Arkoumani E., Tzioras S., Mpougias C., Paraskevaidis E., Efremidis S.C.**
Magnetic resonance imaging in the characterization of ovarian masses, C-0438
- Tsuchiya K., Fujikawa A., Honya K., Nakajima M., Nitatori T., Takemoto S.**
MR digital subtraction angiography using parallel imaging in the diagnosis of vasospasm after subarachnoid hemorrhage (SS 611), B-319

Authors' Index

Tsujioka K., Akino N., Takahashi Y., Niwa M., Uebayashi Y.

Time resolution and phase time resolution in ECG gated reconstruction using multislice CT (SS 1803), B-823

Tucker J.

Battlefield CR: (M-CR, military CR?) (SY 8), E-35

Tuncbilek N., Okten O., Sezer H., Tokatli F., Kaldir M.

Computed tomographic evaluation of serosal invasion and regional lymph node metastasis in colorectal adenocarcinomas, C-0158

Tuncbilek N., Okten O., Sezer H., Tokatli F.

Staging of gastric cancers by computed tomography, C-0159

Tuncbilek N., Kaplan M., Semsi A., Okten O.O., Atakan I., Inci O.

The analytical value of the dynamic MRI semiquantitative parameters in detecting the stage and grade of bladder cancers, C-0520

Tuohy B., Keavey E., Finlay L., McGarrigle A., Daly K., Crowley J., Van Der Putten W.

Evaluation of the performance of two digital "flat panel" cardiac imaging systems using the NEMA cardiac benchmarking phantom, C-0968

Turgut A.T., Cakal E., Birincioglu P., Kosar U., Demirbas B., Aral Y.

Color Doppler ultrasonography findings in hypothyroidism, C-0551

Turgut A.T., Cakal E., Kosar U., Birincioglu P., Demirbas B.

A new parameter for the evaluation of the efficacy of medical treatment in hypothyroidism: Color Doppler measurement of blood flow in the inferior thyroidal artery, C-0552

Tzalonikou M., Athanasopoulou Z.,

Chatzopoulou M., Papoudos M.,

Polymeropoulos V., Papadopoulos V.,

Stringaris K.

MDCT of the acute abdomen: A pictorial essay, C-0076

Tzalonikou M., Foteinos A.,

Athanasopoulou Z., Iliadis C., Mpouchlis G.,

Stringaris K.

Clinically significant cases of wrist pathology: MR appearance. Correlation with surgical findings, C-0706

Tzedakis A., Damilakis J., Perisinakis K., Stratakis J., Gourtsoyiannis N.

Effect of a multislice scanner on patient effective dose: A Monte Carlo study, C-0976

Tzovara J., Papadopoulou F., Anthopoulos A., Siomou E., Arkoumani E., Efremidis S.

Voiding urosonography combined with fluoroscopic voiding cystourethrography in the diagnosis of reflux: Does the order matter? (SS 1812), B-894

U

U-King-Im J.M., Trivedi R.A., Graves M.J.,

Kirkpatrick P.J., Antoun N.M., Gillard J.H.

Characterisation of carotid atheroma in symptomatic and asymptomatic patients using high-resolution gadolinium-enhanced MRI, C-1078

Ucar M., Özdemir A.

Standardization of BMD measurements in different DXA devices, C-0668

Uchida K., Oda K., Kajitani T., Fukuba E., Wada A., Kitagaki H.

High-speed 2D MR cerebral venography using spiral spoiled gradient-echo sequence, C-1034

Uematsu T., Yuen S., Ikuma H., Seki A., Aramaki T., Morimoto N., Endou M., Furukawa H.

The role of CT in local staging of breast cancer, C-0222

Uematsu H.

T1 and T2 characterization in the brain during hyperoxia at 9.4 T, C-0805

Uematsu H., Tsuchida T., Kimura H., Toyooka M., Itoh H.

Assessment of tissue characterization of gliomas: Comparison of tumor blood volume by perfusion-weighted MR imaging and TI-201 SPECT, C-0836

Uffmann M., Ba-Ssalamah A., Schaefer-Prokop C., Mehrain S., Raderer M., Prokop M.

Hydro-multidetector CT in patients with gastric and duodenal lymphoma: Correlation with histopathological results (SS 201a), B-016

Ukimura O.

Feasibility and clinical utility of real-time virtual sonography (RVS) for percutaneous radio frequency ablation of renal tumor (SY 1), E-04

Umarova R.M., Krotenkova M.V., Tanashyan M.M., Chernikova L.A., Konovalov R.

The assessment of early neurorehabilitation effectiveness with MRI, C-0871

Umek W.H., Preyer O., Sora M.C., Ba-ssalamah A., Mlynarik V., Trattning S., Pinker K.

Strategy for self-directed learning of female pelvic floor anatomy from cadaver cross-sections and magnetic resonance images, C-0497

Umetani K., Kobatake M., Yamamoto A., Yamashita T., Imai S., Kajihara Y.

Synchrotron radiation microangiographic imaging of tumor-derived blood vessels in rabbit model of cancer for observation of angiogenic activity, C-0940

Umschaden H.

MR imaging of the small intestine: Clinical results in non-inflammatory small intestinal disorders (SF 13), A-316

Unsinn K.M., Freund M.C., Rieger M., Czermak B., Koenigsrainer A., Margreiter R., Jaschke W.R.

Intestinal transplantation: Imaging findings of posttransplantation anatomy and pathology, C-0087

Urbach H.

Epilepsy, white matter diseases and ageing: A. Epilepsy (CC 817), A-162

Urbanik A., Aleksandrowicz J., Binder M., Chrzan R., Sobiecka B., Kozub J.

The fMRI study of hypnotic suggestion during pain stimulation, C-0808

Usami H., Ikeda M., Ishigaki T., Fukushima H., Shimamoto K.

Influence of liquid crystal display (LCD) monitors on observer performance for detection of nodular lesions on chest radiographs, C-0956

Ustuzhanin D., Kozhuhova M., Sinitsyn V., Pustovitova T., Stukalova O., Chazova I., Ternovoy S.

Quantitative assessment of brain perfusion by MRI in patients with arterial hypertension, C-0872

V

Vakaki M., Pitsoulakis G., Dermentzoglou V., Begli V., Koumanidou C.

Uncomplicated versus tortuous testicular appendages in childhood: Sonographic appearances with embryologic correlation, C-0899

Vakaki M., Pitsoulakis G., Dermentzoglou V., Manoli V., Koumanidou C.

Range of sonographic appearances of the normal breast in children and young adolescents, C-0900

Vakaki M., Pitsoulakis G., Kosmas C., Christopoulos P., Koumanidou C.

Incomplete obliteration of canal of Nuck and processus vaginalis: Sonographic diagnosis with embryological correlation, C-0921

Vakaki M., Pitsoulakis G., Dermentzoglou V., Kosmas C., Koumanidou C.

Abdominal sonographic examination in the pediatric emergency room and incidental findings, C-0932

Vakaki M., Pitsoulakis G., Dermentzoglou V., Tsiarta M., Emmanouil E., Koumanidou C.

Soft tissue swelling of the hand or foot in childhood: The role of sonography, C-0933

Valle M., Bacigalupo L., Pugliese F., Toma' P., Bianchi S., Martinoli C.

High-resolution ultrasound of angled buckle fractures in children, C-0902

Valls C.

Liver imaging: Characterisation and pitfalls: B. Fat (RC 501), A-112

van Beek E.J.R.

Venous imaging and intervention: A. CT of thromboembolic disease (RC 515), A-127

Van Breuseghem I., Van Mieghem I.M., Vandereist L., Bosmans H.T.C.

Validation of tMix estimated T1-T2 values in correlation with relaxometry determined values in a phantom (SS 1510), B-682

Van Breuseghem I., Van Mieghem I.M., Peeters R.R., Bosmans H.T.C., Marchal G.J.

Tmix imaging as alternative for femoro-tibial cartilage T2 mapping at 1.5 T (SS 1813), B-922

van Buchem M.A.

Epilepsy, white matter diseases and ageing: C. Normal ageing and neurodegenerative diseases (CC 817), A-164

van der Molen A.J., Geleijns J.

Extra tube rotations (Z-overscanning) in helical multislice computed tomography of the body: Relative effects on organ doses of the thyroid and testicles, and on effective dose (SS 713), B-447

van der Molen A.J., Geleijns J.

Dose in multislice computed tomography: A comparative study on five scanners and correlation to a recent field study (SS 713), B-448

van der Putten W., Gallagher J., Woulfe P.

A novel method to manufacture anatomically correct phantoms for projection radiography (SS 1513), B-773

Authors' Index

- van der Schaaf I., Hoff R., Rinkel G., van Dijk G., Vethuis B.**
CT perfusion in the acute stage of SAH: Relationship to the development of delayed cerebral ischemia (SS 611), B-313
- Van der Zijden T., De Backer A.I., Vanhoenacker F.M., Parizel P.M.**
Tuberculosis of the spine: CT and MR imaging features, C-0746
- Van Goethem J.W.**
Craniocerebral and spinal trauma: C. Spine trauma (CC 1317), A-309
- Van Goethem M.L.A., Schelfout K., Colpaert C., Kersschot E., Verslegers I., Biltjes I., De Schepper A., Weyler J., Parizel P.**
MR mammography of enhancing breast masses: Can MR predict carcinomas with a fibrotic focus?, C-0191
- Van Mieghem I.M., Frans F., Van Breuseghem I.**
The value of three dimensional dual echo in steady state MR imaging (3D-DESS) as a standard technique in the evaluation of knee internal derangement (SS 1510), B-684
- Van Ongeval C., Van Steen A., Celis V., Van Goethem M., Verslegers I., Joossens K., Marchal G.**
Clinical study to evaluate the diagnostic value of AGFA CR system: Comparison of mammographic hardcopy images to screen-film mammographic images (SS 302), B-159
- van Ooijen P.M.A., ten Bhomer P., Oudkerk M.**
Dicom storage into PACS of out-hospital CD-ROMS (SS 305), B-237
- van Ooijen P.M.A., Dorgelo J., Zijlstra F., Oudkerk M.**
Anomalous coronary anatomy using multi detector computed tomography, C-0275
- Vanbeckevoort D.**
Imaging of the pancreas: Key questions: A. The choice: US/EUS, CT, MRI (RC 1301), A-321
- Vandervliet E.J.M., Özsarlar Ö., Maes M., Van Goethem J., Parizel P.M.**
BOLD functional MRI in simple motor tasks and equivalent motor imagery (SS 1811b), B-931
- Vanhoenacker F.M.H.M., DeBacker A.I., Parizel P.M.**
Gastrointestinal infection: A changing scene: B. Gastrointestinal and abdominal tuberculosis (CC 516), A-134
- VanMetter R., Fletcher-Heath L.**
Characterization of CDMAM image observers (SS 1013), B-548
- Vano E.**
Quality control and dose reduction in digital radiology: B. Managing patient dose in digital radiology (RC 1313), A-348
- Vano E., Fernandez J.M., Ten J.I., Prieto C., Gonzalez L., Rodriguez R.**
A six year follow-up of patient dose values: Transition from conventional to digital in projection radiography (SS 1513), B-770
- Varga A., Forrai G.**
CT diagnosis of pulmonary aspergilloses in hematological diseases, C-0318
- Vasconcelos C., Félix A., Cunha T.M.**
Preoperative assessment of deep myometrial and cervical invasion in endometrial carcinoma: Comparison of magnetic resonance imaging and histopathologic evaluation, C-0423
- Vasic-Vilic J., Prodanovic N., Jovanovic-Nikolic O., Radovinovic-Tasic S., Vukomanovic B.**
The role of bone mineral density and risk factors with gonarthritis patients, C-0676
- Vasilyev A.Y., Vykylyuk M.V., Gipp I.N.**
Radiodiagnosis for hip and shin prosthesis after mine explosion and gunshot wounds, C-0991
- Veillon F.**
Three common neurological problems: Loss of vision, hearing loss, trigeminal and facial nerve palsy: B. Sensorineural hearing loss (CC 917), A-206
- Veillon F.**
Imaging of skull base tumors: A practical approach for your daily practice: C. Temporal bone (RC 1608), A-384
- Veit P., Kuehle C., Herborn C., Stergar H., Beyer T., Bockisch A., Kuehl H., Antoch G.**
Accuracy of combined PET/CT in image-guided interventions of liver malignancies: An ex-vivo study (SS 209b), B-079
- Veit P., Saoudi N., Freudenberg L.S., Kuehl H., Beyer T., Bockisch A., Antoch G.**
Accuracy of whole-body FDG-PET/CT for tumor staging in oncology (SS 1406), B-677
- Veltman J., Boetes C., Blickman J., Barentsz J.O.**
MRI guided localisation of breast lesion (SS 1502), B-731
- Veltman J., Boetes C., Kok T., Obdeijn I., Manoliu R., Besnard P., Zonderland H., Blickman J., Barentsz J.O.**
MRI breast tumor characteristics of BRCA1 and BRCA2 gene mutation carriers (SS 1802), B-837
- Venkatesh S.K., Wang S.**
Severity assessment and quantification of pulmonary embolism with CT pulmonary angiography as a predictor of patient outcome (SS 1404), B-598
- Venkatesh S.K., Lau G.B.H., Wang S.**
Coeliac trunk and its variants: Demonstration with CT, C-1048
- Venturi G., Selvaggio S., Fiumicelli A., Budge A., Bull C., Shaw R., Wilson P., Chippendale A.**
Interoperability solutions for an integrated imaging and information system (IM 1), D-17
- Venturini M., D'Ascenzo F., Bianchi Marzoli S., Simionato F., Scotti G., Del Maschio A.**
Non invasive diagnosis with orbital color Doppler (OCD) of carotid cavernous sinus fistulas (CCSF): Personal experience in 20 cases (SS 1811a), B-907
- Vergendo M., Toso F., Del Frate C., Zuiani C., Padovani R., Bazzocchi M.**
URO-CT vs IVU: Optimisation of URO-CT protocol with multislice CT (MSCT), comparing doses with conventional intravenous urography (SS 1407), B-613
- Verius M., Huttary R., Recheis W., Eisner W., Felber S., zur Nedden D.**
Fused deposition modeling for operation planning, multimodal matching of functional and anatomical data and development of a lung atlas/model (IM 1), D-18
- Verma R.K., Pfeffer J.E., Günther R.W., Schmitz-Rode T.**
Development and experimental testing of a percutaneous temporary pulmonary stent device for severe pulmonary embolism (SS 209b), B-080
- Verma R.K., Pfeffer J.E., Günther R.W., Schmitz-Rode T.**
Development and animal experimental testing of a percutaneous thrombectomy device (SS 309b), B-208
- Verschakelen J.A.**
Airways and infection: A. Airway disorders and hypoluent lungs (E³ 520), A-142
- Vieth V., Langer M., Stehling C., Kraemer S., Kooijmann H., Kugel H., Heindel W., Bachmann R.**
High resolution imaging of the human wrist at 3.0 Tesla: A comparative study of carpal ligaments and TFCC in normal volunteers (SS 1410), B-569
- Vignaux O.**
Cardiomyopathies: B. Restrictive cardiomyopathy (RC 403), A-067
- Vikram R., Ripley C., Zealley I.**
An anatomical study of retro-renal peritoneal extension and implications for safe percutaneous renal intervention (SS 1807b), B-866
- Vilanova J.C., Barcelo J., Villalon M.**
An advanced method of computer aided evaluation applied to breast MRI: A useful tool both for the radiologist analysis and for the diagnostic accuracy, C-0196
- Vilanova J.C., Barceló J., Pujol J., Villalón M.**
Dynamic phono-articulation tract assessment by gated MRI, C-0545
- Vilanova J.C., Barceló J., Villalón M., Miró J.**
Soft-tissue vascular malformations: MR and MR angiographic imaging with pathologic correlation, C-0730
- Vinhais S., Félix A., Cunha T.M.**
Posttreatment complications of gynecologic cancer, C-0424
- Vit A., De Candia A., Piccoli G., Smania S., Marzio A., Bazzocchi M., Gasparini D.**
Intermediate follow-up of stented carotid arteries: Is it possible to define reliable ultrasound velocity criteria? (SS 715), B-457
- Vladica P., Sabharwal R.**
Renal tumours: Technical success and early clinical experience with radio-frequency ablation of 18 tumours, C-0446
- Vladica P., Sabharwal R.**
Multidetector spiral CT renal angiography in the diagnosis of renal artery fibromuscular dysplasia, C-1008
- Vliegenthart R., van Iersel C., Xu D., Wang Y., van Klaveren R.J., de Koning H.J., Prokop M., Mali W.P.T.M., Oudkerk M.**
Trial design and first screening results from the Dutch-Belgian trial on lung cancer screening by spiral CT (NELSON study) (SS 704), B-381

Authors' Index

Vogl T.J., Hammerstingl R.M.
Abdominal MDCT: Protocols and contrast considerations (SY 9), E-43

Vogl T.J.
Rectal carcinoma: Post-treatment follow-up (SF 4a), A-058

Vogl T.J., Mack M.
Interactive image teaching: Paranasal sinuses (E³ 1320), A-350

Vogl T.J., Bisdas S.

How to investigate facial pain: A. Neuralgia and uncommon causes (RC 1708), A-421

Vogl T., Li J., Mack M., Lehnert T., Eichler K., Ghazy H., Wang Y.
MR-guided laser induced thermotherapy (LITT) for retroperitoneal lymph nodal metastases (SS 709), B-408

Vogl T., Li J., Lehnert T., Wang Y., Mack M.
CT-guided radiofrequency ablation (RF) for lung metastases (SS 1409a), B-629

Vogt F.M., Veit P., Freudenberg L., Rühm S.G., Barkhausen J., Antoch G.

Comparison of whole-body PET/CT and whole-body MRI in patients with newly diagnosed non-small cell lung cancer: Initial results (SS 1804), B-840

Volpini F., Ghirardo D., Scarrone A., Mondino I., Grosso M.

Percutaneous treatment of pulmonary arteriovenous malformations (PAVM), C-0570

Vomweg T.W., Hintze C., Mayer D., Faber H., Grossi E., Teifke A., Achenbach T., Rieker O., Thelen M.

A novel non-rigid mono-modal registration algorithm reducing motion artefacts at CE MR investigations (SS 205), B-104

Vomweg T.W., Buscema M., Grossi E., Mayer D., Faber H., Hintze C., Mattiuzzi M., Terzi S., Intraligi M.

CADMRM: A prototype software for automatic computer aided detection and classification of lesions in contrast-enhanced MR-mammography (SS 702), B-376

von Schultheiss G.K.

Imaging of lung cancer: C. Staging and follow-up with PET/PET-CT (RC 804), A-180

von Schultheiss G.K.

Molecular imaging: A. Molecular imaging with PET (RC 1306), A-324

von Tengg-Kobligk H., Ganter M., Boeckler D., Fink C., Zaporozhan J., Giesel F.L., Delorme S., Kauczor H.

Endograft placement for aortic aneurysms and dissections: Pre and post evaluation using MDCT angiography: How to do it, C-1000

Votruba J., Belohlavek O.

The role of FDG PET and PET/CT in differential diagnostics of pancreatic lesions (SS 701b), B-417

Voutetakis A., Sertedaki A.,

Maniati-Christidi M., Kiortsis D., Bossis I., Dacou-Voutetakis C., Argyropoulou M.I.

Magnetization transfer imaging of the pituitary gland in patients with Prop1 gene mutations discloses a well-defined "mass" with normal secretory activity within the pituitary (SS 1412), B-647

W

Waaijer A., van Leeuwen M.S., Olree M., Niessen W., Prokop M.

Grading of carotid artery stenosis: Should we use estimation or measurement? (SS 715), B-451

Waaijer A., Lo T.H., Witkamp T.H., Prokop M.
Occurrence of focal ischaemia after carotid artery stenting without using a neuroprotection device (SS 1009b), B-518

Waaijer A., Velthuis B.K., Bakker C.J.G., de Kort G.A.P., van Leeuwen M.S.

Improvement of CTA of the circle of Willis by using lower tube voltage (SS 1811a), B-903

Wada A., Hayashi T., Katsume T., Fukuba E., Matsuo M., Kitagaki H.

Early diagnosis of postoperative empyema in brain and spine: Use and pitfalls of MR imaging, C-0839

Wade C.K., McEntee M.F., Brennan P.C.
An assessment of the performance of PACS workstation monitors in Ireland, C-0959

Wagner S., Müller-Gerbl M., Weckbach A.

The influence of posterior instrumentation on adjacent and transfixed facet joints in patients with thoracolumbar spinal injuries: A morphological *in vivo* study using computed tomography osteoabsorptiometry (CT-OAM) (SS 610), B-255

Wald C., Bourquain H., Pomposelli J., Peitgen H., Pomfret E.

A novel method for analysis of postoperative liver regeneration in the adult live liver donor (SS 301b), B-179

Waldt S., Woertler K., Metz S., Rummeny E.J.

Variants of the superior labrum and labro-bicipital complex: A comparative study in shoulder specimens using MR arthrography, multi-slice CT arthrography, and anatomic dissection (SS 610), B-259

Walecka A., Sawicki M., Brzosko M., Ostanek L., Fischer K., Kordowski J.

Value of high resistance index - HRI calculated from Doppler spectrum of popliteal arteries in patients with systemic lupus erythematosus (SLE) (SS 615), B-335

Walker W.J., Carpenter T.T.

Pregnancy outcome following uterine artery embolisation (SS 1809), B-872

Wallis M.G.

Diagnostic highlights: B. HRT and other hormone risk markers (RC 902), A-216

Walter C.

Contrast enhanced MRA and perfusion imaging (1) Non invasive assessment of carotid stenosis: MRA and perfusion imaging (SY 6), E-21

Waltering K., Schlosser T., Gaida K., Bruder O., Hunold P., Barkhausen J.

Contrast enhanced magnetic resonance imaging of acute myocardial infarction: Optimization of image contrast (SS 303), B-211

Waltering K., Nassenstein K., Massing S., Schlosser T., Hunold P., Barkhausen J.

Coronary magnetic resonance angiography using parallel acquisition techniques and intravascular contrast media (SS 1403), B-654

Wang Y., Jin Z., Kong L., Jiang J., Xue H., Zhang Z., Ge Q.

The association of low-dose sex hormone replacement therapy and coronary artery disease as determined by multi-slice spiral computed tomography (SS 603), B-303

Wang Y., Jin Z., Kong L., Zhang Z., Zhang S., Lin S.

Coronary angiography with 16-slice spiral computed tomography: Results in 180 patients (SS 703a), B-347

Wang S., Ericson K., Jorgen B.

How much can a negative FDG-PET be trusted? (SS 711), B-437

Wang Y., Cheung P., Shen G.X., Wu E.X., Cao G., Khong P.

Hypoxic-ischemic (HI) brain injury in neonatal rats: The relationship between early post HI apparent diffusion coefficient (ADC) and irreversible infarction (SS 1412), B-642

Wang Z., Yang Z., Shen J., Zhu H., Zhou X., Fang W.

Anomalous origin of coronary arteries: Demonstration with MSCT coronary angiography, C-0261

Warbey V.S., Mullen M., Padley S.P.

Catheter deployed devices in adults with congenital heart disease: A radiological perspective of normal appearances and complications, C-0234

Watanabe Y., Sugimoto H.

Development of collateral channels after successful transcatheter gastric variceal embolization: Assessment by CT and endoscopic examinations, C-0593

Watanabe Y., Kodama Y., Sawada A., Sakuhara Y., Abo D., Funakubo M., Sugimoto H., Miyasaka K.

Interventional procedures of acute retroperitoneal hemorrhage, especially renal and pancreatic hemorrhage, C-0594

Wawrynek W., Baron J., Kasprowska S., Siemianowicz A., Koczy B., Boldysh H.

Advantages of virtual 3D Digital Subtraction Angiography option and "cut" function for imaging of the neck of aneurysm of the Willis' circle with complicated morphology, C-0573

Wawrynek W., Koczy B., Widuchowski J., Kasprowska S., Siemianowicz A., Majer R., Baron J., Krol A.

Routine ultrasound diagnostic of the most frequently injured muscles of professional football players from the transfer list, C-0735

Weaver J.S., Jacobson J.A., De Maeseneer M., Kalume Brigido M., Morag Y., Jamadar D.A.

MR imaging of traumatic elbow injuries with arthrographic, sonographic, clinical and surgical correlation, C-0681

Weber C., Krupski G., Seitz U., Kuhlencordt R., Rogiers X., Adam G.

MRCP in primary sclerosing cholangitis (SS 301b), B-171

Wedegärtner U., Tchirikov M., Schäfer S., Priest A., Schröder H., Adam G.

Functional MRI (BOLD) at 3 Tesla in the brain of fetal sheep: The relation to maternal blood oxygenation during hypoxia and methodological aspects (SS 1512), B-755

Authors' Index

- Wedekind N., Roelofs A.A.J., Beck C., Boehm D., Hendriks J.H.C.L., Skaane P., Karssemeijer N., Everts C.J.G., Peitgen H.**
The impact of training on radiologists' performance in softcopy reading: A study from the European SCREEN-TRIAL project (SS 1802), B-830
- Wehrschatz M., Fritz G., Gallé G., Tillich M., Ruppert-Kohlmayr A.**
Demonstration of ureteral calculus by thick planar reformation of multislice CT (SS 1407), B-616
- Wehrschatz M., Deutschmann H., Aldrian U., Tillich M.**
How many biopsies are necessary in pulmonary nodules to obtain an adequate diagnostic accuracy?, C-0292
- Wei G., Yan F., Xu P., Cheng W., Zeng X., Qian J., Fan L., Liang C.**
Automatic registration of multiphase dynamic contrast multidetector CT (MDCT) studies for the diagnosis of small hepatocellular carcinoma (HCC) (SS 605), B-328
- Weiner G.M., Geiger B., Schulze K., Bilger J., Krebs P., Wolf K., Albrecht T.**
Modified CT-bronchoscopy as a guidance tool for bronchoscopic needle aspiration: A phantom study (SS 1804), B-844
- Weinmann H.**
History of contrast media: MRI contrast agents (SF 4c), A-080
- Weishaupt D.**
High-field body MRI: The new standard?: Musculoskeletal (SF 5), A-107
- Weishaupt D.**
Total imaging solution: Steps toward personalised healthcare: New trends in body MR imaging (SY 6), E-20
- Welsch G., Cavallaro A., Horger W., Menzel M., Bautz W., Mamisch T.C.**
Morphology of the acetabular labrum on MRI in comparison to the quality of corresponding cartilage (SS 710), B-358
- Wessels F.**
Exploiting the power of GPUs in medical imaging (IM 1), D-15
- Wetter A., Engl T., Nadjmabadi D., Lehnert T., Beeken W., Jonas D., Vogl T.J.**
Prospective evaluation of a routine protocol for combined magnetic resonance and ¹H-spectroscopic imaging of the prostate in patients prior to radical prostatectomy (SS 1507), B-723
- Whitby E.**
Emergencies in pediatrics: C. The asphyxiated newborn: Role of new MRI techniques (RC 1612), A-393
- Wick M.C., Rönnellid J., Lampa J., Lindblad S., Nordmark B., Klareskog L., van Vollenhoven R.F.**
Longitudinal analysis of anti-citrulline (anti-CCP) antibodies during 5 years of follow-up in early rheumatoid arthritis: Anti-CCP status is a stable phenotype that predicts greater radiological progression and worse disease activity (SS 1410), B-564
- Wickline S.A., Lanza G.M.**
MR approaches to molecular imaging: C. Targeted MR contrast agents (PR 819), A-203
- Wiener E., Wörtler K., Rechl H., Gerdesmeyer L., Rummey E.**
Labral lesions of the hip: Assessment with MR arthrography in symptomatic patients (SS 310), B-136
- Wikholm G.**
Radiological vascular interventions: B. Acute stroke and transarterial treatment (RC 911), A-226
- Wildberger J.E.**
Higher concentrations - where does it make sense (SY 7), E-28
- Willmann J.K., Baumert B., Schertler T., Wildermuth S., Pfammatter T., Marinsek B., Böhm T.**
Sixteen-row CT angiography for assessment of the aortoiliac and lower extremity arteries in patients with peripheral arterial disease: Prospective comparison with digital subtraction angiography (SS 315), B-241
- Wilms G.**
Cerebral tumors and infections: B. Intra-axial brain tumors (CC 517), A-099
- Wilson D.J.**
Musculoskeletal infection: C. Soft tissue infections (CC 816), A-200
- Wilson D.J., van Kuijk C.**
Interactive image teaching: Cervical spine trauma (E³ 1520), A-365
- Wintersperger B.J., Engelmann M.G., Theiss H., Reiser M.F., Franz W.M., Schoenberg S.O.**
Cine SSFP MR imaging after myocardial infarction: Impact of G-CSF stimulation of peripheral stem cells on cardiac function (SS 303), B-217
- Wintersperger B.J., Nikolaou K., Becker C.R., Ziegler F., Johnson T., Flohr T., Rist C., Knezev M.F.**
64-slice coronary CT angiography: Heart rate dependency of image quality at 0.33 s/360° gantry rotation (SS 703a), B-341
- Wintersperger B.J., Reeder S.B., Schoenberg S.O., Lanz T., Dietrich O., Huber A., Nittka M., Hayes C., Reiser M.F.**
High-resolution multi-slice evaluation of cardiac function with cine SSFP using a dedicated 32-element array-coil and parallel acquisition techniques (PAT) (SS 703b), B-429
- Wirth C., Reimer P., Schima W., Vestring T., Schoenberg S.O., Zech C., Robinson P.J., Study Group D.**
Does dual contrast MRI of the liver with ferucarbotran and gadolinium chelates improve the detection rate of focal liver lesions? Results of an investigator initiated prospective multicenter study (SS 201b), B-050
- Wirth S., Treitl M., Rieger J., Pfeifer K., Reiser M.F.**
Hard disk caches in PACS archives: How big is beautiful? (SS 305), B-233
- Wismueller A., Lange O., Leinsinger G., Meyer-Baese A., Auer D., Reiser M.F.**
How to determine the quality of unsupervised functional MRI data analysis methods? (SS 205), B-103
- Wismueller A., Leinsinger G., Meyer-Baese A., Wiegard R., Lange O., Schlossbauer T., Reiser M.F.**
Machine learning for computer-aided diagnosis in dynamic breast MRI: Can neural network analysis improve the diagnostic accuracy in suspicious lesions? (SS 605), B-321
- Witjes F.**
Imaging of prostate cancer: Present and future: Clinical questions (SA 14), A-352
- Witoszynskyj S., Rauscher A., Reichenbach J.R., Barth M.**
Quality maps for automated phase unwrapping of MR images (SS 205), B-102
- Witzani L., Hoermann M., Kasprian G., Balassy C., Brugge P., Prayer D.**
Investigation of normal renal development with fetal magnetic resonance imaging (SS 1812), B-893
- Woertler K., Settles M., Martinek V., Stollfuss J., Rummey E.J.**
Patellar osteochondral autograft transplantation: Assessment with high-resolution MR imaging at 1.5 T (SS 710), B-354
- Wolberink S.V.R.C., Beets-Tan R.G.H., de Haas-Kock D.F.M., Oudkerk M., Wiggers T.**
Multislice spiral CT for the prediction of an involved circumferential resection margin in primary rectal cancer (SS 301a), B-150
- Wormanns D., Beyer F., Hoffknecht P., Kuhnlk J., Dicken V., Lange T., Thomas M., Heindel W.**
Clinical value of CT-based, software-assisted preoperative prediction of postoperative pulmonary function after lung surgery (SS 704), B-386
- Wu R.H., Ducreux D., Lin R., Guo G., ter Brugge K., Mikulis D.J.**
Outer volume saturation bands improve spatial signal homogeneity in MR 2D chemical shift imaging (SS 1813), B-919
- Wu H., Feng G., Liang H.**
Lipiodol flowing into portal vein after arterial embolization: The influential factors and clinical significance, C-0598
- Wunderbaltinger P.**
Molecular imaging: C. Optical imaging (RC 1306), A-326
- Wuttge-Hannig A.C., Feussner H., Hannig C.E.M.**
Outcome after endoscopic surgical therapy for Zenker's diverticula (SS 1801a), B-812

X

- Xinou E., Boulogianni G., Chourmouzi D., Dedes I., Drevelegas A.**
Primary brain lymphomas: Distinctive imaging features, C-0826
- Ydys V.G., Zikou A.G., Astrakas L., Pantou K., Andronikou S., Argyropoulou M.I.**
Magnetization transfer ratio in the brain of preterm subjects: Age related changes during the first 2 years of life (SS 1412), B-646

Authors' Index

Y

Yagci B., Isik C., Yildirim C., Sabir N., Tatlipinar S.

Color Doppler US in the evaluation of Behçet's disease, C-0526

Yagmurlu B., Tuna H., Erden I.

Malignant vs benign cystic brain masses: Role of perfusion MRI in the differential diagnosis, C-0852

Yalfimov A.N., Ryzhkova D.V., Tyutin L.A., Baranova O.P.

Tc99m-Myoview and Ga-67-Citras combined SPECT imaging for diagnosis of cardiac sarcoidosis, C-0247

Yalfimov A.N., Tyutin L.A., Pozdniakov A.V.

SPECT with HMPAO-Tc99m application to measure the cerebellar blood flow in patients with Chiari malformations, C-0847

Yamagishi T., Höhne K.H., Abe K.

Three-dimensional stereoscopic abdominal MR angiography as an educational tool for medical students, C-0356

Yamaguchi M., Fujita H., Hirano T., Okura Y., Matsumoto M., Johkoh T., Asai Y.

Psychophysical analysis of the DICOM grayscale standard display function, C-0380

Yamamoto S., Motoori K., Ueda T.

Post-radiation malignant tumors in head and neck: A review of the clinical and imaging features, C-0532

Yamaoka T., Inamoto N., Ike K., Nakagawa H.

Image degradation and pseudo-lesions from inappropriate use of post-processing techniques, C-0965

Yamaoka T., Kurita A., Azechi H., Endo Y., Nishikawa H., Noguchi M., Nakano Y.

CT findings and clinical features of portomesenteric thrombosis., C-1054

Yamashita E., Koyama T., Kotani H., Kido A., Umeoka S., Fujiwara T., Fujii S., Imai Y., Togashi K.

MRI features with pathologic correlation of uterine malignant mixed Mullerian tumors, C-0430

Yan F., Xu P., Cheng W., Wei G., Zeng X., Qian J., Fan L.

Computer-assisted evaluation of small hepatocellular carcinoma (HCC) by multiphase dynamic imaging using multidetector helical CT (MDCT) (SS 1801b), B-856

Yanagawa N., Morita F., Ochi S., Funabashi N.

Utility of triple channel injection of contrast material with mixture of saline, with upward acquisition for arterial trees using multislice computed tomography, C-1007

Yanagimachi N., Imai Y., Higashi M.

Nonenhanced peripheral MR angiography using peripheral pulse-triggered three-dimensional half-Fourier fast spin-echo in patients with chronic kidney disease, C-1035

Yang H., Kim A.

Pattern analysis of defecography in patients with chronic constipation: Analysis and its predictive value for the responsiveness of biofeedback therapy (SS 1801a), B-817

Yang H., Do K., Song K., Seo J.

Traumatic diaphragmatic hernia: Comprehensive evaluation using novel MR techniques and multislice CT, C-0310

Yarmenitis S.D., Bakantaki A., Papantoniou Y., Gourtsoyiannis N.

Comparison of B-mode and contrast enhanced ultrasound of the liver in patients undergoing chemotherapy for known primary malignancy (SS 1401b), B-608

Yarmenitis S.D., Kolios G., Papanikolaou N., Maris T., Kouroumalis E., Gourtsoyiannis N.

Integrated sonography of Crohn's disease by combining high-resolution B-mode techniques and contrast enhanced ultrasound (CEUS) perfusion studies of the involved bowel segments, C-0083

Yarmenitis S.D., Bakantaki A., Koulieraki C., Fragos C., Maris T., Gourtsoyiannis N.

Uncommon applications of contrast enhanced ultrasound, C-0400

Yekeler E., Saedi V., Yildirim Donmez F., Tunaci A., Tunaci M., Acunas G.

Evaluation of dynamic contrast enhancement pattern of solitary pulmonary nodules on 3D gradient-echo MR imaging (SS 204), B-035

Yokoyama H., Sanada S., Ohno T.

3D image of Adamkiewicz artery: Preoperative assessment of thoracoabdominal aortic aneurysm, C-1067

Yoon S., Byun J., Park S., Won H., Kim A., Shin Y., Kim P., Ha H., Lee M.

Two-phase CT findings of mass-forming intrahepatic peripheral cholangiocarcinoma in cirrhotic patients: Comparison with those in non-cirrhotic patients (SS 701b), B-419

Yoon J., Cha S., Han S., Lee S., Kang M.

Radiologic findings of gallbladder adenomyomatosis: The importance of showing Rokitansky-Aschoff sinuses, C-0008

Yoon J., Cha S., Han S., Lee S., Kang M.

MR imaging of stomach cancer and ex vivo ¹H MR spectroscopy of the resected stomach, C-0118

Yoon K., Kim E., Hur J., Kim S., Lee Y., Choi K.

Endothelial cell-targeted MR imaging using the anti-VEGFR2 and ICAM-1 antibody-conjugated Gd-DTPA, C-0405

Yoon C., Song H., Shin J.

Covered, retrievable, expandable prostatic stent: Feasibility study in dogs, C-0607

Yoon C., Song H., Shin J.

Malignant duodenal obstructions: Palliative treatment using self-expandable nitinol stents, C-0616

Yoshigi J., Ishida J., Nakamura T., Izaki K., Ando S., Kajitani T., Yoshizako T., Kitagaki H.

MRI findings following radiofrequency ablation(RFA) of lung tumors, C-0629

Yoshikawa H., Ueda T., Myoui A., Tamai N., Araki N., Kudawara I.

Imaging of extraskeletal osteosarcoma, C-0759

Young P.C.

Sacral cementoplasty using combination CT and fluoroscopic guidance: Technical approach, C-0638

Yu C.S., Li K.C.

Quantitative study of fractional anisotropy of the corticospinal tract and corpus callosum in patients with relapsing-remitting MS (SS 211), B-092

Yu J., Zhu X., Yang Z.

Endobronchial tuberculosis: Evaluation with multislice spiral CT (SS 1804), B-847

Yu J., Yang Z., Li Z.

Rare primary mediastinal tumors: Helical CT features and pathological correlation, C-0316

Yudin A.L., Abovich Y.

HRCT in differential diagnosis of types of interstitial pneumonia, C-0302

Z

Zabakis P., Santosh C., Walker L.J., Teasdale E.

Application and efficacy of non-invasive spinal multidetector CT angiography in patients with suspected dural fistula with spinal drainage (SS 1811a), B-908

Zabakis P., Lamin S., Jenkins S., Papanastassiou V., Bhattacharya J.

Cerebral proliferative angiopathy: A distinct subgroup of brain AVMs? A single centre experience, C-0855

Zabakis P., McDonald I., Hadley D., Santosh C.

CE-MRA in the diagnosis of spinal DAVF, C-0883

Zähringer M.

Drug-eluting stents: Drug-eluting stents in renal arteries (NH 10), A-257

Zaleska-Dorobisz U., Weclawek- Tompol J., Kazanowska B.

The imaging findings of primary gastric lymphoma in children, C-0148

Zaleska-Dorobisz U., Jankowski B., Kurcz J., Moron K.

Ultrasound in the diagnosis of acute abdominal pain in children during oncological treatment, C-0892

Zaleska-Dorobisz U., Kazanowska B., Moron K.

Contrast enhanced versus baseline ultrasonography in characterization of enlarged peripheral lymph nodes in children., C-0911

Zaleska-Dorobisz U., Stawarski A., Pytrus T., Iwanczak F., Moron K.

The application of high frequency sonography in the diagnosis and monitoring of inflammatory bowel disease in children, C-0923

Zampa V., Albisinni U., Bargellini I., Odoguardi F., Cioni R., Bartolozzi C.

Osteoid osteoma: Role of dynamic MRI in detection of and definition of success after CT-guided radiofrequency ablation (SS 1010), B-461

Zampa V., Bargellini I., Ortisi S., Odoguardi F., Bartolozzi C.

Diffusion-weighted MRI in differential diagnosis of adrenal masses: Work in progress (SS 1801b), B-850

Zander T., Llorens R., Rostagno R., Zerolo I., Prieto V., Qian Z., Maynar M.

Endovascular treatment of aortoiliac occlusive lesions using a bifurcated endoprothesis, C-0578

Zandrino F., La Paglia E., Benzi L., Musante F.

Assessment of patients with acute mesenteric ischemia (AMI): Multidetector CT (MDCT) signs and clinical performance in a group of patients with surgical correlation, C-0112

Zanetti M.

Wrist: B. MRI and US of chronic pain (RC 910), A-209

Authors' Index

Zangan S.M., Gasparaitis A.E., Giger M.L.

Computerized analysis of abnormal areae gastricae on barium examination, C-0124

Zangos S., Mack M.G., Eichler K., Herzog C., Heller M., Vetter T., Lehnert T., Vogl T.J.

A new cordless coil for MR-guided percutaneous biopsies in a low field system: First clinical experiences (SS 709), B-401

Zangos S., Mayer H., Mayer F., Wetter A., Eichler K., Mack M.G., Schwarz W., Vogl T.J.

MR-guided galvano-therapy in patients with prostate cancer: Technique and first clinical results (SS 1809), B-875

Zaporozhan J., Ley S., Eberhardt R.

Weinheimer O., Fink C., Herth F., Kauczor H.

Influence of different emphysema size classes visualized by quantitative MDCT-analysis on MRA lung perfusion in patients with chronic obstructive pulmonary disease (SS 1504), B-705

Zaspel U., Romano V., Hein P., Hamm B., Rogalla P.

Chest X-ray vs. multislice CT performed at identical radiation doses for detection and characterization of pulmonary nodules (SS 204), B-032

Zavadovskaja V.D., Shoulga O.S., Kilina O.Y., Tonkikh O.S., Nigmatova E.S.

Bone stiffness indices in patients having type I and type II diabetes mellitus based upon ultrasound osteometry of the calcaneum, C-0664

Zavadovskaja V.D., Zorkaltsev M.A., Kilina O.Y., Klimentenko N.L., Perova T.B., Khodashinskaja A.V., Tjuleneva O.

Comparing diagnostic efficacy of sonography and scintigraphy in the diagnosis of rheumatoid arthritis, C-0700

Zdunek P., Gmur A., Wykret M., Pacho R., Wandzel P.

The efficacy of CT-colonography for diagnosis and staging of colon cancer in symptomatic patients, C-0080

Zech C.J., Herrmann K.A., Dietrich O., Menzel M.I., Reiser M.F., Schoenberg S.O.

Black-blood-EPI sequences for the evaluation of focal liver lesion: Comparison to a standard T2-weighted sequence (SS 1801b), B-851

Zhang D.

The study of Gd-labelled liposomes with long circulation time (SS 1406), B-673

Zhang Y., Kang L.Q.

Perfusion CT imaging of angiogenesis in VX2 rabbit brain tumors, C-0781

Zhao X., Li K., Li Y.

MR evaluation of cardiac function in one breath hold with real-time true fast imaging with steady-state precession and parallel acquisition techniques (SS 703b), B-424

Zhao X., Li K., Li Y., Yu C.

MR evaluation of the anisotropic diffusion properties of human heart muscle in vivo using MRDTI with parallel acquisition techniques (SS 1803), B-826

Zhou C., Meng Q., Fan M., Luo B.

Clinical application study of ¹H MRS on bone and soft tissue diseases in the lower limbs (SS 1510), B-681

Zollikofer C.L.

Venous occlusion: B. Vena cava management (RC 1709), A-425

Zompatori M., Battista G., Canini R.

Imaging of lung cancer: B. Staging and follow-up with CT and MRI (RC 804), A-179

Zonderland H.

Open questions: B. Reporting standards (RC 502), A-109

Zoumpoulis P., Vafiadi I., Pahou K.,

Katasounos E., Dalakostas D., Theotokas I., Kyriazi S.

An algorithm-based approach to the sonographic diagnosis of focal liver lesions: A DVD-Rom teaching file with US image and video database, C-0025

Zoumpoulis P.S., Theotokas I., Bechrakis I.,

Kyriazi S., Schizas D., Pahou K., Vafiadi I., Karavitis P.

Ultrasonography of diffuse and focal liver disease: A multimedia DVD-Rom based educational tool and database, C-0044

Zoumpoulis P.S., Theotokas I., Plagou A.,

Schizas D., Tako E., Leli D., Beligiannis C.,

Pahou K.

How to reach the sonographic diagnosis of pancreatic lesions using a simple algorithm: A DVD-Rom based teaching file with US image and video database, C-0056

Zoumpoulis P.S., Theotokas I., Pahou K.,

Dalakostas D., Schizas D., Koratzinos V.,

Filippidou A., Kyriazi S.

An algorithm-based system to facilitate the sonographic diagnosis of renal disease: A DVD-Rom teaching file with US image and video database, C-0443

Alexopoulos D., Prapavesis S., Mastorakou I.,

Leli D., Tako E., Faitaki S., Karavitis P.,

Zoumpoulis P.S.

Transrectal ultrasound (TRUS) of prostate cancer (PRCA): A multimedia DVD Rom-based educational tool and database: Sonographic-pathologic correlation, C-0470

Zoumpoulis P.S., Alexopoulos D., Kyriazi S.,

Beligiannis C., Dalakostas D., Pahou K.,

Kaklamani L.

An efficient way to reach the correct diagnosis on prostate lesions with transrectal ultrasound: DVD-Rom based teaching file with ultrasound images, real-time video display and comparative data, C-0481

Chatzimihail C., Zoumpoulis P., Kyriazi S.,

Mihailidis A., Faitaki S., Pahou K., Bechrakis I.,

Adamakis G., Delibasis G., Tragea H.

Ultrasonography of the musculoskeletal system: Principles of US physics and technology, examination technique, echoanatomy and sonographic features of musculoskeletal disease (a DVD-based teaching file), C-0739

Zuccoli G., Tumiati B., Nicoli F.

Central nervous system involvement in limited forms of Wegener's granulomatosis: CT and MRI findings, C-0865

Zugaro L., Catalucci A., Monina M.,

Di Cesare E., Vicentini C., Masciocchi C.

MR-urography in the evaluation of urinary tract obstruction, C-0511

Zugaro L., Catalucci A., Barile A., Monina M.,

Masciocchi C.

Soft tissues liposarcomas: Relationship between histopathologic features and CT/MRI findings, C-0734

Authors' Index



**List of Authors
and Co-authors**

List of Moderators

List of Authors and Co-authors

A

- Abades Vazquez J.L.: *C-0085*
 Abbasova E.V.: *C-0903*
 Abdala N.: *C-0881*
 Abdul-Khalil H.: *B-423*
 Abe K.: *C-0286, C-0356*
 Abe T.: *C-0010, C-0011*
 Abelairas J.: *B-758*
 Aberle D.R.: *C-0282*
 Abi-Fakher F.: *C-0910*
 Abitbol M.: *B-794*
 Abo D.: *C-0415, C-0594*
 Abolmaali N.D.: *B-650, B-655, B-749*
 Abovich Y.: *C-0302*
 Abraham L.J.: *B-909, C-0160*
 Abramjuk C.: *B-206*
 Aburano T.: *C-0651*
 Acata S.: *C-0286*
 Achenbach S.: *B-662*
 Achenbach T.: *B-104*
 Acitores I.: *C-0588*
 Acquafresca M.: *B-290, C-0620, C-0636*
 Acunas G.: *B-035*
 Adam A.: *A-385, B-334, B-876*
 Adam E.J.: *A-072*
 Adam G.: *B-051, B-053, B-083, B-113, B-114, B-120, B-171, B-213, B-586, B-614, B-652, B-656, B-743, B-755, B-781, B-820, B-918, C-0193, C-0224, C-0757, C-1005, C-1025*
 Adam R.: *C-0007*
 Adamakis G.: *C-0739*
 Adami L.: *C-0447, C-0696, C-0901, C-0922*
 Adams J.E.: *A-101*
 Adamus R.: *B-778*
 Admiraal-Behloul F.: *B-094*
 Adusumilli P.S.: *B-676*
 Afaf A.: *C-0646*
 Agazzi R.: *C-0909*
 Agostinelli A.: *B-061*
 Aguilar M.: *C-0713, C-0731, C-0764, C-0793, C-1044*
 Aguilera-Navarro J.M.: *B-110*
 Aharoni D.: *B-797*
 Ahaus M.: *B-753, B-898*
 Ahl B.: *B-311*
 Ahn B.-H.: *C-0262*
 Ahn J.M.: *C-0663*
 Ahn K.S.: *C-0416*
 Ahovuo J.: *B-231*
 Ahuja G.: *C-0979*
 Aiani L.: *C-0209, C-1066*
 Aigner N.: *B-686*
 Ajaj W.: *B-571, B-813*
 Akalan N.: *B-537*
 Akand M.: *C-0488*
 Akata D.: *B-246*
 Akbas T.: *C-0929*
 Aker S.: *B-404*
 Åkeson P.: *B-700*
 Akgul E.: *C-0515, C-1010*
 Akhmetov Y.A.: *C-0602, C-1036*
 Akhurst T.J.: *B-676*
 Akino N.: *B-823, C-0273*
 Akkerman E.M.: *B-223*
 Aksungur E.: *C-1010*
 Al Bokhrli J.: *B-896*
 Alabau G.: *C-1050*
 Alabiso M.E.: *C-0144*
 Alarcon V.: *C-0106, C-0745*
 Alathiaki A.S.: *C-0841*
 Alberdi I.: *C-0099, C-0100*
 Alberelli C.: *C-0187*
 Alberti G.: *B-422*
- Albisinni U.: *B-461*
 Albiter M.: *C-0459*
 Albrecht T.: *A-041, B-604, B-606, B-844*
 Albucher J.F.: *A-227, B-760*
 Alcaraz-Mexia M.J.: *C-0936*
 Aldescu C.C.: *B-279*
 Aldrian U.: *C-0292*
 Alegre M.I.: *C-0606*
 Aleksandrowicz J.: *C-0808*
 Aleksic M.: *B-456*
 Alexandrino P.: *B-192*
 Alexopoulos D.: *C-0399, C-0470, C-0481, C-0482*
 Alexopoulou E.: *C-0334, C-0584*
 Algeri E.: *C-0238*
 Alhajeri A.: *C-0143, C-0977*
 Alhajeri A.A.: *C-0111*
 Alibek S.: *B-052*
 Aliev M.A.: *C-1036*
 Alijani M.: *C-0103*
 Aliprandi A.: *B-253*
 Alkadhi H.: *B-821, C-0754, C-1053*
 Al-Khaffaf H.: *C-1012*
 Allen C.: *A-387*
 Allen S.: *B-117*
 Allen S.D.: *C-0162*
 Allende H.: *C-0032*
 Alley M.: *C-1030*
 Allona M.: *C-0097, C-1074*
 Allsop J.: *B-117*
 Almén T.: *A-079, B-879, B-882*
 Alonso A.: *C-0086*
 Alonso A.: *C-0576, C-0665*
 Alonso Burgos A.: *B-167*
 Alonso E.: *C-0507*
 Altmeyer K.: *C-0060*
 Alustiza J.M.: *C-0136*
 Alvarez A.: *C-0006, C-0137, C-1049*
 Álvarez A.: *C-0890*
 Alvarez Linera-Prado J.: *C-0813*
 Alvarez Luque A.: *B-758, C-0588, C-0927, C-1074*
 Álvarez-Castells A.: *C-0081, C-0999*
 Alvarez-Sabin J.: *A-002*
 Alves P.: *C-0151*
 Alvey C.: *B-055, B-449, B-796*
 Amberger C.: *B-562*
 Ambrogi C.: *C-0175*
 Amendolia S.R.: *A-119*
 Amadio F.: *C-0614*
 Anagnostara A.: *C-0784*
 Ananthasivan R.: *B-017, B-361*
 Anastopoulos I.: *C-0908*
 Anayama T.: *C-0320*
 Anders K.: *B-280*
 Andersen J.G.: *B-366, B-911*
 Andersson T.: *A-231*
 Andia E.: *C-0763*
 Andic C.: *B-869*
 Ando M.: *B-775*
 Ando S.: *C-0629*
 Andreu J.: *A-213*
 Andreu Navarro F.J.: *B-380*
 Andreu X.: *B-262*
 Andreula C.F.: *A-036, A-401*
 Andrikakos P.: *C-0660*
 Andrísová J.: *C-0042*
 Andriyanicheva H.: *C-0710*
 Andronikou S.: *B-646*
 Ang C.: *B-796*
 Angel A.: *C-0105, C-0166*
 Angelelli G.: *B-475, B-476*
 Angeli E.: *B-066*
 Angeli E.: *B-176, B-862*
 Angeretti M.G.: *B-134*
- Angerson W.: *B-605*
 Anglana F.: *C-0586*
 Angulo E.: *C-0577*
 Anil Kumar B.C.: *B-720*
 Aniq H.: *C-0683*
 Annamalai G.: *C-0327*
 Annibale V.: *C-0188*
 Ansarin M.: *B-184*
 Anselmetti G.C.: *B-283, B-285, B-286*
 Anselmi U.: *C-0980*
 Anslow P.L.: *A-037*
 Anthopoulou A.: *B-894, B-895, B-896*
 Antinori A.: *C-0834*
 Antipa E.: *B-583*
 Antipa E.S.: *C-1071*
 Antoch G.: *B-079, B-553, B-677, B-718, B-840, B-913*
 Antonik M.M.: *C-0544*
 Antonopoulos D.: *C-0334, C-0584, C-0641*
 Antoun N.M.: *C-1077*
 Anzalone N.: *B-764, E-16*
 Apelt D.: *C-0379*
 Aplin M.T.: *B-669*
 Aquerreta J.D.: *C-0665*
 Arabi M.M.S.: *C-0910*
 Arablinskiy A.V.: *C-0465*
 Arakawa H.: *B-074*
 Araki N.: *C-0759*
 Aral Y.: *C-0551*
 Aramaki T.: *C-0222*
 Arana E.: *C-0667*
 Aranda H.: *C-0156*
 Araújo D.: *C-0780*
 Archer J.: *D-14*
 Archiati E.: *B-059, B-125*
 Arcuti P.: *B-127*
 Arenas A.: *C-0067*
 Arenas B.R.: *C-0061*
 Ares J.: *C-0425*
 Argalia G.: *C-0024*
 Argibay P.: *C-0821*
 Argin M.: *B-688*
 Argyropoulou M.I.: *B-560, B-646, B-647*
 Ariche-Maman S.: *A-293*
 Aries P.M.: *B-637*
 Arisaka Y.: *C-0628*
 Arjonilla A.: *B-838*
 Arkoumani E.: *B-894, C-0438*
 Arunk R.: *B-688, C-0215*
 Armstrong P.: *A-248*
 Armstrong S.: *C-0437*
 Arnold S.: *A-282*
 Arredondo F.: *C-0106, C-0745*
 Arrillaga A.: *C-0136*
 Artamonova E.A.: *C-1041*
 Artigues I.: *C-0606*
 Artiko V.: *C-0153*
 Asai Y.: *C-0380*
 Asato R.: *C-0534*
 Ascarelli A.: *B-420, C-0238*
 Aschauer M.: *B-116*
 Aschoff A.J.: *B-108, B-426, B-694, B-827, C-0329, C-0579, C-0783, C-0993, E-50*
 Aschwanden M.: *B-250, B-568*
 Ashiku S.K.: *C-0325*
 Aspelin P.: *B-882*
 Assegnati G.: *B-296, C-0586*
 Astrakas L.: *B-646*
 Astrinaki E.: *C-0860*
 Asvestas P.: *C-0942, C-0963*
 Atakan I.: *C-0520*
 Athanasiou A.: *B-268*
 Athanasopoulou Z.: *C-0076, C-0706*
 Atici A.: *C-0929*

List of Authors and Co-authors

Attanasio S.: *B*-265
 Atzori M.: *C*-0447, *C*-0922
 Aubard Y.: *A*-033
 Aubaud L.: *B*-708
 Aubry R.: *B*-462
 Aubry S.: *C*-0523
 Auci A.: *B*-482, *B*-485
 Auer D.: *B*-103
 Auer F.: *B*-146
 Auerbach M.A.: *B*-187
 Aukett M.: *B*-067, *B*-069
 Auquier M.A.: *C*-1003
 Avigo C.: *B*-059, *B*-609, *C*-0404
 Avinash G.B.: *B*-542
 Avraham E.: *C*-0354
 Avula S.: *C*-0562
 Aw Yeang H.W.: *C*-0489
 Awad N.: *C*-0105
 Aw-Yeang H.W.: *C*-1069
 Aydogdu S.: *B*-688
 Ayed A.: *C*-0007
 Aytekin C.: *C*-1051
 Ayuso C.: *B*-622, *C*-0058, *C*-0232
 Ayuso J.R.: *C*-0058, *C*-0232
 Azavedo E.: *A*-108
 Azechi H.: *C*-1054
 Aziz A.: *C*-0375, *D*-11
 Azoulay D.: *C*-0002
 Azuma S.: *C*-0392

B

Baba Y.: *C*-0381
 Babar J.L.: *C*-0905
 Babar S.A.: *C*-0103, *C*-0442, *C*-0683
 Babaryka G.: *B*-111
 Babic D.: *C*-0565
 Babic N.: *C*-0178
 Babich Y.F.: *C*-0939
 Babiy Y.S.: *C*-0690
 Bach F.: *C*-0747
 Bachelle F.: *B*-734
 Bachinskaya N.Yu.: *B*-230
 Bachmann G.: *B*-594, *B*-839, *C*-0248
 Bachmann R.: *B*-458, *B*-459, *B*-569, *B*-900, *B*-902, *B*-932
 Bacigalupo L.: *B*-026, *B*-270, *B*-589, *B*-800, *C*-0219, *C*-0718, *C*-0902
 Bács É.: *C*-0064
 Badea R.: *B*-193
 Badke A.: *C*-0612
 Bae I.H.: *C*-0533
 Bae Y.-A.: *B*-834
 Baekeland H.: *C*-0378
 Baeten C.G.M.I.: *B*-818
 Baeyaert M.: *B*-441
 Baggio E.: *B*-638
 Baghi M.: *B*-190
 Baglio F.: *B*-229
 Bahépar J.: *B*-591
 Bai R.: *C*-0073
 Baik H.W.: *C*-0567
 Baile E.M.: *C*-1083
 Baimouratov R.: *D*-11
 Baio G.: *B*-026, *B*-589
 Bais B.: *B*-513
 Bajzik G.: *C*-0652
 Bakai A.: *D*-13
 Bakantaki A.: *B*-608, *C*-0400
 Bakker C.J.G.: *B*-903
 Bakon L.: *B*-332
 Baks T.: *B*-308, *B*-342
 Bakshi D.: *C*-1069

Bakshi D.R.: *C*-1062
 Balan K.K.: *B*-465
 Balanika A.: *C*-0726
 Balas B.: *C*-0016
 Balassy C.: *B*-893
 Balcarce P.: *C*-0822
 Balconi G.: *C*-0453, *C*-0454, *C*-0491, *C*-0502
 Baldelli P.: *B*-030
 Bale R.: *A*-270
 Bale R.J.: *B*-060, *B*-101, *D*-03
 Balériaux D.: *A*-038, *A*-367
 Balestrieri A.: *B*-100, *C*-0802, *C*-0863, *C*-0866
 Bali M.A.: *B*-486
 Ballarati C.: *C*-1066
 Ballenilla F.: *C*-0913
 Ballestín Vicente J.: *C*-0704
 Balleguier C.S.: *A*-035, *B*-268
 Baltaci S.: *C*-0479
 Balvay D.: *C*-0390
 Balzer J.O.: *B*-068, *B*-190, *B*-340, *B*-345, *B*-405, *B*-500, *B*-504, *B*-506, *B*-507
 Balzer T.: *B*-048
 Bamberger P.: *B*-151, *B*-152
 Bammer R.: *B*-093, *C*-0915
 Banckwitz R.: *B*-442
 Bandhu S.: *C*-0128
 Bankier A.A.: *A*-017, *A*-187, *A*-247, *B*-595
 Bánkuti A.: *B*-915
 Bansmann P.M.: *B*-213, *B*-652, *B*-656
 Banys R.: *B*-306, *C*-0807
 Bär I.: *B*-282
 Barajas F.: *B*-514
 Baranova O.P.: *C*-0247
 Barbazeni G.: *C*-0190
 Barberini L.: *B*-100, *C*-0802, *C*-0863, *C*-0866
 Barbero S.: *B*-199
 Barbiera F.: *B*-667, *C*-0091, *C*-0167
 Barbieri A.: *B*-215
 Barbieri P.G.: *B*-390
 Barbosa A.: *C*-0061
 Barcelo J.: *C*-0196
 Barceló J.: *C*-0545, *C*-0730
 Bardine A.: *B*-147, *B*-690
 Barentsz J.O.: *A*-351, *A*-354, *B*-490, *B*-493, *B*-497, *B*-725, *B*-731, *B*-837, *C*-0468
 Bares R.: *B*-678
 Bargellini I.: *B*-294, *B*-297, *B*-461, *B*-558, *B*-850
 Barile A.: *B*-129, *B*-137, *B*-140, *C*-0695, *C*-0734, *C*-0767
 Barini M.: *B*-135, *C*-0679, *C*-0707
 Barisone F.: *C*-0463
 Barkhausen J.: *A*-273, *B*-211, *B*-553, *B*-571, *B*-654, *B*-718, *B*-813, *B*-822, *B*-828, *B*-840, *B*-913
 Barkhof F.: *A*-212
 Barlas O.: *C*-0816
 Barlow D.: *B*-796
 Baron J.: *C*-0573, *C*-0675, *C*-0735, *C*-0868
 Barragan-Campos H.M.: *B*-195, *C*-0589
 Barral F.-G.: *B*-462
 Barreau B.: *C*-0184
 Barreau X.: *B*-759
 Barrena R.: *C*-0577
 Barrera C.: *C*-0136, *C*-0249
 Barresi D.: *B*-880
 Barros J.: *C*-0151
 Barsi P.: *A*-251
 Barta M.: *C*-0064
 Bartal G.: *B*-168, *B*-540
 Bartel T.: *B*-828
 Barth M.: *B*-102, *B*-105, *B*-930
 Barth R.A.: *C*-0915
 Bartling S.H.: *B*-276
 Bartolomucci A.: *C*-0296

Bartolotta T.V.: *A*-276, *C*-0027, *C*-0091, *C*-0656, *C*-0727
 Bartolozzi C.: *A*-267, *B*-121, *B*-122, *B*-147, *B*-180, *B*-275, *B*-294, *B*-297, *B*-415, *B*-461, *B*-483, *B*-558, *B*-627, *B*-690, *B*-766, *B*-850, *B*-852, *C*-0054, *C*-0130, *C*-0199, *C*-0708, *C*-0728
 Bartram C.: *B*-149
 Bartram C.I.: *A*-057
 Baruch Y.: *C*-0166
 Baruzzi F.: *B*-283
 Basaran O.: *C*-1011
 Basile A.: *C*-0575
 Basilic R.: *B*-604
 Ba-Ssalalah A.: *B*-011, *B*-012, *B*-016, *B*-789, *B*-935, *C*-0497
 Bassler B.: *B*-570, *B*-576
 Bastarrika Alemán G.: *B*-167, *C*-0455
 Bastarrika G.: *C*-0311
 Bastianello S.: *C*-0804, *C*-0835, *C*-0864, *C*-0947
 Basu S.K.: *B*-663
 Batakis N.: *B*-634, *C*-0349, *C*-0451, *C*-0619
 Batini E.: *B*-852, *C*-0708
 Batista A.: *C*-0606
 Batmaz F.: *C*-0213
 Battaglia G.: *B*-390
 Battista G.: *A*-179
 Battistoni A.: *C*-0190
 Battyány I.: *A*-082
 Bätz L.: *B*-547
 Bauer J.: *B*-251
 Bauer J.S.: *B*-257, *B*-687, *C*-0658
 Bauknecht H.-C.: *C*-0798
 Baum R.P.: *C*-0408
 Baum U.: *B*-280
 Baumert B.: *B*-241, *B*-821
 Baumgartner W.D.: *A*-123
 Baur-Melnyk A.: *A*-046, *B*-464, *B*-466, *B*-717
 Bautista Rodriguez D.: *C*-0874
 Bautz W.: *B*-052, *B*-155, *B*-156, *B*-352, *B*-355, *B*-357, *B*-358
 Bautz W.A.: *B*-280
 Bax J.J.: *A*-272, *B*-214, *B*-220, *B*-428, *C*-0243
 Bazzocchi M.: *C*-0718
 Bazzocchi M.: *B*-266, *B*-397, *B*-457, *B*-613, *B*-618, *B*-805
 Beadsmoore C.J.: *B*-465
 Bearcroft P.W.P.: *A*-311, *B*-465
 Beatovic S.L.: *C*-0466, *C*-0525
 Beauchamp N.: *D*-11
 Beccani D.: *B*-290, *C*-0636
 Bechrakis I.: *C*-0044, *C*-0739
 Bechstein W.-O.: *B*-877
 Beck A.: *B*-407
 Beck C.: *B*-829, *B*-830
 Beck R.: *C*-0293
 Becker C.D.: *A*-139, *A*-219
 Becker C.R.: *A*-010, *A*-174, *B*-341, *B*-343, *B*-346, *B*-691, *B*-846, *E*-30
 Becker H.: *B*-276, *B*-311, *B*-510
 Becker M.: *A*-024
 Beck-Razi N.: *C*-0166
 Bedke J.: *B*-780
 Bednarski M.: *B*-788
 Bedogna V.: *B*-638
 Bedük Y.: *C*-0479
 Beecken W.-D.: *B*-723
 Beer A.J.: *C*-0411
 Beer M.: *B*-897
 Beer M.J.: *A*-240
 Beets-Tan R.G.H.: *A*-016, *B*-150
 Begemann P.G.C.: *B*-614, *B*-820, *C*-1005
 Begli V.: *C*-0899
 Behrens S.: *D*-09

List of Authors and Co-authors

- Beichel R.: A-270, D-04
 Beigelman-Aubry C.: C-1079
 Beisteiner R.: B-930
 Belan V.: C-0042
 Belattar C.: C-0007
 Belcari A.: B-415
 Beleslin B.: C-0595
 Belfiore G.: C-0277
 Belge B.: C-0253
 Belgrano M.: B-342, C-0267, C-0974
 Belgrano M.: B-667
 Belichenko O.: C-0485
 Beligiannis C.: C-0056, C-0481
 Belkind M.B.: B-304
 Bell J.: B-853
 Bell R.E.: B-067, B-069
 Bellan E.: B-546
 Belli A.: B-293
 Belli G.: B-745
 Belli L.: B-914
 Belli P.: B-585, C-0201
 Bellia M.: C-0167
 Bellin M.-F.: C-0002, C-0007
 Bellinck P.: B-441, C-0168
 Bellitti A.: C-0776
 Bellomi M.: A-060, B-037, B-145, B-184, B-369, B-370, B-444
 Belloni E.: B-082
 Belloni G.: C-1066
 Bellussi A.: C-0831
 Belmatoug N.: B-004
 Belohlavek O.: B-417, B-841
 Belysheva E.S.: C-0465
 Ben Achour N.: C-1057
 Ben Amor V.: C-0797
 Benassi M.: C-0338
 Benito A.: C-0330
 Benito A.: C-0516
 Benito J.: C-0882
 Benloch H.: C-0290
 Benos D.J.: B-095
 Benoudiba F.: C-0522
 Bensler S.: B-816
 Benvenuti A.: B-798
 Benzi L.: C-0112
 Berejnoi K.V.: B-739
 Beresnak A.: C-1024, C-1031
 Berger J.: D-02
 Bergh A.: B-495
 Bergmann A.: C-0109
 Bergmann H.: D-01
 Berilgen S.: C-0885
 Berkemeier E.: B-898
 Berlis A.: B-763
 Bermejo A.: C-0067, C-0751, C-0882, C-0913
 Bermudez Bencerrey P.: B-719, C-0792, C-1029
 Bernabeu D.: C-0677, C-0890
 Bernardini A.: B-212, B-219, B-870, C-0493
 Bernasconi T.: C-1003
 Bernathova M.: B-269, C-0225, C-0714, C-1038, C-1039
 Bernd L.: B-139
 Bernerth K.: B-733
 Bernhardi A.: B-737
 Bernhardi P.: B-549
 Bernhardt T.M.: B-038
 Berrettini S.: B-275
 Berrocal T.: A-391, B-758, C-0097, C-0121, C-0886, C-0890, C-0927
 Berry J.: C-0705
 Berry M.G.: C-0733
 Bertaccini P.: B-529
 Bertalanffy H.: B-539
 Bertoletti L.: B-031, B-242, C-0306
- Bertoli E.: B-589
 Bertolotto M.: A-148
 Berton F.: B-127
 Bertuzzi F.: B-176
 Besim A.: B-246
 Besnard P.E.: B-837
 Bessoud B.: A-031
 Bessoud B.: B-362, B-365
 Bettex D.A.: B-821
 Beyer F.: B-038, B-166, B-386
 Beyer T.: B-079, B-677, B-678, B-924
 Beyer T.F.: B-539
 Beyer-Jørgensen P.: A-394
 Beyersdorff D.: B-491
 Bezzi M.: A-386, B-198, B-409
 Bhargava A.: B-676
 Bhat R.: C-0682
 Bhattacharya D.: C-1012
 Bhattacharya J.: C-0855
 Bhattarai N.: C-0147
 Bialek E.J.: B-188, C-0540
 Bianchi C.C.: C-0463
 Bianchi F.: C-0115, C-0145
 Bianchi L.: B-622, C-0610
 Bianchi Marzoli S.: B-907
 Bianchi P.: C-0079
 Bianchi S.: B-800, B-806, C-0719, C-0742, C-0902
 Bibbolino C.: C-0831, C-0834
 Biçakci K.: C-1010
 Bick U.: B-160, B-588
 Biederer J.: B-637
 Bien S.: B-539
 Bieri O.: B-201
 Bigot E.: C-0002
 Bilas K.: C-1071
 Bilbao J.I.: C-0576
 Bilbao Jaureguizar J.-I.: A-028, A-083, B-071
 Bilecen D.: B-201, B-248, B-250, B-568, B-631
 Bilger J.: B-844
 Bilgili M.Y.K.: B-041
 Bilski R.: B-188, C-0540
 Biltjes I.: C-0191
 Binaghi S.: B-318, B-765
 Binder M.: C-0808
 Binokay F.: C-0515, C-1010
 Biondetti P.R.: B-891, C-0335
 Bipat S.: B-142
 Birchall J.D.: B-925
 Birchard K.R.: B-041
 Birincioglu P.: C-0551, C-0552
 Birjawi G.A.: C-0094
 Birkfellner W.: D-01
 Bischof H.: B-260, D-06
 Bisdas S.: A-421, B-311
 Bitsch R.-G.: B-139
 Bitschnau S.: B-368
 Bitsori M.: B-751
 Bittinger F.: B-368
 Bizimi V.: C-1071
 Bizzì A.: A-071
 Bjarnason H.: A-424
 Björkman-Burtscher I.M.: A-328, A-405
 Björnarå B.T.: C-0336
 Blake M.A.: B-010, B-660
 Blake M.M.: B-106
 Blake P.: B-153
 Blanc E.: C-0155
 Blancas C.: C-0284, C-0666
 Blanch J.: C-0935
 Blasco J.: C-0617, C-0645
 Blasetti M.: C-0175
 Blasi V.: A-071
 Blazquez Ortiz J.M.: C-0050
- Bley T.: B-008, B-675
 Blickman J.G.: B-493, B-497, B-731, B-837, C-0469, E-09
 Bloch N.: B-721
 Bloem J.L.: A-396
 Blondin D.: C-0984, C-1019
 Bluemke D.A.: B-421, B-790, C-0420
 Blum A.: A-208
 Blumenkrantz G.: B-565
 Bnà C.: C-0332
 Boan J.F.: C-0516
 Boatta E.: B-509
 Bobin S.: C-0559
 Boccardi A.: C-0830
 Böcher E.: B-506
 Bock E.: B-626, B-870, C-0493
 Bock M.: B-780, B-905, C-0345, C-0386, C-0407
 Böcker W.: B-835
 Bockisch A.: B-079, B-677, B-718, B-913, B-924
 Bode B.: B-351
 Bodewitz S.T.: C-0157
 Bodini M.: C-0189
 Bodner G.: B-269, C-0225, C-0714, C-1038, C-1039, E-70
 Boeckler D.: C-1000
 Boehm D.: B-830
 Boehm H.: B-251, B-256
 Boehm M.: C-0237
 Boehm T.: C-0754
 Boehm T.: B-821
 Boersma E.: B-220
 Boersma E.: B-214
 Boesch C.: B-338
 Boetes C.: B-731, B-837
 Boettcher J.: B-022, B-372, B-670, C-0236, C-0891
 Bogaert J.: A-066, B-084, B-090
 Bogdal J.: C-0807
 Boggi U.: B-415, B-483, C-0054
 Bogner P.: A-250
 Bogoni L.: B-327
 Bogorodzki P.: B-929, C-0844
 Bohl J.: B-532
 Böhlm P.: C-0612
 Böhmt T.: B-241
 Bohndorf K.: A-199, B-129
 Böhner C.: B-156
 Bohner G.: C-0798, C-0799
 Bohrer I.: B-311
 Boikov I.V.: C-0849
 Boiselle P.M.: C-0285, C-0325
 Bojanovic A.: C-0644
 Bojar M.: B-099
 Boke E.: B-246
 Bokeriya L.: C-0912
 Boku N.: B-412
 Bolan P.J.: B-735
 Boldys H.: C-0573
 Bolia A.: A-234
 Boll D.T.: B-108, B-406, C-0329
 Bolte H.: B-637
 Bomma C.: B-421
 Bonaldi G.: B-283, B-286
 Bonanni G.: B-137, C-0767
 Bonasera L.: B-628
 Bonatti H.: C-0053
 Bonavolonta' N.: C-0144
 Bondiau P.-Y.: B-639
 Bonetti M.: B-097, B-284
 Bonetto P.: C-0219
 Bongartz G.M.: A-290, B-248, B-250
 Bongiovanni M.: B-254
 Boniatis I.: C-0370
 Bonini G.: C-0909

List of Authors and Co-authors

- Bonk U.: *B-835*
 Bonnefoy O.: *B-544, C-0684*
 Bonneville J.-F.: *A-265*
 Bonomo L.: *A-027, A-144, A-359, B-173, B-174, B-212, B-219, B-244, B-550, B-577, B-626, B-703, B-707, B-870, C-0340, C-0493, C-0494, C-0503, C-1056*
 Boranga B.: *B-802*
 Boraschi P.: *B-482, B-483, B-485, C-0402*
 Borbély K.: *C-0064*
 Bordes R.: *C-0279, C-0284*
 Borges A.: *A-023, A-207*
 Borghese L.: *B-266*
 Borghi C.: *B-024*
 Borgstede J.P.: *A-338*
 Bornemann L.: *D-09*
 Bornik A.: *A-270, D-04*
 Böröczk A.: *B-915*
 Borowiak H.: *C-0023, C-0564*
 Borowski M.: *B-835*
 Borracini C.: *C-1028*
 Borrego-Gomez J.: *C-0171*
 Borruel S.: *C-0067*
 Borsellino V.: *B-088*
 Borst M.: *B-472*
 Bortone S.: *B-416*
 Borzani I.: *B-411*
 Bose S.: *C-0180*
 Bosk S.: *B-404*
 Boskamp T.: *D-09*
 Bosma G.P.T.: *B-094*
 Bosmans H.T.C.: *B-682, B-769, B-922, C-0978*
 Bosmans J.M.: *C-0243*
 Bosnjakovic P.: *C-0644, C-0812*
 Boss A.: *B-621, C-0611, C-0622*
 Bossis I.: *B-647*
 Bossuyt P.: *B-489*
 Bosurgi F.: *B-265*
 Bosurgi F.: *C-0188*
 Both M.: *B-637*
 Botnar R.M.: *B-307, B-653, B-657, B-658, C-0271*
 Botnar R.M.: *C-0245*
 Bouilleret V.: *B-430*
 Boulahdour H.: *B-462*
 Boulahdour Z.: *C-0523*
 Boulogianni G.: *C-0826*
 Bouomrani S.: *C-1057*
 Bourke G.: *C-0725*
 Bouros D.: *B-843*
 Bourquin H.: *B-179, D-09*
 Bourrier P.: *C-0344, C-0459*
 Boutry N.: *A-006, B-561*
 Bouziane T.: *C-0632, C-0633, C-0647, C-0648*
 Boye R.: *C-0006, C-0137, C-0999, C-1049*
 Boyer C.: *C-0797*
 Boyle G.: *B-559, C-0801*
 Bozgeyik Z.: *C-0885*
 Bozzali M.: *B-229*
 Bozzato A.: *B-052*
 Braat D.D.M.: *C-0435*
 Brader P.: *B-886*
 Brady A.P.: *A-141*
 Braga L.: *B-041*
 Braham R.: *C-1057*
 Bramanti P.: *C-0835*
 Brambilla M.: *C-0535*
 Brambs H.-J.: *B-108, B-694*
 Brammer M.: *B-863*
 Brancaléone C.M.I.: *C-0175*
 Brandl U.: *C-0891*
 Brandstätter J.: *D-02*
 Branera J.: *C-0605*
 Branera Pujol J.: *C-1029*
 Brassel F.: *B-453, B-510, B-901*
- Brat H.: *C-0632, C-0633, C-0647, C-0648*
 Brauer R.: *B-670*
 Bravin A.: *B-030*
 Bravo A.: *C-0097, C-0588, C-0876, C-1074*
 Bravo Rodriguez F.: *C-0794, C-0874*
 Bray A.: *C-0278*
 Brechtel K.: *B-678*
 Breen D.: *B-868*
 Breeuwer M.: *D-07*
 Breitenseher M.J.: *B-686*
 Breitgand A.: *B-540*
 Bremer C.: *A-089, A-299, B-784, B-785, E-58*
 Bremerich J.: *A-277*
 Brennan D.: *B-359*
 Brennan P.: *C-0827*
 Brennan P.C.: *C-0650, C-0959*
 Brestas P.: *C-1071*
 Brestas P.: *C-1065*
 Breuer J.: *B-048, B-748, E-05*
 Brewster J.: *B-724*
 Brillet P.-Y.: *C-1079*
 Brisse H.: *A-431*
 Britten J.: *C-0987*
 Brittenden J.: *C-0490*
 Brizuela C.: *C-0744*
 Brizzi D.: *B-026, B-589*
 Brogna C.: *C-0804*
 Bronisz K.: *C-0321*
 Brook O.R.: *C-0129*
 Brot Q.: *C-0555*
 Brotchi J.: *A-367*
 Brown G.: *B-019, B-143, B-144, C-0164*
 Browne R.: *A-242*
 Bru C.: *A-175, B-622, C-0030, C-0610*
 Bruculeri F.: *B-135, C-0535*
 Bruder O.: *B-211*
 Brueckmann H.: *B-314*
 Bruegel M.: *B-033*
 Bruening R.: *B-314*
 Bruesewitz M.R.: *B-442, B-443*
 Brugger P.C.: *B-221, B-756, B-757, B-889, B-892, B-893*
 Bruhn H.: *B-491*
 Bruining N.: *B-301, B-667*
 Bruix J.: *B-622, C-0610*
 Brunelle F.: *A-193, A-238*
 Bruners P.: *B-520*
 Bruni A.: *B-198, B-299, B-409, B-512*
 Brüning R.: *B-183*
 Brunwall J.: *B-063, B-291, B-456*
 Brunner P.: *B-639*
 Brunner T.: *B-777*
 Bruzzi J.: *B-115*
 Bruzzi J.: *B-477, B-478, B-591*
 Brzsko M.: *B-335*
 Brzozowski K.: *B-871*
 Buchbinder S.: *B-151, B-152*
 Büchler M.W.: *B-414*
 Buchthal S.: *B-095*
 Bücker A.: *A-286*
 Buckley J.: *B-391*
 Buda A.: *B-728*
 Budge A.: *D-17*
 Buecker A.: *B-073, B-203, B-278, B-520, B-522, B-657, B-658*
 Bueno Á.: *C-0657*
 Buerke B.: *B-884*
 Buffa V.: *C-0447, C-0696, C-0901, C-0922*
 Buhmann R.: *C-0345*
 Buhmann S.: *B-164, B-464, B-466, B-815*
 Buhr H.J.: *B-072*
 Bulanova T.V.: *C-0544*
 Bull C.: *D-17*
 Bülow M.: *B-810*
- Bultrini C.: *B-140, C-0767*
 Bunch P.C.: *B-774*
 Buono G.: *B-416*
 Buonomo O.: *B-729*
 Burdese M.: *C-0463*
 Burling D.: *B-696*
 Burney K.: *C-0102, C-0251, C-0450*
 Burrel M.: *C-0617, C-0645*
 Buscema M.: *B-376*
 Busch H.-P.: *A-349*
 Bush B.A.: *B-095*
 Bushby L.H.: *B-579*
 Busi Rizzi E.: *C-0834*
 Bustamante M.: *C-1044*
 Bustos Jiménez M.: *C-0179*
 Buti M.: *C-0031*
 Buttazzi K.: *B-064, B-066*
 Buy X.: *C-0461*
 Buzzio C.: *C-0517*
 Buzzi A.: *C-0106, C-0738, C-0744, C-0745, C-0822*
 Buzzi M.: *C-0744, C-0745*
 Byrne J.V.: *A-054*
 Bytzer P.: *B-600*
 Byun J.H.: *B-419, C-0001, C-0017, C-0022, C-0065*
 Byun J.N.: *C-0062, C-0542*
 Byun J.Y.: *C-0216*
-
- C**
- Cabassa P.: *A-030, B-124, B-125, B-609, C-0404*
 Cabral I.: *B-792*
 Cabrera A.: *C-0249*
 Caccamo N.: *C-0401*
 Cáceres J.: *A-042, A-204, A-211*
 Cáclilia R.S.: *B-730*
 Cademartiri F.: *A-388, B-301, B-308, B-342, B-667, C-0091, C-0167, C-0267, C-0864, C-0947, C-0974*
 Cadi M.: *B-698, C-0043, C-0089*
 Cadioli M.: *B-764*
 Caffarri S.: *B-607*
 Cagnon C.: *B-446*
 Caimmi F.: *B-527*
 Caire-Gana B.: *A-033*
 Cakal E.: *C-0551, C-0552*
 Cakir B.: *C-1051*
 Cakir B.: *C-0817, C-0853*
 Cakirer S.: *A-420, C-0819, C-0878*
 Calabrese F.A.: *B-885, C-1043*
 Calabrese M.: *B-026, B-270, B-589*
 Calbo J.: *C-0214*
 Calbo Maiques J.: *C-0433*
 Calgaro A.: *C-0565*
 Callegari L.: *B-134*
 Calliada F.: *B-127*
 Calvillo Batllés P.: *C-0704*
 Calvisi V.: *B-137, B-140, C-0695*
 Calvo A.: *B-199*
 Calvo N.: *C-0851*
 Camara O.: *B-402*
 Camenzuli A.M.: *C-0471*
 Cammarata R.: *B-528*
 Campagnano S.: *C-0548*
 Campanella D.: *B-377*
 Campanella V.: *C-0371*
 Campani D.: *B-122, B-180, B-415*
 Campbell C.: *C-0327*
 Campi R.: *B-024, C-0209*
 Campion L.: *C-0181*
 Campisi G.: *B-126*
 Camps Herrero J.: *B-378*

List of Authors and Co-authors

- Camps J.: *B-380*
 Canadè A.: *B-707*
 Canalís L.: *B-196*
 Canas C.: *C-0156, C-0741*
 Candia C.: *C-0175*
 Canedo M.: *C-0738*
 Cañete N.: *C-0666*
 Canini R.: *A-179*
 Canis M.: *C-0330*
 Canitano S.: *C-0338*
 Cano D.: *C-0311*
 Cano Rafart D.: *B-167, C-0455*
 Cano Sanchez A.: *C-0874*
 Cano-Rodriguez A.: *B-110*
 Cantwell C.P.: *B-115*
 Canu N.: *B-126*
 Canu T.: *B-422*
 Cañuelo T.: *C-0221*
 Cao G.: *B-642*
 Capdevila A.: *C-0797, C-0935*
 Cappeliez O.: *B-550, C-0632, C-0633, C-0647, C-0648*
 Cappelli C.: *B-297, B-415, C-0054, C-0728*
 Caproni G.: *B-415*
 Capsa R.: *C-0957, C-1072*
 Capuani S.: *C-0653*
 Capuñay C.: *C-0107, C-0268, C-0331, C-0346, C-0347, C-0537, C-1014, C-1015*
 Capurro S.: *C-0172*
 Cara M.: *C-0330*
 Caraballo M.: *C-0061*
 Caramella D.: *A-048, A-154, B-415*
 Carbó S.: *C-0928*
 Carbone I.: *B-420, B-526, C-0238*
 Cardinale L.: *C-0319*
 Cardone G.: *C-0453, C-0454, C-0491, C-0502*
 Carducci S.: *B-287*
 Carizzoni S.: *B-059*
 Carlani M.: *C-0296, C-0297*
 Carlsson P.-O.: *B-881*
 Carnell D.: *C-0304, C-0323*
 Carnero M.: *C-0214*
 Carnero Ruiz M.: *C-0433*
 Carnevale F.: *B-224*
 Carney J.A.: *C-0254, C-0498*
 Caronno R.: *B-062, B-298*
 Carotenuto L.: *B-375*
 Carpegniani P.: *B-283, B-286*
 Carpenter T.T.: *B-872*
 Carpintiero S.: *C-0820*
 Carra L.: *B-265*
 Carrafiello G.: *B-062, B-298*
 Carrascosa J.: *C-0107, C-0268, C-0331, C-0346, C-0347, C-0537, C-1014, C-1015*
 Carrascosa P.M.: *C-0107, C-0268, C-0331, C-0346, C-0347, C-0537, C-1014, C-1015*
 Carrera R.: *C-0751*
 Carreras E.: *C-0894*
 Carrete Jr. H.: *C-0881*
 Carriero A.: *B-135, B-224, B-265, B-527, B-536, C-0188, C-0535, C-0655, C-0679, C-0693, C-0694, C-0707, C-0768, C-0829, C-0830, C-0832, C-1028*
 Carríol I.: *A-390*
 Carrivick L.: *C-0343*
 Caruso G.: *C-0091, C-0401*
 Carvajal A.: *C-0792*
 Casale A.: *C-0548*
 Casali P.: *C-0115, C-0145, C-0769*
 Casanova S.: *C-0255*
 Caseiro-Alves F.: *B-740, C-0039*
 Cassar-Pullicino V.N.: *A-404*
 Casselbrant I.: *B-700*
 Casselman J.W.: *A-021, A-122, A-264*
- Cast J.: *B-868*
 Castaing D.: *C-0002, C-0007*
 Castañeda-Zúñiga W.: *B-514*
 Castaner E.: *C-0326*
 Castañer E.: *C-0289*
 Castaño Duque C.: *C-0778*
 Castela-Murillo A.: *B-110*
 Castell Monsalve F.J.: *C-0179*
 Castellà E.: *C-1023*
 Castellà Fierro E.: *C-0031, C-0250, C-0770*
 Castellazzi G.: *B-185*
 Castelli P.: *B-062, B-298*
 Castelli R.: *C-0335*
 Castellote A.: *C-0894*
 Castelnovo M.M.: *B-891*
 Castiglion I.R.: *C-0107*
 Castoldi M.C.: *B-501*
 Castro Copete M.C.: *C-0433*
 Castro M.C.: *C-0214*
 Castrucci M.: *B-296, C-0586*
 Catala J.: *C-0135*
 Catala M.: *C-0928*
 Catalano C.: *A-220, B-031, B-242, B-267, B-375, B-692, B-857, B-885, C-0192, C-0195, C-0306, C-0371, C-1043*
 Catalucci A.: *C-0428, C-0511, C-0734*
 Cathier P.: *B-161*
 Cattin F.: *A-265*
 Caulo M.: *B-534*
 Causin F.: *C-0768, C-0832*
 Cavacece M.: *B-031, C-0238*
 Cavallaro A.: *B-352, B-355, B-356, B-357, B-358*
 Caverni L.: *B-455*
 Cavouras D.: *C-0355, C-0370, C-0943, C-0955*
 Cecchini S.: *B-798*
 Ceccotti P.: *B-605*
 Cedolini C.: *B-266*
 Ceglédi A.: *C-0064*
 Cejna M.: *A-258*
 Celano T.: *C-0510*
 Celda B.: *C-0475*
 Celebi I.: *C-0456*
 Celedin S.: *C-1017*
 Celestre M.: *B-043, B-044, B-107, B-515, B-710, B-747, C-0019, C-0034, C-0035, C-0090, C-0585*
 Celik V.: *B-584*
 Çeliktaş M.: *C-0515, C-1010*
 Celis V.: *B-159*
 Cenciarini V.: *B-148*
 Centonze M.: *C-0264, C-0360*
 Cenzi D.: *B-638*
 Cercignani M.: *B-229*
 Ceretti E.: *C-0708*
 Cerri G.G.: *B-058*
 Certo M.: *C-0150*
 Cervellini P.: *C-0768*
 Cervera J.: *C-0434*
 Cesare Marincola F.: *C-0802*
 Cestari A.: *C-0453, C-0454*
 Ceugnart L.: *B-734*
 Cha J.G.: *C-0723, C-0736*
 Cha J.H.: *C-0202, C-0203, C-0762*
 Cha S.: *B-439*
 Cha S.H.: *C-0533*
 Cha S.-S.: *C-0008, C-0118*
 Chae E.J.: *C-0022*
 Chai C.-M.: *B-879*
 Chalazonitis A.N.: *C-0396, C-0618*
 Chalkia M.: *C-0075, C-0452, C-1076*
 Chalkia P.: *C-1076*
 Chamalakis K.N.: *B-620*
- Chamberlin P.: *B-917*
 Chammas M.C.: *B-058*
 Chan B.: *B-391*
 Chan F.P.: *C-0263*
 Chan F.P.: *C-0260*
 Chan O.: *A-064, A-261*
 Chandratreya L.: *C-0315, C-0437*
 Chang A.-L.: *C-0004*
 Chang K.-H.: *C-0845*
 Charafeddine R.: *B-392*
 Charlier P.: *B-430*
 Charonitakis E.: *B-620*
 Charonnet J.-M.: *C-0858*
 Chartabilas E.: *C-0075*
 Chassoux F.: *C-0782*
 Chateil J.-F.: *B-544*
 Chaturvedi A.: *B-639*
 Chatzakis G.: *C-1065*
 Chatzimichael K.: *C-0210*
 Chatzimihail C.: *C-0739*
 Chatzopoulou M.: *C-0076*
 Chaudhuri R.: *C-0480*
 Chaustre-Mendoza L.F.: *C-0945*
 Chavan A.: *A-186*
 Chávarri E.: *C-0123*
 Chaveron C.: *B-734*
 Chazova I.: *C-0872*
 Chen C.L.: *C-0412*
 Chen F.: *B-316, B-338*
 Chen J.H.: *B-848*
 Chen S.: *B-933*
 Chen X.: *B-531*
 Chen Y.: *B-555*
 Chenevert T.L.: *B-786*
 Cheng W.: *B-042, B-328, B-856*
 Cheng Y.S.: *B-209, C-0165*
 Cheo Y.H.: *C-0202, C-0203*
 Cheon J.E.: *C-0202, C-0888*
 Cheon J.-E.: *C-0202, C-0888*
 Cheow H.K.: *B-465*
 Chepurov A.: *B-726*
 Chernikova L.A.: *C-0871*
 Chersevani R.: *A-217, B-025*
 Cheung P.-T.: *B-642*
 Chevrot A.: *B-132, B-804, C-0691, C-0747*
 Chiba Y.: *C-0018*
 Chida K.: *C-0228, C-0600*
 Chihara A.: *C-0981*
 Chimenti C.: *B-082*
 Chin C.: *D-14*
 Chin-Aleong J.: *C-0103*
 Chino S.: *B-651*
 Chiocchi M.: *B-519, B-632, B-873*
 Chiodi M.: *B-842*
 Chippendale A.: *D-17*
 Cho E.-S.: *B-714*
 Cho J.H.: *C-0630*
 Cho S.B.: *B-864, C-0416*
 Choe B.-H.: *B-752*
 Choe H.-S.: *B-834*
 Choe K.O.: *C-0229, C-0240, C-0258, C-0274, C-0322*
 Choe Y.H.: *C-0204*
 Choi B.I.: *B-076, B-077, B-178, B-210, B-711*
 Choi B.-I.: *B-695*
 Choi B.W.: *C-0229, C-0240, C-0258, C-0274, C-0301, C-0322*
 Choi C.G.: *B-281*
 Choi C.H.: *B-761*
 Choi C.S.: *B-581*
 Choi D.: *B-418, B-854, C-0048*
 Choi H.W.: *B-761, B-762*
 Choi H.Y.: *C-0755*
 Choi J.-A.: *B-467, B-567, C-0722*

List of Authors and Co-authors

- Choi J.C.: C-0630
 Choi J.W.: B-418, B-854, C-0556
 Choi J.Y.: C-0062, C-0542
 Choi J.-Y.: B-467, B-503, B-567, C-0029, C-0722
 Choi K.H.W.: C-0994
 Choi K.-S.: C-0405
 Choi S.-I.: C-0241
 Choi S.J.: C-0925
 Choi Y.S.: C-0723
 Choke E.: B-293
 Chollet F.: A-227, B-760
 Chollet R.: B-698, C-0089
 Chondros D.: C-0825, C-1016
 Chong P.-N.: C-0877
 Choo H.-J.: B-761, B-762, C-0846
 Choo K.S.: C-0846
 Choo S.W.: C-0621
 Chourmouzi D.: C-0826
 Choury N.: B-708
 Choy E.: C-0705
 Christe A.: B-619
 Christeas N.: C-0613
 Christopoulos A.: C-0660
 Christopoulos P.: C-0921
 Chrysovergis D.: C-0052, C-0962
 Chrzan R.: C-0808
 Chuchalin A.G.: B-709
 Chudácek Z.: C-0082
 Chung E.C.: C-0005, C-0663
 Chung G.-H.: C-0353
 Chung K.B.: B-864
 Chung K.B.C.: C-0416
 Chung M.H.: B-505
 Chung S.: B-831
 Chung S.-H.: C-0353
 Chung S.-Y.: B-834
 Chung S.Y.: C-0217
 Chung S.Y.: C-0322
 Chung S.Y.: C-0301
 Cianci R.: B-712, C-0078
 Ciancibello L.: C-0281
 Ciancio M.L.: C-0209
 Ciarpaglini L.L.: B-389
 Ciatto S.: B-798
 Ciccarelli S.: C-0391
 Ciccarese G.: B-397, B-618
 Cicconi P.: B-254
 Ciecko-Michalska I.: C-0807
 Cieslak B.: C-0003
 Cieszanowski A.: B-929, C-0003, C-0382
 Cila A.: B-537
 Cilotti A.: C-0199
 Cimpeanu A.: C-0957
 Cimpeanu N.: C-0957
 Cina A.: B-244, C-0776, C-1056
 Cina G.: C-1056
 Cinquantini F.: B-492
 Cioffi R.: C-0277
 Cioni D.: B-121, B-122, B-180, B-852
 Cioni R.: B-297, B-461, B-558, C-0054
 Ciosci R.: C-0079
 Cipolletta L.: C-0132
 Ciriello M.: C-1063
 Cirillo M.: B-626, C-0503
 Cirotta N.: C-1018
 Ciszowska-Lyson B.: B-566
 Civardi C.: C-0830
 Clarizia F.: B-024
 Clasen S.: B-621, C-0611, C-0622, C-0623
 Claussen C.D.: B-157, B-310, B-421, B-562,
 B-587, B-621, B-678, B-715, C-0012, C-0257,
 C-0270, C-0293, C-0317, C-0403, C-0612,
 C-0622, C-0623, C-0941, C-0975
 Clément O.: B-779, C-0069, C-0390
 Clevert D.-A.: B-454, B-603, C-0363, C-0569,
 C-1055, C-1064
 Clotet M.: C-0220
 Cobby M.: A-379, C-0315
 Cobelli R.: C-0332, C-0333, C-0517
 Cocco E.: C-0802
 Coche E.E.J.G.: B-479, C-0253
 Cody D.: B-446
 Cognard C.: A-227, B-759, B-760
 Cogollos J.: C-0155
 Cohnen M.: C-0984, C-1019
 Cointepas Y.: C-0782
 Cokkinos D.D.: B-659
 Cokkinos D.V.: B-659
 Colagrande S.: B-745
 Cole H.: B-153, B-545
 Coletta L.: B-043, B-044, B-107, B-515, B-710,
 B-747, C-0019, C-0034, C-0035, C-0585
 Coll D.: C-0185, C-0604
 Colleoni M.L.: B-318, B-765
 Collins C.D.: B-716
 Collins D.: B-144
 Colonnese C.: C-0835
 Colosimo C.: B-292, B-388, B-534, B-644, B-712
 Colpaert C.: C-0191
 Comans E.F.I.: B-142
 Combadiere B.: B-779
 Combadiere C.: B-779
 Comet Segú R.: C-0032
 Como G.: B-397
 Comparetto A.: C-0027
 Connor S.E.J.: C-0528, C-0779
 Conrad L.: B-459
 Constantopoulos S.: B-597
 Conti A.: B-122, B-180, B-852
 Conti G.M.: C-0219
 Contreras J.: B-838
 Cook G.: E-65
 Copeland J.F.: C-0285
 Coppenrath E.: B-615
 Coppenrath E.M.: B-610, B-611
 Corbo G.: B-703
 Cordonnier E.: A-156
 Cormier S.: C-0377
 Cornalba G.: B-185, B-369, B-411, B-455,
 C-0079
 Cornelius P.: B-842
 Corneloup O.: B-087, C-0269
 Cornud F.: A-235
 Cornuz J.: B-596
 Corona M.: B-198, B-299, B-409, B-509, B-512
 Corso R.: B-501, C-0580
 Cortés M.: C-0221
 Cortés P.: C-0886
 Cortese A.: C-0696, C-0901
 Cortet B.: B-561
 Cosin O.: C-0665
 Coskun B.: C-0208
 Coskun M.: C-1011, C-1051
 Cosnard G.: C-0796
 Cosottini M.: B-766
 Cossu E.: B-729
 Cossu M.C.: B-482
 Costa N.: C-0151
 Costa P.: B-296
 Costa S.: C-0667
 Costantini M.: B-585, C-0201
 Costanzi S.: B-870
 Costaridou L.: A-433, B-322, C-0370, C-0954
 Cotroneo A.R.: B-292, B-339
 Cottet A.: B-561
 Cotticelli B.: C-0828
 Coudyzer W.: B-316
 Coulomb M.: B-708
- Courcoutsakis N.A.: C-0254, C-0498
 Courtney H.M.: B-465
 Cova M.: B-602
 Covelli E.M.: C-0277
 Cowan N.C.: A-330, C-0496
 Cowley P.: B-853
 Cowling M.G.: A-428
 Cozcolluela R.: C-0072, C-0099, C-0100
 Craddock A.: B-115
 Cramer M.C.: B-051, B-053
 Cramer M.-J.: B-521
 Cravero F.: C-0655, C-0679, C-0693
 Crawford T.: B-384
 Crean A.: C-0227
 Crecco M.: C-0338
 Crespo A.M.: C-0577
 Crespo Martínez C.: C-0433
 Crinò F.: B-265, C-0188, C-1028
 Cristaudo C.: B-097, B-284
 Cristinelli M.R.: B-059, B-124, B-125, B-609,
 C-0404
 Cristofaro M.: C-0831
 Cristoforetti A.: C-0360
 Crocetti L.: B-121, B-180, B-627, B-852
 Cronin C.G.: C-0364, C-0740, C-0977
 Crowley J.: C-0968
 Crucitti A.: B-626
 Crusco F.: B-633, B-802
 Cserepes É.: C-0064
 Cuadrado M.: C-0928
 Cuéllar H.: C-0006, C-0081, C-0137, C-1049
 Cuéllar i Calàbria H.: C-0999
 Cuénod C.A.: C-0390
 Cunha T.M.: B-792, C-0423, C-0424
 Cunningham P.: B-359
 Cuocolo A.: B-086
 Curati-Alasonatti W.: A-214
 Curti A.: B-185
 Curvo-Semedo L.: C-0039
 Cybulski C.: C-0842
 Cyrylowksi L.: C-0842
 Czarnowska M.: C-0015, C-0149
 Czekajska-Chehab E.: B-274
 Czermak B.: C-0087, C-0898
 Czernin J.: B-187, B-384
 Czerny C.: A-123
 Czyrny Z.: B-566
 Czyszkowski P.: C-0321
-
- D**
- Dabrowiecki S.: C-1040
 Dacou-Voutetakis C.: B-647
 Dagiada K.: C-0766
 D'Agostino A.G.: B-388, B-707
 D'Agostino E.: B-551, C-1045
 Dahl O.E.: C-0336
 Dahmen A.: B-701
 Dahnke H.: B-781, B-784
 Dai D.: B-197
 Daisaki H.: C-0342
 Dakhil A.Z.: B-600
 Dakhno L.: B-054
 Dalakostas D.: C-0025, C-0443, C-0481
 Dalal T.: B-010, B-660
 Daldrup-Link H.E.: A-325, B-739, C-0406
 Dalla Palma F.: C-0360
 Daly K.: C-0968
 D'Amico A.: C-0493
 Damilakis I.: B-649
 Damilakis J.: A-191, B-771, C-0036, C-0976
 Damjanoski G.: C-0596
 Danassi-Afentaki D.: C-0625

List of Authors and Co-authors

- Danchaivijitr N.: *C-0854*
Danes J.: *A-011*
Daniaux M.: *B-803*
Danieli D.: *C-0832*
Daniels D.L.: *C-0856*
Daniels M.D.: *B-139*
Danielsen E.R.: *A-327*
Dannenberg N.: *B-436*
Danti M.: *B-526*
Danza F.M.: *B-626, B-870, C-0493, C-0494, C-0503*
Darge K.: *B-897*
Darnell Martin A.: *B-719, C-1029*
Das M.: *B-169, B-382, B-750, B-819*
D'Ascenzo F.: *B-907*
Dasdemirov E.: *C-0486*
Daskalogiannaki M.: *B-649*
Dassel M.S.: *B-156*
Datir A.P.: *C-0531, C-0547*
Davidson I.: *C-1006*
Davies C.: *C-0164*
Davies N.: *B-853*
Davies R.: *C-0553*
de Albert M.: *C-0156*
De Amicis R.: *C-0786, C-0803*
De Angelis F.: *C-0090*
de Araújo D.B.: *C-0780*
De Backer A.I.: *C-0746*
de Bazelaire C.: *C-0344, C-0459*
de Blieck H.: *D-07*
De Candia A.: *B-457, B-805*
De Caralt T.M.: *C-0232*
De Castro S.: *B-420*
De Catte L.: *C-0906*
De Ceuninck L.: *B-385*
De Cicco E.: *C-0255*
De Cobelli F.: *B-082, B-422*
De Cori S.: *B-766*
De Cristofaro F.: *C-0548*
de Crombrugge R.: *B-479*
De Deurwaerder B.: *B-697*
De España F.: *C-1050*
De Feo C.: *C-0463*
De Feo P.: *C-0473*
de Feyter P.J.: *B-308, B-342*
De Fiori E.: *B-037, B-184*
De Franceschi S.: *B-880*
de Graaf F.: *E-49*
De Graaf N.: *C-0774*
de Haas-Kock D.F.M.: *B-150*
de Haën C.: *A-078*
de Jongh K.: *C-0305*
De Juan C.: *C-0058*
De Juan Delago M.: *C-0778*
de Kerviler E.: *C-0344, C-0459, E-22*
De Keyzer F.: *B-338*
de Koning H.J.: *B-381*
de Kort G.A.P.: *B-903*
De la Iglesia P.: *C-1050*
De la Pedraja Gomez-Ceballos I.: *C-0085*
de Lama E.: *C-0063, C-0507, C-0686, C-0741*
De Lama Salvador E.: *C-0156*
De Leo C.: *B-475, B-476*
De Luca G.: *C-0332*
De Luis E.: *B-071, C-0206, C-0223, C-0665*
De Lutio di Catelguidone E.: *C-0132*
De Maeseneer M.: *C-0681*
De Monti M.: *B-455*
de Monyé C.: *B-452*
De Nicola A.: *B-534*
de Pablo L.: *C-0927*
De Ridder F.: *C-0906*
de Roos A.: *A-173, A-271, B-214, B-220, B-428, C-0243, C-1020*
- De Rosa V.: *C-0132*
De Rubeis M.: *B-409*
De Santis A.: *C-0831*
De Schepper A.: *C-0191*
De Schepper A.M.A.: *B-463*
De Vargas Macciucca M.: *C-0548*
de Vos R.: *B-818*
de Vos S.: *B-521*
de Weert T.T.: *B-452*
De Wever W.F.M.: *B-385, B-845*
de Wilde J.: *A-285*
de Win M.M.L.: *B-222, B-223, C-0815*
Deak P.: *B-445, B-776*
Dearnaley D.: *B-724*
DeBacker A.I.: *A-134*
Debatin J.F.: *A-159, B-175*
Debernardi S.: *B-377*
Debus J.: *B-905*
Deckers S.: *D-07*
Dedes I.: *C-0826*
Deftereos S.: *C-0077*
Deftereos S.P.: *B-640*
Degenhardt C.: *B-610*
Degobbis F.: *B-602*
DeGraef M.: *A-033*
Deguara J.: *B-069*
Dehdashti A.R.: *B-765*
Dehmeshki J.: *C-0291*
Deicke C.: *B-261, B-371*
Deistung A.: *B-105, B-921*
Dekan V.S.: *C-0055, C-0849*
Del Campo L.: *C-0061*
del Cura J.L.: *C-0752*
Del Favero C.: *B-024*
Del Frate C.: *B-266, B-397, B-613, B-618*
Del Greco M.: *C-0264, C-0360*
Del Guerra A.: *A-117*
Del Maschio A.: *B-082, B-176, B-264, B-422, B-862, B-907*
del Valle-Sanz Y.: *C-0936*
Delabrousse E.: *C-0074*
Delaloge S.: *B-268*
DElannoy-Deken V.: *B-477, B-478*
Delfini R.: *C-0804*
Delgado A.: *C-0771*
Delgado Acosta F.: *C-0794, C-0874*
Delgado C.: *C-0657*
Delgado Cordón F.: *C-0704*
Delgado E.: *C-0231*
Delgado J.: *C-0894*
Delgado Sánchez C.: *C-0276*
Delhaye D.: *B-477, B-478*
Delhaye M.: *B-486*
Delibasis G.: *C-0739*
Delibasis K.: *C-0942, C-0963*
Delis H.: *C-0920, C-0954*
Delistamatis A.: *B-238*
Della Pina C.: *C-0199*
Della Sala S.W.: *C-0264*
Dellani P.D.: *B-532*
DellaPina C.: *B-121, B-122, B-180, B-852*
Delorme S.: *B-414, C-0388, C-0395, C-1000*
DeMarco J.: *B-446*
Demelia L.: *C-0863*
Demharter J.: *B-129*
Demirbas B.: *C-0551, C-0552*
den Heeten G.J.: *B-222, B-223, C-0815*
den Hollander J.: *B-095*
Denisov A.: *C-0485*
Denys A.: *A-031, B-596*
Deodhar C.: *B-542*
Dequiedt P.: *B-591*
Derchi L.: *C-0718*
Deridder F.: *B-860*
- Dermentzoglou V.: *C-0899, C-0900, C-0932, C-0933*
Derveenis C.: *C-0052*
Derweesh A.: *B-017, B-361*
Desai S.R.: *A-171, A-376*
deSouza N.M.: *B-724, B-791*
Destro G.: *C-0239*
Deurloo E.E.: *B-379*
Deutschmann H.A.: *B-399, B-886, B-887, C-0292, C-0917*
Deviere J.: *B-486*
Dewey M.: *B-427*
DeYoe E.A.: *C-0856*
Dharaiya E.: *C-0281*
D'Heft C.S.: *C-0650*
Di Bartolomeo M.P.: *B-287*
Di Blasi A.: *C-0586*
Di Cesare E.: *A-068, B-085, C-0428, C-0511, C-1063*
Di Costanzo A.: *B-536, C-0829*
Di Fabio F.: *B-339, B-712, C-0078*
di Maggio C.: *B-546, C-0187*
Di Martino M.: *B-043, B-044, B-107, B-515, B-575, B-699, B-710, B-741, B-747, C-0019, C-0034, C-0035, C-0113, C-0585*
Di Rezze L.: *B-198, B-299, B-512, C-0510*
Di Roma M.: *B-344, B-494, B-528, C-1033*
Di Salle F.: *A-020*
Di Salvo V.: *B-089*
Di Stasi C.: *B-244, C-1056*
Di Terlizzi M.: *B-527*
Di Tolla G.: *C-0626*
Diard F.: *B-544, C-0684*
Dias S.M.: *C-0952*
Díaz Aguilera R.: *C-0874*
Díaz Aguilera R.: *C-0794*
Díaz L.: *C-0223, C-0516, C-0576*
Díaz S.: *B-700*
Dicken V.: *B-386, D-09*
Dickerson R.E.: *B-774*
Dicle O.: *C-0384, C-0448, C-0456*
Diederich S.: *A-417, B-036*
Dieguez S.: *C-0067*
Dieguez-Costa E.M.: *C-0171*
Diehn M.: *B-439*
Diekmann F.: *A-319, B-160, B-588*
Diekmann S.: *B-160*
Dieli F.: *C-0401*
Dietrich M.: *B-350*
Dietrich O.: *B-225, B-226, B-272, B-383, B-429, B-851*
Dietzel M.: *B-261, B-371*
Diez Perez de las Vacas M.I.: *C-0049*
DiFiori J.P.: *B-801*
Digabel-Chabay C.: *C-0211*
Dilhuuyd M.-H.: *C-0184*
Dill T.: *C-0248*
DiMartino E.: *B-278*
Dimitrakopoulou G.: *C-0210*
Dimitriadis A.S.: *B-554, C-0717*
Dimitriadis C.A.: *C-1070*
Dimitropoulos N.: *C-0355, C-0955*
Dimmock M.: *D-14*
Dimopoulos I.: *C-0661*
Dimopoulos P.A.: *C-0660, C-0692, C-0715*
Dina R.: *B-791*
Dinkel H.-P.: *B-693*
Dippel D.W.J.: *C-0774*
Dirk M.: *C-0558*
Dirim Vidinli B.: *C-0558*
Diris B.: *C-0684*
Dirisamer A.: *B-093*
Ditt H.: *D-13*
Dittrich J.: *C-0407*

List of Authors and Co-authors

Dittrich R.: <i>B-458, B-902</i>	Duceux D.: <i>B-430, B-919</i>	Elsner K.: <i>B-247</i>
Divano L.: <i>C-0633, C-0647</i>	Duddalwar V.: <i>B-550</i>	Emmanouil E.: <i>C-0933</i>
Dixon A.K.: <i>A-157, B-465</i>	Duffaut-Andreux C.: <i>C-0691, C-0747</i>	Emmel D.: <i>D-10</i>
Djoa L.: <i>B-697</i>	Duffy G.J.: <i>B-716</i>	Emmer B.J.: <i>B-094</i>
Djuric A.: <i>C-0631, C-0701, C-0702</i>	Duffy P.: <i>C-0327</i>	Enchi Y.: <i>C-0948, C-0949</i>
Djuric-Stefanovic A.: <i>C-0174</i>	Dufour V.: <i>B-004</i>	Endo M.: <i>C-0283</i>
Do H.M.: <i>B-074</i>	Duhamel A.: <i>B-477, B-478, B-591</i>	Endo Y.: <i>C-1054</i>
Do K.-H.: <i>C-0310</i>	Dujardin M.I.: <i>B-860, B-861</i>	Endou M.: <i>C-0222</i>
Doan B.T.: <i>B-779</i>	Dukatz T.: <i>B-539</i>	Engehausen D.: <i>B-722</i>
Dobben A.C.: <i>B-818</i>	Duke D.M.: <i>C-0226</i>	Engel A.: <i>C-0129</i>
Dobriserevic B.: <i>C-0174, C-0631, C-0701, C-0702</i>	Dukic L.: <i>B-414</i>	Engelhard K.: <i>B-722</i>
Dobritz M.: <i>B-364</i>	Dullin C.: <i>B-207, B-333</i>	Engelke C.: <i>B-033, B-163, B-165</i>
Doda E.: <i>B-526</i>	Duman U.: <i>B-246</i>	Engelmann M.G.: <i>B-217</i>
Doenz F.: <i>A-031, B-596</i>	Dunlop D.: <i>C-0521</i>	Engels J.M.L.: <i>A-284</i>
Dogan H.: <i>B-428</i>	Dünser M.: <i>B-269, C-0225</i>	Engl T.: <i>B-723</i>
Dogan O.F.: <i>B-246</i>	Duran C.: <i>C-0597</i>	Enriquez G.: <i>C-0894</i>
Dogliotti L.: <i>B-131, C-0718</i>	Durgan J.: <i>C-0281</i>	Entwistle J.: <i>C-0324</i>
Doi S.: <i>C-0342</i>	Dursun A.: <i>C-0182</i>	Erb G.: <i>C-0403</i>
Dolgova I.: <i>C-0710</i>	Dyce S.: <i>B-909</i>	Erbel R.: <i>B-553</i>
Dolgushin M.B.: <i>B-438</i>	Dymarkowski S.: <i>A-105, B-084, B-090</i>	Ercolani M.: <i>B-375</i>
Dominelli V.: <i>B-299, B-409, B-509</i>	Dyskin D.E.: <i>C-0811</i>	Erden I.: <i>C-0852</i>
Domingo E.: <i>C-0063</i>	Dzienis W.: <i>B-317, C-0698</i>	Erdogan N.: <i>C-0558</i>
Domínguez Echávarri P.: <i>B-167, C-0455</i>	Dzik-Jurasz A.S.: <i>C-0162</i>	Erdugan S.: <i>B-704</i>
Domínguez Ferreras E.: <i>C-0179</i>		Erhard I.: <i>B-216</i>
Domínguez Franjo E.: <i>C-0098</i>		Ericson K.: <i>B-437</i>
Domínguez P.: <i>C-0657</i>		Ermes P.: <i>D-07</i>
Domínguez P.D.: <i>C-0206, C-0223, C-0311, C-0516, C-0576, C-0665</i>		Ernst C.: <i>B-861</i>
Domínguez-Franjo E.: <i>C-0049</i>		Ertel D.: <i>B-668</i>
Dominguez-Marin M.: <i>B-110</i>		Ertzbischoff O.: <i>B-591</i>
Dominguez-Oronoz R.: <i>C-0250, C-0770, C-1023</i>		Eschmann S.M.: <i>B-678</i>
Dominiotto M.: <i>C-0535</i>		Escobar M.: <i>C-0135</i>
Donati F.: <i>B-482, B-483, B-485, C-0402</i>		Escribano Vera J.: <i>C-0813</i>
Donnerstag F.: <i>B-311</i>		Esen G.: <i>B-584</i>
D'Onofrio M.: <i>B-607, C-0026</i>		Esmaeili A.: <i>B-749</i>
Donoso L.: <i>A-093</i>		Espejo Herrero J.J.: <i>C-0794, C-0874</i>
Donuru A.: <i>C-0324</i>		Esposito A.: <i>B-082, B-422</i>
Dorgelo J.: <i>B-309, B-524, C-0275</i>		Esseling R.: <i>B-038</i>
Doria C.: <i>C-0637</i>		Essig M.R.: <i>B-436, B-530, B-905, C-0395</i>
Doriguzzi Breatta A.: <i>B-199</i>		Esslinger M.: <i>B-157</i>
D'Orta G.: <i>B-556</i>		Estenne M.: <i>A-188</i>
Dosdá R.: <i>C-0875</i>		Etechami G.: <i>B-596</i>
Doss M.: <i>B-068</i>		Ettles D.F.: <i>C-1012</i>
Douek P.C.: <i>E-18</i>		Euathrongchit J.: <i>C-0066</i>
Dougeni E.: <i>C-0920</i>		Eun C.K.: <i>C-0925</i>
Doull R.I.: <i>B-720</i>		Eun-A K.: <i>C-0405</i>
Dourado R.: <i>B-876</i>		Eustace S.: <i>B-115</i>
Douskou M.: <i>B-659, C-0246</i>		Eustace S.J.: <i>B-359, B-742</i>
Doutriaux-Dumoulin I.: <i>C-0211</i>		Evaggelidou E.: <i>B-895</i>
Dovas S.: <i>C-1070</i>		Evangelidakis E.: <i>C-0908, C-0931</i>
Downes M.: <i>E-47</i>		Evangelista A.: <i>C-0250, C-1023</i>
Doyle E.: <i>C-0226</i>		Evertsz C.J.G.: <i>B-829, B-830</i>
Drakonaki E.: <i>B-751, C-0508, C-0919</i>		Evlogias N.: <i>C-0934</i>
Draney M.T.: <i>C-1030</i>		Ewenzyck I.: <i>C-0002, C-0007</i>
Drapé J.-L.: <i>B-132, B-804, C-0691, C-0747</i>		Exarhos D.N.: <i>C-1016</i>
Drapkin E.: <i>B-665</i>		Eymann R.: <i>B-205</i>
Drellich-Zbroja A.: <i>B-450</i>		Ezawa H.: <i>C-0351</i>
Drescher R.: <i>C-0599</i>		
Drevelegas A.: <i>A-098, C-0826</i>		
Drewes A.M.: <i>C-0109, C-0110</i>		
Drexl J.: <i>D-09</i>		
Drisis S.: <i>B-551, C-1045</i>		
Drobysheva N.S.: <i>C-0544</i>		
Dromain C.: <i>B-268</i>		
Drop A.: <i>B-112, B-274, B-516</i>		
Drossos C.: <i>C-0775, C-1071</i>		
Drouineau J.: <i>B-759, C-0858</i>		
Dualde D.: <i>C-0434, C-0875</i>		
Duarte A.: <i>B-192</i>		
Dubbins P.A.: <i>A-298</i>		
Düber C.: <i>B-890, C-0930</i>		
Duclos Vallee J.C.: <i>C-0002, C-0007</i>		
Ducou le Pointe H.: <i>A-293</i>		
E		
Ebara H.: <i>C-0339</i>	Eberhard J.: <i>B-663</i>	Ertel D.: <i>B-668</i>
Eberhardt R.: <i>B-704, B-705</i>	Eberhardt R.: <i>B-704, B-705</i>	Ertzbischoff O.: <i>B-591</i>
Ebner F.: <i>B-116, B-572, B-906, B-906</i>	Echeveste J.: <i>B-706, C-0303, C-0876</i>	Eschmann S.M.: <i>B-678</i>
Eckert J.: <i>B-169</i>	Eckstein F.: <i>B-257, B-687, C-0658</i>	Escobar M.: <i>C-0135</i>
Eckstein F.: <i>B-258</i>	Economopoulos N.: <i>C-0726</i>	Escribano Vera J.: <i>C-0813</i>
Eckstein F.: <i>B-257, B-687, C-0658</i>	Economou G.: <i>C-0210</i>	Esen G.: <i>B-584</i>
Eggebrecht H.: <i>B-553</i>	Edyvean S.: <i>B-669</i>	Esmaeili A.: <i>B-749</i>
Egitto M.G.: <i>C-0947</i>	Efremidis S.C.: <i>A-059, A-061, B-597, B-617, B-727, B-894, B-895, C-0438, C-1020</i>	Espejo Herrero J.J.: <i>C-0794, C-0874</i>
Egyed M.: <i>C-0652</i>	Efstathopoulos E.: <i>C-0920</i>	Esposito A.: <i>B-082, B-422</i>
Ehrenstein T.: <i>B-407</i>	Efstathopoulos E.: <i>C-0963</i>	Esseling R.: <i>B-038</i>
Eichinger M.: <i>B-473, B-704</i>	Eggebrecht H.: <i>B-553</i>	Essig M.R.: <i>B-436, B-530, B-905, C-0395</i>
Eichler K.: <i>B-009, B-034, B-302, B-340, B-345, B-401, B-405, B-408, B-410, B-500, B-507, B-875</i>	Egitto M.G.: <i>C-0947</i>	Esslinger M.: <i>B-157</i>
Eikefjord E.: <i>C-0504, C-0518</i>	Egyed M.: <i>C-0652</i>	Estenne M.: <i>A-188</i>
Einsele H.: <i>C-0293</i>	Ehrenstein T.: <i>B-407</i>	Etechami G.: <i>B-596</i>
Eisenberg D.P.: <i>B-676</i>	Eichinger M.: <i>B-473, B-704</i>	Ettles D.F.: <i>C-1012</i>
Eisenberg S.R.: <i>D-05</i>	Eichler K.: <i>B-009, B-034, B-302, B-340, B-345, B-401, B-405, B-408, B-410, B-500, B-507, B-875</i>	Euathrongchit J.: <i>C-0066</i>
Eisner W.: <i>D-18</i>	Eikenberry O.: <i>B-810</i>	Eun C.K.: <i>C-0925</i>
Ekberg O.: <i>B-810</i>	Eklund K.: <i>B-910</i>	Eun-A K.: <i>C-0405</i>
El Bagi M.E.A.: <i>A-135</i>	El Bagi M.E.A.: <i>A-135</i>	Eustace S.: <i>B-115</i>
El Ghali S.: <i>C-0461</i>	El Bagi M.E.A.: <i>A-135</i>	Eustace S.J.: <i>B-359, B-742</i>
El Khoury M.: <i>B-362, B-365</i>	El Ghali S.: <i>C-0461</i>	Evaggelidou E.: <i>B-895</i>
El-Azab M.: <i>B-396</i>	El Khoury M.: <i>B-362, B-365</i>	Evangelidakis E.: <i>C-0908, C-0931</i>
El-Baz M.: <i>B-396</i>	El-Azab M.: <i>B-396</i>	Evangelista A.: <i>C-0250, C-1023</i>
Eldevik P.: <i>B-645, C-0916</i>	El-Baz M.: <i>B-396</i>	Evertsz C.J.G.: <i>B-829, B-830</i>
Eleta F.: <i>C-0821, C-0884</i>	Eldevik P.: <i>B-645, C-0916</i>	Evlogias N.: <i>C-0934</i>
Elfurah M.: <i>B-450</i>	Eleta F.: <i>C-0821, C-0884</i>	Ewenzyck I.: <i>C-0002, C-0007</i>
Elgeti T.: <i>B-427, B-612</i>	Elfurah M.: <i>B-450</i>	Exarhos D.N.: <i>C-1016</i>
El-Hariry I.: <i>C-0460</i>	Elgeti T.: <i>B-427, B-612</i>	Eymann R.: <i>B-205</i>
Eliakim R.: <i>C-0166</i>	El-Hariry I.: <i>C-0460</i>	Ezawa H.: <i>C-0351</i>
Elias D.: <i>C-0252, C-0884</i>	Eliakim R.: <i>C-0166</i>	
Elias D.A.: <i>C-0705</i>	Elias D.: <i>C-0252, C-0884</i>	
Ell P.J.: <i>B-007</i>	Elias D.A.: <i>C-0705</i>	
Ellis S.M.: <i>A-088, A-278, C-0291</i>	Ell P.J.: <i>B-007</i>	
Elmaleh M.: <i>A-239</i>	Ellis S.M.: <i>A-088, A-278, C-0291</i>	
Elmstähli B.A.: <i>B-879</i>	Elmaleh M.: <i>A-239</i>	
F		
Fabbri E.: <i>B-030</i>	Fabbri E.: <i>B-030</i>	Fabbri E.: <i>B-628</i>
Faber H.: <i>B-104, B-376</i>	Faber H.: <i>B-104, B-376</i>	Faber H.: <i>B-104, B-376</i>
Fabiano S.: <i>B-511, B-632, C-0627, C-1033</i>	Fabiano S.: <i>B-511, B-632, C-0627, C-1033</i>	Fabiano S.: <i>B-511, B-632, C-0627, C-1033</i>
Fabregas V.: <i>C-0741</i>	Fabregas V.: <i>C-0741</i>	Fabregas V.: <i>C-0741</i>
Fabri M.: <i>C-0833</i>	Fabri M.: <i>C-0833</i>	Fabri M.: <i>C-0833</i>
Facius M.: <i>B-022, B-263</i>	Facius M.: <i>B-022, B-263</i>	Facius M.: <i>B-022, B-263</i>
Fadeev N.P.: <i>C-0848</i>	Fadeev N.P.: <i>C-0848</i>	Fadeev N.P.: <i>C-0848</i>
Faedda C.: <i>B-026, B-589</i>	Faedda C.: <i>B-026, B-589</i>	Faedda C.: <i>B-026, B-589</i>
Fahrigr R.: <i>B-074, B-888</i>	Fahrigr R.: <i>B-074, B-888</i>	Fahrigr R.: <i>B-074, B-888</i>

italic numbers refer to presentation numbers

A B C D E F G 657

List of Authors and Co-authors

- Faitaki S.: C-0399, C-0470, C-0739
 Falaschi F.: B-482, B-483, B-485, C-0402
 Falchini M.: C-0620, C-0636
 Falcó Fages J.: C-1029
 Falcó J.: C-0605
 Faletti C.: A-312, B-129
 Falini A.: B-229
 Fan G.: B-535, B-643
 Fan L.: B-040, B-328, B-856
 Fan M.: B-681
 Fanelli F.: B-198, B-299, B-409, B-509, B-512
 Fang W.: C-0261
 Fang W.: A-367
 Fantin B.: B-004
 Farber E.: C-0166
 Fargeaudou Y.: B-794
 Farias P.: C-0884
 Farina D.: B-181, B-390
 Farina E.: B-229
 Farina R.: B-363
 Farrell M.: C-0827
 Farrelly C.: C-0785, C-0801, C-1032
 Farsaris D.: C-1016
 Fasano F.: C-0653
 Fasching A.: B-881
 Fataar S.: B-017, B-361
 Fatta G.: C-0401
 Fattori R.: B-064, B-066, B-081, B-529
 Fauser S.: B-432
 Fausto A.: B-021, B-253, B-254, B-264, B-270, C-0198, C-0828
 Fava C.: C-0319
 Favarger N.: B-133
 Fazio F.: B-728
 Fedele F.: C-0238
 Feely J.: B-559
 Fehér E.: B-915
 Feichtinger M.: B-906
 Felber S.: D-18
 Feldman U.: E-33, E-37
 Feldo M.: C-1046, C-1060
 Félix A.: B-792, C-0423, C-0424
 Felix R.: A-411, B-407, B-423, B-491, B-825
 Felten M.K.: B-382
 Femia M.: B-297
 Fenchel M.: C-0270
 Fencl P.: B-841
 Feng F.: C-0824
 Feng G.: C-0598
 Feng X.: B-433, B-434, B-933
 Fenlon H.M.: C-0226
 Feragalli B.: B-388, C-0307
 Fergane B.: B-462, C-0074, C-0523
 Fernández A.: C-0063
 Fernandez Canabal E.: C-0677
 Fernández E.: C-0121
 Fernandez E.: C-0136, C-0249
 Fernández G.C.: C-0276
 Fernández J.: C-0121
 Fernandez J.M.: B-770
 Fernández M.A.: C-0688
 Fernandez P.: C-0171
 Fernández-Carrera M.: C-0123
 Fernandez-Echevarria M.A.: C-0713, C-0731, C-0764
 Fernández-Velilla M.: B-758, C-0303
 Fernández-Zubillaga A.: B-758
 Ferrando J.R.: C-0104
 Ferrando Valls F.: C-0290
 Ferraresi S.: B-215, B-824
 Ferrari A.: C-0830
 Ferrari F.: B-891
 Ferrari M.: B-484
 Ferrari R.: C-0371
 Ferraris F.: C-0319
 Ferreira A.: C-0150
 Ferreiro A.: C-0771
 Ferrer Puchol M.D.: B-378
 Ferrer S.: C-0606
 Ferretti G.R.: B-708
 Ferretti S.: B-037, B-145
 Ferrié J.-C.: C-0858
 Ferrucci J.T.: A-050
 Fettit C.: C-1079
 Feussner H.: B-812
 Fewins H.: C-1062
 Feydy A.: B-004, B-593, C-0673
 Feydy A.: B-132, B-804, C-0747
 Feyer A.: B-310
 Fezoulidis I.V.: B-912
 Fezoulidis J.B.: C-1009
 Fiala P.: B-841
 Fiaschetti V.: C-1033
 Fichele S.: B-702
 Fichte H.: C-0304, C-0323, D-13
 Fiechi D.: C-0454
 Fieguth H.-G.: B-034
 Fiehler J.: B-051
 Field J.: D-14
 Fields S.: B-151, B-152
 Figl M.: D-01
 Figols J.: C-0688
 Figueroa M.T.: C-0106
 Filippidou A.: C-0399, C-0443, C-0482
 Filippone A.: B-339, B-413, B-712, B-745, C-0078
 Filipponi F.: B-122, B-180
 Fink C.: B-398, B-472, B-473, B-704, B-705, B-905, C-0294, C-0345, C-0386, C-1000
 Finke M.: B-453, B-901
 Finlay L.: C-0968
 Fiocchi F.: B-215, B-492, B-824
 Fiore F.: C-0045
 Fiorentino A.: C-1056
 Fiorentino C.: C-0189
 Fiori R.: B-289
 Fiorina P.: B-862
 Firat Z.: B-041
 Fischbach R.: B-307, B-884, C-0245, C-0271
 Fischer D.: C-0105, C-0129, C-0166
 Fischer D.R.: B-261, B-371, B-372
 Fischer H.: B-403
 Fischer K.: B-335
 Fischer M.J.: B-300, B-517, B-633
 Fischer T.: E-63
 Fischer T.: B-816
 Fischmann A.: B-157, B-587
 Fití M.: C-0894
 Fitzek C.: C-0891
 Fitzgerald G.P.: B-909
 Fitzgerald P.: B-663
 Fitzgerald R.: A-260
 Fitzmaurice D.: A-151
 Fiumara C.: B-287, C-0786
 Fiumicelli A.: D-17
 Flach H.Z.: C-0774
 Flanagan F.: C-0226
 Flaris N.: C-0613
 Flatz W.H.: B-183
 Fleischmann D.: B-119, B-888, C-0260, C-0263, C-1013, D-19, E-40
 Fleiter N.: B-506
 Fleiter T.R.: B-694
 Fletcher-Heath L.: B-548
 Flipo R.-M.: B-561
 Flis C.M.: C-0528, C-0779, C-1075
 Flodmark O.: A-419
 Floery D.: B-027, B-836
 Flohr T.G.: B-010, B-341, B-343, B-346, B-349, B-382, B-442, B-660, D-13
 Flor N.: B-185, B-411, B-455
 Flórez-Ordóñez Y.N.: C-0945
 Flöry D.: B-023, B-730
 Foerster B.: B-645, C-0880
 Foerster B.R.: C-0916
 Foki T.: B-930
 Fokin V.A.: C-0849
 Fong Y.: B-676
 Fonseca-Santos J.: C-0924
 Fontana F.: B-297
 Fontana F.: B-298
 Foo L.F.: C-0672
 Foos D.H.: C-0979
 Ford R.: B-772
 Ford S.: C-1047
 Forgács B.: C-0141
 Fork F.-T.: A-056
 Fornara P.: B-135, C-0694, C-0707
 Fornasa F.: C-0190
 Former J.: C-0667
 Forradellas A.: C-0072, C-0099, C-0100
 Forrai G.: C-0064, C-0318
 Forst R.: B-355, B-357
 Forsting M.: B-813
 Forstner R.: A-131
 Forstreuter F.: C-0799
 Forsyth L.: B-916
 Fortis D.: C-0335
 Fortuño Andrés J.R.: C-0605, C-1029
 Fossaceca R.: B-527, C-0768
 Foster A.: B-194
 Fotiinos A.: C-0706
 Fotiadis N.: B-067
 Fotiadou V.: C-0077
 Fotopoulos A.: B-896
 Foussas S.: B-659
 Fousteris A.: C-0482
 Fowler G.: B-334
 Fragos C.: C-0400
 Fraile Moreno E.: C-0098
 Fraile Moreno E.: C-0049
 Fraioli F.: B-031, B-242, C-0306
 Francesca D.: C-0199
 Franceschelli G.: B-185
 Franceschini G.: B-585
 Francone M.: B-084, B-090
 Francone M.: B-420, B-526, C-0238, C-1043
 Franke P.: B-675
 Franken E.M.: C-0367
 Franquet T.: A-043, A-087, A-377, C-0279, C-0284, C-1083
 Frans F.: B-684
 Franz W.M.: B-217
 Fraschini M.: B-100, C-0802, C-0863, C-0866
 Frassani R.: B-065
 Frati A.: C-0804
 Frattini T.: C-1066
 Frauscher F.: A-353, B-130, B-807, B-859
 Frede T.E.: B-833
 Freddy D.: A-283
 Freesmeyer M.G.: B-022
 Freitas D.N.D.: C-0218
 Freling N.J.M.: A-025
 Frericks B.B.: B-072, C-0010, C-0011
 Freudenberg L.: B-840
 Freudenberg L.S.: B-677
 Freund M.: C-0898
 Freund M.C.: B-590, C-0053, C-0087
 Frey H.: E-01
 Frey O.: B-204, B-670
 Freyschmidt J.: A-140
 Friedrich K.: B-353

List of Authors and Co-authors

Fries P.: C-0060, C-0237, C-0659, C-0907	Galazka Z.: B-070	Gaspar T.: B-168
Frigerio L.F.: C-0626	Galesanu C.: B-252	Gasparaitis A.E.: C-0124
Frija G.: C-0069, C-0368, C-0390	Galesanu R.G.: B-252	Gasparini D.: B-065, B-457, B-513
Frija J.: C-0344, C-0459	Galia M.: A-276, B-088, C-0027, C-0167, C-0656, C-0727	Gasparotti R.: A-053, C-0980
Frisoli J.K.: B-074	Galiatsou E.: B-560	Gasser J.: C-1017
Fritzsche A.: C-0012, C-0941	Galina B.: B-583	Gast K.K.: B-701
Fritzsche C.: B-672	Galina P.: C-0295	Gattinoni L.: A-168, A-169
Fritz B.: C-0984, C-1019	Gallacher D.: B-334	Gaudino S.: C-0340
Fritz D.: B-523	Gallagher J.: B-773	Gauglio C.: A-149
Fritz G.A.: B-399, B-616, B-887, C-0917	Gallarato G.: C-0591	Gavelli G.: B-064, B-066, B-081, B-529
Fritz J.: B-421, B-621, C-0612, C-0623	Gallard J.-C.: B-639	Gavrilin A.V.: C-0040
Fröhlich J.: B-746	Gallardo E.: C-0687, C-0688	Gavrilov M.: C-0873
Frokjær J.B.: C-0109, C-0110	Gallardo X.: C-0289, C-0326	Gawehn J.: B-532
Frush D.P.: C-0914	Gallé G.: B-616	Gawenda M.: B-063, B-291, B-456
Frustaci A.: B-082	Gallinat J.: C-0799	Gayle B.: B-392
Fruth M.: B-453, B-901	Gallucci M.: A-366, B-287, C-0786, C-0803	Gazeau F.: B-779
Fu H.H.: C-0824	Galluzzo M.: C-0447, C-0696, C-0901, C-0922	Gazhonova V.: B-726
Fu Y.: D-12	Galuppo C.: B-148	Gazis A.: B-877
Fu Y.: B-739	Gambaccini M.: B-030, B-546	Ge Q.: B-303
Fuchs H.: B-285	Gambaro A.: C-0188	Geiger B.: A-347, B-778
Fuchsjäger M.H.: B-023, B-027, B-730, B-736, C-0678	Gamidov S.: C-0485	Geiger B.: B-844
Fuechsel F.G.: B-189	Gamvroula E.: B-336	Geissler A.: B-930
Fueger B.J.: B-187, B-384	Ganaha F.: C-0601	Geitung J.T.: B-487
Fuerst M.: D-01	Ganatra R.H.: B-925	Geleijns J.: A-396, B-447, B-448
Fugazzola C.: B-134, B-298	Ganau Macias S.: B-380	Genadry R.R.: B-790, C-0420
Führmann A.: D-04	Ganau S.: B-262	Genant H.K.: C-0674, C-0997
Fujii M.: B-470	Gandini G.: B-199, C-0463	Gennaro G.: B-546, C-0187
Fujii N.: C-0560	Gandini R.: B-508, B-511, B-519, B-632, B-635, B-873	Genovese E.: B-134
Fujii S.: C-0422, C-0430, C-0431	Gandolfo N.: C-0718	Geoffray A.: C-0797
Fujikawa A.: B-319	Gandolfo N.G.: B-131	George C.: C-1012
Fujimoto K.: C-0392	Gangi A.: C-0649	Georgescu C.E.: C-0972
Fujimoto S.: C-0788	Gangkofer A.: B-816	Georgescu S.A.: C-0957, C-1072
Fujita H.: C-0380	Gannouni A.: C-0312, C-0313, C-1057	Georgieva B.: B-886
Fujiwara T.: C-0422, C-0430, C-0499	Ganten M.: C-1000	Gerber B.L.: C-0253
Fukasawa H.: C-0308	Ganter C.: B-033	Gerber D.: B-041
Fukuba E.: C-1034	Ganzetti A.: C-0219	Gerdesmeyer L.: B-136
Fukuba E.: C-0806	Garbagnati F.: C-0626	Gerhard R.: B-058
Fukuba E.: C-0839	Garbay J.R.: B-128	German I.: C-0710
Fukunaga T.: C-0308, C-0566	Garcia A.B.: C-0577	Gerritsen F.A.: D-07
Fukushima H.: C-0956	García Casado E.: C-0050	Gershovich M.: C-0671, C-0750
Funabashi N.: C-1007	Garcia Contiente G.: C-0232	Gervas C.: C-0249
Funahashi K.: C-0093	García Criado A.: C-0030	Gervás C.: C-0136
Funakubo M.: C-0415, C-0594	Garcia de Iturraspe C.: C-0136	Ghanem N.A.: B-008, B-247, B-675, C-0127
Fung K.K.L.: C-0994	García de Jalón J.A.: B-071	Ghazy H.: B-408
Funicelli L.: B-145	Garcia del Salto L.: C-0098	Ghiatas A.A.: A-243
Funke M.: B-207, B-333	Garcia del Salto L.: C-0049	Ghirardi C.: B-181
Funovics M.A.: B-671, B-674, B-787	García J.: C-0687	Ghirardo D.: C-0570
Furlan F.: C-1018	Garcia M.: B-622	Ghita O.: B-329
Furmidge I.: C-0160	Garcia Merletti P.: C-0268	Ghysen D.: B-441
Furukawa A.: C-0186	Garcia Morales I.: C-0813	Giacconi C.: C-0199
Furukawa H.: B-412, C-0222	Garcia Pellegrino C.: C-0744, C-0822	Giampietro A.: B-265
Furuya K.: C-0146, C-0170, C-0788	García R.: C-0606	Giancola M.L.: C-0834
Fütterer J.J.: B-490, B-493, B-497, B-725, C-0468	García Rio F.: B-706	Giannakis D.: B-617, B-727
<hr/>		
G		
G. Urbón M.: C-0086	García S.: C-0100	Giannakopoulou C.: C-0919
Gaa J.: B-033	García-Asensio S.: C-0072, C-0099	Giannatempo G.M.: B-536, C-0829
Gabata T.: C-0038	García-Barredo R.: C-0687, C-0688	Giannikouris G.: C-0766
Gackowski A.: B-306	Garcia-Barriga F.J.: C-0156	Giannouli S.: C-0396, C-0618
Gada V.S.: C-0417	García-Medina J.: C-0575	Giannoudi T.: B-640
Gaffuri M.: C-0909	García-Medina V.: C-0575	Giavroglou C.: B-554
Gaggero G.: B-026	Gardeur D.J.: C-0378	Gibney R.G.: B-172
Gagliardi N.: B-367	Gardner E.A.: C-0394	Gibo M.: C-0582
Gahleitner A.: A-422	Garel C.: A-407	Gibo S.: C-0582
Gahr J.: B-473	Garg P.K.: C-0128	Gibson D.: B-117
Gaida K.: B-211	Gargoulaki M.: C-0860	Gielen J.L.M.A.: B-463
Gaignot C.: C-0742	Garmish A.R.: B-680	Giesel F.L.: B-905, C-1000
Gaitanis A.: C-0955	Garmish E.A.: C-0690	Gietema H.A.: B-170
Gaitini D.: C-0166	Garriga V.: C-0928	Gietka-Czernel M.: B-057
Gajewicz W.: C-0869	Gartner L.: B-149	Gigaud M.: B-760
Galanski M.: A-183	Gartus A.: B-930	Giger M.L.: C-0124
	Garvey C.J.: B-909, C-0160, C-0161	Gigli G.L.: B-513
	Garwood M.: B-735	Gigoni R.: B-482, B-483, B-485, C-0402
	Garzón G.: C-0588, C-1074	Gil Bello D.: B-719
		Gil D.: C-0289, C-0326, C-0792
		Gil J.: C-0875

List of Authors and Co-authors

Gil S.: *C-1050*
 Gilabert R.: *C-0030*
 Gilbert L.: *C-0002*
 Gilhuijs K.G.A.: *B-379*
 Gilkeson R.: *C-0281*
 Gilkeson R.C.: *C-0329*
 Gillams A.R.: *A-269, B-481*
 Gillan C.: *B-742*
 Gillard J.H.: *C-1077*
 Gilles R.: *C-0184*
 Gillet B.: *B-779*
 Gil-Nagel Rein A.: *C-0813*
 Gilon R.: *B-003*
 Giménez A.: *C-0279, C-0284*
 Gimson A.: *B-579*
 Gipp I.N.: *C-0991*
 Girard N.: *A-418*
 Girmann M.: *C-0640*
 Girometti R.: *B-618, B-805*
 Gismondi G.: *C-0803, C-1063*
 Gispert S.: *C-0135*
 Giugni E.: *C-0864, C-0947*
 Giulianite F.: *B-173*
 Giunta S.: *C-0338*
 Giuseppetti G.M.: *B-264, C-0024*
 Giusti P.: *C-0130*
 Giusti S.: *C-0130*
 Given M.: *B-194, C-0642*
 Given-Wilson R.M.: *B-832*
 Gjesdal K.I.: *B-487*
 Gkanatsios N.: *B-029*
 Glaser C.: *A-403, B-232, B-683*
 Glaser M.: *B-532*
 Glazer G.M.: *B-074, B-888*
 Glenn D.: *B-627*
 Gleeson T.: *E-46*
 Glotsof D.: *C-0355*
 Glowacki J.: *C-0023, C-0564*
 Gluecker T.: *B-248*
 Glynne-Jones R.: *C-0162*
 Gmür A.: *C-0080, C-0374*
 Gnasso A.: *B-880*
 Gobert P.: *E-26*
 Goddard P.R.: *C-0343*
 Godward S.: *C-0200*
 Goebel M.: *C-0411*
 Goehde S.C.: *B-571, B-813*
 Goffette P.: *A-065*
 Göögüs Ç.: *C-0477, C-0478, C-0479, C-0486, C-0487, C-0488, C-0500*
 Göögüs O.: *C-0487, C-0488*
 Goh P.S.: *C-0096*
 Goh V.: *C-0304, C-0323*
 Goh V.J.: *B-149*
 Gokan T.: *C-0010, C-0011, C-0512*
 Gola G.: *B-127*
 Gola M.: *B-332*
 Golabek W.: *B-274*
 Goldenberg R.: *B-168*
 Goldin J.G.: *C-0282*
 Golding S.J.: *B-055, B-449, B-796*
 Goldman S.M.: *C-0506*
 Goldman S.M.: *C-0881*
 Golebiowski M.: *B-098, C-0003, C-0256, C-0382, C-0844*
 Golebiowski M.: *B-929*
 Golli M.: *C-0312, C-0313*
 Gollini P.: *C-0319*
 Golman K.: *B-879*
 Golovko T.: *C-0732*
 Golpinar F.: *C-0929*
 Gomez A.: *C-0220*
 Gomez E.: *C-1024, C-1031*
 Gómez H.: *C-0072, C-0099, C-0100*
 Gómez León N.: *C-0097, C-0677, C-0927*
 Gomez V.: *C-0793*
 Gomez Zanetta S.: *C-0738*
 Gomez-Dermitt V.: *C-0713, C-0731, C-0764*
 Gomez-Gonzalez E.: *B-110*
 Gómez-León N.: *C-0890*
 Gomi S.: *C-0342*
 Gomi T.: *C-0951*
 Gomis M.: *C-0851*
 Gomori J.M.: *B-168, B-540*
 Gonçalves A.: *B-192*
 Gonzalez A.: *C-0793*
 González Álvarez I.: *C-0433*
 Gonzalez B.: *C-0171*
 Gonzalez C.: *C-0136*
 Gonzalez Crespo I.: *C-0455*
 Gonzalez E.: *C-0063*
 González F.: *C-0009, C-0059*
 Gonzalez Gordaliza C.: *C-0546, C-0561*
 Gonzalez I.: *C-0214*
 Gonzalez L.: *B-770*
 Gonzalez S.: *C-0030*
 González-Crespo I.: *C-0311*
 González-Tutor A.: *C-1044*
 Gooding B.: *B-391*
 Goodman L.R.: *A-170*
 Gopal K.: *C-0527*
 Goraj B.: *C-0772, C-0809, C-0869*
 Goralnik L.: *C-0105*
 Gordeev A.: *C-0710*
 Gordjani N.: *B-897*
 Gorgots O.V.: *C-0602*
 Görkemli H.: *C-0426*
 Gorriño O.: *C-0752*
 Gorska-Chrzastek M.: *C-0809, C-0869*
 Gortenutti G.: *C-0190, C-0239, C-1018*
 Gosek K.: *C-0023*
 Gossrau P.: *B-051*
 Gotfried V.: *E-36*
 Gotovac N.: *C-0178*
 Götz B.: *B-046*
 Gough N.: *C-0445, C-0472, C-0483*
 Goulão A.: *A-003*
 Gould : *C-1062*
 Gould D.A.: *B-202*
 Gouma D.J.: *B-489*
 Gourtsoyannis N.: *A-313, B-091, B-337, B-608, B-649, B-751, B-771, C-0036, C-0083, C-0400, C-0508, C-0800, C-0919, C-0976*
 Gouttefangeas C.: *C-0611*
 Gouvêa M.: *C-0952*
 Gowland P.A.: *A-406*
 Gozzi G.: *C-0219*
 Grabbe E.: *B-207, B-333*
 Grabowska L.: *B-332*
 Graefe S.: *B-204*
 Graells Ferrer M.: *C-0704*
 Graessner J.: *B-053*
 Graessner J.: *B-051*
 Graf H.: *B-621, C-0403, C-0975*
 Graf R.: *A-301*
 Graham R.: *C-0987*
 Grainger A.: *E-69*
 Grampp S.: *A-102*
 Granatelli A.: *B-526*
 Grande D.: *C-0752*
 Granell E.: *C-0666*
 Graser A.: *B-691*
 Grass M.: *B-426, B-820*
 Grassedonio E.: *B-712, B-745, C-0078*
 Grassi R.: *B-363, B-367*
 Gratacós E.: *C-0894*
 Gravano M.: *C-0255*
 Graves M.J.: *C-1077*
 Gray J.E.: *B-772*
 Grazioli L.: *A-147, B-049, B-124, B-125, B-609, C-0404*
 Greco P.: *C-0517*
 Greess H.: *B-052, B-280*
 Gregersen H.: *C-0109*
 Gregersen H.E.: *B-236*
 Grenacher L.: *B-413, B-414*
 Grenier P.: *B-698, C-0043, C-0089, C-1079*
 Grenier P.A.: *A-029, A-097*
 Gress D.: *B-772*
 Grgic A.: *C-0328, C-0387, C-0640*
 Griffith K.: *B-925*
 Grimm C.: *B-315, B-432*
 Grist T.: *E-07*
 Grivé E.: *A-002*
 Gröller E.: *D-19*
 Grolios G.: *C-1070*
 Gromov A.I.: *C-0973*
 Grön G.: *C-0783*
 Gronchi A.: *C-0115, C-0145, C-0769*
 Grüne H.-J.: *B-780*
 Groppo Marchisio F.: *C-0590*
 Gross W.L.: *B-637*
 Grossi E.: *B-104, B-376*
 Großkopf S.: *C-0998*
 Grosso M.: *C-0570, C-0590, C-0591*
 Grosu A.: *C-0411*
 Grothoff M.: *A-411, B-423, B-825*
 Groves A.M.: *B-465, C-0200*
 Groves A.M.: *B-007*
 Gruber G.: *B-288*
 Gruber H.: *C-0714, C-1038, C-1039*
 Gruber M.: *C-0907*
 Gruenhagen J.: *B-732*
 Gruenig E.: *B-472*
 Grunwald I.Q.: *B-205*
 Gruszczyńska K.: *C-0868*
 Gryspeerd S.: *B-697, C-0088*
 Grzelak P.: *B-118, C-0809, C-0869*
 Grzeszczak W.: *C-0023*
 Gstöttner W.: *A-123*
 Guardia Mas E.: *C-0778*
 Guariglia A.: *C-0335*
 Guarise A.: *B-484*
 Guazzoni G.: *C-0453, C-0454, C-0491, C-0502*
 Guccione S.: *B-788*
 Gudlowski Y.: *C-0799*
 Gudmundsen T.E.: *C-0336*
 Guerchicoff M.: *C-0252*
 Guerini H.: *B-132, B-804, C-0691, C-0747*
 Guermazi A.: *C-0460, C-0649, C-0997*
 Guerrisi A.: *B-575, B-741, B-811, C-0084, C-0090, C-0092, C-0391*
 Guettier C.: *C-0002, C-0007*
 Guido F.: *C-0307*
 Guijarro J.: *C-0875*
 Gulati M.S.: *C-0128*
 Gullien R.: *B-154*
 Güllmar D.: *B-648, B-920*
 Guma A.: *C-0156*
 Günaydin I.: *C-0623*
 Gündel L.: *B-169, D-13*
 Gunji Y.: *B-014*
 Guntern D.V.: *B-133*
 Günther R.W.: *B-073, B-080, B-169, B-203, B-208, B-278, B-348, B-349, B-382, B-520, B-522, B-523, B-578, B-653, B-657, B-658, B-750, B-753, B-819, B-898*
 Guo G.: *B-015, B-919*
 Guo Q.: *B-535, B-643*
 Gupta R.: *B-276*
 Gur S.: *B-688*

List of Authors and Co-authors

Gurgan U.: *C-0033*
 Gurses B.: *B-584*
 Gurung J.: *B-324*
 Gutberlet M.: *A-411, B-423, B-423, B-825, D-10*
 Guth S.: *C-0649*
 Gutierrez A.: *C-0252*
 Gutiérrez J.: *C-0121, C-0927*

H

Ha H.K.: *B-419, C-0001, C-0065, C-0119, C-0643*
 Haage P.: *B-578, B-753*
 Haakull A.E.: *B-154*
 Haba D.: *B-279*
 Haberal M.: *C-1051*
 Habermann C.R.: *B-051, B-053*
 Habets R.: *D-07*
 Hacein-Bey L.: *B-927*
 Hatchulla E.: *B-561*
 Haddad M.C.: *C-0094, C-0484, C-0910*
 Haderer A.: *D-10*
 Hadjidekov V.G.: *C-0398*
 Hadjidekova V.B.: *C-0398*
 Hadjigeorgi C.: *C-0784, C-0861, C-0934*
 Hadjipavlou A.: *B-771*
 Hadley D.: *C-0883*
 Haemisch Y.: *E-68*
 Haen S.: *C-0611*
 Haferkamp A.: *B-398*
 Hafsa C.: *C-0312, C-0313*
 Hagiwara A.: *B-665*
 Hahn H.K.: *B-530, D-09*
 Hahn K.: *B-717*
 Haider M.A.: *B-721*
 Hajek M.: *C-0362*
 Halimi P.: *C-0555*
 Halka A.: *C-0733*
 Hall D.E.: *B-786*
 Haller S.: *B-926, B-928*
 Hallett R.L.: *C-0260*
 Halligan S.: *B-149*
 Hallscheidt P.J.: *B-195, B-398, C-0589*
 Halpern B.S.: *B-187, B-384*
 Ham S.-Y.: *B-831*
 Hama Y.: *C-0966*
 Hamann G.F.: *B-314*
 Hamazawa Y.: *C-0760, C-0761*
 Hamers R.: *B-301, B-667*
 Hamm B.: *B-032, B-160, B-427, B-491, B-588, B-612*
 Hamm T.: *B-506*
 Hammami S.: *C-1057*
 Hammerstingl R.M.: *B-045, B-046, B-048, B-855, B-877, E-05, E-43*
 Han B.-K.: *C-0202, C-0203, C-0204*
 Han D.: *C-0376*
 Han D.: *C-0762*
 Han G.S.: *C-0533*
 Han J.K.: *B-076, B-077, B-178, B-210, B-711*
 Han J.-K.: *B-695*
 Han M.H.: *C-0845*
 Han R.: *C-0466*
 Han S.-S.: *C-0008, C-0118*
 Han Y.-M.: *C-0352, C-0353*
 Hanel R.: *D-01*
 Hanisch P.: *B-835*
 Hannig C.E.M.: *B-808, B-809, B-812*
 Hannoun L.: *C-0043*
 Hansch A.: *B-204, B-372, B-670, C-0230, C-0236*
 Hansell D.M.: *A-096*
 Hansell P.: *B-881*
 Hansen J.: *B-036*
 Hansson B.: *A-136*

Hany T.F.: *B-013*
 Hao J.: *B-227, B-228*
 Happel B.: *B-012, C-0509*
 Happel B.M.: *B-400*
 Harada N.: *C-0146*
 Hardit C.: *C-0858*
 Hare C.: *B-305*
 Hargadan G.: *C-1032*
 Hargaden G.C.: *C-0427, C-1021*
 Häring H.-U.: *C-0012, C-0941*
 Harisinghani M.: *A-153*
 Harries-Jones H.: *E-12*
 Harte S.E.: *B-716, C-0013*
 Harth M.: *B-311*
 Hartmann D.: *B-570, B-576*
 Hartmann M.: *B-917*
 Hartmann M.: *C-0395*
 Hartvig Sode A.: *A-394*
 Harvey C.: *B-305*
 Hase M.: *C-0298*
 Hashagen C.: *B-201, B-250*
 Hasiotou M.: *C-0908, C-0931*
 Hatabu H.: *B-387, B-471, C-0285, C-0325*
 Hatano H.: *B-158*
 Hatz R.: *B-383*
 Hatzidakis E.: *C-0919*
 Hatzidakis A.A.: *B-620*
 Hatzimanoli V.: *B-751*
 Hatzimichail K.: *C-0584*
 Haubner R.: *C-0411*
 Haude A.F.: *C-0859*
 Haueisen J.: *B-920*
 Hauenstein O.: *B-169*
 Hauger O.: *B-544, C-0684*
 Hauksson J.: *B-495*
 Haupt C.: *B-510*
 Hausegger K.: *C-1017*
 Hawkes D.: *A-245*
 Hayabuchi N.: *C-0392*
 Hayakawa K.: *C-0601*
 Hayasaka K.: *C-0439*
 Hayashi H.: *C-0837*
 Hayashi N.: *C-0971*
 Hayashi S.: *C-0093, C-0393*
 Hayashi T.: *C-0839*
 Hayes C.: *B-429*
 Hayes C.: *B-218*
 Haykir R.: *C-0138, C-0426*
 He H.: *B-433, B-434*
 Healey A.E.: *B-202*
 Healey P.R.: *B-202*
 Hebart H.: *C-0293, C-0317*
 Heckenkamp J.: *B-063, B-456*
 Heckmann M.: *C-0387*
 Heesakkers R.A.M.: *B-725, C-0468*
 Hegerfeldt S.: *B-114, B-918*
 Heidecker H.G.: *B-568*
 Heidelberger B.: *D-16*
 Heidrich G.: *B-207, B-333*
 Heijmink S.W.T.P.: *B-490, B-493, B-497, C-0468*
 Heiken J.P.: *E-39*
 Hein E.: *B-612*
 Hein P.: *B-032, B-612*
 Heindel W.L.: *B-038, B-166, B-307, B-386, B-458, B-459, B-569, B-784, B-785, B-884, B-900, B-902, B-932, C-0245, C-0271*
 Heinig A.: *B-737*
 Heinrich M.: *C-0328, C-0387, C-0640*
 Heinz A.: *C-0799*
 Heinz-Peer G.: *A-195, B-027, B-400, C-0509, E-29*
 Heiss C.: *C-0997*
 Heiss W.D.: *A-301*
 Helbich T.H.: *A-012, B-023, B-027, B-730, B-736, B-836, E-56*
 Helbig M.: *B-190*
 Heller M.: *B-046, B-401, B-504, B-507*
 Heller M.: *B-637, B-732*
 Hellerhoff P.H.: *B-808, B-809*
 Hellinger J.C.: *B-074, B-888, C-0260, C-0263, C-1013, C-1030*
 Hellström M.: *A-332, B-882*
 Helllund J.C.: *B-487, C-0365*
 Helmberger R.: *B-183*
 Helmberger T.K.: *A-323, A-436, B-502, B-627*
 Hemingway A.: *C-0417*
 Hemminger F.: *B-272*
 Hempel M.J.: *B-183, B-272, B-277*
 Hendl H.: *E-66*
 Hendriks J.H.C.L.: *B-829, B-830*
 Hengst S.A.: *B-407*
 Henk C.B.: *B-331*
 Hen nemuth A.: *D-09*
 Hennessy M.: *B-559*
 Hennig F.F.: *B-356*
 Henriquès C.: *C-0184*
 Henschke C.: *B-039*
 Herber S.: *B-295*
 Herborn C.: *B-034*
 Herborn C.U.: *B-079, B-822*
 Herbreteau D.: *B-759*
 Herfkens R.J.: *C-1030*
 Hericord O.: *B-639*
 Hermann K.P.: *B-156*
 Hermann K.-P.: *B-207, B-333*
 Hermans R.: *A-075, B-338*
 Herman-Sucharska I.: *C-0843*
 Hermus A.R.M.M.: *C-0469*
 Hernalsteen D.: *C-0796*
 Hernandez D.: *C-0135*
 Hernandez G.: *C-0577*
 Herold C.J.: *A-086, A-143, B-892*
 Herold M.: *B-803*
 Herpels V.: *B-697*
 Herralaiz L.: *C-0067, C-0751, C-0882, C-0913*
 Herregods M.C.: *B-084*
 Herrmann C.: *B-543*
 Herrmann K.A.: *B-182, B-383, B-557, B-574, B-851*
 Herrmann K.-H.: *B-923*
 Hershko D.: *C-0105*
 Hertel I.: *C-0379*
 Herth F.: *B-704, B-705*
 Herwadker A.: *C-0795*
 Herzog C.: *B-009, B-302, B-311, B-340, B-345, B-349, B-350, B-401, B-410*
 Herzog H.: *B-407*
 Herzog P.: *A-010, B-161, B-162, B-164, B-611*
 Heuga O.: *B-544*
 Heuschmid M.: *B-310, C-0257, C-0270*
 Heussel C.-P.: *B-701*
 Heyne J.-P.: *C-0230, C-0236*
 Heywang-Köbrunner S.H.: *B-733, B-737*
 Hiatt M.D.: *C-0260, C-0263*
 Hidaka N.: *C-0837*
 Hidalgo A.: *C-0279, C-0284*
 Hieda M.: *C-0581*
 Hierholzer J.: *B-285*
 Hietzschold V.: *B-650, B-655*
 Higashi M.: *C-1035*
 Higashida Y.: *B-158, B-330*
 Higashino T.: *B-387, B-470, B-471, C-0373*
 Higgins C.B.: *B-331*
 Hilger I.: *B-204, B-670, B-672, B-783, C-0409*
 Hill C.: *B-702*
 Hiller N.: *B-797*
 Hillier J.: *B-019*

List of Authors and Co-authors

- Hillit M.: *E-34*
 Himuro K.: *B-158*
 Hindennach M.: *D-09*
 Hine A.L.: *C-0743*
 Hinterleitner C.: *B-101*
 Hinterleitner T.: *B-572*
 Hintze C.: *B-104, B-376*
 Horns M.: *A-340*
 Hirai N.: *C-0581*
 Hiraka K.: *C-0788*
 Hirano T.: *B-651*
 Hirano T.: *C-0380*
 Hirano Y.: *C-0983*
 Hirohashi S.: *A-364*
 Hirota H.: *C-0651*
 Hirsch W.: *A-294, C-0887*
 Hirschfelder H.: *B-282*
 Hirshenbaum A.: *C-0129*
 Hitzke G.: *B-029*
 Hjelt M.: *C-0106, C-0738, C-0744, C-0745, C-0822*
 Hnid N.: *C-0385*
 Ho Y.Y.: *C-0703*
 Hochmuth A.: *B-315, B-763*
 Hochmuth K.: *B-689*
 Hodler J.: *B-351*
 Hoermann M.: *B-893*
 Hoff R.: *B-313*
 Hoffknecht P.: *B-386*
 Hoffman M.H.: *B-108*
 Hoffmann C.W.: *B-606*
 Hoffmann M.H.K.: *B-426, B-827*
 Hoffmann R.-T.: *B-502*
 Hoffmeier A.: *B-307, C-0245, C-0271*
 Hoflehner J.: *B-123, B-803*
 Hofmann S.: *B-686*
 Hofstetter R.: *B-749*
 Hoggard N.: *C-0795*
 Hogstrom B.: *B-644*
 Hoheisel M.: *B-549*
 Hohl C.: *B-578, B-753, B-819, B-898*
 Hoffmann J.: *B-604, B-606*
 Höhn M.: *A-202*
 Höhne K.H.: *C-0356*
 Holden A.: *E-12*
 Hollenbach H.-P.: *B-722*
 Hollerweger A.: *B-123*
 Holloway B.J.: *C-0314*
 Holme E.: *C-0160*
 Holmquist F.: *B-592*
 Holmström A.: *C-0996*
 Holtinkoski T.: *C-0992*
 Honda H.: *B-330*
 Honeyfield L.: *C-0291*
 Hong H.: *B-234*
 Hong H.S.: *C-0736*
 Hong H.-S.: *C-0065*
 Hong S.-C.: *C-0810*
 Hong S.H.: *B-467, B-567, C-0005, C-0722*
 Hong X.: *B-531*
 Hongo N.: *C-1001*
 Honma S.: *C-0983*
 Honnep D.: *B-750*
 Honya K.: *B-319*
 Hopkins R.: *C-0102*
 Hoppe H.: *B-693*
 Hoppel B.: *B-440*
 Hopster D.J.: *C-0480*
 Horgan P.: *B-605*
 Horger M.S.: *B-678, C-0293, C-0317*
 Horger W.: *B-352, B-356, B-357, B-358*
 Horii Y.: *C-0538, C-0838*
 Horii A.: *C-0981*
 Horiuchi T.: *C-0337*
 Horwich A.: *B-724*
 Hoskin P.J.: *C-0304, C-0323*
 Hosono M.: *C-0758*
 Hosten N.: *B-078, B-878, C-0634*
 Hou Z.: *D-11*
 Houghton S.L.: *B-143*
 Hourani M.H.: *C-0910*
 Housden B.: *A-157*
 Houssiau F.A.: *B-003*
 Houwers J.B.: *B-309, B-524*
 Hövels A.: *B-725*
 How T.: *B-202*
 Howling S.J.: *B-305*
 Hrabak M.: *C-1002*
 Hricak H.: *B-498, B-676*
 Hsieh J.: *B-440, B-665, B-666*
 Hsu R.M.: *C-0068*
 Hu Q.: *D-11*
 Huang S.: *D-11*
 Huang Y.H.: *C-0412*
 Hubbe U.: *B-763*
 Huber A.: *B-429*
 Huber A.M.: *B-216, B-218*
 Huber R.: *C-0579*
 Huber W.: *C-0669*
 Huda W.: *C-0958*
 Huelga Zapico E.: *C-0085*
 Hughes C.M.: *C-0650*
 Hughes D.: *C-0795*
 Hughes E.K.: *C-0442*
 Hughes J.L.: *B-793, C-0103, C-0418, C-0436*
 Hughes M.: *C-0880*
 Hugill J.-A.: *B-149*
 Hügli R.: *B-250*
 Huguet M.M.: *C-0231*
 Huguet R.: *C-0935*
 Huh Y.-M.: *C-0721*
 Huisman H.J.: *B-493*
 Huisman T.A.G.M.: *A-052*
 Huizinga T.W.J.: *B-094*
 Hulsbergen van der Kaa C.A.: *B-490, B-493, B-497, C-0468*
 Hummel J.: *D-01*
 Hundt W.: *B-788*
 Hunold P.: *B-211, B-654, B-822, B-828*
 Huo Z.: *B-039*
 Huppert P.: *A-063*
 Huppertz H.-U.: *B-315, B-432*
 Hur J.-M.: *C-0405*
 Hurley M.C.: *B-191, C-0642*
 Hurst R.: *C-0489*
 Hurtier O.: *C-0368*
 Husarik D.B.: *B-013*
 Husband J.E.: *B-143, B-144*
 Huss R.: *B-780*
 Hussain S.M.: *A-106*
 Huttary R.: *D-18*
 Huttner H.B.: *C-0395*
 Huwart L.: *B-362, B-365*
 Huynh I.: *B-430*
 Hwang J.Y.: *C-0755*
 Hwang S.I.: *C-0513*
 Hyland M.: *C-0987*
 Hyodo K.: *B-775*
 Hyung W.J.: *C-0095*
-
- I
- Iabichino C.: *C-0453*
 Iadanza A.: *B-764*
 Iafrancesco M.: *C-0239*
 Iafrate F.: *B-575, B-699, C-0084, C-0092*
 Iannaccone R.: *B-692*
 Iannucci G.: *C-0768, C-0832*
 Ichikawa K.: *C-0981*
 Ichikawa K.: *C-0566*
 Ichikawa Y.: *B-651*
 Ideguchi T.: *B-158*
 Idoate M.A.: *C-0516*
 Iezzi R.: *B-292, B-339*
 Igarashi K.: *C-0018*
 Igci E.: *C-0448, C-0456*
 Ike K.: *C-0965*
 Ikeda M.: *C-0944, C-0948, C-0949, C-0956, C-0981*
 Ikeda N.: *C-0286*
 Ikehira H.: *C-0524*
 Ikuma H.: *C-0222*
 Ikura H.: *C-0339*
 Illea D.: *B-329*
 Iliadis C.: *C-0706*
 Illias W.: *B-288*
 Illic D.: *C-0644*
 Illic M.: *C-0644*
 Ilvan S.: *B-584*
 Imai K.: *C-0948, C-0949*
 Imai S.: *C-0940*
 Imai S.: *C-0429*
 Imai Y.: *A-361, C-1035*
 Imai Y.: *C-0430*
 Imanishi Y.: *C-0147*
 Imbriaco M.: *B-086, B-416*
 Imhof H.: *C-0669, D-06*
 Imhoff K.: *B-155*
 Inal M.: *C-1010*
 Inamoto N.: *C-0965*
 Inaoka T.: *C-0651*
 Ince Y.: *C-1058*
 Inci E.: *C-0558*
 Inci O.: *C-0520*
 Indirinella S.: *B-134*
 Inoue Y.: *C-0348, C-0350, C-0615, C-0758, C-0760, C-0761*
 Inoue Y.: *C-0093, C-0393*
 Intraligi M.: *B-376*
 Ioannidis K.: *C-0766*
 Ioannidou M.: *C-0931*
 Iovane A.: *C-0656*
 Iozzelli A.: *B-556*
 Irace C.: *B-880*
 Irani F.G.: *B-876*
 Irion K.: *C-0173*
 Iriyama M.: *C-0983*
 Iro H.: *B-052*
 Irurzun J.: *C-1050*
 Irwan R.: *C-0383, C-0773*
 Irzyk M.: *C-0807*
 Isbary M.: *B-251*
 Ishak G.E.: *C-0094*
 Ishida J.: *C-0629*
 Ishida T.: *C-0964*
 Ishigaki T.: *A-360, C-0299, C-0944, C-0956, C-0981*
 Ishihara T.: *C-0950, C-0950*
 Ishii K.: *C-0758, C-0760*
 Ishiyama K.: *B-468*
 Ishizuka K.: *C-0147*
 Isik C.: *C-0526*
 Ito D.: *C-0600*
 Ito K.: *C-0581*
 Ito M.: *B-744*
 Itoh H.: *C-0298, C-0536, C-0608, C-0836, C-0867*
 Itoh S.: *C-0944*
 Itoh T.: *C-0499*
 Itskovitch I.E.: *C-0265*

List of Authors and Co-authors

Itrich H.: *B-113, B-120, B-743, B-781, C-1005, C-1025*
 Ivancev K.: *A-287*
 Ivanitsky A.: *C-0912*
 Ivanovic A.: *C-0174, C-0631, C-0701, C-0702*
 Iwanczak F.: *C-0923*
 Iwano S.: *C-0299*
 Iwasaki T.: *E-02*
 Iwasaki Y.: *C-0966*
 Iwinska Zelder J.: *B-539*
 Izaki K.: *C-0629*
 Ibizky G.: *C-0884*
 Izquierdo B.: *C-0577*
 Izquierdo M.A.: *C-0249*
 Izumi J.-I.: *B-538*
 Izycka-Swieszewska E.: *C-0015, C-0016*

J

Jabri K.N.: *B-542*
 Jack L.B.: *A-432*
 Jackowska Z.: *C-0023*
 Jackson A.: *A-155*
 Jackson J.E.: *A-435*
 Jackson V.: *C-0489*
 Jacob D.: *B-794*
 Jacob L.A.: *A-427*
 Jacobs A.H.: *A-301*
 Jacobs F.: *E-67*
 Jacobson J.A.: *B-800, C-0681*
 Jacoulet P.: *B-462*
 Jaeger D.: *B-240*
 Jaeger K.: *B-250*
 Jaehne M.: *B-051, B-053*
 Jager G.J.: *C-0435, C-0469*
 Jäger H.R.: *A-205, C-1075*
 Jäger K.A.: *B-568*
 Jäger L.: *B-183, B-225, B-226, B-271, B-272, B-277*
 Jahnke T.: *B-637*
 Jahntz C.L.: *B-113, B-743, C-1005, C-1025*
 Jain A.K.: *C-0457*
 Jain V.: *C-0128*
 Jakob L.: *B-250*
 Jakobs T.F.: *B-502*
 Jaksic E.: *C-0466, C-0525*
 Jakubowski W.: *B-057, B-188, C-0540*
 Jakupov V.A.: *C-0602, C-1036*
 Jamadar D.A.: *C-0681*
 Jamnig H.: *B-590*
 Janata K.: *B-595*
 Jancewicz P.: *C-0698*
 Janczarek M.: *C-0563*
 Jang K.M.: *C-0048*
 Janica J.: *B-317, C-0698*
 Janica J.R.: *C-0572*
 Janik P.: *B-098*
 Jankharia B.: *C-0272, C-0748*
 Janko-Piatkowska E.: *C-0844*
 Jankowski B.: *C-0892*
 Jansen J.M.: *C-0157*
 Janssen L.W.M.: *B-818*
 Janssens C.H.C.: *B-524*
 Januel A.C.: *A-227, B-759, B-760*
 Januszewicz M.: *B-070, C-0603*
 Jappe U.: *C-0395*
 Jargiello T.: *B-112, B-450, B-516*
 Jaromi S.: *B-027, B-736, B-836*
 Jaron B.: *B-871*
 Jarosz B.: *B-112*
 Jaroszewicz J.: *C-0841*
 Jaschke G.: *B-291*

Jaschke W.R.: *B-060, B-101, B-590, C-0053, C-0087, C-0898, D-03*
 Jastrzebska H.: *B-057*
 Jaworski M.: *B-070, C-0603*
 Jaziri S.: *B-128*
 Je B.-K.: *C-0543*
 Jeffrey R.B.: *C-0068*
 Jelavic-Kojic F.: *C-1042*
 Jeltsch M.: *B-827*
 Jenett M.: *B-604*
 Jenkins P.J.: *B-305*
 Jenkins S.: *C-0855*
 Jensen D.: *C-0504*
 Jensen D.B.: *B-600*
 Jeon S.S.: *C-0621*
 Jeong H.W.: *B-761, B-762, C-0846*
 Jeong S.Y.: *C-0621*
 Jeong Y.J.: *C-0288, C-0300*
 Jeong Y.Y.: *B-018, C-0152*
 Jerbi Ommezine S.: *C-0313*
 Jerebko A.: *B-327*
 Jern M.: *C-0366*
 Jeunehomme F.: *B-160*
 Jevtic V.: *A-198, C-0685*
 Jiang B.: *B-555*
 Jiang J.: *B-303*
 Jimenez del Rio J.: *C-0085*
 Jin G.-Y.: *C-0352, C-0353*
 Jin K.-N.: *B-695*
 Jin Z.: *B-040, B-303, B-347*
 Jin Z.Y.: *C-0824*
 Jing Z.: *B-029*
 Jiricková P.: *C-0529*
 Jochims M.: *B-828*
 Joffre F.G.: *E-26*
 Joglekar G.: *B-542*
 Joh J.H.: *C-0736*
 Johkoh T.: *C-0283*
 Johkoh T.: *C-0380*
 Johnson K.J.: *A-429*
 Johnson S.: *B-202*
 Johnson T.: *B-341, B-346*
 Johnson T.R.C.: *B-846*
 Johnston C.J.: *B-359, B-742, C-1047*
 Jökel M.: *E-13*
 Jonas D.: *B-723*
 Jones G.: *D-14*
 Jones J.R.: *B-495*
 Jones P.A.: *C-0213*
 Jones S.E.: *C-0213*
 Jonsson K.: *B-910*
 Joossens K.: *B-159*
 Jordá J.: *C-0059*
 Jorgen B.: *B-437*
 Josephson L.: *B-671*
 Joshi S.: *B-863*
 Jovanovic-Nikolic O.: *C-0676*
 Juanco C.: *C-0009, C-0059*
 Juchems M.S.: *B-694*
 Juckel G.: *C-0799*
 Jung B.: *B-278*
 Jung E.M.: *B-454, B-603, C-0569, C-1055, C-1064*
 Jung G.: *B-748*
 Jung K.C.: *C-0723*
 Jung N.Y.: *C-0005, C-0216, C-0663*
 Jung S.I.: *C-0513*
 Jung S.S.: *C-0216*
 Jungius K.-P.: *B-603*
 Junkermann H.: *B-829, B-835*
 Junkermann I.: *B-835*
 Juran R.: *B-588*
 Jurik A.-G.: *A-380*
 Jvarsheishvili L.: *C-0070*

K

Kaandorp T.A.M.: *B-214, B-220*
 Kabakci N.: *C-0448, C-0456*
 Kabala J.: *C-0553*
 Kabasawa H.: *C-0867*
 Kachel R.: *C-0023*
 Kachelrieß M.: *B-109, B-445, B-661, B-662, B-668, C-0946*
 Kadohisa S.: *C-0995*
 Kadziolek B.: *C-0572*
 Kagadis G.C.: *C-0369, C-0613*
 Kagaya Y.: *C-0228*
 Kahraman N.: *C-0819, C-0878*
 Kainberger F.: *A-310, B-260, C-0669, D-06*
 Kainuma K.: *C-0964*
 Kaiser G.M.: *B-404*
 Kaiser W.A.: *B-022, B-105, B-204, B-261, B-263, B-371, B-372, B-402, B-403, B-648, B-670, B-672, B-783, B-921, B-923, C-0230, C-0236, C-0409, C-0891*
 Kaji T.: *C-0966*
 Kajihara Y.: *C-0940*
 Kajitani T.: *C-0629, C-0806, C-1034*
 Kakhadze S.: *C-0235*
 Kakizawa H.: *C-0581*
 Kaklamanis L.: *C-0481*
 Kaklis S.: *B-659*
 Kalai A.: *C-0069, C-0555*
 Kalaitzoglou I.: *C-0717*
 Kalamarides M.: *C-0673*
 Kalantzi M.: *B-084, B-090*
 Kalatzis I.: *C-0355*
 Kalden P.: *B-295*
 Kaldir M.: *C-0158*
 Kaloudi E.: *B-238*
 Kale A.: *B-721*
 Kalender W.A.: *A-397, B-109, B-445, B-661, B-662, B-668, B-776, B-777, C-0946, C-0953, D-03*
 Kalhs P.: *C-0857*
 Kalivas N.: *C-0955*
 Kallenberg K.: *B-096*
 Kaloger S.E.: *C-1083*
 Kalogeropoulos I.V.: *B-583*
 Kalogeropoulos J.V.: *C-0295*
 Kalogeropoulos C.: *B-605*
 Kalogeropoulos C.: *B-322, C-0661, C-0920*
 Kalovoulos M.: *C-1070*
 Kalra M.K.: *B-010, B-106, B-369, B-370, B-660*
 Kalume Brigitte M.: *C-0681*
 Kamaya A.: *C-0068, C-1013*
 Kameyama K.: *C-0397*
 Kamiō S.: *C-0372*
 Kamiōka Y.: *C-0299*
 Kampanarou M.: *C-0210, C-0584*
 Kampanarou S.: *C-0625*
 Kamura T.: *C-0020*
 Kanaev S.: *C-0671, C-0750*
 Kandarakis I.: *C-0943, C-0955*
 Kandatsu S.: *B-186, C-0351*
 Kandula V.V.R.: *C-0324*
 Kaneda I.: *C-0018*
 Kaneko K.: *C-0788*
 Kang C.H.: *B-001, B-002, C-0749*
 Kang H.K.: *B-018*
 Kang H.K.: *C-0152*
 Kang H.S.: *B-234*
 Kang H.S.: *B-467, B-567, C-0722*
 Kang J.-S.: *C-0118*
 Kang L.Q.: *C-0781*
 Kang M.-S.: *C-0008*
 Kani H.: *C-0116*
 Kanitsar A.: *D-19*

List of Authors and Co-authors

- Kaniyur S.: *C-0733*
 Kanz K.-G.: *B-006*
 Kapala A.: *C-1040*
 Kapeller B.: *B-674*
 Kaplan M.: *C-0520*
 Kaptoge S.: *B-465*
 Kapustin V.V.: *C-0973*
 Kara E.: *C-0929*
 Karabacakoglu A.: *C-0138*, *C-0426*
 Karadag Z.Ö.: *C-0208*
 Karadeli E.: *C-1011*
 Karadi E.: *C-0652*
 Karadjov A.: *C-0998*
 Karagoz Y.: *C-0819*, *C-0878*
 Karahaliou E.: *C-0349*, *C-0451*, *C-0619*
 Karakas M.H.: *C-1058*
 Karaköse S.: *C-0138*, *C-0426*
 Karam A.R.: *C-0094*, *C-0484*
 Karaman K.: *C-0597*, *C-0816*
 Karamessini M.T.: *C-0369*, *C-0692*, *C-0715*
 Karampeki S.: *A-100*, *B-091*, *C-0800*
 Karan J.B.: *A-184*
 Karanjia N.: *B-144*
 Karantanas A.H.: *A-026*, *A-167*
 Karatapanis S.: *C-1065*
 Karatz A.: *C-0920*
 Karavitis P.: *C-0044*, *C-0470*
 Karaxaliou E.: *B-336*
 Karcaaltincaba M.: *B-246*
 Karch S.: *B-271*
 Kardamakis D.: *C-0661*
 Karkantzia F.: *C-1016*
 Karli Oguz K.: *B-537*
 Karmazanovsky G.G.: *C-0040*
 Karnabatidis D.: *C-0369*, *C-0613*
 Karssemeijer N.: *A-008*, *A-118*, *B-829*, *B-830*
 Kartakis N.: *C-0825*
 Kartel A.: *C-0817*, *C-0853*
 Kasai H.: *B-744*
 Kaserer K.: *B-400*
 Kashiwagi J.: *C-0838*
 Kaskarelis I.: *C-1016*
 Kasperk C.: *B-138*
 Kasprian G.: *B-893*
 Kasprian G.J.: *B-221*, *B-889*
 Kasprowska S.: *C-0573*, *C-0675*, *C-0735*
 Kassubek J.: *B-432*
 Kassymov B.Zh.: *C-1036*
 Kastani D.: *B-560*
 Kastler B.A.C.: *B-462*, *C-0074*, *C-0523*
 Katada K.: *C-0560*
 Kato H.: *C-0286*
 Katoh M.: *B-520*, *B-522*, *B-653*, *B-657*, *B-658*
 Katona G.: *C-0862*
 Katsanos K.: *C-0613*
 Katsaounos E.: *C-0025*
 Katsaros V.K.: *C-0775*
 Katsarou C.: *C-0661*
 Katsiva V.: *C-0246*
 Katsivas A.: *C-0246*
 Katsube T.: *C-0839*
 Katsuda T.: *C-0986*, *C-0995*
 Katz L.: *C-0187*
 Katioti F.: *B-617*, *B-727*, *C-0438*
 Kauczor H.-U.: *B-414*, *B-472*, *B-473*, *B-701*,
 B-704, *B-705*, *B-905*, *C-0294*, *C-0345*, *C-0386*,
 C-0388, *C-0395*, *C-1000*
 Kauffmann G.W.: *B-195*, *B-398*, *B-413*, *B-414*,
 C-0589
 Kaul M.: *C-0193*
 Kaul M.G.: *B-652*, *B-656*
 Kauppinen T.: *B-231*
 Kautznerova D.: *C-0362*
 Kawabe A.: *C-0995*
- Kawahara Y.: *C-0662*, *C-0709*
 Kawamura S.: *C-0601*
 Kawamura Y.: *B-744*
 Kawanishi M.: *C-0840*
 Kawashima A.: *C-0506*
 Kaya A.: *C-0765*
 Kayaçetin E.: *C-0138*
 Kayahan E.M.: *C-1011*, *C-1051*
 Kayani I.: *B-007*
 Kazama T.: *C-0194*
 Kazanowska B.: *C-0148*, *C-0911*
 Keane D.: *C-1021*
 Keane D.: *A-297*
 Keat N.: *B-669*
 Keavey E.: *C-0968*, *C-0969*
 Keeling A.N.: *B-191*
 Kefi A.: *C-0448*
 Kelekis A.D.: *C-0584*, *C-0942*, *C-0963*
 Kelekis D.: *C-0334*, *C-0584*, *C-0624*, *C-0625*,
 C-0641
 Kelekis D.A.: *C-0210*
 Kelekis N.: *C-0942*, *C-0963*
 Kelekis N.L.: *A-410*, *C-0726*
 Kelleher D.: *A-152*
 Kemper J.: *B-213*, *B-614*
 Kenknight B.H.: *D-05*
 Kennedy M.K.: *C-0226*
 Kennedy S.: *B-796*
 Keogan M.: *C-0427*
 Kerr J.: *C-0226*
 Kerschot E.: *C-0191*
 Kettenbach J.: *A-270*, *C-0639*, *D-01*, *D-05*
 Kettunen A.O.: *A-296*, *A-344*, *C-0988*, *C-0992*,
 C-0996
 Khalil R.: *B-611*, *B-615*
 Khalili K.: *B-177*
 Khalili M.: *B-177*
 Khan A.N.: *C-0051*, *C-0139*, *C-0169*, *C-0173*
 Khan M.F.: *B-075*, *B-350*
 Khanna M.: *C-0879*
 Khartchenko V.P.: *C-0903*
 Khodashinskaja A.V.: *C-0700*
 Khong P.-L.: *B-642*
 Khoo L.A.L.: *B-832*
 Khorchidi S.: *B-715*
 Khouri T.: *B-525*
 Khoury N.J.: *C-0484*, *C-0910*
 Kido A.: *C-0422*, *C-0430*, *C-0431*, *C-0534*
 Kiefer B.: *B-722*
 Kiessling F.M.A.: *B-780*, *C-0407*
 Kievit J.: *A-396*
 Kikinis R.: *D-05*
 Kikuchi M.: *C-0194*
 Kilby M.J.: *B-095*
 Kilian A.K.: *B-890*, *C-0930*
 Kilic M.: *C-0033*
 Kiliç Ö.: *C-0477*
 Kilina O.Y.: *C-0664*, *C-0700*
 Kim A.Y.: *B-419*, *B-817*, *C-0001*, *C-0017*, *C-0021*,
 C-0022, *C-0065*, *C-0119*, *C-0643*
 Kim C.-S.: *C-0353*
 Kim C.W.: *C-0300*
 Kim D.B.: *C-0217*
 Kim D.H.: *C-0062*, *C-0542*
 Kim D.H.: *C-0241*, *C-0262*
 Kim D.-I.: *C-0777*
 Kim D.-J.: *C-0777*
 Kim E.: *C-0790*
 Kim E.Y.: *C-0556*, *C-0790*
 Kim G.-H.: *B-834*
 Kim H.: *C-0556*
 Kim H.-D.: *B-831*
 Kim H.H.: *C-0217*
 Kim H.J.: *C-0282*
- Kim H.J.: *B-761*, *B-762*, *C-0870*
 Kim H.J.: *C-0120*, *C-0505*
 Kim I.-O.: *B-641*, *C-0888*
 Kim J.: *B-801*
 Kim J.: *C-0416*, *C-0845*
 Kim J.-H.: *C-0789*
 Kim J.H.: *B-234*
 Kim J.H.: *B-320*
 Kim J.-H.: *C-0029*
 Kim J.J.: *B-864*
 Kim J.-S.: *C-0119*
 Kim J.-Y.: *B-752*
 Kim K.I.: *C-0300*
 Kim K.-I.: *C-0288*
 Kim K.S.: *C-0567*
 Kim K.S.J.: *B-312*
 Kim K.W.: *B-503*, *C-0017*, *C-0021*, *C-0022*,
 C-0029, *C-0065*, *C-0095*, *C-0119*, *C-0643*
 Kim M.: *C-0543*
 Kim M.-J.: *C-0065*
 Kim M.J.: *C-0048*
 Kim M.-J.: *C-0029*, *C-0095*, *C-0643*
 Kim M.S.: *C-0893*
 Kim M.S.: *C-0212*, *C-0309*
 Kim M.Y.: *C-0001*, *C-0217*
 Kim P.N.: *B-419*, *C-0001*, *C-0065*
 Kim S.: *B-394*
 Kim S.: *C-0721*
 Kim S.-B.: *C-0543*
 Kim S.-H.: *C-0405*
 Kim S.-H.: *C-0789*
 Kim S.H.: *B-076*, *B-077*, *B-178*, *B-210*, *B-503*,
 B-711, *C-0029*, *C-0216*, *C-0492*, *C-0492*,
 C-0513, *C-0513*
 Kim S.-H.: *B-695*
 Kim S.H.: *C-0048*
 Kim S.J.: *C-0533*
 Kim S.J.: *C-0846*
 Kim S.J.: *B-281*, *C-0301*, *C-0322*
 Kim S.K.: *C-0005*
 Kim S.M.: *B-001*, *B-002*, *C-0217*, *C-0749*
 Kim S.S.: *C-0556*, *C-0790*
 Kim S.Y.: *C-488*, *C-0017*, *C-0021*, *C-0022*,
 C-0057, *C-0119*
 Kim T.H.: *C-0229*, *C-0258*, *C-0301*, *C-0322*
 Kim T.-K.: *C-0543*
 Kim T.K.: *B-234*
 Kim T.K.: *C-0017*, *C-0643*
 Kim T.U.: *C-0288*
 Kim W.S.: *B-641*, *C-0888*
 Kim Y.: *C-0259*
 Kim Y.C.: *C-0542*
 Kim Y.-G.: *C-0353*
 Kim Y.H.: *C-0152*
 Kim Y.H.: *B-864*, *C-0416*
 Kim Y.J.: *B-505*
 Kim Y.J.: *C-0240*
 Kim Y.-J.: *C-0229*, *C-0258*, *C-0274*
 Kim Y.M.: *C-0699*
 Kim Y.S.: *C-0542*, *C-0723*
 Kim Y.S.: *C-0567*
 Kim Y.-W.: *B-641*, *C-0925*
 Kim Y.W.: *C-0870*
 Kimura H.: *C-0298*, *C-0836*, *C-0867*
 Kimura K.: *C-0283*
 Kindermann I.: *C-0237*
 King B.F.: *C-0506*
 King D.M.: *B-019*
 King S.: *C-0895*
 Kinkel K.: *A-034*
 Kinkel K.: *A-035*
 Kinoshita K.: *C-0608*
 Kinzel S.: *B-073*, *B-203*
 Kiortsis D.N.: *B-647*

List of Authors and Co-authors

Kiraly A.P.: <i>B-325</i>	Koechl A.: <i>D-19</i>	Kotani H.: <i>C-0430</i>
Kirchhoff C.: <i>B-815</i>	Koenigsrainier A.: <i>C-0087</i>	Kotis A.A.: <i>C-1065</i>
Kirchin M.A.: <i>B-644</i>	Koestler H.: <i>A-240</i>	Kotlyarov P.M.: <i>C-0903</i>
Kirimlidis I.: <i>C-0075, C-0452, C-1076</i>	Kofal L.A.: <i>C-0242, C-0265</i>	Kotter E.: <i>B-240, B-247, C-0127</i>
Kiris A.: <i>C-0765</i>	Kofler J.M.: <i>B-443</i>	Kötter I.: <i>B-562, C-0623</i>
Kirk J.: <i>C-0173</i>	Koh D.-M.: <i>B-144</i>	Koukkou P.: <i>C-0962</i>
Kirk M.P.: <i>B-239</i>	Koh S.H.: <i>C-0720</i>	Koulestantios E.: <i>C-0962</i>
Kirkali Z.: <i>C-0456</i>	Koh Y.H.: <i>B-467, B-567, C-0202, C-0203, C-0722, C-0762</i>	Koulieraki C.: <i>C-0400, C-0508</i>
Kirkpatrick P.J.: <i>C-1077</i>	Kohl G.: <i>B-161, B-162</i>	Kouloulias V.E.: <i>C-0942, C-0963</i>
Kirmizis D.: <i>C-1070</i>	Kohle S.: <i>D-09</i>	Koumanidou C.: <i>C-0899, C-0900, C-0921, C-0932, C-0933</i>
Kishimoto R.: <i>B-186, C-0351</i>	Kohlmann S.: <i>B-257</i>	Koumarianos D.: <i>B-912</i>
Kissi A.A.: <i>C-0377</i>	Kohn D.: <i>C-0659</i>	Koumellis P.: <i>B-702</i>
Kitagaki H.: <i>C-1034</i>	Kohzuki M.: <i>C-0228</i>	Kourgeraki R.: <i>C-0860</i>
Kitagaki H.: <i>C-0629, C-0806</i>	Koizumi J.: <i>C-0117, C-0571, C-1026</i>	Kouroumalis E.: <i>C-0083</i>
Kitagaki H.: <i>C-0839</i>	Kojima J.: <i>C-0093</i>	Kouskouras C.: <i>B-554</i>
Kitsakos A.: <i>B-560</i>	Kok T.: <i>B-837</i>	Kovacs E.Z.: <i>B-095</i>
Kivelitz D.: <i>B-427</i>	Kokkinaki A.: <i>B-336, C-0349, C-0451, C-0619</i>	Kovacs P.: <i>B-060, B-101</i>
Kiyosue H.: <i>C-0538, C-0838</i>	Kokkinaki M.: <i>C-0860</i>	Kovalenko Y.: <i>C-0385</i>
Klareskog L.: <i>B-564</i>	Kokkinis C.: <i>C-1009</i>	Kovaleva K.: <i>D-08</i>
Klarhöfer M.: <i>B-928</i>	Koklu B.: <i>C-0819, C-0878</i>	Kownacki L.: <i>C-0256, C-0382</i>
Klaric-Custovic R.: <i>C-0178</i>	Kolios G.: <i>C-0083</i>	Koyama K.: <i>C-0348, C-0350, C-0760, C-0761</i>
Klauser A.: <i>B-129, B-130, B-807, B-859, E-64</i>	Kollar B.: <i>C-0652</i>	Koyama T.: <i>C-0287, C-0422, C-0430, C-0431, C-0499, C-0534</i>
Klauß M.: <i>B-414</i>	Kolli A.: <i>D-04</i>	Koyama T.: <i>C-0337</i>
Klausz R.: <i>E-15</i>	Kolling G.: <i>B-934</i>	Kozhuhova M.: <i>C-0872</i>
Kleen M.: <i>B-111</i>	Kolomodi D.: <i>C-0775</i>	Kozic D.: <i>C-0850, C-0926</i>
Klein G.E.: <i>B-906</i>	Komatsu H.: <i>C-0628</i>	Kozicki I.: <i>B-057</i>
Klein M.: <i>A-301</i>	Komatsu S.: <i>B-186, C-0351</i>	Koziol-Montewka M.: <i>C-1060</i>
Klein S.: <i>B-108</i>	Komatz G.: <i>B-906</i>	Kozub J.: <i>C-0808</i>
Klein W.: <i>D-08</i>	Konda D.: <i>B-508, B-511, B-635, B-873</i>	Kraemer S.: <i>B-458</i>
Kleine P.: <i>B-650, B-655</i>	Kondo K.: <i>C-0964</i>	Kraemer S.: <i>B-569, B-900</i>
Kleinrok J.: <i>C-0563</i>	Kondo S.: <i>C-0758, C-0760</i>	Kralik M.: <i>C-0108</i>
Klempnauer J.: <i>A-185</i>	Kondo Y.: <i>C-0538</i>	Kramann B.: <i>C-0060, C-0328, C-0387, C-0640, C-0907</i>
Klessen C.: <i>B-427</i>	Kong K.M.: <i>C-1027</i>	Kramer H.: <i>B-182, B-249, B-557</i>
Klimeczek P.: <i>B-306</i>	Kong L.: <i>B-303, B-347</i>	Kramer J.: <i>B-686</i>
Klimentenko N.L.: <i>C-0700</i>	König C.W.: <i>C-0612, C-0623</i>	Krämer S.C.: <i>B-459, B-902, B-932</i>
Klimes K.: <i>A-411, B-825, D-10</i>	Konovalov R.: <i>C-0871</i>	Krasilnikova L.A.: <i>C-1068, C-1073</i>
Klingebiel R.: <i>C-0798, C-0799</i>	Konrad-Verse O.: <i>B-530</i>	Krass S.: <i>D-09</i>
Klingler H.C.: <i>C-0509</i>	Konstantinou D.: <i>C-0369</i>	Kraus T.: <i>B-382</i>
Klopp M.: <i>C-0294</i>	Kontopoulou C.: <i>C-0726</i>	Krause J.U.: <i>C-0946</i>
Klose K.-J.: <i>A-007</i>	Koo J.B.: <i>B-467, B-567, C-0722</i>	Krause J.Uwe.: <i>B-661</i>
Klotz E.: <i>B-523, C-0304, C-0323, D-13</i>	Kooijman H.: <i>B-743, B-785, B-900</i>	Krause M.: <i>B-689</i>
Klöw N.E.: <i>C-0365</i>	Kooijmann H.: <i>B-569</i>	Krause M.: <i>B-934</i>
Kluge A.: <i>B-594, B-839</i>	Koops A.: <i>B-083, B-120</i>	Krause T.: <i>B-189</i>
Kluge R.: <i>C-0887</i>	Koos R.: <i>B-522, B-523</i>	Krause U.R.: <i>C-0859</i>
Klüner C.: <i>B-612</i>	Kopp A.: <i>C-0257</i>	Krauss M.: <i>B-282</i>
Klzo L.: <i>C-0244</i>	Kopp A.F.: <i>B-310, C-0270, E-31, E-42</i>	Krausse A.: <i>C-0887</i>
Knaebel H.-P.: <i>B-414</i>	Kopp C.: <i>A-258</i>	Krausz M.: <i>C-0105</i>
Knaup M.: <i>B-661</i>	Koprivsek K.M.: <i>C-0926</i>	Krawczyk M.: <i>C-0003</i>
Knauth M.: <i>B-096</i>	Koratzinos V.: <i>C-0443</i>	Krebs P.: <i>B-844</i>
Knecht R.: <i>B-190</i>	Kordecki K.: <i>C-0572</i>	Kreithner K.-F.: <i>B-245, B-425, B-472, B-685</i>
Knez A.: <i>B-341, B-346, B-846</i>	Kordelle J.: <i>B-355</i>	Kress B.P.J.: <i>B-934</i>
Knoflach M.: <i>B-101</i>	Kordowski J.: <i>B-335</i>	Krestan C.: <i>A-310</i>
Knosp E.: <i>B-935</i>	Koren A.: <i>B-767</i>	Krestin G.P.: <i>A-051, A-084, A-104, A-224, B-308, B-342, C-0267, C-0974</i>
Ko B.-K.: <i>B-831</i>	Koren J.: <i>E-32</i>	Kretzschmar H.A.: <i>B-096</i>
Ko E.: <i>B-834</i>	Körholtz D.: <i>C-0887</i>	Kriaa S.: <i>C-0312, C-0313</i>
Ko H.-K.: <i>B-503</i>	Korhonen P.: <i>B-231</i>	Krishnan A.: <i>B-162, B-164</i>
Ko K.R.: <i>C-0204</i>	Körner M.: <i>B-006, B-543</i>	Krishnan P.: <i>C-0272, C-0748</i>
Ko Y.T.: <i>C-0120, C-0505</i>	Kornienko V.N.: <i>B-438</i>	Kristiansen S.J.: <i>B-154</i>
Kobashi Y.: <i>C-0147</i>	Korzenev A.V.: <i>C-0791</i>	Krivokapic Z.: <i>C-0153</i>
Kobatake M.: <i>C-0940</i>	Kosaka N.: <i>C-0298, C-0536</i>	Kriwanek S.: <i>C-0125</i>
Kobayashi H.: <i>C-0990</i>	Kosar U.: <i>C-0551, C-0552</i>	Krix M.: <i>C-0388, C-0395, E-62</i>
Kobayashi H.: <i>C-0287</i>	Koshida K.: <i>C-0951</i>	Krnic A.: <i>C-1042</i>
Kobayashi M.: <i>C-0337</i>	Koshimoto Y.: <i>C-0867</i>	Kroft L.J.M.: <i>B-428</i>
Kobayashi N.: <i>C-0628</i>	Kösling S.: <i>A-383</i>	Kröger W.: <i>C-0634</i>
Kobayashi T.: <i>C-0971</i>	Kosmas C.: <i>C-0921, C-0932</i>	Krol A.: <i>C-0735</i>
Kobusiewicz W.: <i>C-1046</i>	Kosta P.: <i>B-560</i>	Krolicki L.: <i>C-0256</i>
Kocakoc E.: <i>C-0765, C-0885</i>	Kostanti E.: <i>B-560</i>	Krolo I.: <i>C-0178</i>
Kocaoglu M.: <i>C-0914</i>	Kostenikov N.A.: <i>C-0519, C-0791, C-0848</i>	Krombach G.A.: <i>B-073, B-203, B-278, B-348, B-578, B-753</i>
Koch A.: <i>B-650, B-655</i>	Köster O.: <i>C-0599</i>	Kronreif G.: <i>A-270, D-01</i>
Kochanowicz J.: <i>B-317, C-0572</i>	Kostic V.: <i>C-0850</i>	
Kocher O.N.: <i>C-0325</i>	Kostis W.: <i>B-039</i>	
Koczy B.: <i>C-0573, C-0675, C-0735</i>	Kosuda S.: <i>C-0966</i>	
Kodama Y.: <i>C-0415, C-0594</i>	Kotake H.: <i>C-0286</i>	
Kodera Y.: <i>C-0981</i>		

List of Authors and Co-authors

- Kropatsch W.G.: *D-06*
 Krotenkova M.V.: *C-0871*
 Krueger R.: *B-780*
 Krug D.N.: *B-302*
 Krug R.: *B-258*
 Krüger K.: *B-063, B-456*
 Krumina G.: *A-399*
 Krummenauer F.: *B-425, B-685*
 Krupski G.: *B-171*
 Krupski W.: *C-1046, C-1060*
 Krzystolik K.: *C-0842*
 Ksar J.: *B-645*
 Kubale R.: *B-603*
 Kubas B.: *B-317, C-0698*
 Kubin K.: *B-353*
 Kubo T.: *C-0287*
 Kubova S.Y.: *C-0973*
 Kuchuk P.V.: *C-0465*
 Kuczyk M.: *C-0611*
 Kudawara I.: *C-0759*
 Kuder T.A.: *C-0386*
 Kudo S.: *C-0429*
 Kudryavtseva T.Y.: *C-0040*
 Kuehl H.: *B-079, B-404, B-553, B-677, B-718, B-913, B-924*
 Kuehle C.A.: *B-079, B-571, B-813*
 Kuehnen J.: *B-047*
 Kuettner A.: *B-310, C-0257, C-0270*
 Kugel H.: *B-569, B-900, B-932*
 Kuhagen S.: *D-09*
 Kühl H.P.: *B-522*
 Kuhlenbaumer G.: *B-900*
 Kuhlenbäumer G.: *B-459*
 Kuhlencordt R.: *B-171*
 Kuhlpetter R.: *B-784*
 Kuhnigk J.-M.: *B-386, D-09*
 Kukuk M.: *B-074*
 Kulak W.: *B-317*
 Kumano S.: *C-0014*
 Kumaran M.: *C-0324*
 Kumazaki T.: *C-0308, C-0397, C-0566, C-0837*
 Kumazawa S.: *B-330*
 Kümmerlen B.: *D-09*
 Kuntscherová J.: *C-0082*
 Kunz R.P.: *B-245, B-425*
 Kuo M.D.: *B-391, B-439*
 Küpelí S.: *C-0478*
 Kupesic S.: *C-0419, C-0421*
 Kuramochi A.: *C-0592*
 Kurcz J.: *C-0892*
 Kurita A.: *C-1054*
 Kurjata R.: *B-929, C-0844*
 Kuroki M.: *C-0285*
 Kurth A.: *B-689*
 Kusmierek J.: *C-0809, C-0869*
 Küttner B.: *B-232*
 Kuwahara R.: *B-158*
 Kwak B.K.: *C-0567*
 Kwiatkowski S.: *C-0843*
 Kwon B.J.: *C-0845*
 Kwon S.T.: *C-0699, C-0723*
 Kwon W.: *C-0212, C-0309*
 Kyriakou Y.: *B-661, B-776, B-777, C-0946, C-0953*
 Kyriazi S.: *C-0025, C-0044, C-0443, C-0481, C-0739*
- L**
- La Cruz A.: *D-19*
 La Grassa M.: *C-0187*
 La Mendola C.: *C-0401*
 La Paglia E.: *C-0112*
- La Palombara C.: *B-081*
 La Seta F.: *C-0167*
 La Torre A.: *B-422*
 Labbe-Devilliers C.A.S.: *C-0181, C-0211*
 Labrador T.: *C-0434*
 Ladd M.E.: *B-404*
 Ladurner R.: *B-816*
 Lafite S.: *B-087*
 Lafitte J.-J.: *B-591*
 Lag E.: *C-0183*
 Lagalla R.: *C-0091*
 Laganà D.: *B-062, B-298*
 Lagesen B.: *B-911*
 Laghi A.: *A-268, A-317, A-413, B-043, B-044, B-107, B-515, B-575, B-692, B-699, B-710, B-741, B-747, B-811, C-0019, C-0034, C-0035, C-0084, C-0090, C-0092, C-0113, C-0114, C-0371, C-0391, C-0585*
 Laguillo G.: *C-0101*
 Lai A.: *C-0802*
 Laitt R.: *C-0795*
 Lajaunias P.: *B-430*
 Lakare S.: *B-327*
 Laki A.: *C-0064*
 Lam S.L.: *C-0441*
 Lamas M.: *C-0097, C-0121*
 Lamb H.J.: *A-274, B-214, B-220, C-0243*
 Lambert J.: *C-0647*
 Lambiri I.: *B-337*
 Lambre H.: *C-0820*
 Lameire N.H.: *E-45*
 Laméris J.S.: *B-489*
 Lamin S.: *C-0855*
 Lammer J.: *A-258, A-288, C-0639, D-19*
 Lamp J.: *B-564*
 Lampropoulou P.: *C-0775*
 Lamuraglia M.: *B-128*
 Lamy C.: *C-0796*
 Lanciotti K.: *B-526, C-0238*
 Landrauro Comesaña C.: *C-0794*
 Landenberger K.: *B-350*
 Landeras R.: *C-0009, C-0059, C-0688, C-0713, C-0731, C-0764*
 Landi P.: *B-148*
 Landini A.: *B-798*
 Landuyt W.: *B-338*
 Landwehr P.: *A-292*
 Lang E.K.: *B-392, B-863*
 Lang H.: *C-0461*
 Lang M.: *D-09*
 Lang T.B.: *B-101*
 Lang W.: *C-0953*
 Lang W.: *B-288*
 Lang Z.J.: *C-1027*
 Lange C.: *B-781*
 Lange O.: *B-103, B-321, B-374*
 Lange T.: *B-386*
 Langer M.: *B-008, B-240, B-247, B-675, C-0127*
 Langer M.: *B-569*
 Langhorst J.: *B-571*
 Längle F.: *C-0639*
 Langs G.: *B-260, D-06*
 Lanocita R.: *B-127, E-03*
 Lanz T.: *B-429*
 Lanza G.M.: *A-203*
 Lanzenberger R.: *B-930*
 Lapp R.M.: *B-109*
 Larici A.R.: *B-707*
 Larini P.: *B-061*
 Larkman D.: *B-117*
 Larrache Latasa J.: *B-167, C-0455*
 Larrauri J.: *C-0097*
 Larrue V.: *A-227*
 Larsen E.: *C-0110*
- Larson G.D.: *E-11*
 Larussa D.: *C-0834*
 Lasek W.: *C-1040, C-1059*
 Lassandro F.: *B-367*
 Lassau N.: *B-128*
 Latin B.: *B-899*
 Latkovic Z.: *C-0525*
 Latrabe V.: *C-0269*
 Lattanzio V.: *B-264*
 Latzke D.: *B-400*
 Lau G.B.H.: *C-1048*
 Lau L.: *A-337*
 Lauenstein T.C.: *A-015, B-571, B-813*
 Lauer U.A.: *C-0975*
 Läufle R.: *B-587*
 Laurent F.: *A-178, B-087, C-0269*
 Lautenschläger S.: *B-523*
 Lavdas E.: *B-912*
 Lavergne E.: *B-779*
 Lavery S.: *C-0417*
 Laviani F.: *C-0296*
 Lavini C.: *B-223, C-0815*
 Lavrnic S.: *C-0873*
 Law E.-M.: *E-55*
 Lawinski C.P.: *B-153, B-545*
 Layer G.: *B-570, B-576*
 Lázár I.: *A-253*
 Lazzereschi M.: *B-558*
 Le Bihan D.: *A-221*
 Le Cessie S.: *B-094*
 Le Dref O.: *B-794*
 Le Page L.: *B-004*
 Lea S.: *C-0471*
 Leal-Adán R.: *C-0575*
 Leander P.: *B-879*
 Leblebisatan S.: *C-1010*
 Leclerc J.: *B-128*
 Lecouvet F.: *A-166, B-003*
 Leder U.: *C-0230, C-0236*
 Lederlin M.: *B-087, C-0269*
 Lederman R.: *B-151, B-152*
 Ledermann H.P.: *B-568*
 Lee C.C.: *C-0877*
 Lee D.H.: *B-281, C-0120, C-0505*
 Lee D.Y.: *C-0568, C-0574*
 Lee D.-Y.: *B-503*
 Lee E.J.: *C-0893*
 Lee H.G.: *B-505*
 Lee H.J.: *B-234, B-234*
 Lee H.K.: *C-0736*
 Lee H.Y.: *B-711*
 Lee I.S.: *B-467, B-567, C-0722*
 Lee J.: *B-200*
 Lee J.: *C-0216, C-0259*
 Lee J.B.: *C-0567*
 Lee J.H.: *C-0630*
 Lee J.H.: *C-0810*
 Lee J.J.S.: *C-0412*
 Lee J.M.: *B-076, B-077, B-178, B-210, B-711*
 Lee J.-M.: *B-695*
 Lee J.-S.: *C-0789*
 Lee J.T.: *C-0029*
 Lee J.-T.: *B-503*
 Lee J.W.: *B-394*
 Lee J.W.: *B-467, B-567, C-0722*
 Lee J.-W.: *C-0240, C-0274, C-0721*
 Lee J.Y.: *B-076, B-077, B-178, B-210, B-711*
 Lee J.-Y.: *B-695*
 Lee K.H.: *B-234*
 Lee K.N.: *C-0630*
 Lee K.W.: *B-234*
 Lee M.: *B-194, C-0642*
 Lee M.: *C-0663*
 Lee M.G.: *C-0001*

List of Authors and Co-authors

Lee M.-G.: <i>B</i> -419, <i>C</i> -0017, <i>C</i> -0021, <i>C</i> -0022	Leupold J.: <i>B</i> -247	Litzler J.F.: <i>C</i> -0074
Lee M.H.: <i>C</i> -0005	Leuzzi V.: <i>B</i> -224	Liu G.R.: <i>C</i> -1027
Lee M.J.: <i>A</i> -150, <i>B</i> -191	Levy R.: <i>B</i> -874	Liu J.: <i>D</i> -11
Lee N.J.: <i>C</i> -0543	Lewin J.S.: <i>B</i> -406, <i>C</i> -0329	Livadas G.: <i>A</i> -076
Lee S.: <i>B</i> -394	Lewis M.A.: <i>B</i> -669	Livi U.: <i>B</i> -065
Lee S.G.: <i>C</i> -0790	Lewszuk A.: <i>C</i> -0572	Llauger J.: <i>C</i> -0666
Lee S.H.: <i>B</i> -762	Ley S.: <i>B</i> -472, <i>B</i> -473, <i>B</i> -704, <i>B</i> -705, <i>C</i> -0345,	Llorens P.: <i>C</i> -0657
Lee S.H.: <i>B</i> -001, <i>B</i> -002, <i>B</i> -418, <i>B</i> -581, <i>B</i> -854, <i>C</i> -0749	<i>C</i> -0386	Llorens R.: <i>B</i> -514, <i>C</i> -0578
Lee S.J.: <i>C</i> -0925	Li H.: <i>A</i> -301	Lloret Martí M.T.: <i>B</i> -378
Lee S.-J.: <i>C</i> -0008, <i>C</i> -0118	Li J.: <i>B</i> -408, <i>B</i> -629	Llosa M.A.: <i>C</i> -0061
Lee S.-K.: <i>C</i> -0877	Li J.: <i>B</i> -440	Llovet J.M.: <i>C</i> -0610
Lee S.W.: <i>B</i> -761	Li K.: <i>B</i> -227, <i>B</i> -228, <i>B</i> -424, <i>B</i> -826, <i>B</i> -904	Lo Pinto C.: <i>B</i> -089
Lee S.W.: <i>C</i> -0755	Li K.C.: <i>B</i> -092	Lo Schiavo V.: <i>C</i> -1056
Lee S.-Y.: <i>C</i> -0533	Li M.H.: <i>B</i> -209, <i>C</i> -0165	Lo T.H.: <i>B</i> -518
Lee T.H.: <i>B</i> -761, <i>B</i> -762, <i>C</i> -0846	Li X.Z.: <i>C</i> -0824	Löbel U.: <i>B</i> -648
Lee W.-H.: <i>C</i> -0877	Li Y.: <i>B</i> -424, <i>B</i> -593, <i>B</i> -826	Lobianco R.: <i>B</i> -601
Lee W.J.: <i>B</i> -418, <i>B</i> -854, <i>C</i> -0048	Li Z.-L.: <i>C</i> -0316	Lobo L.: <i>C</i> -0924
Lee W.-Y.: <i>C</i> -0309	Liang C.C.: <i>B</i> -328	Locatelli M.: <i>B</i> -025
Lee Y.: <i>B</i> -834	Liang C.-C.: <i>B</i> -040	Locci E.: <i>C</i> -0802
Lee Y.: <i>C</i> -0372	Liang H.: <i>C</i> -0598	Lochmueller E.-M.: <i>B</i> -257, <i>B</i> -687, <i>C</i> -0658
Lee Y.-C.: <i>C</i> -0353	Liao D.: <i>C</i> -0109	Lodemann K.-P.: <i>B</i> -436, <i>C</i> -0403
Lee Y.-H.: <i>C</i> -0405	Liaparinos P.: <i>C</i> -0943	Loeb T.: <i>C</i> -0069
Lee Y.S.: <i>B</i> -200	Liatsikos E.N.: <i>C</i> -0613	Loevstad M.: <i>B</i> -154
Leen E.: <i>B</i> -605, <i>C</i> -0394	Liberman L.: <i>B</i> -736	Loewe M.: <i>B</i> -288
Leertouwer T.C.: <i>C</i> -0774	Libicher M.: <i>B</i> -138	Löfving A.: <i>C</i> -0358, <i>C</i> -0361
Lees W.: <i>B</i> -481, <i>B</i> -627	Libson E.: <i>B</i> -141	Loggitsi D.: <i>C</i> -0624
Lefere P.: <i>B</i> -697, <i>C</i> -0088	Lichy M.P.: <i>B</i> -562	Lohan D.G.: <i>C</i> -0142, <i>C</i> -0483, <i>C</i> -0635, <i>C</i> -0740, <i>C</i> -1006
Lefort C.: <i>C</i> -0368	Lienemann A.: <i>B</i> -815, <i>B</i> -816	Lohan D.J.: <i>C</i> -0364
Legaszewski T.: <i>C</i> -0564	Liessi G.: <i>B</i> -550	Lohrmann C.: <i>C</i> -0127
Legórburu A.: <i>C</i> -0752	Ligabue G.: <i>B</i> -215, <i>B</i> -492, <i>B</i> -824, <i>E</i> -48	Lomas D.J.: <i>A</i> -177, <i>A</i> -314, <i>B</i> -579
Lehmann K.S.: <i>B</i> -072	Liguori C.: <i>B</i> -174, <i>B</i> -219	Lomazzi C.: <i>B</i> -062
Lehner F.: <i>A</i> -185	Likaki E.: <i>B</i> -322	Lombardi M.: <i>B</i> -088, <i>B</i> -089
Lehnert T.: <i>B</i> -340, <i>B</i> -401, <i>B</i> -405, <i>B</i> -408, <i>B</i> -410, <i>B</i> -500, <i>B</i> -629, <i>B</i> -723, <i>B</i> -877	Lim H.K.: <i>B</i> -418, <i>B</i> -854, <i>C</i> -0048, <i>C</i> -0663	Lombardi R.: <i>B</i> -585
Le-Huu M.: <i>B</i> -436, <i>C</i> -0407	Lim H.S.: <i>C</i> -0152	Lombardi T.: <i>B</i> -842
Leichter I.: <i>B</i> -151, <i>B</i> -152	Lim H.W.: <i>B</i> -505	Lombardo A.: <i>B</i> -212, <i>B</i> -219
Leidecker C.: <i>B</i> -445	Lim J.H.: <i>B</i> -418, <i>B</i> -854, <i>C</i> -0048	Lombardo E.: <i>C</i> -0332
Leinendecker C.: <i>B</i> -819	Lim J.S.: <i>C</i> -0095	Lombardo V.: <i>E</i> -10
Leinsinger G.: <i>B</i> -103, <i>B</i> -321, <i>B</i> -374	Lim J.-S.: <i>C</i> -0029	Lombay B.: <i>A</i> -249
Leite J.P.: <i>C</i> -0780	Lim J.W.: <i>C</i> -0120, <i>C</i> -0505	Londt J.: <i>B</i> -440
Lejoncour R.: <i>B</i> -462	Lim M.K.: <i>B</i> -320	Lonjedo E.: <i>C</i> -0609
Leili D.: <i>C</i> -0056, <i>C</i> -0399, <i>C</i> -0470	Lim P.: <i>C</i> -0253	Loo C.E.: <i>B</i> -379
Lell M.: <i>B</i> -155, <i>B</i> -156, <i>B</i> -280, <i>C</i> -0953	Lim Y.: <i>C</i> -0458	Loose R.W.R.: <i>B</i> -778
Leloutre-Françon B.: <i>C</i> -0797	Lim Y.S.: <i>B</i> -505	Loosemore T.: <i>B</i> -293
Lembcke A.: <i>B</i> -427	Lima J.A.C.: <i>B</i> -421	Lopez Barea F.: <i>C</i> -0677
Lemmi A.: <i>B</i> -842	Limbucci N.: <i>B</i> -085, <i>B</i> -137, <i>B</i> -140, <i>B</i> -287, <i>C</i> -0695, <i>C</i> -0767, <i>C</i> -1063	López C.: <i>C</i> -0221
Lemos A.A.: <i>B</i> -891, <i>C</i> -0335	Lin M.H.: <i>C</i> -0412	Lopez M.: <i>C</i> -0059
Lemos R.R.: <i>C</i> -0886, <i>C</i> -0890	Lin R.: <i>B</i> -919	Lopez-Benitez R.: <i>B</i> -195, <i>C</i> -0589
Lenarz T.: <i>B</i> -276	Lin R.: <i>C</i> -1027	Lopez-Moreno J.L.: <i>C</i> -0507
Lencioni R.: <i>A</i> -335, <i>B</i> -121, <i>B</i> -122, <i>B</i> -180, <i>B</i> -623, <i>B</i> -624, <i>B</i> -625, <i>B</i> -627, <i>B</i> -852, <i>E</i> -61	Lin S.: <i>B</i> -347	Lorente-Ramos R.M.: <i>C</i> -0936
Lengerke C.: <i>C</i> -0317	Lin S.-E.: <i>C</i> -0066	Lorenzen J.: <i>C</i> -0193, <i>C</i> -0757
Leni D.: <i>B</i> -501, <i>C</i> -0580	Lin S.F.: <i>B</i> -848	Lorenzen J.H.: <i>B</i> -586, <i>C</i> -0224
Lenk S.: <i>B</i> -562	Lin Z.: <i>D</i> -12	Lorenzen M.: <i>C</i> -0757
Lenoir M.: <i>A</i> -293	Lin Z.X.: <i>B</i> -015	Lorusso V.: <i>B</i> -885
Lenzen H.: <i>B</i> -038	Lindblad S.: <i>B</i> -564	Losa A.: <i>C</i> -0491
Leedolter S.: <i>B</i> -027	Lindblom G.: <i>B</i> -910	Losert D.: <i>B</i> -282
Leedolter W.: <i>A</i> -230	Lindell E.P.: <i>E</i> -52	Losio C.: <i>B</i> -862
Leonardi A.: <i>B</i> -134	Lindo D.: <i>C</i> -0904	Louredo A.: <i>C</i> -0086
León-Hernández A.: <i>C</i> -0575	Ling C.-M.: <i>C</i> -0877	Loussouarn D.: <i>C</i> -0181
Leotsinidis M.: <i>C</i> -0660	Lingua G.: <i>C</i> -0590	Lovato L.: <i>B</i> -064, <i>B</i> -066, <i>B</i> -081, <i>B</i> -529
Leporace M.: <i>C</i> -0296, <i>C</i> -0297	Link F.: <i>D</i> -09	Lovisolo M.: <i>C</i> -0679, <i>C</i> -0694
Lepori D.: <i>C</i> -0970	Link T.M.: <i>A</i> -103, <i>B</i> -251, <i>B</i> -256, <i>B</i> -257, <i>B</i> -687, <i>C</i> -0658, <i>C</i> -0670	Löwik C.W.G.M.: <i>A</i> -300
Leppert J.D.: <i>B</i> -772	Link T.M.: <i>B</i> -258, <i>B</i> -565	Lozano P.: <i>C</i> -0231
Leprince C.: <i>C</i> -0378	Linn S.: <i>C</i> -0166	Lu J.: <i>B</i> -904
Lera J.: <i>B</i> -121, <i>B</i> -122, <i>B</i> -180, <i>B</i> -852	Linsenmaier U.: <i>B</i> -006	Lubinski J.: <i>C</i> -0842
Lerais J.M.: <i>C</i> -0523	Lirola Cruz M.: <i>C</i> -0050	Luboldt W.: <i>B</i> -034
Leroux G.: <i>E</i> -54	Lisai P.: <i>C</i> -0637	Lucaya J.: <i>C</i> -0894
LeRoy A.J.: <i>C</i> -0506	Lisboa B.W.: <i>B</i> -586, <i>C</i> -0224	Luccicenti G.: <i>C</i> -0804, <i>C</i> -0835, <i>C</i> -0864, <i>C</i> -0947
Lertumnongtum P.: <i>C</i> -0066	Liss P.: <i>B</i> -881	Luciani A.: <i>C</i> -0390
Lesavre A.: <i>C</i> -0756	Lisý J.: <i>B</i> -099	Luciano P.: <i>B</i> -126
Leschka S.: <i>B</i> -821, <i>C</i> -0754, <i>C</i> -1053	Lisy M.R.: <i>B</i> -783, <i>C</i> -0409	Lucic M.: <i>C</i> -0850, <i>C</i> -0926
Lessick J.: <i>B</i> -426	Littera A.: <i>C</i> -0830	Lucidarme O.: <i>B</i> -698, <i>C</i> -0043, <i>C</i> -0089
	Littler P.: <i>C</i> -0161	Luderschmidt S.: <i>C</i> -0411
		Ludwig K.: <i>B</i> -139

List of Authors and Co-authors

- Lufkin R.B.: *B-187*
 Luker J.: *C-0553*
 Lukic-Kostic L.V.: *C-0134*
 Lüleci E.: *B-869*
 Luna A.: *C-0176*
 Lund G.K.: *B-213, B-652*
 Lundin B.: *B-910*
 Luo B.: *B-681*
 Luo S.: *D-11*
 Lupattelli L.: *B-148, B-300, B-517, B-633, B-802, B-842, B-858, C-0494*
 Lupattelli T.: *B-556*
 Lupattelli T.: *B-300, B-517, B-633*
 Lupescu I.: *C-0957, C-1072*
 Lupo A.: *B-638*
 Lusic M.: *C-0108, C-1002*
 Lutomsky B.: *B-083*
 Lüttich A.: *C-0792*
 Lutz J.: *B-225, B-226, B-272, B-277*
 Luypaert R.: *B-860, B-861*
 Luz O.: *C-0257*
 Luzi L.: *B-422*
 Lyakishev A.A.: *B-304*
 Lyburn I.: *C-0102*
 Lynch M.: *B-329*
 Lyon S.: *C-0642*
 Lytras D.: *C-0052*
-
- M**
- Ma J.: *B-314*
 Ma L.: *C-0823*
 Maass J.: *C-0463*
 Maataoui A.: *B-075, B-350*
 Mabiglia C.: *C-0833*
 Macchia R.: *B-392*
 MacDonald S.L.: *C-1083*
 Macfelda K.: *B-674*
 Machann J.: *C-0012, C-0941*
 Machida M.: *C-0308, C-0397*
 Machida N.: *C-0397*
 Mächler H.: *D-08*
 Macho J.: *C-0617, C-0645*
 Maciag R.: *B-070*
 Maciag R.: *C-0603*
 Mack G.M.: *A-073, A-350, B-009, B-068, B-075, B-190, B-340, B-345, B-401, B-405, B-408, B-410, B-500, B-504, B-506, B-507, B-629, B-689, B-875*
 Mackenzie A.: *B-153, B-545*
 MacLachlan J.: *B-853*
 MacPherson L.K.R.: *C-0905*
 Maculotti P.: *B-390*
 Macura K.J.: *B-790, C-0420*
 Maeda H.: *C-0948, C-0949*
 Maeda M.: *C-0758*
 Maeda M.: *C-0549, C-0711, C-0787*
 Maeder P.: *B-318*
 Maes F.: *B-551, C-1045*
 Maes M.: *B-931, C-0168*
 Maffessanti M.: *A-305*
 Maffi P.: *B-176*
 Magistrelli A.: *B-585, B-870, C-0201, C-0494, C-0503, C-0697*
 Magistrelli P.: *B-626*
 Maglaras G.: *B-597*
 Maglione M.: *C-0614*
 Magnusson P.: *B-700*
 Maher M.M.: *B-106, B-369, B-370, B-660*
 Mahfouz A.E.: *B-395, B-865, C-0464, C-1022*
 Mahjoub S.: *C-1057*
 Mahmood U.: *B-787*
 Mahnken A.: *B-203*
- Mahnken A.H.: *B-169, B-348, B-349, B-382, B-520, B-522, B-523, B-750, B-819*
 Mainenti P.P.: *C-0444*
 Maintz D.: *B-307, C-0245, C-0271*
 Mair S.: *B-543*
 Maira G.: *B-534*
 Maj E.: *C-0003*
 Majer R.: *C-0735*
 Majoi C.B.L.M.: *B-222, B-223*
 Majumdar S.: *B-256, B-258, B-565, C-0658, C-0670*
 Makarenko V.: *C-0912*
 Makino K.: *B-651*
 Makkat S.: *B-860, B-861*
 Makó E.K.: *A-176, C-0141*
 Makowiec F.: *C-0127*
 Makris N.: *C-1009*
 Maksan S.M.: *B-368*
 Maksimovic H.: *B-874*
 Maksimovic R.: *C-0248*
 Malagari K.: *A-306, A-378, C-0334, C-0584, C-0624*
 Malago M.: *B-175*
 Malago' R.: *B-607*
 Malan S.: *C-0691*
 Malaspina C.: *B-802*
 Malatara G.: *C-0920*
 Malet Munté A.: *B-719*
 Maléta A.: *B-915*
 Malghem J.: *B-003*
 Mali W.P.T.M.: *B-170, B-381*
 Malich A.: *B-022, B-261, B-263, B-371, B-372, B-402, B-670*
 Mallarini G.: *B-100, C-0802, C-0863, C-0866*
 Mallek R.: *B-736*
 Mallol X.: *C-0063, C-0689, C-0741*
 Mallouhi A.: *C-0898*
 Malone D.E.: *B-172, B-716, C-0013*
 Malone J.: *C-0343*
 Maly P.: *B-645, C-0916*
 Malzy P.: *C-0043*
 Mamisch T.C.: *B-352, B-356, B-357, B-358*
 Mamisch T.C.: *B-355*
 Mamone G.: *C-0027, C-0727*
 Manavis I.: *B-640*
 Manca A.: *B-126, B-196*
 Mancini A.: *C-0106, C-0738, C-0744, C-0745, C-0822*
 Mancini A.P.: *C-0697*
 Mancini L.: *B-085*
 Mancino S.: *B-494*
 Mancinotti A.: *C-0428*
 Manenti G.: *B-494, B-729*
 Manes K.: *C-0052*
 Manestar M.: *B-360*
 Manetta R.: *B-140, C-0767*
 Manfrè L.: *B-097, B-283, B-284, B-286*
 Manfredi M.: *B-525*
 Manfredi R.: *B-173, B-174, B-244*
 Mang T.: *B-327, B-400*
 Mang T.G.: *C-0509, C-0669, C-0857*
 Mangialardi N.: *B-296*
 Mangiapane F.: *B-692*
 Mangili P.: *C-0453, C-0454, C-0491, C-0502*
 Manginas A.: *B-659*
 Mangini M.: *B-298*
 Mangov A.: *B-054*
 Maniati-Christidi M.: *B-647*
 Maniatis P.: *C-0052, C-0962*
 Manitus J.: *C-1040, C-1059*
 Manjon P.: *C-0751*
 Manning W.J.: *B-657, B-658*
 Mano A.: *C-0948, C-0949*
 Manoli E.: *C-0908, C-0931*
- Manoli V.: *C-0900*
 Manolitsas A.: *C-0985, C-0989*
 Manoliu R.A.: *B-837*
 Manopoulou E.: *C-1071*
 Manrique J.: *C-0751*
 Mansueto G.: *B-638, C-0026*
 Mantatzis M.: *B-238, B-843, B-867, C-0036, C-0077*
 Mantzikopoulos G.: *C-0766*
 Mantzios I.: *B-896*
 Manuel D.D.: *C-0180*
 Manzke R.: *B-820*
 Manzoni T.: *C-0833*
 Maragaki E.E.: *B-583*
 Marano G.: *C-1028*
 Marano I.: *C-0144*
 Marantz P.: *C-0252*
 Maratos Y.K.: *C-0069, C-0555*
 Maraviglia B.: *C-0653*
 Marcato C.: *B-061*
 Marcelli G.: *B-373*
 Marcello R.: *B-296, C-0586*
 Marchal G.J.: *B-159, B-316, B-338, B-551, B-922, C-1045*
 Marchenkov Y.V.: *B-709*
 Marchetti L.: *C-0130, C-0728*
 Marchi A.: *C-0190*
 Marchi M.D.: *C-0768, C-0832*
 Marco de Lucas E.: *C-0793*
 Marconi A.: *B-059*
 Marcy P.-Y.: *B-639*
 Mardighian D.: *C-0980*
 Marek I.: *C-0133*
 Maresca L.: *B-508, B-635*
 Margara R.: *C-0417*
 Margreiter R.: *C-0053, C-0087*
 Marin A.: *C-0928*
 Marin B.: *C-0588, C-0876*
 Marin D.: *B-692*
 Marinicek B.: *A-051, B-241, B-360, B-821, C-0754, C-1053*
 Marinelli N.: *B-542*
 Marinelli T.: *B-413*
 Marinelli T.: *B-195, C-0589*
 Marini C.: *C-0199*
 Marini M.: *C-0264*
 Marini U.P.: *C-0189*
 Marinic J.: *C-1002*
 Marino V.: *B-870, C-0503*
 Marinos A.: *C-1065*
 Maris T.: *B-091, C-0083, C-0400, C-0508, C-0800*
 Maritano A.: *C-0718*
 Mark L.P.: *C-0856*
 Mark W.: *C-0053*
 Markey B.: *B-772*
 Markl M.: *C-1030*
 Markovic B.: *B-874*
 Markovic Z.: *B-874, C-0595*
 Marks M.: *B-525*
 Marks M.: *B-074*
 Marlovits S.: *B-353, C-0678*
 Maroldi R.: *A-382, A-400, B-181*
 Maroto A.: *C-0101*
 Marotti M.: *C-0178*
 Marquardt F.: *B-046*
 Marques H.: *C-0151*
 Marques R.: *C-0151*
 Marrelli D.: *B-020*
 Marrosu F.: *B-100, C-0802, C-0863, C-0866*
 Marrosu M.G.: *C-0802*
 Marshall G.: *A-346*
 Marsot-Dupuch K.: *A-241, C-0522, C-0559*
 Martegani A.: *B-024, C-0209, C-1066*
 Martel J.: *C-0657*

List of Authors and Co-authors

Marten K.: <i>A-018, B-033, B-163, B-165</i>	Masulovic D.M.: <i>C-0631, C-0701, C-0702</i>	McDonald I.: <i>C-0883</i>
Martens S.: <i>B-350</i>	Masuyama K.: <i>C-0990</i>	McEntee M.F.: <i>C-0959</i>
Martí M.: <i>C-1074</i>	Mata J.M.: <i>C-0289, C-0326</i>	McGarrigle A.: <i>C-0968</i>
Martí-Bonmatí L.: <i>B-849, B-857, C-0475, C-0667, C-0704, C-0945</i>	Mathieu M.C.: <i>B-128</i>	McGrath A.: <i>C-0280, C-0785</i>
Martin A.: <i>B-331</i>	Mathieu O.: <i>C-0344, C-0459</i>	McInroe G.A.: <i>B-791</i>
Martín Hervas C.: <i>C-0677</i>	Matos C.: <i>B-486</i>	McIntosh A.: <i>B-735</i>
Martin L.: <i>C-0927</i>	Matoussevitch V.: <i>B-456</i>	McIntyre A.: <i>B-055</i>
Martín López E.: <i>C-0268, C-0537, C-1014, C-1015</i>	Matsopoulos G.: <i>C-0942, C-0963</i>	McKenna C.M.: <i>C-0013</i>
Martin M.: <i>C-0882</i>	Matsubara H.: <i>B-014</i>	McKenna D.A.: <i>C-0111</i>
Martin M.A.: <i>C-0751</i>	Matsueda K.: <i>C-0028</i>	McKie S.: <i>C-0725</i>
Martin Olariz A.: <i>B-719</i>	Matsui O.: <i>A-362, C-0038, C-0046, C-0971</i>	McLaren C.: <i>A-194</i>
Martina F.M.: <i>B-244, C-0697</i>	Matsui T.: <i>C-0539, C-0971</i>	McMahon B.P.: <i>C-0109</i>
Martincich L.: <i>B-377</i>	Matsuki M.: <i>C-0116</i>	McMahon C.J.: <i>B-172, B-559</i>
Martinek V.: <i>B-354</i>	Matsumoto K.: <i>C-0982</i>	McNally E.G.: <i>A-402</i>
Martinez A.: <i>C-0913</i>	Matsumoto M.: <i>C-0380</i>	McNicholas M.M.: <i>C-0226</i>
Martinez Alvarez R.: <i>C-0813</i>	Matsumoto S.: <i>C-0373</i>	McNitt-Gray M.F.: <i>B-446, C-0282</i>
Martínez C.: <i>C-0221</i>	Matsumoto S.: <i>C-0538, C-1001</i>	Meaney J.F.M.: <i>A-128, B-559, C-0280, C-0785, C-0801, C-1021, C-1032, C-1047</i>
Martínez C.: <i>C-0123</i>	Matsumura T.: <i>C-0788</i>	Mechtel M.: <i>B-778</i>
Martínez -Cuesta A.: <i>B-071</i>	Matsunami H.: <i>C-0608</i>	Meckle R.: <i>B-201</i>
Martínez de Aragon A.: <i>C-0771</i>	Matsuo M.: <i>C-0839</i>	Meder J.-F.: <i>C-283, C-0782, C-0796</i>
Martínez de Aragón A.: <i>C-0876</i>	Matsuo Y.: <i>C-0429</i>	Medina Portillo S.: <i>C-0884</i>
Martínez de la Haza D.: <i>C-0689</i>	Matsuoka T.: <i>C-0348, C-0350, C-0615</i>	Meding J.: <i>C-1025</i>
Martínez M.J.: <i>C-0122, C-0155</i>	Matusako M.: <i>C-0628</i>	Medrano C.: <i>C-0172, C-0686</i>
Martínez M.-J.: <i>B-924</i>	Matsushita A.: <i>C-0995</i>	Medrano C.: <i>C-0467, C-0476</i>
Martínez Pérez M.J.: <i>B-849</i>	Matsushita S.: <i>C-0392</i>	Medrano S.: <i>C-0928</i>
Martínez Regueira F.: <i>C-0206</i>	Matsuura Y.: <i>C-0539</i>	Meduri A.: <i>B-212, B-219</i>
Martínez Rubio C.: <i>B-378</i>	Matsuya H.: <i>C-0983</i>	Medved M.: <i>B-326</i>
Martínez San Millan J.: <i>C-0546, C-0561</i>	Matsuzaki K.: <i>C-0047, C-0440</i>	Medvedev V.: <i>C-0732</i>
Martínez X.: <i>C-0185</i>	Mattace Raso M.: <i>C-0131, C-0462</i>	Meeder P.J.: <i>B-138</i>
Martínez-Berganza M.T.: <i>C-0072, C-0099</i>	Mattich J.: <i>B-693</i>	Meehan C.P.: <i>C-0364, C-0445, C-0472, C-0740, C-1006</i>
Martínez-Berganza T.: <i>C-0100</i>	Mattiuzzi M.: <i>B-376</i>	Mehanna M.J.: <i>C-0094, C-0484</i>
Martínez-Bisbal M.C.: <i>C-0475</i>	Matuszewski L.: <i>B-784, B-785</i>	Mehrabi S.: <i>B-011, B-012, B-016</i>
Martínez-Cuesta A.: <i>A-083, C-0576</i>	Matute Teresa F.: <i>C-0753, C-0814</i>	Meier R.: <i>C-0406</i>
Martínez-Granados B.: <i>C-0475</i>	Matzek W.: <i>B-400</i>	Meindl T.: <i>B-610, B-611, B-615</i>
Martínez-Miravete P.: <i>C-0183</i>	Matzek W.K.: <i>B-027, B-836</i>	Meingan P.: <i>C-0181, C-0211</i>
Martínez-Miravete P.: <i>B-071</i>	Maubon A.J.M.: <i>A-033</i>	Meissamy S.: <i>B-735</i>
Martínez-Rodrigo J.J.: <i>C-0609</i>	Maurea S.: <i>B-086, B-416</i>	Meissner B.: <i>B-096</i>
Martino V.: <i>B-699, C-0084, C-0092, C-0113</i>	Maurer F.: <i>C-0612</i>	Meissner O.A.: <i>B-111, B-243</i>
Martinoli C.: <i>A-149, B-131, B-800, B-806, C-0719, C-0902</i>	Maurício J.: <i>C-0151</i>	Mejdoubi M.: <i>B-760</i>
Martinoli C.: <i>C-0742</i>	Mauz-Körholz C.: <i>C-0887</i>	Melchert U.H.: <i>C-0859</i>
Martirosian P.: <i>C-0403</i>	Mavrogeni S.: <i>C-0246</i>	Melderis F.: <i>B-333</i>
Martos Becerra J.M.: <i>C-0794, C-0874</i>	Mavrogeni S.I.: <i>B-659</i>	Meli F.J.: <i>C-0820</i>
Maruyama T.: <i>C-0995</i>	Mayer D.: <i>B-104, B-376</i>	Meller G.: <i>B-930</i>
Marx C.: <i>B-261, B-263, B-371, B-402, B-403</i>	Mayer D.: <i>B-788</i>	Melnic G.: <i>B-252</i>
Maryniak R.K.: <i>B-188, C-0540</i>	Mayer F.: <i>B-875</i>	Meloni F.: <i>B-196, C-0637</i>
Marziani M.: <i>B-030</i>	Mayer H.: <i>B-875</i>	Meloni G.B.: <i>C-0637</i>
Marzio A.: <i>B-065, B-457, B-513</i>	Mayerhoefer M.E.: <i>B-686</i>	Meloni T.: <i>C-0707</i>
Mas J.-L.: <i>C-0796</i>	Maynar M.: <i>A-289, B-514, C-0578</i>	Memarsadeghi M.: <i>B-736</i>
Masala S.: <i>B-289</i>	Mayo J.R.: <i>C-1083</i>	Memeo M.: <i>B-475, B-476</i>
Mascarenhas V.M.V.T.: <i>C-0924</i>	Mayumi K.: <i>C-0342</i>	Memis Oktay A.: <i>B-582</i>
Mascaro L.: <i>C-0980</i>	Mazanec R.: <i>B-099</i>	Memmola C.: <i>B-476</i>
Mascheroni F.: <i>C-0209</i>	Mazonakis M.: <i>C-0036</i>	Memmos D.: <i>C-1070</i>
Mascioccchi C.: <i>A-005, B-085, B-129, B-137, B-140, B-287, C-0428, C-0511, C-0695, C-0734, C-0767, C-0786, C-0803, C-1063</i>	Mazur E.: <i>C-1060</i>	Menchini L.: <i>B-173, B-174, B-577</i>
Mase M.: <i>B-744</i>	Mazurenko O.V.: <i>C-0690</i>	Mendlik T.: <i>B-683</i>
Maselli A.: <i>B-517</i>	Mazza E.: <i>B-290, B-628, C-0620, C-0636</i>	Meng Q.: <i>B-555, B-681</i>
Maselli G.: <i>B-300</i>	Mazza G.: <i>B-049</i>	Mengiardi B.: <i>B-351</i>
Maseri A.: <i>B-082</i>	Mazzarella G.: <i>C-0277</i>	Meni A.: <i>C-0655, C-0693</i>
Masetti R.: <i>C-0201</i>	Mazzei M.A.: <i>B-020</i>	Menicagli L.: <i>B-253, B-254</i>
Mashayekhi M.: <i>C-0743</i>	Mazzeo S.: <i>B-415</i>	Mentasti M.: <i>B-914</i>
Masinielli B.M.: <i>B-607</i>	Mazzotta D.: <i>C-0199</i>	Mentzel H.-J.: <i>B-648, C-0891</i>
Masnou P.: <i>B-430</i>	Mc Donnell O.: <i>C-0987</i>	Mentzelopoulou E.: <i>C-0692</i>
Massari F.: <i>B-289</i>	Mc Fadden S.L.: <i>C-0650</i>	Menu Y.: <i>C-0756</i>
Masselli G.: <i>B-577</i>	Mc Gee A.M.: <i>C-0650</i>	Menu Y.: <i>A-113, B-362, B-365</i>
Massing S.: <i>B-404, B-571, B-654, E-14</i>	Mc Hugh J.: <i>B-742</i>	Menzel M.: <i>B-356, B-358</i>
Massuet A.: <i>B-262, C-0289, C-0326, C-0605</i>	Mc Kenna D.A.: <i>C-0143</i>	Menzel M.I.: <i>B-851</i>
Mastantuono M.: <i>A-210</i>	Mc Adams H.P.: <i>E-24</i>	Merchant N.: <i>C-0227</i>
Mastorakou I.: <i>C-0470</i>	McArthur T.: <i>B-305</i>	Mereu M.: <i>B-388, C-0307</i>
Masulovic D.: <i>C-0174, C-0595</i>	McCall I.W.: <i>A-138</i>	Merino E.: <i>C-0507, C-0689</i>
	McCann J.: <i>C-0801, C-1047</i>	Merino P.: <i>C-0009, C-0731, C-0793, C-1044</i>
	McCarthy P.: <i>C-0142, C-0483</i>	Merino X.: <i>C-1023</i>
	McCarthy P.A.: <i>C-0143, C-0364, C-0445, C-0472</i>	Merino-Casabiel X.: <i>C-0250, C-0770</i>
	McCollough C.: <i>B-446</i>	Merisotis T.: <i>B-542</i>
	McCollough C.H.: <i>B-442, B-443</i>	
	McDermott R.: <i>C-0280</i>	

List of Authors and Co-authors

- Merkle E.M.: *B-406*
 Merlin A.: *C-0368*
 Merlino B.: *B-244*
 Meroni R.: *B-455*
 Mertelmeier T.: *B-547, B-549*
 Messa C.: *B-728*
 Messina A.: *C-0115, C-0145, C-0769*
 Mestan H.: *B-355*
 Mesters R.: *B-785*
 Metafratz Z.M.: *B-597, C-1020*
 Metens T.: *B-486*
 Metz S.: *B-259, C-0406*
 Meuli R.: *B-318*
 Meyding-Lamadé U.: *C-0395*
 Meyer J.: *B-472*
 Meyer K.: *C-0193*
 Meyer-Baese A.: *B-103, B-321, B-374*
 Meyers L.: *B-392*
 Meylaerts L.: *B-385*
 Meziti L.: *C-0691, C-0747*
 Miaux Y.: *C-0460*
 Michaely H.J.M.: *B-182, B-454, B-557, B-574*
 Michailidis G.A.: *C-0246, C-0726*
 Michalachis D.: *C-0074*
 Michalakou M.: *C-0860*
 Michelassi M.C.: *B-766*
 Michell M.: *C-0780*
 Midiri M.: *A-276, B-088, B-089, B-667, C-0027, C-0167, C-0656, C-0727*
 Midiri M.: *B-301, C-0267, C-0974*
 Midulla M.: *B-411*
 Miele V.: *C-0447, C-0696, C-0901, C-0922*
 Migaleddu V.: *B-126*
 Miglio C.: *B-043, B-044, B-515, B-710, B-741, B-747, C-0019, C-0034, C-0035, C-0391, C-0585*
 Mihailidis A.: *C-0739*
 Mihajloski D.: *C-0596*
 Mihara F.: *B-330*
 Mikhailova E.A.: *C-0432*
 Miki H.: *C-0014*
 Mikiciuk-Olasik E.: *C-0389*
 Mikulis D.J.: *B-919*
 Milakara D.: *B-930*
 Milcinski M.: *C-0685*
 Milczarek K.: *B-070*
 Mildenberger P.: *A-302, B-368*
 Milicevic M.: *C-0631*
 Miller S.: *B-800*
 Miller S.: *B-157, B-587*
 Millet-Roig J.: *C-0945*
 Mills P.: *C-0213*
 Milne E.N.C.: *B-028, E-59*
 Milz S.: *B-683*
 Minami M.: *C-0028*
 Minamiguchi H.: *C-1037*
 Minar E.: *A-258*
 Mineta M.: *C-0651*
 Minetti E.: *C-0580*
 Minko B.A.: *C-0432*
 Minordi L.M.: *B-577*
 Minoshima S.: *D-11*
 Minota E.: *C-0982*
 Minoui A.: *C-0747*
 Mioduszewski A.: *B-566*
 Miquel A.: *C-0756*
 Miralles M.: *C-0882, C-0913*
 Miranda A.: *C-0999, C-1049*
 Miranda A.M.: *C-0137*
 Mirat A.: *C-0691*
 Miro C.: *B-838*
 Miró J.: *C-0730*
 Miroshnichenko S.I.: *B-541*
 Misciasci T.: *B-244*
 Misra R.R.: *C-0177, C-0733, C-0743*
 Misselwitz B.: *B-113*
 Missiroli C.: *B-185*
 Mitromaras J.: *C-0334, C-0584*
 Mitropoulou M.: *C-0775*
 Mittermayer C.: *B-757, B-892*
 Miyagawa M.: *C-0339*
 Miyamoto A.: *B-883*
 Miyasaka K.: *C-0415, C-0594*
 Miyatani Y.: *C-0983*
 Miyati T.: *B-744, C-0539, C-0951*
 Miyayama S.: *C-0536*
 Mizoe J.: *B-186*
 Mlynarik V.: *B-789, B-935, C-0497, C-0678*
 Moncanu D.: *D-05*
 Mocarski S.: *C-1046*
 Mochizuki T.: *C-0014, C-0339*
 Mocsári Z.: *B-915*
 Moczová J.: *C-0042*
 Mödder U.: *B-748, C-0984, C-1019*
 Modena M.G.: *B-215, B-824*
 Moehler T.: *C-0407*
 Moffat B.A.: *B-786*
 Moffett R.: *D-14*
 Mohiaddin R.H.: *A-389*
 Mohr A.: *C-0674, C-0997*
 Moinard M.: *C-0684*
 Molinari F.: *B-703, C-0340*
 Molinari G.: *C-0255*
 Molino C.: *C-0221*
 Mollá E.: *C-0667*
 Molla Landete M.A.: *C-0290*
 Mollet N.R.: *B-301, B-308, B-342, B-667, C-0267, C-0974*
 Mollica C.: *B-416*
 Monaco D.: *B-061*
 Mondino I.: *C-0570*
 Monedero M.D.: *C-0122, C-0155, C-0609*
 Mones L.: *C-0467, C-0476, C-0686, C-1061*
 Monetti R.: *B-256, C-0670*
 Monina M.: *C-0428, C-0511, C-0734*
 Monnin P.: *C-0970*
 Montagnani S.: *B-121, B-122, B-852*
 Montagne J.-P.: *A-293*
 Montaudon M.: *B-087, C-0269*
 Montemarano E.: *C-0045*
 Montemezzi S.: *C-0190, C-0239, C-1018*
 Montemuro F.: *B-377*
 Montorsi M.: *C-0079*
 Monzón F.: *C-0072, C-0099, C-0100*
 Moon D.: *B-864*
 Moon J.H.: *B-581*
 Moon T.Y.: *C-0288, C-0300*
 Moon T.Y.: *B-394, B-761, C-0846*
 Moon W.K.: *C-0202, C-0203, C-0217*
 Moonen C.: *A-090*
 Moons P.: *B-697*
 Morace F.: *C-0144*
 Morag Y.: *B-800, C-0681*
 Morales J.P.: *B-067, B-069, B-876*
 Morales Olaya J.: *C-0434*
 Morales P.: *B-334*
 Morana G.: *A-039, B-049*
 Moraschi I.: *B-390*
 Moratal-Pérez D.: *C-0945*
 Morbach A.E.: *B-701*
 Moreiras M.: *C-0604*
 Morena M.: *B-049*
 Moreno-Ramos M.D.: *C-0179*
 Morgan R.: *B-293*
 Morhard D.: *B-314*
 Mori H.: *A-363, C-0538, C-0838, C-1001*
 Mori K.: *C-0028*
 Moriarty J.: *B-359*
 Morice P.: *A-035*
 Moriconi E.: *C-0192, C-0195*
 Moriggl B.: *B-807*
 Morimoto N.: *C-0222*
 Morisawa N.: *C-0499*
 Morisetti A.: *B-885*
 Morishita S.: *C-0381*
 Morishita S.: *C-0320*
 Morita F.: *C-1007*
 Morita T.: *C-0582*
 Morita T.: *C-0393*
 Moritz A.: *B-068*
 Moriyama N.: *C-0342, C-0397*
 Moron K.: *C-0892, C-0911, C-0923*
 Morris D.: *B-627*
 Mosbah A.: *B-396*
 Mosca S.: *B-300, B-517*
 Moske-Eick O.: *B-247*
 Mostova M.I.: *C-0242*
 Motamed K.: *B-801*
 Motoori K.: *C-0532*
 Motyl M.: *C-0807*
 Mountzouoglou A.: *C-1076*
 Mounter N.A.: *C-0213*
 Mouravliansky N.: *C-0942, C-0963*
 Moure C.: *C-0231*
 Mourkogiannis N.: *C-0860*
 Mourtopoulos C.: *C-0775*
 Mpatakis N.: *B-336, B-620*
 Mpouchlis G.: *C-0706*
 Mpougias C.: *C-0438*
 Mrklovský M.: *C-0529*
 Mrvic M.: *C-0495, C-0644*
 Mueller C.: *B-839*
 Mueller C.: *B-327, C-0509, C-0669, C-0857*
 Mueller D.: *B-251, B-256, B-257, B-687, C-0670*
 Mueller M.: *C-0407*
 Mueller P.R.: *A-236, A-334*
 Mueller W.M.: *B-435, B-927*
 Muellerleile K.: *B-213*
 Mueller-Lisse U.: *B-611, B-615, B-615*
 Mueller-Lisse U.G.: *A-331, B-111, B-496, B-610, B-611*
 Mueller-Lisse U.L.: *B-610*
 Mühlenbruch G.: *B-169, B-348, B-382*
 Muhr G.: *B-356, B-357*
 Multatieri D.: *C-0172, C-0467, C-0476, C-0686*
 Mulert C.: *B-271*
 Mulkens T.H.E.J.: *B-441*
 Mullen M.: *C-0234*
 Müller C.: *B-008*
 Müller F.-M.: *B-473*
 Müller J.K.E.: *B-689*
 Müller M.: *D-16*
 Müller S.: *B-160*
 Muller S.M.: *B-379*
 Mullerad M.: *B-676*
 Müller-Forell W.: *A-182*
 Müller-Gerbl M.: *B-255*
 Müller-Horvat C.: *B-562, B-715*
 Müller-Hülsbeck S.: *B-637*
 Müller-Schimpfle M.: *B-587*
 Müller-Schimpfle M.: *C-0612*
 Mungan U.: *C-0456*
 Munneke G.J.: *B-293*
 Muñoz Beltran M.: *C-0050*
 Munuera J.L.: *C-0851*
 Murakami R.: *C-0381*
 Muramatsu Y.: *C-0342*
 Muranaka T.: *C-0146, C-0170, C-0788*
 Murano T.: *C-0342*
 Muraoaka N.: *C-0608*
 Murase K.: *B-471*
 Murata K.: *C-0186*

List of Authors and Co-authors

Murata S.: *C-0308, C-0566*
 Murayama S.: *C-0582*
 Murphy J.M.: *C-0111, C-0143*
 Murray D.: *C-0480*
 Murray J.G.: *B-115*
 Murru A.: *C-0863*
 Musante F.: *C-0112*
 Mussack T.: *B-815, B-816*
 Mussagaliев D.T.: *C-0602*
 Mussen E.: *B-441*
 Musset D.: *A-369*
 Musumeci R.: *C-0115, C-0145, C-0769*
 Mutch S.: *B-449*
 Mutignani M.: *B-174*
 Muto M.: *B-283, B-286*
 Mutschler W.: *B-006*
 Muttarak M.: *C-0066*
 Muyor P.: *C-0771*
 Myakinkov V.B.: *B-580*
 Mylona M.D.: *C-0660, C-0692, C-0715*
 Mylona S.: *B-336, B-620, C-0349, C-0451, C-0619*
 Myoui A.: *C-0759*
 Myridis N.E.: *C-0967*
 Mysior M.: *B-118*

N

Na D.G.: *C-0556, C-0790, C-0810, C-0845*
 Nabeya Y.: *B-014*
 Nadjmabadi D.: *B-723*
 Nagabushan N.: *B-007*
 Nagai N.: *B-316*
 Nagami A.: *C-0806*
 Nagareda T.: *C-0339*
 Nagasaka T.: *C-0228*
 Nagasawa H.: *B-468*
 Nagasawa K.: *C-0651*
 Nagel M.: *D-03*
 Nägele T.: *B-715*
 Naidich D.P.: *B-161, B-162, B-164, B-325*
 Naito K.: *C-0560*
 Naito Z.: *C-0397*
 Nakada M.: *C-0600*
 Nakagawa H.: *C-0965*
 Nakagawa R.: *C-0628*
 Nakagiri Y.: *C-0995*
 Nakajima M.: *B-319*
 Nakajima Y.: *C-0147*
 Nakamoto Y.: *C-0982*
 Nakamura K.: *C-0350, C-0615*
 Nakamura S.: *C-0194*
 Nakamura T.: *C-0629*
 Nakamura T.: *C-0299*
 Nakano Y.: *C-1054*
 Nakatani K.: *C-0320*
 Nakayama T.: *C-0582*
 Nakazawa K.: *C-0308, C-0566*
 Nakazono T.: *C-0429*
 Nakos G.: *B-560*
 Nam J.E.: *C-0229, C-0258, C-0274*
 Nam K.J.: *C-0630*
 Nandi A.: *A-432*
 Nani R.: *C-0909*
 Napel S.: *D-19*
 Napoli A.: *B-031, B-119, B-885, C-1043*
 Napoli A.: *C-1013*
 Napoli G.: *B-529*
 Napoli V.: *B-294*
 Narabayashi I.: *C-0116*
 Narayan T.V.: *C-0414*
 Nardini C.: *B-439*
 Nardis G.: *B-373*

Nardis P.G.: *B-031, B-885, C-0306, C-0371, C-0510, C-1043*
 Narita K.: *B-468*
 Narvaez F.J.: *B-563*
 Narvaez J.: *C-0741*
 Narváez J.A.: *B-563, C-0063, C-0507, C-0686, C-0689, C-0741, C-0763*
 Nascimento R.D.: *C-0881*
 Nashan B.: *C-0010, C-0011*
 Nass Ducre M.: *C-0929*
 Nassenstein I.: *B-458, B-459, B-900, B-902*
 Nassenstein K.: *B-654*
 Nasser M.: *B-828*
 Natale L.: *B-212, B-219, B-244*
 Nath A.K.: *B-799*
 Nauck V.: *C-0634*
 Naumov V.G.: *B-304*
 Nava L.: *C-0453, C-0491, C-0502*
 Navalho M.: *B-192*
 Navarro M.: *C-0303*
 Navarro Navarro M.: *C-0433*
 Navarro S.: *C-0058*
 Neelakantan A.: *C-0233*
 Neff K.W.: *B-890, C-0930*
 Nehrke K.: *B-656*
 Neitzel U.: *C-0960, C-0961*
 Nelson M.T.: *B-735*
 Nemec S.F.: *B-273*
 Nemes L.: *C-0064*
 Nemni R.: *B-229*
 Nemore F.: *B-536*
 Neri E.: *B-147, B-275, B-483, B-690, C-0054*
 Neri P.: *B-135*
 Netzer P.: *B-693*
 Neubauer H.: *B-263*
 Neufang A.: *B-295*
 Neuwirth J.: *B-099*
 Nevado M.: *C-0657*
 Nevhasymy A.A.: *B-541*
 Newitt D.C.: *B-258, B-565*
 Neznanov N.G.: *C-0791*
 Ng Q.S.: *C-0304, C-0323*
 Ni Y.: *B-316, B-338*
 Nicholson A.: *A-125*
 Nicolau C.: *B-622, C-0610*
 Nicolazzini S.: *C-0694*
 Nicoli F.: *C-0865*
 Niederle B.: *B-400*
 Niederstadt T.-U.: *B-458, B-902, B-932*
 Niedzwiedek J.: *C-1060*
 Nielsen A.H.: *C-0110*
 Niemi A.: *C-0992*
 Niesen A.: *C-0408*
 Niessen W.: *B-451*
 Nieswand C.: *B-245*
 Nieto M.: *C-0086*
 Nigmatova E.Sh.: *C-0664*
 Niimi T.: *C-0948, C-0949*
 Nikas I.: *C-0934*
 Nikas J.: *C-0784, C-0861*
 Nikiforidis G.: *C-0355*
 Nikiforidis G.: *C-0369*
 Nikita A.: *C-0584, C-0624, C-0625, C-0641*
 Nikolaou A.: *C-0775*
 Nikolaou K.: *B-249, B-341, B-343, B-346, B-846, B-917*
 Nikolopoulos D.: *C-0943, C-0955*
 Nilsen R.A.: *B-665*
 Nin Garaizabal P.: *C-0413*
 Nin P.: *C-0197, C-0425*
 Niño C.: *C-0086*
 Niola R.: *C-0614*
 Nishi N.: *C-0592*
 Nishii T.: *B-768*

Nishikawa H.: *C-1054*
 Nishino M.: *C-0285, C-0325*
 Nishio R.: *C-0286*
 Nishitani H.: *C-0047, C-0440*
 Nitatori T.: *B-319*
 Nitta N.: *C-0186*
 Nittka M.: *B-429*
 Niwa M.: *B-823, C-0273*
 Noeske R.: *B-825*
 Nogami M.: *B-387, B-470, B-471*
 Noguchi M.: *C-0298, C-0536*
 Noguchi M.: *C-1054*
 Nogueira R.G.: *C-0881*
 Noguera J.J.: *B-071, C-0206, C-0223, C-0576, C-0665*
 Nöldige G.: *B-138*
 Nolla J.M.: *B-563*
 Nollo G.: *C-0360*
 Nolte-Ernsting C.C.A.: *A-196, B-083, B-614, B-652, B-656, B-781, B-820*
 Nonent M.: *B-550*
 Nordmark B.: *B-564*
 Noti P.: *C-1071*
 Novak B.: *B-151, B-152*
 Novak C.L.: *B-325*
 Novak D.: *C-0126*
 Novák J.: *C-0529*
 Novello S.: *C-0319*
 Novikov S.: *C-0671, C-0750*
 Novo S.: *C-0171*
 Novotny J.: *C-0362*
 Nowinski W.L.: *C-0375, D-11, D-12*
 Ntziachristos V.: *A-091*
 Nuetter M.: *B-571*
 Numaguchi Y.: *C-0628*
 Numaguchi Y.: *C-0194, C-0337*
 Nunziata A.: *B-601, C-0037, C-0045, C-0131, C-0132, C-0444, C-0462, C-0473*
 Nuyens M.: *B-189*
 Nuzhdina M.A.: *C-0939*
 Nykänen K.: *B-157*
 Nyman U.: *B-592, B-879, B-882*

O

O Gorman P.: *B-742*
 Obata T.: *C-0524*
 Obdeijn I.M.: *B-837*
 Oberdabernig B.: *B-886*
 Oberholzer K.: *B-245, B-425, B-685*
 Oberman B.: *C-1002*
 Obernosterer A.: *B-116*
 Obradovic V.: *C-0153, C-0525*
 O'Brien S.: *C-0280, C-1021, C-1032*
 Occhiato R.: *B-373*
 Ochi S.: *C-1007*
 Ochiai T.: *B-014, C-0163*
 Ochsenkuehn T.: *B-574*
 O'Connell A.-M.: *B-191*
 O'Connell F.: *C-0280*
 O'Connor P.J.: *A-381*
 O'Connor T.: *A-343*
 Oda K.: *C-1034*
 Oda T.: *C-0028*
 O'Daniel J.: *B-446*
 Oder B.: *B-288*
 Odoguardi F.: *B-461, B-483, B-850, C-0708, C-0728*
 Oellig F.: *B-425*
 Officiers F.E.: *A-121*
 Offiah A.: *A-430*
 Ogawa M.: *C-0990*
 Ogino H.: *B-744*

List of Authors and Co-authors

- Ogur E.: *C-0885*
 Oguz M.: *C-1010*
 Oh H.M.L.: *C-0066*
 Oh H.W.: *C-0542*
 Oh J.: *B-018*
 Oh J.H.: *C-0542*
 Oh J.W.: *C-0152*
 Oh J.Y.: *C-0630*
 Oh K.K.: *C-0212*
 Oh Y.-T.: *C-0029*
 Ohgiya Y.: *C-0010, C-0011*
 Ohki M.: *B-158*
 Ohkohchi N.: *C-0028*
 Ohm J.Y.: *C-0699*
 Ohmi N.: *C-0983*
 Ohno T.: *C-1067*
 Ohno Y.: *B-387, B-470, B-471, C-0373*
 Ohnuki T.: *B-056*
 Ohtani Y.: *C-0539*
 Ohtsuka S.: *B-775*
 Ohura D.: *C-0983*
 Oikado K.: *C-0194*
 Oikonomou A.: *A-019, B-843, C-0077*
 Oikonomou A.: *C-1083*
 Oikonomou I.: *B-554*
 Ois A.: *C-0851*
 Okada K.: *B-468*
 Okada T.: *C-0982*
 Okada Y.: *C-0788*
 Okahara M.: *C-0538, C-0838*
 Okamura T.: *C-0348, C-0350, C-0760, C-0761*
 Okazaki N.: *C-0971*
 Okazumi S.: *B-014, C-0163*
 O'Keeffe S.: *C-1032*
 O'Keeffe S.A.: *C-0280*
 Okimoto H.: *B-883*
 Okino K.: *C-0320*
 Oktay O.: *B-582*
 Okten O.O.: *C-0158, C-0159, C-0520, C-1058*
 Okuma T.: *C-0348, C-0350, C-0615, C-0760, C-0761*
 Okumura E.: *C-0046*
 Okumura M.: *C-0964*
 Okuno T.: *C-0601*
 Okura Y.: *C-0380*
 Olalla J.R.: *C-0609*
 Olalla Muñoz J.R.: *B-849*
 Olalla-Muñoz J.R.: *C-0122*
 Oldenburg A.: *B-604*
 O'Leary D.: *B-005*
 Oliveira I.R.: *B-058*
 Oliver T.B.: *C-0682*
 Olivetti L.: *C-0189*
 Oller N.: *C-0231*
 O'Loughlin A.: *B-005*
 Oltre M.: *B-451*
 Olsen Ø.E.: *B-754*
 Ollsson R.: *B-810*
 Olszanski W.: *B-274*
 Onat L.: *C-0597, C-0816*
 O'Neill R.: *B-791*
 Ono N.: *C-0392*
 Onozawa S.: *C-0566*
 Ontahón J.M.: *C-0136*
 Ookubo T.: *C-0093*
 Ookubo T.: *C-0393*
 Op de Beeck B.J.: *C-0168, C-0305, C-0906*
 Opolon P.: *B-128*
 Oppenheim C.: *A-283, C-0782, C-0796*
 Oppermann E.: *B-075*
 Ordonez P.L.: *C-0338*
 O'Regan D.P.: *B-117*
 Orgera G.: *B-198*
 Orguc S.: *C-0033*
- Origgì D.: *B-444*
 Orlacchio A.: *C-0627*
 Orlandi A.: *B-729*
 Oronzo P.: *C-0707, C-1028*
 Ortori S.: *B-850, C-0708, C-0728*
 Ortúñ P.: *C-0101*
 Orvalho L.: *C-0218*
 Orzech M.: *C-0382*
 Orzechowski M.: *B-929, C-0844*
 Osborn A.G.: *A-263*
 Oshima H.: *B-744*
 Osipenko V.I.: *B-474*
 Osorio M.: *C-0101*
 Ostanek L.: *B-335*
 Østergaard L.: *A-281*
 Ostheim-Dzerowycz W.: *B-631*
 Ostojic J.: *C-0850, C-0926*
 Ostojic M.: *C-0595*
 O'Sullivan G.J.: *C-0635, C-1006*
 Oswald M.: *B-111*
 Otake S.: *C-0729*
 Otani H.: *C-0228, C-0600*
 Otani T.: *B-056, B-538, B-768*
 Ottaviani P.: *B-173, C-0503*
 Otten B.J.: *C-0435, C-0469*
 Oudkerk M.: *B-150, B-237, B-309, B-381, B-524, C-0275, C-0383, C-0773*
 Ouwendijk W.J.N.: *B-094*
 Ouzounis D.: *B-238*
 Oyama Y.: *C-0348, C-0350, C-0615*
 Ozaki T.: *C-0020*
 Ozbek O.: *C-1051*
 Özdemir A.: *C-0182, C-0208, C-0668*
 Özdemir H.: *C-0885*
 Özden E.: *C-0477, C-0478, C-0479, C-0486, C-0487, C-0488, C-0500*
 Özdi̇ler E.: *C-0477*
 Ozer C.: *C-0929*
 Ozgocmen S.: *C-0765*
 Ozgun M.: *B-307, C-0245, C-0271*
 Ozretic D.: *B-899*
 Ozretic M.: *B-899*
 Özsarlarak Ö.: *B-931*
 Ozturk A.: *B-537*
-
- P**
- Paasche V.: *B-232*
 Pache G.: *B-008, B-240, B-675, C-0127*
 Pacho R.: *B-332, C-0080, C-0374*
 Paddon A.J.: *B-599*
 Padhani A.R.: *A-201, C-0162, C-0304, C-0323*
 Padley S.P.: *C-0234*
 Padley S.P.G.: *A-415*
 Padovani R.: *B-613*
 Padula S.: *B-267, C-0195*
 Paelinck B.P.: *C-0243*
 Paez de la Torre E.: *C-0822*
 Pafko P.: *B-841*
 Pages M.: *C-0058*
 Pagonas A.: *B-634*
 Pagonidis K.: *B-822*
 Pagonidis K.: *B-337*
 Pahou K.: *C-0025, C-0044, C-0056, C-0443, C-0481, C-0739*
 Paik K.-M.: *C-0574*
 Paik S.H.: *C-0736*
 Pal A.: *B-899*
 Palacio A.: *C-0197, C-0425*
 Palacio Hermoso de Mendoza A.: *C-0413*
 Palczewski P.: *B-332*
 Palkó A.: *A-249*
 Palladino F.: *B-707*
- Pallardo Y.: *C-0326*
 Pallotta F.: *C-0696*
 Pallwein L.: *B-859*
 Palm F.: *B-881*
 Palmberg N.: *B-549*
 Palmberg S.: *C-0366*
 Palmer J.: *C-0666*
 Palmero da Cruz J.: *C-0290*
 Palmero J.: *C-0875*
 Pampana E.: *B-508, B-511, B-632, B-635*
 Pan B.: *B-555*
 Panagiotidou L.: *B-843*
 Panagiotopoulos E.: *C-0370*
 Panayiotakis G.: *B-322, C-0370, C-0920, C-0943, C-0954, C-0955*
 Panebianco V.: *B-699, B-811, C-0092, C-0371, C-0510*
 Pani L.: *B-278*
 Panizza P.: *B-264*
 Pans S.: *B-682, B-684, B-922*
 Pantalone O.: *B-703, C-0493*
 Pantou K.: *B-646*
 Panzironi G.: *C-0548*
 Paolantonio P.: *B-575, B-699, B-741, B-811, C-0084, C-0090, C-0092, C-0113, C-0114, C-0391, C-0510*
 Paolillo A.: *C-0864*
 Papadaki E.: *B-091, C-0800*
 Papadaki P.J.: *C-1009*
 Papadakis A.: *C-0508*
 Papadokostakis G.: *B-771*
 Papadopoulos G.: *B-659*
 Papadopoulos K.: *B-634*
 Papadopoulos V.: *C-0076*
 Papadopoulou F.: *B-894, B-895, B-896*
 Papadopoulou P.: *C-0717*
 Papageorgiou A.: *C-0075, C-0452*
 Papageorgiou P.: *D-14*
 Papagianni A.: *C-1070*
 Papailiou J.: *C-0052, C-0962*
 Papaiaannou G.: *C-0624, C-0625, C-0641*
 Papakonstantinou O.: *A-004, C-0508*
 Papanastassiou V.: *C-0855*
 Papanikolaou N.: *A-014, A-315, B-091, B-751, B-813, C-0083, C-0800, C-1078*
 Papantoniou Y.: *B-608*
 Papke K.: *B-453, B-510, B-901*
 Papoudos M.: *C-0076*
 Paraskevaidis E.: *C-0438*
 Pardo M.: *B-706, C-0303*
 Pardo R.: *C-0221*
 Pardo S.: *C-0091*
 Pare C.: *C-0232*
 Parenti G.: *B-766*
 Parisio A.: *B-127*
 Parizel P.M.: *A-134, A-308, B-463, B-931, C-0168, C-0191, C-0305, C-0746, C-0906*
 Park B.H.: *C-0630*
 Park C.S.: *C-0893*
 Park D.W.: *C-0543*
 Park H.: *C-0005*
 Park H.-H.: *C-0352*
 Park J.G.: *B-018*
 Park J.G.: *C-0152*
 Park J.M.: *C-0217*
 Park J.M.: *C-0810*
 Park J.M.: *C-0202, C-0203*
 Park J.S.: *C-0736*
 Park K.P.: *B-762*
 Park K.S.: *C-0533*
 Park M.H.: *C-0699*
 Park N.H.: *C-0893*
 Park S.-H.: *C-0352*

List of Authors and Co-authors

- Park S.H.: *B-419, C-0017, C-0021, C-0022, C-0643*
 Park S.J.: *B-581*
 Parkhomenko R.A.: *C-0903*
 Parmentier S.: *B-045*
 Parrón M.: *C-0121, C-0303, C-0588, C-0886, C-0890*
 Pascoal A.: *B-153*
 Pascoli S.: *B-389*
 Pashkova T.L.: *B-709*
 Pasowicz M.: *B-306, C-0807*
 Pasquarelli R.: *C-0627*
 Pasquet A.: *C-0253*
 Passariello R.: *B-031, B-043, B-044, B-107, B-198, B-242, B-267, B-299, B-373, B-375, B-409, B-420, B-509, B-512, B-515, B-526, B-575, B-692, B-699, B-710, B-741, B-747, B-811, B-885, C-0019, C-0034, C-0035, C-0084, C-0090, C-0092, C-0113, C-0114, C-0192, C-0195, C-0238, C-0306, C-0371, C-0391, C-0510, C-0585, C-1043*
 Pastor C.: *C-0221*
 Pastor I.: *C-0886*
 Pastor Juan M.: *B-849*
 Pastor P.: *B-838*
 Pastor-Juan M.R.: *C-0122*
 Pastor-Juan R.: *C-0155*
 Patankar T.: *C-0795*
 Patay Z.: *C-0523*
 Patel P.V.: *C-0658*
 Patel U.: *B-393*
 Patlakas G.: *B-843*
 Patrick F.: *B-825*
 Pattynama P.M.T.: *A-237, A-336*
 Paul N.: *B-039, C-0227*
 Paul S.: *B-846*
 Pauls S.: *B-694*
 Pavcev Z.: *B-899*
 Pavelka M.: *C-1039*
 Pechotová M.: *C-0082*
 Pedachenko E.G.: *B-680*
 Pedersen J.F.: *B-600, B-814, B-814*
 Pedicelli A.: *C-0776, C-1056*
 Pedicelli G.: *B-389*
 Pediconi F.: *B-267, B-373, B-375, C-0192, C-0195*
 Pedrazzini F.: *C-0590, C-0591*
 Peeters A.: *C-0796*
 Peeters J.J.M.: *A-345*
 Peeters P.: *B-316*
 Peeters R.R.: *B-922*
 Peh W.C.G.: *A-262, C-0066*
 Pehrson R.: *B-879*
 Peitgen H.-O.: *A-009, A-356, B-179, B-830, D-09*
 Pelage J.-P.: *A-126, B-794*
 Peled N.: *B-168*
 Pellegrino L.: *B-344*
 Pellicer J.M.: *C-0741*
 Peloschek P.: *B-260, D-06*
 Peñaloza F.: *B-849*
 Pendenza G.: *B-519*
 Penning L.: *C-0383*
 Penza G.: *C-0144*
 Pepe A.: *B-088, B-089*
 Pépin J.L.: *B-708*
 Pepino D.: *B-509*
 Perchet D.: *C-1079*
 Perea R.J.: *C-0232*
 Pereira P.: *B-462*
 Pereira P.L.: *A-333, B-621, C-0611, C-0612, C-0622, C-0623*
 Pereira S.: *B-481*
 Perendreu J.: *C-0326, C-0605*
 Perendreu Sans J.: *C-1029*
- Pérez E.: *C-0689*
 Pérez G.: *C-0330*
 Perez Garcia A.: *C-0813*
 Perez L.: *C-0214*
 Pérez López C.: *C-0876*
 Perez M.: *C-0067, C-0913*
 Pérez M.: *C-1061*
 Perez Ortega G.: *C-0874*
 Perez-Lafuente M.: *C-0604*
 Perhoc Z.: *B-899*
 Peric V.: *C-0873*
 Perich X.: *C-0851*
 Perisinakis K.: *A-190, B-649, B-771, C-0976*
 Perkins A.C.: *B-925*
 Perks C.A.: *B-772*
 Perlet C.: *B-733, B-737*
 Pero H.: *A-223*
 Perotto F.: *C-0319*
 Perova T.B.: *C-0700*
 Perrot N.: *A-035*
 Perseghin G.: *B-082, B-422*
 Persigehl T.: *B-784, B-785*
 Persiva Morenza O.: *C-0032*
 Persson A.: *C-0358, C-0361, C-0366*
 Perugini E.: *B-081*
 Pescarini L.: *C-0187*
 Pessis E.: *C-0691, C-0747*
 Petcu S.: *C-0972*
 Peteinelli A.: *C-1009*
 Peter D.: *B-732*
 Peter J.: *C-0407*
 Peterlongo P.: *C-0264*
 Peters J.: *D-07*
 Petersen J.C.: *B-590*
 Petersen K.U.: *B-053*
 Peterson B.: *B-700*
 Petitbon P.: *C-0368*
 Petkovska I.: *C-0282*
 Petralia G.: *B-145*
 Petri S.: *B-120*
 Petritsch W.: *B-572*
 Petrou M.: *B-645, C-0916*
 Petrovic I.: *C-0850*
 Petrovic M.: *C-0153*
 Petrovic N.: *C-0153*
 Petrovic S.S.: *C-0557*
 Petrow P.: *A-132*
 Petrucci L.: *B-409*
 Petrucci P.: *B-294, B-558*
 Petsas T.: *C-0369, C-0661*
 Pettas N.: *C-0908*
 Pettersson G.: *B-700*
 Petzold R.: *D-03*
 Pezeshkmehr A.: *B-119*
 Pezzotta G.: *C-0909*
 Pfammatter T.: *B-241*
 Pfannenberg C.A.: *B-678, B-715, C-0293, C-0317*
 Pfarl G.: *B-836*
 Pfeffer J.E.: *B-073, B-080, B-208*
 Pfeifer B.: *B-570, B-576*
 Pfeifer K.-J.: *B-006, B-233, B-630*
 Pfennig S.: *B-183*
 Pfirrmann C.W.A.: *B-351, B-360*
 Fleiderer S.O.R.: *B-402, B-403*
 Phan C.: *C-0756*
 Phan C.: *C-0658*
 Phan C.M.: *B-258, B-565*
 Phelps M.E.: *B-384*
 Philipp M.: *B-023*
 Philipp M.O.: *C-0678*
 Phoa S.S.K.S.: *B-489*
 Piatkowska-Janko E.: *B-929*
 Piazzalunga B.: *B-181*
 Picazo Escribano N.: *C-0433*
- Picazo N.: *C-0214*
 Picchietti S.: *B-147, B-690*
 Picchio M.: *B-728*
 Piccoli G.: *B-065, B-457, B-513*
 Piccoli T.: *B-097*
 Pichieccio A.: *C-0864*
 Picot V.: *C-0184*
 Picotti A.: *C-0719*
 Piedra T.: *C-0009, C-0059, C-0764, C-0793*
 Pienkowska J.M.: *C-0015, C-0016, C-0133, C-0149*
 Pieroni M.: *B-082*
 Pierot L.: *B-759*
 Pierro A.: *B-292, B-339*
 Pietrani M.A.: *C-0821, C-0884*
 Piffaretti G.: *B-062*
 Pignataro P.: *B-475*
 Piitulainen E.: *B-700*
 Pijl M.E.J.: *B-142*
 Pikoulas K.: *C-0766*
 Pilato E.: *B-529*
 Pilioras N.: *C-0355*
 Pillai A.: *C-1012*
 Pilmer J.: *B-334*
 Pina L.J.: *C-0206, C-0223*
 Pina Vaz C.: *C-0952*
 Pineda V.: *C-0250, C-0770, C-1023*
 Pinker K.: *B-789, B-935, C-0497*
 Pinna V.: *C-0768, C-0832*
 Pintaske J.: *C-0403*
 Pinto A.: *B-363, B-367, C-0614*
 Pinto E.: *B-020*
 Pinto Pabón I.: *A-124*
 Piontek G.: *C-0406*
 Piotrowska D.: *C-0256, C-0382*
 Piperopoulos P.N.: *B-583, C-0295*
 Pipitone V.: *B-508, B-519, B-635, B-873*
 Piqueras J.: *C-0894*
 Pires F.: *B-192*
 Pirovano G.: *B-644*
 Pironti T.: *B-703, C-0340*
 Pirtoli L.: *B-020*
 Pirulli G.: *B-626*
 Pistolese C.: *B-729*
 Pisulska-Otremba A.: *C-0564*
 Pitschner H.: *C-0248*
 Pitsoulakis G.: *C-0861, C-0899, C-0900, C-0908, C-0921, C-0932, C-0933, C-0934*
 Pittiani F.: *B-059*
 Pitton M.B.: *B-295*
 Piver P.: *A-033*
 Piza H.: *C-0898*
 Placidi S.: *C-0909*
 Plagou A.: *C-0056, C-0399, C-0482*
 Plank C.M.: *B-353*
 Plass A.: *B-821*
 Plathow C.: *C-0294, C-0345, C-0386*
 Platten D.J.: *B-669*
 Plavsin B.M.: *C-0419, C-0421*
 Ploder M.: *C-0639*
 Po J.: *C-0915*
 Podestà R.: *A-149, C-0719*
 Pohlman S.: *C-0281*
 Pokieser P.: *B-012, D-02*
 Poldermans D.: *A-272, B-214*
 Poletti Venegoni R.: *B-914*
 Polidura Arruga C.: *C-0085*
 Polimeropoulos V.: *C-0076*
 Politi L.S.: *B-764*
 Pollard L.: *C-0705*
 Pollice S.: *B-224, B-536, C-0829*
 Pöllinger A.: *E-57*
 Polonara G.: *A-145, C-0833*
 Polyviou P.: *C-0295*

List of Authors and Co-authors

- Pomes J.: *C-0645*
 Pomés J.: *C-0617*
 Pomfret E.: *B-179*
 Pomoní M.: *B-634, C-0451, C-0619*
 Pompili G.: *C-0079*
 Pomposelli J.: *B-179*
 Pons M.J.: *C-0206, C-0311, C-0516*
 Pons Renedo M.J.: *B-167*
 Pont J.: *C-0101*
 Pontes-Neto O.M.: *C-0780*
 Pop G.D.: *C-0972*
 Poplaw S.: *C-0263*
 Popolizio T.: *C-0829*
 Popova E.N.: *B-474*
 Popova L.: *C-0398*
 Popp P.: *B-232*
 Porcelli A.: *B-212, B-219*
 Porod V.: *C-0362*
 Porro F.: *C-0335*
 Portalone L.: *B-389*
 Portugaller R.H.: *B-116*
 Portugalli V.: *B-124, B-125, B-609*
 Potocki K.: *C-0108, C-1002*
 Potseluyev D.D.: *C-0602*
 Potter K.C.: *B-143*
 Pourcelot L.: *C-0377*
 Pouwels P.J.W.: *A-329*
 Poves J.I.: *C-0135*
 Powell S.: *C-1062*
 Pozdniakov A.V.: *C-0811, C-0847*
 Pozdniakova O.F.: *C-0055*
 Pozuelo C.: *C-0172, C-0686, C-1061*
 Pozuelo O.: *C-0467, C-0476*
 Pozuelo Segura C.: *C-0467, C-0476*
 Pozzi Mucelli R.: *C-0267, C-0974*
 Pozzilli P.: *B-300, B-517*
 Pozzi-Mucelli F.: *C-0565*
 Pozzi-Mucelli R.: *A-085, B-602, B-607, B-638, C-0565*
 Prabhu S.P.: *C-0102, C-0233, C-0251, C-0343, C-0414, C-0450, C-0521, C-0553, C-0895*
 Prakash B.: *D-11*
 Prapavesis S.: *C-0470, C-0482*
 Prassopoulos P.: *B-238, B-640, B-843, B-867, C-0036, C-0077, C-0254, C-0498*
 Pratali A.: *B-294, C-0054*
 Prause G.: *D-09*
 Prayer D.: *A-408, B-221, B-756, B-757, B-889, B-892, B-893*
 Preda L.: *B-184*
 Prefumo F.: *C-0718*
 Pregarz M.: *C-0026*
 Preim B.: *C-0379*
 Prenafeta M.: *C-0792*
 Preoteasa F.D.: *C-0957*
 Prescod K.: *C-0414, C-0521*
 Preston R.L.: *C-0879*
 Prêteux F.: *C-1079*
 Preusser T.: *D-09*
 Prevrhal S.: *C-0658*
 Preyer O.: *B-789, C-0497*
 Priest A.N.: *B-113, B-114, B-120, B-743, B-755, B-918, C-1005, C-1025*
 Prieto C.: *B-770, C-0886*
 Prieto Del Rei M.J.: *B-719*
 Prieto J.R.: *C-0687*
 Prieto V.: *C-0578*
 Priola A.: *C-0319*
 Priolo F.: *C-0697*
 Priotto R.: *C-0591*
 Prisco A.: *C-0132*
 Prochorec-Sobieszek M.: *B-188, C-0540*
 Prodanovic N.: *C-0676*
 Profanter C.: *B-060*
- Profili S.: *B-196, C-0637*
 Prokesch R.W.: *A-322*
 Prokop M.: *A-116, A-160, A-218, A-291, B-011, B-012, B-016, B-170, B-381, B-451, B-518, B-521, B-595, C-0509, E-38, E-51*
 Prommegger R.: *B-060*
 Pronin I.N.: *B-438*
 Propp S.: *B-271*
 Proscher H.: *C-0125*
 Prost R.W.: *B-435, B-927, C-0856*
 Protopapa E.: *C-0618*
 Provost Y.: *C-0227*
 Prozorovsky K.V.: *C-0432*
 Pruna X.: *C-0928*
 Pruzincová L.: *C-0042*
 Prvulovic N.: *C-0926*
 Przewlocki T.: *B-306*
 Przywara S.: *C-1046, C-1060*
 Psarakis E.: *C-0860*
 Pucci A.: *B-299, B-409, B-512*
 Puderbach M.: *B-472, B-473, C-0294, C-0345, C-0386*
 Puespoek A.: *B-011*
 Puespuik A.: *B-012*
 Puglielli E.: *C-0786*
 Pugliese F.: *B-131, B-806, C-0902*
 Puglioli M.: *B-766*
 Puglisi F.: *B-266*
 Puig Domingo J.: *B-719*
 Puig S.: *A-341, A-398, B-573*
 Pujol J.: *C-0545*
 Puligheddu M.: *B-100, C-0802, C-0863, C-0866*
 Punwani S.: *C-0480*
 Pupillo V.: *B-085, C-0786, C-0803, C-1063*
 Puppi A.: *B-527*
 Puppi A.M.A.: *C-0679, C-0694*
 Puppini G.: *C-0190, C-0239, C-1018*
 Purushothaman H.: *C-0554*
 Puskas Z.: *A-282*
 Pustovitova T.: *C-0872*
 Putz R.: *B-683*
 Putzer D.: *B-101*
 Puy R.: *C-0797*
 Pyanov I.V.: *C-0055*
 Pyrus T.: *C-0923*
-
- Q**
- Qanadli S.: *A-031*
 Qanadli S.-D.: *B-596*
 Qian G.: *D-11*
 Qian J.: *B-075*
 Qian J.-Z.: *B-040, B-328, B-856*
 Qian X.: *B-197*
 Qian Z.: *B-514, C-0578*
 Quaia E.: *B-602, C-1080*
 Quarantelli M.: *B-086*
 Quattropani C.: *B-693*
 Quick H.H.: *B-404*
 Quintarelli S.: *C-0239, C-1018*
 Quintero J.C.: *C-0172, C-1061*
 Quintero J.C.: *C-0467, C-0476*
 Quinto F.: *B-292, B-339*
 Quirico C.: *C-1028*
 Quiroga S.: *C-0006, C-0081, C-0137, C-0999, C-1049*
 Quirós J.: *C-0657*
 Quist M.: *D-07*
-
- R**
- Raabe R.: *B-510*
 Rabadan A.: *C-0821*
- Raby N.: *C-0672*
 Rademakers F.: *B-084*
 Raderer M.: *B-016*
 Radkevich L.A.: *B-438*
 Radny P.: *B-715*
 Rado Y.: *C-0984, C-1019*
 Radovanovic M.: *C-0495*
 Radovanovic-Tasic S.: *C-0676*
 Radtke A.: *B-175*
 Radu E.-W.: *A-163, B-926, B-928*
 Raeth C.: *B-256, C-0670*
 Rafaelsen S.: *A-055*
 Raghu Nath G.: *C-0725*
 Ragozino A.: *B-858*
 Rahbar H.: *C-0880*
 Rainford L.A.: *C-0650*
 Raissaki M.: *A-189, B-649, B-751, C-0919*
 Raith J.: *B-116, B-572*
 Rajan P.S.: *C-0200*
 Rajah P.: *C-0051, C-0139, C-0169, C-0173, C-0458, C-0737, C-0795*
 Rajnics P.: *C-0652*
 Rajpal K.: *C-0272*
 Rakshe T.: *D-19*
 Rakut W.-D.: *E-15*
 Ralleigh G.: *C-0180*
 Ramaekers P.: *C-0906*
 Ramboer K.: *B-697*
 Rami K.: *B-610*
 Ramirez A.: *C-0771*
 Ramírez F.: *C-0185*
 Ramirez J.: *C-0232*
 Ramirez-Urbano F.J.: *C-0770*
 Ramiro E.: *B-838*
 Rammensee H.-G.: *C-0611*
 Ramos A.: *C-0882*
 Ramos Gómez M.: *C-0794*
 Ramos Lopez P.: *C-0098*
 Ramos Lopez P.: *C-0049*
 Ramos Moreno B.: *C-0098*
 Ramos R.: *C-0197*
 Rampinelli C.: *B-037*
 Rampoldi A.: *B-501, C-0580*
 Rand T.: *A-258*
 Rangheard A.-S.: *A-113, B-362, B-365*
 Rankin S.: *B-334*
 Ranlöf M.: *C-0366*
 Ranschaert E.R.: *A-049*
 Rao B.S.: *C-0398*
 Rapezzi C.: *B-081*
 Rapf K.: *B-060*
 Rapoport L.M.: *C-0465*
 Rapp-Bernhardt U.: *B-038*
 Raptopoulos V.: *C-0285*
 Rasche D.: *B-934*
 Rascher-Friesenhausen R.: *D-09*
 Ratib O.: *B-187, B-235, B-384*
 Rauch E.: *B-683*
 Rauhofer U.: *B-889*
 Rauscher A.: *B-102, B-105, B-783, B-921, B-923*
 Ravecca F.: *B-275*
 Ravelli F.: *C-0360*
 Razmadze M.: *C-0235, C-1004*
 Razzaq R.: *C-0527*
 Rea D.: *C-1021*
 Reale C.A.: *B-511, B-635, B-873*
 Reant P.: *B-087*
 Recheis W.: *D-18*
 Rechl H.: *B-136*
 Redaelli C.: *B-746*
 Redchuk A.A.: *B-541*
 Redel T.: *B-111*
 Redl H.: *B-573*
 Reeder S.B.: *B-429*

List of Authors and Co-authors

- Reenders J.W.A.J.: *A-133*
 Reekers J.A.: *A-232, A-255*
 Rees M.R.: *A-275*
 Reft C.: *B-772*
 Regent D.M.: *B-855*
 Reggie D.: *B-283, B-286, B-377, B-627*
 Regi L.: *B-148*
 Regier M.: *B-614*
 Regimenti P.: *B-389*
 Regine G.: *C-0447, C-0696, C-0901, C-0922*
 Regli L.: *B-318, B-765*
 Rehemtulla A.: *B-786*
 Reiber J.H.C.: *A-357*
 Reichenbach J.R.: *B-102, B-105, B-403, B-648, B-672, B-783, B-920, B-921, B-923, C-0230, C-0236, C-0409, C-0891*
 Reidy J.F.: *B-067, B-069*
 Reim S.: *B-111*
 Reimer P.: *A-282, B-047, B-050*
 Reinhardt E.: *A-222*
 Reinsberg S.: *B-724*
 Reiser M.F.: *A-010, A-044, B-006, B-103, B-111, B-182, B-183, B-216, B-217, B-218, B-225, B-226, B-232, B-233, B-243, B-249, B-271, B-272, B-277, B-321, B-341, B-343, B-346, B-374, B-383, B-429, B-454, B-464, B-466, B-496, B-502, B-543, B-550, B-557, B-574, B-610, B-611, B-615, B-630, B-683, B-691, B-717, B-815, B-846, B-851, B-917, C-0363, C-0569, C-1055, C-1064*
 Reiter G.: *D-08*
 Reith W.: *B-205, B-436*
 Reitinger B.: *A-270, D-04*
 Reitmeier F.: *B-051*
 Relea A.: *C-0086*
 Remberger K.: *C-0659*
 Remond A.: *C-1003*
 Rémy J.: *A-114, A-280, A-371, B-477, B-478, B-591*
 Rémy-Jardin M.: *A-114, A-280, A-371, B-477, B-478, B-591*
 Ren B.: *B-029*
 Renard C.: *C-1003*
 Reneman L.: *C-0815*
 Rengo M.: *B-043, B-044, B-107, B-515, B-575, B-699, B-710, B-741, B-747, B-811, C-0019, C-0034, C-0035, C-0084, C-0090, C-0092, C-0113, C-0391, C-0585*
 Renoux J.: *C-0522*
 Renzulli M.: *B-064, B-066, B-081, B-529*
 Reponen J.: *A-094*
 Resch B.: *C-0917*
 Resta M.C.: *B-475*
 Resten A.: *A-372*
 Retkowski M.: *C-0389*
 Rettenbacher T.: *B-123, B-803, E-60*
 Rettl G.: *C-0225*
 Reuchsel C.: *B-261, B-371*
 Reuter M.: *B-637*
 Rexilius J.: *B-530, D-09*
 Reynolds F.: *B-671*
 Reznek R.H.: *B-793, C-0103, C-0418, C-0436*
 Ribeiro A.: *C-0150*
 Ribes R.: *C-0176*
 Ribo J.L.: *C-0935*
 Ricart Selma V.: *B-378*
 Ricaud-Couprise M.: *C-0181, C-0211*
 Riccabona M.: *A-342, C-0917, D-04*
 Ricci F.: *C-0548*
 Richard S.: *C-0559*
 Richter G.M.: *B-195, B-413, B-414, C-0589*
 Rické J.: *B-407, D-10*
 Riddell A.M.: *B-019, B-144, C-0164*
 Ridge C.A.: *B-716*
 Rieber J.: *B-111, B-216*
 Riechling N.: *B-595*
 Riedel T.: *B-776, B-777, C-0953*
 Riedl C.C.: *B-676*
 Riedl C.C.: *B-023, B-027, B-730, B-836*
 Riedmiller H.: *B-897*
 Rieger J.: *B-190*
 Rieger J.: *B-233, B-243, B-630*
 Rieger M.: *C-0053, C-0087, C-0898*
 Rieker O.: *B-104*
 Riemann J.F.: *B-570, B-576*
 Riemer A.: *A-395*
 Rienmüller R.: *A-172, D-08*
 Rienmüller T.: *D-08*
 Righi C.: *B-764*
 Righi D.: *B-199*
 Rikimaru H.: *C-0018*
 Rillardon L.: *C-0673*
 Rimola J.: *C-0605*
 Rinck D.: *B-523, D-13*
 Ringertz H.: *C-0915*
 Rinkel G.: *B-313*
 Ripley C.: *B-866*
 Ripollés T.: *C-0122, C-0155*
 Risso F.: *C-0386*
 Rist C.: *B-341, B-343, B-346, B-846*
 Ristic S.: *C-0644, C-0812*
 Ritchie C.J.: *B-663*
 Ritz J.P.: *B-072*
 Rivlin E.: *B-168*
 Rizzatto G.: *A-375, B-025*
 Rizzo S.M.R.: *B-010, B-106, B-369, B-370, B-660*
 Roach S.: *B-177*
 Robert M.: *B-426*
 Roberts F.: *B-924*
 Roberts T.: *B-370*
 Robertson E.M.: *B-916*
 Robinson K.: *B-329*
 Robinson P.: *C-0725*
 Robinson P.J.: *B-050*
 Robinson P.J.A.: *A-040*
 Robinson S.: *A-423*
 Robl T.: *B-572*
 Robles E.: *C-0086*
 Roca Vanaclocha Y.: *C-0686*
 Roca Y.: *C-1061*
 Roca Y.: *B-563, C-0467, C-0476, C-0507*
 Roche A.: *B-128*
 Roche A.J.: *A-081*
 Roche C.: *C-0111, C-0483*
 Roche C.J.: *C-0143, C-0740, C-0977*
 Roche S.: *C-0006*
 Roche Vallés S.: *C-0031, C-0032*
 Rockall A.: *C-0103, C-0418, C-0436*
 Rodallec M.: *C-0673*
 Roddie M.: *C-0291*
 Rodière E.: *C-0074, C-0523*
 Roditi A.: *C-0215, C-0558*
 Rodrigo S.: *C-0782*
 Rodríguez A.: *C-0851*
 Rodríguez J.I.: *C-0101*
 Rodríguez R.: *B-770*
 Rodriguez-Vigil B.: *B-706, C-0677, C-0876, C-1074*
 Rodt T.: *B-276*
 Roebuck D.: *A-192*
 Roehl F.W.: *B-038*
 Roelandt W.: *B-697*
 Roelofs A.A.J.: *B-829, B-830*
 Roemer F.W.: *C-0674*
 Roemer F.W.: *C-0997*
 Rogalla P.: *B-032, B-612*
 Rogiers X.: *B-171*
 Rogozhyn V.A.: *B-230, B-680*
 Rokhlin G.D.: *C-0811*
 Roldán Romero E.: *C-0794*
 Rollo M.: *C-0776*
 Roma A.: *C-0197, C-0425*
 Roma Dalfo A.: *C-0413*
 Romagnoli A.: *B-344, B-528, C-0297*
 Romagnoli R.: *B-215, B-492, B-824*
 Romaneehsen B.: *B-685*
 Romani M.: *C-0201*
 Romanini L.: *B-049, B-124, B-125, B-609, C-0404*
 Romaniuk C.: *C-0471*
 Romano L.: *B-363, B-367*
 Romano L.: *B-484*
 Romano S.: *B-363*
 Romano V.C.: *B-032, B-588*
 Rombolá S.E.: *C-1024, C-1031*
 Romeike B.: *B-205*
 Romero C.: *C-0820*
 Romero Cique F.L.: *C-0123*
 Romero M.: *C-0617, C-0645*
 Romero-Jaramillo A.: *C-0604*
 Rompa G.: *C-0149*
 Rongen P.M.J.: *C-0367*
 Rönnelid J.: *B-564*
 Roose J.: *B-452*
 Roque A.: *C-0081*
 Roquer J.: *C-0851*
 Rørvik J.: *C-0504, C-0518*
 Ros P.: *C-0176*
 Rösch F.: *C-0408*
 Rose J.: *A-256*
 Roselli A.: *B-267, B-375, C-0192*
 Rosenbaum S.: *B-718, B-913*
 Rosenberg C.: *B-078, B-878, C-0634*
 Rosler R.: *C-0821*
 Roson N.: *C-0928*
 Ross B.D.: *B-786*
 Roß C.J.: *B-687*
 Ross W.R.: *B-663*
 Rosselli del Turco M.: *B-829*
 Rosset A.: *B-235*
 Rossi C.: *C-0653*
 Rossi L.: *B-215, B-824*
 Rossi P.: *B-198, B-299, B-509, B-512*
 Rossi R.: *B-824*
 Rossi S.: *C-0626*
 Rossi S.: *B-602*
 Rossi U.: *B-806*
 Rossini G.: *B-024*
 Rossiter J.: *C-0343*
 Rostagno R.: *B-514, C-0578*
 Rotger R.: *C-0197*
 Rotger Regi R.: *C-0413*
 Roth C.: *B-205*
 Roth E.: *C-0639*
 Rothfuss J.: *B-310, C-0270*
 Rotili A.: *C-0627*
 Rotondo A.: *B-858, C-0494*
 Rotter K.: *B-733*
 Rouanet J.P.: *A-033*
 Rousseau H.: *A-227*
 Roux F.-X.: *C-0782*
 Rovighi L.: *C-0831, C-0834*
 Rovira A.: *C-0792*
 Rovira-Cafèllas A.: *A-002*
 Rovira-Gols A.: *A-002*
 Rowinski O.: *B-070, C-0603*
 Roy C.: *C-0461*
 Roy-Choudhury S.H.: *B-334*
 Royo A.: *B-758*
 Roytberg G.E.: *C-1041*
 Rozengaouz E.V.: *C-0265*
 Rozhková Z.Z.: *B-230, B-680*
 Rozyo T.K.: *C-0563*

List of Authors and Co-authors

- Rozzati D.: *C-0655, C-0693, C-1028*
 Rubin G.D.: *B-119, C-0260, C-1013*
 Rud S.D.: *C-0055, C-0849*
 Rudas M.: *B-730, B-836*
 Rudelius M.: *C-0406*
 Rudenko V.I.: *C-0465*
 Rueckert D.: *A-244*
 Ruehm S.G.: *A-047, A-062, B-175*
 Ruffino A.: *B-199*
 Rüger A.: *A-301*
 Ruhl K.M.: *B-653*
 Rühm S.G.: *B-840*
 Ruiz A.: *C-0122, C-0609*
 Ruiz E.: *C-0059, C-0793*
 Ruiz M.: *C-0221*
 Ruiz Osuna S.: *C-0507*
 Ruiz P.: *C-0793*
 Ruiz S.: *C-0763*
 Ruiz-Hernández P.: *C-0713, C-1044*
 Rumi G.: *C-0652*
 Rummeny E.J.: *B-033, B-136, B-146, B-163, B-165, B-251, B-256, B-257, B-259, B-354, B-364, B-808, B-809, B-857, C-0406, C-0411, C-0670*
 Rumsey M.A.: *B-663*
 Runge V.: *D-11*
 Runza G.: *B-667, C-0027, C-0091, C-0167, C-0727*
 Runza G.: *B-301, B-308, B-342, C-0267, C-0974*
 Rupp N.: *C-0363, C-0569, C-1055, C-1064*
 Rupp R.: *B-139*
 Ruppert-Kohlmayer A.: *B-572, B-906*
 Ruppert-Kohlmayr A.: *B-616*
 Ruscalleda J.: *A-266*
 Ruscalleda N.: *C-0935*
 Ruscalleda Nadal J.: *C-0778*
 Russo F.: *B-377*
 Russo V.: *B-064, B-066, B-081, B-529*
 Ruth C.: *B-029*
 Rutherford E.: *B-868*
 Rutkowska B.: *C-0016, C-0133*
 Rutten A.: *B-521*
 Rybacki C.: *C-0321*
 Rychina I.: *C-0912*
 Rydh A.: *B-495*
 Ryeom H.-K.: *B-752*
 Rymer R.: *B-794*
 Ryoo J.W.: *C-0556, C-0790*
 Ryu C.W.: *B-281*
 Ryu J.A.: *B-001, B-002, C-0749*
 Ryu S.W.: *C-0262*
 Ryzhkova D.V.: *C-0242, C-0247, C-0265, C-0519*
 Rzanny R.: *C-0230, C-0236*
 Rzepko R.: *C-0015*
 Rzeszowska-Sieczka M.: *B-450*
-
- S**
- Saarenmaa I.: *A-215*
 Sabate J.: *C-0220*
 Sabatini U.: *C-0835, C-0947*
 Sabbà C.: *B-476*
 Sabharwal R.: *C-0446, C-1008*
 Sabharwal T.: *A-434, B-067, B-069, B-876*
 Sabin G.: *C-0231*
 Sabir N.: *C-0526*
 Sablayrolles J.L.: *E-23*
 Saccani S.: *B-061*
 Saccardy F.: *C-0858*
 Sacco A.: *B-636*
 Sacco M.: *B-527*
 Sacco R.: *B-388*
 Sadhev A.: *C-0418, C-0436*
- Saeed V.: *B-035*
 Saeed M.: *B-331*
 Saeed R.: *B-055*
 Saez Artacho E.: *B-380*
 Sáez E.: *B-262*
 Saga T.: *C-0287, C-0422, C-0431, C-0499, C-0534*
 Sagan L.: *C-0842*
 Sagara Y.: *C-0838*
 Saghir H.: *B-899*
 Sagoh T.: *C-0536*
 Saguet O.: *B-462*
 Sahdev A.: *B-793*
 Sahin M.: *C-0138*
 Saiani F.: *C-0980*
 Saida Y.: *C-0028*
 Sailer J.: *B-260*
 Saini S.: *B-369, B-370, B-660*
 Saini S.: *B-010, B-106*
 Sainz M.: *C-0183*
 Saito H.: *C-0228, C-0600*
 Saito K.: *C-0286*
 Saito O.: *B-058*
 Saitoh T.: *C-0439*
 Saiz Ayala A.: *C-0753, C-0814*
 Sakai T.: *C-0298*
 Sakaino S.: *C-0147*
 Sakamoto A.C.: *C-0780*
 Sakamoto S.: *C-0982*
 Sakaridis N.: *C-0349*
 Sakellaropoulos P.: *B-322, C-0661*
 Sakino I.: *C-0146, C-0170*
 Sakuhara Y.: *C-0415, C-0594*
 Sakuma H.: *C-0549*
 Sakuma H.: *B-651*
 Sakuma I.: *B-056, B-538, B-768*
 Sala M.: *C-0610*
 Salagierska-Barwinska A.: *C-0772*
 Salaris F.: *B-196*
 Salasky M.: *B-772*
 Saleh A.: *B-740, C-0984, C-1019*
 Salek C.: *B-305*
 Salem R.: *C-1057*
 Salera D.: *C-0024*
 Salgado R.A.: *C-0168, C-0305, C-0906*
 Salganicoff M.: *B-161, B-162, B-164*
 Sali L.: *B-290, B-628, C-0620, C-0636*
 Salinas T.: *C-0220, C-0279*
 Salinas Yeregui T.: *C-0778*
 Salmeron I.: *C-0049*
 Salminen T.: *A-215*
 Salmon I.: *A-367*
 Salomon L.J.: *C-0390*
 Salonikidis P.: *C-0692, C-0715*
 Salovic D.: *B-327, C-0140*
 Salter R.: *B-876*
 Salvador Jr R.: *C-0185*
 Salvador M.: *C-0185*
 Salvador R.: *A-318, C-0185*
 Salvaggio G.: *C-0091, C-0401*
 Salvan C.-V.: *B-435, B-927, C-0856*
 Salvati M.: *C-0804*
 Salvatico R.E.: *C-0820*
 Salvatore M.: *B-086, B-416, C-0444*
 Salvatori F.M.: *B-299, B-509, B-512*
 Salvia R.: *B-484*
 Salvolini U.: *B-536, C-0833*
 Sambrook M.: *C-0672*
 Sampedro I.: *C-1044*
 Samsonov D.: *B-666*
 Samuel D.: *C-0002, C-0007*
 San Juan C.: *C-0475*
 San Roman J.L.: *C-0252, C-0821, C-0884*
 San Roman L.: *C-0135*
- San Roman Manzanera L.: *C-0778*
 San Vicente J.M.: *C-0249*
 Sanabria E.: *B-514*
 Sanada S.: *C-0046, C-0539, C-0971, C-1067*
 Sánchez A.: *C-0686, C-0689, C-0763*
 Sanchez E.: *C-0688, C-0793*
 Sanchez F.: *C-0537*
 Sánchez G.: *C-0284*
 Sanchez M.: *B-622, C-0058*
 Sánchez S.: *C-0183*
 Sanchez-Salmon E.: *C-0731*
 Sánchez-Salmón E.: *C-1044*
 Sancho J.L.: *C-0176*
 Sandler C.M.: *C-0506*
 Sandner A.: *C-0294*
 Sandomenico F.: *B-601, C-0037, C-0045, C-0131, C-0462, C-0473*
 Sanfridsson J.: *B-910*
 Sansoni I.: *B-043, B-044, B-107, B-515, B-710, B-747, C-0019, C-0034, C-0035, C-0585*
 Santamaría N.: *C-0753, C-0814*
 Santana Acosta A.: *C-0098*
 Santocoно S.: *C-0535*
 Santoro L.: *B-745*
 Santos A.C.: *C-0780*
 Santos R.: *C-0150*
 Santos-Armentia E.: *C-0123, C-0276*
 Santosh C.: *B-908, C-0883*
 Sanz de Leon O.M.: *C-0546, C-0561*
 Saoudi N.: *B-677*
 Sapir J.: *E-34*
 Saponjski J.: *C-0595*
 Sapoval M.: *A-233*
 Sarafopoulos A.: *B-554*
 Saranovic D.: *C-0174, C-0631, C-0701, C-0702*
 Sardanelli F.: *B-021, B-185, B-253, B-254, B-264, B-270, B-411, B-455, B-556, C-0198, C-0828*
 Sardella S.S.: *B-294, B-297*
 Sarlieve P.: *C-0074*
 Sarnelli A.: *B-030*
 Sarria L.: *C-0072, C-0099, C-0100*
 Sarrias Guzmán M.J.: *C-0031*
 Sarrias M.: *C-0081*
 Sartor K.: *B-934*
 Sasaguri S.: *C-0320*
 Sasai K.: *C-0020*
 Sasaki H.: *C-0983*
 Sasaki K.: *B-768*
 Sasaki K.: *C-0983*
 Sashi R.: *B-468*
 Satchithananda K.: *C-0554, C-0705*
 Sato H.: *C-0837*
 Sato M.: *C-0337*
 Sato M.: *C-1037*
 Sauer B.: *C-0461*
 Saueressig U.: *B-240*
 Saunders D.E.: *C-0854*
 Saunders M.: *C-0304, C-0323*
 Sauner D.: *B-670*
 Saupe N.: *B-360*
 Sauper T.: *B-060*
 Saur S.C.: *C-0998*
 Saussine c.: *C-0461*
 Savello V.E.: *C-0848*
 Savino G.: *C-0697*
 Sawada A.: *C-0415, C-0594*
 Sawicki M.: *B-335, C-0842*
 Sbuelz M.: *B-805*
 Scaglione M.: *B-363, B-367, B-858, C-0494*
 Scalera G.: *B-300, B-517*
 Scalera G.B.: *B-633, B-802*
 Scarabino T.: *B-224, B-536, C-0829*
 Scardapane A.: *B-475, B-476*
 Scardino P.T.: *B-676*

List of Authors and Co-authors

- Scarrone A.: *C-0570, C-0590, C-0591*
 Scarsbrook A.F.: *C-0496*
 Schaefer P.J.: *C-0997*
 Schaefer-Prokop C.: *B-016, B-595*
 Schaeffter T.: *B-784*
 Schäfer D.: *B-777, C-0953*
 Schäfer J.: *B-562, B-715*
 Schäfer S.: *B-755*
 Schäfers H.-J.: *C-0328*
 Schäfers M.: *A-092*
 Schaffler G.J.: *B-887*
 Schaible T.: *B-890, C-0930*
 Scheenen T.W.J.: *B-490, B-493, B-497, B-725*
 Scheffler K.: *B-201*
 Schekhter A.I.: *B-474*
 Schelfout K.: *C-0191*
 Scheller B.: *B-206*
 Schelling G.: *B-225, B-226*
 Schenk A.: *D-09*
 Scher B.: *B-496*
 Scherr M.K.: *B-374, B-496*
 Schertler T.: *B-241, B-360*
 Scheuerling M.: *B-523*
 Schick F.: *B-562, B-621, C-0012, C-0403, C-0622, C-0941, C-0975*
 Schiemann M.: *B-650, B-655*
 Schiepers C.: *B-384*
 Schild H.: *C-0611*
 Schilham A.M.R.: *B-323*
 Schillaci O.: *C-0296*
 Schilling D.: *B-570, B-576*
 Schilz C.: *A-349*
 Schima W.: *B-011, B-012, B-050, B-327, B-740, B-857*
 Schindera S.: *B-746*
 Schininá V.: *C-0834*
 Schirmer M.: *B-129, B-130*
 Schiza S.: *B-337*
 Schizas D.: *C-0044, C-0056, C-0443*
 Schlager T.: *B-260*
 Schlegel J.: *C-0406*
 Schlemmer H.-P.: *A-045, B-562, B-715*
 Schlef A.T.E.F.: *B-379*
 Schliephake K.: *B-453, B-901*
 Schlossbauer T.: *B-321, B-374*
 Schlosser T.: *B-211, B-654, B-822, B-828*
 Schlüter M.: *B-530, D-09*
 Schmähl A.: *C-0294*
 Schmainda K.M.: *B-435*
 Schmid F.: *B-426*
 Schmid F.T.: *B-827*
 Schmid M.R.: *B-360*
 Schmidt B.: *B-010, B-106, B-660*
 Schmidt B.T.: *B-442*
 Schmidt C.: *C-0997*
 Schmidt D.: *B-621, C-0611, C-0622*
 Schmidt G.P.: *B-717*
 Schmidt S.: *C-1042*
 Schmidt S.A.: *B-694*
 Schmidt T.: *B-578, B-753, B-819, B-898*
 Schmiedt W.: *B-295*
 Schmitt M.: *B-749*
 Schmitz A.M.: *B-663*
 Schmitz B.: *B-827, C-0579, C-0783, C-0993*
 Schmitz S.: *B-117*
 Schmitz-Rode T.: *A-426, B-080, B-208*
 Schmuckenschlager C.: *C-0639*
 Schmücker M.: *C-0408*
 Schneider G.: *B-049*
 Schneider G.K.: *C-0060, C-0237, C-0659, C-0907, E-19*
 Schneider J.: *B-295*
 Schnödt B.: *C-0012, C-0941*
 Schnöring H.: *B-750*
- Schnorr D.: *B-491*
 Schnyder P.: *A-031, A-161, B-133, B-318, B-596*
 Schocke M.: *C-0714, C-1038*
 Schoellnast H.: *B-399, B-886, B-887*
 Schofield J.B.: *C-0213*
 Scholz B.: *B-022*
 Schönberg S.O.: *B-050, B-182, B-183, B-216, B-217, B-218, B-225, B-226, B-243, B-249, B-272, B-383, B-429, B-436, B-454, B-557, B-574, B-717, B-851, B-917, E-08*
 Schoonenberg G.A.F.: *B-326*
 Schoppmann A.: *B-808*
 Schoth F.: *B-348*
 Schöttle P.B.: *B-351*
 Schreer I.: *B-732*
 Schreiber F.: *B-897*
 Schrimmer M.: *B-807*
 Schröder H.: *B-755*
 Schröder M.: *C-0930*
 Schroeder S.: *B-310, C-0257, C-0270*
 Schroeder T.: *B-175*
 Schueler D.: *B-783, C-0409*
 Schuijf J.D.: *B-428*
 Schuknecht B.F.: *A-307*
 Schulze A.C.: *B-568*
 Schulze B.: *B-047*
 Schulz E.: *C-0859*
 Schulz R.: *C-0407*
 Schulz S.: *B-683*
 Schulze K.: *B-844*
 Schulze-Bonhage A.: *B-432*
 Schulz-Wendtland R.: *B-155, B-156*
 Schumacher M.: *A-022*
 Schuncke A.: *C-0960*
 Schütz E.M.: *B-890*
 Schutzner J.: *B-841*
 Schuur K.H.: *C-0157*
 Schwaiger M.: *C-0411*
 Schwark C.: *B-934*
 Schwartz L.H.: *B-498*
 Schwarz J.: *B-248*
 Schwarz M.: *B-008*
 Schwarz W.: *B-009, B-045, B-048, B-340, B-345, B-504, B-507, B-875*
 Schwarz W.V.: *B-046*
 Schwarzbach J.: *B-928*
 Schweitzer H.: *B-295*
 Schweyer M.: *B-216*
 Schwindt W.: *B-932*
 Scialpi M.: *B-148, B-802, B-842, B-858*
 Scialpi M.: *C-0493, C-0494*
 Scifo P.: *B-422*
 Scorsi-Rosset S.: *C-0780*
 Scotti G.: *B-229, B-764, B-907*
 Screaton N.J.: *A-416*
 Scurr E.: *B-144*
 Scurr E.: *B-724*
 Scutt D.: *A-432, C-0489*
 Sebastia C.: *C-0137*
 Sebastià C.: *C-0081, C-0999*
 Sebastià M.C.: *C-0006, C-1049*
 Sebastian A.J.: *B-599*
 Sebie R.: *B-540*
 Sebire N.J.: *B-754*
 Secchi A.: *B-176, B-862*
 Secil M.: *C-0384, C-0448, C-0456*
 Sedivey R.: *B-011, B-012*
 Sedlacik J.: *B-105, B-648, B-783, B-921, B-923*
 Sedonja I.: *C-0685*
 Seeger L.L.: *B-801*
 Seeman P.: *B-099*
 Seemann M.D.: *C-0270*
 Seferovic P.: *C-0248*
 Segarra A.: *C-0604*
- Seghers D.: *B-551, C-1045*
 Segui Palmer M.A.: *B-380*
 Seidel R.M.: *C-0060, C-0237, C-0659, C-0907*
 Seiderer J.: *B-574*
 Seimenis J.: *B-659*
 Seitz J.: *A-032*
 Seitz M.: *B-496*
 Seitz U.: *B-171*
 Seki A.: *C-0222*
 Sekiguchi J.: *C-0337*
 Sekulovic S.Z.: *C-0134*
 Seliger C.: *B-780*
 Sella T.: *B-141, B-498, B-797*
 Selvaggio S.: *D-17*
 Sembritzki O.: *B-924*
 Semela D.: *B-746*
 Semelka R.C.: *B-041*
 Semmler W.: *B-780, C-0407*
 Semnic R.: *C-0926*
 Semsi A.: *C-0520*
 Sen S.: *C-1058*
 Senda M.: *C-0982*
 Sennst D.-A.: *B-668*
 Senoo A.: *C-0393*
 Sentís Crivellé M.: *B-378*
 Sentís M.: *B-262, B-380*
 Seo J.B.: *C-0310*
 Seo J.J.: *B-018*
 Seo J.S.: *C-0229, C-0240, C-0258, C-0274*
 Seo Y.L.: *B-581*
 Seon S.H.J.: *B-312*
 Sequens R.: *C-0082*
 Serafin Z.: *C-1040, C-1059*
 Serafini G.: *A-130, B-131, C-0718*
 Serafin-Krol M.: *B-057, C-0540*
 Sergeeva O.N.: *C-0040*
 Sergiacomi G.: *C-0297*
 Sergiacomi G.L.: *C-0296*
 Serifoglu I.: *C-0853*
 Serikova S.E.: *C-1036*
 Serrallonga M.: *B-563*
 Serrano S.: *B-706*
 Serrano-García C.: *C-0575*
 Serrao E.: *B-296*
 Serres Créixams X.: *C-0031, C-0032*
 Sert G.: *C-0929*
 Sertedaki A.: *B-647*
 Servomaa A.: *C-0988*
 Sessa G.: *C-0655, C-0693*
 Sethu A.U.: *B-799*
 Settles M.: *B-354, B-687*
 Sever A.R.: *C-0213*
 Sevlever G.: *C-0820*
 Seyfarth T.: *B-163, B-165, B-349*
 Sezer H.H.: *C-0158, C-0159*
 Shabbir A.: *C-0096*
 Shah S.K.: *C-0282*
 Shang K.Z.: *C-0165*
 Shanneik K.: *B-662*
 Sharafuddin M.J.: *A-129*
 Sharia M.: *C-0485*
 Sharma B.: *B-143*
 Shatik S.V.: *C-0519*
 Shaughnessy C.: *B-665, B-666*
 Shaw R.: *D-17*
 Sheehan J.J.: *B-716, C-0013*
 Sheehy N.: *C-0785, C-0801, C-0827, C-1032*
 Shelkoplias E.: *C-0671, C-0750*
 Shelton B.: *B-095*
 Shen G.X.: *B-642*
 Shen H.: *B-162, B-164*
 Shen J.: *C-0261*
 Shen T.: *B-433, B-434, B-531*
 Sherif H.: *B-395, B-865, C-0464, C-1022*

List of Authors and Co-authors

Shevchenko H.: C-0205	Simpson E.: B-393	Sorrentino F.: B-088, B-089, C-0656, C-0727
Shibamoto Y.: B-744, B-883	Sindel T.: B-869	Sosna J.: B-141
Shim H.J.: C-0567	Sinha R.: C-0173	Sosnowski P.: A-181
Shimada H.: B-014	Sinitsyn V.: C-0872	Souchay H.: C-0187
Shimada M.: C-0093, C-0393	Sinitsyn V.E.: A-409, B-304	Souftas V.D.: B-867
Shimamoto K.: C-0956	Sinkus R.: C-0193	Soukhov V.Y.: C-0474
Shimizu A.: C-0397	Siomou E.: B-894, B-895, B-896	Sourailidis P.: C-0077
Shimizu K.: C-0339	Siric Z.I.: C-0495	Sourbron S.P.: B-860, B-861
Shimizu T.: C-0415	Sironi S.: B-728	Soutter W.P.: B-791
Shimura H.: C-0600	Sirvanci M.: C-0597	Soyupak B.: C-0515
Shin B.S.: C-0699	Sirvanci M.: C-0816	Soyupak S.: C-0515, C-1010
Shin H.J.: C-0217	Sissopoulos A.: C-0334, C-0641	Spadaro M.: C-0835
Shin J.H.: C-0204, C-0607, C-0616	Sitges M.: C-0232	Spadola L.: B-235
Shin K.S.: B-711	Sivasomboon C.: C-0066	Spagnolo P.: B-525
Shin K.-S.: B-695	Sivberg B.: B-910	Spanidou S.: C-0452
Shin K.S.: B-076	Sjekavica I.: C-1002	Spannagl B.: B-218
Shin K.-S.: B-178	Skaane P.: A-320, B-154, B-830, E-25	Spanos A.: C-0075, C-0452, C-1076
Shin M.J.: B-001, B-002, C-0749	Skarnes W.C.: C-0674	Spanos G.P.: B-554
Shin R.: B-095	Skehan S.J.: B-716	Speck U.: B-206, E-27
Shin S.M.: C-0300	Skiadopoulos S.: B-322, C-0920	Sperandio M.: B-344, B-528, C-0297, C-1033
Shin S.S.: C-0152	Skilakaki M.G.: B-583	Spies L.: D-07
Shin T.B.: C-0630	Skilakaki M.G.: C-0295	Spigonardo F.: B-292
Shin Y.M.: B-419, C-0001, C-0017, C-0022, C-0065	Sklair-Levy M.: B-151	Spilioti M.: B-091
Shinjo H.: C-0512	Skopelitou A.: C-1020	Spilt A.: A-396
Shinmura R.: C-0038	Skoromets T.A.: C-0791	Spina D.: C-0340
Shinohara H.: B-883	Skowronski J.: C-0698	Spinazzi A.: B-644
Shiraki N.: B-744	Srok J.: B-604, B-606	Spinelli A.: B-508, B-511, B-632
Shirato K.: C-0228, C-0600	Skrzelewski S.: C-0023, C-0564	Spirchez Z.: B-193
Shizas D.: C-0334	Slapa R.Z.: B-057	Spirovski M.: C-0926
Shoier K.: B-396	Sloboda V.: C-0529	Spittler A.: C-0639
Shorvon P.J.: C-0177	Sloth M.: B-910	Spitzer D.: C-0529
Shoulga O.S.: C-0664	Slowik A.: C-0807	Spitzerová O.: C-0529
Shrestha R.: B-041	Slowinska-Szednicka J.: B-057	Splendiani A.: C-0803
Shustin V.A.: C-0791	Sluming V.: A-137	Sponza M.: B-065, B-513
Shuto K.: B-014, C-0163	Smania C.: B-457	Spors B.: A-411, B-423, B-825
Shuto R.: C-1001	Smans K.: B-769	Spreafico C.: C-0115
Si Q.: B-040	Smans K.: C-0978	Spreer J.: B-432
Siablis D.: C-0369, C-0613	Smedby Ö.: C-0358, C-0361	Spreng A.: B-619, B-693
Siafakas N.: B-337	Smekal L.: B-776	Spüntrup E.: B-278, B-520, B-522, B-653, B-657, B-658
Siafas I.: C-0052, C-0962	Smevik B.: A-392	Spyridonos P.: C-0355
Siani A.: B-601, C-0037, C-0045, C-0131, C-0132, C-0444, C-0462, C-0473	Smigelski R.: B-566	Spyrou G.: C-0954
Sias A.: B-100, C-0802, C-0863, C-0866	Smirnov P.: B-779	Squarcia M.: C-0610
Siauve N.: C-0390	Smith A.P.: B-029	Squillaci E.: B-494, C-1033
Sica G.: B-086	Smith R.M.: B-925	Sramek M.: D-19
Sidani C.A.: C-0094	Sobiecka B.: C-0808	Srbecký M.: C-0042
Sidhu P.S.: C-0554, C-1075	Sobociński B.: C-1040, C-1059	Srivastav S.: B-277
Sidorowicz M.: C-0389	Soendergaard B.: B-600	Srivastava S.: B-551, C-1045
Siebert S.: B-934	Sofikitis N.: B-617, B-727	Staatz G.: B-578, B-750, B-753, B-898
Siebert U.: B-243	Sohaskey M.L.: C-0674	Stabile Ianora A.A.: B-475, B-476
Siegmann K.C.: B-157, B-587	Soimu U.: B-540	Stähler A.: A-165
Siemianowicz A.: C-0573, C-0675, C-0735	Sokolina I.A.: B-474	Stacchiotti S.: C-0769
Siepmann D.: B-452	Solaiyappan M.: B-421	Stachlewska-Nastfeter E.: B-057
Sigal R.C.: A-035, A-074, B-268	Solano A.: C-0851	Stacul F.: A-197
Sigalas J.: B-640	Solar M.: C-0244	Stadnik T.: B-860, B-861
Signorile P.: C-0586	Soldi E.: C-0219	Stahl R.: B-225, B-226, B-272
Sijens P.: C-0773	Soldi S.: B-185, B-455	Staikidou I.: C-0766
Silakos A.: B-617, B-727	Söllner O.: B-410	Stankovic S.: C-0248
Silberman B.: A-339	Somalvico F.: B-891	Stanzel S.: B-349
Silván M.: C-0009, C-0059	Somuncu I.: C-0914	Stanzhevsky A.A.: C-0791, C-0811
Sim E.K.W.: C-0375	Song B.J.: C-0216	Stathopoulou S.: C-1009
Simal J.: C-0086	Song H.-T.: C-0721	Stauder N.: C-0270
Simaral S.: C-0066	Song H.-Y.: C-0607, C-0616	Stavngaard T.: B-701
Simbrunner J.: B-906	Song I.C.: C-0845	Stavroulis E.: B-085, C-0695
Simonato F.: B-907	Song I.S.: C-0567	Stawarski A.: C-0923
Simon G.H.: B-739	Song K.-S.: C-0310	Stecco A.: B-135, C-0535, C-0655, C-0679, C-0693, C-0694, C-0707, C-0830, C-0832, C-1028
Simoncini A.: C-1024, C-1031	Song S.Y.: C-0893	Stedman B.: B-868
Simonelli G.: B-509	Song W.: B-040	Steen S.C.A.: B-094
Simonetti G.: B-289, B-344, B-494, B-508, B-511, B-519, B-528, B-632, B-635, B-729, B-873, C-0296, C-0297, C-0627, C-1033	Sonka M.: A-270, D-04	Steers J.: B-334
Simonneau G.: A-370	Sonntag A.-K.: B-884	Stefanaki A.: C-0399
Simons P.: B-550	Sonzogni A.: B-145	Stefanczyk L.: B-118, C-0809, C-0869
	Sopransi M.: C-1066	Stefanini M.: B-519, C-0627
	Sora M.C.: B-789, C-0497	
	Sorantin E.: A-270, D-04	
	Sorge I.: C-0887	

List of Authors and Co-authors

- Stefanova R.: *C-0771*
 Steffensen E.: *C-0109, C-0110*
 Stehling C.: *B-458, B-569, B-932*
 Steidle G.: *C-0975*
 Stein H.: *B-809*
 Stein J.: *B-029*
 Steinbrich W.: *B-250, B-568*
 Steiner H.: *B-859*
 Steins R.W.: *C-0394*
 Stenman K.: *B-495*
 Stenzl A.: *C-0611*
 Stepien A.: *C-1046*
 Stergar H.: *B-079*
 Stern Padovan R.: *C-0108, C-1002*
 Sternberg J.M.: *B-891*
 Sterpu M.D.: *C-0474*
 Stessel U.: *B-399, B-887*
 Stetina Z.: *C-0904*
 Steup-Beekman M.G.: *B-094*
 Stevenson W.J.: *C-1012*
 Stieljes B.: *B-530*
 Stiepani H.: *C-0798, C-0799*
 Stikkelbroeck N.M.M.L.: *C-0435, C-0469*
 Stippich C.: *A-070*
 Stix A.: *B-906*
 Stoeckel J.: *B-161, B-162, B-164, B-166*
 Stoeckelhuber B.M.: *C-0859*
 Stoeter P.: *B-532*
 Stoeva M.: *C-0359*
 Stoever T.: *B-276*
 Stojanov D.: *C-0644*
 Stojanov D.A.: *C-0812*
 Stojanovic N.: *C-0812*
 Stojanovska J.: *B-786*
 Stoker J.: *A-414, B-142, B-818*
 Stollberger R.: *B-116*
 Stollfuss J.: *B-354, B-364*
 Stollfuss J.C.: *B-146*
 Storås T.: *B-487*
 Stork A.: *B-083, B-120, B-213, B-614, B-652, B-656, B-820*
 Størmer J.: *A-095*
 Storto M.L.: *A-115, A-146, B-388, B-707, C-0307*
 Stosic-Opincal T.: *C-0873*
 Stoupis C.: *A-111, B-746*
 Straka M.: *D-19*
 Stratakis C.A.: *C-0254, C-0498*
 Stratakis J.: *C-0976*
 Stratta M.: *C-0463*
 Straub R.: *B-075, B-405, B-500*
 Strauss G.: *C-0379*
 Strauss T.: *B-383*
 Strecker R.: *B-247*
 Strickland N.H.: *A-228, A-304*
 Stringaris K.: *C-0076, C-0706*
 Strobel N.: *B-074, B-888*
 Strouhal P.: *C-0314*
 Strozecki P.: *C-1040, C-1059*
 Struelens L.: *B-769, C-0978*
 Struffert T.: *B-205*
 Struwe A.: *B-249*
 Strzesniewski P.: *C-1040*
 Stuber M.: *B-657*
 Studer R.: *B-619*
 Studniarek M.: *C-0015, C-0016, C-0133, C-0149, C-0389*
 Stuifbergen W.N.H.: *C-0157*
 Stukalova O.: *C-0872*
 Su H.S.: *B-787*
 Suasni M.: *C-0509*
 Subramanian K.: *C-0457*
 Subramanyan K.: *C-0281*
 Succio G.: *C-0719*
 Succio G.: *A-149*
- Sucic Z.: *C-1042*
 Suess C.: *B-010, B-106, B-442, B-660, B-691*
 Suetens P.: *A-358*
 Sugimoto H.: *C-0594*
 Sugimoto H.: *C-0593*
 Sugimura K.: *B-387, B-470, B-471, C-0373*
 Suh C.H.: *B-320*
 Suh D.C.: *B-281*
 Suh J.G.: *C-0663*
 Suh J.S.: *C-0721*
 Suh R.: *B-627*
 Suh S.-H.: *C-0568, C-0574, C-0777*
 Suliman H.M.: *C-0435, C-0469*
 Sullo P.: *C-0277*
 Sumanaweera T.S.: *C-0394*
 Sun F.: *C-0824*
 Sun H.: *C-0073*
 Sun R.: *B-780*
 Sun W.: *C-0823*
 Sun X.: *B-316*
 Sunaert S.: *A-069, C-1081*
 Sundgren P.C.: *B-645, C-0880, C-0916*
 Sung D.J.: *B-864, C-0416*
 Sung K.J.: *C-0309*
 Sung M.S.: *B-505*
 Sung S.M.: *B-762*
 Sung Y.M.: *C-0621*
 Sure U.: *B-539*
 Sureda D.: *B-129*
 Süß C.: *D-13*
 Sutton L.: *A-229*
 Suyama J.: *C-0512*
 Suzuki H.: *C-0194*
 Suzuki M.: *C-0046, C-0971*
 Suzuki M.: *C-0342*
 Suzuki Y.: *B-316*
 Svasti-salee : *C-0705*
 Svetel M.: *C-0850*
 Sweeney M.O.: *D-05*
 Sweet J.: *B-721*
 Swierczyna A.: *C-0843*
 Swoboda B.: *B-352*
 Syed R.: *B-007*
 Sylvia J.: *B-023*
 Szafirska M.: *C-0843*
 Szczepanik A.B.: *B-188, C-0540*
 Szczerbo-Trojanowska M.: *B-450, B-516*
 Szczudlik A.: *C-0807*
 Szejnfeld J.: *C-0881*
 Székely G.: *C-0064*
 Szentgyörgyi R.: *A-252*
 Szeszowski W.: *B-098, B-929, C-0844*
 Szikora I.: *A-225*
 Szmidt J.: *B-070*
 Szopinski K.T.: *B-057, B-188*
 Sztantics A.: *B-486*
 Sztuk S.: *C-0843*
 Szurowska E.: *C-0015, C-0016, C-0133, C-0149*
 Szwejda E.: *C-0003*
 Szylberg T.: *C-0321*
 Szyszko T.A.: *C-0904*
-
- T**
- Tabakov S.: *C-0359*
 Táboas J.: *C-0123*
 Taboury J.: *C-0043*
 Tachikake T.: *C-0581*
 Tachizawa N.: *C-0147*
 Tack D.: *A-279*
 Tacke J.: *B-603*
 Tackenberg B.: *B-539*
 Tada T.: *C-0758*
- Tahamtan A.R.: *B-930*
 Taher F.: *B-261, B-371*
 Taibi A.: *B-030*
 Tajima H.: *C-0308, C-0397, C-0566*
 Takada Y.: *C-0758*
 Takada Y.: *C-0983*
 Takagi R.: *B-158*
 Takagi R.: *C-0837*
 Takahashi K.: *C-0651*
 Takahashi M.: *C-0186*
 Takahashi N.: *C-0372*
 Takahashi N.: *C-0028*
 Takahashi S.: *B-056, B-538, B-768*
 Takahashi S.: *C-0228, C-0600*
 Takahashi Y.: *B-823, C-0273*
 Takamura M.: *C-0981*
 Takano T.: *C-0020*
 Takano T.: *C-0566*
 Takao S.: *C-0662, C-0709*
 Takase M.: *C-0628*
 Takasu A.: *C-0560*
 Takeda K.: *C-0549, C-0711, C-0787*
 Takeda K.: *B-651*
 Takeda T.: *C-0608*
 Takeda T.: *B-775*
 Takemoto S.: *B-319*
 Takehana D.: *B-387, B-470, B-471*
 Takeuchi K.: *C-0560*
 Takeuchi M.: *C-0047, C-0440*
 Takeyama N.: *C-0512*
 Tako E.: *C-0056, C-0470*
 Talens A.: *C-0606*
 Tali E.T.: *A-368*
 Taliercio G.: *C-0614*
 Tall P.: *A-227, B-760*
 Tamai K.: *C-0287, C-0422, C-0431, C-0499, C-0534*
 Tamai N.: *C-0759*
 Tamburini S.: *B-880*
 Tamura M.: *C-0524*
 Tan A.G.S.: *C-0066*
 Tan K.T.: *C-1069*
 Tan L.K.A.: *C-0096*
 Tanada S.: *C-0524*
 Tanaka H.: *C-0014*
 Tanaka I.: *B-158*
 Tanaka J.: *C-0592*
 Tanaka R.: *C-0971*
 Tanaka S.: *C-0534*
 Tanaka T.: *C-0186*
 Tanaka Y.: *C-0439*
 Tanashyan M.M.: *C-0871*
 Tancredi D.: *C-0510*
 Tandri H.: *B-421*
 Tang X.: *B-665, B-666*
 Tanghe H.L.J.: *C-0774*
 Tanikake M.: *C-0116*
 Tanoue S.: *C-0538, C-0838*
 Tantau M.: *B-193*
 Tanteles S.: *B-634*
 Tao W.: *C-0824*
 Tapp M.J.F.: *C-0104*
 Tarasow E.: *B-317, C-0698, C-0841*
 Taratuto A.L.: *C-0820*
 Tarazi L.: *C-0985, C-0989*
 Tardáguila F.: *C-0276*
 Tardaguila Montero F.: *B-857*
 Tardivon A.: *A-013*
 Tarhan N.C.: *C-1011, C-1051*
 Tarján Z.: *A-254, C-0141*
 Tarnawski M.: *C-0564*
 Tarragona Hervas V.: *C-0290*
 Tartari S.: *B-636*
 Tartaro A.: *B-534*

List of Authors and Co-authors

- Tastet S.: *C-0184*
 Tasu J.-P.: *C-0858*
 Tatebe T.: *C-0393*
 Tatlipinar S.: *C-0526*
 Tatsch K.: *B-502*
 Távora I.: *B-192*
 Tayev A.M.: *C-1036*
 Taylor A.: *B-090*
 Taylor A.M.: *A-295*
 Taylor C.: *B-702*
 Taylor P.: *B-832*
 Taylor P.R.: *B-067, B-069*
 Taylor S.A.: *A-412*
 Taymoorian C.: *B-491*
 Tchirikov M.: *B-755*
 Teasdale E.: *B-908*
 Teifke A.: *B-104*
 Teisseire A.: *B-477, B-478*
 Tekatas A.: *C-0885*
 ten Berg J.: *B-521*
 ten Bhomer P.: *B-237*
 Ten J.I.: *B-770*
 Tepe G.: *C-0623*
 Tepel M.: *E-44*
 ter Brugge K.: *B-919*
 ter Haar Romeny B.M.: *A-120, A-355, C-0367*
 Terada M.: *C-0628*
 Terada M.: *C-0337*
 Teramoto T.: *C-0093*
 Terlecki P.: *C-1046, C-1060*
 Termote J.-L.: *B-441, C-0168*
 Ternovoy S.: *C-0872*
 Ternovoy S.K.: *B-304, B-474*
 Terra M.P.: *B-818*
 Terzi S.: *B-376*
 Terzis G.: *C-1070*
 Teschner M.: *D-16*
 Tessitore N.: *B-638*
 Testa F.: *C-0590*
 Testembasi H.: *C-1016*
 Testempassi E.: *C-0825*
 Tettoni S.M.: *C-0591*
 Teubl J.: *D-08*
 Teubner J.: *A-374*
 Tezapsidis G.: *C-0985, C-0989*
 Thaler J.: *C-0386*
 Thalhammer A.: *B-068, B-507, B-689, B-877*
 Thalmann G.: *B-619*
 Thamer C.: *C-0012, C-0941*
 Thanos L.: *B-336, B-620, C-0349, C-0451, C-0619, C-0624, C-0625, C-0641*
 Theisen K.: *B-216*
 Theiss H.: *B-217*
 Thelen M.: *B-104, B-245, B-295, B-425, B-685*
 Themudo R.: *C-0150*
 Theocharopoulos N.: *B-771*
 Theofanopoulou M.: *C-0784, C-0861*
 Theotokas I.: *C-0025, C-0044, C-0056, C-0399, C-0443, C-0482*
 Theumann N.H.: *B-133*
 Thibault J.-B.: *B-666*
 Thieke C.: *C-0294*
 Thimmarayappa A.D.: *C-0562*
 Thirunavukarasu A.: *D-11, D-12*
 Thoeny H.C.: *B-338, B-619*
 Thomas A.M.K.: *A-077*
 Thomas L.: *B-009*
 Thomas M.: *B-386*
 Thomas N.: *C-0458*
 Thomas R.: *B-863*
 Thomas S.: *B-067, B-069*
 Thompson D.: *C-0854*
 Thompson M.: *B-293*
 Thornton E.: *B-194*
 Thornton J.: *C-0827*
 Thouveny F.: *B-550*
 Thrall J.H.: *A-303*
 Thuerl C.: *B-013*
 Thurher R.: *C-0325*
 Thurnher M.M.: *A-001, B-093, C-0857*
 Thurnher S.A.: *B-288, E-17*
 Tibballs J.: *B-853*
 Tibishrani M.: *C-0246*
 Tighe M.: *B-305*
 Tilleman E.: *B-489*
 Tillich M.: *B-399, B-616, B-886, B-887, C-0292, E-41*
 Tinazzi Martini P.: *C-0026*
 Tipaldi L.: *C-0175*
 Tissen T.P.: *B-438*
 Titi M.: *C-1012*
 Tiutin L.A.: *C-0265, C-0811*
 Tizon X.: *C-0358, C-0361*
 Tjonneland R.M.: *B-911*
 Tjuleneva O.: *C-0700*
 Tlostanova M.S.: *C-0519*
 Toccafondi F.: *B-290, B-628, C-0620*
 Todd-Pokropek A.: *A-246*
 Todua F.: *C-0070, C-0235, C-1004*
 Tofte T.: *B-366*
 Togashi K.: *C-0287, C-0422, C-0430, C-0431, C-0493, C-0534*
 Toi A.: *B-721*
 Tokat Y.: *C-0033*
 Tokatli F.: *C-0158, C-0159*
 Tokatlı Z.: *C-0487*
 Tókés A.: *B-915*
 TolKKI O.: *B-231*
 Toma' P.: *C-0902*
 Tomà P.: *B-806*
 Tomandl B.F.: *E-53*
 Tomarchio L.: *B-284*
 Tomas M.: *B-838*
 Tomas X.: *C-0617, C-0645*
 Tomaselio A.: *C-0232, C-0617, C-0645*
 Tomasi L.: *C-0239*
 Tomasoni A.: *C-0909*
 Tomassini M.: *B-344, B-528*
 Tombach B.: *B-784, B-785, B-884, E-06*
 Tomei E.: *C-0113*
 Tomitaka E.: *C-0381*
 Tomura N.: *B-056, B-468, B-538, B-768*
 Tonge K.: *C-0879*
 Tonkikh O.S.: *C-0664*
 Torelli L.: *C-1080*
 Torné M.: *C-1061*
 Torreggiani W.: *A-242*
 Torremilans A.: *C-0467, C-0476*
 Torres I.: *B-706, C-0303*
 Torres M.: *C-0183*
 Torres M.: *C-0009*
 Torricelli P.: *B-492*
 Torrione C.: *C-0307*
 Tortajada Giménez L.: *B-378*
 Tortajada Jimenez L.: *B-380*
 Tortajada L.: *B-262*
 Torvund Å.: *B-366*
 Tosetti I.: *C-0463*
 Tosetti M.: *B-224*
 Tosi G.: *B-444*
 Toso F.: *B-397, B-613, B-618, B-805*
 Tosun A.: *C-0817, C-0853*
 Tot T.: *A-373*
 Tóth G.: *C-0141*
 Tóth H.: *B-915*
 Tóth L.: *C-0141*
 Totman J.: *C-0705*
 Tounan T.: *C-0392*
 Tous F.: *C-0172*
 Touzé E.: *C-0796*
 Toyofuku F.: *B-158, B-330*
 Toyooka M.: *C-0836*
 Toyoshima M.: *C-0615*
 Toyota N.: *C-0581*
 Tozzi M.: *B-062*
 Trachtenberg J.: *B-721*
 Tracz W.: *B-306*
 Trafea H.: *C-0739*
 Traid C.: *C-0425*
 Traid Niella C.: *C-0413*
 Tranquart F.: *C-0377*
 Trappe F.: *D-13*
 Trappeniers L.: *C-0305*
 Trattning S.: *B-353, B-789, B-935, C-0497, C-0678*
 Travaglini A.: *C-0307*
 Travaglini F.: *C-0188*
 Treitl M.: *B-233, B-543, B-630*
 Tremoulet M.: *B-760*
 Tresoldi S.: *B-411*
 Treutenaere J.-M.: *C-1003*
 Trew G.: *C-0417*
 Triantafillou L.: *C-0860*
 Triantopoulou C.: *C-0052, C-0962*
 Trinidad C.: *C-0276*
 Trivedi R.A.: *C-1077*
 Trivelli I.: *B-766*
 Triviño F.: *C-0330*
 Trojanowska A.: *B-112, B-274, B-516*
 Trojanowski P.: *B-274*
 Trojsí F.: *B-536*
 Tronnier V.: *B-934*
 Tropine A.: *B-532*
 Trost R.: *B-672, B-783, C-0409*
 Truebenbach J.: *C-0622*
 Trufanov G.E.: *C-0055, C-0849*
 Trumm C.G.: *B-232*
 Truyen R.: *B-326, D-07*
 Trzeszkowska-Rotkegel S.: *C-0023, C-0564*
 Tsai D.-Y.: *C-0372*
 Tsampoulas C.: *B-617, B-727, C-0438*
 Tsanis A.: *B-634*
 Tsantis S.: *C-0355*
 Tsapaki V.: *C-0962*
 Tschampa H.J.: *B-096*
 Tscherney R.: *C-0125*
 Tscholakoff D.: *C-0125*
 Tscholl D.: *C-0328*
 Tsetis D.: *B-337*
 Tsiarta M.: *C-0933*
 Tsifountoudis I.: *B-554*
 Tsikkini A.: *C-1071*
 Tsili A.C.: *B-617, B-727, C-0438*
 Tsinoglou K.: *C-1070*
 Tsitouridis I.: *C-0985, C-0989*
 Tsivtsivadze G.: *C-0070, C-0235, C-1004*
 Tsota I.: *C-0661*
 Tsouroulas M.: *C-1071*
 Tsuchida T.: *C-0836*
 Tsuchiya K.: *C-0186*
 Tsuchiya K.: *B-319*
 Tsuji H.: *B-186, C-0351*
 Tsuijoka K.: *B-823, C-0273*
 Tsukagoshi S.: *C-0964*
 Tsukagoshi S.: *C-0342*
 Tsunoda-Shimizu H.: *C-0194*
 Tsushima Y.: *C-0046*
 Tsvigun B.: *C-0385*
 Tuck J.: *C-0527*
 Tucker J.: *E-35*
 Tuengerthal S.: *B-473*
 Tufarulo L.: *C-0209*
 Tulunay Ö.: *C-0486*

List of Authors and Co-authors

Tumiati B.: *C-0865*
 Tuna B.: *C-0448*
 Tuna H.: *C-0852*
 Tunaci A.: *B-035*
 Tunaci M.: *B-035*
 Tuncbilek N.: *C-0158, C-0159, C-0520, C-1058*

Tuñón Gómez M.: *C-0050*

Tuohy B.: *C-0968, C-0969*

Turchetta S.: *B-484*

Turgut A.T.: *C-0478, C-0486, C-0551, C-0552*

Turhan A.H.: *C-0929*

Turilli D.: *B-126*

Türkölmез K.: *C-0486, C-0500*

Turupoli E.: *B-915*

Tutar N.: *C-1011*

Twarkowski P.: *B-871*

Tybor K.: *C-0869*

Tytin L.A.: *C-0242, C-0247, C-0474, C-0519, C-0791, C-0847, C-0848, C-1068, C-1073*

Tzalonikou M.: *C-0076, C-0706*

Tzanakos G.: *C-0954*

Tzavoulis D.: *B-634*

Tzedakis A.: *B-649, C-0976*

Tziaras S.: *C-0438*

Tzovara J.: *C-0396, C-0618*

Tzovara J.: *B-894, B-895, B-896*

U

Ubeda B.: *C-0197, C-0425*

Ubeda Hernandez B.: *C-0413*

Ucar M.: *C-0668*

Uchida D.: *C-0538*

Uchida K.: *C-1034*

Uchida K.: *C-0806*

Uchida M.: *C-0392*

Uder M.: *C-0328, C-0387, C-0640*

Uebayashi Y.: *B-823, C-0273*

Ueda H.: *C-0287*

Ueda K.: *C-0038*

Ueda T.: *C-0532*

Ueda T.: *C-0759*

Uehara H.: *C-0047, C-0440*

Uehara S.: *C-0788*

Ueki K.: *C-0539*

Uematsu H.: *C-0298, C-0536, C-0608, C-0805, C-0836, C-0867*

Uematsu T.: *C-0222*

Uemura A.: *C-0628*

Ueno K.: *C-0339*

Uesaka K.: *B-412*

Uetani M.: *C-0662, C-0709*

Uffmann M.: *B-016, B-260*

Uggetti C.: *C-0835*

Ugurel M.S.: *C-0914*

Uherek C.: *C-0406*

Uhl M.: *B-008*

Ukimura O.: *E-04*

U-King-Im J.M.: *C-1077*

Ulicheri N.: *B-253*

Ulla M.: *C-0107, C-0268, C-0331, C-0346, C-0347, C-0537, C-1014, C-1015*

Ulmer J.L.: *B-435, B-927, C-0856*

Ulmer S.: *C-0859*

Uluç E.: *C-0558*

Ulus S.: *B-584*

Ulvik N.M.: *C-0504, C-0518*

Umarova R.M.: *C-0871*

Umek W.: *B-789*

Umek W.H.: *C-0497*

Umeoka S.: *C-0287, C-0422, C-0430, C-0431, C-0499, C-0534*

Umetani K.: *C-0940*

Umschaden H.-W.: *A-316*
 Unger B.: *B-399*
 Unsinn K.M.: *C-0053, C-0087*
 Urbach H.: *A-162, B-096*
 Urbani L.: *C-0402*
 Urbanik A.: *A-027, C-0808, C-0843*
 Urigo C.: *B-196*
 Urpolskaya L.: *C-0912*
 Urschler M.: *B-260*
 Ursekar M.: *C-0748*
 Ursone A.: *B-289*
 Usami H.: *C-0956*
 Ushakova G.A.: *C-0432*
 Ushakova T.I.: *C-1041*
 Uské A.: *B-318, B-765*
 Ustuzhanin D.: *C-0872*
 Uthappa M.C.: *C-0733*
 Utz-Billing I.: *B-407*
 Uzhegov T.A.: *C-0465*
 Üzüm N.: *C-0182*
 Uzunoglu N.: *C-0942, C-0963*

V

Vaccaro A.: *C-0199*
 Vafadi I.: *C-0025, C-0044*
 Vagli P.: *B-147, B-690*
 Vaglio A.: *C-0517*
 Vagnarelli S.: *B-198, B-512*
 Vagner J.: *B-403*
 Vaillant J.-C.: *C-0043*
 Vakaki M.: *C-0899, C-0900, C-0921, C-0932, C-0933, C-0934*
 Valdeig S.: *B-072*
 Valdés A.: *C-0031*
 Valencia A.: *C-0450*
 Valente G.: *C-0535*
 Valente S.: *B-703*
 Valentini F.: *C-0184*
 Valentini A.L.: *C-0503*
 Valette P.J.: *B-855*
 Vallati G.: *C-0338*
 Valle M.: *C-0221*
 Valle M.: *B-806, C-0902*
 Vallejos J.: *C-0346, C-0347*
 Vallone P.: *C-0037*
 Vallone S.: *B-283*
 Valls C.: *A-112*
 Valsecchi C.: *B-411*
 Valverde J.: *B-563*
 Valverde S.: *C-0279*
 van Almsick M.A.: *C-0367*
 van Beek E.J.R.: *A-127, B-701, B-702*
 Van Breuseghem I.: *B-682, B-684, B-845, B-922*
 van Buchem M.A.: *A-164, B-094*
 van Delden O.: *B-489*
 van den Bosch H.C.: *B-725*
 van den Brink W.: *C-0815*
 van der Lught A.: *B-452, C-0774*
 van der Molen A.J.: *B-447, B-448*
 van der Putten W.: *B-773, C-0968, C-0969*
 van der Schaaf I.: *B-313*
 van der Wall E.E.: *B-214, B-220*
 Van der Zijden T.: *C-0746*
 Van Dijk X.: *B-441*
 van Dijk G.: *B-313*
 Van Dyck P.: *B-463*
 van Gelder R.E.: *B-326*
 van Ginneken B.: *B-323*
 Van Goethem J.W.: *A-309, B-931*
 Van Goethem M.L.A.: *B-159, C-0191*
 van Iersel C.: *B-381*
 van Klaveren R.J.: *B-381*

van Kuijk C.: *A-365*
 van Leeuwen M.S.: *B-142, B-451, B-903*
 van Lin E.: *B-497*
 Van Loon R.: *C-0978*
 Van Marck E.: *B-463*
 van Mieghem C.: *B-308, B-342*
 Van Mieghem I.M.: *B-682, B-684, B-845, B-922*
 van Milligen-de Wit A.W.M.: *C-0157*
 Van Nostrand L.: *C-0376*
 Van Ongeval C.: *B-159*
 van Ooijen P.M.A.: *B-237, C-0275*
 Van Schuerbeek P.: *B-860, B-861*
 Van Steen A.: *B-159*
 van Stevendaal U.: *B-820*
 van Vollenhoven R.F.: *B-564*
 Van Wetere P.: *B-697*
 van Woudenberg S.: *B-829*
 Vanbeckevoort D.: *A-321*
 VanCauteren M.: *B-651*
 Vance A.: *C-0958*
 Vande Berg B.C.: *B-003*
 Vandecaveye V.: *B-338*
 Vandenbroucke F.: *C-0305*
 Vanderelst L.: *B-682*
 vandermark P.: *C-0858*
 Vandervliet E.J.M.: *B-931*
 Vanhavere F.: *C-0978*
 Vanhoenacker F.: *B-463, C-0906*
 Vanhoenacker F.M.: *C-0746*
 Vanhoenacker F.M.H.M.: *A-134*
 VanMetter R.: *B-548*
 Vannini C.: *B-290, B-628, C-0620, C-0636*
 Vannoni M.: *C-0030*
 Vannozzi F.: *B-147, B-690*
 Vano E.: *A-348, B-770, B-778*
 Vanoverschelde J.-L.: *C-0253*
 Vantali V.: *C-0825*
 Vanzulli A.: *B-501, C-0580*
 Varela M.: *B-622*
 Varga A.: *C-0318*
 Vargas Serrano B.: *C-0179*
 Varzim P.: *C-0150*
 Vasconcelos C.: *C-0423*
 Vashisht S.: *C-0128*
 Vasic-Vilic J.: *C-0676*
 Vasiliadou A.: *C-0508*
 Vasilopoulos C.: *C-0246*
 Vasilyev A.Y.: *C-0544, C-0973*
 Vasilyev A.Yu.: *C-0991*
 Vass K.: *B-093*
 Vassiliou M.: *B-597*
 Vassiliou V.: *C-0661*
 Vassiou K.: *C-1009*
 Vayssettes C.: *C-0390*
 Vazquez E.: *B-838*
 Vázquez-Jiménez J.: *B-750*
 vd Vijver M.: *B-379*
 Vecchioli A.: *B-577*
 Veciana P.: *C-0135*
 Vedlich D.: *C-0362*
 Vega Martínez M.: *C-0704*
 Veillon F.: *A-206, A-384*
 Veit P.: *B-079, B-553, B-677, B-718, B-840, B-913*
 Vejby Soegaard L.: *B-701*
 Velasco M.: *C-0276*
 Velitsista S.: *C-0396*
 Vellodi A.: *C-0854*
 Velthuis B.K.: *B-313, B-903*
 Veltman J.: *B-731, B-837*
 Venditti F.: *B-242, B-267, B-373, B-375, C-0192, C-0195*
 Venkatesh S.K.: *B-598, C-0096, C-0375, C-1048*
 Venstermans C.: *B-441*
 Venturelli F.: *B-124*

List of Authors and Co-authors

- Venturi G.: *D-17*
 Venturini M.: *B-176, B-862, B-907*
 Vera A.: *C-0875*
 Veraldi G.: *C-1018*
 Vera-Valencia M.: *B-110*
 Verbeelen D.: *B-860*
 Vercelli R.: *C-0580*
 Verdu J.: *C-1050*
 Verdun F.R.: *C-0970*
 Vergari V.: *B-741, B-811, C-0391*
 Vergendo M.: *B-613, B-618*
 Vergendo M.: *B-397*
 Vergnaghi D.: *C-0115, C-0145, C-0769*
 Verhaeghe L.: *B-697*
 Verius M.: *D-18*
 Verma R.K.: *B-080, B-208*
 Verschakelen J.A.: *A-142, B-385, B-845*
 Verslegers I.: *B-159, C-0191*
 Vesselova T.N.: *B-709*
 Vestring T.: *B-050*
 Vetter M.: *B-138*
 Vetter T.: *B-401*
 Vezzulli P.: *B-229*
 Vicente Bartulos A.: *C-0546, C-0561*
 Vicentini C.: *C-0428, C-0511*
 Vida J.M.: *C-0176*
 Vidal R.: *C-0604, C-1023*
 Vienne P.: *B-351*
 Viergever E.: *B-214, B-220*
 Vieth V.: *B-569*
 Vignali C.: *B-558*
 Vignaux O.: *A-067*
 Vignot S.: *C-0344*
 Vigorito S.: *B-444*
 Viguier A.: *A-227*
 Vikram R.: *B-866*
 Vilà J.M.: *C-0231*
 Vilà Parera C.: *C-0032*
 Vilana R.: *B-622, C-0610*
 Vilanova J.C.: *C-0196, C-0545, C-0730*
 Vilar J.: *A-204, C-0609*
 Vilgrain V.: *B-004*
 Villa A.: *C-0252*
 Villa G.: *B-444*
 Villalba V.: *C-0220*
 Villalón M.: *C-0196, C-0545, C-0730*
 Villan S.: *C-0213*
 Villanueva A.: *C-0516*
 Villari N.: *B-745*
 Ville Y.: *C-0390*
 Vinhais S.: *C-0424*
 Vinjamuri S.: *C-0489*
 Vinokurov V.L.: *C-0432*
 Viñuela B.: *C-0086*
 Virgilio G.: *B-126*
 Visconti S.: *B-420*
 Visser L.H.: *C-0157*
 Vit A.: *B-065, B-457, B-513*
 Vivas I.: *C-0311*
 Vivas Perez I.: *C-0455*
 Vizcaya S.: *C-0928*
 Vladica P.: *C-0446, C-1008*
 Vlahomitros I.: *C-0715*
 Vlassenbroek A.: *B-479*
 Vlassenbroek A.: *C-0281*
 Vliegenthart R.: *B-381*
 Vlieger E.J.P.: *B-223, C-0815*
 Vlychou M.: *C-1009*
 Vock P.: *B-619, B-746*
 Voegele M.: *D-03*
 Vogel M.: *B-678*
- Vogl T.J.: *A-058, A-073, A-350, A-421, B-009, B-034, B-045, B-046, B-048, B-068, B-075, B-190, B-302, B-311, B-324, B-340, B-345, B-350, B-401, B-405, B-408, B-410, B-500, B-504, B-506, B-507, B-629, B-650, B-655, B-689, B-723, B-749, B-855, B-857, B-875, B-877, E-05, E-43*
 Vogt F.M.: *B-840*
 Vojvodic O.: *B-874*
 Volkau I.: *D-11*
 Vollmar S.: *A-301*
 Volpe M.: *B-416*
 Volpi A.: *C-0402*
 Volpini F.: *C-0570*
 Volterrani L.: *B-020*
 Vomweg T.W.: *B-104, B-376*
 von Rechenberg B.: *B-352*
 von Rothenburg T.: *C-0599*
 von Schulthess G.K.: *A-180, A-324, B-013*
 von Tengg-Kobligk H.: *C-1000*
 von Vopelius-Feldt J.: *B-739*
 von Ziegler F.: *B-346*
 Voormolen M.H.J.: *C-0157*
 Votrubova J.: *B-417*
 Vougioukas V.: *B-763*
 Vougiouklis N.: *C-0075, C-0452, C-1076*
 Voutetakis A.: *B-647*
 Voyvoda N.K.: *C-0182*
 Vrbanec D.: *C-0108*
 Vrints C.J.: *C-0243*
 Vrouhos G.: *C-0860*
 Vucic N.: *C-1042*
 Vukomancic B.: *C-0676*
 Vyklyuk M.V.: *C-0991*
-
- W**
- Waaijer A.: *B-451, B-518, B-903*
 Wada A.: *C-1034*
 Wada A.: *C-0806*
 Wada A.: *C-0839*
 Wada H.: *C-0287*
 Wada Y.: *C-0348, C-0350, C-0758, C-0760, C-0761*
 Wade C.K.: *C-0959*
 Wagner S.: *B-255*
 Wagner T.O.F.: *B-034*
 Wakasa H.: *C-0995*
 Wakasa T.: *C-0761*
 Walach E.: *B-168*
 Wald C.: *B-179*
 Waldt S.: *B-033, B-259*
 Walecka A.: *B-335, C-0842*
 Walecki J.: *B-317, C-0572, C-0698, C-0841*
 Walker L.J.: *B-908*
 Walker W.J.: *B-872*
 Wall A.: *B-038, B-784, B-785*
 Wallis M.G.: *A-216*
 Walsh S.: *C-1006*
 Walsh S.M.: *C-0142, C-0483, C-0635*
 Walter C.: *E-21*
 Waltering K.-U.: *B-211, B-654, B-822, B-828*
 Wandtke J.: *B-039*
 Wandzel P.: *C-0080*
 Wang D.: *B-531*
 Wang D.: *B-439*
 Wang R.Z.: *C-0824*
 Wang S.: *B-437*
 Wang S.: *D-12*
 Wang S.B.: *B-848*
 Wang S.C.: *B-598, C-0096, C-0375, C-1048*
 Wang X.: *C-0979*
 Wang Y.: *B-303, B-347*
- Wang Y.: *B-408, B-629*
 Wang Y.: *B-381*
 Wang Y.: *B-642*
 Wang Z.: *C-0261*
 Warbey V.S.: *C-0234*
 Ward C.: *C-0904*
 Ward E.V.M.: *B-716*
 Warren R.M.L.: *C-0200*
 Wasan R.: *C-0180*
 Wasserman N.F.: *C-0506*
 Wassmer G.: *B-291*
 Watanabe H.: *C-0373*
 Watanabe M.: *C-0093*
 Watanabe Y.: *C-0348, C-0350, C-0758, C-0760*
 Watanabe Y.: *C-0415, C-0593, C-0594*
 Watarai J.: *B-056, B-468, B-538, B-768*
 Watarai J.: *C-0308*
 Watt-Smith S.: *B-055*
 Watura R.: *C-0315*
 Wawrynek W.: *C-0573, C-0675, C-0735*
 Weaver J.S.: *C-0681*
 Weber C.: *B-113, B-114, B-120, B-171, B-652, B-743, C-0757, C-1005, C-1025*
 Weber C.: *B-243, B-630*
 Weber C.: *B-740*
 Weber M.: *B-353*
 Weber M.-A.: *B-530, C-0395*
 Weber O.: *B-331*
 Weber W.A.: *B-187, B-384, C-0411*
 Weckbach A.: *B-255*
 Weclawek-Tompol J.: *C-0148*
 Wedegärtner U.: *B-755, C-0757*
 Wedekind N.: *B-829, B-830*
 Wedel A.K.: *B-586, C-0224*
 Wegenkittl R.: *D-04*
 Wehrschatz M.: *B-616, C-0292*
 Wei G.-Q.: *B-040, B-328, B-856*
 Weigel C.: *B-078, B-878*
 Weihusen A.: *D-09*
 Weiner G.M.: *B-844*
 Weinheimer O.: *B-705*
 Weinmann H.-J.: *A-080, C-0393*
 Weishaupt D.: *A-107, B-360, E-20*
 Weiss F.: *B-053, B-820*
 Weiss W.: *B-364*
 Weissborn K.: *B-311*
 Weissleder R.: *B-671, B-787*
 Weitzer C.: *C-0917*
 Wels W.: *C-0406*
 Welsch G.C.: *B-356, B-358*
 Welsh R.C.: *C-0880*
 Wembacher E.: *B-175*
 Wendland M.F.: *B-739*
 Wendorff J.: *C-0772*
 Weng X.: *C-0823*
 Wenke R.: *B-732*
 Wenkel E.: *B-155, B-156*
 Wenzel S.: *B-207*
 Werber K.-D.: *B-808*
 Werk M.: *D-10*
 Werkgartner G.: *A-270, D-04*
 Wernig M.: *D-02*
 Wersabe A.: *B-157, B-587*
 Wessels F.: *D-15*
 Weßling J.: *B-327*
 Wessner B.: *C-0639*
 Westphalen K.: *B-285*
 Wetter A.: *B-324, B-723, B-875, B-877*
 Weyler J.: *C-0191*
 Whelan P.F.: *B-329*
 Whitby E.: *A-393*
 White L.: *C-0979*
 Whitehouse R.: *C-0737*
 Wichert-Anna L.: *C-0780*

List of Authors and Co-authors

- Wick M.C.: *B-564*
 Wickline S.A.: *A-203*
 Widman A.: *B-058*
 Widuchowski J.: *C-0735*
 Wiebel M.: *B-473*
 Wiegard R.: *B-321*
 Wielage C.: *B-815*
 Wiener E.: *B-136*
 Wienhard K.: *A-301*
 Wiercinska-Drapalo A.: *C-0841*
 Wiersma T.G.: *B-818*
 Wierzba T.: *C-0389*
 Wierzbowski J.M.: *C-0133, C-0149*
 Wieser A.: *B-464, B-466*
 Wiggers T.: *B-150*
 Wikholm G.: *A-226*
 Wiklund G.: *C-0358, C-0361*
 Wild J.: *B-702*
 Wild J.M.: *B-701*
 Wildberger J.E.: *B-169, B-349, B-382, B-520, B-522, B-523, B-750, B-819, E-28*
 Wildermuth S.: *B-241, B-360, B-821, C-0754, C-1053*
 Wilkins J.C.: *C-0705*
 Willatt J.: *C-0496*
 Willems S.: *B-083*
 Willems T.P.: *B-309, B-524*
 Williams E.: *B-666*
 Williams E.C.: *B-665*
 Williamson E.: *C-1013*
 Williamson R.: *C-0417, C-0442*
 Willmann J.K.: *B-241*
 Wilms G.: *A-099*
 Wilson D.J.: *A-200, A-365*
 Wilson M.: *B-331*
 Wilson P.: *D-17*
 Winder J.R.: *C-0650*
 Winkel A.: *B-722*
 Winkeler A.: *A-301*
 Winter H.: *C-0237*
 Winter S.: *B-291*
 Winterbottom S.: *C-0895*
 Winterer J.T.: *B-247, B-675*
 Wintersperger B.J.: *B-217, B-341, B-343, B-346, B-429, B-846*
 Wirth C.: *B-050*
 Wirth S.: *B-233, B-630*
 Wismueller A.: *B-103, B-321, B-374*
 Wisniewska B.: *C-0772*
 Witjes F.: *A-352, B-490*
 Witjes F.A.: *C-0468*
 Witjes J.A.: *B-493, B-497*
 Witkamp T.H.: *B-518*
 Witoszynskyj S.: *B-102, B-105*
 Wittaus H.: *C-0799*
 Witzani L.: *B-893*
 Wlachovská B.: *C-0042*
 Woelmer M.N.: *C-0394*
 Woertler K.: *B-033, B-259, B-354*
 Wójcicka J.: *C-0321*
 Wojczal J.: *B-516*
 Wolak T.: *B-929, C-0844*
 Wolberink S.V.R.C.: *B-150*
 Wolf K.-J.: *B-072, B-604, B-606, B-844*
 Wolf M.: *B-161, B-164*
 Wolfsberger S.: *B-935*
 Wollmer P.: *B-700*
 Wolski A.: *B-516*
 Won H.J.: *B-419, C-0001, C-0017, C-0021, C-0022, C-0065*
 Won J.Y.: *C-0568, C-0574*
 Won J.-Y.: *B-503*
 Woodburn P.: *B-334*
 Woodhead P.M.: *C-1012*
 Woodhouse N.: *B-702*
 Woosley J.T.: *B-041*
 Wormanns D.: *B-036, B-166, B-386*
 Wörtler K.: *B-136, B-146*
 Wotherspoon A.: *B-019, C-0164*
 Woulfe P.: *B-773*
 Wronski J.: *B-112*
 Wronski J.: *C-1046, C-1060*
 Wu E.: *C-0073*
 Wu E.X.: *B-642*
 Wu H.: *C-0598*
 Wu R.H.: *B-015, B-919*
 Wu R.H.: *C-1027*
 Wu T.H.: *C-0412*
 Wu Z.: *B-535, B-643*
 Wucherer M.: *B-778*
 Wülfing C.: *B-785*
 Wunderbalddinger P.: *A-326*
 Wunderlich A.: *B-827*
 Wurdinger S.: *B-263, B-372*
 Wuttge-Hannig A.C.: *B-808, B-809, B-812*
 Wykret M.: *C-0080*
-
- X**
- Xasiotou M.: *C-0934*
 Xiao G.: *C-0375*
 Xiao Z.W.: *C-1027*
 Xie Y.: *B-040*
 Xin M.: *D-12*
 Xinou E.: *C-0826*
 Xu D.M.: *B-381*
 Xu J.: *B-040*
 Xu P.: *B-328, B-856*
 Xue H.: *B-303*
 Xydeas T.: *B-157, B-587*
 Xydis V.G.: *B-646*
-
- Y**
- Yachia D.: *B-874*
 Yagci B.: *C-0526*
 Yagci C.: *C-0478, C-0500*
 Yagmurlu B.: *C-0819, C-0852, C-0878*
 Yakan N.: *D-10*
 Yalfimov A.N.: *C-0247, C-0847*
 Yalinkılıç E.: *C-0426*
 Yamada R.: *C-0615*
 Yamada T.: *C-0651*
 Yamagishi T.: *C-0356*
 Yamaguchi I.: *B-775*
 Yamaguchi M.: *C-0380*
 Yamaguchi T.: *C-0662, C-0709*
 Yamaki T.: *C-0651*
 Yamamoto A.: *C-0940*
 Yamamoto A.: *C-0348, C-0350, C-0615*
 Yamamoto K.: *C-0308*
 Yamamoto N.: *C-0283*
 Yamamoto S.: *C-0532*
 Yamamoto S.: *C-0020*
 Yamamoto T.: *C-0566*
 Yamamoto W.: *C-0651*
 Yaman Ö.: *C-0477, C-0487, C-0488*
 Yamanouchi E.: *C-0608*
 Yamaoka T.: *C-0965, C-1054*
 Yamashita E.: *C-0430*
 Yamashita T.: *C-0940*
 Yamashita Y.: *C-0381*
 Yan F.: *B-042, B-328, B-856*
 Yanagawa N.: *C-0163, C-1007*
 Yanagihara M.: *C-0147*
 Yanagimachi N.: *C-1035*
 Yang C.C.: *C-0412*
-
- Z**
- Zaalberg W.: *B-452*
 Zabakis P.: *B-908, C-0855, C-0883*
 Zabala R.: *C-0752*
 Zabek M.: *C-0572*
 Zaborowski G.: *C-0842*
 Zacherl J.: *B-011, B-012*
 Zagdanski A.-M.: *C-0344, C-0459*
 Zähringer M.: *A-257*

List of Authors and Co-authors

Zaleska-Dorobisz U.: *C-0148, C-0892, C-0911, C-0923*
Zaloff Dakoff J.: *C-0821*
Zamboni G.: *B-607, C-0026*
Zampa V.: *B-461, B-558, B-850, C-0708, C-0728*
Zampedri M.: *B-059*
Zander T.: *B-514, C-0578*
Zandriño F.: *C-0112*
Zanetti M.: *A-209, B-351*
Zang C.H.: *B-015*
Zang P.: *B-535*
Zangan S.M.: *C-0124*
Zangos S.: *B-009, B-302, B-340, B-345, B-401, B-405, B-410, B-500, B-504, B-507, B-875, B-877*
Zankl M.: *B-446*
Zaporozhan J.: *B-472, B-704, B-705, C-1000*
Zappa M.: *B-798*
Zarcero M.: *C-0928*
Zarifi M.: *C-0931, C-0934*
Zaspel U.: *B-032*
Zatloukal P.: *B-841*
Zatttoni L.: *B-636*
Zauner M.: *C-0792*
Zavadovskaja V.D.: *C-0664, C-0700*
Zavaglia C.: *B-501*
Zavras G.M.: *C-1009*
Zayceva A.J.: *B-438*
Zaytsev V.V.: *C-0519*
Zbaeren P.: *B-189*
Zbidi M.: *C-0312, C-0313*
Zdunek P.: *C-0080, C-0374*
Zealley I.: *B-866*
Zech C.: *B-050*
Zech C.J.: *B-574, B-851*
Zeka J.: *B-117*
Zelger B.: *C-0225*
Zeng H.: *B-095*
Zeng M.: *B-042*
Zeng X.: *B-328, B-856*
Zenge M.O.: *B-404*
Zenk J.: *B-052*
Zero I.: *B-514, C-0578*
Zerr I.: *B-096*
Zeytunlu M.: *C-0033*
Zhabina R.M.: *C-0848*
Zhai R.: *B-197*
Zhang D.: *B-673*
Zhang H.X.: *B-209*
Zhang L.: *A-432*
Zhang S.: *B-347*
Zhang Y.: *C-0781*
Zhang Z.: *B-303, B-347*
Zhao X.: *B-424, B-826*
Zhernosekov K.P.: *C-0408*
Zhou C.: *B-681*
Zhou X.: *C-0261*
Zhou X.G.: *B-015*
Zhu H.: *C-0261*
Zhu X.-H.: *B-847*
Zidowitz S.: *D-09*
Ziegler F.: *B-341*
Ziegler S.: *B-924*
Zielinski Z.: *C-0868*
Zieniewicz K.: *C-0003*
Zierott L.: *B-166*
Zijlstra F.: *B-309, B-524, C-0275*
Zikou A.: *B-560*
Zikou A.G.: *B-646*
Zimmermann F.: *B-146*
Zini M.: *B-290, B-628, C-0620, C-0636*
Zink M.: *D-08*
Zivkovic M.: *C-0812*
Ziyeh S.: *B-763*

List of Authors and Co-authors

List of Moderators

A

Adam E.J.: SS 608
 Adam G.B.: SS 310
 Akata D.: SS 301b
 Akyar S.: RC 1704
 Alfke H.: PR 419
 Allison D.J.: WS 818
 Anderson S.: SS 1010
 Armstrong P.: SS 204
 Aspelin P.: SS 707, SY 10
 Azarine A.A.: SS 615

B

Babnik Peskar D.: RC 507
 Bachmann Nielsen M.: SS 301a
 Bader T.: SS 1001
 Barentsz J.O.: SA 14
 Bartolozzi C.: SA 12
 Batakis N.: RC 1709
 Bautz W.: RC 1613
 Bekiesinska-Figatowska M.: SS 1807a
 Bellin M.-F.: RC 106
 Bellomi M.: RC 104
 Bertolotto M.: SS 1807b
 Besenski N.: CC 517
 Besim A.: RC 909
 Bezzu M.: SS 709
 Bigot J.-M.: SS 1409b
 Bilecen D.: SS 215
 Biscaldi E.: SS 1801a
 Björkman-Burtscher I.M.: SF 17, SS 311
 Blickman J.G.: RC 1612, SY 6
 Bongartz G.M.: SY 5
 Bonneville F.: SS 711
 Bonneville J.-F.: SS 611
 Bonomo L.: RC 1604, SY 9
 Boric I.: SS 710
 Boudghène F.P.: SS 715
 Bremer C.: RC 901
 Brennan P.: CC 1317
 Brountzos E.: RC 509
 Brüning R.D.: CC 116
 Brzowski M.: SS 1812
 Buchberger W.: SS 1502

C

Cáceres J.: SF 9a, E³ 820
 Canet Soulas E.: SS 1506b
 Capotondi C.: SS 1409a
 Carmella D.: EF 1, RC 1205, E³ 220a
 Carette M.-F.: CC 416
 Castelijns J.A.: RC 408
 Catalano C.: RC 1215, SS 306
 Chalaoui J.: SS 1404
 Chalazonitis A.N.: SS 1806
 Chevrot A.: SS 310
 Chiesa A.: EM 1, EM 2, EM 3, HL 1, HL 2, HL 3
 Choe Y.H.: SS 203
 Choi B.I.: SS 1001
 Christofides S.: EF 1
 Cieszanowski A.: RC 801
 Claudon M.: RC 1312
 Claussen C.D.: SS 1501a
 Clément O.: RC 1306
 Cognard C.: CC 117
 Copley S.J.: E³ 520
 Couldeau R.: RC 403
 Coutinho D.: SS 208
 Crockford M.: SS 210

Croisille P.: SS 203
 Cuzino D.: SS 608

D

Dalla Palma F.: EM 1
 Dalla Palma L.: SS 1407
 Damilakis J.: EF 2
 De Cobelli F.: SS 303
 de Haan M.W.: RC 515
 de Roos A.: SF 12
 Del Maschio A.: SS 201a
 Desai S.R.: SS 1504
 Devir D.: SY 8
 Diekmann F.: SS 202
 Dimopoulos P.A.: RC 508
 Dixon A.K.: E³ 620a
 Donoghue V.: RC 1214
 Düber C.: WS 1209
 Duceux D.: CC 817

E

Efremidis S.C.: SF 4b
 Egger M.: SY 15
 Eggelsøe H.B.: RC 1608
 Eklund K.: RC 1214
 Elmas N.: SS 1501b
 Ene V.: SS 704
 Erikson U.: SS 1806
 Essig M.: SS 211
 Everse L.: E³ 620b

F

Fabiano S.: SS 1501b
 Fattori R.: RC 1703
 Fausto A.: SS 1402
 Felber A.: SS 1511
 Fenlon H.: SS 701a
 FitzGerald R.: E³ 1020
 Fleischmann D.: E³ 720
 Forgács B.: SS 1810
 Forrai G.: RC 502
 Frauscher F.: SY 1
 Frost R.A.: RC 1701
 FuchsJäger M.H.: SS 301a
 Fujioka M.: RC 1212
 Funovics M.A.: SS 709

G

Galanski M.: SF 8b
 García Figueiras R.: SS 1407
 Garcia-Mónaco R.D.: SS 1009a
 Gattinoni L.: SF 8a
 Geers-van Gemeren S.: RC 1314
 Ghaye B.: SS 1404
 Ghoklar A.: SS 1511
 Given-Wilson R.: SS 1802
 Gleeson F.: SS 704
 Glücker T.: SS 1501a
 Gödeny M.: CC 916
 Golebiowski M.: RC 1314
 Góraj B.: CC 1217
 Gotwald T.F.: SS 308
 Gouliamis A.D.: SS 211
 Gourtsoyannis N.: SF 13
 Grenier P.A.: ER 126
 Gunny R.: SS 1412
 Günther R.W.: SS 609b

H

Hadjidekov G.: SS 1010
 Hájek M.: SS 1813
 Hamm B.: SS 1807a
 Harris K.: SS 201a
 Hartvig Sode A.: RC 1714
 Hatabu H.: SS 1004
 Hatzidakis A.: SS 609b
 Hawkes D.J.: SS 1513
 Healey A.E.: SS 1409b
 Heuser L.: RC 504
 Heywang-Köbrunner S.H.: RC 102
 Ho K.Y.: WS 1615
 Holland R.: SS 1502
 Howarth N.: SS 204
 Hricak H.: SS 1007
 Huber S.: SS 1814
 Huismann T.A.G.M.: RC 912
 Hur G.: CC 917
 Hurley G.D.: SS 305
 Husband J.E.: SS 701b

I

Imhof H.: RC 810
 Ishigaki T.: EM 3

J

Jager G.: RC 807
 Jäger L.: SS 208
 Jargiello T.: SS 715
 Jevtic V.: RC 1610
 Joffre F.G.: SS 1809
 Johansson E.: SS 1506b

K

Kabala J.E.: RC 108
 Kachelrieß M.: RC 913
 Kakhadze S.: SS 201b
 Kalender W.A.: SS 713
 Kämmerer M.: SS 305
 Karani J.B.: WS 418
 Karlinger K.: RC 811
 Karmazanovsky G.G.: SS 1801b
 Kauczor H.-U.: RC 804
 Kekelidze M.: SS 707
 Keleakis D.A.: SS 1009a
 Kettenbach J.: SS 205
 Khong P.-L.: SS 1412
 Kinkel K.: SS 702
 Klose K.-J.: RC 405, SF 1
 Köcher M.: SS 1809
 Kolmannskog N.: RC 1614, SY 4
 Kopp A.F.: RC 1203
 Kramer J.: SS 602
 Krestan C.: SS 610
 Krestin G.P.: ER 926, SF 5, E³ 320
 Kuligowska E.: RC 107

L

Labuscagne J.: SS 711
 Lamb H.J.: SS 1506a
 Laméris J.S.: RC 401
 Laniado M.: SS 306
 Larsson E.-M.B.: SS 1011
 Leconte I.: SS 602
 Lee M.J.: NH 6
 Leidecker C.: SS 1513

List of Moderators

Leonardi M.: *RC 911*

Liermann D.: *WS 1718*

Lim T.-H.: *SS 1803*

Lincender L.: *RC 1301*

Link T.M.: *SS 610*

Livadas G.: *SF 4c*

Lombay B.: *EM 2*

Loose R.W.R.: *SS 1013*

Luciani A.: *SS 1406*

Lucic M.A.: *CC 516*

Lucidarme O.: *SS 1401b*

M

Magnusson A.: *RC 407*

Malone D.E.: *SS 301b*

Maly Sundgren P.C.: *RC 514*

Manelfe C.: *SS 1811a*

Marano R.: *SS 703a*

Marchal G.: *RC 1313*

Marcinski A.J.: *SS 1807b*

Marincek B.: *RC 101*

Maris T.G.: *RC 1213*

Marsot-Dupuch K.: *RC 1708*

Martí-Bonmatí L.: *SS 201b*

Masterson J.: *SS 1804*

Mastorakou I.: *SS 703a*

Matsunaga N.: *SS 615*

Mazonakis M.: *SS 713*

McCall I.W.: *ER 526*

McCloud T.: *E³ 920*

Meaney J.F.M.: *SY 2*

Mechl M.: *SS 1510*

Metz V.M.: *RC 110*

Milne E.N.C.: *SY 13*

Montag B.: *SY 12*

Morcos S.K.: *RC 1614*

Morgan R.: *WS 118*

Mostbeck G.: *SS 1004*

Moussa S.: *SS 1507*

Mueller P.R.: *SS 1409a*

Müller-Hülsbeck S.: *SS 315*

Müller-Schimpfle M.: *SS 1402*

Musset D.: *SF 16*

N

Nakstad P.H.: *RC 111*

Napoli G.: *SS 1009b*

Natale L.: *SS 1403*

Neri E.: *SS 205*

Neuwirth J.: *CC 417*

Noel A.: *SS 1413*

Nyhsen C.: *JRF Highlighted lectures*

O

Oleaga Zufiría L.: *SS 308*

Olsen F.: *RC 514*

Orsi F.: *SS 309a*

Østergaard L.: *SS 611*

Østergaard M.: *SS 1410*

Ostlere S.: *SS 1810*

Otto R.C.: *RC 1302*

Oudkerk M.: *RC 803*

P

Padrón M.: *RC 910*

Palkó A.: *RC 501*

Pallardó Y.: *RC 1204*

Papathanassiou M.: *RC 411*

Pasowicz M.: *SS 303*

Passariello R.: *PR 1219*

Patel U.: *WS 918*

Pavia M.: *SS 609a*

Pavlica P.: *RC 1307*

Pediconi F.: *SS 702*

Peh W.C.G.: *SS 1510*

Petsas T.: *SS 1504*

Pettersson H.: *SS 1410*

Pohjonen H.: *SY 3*

Prassopoulos P.K.: *SS 701b*

Prayer D.: *SS 311*

Pringot J.: *SS 1801a*

Puig Domingo J.: *SS 701a*

R

Rafaelsen S.: *SF 4a*

Ramón Fortuño J.: *SS 209b*

Ramos I.M.: *RC 1602*

Ranschaert E.R.: *E³ 220b*

Reekers J.A.: *NH 10*

Reiser M.F.: *SA 2, SY 7, SY 9*

Rettenbacher T.: *SY 14*

Revel D.: *SS 304*

Riedl C.C.: *SS 302*

Rienmüller R.: *SS 603*

Ringertz H.: *SS 1512*

Roche C.: *SS 1814*

Rosset A.: *SS 605*

Roy C.: *SS 1507*

Rozanes I.: *WS 1609*

Rummenny E.J.: *SS 1506a*

S

Sasiadek M.: *CC 1617*

Sato M.: *RC 1309*

Schaefer-Prokop C.: *E³ 420*

Schick F.: *SS 1413*

Schmidt S.: *SS 1401a*

Semelka R.C.: *SS 1401a*

Semmler W.: *SS 1406*

Sener N.: *RC 1311*

Shahabpour M.: *SS 710*

Silberman B.: *ER 1326*

Skaane P.: *SS 302*

Sorantin E.: *RC 1712*

Sprindrich J.: *SS 210*

Spüntrup E.: *SS 1403*

Staatz G.: *SS 1512*

Stajgis M.: *SS 1015*

Steinke K.: *SS 1804*

Stojanovska J.: *SS 1011*

Strecker E.-P.K.: *SS 309a*

Strickland N.H.: *SF 9b*

Stringaris K.A.: *SS 1801b*

Struyven J.L.: *SS 215*

Stukalova O.: *SS 1803*

Sunaert S.: *SS 1811b*

Svane G.: *RC 902*

Szczerbo-Trojanowska M.: *SS 309b*

T

Tacke J.: *SS 309b*

Tan L.K.A.: *WS 1715*

Tanus Hajj J.: *SS 1401b*

Tardivon A.: *SS 202*

ter Haar Romeny B.M.: *E³ 1420, EF 2*

Tervonen O.: *SS 609a*

Theocharopoulos N.: *SS 1013*

Thurnher M.M.: *RC 1211*

Thurnher S.A.: *SS 1009b*

Torres Tabanera M.: *SS 1802*

Tscholakoff D.: *SS 703b*

Tsetis D.K.: *SS 209a*

Tuma S.: *SS 1003*

Turóczy G.: *JRF Highlighted lectures*

V

van den Hauwe L.: *CC 1717*

van Ooijen P.M.A.: *SS 603*

van Waes P.F.G.M.: *RC 1714*

Vande Berg B.: *RC 510*

Vergesslich K.A.: *RC 1711*

Verstraete K.: *CC 816*

Villeirs G.M.: *SS 1007*

Vlahos L.: *SS 315*

Vock P.: *E³ 120*

Vogl T.J.: *E³ 1320*

Vulev I.P.: *SS 209a*

W

Walchenbach J.: *SY 16*

Walecki J.: *RC 813*

Wein B.B.: *SS 605*

Weishaupt D.: *RC 1310*

Wetzel S.: *SS 1811a*

Willems T.P.: *SS 703b*

Willi U.V.: *SS 1812*

Willmann J.K.: *SS 1015*

Wilson D.J.: *E³ 1520*

Winkels G.: *SY 11*

Wintersperger B.J.: *SS 1003*

Wirestam R.: *SS 1813*

Wormanns D.: *SS 304*

Wunderbaldinger P.: *PR 819*

Y

Yamada R.: *SS 209b*

Z

Zanella F.E.: *SS 1811b*

Zanetti M.: *RC 1710*

Zylak C.J.: *E³ 1220*

Notes
